SANDIA REPORT

SAND92–0700/1 • UC–721
Unlimited Release
Printed December 1992

Preliminary Performance Assessment for the Waste Isolation Pilot Plant, December 1992

Volume 1: Third Comparison with 40 CFR 191, Subpart B

WIPP Performance Assessment Department

Prepared by
Sandia National Laboratories
Albuquerque, New Mexico 87185 and Livermore, California 94550
for the United States Department of Energy
under Contract DE-AC04-76DP00789

Issued by Sandia National Laboratories, operated for the United States Department of Energy by Sandia Corporation.

Available to DOE and DOE contractors from
Office of Scientific and Technical Information
PO Box 62
Oak Ridge, TN 37831

Prices available from (615) 576-8401, FTS 626-8401

Available to the public from
National Technical Information Service
US Department of Commerce
5285 Port Royal Rd
Springfield, VA 22161

NTIS price codes
Printed copy: A10
Microfiche copy: A01

SAND92-0700/1
Unlimited Release
Printed December 1992

Distribution
Category UC-721

Preliminary Performance Assessment for the Waste Isolation Pilot Plant, December 1992

Volume 1: Third Comparison with 40 CFR 191, Subpart B

WIPP Performance Assessment Department
Sandia National Laboratories
Albuquerque, New Mexico 87185

ABSTRACT

Before disposing of transuranic radioactive wastes in the Waste Isolation Pilot Plant (WIPP), the United States Department of Energy (DOE) must evaluate compliance with applicable long-term regulations of the United States Environmental Protection Agency (EPA). Sandia National Laboratories is conducting iterative performance assessments of the WIPP for the DOE to provide interim guidance while preparing for final compliance evaluations.

This volume contains an overview of WIPP performance assessment and a preliminary comparison with the long-term requirements of the *Environmental Radiation Protection Standards for Management and Disposal of Spent Nuclear Fuel, High-Level and Transuranic Radioactive Wastes (40 CFR 191, Subpart B)*. Detailed information about the technical basis for the preliminary comparison is contained in Volume 2. The reference data base and values for input parameters used in the modeling system are contained in Volume 3. Uncertainty and sensitivity analyses related to 40 CFR 191B are contained in Volume 4. Volume 5 contains uncertainty and sensitivity analyses of gas and brine migration for undisturbed performance. Finally, guidance derived from the entire 1992 performance assessment is presented in Volume 6.

Results of the 1992 performance assessment are preliminary, and are not suitable for final comparison with 40 CFR 191, Subpart B. Portions of the modeling system and the data base remain incomplete, and the level of confidence in the performance estimates is not sufficient for a defensible compliance evaluation. Results are, however, suitable for providing guidance to the WIPP Project.

All results are conditional on the models and data used, and are presented for preliminary comparison to the Containment Requirements of 40 CFR 191, Subpart B as mean complementary cumulative distribution functions (CCDFs) displaying estimated probabilistic releases of radionuclides to the accessible environment. Results compare three conceptual models for radionuclide transport in the Culebra Dolomite Member of the Rustler Formation and two approaches to estimating the probability of inadvertent human intrusion into the WIPP by exploratory drilling. The representation for disposal-system performance believed to be most realistic includes intrusion probabilities based on expert-panel judgment and dual-porosity transport with chemical retardation. For intrusions occurring 1000 years after decommissioning, the mean CCDF for this representation lies more than one order of magnitude below the EPA limits. Using the same approach to intrusion probabilities used in the 1991 performance assessment (i.e., not taking expert judgment into account and basing the probability model on the maximum intrusion probability indicated in Appendix B of 40 CFR 191, Subpart B) significantly increases the probability of releases, regardless of the model used for subsurface transport. Assuming the higher intrusion probabilities and dual-porosity transport without chemical retardation, the mean CCDF is approximately one order of magnitude below the EPA limits. For the higher intrusion probabilities and single-porosity, fracture-only transport, the mean CCDF is less than one order of magnitude below the EPA limits.

This volume of the report should be referenced as:

WIPP PA (Performance Assessment) Department. 1992. ***Preliminary Performance Assessment for the Waste Isolation Pilot Plant, December 1992—Volume 1: Third Comparison with 40 CFR 191, Subpart B***. SAND92-0700/1. Albuquerque, NM: Sandia National Laboratories.

ACKNOWLEDGMENTS

The Waste Isolation Pilot Plant (WIPP) Performance Assessment (PA) Department is comprised of both Sandia National Laboratories (SNL) and contractor employees working as a team to produce preliminary comparisons with Environmental Protection Agency (EPA) regulations, assessments of overall long-term safety of the repository, and interim technical guidance to the program. The on-site team, affiliations, and contributions to the 1992 performance assessment are listed in alphabetical order:

Performance Assessment Department

Name	Affil.*	Primary Author of Major Code	Area of Responsibility
R. Anderson	SNL		Department Manager
B. Baker	TEC		SECO2D, Hydrology, Office Manager
J. Bean	UNM		BRAGFLO, 2-Phase Flow
J. Berglund	UNM	CUTTINGS	Task Ldr., Cuttings/Cavings/ Spallings, Engr. Mech.
S. Bertram-Howery	SNL		PA Liaison with DOE, Criteria Document, Test Phase Plan
W. Beyeler	SAI	PANEL, GARFIELD	Geostatistics, Analytical Models, CAMCON Systems Codes
K. Brinster	SAI		Geohydrology, Conceptual Models
R. Blaine	ECO		SECO2D, SECOTP, & CAMCON Systems Codes
T. Blaine	GC		Drilling Technology, Exposure Pathways Data
K. Byle	UNM		Software and Analysis QA
J. Chapman	TRI		Documentation V.3
D. Duncan	MAC		Data QA
K. Economy	ECO		SECO2D, SECOTP, Hydrology &
D. Gallegos	SNL		Transport Task Ldr., Hydrology, Geostatistics, NEA, PSAG
D. Galson	GS		NEA Working Groups, PSAG, PAAG, Human Intrusion
J. Garner	API	PANEL	Source Term, Sens. Anal.
A. Gilkey	UNM		CAMCON Systems Codes
L. Gomez	SNL		Task Ldr., Safety Assessments
M. Gruebel	TRI		EPA Regulations, Documentation V.1, Editor V.1
R. Guzowski	SAI		Geology, Scenario Construction
J. Helton	ASU	CCDFPERM	Task Ldr., Uncert./Sens. Anal., Probability Models, Editor V.4
S. Hora	UHH		Expert Elicitation, Probability Models
H. Iuzzolino	GC	CCDFCALC CCDFPERM	LHS, CAMCON System Codes, Probability Models
R. Klett	SNL		EPA Regulations
P. Knupp	ECO	SECOTP	Comp. Fluid Dyn.
M. LaVenue	INT	GRASP-INV	Hydrology/Geostatistics
C. Leigh	SNL	GENII-S	Exposure Pathways

M. Marietta	SNL		Dep. Dept. Manager, Tech. Coord.
G. de Marsily	UP		Geostatistics Expert Group Chair
R. McCurley	UNM		CAMCON System Codes
B. Napier	PNL	GENII	Safety Assessments
A. Peterson	SNL		Task Ldr., Inventory
B. RamaRao	INT	GRASP-INV	Geostatistics
J. Rath	UNM		CAMCON System Codes
R. Rechard	SNL		Task Ldr., CAMCON, QA
P. Roache	ECO	SECO	Task Ldr., Comp. Fluid Dyn.
D. Rudeen	UNM		STAFF2D, SECOTP, Transport
J. Ruge	ECO		Multigrid Methods/BRAGFLO
T. Russell	ECO		Upscaling
K. Salari	ECO	SECOTP	Transport, Computational Fluid Dynamics
J. Sandha	SAI		INGRES, PA Data Base
J. Schreiber	SAI		BRAGFLO, 2-Phase Flow
D. Scott	TRI		Documentation V.2
P. Swift	TRI		Task Ldr., Geology, Climate Var., Documentation V.1 & 2, Editor V.1, 2, 4, & 5
M. Tierney	SNL		Task Ldr., CDF Constr., Probability Models, Ref. Data, Editor V.2 & 3
K. Trauth	SNL		Task Ldr., Expert Panels
P. Vaughn	API	BRAGFLO	Task Ldr., 2-Phase Flow & Waste Panel Chemistry, Editor V. 4 & 5
T. Zimmerman	GRA		Geostatistics Test Problem

The foundation of the annual WIPP performance assessment is the underlying data set and understanding of the important processes in the engineered and natural barrier systems. Other SNL Departments are the primary source of these data and understanding. Assistance with the waste inventory comes from Westinghouse Electric Corporation and its contractors. We gratefully acknowledge the support of our departmental and project colleagues. Some individuals have worked closely with the performance assessment team, and we wish to acknowledge their contributions individually:

H. Batchelder	WEC	CH & RH Inventories
R. Beauheim	SNL	Natural Barrier System, Hydrologic Parameters
D. Borns	SNL	Geology, Geophysics
B. Butcher	SNL	Engineered Barrier System, Unmodified Waste-Form Parameters, Disposal Room Systems Parameters
L. Brush	SNL	Engineered Barrier System, Source Term (Solubility) and Gas Generation Parameters
L. Clements	ReS	Computer System Support
T. Corbet	SNL	Natural Barrier System, Geologic & Hydrologic Parameters, Conceptual Models
P. Davies	SNL	Natural Barrier System, Hydrologic & Transport Parameters, & 2-Phase Flow Mechanistic Modeling
P. Drez	DE	CH & RH Inventories
R. Finley	SNL	Repository Isolation Systems Parameters
F. Gelbard	SNL	Natural Barrier System, Retardation

E. Gorham	SNL	Natural Barrier System, Fluid Flow & Transport Parameters
R. Holt	CON	Geology
S. Howarth	SNL	Natural Barrier System, Hydrologic Parameters
R. Kehrman	WEC	CH & RH Waste Characterization
K. Lickliter	BEC	EPA Regulations
R. Lincoln	SNL	Room Modeling
F. Mendenhall	SNL	Engineered Barrier System, Unmodified Waste Form Parameters, Waste Panel Closure (Expansion)
D. Munson	SNL	Reference Stratigraphy, Constitutive Models, Physical & Mechanical Parameters
C. Novak	SNL	Natural Barrier Systems, Chemistry
E. Nowak	SNL	Room Modeling, Source Term
J. Orona	ReS	Computer System Support
A. Stevens	SNL	DOE Liaison
J. Tillerson	SNL	Repository Isolation Systems Parameters
W. Wawersik	SNL	Fracturing
S. Webb	SNL	2-Phase Flow Sensitivity Analysis & Benchmarking

* Affiliation

API = Applied Physics Incorporated
ASU = Arizona State University
BEC = Benchmark Environmental Corp.
CON = Consultant
DE = Drez Environmental
ECO = Ecodynamics Research Associates
GC = Geo-Centers Incorporated
GRA = GRAM, Inc.
GS = Galson Sciences
INT = Intera
MAC = MACTEC
PNL = Pacific Northwest Laboratory
ReS = ReSpec
SAI = Scientific Applications International Corporation
SNL = Sandia National Laboratories
TEC = Technadyne Engineering Consultants
TRI = Tech Reps, Inc.
UHH = University of Hawaii at Hilo
UNM = Univ. of New Mexico/New Mexico Engineering Research Institute
UP = University of Paris
WEC = Westinghouse Electric Corporation

Peer Review

Internal/Sandia

A. Lappin
D. Schafer

Management/Sandia

W. Weart

PA Peer Review Panel

R. Heath, Chair	University of Washington
R. Budnitz	Future Resources Associates, Inc.
T. Cotton	JK Research Associates, Inc.
J. Mann	University of Illinois
T. Pigford	University of California, Berkeley
F. Schwartz	Ohio State University

Department of Energy

R. Becker

Expert Panels

Futures

M. Baram	Boston University
W. Bell	Yale University
G. Benford	University of California, Irvine
D. Chapman	The World Bank, Cornell University
B. Cohen	University of Pittsburgh
V. Ferkiss	Georgetown University
T. Glickman	Resources for the Future
T. Gordon	Futures Group
C. Kirkwood	Arizona State University
H. Otway	Joint Research Center (Ispra), Los Alamos National Laboratory
M. Pasqualetti	Arizona State University
D. Reicher	Natural Resources Defense Council
N. Rosenberg	Resources for the Future
M. Singer	The Potomac Organization
T. Taylor	Consultant
M. Vinovski	University of Michigan

Markers

D. Ast	Cornell University
V. Baker	University of Arizona
M. Brill	Buffalo Organization for Social and Technological Innovation
F. Drake	University of California at Santa Cruz
B. Finney	University of Hawaii at Manoa
D. Givens	American Anthropological Association
W. Goodenough	University of Pennsylvania
M. Kaplan	Eastern Research Group
J. Lomberg	Consultant
L. Narens	University of California at Irvine
F. Newmeyer	University of Washington
W. Sullivan	University of Washington
W. Williams	Case Western Reserve University

Source Term

C. Bruton	Lawrence Livermore National Laboratory
I-Ming Chou	U.S. Geological Survey
D. Hobart	Los Alamos National Laboratory
F. Millero	University of Miami

Retardation

R. Dosch	Sandia National Laboratories
C. Novak	Sandia National Laboratories
M. Siegel	Sandia National Laboratories

Geostatistics Expert Group

G. de Marsily, Chair	U. of Paris
R. Bras	Massachusetts Inst. of Tech.

J. Carrera	U. Politécnica de Cataluña
G. Dagan	Tel Aviv U.
A. Galli	Ecole des Mines de Paris
S. Gorlick	Stanford U.
P. Grindrod	Intera Sciences
A. Gutjahr	New Mexico Tech.
D. McLaughlin	Massachusetts Inst. of Tech.
S. Neuman	U. of Arizona
C. Ravenne	Institut Français du Pétrole
Y. Rubin	U. of California, Berkeley

Report Preparation (TRI)

Editors:

Volume 1: M. Minahan (text); D. Marchand (illustrations)
Volume 2: M. Minahan (text); D. Marchand (illustrations)
Volume 3: J. Chapman (text); D. Pulliam (illustrations)

D. Rivard and the Word Processing Department
R. Rohac, R. Andree, and the Illustration and Computer Graphics Departments
S. Tullar and the Production Department

PREFACE

The *Preliminary Performance Assessment for the Waste Isolation Pilot Plant, December 1992* is currently planned to consist of six volumes. The titles of the volumes are listed below. This report is the third in a series of annual reports that document ongoing assessments of the predicted long-term performance of the Waste Isolation Pilot Plant (WIPP); this documentation will continue during the WIPP Test Phase. However, the Test Phase schedule and projected budget may change; if so, the content of the *1992 Preliminary Performance Assessment* report and its production schedule may also change.

Volume 1: Third Comparison with 40 CFR 191, Subpart B

Volume 2: Technical Basis

Volume 3: Model Parameters

Volume 4: Uncertainty and Sensitivity Analyses for 40 CFR 191, Subpart B

Volume 5: Uncertainty and Sensitivity Analyses of Gas and Brine Migration for Undisturbed Performance

Volume 6: Guidance to the WIPP Project from the December 1992 Performance Assessment

TABLE OF CONTENTS

Figures

Tables

1. INTRODUCTION

The Waste Isolation Pilot Plant (WIPP) near Carlsbad, New Mexico, is a research and development project of the United States Department of Energy (DOE). The WIPP is authorized by Congress (Public Law 96-164, 1979) and is designed as a full-scale, mined geologic repository to demonstrate the safe management, storage, and disposal of transuranic (TRU) radioactive wastes generated by DOE defense programs since 1970. In addition to TRU radionuclides, the wastes may contain hazardous (nonradioactive) constituents. Before permanently disposing of radioactive wastes in the WIPP, the DOE must evaluate the repository based on various regulatory criteria for disposal of all the waste components, and the United States Environmental Protection Agency (EPA) must certify that compliance has been satisfactorily demonstrated.

Performance assessments will form the basis for evaluations of compliance with applicable long-term regulations of the EPA, including regulations pertaining to both radioactive and hazardous wastes (see Section 1.2 for a discussion of applicable regulations). This volume provides an overview of WIPP performance assessment and summarizes the December 1992 preliminary comparison with 40 CFR Part 191, Subpart B, which contains the long-term requirements of the *Environmental Radiation Protection Standards for Management and Disposal of Spent Nuclear Fuel, High-Level and Transuranic Radioactive Wastes* (US EPA, 1985). Results presented here are preliminary and are not suitable for final comparison with 40 CFR 191, Subpart B. Portions of the modeling system remain incomplete, and the level of confidence in the performance estimates is not sufficient for a defensible compliance evaluation. Results are suitable for providing interim guidance to the WIPP Project as it prepares for a final compliance evaluation.

Several DOE documents explain the relationship between long-term regulatory information needs and the experimental programs that will fill those needs. The *WIPP Test Phase Plan* (US DOE, 1990a, currently in revision) contains descriptions of experimental programs related to disposal room and drift systems (see also Section 2.4 of this volume and Volumes 2 and 3 of this report), TRU-waste experiments, sealing systems and rock mechanics, hydrology of and transport within the host rock for the WIPP, and flow and transport in rock layers surrounding the WIPP. For each experimental program, the document describes the relevant information needs identified by performance assessments (defined in Section 3.3.1 of this volume) and indicates how the program has been designed to fill those needs.

The technical needs for laboratory and field experiments involving TRU and TRU-mixed waste and simulated waste have been assessed (US DOE, 1992a). These tests are designed to provide information on two topics identified as important for evaluating regulatory compliance: generation of gas from degradation of TRU wastes (defined in Section 2.5.1 of this volume), and the concentration of radionuclides and hazardous constituents within disposal-room brine, both as dissolved species and as colloids.

Extensive laboratory and field studies conducted during the Site Characterization Phase for the WIPP have provided information used to date in performance assessments of the WIPP. References for these studies and discussion of how their results are used in performance assessments are provided in *WIPP Test Phase Activities in Support of Critical Performance Assessment (40 CFR 191 B) Information Needs* (US DOE, 1992b), which is a document prepared by the DOE for the National Academy of Sciences (NAS) WIPP Panel (referred to in Section 1.1.1 of this volume), and in other reports (Tyler et al., 1988; Lappin et al., 1989; US DOE, 1990a).

This report documents the third in a series of preliminary analyses of predicted long-term performance of the WIPP that Sandia National Laboratories (SNL) conducts for the DOE. Preparation for preliminary performance assessments began with the December 1989 *Draft Forecast of the Final Report for the Comparison to 40 CFR Part 191, Subpart B for the Waste Isolation Pilot Plant* (Bertram-Howery et al., 1989) and *Performance Assessment Methodology Demonstration: Methodology Development for Evaluating Compliance with EPA 40 CFR 191, Subpart B, for the Waste Isolation Pilot Plant* (Marietta et al., 1989). The 1990 report (Bertram-Howery et al., 1990) and two supporting volumes (Rechard et al., 1990a; Helton et al., 1991) presented preliminary results of evaluations that addressed only the long-term performance criteria for disposal specified in the radioactive-waste disposal standards (40 CFR 191, Subpart B, US EPA, 1985; see Chapter 3 and Appendix A of this volume). The 1991 version of the report (WIPP PA Division, 1991a,b,c; Helton et al., 1992) presented preliminary evaluations for comparison with the regulatory requirements of 40 CFR 191, Subpart B. A preliminary safety assessment that evaluates possible long-term consequences to the public health as a result of radioactive wastes emplaced in the WIPP is currently being prepared.

This 1992 report updates the preliminary results of the analyses included in the 1991 version of the report. Where data and models are available, the report presents preliminary results that preview a final report. With respect to the disposal of radioactive wastes, this 1992 report is a valid preview only to the extent that 40 CFR 191, Subpart B,

which was promulgated by the EPA in 1985 and remanded by a U.S. Appeals Court in 1987 (NRDC v. US EPA, 1987), is the same as the vacated 1985 version. This report treats the vacated portion of 40 CFR 191 as if it were still effective because the DOE and the State of New Mexico have agreed that compliance planning will continue on that basis until a new Subpart B is promulgated (US DOE and State of New Mexico, 1981, as modified). The *Waste Isolation Pilot Plant Land-Withdrawal Act* (Public Law 102-579, 1992), which mandates specific actions before the Test Phase for the WIPP can begin (see Section 1.1 of this volume), reinstates those portions of 40 CFR 191, Subpart B, that were not the subject of the 1987 remand and requires the EPA to repromulgate the regulation by April 30, 1993. The major quantitative requirement of the regulation addressed in this volume of the report is among those reinstated, and the methodology reported here has not been modified to reflect the EPA's efforts to develop a new Subpart B.

1.1 Description of the WIPP Project

The WIPP is located in semiarid rangeland in southeastern New Mexico. The nearest major population center is Carlsbad (population 25,000 in the 1990 U.S. census), 42 km (26 mi) west of the WIPP (Figure 1-1). Two smaller communities, Loving (population 1,500) and Malaga (population 150), are about 33 km (20 mi) to the southwest. Population density closer to the WIPP is very low; fewer than 30 permanent residents live within a 16-km (10-mi) radius. The nearest residents live 5.6 km (3.5 mi) south of the WIPP surface facility (US DOE, 1990b).

The surface of the land at the WIPP has been leased for cattle grazing. None of the ranches within 10 miles use well water for human consumption because the water contains large concentrations of total dissolved solids. Potash, oil, and gas are the only known important mineral resources. The surrounding area is used primarily for grazing, potash mining, and hydrocarbon exploration and production (US DOE, 1990b).

The WIPP repository is in bedded salt about 655 m (2,150 ft) below the land surface. The location was chosen because features of the regional and local geologic and hydrologic environment are expected to provide excellent natural barriers to radionuclide migration (see Chapter 2 of this volume and Volume 2 of this report).

The *Waste Isolation Pilot Plant Land Withdrawal Act* (Public Law 102-579, 1992) transferred ownership of 16 square miles (41 km^2) at the WIPP (Figure 1-2) from the U.S. Bureau of Land Management to the DOE. The boundary indicated as "WIPP" on illustrations in this volume is the

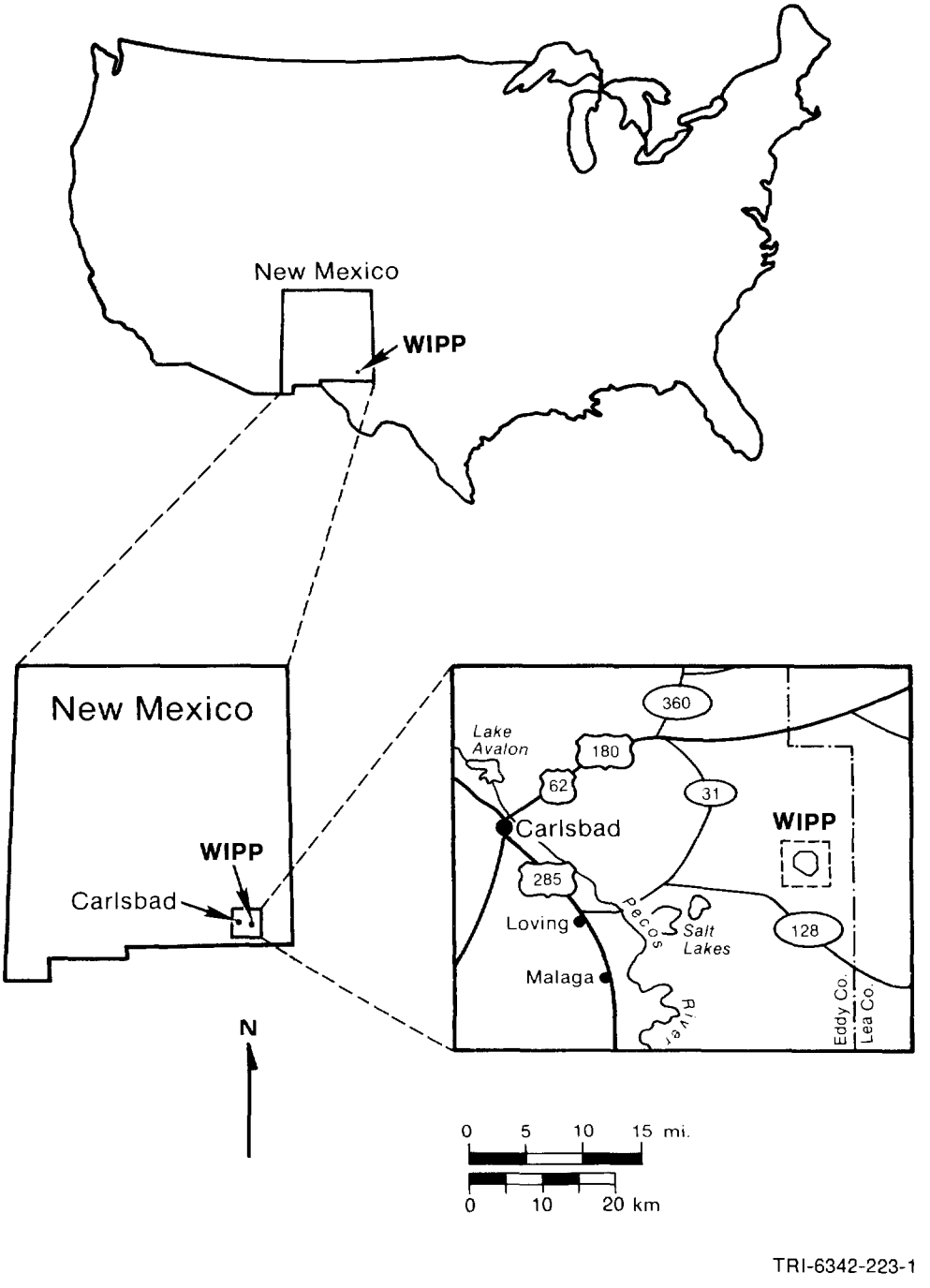

Figure 1-1. WIPP location map (after Bertram-Howery and Hunter, 1989a).

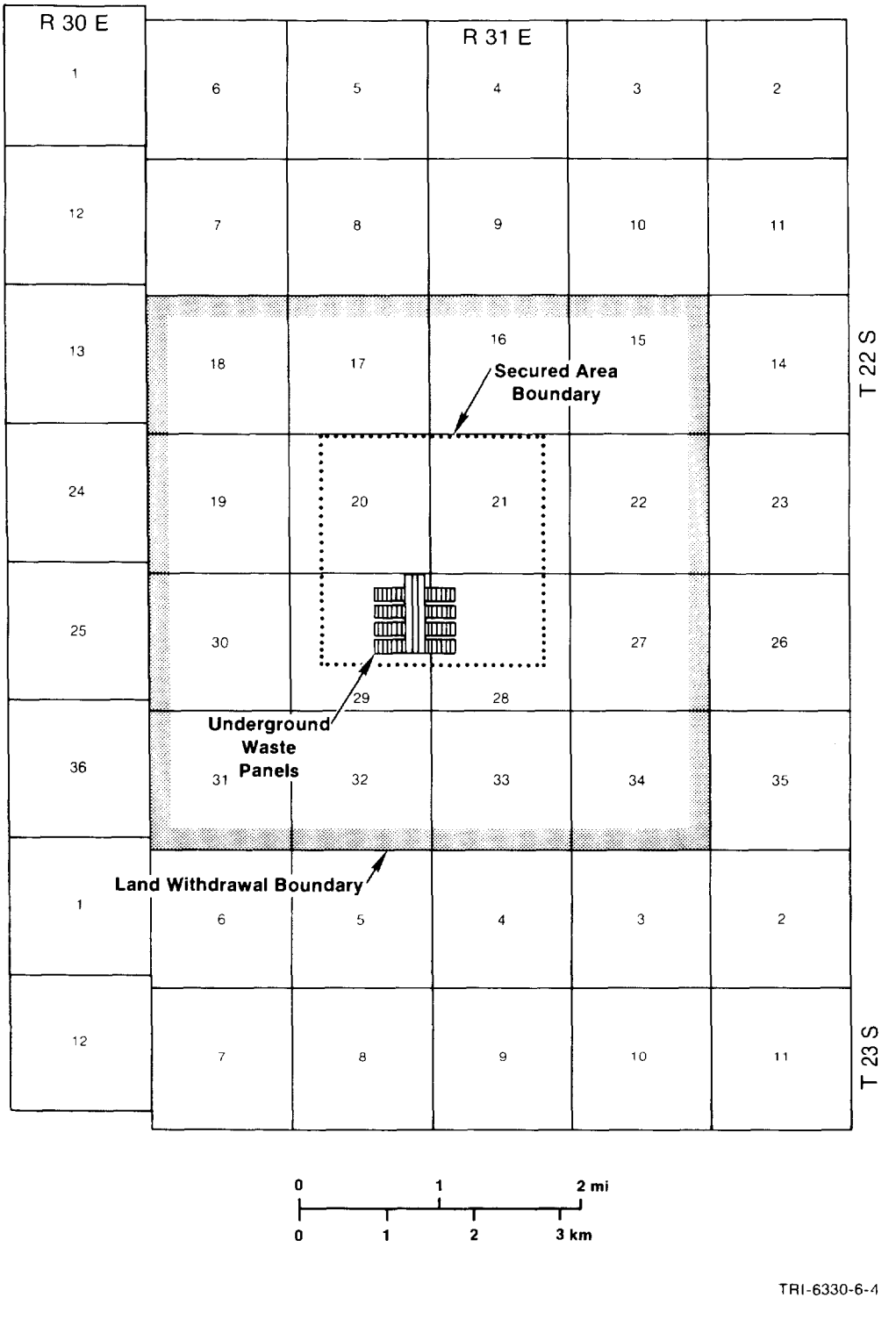

Figure 1-2. Position of the WIPP waste panels relative to WIPP boundaries and surveyed section lines (US DOE, 1989).

boundary of the land-withdrawal area. The legislation also outlined requirements for the Test and Disposal Phases of the WIPP.

The WIPP Test Phase is scheduled to begin when the following criteria, stated in the *WIPP Land Withdrawal Act* (Public Law 102-579, 1992, Section 6), are met: the final 40 CFR 191 regulation is issued and published in the *Federal Register*; the EPA has determined that the DOE has complied with the terms and conditions of the No-Migration Determination for the *Resource Conservation and Recovery Act* (RCRA) (see Section 1.2 of this volume); the EPA has approved the WIPP Test Phase plan and the waste-retrieval plan for the Test Phase; the U.S. Department of Labor has approved training programs for emergency response; the DOE has issued a plan to ensure the safety of Test Phase activities, including using mined rooms that are supported to assure safety during testing, and the Secretary of Labor has reviewed and concurred with the plan; and the DOE has agreed to provide to the EPA biennial performance-assessment reports during the Test Phase that document the analyses of long-term performance of the WIPP. Only EPA-approved transuranic waste in quantities no greater than 1/2 of 1 percent of the total capacity of the WIPP may be emplaced during the Test Phase. Remote-handled (RH) TRU waste (defined in Section 2.5.1 of this volume) may not be emplaced during the Test Phase.

As stated in the *WIPP Land Withdrawal Act* (Public Law 102-579, 1992, Section 7), the DOE may begin disposing of TRU waste in the WIPP when: the EPA has certified that the WIPP facility will comply with 40 CFR 191; the DOE has submitted to Congress plans for decommissioning the WIPP and post-decommissioning management; 180 days have elapsed after notice to Congress that the WIPP has met the provisions of 40 CFR 191, the *Clean Air Act*, the *Solid Waste Disposal Act*, the *Safe Drinking Water Act*, the *Toxic Substances Control Act*, the *Comprehensive Environmental Response, Compensation, and Liability Act of 1980*, and all other applicable Federal laws pertaining to public health and safety or the environment (including the *Resource Conservation and Recovery Act*, see Section 1.2.2); the DOE has acquired oil and gas leases specified by the EPA; the DOE has submitted to Congress comprehensive recommendations and a timetable for disposal of all DOE-controlled transuranic waste; and the DOE has completed a survey that identifies all TRU-waste types at all sites from which wastes are to be shipped to the WIPP.

1.1.1 Participants

The DOE implements the WIPP Project through the WIPP Project Integration Office (Albuquerque, NM), the WIPP Project Site Office (Carlsbad, NM), and its Headquarters in Washington, DC. The WIPP Project Offices are assisted

by two prime contractors: Waste Isolation Division (WID) of Westinghouse Electric Corporation (WEC) and Sandia National Laboratories (SNL). WID is responsible for all facility operations and for compliance with management and storage regulations. SNL, as the scientific program manager, is responsible for developing an understanding of the processes and systems that affect long-term isolation of wastes in the WIPP. That understanding is applied by SNL to the evaluation of the long-term performance of the repository. SNL defines and implements, subsequent to DOE approval, experiments both in laboratories and at the WIPP. In addition, SNL develops and applies models both to interpret experimental data and to assess the performance of the repository.

Federal agencies that provide oversight during the Test and Disposal Phases of the WIPP Project are the U.S. Mine Safety and Health Administration; the U.S. Bureau of Mines; the Occupational Safety and Health Administration; the National Institute for Occupational Safety and Health; and the U.S. Nuclear Regulatory Commission, which oversees transportation of waste to the WIPP.

The *WIPP Land Withdrawal Act* (Public Law 102-579, 1992) provides for review of the assessment of long-term repository performance:

> "The [DOE] shall publish, during the test phase, a biennial performance assessment report, consisting of a documented analysis of the long-term performance of WIPP. Each such report shall be provided to the State [of New Mexico], the [EPA], the National Academy of Sciences, and the EEG [Environmental Evaluation Group] for their review and comment.
>
> If, within 120 days of the publication of a performance assessment report under [the previous] paragraph, the State, the [EPA], the National Academy of Sciences, or the EEG provide written comments on the report, the [DOE] shall submit written responses to the comments to the State, the [EPA], the National Academy of Sciences, and the EEG, and to other appropriate entities or persons after consultation with the State, within 120 days of receipt of the comments" (Public Law 102-579, 1992, Section 6).

The DOE and the State of New Mexico have an Agreement for Consultation and Cooperation (US DOE and State of New Mexico, 1981, as modified). This agreement enables the State, through the Radioactive Waste Consultation Task Force and other agencies, to have an active part in assuring that public safety issues are addressed fully. The New Mexico Environment Department has authority concerning permitting in compliance with the RCRA (see Section 1.2).

The EPA's Office of Radiation and Indoor Air and Office of Solid Waste and Emergency Planning maintain a dialog with the WIPP Project concerning relevant issues. In addition, as explained in Section 1.1 of this volume, the *WIPP Land Withdrawal Act* gave the Administrator of the EPA specified responsibilities regarding approval of the Test and Disposal Phases for the WIPP.

Review of the scientific basis for the WIPP Project is provided by the National Research Council's (of the National Academy of Sciences) Board on Radioactive Waste Management's WIPP Panel.

The Environmental Evaluation Group (EEG) has provided oversight of the WIPP Project since before the WIPP's formal authorization in 1979. The EEG is responsible for independent technical evaluation of the WIPP with regard to the protection of public health and safety and the protection of the environment. Assignment of the EEG to the New Mexico Institute of Mining and Technology occurred with passage of the National Defense Authorization Act (Public Law 100-456, 1988).

Written comments from these reviewers, if provided, and responses about the annual performance assessment are published as Appendix B of this volume.

1.1.2 Wastes

The TRU wastes for which the WIPP is designed are defense-program wastes generated by United States government activities since 1970. The wastes consist of laboratory and production materials contaminated by certain TRU radionuclides and other radioactive and hazardous constituents. If approved, the following 10 DOE TRU-waste generator and/or storage sites are scheduled to ship TRU wastes to the WIPP: Idaho National Engineering Laboratory, Rocky Flats Plant, Hanford Reservation, Savannah River Site, Los Alamos National Laboratory, Oak Ridge National Laboratory, Nevada Test Site, Argonne National Laboratory-East, Lawrence Livermore National Laboratory, and Mound Laboratory (US DOE, 1990c). More information about the wastes scheduled for disposal in the WIPP are in Chapter 2 of this volume and Volume 3 of this report.

1.2 Regulatory Criteria for the WIPP

The EPA regulations applicable to the long-term performance of the WIPP include Subpart B of 40 CFR 191, promulgated in 1985 but remanded to the EPA in 1987 for reconsideration, and the regulations implementing the

Resource Conservation and Recovery Act (Public Law 94-580, 1976). The Council on Environmental Quality promulgated the regulations for implementing the *National Environmental Policy Act* (NEPA) (Public Law 91-190, 1970, as amended; US EPA, 1978); however, the EPA has the responsibility for reviewing and publicly commenting on potential environmental impacts of major federal actions. Additional requirements are specified in the *WIPP Land Withdrawal Act* (see Section 1.1 of this volume).

1.2.1 Radioactive-Waste Disposal Standards (40 CFR 191)

The radioactive-waste disposal standards, *40 CFR Part 191—Environmental Radiation Protection Standards for Management and Disposal of Spent Nuclear Fuel, High-Level and Transuranic Radioactive Wastes* (US EPA, 1985), are divided into two subparts. Subpart A applies to a disposal facility prior to decommissioning and limits annual radiation doses from waste management and storage operations to members of the public in the general environment. Subpart B applies after decommissioning and sets probabilistic limits on cumulative releases of radionuclides to the accessible environment (defined in Section 3.2.2 of this volume) for 10,000 years. Subpart B also sets probabilistic limits on both radiation doses to members of the public in the accessible environment for 1000 years of undisturbed performance (defined in Section 3.5 of this volume) and radioactive contamination of certain sources of groundwater within or near the controlled area (defined in Section 3.2.3 of this volume) for 1000 years after disposal. The DOE must provide a reasonable expectation that the WIPP will comply with the quantitative requirements of Subpart B of 40 CFR 191. Appendix A of 40 CFR 191 specifies how to determine release limits; Appendix B of 40 CFR 191 provides nonmandatory guidance for implementing Subpart B. The regulation is reproduced as Appendix A of this volume, and the specific requirements of 40 CFR 191, Subpart B, are discussed in Chapter 3 of this volume.

Volumes 1 through 4 of this report document the preliminary results of the evaluations of the long-term performance of the WIPP for the third comparison with the requirements of 40 CFR 191, Subpart B. The quantitative evaluation of the long-term performance of the WIPP with respect to Subpart B of 40 CFR 191 also forms the basis for safety assessments and for uncertainty and sensitivity analyses to identify parameters and processes that are important for evaluating transport of nonradioactive hazardous wastes regulated under 40 CFR 268 (see Section 1.2.2).

1.2.2 Resource Conservation and Recovery Act (RCRA)

The *Resource Conservation and Recovery Act* (RCRA) (Public Law 94-580, 1976) was enacted to provide management of hazardous wastes. The long-term regulations promulgated for implementing the RCRA, specifically 40 CFR 268 (US EPA, 1986) for the WIPP, prohibit land disposal of specified hazardous wastes, including volatile organic compounds and heavy metals, unless the owner or operator of the facility petitions for a variance and successfully demonstrates "to a reasonable degree of certainty, that there will be no migration of hazardous constituents from the disposal unit or injection zone for as long as the wastes remain hazardous" or the waste is treated in accordance with applicable treatment standards (40 CFR 268.6(a), US EPA, 1986). Guidance provided by the EPA on the interpretation of this wording indicates that "no migration" will be defined to be concentrations of hazardous constituents below health-based or environmentally based levels at the disposal-unit boundary (US EPA, 1992).

In March 1990, the DOE petitioned the EPA for a "no-migration" determination for a Test Phase for the WIPP (US DOE, 1990d). The DOE submitted the results of modeling to demonstrate, to a reasonable degree of certainty, that the emplaced test wastes would not migrate from the disposal unit during the WIPP Test Phase. The EPA issued a conditional "no-migration" determination, for the WIPP Test Phase only, in November 1990 (US EPA, 1990a). In July 1990 the EPA authorized the State of New Mexico to apply the RCRA regulations to facilities in the state that manage radioactive mixed wastes (US EPA, 1990b). Evaluation strategies are currently being developed for RCRA compliance after the Test Phase is completed. Analyses have been initiated to support evaluations of long-term compliance with the RCRA regulations at the WIPP (WIPP PA Department, 1992).

1.2.3 National Environmental Policy Act (NEPA)

The *National Environmental Policy Act* (NEPA) (Public Law 91-190, 1970, as amended) is enforced by regulations that are not specific regulatory guidelines, but contain a mandate for evaluating the environmental consequences of all significant aspects of a project (US EPA, 1978). The DOE has prepared several environmental impact statements (EISs) that have addressed the predicted experimental, operational, and long-term behavior of the repository (US DOE, 1979, 1980a, 1990c). In addition, the DOE has committed to complete another supplemental EIS at or near the end of the WIPP Test Phase, before disposal in the WIPP may begin. The potential health risks posed by estimated groundwater releases of TRU radionuclides

and by direct removal of radionuclides to the surface as a result of drilling have been assessed in the NEPA documentation for the WIPP.

The regulations that implement the NEPA do not specifically require calculating doses of radionuclides to members of the public. However, the WIPP Panel of the National Academy of Sciences, a panel that reviews the scientific basis for the WIPP, has requested safety assessments that present dose calculations for 10,000 years or peak arrival times of radionuclides, whichever occurs first. In accordance with the WIPP Panel's request, preliminary probabilistic safety assessments in which doses have been calculated for hypothetical exposure pathways are part of the analyses that evaluate long-term performance of the WIPP; safety assessments will be prepared periodically.

2. OVERVIEW OF THE DISPOSAL SYSTEM

The characteristics of the WIPP disposal system and its geologic setting are described in detail in other reports (Powers et al., 1978a,b; the WIPP *Final Environmental Impact Statement* [US DOE, 1980a]; Bechtel, 1986; Lappin et al., 1989; the WIPP *Final Safety Analysis Report* [US DOE, 1990b]; and the WIPP *Supplement Environmental Impact Statement* [US DOE, 1990c]). Additional detailed discussion is contained in Volumes 2 and 3 of this report and references cited therein.

2.1 Physical Setting

The WIPP is located in southeastern New Mexico east of the Pecos River and west of the high plains of West Texas, in a region of sand dunes known locally as Los Medaños (The Dunes). Most dunes in the area are stabilized by vegetation, and there is relatively little local topographic relief. Major regional features (Figures 2-1 and 2-2) include Nash Draw, Laguna Grande de la Sal, and the Pecos River.

The land surface within Los Medaños slopes gradually upward to the northeast from Livingston Ridge on the eastern boundary of Nash Draw to a low ridge called "The Divide." Nash Draw, 8 km (5 mi) west of the WIPP, is a broad, shallow topographic depression with no external surface drainage. Nash Draw extends northeast about 35 km (22 mi) from the Pecos River east of Loving, New Mexico, to the Maroon Cliffs area. This feature is bounded on the east by Livingston Ridge and on the west by Quahada Ridge.

Laguna Grande de la Sal, about 9.5 km (6 mi) west-southwest of the WIPP, is a large playa about 3.2 km (2 mi) wide and 4.8 km (3 mi) long, formed by coalesced collapse sinks that were created by dissolution of evaporite deposits. In the geologic past, a relatively permanent, saline lake occupied the playa. In recent history, however, the lake has undergone numerous cycles of filling and evaporation in response to wet and dry seasons, and effluent from the potash and oil and gas industries has enlarged the lake.

The Pecos River, the principal surface-water feature in southeastern New Mexico, flows southeastward, draining into the Rio Grande in western Texas. At its closest point, the river is about 20 km (12 mi) southwest of the WIPP. Surface drainage from the WIPP does not reach the river or its ephemeral tributaries.

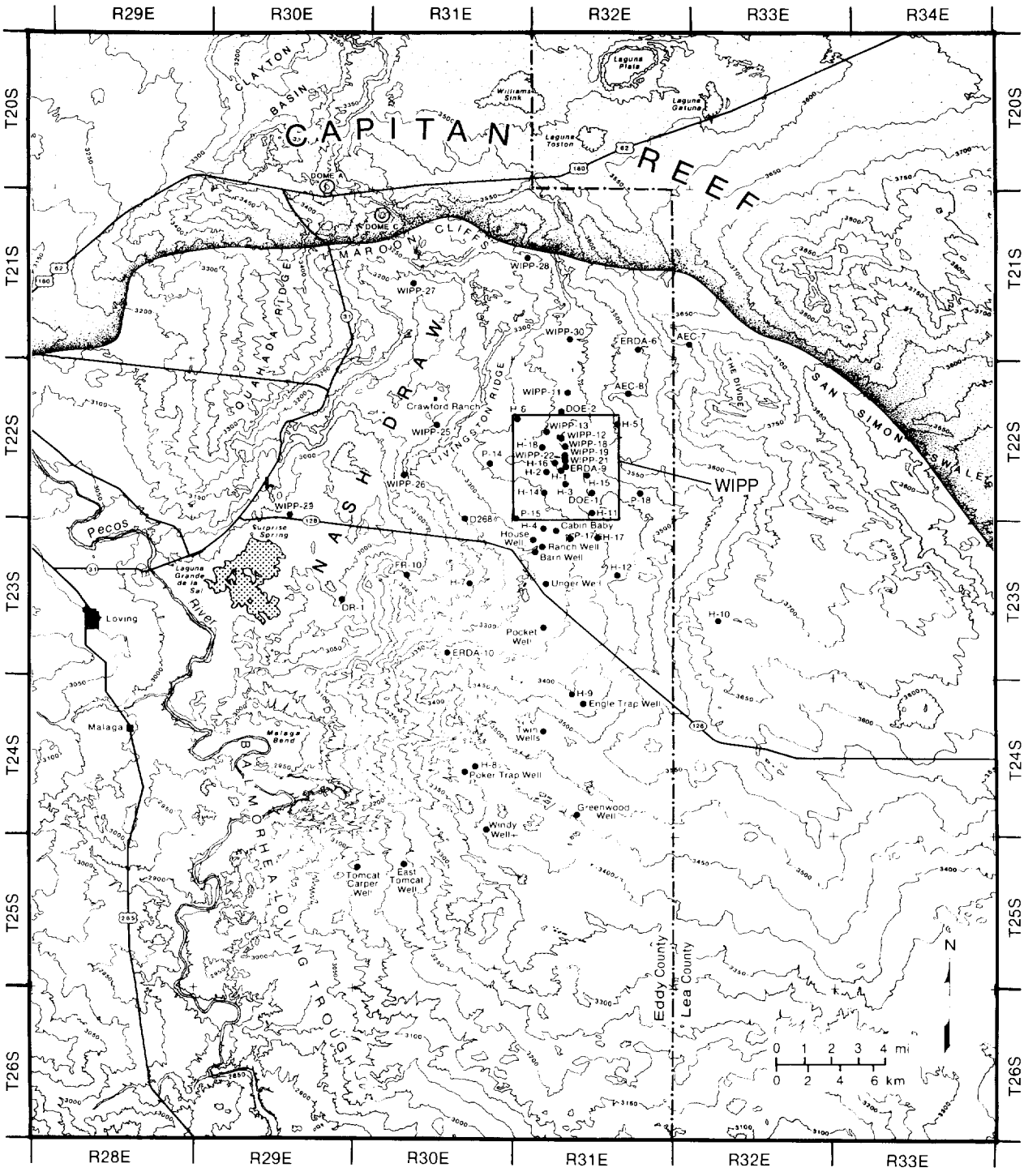

TRI-6342-612-9

Figure 2-1. Topographic map of the WIPP area (Bertram-Howery et al., 1990).

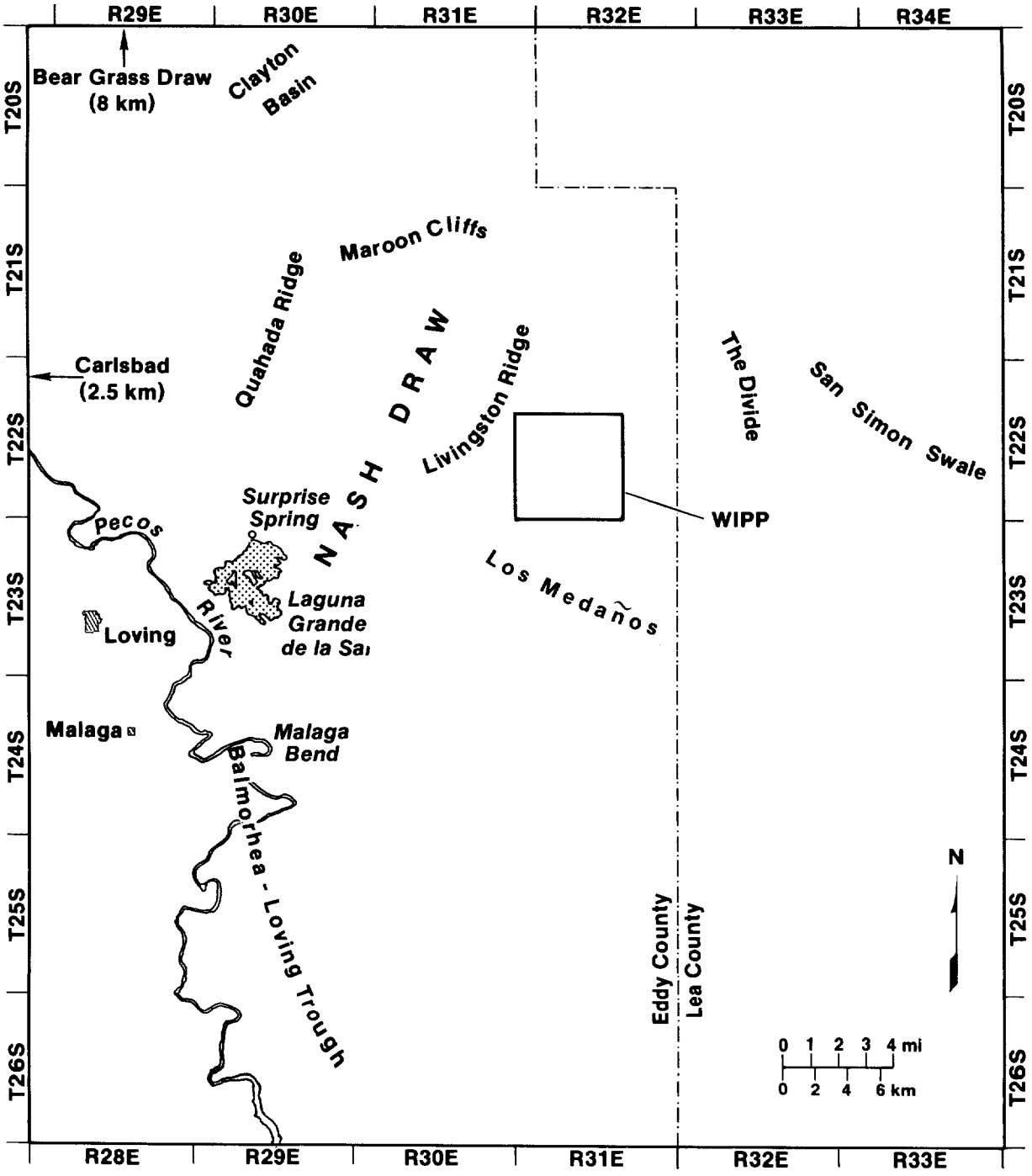

TRI-6342-134-1

Figure 2-2. Map of the WIPP area, showing physiographic features (Bertram-Howery et al., 1990).

2.2 Natural Resources

Potash, oil, and gas are the only known important mineral resources in the vicinity of the WIPP. Estimates of the volumes and locations of these resources are reported by US DOE (1980a).

About 56 productive oil and gas wells are located within a radius of 16 km (10 mi) from the WIPP; the wells generally tap Pennsylvanian strata, about 4,200 m (14,000 ft) deep. The hydrocarbon well closest to the land-withdrawal boundary is about 3 km (2 mi) to the south-southwest of the waste panels, and has produced natural gas since 1982 (Silva and Channell, 1992). The surface location of the well is outside the land-withdrawal boundary, but the borehole is slanted to withdraw gas from rocks below the WIPP horizon within the boundary. Except for this well, resource extraction is not allowed within the proposed land-withdrawal boundary.

Three potash mines and two associated chemical-processing plants are located between 8 and 16 km (5 and 10 mi) from the WIPP (US DOE, 1990b). As discussed further in Section 2.3 of this volume, potash-enriched beds are found stratigraphically above the repository horizon; neither mining of potash nor exploratory drilling for potash reserves reaches the repository horizon. The nearest economically exploitable potash reserves are approximately 1 km (0.6 mi) from the waste panels (Brausch et al., 1982; Guzowski, 1991).

2.3 Summary of Regional Geology

Geologically, the WIPP is located in the Delaware Basin, which is an elongated depression that extends from just north of Carlsbad, New Mexico, southward into Texas (Figure 2-3). The basin covers over 33,000 km^2 (12,750 mi^2) and is filled with sedimentary rocks to depths as great as 7,300 m (24,000 ft) (Hills, 1984).

2.3.1. Geologic History

The geologic history of the Delaware Basin is described in more detail elsewhere (Hiss, 1975; Powers et al., 1978a,b; Cheeseman, 1978; Williamson, 1978; Hills, 1984; Ward et al., 1986; Harms and Williamson, 1988; Volume 2, Chapter 2 of this report). Rock units of the Delaware Basin representing the Permian System through the Quaternary System are shown in Table 2-1. Simplified stratigraphy at the WIPP is shown in Figure 2-4.

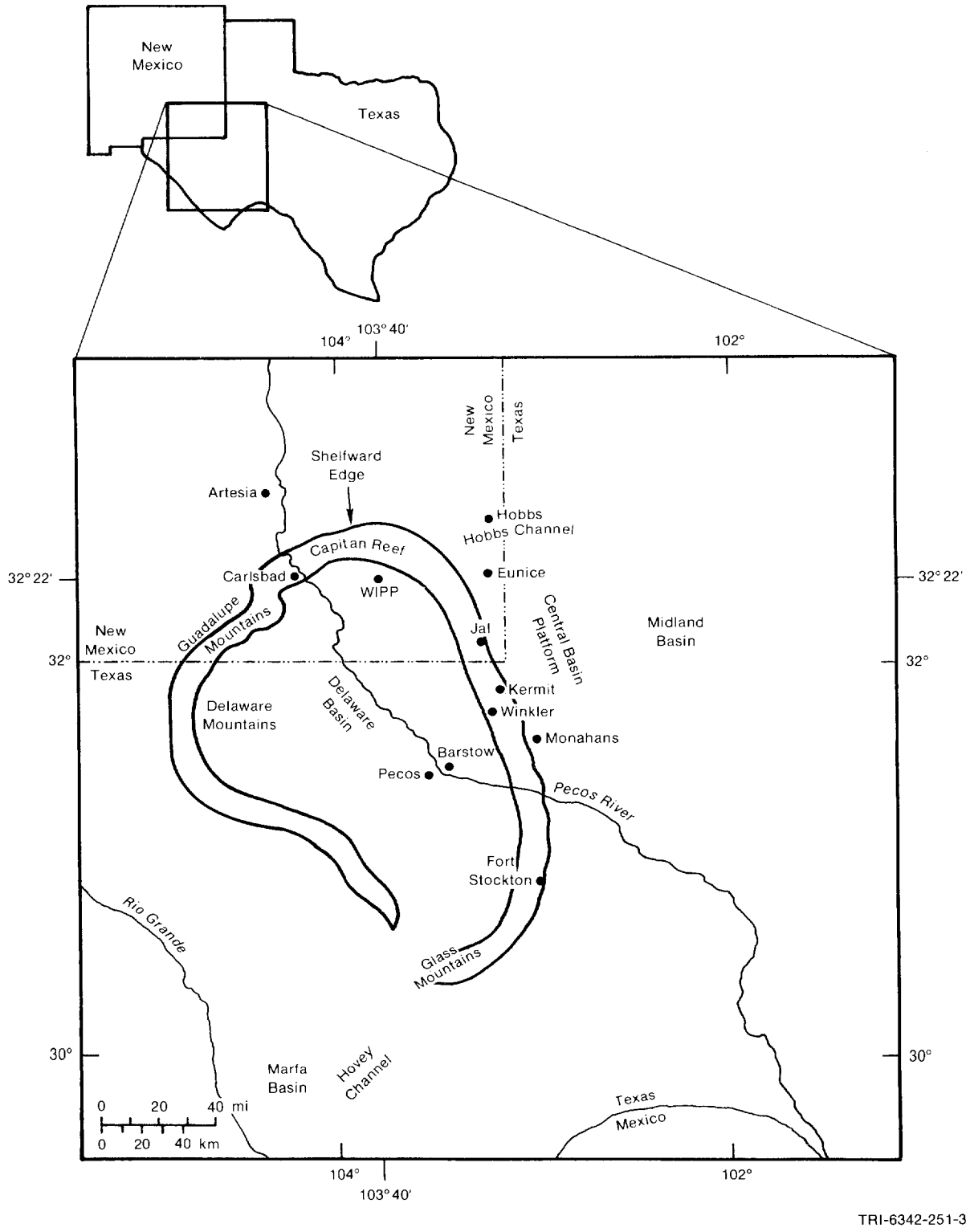

Figure 2-3. Location of the WIPP in the Delaware Basin (modified from Richey et al., 1985).

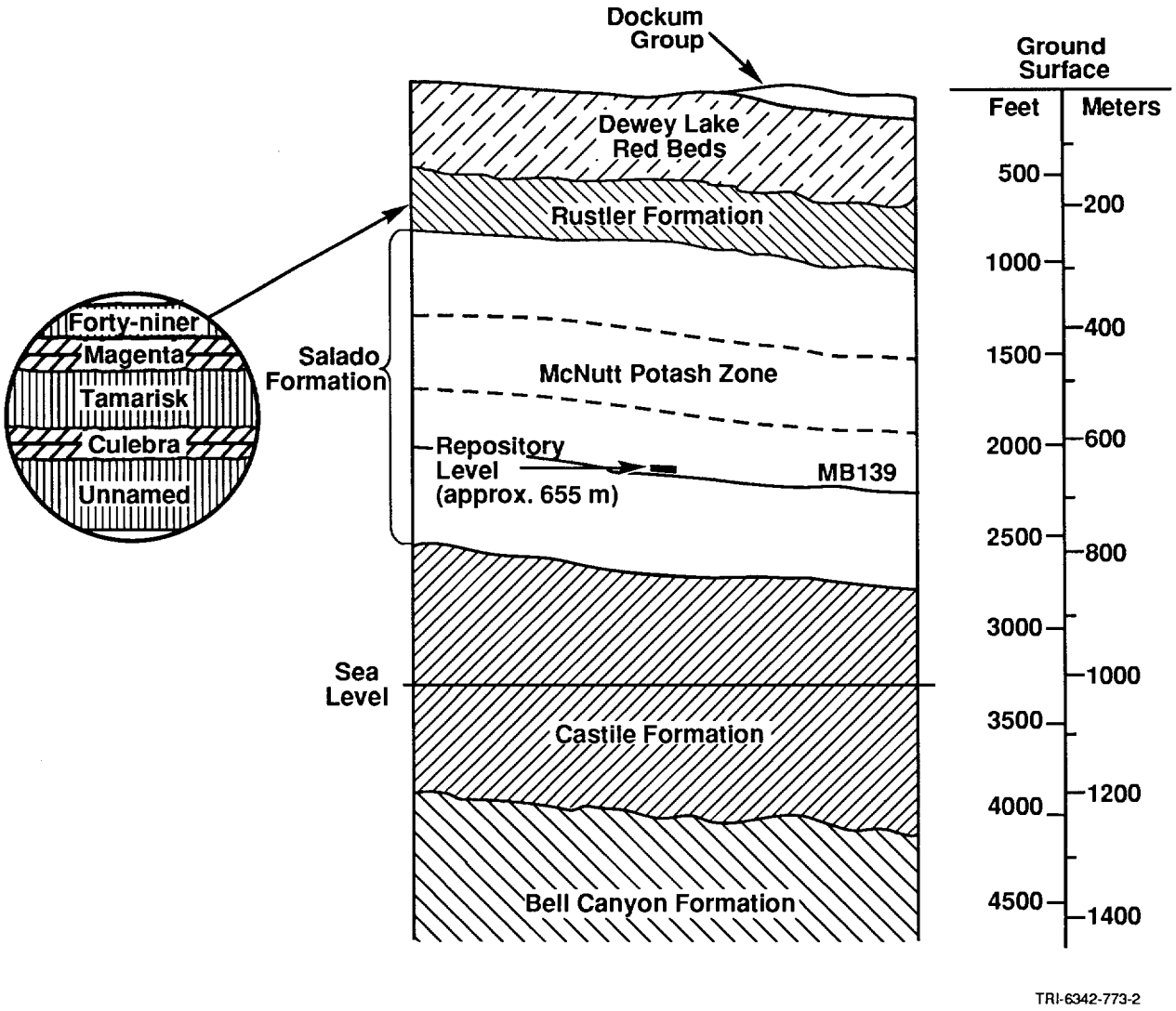

Figure 2-4. Generalized WIPP stratigraphy (modified from US DOE, 1980b).

Table 2-1. Major Stratigraphic Divisions, Southeastern New Mexico

Erathem	System	Series	Lithostratigraphic Unit	Age Estimate (yr)
Cenozoic	Quaternary	Holocene	Windblown sand	
		Pleistocene	Mescalero caliche	~500,000
			Gatuña Formation	~600,000±
	Tertiary	Pliocene	Ogallala Formation	5.5 million
		Miocene		24 million
		Oligocene Eocene Paleocene	Absent in Southeastern New Mexico	66 million
Mesozoic	Cretaceous	Upper	Absent in Southeastern New Mexico	
		Lower	Detritus preserved	144 million
	Jurassic		Absent in Southeastern New Mexico	208 million
	Triassic	Upper Lower	Dockum Group Absent in Southeastern New Mexico	245 million
Paleozoic	Permian, Upper	Ochoan	Dewey Lake Red Beds Rustler Formation Salado Formation Castile Formation	
	Permian, Lower	Guadalupian	Capitan Limestone and Bell Canyon Formation	
		Leonardian Wolfcampian	Bone Springs Wolfcamp (informal)	286 million

Source: Modified from Bachman, 1987

The Delaware Basin began forming by crustal subsidence during the Pennsylvanian Period, approximately 300 million years ago. Relatively rapid subsidence during the Early and mid-Permian, between approximately 286 and 260 million years ago, resulted in the deposition of a sequence of deep-water sandstones, shales, and limestones rimmed by shallow-water limestone

reefs (Figure 2-3). The thickest of the reef deposits, the Capitan Limestone, is buried under younger rocks north and east of the WIPP but is exposed at the surface in the Guadalupe Mountains to the west. Subsidence slowed during the Late Permian; evaporite deposits of the Castile Formation and the Salado Formation, which hosts the WIPP, filled the basin and extended over the reef margins. Evaporites, carbonates, and clastic rocks of the Rustler Formation and the Dewey Lake Red Beds were deposited above the Salado Formation before the end of the Permian Period.

Beginning with the Triassic Period and continuing to the present, the geologic record for the area indicates long periods of nondeposition or erosion. Those formations that are present are either relatively thin or discontinuous and are not included in the performance assessment of the WIPP. Near the repository, the older, Permian-age deposits below the Dewey Lake Red Beds have not been affected by erosional processes during the past 250 million years (Lappin, 1988).

Minimal tectonic activity has occurred in the region since the Permian Period (Hayes, 1964; Williamson, 1978; Hills, 1984; Powers et al., 1978a). Faulting during the late Tertiary Period formed the Guadalupe and Delaware Mountains along the western edge of the basin. The most recent igneous activity in the area was during the mid-Tertiary Period about 35 million years ago and is evidenced by a dike in the subsurface 16 km (10 mi) northwest of the WIPP (Powers et al., 1978a,b). Major volcanic activity last occurred more than 1 billion years ago during Precambrian time (Powers et al., 1978a,b). None of these processes affected the Salado Formation at the WIPP.

2.3.2 Stratigraphy and Geohydrology

The Bell Canyon Formation of the Delaware Mountain Group is the deepest hydrostratigraphic unit being considered in the performance assessment (Figure 2-4). Understanding hydrologic conditions in the Bell Canyon is potentially important because oil and gas drilling into deeper Pennsylvanian strata could first penetrate the WIPP and brine-saturated sandstones of the Bell Canyon Formation. Available pressure data from wells indicate that brine flow from the Bell Canyon Formation is not a likely mechanism for radionuclide release (Volume 2, Section 2.2.1 of this report), however, and the Bell Canyon Formation is not included explicitly in performance-assessment modeling.

The Castile Formation near the WIPP consists of anhydrite and lesser amounts of halite. The Castile Formation is of interest because it contains discontinuous reservoirs of pressurized brine that could affect repository performance if penetrated by an exploratory borehole. Except where brine reservoirs are present, permeability of the Castile Formation is extremely low, and rates of groundwater flow are too low to affect the disposal system within the next 10,000 years.

The 250-million-year-old Salado Formation, which hosts the repository, is about 600 m (2,000 ft) thick and consists of the following three informal members:

- a lower member, which is mostly halite with lesser amounts of anhydrite, polyhalite, and glauberite, with some layers of fine clastic material. The unit is 296 to 354 m (960 ft to 1160 ft) thick, and the WIPP repository is located within it, 655 m (2,150 ft) below the land surface (Jones, 1978). Anhydrite layers near the WIPP horizon that are modeled in performance assessment include Marker Beds 138 and 139 and anhydrites A and B (Figure 2-5). Because anhydrite is more brittle than halite, fracturing within these interbeds has the potential to provide a pathway for gas and brine (and, therefore, contaminants) to migrate from the repository

- a middle member, the McNutt Potash Zone, which is reddish-orange and brown halite with deposits of sylvite and langbeinite from which potassium salts are mined (Jones, 1978)

- an upper member, which is reddish-orange to brown halite interbedded with polyhalite, anhydrite, and sandstone (Jones, 1978)

These lithologic layers are nearly horizontal at the WIPP, with a regional dip of less than one degree. The Salado Formation has not been disturbed by post-depositional processes in the WIPP area, and groundwater flow within it is extremely slow because primary porosity and open fractures are lacking in the plastic salt (Mercer, 1983). The formation is assumed to be brine-saturated throughout the WIPP area, but low permeability allows for little groundwater movement. The Salado Formation is discussed in more detail in Volumes 2 and 3 of this report.

The Rustler Formation, the youngest formation of the Late Permian evaporite sequence, includes units that provide potential pathways for radionuclide migration away from the WIPP. The following five units of the Rustler, in ascending order, have been described (Vine, 1963; Mercer, 1983):

- an unnamed lower member, composed mostly of fine-grained, silty sandstones and siltstones interbedded with anhydrite west of the WIPP but with increasing amounts of halite to the east

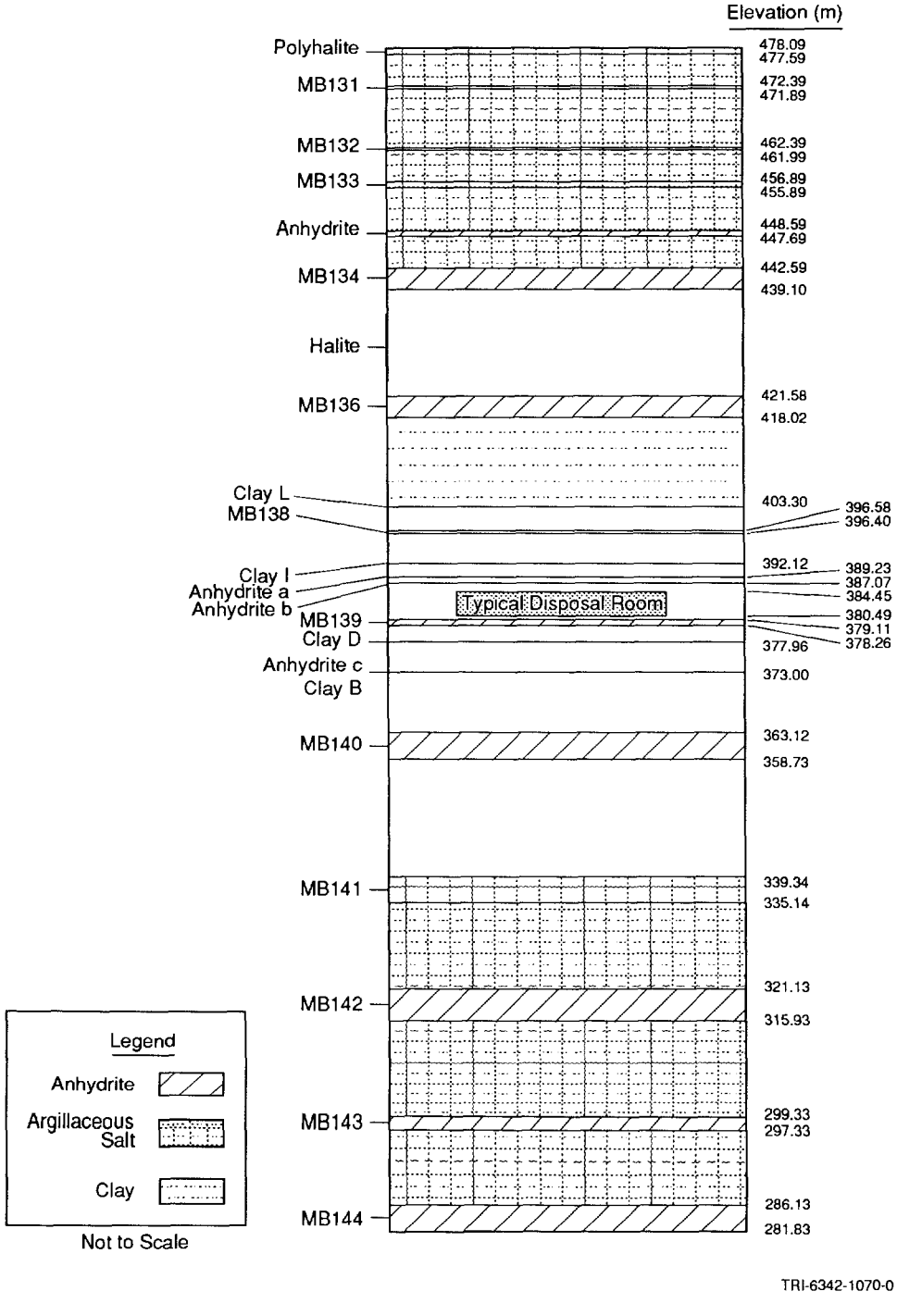

Figure 2-5. Reference local stratigraphy near repository (after Munson et al., 1989a, Figure 3-3; elevations from Bechtel, 1986).

- the Culebra Dolomite Member, a microcrystalline, grayish dolomite or dolomitic limestone with solution cavities containing some gypsum and anhydrite filling

- the Tamarisk Member, composed of anhydrite interbedded with thin layers of claystone and siltstone, with some halite east of the WIPP

- the Magenta Dolomite Member, a very-fine-grained, greenish-gray dolomite with reddish-purple layers

- the Forty-niner Member, consisting of anhydrite interbedded with a layer of siltstone, with halite present east of the WIPP

Most groundwater flow in the Rustler Formation occurs in the Culebra Dolomite and Magenta Dolomite Members. The intervening units (the unnamed lower member, the Tamarisk Member, and the Forty-niner Member) are considered aquitards because of their low permeability throughout the area.

Groundwater flow in the Culebra Dolomite Member near the WIPP is north to south (see Volume 2, Chapter 2 of this report). Recharge apparently occurs north of the WIPP, possibly at Bear Grass Draw where the Rustler Formation is near the surface and at Clayton Basin where karst activity has disrupted the Culebra Dolomite (Mercer, 1983). Discharge occurs west-southwest of the WIPP, either into the Pecos River at Malaga Bend (Hale et al., 1954; Hale and Clebsch, 1958; Havens and Wilkens, 1979; Mercer, 1983), or into Cenozoic alluvium in the Balmorhea-Loving Trough, which is a series of coalesced, lens-shaped solution troughs formed by an ancestral Pecos River, or into both (Brinster, 1991). Culebra water near the WIPP contains large concentrations of total dissolved solids (Siegel et al., 1991). Currently, no wells in the WIPP vicinity produce water from the Culebra for human consumption. The nearest well that has produced water from the Culebra for livestock is 6 km (4 mi) from the waste panels (Bodine et al., 1991).

Small amounts of water can be produced from the Magenta Dolomite Member from a thin, silty dolomite, along bedding planes of rock units, and along fractures (Mercer, 1983). Regionally, the direction of groundwater flow is similar to that in the Culebra, either toward Malaga Bend or more directly southward to the Balmorhea-Loving Trough. Near the WIPP, available well data indicate that flow in the Magenta is locally from east to west, perpendicular to flow in the Culebra (see Section 2.2.3.6 of Volume 2 of this report). No wells in the WIPP vicinity produce water from the Magenta for human or livestock consumption.

Overlying the Rustler Formation are the Dewey Lake Red Beds, which are the youngest Permian rocks and which consist of alternating layers of reddish-brown, fine-grained sandstone and siltstone cemented with calcite and gypsum (Vine, 1963). Several wells in the WIPP area produce small amounts of water from the Dewey Lake Red Beds for livestock (Cooper and Glanzman, 1971). The closest such well is at the J.C. Mills (James) Ranch, 4 km (2.5 mi) south of the waste panels. In general, however, the unit is not a productive source of water; drilling has identified only a few localized zones of relatively high permeability (Mercer, 1983; Beauheim, 1987a).

From the WIPP eastward, the Dewey Lake Red Beds are unconformably overlain by Triassic rocks of the undifferentiated Dockum Group (Figure 2-4). The lower Dockum is composed of poorly sorted, angular, coarse-grained to conglomeratic, thickly bedded clastic material interfingering with shales. At the WIPP, the unit is relatively thin (approximately 10 m [33 ft] thick), and unsaturated. Further east, where the Triassic rocks are thicker, they are the chief source of water for domestic and livestock use in eastern Eddy County and western Lea County (Nicholson and Clebsch, 1961; Richey et al., 1985). Recharge to the Triassic rocks is mainly downward flow from overlying alluvium.

No rocks of Jurassic or Cretaceous age are present east of the Pecos River near the WIPP. The Tertiary Period is represented by a thin remnant of the Ogallala Formation at The Divide west of San Simon Swale. The Quaternary Period is represented by discontinuous sandstones and conglomerates of the Gatuña Formation, the informally named Mescalero caliche, and localized accumulations of alluvium and dune sands (Bachman, 1980, 1984; Mercer, 1983).

2.4 Repository/Shaft System

The WIPP repository is about 655 m (2,150 ft) below the land surface in bedded salt of the Salado Formation. Present plans call for mining eight panels of seven rooms each and two equivalent panels in the central drifts (Figure 2-6 and 2-7). As each panel is filled with waste, the next panel will be mined. Before the repository is closed permanently, each panel will be backfilled and sealed, waste will be placed in the drifts between the panels and backfilled, to create two additional panel volumes, and access ways will be sealed off from the shafts. Because the WIPP is a research and development facility, an extensive experimental area is also in use north of the waste-disposal area (US DOE, 1990a). Additional information on the repository design is in Volumes 2 and 3 of this report.

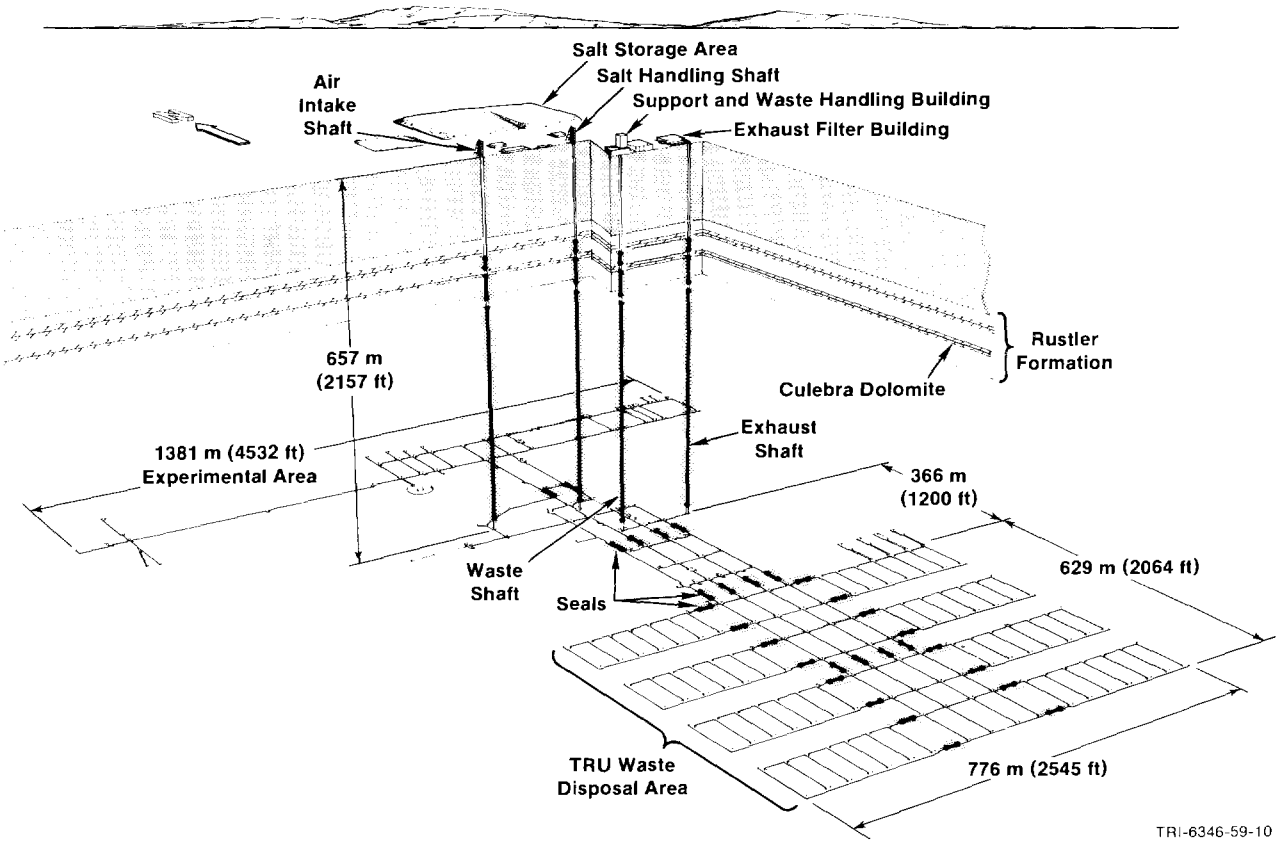

Figure 2-6. Proposed WIPP repository, showing both TRU-waste disposal areas and experimental areas (after Waste Management Technology Dept., 1987).

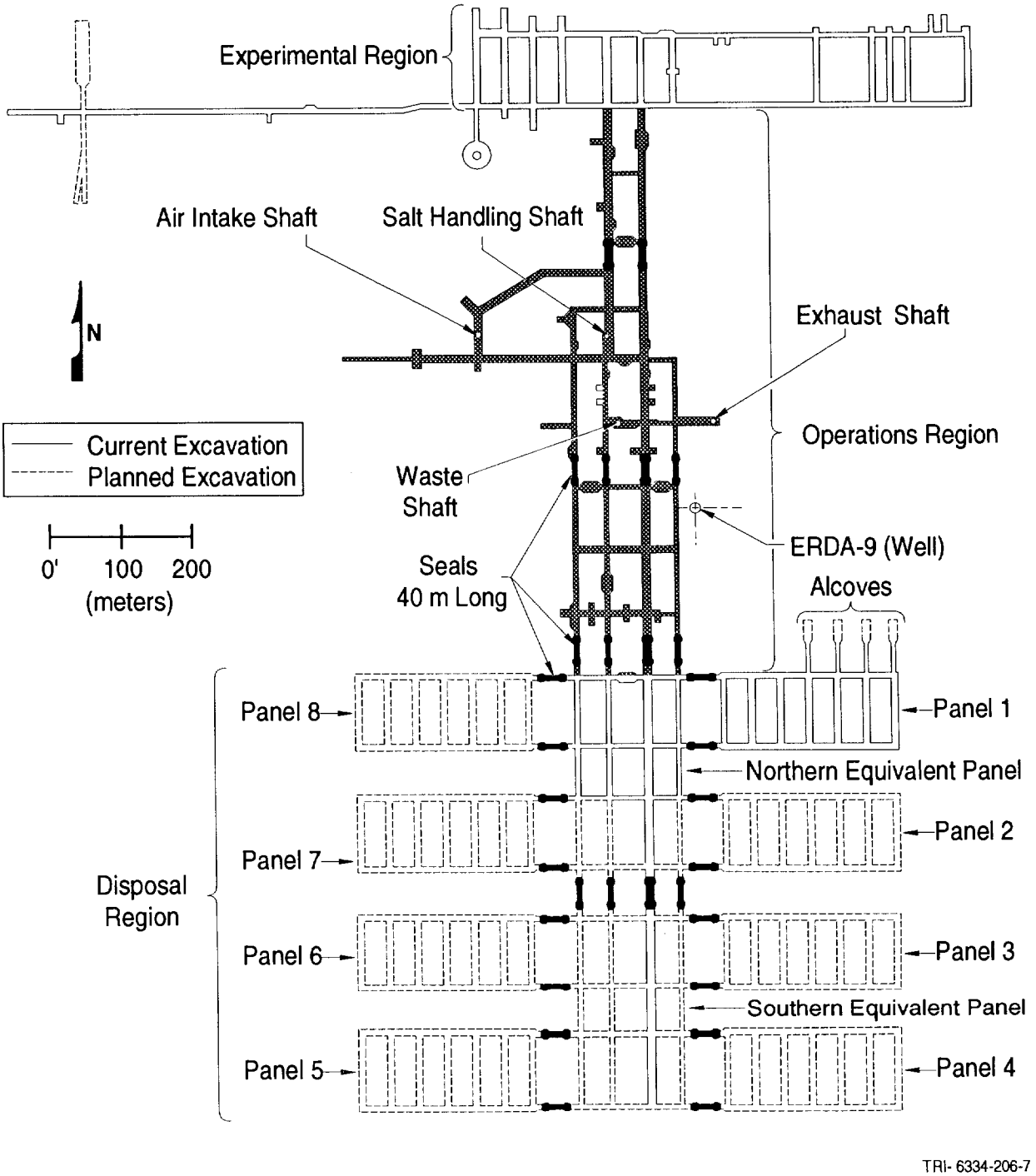

Figure 2-7. Excavated areas and planned seals in the WIPP repository (modified from Bechtel, 1986; Nowak et al., 1990).

2.5 Waste

As noted in Section 1.1.2 of this volume, the WIPP is designed for transuranic waste generated by United States government defense-related activities since 1970. The waste consists of laboratory and production materials such as glassware, metal pipes, sorbed or solidified spent solvents, disposable laboratory clothing, cleaning rags, and solidified sludges. Along with other contaminants, the waste is contaminated by alpha-emitting transuranic (TRU) elements with atomic numbers greater than 92 (uranium), half-lives greater than 20 years, and curie contents greater than 100 nCi/g. Additional contaminants include other radionuclides of uranium and several contaminants with half-lives less than 20 years. Approximately 60 percent of the TRU waste may be co-contaminated with hazardous constituents as defined under the Resource Conservation and Recovery Act (RCRA). The waste scheduled for disposal in the WIPP is described in more detail in Volume 3 of this report.

In accordance with DOE Order 5820.2A (US DOE, 1990a), heads of DOE Field Organizations can determine that other alpha-contaminated wastes, peculiar to a specific waste-generator site, must be managed as TRU wastes. The WIPP Waste Acceptance Criteria (WAC) determine which TRU wastes will be accepted for emplacement in the WIPP (US DOE, 1991a). Under current plans, most TRU waste generated since 1970 will be disposed of in the WIPP, but some will be disposed of on-site at other DOE facilities. Inventories of the waste to be disposed of in the WIPP are in Volume 3 of this report.

2.5.1 Waste Form

Alpha-emitting TRU waste, although dangerous if inhaled or ingested, is not dangerous externally and can be handled safely if confined in a sealed container. Most of the waste, therefore, can be contact handled (CH) because the external dose rate (200 mrem/h or less) permits people to handle properly sealed drums and boxes without any special shielding. The only containers that can currently be shipped to the WIPP in a TRUPACT-II truck-transport container (NuPac, 1989) are 55-gallon steel drums, metal standard waste boxes (SWBs), 55-gallon drums overpacked in an SWB, and an experimental bin overpacked in an SWB (US DOE, 1990c). Additional information on waste containers is in Volume 3 of this report.

A portion of the TRU waste must be remotely handled (RH). Because the surface dose rate exceeds 200 mrem/h, the waste canisters must be packaged for handling and transportation in specially shielded casks. The surface dose rate of RH-TRU canisters cannot exceed 1,000 rem/h, and no more than 5

percent of the canisters can exceed 100 rem/h. RH-TRU waste in canisters will be emplaced in holes drilled into the walls of the rooms (US DOE, 1990b).

As stated in the *WIPP Land Withdrawal Act* (Public Law 102-579, 1992), the WIPP's current design capacity for all radionuclides is 6.2 million ft^3 (approximately 175,600 m^3), of which no more than 5.1 million curies (Ci) may be RH-TRU waste. The complex analyses for evaluating regulatory compliance require knowledge of the waste inventory. Therefore, all analyses will be based on current projections of a design volume inventory, estimated at about 532,500 drums and 33,500 boxes of CH-TRU waste (WIPP PA Division, 1991c). The wastes are classified as either retrievably stored or newly generated (future generated). Additional information on inventory estimates is in Volume 3 of this report.

A hazardous constituent of CH-TRU waste is lead that is present as incidental shielding, glovebox parts, and linings of gloves and aprons. Trace quantities of mercury, barium, chromium, silver, and cadmium have also been reported (US DOE, 1990d). Estimates of the quantities of metals and combustibles are discussed in Volume 3 of this report. Sludges may contain a solidifier (such as cement), absorbent materials, inorganic compounds, complexing agents, and organic compounds including oils, solvents, alcohols, emulsifiers, surfactants, and detergents. The WAC (US DOE, 1991a) waste-form requirements state that the waste material shall be immobilized if greater than 1 percent by weight is particulate material less than 10 microns in diameter or if greater than 15 percent by weight is particulate material less than 200 microns in diameter. Only residual liquids in well-drained containers (e.g., bottles, cans, etc.) in quantities less than approximately 1 percent of the container's volume are allowed. The total liquid shall be less than one volume percent of the waste container (e.g., drum or SWB). Radionuclides in pyrophoric form are limited to less than 1 percent by weight of the waste package, and no explosives or compressed gases are allowed. These hazardous constituents are not regulated under 40 CFR Part 191, but some are regulated separately by the EPA and New Mexico under the *Resource Conservation and Recovery Act* (RCRA). Many of these chemicals (hazardous and nonhazardous), if present in significant quantities, could affect the ability of radionuclides to migrate out of the repository by influencing rates of degradation of the organics, microbial activity, and gas generation. The effects of these processes are being studied.

2.5.2 Radionuclide Inventory

The radionuclide composition of CH- and RH-TRU waste varies depending upon the facility and process that generate the waste. An estimate of the CH- and RH-TRU radionuclide inventories is in Volume 3 of this report.

The fissile material content in equivalent grams of plutonium-239 allowed by the WAC for CH-TRU waste is less than 200 g for a 55-gallon drum and less than 25 g for a SWB. It is expected that the fissile material for TRU waste in a remotely handled cask will be limited to less than 325 g (US DOE, 1991a).

As discussed further in Section 3.3.2 of this volume, the EPA has set cumulative release limits in curies per 10,000 years for isotopes of americium, carbon, cesium, iodine, neptunium, plutonium, radium, strontium, technetium, thorium, tin, and uranium, as well as for certain other radionuclides (Appendix A of 40 CFR 191, Subpart B). Although the initial WIPP inventory contains little or none of some of the listed nuclides, they will be produced as a result of radioactive decay and must be accounted for in the compliance evaluation. Moreover, for compliance with the Individual Protection Requirements of 40 CFR 191, Subpart B, any radionuclides not listed in Appendix A must be accounted for if those radionuclides could contribute to doses.

2.5.3 Possible Modifications to Waste Form

If ongoing research does not establish sufficient confidence in acceptable performance or indicates a potential for unacceptable performance, modifications to the waste form or backfill could be required. SNL has conducted preliminary research on possible modifications (Butcher, 1990). The Engineered Alternatives Task Force (EATF) identified specific alternatives, ranked alternatives according to specific feasibility criteria, and recommended further research (US DOE, 1990e, 1991b). The DOE will make decisions about testing and, if necessary, implementing alternatives based on the recommendations of the EATF and performance-assessment considerations provided by SNL.

3. APPLICATION OF 40 CFR PART 191, SUBPART B, TO THE WIPP

The radioactive-waste disposal regulations, *40 CFR Part 191—Environmental Radiation Protection Standards for Management and Disposal of Spent Nuclear Fuel, High-Level and Transuranic Radioactive Wastes* (US EPA, 1985), referred to in this volume of the report as the Standard, are divided into two subparts.

Subpart A limits the radiation doses that may be received by members of the public in the general environment (see Section 3.2.2 of this volume), as a result of management and storage of TRU wastes at DOE disposal facilities not regulated by the Nuclear Regulatory Commission (NRC). Subpart A requires that "the combined annual dose equivalent to any member of the public in the general environment resulting from discharges of radioactive material and direct radiation from such management and storage shall not exceed 25 millirems to the whole body and 75 millirems to any critical organ" (§ 191.03(b)). Subpart A does not apply to long-term disposal of radioactive wastes. Subpart A is discussed in the *Technical Needs Assessment* report (US DOE, 1992a), and in the "Test Phase Plan" currently being prepared by the DOE. Except for discussion of a few terms that are important in understanding Subpart B, Subpart A is not considered further in this report.

Subpart B of the Standard (Figure 3-1) specifies probabilities of cumulative releases of radionuclides to the accessible environment (see Section 3.2.2 of this volume) for 10,000 years (Containment Requirements, § 191.13) and annual radiation dose limits to members of the public in the accessible environment for 1000 years (Individual Protection Requirements, § 191.15) as a result of TRU-waste disposal. Actions and procedures are required to increase confidence that the probabilistic release limits specified in the Containment Requirements will be met (Assurance Requirements, § 191.14). Radioactive contamination of certain sources of groundwater near the WIPP disposal system from such TRU wastes is also regulated (Groundwater Protection Requirements, § 191.16), if any of these sources of groundwater are found to be present (US DOE, 1989). Each of the four requirements of Subpart B and their method of evaluation by the WIPP Project are discussed in this chapter.

Subpart B of the Standard was vacated and remanded to the EPA by the United States Court of Appeals for the First Circuit in July 1987 (NRDC v. US EPA, 1987). A proposed revision of the Standard was prepared for discussion within the EPA in February 1992. The *WIPP Land Withdrawal Act* (Public Law 102-579, 1992) reinstated those portions of the 40 CFR 191,

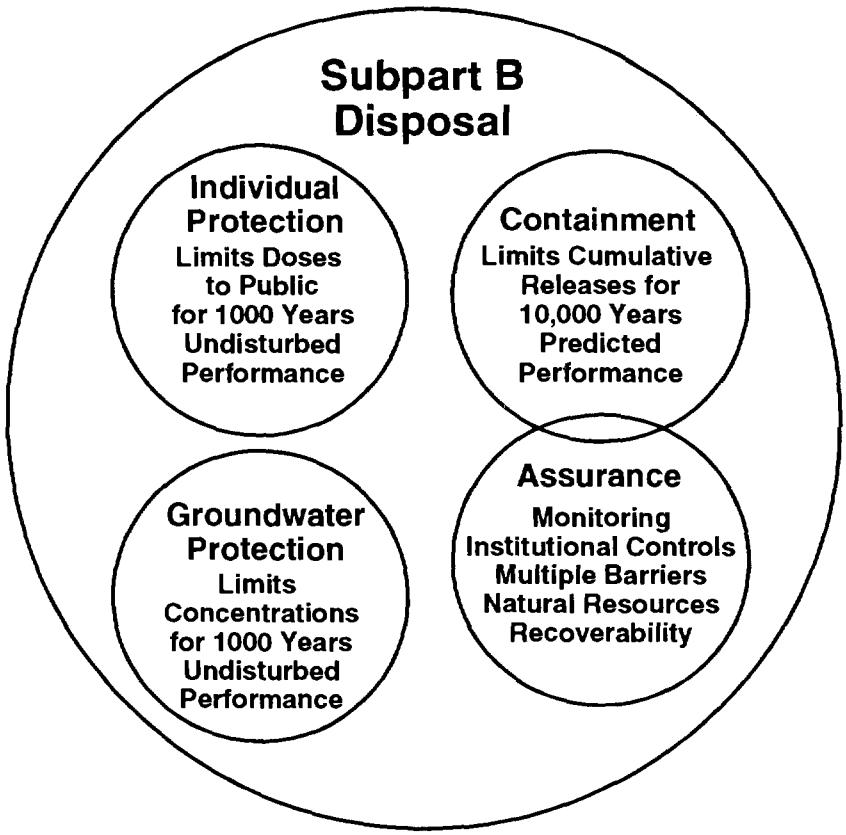

Figure 3-1. Graphical representation of Subpart B of *40 CFR Part 191—Environmental Radiation Protection Standards for Management and Disposal of Spent Nuclear Fuel, High-Level and Transuranic Radioactive Wastes* (after US DOE, 1989). The overlapping of the Assurance Requirements with the Containment Requirements indicates that the Assurance Requirements specify actions and procedures to increase confidence that the probabilistic release limits in the Containment Requirements will be met.

Subpart B that were not the subject of the remand, and requires the EPA to repromulgate the standard by April 30, 1993, with appropriate revisions to §191.15 and §191.16. The Second Modification to the Consultation and Cooperation Agreement (US DOE and State of New Mexico, 1981, as modified) commits the WIPP Project to proceed with compliance planning using the Standard as first promulgated until a revised Standard becomes available. Therefore, this report discusses the Standard as first promulgated. Compliance plans for the WIPP will be revised as necessary in response to changes in the Standard resulting from the repromulgation. The current DOE approach to compliance with the Standard is described in the WIPP *Compliance Strategy* (US DOE, 1989; also see US DOE, 1990d). Additional discussion of some aspects of the current compliance approach is in the *Technical Needs Assessment* report (US DOE, 1992a), and in the "Test Phase Plan" currently being prepared by the DOE.

The full text of the Standard is reproduced as Appendix A of this volume.

3.1 Guidance for Implementation of the Standard

Appendix B of the Standard is EPA's guidance to the implementing agency (in this case, the DOE). Although it is not formal regulatory criteria within the Standard, Appendix B describes the EPA's assumptions regarding the implementation of Subpart B. In the supplementary information published with the Standard, the EPA states that it intends the guidance to be followed:

> "...Appendix B...describes certain analytical approaches and assumptions through which the [EPA] intends the various long-term numerical standards of Subpart B to be applied. This guidance is particularly important because there are no precedents for the implementation of such long-term environmental standards, which will require consideration of extensive analytical projections of disposal system performance" (US EPA, 1985, p. 38069).

The EPA based Appendix B on analytical assumptions it used to develop the technical basis for the numerical disposal standards. Thus, the EPA "believes it is important that the assumptions used by the [DOE] are compatible with those used by EPA in developing this rule. Otherwise, implementation of the disposal standards may have effects quite different than those anticipated by EPA" (US EPA, 1985, p. 38074).

3.2 Terminology

The concept of "site" is integral to limits established by Subparts A and B for releases of radionuclides from the repository, during disposal, decommissioning, and post-closure phases. "Site" is used differently in the two subparts. The differences in the meaning of "site" for the two subparts must be understood in order to avoid confusion in applying the Standard to the WIPP. The definitions of "general environment," "accessible environment," and "controlled area," which are also important in assessing compliance with the Standard, depend on the definition of "site." "Site" has also been used generically for many years by the waste-management community (e.g., in the phrases "site characterization" or "site specific"); few uses of the word correspond to either of the EPA's usages in the Standard (Bertram-Howery and Hunter, 1989a; also see US DOE, 1989). Other terms that are important in understanding the application of the Standard to the WIPP also are explained in this section.

3.2.1 "Site"

The "**site**" as defined for Subpart A is "an area contained within the boundary of a location under the effective control of persons possessing or using...radioactive waste that are involved in any activity, operation, or process covered by this Subpart" (§ 191.02(n)). **Site** for the purposes of Subpart A of the WIPP is the secured-area boundary shown in Figure 1-2. This area will be under the effective control of the security force at the WIPP, and only authorized persons will be allowed within the boundary (US DOE, 1989). In addition, the DOE has control over the area contained within the land-withdrawal boundary, designated by the U.S. Congress (Public Law 102-579, 1992) as the 16 sections (16 mi^2 [41 km^2]) shown in Figure 1-2. The land-withdrawal boundary is referred to in the agreement with New Mexico (US DOE and State of New Mexico, 1981, as modified) and in the WIPP ***Final Safety Analysis Report*** (US DOE, 1990b) as the "WIPP **site** boundary." Control by the DOE prohibits habitation within the land-withdrawal boundary. Consequently, for the purposes of assessing operational doses to nearby residents for Subpart A, the assumption can be made that no one lives closer than the latter boundary (Bertram-Howery and Hunter, 1989a).

The term "disposal **site**" is used frequently in Subpart B and in Appendix B of the Standard, although it is not defined in the regulation. The **site** for the purposes of Subpart A and the "disposal **site**" for the purposes of Subpart B are not the same. For the purposes of the WIPP strategy for compliance with Subpart B, the "disposal **site**" and the "controlled area" (defined in Section 3.2.3) are the same (US DOE, 1989).

The boundary indicated as "WIPP" on illustrations in this volume is the boundary of the land-withdrawal area and is the same as the "controlled area" boundary used in the 1992 preliminary performance assessment of the WIPP. The subsurface projection of the land-withdrawal boundary within the Salado Formation also forms the lateral boundary of the disposal-unit for evaluating compliance with 40 CFR 268.6 (US EPA, 1990a).

3.2.2 "General Environment" and "Accessible Environment"

The term "**general environment**" is used in Subpart A and is defined as the "total terrestrial, atmospheric, and aquatic environments outside sites within which any activity, operation, or process associated with the management and storage of...radioactive waste is conducted" (§ 191.02(o)). "**Accessible environment**" is used in Subpart B and is defined as "...(1) the atmosphere; (2) land surfaces; (3) surface waters; (4) oceans; and (5) all of the lithosphere that is beyond the controlled area" (see Section 3.2.3) (§ 191.12(k)).

3.2.3 "Controlled Area"

The "**controlled area**" as defined in Subpart B of the Standard is

> "(1) A surface location, to be identified by passive institutional controls, that encompasses no more than 100 square kilometers and extends horizontally no more than five kilometers in any direction from the outer boundary of the original location of the radioactive wastes in a disposal system; and (2) the subsurface underlying such a surface location" (§ 191.12(g)).

The **controlled area** is limited to the lithosphere and the surface within no more than 5 km (approximately 3 mi) from the outer boundary of the WIPP waste-emplacement panels. The boundary of this maximum-allowable **controlled area** does not coincide with the secured-area boundary (Figure 1-2) or with the land-withdrawal boundary (Figure 3-2). According to the definition of "accessible environment," the surface of the **controlled area** is in the accessible environment; the underlying subsurface of the **controlled area** is not part of the accessible environment (Figure 3-2). Any radionuclides that reached the surface would be subject to the limits, as would any that reached the lithosphere outside the subsurface portion of the **controlled area**.

The surface of the **controlled area** is to be identified by passive institutional controls, including permanent markers designating the "disposal site." Additional passive institutional controls are public

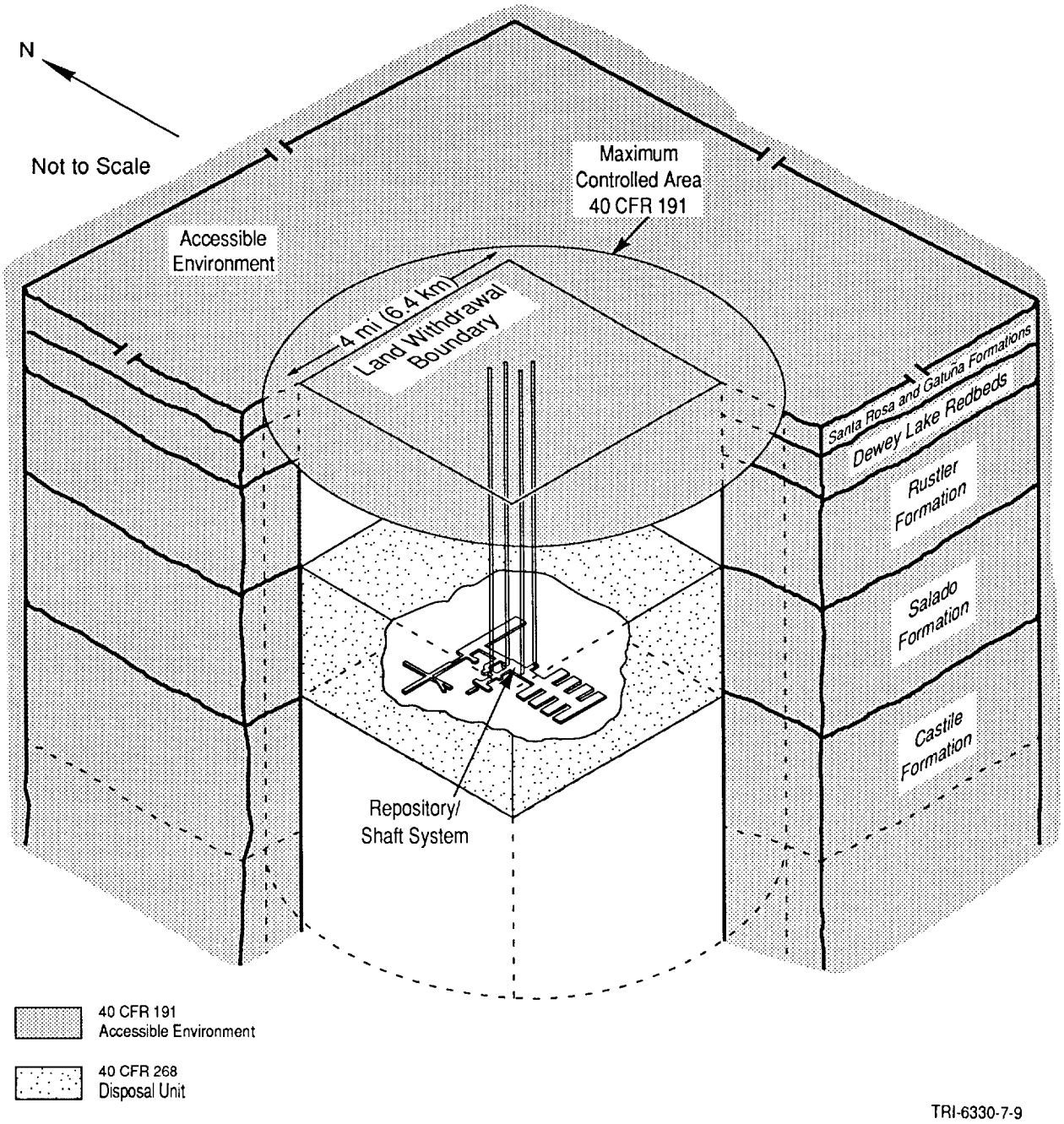

Figure 3-2. Artist's concept of the WIPP disposal system showing the controlled area and accessible environment for 40 CFR 191, Subpart B, and the repository/shaft system. The repository/shaft system scale is exaggerated. On the land surface, the land-withdrawal boundary is shown at the same scale as the maximum extent of the controlled area (modified from Bertram-Howery and Hunter, 1989b). The disposal-unit boundaries for 40 CFR 268 for the WIPP Test Phase are shown for reference (US EPA, 1990a).

records, government ownership, and other methods of preserving knowledge about the disposal system (see Section 3.2.4). Permanent markers and other passive institutional controls are intended to indicate the dangers of the wastes and their location (§ 191.12(e); § 191.12(g)).

3.2.4 "Disposal System" and "Barriers"

The Standard defines "**disposal system**" to mean "any combination of engineered and natural barriers that isolate...radioactive waste after disposal" (§ 191.12(a)). Additionally,

> "'[b]arrier' means any material or structure that prevents or substantially delays movement of water or radionuclides toward the accessible environment. For example, a barrier may be a geologic structure, a canister, a waste form with physical and chemical characteristics that significantly decrease the mobility of radionuclides, or a material placed over and around waste, provided that the material or structure substantially delays movement of water or radionuclides" (§ 191.12(d).

For the WIPP, the **disposal system** is the combination of the engineered **barriers** of the repository/shaft system and the natural **barriers** of the "disposal site" (Figure 3-2) that isolate the wastes from the accessible environment. The engineered barriers are seals in drifts and panel entries' backfill in drifts and panels, seals in shafts, and plugs in boreholes. Engineered modifications to the repository design could include making the waste itself form a **barrier**. Natural **barriers** are the subsurface geologic and hydrologic systems within the controlled area that inhibit release and migration of hazardous materials. **Barriers** are not limited to the examples given in the Standard's definition, nor are those examples mandatory for the WIPP. As recommended by the EPA in Appendix B, "...reasonable projections for the protection expected from all of the engineered and natural barriers...will be considered" (US EPA, 1985, p. 38088). No portion will be disregarded, unless that portion of the system makes a "negligible contribution to the overall isolation provided" by the WIPP (US DOE, 1989).

3.3 Containment Requirements

The primary objective of Subpart B is "to isolate most of the wastes from man's environment by limiting long-term releases and the associated risks to populations" (US EPA, 1985, p. 38070). This objective is reflected quantitatively in the Containment Requirements (§ 191.13).

3.3.1 Performance Assessment

Quantitatively evaluating compliance with the Containment Requirements requires a performance assessment, which has specific meaning within the Standard:

> "'Performance assessment' means an analysis that: (1) identifies the processes and events that might affect the disposal system; (2) examines the effects of these processes and events on the performance of the disposal system; and (3) estimates the cumulative releases of radionuclides, considering the associated uncertainties, caused by all significant processes and events. These estimates shall be incorporated into an overall probability distribution of cumulative release to the extent practicable" (§ 191.12(q)).

Identification of processes and events that might affect the disposal system is part of scenario development and screening for the WIPP and is discussed in Chapter 4 of this volume and Volume 2 of this report. Examining the effects of the processes and events and estimating cumulative releases of radionuclides are part of the performance-assessment consequence modeling and are also discussed in Chapter 4 of this volume and Volume 2 of this report.

The Containment Requirements state that performance must be measured in probabilistic terms. The allowable radionuclide release is not a single, fixed quantity, but rather is a function of the probability that the events and parameter values that contribute to the release will occur (Bertram-Howery and Swift, 1990). Specifically,

> "cumulative releases of radionuclides to the accessible environment for 10,000 years after disposal from all significant processes and events that may affect the disposal system shall:
>
> (1) Have a likelihood of less than one chance in 10 of exceeding the quantities calculated according to Table 1 (Appendix A) [see Section 3.3.2 of this volume], and
>
> (2) Have a likelihood of less than one chance in 1,000 of exceeding ten times the quantities calculated according to Table 1 (Appendix A) [see Section 3.3.2 of this volume]" (§ 191.13(a)).

Numerical limits have been placed not on the predicted cumulative radionuclide releases, but rather on the probability that cumulative releases will exceed quantities calculated as prescribed.

With the minor modifications of a 1000-year time period and the addition of a water withdrawal well to provide a potential pathway for radionuclides to reach humans, the performance-assessment methodology developed for the Containment Requirements can be used to assess compliance with undisturbed

performance for the Individual Protection Requirements (see Section 3.5 and Chapter 4 of this volume). This volume will refer to the assessment of compliance with both § 191.13(a) of the Containment Requirements and the Individual Protection Requirements as the "performance assessment."

3.3.2 Release Limits

Appendix A of the Standard establishes release limits for all regulated radionuclides. Table 1 in that appendix gives the limit for cumulative releases to the accessible environment for 10,000 years after disposal for each radionuclide per unit of waste. Note 1(e) to Table 1 defines the unit of waste as an amount of TRU wastes containing one million curies of alpha-emitting transuranic radionuclides with half-lives greater than 20 years. Note 2(b) describes how to develop release limits for a TRU-waste disposal system by determining the waste-unit factor, which is the inventory (in curies) of transuranic alpha-emitting radionuclides in the wastes with half-lives greater than 20 years, divided by one million curies, where transuranic is defined as radionuclides with atomic weights *greater* than 92 (uranium). Consequently, as currently defined in the Standard, all radioactivity in the wastes cannot be included when calculating the waste-unit factor, and release limits are lower than they would be if the waste-unit factor were based on the entire inventory. For the WIPP, 4.3×10^6 curies of the 1992 radioactivity design total of 10.0×10^6 curies are estimated to come from transuranic alpha-emitting radionuclides with half-lives greater than 20 years (memorandum by Peterson in Volume 3, Appendix A of this report). This number is based on the design radionuclide inventories by waste generator for contact-handled (CH) and remotely handled (RH) TRU wastes (see memorandum by Peterson in Volume 3, Appendix A of this report). By definition, isotopes of uranium (atomic weight of 92) and those that are short-lived (half-lives less than 20 years) cannot be included in determining the waste-unit factor. The most important such isotope for the WIPP is Pu-241, which has a half-life of 14.4 years (see Volume 3 of this report). Although Pu-241 and other isotopes in the design radionuclide inventories cannot be included in calculating the waste-unit factor, performance assessments for the WIPP do consider these radionuclides and their decay products in consequence calculations.

Note 6 of Table 1 in the Standard's Appendix A describes the manner in which the release limits are to be used to determine compliance with § 191.13(a): for each radionuclide released, the ratio of the estimated cumulative release to the release limit for that radionuclide must be determined; ratios for all radionuclides are then summed for comparison to

the requirements of § 191.13(a). Thus, the quantity of a radionuclide that may be released depends on the quantities of all other radionuclides projected to be released but cannot exceed its own release limit. The summed normalized release cannot exceed 1 for probabilities greater than 0.1, and cannot exceed 10 for probabilities greater than 0.001 but less than 0.1 (§ 191.13(a)). Potential releases estimated to have probabilities less than 0.001 are not limited (§ 191.13(a)). Calculation methods for summed normalized releases are described in more detail in Volume 2 of this report.

3.3.3 Human Intrusion

Determining compliance with the Standard requires performance assessments that include the probabilities and consequences of disruptive events. Appendix B of the Standard indicates that "inadvertent and intermittent intrusion by exploratory drilling for resources ... can be the most severe intrusion scenario assumed by the [DOE]" (US EPA, 1985, p. 38089).

In the Second Modification to the Consultation and Cooperation Agreement (US DOE and State of New Mexico, 1981, as modified), the DOE agreed to prohibit further subsurface mining, drilling, slant drilling under the withdrawal area, or resource exploration unrelated to the WIPP Project from the land surface to 6000 feet (1830 m) in the subsurface for the 16 square miles under DOE control. The Standard limits reliance on future institutional control in that "performance assessments... shall not consider any contributions from active institutional controls for more than 100 years after disposal" (§ 191.14(a)). The Standard further requires that "disposal sites shall be designated by the most permanent markers, records, and other passive institutional controls practicable to indicate the dangers of the wastes and their location" (§ 191.14(c)). The possibility of inadvertent human intrusion into repositories in salt formations during resource evaluation must be considered, and the use of passive institutional controls to deter such intrusion should be "taken into account" in performance assessments (US EPA, 1985, p. 38080).

The EPA gives specific guidance in Appendix B of the Standard for considering inadvertent human intrusion. The EPA indicates that only realistic possibilities for human intrusion that may be mitigated by design, site selection, and passive institutional controls need be considered. Additionally, the EPA assumes that passive institutional controls should "...reduce the chance of inadvertent intrusion compared to the likelihood if no markers and records were in place." Exploring for subsurface resources requires extensive and organized effort. Because of

this effort, information from passive institutional controls is likely to reach resource explorers and deter intrusion into the disposal system (US EPA, 1985, p. 38080). In particular, as long as passive institutional controls "endure and are understood," the guidance states that they can be assumed to deter "systematic or persistent exploitation" of the disposal site, and furthermore, "can reduce the likelihood of inadvertent, intermittent human intrusion." The EPA indicates in Appendix B of the Standard that exploratory drilling for resources is the most severe intrusion that must be considered (US EPA, 1985, p. 38089). Because of the Standard's emphasis on exploratory drilling for resources as the most severe type of human intrusion to be considered at a disposal site, mining within the controlled area has not been included in performance assessment for the WIPP (Guzowski, 1990). Mining outside the WIPP boundary was retained for scenario development because of the possible effects on recharge and groundwater flow of subsidence over mined areas (Guzowski, 1990; Guzowski and Helton, 1991, Section 4.1.4). Consequences of such potash mining have not yet been included in performance-assessment modeling and will be addressed in future analyses when a three-dimensional model for regional groundwater flow is available.

Effects of site location, repository design, and passive institutional controls can be used in judging the likelihood and consequences of inadvertent drilling intrusion. The EPA suggests in Appendix B of the Standard that intruders will soon detect or be warned of the incompatibility of their activities with the disposal site by their own exploratory procedures or by passive institutional controls (US EPA, 1985, p. 38089).

Appendix B specifies that credit for using active institutional controls to prevent or reduce radionuclide releases cannot be taken for more than 100 years after decommissioning (US EPA, 1985, p. 38088). In previous performance assessments (Bertram-Howery et al., 1990; WIPP PA Division, 1991a), the WIPP Project has assumed that no human intrusion of the repository would occur during the 100-year period of active institutional controls, but that site-specific exploitation outside the controlled area might occur. For the 1992 performance assessment, the probabilities of human intrusion were also considered based on the judgments of an expert panel (see memorandum by Hora in Volume 3, Appendix A of this report). Comparisons of performance estimated using both the probabilities based on expert judgment and the probability model used in 1991 are provided in Chapter 5 of this volume.

Appendix B of the Standard (US EPA, 1985, p. 38089) specifies that after the period of active institutional control, the predicted number of exploratory boreholes assumed to be drilled inside the controlled area

through inadvertent human intrusion is to be based on site-specific information and need not exceed 30 boreholes/km^2 (0.4 mi^2) per 10,000 years. No more severe scenarios for human intrusion inside the controlled area need be considered. Appendix B also indicates that while passive institutional controls endure, they can reduce the likelihood of inadvertent human intrusion to a degree to be determined by the DOE, although the possibility of inadvertent intrusion cannot be eliminated (US EPA, 1985, p. 38088).

Given the approach chosen by the EPA for defining the disposal standards, repository performance must be predicted probabilistically to evaluate compliance quantitatively. Determining the probability of intrusion poses questions that cannot be answered by numerical modeling or experimentation. Projecting future drilling activity requires unattainable knowledge about complex variables such as economic demand for natural resources, institutional control over the site, public awareness of radiation hazards, and changes in exploration technology. The 1992 preliminary performance assessment uses estimates of the probability of human intrusion that are based on guidance from expert panels on possible future societies and on the potential effectiveness and duration of passive institutional controls to deter intrusion into the WIPP (Hora et al., 1991; also see Volume 2 of this report and the memorandum by Hora in Volume 3, Appendix A of this report).

3.3.4 Uncertainties

The EPA recognizes in the preamble to the Standard that "standards must be implemented in the design phase for ... disposal systems because active surveillance cannot be relied upon" over the long time of interest. The EPA further notes that "standards must accommodate large uncertainties, including uncertainties in our current knowledge about disposal-system behavior and the inherent uncertainties regarding the distant future" (US EPA, 1985, p. 38070). Within the text of the Standard, the definition of performance assessment requires "considering the associated uncertainties" (§ 191.12(q); see Section 3.3.1 of this volume).

"Uncertainties in parameters" are the only source of uncertainty specifically identified in the Standard (US EPA, 1985, Appendix B, p. 38088). Uncertainty in input parameters used in predictive models may result from several sources, including incomplete data, intrinsic spatial variability of the property in question, measurement uncertainty, and uncertainty resulting from differences in scale between data acquisition and model application. Uncertainty in input parameters is not, however, the only potential source of uncertainty in performance assessment. As

indicated in the following definitions adopted from Gallegos et al. (1992) and the NEA (1992a), additional uncertainty may enter the analysis through the choice of conceptual models used to represent the disposal system.

> Conceptual Model: A set of qualitative assumptions used to describe a system or subsystem for a given purpose. At a minimum, these assumptions concern the geometry and dimensionality of the system, initial and boundary conditions, time dependence, and the nature of the relevant physical and chemical processes. The assumptions should be consistent with one another and with existing information within the context of the given purpose.
>
> Alternative Conceptual Models: Alternative sets of assumptions that describe the same system for the same purpose, where each set of assumptions is consistent with the existing information.
>
> Conceptual Model Uncertainty: The lack of knowledge about the system resulting from limited information available to support or refute alternative conceptual models.

Uncertainty may exist also in the computational models used to perform quantitative analyses based on the chosen conceptual models. As used here, computational models include the mathematical models used to represent the physical processes, the numerical models used to solve the mathematical models, and the computer codes used to implement the solution.

The selection of scenarios to be analyzed also may introduce uncertainty into the estimated performance. Scenario uncertainty may be further subdivided into uncertainty in the completeness of the scenarios considered, uncertainty in the way in which computational results are aggregated to represent scenario consequences, and uncertainty in the probabilities associated with their occurrence.

Performance assessment thus requires considering numerous uncertainties in the projected performance of the disposal system. The WIPP Performance Assessment Department's methodology for uncertainty analysis (described in Chapter 4 of this volume and Volume 2, Chapters 3 and 4 of this report) relies on the selection of scenarios to be analyzed, the determination of scenario probabilities, and the calculation of scenario consequences using a Monte Carlo simulation technique (Pepping et al., 1983; Hunter et al., 1986; Cranwell et al., 1987, 1990; Campbell and Cranwell, 1988; Rechard, 1989; Helton, 1991). The Performance Assessment Department will assess and reduce uncertainty to the extent practicable using a variety of techniques (Table 3-1). For example, the WIPP Project uses uncertainty analyses to evaluate the amount of variability in the results of a model that can be attributed to uncertainty in the parameter input data.

Table 3-1. Techniques for Assessing or Reducing Uncertainty in the WIPP Performance Assessment

Type of Uncertainty	Technique for Assessing or Reducing Uncertainty	References to Performance Assessment Reports (also see references cited within these reports)
Scenarios (Completeness, Aggregation, and Probabilities)	Expert Judgment and Peer Review	Marietta et al., 1989; Bertram-Howery et al., 1990, Chapter 4; Guzowski, 1990; Tierney, 1990; Helton, 1991; Guzowski and Helton, 1991; Hora et al., 1991; memorandum by Hora in Volume 3, Appendix A of this report
	Quality Assurance	Rechard et al., 1992a, 1992b
Conceptual Models	Expert Judgment and Peer Review	Marietta et al., 1989; Bertram-Howery et al., 1990; WIPP PA Division, 1991b; Volume 2 of this report
	Sensitivity Analysis	Helton et al., 1991, 1992; Volume 4 of this report
	Uncertainty Analysis	Helton et al., 1991, 1992; Volume 4 of this report
	Quality Assurance	Rechard et al., 1992b
Computational Models	Expert Judgment and Peer Review	Marietta et al., 1989; Bertram-Howery et al., 1990; WIPP PA Division, 1991b; Volume 2 of this report
	Verification and Validation*	Marietta et al., 1989; Bertram-Howery et al., 1990; WIPP PA Division, 1991b; Volume 2 of this report
	Sensitivity Analysis	Helton et al., 1991, 1992; Volume 4 of this report
	Quality Assurance	Rechard et al., 1991

* to the extent possible

Table 3-1. Techniques for Assessing or Reducing Uncertainty in the WIPP Performance Assessment (continued)

Type of Uncertainty	Technique for Assessing or Reducing Uncertainty	References to Performance Assessment Reports (also see references cited within these reports)
Parameter Values and Variability	Expert Judgment and Peer Review	Rechard et al., 1990a, 1990b; WIPP PA Division, 1991c; Trauth et al., 1992; Volume 3 of this report
	Data-Collection Programs	Annual program plans for the WIPP
	Sampling Techniques	Helton, 1991
	Sensitivity Analysis	Helton et al., 1991, 1992; Volume 4 of this report
	Uncertainty Analysis	Helton et al., 1991, 1992; Volume 4 of this report
	Quality Assurance	Rechard et al., 1992a

Source: After Bertram-Howery and Hunter, 1989b

Sensitivity analyses identify the main contributors to the observed variation in the results. These techniques typically are applied iteratively. The first iteration can include rather general assumptions leading to preliminary results that help focus these techniques in subsequent iterations. In this manner, the resources required to implement the techniques in Table 3-1 can be directed at the areas of the WIPP performance assessment where the benefits of understanding uncertainty and reducing it (where possible) would be the greatest.

Modeling the behavior of a hydrogeologic system such as the WIPP disposal system necessarily will be uncertain because knowledge about its real behavior is uncertain. Many of the parameters used as inputs to a model of the system are obtained only by a data-collection process. Investigators knowledgeable about the data they collect make a finite number of observations, choosing what parameters to measure, how to measure them, where to measure them, and when to measure them. However, the collection process itself can introduce uncertainty through measurement error, the system's inherent randomness, and limited sampling of the variable physical, chemical, and biological properties of the system. In many aspects of data collection, the professional judgment of an analyst with expertise in the area of investigation often enters into the scientific process. For example, selection of methods to collect data, interpretation of data, development of conceptual models, and selection of model parameters all require professional analysis and judgment. The analyst's final data set is based on available data, use of the parameter in the computational model, behavior of analogous systems, and the analyst's own expert judgment.

The WIPP Project will use more formalized expert judgment for some parameters or models identified as being important to WIPP performance in cases where significant uncertainty exists in the available data and conceptual models and experimental or field data cannot be practicably obtained. In these instances, formal elicitations will provide probability distributions for model parameters. These distributions may be used to provide guidance to the Project until experimental or field data become available, or, in those cases where direct acquisition of data is impossible or unrealistic, the elicited distributions may form part of the basis for compliance evaluation. Expert panels may also be used to provide independent evaluation.

Formal elicitation offers a structured procedure for gathering opinions from a panel of professionals with the recognized training and experience to address a specific problem. The process encourages diversity in opinions and thus guards against understating uncertainty. In addition, formal elicitation promotes clear and thorough documentation of the manner

in which results are achieved (Hora and Iman, 1989). The judgments that result from formal elicitation represent the current state of knowledge and provide a consensus of understanding, but they do not create information. An important aspect of elicitation, either during or following the process, is examining the manner in which new data may improve understanding. As new observations are made, the state of knowledge is refined. Thus far, expert panels have provided estimates of solubility and sorption parameters for selected radionuclides (Trauth et al., 1992). Additional expert panels may be convened to quantify other parameters and thus address the uncertainty in using those important data sets and associated conceptual models.

WIPP performance assessment must also address the potential for human intrusion and the effectiveness of passive institutional controls to deter such intrusion. An expert panel has already provided judgment on future societies' possible technical capabilities, needs, and social structures (Hora et al., 1991). An additional panel has developed marker characteristics to maximize both marker lifetimes and information that could be communicated to future generations. These panel judgments were used in the 1992 performance assessment and are discussed in Volumes 2 and 3 of this report. Another expert panel is under consideration to develop strategies for barriers to intrusion-by-drilling.

One type of uncertainty that cannot be completely resolved is the validity of various conceptual and computational models for predicting disposal-system behavior 10,000 years into the future. Although models will be validated using available site or analog data to the extent possible, expert judgment will be relied upon where validation is not possible. Uncertainties arising from the numerical solutions of a mathematical model are resolved in the process of verification (checking for numerical accuracy) of computer programs. Uncertainty resulting from the scenarios selected for modeling is most appropriately addressed in scenario development through a systematic and thorough examination of possible scenario components (events and processes); in scenario screening based on probability, consequence, physical reasonableness, and regulatory guidance; and in probability assignment by the techniques used for evaluation or estimation. Expert judgment to evaluate completeness and provide estimates of probabilities for events and processes may also be necessary (US DOE, 1990a).

Quality assurance (QA) procedures for performance assessment control analysis results in three areas—data, software, and analysis—and two subareas—elicitation of judgments from expert panels and documentation. QA procedures for data on facility design and geologic model parameters control traceability and documentation of data (Rechard et al., 1992a). QA

procedures for software ensure that it performs as expected during the analysis by controlling traceability, retrievability, verification, and documentation (Rechard et al., 1991). QA procedures for analysis provide a framework and process so that analysis results present a reliable view of WIPP performance based on the present knowledge by controlling traceability, validation, personnel qualifications, data use, and peer review (Rechard et al., 1992b). QA procedures for documentation ensure that sufficient documented information is available to record how analyses were performed and how decisions were reached by specifying technical, management, and critical peer reviews (Rechard et al., 1992b).

3.3.5 Compliance Assessment

The Standard assumes that the results of the performance assessment for § 191.13(a) will be incorporated, to the extent practicable, into an overall probability distribution of cumulative release. In Appendix B of the Standard, the EPA assumes that, whenever practicable, results can be assembled into a single complementary cumulative distribution function (CCDF) that indicates the probability of exceeding various levels of summed normalized cumulative releases (US EPA, 1985, p. 38088) (Figure 3-3).

Descriptions of a procedure for performance assessment based on the construction of a CCDF are available (Pepping et al., 1983; Hunter et al., 1986; Cranwell et al., 1987, 1990; Campbell and Cranwell, 1988; Rechard, 1989; Helton, in press). The construction of CCDFs follows from the development of scenario probabilities and the calculation of scenario consequences. Further, the effects of different types of uncertainties can be shown by constructing families of CCDFs and then reducing each family to a single CCDF. The construction of families of CCDFs and various summary CCDFs is described in Volume 2 of this report.

Currently, CCDF curves for single scenarios and single conceptual models are used extensively in performance-assessment sensitivity analysis for comparing alternative conceptual models (Helton et al., 1991, 1992). Such CCDF curves do not establish compliance or noncompliance, but they convey vital information about how changes in model assumptions or parameter distributions may influence performance (Bertram-Howery and Swift, 1990).

Preliminary performance assessments are performed periodically for the WIPP to provide interim guidance to the Project as it prepares for final compliance evaluations. No "final" CCDF curves yet exist because the

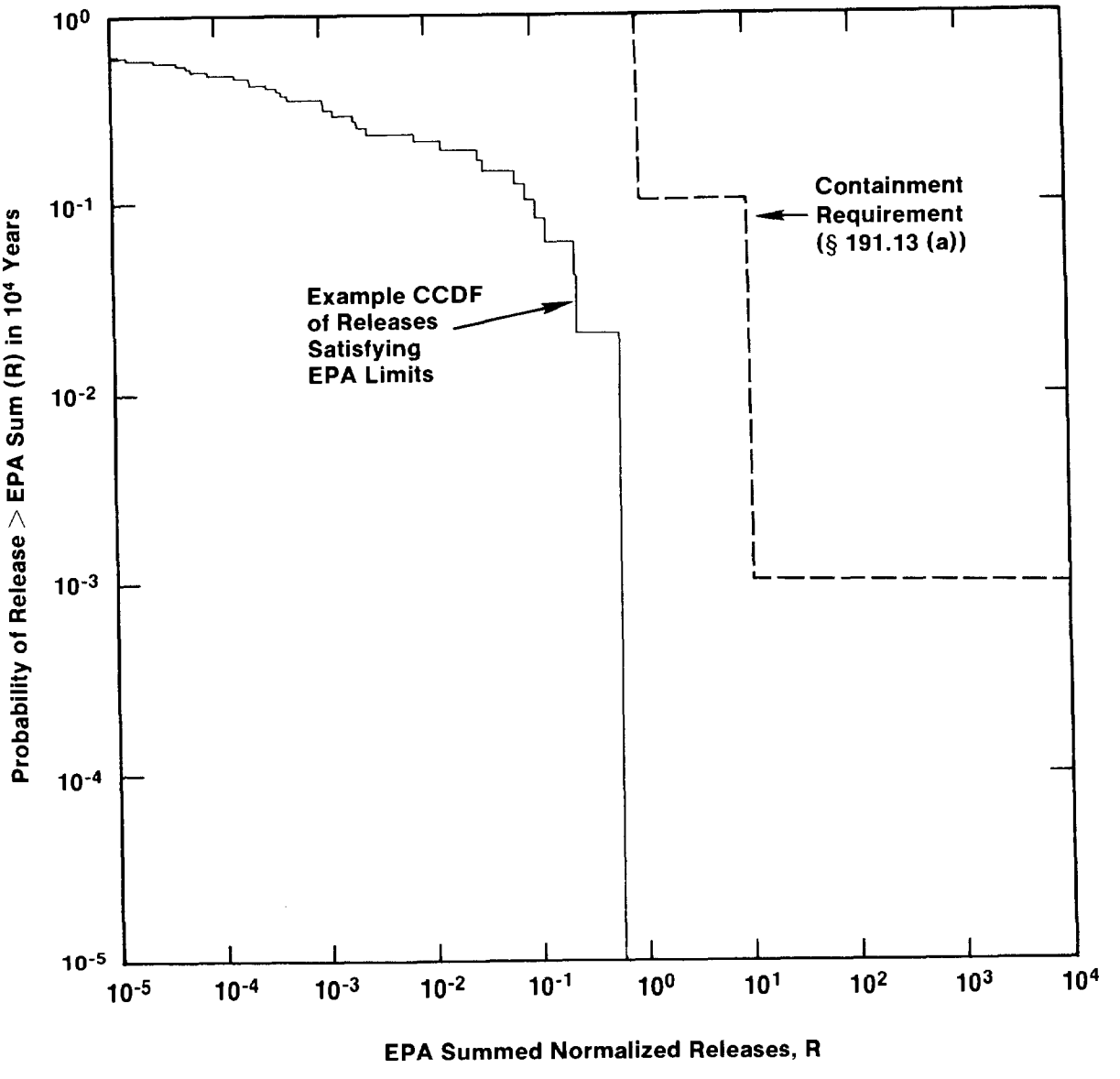

Figure 3-3. Hypothetical CCDF illustrating compliance with the Containment Requirements (after Marietta et al., 1989).

modeling system is incomplete and some input parameters have yet to be fully specified. Final probabilities for specific scenarios and many parameter-value distribution functions are still undetermined (see Volumes 2 and 3 of this report); therefore all CCDF curves presented in this report are preliminary. Although the compliance limits are routinely included on plots as reference points, the currently available curves should not be used to judge compliance with the Containment Requirements because the curves reflect an incomplete modeling system (Volume 2 of this report) and incomplete data (Volume 3 of this report) and because the Standard has not been repromulgated.

3.3.6 "Reasonable Expectation" of Compliance

The EPA assumes that a single CCDF will incorporate all uncertainty (US EPA, 1985, p. 38088). The Containment Requirements (§ 191.13(a)) state that, based upon performance assessment, releases shall have probabilities not exceeding specified limits. Appendix B of the Standard states that "the [EPA] assumes that a disposal system can be considered to be in compliance with § 191.13 if this single distribution function meets the requirements of § 191.13(a)" (US EPA, 1985, p. 38088). However, § 191.13(b) states:

> "Performance assessments need not provide complete assurance that the requirements of 191.13(a) will be met. Because of the long time period involved and the nature of the events and processes of interest, there will inevitably be substantial uncertainties in projecting disposal system performance. Proof of the future performance of a disposal system is not to be had in the ordinary sense of the word in situations that deal with much shorter time frames. Instead, what is required is a reasonable expectation, on the basis of the record before the implementing agency, that compliance with 191.13(a) will be achieved."

Given the discussions on use of qualitative judgment in Appendix B to the Standard, the EPA means the entire record, including qualitative judgments. The guidance states:

> "The [EPA] believes that the implementing agencies must determine compliance with §§ 191.13, 191.15, and 191.16 of Subpart B by evaluating long-term predictions of disposal system performance. Determining compliance with § 191.13 will also involve predicting the likelihood of events and processes that may disturb the disposal system. In making these various predictions, it will be appropriate for the implementing agencies to make use of rather complex computational models, analytical theories, and prevalent expert judgment relevant to the numerical predictions. Substantial uncertainties are likely to be encountered in making these predictions. In fact, sole reliance on these numerical

predictions to determine compliance may not be appropriate; the implementing agencies may choose to supplement such predictions with qualitative judgments as well."

Thus, the EPA assumes that satisfying the numeric requirements is sufficient to demonstrate compliance with § 191.13(a) but not mandatory. A basis for concluding that a system provides good isolation can include qualitative judgment as well as quantitative results and thus does not totally depend upon the calculated CCDF. As discussed in the "Test Phase Plan" currently being prepared by the DOE, and in the *Technical Needs Assessment* report (US DOE, 1992a), the likelihood that excess releases will occur must be considered in the qualitative decision about a "reasonable expectation" of compliance but is not necessarily the deciding factor.

In the supplementary information published with the Standard, the EPA states that "the numerical standards chosen for Subpart B, by themselves, do not provide either an adequate context for environmental protection or a sufficient basis to foster public confidence..." (US EPA, 1985, p. 38079). The EPA also states that "factors such as [food chains, ways of life, and the size and geographical distributions of populations] cannot be usefully predicted over [10,000 years]....The results of these analyses should not be considered a reliable projection of the 'real' or absolute number of health effects resulting from compliance with the disposal standards" (US EPA, 1985, p. 38082).

The EPA recognizes that too many uncertainties exist in projecting the behavior of natural and engineered components for 10,000 years and that too many opportunities for errors in calculations or judgments are possible for the numerical requirements to be the sole basis for determining the acceptability of a disposal system (US EPA, 1985, p. 38079). Qualitative Assurance Requirements (discussed further in Section 3.4 of this volume) were included in the Standard to ensure that "cautious steps are taken to reduce the problems caused by these uncertainties." These qualitative Assurance Requirements are "an essential complement to the quantitative containment requirements" (US EPA, 1985, p. 38079). Each qualitative requirement was chosen to compensate for some aspect of the inherent uncertainty in projecting the future performance of a disposal system (see Section 3.4 of this volume). The Assurance Requirements begin by declaring that compliance with their provisions will "provide the confidence needed for long-term compliance with the requirements of 191.13" (§ 191.14).

Determining compliance with Subpart B depends on the estimated overall probability distribution of cumulative releases and on the estimated annual doses; however, it also depends on the strength of the assurance strategies (US DOE, 1987, currently in revision) that will be implemented and on the qualitative judgment of the DOE and its analysts. The preceding discussion demonstrates the EPA's recognition of the difficulties involved in predicting the future and in quantifying the outcomes of future events. The EPA expects the DOE to understand the uncertainties in the disposal system's behavior to the extent practical, while recognizing that substantial uncertainties will nevertheless remain.

3.4 Assurance Requirements

The EPA included Assurance Requirements (§ 191.14) in the 1985 Standard to provide confidence the agency believes is needed for long-term compliance with the Containment Requirements. These requirements apply only to disposal systems not regulated by the NRC, because comparable provisions exist in NRC regulations. The Assurance Requirements are designed to complement the Containment Requirements because of the uncertainties involved in predicting long-term performance of disposal systems (US EPA, 1985, p. 38072).

Each Assurance Requirement applies to some aspect of uncertainty about long-term containment:

> Limiting reliance on active institutional controls to 100 years precludes relying on future generations to maintain surveillance;
>
> Carefully planned monitoring will reduce the likelihood of unexpectedly poor system performance going undetected;
>
> Using passive institutional controls such as markers and records will reduce the chances of inadvertent or systematic intrusion;
>
> Including multiple barriers, both engineered and natural, will reduce the risk should one type of barrier not perform as expected;
>
> Considering future resource potential and demonstrating that the favorable characteristics of the disposal site compensate for the likelihood of disturbance will add to the confidence that the chosen site is appropriate;
>
> Selecting a disposal system that permits possible future recovery of most of the wastes for a reasonable period of time after disposal will allow future generations the option of relocating the wastes should new developments warrant such recovery (US DOE,

1990d). In promulgating the Standard, the EPA stated that "the intent of this provision was not to make recovery of waste easy or cheap, but merely possible...because the [EPA] believes that future generations should have options to correct any mistakes that this generation might unintentionally make" (US EPA, 1985, p. 38082). The EPA also stated that "*any* current concept for a mined geologic repository meets this requirement *without* any additional procedures or design features" (US EPA, 1985, p. 38082, emphasis in original).

3.5 Individual Protection Requirements

The Individual Protection Requirements (§ 191.15) of the Standard require predicting potential doses to humans resulting from releases to the accessible environment for undisturbed performance during the first 1000 years after decommissioning of the repository, in the event that performance assessments predict such releases. Although challenges to this requirement contributed to the remand of Subpart B to the EPA, the WIPP Project has made no assumptions about how the requirement may change when the Standard is repromulgated.

The methodology developed for assessing compliance with the Containment Requirements can be used to estimate doses as specified by the Individual Protection Requirements. One of the products of scenario development for the Containment Requirements is a base-case scenario for the WIPP that describes undisturbed conditions. The undisturbed performance of the repository is its design-basis behavior, including variations in that behavior resulting from uncertainties in the 10,000-year performance of natural and engineered barriers and excluding human intrusion and unlikely natural events, as defined in §191.12(p):

> "'Undisturbed performance' means predicted behavior of a disposal system, including consideration of the uncertainties in predicted behavior, if the disposal system is not disrupted by human intrusion or the occurrence of unlikely natural events."

Undisturbed performance for the WIPP is understood to mean that uncertainties in such repository features as engineered barriers (seals and plugs) must be specifically included in the analysis of the predicted behavior (US DOE, 1990a). Human intrusion means any human activity other than those directly related to repository characterization, construction, operation, or monitoring. The effects of intrusion are specifically excluded from the undisturbed-performance analysis (US DOE, 1989).

Because of the relative stability of the natural systems within the region of the WIPP disposal system, all events and processes that are

expected to occur naturally are part of the base-case scenario and are assumed to represent undisturbed performance (Marietta et al., 1989). Unlikely natural events not included in undisturbed performance of the WIPP are those events and processes that have not occurred in the past at a sufficient rate to affect the Salado Formation at the repository horizon within the controlled area and potentially cause the release of radionuclides.

The EPA assumes in Appendix B to the Standard that compliance with the Individual Protection Requirements "can be determined based upon best estimate predictions" rather than a probabilistic analysis. Thus, according to the EPA, when uncertainties are considered, only "the mean or median of the appropriate distribution, whichever is higher," need fall below the limits (US EPA, 1985, p. 38088).

The Individual Protection Requirements state that "the annual dose equivalent from the disposal system to any member of the public in the accessible environment" shall not exceed "25 millirems to the whole body or 75 millirems to any critical organ" (§ 191.15). These requirements apply to undisturbed performance of the disposal system, considering all potential release and dose pathways, for 1000 years after disposal. A specifically stated requirement is that modeled individuals be assumed to consume 2 L (0.5 gal) per day of drinking water from a significant source of groundwater, as defined in the Standard:

> "'Significant source of ground water'...means: (1) An aquifer that: (i) Is saturated with water having less than 10,000 milligrams per liter of total dissolved solids; (ii) is within 2,500 feet of the land surface; (iii) has a transmissivity greater than 200 gallons per day per foot, provided that any formation or part of a formation included within the source of ground water has a hydraulic conductivity greater than 2 gallons per day per square foot...; and (iv) is capable of continuously yielding at least 10,000 gallons per day to a pumped or flowing well for a period of at least a year; or (2) an aquifer that provides the primary source of water for a community water system as of [November 18, 1985]" (§ 191.12(n)).

No water-bearing unit at the WIPP meets the first definition of significant source of groundwater at tested locations within the land-withdrawal area. At most well locations, water-bearing units meet neither requirement (i) nor (iii): total dissolved solids exceed 10,000 mg/L and transmissivity is less than 200 gallons per day per foot (26.8 $ft^3/ft \cdot day$ or 2.9×10^{-5} $m^3/m \cdot sec$) (Siegel et al., 1991; Brinster, 1991). Outside the land-withdrawal area, however, portions of the Culebra Dolomite Member do meet the requirements of the first definition. The WIPP Project will

assume that any *portion* of an aquifer that meets the first definition is a significant source of groundwater and will examine communication between nonqualifying and qualifying portions. No community water system is being supplied by any aquifer near the WIPP; therefore, no aquifer meets the second definition of significant source of groundwater (US DOE, 1989).

Based on current evaluations, no units near the WIPP appear to meet the entire definition of a significant source of groundwater. The nearest aquifer that meets the first definition of a significant source of groundwater over its entire extent is the alluvial and valley-fill aquifer along the Pecos River. Communication between this aquifer and any other aquifers near the WIPP will be evaluated in future analyses when an improved model for regional groundwater flow is available (US DOE, 1989). Studies will include reviewing and assessing regional and WIPP drilling records and borehole histories for pertinent hydrologic information (US DOE, 1990a).

No releases from the undisturbed repository/shaft system are expected to occur within the 1000-year period of the Individual Protection Requirements, nor within the 10,000-year period of the Containment Requirements (Lappin et al., 1989; Marietta et al., 1989; WIPP PA Division, 1991b; WIPP PA Department, 1992; Chapter 5 of this volume). Therefore, dose predictions for undisturbed performance are not expected to be necessary. To date, analyses of undisturbed conditions indicate successful long-term isolation of the wastes (see Chapter 5 of this volume).

3.6 Groundwater Protection Requirements

Special sources of groundwater are protected by the Groundwater Protection Requirements (§ 191.16) from contamination at levels greater than certain limits. "Special sources of groundwater" are defined as

> "those Class I ground waters identified in accordance with the [EPA's] Ground-Water Protection Strategy published in August 1984 that: (1) Are within the controlled area encompassing a disposal system or are less than five kilometers beyond the controlled area; (2) are supplying drinking water for thousands of persons as of the date that the [DOE] chooses a location within that area for detailed characterization as a potential site for a disposal system (e.g., in accordance with Section 112(b)(1)(B) of the NWPA); and (3) are irreplaceable in that no reasonable alternative source of drinking water is available to that population" (§ 191.12(o)).

Class I groundwaters are defined as follows (US EPA, 1984):

> "Certain ground-water resources are in need of special protective measures. These resources are defined to include those that are highly vulnerable to contamination because of the hydrogeological characteristics of the areas under which they occur. Examples of hydrogeological characteristics that cause groundwater to be vulnerable to contamination are high hydraulic conductivity (karst formations, sand and gravel aquifers) or recharge conditions (high water table overlain by thin and highly permeable soils). In addition, special groundwaters are characterized by one of the following two factors:
>
> (1) Irreplaceable source of drinking water. These include groundwater located in areas where there is no practical alternative source of drinking water (islands, peninsulas, isolated aquifers over bed rock) or an insufficient alternative source for a substantial population; or
>
> (2) Ecologically vital, in that the groundwater contributes to maintaining either the base flow or water level for a particularly sensitive ecological system that, if polluted, would destroy a unique habitat (e.g., those associated with wetlands that are habitats for unique species of flora and fauna or endangered species)."

As defined in the Groundwater Protection Requirements, no special sources of groundwater exist at the WIPP within the maximum area allowed (Figure 3-4); therefore, the requirement to estimate radionuclide concentrations in such groundwater is not relevant to the WIPP (see Chapter 5 of this volume).

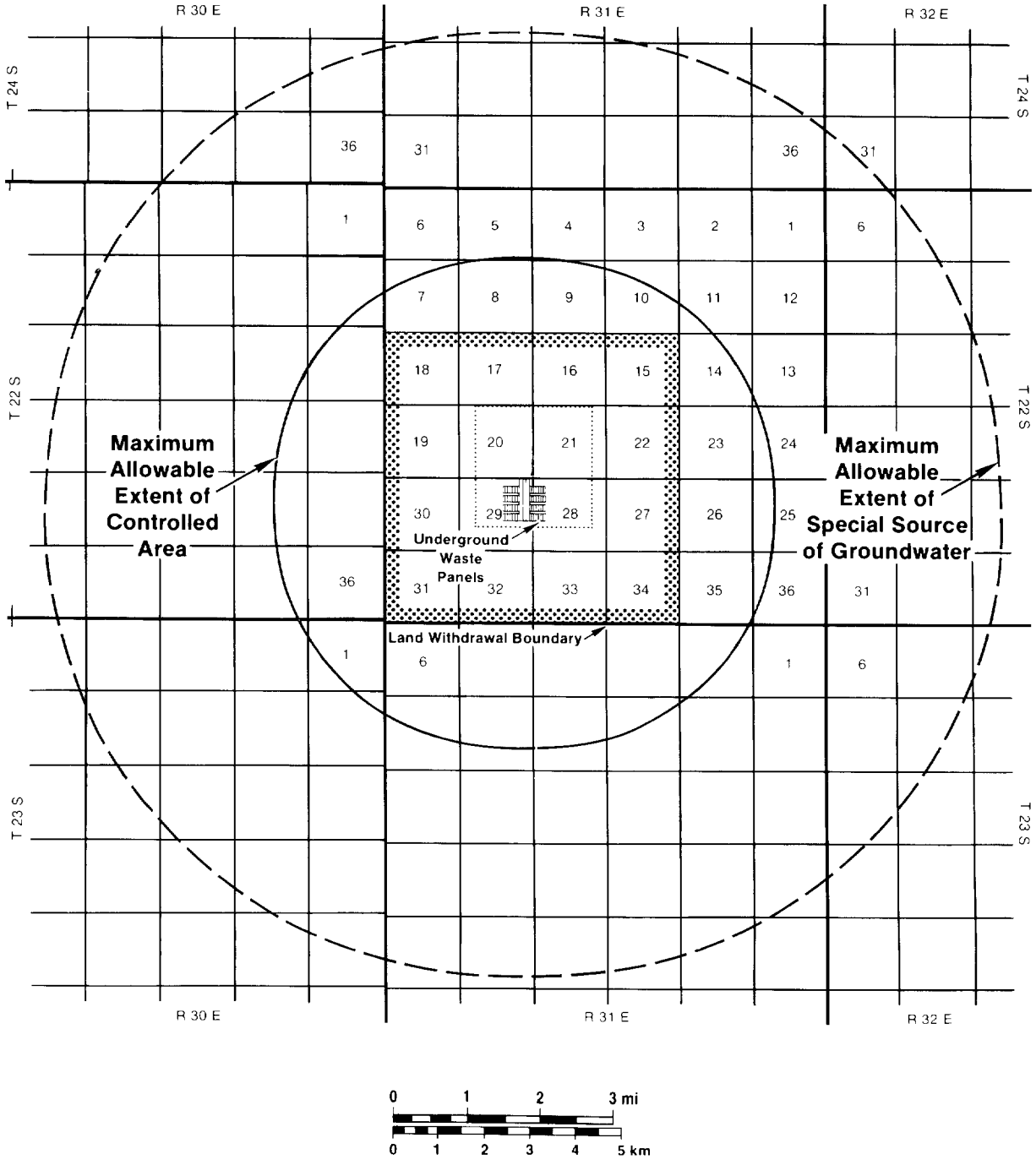

Figure 3-4. Illustration of boundary definitions pertaining to the Groundwater Protection Requirements (after US DOE, 1989). The dashed line, drawn 5 km (3 mi) from the maximum allowable extent of the controlled area (§ 191.12(g)), shows the maximum area in which the occurrence of a special source of groundwater (§ 191.12(o)) is of regulatory interest.

4. PERFORMANCE-ASSESSMENT METHODOLOGY

This chapter contains a brief and simplified overview of the methodology used in WIPP performance assessment. A more complete discussion is presented in Volume 2 of this report and in references cited therein.

The WIPP performance assessment represents risk as a triplet consisting of the answers to the following three questions (Kaplan and Garrick, 1981):

(1) What can happen? (scenarios)

(2) How likely are things to happen? (probabilities of scenarios)

(3) What are the consequences of these things (scenarios) happening?

The first question is answered by a systematic scenario construction procedure that results in a set of comprehensive and mutually exclusive scenarios for consequence analysis (Guzowski, 1990; Cranwell et al., 1990; NEA, 1992b). Answering the second question requires that probability estimates be made for the scenarios retained for analysis. A formal elicitation procedure using expert panels has been recommended by other programs (Hora and Iman, 1989; Andersson et al., 1989; Stephens and Goodwin, 1989; Bonano et al., 1990) and employed by WIPP performance assessment. Answering the third question requires a modeling system to estimate consequences, expressed in terms of the performance measures of interest. The WIPP performance assessment uses a Monte Carlo technique to examine uncertainty in performance estimates and to perform sensitivity analyses that provide guidance to the Project.

The WIPP performance assessment is iterative, and answers to each of these three questions will be reexamined as the Project moves toward a final regulatory compliance evaluation. Thus, the set of scenarios selected for consequence analysis may change as new information dictates (although the scenarios examined in 1992 are essentially unchanged from 1991). Scenario probabilities have changed as expert judgment is incorporated, and the modeling system continues to change as new models and data become available.

4.1 Scenarios

WIPP performance assessment uses a formal scenario-selection procedure consisting of five steps (Cranwell et al., 1990): (1) compiling or adopting a comprehensive set of events and processes that potentially could affect the disposal system, (2) classifying the events and processes to aid in

completeness arguments, (3) screening the events and processes to identify those that can be eliminated from consideration in the performance assessment, (4) developing scenarios by combining events and processes that remain after screening, and (5) screening scenarios to identify those that have little or no effect on the performance estimate. In the application of this scenario-selection process to the WIPP, events and processes were screened according to probability, consequence, and physical reasonableness. Following guidance from the Containment Requirements of the Standard (§ 191.13), those events and processes with a probability of less than 10^{-4} in 10,000 years were eliminated, as were those which would have little or no consequence on performance or which would be physically unreasonable. This screening process is summarized in Volume 2, Chapter 4 of this report, and is described in detail in the 1991 documentation (Guzowski and Helton, 1991).

For the WIPP, the result of the scenario-selection process is a set of eight scenarios constructed from three retained events (Figure 4-1). No scenarios resulting from the selection process have been screened out. Scenarios shown in Figure 4-1 that include the effects of subsidence due to potash mining have not been included in the 1992 or previous performance assessments, but the impact of subsidence events will be examined in future analyses. The four scenarios analyzed in 1992 are discussed in the following sections.

4.1.1 Undisturbed Performance (Base Case)

As defined in the Standard (§ 191.12(p)) and discussed in Section 3.5 of this volume, "'undisturbed performance' means the predicted behavior of a disposal system, including consideration of the uncertainties in predicted behavior, if the disposal system is not disrupted by human intrusion or the occurrence of unlikely natural events." The Standard does not define "unlikely," but the WIPP Performance Assessment Department interprets the probability cutoff of 10^{-4} in 10,000 years proposed in Appendix B of the Standard for the Containment Requirements (§ 191.13) to be a suitable working definition for the term.

No disruptive natural events with probabilities greater than 10^{-4} in 10,000 years were identified during the scenario-selection procedure, so "undisturbed performance" is the same as the "base case" scenario in Figure 4-1. Because of the relative stability of the natural systems within the region of the WIPP disposal system, all naturally occurring events and processes retained for scenario construction (e.g., climate variability) (1) will occur, (2) are part of the base-case scenario, and (3) are nondisruptive. The base-case scenario (Figure 4-2a) describes the disposal

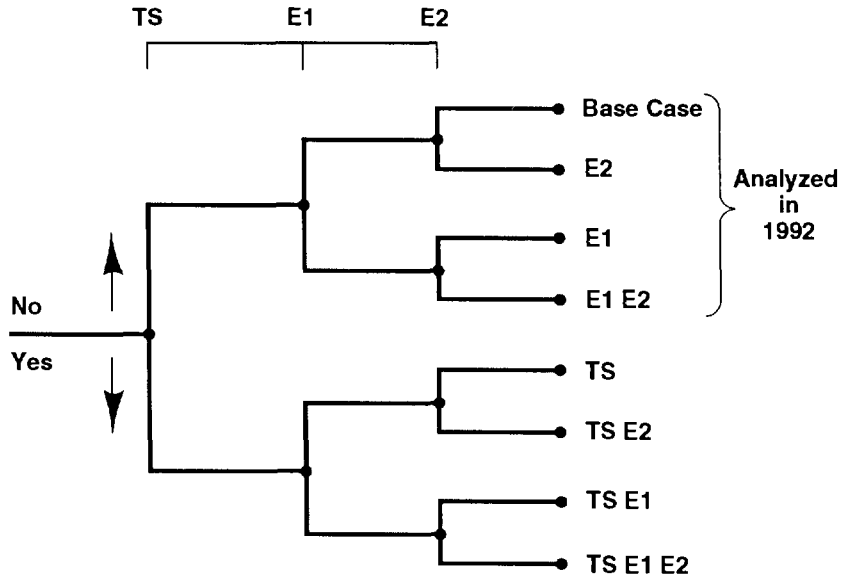

Figure 4-1. Potential scenarios for the WIPP disposal system. Each scenario is a set of similar occurrences and a subset of all possible 10,000-year histories beginning at decommissioning of the WIPP.

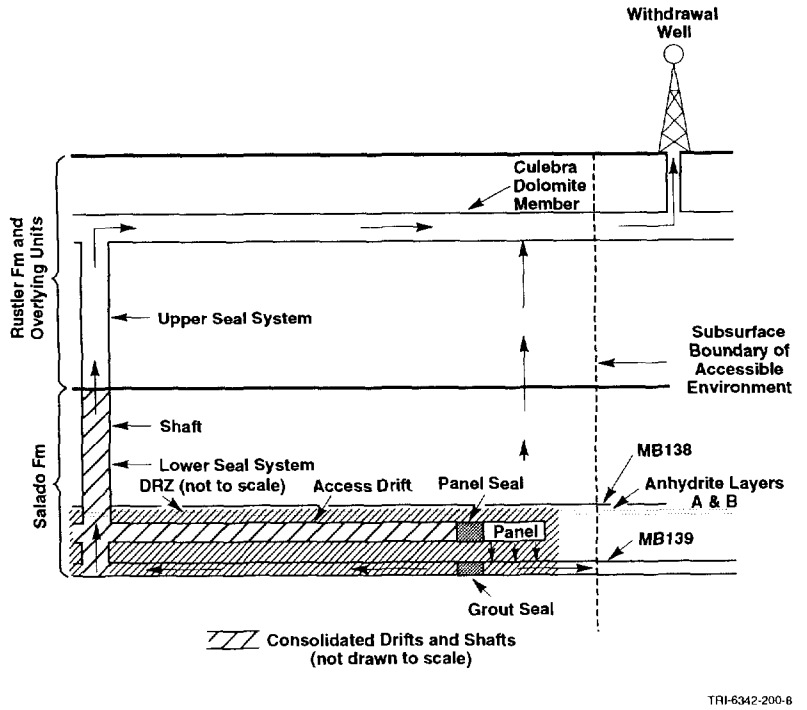

(a)

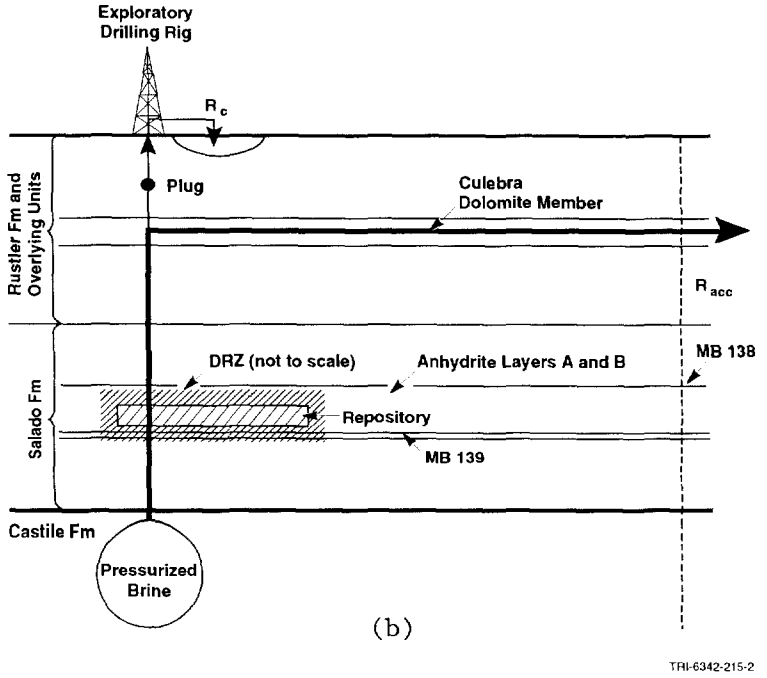

(b)

Figure 4-2. Conceptual models for (a) the undisturbed performance scenario and (b) the E1 scenario. Arrows indicate assumed direction and relative magnitude of flow. R_c is the release of cuttings and eroded material. R_{acc} is the release at the subsurface boundary of the accessible environment. Illustrated plugs are assumed to remain intact for 10,000 years.

system from the time of decommissioning and incorporates all expected changes in the system and associated uncertainties for the 10,000 years of concern for the Containment Requirements (§ 191.13). Two potential pathways for migration of radionuclides dissolved in brine are considered. In the first path, brine may migrate either through drifts or through the disturbed rock zone (DRZ) surrounding the excavation and anhydrite interbeds (primarily MB139) to the shafts and then upward toward the Culebra Dolomite Member of the Rustler Formation, which is the most permeable water-saturated unit overlying the repository. Transport may then occur laterally in the Culebra toward the subsurface boundary of the accessible environment. In the second path, brine may migrate laterally toward the subsurface boundary of the accessible environment within anhydrite interbeds in the Salado Formation. Considered for only 1000 years, and with the addition of a water withdrawal well to provide a potential pathway for radionuclides to reach humans, the base-case scenario is also suitable for evaluations of undisturbed performance for the Individual Protection Requirements (§ 191.15). Considering gas migration pathways to the disposal-unit boundary and, if necessary, transport of hazardous constituents in both gas and brine phases, the base-case scenario is suitable for evaluations of undisturbed performance for 40 CFR 268.6 (RCRA) (see Volume 5 of this report).

4.1.2 Inadvertent Human Intrusion

Performance assessments for 40 CFR 191, Subpart B, presently concentrate on inadvertent human intrusion during exploratory drilling for resources, which has been demonstrated by past analyses (Marietta et al., 1989; Bertram-Howery et al., 1990; WIPP PA Division, 1991a,b,c; WIPP PA Department, 1992; see also Section 5.2 of this volume) to be the only event likely to lead to radionuclide releases close to or in excess of regulatory limits. Future drilling technology is assumed for these analyses to be comparable to technology presently in use in the region around the WIPP.

If the waste-emplacement panels are penetrated by an exploratory borehole, radionuclides may reach the accessible environment by two principal pathways. First, some radionuclides will be transported up the borehole directly to the ground surface. Second, additional radionuclides transported up the borehole will migrate into overlying strata and may be transported laterally in groundwater to the subsurface boundary of the accessible environment.

Most releases at the ground surface will be in the form of particulate waste entrained in the drilling fluid, including components from cuttings (material removed by the drill bit), cavings (material eroded from the

borehole wall by the circulating drilling fluid), and spallings (material that enters the borehole as the repository depressurizes). For convenience, these particulate releases are collectively referred to in performance-assessment documentation as cuttings. For the 1992 calculations, results referred to as cuttings include cavings but do not include spallings. If important, spallings will be included in future performance assessments when models and data are available. Additional discussion of the modeling of particulate releases at the ground surface during drilling is provided in Volume 2, Section 7.7 of this report. Release of radionuclides dissolved in brine that may flow up the borehole to the ground surface both during drilling and after degradation of plugs has not been included either in past performance assessments or in the results presented in this volume. Volume 4 of the 1992 documentation will contain preliminary analyses of the potential for releases by this mechanism.

Subsurface releases of radionuclides following lateral transport in groundwater are believed to be most likely to occur in the Culebra Dolomite Member of the Rustler Formation overlying the repository. For analysis purposes, subsurface transport is assumed to occur only in the Culebra, maximizing the potential for releases by this pathway. Additional discussion of flow and transport in the Culebra is provided in Volume 2, Section 7.6 of this report.

Figures 4-2b and 4-3 illustrate the three representative intrusion scenarios shown in Figure 4-1. In the E1 scenario (Figure 4-2b), a borehole penetrates the repository and a hypothetical pressurized brine reservoir in the underlying Castile Formation. In the E2 scenario (Figure 4-3a), a borehole penetrates the repository and misses the hypothetical brine reservoir. In the E1E2 scenario (Figure 4-3b), one borehole penetrates the repository and the hypothetical brine reservoir and a second borehole penetrates the repository but misses the pressurized brine reservoir.

In all three of these intrusion scenarios, borehole plugs are assumed to be emplaced and to perform so as to maximize fluid flow into the Culebra Dolomite Member of the Rustler Formation. These plug configurations have been chosen to facilitate examination of the specific scenarios, and do not reflect the most realistic conditions expected. In the E1 and E2 scenarios, any plugs between the repository and the Culebra are assumed to fail immediately, whereas plugs above the Culebra remain effective for 10,000 years. In the E1E2 scenario, a plug in the E1-type borehole between the repository and the Culebra remains effective and forces flow through the waste and up the E2-type hole, where a plug above the Culebra forces flow laterally toward the accessible-environment boundary. As noted above,

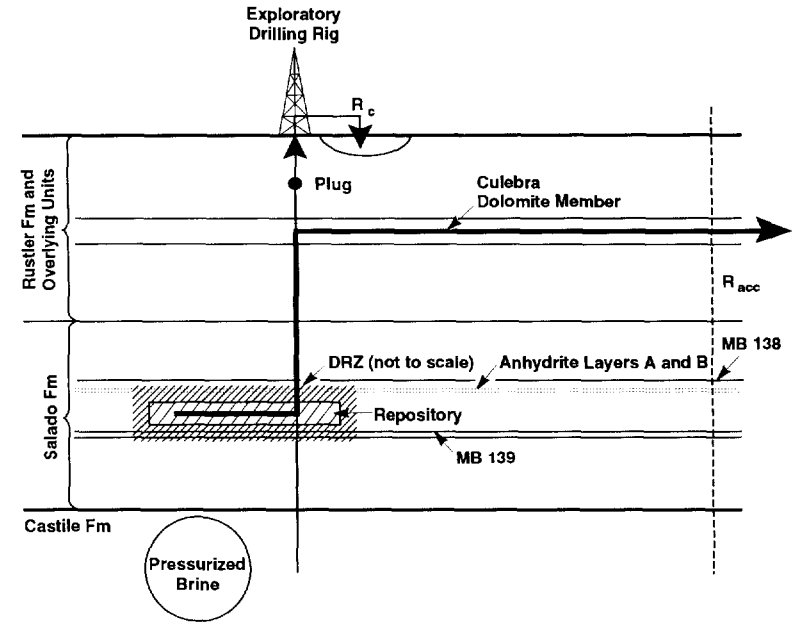

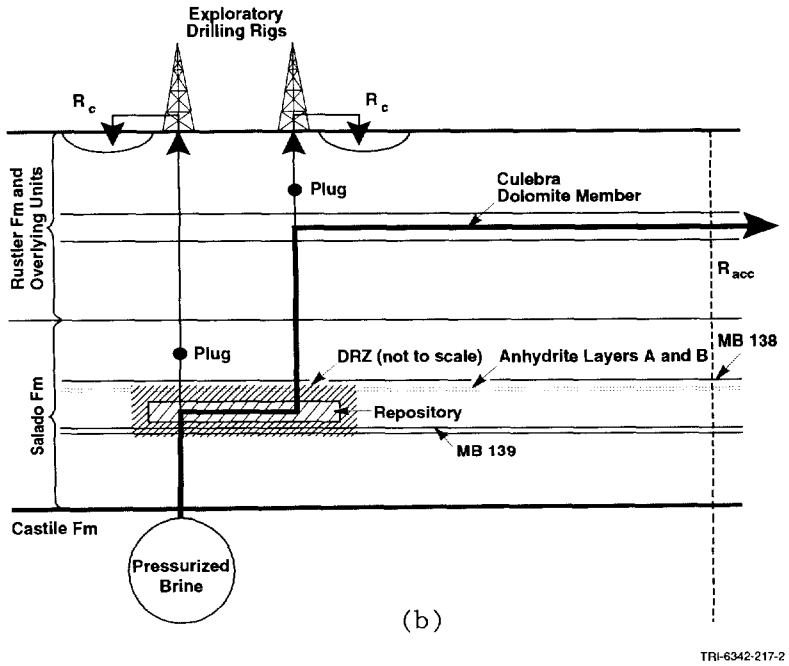

Figure 4-3. Conceptual models for (a) the E2 scenario and (b) the E1E2 scenario. Arrows indicate assumed direction and relative magnitude of flow. R_c is the release of cuttings and eroded material. R_{acc} is the release at the subsurface boundary of the accessible environment. Illustrated plugs are assumed to remain intact for 10,000 years.

consequences of alternative assumptions about plugging in which all plugs degrade to a material with relatively high permeability (as suggested in Appendix B of the Standard [US EPA, 1985, p. 38089]) and brine is allowed to flow at the ground surface will be examined and documented in a subsequent volume.

For improved computational resolution, the E1, E2, and E1E2 scenarios have been subdivided further into computational scenarios on the basis of time of intrusion and activity of the waste intersected. As discussed in Volume 2, Chapter 4 of this report, subsurface radionuclide releases following groundwater transport in the Culebra are calculated in the 1992 performance assessment only for intrusions occurring 1000 years after decommissioning. Because of the decreased time available for transport, later intrusions are expected to result in smaller releases. As in 1991, for computational efficiency, E1-type intrusions are not analyzed explicitly, but rather are assumed to have the same consequences as E2-type intrusions (WIPP PA Division, 1991b). Releases of cuttings are calculated for six time intervals, including intrusions at 125, 175, 350, 1000, 3000, and 7250 years. Multiple intrusions are allowed, with a maximum number of 10 occurring in simulations used in the 1992 analyses.

4.2 Probabilities of Scenarios

Identifying the probability of future human intrusion is at best a qualitative task. Preliminary performance assessments for the WIPP prior to 1990 considered a fixed number of human intrusions with fixed and arbitrary probabilities (Marietta et al., 1989; Guzowski, 1991). The 1990 preliminary assessment (Bertram-Howery et al., 1990) compared performance assuming fixed probabilities for intrusion events with performance estimated assuming that intrusion through the repository follows a Poisson process (i.e., intrusion events are random in time and space) with a rate constant, λ. The 1991 assessment (WIPP PA Division, 1991a,b) included a probability model based on the Poisson assumption and also included effects of variable activity loading with boreholes intersecting waste of five different levels of radioactivity (Helton et al., 1992). Based on guidance in Appendix B of the Standard, a maximum of 30 boreholes/km^2 were allowed in 10,000 years, although the largest number to occur in any realization was 10 per 0.5 km^2.

The 1992 preliminary performance assessment marks the first use for the WIPP of external expert judgment to estimate the probability of future intrusion. Teams of experts from outside the WIPP Project were selected and organized into two panels to address (1) the nature of future societies and the possible modes of intrusion, and (2) types of markers and their

potential effectiveness in deterring intrusion (Hora et al., 1991; memorandum by Hora in Volume 3, Appendix A of this report). The judgments elicited from these panels were used to construct an algorithm describing possible changes in the Poisson rate constant, λ, with time (memorandum by Hora in Volume 3, Appendix A of this report). The 1992 preliminary performance assessment presents results calculated both using the 1991 time-invariant formulation for λ and the time-dependent formulation based on external expert judgment. Both formulations used the same representation for variable activity loading used in the 1991 performance assessment (Helton et al., 1992). The time-dependent formulation including the deterrence effect of markers resulted in significantly fewer intrusions (a maximum of 3 for intrusions occurring at 1000 years and 4 for the 6 intrusion times) than the time-invariant formulation (a maximum of 8 for intrusions occurring at 1000 years and 10 for 6 intrusion times).

4.3 Scenario Consequence Modeling

Consequence modeling for WIPP performance assessment uses a linked system of computational models to describe the disposal system and a Monte Carlo technique that relies on multiple simulations using sampled values for selected input parameters to quantify uncertainty in the performance estimate. A full analysis includes selecting imprecisely known parameters to be sampled, constructing distributions for each of these parameters incorporating available data and subjective information, generating a sample from these variables, and calculating consequences for each sample element. Consideration of alternative conceptual models (defined in Section 3.3.4 of this volume), which may require different input parameters and perhaps different computational models, at present is included by repeating the full analysis for each conceptual model to assess uncertainty among alternative models. Results for preliminary comparison with 40 CFR 191, Subpart B, are usually displayed in terms of complementary cumulative distribution functions (CCDFs), which are plots of exceedance probability versus consequence. The consequence measure for § 191.13 is the EPA normalized sum, as discussed in Section 3.3.2 of this volume and in Volume 3, Section 3.3.4 of this report. Construction of CCDFs is discussed in Volume 2, Chapter 3 of this report.

Uncertainty and sensitivity analyses use a Latin hypercube sampling technique followed by stepwise rank regression analysis (Iman and Helton, 1985; Helton et al., 1991, 1992). In other sensitivity analyses for alternative conceptual models, specific parameter groups are assigned fixed values corresponding to extreme and median values, and all other parameters in the data base are sampled probabilistically over the full range of possible values. A parameter or group of parameters is thus tested *ceteris*

paribus (all other things being equal) within a Monte Carlo simulation (Helton et al., 1991). To compare with the Standard for each conceptual model, results are assembled into CCDF plots of probability versus 10,000-year normalized cumulative radionuclide release, as recommended in the guidance to the Standard. The technique isolates effects of variations in parameter groups (used to represent alternative conceptual models) on predicted performance. Priorities can then be suggested for future modeling and experimental research.

4.3.1 Computational Models

Major computer programs (codes) used in the computational models for the 1992 preliminary performance assessment (Figure 4-4) are described in detail in Volume 2 of this report. They reflect improvements in the conceptual and numerical models used in the 1991 and previous performance assessments, and permit the replacement of simplifying assumptions with more realistic models. Three of the most significant improvements in 1992 are discussed here.

The 1992 calculations mark the first time the effects of salt creep have been explicitly included in performance assessments. Salt will deform over time by creep in response to a pressure gradient, and, if the repository remained at atmospheric pressure, lithostatic stresses would cause it to close almost completely within 100 years (Tyler et al., 1988; Munson et al., 1989a,b). Gas will be generated within the repository by degradation of the waste, however, and pressure within the repository will rise to elevated levels that will retard complete creep closure and may perhaps partially reverse the process. In 1991, no model was available to describe the coupled interaction of creep closure and gas pressurization, and the performance-assessment calculations used a simplifying assumption that porosity within the disposal region would remain constant through time. As discussed in detail in Volume 2, Section 7.3 of this report, the 1992 calculations use output from the geomechanical code SANCHO (Stone et al., 1985) to define the porosity of the waste as a function of pressure. Although this method does not represent a full coupling of creep closure and gas generation, the modeling improvement allows the performance assessment to evaluate the importance of changing void volume in the repository. An analysis of the impact on performance of including salt creep is included in Volume 4 of this report.

The method used to incorporate spatial variability in the transmissivity field in the Culebra has been modified significantly from that used in 1991. The Performance Assessment Department now uses an automated inverse approach to calibrate a two-dimensional model to both

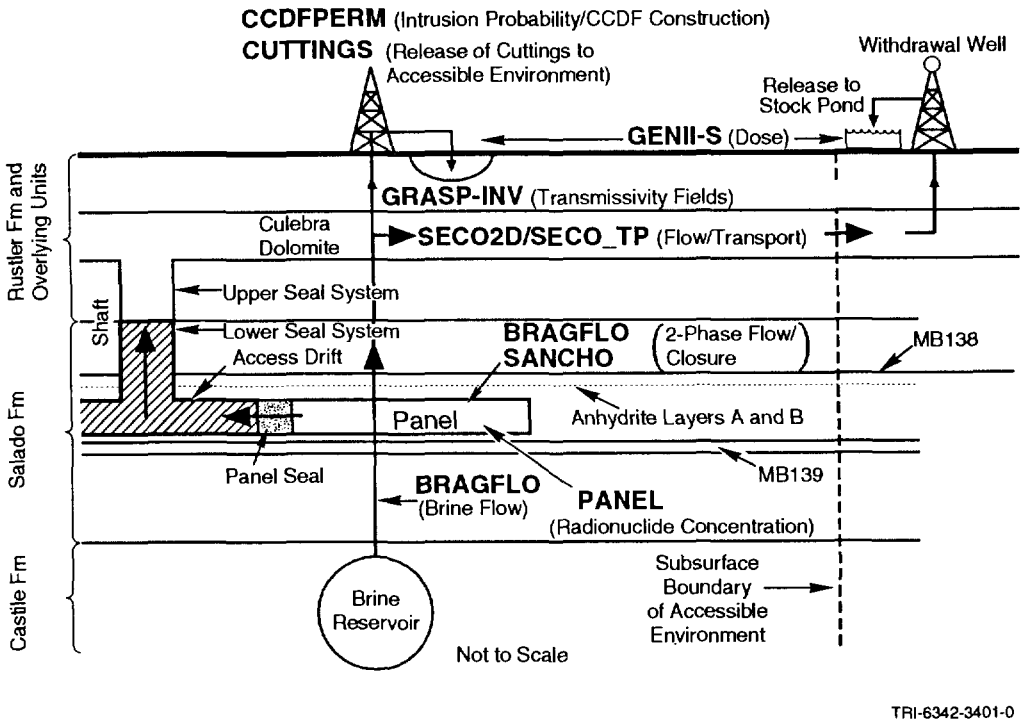

Figure 4-4. Major codes used in the 1992 performance assessment.

steady-state and transient pressure data generating multiple realizations of the transmissivity field (Volume 2, Section 7.5 of this report; LaVenue and RamaRao, 1992). Seventy calibrated fields were sampled for use in the 1992 performance assessment.

Radionuclide transport in the Culebra, which had been simulated using STAFF2D (Huyakorn et al., 1991) in the 1991 performance assessment, is now simulated by the SECO-TP code (Volume 3, Section 1.4.6 of this report). SECO-TP is a dual-porosity model in which advective transport is allowed only in fractures, and diffusion of solute occurs into the rock matrix surrounding the fracture. The fracture system is idealized as planar and parallel, and each fracture wall may be coated with a layer of clay of uniform thickness and porosity. The model is capable of simulating both physical retardation by diffusion and chemical retardation by sorption in both clay fracture-linings and dolomite matrix.

Several significant improvements remain to be made in the performance-assessment modeling system. Specifically, the model used in 1992 for groundwater flow in the Culebra does not include possible effects of subsidence related to potash mining or a representation of recharge that includes present or future vertical groundwater flow within the Rustler Formation (leakage). The model used to represent the response of the repository and the surrounding strata to the generation of gas by waste degradation does not include effects of possible pressure-dependent fracturing of anhydrite layers within the Salado Formation. Modeling system improvements also remain to be made with respect to gas generation, the conceptual three-dimensional model for regional groundwater flow, the impact of spallings and direct flow of brine up a borehole to the surface, transport of radionuclides as colloids, and possible correlations between input parameters used in computational models. Consequences of these aspects of disposal-system performance will be examined in future analyses as additional information becomes available.

4.3.2 Distributions for Imprecisely Known Variables

The complete data base used in the 1992 preliminary performance assessment is presented in Volume 3 of this report, and includes ranges and cumulative distribution functions (cdfs) for all sampled parameters and median values for all non-sampled parameters. Ranges for parameter values have been selected by WIPP Project researchers in their respective fields. The selection of parameters to be sampled is based on previous sensitivity analyses and, to some extent, on subjective judgment by the researchers on the importance of the parameters. Distribution functions for parameters have been assigned by the Performance Assessment Department using available

data and the maximum entropy formalism (MEF), which minimizes the amount of spurious information that enters into cdf construction from sparse data or limited quantitative information (Tierney, 1990). For WIPP performance assessment, the MEF serves as a consistent mathematical procedure for deriving cdfs for imprecisely known variables from a set of quantitative constraints on the form of the distribution (e.g., range, mean, variance, or different percentiles). Two empirical distributions are particularly important. When measured data are available, the empirical cdf is piecewise uniform. Following the MEF, the empirical cdf is modified by joining the empirical percentile points (including extrapolated end points) with straight lines, resulting in a piecewise linear cdf. When data are not available and subjective point estimates are supplied by experts, the cdf is again piecewise linear and constructed by linearly connecting the subjective point estimates. Judgments that are made by experts are a snapshot of the current state of knowledge. As new observations are made for important parameters, this state of knowledge and the cdf are refined.

To supplement the available information for constructing the required cdfs, several expert panels were convened and a formal elicitation process was used (Bonano et al., 1990; Hora and Iman, 1989). A formal elicitation of expert opinion includes five components: selection of issue and issue statement, selection of experts, elicitation sessions, recomposition of an expert's opinion and aggregation of group opinion, and documentation. As did the 1991 performance assessment, the 1992 analyses include the outcomes of formal elicitations from two expert panels on important geochemical parameters. A source-term panel provided subjective point estimates for constructing logarithmic piecewise linear cdfs of radionuclide solubilities in disposal-room brine, and a second panel on radionuclide retardation in the Culebra provided estimates for distribution coefficients (Trauth et al., 1992). Members of the source-term panel concluded they could not make judgments about suspended-solids concentrations because of a lack of experimental data and consequently limited knowledge on colloids and their formation. The retardation panel estimated distribution coefficients (K_ds) for fracture clays and matrix dolomite using available data. Experimental programs have been initiated that will provide WIPP-specific data on both the source term (dissolved species and colloids) and retardation in the Culebra (US DOE 1992a,b).

The 1992 WIPP performance assessment selected 49 imprecisely known variables (including, for example, uncertain material properties of the waste, the Salado Formation, and the Culebra Dolomite) for consideration in the human-intrusion scenarios (Volume 3, Tables 6.0-1, 6.0-2, and 6.0-3 of this report). Values sampled from the distributions assigned to these 49 variables were used to construct 70 vectors of sampled parameters to use in Monte Carlo simulations. Sampled values for each of the 70 vectors are

presented in Volume 4 of this report. Because 2 different scenarios were analyzed explicitly (E2 and E1E2), performance estimates reported for each conceptual model considered are based on 140 realizations of the full modeling system.

4.3.3 Generation of the Sample Elements

WIPP performance assessment uses a stratified sampling technique called Latin hypercube sampling (LHS) that ensures full coverage of the range of each sampled variable (McKay et al., 1979). The range of each variable is divided into N intervals of equal probability, and one value is randomly selected from each interval. The N values of the first parameter are randomly paired with the N values of the second parameter, and so on, until N sample elements (vectors) are obtained. This procedure ensures that the distribution tails are sampled and is a more efficient technique than simple random sampling in that fewer sample elements are required for a Monte Carlo analysis. The size of N (70 for the 1992 performance assessment) is selected based on the observation that a sample size of 4/3 times the number of sampled parameters is generally sufficient to capture variability in independent input parameters (Iman and Helton, 1985).

Most of the uncertain variables that were sampled during the 1992 performance assessment were assumed to be independent, although some are expected to be correlated in some way. For example, local porosity is probably correlated with local permeability in most media, but the correlation structure is unknown. Controlling correlation within a sample for Monte Carlo analysis is important to ensure that uncertainty and sensitivity analysis results are meaningful. WIPP performance assessment uses a rank correlation (i.e., on rank-transformed variables instead of on the original raw data) technique that effectively captures variable linkage while maintaining the integrity of the LHS intervals (Iman and Conover, 1982; Helton et al., 1991). However, the correlation structure for most of the uncertain variables that are expected to be correlated has not yet been adequately addressed. Future performance assessments will test approaches for dealing with these unknown correlations.

5. RESULTS OF THE 1992 PRELIMINARY COMPARISON WITH 40 CFR 191, SUBPART B

Results from the 1992 preliminary performance assessment are presented for informal comparison with the Containment Requirements and the Individual Protection Requirements of the Standard. Although not based on the 1992 preliminary performance assessment, the status of preliminary compliance with the Assurance Requirements and the Groundwater Protection Requirements is also discussed.

5.1 Containment Requirements

Compliance with the Containment Requirements is evaluated using CCDF curves that graph exceedance probability versus cumulative radionuclide releases for all significant scenarios. Results presented here are not suitable for final compliance evaluations because portions of the modeling system and data base are incomplete, conceptual-model uncertainties are not included, final scenario probabilities remain to be determined, the level of confidence in the results remains to be established, and the final version of the Standard has not been promulgated. Uncertainty analyses required to establish the level of confidence in results will be included in future performance assessments as advances permit quantification of uncertainties in the modeling system and the data base.

5.1.1 Previous Studies

Preliminary comparisons of the estimated performance of the WIPP with the Containment Requirements have been published iteratively since 1989 (Marietta et al., 1989; Bertram-Howery et al., 1990; WIPP PA Division 1991a). Annual sensitivity analyses have helped identify areas where improvements in the modeling system can increase overall confidence in the performance estimate (Helton et al., 1991, 1992), and each subsequent iteration of performance assessment has represented a significant advance over the preceding iteration.

The 1991 preliminary comparison indicated that, for the conceptual and computational models, parameter values, and scenario probabilities believed by the WIPP PA Department at that time to best represent the behavior of the disposal system, the mean CCDF lay an order of magnitude or more below the EPA compliance limits (WIPP PA Division, 1991a). As is also true for the 1992 preliminary comparison, the 1991 performance estimate could not be considered defensible for a final compliance evaluation. Results of

uncertainty and sensitivity analyses conducted as part of the 1991 performance assessment have, however, provided valuable guidance to the Project as it moves toward a final compliance evaluation.

5.1.2 1992 Preliminary Comparison

The 1992 performance assessment has concentrated resources on analyzing the impact of specific sources of uncertainty on the performance estimate. Fewer times of intrusion have been considered (to allow allocating resources to simulation of alternative conceptual models), and the 1992 results are therefore less suitable in that sense for direct comparison to the EPA limits than were the 1991 results. In all other ways, however, the 1992 performance assessment reflects a more realistic representation of the future behavior of the disposal system. As described in Chapter 4 of this volume and Volume 2 of this report, major modeling improvements have been made in coupling creep closure of the repository to gas pressurization, in accounting for spatial variability of transmissivity in the Culebra Dolomite Member of the Rustler Formation, and in simulating radionuclide transport in the Culebra. As described in Volumes 2 and 3 of this report, other improvements have been made throughout the modeling system and the data base. As described in Chapter 4 of this volume, improvements remain to be made in many areas, including modeling of possible pressure-dependent fracturing of anhydrite interbeds in the Salado Formation, modeling of three-dimensional groundwater flow in the Rustler Formation, modeling of gas-generation processes, and acquisition of experimental data for actinide solubilities and retardations.

The 1992 preliminary comparison examines uncertainty resulting from imprecisely known values for input parameters and the impact of two additional sources of uncertainty: the probability of human intrusion, and the choice of conceptual model for transport in the Culebra. Past preliminary comparisons have shown that the location of the mean CCDF is sensitive to assumptions made about both sources (Bertram-Howery et al., 1990; Helton et al., 1992). Because the emphasis here is on the relative position of the CCDFs calculated with each set of assumptions, all figures shown here are comparisons of two or more CCDFs calculated using either different probabilities or alternative conceptual models (see Section 3.3.4 of this volume for definitions of conceptual model and alternative conceptual models). For simplicity, only mean curves are shown. The complete families of CCDFs (with a single curve for each of the 70 vectors) will be shown in an appendix of Volume 4 of this report for each case considered, together with summary plots showing the mean, median, 10th percentile, and 90th percentile curves. Analyses of uncertainty resulting

from imprecisely known values for input parameters are provided in Volume 4 of this report.

5.1.2.1 CASES CONSIDERED FOR ANALYSIS IN 1992

Cases considered for analysis were defined on the basis of the choice of probability model for human intrusion (fixed rate constant versus time-dependent rate constant based on expert-panel judgment), the mode of release (cuttings versus subsurface transport), and the choice of conceptual model for radionuclide transport in the Culebra (single porosity versus dual porosity, with and without chemical retardation). All cases are compared *ceteris paribus*, and all computational models and parameter values (both fixed and sampled), except those used in the conceptual models being compared, are identical throughout. All releases from groundwater transport are calculated at the subsurface projection of the land-withdrawal boundary (see Section 1.1 of this volume), 2.4 km south of the southern waste panels. Travel paths in the sampled transmissivity fields are not straight lines, and are somewhat greater in length than the minimum 2.4 km (LaVenue and RamaRao, 1992).

5.1.2.1.1 Intrusion Probability Models

The intrusion probability models are described in detail in Volume 2, Chapter 5 of this report. Both are based on the assumption that intrusion events will follow a Poisson process, and be random in time and space. One model, referred to as the "constant λ" model, is identical to that used in 1991 (WIPP PA Division, 1991a,b). The rate constant λ used in the Poisson model is assumed to be time-invariant, and is sampled from a uniform distribution with a range from zero to a maximum value that allows 30 boreholes/km^2 in 10,000 years. This upper limit is the number suggested by the EPA in Appendix B of the Standard as the largest probability of intrusion that need be considered (US EPA, 1985, p. 38089), which occurs in the Poisson model with a low probability. For the 70 vectors used in the 1992 analyses, the largest number of intrusions in the 0.5 km^2 of the waste-disposal area was 10, rather than the potential maximum of 15.

Guidance from the EPA in Appendix B of the Standard indicates that the DOE "should consider the effects of each particular disposal system's site, design, and passive institutional controls in judging the likelihood and consequences of ... inadvertent exploratory drilling" (US EPA, 1985, p. 38089). The second probability model, referred to as the "time-dependent λ" model, reflects the judgment of two expert panels convened by the WIPP

Performance Assessment Department to evaluate the likelihood of intrusion (Hora et al., 1991; memorandum by Hora in Volume 3, Appendix A of this report). Specifically, these panels considered (1) future societies and their means and motives for intruding into the WIPP, and (2) the design and potential efficacy of passive markers that might deter such intrusion. Judgment elicited from these panels was used to construct an alternative probability model for human intrusion (memorandum by Hora in Volume 3, Appendix A of this report). Two important aspects of the model need emphasis. First, the expert panels did not believe intrusions were equally likely at all times during the 10,000-year period; the rate constant λ therefore varies as a function of time. Intrusions are in general more likely at early times. The panel judged that exploratory drilling and hydrocarbon development would be likely to end in the next 300 to 500 years because of resource depletion and/or shifting from a hydrocarbon-based economy. Second, the expert panels concluded that intrusion was not as likely as suggested by the EPA's guidance on the maximum number of boreholes. The overall probability of intrusion based on the expert judgment is significantly less than that predicted by the constant λ model; the largest number of intrusions occurring in 10,000 years in any of the 70 vectors using the time-dependent λ model was 4.

5.1.2.1.2 Mode of Release

As in previous performance assessments, the 1992 results include two modes of radionuclide release following human intrusion. Particulate waste intersected by the drill bit (cuttings) and eroded from the borehole wall by circulating drilling fluid (cavings) will be brought directly to the ground surface. The radionuclides contained in this material are collectively referred to here as cuttings. Radionuclide releases to the accessible environment may also occur in the subsurface, as a result of brine flow up the borehole and laterally through the Culebra. Modeling of both pathways is described in detail in Volume 2 of this report.

Cuttings releases, which reach the accessible environment immediately following intrusion, are sensitive to the radioactive decay history of the inventory during the first 1000 years after decommissioning. Subsurface releases, which require a relatively long period of transport to the accessible environment, are believed to be less sensitive to the time of intrusion because decay will continue to occur during transport. The 1992 performance assessment therefore uses different times of intrusion for cuttings and subsurface releases. Greater resolution is provided for cuttings releases, with intrusions considered at six times (100, 175, 350, 1000, 3000, and 7250 years after decommissioning). Only a single intrusion

time (1000 years after decommissioning) is considered for subsurface releases. This is the same intrusion time used in sensitivity analyses for groundwater transport used in the 1991 performance assessment (Helton et al., 1992).

5.1.2.1.3 Alternative Conceptual Models for Radionuclide Transport in the Culebra

Radionuclide transport in the Culebra is described in detail in Volume 2, Section 7.6 of this report. Three alternative conceptual models are considered here. These alternative conceptual models are defined on the basis of the presence or absence of chemical retardation, the presence or absence of clay linings in fractures, and the presence or absence of effective matrix porosity.

In the first conceptual model, referred to as the "fracture-only, K_d=0" model, the Culebra is treated as a single-porosity medium with transport occurring only in fractures without clay linings. Distribution coefficients (K_ds) are assumed to be zero, and neither physical nor chemical retardation occurs. This model is not believed to be realistic and is not supported by available data (Kelley and Pickens, 1986; Saulnier, 1987; Beauheim, 1987a,b, 1989; Jones et al., 1992). The model represents one endpoint of a continuum of possible models, and is examined to provide insights about the potential uncertainty introduced into the performance assessment by the lack of knowledge about transport processes in the Culebra.

The second conceptual model, referred to as the "dual-porosity, K_d=0" model, treats the Culebra as a dual-porosity medium, with transport occurring in clay-lined fractures and diffusion occurring into the pore volume of both the clay lining and the dolomite matrix. Distribution coefficients (K_ds) are assumed to be zero, and no chemical retardation occurs. The dual-porosity model is supported by available data from well tests (Kelley and Pickens, 1986; Saulnier, 1987; Beauheim, 1987b,c, 1989; Jones et al., 1992). Chemical retardation is believed likely to occur (Trauth et al., 1992), but experimental data are not available to provide defensible estimates of K_ds. This model is examined in part in fulfillment of the requirements of the Agreement for Consultation and Cooperation between the Department of Energy and the State of New Mexico (US DOE and the State of New Mexico, 1981, as modified), which states that "[i]n the absence of experimentally justifiable values, K_d will equal zero, i.e., no credit for retardation will be taken in the performance assessment calculations."

The third conceptual model, referred to as the "dual-porosity, $K_d \neq 0$" model, is identical to the second conceptual model except that chemical retardation does occur by sorption in both the clay linings and the dolomite matrix. The WIPP Performance Assessment Department believes that this model provides the most realistic representation of radionuclide transport in the Culebra. The model cannot, however, be fully supported by available data, nor can the alternative conceptual models presented above be fully refuted at this time. Experimental programs, including laboratory-scale radioactive tracer tests in progress in core samples from the Culebra (US DOE, 1992b, and references cited therein) and nonradioactive tracer tests planned for well locations in the Culebra (Beauheim and Davies, 1992), will provide data to reduce uncertainty in the conceptual model for transport in the Culebra.

These three conceptual models do not represent all possible combinations of the three criteria used to define the transport model. Dual-porosity models are also possible in which either clay linings or matrix porosity are absent. Results calculated using these models are discussed in Volume 4 of this report, together with more detailed analysis of the three conceptual models examined here.

5.1.2.2 RESULTS OF THE PRELIMINARY COMPARISON WITH THE CONTAINMENT REQUIREMENTS

The uncertainty introduced into cuttings releases by the choice of intrusion probability model is displayed in Figure 5-1. Cuttings are calculated for six times of intrusion. Probabilities are lower for the time-dependent λ (λ_t) case. As in previous performance assessments, plateau-shaped steps in both curves reflect the use of different activity-load categories (Helton et al., 1992). The larger number of intrusions occurring for the constant λ (λ_o) case results in a smoother appearance. Curves converge at low probabilities because those portions of the mean CCDFs are dominated by releases from the low-permeability intrusions that intersect waste of the highest activity levels.

Cuttings releases were recalculated for a single time of intrusion 1000 years after decommissioning to permit useful comparisons and combinations with the subsurface releases calculated for intrusion at the same time. Comparison of the cuttings-only CCDFs calculated for the constant λ case for six times of intrusion and a single time of intrusion provides a measure of the information gained by considering releases from intrusions at multiple times (Figure 5-2). Both probability and magnitude of normalized releases are increased by less than one order of magnitude when

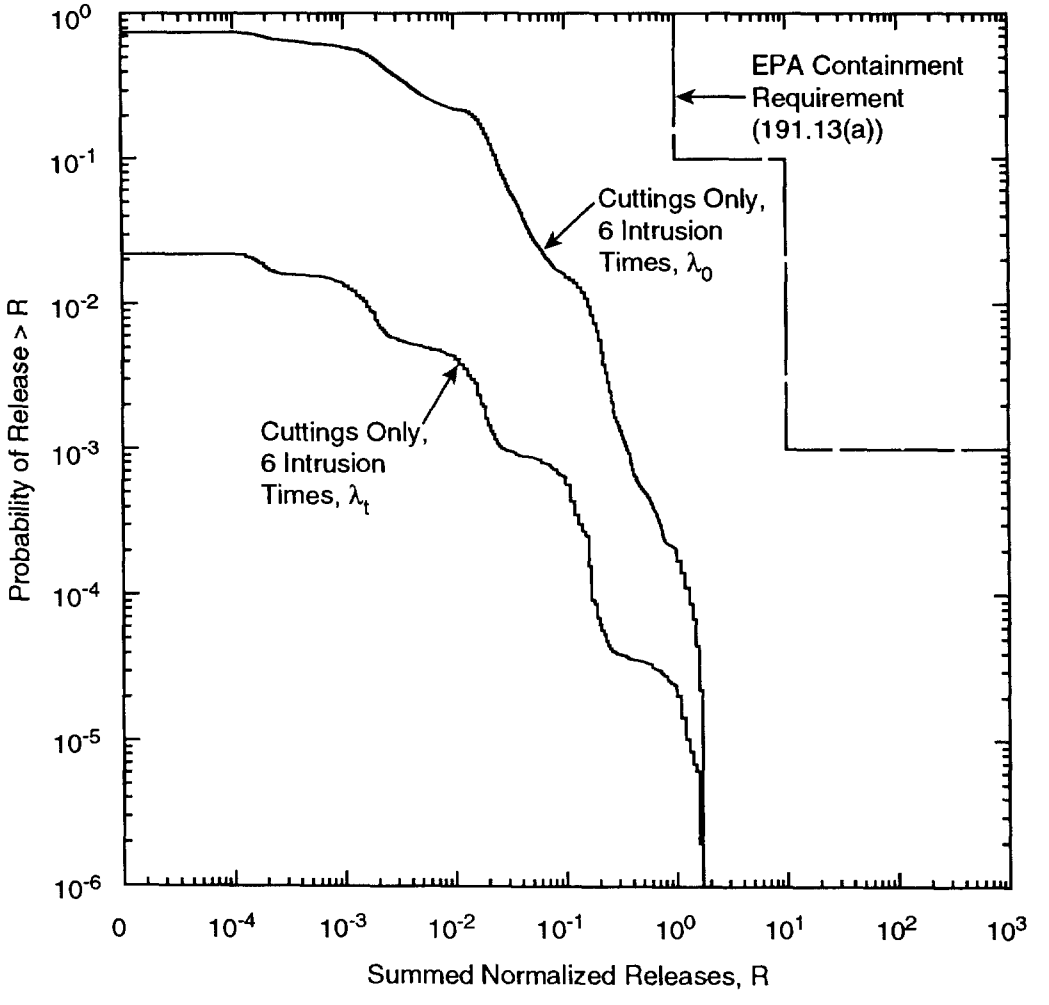

Figure 5-1. Mean CCDFs calculated for cuttings releases only for six intrusion times. Two Poisson models for the probability of human intrusion are compared: one (λ_0) is a constant λ model in which a maximum of 30 boreholes/km^2 may occur in 10,000 years; the other (λ_t) is a time-dependent λ model in which the Poisson rate constant λ was based on expert panel judgment. In both cases λ was specified using a sampled variable that was different for each of the 70 vectors used to construct the CCDFs. Summed normalized releases are displayed using an inverse hyperbolic sine scale, which differs from a logarithmic scale only in the interval between 0 and 10^{-4}.

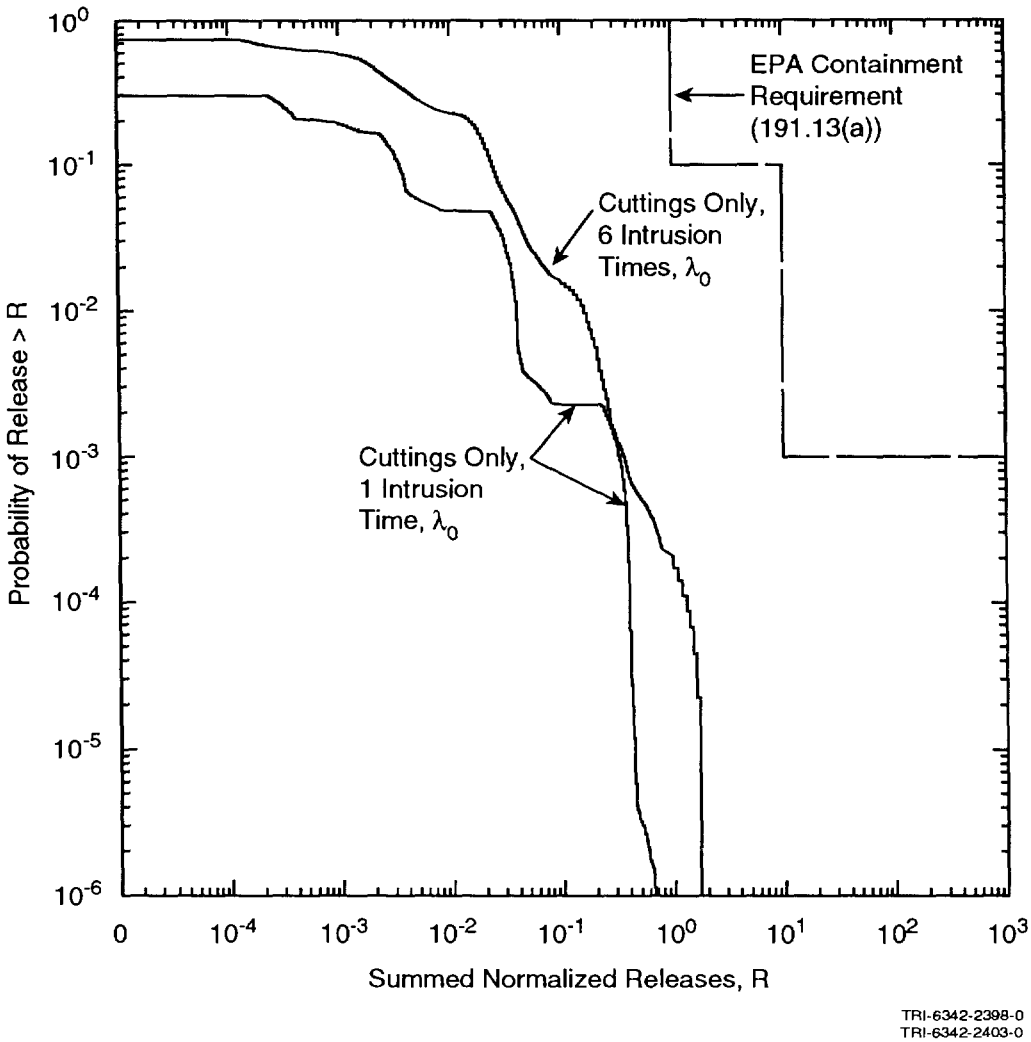

Figure 5-2. Mean CCDFs calculated for cuttings releases only, displaying the effect of considering a single time of intrusion versus six intrusion times. Both CCDFs were calculated using the constant λ model. Summed normalized releases are displayed using an inverse hyperbolic sine scale, which differs from a logarithmic scale only in the interval between 0 and 10^{-4}.

intrusions at multiple times are considered. Although releases from groundwater transport were not calculated for multiple time intervals in 1992, a similar comparison was made for subsurface releases from a dual-porosity model in the 1991 performance assessment. Examination of Figures 4.1-2 (lower right frame) and Figure 5.1-4 (lower right frame) in Helton et al. (1992) indicates that considering multiple time of intrusion (five intervals in 1991) increases both probability and magnitude of low-consequence releases less than one order of magnitude.

For the single-porosity, fracture-only conceptual model for transport used in 1992, subsurface releases exceed cuttings releases in the low-probability, high-consequence portion of the CCDF (Figure 5-3). The smaller subsurface releases occur at a lower probability than the comparable cuttings releases because not all intrusions resulted in releases into the Culebra. No releases occurred in vectors where the repository was not brine saturated at the time of intrusion and did not completely resaturate with brine following intrusion, because brine from the waste-disposal area did not flow up the borehole. Comparison of the CCDFs for cuttings and subsurface releases indicates that, if the effects of neither physical nor chemical retardation in the Culebra are included in the analysis, radionuclide transport in the Culebra may be the mechanism most likely to affect compliance with § 191.13 (Figure 5-3a). Even for the higher probability, constant λ case, however, the mean CCDF for cuttings and subsurface combined transport lies below the EPA limits (Figure 5-3b).

Use of the dual-porosity, K_d=0 conceptual model for radionuclide transport results in a reduction of subsurface releases compared to those estimated using the single-porosity model (Figure 5-4). For the constant λ case, the inclusion of physical retardation (but not, in this example, chemical retardation) shifts the location of the mean CCDF significantly in the region likely to affect regulatory compliance. For the time-dependent λ case, the lower overall probability of intrusions causes the main divergence between the single- and dual-porosity curves to occur at low probabilities, off the scale used here. This observation suggests that compliance with § 191.13 may be less sensitive to assumptions about the conceptual model for transport in the Culebra for lower intrusion probabilities.

Including the effects of chemical retardation as well as physical retardation (the dual-porosity, $K_d \neq 0$ conceptual model for transport) results in releases that are further reduced below those estimated assuming only physical retardation (Figure 5-5). Subsurface releases for the $K_d \neq 0$ conceptual model are less than the estimated cuttings releases at all probabilities (for the time-dependent λ case, the mean CCDF indicates no releases at this scale); the location of the mean CCDFs is determined

(a)

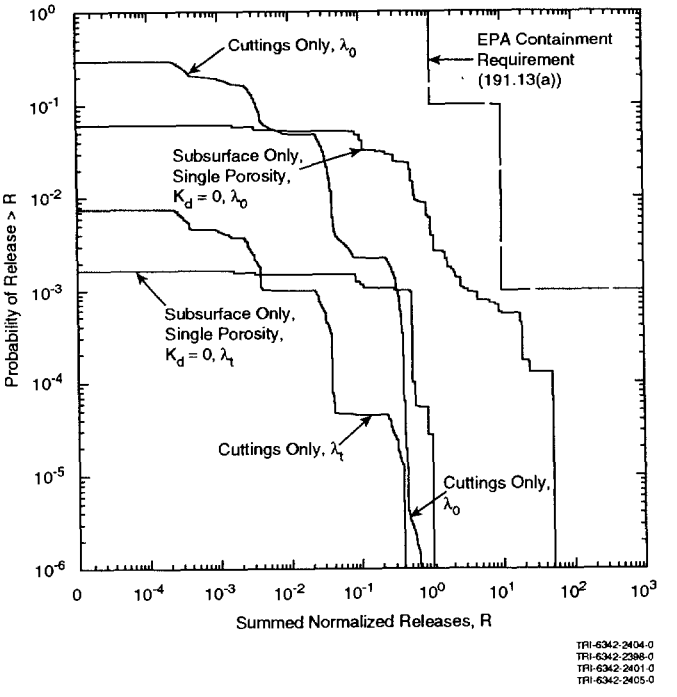

(b)

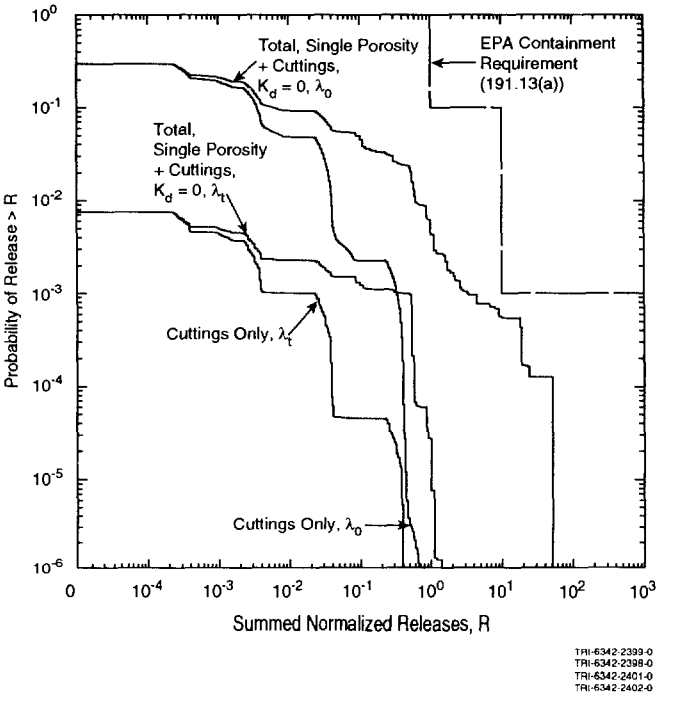

Figure 5-3. Comparison of mean CCDFs for cuttings releases and releases resulting from subsurface transport in the Culebra from intrusions occurring at 1000 years assuming a single-porosity, fracture-only conceptual model for transport. Figure 5-3a compares cuttings-only and subsurface-only releases. Figure 5-3b compares cuttings-only releases with total releases. Both constant λ and time-dependent λ cases are shown. Summed normalized releases are displayed using an inverse hyperbolic sine scale, which differs from a logarithmic scale only in the interval between 0 and 10^{-4}.

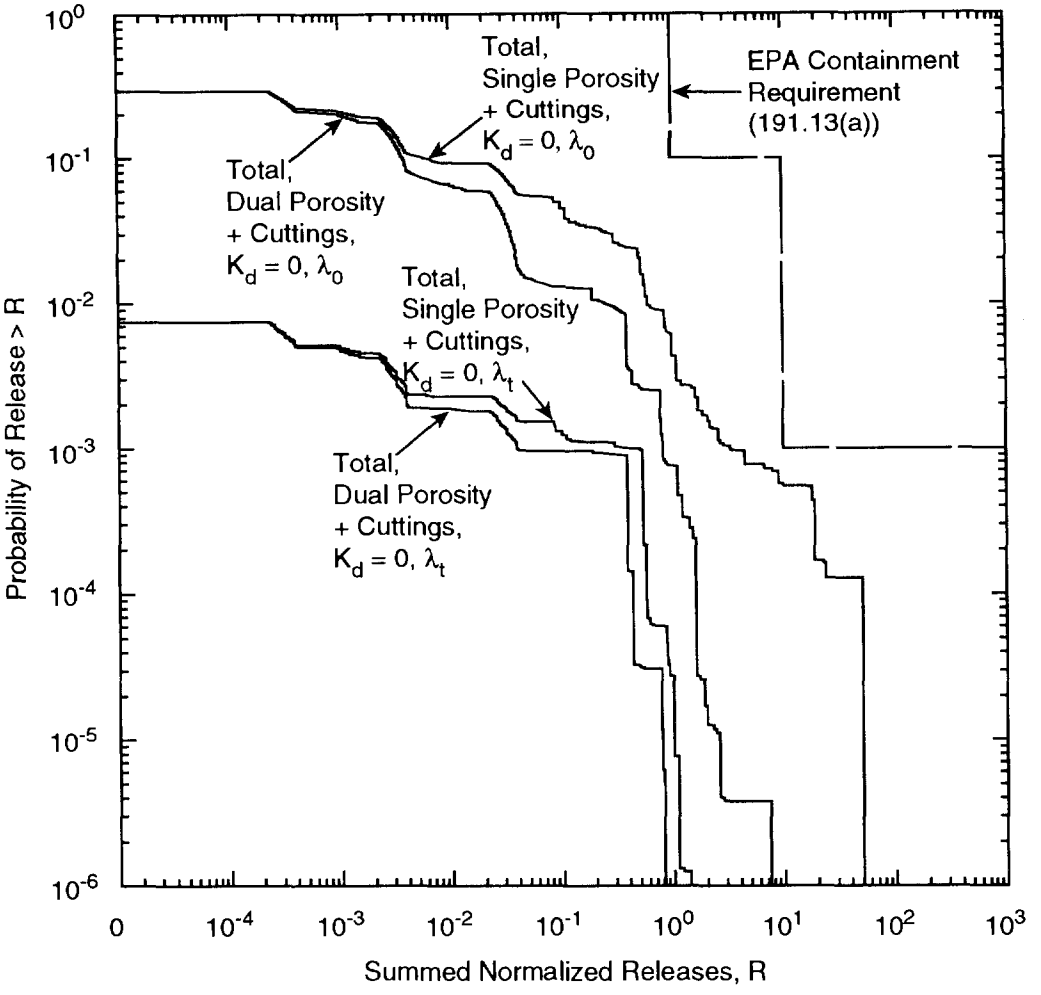

Figure 5-4. Comparison of mean CCDFs for total (cuttings plus subsurface) releases from intrusions occurring at 1000 years for single-porosity and dual-porosity, K_d=0 conceptual models for transport in the Culebra. Both constant λ and time-dependent λ cases are shown. Summed normalized releases are displayed using an inverse hyperbolic sine scale, which differs from a logarithmic scale only in the interval between 0 and 10^{-4}.

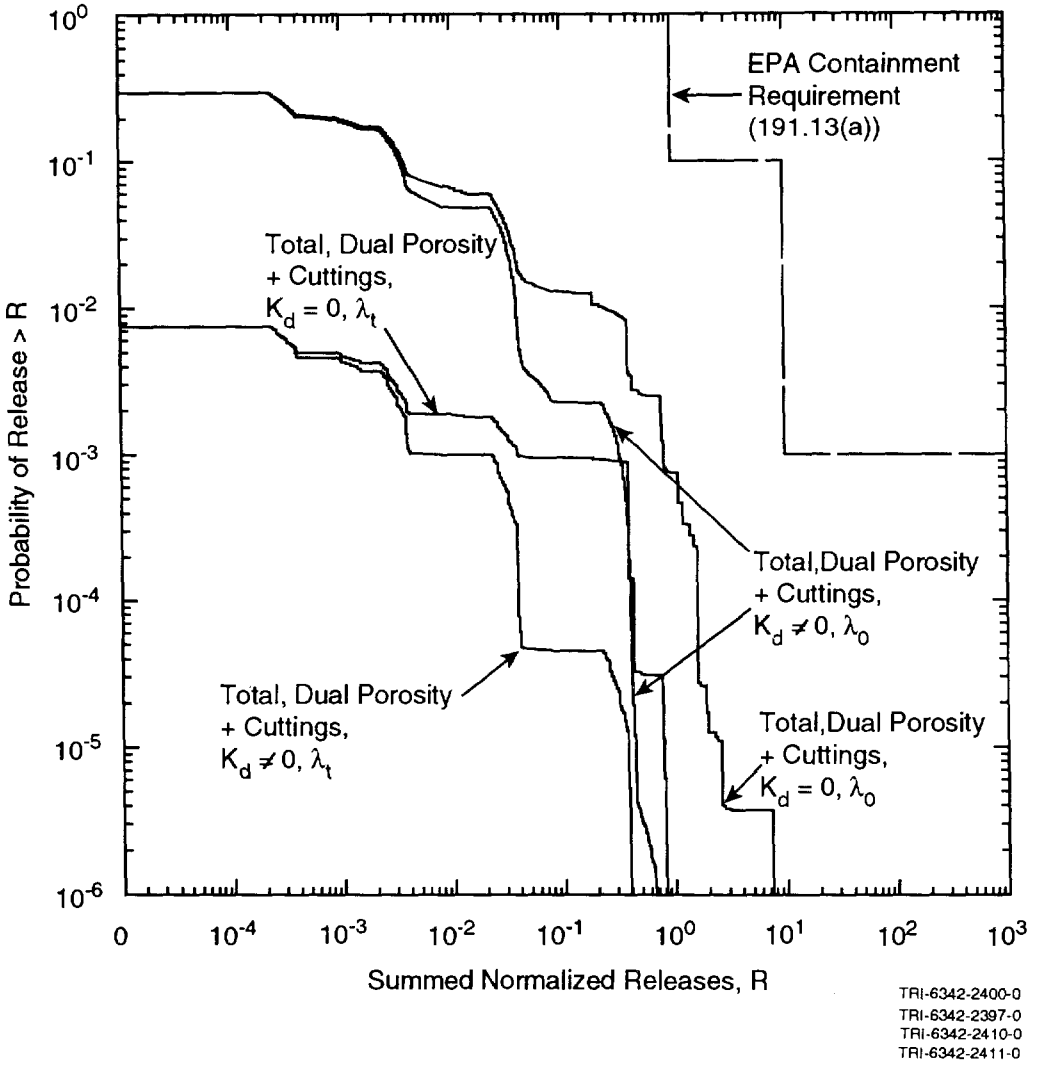

Figure 5-5. Comparison of mean CCDFs for total (cuttings plus subsurface) releases from intrusions occurring at 1000 years for dual-porosity, $K_d=0$ and dual-porosity, $K_d\neq0$ conceptual models for transport in the Culebra. Both curves shown for $K_d\neq0$ are dominated completely by cuttings releases. Both constant λ and time-dependent λ cases are shown. Summed normalized releases are displayed using an inverse hyperbolic sine scale, which differs from a logarithmic scale only in the interval between 0 and 10^{-4}.

entirely by the cuttings releases (compare to Figure 5-3a). K_d values used in these calculations were sampled from the same ranges used in the 1991 performance assessment, and are based on judgment elicited from a panel of SNL experts. K_d values used in a final compliance evaluation will be based on experimental data (US DOE, 1992b, and references cited therein).

5.1.2.3 DISCUSSION OF THE 1992 PRELIMINARY COMPARISON WITH THE CONTAINMENT REQUIREMENTS

Results presented in the preceding section are consistent with the conclusion made in previous preliminary comparisons that performance estimates for the WIPP lie below the limits set by the Containment Requirements (Bertram-Howery et al., 1990; WIPP PA Division, 1991a). As illustrated in Figure 5-6, consideration of alternative models for the probability of human intrusion and radionuclide transport in the Culebra provides insights into the relative impacts on performance of specific components of the natural barrier system and institutional controls at the WIPP.

The uppermost CCDF in Figure 5-6, labeled "Total, Single Porosity + Cuttings, λ_0" and calculated using the single-porosity and constant λ models, represents an estimate of the performance of the disposal system with very little contribution from the natural barrier provided by retardation in the Culebra and no contribution from the potential institutional barrier that could be provided by passive markers, as required by the Assurance Requirements. For the modeling system and data base used in 1992, the mean CCDF for this case lies below the EPA limits.

The segments of a CCDF shown with a dotted line and labeled "Total, Discharge from Borehole + Cuttings, λ_0" display performance with *no* contribution whatsoever from retardation in the Culebra. This CCDF is unlike all others shown in this volume in that releases are not calculated at the accessible environment, and therefore is not suitable for comparison, preliminary or otherwise, with the Containment Requirements. The curve displays releases directly into the Culebra (with cuttings also included) from boreholes occurring at 1000 years, and therefore provides an estimate of total releases if subsurface transport to the accessible environment were instantaneous and complete. The curve shows repository performance estimated with contributions from only the natural barrier provided by the Salado Formation and the engineered barrier system. Instantaneous and complete transport in the Culebra is physically unrealistic, and this curve is displayed only for the purpose of comparison with the curve described in the previous paragraph, which was calculated

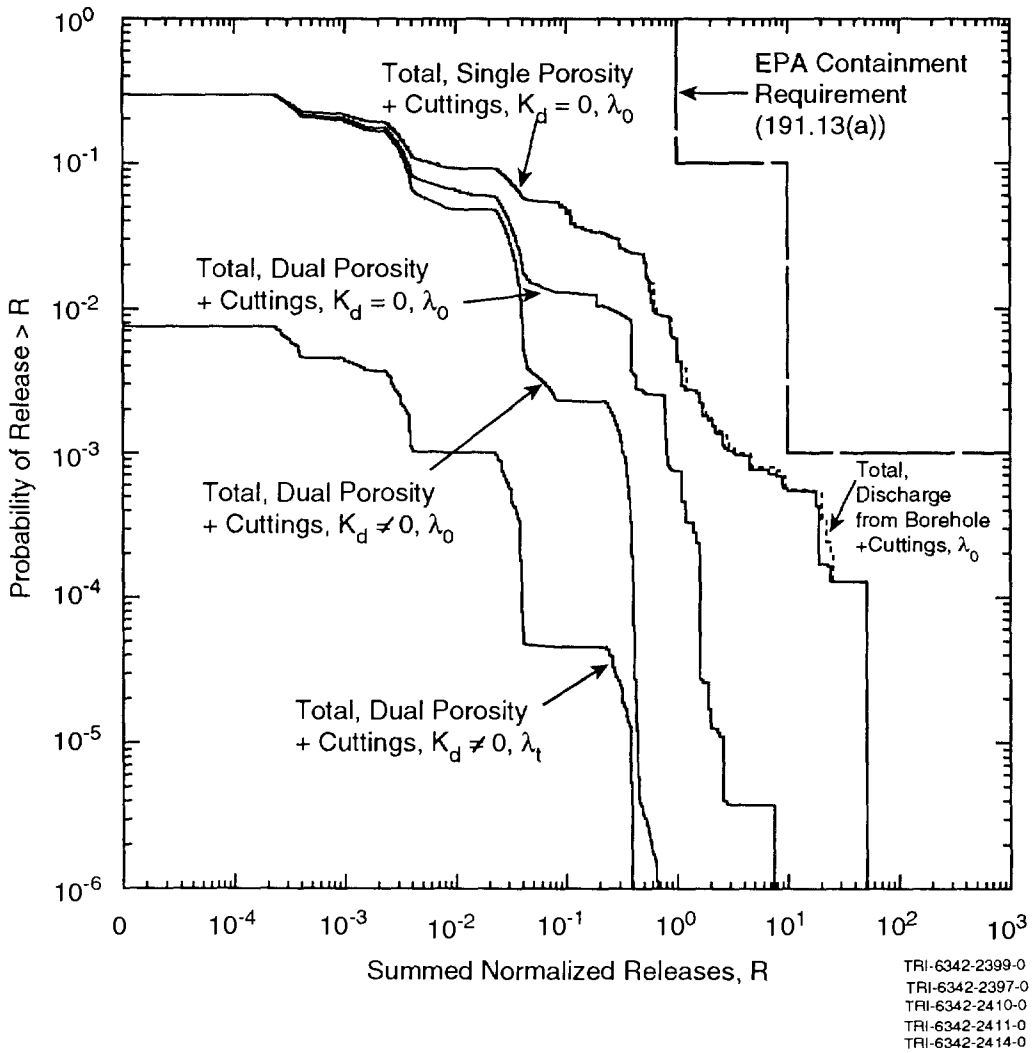

Figure 5-6. Comparison of mean CCDFs for total (cuttings plus subsurface) releases from intrusions occurring at 1000 years showing the impact of including specific components of the natural and institutional barrier systems. Both curves shown for $K_d \neq 0$ are dominated completely by cuttings releases. Summed normalized releases are displayed using an inverse hyperbolic sine scale, which differs from a logarithmic scale only in the interval between 0 and 10^{-4}.

using the single-porosity and constant λ models. The two curves are identical for most of their lengths. The differences between the curves are caused by radioactive decay during transport, and rapid transport in the single-porosity transport model in effect allows all sufficiently long-lived radionuclides that enter the Culebra to be released to the accessible environment within the 9000 years following intrusion.

The CCDF in Figure 5-6 labeled "Total, Dual Porosity + Cuttings, K_d=0, λ_o," represents an estimate of the performance of the disposal system if physical retardation by diffusion into the pore volume of the Culebra is included as a part of the natural barrier system. The area between the first and second CCDFs is a measure of the potential regulatory impact of including physical retardation. Similarly, the next CCDF in Figure 5-6, calculated using the dual-porosity, $K_d \neq 0$, and constant λ models, represents an estimate of the performance of the disposal system if both physical and chemical retardation in the Culebra are included in the natural barrier system. The location of this third curve is determined entirely by cuttings releases.

The final CCDF in Figure 5-6, calculated using the dual-porosity, $K_d \neq 0$, and time-dependent λ models, shows the effect of including expert judgment on the efficacy of passive markers in reducing the probability of human intrusion. This final CCDF, also determined entirely by cuttings releases, was calculated using what the WIPP Performance Assessment Department believes at this time to be the most realistic conceptual model for the disposal system, based on models and data available in 1992. As indicated previously, results are preliminary, and none of the curves shown in Figure 5-6 are believed sufficiently defensible for use in a final compliance evaluation.

5.2 Individual Protection Requirements

The Standard requires that an uncertainty analysis of undisturbed conditions be performed to assess compliance with the Individual Protection Requirements. In the case of the WIPP, the performance measure is dose to humans in the accessible environment.

Thus far, evaluations indicate that radionuclides will not migrate to the accessible environment boundary during 1000 years. Therefore, dose calculations are not expected to be a part of the WIPP assessment of compliance with the Standard. However, Subpart B is in remand. Performance assessments will continue to evaluate compliance with the Individual Protection Requirements of the 1985 Standard until a revised Standard is promulgated.

5.2.1 Previous Studies

Three previous studies reported doses to humans resulting from hypothetical releases from the WIPP for selected scenarios (US DOE, 1980a; Lappin et al., 1989, 1990). Although these studies employed deterministic calculations and were not concerned with assessing compliance with the Individual Protection Requirements, they had an important influence on the design of probability-based dose calculations. An uncertainty analysis of undisturbed performance was performed in a methodology demonstration for WIPP performance assessment (Marietta et al., 1989). The relative importance of various phenomena and system components was examined through sensitivity analyses of four different repository/shaft models for undisturbed conditions (Rechard et al., 1990b). Calculations for undisturbed performance of the repository were not updated in the 1990 preliminary performance assessment (Bertram-Howery et al., 1990). However, information about possible effects of gas generated within the repository was obtained from the assessment of disturbed performance.

The approach adopted for the 1991 preliminary performance assessment was to perform deterministic calculations to verify that, using the 1991 modeling system, previous conclusions of no releases in 10,000 years were still valid. First, a two-dimensional horizontal simulation to assess the migration of brine from the repository into the intact portion of MB139 was performed. The calculation estimated the spatial scale that passive, neutrally buoyant particles would be transported in advecting brine as a result of maximum gas-generation rates in a waste panel. Second, a two-dimensional simulation of a vertical section of the repository from waste panels to the closest shaft was performed to assess migration of radionuclides through the DRZ, panel seals, and backfilled excavations. The calculation estimated the extent that radionuclides would be transported in brine flowing toward and upward through sealed shafts as a result of the pressure gradient between the Culebra Dolomite and a waste panel that is pressurized with waste-generated gas. Least favorable bounds for important parameter values (e.g., an inexhaustible source, no decay, no retardation, the same solubility limit for all radionuclides, etc.) were assumed.

Results of the horizontal simulation showed concentrations at 120 m from the panels in the intact MB139 after 10,000 years to be 1 percent of the source. Results of the vertical simulation including the shaft showed EPA normalized sums (consequences) at 10,000 years of less than 10^{-2} at 20 m up the shaft and less than 10^{-3} at 50 m up the shaft. The 1991 preliminary performance assessment indicated that no significant releases occur at the shaft/Culebra intersection at 10,000 years.

Sensitivity analyses of gas and brine migration provide further support for the preliminary conclusion that radionuclides will not migrate to the accessible environment from the undisturbed repository (WIPP PA Department, 1992). These analyses of 10,000-year undisturbed performance used a two-dimensional vertical cross-section of the repository that included a simplified representation of the shaft and shaft-seal system, and examined flow of both brine and gas up the shaft and horizontally through anhydrite interbeds toward the accessible environment. Analyses did not include salt creep or pressure-dependent fracturing of anhydrite interbeds. Because these analyses were primarily designed to provide guidance to the WIPP Project for use in developing a strategy for evaluating compliance with the RCRA (specifically, with 40 CFR 268.6, which states the conditions for land disposal of hazardous wastes), emphasis was placed on gas migration, and radionuclide transport was not included in the calculations. However, in the selected analyses in which brine flow was tracked from the waste panels, no brine that had been in contact with waste migrated past the disturbed rock zone in 10,000 years. Because the only significant transport of radionuclides from the WIPP will occur in brine, analyses of brine migration provide an approximation of the maximum distance radionuclides may travel.

5.2.2 1992 Preliminary Comparison

Results of the 1992 preliminary performance assessment for informal comparison with the Individual Protection Requirements will be reported in Volume 4 of this report.

5.3 Assurance Requirements

As prescribed in the Agreement for Consultation and Cooperation with the State of New Mexico (US DOE and State of New Mexico, 1981, as modified), the WIPP Project has prepared a plan for implementing the Assurance Requirements of the 1985 Standard (US DOE, 1987). The plan is preliminary because methods and technologies could evolve over the waste-emplacement time frame. A draft of the revised *Assurance Requirements Plan* (US DOE, 1987) is in review; however, the information in the following sections is from the 1987 version unless otherwise noted. In accordance with the Project's interpretation of the EPA's intention, the Project will select assurance measures based on the uncertainties in the final performance assessment. The current plan includes definitions and clarifications of the Standard as it applies to the WIPP, the implementation objective for each requirement, an outline of the

implementation steps for each requirement, and a schedule of activities leading to final compliance. Additional information on markers as passive institutional controls comes from performance-assessment activities using expert panels.

5.3.1 Active Institutional Controls

Active institutional controls are expected to include evaluation of land use in the WIPP area; maintaining fences and buildings and guarding the facility during active cleanup; decontamination and decommissioning; land reclamation; and post disposal-phase monitoring. The objectives of these activities are to provide a facility and presence at the site during active cleanup; to restore the land surface as closely to its original condition as possible to avoid future preferential selection of the area for incompatible uses, if restoration is deemed desirable after consideration of the results of the expert panel on markers (see Section 5.3.3 of this volume); and to monitor the disposal system.

Performance assessments may assume that active control is maintained for 100 years; in the 1992 calculations, no intrusions are assumed to occur during the first 100 years after decommissioning.

5.3.2 Disposal-System Monitoring

Monitoring is required until no significant concerns need to be addressed by further monitoring. The objective of the monitoring program is "to detect substantial and detrimental deviation from the expected performance of the disposal system" (§ 191.14(b)). Monitoring activities will be identified during the course of the performance assessment, but are likely to include monitoring of hydrological, geological, geochemical, and structural performance. Monitoring that jeopardizes the isolation capabilities of the disposal system is not allowed. Numerous survey monuments have been installed to monitor subsidence as an indicator of unexpected changes in the disposal system.

5.3.3 Passive Institutional Controls

The Project will implement passive institutional controls over the entire controlled area of the WIPP. Passive institutional controls include markers warning of the presence of buried nuclear waste and identifying the boundary of the controlled area, external records about the WIPP repository, and continued federal ownership. The EPA assumes in the

guidance to the Standard that passive institutional controls will reduce the possibility of inadvertent human intrusion into the repository. Compliance evaluation for the Standard must address the potential for human intrusion and the effectiveness of passive institutional controls to deter such intrusion.

To address the issues of markers for the WIPP, two expert panels were established. Members of the first panel identified possible future societies and how they may intrude the repository, and also developed probabilities of future society development and of various intrusions (Hora et al., 1991). The possible modes of intrusion identified by the first panel were provided to a second panel as an aid in developing design characteristics for permanent markers and judging the efficacy of the markers in deterring human intrusion. A report about the "markers" panel is currently being prepared. In addition, a report is in preparation that describes past efforts at developing barriers to human intrusion, as a complement to the markers.

Records will be preserved of the disposal site and its contents. The expert panel on intrusion into the repository considered the impact of records preservation on intrusion rates and probabilities (Hora et al., 1991). The panel indicated that records should specify techniques for borehole plugging in the event that exploratory drilling caused an intrusion. Such techniques could be incorporated into legal records together with the description and location of the disposal system. The records could also contain a warning about the potential effects of drilling through the repository and into pressurized brine in the Castile Formation.

In accordance with Appendix B of the Standard, the DOE or some successor agency is assumed to retain ownership and administrative control over the WIPP area. The federal agency responsible for the land will institute regulations that appropriately restrict land use and development. Acreage around the WIPP is owned by the Federal government and currently administered by the DOE. The area within the land-withdrawal boundary for the WIPP is withdrawn from all forms of entry, appropriation, and disposal under the public land laws, including the mineral leasing laws, the geothermal leasing laws, the material sale laws, and the mining laws (Public Law 102-579, 1992, Section 3). With respect to drilling, the DOE has control of the acreage within the land-withdrawal boundary from the surface to 6000 ft (1830 m) in the subsurface. Additionally, grazing may continue to the extent that it is compatible with WIPP activities.

5.3.4 Multiple Barriers

The Standard requires that both natural and engineered barriers be used as part of the isolation system. At the WIPP, natural barriers include the favorable characteristics of the salt formation and the geohydrologic setting. Engineered barriers that will isolate wastes from the accessible environment will include seals in repository excavations and bentonite and crushed-salt backfill in waste-emplacement panels. The effectiveness of these barriers is being modeled for the performance assessment to determine if they will provide a disposal system that isolates the radioactive wastes to the levels required in the Standard. In addition, the Engineered Alternatives Task Force has evaluated additional engineering measures for the WIPP, should such measures be necessary (US DOE, 1990e, 1991d).

5.3.5 Natural Resources

The Standard requires that locations containing recoverable resources not be used for repositories unless the favorable characteristics of a proposed location can be shown to compensate for the greater likelihood of being disturbed in the future. Evaluation of the natural resources in the WIPP area centers on two issues: (1) the denial of resources that could not be developed because such development might conflict with the long-term goal of waste isolation, and (2) the attractiveness to future generations of resources associated with the location. Future societies might attempt to exploit natural resources near the WIPP and thereby create the potential for a release of radionuclides into the accessible environment. These issues have been evaluated in several reports (US DOE, 1980a, 1981; US DOE and State of New Mexico, 1981, as modified; Brausch et al., 1982; Weart, 1983; US DOE, 1990d). A recent report summarizes these earlier reports (US DOE, 1991c), and the DOE will continue to document information about natural resources that was used in making the decision to proceed with the WIPP Project.

5.3.6 Waste Removal

The Standard requires that disposal systems be selected so that removal of most of the wastes is not precluded for a reasonable period of time after disposal (§ 191.14(f)). A primary plan for waste removal during the disposal phase of the WIPP (Subpart A of the Standard) has been prepared (US DOE, 1980a). In promulgating the Standard, the EPA stated that to meet the waste-removal requirement for the post-closure phase (Subpart B of the Standard), it only need be technologically feasible to be able to mine the sealed repository and recover the waste, even at substantial cost and

occupational risk (US EPA, 1985, p. 38082). The EPA also stated that "*any* current concept for a mined geologic repository meets this requirement *without* any additional procedures or design features" (US EPA, 1985, p. 38082, emphasis in original). Thus, the WIPP satisfies this requirement.

5.4 Groundwater Protection Requirements

The WIPP must comply with the Groundwater Protection Requirements of the Standard by providing a reasonable expectation that radionuclide concentrations in a "special source of ground water" will not exceed specified values (§ 191.16; also see Section 3.6 of this volume). Evaluations have indicated that the requirement is not relevant to the WIPP because no groundwater near the WIPP within the maximum areal extent designated by the Standard (Figure 3-4) satisfies the definition of a "special source of groundwater."

Based upon the EPA definition of Class I groundwater (US EPA, 1984) as used in the definition of special source of groundwater, for Class I groundwater to be present at the WIPP, the groundwater resource must be highly vulnerable to contamination because of the hydrogeological characteristics of the areas under which the resource occurs, including areas of high hydraulic conductivity or areas of groundwater recharge. Either of the following must also be true: the groundwater must be an irreplaceable source of drinking water, or the groundwater must be ecologically vital.

The hydrogeological characteristics of the WIPP have been evaluated through extensive ongoing investigations dating to 1975 (US DOE, 1990c). Groundwater quality and the hydrologic conductivity of water-bearing units at the WIPP are monitored and reported annually (Lyon, 1989). The most transmissive hydrologic unit in the WIPP area is the Culebra Dolomite Member of the Rustler Formation (see Chapter 2 of this volume and Volume 2 of this report). Hydraulic properties of the Culebra Dolomite have been calculated from test holes in the vicinity of the WIPP (summarized in Cauffman et al., 1990, and Brinster, 1991). Horizontal groundwater flow in the Culebra away from the WIPP is generally to the south along a decreasing gradient at a very slow rate. Based on hydrogeological studies in the WIPP area, no geological units with high hydraulic conductivities that would require special protective measures appear to be present (Marietta et al., 1989; Lappin et al., 1989; US DOE, 1990c). If groundwater that is highly vulnerable to contamination were present near the WIPP, it would not be classified as Class I because it is neither an irreplaceable source of

drinking water for a substantial population (Lappin et al., 1989) nor ecologically vital (US DOE, 1980a, 1991c).

Even if Class I groundwater were present at the WIPP, the Groundwater Protection Requirements would be relevant only if the groundwater were supplying drinking water to thousands of persons at the date DOE selected the site for development of the WIPP *and* if these groundwaters were irreplaceable. At the time the DOE chose the WIPP location, and currently, no source of water (including Class I groundwater) within 5 km (3 mi) beyond the maximum allowable extent of the controlled area was supplying drinking water for thousands (or even tens) of persons. Thus, even if Class I groundwater were present, the Groundwater Protection Requirements would not be relevant to the WIPP.

6. CONCLUSIONS

The 1992 preliminary comparison with 40 CFR 191, Subpart B, for the WIPP is consistent with the conclusions from the 1990 and 1991 preliminary comparisons (Bertram-Howery et al., 1990; WIPP PA Division, 1991a): based on the presently available conceptual models, computational models, and data describing disposal-system performance, the WIPP Performance Assessment Department has a high level of confidence that the WIPP will be able to comply with the quantitative requirements of the Standard as promulgated in 1985 (US EPA, 1985). As summarized in the following discussion, however, the modeling system and data base are still incomplete; results therefore remain preliminary and should not be used for a formal comparison with the Standard. Furthermore, the Standard has been vacated by a Federal Court of Appeals (NRDC v. US EPA, 1987). The Standard will be repromulgated in 1993, as specified by the *WIPP Land Withdrawal Act* (Public Law 102-579, 1992), and may differ in some aspects from the 1985 version on which the 1992 preliminary comparison is based. The WIPP Performance Assessment Department anticipates that a final, defensible performance assessment suitable for compliance evaluation will be completed following additional iterations of preliminary performance assessments.

The 1992 performance-assessment calculations reflect improvements in several important portions of the modeling system. Specific major improvements in the modeling system for 1992 (described in detail in Volume 2 of this report) are: the inclusion of the effects of salt creep in the modeling of disposal-room behavior; the use of an advanced geostatistical procedure to account for spatial variability in the transmissivity of the Culebra Dolomite Member of the Rustler Formation; and the use of a computational model for radionuclide transport in the Culebra that allows consideration of alternative conceptual models for dual-porosity and single-porosity transport. The 1992 performance assessment also marks the first use of judgment elicited from expert panels to determine the probability of future inadvertent human intrusion into the WIPP (see Volume 2, Chapter 5 of this report, and the memorandum by Hora in Volume 3, Appendix A of this report).

Results of the 1992 preliminary comparison with the Containment Requirements of the Standard (§ 191.13) are presented as mean complementary cumulative distribution functions (CCDFs) displaying estimated probabilistic releases of radionuclides to the accessible environment for 10,000 years. Results compare three conceptual models for radionuclide transport in the Culebra and two approaches to estimating the probability of inadvertent human intrusion into the WIPP by exploratory drilling. The representation

for disposal-system performance believed by the WIPP Performance Assessment Department to be most realistic includes intrusion probabilities based on expert-panel judgment and dual-porosity transport with chemical retardation. For intrusions occurring 1000 years after decommissioning, the mean CCDF for this representation lies more than one order of magnitude below the EPA limits. Using the same approach to intrusion probabilities used in the 1991 performance assessment (i.e., not taking expert judgment into account and basing the probability model on the maximum intrusion probability indicated in Appendix B of 40 CFR 191) significantly increases the probability of releases, regardless of the model used for subsurface transport. Assuming the higher intrusion probabilities and dual-porosity transport without chemical retardation, the mean CCDF is approximately one order of magnitude below the EPA limits. For the higher intrusion probabilities and single-porosity, fracture-only transport (which assumes very little contribution from the natural barrier provided by retardation in the Culebra), the mean CCDF is less than one order of magnitude below the EPA limits.

Performance estimates for the 1992 preliminary comparison with the Individual Protection Requirements of the Standard (§ 191.15) have not been included in this volume. Previous analyses indicate that no radionuclides will reach the accessible environment from the undisturbed repository for 10,000 years (Marietta et al., 1989). Calculations of brine and gas migration from the undisturbed repository completed using the 1991 performance-assessment modeling system suggest that brine (the only medium in which significant radionuclide transport will occur at the WIPP) that has been in contact with waste will not migrate more than a few tens of meters from the waste-emplacement panels in 10,000 years (WIPP PA Department, 1992). Determination of compliance with the Individual Protection Requirements as promulgated in 1985 will be based on estimates of doses to humans in the accessible environment for 1000 years (rather than 10,000 years) of undisturbed performance. Because no releases whatsoever to the accessible environment are predicted for 1000 years of undisturbed performance, no doses to humans are anticipated and determination of compliance with the Individual Protection Requirements should be straightforward.

The third quantitative requirement of the Standard, the Groundwater Protection Requirements (§ 191.16), does not apply to the WIPP because no "special source of ground water," as defined in the Standard, is present at the WIPP. All groundwater at the WIPP fails to meet more than one of the specified criteria, including the requirement that a "special source of ground water" be "supplying drinking water for thousands of persons as of the date that the [DOE] chooses a location..." and that the source of water be "irreplaceable" (§ 191.12(o)).

As noted above, several aspects of the modeling system and data base can be identified now as requiring additional work before the performance assessment can be considered defensible for a final comparison to the Standard. Information will be provided for specific needs (e.g., conceptual models or distributions for important parameters that are insufficiently supported by experimental data) by ongoing and planned laboratory and field experimental programs described in the *Test Phase Plan* (US DOE, 1990a, currently in revision). These needs include include the following: defensible values for radionuclide solubilities in repository brine; retardation factors for radionuclides in the Culebra; additional support for the dual-porosity model for transport in the Culebra; and an improved model for the generation of gas as waste and containers degrade. Other needs will be met by improvements in performance-assessment modeling. Conceptual and computational models will be developed for pressure-dependent fracturing of the anhydrite interbeds above and below the repository. Spalling of waste into an intruding borehole as the repository depressurizes will be examined and, if important, included in performance-assessment modeling. The consequences of brine flow to the surface following borehole intrusion will be modeled. Several aspects of groundwater flow in the Culebra will be examined as a three-dimensional model for regional groundwater flow becomes available, including the possible effects of subsidence related to potash mining, uncertainty resulting from the incomplete understanding of present recharge and vertical flow between units, and additional analyses of the effects of climatic change. Future analyses will also examine the effect on estimated performance of correlations that may exist between physical parameters that are currently assumed for the Monte Carlo simulations to be uncorrelated.

The WIPP Performance Assessment Department believes that future analyses will indicate that none of these identified needs will have a major impact on compliance with the quantitative requirements of the Standard. This belief cannot be supported defensibly at this time and is offered here as an opinion of the Performance Assessment Department, rather than as fact. It is based on the premise that the major processes that will contribute to radionuclide releases have already been identified and included in the performance-assessment modeling system. Although the performance-assessment needs identified now and listed above contribute to uncertainty in estimated performance, resolution of those needs is unlikely to shift the location of the mean CCDF beyond the range displayed in the 1992 results. Additional needs may be identified by future performance-assessment iterations and laboratory and field studies, but none is foreseen at this time to have an impact as great as that of those already identified.

7. REFERENCES

Andersson, J., T. Carlsson, T. Eng, F. Kautsky, E. Soderman, and S. Wingefors. 1989. *The Joint SKI/SKB Scenario Development Project*. TR89-35. Stockholm, Sweden: Svensk Kärnbränslehantering AB.

Bachman, G.O. 1980. *Regional Geology and Cenozoic History of the Pecos Region, Southeastern New Mexico*. US Geological Survey Open-File Report 80-1099. Denver, CO: US Geological Survey.

Bachman, G.O. 1984. *Regional Geology of Ochoan Evaporites, Northern Part of Delaware Basin*. New Mexico Bureau of Mines and Mineral Resources Circular 184. Socorro, NM: New Mexico Bureau of Mines and Mineral Resources.

Bachman, G.O. 1987. *Karst in Evaporites in Southeastern New Mexico*. SAND86-7078. Albuquerque, NM: Sandia National Laboratories.

Beauheim, R.L. 1987a. *Interpretations of Single-Well Hydraulic Tests Conducted At and Near the Waste Isolation Pilot Plant (WIPP) Site, 1983-1987*. SAND87-0039. Albuquerque, NM: Sandia National Laboratories.

Beauheim, R.L. 1987b. *Analysis of Pumping Tests of the Culebra Dolomite Conducted at the H-3 Hydropad at the Waste Isolation Pilot Plant (WIPP) Site*. SAND86-2311. Albuquerque, NM: Sandia National Laboratories.

Beauheim, R.L. 1987c. *Interpretation of the WIPP-13 Multipad Pumping Test of the Culebra Dolomite at the Waste Isolation Pilot Plant (WIPP) Site*. SAND87-2456. Albuquerque, NM: Sandia National Laboratories.

Beauheim, R.L. 1989. *Interpretation of H-11b4 Hydraulic Tests and the H-11 Multipad Pumping Test of the Culebra Dolomite at the Waste Isolation Pilot Plant (WIPP) Site*. SAND89-0536. Albuquerque, NM: Sandia National Laboratories.

Beauheim, R.L., and P.B. Davies. 1992. "Experimental Plan for Tracer Testing in the Culebra Dolomite at the WIPP Site." Revision A. Albuquerque, NM: Sandia National Laboratories.

Bechtel, Inc. 1986. *Design Validation Final Report*. DOE/WIPP-86-010. Prepared for US Department of Energy. San Francisco, CA: Bechtel National, Inc.

Bertram-Howery, S.G., and R.L. Hunter. 1989a. *Plans for Evaluation of the Waste Isolation Pilot Plant's Compliance with EPA Standards for Radioactive Waste Management and Disposal*. SAND88-2871. Albuquerque, NM: Sandia National Laboratories.

Bertram-Howery, S.G., and R.L. Hunter, eds. 1989b. *Preliminary Plan for Disposal-System Characterization and Long-Term Performance Evaluation of the Waste Isolation Pilot Plant*. SAND89-0178. Albuquerque, NM: Sandia National Laboratories.

Bertram-Howery, S.G., and P.N. Swift. 1990. *Status Report: Potential for Long-Term Isolation by the Waste Isolation Pilot Plant Disposal System*. SAND90-0616. Albuquerque, NM: Sandia National Laboratories.

Bertram-Howery, S.G., M.G. Marietta, D.R. Anderson, K.F. Brinster, L.S. Gomez, R.V. Guzowski, and R.P. Rechard. 1989. *Draft Forecast of the Final Report for the Comparison to 40 CFR Part 191, Subpart B, for the Waste Isolation Pilot Plant*. SAND88-1452. Albuquerque, NM: Sandia National Laboratories.

Bertram-Howery, S.G., M.G. Marietta, R.P. Rechard, P.N. Swift, D.R. Anderson, B.L. Baker, J.E. Bean, Jr., W. Beyeler, K.F. Brinster, R.V. Guzowski, J.C. Helton, R.D. McCurley, D.K. Rudeen, J.D. Schreiber, and P. Vaughn. 1990. *Preliminary Comparison with 40 CFR Part 191, Subpart B for the Waste Isolation Pilot Plant, December 1990*. SAND90-2347. Albuquerque, NM: Sandia National Laboratories.

Bodine, M.W., Jr., B.F. Jones, and S.J. Lambert. 1991. "Chapter 4: Normative Analysis of Groundwaters from the Rustler Formation Associated with the Waste Isolation Pilot Plant, Southeastern New Mexico," *Hydrogeochemical Studies of the Rustler Formation and Related Rocks in the Waste Isolation Pilot Plant Area, Southeastern New Mexico*. Eds. M.D. Siegel, S.J. Lambert, and K.L. Robinson. SAND88-0196. Albuquerque, NM: Sandia National Laboratories.

Bonano, E.J., S.C. Hora, R.L. Keeney, and D. von Winterfeldt. 1990. *Elicitation and Use of Expert Judgement in Performance Assessment for High-Level Radioactive Waste Repositories*. NUREG/CR-5411, SAND89-1821. Albuquerque, NM: Sandia National Laboratories.

Brausch, L.M., A.K. Kuhn, and J.K. Register. 1982. *Natural Resources Study, Waste Isolation Pilot Plant (WIPP) Project, Southeastern, New Mexico*. WTSD-TME-3156. Albuquerque, NM: D'Appolonia Consulting Engineers.

Brinster, K.F. 1991. *Preliminary Geohydrologic Conceptual Model of the Los Medaños Region near the Waste Isolation Pilot Plant for the Purpose of Performance Assessment*. SAND89-7147. Albuquerque, NM: Sandia National Laboratories.

Butcher, B.M. 1990. *Preliminary Evaluation of Potential Engineered Modifications for the Waste Isolation Pilot Plant (WIPP)*. SAND89-3095. Albuquerque, NM: Sandia National Laboratories.

Campbell, J.E., and R.M. Cranwell. 1988. "Performance Assessment of Radioactive Waste Repositories," *Science*. Vol. 239, no. 4846, 1389-1392.

Cauffman, T.L., A.M. LaVenue, and J.P. McCord. 1990. *Ground-Water Flow Modeling of the Culebra Dolomite. Volume II: Data Base.* SAND89-7068/2. Albuquerque, NM: Sandia National Laboratories.

Cheeseman, R.J. 1978. "Geology and Oil/Potash Resources of the Delaware Basin, Eddy and Lea Counties, New Mexico," *Geology and Mineral Deposits of Ochoan Rocks in Delaware Basin and Adjacent Areas.* Ed. G.S. Austin. New Mexico Bureau of Mines and Mineral Resources Circular 159. Socorro, NM: New Mexico Bureau of Mines and Mineral Resources. 7-14.

Cooper, J.B., and V.M. Glanzman. 1971. "Geohydrology of Project GNOME Site, Eddy County, New Mexico," *Hydrology of Nuclear Test Sites.* US Geological Survey Professional Paper 712-A. Washington, DC: US Government Printing Office.

Cranwell, R.M., J.E. Campbell, J.C. Helton, R.L. Iman, D.E. Longsine, N.R. Ortiz, G.E. Runkle, and M.J. Shortencarier. 1987. *Risk Methodology for Geologic Disposal of Radioactive Waste: Final Report.* NUREG/CR-2452, SAND81-2573. Albuquerque, NM: Sandia National Laboratories.

Cranwell, R.M., R.V. Guzowski, J.E. Campbell, and N.R. Ortiz. 1990. *Risk Methodology for Geologic Disposal of Radioactive Waste: Scenario Selection Procedure.* NUREG/CR-1667, SAND80-1429. Albuquerque, NM: Sandia National Laboratories.

Gallegos, D.P., P.I. Pohl, and C.D. Updegraff. 1992. *An Investigation of the Impact of Conceptual Model Uncertainty on the Estimated Performance of a Hypothetical High-Level Nuclear Waste Repository Site in Unsaturated, Fractured Tuff.* SAND90-2882. Albuquerque, NM: Sandia National Laboratories.

Guzowski, R.V. 1990. *Preliminary Identification of Scenarios That May Affect the Escape and Transport of Radionuclides From the Waste Isolation Pilot Plant, Southeastern New Mexico.* SAND89-7149. Albuquerque, NM: Sandia National Laboratories.

Guzowski, R.V. 1991. *Evaluation of Applicability of Probability Techniques to Determining the Probability of Occurrence of Potentially Disruptive Intrusive Events at the Waste Isolation Pilot Plant.* SAND90-7100. Albuquerque, NM: Sandia National Laboratories.

Guzowski, R.V., and J.C. Helton. 1991. "Chapter 4: Scenarios for Compliance Assessment," *Preliminary Comparison with 40 CFR Part 191, Subpart B for the Waste Isolation Pilot Plant, December 1991—Volume 1: Methodology and Results.* WIPP Performance Assessment Division (Report Author). SAND91-0893/1. Albuquerque, NM: Sandia National Laboratories.

Hale, W.E., and A. Clebsch, Jr. 1958. *Preliminary Appraisal of Groundwater Conditions in Southeastern Eddy County and Southwestern Lea County, New Mexico*. Trace Elements Memorandum Report 1045. United States Department of the Interior, Geological Survey. (Copy on file in the Waste Management and Transportation Library, Sandia National Laboratories, Albuquerque, NM.)

Hale, W.E., L.S. Hughes, and E.R. Cox. 1954. *Possible Improvement of Quality of Water of the Pecos River by Diversion of Brine at Malaga Bend, Eddy County, New Mexico*. Carlsbad, NM: Pecos River Commission, New Mexico and Texas, in cooperation with USGS Water Resources Division.

Harms, J.C., and C.R. Williamson. 1988. "Deep-Water Density Current Deposits of Delaware Mountain Group (Permian), Delaware Basin, Texas and New Mexico," *American Association of Petroleum Geologists Bulletin*. Vol. 72, no. 3, 299-317.

Havens, J.S., and D.W. Wilkins. 1979. *Experimental Salinity Alleviation at Malaga Bend of the Pecos River, Eddy County, New Mexico*. US Geological Survey Water-Resources Investigations 80-4. Albuquerque, NM: US Department of the Interior, Geological Survey.

Hayes, P.T. 1964. *Geology of the Guadalupe Mountains, New Mexico*. US Geological Survey Professional Paper 446. Washington, DC: US Government Printing Office.

Helton, J.C. 1991. "Chapter 3: Performance-Assessment Overview," *Preliminary Comparison with 40 CFR Part 191, Subpart B for the Waste Isolation Pilot Plant, December 1991—Volume 1: Methodology and Results*. WIPP Performance Assessment Division (Report Author). SAND91-0893/1. Albuquerque, NM: Sandia National Laboratories.

Helton, J.C. In press. "Risk, Uncertainty in Risk and the EPA Release Limits for Radioactive Waste Disposal," *Nuclear Technology*. (To appear in 1993 in Vol. 101, no. 1, 18-39.)

Helton, J.C., J.W. Garner, R.D. McCurley, and D.K. Rudeen. 1991. *Sensitivity Analysis Techniques and Results for Performance Assessment at the Waste Isolation Pilot Plant*. SAND90-7103. Albuquerque, NM: Sandia National Laboratories.

Helton, J.C., J.W. Garner, R.P. Rechard, D.K. Rudeen, and P.N. Swift. 1992. *Preliminary Comparison with 40 CFR Part 191, Subpart B for the Waste Isolation Pilot Plant, December 1991—Volume 4: Uncertainty and Sensitivity Analysis Results*. SAND91-0893/4. Albuquerque, NM: Sandia National Laboratories.

Hills, J.M. 1984. "Sedimentation, Tectonism, and Hydrocarbon Generation in the Delaware Basin, West Texas and Southeastern New Mexico," *American Association of Petroleum Geologists Bulletin*. Vol. 68, no. 3, 250-267.

Hiss, W.L. 1975. "Stratigraphy and Ground-Water Hydrology of the Capitan Aquifer, Southeastern New Mexico and West Texas." PhD dissertation. Boulder, CO: University of Colorado.

Hora, S.C., and R.L. Iman. 1989. "Expert Opinion in Risk Analysis: The NUREG-1150 Methodology," *Nuclear Science and Engineering*. Volume 102, no. 4, 323-331.

Hora, S.C., D. von Winterfeldt, and K.M. Trauth. 1991. *Expert Judgment on Inadvertent Human Intrusion into the Waste Isolation Pilot Plant*. SAND90-3063. Albuquerque, NM: Sandia National Laboratories.

Hunter, R.L., R.M. Cranwell, and M.S.Y. Chu. 1986. *Assessing Compliance With the EPA High-Level Waste Standard: An Overview*. NUREG/CR-4510, SAND86-0121. Albuquerque, NM: Sandia National Laboratories.

Huyakorn, P.S., H.O. White, Jr., and S. Panday. 1991. *STAFF2D Solute Transport and Fracture Flow in Two Dimensions. Version 3.1*. Herndon, VA: Hydrogeologic, Inc. (Copy on file in Waste Management and Technology Library, Sandia National Laboratories, Albuquerque, NM.)

Iman, R.L., and W.J. Conover. 1982. "A Distribution-Free Approach to Inducing Rank Correlation Among Input Variables," *Communications in Statistics: Simulation and Computation*. Vol. B11, no. 3, 311-334.

Iman, R.L., and J.C. Helton. 1985. *A Comparison of Uncertainty and Sensitivity Analysis Techniques for Computer Models*. NUREG/CR-3904, SAND84-1461. Albuquerque, NM: Sandia National Laboratories.

Jones, C.L. 1978. *Test Drilling for Potash Resources: Waste Isolation Pilot Plant Site, Eddy County, New Mexico*. US Geological Survey Open-File Report 78-592. Denver, CO: US Geological Survey.

Jones, T.L., V.A. Kelley, J.F. Pickens, D.T. Upton, R.L. Beauheim, and P.B. Davies. 1992. *Integration of Interpretation Results of Tracer Tests Performed in the Culebra Dolomite at the Waste Isolation Pilot Plant Site*. SAND92-1579. Albuquerque, NM: Sandia National Laboratories.

Kaplan, S., and B.J. Garrick. 1981. "On the Quantitative Definition of Risk," *Risk Analysis*. Vol. 1, no. 1, 11-27.

Kelley, V.A., and J.F. Pickens. 1986. *Interpretation of the Convergent-Flow Tracer Tests Conducted in the Culebra Dolomite at the H-3 and H-4 Hydropads at the Waste Isolation Pilot Plant (WIPP) Site*. SAND86-7161. Albuquerque, NM: Sandia National Laboratories.

Lappin, A.R. 1988. *Summary of Site-Characterization Studies Conducted from 1983 through 1987 at the Waste Isolation Pilot Plant (WIPP) Site, Southeastern New Mexico*. SAND88-0157. Albuquerque, NM: Sandia National Laboratories.

Lappin, A.R., R.L. Hunter, D.P. Garber, P.B. Davies, R.L. Beauheim, D.J. Borns, L.H. Brush, B.M. Butcher, T. Cauffman, M.S.Y. Chu, L.S. Gomez, R.V. Guzowski, H.J. Iuzzolino, V. Kelley, S.J. Lambert, M.G. Marietta, J.W. Mercer, E.J. Nowak, J. Pickens, R.P. Rechard, M. Reeves, K.L. Robinson, and M.D. Siegel, eds. 1989. *Systems Analysis, Long-Term Radionuclide Transport, and Dose Assessments, Waste Isolation Pilot Plant (WIPP), Southeastern New Mexico; March 1989*. SAND89-0462. Albuquerque, NM: Sandia National Laboratories.

Lappin, A.R., R.L. Hunter, P.B. Davies, D.J. Borns, M. Reeves, J. Pickens, and H.J. Iuzzolino. 1990. *Systems Analysis, Long-Term Radionuclide Transport, and Dose Assessments, Waste Isolation Pilot Plant (WIPP), Southeastern New Mexico; September 1989*. SAND89-1996. Albuquerque, NM: Sandia National Laboratories.

LaVenue, A.M., and B.S. RamaRao. 1992. *A Modeling Approach To Address Spatial Variability within the Culebra Dolomite Transmissivity Field*. SAND92-7306.

Lyon, M.L. 1989. *Annual Water Quality Data Report for the Waste Isolation Pilot Plant*. DOE/WIPP 89-001. Carlsbad, NM: Westinghouse Electric Corporation.

Marietta, M.G., S.G. Bertram-Howery, D.R. Anderson, K.F. Brinster, R.V. Guzowski, H. Iuzzolino, and R.P. Rechard. 1989. *Performance Assessment Methodology Demonstration: Methodology Development for Evaluating Compliance with EPA 40 CFR 191, Subpart B, for the Waste Isolation Pilot Plant*. SAND89-2027. Albuquerque, NM: Sandia National Laboratories.

McKay, M.D., R.J. Beckman, and W.J. Conover. 1979. "A Comparison of Three Methods for Selecting Values of Input Variables in the Analysis of Output from a Computer Code," *Technometrics*. Vol. 21, no. 2, 239-245.

Mercer, J.W. 1983. *Geohydrology of the Proposed Waste Isolation Pilot Plant Site, Los Medanos Area, Southeastern New Mexico*. US Geological Survey Water-Resources Investigations Report 83-4016. Albuquerque, NM: US Geological Survey.

Munson, D.E., A.F. Fossum, and P.E. Senseny. 1989a. *Advances in Resolution of Discrepancies Between Predicted and Measured In Situ WIPP Room Closures*. SAND88-2948. Albuquerque, NM: Sandia National Laboratories.

Munson, D.E., A.F. Fossum, and P.E. Senseny. 1989b. *Approach to First Principles Model Prediction of Measured WIPP In Situ Room Closure in Salt*. SAND88-2535. Albuquerque, NM: Sandia National Laboratories.

NEA (Nuclear Energy Agency). 1992a. *PSACOIN Level 2 Exercise: Problem Specification and Questionnaire for Stage 1*. NEA/PSAG/DOC(92)2. Paris: NEA Probabilistic System Assessment Group (PSAG), Radioactive Waste Management Committee, Steering Committee for Nuclear Energy, Organization for Economic Co-Operation and Development, Nuclear Energy Agency. (Copy on file in the Waste Management and Transportation Library, Sandia National Laboratories, Albuquerque, NM.)

NEA (Nuclear Energy Agency). 1992b. *Safety Assessment of Radioactive Waste Repositories: Systematic Approaches to Scenario Development*. Paris: Organization for Economic Co-Operation and Development, Nuclear Energy Agency.

Nicholson, A., Jr., and A. Clebsch, Jr. 1961. *Geology and Ground-Water Conditions in Southern Lea County, New Mexico*. New Mexico Bureau of Mines and Mineral Resources Ground-Water Report No. 6. Socorro, NM: New Mexico Bureau of Mines and Mineral Resources.

Nowak, E.J., J.R. Tillerson, and T.M. Torres. 1990. *Initial Reference Seal System Design: Waste Isolation Pilot Plant*. SAND90-0355. Albuquerque, NM: Sandia National Laboratories.

NRDC (National Resources Defense Council) v. US EPA (United States Environmental Protection Agency). 1987. *824 Federal Reporter, 2d Series (1st Circuit 1987)*. 1258-1294.

NuPac (Nuclear Packaging, Inc.). 1989. *Safety Analysis Report for the TRUPACT-II Shipping Package*. NuPac TRUPACT-II SAR Rev. 4. Washington, DC: Nuclear Packaging, Inc.

Pepping, R.E., M.S.Y. Chu, and M.D. Siegel. 1983. "A Simplified Analysis of a Hypothetical Repository in a Basalt Formation," *Technical Assistance for Regulatory Development: Review and Evaluation of the Draft EPA Standard 40 CFR 191 for Disposal of High-Level Waste*. NUREG/CR-3235, SAND82-1557. Albuquerque, NM: Sandia National Laboratories. Vol. 2.

Powers, D.W., S.J. Lambert, S-E. Shaffer, L.R. Hill, and W.D. Weart, eds. 1978a. *Geological Characterization Report, Waste Isolation Pilot Plant (WIPP) Site, Southeastern New Mexico*. SAND78-1596. Albuquerque, NM: Sandia National Laboratories. Vol. 1.

Powers, D.W., S.J. Lambert, S-E. Shaffer, L.R. Hill, and W.D. Weart, eds. 1978b. *Geological Characterization Report, Waste Isolation Pilot Plant (WIPP) Site, Southeastern New Mexico*. SAND78-1596. Albuquerque, NM: Sandia National Laboratories. Vol. 2.

Public Law 91-190. 1970. *National Environmental Policy Act of 1969*, as amended by Public Law 94-52 (July 3, 1975) and Public Law 94-83 (August 9, 1975).

Public Law 94-580. 1976. *Resource Conservation and Recovery Act of 1976.*

Public Law 96-164. 1979. *Department of Energy National Security and Military Applications of Nuclear Energy Authorization Act of 1980.*

Public Law 100-456. 1988. *National Defense Authorization Act, Fiscal Year 1989.*

Public Law 102-579. 1992. *Waste Isolation Pilot Plant Land Withdrawal Act.*

Rechard, R.P. 1989. *Review and Discussion of Code Linkage and Data Flow in Nuclear Waste Compliance Assessments.* SAND87-2833. Albuquerque, NM: Sandia National Laboratories.

Rechard, R.P., H. Iuzzolino, and J.S. Sandha. 1990a. *Data Used in Preliminary Performance Assessment of the Waste Isolation Pilot Plant (1990).* SAND89-2408. Albuquerque, NM: Sandia National Laboratories.

Rechard, R.P., W. Beyeler, R.D. McCurley, D.K. Rudeen, J.E. Bean, and J.D. Schreiber. 1990b. *Parameter Sensitivity Studies of Selected Components of the Waste Isolation Pilot Plant Repository/Shaft System.* SAND89-2030. Albuquerque, NM: Sandia National Laboratories.

Rechard, R.P., P.J. Roache, R.L. Blaine, A.P. Gilkey, and D.K. Rudeen. 1991. *Quality Assurance Procedures for Computer Software Supporting Performance Assessments of the Waste Isolation Pilot Plant.* SAND90-1240. Albuquerque, NM: Sandia National Laboratories.

Rechard, R.P., K.M. Trauth, and R.V. Guzowski. 1992a. *Quality Assurance Procedures for Parameter Selection and Use of Expert Judgment Panels Supporting Performance Assessments of the Waste Isolation Pilot Plant.* SAND91-0429. Albuquerque, NM: Sandia National Laboratories.

Rechard, R.P., D.K. Rudeen, and P.J. Roache. 1992b. *Quality Assurance Procedures for Analyses and Report Reviews Supporting Performance Assessments of the Waste Isolation Pilot Plant.* SAND91-0428. Albuquerque, NM: Sandia National Laboratories.

Richey, S.F., J.G. Wells, and K.T. Stephens. 1985. *Geohydrology of the Delaware Basin and Vicinity, Texas and New Mexico.* US Geological Survey Water Resources Investigations Report 84-4077. Washington, DC: US Geological Survey.

Saulnier. G.J., Jr. 1987. *Analysis of Pumping Tests of the Culebra Dolomite Conducted at the H-11 Hydropad at the Waste Isolation Pilot Plant (WIPP) Site.* SAND87-7124. Albuquerque, NM: Sandia National Laboratories.

Siegel, M.D., S.J. Lambert, and K.L. Robinson, eds. 1991. *Hydrogeochemical Studies of the Rustler Formation and Related Rocks in the Waste Isolation Pilot Plant Area, Southeastern New Mexico.* SAND88-0196. Albuquerque, NM: Sandia National Laboratories.

Silva, M.K., and J.K. Channell. 1992. *Implications of Oil and Gas Leases at the WIPP on Compliance with EPA TRU Waste Disposal Standards.* EEG-50. Albuquerque, NM: Environmental Evaluation Group.

Stephens, M.E., and B.W. Goodwin. 1989. "Scenario Analysis for the Postclosure Assessment of the Canadian Concept for Nuclear Fuel Waste Disposal," *Proceedings of the Symposium on Safety Assessment of Radioactive Waste Repositories, Paris, October 9-13, 1989.* Paris: Organization for Economic Co-Operation and Development, Nuclear Energy Agency. 405-415.

Stone, C.M., R.D. Krieg, and Z.E. Beisinger. 1985. *SANCHO: A Finite Element Computer Program for the Quasistatic, Large Deformation, Inelastic Response of Two-Dimensional Solids.* SAND84-2618. Albuquerque, NM: Sandia National Laboratories.

Tierney, M.S. 1990. *Constructing Probability Distributions of Uncertain Variables in Models of the Performance of the Waste Isolation Pilot Plant: The 1990 Performance Simulations.* SAND90-2510. Albuquerque, NM: Sandia National Laboratories.

Trauth, K.M., S.C. Hora, R.P. Rechard, and D.R. Anderson. 1992. *The Use of Expert Judgment to Quantify Uncertainty in Solubility and Sorption Parameters for Waste Isolation Pilot Plant Performance Assessment.* SAND92-0479. Albuquerque, NM: Sandia National Laboratories.

Tyler, L.D., R.V. Matalucci, M.A. Molecke, D.E. Munson, E.J. Nowak, and J.C. Stormont. 1988. *Summary Report for the WIPP Technology Development Program for Isolation of Radioactive Waste.* SAND88-0844. Albuquerque, NM: Sandia National Laboratories.

US DOE (Department of Energy). 1979. *Draft Environmental Impact Statement, Management of Commercially Generated Radioactive Waste.* DOE/EIS-0046-D. Washington, DC: US Department of Energy.

US DOE (Department of Energy). 1980a. *Final Environmental Impact Statement: Waste Isolation Pilot Plant.* DOE/EIS-0026. Washington, DC: US Department of Energy. Vols. 1-2.

US DOE (Department of Energy). 1980b. *Waste Isolation Pilot Plant Safety Analysis Report.* Washington, DC: US Department of Energy. Vols. 1-5.

US DOE (Department of Energy). 1981. "Waste Isolation Pilot Plant (WIPP): Record of Decision," *Federal Register.* Vol. 46, no. 18, 9162-9164.

US DOE (Department of Energy). 1987. *A Plan for the Implementation of Assurance Requirements in Compliance with 40 CFR Part 191.14 at the Waste Isolation Pilot Plant*. DOE/WIPP 87-016. Carlsbad, NM: Westinghouse Electric Corporation.

US DOE (Department of Energy). 1989. *Waste Isolation Pilot Plant Compliance Strategy for 40 CFR Part 191*. WIPP-DOE 86-013. Carlsbad, NM: WIPP Project Office.

US DOE (Department of Energy). 1990a. *WIPP Test Phase Plan: Performance Assessment*. DOE/WIPP 89-011, Rev. 0. Carlsbad, NM: US Department of Energy.

US DOE (Department of Energy). 1990b. *Final Safety Analysis Report, Waste Isolation Pilot Plant*. WP 02-9, Rev. 0. Carlsbad, NM: Westinghouse Electric Corporation.

US DOE (Department of Energy). 1990c. *Final Supplement Environmental Impact Statement, Waste Isolation Pilot Plant*. DOE/EIS-0026-FS. Washington, DC: US Department of Energy, Office of Environmental Restoration and Waste Management.

US DOE (Department of Energy). 1990d. *Waste Isolation Pilot Plant No-Migration Variance Petition*. DOE/WIPP 89-003, Revision 1. Carlsbad, NM: Westinghouse Electric Corporation.

US DOE (Department of Energy). 1990e. *Recommended Initial Waste Forms for the WIPP Experimental Test Program, May 1990, Engineered Alternatives Task Force*. DOE/WIPP 90-009. Carlsbad, NM: Westinghouse Electric Corporation.

US DOE (Department of Energy). 1991a. *Waste Acceptance Criteria for the Waste Isolation Pilot Plant, December 1991*. DOE/WIPP-069, Rev. 4. Carlsbad, NM: Westinghouse Electric Corporation.

US DOE (Department of Energy). 1991b. *Draft Report: Evaluation of the Effectiveness and Feasibility of the Waste Isolation Pilot Plant Engineered Alternatives: Final Report of the Engineered Alternatives Task Force*. DOE/WIPP 91-007, Revision 0. Carlsbad, NM: Westinghouse Electric Corporation.

US DOE (Department of Energy). 1991c. *Implementation of the Resource Disincentive in 40 CFR Part 191.14(e) at the Waste Isolation Pilot Plant*. DOE/WIPP 91-029. Carlsbad, NM: Westinghouse Electric Corporation.

US DOE (Department of Energy). 1992a. *Gas-Generation and Source-Term Programs: Technical Needs Assessment for the Waste Isolation Pilot Plant Test Phase*. DOE/WPIO/001-92, Revision 0 (Draft). Albuquerque, NM: WIPP Project Integration Office. (Copy on file at the Waste Management and Transportation Library, Sandia National Laboratories, Albuquerque, NM.)

US DOE (Department of Energy). 1992b. *WIPP Test Phase Activities in Support of Critical Performance Assessment (40 CFR 191 B) Information Needs (40 CFR 191, Subpart B)*. Attachment I. Washington, DC: US Department of Energy.

US DOE (Department of Energy) and State of New Mexico. 1981, as modified. "Agreement for Consultation and Cooperation" on WIPP by the State of New Mexico and US Department of Energy, modified 11/30/84, 8/4/87, and 4/18/88.

US EPA (Environmental Protection Agency). 1978. "40 CFR Parts 1500-1508: Regulations for Implementing the Procedural Provisions of the National Environmental Policy Act," as amended and published in the most recent *Code of Federal Regulations*. Washington DC: Office of the Federal Register, National Archives and Records Administration.

US EPA (Environmental Protection Agency). 1984. *Ground-Water Protection Strategy*. Washington, DC: Office of Ground-Water Protection, US Environmental Protection Agency.

US EPA (Environmental Protection Agency). 1985. "40 CFR Part 191: Environmental Standards for the Management and Disposal of Spent Nuclear Fuel, High-Level and Transuranic Radioactive Wastes; Final Rule," *Federal Register*. Vol. 50, no. 182, 38066-38089.

US EPA (Environmental Protection Agency). 1986. "40 CFR Part 268: Land Disposal Restrictions," as amended and published in the most recent *Code of Federal Regulations*. Washington DC: Office of the Federal Register, National Archives and Records Administration.

US EPA (Environmental Protection Agency). 1990a. "Conditional No-Migration Determination for the Department of Energy Waste Isolation Pilot Plant (WIPP)," *Federal Register*. Vol. 55, no. 220, 47700-47721.

US EPA (Environmental Protection Agency). 1990b. "40 CFR Part 271: State of New Mexico: Final Authorization of State Hazardous Waste Management Program," *Federal Register*. Vol. 55, no. 133, 28397-28398.

US EPA (Environmental Protection Agency). 1992. *"No Migration" Variances to the Hazardous Waste Land Disposal Prohibitions: A Guidance Manual for Petitioners, Draft, July 1991*. EPA/S30/R-92/03. Washington, DC: US Environmental Protection Agency, Office of Solid Waste. (Copy on file at the Waste Management and Transportation Library, Sandia National Laboratories, Albuquerque, NM).

Vine, J.D. 1963. "Surface Geology of the Nash Draw Quadrangle, Eddy County, New Mexico," *U.S. Geological Survey Bulletin 1141-B*. Washington, DC: US Government Printing Office.

Ward, R.F., C.G./St.C. Kendall, and P.M. Harris. 1986. "Upper Permian (Guadalupian) Facies and Their Association with Hydrocarbons - Permian Basin, West Texas and New Mexico," *American Association of Petroleum Geologists Bulletin*. Vol. 70, no. 3, 239-262.

Waste Management Technology Department. 1987. *The Scientific Program at the Waste Isolation Pilot Plant*. SAND85-1699. Albuquerque, NM: Sandia National Laboratories.

Weart W.D. 1983. *Summary Evaluation of the Waste Isolation Pilot Plant (WIPP) Site Suitability*. SAND83-0450. Albuquerque, NM: Sandia National Laboratories.

Williamson, C.R. 1978. "Depositional Processes, Diagenesis and Reservoir Properties of Permian Deep-Sea Sandstones, Bell Canyon Formation, Texas-New Mexico." PhD dissertation. Austin, TX: University of Texas.

WIPP PA (Performance Assessment) Department. 1992. *Long-Term Gas and Brine Migration at the Waste Isolation Pilot Plant: Preliminary Sensitivity Analyses for Post-Closure 40 CFR 268 (RCRA), May 1992*. SAND92-1933. Albuquerque, NM: Sandia National Laboratories.

WIPP PA (Performance Assessment) Division. 1991a. *Preliminary Comparison with 40 CFR Part 191, Subpart B for the Waste Isolation Pilot Plant, December 1991—Volume 1: Methodology and Results*. SAND91-0893/1. Albuquerque, NM: Sandia National Laboratories.

WIPP PA (Performance Assessment) Division. 1991b. *Preliminary Comparison with 40 CFR Part 191, Subpart B for the Waste Isolation Pilot Plant, December 1991—Volume 2: Probability and Consequence Modeling*. SAND91-0893/2. Albuquerque, NM: Sandia National Laboratories.

WIPP PA (Performance Assessment) Division. 1991c. *Preliminary Comparison with 40 CFR Part 191, Subpart B for the Waste Isolation Pilot Plant, December 1991—Volume 3: Reference Data*. SAND91-0893/3. Albuquerque, NM: Sandia National Laboratories.

APPENDIX A:
TITLE 40, CODE OF FEDERAL REGULATIONS, SUBCHAPTER F, PART 191

APPENDIX A:
TITLE 40, CODE OF FEDERAL REGULATIONS
SUBCHAPTER F—RADIATION PROTECTION PROGRAMS

PART 191—ENVIRONMENTAL RADIATION PROTECTION STANDARDS FOR MANAGEMENT AND DISPOSAL OF SPENT NUCLEAR FUEL, HIGH-LEVEL AND TRANSURANIC RADIOACTIVE WASTES

Subpart A—Environmental Standards for Management and Storage

Subpart B—Environmental Standards for Disposal

Authority: The Atomic Energy Act of 1954, as amended; Reorganization Plan No. 3 of 1970; and the Nuclear Waste Policy Act of 1982.

Subpart A—Environmental Standards for Management and Storage

§ 191.01 Applicability.

This Subpart applies to:

(a) Radiation doses received by members of the public as a result of the management (except for transportation) and storage of spent nuclear fuel or high-level or transuranic radioactive wastes at any facility regulated by the

Nuclear Regulatory Commission or by Agreement States, to the extent that such management and storage operations are not subject to the provisions of Part 190 of title 40; and

(b) Radiation doses received by members of the public as a result of the management and storage of spent nuclear fuel or high-level or transuranic wastes at any disposal facility that is operated by the Department of Energy and that is not regulated by the Commission or by Agreement States.

§ 191.02 Definitions.

Unless otherwise indicated in this Subpart, all terms shall have the same meaning as in Subpart A of Part 190.

(a) "Agency" means the Environmental Protection Agency.

(b) "Administrator" means the Administrator of the Environmental Protection Agency.

(c) "Commission" means the Nuclear Regulatory Commission.

(d) "Department" means the Department of Energy.

(e) "NWPA" means the Nuclear Waste Policy Act of 1982 (Pub. L. 97-425).

(f) "Agreement State" means any State with which the Commission or the Atomic Energy Commission has entered into an effective agreement under subsection 274b of the Atomic Energy Act of 1954, as amended (68 Stat. 919).

(g) "Spent nuclear fuel" means fuel that has been withdrawn from a nuclear reactor following irradiation, the constituent elements of which have not been separated by reprocessing.

(h) "High-level radioactive waste," as used in this Part, means high-level radioactive waste as defined in the Nuclear Waste Policy Act of 1982 (Pub. L. 97-425).

(i) "Transuranic radioactive waste," as used in this Part, means waste containing more than 100 nanocuries of alpha-emitting transuranic isotopes, with half-lives greater than twenty years, per gram of waste, except for: (1) High-level radioactive wastes; (2) wastes that the Department has determined, with the concurrence of the Administrator, do not need the degree of isolation required by this Part; or (3) wastes that the Commission has approved for disposal on a case-by-case basis in accordance with 10 CFR Part 61.

(j) "Radioactive waste," as used in this Part, means the high-level and transuranic radioactive waste covered by this Part.

(k) "Storage" means retention of spent nuclear fuel or radioactive wastes with the intent and capability to readily retrieve such fuel or waste for subsequent use, processing, or disposal.

(l) "Disposal" means permanent isolation of spent nuclear fuel or radioactive wastes from the accessible environment with no intent of recovery, whether or not such isolation permits the recovery of such fuel or waste. For example, disposal of waste in a mined geologic repository occurs when all of the shafts to the repository are backfilled and sealed.

(m) "Management" means any activity, operation, or process (except for transportation) conducted to prepare spent nuclear fuel or radioactive waste for storage or disposal, or the activities associated with placing such fuel or waste in a disposal system.

(n) "Site" means an area contained within the boundary of a location under the effective control of persons possessing or using spent nuclear fuel or radioactive waste that are involved in any activity, operation, or process covered by this Subpart.

(o) "General environment" means the total terrestrial, atmospheric, and aquatic environments outside sites within which any activity, operation, or process associated with the management and storage of spent nuclear fuel or radioactive waste is conducted.

(p) "Member of the public" means any individual except during the time when that individual is a worker engaged in any activity, operation, or process that is covered by the Atomic Energy Act of 1954, as amended.

(q) "Critical organ" means the most exposed human organ or tissue exclusive of the integumentary system (skin) and the cornea.

§ 191.03 Standards.

(a) Management and storage of spent nuclear fuel or high-level or transuranic radioactive wastes at all facilities regulated by the Commission or by Agreement States shall be conducted in such a manner as to provide reasonable assurance that the combined annual dose equivalent to any member of the public in the general environment resulting from: (1) Discharges of radioactive material and direct radiation from such management and storage and (2) all operations covered by Part 190; shall not exceed 25 millirems to the

whole body, 75 millirems to the thyroid, and 25 millirems to any other critical organ.

(b) Management and storage of spent nuclear fuel or high-level or transuranic radioactive wastes at all facilities for the disposal of such fuel or waste that are operated by the Department and that are not regulated by the Commission or Agreement States shall be conducted in such a manner as to provide reasonable assurance that the combined annual dose equivalent to any member of the public in the general environment resulting from discharges of radioactive material and direct radiation from such management and storage shall not exceed 25 millirems to the whole body and 75 millirems to any critical organ.

§ 191.04 Alternative standards.

(a) The Administrator may issue alternative standards from those standards established in 191.03(b) for waste management and storage activities at facilities that are not regulated by the Commission or Agreement States if, upon review of an application for such alternative standards:

(1) The Administrator determines that such alternative standards will prevent any member of the public from receiving a continuous exposure of more than 100 millirems per year dose equivalent and an infrequent exposure of more than 500 millirems dose equivalent in a year from all sources, excluding natural background and medical procedures; and

(2) The Administrator promptly makes a matter of public record the degree to which continued operation of the facility is expected to result in levels in excess of the standards specified in 191.03(b).

(b) An application for alternative standards shall be submitted as soon as possible after the Department determines that continued operation of a facility will exceed the levels specified in 191.03(b) and shall include all information necessary for the Administrator to make the determinations called for in 191.04(a).

(c) Requests for alternative standards shall be submitted to the Administrator, U.S. Environmental Protection Agency, 401 M Street, SW., Washington, DC 20460.

§ 191.05 Effective date.

The standards in this Subpart shall be effective on November 18, 1985.

Subpart B—Environmental Standards for Disposal

§ 191.11 Applicability.

(a) This Subpart applies to:

(1) Radioactive materials released into the accessible environment as a result of the disposal of spent nuclear fuel or high-level or transuranic radioactive wastes;

(2) Radiation doses received by members of the public as a result of such disposal; and

(3) Radioactive contamination of certain sources of ground water in the vicinity of disposal systems for such fuel or wastes.

(b) However, this Subpart does not apply to disposal directly into the oceans or ocean sediments. This Subpart also does not apply to wastes disposed of before the effective date of this rule.

§ 191.12 Definitions.

Unless otherwise indicated in this Subpart, all terms shall have the same meaning as in Subpart A of this Part.

(a) "Disposal system" means any combination of engineered and natural barriers that isolate spent nuclear fuel or radioactive waste after disposal.

(b) "Waste," as used in this Subpart, means any spent nuclear fuel or radioactive waste isolated in a disposal system.

(c) "Waste form" means the materials comprising the radioactive components of waste and any encapsulating or stabilizing matrix.

(d) "Barrier" means any material or structure that prevents or substantially delays movement of water or radionuclides toward the accessible environment. For example, a barrier may be a geologic structure, a canister, a waste form with physical and chemical characteristics that significantly decrease the mobility of radionuclides, or a material placed over and around waste, provided that the material or structure substantially delays movement of water or radionuclides.

(e) "Passive institutional control" means: (1) Permanent markers placed at a disposal site, (2) public records and archives, (3) government ownership and regulations regarding land or resource use, and (4) other methods of preserving knowledge about the location, design, and contents of a disposal system.

(f) "Active institutional control" means: (1) Controlling access to a disposal site by any means other than passive institutional controls; (2) performing maintenance operations or remedial actions at a site, (3) controlling or cleaning up releases from a site, or (4) monitoring parameters related to disposal system performance.

(g) "Controlled area" means: (1) A surface location, to be identified by passive institutional controls, that encompasses no more than 100 square kilometers and extends horizontally no more than five kilometers in any direction from the outer boundary of the original location of the radioactive wastes in a disposal system; and (2) the subsurface underlying such a surface location.

(h) "Ground water" means water below the land surface in a zone of saturation.

(i) "Aquifer" means an underground geological formation, group of formations, or part of a formation that is capable of yielding a significant amount of water to a well or spring.

(j) "Lithosphere" means the solid part of the Earth below the surface, including any ground water contained within it.

(k) "Accessible environment" means: (1) The atmosphere; (2) land surfaces; (3) surface waters; (4) oceans; and (5) all of the lithosphere that is beyond the controlled area.

(l) "Transmissivity" means the hydraulic conductivity integrated over the saturated thickness of an underground formation. The transmissivity of a series of formations is the sum of the individual transmissivities of each formation comprising the series.

(m) "Community water system" means a system for the provision to the public of piped water for human consumption, if such system has at least 15 service connections used by year-round residents or regularly serves at least 25 year-round residents.

(n) "Significant source of ground water," as used in this Part, means: (1) An aquifer that: (i) Is saturated with water having less than 10,000 milligrams per liter of total dissolved solids; (ii) is within 2,500 feet of the land surface; (iii) has a transmissivity greater than 200 gallons per day per foot, provided that any formation or part of a formation included within the source of ground water has a hydraulic conductivity greater than 2 gallons per day per square foot; and (iv) is capable of continuously yielding at least 10,000 gallons per day to a pumped or flowing well for a period of at least a

year; or (2) an aquifer that provides the primary source of water for a community water system as of the effective date of this Subpart.

(o) "Special source of ground water," as used in this Part, means those Class I ground waters identified in accordance with the Agency's Ground-Water Protection Strategy published in August 1984 that: (1) Are within the controlled area encompassing a disposal system or are less than five kilometers beyond the controlled area; (2) are supplying drinking water for thousands of persons as of the date that the Department chooses a location within that area for detailed characterization as a potential site for a disposal system (e.g., in accordance with Section 112(b)(1)(B) of the NWPA); and (3) are irreplaceable in that no reasonable alternative source of drinking water is available to that population.

(p) "Undisturbed performance" means the predicted behavior of a disposal system, including consideration of the uncertainties in predicted behavior, if the disposal system is not disrupted by human intrusion or the occurrence of unlikely natural events.

(q) "Performance assessment" means an analysis that: (1) Identifies the processes and events that might affect the disposal system; (2) examines the effects of these processes and events on the performance of the disposal system; and (3) estimates the cumulative releases of radionuclides, considering the associated uncertainties, caused by all significant processes and events. These estimates shall be incorporated into an overall probability distribution of cumulative release to the extent practicable.

(r) "Heavy metal" means all uranium, plutonium, or thorium placed into a nuclear reactor.

(s) "Implementing agency," as used in this Subpart, means the Commission for spent nuclear fuel or high-level or transuranic wastes to be disposed of in facilities licensed by the commission in accordance with the Energy Reorganization Act of 1974 and the Nuclear Waste Policy Act of 1982, and it means the Department for all other radioactive wastes covered by this Part.

§ 191.13 Containment requirements.

(a) Disposal systems for spent nuclear fuel or high-level or transuranic radioactive wastes shall be designed to provide a reasonable expectation, based upon performance assessments, that cumulative releases of radionuclides to the accessible environment for 10,000 years after disposal from all significant processes and events that may affect the disposal system shall:

(1) Have a likelihood of less than one chance in 10 of exceeding the quantities calculated according to Table 1 (Appendix A); and

(2) Have a likelihood of less than one chance in 1,000 of exceeding ten times the quantities calculated according to Table 1 (Appendix A).

(b) Performance assessments need not provide complete assurance that the requirements of 191.13(a) will be met. Because of the long time period involved and the nature of the events and processes of interest, there will inevitably be substantial uncertainties in projecting disposal system performance. Proof of the future performance of a disposal system is not to be had in the ordinary sense of the word in situations that deal with much shorter time frames. Instead, what is required is a reasonable expectation, on the basis of the record before the implementing agency, that compliance with 191.13(a) will be achieved.

§ 191.14 Assurance requirements.

To provide the confidence needed for long-term compliance with the requirements of 191.13, disposal of spent nuclear fuel or high-level or transuranic wastes shall be conducted in accordance with the following provisions, except that these provisions do not apply to facilities regulated by the Commission (see 10 CFR Part 60 for comparable provisions applicable to facilities regulated by the Commission):

(a) Active institutional controls over disposal sites should be maintained for as long a period of time as is practicable after disposal; however, performance assessments that assess isolation of the wastes from the accessible environment shall not consider any contributions from active institutional controls for more than 100 years after disposal.

(b) Disposal systems shall be monitored after disposal to detect substantial and detrimental deviations from expected performance. This monitoring shall be done with techniques that do not jeopardize the isolation of the wastes and shall be conducted until there are no significant concerns to be addressed by further monitoring.

(c) Disposal sites shall be designated by the most permanent markers, records, and other passive institutional controls practicable to indicate the dangers of the wastes and their location.

(d) Disposal systems shall use different types of barriers to isolate the wastes from the accessible environment. Both engineered and natural barriers shall be included.

(e) Places where there has been mining for resources, or where there is a reasonable expectation of exploration for scarce or easily accessible resources, or where there is a significant concentration of any material that is not widely available from other sources, should be avoided in selecting disposal sites. Resources to be considered shall include minerals, petroleum or natural gas, valuable geologic formations, and ground waters that are either irreplaceable because there is no reasonable alternative source of drinking water available for substantial populations or that are vital to the preservation of unique and sensitive ecosystems. Such places shall not be used for disposal of the wastes covered by this Part unless the favorable characteristics of such places compensate for their greater likelihood of being disturbed in the future.

(f) Disposal systems shall be selected so that removal of most of the wastes is not precluded for a reasonable period of time after disposal.

§ 191.15 Individual protection requirements.

Disposal systems for spent nuclear fuel or high-level or transuranic radioactive wastes shall be designed to provide a reasonable expectation that, for 1,000 years after disposal, undisturbed performance of the disposal system shall not cause the annual dose equivalent from the disposal system to any member of the public in the accessible environment to exceed 25 millirems to the whole body or 75 millirems to any critical organ. All potential pathways (associated with undisturbed performance) from the disposal system to people shall be considered, including the assumption that individuals consume 2 liters per day of drinking water from any significant source of ground water outside of the controlled area.

§ 191.16 Ground water protection requirements.

(a) Disposal systems for spent nuclear fuel or high-level or transuranic radioactive wastes shall be designed to provide a reasonable expectation that, for 1,000 years after disposal, undisturbed performance of the disposal system shall not cause the radionuclide concentrations averaged over any year in water withdrawn from any portion of a special source of ground water to exceed:

(1) 5 picocuries per liter of radium-226 and radium-228;

(2) 15 picocuries per liter of alpha-emitting radionuclides (including radium-226 and radium-228 but excluding radon); or

(3) The combined concentrations of radionuclides that emit either beta or gamma radiation that would produce an annual dose equivalent to the total body or any internal organ greater than 4 millirems per year if an individual

consumed 2 liters per day of drinking water from such a source of ground water.

(b) If any of the average annual radionuclide concentrations existing in a special source of ground water before construction of the disposal system already exceed the limits in 191.16(a), the disposal system shall be designed to provide a reasonable expectation that, for 1,000 years after disposal, undisturbed performance of the disposal system shall not increase the existing average annual radionuclide concentrations in water withdrawn from that special source of ground water by more than the limits established in 191.16(a).

§ 191.17 Alternative provisions for disposal.

The Administrator may, by rule, substitute for any of the provisions of Subpart B alternative provisions chosen after:

(a) The alternative provisions have been proposed for public comment in the **Federal Register** together with information describing the costs, risks, and benefits of disposal in accordance with the alternative provisions and the reasons why compliance with the existing provisions of Subpart B appears inappropriate;

(b) A public comment period of at least 90 days has been completed, during which an opportunity for public hearings in affected areas of the country has been provided; and

(c) The public comments received have been fully considered in developing the final version of such alternative provisions.

§ 191.18 Effective date.

The standards in this Subpart shall be effective on November 18, 1985.

Appendix A—Table for Subpart B

TABLE 1.—RELEASE LIMITS FOR CONTAINMENT REQUIREMENTS

(Cumulative releases to the accessible environment for 10,000 years after disposal)

Radionuclide	Release limit per 1,000 MTHM or other unit of waste (see notes) (curies)
Americium-241 or -243	100
Carbon-14	100
Cesium-135 or -137	1,000
Iodine-129	100
Neptunium-237	100
Plutonium-238, -239, -240, or -242	100
Radium-226	100
Strontium-90	1,000
Technetium-99	10,000
Thorium-230 or -232	10
Tin-126	1,000
Uranium-233, -234, -235, -236, or -238	100
Any other alpha-emitting radionuclide with a half-life greater than 20 years	100
Any other radionuclide with a half-life greater than 20 years that does not emit alpha particles	1,000

Application of Table 1

Note 1: *Units of Waste.* The Release Limits in Table 1 apply to the amount of wastes in any one of the following:

(a) An amount of spent nuclear fuel containing 1,000 metric tons of heavy metal (MTHM) exposed to a burnup between 25,000 megawatt-days per metric ton of heavy metal (MWd/MTHM) and 40,000 MWd/MTHM;

(b) The high-level radioactive wastes generated from reprocessing each 1,000 MTHM exposed to a burnup between 25,000 MWd/MTHM and 40,000 MWd/MTHM;

(c) Each 100,000,000 curies of gamma or beta-emitting radionuclides with half-lives greater than 20 years but less than 100 years (for use as discussed in Note 5 or with materials that are identified by the Commission as high-level radioactive waste in accordance with part B of the definition of high-level waste in the NWPA);

(d) Each 1,000,000 curies of other radionuclides (i.e., gamma or beta-emitters with half-lives greater than 100 years or any alpha-emitters with half-lives greater than 20 years) (for use as discussed in Note 5 or with materials that are identified by the Commission as high-level radioactive waste in accordance with part B of the definition of high-level waste in the NWPA); or

(e) An amount of transuranic (TRU) wastes containing one million curies of alpha-emitting transuranic radionuclides with half-lives greater than 20 years.

Note 2: *Release Limits for Specific Disposal Systems.* To develop Release Limits for a particular disposal system, the quantities in Table 1 shall be adjusted for the amount of waste included in the disposal system compared to the various units of waste defined in Note 1. For example:

(a) If a particular disposal system contained the high-level wastes from 50,000 MTHM, the Release Limits for that system would be the quantities in Table 1 multiplied by 50 (50,000 MTHM divided by 1,000 MTHM).

(b) If a particular disposal system contained three million curies of alpha-emitting transuranic wastes, the Release Limits for that system would be the quantities in Table 1 multiplied by three (three million curies divided by one million curies).

(c) If a particular disposal system contained both the high-level wastes from 50,000 MTHM and 5 million curies of alpha-emitting transuranic wastes, the Release Limits for that system would be the quantities in Table 1 multiplied by 55:

$$\frac{50{,}000 \text{ MTHM}}{1{,}000 \text{ MTHM}} + \frac{5{,}000{,}000 \text{ curies TRU}}{1{,}000{,}000 \text{ curies TRU}} = 55$$

Note 3: *Adjustments for Reactor Fuels with Different Burnup.* For disposal systems containing reactor fuels (or the high-level wastes from reactor fuels) exposed to an average burnup of less than 25,000 MWd/MTHM or greater than 40,000 MWd/MTHM, the units of waste defined in (a) and (b) of Note 1 shall be adjusted. The unit shall be multiplied by the ratio of 30,000 MWd/MTHM divided by the fuel's actual average burnup, except that a value of 5,000

MWd/MTHM may be used when the average fuel burnup is below 5,000 MWd/MTHM and a value of 100,000 MWd/MTHM shall be used when the average fuel burnup is above 100,000 MWd/MTHM. This adjusted unit of waste shall then be used in determining the Release Limits for the disposal system.

For example, if a particular disposal system contained only high-level wastes with an average burnup of 3,000 MWd/MTHM, the unit of waste for that disposal system would be:

$$1{,}000 \text{ MTHM} \times \frac{(30{,}000)}{(5{,}000)} = 6{,}000 \text{ MTHM}$$

If that disposal system contained the high-level wastes from 60,000 MTHM (with an average burnup of 3,000 MWd/MTHM), then the Release Limits for that system would be the quantities in Table 1 multiplied by ten:

$$\frac{60{,}000 \text{ MTHM}}{6{,}000 \text{ MTHM}} = 10$$

which is the same as:

$$\frac{60{,}000 \text{ MTHM}}{1{,}000 \text{ MTHM}} \times \frac{(5{,}000 \text{ MWd/MTHM})}{(30{,}000 \text{ MWd/MTHM})} = 10$$

Note 4: ***Treatment of Fractionated High-Level Wastes.*** In some cases, a high-level waste stream from reprocessing spent nuclear fuel may have been (or will be) separated into two or more high-level waste components destined for different disposal systems. In such cases, the implementing agency may allocate the Release Limit multiplier (based upon the original MTHM and the average fuel burnup of the high-level waste stream) among the various disposal systems as it chooses, provided that the total Release Limit multiplier used for that waste stream at all of its disposal systems may not exceed the Release Limit multiplier that would be used if the entire waste stream were disposed of in one disposal system.

Note 5: ***Treatment of Wastes with Poorly Known Burnups or Original MTHM.*** In some cases, the records associated with particular high-level waste streams may not be adequate to accurately determine the original metric tons of heavy metal in the reactor fuel that created the waste, or to determine the average burnup that the fuel was exposed to. If the uncertainties are such that the original amount of heavy metal or the average fuel burnup for particular high-level waste streams cannot be quantified, the units of waste derived from (a) and (b) of Note 1 shall no longer be used. Instead, the units of waste defined in (c) and (d) of Note 1 shall be used for such high-level waste streams. If the uncertainties in such information allow a range of values to be associated with the original amount of heavy metal or the average fuel

burnup, then the calculations described in previous Notes will be conducted using the values that result in the smallest Release Limits, except that the Release Limits need not be smaller than those that would be calculated using the units of waste defined in (c) and (d) of Note 1.

Note 6: *Uses of Release Limits to Determine Compliance with 191.13.* Once release limits for a particular disposal system have been determined in accordance with Notes 1 through 5, these release limits shall be used to determine compliance with the requirements of 191.13 as follows. In cases where a mixture of radionuclides is projected to be released to the accessible environment, the limiting values shall be determined as follows: For each radionuclide in the mixture, determine the ratio between the cumulative release quantity projected over 10,000 years and the limit for that radionuclide as determined from Table 1 and Notes 1 through 5. The sum of such ratios for all the radionuclides in the mixture may not exceed one with regard to 191.13(a)(1) and may not exceed ten with regard to 191.13(a)(2).

For example, if radionuclides A, B, and C are projected to be released in amounts Q_a, Q_b, and Q_c, and if the applicable Release Limits are RL_a, RL_b, RL_c, then the cumulative releases over 10,000 years shall be limited so that the following relationship exists:

$$\frac{Q_a}{RL_a} + \frac{Q_b}{RL_b} + \frac{Q_c}{RL_c} < 1$$

Appendix B—Guidance for Implementation of Subpart B

[Note: The supplemental information in this appendix is not an integral part of 40 CFR Part 191. Therefore, the implementing agencies are not bound to follow this guidance. However, it is included because it describes the Agency's assumptions regarding the implementation of Subpart B. This appendix will appear in the Code of Federal Regulations.]

The Agency believes that the implementing agencies must determine compliance with §§ 191.13, 191.15, and 191.16 of Subpart B by evaluating long-term predictions of disposal system performance. Determining compliance with § 191.13 will also involve predicting the likelihood of events and processes that may disturb the disposal system. In making these various predictions, it will be appropriate for the implementing agencies to make use of rather complex computational models, analytical theories, and prevalent expert judgment relevant to the numerical predictions. Substantial uncertainties are likely to be encountered in making these predictions. In fact, sole reliance on these numerical predictions to determine compliance may not be appropriate; the implementing agencies may choose to supplement such predictions with

qualitative judgments as well. Because the procedures for determining compliance with Subpart B have not been formulated and tested yet, this appendix to the rule indicates the Agency's assumptions regarding certain issues that may arise when implementing §§ 191.13, 191.15, and 191.16. Most of this guidance applies to any type of disposal system for the wastes covered by this rule. However, several sections apply only to disposal in mined geologic repositories and would be inappropriate for other types of disposal systems.

Consideration of Total Disposal System. When predicting disposal system performance, the Agency assumes that reasonable projections of the protection expected from all of the engineered and natural barriers of a disposal system will be considered. Portions of the disposal system should not be disregarded, even if projected performance is uncertain, except for portions of the system that make negligible contributions to the overall isolation provided by the disposal system.

Scope of Performance Assessments. Section 191.13 requires the implementing agencies to evaluate compliance through performance assessments as defined in § 191.12(q). The Agency assumes that such performance assessments need not consider categories of events or processes that are estimated to have less than one chance in 10,000 of occurring over 10,000 years. Furthermore, the performance assessments need not evaluate in detail the releases from all events and processes estimated to have a greater likelihood of occurrence. Some of these events and processes may be omitted from the performance assessments if there is a reasonable expectation that the remaining probability distribution of cumulative releases would not be significantly changed by such omissions.

Compliance with Section 191.13. The Agency assumes that, whenever practicable, the implementing agency will assemble all of the results of the performance assessments to determine compliance with § 191.13 into a "complementary cumulative distribution function" that indicates the probability of exceeding various levels of cumulative release. When the uncertainties in parameters are considered in a performance assessment, the effects of the uncertainties considered can be incorporated into a single such distribution function for each disposal system considered. The Agency assumes that a disposal system can be considered to be in compliance with § 191.13 if this single distribution function meets the requirements of § 191.13(a).

Compliance with Sections 191.15 and 191.16. When the uncertainties in undisturbed performance of a disposal system are considered, the implementing agencies need not require that a very large percentage of the range of estimated radiation exposures or radionuclide concentrations fall below limits established in §§ 191.15 and 191.16, respectively. The Agency assumes that

compliance can be determined based upon "best estimate" predictions (e.g., the mean or the median of the appropriate distribution, whichever is higher).

Institutional Controls. To comply with § 191.14(a), the implementing agency will assume that none of the active institutional controls prevent or reduce radionuclide releases for more than 100 years after disposal. However, the Federal Government is committed to retaining ownership of all disposal sites for spent nuclear fuel and high-level and transuranic radioactive wastes and will establish appropriate markers and records, consistent with § 191.14(c). The Agency assumes that, as long as such passive institutional controls endure and are understood, they: (1) can be effective in deterring systematic or persistent exploitation of these disposal sites; and (2) can reduce the likelihood of inadvertent, intermittent human intrusion to a degree to be determined by the implementing agency. However, the Agency believes that passive institutional controls can never be assumed to eliminate the chance of inadvertent and intermittent human intrusion into these disposal sites.

Consideration of Inadvertent Human Intrusion into Geologic Repositories. The most speculative potential disruptions of a mined geologic repository are those associated with inadvertent human intrusion. Some types of intrusion would have virtually no effect on a repository's containment of waste. On the other hand, it is possible to conceive of intrusions (involving widespread societal loss of knowledge regarding radioactive wastes) that could result in major disruptions that no reasonable repository selection or design precautions could alleviate. The Agency believes that the most productive consideration of inadvertent intrusion concerns those realistic possibilities that may be usefully mitigated by repository design, site selection, or use of passive controls (although passive institutional controls should not be assumed to completely rule out the possibility of intrusion). Therefore, inadvertent and intermittent intrusion by exploratory drilling for resources (other than any provided by the disposal system itself) can be the most severe intrusion scenario assumed by the implementing agencies. Furthermore, the implementing agencies can assume that passive institutional controls or the intruders' own exploratory procedures are adequate for the intruders to soon detect, or be warned of, the incompatibility of the area with their activities.

Frequency and Severity of Inadvertent Human Intrusion into Geologic Repositories. The implementing agencies should consider the effects of each particular disposal system's site, design, and passive institutional controls in judging the likelihood and consequences of such inadvertent exploratory drilling. However, the Agency assumes that the likelihood of such inadvertent and intermittent drilling need not be taken to be greater than 30 boreholes

per square kilometer of repository area per 10,000 years for geologic repositories in proximity to sedimentary rock formations, or more than 3 boreholes per square kilometer per 10,000 years for repositories in other geologic formations. Furthermore, the Agency assumes that the consequences of such inadvertent drilling need not be assumed to be more severe than: (1) Direct release to the land surface of all the ground water in the repository horizon that would promptly flow through the newly created borehole to the surface due to natural lithostatic pressure—or (if pumping would be required to raise water to the surface) release of 200 cubic meters of ground water pumped to the surface if that much water is readily available to be pumped; and (2) creation of a ground water flow path with a permeability typical of a borehole filled by the soil or gravel that would normally settle into an open hole over time—not the permeability of a carefully sealed borehole.

APPENDIX B:
RESPONSE TO REVIEW COMMENTS ON THE 1991 PERFORMANCE ASSESSMENT

APPENDIX B: RESPONSE TO REVIEW COMMENTS ON THE 1991 PERFORMANCE ASSESSMENT

As stated in the *Waste Isolation Pilot Plant Land Withdrawal Act* (Public Law 102-579, 1992), performance assessment (PA) analyses shall be provided every two years "to the State [of New Mexico], the [EPA], the National Academy of Sciences, and the EEG [Environmental Evaluation Group] for their review and comment."

The inclusion of this appendix in the 1992 *Preliminary Performance Assessment* marks the third year that the Sandia National Laboratories' (SNL) PA Department has published the complete text of formal comments received from these groups together with responses indicating how comments will be addressed in future PA iterations (Bertram-Howery et al., 1990; WIPP PA Division, 1991a). In previous years this appendix has included comments from the New Mexico Environment Department (1990, 1991), the EPA Office of Radiation Programs (1990), and the EEG (1990, 1991). Comments have been received in 1992 only from the EEG. These comments pertain to the 1991 preliminary PA, as published in the first four volumes of SAND91-0893 (WIPP PA Division, 1991a,b,c; Helton et al., 1992).

Text of comments from the EEG and responses from the SNL Waste Isolation Pilot Plant (WIPP) PA Department follow. Organization of the responses is based on the organization of the comments. The EEG has provided both general comments in which they discuss important issues in the documents and state the conclusions of their review, and specific, page-by-page comments referenced directly to SAND91-0893. The PA Department has numbered EEG comments and inserted responses directly following each comment. EEG's general observations about important issues and conclusions are contained in comments 1 through 18. Page-by-page comments are numbered 19 through 96. In cases where page-by-page comments address points already covered in the general comments, responses are brief, and refer the reader back to the more detailed discussion.

EEG has also provided comments on the WIPP PA Department's responses to comments published in 1991 on the 1990 preliminary performance assessment. These comments are presented with PA responses following the comments on the 1991 documents, beginning on page B-53. Numbers assigned to these comments reflect the numbering used in Appendix B of the 1991 documentation (WIPP PA Division, 1991a). Readers should consult that volume for the original text of the comments and responses.

Comments on SAND91-0893 from the Environmental Evaluation Group, with Responses from the WIPP Performance Assessment Department

Comments dated July 31, 1992

I. Introduction

The Environmental Evaluation Group (EEG) is impressed by the productivity of the Sandia National Laboratories (SNL) WIPP Performance Assessment Group in the second year of detailed performance assessment for WIPP. The four volumes of SAND91-0893 display a massive effort to continue to synthesize a large amount of work and data in the areas of site characterization; in situ hydrologic and rock mechanics studies underground; waste characterization; conceptual models of natural phenomena; and expected behavior of geologic and engineered barriers. A workable mechanism is developing to document the expected evolution of conditions in the repository after decommissioning. Although much work remains to be done, we share the Sandia scientists' optimism that this continued effort will result in providing the best possible basis to assess WIPP's compliance with the EPA disposal standards for high-level and transuranic nuclear waste repositories (40 CFR 191, Subpart B).

This review is organized in four sections. Following the Introduction, Major Conclusions are provided. Certain important issues are identified for consideration in future P.A. efforts in the third section. This is followed by "page by page" comments. The last section of these review comments consists of the EEG reply to the SNL response to the EEG's comments on the 1990 reports. This arrangement has caused some duplication, but in the interest of clarity, it should be acceptable.

COMMENT 1. EEG review of the 1991 P.A. is not complete. For example, detailed comments are provided only on the first four chapters of volume 1, and volume 4. However, these comments are being provided at this time to enable SNL to utilize our thoughts and concerns as they begin to make decisions on the selection of data, scenarios and models, before the calculations begin for the 1992 iteration.

RESPONSE 1. In order to produce an iteration of WIPP PA by the end of each calendar year, the design of the analyses for that year must be decided by April 1. Comments received after that date cannot, in general, be addressed

until the following year's PA. For future PAs, the 1992 *WIPP Land Withdrawal Act* states that formal comments from the EEG (as well as EPA, NMED, and NAS) should be received within 120 days of publication of the PA documentation if a formal response is required.

COMMENT 2. We have mixed feelings about the organization of the Sandia reports (4 volumes of SAND91-0893). The organization appears quite logical, but still it requires much effort to gather all the information about a particular scenario analysis or to track all the steps of a calculation. For example, the possibility of direct release of waste to the surface through drill-cuttings is first mentioned in Chapter 4 of Vol. 1. Some of the assumptions and considerations as well as the results are provided in Chapter 7 of Volume 2, but one has to search in volume 3 for the input data used for this analysis, even though the input data used in the cuttings code to characterize the drilling mud, drill string, and waste properties was fixed for all cases. However, the fact that four activity levels in the waste were used for this analysis does not become clear until one studies the sensitivity analysis in Volume 4 (Chapter 4). Similarly, the fact that the gas effects considered in the analyses are limited only to the retardation of brine inflow and the structural effects are not considered is not clearly stated anywhere in the scattered discussion of gas effects. We have no specific suggestions to improve the organization except to recommend that the needs of the reviewer should be kept in mind and information should be presented and cross-referenced (by Chapter, Section, and page) so that related information is easily found. In addition, it may be helpful to provide a much expanded Executive Summary (an entire chapter or perhaps a full volume) in which the assumptions, data, scenarios and procedures are more clearly presented in one place.

RESPONSE 2. In general, the PA Department agrees with the comment. The reports have been reorganized for 1992 to improve the presentation. Efforts have been made to provide better referencing and cross-referencing between volumes, and Volume 1 is briefer and presents a clearer overview of the PA.

II. Major Conclusions

COMMENT 3. The 1991 P.A. calculations lack conservatism in assumptions of scenarios, use of parameters and assignment of probabilities, even compared with the 1990 effort. Examples of non-conservative assumptions include: use of 5 km distance for the Culebra transport rather than the site boundary, use

of drilling rate median value of one-half of the maximum in 40 CFR 191, not considering any intrusion for the first 1000 years, not considering a scenario involving contaminated brine flows to the surface, use of unjustified K_d values, assumption of double-porosity flow with matrix diffusion to calculate travel times through the Culebra, undisturbed performance analyses only for the expected case, etc. In this sense, the 1991 P.A. reports are not an improvement over the 1990 effort.

RESPONSE 3. With respect to 40 CFR 191B, the purpose of PA is to provide probabilistic uncertainty analyses of realistic estimates of disposal-system performance. Modeling assumptions in general should not made in the context of "conservative" or "nonconservative" but rather in the context of acceptable approximation of reality.

With respect to interim guidance to the Project from preliminary PAs, uncertainty and sensitivity analyses are most useful if performed on the most realistic modeling system available, rather than on artificially conservative assumptions.

The PA Department recognizes that it is possible to characterize some assumptions as "nonconservative." Other assumptions could be characterized as "conservative." (See, for example, Response 44.) We are responsive to comments about specific assumptions, and will work to increase realism in assumptions.

The specific points are addressed individually.

3.1 "The use of 5 km distance for the Culebra transport rather than the site boundary."

The 1992 PA uses the land-withdrawal boundary, 2.4 km from the waste panels.

3.2 "Use of drilling rate median value of one-half of the maximum in 40 CFR 191.

Expert judgment on the probability of human intrusion and the potential effectiveness of passive markers has been incorporated in the 1992 PA. CCDFs are presented comparing releases calculated using these probabilities with releases calculated using the same approach to determining intrusion probabilities used in 1991.

3.3 "Not considering any intrusion for the first 1000 years."

This assumption in 1991 did affect direct releases through cuttings and cavings. The 1992 PA uses better resolution in time for direct releases. Subsurface releases are not believed to be particularly different for intrusions prior to 1000 yr (radioactive decay continues to occur during transport in the Culebra), and because limited resources require the PA Department to balance the total number of calculations with the need to improve model physics and accuracy, we do not provide further resolution of intrusion times for subsurface transport. We acknowledge that the final compliance assessment should have sufficient resolution to demonstrate that the shape of the summary CCDF is adequately captured.

3.4 "Not considering a scenario involving contaminated brine flows to the surface."

The PA Department has performed single-phase calculations for drilling fluid and Castile brine flow to the surface during drilling, and consequences were not important compared to direct removal of cuttings and cavings. We will repeat these subsidiary simulations using BRAGFLO for both release during drilling and long-term releases through abandoned boreholes. Results will be presented in a later volume of the 1992 PA documentation.

3.5 "Use of unjustified K_d values."

Results of calculations assuming K_d=0 were published in Volume 4 of the 1991 documentation (Helton et al., 1992, Section 5.4). The PA Department will continue to examine performance for both K_d=0 and estimates of K_d based on expert judgment until defensible K_d values are available.

3.6 "Assumption of double-porosity flow with matrix diffusion to calculate travel times through the Culebra."

The PA Department's preferred conceptual model for the disposal system, based on available information, continues to include dual-porosity transport in the Culebra, as wells as non-zero K_ds, waste-generated gas, creep closure (included for the first time in 1992), and variable climate. For comparison purposes, Volume 1 of the 1992 documentation (this volume) also contains results calculated for the preferred model assuming single-porosity, fracture-only transport with K_d=0.

COMMENT 4. We continue to remain unconvinced about zero releases following undisturbed performance scenarios. We believe this is due to a combination of misinterpretation of the 40 CFR 191 definition of undisturbed performance and use of non-conservative values of certain input parameters.

RESPONSE 4. The PA Department believes the interpretation of 40 CFR 191 used in the 1991 (and 1992) PA is correct. Screening of events and processes for § 191.13 has identified no natural events with probabilities greater than 10^{-4} in 10^{4} yr that will disrupt the disposal system (WIPP PA Division, 1991a, Chapter 4). Non-disruptive natural processes (e.g., climate change) are included in the base-case scenario for § 191.13. This base-case scenario also describes undisturbed performance, as defined for §191.15 in § 191.12(p).

With regard to "non-conservative values for certain input parameters," the PA Department notes that Appendix B of 40 CFR 191 indicates that "compliance [with § 191.15] can be determined based on "best estimate" predictions" (US EPA, 1985, p. 38088). Probabilistic analyses are used for 40 CFR 191B to examine uncertainty in realistic predictions, not to provide conservative performance estimates. (See Response 3.)

The preliminary analyses of undisturbed performance reported in the 1991 PA (WIPP PA Division, 1991b) used realistic estimates of parameter values, rather than probabilistically sampled values. Sensitivity and uncertainty analyses of undisturbed performance conducted during 1991 (WIPP PA Department, 1992; not published at the time of the EEG review) use sampled values for input parameters and confirm the conclusion of the previous analyses. For undisturbed conditions, brine that has been in contact with waste does not migrate to the accessible environment. (Or even a small fraction of the distance to it: in the analyses reported in WIPP PA Department, 1992, potentially contaminated brine did not leave the DRZ.)

COMMENT 5. With respect to the analysis of human intrusion scenarios, it appears that the releases from direct removal of drill-cuttings to the surface would be much more severe if a more realistic distribution of radionuclide concentrations in the waste planned for WIPP is sampled and the first intrusion is assumed to occur at a realistic time interval before 1000 years.

RESPONSE 5. Releases at the surface from earlier intrusions are examined in 1992: see Response 3.3. Radionuclide content of the waste is based on the IDB (US DOE, 1991). We are unsure what is meant by "a more realistic distribution of radionuclide concentrations"; see Comment 15, where EEG

observes that the "four activity levels chosen seem reasonable (and probably slightly conservative)...".

COMMENT 6. The 1991 performance assessment has assumed several parameters and physical and chemical processes which have helped to keep CCDFs within the Standards' Containment Requirement limits, but no clear justification is provided for these very non-conservative choices. Expert judgment has been used in lieu of experimentally determined values.

RESPONSE 6. As does the 1992 PA, the 1991 PA presented performance estimates for the preferred conceptual model based on available information about the disposal system (see Response 3.6). Alternative conceptual models were presented in Volume 4 (Helton et al., 1992). The goal of PA is to provide a realistic estimate of disposal-system performance with an understanding of the uncertainty in that estimate, rather than simply a conservative estimate (see Response 3). We disagree that the modeling choices are unjustified, and we note that the implication in Comment 6 that expert judgment is unavoidably non-conservative is incorrect.

COMMENT 7. Another area of EEG concern with the 1991 P.A. calculation is the apparent discrepancies in the estimates of the WIPP inventory of various radionuclides. Uranium-233 inventory assumption provides perhaps the most glaring example that would dramatically affect the total integrated discharges for various scenarios.

RESPONSE 7. See Comment 13 for an expanded discussion of this point by the EEG. The PA Department also notes difficulties in obtaining consistent estimates of waste that will be generated in the future. PAs will continue to use the inventory given in the IDB (US DOE, 1991).

COMMENT 8. As we did in 1991, we would again like to recommend that the 1992 and subsequent P.A. iterations include simulations of engineered modified waste forms to provide guidance to the DOE planners.

RESPONSE 8. The PA Department will do so if resources for additional sensitivity analyses are available.

COMMENT 9. And, to conclude this listing of EEG's major concerns with the 1991 P.A. effort, statements such as "Summary of CCDFs (mean and median curves) lie an order of magnitude or more below the regulatory limits" (p.

ES-6, etc.), are misleading at this stage of performance assessment. Portions of the modeling system and data base are incomplete, conceptual model uncertainties are not fully included, final scenario probabilities remain to be estimated, and the level of confidence in the results has not been established.

RESPONSE 9. The PA Department believes that it is important (rather than "misleading") to present preliminary results conditional on clearly stated assumptions and caveats. We agree that preliminary results should not be used out of context. The full quote from pages ES-6 and ES-7 of the 1991 Volume 1 was "Informal comparison of these preliminary results with the Containment Requirements indicates that, for the assumed models, parameter values, and scenario probabilities, summary CCDFs (mean and median curves) lie an order of magnitude or more below the regulatory limits."

III. Important Issues

Input Data

COMMENT 10. EEG has not yet thoroughly reviewed Volume 3: Reference Data to check the reasonableness of the range of various parameters proposed by individual SNL investigators and the connection between the ranges proposed and the results of the experiments on which they are based. We have serious concerns, however, about the values used for some of the more sensitive parameters which directly affect the outcome of the performance assessment.

Retardation of various radionuclides during transport through the Culebra aquifer is a case in point. For last year's effort, P.A. has relied on the "expert judgement elicitation" of two Sandia lab employees. The only existing k_d measurements on the Culebra rock were made using powdered samples which EEG criticized and rejected in 1979. However, one of the two experts used those data for his expert judgement in 1991! And even though the numbers suggested by the third expert (also a SNL employee) are between 1 and 3 orders of magnitude more conservative, his assumptions of 1% clay in the matrix of the Culebra dolomite and 100% clay filled fractures has no demonstrated scientific basis. It is interesting to note that the P.A. group disregarded the numbers provided by this third expert, but accepted his recommendation to assume a median value of 50% of fractures filled with clay based on a suggested normal distribution between 10% and 90%. No scientific justification for this distribution has been provided.

RESPONSE 10. PA modeling of transport in the Culebra will be revised appropriately when results are available from ongoing tracer column experiments. Until such time, PA will continue to examine alternative conceptual models in which K_d=0. The description of clay linings in fractures and the approach to modeling their impact on transport has been revised for 1992 (See Volumes 2 and 3).

COMMENT 11. The P.A. calculations of scenarios with releases through the Culebra dolomite have also relied on the assumption of double porosity flow with matrix diffusion. While the mechanism of matrix diffusion has been successfully assumed in the interpretation and modeling of hydrologic flow tests data, it has never been demonstrated to exist either experimentally or through modeling. The CCDF plots are highly sensitive to the combined assumptions of (1) the presence of clay in the matrix and in the fractures of the Culebra dolomite, (2) mechanics of double porosity flow with matrix diffusion, and (3) high degree of physical and chemical retardation of radionuclides during such transport. In fact, the sensitivity analyses indicate that without these assumptions, the CCDF curves for the scenarios involving flow through the Culebra would violate the containment standards. It is essential, therefore, that very good experimental and theoretical demonstration of the occurrence of these processes be provided.

RESPONSE 11. The PA Department agrees that experimental and theoretical demonstration of these processes is important. We disagree that "matrix diffusion ... has never been demonstrated." Existing hydropad tests indicate that dual-porosity transport on the scales of the tests is the most realistic conceptual model for fractured portions of the Culebra (Kelley and Pickens, 1986; Saulnier, 1987; Beauheim, 1987a,b, 1989; Jones et al., 1992). Planned hydraulic testing will further examine this question (Beauheim and Davies, 1992).

Undisturbed Performance of Repository/Shaft

COMMENT 12. Chapter 4 in Volume 2 devotes 83 pages to a description of the evaluations that have been performed to date. The calculations have been extensive and have involved 4 computational models (Boast II, Panel, Sutra, and Staff2D). The objectives of the calculations this year (summarized on page 4-81 of Volume 2) are primarily cross verification between models and initial approximations of gas generation effects.

All results indicate that migration of nuclides even a few meters up a shaft are orders of magnitude less than the allowable releases in 40 CFR 191. The assumptions are considered conservative but are not claimed to be bounding. These preliminary findings reinforce earlier conclusions that no non-human intrusion scenarios will result in releases and will thus never be a factor in showing compliance with the Standard.

EEG believes a conclusion that non-human intrusion scenarios will never be a problem and can thus be ignored is still unproven. Our reasons for this are discussed below.

This section is entitled "undisturbed performance." The discussion on page 4-63 of Volume 1 about undisturbed performance is misleading. The definition of undisturbed performance is quoted from the 1985 Standard as not including unlikely natural events. This is the correct definition, but it is to be applied only to the Individual Protection Requirements (191.15) and the Groundwater Protection Requirements (191.16). The Containment Requirements (191.13) apply the same probability limits to natural events as they do to disruptive events such as human intrusion. Therefore, the Performance Assessment needs to consider events with probabilities as low as 0.0001 in 10,000 years when constructing the CCDF.

The evaluation of "undisturbed performance" in the 1991 Preliminary Comparison clearly does not consider low probability conditions. For example, all modeling was done with the assumption that the degree of brine saturation in the wastes was 30% or less. The result was relative permeabilities in the waste that are orders of magnitude less than in the surrounding formation.

The values used for permeability in the anhydrite and halite were those from the median/average of the range used for human intrusion scenarios and sampling was apparently not done from the distribution. Likewise the solubility values used were around the center of the range and orders of magnitude below the 90-percentile levels shown in Table 3.3-11 of Volume 3.

It may turn out that calculations will show that truly bounding (or very low probability) conditions will still result in trivial releases from non-human intrusion events. SNL should, however, perform uncertainty and sensitivity analyses for the undisturbed case. An alternate approach might be to calculate truly bounding scenarios to see if it is possible to dispense with non-human-intrusion scenarios without further refining of calculations. These calculations should include a fully saturated room with solubility, and the formation and shaft permeability values at or near the 1.0 cumulative probability level.

RESPONSE 12. Points raised here are addressed individually.

12.1 "Non-human intrusion scenarios [should not be ignored]."

The PA Department agrees. They are included in the base-case scenario for § 191.13. If analyses of undisturbed performance for § 191.15 and 40 CFR 268.6 show a potential for 10,000-yr releases to the accessible environment, these releases will be included in CCDFs for § 191.13. As noted in the 1992 PA and previous iterations, the WIPP PA Department has high confidence that realistic models will continue to show that human intrusion is the only likely event with the potential to result in any releases to the accessible environment.

12.2 Definition of undisturbed performance.

See Response 4. The PA Department believes its usage is correct.

12.3 "The evaluation of 'undisturbed performance' in the 1991 Preliminary Comparison clearly does not consider low-probability conditions. For example, all modeling was done with the assumption that brine saturation in the wastes was 30% or less."

This comment suggests a misunderstanding of the PA modeling system. Brine saturation in the waste is "assumed" only for initial conditions. At all other times, it is a model-calculated quantity dependent on the material properties used in the model, the initial and boundary conditions, and the fundamental equations used to describe two-phase fluid flow. PA makes no *a priori* assumptions about the probability of model outcomes.

12.4 "The values used for permeability ... were ... median/average."

See Response 4. The comment is correct.

12.5 Implied request for "truly bounding (or very low probability) conditions."

See Responses 3, 4, and 6. The goal of PA for 40 CFR 191B is uncertainty analysis of realistic conditions, not worst-case analysis. The PA Department has completed uncertainty and sensitivity analyses for the undisturbed case (WIPP PA Department, 1992) and will continue to perform them in the future.

Uranium-233 Inventory

COMMENT 13. The 1991 Comparison lists a design inventory for Uranium-233 of 305 Ci (103.7 Ci CH and 201.5 Ci RH). This value is derived from the 1990 IDB (Integrated Data Base) where weight fractions of the major radionuclides of the mixes are reported. The IDB did not report the inventory of each radionuclide. The value in the 1987 IDB was about 7800 Ci.

The only detailed inventory document we are aware of is DOE/WIPP 88-005 ("Radionuclide Source Terms for the Waste Isolation Pilot Plant"). This report was never, to our knowledge, issued as a final report. However, we have been told by Westinghouse personnel that it is the major data base that was used to develop subsequent IDB reports. This document gives the following values:

CURIES OF URANIUM-233

Facility	CH - TRU		RH - TRU		
	stored	NG	stored	NG	
ORNL	2608.0	4459.0	0.0	0.0	
INEL	574.0	1.0	18.9	4.0	
LANL	48.0	0.0	0.0	0.0	
	3230.0	4460.0	18.9	4.0	= 7713 ci TOTAL

Also in 1983, EEG obtained an estimated radionuclide composition for all TRU stored at INEL. The estimate for U-233 was 862 Ci total, with less than one curie of this in RH-TRU.

It has been our experience that it is difficult to "back numbers out" of the IDB. The various tables are summaries of data and are not internally consistent. In order to calculate the curies of a radionuclide one has to assume that the grams per cubic meter of transuranics in each mix are the same. For example, when this assumption is made in Tables 3.5 and 3.8 of the 1990 IDB for ORNL CH-TRU, one calculates 25,400 Ci of alpha radioactivity. Table 3.5 lists 17,500 Ci.

Uranium-233 is one of the more critical radionuclides for performance assessment because of its expected greater solubility and lower retardation coefficient. The importance of uranium radionuclides to the Performance Assessment is indicated in Table B-4 (Volume 2) where 94.5% of the Total Integrated Discharge is attributed to U-234 and 4.3% is attributed to U-233.

The U-234 inventory of 3315 Ci is from the decay of 9.26 million curies of Pu-238. A U-233 inventory 25 times greater than that used in this report would increase the Total Integrated Discharge from 0.065 to 0.13.

SNL needs to carefully review estimates of the inventory for Uranium-233 and other radionuclides. Data should continue to be updated and obtained more directly than from the IDB values.

RESPONSE 13. The PA Department has little to add to this comment, except to note that the effects on regulatory compliance of changes in the radioactive inventory may be somewhat muted because allowable releases are normalized to the total inventory. We recognize the potential for discrepancies in estimates of waste not yet generated. Radionuclide inventories for PA will continue to be based on the IDB, however, unless or until an alternative approach is identified.

Cuttings Removal

COMMENT 14. EEG recommended in 1991 that the highly variable radionuclide concentrations in the waste be considered in evaluating the curies of TRU waste brought to the surface in borehole cuttings. The 1991 comparison responded to this recommendation by dividing the waste into four activity levels. An average activity was obtained from sampling on this activity distribution. This average activity was used in Appendix B, Volume 2 for the 60 vector runs with the 45 sampled parameters (which included drill bit diameter). Since the sampled average values differed very little from the simple average (about +2.2% at 1,000 years and +4.0% at 3,000 years), the end result of using a sampled average value was negligible in the Appendix B Tables. However, the activity levels were factored into the CCDF construction and the results appear reasonable.

The sensitivity analysis for cutting removal (in Chapter 4 of Volume 4) concludes that drill bit diameter is not a very sensitive parameter. We agree and recommend that in the future consideration be given to sampling directly on the four activity levels in the waste and use a constant drill bit diameter of about 0.34 m. Also, the quantity of waste removable under various room and brine conditions needs to be better understood (see page by page comments for Volume 4).

RESPONSE 14. The PA Department agrees that the quantity of waste removed under various room conditions needs to be better understood.

COMMENT 15. The four activity levels chosen seem reasonable (and probably slightly conservative) when compared to the waste inventory curies in Table 3.3-5 (Volume 3) and volumes in Table 3.4-5 (Volume 3). However, it is noted that the level 4 activity at 3,000 years and later could not be attained by containers that met the initial criticality limits (200 FGE for a 208 liter drum) because most of the activity would have to come from Pu-239 or Pu-240.

RESPONSE 15. Note that the CUTTINGS code includes radioactive decay, and that the activity levels are based on activity at the time of emplacement.

COMMENT 16. The statement is made on page 4-7, lines 34-37 of Volume 4 that a single borehole would not result in a normalized release that exceeds 1.0 and that an intrusion at an earlier time might exceed 1.0. It would be more accurate to say that a single borehole at 1,000 years could theoretically reach 1.0 and that earlier intrusions could definitely exceed 1.0. This is because drums loaded to the maximum permitted PE-Ci and FGE levels with (for example) 987 Ci Am-241, and 11.4 Ci Pu-239, and 1.1 Ci Pu-240 would have 1262 Ci brought to the surface (1.06 normalized release) from a .944-m (eroded diameter) borehole. Also, permissible loading levels of Pu-238 (1100 Ci in a 208 liter drum) could result in normalized releases exceeding 1.0 for greater than 210 years. Because of the early time effect of cuttings and brine flows brought to the surface, EEG believes that SNL should sample on time as they did in the 1990 comparison and not make the first intrusion at 1000 years in all 60 vectors.

RESPONSE 16. See Response 3.3. Releases at the surface are evaluated for earlier intrusions. PA has not sampled on time of intrusion in 1992, however, and will not in future analyses. As discussed in Section 3.1.3 of Volume 1 of the 1991 PA documentation, stochastic uncertainty (e.g., time of intrusion) and subjective uncertainty (e.g., uncertainty in values for imprecisely known model parameters) are fundamentally different. Confusing the two types of uncertainty complicates parametric uncertainty analyses.

Gas Effects

COMMENT 17. DOE has maintained since 1988 that data on gas generation from TRU waste is needed to narrow uncertainties in the performance assessment. In fact, almost the entire justification for starting waste emplacement at WIPP has been based on the need for data to assess compliance with 40 CFR 191

Subpart B. Naturally, one would look to the performance assessment analyses to verify these claims. The P.A. reports so far have not supported the DOE assertion that in situ gas generation data is needed to narrow or remove uncertainties in performance assessment. In fact, although it is not clearly mentioned in any of the 1991 P.A. reports, the only effects of gas generation used are those that are beneficial to P.A. (reduces the releases to the environment). This is because the gas effects have been used only to further reduce the assumed rates of brine inflow, which proves to be beneficial to P.A. The structural effects of gas production that could result in opening of fractures and providing new pathways and mechanisms for releases have not been considered in the P.A. calculations so far.

The net result of assuming the "good" effects of gas and not the "bad" ones, yields results which counter the DOE claims of the need for more in situ gas data. What is the point in undertaking the expense of gas generation tests when the gas generation from waste is actually beneficial in demonstrating compliance with 40 CFR 191? Would it not be better to use these resources to obtain experimental data on radionuclide retardation, solubility, and the nature of porous media flow through the Culebra, the parameters that have the maximum impact on P.A.?

Of course, the assumption that the gas generation would retard brine inflow and thus would help in reducing the releases to the environment is simplistic. The conditions in the repository are expected to evolve as a result of complex interplay of brine inflow, salt creep, disturbed rock zone (DRZ) development, physical disintegration and chemical decomposition of the waste, and gas generation. To predict the range of possible future conditions, and various pathways of development of such conditions, would require complex modeling of coupled processes such as that presented by Davies, Brush and Mendenhall in SAND91-2378.

EEG recommends that the 1992 P.A. should include gas generation effects and the results should be used to assess the need to collect more gas generation data in situ "to reduce uncertainties in performance assessment."

RESPONSE 17. See Response 12.3. The PA Department does not "assume" that gas generation retards brine inflow. Rather, the retardation of brine inflow by elevated gas pressures is calculated by a sophisticated computational model based on fundamental principles of physics and available data and conceptual models.

Pressure-dependent fracturing of anhydrite marker beds has not been included in the 1992 PA. It will be included in future PAs when adequate conceptual and computational models are available.

Comments by the EEG about the relative importance of additional information about gas generation effects for assessing regulatory compliance apparently apply only to 40 CFR 191B. The PA Department notes that analyses with regard to 40 CFR 268.6 (WIPP PA Department, 1992) were not complete at the time of the EEG review.

Waste Form Modification

COMMENT 18. The calculations published by the WIPP Engineered Alternatives Task Force (EATF - DOE/WIPP91-007) indicate that waste form modification could improve repository performance by reducing radionuclide releases into the accessible environment by up to four orders of magnitude, depending on the release scenario and the waste form modification. However, the EATF was unable to make specific recommendations for waste treatment, noting that more work needed to be completed by the SNL performance-assessment effort. The 1991 performance assessment calculations by SNL did not include simulations of the engineered alternatives to the waste form, although the need for performing those calculations was acknowledged. EEG recommends that the 1992 and future P.A. iterations should include assumed waste-form modifications to better assess the merits of such modifications in demonstrating compliance with 40 CFR 191.

RESPONSE 18. See Response 8.

IV. Page by Page Comments

Volume 1, Executive Summary

COMMENT 19. Page (ES-3), lines 12,17. The statement that computational scenarios are distinguished by the time and number of intrusions does not reflect the methodology presented in Volume 2 (Chapter 2), in that "time periods" 2000 years in duration and not exact times are utilized. The mid-point of each interval is a mean average intrusion time estimated by assuming equal likehood across it. Also, it should be mentioned that the historical drilling rate at the site is the maximum rate required by the Standard, whereas the 1991 P.A. samples on a uniform distribution between zero and the maximum required rate. More detailed concerns with this section will be addressed in later comments.

RESPONSE 19. See Responses 3.1, 3.3, and 16.

COMMENT 20. Page (ES-4), lines 2-8. Without mentioning the fact that many parameter distributions are based on subjective judgements formulated by expert panels, which are not readily amenable to uncertainty and (to a lesser extent) sensitivity analysis, one is led to believe that all parameters utilized are derived from experimental measurements. The use of subjective judgement for this purpose, or the use of expert panels to derive such distributions, should be mentioned somewhere in the Executive Summary to convey this type of existing uncertainty in the P.A.

RESPONSE 20. The 1992 documentation makes the point more clearly.

COMMENT 21. Page (ES-4-5), lines 42-45;1-2. Simulations of undisturbed performance indicate zero releases to the accessible environment. This result is based on current parameter uncertainties, incomplete utilization and understanding of certain processes such as structural effects of gas generation, climate and subsidence effects, and an apparent misinterpretation of the definition of undisturbed performance in the 1985 Standard. Therefore, the absence of an analysis of the "base" scenario together with its sensitivity to parameters is of some concern to EEG. Without such a summary, it is not possible to judge the relative effectiveness of containment, and to determine which parameters have controlling influence, and whether their distributions are derived from subjective or experimental process. All of this information should be available for review in future iterations of P.A.

RESPONSE 21. See Responses 4 and 12.

COMMENT 22. Page (ES-5), lines 8-10. The upper bound of 30 boreholes/km^2/10,000 years mentioned in the EPA Standard was based on the observed frequency of drilling in the vicinity of the WIPP site. Therefore, what is the justification for the use of a rate constant with the observed frequency at the site to be the upper bound and a lower bound of zero? The drilling rate appears to have increased in recent years. It may increase or decrease in the future. A more conservative distribution should be used for the future P.A. calculations and a justification should be provided for the distribution used.

RESPONSE 22. See Response 3.2. Note that the expert panels did not agree that "a more conservative distribution should be used."

COMMENT 23. Page (ES-5), lines 10-13. The use of five disjoint time intervals of 2000 years is apparently based on the need to keep computer simulation costs to an acceptable value, and not on any scientific analysis of the impact of these specific intervals and size on the overall CCDF formulation. As was mentioned earlier, the choice of a midpoint for these intervals is based on a mean expectation within a given interval, but the presence of more than one event within a given interval is seemingly meaningless if tracking of repository history is to be taken into consideration. If the time(s) of intrusion are truly independent from one another, then sampling of any number of intrusion singlets, doublets, triplets, ..., etc., from a uniform distribution of 10,000 years, coupled with a calculation of probabilities of occurrence for these intrusions using the Poisson distributions derived within the text, would have possibly been more representative and less arbitrary than the methodology used in P.A. for this purpose. Hence, the five time intervals selected by this methodology would have been of unequal length with possible overlaps.

RESPONSE 23. See Responses 3.3 and 16.

COMMENT 24. Page (ES-5), lines 13-15. Geophysical (TDEM) anomalies at the level of the upper Castile Formation underlying the waste panels indicate the presence of a brine reservoir. However, short of extensive drilling down to that horizon, one can never be certain about the presence or absence of a brine reservoir at that depth or the fraction of the area underlain by the waste panels to be occupied by brine. EEG recommends that while credit may be taken for the uncertainties of a future drillhole reaching that depth, it should be assumed that any hole reaching the upper Castile would encounter pressurized brine reservoir with properties similar to the one encountered by the borehole WIPP-12. To attempt to delineate the fraction occupied by brine on the basis of the TDEM contours is not a valid exercise.

RESPONSE 24. The WIPP PA Department agrees that "one can never be certain about the presence or absence of a brine reservoir." Therefore, we have used available information to provide a reasonable estimate of the uncertainty in our knowledge about the absence or presence of a brine reservoir. The purpose of PA is to provide realistic estimates of performance, not worst-case estimates (See Responses 4 and 12).

COMMENT 25. Page (ES-5), lines 15-18. The four activity levels chosen appear to be reasonable, and probably slightly conservative, when compared to the waste inventory curies in Table 3.3-5 (vol. 3) and the volumes of waste

in Table 3-4-5 (vol. 3). It should be noted, however, that the level four activity at 3000 years and later could not be attained by containers that met the initial criticality limits (200 FGE for a 208 liter drum), because most of the activity would have to come from Pu-239 or Pu-240.

RESPONSE 25. See Responses 5 and 15.

COMMENT 26. Page (ES-5), lines 28-38. It is not mentioned that the dual-porosity model being employed, and the consequently large retardations ascribed to the fractures and the matrix (both chemical and physical) have not been proven to be representative at the site. EEG voiced concern in the 1990 P.A. over the use of unjustifiably large retardation factors ascribed to the fractures and matrix. The 1991 P.A. which shows even larger maximum retardation factors only exacerbates our concerns that these factors have not been experimentally justified. Finally, we are still concerned over the use of Expert Panels to derive parameter distributions that can be measured experimentally. Any potential impact that such use will have on the C&C agreement between DOE and the State has been ignored. This Summary should reflect these uncertainties.

RESPONSE 26. See Responses 3.5, 3.6, and 10.

COMMENT 27. Page (ES-6), lines 13-27. This section does not state that the cuttings/corings removal scenarios are not completely modeled, which is important because these types of events dominate the CCDF. Furthermore, it appears that these scenarios would result in much higher releases if a more realistic distribution of radionuclide concentrations is sampled and the first intrusion is assumed to occur much sooner than 1000 years. It is important to know the magnitude of the low probability significant releases and the parameter sensitivity for such releases. This should be provided.

RESPONSE 27. See Responses 3.3, 5, and 15. Emphasis on the importance of cuttings and cavings is more carefully noted in the 1992 documentation. Consequences of core drilling have not been analyzed explicitly because this type of drilling is not commonly used in exploratory boreholes that reach the WIPP horizon. Total volume of waste removed by coring, like that removed as cuttings, would probably be most sensitive to the diameter of the drill bit.

COMMENT 28. Page (ES-6,7), lines 24-2. Statements such as, "summary of CCDFs (mean and median curves) lie an order of magnitude or more below the regulatory limits" are misleading at this stage of performance assessment for reasons summarized in lines 37 to 42 of p. ES-6 and in our major conclusions.

RESPONSE 28. The PA Department disagrees. See Response 9.

COMMENT 29. Page (ES-7), lines 10-11. EEG disagrees with the statement that the WIPP project has satisfied the natural resources assurance requirement outlined in 40 CFR 191.14(e). A review of the referenced DOE report (DOE/WIPP 91-029, August 1991) was provided to WPIO on December 27, 1991. The EEG letter made constructive suggestions towards achieving compliance with the requirement. We have not yet received a reply to our letter. Our position is that the determination that this mineral-rich site is acceptable will be made by the results of the P.A. with drilling rates applicable to a mineral-rich site.

RESPONSE 29. With regard to drilling rates, see Response 3.2. The PA Department is not familiar with the status of the DOE's response to the letter mentioned in the comment.

Volume 1, Chapter 1 - Introduction

COMMENT 30. Page (1-13), lines 4-8. The Consultation and Cooperation Agreement requires DOE to consult and cooperate with various branches of the New Mexico State government and with EEG and not just with the N.M. Environment Department. This change from the 1990 report (SAND90-2347, page I-20) is obviously deliberate, but wrong. In fact, the C and C agreement mentions no particular State agency, but does mention EEG.

RESPONSE 30. Text describing the participants in the WIPP Project has been revised in the 1992 documentation to reflect the 1992 Land Withdrawal Act, which clarifies the EEG's role as a reviewer.

COMMENT 31. Page (1-13), lines 8-18. The Environmental Evaluation Group (EEG) is the only full-time independent review group for the WIPP project and has been conducting this work since 1978. The ACNFS is now defunct and the DNFSB has only commented on the clarification of some DOE Orders' applicability to WIPP. This paragraph and the Synopsis (page 1-32) should appropriately describe the role of the review groups, and list them in the

order of their importance and involvement with the WIPP project.

RESPONSE 31. See Response 30.

COMMENT 32. Page (1-15), lines 5-9. The well that bottoms within the WIPP site (James Ranch Unit No. 13) is not only "capable of producing gas," but has been producing gas and condensate since January 1983, except for a shut-in period of one month in July 1985 and for three extended periods of several months beginning in April 1987. This well has produced over 3 million MCF of gas to date.

RESPONSE 32. The text has been revised, and now cites the report by the EEG documenting production from this well.

COMMENT 33. Page (1-25), lines 43-5. What is "an extensive experimental area ... under construction north of the waste disposal area"?

RESPONSE 33. This refers to the underground experimental area excavated north of the waste-disposal area.

Volume 1, Chapter 2 - Application of Subpart B

COMMENT 34. Page (2-4), lines 18-21. This agreement has already been broken by allowing resource extraction from the WIPP site through slant drilling. What are the plans to correct the situation?

RESPONSE 34. The question should be addressed directly to the DOE.

COMMENT 35. Page (2-7) lines 32-44. EEG does not consider it appropriate to use expert panel judgement on parameter distributions, which can be determined experimentally as was indicated in the review of the 1990 P.A. This is particularly true for parameters which have great impact on the resulting CCDFs, such as radionuclide solubility and chemical retardation. The P.A. has not addressed the conflict between using retardation values derived in this manner and the current C & C agreement between DOE and the State. Furthermore, EEG questions whether the current use of expert panels and "expert judgement" by SNL goes beyond the intent of the Standard. Clearly, this is an unresolved policy issue.

RESPONSE 35. Parameter values for solubility and retardation are being examined experimentally. Expert judgment is used for these parameters in the 1992 PA to provide interim guidance to the Project until experimental data are available. We note that the evidence that these parameters "have great impact on the resulting CCDFs" comes from analyses using expert judgment. Without the guidance provided by expert judgment, conclusions about relative importance of these parameters would be unsupported.

Although the PA Department agrees with the EEG about the importance of experimental data for all important parameters, and particularly for solubilities and retardations, we question the usefulness of a philosophy that demands in an absolute sense that all distributions which can be determined experimentally must be so determined. First, it should be noted that relatively few parameters in a natural system can be known completely from experimentation. Second, the philosophy presupposes that all parameters are of equal importance and that there are unlimited resources and time for experimentation. One of the purposes of iterative PA is to identify important parameters so that resources may be allotted sensibly. The EEG acknowledges this purpose: see, for example, Comment 17.

Volume 1, Chapter 3 - Performance Assessment Overview

COMMENT 36. Page (3-8), lines 26-30. If the statement is true that most parameter distributions will be of the subjective type as opposed to distributions obtained by classical statistical techniques, then the resulting CCDFs obtained from such an analysis will be mostly subjective as well. While it is possible to perform uncertainty analysis of a subjectively derived CCDF, the meaning of such an exercise is questionable from a quantitative point of view. Also, the statement of the possibility that some distributions will be obtained experimentally is contrary to what is expected for assessing WIPP in a quantitative sense to the greatest degree possible. Does the Standard allow such a procedure for highly sensitive parameters for which it is possible to obtain experimental data to perform statistical analysis? EEG has already noted problems of this type in the 1990 P.A. comparison to the Standard, along with attendant problems in devising uncertainty analyses with this approach. The current P.A. comparison increases this concern because it appears to be adding more uncertainty (subjective) to the results by design than it is explaining.

RESPONSE 36. See Response 35. Few, if any, parameters in a complex, spatially varying natural system can ever be known well enough from experiments or field observations to provide a meaningful basis for pure classical statistical analysis. Informed, subjective judgment of analysts

invariably enters into the interpretation of data at many stages, from field and laboratory measurement to the construction of distributions for model parameters. Because data often cannot be collected specifically for the parameters used in models, and can only rarely be collected at the scale at which they are used in models, subjective judgment fills an important and valuable role in performance assessment. The PA Department acknowledges the preeminent importance of experimental data, but does not wish to obscure the role of subjective judgment in PA.

COMMENT 37. Page (3-16), lines 21-38. The explanation of Type A and Type B uncertainty for stochastic and subjective variations, respectively, seemingly attempts to legitimize the use of subjective uncertainty over uncertainty derived from classical statistical measurements of experimental data. Also, subjectivity is extended to represent stochastic uncertainty as well. In fact the CCDFs presented in the current P.A. use subjective distributions to construct both ordinate and abscissa. Furthermore, these CCDFs have been derived through the use of Latin Hypercube Sampling of the subjective distribution(s) for both axes. An important question arises as to what is being measured in uncertainty analysis when the CCDFs have been constructed from such a large number of subjectively derived distributions. Is there such a thing as a "subjective" mean or median? Are some subjective distributions more "real" than others? Do they all receive equal "weighting," including the "few" that have been derived from experimental measurements at the site? EEG questioned the meaning of such analyses when experimentally derived distributions were "mixed" with those of subjective origin in the 1990 P.A. The reply (and one which is reflected in the current P.A.) is that very few of the distributions were of the experimental type. How then do site-specific measurements and observations enter into the P.A. process? If site-specific information is important and is being (or will be in the future) utilized, then this report should give a clear and concise statement as to how this type of information is being (or will be) used to formulate the subjectively derived distributions, and experimental measurements should be displayed on the distributions being utilized. A plot of distributions without real data-points such as are presented in Volume 3 are not very supportive. EEG realizes that some parameter distributions are not amenable to experimental derivation, but for those which can be measured on a site-specific basis, every attempt should be made to determine parameter distributions by this approach.

RESPONSE 37. See Responses 35 and 36. See also the discussion of cdf construction in Chapter 1 of Volume 3 of the 1992 documentation.

COMMENT 38. Page (3-17), lines 38-43. The term, nR, is defined as the "normalized release" for TRU waste. It should more appropriately be defined as the "normalized fractional release" for CCDF construction purposes.

RESPONSE 38.

The PA Department will continue its usage, which we believe to be correct and unambiguous.

COMMENT 39. Page (3-35), lines 22-28. What is the basis for the assumption that the TS scenario has no impact on releases from the repository? There is no information in the current or previous P.A. indicating that this is the case, and it was not excluded in earlier screening efforts to be of no great consequence. In a response to an EEG concern in the 1990 P.A., it was stated that a modeling strategy had not been developed. Is this still the case in 1991? If this is the case, then how was the assumption about TS events made? If the modeling strategy is now complete, then what are the test results to justify the assumption on TS events in 1991? Also, there is no mention of climatic change as part of the scenario characterizations, although this parameter is mentioned at other locations in the current P.A. reports.

RESPONSE 39. The statement in question about the TS event was misleading. PA will examine the effects of subsidence related to potash mining when conceptual and computational models are available. Climatic change is included in the base-case scenario.

COMMENT 40. Page (3-35), lines 30-45. Computational scenario probabilities and consequences for the 1991 P.A. are based on:

1) number of drilling intrusions
2) time of drilling intrusions
3) whether or not a single panel is penetrated by two or more boreholes, of which at least one penetrates a brine pocket and at least one does not
4) the activity level of waste penetrated by the boreholes.

The third condition presumably refers to an E1E2-type scenario, where any number of penetrations could intercept both a waste panel alone or both a waste panel and an underlying brine pocket. It excludes the following:

a) whether or not a single panel is penetrated by two or more boreholes, none of which intercept a brine pocket
b) whether or not a single panel is penetrated by two or more boreholes, all of which intercept a brine pocket
c) whether or not a single panel is penetrated by one borehole which intercepts a brine pocket (E1).

Cases (a) and (c) differ primarily in the amount of cuttings released to the surface (assuming an intact plug above the Rustler Formation). Cases (b) and (c) differ primarily in the amount of cuttings released to the surface by drilling and by shearing of material from the borehole by the extruding brine (assuming an intact plug within the Salado Formation). It is not clear whether case (3) above takes into account the extra cuttings from multiple intrusions or takes into consideration single-intrusion events in its definition of computational scenarios. Does case (3) apply only to groundwater transport in the Culebra Dolomite? If not, how are the above exclusions (a,b,c) justified in the definition of computational scenarios?

RESPONSE 40. The text apparently should have been clearer. The calculations did address all of the points raised, and did not exclude the listed cases. Multiple intrusions were allowed, and cuttings were calculated for each.

COMMENT 41. Page (3-36), lines 1-52. In the selection of discrete time intervals, why must they be:

a. of equal duration (this P.A. uses 2000-year intervals)
b. disjoint (100-2000, 2000-4000, 4000-6000, 6000-8000, 8000-10000)
c. only 5 intervals?

What are the implications of these conditions on the construction of the CCDFs for P.A., as opposed to more stochastic variation of (a), and the use of more intervals(c), which may or may not be disjointed? Would it not have been more consistent to have selected a given year at random from each interval using LHS, since in effect the division of the "even" distribution of year numbers from 1 to 10000 was partitioned into equal probability areas by this approach: instead of assuming that intrusions occurred at 1000, 3000, 5000, 7000, and 9000 years, say at 656, 3200, 4800, 7800, and 9100 could have been selected at random from within each interval of the distribution. Hence, the time intervals utilized in Eq. 3-23 would not necessarily be equal, and would reflect the LHS methodology utilized for other parameters. The latter would still conserve disjoint (but possibly unequal) intervals. Another approach would have been to sample single,

doublet, triplet,... years of intrusion from the even distribution of years between 1 to 10000 years (possibly excluding any intrusion occurrences below 100 years), and calculating intrusion probabilities using Eq. 3-27. This would result in possible disjoint and unequal time intervals. Such an approach would minimize any bias that repository history would have on the resulting CCDFs. Why were these (or other) approaches not considered? Finally, it is not clear that in the definition of n(1), n(2), n(3)... that these values are not necessarily equal to 1, 2, 3,.., respectively. An analysis of Eq. 3-27 indicates that they do not have to equal these values when calculating the values in Table 3-2 using Eq. 3-27. The definition needs to be clarified in this respect.

RESPONSE 41. See Response 3.3. The 1992 PA provides better resolution for surface releases from early intrusions. Subsurface releases are believed to be less sensitive to the time of intrusion because decay continues to occur during groundwater transport. The five time intervals were selected for computational efficiency.

COMMENT 42. Page (3-37), lines 1-5. What is the basis for the statement that subsidence events and single borehole penetrations into pressurized brine pockets "do not appear to be important" in the determination of scenario consequences, and therefore are not considered in the 1991 P.A.? One of EEG's concerns for the 1990 P.A. was the exclusion of subsidence events (TS) from consideration. One of the replies to this concern was that such an event was not yet modeled. Was it modeled for inclusion in the 1991 P.A., but not considered? If so, where is the documentation that such an event may not be important in P.A. If the modeling of this event is not complete, then how can such a statement be supported? Also, why was it not originally screened out as being of little consequence at an earlier stage of P.A.? It is still part of the event tree in Figure 3-14. Also, why is the E1 event not considered important in lieu of the release of cuttings and eroded materials to the surface? Is the E2 scenario also not important on this basis? Does the scenario have to be of the form described by Eq. 3-23 (E1E2 related) to be important enough for consideration?

RESPONSE 42. See Response 39 with regard to TS. Surface releases from E1 and E2 were included in the 1991 and 1992 PA and will continue to be included. Note that, as modeled, the quantity of cuttings/cavings released from the two types of intrusions is the same, and that the total release of cuttings and cavings dominates the summary CCDFs for the preferred conceptual model.

COMMENT 43. Page (3-38), lines 1-31. Equation 3-28 is a versatile equation for estimating the probability of any combination of intrusions within designated time intervals, including multiple intrusions in combination with a variety of intrusions in other intervals. Since n(i) can take on any value including zero (although not clearly explained in the text) in any of the intervals, all of the intrusion combinations in Table 3-2 can be obtained with this single equation. However, Eq. 3-29, which expresses the probability of the specified intrusions having penetrated specific activity levels of waste, needs more explanation or at least an example of its use to make it clearer. For instance, suppose there are two activity levels of waste, each with a probability of 0.5, and two boreholes are specified; one in time interval 2 and one in time interval 3. Then the probability of occurrence using Eq. 3-28 equals 0.01673 as shown in Table 3-2. Secondly, assume that one wants to know the probability of both boreholes hitting activity level 2, then the product series in Eq. 3-29 will predict 0.25 correctly. The same would be true for both boreholes striking activity level 1. However, some confusion arises when this equation is used to predict the boreholes striking activity level 1 and 2 since there are two ways to arrive at this possibility. Equation 3-29 gives the correct probability because Eq. 3-28 accounts for the number of permutations: any value in Table 3-2 can be computed as the product of the number of permutations of the intrusion combination times the probability of the intrusions occurring in the same time interval. Thus, the probability of three intrusions in time intervals 2, 3, and 4 (1.098E-02, Table 3-2) can be calculated as the product of the probability of three intrusions in a single time interval (such as for 2, 2, 2;3, 3, 3;4, 4, 4) times the number of permutations of 2, 3, and 4 time intervals (6): 6 x 1.829E-03 = 1.098E-02.. etc. In fact, Eq. 3-28 is not required in its product form (II) to obtain the values in Table 3-2 if the permutations of the intrusion combinations are utilized in this manner and the time intervals are equal:

$$p(n) = cf*j!*(\lambda^n*\Delta t^n/n!)*(\exp(-\lambda*(b-a)), \text{ where}$$

n	=	number of intrusions
j	=	permutation number (j less than or equal to n)
Δt	=	time interval (less than or equal to (b-a)
b	=	time at end of total time interval
a	=	time at beginning of total time interval.
cf	=	correction factor for presence of first time interval in permutation number.. (1, 2), (1, 1, 3).. etc., (cf=1.0 if all time intervals are equal, see below).

The correction factor (cf) for the first time interval (1900 years) as opposed to 2000 years for all other time intervals (2, 3, 4, 5) depends on how many times it appears in the permutation:

$$cf = (1900/2000)^a, \text{ where}$$

a = number of times interval 1 appears in permutation number.. a=1 for (1, 2); a=2 for (1, 1, 2); a=3 for (1, 1, 1, 4); a=0 for (2, 3, 4); a=2 for (1, 1, 2, 4)..etc.

This equation can be extended to include other unequal intervals as well.

RESPONSE 43. The author of this comment has noted correctly that probability computations with Equation 3-28 (which applies to a constant drilling intensity λ) can be considerably simplified, particularly for the case of equal time intervals, if the number of permutations of distinct time intervals is taken into account. The PA Department has not determined whether similar simplifications are possible when the drilling intensity is a function of time, $\lambda(t)$, as occurs in the 1992 PA calculations (see Section 5.1 of the 1992 Volume 2). In any case, Equations 3-28 and 3-29 were derived (in Sections 2.4 and 3.2, respectively, of the 1991 Volume 2) in a way that guarantees applicability to situations where the drilling intensity is any bounded, integrable function of time on the interval (0, 10,000 years). Because constant λ is such a function, Equations 3-28 and 3-29 are correct, although possibly computationally inefficient.

COMMENT 44. Page (3-45), lines 22-37. It is not clear how rCi releases are incorporated into CCDF construction if it is assumed that there are five different activity levels for TRU wastes in the 1991 P.A.? Does this statement mean that they could be used if only one activity level (such as the mean) were used? More explanation is needed. Also, please explain the basis for the assumption that an E1E2 scenario can only take place when the necessary boreholes occur within the same time interval (2000-year duration, as opposed to over a 10000-year duration)? The result of this assumption is to lower the probability of such an occurrence as illustrated in Table 3-1, because multiple intrusions involving different time intervals have higher occurrence probabilities (greater than 2000 years between occurrences). In lieu of the fact that two or more intrusions (one of which penetrates pressurized brine, and one does not) can occur over the entire 10000-year period with higher probabilities (1, 1, 1, 1 has a lower probability of occurrence than 1, 2, 3, 4 for 4 intrusions, see Table 3-2), why are they excluded? Furthermore, how is the time interval between intrusions defined under this assumption? Does not the repository history have any bearing on

the ultimate releases, or is this history assumed to be constant for the 1991 P.A.? The third assumption that an E1E2 scenario involving more than two boreholes will have the same release as one involving only two is clearly incorrect if cutting releases are to be incorporated into the scenarios. This assumption would lead one to believe that all cutting releases for multiple intrusions are not being considered in this P.A. Is this true? Why?

RESPONSE 44. More explanation is provided in Volume 4 of the 1991 documentation on the use of varying activity levels to determine releases of cuttings/cavings (Helton et al., 1992). The decision to calculate possible effects of flow between boreholes within a single panel only for those holes that occur within the same 2000-yr period is a simplification made for computational efficiency. Note, however, that the E1E2 flow pattern will persist only as long as a plug between the repository and the Culebra remains intact in one of the boreholes. Although the PA Department assumes other plugs will degrade within a short time, this plug (and others used to maximize brine flow into the Culebra in the E1, E2, and E1E2 scenarios) is assumed to remain intact for the balance of the 10,000 yr. The EEG is correct in observing that some assumptions used to construct the E1E2 scenario are simplistic. With regard to the final question, cuttings/cavings releases from multiple intrusions were included in the 1991 (and 1992) PAs.

COMMENT 45. Page (3-46), lines 49-54. This a very confusing statement in that type B uncertainty (scenario consequences) does not have to be subjective: the more quantitatively meaningful uncertainty in this case would be statistically derived. In fact subjective uncertainty should be the last resort, and parameters should be based on "site-specific" data if at all possible. This statement appears as an attempt to legitimize the use of subjective uncertainty for P.A. as a substitute (rather than as an alternative) for experimentally derived distributions. EEG has expressed concern over the use of subjective parameter distributions for the 1990 P.A. and reiterates that same concern for the 1991 P.A. The same argument can be applied to stochastic (scenario probabilities) uncertainty; however, it must be admitted that some of these characterizations are not amenable to the experimental method and must remain subjective.

RESPONSE 45. See Responses 35 and 36.

COMMENT 46. Page (3-47), lines 30-37. The differential analysis techniques review is very clear as to what methodologies will be used to perform both sensitivity and uncertainty analysis. However, the methods employed are most informative and precise when:

1. All of the parameters used in CCDF construction are sampled from known statistically derived distributions.

2. The LHS sampling technique samples the necessary parameters in a way that the variables in the set (v1, v2, v3,..., n) are a representative n-tuple set of the actual sample space.

3. Variable covariance effects on sensitivity and uncertainty effects are not significant.

Whereas the problems that may be associated with covariance among the parameters sampled by LHS was mentioned in the 1990 P.A., there is no mention of any attempts to determine where (and if) such relationships exist in either the 1990 or 1991 P.A. documents. Also, the effect of subjective judgement on any "actual" covariance among parameters has not been addressed. Are there any field measurements being employed to test for this property at least among some of the important parameters being employed in P.A.? Is it possible to measure covariance from a set of subjectively derived parameter distributions?

It is unclear how the LHS methodology being employed takes into account (or will) possible covariances among some of the parameters. At present 60 samples are obtained from 45 parameter distributions; however, the sequence (from which of the 60 subdivisions of equal probability) of each parameter is not presented in the text. For instance, in the first sampling of the 45 parameters, do all of them come from the first equal probability segment of each distribution 1, 1, 1, 1, 1,..etc., or is each parameter possibly sampled from a random set of probability intervals.. 1, 3, 56, 22, 44,..etc.? If the sampling is taken from different equal probability intervals, then that sequence should be recorded for review, particularly if covariance effects are expected between some of the parameters. Is there a specific methodology for sampling to obtain non-biased samples from such a large number of parameters with (and without) covariance among some of the parameters?

RESPONSE 46. In general, correlations are not included in the PA LHS sampling because available information is insufficient to define meaningful correlations. Some parameters are correlated, and others will be in future PAs as new data become available. For uncorrelated parameters, samples are selected from uncorrelated intervals of equal probability. These sequences are recorded for review in Appendices included in the 1990, 1991, and 1992 PA documentation. For additional information on the methodology for obtaining unbiased samples from a large number of parameters, the reviewer is referred to Section 3.5 of Volume 1 of the 1991 PA documentation (WIPP PA Division, 1991a) and to the references cited therein.

COMMENT 47. Page (3-54), lines 20-45. EEG agrees with the statement on using crude characterization of ranges and distributions as input for P.A. if the analysis is primarily of an "exploratory" nature. However, this message is not conveyed in the Executive Summary, which states that "reasonable confidence" exists in meeting the Standard. In fact a direct contradiction exists with the statement "..care should be taken to avoid assigning unreasonably large ranges to variables" with what has actually taken place with respect to retardation factors and radionuclide solubilities in the 1991 P.A., even when compared to the 1990 P.A. EEG in its comments on the 1990 P.A. addressed the issue of CCDF output and associated sensitivity results as being highly dependent on the ranges assigned to input variables as is discussed in this section and is in agreement. However, this philosophy is not clearly evident in this P.A. What is the reason for this discrepancy? If the 1991 P.A. is still of an exploratory nature, then it should be stated as such, and conclusions drawn from it should be stated in this manner.

EEG also agrees that "often, most of the variation in an output variable will be caused by a relatively small subset of the input variables" as the basis for using rather crude range and distribution assumptions for the parameters to find the most sensitive parameters upon which to direct more resources in characterization. However, this approach may be questionable if some of these ranges and distributions have been grossly overestimated or improperly characterized. In fact "expert panels" were convened to address both solubility and retardation characterizations in 1991 with very little experimental research to justify their use.

RESPONSE 47. See Response 6, 35, and 36.

COMMENT 48. Page (3-57), lines 11-45. It appears that the under-pinnings of P.A. are being discussed in this section. Variables for which experimental designs can be constructed to determine parameter distributions by formal statistical procedures are stated to be in the minority. According to this analysis the majority of parameters are not amenable to this type of formulation for seven reasons. What is the impact of this conclusion on the interpretation of the resultant CCDFs from the viewpoint of the Standard? Does the Standard allow such lack of statistical formalism to practically all of the parameters employed in this exercise? Does it imply that "expert panel" judgement can be used to substitute for "site-specific" data for important "quantitative" parameters? Has this approach been legitimized by EPA? Of the seven reasons stated for proceeding with this approach, only the last two (6, 7) appear to be totally justified: rare geological events are

not amenable to experiment, and predicting future human behavior (including human intrusion) over 10000 years is of a speculative nature. The first reason (time-scale problem) is peculiar to long-term trends such as future climatic patterns, geochemical equilibrium, etc., but, in addition, it represents the predictive or extrapolative nature of the Standard as a whole from known properties and processes. Physical and chemical properties of the repository which have controlling influence on repository behavior are mostly time-invariant, and are amenable to statistical formalism. Stated reasons (3-5) are not, strictly speaking, "reasons," but "problems" which must be overcome by experimental design. Problems of scale and heterogeneity can be resolved to an acceptable level of resolution without resorting to subjective judgement, which insures that the level of uncertainty has its roots exclusively in site-specific measurements. In some cases, the concerns for repository integrity due to extra boreholes could be avoided by examining adjacent or upstream locations that have properties similar to the withdrawal area.

RESPONSE 48. See Responses 35 and 36. The PA Department disagrees with the argument presented here. For example, we do not believe that "problems of scale and heterogeneity can be resolved to an acceptable level without resorting to subjective judgment." Note that the suggested extrapolation of data from "adjacent or upstream locations" requires subjective judgment.

COMMENT 49. Page (3-60), lines 17-20. Has the approach of avoiding the use of established distributions (e.g., normal, lognormal, beta) in P.A. been utilized in 1991 (Table 6.0-1, 2, 3, Volume 3 of this P.A.)? If true, then this is a significant departure from the 1990 P.A. Why was this philosophy not followed previously, and what advantage is there to such avoidance?

RESPONSE 49. Assigning "established distributions" to sparse data can result in the introduction of spurious information in the cdf. See the discussion of the Maximum Entropy Formalism by Tierney (1990).

COMMENT 50. Page (3-61) , Figure 3-17. Under the description of the figure: should the word be "quantiles" rather than "quantities"?

RESPONSE 50. Yes.

COMMENT 51. Page 3-74, Figure 3-22. What do the unit marks on the ordinate represent? Are they necessary?

RESPONSE 51. The marks are included to provide a convenient visual frame of reference for the reader. Neither a scale nor units are stated or implied.

COMMENT 52. Page (3-75), lines 25-40. The use of Eq. 3-53 as stated assumes that each input variable is linear with respect to the dependent variable which may not be the case. A multiple curvilinear or linear-curvilinear model could give a better fit to the data. Secondly, the number of variables (45) will probably exceed the utility of this type of equation when trying to distinguish the contribution of each parameter to the total regression sum of squares. Thirdly, the fit should be tested for significance using F-test criteria before any further elaboration should be attempted. Fourthly, each partial regression coefficient should be tested for significance using the t-test to determine the number of input parameters which significantly affect the regression sum of squares, and a step-wise regression approach utilized to derive the final relationship. After the final multiple regression equation is developed (assuming an acceptable multiple-R which is significant at an acceptable confidence level, and all partial regression coefficients are significantly different from zero at an acceptable confidence level), then the individual regression sum of squares for the remaining parameters can be determined (it is not necessary that the relationship of any or all the remaining input parameters be linear related to the dependent variable; there may also be cross-product effects). However, the rather large injected "subjective" variances for most of the input parameters which have been made (in combination with LHS) may not allow most of the partial regression coefficients to be significantly different from zero at an established confidence level, and the resultant total error sum of squares may be overwhelmingly large in comparison with the total regression sum of squares. Any significant relationships for particularly important input parameters such as chemical retardations may be masked by the rather large variances "subjectively" arrived at by external and internal experts. It will be surprising if more than a handful of the input parameters will significantly correlate with the dependent variable, and even then, interpretation of the results will be confounded by the subjective component. All other developments in the remaining sections of Chapter 3 (which are very concise and well written) pertaining to sensitivity and uncertainty analysis may be compromised by artificially injected variances using the subjective approach.

RESPONSE 52. These topics are discussed in detail in Chapter 3 of Volume 1 of the 1991 documentation (WIPP PA Division, 1991a, Section 3.5.2), in Helton et al. (1991), and in references cited therein. With regard to the ranges used for "particularly important input parameters such as chemical retardations," see Response 35.

Volume 1, Chapter 4 - Scenarios for Compliance Assessment

COMMENT 53. Page (4-2), lines 35-39. The statement that base-case scenario leads to zero release from the containment area is "apparently true" is made on the basis of a great deal of uncertainty in both parameter and conceptual model determinations. For instance, the effect of colloidal materials and chelation on radionuclide transport has not been addressed in P.A. to date, nor has the full interaction of gas pressurization on transport down MB139 been fully conceptualized. Statements of this type are misleading and should be avoided in P.A. unless they are fully justified.

RESPONSE 53. See Responses 4 and 9.

COMMENT 54. Page (4-7), lines 2-7. This statement should indicate that while drilling intrusions are based on four conditions, the actual sampling scheme is not a generalized process as might be implied, but is only approximated by a sampling design that contains a significant number of assumptions in the use of a Poisson distribution. The impact of this design on CCDFs, which would be obtained from a more stochastic approach, should be included in this report.

RESPONSE 54. See Response 3.3.

COMMENT 55. Page (4-13), lines 9-13. The statement on how screening decisions using qualitative judgment are made for certain events is true only if they can remain unbiased. While it is a simple thing to do in theory, it can be very difficult to do in practice, and a methodology should be developed to deal with investigator bias in making qualitative judgments. Also, the P.A. should indicate where this type of judgment has been used to separate it from those which are based on sufficiently detailed data bases. In general, EEG is not in favor of using "expert judgement" in place of data that can be obtained by laboratory and field experiments.

RESPONSE 55. The PA Department acknowledges that qualitative judgments should identified as such. A methodology has been developed for dealing with investigator bias in making qualitative judgments, and has been applied by the PA Department with panels on solubility, retardation, and the probability of human intrusion.

COMMENT 56. Page (4-14), lines 35-45. Since the predominant shrub in the immediate WIPP area is mesquite (Prosopis sp.), which is usually an invader species and is very inefficient in water utilization if supply is ample (phreatophyte), it is not clear that this species will prevail in the future. Many areas of New Mexico rangeland have been invaded by mesquite as result of overgrazing and it has been very difficult to eradicate once established. Mesquite has both a shallow diffuse root system and a much deeper taproot which "mines" water at relatively impervious interfaces such as the caliche "hardpan," which keeps it relatively dry. If the rangeland area around the WIPP has been overgrazed to the point that invader species such as mesquite have become dominant, then recovery of that rangeland in the future may eventually eradicate this phreatophyte resulting in greater soil moisture at the hardpan interface (hence, greater infiltration losses to lower strata below the rooting zone). Such recovery could occur during a wet cycle. Are there any studies indicating what the climatic climax species may have been in the past? Has overgrazing been a factor in allowing invasion by mesquite, or has this plant been endemic in the area as an arrested seral stage for a long period of time? Also, has the caliche layer in the WIPP area been breached significantly by removal for road construction, other uses, or by sinkholes and playa lakes? (see Environ. Geol. Water Sci., Vol. 19, No. 1, 21-32, 1992)

RESPONSE 56. See Response 57, Comment 91, and Response 91. The PA Department acknowledges that many unresolved questions remain about the effects of plant communities on infiltration and about the changes in plant communities over long periods of time. (See Grover and Musick, 1990, for an analysis of changes in southern New Mexico plant communities during the last century.) However, the PA Department believes it is possible to capture the effects of variations in recharge by directly varying boundary conditions on the groundwater-flow model. The caliche layer is not present in all of the area in which groundwater flow is modeled. For example, it is absent in Nash Draw. The effects of vertical leakage throughout the model domain (with and without caliche) will be considered in future PAs when a three-dimensional regional groundwater-flow model is available.

COMMENT 57. Page (4-15), lines 33-42. These statements are misleading in that the modeling of climate for P.A. in 1991 is more or less a ploy, rather than actual modeling. None of the basic features of temperature and moisture patterns are being used to model precipitation, infiltration, evapotranspiration and runoff (surface and return flow, etc.). The use of injection wells on the northern WIPP boundary to represent climate is hardly representative of near field effects, particularly those which might be

interactive with land subsidence. The limitations of the current climate modeling should be presented clearly and concisely in this section, particularly because the base case scenario was not analyzed in the 1991 P.A.

RESPONSE 57. As the documentation clearly indicates, WIPP PA does not contain direct modeling of climate change, but instead approximates possible effects of climate change by varying boundary conditions on the regional groundwater-flow model (see, for example, p. 5-23, lines 5-21 and p. 5-37, line 35 through p. 5-38, line 34 of Volume 1 of the 1991 documentation [WIPP PA Division, 1991a]). See Comment 91 and Response 91 for additional information.

COMMENT 58. Page (4-21), lines 7-9. This section should also describe the 4.8 magnitude earthquake of 1/2/92.

RESPONSE 58. This event occurred after the document was printed.

As a general response that will be referenced below in response to other comments on the screening of events and processes, the PA Department acknowledges that screening of events and processes must be updated iteratively to reflect concerns of reviewers and new information. This portion of the PA has not been updated for 1992 because of limited resources. The PA Department encourages constructive comments on the screening of events and processes and will respond in future PAs.

COMMENT 59. Page (4-25), lines 22-26. The Snyder and Gard (1982) hypothesis of breccia chimney formation was effectively countered by another conceptual model involving dissolution of the Salado salt (Peter Davies, Ph.D. thesis, pp. 104-108 and Proc. Int. Symp. on Salt, May 24-28, 1983, vol. 1, pp. 331-350, publ. 1985). After drilling of DOE-2, EEG accepted the lack of threat to the WIPP site from deep dissolution within the Salado. The discussion should nevertheless include Davies' hypothesis.

RESPONSE 59. See Response 58. The comment will be addressed when event and process screening is updated.

COMMENT 60. Page (4-26), lines 11-14. Dewey Lake Redbeds hydrology has never been properly studied in spite of repeated suggestions by EEG and other review groups that it should be. Dewey Lake Redbeds do not have "low water content." James Ranch wells are completed in this Formation.

RESPONSE 60. See Response 58. The PA Department is aware of the livestock wells producing from the Dewey Lake Red Beds. Text will be revised when event and process screening is updated.

COMMENT 61. Page (4-26), lines 14-29. Recharge and infiltration of water at and in the vicinity of the WIPP site has never been properly studied in spite of repeated suggestions by EEG and other review groups to do so. Because of the lack of information in this area, EEG cannot accept assertions of low consequence of water infiltration now or in the future. This process should not be eliminated from the P.A. process.

RESPONSE 61. See Responses 56 and 58. Text will be revised when event and process screening is updated.

COMMENT 62. Page (4-26), lines 44-45. The statement, "brine concentration generally becomes greater to the southwest" of the WIPP site, is wrong. The Culebra water at H-7 has 3,200 mg/l TDS. The reason for the Culebra water being much fresher (very low TDS) south and southwest of the WIPP site has never been adequately explained.

RESPONSE 62. The EEG's observations about chemistry of the Culebra water are correct. The text in question, however, refers to water in the contact zone between the Salado and Rustler Formations.

COMMENT 63. Page (4-27), lines 8-11. DOE has not physically investigated the nature of the Mescalero Caliche layer at and in the vicinity of the WIPP site, although the argument of this layer acting as a barrier to water infiltration has often been advanced. A private citizen, Richard Hayes Phillips, dug trenches to the Caliche layer near the WIPP site in 1986. These trenches clearly demonstrated that the caliche layer has many gaps through which water can infiltrate. DOE has photographs and videorecordings of these trenches.

RESPONSE 63. See Response 58. The PA Department is aware of Phillips' work. Text will be revised when event and process screening is updated.

COMMENT 64. Page (4-27), lines 12-13. It is not correct to say that the anhydrite layers in the Rustler Formation tend to be unfractured. WIPP shafts have demonstrated the existence of many open fractures in all the zones of the Rustler Formation. See, for example, Plate 1 (p. 80) in EEG-32.

RESPONSE 64. See Response 58. The PA Department is aware of the referenced work. Text will be revised when event and process screening is updated.

COMMENT 65. Page (4-27), lines 36-40. What is the basis for the statement, "the dissolution that formed Nash Draw was a relatively short-lived process that is not continuing at present"? Every other document on the subject concludes that the process is continuing. One can witness the "solution and fill" process, first described by Lee (USGS Bull. 760-D, 1925) and accepted by George Bachman, at 50 sinkholes in the Nash Draw.

RESPONSE 65. See Response 58. The PA Department is aware of the referenced work. Text will be revised when event and process screening is updated. Note, however, that the text discusses an alternative hypothesis for the cause of the large-scale dissolution that created the Draw, and was not intended to deny ongoing local dissolution.

COMMENT 66. Page (4-28), lines 21-34. The conclusion of this summary, that the Nash Draw type dissolution most likely will not reach the WIPP repository in 10,000 years, is acceptable, but the preceding discussion that leads to this conclusion has many inaccuracies and new hypotheses that have never been discussed in the scientific community or the scientific literature.

RESPONSE 66. See Response 58. Text will be revised when event and process screening is updated.

COMMENT 67. Page (4-33), lines 24-31. Was the panel of experts told that EPA's "30 boreholes/km^2 in 10,000 years" number is based on the drilling frequency in the WIPP site area?

RESPONSE 67. The panel was not provided this information in formal documentation. The PA Department agrees that the EPA's upper bound is comparable to past drilling frequency in the Delaware Basin. The panel was provided extensive information about past drilling in the WIPP vicinity, and was encouraged to come to its own conclusions about the relevance of this information to future drilling frequency. They were informed as to the

guidance provided by the Standard, but they were asked not to limit their considerations to regulatory issues. For example, they considered modes of intrusion other than exploratory drilling for natural resources. See Hora et al. (1991) and Guzowski and Gruebel (1991) for additional information.

COMMENT 68. Page (4-38), lines 12-15. Since the total dissolved solids (TDS) in water from the H-2 wells is so close to 10,000 mg/l, it cannot be concluded that the Culebra water at the WIPP site is all greater than 10,000 mg/l.

RESPONSE 68. See Response 58. The text will be revised when event and process screening is updated. Note, however, that no claim is made that all Culebra water at the site has a TDS content greater than 10,000 mg/ℓ. Rather, the argument is made that Culebra water within 5 km of the waste panels is not potable. The PA Department believes this to be a reasonable assertion. Reference in the paragraph in question to the definition in 40 CFR 191B of "significant source of groundwater" is misleading, and will be corrected. See Section 2.3 of Volume 1 of the 1991 documentation (WIPP PA Division, 1991a) for a discussion of "significant source of groundwater."

COMMENT 69. Page (4-40), lines 38-43. The statement regarding appropriation of available water supplies to areas with better soils than present at WIPP is dependent on the current climate and the potential water storage capacity of the region. Incorporation of higher rainfall (and distribution pattern conducive to greater storage capacity) may indeed make it economically possible to convert the area surrounding WIPP toward agricultural pursuits. While it may be possible to exclude irrigation as a process in scenario development for other reasons, the argument presented here is not very convincing. A factor of two increase in precipitation may transform the region into a potential "dry-farming" region requiring irrigation only as a supplement during periods of soil moisture deficits. This argument was presented in the 1990 P.A.

RESPONSE 69. See Response 58. Irrigation will be reexamined when event and process screening is updated.

COMMENT 70. Page (4-42), lines 8-40. These statements ignore the probable doubling of precipitation in the study area and the consequent increase of water storage capacity of the region. The requirement of a sufficiently large source of water (line 32) to replace leakage and evaporation losses may be accounted for by the increased amount of rainfall in the form of increased

soil moisture and available surface water for agricultural purposes. Why is it unrealistic to consider the use of the Ogallala aquifer northeast of WIPP for agricultural purposes in the area? There is a potential for recharging the aquifer by either natural or man-made activities. Also, is it not conceivable that "pan-evaporation" could be reduced in the future by the use of chemical surface coating of reservoir surfaces if necessary? Potential and actual evaporation and/or evapotranspiration from soil surfaces and consequent natural biomass density increases also need to be discussed from the viewpoint of increased precipitation projected for the study area. The arguments presented in this section are not very convincing because of the omission of potential precipitation increases.

RESPONSE 70. See Response 58. Text will be revised when event and process screening is updated.

COMMENT 71. Pages (4-48,49) lines 33-43-3. There appear to be good reasons why a local "rapid" removal of salt to excavate the WIPP repository may have a possibly significant effect on the overlying units. Effects of salt removal have occurred over a long period of time, and are both a local and a far-field phenomenon. Self-healing could have occurred to further mitigate the response. The response may be more similar to subsidence that has occurred in the area as a result of potash removal, than to long term events. Why was such a comparison and analysis omitted? However, if one is going to be concerned about subsidence due to WIPP excavations, then that due to solution mining of potash in the McNutt zone above the repository should also be considered even though it is not required by the Standard. The conclusions presented in this section do not do justice to the excellent analysis of "subsidence and cavings" presented in previous statements of this section and use a bad example for comparison.

RESPONSE 71. See Response 58. Text will be revised when event and process screening is updated.

COMMENT 72. Page (4-50), lines 15-16. The WIPP waste is not "low level," and there will be some thermal loading by the RH-TRU waste.

RESPONSE 72. See Response 58. The error is noted and will be corrected when event and process screening is updated.

COMMENT 73. Page (4-51, 52), lines 17-45, 1-3. This section on gas generation should state that the PA so far has not considered the structural

effects of gas generation, but has limited the consideration to reducing the amount of brine that will flow into the rooms and drifts. The effect of this limited consideration has generally been beneficial for PA demonstration in that the releases with gas generation are less than without.

RESPONSE 73. See Responses 12.3 and 17 for a discussion of the distinction between modeling assumptions and and model outcomes.

It is correct that the 1991 (and 1992) PA did not include conceptual or computational models for possible pressure-dependent fracturing of anhydrite marker beds. This process will be included in PA when conceptual and computational models are available.

The purpose of the discussion here is to determine whether or not an event or process should be included in the development of scenarios for analysis. As such, the discussion need not and should not include a discussion of modeling capability. The PA Department does not screen events or processes on the basis of modeling capability.

COMMENT 74. Pages (4-54), lines 29-31. In lines (14-16) of this section climatic change is recognized as part of the base-case scenario. In the lines commented on it appears that the effect of increased precipitation and possibly changed precipitation throughout the year are not taken into consideration in arriving at conclusions about irrigation and damming considerations. This has occurred in several other sections of this report. Why? Also, Table 4-2 (Page 4-56) indicates that these processes have been screened out because of low probability of occurrence or low consequence. Yet it appears that inclusion of a wetter period has not been considered in arriving at these conclusions. If climate change has been considered in these deliberations, then it should be documented in this report at all locations where these events or processes are discussed.

RESPONSE 74. See Response 58. The text will be revised when event and process screening is updated.

COMMENT 75. Page (4-58), lines 14-17. What is the basis for the statement that subsidence caused by mine openings and explosions caused by waste degradation have no effect on the performance of the disposal system? If this conclusion(s) has been documented elsewhere, then it should be referenced.

RESPONSE 75. See Response 58. The text will be revised when event and process screening is updated.

COMMENT 76. Page (4-66), lines 1-7. It is stated that gas will flow through the upper portions of the drifts and the anhydrite layers A and B and saturate the shaft seals, thereby inhibiting brine migration up the shaft to the Culebra Dolomite. This conclusion must be based on modeling efforts; however, has the large areal expanse of anhydrite layers A and B been taken into consideration in arriving at this conclusion? What was the extent of horizontal gas transport, and what effect does it have on the saturation rate and time of transit to the shaft seals?

RESPONSE 76. Additional analysis relevant to this comment is provided in WIPP PA Department (1992). As the comment correctly notes, the conclusion is model-based, and is therefore not an essential part of the scenario definition. The text has been revised.

COMMENT 77. Page (4-67), lines 11-14. The statement that no radionuclides are released to the Culebra in 1000 years under undisturbed conditions is based on current P.A. modeling efforts. It should be qualified to reflect these uncertainties, and that it is based on current modeling strategies which are not exhaustive.

RESPONSE 77. See Responses 4 and 12.

COMMENT 78. Pages (4-63-73), lines 17 through line 33 on page-4-73. The discussion of the base-case, E2, E1, and E1E2 scenarios is very well written and comprehensive with respect to the current modeling strategies. However, none of the scenarios indicate a flow down MB139 to the accessible environment. In view of the gas pressurization effects which makes this pathway more important, it should be included in this and future modeling strategies.

RESPONSE 78. This pathway is discussed in the cited pages (p 4-66, lines 10-20, WIPP PA Division, 1991a). Simulations of flow along this pathway are referenced in these lines and described in detail in Volume 2 of the 1991 documentation (WIPP PA Division, 1991c, Section 4.2.3.3, p. 4-46/81). Additional analyses have been performed since this review was completed (WIPP PA Department, 1992).

Volume 4 Comments

This uncertainty and sensitivity analysis is very important to the performance assessment effort because it indicates the relative importance of certain model and parameter value assumptions to the outcome. The results are valuable guidance to laboratory and field studies that need to be performed, to reevaluations of conceptual models, and to calculations that should be performed in subsequent iterations of the Performance Assessment.

EEG has reviewed this volume and page by page comments are included. We also respond to each item under the headings insights, possibilities for additional investigations, and possible improvements to the 1992 performance assessments in Chapter 6.

COMMENT 79. A generic comment is that EEG believes these types of analyses should also be applied to the undisturbed performance of the repository. The analysis in Chapter 4 of Volume 2 considers only best-estimate conceptual model conditions. We believe (see our comments elsewhere) that models involving no gas generation and fully saturated storage rooms also need to be considered.

RESPONSE 79. The PA Department agrees that uncertainty analyses should include undisturbed performance. The first such analyses are now complete (WIPP PA Department, 1992). Simulations of disturbed performance without gas generation were included in the 1991 PA to provide a useful comparison to the single-phase results presented in previous years. The PA Department does not plan, however, to continue simulations without gas generation. No conceptual model has been proposed to suggest that degrading waste will not generate gas. See comment 3 for a discussion of realism in PA. Note that brine saturation in the waste panels is calculated by the two-phase flow model. See Responses 12.3 and 17.

Volume 4, Chapter 2 - Structure of WIPP Performance Assessment

COMMENT 80. Page (2-15), line 12. The accessible environment is assumed to begin 5 km from the waste panels. The present definition of the accessible environment in 40 CFR 191 is the site boundary, which is less than 3 km from some portions of the waste panels. The four volumes are misleading about using the 5-km distance for the accessible environment. The titles of Tables B-4 and B-5 in Volume 2 refer to the Accessible Environment without qualification. A reviewer is required to search through these 4 inches of reports to find out what has been done. Page 6-53 of Volume 2 implies that

computations have been made at 3 km. Why weren't the results at 3 km used in Tables B-4 and B-5 and in the Summary CDF? Are the results at 3 km presented anywhere in the 4 volumes?

This is an important issue. The values are probably somewhat greater at the site boundary.

RESPONSE 80. See Response 3.1. Subsurface releases are calculated at the land withdrawal boundary in the 1992 PA, 2.4 km south of the panels.

COMMENT 81. Page (2-16), lines 21-26. Assumptions (2) [E1E2 holes happen in the same time interval] and (3) [more than 2 holes in E1E2 scenario are the same as 2 holes] are not conservative, and without calculations, it is uncertain whether this non-conservatism is significant.

RESPONSE 81. See Response 3 on the question of realism versus conservatism. See Response 44 for observations on the assumptions used in the E1E2 scenario. Note that more than two holes in an E1E2 scenario are the same as two holes only for subsurface releases. Cuttings from multiple hits are included.

COMMENT 82. Page (2-20). As mentioned under the cuttings topic, we believe the activity levels are reasonable and probably slightly conservative. However, the activity Level 4 values could not be obtained for WIPP wastes after 3,000 years if the initial criticality requirements were met.

RESPONSE 82. See Response 15.

COMMENT 83. Pages (3-8) and (3-9). The six cases chosen represent a wide range of cases that could affect uncertainty, and it is appropriate to examine them as has been done in this report. However, it is noted that two cases which probably are more severe than these six have been excluded. These are: (a) gas generation, single porosity, no retardation; and (b) no gas generation, single porosity, no retardation. We recommend that these two cases be examined in the 1992 comparison.

RESPONSE 83. Case (a) is included in the 1992 PA. Case (b) is not: no conceptual model has been proposed in which degrading waste does not generate gas. See Response 79.

COMMENT 84. Pages (4-1,2). Figure 2.1-2 is incorrectly referred to as 2.1-1 on several occasions in these two pages.

RESPONSE 84. The error has been noted.

COMMENT 85. Page (4-10). The importance of uranium radionuclides in groundwater transport is not surprising to EEG. In EEG-9 (September 1981), we concluded that uranium-233 would be the most important radionuclide from the well water pathway.

RESPONSE 85. Results are preliminary, and may be sensitive to distributions used for solubility and retardation that were based on expert panel judgment.

COMMENT 86. Page (4-11). The caption to Figure 4.4-1 should indicate whether the accessible environment is at the site boundary or at 5 km.

RESPONSE 86. See Response 3.1. The omission has been noted.

COMMENT 87. Page (4-17). The ranges of total brine flow into the Culebra Dolomite shown in Figure 4.4-8 appear reasonable. The extensive testing of the WIPP-12 brine reservoir in 1981 and 1982 led to a prediction that WIPP-12 would produce (through an open borehole) 382,000 m^3 at the repository level, 126,000 m^3 at the Culebra, and 56,000 m^3 at the surface.

RESPONSE 87. Data from WIPP 12 was used to construct the PA brine-reservoir model (see Section 4.3 of Volume 3 of the 1991 documentation, WIPP PA Division, 1991c).

COMMENT 88. Page (4-38), Figure 4.5-9. The CCDF plotted on this figure indicates that the mean of releases into the Culebra exceeds the Standard at that location. This figure illustrates clearly why EEG believes it to be very important that brine-flows to the surface from an E1E2 scenario need to be modeled. The WIPP-12 brine reservoir had pressure and compressibility characteristics that would produce (through an open borehole) a flow at the surface that was about 0.45 of that at the Culebra.

RESPONSE 88. See Response 3.4. Note, however, that brine flowing at the surface from a single borehole (as at WIPP 12) will not have circulated through the waste, and will not have the same radionuclide content estimated

for the brine entering the Culebra for the E1E2 scenario. The comparison is inappropriate.

COMMENT 89. Page (4-38), Line 22. Is it appropriate to call a release that exceeds the standard at a point as "already a small release"?

RESPONSE 89. No.

COMMENT 90. Page (5-37), lines 2,3. The mean value of the single porosity, no gas CCDF is about 2.5 times the mean value for single porosity with gas. This difference may not be negligible as the curves approach the Standard limit.

RESPONSE 90. See Responses 79 and 83 with regard to the no-gas-generation case.

COMMENT 91. Page (5-56), lines 38-40. Modeling the effects of enhanced recharge, rather than predicting climate change per se, appears to be a reasonable approach. Also, the use of the ground surface at the recharge area as the boundary head (Page 5-57, lines 15-19) is a good way to address bounding conditions.

RESPONSE 91. The PA Department agrees with the comment. See Comments 56 and 57. The 1992 approach is similar to that used in 1991. Future PAs will continue to use variable boundary conditions to approximate effects of enhanced recharge related to climatic change.

COMMENT 92. Page (5-60), lines 20-22 and 29-30. The explanation of why maximum recharge has minimum impact on releases to the accessible environment in 10,000 years for single porosity flow appears plausible for scenarios that occur at 1,000 years. However, isn't it likely there will be greater releases from maximum recharge for scenarios that occur later?

RESPONSE 92. Yes. Simulations were restricted to the first time interval by resource limitations. Note, however, that regardless of climate change releases from late-time intrusions will not exceed those from the 1000-yr intrusion.

COMMENT 93. Page (6-3), lines 8-32. This is a well-written paragraph that clearly points out the importance of solubility and distribution coefficient

values for americium, plutonium, and uranium. An important uncertainty that is not addressed in Volume 4 is changes in the number of curies and the radionuclide distribution in the inventory. Such changes could significantly change the number of waste units and drastically change the fraction of the inventory that reaches the accessible environment.

An example of the effect of plausible inventory changes is the following: (1) the Uranium-233 inventory is 7800 Ci (the best estimate prior to your current assumptions); and (2) the quantity of Plutonium-238 coming from the Savannah River Site is reduced by 7 million curies. A drastic reduction in the Plutonium-238 inventory is possible for several reasons: (a) the existing inventory (end of 1990) is only 666,000 alpha curies; (b) there has been consideration of not bringing some of the high-curie Plutonium-238 wastes to WIPP because of shipping problems; and (c) there has been talk of obtaining future Plutonium-238 requirements from Russia or elsewhere. With these inventory changes, the number of waste units drops to 4.87 and the quantity of Uranium-234 produced from Plutonium-238 decay is reduced from 3315 Ci to 809 Ci. However, with the increase in Uranium-233, the integrated discharge for vector 9 in Table B-5 (volume 2) increases from 0.14 to 0.49 at 5 km. The curies of cuttings brought to the surface would remain about the same, and hence their fraction of the integrated discharge would also increase.

The variability in inventory needs to be treated as an important uncertainty that has to be determined as accurately as possible and upgraded constantly throughout the Performance Assessment.

RESPONSE 93. See Response 13. Radionuclide inventories for PA will continue to be based on the IDB unless or until an alternative approach is identified.

COMMENT 94. Page (6-14). We have the following comments on the "insights (that) have emerged from these analyses."

1) The drilling rate constant is certainly very important. The expert review process is one way of trying to better predict the future. However, EEG is not completely comfortable with this approach and is not convinced that this is the appropriate way to interpret EPA Guidance. It appears this approach is an attempt to avoid treating the WIPP site as a mineral rich area with underlying brine reservoirs.

2) EEG agrees that the interplay between Salado permeability and gas generation is very important and supports the research programs that are underway.

3) Elemental solubilities are very important. The laboratory work underway is already yielding useful preliminary work. Both laboratory and drum-size solubility tests need to be pursued vigorously.

4) Distribution coefficients are very important and the best way to obtain defensible numbers is with the planned experiments in the laboratory with Culebra cores. An appropriate sorbing tracer field study may also provide useful confirmatory information and should be conducted.

5) A better determination of whether single or dual-porosity is the appropriate transport model in the Culebra is definitely needed. A field tracer test, such as the one recently proposed by SNL, needs to be pursued.

6) EEG believes that the transmissivity fields study for the Culebra is important and should be continued.

RESPONSE 94. With regard to point 1), see Response 3.2 and 67. With regard to points 2) through 6), the PA Department notes that the recognition of the importance of these studies demonstrates the usefulness of preliminary PAs using available data, realistic models, and subjective judgment. See, for example, Responses 3, 4, 6, 9, 12.5, 35, and 36

COMMENT 95. Pages (6-17). Three possibilities for additional investigations are mentioned. Our views on these investigations follow.

1) The 1991 Preliminary Comparison has concluded that cuttings removal is the major component of the likely release to the accessible environment. Therefore, processes that could affect these releases do need to be considered in more detail. During their original scoping studies in 1987-88, SNL used an assumption that in an unconsolidated room the waste in containers would also be unconsolidated and an intrusion borehole would bring all the contents of an intercepted container to the surface. This seems to be a reasonable assumption for those cases where gas generation has prevented room closure and it should be reevaluated.

2) Borehole permeability is indeed an important parameter that needs to be better understood. EEG has taken the position that the Guidance in 40 CFR 191 ("... with a permeability typical of a borehole filled by soil or gravel that would normally settle into an open hole over time ... not the permeability of a carefully sealed borehole") is reasonable and not conservative since recent experience indicates that in practice many inactive boreholes have not been sealed as required by regulations. Therefore, we believe your evaluations should address the permeability of boreholes being filled over time by soil or gravel, and not engineered seals.

3) EEG's views on the manner of addressing pressurized brine pockets in the Castile Formation are discussed elsewhere in the comments.

RESPONSE 95. The points are addressed individually.

95.1 The PA model for borehole erosion results in a borehole diameter greater than the 0.6-m diameter of a 55-gallon drum (see p. 7-16 of Volume 2 of the 1991 documentation (WIPP PA Division, 1991b)).

95.2 Engineered seals are not assumed in boreholes, except as necessary to maximize brine flow into the Culebra for the E1, E2, and E1E2 scenarios (see Response 44). The PA Department has otherwise implemented EPA guidance on borehole permeability consistently since 1989 (Marietta et al., 1989, p. III-53; Rechard et al., 1990, p. IV-7/8; WIPP PA Division, 1991a, p. 6-10, line 55-56; WIPP PA Division 1991c, Section 4.2). Borehole permeability is assumed to be similar to that reported by Freeze and Cherry (1979, p. 29) for silty sand.

95.3 See Response 24.

COMMENT 96. Page (6-18). Possible improvements to the 1992 Performance Assessment are identified. Our views on these follow.

1) Drilling intrusions at times earlier than 1000 years should definitely be considered, as was done in 1990.

2) More thought should be given to how clusters of high activity containers might be located in repository storage rooms. In 1988, EEG evaluated the effects of drilling into an average stack of drums from SRP and LANL because of the reasonable assumption they would arrive in a TRUPACT trailer load and be stacked together.

(Waste Management '88, pp 355-364; also reprinted in EEG-42, Appendix B). Other schemes could also be developed.

3) E2-type scenarios should be considered separately.

4) Direct release of brine to the surface should definitely be modeled. This scenario is perhaps the most critical, is plausible, and has been urged by EEG for years. Note our statements elsewhere in these comments.

5) We agree that E1E2 probability estimates should be improved. The inclusion of this scenario when the second borehole falls in a later time period should be considered. Also, the assumption that panel seal plugs will be effective enough to preclude an E1E2 scenario from developing from boreholes in adjacent panels should be reevaluated.

RESPONSE 96. Points are addressed individually.

96.1 See Response 3.2

96.2 The method used in the 1991 PA (see Section 2.4 of Volume 4 of the 1991 documentation, Helton et al., 1992) assumes some "clustering" of waste--all waste intercepted by a single borehole is assumed to be of a single activity level. This would be unlikely if waste were randomly distributed in the panels.

96.3 E2 scenarios will be modeled separately from E1 when resources permit. Note the discussion in Volume 2 of the 1991 PA (WIPP PA Division, 1991b, section 5.2.5.1, p. 5-25/27) comparing flows from E1, E2, and E1E2-type intrusions.

96.4 See Responses 3.4, 88.

96.5 See Responses 44 and 81.

V. EEG Reply to SNL Responses to EEG's Comments on 1990 Preliminary Comparison

SNL's responses to EEG's comments on the 1990 Preliminary Comparison (SAND 90 - 2347) are included in Appendix B (pages 5 to 43) of Volume 1 of SAND 91-0893. The following reply addresses only those comments that were not satisfactorily answered in the SNL Response or in SAND 91-0893 or those that are still not being addressed in a satisfactory manner. Also, some of the responses are discussed elsewhere in our comments.

COMMENT 5. The question on the use of the 1987 IDB was answered satisfactorily. However, we emphasize that the inventory needs to be as accurate and detailed as possible and constantly updated.

RESPONSE. See Response 13 above to the comments on the 1991 documentation.

COMMENT 8. The section 2.1.6 in SAND 91-0893 (Modifying the Requirements) adds the sentence: "An impact study was recently initiated for TRU-waste repositories, but findings are not yet available." We are very interested in obtaining details of this study as soon as possible. Is this a study related to the TRU waste unit that is attempting to develop a rationale for justifying less stringent containment requirements for WIPP than for a commercial HLW repository?

RESPONSE. The 1985 version of 40 CFR 191 contains a risk/benefit criterion for high-level waste (HLW) and spent fuel (SF). However, there are no such criteria for TRU-waste disposal, and no safety requirements were established that apply to TRU waste. Several recent studies (Klett, 1991; Numark and Phelps, 1992; Klett and Gruebel, 1992) and presentations by J. K. Channell of the EEG and others in late 1991 and early 1992 at the Electric Power Research Institute conferences on the technical basis for EPA HLW disposal criteria have offered approaches to developing criteria for TRU-waste disposal that are different from those in the current version of 40 CFR 191. None, however, have advanced a definitive method of developing a risk/benefit criterion for TRU waste.

COMMENT 19a. Approximately 8 pages are devoted to answering our question about the existence of a disturbed area in MB-139 horizontally from excavated waste storage rooms. A good argument is made for the position that the drop off in permeability is very rapid at the Far Field/Disturbed Rock Zone Interface. Apparently (from line 14 of page B-19), this boundary is assumed

to be no farther than the horizontal limits of the excavation. This far field is then taken to have a permeability of 2.87 E-20 m^2 (Table 1, page B-23). This description is not consistent with material presented elsewhere in SAND 91-0893. For example, data plotted on page 2-59 of Volume 3 shows anhydrite permeabilities of 1.0E-18 m^2 at 7.3 m and about 8E-20 m^2 at 10 m and 12.6 m. Also, the statement on page 5-41 of Volume 1 says that the ultimate extent of the DRZ is unknown. Furthermore, on page 4-46 (line 29) of Volume 2 it is stated that brine in the repository will flow in all directions. One would expect movement in all directions if MB-139 is effectively sealed beneath the panel seals and the brine movement from the repository rooms to the shafts (that was modeled for undisturbed performance) was blocked.

EEG still has a concern that contaminated brine could be present in a disturbed zone of MB-139 that extends several meters horizontally from the excavated rooms. This contaminated brine would be brought to the surface with drilling fluid if intercepted by a borehole. Also, depending on the permeability at the point of intrusion, a greater volume of contaminated MB-139 brine could be involved in an E1 or E1E2 scenario event.

RESPONSE. Additional analyses of brine migration from the undisturbed repository are presented in WIPP PA Department (1992). Uncertainty and sensitivity analyses of undisturbed performance will continue to examine the extent of brine migration into the anhydrite marker beds.

The PA Department notes that although the area in which intrusions may intersect radionuclides increases as contaminated brine migrates laterally, the rate at which radionuclides may flow into the hole will be substantially less away from the excavated area in which the waste was originally emplaced. The probability of intrusion will increase if "near misses" are included. Probability of "direct hits" will be unchanged, however, and consequences of "near misses" will be less than the consequences of direct hits already considered in PA.

COMMENT 19b. Merely specifying permeabilities in an engineering design does not prove they will be achieved over periods of thousands of years. Hopefully, the seal test program will provide "justification" of the claimed permeabilities. We have found considerable discussion of borehole permeability effects in Volume 4, but have not found a discussion of shaft seal requirements.

RESPONSE. Uncertainty and sensitivity analyses of undisturbed performance now provide preliminary guidance on seal permeabilities (WIPP PA Department, 1992). Additional guidance will be provided from future such analyses.

COMMENTS 19c and 19d. The issues of climatic change and vertical recharge into the Culebra are recognized by SNL and are still being investigated. We have no further comment at this time.

RESPONSE. Work continues on regional geohydrology.

COMMENT 19e. The response to our comment about uncertainty in the source term is satisfactory for now. However, sometime between now and your final P.A. report, it will be necessary to calculate CCDFs over the possible range of the radionuclide composition in the inventory.

RESPONSE. See Response 13 above to the comments on the 1991 documentation.

COMMENT 19, Brine Slurry Filled Room. The response to this comment (p. 13-36) gives credit to "EEG and others" for raising this issue. Actually the issue was raised by the SNL Performance Assessment Group in a memo titled "Early P.A. Scoping Calculations..." dated April 7, 1987. EEG was presented these calculations in June, 1987 as a serious matter and a presentation was made by SNL to the NAS WIPP Panel on September 22, 1987 in Idaho. The expression "brine-slurry filled room" was first used in the above-referenced memo and in the presentations.

EEG is not persuaded that the existence of a brine slurry filled room can be ignored. In fact, your statement on page B-37, line 1, says that in "the vast majority of simulations.....there is insufficient brine entering the room to fill the pores...." Since 40 CFR 191 is concerned with low probability events, the cases where this could occur need to be considered. The brine could also come from the Castile brine reservoir intercepted in the E1 Scenario. Since the expected condition of the undisturbed repository (Chapter 4, Volume 2) would appear to result in an unconsolidated waste form, we are pleased to see that you are studying waste removal with both consolidated and unconsolidated wastes.

RESPONSE. See the Responses 4 and 12.3 above to the comments on the 1991 documentation. Brine saturations within the waste panels are not assumed, they are calculated based on available realistic models and parameter distributions. The PA Department does not make *a priori* assumptions about

the probability of model outcomes. Present modeling does not indicate that the volume of brine in the panels will be sufficient to create a slurry (WIPP PA Department, 1992). Uncertainty and sensitivity analyses will continue to examine brine saturation within the waste.

COMMENT 19, Radionuclide Quantities in Drill Cuttings. You have not responded to our comments on this issue. However, it is noted that the 1991 comparison uses (in Chapter 2 of Volume 2) an average concentration determined by sampling on four activity levels. We will not comment in detail on this methodology at this time except to note that somewhat different results would probably be obtained if random sampling had been conducted on each vector. Also, the fact that much greater quantities of radionuclides could be brought to the surface during the first few hundred years is obscured by arbitrarily having the first borehole occur at 1,000 years.

RESPONSE. See Response 3.2 above to the comments on the 1991 documentation.

COMMENT 19, Contaminated Brine Flows to the Surface. This issue has been discussed with SNL and others for several years. SNL has not denied that there is a need to model this scenario but have not done so, have not explained the reason for the delay, nor given a schedule for when modeling will be done.

EEG believes this scenario may be the most critical one for the PA and that it should be modeled in the 1992 Preliminary Comparison. We do not understand why its modeling is being delayed.

Our arguments for including this scenario have been included in our 1991 comments on SAND 90-2347 and elsewhere and will not be repeated here. We do have two comments on your response: (1) The effect that the "relatively low permeability waste and backfill" will have on the flow of brine at the surface will be uncertain until it is modeled quantitatively. Also, the permeability of a brine-filled room that was unconsolidated at the time of flooding may not be too low; and (2) the statement is made that "unrestricted artesian flow from a Castile brine pocket would normally not be permitted." EEG has presented the only data we were aware of about drilling practices in the Delaware Basin and these data indicate that varying amounts of flow are invariably allowed. We would appreciate receiving any additional data available.

RESPONSE. See Responses 3.4 and 88 above to the comments on the 1991 documentation.

COMMENT 20. The PA team's plans "to examine the effects of varying recharge directly, with uncertainty in the recharge factor..." appears reasonable. There is no need to get bogged down in modeling specific causes of recharge as long as a conservatively chosen range of value is examined.

RESPONSE. See Comments and Responses 56, 57, and 91 above in the discussion of the 1991 documentation.

COMMENT 22. SNL is addressing the issue of retardation factors experimentally at this time. We will follow work on this very important issue closely. SNL does not need to continue to use expert-judgement-provided numbers for retardation "in order to provide guidance to the data-acquisition work." The sensitivity of this parameter has been established by the PA work performed to-date and the importance of experimentally establishing the ranges of K_d and retardation factors for various radionuclides has been well recognized. What more guidance is needed?

RESPONSE. See Responses 3 and 3.5 above to the comments on the 1991 documentation.

COMMENT 23. We are pleased to see continued work in the geostatistics area.

RESPONSE. Initial results from the geostatistics program are incorporated in the 1992 PA. Work continues in this area.

References for Appendix B

Beauheim, R.L. 1987a. *Analysis of Pumping Tests of the Culebra Dolomite Conducted at the H-3 Hydropad at the Waste Isolation Pilot Plant (WIPP) Site*. SAND86-2311. Albuquerque, NM: Sandia National Laboratories.

Beauheim, R.L. 1987b. *Interpretation of the WIPP-13 Multipad Pumping Test of the Culebra Dolomite at the Waste Isolation Pilot Plant (WIPP) Site*. SAND87-2456. Albuquerque, NM: Sandia National Laboratories.

Beauheim, R.L. 1989. *Interpretation of H-11b4 Hydraulic Tests and the H-11 Multipad Pumping Test of the Culebra Dolomite at the Waste Isolation Pilot Plant (WIPP) Site*. SAND89-0536. Albuquerque, NM: Sandia National Laboratories.

Beauheim. R.L., and P.B. Davies. 1992. "Experimental Plan for Tracer Testing in the Culebra Dolomite at the WIPP Site." Revision A. Albuquerque, NM: Sandia National Laboratories.

Bertram-Howery, S.G., M.G. Marietta, R.P. Rechard, P.N. Swift, D.R. Anderson, B.L. Baker, J.E. Bean, Jr., W. Beyeler, K.F. Brinster, R.V. Guzowski, J.C. Helton, R.D. McCurley, D.K. Rudeen, J.D. Schreiber, and P. Vaughn. 1990. *Preliminary Comparison with 40 CFR Part 191, Subpart B for the Waste Isolation Pilot Plant, December, 1990*. SAND90-2347. Albuquerque, NM: Sandia National Laboratories.

Freeze, R.A., and J.A. Cherry. 1979. *Groundwater*. Englewood Cliffs, NJ: Prentice-Hall, Inc.

Grover, H.D., and H.B. Musick. 1990. "Shrubland Encroachment in Southern New Mexico, U.S.A.: An Analysis of Desertification Processes in the American Southwest," *Climatic Change*. Vol. 17, no. 2-3, 305-330.

Guzowski, R.V., and M.M. Gruebel, eds. 1991. *Background Information Presented to the Expert Panel on Inadvertent Human Intrusion into the Waste Isolation Pilot Plant*. SAND91-0928. Albuquerque, NM: Sandia National Laboratories.

Helton, J.C., J.W. Garner, R.D. McCurley, and D.K. Rudeen. 1991. *Sensitivity Analysis Techniques and Results for Performance Assessment at the Waste Isolation Pilot Plant*. SAND90-7103. Albuquerque, NM: Sandia National Laboratories.

Helton, J.C., J.W. Garner, R.P. Rechard, D.K. Rudeen, and P.N. Swift. 1992. *Preliminary Comparison with 40 CFR Part 191, Subpart B for the Waste Isolation Pilot Plant, December 1991. Volume 4: Uncertainty and Sensitivity Analysis Results*. SAND91-0893/4. Albuquerque, NM: Sandia National Laboratories.

Hora, S.C., D. von Winterfeldt, and K.M. Trauth. 1991. *Expert Judgment on Inadvertent Human Intrusion into the Waste Isolation Pilot Plant.* SAND90-3063. Albuquerque, NM: Sandia National Laboratories.

Jones, T.L., V.A. Kelley, J.F. Pickens, D.T. Upton, R.L. Beauheim, and P.B. Davies. 1992. *Integration of Interpretation Results of Tracer Tests Performed in the Culebra Dolomite at the Waste Isolation Pilot Plant Site.* SAND92-1579. Albuquerque, NM: Sandia National Laboratories.

Kelley, V.A., and J.F. Pickens. 1986. *Interpretation of the Convergent-Flow Tracer Tests Conducted in the Culebra Dolomite at the H-3 and H-4 Hydropads at the Waste Isolation Pilot Plant (WIPP) Site.* SAND86-7161. Albuquerque, NM: Sandia National Laboratories.

Klett, R.D. 1991. *Proposed Extensions of United States Fundamental and Derived Standards for High-Level and Transuranic Radioactive Waste Disposal.* SAND91-0211. Albuquerque, NM: Sandia National Laboratories.

Klett, R.D., and M.M. Gruebel. 1992. *Evaluation of Alternatives for High-Level and Transuranic Radioactive-Waste Disposal Standards.* SAND92-0556. Albuquerque, NM: Sandia National Laboratories.

Marietta, M.G., S.G. Bertram-Howery, D.R. Anderson, K.F. Brinster, R.V. Guzowski, H. Iuzzolino, and R.P. Rechard. 1989. *Performance Assessment Methodology Demonstration: Methodology Development for Evaluating Compliance with EPA 40 CFR 191, Subpart B, for the Waste Isolation Pilot Plant.* SAND89-2027. Albuquerque, NM: Sandia National Laboratories.

Numark, N.J., and S.R. Phelps. 1992. "Equivalence to 1,000 MTHM of Spent Fuel: Application of 40 CFR 191 to Other Wastes," *Proceedings of the International High-Level Radioactive Waste Management Conference, Las Vegas, NV, April 12-16, 1992.* LaGrange Park, IL: American Nuclear Society, Inc. Vol. 1, 1074-1081.

Public Law 102-579. 1992. *Waste Isolation Pilot Plant Land Withdrawal Act.*

Rechard, R.P., H.J. Iuzzolino, and J.S. Sandha. 1990. *Data Used in Preliminary Performance Assessment of the Waste Isolation Pilot Plant (1990).* SAND89-2408. Albuquerque, NM: Sandia National Laboratories.

Saulnier, G.J., Jr. 1987. *Analysis of Pumping Tests of the Culebra Dolomite Conducted at the H-11 Hydropad at the Waste Isolation Pilot Plant (WIPP) Site.* SAND87-7124. Albuquerque, NM: Sandia National Laboratories.

Tierney, M.S. 1990. *Constructing Probability Distributions of Uncertain Variables in Models of the Performance of the Waste Isolation Pilot Plant: The 1990 Performance Simulations.* SAND90-2510. Albuquerque, NM: Sandia National Laboratories.

US DOE (Department of Energy). 1991. *Integrated Data Base for 1991: U.S. Spent Fuel and Radioactive Waste Inventories, Projections, and Characteristics*. DOE/RW-0006, Rev. 7. Oak Ridge, TN: Oak Ridge National Laboratory.

US EPA (Environmental Protection Agency). 1985. "40 CFR 191: Environmental Standards for the Management and Disposal of Spent Nuclear Fuel, High-Level and Transuranic Radioactive Wastes, Final Rule." *Federal Register*. Vol. 50, no. 182, 38066-38089.

WIPP PA (Performance Assessment) Department. 1992. *Long-Term Gas and Brine Migration at the Waste Isolation Pilot Plant: Preliminary Sensitivity Analyses for Post-Closure 40 CFR 268 (RCRA), May 1992*. SAND92-1933. Albuquerque, NM: Sandia National Laboratories.

WIPP PA (Performance Assessment) Division. 1991a. *Preliminary Comparison with 40 CFR Part 191, Subpart B for the Waste Isolation Pilot Plant, December 1991. Volume 1: Methodology and Results*. SAND91-0893/1. Albuquerque, NM: Sandia National Laboratories.

WIPP PA (Performance Assessment) Division. 1991b. *Preliminary Comparison with 40 CFR Part 191, Subpart B for the Waste Isolation Pilot Plant, December 1991. Volume 2: Probability and Consequence Modeling*. SAND91-0893/2. Albuquerque, NM: Sandia National Laboratories.

WIPP PA (Performance Assessment) Division. 1991c. *Preliminary Comparison with 40 CFR Part 191, Subpart B for the Waste Isolation Pilot Plant, December 1991. Volume 3: Reference Data*. SAND91-0893/3. Albuquerque, NM: Sandia National Laboratories.

DISTRIBUTION

(Send Distribution list changes to M.M. Gruebel, Dept. 6342, Sandia National Laboratories, PO Box 5800, Albuquerque, NM 87185-5800)

Federal Agencies

US Department of Energy (2)
Office of Environmental Restoration
and Waste Management
Attn: L.P. Duffy, EM-1
C. Frank, EM-50
Washington, DC 20585

US Department of Energy (3)
Office of Environmental Restoration
and Waste Management
Attn: M. Frei, EM-34 (Trevion II)
Director, Waste Management Projects
Washington, DC 20585-0002

US Department of Energy
Office of Environmental Restoration
and Waste Management
Attn: J. Lytle, EM-30 (Trevion II)
Washington, DC 20585-0002

US Department of Energy
Office of Environmental Restoration
and Waste Management
Attn: S. Schneider, EM-342
(Trevion II)
Washington, DC 20585-0002

US Department of Energy (3)
WIPP Task Force
Attn: G.H. Daly
S. Fucigna
B. Bower
12800 Middlebrook Rd.
Suite 400
Germantown, MD 20874

US Department of Energy (4)
Office of Environment, Safety and
Health
Attn: R.P. Berube, EH-20
C. Borgstrum, EH-25
R. Pelletier, EH-231
K. Taimi, EH-232
Washington, DC 20585

US Department of Energy (5)
WIPP Project Integration Office
Attn: W.J. Arthur III
R. Becker
P. Dickman
L.W. Gage
P.J. Higgins
D.A. Olona
PO Box 5400
Albuquerque, NM 87115-5400

US Department of Energy (10)
WIPP Project Site Office (Carlsbad)
Attn: A. Hunt (4)
V. Daub (4)
J. Lippis
K. Hunter
PO Box 3090
Carlsbad, NM 88221-3090

US Department of Energy, (5)
Office of Civilian Radioactive Waste
Management
Attn: Deputy Director, RW-2
Associate Director, RW-10
Office of Program
Administration and
Resources Management
Associate Director, RW-20
Office of Facilities
Siting and Development
Associate Director, RW-30
Office of Systems
Integration and
Regulations
Associate Director, RW-40
Office of External
Relations and Policy
Office of Geologic Repositories
Forrestal Building
Washington, DC 20585

US Department of Energy
Attn: National Atomic Museum Library
Albuquerque Operations Office
PO Box 5400
Albuquerque, NM 87185

US Department of Energy
Research & Waste Management Division
Attn: Director
PO Box E
Oak Ridge, TN 37831

US Department of Energy (2)
Idaho Operations Office
Fuel Processing and Waste
Management Division
785 DOE Place
Idaho Falls, ID 83402

US Department of Energy
Savannah River Operations Office
Defense Waste Processing
Facility Project Office
Attn: W.D. Pearson
PO Box A
Aiken, SC 29802

US Department of Energy (2)
Richland Operations Office
Nuclear Fuel Cycle & Production
Division
Attn: R.E. Gerton
825 Jadwin Ave.
PO Box 500
Richland, WA 99352

US Department of Energy (3)
Nevada Operations Office
Attn: J.R. Boland
D. Livingston
P.K. Fitzsimmons
2753 S. Highland Drive
Las Vegas, NV 89183-8518

US Department of Energy (2)
Technical Information Center
PO Box 62
Oak Ridge, TN 37831

US Department of Energy (2)
Chicago Operations Office
Attn: J.C. Haugen
9800 South Cass Avenue
Argonne, IL 60439

US Department of Energy
Los Alamos Area Office
528 35th Street
Los Alamos, NM 87544

US Department of Energy (3)
Rocky Flats Area Office
Attn: W.C. Rask
G. Huffman
T. Lukow
PO Box 928
Golden, CO 80402-0928

US Department of Energy
Dayton Area Office
Attn: R. Grandfield
PO Box 66
Miamisburg, OH 45343-0066

US Department of Energy
Attn: E. Young
Room E-178
GAO/RCED/GTN
Washington, DC 20545

US Bureau of Land Management
101 E. Mermod
Carlsbad, NM 88220

US Bureau of Land Management
New Mexico State Office
PO Box 1449
Santa Fe, NM 87507

US Environmental Protection
Agency (2)
Office of Radiation Protection
Programs (ANR-460)
Washington, DC 20460

US Nuclear Regulatory Commission
Division of Waste Management
Attn: H. Marson
Mail Stop 4-H-3
Washington, DC 20555

US Nuclear Regulatory Commission (4)
Advisory Committee on Nuclear Waste
Attn: D. Moeller
M.J. Steindler
P.W. Pomeroy
W.J. Hinze
7920 Norfolk Avenue
Bethesda, MD 20814

Defense Nuclear Facilities Safety
Board
Attn: D. Winters
625 Indiana Avenue, NW
Suite 700
Washington, DC 20004

Nuclear Waste Technical Review
Board (2)
Attn: Library
Suite 910
1100 Wilson Blvd.
Arlington, VA 22209-2297

Energy and Science Division
Office of Management and Budget
Attn: K. Yuracko
725 17th Street NW
Washington, DC 20503

US Geological Survey (2)
Water Resources Division
Attn: C. Peters
Suite 200
4501 Indian School NE
Albuquerque, NM 87110

New Mexico Concressional Delegation

Jeff Bingaman
U.S. Senate
110 Hart SOB
Washington, DC 20510-3102

Pete V. Domenici
U.S. Senate
427 Dirksen Bldg.
Washington, DC 20510-3101

Bill Richardson
House of Representatives
2349 Rayburn HOB
Washington, DC 20515

Steven H. Schiff
House of Representatives
1009 Longworth HOB
Washington, DC 20515

Joe Skeen
House of Representatives
2367 Rayburn HOB
Washington, DC 20515

State Agencies

New Mexico Bureau of Mines
and Mineral Resources
Socorro, NM 87801

New Mexico Energy, Minerals and
Natural Resources Department
Attn: Librarian
2040 South Pacheco
Santa Fe, NM 87505

New Mexico Energy, Minerals and
Natural Resources Department
New Mexico Radioactive Task Force (2)
(Governor's WIPP Task Force)
Attn: A. Lockwood, Chairman
C. Wentz, Coordinator/Policy
Analyst
2040 South Pacheco
Santa Fe, NM 87505

Bob Forrest
Mayor, City of Carlsbad
PO Box 1569
Carlsbad, NM 88221

Executive Director
Carlsbad Department of Development
Attn: C. Bernard
PO Box 1090
Carlsbad, NM 88221

New Mexico Environment Department
Secretary of the Environment (3)
Attn: J. Espinosa
PO Box 968
1190 St. Francis Drive
Santa Fe, NM 87503-0968

New Mexico Environment Department
Attn: P. McCasland
WIPP Project Site Office
PO Box 3090
Carlsbad, NM 88221-3090

New Mexico State Engineer's Office
Attn: M. Chudnoff
PO Box 25102
Santa Fe, NM 87504-5102

Environmental Evaluation Group (5)
Attn: R. Neill
Suite F-2
7007 Wyoming Blvd. NE
Albuquerque, NM 87109

Advisory Committee on Nuclear Facility Safety

John F. Ahearne
Executive Director, Sigma Xi
99 Alexander Drive
Research Triangle Park, NC 27709

James E. Martin
109 Observatory Road
Ann Arbor, MI 48109

WIPP Panel of National Research Council's Board on Radioactive Waste Management

Charles Fairhurst, Chairman
Department of Civil and
Mineral Engineering
University of Minnesota
500 Pillsbury Dr., SE
Minneapolis, MN 55455-0220

John O. Blomeke
3833 Sandy Shore Drive
Lenoir City, TN 37771-9803

John D. Bredehoeft
Western Region Hydrologist
Water Resources Division
US Geological Survey (M/S 439)
345 Middlefield Road
Menlo Park, CA 94025

Fred M. Ernsberger
1325 NW 10th Avenue
Gainsville, FL 32601

Rodney C. Ewing
Department of Geology
University of New Mexico
200 Yale, NE
Albuquerque, NM 87131

B. John Garrick
PLG, Inc.
Suite 400
4590 MacArthur Blvd.
Newport Beach, CA 92660-2027

Leonard F. Konikow
US Geological Survey
431 National Center
Reston, VA 22092

Jeremiah O'Driscoll
505 Valley Hill Drive
Atlanta, GA 30350

Christopher Whipple
Clement International Corp.
160 Spear St.
Suite 1380
San Francisco, CA 94105-1535

National Research Council (3)
Board on Radioactive
Waste Management
RM HA456
Attn: P.B. Myers,
Staff Director (2)
G.J. Grube
2101 Constitution Avenue
Washington, DC 20418

Performance Assessment Peer Review Panel

G. Ross Heath
College of Ocean and
Fishery Sciences HN-15
583 Henderson Hall
University of Washington
Seattle, WA 98195

Thomas H. Pigford
Department of Nuclear Engineering
4159 Etcheverry Hall
University of California
Berkeley, CA 94720

Thomas A. Cotton
JK Research Associates, Inc.
4429 Butterworth Place, NW
Washington, DC 20016

Robert J. Budnitz
President, Future Resources
Associates, Inc.
2000 Center Street
Suite 418
Berkeley, CA 94704

C. John Mann
Department of Geology
245 Natural History Bldg.
1301 West Green Street
University of Illinois
Urbana, IL 61801

Frank W. Schwartz
Department of Geology and Mineralogy
The Ohio State University
Scott Hall
1090 Carmack Rd.
Columbus, OH 43210

National Laboratories

Argonne National Laboratory (2)
Attn: A. Smith
D. Tomasko
9700 South Cass, Bldg. 201
Argonne, IL 60439

Battelle Pacific Northwest Laboratory (3)
Attn: R.E. Westerman
S. Bates
H.C. Burkholder
Battelle Boulevard
Richland, WA 99352

Idaho National Engineering Laboratory (2)
Attn: H. Loo
R. Klinger
Mail Stop 5108
Idaho Falls, ID 83403-4000

Los Alamos National Laboratory
Attn: B. Erdal, CNC-11
PO Box 1663
Los Alamos, NM 87545

Los Alamos National Laboratory
Attn: A. Meijer
PO Box 1663, Mail Stop J514
Los Alamos, NM 87545

Los Alamos National Laboratory (3)
HSE-8
Attn: M. Enoris
L. Soholt
J. Wenzel
PO Box 1663
Los Alamos, NM 87545

Los Alamos National Laboratory
EM-7
Attn: S. Kosiewicz
PO Box 1663, Mail Stop J595
Los Alamos, NM 87545

Oak Ridge National Laboratory
Transuranic Waste Manager
Attn: D.W. Turner
PO Box 2008, Bldg. 3047
Oak Ridge, TN 37831-6060

Pacific Northwest Laboratory
Attn: B. Kennedy
PO Box 999
Richland, WA 99352

Savannah River Laboratory (3)
Attn: N. Bibler
M.J. Plodinec
G.G. Wicks
Aiken, SC 29801

Savannah River Plant (2)
Attn: R.G. Baxter
Bldg. 704-S
K.W. Wierzbicki
Bldg. 703-H
Aiken, SC 29808-0001

Corporations/Members of the Public

Benchmark Environmental Corp.
Attn: C. Frederickson
4501 Indian School NE
Suite 105
Albuquerque, NM 87110

City of Albuquerque
Public Works Department
Utility Planning Division
Attn: W.K. Summers
PO Box 1293
Albuquerque, NM 87103

Deuel and Associates, Inc.
Attn: R.W. Prindle
7208 Jefferson NE
Albuquerque, NM 87109

Disposal Safety, Inc.
Attn: B. Ross
1660 L Street NW
Suite 314
Washington, DC 20036

Ecodynamics (2)
Attn: P. Roache
R. Blaine
PO Box 9229
Albuquerque, NM 87119-9229

EG & G Idaho (3)
1955 Fremont Street
Attn: C. Atwood
C. Hertzler
T.I. Clements
Idaho Falls, ID 83415

Geomatrix
Attn: K. Coppersmith
100 Pine Street, Suite 1000
San Francisco, CA 94111

Golder Associates, Inc. (3)
Attn: M. Cunnane
R. Kossik
I. Miller
4104 148th Avenue NE
Redmond, WA 98052

INTERA, Inc. (2)
Attn: J.F. Pickens
A.M. LaVenve
6850 Austin Center Blvd.
Suite 300
Austin, TX 78731

INTERA, Inc.
Attn: W. Stensrud
PO Box 2123
Carlsbad, NM 88221

INTERA, Inc.
Attn: W. Nelson
101 Convention Center Drive
Suite 540
Las Vegas, NV 89109

IT Corporation (2)
Attn: R.F. McKinney
J. Myers
Regional Office, Suite 700
5301 Central Avenue NE
Albuquerque, NM 87108

John Hart and Associates, P.A.
Attn: J.S. Hart
2815 Candelaria Road NW
Albuquerque, NM 87107

John Hart and Associates, P.A.
Attn: K. Lickliter
1009 North Washington
Tacoma, WA 98406

MACTEC (2)
Attn: J.A. Thies
D.K. Duncan
8418 Zuni Road SE, Suite 200
Albuquerque, NM 87108

Newman and Holtzinger
Attn: C. Mallon
1615 L Street NW, Suite 1000
Washington, DC 20036

RE/SPEC, Inc. (2)
Attn: W. Coons
4775 Indian School NE, Suite 300
Albuquerque, NM 87110

RE/SPEC, Inc.
Attn: J.L. Ratigan
PO Box 725
Rapid City, SD 57709

Reynolds Elect/Engr. Co., Inc.
Attn: E.W. Kendall
Building 790, Warehouse Row
PO Box 98521
Las Vegas, NV 89193-8521

Roy F. Weston, Inc.
CRWM Tech. Supp. Team
Attn: C.J. Noronha
955 L'Enfant Plaza SW
North Building, Eighth Floor
Washington, DC 20024

Science Applications International
Corporation (SAIC)
Attn: H.R. Pratt
10260 Campus Point Drive
San Diego, CA 92121

Science Applications International
Corporation (2)
Attn: D.C.Royer
C.G. Pflum
101 Convention Center Dr.
Las Vegas, NV 89109

Science Applications International
Corporation (2)
Attn: M. Davis
J. Tollison
2109 Air Park Road SE
Albuquerque, NM 87106

Science Applications International
Corporation (2)
Attn: J. Young
D. Lester
18706 North Creek Parkway, Suite 110
Bothell, WA 98011

Southwest Research Institute
Center for Nuclear Waste Regulatory
Analysis (2)
Attn: P.K. Nair
6220 Culebra Road
San Antonio, TX 78228-0510

Systems, Science, and Software (2)
Attn: E. Peterson
P. Lagus
Box 1620
La Jolla, CA 92038

TASC
Attn: S.G. Oston
55 Walkers Brook Drive
Reading, MA 01867

Tech Reps, Inc. (6)
Attn: J. Chapman
C. Crawford
D. Marchand
J. Stikar
P. Oliver
D. Scott
5000 Marble NE, Suite 222
Albuquerque, NM 87110

Tolan, Beeson & Associates
Attn: T.L. Tolan
2320 W. 15th Avenue
Kennewick, WA 99337

TRW Environmental Safety Systems
Attn: I. Sacks
2650 Park Tower Drive, Suite 800
Vienna, VA 22180

Westinghouse Electric Corporation (5)
Attn: Library
L. Trego
C. Cox
L. Fitch
R.F. Kehrman
PO Box 2078
Carlsbad, NM 88221

Westinghouse Hanford Company
Attn: D. E. Wood
MSIN HO-32
PO Box 1970
Richland, WA 99352

Western Water Consultants
Attn: D. Fritz
1949 Sugarland Drive #134
Sheridan, WY 82801-5720

Western Water Consultants
Attn: P.A. Rechard
PO Box 4128
Laramie, WY 82071

P. Drez
8816 Cherry Hills Road, NE
Albuquerque, NM 87111

D.W. Powers
Star Route Box 87
Anthony, TX 79821

Shirley Thieda
PO Box 2109, RR1
Bernalillo, NM 87004

Jack Urich
c/o CARD
144 Harvard SE
Albuquerque, NM 87106

Universities

University of California
Mechanical, Aerospace, and
Nuclear Engineering Department (2)
Attn: W. Kastenberg
D. Browne
5532 Boelter Hall
Los Angeles, CA 90024

University of California
Mine Engineering Dept.
Attn: Neville Cook
Rock Mechanics Engineering
Berkeley, CA 94720

University of Hawaii at Hilo
Attn: S. Hora
Business Administration
Hilo, HI 96720-4091

University of New Mexico
Geology Department
Attn: Library
Albuquerque, NM 87131

University of New Mexico
Research Administration
Attn: H. Schreyer
102 Scholes Hall
Albuquerque, NM 87131

University of Wyoming
Department of Civil Engineering
Attn: V.R. Hasfurther
Laramie, WY 82071

University of Wyoming
Department of Geology
Attn: J.I. Drever
Laramie, WY 82071

University of Wyoming
Department of Mathematics
Attn: R.E. Ewing
Laramie, WY 82071

Libraries

Thomas Brannigan Library
Attn: D. Dresp
106 W. Hadley St.
Las Cruces, NM 88001

Hobbs Public Library
Attn: M. Lewis
509 N. Ship Street
Hobbs, NM 88248

New Mexico State Library
Attn: N. McCallan
325 Don Gaspar
Santa Fe, NM 87503

New Mexico Tech
Martin Speere Memorial Library
Campus Street
Socorro, NM 87810

New Mexico Junior College
Pannell Library
Attn: R. Hill
Lovington Highway
Hobbs, NM 88240

Carlsbad Municipal Library
WIPP Public Reading Room
Attn: L. Hubbard
101 S. Halagueno St.
Carlsbad, NM 88220

University of New Mexico
General Library
Government Publications Department
Albuquerque, NM 87131

NEA/Performance Assessment Advisory Group (PAAG)

P. Duerden
ANSTO
Lucas Heights Research Laboratories
Private Mail Bag No. 1
Menai, NSW 2234, AUSTRALIA

Gordon S. Linsley
Division of Nuclear Fuel Cycle and
Waste Management
International Atomic Energy Agency
PO Box 100
A-1400 Vienna, AUSTRIA

Nicolo Cadelli
Commission of the European Communities
200, Rue de la Loi
B-1049 Brussels, BELGIUM

R. Heremans
Organisme Nationale des Déchets
Radioactifs et des Matiéres
Fissiles
ONDRAF
Place Madou 1, Boitec 24/25
B-1030 Brussels, BELGIUM

J. Marivoet
Centre d'Etudes de l'Energie Nucléaire
CEN/SCK
Boeretang 200
B-2400 Mol, BELGIUM

P. Conlon
Waste Management Division
Atomic Energy Control Board (AECB)
PO Box 1046
Ottawa, Canada KIP 559, CANADA

A.G. Wikjord
Manager, Environmental and Safety Assessment Branch
Atomic Energy of Canada Limited
Whiteshell Nuclear Research Establishment
Pinewa, Manitoba ROE 1LO, CANADA

Jukka-Pekka Salo
Teollisuuden Voima Oy (TVO)
Fredrikinkatu 51-53 B
SF-00100 Helsinki, FINLAND

Timo Vieno
Technical Research Centre of Finland (VTT)
Nuclear Energy Laboratory
PO Box 208
SF-02151 Espoo, FINLAND

Timo Äikäs
Teollisuuden Voima Oy (TVO)
Fredrikinkatu 51-53 B
SF-00100 Helsinki, FINLAND

M. Claude Ringeard
Division de la Sécurité et de la Protection de l'Environment (DSPE)
Commissariat á l'Energie Atomique
Agence Nationale pour la Gestion des Déchets Radioactifs (ANDRA)
Route du Panorama Robert Schuman
B. P. No. 38
F-92266 Fontenay-aux-Roses Cedex
FRANCE

Gérald Ouzounian
Agence Nationale pour la Gestion des Déchets Radioactifs (ANDRA)
Route du Panorama Robert Schuman
B. P. No. 38
F-92266 Fontenay-aux-Roses Cedex
FRANCE

Claudio Pescatore
Division of Radiation Protection and Waste Management
OECD Nuclear Energy Agency
38, Boulevard Suchet
F-75016 Paris, FRANCE

M. Dominique Greneche
Commissariat á l'Energie Atomique
IPSN/DAS/SASICC/SAED
B. P. No. 6
F-92265 Fontenay-aux-Roses Cedex,
FRANCE

Robert Fabriol
Bureau de Recherches Géologiques et Miniéres (BRGM)
B. P. 6009
45060 Orléans Cedex 2, FRANCE

P. Bogorinski
Gesellschaft für Reaktorsicherheit (GRS) mbH
Schwertnergasse 1
D-5000 Köln 1, GERMANY

R. Storck
GSF - Institut für Tieflagerung
Theodor-Heuss-Strabe 4
D-3300 Braunschweig, GERMANY

Ferrucio Gera
ISMES S.p.A
Via del Crociferi 44
I-00187 Rome, ITALY

Hiroyuki Umeki
Isolation System Research Program
Radioactive Waste Management Project
Power Reactor and Nuclear Fuel Development Corporation (PNC)
1-9-13, Akasaka
Minato-ku
Tokyo 107, JAPAN

P. Carboneras Martinez
ENRESA
Calle Emilio Vargas 7
R-28043 Madrid, SPAIN

Tönis Papp
Swedish Nuclear Fuel and Waste Management Co.
Box 5864
S 102 48 Stockholm, SWEDEN

Conny Hägg
Swedish Radiation Protection Institute
(SSI)
Box 60204
S-104 01 Stockholm, SWEDEN

J. Hadermann
Paul Scherrer Institute
Waste Management Programme
CH-5232 Villigen PSI, SWITZERLAND

J. Vigfusson
USK- Swiss Nuclear Safety Inspectorate
Federal Office of Energy
CH-5303 Würenlingen, SWITZERLAND

D.E. Billington
Departmental Manager - Assessment
Studies
Radwaste Disposal R&D Division
AEA Decommissioning & Radwaste
Harwell Laboratory, B60
Didcot Oxfordshire OX11 ORA
UNITED KINGDOM

P. Grimwood
Waste Management Unit
BNFL
Sellafield
Seascale, Cumbria CA20 1PG
UNITED KINGDOM

Alan J. Hooper
UK Nirex Ltd
Curie Avenue
Harwell, Didcot
Oxfordshire, OX11 ORH
UNITED KINGDOM

Jerry M. Boak
Yucca Mountain Project Office
US Department of Energy
PO Box 98608
Las Vegas, NV 89193

Seth M. Coplan (Chairman)
US Nuclear Regulatory Commission
Division of High-Level Waste
Management
Mail Stop 4-H-3
Washington, DC 20555

A.E. Van Luik
INTERA/M&O
The Valley Bank Center
101 Convention Center Dr.
Las Vegas, NV 89109

NEA/PSAG User's Group

Shaheed Hossain
Division of Nuclear Fuel Cycle and
Waste Management
International Atomic Energy Agency
Wagramerstrasse 5
PO Box 100
A-1400 Vienna, AUSTRIA

Alexander Nies (PSAC Chairman)
Gesellschaft für Strahlen- und
Institut für Tieflagerung
Abteilung für Endlagersicherheit
Theodor-Heuss-Strasse 4
D-3300 Braunschweig, GERMANY

Eduard Hofer
Gesellschaft für Reaktorsicherheit
(GRS) MBH
Forschungsgelände
D-8046 Garching, GERMANY

Andrea Saltelli
Commission of the European Communities
Joint Resarch Centre of Ispra
I-21020 Ispra (Varese), ITALY

Alejandro Alonso
Cátedra de Tecnología Nuclear
E.T.S. de Ingenieros Industriales
José Gutiérrez Abascal, 2
E-28006 Madrid, SPAIN

Pedro Prado
CIEMAT
Instituto de Tecnología Nuclear
Avenida Complutense, 22
E-28040 Madrid, SPAIN

Miguel Angel Cuñado
ENRESA
Emilio Vargas, 7
E-28043 Madrid, SPAIN

Francisco Javier Elorza
ENRESA
Emilio Vargas, 7
E-28043 Madrid, SPAIN

Nils A. Kjellbert
Swedish Nuclear Fuel and Waste
Management Company (SKB)
Box 5864
S-102 48 Stockholm, SWEDEN

Björn Cronhjort
Swedish National Board for Spent
Nuclear Fuel (SKN)
Sehlsedtsgatan 9
S-115 28 Stockholm, SWEDEN

Richard A. Klos
Paul-Scherrer Institute (PSI)
CH-5232 Villingen PSI
SWITZERLAND

NAGRA (2)
Attn: C. McCombie
F. Van Dorp
Parkstrasse 23
CH-5401 Baden, SWITZERLAND

N. A. Chapman
Intera Information Technologies
Park View House, 14B Burton Street
Melton Mowbray
Leicestershire, LE13 1AE
UNITED KINGDOM

Daniel A. Galson
Galson Sciences Ltd.
35, Market Place
Oakham
Leicestershire LE15 6DT
UNITED KINGDOM

David P. Hodgkinson
Intera Information Technologies
Chiltern House
45 Station Road
Henley-on-Thames
Oxfordshire RG9 1AT, UNITED KINGDOM

Brian G.J. Thompson
Department of the Environment: Her
Majesty's Inspectorate of Pollution
Room A5.33, Romney House
43 Marsham Street
London SW1P 2PY, UNITED KINGDOM

Intera Information Technologies
Attn: M.J.Apted
3609 South Wadsworth Blvd.
Denver, CO 80235

US Nuclear Regulatory Commission (2)
Attn: R. Codell
N. Eisenberg
Mail Stop 4-H-3
Washington, DC 20555

Battelle Pacific Northwest
Laboratories
Attn: P.W. Eslinger
PO Box 999, MS K2-32
Richland, WA 99352

Center for Nuclear Waste Regulatory
Analysis (CNWRA)
Southwest Research Institute
Attn: B. Sagar
PO Drawer 28510
6220 Culebra Road
San Antonio, TX 78284

Geostatistics Expert Working Group (GXG)

Rafael L. Bras
R.L. Bras Consulting Engineers
44 Percy Road
Lexington, MA 02173

Jesus Carrera
Universidad Politécnica de Cataluña
E.T.S.I. Caminos
Jordi, Girona 31
E-08034 Barcelona, SPAIN

Gedeon Dagan
Department of Fluid Mechanics and Heat
Transfer
Tel Aviv University
PO Box 39040
Ramat Aviv, Tel Aviv 69978, ISRAEL

Ghislain de Marsily (GXG Chairman)
University Pierre et Marie Curie
Laboratorie de Geologie Applique
4, Place Jussieu - T.26 - 5^{e} etage
75252 Paris Cedex 05, FRANCE

Alain Galli
Centre de Geostatistique
Ecole des Mines de Paris
35 Rue St. Honore
77035 Fontainebleau, FRANCE

Steve Gorelick
Department of Applied Earth Sciences
Stanford University
Stanford, CA 94305-2225

Peter Grindrod
INTERA Information Technologies Ltd.
Chiltern House, 45 Station Road
Henley-on-Thames
Oxfordshire, RG9 1AT
UNITED KINGDOM

Alan Gutjahr
Department of Mathematics
New Mexico Institute of Mining and Technology
Socorro, NM 87801

C. Peter Jackson
Harwell Laboratory
Theoretical Studies Department
Radwaste Disposal Division
Bldg. 424.4
Oxfordshire Didcot Oxon OX11 ORA
UNITED KINDGOM

Peter Kitanidis
60 Peter Coutts Circle
Stanford, CA 94305

Rae Mackay
Department of Civil Engineering
University of Newcastle Upon Tyne
Newcastle Upon Tyne NE1 7RU
UNITED KINGDOM

Dennis McLaughlin
Parsons Laboratory
Room 48-209
Department of Civil Engineering
Massachusetts Institute of Technology
Cambridge, MA 02139

Shlomo P. Neuman
College of Engineering and Mines
Department of Hydrology and Water Resources
University of Arizona
Tucson, AZ 85721

Christian Ravenne
Geology and Geochemistry Division
Institut Francais du Pétrole
1 & 4, av. de Bois-Préau BP311
92506 Rueil Malmaison Cedex
FRANCE

Yoram Rubin
Department of Civil Engineering
University of California
Berkeley, CA 94720

Foreign Addresses

Studiecentrum Voor Kernenergie
Centre D'Energie Nucleaire
Attn: A. Bonne
SCK/CEN
Boeretang 200
B-2400 Mol, BELGIUM

Atomic Energy of Canada, Ltd. (3)
Whiteshell Research Estab.
Attn: M.E. Stevens
B.W. Goodwin
D. Wushke
Pinewa, Manitoba
ROE 1LO, CANADA

Esko Peltonen
Industrial Power Company Ltd.
TVO
Fredrikinkatu 51-53
SF-00100 Helsinki 10, FINLAND

Jean-Pierre Olivier
OECD Nuclear Energy Agency (2)
38, Boulevard Suchet
F-75016 Paris, FRANCE

D. Alexandre, Deputy Director
ANDRA
31 Rue de la Federation
75015 Paris, FRANCE

Claude Sombret
Centre D'Etudes Nucleaires
De La Vallee Rhone
CEN/VALRHO
S.D.H.A. BP 171
30205 Bagnols-Sur-Ceze, FRANCE

Bundesministerium fur Forschung und Technologie
Postfach 200 706
5300 Bonn 2, GERMANY

Bundesanstalt fur Geowissenschaften und Rohstoffe
Attn: M. Langer
Postfach 510 153
3000 Hanover 51, GERMANY

Gesellschaft fur Reaktorsicherheit (GRS) (2)
Attn: B. Baltes
W. Muller
Schwertnergasse 1
D-5000 Cologne, GERMANY

Institut fur Tieflagerung (2)
Attn: K. Kuhn
Theodor-Heuss-Strasse 4
D-3300 Braunschweig, GERMANY

Physikalisch-Technische Bundesanstalt
Attn: P. Brenneke
Postfach 33 45
D-3300 Braunschweig, GERMANY

Shingo Tashiro
Japan Atomic Energy Research Institute
Tokai-Mura, Ibaraki-Ken
319-11, JAPAN

Netherlands Energy Research Foundation (ECN)
Attn: L.H. Vons
3 Westerduinweg
PO Box 1
1755 ZG Petten, THE NETHERLANDS

Johan Andersson
Swedish Nuclear Power Inspectorate
Statens Kärnkraftinspektion (SKI)
Box 27106
S-102 52 Stockholm, SWEDEN

Fred Karlsson
Svensk Karnbransleforsorjning AB SKB
Box 5864
S-102 48 Stockholm, SWEDEN

Nationale Genossenschaft fur die Lagerung Radioaktiver Abfalle (NAGRA) (2)
Attn: S. Vomvoris
P. Zuidema
Hardstrasse 73
CH-5430 Wettingen, SWITZERLAND

AEA Technology
Attn: J.H. Rees
D5W/29 Culham Laboratory
Abington
Oxfordshire OX14 3DB, UNITED KINGDOM

AEA Technology
Attn: W.R. Rodwell
044/A31 Winfrith Technical Centre
Dorchester
Dorset DT2 8DH, UNITED KINGDOM

AEA Technology
Attn: J.E. Tinson
B4244 Harwell Laboratory
Didcot, Oxfordshire OX11 ORA
UNITED KINGDOM

D.R. Knowles
British Nuclear Fuels, plc
Risley, Warrington
Cheshire WA3 6AS, 1002607
UNITED KINGDOM

Internal

1 A. Narath
20 O.E. Jones
1502 J.C. Cummings
1511 D.K. Gartling
6000 D.L. Hartley
6115 P.B. Davies
6119 E.D. Gorham
6119 Staff (14)
6121 J.R. Tillerson
6121 Staff (7)
6233 J.C. Eichelberger
6300 D.E. Ellis
6302 L.E. Shephard
6303 S.Y. Pickering
6303 W.D. Weart
6305 S.A. Goldstein
6306 A.L. Stevens
6312 F.W. Bingham
6313 L.S. Costin
6331 P.A. Davis

6341 Sandia WIPP Central Files (300)
6342 D.R. Anderson
6342 Staff (30)
6343 S.A. Orrell, Acting
6343 Staff (3)
6345 R.C. Lincoln
6345 Staff (9)
6347 D.R. Schafer
6348 J.T. Holmes
6351 R.E. Thompson
6352 D.P. Garber
6352 S.E. Sharpton
6400 N.R. Ortiz
6613 R.M. Cranwell
6613 R.L. Iman
6613 C. Leigh
6622 M.S.Y. Chu
6641 R.E. Luna, Acting
7141 Technical Library (5)
7151 Technical Publications
7613-2 Document Processing for
DOE/OSTI (10)
8523-2 Central Technical Files
9300 J.E. Powell
9310 J.D. Plimpton
9330 J.D. Kennedy

☆ U.S. GOVERNMENT PRINTING OFFICE 1992—774-122/80123

SANDIA REPORT

SAND92–0700/2 • UC–721
Unlimited Release
Printed December 1992

Preliminary Performance Assessment for the Waste Isolation Pilot Plant, December 1992

Volume 2: Technical Basis

WIPP Performance Assessment Department

Prepared by
Sandia National Laboratories
Albuquerque, New Mexico 87185 and Livermore, California 94550
for the United States Department of Energy
under Contract DE-AC04-76DP00789

Issued by Sandia National Laboratories, operated for the United States Department of Energy by Sandia Corporation.

Available to DOE and DOE contractors from
Office of Scientific and Technical Information
PO Box 62
Oak Ridge, TN 37831

Prices available from (615) 576-8401, FTS 626-8401

Available to the public from
National Technical Information Service
US Department of Commerce
5285 Port Royal Rd
Springfield, VA 22161

NTIS price codes
Printed copy: A12
Microfiche copy: A01

SAND92-0700/2
Unlimited Release
Printed December 1992

Distribution
Category UC-721

Preliminary Performance Assessment for the Waste Isolation Pilot Plant, December 1992

Volume 2: Technical Basis

WIPP Performance Assessment Department
Sandia National Laboratories
Albuquerque, New Mexico 87185

ABSTRACT

Before disposing of transuranic radioactive waste in the Waste Isolation Pilot Plant (WIPP), the United States Department of Energy (DOE) must evaluate compliance with applicable long-term regulations of the United States Environmental Protection Agency (EPA). Sandia National Laboratories is conducting iterative performance assessments (PAs) of the WIPP for the DOE to provide interim guidance while preparing for a final compliance evaluation. This volume contains the technical basis for the 1992 PA. Specifically, it describes the conceptual basis for consequence modeling and the PA methodology, including the selection of scenarios for analysis, the determination of scenario probabilities, and the estimation of scenario consequences using a Monte Carlo technique and a linked system of computational models.

Additional information about the 1992 PA is provided in other volumes. Volume 1 contains an overview of WIPP PA and results of a preliminary comparison with the long-term requirements of the EPA's *Environmental Protection Standards for Management and Disposal of Spent Nuclear Fuel, High-Level and Transuranic Radioactive Wastes* (40 CFR 191, Subpart B). Volume 3 contains the reference data base and values for input parameters used in consequence and probability modeling. Volume 4 contains uncertainty and sensitivity analyses related to the preliminary comparison with 40 CFR 191B. Volume 5 contains uncertainty and sensitivity analyses of gas and brine migration for undisturbed performance. Finally, guidance derived from the entire 1992 PA is presented in Volume 6.

This volume of the report should be referenced as:

WIPP PA (Performance Assessment) Department. 1992. *Preliminary Performance Assessment for the Waste Isolation Pilot Plant, December 1992 — Volume 2: Technical Basis.* SAND92-0700/2. Albuquerque, NM: Sandia National Laboratories.

ACKNOWLEDGMENTS

The Waste Isolation Pilot Plant (WIPP) Performance Assessment (PA) Department is comprised of both Sandia National Laboratories (SNL) and contractor employees working as a team to produce preliminary comparison with Environmental Protection Agency (EPA) regulations, assessments of overall long-term safety of the repository, and interim technical guidance to the program. The on-site team, affiliations, and contributions to the 1992 performance assessment are listed in alphabetical order:

Performance Assessment Department

Name	Affil.*	Primary Author of Major Code	Area of Responsibility
R. Anderson	SNL		Department Manager
B. Baker	TEC		SEC02D, Hydrology, Office Manager
J. Bean	UNM		BRAGFLO, 2-Phase Flow
J. Berglund	UNM	CUTTINGS	Task Ldr., Cuttings/Cavings/Spallings, Engr. Mech.
S. Bertram-Howery	SNL		PA Liaison with DOE, Criteria Document, Test Phase Plan
W. Beyeler	SAI	PANEL, GARFIELD	Geostatistics, Analytical Models, CAMCON Systems Codes
K. Brinster	SAI		Geohydrology, Conceptual Models
R. Blaine	ECO		SEC02D, SECOTP, & CAMCON Systems Codes
T. Blaine	GC		Drilling Technology, Exposure Pathways Data
K. Byle	UNM		Software and Analysis QA
J. Chapman	TRI		Documentation V.3
D. Duncan	MAC		Data QA
K. Economy	ECO		SEC02D, SECOTP, Hydrology & Transport
D. Gallegos	SNL		Task Ldr., Hydrology, Geostatistics, NEA, PSAG
D. Galson	GS		NEA Working Groups, PSAG, PAAG, Human Intrusion
J. Garner	API	PANEL	Source Term, Sens. Anal.
A. Gilkey	UNM		CAMCON Systems Codes
L. Gomez	SNL		Task Ldr., Safety Assessments
M. Gruebel	TRI		EPA Regulations, Documentation V.1, Editor V.1
R. Guzowski	SAI		Geology, Scenario Construction
J. Helton	ASU	CCDFPERM	Task Ldr., Uncert./Sens. Anal., Probability Models, Editor V.4
S. Hora	UHH		Expert Elicitation, Probability Models
H. Iuzzolino	GC	CCDFCALC, CCDFPERM	LHS, CAMCON System Codes, Probability Models
R. Klett	SNL		EPA Regulations
P. Knupp	ECO	SECOTP	Comp. Fluid Dyn.
M. LaVenue	INT	GRASP-INV	Hydrology/Geostatistics
C. Leigh	SNL	GENII-S	Exposure Pathways
M. Marietta	SNL		Dep. Dept. Manager, Tech. Coord.
G. de Marsily	UP		Geostatistics Expert Group Chair
R. McCurley	UNM		CAMCON System Codes
B. Napier	PNL	GENII	Safety Assessments
A. Peterson	SNL		Task Ldr., Inventory

B. RamaRao	INT	GRASP-INV	Geostatistics
J. Rath	UNM		CAMCON System Codes
R. Rechard	SNL		Task Ldr., CAMCON, QA
P. Roache	ECO	SECO	Task Ldr., Comp. Fluid Dyn.
D. Rudeen	UNM		STAFF2D, SECOTP, Transport
J. Ruge	ECO		Multigrid Methods/BRAGFLO
T. Russell	ECO		Upscaling
K. Salari	ECO	SECOTP	Transport, Computational Fluid Dynamics
J. Sandha	SAI		INGRES, PA Data Base
J. Schreiber	SAI		BRAGFLO, 2-Phase Flow
D. Scott	TRI		Documentation V.2
P. Swift	TRI		Task Ldr., Geology, Climate Var., Documentation V.1 & 2, Editor V.1, 2, 4, & 5
M. Tierney	SNL		Task Ldr., CDF Constr., Probability Models, Ref. Data, Editor V.2 & 3
K. Trauth	SNL		Task Ldr., Expert Panels
P. Vaughn	API	BRAGFLO	Task Ldr., 2-Phase Flow & Waste Panel Chemistry, Editor V.4 & 5
T. Zimmerman	GRA		Geostatistics Test Problem

The foundation of the annual WIPP performance assessment is the underlying data set and understanding of the important processes in the engineered and natural barrier systems. Other SNL Departments are the primary source of these data and understanding. Assistance with the waste inventory comes from Westinghouse Electric Corporation and its contractors. We gratefully acknowledge the support of our departmental and project colleagues. Some individuals have worked closely with the performance assessment team, and we wish to acknowledge their contributions individually:

H. Batchelder	WEC	CH & RH Inventories
R. Beauheim	SNL	Natural Barrier System, Hydrologic Parameters
D. Borns	SNL	Geology, Geophysics
B. Butcher	SNL	Engineered Barrier System, Unmodified Waste-Form Parameters, Disposal Room Systems Parameters
L Brush	SNL	Engineered Barrier System, Source Term (Solubility) and Gas Generation Parameters
L. Clements	ReS	Computer System Support
T. Corbet	SNL	Natural Barrier System, Geologic & Hydrologic Parameters, Conceptual Models
P. Davies	SNL	Natural Barrier System, Hydrologic & Transport Parameters, & 2-Phase Flow Mechanistic Modeling
P. Drez	DE	CH & RH Inventories
R. Finley	SNL	Repository Isolation Systems Parameters
F. Gelbard	SNL	Natural Barrier System, Retardation
E. Gorham	SNL	Natural Barrier System, Fluid Flow & Transport Parameters
R. Holt	CON	Geology
S. Howarth	SNL	Natural Barrier System, Hydrologic Parameters
R. Kehrman	WEC	Ch & RH Waste Characterization
K. Lickliter	BEC	EPA Regulations
R. Lincoln	SNL	Room Modeling
F. Mendenhall	SNL	Engineered Barrier System, Unmodified Waste Form Parameters, Waste Panel Closure (Expansion)
D. Munson	SNL	Reference Stratigraphy, Constitutive Models, Physical & Mechanical Parameters
C. Novak	SNL	Natural Barrier Systems, Chemistry
E. Nowak	SNL	Room Modeling, Source Term
J. Orona	ReS	Computer System Support
A. Stevens	SNL	DOE Liaison
J. Tillerson	SNL	Repository Isolation Systems Parameters

W. Wawersik	SNL	Fracturing
S. Webb	SNL	2-Phase Flow Sensitivity Analysis & Benchmarking

* Affiliation

API = Applied Physics Incorporated
ASU = Arizona State University
BEC = Benchmark Environmental Corp.
CON = Consultant
DE = Drez Environmental
ECO = Ecodynamics Research Associates
GC = Geo-Centers Incorporated
GRA = GRAM, Inc.
GS = Galson Sciences
INT = Intera
MAC = MACTEC
PNL = Pacific Northwest Laboratory
ReS = ReSpec
SAI = Scientific Applications International Corporation
SNL = Sandia National Laboratories
TEC = Technadyne Engineering Consultants
TRI = Tech Reps, Inc.
UHH = University of Hawaii at Hilo
UNM = University of New Mexico/New Mexico Engineering Research Institute
UP = University of Paris
WEC = Westinghouse Electric Corporation

Peer Review

Internal/Sandia
L. Gomez
D. Schafer

Management/Sandia
W. Weart

PA Peer Review Panel

R. Heath, Chair	University of Washington
R. Budnitz	Future Resources Associates, Inc.
T. Cotton	JK Research Associates, Inc.
J. Mann	University of Illinois
T. Pigford	University of California, Berkeley
F. Schwartz	Ohio State University

Department of Energy
R. Becker

Expert Panels

Futures

M. Baram	Boston University
W. Bell	Yale University
G. Benford	University of California, Irvine
D. Chapman	The World Bank, Cornell University
B. Cohen	University of Pittsburgh
V. Ferkiss	Georgetown University
T. Glickman	Resources for the Future
T. Gordon	Futures Group
C. Kirkwood	Arizona State University
H. Otway	Joint Research Center (Ispra), Los Alamos National Laboratory

M. Pasqualetti	Arizona State University
D. Reicher	Natural Resources Defense Council
N. Rosenberg	Resources for the Future
M. Singer	The Potomac Organization
T. Taylor	Consultant
M. Vinovskis	University of Michigan

Markers

D. Ast	Cornell University
V. Baker	University of Arizona
M. Brill	Buffalo Organization for Social and Technological Innovation
F. Drake	University of California at Santa Cruz
B. Finney	University of Hawaii at Manoa
D. Givens	American Anthropological Association
W. Goodenough	University of Pennsylvania
M. Kaplan	Eastern Research Group
J. Lomberg	Consultant
L. Narens	University of California at Irvine
F. Newmeyer	University of Washington
W. Sullivan	University of Washington
W. Williams	Case Western Reserve University

Source Term

C. Bruton	Lawrence Livermore National Laboratory
I-Ming Chou	U.S. Geological Survey
D. Hobart	Los Alamos National Laboratory
F. Millero	University of Miami

Retardation

R. Dosch	Sandia National Laboratories
C. Novak	Sandia National Laboratories
M. Siegel	Sandia National Laboratories

Geostatistics Expert Group

G. de Marsily, Chair	U. of Paris
R. Bras	Massachusetts Inst. of Tech.
J. Carrera	U. Politécnica de Cataluña
G. Dagan	Tel Aviv U.
A. Galli	Ecole des Mines de Paris
S. Gorlick	Stanford U.
P. Grindrod	Intera Sciences
A. Gutjahr	New Mexico Tech
D. McLaughlin	Massachusetts Inst. of Tech.
S. Neuman	U. of Arizona
C. Ravenne	Institut Français du Pétrole
Y. Rubin	U. of California, Berkeley

Report Preparation (TRI)

Volume 1: M. Minahan (text); D. Marchand (illustrations)
Volume 2: M. Minahan (text); D. Marchand (illustrations)
Volume 3: J. Chapman (text); D. Marchand (illustrations)

D. Rivard and the Word Processing Department
R. Rohac, R. Andree, and the Illustration and Computer Graphics Departments
S. Tullar and the Production Department

CONTENTS

Figures

Tables

1. INTRODUCTION

The Waste Isolation Pilot Plant (WIPP) is planned as a research and development facility to demonstrate the safe disposal of transuranic (TRU) wastes generated by defense programs of the United States Department of Energy (DOE). Before disposing of waste in the WIPP, the DOE must evaluate compliance with applicable long-term regulations of the United States Environmental Protection Agency (EPA), including 40 CFR 191 Subpart B *(Environmental Radiation Protection Standards for Management and Disposal of Spent Nuclear Fuel, High-Level and Transuranic Radioactive Wastes)* [U.S. EPA, 1985]) and 40 CFR 268.6 (U.S. EPA, 1986), which is the portion of the *Land Disposal Restrictions* of the *Hazardous and Solid Waste Amendments* to the *Resource Conservation and Recovery Act* (RCRA) that states the conditions for disposal of specified hazardous wastes. Performance assessments (PAs) will form the basis for evaluating compliance with all applicable long-term regulations of the EPA. The WIPP Performance Assessment (PA) Department of Sandia National Laboratories (SNL) is performing annual iterative preliminary PAs to provide guidance to the Project while preparing for final compliance evaluation. The 1991 preliminary performance assessment for comparison with 40 CFR 191B was documented in 4 volumes (WIPP PA Division, 1991 a, b, c; Helton et al., 1992).

1.1 Purpose of Volume 2

This volume describes the technical basis for the 1992 WIPP preliminary PA: conceptual model development, probability modeling, and consequence modeling of the WIPP disposal system for evaluating compliance with the quantitative requirements of applicable long-term regulations. Volume 1 deals primarily with the regulations in Subpart B of 40 CFR Part 191 and their application to the WIPP, but also summarizes aspects of this volume and explains the 1992 status of the WIPP PA. Volume 3 compiles model parameters, constructs cumulative distribution functions (cdfs) and discusses their derivation from the pertinent data of disposal system characterization. Uncertainty and sensitivity analysis results related to 40 CFR 191B are discussed in Volume 4. Uncertainty and sensitivity analysis results of gas and brine migration for undisturbed performance are discussed in Volume 5. Finally, guidance derived from the entire 1992 PA is presented in Volume 6.

1.2 Organization of Volume 2

Volume 2 consists of seven chapters and four appendices. This chapter (Chapter 1) describes the organization of Volume 2. The remaining six chapters are organized following the PA methodology described in Volume 1.

- Chapter 2 (Conceptual Basis for Consequence Modeling) describes the conceptual basis for consequence modeling. This chapter is a detailed expansion of the brief discussion in Chapter 2 of Volume 1, and provides a bibliographic mapping into the published literature of the site characterization and engineered design programs.

- Chapter 3 (Performance Assessment Methodology) describes the conceptual model for risk that forms the framework (scenarios, frequency or probability of scenarios, and consequences of scenarios) for the WIPP

PA, presents an outline of the Monte Carlo technique that is used for uncertainty and sensitivity analyses, and discusses the construction of complementary cumulative distribution functions (CCDFs). This chapter is a detailed expansion of Chapter 4 of Volume 1, and is generally unchanged from the 1991 PA.

- Chapter 4 (Scenario Construction) examines the first element (scenarios) of the conceptual model for risk. This chapter discusses the application of the methodology for scenario construction—identifying, screening, and classifying events and processes; developing scenarios using a logic diagram; and screening of scenarios —for the WIPP. Retained scenarios that are analyzed in the 1992 PA are described. This material is generally unchanged from the 1991 PA and therefore references previous documents extensively. Scenarios included in the Monte Carlo analysis in 1991 are included again in 1992.

- Chapter 5 (Drilling Intrusion Probabilities) examines the second element (probabilities or frequencies of scenarios) of the conceptual model for risk. The probability model that is used for the 1992 analysis was presented in the 1991 documentation, so this chapter is a much briefer description that references previous documentation. The significant difference in the application of this model is that time-varying drilling intensities were used in 1992, whereas in 1991 only constant, but imprecisely known, drilling intensities were used. A brief discussion of how these new drilling intensity functions were derived from expert panel output that references material in Volume 3 is included.

- Chapter 6 (Data and cdfs) begins the description of the different steps of the Monte Carlo technique: selection of imprecisely known parameters, construction of ranges and distributions for these parameters, generation of the sample, propagation of uncertainty through the system model, uncertainty analysis, and sensitivity analysis. This chapter briefly describes the first steps: selection of imprecisely known parameters and construction of their ranges and distributions. The entire data base, especially model parameters, is the subject of Volume 3.

- Chapter 7 (Consequence Modeling) describes the modeling system that is used to calculate consequences of scenarios. The Latin hypercube sampling technique that is used to generate the sample for Monte Carlo analysis is described elsewhere (Helton et al., 1991) and is not repeated. This chapter focuses on the 1992 modeling system through which uncertainty is propagated for the uncertainty and sensitivity analysis. Each major module of this system is described in terms of governing equations and modeling assumptions. More detailed code descriptions are contained in the four appendices as follows:

Appendix A. A repository and shaft seal module is used that simulates two-phase (gas and brine) flow through the repository, shaft seals, and surrounding environs (BRAGFLO) with an equilibrium-mixing cell for calculating radionuclide concentrations in the brine phase (PANEL). These codes were used in the 1991 PA.

Appendix B. A module (SANCHO) for simulating quasistatic, large-deformation, inelastic response of the halite is used to provide waste porosity as a function of time. These calculations incorporate the effect of creep closure and of halite response to waste-generated gas into the PA; they are performed outside the Monte Carlo analysis. Only the waste porosity functions are used during

consequence calculations. This is the first year that the effects of halite creep have been included in PA calculations.

Appendix C. Groundwater flow and transport models (SECO-2DH and SECO-TP) are used to calculate subsurface transport through the Culebra Dolomite Member of the Rustler Formation to the land-withdrawal boundary. First, the groundwater flow is calculated for a single-porosity, matrix-only, porous medium (dolomite). The flow calculation is performed first on a regional scale and second on a local scale with boundary conditions derived from the regional-scale distribution. Climate variability enters through time-varying boundary conditions that are based on a simple precipitation/recharge conceptualization. Spatial variability enters by drawing one field from a set of multiple, plausible transmissivity fields that are generated outside the Monte Carlo analysis (GRASP-INV). SECO-2DH was used in the 1991 PA.

Second, the flow field is used for a radionuclide-transport simulation. The transport simulator SECO-TP was used for the first time in 1992. It models single- or dual-porosity transport through an idealized, fractured medium. Retardation in pore volume of the dolomite matrix and/or the fracture-lining clay can be included simultaneously or separately. SECO-TP is a further improvement over previous capability in that it is more accurate and numerically efficient, allowing higher-resolution, higher-accuracy simulations in the same time.

Appendix D. A module (GRASP-INV) for generating multiple, plausible transmissivity fields to be used by SECO2-DH is used for the first time in 1992. This module is an improvement over previous capability in that it produces transmissivity fields that reproduce the measured values of transmissivity at well locations and that are calibrated, i.e., flow calculations with these fields reproduce (to within a pre-selected criterion) steady-state and transient pressure data at the well locations. Therefore, each field is a plausible realization of the true but unknown transmissivity field. One entire field is drawn and used for a single consequence calculation during the Monte Carlo analysis.

1.3 Code Linkage and Data Flow

The complexity of the compliance-assessment modeling system for the WIPP requires that calculations be controlled by an executive program (Rechard, 1989; Rechard et al., 1989; Rechard, 1992). CAMCON (Compliance Assessment Methodology CONtroller) controls code linkage and data flow during lengthy and iterative consequence analyses, minimizes analyst intervention during data transfer, and automatically handles quality assurance during the calculations. CAMCON currently consists of about 75 codes and FORTRAN object libraries; it includes approximately 293,000 lines of FORTRAN software written specifically for the WIPP Project and another 175,000 lines of software adapted from other applications.

The controller allows easy examination of intermediate diagnostics and final results. Computer modules within the executive program can be easily replaced for model comparisons. CAMCON modularizes tasks so computer programs for a particular module are interchangeable. CAMCON is fully described in Rechard (1992).

1.3.1 Data Bases

Three data bases, primary, secondary, and computational, are included in CAMCON. The primary data base contains measured field and laboratory data gathered during the disposal-system and regional characterization. Because the analysis can be no better than these data, the data base should contain all necessary data for the compliance assessment and repository design, have as little subjective interpretation as possible, and be quality assured. Data base structure must be flexible to accommodate different organizations and unforeseen types of data. Practical experience suggests that a relational data base is best.

The secondary data base contains interpreted data, usually interpolated onto a regular grid, and incorporates information that comprises the conceptual model of the disposal system. Levels of interpretation can vary from objective interpolation of data combined with subjective judgments to totally subjective extrapolations of data; all interpretations are well documented to ensure the secondary data is reproducible by others. Data from literature or professional judgment are used to fill knowledge gaps to complete the conceptual model. The secondary data base must be accessible to both the analyst and the executive package controlling the system.

The computational data base is CAMDAT (Compliance Assessment Methodology DATa). CAMDAT uses a neutral-file format so that a series of computer programs can be linked by a "zig-zag" connection rather than the usual serial connection. The file format chosen for CAMDAT was based on GENESIS (Taylor et al., 1987) and EXODUS and their associated data manipulation and plotting programs (Gilkey, 1986a,b, 1988; Gilkey and Flanagan, 1987). CAMDAT is fully described in Rechard (1992).

1.3.2 Program Linkage and Model Applications

Program linkage and data flow through CAMDAT are controlled by CAMCON. Computer programs that make up the CAMCON system are major program modules, support program modules, and translators. Major program modules refer to programs that represent major tasks of the consequence modeling. Support program modules refer to programs such as interpolators that are necessary to facilitate use of major program modules. Translator program modules refer to programs that translate data either into or out of the computational data base. Figure 1-1 shows how programs are used in the 1992 PA to evaluate human-intrusion scenarios. BRAGFLO, GRASP-INV, SECO-TP, and CUTTINGS were run outside of CAMCON, with manual data transfer. GENII-S was not used because a safety assessment was not included in the 1992 PA. All other codes were used within CAMCON as shown (Figure 1-1).

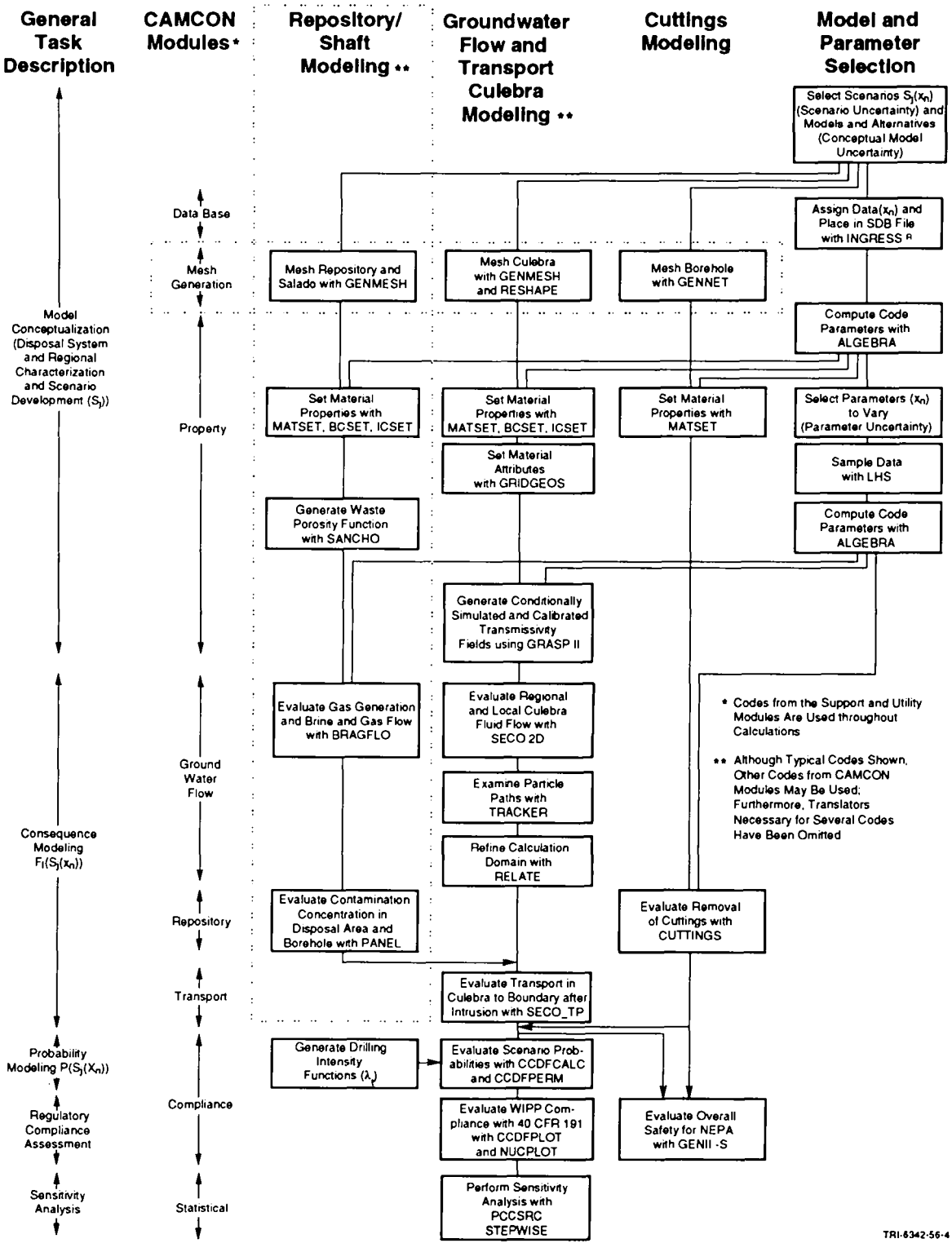

Figure 1-1. 1992 Organization of Programs in CAMCON (after Rechard, 1992).

2. CONCEPTUAL BASIS FOR CONSEQUENCE MODELING

2.1 Introduction

2.1.1 Conceptual Models

This chapter describes the conceptual basis for modeling the performance of the WIPP repository, the waste it contains, and the surrounding geology and hydrology, and summarizes the available knowledge of the site and the physical processes that operate there. This knowledge forms the framework for the preferred conceptual model used in WIPP PA (i.e., the model believed by the WIPP PA Department to be the most realistic representation for the behavior of the disposal system), and for alternative conceptual models. Conceptual model and alternative conceptual models are defined as follows (Gallegos et al., 1992; NEA, 1992):

- Conceptual model: A set of qualitative assumptions used to describe a system or subsystem for a given purpose. At a minimum, these assumptions concern the geometry and dimensionality of the system, initial and boundary conditions, time dependence, and the nature of the relevant physical and chemical processes. The assumptions should be consistent with one another and with existing information within the context of the given purpose.

- Alternative conceptual models: Alternative sets of assumptions that describe the same system for the same purpose, where each set of assumptions is consistent with the existing information.

Each alternative conceptual model identifies the processes that the mathematical models must characterize and provides the context within which the mathematical models must operate.

As an example of the role alternative conceptual models play in performance assessment, Volume 1 of the 1992 WIPP PA documents the use of three alternative conceptual models for the subsurface transport of radionuclides in the Culebra Dolomite Member of the Rustler Formation. (See Section 2.2 for an explanation of the regional geohydrology, Section 4.2 for an explanation of the transport pathway, and Section 7.6 for a discussion of the transport model. See Section 5.1 of Volume 1 of this report for a comparison of disposal-system performance estimated using each of the three conceptual models. See Volume 4 of this report for additional analysis of these and other alternative conceptual models.) In the first conceptual model, transport occurs only in clay-lined fractures in a single-porosity medium, and chemical retardation does not occur. In the second conceptual model, transport occurs in a dual-porosity medium (clay-lined fractures and matrix); radionuclides may diffuse into the pore volume of both the clay linings and the rock matrix. Chemical retardation does not occur. In the third conceptual model, believed by the WIPP PA Department to be the most realistic representation for the behavior of the system, transport occurs in a dual-porosity medium, as in the second conceptual model, except that chemical retardation does occur as a result of sorption of radionuclides in both clay linings and rock matrix.

The first of these three alternative conceptual models is not supported by available information (see Section 2.2.4), and is included in the analysis as an unrealistic, but known, endpoint of a continuum on which a realistic endpoint is unknown. As such, it provides useful guidance on the largest releases that may be anticipated as a result of groundwater transport in the Culebra. Comparison of all three conceptual models provides insight into the uncertainty in performance estimates resulting from an incomplete understanding of the dual-porosity behavior of the Culebra and the lack of defensible data describing chemical retardation of radionuclides (see Section 2.2.4).

Other major aspects of the conceptual model for the WIPP used in the 1992 PA include the following: generation of gas in the waste-emplacement panels by degradation of waste and containers; closure and re-expansion of the panels by salt creep; the release of radionuclides at the ground surface and into the Culebra as a result of borehole intrusion during exploratory drilling; changes in groundwater flow resulting from future climatic changes; and the effect of passive marker systems on intrusion rates.

2.1.2 Chapter Organization

The WIPP and surrounding environment provide multiple barriers to radionuclide migration. This chapter explains the WIPP PA's present understanding of the conceptual basis of these barriers. The chapter is organized into two major parts:

- natural barrier system (Section 2.2)—the regional geology and hydrology surrounding the WIPP (Section 2.2.1); the stratigraphy below and above the repository (Section 2.2.2); climate, water balance, and groundwater flow in the WIPP vicinity (Section 2.2.3); and radionuclide transport in the Culebra Dolomite (Section 2.2.4)

- engineered barrier system (Section 2.3)— the repository and seal design (Section 2.3.2); the waste itself (Section 2.3.3); the radionuclide source term (Section 2.3.4); and closure, flow, and room/waste interactions (Section 2.3.5)

2.2 Natural Barrier System

2.2.1 Regional Geology

The geology of the WIPP and the surrounding area has been introduced briefly in Chapter 2 of Volume 1, and is described elsewhere in detail (e.g., Hiss, 1975; Powers et al., 1978a,b; Cheeseman, 1978; Williamson, 1978; Hills, 1984; Ward et al., 1986; Harms and Williamson, 1988; Holt and Powers, 1988, 1990; Beauheim and Holt, 1990; Brinster, 1991). The brief review presented here describes regional structural features and introduces the major stratigraphic units. Specific geologic features that affect compliance-assessment modeling are described in subsequent sections of this chapter.

The WIPP is located near the northern end of the Delaware Basin, a structural depression that formed during the Late Pennsylvanian and Permian Periods, approximately 300 to 245 million years ago (Figures 2-1 and 2-2). Sedimentation within the subsiding basin resulted in the deposition of up to 4,000 m (13,000 ft) of marine strata. Organic activity at the basin margins produced massive carbonate reefs that separated deep-water facies from the shallow-water shelf sediments deposited landward.

Permian-age rocks of importance to WIPP performance-assessment modeling are those of the Guadalupian and Ochoan Series, deposited between approximately 265 and 245 million years ago (Figure 2-3). During this time subsidence in the Delaware Basin was initially rapid, resulting in deposition of deep-water shales, sandstones, and limestones of the Delaware Mountain Group. Intermittent connection with the open ocean and a decrease in clastic sediment supply, possibly in response to regional tectonic adjustments, led to the deposition of a thick evaporite sequence. Anhydrites and halites of the Castile Formation are limited to the structurally deeper portion of the basin, enclosed within the reef-facies rocks of the Capitan Limestone. Subsidence within the basin slowed in Late Permian time, and the halites of the Salado Formation, which include the host strata for the WIPP, extend outward from the basin center over the Capitan Reef and the shallow-water shelf facies. Latest Permian-age evaporites, carbonates, and clastic rocks of the Rustler Formation and the Dewey Lake Red Beds record the end of regional subsidence and include the last marine rocks deposited in southeastern New Mexico during the Paleozoic. The overlying sandstones of the Triassic-age Dockum Group reflect continental deposition and mark the onset of a period of regional tectonic stability that lasted approximately 240 million years, until late in the Tertiary Period.

Permian-age strata of the Delaware Basin now dip gently (generally less than 1^{o}) to the east, and erosion has exposed progressively older units toward the western edge of the basin (Figures 2-1 and 2-4). This tilting reflects the Late Pliocene and early Pleistocene (approximately 3.5 million to 1 million years ago) uplift of the Capitan Reef to form the Guadalupe Mountains more than 60 km (37 miles) west of the WIPP (Figures 2-1, 2-4). Field evidence suggests that additional uplift may have occurred during the late Pleistocene and Holocene, and some faults of the Guadalupe Mountains may have been active within the last 1,000 years (Powers et al., 1978a,b). North and east of the WIPP, the Capitan Reef has not been uplifted and remains in the subsurface (Figure 2-5).

The present landscape of the Delaware Basin has been influenced by near-surface dissolution of the evaporites (Bachman, 1984, 1987). Karst features created by dissolution include sinkholes, subsidence valleys, and breccia pipes. Most of these features formed during wetter climates of the Pleistocene, although active dissolution is still occurring wherever evaporites are exposed at the surface. Some dissolution may also be occurring in the subsurface where circulating groundwater comes in contact with evaporites: for example, modern subsidence in San Simon Swale east of the WIPP (Figure 2-6) may be related to localized dissolution of the Salado Formation (Anderson, 1981; Bachman, 1984; Brinster, 1991). Nash Draw, which formed during the Pleistocene by dissolution and subsidence, is the most prominent karst feature near the WIPP. As discussed again in Section 2.2.2.6 following, evaporites in the Rustler Formation have been affected by dissolution near Nash Draw.

The largest karst feature in the Delaware Basin is the Balmorhea-Loving Trough, south of the WIPP along the axis of the basin (Figure 2-6). Dissolution of evaporites, perhaps along the course of a predecessor of the modern Pecos River, resulted in subsidence and the deposition of Cenozoic alluvium up to 300 m (984 ft) thick in south-

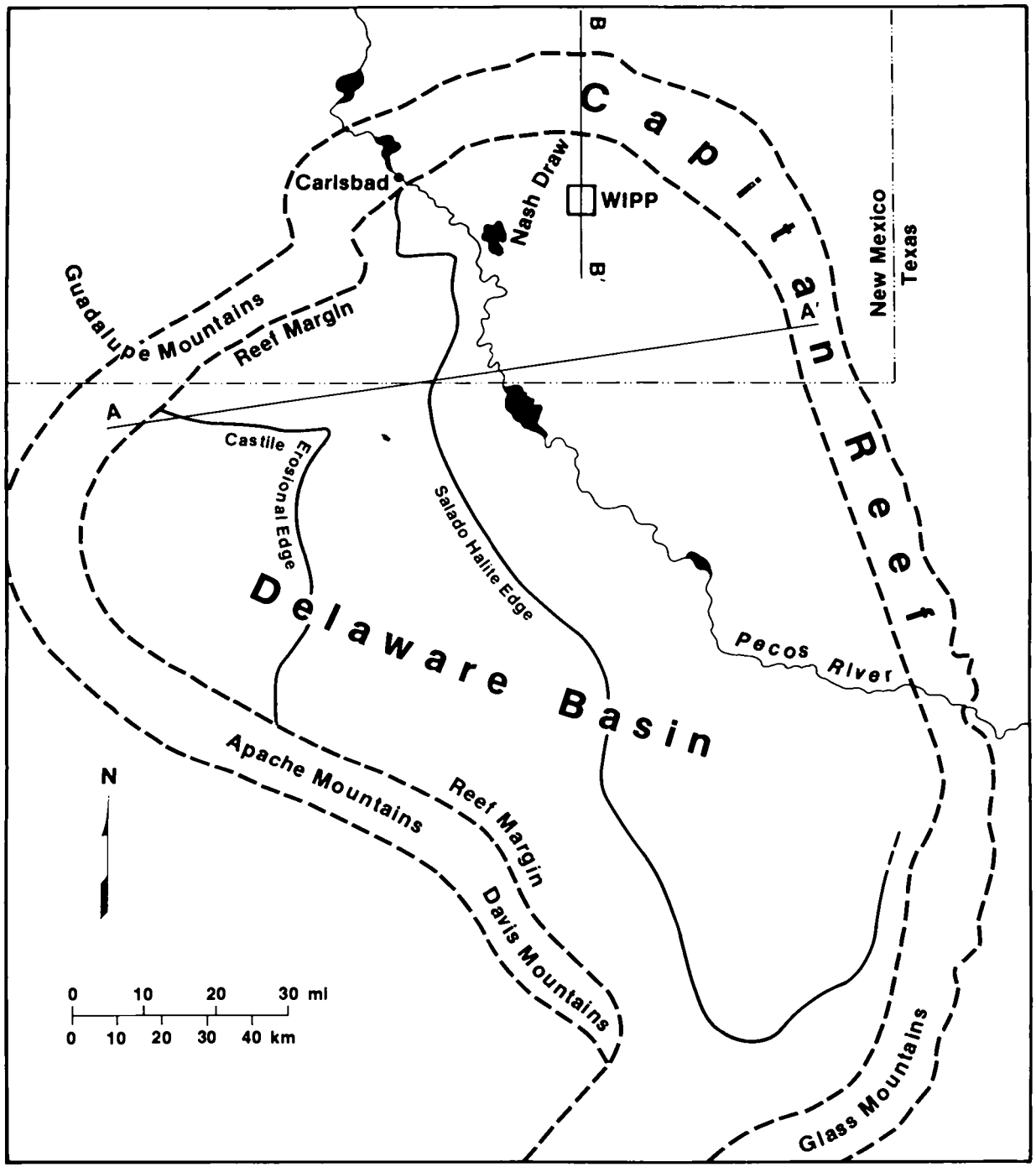

TRI-6342-237-4

Figure 2-1. Generalized geology of the Delaware Basin, showing the location of the Capitan Reef and the erosional limits of the basinal formations (Lappin, 1988).

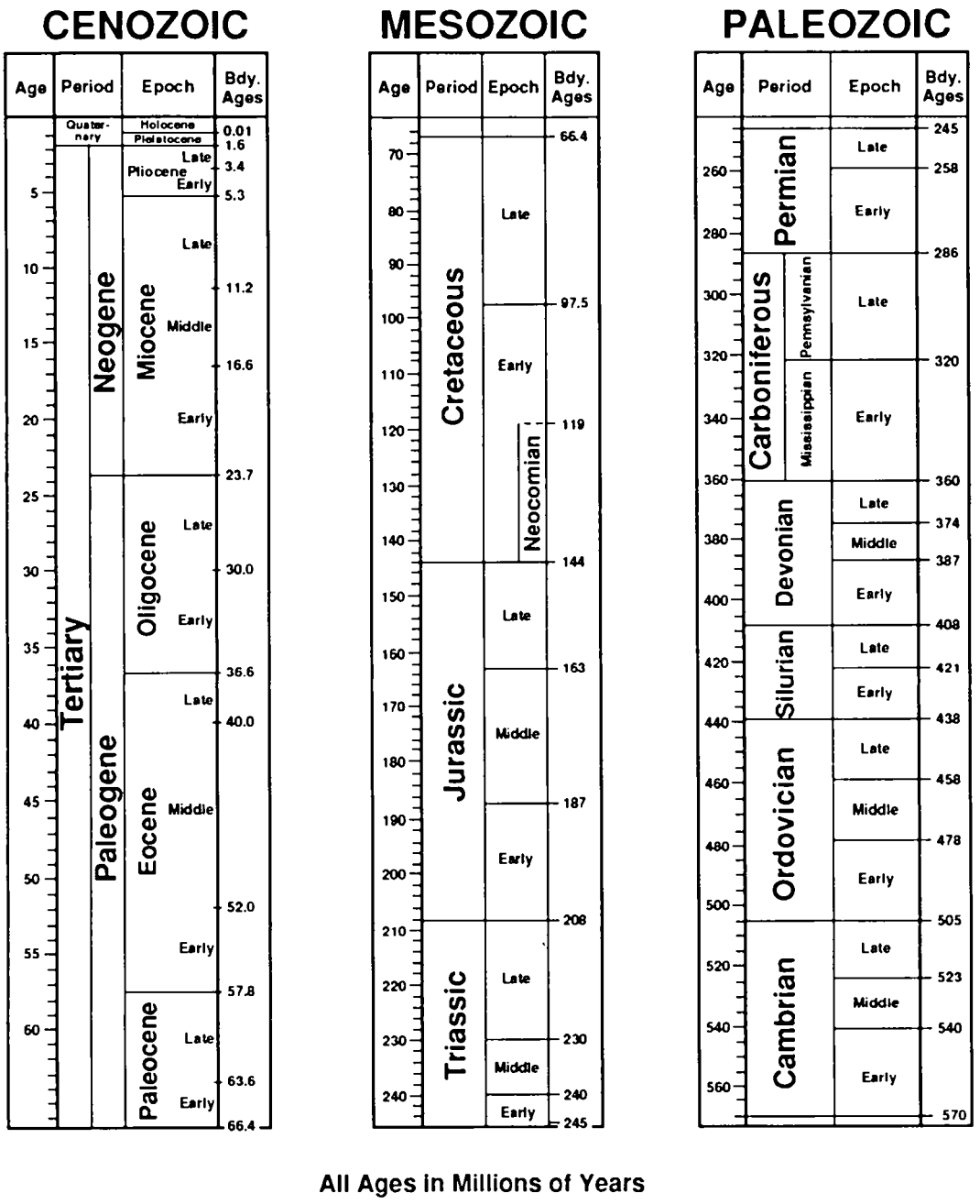

Figure 2-2. Geologic time scale (simplified from Geological Society of America, 1984).

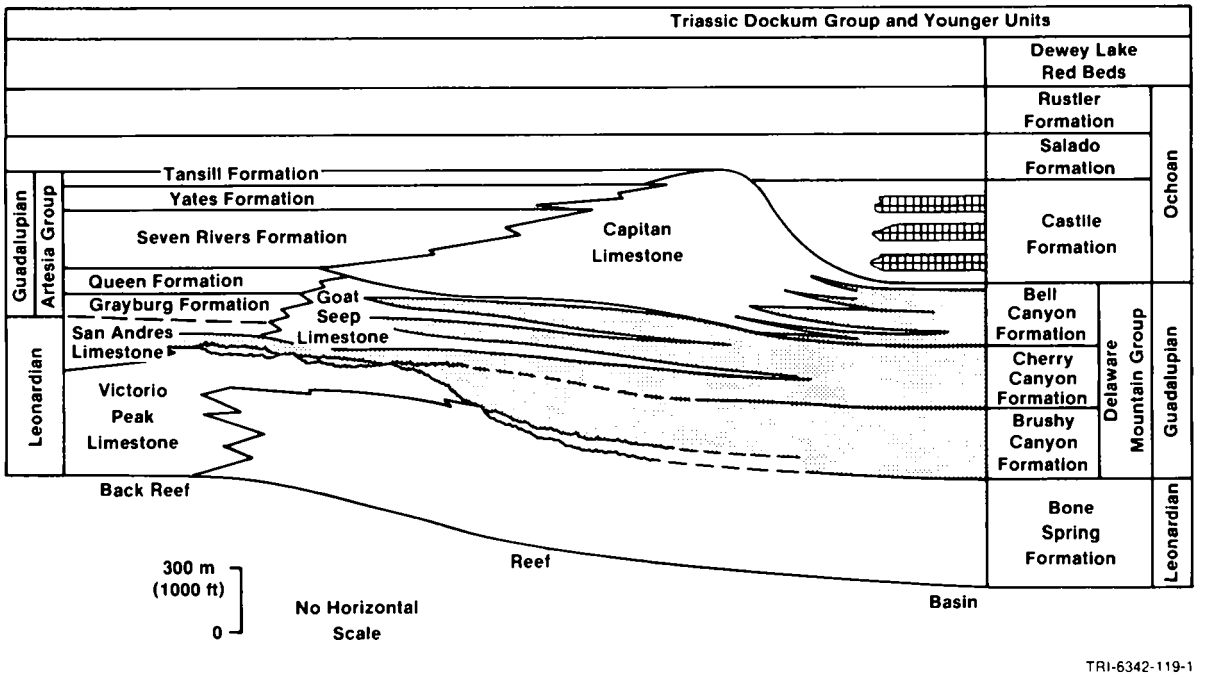

Figure 2-3. Stratigraphy of the Delaware Basin (modified from Mercer, 1983; Brinster, 1991)

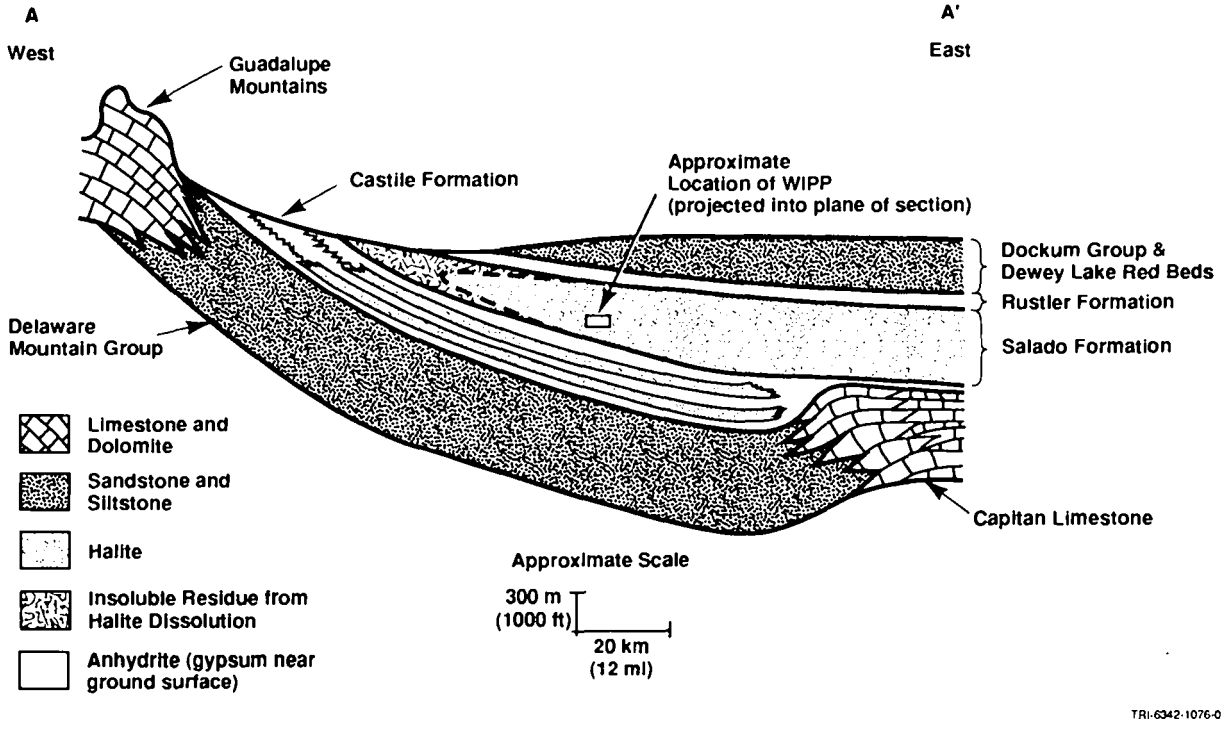

Figure 2-4. Schematic east-west cross section through the northern Delaware Basin (modified from Davies, 1984). Note extreme vertical exaggeration. Approximate location of line of section shown on Figure 2-1.

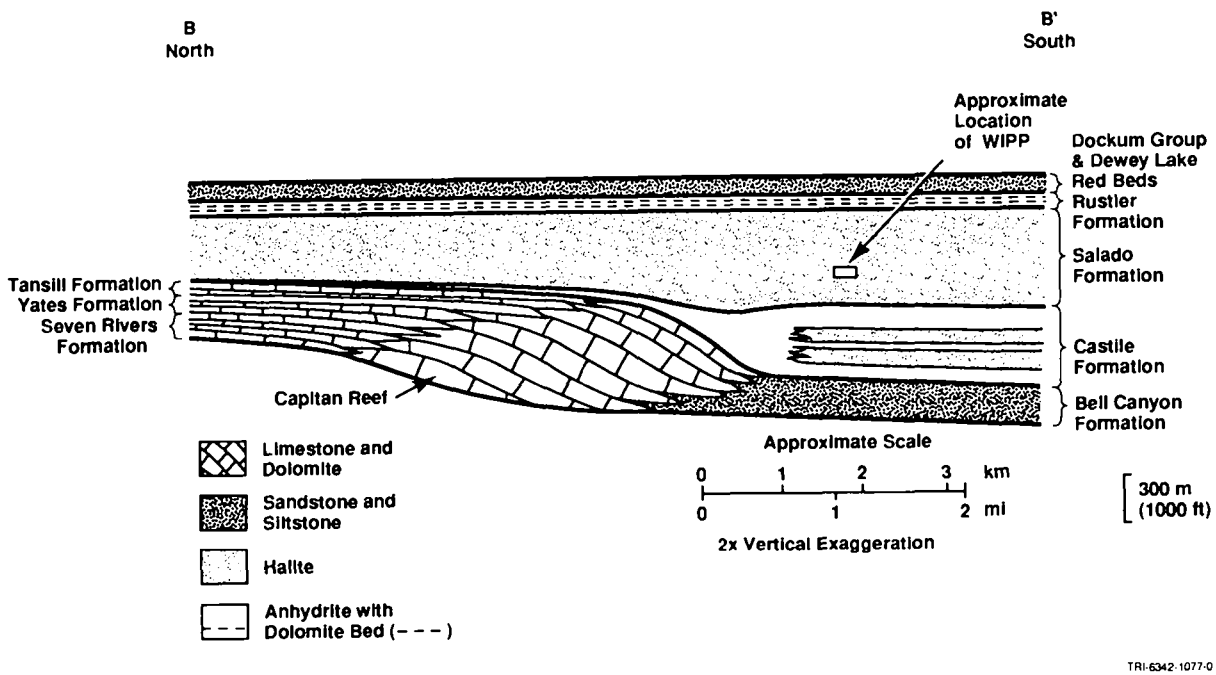

Figure 2-5. Schematic north-south cross section through the Northern Delaware Basin (modified from Davies, 1984). Note extreme vertical exaggeration. Approximate location of line of section shown on Figure 2-1.

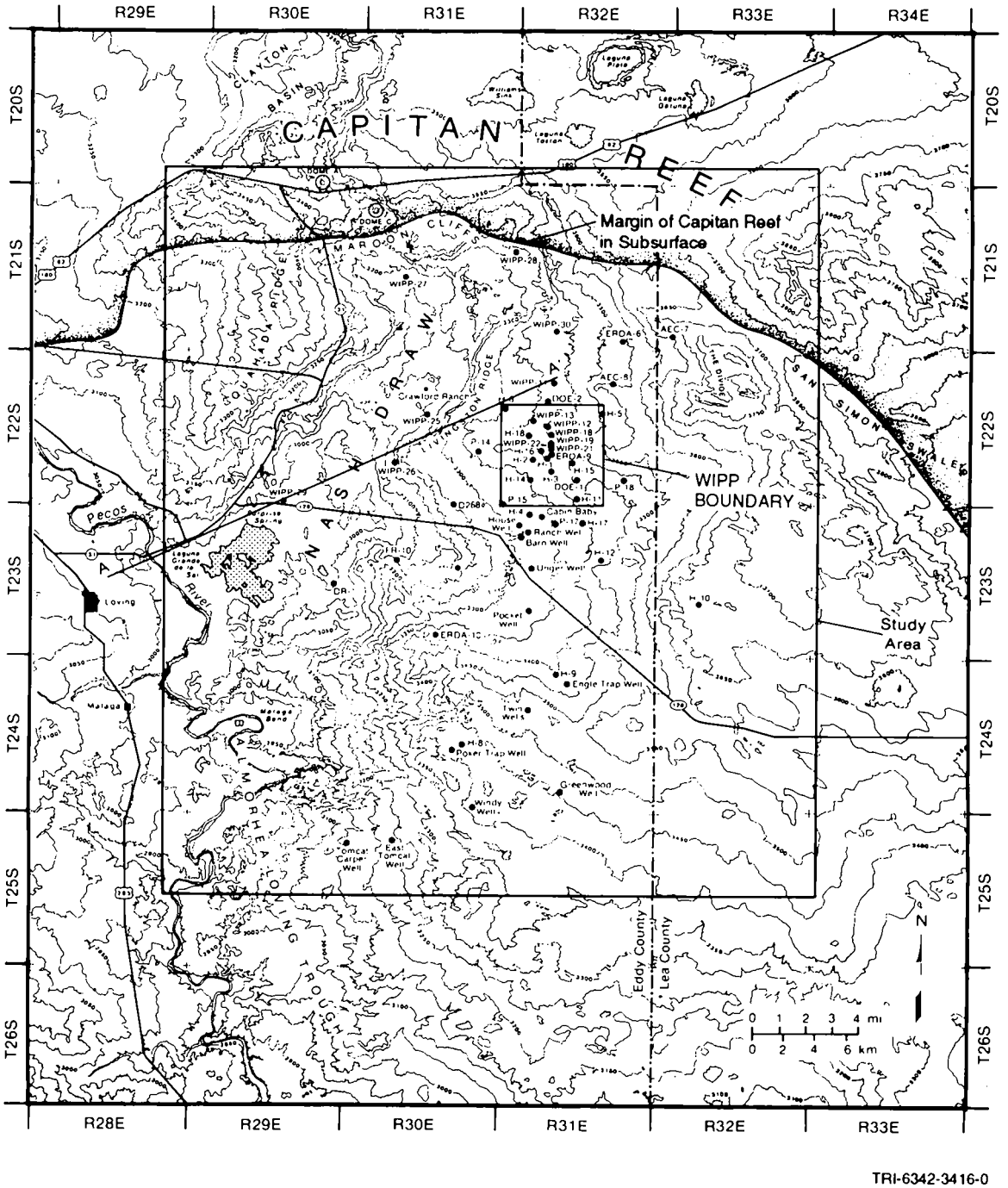

TRI-6342-3416-0

Figure 2-6. Map of the WIPP vicinity showing the land-withdrawal area (labeled "WIPP Boundary"), the study area of Brinster (1991), and the location of observation wells (Haug et al., 1987; Brinster, 1991).

ern Eddy County, and up to almost 600 m (1970 ft) thick across the state line in Texas (Bachman, 1984, 1987; Brinster, 1991).

2.2.2 Stratigraphy

This review is based primarily on the summary presented by Brinster (1991), and is limited to those units that may have an important role in future performance of the disposal system. Hydrologic data about the units have been summarized by Brinster (1991), and are, in general, not repeated here. Stratigraphic relationships between the units are shown in Figure 2-3. Figure 2-6 shows the region examined in detail by Brinster (1991) and the location of wells that provide basic data.

2.2.2.1 BELL CANYON FORMATION

The Bell Canyon Formation consists of 210 to 260 m (690 to 850 ft) of sandstones and siltstones with minor limestones, dolomites, and conglomerates (Williamson, 1978; Mercer, 1983; Harms and Williamson, 1988). Sandstones within the upper portion of the Bell Canyon Formation occur as long, sinuous channels separated by siltstones, reflecting their deposition by density currents that flowed into the deep basin from the Capitan Reef (Harms and Williamson, 1988). These sandstones have been targets for hydrocarbon exploration elsewhere in the Delaware Basin and are also of interest for the WIPP performance assessment because they are the first aquifers below the evaporite sequence that hosts the repository.

Simulations of undisturbed repository performance do not include the Bell Canyon Formation because a thick sequence of evaporites with very low permeability separates the formation from the overlying units. Simulations of human intrusion scenarios do not include a borehole pathway for fluid migration between the Bell Canyon Formation (or deeper units) and the repository. Relatively little is known about the head gradient that would drive flow along this pathway, but data from five wells in the Bell Canyon Formation suggest that flow would be slight, and, in an uncased hole, downward because of brine density effects (Mercer, 1983; Beauheim, 1986; Lappin et al., 1989).

2.2.2.2 CAPITAN LIMESTONE

The Capitan Limestone is not present at the WIPP, but is a time-stratigraphic equivalent of the Bell Canyon Formation to the west, north, and east (Figures 2-1, 2-3). The unit is a massive limestone ranging from 76 to 230 m (250 to 750 ft) thick. Dissolution and fracturing have enhanced effective porosity, and the Capitan is a major aquifer in the region, providing the principal water supply for the city of Carlsbad. Upward flow of groundwater from the Capitan aquifer may be a factor in dissolution of overlying halite and the formation of breccia pipes. Existing breccia pipes are limited to the vicinity of the reef, as is the active subsidence in San Simon Swale (Figure 2-6) (Brinster, 1991).

2.2.2.3 CASTILE FORMATION

The Castile Formation is approximately 470 m (1540 ft) thick at the WIPP and contains anhydrites with intercalated limestones near the base and halite layers in the upper portions. Primary porosity and permeability in the Castile Formation are extremely low. However, approximately 18 wells in the region have encountered brine reservoirs in fractured anhydrite in the Castile Formation (Brinster, 1991). Hydrologic and geochemical data have been interpreted as indicating that these brine occurrences are hydraulically isolated (Lambert and Mercer, 1978; Lappin, 1988). Fluid may have been derived from interstitial entrapment of connate water after deposition (Popielak et al., 1983), dehydration of the original gypsum to anhydrite (Popielak et al., 1983), or intermittent movement of meteoric waters from the Capitan aquifer into the fractured anhydrites between 360,000 and 880,000 years ago (Lambert and Carter, 1984). Pressures within these brine reservoirs are greater than those at comparable depths in other relatively permeable units in the region and range from 7 to 17.4 MPa (Lappin et al., 1989).

Pressurized brine in the Castile Formation is of concern for performance assessment because occurrences have been found at WIPP-12 within the WIPP land-withdrawal area and at ERDA-6 and other wells in the vicinity. The WIPP-12 reservoir is at a depth of 918 m (3012 ft), about 250 m (820 ft) below the repository horizon, and is estimated to contain 2.7×10^{6} m^3 (1.7×10^{7} barrels) of brine at a pressure of 12.7 MPa (Lappin et al., 1989). This pressure is greater than the nominal freshwater hydrostatic pressure at that depth (9 MPa) and is slightly greater than the nominal hydrostatic pressure for a column of equivalent brine at that depth (11.1 MPa). The brine is saturated, or nearly so, with respect to halite, and has little or no potential to dissolve the overlying salt (Lappin et al., 1989). Brine could, however, reach the repository, overlying strata, and the ground surface through an intrusion borehole.

Early geophysical surveys mapped a structurally disturbed zone in the vicinity of the WIPP that may correlate with fracturing or development of secondary porosity within the Castile Formation; this zone could possibly contain pressurized brine (Borns et al., 1983). Later electromagnetic surveys indicated that the brine present at WIPP-12 could underlie part of the waste panels (Earth Technology Corporation, 1988). WIPP-12 data are therefore used to develop a conceptual model of the brine reservoir for analyzing scenarios that include the penetration of pressurized brine. Data describing the Castile Formation brine reservoir are summarized in Volume 3, Section 4.3 of this report.

2.2.2.4 SALADO FORMATION

The Salado Formation is about 600 m (1970 ft) thick at the WIPP and contains halite interbedded with anhydrite, polyhalite, glauberite, and some thin mudstones (Adams, 1944; Bachman, 1981; Mercer, 1983). Unlike the underlying Castile Formation, the Salado Formation overlaps the Capitan Limestone and extends eastward beyond the reef for many kilometers into west Texas (Figure 2-3). Erosion has removed the Salado Formation from the western portion of the basin (Figure 2-1).

Where the Salado Formation is intact and unaffected by dissolution, natural groundwater flow is negligible because primary porosity and open fractures are lacking in the plastic salt (Mercer, 1983; Brinster, 1991). The formation is not dry, however. Interstitial brine seeps into the repository at rates up to approximately 0.01

ℓ/day/for each m (in length) of excavation (Bredehoeft, 1988; Nowak et al., 1988), and the Salado is assumed to be saturated (Brinster, 1991). Porosity is estimated to be approximately 0.01 (expressed as void volume per unit volume of rock). Permeability of the formation is very low but measurable, with an average value of 0.05 microdarcies (5×10^{-20} m^2) reported by Powers et al. (1978a,b) from well tests. This value corresponds approximately to a hydraulic conductivity 5×10^{-13} m/s (1×10^{-7} ft/d) (Freeze and Cherry, 1979, Table 2.3). In situ testing of halite in the repository indicates lower permeabilities ranging from 1 to 100 nanodarcies (10^{-22} to 10^{-20} m^2) (Stormont et al., 1987; Beauheim et al., 1991). Additional information about the geology of the Salado Formation at the repository is provided in Section 2.3.1, and in Volume 3, Section 2.3 of this report.

2.2.2.5 RUSTLER-SALADO CONTACT ZONE

In the vicinity of Nash Draw, the contact between the Rustler and Salado Formations is an unstructured residuum of gypsum, clay, and sandstone created by dissolution of halite. The residuum becomes thinner to the east and intertongues with clayey halite of the unnamed lower member of the Rustler Formation. Mercer (1983) concluded, on the basis of brecciation at the contact, that dissolution in Nash Draw occurred after deposition of the Rustler Formation. In shafts excavated at the WIPP, the residuum shows evidence of channeling and filling, fossils, and bioturbation, indicating that some dissolution occurred before Rustler deposition (Holt and Powers, 1988).

The residuum ranges in thickness in the vicinity of the WIPP from 2.4 m (7.9 ft) in P-14 east of Nash Draw to 33 m (108 ft) in WIPP-29 within Nash Draw (Mercer, 1983). Measured hydraulic conductivity values for the residuum are highest at Nash Draw (up to 10^{-6} m/s [10^{-1} ft/d]), and three to six orders of magnitude lower to the east (Brinster, 1991). Porosity estimates range from 0.15 to 0.33 (Robinson and Lang, 1938; Hale and Clebsch, 1958; Geohydrology Associates, Inc., 1979; Mercer, 1983).

2.2.2.6 RUSTLER FORMATION

The Rustler Formation is of particular importance for WIPP PA because it contains the most transmissive units above the repository and therefore provides the most likely pathway for the subsurface transport of radionuclides to the accessible environment.

The Rustler Formation is 95 m (312 ft) thick at the WIPP (as measured in ERDA-9) and ranges in the area from a minimum of 8.5 m (28 ft) where thinned by dissolution and erosion west of the repository to a maximum of 216 m (709 ft) to the east (Brinster, 1991). Overall, the formation is composed of about 40 percent anhydrite, 30 percent halite, 20 percent siltstone and sandstone, and 10 percent anhydritic dolomite (Lambert, 1983). On the basis of outcrops in Nash Draw west of the WIPP, the formation is divided into four formally named members and a lower unnamed member (Vine, 1963). These five units (Vine, 1963; Mercer, 1983) are, in ascending order, the unnamed lower member (oldest), the Culebra Dolomite Member, the Tamarisk Member, the Magenta Dolomite Member, and the Forty-niner Member (youngest) (Figure 2-7, Table 2-1).

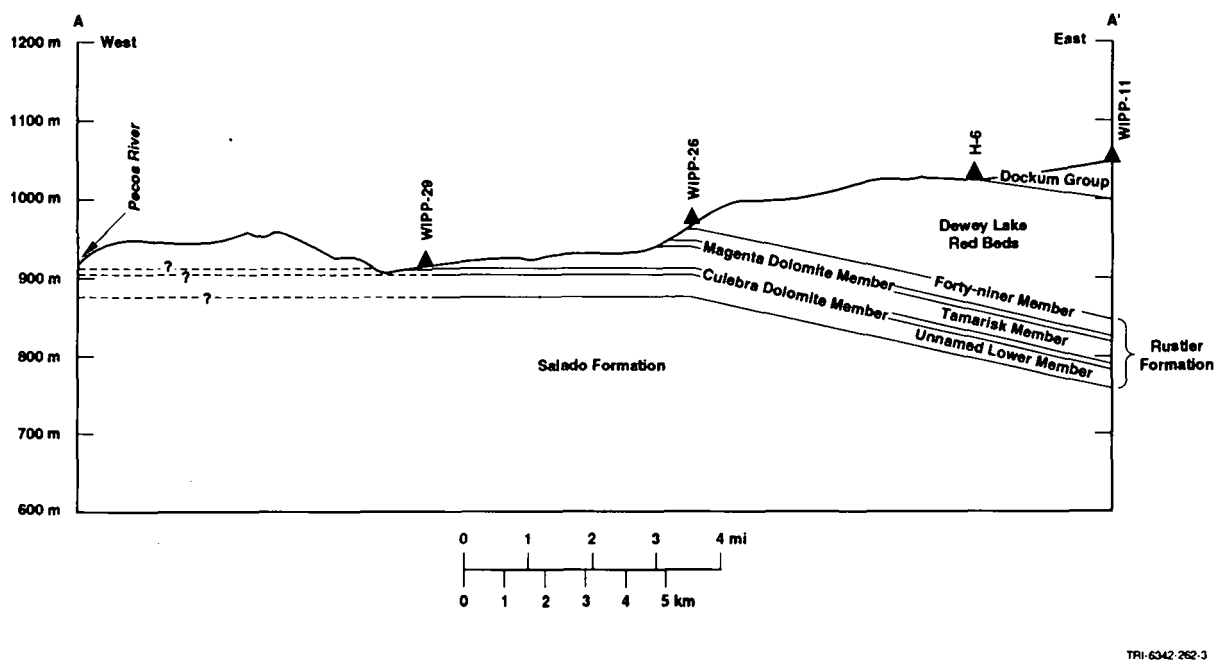

Figure 2-7. East-west cross section showing stratigraphy of the Rustler Formation and the Dewey Lake Red Beds (modified from Brinster, 1991). Note vertical exaggeration. Location of cross section is shown on Figure 2-6.

Table 2-1. Properties of the Rustler Formation Units and Rustler-Salado Contact Zone. (Sources for data provided in text.)

Member Name	Thickness (max/min) (m)	Hydraulic Conductivity (max/min) (m/s)	Porosity (max/min)
Forty-niner	20	5.0×10^{-9} 5.0×10^{-10}	—
Magenta	8 4	5.0×10^{-5} 5.0×10^{-10}	—
Tamarisk	84 8		—
Culebra	11.6 4	1×10^{-4} 2×10^{-10}	0.30 0.03
Unnamed	36	1×10^{-11} 6×10^{-15}	—
Rustler-Salado Contact Zone	33 2.4	1×10^{-6} 1×10^{-12}	0.33 0.15

The Unnamed Lower Member

The unnamed lower member is about 36 m (118 ft) thick at the WIPP and thickens slightly to the east. The unit is composed mostly of fine-grained silty sandstones and siltstones interbedded with anhydrite (converted to gypsum at Nash Draw) west of the WIPP. Increasing amounts of halite are present to the east. Halite is present over the WIPP (Figure 2-8), but is absent north and south of the WIPP where the topographic expression of Nash Draw extends eastward. Distribution of halite within this and other members of the Rustler Formation is significant because, as is discussed in the following section, an apparent correlation exists between the absence of halite and increased transmissivity in the Culebra Dolomite Member.

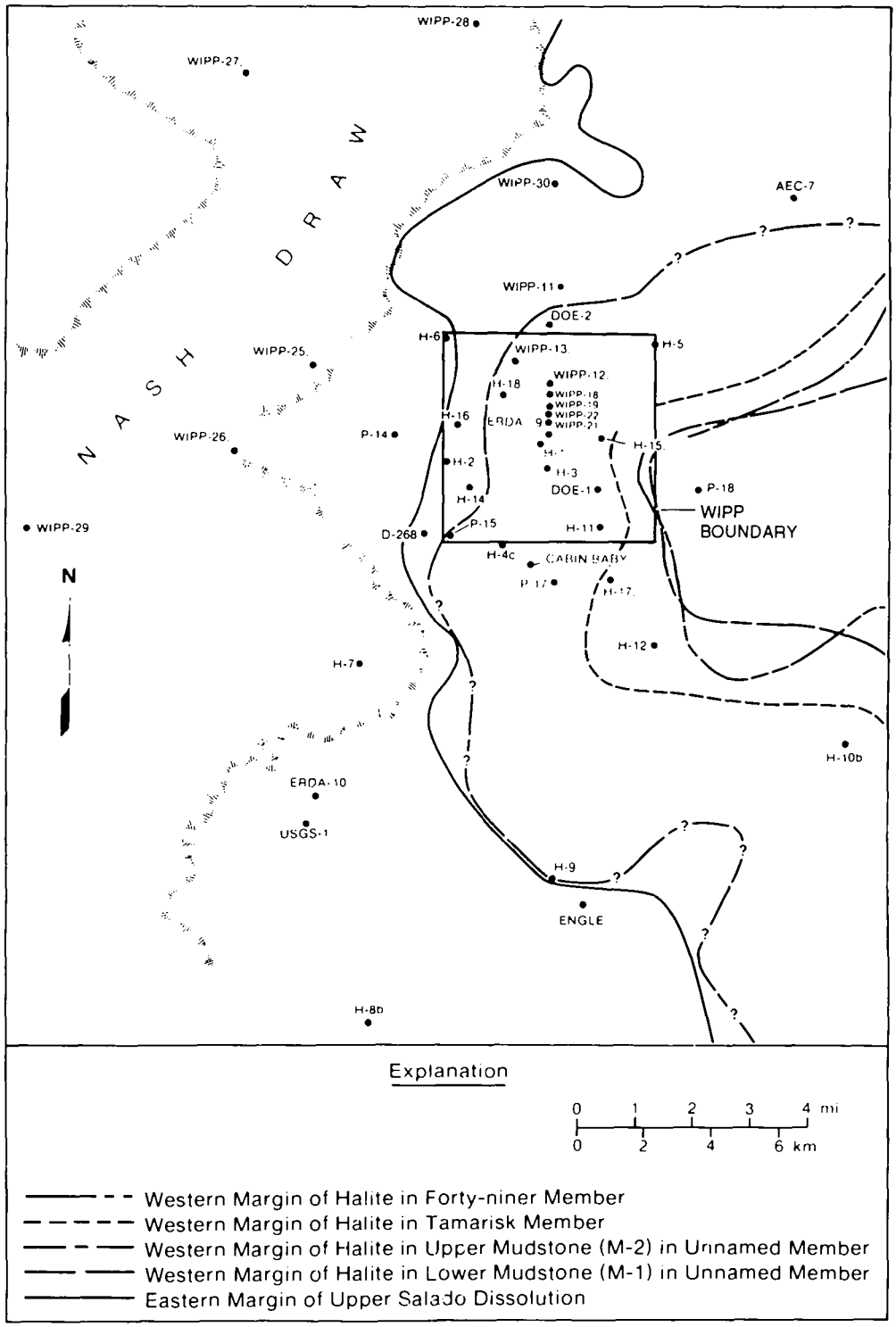

Figure 2-8. Rustler Formation halite around the WIPP (Lappin et al., 1989).

The basal interval of the unnamed lower member contains siltstone and sandstone of sufficient transmissivity to allow groundwater flow. Transmissivities of 2.9×10^{-10} m^2/s (2.7×10^{-4} ft^2/d) and 2.4×10^{-10} m^2/s (2.2×10^{-4} ft^2/d) were calculated from tests at H-16 that included this interval (Beauheim, 1987a). Assuming all flow in the 34-m (112-ft) test interval came from the 20 m (64 ft) of the basal interval, these transmissivity values correspond to hydraulic conductivities of 1.5×10^{-11} m/s (4.2×10^{-6} ft/d) and 1.2×10^{-11} ms (3.4×10^{-6} ft/d). Hydraulic conductivity in the lower portion of the unnamed member is believed to increase to the west in and near Nash Draw, where dissolution in the underlying Rustler-Salado contact zone has caused subsidence and fracturing of the sandstone and siltstone (Beauheim and Holt, 1990).

The remainder of the unnamed lower member contains mudstones, anhydrite, and variable amounts of halite. Hydraulic conductivity of these lithologies is extremely low: tests of mudstones and claystones in the waste-handling shaft gave hydraulic conductivity values ranging from 6×10^{-15} m/s (2×10^{-9} ft/d) to 1×10^{-13} m/s (3×10^{-8} ft/d) (Saulnier and Avis, 1988; Brinster, 1991).

Culebra Dolomite Member

The Culebra Dolomite Member of the Rustler Formation is microcrystalline dolomite or dolomitic limestone with solution cavities (Vine, 1963). In the vicinity of the WIPP, it ranges in thickness from 4 to 11.6 m (13 to 38.3 ft) and has a mean thickness of about 7 m (23 ft). Outcrops of the Culebra Dolomite occur in the southern part of Nash Draw and along the Pecos River.

The Culebra Dolomite has been identified as the most likely pathway for release of radionuclides to the accessible environment because of its relatively high hydraulic conductivity near the WIPP, and hydrologic research has concentrated on the unit for over a decade (Mercer and Orr, 1977, 1979; Mercer, 1983; Mercer et al., 1987; Beauheim, 1987a,b; LaVenue et al., 1988, 1990; Davies, 1989; Cauffman et al., 1990). Hydraulic data are available from 41 well locations in the WIPP vicinity (Cauffman et al., 1990).

Hydraulic conductivity of the Culebra varies six orders of magnitude from east to west in the vicinity of the WIPP (Figure 2-9), ranging from 2×10^{-10} m/s (6×10^{-5} ft/d) at P-18 east of the WIPP to 1×10^{-4} m/s (6×10^{1} ft/d) at H-7 in Nash Draw (Brinster, 1991). Present understanding of the geologic controls on this variation in conductivity is based primarily on studies of core samples from 17 boreholes, exposures in the walls of three shafts excavated at the WIPP, and approximately 600 geophysical logs from boreholes throughout the vicinity (Figure 2-10) (Holt and Powers, 1988; Powers and Holt, 1990; Beauheim and Holt, 1990).

Measured matrix porosities of the Culebra Dolomite range from 0.03 to 0.30 (Lappin et al., 1989; Kelley and Saulnier, 1990). Fracture porosity values have not been measured directly, but interpreted values from tracer tests at the H-3 and H-11 hydropads are 2×10^{-3} and 1×10^{-3}, respectively (Kelley and Pickens, 1986). Data are insufficient to map spatial variability of porosity.

Variations in hydraulic conductivity in the Culebra are believed to be controlled by the relative abundance of open fractures (Snyder, 1985; Beauheim and Holt, 1990; Brinster, 1991) rather than by primary (i.e., depositional) features of the unit. Lateral variations in depositional environments were small within the mapped region, and

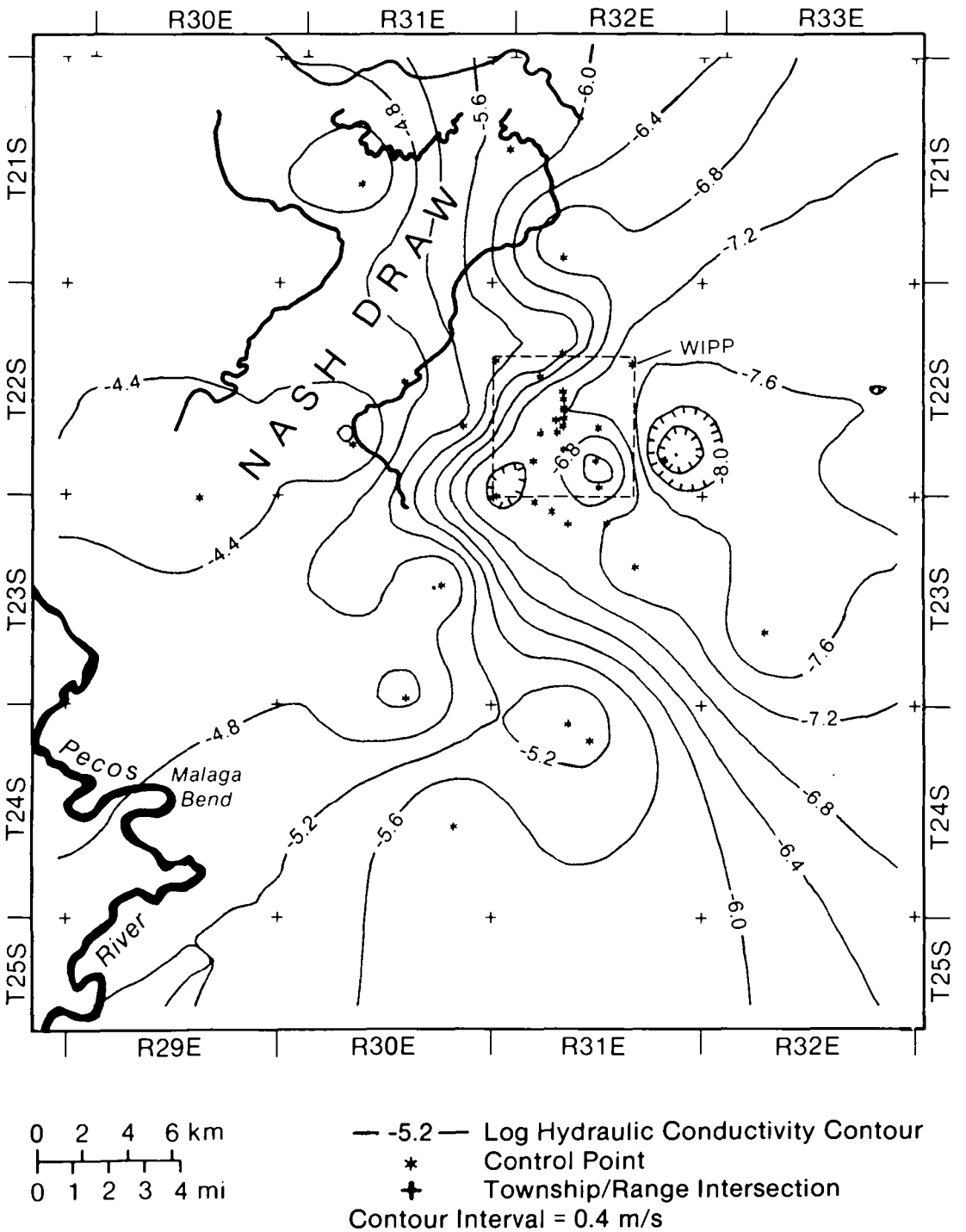

Figure 2-9. Log hydraulic conductivities (measured in m/s) of the Culebra Dolomite Member of the Rustler Formation (Brinster, 1991).

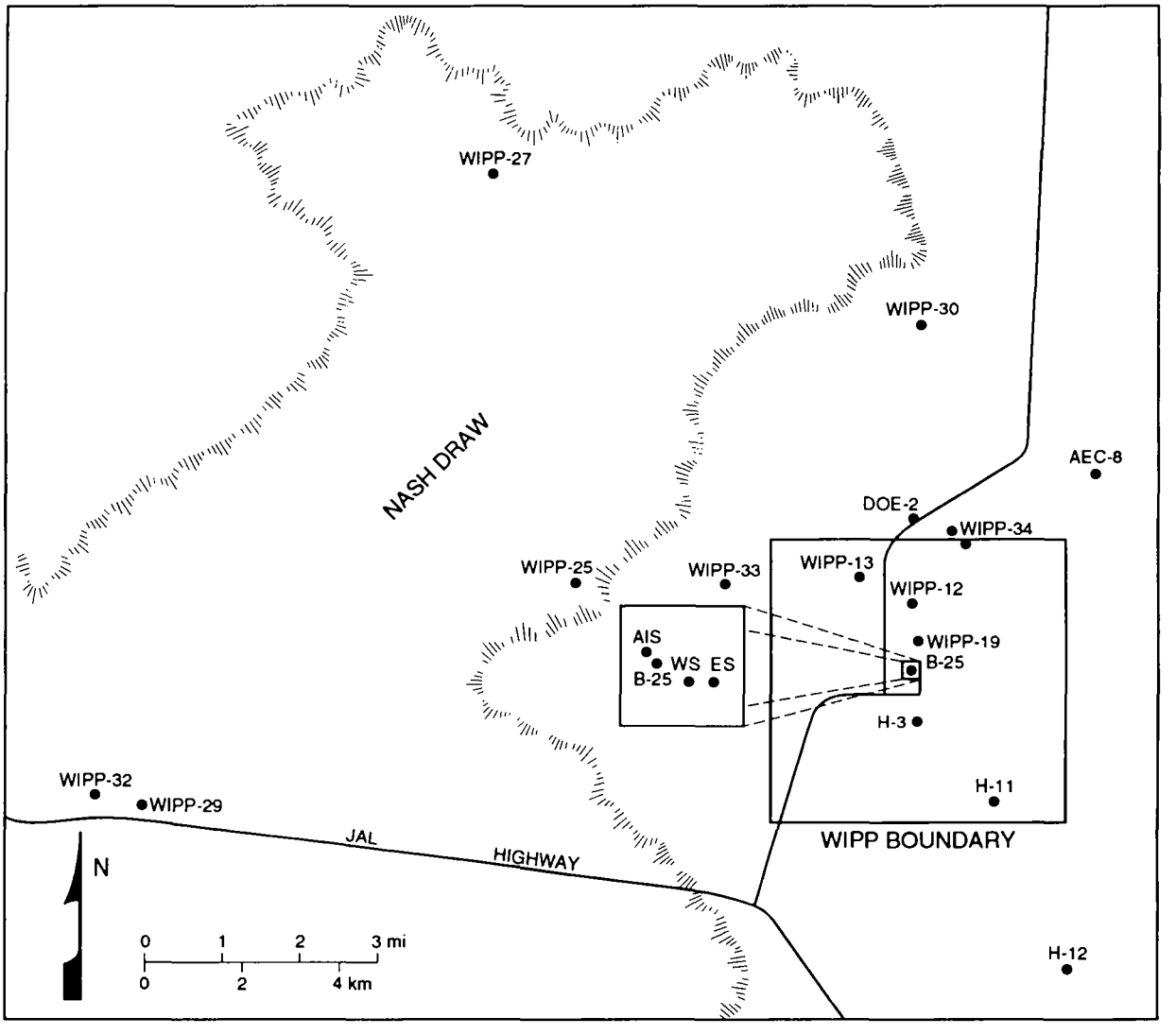

TRI-6342-3431-0

Figure 2-10. Sources of geologic information about the Culebra Dolomite, including boreholes from which core samples are available, and shafts studied during excavation. AIS, ES, and WS refer to the air intake, exhaust, and waste shafts, respectively.

primary features of the Culebra show little map-scale spatial variability (Holt and Powers, 1988). Direct measurements of the density of open fractures are not available from core samples because of incomplete recovery and fracturing during drilling, but comparisons between highly fractured outcrops of the Culebra in southern Nash Draw and the relatively unfractured exposures in the WIPP shafts suggests that density of open fractures in the Culebra decreases to the east. Qualitative correlations have been noted between hydraulic conductivity and several geologic features possibly related to open-fracture density, including (1) the distribution of overburden above the Culebra (Figure 2-11) (Holt and Powers, 1988; Beauheim and Holt, 1990); (2) the distribution of halite in other members of the Rustler Formation (compare Figures 2-8 and 2-9) (Snyder, 1985); (3) the dissolution of halite in the upper portion of the Salado Formation (Figure 2-12) (Beauheim and Holt, 1990); and (4) the distribution of gypsum fillings in fractures in the Culebra (Figure 2-13) (Beauheim and Holt, 1990).

Regional tilting of the Delaware Basin during the Late Pliocene and early Pleistocene (see Section 2.2.1) and subsequent erosion have resulted in a westward decrease in overburden above the Culebra (Figure 2-13). The decrease in confining stress during erosional unloading may have caused fracturing in the Culebra (Beauheim and Holt, 1990), and may also have controlled the degree to which fractures opened. Locally, however, variations in conductivity do not correlate precisely with variations in overburden thickness, and other geologic phenomena must contribute (Beauheim and Holt, 1990).

Where the present distribution of halite in the Rustler Formation (Figure 2-8) results from post-depositional dissolution, subsidence over areas of dissolution may have caused fracturing in the Culebra (Snyder, 1985). Mapping of depositional environments in the Rustler Formation indicates, however, that the present limits of halite in the formation coincide, in general, with a depositional transition from evaporites to mudstones near the margins of a saline pan (Holt and Powers, 1988; Powers and Holt, 1990). Dissolution of the upper portion of the Salado Formation (Figure 2-12), as inferred from stratigraphic thinning observed in geophysical logs, may also have caused subsidence and fracturing in the Culebra (Beauheim and Holt, 1990).

Detailed examination of core samples from the Culebra shows that the percentage of fractures that are filled with post-depositional gypsum crystals increases eastward across the site (Figure 2-13) (Beauheim and Holt, 1990). Furthermore, the crystalline structure of the fracture fillings changes across the site, suggesting that the present conductivity distribution may reflect spatial variability in the processes that formed fracture fillings. East of the WIPP, fracture-filling crystals have predominantly incremental growth forms, indicating gradual growth as the fractures opened and no subsequent dissolution. Fractures with incremental fillings probably have had relatively small apertures and little groundwater flow through them throughout their history. From the WIPP west, fracture fillings, where present, are predominantly passive gypsum crystals that grew in pre-existing void spaces. By implication, any early, incremental fillings in these fractures must have been dissolved at some time in the past, and the fractures may have had relatively large groundwater flow through them before passive crystal growth. In places where early, incremental fillings have been removed by dissolution and passive crystal growth have not formed, or where they have been removed by further dissolution, conductivity is high. In places where either passive or incremental crystals fill most fractures, conductivity is low.

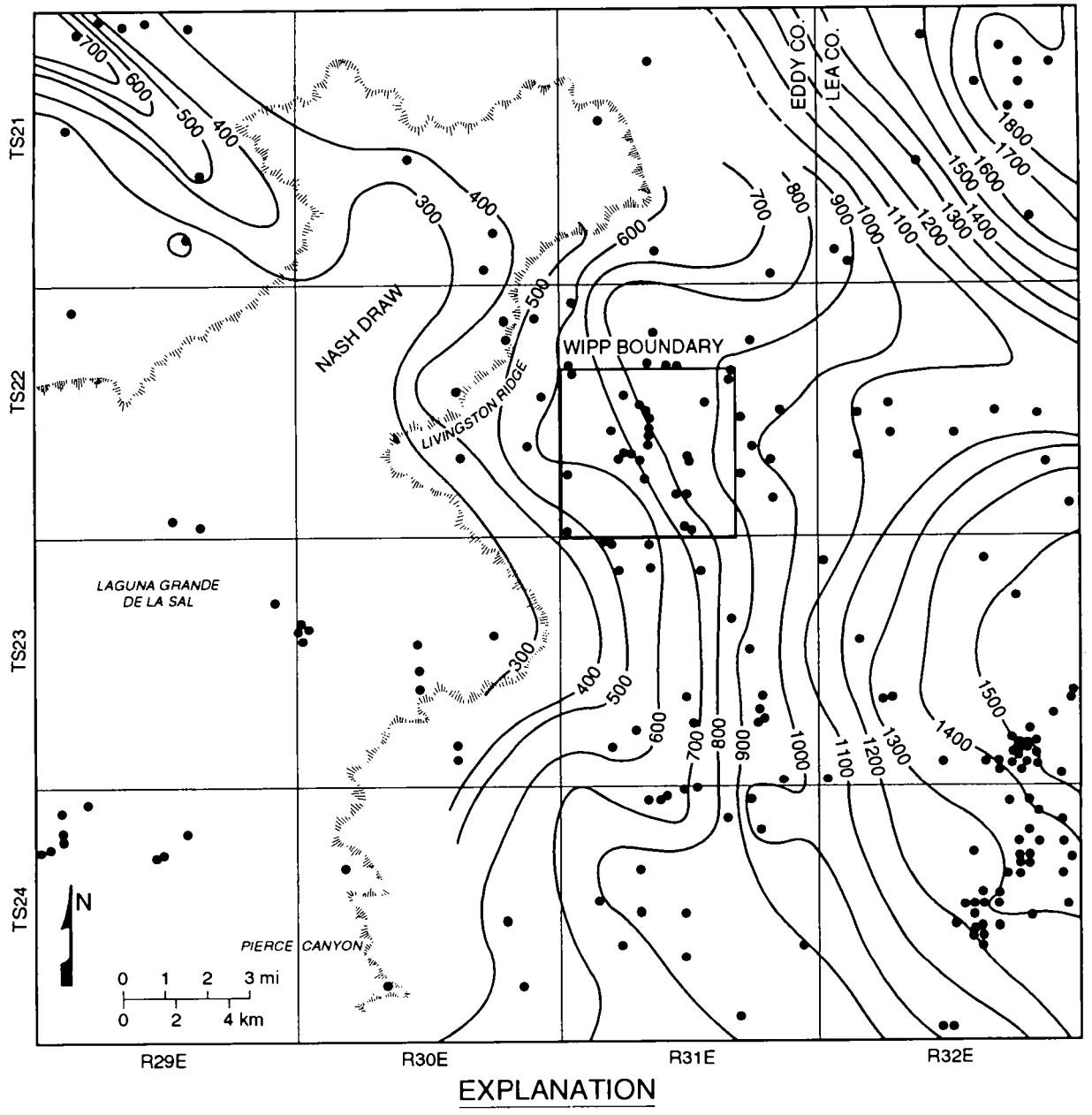

Figure 2-11. Isopach of overburden for the Culebra Dolomite Member (Beauheim and Holt, 1990).

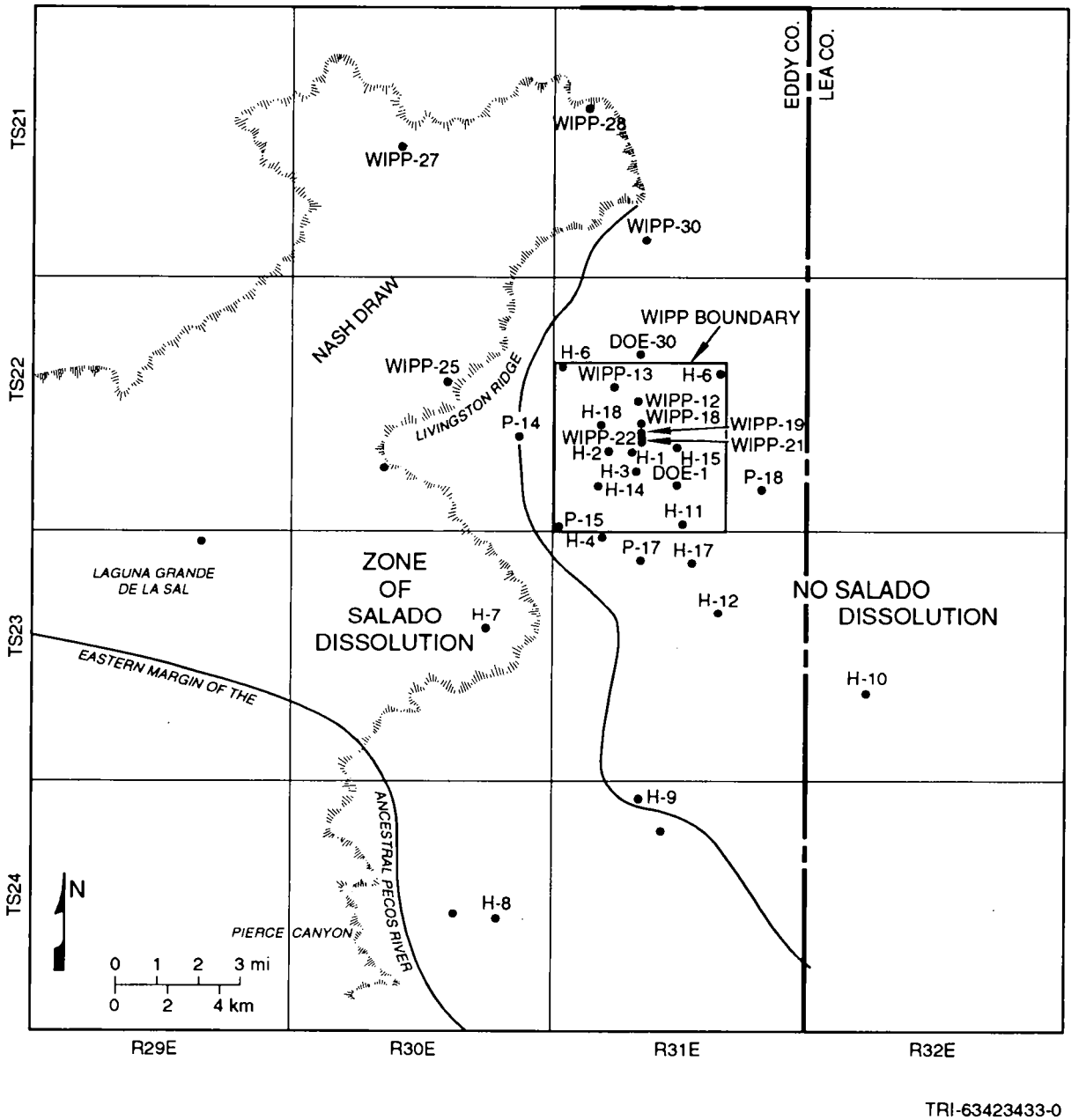

Figure 2-12. Interpreted extent of Salado dissolution (Beauheim and Holt, 1990).

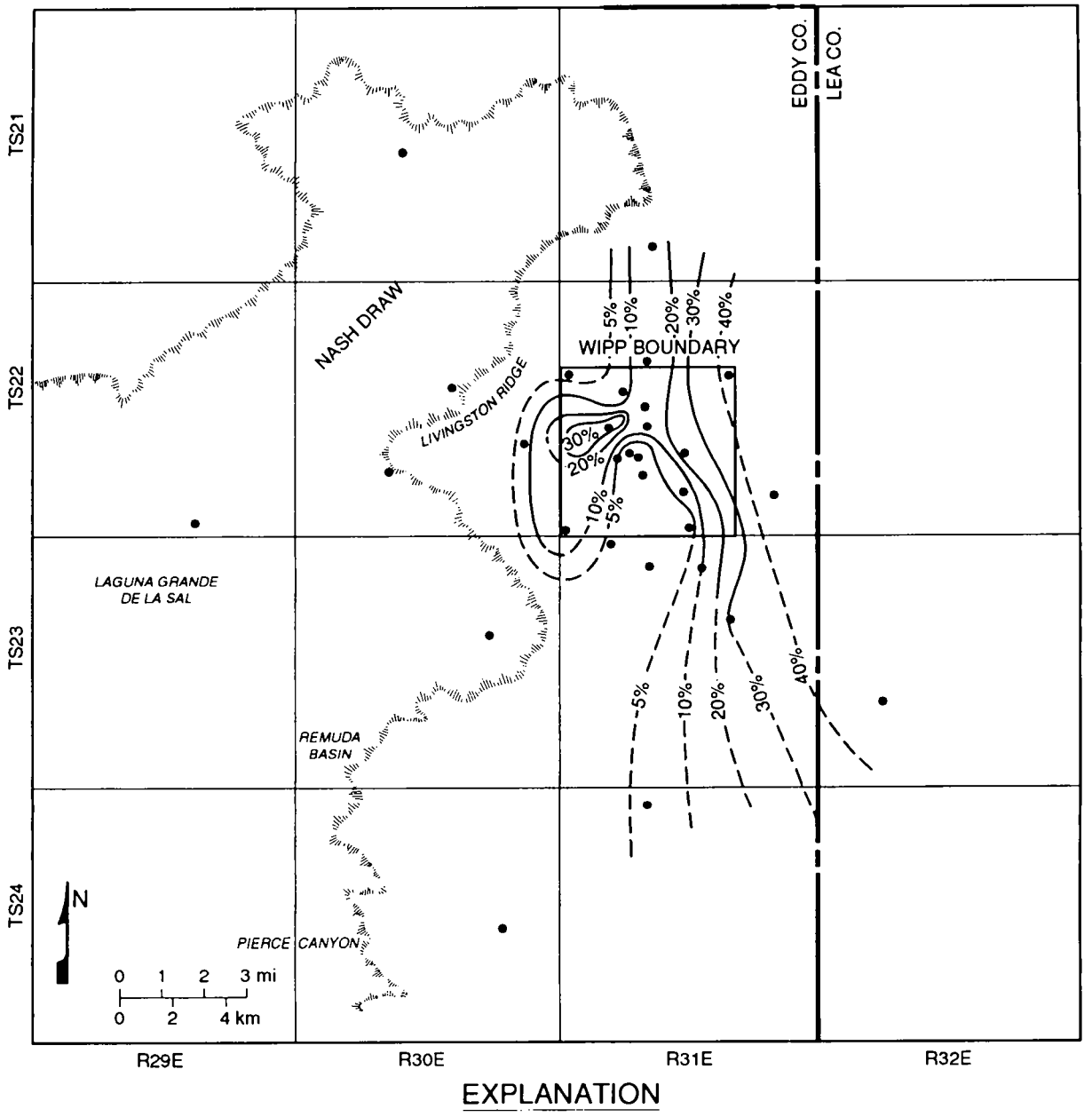

TRI-6342-3434-0

Figure 2-13. Percentage of natural fractures in the Culebra Dolomite Member filled with gypsum (Beauheim and Holt, 1990).

As observed in core samples from the Culebra, clay minerals commonly occur on the surfaces of subhorizontal fractures in dolomite (Sewards, 1991; Sewards et al., 1991a,b). Present distribution and composition of clay in the Culebra (and other members of the Rustler Formation) reflect both depositional and diagenetic processes (Sewards et al., 1992). Clays are most abundant in horizontal layers that represent original bedding planes in the evaporite sequences. These clay-rich layers are found within the Culebra throughout the WIPP vicinity. Because they are less competent than the dolomite above and below, clay-rich layers are preferentially opened during fracturing, creating clay-lined subhorizontal fractures. Clay minerals identified by x-ray diffraction analysis include corrensite (ordered mixed-layer chlorite/saponite) and illite, with minor amounts of serpentine and chlorite. Corrensite is the most abundant of the clay minerals, usually constituting about 50 percent of the clay assemblage (Sewards et al., 1991a). Original detrital clays were illite and smectite; alternation of smectite into corrensite occurred during early diagenesis as magnesium-rich pore waters migrated through the formation (Sewards et al., 1992). Isotopic analyses (Rb/Sr) indicate that clay minerals reached their present composition during the Late Permian (Brookins et al., 1990).

Because the cation exchange capacity of clay minerals in general and corrensite in particular is higher than that of dolomite or gypsum, clay fracture-linings may play an important role in the chemical retardation of radionuclides during potential transport (Siegel et al., 1990; Sewards et al., 1992). Clay fracture-linings may also affect physical retardation of radionuclides by diffusion into the pore volume of both dolomite matrix and the clay linings during transport (Section 7.6.2 of this volume; Volume 3, Section 2.6 of this report; memorandum by Novak et al. in Volume 3, Appendix A of this report).

Tamarisk Member

Where present in southeastern New Mexico, the Tamarisk Member ranges in thickness from 8 to 84 m (26 to 276 ft) in southeastern New Mexico, and is about 36 m (118 ft) thick at the WIPP. The Tamarisk consists of mostly anhydrite or gypsum interbedded with thin layers of claystone and siltstone. Near Nash Draw, dissolution has removed evaporites from the Tamarisk Member, and the Magenta and Culebra Dolomites are separated only by a few meters of residue (Brinster, 1991).

Unsuccessful attempts were made in two wells, H-14 and H-16, to test a 2.4-m (7.9-ft) sequence of the Tamarisk Member that consists of claystone, mudstone, and siltstone overlain and underlain by anhydrite. Permeability was too low to measure in either well within the time allowed for testing, but Beauheim (1987a) estimated the transmissivity of the claystone sequence to be one or more orders of magnitude less than that of the tested interval in the unnamed lower member, which yielded transmissivity values of 2.9×10^{-10} m^2/s (2.7×10^{-4} ft^2/d) and 2.4×10^{-10} m^2/s (2.2×10^{-4} ft^2/d), corresponding to hydraulic conductivities in the basal siltstone of the unnamed lower member of 1.5×10^{-11} m/s (4.2×10^{-6} ft/d) and 1.2×10^{-11} m/s (3.4×10^{-6} ft/d).

Magenta Dolomite Member

The Magenta Dolomite Member of the Rustler Formation is a fine-grained dolomite that ranges in thickness from 4 to 8 m (13 to 26 ft) and is about 6 m (19 ft) thick at the WIPP. The Magenta is saturated except near

outcrops along Nash Draw, and hydraulic data are available from 14 wells. Hydraulic conductivity ranges over five orders of magnitude from 5.0×10^{-10} to 5.0×10^{-5} m/s (1×10^{-4} to 1×10^{1} ft/d).

A contour map of log hydraulic conductivities of the Magenta Dolomite Member based on sparse data (Figure 2-14) shows a decrease in conductivity from west to east, with slight indentations of the contours north and south of the WIPP that correspond to the topographic expression of Nash Draw (Brinster, 1991). Comparison of Figures 2-9 and 2-14 show that in most locations conductivity of the Magenta is one to two orders of magnitude less than that of the Culebra.

No porosity measurements have been made on the Magenta Dolomite Member. Beauheim (1987a) assumed a representative dolomite porosity of 0.20 for interpretations of well tests.

Forty-niner Member

The uppermost member of the Rustler Formation, the Forty-niner Member, is about 20 m (66 ft) thick throughout the WIPP area and consists of low-permeability anhydrite and siltstone. Tests in H-14 and H-16 yielded hydraulic conductivities of about 5×10^{-9} m/s (1×10^{-3} ft/d) and 5×10^{-10} m/s (1×10^{-4} ft/d) respectively (Beauheim, 1987a).

2.2.2.7 SUPRA-RUSTLER ROCKS

Strata above the Rustler Formation are not believed to represent a significant pathway for the migration of radionuclides from the repository to the accessible environment because of relatively low transmissivities within the saturated zone. These units are important to performance assessment, however, because vertical flux through them may play an important role in the inflow and outflow of water from the Rustler Formation. Available models of groundwater flow in the Culebra do not incorporate the effects of vertical flux.

Where present, the supra-Rustler units collectively range in thickness from 4 to 536 m (13 to 1758 ft). Regionally, the supra-Rustler units thicken to the east and form a uniform wedge of overburden across the region (Brinster, 1991). Fine-grained sandstones and siltstones of the Dewey Lake Red Beds (Pierce Canyon Red Beds of Vine, 1963) conformably overlie the Rustler Formation at the WIPP and are the uppermost Permian rocks in the region. The unit is absent in Nash Draw, is as much as 60 m (196 ft) thick where present west of the WIPP, and can be over 200 m (656 ft) thick east of the WIPP (Figures 2-4, 2-7). East of the WIPP, the Dewey Lake Red Beds are unconformably overlain by Mesozoic rocks of the Triassic Dockum Group. These rocks are absent west of the repository and reach a thickness of over 100 m (328 ft) in western Lea County. East of the WIPP, Triassic and, in some locations, Cretaceous rocks are unconformably overlain by the Pliocene Ogallala Formation. At the WIPP, Permian strata are overlain by 8 m (25 ft) of the Triassic Dockum Group, discontinuous sands and gravels of the Pleistocene Gatuña Formation, the informally named Pleistocene Mescalero caliche, and Holocene soils (Holt and Powers, 1990).

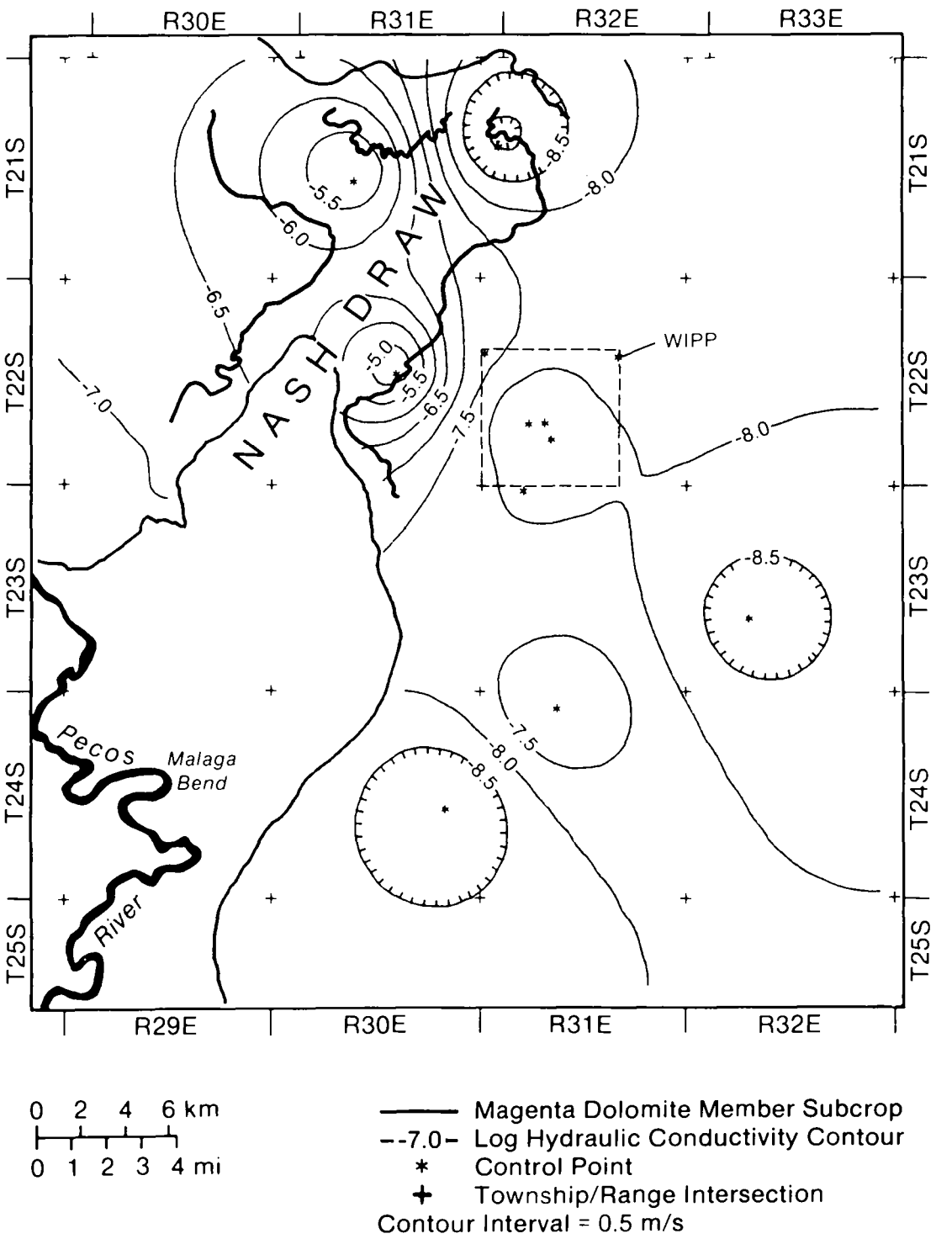

Figure 2-14. Log hydraulic conductivities (measured in m/s) of the Magenta Dolomite Member of the Rustler Formation (Brinster, 1991).

Drilling in the Dewey Lake Red Beds has not identified a continuous zone of saturation. Some localized zones of relatively high permeability were identified by loss of drilling fluids at DOE-2 and H-3d (Mercer, 1983; Beauheim, 1987a). Thin and apparently discontinuous saturated sandstones were identified in the upper Dewey Lake Red Beds at H-1, H-2, and H-3 (Mercer and Orr, 1979; Mercer, 1983). Several wells operated by the J. C. Mills Ranch (James Ranch) south of the WIPP produce sufficient quantities of water from the Dewey Lake Red Beds to supply livestock (Brinster, 1991).

Hydrologic properties of supra-Rustler rocks are relatively poorly understood because of the lack of long-term hydraulic tests and the difficulty of making those measurements. Hydraulic conductivity of the Dewey Lake Red Beds, assuming saturation, is estimated to be 10^{-8} m/s (10^{-3} ft/d), corresponding to the hydraulic conductivity of fine-grained sandstone and siltstone (Mercer, 1983; Davies, 1989). Porosity is estimated to be about 0.20, which is representative of fine-grained sandstone (Brinster, 1991).

2.2.3 Hydrology

2.2.3.1 PRESENT CLIMATE

The present climate of southeastern New Mexico is arid to semi-arid (Swift, 1992). Annual precipitation is dominated by a late summer monsoon, when solar warming of the continent creates an atmospheric pressure gradient that draws moist air inland from the Gulf of Mexico (Cole, 1975). Winters are cool and generally dry.

Mean annual precipitation at the WIPP has been estimated to be between 28 and 34 cm/yr (10.9 and 13.5 in/yr) (Hunter, 1985). At Carlsbad, 42 km (26 mi) west of the WIPP and 100 m (330 ft) lower in elevation, 53-year (1931-1983) annual means for precipitation and temperature are 32 cm/yr (12.6 in/yr) and 17.1°C (63°F) (University of New Mexico, 1989). Freshwater pan evaporation in the region is estimated to be 280 cm/yr (110 in/yr) (U.S. DOE, 1980).

Short-term climatic variability can be considerable in the region. For example, the 105-year (1878 to 1982) precipitation record from Roswell, 135 km (84 mi) northwest of the WIPP and 60 m (200 ft) higher in elevation, shows an annual mean of 27 cm/yr (10.6 in/yr) with a maximum of 84 cm/yr (32.9 in/yr) and a minimum of 11 cm/yr (4.4 in/yr) (Hunter, 1985).

2.2.3.2 PALEOCLIMATES AND CLIMATIC VARIABILITY

Based on the past record, it is reasonable to assume that climate will change at the WIPP during the next 10,000 years, and the performance-assessment hydrologic model must allow for climatic variability. Presently available long-term climate models are incapable of resolution on the spatial scales required for numerical predictions of future climates at the WIPP (e.g., Hansen et al., 1988; Mitchell, 1989; Houghton et al., 1990), and simulations using these models are of limited value beyond several hundreds of years into the future. Direct modeling of climates during the next 10,000 years has not been attempted for WIPP performance assessment.

Instead, performance-assessment modeling uses past climates to set limits for future variability (Swift, 1991, 1992). The extent to which unprecedented climatic changes caused by human-induced changes in the composition of the Earth's atmosphere may invalidate this assumption is uncertain. Presently available models of climatic response to an enhanced greenhouse effect (e.g., Mitchell, 1989; Houghton et al., 1990) do not predict changes of a larger magnitude than those of the Pleistocene (although predicted rates of change are greater), suggesting the choice of a Pleistocene analog for future climatic extremes will remain appropriate.

Geologic data from the American Southwest show repeated alternations of wetter and drier climates throughout the Pleistocene, which correspond to global cycles of glaciation and deglaciation (Swift, 1992). Climates in southeastern New Mexico have been coolest and wettest during glacial maxima, when the North American ice sheet reached its southern limit roughly 1200 km (750 mi) north of the WIPP. Mean annual precipitation at these extremes was approximately twice that of the present. Mean annual temperatures may have been as much as 5°C (9°F) cooler than at present. Modeling of global circulation patterns suggests these changes resulted from the disruption and southward displacement of the winter jet stream by the ice sheet, causing an increase in the frequency and intensity of winter storms throughout the Southwest (COHMAP Members, 1988).

Data from plant and animal remains and paleo-lake levels permit quantitative reconstructions of precipitation in southeastern New Mexico during the advance and retreat of the last major ice sheet in North America. Figure 2-15 shows estimated mean annual precipitation for the WIPP for the last 30,000 years, based on an estimated present precipitation of 30 cm/yr (11.8 in/yr). The precipitation maximum coincides with the maximum advance of the ice sheet 22,000 to 18,000 years ago. Since the final retreat of the ice sheet approximately 10,000 years ago, conditions have been generally dry, with intermittent and relatively brief periods when precipitation may have approached glacial levels. Causes of these Holocene fluctuations are uncertain (Swift, 1992).

Glacial periodicities have been stable for the last 800,000 years, with major peaks occurring at intervals of 19,000, 23,000, 41,000 and 100,000 years, corresponding to variations in the Earth's orbit (Milankovitch, 1941; Hays et al., 1976; Imbrie et al., 1984; Imbrie, 1985). Barring anthropogenic changes in the Earth's climate, relatively simple modeling of the nonlinear climatic response to astronomically controlled changes in the amount of solar energy reaching the Earth suggests that the next glacial maximum will occur in approximately 60,000 years (Imbrie and Imbrie, 1980). Regardless of anthropogenic effects, short-term, non-glacial climatic fluctuations comparable to those of the last 10,000 years are probable during the next 10,000 years and must be included in performance-assessment modeling.

Climatic variability will be incorporated into the modeling system conceptually by varying groundwater flow into the Culebra Dolomite Member of the Rustler Formation as a scaled function of precipitation (Swift, 1991). Short-term variability in precipitation is approximated with a periodic function that generates peaks of twice present precipitation three times during the next 10,000 years and with a future climate that is wetter than that of the present approximately one half of the time. Long-term, glacial increase in precipitation is approximated with a periodic function that reaches a maximum of twice present precipitation in 60,000 years. For this performance assessment, climatic variability has been included in the consequence analysis by varying boundary conditions of the Culebra groundwater-flow model as a scaled function of future precipitation. Potentiometric heads along a portion of the northern boundaries of the regional model domain were varied between present elevation and approximately the ground surface, reaching maximum elevations at times of maximum precipitation.

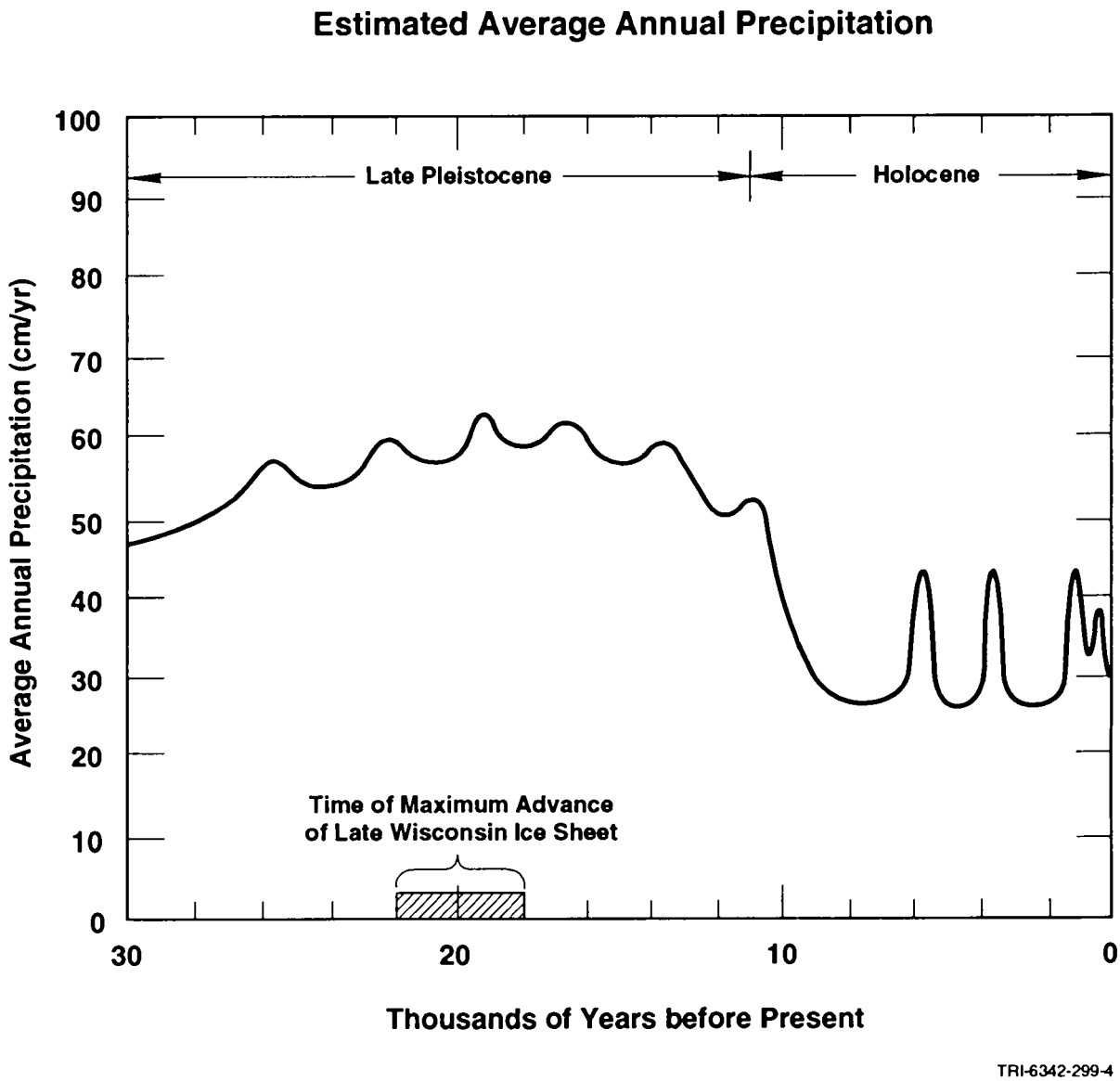

Figure 2-15. Estimated mean annual precipitation at the WIPP during the Late Pleistocene and Holocene (modified from Swift, 1992).

2.2.3.3 SURFACE WATER

The Pecos River, the principal surface-water feature in southeastern New Mexico, flows southeastward in Eddy County approximately parallel to the axis of the Delaware Basin (Figure 2-1) and drains into the Rio Grande in western Texas. In the vicinity of the WIPP, the drainage system includes small ephemeral creeks and draws and has a drainage area of about 50,000 km^2 (20,000 mi^2). At its closest point, the Pecos River is about 20 km (12 mi) southwest of the WIPP (Brinster, 1991).

Very little, if any, of the surface water from Nash Draw reaches the Pecos River (Robinson and Lang, 1938; Lambert, 1983). Several shallow, saline lakes in Nash Draw cover an area of about 16 km^2 (6 mi^2) southwest of the WIPP (Figure 2-6) and collect precipitation, surface drainage, and groundwater discharge from springs and seeps. The largest lake, Laguna Grande de la Sal, has existed throughout historic time. Since 1942, smaller, intermittent, saline lakes have formed in closed depressions north of Laguna Grande de la Sal as a result of effluent from potash mining and oil-well development in the area (Hunter, 1985). Effluent has also enlarged Laguna Grande de la Sal.

2.2.3.4 THE WATER TABLE

No maps of the water table are available for the vicinity of the WIPP. Outside of the immediate vicinity of the Pecos River, where water is pumped for irrigation from an unconfined aquifer in the alluvium, near-surface rocks are either unsaturated or of low permeability and do not produce water in wells. Tests of the lower Dewey Lake Red Beds in H-14 that were intended to provide information about the location of the water table proved inconclusive because of low transmissivities (Beauheim, 1987a). Livestock wells completed south of the WIPP in the Dewey Lake Red Beds at the J. C. Mills Ranch (James Ranch) may produce from perched aquifers (Mercer, 1983; Lappin et al., 1989), or they may produce from transmissive zones in a continuously saturated zone that is elsewhere unproductive because of low transmissivities.

Regionally, water-table conditions can be inferred for the more permeable units where they are close to the surface and saturated. The Culebra Dolomite may be under water-table conditions in and near Nash Draw and near regions of the Rustler Formation outcrop in Bear Grass Draw and Clayton Basin north of the WIPP (Figure 2-6). The Magenta Dolomite is unsaturated and presumably above the water table at WIPP-28 and H-7 near Nash Draw. Water-table conditions exist in the Rustler-Salado contact zone near where it discharges into the Pecos River at Malaga Bend (Brinster, 1991).

2.2.3.5 REGIONAL WATER BALANCE

Hunter (1985) examined the overall water budget of approximately 5180 km^2 (2000 mi^2) surrounding the WIPP. Water inflow to the area comes from precipitation, surface-water flow in the Pecos River, groundwater flow across the boundaries of the region, and water imported to the region for human use. Outflow from the water-budget model occurs as stream-water flow in the Pecos River, groundwater flow, and evapotranspiration. Volumes of water gained by precipitation and lost by evapotranspiration are more than one order of magnitude larger than volumes gained or lost by other means.

Uncertainties about precipitation, evapotranspiration, and water storage within the system limit the usefulness of estimates of groundwater recharge based on water-budget analyses. Regionally, Hunter (1985) concluded that approximately 96 percent of precipitation was lost directly to evapotranspiration, without entering the surface or groundwater flow systems. Within the 1000 km^2 (386 mi^2) immediately around the WIPP, where no surface runoff occurs and all precipitation not lost to evapotranspiration must recharge groundwater, a separate analysis suggested evapotranspiration may be as high as 98 to 99.5 percent (Hunter, 1985). Direct measurements of infiltration rates are not available from the WIPP vicinity.

2.2.3.6 GROUNDWATER FLOW ABOVE THE SALADO FORMATION

Well tests indicate that the three most permeable units in the vicinity of the WIPP above the Salado Formation are the Culebra Dolomite and Magenta Dolomite Members of the Rustler Formation and the residuum at the Rustler-Salado contact zone. The vertical permeabilities of the strata separating these units are not known, but lithologies and the potentiometric and geochemical data summarized below suggest that for most of the region, vertical flow between the units is very slow. Although preliminary hydrologic modeling indicates that some component of vertical flow between units can be compatible with observed conditions (Haug et al., 1987; Davies, 1989), the Culebra is assumed to be perfectly confined for the 1992 performance-assessment calculations.

Potentiometric Surfaces

Mercer (1983) and Brinster (1991) have constructed potentiometric-surface maps for the Rustler-Salado residuum, the Culebra Dolomite, and the Magenta Dolomite; Brinster's (1991) maps are reproduced here (Figures 2-16, 2-17, and 2-18). These maps show the elevation above sea level to which fresh water would rise in a well open to each unit. Contours are based on measured heads (water elevations in wells) that have been adjusted to freshwater-equivalent heads (the level to which fresh water would rise in the same well). Maps for the Culebra and the Magenta Dolomites are based on data from 31 and 16 wells, respectively. The map for the Rustler-Salado residuum includes data from 14 wells and water elevations in the Pecos River, reflecting an assumption that water-table conditions exist in the unit near the river.

Because the data used to construct the potentiometric maps are sparse and unevenly distributed, interpretations must be made with caution. For example, the "bull's-eye" patterns visible in all three maps are controlled by single data points, and would probably disappear from the maps if sufficient data were available. Contours are most reliable where data are closely spaced, particularly in the immediate vicinity of the WIPP, and are least reliable where they have been extrapolated into areas of no data, such as the southeast portion of the mapped area. With these caveats noted, however, the potentiometric maps can be useful in drawing conclusions about flow both within and between the three units.

Flow of a constant-density liquid within an isotropic medium would be perpendicular to the potentiometric contours. Near the WIPP, localized regions have been identified where variations in brine density result in non-uniform gravitational driving forces and anomalous flow directions (Davies, 1989), and the effects of anisotropy on flow patterns are not fully understood. In general, however, flow in the Rustler-Salado contact zone is from

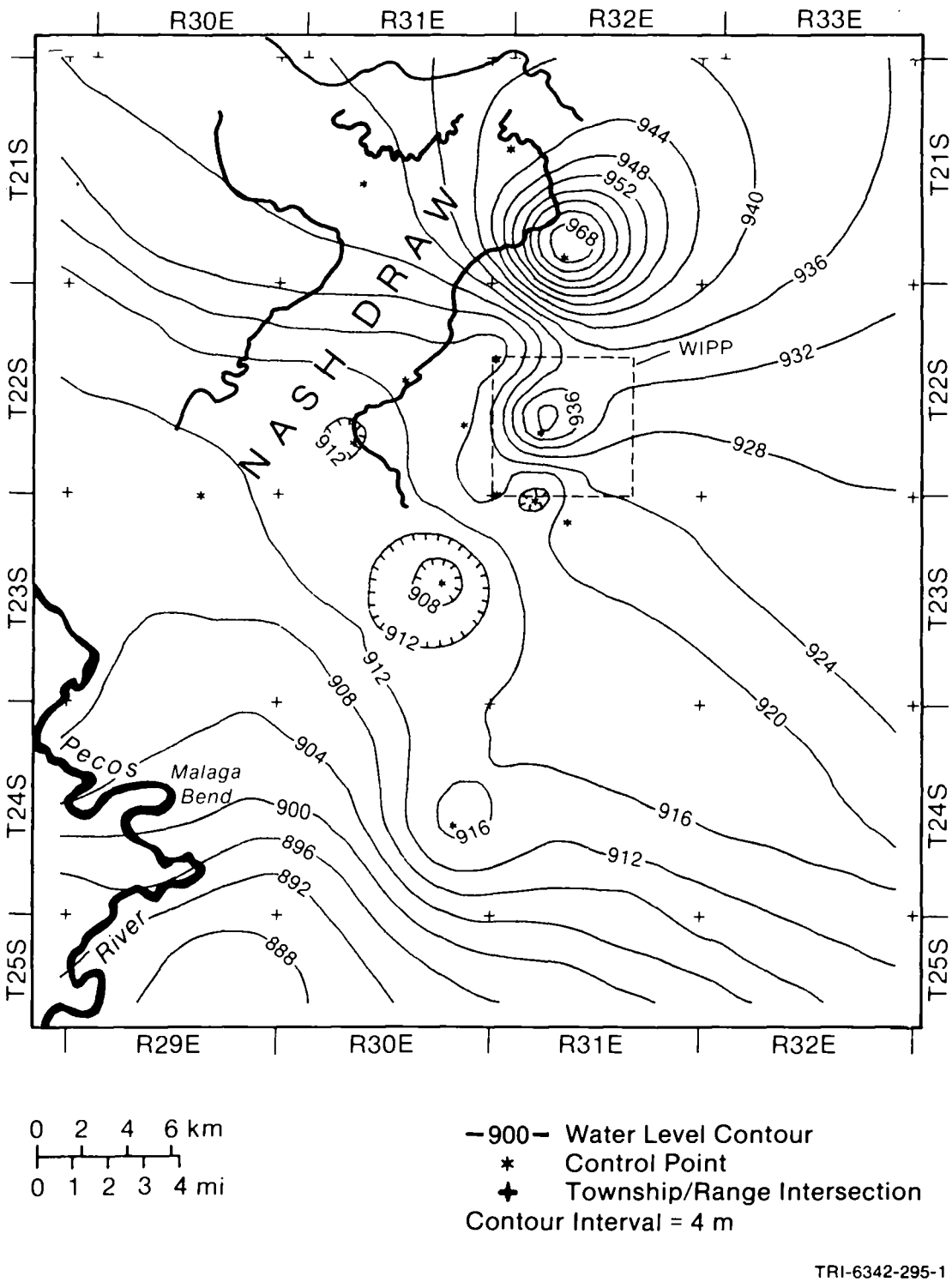

Figure 2-16. Adjusted potentiometric surface of the Rustler-Salado contact zone in the WIPP vicinity (Brinster, 1991). Contours based on head data from indicated wells and water elevations in the Pecos River.

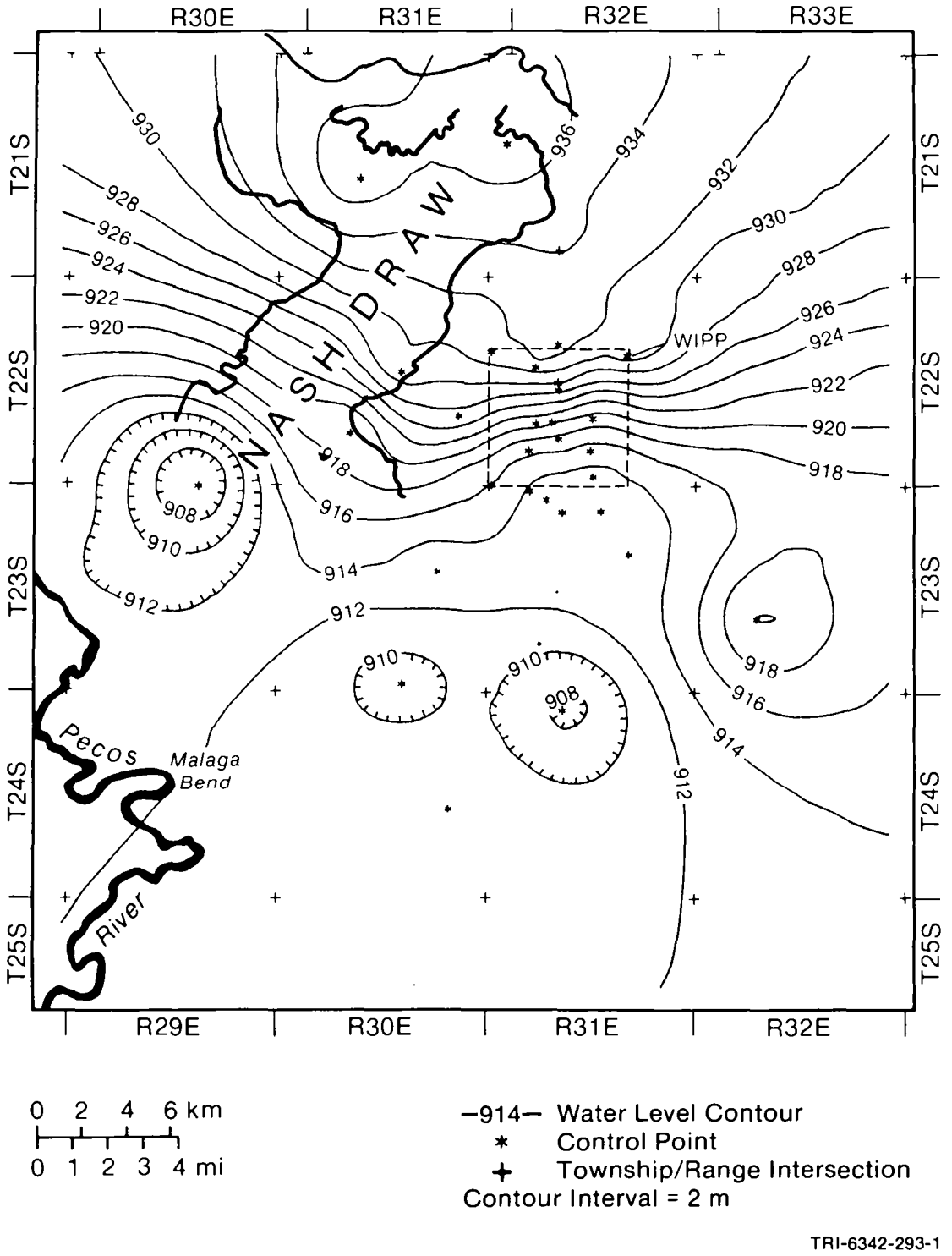

Figure 2-17. Adjusted potentiometric surface of the Culebra Dolomite Member of the Rustler Formation in the WIPP vicinity (Brinster, 1991). Contours based on head data from indicated wells.

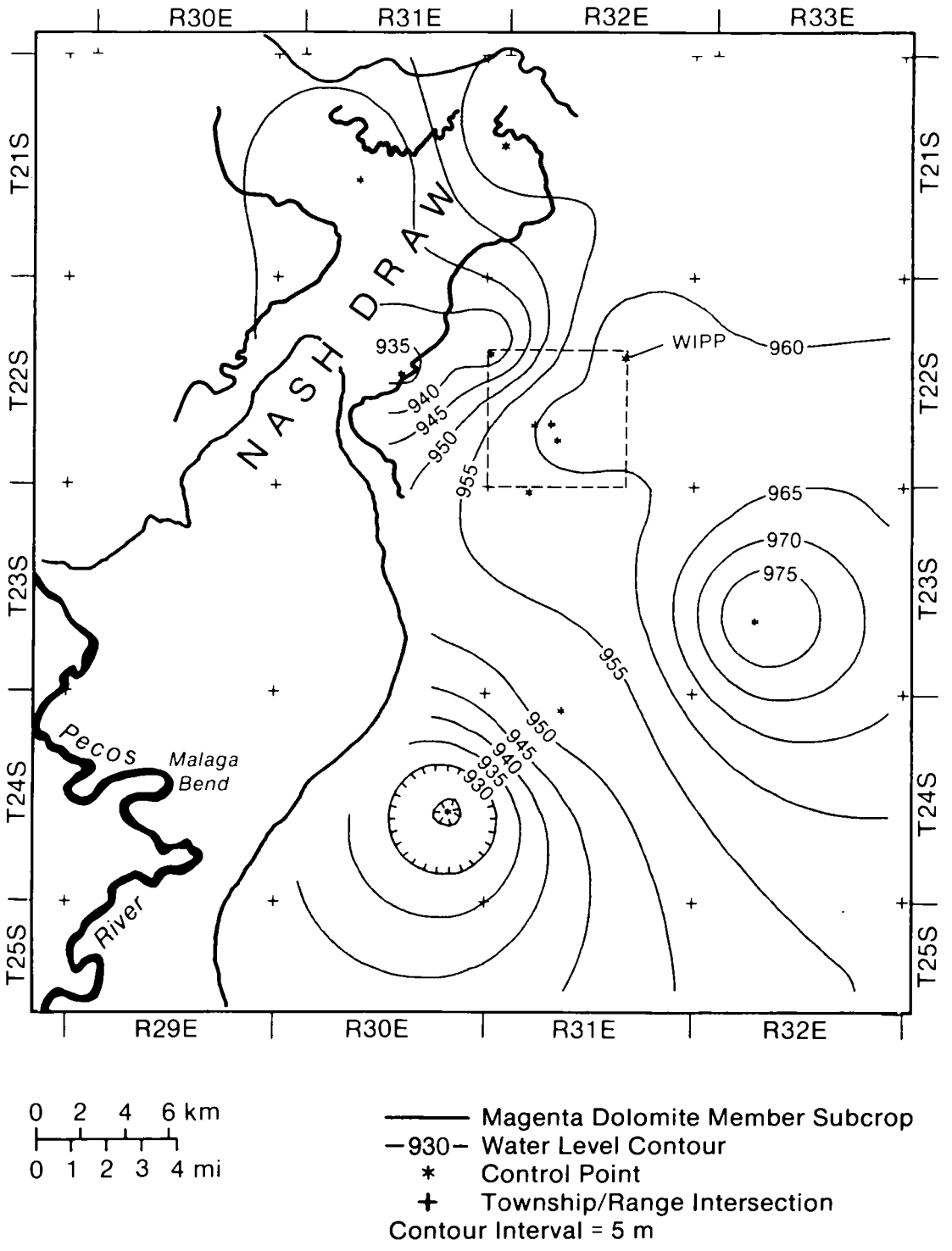

Figure 2-18. Adjusted potentiometric surface of the Magenta Dolomite Member of the Rustler Formation in the WIPP vicinity (Brinster, 1991). Contours based on head data from indicated wells.

northeast to southwest. Flow in the Culebra is from north to south, and flow in the Magenta is from east to west in that portion of the study area where data are sufficient to permit interpretation (i.e., near the WIPP). Differences in flow directions may reflect long-term transient conditions (see "Recharge and Discharge" in Section 2.2.3.6) and indicate low permeability of the strata separating the three units; that is, if the three functioned as a single aquifer, potentiometric maps would be similar.

Flow between units also is a function of hydraulic gradient and can be interpreted qualitatively from the potentiometric maps. Like lateral flow within units, vertical flow between units is from higher potentiometric levels to lower levels. Differences between the elevations of the potentiometric surfaces reflect low permeabilities of the intervening strata and slow rates of vertical leakage relative to rates of flow within the aquifers. Brinster (1991), and Beauheim (1987a) present analyses of vertical hydraulic gradients on a well-by-well basis. These analyses suggest that, if flow occurs, the direction of flow between the Magenta and the Culebra is downward throughout the WIPP area. Directly above the repository, flow may be upward from the Rustler-Salado residuum to the Culebra Dolomite. Elsewhere in the region, both upward and downward flow directions exist between the two units.

Groundwater Geochemistry

Major solute geochemical data are available for groundwater from the Rustler-Salado contact zone from 20 wells, from the Culebra Dolomite from 32 wells, and from the Magenta Dolomite from 12 wells (Siegel et al., 1991). Groundwater quality in all three units is poor, with total dissolved solids (TDS) exceeding 10,000 mg/L (the concentration specified for regulation by the Individual Protection Requirements of 40 CFR 191B) in most locations.

Waters from the Rustler-Salado contact zone have the highest TDS concentrations of any groundwaters in the WIPP area. The lowest concentration reported from the unit is 70,000 mg/L from H-7c southwest of the WIPP, and the highest is 410,000 mg/L from H-5 at the northeast corner of the land-withdrawal area (Siegel et al., 1991).

Waters from the Magenta Dolomite are the least saline of those in the confined units. Within the land-withdrawal area, TDS concentrations range from approximately 4000 to 25,000 mg/L. Higher values are reported from H-10 southeast of the WIPP, where the sample is of uncertain quality, and from WIPP 27 in Nash Draw, where groundwater chemistry has been altered by dumping of effluent from potash mines (Siegel et al., 1991).

Groundwater chemistry is variable in the Culebra Dolomite. A maximum TDS concentration of 324,100 mg/L is reported from WIPP-29 west of the repository in Nash Draw, and a minimum value of 2830 mg/L is reported from H-8, 14 km (9 mi) southwest of the repository. Three other wells (H-7, H-9, and the Engle well), all south of the WIPP, also contain water with less than 10,000 mg/L TDS (Siegel et al., 1991).

Relative concentrations of major ions vary spatially within the Culebra Dolomite. Siegel et al. (1991) recognized four zones containing distinct hydrochemical facies (Figure 2-19) and related water chemistry to the distribution of halite in the Rustler Formation. Zone A contains a saline (about 2 to 3 molal) sodium chloride brine with a magnesium/calcium molar ratio greater than 1.2. Zone A waters occur eastward from the repository,

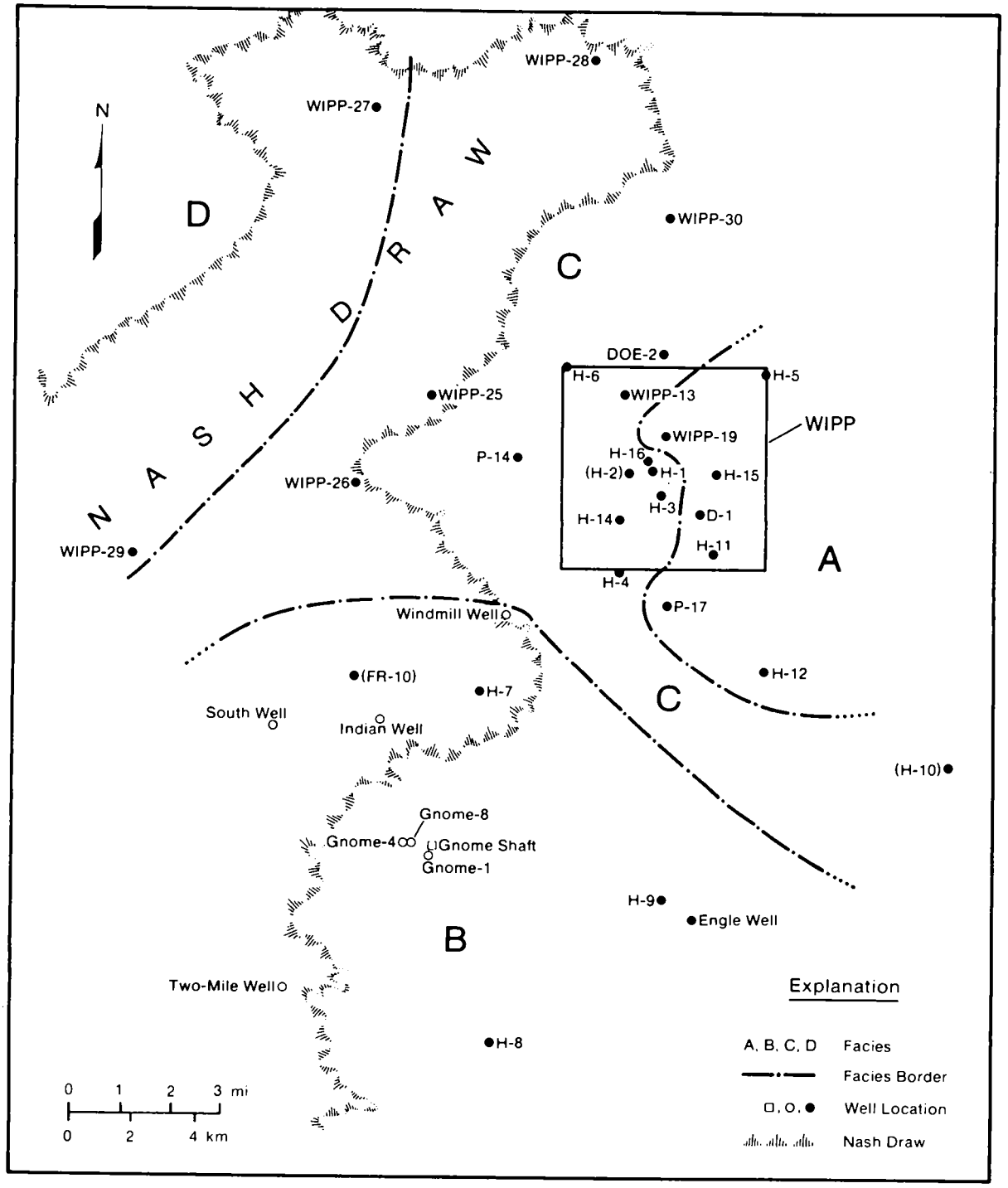

TRI-6331-78-0

Figure 2-19. Hydrochemical facies in the Culebra Dolomite Member of the Rustler Formation (Siegel et al., 1991).

in a region that corresponds roughly with the area of lowest transmissivity in the Culebra Dolomite. Halite is present in the unnamed lower member of the Rustler Formation throughout Zone A, and in the eastern portion of the region halite occurs in the upper members as well. Zone B is an area of dilute, calcium sulfate-rich water (ionic strength less than 0.1 molal) south of the repository. This region generally has high transmissivity in the Culebra Dolomite, and halite is absent from all members of the Rustler Formation. Zone C, extending from the repository west to Nash Draw, contains waters of variable composition with low to moderate ionic strength (0.3 to 1.6 molal), with magnesium/calcium molar ratios less than 1.2. Transmissivity is variable in this region, and halite is present in the Rustler Formation only to the east, in the unnamed lower member. Salinities are highest near the eastern edge of the zone. Zone D waters, found only in two wells in Nash Draw, are anomalously saline (3 to 6 molal) and have high potassium/sodium ratios that reflect contamination by effluent from potash mines.

Distribution of the hydrochemical facies may not be consistent with the inferred north-to-south flow of groundwater in the Culebra Dolomite. Specifically, less saline waters of Zone B are down-gradient from more saline waters in Zones A and C. Chapman (1988) suggested that direct recharge of fresh water from the surface could account for the characteristics of Zone B. As discussed in more detail below ("Recharge and Discharge" section), the inconsistency between chemical and potentiometric data could also result from a change in location and amount of recharge since the wetter climate of the last glacial maximum (Lambert, 1991). Present flow in the Culebra could be transient, reflecting gradual drainage of a groundwater reservoir filled during the Pleistocene (Lambert and Carter, 1987; Davies; 1989; Lambert, 1991). Regional hydrochemical facies may not have equilibrated with the modern flow regime and instead may reflect geographic distribution of halite during a past flow regime (Siegel and Lambert, 1991).

Recharge and Discharge

The only documented points of naturally occurring groundwater discharge in the vicinity of the WIPP are the saline lakes in Nash Draw and the Pecos River, primarily near Malaga Bend (Hunter, 1985; Brinster, 1991). Discharge into the lakes from Surprise Spring was measured at a rate of less than 0.01 m^3/s (0.35 ft^3/s) in 1942 (Hunter, 1985). Estimated total groundwater discharge into the lakes is 0.67 m^3/s (24 ft^3/s) (Hunter, 1985). Based on chemical and potentiometric data, Mercer (1983) concluded that discharge from the spring was from fractured and more transmissive portions of the Tamarisk Member of the Rustler Formation, and that the lakes were hydraulically isolated from the Culebra Dolomite and lower units. Lambert and Harvey's (1987) analysis of stable isotopes in water from Surprise Spring supports the conclusion that Surprise Spring and Laguna Grande de la Sal are not discharge points for the Culebra Dolomite.

Groundwater discharge into the Pecos River is larger than discharge into the saline lakes. Based on 1980 stream-flow gage data, Hunter (1985) estimated that groundwater discharge into the Pecos River between Avalon Dam north of Carlsbad and a point south of Malaga Bend was no more than approximately 0.92 m^3/s (33 ft^3/s). Most of this gain in stream flow occurs near Malaga Bend and is the result of groundwater discharge from the residuum at the Rustler-Salado contact zone (Hale et al., 1954; Kunkler, 1980; Hunter, 1985; Brinster, 1991).

The only documented point of groundwater recharge is also near Malaga Bend, where an almost immediate water-level rise has been reported in a Rustler-Salado residuum well following a heavy rainstorm (Hale et al.,

1954). This location is hydraulically down-gradient from the repository, and recharge here has little relevance to flow near the WIPP. Examination of the potentiometric-surface map for the Rustler-Salado contact zone (Figure 2-16) indicates that some inflow may occur north of the WIPP, where freshwater-equivalent heads are highest. Additional inflow to the contact zone may occur as leakage from overlying units, particularly where the units are close to the surface and under water-table conditions. Brinster (1991) proposed that inflow to the contact zone (and other units in the Rustler Formation) could also come from below, upward through breccia pipes from the Capitan aquifer north and east of the repository.

No direct evidence exists for the location of either recharge to or discharge from the Culebra Dolomite. The potentiometric-surface map (Figure 2-17) implies inflow from the north and outflow to the south. Mercer (1983) suggested that recharge from the surface probably occurred 15 to 30 km (9 to 19 mi) northwest of the WIPP in and north of Clayton Basin (Figure 2-6), where the Rustler Formation crops out. An undetermined amount of inflow may also occur as leakage from overlying units throughout the region.

The potentiometric-surface map (Figure 2-17) indicates that flow in the Culebra Dolomite is toward the south. Some of this southerly flow may enter the Rustler-Salado contact zone under water-table conditions near Malaga Bend and ultimately discharge into the Pecos River. Additional flow may discharge directly into the Pecos River or into alluvium in the Balmorhea-Loving Trough to the south (Figure 2-6) (Brinster, 1991).

Recharge to the Magenta Dolomite may also occur north of the WIPP in Bear Grass Draw and Clayton Basin (Mercer, 1983). The potentiometric-surface map indicates that discharge is toward the west in the vicinity of the WIPP, probably into the Tamarisk Member and the Culebra Dolomite near Nash Draw. Some discharge from the Magenta Dolomite may ultimately reach the saline lakes in Nash Draw. Additional discharge probably reaches the Pecos River at Malaga Bend or alluvium in the Balmorhea-Loving Trough (Brinster, 1991).

Isotopic data from groundwater samples suggest that groundwater travel time from the surface to the Dewey Lake Red Beds and the Rustler Formation is long and rates of flow are extremely slow. Low tritium levels in all WIPP-area samples indicate minimal contributions from the atmosphere since 1950 (Lambert and Harvey, 1987). Four modeled radiocarbon ages from Rustler Formation and Dewey Lake Red Beds groundwater are between 12,000 and 16,000 years (Lambert, 1987). Observed uranium isotope activity ratios require a conservative minimum residence time in the Culebra Dolomite of several thousands of years and more probably reflect minimum ages of 10,000 to 30,000 years (Lambert and Carter, 1987). Stable-isotope data are more ambiguous: Lambert and Harvey (1987) concluded that compositions are distinct from modern surface values and that the contribution of modern recharge to the system is slight, whereas Chapman (1986, 1988) concluded that available stable-isotope data do not permit interpretations of groundwater age. Additional stable-isotope research is in progress and may resolve some uncertainty about groundwater age.

Potentiometric data from four wells support the conclusion that little infiltration from the surface reaches the transmissive units of the Rustler Formation. Hydraulic head data are available for a claystone in the Forty-niner Member from DOE-2, H-3, H-4, H-5, and H-6. Comparison of these heads to Magenta heads in surrounding wells shows that flow between the units at all four wells may be upward (Beauheim, 1987a). This observation offers no insight into the possibility of infiltration reaching the Forty-niner Member, but it rules out the possibility of infiltration reaching the Magenta Dolomite or any deeper units at these locations.

Location and amount of groundwater recharge and discharge in the area may have been substantially different during wetter climates of the Pleistocene. Gypsiferous spring deposits on the east side of Nash Draw are of late Pleistocene age and reflect discharge from an active water table in the Rustler Formation (Bachman, 1981, 1987; Davies, 1989; Brinster, 1991). Coarse sands and gravels in the Pleistocene Gatuña Formation indicate deposition in high-energy, through-going drainage systems unlike those presently found in the Nash Draw area (Bachman, 1987). Citing isotopic evidence for a Pleistocene age for Rustler Formation groundwater, Lambert and Carter (1987) and Lambert (1991) have speculated that during the late Pleistocene, Nash Draw may have been a principal recharge area, and flow in the vicinity of the WIPP may have been eastward. In this interpretation, there is essentially no recharge at the present, and the modern groundwater-flow fields reflect the gradual draining of the strata. Preliminary modeling of long-term transient flow in a two-dimensional, east-west cross section indicates that, although the concept remains unproven, it is not incompatible with observed hydraulic properties (Davies, 1989). As the performance-assessment groundwater-flow model is further developed and refined, the potential significance of uncertainty in the location and amount of future recharge will be re-evaluated.

2.2.4 Radionuclide Transport in the Culebra Dolomite

Hydraulic tests using nonreactive tracers have been conducted in the Culebra Dolomite Member of the Rustler Formation near the WIPP at the H-2, H-3, H-4, H-6, and H-11 hydropad well locations (Kelley and Pickens, 1986; Saulnier, 1987; Beauheim, 1987b,c; Jones et al., 1992) (see Figures 2-6 and 2-8 for well locations). At the H-2 and H-4 hydropads, transmissivity in the Culebra is low, and tracer test results are best explained by characterizing the Culebra as a single-porosity, matrix-only medium in which interconnected open fractures are not present (see Section 2.2.2.6 for a discussion of fractures in the Culebra). At the H-3, H-6, and H-11 hydropads, a dual-porosity, fracture-plus-matrix model for transport provides the best agreement with the tracer test data. Neither a single-porosity, fracture-only nor a single-porosity, matrix-only model provides a suitable interpretation of the tracer test data at these locations (Jones et al., 1992). The H-3 and H-11 hydropad locations lie south and southeast of the waste panels, within the predicted flow paths from the panels (LaVenue and RamaRao, 1992), and the WIPP PA Department therefore believes that a dual-porosity transport model provides the most realistic estimate of subsurface releases at the accessible environment boundary. Alternative conceptual models for both single-porosity, fracture-only transport (believed to be an unrealistic but known endpoint of a continuum of models on which a realistic endpoint is uncertain) and dual-porosity, matrix-plus-fracture transport (believed to be realistic) were used in the 1992 PA. Results are compared in Volume 1, Chapter 5 of this report.

Unlike the nonreactive materials used in tracer tests, radionuclides may be retarded during transport by chemical interactions with the rock. Distribution coefficients (K_ds, mL/g), defined for a given element as the concentration sorbed per gram of rock divided by the concentration per a milliliter of solution, are used to describe the partitioning of radionuclides between groundwater and rock. As described in Section 7.6, K_ds are then used to derive retardation factors, defined as mean fluid velocity divided by mean radionuclide velocity, which take into account pore space geometry and the thickness of clay linings that line pores and fractures as well as K_d values. Distribution coefficients may be determined experimentally for individual radionuclides in specific water/rock systems (e.g., Lappin et al., 1989), but because values are strongly dependent on water chemistry and rock mineralogy and the nature of the flow system, experimental data cannot be extrapolated directly to a complex natural system. For the 1992 (and 1991) preliminary performance assessments, cumulative distribution functions

(cdfs) for K_ds were based on judgment elicited from an expert panel as described in the following section. In keeping with the agreement between the DOE and the State of New Mexico (U.S. DOE and the State of New Mexico, 1981, as modified), K_ds used in final compliance evaluations will be based on experimentally justified data.

Sensitivity analyses performed as part of the 1990 PA indicated that, conditional on the models and distributions used in the 1990 calculations, variability in distribution coefficients was one of the most important contributors to overall variability in cumulative releases through groundwater transport (Helton et al., 1991), and that overall performance was sensitive to the choice of conceptual model (single porosity versus dual porosity) for transport (Bertram-Howery et al., 1990). Sensitivity analyses performed as part of the 1991 PA confirmed the importance of both chemical retardation and physical retardation (Helton et al., 1992). The potential impact of uncertainty in the conceptual model for transport is examined again in the 1992 PA.

2.2.4.1 EXPERT JUDGMENT ELICITATION FOR K_ds

Unlike other expert panels organized for WIPP performance assessment, which consisted of experts with no formal affiliation with SNL (e.g., the future intrusion and markers panels discussed in Chapter 5 of this volume and the source term panel discussed later in this chapter), the Radionuclide Retardation Expert Panel consisted of SNL staff members who are currently working or have worked on retardation in the Culebra. In other regards, procedures for the presentation of the issues and the elicitation of results were as suggested by Hora and Iman (1989) and Bonano et al. (1990).

The Radionuclide Retardation Expert Panel was requested to provide probability distributions for distribution (sorption) coefficients for eight elements (americium, curium, uranium, neptunium, plutonium, radium, thorium, and lead) that represent a spatial average over the total area of concern (from a hypothetical intrusion borehole to the boundary of the accessible environment). This was to be done for two separate cases: (1) the coefficients that result from the clay that lines the fractures in the Culebra Dolomite, and (2) the coefficients that result from the matrix pore space of the Culebra Dolomite. During the meetings, the panelists decided to further break down the problem by examining the coefficients that would result from the particular rock species and two different transport fluids: (1) transport fluid that is predominantly relatively low-salinity Culebra brine, or (2) transport fluid that is predominantly high-salinity Salado brine. Probability distributions were thus provided for four situations for each radionuclide.

Two short meetings were held in April 1991 to discuss the physical situation and the issue statement. The period between the second and third meetings (approximately one month) was available for the panelists to examine the existing data base and discuss the results with each other. The third meeting, held at the end of May 1991, involved the expert judgment elicitation training, a discussion among the panelists as to the cases and assumptions to be used during the elicitation, and the actual elicitation sessions. At the request of one of the panelists, judgments were elicited separately from the experts. Each panelist provided distributions where they were able. Incompleteness resulted in some cases from a lack of knowledge about a particular radionuclide. Specific distributions provided by each panelist are presented in Volume 3 of the 1991 edition of this report

(Section 2.6.10 of WIPP PA Division [1991c]). The composite distributions used in the 1992 performance-assessment calculations are provided in Volume 3 of this report (Section 2.6.4).

The panelists judgments were based on a body of data generated largely by experiments with rock samples taken from boreholes in the vicinity of the WIPP (Trauth et al., 1992):

- plutonium K_ds (Dosch and Lynch, 1978; Lynch and Dosch, 1980; Dosch, 1980; Nowak, 1980; Serne et al., 1977; Tien et al., 1983)
- americium K_ds (Dosch and Lynch, 1978; Lynch and Dosch, 1980; Nowak, 1980; Serne et al., 1977; Tien et al., 1983)
- curium K_ds (Dosch and Lynch, 1978; Serne et al., 1977; Tien et al., 1983)
- neptunium K_ds (Dosch and Lynch, 1978; Serne et al., 1977; Tien et al., 1983)
- uranium K_ds (Dosch, 1981; Dosch, 1980; Serne et al., 1977; Tien et al., 1983)
- strontium K_ds (as analog for radium) (Dosch and Lynch, 1978; Lynch and Dosch, 1980; Dosch, 1980; Serne et al., 1977)
- radium and lead K_ds (Tien et al., 1983)
- thorium K_ds (Tien et al., 1983).

The K_d values reported in these references were calculated by indirect means: Measurements were not taken of the activity sorbed to the rock. Rather, measurements were taken as to the activity lost from the solution contacting the rock.

Tien et al. (1983) differed in their experimental approach from the other experimenters cited above. Tien et al. (1983) compiled experimental distribution coefficients from open literature that might be applicable to investigations of a potential repository site in bedded salt in the Palo Duro Basin of Texas.

2.2.4.2 PLANNED AND ONGOING EXPERIMENTAL WORK RELATED TO RADIONUCLIDE TRANSPORT IN THE CULEBRA

The WIPP Test Phase Plan (U.S. DOE, 1990a, currently in revision) contains experimental programs that will provide additional information on both chemical and physical retardation.

Chemical retardation will be addressed through laboratory experiments that will measure adsorption of radionuclides as a function of water composition to characterize adsorption in the wide range of groundwater compositions expected in the Culebra. Batch sorption experiments, in which crushed Culebra rock will be placed

in a brine solution containing the radionuclides of interest, will provide K_d values for many different conditions, but will provide little information about retardation in natural fractures. K_ds based on these experiments will provide an upper bound on the amount of sorption that can be expected. A set of column-flow experiments is therefore in progress that will measure radionuclide sorption in columns of intact Culebra rock (core samples from the Air Intake Shaft at the WIPP), thus providing a more direct determination of natural (both chemical and physical) retardation in the Culebra (see U.S. DOE, 1992, and references cited therein for additional information about these experiments).

Retardation could also be addressed through tracer tests at a proposed new seven-well hydropad, to be called H-19 (Beauheim and Davies, 1992). The test may be conducted at the site of an existing well (e.g., H-3), or a new location may be selected. In either case H-19 will be in a region of relatively high transmissivity south or southeast of the waste panels, within the envelope of predicted flow paths to the accessible environment. Tests with both conservative and reactive (but not radioactive) tracers will examine transport along various paths between a central well and six outer wells drilled at different radii from the central location. Specific objectives of these tests are to: address questions about vertical heterogeneity in the Culebra (tests will isolate specific horizontal layers within the Culebra in different wells to examine vertical flow and transport between layers); to provide data to allow evaluation of alternative conceptual models for transport in the Culebra, including anisotropic, heterogeneous, and channeling models; to provide information about chemical retardation processes on a field scale; to provide additional evidence that matrix diffusion is an important process in retardation; and to provide core samples for additional laboratory tests from the region of predicted flow paths to the accessible environment. Results of the field tracer tests are anticipated to be available for use in performance assessment beginning in 1995 (Beauheim and Davies, 1992).

2.3 Engineered Barrier System

The WIPP disposal system includes engineered barriers that minimize the rate at which radionuclides may migrate through the hydrogeologic setting to the accessible environment. As presently designed, the repository relies on seals in panels, drifts, and shafts to prevent migration through the excavated openings. If performance assessments indicate additional barriers are needed to reduce potential radionuclide transport up an intrusion borehole, modifications can be made to the form of the waste and backfill or to the design of the waste-emplacement areas that will enhance long-term performance. Section 2.3 contains descriptions of the repository and seal design, the waste, the radionuclide source term, and the room/waste interactions. Because the performance of engineered barriers is dependent on the properties of the surrounding strata, Section 2.3 also contains additional information about the Salado Formation at the repository horizon.

2.3.1 The Salado Formation at the Repository Horizon

Depositional processes that created the Salado Formation were laterally persistent over large areas, and individual stratigraphic horizons within the formation can be recognized in potash mines and boreholes throughout the WIPP region (Lowenstein, 1988). Forty-four anhydrite and polyhalite "marker beds" in the Salado Formation have been identified and numbered within the approximately 2700 km^2 (1050 mi^2) of the Carlsbad potash mining

district (Jones et al., 1960). Thinner interbeds of anhydrite, clay, and polyhalite occur throughout the formation, and are also laterally persistent.

Lithologic layers in the Salado Formation dip less than 1° to the southeast at the WIPP, and the waste-emplacement area is being excavated at a constant stratigraphic horizon rather than at a constant elevation so that all waste panels will share the same local stratigraphy. This slight slope of the repository will result in a difference in floor elevation between the highest and lowest panels of less than 10 m.

Panels are excavated entirely within a 7.3-m (24-ft) thick section of halite and polyhalite between anhydrite marker beds 138 (MB138) and 139 (MB139), approximately 380 m (1250 ft) below the top of the Salado Formation (Figure 2-20a). Waste-emplacement panels are excavated in the lower portion of this section, approximately 1.4 m (4.6 ft) above MB139 (Figure 2-20b). Excavation has penetrated MB139 in sumps of all four shafts, and in other locations. Experimental rooms, located in a separate part of the repository north of the waste-emplacement area (see Section 2.3.2), have been excavated at a stratigraphic level higher than that of the waste-emplacement panels, in part, so that borehole tests can be conducted beneath the room floors in undisturbed strata of the waste-emplacement horizon.

Anhydrite interbeds are of importance for performance assessment because they are more permeable than the halite layer containing the disposal room, and therefore provide the dominant pathway for fluid migration. As discussed in more detail in Volume 3, presently available WIPP test data indicate undisturbed permeabilities ranging between 10^{-16} and 10^{-21} m^2 for anhydrite and between 10^{-19} and 10^{-24} m^2 for halite (Gorham et al. memo in Volume 3, Appendix A of this report). Interbeds included in the 1992 performance assessment are MB139, and anhydrites A and B and MB138 located above the waste-emplacement panels (Figures 2-20a and 2-20b).

Excavation of the repository and the consequent release of lithostatic stress has created a disturbed rock zone (DRZ) around the underground openings. The DRZ at the WIPP has been confirmed by borehole observations, geophysical surveys, and gas-flow tests, and varies in extent from 1 to 5 m (3.3 to 16.4 ft) (Stormont et al., 1987; Peterson et al., 1987; Lappin et al., 1989). Fractures and microfractures within the DRZ have increased porosity and permeability of the rock and increased brine flow from the DRZ to the excavated openings (Borns and Stormont, 1988, 1989). Fracturing has occurred in MB139 below the waste-emplacement panels and in both anhydrites A and B above the waste-emplacement panels. It is not known how far fracturing in the anhydrite interbeds extends laterally from the excavations at this time, nor is the ultimate extent of the DRZ known. Most deformation related to development of the DRZ is believed to occur in the first five years after excavation (Lappin et al., 1989).

Fracturing in the DRZ, particularly in the anhydrite interbeds, may provide an enhanced pathway for fluid migration out of the repository and possibly around panel and drift seals. Characterization of fracture-related permeability in these layers is essential to modeling of two-phase (gas and brine) fluid flow into and out of the repository. Work is in progress on modeling the possible pressure dependency of fracture permeability in anhydrite interbeds, and results will be incorporated in future PAs.

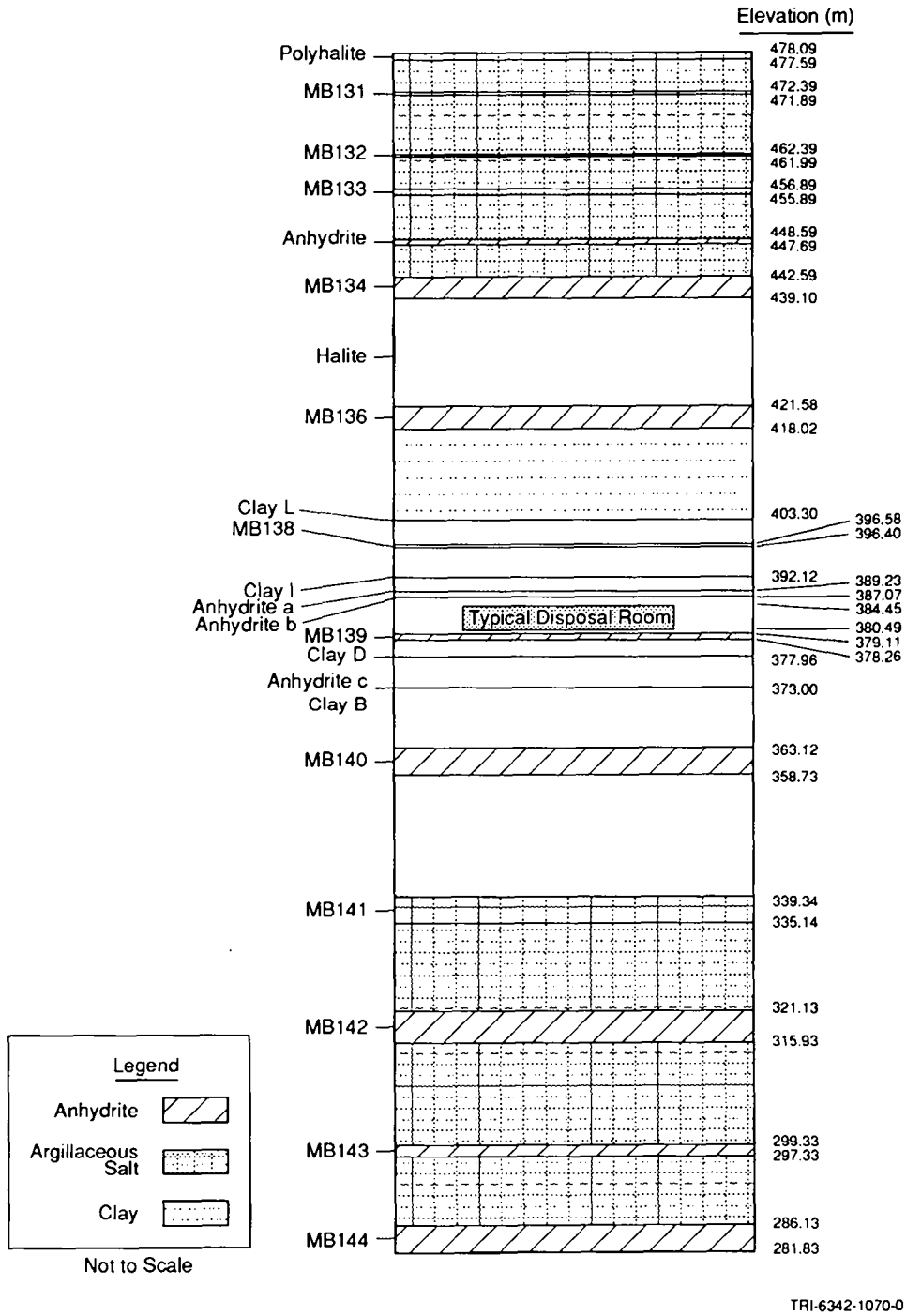

Figure 2-20a. Reference local stratigraphy near repository (after Munson et al., 1989a, Figure 3-3).

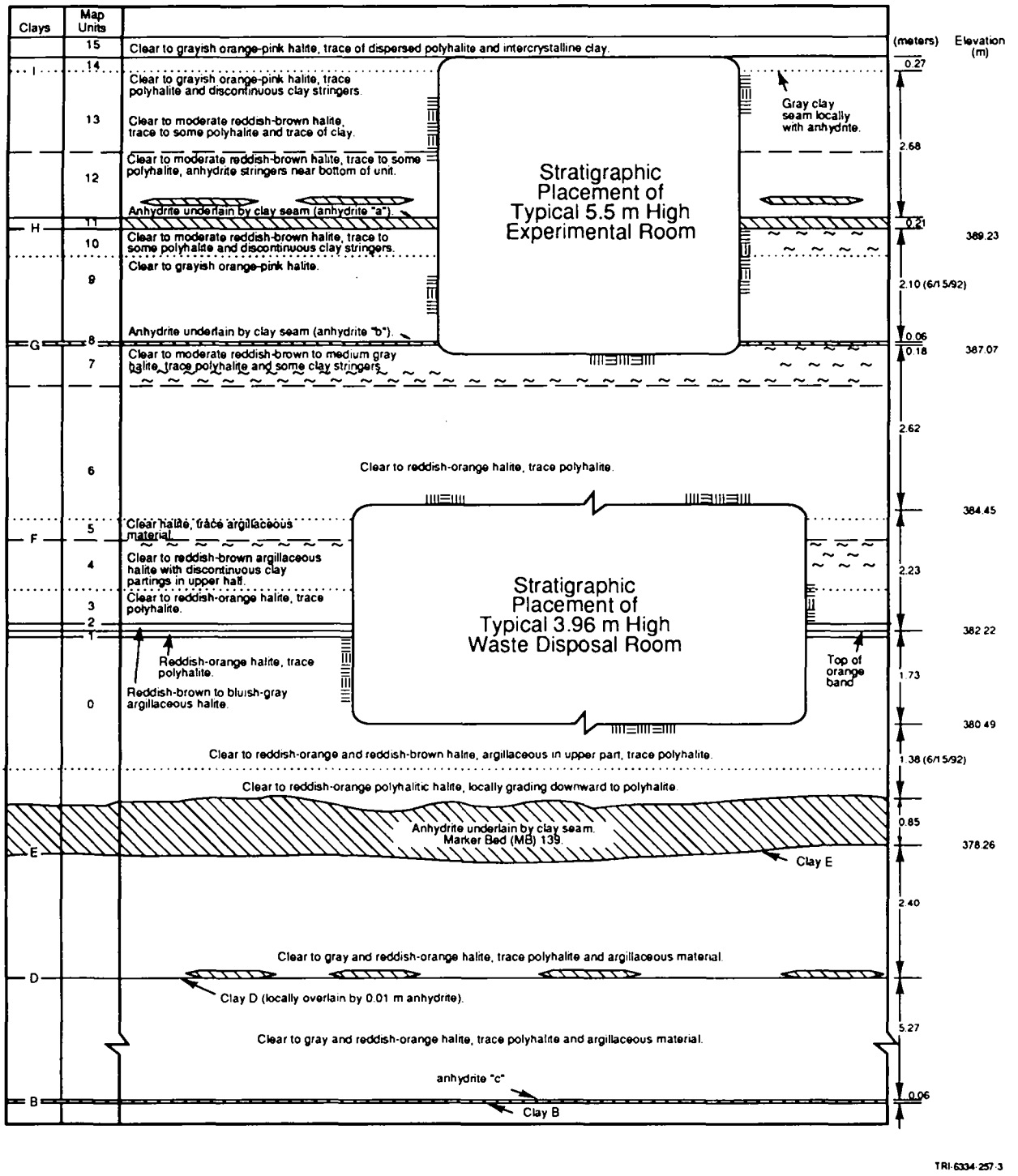

Figure 2-20b. Stratigraphy at the repository horizon (after Bechtel National, Inc., 1986, Figures 6-2, 6-3, and Lappin et al., 1989, Figure 4-12). Units in the disposal area dip slightly to the south, but disposal excavations are always centered about the orange marked band (reddish-orange halite).

Borehole observations of pore-fluid pressure and permeability suggest that there may be a transition zone extending outward beyond the DRZ. Within this transition zone pore-fluid pressures have dropped from their undisturbed, pre-excavation level, apparently without irreversible rock damage and large permeability changes (Gorham et al. memo in Volume 3, Appendix A of this report). The full extent of the transition zone is uncertain, as are its material properties. Properties of the transition zone used in the 1992 PA calculations are discussed in a memorandum of July 14, 1992 by Davies et al. in Volume 3, Appendix A of this report.

2.3.2 Repository and Seal Design

Major components of repository design that affect performance assessment are the waste itself, the underground waste-emplacement area and its access drifts and shafts, and the seals that will be used to isolate the emplacement area when the repository is decommissioned. The underground workings will ultimately consist of eight waste-emplacement panels, access drifts and shafts, and an experimental area (Figure 2-21). Drifts in the central portion of the repository will also be used for waste emplacement, providing the equivalent of an additional two panels for waste emplacement. A more detailed discussion of repository design is available in Volume 3 of this report.

All underground horizontal openings are rectangular in cross section. The emplacement area drifts are 4.0 m (13 ft) high by 7.6 m (25 ft) wide; the disposal rooms are 4.0 m (13 ft) high, 10.1 m (33 ft) wide, and 91.4 m (300 ft) long. Pillars between rooms are 30.5 m (100 ft) wide. The eight waste-emplacement panels will each have an initial volume of 46,000 m^3 (1.6×10^6 ft^3). The northern drift emplace area will have an initial volume of 34,000 m^3 (1.2×10^6 ft^3), and the southern drift emplacement area will have an initial volume of 33,000 m^3 (1.2×10^6 ft^3) (Rechard et al., 1990a). Overall, the waste-emplacement areas will have an initial volume of about 435,000 m^3 (1.5×10^7 ft^3).

The four vertical access shafts are cylindrical and range in diameter from 5.8 m (19 ft) to 3.0 m (10 ft). Shafts are lined in the units above the Salado Formation to prevent groundwater inflow and provide stability; they are unlined in the salt.

Excavation of the first waste-emplacement panel is complete; the remaining panels will be excavated as needed. Waste will be emplaced within the panels in drums or metal boxes, and panels will be backfilled and sealed as they are filled. Seals will be installed in panels, drifts, and the vertical shafts before the repository is decommissioned. Waste, backfill, and seals will be consolidated by creep closure after decommissioning.

2.3.2.1 WASTE CHARACTERIZATION

The waste that will be emplaced in the WIPP must meet the Waste Acceptance Criteria for the Waste Isolation Pilot Plant (U.S. DOE, 1991a) as explained in Volume 1 of this report (Chapter 3). These acceptance criteria specify that waste material containing particulates in certain size and quantity ranges will be immobilized,

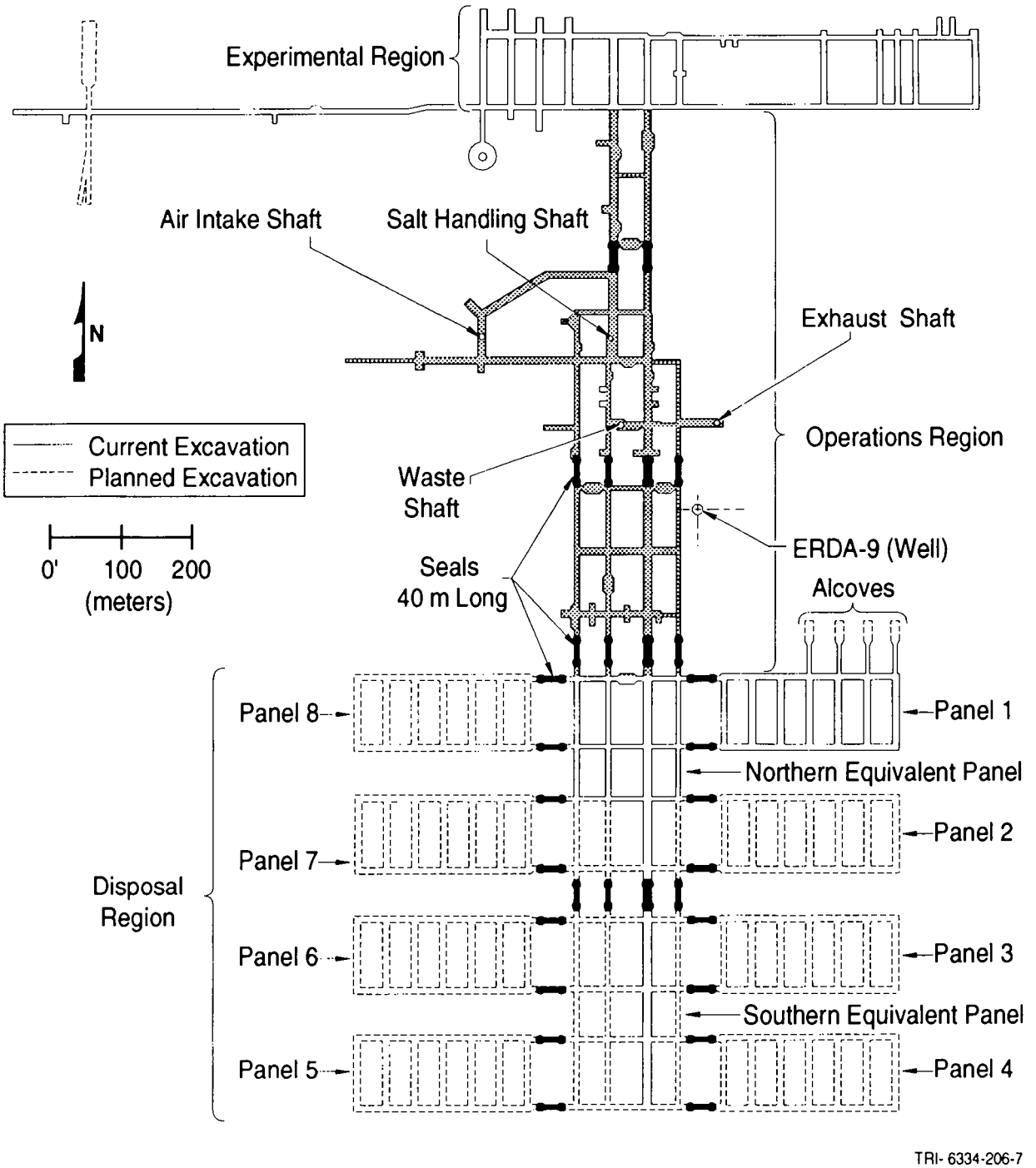

Figure 2-21. Plan view of waste-disposal horizon showing shaft, drift, and panel seal locations (after Nowak et al., 1990).

that waste liquid content be restricted to that remaining in well-drained containers and be less than one volume percent of the waste container, and that radionuclides in phyrophoric form be limited to less than one percent by weight of the external container. The requirements also prohibit disposal at the WIPP of wastes containing explosives, compressed gases, and ignitable, corrosive or reactive materials.

The current design of the WIPP has a total emplacement volume for contact-handled transuranic (CH-TRU) waste of 6.2×10^6 ft^3 (approximately 175,600 m^3) (U.S. DOE, 1980; Public Law 102-579, 1992). The estimated volume of CH-TRU waste supplied by the 10 waste-generator and/or storage sites for the 1991 Integrated Data Base (IDB, US DOE 1991b) was approximately 53,700 m^3 of stored waste and an additional 42,800 m^3 of waste to be generated by 2013. Estimates of the volume of waste to be generated may change in the future. Rather than revise the volume of waste emplaced in the WIPP each year, the current performance-assessment calculations are based on an initial CH-TRU-waste volume of approximately 175,600 m^3, the design volume. This is mostly for modeling convenience and will not have a significant effect on comparisons to 40 CFR 191B.

The current estimate of the stored and projected waste total about 96,500 m^3. Therefore, an additional 79,000 m^3 of waste could be emplaced in the WIPP. The characteristics of the additional 79,000 m^3 of waste were estimated from the characteristics of the projected waste of the five largest future generators. Because of changes that are occurring in weapons production and waste processing the waste that has not been generated cannot be characterized precisely. Estimates of waste characterization currently used in performance assessment have the potential for a large uncertainty. As discussed in Section 3.3.5 of Volume 3 of this report, uncertainty in the constituents that affect gas generation from corrosion of iron-based materials and from biodegradation of cellulosics and rubbers have been included in the 1992 preliminary performance assessment.

Characterization of the CH-TRU waste for the current performance-assessment calculations was based on a scale-up of masses estimated from expanded waste-characterization information. Based on 175,600 m^3 of CH-TRU waste emplaced in the WIPP, estimates of a total of about 12,000,000 kg of combustibles, 20,000,000 kg of metals and glass, and 25,000,000 kg of sludges were calculated. The total masses of iron-based metals, cellulosics, and rubbers were also calculated, and are provided in the memorandum by Peterson in Volume 3, Appendix A of this report. The masses of these materials are required for performance assessment because they influence gas generation and potential radionuclide transport.

The weight of the waste containers, drums and boxes, and of container liners were estimated because they also effect gas-generation potential. It was assumed in the estimation of the container weights that only steel 55-gallon drums and standard waste boxes (SWBs) will be emplaced in the WIPP. Other than test bins, these are the only containers that can currently be transported in a TRUPACT-II (NuPac, 1989). Based on emplacing 175,600 m^3 of CH-TRU-waste in drums and SWBs, it was estimated that about 518,000 drums and 35,600 SWBs would be disposed of in the WIPP. The total weight of the low-carbon steel in the drums and SWBs is larger that the estimated weight of corrodible iron-based materials in the waste.

The estimates of the total weight of the metals and glass and combustibles were nearly the same as were estimated for the 1991 PA analyses (WIPP PA Division, 1991a). The weight of sludge decreased significantly from the 1991 estimate. The weight of sludge in 1991 was based on the total weight of waste and average

weights of combustibles and metals and glass. The current estimate of the weight of sludge was based on expanded input from the sites. The estimates of the weights of iron-based corrodible metals and biodegradable materials were slightly decreased from the 1991 estimates.

2.3.2.2 SEALS

Seals will be emplaced in the entrance to each panel, in two locations within the drifts between the panels and the vertical shafts in the drifts between the experimental area and the vertical shafts, and in each of the four vertical shafts (Figure 2-21, 2-22) (Nowak et al., 1990). Design of these seals reflects specific functions for each type of seal. Seals in the upper portion of the shafts must prevent groundwater flow from the transmissive units of the Rustler Formation from reaching the lower portions of the shafts and the waste-emplacement areas. Seals in the lower portion of the shafts must provide a long-term, low-permeability barrier that will prevent Salado Formation brine and gas from migrating up the shaft. Panel seals (and drift seals) will inhibit long-term migration of radionuclide-contaminated brine through the drifts to the base of the shafts and must also provide safe isolation of radionuclides during the operational phase of the repository.

The primary long-term component of both lower shaft and panel seals will be crushed salt, confined between short-term rigid bulkheads until creep closure reconsolidates it to properties comparable to those of the intact Salado Formation. The short-term seals will be concrete in the panels and drifts, and composite barriers of concrete, bentonite, and consolidated crushed salt in the shafts. Crushed salt in the long-term portion of the seals will be preconsolidated to approximately 80% of the density of the intact formation and will compact further to approximately 95% of initial density within 100 years, at which time permeabilities are expected to be comparable to those of the undisturbed rock (Nowak and Stormont, 1987). Panel seals will be 40 m (131 ft) long, with 20 m (66 ft) of preconsolidated crushed salt between two 10-m (33-ft) concrete barriers. Shaft-seal systems will extend from the repository horizon in the Salado Formation to the surface, and will include composite barriers at the appropriate depths for individual lithologic units, including the Culebra Dolomite Member of the Rustler Formation (Nowak et al., 1990). Additional information about seal design is presented in Volume 3 of this report.

Marker Bed 139 will be sealed below each panel and drift seal by grouting, either with crushed-salt-based grout, cementitious material, bitumen, or other appropriate materials. Other anhydrite layers will be sealed similarly. Salt creep is expected to close fractures in halite in the DRZ over time, and engineered seals are not planned for the DRZ outside of MB139 and other interbeds.

2.3.2.3 BACKFILL

Void space between waste containers and elsewhere in the underground workings will be backfilled before sealing and decommissioning (Tyler et al., 1988; Lappin et al., 1989). The primary function of backfill will be to reduce initial void space in the excavated regions and to accelerate the entombment of the waste by creep closure. Consolidation of backfill by salt creep may reduce permeability in the waste-emplacement regions and limit brine flow through the waste; long-term properties of the backfill are uncertain, however, and will depend on

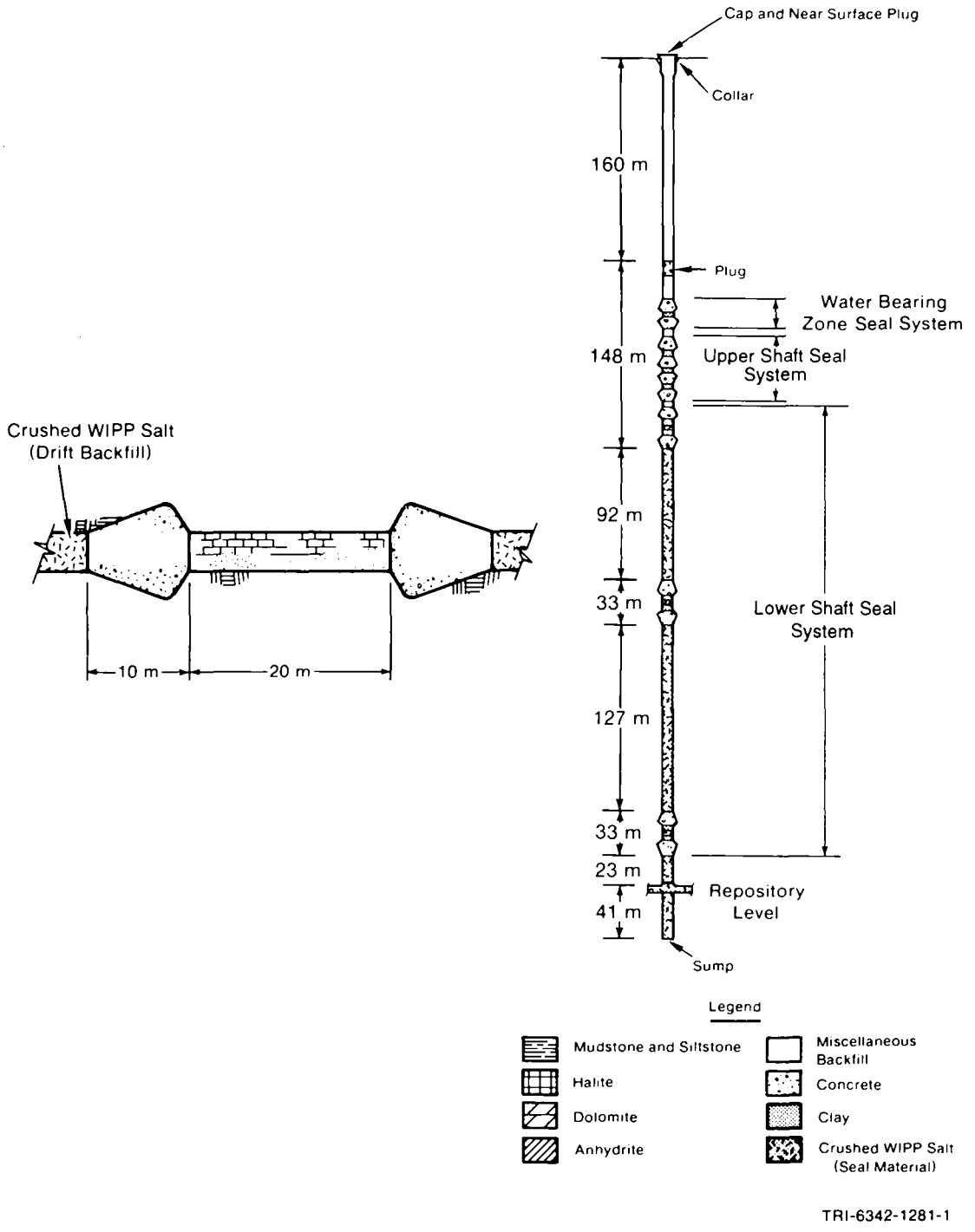

Figure 2-22. Representative shaft and plug seals (after Nowak et al., 1990). Vertical distances based on stratigraphy in ERDA-9.

fluid pressures within the panels. As discussed in Section 2.3.5, the pressure history of the repository will depend on the complexly coupled processes of salt creep, gas generation within the waste, and brine inflow from the surrounding Salado Formation. Performance-assessment calculations for 1992 assume a backfill of pure, unconsolidated crushed salt, with a relatively high permeability that provides little resistance to fluid flow. Pure salt will not sorb radionuclides, and retardation of radionuclides within the repository environment is not simulated. Design alternatives for backfill that contains bentonite as an additional barrier to retard radionuclides have been examined (U.S. DOE, 1990b, 1991c; Butcher et al., 1991; Pfeifle and Brodsky, 1991; Brodsky and Pfeifle, 1992) and will be available if needed.

2.3.2.4 ENGINEERED ALTERNATIVES

The WIPP has been designed to dispose of waste in the form in which it is shipped from the TRU-waste-generator and/or storage sites. Preliminary performance-assessment calculations indicate that modifications to the waste form that limit dissolution of radionuclides in brine have the potential to improve predicted performance of the repository (Marietta et al., 1989; Bertram-Howery and Swift, 1990). Modifications to the backfill and design of the room could also reduce radionuclide releases. Modifications could also, if needed, mitigate the effects of gas generated within the repository. Present performance assessments are not complete enough to determine whether or not such modifications will be needed for regulatory compliance, but the DOE has investigated engineered alternatives to waste form and repository design so that alternatives will be available if needed (U.S. DOE, 1990b). The Engineered Alternatives Task Force (EATF) has identified 19 possible modifications to waste form, backfill, and room design that merit additional investigation (U.S. DOE, 1990b, 1991c). The 1992 performance-assessment calculations do not include simulations of these alternatives. Selected alternatives may be examined in future performance-assessment calculations, however, to provide guidance to DOE on possible effectiveness of modifications.

2.3.3 Radionuclide Inventory

As described in additional detail in Volume 3, Chapter 3 of this report, the radionuclide inventory for the 1992 performance assessment is estimated from input to the 1991 Integrated Data Base (IDB, U.S. DOE, 1991b). The 1991 IDB inventory of contact-handled transuranic (CH-TRU) waste (defined as transuranic waste with a surface dose rate not greater than 200 mrem/hr [Public Law 102-579, 1992]) identifies approximately 53,700 m^3 of waste as currently stored at generator sites, and projects an additional volume of 42,800 m^3 that will be generated in the future. The design volume of the WIPP (175,600 m^3) will accommodate an additional approximately 79,100 m^3 of waste that is not described in the IDB. Performance assessments use an inventory in which the amount of CH-TRU is scaled up from the IDB volume to the design volume. CH-TRU activity of the initial design-volume inventory, expressed in curies, is estimated by scaling the curie inventory of the projected CH-TRU waste from each of the five sites that will generate the most waste in the future by a factor of 1.89 (the ratio of design volume to IDB volume) (Volume 3, Sections 3.3 and 3.4 of this report). This scaling of the inventory to a standard volume is done for modeling convenience, primarily to ensure the commensurability of analysis results from one iteration of performance assessment to the next. Because the releases allowed by the EPA are normalized using a waste unit factor based on the total inventory of transuranic waste (U.S. EPA, 1985; see Volume 1, Appendix A,

and Volume 3, Section 3.3.4 of this report), scaling of the inventory does not have a proportional effect on the location of the CCDF used for preliminary comparison with 40 CFR 191.13 (Volume 1, Section 5.1 of this report).

The initial design-volume inventory of CH-TRU waste used in the 1992 performance assessment contains 8.2×10^6 Ci (memorandum by Peterson in Volume 3, Appendix A of this report). Uncertainty in this inventory is large, particularly given the potential changes in the sources of CH waste due to changes in weapons production. Existing legislation, regulations, and agreements do not limit the total curie inventory of CH-TRU waste that may be emplaced, but do limit the total volume of waste that may be emplaced in the WIPP (6.2×10^6 ft^3, or 175,600 m^3) (Public Law 102-579, 1992).

Remotely-handled transuranic waste (RH-TRU), defined to have a surface dose rate greater than 200 mrem/hr but less than 1,000 rem/hr, will also be emplaced in the WIPP. The total RH-TRU inventory is limited to 5.1×10^6 Ci; no more than five percent of the RH-TRU canisters emplaced at the WIPP may have surface dose rates that exceed 100 rem/hr, and the activity of the RH-TRU waste shall not exceed 23 Ci/liter averaged over the volume of a canister (Public Law 102-579, 1992). Existing and projected RH-TRU waste in the IDB (US DOE, 1991b) has a volume of 6,667 m^3. This is slightly less than the WIPP design volume for RH-TRU waste (7080 m^3), but is predicted by the IDB to require 8071 canisters, somewhat more than the design capacity of 7950 canisters. The discrepancy occurs because the volume of waste placed in each canister differs depending on the generator site, and not all canisters will be filled to the capacity assumed for the WIPP design criteria. The 1991 IDB also indicates that there may be a considerable volume of uncharacterized waste that will probably be classified as RH-TRU. Given these uncertainties, the RH-TRU inventory is not scaled to design volume, and is used in the 1992 PA as reported in the 1991 IDB. The total remotely-handled inventory for 1992 is approximately 3.5×10^6 Ci, of which 1.8×10^6 Ci result from transuranic radionuclides and isotopes of uranium (i.e., radionuclides with atomic number greater than or equal to 92) (memorandum from Peterson, Volume 3, Appendix A of this report).

Radioactive decay within the repository is simulated with a simplified set of decay chains, provided in Volume 3, Section 3.3.3 of this report. Of the 70 radionuclides identified as present either in the initial WIPP inventory or as decay products, 26 are considered explicitly in PA analyses of direct releases from the repository to the ground surface. (See Section 4.2 of this volume for a discussion of human intrusion scenarios and Section 7.7 of this volume for a discussion of modeling of releases during drilling.) Radionuclides omitted from the simplified decay chains are those that have very short half-lives, very low activities, or both. Subsurface transport within the Culebra Dolomite Member of the Rustler Formation (see Sections 4.2 and 7.6 of this volume) is simulated for the nine most important radionuclides, identified in Volume 3, Section 3.3.3 of this report.

The only radioactive gas expected in the repository is radon-222, created from decay of radium-226. Decay of thorium-230 will cause the activity of radium-226 in a panel to increase from about 0 Ci at the time of emplacement to 8 Ci at 10,000 years. Because radon-222, with a half-life of only 3.8 days, will exist in secular equilibrium (equal activity) with radium-226, with a half-life of 1600 years, its activity will also be insignificant throughout the 10,000-year period. At 100,000 years the activity of radium-226 would increase to about 58 Ci in a panel, and the activity of radon-222 would still not be significant. Not including release of volatile radionuclides does not significantly affect the total radionuclide release.

2.3.4 Radionuclide Solubility and the Source Term for Transport Calculations

Before 1991, WIPP performance assessments calculated the source term for transport modeling* using the same estimated range and distribution (loguniform from 10^{-9} to 10^{-3} M) for the solubility limit of all radionuclide species in repository brine (Lappin et al., 1989; Brush and Anderson, 1989a). A fixed distribution was applied to all radionuclides for PA calculations before 1991 because, as is explained below, the state of knowledge at that time did not allow for the differentiation of radionuclides.

During the first meeting of the WIPP PA Source Term Group (in June of 1988), Choppin reported that estimates of the speciation and solubilities of americium, neptunium, plutonium, uranium, and thorium in both the Salado and Castile brines for expected concentrations of organic ligands were not possible because there are no thermodynamic data (solubility products for solid phases, or stability constants for dissolved organic or inorganic complexes) for these elements in solutions with ionic strengths equal to those of the Salado and Castile brines (Brush and Anderson, 1989b). In addition, Choppin observed that data reported by different groups using different experimental techniques are often contradictory, making the use of subjective expert judgment necessary for preliminary data selection for PA use until data from WIPP-specific experimental programs are available (see Section 2.3.4.2).

In lieu of data from laboratory experiments, the Source Term Group recommended a "best estimate" of 10^{-6} M for the concentration of plutonium and americium in any brine that resaturates the WIPP disposal rooms (Brush and Anderson, 1989a). This is the intermediate value (on a logarithmic scale) of the range of dissolved radionuclide concentrations (10^{-9} to 10^{-3} M) that have been used for sensitivity studies of the source term. Because the PA calculations require the input of a probability distribution, the entire range discussed above was used as a loguniform distribution. Because of the lack of applicable experimental data, there was no differentiation between the concentrations of various radionuclides in the 1989 PA. The 1990 estimated range in effective radionuclide solubilities was intended to include the effects of possible colloid formation within the repository (Rechard et al., 1990a). The conservative assumption was that colloidal materials would be completely transportable (i.e., that they would not be sorbed or precipitated within the repository).

2.3.4.1 EXPERT JUDGMENT ELICITATION

Since the beginning of the WIPP PA effort, it has been recognized that assuming a fixed solubility distribution for all radionuclides does not adequately capture the considerable uncertainty in radionuclide concentrations expected in the repository. The need for a better understanding of the source term was further highlighted by sensitivity analyses performed as part of the 1990 preliminary performance assessment. These sensitivity analyses indicated that, conditional on the models and distributions used in the 1990 calculations, uncertainty in the solubility limit was the most important single contributor to variability in total cumulative releases to the accessible environment resulting from groundwater transport (Helton et al., 1991).

---

* The source term for transport modeling for the PA is based an analytical model that calculates the equilibrium concentration of the radionuclide species in the repository brine. See Section 7.4 and Appendix A.

Because of the paucity of experimental data for the conditions and solutions expected specifically at the WIPP, a panel of experts external to the WIPP Project, called the Source Term Expert Panel, was convened in the spring of 1991 to provide the performance-assessment team with judgment about both dissolved and suspended radionuclides* for specific elements under variable Eh and pH conditions. Their judgments have been used to develop radionuclide solubilities that vary by radionuclide and type of brine solution. The resulting solubility ranges have been used in the 1991 and 1992 PA calculations.

Selection of the Source Term Expert Panel and elicitation of their judgment on solubility limits followed the procedure suggested by Hora and Iman (1989). Candidates for the expert panel on source term were gathered by a two-tiered nomination process. Initial nominations were solicited from an SNL staff member and an external consultant, as well as from members of the Performance Assessment Peer Review Panel and the National Research Council's WIPP Panel. Additional nominations were requested from all those contacted. Curricula vitae from those who were interested in participating in such a panel and available during the entire study period were reviewed by a two-member selection committee external to SNL. Some individuals removed themselves from consideration because of prior time commitments, current contracts with SNL, a self-determined lack of expertise, or involvement in an oversight organization. Nominees were evaluated on the basis of expertise and professional reputation; four experts were selected whose complementary areas of specialization provided the needed breadth and balance to the panel.**

During the first meeting of the Source Term Expert Panel (March 1991), the Panel members were presented with published papers and reports identified from a comprehensive literature search that focused on radionuclide solubility in high-ionic-strength solutions in salt formations, covering the United States repository program as well as experiments conducted in Germany, Canada, Finland, Sweden, and at the Commission of the European Communities, Joint Research Center at Ispra, Italy. Other issues discussed in these publications were speciation, colloids, the leaching of radionuclides from high-level waste (HLW) glass, and the impact of backfill materials.

A summary of the expert judgment elicitation procedure and results, presented in detail in Trauth et al. (1992), follows. A final report on this effort by the members the Source Term Expert Panel will be available in 1993.

As stated above, the Source Term Expert Panel was selected to include a balance in the required areas of expertise (experience in actinide chemistry and with high-ionic-strength solutions). At the first meeting, the panelists divided the problem into areas of specific responsibility and provided a structure for assembling the individual judgments to obtain a single distribution codifying the collective judgment of the panel. In addition, the group of experts decided to be elicited together to produce one set of results. A consequence of the group elicitation is that the uncertainty expressed by specific experts could not be assessed. However, many of the inter-expert differences were captured during the elicitation process resulting in more widely dispersed probability functions.

---

* Because of the limited state of knowledge regarding colloids, the Source Term Expert Panel chose to limit their judgments to dissoloved radionuclides (solubility).

** In the case of the Source Term Expert Panel, expertise was required in actinide chemistry and high-ionic-strength chemistry. Therefore, experts from both these disciplines were selected. These individuals used their complementary expertise to arrive at judgments that satisfy all the pertinent constraints of the solubility problem.

In addition to a literature review (discussed above), preparation for elicitation involved computer calculations by the panel members using a standard brine that simulates the brine in the Salado Formation as the solvent (WIPP Brine A) (Lappin et al., 1989). These efforts resulted in the determination of the oxidation state(s) in which the radionuclides would exist in the WIPP rooms and drifts. Moreover, the solution and solid species that would coexist with that particular oxidation state were identified using two regimes: (1) one regime based on solid species with the highest solubility and therefore highest radionuclide concentration, and (2) another regime based on solid species with the lowest solubility and therefore lowest radionuclide concentration. Which regime predominates depends on the chemical properties within the repository, which in turn may depend on pH and ionic strength of the brine and the presence of carbonates and/or sulfates. Furthermore, the factors controlling each regime may differ for different radionuclides.

The experts' judgments on the solubility distributions were elicited at the second meeting (in April of 1991). The assessment for each distribution began by establishing the upper and lower solubility regimes and the calculated solubility of each radionuclide within each regime. The resulting probability distributions for the radionuclides used in the 1992 calculations are presented in Volume 3 of this report (Section 3.3.5). Because the calculated solubility is a single number that does not incorporate any uncertainty, it was necessary to account for uncertainty in both the calculated value and the underlying conditions, such as pH.

Typically, the calculated value would be used to establish a fractile, often either the 0.10 or 0.90 fractile, of the distribution. The absolute lower limit of the distribution was obtained by considering the sensitivity of solubility to the underlying brine chemistry. The interior fractiles were obtained after the 0.10 and 0.90 fractiles and the endpoints were established. Where possible, concentration data from well water from the Nevada Yucca Mountain site (J-13) was used with a correction for the ionic-strength difference between the J-13 water and the WIPP Brine A to determine the 0.50 fractile. For the determination of the 0.25 and 0.75 fractiles, one speciation was thought in some cases to be more likely, resulting in a skewed distribution. In other cases, both speciations were thought to be likely, resulting in a more symmetrical distribution.

The Source Term Expert Panel had considerable difficulty dealing with colloids because of a lack of experimental data and limited knowledge of the physical principles governing their formation. Some diversity of opinion existed about the significance of colloids. The panel did not believe that they could make judgments about suspended-solids concentrations at the present time. They planned to include recommendations for future experiments related specifically to colloids in a final panel report. Transport of radionuclides in colloids has not been included in the 1992 PA.

Correlations between the concentrations assigned to the radionuclides were discussed briefly by the panel. The consensus was that correlations do exist, possibly between americium(III) and curium(III), and between neptunium(IV) and plutonium(IV). The panel is expected to address this issue in a forthcoming report on their findings.

2.3.4.2 EXPERIMENTAL WORK

Future WIPP performance assessments will rely increasingly on data from planned solubility tests of actual waste. These tests will complement the laboratory studies of radionuclide chemistry. The laboratory program is currently determining solubilities and sorption coefficients of plutonium and its oxidation state analogues in synthetic brines under various conditions of pH, and will soon examine actinide speciation and measure stability constants for complex ions (Brush, 1990). As currently planned, the actinide source-term program will involve filling test containers with a mixture of natural and synthetic brines with compositions chemically similar to those of intergranular brines found in the Salado Formation. Container size will depend on waste homogeneity; heterogeneous waste types such as combustibles will use "drum scale" vessels of 210 L volume, while more homogeneous types such as process sludges will use "liter scale" test containers. The containers will permit regular brine sampling, and gas monitoring and venting.

2.3.5 Creep Closure, Fluid Flow, and Room/Waste Interactions

When the repository is decommissioned, free brine initially will not be present within the emplacement area, and void space above the backfilled waste will be air-filled. Brine seepage from the Salado Formation will have filled fractures in anhydrite interbeds above and below the emplacement area (Lappin et al., 1989; Rechard et al., 1990b).

Following excavation salt creep will begin to close the repository. In the absence of elevated gas pressures within the repository, modeling of salt creep indicates that consolidation of the waste in unreinforced rooms would be largely complete within 100 years (Tyler et al., 1988; Munson et al., 1989a,b). Brine will seep into the emplacement area from the surrounding salt, however, and gas will be generated in the humid environment by corrosion of metals, radiolysis of brine, and microbial decomposition of organic material. Some gas will disperse into the surrounding anhydrite layers. Continued gas generation could increase pressure within the repository sufficiently to reverse brine inflow and partially or completely desaturate the waste-emplacement area. Pressure may be high enough to open fractures in the anhydrite interbeds above and below the repository, allowing additional lateral migration of gas from the waste-emplacement area. High pressure may also halt and partially reverse closure by salt creep. In the undisturbed final state, the emplacement area could be incompletely consolidated and gas-filled rather than brine-filled.

All of the major processes active in the waste-emplacement area are linked, and all are rate- and time-dependent. For example, creep closure will be, in part, a function of pressure within the repository. Pressure will be in turn a function of the amount of gas generated and the volume available within the repository and the surrounding Salado Formation for gas storage. Gas-storage volume will be a function of closure rate and time, with storage volume decreasing as consolidation continues. Time and rate of gas generation, therefore, will strongly influence repository pressurization and closure. Gas-generation rates will be dependent on specific reaction rates and the availability of reactants, including water. Some water can be generated by microbial activity (Brush and Anderson, 1989b). Additional water will be provided by brine inflow, which, is assumed to occur according to two-phase immiscible flow through a porous medium and which will depend in large part on repository pressure, so that some gas-generation reactions could be partially self-buffering.

Responses of the disposal system to human intrusion are equally complicated. Consequences will depend on the time of intrusion, the degree to which the repository has closed, and the amount of gas generated. If intrusion occurs into a fully pressurized, dry, and partially unconsolidated waste-emplacement area, venting of gas up the borehole will permit brine to resaturate available void space. Following eventual deterioration of plugs in an intrusion borehole, brine may flow from the emplacement area into the borehole, transporting radionuclides upward toward the accessible environment. Upward flow from a pressurized brine pocket in the Castile Formation may contribute to flow and radionuclide transport.

3. PERFORMANCE ASSESSMENT METHODOLOGY

This chapter contains an overview of WIPP performance-assessment methodology. Additional information about this subject is provided in other published sources (Helton et al., 1991; WIPP PA Division, 1991a).

3.1 Conceptualization of Risk for the WIPP Performance Assessment

The WIPP performance assessment uses a conceptualization for risk similar to that developed for risk assessments for nuclear power plants. This conceptualization characterizes risk in terms of what can go wrong, how likely things are to go wrong, and what the consequences are of things going wrong. This description provides a structure on which both the representation and calculation of risk can be based.

Kaplan and Garrick (1981) have presented this representation of risk as a set of ordered triples. The WIPP performance assessment uses their representation, and defines risk to be a set $\mathcal{R}$ of the form

$$\mathcal{R} = \left\{ \left(S_i, pS_i, \mathbf{cS}_i \right), \; i = 1, \ldots, nS \right\}, \tag{3-1}$$

where

S_i = a set of similar occurrences,

pS_i = probability that an occurrence in set S_i will take place,

$\mathbf{cS}_i$ = a vector of consequences associated with S_i,

nS = number of sets selected for consideration,

and the sets S_i have no occurrences in common (i.e., the S_i are disjoint sets). This representation formally decomposes risk into what can happen (the S_i), how likely things are to happen (the pS_i), and the consequences of what can happen (the $\mathbf{cS}_i$). The S_i are scenarios in the WIPP performance assessment, the pS_i are scenario probabilities, and the vector $\mathbf{cS}_i$ contains the normalized EPA releases and other performance measures associated with scenario S_i. Other performance measures of interest are dose and health effects for safety assessments, and concentrations of heavy metals and volatile organic compounds (VOCs) for hazardous waste assessments.

Risk results in $\mathcal{R}$ can be summarized with complementary cumulative distribution functions (CCDFs). These functions provide a display of the information contained in the probabilities pS_i and the consequences $\mathbf{cS}_i$. With the assumption that a particular consequence result cS in the vector $\mathbf{cS}$ has been ordered so that $cS_i \le cS_{i+1}$ for $i = 1, \ldots, nS$, the CCDF for this consequence result is the function F defined by

$F(x)$ = probability that cS exceeds a specific consequence value x

$$= \sum_{j=i}^{nS} pS_j \tag{3-2}$$

where i is the smallest integer such that $\mathbf{cS}_i > x$. As illustrated in Figure 3-1, F is a step function that represents the probabilities that consequence values on the abscissa will be exceeded. To avoid a broken appearance, CCDFs are usually plotted with vertical lines added at the discontinuities.

The steps in the CCDFs shown in Figure 3-1 result from the discretization of all possible occurrences into the sets $S_i,\ldots S_{nS}$. Unless the underlying processes are inherently disjoint, the use of more sets S_i will tend to reduce the size of these Ssteps and, in the limit, will lead to a smooth curve.

3.1.1 Calculation of Risk

The calculation of risk and its associated uncertainty begins with the determination of the sets S_i, which are the scenarios to be analyzed. Once these sets are determined, their probabilities pS_i and associated consequences $\mathbf{cS}_i$ must be determined. In practice, development of the S_i is an iterative process that must take into account the procedures required to determine the probabilities pS_i and the consequences $\mathbf{cS}_i$. For the WIPP performance assessment, the overall process is organized so that pS_i and $\mathbf{cS}_i$ are calculated by various models, the configuration of which depends on the individual S_i.

Use of these models requires values for imprecisely known variables that can be represented by a vector

$$\mathbf{x} = [x_1, x_2, \ldots, x_{nV}], \tag{3-3}$$

where each x_j is an imprecisely known input required in the analysis and nV is the total number of such inputs. If the analysis has been developed so that each x_j is a real-valued quantity for which the overall analysis requires a single value, the representation for risk in Equation 3-1 can be restated as a function of $\mathbf{x}$:

$$\mathcal{R}(\mathbf{x}) = \{[S_i(\mathbf{x}), pS_i(\mathbf{x}), \mathbf{cS}_i(\mathbf{x})],\ i = 1,\ldots,nS(\mathbf{x})\} \tag{3-4}$$

As $\mathbf{x}$ changes, so will $\mathcal{R}(\mathbf{x})$ and all summary measures that can be derived from $\mathcal{R}(\mathbf{x})$. Thus, rather than a single CCDF for each consequence contained in the vector $\mathbf{cS}$ shown in Equation 3-1, a distribution of CCDFs results from the possible values that $\mathbf{x}$ can represent (Figure 3-2).

The distribution assigned to the individual variables x_j in $\mathbf{x}$ reflect uncertainty in the modeling system. Factors that affect uncertainty in risk results can be subdivided into those that affect imprecisely known variables, those related to the selection of conceptual and computational models, and those related to scenario selection. Factors related to scenario selection can be further subdivided into completeness, aggregation, and stochastic

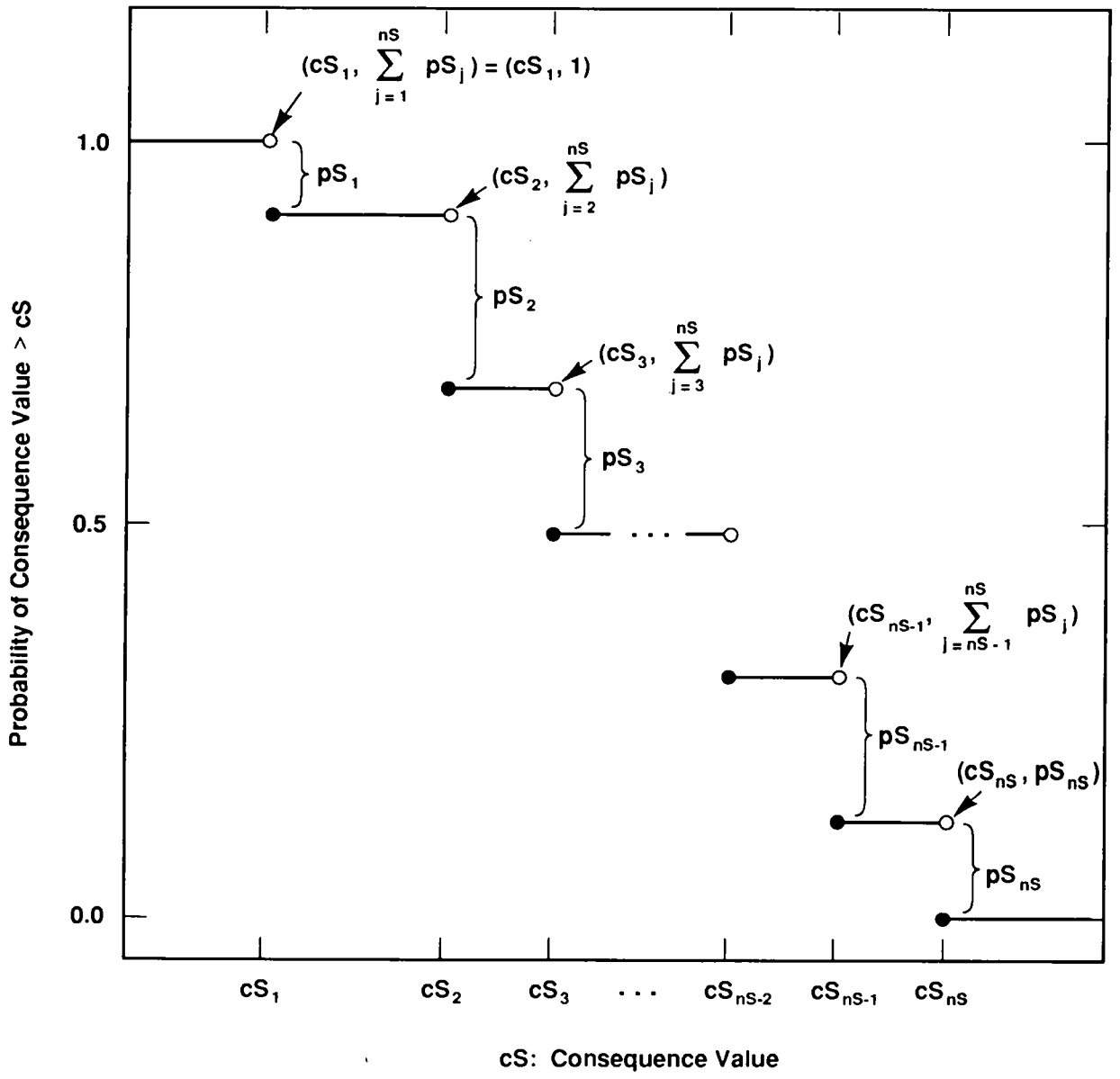

TRI-6342-730-5

Figure 3-1. Estimated CCDF for consequence result **cS** (Helton et al., 1991; Helton, in press). The open and solid circles at the discontinuities indicate the points included on (solid circles) and excluded from (open circles)the CCDF.

variation. Uncertainty about imprecisely known variables may result from incomplete data or measurement uncertainty, and can affect all three elements of the triple introduced in Equation 3-1. Uncertainty about the appropriate choices of models can affect both pS_i and $\mathbf{cS}_i$. Due to the complex nature of risk assessments, model selection can also affect the definition of the S_i. Completeness refers to the extent that a performance assessment includes all possible occurrences for the system under consideration. In terms of the risk representation in Equation 3-1, completeness deals with whether or not all possible occurrences are included in the union of the sets S_i. Aggregation refers to the division of the possible occurrences into the sets S_i. Resolution is lost if the S_i are defined too coarsely (e.g., nS is too small) or in some other inappropriate manner. Computational efficiency is lost if nS is too large. Model selection refers to the actual choice of the models used in a risk assessment. Uncertainty about the appropriate model choice can affect both pS_i and $\mathbf{cS}_i$. Due to the complex nature of risk assessments, model selection can also affect the definition of the S_i. Uncertainty about imprecisely known variables, which may result from incomplete data or measurement uncertainty, can also affect all three elements of the risk triple. Stochastic variation is represented by the probabilities pS_i, which are functions of the many factors that affect the occurrence of the individual sets S_i.

Individual variables x_j may relate to each of these different types of uncertainty. For example, individual variables might relate to completeness uncertainty (e.g., the value for a cutoff used to drop low-probability occurrences from the analysis), aggregation uncertainty (e.g., a bound on the value for nS), model uncertainty (e.g., a 0-1 variable that indicates which of two alternative models should be used), variable uncertainty (e.g., a solubility limit or a retardation for a specific element), or stochastic uncertainty (e.g., a variable that helps define the probabilities for the individual S_i).

3.1.2 Characterization of Uncertainty in Risk

Characterization of the uncertainty in the results of a performance assessment requires characterization of the uncertainty in $\mathbf{x}$, the vector of imprecisely known variables. This uncertainty can be described with a sequence of probability distributions

$$D_1, D_2, \ldots, D_{nV}, \tag{3-5}$$

where D_j is the distribution developed for the variable x_j, j=1, 2, ..., nV, contained in $\mathbf{x}$. The definition of these distributions may also be accompanied by the specification of correlations and various restrictions that further define the possible relations among the x_j. These distributions and other restrictions probabilistically characterize where the appropriate input to use in the performance assessment might fall, given that the analysis is structured so that only one value can be used for each variable under consideration.

Once the distributions in Equation 3-5 have been developed, Monte Carlo techniques can be used to determine the uncertainty in $\mathcal{R}(\mathbf{x})$ from the uncertainty in $\mathbf{x}$. First, a sample

$$\mathbf{x}_k = \left[x_{k1}, x_{k2}, \ldots, x_{k,nV}\right],\ k = 1, \ldots, nK \tag{3-6}$$

is generated according to the specified distributions and restrictions, where nK is the size of the sample. Performance-assessment calculations are then performed for each sample element $\mathbf{x}_k$, which yields a sequence of risk results of the form

$$\mathcal{R}(\mathbf{x}_k) = \left\{\left[S_i(\mathbf{x}_k), pS_i(\mathbf{x}_k), \mathbf{cS}_i(\mathbf{x}_k)\right],\ i = 1,\ldots,nS(\mathbf{x}_k)\right\}, \tag{3-7}$$

for $k = 1, \ldots, nK$. Each set $\mathcal{R}(\mathbf{x}_k)$ is the result of one complete set of calculations performed with a set of inputs (i.e., $\mathbf{x}_k$) that the review process producing the distributions in Equation 3-5 concluded was possible. Further, associated with each risk result $\mathcal{R}(\mathbf{x}_k)$ in Equation 3-7 is a probability or weight* that can be used in making probabilistic statements about the distribution of $\mathcal{R}(\mathbf{x})$.

A single CCDF can be produced for each set $\mathcal{R}(\mathbf{x}_k)$ of results shown in Equation 3-7, yielding a family of CCDFs of the form shown in Figure 3-2. This distribution of CCDFs can be summarized by plotting the mean value and selected percentile values of the exceedance probabilities shown on the ordinate for each consequence value on the abscissa. For example, the mean plus the 10th, 50th (i.e., median), and 90th percentile values might be used (Figure 3-3). The mean and percentile values can be obtained from the exceedance probabilities associated with the individual consequence values and the weights or "probabilities" associated with the individual sample elements.

Consideration of a family of CCDFs allows a distinction between the uncertainty that controls the shape of a single CCDF and the uncertainty that results in a distribution of CCDFs. The stepwise shape of a single CCDF reflects the fact that a number of different occurrences have a real possibility of taking place. This type of uncertainty is referred to as stochastic variation in this report. A family of CCDFs arises from the fact that fixed, but unknown, quantities are needed in the estimation of a CCDF. The distributions that characterize what the values for these fixed quantities might be lead to a distribution of CCDFs, with each single CCDF reflecting a specific sample element $\mathbf{x}_k$.

Both Kaplan and Garrick (1981) and the International Atomic Energy Agency (IAEA, 1989) distinguish between these two types of uncertainty. Specifically, Kaplan and Garrick distinguish between probabilities derived from frequencies and probabilities that characterize degrees of belief. Probabilities derived from frequencies correspond to the probabilities pS_i in Equation 3-1, while probabilities that characterize degrees of belief (i.e., subjective probabilities) correspond to the distributions indicated in Equation 3-5. The IAEA report distinguishes between what it calls Type-A uncertainty and Type-B uncertainty. The IAEA report defines Type-A uncertainty to be stochastic variation; as such, this uncertainty corresponds to the frequency-based probability of Kaplan and Garrick and the pS_i of Equation 3-1. Type-B uncertainty is defined to be uncertainty that is due to lack of knowledge about fixed quantities; thus, this uncertainty corresponds to the subjective probability of Kaplan and

* In random or Latin hypercube sampling, this weight is the reciprocal of the sample size (i.e., $1/nK$) and can be used in estimating means, cumulative distribution functions, and other statistical properties. This weight is often referred to as the probability for each observation (i.e., sample $\mathbf{x}_k$). However, this association is not technically correct. If continuous distributions are involved, the actual probability of each observation is zero.

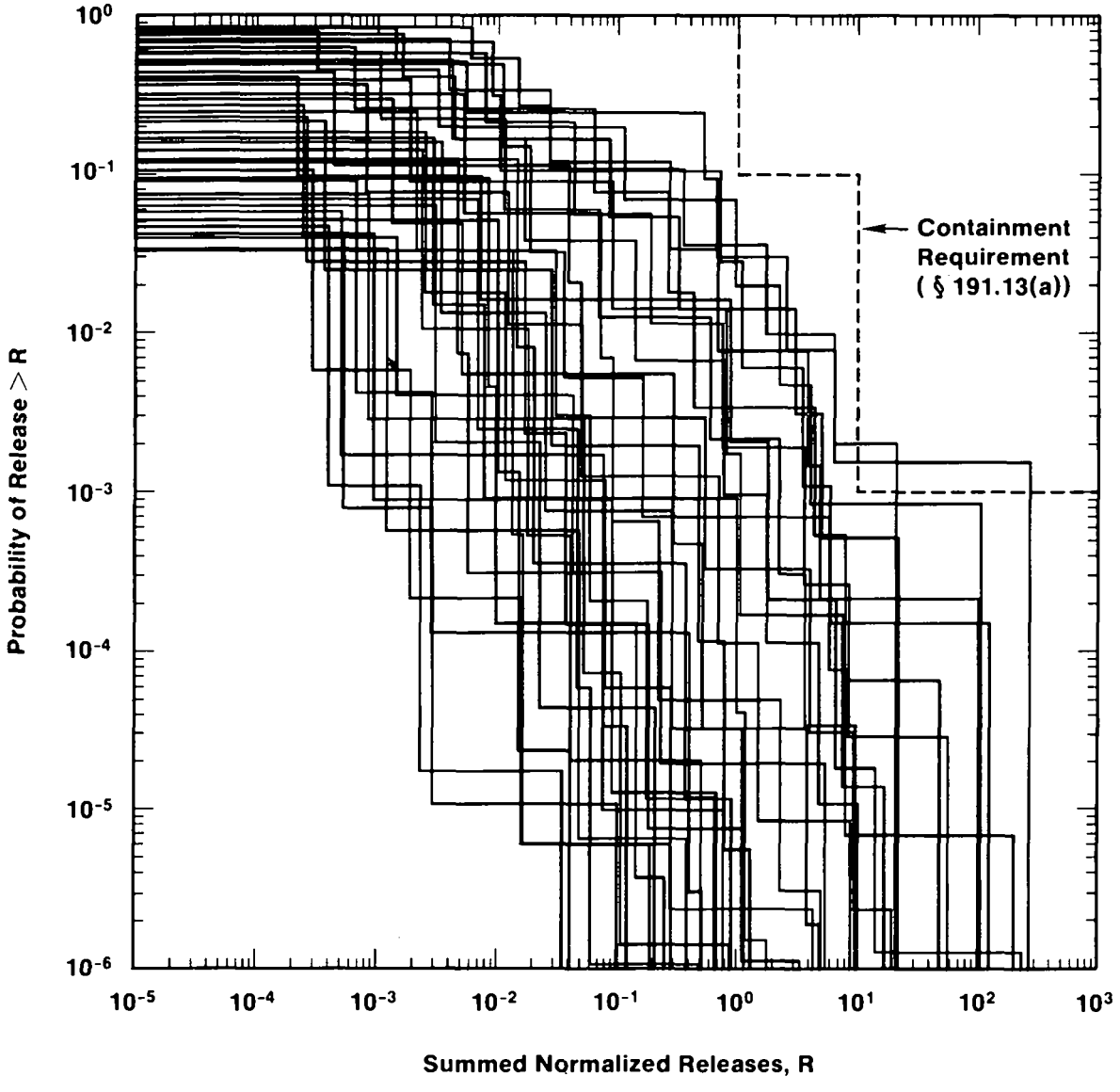

Figure 3-2. Example distribution of CCDFs obtained by sampling imprecisely known variables.

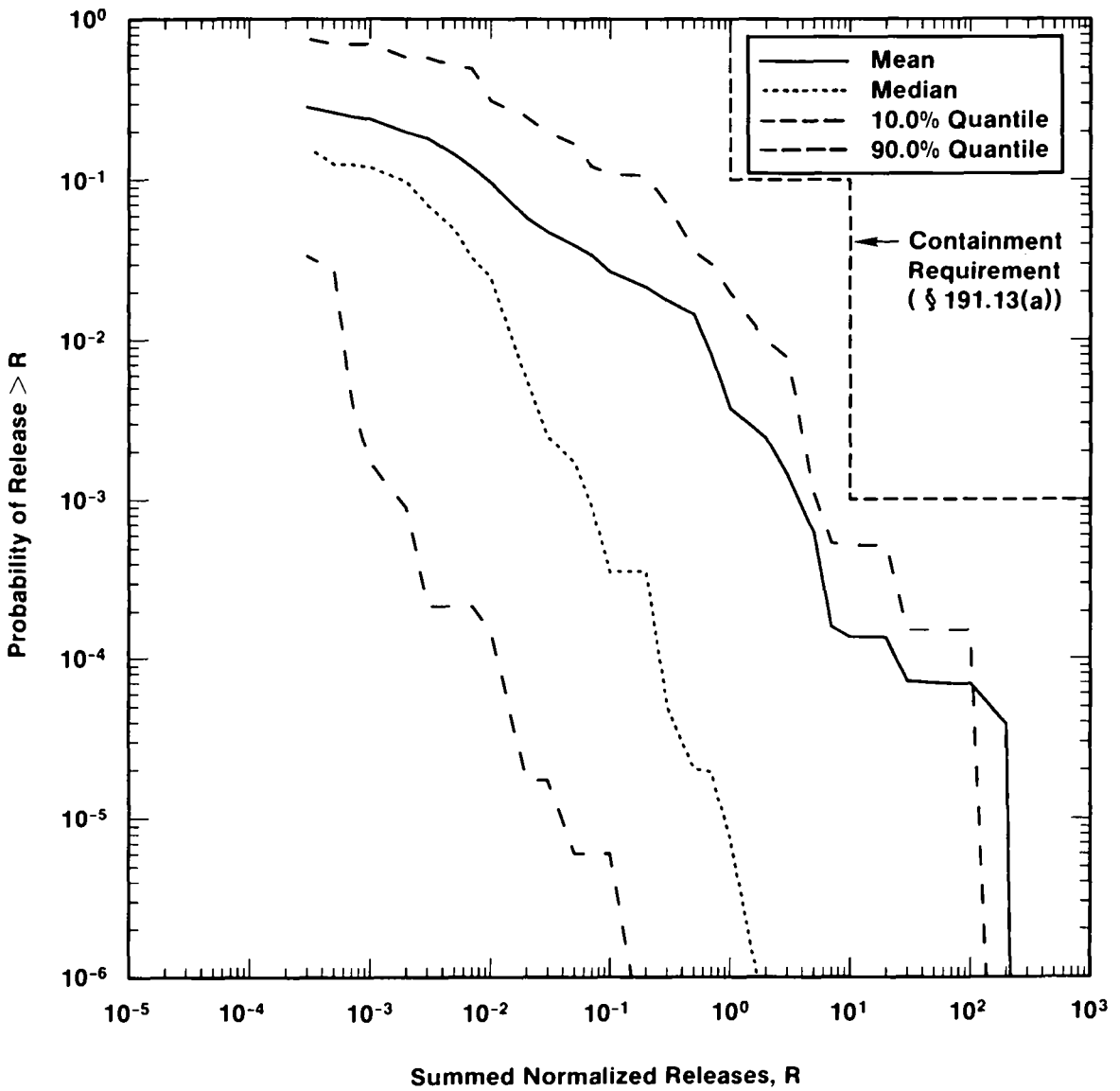

TRI-6342-1501-0

Figure 3-3. Example summary curves derived from an estimated distribution of CCDFs. The curves in this figure were obtained by calculating the mean and the indicated percentiles for each consequence value on the abscissa in Figure 3-2. The 90th-percentile curve crosses the mean curve due to the highly skewed distributions for exceedance probability. This skewness also results in the mean curve being above the median curve.

Garrick and the distributions indicated in Equation 3-5. This distinction has also been made by other authors, including Vesely and Rasmuson (1984), Paté-Cornell (1986), and Parry (1988).

For a given conceptual model in the WIPP performance assessment, subjective uncertainty enters the analysis due to lack of knowledge about quantities such as solubility limits, retardation factors, and flow fields. Stochastic uncertainty enters the analysis through the assumption that future exploratory drilling will be random in time and space (i.e., follows a Poisson process). However, the rate constant λ in the definition of this Poisson process is assumed to be imprecisely known. Thus, subjective uncertainty exists in a quantity used to characterize stochastic uncertainty.

3.1.3 Risk and the EPA Limits

The EPA expressly identifies the need to consider the impact of uncertainties in calculations performed to show compliance with the Containment Requirements. Specifically, Appendix B of 40 CFR 191 suggests that

> ...whenever practicable, the implementing agency will assemble all of the results of the performance assessments to determine compliance with § 191.13 into a "complementary cumulative distribution function" that indicates the probability of exceeding various levels of cumulative release. When the uncertainties in parameters are considered in a performance assessment, the effects of the uncertainties considered can be incorporated into a single such distribution function for each disposal system considered. The Agency assumes that a disposal system can be considered to be in compliance with [section] 191.13 if this single distribution function meets the requirements of [section] 191.13(a) (U.S. EPA, 1985, p. 38088).

The representation for risk in Equation 3-1 provides a conceptual basis for the calculation of the complementary cumulative distribution function (CCDF) for normalized releases specified in 40 CFR 191B. Further, this representation provides a structure that can be used for both the incorporation of uncertainties and the representation of the effects of uncertainties.

Each CCDF in the family of CCDFs that results from Eq. 3-7 would be the appropriate choice for comparison against the EPA requirements, *if* $\mathbf{x}_k$ contained the correct variable values for use in determining the pS_i and $\mathbf{cS}_i$ *and if* the assumed conceptual models correctly characterize the disposal system. Increasing the sample size nK will, in general, produce a better approximation of the true distribution of CCDFs, but will not alter the fact that the distribution of CCDFs is conditional on the assumptions of the analysis.

If nK is large, displays of the complete family of CCDFs can be difficult to interpret. As discussed in the previous section, mean and percentile curves can be used to summarize the information contained in the family. Appendix B of 40 CFR 191 suggests that "the effects of the uncertainties considered can be incorporated into a single [CCDF]" (U.S. EPA, 1985; p. 38088), but 40 CFR 191 does not contain specific guidance on which curve should be compared to the Containment Requirements. In previous work, the mean curve has generally been proposed for showing compliance with § 191.13(a) (e.g., Cranwell et al., 1987, 1990; Hunter et al., 1986). Only mean curves are shown in Volume 1 of this report. Complete families of curves and the associated summary curves are presented in Volume 4 of this report.

Whenever a distribution of curves is reduced to a single curve, information on uncertainty is lost. Replicated Monte Carlo analyses can characterize the uncertainty in an estimated mean CCDF or other summary curve. However, representing the uncertainty in an estimated value in this way is quite different from displaying the variability or uncertainty in the population from which the estimate is derived. For example, the uncertainty in the estimated mean curve in Figure 3-3 is less than the variability in the population of CCDFs that was averaged to obtain this mean. Therefore, results of the preliminary WIPP performance assessments are displayed as both complete families of CCDFs (as illustrated in Figure 3-2) and summary curves (as illustrated in Figure 3-3).

Because CCDFs are conditional on the assumptions of the analysis, no single curve or family of curves from a single analysis can display conceptual model uncertainty. The WIPP performance assessment examines conceptual model uncertainty by repeating the complete Monte Carlo analysis for each alternative conceptual model, and comparing mean CCDFs. Only those portions of the analysis specific to the alternative conceptual models (e.g., selected parameter values or computational models) are altered. All other models and parameter values are the same in each analysis, and the two conceptual models are thus compared *ceteris paribus* (all other things being equal). The shift in the location of the CCDF provides a measure of the uncertainty introduced by the existence of alternative conceptual models, and provides the Project guidance on which alternative conceptual models have the greatest potential to affect disposal-system performance.

3.2 Selection of Scenarios

40 CFR 191 does not include the term scenario in its definition of performance assessment, referring instead only to events and processes that might affect the disposal system during the next 10,000 years. Considering the consequences of isolated events and processes, however, is not sufficient; the various combinations of events and processes that define possible future states of the disposal system must be considered in a complete analysis. Combinations of events and processes are referred to as scenarios in Bertram-Howery and Hunter (1989), Marietta et al. (1989), Cranwell et al. (1990), Bertram-Howery et al. (1990), and WIPP PA Division (1991a).

3.2.1 Conceptual Basis for Scenario Development

The scenarios S_i are obtained by subdividing a set S (the sample space) that contains all possible 10,000-year time histories at the WIPP beginning at the decommissioning of the facility. Because resources for analysis are finite and the set S has infinitely many elements, an important goal of scenario development is to recognize and remove from full consideration those scenarios for which the impact on compliance with 40 CFR 191B can be reasonably anticipated to be negligible due to low probability, low consequences, or regulatory exclusion.

Five subsets of S provide a starting point for scenario development (Figure 3-4). The reasoning behind selecting these subsets is provided in Section 4.2.3 of this volume. First, the base-case subset S_B consists of all elements in S that fall within the bounds of what can be reasonably anticipated to occur at the WIPP over

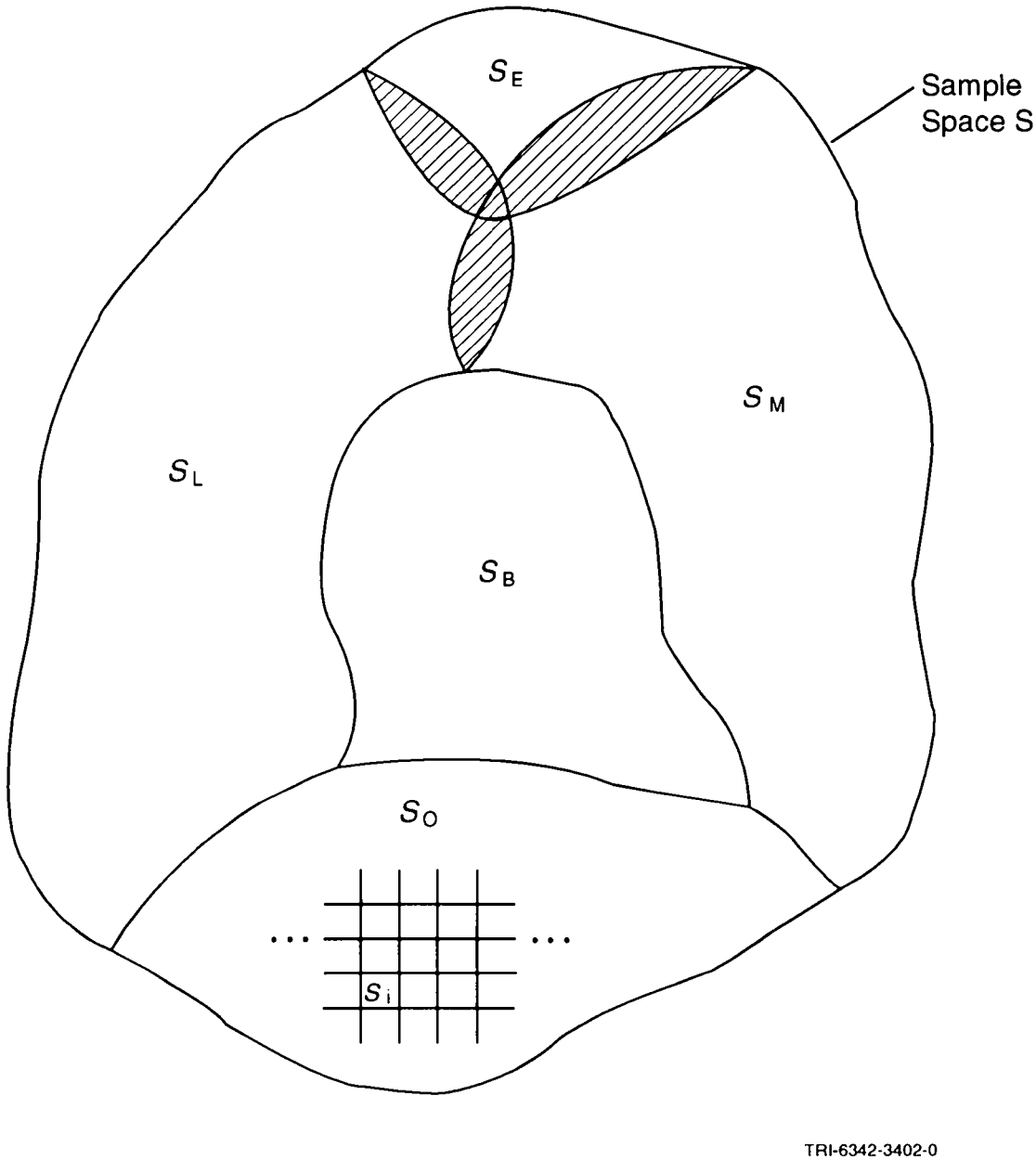

Figure 3-4. Decomposition of the sample space S into high-level subsets, where S_B designates the base-case subset, S_M designates a minimal disruption subset, S_E designates a regulatory exclusion subset, S_L designates a low-probability subset, and S_O designates $\left(S_B \cup S_M \cup S_E \cup S_L\right)^c$.

10,000 years, and represents the undisturbed performance of the disposal system. Second, a minimal disruption subset S_M consists of all elements in S that involve disruptions that result in no significant perturbation to the consequences associated with the corresponding elements in the base-case subset S_B. Third, a regulatory exclusion subset S_E consists of all elements in S that are excluded from consideration by regulatory directive (e.g., human intrusions more severe than the drilling of exploratory boreholes). Fourth, a low-probability subset S_L consists of elements of S not contained in S_B whose collective probability is small (e.g., the probability of S_L is less than 0.0001) regardless of their potential consequences. Everything that remains in S after the identification of S_B, S_M, S_E, and S_L now becomes a fifth subset S_O, where the subscript O represents "Other." In set notation,

$$S_O=\left(S_B\cup S_M\cup S_E\cup S_L\right)^c \tag{3-8}$$

where the superscript c is used to designate the complement of a set.

Evaluation of compliance with the Containment Requirements of 40 CFR 191B does not depend equally on each of the five subsets of S. By definition, elements of S_E are excluded from consideration. The relative contributions of the other four subsets to a hypothetical CCDF for the WIPP are shown in Figure 3-5. Releases associated with the base case S_B for the WIPP are zero for this analysis (see Chapter 5 of Volume 1 and references cited there), and the consequences of both S_B and S_M therefore plot well below the EPA limits, at the extreme upper left of the CCDF. Consequences of S_L are by definition of sufficiently low probability (less than 10^{-4} in 10^4 years) that they plot below the EPA limits. High-consequence elements of S_L plot at the lower right of the CCDF. Compliance depends primarily therefore on the examination of S_O, and specifically on a set of additional scenarios S_i, i=1, ..., nS, obtained by further refining (i.e., subdividing) the subset S_O. S_E, S_L, and S_M could be defined to be mutually exclusive, but this distinction is not important here so they are represented in Figure 3-4 with non-empty intersections. As described in Section 4.2.1, S_B and S_O are constructed to be mutually exclusive and to have empty intersections with S_M and S_L.

Although the scenarios that affect compliance for the WIPP come from the set S_i, performance assessments must also include S_B. The overall pattern of Figure 3-5 can be seen in the results of the WIPP preliminary performance assessments, with S_B determining the upper left of the CCDF and the remainder being determined by the S_i.

This analysis does not exclude S_L from consideration in the comparison with the EPA release limits. The contribution from S_L would always plot to the lower right of the CCDF, well below the EPA probability limits, and therefore would not matter in a compliance decision. S_M is not included in WIPP PA so the probability of S_M is not accumulated as shown in Figure 3-5, i.e., only the probability of S_B is included. The net effect of excluding S_M is to raise the CCDF toward the probability limits; therefore, including S_M would not negate a compliance decision.

Consequences of S_M cannot be seen on the CCDF for the WIPP because releases from S_B are zero. Consequences of S_L, which, if calculated, would appear as an extension on the extreme lower right of the CCDF, are also not displayed directly in the results of the WIPP performance assessments.

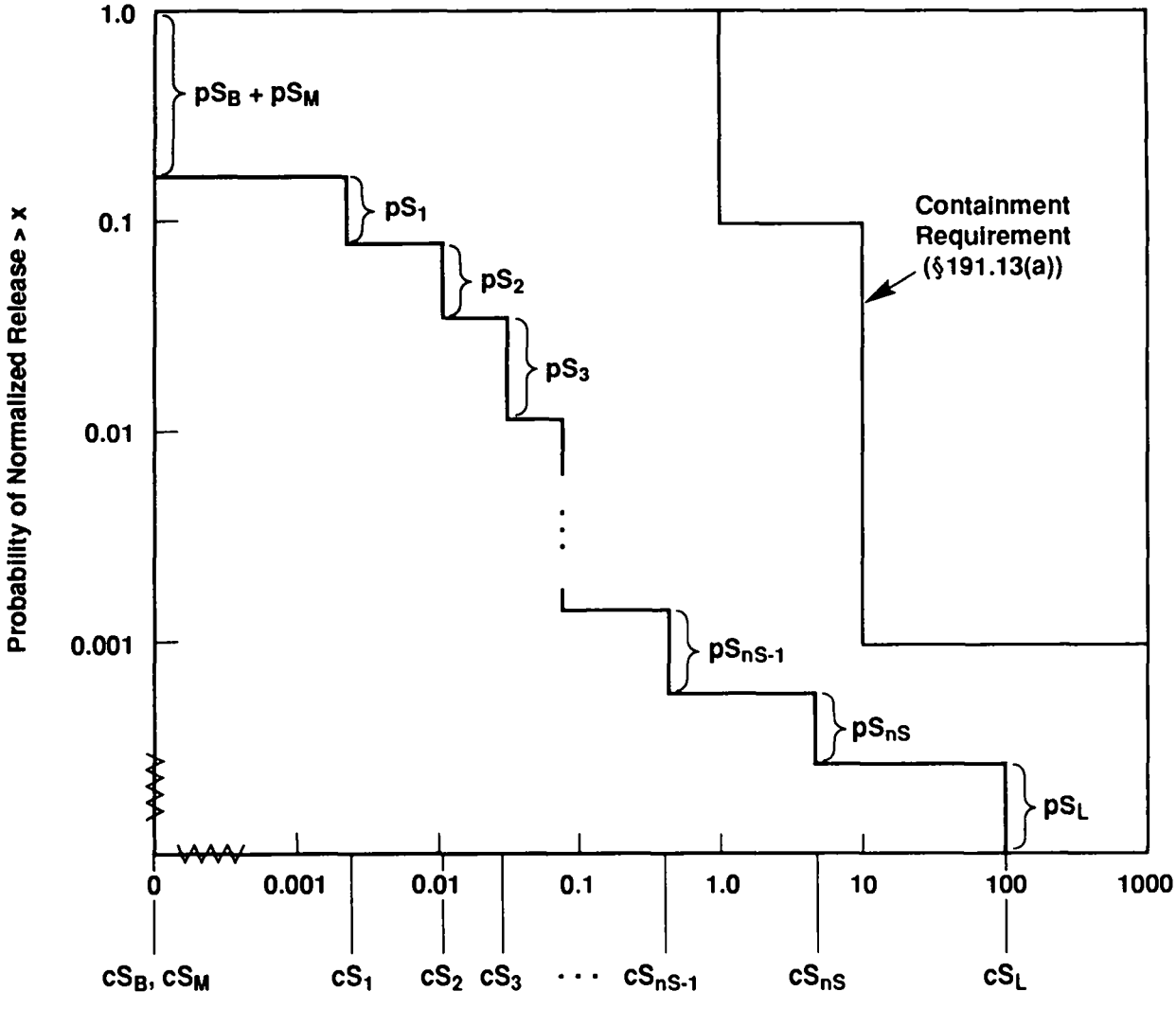

Notation: $pS_B, pS_M, pS_1, pS_2, \ldots, pS_{nS}, pS_L$ probability for corresponding scenario

$cS_B, cS_M, cS_1, cS_2, \ldots, cS_{nS}, cS_L$ consequence for corresponding scenario

$S_1, S_2, \ldots, S_{nS}$ assumed to be ordered so that $cS_1 \leq cS_2 \leq \ldots \leq cS_{nS}$

TRI-6342-1278-0

Figure 3-5. Construction of a CCDF for comparison with the EPA release limits. Note that the location of $\mathbf{cS_B}$ at the lower left of the plot is correct for the WIPP—where no releases are predicted from the undisturbed base case—but is not a generic requirement for all sites.

The WIPP performance assessment does not follow the exact EPA guidance in defining S_L. Appendix B of 40 CFR 191 suggests that "... performance assessments need not consider categories of events or processes that are estimated to have less than one chance in 10,000 of occurring over 10,000 years" (U.S. EPA, 1985, p. 38088). By suitably defining the events and processes selected for consideration (i.e., by making nS sufficiently large), all probabilities can theoretically be made less than the specified bound. Conceptually, the WIPP performance assessment avoids the potential problems raised by the wording of the guidance by placing a bound on the total probability of all occurrences that are removed from detailed consideration (i.e., the probability pS_L for S_L) rather than the individual probabilities for a number of different scenarios. In practice, the distinction has little impact because, as discussed later in Chapter 4 of this volume, probabilities estimated for elements of S_L are substantially below the suggested cutoff.

3.2.2 WIPP Performance-Assessment Approach to Scenario Development

Recognition of the five subsets of S provides the basis for the WIPP performance assessment's approach to scenario development. Because S_B, S_E, S_L, and S_M may account for a large part of the sample space S and also have readily predicted effects on the CCDF used for comparison with the EPA release limits, S_B, S_E, S_L, and S_M are determined in the first stage of development before S_O is subdivided into the scenarios S_i shown in Figure 3-4.

The WIPP performance assessment uses a two-stage procedure for scenario development and the determination of scenario probabilities. The purpose of the first stage is to develop a comprehensive set of scenarios that includes all occurrences that might reasonably take place at the WIPP, and to determine the probabilities of these scenarios. The result of this stage is a set of scenarios that summarize what might happen at the WIPP. These scenarios provide a basis for discussing the future behavior of the WIPP and a starting point for the second stage of the procedure, which is the definition of scenarios S_i and the determination of the probabilities pS_i at a level of detail that is appropriate for use with the conceptual and computational models employed in the performance assessment.

The first stage of the analysis focuses on the determination of the sample space S and the subsets S_B, S_E, S_L, S_M and S_O. Major groupings of scenarios within S_O are also recognized at this time, and defined for reference purposes as summary scenarios. This stage of the analysis uses a scenario-selection procedure suggested by Cranwell et al. (1990) that consists of the following five steps: (1) compiling or adopting a "comprehensive" list of events and processes that potentially could affect the disposal system, (2) classifying the events and processes to aid in completeness arguments, (3) screening the events and processes to identify those that can be eliminated from consideration in the performance assessment, (4) developing scenarios by combining the events and processes that remain after screening, and (5) screening scenarios to identify those that have little or no effect on the shape or location of the mean CCDF.

The purpose of the first step is to develop the sample space S, which consists of all possible 10,000-year time histories that involve the identified events and processes. The sample space S is subdivided into the subsets S_B, S_E, S_L, S_M, and S_O in Steps 2 and 3. The screening associated with Steps 2 and 3 also removes time

histories from S that are physically unreasonable. In Step 4, a preliminary subdivision of the subset S_O into additional summary scenarios is accomplished through a two-part process. In the first part, subsets of S_O (i.e., scenarios) are defined that involve specific events or processes. However, these scenarios are not mutually exclusive. In the second part, a subdivision of S_O into mutually exclusive scenarios S_i is accomplished by forming all possible intersections of the single event/process scenarios and their complements. The fifth and final step in the process is a screening of the scenarios S_i on the basis of probability, consequence, and physical reasonableness. The purpose of this screening is to determine if some of the S_i can be removed from the analysis.

A second stage of scenario development is necessary because the summary scenarios developed in the first stage are, in general, not defined at sufficiently fine levels of resolution for use in the construction of a CCDF that adequately displays the effects of stochastic, or Type-A, uncertainty (Section 3.1.2). The computational scenarios described in Section 4.4 of this volume represent a substantially finer subdivision of S_O than that used to construct the summary scenarios, but they are based on the same screening of events and processes conducted during the first stage of scenario development. As in previous scenario construction for preliminary performance assessments of the WIPP, inadvertent intrusion into the repository during exploratory drilling is the only disruptive event considered in the 1992 assessment, and the computational scenarios reflect subdivisions based on time and number of intrusion, the activity of the waste intersected, and whether or not pressurized brine is encountered in the Castile Formation below the repository.

The determination of both scenarios and scenario probabilities is a complex process with significant uncertainties. To help assure that the WIPP performance assessment brings a broad perspective to this task, expert panels have been formed to provide a diversity of views with respect to possible futures at the WIPP and the probability of human intrusion. The formation of these panels and the results obtained from their deliberations are documented in Hora et al. (1991) and the memorandum by Hora in Volume 3, Appendix A of this report.

No inherently correct grouping exists of the possible time histories into scenarios; the probabilities associated with individual scenarios S_i can always be reduced by using a finer grouping. As long as low-probability S_i are not discarded, the use of more but lower probability S_i will improve the resolution in the estimated CCDF shown in Figure 3-1. Because a consequence must be calculated for each scenario S_i, the use of more S_i results in more detailed specification of the calculations that must be performed for each scenario.

For example, a scenario S_i for the WIPP might be defined by

$$S_i = \{x : x \text{ a single 10,000-year time history beginning at decommissioning of the facility under consideration in which a single borehole occurs}\}. \quad (3\text{-}9)$$

A more refined definition would be

$S_{ik} = \{x : x$ a 10,000-year history at the WIPP beginning at decommissioning in which a single borehole occurs between $(i-1)\times 10^3$ and $i\times 10^3$ years and no boreholes occur during any other time interval$\}$. (3-10)

Then,

$$S_{ik} \subset S_i, i = 1,\ldots,10, \text{ and } S_i = \bigcup_{k=1}^{10} S_{ik} \quad (3\text{-}11)$$

Thus, S_i and $\cup_k S_{ik}$ contain the same set of time histories. However, the individual S_{ik} are smaller sets of time histories that are included in the larger set S_i. In terms of performance assessment, each S_{ik} describes a more specific set of conditions that must be modeled than does S_i. The estimated CCDF in Figure 3-1 could be constructed with either S_i or the S_{ik}, although the use of the S_{ik} would result in less aggregation error, and thus, provide better resolution in the resultant CCDF.

The S_i appearing in the definition of risk in Equation 3-1 should be developed to a level of resolution at which it is possible to view the analysis for each S_i as requiring a fixed, but possibly imprecisely known, vector $\mathbf{x}$ of variable values. When a set S_i is appropriately defined, it should be possible to use the same model or models and the same vector of variable values to represent every occurrence (e.g., a 10,000-year time history for the WIPP) in S_i. Scenario definition must permit the consequences $\mathbf{cS}_i$ appearing in Equation 3-1 to be calculated with reasonable efficiency, while holding the amount of aggregation error that enters the analysis to a reasonable level. Thus, although subdivision of S into a large number of S_i (e.g., on the basis of time of intrusion) may result in increased resolution in the estimate of $\mathbf{cS}$, it may also result in a computationally impractical analysis. Performance assessments must balance these competing requirements.

3.3 Determination of Scenario Probabilities

The second element of the ordered triples shown in Equation 3-1 is the scenario probability pS_i. As with scenario definition, the probabilities pS_i have been developed at two levels of detail.

Preliminary probabilities for the summary scenarios have been developed by Marietta et al. (1989) and Guzowski (1991). Apostolakis et al. (1991) provide an additional discussion of techniques for determining probabilities in the context of performance assessment for radioactive-waste disposal.

Probabilities for the computational scenarios used in the construction of CCDFs are discussed in Chapter 5 of this volume, and are based on the assumption that the occurrence of boreholes through the repository follows a Poisson process (i.e., are random in time and space) with a rate constant λ. Formulas for determining pS_i dependent on this assumption are derived in Chapter 5. The derivations are general and include both the stationary (i.e., constant λ) and nonstationary (i.e., time-dependent λ) cases. The 1992 performance assessment estimates consequences using both constant values for λ and time-dependent values derived from expert judgment.

3.4 Calculation of Scenario Consequences

The third element of the ordered triples shown in Equation 3-1 is the scenario consequence, $\mathbf{cS}_i$. Estimation of $\mathbf{cS}_i$ is done using a linked system of computational models described in greater detail in Chapters 7 and 8 of this volume.

The models used in the WIPP performance assessment, as in other complex analyses, exist at four different levels. First, conceptual models provide a framework in which information about the disposal system can be organized and linked to processes that can be simulated with quantitative models. An adequate conceptual model is essential for both the development of the sample space $\mathcal{S}_O$ appearing in Equation 3-8 and the division of $\mathcal{S}_O$ into the scenarios $\mathcal{S}_i$ appearing in Equation 3-1. As defined in Chapter 2, alternative conceptual models may exist that are equally consistent with the available information. Consequences for each scenario must be estimated separately for each alternative conceptual model included in the analysis.

Second, mathematical models are developed to represent the processes at the site. The conceptual models provide the context within which these mathematical models must operate and define the processes they must characterize. The mathematical models are predictive in the sense that, given known properties of the system and possible perturbations to the system, they predict the response of the system. Among the processes represented by these mathematical models are fluid flow, mechanical deformation, radionuclide transport in groundwater, removal of waste through intruding boreholes, and human exposure to radionuclides released to the surface environment. Mathematical models for these processes, and others, are described in Chapter 7 of this volume.

Third, numerical models are developed to approximate the mathematical models. Most mathematical models do not have closed-form solutions, and numerical procedures must be developed to provide approximations to the solutions of the mathematical models. In essence, these approximations provide "numerical models" that calculate results that are close to the solutions of the original mathematical models. For example, Runge-Kutta procedures are often used to solve ordinary differential equations, and finite difference and finite element methods are used to solve partial differential equations. In practice, it is unusual for a mathematical model to have a solution that can be determined without the use of an intermediate numerical model. Numerical models used in the WIPP performance assessment are described in appendices to this volume.

Fourth, the complexity of the system requires the use of computer codes to implement the numerical models. Figure 3-6 illustrates the sequence of linked codes used in the 1992 WIPP performance assessment. Each of the models appearing in this figure is briefly described in Table 3-1; more information is available in Chapter 7 and appendices to this volume, and in references cited there.

3.5 Monte Carlo Analysis Techniques

As discussed in more detail by Helton et al. (1991) and in Volume 4 of this report, the WIPP performance assessment uses Monte Carlo techniques for uncertainty and sensitivity analyses. In the context of this report, uncertainty analyses evaluate uncertainty in performance estimates that results both from the existence of alternative conceptual models and from the uncertainty about imprecisely known input variables. Sensitivity anal-

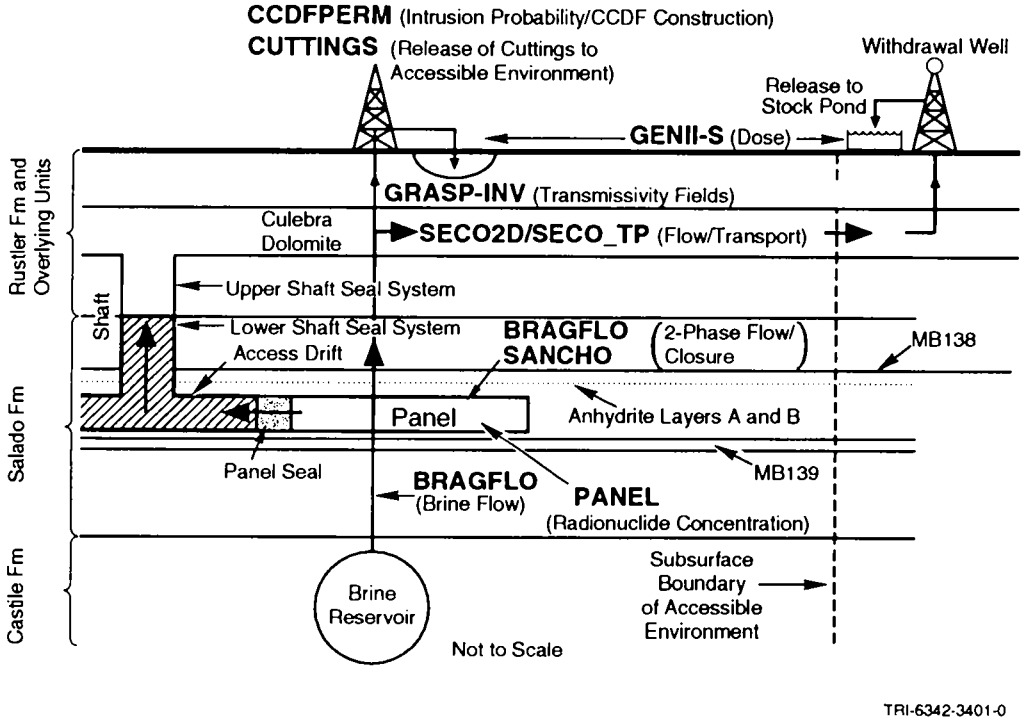

Figure 3-6. Models used in 1992 WIPP performance assessment. The names for computer models (i.e., computer codes) are shown in capital letters.

Table 3-1. Summary of Computer Models Used in the 1992 WIPP Performance Assessment

Model	Description
BRAGFLO	Describes the multiphase flow of gas and brine through a porous, heterogenous reservoir. BRAGFLO solves simultaneously the coupled partial differential equations that describe the mass conservation of gas and brine along with appropriate constraint equations, initial conditions, and boundary conditions (Chapter 7).
CCDFPERM	Constructs probabilities for various computational scenarios associated with human intrusion by exploratory drilling (Section 1.4.2 of Volume 3).
CUTTINGS	Calculates the quantity of radioactive material (in curies) brought to the surface as cuttings and cavings generated by an exploratory drilling operation that penetrates a waste panel (Chapter 7).
GENII-S	Estimates potential radiation doses to humans from radionuclides in the environment (Leigh et al., in review).
GRASP-INV	Automatically generates simulations of transmissivity fields (estimates of transmissivity values) conditioned on measured transmissivity values and calibrated to steady-state and transient pressure data at well locations using an adjoint sensitivity and pilot-point technique (LaVenue and RamaRao, 1992).
PANEL	Calculates rate of discharge and cumulative discharge of radionuclides from a repository panel through an intrusion borehole. Discharge is a function of fluid flow rate, nuclide solubility, and remaining inventory (Chapter 7).
SANCHO	Finite element program that solves quasistatic, large deformation, inelastic response of two-dimensional solids (Stone et al., 1985). Used in the 1992 performance assessment to determine porosity of the waste as a function of time and moles of gas generated (Section 1.4.7 of Volume 3).
SECO2D	Calculates single-phase Darcy flow for groundwater-flow problems in two dimensions. The formulation is based on a single partial differential equation for hydraulic head using fully implicit time differencing (Chapter 7).
SECOTP	Simulates fluid flow and transport of radionuclides in fractured porous media (Chapter 7).

yses determine the contribution of individual input variables to the uncertainty in model predictions. As used here, both these types of analyses provide information about the effects of subjective, or Type-B, uncertainty. The effects of stochastic, or Type-A, uncertainty are incorporated into the performance assessment through the scenario probabilities pS_i appearing in Equation 3-1.

Monte Carlo analyses involve five steps: (1) selection of the variables to be examined and the ranges and distributions for their possible values; (2) generation of the samples to be analyzed; (3) propagation of the samples through the analysis; (4) uncertainty analysis; and (5) sensitivity analysis. These steps are described briefly in the following sections. A more complete discussion can be found in Helton et al. (1991).

3.5.1 Selection of Variables and Their Ranges and Distributions

Monte Carlo analyses use a probabilistic procedure for the selection of model input. Therefore, the first step in a Monte Carlo analysis is the selection of uncertain variables and of ranges and distributions that characterize the uncertainty in their possible values. These variables are typically input parameters to computer models, and the impact of the assigned ranges and distributions can be great: analysis results are controlled in large part by the choice of input. Results of uncertainty and sensitivity analyses, in particular, strongly reflect the characterization of uncertainty in the input data.

As discussed in detail in Volume 3 of this report, information about the ranges and distributions of possible values is drawn from a variety of sources, including field data, laboratory data, literature, and, in instances where significant uncertainty exists and site-specific information is unavailable or insufficient at the time of the analyses, subjective expert judgment. In general, data from these sources cannot be examined statistically and incorporated directly in performance-assessment analyses, because data are rarely gathered with the specific model application in mind. Spatial and temporal scales over which the data are valid often do not match those of the models' applications, and in many cases, real site-specific data are simply not available. Data may be sparse or unavailable because measurements are infeasible (e.g., drilling sufficient boreholes to determine the regional heterogeneity of transmissivity in overlying aquifers), because direct measurements would in themselves create risk (e.g., drilling of boreholes through the repository to determine the extent of an underlying brine reservoir), because measurements are impossible (e.g., measuring future drilling technology), or for other reasons.

The review process that leads from the available data to the construction of the cumulative distribution functions (cdfs) used in the performance-assessment analyses is described in detail in Volume 3 of this report. Because of the nature of the available data and the type of analysis, this review process is unavoidably subjective, and involves the expert judgment of the investigators and performance-assessment analysts.

The ultimate outcome of the review process is a distribution function $F(x)$ of the form shown in Figure 3-7 for each independent variable of interest. For a particular variable x_j, the function F is defined such that

$$\text{prob}\left(x < x_j \leq x + \Delta x\right) = F(x + \Delta x) - F(x) \tag{3-12}$$

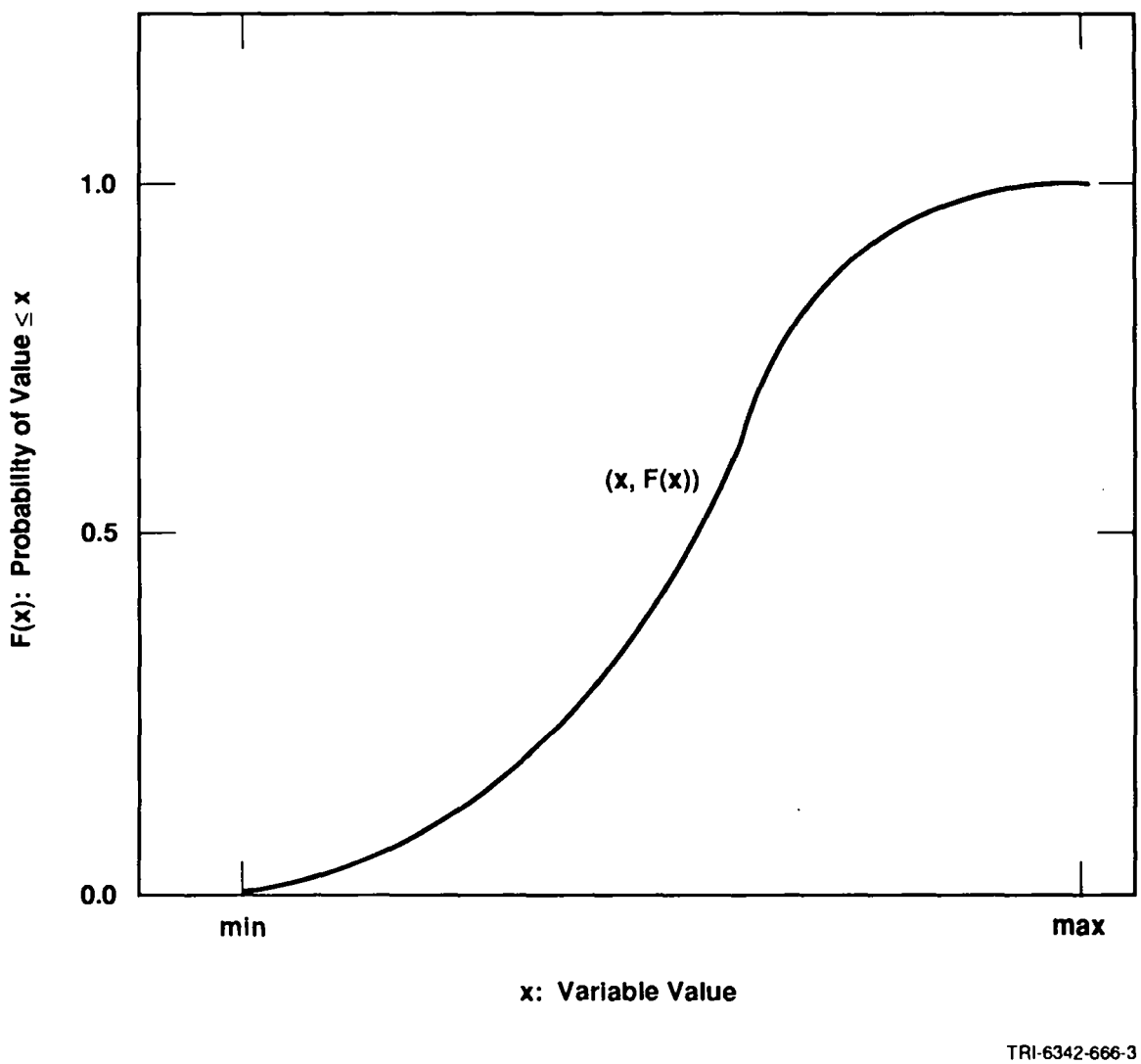

Figure 3-7. Distribution function for an imprecisely known analysis variable. For each value x on the abscissa, the corresponding value $F(x)$ on the ordinate is the probability that the appropriate value to use in the analysis is less than or equal to x (Helton et al., 1991).

That is, $F(x+\Delta x) - F(x)$ is equal to the probability that the appropriate value to use for x_j in the particular analysis under consideration falls between x and $(x + \Delta x)$.

3.5.2 Generation of the Sample

Various techniques are available for generating samples from the assigned distribution functions for the variables (McGrath et al., 1975; McGrath and Irving, 1975a,b), including random sampling, stratified sampling, and Latin hypercube sampling. As discussed in more detail in Helton et al. (1991), the WIPP performance assessment uses stratified sampling and Latin hypercube sampling.

Stratified sampling is a modification of random sampling in which a systematic coverage of the full range of possible values is forced by subdividing the sample space into strata with assigned probabilities. The decomposition of the subset S_O shown in Equation 3-8 into scenarios S_i as indicated in Equation 3-1 is a form of stratified sampling in which the scenario probabilities pS_i are the strata probabilities. Stratified sampling forces the inclusion of low-probability, but possibly high-consequence, scenarios, and is used to incorporate stochastic, or Type-A, uncertainty into the WIPP performance assessment.

Latin hypercube sampling (McKay et al., 1979), in which the full range of each variable is subdivided into intervals of equal probability and samples are drawn from each interval, is used to incorporate subjective, or Type-B, uncertainty, into the WIPP performance assessment. Specifically, a Latin hypercube sample of size 70 was generated from the 49 variables in Tables 6.0-1, -2, and -3 in Volume 3 of this report. The restricted pairing technique of Iman and Conover (1982) was used to prevent spurious correlations within the sample. The resultant sample is listed in Volume 4 of this report.

3.5.3 Propagation of the Sample through the Analysis

The next step is the propagation of the sample through the analysis. Each element of the sample is supplied to the model as input, and the corresponding model predictions are saved for use in later uncertainty and sensitivity studies. The Compliance Assessment Methodology Controller (CAMCON) has been developed to facilitate the complex calculations and storage of the input and output files from each program (Rechard, 1989, 1992). This methodology incorporates data bases, sampling procedures, model evaluations, data storage, uncertainty and sensitivity analysis procedures, and plotting capabilities into a unified structure. The structure and operation of CAMCON is illustrated in Figure 1-1.

Additional information on CAMCON and its use in the 1992 WIPP performance assessment is given in Chapter 1 of this volume and in Rechard (1992).

3.5.4 Uncertainty Analysis

Once a sample has been generated and propagated through a model, uncertainty in the model predictions can be interpreted directly from the CCDF. Stochastic, or Type-A, uncertainty, is represented by the steps in an individual CCDF. Subjective, or Type-B, uncertainty, can be represented either with a family of CCDFs or with a summary diagram showing mean and quantile curves, as shown in Figures 3-2 and 3-3.

Uncertainty in a predicted performance measure can be characterized with an estimated distribution function, which can be displayed either as the above CCDF, a density function, a cumulative distribution function, or as box plots (Iman and Conover, 1982), as shown in Figure 3-8. The endpoints of the boxes in Figure 3-8 are formed by the lower and upper quartiles of the data, that is, $x_{.25}$ and $x_{.75}$. The vertical line within the box represents the median, $x_{.50}$. The sample mean is identified by the large dot. The bar on the right of the box extends to the minimum of $x_{.75} + 1.5(x_{.75} - x_{.25})$ and the maximum observation. In a similar manner, the bar on the left of the box extends to the maximum of $x_{.25} - 1.5(x_{.75} - x_{.25})$ and the minimum observation. The observations falling outside of these bars are shown with x's. Box plots display the same information as a distribution function in a reduced form (without explicit probabilities). They are convenient for presenting and comparing different distributions in a single figure, especially for displaying outliers (high consequence values).

3.5.5 Sensitivity Analysis

The final step in a Monte Carlo study is sensitivity analysis, which provides information about the sensitivity of the modeling system to uncertainty in specific input parameters. Sensitivity analyses can identify those parameters for which reductions in uncertainty (i.e., narrowing of the range of values from which the sample used in the Monte Carlo analysis is drawn) have the greatest potential to increase confidence in the estimate of disposal-system performance. Identification of sensitive parameters can help set priorities for additional research; however, because results of these analyses are inherently conditional on the models, data distributions, and techniques used to generate them, the analyses cannot provide insight about the correctness of the conceptual models and data distributions used. Qualitative judgment about the modeling system must be used in conjunction with sensitivity analyses to set priorities for performance-assessment data acquisition and model development.

Sensitivity analysis techniques used in the WIPP performance assessment include scatterplots and regression analysis, and are described in detail by Helton et al. (1991). Results of the 1992 sensitivity analyses are presented in Volume 4 of this report.

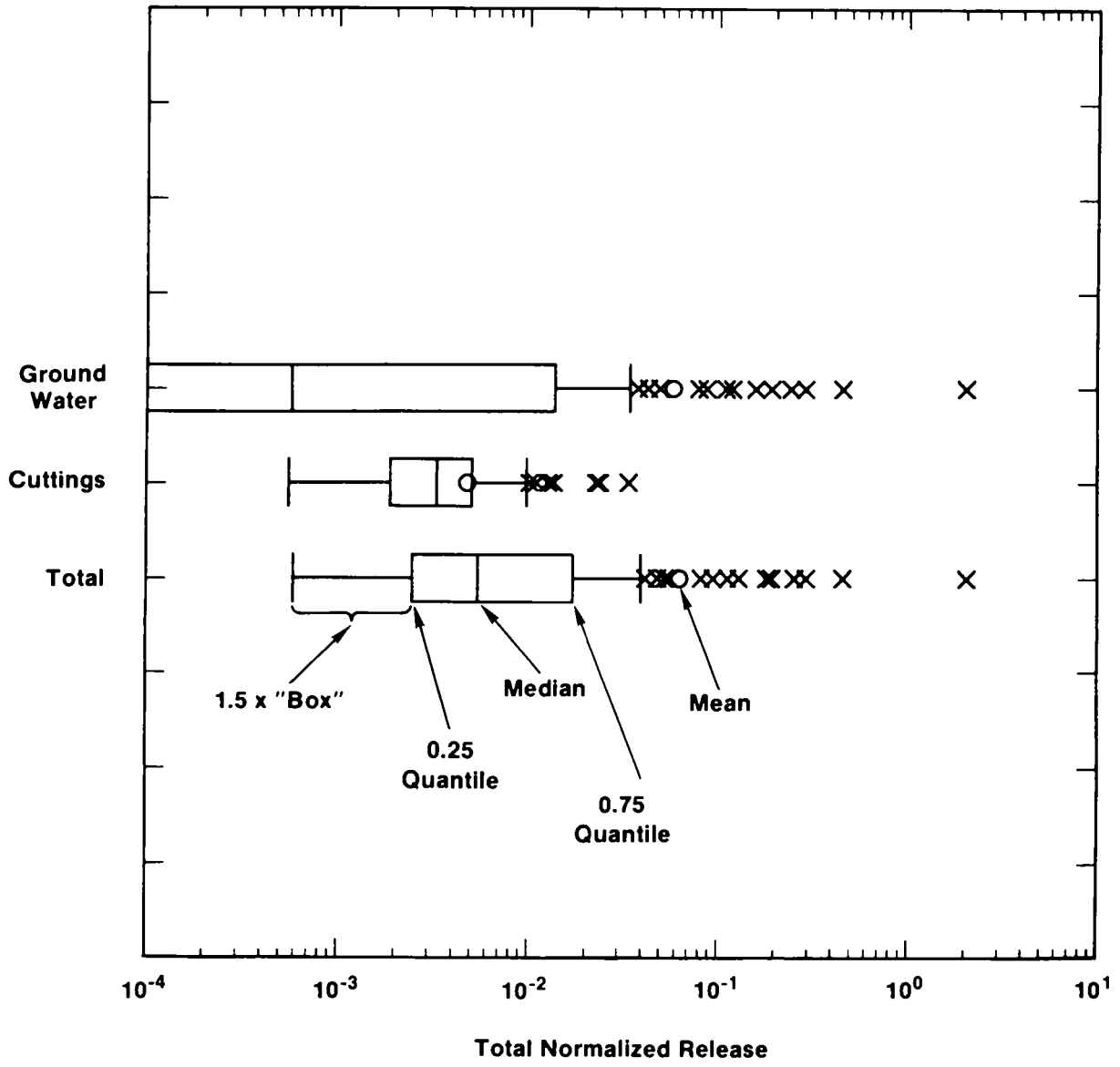

Figure 3-8. Example of box plots (hypothetical results).

4. SCENARIO CONSTRUCTION

4.1 Evaluation of Events and Processes

The selection of scenarios for consideration in WIPP PA is based on the formal five-step procedure described by Cranwell et al. (1990). The five steps are (1) compiling or adopting a comprehensive set of events and processes* that potentially could affect the disposal system, (2) classifying the events and processes to aid in completeness arguments, (3) screening the events and processes to identify those that can be eliminated from consideration in the PA, (4) developing scenarios by combining the events and processes that remain after screening, and (5) screening scenarios to identify those that have little or no effect on the shape or location of the CCDFs. Section 4.1 summarizes work done on the first three of these steps: the identification, classification, and screening of events and processes, referred to jointly as "evaluation of events and processes." Evaluation of events and processes has not been significantly revised since 1991, and more complete discussions of specific events and processes are available elsewhere (Guzowski, 1990; WIPP PA Division, 1991a). Additional work is in progress on evaluation of events and processes in response to reviewers' comments (e.g., Appendix B of Volume 1 of this report), and will be incorporated in future PAs.

4.1.1 Identifying Events and Processes

The WIPP PA uses the list of potentially disruptive events and processes provided by Cranwell et al. (1990) as a starting point for scenario development (Table 4-1). This list was developed by a panel of experts that met in 1976 and again in 1977 under the auspices of the U.S. Nuclear Regulatory Commission to identify events and processes that could compromise the performance of an engineered disposal system for nuclear waste constructed in deep geologic media.** Concerns raised during the development of the WIPP have led to the inclusion of three additional events and processes not identified by the panel: gas generation by the degradation of the waste, waste-related explosions, and nuclear criticality.

---

* Note that classification of a phenomenon as an event rather than a process, or vice versa, has no affect on scenario development. The distinction in terminology is based on 40 CFR 191B (§191.13(a)), and has been interpreted to describe the time interval over which a phenomenon occurs relative to the time interval of interest. Events are relatively brief whereas processes may occur during a large portion of the time interval of interest. The distinction is not rigid, however, and the terms are functionally interchangeable in scenario development.

** As listed in Cranwell et al. (1990), the Scenario Identification Panel Members and their affiliations were William S. Twenhofel, United States Geological Survey (USGS), Denver, CO; William W. Dudley, USGS, Denver, Co; Randolph Stone, Lawrence Livermore National Laboratory, Livermore, CA; Frederick J. Pearson, USGS, Reston, VA; Herbert R. Shaw, USGS, Menlo Park, CA; Donald Caldwell, United States Nuclear Regulatory Commission (USNRC), Washington, DC; Ben Ross, The Analytical Sciences Corp., Reading, MA; Edward Hawkins, USNRC, Washington, DC; and Martin Tierney, Sandia National Laboratories, Albuquerque, NM. Working sessions of this panel were held on December 7-8, 1976, at Grand Canyon, AZ, and again on April 13, 1977, in Carlsbad, NM.

Table 4-1. Potentially Disruptive Events and Processes

Natural Events and Processes	
Celestial Bodies	Meteorite Impact
Surficial Events and Processes	Erosion/Sedimentation Glaciation Pluvial Periods Sea-Level Variations Hurricanes Seiches Tsunamis Regional Subsidence or Uplift Mass Wasting Flooding
Subsurface Events and Processes	Diapirism Seismic Activity Volcanic Activity Magmatic Activity Formation of Dissolution Cavities Formation of Interconnected Fracture Systems Faulting
Human-Induced Events and Processes	
Inadvertent Intrusions	Explosions Drilling Mining Injection Wells Withdrawal Wells
Hydrologic Stresses	Irrigation Damming of Streams and Rivers
Repository- and Waste-Induced Events and Processes	Caving and Subsidence Shaft and Borehole Seal Degradation Thermally Induced Stress Fracturing in Host Rock Excavation-Induced Stress Fracturing in Host Rock Gas Generation Explosions Nuclear Criticality

Source: Modified from Cranwell et al., 1990.

4.1.2 Classifying Events and Processes

This step is optional, and has not been carried out explicitly for WIPP PA. Cranwell et al. (1990) included classification in the procedure to assist in organizing the events and processes, to assist in completeness arguments, and to provide insights when developing conceptual models of the disposal system.

4.1.3 Screening Events and Processes

Events and processes are screened using three criteria developed by Cranwell et al. (1990): probability of occurrence, consequence, and physical reasonableness; and a fourth criteria specific to PAs conducted for 40 CFR 191B, regulatory requirements. All four are applied in the context of the 1985 version of 40 CFR 191B (U.S. EPA, 1985), and screening will be reexamined when the regulation is repromulgated.

The "probability of occurrence" and "consequence" criteria are based directly on guidance provided in Appendix B of 40 CFR 191:

> The [EPA] assumes that . . . performance assessments need not consider categories of events or processes that are estimated to have less than one chance in 10,000 of occurring over 10,000 years. Furthermore, the performance assessments need not evaluate in detail the releases from all events and processes estimated to have a greater likelihood of occurrence. Some of these events and processes may be omitted from the performance assessments if there is a reasonable expectation that the remaining probability distribution of cumulative releases would not be significantly changed by such omissions (U.S. EPA, 1985, p. 38088).

As interpreted by the WIPP PA Department, individual events and processes (as well as "categories of events and processes") that have a probability of more than 1 chance in 10,000 of occurring over 10,000 years will be retained for further evaluation. Lower-probability phenomena are identified but not considered further. Low-consequence phenomena (i.e., those that would not significantly change the CCDF) are identified qualitatively in the WIPP PA methodology and are eliminated regardless of probability (WIPP PA Division, 1991a). Consequences of these phenomena can be evaluated quantitatively if uncertainties warrant.

The final screening criterion described by Cranwell et al. (1990), "physical reasonableness," is not explicitly described in 40 CFR 191B. As used in WIPP PA, this criterion distinguishes between those phenomena to which a meaningful probability can be assigned (e.g., meteorite impacts) and those phenomena for which scientific understanding is insufficient to assign meaningful and defensible quantitative probabilities (e.g., the occurrence of volcanic activity in a geologic setting where such an event is unprecedented). The distinction between "physical reasonableness" and "probability of occurrence" is not rigid, and phenomena identified as "physically unreasonable" could also be eliminated on the basis of extremely low probability.

The "regulatory requirements" criterion is used only to screen events related to human activities, and is based directly on guidance in Appendix B of 40 CFR 191:

> . . . inadvertent and intermittent intrusion by exploratory drilling for resources (other than any provided by the disposal system itself) can be the most severe intrusion scenario assumed by the implementing agencies (U.S. EPA, 1985, p. 38089).

As interpreted by the WIPP PA Department, this allows the exclusion of all deliberate human activities that disrupt the repository, as well as those inadvertent human activities that could result in consequences (e.g., EPA normalized cumulative releases to the accessible environment, or other performance measures) greater than those of exploratory drilling. Specifically, this criterion is used to screen acts of war, direct mining of the waste, systematic drilling of multiple boreholes for resource production or other purposes, and modes of intrusion other than exploratory drilling identified by an expert panel on inadvertent human intrusion into the WIPP (Hora et al., 1991; memorandum by Hora in Volume 3, Appendix A of this report).

4.1.4 Summary of Screened Events and Processes

The following summary is taken from the 1991 PA (WIPP PA Division, 1991a), where each of the events and processes listed in Table 4-1 are described in detail. As shown in Table 4-2, events and processes are either retained for consideration in PA or screened out on the basis of the four criteria described in the previous section. Events and processes retained for consideration are either included in the base-case scenario for the system or used for developing scenarios describing disturbed performance.

All of the natural events and processes listed in Table 4-1 that have been retained are part of the undisturbed performance of the system, and none are included in the development of disturbed-performance scenarios. Phenomena such as erosion, sedimentation, climatic change (pluvial periods), seismic activity, and some shallow dissolution are certain to occur during the next 10,000 years, and are part of the conceptual model for the base-case scenario. Several other listed events (i.e., sea-level variations, hurricanes, seiches, and tsunamis) are restricted to coastal areas, and are physically unreasonable at the WIPP location. Surficial geologic events, including regional subsidence or uplift, mass wasting, glaciation, and flooding, and all subsurface events except seismic activity and shallow dissolution of the Rustler-Salado contact are screened out as physically unreasonable or of low probability.

Of the human-induced events and processes, inadvertent explosions at the location of the waste panels are excluded by regulatory requirements; inadvertent explosions near the waste panels during warfare and nuclear testing are screened out on the basis of low probability. Irrigation and damming of valleys close enough to the WIPP to have an impact are low-probability events because of poor water and soil quality and limited water supplies. Based on the geologic setting and previous resource evaluations, both exploratory drilling for resources and the drilling of injection wells are realistic events for the WIPP, and are retained for scenario development. Intrusion of injection wells into the waste-emplacement region is not modeled explicitly in PA, because drilling technology and therefore consequences are assumed to be the same as for exploratory drilling. Expert judgment on the probability of intrusion by injection wells is not available (Hora, memo in Appendix A of Volume 3). Injection wells that do not penetrate the repository are screened out on the basis of low consequence.

Table 4-2. Summary of Screened Events and Processes (from WIPP PA Division, 1991a)

Events and Processes	RETAINED		SCREENED OUT			
	Base-Case Conditions	For Scenario Development	Low Probability	Physically Unreasonable	Low Consequence	Regulatory Requirements
Natural						
Meteorite Impact			×			
Erosion/Sedimentation	×					
Glaciation				×		
Pluvial Periods (Climate Change)	×					
Sea-Level Variations				×		
Hurricanes				×		
Seiches				×		
Tsunamis						
"Conventional"				×		
Meteorite Impact			×			
Regional Subsidence or Uplift				×		
Mass Wasting				×		
Flooding				×		
Diapirism				×		
Seismic Activity	×					
Volcanic Activity				×		
Magmatic Activity				×		
Formation of Dissolution Cavities						
Deep Dissolution				×		
Shallow Dissolution						
Rustler-Salado Contact	×					
Nash Draw*			×		×	
Formation of Interconnected Fracture Systems				×		
Faulting				×		

*Screening criterion depends on which possible mechanisms considered for origin of Nash Draw

Table 4-2. Summary of Screened Events and Processes (from WIPP PA Division, 1991a) (continued)

Events and Processes	RETAINED		SCREENED OUT			
	Base-Case Conditions	For Scenario Development	Low Probability	Physically Unreasonable	Low Consequence	Regulatory Requirements
Human-Induced						
Explosions						
At Waste-Panels Location						×
Near Waste-Panels Location						
At Surface/Warfare			×			
Deep Testing			×			
Drilling (Exploratory)		×				
Mining						
At Waste-Panels Location						×
Near Waste-Panels Location		×				
Injection Wells					×	
Withdrawal Wells						
Water Wells		×				
Oil and Gas Wells						
At Waste-Panels Location						×
Near Waste-Panels Location					×	
Geothermal Wells					×	
Irrigation			×			
Damming of Streams and Rivers						
At Pecos River					×	
Near Nash Draw			×			
Repository- and Waste-Induced						
Subsidence and Caving					×	
Shaft & Borehole Seal Degradation	×					
Thermally Induced Fractures				×		
Excavation-Induced Fractures	×					
Gas Generation	×					
Explosions (Gas Ignition)					×	
Near Criticality						
Critical Mass (Explosion)			×			
Sustained Reaction**						

** Retained for additional evaluation

In the category of waste- and repository-induced events and processes, gas generation and shaft-seal degradation are part of the conceptual model of the base-case scenario. Borehole seal degradation is addressed through parameter uncertainty during modeling. Excavation-induced fracturing in the host rock is handled by including the disturbed zone surrounding mined openings in the conceptual model of the base-case scenario. Caving into the rooms or drifts may occur in the short term after decommissioning, but this process has no long-term consequences on performance because of the mechanical behavior of salt. Thermally induced fracturing of the host rock is not a physically reasonable phenomenon because of the low thermal output of WIPP waste. Subsidence caused by the mined openings and explosions caused by the ignition of gases created by waste degradation have no effect on the long-term performance of the disposal system and can be eliminated from scenario development. Nuclear criticality requires additional evaluation before a screening decision is made.

As shown in Table 4-2, a total of 10 events and processes are retained for consideration following screening. Seven of these are essentially certain to occur, and are included in the conceptual model for the base-case scenario (see Section 4.2.3.1). The other three—exploratory drilling, potash mining near the waste panels, and water wells—are used to develop summary scenarios describing disturbed performance of the system. Exploratory drilling is subdivided into two possibilities: drilling into a waste-filled room or drift and a brine reservoir in the underlying Castile Formation (Event E1), and drilling into a waste-filled room or drift without penetrating a brine reservoir (Event E2). Mining (Event E3) is limited to potash extraction by either conventional or solution methods in areas beyond the boundaries of the waste panels; drilling of withdrawal wells (Event E3) is limited to water wells in areas where water quantity and quality will permit water use. Both mining and water wells will be evaluated in future performance assessments for their effects on groundwater flow in the WIPP area.

4.2 Summary Scenarios

4.2.1 Development of Summary Scenarios

As explained in the 1991 PA documentation (WIPP PA, 1991a, Section 4.1.7), logic diagrams based on the approach defined by Cranwell et al. (1990) are used to combine events and processes that remain after screening into summary scenarios. As the logic diagram for the WIPP performance assessment (Figure 4-1) shows, no temporal relationship between events and processes is implied by their sequence across the top of the diagram; at each junction within the diagram a yes/no decision is made as to whether the next event or process is added to the scenario. As a result, each scenario consists of a combination of occurrence and nonoccurrence of all events and processes that survive screening (Cranwell et al., 1990). To simplify scenario notation, only the events and processes that occur are used to identify the scenario. Based on the assumption that the events and processes remaining after screening define all possible futures of the disposal system that are important for a probabilistic assessment, the logic diagram produces scenarios that are comprehensive and mutually exclusive because all possible combinations of events and processes are developed, and each scenario is a unique set of events and processes.

Figure 4-1 shows all of the scenarios (the possible combinations of the four events) that survived the screening process for the WIPP (Section 4.1.4):

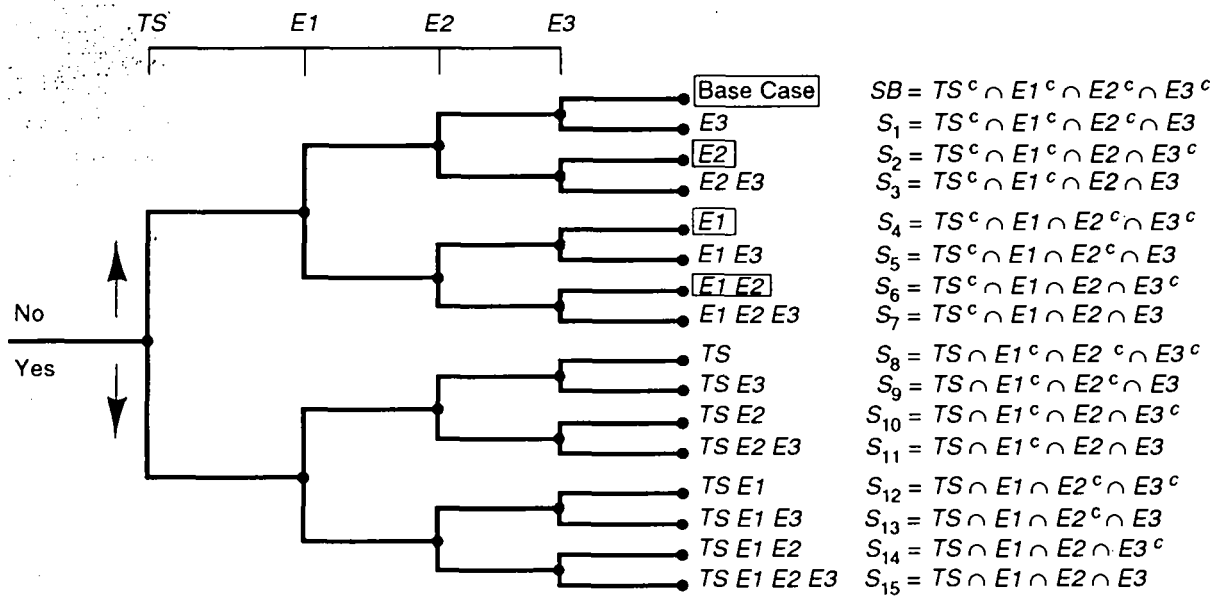

x = 10,000 yr Time History

TS = {x: Subsidence Resulting from Solution Mining of Potash}

E1 = {x: One or More Boreholes Pass Through a Waste Panel and into a Brine Pocket}

E2 = {x: One or More Boreholes Pass Through a Waste Panel Without Penetrating a Brine Pocket}

E3 = {x: One or More Withdrawal Wells near Repository Where Water Quality Will Permit Water Use}

Superscript c (e.g., TS^c) Denotes Set Complement

TRI-6342-3436-0

Figure 4-1. Potential scenarios for the WIPP disposal system.

- E1, the inadvertent drilling of an exploratory borehole into a waste-filled room or drift and a brine reservoir in the underlying Castile Formation,

- E2, the inadvertent drilling of an exploratory borehole into a waste-filled room or drift that does not intersect a brine reservoir in the underlying Castile Formation,

- E3, drilling of water withdrawal wells in areas where water quality will permit water use, and

- TS, mining for potash by either conventional or solution methods in areas beyond the boundaries of the waste panels.

For the 1992 PA calculations, only the base-case scenario and scenarios containing the E1 and E2 events were considered; therefore, only four summary scenarios were evaluated this year: the base case (expected behavior of the disposal system without disruption by human intrusion), E1, E2, and E1E2. The TS event will be added to later PA calculations for 40 CFR 191B. The E3 event will be evaluated in safety assessments because it provides a potential pathway through which human doses could occur.

4.2.2 Screening of Summary Scenarios

The purpose of scenario screening is to identify those scenarios that will have no or a minimal impact on the shape and/or location of the mean CCDF. The criteria used to screen combinations of events and processes (scenarios) are similar to those criteria used to screen individual events and processes (Section 4.1.3). These criteria are physical reasonableness of the combinations of events and processes, probability of occurrence of the scenario, and consequence.

The probability of occurrence for a scenario is determined by combining the probabilities of occurrence and nonoccurrence from the events and processes that make up the scenario. A mechanical approach to determining scenario probabilities can be implemented by assigning the probability of occurrence and nonoccurrence for each event and process to the appropriate "yes" and "no" legs at each bifurcation in the logic diagram (Figure 4-1). The probability of a scenario is the product of the probabilities along the pathway through the logic diagram that defines that scenario. Based on the probability criterion in Appendix B of 40 CFR 191 for screening out individual events and processes, scenarios with probabilities of occurrence of less than 1 chance in 10,000 in 10,000 years need not be considered in determining compliance with 40 CFR 191B, and therefore, consequence calculations are not necessary.

Consequence in this step of the procedure means integrated discharge to the accessible environment for 10,000 years. By inferring that the guidance in Appendix B of 40 CFR 191 for individual events and processes also applies to scenarios, scenarios whose probability of occurrence is greater than the cutoff in Appendix B can be eliminated from further consideration if their omission would not significantly change the remaining probability distribution of cumulative releases. Because the degree to which the mean CCDF will be affected by omitting such scenarios is difficult to estimate prior to constructing CCDFs, only those scenarios that have no releases or very small, low-probability releases should be screened out from additional consequence calculations. If

significant changes are made to the data base, the conceptual models, or mathematical models of the disposal system, the omitted scenarios should be rescreened.

In implementing this step of the procedure for this preliminary WIPP performance assessment, no scenarios were screened out. Because parameter values did not define the events, all combinations of events in the scenarios are physically reasonable. Because final scenario probabilities have not been estimated, no scenarios were screened out on the basis of low probability of occurrence. Final calculations of consequences have not been completed, so no scenarios were screened out on the basis of this criterion.

4.2.3 Retained Summary Scenarios

This section describes the scenarios retained for consequence analysis that are considered in the 1992 PA calculations.

4.2.3.1 UNDISTURBED SUMMARY SCENARIO (S_B)

Guidance from 40 CFR 191

The Individual Protection Requirements of 40 CFR 191B (§191.15) call for a reasonable expectation that the disposal system will limit annual doses to individuals for 1,000 years after disposal, assuming undisturbed performance of the disposal system. Undisturbed performance is defined in 40 CFR 191B to mean "the predicted behavior of a disposal system, including consideration of the uncertainties in predicted behavior, if the disposal system is not disrupted by human intrusion or the occurrence of unlikely natural events" (§191.12(p)). Duration of this performance is not limited by the definition.

Although undisturbed performance is not mentioned in the Containment Requirements (§191.13), undisturbed performance is not precluded from the containment calculations and, for the WIPP, is the base case of the scenario-development methodology (Cranwell et al., 1990; Guzowski, 1990). The base-case scenario describes the disposal system from the time of decommissioning and incorporates all expected changes in the system and associated uncertainties for the 10,000 years of concern for §191.13. Subpart B of 40 CFR 191 does not provide a definition of unlikely natural events to be excluded from undisturbed performance nor, by implication, likely natural events to be included. Because of the relative stability of the natural systems within the region of the WIPP disposal system, all naturally occurring events and processes that will occur are part of the base-case scenario and are nondisruptive. These conditions represent undisturbed performance (Marietta et al., 1989; Bertram-Howery et al., 1990). They include the events and processes retained for undisturbed conditions, which are listed in Table 4-2.

Base-Case Description

After the repository is filled with waste, the disposal rooms and drifts in the panels are backfilled and seals are emplaced in the shafts and access drifts to the panels (Figure 4-2). While excavations are open, the salt creeps inward because of the decrease in confining pressure on the salt around the rooms. Portions of the access drifts and the lower parts of shafts are filled with preconsolidated, crushed salt (Stormont et al., 1987; Borns and Stormont, 1988; Nowak et al., 1990). Because of the high lithostatic pressures at the repository depth, salt creep is expected to exert sufficient pressure on the crushed salt to consolidate the material into low-conductivity seals with properties similar to those of the host rock. Portions of the upper parts of the shafts are also filled with salt, but pressure is not expected to be sufficient here to cause the same degree of consolidation as is expected in lower portions of the shafts.

Gas generation is an important process for the undisturbed case. Some waste and some waste containers will be composed of organic material. Because microbes transported into the repository with the waste are expected to be viable under sealed-repository conditions (Brush and Anderson, 1989b), organic material in the repository will biodegrade with concomitant generation of gases. In addition, moisture in the repository, either brought in with waste or seeping in from the Salado Formation, can corrode metals in the waste and metallic waste containers themselves, with gas generated as a by-product. Radiolysis also will generate gases.

Sufficient quantities of gas will be generated to result in elevated pressures in the repository, approaching and perhaps exceeding lithostatic pressure (approximately 15 MPa). Elevated pressures may open fractures in anhydrite layers above and below the waste-disposal panels, which are relatively more brittle than the plastic halite.

Two potential pathways for groundwater flow and radionuclide transport dominate the undisturbed disposal system (Figure 4-2):

- In the first path, the pressure gradient between the waste-disposal panels and the Culebra causes brine and radionuclides to migrate from the waste-disposal panels to the base of the shafts and up the shafts toward the Culebra. This migration may occur directly through panel seals and the backfill in access drifts, but is more likely to occur through anhydrite interbeds (primarily MB139 below the panels, but possibly also MB138 and interbeds A and B above the panels). Contaminated brine may enter the interbeds either through fractures in salt in the DRZ, or directly as a result of rooms and drifts intersecting the interbeds during construction or room closure. Migration to the base of the shafts could then occur in fractures in the anhydrite layers. Migration up the shafts occurs through the shaft-seal system.

- The second major path for brine and radionuclide migration from the undisturbed repository is laterally through anhydrite interbeds toward the subsurface boundary of the accessible environment in the Salado Formation. Brine enters the interbeds as described for the first path, and is driven outward from the panels by elevated pressures in the waste resulting from gas generation.

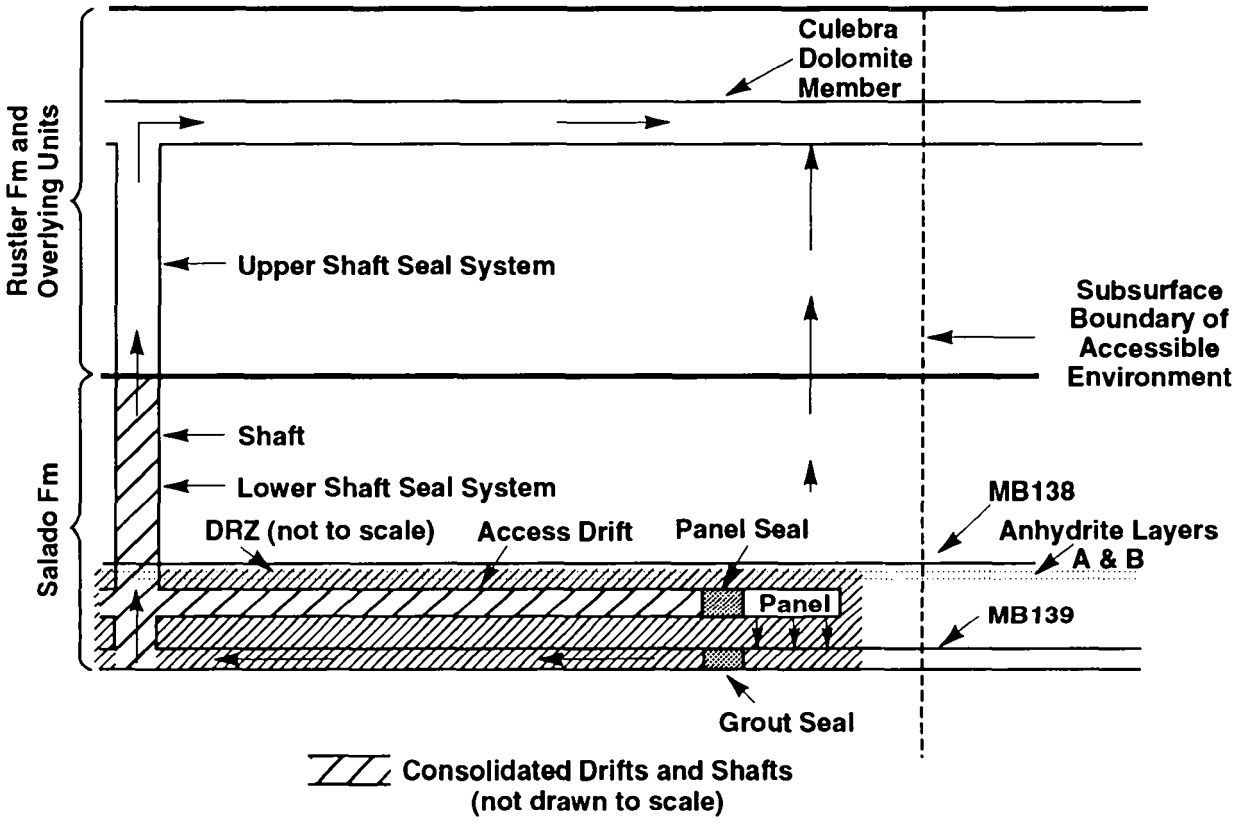

Figure 4-2. Conceptual model used in simulating undisturbed performance.

A third pathway for radionuclide transport from the undisturbed disposal system was considered in previous analyses (Lappin et al., 1989), in which brine migrated vertically from the panels through the intact Salado Formation toward the Culebra. Although this pathway has a larger pressure decline over the shortest distance than either of those discussed above, and also has the largest cross-sectional area through which migration could occur, low permeabilities of the intact halite result in extremely long travel times (400,000 years for the first arrival of radionuclides at the Culebra, as calculated by Lappin et al. [1989]). Because of the improbability of developing interconnected, vertical fractures in the plastic halite, this pathway is not modeled in performance assessment.

4.2.3.2 HUMAN-INTRUSION SUMMARY SCENARIOS

Guidance from 40 CFR 191

Appendix B of 40 CFR 191 provides guidance on a number of factors concerning human intrusion. Active controls cannot be assumed to prevent or reduce radionuclide releases for more than 100 years after disposal (U.S. EPA, 1985, p. 38088). Passive institutional controls can be assumed to deter systematic and persistent exploitation and to reduce the likelihood of inadvertent intrusion, but these controls cannot eliminate the chance of inadvertent intrusion. As discussed in Section 4.1.3, Appendix B (U.S. EPA, 1985, p. 38088) also suggests that exploratory drilling for resources can be the most severe form of human intrusion considered, and that the likelihood and consequence of drilling should be based on site-specific factors. In keeping with the guidance, this assessment includes scenarios that contain human-intrusion events.

Intrusion Borehole through a Room or Drift into Pressurized Brine in the Castile Formation (Summary Scenario E1)

Scenario E1 (Figure 4-3) consists of one or more boreholes that penetrate through a waste-filled room or drift and continue into or through a brine reservoir in the underlying Castile Formation in which brine pressure is between hydrostatic and lithostatic for that depth (Marietta et al., 1989). Radionuclides may be released to the accessible environment in two ways: some radionuclides will be brought to the ground surface during drilling as particulate material entrained in drilling fluid; additional radionuclides may reach the subsurface boundary of the accessible environment following long-term groundwater transport up the borehole and laterally down a potentiometric gradient in the Culebra Dolomite Member of the Rustler Formation.

Radionuclides released during drilling result from the drill bit directly intersecting waste. Material ground up by the drill bit (cuttings) is transported to the surface by the circulating drilling fluid. Additional material may be eroded from the walls of the borehole by the circulating drilling fluid (cavings) or by the spalling of solid material into the hole as the panel depressurizes. Cuttings, cavings, and spallings are collectively referred to as cuttings in performance-assessment documentation.

After drilling is complete, the hole is assumed to be plugged and abandoned. All borehole plugs and drilling mud remaining in the borehole, except for a plug above the Culebra, are assumed to degrade into material with

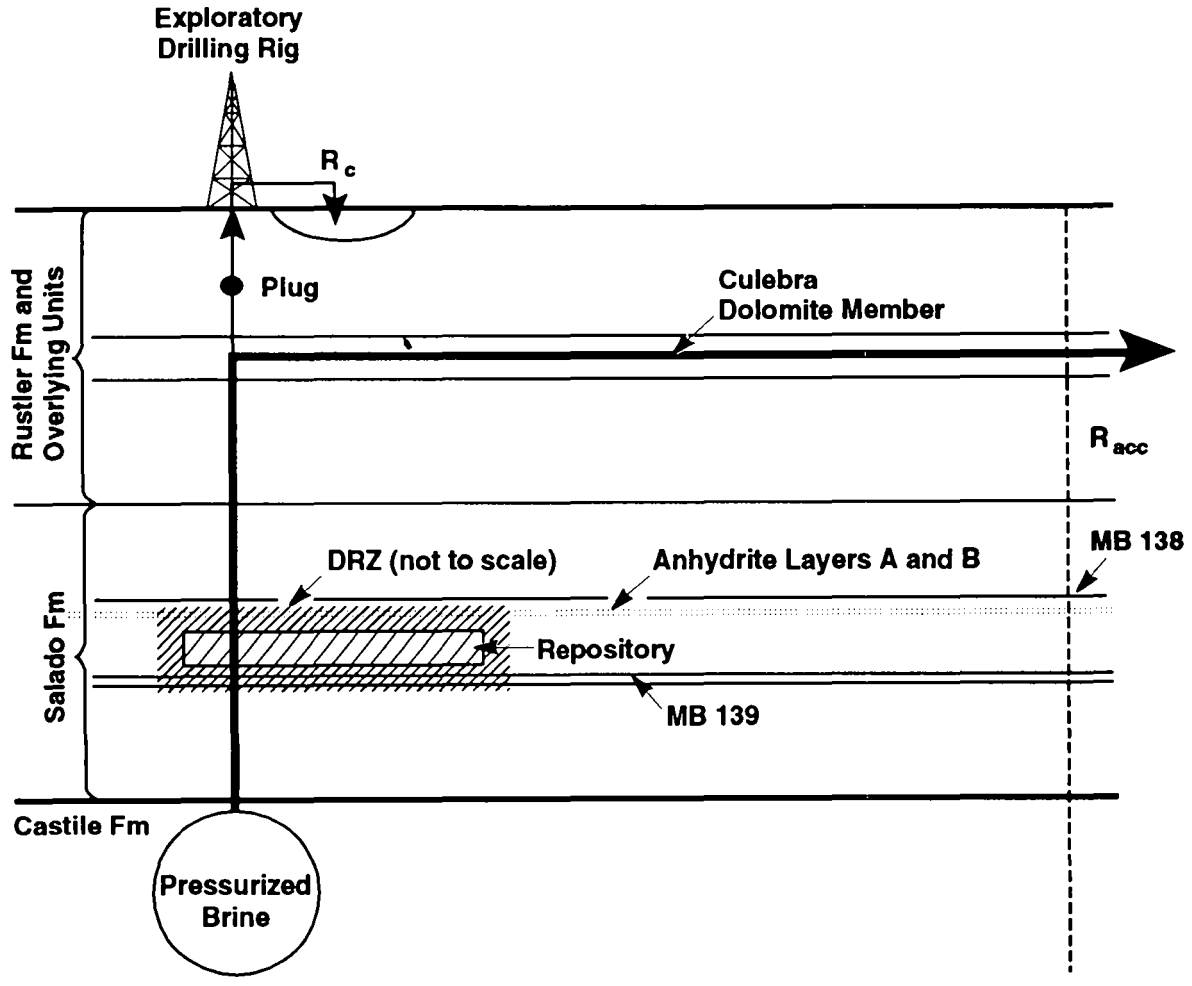

Figure 4-3. Conceptual model for scenario E1. Arrows indicate assumed direction of flow. Exploratory borehole penetrates pressurized brine below the repository horizon. R_c is the release of material directly from the drilling operation. R_{acc} is the release at the subsurface boundary of the accessible environment. A plug above the Culebra Dolomite Member is assumed to remain intact for 10,000 years.

properties similar to those of silty sand. Plug degradation is in keeping with guidance provided by Appendix B of 40 CFR 191: "consequences of ... inadvertent drilling need not be more severe than ... creation of a groundwater flow path with a permeability typical of a borehole filled by the soil or gravel that would normally settle into an open hole over time—not the permeability of a carefully sealed borehole" (U.S. EPA, 1985, p. 38089). The borehole is assumed to remain propped open by the material filling it, preventing closure of the hole by salt creep in the Salado Formation. A single plug above the Culebra is assumed to remain intact for Scenario E1, diverting all upward flow into the Culebra and maximizing radionuclide transport into that unit and toward the subsurface boundary of the accessible environment. Rate of flow depends on the head difference between the Culebra and the injected brine and on the hydraulic properties of the borehole fill. Radionuclides from the room may be incorporated into the Castile brine if it circulates through the waste adjacent to the borehole.

Intrusion Borehole into a Room or Drift (Summary Scenario E2)

Scenario E2, like Scenario E1 (described above), also consists of one or more boreholes that penetrate to or through a waste-filled room or drift (Figure 4-4). Unlike Scenario E1, however, the borehole does not intersect pressurized brine or any other important source of water (Marietta et al., 1989). Releases of cuttings at the ground surface during drilling are identical to those described for Scenario E1, as are the assumptions about borehole plugging. Rate of flow into the Culebra is determined in Scenario E2 by the head gradient between the repository and the Culebra and the hydraulic properties of the borehole fill.

Intrusion Borehole through a Room or Drift into Pressurized Brine in the Castile Formation and Another Intrusion Borehole into the Same Panel (Summary Scenario E1E2)

Scenario E1E2 consists of exactly two boreholes that penetrate waste-filled rooms or drifts in the same panel (Figure 4-5) (Marietta et al., 1989). One borehole also penetrates pressurized brine in the Castile Formation, whereas the other borehole does not. Assumptions about the degradation of borehole plugs are the same as those described for Scenarios E1 and E2, except that in this case specific plugs are assumed to remain intact so as to maximize flow from the Castile brine reservoir through the waste and into the Culebra. The borehole that penetrates the pressurized brine (the E1-type borehole) remains plugged between the waste and the Culebra; the other borehole (the E2-type borehole) remains plugged above the Culebra. Brine flow in Scenario E1E2 is driven by the head difference between the Castile brine reservoir and the Culebra.

Radionuclides are released directly to the surface during drilling of the two holes as described with E1 and E2; additional releases from this system are dependent on the sequence in which the holes are drilled. The plug in the borehole that penetrates the pressurized brine reservoir allows brine flowing up the hole to enter the repository but not leave the repository until the second hole penetrates the same panel. Once the second hole is drilled, a pathway is formed for brine and gas from the pressurized brine reservoir to flow through waste panels and nearby members to this new hole and up to the Culebra Dolomite Member. If the hole that does not penetrate pressurized brine is drilled first, gas and/or fluid pressure is relieved; this is followed by brine flow and radionuclide transport up the hole as a result of brine inflow into the panel from the host rock, possibly enhanced by creep

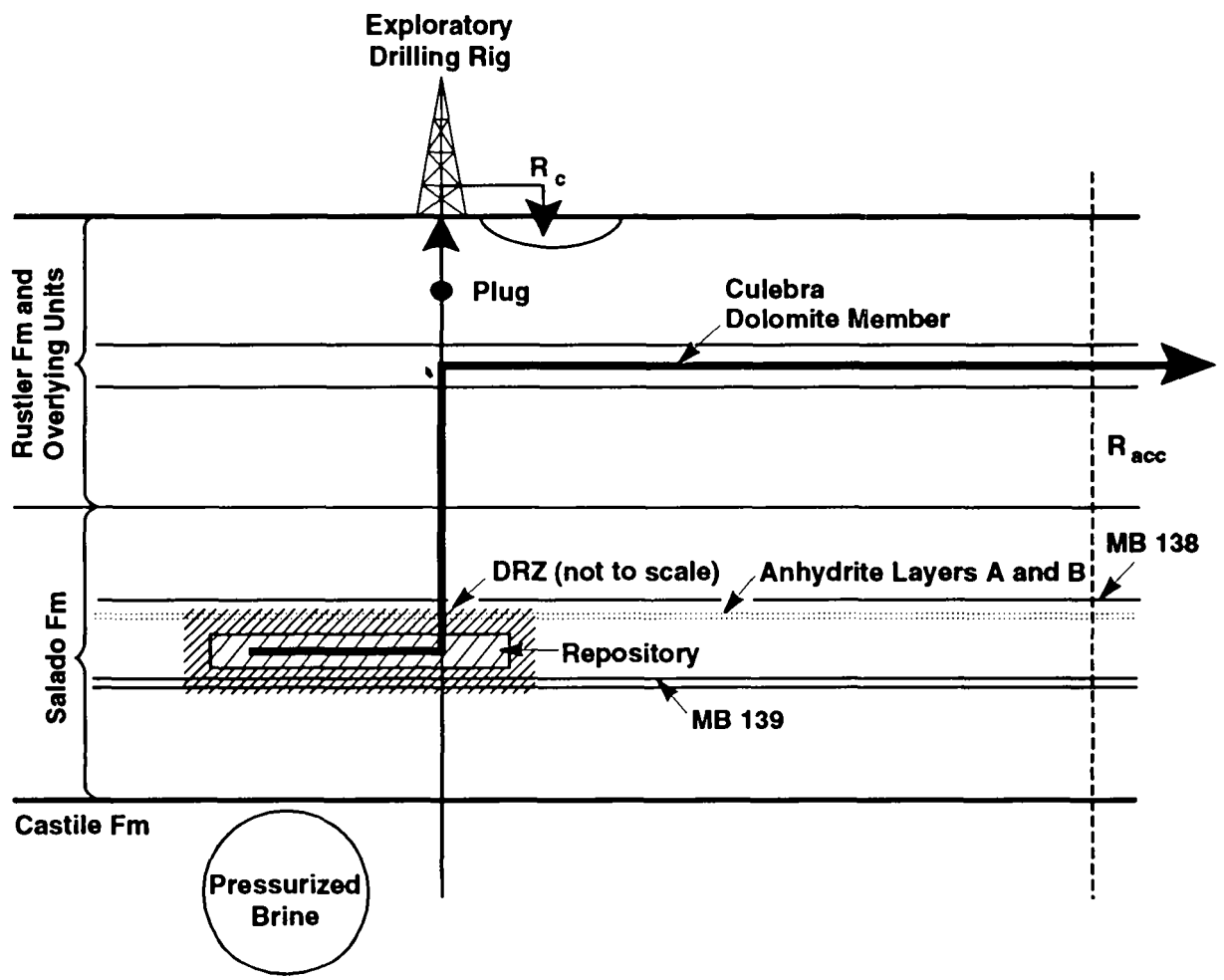

Figure 4-4. Conceptual model for scenario E2. Arrows indicate assumed direction of flow. Exploratory borehole does not penetrate pressurized brine below the repository horizon. R_c is the release of material directly from the drilling operation. R_{acc} is the release at the subsurface boundary of the accessible environment. A plug above the Culebra Dolomite Member is assumed to remain intact for 10,000 years.

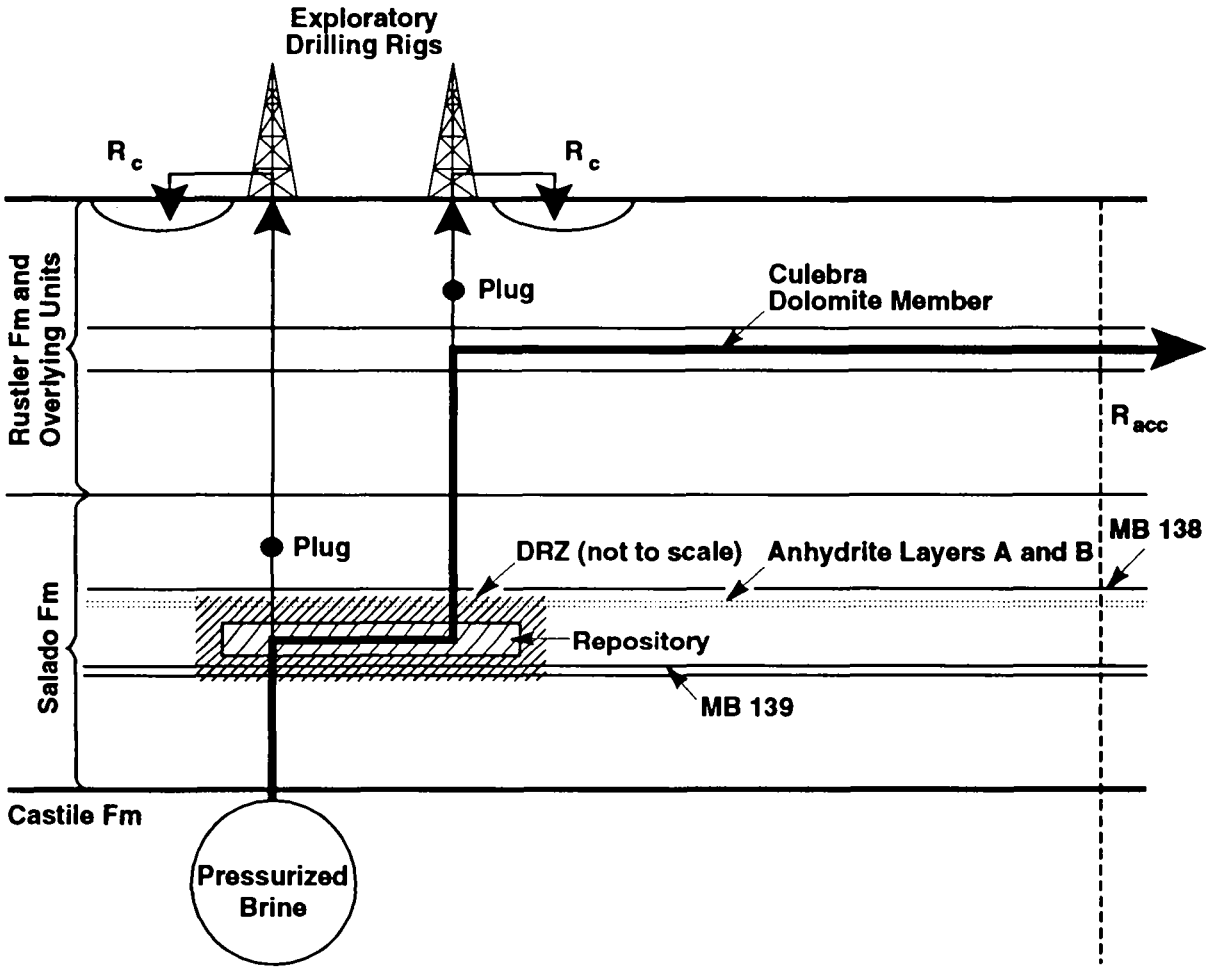

Figure 4-5. Conceptual model for scenario E1E2. Arrows indicate assumed direction of flow. One exploratory borehole penetrates pressurized brine below the repository horizon a plug between the repository and the Culebra Dolomite Member is assumed to remain intact for 10,000 years. The second borehole does not penetrate pressurized brine below the repository; a plug above the Culebra Dolomite Member is assumed to remain intact for 10,000 years. R_c is the release of material directly from the drilling operation. R_{acc} is the release at the subsurface boundary of the accessible environment.

closure of rooms and drifts. Flow is diverted into the Culebra by the plug located above this unit. The subsequent drilling and plugging of the borehole that penetrates the pressurized brine reservoir results in flow through the repository and up the other borehole. If driving pressure is depleted, Scenario E1E2 reverts to Scenario E2, because the borehole that penetrates the pressurized brine no longer contributes to flow and transport (Marietta et al., 1989). For modeling convenience, analyses of Scenario E1E2 assume that both boreholes are drilled at or close to the same time.

4.2.4 Computational Approximations of Scenarios E1, E2, and E1E2

The 1992 PA calculations use the same conceptual approximations for Scenarios E1, E2, and E1E2 that were used in the 1991 calculations (WIPP PA Division, 1991b, Sections 5.1.1 and 5.1.2). E2-type intrusions are simulated explicitly using the BRAGFLO, SANCHO, and PANEL codes (Sections 7.2, 7.3, and 7.4, and Appendices A and B of this volume).

E1E2-type intrusions are not simulated explicitly because the axisymmetric cylindrical geometry used for BRAGFLO cannot readily accommodate two intrusion boreholes (WIPP PA Division, 1991b, Section 5.1.1). E1E2-type boreholes are simulated therefore using a single borehole and the assumption that all brine in the panel mixes with all Castile brine flowing up the borehole. This assumption duplicates the primary feature of Scenario E1E2—all radionuclides in a single panel are potentially available for transport up the borehole. Because the flow path between the two boreholes is omitted, the simplification may somewhat overestimate both the amount of waste dissolved and the rate at which flow occurs through the waste and up the borehole.

E1-type intrusions are also not simulated explicitly, in this case for computational efficiency. Consequences of E1-type intrusions are instead assumed to be the same as the consequences for E2-type intrusions occurring at the same time. Probabilities are determined separately for the two types of intrusions (Section 5.3 of this volume); the contributions of Scenarios E1 and E2 to the overall CCDF are therefore not identical.

Justification for this approximation is based on the assumption that brine flowing up the E1 borehole from the Castile reservoir does not circulate through the waste. All radionuclides entering the borehole are assumed to be dissolved in brine that entered the waste from the far field of the Salado Formation or that was initially present in the panels. Comparison in the 1991 PA (WIPP PA Division, 1991b, Section 5.1.2) of the consequences of E1- and E2-type intrusions for 60 realizations indicates that cumulative flow of brine from the panel into the borehole is in most (but not all) realizations greater for the E2 borehole than for the E1 borehole. Larger brine flows from the waste (and therefore larger potential radionuclide releases) occur for the E2 borehole because the elevated Castile brine pressure present in the E1 borehole retards brine inflow into the waste from the far field of the Salado Formation. Brine flows from the waste into the E1 borehole exceed those into the E2 borehole only for those realizations in which total flow is small because the panel was not brine-saturated at the time of intrusion. These small total flows make only a small contribution to the total radionuclide release, and do not invalidate the approximation.

5. DRILLING INTRUSION PROBABILITIES

5.1 Introduction

Representation of a performance assessment as a set of ordered triples and the construction of CCDFs (Section 3.1) both involve the idea of scenario probabilities; in turn, the idea of scenario probabilities makes sense only if an underlying sample space is defined. Current performance assessments that address the EPA release limits use a sample space $\mathcal{S}$ defined by

$$\mathcal{S} = \{x : x \text{ a single 10,000-year history of the facility under consideration, beginning at decommissioning}\}. \quad (5\text{-}1a)$$

Each history, x, is assumed to be complete in the sense that it provides a full specification, including time of occurrence, for everything of importance to performance assessment. The summary scenarios (base case, E1, E2, and E1E2) are then defined as subsets of $\mathcal{S}$. Specifically,

$$E1 = \{x : x \text{ a single 10,000-year history in which at least one borehole penetrates a waste-filled room or drift } \textit{and} \text{ a pressurized brine reservoir}\}, \quad (5\text{-}1b)$$

$$E2 = \{x : x \text{ a single 10,000-year history in which at least one borehole penetrates a waste-filled room or drift without penetrating a pressurized brine reservoir}\}, \text{ and} \quad (5\text{-}1c)$$

$$E1E2 = \{x : x \text{ a single 10,000-year history in which at least one pair of boreholes penetrates waste-filled rooms or drifts in the same panel; one of the boreholes in this pair penetrates a pressurized brine reservoir while the other does not}\}. \quad (5\text{-}1d)$$

Each summary scenario is further divided into disjoint subset $\mathcal{S}_i$ called computational scenarios. For example,

$$E1 \triangleq \bigcup_i \mathcal{S}_i, \quad (5\text{-}2)$$

where the $\mathcal{S}_i$ appear in the ordered-triple representation in Equation (3-1). In the terminology of probability theory, the $\mathcal{S}_i$ are events (as are the summary scenarios: base case, E1, E2, and E1E2), and the pS_i are probabilities for these events. However, to avoid confusion engendered by the different disciplines' use of the word "event," the $\mathcal{S}_i$ will be called scenarios and the pS_is will simply be called probabilities. The purpose of this chapter is to show how the pS_is are calculated in the 1992 performance-assessment exercise; but before proceeding, it is important to recognize several properties of the $\mathcal{S}_i$s (computational scenarios) and the pS_is (computational scenario probabilities).

It is the discretization of the sample space S_i into the sets S_i that leads to the steps in the estimated CCDFs (Section 3.2). To construct CCDFs of the form shown in Section 3.2, the time histories associated with a given summary scenario must be sorted into disjoint sets such that

- each S_i is sufficiently homogeneous that it is reasonable to use the same consequence result $\mathbf{cS}_i$ for all elements of S_i
- a probability pS_i can be determined for each S_i
- the computational costs for estimation of pS_is and $\mathbf{cS}_i$s are acceptable.

5.2 Probability Computations

This section describes a decomposition of summary scenarios involving drilling intrusions into computational scenarios on the basis of number of intrusions and their times of occurrence and derives formulas necessary to convert from drilling rates to scenario probabilities. For these derivations, the occurrence of individual drilling intrusions is assumed to be random in time and space, although the drilling rate need not be assumed constant or, for that matter, continuous through time.

The symbol $S_k(a,b)$ will be used to denote subsets of the sample space defined by

$$S_k(a,b)=\{x: x \text{ an element of } S \text{ that involves exactly k drilling intrusions in the time interval } [a,b]\}. \tag{5-3}$$

One objective of this section is to present the probability $p[S_k(a,b)]$ for $S_k(a,b)$. Membership in $S_k(a,b)$ only places a restriction on intrusions in the time interval $[a,b]$ and thus does not preclude intrusions in other time intervals. As a result, an additional objective will be to present the probability $p\left[\bigcap_{i=1}^{n} S_{n(i)}(t_{i-1},t_i)\right]$ for the set $\bigcap_{i=1}^{n} S_{n(i)}(t_{i-1},t_i)$, where $t_0 < t_1 < \cdots < t_n$ and each $n(i)$, $i=1,2,\ldots,n$, is a nonnegative integer. This corresponds to determining the present of a scenario in which exactly $n(1)$ intrusions occur in time interval $[t_0,t_1]$, exactly $n(2)$ intrusions occur in time interval $[t_1,t_2]$, and so on. Helton (in press) has suggested a general form for these intrusion probabilities; the core of ideas behind his suggestion is outlined below.

The probability of having exactly one intrusion in the time interval $[u,v]$ is approximated by a function F such that

$$p[S_1(u,v)] = F(u,v) + O\left[(v-u)^2\right], \tag{5-4}$$

where the preceding notation is a shorthand for the statement that the ratio

$$\frac{p[S_1(u,v)] - F(u,v)}{(v-u)^2} \tag{5-5}$$

is bounded as $v-u$ approaches zero. More precisely, the statement in Equation 5-4 is satisfied on a time interval $[a,b]$ if there exists a number B and a sequence of times $a=t_0<t_1<\cdots<t_n=b$ such that, if $1\le i\le n$ and $t_{i-1}\le u<v\le b$, then

$$\left|\frac{p[S_1(u,v)]-F(u,v)}{(v-u)^2}\right|<B. \tag{5-6}$$

The expressions in Equations 5-4 and 5-6 are providing a mathematical form for the statement "$F(u,v)$ is a good approximation to $p[S_1(u,v)]$ when $v-u$ is small."

The function F in Equation 5-4 can be defined in a number of ways. The simplest definition is

$$F(u,v)=\lambda(v-u). \tag{5-7}$$

In this case, F corresponds to a Poisson process with a time-independent rate constant λ (i.e., a homogeneous Poisson process) and

$$p[S_k(a,b)]=\frac{[\lambda(b-a)]^k}{k!}\exp[-\lambda(b-a)]. \tag{5-8}$$

The probability of intrusion by drilling was modeled as a homogeneous Poisson process in the 1991 series of PA calculations. The constant λ was taken as an imprecisely known parameter with upper bound equal to the maximum drilling rate required by EPA standards; i.e., λ was uniformly distributed between zero and λ_{max}, with

$$\begin{aligned}\lambda_{max}&=\left(\frac{30}{\text{km}^2\bullet 10{,}000\text{ yr}}\right)\bullet(\text{area of waste panels})\\&=3.28\times10^{-4}\text{ yr}^{-1}\end{aligned} \tag{5-9}$$

The next step in generalizing beyond Equation 5-7 is

$$F(u,v)=\lambda(u)(v-u), \tag{5-10}$$

in which case F corresponds to a Poisson process with a time-dependent rate constant (i.e., a nonhomogeneous Poisson process) and

$$p[S_k(a,b)]=\frac{1}{k!}\left(\int_a^b\lambda(s)ds\right)^k\exp\left[-\int_a^b\lambda(s)ds\right]. \tag{5-11}$$

This result can be used to compute the probability of a general scenario in which exactly $n(1)$ intrusions occur in time interval $[t_0, t_1]$, exactly $n(2)$ intrusions occur in time interval $[t_1, t_2]$, and so on. If this general scenario is denoted by $\mathcal{S}(\mathbf{n})$, where

$$\mathbf{n} = [n(1), n(2), ..., n(n)] \text{ and } t_0 = a, t_n = b,$$

then

$$p[\mathcal{S}(\mathbf{n})] = \prod_{i=1}^{n} \left[\frac{1}{n(i)!} \left(\int_{t_{i-1}}^{t_i} \lambda(s) ds \right)^{n(i)} \right] \exp\left[- \int_a^b \lambda(s) ds \right] . \quad (5\text{-}12)$$

Computational scenarios and corresponding probabilities for summary scenarios E1 and E2 can be generated by specification of the time intervals $[t_{i-1}, t_i]$ and the $n(i)$ appearing in Equation 5-12, and by suitably defining the function $\lambda(t)$ appearing in that equation.

In the preferred conceptual model for the 1992 series of PA calculations, probability of intrusion by drilling is modeled as an inhomogeneous Poisson process using Equations 5-11 and 5-12; for comparison, the 1992 PA also uses a homogeneous Poisson process (Equation 5-9) as an alternative conceptual model for drilling intrusions. For the preferred conceptual model, the time-dependent drilling rates, $\lambda(t)$, are calculated with an algorithm proposed by Hora (see Section 5.2; also Hora's memo in Appendix A of Volume 3 of this report) using information obtained in an expert judgment process concerning effects of human intrusion into the WIPP. Note that Hora's algorithm gives drilling rates in units of

$$\frac{\text{number of boreholes}}{\text{km}^2 \bullet 10{,}000\ \text{yr}}$$

and the time-dependent drilling rates used in Equations 5-11 and 5-12 are scaled from Hora's values by multiplying by area of the waste panels (Equation 5-9). As stated above, $\lambda(t)$ may also have to be scaled to reflect, for example, the fraction of the area of waste panels that overlaps brine pockets.

Computational scenarios for the E1E2 summary scenario can be defined in a manner similar to the ones employed for the E1 and E2 scenarios. Once defined, the probabilities of these computational scenarios are best calculated using the basic result in Equation 5-11 together with the scenario

$$\mathcal{BP}^{+-}(t_{i-1}, t_i) = \{x : x \text{ an element of } \mathcal{S} \text{ in which a waste panel is penetrated by one or more boreholes that pass through a pressurized brine pocket in the time interval } (t_{i-1}, t_i) \text{ and by one or more boreholes that do not pass through a pressurized brine pocket in the time interval } (t_{i-1}, t_i)\}.$$

Then, in extension of the derivations on pages 2-23 to 2-27 of the 1991 Volume 2 (WIPP PA Division, 1991b),

$$p\left[\mathcal{BP}^{+-}(t_{i-1}, t_i)\right] \bullet \sum_{\ell=1}^{nP} \left\{1 - \exp\int_{t_{i-1}}^{t_i} \lambda_\ell^+(t)dt\right\}\left\{1 - \exp\int_{t_{i-1}}^{t_i} \lambda_\ell^-(t)dt\right\}, \tag{5-13}$$

where

nP = the number of waste panels

$$\lambda_\ell^+(t) = \left(\frac{aBP}{nP \bullet aTOT}\right)\lambda(t)$$

$$\lambda_\ell^-(t) = \left(\frac{aTOT(\ell) - aBP / nP}{aTOT}\right)\lambda(t)$$

aBP = area of pressurized brine pocket under waste panels (m^2)

$aTOT(\ell)$ = area of ℓ^{th} waste panel (m^2)

$aTOT$ = total area of waste panels (m^2).

Variable activity loading in the repository was described using the same representation used in the 1991 PA (Helton et al., 1992, Chapter 2). Intrusion probabilities were calculated using the code CCDFPERM (Volume 3, Section 1.4.2 of this report).

5.3 Lambda Function Generation

The 1992 performance assessment is the first to incorporate the judgments of experts on possible future modes of intrusion into the WIPP and on how markers may mitigate the effects of these intrusions; 40 CFR 191, Subpart B, (U.S. EPA, 1985) requires consideration of both these questions. Specifically, 40 CFR 191, Subpart B, indicates that the DOE "should consider the effects of each particular disposal system's site, design, and passive institutional controls in judging the likelihood and consequence of . . . inadvertent human intrusion" (Appendix B of U.S. EPA, 1985). The discussion that follows in Sections 5.3.1, 5.3.2, and 5.3.3 describes WIPP PA's methodology for addressing the mitigating effect of passive markers. This approach may be refined and modified as the performance assessment process matures. The following material, largely excerpted from Hora (memo in Appendix A, Volume 3 of this report), is intended to give an overview of the expert-judgment processes and reasoning that entered into the construction of a probabilistic model of inadvertent intrusion by exploratory drilling.

5.3.1 The Expert Judgment Process

During 1990-1992, experts external to SNL were assembled to study the likelihood of potential inadvertent human intrusion into the WIPP. These experts formed two groups—one group (called the Futures Panel) studied

what future societies might be like and how they might inadvertently intrude into nuclear waste (Hora et al., 1991). The second group (called the Markers Panel), after considering the findings of the first group, studied how markers might be used to warn future societies about the presence and danger of the buried waste (memorandum by Hora in Volume 3, Appendix A of this report). Both groups provided probabilities and probability distributions for critical aspects of the human intrusion problem.

The Futures Panel was divided into four teams. Each team was composed of four experts from various fields of social and physical science. Each team was asked to address the same set of questions. The results of their work suggests that future societies may undertake activities that could lead to inadvertent intrusion into the WIPP. These teams judged that a number of factors (such as level of technology, demand for resources, population level, and ability to retain knowledge about nuclear waste) would influence the likelihood of inadvertent intrusion. Because the teams used different structures for analysis and considered different factors that would influence the likelihood of inadvertent intrusion, the results of their endeavors had to be interpreted individually in order to be used in the construction of Lambda Functions.

As the Futures Panel was completing its effort, the Markers Panel, consisting of 13 experts, was organized into two teams to study markers for the WIPP site. These markers may be incorporated into the repository design to serve as warnings to future societies about the presence of nuclear waste. Each team was asked to consider the findings of the Futures teams, to suggest design characteristics for a marker system, and to assess the efficacy of such a system of markers in deterring inadvertent human intrusion. Based on the assumption that the ability of a marker system to deter intrusions rests on the survival of the marker system over an extended period of time and the ability of potential intruders to detect the markers and to understand the messages that they carry, the Markers Panel members were asked to provide estimates of probabilities for several events:

- First, the probability that a marker and its message(s) would remain intact. (This first probability estimate was requested for various times in the future.)

- Second, if the marker and its messages remain intact, the probability that the potential intruders are able to understand the message and thus become forewarned of the inherent dangers of intrusion. (This second probability estimate was requested for several different types of intrusion.)

The above two probability estimates were made under various assumptions about the state of technology in the future.

As noted above, the Futures Panel posed several types of activities that could lead to inadvertent intrusion into the WIPP (drilling, mining, archaeological investigation); but on the basis of guidance in Appendix B of 40 CFR Part 191 (U.S. EPA, 1985), it was concluded that the preliminary performance assessment need not consider intrusion modes such as mining or archaeological investigation that may result in more severe consequences than exploratory drilling for resources. Moreover, the guidance also provides an upper bound for the drilling intensity to be used in the performance assessment. Three modes of exploratory drilling were identified by the experts examining human intrusion issues. These modes are exploratory drilling for mineral resources (primarily fossil fuels), drilling water wells, and drilling for injection disposal wells. Because the repository is well below the water table in an area where water quality is poor, drilling for water was judged to be an insignificant threat when

compared to drilling for mineral resources (see Section 4.1.3 of this volume). Drilling for disposal wells was identified as a possible threat by one of the four Futures teams, but probabilities were not provided. Thus, exploratory drilling for resources is the only mode of intrusion considered in the 1992 preliminary comparison.

5.3.2 Algorithm for Generating Lambda Functions

The time-dependent drilling rates, or lambda functions, that arise in modeling the probability of drilling (Section 5.2 of this volume) were calculated in the 1992 PA exercise using an algorithm constructed by Hora (memo in Volume 3, Appendix A of this report). The purpose of this algorithm was to assemble quantitative expert judgments concerning future human intrusion into the WIPP.

The existence of markers and the ability of a society to interpret the warnings left at the WIPP may depend upon the state of development of that society. In this exercise, the state of development of the society was represented by the level of the technological development of the society. The level of technological development (high, medium, or low) was randomly generated from probability distributions provided by the Futures teams. Prior to this step, however, the Futures team whose level of technology was to be sampled had to be chosen. This was necessary because the four teams studying potential futures developed analyses independently and in different ways and there was no simple way to combine their findings. For this reason, a team was randomly selected on each generation of a lambda function. The assessments from each team represent their collective judgment. In contrast, members of one of the Markers teams individually provided probability assessments while the other team provided a consensus set of probability distributions. Thus, when one of the two Markers teams was randomly chosen, it could also be necessary to select randomly one of the team members for that iteration. This procedure avoided making unfounded assumptions about how to combine disparate distributions.

Next, using a given level of technology, the frequency (f) at which attempted inadvertent intrusion occurs in the absence of markers or monuments was elicited from the Futures experts. This time-dependent frequency is called the raw drilling intensity; it does not take into account deterrence by markers. Thus, to gain an estimate of the effective drilling intensity λ, the raw drilling intensity was modified in the following way: For each of the several points in time that the raw drilling intensity was evaluated, the probability of the markers existing (p_1) and the probability of the markers deterring an intrusion attempt given that the markers exist (p_2) were evaluated. These two probabilities modify the raw drilling intensity to give the effective drilling intensity,

$$\lambda = f(1 - p_1 p_2).$$

The algorithm for generating inadvertent intrusion can then be succinctly described by the following steps:

1. Randomly select one of the four Futures teams.

The following steps use distributions conditional on the outcome of step 1:

2. Randomly select a level of technology in the future. When probabilities of levels of technology are time-dependent, a rank correlation of 1 will be used to generate the level of technology in the several time periods.

3. Generate a random variable to determine the intrusion intensity. When intrusion intensities vary with time periods, a rank correlation of 1 will be used to generate the intrusion intensities in the several time periods.

4. Randomly select one of the Markers teams and a Marker team member, if necessary.

5. For each time period generate the probability that markers are extant given the level of technology.

6. For each time period, generate the probability that the markers deter intrusion given that the markers are extant, the level of technology, and the mode of intrusion.

7. Compute the effective drilling intensity for each time period.

Note that in step 3, a single random number is used to select an intrusion intensity for all periods. This assumption results in the variability of the performance measure being maximized among the Monte Carlo iterations.

5.3.3 Use of the Lambda Functions

The effective drilling intensity, $\lambda(t)$, is used to generate probabilities of computational scenarios for human intrusion by drilling in the manner described in Section 5.2. However, the algorithm described in Section 5.3.2 does not provide direct input to sensitivity and uncertainty analyses; instead, the code implementing the algorithm is run many times in order to generate a family of equally likely realizations of the lambda functions, and it is this family of realizations that is sampled in the Monte Carlo calculations (see Section 5.2, Volume 3 of this report). A family of 70 realizations was generated for the 1992 series of calculations; one of these realizations is shown on Figure 5-1 and the remainder are displayed in Appendix D of Volume 3. The realizations of $\lambda(t)$ can be regarded as a random sample from an effectively infinite population of drilling intensities implicitly defined by the expert-judgment data and the reasoning that went into the construction of Hora's algorithm (Section 5.3.2). The variability shown by members of this artificial population (see Appendix D, Volume 3) represents the assessed uncertainty in future drilling intensities and the effectiveness of markers.

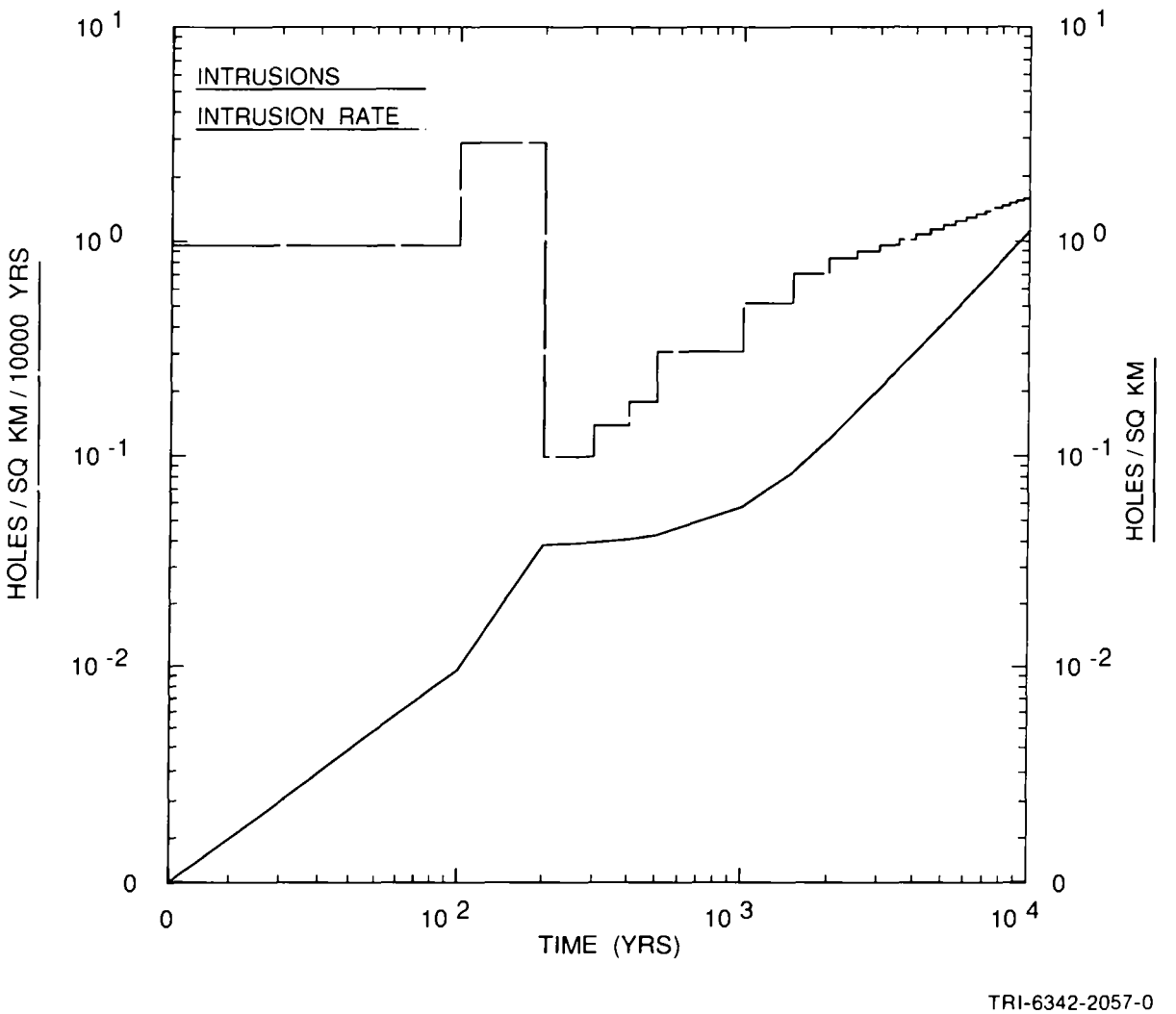

Figure 5-1. A realization of effective drilling intensity $\lambda(t)$ (dashed line) and its associated integrated effective drilling intensity (solid line) as functions of time. This is one of 70 realizations used in 1992 sensitivity and uncertainty analyses.

6. DATA AND CDFS

6.1. Conventions

Volume 3 of this report provides distribution functions for parameter values used as input to the 1992 PA calculations, and references for the primary data sources on which the distributions are based. Volume 3 uses standard terms of probability theory and statistics or nonstandard terms to characterize model parameters. Very brief explanations of these terms are provided below; more detailed explanations are provided in Section 1.2 of Volume 3.

6.1.1 Probability Distribution Functions

For a continuous, uncertain parameter, say X, the *probability density function* (pdf) is a function $f(x) \geq 0$ with the properties

$\int_a^b f(x)dx =$ probability that uncertain *parameter* X lies in interval (a,b):

$$\int_{-\infty}^{+\infty} f(x)dx = 1$$

The *cumulative distribution function* (cdf) associated with $f(x)$ is defined by

$F(x) = \int_{-\infty}^{x} f(s)ds =$ probability that uncertain parameter X is less than or equal to x.

Uncertain parameters may also be called "imprecisely known parameters" elsewhere in this series of reports.

Probability density functions (pdfs) and cdfs can be similarly defined for uncertain parameters that take on a denumerable number of values, $x_i, i = 1,2,....$ The sequence $\{f_i\}, i = 1,2,...,$ such that $f_i > 0$ and

$$\sum_i f_i = 1,$$

is the discrete analogue of the continuous pdf, and

$$F(x) = \sum_{all\ x_i < x} f_i$$

is the discrete analogue of the continuous cdf.

6.1.2 Empirical Distribution Functions

Empirical cdfs are histograms or piecewise-constant functions that are based on percentiles derived from a set of measurements (data), or a set of subjective estimates of experts. For independent measurements (data) of some quantity, the empirical cdf is an unbiased estimator of the unknown population cdf of that quantity (Blom, 1989, p. 216); this property does not always apply to empirical cdfs derived from subjective estimates of experts.

6.1.3 Range

The *range* of a distribution is denoted by (a,b), the pair of numbers in which a and b are respectively the minimum and maximum values that can reasonably be taken by the uncertain parameter X.

6.1.4 Mean and Sample Mean

The mean value (or, simply, *mean*) of a distribution is one measure of the central tendency of a distribution; it is analogous to the arithmetic average of a series of numbers. The population mean, μ, is defined by

$$\mu = \int_{-\infty}^{\infty} xf(x)dx \text{ for continuous distributions, or}$$

$$\sum_{\text{all } x_i} x_i f_i \text{ for discrete distributions.}$$

The sample mean, denoted by $\bar{x}$, is the arithmetic average of values in an empirical data set. A sample mean can also be assigned to empirical cdfs derived from subjective estimates of experts.

6.1.5 Median and Sample Median

The median value of a cdf is denoted by x_{50} and is that value in the range at which 50% of all values lie above and below (i.e., the 0.5 quantile). Sample medians, here denoted by $\bar{x}_{50}$, can be obtained directly from empirical cdfs.

6.1.6 Variance and Coefficient of Variation

The *variance* of a distribution, σ^2, is the second moment of the distribution about its mean, i.e.,

$$\sigma^2 = \int_{-\infty}^{\infty} (x-\mu)^2 f(x)dx \text{ for continuous distributions, or}$$

$$\sum_{\text{all } x_i} (x_i - \mu)^2 f_i \text{ for discrete distributions.}$$

The *standard deviation*, σ, is the positive square root of the variance. The coefficient of variation, the ratio of standard deviation to mean, σ/μ, is a convenient measure of the relative width of a distribution.

The *sample variance*, S^2, of a set of measurements of parameter X, say $X_1, X_2, \ldots, X_N$ is the sum

$$\frac{1}{N-1} \sum_{n=1}^{N} (X_n - \bar{x})^2 .$$

The sample variance of independent measurements of some quantity is an unbiased estimator of the population variance of that quantity (Blom, 1989, p. 197). (A variance can also be formally calculated for empirical cdfs derived from subjective estimates of experts; this is not a sample variance, however.)

6.1.7 Categories of Distributions

Distributions used in the 1992 PA are grouped into five categories:

- continuous, analytical distributions (normal, lognormal, uniform, or loguniform)
- discrete, analytical distributions (Poisson, binomial)
- constructed empirical distributions based on measurements
- constructed empirical distributions based on expert judgment
- miscellaneous categories (null distributions; i.e., constants and tabular functions).

6.1.7.1 CONTINUOUS DISTRIBUTIONS

Four continuous, analytical distributions are frequently used in the 1992 PA:

- **Normal.** Normal designates the normal pdf, a good approximation to the distribution of many physical parameters.
- **Lognormal.** Lognormal designates a lognormal pdf, a distribution of a variable whose logarithm follows a normal distribution.
- **Uniform.** Uniform designates a pdf that is constant in the interval (a, b) and zero outside of that interval.

- **Loguniform.** Loguniform designates a loguniform pdf, a distribution of a variable whose logarithm follows a uniform distribution.

6.1.7.2 DISCRETE DISTRIBUTIONS

A frequently used discrete distribution is the Poisson distribution. The Poisson pdf is often used to model processes taking place over continuous intervals of time such as the arrival of telephone calls at a switch station (queuing problem) or the number of imperfections per unit length produced in a bolt of cloth. The Poisson pdf was used in the 1991 probability model for human intrusion by exploratory drilling. The 1992 probability model for human intrusion incorporates effects of deterrence by markers; this model is based on generalized Poisson distributions.

6.1.7.3 CONSTRUCTED DISTRIBUTIONS (DATA)

A *constructed distribution* of the *Data* type is simply an empirical cdf constructed from sets of measured data points in the data base. For intrinsically discrete data, the empirical cdf is a piecewise-constant function resembling a histogram. For intrinsically continuous data, the empirical cdf is always converted to a piecewise-linear function by joining the empirical percentile points with straight lines; this is done to ensure that, in Monte Carlo sampling, the distribution of sampled parameter values will cover all of the range of the distribution (Tierney, 1990, p. II-5).

In some cases, the PA Department may modify constructed distributions of the Data type by extending the range of the data set to include estimated 0.01 and 0.99 quantiles. Because the range of measurements in a data set may not reflect the true range of the random variable underlying the measurements, the PA Department may estimate the range by $\bar{x} + 2.33s$, where $\bar{x}$ is the sample mean and s is the sample standard deviation.

6.1.7.4 CONSTRUCTED DISTRIBUTIONS (SUBJECTIVE)

Constructed distributions of the *Subjective* type are histograms based on subjective estimates of range (the 0 and 100 percentile) and at least one interior percentile point (usually the 50 percentile or median). The subjective estimates of percentile points are usually obtained directly from experts in the subject matter of the parameter of concern. Histograms for intrinsically continuous parameters are always converted to piecewise linear cdfs by joining the subjective percentile points with straight lines.

6.1.7.5 MISCELLANEOUS CATEGORIES

Null categories of distributions are described below:

- **Constant.** When a distribution type is listed as constant, a distribution has not been assigned and a constant value is used in all PA calculations.

- **Spatial.** The spatial category indicates that the parameter varies spatially. This spatial variation is usually shown on an accompanying figure. The median value recorded is a typical value for simulations that use the parameter as a lumped parameter in a model; however, the value varies depending upon the scale of the model. The range of a spatially varying parameter is also scale dependent.

- **Table.** The table category indicates that the parameter varies with another property and the result is a tabulated value. For example, relative permeability varies with saturation; its distribution type is listed as table (also, the median value is not meaningful and is therefore omitted in the table).

6.2 Selection of Parameter Distributions

6.2.1 Requests for Data from Sandia Investigators and Analysts

The PA Department follows a well-defined procedure for acquiring and controlling the parameter distributions used in consequence and probability models:

- **Identify Necessary Data.** Each year, the PA Department identifies data that are necessary to construct parameter distributions for the preliminary performance assessment. Members of the department may compile data from published reports, personal communications with investigators, and other sources.

- **Request Median Value and Distribution.** The PA Department then requests that the investigators provide either new data or a median value and distribution for each parameter in a large subset of the parameters. Some model parameters are specific to the PA calculations and so individuals in the PA Department are considered the experts for these parameters (e.g., probability model parameters). Initially, Sandia investigators are responsible for providing data, or if data are unavailable, distributions for all parameters. As this procedure for acquiring data is repeated, a few parameters are evaluated through formal elicitation.

- **Update Secondary Data Base.** The PA Department enters the endorsed or elicited data for all parameters into the secondary data base. The PA Department then either constructs parameter distributions or uses distributions provided by the investigator; the PA Department selects a subset of these parameters to sample in each annual PA exercise, keeping all other values constant at their median values, unless specifically noted.

- **Perform Consequence Simulations and Sensitivity Analyses.** The PA Department runs consequence simulations and sensitivity analyses with selected subsets of parameters from the updated secondary data base. The sensitivity analysis evaluates the sensitivity of a parameter in determining variation of the result (i.e., CCDF).

- **Determine Whether Parameter Is Important in Analysis.** By means of the sensitivity analyses, the PA Department can determine whether the parameter as specified is significant in the calculations.

6.2.2 Construction of Distributions

The PA Department follows the five-step procedure outlined below to construct probability distributions (cdfs):

1. Determine whether site-specific data for the parameter in question exist. If data exist, go to step 3.

2. Request that the investigator supply a specific shape (e.g., normal, lognormal) and associated numerical parameters for the distribution of the parameter. If specific shape and distribution parameters cannot be supplied, go to step 4; otherwise go to step 5.

3. Determine the size of the combined data sets. Is sample size is sufficiently large, PA staff constructs distribution (go to step 5).

4. If sample size is small, or investigator cannot provide a specific distribution, request that the investigator provide subjective estimates of the range and details on the distribution of the parameter.

5. Assign distribution.

6.2.3 Some Limitations on Distributions

The major limitations on the validity of the probability distributions assigned to parameters in the 1992 PA are believed to be a consequence of two things:

- The equating of spatial variability with model parameter uncertainty, particularly for that class of parameters called material-property parameters.

- The neglect of correlations between model parameters.

These limitations are discussed in detail in Volume 3 (Section 1.3.3).

7. CONSEQUENCE MODELING

7.1 Radioactive Decay

The quantity of radioactive material that reaches the accessible environment depends in part on the growth and decay of the component radionuclides in the waste. The Bateman equations (Wehr et al., 1984) are used to calculate this decay within the repository. The Bateman equations in terms of activity are:

$$\frac{dN_i}{dt} = -\lambda_i N_i + \lambda_i N_{i-1}, \tag{7-1}$$

where N_i is the activity of radionuclide i, t is time, and λ_i is the disintegration constant of radionuclide i.

For given initial inventories $N_i^{(0)}$, the solution can be written as

$$N_i(t) = \sum_{j=1}^{i} a_{i,j} e^{-\lambda_j t}, \tag{7-2}$$

where the coefficients $a_{i,j}$ are defined by the recurrence relations

$$a_{i,i} = N_i^{(0)} - \sum_{j=1}^{i-1} a_{i,j} \tag{7-3}$$

and

$$a_{i,j} = \frac{\lambda_i}{\lambda_i - \lambda_j} a_{i-1,j} \qquad i > j. \tag{7-4}$$

7.2 Multiphase Flow Through Porous Media

A computational model called BRAGFLO (BRine And Gas FLOw) that simulates two-phase fluid flow through porous, heterogeneous reservoirs has been developed for WIPP PA. As discussed in Appendix A of this volume, BRAGFLO uses finite-difference methods to solve the coupled nonlinear partial differential equations (PDEs) describing the mass conservation of the gas and brine components distributed between the gas and liquid phases.

The PA Department uses BRAGFLO in Monte Carlo consequence analyses to quantify the flow of brine and gas through the repository and surrounding strata for both the undisturbed, base-case scenario and human-intrusion scenarios. For the 1992 PA, the code is used to model fluid flow within the Salado Formation and the repository, including a representation of the shaft system for undisturbed performance. The Culebra Dolomite Member of the

Rustler Formation and a hypothetical pressurized brine reservoir in the Castile Formation are included in the model because of their potential roles as a sink and a source, respectively, for fluid flow.

7.2.1 Features and Capabilities of BRAGFLO

BRAGFLO is capable of describing three-phase (e.g., water, gas, and oil) fluid flow through porous media in one, two, or three dimensions. Only two phases (brine and gas) are modeled for WIPP PA; calculations to date have only been performed in one and two dimensions. The code uses spatially varying meshes and solves the coupled nonlinear PDEs using nonlinear Newton-Raphson iteration, automatic time-stepping, and direct or iterative solvers.

Additional features of BRAGFLO are the capability to incorporate the following: the effect of halite creep on waste porosity using output from the SANCHO code (see Section 7.3 and Appendix B of this volume); anisotropic permeabilities; nonideal gas behavior (Redlich-Kwong-Soave); rock compressibility; and kinetic or reactant-dependent gas generation as a function of fluid saturations.

Multiphase flow is simulated as simultaneous immiscible displacement in porous media. Regions within the model domain (e.g., waste, seals, and lithologic units) are represented as solid continua of interconnected void space, and porosity is expressed as the ratio of void volume to total volume for each region. Flow occurs according to heuristic extensions of Darcy's Law, in that the rate of flow of a homogeneous fluid through a porous medium is proportional to the hydraulic gradient and to the cross-sectional area normal to the direction of flow, and inversely proportional to fluid viscosity (see Appendix A of this volume for additional discussion). Permeability is the constant of proportionality in Darcy's law. Flow is assumed to be laminar, and fluids are viscous and Newtonian. Forces that affect fluid flow are those due to pressure, gravity, capillarity, and viscous shear. Fluid saturation is defined to be the ratio of fluid volume to void volume. At least one fluid phase is present at all times, and all void volume is occupied by fluid.

Effects of capillary pressure and relative permeability occur when two (or more) fluid phases are present in a porous medium. Curvature of the interface separating fluid phases and surface tension cause a capillary pressure difference across the interface. During fluid flow, interference between the phases deforms the interface. Relative permeability describes this interference on a macroscopic scale, and varies with fluid saturation. Relative permeability is expressed as the ratio of the permeability of the rock (or other material) with the fluid in question at a given saturation to the permeability of the rock when 100 percent saturated with the fluid.

Residual saturation of a fluid phase is defined as the smallest saturation of fluid required to form continuous pathways through the medium. It is the minimum saturation at which the phase will flow in response to a pressure gradient. Below residual brine saturation, brine exists as a thin film around rock grains or as isolated pockets, and gas is present in sufficient volume to form an interconnected pathway. The relative permeability for brine is zero. Above residual brine saturation and below residual gas saturation, both brine and gas form continuous pathways through the porous network, and relative permeabilities for both phases are greater than zero.

When brine saturation is sufficiently high that gas saturation falls below residual, gas exists only as isolated pockets surrounded by brine. Gas flow does not occur, and relative permeability for gas is zero.

7.2.2 Interaction of Important Repository Processes

The coupling of processes simulated by BRAGFLO is illustrated schematically in Figure 7-1. The material properties that describe the repository system are represented in the center of a triangle, the apices of which represent the physical processes that operate within the system. Arrows indicate the major interactions. Thus, the amount of brine present in the room is a function of two-phase flow, and is a contributing factor in the rate and amount of gas generation. The rate and amount of gas generation are contributing factors to two-phase flow, as is brine consumption by corrosion reactions that generate gas. Changes in waste porosity result from halite creep; it affects both two-phase flow and, therefore, gas generation through its influence on brine solubility. Completing the coupled interactions, both two-phase flow and gas generation affect halite creep (through their impact on pressure within the panels) and therefore have an effect on changes in waste porosity.

7.2.3 General Assumptions Used in 1992 PA Two-Phase Flow Modeling

The following is a list of major assumptions used in two-phase flow modeling for the 1992 PA:

- Rock permeabilities (1) varied with material type, (2) were uniform within a material, and (3) did not vary with time.

- Void volume of waste was estimated as a function of pressure using SANCHO (Section 7.3 of this volume).

- Gas potential was based on an extrapolation of inventory volume fractions of combustibles and metals/glasses to design capacity (Section 2.3.2.1 of this volume; Volume 3, Section 3.4 of this report).

- Gas generation occurs by corrosion of ferrous metals and biodegradation of combustible materials only, and the contribution of radiolysis is assumed to be negligible (Volume 3, Section 3.3 of this report; WIPP PA Division, 1991c, Section 3.3).

- All gas was assumed to have the physical properties of hydrogen, which will be a principal component resulting from corrosion of ferrous metals (Volume 3, section 1.4.1 of this report).

- As long as corrodible or biodegradable waste remains, gas generation is a function only of brine saturation (WIPP PA Division, 1991c, Section 3.3).

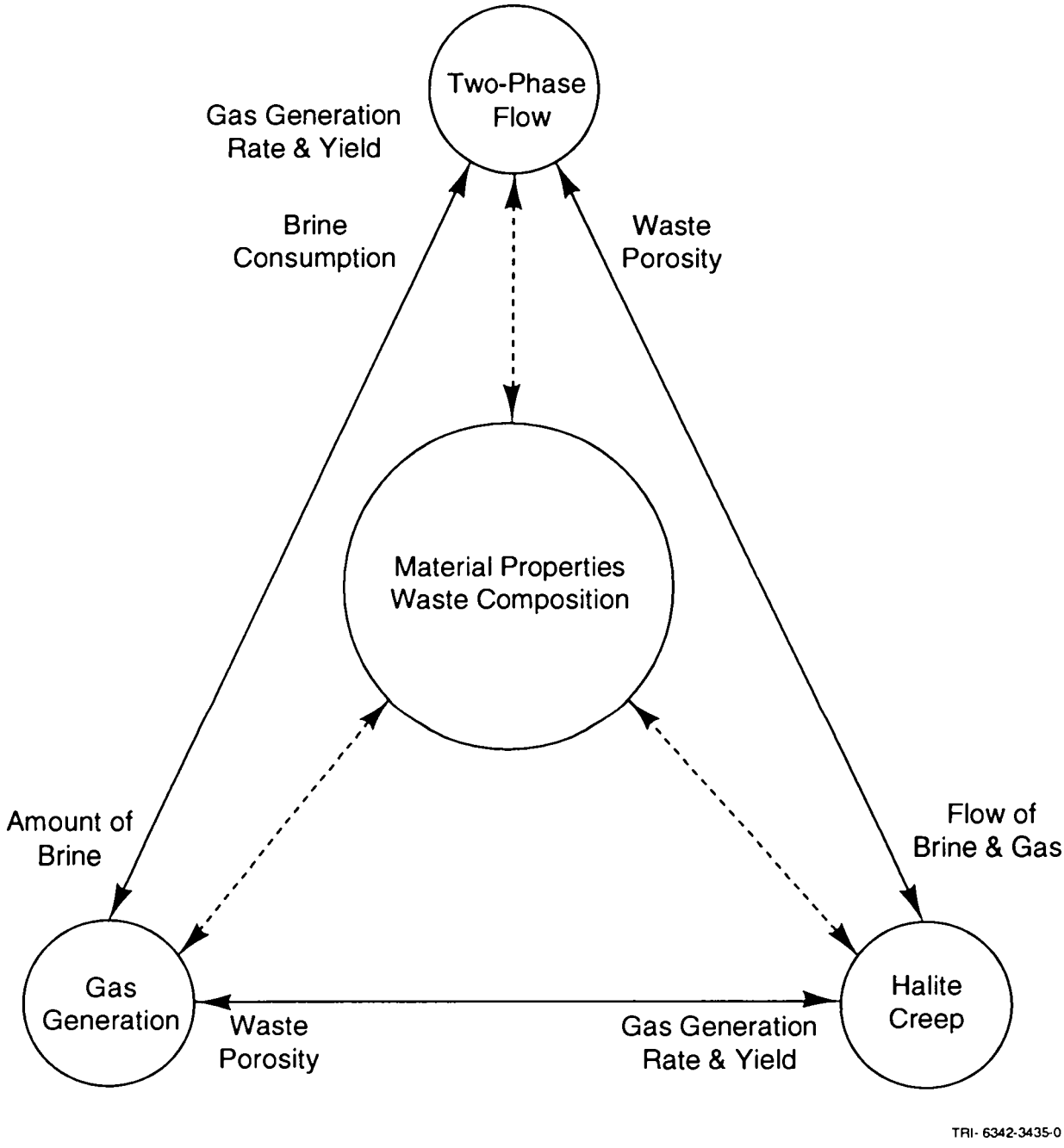

Figure 7-1. Interaction of some important repository processes.

- Water is consumed during corrosion of ferrous metals; biodegradation reactions require the presence of water to occur but have no effect on the net water balance (WIPP PA Division, 1991c, Section 3.3).
- No reactions affect gas after it is generated (WIPP PA Division, 1991c, Section 3.3).
- The solubility of gas in brine is assumed to be negligible.
- The Salado Formation is assumed to be initially 100 percent brine saturated.
- Initial pressures in the Salado Formation vary hydrostatically from a sampled pressure at the elevation of MB139 (Volume 3, Section 2.4.3 of this report).

7.3 Waste-Filled Room Deformation

Consequence models of multiphase flows within a waste-filled room (Section 7.2) require that the effective porosity and permeability of waste and backfill materials be specified. Realistic estimates of effective porosity and permeability must in turn account for three phenomena:

- waste-material composition (metallics, sludges, combustibles)
- geomechanical closure of the room
- backpressure of gases generated in the room by chemical and biological degradation of waste materials.

Thus, the ideal model of multiphase flow within a waste-filled room would couple the two-phase flow model described in Section 7.2 and Appendix A with a model that can simulate the geomechanical closure of the room.

This ideal model, however, is not practically achievable. Direct solution of the fully coupled equations of two-phase flow and geomechanical closure in the repetitive manner required by the PA methodology is unrealistic using present resources; the PA Department instead has chosen to examine the sensitivity of the system to closure using simplifications of the coupling that capture closure approximately while keeping calculations of two-phase flow manageable. In the 1991 series of PA calculations, a simple approximation was made: Effects of room closure and gas pressure were ignored and room material-property parameters were assigned time-independent values that were based on the assumed waste-material composition. (See Sections 3.4.7 and 3.4.8 of WIPP PA Division [1991c]).

The present (1992) series of calculations includes effects of room closure and gas generation in an indirect way. A *separate* (i.e., uncoupled) calculation of the effective porosity of a waste-filled room as a function of time and total moles of gas generated was made (Mendenhall and Lincoln, February 28, 1992, memo in Appendix A, Volume 3 of this report); data from this calculation were used to fit a porosity "surface" (Figure 7-2) that was then used as a constraint on room porosity in the equations of two-phase flow (see Appendix A on BRAGFLO).

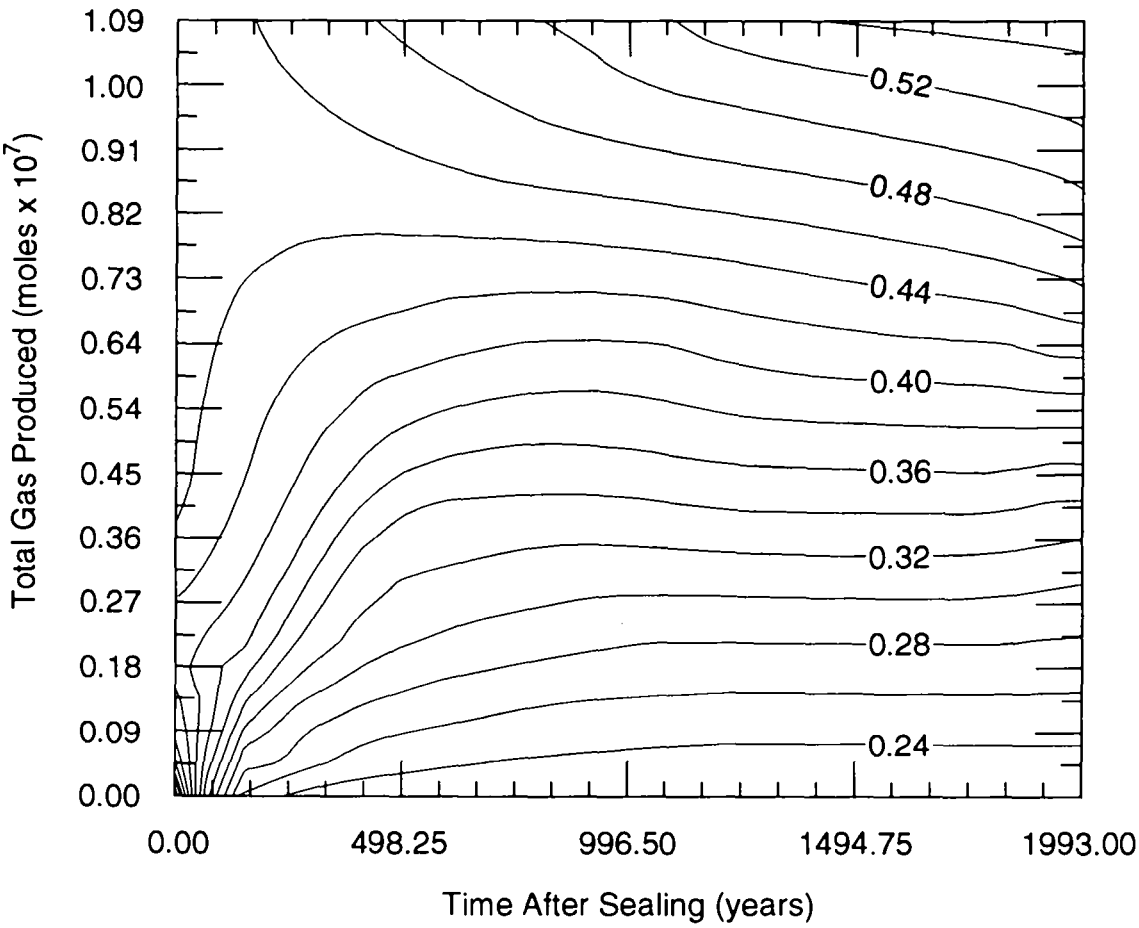

Figure 7-2. Surface giving porosity of waste-filled disposal room as a function of total volume of gas produced and time after sealing. Pore space is assumed to be fully saturated with gas. Porosity is expressed as void volume per unit volume of waste.

The room deformation component of the separate calculation was accomplished with SANCHO, a finite element computer program for simulating the quasistatic, large-deformation, inelastic response of two-dimensional solids; a brief description of the SANCHO code is provided in Appendix B. Details of room-deformation and gas-generation components of the separate calculation and values of mechanical and material-property parameters used in the separate calculation are provided in Volume 3 of this report.

7.4 Waste Mobilization

Following the occurrence of an E2 or E1E2 scenario (Section 4.2.3.2), flow of brine through a collapsed WIPP panel and up an intrusion borehole may result in mobilization of dissolved, radionuclide-bearing compounds and their transport towards the Culebra Dolomite Member of the Rustler Formation. The consequence model that simulates the process of waste mobilization is currently implemented in part of a computer code called PANEL. The mathematical model on which PANEL is based is described in Section 1.4.4 of Volume 3 of this series of reports, and represents an extreme simplification of a potentially complex situation that in reality involves a mixture of waste forms having widely varying physical and chemical compositions in contact with inhomogeneous flows of brine. The discussion that follows (1) details the assumptions that were made in order to arrive at the simplified mathematical model of waste mobilization (Section 7.4.1) and (2) briefly presents the simplified model of waste mobilization (Section 7.4.2).

7.4.1 Assumptions

Eight assumptions about panel geometry, waste and backfill composition, brine discharge, and brine-waste chemical reactions are implicit in the PA Department's current model of waste mobilization:

1. A collapsed WIPP panel (rooms and drifts) is idealized as a single, connected cavity of constant volume (Figure 7-3).

2. Waste and backfill within the collapsed WIPP panel (cavity) are treated as a homogeneous porous medium of constant porosity and infinite permeability; radionuclide-bearing compounds are uniformly distributed throughout the cavity.

3. The idealized panel (cavity) is connected to sources and sinks for brine by one or more discrete inlets or outlets (boreholes); brine may also flow across walls of the cavity (Figure 7-3).

4. Steady-state discharge of brine through the idealized panel is assumed to hold for all time; that is,

$$\sum Q_{in} = \sum Q_{out} = Q(t),$$

where the net discharge, $Q(t)$, is calculated with the model for multiphase flow (Section 7.2).

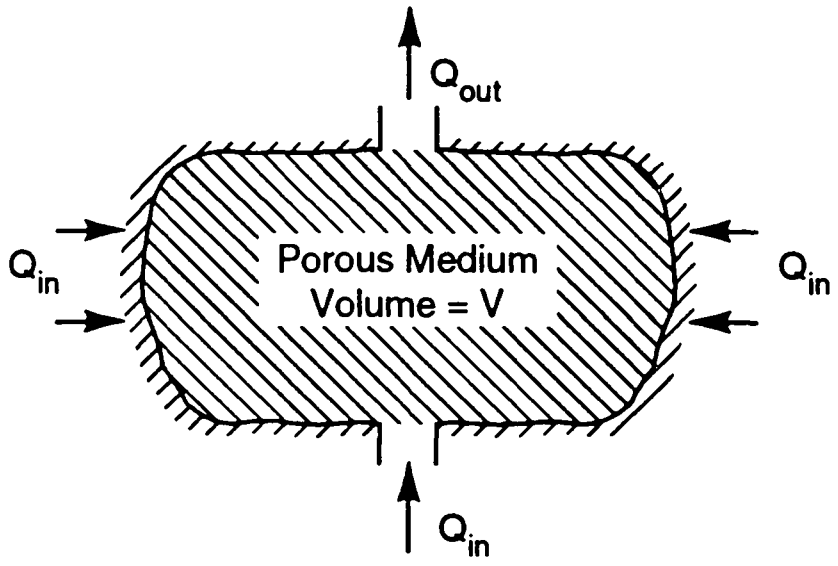

TRI-6342-1435-0

Figure 7-3. Idealized collapsed WIPP panel in PANEL model.

5. The pore spaces of the idealized panel are fully saturated with brine at all times; that is, mobilization of radionuclide-bearing compounds in the gas phase is ignored.

6. Chemical equilibrium and uniform mixing of liquid-phase compounds throughout the idealized panel are achieved on time scales that are much smaller than the mean residence time of the brine in the cavity.

7. The solubility limit for a given isotope (e.g., U-234) of a given element (e.g., uranium) is assumed to be proportional to the solubility limit of the element; the constant of proportionality is taken as the ratio of the mass of the isotope that currently remains in the cavity to the sum of the masses of all currently remaining isotopes of the element.

8. Mobilization is limited to dissolved radionuclides; suspended radionuclides (colloids) are not considered to be mobilized by the brine.

Assumptions 1 and 2 imply that the total pore space in the idealized, collapsed WIPP panel is constant and equal to ϵV, where ϵ is the constant porosity and V is the cavity volume; assumption 5 implies that the total pore space is filled with brine at all times. Assumptions 3 and 4 imply that the mean residence time of brine in the repository is given by

$$\tau = \frac{\epsilon V}{Q},$$

regardless of the stated time dependence of Q. Assumption 6 implies that characteristic times to reach chemical equilibrium and characteristic times for complete mixing of dissolved species by diffusion through cavity pore spaces are always much smaller than τ. Because the rates of chemical reactions between dissolved and immobile species are unknown, the validity of assumption 6 cannot be tested at this time; times for complete mixing by diffusion can be estimated but have not yet been compared with mean residence times for brine.

Assumption 7 was made in order to simplify the equations that describe the masses of the various radioactive isotopes of an element that remain in the cavity at any time after occurrence of an E2 or E1E2 scenario (see Section 7.4.2 below and Section 1.4.4 of Volume 3). An alternative assumption would set isotope solubility limits equal to the element solubility limit.

7.4.2 Simplified Mathematical Model

The simplified mathematical model of waste mobilization is expressed as a system of coupled, ordinary differential equations, with each system applying to a radioactive decay chain:

$$\dot{M}_i = -S_i\left(\frac{M_i}{\sum_j M_j}\right)Q(t) - \lambda_i M_i + \left(\lambda_{i-1}M_{i-1}\right)\left(\frac{atomic\ \ wt_i}{atomic\ \ wt_{i-1}}\right), \tag{7-5}$$

where $i = 1, 2, \ldots, N$ numbers the N radionuclides in a given decay chain, a dot ($\bullet$) over a quantity means the time derivative, and

$M_i(t)$ = mass of i^{th} radionuclide remaining in cavity at time $t > t_0$ (kg),

$Q(t)$ = discharge of brine through cavity at $t > t_0$ (m^3/s),

S_i = solubility limit for *element* associated with i^{th} radionuclide (kg/m^3),

λ_i = decay constant for i^{th} radionuclide (s^{-1}), and

t_0 = the time of initiation of a disruptive scenario (s).

In Equation 7-5, ΣM_j signifies summation over the remaining masses of all radionuclides (including the i^{th} radionuclide) associated with a given element. The initial conditions of Equation 7-5 are

$$M_i(t_0) = M_{i0}(t_0), \tag{7-6}$$

where $M_{i0}(t_0)$ is the initial ($t = 0$) inventory of the i^{th} radionuclide (kg) aged by the Bateman equations (Section 7.1) to reflect mass remaining at $t_0 > 0$.

7.5 Groundwater Transmissivity Fields

The WIPP PA Department employs a multiple-realization technique to account for spatial variability of the transmissivity field within the Culebra Dolomite (LaVenue and RamaRao, 1992). The technique uses an automated inverse approach to calibrate a two-dimensional model to both steady-state and transient pressure data. The multiple-realization technique can be broken down into three steps:

1. **Unconditional Simulation.** An unconditional simulation of the WIPP transmissivity fields is generated. This is a random field that has the same spatial correlation structure as the transmissivity measurements, but does not necessarily match measured transmissivities at the location of their measurements.

2. **Conditional Simulation.** The random field produced in Step 1 is conditioned in this step so that it honors exactly the measured transmissivities at the locations of their measurements. The resulting field, called a "conditional simulation" of the transmissivity field, is used as the initial estimate of the Culebra transmissivity field.

3. **Automated Calibration.** The conditional simulation of the transmissivity field is then calibrated so that the pressures computed by the groundwater-flow model (both steady and transient state) agree closely (calibrated within the uncertainty in head measurements, i.e., between 1 and 2 m) with the measured pressures in a least-square sense. Calibration is achieved by placing synthetic transmissivity values (pilot points) automatically where the sensitivity of the difference between observed and calculated pressure to changes in the transmissivity field is greatest. When calibration is completed, a conditionally simulated transmissivity field is obtained that conforms with all head and transmissivity data at the WIPP site and may be regarded therefore as a plausible version of the true distribution of transmissivity.

This process is repeated to produce the desired number of calibrated, conditionally simulated fields. (Seventy of these fields were calculated in this manner for the 1992 PA calculations.) A description of this methodology, extracted from LaVenue and RamaRao (1992), follows. (A more complete discussion of the methodology is provided in Appendix D of this volume.)

7.5.1 Unconditional Simulation

The following methods have been used earlier in groundwater hydrology for generating unconditional simulations: nearest-neighbor method (Smith and Freeze, 1979; Smith and Schwartz, 1981), matrix decomposition (de Marsily, 1986), multidimensional spectral analysis (Shinozuka and Jan, 1972; Mejía and Rodríguez-Iturbe, 1974), turning-bands method (Matheron, 1971, 1973; Mantoglou and Wilson, 1982; Zimmerman and Wilson, 1990). Here the turning-bands method is used.

In the turning-bands method, a two-dimensional stochastic process is generated by the summation of a series of equivalent one-dimensional processes (Mantoglou and Wilson, 1982):

$$Z_s(N) = \frac{\sum_{i=1}^{L} Z_i\left(\zeta_{N_i}\right)}{\sqrt{L}}, \tag{7-7}$$

where $Z_s(N)$ is the two-dimensional field to be simulated, $Z_i\left(\zeta_{N_i}\right)$ is the one-dimensional process in the line interval (band) of line i measured by ζ_i and containing N_i (the projection of point N onto line i), and L is the number of lines selected. As in LaVenue et al. (1990), the 1992 calculations model the WIPP transmissivity data as a two-dimensional field with an intrinsic random function of order zero (IRF-0), making it possible to use the Weiner-Levy Process to generate the line process $Z_i\left(\zeta_{N_i}\right)$ in Equation 7-7.

7.5.2 Conditional Simulation

The procedure for conditioning is based on the following relationship:

$$Z(x) \approx Z_{ok}(x) + \left[Z_{uc}(x) - Z_{uk}(x)\right], \tag{7-8}$$

where $Z(x)$ is the true (but unknown) value of the field at point x, $Z_{ok}(x)$ is the kriged estimate of Z at x based on the observed values of Z at the locations of the observations, $Z_{uc}(x)$ is the unconditionally simulated value of the field at point x, and $Z_{uk}(x)$ is value of the kriged estimate at x based on the unconditionally simulated values of Z_{uc} at the locations of the observations. Equation 7-8 clarifies the conditioning step as one of adding a simulated kriging error on a kriged field using the measured data. This step involves kriging twice, once with the measured transmissivities and another time with the unconditionally simulated transmissivities, both at the location of the observations. The simulated kriging error is rendered zero at all observation points.

7.5.3 Automated Calibration

In the 1992 calculations, model calibration is done by an indirect approach. Synthetic transmissivity values, referred to as pilot points, are automatically placed in regions of the conditionally simulated transmissivity field where an objective function (Equation 7-9) is most sensitive to changes in the this transmissivity field. This objective function is defined as the weighted sum of the squared deviations between the model computed pressures and the observed pressures, with the summation being extended in the spatial and temporal domain where pressure measurements are taken:

$$J(\underline{u}) = \sum_{k=1}^{L} \underline{e}_p^T(k)\underline{\underline{R}}^{-1}(k)\underline{e}_p(k), \tag{7-9}$$

where $J(\underline{u})$ is the weighted least square (WLS) error criterion function, $\underline{u}$ is the vector of parameters ($Y_p = \log_{10} T_p$), T_p is the pilot-point transmissivity, $\underline{e}_p$ is the difference between the computed and observed pressures, $\underline{\underline{R}}$ is the covariance matrix of errors in the observed pressure, k is the time step number, L is the number of time steps, and T is the transpose.

Pilot points are added to the existing measured transmissivity data set during the course of calibration. After a pilot point is added to the transmissivity data set, the augmented data set is used to obtain a revised, conditionally simulated transmissivity field for a subsequent iteration in calibration. With the addition of a pilot point, the transmissivity distribution in the neighborhood of the pilot point gets modified with dominant modifications being closer to the pilot-point location.

Pilot points are placed at locations where their potential for reducing the objective function (Equation 7-9) is highest. This potential is quantified by the sensitivity coefficients (dJ/dY) of the objective function J with respect to Y, the logarithm (to base 10) of pilot-point transmissivity. Coupled adjoint sensitivity analysis and kriging are used to compute the required derivatives (RamaRao and Reeves, 1990). The transmissivities at pilot points are assigned by an unconstrained optimization algorithm and a subsequent imposition of constraints. The optimization algorithm, which belongs to a class of iterative search algorithms, involves the repeated application of the following equation until convergence is achieved:

$$\underline{Y}_{i+1} = \underline{Y}_i + \beta_i \underline{d}_i, \tag{7-10}$$

where i is the iteration index, $\underline{d}_i$ is the direction vector, β_i is the step length (a scalar), and $\underline{Y}_i$ is a vector of parameters to be optimized (i.e., logarithms of pilot point transmissivities to base 10).

There are two levels of iteration used in the calibration process, designated as "inner" and "outer" iterations. An inner iteration relates to the iterations needed to optimize the transmissivities of the pilot points. When the convergence of an inner iteration is achieved, the pilot points are added to the transmissivity data set, and then the outer iteration may proceed. During the outer iteration, optimal location of the next set of pilot points is determined using coupled kriging and adjoint sensitivity analysis. Subsequently, their transmissivities are optimized by a sequence of inner iterations.

Convergence criteria for the inner iterations are as follows:

- The performance measure J drops below a prescribed minimum value.
- The number of iterations equals a prescribed maximum for the inner iterations.
- The ratio of the norm of the gradient to the initial gradient norm reduces below a prescribed value.
- The gradient norm is less than a prescribed minimum.
- The relative change in the objective function falls below a prescribed value.

Outer iterations cease once the performance measure J drops below a prescribed minimum value or the number of iterations equals a prescribed maximum for the outer iterations.

7.6 Groundwater Flow and Transport

Following the occurrence of an E2 or E1E2 scenario (Section 4.2.3.2), flow of brine through a collapsed WIPP panel may result in mobilization of dissolved, radionuclide-bearing compounds from waste (Section 7.4), the transport of these compounds up an intrusion borehole, and eventually their injection into the Culebra Dolomite Member of the Rustler Formation (Section 2.2.2.6). Dissolved compounds that reach the Culebra could then be carried to the accessible-environment boundary by advection and diffusion in groundwater flowing in the Culebra. Thus, to estimate consequences of certain disturbed-case scenarios, models of groundwater flow and solute transport through the Culebra are needed.

The consequence model that simulates groundwater flow in the Culebra is currently implemented by a computer code called SECO_2DH (Appendix C). The mathematical model on which SECO_2DH is based is described in Section 7.6.1 (below), which details assumptions that were made in order to arrive at the current model of groundwater flow; this section also contains discussions of modeling the effects of climate change on boundary conditions for the Culebra flow model.

Simulations of solute transport in groundwater flowing through the Culebra are currently implemented by a companion to the SECO_2DH code called SECO_TP (Appendix C). The mathematical model on which SECO_TP is based is described in Section 1.4.6 of Volume 3 of the present series of reports. Section 7.6.2 (following) contains discussion of the assumptions that were made in order to arrive at the current model of solute transport; it also contains discussion of the 1992 treatments of hydrodynamic dispersion (Section 7.6.2.1) and chemical sorption in fracture flows (Section 7.6.2.2).

The mathematical models of groundwater flow and solute transport are based on a common, highly simplified conceptual model of the Culebra Dolomite Member of the Rustler Formation: The Culebra Dolomite Member is imagined to be a sheet-like mass of rock having lateral dimensions of the order of tens of kilometers and uniform thickness of about 8 meters. Sets of planar fractures, all parallel to the plane of bedding, run continuously throughout the rock mass (Figure 7-4, top) and it is assumed that all water flow through the Culebra is sustained by the fracture sets, i.e., there is no flow through matrix blocks separating fractures (Figure 7-4, lower left) even though the matrix blocks are assumed to be saturated and have a finite kinematic porosity. The surfaces of fractures are assumed to be uniformly coated with layers of clay of constant thickness greater than or equal to 0 (Figure 7-4, lower right) that are never allowed to entirely fill the void space of a fracture; these clay layers are assumed to be saturated and to have finite kinematic porosity, but as in the matrix material, no advective flow is allowed through a clay layer.

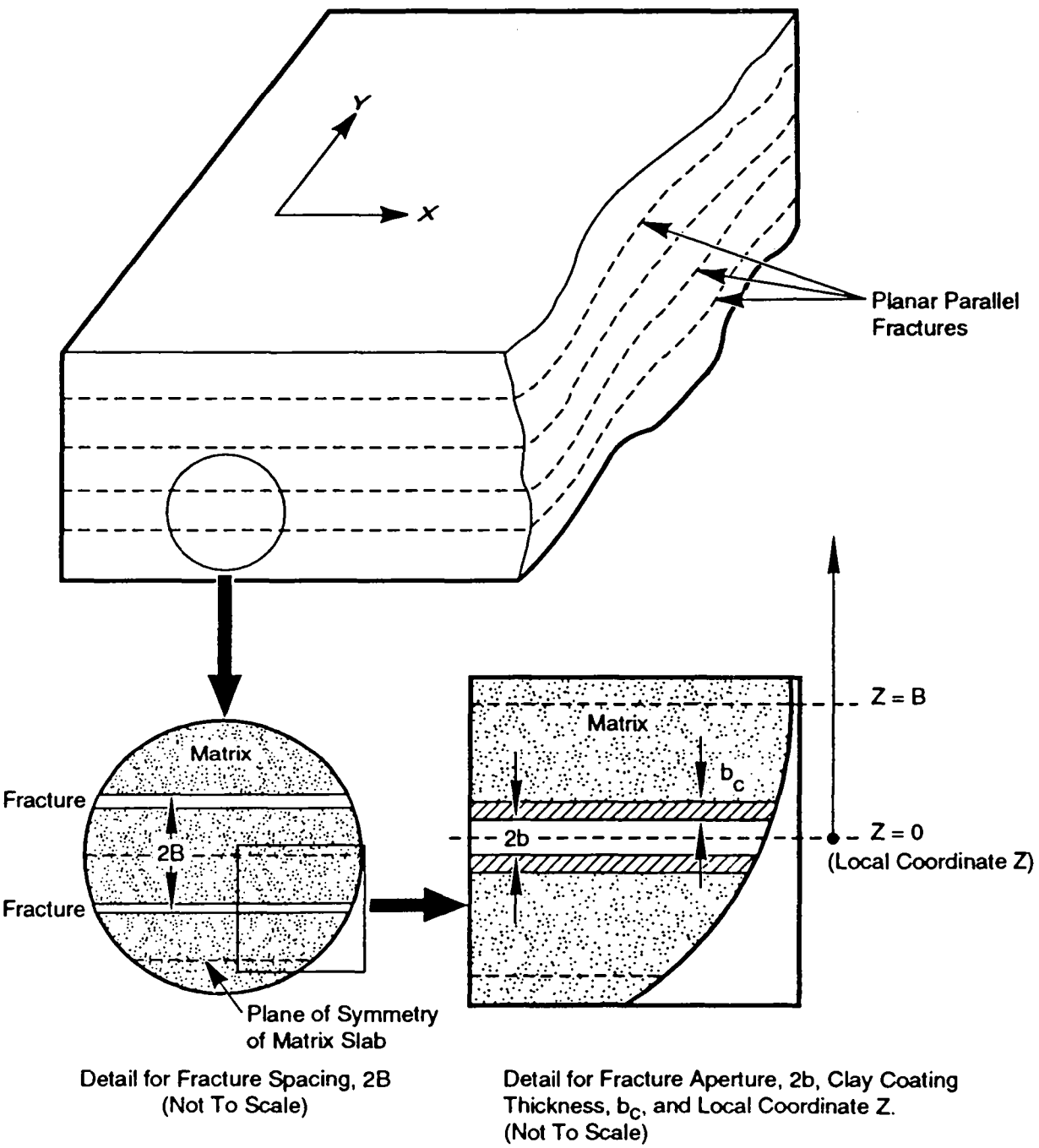

Figure 7-4. Conceptual hydrologic model of the Culebra Dolomite Member.

7.6.1 Groundwater Flow in the Culebra

Groundwater flow at regional and local scales within the Culebra Dolomite is simulated by solving the following partial differential equation in two dimensions (x,y):

$$S_s \frac{\partial h}{\partial t} = \nabla \bullet \left(\overline{K} \bullet \nabla h \right) \tag{7-11}$$

where

h = $h(x,y,t)$, the hydraulic head(m),

S_s = $S_s(x,y,t)$, the specific storage of the Culebra (m^{-1}),

$\overline{K}$ = $\overline{K}(x,y,t)$, the hydraulic conductivity tensor (m/s).

The specific storage and hydraulic conductivity tensors are obtained from more directly measurable quantities.

$$S_s = \frac{S(x,y)}{\Delta Z}, \quad \overline{K} = \frac{\overline{T}(x,y)}{\Delta Z}, \tag{7-12}$$

where

$S(x,y)$ = storage coefficient in the Culebra (dimensionless),

ΔZ = $Z(x,y)$, Culebra thickness (m),

$\overline{T}(x,y)$ = one of a set of simulated transmissivity tensors (units: m^2/s). See Section 2.6.9 of Volume 3 for a discussion of how transmissivity fields are generated. Also see Section 7.5 of this report.

Given appropriate initial and boundary conditions, the SECO_2DH code is used to solve Equation 7-11 numerically to yield a potentiometric head field, $h(x,y,t)$, which may be used to compute specific discharge (or Darcy velocity) at any point in the Culebra:

$$\vec{q}(x,y,t) = -\overline{K} \bullet \nabla h \,(\mathrm{m/s}). \tag{7-13}$$

The storage coefficients $S(x,y)$, and the Culebra thickness ΔZ are treated as constants (as opposed to functions of position) in the 1992 series of calculations.

7.6.1.1 BOUNDARY CONDITIONS

Groundwater flow is modeled separately in regional and local grids (Figure 7-5) to provide increased resolution in the area of primary interest around the WIPP. In solving Equation (7-11), boundary conditions are specified on the outer edges of the regional grid; these boundary conditions may be a mix of the following kind, depending upon geological and hydrological conditions at a point on the regional boundary: (1) Dirichlet (specified h on boundary); (2) inhomogeneous Neuman (specified gradients of h on boundary); (3) Robin boundary conditions [a mixture of (1) and (2)]; and (4) adaptive boundary conditions, in which flux ($\vec{q}$) is specified at inflow boundaries and head (h) is specified at outflow boundaries. Boundary conditions for the local grid, in which radionuclide transport is modeled, are determined by the groundwater flow calculated for the regional grid. The actual problem geometry and specifications for boundary conditions that were used in the 1992 series of calculations can be found in Volume 4 of this report.

7.6.1.2 EFFECTS OF CLIMATE CHANGE

The effects of climate change are simulated through inclusion of time-dependent Dirichlet boundary conditions. Specifically, potentiometric heads on portions of the northwestern and northeastern edges of the regional grid (closest to the assumed recharge area for the Culebra) are set according to the formula (Swift, 1992, 1991)

$$h_f(x,y,t) = h_p(x,y)\left[\frac{3A_R+1}{4} - \left(\frac{A_R-1}{2}\right)\left(\cos\theta t - \sin\frac{\Phi}{2}t + \frac{1}{2}\cos\Phi t\right)\right] \tag{7-14}$$

where

h_f = future potentiometric head (m)

h_p = present potentiometric head (m)

A_R = Recharge amplitude factor (dimensionless)

θ = Pleistocene glaciation frequency (Hz)

Φ = frequency of Holocene-type climatic fluctuations (Hz).

The recharge amplitude factor, A_R, is a number to be chosen between 1 and $\gamma > 1$. If $A_R = 1$, it is seen that there are no effects of climatic change. If $A_R > 1$, the maximum future head, h_f, will be greater than the present head. The constant γ is a scaling factor that is chosen to ensure physically reasonable head values on the portion of the recharge boundary where boundary conditions are applied.

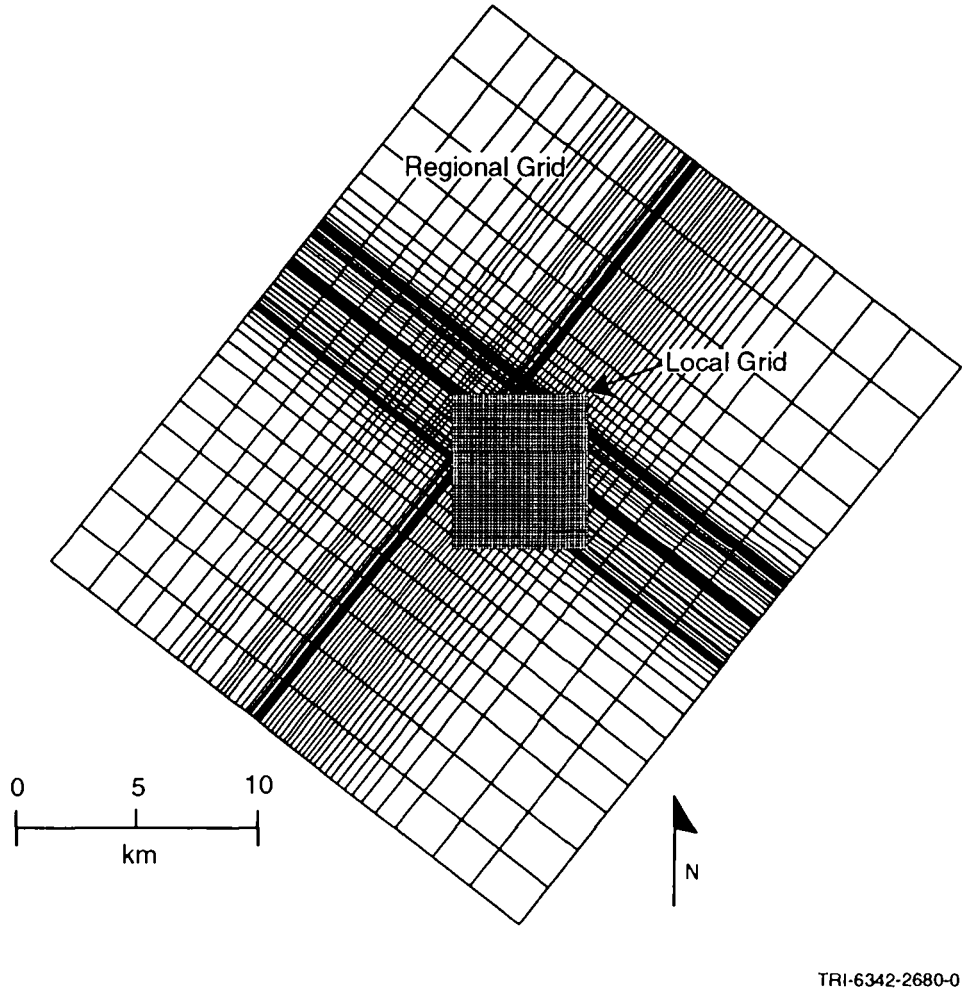

Figure 7-5. Example of regional and local grids used for disturbed fluid flow and transport calculations.

7-17

7.6.2 Solute Transport in the Culebra

The mathematical model of solute transport at the local scale is described in Section 1.4.6 of Volume 3 of the present series of reports. The physical assumptions and limitations of the 1992 version of the solute transport model are the same as those of the 1991 version (see 6.5.2.3 in WIPP PA Division, 1991b), namely:

1. The numerical solution is limited to two dimensions, reflecting the conceptual model of the Culebra Dolomite member (Figure 7-4).

2. Hydrodynamic dispersion is quantified with a Fick's law term.

3. Fracture flow is modeled as an equivalent porous medium of constant porosity.

4. No advective transport exists through the Culebra matrix; however, one-dimensional diffusion of solutes across fracture-matrix interfaces are allowed (Figure 7-4).

5. Adsorption of solutes on solid phases obeys a linear isotherm.

6. Local chemical equilibrium always exists between solutes and solid phases.

7. Material-property parameters are treated as constants over distinct material regions; in other words, intramaterial spatial variability is ignored.

The purpose of assumption 4 is to permit simple simulation of the phenomenon of dynamic solute storage within porous materials surrounding fractures. As solute concentration in fractures increases, solute will diffuse into and become immobilized within the matrix; if concentrations in fractures decreases with time, solute is returned to fractures by diffusion out of the matrix.

The major differences between the 1992 and 1991 versions of the solute transport model lie in the former's treatment of dispersivity parameters and adsorption effects in fracture flows. Details of changes in the way these important physical effects are implemented in the model are presented in the remainder of this section.

7.6.2.1 MODELING HYDRODYNAMIC DISPERSION

The components of the hydrodynamic dispersion tensor for the fracture system D_{ij}, are (Scheidegger, 1960)

$$D_{11} = \alpha_L \frac{(V_1)^2}{|V|} + \alpha_T \frac{(V_2)^2}{|V|} + D^*,$$

1 $$D_{22} = \alpha_L \frac{(V_2)^2}{|V|} + \alpha_T \frac{(V_1)^2}{|V|} + D^*,$$

$$D_{12} = D_{21} = (\alpha_L - \alpha_T)\frac{V_1 V_2}{|V|},$$

2 where V_i, i = 1,2, are the components of the average linear velocity vector in the fracture system (m/s), α_L and
3 α_T are respectively longitudinal and transverse dispersivities (m), D^* is the molecular diffusion coefficient of the
4 "average" solute species (m^2/s), and

5 $$|V| = \left(V_1^2 + V_2^2\right)^{1/2}$$

6 The dispersivities, α_L and α_T, are measures of the dispersion of the true linear velocity vector about the
7 average value. Ideally, these parameters would be estimated by fitting transport model calculations to results of
8 tracer tests conducted in the Rustler Formation at an appropriate scale; but, in the absence of tracer-test results
9 suitable for parameter estimation, the PA Department has had to rely on subjective judgments and results from
10 stochastic transport theory to form the necessary estimates. In 1991, it was assumed that α_L, α_T were
11 imprecisely known constants (WIPP PA Division, 1991c, Section 2.6.2), with longitudinal dispersivity varying
12 between 50 and 300 meters and transverse dispersivity varying between 5 and 30 meters (i.e., one-tenth of
13 longitudinal dispersivity).

14 The treatment of Culebra dispersivity in the present (1992) series of PA calculations relies heavily on
15 stochastic transport theory, exemplified by the universal scaling approach used by Neuman (1990) to investigate
16 the compatibility of fractal transmissivity fields with the observed scale dependence of dispersivity. Neuman
17 provides an expression that relates longitudinal dispersivity to the mean value of the variogram of ln T variance at
18 the scale S and the travel distance L, namely

19 $$\alpha_L = C_o \, L \, \sigma_y^2(S), \tag{7-15}$$

20 where C_o is a constant ~ 1 in isotropic media; and

21 $$\sigma_y^2(S) = \bar{\gamma}(v, v) \simeq \frac{1}{v^2} \int_v \int_v \gamma(x - y)\, dx\, dy, \tag{7-16}$$

22 where $\gamma(h)$ is the variogram of ln T, $h = |\mathbf{x}\text{-}\mathbf{y}|$, and each integration in the above expression is carried over a
23 fixed area v, ~ L^2. In current (1992) PA calculations, C_o = 1 and L is taken to be the size of the model block in
24 which α_L is being evaluated.

The variogram, $\gamma(h)$, is taken to be the one used in the "local" scale generation of the 1992 random transmissivity fields (Section 7.5 and Appendix D, Volume 3),

$$\gamma(h) = 1.2 \times 10^{-3}\, h\,. \tag{7-17}$$

Here, the "local" scale is defined as that appropriate for the transmissivity measurements, i.e., a scale length between slug tests radii of influence and pump tests radii of influence; such a scale length is of the order of 10 meters. Note that Equation (7-17) is a linear variogram, for which the concepts of "correlation length" and "integral scale" have no meaning.

The integral in Equation (7-16) has been evaluated by Journel and Huijlbregts (1978, p. 113) for a linear variogram $\gamma(h) = h$ and a rectangular mesh with dimensions L and ℓ. Their result is analytically messy, but in the case where $L = \ell$ (v = area of a square of side L), their expression reduces to

$$\bar{\gamma}(v, v) = 0.5213\, L\,.$$

Multiplying this expression by the constant in Equation (7-17), 1.2×10^{-3}, and substituting for $\bar{\gamma}(v, v)$ in Equation (7-13) gives an expression for the longitudinal dispersivity in terms of the size of the model block in which α_L is being evaluated:

$$\alpha_L \simeq 6.2 \times 10^{-4}\, L^2 \text{ (m)}\,. \tag{7-18}$$

In practice, a value of 1.5 meters is added to the α_L obtained by Equation (7-18) in order to account for microscale dispersion that must occur below the "local" scale.

The ratio of longitudinal to transverse dispersivity does not seem to be scale dependent; data from Gelhar et al. (1992) suggest that this ratio is almost always between 10 and 50. In the present (1992) series of calculations, the fixed relation

$$\alpha_T = \frac{1}{10}\,\alpha_L \tag{7-19}$$

was adopted.

Note that using model block size as travel distance in obtaining Equation (7-18) is equivalent to the assumption that dispersivity reaches its asymptotic limit at the scale of a model block, and any other non-asymptotic behavior is taken care of by variability of the simulated transmissivity fields (Section 7.5 and Appendix D, Volume 3).

7.6.2.2 MODELING CHEMICAL SORPTION IN FRACTURE FLOWS

Chemical retardation of solutes by sorption on fracture surfaces was modelled in 1990-1991 PA calculations with a formula proposed by M. D. Siegel (1990). Siegel suggested that the effective solute velocity in a clay-lined fracture, V_{eff}, is related to the average linear velocity of groundwater in the fracture, V, by

$$\frac{V}{V_{eff}} = 1 + \rho_c \, K_{dc} \left(b_c / b \right), \tag{7-20}$$

where

ρ_c = density of clay liner (kg/m^3),

K_{dc} = partition coefficient of solute in clay (m^3/kg),

$2b_c$ = total thickness of clay layer in a fracture (m), and

$2b$ = fracture aperture (m).

The expression on the right side of Equation (7-20) is called R, the retardation factor; the partition coefficient K_{dc} is also called the distribution coefficient.

Consideration of Equation (7-20) will show that it cannot generally describe retardation of solutes being transported through an *open*, saturated fracture; in this case, retardation of solute molecules must proceed by reactions between the mobilized species and stationary species located on the solid surface facing the fracture void space. In contrast, Equation (7-20) turns out to be a "thin-skin" approximation to retardation of mobile solutes *within* pore spaces of the clay layer, which is valid only after solute molecules have diffused or been advected into the clay layer and concentrational equilibrium is nearly established. In other words, Equation (7-20) is appropriate for concentrational equilibrium; note, however, that it may take a long time to reach concentrational equilibrium by diffusion of solute through highly sorbing clay and that, by assuming instantaneous equilibrium, the retardation of solutes in fracture flows may have been overestimated in the 1990-1991 calculations.

The PA Department abandoned use of Equation (7-20) in 1992 and, for reasons provided below, has set $R = 1$ in fracture flows (see Equation 1.4.6-1 in Section 1.4.6, Volume 3 of this report). An approximate, but physically motivated expression for the retardation of solutes in fracture flows is derived in the remainder of this subsection and used to justify the choice of $R = 1$.

Freeze and Cherry (1979, p. 411) give an expression for the retardation factor in solute transport through a planar fracture of aperture $2b$:

$$R = 1 + \frac{1}{b} K_a, \tag{7-21}$$

where

$$K_a = \frac{\text{mass of solute on solid phase per unit area of solid phase}}{\text{concentration of solute in solution}} \quad (\text{m}).$$

Equation (7-21) should be valid when time scales for (1) diffusion across a fracture aperture and (2) achievement of equilibrium in surficial chemical reactions are always much smaller than other problem time scales (e.g., time required to advect a solute molecule across a grid cell, time required to diffuse into clay layers).

The surficial distribution coefficient, K_a, can be related to the familiar mass-based distribution coefficient (Freeze and Cherry, 1979, p. 405),

$$K_d = \frac{\text{mass of solute on solid phase per unit mass of solid phase}}{\text{concentration of solute in solution}} \quad (\text{m}^3/\text{kg}).$$

by

$$K_a = K_d / \sigma_m ,$$

where σ_m is the surface area per unit mass of the solid phase (m^2/kg). Obviously, σ_m depends upon the physical nature of the solid phase, here a natural aggregation of clay grains on the surfaces of saturated fractures in the Culebra Dolomite. No measurements or estimates of σ_m for these clays seem to be available, but an order-of-magnitude estimate of this quantity can be rapidly made if the clay is visualized as an aggregation of regularly packed spheres of radius a (i.e., spheres centered on vertices of a cubic lattice of elemental size $2a$). To begin making this estimate, consider M kg of bulk clay having *grain-density* ρ_g; then the number of spheres in this mass is

$$n_p \simeq (3M)/\left(4\pi a^3 \rho_g\right),$$

and the surface area of the solid phase that is presented to the pore space of the M kg of clay is

$$A \simeq 4\pi a^2 n_p = \frac{3M}{a\rho_g}.$$

It follows that

$$\sigma_m = \frac{A}{M} \approx \frac{3}{a\rho_g}, \quad \text{and so } K_a \simeq \frac{a\rho_g K_d}{3}.$$

Substitution of this result in Equation (7-21) gives the promised order-of-magnitude estimate of the fracture retardation factor:

$$R \simeq 1 + \frac{\rho_g}{3} K_d \, (a/b). \qquad (7\text{-}22)$$

Note the superficial similarity of expressions in Equations (7-20) and (7-22). Their relative magnitudes are nevertheless always different as can be seen by forming the ratio of (R-1)s from the respective formulas; for instance, the ratio of (R-1) for Equation (7-22) to (R-1) for Equation (7-20) is of the order of a/b_c, the ratio of clay particle size to clay layer thickness. In all but the narrowest of fracture apertures, a/b_c should be of the order of 10^{-2} or less (take a = 1 μm, b = 100 μm). Thus, retardations computed from Equation (7-22) should be much less than retardations computed from Equation (7-20), justifying the earlier claim that retardation in fracture flows (i.e., "single porosity" model) may have been overestimated in the 1990-1991 series of PA calculations.

Clay layers on fracture surfaces actually played two roles in 1990-1991 PA models of solute transport in the Culebra Dolomite: (1) the role described above, i.e., as agents of retardation of solutes in fracture flows, and (2) as barriers to mass transfer of solutes across the matrix-fracture interface (the "matrix skin resistance" of Section 2.6.7 in WIPP PA Division, 1991c). The PA Department has also abandoned the second of these roles for clay linings in 1992 versions of the solute-transport models. Clay linings are now treated as extensions of the matrix and a single diffusion equation [Equation (1.4.6-5), Section 1.4.6, Volume 3 of this series] is used to model solute mass transport in an effective porous media comprised of Culebra matrix blocks and their adjacent clay linings.

7.7 Direct Removal of Waste

Of the possible pathways for release during the 10,000-year regulatory period, one of the most important is that caused by the direct removal of waste that would result when an exploratory drill bit inadvertently penetrates a waste storage room. To quantify the extent of radioactive release resulting from direct removal of waste, the model described below, extracted from Berglund (1992), has been developed. The current performance assessment model assumes that future drilling techniques will be similar to those in use today. This assumption is necessary to provide a basis on which predictions of release can be estimated.

In rotary drilling, a cutting bit attached to a series of hollow drill collars and drill pipes is rotated at a fixed angular velocity and is directed to cut downward through underlying strata. To remove the material loosened by the drilling action, a drilling fluid ("mud") is pumped down the drill pipe, through and around the drill bit, and up to the surface within the annulus formed by the drill pipe and the borehole wall (Figure 7-6).

If an exploratory drill bit penetrates a waste-filled room, waste resulting from three separate physical processes can mix with the drilling fluid and be transported to the surface:

- cuttings—waste contained in the cylindrical volume created by the cutting action of the drill bit through the waste,
- cavings—waste that erodes from the borehole in response to the upward-flowing drilling fluid within the annulus, and
- spallings—waste surrounding the eroded borehole that is transported by waste-generated gas escaping to the lower-pressure borehole.

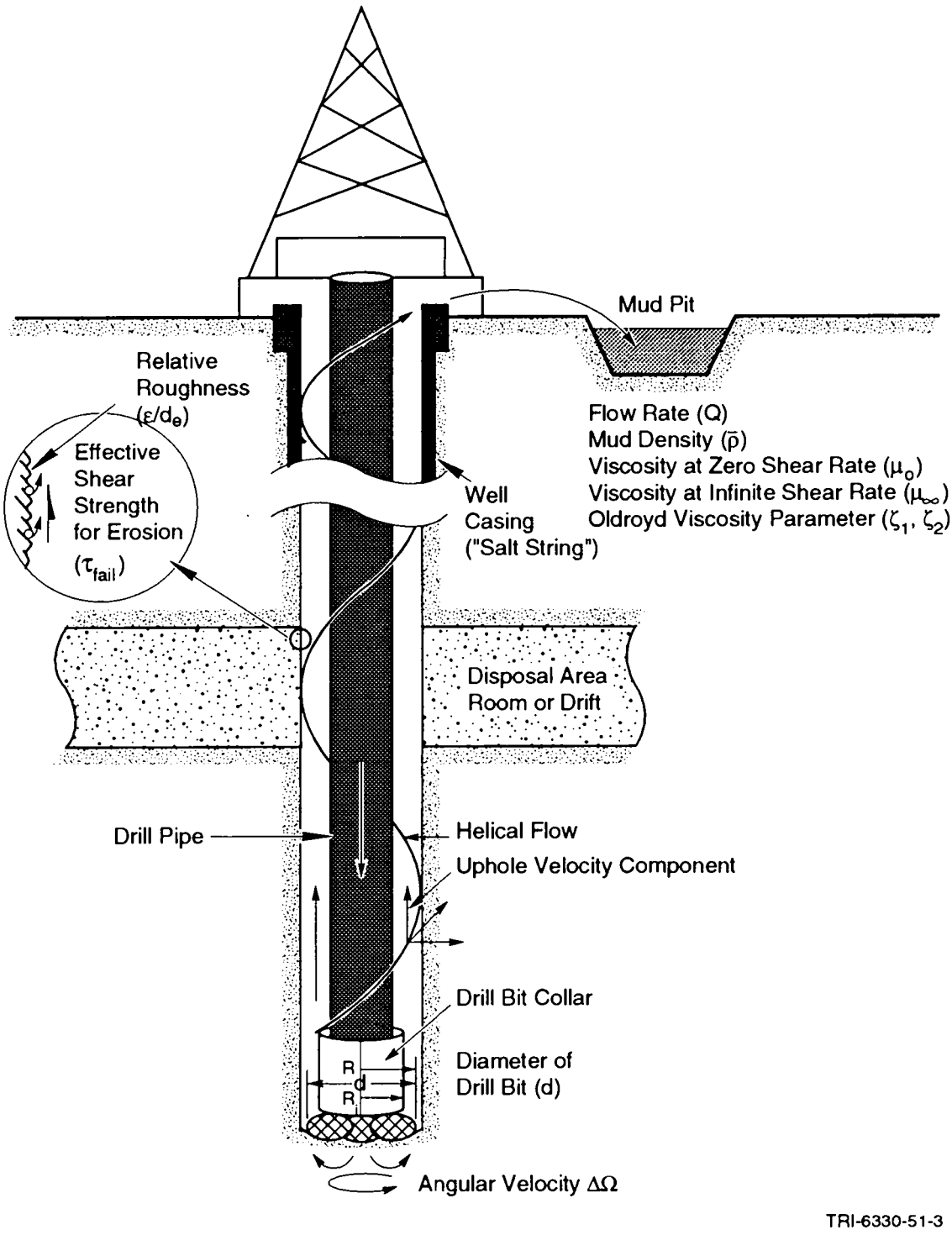

Figure 7-6. Rotary drilling.

A discussion of these three processes follows.

7.7.1 Cuttings

For a gauge borehole, the volume of cuttings removed and transported to the surface is equal to the product of the drill bit area and the drill depth. Thus, to estimate the total volume of waste removed due to the cutting action of the drill bit (V), it is only necessary to know the compacted repository height (h) and the drill-bit area (A):

$$V = Ah. \tag{7-23}$$

The cuttings volume calculated in this manner is a lower bound to the total quantity of waste removed by drilling.

7.7.2 Cavings

While a number of factors that influence drillhole wall erosion have been identified in the literature (Broc, 1982), industry opinion singles out fluid shear stress as the most important factor (Walker and Holman, 1971; Darley, 1969). This analysis therefore assumes that borehole erosion is caused primarily by the magnitude of fluid shear stress acting on the borehole wall. This analysis also assumes that erosion of wall material occurs when the fluid shear stress at the wall exceeds the effective shear strength for erosion of the wall material (the surrounding compacted repository wastes) and that the diameter of the bored hole increases until this condition no longer exists. In this process, it is assumed that sufficient time is available to complete the erosion process. All the eroded material is assumed to pass to the surface in the flowing drilling fluid.

Flow in the annulus between the drill pipe and borehole wall is usually laminar (Darley and Gray, 1988). Adjacent to the collars, however, the smaller annular volume created by the larger collar diameter (Figure 7-6) causes higher mud velocities, making flow either laminar or turbulent (Berglund, 1990; Pace, 1990). For laminar flow, the analysis lends itself to classical solution methods. Turbulent flow, where the flow is assumed to be axial with no rotational component, requires a more approximate approach.

7.7.2.1 LAMINAR FLOW

Below Reynolds numbers of about 2100 for Newtonian fluids and 2400 for some non-Newtonian fluids (Walker, 1976), experiments have shown that the flow of a fluid in a circular pipe or annulus is well behaved and can be described using a well-defined relationship between the velocity field and the fluid shear stress. This type of flow is called laminar. Drilling fluids exhibit non-Newtonian fluid behavior, making it necessary to choose a functional form for the variation of viscosity with shear rate for the fluid. Of the several different functional forms that can be used to account for the varying viscosity, this analysis uses a form chosen by Oldroyd (1958) and further developed by Savins and Wallick (1966).

Savins and Wallick (1966) have shown that the solution for laminar helical flow of a non-Newtonian fluid in an annulus could be written in terms of three nonlinear integral equations:

$$F_1 = \int_{\alpha}^{1} \left(\frac{\rho^2 - \lambda^2}{\rho} \right) \frac{d\rho}{\eta} = 0$$

$$F_2 = C \int_{\alpha}^{1} \frac{d\rho}{\rho^3 \eta} - \Delta\Omega = 0$$

$$F_3 = \frac{4Q}{\pi R^3} + 4\left(\frac{RJ}{2} \right) \int_{\alpha}^{1} \left(\frac{\alpha^2 - \rho^2}{\eta} \right) \left(\frac{\rho^2 - \lambda^2}{\rho} \right) d\rho = 0, \quad (7\text{-}24)$$

where Q is the drilling fluid (mud) flow rate; r is the radial coordinate; α is the ratio of the collar radius over the cutting radius (R_i/R) (Figure 7-6); $\Delta\Omega$ is the drill string angular velocity; η is the viscosity of the drilling fluid; ρ is the non-dimensional radial coordinate representing the ratio r/R; and λ^2, $RJ/2$, and C are parameters related to the fluid shear stresses. As long as annular flow remains in the laminar regime, the above three nonlinear integral equations can be solved numerically to determine the final eroded volume of the borehole (a function of the effective shear strength for erosion, τ_{fail}) and the resulting total cavings volume.

7.7.2.2 TURBULENT FLOW

At a Reynolds number of about 3000, flow becomes fully turbulent; momentum effects dominate and fluid viscosity is no longer as important in characterizing pressure losses. A far more important parameter is the surface roughness past which the fluid must flow.

The increased complexity of turbulent flow makes empirical procedures necessary. For axial flow in an annulus, the pressure loss under turbulent conditions can be approximated by (Broc, 1982)

$$\Delta P = \frac{2fL\bar{\rho}\bar{V}^2}{(0.8165)D}, \quad (7\text{-}25)$$

where f is the coefficient of pressure head loss (Fanning friction factor), D is the hydraulic diameter, L is the borehole length, $\bar{V}$ is the average fluid velocity, and $\bar{\rho}$ is the drill fluid density.

If the shear stress due to the flowing fluid is assumed to be uniformly distributed on the inner and outer surfaces of the annulus, it can be easily shown using Equation 7-25 that the shear stress is related to the average fluid velocity through the relation

$$\tau = \frac{f\rho\bar{V}^2}{2(0.8165)}, \tag{7-26}$$

The Fanning friction factor is empirically related to the Reynolds number and relative roughness by the equation (Whittaker, 1985)

$$\frac{1}{\sqrt{f}} = -4\log_{10}\left[\frac{\varepsilon}{3.72D} + \frac{1.255}{R_e\sqrt{f}}\right], \tag{7-27}$$

where ε/D is the relative roughness and R_e is the Reynolds number. For circular pipes, D in this equation represents the inside diameter and ε is the absolute roughness or the average depth of pipe wall irregularities. In the absence of a similar equation for flow in an annulus, it is assumed that this equation also applies here, where D is the hydraulic diameter, and ε is the absolute roughness of the waste-borehole interface.

The above three equations can be used to obtain the final eroded borehole radius under turbulent flow conditions by forcing the fluid shear stress acting on the borehole wall to equal the shear strength for erosion of the repository waste (τ_{fail}).

7.7.3 Spallings

The spalling of borehole walls is a common occurrence in oil and gas drilling and can be caused by an encounter with a geopressurized formation; a similar event may occur if an exploratory drill bit penetrates a waste-filled, pressurized room at the WIPP. Corrosion and biodegradation of the waste will generate gas, raising the gas pore pressure in the waste to values approaching and perhaps exceeding the lithostatic level within the next 700 to 2,000 years. Because the permeability of the surrounding Salado Formation is expected to be 1 to 7 orders of magnitude less than that of the compacted waste, the Salado can be considered impermeable compared to the waste. The intrusion of a drill bit into the waste could therefore "suddenly" expose the waste with its high pore pressure (for example, 14.8 MPa) to the borehole hydrostatic pressure of 7.7 MPa (assuming a saturated salt solution is used while drilling), causing gas to escape to the borehole after flowing through the compacted waste. The escaping gas may compromise the stability of the borehole wall and contribute to the quantity of waste material that reaches the surface environment.

Spalling is a complex process that involves the flow of gas in a moving waste matrix, changing stress states, changing porosity and permeability of the waste, waste failure, and when the waste interacts with the drill bit, turbulent mixing of the three phases—solid waste, drilling fluid, and gas. The approach for modeling spalling caused by the intrusion of an exploratory drill bit is still being developed.

The current state of understanding for spall as related to WIPP is treated in Berglund (1992). In addition to a discussion of related literature, Berglund (1992) describes several types of calculations, each of which addresses a different aspect of gas flow and waste response from a penetrated, gas-pressurized, waste storage room. The waste response is found to be very dependent on the constitutive nature of the compacted composite waste, a feature

that is currently unknown. If the waste is assumed to behave as a granular, soil-like material with a nonlinear constitutive character and a small cohesive strength, the behavior of the waste subject to gas flow indicates a movement toward the borehole after penetration. In both the one- and two-dimensional computational models, where an instantaneous borehole pressure drop is assumed, the inward motion of the waste-borehole boundary would quickly (in milliseconds) be blocked by the presence of the drill string and would remain impressed against the drill string while a sufficient pore pressure gradient is maintained.

What happens to the waste as it is impressed against the drill string is not known because the interface between the waste and drill stem is very difficult to characterize without experimental verification. One possibility is the compressed waste will completely block the flow of drilling mud. Whether the drilling operation can proceed in such circumstances is unknown. Certainly the flow of gas out of the waste will be further restricted if not completely blocked. Such a restriction would prolong the compressive stresses acting between the drill string and the waste. Another possibility is that some drilling fluid may be able to channel its way through the waste-drill string boundary carrying eroded waste up into the upper borehole.

The driller may, however, be able to detect the resistance afforded by the waste pressing against the drill stem by the increase in torque, circulation pressure, and by a drop in mud flowrate (Austin, 1983). Under such conditions the driller may raise the cutting bit and allow the "spall" to continue naturally, eventually proceeding after the process diminishes (Short, 1982). Often under these conditions a repetitive process is undertaken of cleaning out, drilling ahead a few feet of new hole, picking up the drill bit to check for fill, then cleaning out again. This is repeated until spalling slows. The cleanout procedure can be used for 12 to 24 hours, or longer, if it shows sign of becoming effective (Short, 1982).

If drilling can proceed with the waste impressed against the drilling equipment, erosion will probably occur at the interface and could continue until a significant portion of the gas has leaked from the penetrated room or the target drill depth is reached. Based on leakage rates from the waste with uniform permeabilities, significant volumes of gas will be removed from the room only after several hours for the greatest waste permeability and hundreds of days for the least permeability. Moreover, the decrease in waste permeability caused by the compressive stress field at the drill string-waste interface is likely to decrease the gas leakage rates significantly.

In the analyses considered in Berglund (1992), actions to prevent a blowout taken by the driller after encountering a gas-pressurized formation are also discussed. When formation gas flow into a borehole is detected at the surface, such as by an increase in return mud volume, the driller usually will "close in" the well by engaging blowout preventers (BOPs) to prevent serious injury to personnel and damage to equipment. This action is usually taken within a minute or two after the "kick" is first observed, and the effect is that the gas flow from the formation to the borehole is effectively curtailed (Mills, 1984). The well is then "killed" by increasing the mud density in the borehole so that the formation (waste) pore pressure is in balance with the mud pressure. The drilling can then safely continue. With the pressure gradient in the borehole wall thus reduced to zero, spallation will cease and waste will be brought to the surface by erosion only. BOPs are engaged only if a blowout condition is detected. For high-permeability wastes ($k = 1 \times 10^{-13}$ m^2), the rate of flow of gas to the borehole will increase the mud volume in the annulus significantly, and it is very likely that the well will be "killed." However, for lower permeabilities, the gas flowrate is much reduced; the driller may not engage BOPs but continue drilling, thus allowing spall into the borehole to occur.

Estimating the amount of material that may eventually be passed into the borehole as the result of gas generation in the repository is difficult and speculative. However, based upon the analysis performed and the literature examined to date, it does not appear to be unreasonable that a volume of waste greater than the lower bound cuttings volume (bit area × waste depth) could eventually reach the ground surface. Currently, little data are available that predict the constitutive nature of the compacted, decomposed waste at the time of intrusion, nor have there been any experiments performed that could confirm the mechanisms for borehole spall as discussed. These data are currently being developed.

8. REFERENCES

Adams, J.E. 1944. "Upper Permian Ochoa Series of Delaware Basin, West Texas and Southeastern New Mexico," *Bulletin of the American Association of Petroleum Geologists.* Vol. 28, no. 11, 1596-1625.

Anderson, R.Y. 1981. "Deep-Seated Salt Dissolution in the Delaware Basin, Texas and New Mexico," *Environmental Geology and Hydrology in New Mexico.* Eds. S. G. Wells and W. Lambert. New Mexico Geological Society Special Publication No. 10. Roswell, NM: New Mexico Geological Society, 133-145.

Apostolakis, G., R. Bras, L. Price, J. Valdes, K. Wahi, and E. Webb. 1991. *Techniques for Determining Probabilities of Events and Processes Affecting the Performance of Geologic Repositories: Suggested Approaches.* NUREG/CR-3964, SAND86-0196. Albuquerque, NM: Sandia National Laboratories. Vol. 2.

Austin, E.H. 1983. *Drilling Engineering Handbook.* Boston, MA: International Human Resources Development Corporation.

Bachman, G.O. 1981. *Geology of Nash Draw, Eddy County, New Mexico.* U.S. Geological Survey Open-File Report 81-31. Denver, CO: U. S. Geological Survey.

Bachman, G.O. 1984. *Regional Geology of Ochoan Evaporites, Northern Part of Delaware Basin.* New Mexico Bureau of Mines and Mineral Resources Circular 184. Socorro, NM: New Mexico Bureau of Mines and Mineral Resources.

Bachman, G.O. 1987. *Karst in Evaporites in Southeastern New Mexico.* SAND86-7078. Albuquerque, NM: Sandia National Laboratories.

Beauheim, R.L. 1986. *Hydraulic-Test Interpretations for Well DOE-2 at the Waste Isolation Pilot Plant (WIPP) Site.* SAND86-1364. Albuquerque, NM: Sandia National Laboratories.

Beauheim, R.L. 1987a. *Interpretations of Single-Well Hydraulic Tests Conducted At and Near the Waste Isolation Pilot Plant (WIPP) Site, 1983-1987.* SAND87-0039. Albuquerque, NM: Sandia National Laboratories.

Beauheim, R.L. 1987b. *Analysis of Pumping Tests of the Culebra Dolomite Conducted At the H-3 Hydropad at the Waste Isolation Pilot Plant (WIPP) Site.* SAND86-2311. Albuquerque, NM: Sandia National Laboratories.

Beauheim, R.L. 1987c. *Interpretation of the WIPP-13 Multipad Pumping Test of the Culebra Dolomite at the Waste Isolation Pilot Plant (WIPP) Site.* SAND87-2456. Albuquerque, NM: Sandia National Laboratories.

Beauheim, R.L., and P.B. Davies. 1992. "Experimental Plan for Tracer Testing in the Culebra Dolomite at the WIPP Site." Revision A. Albuquerque, NM: Sandia National Laboratories.

Beauheim, R.L., and R.M. Holt. 1990. "Hydrogeology of the WIPP Site," *Geological and Hydrological Studies of Evaporites in the Northern Delaware Basin for the Waste Isolation Pilot Plant (WIPP), New Mexico.* Geological Society of America 1990 Annual Meeting Field Trip #14 Guidebook. Dallas, TX: Dallas Geological Society. 131-179.

Beauheim, R.L., G.J. Saulnier, Jr., and J. D. Avis. 1991. *Interpretation of Brine-Permeability Tests of the Salado Formation at the Waste Isolation Pilot Plant Site: First Interim Report.* SAND90-0083. Albuquerque, NM: Sandia National Laboratories.

Bechtel National, Inc. 1986. *Waste Isolation Pilot Plant Design Validation Final Report.* DOE/WIPP-86-010. Prepared for U.S. Department of Energy. San Fransisco, CA: Bechtel National, Inc.

Berglund, J.W. 1990. Appendix A, "Letter 1a: Bar Graphs Representing Range of Values for Drilling Operations Near WIPP Site," *Data Used in Preliminary Performance Assessment of the Waste Isolation Pilot Plant (1990).* R.P. Rechard, H. Iuzzolino, and J. S. Sandha (Report Authors). SAND89-2408. Albuquerque, NM: Sandia National Laboratories. A-157 through A-164.

Berglund, J.W. 1992. *Mechanisms Governing the Direct Removal of Wastes from the Waste Isolation Pilot Plant Repository Caused by Exploratory Drilling.* SAND92-7295. Albuquerque, NM: Sandia National Laboratories.

Bertram-Howery, S.G., and R.L. Hunter, eds. 1989. *Preliminary Plan for Disposal-System Characterization and Long-Term Performance Evaluation of the Waste Isolation Pilot Plant.* SAND89-0178. Albuquerque, NM: Sandia National Laboratories.

Bertram-Howery, S.G., and P.N. Swift. 1990. *Status Report: Potential for Long-Term Isolation by the Waste Isolation Pilot Plant Disposal System.* SAND90-0616. Albuquerque, NM: Sandia National Laboratories.

Bertram-Howery, S.G., M.G. Marietta, R.P. Rechard, P.N. Swift, D.R. Anderson, B.L. Baker, J.E. Bean, Jr., W. Beyeler, K.F. Brinster, R.V. Guzowski, J.C. Helton, R.D. McCurley, D.K. Rudeen, J.D. Schreiber, and P. Vaughn. 1990. *Preliminary Comparison with 40 CFR Part 191, Subpart B for the Waste Isolation Pilot Plant, December 1990.* SAND90-2347. Albuquerque, NM: Sandia National Laboratories.

Blom, G. 1989. *Probability and Statistics: Theory and Applications.* New York, NY: Springer-Verlag.

Bonano, E.J., S.C. Hora, R.L. Keeney, and D. von Winterfeldt. 1990. *Elicitation and Use of Expert Judgement in Performance Assessment for High-Level Radioactive Waste Repositories.* NUREG/CR-5411, SAND89-1821. Albuquerque, NM: Sandia National Laboratories.

Borns, D.J., and J.C. Stormont. 1988. *An Interim Report on Excavation Effect Studies at the Waste Isolation Pilot Plant: The Delineation of the Disturbed Rock Zone.* SAND87-1375. Albuquerque, NM: Sandia National Laboratories.

Borns, D.J., and J.C. Stormont. 1989. "The Delineation of the Disturbed Rock Zone Surrounding Excavations in Salt," *Rock Mechanics as a Guide for Efficient Ulilization of Natural Resources, Proceedings of the 30th U.S. Symposium, West Virginia University, Morgantown, WV. June 19-22, 1989.* Ed. A.W. Rhair. Brookfield, VT: A.A. Balkema. 353-360.

Borns, D.J., L.J. Barrows, D.W. Powers, and R.P. Snyder. 1983. *Deformation of Evaporites Near the Waste Isolation Pilot Plant (WIPP) Site.* SAND82-1069. Albuquerque, NM: Sandia National Laboratories.

Bredehoeft, J.D. 1988. "Will Salt Repositories Be Dry?" *EOS, Transactions, of the American Geophysical Union.* Vol. 69, no. 9.

Brinster, K.F. 1991. *Preliminary Geohydrologic Conceptual Model of the Los Medaños Region Near the Waste Isolation Pilot Plant for the Purpose of Performance Assessment.* SAND89-7147. Albuquerque, NM: Sandia National Laboratories.

Broc, R., ed. 1982. *Drilling Mud and Cement Slurry Rheology Manual.* Houston, TX: Gulf Publishing Company.

Brodsky, N.S., and T.W. Pfeifle. 1992. *Consolidation of the Waste Isolation Pilot Plant Crushed Salt/Bentonite Mixtures as a Function of Confining Pressure and Moisture Content as Compared With Constitutive Model Predictions.* SAND91-7071. Albuquerque, NM: Sandia National Laboratories.

Brookins, D.G., S.J. Lambert, and D.B. Ward. 1990. *Authigenic Clay Minerals in the Rustler Formation, WIPP Site, New Mexico.* SAND89-1405. Albuquerque, NM: Sandia National Laboratories.

Brush, L.H. 1990. *Test Plan for Laboratory and Modeling Studies of Repository and Radionuclide Chemistry for the Waste Isolation Pilot Plant.* SAND90-0266. Albuquerque, NM: Sandia National Laboratories.

Brush, L.H., and D.R. Anderson. 1989a. Appendix E: "Estimates of Radionuclide Concentrations in Brines," *Performance Assessment Methodology Demonstration: Methodology Development for Purposes of Evaluating Compliance with EPA 40 CFR 191, Subpart B, for the Waste Isolation Pilot Plant.* M.G. Marietta, S.G. Bertram-Howery, D.R. Anderson, K.F. Brinster, R.V. Guzowski, H. Iuzzolino, and R.P. Rechard (Report Authors). SAND89-2027. Albuquerque, NM: Sandia National Laboratories. E-1 through E-14.

Brush, L.H., and D.R. Anderson. 1989b. Appendix A.2: "Effects of Microbial Activity on Repository Chemistry, Radionuclide Speciation, and Solubilities in WIPP Brines," *Systems Analysis, Long-Term Radionuclide Transport, and Dose Assessments, Waste Isolation Pilot Plant (WIPP), Southeastern New Mexico; March 1989.* Eds. A.R. Lappin, R.L. Hunter, D.P. Garber, and P.B. Davies. SAND89-0462. Albuquerque, NM: Sandia National Laboratories. A-31 through A-50.

Butcher, B.M., C.F. Novak, and M. Jercinovic. 1991. *The Advantages of a Salt/Bentonite Backfill for Waste Isolation Pilot Plant Disposal Rooms.* SAND90-3074. Albuquerque, NM: Sandia National Laboratories.

Cauffman, T.L., A.M. LaVenue, and J.P. McCord. 1990. *Ground-Water Flow Modeling of the Culebra Dolomite. Volume II: Data Base.* SAND89-7068/2. Albuquerque, NM: Sandia National Laboratories.

Chapman, J.B. 1986. *Stable Isotopes in the Southeastern New Mexico Groundwater: Implications for Dating Recharge in the WIPP Area.* EEG-35. Santa Fe, NM: Environmental Evaluation Group, Environmental Improvements Division, Health and Environment Department, State of New Mexico.

Chapman, J.B. 1988. *Chemical and Radiochemical Characteristics of Groundwater in the Culebra Dolomite, Southeastern New Mexico.* EEG-39. Santa Fe, NM: Environmental Evaluation Group, Environmental Improvement Division, Health and Environment Department, State of New Mexico.

Cheeseman, R.J. 1978. "Geology and Oil/Potash Resources of the Delaware Basin, Eddy and Lea Counties, New Mexico," *Geology and Mineral Deposits of Ochoan Rocks in Delaware Basin and Adjacent Areas.* Ed. G.S. Austin. New Mexico Bureau of Mines and Mineral Resources Circular 159. Socorro, NM: New Mexico Bureau of Mines and Mineral Resources. 7-14.

COHMAP (Cooperative Holocene Mapping Project) Members. 1988. "Climatic Changes of the Last 18,000 Years: Observations and Model Simulations," *Science.* Vol. 241, no. 4869, 1043-1052.

Cole, F.W. 1975. *Introduction to Meteorology.* 2nd. ed. New York, NY: John Wiley and Sons, Inc.

Cranwell, R.M., J.E. Campbell, J.C. Helton, R.L. Iman, D.E. Longsine, N.R. Ortiz, G.E. Runkle, and M.J. Shortencarier. 1987. *Risk Methodology for Geologic Disposal of Radioactive Waste: Final Report.* NUREG/CR-2452, SAND81-2573. Albuquerque, NM: Sandia National Laboratories.

Cranwell, R.M., R.V. Guzowski, J.E. Campbell, and N.R. Ortiz. 1990. *Risk Methodology for Geologic Disposal of Radioactive Waste: Scenario Selection Procedure.* NUREG/CR-1667, SAND80-1429. Albuquerque, NM: Sandia National Laboratories.

Darley, H.C.H. 1969. "A Laboratory Investigation of Borehole Stability," *JPT, Journal of Petroleum Technology.* Vol. 21, no. 7, 883-892.

Darley, H.C.H., and G.R. Gray. 1988. *Composition and Properties of Drilling and Completion Fluids.* Houston, TX: Gulf Publishing Company. 243.

Davies, P.B. 1984. "Deep-Seated Dissolution and Subsidence in Bedded Salt Deposits." Ph.D. dissertation. Stanford, CA: Department of Applied Earth Sciences, Stanford University.

Davies, P.B. 1989. *Variable-Density Ground-Water Flow and Paleohydrology in the Waste Isolation Pilot Plant (WIPP) Region. Southeastern New Mexico.* U.S. Geological Survey Open-File Report 88-490. Albuquerque, NM: U.S. Geological Survey.

de Marsily, G. 1986. *Quantitative Hydrogeology: Groundwater Hydrology for Engineers.* Orlando, FL: Academic Press, Inc.

Dosch, R.G. 1980. *Assessment of Potential Radionuclide Transport in Site-Specific Geologic Formations.* SAND79-2468. Albuquerque, NM: Sandia National Laboratories.

Dosch, R.G. 1981. *Solubility and Sorption Characteristics of Uranium (VI) Associated with Rock Samples and Brines/Groundwaters from WIPP and NTS.* SAND80-1595. Albuquerque, NM: Sandia National Laboratories.

Dosch, R.G., and A.W. Lynch. 1978. *Interaction of Radionuclides with Geomedia Associated with the Waste Isolation Pilot Plant (WIPP) Site in New Mexico.* SAND78-0297. Albuquerque, NM: Sandia National Laboratories.

Earth Technology Corporation. 1988. *Final Report for Time Domain Electromagnetic (TDEM) Surveys at the WIPP Site.* SAND87-7144. Albuquerque, NM: Sandia National Laboratories.

Freeze, R.A., and J.A. Cherry. 1979. *Groundwater.* Englewood Cliffs, NJ: Prentice-Hall, Inc.

Gallegos, D.P., P.I. Pohl, and C.D. Updegraff. 1992. *An Investigation of the Impact of Conceptual Model Uncertainty on the Estimated Performance of a Hypothetical High-Level Nuclear Waste Repository Site in Unsaturated, Fractured Tuff.* SAND90-2882. Albuquerque, NM: Sandia National Laboratories.

Gelhar, L.W., C. Welty, and K.R. Rehfeldt. 1992. "A Critical Review of Data on Field-Scale Dispersion in Aquifers," *Water Resources Research.* Vol. 28, no. 7, 1955-1974.

Geohydrology Associates, Inc. 1979. *Water-Resources Study of the Carlsbad Potash Area, New Mexico.* Consultant Report for the U.S. BLM. Contract No. YA-S12-CT8-195. (Copy on file in the Waste Management and Transportation Library, Sandia National Laboratories, Albuquerque, NM.)

Geological Society of America, Inc. 1984. *Decade of North American Geology Geologic Time Scale.* Geological Society of America Map and Chart Series MCH050. Boulder, CO: Geological Society of America, Inc.

Gilkey, A.P. 1986a. *SPLOT — A Distance-versus-Variable Plot Program for the Output of a Finite Element Analysis.* SAND86-0882. Albuquerque, NM: Sandia National Laboratories.

Gilkey, A.P. 1986b. *TPLOT — A Time History or X-Y Plot Program for the Output of a Finite Element Analysis.* SAND86-0883. Albuquerque, NM: Sandia National Laboratories.

Gilkey, A.P. 1988. *ALGEBRA - A Program That Algebraically Manipulates the Output of a Finite Element Analysis.* SAND88-1431. Albuquerque, NM: Sandia National Laboratories.

Gilkey, A.P., and D.P. Flanagan. 1987. *DETOUR — A Deformed Mesh/Contour Plot Program.* SAND86-0914. Albuquerque, NM: Sandia National Laboratories.

Guzowski, R.V. 1990. *Preliminary Identification of Scenarios That May Affect the Escape and Transport of Radionuclides From the Waste Isolation Pilot Plant, Southeastern New Mexico.* SAND89-7149. Albuquerque, NM: Sandia National Laboratories.

Guzowski, R.V. 1991. *Evaluation of Applicability of Probability Techniques to Determining the Probability of Occurrence of Potentially Disruptive Intrusive Events at the Waste Isolation Pilot Plant.* SAND90-7100. Albuquerque, NM: Sandia National Laboratories.

Hale, W.E., and A. Clebsch, Jr. 1958. *Preliminary Appraisal of Ground-Water Conditions in Southeastern Eddy County and Southwestern Lea County, New Mexico.* Trace Elements Memorandum Report 1045. United States Department of the Interior, Geological Survey. (Copy on file in the Waste Management and Transportation Library, Sandia National Laboratories, Albuquerque, NM.)

Hale, W.E., L.S. Hughes, and E.R. Cox. 1954. *Possible Improvement of Quality of Water of the Pecos River by Diversion of Brine at Malaga Bend, Eddy County, New Mexico.* Carlsbad, NM: Pecos River Commission, New Mexico and Texas, in cooperation with United States Department of the Interior, Geological Survey, Water Resources Division.

Hansen, J., I. Fung, A. Lacis, D. Rind, S. Lebedeff, R. Ruedy, and G. Russell. 1988. "Global Climate Changes as Forecast by Goddard Institute for Space Studies Three-Dimensional Model," *Journal of Geophysical Research.* Vol. 93, no. D8, 9341-9364.

Harms, J.C., and C.R. Williamson. 1988. "Deep-Water Density Current Deposits of Delaware Mountain Group (Permian), Delaware Basin, Texas and New Mexico," *American Association of Petroleum Geologists Bulletin* . Vol. 72, no. 3, 299-317.

Haug, A., V.A. Kelley, A.M. LaVenue, and J.F. Pickens. 1987. *Modeling of Ground-Water Flow in the Culebra Dolomite at the Waste Isolation Pilot Plant (WIPP) Site: Interim Report.* SAND86-7167. Albuquerque, NM: Sandia National Laboratories.

Hays, J.D., J. Imbrie, and N.J. Shackleton. 1976. "Variations in the Earth's Orbit: Pacemaker of the Ice Ages," *Science.* Vol. 194, no. 4270, 1121-1132.

Helton, J.C. In press. "Drilling Intrusion Probabilities for Use in Performance Assessment for Radioactive Waste Disposal," *Reliability Engineering and System Safety.* (Copy on file as SAND93-7001J in Waste Management and Transportation Library, Sandia National Laboratories, Albuquerque, NM.)

Helton, J.C., J.W. Garner, R.D. McCurley, and D.K. Rudeen. 1991. *Sensitivity Analysis Techniques and Results for Performance Assessment at the Waste Isolation Pilot Plant.* SAND90-7103. Albuquerque, NM: Sandia National Laboratories.

Helton, J.C., J.W. Garner, R.P. Rechard, D.K. Rudeen, and P.N. Swift. 1992. *Preliminary Comparison with 40 CFR Part 191, Subpart B for the Waste Isolation Pilot Plant, December 1991—Volume 4: Uncertainty and Sensitivity Analysis Results.* SAND91-0893/4. Albuquerque, NM: Sandia National Laboratories.

Hills, J.M. 1984. "Sedimentation, Tectonism, and Hydrocarbon Generation in Delaware Basin, West Texas and Southeastern New Mexico," *American Association of Petroleum Geologists Bulletin.* Vol. 68, no. 3, 250-267.

Hiss, W.L. 1975. "Stratigraphy and Ground-Water Hydrology of the Capitan Aquifer, Southeastern New Mexico and West Texas." Ph.D. dissertation. Boulder, CO: University of Colorado.

Holt, R.M., and D.W. Powers. 1988. *Facies Variability and Post-Depositional Alteration Within the Rustler Formation in the Vicinity of the Waste Isolation Pilot Plant, Southeastern New Mexico.* DOE/WIPP-88-004. Carlsbad, NM. Westinghouse Electric Corporation.

Holt, R.M., and D.W. Powers. 1990. *Geologic Mapping of the Air Intake Shaft at the Waste Isolation Pilot Plant.* DOE-WIPP 90-051. Carlsbad, NM: Westinghouse Electric Corporation.

Hora, S.C., and R.L. Iman. 1989. "Expert Opinion in Risk Analysis: The NUREG-1150 Methodology." *Nuclear Science and Engineering.* Vol. 102, no. 4, 323-331.

Hora, S.C., D. von Winterfeldt, and K.M. Trauth. 1991. *Expert Judgment on Inadvertent Human Intrusion into the Waste Isolation Pilot Plant.* SAND90-3063. Albuquerque, NM: Sandia National Laboratories.

Houghton, J.T., G.J. Jenkins, and J.J. Ephraums. 1990. *Climate Change: The IPCC Scientific Assessment.* New York, NY: Cambridge University Press.

Hunter, R.L. 1985. *A Regional Water Balance for the Waste Isolation Pilot Plant (WIPP) Site and Surrounding Area.* SAND84-2233. Albuquerque, NM: Sandia National Laboratories.

Hunter, R.L., R.M. Cranwell, and M.S.Y. Chu. 1986. *Assessing Compliance with the EPA High-Level Waste Standard: An Overview.* SAND86-0121, NUREG/CR-4510. Albuquerque, NM: Sandia National Laboratories.

IAEA (International Atomic Energy Agency). 1989. *Evaluating the Reliability of Predictions Made Using Environmental Transfer Models.* Safety Series Report No. 100. Vienna: International Atomic Energy Agency.

Iman, R.L., and W.J. Conover. 1982. "A Distribution-Free Approach to Inducing Rank Correlation Among Input Variables," *Communications in Statistics: Simulation and Computation.* Vol. B11, no. 3, 311-334.

Iman, R.L. and W.J. Conover. 1983. *A Modern Approach to Statistics.* New York, NY: John Wiley & Sons, Inc.

Imbrie, J. 1985. "A Theoretical Framework for the Pleistocene Ice Ages," *Journal of the Geological Society.* Vol. 142, pt. 3, 417-432.

Imbrie, J., and J.Z. Imbrie. 1980. "Modeling the Climatic Response to Orbital Variations," *Science.* Vol. 207, no. 4334, 943-953.

Imbrie, J., J.D. Hays, D.G. Martinson, A. McIntyre, A.C. Mix, J.J. Morley, N.G. Pisias, W.L. Prell, and N.J. Shackleton. 1984. "The Orbital Theory of Pleistocene Climate: Support from a Revised Chronology of the Marine $\delta^{18}O$ Record," *Milankovitch and Climate, Proceedings of the NATO Advanced Research Workshop on Milankovitch, Palisades, NY, November 30-December 4, 1982.* Eds. A.L. Berger, J. Imbrie, J. Hays, G. Kukla, and B. Saltzman. Boston, MA: D. Reidel Publishing Co. Pt. 1, 269-305.

Jones, C.L., C.G. Bowles, and K.G. Bell. 1960. *Experimental Drill Hole Logging in Potahs Deposits of the Carlsbad District, New Mexico.* U.S. Geological Survey Open File Report 60-84. Denver, CO: U.S. Geological Survey.

Jones, T.L., V.A. Kelley, J.F. Pickens, D.T. Upton, R.L. Beauheim, and P.B. Davies. 1992. *Integration of Interpretation Results of Tracer Tests Performed in the Culebra Dolomite at the Waste Isolation Pilot Plant Site.* SAND92-1579. Albuquerque, NM: Sandia National Laboratories.

Journel, A.G., and Ch.J. Huijbregts. 1978. *Mining Geostatistics.* Orlando, FL: Academic Press, Inc.

Kaplan, S., and B.J. Garrick. 1981. "On the Quantitative Definition of Risk," *Risk Analysis.* Vol. 1, no. 1, 11-27.

Kelley, V.A., and J.F. Pickens. 1986. *Interpretation of the Convergent-Flow Tracer Tests Conducted in the Culebra Dolomite at the H-3 and H-4 Hydropads at the Waste Isolation Pilot Plant (WIPP) Site.* SAND86-7161. Albuquerque, NM: Sandia National Laboratories.

Kelley, V.A., and G.J. Saulnier, Jr. 1990. *Core Analyses for Selected Samples from the Culebra Dolomite at the Waste Isolation Pilot Plant.* SAND90-7011. Albuquerque, NM: Sandia National Laboratories.

Kunkler, J.L. 1980. *Evaluation of the Malaga Bend Salinity Alleviation Project, Eddy County, New Mexico.* U.S. Geological Survey Open-File Report 80-1111. Albuquerque, NM: U.S. Geological Survey/Water Resources Division and the Pecos River Commission.

Lambert, S.J. 1983. *Dissolution of Evaporites in and Around the Delaware Basin, Southeastern New Mexico and West Texas.* SAND82-0461. Albuquerque, NM: Sandia National Laboratories.

Lambert S.J. 1987. *Feasability Study: Applicability of Geochronologic Methods Involving Radiocarbon and Other Nuclides to the Groundwater Hydrology of the Rustler Formation, Southeastern New Mexico.* SAND86-1054. Albuquerque, NM: Sandia National Laboratories.

Lambert, S.J. 1991. Chapter 5: "Isotopic Constraints on the Rustler and Dewey Lake Groundwater Systems," *Hydrogeochemical Studies of the Rustler Formation and Related Rocks in the Waste Isolation Pilot Plant Area, Southeastern New Mexico.* Eds. M.D. Siegel, S.J. Lambert, and K.L. Robinson. SAND88-0196. Albuquerque, NM: Sandia National Laboratories. 5-1 through 5-79.

Lambert, S.J., and J.A. Carter. 1984. *Uranium-Isotope Disequilibrium in Brine Reservoirs of the Castile Formation, Northern Delaware Basin, Southeastern New Mexico, I: Principles and Methods.* SAND83-0144. Albuquerque, NM: Sandia National Laboratories.

Lambert, S.J., and J.A. Carter. 1987. *Uranium-Isotope Systematics in Groundwaters of the Rustler Formation, Northern Delaware Basin, Southeastern New Mexico. I. Principles and Preliminary Results.* SAND87-0388. Albuquerque, NM: Sandia National Laboratories.

Lambert, S.J., and D.M. Harvey. 1987. *Stable-Isotope Geochemistry of Groundwaters in the Delaware Basin of Southeastern New Mexico.* SAND87-0138. Albuquerque, NM: Sandia National Laboratories.

Lambert, S.J., and J.W. Mercer. 1978. *Hydrologic Investigations of the Los Medaños Area, Southeastern New Mexico, 1977.* SAND77-1401. Albuquerque, NM: Sandia National Laboratories.

Lappin, A.R. 1988. *Summary of Site-Characterization Studies Conducted from 1983 through 1987 at the Waste Isolation Pilot Plant (WIPP) Site, Southeastern New Mexico.* SAND88-0157. Albuquerque, NM: Sandia National Laboratories.

Lappin, A.R., R.L. Hunter, D.P. Garber, P.B. Davies, R.L. Beauheim, D.J. Borns, L.H. Brush, B.M. Butcher, T. Cauffman, M.S.Y. Chu, L.S. Gomez, R.V. Guzowski, H.J. Iuzzolino, V. Kelley, S.J. Lambert, M.G. Marietta, J.W. Mercer, E.J. Nowak, J. Pickens, R.P. Rechard, M. Reeves, K.L. Robinson, and M.D. Siegel. 1989. *Systems Analysis, Long-Term Radionuclide Transport, and Dose Assessments, Waste Isolation Pilot Plant (WIPP), Southeastern New Mexico; March 1989.* SAND89-0462. Albuquerque, NM: Sandia National Laboratories.

LaVenue, A.M., and B.S. RamaRao. 1992. A *Modeling Approach to Address Spatial Variability within the Culebra Dolomite Transmissivity Field.* SAND92-7306. Albuquerque, NM: Sandia National Laboratories.

LaVenue, A.M., A. Haug, and V.A. Kelley. 1988. *Numerical Simulation of Groundwater Flow in the Culebra Dolomite at the Waste Isolation Pilot Plant (WIPP) Site; Second Interim Report.* SAND88-7002. Albuquerque, NM: Sandia National Laboratories.

LaVenue, A.M., T.L. Cauffman, and J.F. Pickens. 1990. *Ground-Water Flow Modeling of the Culebra Dolomite: Volume I - Model Calibration.* SAND89-7068/1. Albuquerque, NM: Sandia National Laboratories.

Leigh, C.D., B.M. Thompson, J.E. Campbell, D.E. Longsine, R.A. Kennedy, and B.A. Napier. (In review). *User's Guide for GENII-S: A Code for Statistical and Deterministic Simulations of Radiation Doses to Humans from Radionuclides in the Environment.* SAND91-0561. Albuquerque, NM: Sandia National Laboratories. (Copy on file in the Waste Management and Transportation Library, Sandia National Laboratories, Albuquerque, NM.)

Lowenstein, T.K. 1988. "Origin of Depositional Cycles in a Permian "Saline Giant": The Salado (McNutt Zone) Evaporites of New Mexico and Texas," *Geological Society of America Bulletin.* Vol. 100, no. 4, 592-608.

Lynch, A.W., and R.G. Dosch. 1980. *Sorption Coefficients for Radionuclides on Samples from the Water-Bearing Magenta and Culebra Members of the Rustler Formation.* SAND80-1064. Albuquerque, NM: Sandia National Laboratories.

Mantoglou, A., and J.L. Wilson. 1982. "Turning Bands Method for Simulation of Random Fields Using Line Generation by a Spectral Method," *Water Resources Research.* Vol. 18, no. 5, 1379-1394.

Marietta, M.G., S.G. Bertram-Howery, D.R. Anderson, K.F. Brinster, R.V. Guzowski, H. Iuzzolino, and R.P. Rechard. 1989. *Performance Assessment Methodology Demonstration: Methodology Development for Evaluating Compliance With EPA 40 CFR Part 191, Subpart B, for the Waste Isolation Pilot Plant.* SAND89-2027. Albuquerque, NM: Sandia National Laboratories.

Matheron, G. 1971. *The Theory of Regionalized Variables and its Applications.* Fontainebleau, France: École National Supériéure des Mines.

Matheron, G. 1973. "The Intrinsic Random Functions and Their Applications," *Advances in Applied Probability.* Vol. 5, no. 3, 439-468.

McGrath, E.J., and D.C. Irving. 1975a. *Techniques for Efficient Monte Carlo Simulation. Volume II. Random Number Generation for Selected Probability Distributions.* ORNL-RSIC-38 (Vol. 2). Oak Ridge, TN: Oak Ridge National Laboratory.

McGrath, E.J., and D.C. Irving. 1975b. *Techniques for Efficient Monte Carlo Simulation. Volume III. Variance Reduction.* ORNL-RSIC-38 (Vol. 3). Oak Ridge, TN: Oak Ridge National Laboratory.

McGrath, E.J., S.L. Basin, R.W. Burton, D.C. Irving, and S.C. Jaquette. 1975. *Techniques for Efficient Monte Carlo Simulation. Volume I. Selecting Probability Distributions.* ORNL-RSIC-38. (Vol. 1). Oak Ridge, TN: Oak Ridge National Laboratory.

McKay, M.D., R.J. Beckman, and W.J. Conover. 1979. "A Comparison of Three Methods for Selecting Values of Input Variables in the Analysis of Output from a Computer Code," *Technometrics.* (Vol. 21). no. 2, 239-245.

Mejía, J.M., and I. Rodríguez-Iturbe. 1974. "On the Synthesis of Random Fields From the Spectrum: An Application to the Generation of Hydrologic Spatial Processes," *Water Resources Research.* Volume 10, no. 4, 705-711.

Mercer, J.W. 1983. *Geohydrology of the Proposed Waste Isolation Pilot Plant Site, Los Medaños Area, Southeastern New Mexico.* U.S. Geological Survey Water-Resources Investigations Report 83-4016. Albuquerque, NM: U.S. Geological Survey.

Mercer, J.W., and B.R. Orr. 1977. *Review and Analysis of Hydrogeologic Conditions Near the Site of a Potential Nuclear-Waste Repository, Eddy and Lea Counties, New Mexico.* U.S. Geological Survey Open-File Report 77-123. Albuquerque, NM: U.S. Geological Survey.

Mercer, J.W., and B.R. Orr. 1979. *Interim Data Report on Geohydrology of the Proposed Waste Isolation Pilot Plant Site, Southeast New Mexico.* U.S. Geological Survey Water-Resources Investigations 79-98. Albuquerque, NM: U.S. Geological Survey.

Mercer, J.W., R.L. Beauheim, R.P. Snyder, and G.M. Fairer. 1987. *Basic Data Report for Drilling and Hydrologic Testing of Drillhole DOE-2 at the Waste Isolation Pilot Plant (WIPP) Site.* SAND86-0611. Albuquerque, NM: Sandia National Laboratories.

Milankovitch, M. 1941. *Canon of Insolation and the Ice-age Problem.* Koniglich Serbische Akademie, Beograd. (English translation by the Israel Program for Scientific Translations; published by the U.S. Department of Commerce and the National Science Foundation, Washington, D.C.).

Mills, P.G. 1984. *Blowout Prevention Theory and Applications.* Boston, MA: International Human Resources Development Corporation. 27-28.

Mitchell, J.F.B. 1989. "The 'Greenhouse Effect' and Climate Change," *Reviews of Geophysics.* Vol. 27, no. 1, 115-139.

Munson, D.E., A.F. Fossum, and P.E. Senseny. 1989a. *Advances in Resolution of Discrepancies Between Predicted and Measured In Situ WIPP Room Closures.* SAND88-2948. Albuquerque, NM: Sandia National Laboratories.

Munson, D.E., A.F. Fossum, and P.E. Senseny. 1989b. *Approach to First Principles Model Prediction of Measured WIPP In Situ Room Closure in Salt.* SAND88-2535. Albuquerque, NM: Sandia National Laboratories.

NEA (Nuclear Energy Agency). 1992. *Safety Assessment of Radioactive Waste Repositories: Systematic Approaches to Scenario Development.* Paris: Nuclear Energy Agency, Organisation for Economic Co-Operation and Development.

Neuman, S.P. 1990. "Universal Scaling of Hydraulic Conductivities and Dispersivities in Geologic Media," *Water Resources Research.* Vol. 26, no. 8, 1749-1758.

Nowak, E.J. 1980. *Radionuclide Sorption and Migration Studies of Getters for Backfill Barriers.* SAND79-1110. Albuquerque, NM: Sandia National Laboratories.

Nowak, E.J., and J.C. Stormont. 1987. *Scoping Model Calculations of the Reconsolidation of Crushed Salt in WIPP Shafts.* SAND87-0879. Albuquerque, NM: Sandia National Laboratories.

Nowak, E.J., D.F. McTigue, and R. Beraun. 1988. *Brine Inflow to WIPP Disposal Rooms: Data, Modeling, and Assessment.* SAND88-0112. Albuquerque, NM: Sandia National Laboratories.

Nowak, E.J., J.R. Tillerson, and T.M. Torres. 1990. *Initial Reference Seal System Design: Waste Isolation Pilot Plant.* SAND90-0355. Albuquerque, NM: Sandia National Laboratories.

NuPac (Nuclear Packaging, Inc.). 1989. *Safety Analysis Report for the TRUPACT-II Shipping Package.* NuPac TRUPACT-II SAR Rev. 4. Washington, DC: Nuclear Packaging, Inc.

Oldroyd, J.G. 1958. "Non-Newtonian Effects in Steady Motion of Some Idealized Elastico-Viscous Liquids," *Proceedings of the Royal Society of London.* Series A, Vol. 245, no. 1241, 278-297.

Pace, B.O. 1990. Appendix A, "Letter 1b: Changes to Bar graphs," *Data Used in Preliminary Performance Assessment of the Waste Isolation Pilot Plant (1990).* R.P. Rechard, H. Iuzzolino, and J.S. Sandha (Report Authors). SAND89-2408. Albuquerque, NM: Sandia National Laboratories. A-165 through A-170.

Parry, G.W. 1988. "On the Meaning of Probability in Probabilistic Safety Assessment," *Reliability Engineering and System Safety.* Vol. 23, no. 4, 309-314.

Paté-Cornell, M.E. 1986. "Probability and Uncertainty in Nuclear Safety Decisions," *Nuclear Engineering and Design.* Vol. 93, no. 3, 319-327.

Peterson, E.W., P.L. Lagus, and K. Lie. 1987. *Fluid Flow Measurements of Test Series A and B for the Small Scale Seal Performance Tests.* SAND87-7041. Albuquerque, NM: Sandia National Laboratories.

Pfeifle, T.W., and N. S. Brodsky. 1991. *Swelling Pressure, Water Uptake, and Permeability of 70/30 Crushed Salt Bentonite.* SAND91-7070. Albuquerque, NM: Sandia National Laboratories.

Popielak, R.S., R.L. Beauheim, S.R. Black, W.E. Coons, C.T. Ellingson, and R.L. Olsen. 1983. *Brine Reservoirs in the Castile Fm., Waste Isolation Pilot Plant (WIPP) Project, Southeastern New Mexico.* TME-3153. Carlsbad, NM: U.S. Department of Energy.

Powers, D.W., and R.M. Holt. 1990. "Sedimentology of the Rustler Formation near the Waste Isolation Pilot Plant (WIPP) Site," *Geological and Hydrological Studies of Evaporites in the Northern Delaware Basin for the Waste Isolation Pilot Plant (WIPP), New Mexico, Geological Society of America 1990 Annual Meeting, Dallas, TX, October 29-November 1, 1990.* Geological Society of America 1990 Annual Meeting, Field Trip #14 Guidebook. Dallas, TX: Dallas Geological Society. 79-106.

Powers, D.W., S.J. Lambert, S-E. Shaffer, L.R. Hill, and W.D. Weart, eds. 1978a. *Geological Characterization Report, Waste Isolation Pilot Plant (WIPP) Site, Southeastern New Mexico.* SAND78-1596. Albuquerque, NM: Sandia National Laboratories. Vol. I.

Powers, D.W., S.J. Lambert, S-E. Shaffer, L.R. Hill, and W.D. Weart, eds. 1978b. *Geological Characterization Report, Waste Isolation Pilot Plant (WIPP) Site, Southeastern New Mexico.* SAND78-1596. Albuquerque, NM: Sandia National Laboratories. Vol. II.

Public Law 102-579. 1992. *Waste Isolation Pilot Plant Land Withdrawal Act.*

RamaRao, B.S., and M. Reeves. 1990. *Theory and Verification for the GRASP II Code for Adjoint-Sensitivity Analysis of Steady-State and Transient Ground-Water Flow.* SAND89-7143. Albuquerque, NM: Sandia National Laboratories.

Rechard, R.P. 1989. *Review and Discussion of Code Linkage and Data Flow in Nuclear Waste Compliance Assessments.* SAND87-2833. Albuquerque, NM: Sandia National Laboratories.

Rechard, R.P., ed. 1992. *User's Reference Manual for CAMCON: Compliance Assessment Methodology Controller Version 3.0.* SAND90-1983. Albuquerque, NM: Sandia National Laboratories.

Rechard, R.P., H.J. Iuzzolino, J.S. Rath, A.P. Gilkey, R.D. McCurley, and D.K. Rudeen. 1989. *User's Manual for CAMCON: Compliance Assessment Methodology Controller.* SAND88-1496. Albuquerque, NM: Sandia National Laboratories.

Rechard, R.P., H. Iuzzolino, and J.S. Sandha. 1990a. *Data Used in Preliminary Performance Assessment of the Waste Isolation Pilot Plant (1990).* SAND89-2408. Albuquerque, NM: Sandia National Laboratories.

Rechard, R.P., W. Beyeler, R.D., McCurley, D.K. Rudeen, J.E. Bean, and J.D. Schreiber. 1990b. *Parameter Sensitivity Studies of Selected Components of the Waste Isolation Pilot Plant Repository/Shaft System.* SAND89-2030. Albuquerque, NM: Sandia National Laboratories.

Robinson, T.W., and W.B. Lang. 1938. *Geology and Ground-Water Conditions of the Pecos River Valley in the Vicinity of Laguna Grande de la Sal, New Mexico, With Special Reference to the Salt Content of the River Water.* New Mexico State Engineer 12th-13th Biennial Reports 1934-1938. Santa Fe, NM: State Engineer. 77-100.

Saulnier, G.J., Jr. 1987. *Analysis of Pumping Tests of the Culebra Dolomite Conducted at the H-11 Hydropad at the Waste Isolation Pilot Plant (WIPP) Site.* SAND87-7124. Albuquerque, NM: Sandia National Laboratories.

Saulnier, G.J., Jr., and J.D. Avis. 1988. *Interpretation of Hydraulic Tests Conducted in the Waste-Handling Shaft at the Waste Isolation Pilot Plant (WIPP) Site.* SAND88-7001. Albuquerque, NM: Sandia National Laboratories.

Savins, J.G., and G.C. Wallick. 1966. "Viscosity Profiles, Discharge Rates, Pressures, and Torques for a Rheologically Complex Fluid in a Helical Flow," *A.I.Ch.E. Journal.* Vol. 12, no. 2, 357-363.

Scheidegger, A.E. 1960. *The Physics of Flow Through Porous Media.* Rev. ed. Toronto, Canada: University of Toronto Press.

Serne, R.J., D. Rai, M.J. Mason, and M.A. Molecke. 1977. *Batch Kd Measurements of Nuclides to Estimate Migration Potential at the Proposed Waste Isolation Pilot Plant in New Mexico.* PNL-2448. Richland, WA: Battelle Pacific Northwest Laboratories.

Sewards, T. 1991. *Characterization of Fracture Surfaces in Dolomite Rock, Culebra Dolomite Member, Rustler Formation.* SAND90-7019. Albuquerque, NM: Sandia National Laboratories.

Sewards, T., M.L. Williams, and K. Keil. 1991a. *Mineralogy of the Culebra Dolomite Member of the Rustler Formation.* SAND90-7008. Albuquerque, NM: Sandia National Laboratories.

Sewards, T., R. Glenn, and K. Keil. 1991b. *Mineralogy of the Rustler Formation in the WIPP-19 Core.* SAND87-7036. Albuquerque, NM: Sandia National Laboratories.

Sewards, T., A. Brearley, R. Glenn, I.D.R. MacKinnon, and M.D. Siegel. 1992. *Nature and Genesis of Clay Minerals of the Rustler Formation in the Vicinity of the Waste Isolation Pilot Plant in Southeastern New Mexico.* SAND90-2569. Albuquerque, NM: Sandia National Laboratories.

Shinozuka, M., and C-M. Jan. 1972. "Digital Simulation of Random Processes and Its Applications," *Journal of Sound and Vibration.* Vol. 25, no. 1, 111-128.

Short, J.A. 1982. *Drilling and Casing Operations.* Tulsa, OK: PennWell Books. 183-184.

Siegel, M.D. 1990. Appendix A, "Memo 3a: Representation of Radionuclide Retardation in the Culebra Dolomite in Performance Assessment Calculations," *Data Used in Preliminary Performance Assessment of the Waste Isolation Pilot Plant* (1990). R.P. Rechard, H. Iuzzolino, and J.S. Sandha (Report Authors). SAND89-2408. Albuquerque, NM: Sandia National Laboratories. A-43 through A-62.

Siegel, M.D., J.O. Leckie, S.W. Park, S.L. Phillips, and T. Sewards. 1990. *Studies of Radionuclide Sorption by Clays in the Culebra Dolomite at the Waste Isolation Pilot Plant Site, Southeastern New Mexico.* SAND89-2387. Albuquerque, NM: Sandia National Laboratories.

Siegel, M.D., and S.J. Lambert. 1991. Chapter 1: "Summary of Hydrogeochemical Constraints on Groundwater Flow and Evolution in the Rustler Formation," *Hydrogeochemical Studies of the Rustler Formation and Related Rocks in the Waste Isolation Pilot Plant Area, Southeastern New Mexico.* Eds. M.D. Siegel, S.J. Lambert, and K.L. Robinson. SAND88-0196. Albuquerque, NM: Sandia National Laboratories. 1-1 through 1-109.

Siegel, M.D., K.L. Robinson, and J. Myers. 1991. Chapter 2: "Solute Relationships in Groundwaters from the Culebra Dolomite and Related Rocks in the Waste Isolation Pilot Plant Area, Southeastern New Mexico," *Hydrogeochemical Studies of the Rustler Formation and Related Rocks in the Waste Isolation Pilot Plant Area, Southeastern New Mexico.* Eds. M. D. Siegel, S.J. Lambert, and K.L. Robinson. SAND88-0196. Albuquerque, NM: Sandia National Laboratories.2-1 through 2-164.

Skokan, C., J. Starrett, and H.T. Anderson. 1988. *Final Report: Feasibility Study of Seismic Tomography to Monitor Underground Pillar Integrity at the WIPP Site.* SAND88-7096. Albuquerque, NM: Sandia National Laboratories.

Smith, L., and R.A. Freeze. 1979. "Stochastic Analysis of Steady State Groundwater Flow in a Bounded Domain, 2. Two-Dimensional Simulations," *Water Resources Research.* Vol. 15, no. 6, 1543-1559.

Smith, L., and F.W. Schwartz. 1981. "Mass Transport, 2. Analysis of Uncertainty in Prediction," *Water Resources Research.* Vol. 17, no. 2, 351-369.

Snyder, R.P. 1985. *Dissolution of Halite and Gypsum, and Hydration of Anydrite to Gypsum, Rustler Formation, in the Vicinity of the Waste Isolation Pilot Plant, Southeastern New Mexico.* Open-File Report 85-229. Denver, CO: U.S. Geological Survey.

Stone, C.M., R.D. Krieg, and Z.E. Beisinger. 1985. *SANCHO: A Finite Element Computer Program for the Quasistatic, Large Deformation, Inelastic Response of Two-Dimensional Solids.* SAND84-2618. Albuquerque, NM: Sandia National Laboratories.

Stormont, J.C. 1988. *Preliminary Seal Design Evaluation for the Waste Isolation Pilot Plant.* SAND87-3083. Albuquerque, NM: Sandia National Laboratories.

Stormont, J.C., E.W. Peterson, and P.L. Lagus. 1987. *Summary of and Observations About WIPP Facility Horizon Flow Measurements Through 1986.* SAND87-0176. Albuquerque, NM: Sandia National Laboratories.

Swift, P.N. 1991. "Appendix A: Climate and recharge variability parameters for the 1991 WIPP PA calculations," *Preliminary Comparison with 40 CFR Part 191, Subpart B for the Waste Isolation Pilot Plant, December 1991 — Volume 3: Reference Data.* WIPP Performance Assessment Division (Report Author). SAND91-0893/3. Albuquerque, NM: Sandia National Laboratories. A-107 through A-122.

Swift, P.N. 1992. *Long-Term Climate Variability at the Waste Isolation Pilot Plant, Southeastern New Mexico, USA.* SAND91-7055. Albuquerque, NM: Sandia National Laboratories.

Taylor, L.M., D.P. Flanagan, and W.C. Mills-Curran. 1987. The GENESIS Finite Element Mesh File Format. SAND86-0910. Albuquerque, NM: Sandia National Laboratories.

Tien, P-L., F.B. Nimick, A.B. Muller, P.A. Davis, R.V. Guzowski, L.E. Duda, and R.L. Hunter. 1983. *Repository Site Data and Information in Bedded Salt: Palo Duro Basin, Texas.* SAND82-2223, NUREG/CR-3129. Albuquerque, NM: Sandia National Laboratories.

Tierney, M.S. 1990. *Constructing Probability Distributions of Uncertain Variables in Models of the Performance of the Waste Isolation Pilot Plant: The 1990 Performance Simulations.* SAND90-2510. Albuquerque, NM: Sandia National Laboratories.

Trauth, K.M., S.C. Hora, R.P. Rechard, and D.R. Anderson. 1992. *The Use of Expert Judgment to Quantify Uncertainty in Solubility and Sorption Parameters for Waste Isolation Pilot Plant Performance Assessment.* SAND92-0479. Albuquerque, NM: Sandia National Laboratories.

Tyler, L.D., R.V. Matalucci, M.A. Molecke, D.E. Munson, E.J. Nowak, and J.C. Stormont. 1988. *Summary Report for the WIPP Technology Development Program for Isolation of Radioactive Waste.* SAND88-0844. Albuquerque, NM: Sandia National Laboratories.

U.S. DOE (Department of Energy). 1980. *Final Environmental Impact Statement: Waste Isolation Pilot Plant.* DOE/EIS-0026. Washington, DC: U.S. Department of Energy. Vols. 1-2.

U.S. DOE (Department of Energy). 1990a. *WIPP Test Phase Plan: Performance Assessment.* DOE/WIPP 89-011, Rev. 0. Carlsbad, NM: U.S. Department of Energy, Waste Isolation Pilot Plant.

U.S. DOE (Department of Energy). 1990b. *Recommended Initial Waste Forms for the WIPP Experimental Test Program, May 1990, Engineered Alternatives Task Force.* DOE/WIPP 90-009. Carlsbad, NM: Westinghouse Electric Corporation.

U.S. DOE (Department of Energy). 1991a. *Waste Acceptance Criteria for the Waste Isolation Pilot Plant.* WIPP-DOE-069, Rev. 4.0. Carlsbad, NM: Westinghouse Electric Corporation.

U.S. DOE (Department of Energy). 1991b. *Integrated Data Base for 1991: U.S. Spent Fuel and Radioactive Waste Inventories, Projections, and Characteristics.* DOE/RW-0006, Rev. 7. Oak Ridge, TN: Oak Ridge National Laboratory.

U.S. DOE (Department of Energy). 1991c. *Draft Report: Evaluation of the Effectiveness and Feasibility of the Waste Isolation Pilot Plant Engineered Alternatives: Final Report of the Engineered Alternatives Task Force.* DOE/WIPP 91-007, Revision 0. Carlsbad, NM: Westinghouse Electric Corporation.

U.S. DOE (Department of Energy). 1992. *WIPP Test Phase Activities in Support of Critical Performance Assessment Information Needs (40 CFR 191, Subpart B).* Attachment I. Washington, DC: U.S. Department of Energy.

U.S. DOE (Department of Energy) and State of New Mexico. 1981, as modified. "Agreement for Consultation and Cooperation" on WIPP by the State of New Mexico and U.S. Department of Energy, modified 11/30/84, 8/4/87, and 4/18/88.

U.S. EPA (Environmental Protection Agency). 1985. "40 CFR Part 191: Environmental Standards for the Management and Disposal of Spent Nuclear Fuel, High-Level and Transuranic Radioactive Wastes Final Rule," *Federal Register.* Vol. 50, no. 182, 38066-38089.

U.S. EPA (Environmental Protection Agency). 1986. "40 CFR Part 268 Land Disposal Restrictions," as amended and published in the most recent *Code of Federal Regulations.* Washington, DC: Office of the Federal Register, National Archives and Records Administration.

University of New Mexico. 1989. *New Mexico Statistical Abstract 1989.* Albuquerque, NM: Bureau of Business and Economic Research, University of New Mexico.

Vesely, W.E., and D.M. Rasmuson. 1984. "Uncertainties in Nuclear Probabilistic Risk Analyses," *Risk Analysis.* Vol. 4, no. 4, 313-322.

Vine, J.D. 1963. *Surface Geology of the Nash Draw Quadrangle, Eddy County, New Mexico.* U.S. Geological Survey Bulletin 1141-B. Washington, DC: U.S. Government Printing Office.

Walker, R.E. 1976. "Hydraulic Limits are Set by Flow Restrictions," *Oil and Gas Journal.* Vol. 74, no. 40, 86-90.

Walker, R.E., and W.E. Holman. 1971. "Computer Program Predicting Drilling-Fluid Performance," *Oil and Gas Journal.* Vol. 69, no. 13, 80-90.

Ward, R.F., C.G. St. C. Kendall, and P.M. Harris. 1986. "Upper Permian (Guadalupian) Facies and Their Association with Hydrocarbons - Permian Basin, West Texas and New Mexico," *American Association of Petroleum Geologists Bulletin.* Vol. 70, no. 3, 239-262.

Wehr, R.M., J.A. Richards, Jr., and T.W. Adair III. 1984. *Physics of the Atom.* 4th ed. Reading, MA. Addison-Wesley Publishing Company.

Whittaker, A., ed. 1985. *Theory and Application of Drilling Fluid Hydraulics.* Boston, MA: International Human Resources Development Corporation.

Williamson, C.R. 1978. "Depositional Processes, Diagenesis and Reservoir Properties of Permian Deep-Sea Sandstone Bell Canyon Formation." Ph.D. dissertation. Austin, TX: University of Texas.

WIPP PA (Performance Assessment) Division. 1991a. *Preliminary Comparison with 40 CFR Part 191, Subpart B for the Waste Isolation Pilot Plant, December 1991 — Volume 1: Methodology and Results.* SAND91-0893/1. Albuquerque, NM: Sandia National Laboratories.

WIPP PA (Performance Assessment) Division. 1991b. *Preliminary Comparison with 40 CFR Part 191, Subpart B for the Waste Isolation Pilot Plant, December 1991— Volume 2: Probability and Consequence Modeling.* SAND91-0893/2. Albuquerque, NM: Sandia National Laboratories.

WIPP Performance Assessment Division (WIPP PA Division). 1991c. *Preliminary Comparison with 40 CFR Part 191, Subpart B for the Waste Isolation Pilot Plant, December 1991 — Volume 3: Reference Data.* SAND91-0893/3. Albuquerque, NM: Sandia National Laboratories.

Zimmerman, A., and J.L. Wilson. 1990. *Description of and User's Manual for TUBA: A Computer Code for Generating Two-Dimensional Random Fields via the Turning Bands Method.* Albuquerque, NM: Gram, Inc.

APPENDIX A:
BRAGFLO AND PANEL

APPENDIX A: BRAGFLO AND PANEL

A.1 Background

The WIPP PA Department has developed a computational model called BRAGFLO (BRine And Gas FLOw) to simulate two-phase flow through porous, heterogeneous reservoirs. BRAGFLO numerically solves the coupled nonlinear partial differential equations (PDEs) describing the mass conservation of the gas and brine components distributed between the gas and liquid phases. Finite difference methods are used to develop analogs of the mass conservation PDEs in two spatial dimensions. These analogs are integrated over time using a modified Newton-Raphson method and variable time spacing.

BRAGFLO output is used to provide input for an equilibrium-mixing cell mathematical model called PANEL to evaluate radionuclide concentrations resulting from the mixing of brine with waste. PANEL has no geometry; it can be thought of as a point. The brine flow up the borehole that is calculated by BRAGFLO is input to PANEL so that appropriate amounts of radionuclides determined by their respective solubilities can be added to the brine flow.

A.1.1 BRAGFLO Features and Limitations

BRAGFLO is a modeling tool that can accommodate conceptual model changes and is therefore well suited to test various alternative conceptual models. This flexibility results, in part, from the highly structured and modular coding style used. BRAGFLO is also designed to be robust and numerically stable when simulating multiphase flow over a wide range of conditions and input property values.

Current limitations of BRAGFLO include:

- Only isothermal two-phase flow is modeled.
- Only two components or chemical species are modeled, and only one of the components can be distributed between both phases, such as a gas component existing in the gas phase and a water or oil phase as dissolved gas. In the case of the WIPP performance assessment, the waste-generated gas exists in both the gas phase and the brine phase, but the brine exists only in the brine phase (the brine has zero vapor pressure).
- The porous medium within each numerical grid block is treated as a single continuum; discrete fracturing or dual porosity is not considered.
- Grid block connectivity is not arbitrary and is fixed by spatial constraints. The solution domain cannot be modeled by mixed dimensionality.

- If two phases or components exist anywhere in the repository, both component mass balances must be solved everywhere in the repository even though isolated areas may be governed solely by single-phase flow.

- Non-Darcy flow, where flow is proportional to a potential gradient (for example, molecular diffusion) is not modeled.

- Fluids are assumed to exhibit Newtonian behavior (fluid viscosity does not vary with rate or time of shear).

A.1.2 Performance Assessment Role of BRAGFLO and PANEL

The WIPP PA Department is using BRAGFLO to study the effects of gas on the flow of brine through the repository and up an intrusion borehole. Specifically, BRAGFLO models the effects of the interaction of the following phenomena:

- gas generation from corrosion and microbiological degradation of the waste,

- brine movement from the surrounding rock through the waste over time,

- possible saturation of the waste by mixing with brine from an underlying pressurized reservoir that reaches the waste through a borehole created by an exploratory drill bit, and

- creep closure of the surrounding host rock.

BRAGFLO uses wells to model gas generation from corrosion and microbiological degradation of the waste, the brine flow from a breached underlying pressurized brine pocket, and brine influx from the surrounding host rock. In BRAGFLO, wells may be accommodated by using simple well models or by directly including well geometry and properties in the numerical mesh. This process is described in detail in the 1991 performance assessment documentation (see Section 5.2.2.5 of WIPP PA Division, 1991).

PANEL uses the results of BRAGFLO to predict mixing of radionuclides with brine (see Section A.3).

Creep closure of the host rock surrounding the repository will result in pressurization or rock deformation, changing material porosities and permeabilities. Presently, BRAGFLO is capable of using as input varying room porosity, which changes with closure as predicted by SANCHO (Appendix B). Porosities and absolute permeabilities of all other materials in the modeled waste room are currently treated as imprecisely known constants.

A.2 Flow (BRAGFLO)

A.2.1 Fundamental Equations

The BRAGFLO flow model simultaneously solves five equations:

- a partial differential equation that describes the mass conservation of gas in the repository and surrounding formation,
- a partial differential equation that describes the mass conservation of the brine in the repository and surrounding formation,
- a saturation constraint equation,
- a mass fraction constraint equation on the components making up the brine phase, and
- a capillary pressure constraint equation.

The above equations, along with appropriate boundary and initial conditions and material property relationships, form the basis of the model's fundamental equations. These equations are described in detail in Volume 3 of this report (Section 1.4.1) and the 1991 performance assessment documentation (see Section 5.2 of WIPP PA Division, 1991).

A.2.2 General Conceptualization

BRAGFLO can simulate the simultaneous flow of two immiscible phases through a porous anisotropic reservoir. The reservoir may consist of many materials with widely differing characteristics. Reservoir properties may also vary spatially within a particular material type.

A description of multiphase porous media flow is necessary to understand the assumptions involved in modeling multiphase flow through porous media. Details of the equations of motion for multiphase flow describing assumptions, derivations, and implementation are wide-spread throughout the petroleum literature (Bear et al., 1968; Bear, 1975, 1979; Dake, 1978; Crichlow, 1977; Collins, 1961; Aziz and Settari, 1979; Peaceman, 1977; Crookston et al., 1979; Coats, 1980; Vaughn, 1986; Rubin and Vinsome, 1979; Scheidegger, 1960). The nomenclature, assumptions, and conceptualization used here are typical of those found in much of the multiphase reservoir modeling literature referenced above.

BRAGFLO is based on a description of porous media presented by Bear (1975), Bear et al. (1968), and Bear and Bachmat (1967). The porous media is characterized as a portion of space occupied by heterogeneous matter made up of a solid phase and at least one fluid phase. The space that is occupied by the fluid phases is called the

pore or void space. Some of the pores are interconnected (effective porosity) and others are not. This void space forms a tortuous network of randomly sized and located channels. The porous medium forms a continuum with the solid matrix present in each representative volume.

The conceptualization of fluid flow through such a porous media is consistent with assumptions and descriptions presented in Bear (1975). The fluids are assumed to be Newtonian and may be compressible. The flow in the void space is laminar and confined to well-defined channels with fluid particles moving parallel to the channel walls. The forces acting on the fluid particles result only from pressure, gravity, capillary action, and shear. Flow in the network of channels contained in a given volume gives rise to average gradients that are independent of the geometry of individual channels.

BRAGFLO simulates multiphase flow through porous media. Two types of multiphase flow are possible, miscible and immiscible. BRAGFLO considers immiscible displacement only. In this case, both fluids flow simultaneously through the porous network. The two fluid phases are separated by an interface whose curvature and surface tension give rise to a capillary pressure difference across the interface (Brooks and Corey, 1964; Corey, 1986; Peaceman, 1977; Dake, 1978; Crichlow, 1977; Collins, 1961). The interface is assumed to be abrupt and any transitions from one phase to another occur over a distance of negligible length compared to the channel diameter (Bear, 1975).

The concept of saturation is introduced to describe the occupation of void space by more than one fluid. Saturation is defined as the volume fraction of void space occupied by a particular fluid. Interfacial tension exists where the two immiscible fluids contact each other. The shape of the resulting meniscus defines the wettability of the system (Brooks and Corey, 1964; Bear, 1975). For example, the convex side of the meniscus faces toward the wetting phase, while the concave side faces toward the non-wetting phase. Interfacial tension and wettability may depend on the direction the interface is moving. This phenomenon is called hysteresis. Hysteresis is a secondary effect and is not currently modeled (Brooks and Corey, 1964).

Three saturation regions are differentiated in the two-phase system, brine and gas, for example. Assuming a brine-wet reservoir, at low brine saturations, brine forms in isolated rings or exists as a thin film. As brine saturation increases, a condition is reached where the brine forms a continuous phase that is capable of transmitting pressure. Above this critical saturation or "irreducible saturation," brine flow is possible. Potential flow of brine below the irreducible brine saturation will not occur. At high brine saturations, brine isolates the gas and the gas no longer forms a continuous phase. This occurs at the irreducible gas saturation.

Bear's continuum approach is assumed for multiphase flow (Bear, 1975). Each fluid is a continuum and the various continua occupy the void space simultaneously. The equations of motion for multiphase flow used here are based on heuristic extensions of Darcy's law (Hubbert, 1956; Bear, 1975, 1979; Dake, 1978; Crichlow, 1977; Collins, 1961; Dullien, 1979; Hiatt, 1968; de Marsily, 1986; De Wiest, 1965; Aziz and Settari, 1979).

The following is a statement of Darcy's law in differential form:

$$q_v = -\frac{k}{\mu}[\nabla P - \rho g] \qquad \text{(A-1)}$$

where q_v is the volumetric flow rate per unit cross-sectional area, k is the absolute or intrinsic permeability of the porous media, μ is the fluid viscosity, ρ is the fluid density, g is the gravitational constant, and P is the fluid pressure.

Darcy's original observations were made on the one-dimensional vertical flow of water through a fully saturated porous medium (Hubbert, 1956). Darcy postulated the law, which states that the flow of water under these conditions is proportional to the change in potential. Many generalizations of Darcy's law can be found in the literature (Bear, 1975, 1979; Bear et al., 1968; Bear and Bachmat, 1967; Dake, 1978; Crichlow, 1977; Collins, 1961; Dullien, 1979; Hiatt, 1968; de Marsily, 1986; De Wiest, 1965; Aziz and Settari, 1979). These generalizations extend Darcy's observation to other fluids, to the simultaneous flow of immiscible fluids, to multiple dimensions, and to compressible fluids. These generalizations are used in obtaining the equations of motion governing the two-phase flow assumed in BRAGFLO.

The first extension is a generalization from an isotropic to an anisotropic medium. This extension is developed heuristically as well as theoretically in Bear (1975). Implicit in this generalization is the extension to two and three dimensions.

The second extension is that of accounting for fluid compressibility effects. Hubbert (1940) shows that extensions of Darcy's law to compressible fluids, such as gas, are valid provided the density of the fluid is a function of pressure only and the flow is irrotational.

The third extension of Darcy's law accounts for the presence and flow of multiple immiscible phases. Once steady-state flow is achieved, Darcy's law may be extended to describe the separate flow of each phase (Bear, 1975). This extension introduces the concept of effective permeabilities, relative permeabilities, and capillary pressure.

For each phase, the absolute permeability of Equation A-1 is replaced by the effective phase permeability, and the pressure of Equation A-1 is replaced by the phase pressure. These effective permeabilities are empirically determined by pressure drop and flow measurements. Numerous experiments verify the validity of this extension and suggest that the effective permeability depends on characteristics of the rock, the wettability characteristics, surface tension, the shape of the interface separating the phases, and phase saturation. The effective permeabilities do not appear to depend on fluid viscosities or their specific discharges (Bear, 1975; Scheidegger, 1960). Instead of using effective permeabilities, it is more convenient to refer to relative permeabilities, which are defined for each phase as the ratio of the effective phase permeability to the absolute or intrinsic permeability of the medium (measured when the medium is saturated with a single fluid).

A.2.3. Geometry

BRAGFLO is developed in terms of a one-, two- or three-dimensional block-centered grid system. In general, the three-dimensional numerical methods are normally based on Cartesian xyz coordinates. The finite difference formulations in BRAGFLO are sufficiently general to handle grid block "stretching" (variable grid spacing) in the directions of flow, as well as variable grid thickness or cross-sectional area in directions normal to flow. In

addition, the coordinate system may be rotated in three-dimensional space, with respect to the direction of gravity resulting in the generalized case of gravity components in each of the coordinate directions.

Because of these generalities, many geometries may be considered. Some of these include the following:

- Cartesian geometry (one-dimensional linear vertical, horizontal, or inclined flow; two-dimensional planar areal sweep, vertical or inclined flow; three-dimensional flow),
- Cylindrical geometry (two-dimensional axisymmetric cylindrical geometry with axis of symmetry oriented parallel, normal, or inclined to the direction of gravity),
- Spherical symmetry, and
- Non-Cartesian geometry (variable grid thickness and cross-sectional areas normal to flow).

To model in axisymmetric cylindrical geometry or spherical symmetry requires only an external transformation to obtain the equivalent Cartesian grid block sizes required for BRAGFLO. For example, consider the two-dimensional convergent flow toward a well in radial coordinates r and z (Figure A-1) (symmetry is assumed in the angular direction, θ).

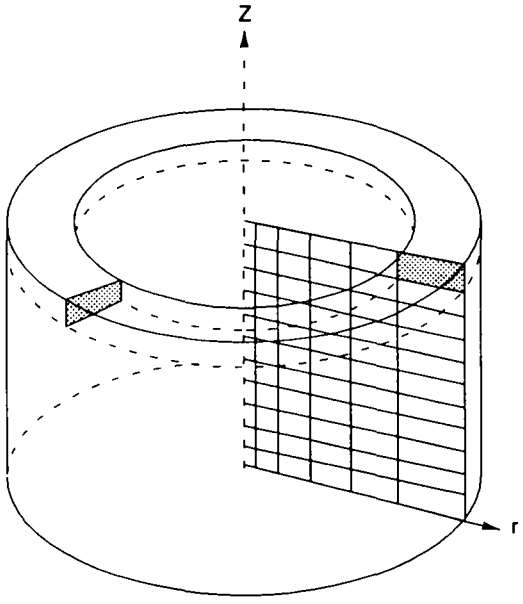

TRI-6342-1476-1

Figure A-1. Schematic representation of an axisymmetric cylindrical model.

If the coordinate transformations of $x(x,z) = r$, $y(x,z) = 2\pi r$ and $z(x,z) = z$, then an equivalent Cartesian system of the cylindrical geometry is defined. In the Cartesian system, flow is in the x and z directions. The length in the non-flow or symmetric direction, y, varies with x and accounts for the increase in cross-sectional area (normal to radial flow) with radial distance from the well. The transformation are justified by the equivalence of the volume integration in the two coordinate systems. An arbitrary function of r and z, $f(r,z)$ is integrated over the cylindrical element volume as

$$F = \int_{z_k}^{z_{k+1}} \int_{r_i}^{x_{i+1}} \int_{0}^{2\pi} f(r,z) r \, d\Theta \, dr \, dz \tag{A-2}$$

When the above transformations are defined, Equation A-2 is identical to the integration in Cartesian coordinates carried out below:

$$G = \int_{z_k}^{z_{k+1}} \int_{x_i}^{x_{i+1}} \int_{0}^{2\pi r} g(x,z) \, dx \, dy \, dz \tag{A-3}$$

Therefore, the conversion from radial geometry to the BRAGFLO Cartesian formulation requires only setting the mesh width (y) of each grid block equal to the circumference of a circle passing through the center of that grid block.

The way in which grid block sizes may vary is not arbitrary and depends on restrictions concerning grid block connectivity and interface cross-sectional areas. In BRAGFLO, two criteria determine valid grid block stretchings. First, grid-block stretchings are confined to certain directions dependent on the dimensionality of the flow. For example, in one-dimensional flow, the length of all grid blocks (Δx, Δy, and Δz) may vary in the direction of flow. In two-dimensional flow (x and y directions), the length Δx can vary only in the x-direction while the length Δy can vary only in the y-direction. For three-dimensional flow, the length of the grid blocks can only vary in the direction of flow coincident to their respective orientations. That is, Δx varies only in x, Δy varies only in y, and Δz = varies only in z. The reasons for these restrictions arise when determining appropriate averages for flows across block interfaces, given values evaluated at the centers of adjacent blocks. Secondly, grid block sizes may vary only in a way that results in a one-to-one connectivity between grid blocks in each direction starting from the origin. Grid block stretchings that violate only the first criterion may or may not be physically valid and are acceptable by BRAGFLO, although a warning message alerts the user to possible problems. Stretchings that violate criterion two above will not run. The grid patterns of Figure A-2 (a, b, and c) depict grid stretchings in one, two, and three dimensions, respectively, which are consistent with both criteria above.

The reason that some violations of the first criterion above present problems is that they may require restrictive assumptions concerning the average cross-sectional area between adjacent grid blocks for calculating interblock transmissibilities, flow rates, and velocities. The reason violations of the second criterion are not acceptable is because they are inconsistent with the bookkeeping assumed in BRAGFLO for mapping the coordinates of the grid block centers from their spatial positions to their locations in the numerical space.

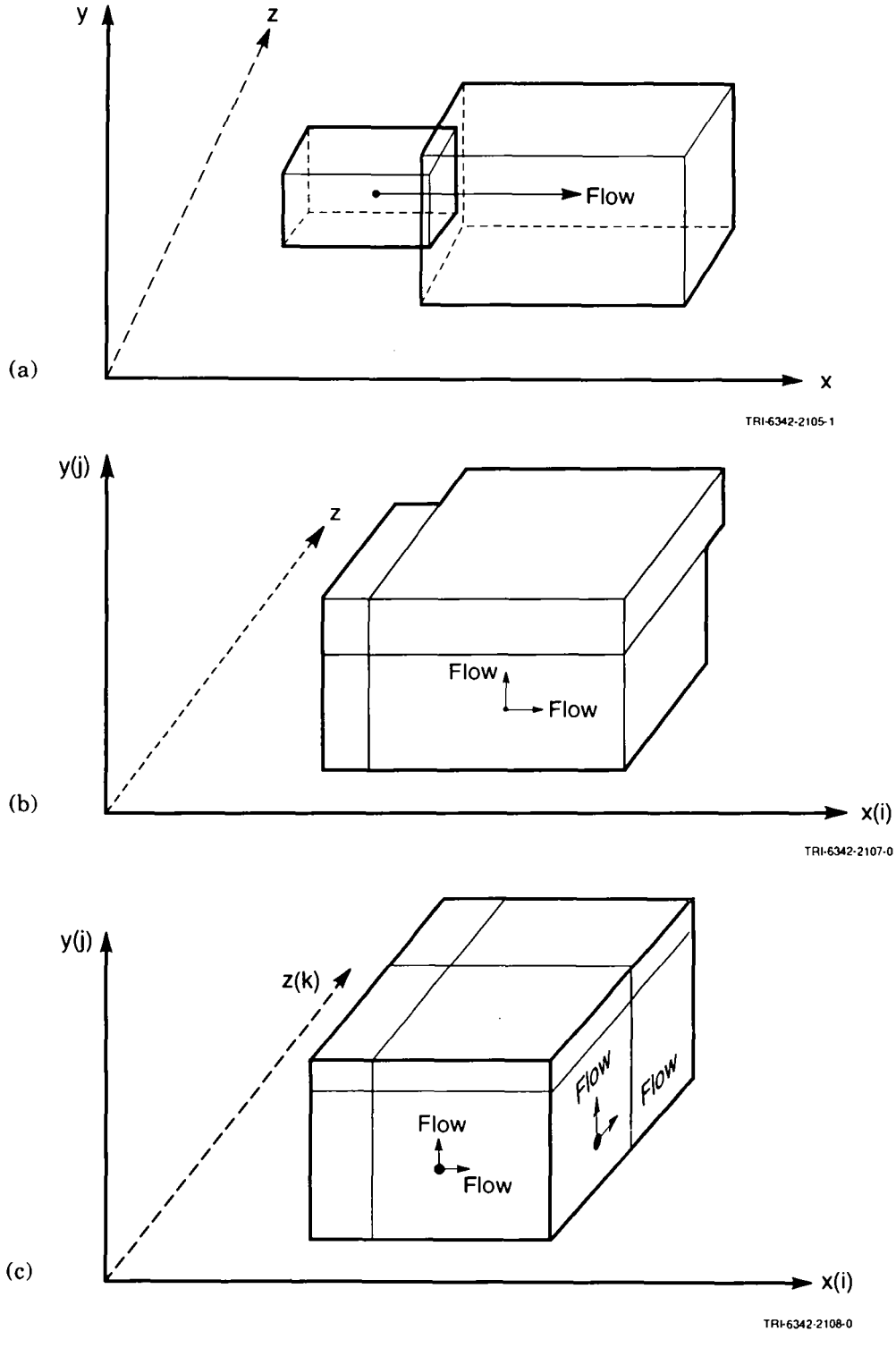

Figure A-2. Grid-block stretching for flow in (a) one, (b) two, or (c) three dimensions.

A.2.4 Derivation of Flow Equations

The derivation of the flow equations begins by consideration of mass conservation in a differential volume element. The derivation will initially be presented for one-dimensional compressible flow and then generalized to other dimensionalities. The derivation is generalized to allow for the cross-sectional area normal to flow to vary in the direction of flow.

Consider the mass conservation of a single component in a two-phase system about the control volume depicted in Figure A-3.

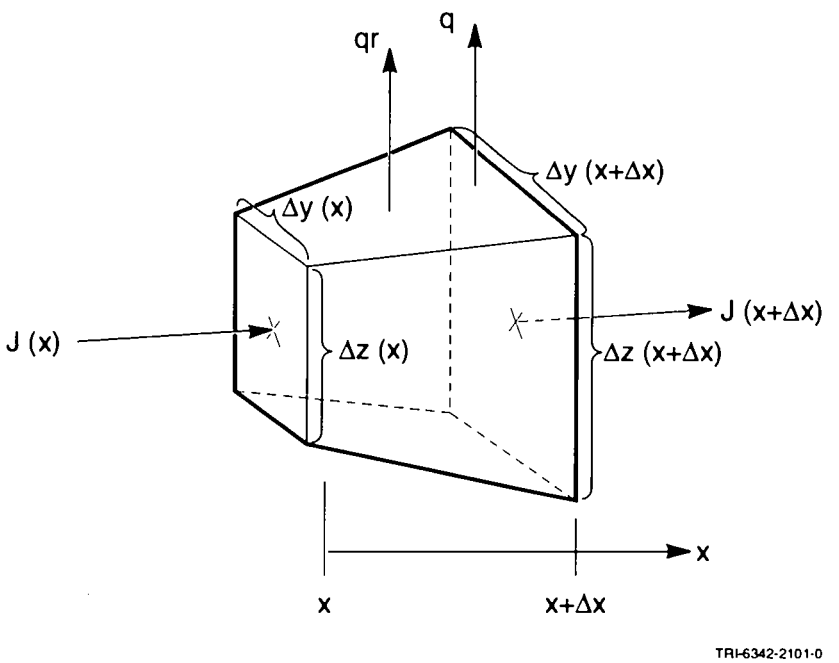

Figure A-3. Control volume for derivation of flow equations.

Flow is in the x direction across a length Δx. The cross-sectional area normal to flow varies with x as $A(x) = \Delta y(x) \bullet \Delta z(x)$. Therefore, the cross-section areas at the left boundary and right boundary are $\Delta y(x) \bullet \Delta z(x)$ and $\Delta y(x + \Delta x) \bullet \Delta z(x + \Delta x)$ respectively. The mass flux entering the element at the left face is $J(x)$, while the mass flux leaving at the right face is $J(x + \Delta x)$. Included in the mass balance are terms for mass rate of injection (per unit volume of reservoir) due to wells, q, and chemical reaction, q_r. We also acknowledge that the density and saturation of the component, as well as the porosity of the reservoir, may change with time.

The mass conservation equation simply states that

[rate in] - [rate out] + [rate injected] + [rate reacted] = [rate accumulated] (A-4)

The rate at which mass enters the element from the left boundary is

$$J(x) \bullet \Delta y(x) \bullet \Delta z(x)$$

The rate at which mass exits the element at the right boundary is

$$J(x + \Delta x) \bullet \Delta y(x + \Delta x) \bullet \Delta z(x + \Delta x)$$

The rate at which mass is injected or produced by or from a well into the element is

$$q \bullet \overline{\Delta y \bullet \Delta z} \bullet \Delta x = q \bullet \overline{A} \bullet \Delta x,$$

where $\overline{A}$ is an average value of the product of Δy and Δz across the block length Δx, the volume of the block being $\overline{\Delta y \bullet \Delta z} \bullet \Delta x$.

Similarly, the rate at which mass is reacted in the element is

$$q_r \bullet \overline{\Delta y \bullet \Delta z} \bullet \Delta x = q_r \bullet \overline{A} \bullet \Delta x$$

The rate at which mass is accumulated in the element volume is

$$\frac{\partial}{\partial t}\left(\overline{\phi}\overline{\rho}\overline{S}\right) \bullet \overline{A}\Delta x,$$

because $\overline{\phi} \bullet \overline{\rho} \bullet \overline{S} \bullet \overline{A}\ \Delta x$ is the mass contained in the element. The bars signify an average of the value in the element. We have assumed that the size of the element does not change with time.

The statement of component mass conservation (Equation A-4) is written as

$$\left[J_x \Delta y \Delta z\right]_x - \left[J_x \Delta y \Delta z\right]_{x+\Delta x} + \left[q\overline{\Delta y \Delta z}\Delta x\right] + \left[q_r \overline{\Delta y \Delta z}\Delta x\right] = \overline{\Delta y \Delta z}\Delta x \frac{\partial}{\partial t}\left(\overline{\phi}\overline{\rho}\overline{S}\right) \tag{A-5}$$

Dividing Equation A-5 by Δx gives

$$\frac{-\left[J_x \Delta y \Delta z\right]_{x+\Delta x} + \left[J_x \Delta y \Delta z\right]_x}{\Delta x} + \left[q\overline{\Delta y \Delta z}\right] + \left[q_r \overline{\Delta y \Delta z}\right] = \overline{\Delta y \Delta z} \frac{\partial\left(\overline{\phi}\overline{\rho}\overline{S}\right)}{\partial t} \tag{A-6}$$

If we define a derivative to be

$$\frac{\partial f(x)}{\partial x} = \lim_{\Delta x \to 0} \frac{f(x + \Delta x) - f(x)}{\Delta x},$$

then in this limit, the differential form of the component mass conservation equation is

$$-\frac{\partial(J_x \Delta y \Delta z)}{\partial x} + q\Delta y\Delta z + q_r \Delta y \Delta z = \Delta y \Delta z \frac{\partial(\phi \rho S)}{\partial t} \tag{A-7}$$

where we have noted in the limit as $\Delta x \to 0$ that $\overline{\Delta y \Delta z} \to \Delta y(x)\Delta z(x)$, $\overline{\rho} \to \rho(x)$, $\overline{\phi} \to \phi(x)$, and $\overline{S} \to S(x)$.

Following a similar procedure in considering two-dimensional and three-dimensional flow results in the following differential forms of the component mass conservation equations:

Two-dimensional form:

$$-\frac{\partial(J_x \Delta z)}{\partial x} - \frac{\partial(J_y \Delta z)}{\partial y} + q\Delta z + q_r \Delta z = \Delta z \frac{\partial(\phi \rho S)}{\partial t} \tag{A-8}$$

Three-dimensional form:

$$-\frac{\partial(J_x)}{\partial x} - \frac{\partial(J_y)}{\partial y} - \frac{\partial(J_z)}{\partial z} + q + q_r = \frac{\partial(\phi \rho S)}{\partial t} \tag{A-9}$$

We have generalized to allow flux in the y and z directions, J_y and J_z respectively.

If Equations A-7, A-8, and A-9 are compared, the differential component mass conservation equations may be generalized for arbitrary dimensionality as follows:

$$-\nabla \bullet \alpha \vec{J} + \alpha(q + q_r) = \alpha \frac{\partial(\phi \rho S)}{\partial t} \tag{A-10}$$

where α is a geometric factor and depends on dimensionality as follows:

one dimension: $\alpha(x, y, z) = \Delta y(x)\Delta z(x)$,
two dimensions: $\alpha(x, y, z) = \Delta z(x, y)$,
three dimensions: $\alpha(x, y, z) = 1$,
and $\nabla \bullet \alpha \vec{J}$ is shorthand for $\frac{\partial(\alpha J_x)}{\partial x} + \frac{\partial(\alpha J_y)}{\partial y} + \frac{\partial(\alpha J_z)}{\partial z}$.

It is important to note that, in general, α varies spatially and, therefore, remains inside the above derivative terms. In two-dimensional flow, J_z is zero, and in one-dimensional flow, both J_y and J_z are zero.

Equation (A-11) is written for one component. In multicomponent systems, the mass of each component must be conserved. This results in multiple conservation equations (one for each component) similar to Equation A-11.

The development leading up to Equation A-11 assumed that the component exists in one phase because its mass is assumed equal to the product $\phi\rho S$. We now relax this assumption and write the two mass conservation equations for a two-phase, two-component system in which each component may be distributed between each of the phases. Such conditions arise when gas dissolves in liquid or liquid vaporizes into gas.

For convenience and generality, the two phases will consist of a wetting and a non-wetting phase denoted by lowercase w and n, respectively. The two components will be distinguished according to wetting and non-wetting and denoted by uppercase W and N. We recognize that wettability is a characteristic of the phase and not a component property. The nomenclature "wetting component" is used to indicated that this component in general dominates the wetting phase and similarly for the non-wetting component.

Component concentrations are required when a phase may consist of more than one component. Define C_{Ij} as the mass fraction of the Ith component in the jth phase. Using the above nomenclature, four concentration terms can be defined for the general two-component, two-phase system: C_{Nw}, C_{Ww}, C_{Nn}, and C_{Wn}. Because all the mass in a phase must come from the two components, then the component concentrations in each phase are related as

$$C_{Nw} + C_{Ww} = 1.0 \text{ and } C_{Nn} + C_{Wn} = 1.0 \tag{A-11}$$

With the above concepts and nomenclature defined, Equation A-10 is applied to both the wetting and non-wetting components as follows:

Non-wetting component mass balance:

$$-\nabla \bullet \alpha \vec{J}_N + \alpha(q_N + q_{rN}) = \alpha \frac{\partial}{\partial t}(\phi\rho_n S_n C_{Nn} + \phi\rho_w S_w C_{Nw}) \tag{A-12}$$

Wetting component mass balance:

$$-\nabla \bullet \alpha \vec{J}_W + \alpha(q_W + q_{rW}) = \alpha \frac{\partial}{\partial t}(\phi\rho_n S_n C_{Wn} + \phi\rho_w S_w C_{Ww}) \tag{A-13}$$

Comparison of Equations A-12 and A-13 with A-10 shows that aside from the addition of some subscripts, the major differences come from allowing for the possibility of component mass in the element volume to be distributed between the two phases. For example, in the wetting component mass balance (Equation A-13), the first term in the time derivative, $\phi\rho_n S_n C_{Wn}$ is the mass of the wetting component distributed to the non-wetting phase in the element volume. The second term in the time derivative, $\phi\rho_w S_w C_{Ww}$ is the mass of the wetting component distributed to the wetting phase in the element volume.

The component mass flux vectors $\vec{J}_N$ and $\vec{J}_W$ consist of contributions from both phases. The flux can be expanded and written to account for these contributions as follows:

$$\vec{J}_N = C_{Nn}\rho_n\vec{V}_n + C_{Nw}\rho_w\vec{V}_w \tag{A-14}$$

$$\vec{J}_W = C_{Wn}\rho_n\vec{V}_n + C_{Ww}\rho_w\vec{V}_w. \tag{A-15}$$

$\vec{V}_n$ and $\vec{V}_w$ are the superficial velocities for the non-wetting and wetting phases, respectively.

So far in this development, no assumptions have been made concerning the velocities or their relationships to pressure or potential. In BRAGFLO, Darcy's original law, extended to multiphase and multidimensional flow and accounting for gravity and capillary forces, relates superficial velocities to potential.

As mentioned in Section A.2.2, when two immiscible fluids occupy the pore space, they become separated by an interface. The curvature and surface tension of this interface produces a pressure difference called the capillary pressure. This capillary pressure has been experimentally observed to vary with saturation. In BRAGFLO, the capillary pressure is defined by Equation A-16 as the difference between non-wetting phase pressure and wetting phase pressure.

$$P_C(S_w) = P_n - P_w \tag{A-16}$$

Assuming each phase pressure is partially responsible for the flow of only that phase, Darcy's law in differential form becomes

$$\vec{V}_n = -\frac{K_n}{\mu_n}(\nabla P_n - \rho_n g \nabla D) \tag{A-17}$$

$$\vec{V}_w = -\frac{K_w}{\mu_w}(\nabla P_w - \rho_w g \nabla D), \tag{A-18}$$

where g is the gravitational constant of acceleration and D is the depth, which may vary spatially with all three coordinates.

In Equation A-17 and A-18, K_n and K_w are the effective permeabilities to flow for each phase. Unlike the absolute permeability of a porous medium in Darcy's original law that is independent of the flowing fluid (except for gas at low pressures), the effective permeability depends on the characteristics of the rock and fluid and has been experimentally observed to vary with the type and amount of fluid present (i.e., to vary with saturation). Instead of effective permeability, it is more common to encounter relative permeabilities in the reservoir literature. The relative permeabilities are defined as the ratio of the effective permeability of a phase to the absolute permeability (or single fluid permeability) of the porous medium.

$$k_{rn} = \frac{K_n}{K} \tag{A-19}$$

$$k_{rw} = \frac{K_w}{K} \tag{A-20}$$

The dependence of capillary pressure and relative permeability on fluid saturation is described in more detail in Volume 3, Section 2.3.1 of this report.

Substitution of Equations A-14, A-15, A-17, A-18, A-19, and A-20 into A-12 and A-13 results in the two-component mass conservation equations, A-21 and A-22.

$$-\nabla \bullet \left[\frac{\alpha C_{Nn} \rho_n k_{rn} K}{\mu_n} (\nabla P_n - \rho_n g \nabla D) + \frac{\alpha C_{Nw} \rho_w k_{rw} K}{\mu_w} (\nabla P_w - \rho_w g \nabla \mathrm{D}) \right] + \alpha (q_N + q_{rN})$$

$$= \alpha \frac{\partial}{\partial t} [\phi \rho_n S_n C_{Nn} + \phi \rho_w S_w C_{Nw}] \tag{A-21}$$

$$-\nabla \bullet \left[\frac{\alpha C_{Wn} \rho_n k_{rn} K}{\mu_n} (\nabla P_n - \rho_n g \nabla \mathrm{D}) + \frac{\alpha C_{Ww} \rho_w k_{rw} K}{\mu_w} (\nabla P_w - \rho_w g \nabla D) \right] + \alpha (q_N + q_{rN})$$

$$= \alpha \frac{\partial}{\partial t} [\phi \rho_n S_n C_{Wn} + \phi \rho_w S_w C_{Ww}] \tag{A-22}$$

Equations A-21 and A-22, along with A-11, A-16, and the phase saturation constraint, Equation A-23, form the system of equations solved simultaneously in BRAGFLO.

$$S_n + S_w = 1.0 \tag{A-23}$$

The constraint on saturation simply states that all of the pore space volume is occupied by the fluid phases.

The absolute permeability that appears in Equations A-21 and A-23 is directional and may be in general viewed as a second-order tensor. When the permeability of a porous medium depends on direction, the medium is characterized as being anisotropic. In BRAGFLO, the anisotropic porous medium is assumed to be orthotropic with the three orthogonal axes of the medium being aligned with the three coordinate axes. The off-diagonal elements of the permeability tensor are zero for an orthotropic porous medium. The diagonal permeabilities are K_x, K_y, and K_z. Some pre-processing of permeability data may be required if the data is taken in directions not aligned with the model's coordinate axes.

Assuming the concentrations and all of the physical properties of the fluids and the porous media are defined, the system of equations defines the spatial and temporal variation in the four dependent variables S_n, S_w, P_n, and P_w. The saturation constraint (Equation A-23) and the definition of capillary pressure (Equation A-16) are used to eliminate two of the dependent variables.

Theoretically, any two of the variables may be eliminated from the system, leaving two primary dependent variables. Some combinations may be numerically more advantageous than others. Selecting both phase pressures as primary dependent variables is not appropriate because saturation would then be obtained from the capillary pressure dependence on saturation, which may not be defined below residual saturations or capillary pressure may not uniquely specify a saturation.

In BRAGFLO, the primary dependent variables are selected as S_n and P_w. S_n is aligned with the non-wetting mass conservation partial differential equation (Equation A-21), while P_w is aligned with Equation A-22. Equation A-23 determines S_w from S_n, and Equation A-16 is used to obtain P_n once S_w and P_w are known. No fundamental difference was observed when the primary dependent variables of P_n and S_w were used during simple test problems. Nevertheless, the current BRAGFLO formulation assumes S_n and P_w as primary dependent variables.

A.2.5 Initial and Boundary Conditions

S_n, S_w, P_n, and P_w

Specification of boundary and initial conditions is required to complete the formulation. Upon examination of Equations A-21 and A-22, it is evident that they are second-order with respect to non-wetting phase pressure (P_n) and wetting phase pressure (P_w). Thus, two boundary conditions are required for each phase pressure in each dimension (two for P_n and P_w in x, two for P_n and P_w in y, and two for P_n and P_w in z). BRAGFLO handles boundary conditions in a way that typifies reservoir models; that is, the reservoir of interest in enclosed by a boundary across which there is no flow in the direction normal to it. Mathematically, these types of conditions are Neumann boundary conditions in which the normal derivative of pressure to the boundary is zero. In BRAGFLO, this is accomplished by assigning a zero value to the normal transmissibilities along each of the boundaries for both the gas and brine phases.

Through the use of wells, BRAGFLO has the capability to override the no-flow conditions. By locating pressure-constrained or flow-constrained fictitious wells along the boundaries, fixed pressures along the boundary or non-zero flow into or out of the reservoir across the boundary can be approximated.

No-flow boundary conditions may occur on two types of boundaries: one is the physical boundary of the reservoir being modeled; the other is along a line of symmetry. An implicit assumption in the use of no-flow boundaries is that the boundaries are located far enough away from the wells or other regions of interest that the boundaries exert negligible influence on the flow behavior in the reservoir over the duration of simulation time.

A number of variables and properties must be specified at time $t = 0$. These initial conditions consist of: (1) the two dependent variables aligned with Equation A-21 and Equation A-22 (S_n and P_w), (2) the reservoir properties of porosity and the directional permeabilities, and (3) the concentrations of metal and cellulose. These variables must be specified throughout the simulation volume and along the boundaries. All other material properties (fluid and reservoir properties) must also be specified; however, properties such as relative

permeabilities, capillary pressures, densities, viscosities, dissolved gas, etc., are functions of the previously specified dependent variables and are calculated in BRAGFLO.

A.2.6 Numerical Solution Techniques

The numerical techniques in the BRAGFLO flow model are based on a fully implicit finite difference representation of the nonlinear conservation equations. In implicit methods, the dependent variable at a particular location is evaluated as a function of the current values of its neighbors and the current value of any coefficients. In explicit methods, current values of the dependent variables are evaluated as a function of previously determined (or past-dated) values of dependent variables and coefficients. Implicit methods are inherently more numerically stable compared to their explicit or hybrid (IMPES) counterparts (Fanchi et al., 1982; Carnahan et al., 1969; Smith, 1965). The penalty for this increased stability is the increased computational effort associated with the simultaneous solution of the resulting finite difference analogs of the conservation equations at each grid block center. A complete discussion of numerical solution techniques is provided in the 1991 performance assessment documentation (see Section 5.2 of WIPP PA Division, 1991).

A.2.7 Benchmark Results

BRAGFLO has been benchmarked against two other multiphase reservoir codes (BOAST II and TOUGII). The results of four one-dimensional, radial benchmarks (with/without dissolved gas and with/without gas generation) showed excellent agreement among the three codes. Benchmark results are provided in the 1991 performance assessment documentation (see Section 5.2.2.3 of WIPP PA Division, 1991).

A.2.8 Postprocessing

BRAGFLO output has in the past consisted solely of various distributions—pressures, saturations, interblock, flows, etc. However, detailed analyses of the results, such as those discussed in the RCRA report (WIPP PA Department, 1992) and the 1991 sensitivity analysis report (Helton et al., 1992), require more detailed output. Examples include extents of gas flow in particular regions (such an the anhydrite layers) and especially numerous integrated quantities, such as integrated flows up intrusion boreholes or flows through drift or shaft seals.

Last year, these integrations and summary types of calculations were done externally to BRAGFLO using CAMCON postprocessing tools, in particular, ALGEBRA. However, the postprocessors can deal only with data in the BRAGFLO output files. Because the quantity of output from BRAGFLO can be vast, results are generally printed out only every 15 or 20 time steps. For most purposes, this provides an adequate amount of detail. However, some of the integrations are done on quantities that can vary extremely rapidly. For example, the rate of brine flow up an intrusion borehole can sometimes be very high immediately following the intrusion, but last for only a few time steps. Assuming that the high rate lasts for 15 or 20 steps, rather than just two steps, can seriously overestimate the quantity of brine that flowed up the borehole in that time period.

This shortcoming was corrected in 1992 by performing these integrations internally to BRAGFLO. All integrations and summary statistics used in detailed analysis of BRAGFLO output are now calculated at each step of a performance calculation. Thus, these results are as accurate as the fundamental solution quantities calculated in BRAGFLO (brine pressures and gas saturations). No additional errors are introduced by postprocessing partial results.

A drawback to performing these integrations internally to BRAGFLO is that portions of the code become mesh specific. In order to integrate flows up an intrusion borehole, for example, the location of the borehole must be "hardwired" into the code. In addition, quantities that are of interest in one mesh do not even exist in another mesh because the conceptual model differs. To program the integration and summary calculations to be completely general to enable it to perform on any mesh is not feasible under the PA time constraints. Thus, multiple versions of BRAGFLO currently are used, each one differing only in the number and type of output summary calculations that are done for the particular mesh and conceptual model being used. All other internal workings of the different versions are identical.

A.3 Waste Mobilization (PANEL)

PANEL's waste mobilization model mathematically computes the radionuclide concentrations in the brine that result from the waste mixing with the brine. This model assumes that the concentrations of all species are uniform through the waste room, that the concentrations of all species are always in equilibrium, and that solubility limits for a given element are allocated among its isotopes on the basis of relative abundance. Radioactive decay based on the Bateman equations (Section 7.1 of this volume; WIPP PA Division 1991, Section 7.2.3) is also taken into consideration. A complete description of the waste mobilization model is provided in the PANEL discussions found in Volume 3 of this report (Section 1.4.4) and in the 1991 performance assessment documentation (see Section 5.3.2 of WIPP PA Division, 1991).

Appendix A References

Aziz, K., and A. Settari. 1979. *Petroleum Reservoir Simulation.* London: Applied Science Publishers.

Bear, J. 1975. *Dynamics of Fluids in Porous Media.* New York, NY: Elsevier Publishing Company.

Bear, J. 1979. *Hydraulics of Groundwater.* New York, NY: McGraw-Hill, Inc.

Bear, J., and Y. Bachmat. 1967. "A Generalized Theory on Hydrodynamic Dispersion in Porous Media," *I.A.S.H. Symp. Artificial Recharge and Management of Aquifers.* IASH, P.N. 72. Haifa, Israel. 7-16.

Bear, J., D., I. H. Zaslovskii, and S. Irmay. 1968. *Physical Principles of Water Percolation and Seepage.* Paris: UNESCO.

Brooks, R.H., and A.T. Corey. 1964. *Hydraulic Properties of Porous Media.* Hydrology Paper No. 3. Fort Collins, CO: Civil Engineering Department, Colorado State University.

Carnahan, B., H.A. Luther, and J.O. Wilkes. 1969. *Applied Numerical Methods.* New York, NY: John Wiley & Sons, Inc.

Coats, K.H. 1980. "In-Situ Combustion Model," *Society of Petroleum Engineers Journal.* Vol. 26, no. 6, 533-554.

Collins, R.E. 1961. *Flow of Fluids Through Porous Materials.* New York, NY: Reinhold Publishing Corporation.

Corey, A.T. 1986. *Mechanics of Immiscible Fluids in Porous Media.* Littleton, CO: Water Resources Publications.

Crichlow, H.B. 1977. *Modern Reservoir Engineering - A Simulation Approach.* Englewood Cliffs, NJ: Prentice-Hall, Inc.

Crookston, R.B., W.E. Culham, and W.H. Chen. 1979. "Numerical Simulation Model for Thermal Recovery Processes," *Society of Petroleum Engineers Journal.* Vol. 19, no. 1, 37-58.

Dake, L.P. 1978. *Fundamentals of Reservoir Engineering.* New York, NY: Elsevier Scientific Publishing Company.

de Marsily, G. 1986. *Quantitative Hydrogeology: Groundwater Hydrology for Engineers.* Orlando, FL: Academic Press, Inc.

De Wiest, R.J.M. 1965. *Geohydrology.* New York, NY: John Wiley and Sons.

Dullien, F.A.L. 1979. *Porous Media Fluid Transport and Pore Structure.* New York, NY: Academic Press, Inc.

Fanchi, J.R., K.J. Harpole, and S.W. Bujnowsky. 1982. *BOAST: A Three-Dimensional Three-Phase Black Oil Applied Simulation Tool (Version 1).* DOE/BC/10033-3. Tulsa, OK: Keplinger and Associates, Inc.

Helton, J.C., J.W. Garner, R.P. Rechard, D.K. Rudeen, and P.N. Swift. 1992. *Preliminary Comparison with 40 CFR Part 191, Subpart B for the Waste Isolation Pilot Plant, December 1991—Volume 4: Uncertainty and Sensitivity Analysis Results.* SAND91-0893/4. Albuquerque, NM: Sandia National Laboratories.

Hiatt, W.N. 1968. "Mathematical Basis of Two-Phase, Incompressible, Vertical Flow Through Porous Media and Its Implications in the Study of Gravity-Drainage-Type Petroleum Reservoirs," *Society of Petroleum Engineers Journal.* Vol. 8, no. 3, *225-230.*

Hubbert, M.K. 1940. "The Theory of Ground-Water Motion," *The Journal of Geology.* Vol. 48, no. 8, pt. 1, 785-944.

Hubbert, M.K. 1956. "Darcy's Law and the Field Equations of the Flow of Underground Fluids," *Journal of Petroleum Technology.* Vol. 8, 222-239.

Peaceman, D.W. 1977. *Fundamentals of Numerical Reservoir Simulation.* New York: Elsevier Scientific Publishing Company.

Rubin, B., and P.K.W. Vinsome. 1979. "Simulation of the In-Situ Combusion Process in One Dimension Using a Highly Implici Finite Difference Scheme," *Preprint, 30th Annual Meeting of the Canadian Institute of Mining and Metallurgy, Banft, Canada, May 8-11, 1979.* Paper 79-30-14. Montreal, Quebec: Canadian Institute of Mining and Metallurgy, Petroleum Society.

Scheidegger, A. E. 1960. *The Physics of Flow Through Porous Media.* Rev. ed. Toronto, Canada: University of Toronto Press.

Smith, G.D. 1965. *Numerical Solution of Partial Differential Equations, with Exercises and Worked Solutions.* New York, NY: Oxford University Press.

Vaughn, P. 1986. *A Numerical Model for Thermal Recovery Processes in Tar Sand: Description and Application.* DOE/FE/60177-2219. (Available from National Technical Information Service, Springfield, VA.)

WIPP Performance Assessment (PA) Department. 1992. *Long-Term Gas and Brine Migration at the Waste Isolation Pilot Plant: Preliminary Sensitivity Analyses for Post-Closure 40 CFR 268 (RCRA), May 1992.* SAND92-1933. Albuquerque, NM: Sandia National Laboratories.

WIPP Performance Assessment (PA) Division. 1991. *Preliminary Comparison with 40 CFR Part 191, Subpart B for the Waste Isolation Pilot Plant, December 1991 - Volume 2: Probability and Consequence Modeling.* SAND91-0893/2. Albuquerque, NM: Sandia National Laboratories.

APPENDIX B:
SANCHO

APPENDIX B: SANCHO

B.1 Overview

SANCHO is a special purpose, finite-element computer program developed at Sandia National Laboratories to solve problems of the quasistatic, large-deformation, inelastic response of two-dimensional (i.e., planar or axisymmetric) solids (Stone et al., 1985). This program numerically solves the general, nonlinear partial differential equations that govern relaxation to equilibrium between stresses and applied loads in a solid body. Because the general equations are an underdetermined system, they must be supplemented with constitutive equations for up to three optional material models: a finite strain, elastic-plastic strain-hardening model; a volumetric plasticity model; and a metallic creep model. The material models actually used in the 1992 series of PA calculations are described in Section 1.4.7 of Volume 3.

SANCHO uses a finite-element method to obtain a numerical solution; the elements are bilinear, isoparametric quadrilaterals with constant bulk strain. The solution strategy for obtaining equilibrium includes the use of an iterative scheme designed around a self-adaptive, dynamic relaxation algorithm; the iterative scheme is an explicit, central-difference, pseudo-time integration with artificial damping. Because the scheme is explicit, no stiffness matrix is formed or factored — a feature that can reduce computer storage requirements.

B.2 Summary of Theory and Fundamental Equations

The theory underlying SANCHO is that of the motion of point-like particles that are imbedded within a solid body V, which occupies a region of three-dimensional space and is subject to deformation under the influence of prescribed body and surface forces. These particles usually occupy the corners or centers of elements of a mesh that is placed over the volume V at the time ($t = 0$) that deformation begins; the configuration at this time is called the *reference configuration* and the position of a particle is specified by its vector of material coordinates, $\mathbf{X}$. In the reference configuration, the solid body is assumed to be strain free, though not necessarily stress free. As time increases and the body deforms, the particles move with the material along trajectories denoted by

$$x = \xi(\mathbf{X}, t). \tag{B-1}$$

The vector function ξ describes the motion of a particle that starts at $\mathbf{X}$ at $t = 0$; clearly

$$\xi(\mathbf{X}, 0) = \mathbf{X}.$$

It is the vector function ξ that is the basic dependent variable in problems of this kind because knowledge of it permits graphic visualization of the change in shape of the deforming body. For purposes of computing the dynamics of deformation, however, it is more convenient to view the flow of the particles through three-dimensional space as though they were imbedded in a continuous fluid moving with a velocity field,

$$\mathbf{v} = \frac{\partial}{\partial t}\xi(\mathbf{X}, t) = \eta(\mathbf{x}, t), \tag{B-2}$$

defined for $t \geq 0$ and *any* point $\mathbf{x} \in R^3$ (note that $\mathbf{x}$ is now an arbitrary point in space); this is called the *Eulerian point of view.*

The Eulerian point of view permits the calculation of the true acceleration of an element of mass that is instantaneously located at $\mathbf{x}$: from (B-1) and (B-2) and the chain rule of calculus, it is seen that the true acceleration is just the material derivative of V,

$$\frac{d\mathbf{v}}{dt} = \frac{\partial \mathbf{v}}{\partial t} + v \bullet \nabla v \tag{B-3}$$

The fundamental equation governing the deformation of the solid body V follows by application of Newton's Laws of Motion to an arbitrary element of mass in volume V (see Malvern, 1969 Section 5.3):

$$\rho \frac{d\mathbf{v}}{dt} = \nabla \bullet \mathbf{T} + \rho \mathbf{b} \tag{B-4}$$

where

ρ = mass density (kg/m^3)

$\mathbf{T}$ = the Canchy stress tensor $\left(kg/m \cdot s^2\right)$

$\mathbf{b}$ = sum of specific body forces (i.e., forces per unit mass: usually, gravity; m/s^2).

The mass density must also satisfy the continuity equation:

$$\frac{d\rho}{dt} = -\rho \nabla \bullet \mathbf{v} \tag{B-5}$$

SANCHO was actually designed to solve the equilibrium equations associated with (B-4) and (B-5), i.e., the dynamical equations that apply when $|\mathbf{v}|$ and the time rate-of-change of density are small or zero [but in numerical practice a "quasistatic" approximation is employed that requires the re-introduction of artificial time derivatives having much the same form as the left-hand sides of (B-4) and (B-5)]. The quasistatic approximation to the equations of motion takes the form (Stone et al., 1985)

$$\nabla \bullet \mathbf{T} + \rho \mathbf{b} = 0, \tag{B-6}$$

and allows for three kinds of boundary conditions:

1. Jump condition at a contact discontinuity defined by some *internal* surface S_0; this condition requires that

$$\left(\mathbf{T}^+ - \mathbf{T}^-\right) \bullet \mathbf{n}_0 = 0 \quad on\ S_0 \tag{B-7}$$

where $\mathbf{n}_0$ is the outward unit normal on S_0, and the (+) and (-) signs on the stress tensors signify respectively values taken on the outer and inner sides of S_0.

2. Traction boundary conditions on some *external* surface S_1, of the form

$$\mathbf{T} \bullet \mathbf{n}_1 = \mathbf{S}(t) \quad on\ S_1 \tag{B-8}$$

where $\mathbf{n}_1$ is the outward unit normal on S_1, and $S(t)$ is a prescribed vector function of time.

3. Displacement boundary conditions on some *external* surface S_2;

$$\xi(\mathbf{X}, t) = \mathbf{k}(t) \quad on\ S_2 \tag{B-9}$$

where $\mathbf{k}(t)$ is a prescribed vector function of time.

Taken alone, equations (B-6) and the boundary conditions (B-7) through (B-9) obviously do not determine stress distributions. In the two-dimensional geometries of the SANCHO code, the stress tensor has three independent components; in matrix notation,

$$\mathbf{T} = \begin{pmatrix} t_{11} & t_{12} \\ t_{21} & t_{22} \end{pmatrix}, \text{ with } t_{12} = t_{21},$$

and so one more relation is needed in order to make a determinate system of equations. The *constitutive equations* or the stress-strain relations defining the nature of the material under consideration are usually chosen in a way that supplies the required, addition relationships (note, however, that the form of the constitutive equations may vary in space because different kinds of materials may occupy different parts of the solid body V).

The constitutive equations in SANCHO are usually expressed as ordinary differential equations (ODEs) for the components of the stress tensor or the components of the deviatoric stress tensor,

$$\mathbf{T}' = \mathbf{T} - \sigma\mathbf{I} = \mathbf{T} + p\mathbf{I} \tag{B-10}$$

where σ denotes the mean normal stress and p is the mean normal pressure. For examples of the ODEs governing material models used in the 1992 PA calculations, see Section 1.4.7 of Volume 3.

Appendix B References

Malvern, L.E. 1969. *Introduction to the Mechanics of a Continuous Medium.* Englewood Cliffs, NJ: Prentice-Hall, Inc.

Stone, C.M., R.D. Kreig, and Z.E. Besinger. 1985. *SANCHO — A Finite Element Computer Program for the Quasistatic, Large Deformation, Inelastic Response of Two-Dimensional Solids.* SAND84-2618. Albuquerque, NM: Sandia National Laboratories.

APPENDIX C:
SECO FLOW AND TRANSPORT MODEL

APPENDIX C: SECO FLOW AND TRANSPORT MODEL

C.1 Flow

SECO_2DH calculates single-phase Darcy flow for groundwater flow problems in two dimensions. The formulation is based on a single partial differential equation for a hydraulic head using fully implicit time differencing. Both confined and unconfined aquifer conditions are simulated. The flow is solved in both a regional and a local grid, each of which is defined independently of the grid that defines the aquifer properties. A semi-coarsening multigrid solvers is used to increase solution efficiency for large array dimensions. High-order accuracy particle tracking is available for both grids. The codes are written in DEC VMS FORTRAN. The codes are designed specifically for execution on VAX computers operating under the VMS operating system. The guiding philosophy for the SECO codes is to make the problem definition convenient and to facilitate as much as possible the running of grid-convergence tests and local-area simulations within the larger regional-area simulation. The codes are particularly well suited for testing alternative conceptual models for flow and transport.

C.1.1 Governing Equation

SECO_2DH simulates groundwater flow at regional and local scales within the Culebra Dolomite by solving the following partial differential equation in two dimensions (x,y) in time (t) for potentiometric head, h:

$$S_s \frac{\partial h}{\partial t} = \nabla \bullet (K \nabla h) - W \tag{C-1}$$

where K is the (tensor) hydraulic conductivity, S_s is the specific storage of the porous material (the Culebra), t is time, and W is a volumetric flux (out of the Culebra) per unit volume of formation (used to simulate wells or recharge). The principal axes of K must be aligned along the coordinate directions x and y. S_s, K, and W may be functions of (x, y, t). For a derivation of this equation from Darcy's flow and the equation of mass conservation, see McDonald and Harbaugh (1988).

C.1.2 Discretization and Solvers

Equation C-1 (or the steady-state version with $\partial h/\partial t = 0$) is discretized using standard second-order differences in space and first-order backward (fully implicit) differences in time (McDonald and Harbaugh, 1988; Roache, 1976). The fully implicit time differencing produces unconditional stability for this linear equation, but requires solution of an elliptic equation at each time step. In MODFLOW and other common groundwater hydrology codes, this linear, elliptic equation is solved by either the two-line successive over-relaxation (SOR) iterative method or by a direct solver. The direct solver is not considered to be practical for realistic grids (sufficiently fine resolution), being excessively sensitive to computer round-off error (especially on VAX-class computers) and very slow. In SECO_2DH, the solver options are point SOR, (single) line SOR (e.g., see Roache, 1976), and the

semi-coarsening multigrid solver MGSS2, which was developed at Ecodynamics (personal communication with P. Knapp, Ecodynamics Research Associates, Albuquerque, NM).

The semi-coarsening multigrid solver (MGSS2) is the default option. For very coarse resolution (e.g., a 6×6 grid that might be used for development of code enhancements), the point SOR solver is fastest. However, MGSS2 results in significantly increased efficiency for problems with fine resolution and strongly varying conductance (due to either hydraulic conductivity variations or highly stretched grids). Further, the MGSS2 solver does not require that the user estimate an optimum relaxation factor, as SOR solvers do.

C.1.3 Block-Centered Discretization

SECO_2DH has been written with an option flag called MAC to select either the most common block-centered discretization (MAC=1), with the cell edge coincident with the aquifer edge, or node-centered discretization (MAC=0), with the cell center (or node) on the aquifer edge. Unless required by a specific study, the default cell configuration is MAC=1. This configuration clearly more accurately locates the aquifer edge for both Dirichlet (fixed-head) and Neumann (fixed-gradient) boundary conditions. For QA purposes, MAC=0 is unsupported in SECO_2DH.

C.1.4 Problem Decoupling

To make the problem definition convenient and to facilitate the running of grid convergence tests and local-area simulations within the larger regional-area simulation, the problem definition is decoupled from the computational grid. The aquifer properties are defined on a discrete data base that can be independent of the computational grids. A sequence of grid solutions does not require the user to define aquifer properties point by point in each computational grid; likewise, the regional computational grid is decoupled from the local computational grid, both in space and time. A number of parameters, including the boundaries of the computational regions, the spatial increments (cell sizes), the simulation times, and the time steps, are all decoupled in both space and time. The only requirement is that the local grid-problem domain of definition must lie within the regional grid-problem domain of definition. Likewise, definition of boundary conditions (types and values) and wells (locations and pumping schedules) are decoupled from the computational grid and are defined in the continuum.

C.2 Transport

SECO_TP uses a total variational diminishing (TVD) scheme to solve the two-dimensional radionuclide transport equation in a fractured porous medium (Salari et al., 1992). The TVD scheme employed by SECO_TP uses three-level time differencing and directional splitting to improve accuracy and execution time.

An overview theoretical development of SECO_TP that follows has been extracted from Salari et al. (1992). A more detailed explanation is available from Salari et al. (1992) and the work cited below.

C.2.1 Governing Equation

The relevant partial differential equation contains advection, dispersion, absorption, source, and decay terms. The radionuclide transport problem consists of N species equations, $k = 1,\ldots, N$:

$$\nabla \bullet \left[\mathrm{D} \nabla C_k - \mathrm{V} C_k \right] = \phi R_k \frac{\partial C_k}{\partial t} + \phi R_k \lambda_k C_k - \phi R_{k-1} \lambda_{k-1} C_{k-1} - Q \hat{C}_k - \Gamma_k, \tag{C-2}$$

where the dependent variables are C_k, the concentration of the kth radionuclide. Physical parameters include $D(x,t)$, a 2×2 hydrodynamic dispersion tensor (velocity-dependent); $V(\mathbf{x})$, the Darcy velocity; $\phi(\mathbf{x})$, the fracture porosity; R_k, the retardation coefficient; λ_k, the species decay constant; and $\hat{C}_k$, the concentration of the kth injected radionuclide. The well injection rate is Q. Detailed physical descriptions of these terms can be found in Huyakorn and Pinder (1983) and Bear and Bachmat (1990). A dual-continuum model requires the additional source term Γ_k to represent the flux due to the exchange of contaminant between the fracture and matrix domain. Fracture flow (single-porosity) and fracture/matrix-flow (dual-porosity) versions of Equation C-2 are presented and discussed in detail in Volume 3 of this report (Section 1.4.6). The N equations are linear and sequentially coupled.

A general Robin boundary condition is assumed:

$$\alpha C_k + \beta \frac{\partial C_k}{\partial n} = \gamma \tag{C-3}$$

on a planar rectangular domain Ω. For various choices of $\alpha(\mathbf{x})$, $\beta(\mathbf{x})$, and $\gamma(\mathbf{x})$, one may obtain Dirichlet, Neumann, or Cauchy boundary conditions on different portions of the boundary. The flow field is obtained from SECO_2DH.

The two-dimensional governing equation is solved using an approximate factorization (Fletcher, 1988) with an implicit treatment of boundary conditions. The convective terms are modeled by TVD (Yee, 1987) and the remaining terms by central differencing. Solution of the governing equation is explained in detail in Salari et al. (1992).

C.2.2 Code Verification

The SECO_TP code has been applied to test problems and is shown to be accurate for both high and low mesh Peclet numbers. SECO_TP has been verified for temporal and spatial accuracy using the following unsteady equation and its solution, with $V = ui$:

$$C_t + uC_x = \alpha_L u C_{xx} + \alpha_T u C_{yy} - g(x,y,t), \tag{C-4}$$

where

$$g(x,y,t) = (x-ut)^2 + y^2,$$

and $0 < x < 1$, $0 < y < 1$. The initial condition is given by

$$C(x,y,0) = \frac{1}{12u}\left[\frac{x^4}{\alpha_L} + \frac{y^4}{\alpha_T}\right] \tag{C-5}$$

The exact solution to Equation C-4 is

$$C(x,y,t) = \frac{1}{12u}\left[\frac{(x-ut)^4}{\alpha_L} + \frac{y^4}{\alpha_T}\right]. \tag{C-6}$$

Because the computational domain is finite, the Dirichlet boundary conditions are time dependent and may be obtained from the exact solution.

Table C-1 presents the computed solution to Equation C-4 at time = 25 for four different grid sizes and time steps. The magnitude of the coefficients are $u = 0.1$, $\alpha_L = 0.1$, and $\alpha_T = 0.1$. Examination of the ratio of root mean square (RMS) of errors shows that the overall solution is second-order accurate in time and space.

The SECO_TP code has also been benchmarked against exact transport solutions in Javandel et al. (1984), Tang et al. (1981), and Knupp and Salari (1992).

Table C-1. Convergence Results, Uniform Grid

Size	Δx	Δy	RMS	RMS Ratio
20×20	0.05	0.25	7.697E-3	
40×40	0.025	0.125	1.954E-3	3.94
80×80	0.0125	0.0625	4.921E-4	3.97
160×160	0.00625	0.03125	1.234E-4	3.99

Appendix C References

Bear, J., and Y. Bachmat. 1990. *Introduction to Modeling of Transport Phenomena in Porous Media.* Dordrecht, Netherlands: Kluwer Academic Publishers.

Fletcher, C.A.J. 1988. *Computational Techniques for Fluid Dynamics.* New York, NY: Springer-Verlag. Vols. 1-2.

Huyakorn, P.S., and G.F. Pinder. 1983. *Computational Methods in Subsurface Flow.* New York, NY: Academic Press.

Javandel, I., C. Doughty, and C-F. Tsang. 1984. *Groundwater Transport: Handbook of Mathematical Models.* Water Resources Monograph No. 10. Washington, DC: American Geophysical Union.

Knupp, P.M., and K. Salari. 1992. *Contributions of an Analytical Solution to a 2D Radionuclide Transport Problem for Site Performance Assessment.* Albuquerque, NM: Ecodynamics Research Associates Technical Report. (Copy on file in Waste Management and Transportation Library, Sandia National Laboratories, Albuquerque, NM.)

McDonald, M.G., and A.W. Harbaugh. 1988. *A Modular Three-Dimensional Finite-Difference Ground-Water Flow Model.* Techniques of Water-Resources Investigations of the United States Geological Survey, Book 6, Modeling Techniques. Reston, VA: U.S. Geological Survey.

Roache, P.J. 1976. *Computational Fluid Dynamics.* Rev. printing. Albuquerque, NM: Hermosa Publishers.

Salari, K., P. Knupp, P. Roache, and S. Steinberg. 1992. "TVD Applied to Radionuclide Transport in Fractured Porous Media," *Proceedings of IX International Conference on Computational Methods in Water Resources, Denver, Colorado.* 141-148. (Copy on file in Waste Management and Transportation Library, Sandia National Laboratories, Albuquerque, NM.)

Tang, D.H., E.O. Frind, and E.A. Sudicky. 1981. "Contaminant Transport in Fractured Porous Media: Analytical Solution for a Single Fracture," *Water Resources Research.* Vol. 17, no. 3, 555-564.

Yee, H.C. 1987. "Construction of Explicit and Implicit Symmetric TVD Schemes and Their Applications," *Journal of Computational Physics.* Vol. 68, no. 1, 151-179.

APPENDIX D:
CULEBRA TRANSMISSIVITY FIELD SIMULATIONS

APPENDIX D: CULEBRA TRANSMISSIVITY FIELD SIMULATIONS

The information presented in this appendix is extracted from LaVenue and RamaRao (1992).

D.1 Background

Efforts to incorporate uncertainty in the Culebra transmissivity field into PA calculations have been somewhat evolutionary. In the 1990 PA calculations, the Culebra was divided into seven zones or regions. A mean transmissivity value and an associated standard deviation was assigned to each zone. By sampling from the distributions associated with each zone, multiple realizations of zonal transmissivity values were subsequently used as input to the flow and transport calculations. Although computationally elegant, the specification of zones significantly reduces the spatial variability within a given realization because each zone has a constant value. In addition, large differences in the values assigned to each zone in a given realization may occur generating severe step changes in the permeability field.

In an effort to improve the transmissivity field used in the 1991 PA calculations, conditional simulations (CS) of Culebra transmissivity fields were produced by conditioning upon the observed transmissivity values and the pilot points which were added in the LaVenue et al. (1990) model. The CS transmissivity fields were then used in a groundwater flow model (WIPP PA Division, 1991). The boundary conditions necessary to reduce the differences between the observed and calculated steady-state heads were then determined. Those realizations that did not meet a minimum error criteria were not considered adequate and were discarded. This work resulted in over 60 conditional simulations that had acceptable fits to the observed steady-state freshwater heads. These 60 fields were subsequently used in the calculations by sampling on a uniformly distributed variable assigned to each CS field (WIPP PA Division, 1991). The differences between each realization is depicted by a groundwater travel-time cumulative-distribution function, where travel times range from approximately 10,000 years to 30,000 years. These travel times are used as an internal diagnostic measure in the generation of CS transmissivity fields. Travel times used in the calculation of Environmental Protection Agency (EPA) normalized releases of radionuclides to the accessible environment are calculated using the CS transmissivity fields and the SECO flow and transport codes.

In March of 1991, a geostatistics/stochastic-hydrology expert panel (GXG) was convened to provide guidance for adequately incorporating the uncertainty of the Culebra transmissivity field into the PA calculations. After reviewing the previous work, the GXG had several concerns regarding the approach taken in LaVenue et al. (1990). One of the principal concerns raised by the GXG panel members related to the subjectivity inherent in the manual calibration approach. For example, the model was calibrated in a piecewise fashion by sequentially selecting regions to be calibrated, instead of calibrating the whole model area at the same time. The model was sequentially calibrated in the northwest (upgradient) region, southwest region, southern region, and central region or WIPP-site boundary area. As mentioned in the 1990 study, the regions upgradient and downgradient from the WIPP-site area were calibrated prior to making any changes within the WIPP-site boundary. This approach was employed in order to reproduce the regional hydraulic gradients across the northern and southern WIPP-site boundaries; it is analogous to producing a regional flow model to provide boundary conditions for a local scale

model. The GXG panel wondered whether there would be any major differences in the calibrated transmissivity field had the entire model area been calibrated at the same time.

Several recommendations were proposed by the GXG panel members and are described in detail in Gallegos (1992). One of their recommendations included repeating the modeling performed by LaVenue et al. (1990), which included steady-state and transient model calibration, numerous times. However, instead of simply kriging the transmissivities, conditional simulations would be generated and subsequently calibrated. The conditional simulations would allow for different transmissivity fields to be used as the initial fields for the model. These fields would initially be conditioned on the observed transmissivity data only. Subsequent model calibration would then condition each of the conditionally simulated fields to the observed steady-state and transient heads. Because the GXG panel also expressed concerns regarding the manual assignment of transmissivities to the pilot points, the approach used in LaVenue et al. (1990) was also enhanced to include optimization routines that were needed to assign transmissivity values to the pilot points once their location was selected.

The present study addresses the uncertainty in the travel time by embedding the problem in a probabilistic framework. The true transmissivity distribution at the WIPP site is conceptualized to be one realization of a stochastic process. Accordingly, a large number of realizations of this stochastic process, which are very plausible versions of the true transmissivity at the WIPP site, are generated. This ensemble of realizations is thus used with the groundwater flow model to generate an ensemble of the corresponding travel times. The distribution of the travel times provides an understanding of the uncertainty. While several statistical measures can be used to quantify the uncertainty, a complimentary cumulative distribution function (CCDF) is commonly used for a graphical display of the uncertainty in travel time.

This appendix describes the methodology of this new approach as it is used in the Culebra system. (A more complete explanation of this new approach and its application is provided in LaVenue and RamaRao [1992].) Seventy calibrated conditionally simulated (CCS) transmissivity fields were produced using this approach; these fields are discussed in Section 2.6.3 of Volume 3 of this report and are presented in Appendix C of Volume 3 of this report.

D.2 Overview of Methodology

The solution methodology involves the generation of a large number of random transmissivity fields, each of which is in close agreement with all the measured data at the WIPP site. The collected data at the WIPP site is comprised of (1) transmissivity measurements, and (2) pressure measurements (both steady state and transient state). Conformity between a random transmissivity field and the measured data is achieved in stages, as described below. Figure D-1 presents an overview of the different steps in this study.

First, unconditional simulations of the WIPP transmissivity fields are generated. These are random fields, having the same statistical moments (the mean and the variance) and the same spatial correlation structure, as indicated by the transmissivity measurements. (These fields need not, however, match the measured transmissivities at the location of their measurements.)

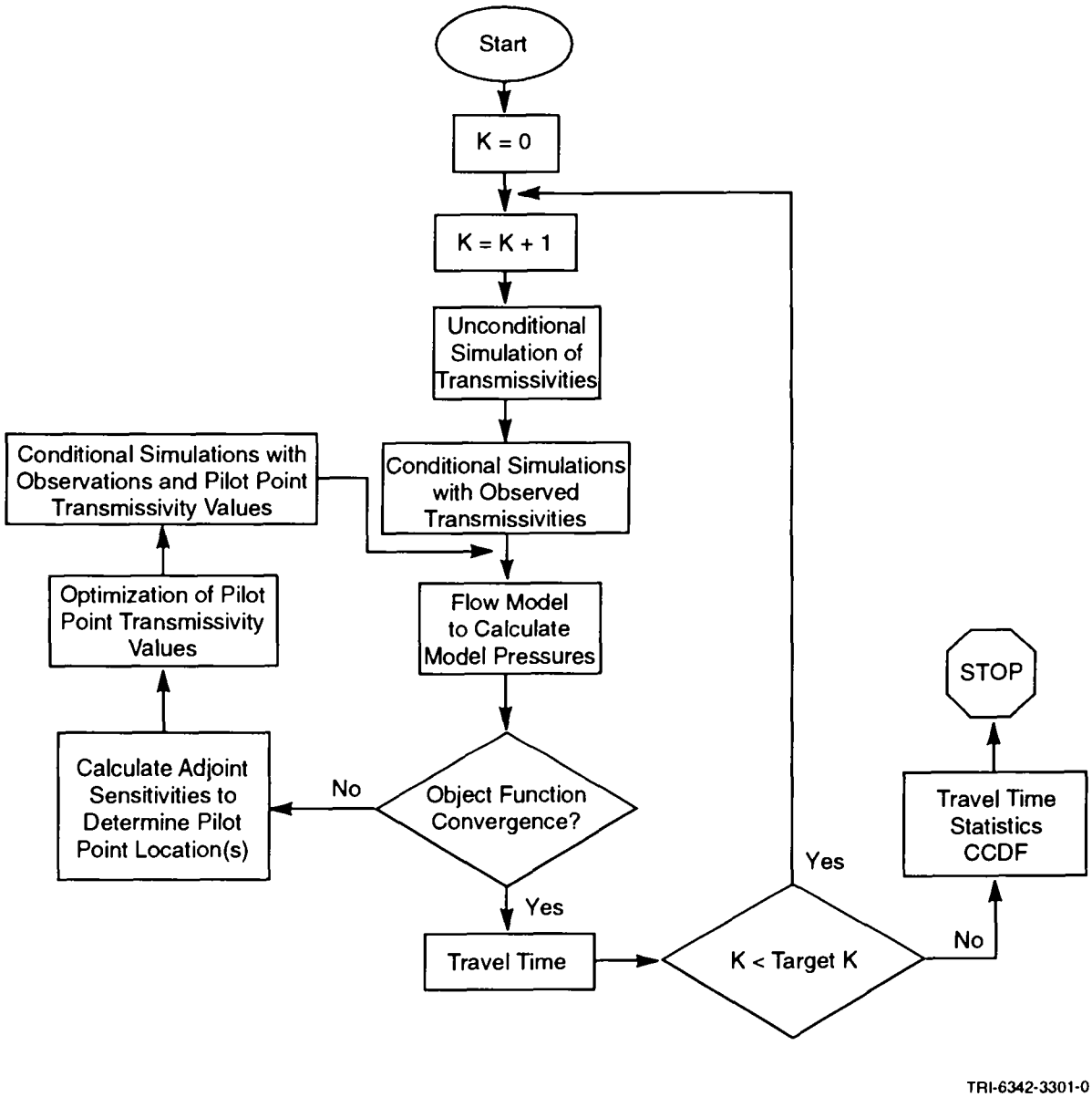

Figure D-1. Calibration of conditionally simulated transmissivity fields: flow chart.

These transmissivity fields are then conditioned, so that they honor exactly the measured transmissivities at the locations of their measurements. The resulting fields are called conditional simulations of the transmissivity fields.

The conditional simulations of transmissivity field are then further conditioned, such that the pressures computed by the groundwater flow model (both steady and transient state) agree closely with the measured pressures, in a least-square sense. This phase is known as calibration or the solution of inverse problem, and accounts for a large part of the time and effort in this study. When the calibration is completed, one obtains a random transmissivity field that is in conformity with all the data at the WIPP site, and may therefore be regarded as a plausible version of the true distribution of transmissivity at the WIPP site.

In this study model calibration is done by an indirect approach. An objective function is defined as the weighted sum of the squared deviations between the model computed pressures and the observed pressures, with the summation being extended in the spatial and temporal domain where pressure measurements are taken. The classical formulation of the calibration then requires the minimization of the objective function, subject to the constraints of the groundwater flow equations in the steady and transient state. This approach is implemented by iteratively adjusting the transmissivity distribution until the objective function is reduced to a prescribed minimum value.

A common approach to calibration consists in dividing the model domain into a few zones, in each of which the transmissivity is treated as constant. The transmissivities in the different zones constitute the parameters to be adjusted in the optimization process. Clearly, the delineation of zones is a subjective process and does affect the results of the calibration. Thus, it may become necessary to consider several alternative zonation patterns for calibration. Also, in this approach, uniform transmissivities are assigned to each zone. This representation may be considered as inadequate, particularly while addressing the issues of spatial variability (within a zone).

To avoid the above difficulties of the zonation approach, an approach using pilot points as parameters is adopted here. A pilot point is a synthetic transmissivity data point, that is added to an existing measured transmissivity data set during the course of calibration. A pilot-point is defined by its spatial location and by the transmissivity value assigned to it. After a pilot point is added to the transmissivity data set, the augmented data set is used to obtain kriged or conditionally simulated transmissivity fields, for a subsequent iteration in calibration. With the addition of a pilot point, the transmissivity distribution in the neighborhood of the pilot point gets modified with dominant modifications being closer to the pilot-point location. The modifications in the different grid blocks are determined by kriging weights and are not uniform (as in the zonation approach). Conceptually, a pilot point may be viewed as a simple model to effect realistic modifications of transmissivity in a large region of the model.

A coupled kriging-and-adjoint sensitivity analysis is used for the location of the pilot point; optimization algorithms are used for assigning the transmissivity of a pilot point. Thus, the pilot-point approach to calibration has been rendered objective, a feature considered very desirable for the WIPP site. Further, a multistage approach has been used in implementing this methodology. This aspect bears similarity to the dynamic programming method of optimization.

D.3 Code Development: An Overview

A comprehensive code package has been assembled using many of the codes already developed and frequently used in groundwater flow simulations. They are listed below. For details of the theory and application of these codes, the following references cited may be consulted:

- TUBA, unconditional simulation of transmissivity field (Zimmerman and Wilson, 1990),
- AKRIP, generalized kriging (Kafritsas and Bras, 1981),
- SWIFT II, modeling pressures (steady and transient state) (Reeves et al., 1986a,b,c)
- GRASP II, adjoint sensitivity analysis (steady and transient state) (Wilson et al., 1986; RamaRao and Reeves, 1990), and
- STLINE, groundwater travel time and travel paths (Intera, Inc., 1989).

In addition to using the above codes, the following new codes have been developed in the present task. The details of the new codes are provided in LaVenue and RamaRao (1992).

- MAIN—drives the different modules
- CONSIM—generates conditional simulations of transmissivity from the unconditional simulations of transmissivity
- PILOTL—locates the pilot points based on sensitivity analysis
- PAREST—assigns the pilot point transmissivities by minimization of a least square objective function

D.4 Simulated Transmissivities

In the earlier modeling efforts for WIPP (LaVenue et al., 1990), kriging has been employed to address the issue of spatial variability in transmissivity. In an effort where only one calibrated field is to be produced, kriging becomes an obvious choice. Kriging provides optimal estimate of the transmissivity at a point, thereby necessarily smoothing out the true variability between measurement points. On the contrary, simulated values reproduce the fluctuation patterns in transmissivity, which may lead to extreme values in travel times. Thus, simulated fields are useful to resolve the residual uncertainty not addressed by kriging.

D.4.1 Unconditional Simulation

An unconditional simulation of transmissivity field is a random field having the same statistical moments (mean and variance) and the same spatial correlation structure as indicated by the measured transmissivities in the field. An unconditionally simulated transmissivity field is said to be isomorphic with the true field, and is independent of the true field. The following methods have been used earlier in groundwater hydrology for generating unconditional simulations:

- nearest neighbor method (Smith and Schwartz, 1981; Smith and Freeze, 1979),
- matrix decomposition,
- multidimensional spectral analysis (Shinozuka and Jan, 1972; Mejía and Rodríguez-Iturbe, 1974), and
- turning bands method (Matheron, 1971, 1973; Mantoglou and Wilson, 1982; Zimmerman and Wilson, 1990).

In this study, the turning bands method has been used. It is an extremely fast and efficient algorithm and the code TUBA to implement this, is available in public domain.

A two-dimensional (or a three-dimensional) stochastic process is generated in this method by the summation of a series of equivalent one-dimensional processes. Figure D-2 shows a definition sketch taken from Mantoglou and Wilson (1982). The region P shows a grid of points at each of which the two-dimensional field is to be generated. In particular, consider a point N in the grid where the two-dimensional field $[Z_s(N)]$ is to be simulated.

Consider a particular line i, the length along which, from the origin O, is measured by ζ_i. This line is divided into a number of intervals (bands), of length $\Delta\zeta_i$, in each of which the one-dimensional process Z_i is computed. Let N_i be the projection of the point N onto the line i. Let $Z_i(\zeta_i)$ be the one-dimensional process in the band containing N_i. Then the two-dimensional process $[Z_s(N)]$ is obtained by summing the contributions from the different lines, by the relation

$$Z_s(N) = \frac{\sum_{i=1}^{L} Z_i\left(\zeta_{N_i}\right)}{\sqrt{L}}, \qquad \text{(D-1)}$$

where L is the number of lines selected. Usually L is between 16 and 20.

LaVenue et al. (1990) analyzed the WIPP transmissivity data and identified the spatial structure of the two-dimensional transmissivity field. They modeled it as an isotropic process and as an intrinsic random function of order zero (IRF-0), with the generalized covariance function (GCF) given by

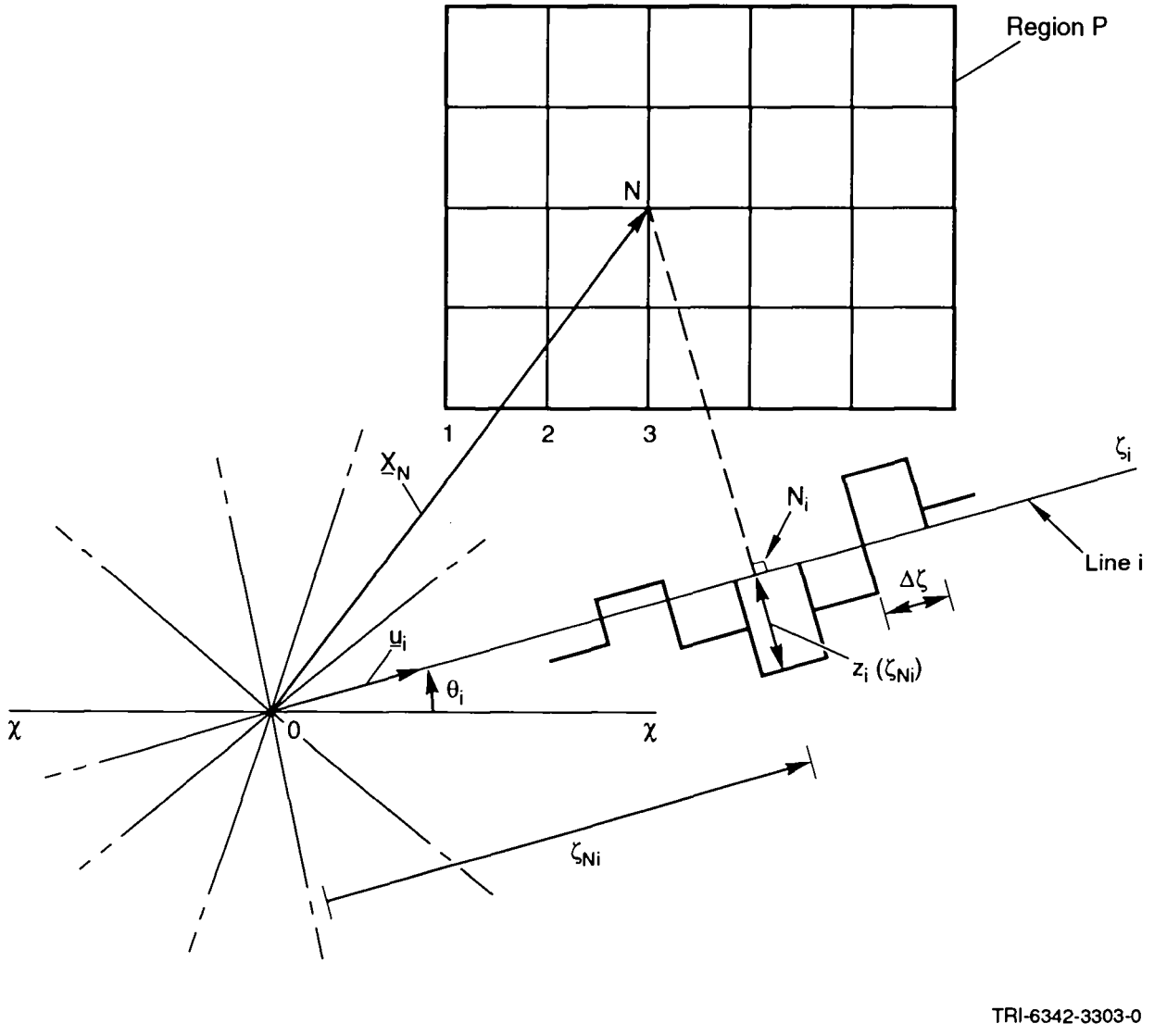

Figure D-2. Schematic representation of the field and turning bands lines (Mantoglou and Wilson, 1982).

$$k_2(r) = -a_0 r \quad \text{(GCF)}$$

r = a radial distance (D-2)

a_0 = a constant

The subscript 2 denotes a two-dimensional process.

If $k_1(r)$ is the GCF for an equivalent one-dimensional process,

$$k_1(r) = -\left(\frac{\pi}{2}\right) a_0 r . \tag{D-3}$$

The Weiner-Levy process is known to be an IRF-0 process and is accordingly used to generate the line process. The relevant equations are given below.

$$Z_i(\zeta) = W(\zeta), \tag{D-4}$$

where $W(\zeta)$ is the Weiner-Levy Process.

$$W(0) = 0, \tag{D-5}$$

$$W(\zeta + \Delta\zeta) = W(\zeta) + gU(\zeta), \tag{D-6}$$

$$U(\zeta) = U\left[-\frac{1}{2}, \frac{1}{2}\right], \tag{D-7}$$

and

$$g = \sqrt{12\pi a_0 \Delta\zeta}, \tag{D-8}$$

where $U(\zeta)$ is a uniformly distributed random variable.

D.4.2 Conditional Simulation

An unconditionally simulated transmissivity field, which is made to honor exactly the measured transmissivity at the locations of the measurements, is called a conditionally simulated transmissivity field. The procedure of conditioning is described below.

Let $Z(x)$ be the true value (not known) of the field at a point x. One may decompose $Z(x)$ as below:

$$Z(x) = Z_{ok}(x) + [Z(x) - Z_{ok}(x)], \tag{D-9}$$

where $Z_{ok}(x)$ is the kriged estimate of Z, at x, based on the observed values of Z at the locations of the observations.

Here, $[Z(x) - Z_{ok}(x)]$ is a true kriging error and is unknown, since the true value of $Z(x)$ is unknown. It is possible to simulate this error.

Using the unconditionally simulated values (Z_{uc}) at the locations of the observations (not the actual observations), a kriged field (Z_{uk}) is generated. One may write, using a similar decomposition as above,

$$Z_{uc}(x) = Z_{uk}(x) + [Z_{uc}(x) - Z_{uk}(x)] \tag{D-10}$$

where $[Z_{uc}(x) - Z_{uk}(x)]$ is also a kriging error, and is known and may be called a simulated kriging error. This error is isomorphic with the true kriging error. More importantly, this error is independent of the kriged values:

$$E[Z_{ok}(x), \{Z_{uc}(y) - Z_{uk}(y)\}] = 0 \text{ for all } x,y \tag{D-11}$$

Substituting the known simulated kriging error for the true but unknown kriging error, in Equation D-9, one obtains:

$$Z(x) \approx Z_{ok}(x) + [Z_{uc}(x) - Z_{uk}(x)] \tag{D-12}$$

Equation D-12 clarifies the conditioning step as one of adding of simulated kriging error on a kriged field using the measured data. This step involves kriging twice, once with the measured transmissivities and another time with the unconditionally simulated transmissivities, both at the location of the observations. The superposition of the three different transmissivity fields is graphically illustrated in Figure D-3.

The (average) transmissivity of each grid block is obtained here, using Gaussian quadrature. A 2×2 Gauss point scheme is used for quadrature in each grid block.

The conditional simulations constitute the most important input to the groundwater flow model. It is useful to appreciate the following properties of a conditional simulation (CS):

1. **The CS field honors the measured values exactly at the measurement locations.** This follows from the fact the kriging is an exact interpolator, so that the simulated kriging error is zero at measurement locations and, further, the kriged value from observations (Z_{ok}) reduces to the measured value, for the same reason.

$$Z_{CS}(x) \simeq Z_{OK}(x) + [Z_{UC}(x) - Z_{UK}(x)]$$

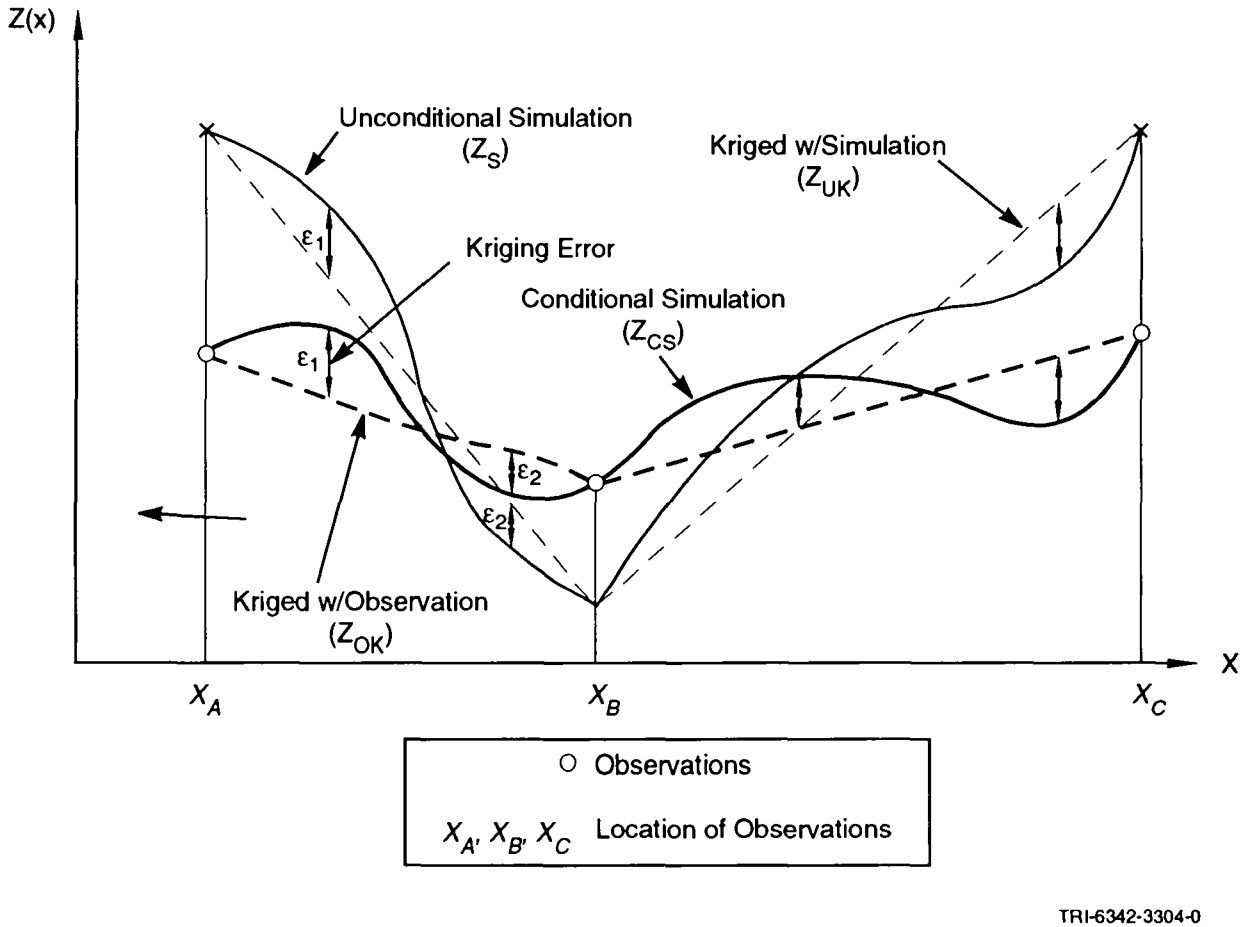

Figure D-3. Conditional and unconditional simulation: relationships.

2. **The CS field has the same spatial correlation structure as indicated by the measured data.** This follows from an orthogonality property of the kriging errors (Equation D-11), which states that the kriging errors (both true and simulated) are uncorrelated with any kriged values for stationary field and with generalized increments for the intrinsic fields (Delfiner, 1976; Delhomme, 1979). Accordingly, the addition of simulated kriging error field to a kriged field does not alter the spatial correlation structure of the kriged field. It may be recalled that the kriged field itself has the same correlation structure as implied by the data.

3. **The average of many CS fields at a location x, is merely the kriged estimate at x** $[Z_{ok}(x)]$.

4. **The variance of many CS fields at a location x is given by the kriging variance.**

5. **The CS fields reproduce the true variability of the field, in contrast to a smoothed field given by kriging.**

6. **The conditioning step introduces a robustness with respect to the features of the reality that are not specifically known or imposed on the (unconditionally) simulated field.** This robustness increases with the amount of the conditioning data.

D.4.3 Computational Options for Simulated Fields

The simulated kriging error is rendered zero at all observation points (see Figure D-4). When a pilot point is added to the observed transmissivity data set, two options exist:

- The pilot point may be given the full status of an observed data point. Then the simulated kriging error at the pilot point is also rendered zero. In this case, the simulated kriged error field varies from one iteration to the other, and needs to be computed at every iteration.

- The simulated kriging error is rendered zero only at the observed data point and not at the pilot points. Thus, the pilot points are used to obtain the kriged field using the 'augmented' data. But the simulated kriged error field remains the same as the initial field through all the iterations. It does not need to be recomputed during the various iterations.

While obtaining the kriged field using the simulated data at the measurement locations, two options exist:

- Assume that the simulated value (Z_{uc}) has the same errors as the actual measurements.

- Assume that the simulated value (Z_{uc}) has no errors.

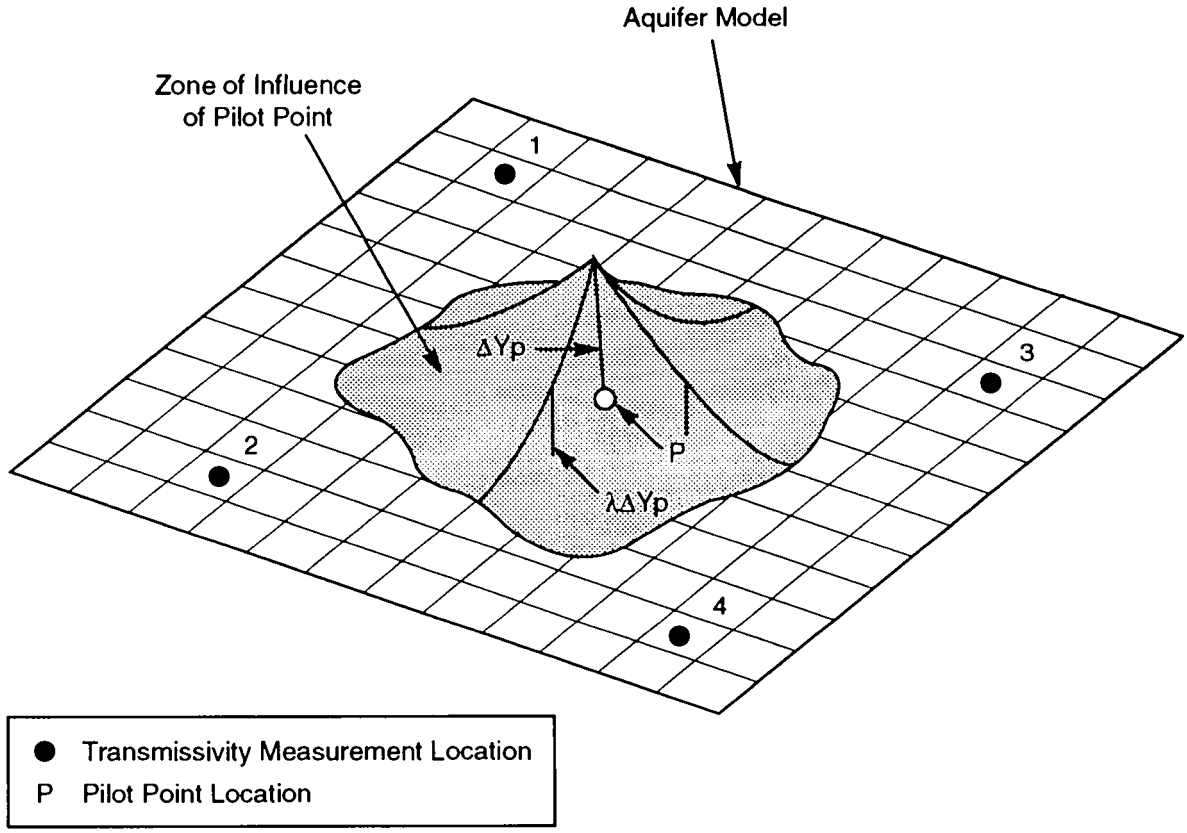

Pilot Point - Schematic

		X	Y	T	y	σ_y
Measured Transmissivity	1 2 ⋮ 4	150	1050	$10^{-3.1}$	-3.1	0.5
Pilot Points added in Calibration	P_1 P_2 ⋮ P_n	650	620	$10^{-4.81}$	-4.81	0.84

TRI-6342-3305-0

Figure D-4. Pilot point: schematic.

D.4.4 Validation of Simulations

For every CS field, the mean and variance of the transmissivity are computed and compared with that of the WIPP data. Also, using the code AKRIP, the generalized covariance function (GCF) of the field is obtained and is compared with that obtained from measured data at the WIPP. A close agreement between the two provides verification that the generated CS field is a plausible version of the reality at the WIPP site. The procedure is repeated for all the CS fields.

A collection of all the CS fields generated constitutes an ensemble. For any one location in the field, transmissivity values across all the fields in the ensemble are studied and their mean and variance computed. A spatial distribution of the ensemble mean and variance should closely agree with the spatial distribution of kriged values and kriging variance obtained from the kriging exercise itself.

D.5 Automated Calibration

In an automatic algorithm, it becomes necessary to restrict the number of parameters (to be identified) to a small number; this step is called parameterization. The zonation approach and the pilot-point methodology can both be viewed as two alternative paths for parameterization. As shown above, the pilot-point approach eliminates an inherent subjectivity in the zonation approach and provides for the most objective inverse algorithm.

D.5.1 Objective Function

The objective function that is to be minimized in the calibration is a weighted least-square-error criterion function. It comprises of two components, a model-fit criterion and a plausibility criterion. The model-fit criterion is a weighted sum of the squared deviations between the computed and measured pressures taken over all points in spatial and temporal domains, where pressure measurements have been made. The plausibility criterion demands that the calibrated transmissivities be not too far from their prior estimates. A relative weight η between the plausibility criterion and the model-fit criterion has been used. In the present study, due to the nature of the pilot point methodology (de Marsily et al., 1984), the plausibility criterion is disregarded by setting $\eta = 0$; the code, however, has the capability to use it.

Equation D-13 defines the objective function in general terms:

$$J(\underline{u}) = \sum_{k=1}^{L} \underline{e}_p^T(k)\underline{\underline{R}}^{-1}(k)\underline{e}_p(k) \quad \text{(model fit)}$$

$$+\eta \bullet \underline{e}_u^T \bullet \underline{\underline{U}}^{-1} \bullet \underline{e}_u \qquad \text{(plausibility)}, \qquad \text{(D-13)}$$

where:

$J(\underline{u})$ = weighted least square (WLS) error criterion function

$\underline{e}_p = \left\{\underline{p}(k) - \underline{p}_{ob}(k)\right\}$

$\underline{e}_u = \left\{\underline{u} - \underline{u}_{est}\right\}$

$\underline{\underline{R}}$ = covariance matrix of errors in $\underline{p}_{ob}$

$\underline{\underline{U}}$ = covariance matrix of errors in $\underline{u}$

$\underline{u}$ = vector of parameters ($Y_p = \log_{10} T_p$)

η = relative weight of the plausibility criterion to model fit criterion

k = time step number

$\underline{p}(k)$ = pressures computed

$\underline{p}_{ob}(k)$ = pressures observed

T = transpose

T_p = pilot point transmissivity

L = number of time steps.

After optimal estimates of $\underline{u}$ are obtained, the posterior covariance matrix of the parameters is given by

$$\underline{\underline{P}}_{uu} = \left\{\sum_{k=1}^{L} \underline{\underline{S}}^T(k)\underline{\underline{R}}^{-1}(k)\underline{\underline{S}}(k) + \underline{\underline{U}}^{-1}\right\}^{-1} \tag{D-14}$$

$$\underline{\underline{S}}^T(k) = \text{Jacobian Matrix} = \left[\frac{dp(k)}{d\underline{u}'}\right],$$

where $\underline{\underline{P}}_{uu}$ is the posterior covariance matrix of the parameters.

D.5.2 Parameters of Calibration

The pilot-point transmissivities are the parameters that are adjusted for calibration. However, in the mathematical implementation, the logarithms (to base 10) of the transmissivities (and not the transmissivity) are treated as parameters. The calibration parameters are given by

$$Y_p = \log_{10} T_p$$

where T_p is the transmissivity at a pilot point (suffix p denotes pilot point). Figure D-4 illustrates the concepts of pilot points presented above.

D.5.3 Pilot-Point Location

Pilot points are placed at locations where their potential for reducing the objective function is the highest. This potential is quantified by the sensitivity coefficients (dJ/dY) of the objective function J, with respect to Y, the logarithm (to base 10) of pilot-point transmissivity. A large number of candidate pilot points are considered, usually the centroids of all the grid blocks in the flow-model grid. The selected candidate pilot points are ranked in the descending order of the magnitude of their absolute sensitivity coefficients, i.e., $|dJ/dY|$. The required number of pilot points is chosen from the top of the ranked list of points.

Coupled adjoint sensitivity analysis and kriging is used to compute the required derivatives, and the procedure is documented in RamaRao and Reeves (1990). It is described briefly here.

Let P be a pilot point added to a set of N observation points. Let T_p be the transmissivity assigned to pilot point P. Kriging is done using Y_p, where

$$Y_p = \log_{10} T_p \tag{D-15}$$

The kriged estimate (Y^*) at the centroid of a gridblock m, is given by

$$Y_m^* = \sum_{k=1}^{N} Y_k \bullet \gamma_{m,k} + Y_p \bullet \gamma_{m,p}\,, \tag{D-16}$$

where k is the subscript for observation point, p is the subscript for pilot point, and $\gamma_{m,k}$ and $\gamma_{m,p}$ are the kriging weights for the interpolation point m and data point k and interpolation point m and data point p, respectively.

When a pilot point transmissivity is perturbed, the kriged transmissivities and, hence, the permeabilities in all gridblocks are altered, causing the objective function J to change. Accordingly, using the chain rule,

$$\frac{dJ}{dY_p} = \sum_{m=1}^{M} \frac{dJ}{dY_m^*} \frac{dY_m^*}{dY_p} \tag{D-17}$$

where M is the total number of grid blocks in the flow model.

$$\frac{dY_m^*}{dY_p} = \gamma_{m,p} \quad \text{(from Equation D-16)}$$

$$\frac{dJ}{dY_p} = \sum_{m=1}^{M} \frac{dJ}{dY_m^*} \bullet \gamma_{m,p} \tag{D-18}$$

$$Y_m^* = \log_{10}\left(T_m^*\right)$$

$$T_m^* = K_m \frac{\rho_m}{\mu_m} g b_m$$

$$\frac{dJ}{dY_m^*} = \ln(10) K_m \frac{dJ}{dK_m} \tag{D-19}$$

where T^* is the estimated transmissivity, K^* is the estimated permeability, ρ is fluid density, μ is fluid viscosity, g is acceleration due to gravity, b is gridblock thickness, and m is the subscript denoting gridblock.

Combining Equations D-18 and D-19

$$\frac{dJ}{dY_p} = \ln(10) \sum_{m=1}^{M} \gamma_{m,p} K_m \frac{dJ}{dK_m} \tag{D-20}$$

The sensitivity coefficient, dJ/dK_m of the objective function with respect to the permeability in a gridblock m is obtained by adjoint sensitivity analysis.

Adjoint sensitivity analysis provides an extremely fast algorithm, particularly when, for a given objective function J, the sensitivity coefficients are to be computed for a large number of parameters (permeabilities in thousands of grid blocks, as is the case here).

Let the groundwater flow model be represented by the following matrix equation:

$$\underline{\underline{A}}\,\underline{p}^n = \underline{\underline{B}}\,\underline{p}^{n-1} + \underline{f}^n \tag{D-21}$$

where for a fully implicit scheme of time integration adopted here,

$\underline{p}$ = vector of gridblock pressures
$\underline{\underline{A}}$ = $\underline{\underline{C}} + \underline{\underline{B}}$
$\underline{\underline{B}}$ = $\underline{\underline{S}}/\Delta t$
$\underline{\underline{C}}$ = conductance matrix
$\underline{\underline{S}}$ = storativity matrix
$\underline{f}^n$ = vector of source terms
Δt = $t^n - t^{n-1}$
t = time
n = time level (1,2,3 .... L)

L = maximum time level of the simulation.

First, an adjoint state vector $\{\lambda\}$ is obtained by the solution of the following equation:

$$\underline{\underline{A}}\underline{\lambda}^{n-1} = \underline{\underline{B}}\underline{\lambda}^{n} + \left[\frac{\partial J}{\partial \underline{p}^{n}}\right]^{T} \tag{D-22}$$

where T denotes the transpose of the matrix.

Equation D-22 is solved backwards in time, from $n = L$ to $n = 1$ with

$$\underline{\lambda}^{L} = 0 \tag{D-23}$$

If α_i is a generic sensitivity parameter in the gridblock i, the sensitivity coefficient $dJ/d\alpha_i$ is evaluated by the expression:

$$\frac{dJ}{d\alpha_i} = \frac{\partial J}{\partial \alpha_i} + \sum_{n=1}^{L} \underline{\lambda}^{nT} \bullet \left[\frac{\partial \underline{\underline{A}}}{\partial \alpha_i}\underline{p}^{n} - \frac{\partial \underline{\underline{B}}}{\partial \alpha_i}\underline{p}^{n-1} - \frac{\partial \underline{f}^{n}}{\partial \alpha_i}\right] \tag{D-24}$$

Here, the Equation D-24 is evaluated with $\alpha_i = K_i$, the permeability in the i^{th} gridblock.

D.5.4 Pilot Points: Transmissivities

The transmissivities at pilot points are assigned by an unconstrained optimization algorithm and a subsequent imposition of constraints.

The optimization algorithm chosen here belongs to a class of iterative search algorithms. It involves a repeated application of the following equation until convergence is achieved:

$$\underline{Y}_{i+1} = \underline{Y}_i + \beta_i \bullet \underline{d}_i, \tag{D-25}$$

where i is the iteration index, $\underline{d}_i$ is the direction vector, β_i is the step length (a scalar), and $\underline{Y}_i$ is the vector of parameters to be optimized (i.e., logarithms of pilot-point transmissivities to base 10).

The steps in the implementation of this algorithm are as follows:

1. For the selected number of pilot points, choose the initial estimates of the parameters ($Y_p = \log_{10} T_p$). These are taken to be the kriged or the conditionally simulated values in the gridblocks, where pilot points are located depending upon the option chosen.

2. Compute the direction vector, $\underline{d}_i$, as per one of the three algorithms discussed below (Fletcher-Reeves, Broyden's, or Davidon-Fletcher-Powell). The direction vector constitutes a direction in the hyperspace of the parameters, and advancing along this direction, yields new values of the parameters. The step-length β determines the actual advance along this direction.

3. Determine the optimal step-length β, which minimizes the objective function. (How the step length is determined is explained in detail in LaVenue and RamaRao [1992].)

4. Update the parameters:

$$\underline{Y}_{i+1} = \underline{Y}_i + \beta_i \underline{d}_i$$

5. Impose the constraints, as explained in Section D.5.5.

6. Check for convergence.

7. If convergence is achieved, the optimization algorithm is completed, the pilot points are added to the data, and execution of the main algorithm continues.

8. If convergence is not achieved, let $i = i + 1$, and go to Step 9.

9. Using the augmented data set, generate a new conditional simulation of transmissivity field, derive the corresponding pressure field, and recompute the gradient vector using the already selected pilot-point locations. (The pilot-point selection process will be skipped.)

10. Go to Step 2.

The code includes three options for the computation of the direction vector $\underline{d}_i$. They are the algorithms due to (1) Fletcher-Reeves, (2) Broyden, and (3) Davidon-Fletcher-Powell (Luenberger, 1973; Gill et al., 1981; Carrera and Neuman, 1986). (These options are explained in detail in LaVenue and RamaRao [1992].)

D.5.5 Pilot Point Transmissivities: Constraints

It is possible that the optimization algorithms may dictate large changes in the parameters and bring about an impressive reduction in the objective function. Such recommended large changes may be viewed as undesirable for several reasons. At any point in the field, one can obtain a kriged estimate of transmissivity and its variance (kriging variance). One may construct a confidence interval (assuming a normal distribution of kriging errors) for the transmissivity. It is reasonable to expect the calibrated value to be within the confidence band. A constraint may be imposed to achieve this.

Further, situations may exist where the confidence band may be large. A large change in the parameter value, even if contained within the confidence band, can cause a large change in the spatial-correlation structure of

the transmissivity field. One of the objectives in calibration can then be to limit the maximum charge to a specified value, so that the geostatistical structure is not altered significantly.

Consider the kth parameter, whose value is Y_k (kth element in the vector of parameters, $\underline{Y}$). Then,

$$\begin{aligned} \Delta Y_{k,i} &= \left(Y_{k,i+1} - Y_{k,i}\right) \\ &= \beta_i \bullet d_{k,i} \end{aligned} \quad , \tag{D-26}$$

where i is an iteration index.

Constraint 1: The parameter value should lie within the confidence band.

$$Y_{k,o} - m\sigma_{yo} \le Y_{k,i} \le Y_{k,o} + m\sigma_{yo}, \tag{D-27}$$

where the subscript o indicates initially kriged value, based on the measured data only. Thus $Y_{k,o}$ gives the initially kriged value at the location of the k^{th} pilot point, and σ^2_{yo} gives the initially computed kriging variance at the same location, m is the multiplier of the standard deviation, which gives the semi width of the confidence band. If normal distribution is assumed for kriging errors, and if 95% confidence levels are desired; $m = 2$.

Constraint 2: The change in any parameters must be limited to ΔY_{max}.

$$\Delta Y_{k,i} \le \Delta Y_{max} \tag{D-28}$$

After the optimization, these constraints are implemented for each parameter. In reality, only one constraint is active for a pilot-point. Also, in implementation, the optimal step length computed is reduced if the constraint became active, still preserving the direction.

D.5.6 Convergence Criteria

It may be noted that there are two levels of iteration, designated as inner and outer iterations. An inner iteration relates to the iterations needed to optimize the transmissivities of the pilot points. Thus, when an inner iteration is repeated, the pilot-point locations are fixed as at the beginning of the sequence of inner iterations. When the convergence of an inner iteration is achieved, the pilot points are added to the transmissivity data set. This then sets the stage for an outer iteration. During the course of outer iteration, optimal location of the next set of pilot points is done using coupled kriging and adjoint sensitivity analysis. Subsequently, their transmissivities are optimized by a sequence of inner iterations. Figure D-5 clarifies these points.

It may be noted that both inner and outer iterations go through all phases of the algorithm, except that inner iterations skip the phase of selecting pilot points from a grid of candidate pilot points.

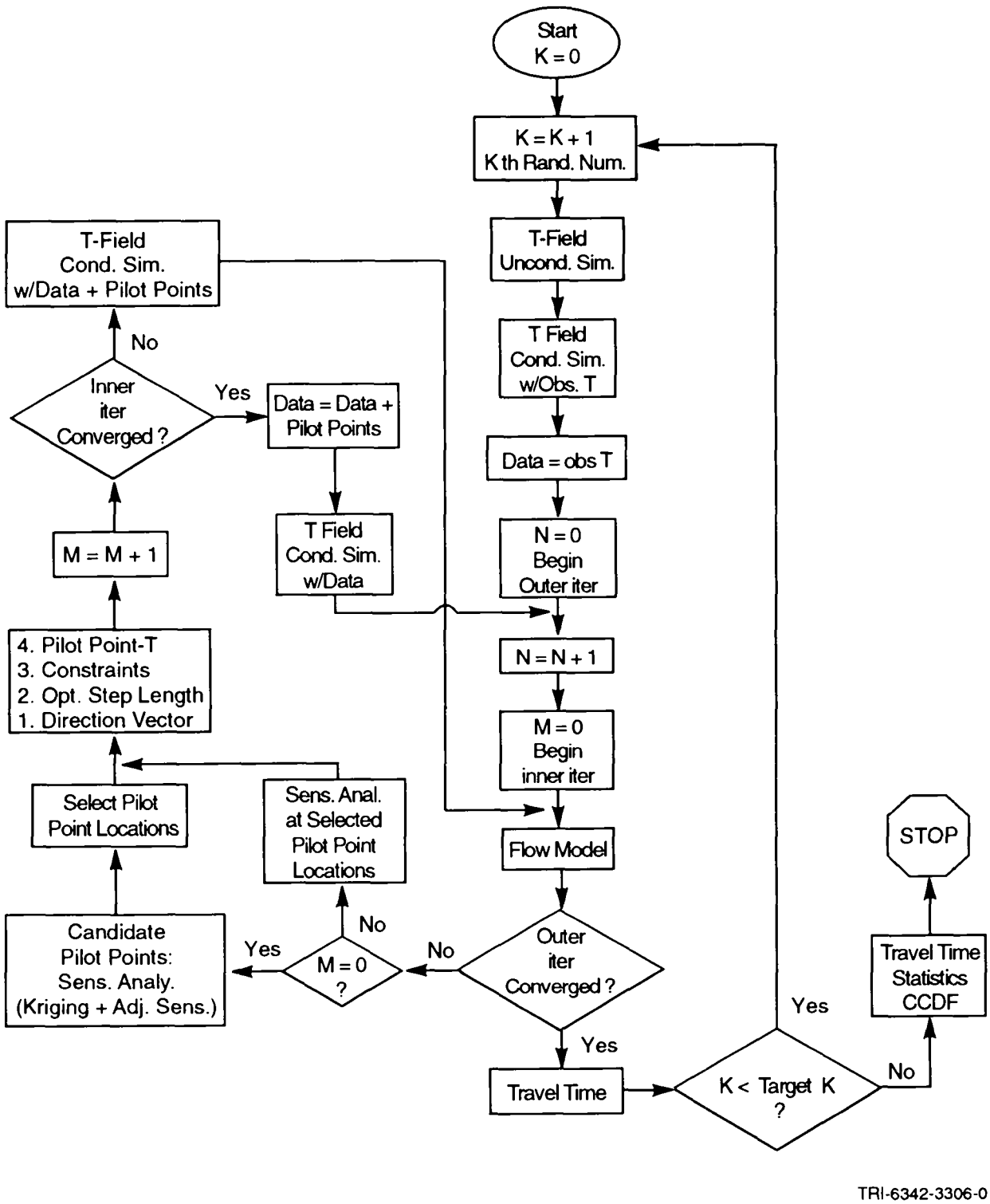

Figure D-5. Inner and outer iterations of calibration.

D.5.6.1 CONVERGENCE CRITERIA: INNER ITERATIONS.

1. The performance measure J drops below a prescribed minimum value (JMIN):

$$J \leq \text{JMIN} \tag{D-29}$$

2. The number of iterations (NITER) equals a prescribed maximum number of iterations, for the inner iterations (ITERMX1):

$$\text{NITER} \geq \text{ITERMX1} \tag{D-30}$$

3. The ratio of the norm of the gradient, to the initial-gradient norm reduces below a prescribed value (GRNR):

$$\frac{\|\underline{g}\|}{\|\underline{g}_o\|} \leq \underset{(\text{gradient norm ratio})}{\text{GRNR}} \tag{D-31}$$

4. The gradient norm $\|\underline{g}\|$ is less than a prescribed minimum (GRMIN):

$$\|\underline{g}\| \leq \text{GRMIN} \tag{D-32}$$

5. The relative change in objective function is defined, as $\Delta J/J$, where ΔJ is the change in the objective function during one iteration. Iterations are terminated if this relative change falls below a prescribed value (RELCJ):

$$\frac{\Delta J}{J} \leq \text{RELCJ} \tag{D-33}$$

D.5.6.2 CONVERGENCE CRITERIA: OUTER ITERATIONS.

Outer iterations are terminated essentially on criteria (1) and (2) of inner iterations. They are not repeated.

Appendix D References

Carrera, J., and S.P. Neuman. 1986. "Estimation of Aquifer Parameters Under Transient and Steady State Conditions 2, Uniqueness, Stability, and Solution Algorithms," *Water Resources Research.* Vol. 22, no. 2, 211-227.

Delfiner, P. 1976. "Linear Estimation of Non Stationary Spatial Phenomena," *Advanced Geostatistics in the Mining Industry, Proceedings of the NATO Advanced Study Institute, University of Rome, October 13-25, 1975.* Eds. M. Guarescio, M. David, and C. Huijbregts. Hingham, MA: D. Reidel, 49-68.

Delhomme, J.P. 1979. "Spatial Variability and Uncertainty in Groundwater Flow Parameters: A Geostatistical Approach," *Water Resources Research.* Vol. 15, no. 2, 269-280.

de Marsily, G, G. Lavedan, M. Boucher, and G. Fasanino. 1984. "Interpretation of Interference Tests in a Well Feild Using Geostatistical Techniques to Fit the Permeability Distribution in a Reservoir Model," *Geostatistics for Natural Resources Characterization, South Lake Tahoe, CA, Sept. 6-17, 1983.* Eds. G. Verly, M. David, A.G. Journel, and A. Marechai. Hingham, MA: D. Reidel, Pt. 2, 831-849.

Gallegos, D.P., P.I. Pohl , and C.D. Updegraff. 1992. *An Investigation of the Impact of Conceptual Model Uncertainty on the Estimated Performance of a Hypothetical High-Level Nuclear Waste Repository Site in Unsaturated, Fractured Tuff.* SAND90-2882. Albuquerque, NM: Sandia National Laboratories.

Gill, P.E., W. Murray, and M.H. Wright. 1981. *Practical Optimization.* New York, NY: Academic Press, Inc.

Intera, Inc. 1989. *Users Manual for STLINE.* 097B-12C-001B.

Kafritsas, J., and R.L. Bras. 1981. *The Practice of Kriging.* Technical Report 263. Cambridge, MA: Ralph M. Parsons Laboratory, Massachusetts Institute of Technology.

LaVenue, A.M., T.L. Cauffman, and J.F. Pickens. 1990. *Ground-Water Flow Modeling of the Culebra Dolomite. Volume I: Model Calibration.* SAND89-7068/1. Albuquerque, NM: Sandia National Laboratories.

LaVenue, A.M., and B.S. RamaRao. 1992. *A Modeling Attempt to Address Spatial Variability within the Culebra Dolomite Transmissivity Field.* SAND92-7306. Albuquerque, NM: Sandia National Laboratories.

Luenberger, D.G. 1973. *Introduction to Linear and Nonlinear Programming.* Reading, MA: Addison-Wesley Publishing Co.

Mantoglou, A., and J.L. Wilson. 1982. "Turning Bands Method for Simulation of Random Fields Using Line Generation by a Spectral Method," *Water Resources Research.* Vol. 18, no. 5, 1379-1394.

Matheron, G. 1971. *The Theory of Regionalized Variables and its Applications.* Paris, France: École National Supérieure des Mines.

Matheron, G. 1973. "The Intrinsic Random Functions and Their Applications," *Advances in Applied Probability.* Vol. 5, no. 3, 439-468.

Mejía, J. M., and I. Rodríguez-Iturbe. 1974. "On the Synthesis of Random Fields Sampling From the Spectrum: An Application to the Generation of Hydrologic Spatial Processes," *Water Resources Research.* Vol. 10, no. 4, 705-711.

RamaRao, B.S., and M. Reeves. 1990. *Theory and Verification for the GRASP II Code for Adjoint-Sensitivity Analysis of Steady-State and Transient Ground-Water Flow.* SAND89-7143. Albuquerque, NM: Sandia National Laboratories.

Reeves, M., D.S. Ward, N.D. Johns, and R.M. Cranwell. 1986a. *Theory and Implementation for SWIFT II, the Sandia Waste-Isolation Flow and Transport Model for Fractured Media, Release 4.84.* NUREG/CR-3328. SAND83-1159. Albuquerque, NM: Sandia National Laboratories.

Reeves, M., D.S. Ward, N.D. Johns, and R.M. Cranwell. 1986b. *Data Input Guide for SWIFT II, The Sandia Waste-Isolation Flow and Transport Model for Fractured Media, Release 4.84.* NUREG/CR-3162. SAND83-0242. Albuquerque, NM: Sandia National Laboratories.

Reeves, M., D.S. Ward, P.A. Davis, and E.J. Bonano. 1986c. *Swift II Self-Teaching Curriculum: Illustrative Problems for the Sandia Waste Isolation Flow and Transport Model for Fractured Media.* NUREG/CR-3925. SAND84-1586. Albuquerque, NM: Sandia National Laboratories.

Shinozuka, M., and C-M. Jan. 1972. "Digital Simulation of Random Processes and Its Applications," *Journal of Sound and Vibration.* Vol. 25, no. 1, 111-128.

Smith, L., and R.A. Freeze. 1979. "Stochastic Analysis of Steady State Groundwater Flow in a Bounded Domain. 2. Two-dimensional Simulations," *Water Resources Research.* Vol. 15, no. 6, 1543-1559.

Smith, L., and F.W. Schwartz. 1981. "Mass Transport. 2. Analysis of Uncertainty in Prediction," *Water Resources Research.* Vol. 17, no. 2, 351-369.

Wilson, J.L., B.S. RamaRao, and J.A. McNeish. 1986. *GRASP: A Computer Code to Perform Post-SWENT Adjoint Sensitivity Analysis of Stead-State Ground-Water Flow.* BMI/ONWI-625. Columbus, OH: Office of Nuclear Waste Isolation, Battelle Memorial Institute.

WIPP Performance Assessment (PA) Division. 1991. *Preliminary Comparison with 40 CFR Part 191, Subpart B for the Waste Isolation Pilot Plant, December 1991 — Volume 2: Probability and Consequence Modeling.* SAND91-0893/2. Albuquerque, NM: Sandia National Laboratories.

Zimmerman, D.A., and J.L. Wilson. 1990. *Description of and User's Manual for TUBA: A Computer Code for Generating Two-Dimensional Random Fields via the Turning Bands Method.* Albuquerque, NM: Gram, Inc.

DISTRIBUTION

(Send Distribution list changes to M.M. Gruebel, Dept. 6342, Sandia National Laboratories, PO Box 5800, Albuquerque, NM 87185-5800)

Federal Agencies

US Department of Energy (2)
Office of Environmental Restoration and Waste Management
Attn: L.P. Duffy, EM-1
C. Frank, EM-50
Washington, DC 20585

US Department of Energy (3)
Office of Environmental Restoration and Waste Management
Attn: M. Frei, EM-34 (Trevion II)
Director, Waste Management Projects
Washington, DC 20585-0002

US Department of Energy
Office of Environmental Restoration and Waste Management
Attn: J. Lytle, EM-30 (Trevion II)
Washington, DC 20585-0002

US Department of Energy
Office of Environmental Restoration and Waste Management
Attn: S. Schneider, EM-342 (Trevion II)
Washington, DC 20585-0002

US Department of Energy (3)
WIPP Task Force
Attn: G.H. Daly
S. Fucigna
B. Bower
12800 Middlebrook Rd.
Suite 400
Germantown, MD 20874

US Department of Energy (4)
Office of Environment, Safety and Health
Attn: R.P. Berube, EH-20
C. Borgstrum, EH-25
R. Pelletier, EH-231
K. Taimi, EH-232
Washington, DC 20585

US Department of Energy (5)
WIPP Project Integration Office
Attn: W.J. Arthur III
R. Becker
P. Dickman
L.W. Gage
P.J. Higgins
D.A. Olona
PO Box 5400
Albuquerque, NM 87115-5400

US Department of Energy (10)
WIPP Project Site Office (Carlsbad)
Attn: A. Hunt (4)
V. Daub (4)
J. Lippis
K. Hunter
PO Box 3090
Carlsbad, NM 88221-3090

US Department of Energy, (5)
Office of Civilian Radioactive Waste Management
Attn: Deputy Director, RW-2
Associate Director, RW-10
Office of Program Administration and Resources Management
Associate Director, RW-20
Office of Facilities Siting and Development
Associate Director, RW-30
Office of Systems Integration and Regulations
Associate Director, RW-40
Office of External Relations and Policy
Office of Geologic Repositories
Forrestal Building
Washington, DC 20585

US Department of Energy
Attn: National Atomic Museum Library
Albuquerque Operations Office
PO Box 5400
Albuquerque, NM 87185

US Department of Energy
Research & Waste Management Division
Attn: Director
PO Box E
Oak Ridge, TN 37831

US Department of Energy (2)
Idaho Operations Office
Fuel Processing and Waste
Management Division
785 DOE Place
Idaho Falls, ID 83402

US Department of Energy
Savannah River Operations Office
Defense Waste Processing
Facility Project Office
Attn: W.D. Pearson
PO Box A
Aiken, SC 29802

US Department of Energy (2)
Richland Operations Office
Nuclear Fuel Cycle & Production
Division
Attn: R.E. Gerton
825 Jadwin Ave.
PO Box 500
Richland, WA 99352

US Department of Energy (3)
Nevada Operations Office
Attn: J.R. Boland
D. Livingston
P.K. Fitzsimmons
2753 S. Highland Drive
Las Vegas, NV 89183-8518

US Department of Energy (2)
Technical Information Center
PO Box 62
Oak Ridge, TN 37831

US Department of Energy (2)
Chicago Operations Office
Attn: J.C. Haugen
9800 South Cass Avenue
Argonne, IL 60439

US Department of Energy
Los Alamos Area Office
528 35th Street
Los Alamos, NM 87544

US Department of Energy (3)
Rocky Flats Area Office
Attn: W.C. Rask
G. Huffman
T. Lukow
PO Box 928
Golden, CO 80402-0928

US Department of Energy
Dayton Area Office
Attn: R. Grandfield
PO Box 66
Miamisburg, OH 45343-0066

US Department of Energy
Attn: E. Young
Room E-178
GAO/RCED/GTN
Washington, DC 20545

US Bureau of Land Management
101 E. Mermod
Carlsbad, NM 88220

US Bureau of Land Management
New Mexico State Office
PO Box 1449
Santa Fe, NM 87507

US Environmental Protection
Agency (2)
Office of Radiation Protection Programs
(ANR-460)
Washington, DC 20460

US Nuclear Regulatory Commission
Division of Waste Management
Attn: H. Marson
Mail Stop 4-H-3
Washington, DC 20555

US Nuclear Regulatory Commission (4)
Advisory Committee on Nuclear Waste
Attn: D. Moeller
M.J. Steindler
P.W. Pomeroy
W.J. Hinze
7920 Norfolk Avenue
Bethesda, MD 20814

Defense Nuclear Facilities Safety Board
Attn: D. Winters
625 Indiana Avenue, NW
Suite 700
Washington, DC 20004

Nuclear Waste Technical Review
Board (2)
Attn: Library
Suite 910
1100 Wilson Blvd.
Arlington, VA 22209-2297

Energy and Science Division
Office of Management and Budget
Attn: K. Yuracko
725 17th Street NW
Washington, DC 20503

US Geological Survey (2)
Water Resources Division
Attn: C. Peters
Suite 200
4501 Indian School NE
Albuquerque, NM 87110

New Mexico Congressional Delegation

Jeff Bingaman
U.S. Senate
110 Hart SOB
Washington, DC 20510-3102

Pete V. Domenici
U.S. Senate
427 Dirksen Bldg.
Washington, DC 20510-3101

Bill Richardson
House of Representatives
2349 Rayburn HOB
Washington, DC 20515

Steven H. Schiff
House of Representatives
1009 Longworth HOB
Washington, DC 20515

Joe Skeen
House of Representatives
2367 Rayburn HOB
Washington, DC 20515

State Agencies

New Mexico Bureau of Mines
and Mineral Resources
Socorro, NM 87801

New Mexico Energy, Minerals and Natural
Resources Department
Attn: Librarian
2040 South Pacheco
Santa Fe, NM 87505

New Mexico Energy, Minerals and Natural
Resources Department
New Mexico Radioactive Task Force (2)
(Governor's WIPP Task Force)
Attn: A. Lockwood, Chairman
C. Wentz, Coordinator/Policy Analyst
2040 South Pacheco
Santa Fe, NM 87505

Bob Forrest
Mayor, City of Carlsbad
PO Box 1569
Carlsbad, NM 88221

Executive Director
Carlsbad Department of Development
Attn: C. Bernard
PO Box 1090
Carlsbad, NM 88221

New Mexico Environment Department
Secretary of the Environment (3)
Attn: J. Espinosa
PO Box 968
1190 St. Francis Drive
Santa Fe, NM 87503-0968

New Mexico Environment Department
Attn: P. McCasland
WIPP Project Site Office
PO Box 3090
Carlsbad, NM 88221-3090

New Mexico State Engineer's Office
Attn: M. Chudnoff
PO Box 25102
Santa Fe, NM 87504-5102

Environmental Evaluation Group (5)
Attn: R. Neill
Suite F-2
7007 Wyoming Blvd. NE
Albuquerque, NM 87109

Advisory Committee on Nuclear Facility Safety

John F. Ahearne
Executive Director, Sigma Xi
99 Alexander Drive
Research Triangle Park, NC 27709

James E. Martin
109 Observatory Road
Ann Arbor, MI 48109

WIPP Panel of National Research Council's Board on Radioactive Waste Management

Charles Fairhurst, Chairman
Department of Civil and
Mineral Engineering
University of Minnesota
500 Pillsbury Dr., SE
Minneapolis, MN 55455-0220

John O. Blomeke
3833 Sandy Shore Drive
Lenoir City, TN 37771-9803

John D. Bredehoeft
Western Region Hydrologist
Water Resources Division
US Geological Survey (M/S 439)
345 Middlefield Road
Menlo Park, CA 94025

Fred M. Ernsberger
1325 NW 10th Avenue
Gainsville, FL 32601

Rodney C. Ewing
Department of Geology
University of New Mexico
200 Yale, NE
Albuquerque, NM 87131

B. John Garrick
PLG, Inc.
Suite 400
4590 MacArthur Blvd.
Newport Beach, CA 92660-2027

Leonard F. Konikow
US Geological Survey
431 National Center
Reston, VA 22092

Jeremiah O'Driscoll
505 Valley Hill Drive
Atlanta, GA 30350

Christopher Whipple
Clement International Corp.
160 Spear St.
Suite 1380
San Francisco, CA 94105-1535

National Research Council (3)
Board on Radioactive
Waste Management
RM HA456
Attn: P.B. Myers,
Staff Director (2)
G.J. Grube
2101 Constitution Avenue
Washington, DC 20418

Performance Assessment Peer Review Panel

G. Ross Heath
College of Ocean and
Fishery Sciences HN-15
583 Henderson Hall
University of Washington
Seattle, WA 98195

Thomas H. Pigford
Department of Nuclear Engineering
4159 Etcheverry Hall
University of California
Berkeley, CA 94720

Thomas A. Cotton
JK Research Associates, Inc.
4429 Butterworth Place, NW
Washington, DC 20016

Robert J. Budnitz
President, Future Resources
Associates, Inc.
2000 Center Street
Suite 418
Berkeley, CA 94704

C. John Mann
Department of Geology
245 Natural History Bldg.
1301 West Green Street
University of Illinois
Urbana, IL 61801

Frank W. Schwartz
Department of Geology and Mineralogy
The Ohio State University
Scott Hall
1090 Carmack Rd.
Columbus, OH 43210

National Laboratories

Argonne National Laboratory (2)
Attn: A. Smith
D. Tomasko
9700 South Cass, Bldg. 201
Argonne, IL 60439

Battelle Pacific Northwest Laboratory (3)
Attn: R.E. Westerman
S. Bates
H.C. Burkholder
Battelle Boulevard
Richland, WA 99352

Idaho National Engineering Laboratory (2)
Attn: H. Loo
R. Klinger
Mail Stop 5108
Idaho Falls, ID 83403-4000

Los Alamos National Laboratory
Attn: B. Erdal, CNC-11
PO Box 1663
Los Alamos, NM 87545

Los Alamos National Laboratory
Attn: A. Meijer
PO Box 1663, Mail Stop J514
Los Alamos, NM 87545

Los Alamos National Laboratory (3)
HSE-8
Attn: M. Enoris
L. Soholt
J. Wenzel
PO Box 1663
Los Alamos, NM 87545

Los Alamos National Laboratory
EM-7
Attn: S. Kosiewicz
PO Box 1663, Mail Stop J595
Los Alamos, NM 87545

Oak Ridge National Laboratory
Transuranic Waste Manager
Attn: D.W. Turner
PO Box 2008, Bldg. 3047
Oak Ridge, TN 37831-6060

Pacific Northwest Laboratory
Attn: B. Kennedy
PO Box 999
Richland, WA 99352

Savannah River Laboratory (3)
Attn: N. Bibler
M.J. Plodinec
G.G. Wicks
Aiken, SC 29801

Savannah River Plant (2)
Attn: R.G. Baxter
Bldg. 704-S
K.W. Wierzbicki
Bldg. 703-H
Aiken, SC 29808-0001

Corporations/Members of the Public

Benchmark Environmental Corp.
Attn: C. Frederickson
4501 Indian School NE
Suite 105
Albuquerque, NM 87110

City of Albuquerque
Public Works Department
Utility Planning Division
Attn: W.K. Summers
PO Box 1293
Albuquerque, NM 87103

Deuel and Associates, Inc.
Attn: R.W. Prindle
7208 Jefferson NE
Albuquerque, NM 87109

Disposal Safety, Inc.
Attn: B. Ross
1660 L Street NW
Suite 314
Washington, DC 20036

Ecodynamics (2)
Attn: P. Roache
R. Blaine
PO Box 9229
Albuquerque, NM 87119-9229

EG & G Idaho (3)
1955 Fremont Street
Attn: C. Atwood
C. Hertzler
T.I. Clements
Idaho Falls, ID 83415

Geomatrix
Attn: K. Coppersmith
100 Pine Street, Suite 1000
San Francisco, CA 94111

Golder Associates, Inc. (3)
Attn: M. Cunnane
R. Kossik
I. Miller
4104 148th Avenue NE
Redmond, WA 98052

INTERA, Inc. (2)
Attn: J.F. Pickens
A.M. LaVenve
6850 Austin Center Blvd.
Suite 300
Austin, TX 78731

INTERA, Inc.
Attn: W. Stensrud
PO Box 2123
Carlsbad, NM 88221

INTERA, Inc.
Attn: W. Nelson
101 Convention Center Drive
Suite 540
Las Vegas, NV 89109

IT Corporation (2)
Attn: R.F. McKinney
J. Myers
Regional Office, Suite 700
5301 Central Avenue NE
Albuquerque, NM 87108

John Hart and Associates, P.A.
Attn: J.S. Hart
2815 Candelaria Road NW
Albuquerque, NM 87107

John Hart and Associates, P.A.
Attn: K. Lickliter
1009 North Washington
Tacoma, WA 98406

MACTEC (2)
Attn: J.A. Thies
D.K. Duncan
8418 Zuni Road SE, Suite 200
Albuquerque, NM 87108

Newman and Holtzinger
Attn: C. Mallon
1615 L Street NW, Suite 1000
Washington, DC 20036

RE/SPEC, Inc. (2)
Attn: W. Coons
4775 Indian School NE, Suite 300
Albuquerque, NM 87110

RE/SPEC, Inc.
Attn: J.L. Ratigan
PO Box 725
Rapid City, SD 57709

Reynolds Elect/Engr. Co., Inc.
Attn: E.W. Kendall
Building 790, Warehouse Row
PO Box 98521
Las Vegas, NV 89193-8521

Roy F. Weston, Inc.
CRWM Tech. Supp. Team
Attn: C.J. Noronha
955 L'Enfant Plaza SW
North Building, Eighth Floor
Washington, DC 20024

Science Applications International Corporation (SAIC)
Attn: H.R. Pratt
10260 Campus Point Drive
San Diego, CA 92121

Science Applications International Corporation (2)
Attn: D.C.Royer
C.G. Pflum
101 Convention Center Dr.
Las Vegas, NV 89109

Science Applications International Corporation (2)
Attn: M. Davis
J. Tollison
2109 Air Park Road SE
Albuquerque, NM 87106

Science Applications International Corporation (2)
Attn: J. Young
D. Lester
18706 North Creek Parkway, Suite 110
Bothell, WA 98011

Southwest Research Institute
Center for Nuclear Waste Regulatory Analysis (2)
Attn: P.K. Nair
6220 Culebra Road
San Antonio, TX 78228-0510

Systems, Science, and Software (2)
Attn: E. Peterson
P. Lagus
Box 1620
La Jolla, CA 92038

TASC
Attn: S.G. Oston
55 Walkers Brook Drive
Reading, MA 01867

Tech Reps, Inc. (6)
Attn: J. Chapman
C. Crawford
D. Marchand
J. Stikar
P. Oliver
D. Scott
5000 Marble NE, Suite 222
Albuquerque, NM 87110

Tolan, Beeson & Associates
Attn: T.L. Tolan
2320 W. 15th Avenue
Kennewick, WA 99337

TRW Environmental Safety Systems
Attn: I. Sacks
2650 Park Tower Drive, Suite 800
Vienna, VA 22180

Westinghouse Electric Corporation (5)
Attn: Library
L. Trego
C. Cox
L. Fitch
R.F. Kehrman
PO Box 2078
Carlsbad, NM 88221

Westinghouse Hanford Company
Attn: D. E. Wood
MSIN HO-32
PO Box 1970
Richland, WA 99352

Western Water Consultants
Attn: D. Fritz
1949 Sugarland Drive #134
Sheridan, WY 82801-5720

Western Water Consultants
Attn: P.A. Rechard
PO Box 4128
Laramie, WY 82071

P. Drez
8816 Cherry Hills Road, NE
Albuquerque, NM 87111

D.W. Powers
Star Route Box 87
Anthony, TX 79821

Shirley Thieda
PO Box 2109, RR1
Bernalillo, NM 87004

Jack Urich
c/o CARD
144 Harvard SE
Albuquerque, NM 87106

Universities

University of California
Mechanical, Aerospace, and
Nuclear Engineering Department (2)
Attn: W. Kastenberg
D. Browne
5532 Boelter Hall
Los Angeles, CA 90024

University of California
Mine Engineering Dept.
Attn: Neville Cook
Rock Mechanics Engineering
Berkeley, CA 94720

University of Hawaii at Hilo
Attn: S. Hora
Business Administration
Hilo, HI 96720-4091

University of New Mexico
Geology Department
Attn: Library
Albuquerque, NM 87131

University of New Mexico
Research Administration
Attn: H. Schreyer
102 Scholes Hall
Albuquerque, NM 87131

University of Wyoming
Department of Civil Engineering
Attn: V.R. Hasfurther
Laramie, WY 82071

University of Wyoming
Department of Geology
Attn: J.I. Drever
Laramie, WY 82071

University of Wyoming
Department of Mathematics
Attn: R.E. Ewing
Laramie, WY 82071

Libraries

Thomas Brannigan Library
Attn: D. Dresp
106 W. Hadley St.
Las Cruces, NM 88001

Hobbs Public Library
Attn: M. Lewis
509 N. Ship Street
Hobbs, NM 88248

New Mexico State Library
Attn: N. McCallan
325 Don Gaspar
Santa Fe, NM 87503

New Mexico Tech
Martin Speere Memorial Library
Campus Street
Socorro, NM 87810

New Mexico Junior College
Pannell Library
Attn: R. Hill
Lovington Highway
Hobbs, NM 88240

Carlsbad Municipal Library
WIPP Public Reading Room
Attn: L. Hubbard
101 S. Halagueno St.
Carlsbad, NM 88220

University of New Mexico
General Library
Government Publications Department
Albuquerque, NM 87131

NEA/Performance Assessment Advisory Group (PAAG)

P. Duerden
ANSTO
Lucas Heights Research Laboratories
Private Mail Bag No. 1
Menai, NSW 2234, AUSTRALIA

Gordon S. Linsley
Division of Nuclear Fuel Cycle and Waste Management
International Atomic Energy Agency
PO Box 100
A-1400 Vienna, AUSTRIA

Nicolo Cadelli
Commission of the European Communities
200, Rue de la Loi
B-1049 Brussels, BELGIUM

R. Heremans
Organisme Nationale des Déchets Radioactifs et des Matiéres Fissiles
ONDRAF
Place Madou 1, Boitec 24/25
B-1030 Brussels, BELGIUM

J. Marivoet
Centre d'Etudes de l'Energie Nucléaire
CEN/SCK
Boeretang 200
B-2400 Mol, BELGIUM

P. Conlon
Waste Management Division
Atomic Energy Control Board (AECB)
PO Box 1046
Ottawa, Canada KIP 559, CANADA

A.G. Wikjord
Manager, Environmental and Safety Assessment Branch
Atomic Energy of Canada Limited
Whiteshell Nuclear Research Establishment
Pinewa, Manitoba ROE 1LO, CANADA

Jukka-Pekka Salo
Teollisuuden Voima Oy (TVO)
Fredrikinkatu 51-53 B
SF-00100 Helsinki, FINLAND

Timo Vieno
Technical Research Centre of Finland (VTT)
Nuclear Energy Laboratory
PO Box 208
SF-02151 Espoo, FINLAND

Timo Äikäs
Teollisuuden Voima Oy (TVO)
Fredrikinkatu 51-53 B
SF-00100 Helsinki, FINLAND

M. Claude Ringeard
Division de la Sécurité et de la Protection de l'Environment (DSPE)
Commissariat á l'Energie Atomique
Agence Nationale pour la Gestion des Déchets Radioactifs (ANDRA)
Route du Panorama Robert Schuman
B. P. No. 38
F-92266 Fontenay-aux-Roses Cedex
FRANCE

Gérald Ouzounian
Agence Nationale pour la Gestion des Déchets Radioactifs (ANDRA)
Route du Panorama Robert Schuman
B. P. No. 38
F-92266 Fontenay-aux-Roses Cedex
FRANCE

Claudio Pescatore
Division of Radiation Protection and Waste Management
OECD Nuclear Energy Agency
38, Boulevard Suchet
F-75016 Paris, FRANCE

M. Dominique Greneche
Commissariat á l'Energie Atomique
IPSN/DAS/SASICC/SAED
B. P. No. 6
F-92265 Fontenay-aux-Roses Cedex,
FRANCE

Robert Fabriol
Bureau de Recherches Géologiques et Miniéres (BRGM)
B. P. 6009
45060 Orléans Cedex 2, FRANCE

P. Bogorinski
Gesellschaft für Reaktorsicherheit (GRS) mbH
Schwertnergasse 1
D-5000 Köln 1, GERMANY

R. Storck
GSF - Institut für Tieflagerung
Theodor-Heuss-Strabe 4
D-3300 Braunschweig, GERMANY

Ferrucio Gera
ISMES S.p.A
Via del Crociferi 44
I-00187 Rome, ITALY

Hiroyuki Umeki
Isolation System Research Program
Radioactive Waste Management Project
Power Reactor and Nuclear Fuel Development Corporation (PNC)
1-9-13, Akasaka
Minato-ku
Tokyo 107, JAPAN

P. Carboneras Martinez
ENRESA
Calle Emilio Vargas 7
R-28043 Madrid, SPAIN

Tönis Papp
Swedish Nuclear Fuel and Waste Management Co.
Box 5864
S 102 48 Stockholm, SWEDEN

Conny Hägg
Swedish Radiation Protection Institute (SSI)
Box 60204
S-104 01 Stockholm, SWEDEN

J. Hadermann
Paul Scherrer Institute
Waste Management Programme
CH-5232 Villigen PSI, SWITZERLAND

J. Vigfusson
USK- Swiss Nuclear Safety Inspectorate
Federal Office of Energy
CH-5303 Würenlingen, SWITZERLAND

D.E. Billington
Departmental Manager - Assessment Studies
Radwaste Disposal R&D Division
AEA Decommissioning & Radwaste
Harwell Laboratory, B60
Didcot Oxfordshire OX11 ORA
UNITED KINGDOM

P. Grimwood
Waste Management Unit
BNFL
Sellafield
Seascale, Cumbria CA20 1PG
UNITED KINGDOM

Alan J. Hooper
UK Nirex Ltd
Curie Avenue
Harwell, Didcot
Oxfordshire, OX11 ORH
UNITED KINGDOM

Jerry M. Boak
Yucca Mountain Project Office
US Department of Energy
PO Box 98608
Las Vegas, NV 89193

Seth M. Coplan (Chairman)
US Nuclear Regulatory Commission
Division of High-Level Waste Management
Mail Stop 4-H-3
Washington, DC 20555

A.E. Van Luik
INTERA/M&O
The Valley Bank Center
101 Convention Center Dr.
Las Vegas, NV 89109

NEA/PSAG User's Group

Shaheed Hossain
Division of Nuclear Fuel Cycle and Waste Management
International Atomic Energy Agency
Wagramerstrasse 5
PO Box 100
A-1400 Vienna, AUSTRIA

Alexander Nies (PSAC Chairman)
Gesellschaft für Strahlen- und
Institut für Tieflagerung
Abteilung für Endlagersicherheit
Theodor-Heuss-Strasse 4
D-3300 Braunschweig, GERMANY

Eduard Hofer
Gesellschaft für Reaktorsicherheit (GRS) MBH
Forschungsgelände
D-8046 Garching, GERMANY

Andrea Saltelli
Commission of the European Communities
Joint Resarch Centre of Ispra
I-21020 Ispra (Varese), ITALY

Alejandro Alonso
Cátedra de Tecnología Nuclear
E.T.S. de Ingenieros Industriales
José Gutiérrez Abascal, 2
E-28006 Madrid, SPAIN

Pedro Prado
CIEMAT
Instituto de Tecnología Nuclear
Avenida Complutense, 22
E-28040 Madrid, SPAIN

Miguel Angel Cuñado
ENRESA
Emilio Vargas, 7
E-28043 Madrid, SPAIN

Francisco Javier Elorza
ENRESA
Emilio Vargas, 7
E-28043 Madrid, SPAIN

Nils A. Kjellbert
Swedish Nuclear Fuel and Waste Manageme
Company (SKB)
Box 5864
S-102 48 Stockholm, SWEDEN

Björn Cronhjort
Swedish National Board for Spent Nuclear Fuel (SKN)
Sehlsedtsgatan 9
S-115 28 Stockholm, SWEDEN

Richard A. Klos
Paul-Scherrer Institute (PSI)
CH-5232 Villingen PSI
SWITZERLAND

NAGRA (2)
Attn: C. McCombie
F. Van Dorp
Parkstrasse 23
CH-5401 Baden, SWITZERLAND

N. A. Chapman
Intera Information Technologies
Park View House, 14B Burton Street
Melton Mowbray
Leicestershire, LE13 1AE
UNITED KINGDOM

Daniel A. Galson
Galson Sciences Ltd.
35, Market Place
Oakham
Leicestershire LE15 6DT
UNITED KINGDOM

David P. Hodgkinson
Intera Information Technologies
Chiltern House
45 Station Road
Henley-on-Thames
Oxfordshire RG9 1AT, UNITED KINGDO

Brian G.J. Thompson
Department of the Environment: Her Majesty's Inspectorate of Pollution
Room A5.33, Romney House
43 Marsham Street
London SW1P 2PY, UNITED KINGDOM

Intera Information Technologies
Attn: M.J.Apted
3609 South Wadsworth Blvd.
Denver, CO 80235

US Nuclear Regulatory Commission (2)
Attn: R. Codell
N. Eisenberg
Mail Stop 4-H-3
Washington, DC 20555

Battelle Pacific Northwest Laboratories
Attn: P.W. Eslinger
PO Box 999, MS K2-32
Richland, WA 99352

Center for Nuclear Waste Regulatory Analysis (CNWRA)
Southwest Research Institute
Attn: B. Sagar
PO Drawer 28510
6220 Culebra Road
San Antonio, TX 78284

Geostatistics Expert Working Group (GXG)

Rafael L. Bras
R.L. Bras Consulting Engineers
44 Percy Road
Lexington, MA 02173

Jesus Carrera
Universidad Politêcnica de Cataluña
E.T.S.I. Caminos
Jordi, Girona 31
E-08034 Barcelona, SPAIN

Gedeon Dagan
Department of Fluid Mechanics and Heat Transfer
Tel Aviv University
PO Box 39040
Ramat Aviv, Tel Aviv 69978, ISRAEL

Ghislain de Marsily (GXG Chairman)
University Pierre et Marie Curie
Laboratorie de Geologie Applique
4, Place Jussieu - T.26 - 5^{e} etage
75252 Paris Cedex 05, FRANCE

Alain Galli
Centre de Geostatistique
Ecole des Mines de Paris
35 Rue St. Honore
77035 Fontainebleau, FRANCE

Steve Gorelick
Department of Applied Earth Sciences
Stanford University
Stanford, CA 94305-2225

Peter Grindrod
INTERA Information Technologies Ltd.
Chiltern House, 45 Station Road
Henley-on-Thames
Oxfordshire, RG9 1AT
UNITED KINGDOM

Alan Gutjahr
Department of Mathematics
New Mexico Institute of Mining and Technology
Socorro, NM 87801

C. Peter Jackson
Harwell Laboratory
Theoretical Studies Department
Radwaste Disposal Division
Bldg. 424.4
Oxfordshire Didcot Oxon OX11 ORA
UNITED KINDGOM

Peter Kitanidis
60 Peter Coutts Circle
Stanford, CA 94305

Rae Mackay
Department of Civil Engineering
University of Newcastle Upon Tyne
Newcastle Upon Tyne NE1 7RU
UNITED KINGDOM

Dennis McLaughlin
Parsons Laboratory
Room 48-209
Department of Civil Engineering
Massachusetts Institute of Technology
Cambridge, MA 02139

Shlomo P. Neuman
College of Engineering and Mines
Department of Hydrology and Water Resources
University of Arizona
Tucson, AZ 85721

Christian Ravenne
Geology and Geochemistry Division
Institut Francais du Pétrole
1 & 4, av. de Bois-Préau BP311
92506 Rueil Malmaison Cedex
FRANCE

Yoram Rubin
Department of Civil Engineering
University of California
Berkeley, CA 94720

Foreign Addresses

Studiecentrum Voor Kernenergie
Centre D'Energie Nucleaire
Attn: A. Bonne
SCK/CEN
Boeretang 200
B-2400 Mol, BELGIUM

Atomic Energy of Canada, Ltd. (3)
Whiteshell Research Estab.
Attn: M.E. Stevens
B.W. Goodwin
D. Wushke
Pinewa, Manitoba
ROE 1L0, CANADA

Esko Peltonen
Industrial Power Company Ltd.
TVO
Fredrikinkatu 51-53
SF-00100 Helsinki 10, FINLAND

Jean-Pierre Olivier
OECD Nuclear Energy Agency (2)
38, Boulevard Suchet
F-75016 Paris, FRANCE

D. Alexandre, Deputy Director
ANDRA
31 Rue de la Federation
75015 Paris, FRANCE

Claude Sombret
Centre D'Etudes Nucleaires
De La Vallee Rhone
CEN/VALRHO
S.D.H.A. BP 171
30205 Bagnols-Sur-Ceze, FRANCE

Bundesministerium fur Forschung und
Technologie
Postfach 200 706
5300 Bonn 2, GERMANY

Bundesanstalt fur Geowissenschaften
und Rohstoffe
Attn: M. Langer
Postfach 510 153
3000 Hanover 51, GERMANY

Gesellschaft fur Reaktorsicherheit (GRS) (2)
Attn: B. Baltes
W. Muller
Schwertnergasse 1
D-5000 Cologne, GERMANY

Institut fur Tieflagerung (2)
Attn: K. Kuhn
Theodor-Heuss-Strasse 4
D-3300 Braunschweig, GERMANY

Physikalisch-Technische
Bundesanstalt
Attn: P. Brenneke
Postfach 33 45
D-3300 Braunschweig, GERMANY

Shingo Tashiro
Japan Atomic Energy Research Institute
Tokai-Mura, Ibaraki-Ken
319-11, JAPAN

Netherlands Energy Research
Foundation (ECN)
Attn: L.H. Vons
3 Westerduinweg
PO Box 1
1755 ZG Petten, THE NETHERLANDS

Johan Andersson
Swedish Nuclear Power Inspectorate
Statens Kärnkraftinspektion (SKI)
Box 27106
S-102 52 Stockholm, SWEDEN

Fred Karlsson
Svensk Karnbransleforsorjning
AB SKB
Box 5864
S-102 48 Stockholm, SWEDEN

Nationale Genossenschaft fur die Lagerung
Radioaktiver Abfalle (NAGRA) (2)
Attn: S. Vomvoris
P. Zuidema
Hardstrasse 73
CH-5430 Wettingen, SWITZERLAND

AEA Technology
Attn: J.H. Rees
D5W/29 Culham Laboratory
Abington
Oxfordshire OX14 3DB, UNITED KINGDO

AEA Technology
Attn: W.R. Rodwell
O44/A31 Winfrith Technical Centre
Dorchester
Dorset DT2 8DH, UNITED KINGDOM

AEA Technology
Attn: J.E. Tinson
B4244 Harwell Laboratory
Didcot, Oxfordshire OX11 ORA
UNITED KINGDOM

D.R. Knowles
British Nuclear Fuels, plc
Risley, Warrington
Cheshire WA3 6AS, 1002607
UNITED KINGDOM

Internal

1	A. Narath
20	O.E. Jones
1502	J.C. Cummings
1511	D.K. Gartling
6000	D.L. Hartley
6115	P.B. Davies
6119	E.D. Gorham
6119	Staff (14)
6121	J.R. Tillerson
6121	Staff (7)
6233	J.C. Eichelberger
6300	D.E. Ellis
6302	L.E. Shephard
6303	S.Y. Pickering
6303	W.D. Weart
6305	S.A. Goldstein
6306	A.L. Stevens
6312	F.W. Bingham
6313	L.S. Costin
6331	P.A. Davis
6341	Sandia WIPP Central Files (300)
6342	D.R. Anderson
6342	Staff (30)
6343	S.A. Orrell, Acting
6343	Staff (3)
6345	R.C. Lincoln
6345	Staff (9)
6347	D.R. Schafer
6348	J.T. Holmes
6351	R.E. Thompson
6352	D.P. Garber
6352	S.E. Sharpton
6400	N.R. Ortiz
6613	R.M. Cranwell
6613	R.L. Iman
6613	C. Leigh
6622	M.S.Y. Chu
6641	R.E. Luna, Acting
7141	Technical Library (5)
7151	Technical Publications
7613-2	Document Processing for DOE/OSTI (10)
8523-2	Central Technical Files
9300	J.E. Powell
9310	J.D. Plimpton
9330	J.D. Kennedy

☆ U.S. GOVERNMENT PRINTING OFFICE 1992—774-122/80126

THIS PAGE INTENTIONALLY LEFT BLANK

SANDIA REPORT

SAND92–0700/3 • UC–721
Unlimited Release
Printed December 1992

Preliminary Performance Assessment for the Waste Isolation Pilot Plant, December 1992

Volume 3: Model Parameters

Sandia WIPP Project

Prepared by
Sandia National Laboratories
Albuquerque, New Mexico 87185 and Livermore, California 94550
for the United States Department of Energy
under Contract DE-AC04-76DP00789

Issued by Sandia National Laboratories, operated for the United States Department of Energy by Sandia Corporation.

Available to DOE and DOE contractors from
Office of Scientific and Technical Information
PO Box 62
Oak Ridge, TN 37831

Prices available from (615) 576-8401, FTS 626-8401

Available to the public from
National Technical Information Service
US Department of Commerce
5285 Port Royal Rd
Springfield, VA 22161

NTIS price codes
Printed copy: A99
Microfiche copy: A01

SAND92-0700/3
Unlimited Release
Printed December 1992

Distribution
Category UC-721

Preliminary Performance Assessment for the Waste Isolation Pilot Plant, December 1992

Volume 3: Model Parameters

Sandia WIPP Project
Sandia National Laboratories
Albuquerque, New Mexico 87185

ABSTRACT

This volume documents model parameters chosen as of July 1992 that were used by the Performance Assessment Department of Sandia National Laboratories in its 1992 preliminary performance assessment of the Waste Isolation Pilot Plant (WIPP). Ranges and distributions for about 300 modeling parameters in the current secondary data base are presented in tables for the geologic and engineered barriers, global materials (e.g., fluid properties), and agents that act upon the WIPP disposal system such as climate variability and human-intrusion boreholes. The 49 parameters sampled in the 1992 Preliminary Performance Assessment are given special emphasis with tables and graphics that provide insight and sources of data for each parameter.

This volume of the report should be referenced as:

Sandia WIPP Project. 1992. *Preliminary Performance Assessment for the Waste Isolation Pilot Plant, December 1992. Volume 3: Model Parameters.* SAND92-0700/3. Albuquerque, NM: Sandia National Laboratories.

ACKNOWLEDGMENTS

The Waste Isolation Pilot Plant (WIPP) Performance Assessment (PA) Department is comprised of both Sandia National Laboratories (SNL) and contractor employees working as a team to produce these annual preliminary comparisons with Environmental Protection Agency (EPA) regulations, assessments of overall long-term safety of the repository, and interim technical guidance to the program. The on-site team, affiliations, and contributions to the 1992 performance assessment are listed in alphabetical order:

Performance Assessment Department

Name	Affil.*	Primary Author of Major Code	Area of Responsibility
R. Anderson	SNL		Department Manager
B. Baker	TEC		SEC02D, Hydrology, Office Manager
J. Bean	UNM		BRAGFLO, 2-Phase Flow
J. Berglund	UNM	CUTTINGS	Task Ldr., Cuttings/Cavings/Spallings, Engr. Mech.
S. Bertram-Howery	SNL		PA Liaison with DOE, Criteria Document, Test Phase Plan
W. Beyeler	SAI	PANEL, GARFIELD	Geostatistics, Analytical Models, CAMCON Systems Codes
K. Brinster	SAI		Geohydrology, Conceptual Models
R. Blaine	ECO		SEC02D, SECOTP, & CAMCON Systems Codes
T. Blaine	GC		Drilling Technology, Exposure Pathways Data
K. Byle	UNM		Software and Analysis QA
J. Chapman	TRI		Documentation V.3
D. Duncan	MAC		Data QA
K. Economy	ECO		SEC02D, SECOTP, Hydrology & Transport
D. Gallegos	SNL		Task Ldr., Hydrology, Geostatistics, NEA, PSAG
D. Galson	GS		NEA Working Groups, PSAG, PAAG, Human Intrusion
J. Garner	API	PANEL	Source Term, Sens. Anal.
A. Gilkey	UNM		CAMCON Systems Codes
L. Gomez	SNL		Task Ldr., Safety Assessments
M. Gruebel	TRI		EPA Regulations, Documentation V.1, Editor V.1
R. Guzowski	SAI		Geology, Scenario Construction
J. Helton	ASU	CCDFPERM	Task Ldr., Uncert./Sens. Anal., Probability Models, Editor V.4
S. Hora	UHH		Expert Elicitation, Probability Models
H. Iuzzolino	GC	CCDFCALC, CCDFPERM	LHS, CAMCON System Codes, Probability Models
R. Klett	SNL		EPA Regulations
P. Knupp	ECO	SECOTP	Comp. Fluid Dyn.
M. LaVenue	INT	GRASP-INV	Hydrology/Geostatistics

C. Leigh	SNL	GENII-S	Exposure Pathways
M. Marietta	SNL		Dep. Dept. Manager, Tech. Coord.
G. de Marsily	UP		Geostatistics Expert Group Chair
R. McCurley	UNM		CAMCON System Codes
B. Napier	PNL	GENII	Safety Assessments
A. Peterson	SNL		Task Ldr, Inventory
B. RamaRao	INT	GRASP-INV	Geostatistics
J. Rath	UNM		CAMCON System Codes
R. Rechard	SNL		Task Ldr. CAMCON, QA
P. Roache	ECO	SECO	Task Ldr., Comp. Fluid Dyn.
D. Rudeen	UNM		STAFF2D, SECOTP, Transport
J. Ruge	ECO		Multigrid Methods/BRAGFLO
T. Russell	ECO		Upscaling
K. Salari	ECO	SECOTP	Transport, Computational Fluid Dynamics
J. Sandha	SAI		INGRES, PA Data Base
J. Schreiber	SAI		BRAGFLO, 2-Phase Flow
D. Scott	TRI		Documentation V.2
P. Swift	TRI		Task Ldr., Geology, Climate Var., Documentation V.1 & 2, Editor V.1, 2, 4, & 5
M. Tierney	SNL		Task Ldr., CDF Constr., Probability Models, Ref. Data, Editor V.2 & 3
K. Trauth	SNL		Task Ldr., Expert Panels
P. Vaughn	API	BRAGFLO	Task Ldr., 2-Phase Flow & Waste Panel Chemistry, Editor V.4 & 5
T. Zimmerman	GRA		Geostatistics Test Problem

The foundation of the annual WIPP performance assessment is the underlying data set and understanding of the important processes in the engineered and natural barrier systems. Other SNL Departments are the primary source of these data and understanding. Assistance with the waste inventory comes from WEC and its contractors. We gratefully acknowledge the support of our departmental and project colleagues. Some individuals have worked closely with the performance assessment team, and we wish to acknowledge their contributions individually:

H. Batchelder	WEC	CH & RH Inventories
R. Beauheim	SNL	Natural Barrier System, Hydrologic Parameters
D. Borns	SNL	Geology, Geophysics
B. Butcher	SNL	Engineered Barrier System, Unmodified Waste-Form Parameters, Disposal Room Systems Parameters
L Brush	SNL	Engineered Barrier System, Source Term (Solubility) and Gas Generation Parameters
L. Clements	ReS	Computer System Support
T. Corbet	SNL	Natural Barrier System, Geologic & Hydrologic Parameters, Conceptual Models
P. Davies	SNL	Natural Barrier System, Hydrologic & Transport Parameters, & 2-Phase Flow Mechanistic Modeling
P. Drez	DE	CH & RH Inventories
R. Finley	SNL	Repository Isolation Systems Parameters
F. Gelbard	SNL	Natural Barrier System, Retardation
E. Gorham	SNL	Natural Barrier System, Fluid Flow & Transport Parameters

R. Holt	CON	Geology
S. Howarth	SNL	Natural Barrier System, Hydrologic Parameters
R. Kehrman	WEC	Ch & RH Waste Characterization
K. Lickliter	BEC	EPA Regulations
R. Lincoln	SNL	Room Modeling
F. Mendenhall	SNL	Engineered Barrier System, Unmodified Waste Form Parameters, Waste Panel Closure (Expansion)
D. Munson	SNL	Reference Stratigraphy, Constitutive Models, Physical & Mechanical Parameters
C. Novak	SNL	Natural Barrier Systems, Chemistry
E. Nowak	SNL	Room Modeling, Source Term
J. Orona	ReS	Computer System Support
A. Stevens	SNL	DOE Liaison
J. Tillerson	SNL	Repository Isolation Systems Parameters
W. Wawersik	SNL	Fracturing
S. Webb	SNL	2-Phase Flow Sensitivity Analysis & Benchmarking

---

* Affiliation

API = Applied Physics Incorporated
ASU = Arizona State University
BEC = Benchmark Environmental Corp.
CON = Consultant
DE = Drez Environmental
ECO = Ecodynamics Research Associates
GC = Geo-Centers Incorporated
GRA = GRAM, Inc.
GS = Galson Sciences
INT = Intera
IT = International Technology
MAC = MACTEC
PNL = Pacific Northwest Laboratory
ReS = ReSpec
SAI = Scientific Applications International Corporation
SNL = Sandia National Laboratories
TEC = Technadyne Engineering Consultants
TRI = Tech Reps, Inc.
UHH = University of Hawaii at Hilo
UNM = University of New Mexico/New Mexico Engineering Research Institute
UP = University of Paris
WEC = Westinghouse Electric Corporation

Peer Review

Internal/Sandia
L. Gomez
D. Schafer

Management/Sandia
W. Weart

PA Peer Review Panel

R. Heath, Chair	University of Washington
R. Budnitz	Future Resources Associates, Inc.
T. Cotton	JK Research Associates, Inc.
J. Mann	University of Illinois
T. Pigford	University of California, Berkeley
F. Schwartz	Ohio State University

Department of Energy
R. Becker

Expert Panels

Futures

M. Baram	Boston University
W. Bell	Yale University
G. Benford	University of California, Irvine
D. Chapman	The World Bank, Cornell University
B. Cohen	University of Pittsburgh
V. Ferkiss	Georgetown University
T. Glickman	Resources for the Future
T. Gordon	Futures Group
C. Kirkwood	Arizona State University
H. Otway	Joint Research Center (Ispra), Los Alamos National Laboratory
M. Pasqualetti	Arizona State University
D. Reicher	Natural Resources Defense Council
N. Rosenberg	Resources for the Future
M. Singer	The Potomac Organization
T. Taylor	Consultant
M. Vinovskis	University of Michigan

Markers

D. Ast	Cornell University
V. Baker	University of Arizona
M. Brill	Buffalo Organization for Social and Technological Innovation
F. Drake	University of California at Santa Cruz
B. Finney	University of Hawaii at Manoa
D. Givens	American Anthropological Association
W. Goodenough	University of Pennsylvania
M. Kaplan	Eastern Research Group
J. Lomberg	Consultant
L. Narens	University of California at Irvine
F. Newmeyer	University of Washington
W. Sullivan	University of Washington
W. Williams	Case Western Reserve University

Source Term

C. Bruton	Lawrence Livermore National Laboratory
I-Ming Chou	U.S. Geological Survey
D. Hobart	Los Alamos National Laboratory
F. Millero	University of Miami

Retardation

R. Dosch	Sandia National Laboratories
C. Novak	Sandia National Laboratories
M. Siegel	Sandia National Laboratories

Geostatistics Expert Group

G. de Marsily, Chair	U. of Paris
R. Bras	Massachusetts Inst. of Tech.
J. Carrera	U. Politécnica de Cataluña
G. Dagan	Tel Aviv U.
A. Galli	Ecole des Mines de Paris
S. Gorlick	Stanford U.
P. Grindrod	Intera Sciences
A. Gutjahr	New Mexico Tech
D. McLaughlin	Massachusetts Inst. of Tech.
S. Neuman	U. of Arizona
C. Ravenne	Institut Français du Pétrole
Y. Rubin	U. of California, Berkeley

Report Preparation (TRI)

Illustration Editors

Volume 1: D. Marchand
Volume 2: D. Marchand
Volume 3: D. Pulliam

Dolores Miera and Leona Tartaglia of the Word Processing Department
R. Rohac, R. Andree, and the Illustration and Computer Graphics Departments
S. Tullar and the Production Department

PREFACE

This volume documents model parameters that were used in sensitivity and uncertainty studies by the Performance Assessment (PA) Department of Sandia National Laboratories in its 1992 preliminary comparison of the Waste Isolation Pilot Plant (WIPP) with the Environmental Protection Agency's (EPA's) *Environmental Standards for the Management and Disposal of Spent Nuclear Fuel, High-Level, and Transuranic Radioactive Wastes (40 CFR 191).*

Besides the DOE Project Integration and Site Offices in New Mexico, which oversee the project, the WIPP currently has two major participants: Sandia National Laboratories in Albuquerque, New Mexico, which functions as scientific investigator; and Westinghouse Electric Company, which is responsible for the management of WIPP operations. The specific tasks of Sandia are (1) characterizing the disposal system and surrounding region and responding to specific concerns of the State of New Mexico, (2) assessing the performance of the WIPP (e.g., assessing regulatory compliance with *40 CFR 191, Subpart B*, except the Assurance Requirements), (3) performing analytic, laboratory, field experiments, and applied research to nuclear waste disposal in salt, relevant to support tasks 1 and 2 (disposal system characterization and performance assessment), and (4) providing ad hoc scientific and engineering support (e.g., supporting environmental assessments such as Resource Conservation and Recovery Act (RCRA, 1976) and the National Environmental Policy Act (NEPA, 1969). This volume helps fulfill the performance assessment task.

For the performance assessment, the PA Department at Sandia maintains a data base, the secondary data base (SDB), which contains interpreted data from many primary sources. The data are used to form a conceptual model of the WIPP disposal system. The SDB provides a set of parameter values (median, range, and distribution type where appropriate) and the source of these values. As better information becomes available, the parameter values reported herein will be updated. Thus, this volume is only a snapshot of the data that supports parameters in the SDB compiled as of April 1992. Updated parameter reports will be issued annually as a separate volume of the *Preliminary Performance Assessment for the Waste Isolation Pilot Plant.* A previous data report was published in December 1991 (WIPP PA Division, 1991).

The 1992 comparison and background information on the comparison are reported in Volumes 1, 2, and 4 of this report:

> SNL (Sandia National Laboratories) WIPP PA Department. 1992. *Preliminary Performance Assessment for the Waste Isolation Pilot Plant, December 1992—Volume 1: Third Comparison with 40 CFR 191, Subpart B.* SAND92-0700/1. Albuquerque, NM: Sandia National Laboratories.
>
> SNL (Sandia National Laboratories) WIPP PA Department. 1992. *Preliminary Performance Assessment for the Waste Isolation Pilot Plant, December 1992—Volume 2: Technical Basis.* SAND92-0700/2. Albuquerque, NM: Sandia National Laboratories.
>
> SNL (Sandia National Laboratories) WIPP PA Department. 1993. *Preliminary Performance Assessment for the Waste Isolation Pilot Plant, December 1992—Volume 4: Sensitivity Analyses for 40 CFR 191, Subpart B.* SAND92-0700/4. Albuquerque, NM: Sandia National Laboratories.

The present volume documents parameter values used in models described in Volume 2; in turn, sensitivity and uncertainty analyses employing the models of Volume 2 are reported in Volumes 1 and 4.

Transforming data into distributions of model parameters is a major PA Department task. Although the PA Department is responsible for comparing the WIPP with *40 CFR 191, Subpart B*, the majority of data used for these comparisons is supplied by experimenters and analysts characterizing the disposal system and surrounding regional geology as noted in the acknowledgments.

In addition to individual contributors who established current data, earlier contributors are also acknowledged. Much of the data provided prior to 1991 is summarized in *Systems Analysis, Long-Term Radionuclide Transport, and Dose*

Assessments, Waste Isolation Pilot Plant (WIPP), Southeastern New Mexico; March 1989, edited by Lappin et al. (1989). Because of this report's wide circulation, we found it convenient to refer to this report as a data source, although in many cases it only summarizes others' work. Its selection as a source is not meant to diminish the contributions of the original authors. However, Lappin et al. (1989) is the first report in which ranges were assigned for many parameters, so it does provide a primary reference for these ranges. Furthermore, some of the data has not yet been published and thus Lappin et al. (1989) may be the only source until documentation is complete.

We appreciate the time and suggestions supplied by the final peer reviewers: D. R. Anderson (6342), E. D. Gorham (6119), R. C. Lincoln (6345), and J. R. Tillerson (6121). In addition, the editorial help on the text and over 100 illustrations provided respectively by J. Chapman and D. Pulliam of Tech Reps, Inc., Albuquerque, New Mexico, greatly improved the report.

CONTENTS

Figures

Figure

Figure

Figure

Tables

Table

1. INTRODUCTION

1.1 Purpose and Organization of Report

The purpose of this volume is to describe parameters of mathematical models chosen as of July 1992 for use by the Performance Assessment (PA) Department of Sandia National Laboratories in its 1992 evaluation of the long-term performance ("performance assessment") of the Waste Isolation Pilot Plant (WIPP). In this volume, performance assessment refers to the prediction of all long-term performance. For example, the models and parameters can be used to compare WIPP performance with the requirements of the Environmental Protection Agency's (EPA's) *Environmental Standards for the Management and Disposal of Spent Nuclear Fuel, High-Level, and Transuranic Radioactive Wastes (40 CFR 191)*, with long-term safety goals for individual exposure (doses) that may be necessary for environmental impact statements (National Environmental Policy Act [NEPA, 1969]), and with long-term requirements of hazardous waste regulations (Resource Conservation and Recovery Act of 1976 [RCRA, 1976]).

About 300 distinct parameters are listed in this report for use in the consequence and probability models used in simulations of the WIPP. Data bases, sources, and reasoning that supported the choices of probability distributions for each of the 300 parameters were described in the 1991 counterpart of the present volume (i.e., WIPP PA Division, 1991, Vol. 3). In the present volume, emphasis is placed upon sources and reasoning behind the 49 parameters that were sampled in the 1992 PA calculations for purposes of sensitivity and uncertainty analyses; these 49 parameters are given extended discussion in the form of data tables andgraphics. Most of these parameters specify the physical, chemical, or hydrologic properties of the rock formations (geologic barriers) in which the WIPP is placed; a substantial number of the parameters specify physical, chemical, or hydrologic properties of the seals, backfill, and waste form (engineered barriers); and some pertain to future climatic variability or future episodes of exploratory drilling at the WIPP. Dimensions of selected engineered features of the WIPP underground facility are also listed, although these dimensions are not counted as part of the 300 parameters.

The EPA Standard, *40 CFR 191*, explicitly acknowledges the uncertainties associated with scientific predictions, especially when predictions cover thousands of years, and mandates that this uncertainty be reported when making comparisons with the Standard, Subpart B. One of several sources of uncertainty in scientific predictions is uncertainty in the values of the parameters in mathematical models used to make those predictions; consequently, this report also lists estimates of the range and distribution (uncertainty) of the parameters.

The organization of this volume is as follows:

- The remainder of Chapter 1 presents conventions used in the data tables, and background information on the selection of distributions, performance assessments, and the WIPP. Chapter 1 is arranged so that information specific to the data is presented first, followed by more general information (e.g., background on the WIPP consequence models).
- Chapter 2 provides consequence-model parameters for geologic barriers.
- Chapter 3 provides consequence-model parameters for the engineered barriers and source terms.
- Chapter 4 provides consequence-model parameters for global materials such as fluid properties (e.g., Salado Formation brine compressibility) and properties of agents that act upon the WIPP disposal system such as climate variability and human-intrusion boreholes.
- Chapter 5 provides parameters for human-intrusion probability models.
- Chapter 6 lists the specific parameters that were varied for the December 1992 preliminary comparison of the WIPP with *40 CFR 191, Subpart B*.

- Appendix A is a compilation of memoranda from principal investigators; each memorandum documents either data or recommendations concerning the choice of a parameter's distribution or use of the parameter in a consequence model.
- Appendix B is tabulated data for existing wells near the WIPP site (i.e., data on Well ID, location, and formations penetrated).
- Appendices C and D provide graphic and tabular representations of certain parameters that are not conveniently placed in the main body of the report.
- Following the cited references is a table of conversion factors between SI and common English units; a glossary of terms; and a list of variables, acronyms, and initialisms.

1.2 Conventions

Chapters 2 through 5 provide data and information used in the PA Department's 1992 mathematical models of the WIPP system. The parameter sheets, graphs, and discussions in these chapters may use standard terms of probability theory and statistics or non-standard terms to characterize model parameters; brief explanations of these terms are provided below, along with a key to the parameter sheets.

1.2.1 Probability Distribution Functions

For a continuous parameter, say X, the *probability density function* (pdf) is a function $f(x) > 0$ with the properties

$$\int_a^b f(x)\,dx = \text{probability that uncertain } \textit{parameter } X \text{ lies in interval (a,b):}$$

$$\int_{-\infty}^{+\infty} f(x)\,dx = 1 .$$

The *cumulative distribution function* (cdf) associated with f(x) is defined by

$$F(x) = \int_{-\infty}^{x} f(s)\,ds = \text{probability that uncertain parameter X is less than or equal to x.}$$

Probability density functions (pdfs) and cdfs can be similarly defined for uncertain parameters that take on a denumerable number of values, x_i, i=1,2, ... The sequence $\{f_i\}$, i=1,2, ..., such that $f_i > 0$ and

$$\sum_i f_i = 1,$$

is the discrete analogue of the continuous pdf, and

$$F(x) = \sum_{\text{all } x_i < x} f_i$$

is the discrete analogue of the continuous cdf.

Examples of common, analytic, continuous and discrete probability distributions are shown in Table 1.2-1.

Table 1.2-1. Description of Several Probability Distributions

	Probability Density Function f(x)	Cumulative Distribution Function F(x)	Expected Value μ	Variance σ^2
1.	Beta $\frac{\frac{1}{B(\alpha,\lambda)}(x-a)^{\alpha-1}(b-x)^{\lambda-1}}{(b-a)^{\alpha+\lambda-2}}$ $a<x<b,\ \alpha>0,\ \lambda>0$ where $B(\alpha,\lambda)=\frac{\Gamma(\alpha)\ \Gamma(\lambda)}{\Gamma(\alpha+\lambda)}$ and $\Gamma(\gamma)=\int_0^\infty x^{\gamma-1}e^{-x}dx$ $=\frac{\alpha!\ \lambda!}{(\alpha+\lambda-1)!}$ if α and λ are integers	$\int_a^x f(x)\ dx$	$a=\frac{\alpha}{\alpha+\lambda}$	$\frac{(b-a)^2\ \alpha\lambda}{(\alpha+\lambda)^2(\alpha+\lambda+1)}$
2.	Gamma $\frac{\lambda^\alpha x^{\alpha-1}e^{-\lambda x}}{\Gamma(\alpha)}$	$\int_0^x f(x)\,dx$	$\frac{\alpha}{\lambda}$	$\frac{\alpha}{\lambda^2}$
3.	Exponential $\lambda e^{-\lambda x} x\geq 0$	$1-e^{-\lambda x}$	$\frac{1}{\lambda}$	$\frac{1}{\lambda^2}$

Table 1.2-1. Description of Several Probability Distributions (Continued)

	Probability Density Function f(x)	Cumulative Distribution Function F(x)	Expected Value μ	Variance σ^2
4.	Normal $N(\mu, \sigma^2)$			
	$\frac{1}{\sigma\sqrt{2\pi}} \exp\left[-\frac{(x-\mu)^2}{2\sigma^2}\right]$	$\int_{-\infty}^{x} f(\chi)\, d\chi$	μ	σ^2
	$-\infty \le x \le \infty$			
	but for WIPP PA			
	$a \le x \le b$ where $P(x > a) = 0.99$ and			
	$P(x > b) = 0.01$		$\mu = \frac{a+b}{2}$	$\left(\frac{b-a}{4.66}\right)^2$
5.	Lognormal		$\exp\left[\mu(y) + \frac{\sigma^2(y)}{2}\right]$	
	$\frac{1}{\sigma x\sqrt{2\pi}} \exp\left[-\frac{1}{2\sigma^2} (\ln x - \mu)^2\right]$	$\int_{o}^{x} f(\chi)\, d\chi$	Median $= e^{\mu(y)}$	$e^{2\mu(y)+\sigma^2}\left(e^{\sigma^2(y)} - 1\right)$
	$x \ge 0$			
	$x = e^y$ where $y = N(\mu, \sigma^2)$			
	but for WIPP PA			
	P(y>a) = 0.99 and			
	P(y>b) = 0.01		$\mu(y) = \frac{a+b}{2}$	$\sigma^2(y) = \left(\frac{b-a}{4.66}\right)^2$

Table 1.2-1. Description of Several Probability Distributions (Concluded)

	Probability Density Function f(x)	Cumulative Distribution Function F(x)	Expected Value μ	Variance σ^2
6.	Uniform		$\frac{a+b}{2} = \mu$	$\frac{(b-a)^2}{12}$
	$\frac{1}{b-a}$ $a \le x \le b$	$\frac{x-a}{b-a}$	$a = \mu - \sqrt{3\sigma}$ $b = \mu + \sqrt{3\sigma}$	
7.	Loguniform			
	$\frac{1}{x(\ln b - \ln a)}$	$\frac{\ln x - \ln a}{\ln b - \ln a}$	$\frac{b-a}{\ln b - \ln a}$	$(b-a)\left[\frac{(\ln b - \ln a)(b+a) - 2(b-a)}{2(\ln b - \ln a)^2}\right]$
	$a < x < b$		Median = $\sqrt{ab}$	
8.	Binomial (discrete)			
	$\frac{n!}{x!(n-x)!} p^x (1-p)^{n-x}$	$\sum_{\chi=0}^{x} f(\chi)$	np	np(1-p)
	x = 0,1,2,...,N;			
9.	Poisson (discrete)			
	$\frac{\mu^x e^{-\mu}}{x!}$ $x = 0, 1, 2, ..., \infty$	$\sum_{\chi=0}^{x} f(\chi)$	μ	μ

1.2.2 Empirical Distribution Functions

Empirical cdfs are histograms or piecewise constant functions based on percentiles derived from a set of measurements (data), or a set of subjective estimates of experts. For independent measurements (data) of some quantity, the empirical cdf is an unbiased estimator of the unknown population cdf of that quantity (Blom, 1989, p. 216); this property does not rigorously apply to empirical cdfs derived from subjective estimates of experts.

1.2.3 Range

The range of a distribution is denoted by (a,b), the pair of numbers in which a and b are respectively the minimum and maximum values that can reasonably be taken by the uncertain parameter X.

1.2.4 Mean and Sample Mean

The mean value (or, simply, *mean*) of a distribution is one measure of the central tendency of a distribution; it is analogous to the arithmetic average of a series of numbers. The population mean, μ, is defined by

$$\mu = \int_{-\infty}^{\infty} x f(x)\, dx \text{ for continuous distributions, or}$$

$$\sum_{\text{all } x_i} x_i f_i \text{ for discrete distributions.}$$

The *sample mean*, denoted by $\bar{x}$, is the arithmetic average of values in an empirical data set. A sample mean can also be assigned to empirical cdfs derived from subjective estimates of experts.

1.2.5 Median and Sample Median

The *median* value of a cdf is denoted by x_{50} and is that value in the range at which 50% of all values lie above and below (i.e., the 0.5 quantile). *Sample medians*, here denoted by $\bar{x}_{50}$, can be obtained directly from empirical cdfs in the obvious way.

1.2.6 Variance and Coefficient of Variation

The *variance* of a distribution, σ^2, is the second moment of the distribution about its mean, i.e.,

$$\sigma^2 = \int_{-\infty}^{\infty} (x-\mu)^2 f(x)\, dx \text{ for continuous distributions, or}$$

$$\sum_{\text{all } x_i} (x_i-\mu)^2 f_i \text{ for discrete distributions.}$$

The *standard deviation*, σ, is the positive square root of the variance. The coefficient of variation, the ratio of standard deviation to mean, σ/μ, is a convenient measure of the relative width of a distribution.

The *sample variance* of a set of measurements of parameter X, say X_1, X_2, X_3, ...X_N is the sum

$$\frac{1}{(N-1)} \sum_{n=1}^{N} (X_n - \bar{x})^2.$$

The sample variance of independent measurements of some quantity is an unbiased estimator of the population variance of that quantity (Blom, 1989, p. 197). (A variance can also be formally calculated for empirical cdfs derived from subjective estimates of experts; this is not a sample variance, however.)

1.2.7 Categories of Distributions

Distributions used in this report are grouped into five categories:

1. Continuous analytical distributions: beta, normal, lognormal, uniform or loguniform (Figure 1.2-1a),
2. Discrete analytical distributions: Poisson (Figure 1.2-1b), binomial,
3. Constructed empirical distributions based on measurements (Figure 1.2-1b),
4. Constructed empirical distributions based on expert judgment ("Subjective Estimates," Figure 1.2-1b),
5. Miscellaneous categories (null distributions): constant, spatial, and table.

CONTINUOUS DISTRIBUTIONS

Four continuous, analytical distributions frequently used in this report are described below.

Normal

Normal designates the normal pdf, a good approximation to the distribution of many physical parameters. The normal distribution arises naturally from the central limit theorem (Johnson and Kotz, 1970a, p. 40; Miller and Freund, 1977, p. 104). For purposes of performance assessment, the distribution is arbitrarily truncated at the 0.01 and 0.99 quantities (i.e., the probability that the parameter will be smaller or larger is 1%), which corresponds to $\bar{x} \pm 2.33s$, where s is the sample standard deviation.

Lognormal

Lognormal designates a lognormal pdf, a distribution of a variable whose logarithm follows a normal distribution. The distribution is arbitrarily truncated at the 0.01 and 0.99 quantiles.

Uniform

Uniform designates a pdf that is constant in the interval (a,b) and zero outside of that interval.

Loguniform

Loguniform designates a loguniform pdf, a distribution of a variable whose logarithm follows a uniform distribution.

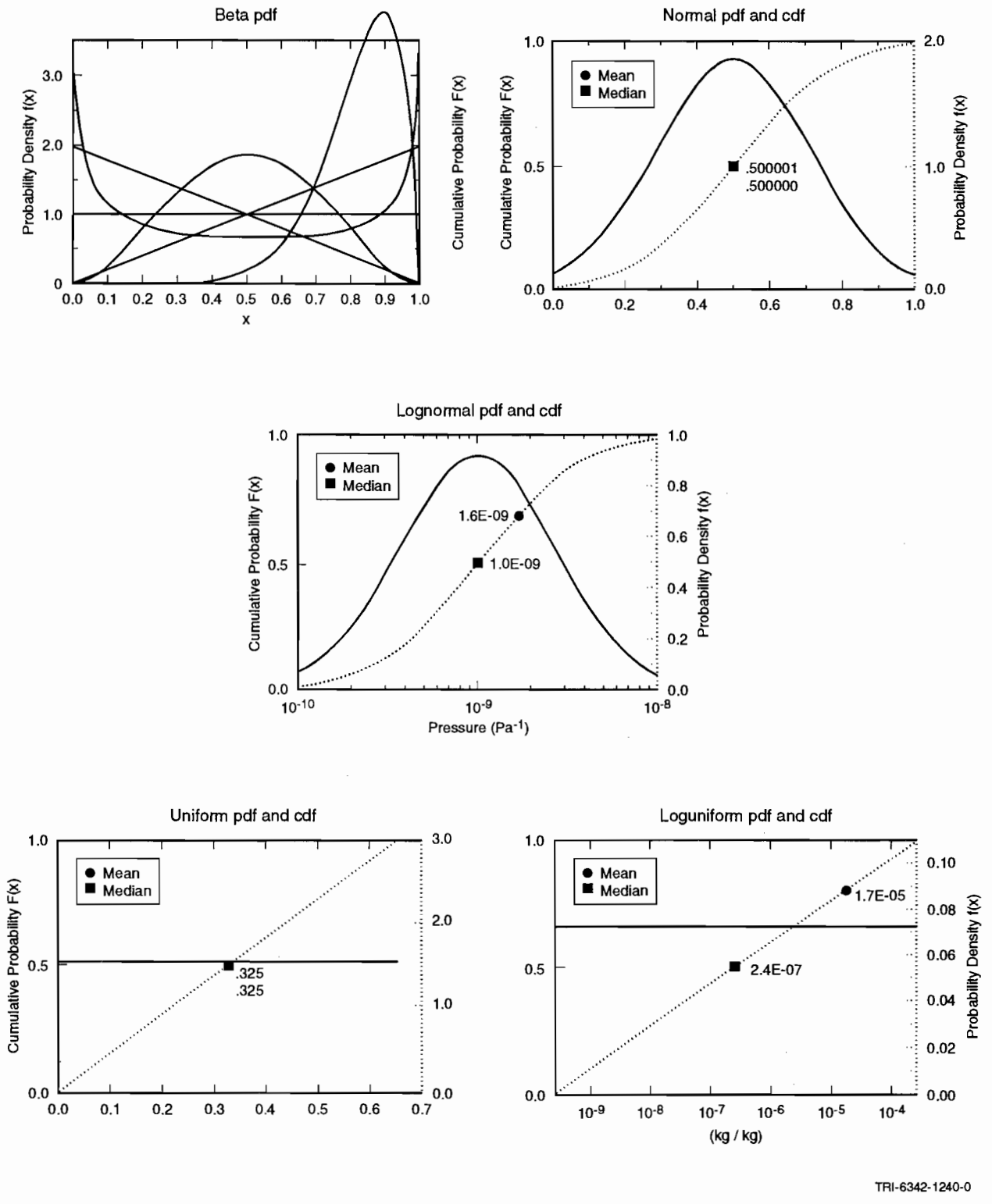

(a) Continuous Distribution Plots

Figure 1.2-1. Examples of distribution plots.

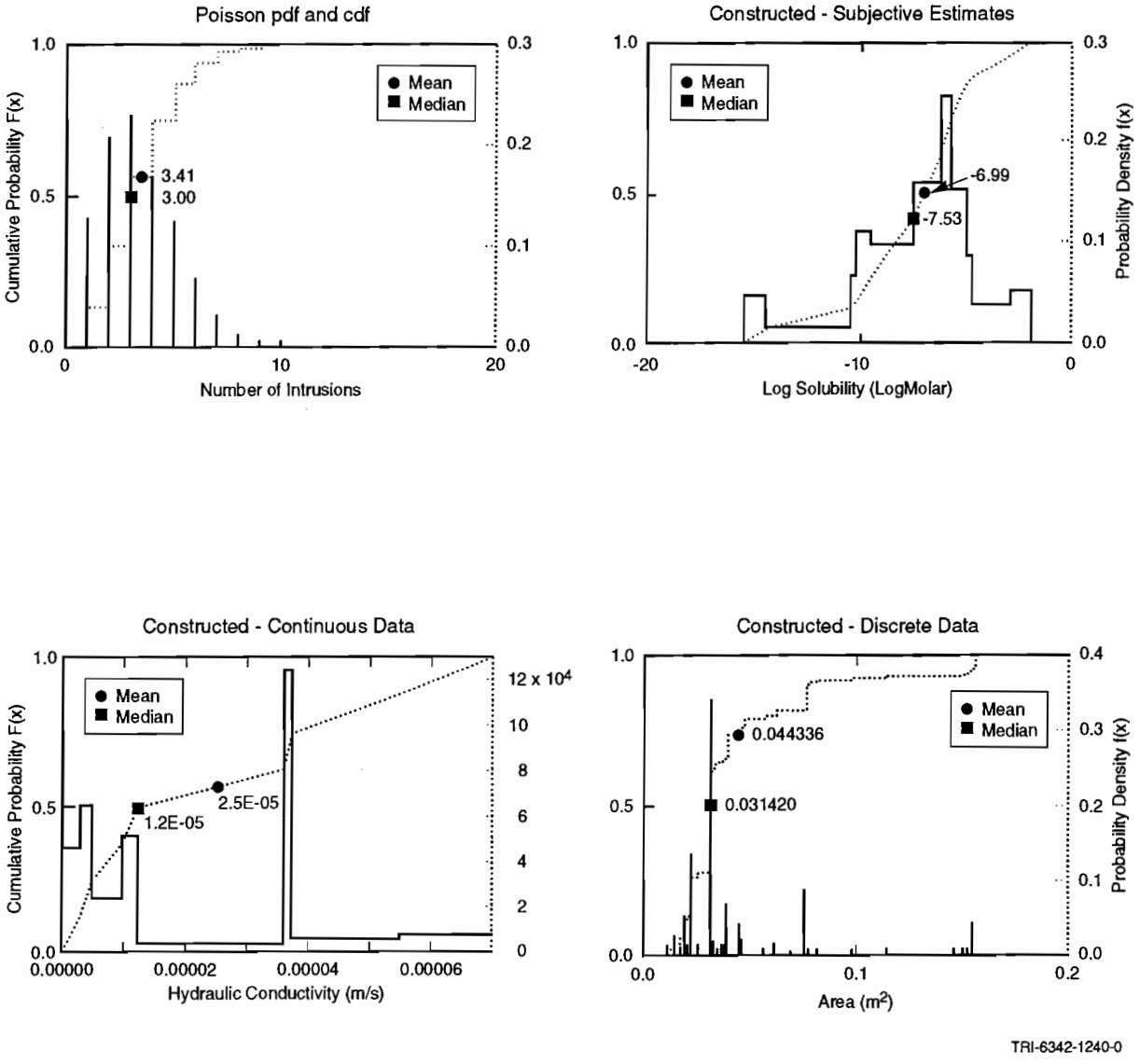

(b) Discrete and Constructed Distribution Plots

Figure 1.2-1. Examples of distribution plots (concluded).

DISCRETE DISTRIBUTIONS

A frequently used discrete distribution is the Poisson distribution (Figure 1.2-1b). The Poisson pdf is often used to model processes taking place over continuous intervals of time, such as the arrival of telephone calls at a switch station (queuing problem) or the number of imperfections per unit length produced in a bolt of cloth. The Poisson pdf was used in the 1991 probability model for human intrusion by exploratory drilling. The 1992 probability model for human intrusion incorporates effects of deterrence of markers and monuments; this model is based on generalized Poisson distributions (see Section 1.4.2).

CONSTRUCTED DISTRIBUTIONS (DATA)

A constructed distribution of the Data type is simply an empirical cdf constructed from sets of measured data points in the data base. For intrinsically discrete data, the empirical cdf is a piecewise-constant function resembling a histogram. For intrinsically continuous data, the empirical cdf is always converted to a piecewise-linear function by joining the empirical percentile points with straight lines; this is done to ensure that, in Monte Carlo sampling, the distribution of sampled parameter values will cover all of the range of the distribution (Tierney, 1990, p. II-5).

In some cases, the PA Department may modify constructed distributions of the Data type by extending the range of the data set to include estimated 0.01 and 0.99 quantiles. Since the range of measurements in a data set may not reflect the true range of the random variable underlying the measurements, the PA Department may estimate the range by $\bar{x} + 2.33s$, where $\bar{x}$ is the *sample* mean and s is the *sample* standard deviation. (The lower limit of this estimate is not allowed to be less than zero for an intrinsically positive variable: both the upper and lower limit are not allowed to exceed physical limits.) This estimate of range is justified by the fact that the indicated end-points are estimates of the 0.01 and 0.99 quantiles if the variable is normally distributed. If the variable is not normally distributed, the quantiles will differ in inessential ways (Table 1.2-2). For any distribution with finite mean and variance, Chebyshev's inequality states that the probability that the random variable x lies outside the interval $(\bar{x} - hs, \bar{x} + hs)$, $h > 0$, is a quantity less than $1/h^2$ (Blom, 1989, p. 121); i.e.,

$$P(|x - \bar{x}| \geq hs) \leq \frac{1}{h^2} . \qquad (1.2\text{-}1)$$

If the pdf of the unknown distribution is known to be unimodal and symmetric about the mean value, then the right-hand side of Eq. 1.2-1 can be replaced with $4/(9h^2)$ (Gauss' inequality); i.e.,

$$P(|x - \bar{x}| \geq hs) \leq \frac{4}{9h^2} . \qquad (1.2\text{-}2)$$

CONSTRUCTED DISTRIBUTIONS (SUBJECTIVE)

Constructed distributions of Subjective type are histograms based on subjective estimates of range (the 0 and 100 percentile) and at least one interior percentile point (usually the 50 percentile or median). The subjective estimates of percentile points are usually obtained directly from experts in the subject matter of the parameter of concern (see Section 1.3.1). Histograms for intrinsically continuous parameters are always converted to piecewise linear cdfs by joining the subjective percentile points with straight lines.

Whether a constructed distribution is of the subjective or data type should be evident from the discussion material on a parameter sheet.

Table 1.2-2. Probability of Parameters Lying within Range Defined by $\bar{x} \pm hs$ (after Harr, 1987, Table 1.8.2)

h	Chebyshev's Inequality	Gauss' Inequality	Exponential pdf	Normal pdf	Uniform pdf
1	0	0.56	0.86	0.68	0.58
2	0.75	0.89	0.95	0.96	1.00
2.33	0.82	0.92	0.964	0.9802	1.00
3	0.89	0.95	0.982	0.9973	1.00
4	0.94	0.97	0.993	0.99993	1.00

MISCELLANEOUS CATEGORIES

Other "null" categories of distributions are described below:

Constant

When a distribution type is listed as constant, a distribution has not been assigned and a constant value is used in all PA calculations.

Spatial

The spatial category of data indicates that the parameter varies spatially. This spatial variation is usually shown on an accompanying figure. The median value recorded is a typical value for simulations that use the parameter as a lumped parameter in a model; however, the value varies depending upon the scale of the model. The range of a spatially varying parameter is also scale dependent.

Table

The table category of data indicates that the parameter varies with another property and the result is a tabulated value. For example, relative permeability varies with saturation; its distribution type is listed as table (also, the median value is not meaningful and is therefore omitted in the table).

1.2.8 Key to Parameter Sheets

Characteristics of each of the 49 parameters sampled in the 1992 PA calculations are summarized in Parameter Sheets (Figure 1.2-2) for the convenience of the reader. Many other important parameters may also receive treatment in these Parameter (or Data) Sheets. A key to the meaning of the entries in a Parameter Sheet is provided below.

Parameter Sheets are divided by horizontal lines into four boxes. In the first box (top of page), there can be up to seven entries.

Parameter Sheet

Parameter:	**Threshold displacement pressure (p_t)**
Material:	halite and polyhalite within Salado Formation, [Salado, Press CTD]
Definition, Units:	Pa
Values:	Range: (2.3×10^5, 2.3×10^9) Median: 2.3×10^7
Distribution:	Lognormal
Correlation:	

Data Source(s):

Davies, P. B. 1991a. *Evaluation of the Role of Threshold Pressure in Controlling Flow of Waste-Generated Gas into Bedded Salt at the Waste Isolation Pilot Plant.* SAND90-3246. Albuquerque, NM: Sandia National Laboratories. (Investigator Judgment)

Davies, P. B. 1991b. Appendix A: "Uncertainty Estimates for Threshold Pressure for 1991 Performance Assessment Calculations Involving Waste-Generated Gas," *Preliminary Comparison with 40 CFR Part 191, Subpart B for the Waste Isolation Pilot Plant, December 1991. Volume 3: Reference Data.* WIPP Performance Assessment Division. Eds. R. P. Rechard, A. C. Peterson, J. D. Schreiber, H. J. Iuzzolino, M. S. Tierney, and J. S. Sandha. SAND91-0893/3. Albuquerque, NM: Sandia National Laboratories. A-37 through A-41. (Investigator Judgment)

Usage:

Mathematical model:

Section 1.4.1, this volume.

Equation 1.4.1-6.

Computational models:

BRAGFLO

Ranking in Past Sensitivity Analyses:

40 CFR 191	Low
40 CFR 268	Not tested
NEPA	Not tested
Other	Not applicable

Figure 1.2-2. Example of a parameter sheet.

- **Parameter:** The name of the parameter (e.g., "threshold displacement pressure"), followed by its mathematical symbol (e.g., "p_t") if appropriate.
- **Material:** The materials or subsystems in which the parameter applies (e.g. "halite and polyhalite within Salado Fm.) followed by the current (1992) names for the parameter in the secondary data base (e.g., "[Salado, Press CTD]").
- **Definition:** A short definition of the parameter may appear in this entry if there is the possibility of confusing the parameter with other quantities; usually, this entry is blank.
- **Units:** The physical units in which the parameter is measured (e.g., "Pa" or Pascals). Only SI units are used in the tables and secondary data base (except for radionuclide inventory activity, which is expressed in curies). Occasionally, for the sake of clarity, the parameter may also be expressed in the Values entry (see below) in terms of more familiar or intuitive units, e.g., years instead of seconds.
- **Values:** The values entry gives a snapshot of the range and median of the distribution of the parameter; e.g., in the values entry of the example,

$$\text{Range: } (2.3 \times 10^5, 2.3 \times 10^9) \text{ Median: } 2.3 \times 10^7.$$

- **Distribution:** The type of the distribution of the parameter using type names defined in Section 1.2.7. For example, "lognormal" is the continuous, analytical distribution defined in entry 5 of Table 1.2-1.
- **Correlation:** Names of other parameters with which the parameter in question is correlated. If this entry is blank, the parameter in question is assumed to be functionally and statistically independent of all other parameters.

The second box (from top of page) contains only one type of information.

- **Data Source(s):** A list of the primary documents supplying data and information used by PA Department staff in constructing the parameters distribution. (Documents judged to be secondary sources may be cited in Discussions that may follow each parameter sheet.) Each data-source entry is followed by a parenthetical characterization of the nature of the evidence or arguments in the source: the possible categories are

  1. *WIPP Observational Data.* Data from observational measurements made on site at the WIPP or in a laboratory in connection with the WIPP Project. These data are usually published as a formal report or a journal article, but in some cases may take the form of an internal Sandia memorandum.
  2. *Non-WIPP Literature Data.* General data for systems or processes that are similar to those occurring at the WIPP. These data may be found in formal non-WIPP reports, journal articles, or handbooks.
  3. *Investigator Judgment.* Evidence or arguments provided by Investigators within the WIPP Project after review of available observational data and relevant literature. Investigator judgment is often necessary because few hard quantitative data exist or existing data were measured on spatial and temporal scales that differ from PA model requirements.
  4. *Expert Panel Judgment.* Evidence or arguments provided by an Expert Judgment Panel, rather than an individual Investigator, after a comprehensive review of related information (e.g., WIPP reports, relevant literature).
  5. *General Engineering Knowledge.* Evidence or arguments based on engineering "rules of thumb," i.e., accepted engineering rules and practice whose validity has been endorsed by years of successful application but for which there are no consensuable (scientific) explanations.

The third box (from top of page) in a parameter sheet contains information on the use of the parameter in the several consequence or probability models employed by the PA Department.

- **Mathematical model:** General statements on use of the parameter are supplied in this entry. In the present volume on Model Parameters, the reader will be directed towards the appropriate subsections and equations in Section 1.4, "Background on 1992 Probability and Consequence Models."
- **Computational models:** A list of current computational models used by the PA Department that generally require specification of the parameter, starting with the name of the model that uses the parameter in the 1992 Preliminary Performance Assessment.

The last box of a Parameter Sheet (bottom of page) states the ranking of the sensitivity of a parameter with respect to sensitivity studies addressing three standards or regulations: 40 CFR 191, Subpart B; 40 CFR 268 (RCRA); and NEPA. The rankings are based largely on limited, formal sensitivity analyses performed in past years. Sensitivity analyses conducted during *40 CFR 191* studies are described in Helton et al., 1991, 1992; the *40 CFR 191* entries in the last box of a parameter sheet are based on rankings established in these studies. A recent sensitivity analysis conducted specifically for the *40 CFR 268* (RCRA) models (WIPP PA Department, 1992) was used to establish the entries under *40 CFR 268* in the last box of the parameter sheets. In these kinds of analyses, a parameter's sensitivity can be measured by the frequency-of-appearance and relative position of the parameter in rank-regression tables (see Helton et al., 1991, pg. III-45). A sampled parameter that does not appear in a rank-regression table could be termed insensitive; a parameter that appears frequently in the tables could be called sensitive, etc. This suggests the following notation for the ranking of a parameter.

- **Not applicable**: To mean that the parameter is judged not to be uncertain (or imprecisely known); the parameter is usually a high-precision constant such as a dimension of an engineered feature or a universal physical constant.
- **Not tested**: To mean that the parameter is judged to be uncertain but has not yet been selected for sampling, i.e., tested, in a sensitivity study. (See Chapter 6 for procedures used in selecting parameters for sampling in sensitivity studies.)
- **Low:** To mean that the parameter has been tested in sensitivity studies and either did not appear, or appeared infrequently and in low-order, in the studies' rank-regression tables.
- **Medium:** To mean that the parameter has been tested in sensitivity studies and appeared frequently in the studies' rank-regression tables.
- **High:** To mean that the parameter has been tested in sensitivity studies and has consistently appeared as one of the top-ranking entries in the studies' rank-regression tables.

1.3 Background on Selecting Parameter Distributions

1.3.1 Requests for Data from Sandia Investigators and Analysts

When evaluating long-term performance, the PA Department follows a well-defined procedure for acquiring and controlling the data used in consequence and probability models. A data base, called the secondary data base, contains the interpreted data and in essence embodies the PA Department's conceptual model(s) of the disposal system (Rechard, 1992). The data provided in this report are from the secondary data base as of April 1992 and are used in the 1992 preliminary performance assessment of the WIPP (Volume 1 of this report).

The major sources of the data are the task leaders and investigators at Sandia and Westinghouse Electric Corporation.

IDENTIFY NECESSARY DATA

Each year, the PA Department identifies data that are necessary to perform the calculations for the preliminary performance assessment. Members of the department may informally compile data from published reports, personal communications with investigators, and other sources.

REQUEST MEDIAN VALUE AND DISTRIBUTION

The PA Department then requests that the investigators provide either new data or a median value and distribution for each parameter in a large subset of the parameters. Some model parameters are specific to the PA calculations and so individuals in the PA Department are considered the experts for these parameters (e.g., probability model parameters).

Initially, Sandia investigators are responsible for providing data or--if data are unavailable--distributions for all parameters. As this procedure for acquiring data is repeated, a few parameters are evaluated through formal elicitation.

UPDATE SECONDARY DATA BASE

The PA Department enters the endorsed or elicited data for all parameters into the secondary data base. The PA Department then either constructs parameter distributions or uses distributions provided by investigators; the PA Department selects a subset of these parameters to sample, keeping all other values constant at their *median* values, unless specifically noted.

PERFORM CONSEQUENCE SIMULATIONS AND SENSITIVITY ANALYSES

The PA Department runs consequence simulations and sensitivity analyses with selected subsets of data from the updated secondary data base. The sensitivity analysis evaluates the sensitivity of a parameter in determining variation of the result (i.e., a complementary cumulative distribution function [CCDF]). During this time, the PA Department prepares a report that lists parameters in the secondary data base at the time of these calculations (i.e., this data report).

DETERMINE WHETHER PARAMETER IS IMPORTANT IN ANALYSIS

By means of the sensitivity analyses, the PA Department can determine whether the parameter is significant in the calculations. If the parameter does not appear to be significant in the sensitivity analyses, and the review process of the Parameter Report does not question the parameter value, then a flag is set in the secondary data base for that parameter to indicate that it is not likely either to change or be sampled in forthcoming sensitivity studies.

1.3.2 Construction of Distributions

The steps below describe the procedure developed by the PA Department to construct probability distributions (cdfs) for the uncertain parameters in consequence and probability models (Figure 1.3-1) (modified from Tierney, 1990).

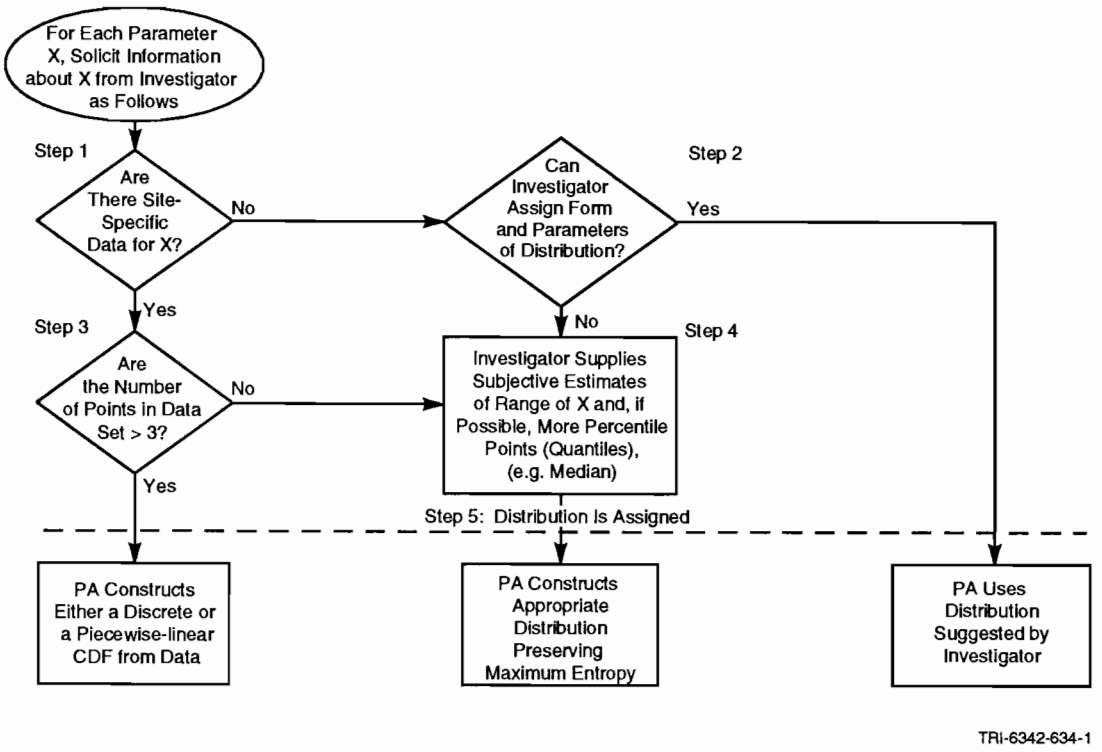

Figure 1.3-1. Five-step procedure used to construct cumulative distribution functions (cdfs) for the 1992 performance simulations. Investigator refers to expert in subject matter (after Tierney, 1990).

STEP 1

Determine whether site-specific data for the parameter in question exist, i.e., find a set of site-specific sample values of the parameter. Data and information are usually either documented in a formal report or are described in an internal memorandum (see Appendix A). If data sets exist, go to Step 3; if no data sets are found, go to Step 2.

STEP 2

Request that the investigator supply a specific shape (e.g., normal, lognormal) and associated numerical parameters for the distribution of the parameter. If the investigator assigns a specific shape and numerical values for the distribution's parameters, go to Step 5; if the investigator cannot assign a specific shape and appropriate parameters, go to Step 4. In responding to this request, the investigator may use his or her knowledge of global data to form an answer. Distributions supplied by investigators may be documented by a memorandum (see Appendix A).

STEP 3

Determine the size of the combined data sets. If the number of values in the combined data set is >3, use the combined data to construct a piecewise-linear cumulative distribution function or, alternatively, a discrete cumulative distribution function, and then go to Step 5. If the number of variables in the combined data set is ≤3, go to Step 4.

STEP 4

Request that the investigator provide subjective estimates of (a) the range of the variable (i.e., the minimum and maximum values taken by the variable with at least 99% confidence and preferably 100% confidence) and (b) if possible, one of the following (in decreasing order of preference): (1) percentile points for the distribution of the variable (e.g., the 25th, 50th [median], and 75th percentiles), (2) the mean value and standard deviation of the distribution, or (3) the mean value. Again, in responding to this request, the investigator may use his or her knowledge of global data to form an answer and may document that answer in a memorandum (see Appendix A). Then, using the maximum entropy formalism (MEF), construct one of the following distributions depending upon the kind of subjective estimate that has been provided (Tierney, 1990; Harr, 1987):

- Uniform probability distribution function (pdf) over the range of the variable,
- Piecewise-linear cdf based on the subjective percentiles,
- Exponential pdf (truncated) based on the subjective range and mean value,
- Normal pdf based on subjective mean value and standard deviation.

Then go to Step 5.

STEP 5

End of procedure; distribution is assigned. Computational considerations and limitations on the data itself may require later modification to some distributions. Some of these limitations are discussed in the next section.

1.3.3 Some Limitations on Distributions

The major limitations on ensuring the validity of the probability distributions assigned to parameters in the 1992 Preliminary Performance Assessment are thought to be a consequence of two acts:

- The equating of spatial variability with model parameter uncertainty, particularly for that class of parameters called material-property parameters.
- The neglect of obvious correlations between model parameters.

The following arguments attempt to explain these limitations, i.e., they show why some of the current assignments of probability distributions to material-property parameters of WIPP performance models may be unnecessarily conservative, given the present level of detail and spatial resolution of the models. Current methods of assigning uncertainty to some of the material-property parameters (e.g., including small-scale spatial variability as a source of uncertainty) may distort results of sensitivity analyses and entail unnecessary expense, but will probably not affect validity of results of the uncertainty analyses that are used to make preliminary comparisons with EPA standards.

NO SCALING OF VARIABILITY FOR MATERIAL-PROPERTY PARAMETERS

WIPP performance models described in Volume 2 of this report are based on the numerical solution of one or more of three types of equations:

(a) Partial differential equations - which are reduced to a set of algebraic equations or ordinary differential equations in order to effect a solution by finite-difference or finite-element methods. Examples: the equations of groundwater and brine flow, solute transport, gas flow, and salt creep (see Sections 1.4.1, 1.4.5, and 1.4.6).

(b) Ordinary differential equations - which may be the result of a reduction of a partial differential equation or may directly model the dynamics of a lumped-parameter system, e.g., punctured brine reservoirs, leaching and decay of radioactive waste stored in a panel (see Section 1.4.4).

(c) Algebraic equations of the form

$$F(x_1, x_2, x_3, ..., x_n; y) = 0$$

which may arise indirectly from equilibrium solutions of ordinary differential equations (i.e., solutions for time $\rightarrow \infty$) or may directly express a model of some physical relationship between WIPP performance-model variables (x_1, x_2, x_3, ..., x_n) and y (see Section 1.4.3).

In addition to dependent variables and independent variables of position and time, certain constant quantities will appear in each of the three types of equations. Such constants can be called "free" parameters because they may freely be specified by the user of the equations in which they appear. In most cases, these free parameters are intended to represent physical and chemical properties of real materials of the WIPP system: e.g., the hydraulic conductivity, porosity, and specific storage in models of fluid flow in the Salado Formation; the fracture spacing, dispersivity, diffusivity, and chemical distribution coefficients in models of solute transport in the Culebra Formation; the porosity, permeability and solubility of waste forms emplaced in a typical WIPP panel. This kind of parameter will be called a *material-property parameter* in the remainder of this section.

Many of the material-property parameters of WIPP performance models have been included in the set of uncertain variables sampled in recent studies of variable sensitivity of performance models (for example, Helton et al., 1991). (Note: In these studies, all uncertain model parameters were usually called "variables" or "independent variables.") In these studies, uncertainty associated with a sampled parameter was quantified by assigning an empirical or subjective probability distribution to the values taken on by that parameter within a predetermined range of values. Current procedures for the assignment of probability distributions were described in the previous section.

The distribution of a material-property parameter needs to reflect spatial variability of the material property and also the scale of the model. The zones or cells of numerical models (finite-element, finite-difference, or lumped-parameter models) must be few in number in order to minimize computational time and expense; in a typical problem involving geologic media, these cells will have dimensions of tens of meters or more and volumes of thousands of cubic meters. Material-property parameters must therefore represent the effects of a physical or chemical property of matter in these relatively large, arbitrarily defined volumes of space. It follows that material-property parameters are model dependent and usually not observable quantities, i.e., quantities that can be measured in the field or in the laboratory. On the other hand, with few exceptions (e.g., formation transmissivity measured by pumping tests) most physical and chemical properties of geologic or anthropogenic materials are actually measured on spatial scales typical of the laboratory or an exploratory borehole, a matter of at most a few tens of centimeters. In addition, natural materials and many man-made materials (e.g., defense waste) tend to be inhomogeneous on spatial scales that are smaller than the scales that characterize model cell sizes; accordingly, a set of measurements of a material property taken randomly from large volumes of real material may show wide variability. The question is: How to assign values to material-property parameters in a way that correctly reflects both cell size and the small-scale variability that may appear in measurements of the corresponding material property?

One way of approaching the problem of scaling is as follows. Assume that the material property can be represented as a scalar field in space, say $\phi(x)$, where $\mathbf{x} = (x,y,z)$ denotes position in space. (The assumptions of a scalar quantity in three dimensions are for the sake of simplicity of argument and involve no loss of generality; the property could be a vector or tensor.) It is argued in some modern textbooks that the material-property parameter, say Φ, to be used in type (a) equations (above) should be taken as a spatial average of ϕ over the cell or zone; for instance, in a cell or zone of volume V,

$$\Phi(V) = \frac{1}{V}\int_V \phi(\mathbf{x})\, d\mathbf{x} \tag{1.3-1}$$

where $d\mathbf{x}$ is the volume element dxdydz. (Again, no loss of generality is involved; a line or surface average could replace the volume average.) The arguments for this choice of material-property parameter are highly technical and limitations of time and space preclude their inclusion in this note; however, see the discussion in de Marsily (1986, Chapter 3 and Section 4.4).

To account for spatial variability of $\phi(\mathbf{x})$, it can be assumed that ϕ is a *stationary, random scalar field* within a cell volume V, with realizations $\phi(\mathbf{x},\mu)$ and the following statistical properties:

$$\text{Expectation of } \phi(\mathbf{x}, \mu) = E[\phi(\mathbf{x})] = \bar{\phi}, \text{ a constant,} \tag{1.3-2}$$

and

$$\begin{aligned}\text{Covariance of } \phi(\mathbf{x}, \mu) &= E\{ [\phi(\mathbf{x}) - \bar{\phi}] [\phi(\mathbf{y}) - \bar{\phi}] \} \\ &= \sigma^2 \rho(|\mathbf{x} - \mathbf{y}|) \quad ,\end{aligned} \tag{1.3-3}$$

where σ^2 is a constant (called the *variance* of ϕ), and $\rho(\bullet)$ is a function of $r = |\mathbf{x} - \mathbf{y}|$ with the properties,

$$\begin{aligned}&\rho(r) \geq 0 \text{ for } r \in (0,\infty) \ , \\ &\rho(r) \to 1 \text{ as } r \to 0 \ , \\ &\rho(r) \to 0 \text{ as } r \to \infty \ .\end{aligned} \tag{1.3-4}$$

The function $\rho(\bullet)$ is called the *autocorrelation function* (Yaglom, 1962); it is a measure of the statistical dependence of the values of ϕ measured at two different points $\mathbf{x}$ and $\mathbf{y}$. The stationarity assumptions of constant mean value $\bar{\phi}$ and variance σ^2 can be slightly weakened by allowing these quantities to depend on the coordinates of the center of the volume V, i.e., $\bar{\phi}$ and σ^2 may vary from cell to cell.

Treating $\phi(\mathbf{x})$ as a stationary random field with statistical properties 1.3-2 through 1.3-4 allows estimates of the mean value and variance of the volume average of ϕ, $\Phi(V)$, to be made. It is shown in textbooks (see for instance Yaglom, 1962, pgs. 23-24) that

$$\text{Expectation of } \Phi(V) = E[\Phi(V)] = \bar{\phi}, \tag{1.3-5}$$

and

$$\text{Variance of } \Phi(V) = \frac{\sigma^2}{V^2}\int_V\int_V \rho(|\mathbf{x} - \mathbf{y}|)\, d\mathbf{x}\, d\mathbf{y}. \tag{1.3-6}$$

If $\bar{\phi}$, σ^2 and $\rho(r)$ were known, the problem would be essentially solved in that the distribution of the material-property parameter, $\Phi(V)$, could be approximated by a normal distribution with mean and variance given respectively by Eqs. 1.3-5 and 1.3-6. In general, $\bar{\phi}$, σ^2 and the function $\rho(r)$ must be estimated using sets of spatially coordinated measurements of the material property ϕ, say $(\phi_1, \phi_2, ..., \phi_N)$. The estimators of $\bar{\phi}$ and σ^2 are the usual unbiased estimators of mean and variance (see Tierney, 1990, pp. II-4,5) and, given a sufficiently large set of spatially coordinated measurements of ϕ, approximations to the autocorrelation function could be constructed and used in

numerical evaluations of the volume integrals in Eq. 1.3-6. This ideal solution to the problem cannot be implemented, however, since there are few measurements of the material properties appearing in WIPP performance models (and most are not spatially indexed; measured transmissivity, grain density, porosity, and tortuosity of the Culebra Formation are exceptions). Thus, one must try to use available measurements and insight to infer the statistical properties, given by Eqs. 1.3-5 and 1.3-6, of material-property parameters, $\Phi(V)$. Examples of attempts to treat uncertainty in material-property parameters are given in the treatments of Salado Formation permeabilities and far-field pore pressures in Sections 2.3 and 2.4 of this volume. The following general observations may also be useful in inferring statistical properties of material-property parameters.

(1) The variance of a material-property parameter is less than or equal to the apparent variance of the material property. Note that because of the properties of $\rho(r)$ (Eq. 1.3-4), the integrand in the double volume integral of Eq. 1.3-6 is always less than one so that

$$\text{Variance of } \Phi(V) \leq \sigma^2 .$$

In particular, if the special form of autocorrelation function is taken ("cookie cutter"),

$$\rho(|x-y|) = 1 \text{ if } |x-y| \leq a, \qquad (1.3\text{-}7)$$
$$= 0 \text{ otherwise,}$$

then

$$\text{Variance of } \Phi(V) \approx \frac{\upsilon}{v}\sigma^2 , \qquad (1.3\text{-}8)$$

where $v = \frac{4\pi}{3} a^3$ can be called the *volume of correlation*. Equation 1.3-8 suggests that if the volume of correlation is <<V, then the distribution of $\Phi(V)$ is peaked about the mean value of the material property, $\bar{\phi}$. If the coefficient of variation of the material property, $\sigma/\bar{\phi}$, is not large (say, of the order of one), the distribution of $\Phi(V)$ is more sharply peaked about the mean value, $\bar{\phi}$, than is the distribution of the material property, $\phi(x)$. If this tendency is strong enough, then $\Phi(V)$ can simply be assigned the mean value,

$$\Phi(V) \approx \bar{\phi} .$$

This is what is usually done in studies with numerical models that are not probabilistic; that is, not directed explicitly towards sensitivity and uncertainty analyses.

(2) If, as suggested above, $\Phi(V) \approx \bar{\phi}$, then one must consider the uncertainty inherent in estimating the mean value $\bar{\phi}$, that arises from (a) a limited number of measurements of the material property, and (b) relationships between $\bar{\phi}$ and other uncertain problem parameters. Uncertainty of type (a) can be handled by fitting available data to a "t-distribution" (Blom, 1989) which, in a Bayesian approach, gives the distribution of the true mean of the material property about the sample mean of measurements. However, this was not done in assigning ranges to parameters in the 1992 exercise. Uncertainty of type (b) is usually model dependent and must be handled on a case-by-case basis (see remarks on correlations below).

The standard techniques of statistical estimation cannot be directly applied when the distribution of the material property, $\phi(x)$, must be gained by subjective means, i.e., the elicitation of expert judgment. In such cases, the PA Department must make the assumption that the distribution of the material property, $\phi(x)$, is also the distribution of the material-property parameter, $\Phi(V)$. Instances where this assumption was made are found in the sections on waste-form solubility (3.3.5) and Culebra sorption coefficients (2.6).

GENERAL ABSENCE OF CORRELATIONS AMONG PARAMETERS

Most of the 49 parameters varied during the 1992 Preliminary Performance Assessment exercise were assumed to be independent random variables even though it was known that some were dependent upon others, i.e., correlated in some way. Correlations of the model variables may arise from the fact that there are natural correlations between the local quantities used to determine the form of the model variable (e.g., local porosity could be strongly correlated with local permeability); or correlations of model variables may be implicit in the form of the mathematical model in which they are used. The effects of neglecting correlations on the sensitivity/uncertainty analyses are generally unknown.

In some instances (Sections 2.3.5, 2.4.5) an attempt was made to induce known correlations by the adjustment of the ranges of distributions; in other cases (threshold displacement pressure in Section 2.4.1), perfect correlation was simply assumed.

1.3.4 Selection of Parameters for Sampling

For the 1992 preliminary performance assessment of the WIPP, the 49 parameters that were selected for variation (sampling) together with a brief description of why they were selected are discussed in Chapter 6. Other studies on subsystems of the WIPP disposal system (e.g., sensitivity of the repository to gas generation) may use different subsets of the approximately 300 parameters for which distributions are reported herein.

1.4 Background on 1992 Probability and Consequence Models

A majority of the parameters described in the present volume specify constants or material-property parameters (Section 1.3.3) that appear in the mathematical formulations of seven consequence or probability models used in the 1992 Preliminary Comparison exercise. The models are described in detail in Volume 2 of this report. In the present section, a link between Volume 2 and the data and distributions of Volume 3 is made by providing brief descriptions of the governing equations for each model and later noting in a Parameter Sheet where each parameter fits in a numbered model equation. The seven models to be described are

- A model of two-phase flow in backfilled repository openings and the Salado Formation (BRAGFLO),
- A model of human intrusion in the presence of markers and monuments (a part of the CCDFPERM code),
- A model of borehole cuttings removal (CUTTINGS),
- A model of radionuclide discharge from a brine-flooded panel (PANEL),
- A model of fluid flow in the Culebra (SECO2D),
- A model of solute transport in the Culebra (SECO/TP),
- A model of deformation of waste-filled room (SANCHO).

1.4.1 Two-Phase Flow: BRAGFLO

Study of the effects of gas on the flow of brine through the repository and up an intrusion borehole require a computational model that simulates two-phase flows through porous, heterogeneous reservoirs. The PA Department uses a model developed in-house for Sandia National Laboratories and called BRAGFLO. The governing equations for BRAGFLO are presented in this section. Conceptual models of two-phase flow are further described in Section 7.2 and Appendix A of Volume 2 of this series of reports.

BRAGFLO solves simultaneously the partial differential equations (PDEs) that describe the mass conservation of each mobile component (gas and brine) along with appropriate constraint equations, initial conditions, and boundary conditions. The fundamental equations can be found in Peaceman (1977) and Crichlow (1977). A total of five independent equations (two component mass conservation PDEs and three constraints) can be written to define the two-phase flow phenomena:

Gas Component Conservation:

$$\nabla \bullet \left[\frac{\alpha \rho_n K k_{rn}}{\mu_n} \left(\nabla P_n - \rho_n g \nabla D \right) + \frac{\alpha C_{Nw} \rho_w K k_{rw}}{\mu_w} \left(\nabla P_w - \rho_w g \nabla D \right) \right] + \alpha q_n + \alpha q_{rn} \qquad (1.4.1\text{-}1)$$

$$= \alpha \frac{\partial \left(\phi \rho_n S_n + \phi C_{Nw} \rho_w S_w \right)}{\partial t} \ ,$$

Brine Component Conservation:

$$\nabla \bullet \left[\frac{\alpha C_{Ww} \rho_w K k_{rw}}{\mu_w} \left(\nabla P_w - \rho_w g \nabla D \right) \right] + \alpha q_w + \alpha q_{rw} = \alpha \frac{\partial \left(\phi C_{Ww} \rho_w S_w \right)}{\partial t} \ , \qquad (1.4.1\text{-}2)$$

Saturation Constraint:

$$S_n + S_w = 1 \ , \qquad (1.4.1\text{-}3)$$

Mass Fraction Constraint:

$$C_{Nw} + C_{Ww} = 1.0 \ , \qquad (1.4.1\text{-}4)$$

Capillary Pressure Constraint:

$$P_n - P_w = P_c \ , \qquad (1.4.1\text{-}5)$$

where the quantities in Eqs. 1.4.1-1 through 1.4.1-5 have the following meanings:

(Note that starred [*] quantities are given extended discussion below.)

	$C_{M\ell}$	mass fraction of component M dissolved or miscible in phase ℓ,
	g	gravitational acceleration constant [Lt^2], [m s^{-2}],
	K	absolute permeability of the reservoir [L^2], [m^2],
*	$k_{r\ell}$	relative permeability to phase ℓ [dimensionless],
*	P_c	capillary pressure [$ML^{-1}t^{-2}$], [Pa],
	P_ℓ	pressure of phase ℓ [$ML^{-1}t^{-2}$], [Pa],
	q_ℓ	mass rate of well injection (or production, if negative) per unit volume of reservoir [$ML^{-3}t^{-1}$], [kg m^{-3} s^{-1}],
*	$q_{r\ell}$	mass rate of products produced (or reactant consumed, if negative) per unit volume of reservoir due to chemical reaction [ML^{-3} t^{-1}], [kg m^{-3} s^{-1}],
	S_ℓ	saturation of phase ℓ [dimensionless],

	x,y	spatial dimensions (x-horizontal, y-vertical),
	α	geometric factor (in three dimensions, $\alpha = 1$; in two dimensions, α = length; in one dimension, α = area,
	∇	gradient, shorthand for vector $\partial/\partial x$, $\partial/\partial y$ in two dimensions,
	$\nabla\bullet$	divergence, shorthand for $\partial/\partial x + \partial/\partial y$ in two dimensions,
*	ϕ	reservoir porosity [dimensionless],
	ρ_ℓ	density of phase ℓ [$M^1 L^{-3}$], [$kg^1 m^{-3}$],
	μ_ℓ	viscosity of phase ℓ [$ML^{-1} t^{-1}$], [cp].

Subscripts:

N	nonwetting component (gas component),
n	nonwetting phase (gas phase),
W	wetting component (brine component),
w	wetting phase (brine phase).

NOTES ON RELATIVE PERMEABILITY AND CAPILLARY PRESSURE

Brooks and Corey (1964) observed that the effective saturation of a porous material, s_e, can be related to the capillary pressure, p_c, by

$$p_c = \frac{p_t}{s_e^{1/\lambda}}, \qquad (1.4.1\text{-}6a)$$

where

p_t = threshold displacement pressure,

λ = Brooks and Corey exponent.

Brooks and Corey defined s_e as

$$s_e = \frac{s_\ell - s_{\ell r}}{1 - s_{\ell r}},$$

where s_ℓ is the wetting phase saturation (brine) and $s_{\ell r}$ is the residual wetting phase saturation, below which the wetting phase no longer forms a continuous network through the pore network and therefore does not flow, regardless of the pressure gradient. This has been modified to account for residual (or critical) gas saturation, s_{gr}:

$$s_e = \frac{s_\ell - s_{\ell r}}{1 - s_{gr} - s_{\ell r}}. \qquad (1.4.1\text{-}7a)$$

The relative permeability of the wetting phase ($k_{r\,\ell}$) is obtained from

$$k_{r\ell} = s_e^{\frac{2+3\lambda}{\lambda}} \quad . \tag{1.4.1-8a}$$

For the gas phase, the relative permeability (k_{rg}) is

$$k_{rg} = (1 - s_e)^2 \left(1 - s_e^{\frac{2+\lambda}{\lambda}}\right) . \tag{1.4.1-9a}$$

Alternative analytic forms for effective saturation, capillary pressure, and relative permeabilities were suggested by Webb (April 30, 1992, Memo in Appendix A) and were tested in the 1992 sensitivity analyses. These forms are based on the Van Genuchten-Parker model of two-phase characteristic curves (Van Genuchten, 1978; Parker et al., 1987). The effective saturation takes the form

$$s_e = \frac{s_\ell - s_{\ell r}}{s_{\ell s} - s_{\ell r}} \quad , \tag{1.4.1-7b}$$

where $s_{\ell s}$ is the maximum wetting-phase saturation (taken as 1 - s_{gr} by the PA Department, where s_{gr} is critical gas saturation). The capillary pressure takes the form,

$$P_c = P_o \left[S_e^{-1/m} - 1\right]^{1-m} \quad , \tag{1.4.1-6b}$$

where $m = \lambda/(1+\lambda)$, λ is the Brooks and Corey exponent (Eq. 1.4.1-6a), and P_o is a constant determined by equating Eq. 1.4.1-6b to Eq. 1.4.1-6a at $S_e = 0.5$. The alternative relative permeabilities take the forms:

$$k_{r\ell} = s_e^{1/2} \left[1 - \left(1 - s_e^{1/m}\right)^m\right]^2 \quad , \tag{1.4.1-8b}$$

$$k_{rg} = \left(1 - s_e\right)^{1/2} \bullet \left(1 - s_e^{1/m}\right)^{2m} \quad . \tag{1.4.1-9b}$$

NOTES ON GAS-GENERATION TERMS

The terms q_{rn}, q_{rw} appearing in Eqs. 1.4.1-1 and 1.4.1-2 are sums of production (or consumption) terms for two processes: corrosion and microbial degradation. The contributing terms for each process are discussed below.

Gas Production and Brine Consumption from Corrosion of Steel

Let

q_{CH_2} = rate of H_2 production by corrosion per unit volume of panel (kg/m^3•s),

q_{CH_2O} = rate of H_2O consumption by corrosion per unit volume of panel (kg/m^3•s).

These rates are calculated by Eqs. 1.4.1-10 and 1.4.1-11 below,

$$q_{CH_2} = (k_{CI}\ S_\ell + k_{CH}\ S_g)\ (X_{CH_2})\ (M_{H_2}), \tag{1.4.1-10}$$

$$q_{CH_2O} = \frac{q_{CH_2} \bullet (X_{CH_2O})\ (M_{H_2O})}{(X_{CH_2})\ (M_{H_2})}, \tag{1.4.1-11}$$

where

k_{CI} = rate constant for corrosion under inundated conditions [mole Fe/(m^3-panel•s)],

k_{CH} = rate constant for corrosion under humid conditions [mole Fe/(m^3-panel•s)],

S_ℓ, S_g = liquid (brine) and gas saturations (dimensionless),

X_{CH_2} = corrosion stoichiometry factor for H_2 (mol H_2/mol Fe),

X_{CH_2O} = corrosion stoichiometry factor for H_2O (mol H_2O/mol Fe),

M_{H_2} = molecular weight for H_2 expressed as (kg/mole),

M_{H_2O} = molecular weight for H_2O expressed as (kg/mole).

The quantities k_{CI}, k_{CH}, X_{CH_2} and X_{CH_2O} are expressed in terms of secondary data base parameters by the relations

$$k_{CI} = \frac{\dot{n}'_{CI}\ A_d\ n_d}{X_{CH_2}\ V_{pf}}\ , \quad k_{CH} = f\ k_{CI}\ , \tag{1.4.1-12}$$

and

$$X_{CH_2} = \frac{(4-x)}{3}\ , \quad X_{CH_2O} = -\frac{(4+2x)}{3}\ . \tag{1.4.1-13}$$

In Eq. 1.4.1-12,

$$f = \dot{n}'_{CH}/\dot{n}'_{CI} = \text{the relative humid gas production rate by corrosion,} \tag{1.4.1-14}$$

and

$\dot{n}'_{CI}$ = rate of H_2 production by corrosion, inundated conditions [mol H_2/(m^2-surface steel)•s],

$\dot{n}'_{CH}$ = rate of H_2 production by corrosion, humid conditions [mol H_2/(m^2-surface steel)•s],

A_d = surface area of steel in an equivalent drum, including both drum and its contents (m^2),

n_d = number of equivalent drums in a generalized waste region (dimensionless),

V_{pf} = volume of generalized waste region.

Note: A "generalized waste region" can be either a room, a panel, or the entire repository, depending upon the purposes of the calculation. The parameters A_d, n_d, and V_{pf} were constants in the 1992 calculations with BRAGFLO.

In Eq. 1.4.1-13,

x = the anoxic, iron-corrosion stoichiometric factor, a dimensionless number between zero and one. (1.4.1-15)

Gas Production from Microbial Degradation

Let

q_{BH_2} = rate of H_2 production by biodegradation of cellulosics per unit volume of panel ($kg/m^3 \cdot s$).

This rate is calculated from Eq. 1.4.1-16 below,

$$q_{BH_2} = k_{BI}\, S_\ell + k_{BH}\, S_g \left(S_{BH_2}\right)\left(M_{H_2}\right) \quad , \tag{1.4.1-16}$$

where

k_{BI} = rate constant for biodegradation of cellulosics under inundated conditions [mole cellulosics/(m^3 panel•s)],

k_{BH} = rate constant for biodegradation of cellulosics under humid conditions [mole cellulosics/(m^3 panel•s)],

S_{BH_2} = biodegradation stoichiometric factor for H_2 (mole H_2/mole cellulosics),

and other quantities appearing in Eq. 1.4.1-16 have been defined in Part A. The quantities k_{BI} and k_{BH} are expressed in terms of other secondary data base parameters in a manner similar to Part A:

$$k_{BI} = \frac{\dot{n}_{BI} \bullet n_d \bullet v_d \bullet f_c \bullet \rho_c}{S_{BH_2} \bullet V_{pf}}, \qquad k_{BH} = \xi\, k_{BI} \tag{1.4.1-17}$$

New quantities in Eq. 1.4.1-17 are

v_d = internal volume of equivalent drum (m^3),

f_c = volume fraction of cellulosics in undisturbed drum (dimensionless),

ρ_c = effective density of cellulosics in undisturbed drum (kg/m^3),

$\dot{n}_{BI}$ = rate of gas production by biodegradation, inundated conditions [mole gas/(kg-cellulosics•s)],

$\dot{n}_{BH}$ = rate of gas production by biodegradation, humid conditions [mole gas/(kg-cellulosics•s)], which is implicitly defined by

$$\xi = \dot{n}_{BH}/\dot{n}_{BI} = \text{relative humid gas production rate by microbial degradation.} \qquad (1.4.1\text{-}18)$$

NOTE ON RESERVOIR POROSITY

The "reservoir" in the two-phase flow model can be comprised of many different materials (named on Figure 1.4-1), each of which is assigned usually different porosities and absolute permeabilities. With one exception, material porosities and absolute permeabilities are assumed to be imprecisely known constants because the present version of the two-phase flow model cannot account for changes in material properties owing to pressurization or rock deformation. The one exception is the porosity of the generalized waste region, which was independently modeled in 1992 as a function of time and total volumes of gas generated by corrosion and microbial action (Figure 1.4-2).

Mendenhall and Lincoln (February 28, 1992, Memo in Appendix A) estimated waste region porosity as a function of time and volume-of-gas space using the SANCHO code (Stone et al., 1985) and baseline data provided by Beraún and Davies (September 2, 1991, Memo in Appendix A). SANCHO is a finite-element computer program for simulating the quasistatic, large-deformation, inelastic response of two-dimensional solids. In the present application, the two-dimensional solid is a waste-filled disposal room imbedded in a much larger block of bedded salt.

The addition of SANCHO to the set of models used by the PA Department has triggered a need to include a host of mechanical parameters for waste and Salado materials in the Secondary Data Base (SDB). A brief discussion of the constitutive equations used in SANCHO is provided in Section 1.4.7; values of waste and Salado-material mechanical parameters that were used by Mendenhall and Lincoln, and Beraún and Davies, are presented in Section 2.5.

1.4.2 Human Intrusion: CCDFPERM

The event "unintentional intrusion into WIPP repository by exploratory drilling" forms the basis for the major disturbed-case scenario class in WIPP performance assessment. Since 1990, the PA Department has used a probability model for this event that is based on the assumption that future episodes of exploratory drilling are a Poisson counting process with constant intensity: in other words, the probability that a portion of the repository is drilled exactly n times in a period of T years is

$$\Pr\{N = n\} = \frac{(\lambda T)^n}{n!} e^{-\lambda T}, \quad n = 0, 1, 2, \ldots$$

where λ is an imprecisely known parameter called the intensity of drilling. Physically speaking, λ is the expected frequency of drilling per unit area (units: events/m^2 • s) times the projected area (in m^2) of the portion of the repository of concern, e.g., that part of the repository underlain by brine reservoirs. Tierney (1991, pg. C-8) observed that treating λ as a constant over the 10,000-yr period of performance is unrealistic since it is equivalent to ignoring potential deterring effects of markers/monuments on future explorers.

During 1990-1992, Sandia National Laboratories assembled two groups of external experts with the purpose of formally addressing questions of future human intrusion into the WIPP through the Expert Judgment Panel process. Deliberations of these experts have led to insights concerning future human intrusion and, in particular, subjective probabilities of human intrusion in the presence of markers and monuments. One insight is that realistic drilling intensities are functions of time whose functional form can be inferred from subjective probabilities obtained from the expert panels (Hora, August 25, 1992, Memo in Appendix A).

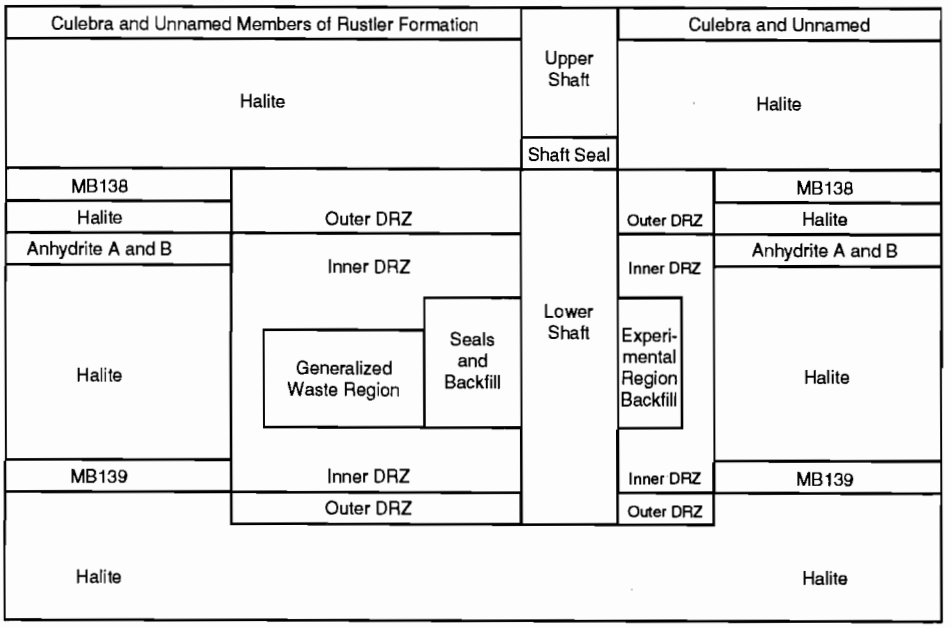

Figure 1.4-1. Idealization of waste-disposal reservoir used in BRAGFLO calculation of two-phase flow in repository and surroundings. Possible material types are shown in a planar (x, y) geometry.

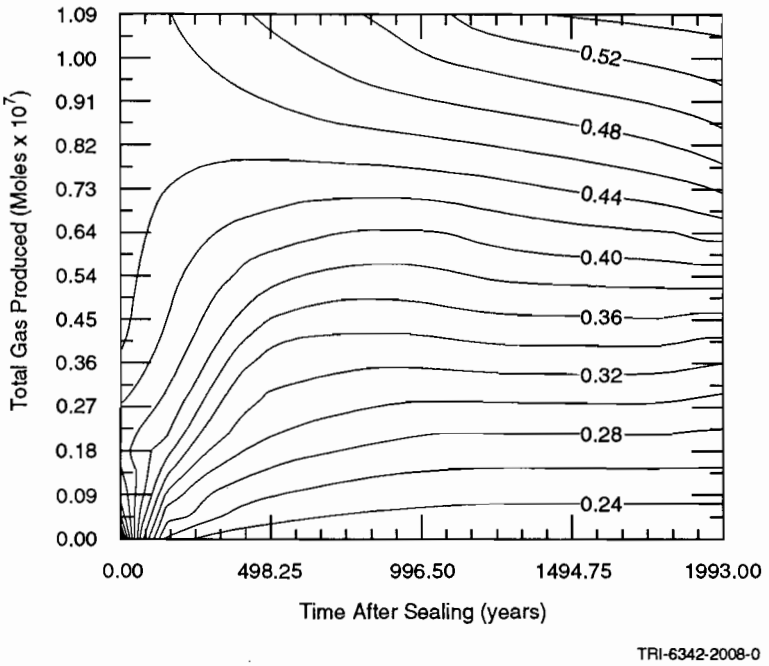

Figure 1.4-2. Isopleths of porosity of waste-filled disposal room as a function of total volume of gas produced and time after sealing. Pore space is assumed to be fully saturated with gas.

This section shows how the time-dependent drilling intensities generated by Hora (see Section 5.2) are used in the code CCDFPERM to construct probabilities for the various computational scenarios associated with human intrusion by exploratory drilling (see Helton, 1991, Chapter 2, for a complete discussion of computational scenarios and the construction of probabilities). The following material is largely taken from Ross (1985, pg. 220) and differs from Helton's treatment of the subject only in notation and style. Further discussion of the human-intrusion model can be found in Chapter 5 of Volume 2 of this series of reports.

INHOMOGENEOUS POISSON PROCESS

A *counting process* is a random process, $\{N(t), t \geq 0\}$, representing (in the present application) the cumulative number of drilling events that have occurred up to some time $t \geq 0$ after closure of the WIPP. A counting process is said to be an inhomogeneous Poisson process with intensity function $\lambda(t)$, $t \geq 0$, if

(i) $N(0) = 0$,
(ii) $\{N(t), t \geq 0\}$ has independent increments,
(iii) $\Pr\{N(t+h) - N(t) \geq 2\} = o(h)$,
(iv) $\Pr\{N(t+h) - N(t) = 1\} = \lambda(t)h + o(h)$.

In conditions (iii) and (iv), Pr {...} stands for the probability that statement {...} is true, and o(h) stands for any function f(h) with the property,

$$\lim_{h \to 0} \frac{f(h)}{h} = 0 .$$

In simple terms, o(h) is any function that tends to zero faster than the function f(h) = h as h tends to zero. The meaning of the notation {N(t+h)-N(t) = n} should be clear: exactly n drillings occur between the time t and the time t+h.

If conditions (i) - (iv) hold, it can be proven that, for any $n \geq 0$ and any integrable $\lambda(t)$,

$$\Pr\{N(t+s) - N(t) = n\} = \frac{[m(t+s) - m(t)]^n}{n!} \exp\{-[m(t+s) - m(t)]\}, \quad (1.4.2\text{-}1)$$

where

$$m(t) = \int_0^t \lambda(x)\, dx . \quad (1.4.2\text{-}2)$$

APPLICATION TO COMPUTATIONAL-SCENARIO PROBABILITIES

Calculation of computational-scenario probabilities usually begins by dividing the 10,000-yr period of performance into nT intervals,

$$[t_{i-1}, t_i], t_i > t_{i-1}, i = 1, 2, \ldots, nT .$$

Let N_i be the random variable counting the number of drillings that occurs in the interval $[t_{i-1}, t_i]$. Then, by Eq. 1.4.2-1, the probability that exactly n drillings occur in the i^{th} interval is

$$P_i[n] = \frac{[m_i]^n}{n!} e^{-m_i}, \quad (1.4.2\text{-}3)$$

where, by Eq. 1.4.2-2, m_i is shorthand for the quantity

$$\left[m(t_i) - m(t_{i-1})\right] = \int_{t_i}^{t_{i-1}} \lambda(x)\,dx \quad . \tag{1.4.2-4}$$

Given an intensity function, $\lambda(t)$, defined on the period of performance (0 to 10,000 yr), Eqs. 1.4.2-3 and 1.4.2-4 are sufficient for the computation of all necessary computational-scenario probabilities by CCDFPERM. In practice, the intensity function used to compute the m_i by Eq. 1.4.2-4 is randomly selected (or "sampled") from a finite set of intensity functions that has been generated prior to the PA calculations with CCDFPERM. The sample intensity function is then modified by multiplication with other parameters, e.g., fraction of repository area that is underlain by brine reservoirs:

$$\lambda(t) = p \bullet \lambda_s(t) \ , \tag{1.4.2-5}$$

where λ_s is the sampled intensity function (represented by a piecewise-linear function defined on the interval [0 to 10,000 yr]) and p stands for the product of the other necessary parameters. The set of intensity functions from which samples are taken has been ordered in a way that guarantees that each of its members is equally likely to be sampled (see Section 5.2 for details and Appendix D).

1.4.3 Cuttings Removal: CUTTINGS

One of the more important considerations in assessing the long-term behavior of the WIPP repository involves the transport of radionuclides from the WIPP repository as the result of penetrating a panel by an exploratory borehole. If a borehole intrudes the repository, waste will be brought directly to the surface as particulates suspended in the circulating drilling fluid. This section briefly addresses the basic equations governing direct waste removal due to drilling as they are formulated in the CUTTINGS model. The CUTTINGS code, developed specifically for the WIPP, calculates the quantity of radioactive material (in curies) brought to the surface as cuttings generated by an exploratory drilling operation that penetrates the repository during the human intrusion type scenario. The code determines the amount of cuttings removed by drilling and mud erosion, and accounts for radioactive decay that has occurred up to the intrusion time.

In the human-intrusion type scenario, a hydrocarbon exploration well is drilled through a WIPP repository panel and into the underlying pressurized brine Castile Formation (Figure 1.4-3). If rotary drilling is assumed, a volume of repository wastes is removed from the breached panel and is transported to the surface as cuttings and cavings suspended in the drilling fluid. The minimum volume of repository material removed is equal to the cross-sectional area of the drill bit multiplied by the repository thickness (cuttings). This minimum volume must be increased by material eroded from the borehole wall (cavings) by the scouring action of the swirling drilling fluid. Both cuttings and cavings will be released to the accessible environment in a settling pit at the surface.

Although the amount of waste removed by direct cutting is simple to calculate, calculating the amount of waste eroded from the borehole wall is more difficult. A number of factors may influence borehole erosion (e.g., eccentricity of pipe and hole, impact of solid particles in mud on the walls, physical and chemical interaction between mud and walls, and time of contact between the mud and walls [Broc, 1982]); however, industry opinion singles out fluid shear stress as the most important factor (Darley, 1969; Walker and Holman, 1971). A full discussion of the mathematical model of erosion of the borehole wall is presented in Section 7.7 of Volume 2 of this report; here, it is sufficient to note that drill hole wall erosion is probably largely determined by the effects of fluid shear stress acting on the wall and the character of the fluid-flow regime.

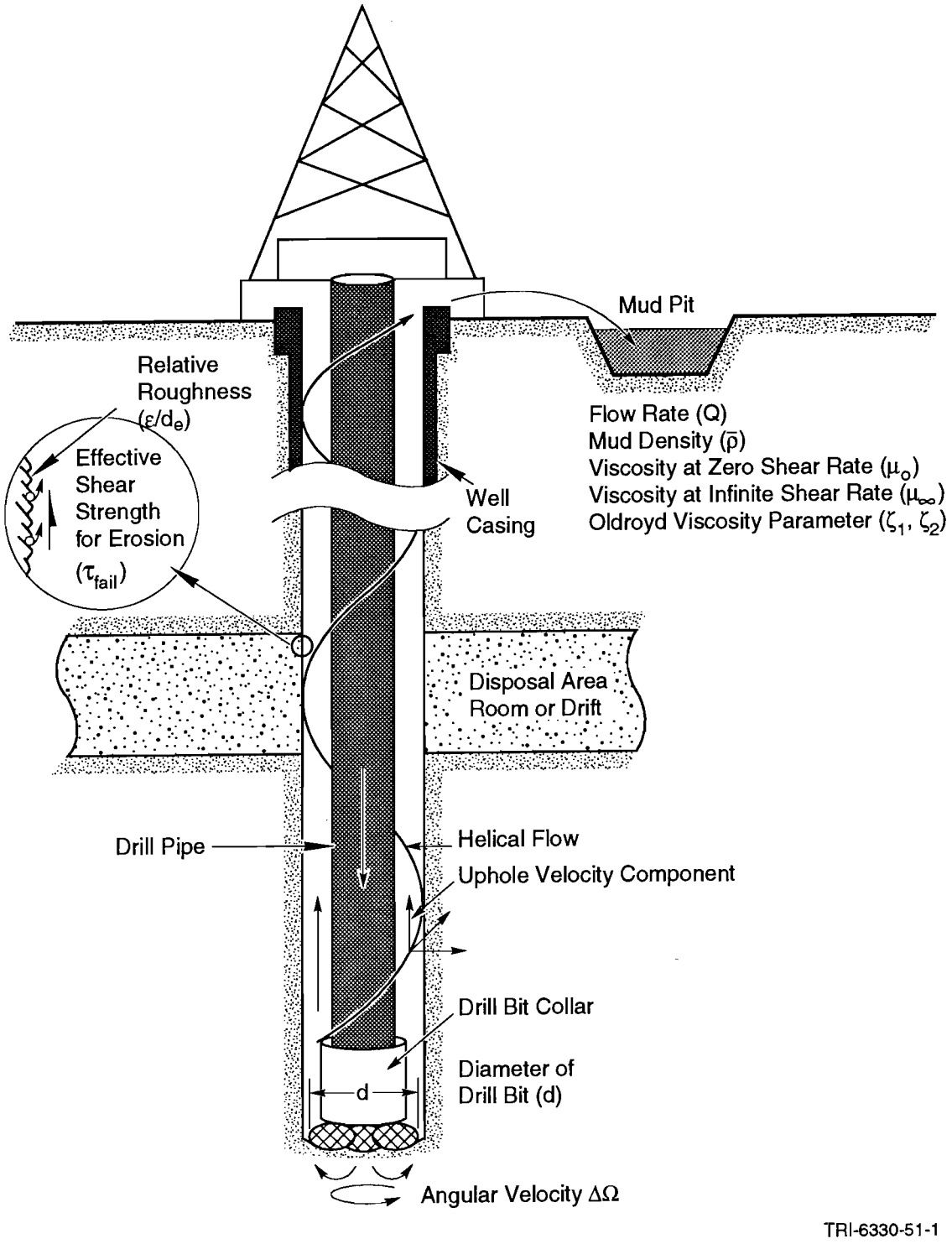

Figure 1.4-3. Some features of the CUTTINGS model.

Three drilling mud properties (density, viscosity, and yield stress) are necessary to evaluate the fluid shear stress, which in turn is one of several parameters used to evaluate the amount of material eroded from the borehole wall by scouring from the swirling drilling fluid.

FLOW REGIME

Whether the flow regime within the annulus is laminar or turbulent is governed by the Reynolds number, N_R. The Reynolds number is dependent upon the properties of the drilling mud (density, viscosity, and velocity) and the size of the annulus. The Reynolds number is defined as

$$N_R = \frac{\bar{\rho}\ \bar{V} d_e}{\bar{\mu}}, \qquad (1.4.3\text{-}1)$$

where

d_e = length dimension = equivalent hydraulic diameter for annulus $= d_{hole} - d_{collar}$,
$\bar{\rho}$ = average fluid density,
$\bar{V}$ = average fluid velocity,
$\bar{\mu}$ = average fluid viscosity (for non-newtonian fluids, the average viscosity will depend upon the viscosity model used).

SHEAR STRESS

For both laminar and turbulent axial flow in an annulus, the shear stress can be expressed as (Vennard and Street, 1975, p. 381):

$$\tau = \frac{f\bar{\rho}\bar{V}^2}{2}. \qquad (1.4.3\text{-}2)$$

The fanning friction factor, f, is discussed below for turbulent and laminar shear stress.

Turbulent Shear Stress

In turbulent flow (Reynolds number $N_R > N_{R_{crit}}$ where $N_{R_{crit}} = 2{,}100$ for newtonian fluids and 2,400 for some non-newtonian fluids [Vennard and Street, 1975, p. 384; Walker, 1976, p. 89]) the fanning friction factor is dependent on both N_R, and surface roughness (e.g., Moody diagram [Vennard and Street, 1975, Figure 9.5; Streeter and Wylie, 1975, Figure 5.32]), with N_R having a minor influence. Consequently, the shear stress is dependent primarily upon absolute surface roughness, ε, and kinetic energy $\frac{\bar{\rho}\bar{V}^2}{2}$. An empirical expression for f is (Colebrook, 1939):

$$\frac{1}{\sqrt{f}} = -4 \log \left[\frac{\varepsilon/d}{3.72} + \frac{1.255}{N_R\sqrt{f}} \right] \qquad (1.4.3\text{-}3)$$

where

ε = absolute roughness of material,

d = hydraulic diameter = difference between borehole diameter and collar diameter and N_R is calculated using the limiting viscosity μ_∞ (Figure 1.4-4).

Laminar Shear Stress

For laminar flow, the fanning friction factor, f, is a function of only N_R. The shear stress in laminar flow (Reynolds number $N_R < 2{,}100$ [Vennard and Street, 1975, p. 384]) depends solely on the fluid viscosity and strain rate (velocity gradient); however, for a non-newtonian fluid such as drilling mud, the viscosity varies with strain rate (Figure 1.4-4). Several functional forms are used to model this variation (Ideal Bingham Plastic, Power Law, and Oldroyd Model). The PA Department currently uses the Oldroyd model. For the laminar flow regime both the axial and circumferential motion of the drilling mud are considered.

Oldroyd Model

Oldroyd's (1958) shear softening model of the viscosity can approximate the drilling fluid behavior away from the yield stress (τ_0) by the appropriate choice of parameters:

$$\tau = \mu_0 \left[\frac{1 + \zeta_2 \Gamma^2}{1 + \zeta_1 \Gamma^2} \right] \Gamma , \qquad (1.4.3\text{-}4)$$

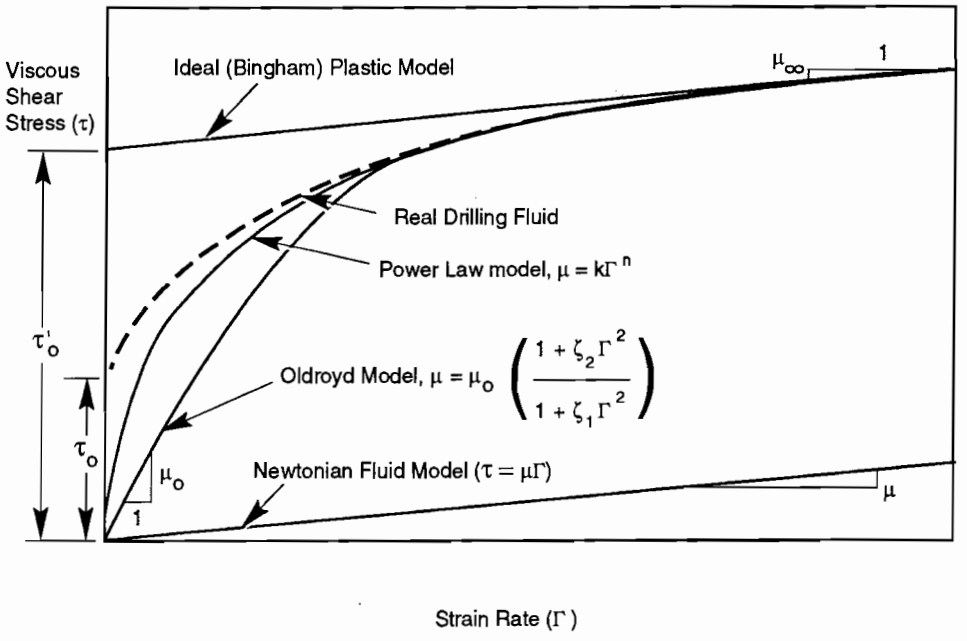

Figure 1.4-4. Various models for modeling drilling fluid shear stress.

where

μ_∞ = $\mu_o (\zeta_2/\zeta_1)$ = limiting viscosity at infinite strain rate,
Γ = strain rate,
$\zeta_1 \zeta_2$ = Oldroyd model parameters,
μ_0 = limiting viscosity at zero rate of strain.

Note that for the PA calculations, ζ_1 was assumed equal to 2 ζ_2, based on viscosity measurements for an oil-based, 1.7-kg/m^3 (14-lb/gal) mud (Darley and Gray, 1988, Table 5-2). The assumption can be somewhat arbitrary since the behavior at high strain rate (away from the yield point) is of primary interest.

Using the above assumption, the parameter ζ_2 was estimated by equating the linear ideal plastic model, with the Oldroyd model at a high strain rate (Figure 1.4-4). Simple algebraic manipulation gives

$$\zeta_2 = (\mu_\infty \Gamma_m - \tau'_o)/2\Gamma^2_m \tau'_o . \qquad (1.4.3\text{-}5)$$

The high strain rate selected for the match point (Γ_m) was 1020 s^{-1}.

1.4.4 Repository Discharge: PANEL

Flow of brine through a collapsed WIPP panel and up an intrusion borehole may result in mobilization of dissolved, radionuclide-bearing compounds and their transport towards the Culebra. The PA Department models these effects with a code called PANEL. Governing equations for that part of PANEL model concerned with waste mobilization and transport are presented in this section.

In the PANEL model, a collapsed WIPP panel (rooms and drifts) is treated as a single, hydraulically connected cavity of volume V that contains a porous medium (waste and backfill). The cavity is connected to sources and sinks for brine by one or more inlets or outlets (Figure 1.4-5).

Quasi-steady discharge of brine through the panel is assumed, i.e.,

$$Q(t) = Q_{out} = Q_{in} , \qquad (1.4.4\text{-}1)$$

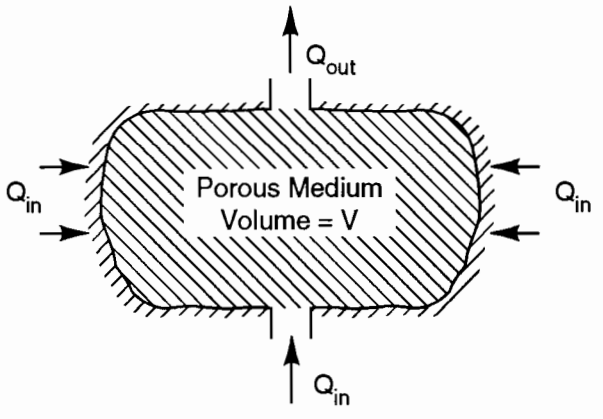

Figure 1.4-5. Idealized collapsed WIPP panel in PANEL model.

where Q(t) is the brine discharge through volume V in units of m^3/s. (Note: the PANEL model receives Q(t) from the BRAGFLO model; see Section 1.4.1.)

WASTE MOBILIZATION

The mobilization of radioactivity in the waste form can be modeled by considering the dynamics of three variables:

$M_{ui}(t)$ = mass of i^{th} nuclide in undissolved form in volume V at time t,
$M_{di}(t)$ = mass of i^{th} nuclide in dissolved form in volume V at time t,
$M_{ai}(t)$ = mass of i^{th} nuclide adsorbed on solids in volume V at time t.

Thus,

$$M_i(t) = M_{ui} + M_{di} + M_{ai} \qquad (1.4.4\text{-}2)$$

= total mass of i^{th} nuclide in volume V at time t.

The dynamics of these mass components follow from three ordinary differential equations (three for each nuclide species). The first dynamical equation is

$$\dot{M}_{ui} = -k_i M_{ui}\left[S_i - \frac{M_{di}}{w}\right] - \lambda_i M_{ui} + \lambda_{i-1} M_{ui-1}\,, \qquad (1.4.4\text{-}3)$$

where a dot ($\dot{}$) means the time derivative and

$$w = \bar{\phi}\,\bar{S}_\ell\, V = \text{volume of brine in cavity.} \qquad (1.4.4\text{-}4)$$

In Eq. 1.4.4-4, $\bar{\phi}$ and $\bar{S}_\ell$ are respectively the average porosity and the average saturation of the medium filling V (i.e., the compressed WIPP wastes and backfill).

The first term on the right side of Eq. 1.4.4-3 models dissolution of undissolved mass: the rate of dissolution is assumed to be proportional to M_{ui} and the difference between the concentration of a saturated solution (S_i) and the concentration of dissolved mass (M_{di}/w); the constant of proportionality k_i is a rate constant (units: $m^3/kg{\cdot}s$). The second and third terms on the right side of Eq. 1.4.4-3 respectively represent loss of mass through radioactive decay of undissolved mass, and gain of mass through the decay of a parent species.

The second dynamical equation is

$$\dot{M}_{di} = k_i M_{ui}\left[S_i - \frac{M_{di}}{w}\right] - Q\frac{M_{di}}{w} - \frac{\bar{\rho}_b}{\bar{\phi}} K_{di}\dot{M}_{di} - \lambda_i M_{di} + \lambda_{i-1} M_{di-1}\,. \qquad (1.4.4\text{-}5)$$

The first term on the right side of Eq. 1.4.4-5 was explained above; mass lost from the undissolved component is gained by the dissolved component. The second term on the right side of Eq. 1.4.4-5 represents mass lost from volume V by advection in the brine discharge through the panel (Q is never negative). The third term on the right side represents loss of dissolved mass by chemical sorption processes; it is assumed that sorption/desorption processes are rapid and follow a linear isotherm so that

$$M_{ai} \cong \frac{\bar{\rho}_b}{\bar{\phi}} \bar{K}_{di} M_{di}, \qquad (1.4.4\text{-}6)$$

where $\bar{\rho}_b$ is the average bulk density of compressed wastes and backfill (kg/m^3) and $\bar{K}_{di}$ is the average distribution coefficient for the i^{th} nuclide in wastes and backfill (Freeze and Cherry, 1979, p. 405). Meanings of the fourth and fifth terms on the right side of Eq. 1.4.4-5 were explained above for the undissolved mass component.

The third dynamical equation is

$$\dot{M}_{ai} = \frac{\bar{\rho}_b}{\bar{\phi}} \bar{K}_{di} \dot{M}_{di} - \lambda_i M_{ai} + \lambda_{i-1} M_{ai-1}, \qquad (1.4.4\text{-}7)$$

where all terms on the right of Eq. 1.4.4-7 have been explained.

The three dynamical equations, 1.4.4-3, 1.4.4-5, and 1.4.4-7, can be somewhat simplified by defining

$R_i = 1 + \frac{\bar{\rho}_b}{\bar{\phi}} \bar{K}_{di}$ the effective retardation coefficient for the i^{th} nuclide species (dimensionless),

$C_{di} = M_{di}/w$ dissolved concentration of i^{th} nuclide species in brine (kg/m^3).

The three dynamical equations become

$$\dot{M}_{ui} = -k_i M_{ui} [S_i - C_{di}] - \lambda_i M_{ui} + \lambda_{i-1} M_{ui-1} \qquad (A),$$

$$R_i \dot{M}_{di} = k_i M_{ui} [S_i - C_{di}] - QC_{di} - \lambda_i M_{di} + \lambda_{i-1} M_{di-1} \qquad (B),$$

$$\dot{M}_{ai} = (R_i - 1) \dot{M}_{di} - \lambda_i M_{ai} + \lambda_{i-1} M_{ai-1} \qquad (C).$$

The initial conditions for the system (A)-(C) are usually taken at a time $t_o > 0$, the time of borehole penetration. At this time,

$M_{ui}(t_o) = M_o(t_o)$ the inventory at closure (t = 0) of the i^{th} nuclide species aged to time $t_o > 0$ (in kg),

$M_{di}(t_o) = o$ $M_{ai}(t_o) = 0.$ (1.4.4-8)

Furthermore, $Q(t_o) = 0$ but Q(t), is a non-negative function (≥ 0) of time for $t > t_o$.

The rate at which mass of the i^{th} nuclide is discharged from the panel is obviously

$$Q(t) C_{di}(t) \text{ (kg/s)}, \quad t > t_o. \qquad (1.4.4\text{-}9)$$

APPROXIMATIONS IN PANEL

The full set of dynamical equations, (A)-(C), are not directly solved in the PANEL model; instead, (A)-(C) are first added to give

$$\dot{M}_i = -Q C_{di} - \lambda_i M_i + \lambda_{i-1} M_i$$

$$M_i(t_o) = M_o(t_o) \ . \qquad (1.4.4\text{-}10)$$

This equation is solved with the simplifying assumption that

$$C_{di}(t) = \frac{M_i}{\sum_j M_j} S_i, \ t > t_o \ . \qquad (1.4.4\text{-}11)$$

and the sum in the denominator is taken over all isotopes of the same element as that of species i.

1.4.5 Fluid Flow in Culebra: SECO2D

Studies of potential releases of radionuclides from the WIPP to the accessible environment along liquid pathways require computational models of the flow of groundwater through the Culebra Dolomite Member, and models of how flow in the Culebra would be affected by climatic change. The PA Department uses a model of these phenomena called SECO2D. The governing equations for SECO2D are summarized in this section: first, the equation of groundwater flow is presented, then the effects of climate change on boundary conditions for the flow equation are briefly described. Further discussion of the model of fluid flow in the Culebra is found in Sections 7.5, 7.6, and Appendix C of Volume 2 of the present series of reports.

GROUNDWATER FLOW

SECO2D simulates groundwater flow at regional and local scales within the Culebra Dolomite by solving the following partial differential equation in two dimensions (x,y):

$$S_s \frac{\partial h}{\partial t} = \nabla \bullet (\bar{K} \bullet \nabla h) - W \ , \qquad (1.4.5\text{-}1)$$

where

- h = $h(x,y,t)$, the potentiometric head (m),
- S_s = $S_s(x,y,t)$, the specific storage of the Culebra (m^{-1}),
- $\bar{K}$ = $\bar{K}(x,y,t)$, the hydraulic conductivity tensor (m/s),
- W = $W(x,y,t)$, a volumetric flux per unit volume of formation (s^{-1}), (used to simulate wells or recharge).

The specific storage and hydraulic conductivity tensor are obtained from more directly measurable quantities, i.e., in the present version of SECO2D,

$$S_s = \frac{S(x,y)}{\Delta Z} \ , \quad \bar{K} = \frac{\bar{T}(x,y)}{\Delta Z} \ , \qquad (1.4.5\text{-}2)$$

where

- $S(x,y)$ = storage coefficient in the Culebra (dimensionless),
- ΔZ = $\Delta Z(x,y)$, Culebra thickness (m),

$\bar{T}(x, y)$ = one of a set of simulated transmissivity tensors (units: m^2/s). See Section 2.6.9 for a discussion of how transmissivity fields are generated. Also see Section 7.5 of Volume 2 of the present series of reports.

Given appropriate initial and boundary conditions, Eq. 1.4.5-1 is solved numerically to yield a potentiometric head field, h(x,y,t), which may be used to compute specific discharge (or Darcy velocity) at any point in the Culebra:

$$\vec{q}(x, y, t) = -\bar{K} \bullet \nabla h \quad (m/s) \ . \tag{1.4.5-3}$$

In SECO2D, boundary conditions are specified on the outer edges of the regional (or, in some cases, local) grid; these boundary conditions may be a mix of the following kinds: (1) Dirichlet (specified h on boundary); (2) inhomogeneous Neuman (specified gradients of h on boundary); (3) Robin boundary conditions [a mixture of (1) and (2)]; and (4) adaptive boundary conditions, in which flux ($\vec{q}$) is specified at inflow boundaries and head (h) is specified at outflow boundaries.

EFFECTS OF CLIMATE CHANGE

The 1992 version of SECO2D simulates effects of climate change through inclusion of time-dependent Dirichlet boundary conditions. Specifically, potentiometric heads on the northwestern edges of the regional grid (the suspected recharge area for the Culebra) are set according to the formula

$$h_f(x,y,t) = h_p(x,y)\left[\frac{3A_R+1}{4} - \left(\frac{A_R-1}{2}\right)\left(\cos\theta t - \sin\frac{\phi}{2}t + \frac{1}{2}\cos\phi t\right)\right] \ , \tag{1.4.5-4}$$

where

h_f = future potentiometric head (m),
h_p = present potentiometric head (m), given a realization of regional transmissivities (see Section 2.6.3),
A_R = Amplitude factor (dimensionless),
θ = Pleistocene glaciation frequency (Hz),
ϕ = frequency of Holocene-type climatic fluctuations (Hz).

The recharge amplitude factor, A_R, is a number to be chosen between 1 and $\gamma > 1$ and is scaled from the sampled index factor (Section 4.4). If $A_R = 1$, it is seen that there are no effects of climatic change. If $A_R > 1$, the maximum future head, h_f, will be greater than the present head. The constant γ is a scaling factor that is chosen by the PA analyst to ensure physically reasonable head values on the portion of the recharge boundary where boundary conditions are applied. The origins of the climate change model are treated in detail in Chapter 6 of Volume 4 of the present series of reports.

1.4.6 Solute Transport in Culebra: SECO/TP

Studies of potential releases of radionuclides from the WIPP to the accessible environment along liquid pathways require a computational model of solute transport in groundwater flowing through the Culebra Dolomite Member. In 1992, the PA Department is using a model developed specifically for Sandia National Laboratories and called SECO/TP. This section summarizes the governing equations for that model. Solute transport in the Culebra is discussed in more detail in Section 7.6 and Appendix C of Volume 2 of the present series of reports.

SECO/TP is a "dual porosity" model of solute transport in the Culebra in the sense that advective transport is allowed only through the fracture system but diffusion of solute into the rock matrix surrounding a fracture is possible. The fracture system is idealized as planar and parallel (Figure 1.4-6); each fracture wall may be coated with a layer of clay of uniform thickness.

MASS TRANSPORT IN FRACTURE SYSTEM

The governing equation for mass transport in a single fracture is

$$\frac{\partial C_\ell}{\partial t} = -\frac{\partial}{\partial x_i}\left(V_i C_\ell - D_{ij}\frac{\partial C_\ell}{\partial x_j}\right) - \lambda_\ell C_\ell + \sum_{m=1}^{m} \xi_{\ell m}\lambda_m C_\ell + Q\left(C_\ell^o - C_\ell\right) + \Gamma_\ell \quad , \tag{1.4.6-1}$$

where the summation convention has been used ($x_1 = x$, $x_2 = y$) and ℓ, m = 1, 2, ..., m, label the solute species (radionuclide mass). The quantities in Eq. 1.4.6-1 have the following meanings [starred (*) items are explained below].

	C_ℓ	=	trace concentration of ℓ^{th} solute specie in fracture fluid (kg/m^3),
*	V_i	=	average linear velocity vector in fracture system (m/s),
*	D_{ij}	=	hydrodynamic dispersion tensor (m^2/s),
	λ_ℓ	=	decay constant for ℓ^{th} solute species (radionuclide, s^{-1}),
	$\xi_{\ell m}$	=	fraction of m^{th} parent species that decays into ℓ^{th} solute species (dimensionless),
	Q	=	rate of fluid injection per unit volume of formation (s^{-1}),
	C_ℓ^o	=	concentration of ℓ^{th} solute species in injected fluid (kg/m^3),
	Γ_ℓ	=	rate of mass transfer of ℓ^{th} species from matrix system to fracture system (kg/m^3•s).

The average linear velocity vector, V_i, is related to the specific discharge in the Culebra by

$$V_i = q_i/\phi_f \, , \tag{1.4.6-2}$$

where the specific discharge, q_i, is provided by the SECO2D model [see Eq. 1.4.5-3] and ϕ_f is the fracture porosity of the Culebra. For planar parallel fractures (Figure 1.4-6) and b<<B,

$$\phi_f = \frac{b}{b+B} \, . \tag{1.4.6-3}$$

In practical modeling of solute transport in the Culebra, ϕ_f and 2B are taken as known quantities and Eq. 1.4.6-3 is used to calculate the fracture aperture 2b. The ratio b_c/b is also assumed to be known; given b, b_c can be calculated from this ratio.

The components of the hydrodynamic dispersion tensor for the fracture system, D_{ij}, are

$$D_{11} = \alpha_L \frac{(V_1)^2}{|V|} + \alpha_T \frac{(V_2)^2}{|V|} + D^*, \tag{1.4.6-4a}$$

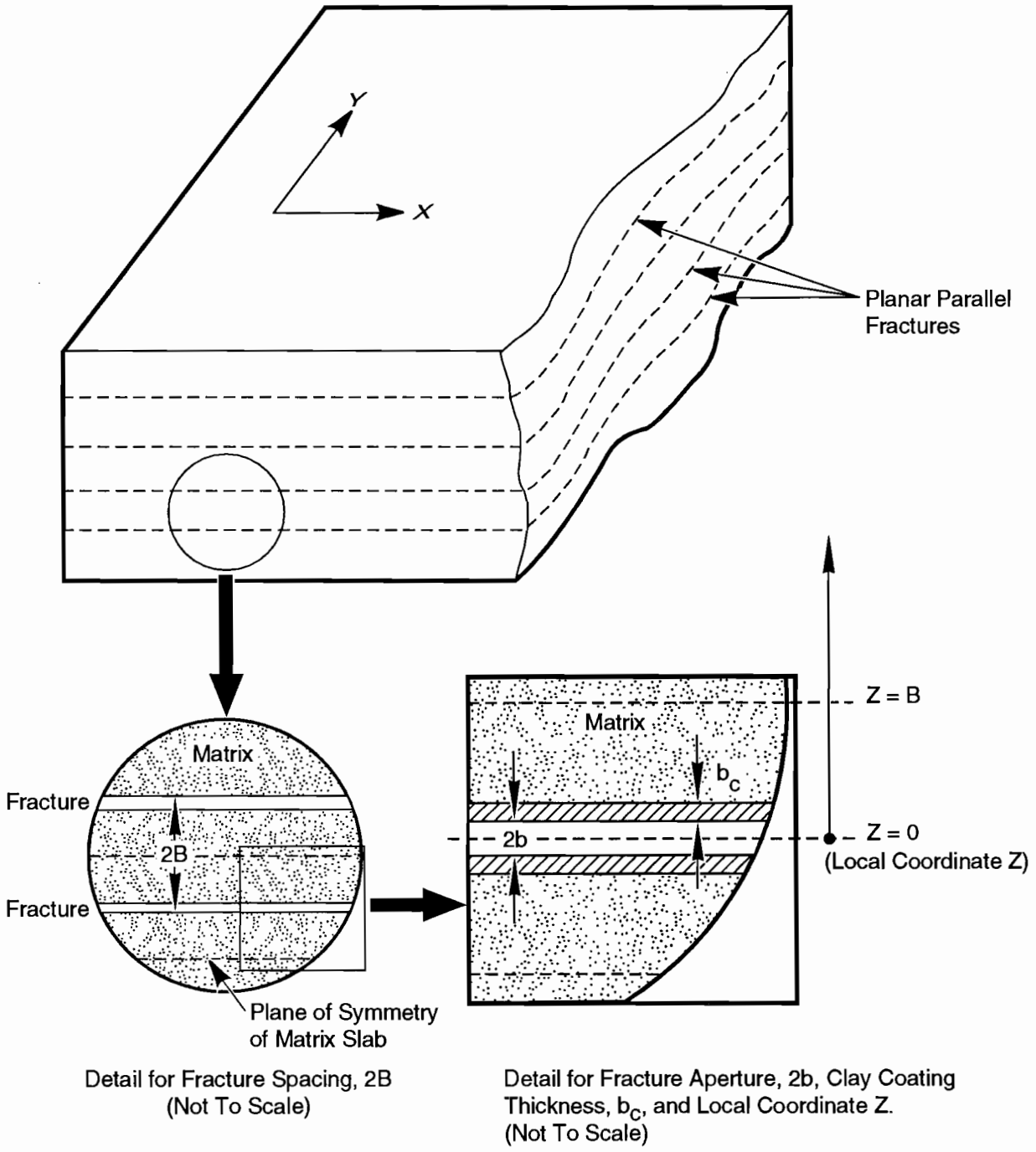

Figure 1.4-6. Idealized section of Culebra Dolomite Member.

$$D_{22} = \alpha_L \frac{(V_2)^2}{|V|} + \alpha_T \frac{(V_1)^2}{|V|} + D^*, \qquad (1.4.6\text{-}4b)$$

$$D_{12} = D_{21} = (\alpha_L - \alpha_T) \frac{V_1 V_2}{|V|}, \qquad (1.4.6\text{-}4c)$$

where α_L, α_T are respectively longitudinal and transverse dispersivities (m), D^* is the molecular diffusion coefficient of the "average" solute species (m^2/s), and

$$|V| = (V_1^2 + V_2^2)^{1/2}.$$

The rate of mass transfer from the matrix to the fracture system, Γ_ℓ, will be explained after mass storage in the matrix is described.

MASS STORAGE IN CLAY COATINGS AND MATRIX

Mass storage in clay coatings and matrix slabs occurs by diffusion of solute mass across the fracture facings; only diffusion perpendicular to the fracture facings (i.e., along the local coordinate Z, Figure 1.4-6) is allowed. The governing diffusion equation is

$$\phi R_\ell \frac{\partial C'_\ell}{\partial t} = \frac{\partial}{\partial z} D' \frac{\partial C'_\ell}{\partial z} - \phi R_\ell \lambda_\ell C'_\ell + \sum_{m=1}^{m} \xi_{\ell m} \phi R_m \lambda_m C'_m \quad , \qquad (1.4.6\text{-}5)$$

where new quantities have the following meanings (again, starred items [*] are explained below).

$C'_\ell(z,t)$ = trace concentration of ℓ^{th} solute species in pore fluid of clay coating or matrix (kg/m^3),
* $\phi(z)$ = porosity of clay coating or matrix (dimensionless),
* $R_\ell(z)$ = retardation coefficient of ℓ^{th} solute species in pores of clay coating or matrix (dimensionless),
* $D'(z)$ = effective molecular diffusion coefficient in pores of clay coating or matrix (m^2/s).

The porosity of clay coating or matrix depends on location:

$$\phi(z) = \begin{cases} \phi_c \text{ (constant clay porosity)}, & b \le z < b + b_c \\ \phi_m \text{ (constant matrix porosity)}, & b + b_c \le z \le B \end{cases} , \qquad (1.4.6\text{-}6)$$

The effective molecular diffusion coefficient in pores of clay coating or matrix also depends on location:

$$D'(z) = \begin{cases} \tau_c D^*, & b \le z < b + b_c \\ \tau_m D^*, & b + b_c \le z \le B \end{cases} , \qquad (1.4.6\text{-}7)$$

where τ_c and τ_m are the (constant) tortuousities of clay and matrix respectively (dimensionless).

In a similar fashion, the retardation coefficient of the ℓ^{th} solute species takes two values:

$$R_\ell(z) = 1 + \begin{cases} \left(\dfrac{\rho_g(1-\phi)k_{d,\ell}}{\phi}\right)_c, & b \le z < b + b_c \\ \left(\dfrac{\rho_g(1-\phi)k_{d,\ell}}{\phi}\right)_m, & b + b_c \le z \le B \end{cases} \qquad (1.4.6\text{-}8)$$

where

ρ_g stands for grain density (kg/m^3) of the material,
$k_{d,\ell}$ is the distribution coeffient of the ℓ^{th} solute species in the pores of the material (m^3/kg),
ϕ is the porosity of the material (dimensionless).

The notation,

$$(...)_{c \text{ or } m},$$

indicates qualities in either clay coating (c) or matrix (m).

THE MASS TRANSFER TERM

The term Γ_ℓ specifying the rate of mass transfer of the ℓ th solute species from the matrix to the fracture system takes the form

$$\Gamma_\ell(x,y,t) = -\frac{2}{b}\left(D'\frac{\partial C'_\ell}{\partial z}\right)_{z=b}, \qquad (1.4.6\text{-}9)$$

where all quantities have been defined.

INITIAL AND BOUNDARY CONDITIONS

Equation 1.4.6-1 can be solved subject to a variety of boundary conditions (prescribed input flux, constant concentrations on boundary). The usual initial condition is $C_\ell(x,y,o) = 0$.

Equation 1.4.6-5 is solved subject to the initial condition $C_\ell(x,y,z,o) = 0$ ($b \le z \le B$) and the boundary conditions,

$$\frac{\partial C'_\ell}{\partial z}(x,y,B,t) = 0, \qquad (1.4.6\text{-}10)$$

(i.e., no mass flux across plane of symmetry of matrix slab),

$$C'_\ell(x,y,b,t) = C_\ell(x,y,t), \qquad (1.4.6\text{-}11)$$

(i.e., concentrations match at interfaces between fracture void space and clay coatings).

1.4.7 Waste-Filled Room Deformation: SANCHO

Realistic estimates of the effective porosity and permeability of a closed, waste-filled room require that the effects of room deformation and internal gas generation be taken into account. In 1991, the PA Department largely

ignored the latter effects and assigned constant porosity and permeability based on waste-material composition (WIPP PA Division, 1991, Vol. 3, Sections 3.4.7 and 3.4.8). In the present (1992) series of PA calculations, the effects of deformation and gas generation have been included only indirectly through the use of a separate calculation of a porosity "surface" which gives room porosity as a function of time and total volumes of gas generated by corrosion and microbial action (Mendenhall and Lincoln, February 28, 1992, Memo in Appendix A). The room-deformation component of this calculation employed SANCHO, a finite-element computer program for simulating the quasistatic, large-deformation, inelastic response of two-dimensional solids (Stone et al., 1985). Gas generation was calculated in much the same way as the gas-generation terms in the BRAGFLO code; see Section 1.4.1. This section emphasizes the constitutive equations used in SANCHO to model room deformation.

SANCHO is a special purpose, finite-element program that was developed in response to some of the perceived drawbacks with existing finite element software for nonlinear analysis. SANCHO was developed to solve the quasistatic, large deformation, inelastic response of two dimensional solids. The element library is based on a bilinear isoparametric quadrilateral with a constant bulk strain. The equilibrium solution strategy uses an iterative scheme designed around a self-adaptive dynamic relaxation algorithm. The iterative scheme is based on explicit central difference pseudo-time integration with artificial damping. The code is explicit in nature so that no stiffness matrix is formed or factorized that reduces the amount of computer storage necessary for execution. The explicit nature of the program also makes it attractive for vectorization on vector processing machines. The code has a standard material model interface that is used with three material models incorporated within the code. A finite strain elastic-plastic strain hardening model, a volumetric plasticity model, and a metallic creep material model are presently included. (Recent modifications allow the SANCHO user to employ his or her own material models.) A sliding interface capability, based on a master-slave algorithm, is also incorporated within SANCHO (Stone et al., 1985, p. 12).

The fundamental SANCHO equations will not be discussed here; the relevant physical assumptions are best expressed in terms of the constitutive equations of the material models selected by the SANCHO user. Three material models were used in calculating the porosity surface for a deformed room: (1) an elastic/secondary creep model for intact salt surrounding room opening; (2) an elastic/secondary creep model for crushed-salt room backfill; and (3) a volumetric plasticity model of mechanical response of waste contained within a room.

ELASTIC/SECONDARY CREEP MODEL FOR INTACT SALT

The constitutive equations for the intact-salt components of the model repository are (Mendenhall et al., 1991):

$$\dot{s}_{ij} = 2G\left[\dot{e}'_{ij} - (1.5)^{(N+1)/2} \bullet A \ \exp(Q/RT) \bullet \left(s_{k\ell} \ s_{k\ell}\right)^{(N-1)/2} s_{ij}\right] , \qquad (1.4.7\text{-}1)$$

$$\dot{\sigma}_{kk} = 3K e_{kk} \ , \qquad (1.4.7\text{-}2)$$

where the summation convention is used, i.e.,

$$e_{kk} = e_{11} + e_{22} .$$

A dot over a quantity signifies time derivative and

σ_{ij} = stress tensor (Pa),

s_{ij} = $\sigma_{ij} - \frac{1}{3} \ \sigma_{kk}$ = deviatoric stress tensor,

e_{ij} = deviatoric strain tensor,

$\dot{e}'_{ij}$ = deviatoric strain rate (treated as constant over a time step),

* G = elastic shear modulus (Pa),

A = an experimentally determined constant,

N = an experimentally determined constant,

Q/RT = exponential constant for deviatoric creep model,

* K = elastic bulk modulus (Pa).

Starred (*) quantities are described below.

The elastic shear modulus, G, is approximated by

$$G = G_o \exp(G_1 \rho) \ , \tag{1.4.7-3}$$

and the elastic bulk modulus is approximated by

$$K = K_o \exp(K_1 \rho) \ , \tag{1.4.7-4}$$

where G_0, G_1, K_0, K_1 are experimentally determined constants.

CRUSHED SALT BACKFILL MODEL

The constitutive equations for crushed-salt backfill component of the model repository are (Mendenhall et al., 1991):

$$\dot{s}_{ij} = 2G\left[\dot{e}'_{ij} - A_c\left(\rho_{int.}/\rho\right)^N \exp\left(Q/RT\right)\left(s_{k\ell}\ s_{k\ell}\right)^{(N-1)/2} s_{ij}\right] \ , \tag{1.4.7-5}$$

$$\dot{\rho} = B_o\left[\exp\left(B, P\right) - 1\right]\exp\left(A\rho\right) \ , \tag{1.4.7-6}$$

where G is the elastic shear modulus (Eq. 1.4.7-3), summation convention is implied in the term $\left(s_{k\ell},\ s_{k\ell}\right)$, and the other quantities appearing in Eq. 1.4.7-5 have the same meanings as in Eq. 1.4.7-1. In Eq. 1.4.7-6,

ρ = local density
$\dot{\rho}$ = rate of change of density ($kg/m^3 \cdot s$),
P = pressure (Pa),
A_c, A, B_0, B_1 and ρ_{int} are experimentally determined constants.

In addition, the elastic bulk modulus, K, is given by Eq. 1.4.7-4.

VOLUMETRIC PLASTICITY MODEL FOR WASTE

The constitutive equations for the waste component of the model repository are identical to the equations for the model of soil and crushable foam material specified in the SANCHO manual (Stone et al., 1985, pgs. 40-46; see Eqs. 47-50 in particular). The SANCHO model of soils and crushable foams requires that the following parameters be specified by the user of the code (Stone et al., 1985, p. 67):

μ = shear modulus,
K_0 = bulk unloading modulus,
a_0 = yield function constant,
a_1 = yield function constant,
a_2 = yield function constant. (1.4.7-7)

In addition, the model requires that the user specify volumetric strain [essentially $\ln(\rho/\rho_o)$] as a function of pressure, i.e.,

$$\ln(\rho/\rho_o) = F(P) \quad , \tag{1.4.7-8}$$

where ρ is waste density (kg/m^3) and ρ_0 is initial waste density (before any significant compaction by repository deformation has begun).

NOTE ON PROBLEM GEOMETRY

Typical geometry, modeling mesh, and boundary conditions for the calculation of a porosity surface with SANCHO are illustrated in Figure 1.4-7. Boundary conditions apply to a single room assumed to be imbedded in an infinite lattice of similar rooms spaced uniformly on 40-m centerlines.

Each mined room is 4 m high by 10 m wide by 100 m long. A room is assumed to contain 6804 drums filled with unprocessed waste. Other details of room geometry and composition are found in Beraún and Davies (September 12, 1991, Memo in Appendix A).

NOTE ON GAS GENERATION

Gas pressure in the model disposal room was computed from the ideal gas law based on the instantaneous "void" volume in the room (i.e., the volume not occupied by liquids or solids) and the total amount of gas in the room.

$$P_g = \frac{NRT}{V - V_s} \tag{1.4.7-9}$$

where

P_g = gas pressure,
N = $f \cdot D \cdot \int_0^t \frac{\partial N}{\partial t}\, dt$ = total moles of gas produced per room up to time t,
$\partial N / \partial t$ = rate of gas production (moles / s - drum),
R = 8.23 $(m^3 \cdot Pa)/(g - moles \cdot K)$,
T = 300K,
V = current void volume (m^3), (1.4.7-10)

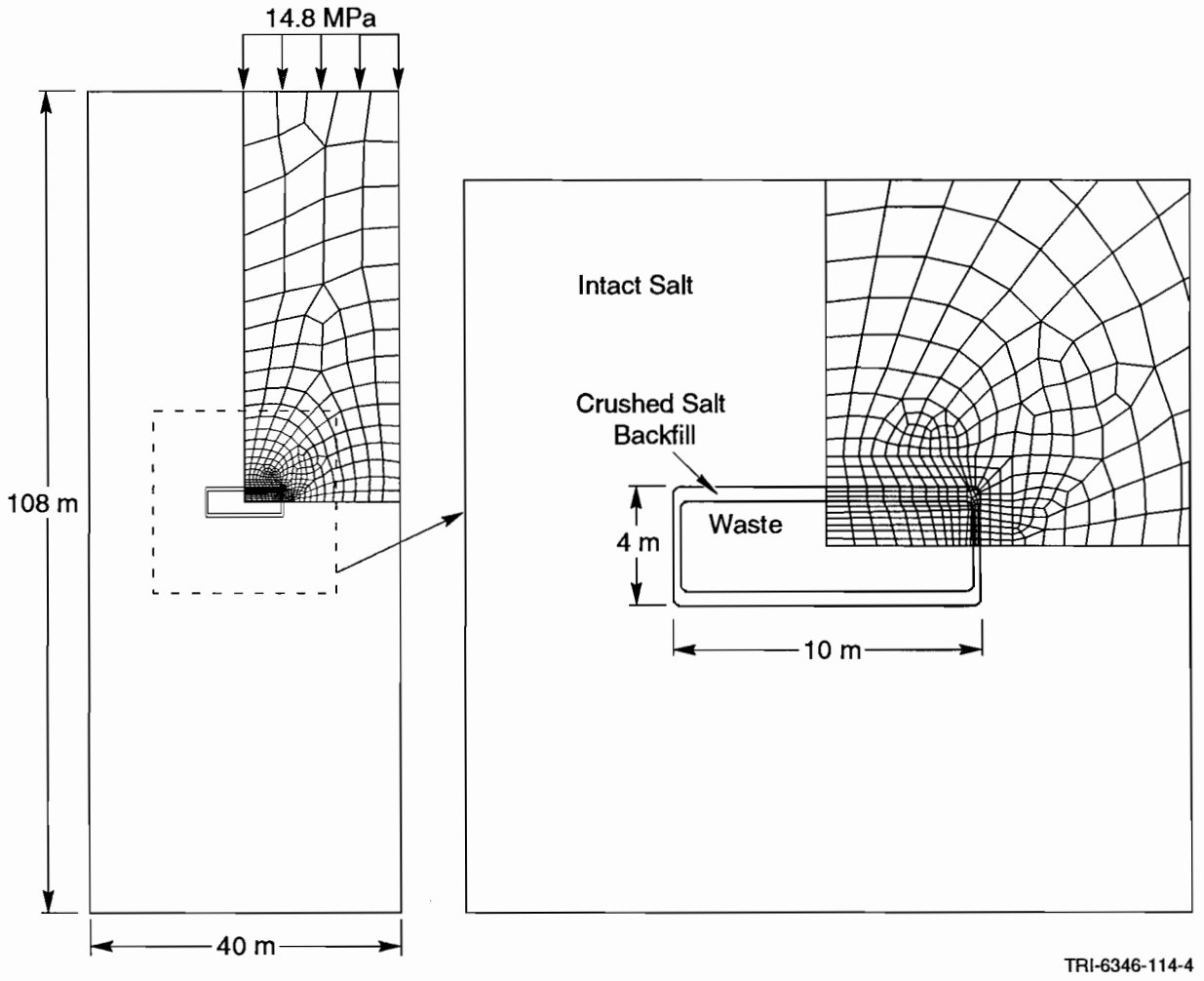

Figure 1.4-7. Modeling mesh and boundary conditions for calculation of porosity surface with SANCHO (adopted from Mendenhall et al., 1991, Figure 3-2).

V_s = volume of solids per storage room,
f = percentage of waste generating gas,
D = number of drums.

In these geomechanical simulations, gas pressure acts outward on the walls, floor, and ceiling of the storage room providing a backstress opposing closure (Mendenhall et al., 1991).

1.5 Background on WIPP

1.5.1 Purpose

The DOE was authorized by Congress in 1979 to build the WIPP as a research and development facility to demonstrate the safe management, storage, and eventual disposal of transuranic (TRU) waste generated by DOE defense

programs (WIPP Act, 1979). Only after demonstrating compliance with *40 CFR 191* and other laws and regulations (e.g., RCRA [1976] and NEPA [1969]) will the DOE permanently dispose of TRU waste at the WIPP repository.

1.5.2 Location

The WIPP is located within a large sedimentary basin, the Delaware Basin, in southeastern New Mexico, an area of low population density approximately 38 km (24 mi) east of Carlsbad (Figure 1.5-1). Geographically, the WIPP is between the high plains of West Texas and the Guadalupe and Sacramento Mountains of southeastern New Mexico.

Four prominent surface features are found in the area--Los Medaños ("The Dunes"), Nash Draw, Laguna Grande de la Sal, and the Pecos River. Los Medaños is a region of gently rolling hills that slopes upward to the northeast from the eastern boundary of Nash Draw to a low ridge called "The Divide." The WIPP is in Los Medaños. Nash Draw, 8 km (5 mi) west of the WIPP, is a broad shallow topographic depression with no external surface drainage. Laguna Grande de la Sal, about 9.5 km (6 mi) west-southwest of the WIPP, is a large playa about 3.2 km (2 mi) wide and 4.8 km (3 mi) long formed by coalesced collapse sinks that were created by dissolution of evaporate deposits. The Pecos River, the principal surface-water feature in southeastern New Mexico, flows southeastward, draining into the Rio Grande in western Texas.

1.5.3 Geologic History of the Delaware Basin

The Delaware Basin, an elongated, geologically confined depression, extends from just north of Carlsbad, New Mexico, into Texas west of Fort Stockton (Figure 1.5-2). The basin covers 33,000 km^2 (12,750 mi^2) and is filled with sedimentary rocks to depths as great as 7,300 m (24,000 ft) (Hills, 1984). Geologic history of the Delaware Basin began about 450 to 500 million years ago when a broad, low depression formed during the Ordovician Period as transgressing seas deposited clastic and carbonate sediments (Hiss, 1975; Powers et al., 1978; Cheeseman, 1978; Williamson, 1978; Hills, 1984; Ward et al., 1986; Harms and Williamson, 1988). After a long period of accumulation and subsidence, the depression separated into the Delaware and Midland Basins when the area now called the Central Basin Platform uplifted during the Pennsylvanian Period, about 300 million years ago.

During the Early and Middle Permian Period, the Delaware Basin subsided rapidly, resulting in a sequence of clastic rocks rimmed by reef limestone. The thickest of the reef deposits, the Capitan Limestone, is buried north and east of the WIPP but is exposed at the surface in the Guadalupe Mountains to the west (Figure 1.5-2). Evaporite deposits (marine bedded salts) of the Castile Formation and the Salado Formation, which hosts the WIPP, filled the basin during the late Permian Period and extended over the reef margins. Evaporites, carbonates, and clastic rocks of the Rustler Formation and the Dewey Lake Red Beds were deposited above the Salado Formation before the end of the Permian Period.

1.5.4 Repository

The repository is located in the Delaware Basin in the 600-m- (2,000-ft-) thick Salado Formation of marine bedded salts (Late Permian Period). The repository level is located within these bedded salts 655 m (2,150 ft) below the surface and 384 m (1,260 ft) above sea level. The WIPP repository is composed of a single underground disposal level connected to the surface by four shafts (Figure 1.5-3). The repository level consists of an experimental area at the north end and a disposal area at the south end.

1.5.5 WIPP Waste Disposal System

The WIPP relies on three approaches to contain waste: geologic barriers, engineered barriers, and institutional controls. The third approach, institutional controls, consists of many parts, e.g., the legal ownership and regulations

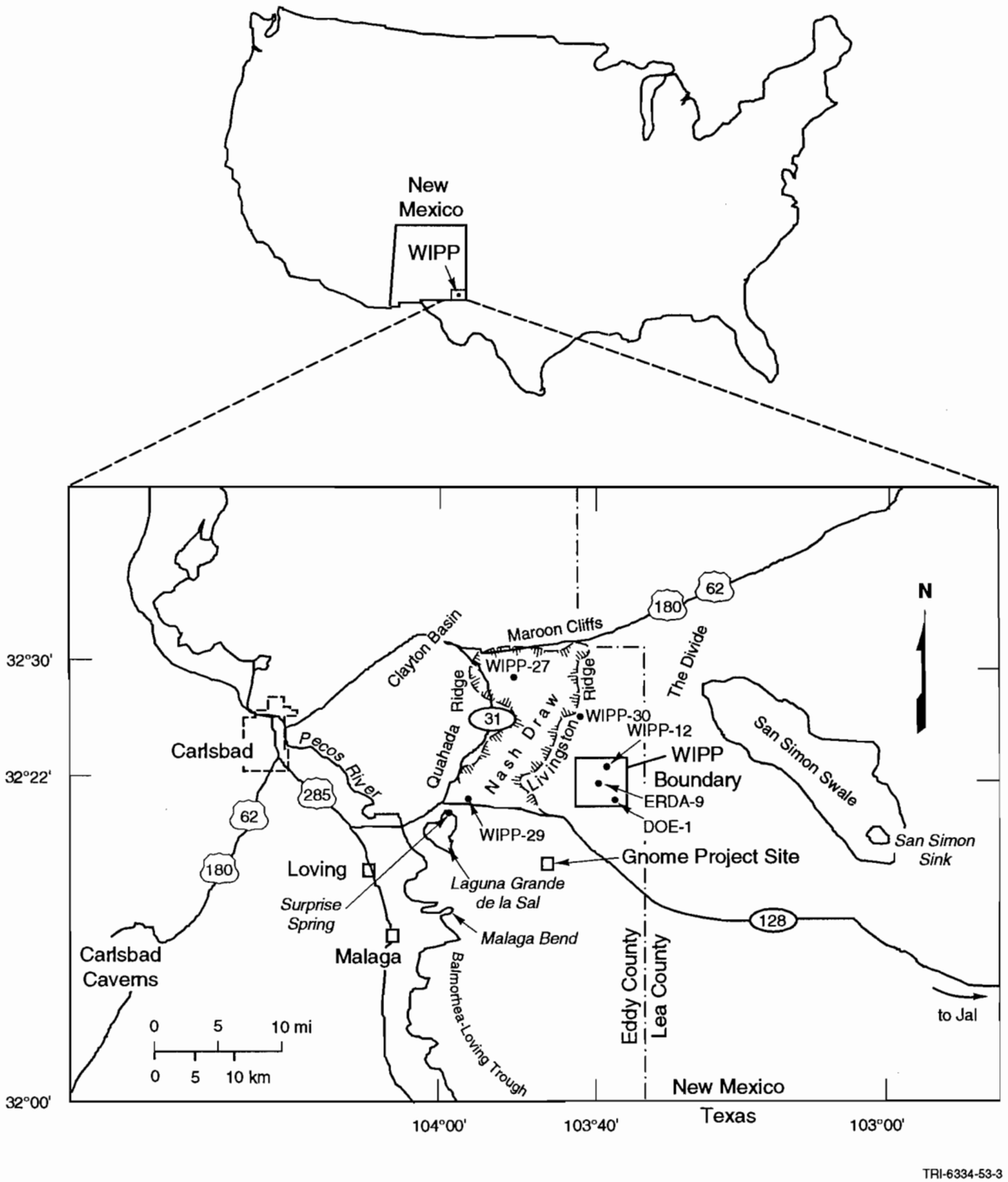

Figure 1.5-1. WIPP location in southeastern New Mexico (after Rechard, 1989, Figure 1.2).

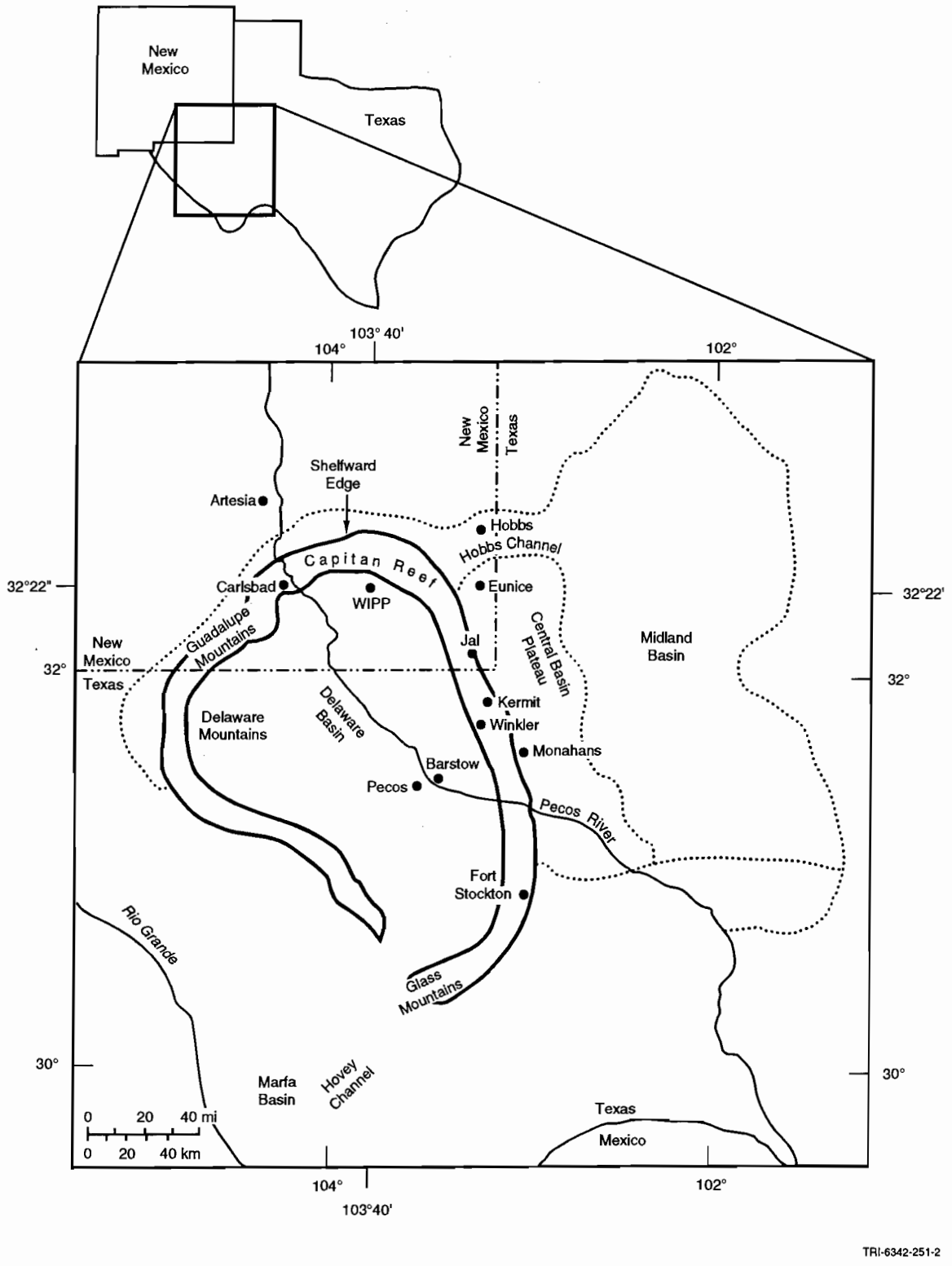

Figure 1.5-2. Location of the WIPP in the Delaware Basin (modified from Richey et al., 1985 and Lappin, 1988, Figure 1.4).

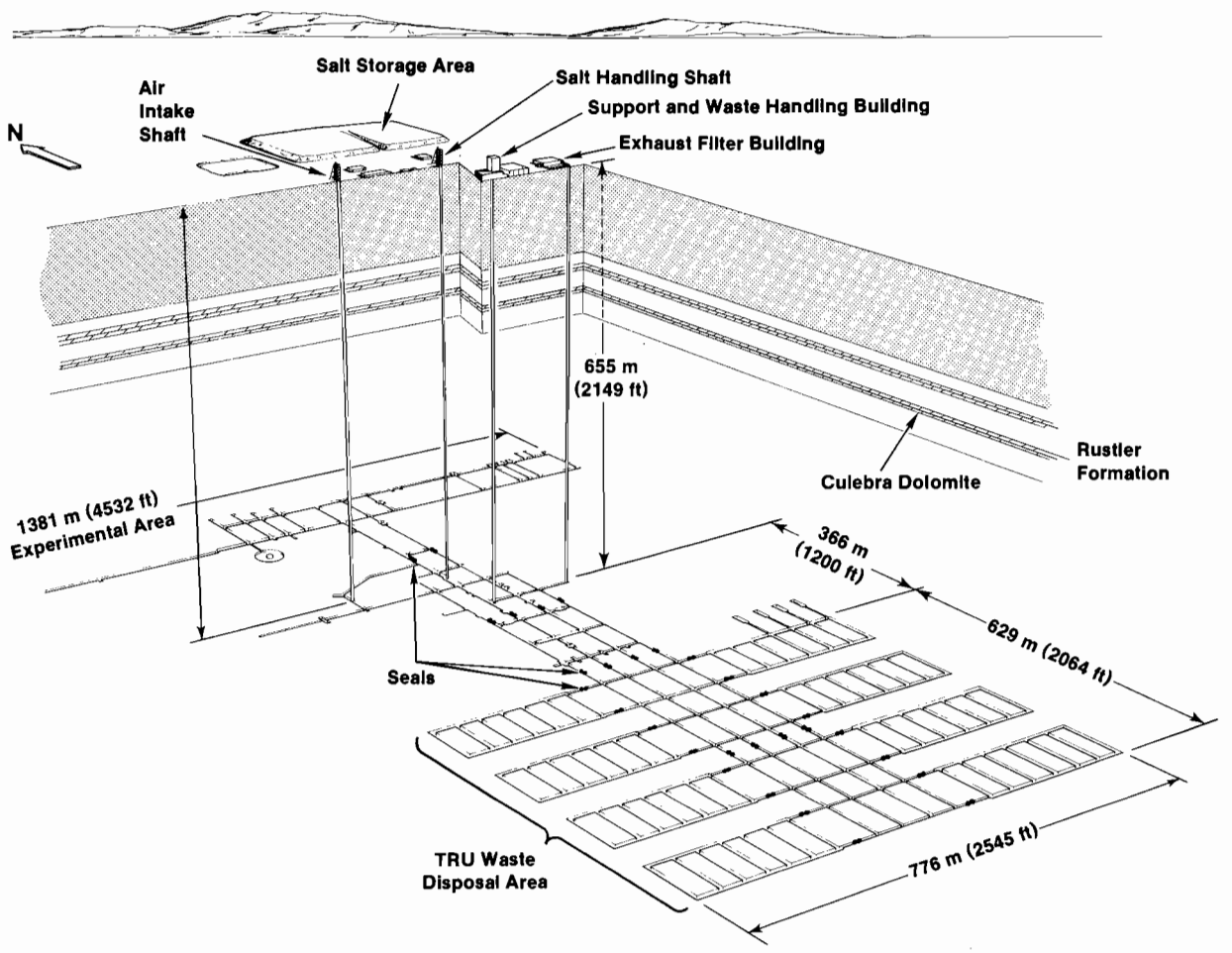

Figure 1.5-3. WIPP repository, showing surface facilities, proposed TRU disposal areas, and experimental areas (after Nowak et al., 1990, Figure 2).

of the land and resources by the U.S. Government, the fencing and signs around the property, permanent markers, public records and archives, and other methods of preserving knowledge about the disposal system.

The WIPP disposal system, as defined by *40 CFR 191*, includes the geologic and engineered barriers. The physical features of the repository (e.g., design of repository, waste form) are components of these barriers.

The geologic barriers are limited to the lithosphere up to the surface and no more than 5 km (3 mi) from the outer boundary of the WIPP waste-emplacement panels (Figure 1.5-4). The boundary of this maximum-allowable geologic subsystem is greater than the current boundary of the WIPP land withdrawal. The extent of the WIPP controlled area will be defined during performance assessment but will not be less than the area withdrawn, which is under U.S. DOE administrative control (Bertram-Howery and Hunter, 1989).

Data for components of the geologic and engineered barriers are the subject of this volume. No data on institutional controls are contained in this volume.

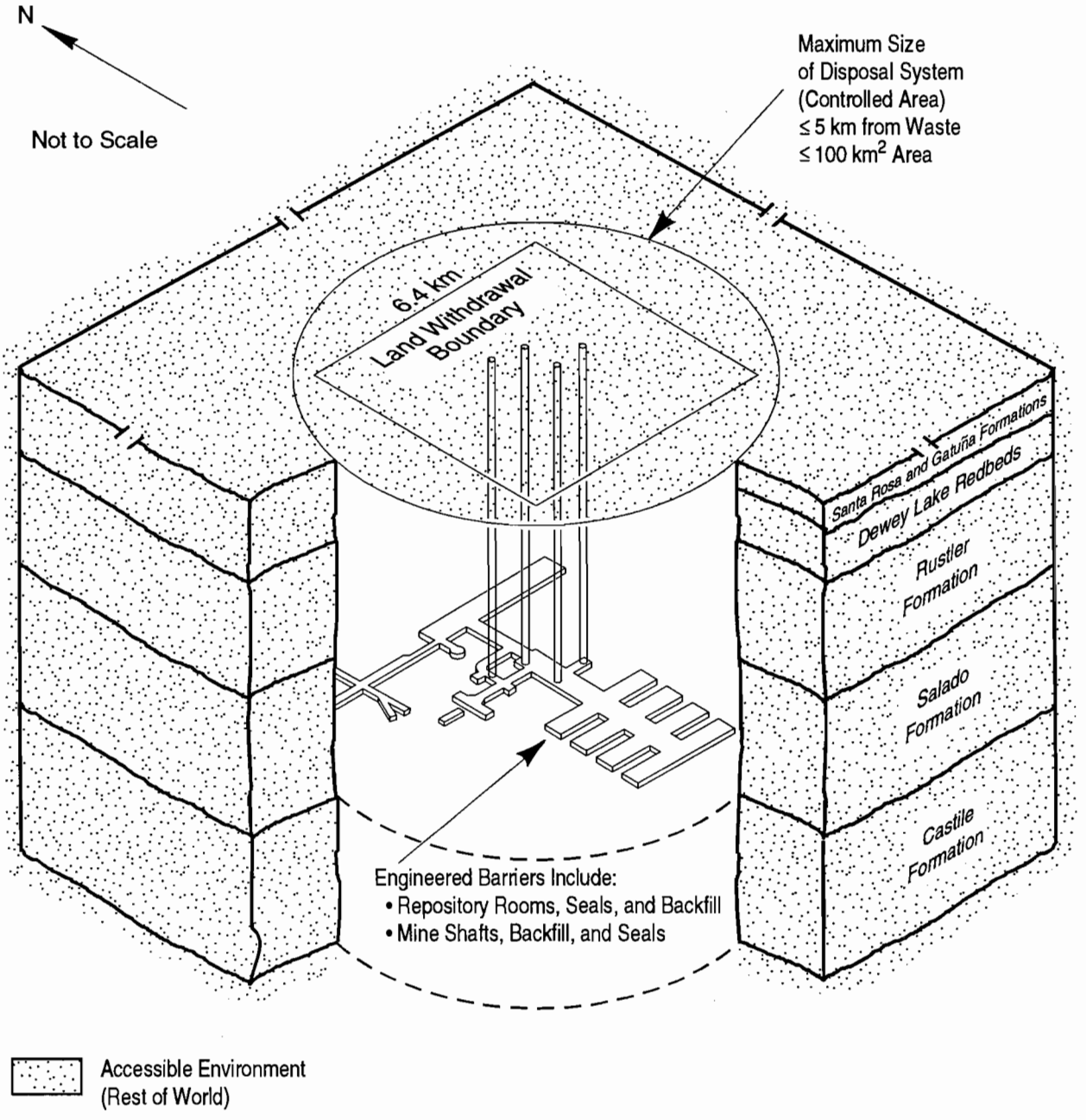

Figure 1.5-4. Geologic and engineered barriers of the WIPP disposal system (after Bertram-Howery and Hunter, 1989, Figure II-1).

2. GEOLOGIC BARRIERS

The geologic barriers consist of the physical features of the repository, such as stratigraphy and geologic components.

2.1 Areal Extent of Geologic Barriers

Figure 2.1-1 shows the maximum areal extent of the geologic barriers. Figure 2.1-2 shows the universal transverse mercator (UTM) coordinates of the modeling domains. The UTM coordinates for the northeast and southeast corners of the land-withdrawal boundary were derived from values reported in Gonzales (1989). Because the township ranges shift at the land-withdrawal border, the UTM coordinates for the northwest and southwest corners were derived from information on the wells nearest the corners (i.e., Well H-6A for the northwest corner and Well D-15 for the southwest corner).

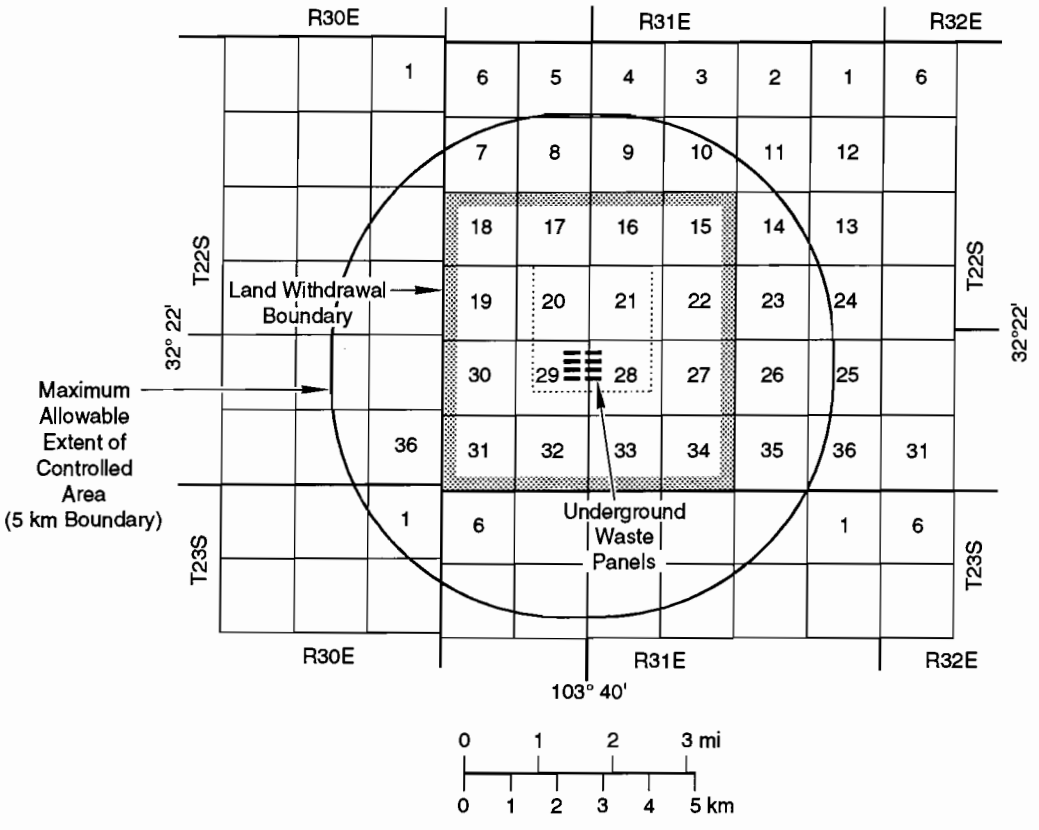

Figure 2.1-1. Position of the WIPP waste panels relative to land-withdrawal boundary (16 contiguous sections), 5-km boundary (40 CFR 191.12y), and surveyed section lines (after U.S. DOE, 1989, Figure 2.2).

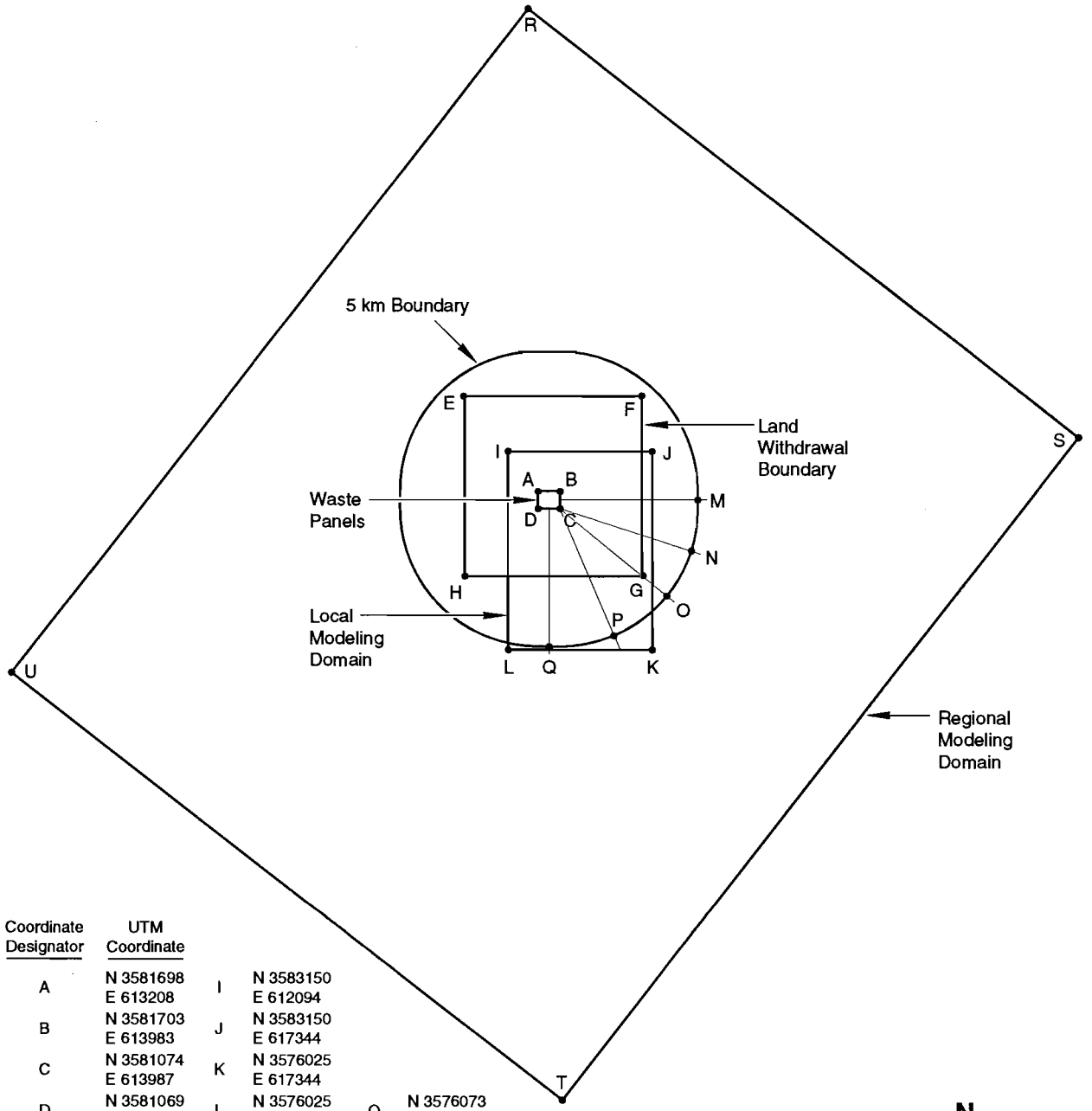

Coordinate Designator	UTM Coordinate				
A	N 3581698 E 613208	I	N 3583150 E 612094		
B	N 3581703 E 613983	J	N 3583150 E 617344		
C	N 3581074 E 613987	K	N 3576025 E 617344		
D	N 3581069 E 613212	L	N 3576025 E 612094	Q	N 3576073 E 613631
E	N 3585057 E 610496	M	N 3581420 E 618984	R	N 3598943 E 612819
F	N 3585109 E 616941	N	N 3579579 E 618791	S	N 3583551 E 632519
G	N 3578681 E 617015	O	N 3577945 E 617856	T	N 3559911 E 614049
H	N 3578612 E 610566	P	N 3576436 E 615991	U	N 3575303 E 594349

Figure 2.1-2. UTM coordinates of the modeling domains.

Figure 2.1-3 shows the topography, the locations of wells used for defining the general stratigraphy, and the modeling domains near the WIPP typically plotted in the report. The well locations by UTM, state plan coordinates, and survey sections are provided in Table B.1 (Appendix B). The elevations of the stratigraphic layers in each of the wells are tabulated in Table B.2 (Appendix B).

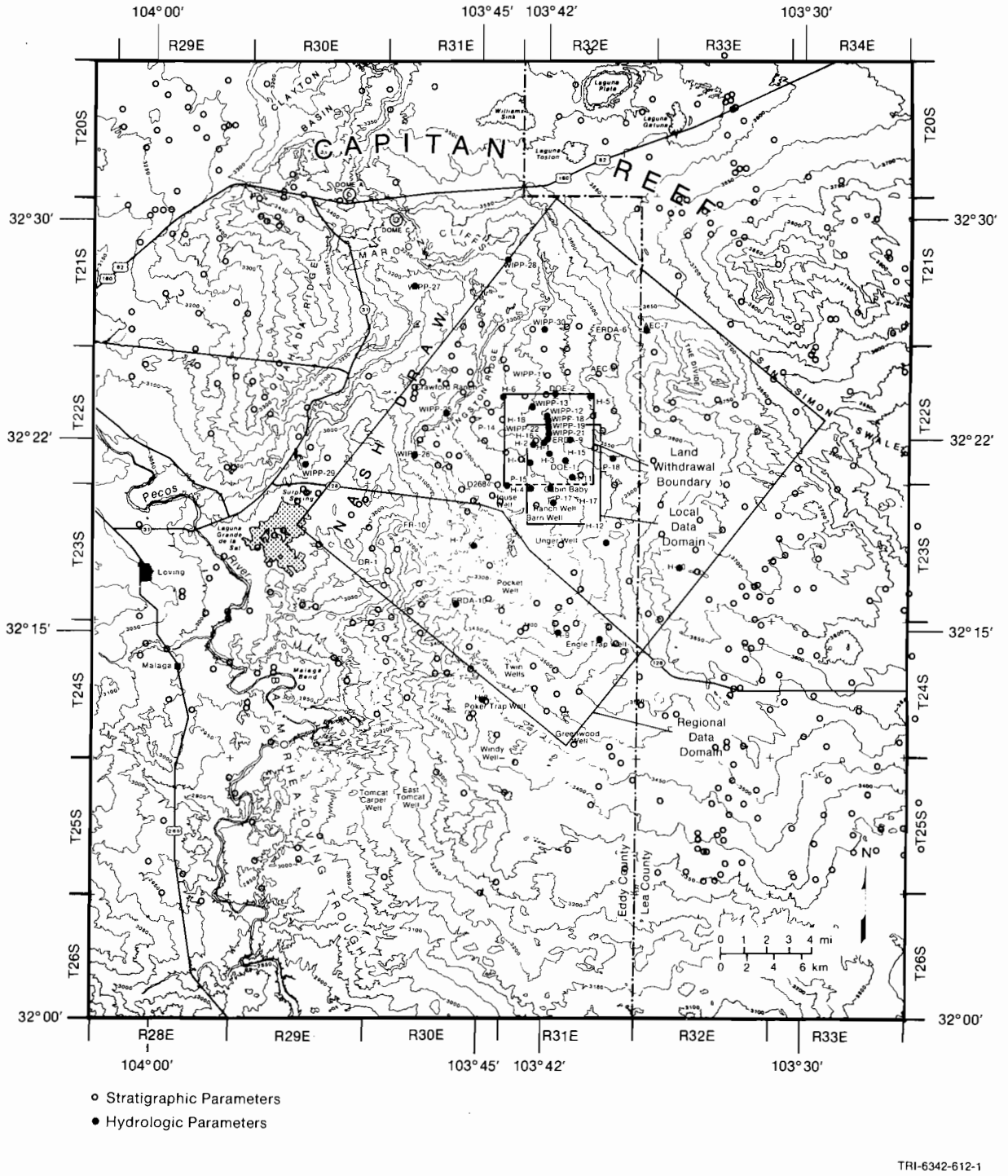

Figure 2.1-3. Locations of wells for defining general stratigraphy and regional and local data domains typically plotted in this volume.

2.2 Stratigraphy at the WIPP

The level of the WIPP repository is located within bedded salts (Figures 2.2-1 and 2.2-2), which consist of thick halite and interbeds of minerals such as clay and anhydrites of the Late Permian Period (Ochoan Series) (approximately 255 million yr old)* (Figure 2.2-3). A polyhalitic anhydrite interbed that forms a potential transport pathway, Marker Bed 139 (MB139), is located about 1 m (3 ft) below the repository interval (Figure 2.2-3). This unit is about 1 m (3 ft) thick and is one of about 45 siliceous or sulfatic units within the Salado Formation (Figure 2.2-4) (Lappin, 1988; Tyler et al., 1988).

For most strata above the repository, the elevations (though varying) are well known because of numerous wells; however, directly below the repository the elevations of the base of Anhydrite III in the Castile Formation and the top of Bell Canyon can only be inferred from a geologic cross section (Figure 2.2-1). The geologic structure is uncomplicated, thus the uncertainty is likely to be small on the regional geologic scale. Because the information is important to evaluating the potential for and size of brine reservoirs under the repository, uncertainty bounds have been placed on these two elevations inferred from the geologic cross section. In the 1992 PA calculations, elevations of the two contacts at ERDA-9 were assumed to vary uniformly between the elevations reported from the closest wells that provide data (Cabin Baby-1 and WIPP-12 for the base of Anhydrite III, and Cabin Baby-1 and DOE-2 for the top of the Bell Canyon Formation).

*This age reflects the 1983 Geological Society of America time scale (Geological Society of America, Inc., 1984).

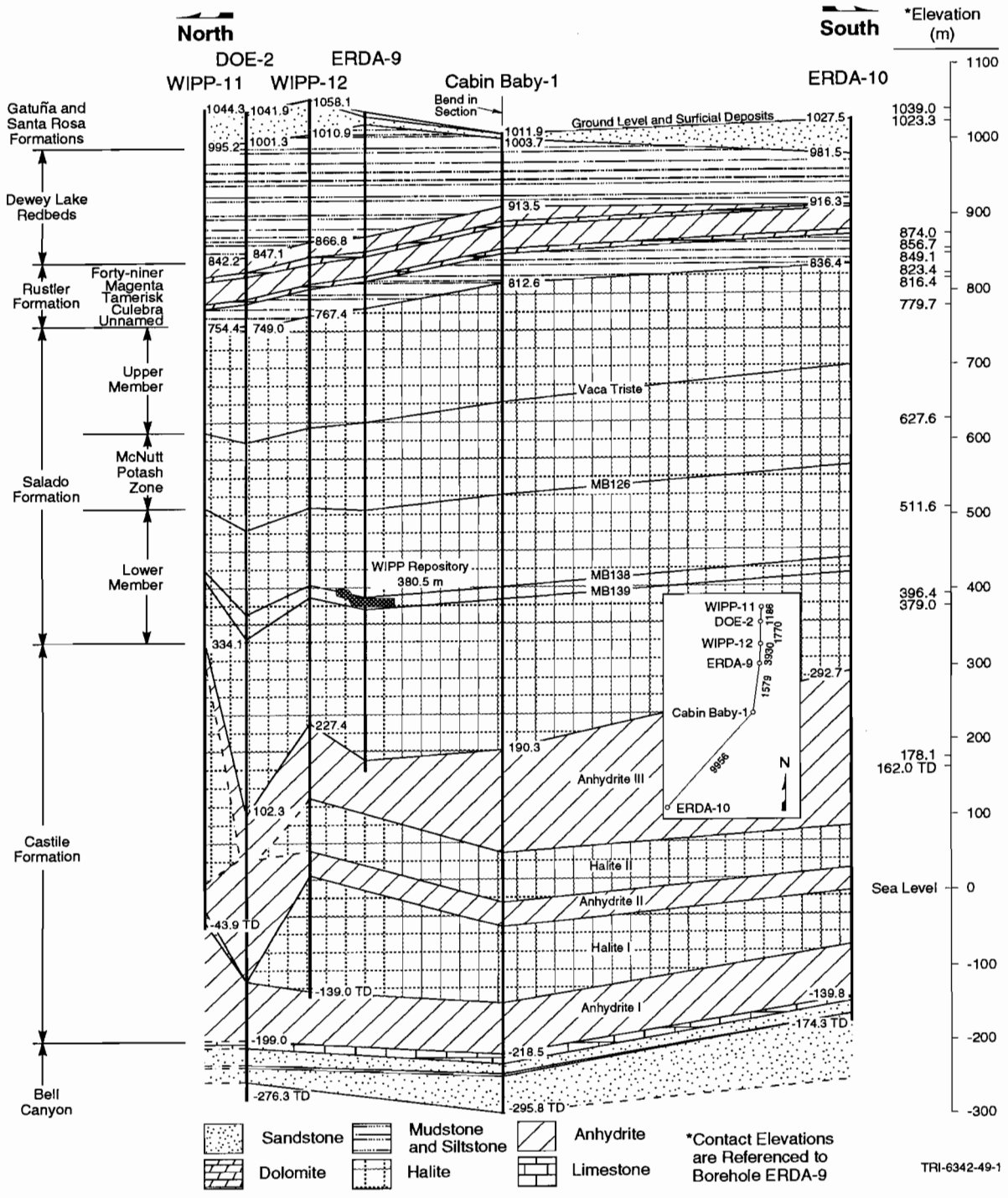

Figure 2.2-1. Level of WIPP repository, located in the Salado Formation. The Salado Formation is composed of thick halite with thin interbeds of clay and anhydrite deposited as marine evaporites about 255 million years ago (Permian period) (after Lappin, 1988, Figure 3.1 based on Borns, 1987).

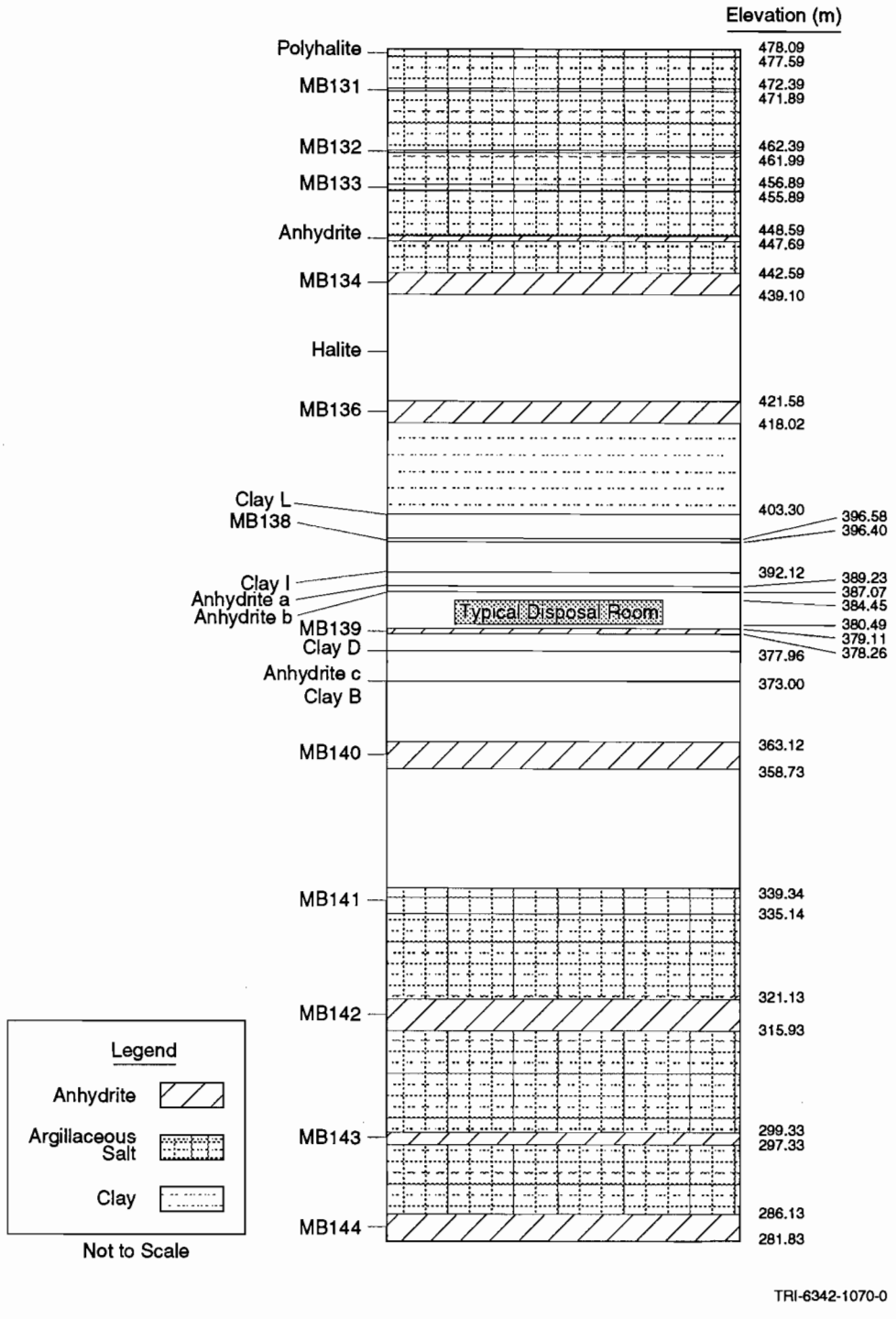

Figure 2.2-2. Reference local stratigraphy near repository (after Munson et al., 1989, Figure 3-3).

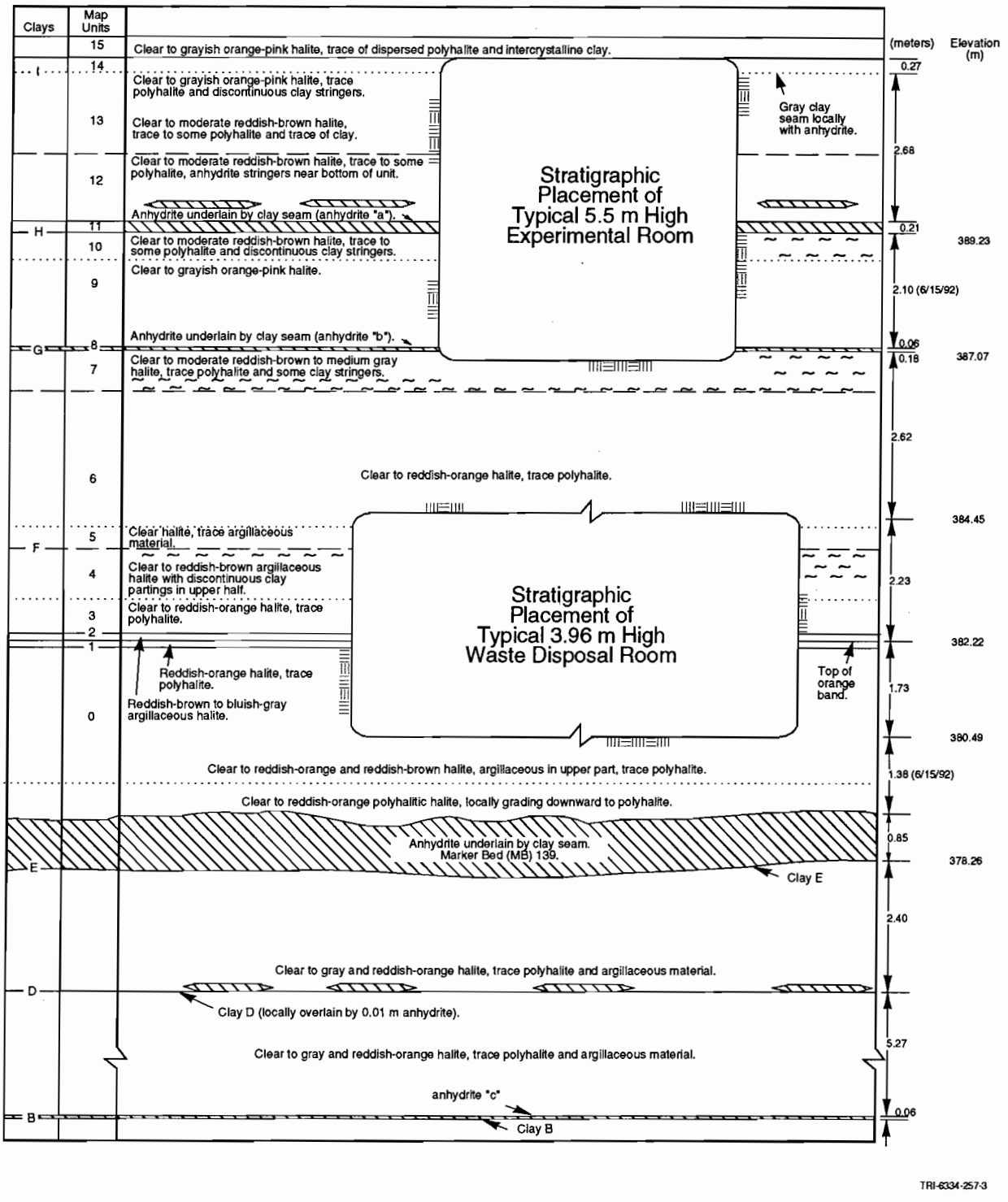

Figure 2.2-3. Stratigraphy at the repository horizon (after Bechtel National, Inc., 1986, Figures 6-2, 6-3 and Lappin et al., 1989, Figure 4-12). Units in the disposal area dip slightly to the south, but disposal excavations are always centered about the orange marked band (reddish-orange halite).

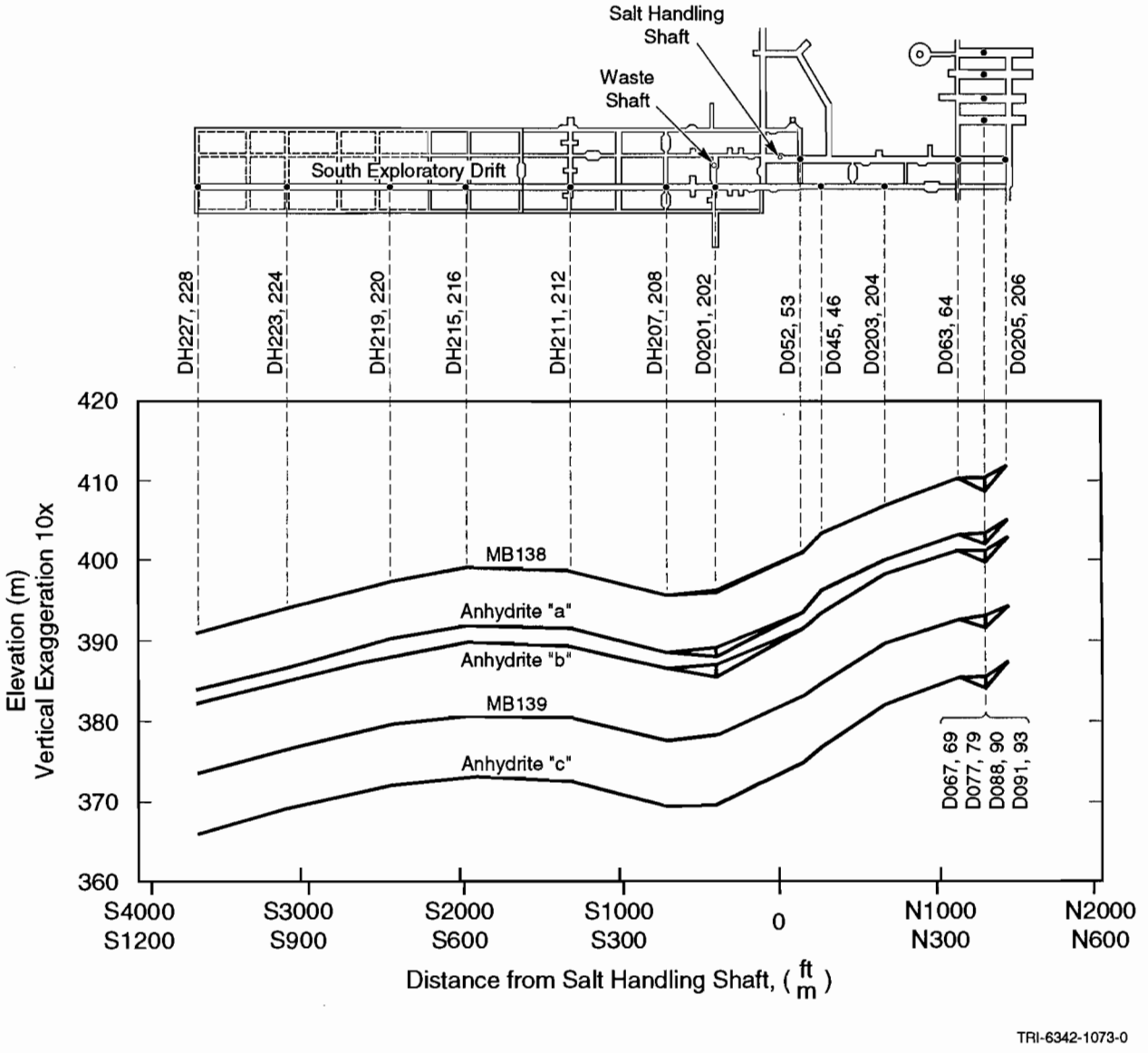

Figure 2.2-4. North-south cross-section showing Salado Formation stratigraphy near repository (after Krieg, 1984, Figure 2).

Anhydrite III Elevation*

Parameter: **Base of Anhydrite III elevation above mean sea level @ ERDA-9**
Material: Anhydrite within Castile Formation (Anhydrt3, Elevat)

Definition, Units: m

Values: Range: (53, 127) Median: 90

Distribution: Uniform
Correlation:

Data Source(s): See Discussion.
(WIPP Observational Data; Investigator Judgment)

Usage:

Mathematical model:
Area of Castile Brine Reservoir below WIPP Disposal Area (Section 5.1, this volume).

Equation (NA).

Computational models:
CCDFPERM

Ranking in Past Sensitivity Analyses:

40 CFR 191	Not tested
40 CFR 268	Not applicable
NEPA	Not applicable
Other	Not applicable

*Key to Parameter Sheets is provided in Section 1.2.8.

Bell Canyon Elevation @ ERDA-9*

Parameter: **Top of Bell Canyon elevation above mean sea level @ ERDA-9**
Material: Bell Canyon Formation (BCanyon, All, Elevat)

Definition, Units: m

Values: Range: (-228, -198) Median: -213

Distribution: Uniform
Correlation:

Data Source(s): See Discussion.
(WIPP Observational Data; Investigator Judgment)

Usage:

Mathematical model:
Area of Castile Brine Reservoir below WIPP Disposal Area (Section 5.1, this volume).

Equation (NA).

Computational models:
CCDFPERM

Ranking in Past Sensitivity Analyses:

40 CFR 191	Not tested
40 CFR 268	Not applicable
NEPA	Not applicable
Other	Not applicable

*Key to Parameter Sheets is provided in Section 1.2.8.

2.3 Hydrologic Parameters for Halite and Polyhalite within Salado Formation

The Salado Formation is composed of thick halite with thin interbeds of clay and anhydrite deposited as marine evaporites about 255 million years ago (Permian Period). A summary of the parameters for the Salado Formation near the repository are given in Table 2.3-1.

Table 2.3-1. Parameter Values for Halite and Polyhalite within Salado Formation near Repository

Parameter[a]	Median	Range		Units	Distribution Type	Source
Capillary pressure (p_c) and relative permeability (k_{rw})						
Threshold displacement pressure (p_t)	2.3×10^7	2.3×10^5 (correlated with permeability in 1992)	2.3×10^9	Pa	Lognormal	Davies, 1991a, 1991b
Residual saturations						
Wetting phase (Swr)	**2×10^{-1}**	**0**	**4×10^{-1}**	**none**	**Uniform**	**Webb, 1992a, 1992b, Memos in Appendix A; Davies and LaVenue, 1990b**
Gas phase (Sgr)	**2×10^{-1}**	**0**	**4×10^{-1}**	**none**	**Uniform**	**Davies and LaVenue, 1990b; Webb, 1992a, 1992b, Memos in Appendix A**
Brooks-Corey exponent (λ)	**0.7**	**0.2**	**10.0**	**none**	**Constructed**	**Davies and LaVenue, 1990b; Webb, 1992a, 1992b, Memos in Appendix A**
Density						
Grain (ρ_g) halite	2.163×10^3			kg/m^3	Constant	Carmichael, 1984, Table 2; Krieg, 1984, p. 14; Clark, 1966, p. 44
Grain (ρ_g) polyhalite	2.78×10^3			kg/m^3	Constant	Hume and Shakoor, 1981, p. 103-203
Bulk (ρ_{bulk})	2.14×10^3			kg/m^3	Constant	Holcomb and Shields, 1987, p.17
Average (ρ_{ave})	2.3×10^3			kg/m^3	Constant	Krieg, 1984, Table 4
Dispersivity						
Longitudinal (α_L)	1.5×10^1	1	4×10^1	m	Constructed	Pickens and Grisak, 1981; Lappin et al., 1989, Table D-2
Ratio (α_L/α_T)	10	3	25	none	Constructed	Pickens and Grisak, 1981; Freeze and Cherry, 1979, Figure 9.6
Partition coefficient						
All species	0			m^3/kg	Constant	Lappin et al., 1989, p. D-17
Permeability (k)						
Log undisturbed	**-21.2**	**-24.0**	**-19.0**	**log (m^2)**	**Constructed**	**Gorham et al., June 15, 1992, Memo in Appendix A; Howarth et al., 1991; Beauheim et al., 1991a**
Log disturbed	-20.7	-22.0	-15.0	log (m^2)	Constructed	Gorham et al., June 15, 1992, Memo in Appendix A; Howarth et al., 1991; Beauheim et al., 1991a
Pore pressure (p)	9.5	9.0	10.0	MPa	Uniform	Gorham et al., June 15, 1992, Memo in Appendix A; Howarth et al., 1991; Beauheim et al., 1991a
Porosity (ϕ)						
Undisturbed	1×10^{-2}	1×10^{-3}	3×10^{-2}	none	Constructed	See text; Powers et al.,1978; U.S. DOE, 1983
Disturbed	6×10^{-2}			none	Constant	See text.
Specific storage	9.5×10^{-8}	2.8×10^{-8}	1.4×10^{-6}	m^{-1}	Constructed	Beauheim, 1991
Tortuosity	1.4×10^{-1}	1×10^{-2}	6.67×10^{-1}	none	Constructed	Freeze and Cherry, 1979, p. 104; Kelley and Saulnier, 1990, Table 4.6; Lappin et al., 1989, Table E-9

[a]Parameters in bold were sampled in the 1992 calculations.

2.3.1 Capillary Pressure and Relative Permeability

Two-phase characteristic curves (capillary pressure and relative permeability) for Salado halite, Salado anhydrite, and waste have not been measured. In modeling two-phase phenomena (Section 1.4.1), the PA Department has adopted suggestions of Davies (1991b) and Webb (1992b, Memo in Appendix A) that characteristic curves be calculated using either the Brooks-Corey formulae (Brooks and Corey, 1964) or the Van Genuchten-Parker formulae (Van Genuchten, 1978). Use of either formulae requires knowledge of four material-property parameters:

- p_t - threshold displacement pressure (Pa),
- $S_{\ell r}$ - residual wetting phase saturation (dimensionless),
- S_{gr} - residual (or critical) gas saturation (dimensionless),
- λ - the Brooks-Corey exponent (dimensionless).

None of these parameters has been measured for materials of interest (halite, anhydrite, waste); for purposes of sensitivity analyses, their ranges, distributions and correlations are estimated from natural-analog data (Davies and LaVenue, 1990b; Davies, 1991b; Webb, 1992a, Memo in Appendix A). The natural analogs consist of materials that possess some of the same characteristics (i.e., permeability and porosity) as the anhydrite, halite, and waste room. The natural analogs applicable to the very low permeability of the halite and anhydrite were sands that were investigated during the Multiwell Tight Gas Sands Project (Ward and Morrow, 1985). The permeability for these sands typically ranges from 1×10^{-16} to 1×10^{-19} m^2 (1×10^{-1} to 1×10^{-4} mD). Although these permeabilities are higher than those of the anhdyrites and halites, no other material was found with a lower permeability for which capillary pressure and relative permeability curves had been measured. Parameters selected for the anhydrites and waste room are discussed in later sections.

The uncertainty surrounding these parameters is unknown. An initial range was selected for the purpose of being able to run sensitivity studies. The ranges shown for the parameters are arbitrary, corresponding to a simple doubling and halving of the median values. A family of curves produced by sampling 20 times from the assigned distributions using the Brooks-Corey formulae is shown in Figure 2.3-1. Sample curves for capillary pressure and relative permeability are also shown in Figure 2.3-2.

a)

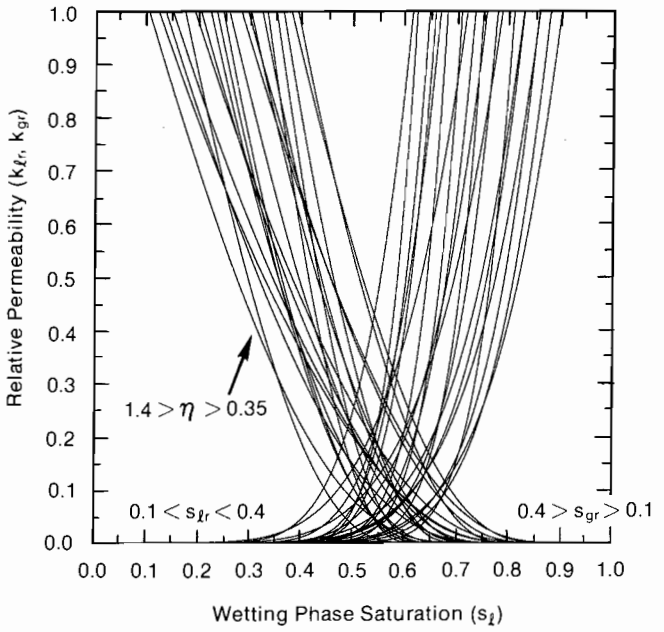

b)

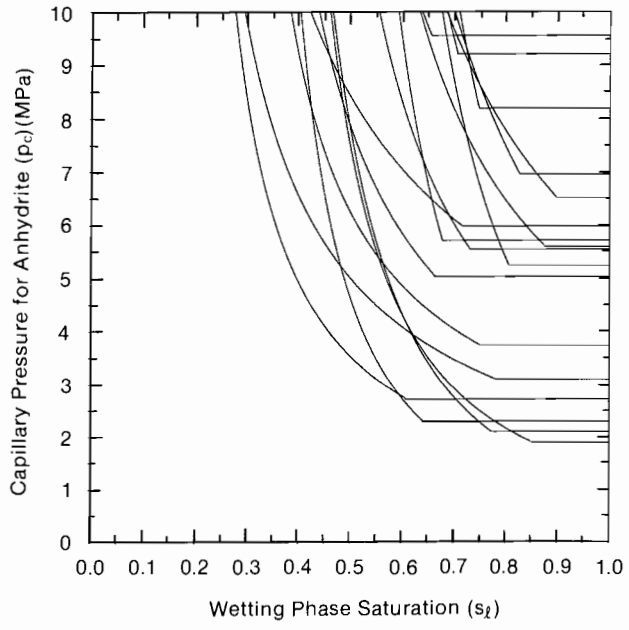

TRI-6342-1465-0

Figure 2.3-1. Example of variation in relative permeability and capillary pressure when Brooks and Corey parameters are varied.

a)

b)

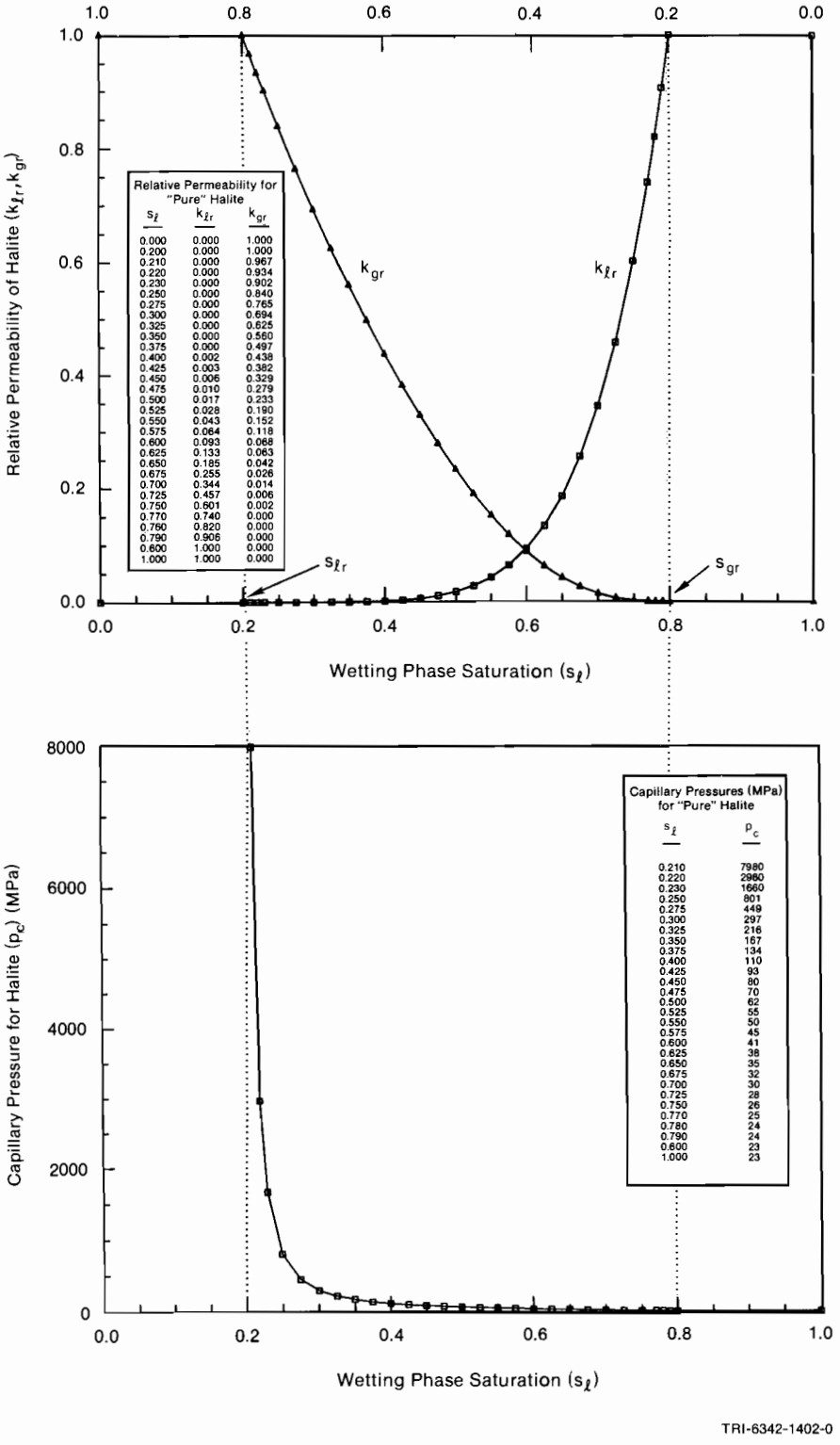

Figure 2.3-2. Estimated relative permeability and capillary pressure curves (source: Davies, 1991a).

Threshold Displacement Pressure, p_t*

Parameter: **Threshold displacement pressure (p_t)**
Material: Halite and polyhalte within Salado Formation, (Salado, PressCTD)

Definition, Units: Pa

Values: Range: (2.3×10^5, 2.3×10^9) Median: 2.3×10^7

Distribution: Lognormal
Correlation: Correlated with halite permeability (see Discussion)

Data Source(s): Davies, P. B. 1991a. *Evaluation of the Role of Threshold Pressure in Controlling Flow of Waste-Generated Gas into Bedded Salt at the Waste Isolation Pilot Plant.* SAND90-3246. Albuquerque, NM: Sandia National Laboratories. (Investigator Judgment)

Davies, P. B. 1991b. Appendix A: "Uncertainty Estimates for Threshold Pressure for 1991 Performance Assessment Calculations Involving Waste-Generated Gas," *Preliminary Comparison with 40 CFR Part 191, Subpart B for the Waste Isolation Pilot Plant, December 1991. Volume 3: Reference Data.* WIPP Performance Assessment Division. Eds. R. P. Rechard, A. C. Peterson, J. D. Schreiber, H. J. Iuzzolino, M. S. Tierney, and J. S. Sandha. SAND91-0893/3. Albuquerque, NM: Sandia National Laboratories. A-37 through A-41. (Investigator Judgment)

Usage:

Mathematical model:
Section 1.4.1, this volume.

Equation 1.4.1-6.

Computational models: 2-Phase Fluid Flow
BRAGFLO

Ranking in Past Sensitivity Analyses:

40 CFR 191	Low
40 CFR 268	Not tested
NEPA	Not tested
Other	Not applicable

*Key to Parameter Sheets is provided in Section 1.2.8.

Discussion:

Threshold Pressure: Threshold pressure plays an important role in controlling which Salado lithologies are accessible to gas and at what pressure gas will flow. Some investigators define threshold pressure as the capillary pressure associated with first penetration of a nonwetting phase into the largest pores near the surface of the medium, which means that threshold pressure is equal to the capillary pressure at a water saturation of 1.0 (Davies, 1991a, p. 9). Others define threshold pressure as the capillary pressure associated with the incipient development of a continuum of the nonwetting phase through a pore network, providing gas pathways not only through relatively large pores, but also through necks between pores. This latter definition means that threshold pressure is equal to the capillary pressure at a saturation equal to the residual gas saturation (dashed lines in Figure 2.3-2). Because flow of waste-generated gas outward from the WIPP repository will require that outward flowing gas penetrate and establish a gas-filled network of flow paths in the surrounding bedded salt, the latter definition has been adopted here.

The Salado Formation's thick halite beds with anhydrite and clay interbeds are similar in many respects to the consolidated lithologies presented in Figure 2.3-3. Similarities in pore structure exist between halite, anhydrite, and low-permeability carbonates; low-permeability sandstones and crystalline cements; and clay interbeds and shales. Given the general similarities, a best-fit power curve through the combined data set for consolidated lithologies was judged to provide the best available correlation for estimates of threshold pressure for the Salado Formation (Figure 2.3-3). Threshold pressure is also a key parameter in the Brooks and Corey (1964) model used to characterize the 2-phase properties of analogue materials for preliminary gas calculations (Davies and LaVenue, 1990a). Because threshold pressure is strongly related to intrinsic permeability, an empirical estimate is used as follows (Davies, 1991a, p. 25):

$$p_t\,(\text{MPa}) = 5.6 \times 10^{-7}\,[k\,(m^2)]^{-0.346}\,.$$

Capillary Pressure and Relative Permeability. Figure 2.3-2a shows the values estimated for relative permeability for Salado salt using only the Brooks-Corey model. Figure 2.3-2b shows the estimated capillary pressure curve for Salado salt. Figures 2.3-1a and 2.3-1b are examples of variation in relative permeability and capillary pressure when the Brooks and Corey parameter is varied.

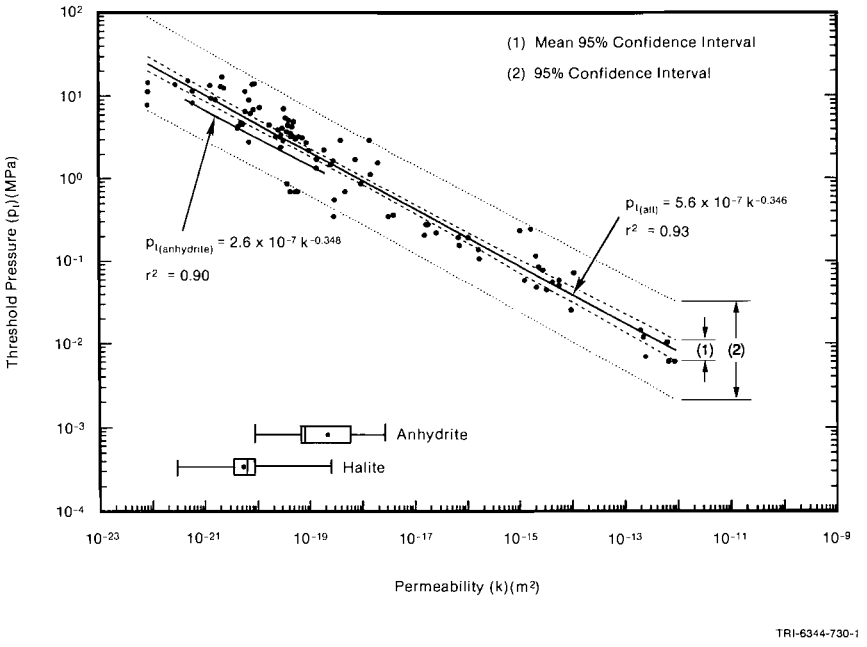

Figure 2.3-3. Correlation of threshold pressure with permeability for a composite of data from all consolidated rock lithologies. Data from Rose and Bruce, 1949; Wyllie and Rose, 1950; Thomas et al., 1968; and Ibrahim et al., 1970 (after Davies, 1991a, Figures 5 and 8).

Residual Wetting Phase (Liquid) Saturation*

Parameter: **Residual wetting phase (liquid) saturation ($S_{\ell r}$)**
Material: Halite and polyhalite within Salado Formation, (Salado, Sat RWP)

Definition, Units: Dimensionless

Values: Range: $(0, 4 \times 10^{-1})$ Median: 2×10^{-1}

Distribution: Uniform
Correlation:

Data Source(s):

Webb, S. W. 1992a. "Uncertainty Estimates for Two-Phase Characteristic Curves for 1992 RCRA Calculations" (see Appendix A, pp. A-141 through A-146). (Investigator Judgment)

Webb, S. W. 1992b. "Uncertainty Estimates for Two-Phase Characteristic Curves for 1992 40 CFR 191 Calculations" (see Appendix A, pp. A-147 through A-155). (Investigator Judgment)

Davies, P. B., and A. M. LaVenue. 1990b. Appendix A: "Additional Data for Characterizing 2-Phase Flow Behavior in Waste-Generated Gas Simulations and Pilot Point Information for Final Culebra 2-D Model (SAND89-7068/1)," *Data Used in Preliminary Performance Assessment of the Waste Isolation Pilot Plant (1990).* R. P. Rechard, H. Iuzzolino, and J. S. Sandha. SAND89-2408. Albuquerque, NM: Sandia National Laboratories. A-139 through A-156. (Investigator Judgment)

Usage:

Mathematical model:
Section 1.4.1, this volume.

Equation 1.4.1-7.

Computational models:
BRAGFLO

Ranking in Past Sensitivity Analyses:

40 CFR 191	Not tested
40 CFR 268	Low
NEPA	Not tested
Other	Not tested

*Key to Parameter Sheets is provided in Section 1.2.8.

Residual Gas Saturation*

Parameter: **Residual gas saturation (S_{gr})**
Material: Halite and polyhalite within Salado Formation, (Salado, SatRGP)

Definition, Units: Dimensionless

Values: Range: $(0, 4 \times 10^{-1})$ Median: 2×10^{-1}

Distribution: Uniform
Correlation:

Data Source(s):

Webb, S. W. 1992a. "Uncertainty Estimates for Two-Phase Characteristic Curves for 1992 RCRA Calculations" (see Appendix A, pp. A-141 through A-146). (Investigator Judgment)

Webb, S. W. 1992b. "Uncertainty Estimates for Two-Phase Characteristic Curves for 1992 40 CFR 191 Calculations" (see Appendix A, pp. A-147 through A-155). (Investigator Judgment)

Davies, P. B., and A. M. LaVenue. 1990b. Appendix A: "Additional Data for Characterizing 2-Phase Flow Behavior in Waste-Generated Gas Simulations and Pilot Point Information for Final Culebra 2-D Model (SAND89-7068/1)," *Data Used in Preliminary Performance Assessment of the Waste Isolation Pilot Plant (1990).* R. P. Rechard, H. Iuzzolino, and J. S. Sandha. SAND89-2408. Albuquerque, NM: Sandia National Laboratories. A-139 through A-156. (Investigator Judgment)

Usage:

Mathematical model:
Section 1.4.1, this volume.

Equation 1.4.1-7.

Computational models:
BRAGFLO

Ranking in Past Sensitivity Analyses:

40 CFR 191	Not tested
40 CFR 268	Low
NEPA	Not tested
Other	Not tested

*Key to Parameter Sheets is provided in Section 1.2.8.

Brooks and Corey Exponent*

Parameter: **Brooks and Corey exponent (λ)**
Material: Halite and polyhalite within Salado Formation, (Salado, BrkCorEx)

Definition, Units: Dimensionless

Values: Range: (0.2, 10.0) Median: 0.7

Distribution: Constructed
Correlation:

Data Source(s):

Webb, S. W. 1992a. "Uncertainty Estimates for Two-Phase Characteristic Curves for 1992 RCRA Calculations" (see Appendix A, pp. A-141 through A-146). (Investigator Judgment)

Webb, S. W. 1992b. "Uncertainty Estimates for Two-Phase Characteristic Curves for 1992 40 CFR 191 Calculations" (see Appendix A, pp. A-147 through A-155). (Investigator Judgment)

Davies, P. B., and A. M. LaVenue. 1990b. Appendix A: "Additional Data for Characterizing 2-Phase Flow Behavior in Waste-Generated Gas Simulations and Pilot Point Information for Final Culebra 2-D Model (SAND89-7068/1)," *Data Used in Preliminary Performance Assessment of the Waste Isolation Pilot Plant (1990).* R. P. Rechard, H. Iuzzolino, and J. S. Sandha. SAND89-2408. Albuquerque, NM: Sandia National Laboratories. A-139 through A-156. (Investigator Judgment)

Usage:

Mathematical model:
Section 1.4.1, this volume.

Equation 1.4.1-6.

Computational models:
BRAGFLO

Ranking in Past Sensitivity Analyses:

40 CFR 191	Not tested
40 CFR 268	Low
NEPA	Not tested
Other	Not applicable

*Key to Parameter Sheets is provided in Section 1.2.8.

2.3.2 Density

Grain Density of Halite in Salado Formation*

Parameter: **Density, grain (ρ_g)**
Material: Halite within Salado Formation (Halite, DnsGrain)

Definition, Units: kg/m^3

Values: 2.163×10^3

Distribution: Constant
Correlation:

Data Source(s):
Carmichael, R. S., ed. 1984. *CRC Handbook of Physical Properties of Rocks*. Boca Raton, FL: CRC Press, Inc. Vol. III. (Table 2)

Krieg, R. D. 1984. *Reference Stratigraphy and Rock Properties for the Waste Isolation Pilot Plant (WIPP) Project*. SAND83-1908. Albuquerque, NM: Sandia National Laboratories. (p. 14)

Clark, S. P., Jr., ed. 1966. *Handbook of Physical Constants*. Memoir 97. New York, NY: The Geological Society of America, Inc. (p. 44)

Usage:

Mathematical model:
(Value recommended for exploratory modeling.)

Equation (NA).

Computational models:
(NA)

Ranking in Past Sensitivity Analyses:

40 CFR 191	Not applicable
40 CFR 268	Not applicable
NEPA	Not applicable
Other	Not applicable

*Key to Parameter Sheets is provided in Section 1.2.8.

Grain Density of Polyhalite in Salado Formation*

Parameter: **Density, grain (ρ_g)**
Material: Polyhalite within Salado Formation (PHalite, All, DnsGrain)

Definition, Units: kg/m^3

Values: 2.78×10^3

Distribution: Constant
Correlation:

Data Source(s): Hume, H. R., and A. Shakoor. 1981. "Mechanical Properties," *Physical Properties Data for Rock Salt*. NBS Monograph 167. Washington, DC: National Bureau of Standards. (p. 103-203)

Usage:

Mathematical model:
(Value recommended for exploratory modeling.)

Equation (NA).

Computational models:
(NA)

Ranking in Past Sensitivity Analyses:

40 CFR 191	Not applicable
40 CFR 268	Not applicable
NEPA	Not applicable
Other	Not applicable

*Key to Parameter Sheets is provided in Section 1.2.8.

Bulk Density of Halite in Salado (Halite)*

Parameter: **Density, bulk (ρ_{bulk})**
Material: Halite within Salado Formation (Salado, All, DnsBlk)

Definition, Units: kg/m^3

Values: 2.14×10^3

Distribution: Constant
Correlation:

Data Source(s): Holcomb, D. J., and M. Shields. 1987. *Hydrostatic Creep Consolidation of Crushed Salt With Added Water.* SAND87-1990. Albuquerque, NM: Sandia National Laboratories. (p. 17)

Usage:

Mathematical model:

The PA Department has used a bulk density of halite near the repository of 2,140 kg/m^3 as reported by Holcomb and Shields (1987, p. 17). This value corresponds to a porosity of 0.01.

$$\rho_{bulk} = (\rho_g (1-\phi))$$

Computational models:

(NA)

Ranking in Past Sensitivity Analyses:

40 CFR 191	Not applicable
40 CFR 268	Not applicable
NEPA	Not applicable
Other	Not applicable

*Key to Parameter Sheets is provided in Section 1.2.8.

Average Density near Repository*

Parameter: **Density, average (ρ_{ave})**
Material: Material near repository (Salado Formation) (Salado, All, DnsAvg)

Definition, Units: kg/m^3

Values: 2.3×10^3

Distribution: Constant
Correlation:

Data Source(s): Krieg, R. D. 1984. *Reference Stratigraphy and Rock Properties for the Waste Isolation Pilot Plant (WIPP) Project.* SAND83-1908. Albuquerque, NM: Sandia National Laboratories. (Table 4)

Usage:

Mathematical model:
(Value used by PA Department in past exploratory modeling.)

Equation (NA).

Computational models:
(NA)

Ranking in Past Sensitivity Analyses:

40 CFR 191	Not applicable
40 CFR 268	Not applicable
NEPA	Not applicable
Other	Not applicable

*Key to Parameter Sheets is provided in Section 1.2.8.

2.3.3 Dispersivity

Dispersivity, Longitudinal*

Parameter: **Dispersivity, longitudinal (α_L)**
Material: Halite and polyhalite within Salado Formation (Salado, All, Disp_lng)

Definition, Units: m

Values: Range: (1, 40) Median: 15

Distribution: Constructed
Correlation:

Data Source(s): Pickens, J. F., and G. E. Grisak. 1981. "Modeling of Scale-Dependent Dispersion in Hydrogeologic Systems," *Water Resources Research*. Vol. 17, no. 6, 1701-1711. (Engineering Lore)

Lappin, A. R., R. L. Hunter, D. P. Garber, and P. B. Davies, eds. 1989. *Systems Analysis, Long-Term Radionuclide Transport, and Dose Assessments, Waste Isolation Pilot Plant (WIPP), Southeastern New Mexico; March 1989*. SAND89-0462. Albuquerque, NM: Sandia National Laboratories. (Table D-2) (Investigator Judgment)

Usage:

Mathematical model:
(Value recommended for exploratory modeling.)

Equations 1.4.6-4a to 1.4.6-4b (definition of hydrodynamic dispersion tensor) in Section 1.4.6, this volume.

Computational models: Transport
STAFF2D

Ranking in Past Sensitivity Analyses:

40 CFR 191	Low (see Discussion)
40 CFR 268	Not tested
NEPA	Not tested
Other	Not applicable

*Key to Parameter Sheets is provided in Section 1.2.8.

Dispersivity Ratio*

Parameter: **Dispersivity ratio (α_L/α_T)**
Material: Halite and polyhalite within Salado Formation (Salado, All, Disp_trn)

Definition, Units: Ratio of longitudinal dispersivity to transverse dispersivity (dimensionless)

Values: Range: (3, 25) Median: 10

Distribution: Constructed
Correlation: Dispersivity, longitudinal

Source(s): PA Judgment based on the following sources:
Pickens, J. F., and G. E. Grisak. 1981. "Modeling of Scale-Dependent Dispersion in Hydrogeologic Systems," *Water Resources Research*. Vol. 17, no. 6, 1701-1711. (Engineering Lore)
Freeze, R. A., and J. A. Cherry. 1979. *Groundwater*. Englewood Cliffs, NJ: Prentice-Hall, Inc. (Figure 9.6) (Non-WIPP Literature Data)

Usage:

Mathematical model:
(Value recommended for exploratory modeling.)

Equations 1.4.6-4a to 1.4.6-4b (definition of hydrodynamic dispersion tensor) in Section 1.4.6, this volume.

Computational models:
STAFF2D

Ranking in Past Sensitivity Analyses:

40 CFR 191	Low (see Discussion)
40 CFR 268	Not tested
NEPA	Not tested
Other	Not applicable

*Key to Parameter Sheets is provided in Section 1.2.8.

Discussion:

No solute transport tests have been run in the Salado Formation, and no relevant solute transport data exist for very low permeability media from which to estimate dispersivity (α). Exploratory calculations of brine flows near the repository in the Salado show that linear fluid velocities are small and that solute transport proceeds mainly by diffusion (WIPP PA Division, 1991, vol. 2, Section 4.2.3). At these small velocities, the rule of thumb applied in standard porous media (Pickens and Grisak, 1981) is assumed to apply, that is, the longitudinal dispersivity α_L is approximately equal to $0.1d_s$ where d_s is the distance traveled by the solute. For typical distances traveled, α_L is between 1 and 40 m (3 and 130 ft). The distribution for α_L is shown in Figure 2.3-4.

Transverse dispersivity (α_T) is usually linearly related to α_L. The ratio of α_L to α_T typically varies between 5 and 20 (see, for example, Freeze and Cherry, 1979, Figure 9.6; Dullien, 1979, Figure 7.13; Bear and Verruijt, 1987). However, at very low velocities the ratio can approach 1, while in some strata the ratio has been reported to approach 100 (Marsily, de, 1986). The current range chosen by PA Analysts for sensitivity studies is 3 to 25 (Figure 2.3-5).

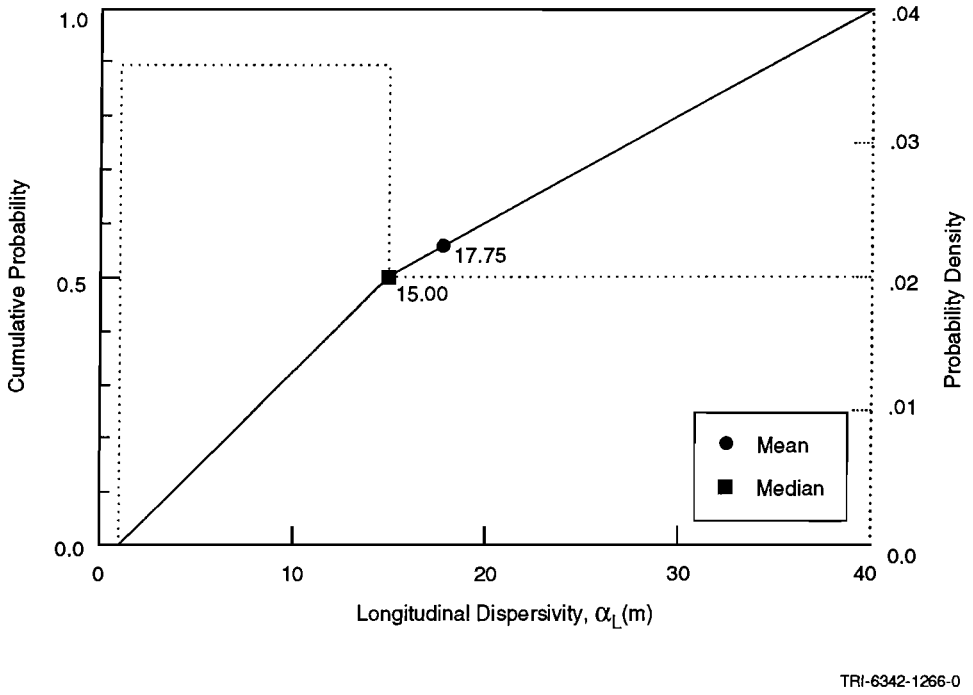

Figure 2.3-4. Estimated distribution for longitudinal dispersivity in halite, Salado Formation.

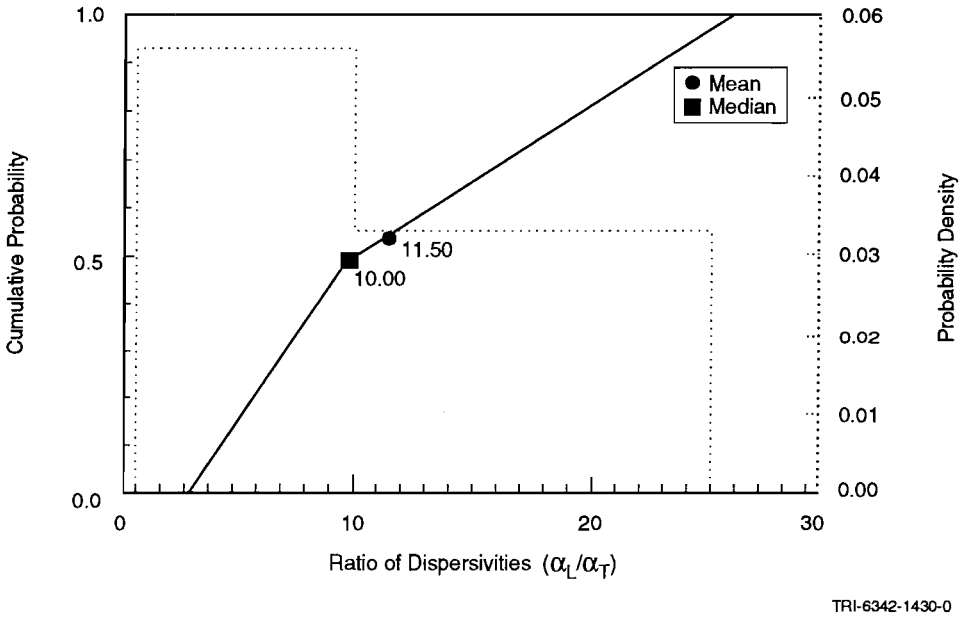

Figure 2.3-5. Estimated distribution for dispersivity ratio in halite, Salado Formation.

2.3.4 Partition Coefficients and Retardation

Partition Coefficient for Halite and Polyhalite*

Parameter: **Partition coefficient for halite and polyhalite (Kd), all species**
Material: Halite and polyhalite within Salado Formation (Salado, Kd_All)

Definition, Units: m^3/kg

Values: 0

Distribution: Constant
Correlation:

Data Source(s): Lappin, A. R., R. L. Hunter, D. P. Garber, and P. B. Davies, eds. 1989. *Systems Analysis, Long-Term Radionuclide Transport, and Dose Assessments, Waste Isolation Pilot Plant (WIPP), Southeastern New Mexico; March 1989.* SAND89-0462. Albuquerque, NM: Sandia National Laboratories. (p. D-17) (Investigator Judgment)

Usage:

Mathematical model:

The halite and polyhalite in the Salado Formation are assumed by PA Analysts not to interact chemically with any contaminants.

Equation (NA).

Computational models:

(NA)

Ranking in Past Sensitivity Analyses:

40 CFR 191	Not applicable
40 CFR 268	Not applicable
NEPA	Not applicable
Other	Not applicable

*Key to Parameter Sheets is provided in Section 1.2.8.

2.3.5 Permeability

Undisturbed Permeability*

Parameter: **Permeability, undisturbed (k)**
Material: Halite and polyhalite within Salado Formation, (Salado, LogPrmU)

Definition, Units: Log permeability values given (dimensionless); permeability has units of m^2.

Values: Range: (-24.0, -19.0) Median: -21.2 (log_{10} of values)

Distribution: Constructed (see Discussion)
Correlation:

Data Source(s):

Gorham, E., R. Beauheim, P. Davies, S. Howarth, and S. Webb. 1992. "Recommendations to PA on Salado Formation Intrinsic Permeability and Pore Pressure for 40 CFR 191 Subpart B Calculations" (see Appendix A, pp. A-47 through A-67). (Investigator Judgment based on WIPP data)

Howarth, S. M., E. W. Peterson, P. L. Lagus, K. Lie, S. J. Finley, and E. J. Nowak. 1991. "Interpretation of In-Situ Pressure and Flow Measurements of the Salado Formation at the Waste Isolation Pilot Plant," *Society of Petroleum Engineers Rocky Mountain Regional Meeting and Low-Permeability Reservoir Symposium, Denver, CO, April 15-17, 1991.* SPE-21840. Richardson, TX: Society of Petroleum Engineers. (Investigator Judgment based on WIPP data)

Beauheim, R. L., G. J. Saulnier, Jr., and J. D. Avis. 1991a. *Interpretation of Brine-Permeability Tests of the Salado Formation at the Waste Isolation Pilot Plant Site: First Interim Report.* SAND90-0083. Albuquerque, NM: Sandia National Laboratories. (Investigator Judgment based on WIPP data)

Usage:

Mathematical model:

Section 1.4.1, this volume.

Equations 1.4.1-1 and 1.4.1-2 in Section 1.4.1, this volume.

Computational models:

BRAFGLO

Ranking in Past Sensitivity Analyses:

40 CFR 191	High
40 CFR 268	Medium
NEPA	Not tested
Other	Not applicable

*Key to Parameter Sheets is provided in Section 1.2.8.

Discussion:

The permeability of undisturbed halite was a highly sensitive parameter in determining releases of Pu-239 during the 1991 series of calculations. Calling this parameter SALPERM, it is seen from the scatterplot in Figure 2.3-6 that there is a threshold in SALPERM such that, in a scenario that includes gas generation in the repository and intrusion by drilling at 1000 yr, there is essentially no release if SALPERM $< 5 \times 10^{-21}$ m^2, and finite release if SALPERM $> 5 \times 10^{-21}$ m^2. The undisturbed halite permeability determines how long it will take for a waste panel to be filled with brine; if the pore space in a panel cannot fill with brine due to very low halite permeability, then there can be no fluid flow up the intrusion borehole and hence no radionuclide release (Helton et al., 1992, p. 4-20). The distribution of SALPERM that was used in the 1991 series of calculations is shown on Figure 2.3-7; note that more than 50% of the values exceed 5×10^{-21} m^2.

The distribution of SALPERM used in the 1992 series of calculations (Figure 2.3-8) differs from the 1991 distribution (Figure 2.3-7) in two ways: in 1992, only about 18% of values exceed the threshold of 5×10^{-21} m^2, and the upper limit of permeability is now set at 10^{-19} m^2. A rationale for these changes is supplied by Gorham et al. (June 15, 1992, Memo in Appendix A).

The PA Department judges that both distributions are adequate for the purpose of testing sensitivity of far-field permeability in the two-phase flow model (Section 1.4.1) but that neither distribution really represents uncertainty in the *average* far-field permeability, the quantity that should be used in the current version of the two-phase flow model. Because average halite permeability is (and is likely to remain) a sensitive determinant of releases of radionuclides from a disturbed waste panel, a direct approach to inferring uncertainty in average halite permeability, an approach that uses only measurements of that quantity, seems desirable. One such approach, based on "bootstrap" statistical methods (see Efron and Tibshirani, 1991, for a review), is outlined below and applied to the inference of averages of far-field permeability and pore pressure in sections that follow. The data used in these applications arises from three experimental programs; the three programs (Permeability Tests, Small-Scale Brine Inflow, and Room Q described in the draft of the "Sandia National Laboratories Waste Isolation Pilot Plant Program Plan for Fiscal Year 1992") are evaluating permeability, storativity, and pore pressure in halite and anhydrite layers of the Salado Formation. Results of these programs available in April, 1992, are summarized in Table 2.3-2.

Estimating far-field parameters by non-linear regression: Let $(y_1, y_2, ..., y_N)$ be logarithms of permeabilities, or pore pressures, that are measured at corresponding distances $(x_1, x_2, ..., x_N)$ into the Salado Formation from the walls of an open excavation. Data, such as that given in Table 2.3-2, can be used to fit by least squares an expression of the form:

$$y(x) = a + b \exp(-x/c), \qquad (2.3.5\text{-}1)$$

where the coefficients (a, b, c) have the following physical meanings:

- a = an estimate of $\log_{10}$ of undisturbed permeability or an estimate of undisturbed pore pressure at repository level (to see that this is plausible, let $x \rightarrow \infty$ in Eq. 2.3.5-1);
- c = an estimate of the characteristic depth of the disturbed permeability zone or the (possibly different) characteristic depth of the disturbed pore-pressure zone (m);
- a+b = an estimate of $\log_{10}$ of disturbed permeability near the wall of an excavation (let $x \rightarrow o$ in Eq. 2.3.5-1). Since permeability is expected to decrease with increasing distance into the Salado, $b > 0$ in this case. Alternatively, if y(x) measures pore pressure, a+b is an estimate of disturbed pore pressure near the wall; $(a + b) \simeq 0$, so $b < 0$ in this case.

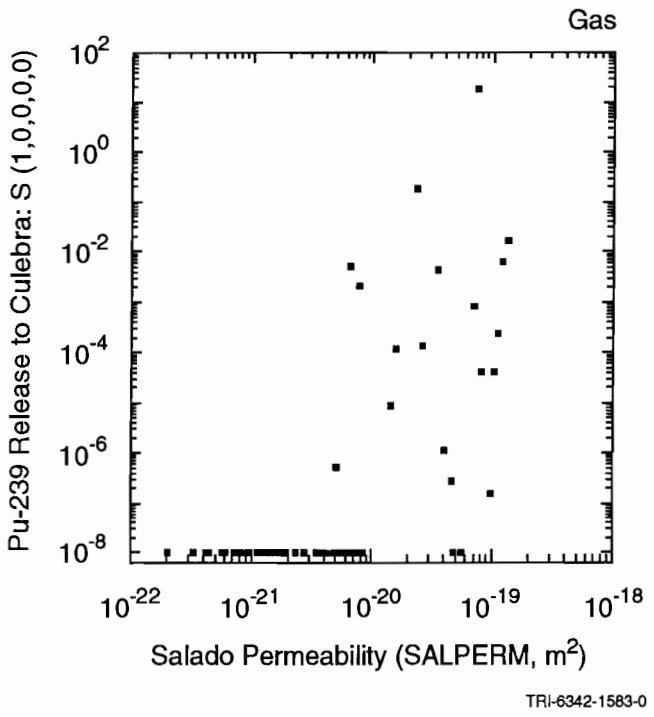

Figure 2.3-6. Scatterplot for normalized release of Pu-239 to the Culebra Dolomite with gas generation in the repository and intrusion occurring at 1000 yr for variable SALPERM (Salado permeability) (after Helton et al., 1992, Figure 4.5-1).

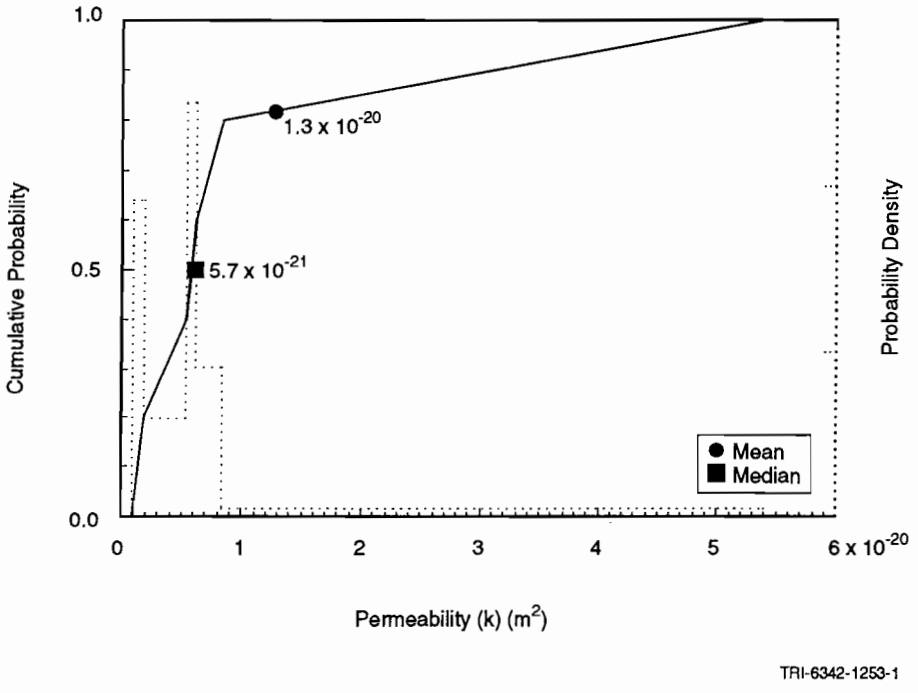

Figure 2.3-7. Estimated distribution (in 1991) for Salado undisturbed permeability.

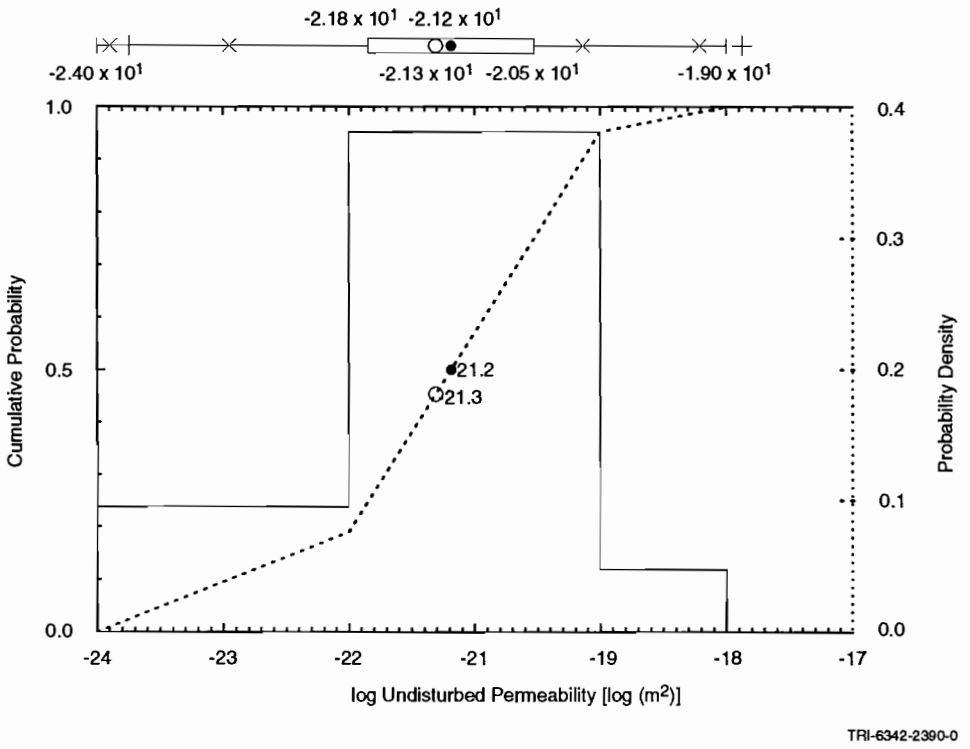

Figure 2.3-8. Estimated distribution in 1992 for Salado undisturbed permeability.

The choice of functional form (Eq. 2.3.5-1) is not entirely arbitrary. Because of excavation disturbance and depressurization, it is expected that pore pressure (or permeability) should increase (or decrease) with increasing distance x into the Salado Formation in the manner indicated in Figure 2.3-9, and – ignoring natural inhomogeneities and errors of measurement – should asymptotically approach constant values corresponding to the average far-field values as $x \rightarrow \infty$. Equation 2.3.5-1 is but one of many functions that, with proper choice of constants, will mimic the expected spatial distributions of pore pressure and permeability near the wall of an open excavation. Another possible functional form is

$$y(x) = a + (b/(c + x^d)) \quad . \tag{2.3.5-2}$$

The constant a in Eq. 2.3.5-2 has the same physical meaning as constant a in Eq. 2.3.5-1, but other constants in Eq. 2.3.5-2 will obviously take a different meaning.

Interest centers primarily on the coefficient a and the uncertainty associated with that coefficient. The other coefficients, b and c, are probably not meaningful as estimators of disturbed-zone parameters of a waste-loaded excavation that has undergone some collapse and compaction; in other words, measurements of the material parameters of contemporary disturbed zones of WIPP excavations should probably not be used to infer the parameters of the disturbed zone of the same excavation after it has been filled with waste and backfill, closed, and allowed to subside for hundreds to thousands of years.

To infer the uncertainty of the coefficient a, "bootstrap" methods described in Section 14.5 of Press et al., 1986, have been adopted. The methods are based on a recognition that a given data set,

$$Y = (y_1, y_2, ..., y_N),$$

Table 2.3-2. Summary of Measurements of Salado Halite Permeabilities and Pore Pressures

Test No.	Lithology	Distance[b] (m)	Measured Permeability (m^2)	log_{10} Permeability[c]	Pressure (MPa)[d]	Orientation	Sources[e]
QPP12(pre)[a]	Halite	26.7	6.8×10^{-22}	-21.2 ± 0.7	9.5 ± 0.5	vertical, down	1, 2
C2H03	pure halite	7.76 - 9.14	too low to measure	–	–	horizontal	1, 3
SCP01-GZ	halite ?	?	too low to measure	–	–	angle, down 13°	1
QPP05 (pre)	halite	23.0	too low to measure	–	–	vertical, up	1, 2
QPP02 (pre)	halite	26.7	too low to measure	–	–	vertical, up	1, 2
S1P72-A-GZ	halite	?	8.6×10^{-22}	-21.1	5.1	angle, down 32°	1, 3
QPP21 (post)	halite	12.2	1.9×10^{-22}	-21.7	4.8	horizontal	1, 2
C2H01-B	avg. halite	4.50 - 5.58	5.3×10^{-21}	-20.3	3.1	vertical, down	1, 3
C2H01-B-GZ	avg. halite	2.92 - 4.02	1.9×10^{-21}	-20.7	4.1	vertical, down	1, 3
L4P51-A	avg. halite & clay	3.33 - 4.75	6.1×10^{-21}	-20.2	2.7	vertical, down	1, 3
SOP01	avg. halite & clay	3.74 - 5.17	8.3×10^{-21}	-20.1	4.4	vertical, down	1, 3
S1P71-A	avg. halite & clay	3.12 - 4.56	6.1×10^{-20}	-19.2	2.9	vertical, down	1, 3
QPP15	halite	23 ?	2.2×10^{-21}	-20.7	3.1	vertical, down	1, 2
DBT10	halite	3.0 - 6.0	5.8×10^{-22}	-21.2	(5.0 assumed)	vertical, down	1, 4
DBT11	halite	3.0 - 6.0	2.3×10^{-21}	-20.6	(5.0 assumed)	vertical, down	1, 4
DBT12	halite	3.0 - 6.0	1.3×10^{-21}	-20.9	(5.0 assumed)	vertical, down	1, 4
DBT13	halite	3.0 - 6.0	3.4×10^{-22}	-21.5	(5.0 assumed)	vertical, down	1, 4
DBT14A/B	halite	3.0 - 6.0	3.1×10^{-21}	-20.5	(5.0 assumed)	vertical, down	1, 4
DBT15A/B	halite	3.0 - 6.0	5.0×10^{-22}	21.3	(5.0 assumed)	vertical, down	1, 4
L4B01	halite	3.0 - 6.0	1.3×10^{-22}	-21.9	(5.0 assumed)	vertical, down	1, 4
DBT31A	–	–	–	–	–	–	not used, 1
QPP12 (post)	halite	6.1	4.4×10^{-22}	-21.4	9.4	vertical, down	1, 2
C2H01-A	avg. halite	2.09 - 5.58	2.7×10^{-18}	-17.6	0.5	vertical, down	1, 3
C2H01-A-GZ	halite	0.50 - 1.64	(unmeasurable)	–	0.0	vertical, down	1, 3
S1P73-B-GZ	?	?	(unmeasurable)	–	2.5	?	1

a - "Pre" and "post" mean pre- and post-mineby for Q tunnel tests.
b - Estimated distance of apparatus from wall of excavation
c - A standard error of one-half order of magnitude assumed for all permeabilities
d - A standard error of 0.5 MPa assumed for all measured or inferred pressures
e - Sources: 1 - Gorham et al., June 15, 1992, Memo (Appendix A, this volume),
2 - Howarth et al., 1991,
3 - Beauheim et al., 1991b,
4 - Finley and McTigue, 1991.

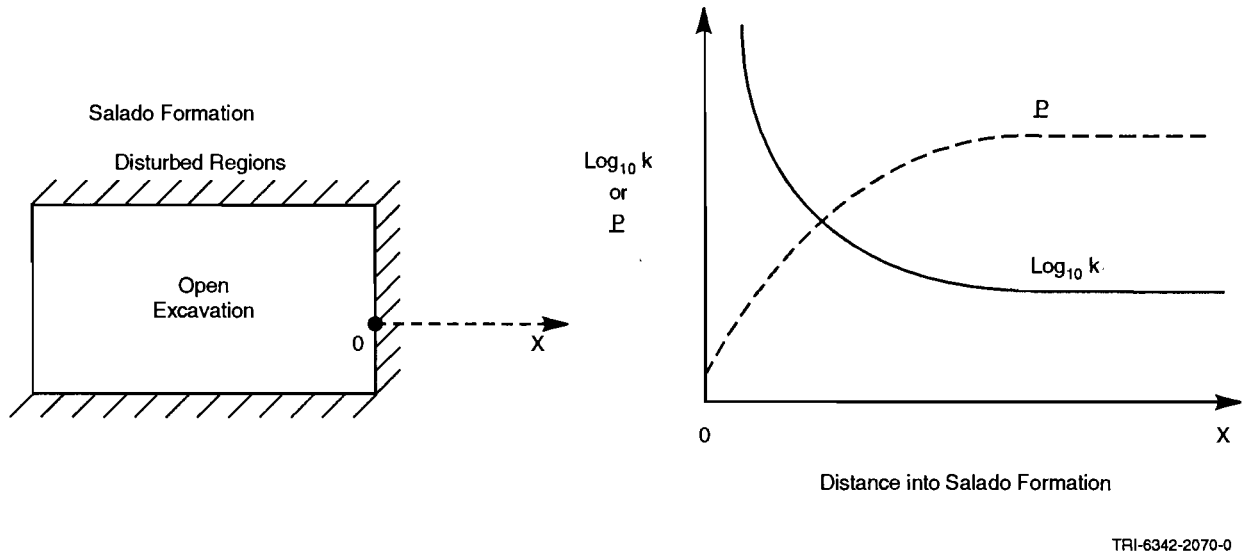

Figure 2.3-9. Expected qualitative behavior of pore pressure (P) and log permeability ($\log_{10}$k) near wall of an open excavation.

can yield at best a single *estimate* of the coefficients,

$$A_o = (a_o, b_o, c_o),$$

when the data are fitted to an expression like Eq. 2.3.5-1. However, if the standard error of each datum is known and can be interpreted in terms of a standard deviation of the measurement, it becomes possible to obtain an arbitrary number of *synthetic data sets* by Monte Carlo simulations. These synthetic data sets can then be used in the regression formula to obtain new estimates of the coefficients, i.e.,

$$A_1, A_2, ..., A_m,$$

which can be treated as though they were data concerning the coefficients themselves; in other words, the empirical cdfs and correlations between the coefficients a, b, and c can be constructed by standard statistical techniques. The method described here has the advantage that empirical cdfs of parameters can be inferred directly from measurements of the fitted quantity and its presumed measurement errors; the need for subjective judgments on the part of investigators–such as the judgments giving Figures 2.3-7 and 2.3-8–is minimized. Furthermore, the method effectively averages over small-scale spatial variations in the material properties and therefore gives a better description of uncertainty in the *average* value of those properties (i.e., a better estimate of the material-property parameter used in PA consequence model[s]; see Section 1.3.3 for a discussion of this issue). The method has the disadvantage that the functional forms used in the non-linear regression (e.g., Eqs. 2.3.5-1 and 2.3.5-2) are in general not unique; the use of different functional forms in the regression analyses can yield quite different distributions for the coefficients (or parameters) a, b, and c. The robustness of different functional forms needs to be examined before the method can be applied with confidence to any given problem. Furthermore, robustness of results with respect to assumptions about the size of the standard deviations of measurements needs to be examined since quoted standard deviations are more often than not guesses of the investigators.

As an example of this technique for estimating the distributions of far-field quantities, data from Table 2.3-2 have been used to generate a simulated distribution of the mean, far-field halite permeability (Figure 2.3-10). Note that only about 3% of average SALPERM values exceed the threshold of 5×10^{-21} m^2.

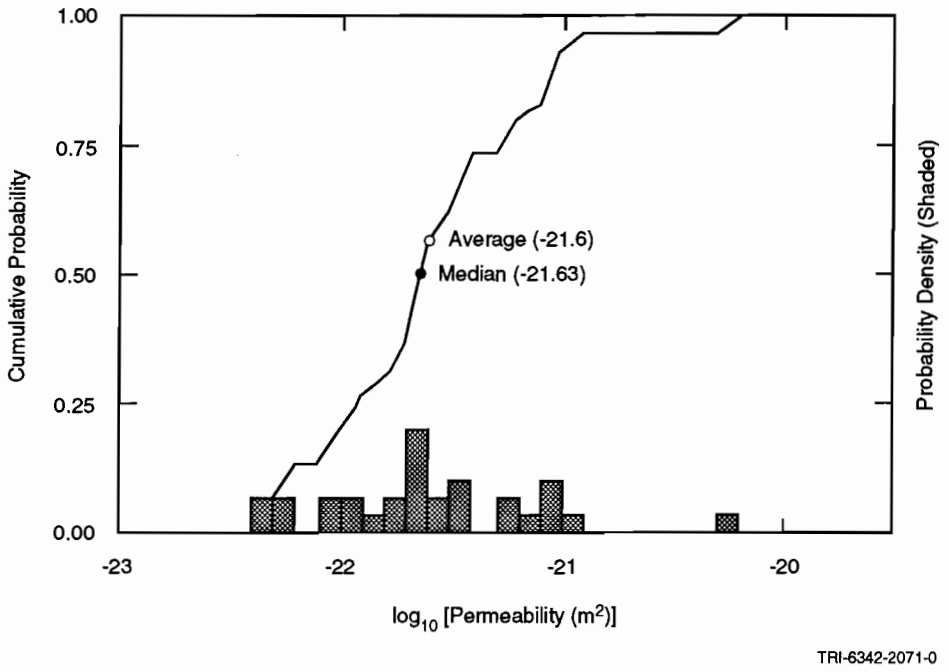

Figure 2.3-10. Simulated undisturbed (far-field) halite permeability. Coefficient "a" in non-linear least square fit to Eq. 2.3.5-1; 30 samples.

Disturbed Permeability*

Parameter: **Permeability, disturbed (k)**
Material: Halite and polyhalite within Salado Formation, (Salado, LogPrmD)

Definition, Units: Log permeability values given (dimensionless); permeability has units of m^2.

Values: Range: (-22.0, -15.0) Median: -20.7

Distribution: Constructed (see Discussion)
Correlation:

Data Source(s):

Gorham, E., R. Beauheim, P. Davies, S. Howarth, and S. Webb. 1992. "Recommendations to PA on Salado Formation Intrinsic Permeability and Pore Pressure for 40 CFR 191 Subpart B Calculations" (see Appendix A, pp. A-47 through A-67). (Investigator Judgment based on WIPP data)

Howarth, S. M., E. W. Peterson, P. L. Lagus, K. Lie, S. J. Finley, and E. J. Nowak. 1991. "Interpretation of In-Situ Pressure and Flow Measurements of the Salado Formation at the Waste Isolation Pilot Plant," *Society of Petroleum Engineers Rocky Mountain Regional Meeting and Low-Permeability Reservoir Symposium, Denver, CO, April 15-17, 1991.* SPE-21840. Richardson, TX: Society of Petroleum Engineers. (Investigator Judgment based on WIPP data)

Beauheim, R. L., G. J. Saulnier, Jr., and J. D. Avis. 1991a. *Interpretation of Brine-Permeability Tests of the Salado Formation at the Waste Isolation Pilot Plant Site: First Interim Report.* SAND90-0083. Albuquerque, NM: Sandia National Laboratories. (Investigator Judgment based on WIPP data)

Usage:

Mathematical model:
Section 1.4.1, this volume.

Equations 1.4.1-1 and 1.4.1-2 in Section 1.4.1, this volume.

Computational models:
BRAGFLO

Ranking in Past Sensitivity Analyses:

40 CFR 191	Not tested
40 CFR 268	Low
NEPA	Not tested
Other	Not tested

*Key to Parameter Sheets is provided in Section 1.2.8.

Discussion:

The disturbed permeability and porosity of the Salado Formation and interbeds vary from the intact properties to large, open fractures. These two disturbed properties also change as the stress field around the excavations change with time. Furthermore, the halite will likely heal to intact conditions over time (Sutherland and Cave, 1978; Lappin et al., 1989, p. 4-45). For these reasons, disturbed permeability is treated as an independent parameter when it is not possible to predict changes in halite permeability due to changes in the stress field. In the 1992 data base, the disturbed permeability is assumed to be distributed according to the empirical cdf of the non-far-field data points listed in Table 2.3-2. Figure 2.3-11 shows the resulting distribution.

Disturbed permeability of halite was not sampled in 1992 calculations.

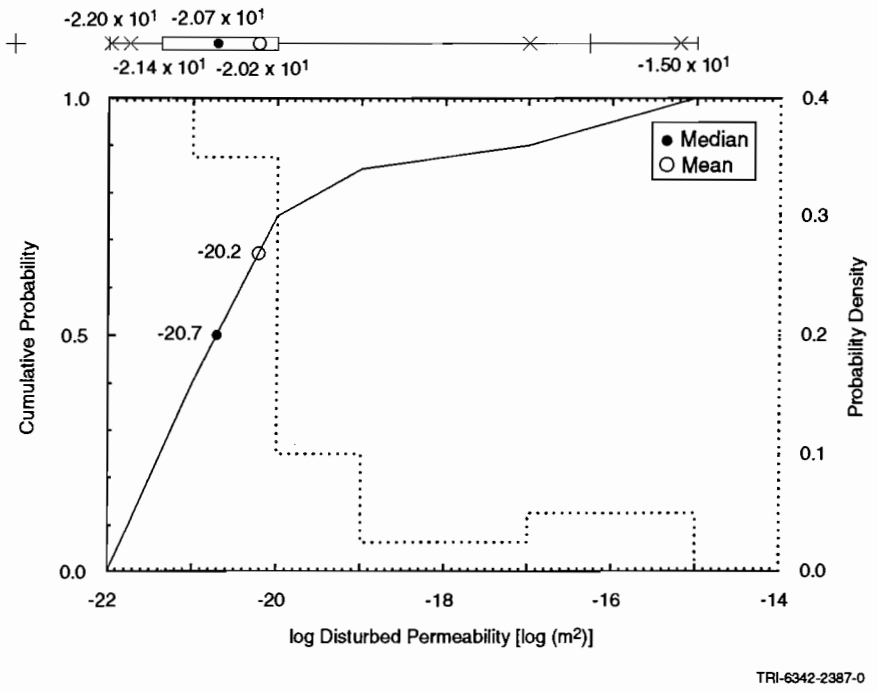

Figure 2.3-11. Estimated distribution (in 1992) for Salado halite disturbed permeability.

2.3.6 Pore Pressure at Repository Level in Halite

Pore Pressure*

Parameter: **Pore pressure (p)**
Material: Halite and polyhalite within Salado Formation, (Salado, Pressure)

Definition, Units: MPa

Values: Range: (9.0, 10.0) Median: 9.5

Distribution: Uniform
Correlation:

Data Source(s):

Gorham, E., R. Beauheim, P. Davies, S. Howarth, and S. Webb. 1992. "Recommendations to PA on Salado Formation Intrinsic Permeability and Pore Pressure for 40 CFR 191 Subpart B Calculations" (see Appendix A, pp. A-47 through A-67). (Investigator Judgment based on WIPP data)

Howarth, S. M., E. W. Peterson, P. L. Lagus, K. Lie, S. J. Finley, and E. J. Nowak. 1991. "Interpretation of In-Situ Pressure and Flow Measurements of the Salado Formation at the Waste Isolation Pilot Plant," *Society of Petroleum Engineers Rocky Mountain Regional Meeting and Low-Permeability Reservoir Symposium, Denver, CO, April 15-17, 1991.* SPE-21840. Richardson, TX: Society of Petroleum Engineers. (Investigator Judgment based on WIPP data)

Beauheim, R. L., G. J. Saulnier, Jr., and J. D. Avis. 1991. *Interpretation of Brine-Permeability Tests of the Salado Formation at the Waste Isolation Pilot Plant Site: First Interim Report.* SAND90-0083. Albuquerque, NM: Sandia National Laboratories. (Investigator Judgment based on WIPP data)

Usage:

Mathematical model:
Section 1.4.1, this volume.

Equations: Boundary condition on fluid pressure in Eqs. 1.4.1-1 and 1.4.1-2.

Computational models:
BRAGFLO

Ranking in Past Sensitivity Analyses:

40 CFR 191	Not tested
40 CFR 268	Not tested
NEPA	Not tested
Other	Not tested

*Key to Parameter Sheets is provided in Section 1.2.8.

Discussion:

In 1992, far-field pore pressure in halite is assumed to be uniformly distributed on the interval (9,10) MPa, based on the single measurement (9.4 ± 0.5 MPa, test QPP12 [pre] in Table 2.3-2) that was endorsed as a far-field value (Gorham et al., June 15, 1992, Memo in Appendix A, this volume).

As another example of the technique for estimating average far-field quantities, data from Table 2.3-2 and regression techniques described in Section 2.3.5 have been used to generate a simulated distribution for far-field pore pressure in halite (Figure 2.3-12). Results of this trial simulation suggest that halite pore pressure at the repository level is approximately the hydrostatic pressure of Castile brines, as measured from the surface (Figure 2.3-13).

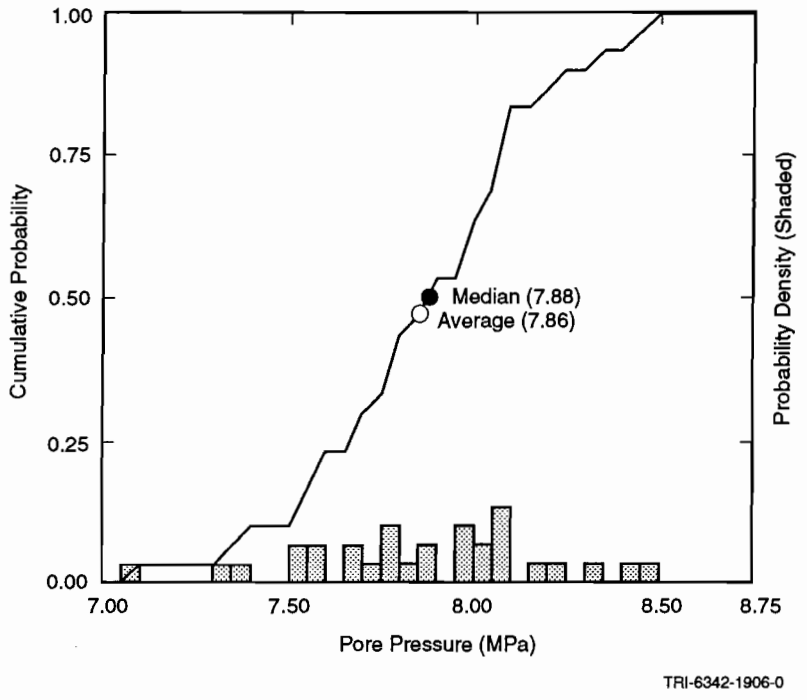

Figure 2.3-12. Simulated undisturbed (far-field) pore pressure at repository depth in halite. Coefficient "a" in nonlinear least squares fit to Eq. 2.3.5-1; 30 samples.

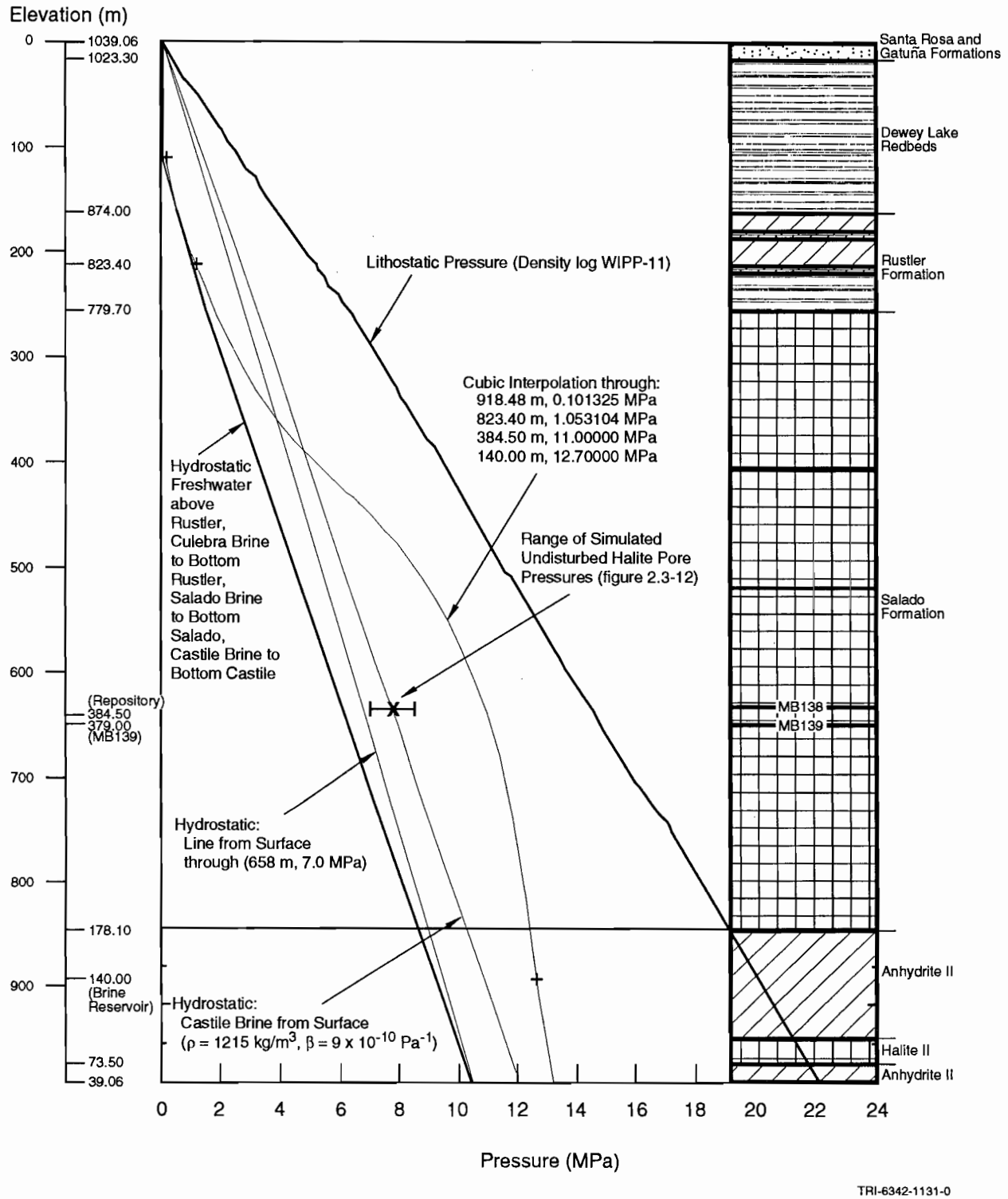

Figure 2.3-13. Calculated lithostatic and hydrostatic pressures with depth.

2.3.7 Porosity

Undisturbed Porosity*

Parameter:	**Porosity, undisturbed (ϕ)**
Material:	Halite and polyhalite within Salado Formation, (Salado, Pore_U)
Definition, Units:	Dimensionless
Values:	Range: (1×10^{-3}, 3×10^{-2}) Median: 1×10^{-2}
Distribution:	Constructed (see Discussion)
Correlation:	

Data Source(s): Investigator Judgment (see Discussion).

Powers, D. W., S. J. Lambert, S-E. Shaffer, L. R. Hill, and W. D. Weart, eds. 1978. *Geological Characterization Report, Waste Isolation Pilot Plant (WIPP) Site, Southeastern New Mexico*. SAND78-1596. Albuquerque, NM: Sandia National Laboratories. Vols. 1-2.

U.S. Department of Energy. 1983. "Brine Content of Facility Interval Strata," *Results of Site Validation Experiments*. TME 3177. [Carlsbad, NM]: Waste Isolation Pilot Plant. Vol. II, Supporting Document 10.

Usage:

Mathematical model:

Section 1.4.1, this volume.

Equations 1.4.1-1 and 1.4.1-2; specifies porosity of part of reservoir that is undisturbed halite.

Computational models:

BRAGFLO

Ranking in Past Sensitivity Analyses:

40 CFR 191	Not tested
40 CFR 268	Not tested
NEPA	Not tested
Other	Not tested

*Key to Parameter Sheets is provided in Section 1.2.8.

Discussion:

The PA assumed the median porosity to be 0.01 based on an unpublished report about electromagnetic and DC resistivity measurements (Skokan, C., J. Starrett, and H. T. Andersen. 1988. *Final Report: Feasibility Study of Seismic Tomography to Monitor Underground Pillar Integrity at the WIPP Site.* Contractor Report. Albuquerque, NM: Sandia National Laboratories). This median value is identical to that calculated from a grain density of 2,163 kg/m^3 (135 lb/ft^3) for halite, and a bulk density of 2,140 kg/m^3 (133.6 lb/ft^3) ($\rho_b = (1-\phi)\rho_g$). The low value of 0.001 is based on drying experiments (Powers et al., 1978), while the high value of 0.03 is suggested by the low end of DC resistivity measurements in the unpublished report by Skokan et al., cited above.

Figure 2.3-14 shows the estimated distribution for the undisturbed porosity.

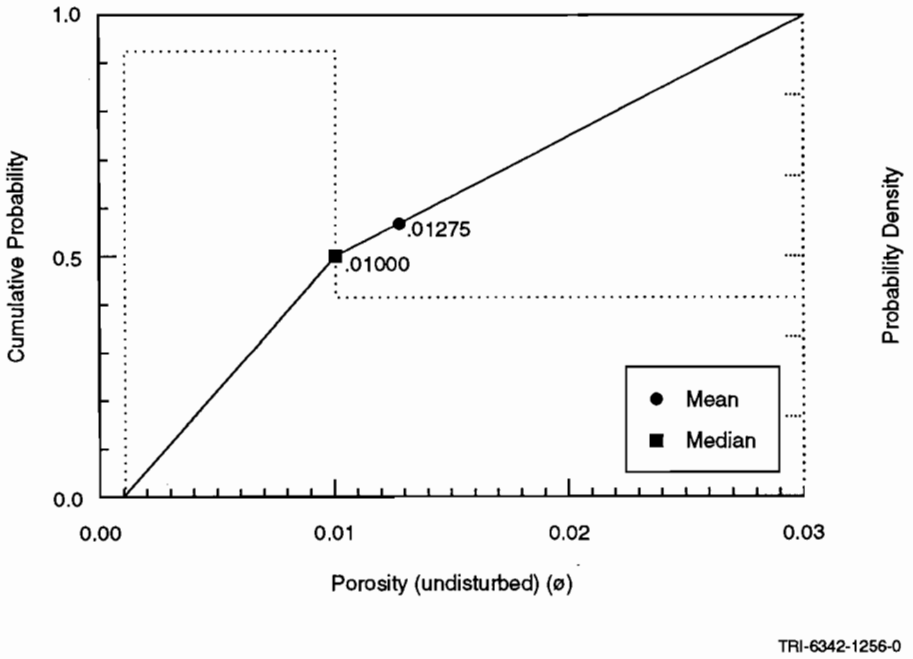

Figure 2.3-14. Estimated distribution for undisturbed porosity in halite, Salado Formation.

Disturbed Porosity*

Parameter: **Porosity, disturbed (ϕ)**
Material: Halite and polyhalite within Salado Formation, (Salado, Pore_D)

Definition, Units: Dimensionless

Values: 6×10^{-2}

Distribution: Constant
Correlation:

Data Source(s): The disturbed porosity of 0.06 is calculated by assuming that the final (disturbed) density of halite is 0.95 of the intact density, i.e., ϕ is such that

$$0.95\rho_b = (1 - \phi)\,\rho_g$$

where ρ_g is grain density of halite (Section 2.3.2) and
ρ_b is bulk density of halite (Section 2.3.2).

Usage:

Mathematical model:
Section 1.4.1, this volume.

Equations 1.4.1-1 and 1.4.1-2; specifies porosity of part of reservoir that is disturbed halite.

Computational models:
BRAGFLO

Ranking in Past Sensitivity Analyses:

40 CFR 191	Not applicable
40 CFR 268	Not applicable
NEPA	Not applicable
Other	Not applicable

*Key to Parameter Sheets is provided in Section 1.2.8.

2.3.8 Specific Storage

Specific Storage*

Parameter: **Specific storage (S_s)**
Material: Halite and polyhalite within Salado Formation, (Salado, Sp_Stor)

Definition, Units: m^{-1}

Values: Range: (2.8×10^{-8}, 1.4×10^{-6}) Median: 9.5×10^{-8}

Distribution: Constructed
Correlation:

Data Source(s): Beauheim, R. [L.] 1991. Appendix A: "Review of Salado Parameter Values to be Used in 1991 Performance Assessment Calculations," *Preliminary Comparison with 40 CFR Part 191, Subpart B for the Waste Isolation Pilot Plant, December 1991. Volume 3: Reference Data.* WIPP Performance Assessment Division. Eds. R. P. Rechard, A. C. Peterson, J. D. Schreiber, H. J. Iuzzolino, M. S. Tierney, and J. S. Sandha. SAND91-0893/3. Albuquerque, NM: Sandia National Laboratories. A-19 through A-23. (Investigator Judgment)

Usage:

Mathematical model:

Specific storage is used to specify solid compressibility, β_s, which in turn constrains changes in solid porosity by the relationship,

$$\beta_s = \frac{1}{\phi}\frac{\partial \phi}{\partial p}$$

where p is pore pressure (brine pressure). Such a relationship, or one similar to it, is used in BRAGFLO (Section 1.4.1) and other two-phase flow models. See Discussion.

Computational models:

BRAGFLO

Ranking in Past Sensitivity Analyses:

40 CFR 191	Not tested
40 CFR 268	Not tested
NEPA	Not tested
Other	Not tested

*Key to Parameter Sheets is provided in Section 1.2.8.

Figure 2.3-15 shows the estimated distribution for specific storage. The median and range of this distribution were recommended by Beauheim (1991).

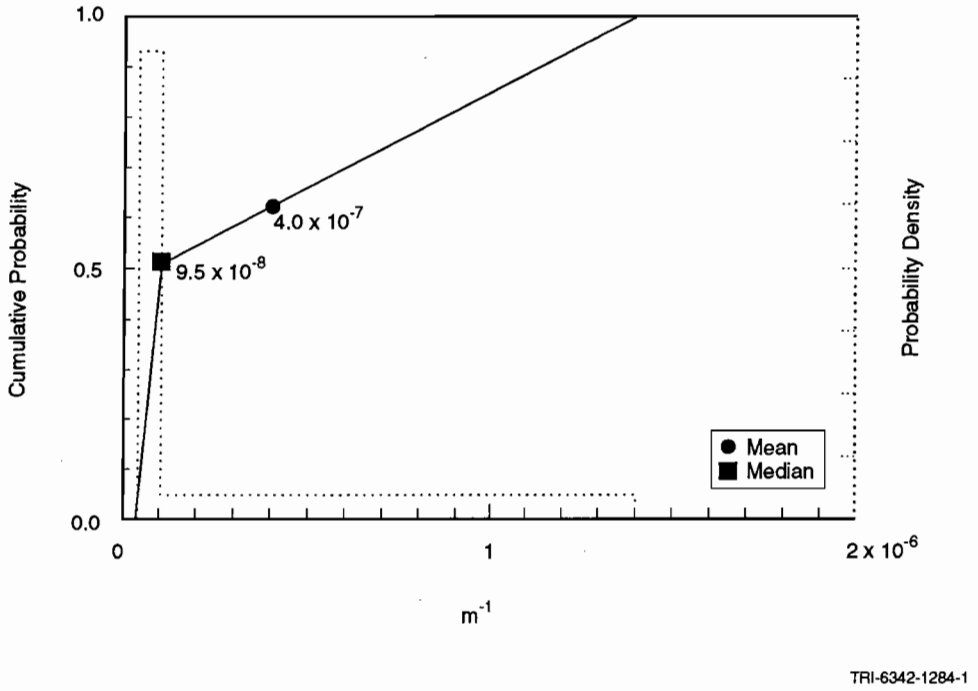

Figure 2.3-15. Estimated distribution for specific storage of halite, Salado Formation.

Discussion:

Specific storage is usually defined by the relationship,

$$S_s = \rho_f g (\beta_s + \phi\beta_f) . \qquad (2.3\text{-}6)$$

where

ρ_f = mass density of fluid (kg/m^3),
g = acceleration of gravity (m/s^2),
β_s = compressibility of solid matrix (Pa^{-1}),
ϕ = porosity of solid matrix (dimensionless),
β_f = compressibility of fluid (Pa^{-1}).

The above relationship can be solved for β_s to give

$$\beta_s = (S_s/\rho_f g) - \phi\beta_f , \qquad (2.3\text{-}7)$$

which can then be used to constrain changes in solid porosity with pressure through relationships of the form

$$\beta_s = \text{a function of } \phi \text{ and } \partial\phi/\partial\rho .$$

Some confusion may result because groundwater models often employ different definitions for the matrix compressibility β_s. For example SUTRA (Voss, 1984) defines β_s as

$$\beta_s = \frac{1}{1-\phi}\frac{\partial \phi}{\partial p},$$

but defines capacitance (specific pressure storativity) as

$$c = (1-\phi)\beta_s + \phi\beta_f,$$

thus

$$c = \frac{\partial \phi}{\partial p} + \phi\beta.$$

STAFF 2D (Huyakorn et al., 1991) and HST3D (Kipp, 1987) defines β_s as

$$\beta_s = \frac{\partial \phi}{\partial p},$$

while BOAST II (Fanchi et al., 1987) and BRAGFLO (Section 1.4.1, this volume) use

$$\beta_s = \frac{1}{\phi}\frac{\partial \phi}{\partial p}.$$

It is important to recognize that each code uses a different definition of matrix compressibility and all ignore solid compressibility.

2.3.9 Tortuosity

Tortuosity*

Parameter: **Tortuosity (τ)**
Material: Halite and polyhalite within Salado Formation, (Salado, Tortusty)

Definition, Units: Dimensionless

Values: Range: (1×10^{-2}, 6.67×10^{-1}) Median: 1.4×10^{-1}

Distribution: Constructed
Correlation:

Data Source(s):
Freeze, R. A., and J. A. Cherry. 1979. *Groundwater.* Englewood Cliffs, NJ: Prentice-Hall, Inc. (p. 104)

Kelley, V. A., and G. J. Saulnier, Jr. 1990. *Core Analyses for Selected Samples from the Culebra Dolomite at the Waste Isolation Pilot Plant Site*. SAND90-7011. Albuquerque, NM: Sandia National Laboratories. (Table 4.6)

Lappin, A. R., R. L. Hunter, D. P. Garber, and P. B. Davies, eds. 1989. *Systems Analysis, Long-Term Radionuclide Transport, and Dose Assessments, Waste Isolation Pilot Plant (WIPP), Southeastern New Mexico; March 1989.* SAND89-0462. Albuquerque, NM: Sandia National Laboratories. (Table E-9)

Usage:

Mathematical model:

Intact matrix tortuosity is used to evaluate the effective molecular diffusion coefficient (D_m) from the coefficient of molecular diffusion ($D^{\square}$) in the pure saturating fluid ($D_m = \tau D^{\square}$), where τ equals $(\ell / \ell_{path})^2$, ℓ is the linear length, and ℓ_{path} is the length of the [tortuous] path that a fluid particle would take (Bear, 1972, p. 111).

Computational models:

SUTRA (used only in 1991 calculations)

Ranking in Past Sensitivity Analyses:

40 CFR 191	Not tested
40 CFR 268	Not tested
NEPA	Not tested
Other	Not tested

*Key to Parameter Sheets is provided in Section 1.2.8.

Discussion:

No direct measurements of tortuosity are available in the halite or anhydrite layers of the Salado Formation. The range reported is the theoretical value of 0.667 for uniform-sized grains at low Peclet numbers (N_p) (Dullien, 1979, Figure 7.12) down to 0.01 observed in laboratory experiments of nonadsorbing solutes in porous materials (Freeze and Cherry, 1979, p. 104). The PA Department selected a median value equal to that of the Culebra Dolomite Member (see Table 2.6-1).

2.4 Hydrologic Parameters for Anhydrite Layers within Salado Formation

Table 2.4-1 provides a summary of all parameter values for anhydrite layers near the repository within the Salado Formation. Marker Bed 139 (MB139), a potential transport pathway, is an interbed located about 1 m (3.3 ft) below the repository interval and thus is an anhydrite layer of particular interest. Figure 2.4-1 shows a cross section of MB139.

Table 2.4-1. Hydrologic Parameter Values for Anhydrite Layers within Salado Formation

Parameter[a]	Median	Range		Distribution Units	Type	Discussion and Sources in:
Capillary pressure (p_c) and relative permeability (k_{rw})						
Threshold displacement pressure (p_t)	(Perfectly correlated with anhydrite permeability)			Pa	Function	Section 2.3.1
Residual saturations						
Wetting phase ($S_{\ell r}$)	2×10^{-1}	0.0	4×10^{-1}	none	Uniform	Section 2.3.1
Gas phase (Sg_r)	2×10^{-1}	0.0	4×10^{-1}	none	Uniform	Section 2.3.1
Brooks-Corey exponent (λ)	7×10^{-1}	2×10^{-1}	1×10^{1}	none	Constructed	Section 2.3.1
Density, grain (ρ_g)	2.963×10^{3}			kg/m^3	Constant	WIPP PA Division, 1991, Vol. 3, 2.4.2
Dispersivity						
Longitudinal (α_L)	1.5×10^{1}	1	4×10^{1}	m	Constructed	WIPP PA Division, 1991, Vol. 3, 2.4.3
Ratio (α_L/α_T)	10	3	25	none	Constructed	WIPP PA Division, 1991, Vol. 3, 2.4.3
Partition coefficient						
Am	2.5×10^{-2}			m^3/kg	Constant	WIPP PA Division, 1991, Vol. 3, 2.4.4
Np	1×10^{-3}			m^3/kg	Constant	WIPP PA Division, 1991, Vol. 3, 2.4.4
Pb	1×10^{-3}			m^3/kg	Constant	WIPP PA Division, 1991, Vol. 3, 2.4.4
Pu	1×10^{-1}			m^3/kg	Constant	WIPP PA Division, 1991, Vol. 3, 2.4.4
Ra	1×10^{-3}			m^3/kg	Constant	WIPP PA Division, 1991, Vol. 3, 2.4.4
Th	1×10^{-1}			m^3/kg	Constant	WIPP PA Division, 1991, Vol. 3, 2.4.4
U	1×10^{-3}			m^3/kg	Constant	WIPP PA Division, 1991, Vol. 3, 2.4.4
Log Permeability (k)						
Undisturbed	**-19.3**	**-21.0**	**-16.0**	**log (m^2)**	**Constructed**	**Section 2.4.2**
Disturbed	-15.0			log (m^2)	Constant	Section 2.4.2
Pore pressure	**12.5**	**12.0**	**13.0**	**MPa**	**Uniform**	**Section 2.4.3**
Porosity (ϕ)						
Undisturbed	**1×10^{-2}**	**1×10^{-3}**	**3×10^{-2}**	**none**	**Constructed**	**Section 2.4.4**
Disturbed	(correlated with undisturbed porosity)			none	Uniform	Section 2.4.4
Specific storage	1.4×10^{-7}	9.7×10^{-8}	1×10^{-6}	m^{-1}	Constructed	WIPP PA Division, 1991, Vol. 3, 2.4.8
Thickness (Δz)	9×10^{-1}	4×10^{-1}	1.25	m	Constructed	WIPP PA Division, 1991, Vol. 3, 2.4.9
Tortuosity	1.4×10^{-1}	1×10^{-2}	6.67×10^{-1}	none	Constructed	WIPP PA Division, 1991, Vol. 3, 2.4.10

[a]Parameters in bold were sampled in the 1992 calculations.

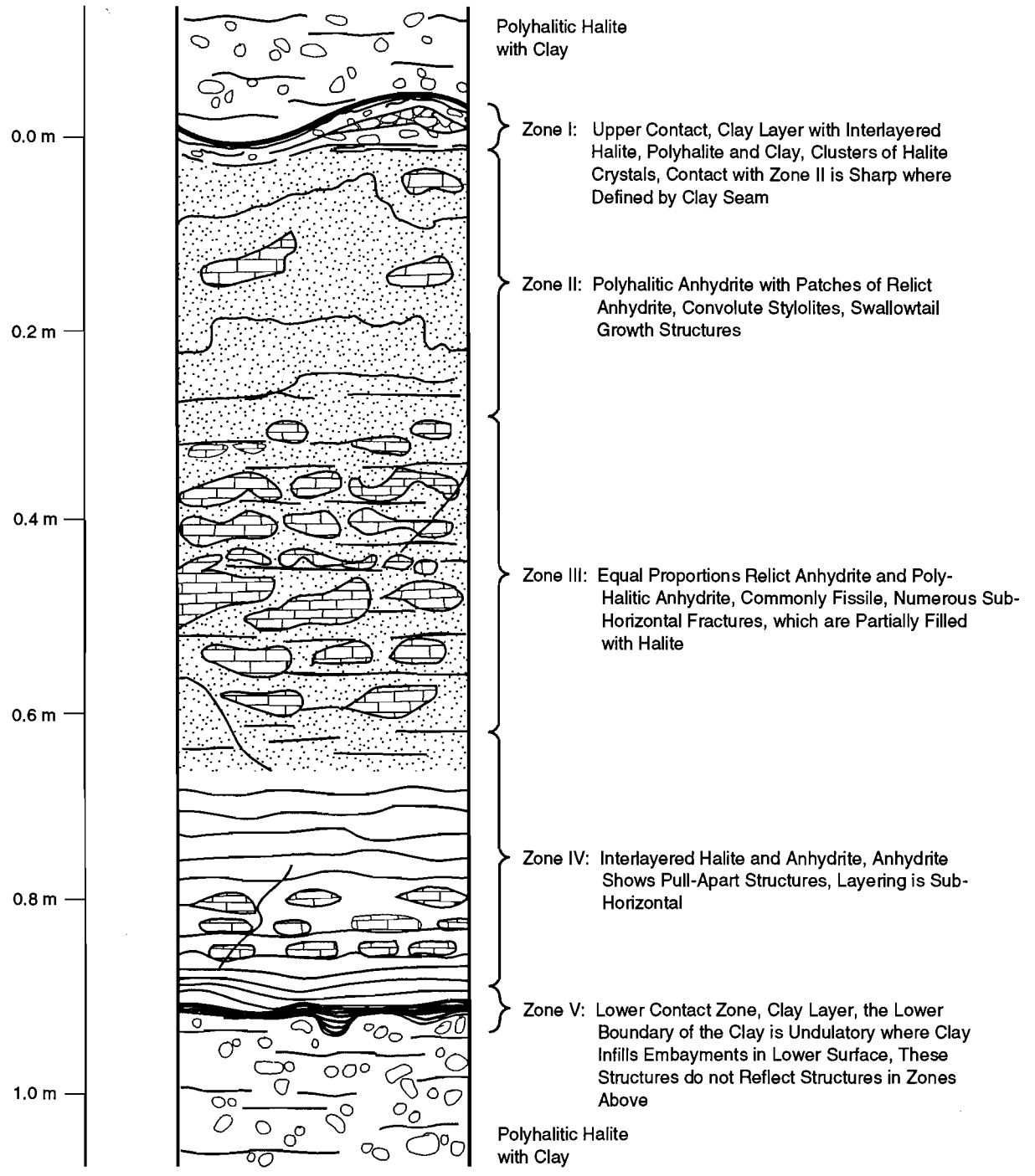

Figure 2.4-1. Generalized cross section of Marker Bed 139 near repository. The figure shows the internal variability of the unit and the character of both the upper and lower contacts (after Borns, 1985). The thickness varies spatially between 0.4 and 1.25 m with a reference thickness of 0.99 m (Krieg, 1984, Table I).

2.4.1 Capillary Pressure and Relative Permeability

Threshold Displacement Pressure, P_t*

Parameter: **Threshold displacement pressure (p_t)**
Material: Anhydrite layers within Salado Formation (MB139, PressCTD)

Definition Units: Pa

Values: P_t (MPa) = $2.6 \times 10^{-7}\ k^{-0.348}$

Distribution: Function (above)
Correlation: Perfectly correlated with anhydrite permeability.

Data Source(s): Davies, P. B. 1991a. *Evaluation of the Role of Threshold Pressure in Controlling Flow of Waste-Generated Gas into Bedded Salt at the Waste Isolation Pilot Plant.* SAND90-3246. Albuquerque, NM: Sandia National Laboratories. (Investigator Judgment)

Davies, P. B. 1991b. Appendix A: "Uncertainty Estimates for Threshold Pressure for 1991 Performance Assessment Calculations Involving Waste-Generated Gas," *Preliminary Comparison with 40 CFR Part 191, Subpart B for the Waste Isolation Pilot Plant, December 1991. Volume 3: Reference Data.* WIPP Performance Assessment Division. Eds. R. P. Rechard, A. C. Peterson, J. D. Schreiber, H. J. Iuzzolino, M. S. Tierney, and J. S. Sandha. SAND91-0893/3. Albuquerque, NM: Sandia National Laboratories. A-37 through A-41. (Investigator Judgment)

Usage:

Mathematical model:
Two-Phase Flow (Section 1.4.1, this volume).

Equation 1.4.1-6.

Computational models:
BRAGFLO

Ranking in Past Sensitivity Analyses:

40 CFR 191	Low
40 CFR 268	Not tested
NEPA	Not tested
Other	Not tested

*Key to Parameter Sheets is provided in Section 1.2.8.

Residual Wetting Phase Saturation*

Parameter: **Residual wetting phase (liquid) saturation ($S_{\ell r}$)**
Material: Anhydrite layers within Salado Formation (MB139, SatRWP)

Definition Units: Dimensionless

Values: Range: $(0.0, 4 \times 10^{-1})$ Median: 2×10^{-1}

Distribution: Uniform
Correlation:

Data Source(s):

Davies, P. B., and A. M. LaVenue. 1990b. Appendix A: "Additional Data for Characterizing 2-Phase Flow Behavior in Waste-Generated Gas Simulations and Pilot Point Information for Final Culebra 2-D Model (SAND89-7068/1)," *Data Used in Preliminary Performance Assessment of the Waste Isolation Pilot Plant (1990).* R. P. Rechard, H. Iuzzolino, and J. S. Sandha. SAND89-2408. Albuquerque, NM: Sandia National Laboratories. A-139 through A-156. (Investigator Judgment)

Webb, S. W. 1992a. "Uncertainty Estimates for Two-Phase Characteristic Curves for 1992 RCRA Calculations" (see Appendix A, pp. A-141 through A-146). (Investigator Judgment)

Webb, S. W. 1992b. "Uncertainty Estimates for Two-Phase Characteristic Curves for 1992 40 CFR 191 Calculations" (see Appendix A, pp. A-147 through A-155). (Investigator Judgment)

Usage:

Mathematical model:
Two-Phase Flow, Section 1.4.1, this volume.

Equation 1.4.1-7.

Computational models:
BRAGFLO

Ranking in Past Sensitivity Analyses:

40 CFR 191	Not tested
40 CFR 268	Low
NEPA	Not tested
Other	Not tested

*Key to Parameter Sheets is provided in Section 1.2.8.

Residual Gas Saturation*

Parameter: **Residual gas saturation (S_{gr})**
Material: Anhydrite layers within Salado Formation (MB139, SatRGP)

Definition Units: Dimensionless

Values: Range: $(0.0, 4 \times 10^{-1})$ Median: 2×10^{-1}

Distribution: Uniform
Correlation:

Data Source(s):

Davies, P. B., and A. M. LaVenue. 1990b. Appendix A: "Additional Data for Characterizing 2-Phase Flow Behavior in Waste-Generated Gas Simulations and Pilot Point Information for Final Culebra 2-D Model (SAND89-7068/1)," *Data Used in Preliminary Performance Assessment of the Waste Isolation Pilot Plant (1990).* R. P. Rechard, H. Iuzzolino, and J. S. Sandha. SAND89-2408. Albuquerque, NM: Sandia National Laboratories. A-139 through A-156. (Investigator Judgment)

Webb, S. W. 1992a. "Uncertainty Estimates for Two-Phase Characteristic Curves for 1992 RCRA Calculations" (see Appendix A, pp. A-141 through A-146). (Investigator Judgment)

Webb, S. W. 1992b. "Uncertainty Estimates for Two-Phase Characteristic Curves for 1992 40 CFR 191 Calculations" (see Appendix A, pp. A-147 through A-155). (Investigator Judgment)

Usage:

Mathematical model:
Two-Phase Flow, Section 1.4.1, this volume.

Equation 1.4.1-7.

Computational models:
BRAGFLO

Ranking in Past Sensitivity Analyses:

40 CFR 191	Not tested
40 CFR 268	Low
NEPA	Not tested
Other	Not tested

*Key to Parameter Sheets is provided in Section 1.2.8.

Brooks and Corey Exponent*

Parameter: **Brooks and Corey exponent (λ)**
Material: Anhydrite layers within Salado Formation (MB139, BrkCorEx)

Definition Units: Dimensionless

Values: Range: (0.2, 10.0) Median: 0.7

Distribution: Constructed
Correlation:

Data Source(s):

Davies, P. B., and A. M. LaVenue. 1990b. Appendix A: "Additional Data for Characterizing 2-Phase Flow Behavior in Waste-Generated Gas Simulations and Pilot Point Information for Final Culebra 2-D Model (SAND89-7068/1)," *Data Used in Preliminary Performance Assessment of the Waste Isolation Pilot Plant (1990).* R. P. Rechard, H. Iuzzolino, and J. S. Sandha. SAND89-2408. Albuquerque, NM: Sandia National Laboratories. A-139 through A-156. (Investigator Judgment)

Webb, S. W. 1992a. "Uncertainty Estimates for Two-Phase Characteristic Curves for 1992 RCRA Calculations" (see Appendix A, pp. A-141 through A-146). (Investigator Judgment)

Webb, S. W. 1992b. "Uncertainty Estimates for Two-Phase Characteristic Curves for 1992 40 CFR 191 Calculations" (see Appendix A, pp. A-147 through A-155). (Investigator Judgment)

Usage:

Mathematical model:
Two-Phase Flow, Section 1.4.1, this volume.

Equation 1.4.1-6.

Computational models:
BRAGFLO

Ranking in Past Sensitivity Analyses:

40 CFR 191	Not tested
40 CFR 268	Low
NEPA	Not tested
Other	Not tested

*Key to Parameter Sheets is provided in Section 1.2.8.

Discussion:

Relationships between these parameters are discussed in Section 1.4.1. Preliminary parameter values selected for MB139 and other anhydrite beds are the same as for Salado halite (Section 2.3.1), except for a lower threshold displacement pressure (p_t), and were taken from experimental data measured for the tight gas sands (Ward and Morrow, 1985; Davies and LaVenue, 1990b).

2.4.2 Permeability

Undisturbed Permeability*

Parameter: **Log permeability, undisturbed**
Material: Anhydrite layers within Salado Formation (MB139, LogPrmU)

Definition Units: log (m^2)

Values: Range: (-21.0, -16) Median: -19.3

Distribution: Constructed
Correlation:

Data Source(s): Davies, P. B., R. L. Beauheim, and E. D. Gorham. 1992b. "Additional Comments on Far-Field Anhydrite Permeability Distribution in 'PA Modeling Using BRAGFLO -- 1992' 7-8-92 Memo by J. Schreiber" (see Appendix A, pp. A-39 through A-45). (Investigator Judgment)

(Source #1)
Davies, P. B., S. W. Webb, and E. D. Gorham. 1992a. "Feedback on 'PA Modeling Using BRAGFLO -- 1992' 7-8-92 Memo by J. Schreiber" (see Appendix A, pp. A-21 through A-37). (Investigator Judgment)

Usage:

Mathematical model:
Two-Phase Flow, Section 1.4.1, this volume.

Equations 1.4.1-1 and 1.4.1-2.

Computational models:
BRAGFLO

Ranking in Past Sensitivity Analyses:

40 CFR 191	Medium (see discussion)
40 CFR 268	High
NEPA	Not tested
Other	Not tested

*Key to Parameter Sheets is provided in Section 1.2.8.

Discussion:

In 1991, the permeability of undisturbed anhydrite was shown to be a moderately sensitive parameter in determining releases of radioactivity to Culebra Dolomite under conditions of gas generation within the repository.

The 1992 distribution of anhydrite permeability in the far field (Figure 2.4-2) is based on recommendations given in Davies et al. (1992b, Memo in Appendix A). The 1992 distribution differs from the 1991 distribution (Figure 2.4-3) in the assignment of significant probability to values of permeability greater than 10^{-18} m^2 and less than 10^{-20} m^2; the median values of the 1991 and 1992 distributions, 7.8 x 10^{-20} m^2 and 5.0 x 10^{-20} m^2 respectively, are not significantly different.

According to Davies et al. (1992b, Memo in Appendix A), the 1992 distribution does not capture permeabilities representative of interbed fracturing due to pressurization by gas that could be generated by WIPP wastes.

An Estimate of Average Undisturbed Anhydrite Permeability. The method for estimating far-field halite parameters by non-linear regression described in Section 2.3.2 has also been used to make preliminary estimates of the distribution of the average anhydrite permeability in the far field. Available results of experiments that measured anhydrite permeability and pore pressure are summarized in Table 2.4-2. Eight measurements from this series of results were used as the basis for generating artificial data sets in the manner indicated in Section 2.3.2; the regression curves fitted to 30 artificial data sets are shown on Figure 2.4-4. (Note that the form of the regression curve is the same as the one described in Section 2.3.2:

$$y(x) = a + be^{-x/c}$$

in which the parameter a estimates the far-field $[x \rightarrow \infty]$ material-property parameter.) The empirical cdf for the average of undisturbed anhydrite permeability that results from this procedure is sketched on Figure 2.4-5.

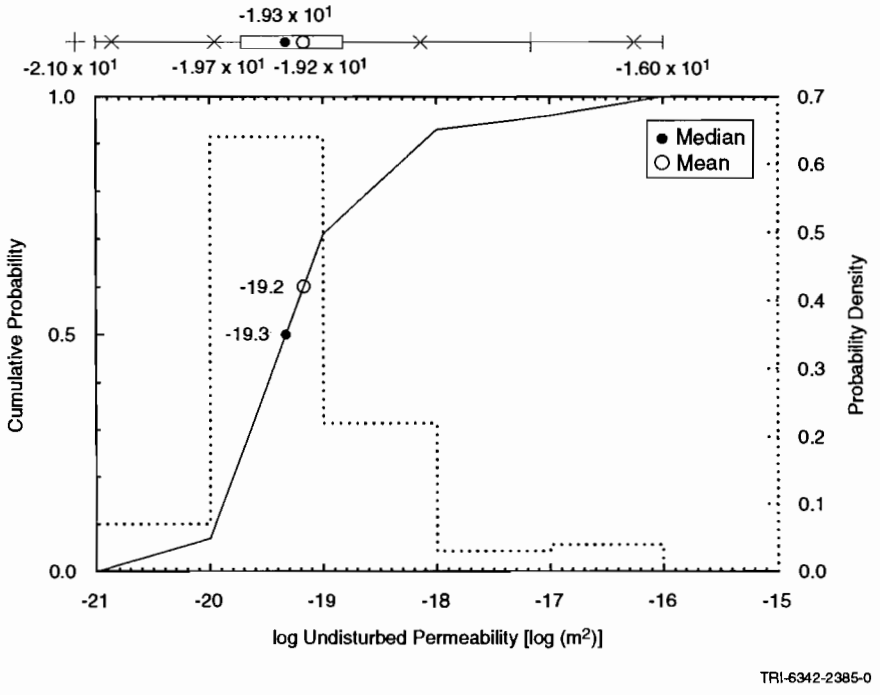

Figure 2.4-2. Estimated distribution in 1992 for undisturbed permeability of anhydrite layers in Salado Formation. (See discussion.)

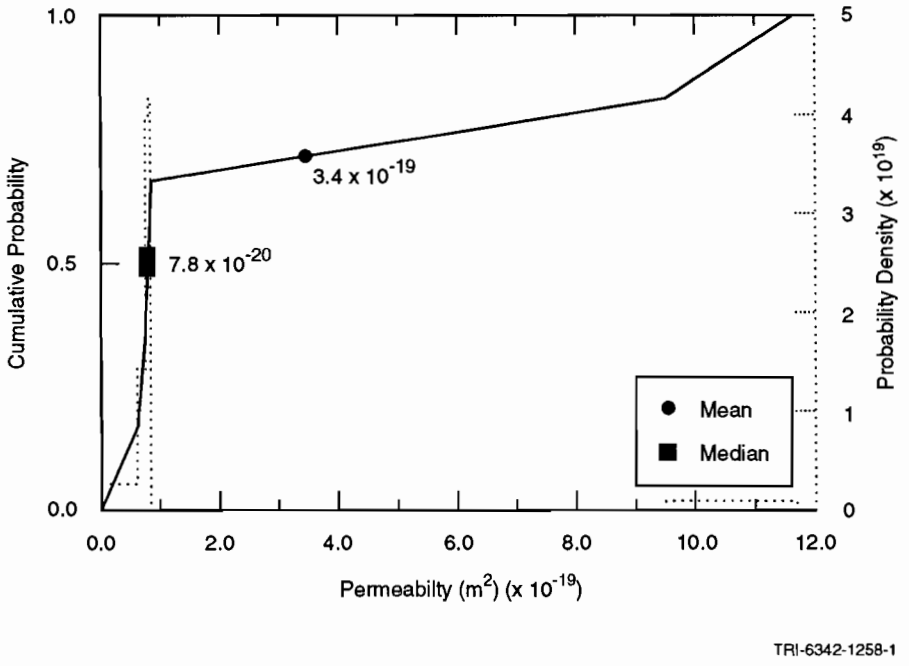

Figure 2.4-3. Estimated 1991 distribution for undisturbed permeability, anhydrite layers in Salado Formation.

Table 2.4-2. Summary of Measurements of Salado Anhydrite Permeabilities and Pore Pressures

Test No.	Lithology	Distance[b] (m)	Measured Permeability (m^2)	log_{10} Permeability	Pressure (MPa)	Orientation	Sources[e]
SCP01	MB139	10.50 - 14.78	3.0×10^{-20}	-19.5 ± 0.7[c]	12.4 ± 0.5[d]	vertical, down	1, 3
[a]QPP13 (pre)	MB139	23.4	4.1×10^{-20}	-19.4	12.5	vertical down	1, 2
QPP03 (pre)	anhydrite	23.4	4.4×10^{-20}	-19.4	12.6	vertical, up	1, 2
C2H02	MB139	9.47 - 10.86	7.8×10^{-20}	-19.1	9.3	45°, down	1, 3
L4P51-B	anhydrite "c"	9.62 - 9.72	5.0×10^{-20}	-19.3	5.1	vertical, down	1, 3
S1P71-B	anhydrite "c"	9.48 - 9.80	6.8×10^{-20}	-19.2	4.9	vertical, down	1, 3
C2H01-C	MB139	6.63 - 8.97	9.5×10^{-19}	-18.0	8.0	vertical, down	1, 3
C1X10	MB139	?	5.0×10^{-17}	-16.3	7.3	?	1
QPP03 (post)	anhydrite "b"	3.07	7.9×10^{-20}	-19.1	7.0	vertical, up	1, 2
QPP13 (post)	MB139	3.07	4.7×10^{-20}	-19.3	8.1	vertical, down	1, 2
L4P52-A	anhydrite "a"	?	1.0×10^{-19}	-19.0	6.4	?	1
QPB01	?	?	9.6×10^{-21}	-20.0	(5.0 assumed)	?	1
QPB02	?	?	1.6×10^{-19}	-18.8	(5.0 assumed)	?	1
QPB03	?	?	1.2×10^{-20}	-19.9	(5.0 assumed)	?	1
S1P72	MB139	4.40 - 6.00	unmeasurable	-	1.2	?	1, 3
S1P73-B	MB138	10.86 - 11.03	2.9×10^{-19}	-18.5	4.5	?	1, 3
S0P01-GZ	MB139	1.86 - 2.91	5.7×10^{-18}	-17.2	0.5	vertical, down	1, 3
S1P73-A	?	?	too high to measure ($\sim 10^{-15}$)	-	0.5	?	1
S1P73-A-GZ	?	?	too high to measure ($\sim 10^{-15}$)	-	0.0	?	1
S1P71-A-GZ	?	?	too high to measure ($\sim 10^{-14}$)	-	0.0	?	1
L4P51-A-GZ	MB139	1.86 - 2.91	too high to measure ($\sim 10^{-15}$)	-	0.3	?	1, 3

Key to Table 2.4-2:

a - "Pre" and "post" mean pre- and post-minebye for Q tunnel tests.

b - Estimated distance of apparatus from wall of excavation

c - A standard error of one-half order of magnitude assumed for all permeability measurements

d - A standard error of 0.5 MPa assumed for all measured or inferred pressures

e - Sources: 1 - Gorham et al., June 15, 1992 (Memo in Appendix A),
2 - Howarth et al., 1991,
3 - Beauheim et al., 1991a,
4 - Finley and McTigue, 1991.

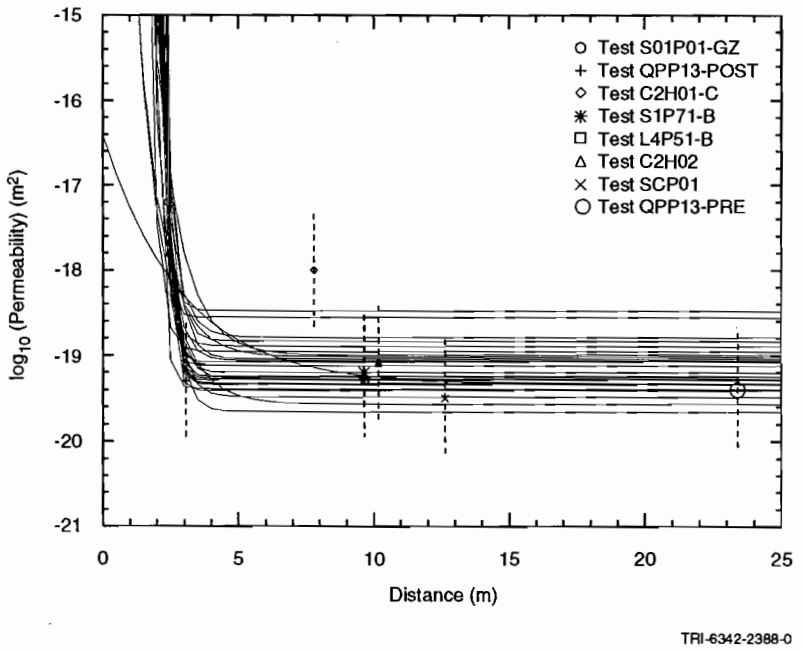

Figure 2.4-4. Regression curves fitted to artificial data sets for undisturbed anhydrite permeability (30 samples).

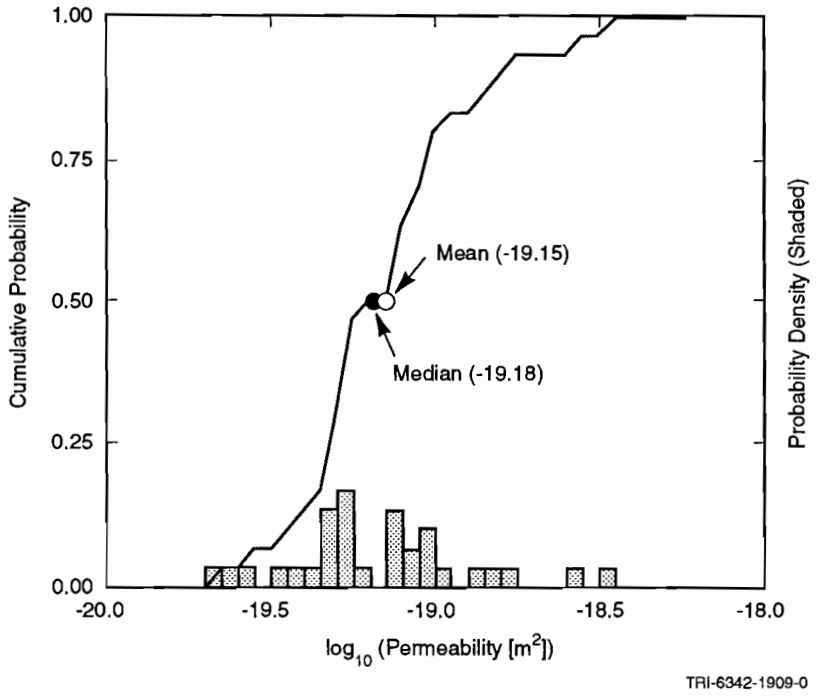

Figure 2.4-5. Simulated distribution of average, undisturbed permeability of anhydrite (30 samples).

Disturbed Permeability*

Parameter:	**Log permeability, disturbed (k)**
Material:	Anhydrite layers within Salado Formation (Salado, LogGPrm)
Definition Units:	log (m^2)
Values:	-15.0
Distribution:	Constant
Correlation:	

Data Source(s): None: PA analyst's choice (see Section 2.3.2).

Usage:

Mathematical model:

Two-Phase Flow, Section 1.4.1, this volume.

Equations 1.4.1-1 and 1.4.1-2.

Computational models:

BRAGFLO

Ranking in Past Sensitivity Analyses:

40 CFR 191	Not tested
40 CFR 268	Low
NEPA	Not tested
Other	Not tested

*Key to Parameter Sheets is provided in Section 1.2.8.

2.4.3 Pore Pressure at Repository Level in Anhydrite

Pore Pressure*

Parameter: **Pore pressure at repository level (p)**
Material: Anhydrite layers within Salado Formation (MB139, Pressure)

Definition Units: MPa

Values: Range: (12.0, 13.0) Median: 12.5

Distribution: Uniform
Correlation:

Data Source(s): Davies, P. B., R. L. Beauheim, and E. D. Gorham. 1992b. "Additional Comments on Far-Field Anhydrite Permeability Distribution in 'PA Modeling Using BRAGFLO -- 1992' 7-8-92 Memo by J. Schreiber" (see Appendix A, pp. A-39 through A-45). (Investigator Judgment)

Usage:

Mathematical model:
Two-Phase Flow, Section 1.4.1, this volume.

Equation: (Boundary condition on fluid pressure in Eqs. 1.4.1-1 and 1.4.1-2.)

Computational models:
BRAGFLO

Ranking in Past Sensitivity Analyses:

40 CFR 191	Medium
40 CFR 268	High
NEPA	Not tested
Other	Not tested

*Key to Parameter Sheets is provided in Section 1.2.8.

Discussion:

The 1991 distribution of brine pore pressure at repository level in anhydrite is shown in Figure 2.4-6. This distribution was used to express variability in pore pressure in both halite and anhydrite in the 1991 PA exercises. Brine pore pressure proved to be a moderately sensitive parameter in determining releases to the Culebra (and beyond) in scenarios that took account of gas generation in the repository (Helton et al., 1992, Table 4.5-1).

The 1992 distribution of brine pore pressure at repository level (in both halite and anhydrite) is taken to be uniform on the interval 12 MPa to 13 MPa and is based on test results quoted in the Davies et al., July 22, 1992b (Memo in Appendix A). Three measurements were available from regions in which fluid depressurization was judged to be small; all three measurements yielded pressure values in the range 12 to 13 MPa.

An Estimate of Average Undisturbed Pore Pressure in Anhydrite. The method for estimating far-field halite parameters that was described in Section 2.3.2 has also been used to make preliminary estimates of the distribution of the average of undisturbed pore pressure in anhydrite. Eight measurements from the series of test results listed in Table 2.3-2 were used as the basis for generating artificial data sets; the resulting regression curves fitted to 30 artificial data sets are shown on Figure 2.4-7. (The form of the regression curve is the same as in Section 2.3.2.) The resulting empirical cdf for the average of undisturbed pore pressure in anhydrite is shown on Figure 2.4-8. This figure should be compared with Figure 2.3-10, the simulated distribution of the average of undisturbed pressure in halite at the repository level. Whether these results make physical sense remains to be determined.

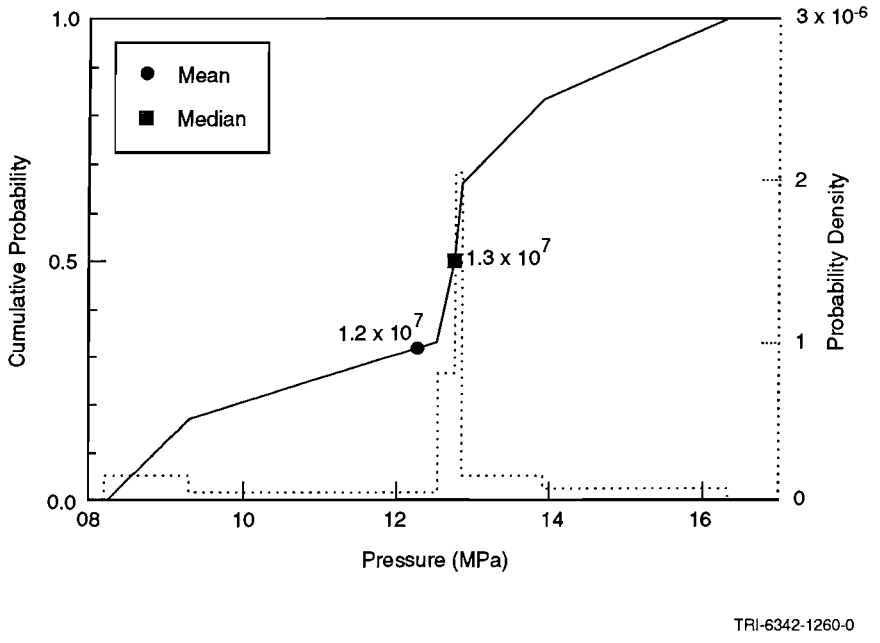

Figure 2.4-6. Distribution used in 1991 for brine pore pressure in anhydrite MB139 at repository level.

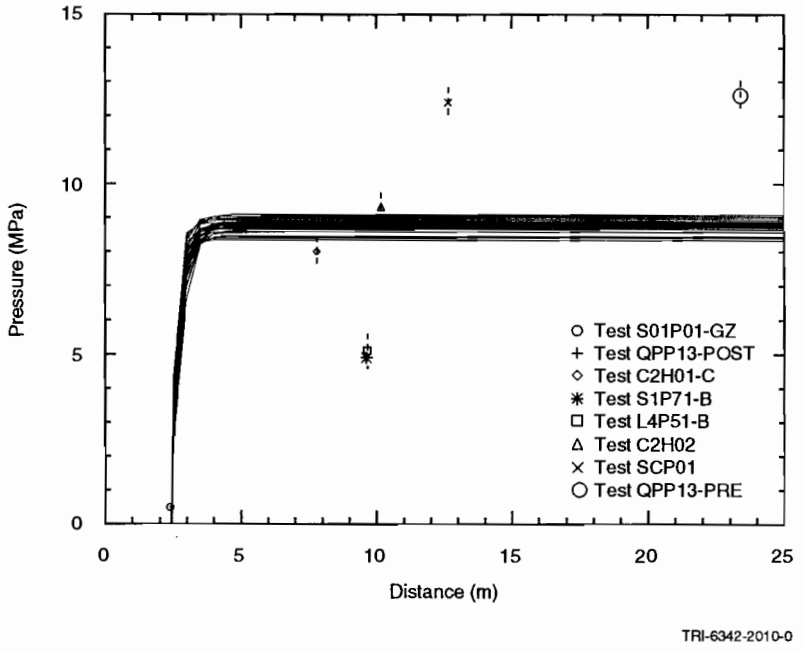

Figure 2.4-7. Regression curves fitted to artificial data sets for undisturbed anhydrite pore pressure (30 samples).

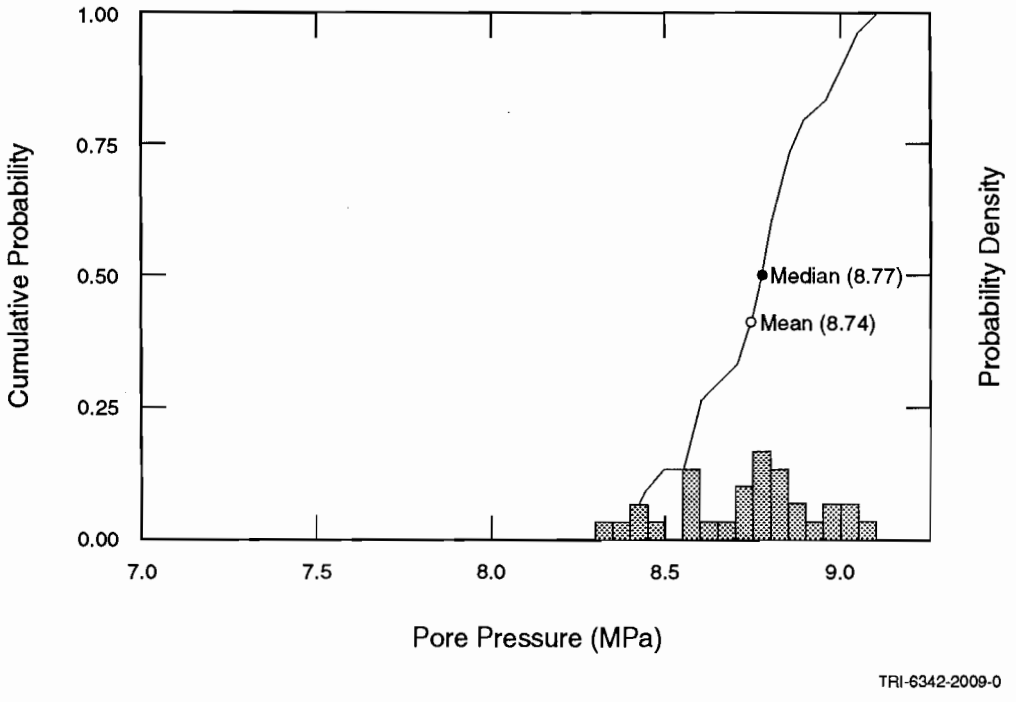

Figure 2.4-8. Simulated distribution of average undisturbed pore pressure at repository depth in anhydrite (30 samples).

2.4.4 Porosity

Undisturbed Porosity*

Parameter:	**Porosity, undisturbed (ϕ)**
Material:	Anhydrite layers within Salado Formation (MB139, Pore_U)
Definition Units:	Dimensionless
Values:	Range: (1×10^{-3}, 3×10^{-2}) Median: 1×10^{-2}
Distribution:	Constructed
Correlation:	

Data Source(s): Investigator Judgment (see Discussion).

Powers, D. W., S. J. Lambert, S-E. Shaffer, L. R. Hill, and W. D. Weart, eds. 1978. *Geological Characterization Report, Waste Isolation Pilot Plant (WIPP) Site, Southeastern New Mexico*. SAND78-1596. Albuquerque, NM: Sandia National Laboratories. Vols. 1-2.

U.S. Department of Energy. 1983. "Brine Content of Facility Interval Strata," *Results of Site Validation Experiments*. TME 3177. [Carlsbad, NM]: Waste Isolation Pilot Plant. Vol. II, Supporting Document 10.

Usage:

Mathematical model:

Two-Phase Flow, Section 1.4.1 of this volume

Equations 1.4.1-1 and 1.4.1-2.

Computational models:

BRAGFLO

Ranking in Past Sensitivity Analyses:

40 CFR 191	Low
40 CFR 268	Low
NEPA	Not tested
Other	Not tested

*Key to Parameter Sheets is provided in Section 1.2.8.

Discussion:

PA calculations have assumed an undisturbed anhydrite porosity similar to the undisturbed porosity of the Salado Formation as a whole. The PA Department assumed the median porosity to be 0.01 based on an unpublished report on electromagnetic and DC resistivity measurements (Skokan, C., J. Starrett, and H. T. Andersen. 1988. *Final Report: Feasibility Study of Seismic Tomography to Monitor Underground Pillar Integrity at the WIPP Site.* Contractor Report. Albuquerque, NM: Sandia National Laboratories). This median value is identical to that calculated from a grain density of 2,163 kg/m^3 (135 lb/ft^3) for halite and a bulk density of 2,140 kg/m^3 (133.6 lb/ft^3) ($\rho_b = (1 - \phi)\rho_g$). The low value of 0.001 is based on drying experiments (Powers et al., 1978), whereas the high of 0.03 was suggested by the low end of the DC resistivity measurements in the unpublished report by Skokan et al., cited above.

Figure 2.4-9 shows the estimated distribution for undisturbed porosity for the anhydrite layers.

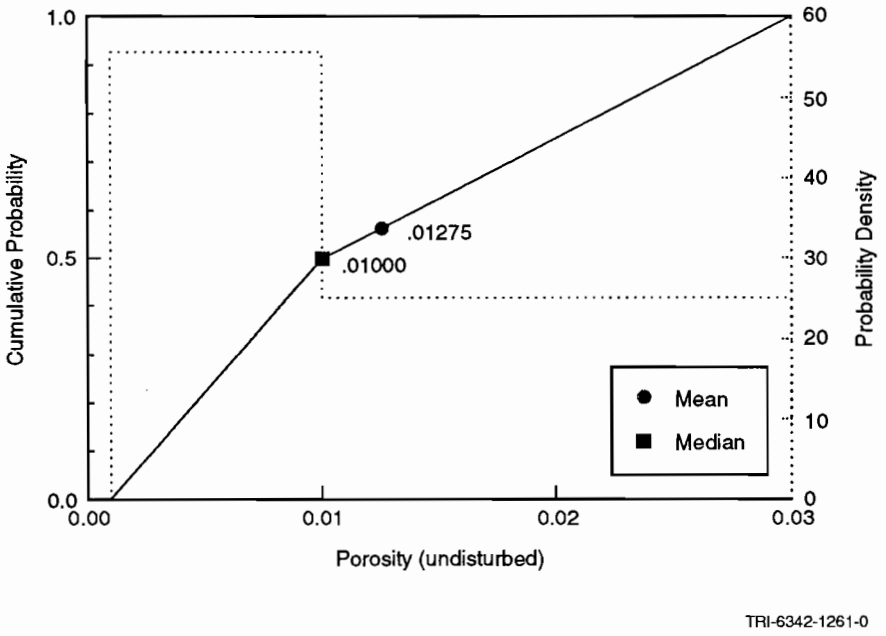

Figure 2.4-9. Estimated distribution for undisturbed porosity for anhydrite layers in Salado Formation.

Disturbed Porosity*

Parameter:	**Porosity, disturbed (ϕ)**
Material:	Disturbed anhydrite and halite layers within Salado Formation (MB139, Uniform1)
Definition Units:	Dimensionless
Values:	0.06 (maximum value; see Discussion)
Distribution:	Uniform between maximum value and value of undisturbed porosity
Correlation:	Correlated with undisturbed porosity (see Discussion)

Data Source(s): None; PA analyst's choice.

Usage:

Mathematical model:

Two-Phase Flow, Section 1.4.1 of this volume.

Equations 1.4.1-1 and 1.4.1-2.

Computational models:

BRAGFLO

Ranking in Past Sensitivity Analyses:

40 CFR 191	Not tested
40 CFR 268	Not tested
NEPA	Not tested
Other	Not tested

*Key to Parameter Sheets is provided in Section 1.2.8.

Discussion:

The porosity of regions of both disturbed anhydrite and halite are modeled by the following relation:

$$\phi(\text{disturbed}) = 0.06\ U + [\phi\ (\text{undisturbed})]\ (1 - U)\ .$$

where ϕ (undisturbed) is itself a sampled parameter (see previous data table), and U is a number uniformly distributed on the interval (0,1).

The maximum value of disturbed porosity (0.06) is rationalized in WIPP PA Division, 1991, Vol. 3, p. 2-37.

2.5 Mechanical Parameters for Materials in Repository and Salado Formation

The 1992 attempt to incorporate effects of disposal-room deformation in a calculation of average room porosity and permeability has triggered the need to include 23 new parameters in the PA Department's Secondary Data Base. These new parameters are primarily mechanical or material properties that appear in constitutive equations for the behavior of intact salt, crushed-salt backfill, or composite waste materials (Section 1.4.7); the 23 parameters and the values assigned to them are summarized in Tables 2.5-1 and 2.5-2. The uncertainty associated with these mechanical or material properties is presently unknown, so they have been assigned fixed values in the 1992 series of PA calculations.

Other, non-mechanical parameters have arbitrarily been included in Table 2.5-1, and may be redundant with similar quantities appearing elsewhere in this report: for example, parameters for the gas-generation model used in the porosity surface calculations have been included in Table 2.5-1 for the sake of completeness even though they are similar to (but do not generally have the same values as) the gas generation rates described in Section 3.3.5.

Discussion of Sources:

The primary source for values assigned to the 23 mechanical or material properties in 1992 calculations is Mendenhall et al., 1991. This citation is confirmed by Butcher in his September 9, 1992 memo (Appendix A). Most of these values are taken from the much earlier work of Krieg (1984) or Sjaardema and Krieg (1987) according to Munson in his October 26, 1992 memo (Appendix A). Mendenhall et al. modified the Sjaardema and Krieg values of elastic shear modulus and elastic bulk modulus of intact and crushed salt to conform with the "Reduced Modulus" model frequently used in WIPP problems (Munson, October 26, 1992, Memo in Appendix A) by dividing the Sjaardema and Krieg values by 12.5.

According to Butcher (September 9, 1992, Memo in Appendix A), the function giving volumetric strain as a function of pressure (Table 2.5-2) was derived from the solid line axial compaction stress versus porosity curve in Figure 2 of the September 12, 1991 memo of Beraún and Davies (Appendix A). Actual data points from which the Beraún-Davies curve was derived are given in Table 3-2 of Butcher et al., 1991: Table 2.5-2 was constructed by dividing each axial stress datum by 3 and converting porosity to the ratio ρ/ρ_o, where ρ is current density of waste and ρ_o is waste initial density. The curve implicit in Table 2.5-2 assumes an initial waste density of 426 kg/m^3 and a theoretical solid density of 2000 kg/m^3.

Table 2.5-1. Summary of Parameters Used in Mechanical Models of Repository and Salado Formation Materials.

Parameter	Median[a]	Units	Section 1.4.7 Eq. No.	Source[b]
• Model of intact salt				
G - elastic shear modulus	0.992	GPa	1.4.7-1	1, see discussion
K - elastic bulk modulus	1.656	GPa	1.4.7-2	1, see discussion
A - experimental constant	5.79×10^{-36}	Pa-4.9/s	1.4.7-2	1
N - experimental constant	4.9	none	1.4.7-1	1, 3
Q/RT - exponential constant	20.13	none	1.4.7-1	1, 3 (@ 300°K)
• Model of crushed salt backfill				
G_0 - elastic shear modulus	864.0	Pa	1.4.7-3	1, see discussion
G_1 - experimental constant	6.53×10^{-3}	m^3/kg	1.4.7-3	1, 2
K_0 - elastic bulk modulus	1.41	kPa	1.4.7-4	1, see discussion
K_1 - experimental constant	6.53×10^{-3}	m^3/kg	1.4.7-4	1, 2
A_c - experimental constant	5.79×10^{-36}	$Pa^{-4.9}/s$	1.4.7-5	1
ρ_{int} - density of intact halite	2.14×10^{3}	kg/m^3	1.4.7-5	2
N - experimental constant	4.9	none	1.4.7-5	1
Q/RT - exponential constant	20.13	none	1.4.7-5	1
B_0 - experimental constant	1.3×10^{8}	$kg/(m^3 \cdot s)$	1.4.7-6	1, 2
B_1 - experimental constant	0.82×10^{-6}	Pa^{-1}	1.4.7-6	1, 2
A - experimental constant	-17.3×10^{-3}	m^3/kg	1.4.7-6	1, 2
• Volumetric plasticity model for waste				
μ - shear modulus	333	MPa	1.4.7-7	1
K_0 - bulk unloading modulus	222	MPa	1.4.7-7	1
a_0 - yield function constant	0	none	1.4.7-7	1
a_1 - yield function constant	0	none	1.4.7-7	1
a_2 - yield function constant	3	none	1.4.7-7	1
ρ_0 - initial waste density	426	kg/m^3	1.4.7-8	4
F(P) - volumetric strain as a function of pressure	(see Table 2.5-2 and discussion)		1.4.7-8	4
• Gas generation model for porosity-surface calculation gas production rates (inundated)				
Anoxic corrosion rate	3.17×10^{-8}	mole/(drum • s)	1.4.7-10	5
Anoxic corrosion potential	1050	mole/drum	1.4.7-10	5
Microbial rate	3.17×10^{-8}	mole/(drum • s)	1.4.7-10	5
Microbial potential	550	mole/drum	1.4.7-10	5
Radiolysis rate	0	mole/(drum • s)	1.4.7-10	5
Radiolysis potential	0	mole/drum	1.4.7-10	5
D - number of drums	6804	none	1.4.7-10	5

[a] All parameters are constants unless otherwise noted.

[b] Key to sources:

1. Mendenhall et al., 1991
2. Sjaardema and Krieg, 1987
3. Munson (October 26, 1992, Memo in Appendix A)
4. Butcher (September 9, 1992, Memo in Appendix A)
5. Beraún and Davies (September 12, 1991, Memo in Appendix A)

Table 2.5-2. Volumetric Strain as a Function of Pressure: Relationship Used in Volumetric Plasticity Model for Waste in Disposal Room (from Butcher, September 9, 1992, Memo in Appendix A).

Pressure (MPa)	log Density Ratio ln ρ/ρ_o
0.028	0.032
0.733	0.741
1.133	0.898
1.667	1.029
2.800	1.180
10.17	1.536

2.6 Parameters for Culebra Dolomite Member of Rustler Formation

The Culebra Dolomite Member of the Rustler Formation is a finely crystalline, locally argillaceous (containing clay) and arenaceous (containing sand), vuggy dolomite ranging in thickness near the WIPP from about 7 m (23 ft) (at DOE-1 and other locations) to 14 m (46 ft) (at H-7). The PA Department has chosen 7.7 m as a reference thickness. Figure 2.6-1 shows a detailed lithology of the Rustler Formation. Figure 2.6-2 is a cross-section across the WIPP disposal system. The Culebra Dolomite is generally considered to provide the most important potential groundwater-transport pathway for radionuclides that may be released to the accessible environment provided human intrusion occurs. Accordingly, the WIPP Project has devoted much attention to understanding the hydrogeology and hydraulic properties of the Culebra. Figure 2.6-3 shows the locations of wells used to define the hydrologic parameters for the Culebra Dolomite. Detailed hydrogeologic information is available in reports by Brinster (1991) and Holt and Powers (1988). The Culebra Dolomite has been tested at 41 locations in the vicinity of the WIPP. Results of these tests and interpretations have been reported by Beauheim (1987a,b,c; 1989), Saulnier (1987), and Avis and Saulnier (1990).

One early observation (Mercer and Orr, 1979) was that the transmissivity of the Culebra Dolomite varies by six orders of magnitude in the vicinity of the WIPP. This variation in transmissivity appears to be the result of differing degrees of fracturing within the Culebra Dolomite. The cause of the fracturing, however, is unresolved. Culebra transmissivities of about 1 x 10^{-6} m^2/s (0.93 ft^2/d) or greater appear to be related to fracturing. Where the transmissivity of the Culebra Dolomite is less than 1 x 10^{-6} m^2/s (0.93 ft^2/d), few or no open fractures have been observed in core, and the Culebra's hydraulic behavior during pumping or slug tests is that of a single-porosity medium. Where transmissivities are between 1 x 10^{-6} m^2/s (0.93 ft^2/d) and at least 1 x 10^{-4} m^2/s (93 ft^2/d), open fractures are observed in core, and the hydraulic behavior of the Culebra Dolomite during pumping tests is that of a dual-porosity medium (Beauheim, 1987a, b, c; Saulnier, 1987).

Parameter values for the Culebra Dolomite Member are given in Table 2.6-1.

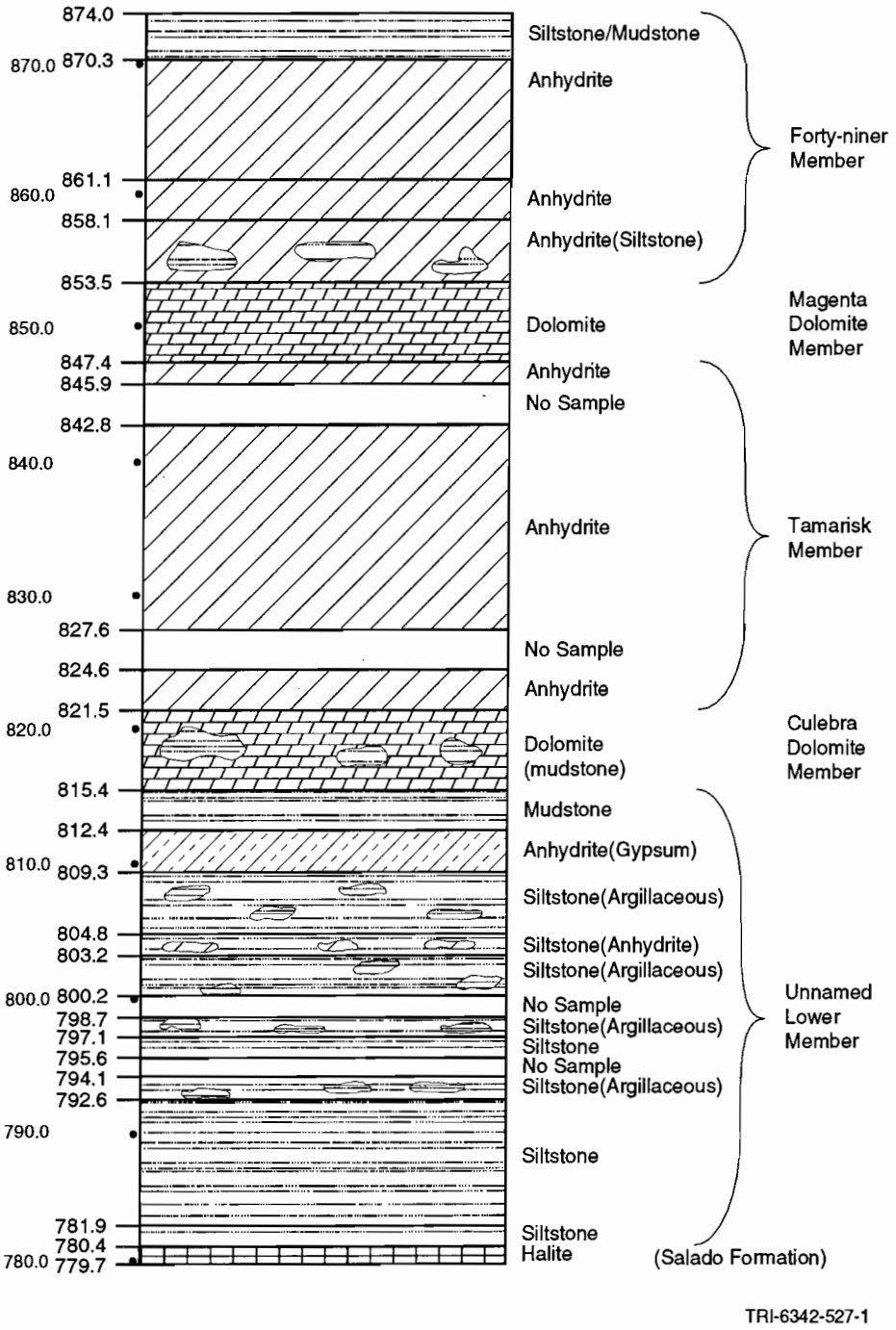

Figure 2.6-1. Detailed lithology of Rustler Formation at ERDA-9 (after SNL and U.S. Geological Survey, 1983).

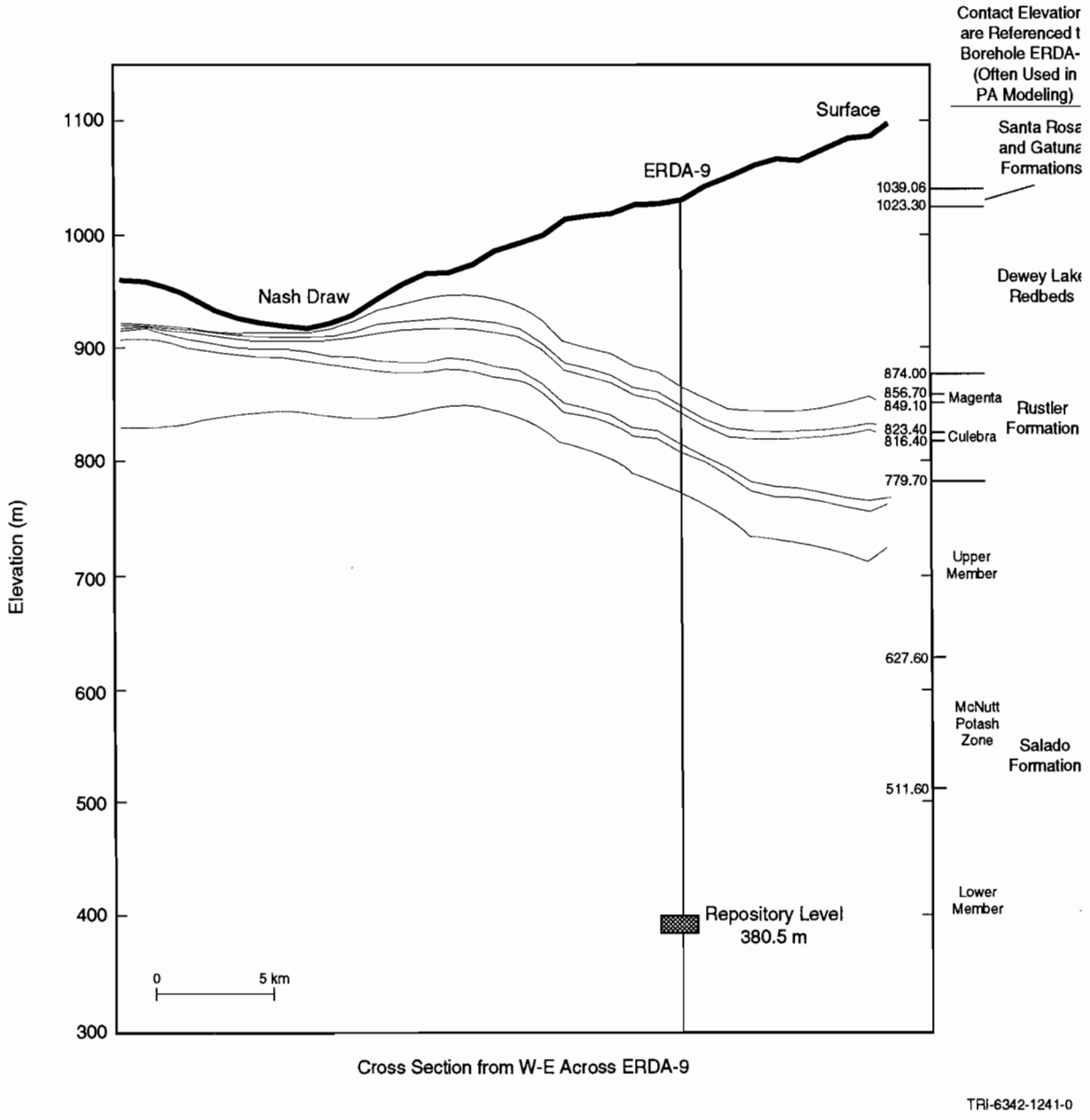

Figure 2.6-2. Interpolated geologic west-east cross section across the WIPP disposal system (after Mercer, 1983; Davies, 1989, Figure 53).

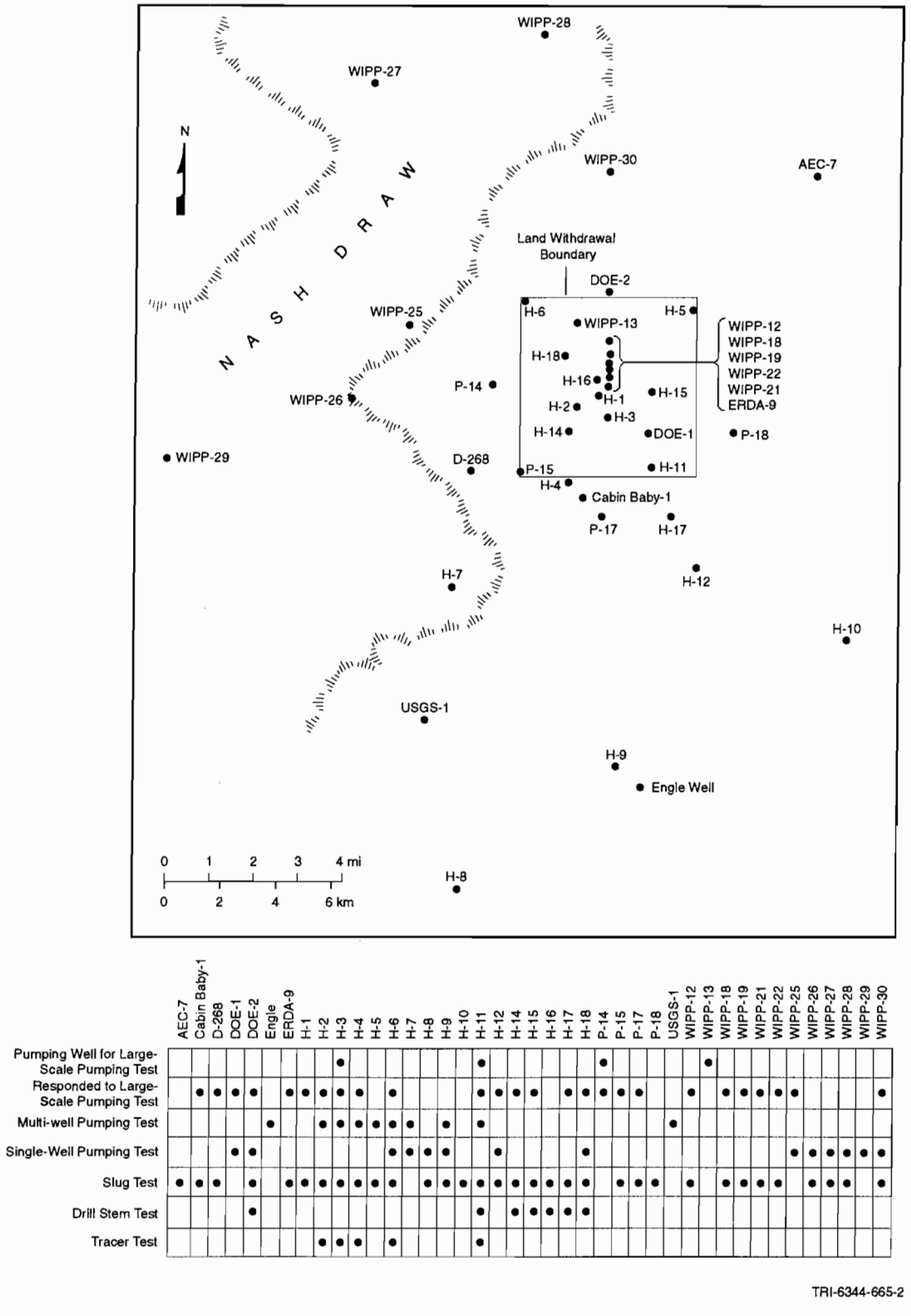

Figure 2.6-3. Location of wells used to define hydrologic parameters for Culebra Dolomite.

Table 2.6-1. Summary of Parameter Values for Culebra Dolomite Member of Rustler Formation

Parameter[a]	Median	Range		Distribution Units	Type	Discussion and Sources in:
Density						
Dolomite, grain (ρ_g)	2.82×10^3	2.78×10^3	2.86×10^3	kg/m^3	Normal	WIPP PA Division, 1991, Vol. 3, Section 2.6.1
Clay, bulk (ρ_b)	2.5×10^3			kg/m^3	Constant	WIPP PA Division, 1991, Vol. 3, Section 2.6.1
Dispersivity[b]						
Longitudinal (α_L)	1×10^2	5×10^1	3×10^2	m	Constructed	WIPP PA Division, 1991, Vol. 3, Section 2.6.2
Ratio (α_L/α_T)	10	1	25	none	Constructed	WIPP PA Division, 1991, Vol. 3, Section 2.6.2
Fracture spacing (2B)	**4×10^{-1}**	**6×10^{-2}**	**8**	**m**	**Constructed**	**Section 2.6.2**
Clay filling fraction (b_c/b)	**0.0**	**0.0**	**0.5**	**none**	**Constructed**	**Section 2.6.1**
Log Partition coefficients						
Matrix						
Am	**-0.730**	**-4.0**	**2.0**	**log (m^3/kg)**	**Constructed**	**Section 2.6.4**
Cm	-0.730	-4.0	2.0	log (m^3/kg)	Constructed	Section 2.6.4
Np	**-1.32**	**-4.0**	**2.0**	**log (m^3/kg)**	**Constructed**	**Section 2.6.4**
Pb	-1.99	-4.0	0.0	log (m^3/kg)	Constructed	Section 2.6.4
Pu	**-0.584**	**-4.0**	**2.0**	**log (m^3/kg)**	**Constructed**	**Section 2.6.4**
Ra	**-2.00**	**-4.0**	**1.0**	**log (m^3/kg)**	**Constructed**	**Section 2.6.4**
Th	**-2.00**	**-4.0**	**0.0**	**log (m^3/kg)**	**Constructed**	**Section 2.6.4**
U	**-1.54**	**-4.0**	**0.0**	**log (m^3/kg)**	**Constructed**	**Section 2.6.4**
Clay						
Am	**1.97**	**-4.0**	**3.0**	**log (m^3/kg)**	**Constructed**	**Section 2.6.4**
Cm	1.97	-4.0	3.0	log (m^3/kg)	Constructed	Section 2.6.4
Np	**0.0**	**-4.0**	**3.0**	**log (m^3/kg)**	**Constructed**	**Section 2.6.4**
Pb	-1.00	-4.0	2.0	log (m^3/kg)	Constructed	Section 2.6.4
Pu	**2.31**	**-4.0**	**3.0**	**log (m^3/kg)**	**Constructed**	**Section 2.6.4**
Ra	**-1.47**	**-4.0**	**2.0**	**log (m^3/kg)**	**Constructed**	**Section 2.6.4**
Th	**-1.00**	**-4.0**	**1.0**	**log (m^3/kg)**	**Constructed**	**Section 2.6.4**
U	**-2.12**	**-4.0**	**0.0**	**log (m^3/kg)**	**Constructed**	**Section 2.6.4**
Porosity						
Fracture (ϕ_f)	**1×10^{-3}**	**1×10^{-4}**	**1×10^{-2}**	**none**	**Lognormal**	**Section 2.6.2**
Matrix (ϕ_m)	**1.39×10^{-1}**	**9.6×10^{-2}**	**2.08×10^{-1}**	**none**	**Data**	**Section 2.6.2**
Clay (ϕ_c)	**0.275**	**0.05**	**0.5**	**none**	**Uniform**	**Section 2.6.2**
Storage coefficient (S)	2×10^{-5}	5×10^{-6}	5×10^{-4}	none	Constructed	WIPP PA Division, 1991, Vol. 3, Section 2.6.5
Thickness (Δz)	7.7	5.5	1.13×10^1	m	Spatial	WIPP PA Division, 1991, Vol. 3, Section 2.6.6
Tortuosity (τ)						
Dolomite	1.2×10^{-1}	3×10^{-2}	3.3×10^{-1}	none	Data	WIPP PA Division, 1991, Vol. 3, Section 2.6.7
Clay	1.2×10^{-2}	3×10^{-3}	3.3×10^{-2}	none	Constructed	WIPP PA Division, 1991, Vol. 3, Section 2.6.7
Index for transmissivity fields	**0.5**	**0.0**	**1.0**	**none**	**Uniform**	**Section 2.6.3**

[a] Parameters in bold were sampled in the 1992 calculations.
[b] Not used in 1992; see Volume 2 of this report, Section 7.6, for a discussion of the 1992 model of hydrodynamic dispersion.

2.6.1 Fraction of Clay Filling in Fractures

Clay Filling Fraction*

Parameter:	**Clay filling fraction (b_c/b)**
Material:	Culebra Dolomite Member of Rustler Formation (Culebra, FClayFll)
Definition Units:	Dimensionless
Values:	Range: (0.0, 0.5) Median: 0.0
Distribution:	Constructed (see Discussion)
Correlation:	

Data Source(s): Siegel, M. D. 1990. Appendix A: "Representation of Radionuclide Retardation in the Culebra Dolomite in Performance Assessment Calculations." *Data Used in Preliminary Performance Assessment of the Waste Isolation Pilot Plant (1990).* R. P. Rechard, H. Iuzzolino, and J. S. Sandha. SAND89-2408. Albuquerque, NM: Sandia National Laboratories. A-43 through A-62. (Investigator Judgment)

Novak, C. F., F. Gelbard, and H. W. Papenguth. 1992. "Parameter Recommendations for Porosity and Thickness of Clay Fracture Linings for the 1992 WIPP Performance Assessment Calculations" (see Appendix A, pp. A-125 through A-131). (Investigator Judgment)

Usage:

Mathematical model:

Solute transport in Culebra, Section 1.4.6, this volume.

Equation 1.4.6-3 and text following that equation (see Figure 1.4-4).

Computational models:

SECO/TP
STAFF2D (1991)

Ranking in Past Sensitivity Analyses:

40 CFR 191	Not tested
40 CFR 268	Not tested
NEPA	Not tested
Other	Not tested

*Key to Parameter Sheets is provided in Section 1.2.8.

Discussion:

Within fractures of the Culebra Dolomite Member, gypsum and corrensite (alternating layers of chlorite and smectite) are observed. To evaluate the retardation of radionuclides within the fractures (caused by interaction with this material lining the fractures), the fraction of lining material (b_c/b) is needed, where $2b_c$ is the total thickness of clays and 2b is fracture aperture. At present, data are not available to estimate the true range or distribution of b_c/b in the Culebra. Siegel (1990) recommended a normal distribution with a maximum of 0.9 and a minimum of 0.1. Current PA calculations have adopted the recommendations of Novak et al. (July 20, 1992, Memo in Appendix A) who note that clays do not invariably occur in all fractures, and that the absence of clays should be accounted for by a cdf of the form

$$\Pr\left\{\frac{bc}{b} \le x\right\} = \begin{cases} 0.5U(x)+x & \text{if } 0 \le x \le 0.5 \\ 1 & \text{if } 0.5 < x \end{cases},$$

where U(x) is the unit step function. This distribution is plotted on Figure 2.6-4. Sampling from the distribution will give zero clay-layer thickness 50% of the time, and non-zero clay layer thickness 50% of the time.

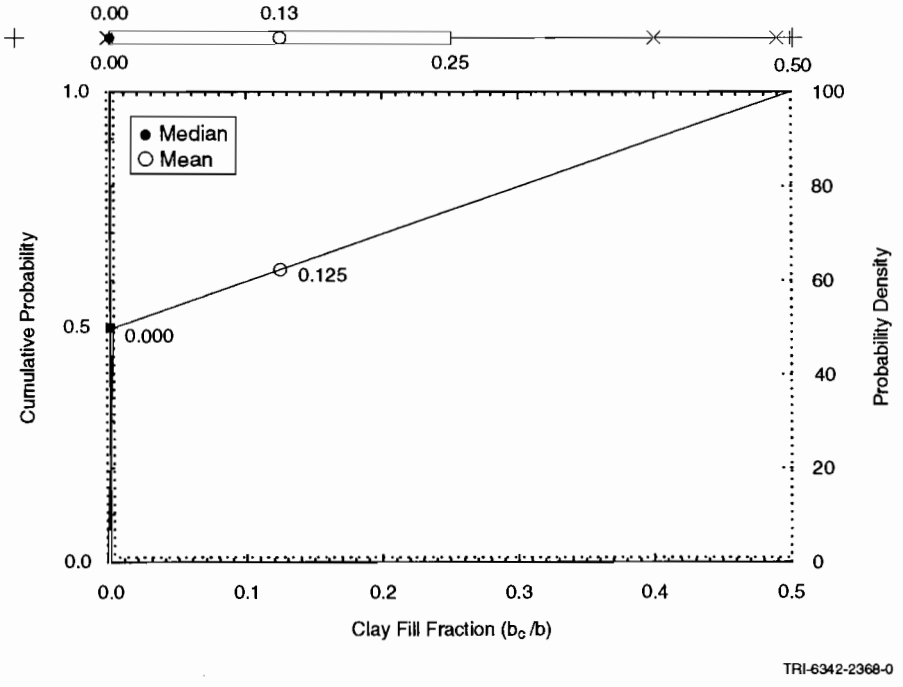

Figure 2.6-4. Estimated distribution for clay filling fraction, Culebra Dolomite Member.

2.6.2 Porosity

Fracture Porosity*

Parameter: **Fracture porosity (ϕ_f)**
Material: Culebra Dolomite Member of Rustler Formation (Culebra, FPore)

Definition Units: Dimensionless

Values: Range: (1×10^{-4}, 1×10^{-2}) Median: 1×10^{-3}

Distribution: Lognormal
Correlation:

Data Source(s): Lappin, A. R., R. L. Hunter, D. P. Garber, and P. B. Davies, eds. 1989. *Systems Analysis, Long-Term Radionuclide Transport, and Dose Assessments, Waste Isolation Pilot Plant (WIPP), Southeastern New Mexico; March 1989*. SAND89-0462. Albuquerque, NM: Sandia National Laboratories. (Table 1-2; Table E-6) (Investigator Judgment)

Usage:

Mathematical model:
Solute transport in Culebra, Section 1.4.6, this volume.

Equation 1.4.6-3 and text following that equation.

Computational models:
SECO/TP
STAFF2D (1991)

Ranking in Past Sensitivity Analyses:

40 CFR 191	High
40 CFR 268	Not tested
NEPA	Not tested
Other	Not tested

*Key to Parameter Sheets is provided in Section 1.2.8.

Discussion:

The fracture porosities interpreted from the tracer tests at the H-3 and H-11 hydropads are 2 x 10^{-3} (Kelley and Pickens, 1986) and 1 x 10^{-3}, respectively.

Both H-3 and H-11 lie near the expected transport pathway. The average value rounded to one significant figure was selected as the median and used for PA calculations. Similar to Lappin et al. (1989), the PA Department set the minimum and maximum one order of magnitude to either side of this median.

Figure 2.6-5 shows the estimated distribution for the fracture porosity.

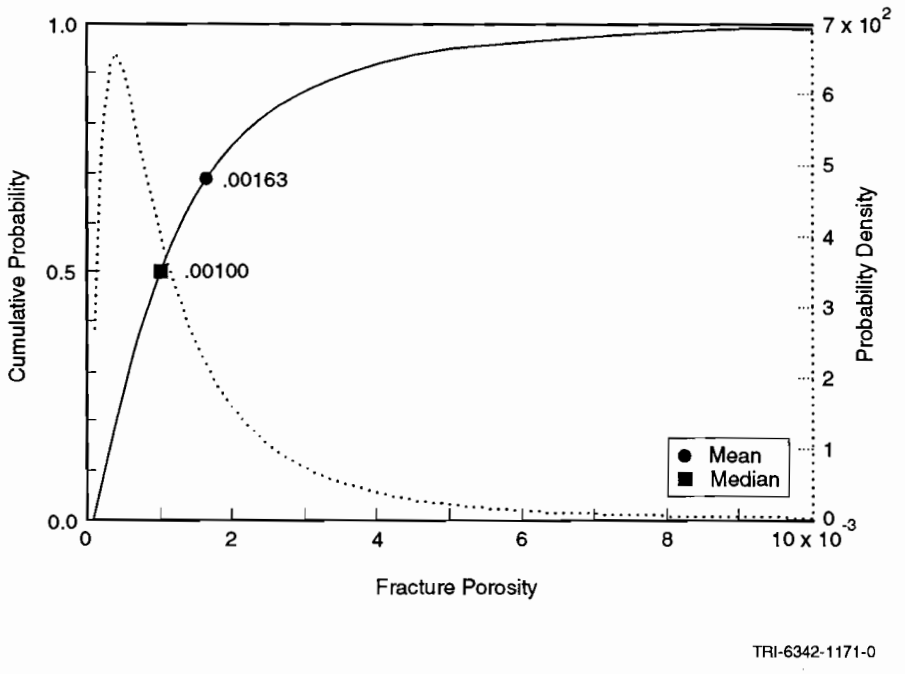

Figure 2.6-5. Estimated distribution for fracture porosity, Culebra Dolomite Member.

Clay Porosity*

Parameter: **Clay porosity (ϕ_c)**
Material: Clays lining fractures of Culebra Dolomite Member of Rustler Fm. (Culebra, PoreClay)

Definition, Units: Dimensionless

Values: Range: (0.05, 0.5) Median: 0.275

Distribution: Uniform
Correlation:

Data Source(s): The 1992 distribution of clay porosity is based on recommendations of the authors of the following memo:
Novak, C.F., F. Gelbard, and H.W. Papenguth. 1992. "Parameter Recommendations for Porosity and Thickness of Clay Fracture Linings for the 1992 WIPP Performance Assessment Calculations" (see Appendix A, pp. A-125 through A-131). (Investigator Judgment based on non-WIPP literature)

Usage:

Mathematical model:
Solute transport in Culebra, Section 1.4-6, this volume.

Equation 1.4.6-6 (also see Figure 1.4-4).

Computational models:
SECO/TP
STAFF2D (1991)

Ranking in Past Sensitivity Analyses:

40 CFR 191	Not tested
40 CFR 268	Not tested
NEPA	Not tested
Other	Not tested

*Key to Parameter Sheets is provided in Section 1.2.8.

Matrix Porosity*

Parameter: **Matrix porosity (ϕ_m)**
Material: Matrix of Culebra Dolomite Member of Rustler Formation (Culebra, Porosity)

Definition Units: Dimensionless

Values: Range: (0.095, 0.252) Median: 0.145

Distribution: Data
Correlation:

Data Source(s):

Kelley, V. A., and G. J. Saulnier, Jr. 1990. *Core Analyses for Selected Samples from the Culebra Dolomite at the Waste Isolation Pilot Plant Site.* SAND90-7011. Albuquerque, NM: Sandia National Laboratories. (Table 4.4) (WIPP Observational Data)

Lappin, A. R., R. L. Hunter, D. P. Garber, and P. B. Davies, eds. 1989. *Systems Analysis, Long-Term Radionuclide Transport, and Dose Assessments, Waste Isolation Pilot Plant (WIPP), Southeastern New Mexico; March 1989.* SAND89-0462. Albuquerque, NM: Sandia National Laboratories. (Table E-8) (Investigator Judgment)

Usage:

Mathematical model:

Solute transport in Culebra, Section 1.4-6 of this volume.

Equation 1.4.6-6 (also see Figure 1.4-4).

Computational models:

SECO/TP
STAFF2D (1991)

Ranking in Past Sensitivity Analyses:

40 CFR 191	Medium
40 CFR 268	Not tested
NEPA	Not tested
Other	Not tested

*Key to Parameter Sheets is provided in Section 1.2.8.

Discussion:

Matrix porosity has been evaluated by the Boyles' law technique using helium or air on 79 samples taken from the intact portion of core from 20 borehole or hydropad locations near the WIPP and also by water-resaturation for 30 of the samples. The agreement between the two techniques was excellent with an r^2 of 0.99 (Kelley and Saulnier, 1990, p. 4-7). From the Boyles' law technique, an average porosity for the 20 wells of 0.139 was obtained, with a range of 0.096 to 0.208 (Kelley and Saulnier, 1990, Table 4.4). (Lappin et al. [1989, Table E-8] report an average of 0.153 with a range of 0.028 and 0.303 assuming each of the 79 measurements is independent.) For many of the wells, a large amount of core was lost in porous (vuggy) and/or fractured portions of the Culebra Dolomite Member. Thus only intact matrix porosity is reported here.

Figure 2.6-6 shows the empirical distribution function for porosity of the Culebra Dolomite member.

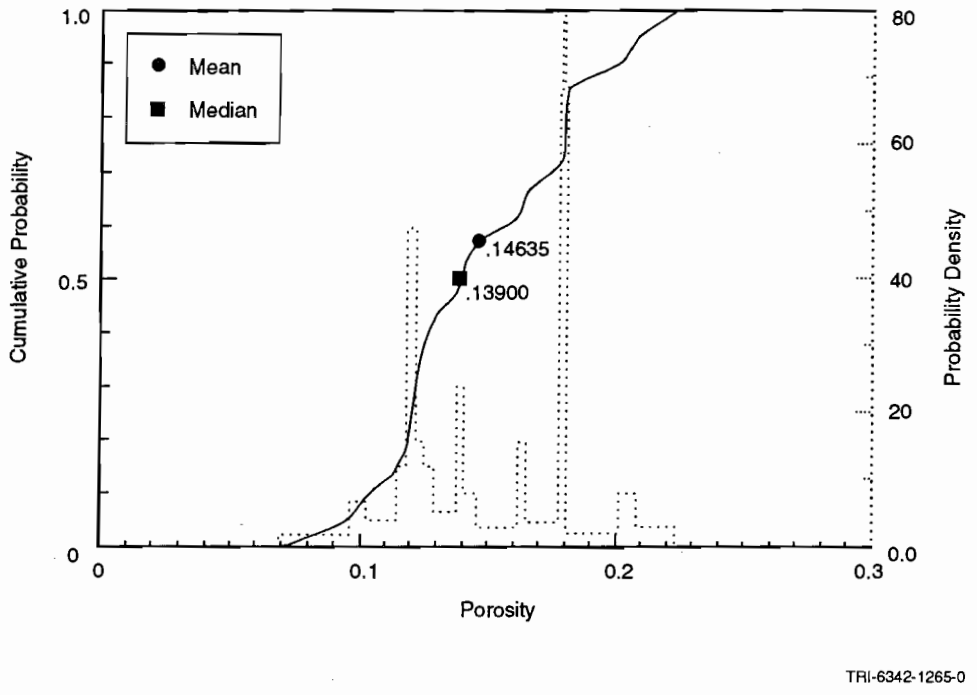

Figure 2.6-6. Empirical distribution for intact matrix porosity of Culebra Dolomite Member assuming no spatial correlation.

Fracture Spacing*

Parameter: **Fracture spacing (2B)**
Material: Culebra Dolomite Member of Rustler Formation (Culebra, FrctrSp)

DefinitionUnits: m

Values: Range: $(6 \times 10^{-2}, 8)$ Median: 4×10^{-1}

Distribution: Constructed
Correlation:

Data Source(s): Beauheim, R. L., T. F. Corbet, P. B. Davies, and J. F. Pickens. 1991b. Appendix A: "Recommendations for the 1991 Performance Assessment Calculations on Parameter Uncertainty and Model Implementation for Culebra Transport Under Undisturbed and Brine-Reservoir-Breach Conditions," *Preliminary Comparison with 40 CFR Part 191, Subpart B for the Waste Isolation Pilot Plant, December 1991. Volume 3: Reference Data.* WIPP Performance Assessment Division. Eds. R. P. Rechard, A. C. Peterson, J. D. Schreiber, H. J. Iuzzolino, M. S. Tierney, and J. S. Sandha. SAND91-0893/3. Albuquerque, NM: Sandia National Laboratories. A-7 through A-18. (Investigator Judgment)

Usage:

Mathematical model:

Solute transport in Culebra, Section 1.4-6, this volume.

Equations 1.4.6-3 and 1.4.6-10, establishes no-diffusion boundary (see also Figure 1.4-4).

Computational models:

SECO/TP
STAFF2D

Ranking in Past Sensitivity Analyses:

40 CFR 191	High
40 CFR 268	Not tested
NEPA	Not tested
Other	Not tested

*Key to Parameter Sheets is provided in Section 1.2.8.

Discussion:

Both horizontal and vertical fracture sets have been observed in core samples, shaft excavations, and outcrops (however, PA models use only horizontal fracture sets). A fracture spacing varying between 0.23 and 1.2 m (0.75 and 3.9 ft) has been interpreted for two travel paths at the H-3 borehole (Kelley and Pickens, 1986). Preliminary evaluation of the breakthrough curves for the H-6 borehole tracer test suggests a fracture spacing between 0.056 and 0.44 m (0.18 and 1.44 ft), and the H-11 borehole tracer test suggests a fracture spacing between 0.11 and 0.32 m (0.36 and 1.05 ft) (Beauheim et al., 1991b). From these data, Beauheim et al. (1991b) suggested a minimum of 0.06 m (0.2 ft) and a maximum equivalent to the assumed uniform thickness of the Culebra (8 m [26.2 ft]). Finally, the average fracture spacing at the three wells (H-3, H-6, and H-11) is 0.4 m (1.3 ft); the PA Department has chosen 0.4 m as median fracture spacing.

In the 1991 sensitivity analyses, fracture spacing in the Culebra Dolomite proved to be a moderate to highly sensitive parameter in determining releases of most radionuclides to the accessible environment. This sensitivity was independent of gas generation in the repository but (of course) was dependent on whether or not a dual-porosity transport model was used in the analysis.

The constructed distribution of Culebra fracture spacing is shown on Figure 2.6-7.

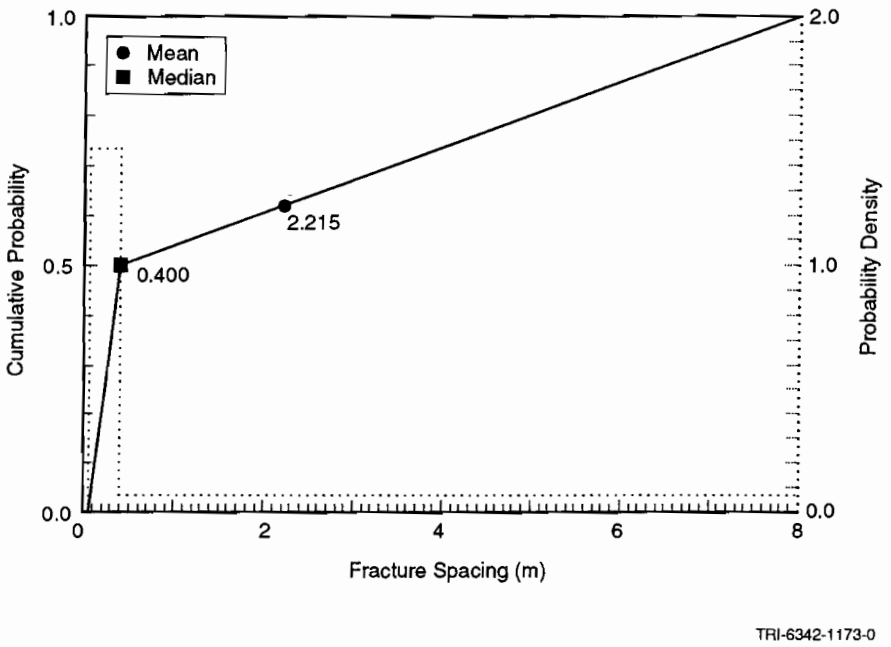

Figure 2.6-7. Constructed distribution for Culebra fracture spacing.

2.6.3 Transmissivity

Index for Culebra Transmissivity Fields*

Parameter: **Index for Culebra transmissivity fields**
Material: Culebra Dolomite Member of Rustler Formation (Global, IdxTrans)

Definition Units: Dimensionless

Values: Range: (0, 1) Median: 0.5

Distribution: Uniform
Correlation:

Data Source(s): See Discussion.

Usage:

Mathematical model:

Fluid flow in Culebra, Section 1.4.5, this volume.

Equation: This parameter labels realizations of transmissivity fields T(x,y) that appear in Eq. 1.4.5-2; see Discussion.

Computational models:

SECO2D

Ranking in Past Sensitivity Analyses:

40 CFR 191	Medium
40 CFR 268	Not tested
NEPA	Not tested
Other	Not tested

*Key to Parameter Sheets is provided in Section 1.2.8.

Discussion of Transmissivity Fields:

The 1990 WIPP Performance Assessment used a simple zonal approach for including uncertainty in the transmissivity *(T)* field within the Culebra Dolomite Member of the Rustler Formation. The zonal method divides the regional and local computational domains into geographic regions; 8, 13, and 15 regions have been used for different analyses reported in Marietta et al. (1989) and Bertram-Howery et al. (1990). In each region, a distribution was constructed using transmissivity measurements from available wells (Tables 2.6-2 and 2.6-3). This empirical distribution was sampled and one constant value used for the transmissivity in each zone. Each zone was sampled independently, so a single simulation used 8 (or 13 or 15) transmissivity values to represent the regional *T* field. Some simulations used distributions constructed from pilot point values (LaVenue et al., 1990) at locations assigned during calibration in addition to actual measurements at well locations.

The early (1990) approach was improved in 1991 in two ways:

- The reason for varying transmissivity over geographic zones is to include spatial variability in the *T* field. Correlations exist in the *T* field over distances greater than five kilometers; thus, assuming that the 8 (or 13 or 15) zones are independent during sampling is only a first approximation. Spatial dependence has been included over the whole model domain.
- The *T* fields generated by the simple zonal approach directly used transmissivity measurements whereas other information was included only indirectly through pilot point values. Many other data are available, and it has been possible to incorporate some of these data directly, e.g., hydraulic head measurements (Table 2.6-4) and geologic information.

Transmissivities display a variability in space that can be characterized using measured data, e.g., pump tests, by geostatistical analyses. This spatial variability was found to be stationary in the mean (LaVenue et al., 1990), but intrinsic in the second moment (IRF = 0) with a linear variogram without nugget effect (i.e., locally described by a constant with random perturbations that increase in variance with distance). Several techniques are available to generate random fields having this spatial structure: turning bands, inversion of the full covariance matrix, and spectral methods. Many such realizations could be generated and each realization could be used as one input for a system simulation. Each realization would than have the correct spatial structure of the true field, and would satisfy the first objective above.

However, these realizations would not be fully coherent with the actual measurements, and would overestimate the uncertainty in the *T* field. Making realizations of random fields coherent with measured information is called "conditioning". For WIPP PA, conditioning can be performed on at least four types of information:

- Measured *T* values at the wells.
- Measured or estimated head values at the wells in pre-excavation steady-state conditions.
- Measured head values during various transient hydraulic tests (e.g., long-term pump tests, shaft excavation).
- Indirect geologic data that can be correlated with transmissivity (such as overburden thickness, or presence of evaporites in the Culebra or Rustler).

Of the half-dozen methods available for conditioning on head data, two have been used to date in WIPP PA work. In 1991, random fields conditioned on *T* measurements at well locations and on values assigned during manual calibration were assigned to pilot point locations where no measurements were available (LaVenue et al., 1990). Forty-one measured-*T* and 41 pilot-point values are available. The pilot point values were assigned to insure coherence of the calibrated *T* field with the measured head data (both steady-state and transient conditions) so conditioning on head data is indirectly included. An advantage of this method is that it does not require any assumption on the acceptable range of variability of *T* (Var(*T*)). Many methods require that the Var(ln*T*)>1, and in the Culebra the Var(ln*T*) is about 3.5. This first method also allows using a variable-density fluid-flow model which may be important in the Culebra (Davies, 1989). Other methods are linear, but can only accommodate constant-density fluid-flow

Table 2.6-2. Logarithms of Selected Transmissivity Measurements in Culebra Dolomite Member (after Cauffman et al., 1990, Table C.1)

Well ID	Median	Low Range	High Range
AEC7	-6.5535	-7.7185	-5.3885
CABIN1	-6.5213	-7.6863	-5.3563
D268	-5.6897	-6.8547	-4.5247
DOE1	-4.4271	-5.0096	-3.8466
DOE2	-4.0191	-4.6016	-3.4366
ENGLE	-4.3350	-4.9175	-3.7525
ERDA9	-6.2964	-7.4614	-5.1314
H1	-6.0290	-7.1940	-4.8640
H10B	-7.1234	-8.2884	-5.9584
H11B1	-4.5057	-5.0882	-3.9232
H12	-6.7132	-7.8782	-5.5482
H14	-6.4842	-7.6492	-5.3192
H15	-6.3804	-7.5454	-5.2154
H16	-6.1149	-7.2799	-4.9499
H17	-6.6361	-7.8011	-5.4471
H18	-5.7775	-6.3600	-5.1950
H2B1	-6.2005	-6.7830	-5.6180
H3	-5.6089	-6.1914	-5.0264
H4B	-5.9960	-6.5785	-5.4135
H5B	-7.0115	-7.5940	-6.4290
H6B	-4.4500	-5.0325	-3.8675
H7B1	-2.8125	-3.3950	-2.2300
H8B	-5.0547	-5.6372	-4.4722
H9B	-3.9019	-4.4844	-3.3194
USGS1	-3.2584	-3.8409	-2.6759
WIPP12	-6.9685	-8.1355	-5.8035
WIPP13	-4.1296	-5.2946	-2.9646
WIPP18	-6.4913	-7.6563	-5.3263
WIPP19	-6.1903	-7.3553	-5.0253
WIPP21	-6.5705	-7.7355	-5.4055
WIPP22	-6.4003	-7.5653	-5.2353
WIPP25	-3.5412	-4.1237	-2.9587
WIPP26	-2.9136	-3.4961	-2.3311
WIPP27	-3.3692	-3.9517	-2.7867
WIPP28	-4.6839	-5.2664	-4.1014
WIPP29	-2.9685	-3.5510	-2.3860
WIPP30	-6.6023	-7.7673	-5.4373
P14	-3.5571	-4.5124	-2.6018
P15	-7.0354	-8.2004	-5.8704
P17	-5.9685	-7.1335	-4.8035
P18	-1.0123×10^{1}	-1.1288×10^{1}	-8.9584

Table 2.6-3. Logarithms of Transmissivity of Calibrating Points (Pilot Points) for Culebra Dolomite Member (after Davies and LaVenue, 1990b)

Well ID	Median	Low Range	High Range
PP1	-2.0700	-4.4233	2.833×10^{-1}
PP2	-2.2500	-4.5334	3.340×10^{-2}
PP3	-2.3200	-4.6267	-1.330×10^{-2}
PP4	-3.6200	-5.3442	-1.8958
PP5	-3.5800	-5.2576	-1.9024
PP6	-6.0200	-7.7675	-4.2725
PP7	-6.4200	-8.0044	-4.5656
PP8	-3.4100	-4.8779	-1.9421
PP9	-2.7100	-3.8913	-1.5217
PP11	-7.7200	-9.1413	-6.2987
PP12	-8.0800	-9.0353	-7.1247
PP13	-5.6400	-6.5953	-4.6847
PP14	-8.3400	-9.7846	-6.8954
PP15	-6.4900	-7.7482	-5.2318
PP16	-5.1300	-6.5280	-3.7320
PP17	-6.6000	-8.1378	-5.0622
PP18	-2.6300	-4.5173	-7.427×10^{-1}
PP19	-2.8600	-4.7939	-9.261×10^{-1}
PP20a	-2.9400	-4.8972	-9.828×10^{-1}
PP21a	-3.0000	-4.8407	-1.1593
PP23	-3.8500	-5.1548	-2.5452
PP24	-3.5000	-4.2689	-2.7311
PP25	-6.0000	-7.0718	-4.9282
PP26	-5.5000	-6.3388	-4.6612
PP27	-4.2500	-5.3684	-3.1316
PP28	-3.5000	-4.7582	-2.2418
PP29	-3.2500	-4.3451	-2.1549
PP30	-6.1600	-7.3250	-4.9950
PP31	-5.8700	-7.0350	-4.7050
PP32	-5.0000	-5.7223	-4.2777
PP34	-3.5900	-4.5453	-2.6347
PP35	-2.6700	-3.6253	-1.7147
PP36	-5.1700	-6.0787	-4.2613
PP37	-4.3100	-6.0342	-2.5858
PP38	-3.9000	-5.3446	-2.4554
PP39	-3.9000	-5.3446	-2.4554
PP40	-5.9300	-6.8853	-4.9747
PP41	-4.0000	-4.9553	-3.0447
PP42	-3.5000	-4.5951	-2.4049
PP43	-5.0000	-5.9553	-4.0447
PP44	-5.0000	-5.9553	-4.0447

Table 2.6-4. Summary of Selected Steady-State Freshwater Head Measurements in Culebra Dolomite Member (after Cauffman et al., 1990, Table 6.2)

Well ID	Median (m)	Low Range (m)	High Range (m)
AEC7	9.3200×10^2	9.3014×10^2	9.3386×10^2
CABIN1	9.1120×10^2	9.0980×10^2	9.1260×10^2
D268	9.1520×10^2	9.1462×10^2	9.1578×10^2
DOE1	9.1390×10^2	9.0831×10^2	9.1949×10^2
DOE2	9.3530×10^2	9.3181×10^2	9.3880×10^2
H1	9.2330×10^2	9.1860×10^2	9.2796×10^2
H10B	9.2140×10^2	9.1627×10^2	9.2653×10^2
H11B1	9.1280×10^2	9.1000×10^2	9.1560×10^2
H12	9.1360×10^2	9.1080×10^2	9.1640×10^2
H14	9.1550×10^2	9.1457×10^2	9.1643×10^2
H15	9.1560×10^2	9.1234×10^2	9.1886×10^2
H17	9.1100×10^2	9.0890×10^2	9.1310×10^2
H18	9.3190×10^2	9.2887×10^2	9.3493×10^2
H2C	9.2400×10^2	9.2167×10^2	9.2633×10^2
H3B1	9.1710×10^2	9.1267×10^2	9.2153×10^2
H4B	9.1280×10^2	9.1140×10^2	9.1420×10^2
H5B	9.3400×10^2	9.3074×10^2	9.3726×10^2
H6B	9.3260×10^2	9.3027×10^2	9.3493×10^2
H7B1	9.1270×10^2	9.1200×10^2	9.1340×10^2
H8B	9.1240×10^2	9.1147×10^2	9.1333×10^2
H9B	9.0820×10^2	9.0680×10^2	9.0960×10^2
P14	9.2690×10^2	9.2480×10^2	9.2900×10^2
P15	9.1680×10^2	9.1494×10^2	9.1866×10^2
P17	9.1160×10^2	9.0997×10^2	9.1323×10^2
USGS1	9.0980×10^2	9.0922×10^2	9.1038×10^2
USGS4	9.0970×10^2	9.0947×10^2	9.0993×10^2
USGS8	9.1110×10^2	9.1087×10^2	9.1133×10^2
WIPP12	9.3310×10^2	9.3147×10^2	9.3473×10^2
WIPP13	9.3400×10^2	9.3120×10^2	9.3680×10^2
WIPP18	9.3000×10^2	9.2720×10^2	9.3280×10^2
WIPP25	9.2870×10^2	9.2637×10^2	9.3103×10^2
WIPP26	9.1940×10^2	9.1882×10^2	9.1998×10^2
WIPP27	9.3810×10^2	9.3647×10^2	9.3973×10^2
WIPP28	9.3700×10^2	9.3467×10^2	9.3933×10^2
WIPP29	9.0540×10^2	9.0482×10^2	9.0598×10^2
WIPP30	9.3510×10^2	9.3254×10^2	9.3766×10^2

models. A second advantage is computational efficiency because the Cholesky decomposition only needs to be performed once regardless of the number of simulations.

The approach in 1992 is an extension of the pilot point approach used for the calibration of the Culebra T field. This method generates random fields conditioned on T measurements, steady-state, and transient head data without restriction on Var(ln$T$) and with variable-density fluid-flow models.

In this method, random T fields conditioned only on the measured T values are first generated. These fields are further conditioned on the head data by calibrating them with the pilot point approach both on steady-state and transient data. The procedure has been automated to generate a large number of calibrated random fields. Order of pilot point selection and the uniqueness of the resulting T field were issues to be examined during operational tests and sensitivity analyses.

In 1992, application of the procedures described above produced 70 realizations of the transmissivity field in Culebra Dolomite (plots of these realizations are presented in Appendix C). These 70 realizations were then ordered by travel time to the accessible environment (3.5 km from center of repository area): each realization was converted to a flow field (assuming uniform Culebra thickness of 8 m and 16% effective porosity) and the travel time associated with that field was calculated with the program TRACKER. The 70 realizations were then ranked according to their associated travel times (Figure 2.6-8). Flow fields in the 1992 PA calculations were selected by sampling a uniform random variable on the interval (0,1), mapping this result onto the integers 1-70, and using the resulting integer to choose a flow field. Because the flow fields are considered to be equally likely, the rank of the sampled index value can be used as the index of the flow fields.

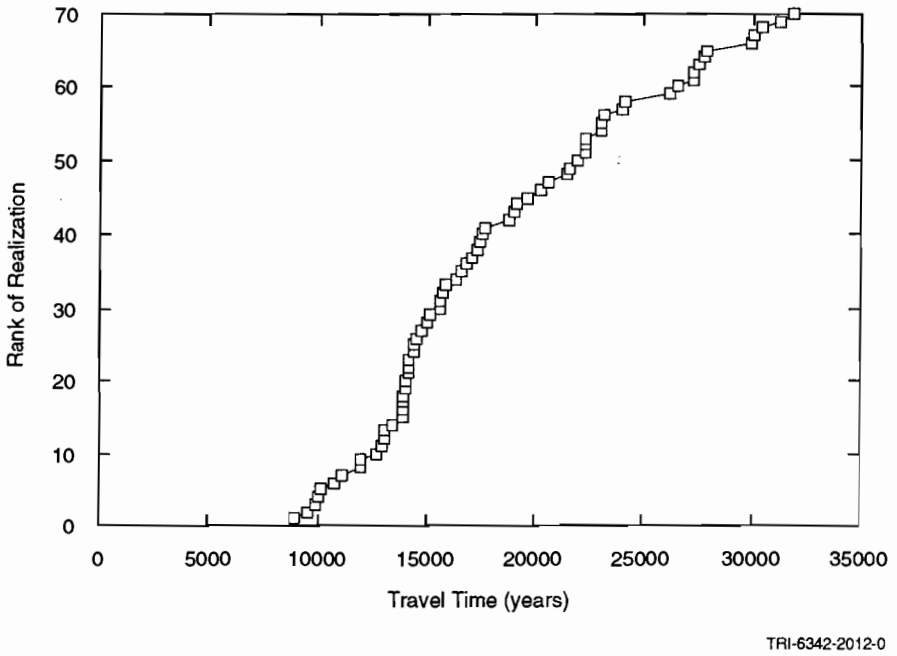

Figure 2.6-8. Empirical travel time distribution associated with the 70 realizations of Culebra transmissivity fields (see text).

2.6.4 Partition Coefficients and Retardations

A partitioning or distribution coefficient (K_d), which describes the intensity of sorption, is used to calculate the partitioning of species such as radionuclides between the groundwater and rock and, thereby, calculate the sorption capacity or retardation (R).

The logarithmic K_d distributions used in 1991 and 1992 are reported in Tables 2.6-5 and 2.6-6 and are considered to be realistic in light of available data; however, these distributions require a number of subjective assumptions that ongoing experiments may invalidate. The distributions were derived from an internal expert-judgment process regarding radionuclide retardation in the Culebra, which convened in April and May, 1991 (Trauth et al., 1992). The three Sandia experts involved were Robert G. Dosch (6212), Craig F. Novak (6119), and Malcolm D. Siegel (6115). The three experts participated in individual elicitation sessions for the purpose of developing probability distributions for the distribution coefficients for americium, curium, lead, neptunium, plutonium, radium, thorium, and uranium, for two sets of conditions. The first is the nature of the transport fluid: essentially Culebra or Salado brine. The second is whether the retardation takes place in the dolomite matrix or in the clay lining the fractures.

The K_d distributions that actually resulted from this panel are discussed in Section 2.6.10 of the WIPP PA Division, 1991, vol. 3. The distributions are derived from a combination of values from Dosch and Novak. The rationales behind Dosch' and Novak's values are briefly described below; a more thorough description of Novak's values is provided in Novak, 1991. The K_d distributions were converted to logarithmic form in 1992.

Dosch reviewed data from several experiments on distribution coefficients for various actinides in a variety of media. His own work (Lynch and Dosch, 1980) was included in his data set. He believed that even though some experiments were conducted using media different from the Culebra matrix and the Culebra clay, most of the data could not be discounted (personal communication from S. Hora, September 1991 regarding expert panel elicitation on May 1991). His justification for this was that experimental data directly applicable to the issue at hand were so scarce that no relevant data should be disregarded. In general, Dosch remarked that most of the experimental data deserved equal weight in any judgments about the behavior of actinides in the Culebra matrix and clay. Dosch declined to give any probability distributions for thorium and lead because he did not believe himself qualified to make enlightened assessments for those elements.

Novak examined available research that detailed the experimental measurement of K_ds using substrates and water compositions pertinent to transport in the WIPP system (Novak, 1992). He showed that (1) data are not available for all elements of interest, (2) almost no data exist for clay substrates in the Culebra, and (3) existing data may not be applicable to current human-intrusion scenarios. In this study (Novak, 1992), Novak also questioned the use of the K_d model for estimating radionuclide retardation in the Culebra.

Novak believes that the water composition called "Culebra H_2O" is the least dissimilar to Case One among available data for Case One, which assumed that water reaching the Culebra would not change the composition of Culebra water significantly, except for the presence of radionuclides. Brine A best represented Case Two, which assumed that water reaching the Culebra would not be diluted and a concentrated brine contaminated with radionuclides would flow through the Culebra. Within each case, K_d estimates were needed for radionuclide sorption on the matrix (i.e., the dolomitic Culebra substrates), and in the fractures (i.e., on clay materials lining fractures). Each type of water was used for both matrix and fractures. Thus, for Case One, data from "Culebra H_2O" studies were used to estimate K_d values where actual data were not available. Similarly, Brine A data were used to estimate K_ds for Case Two.

Novak offered K_ds of 0 m^3/kg for all cdfs because he thought it possible that any of the elements could be transported with the fluid velocity. Upper bounds represent Novak's opinions on maximum values for K_ds observable under human-intrusion scenarios (Novak, 1991). Novak chose different sets of fractiles for different radionuclides. These represent his best estimates resulting from his studies of existing data and literature.

Novak further states that values obtained through the expert elicitation process are subjective estimates only because of large uncertainties in water composition, mixing within the Culebra, and the questionable utility of the K_d

Table 2.6-5. Summary of 1992 Partition Coefficients of Radionuclides for Culebra Dolomite Member within Matrix Dominated by Culebra Brine.

Element	Median	Range		Units	Value of Additional Information
Am	-0.730	-4.0	2.0	$\log_{10}$ (m^3/kg)	High
Cm	-0.730	-4.0	2.0	$\log_{10}$ (m^3/kg)	Not tested
Np	-1.32	-4.0	2.0	$\log_{10}$ (m^3/kg)	High
Pb	-1.99	-4.0	0.0	$\log_{10}$ (m^3/kg)	Not tested
Pu	-0.584	-4.0	2.0	$\log_{10}$ (m^3/kg)	High
Ra	-2.00	-4.0	1.0	$\log_{10}$ (m^3/kg)	Not tested
Th	-2.00	-4.0	0.0	$\log_{10}$ (m^3/kg)	High
U	-1.54	-4.0	0.0	$\log_{10}$ (m^3/kg)	High

Table 2.6-6. Summary of 1992 Partition Coefficients of Radionuclides for Culebra Dolomite Member within Fracture Clays Dominated by Culebra Brine.

Element	Median	Range		Units	Value of Additional Information
Am	1.97	-4.0	3.0	$\log_{10}$ (m^3/kg)	High
Cm	1.97	-4.0	3.0	$\log_{10}$ (m^3/kg)	Not tested
Np	0.00	-4.0	3.0	$\log_{10}$ (m^3/kg)	High
Pb	-1.00	-4.0	2.0	$\log_{10}$ (m^3/kg)	Not tested
Pu	2.31	-4.0	3.0	$\log_{10}$ (m^3/kg)	High
Ra	-1.47	-4.0	2.0	$\log_{10}$ (m^3/kg)	Not tested
Th	-1.00	-4.0	1.0	$\log_{10}$ (m^3/kg)	High
U	-2.12	-4.0	0.0	$\log_{10}$ (m^3/kg)	High

model. Finally, Novak argues that these cdfs for K_ds do not substitute for actual data, and believes that additional study is needed to quantify the potential for radionuclide retardation in the Culebra (Novak, 1991).

In the 1991 series of sensitivity analyses (Helton et al., 1992), the partition coefficients for Am, Np, Pu, Th and U were highly sensitive parameters in the determination of radionuclide releases to the accessible environment; the clay partition coefficients for Am, Pu, and U were the most sensitive among the ten parameters of this kind that were tested.

Partition Coefficients in Matrix of Culebra Dolomite*

Parameter: **Partition coefficients (K_d) for Am, Cm, Np, Pb, Pu, Ra, Th, U**
Material: Matrix of Culebra Dolomite Member of Rustler Formation Culebra Brine

Definition, Units: Log (m^3/kg)

Values: See Table 2.6-5.

Distribution: Constructed (see Figures 2.6-9[a] through 2.6-9[h])
Correlation:

Data Source(s): Trauth, K. M., S. C. Hora, R. P. Rechard, and D. R. Anderson. 1992. *The Use of Expert Judgment to Quantify Uncertainty in Solubility and Sorption Parameters for Waste Isolation Pilot Plant Performance Assessment.* SAND92-0479. Albuquerque, NM: Sandia National Laboratories. (Expert Panel Judgment)

Usage:

Mathematical model:
Solute Transport in Culebra, Section 1.4.6, this volume.

Equation 1.4.6-8.

Computational models:
SEC0/TP
STAFF2D

Ranking in Past Sensitivity Analyses:

40 CFR 191	High for Am, Np, Pu, Th, U; others not tested
40 CFR 268	Not tested
NEPA	Not tested
Other	Not tested

*Key to Parameter Sheets is provided in Section 1.2.8.

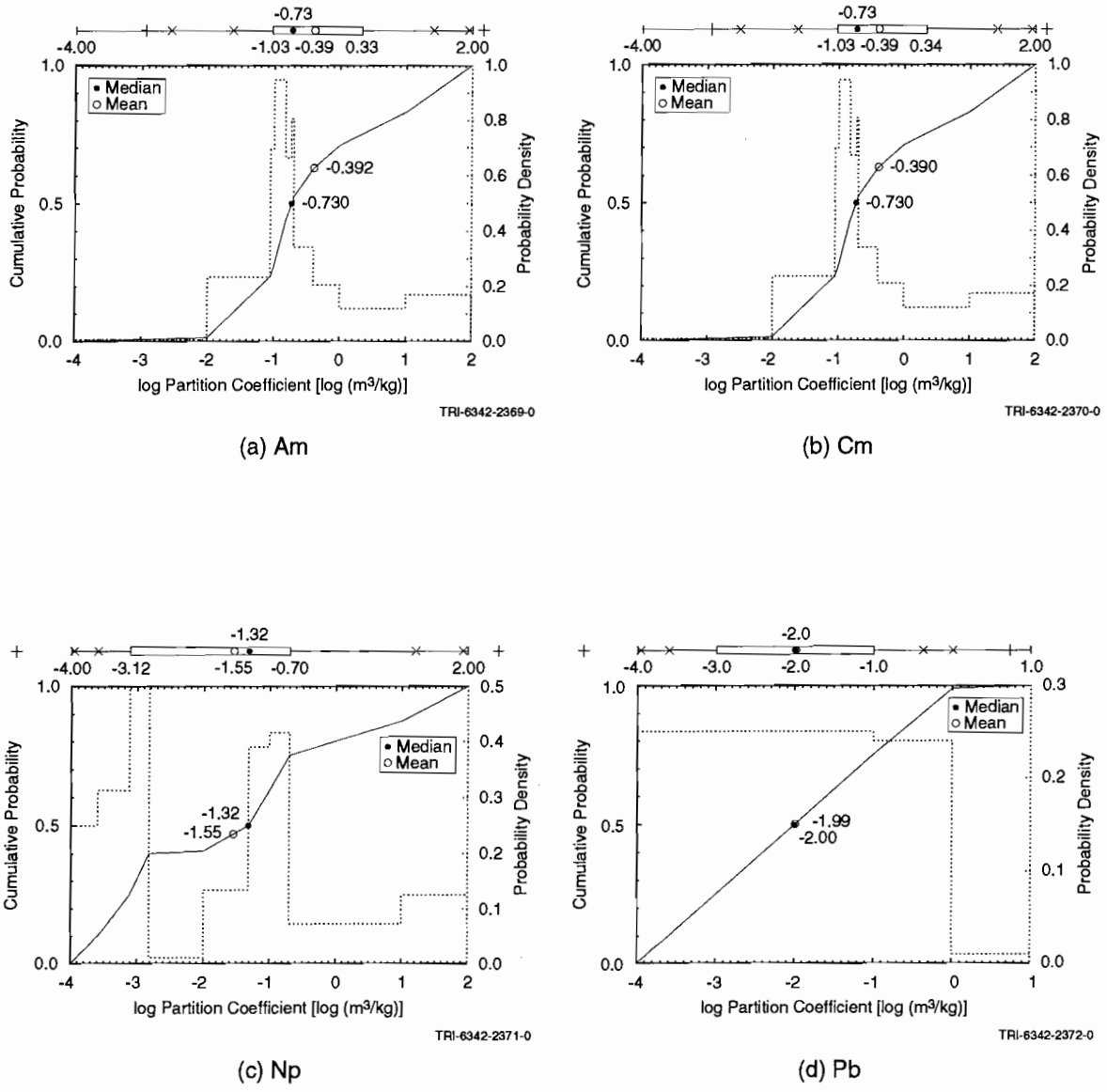

Figure 2.6-9. Constructed distribution for partition coefficient in matrix for (a) americium (Am), (b) curium (Cm), (c) neptunium (Np), (d) lead (Pb), (e) plutonium (Pu), (f) radium (Ra), (g) thorium (Th), and (h) uranium (U).

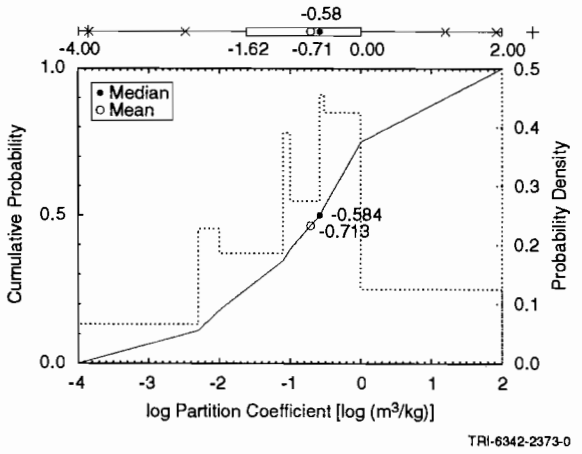

(e) Pu

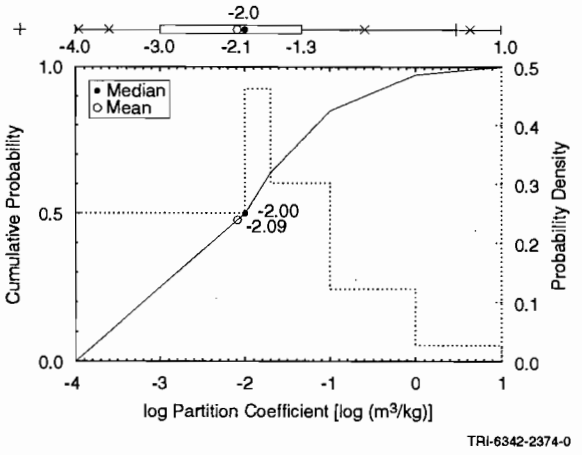

(f) Ra

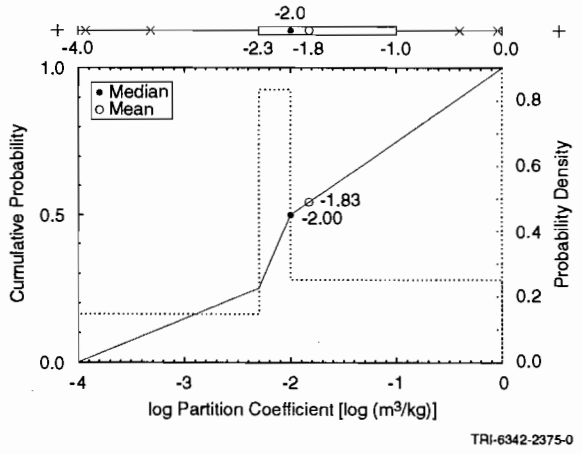

(g) Th

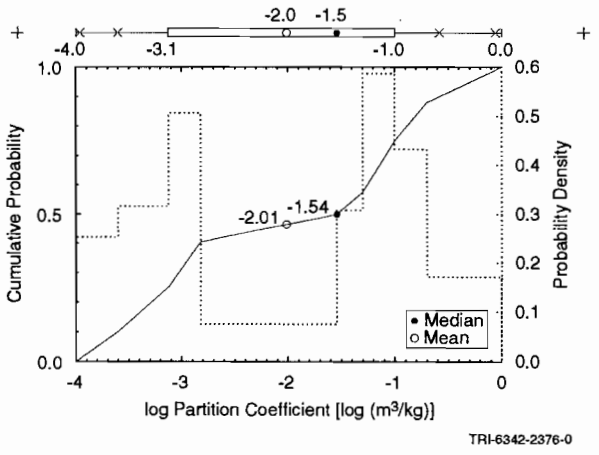

(h) U

Figure 2.6-9. Constructed distribution for partition coefficient in matrix for (a) americium (Am), (b) curium (Cm), (c) neptunium (Np), (d) lead (Pb), (e) plutonium (Pu), (f) radium (Ra), (g) thorium (Th), and (h) uranium (U) (continued).

Partition Coefficients in Clay Lining Fractures of Culebra Dolomite*

Parameter: **Partition coefficients (K_d) for Am, Cm, Np, Pb, Pu, Ra, Th, U**
Material: Clay lining fractures of Culebra Dolomite Member of Rustler Formation Culebra brine

Definition, Units: Log (m^3/kg)

Values: See Table 2.6-6.

Distribution: Constructed (see Figures 2.6-10 [a] through 2.6-10[h])
Correlation:

Data Source(s): Trauth, K. M., S. C. Hora, R. P. Rechard, and D. R. Anderson. 1992. *The Use of Expert Judgment to Quantify Uncertainty in Solubility and Sorption Parameters for Waste Isolation Pilot Plant Performance Assessment.* SAND92-0479. Albuquerque, NM: Sandia National Laboratories. (Expert Panel Judgment)

Usage:

Mathematical model:
Solute Transport in Culebra, Section 1.4.6, this volume.

Equation 1.4.6-8.

Computational models:
SECO/TP
STAFF2D

Ranking in Past Sensitivity Analyses:

40 CFR 191	High for Am, Np, Pu, Th, U; others not tested
40 CFR 268	Not tested
NEPA	Not tested
Other	Not tested

*Key to Parameter Sheets is provided in Section 1.2.8.

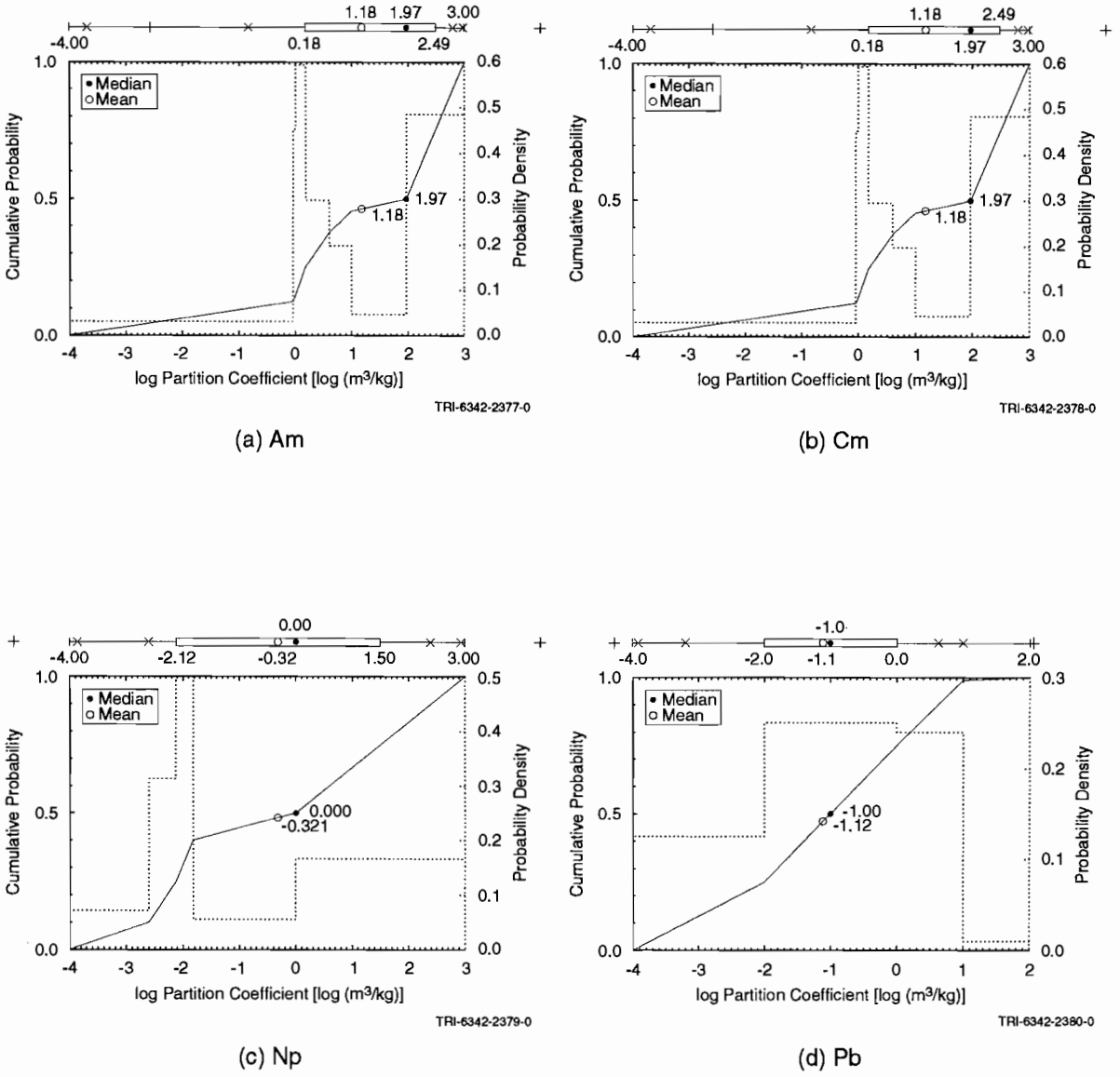

Figure 2.6-10. Constructed distribution for partition coefficient in clay for (a) americium (Am), (b) curium (Cm), (c) neptunium (Np), (d) lead (Pb), (e) plutonium (Pu), (f) radium (Ra), (g) thorium (Th), and (h) uranium (U).

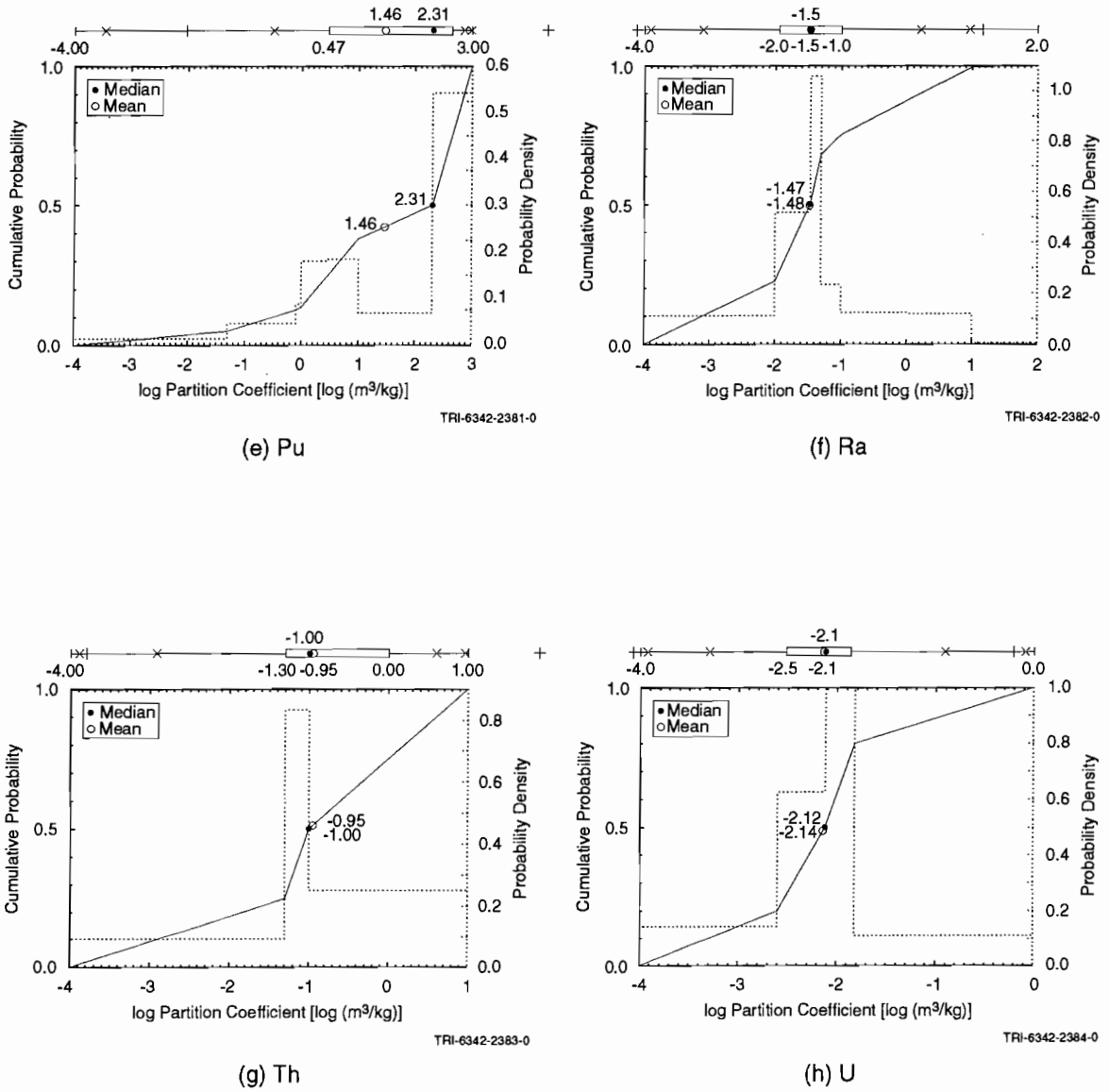

Figure 2.6-10. Constructed distribution for partition coefficient in clay for (a) americium (Am), (b) curium (Cm), (c) neptunium (Np), (d) lead (Pb), (e) plutonium (Pu), (f) radium (Ra), (g) thorium (Th), and (h) uranium (U) (continued).

3. ENGINEERED BARRIERS AND SOURCE TERM

The engineered barriers consist of the repository design, waste form, seals, and backfill. Also discussed in this chapter are characteristics of the waste such as inventory of radionuclides and hazardous chemicals, solubility, and gas production potential.

3.1 Dimensions of Underground Facility

The WIPP repository is composed of a single 15-ha (38-acre) underground disposal level constructed in one stratigraphic interval, which dips slightly to the south. The repository level consists of an experimental region at the north end, the operations region in the center for waste-handling and repository equipment maintenance, and a disposal region at the south end (Figures 3.1-1 and 3.1-2). The UTM coordinates shown in Figure 3.1-2 are derived from the state plane coordinates reported in Gonzales, 1989. To maintain consistency with coordinate values reported elsewhere in this volume, the UTM coordinates were computed by the Technology Application Center, University of New Mexico, Albuquerque, New Mexico 87106. Table 3.1-1 provides a summary of the excavated and enclosed areas (see Figure 3.1-1 for a visual appreciation of these terms) and initial volumes of excavated regions (not considering disturbed rock zone [DRZ] or closure). At present, only the first panel has been excavated.

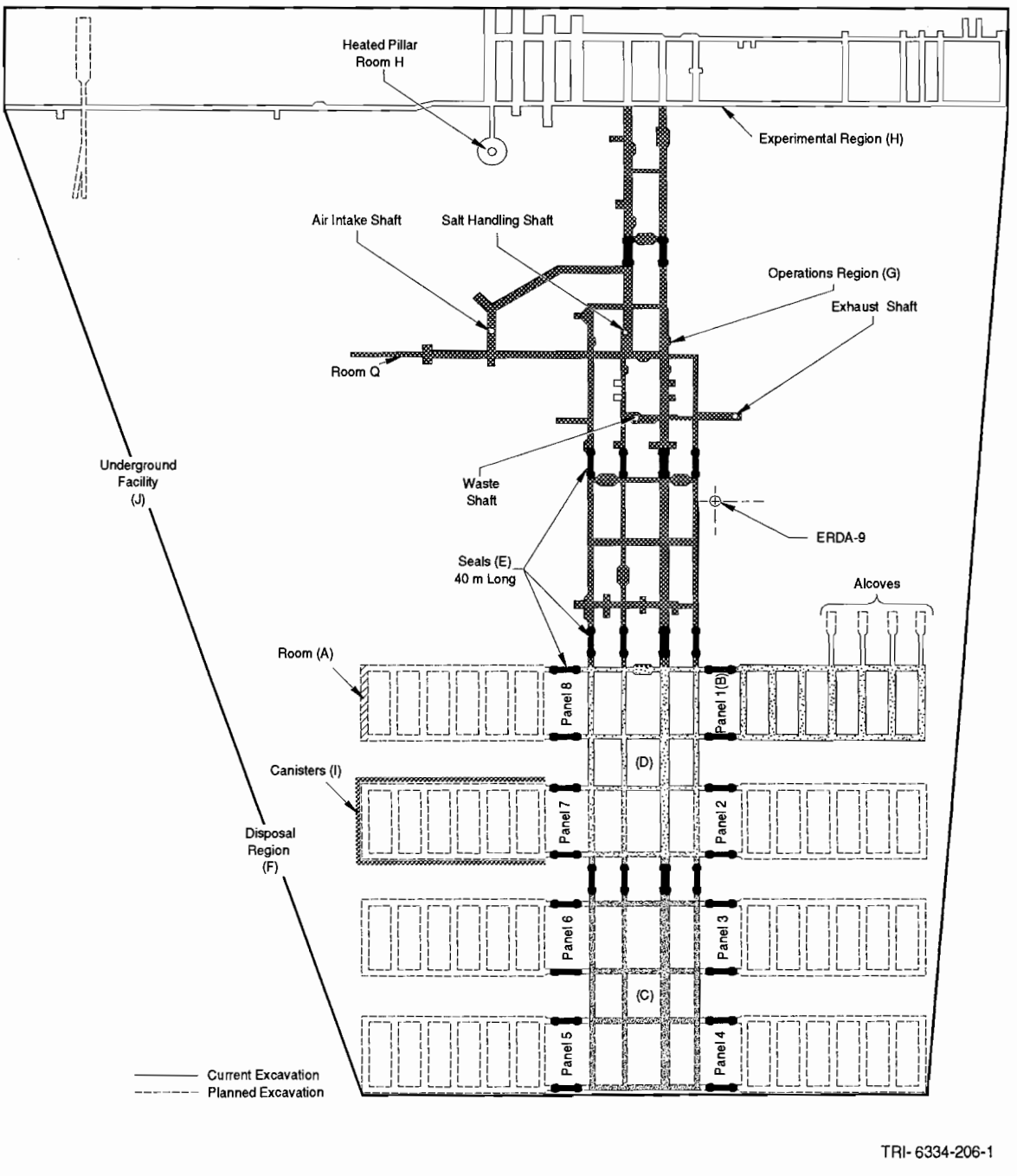

Figure 3.1-1. Excavated and enclosed areas in the WIPP repository.

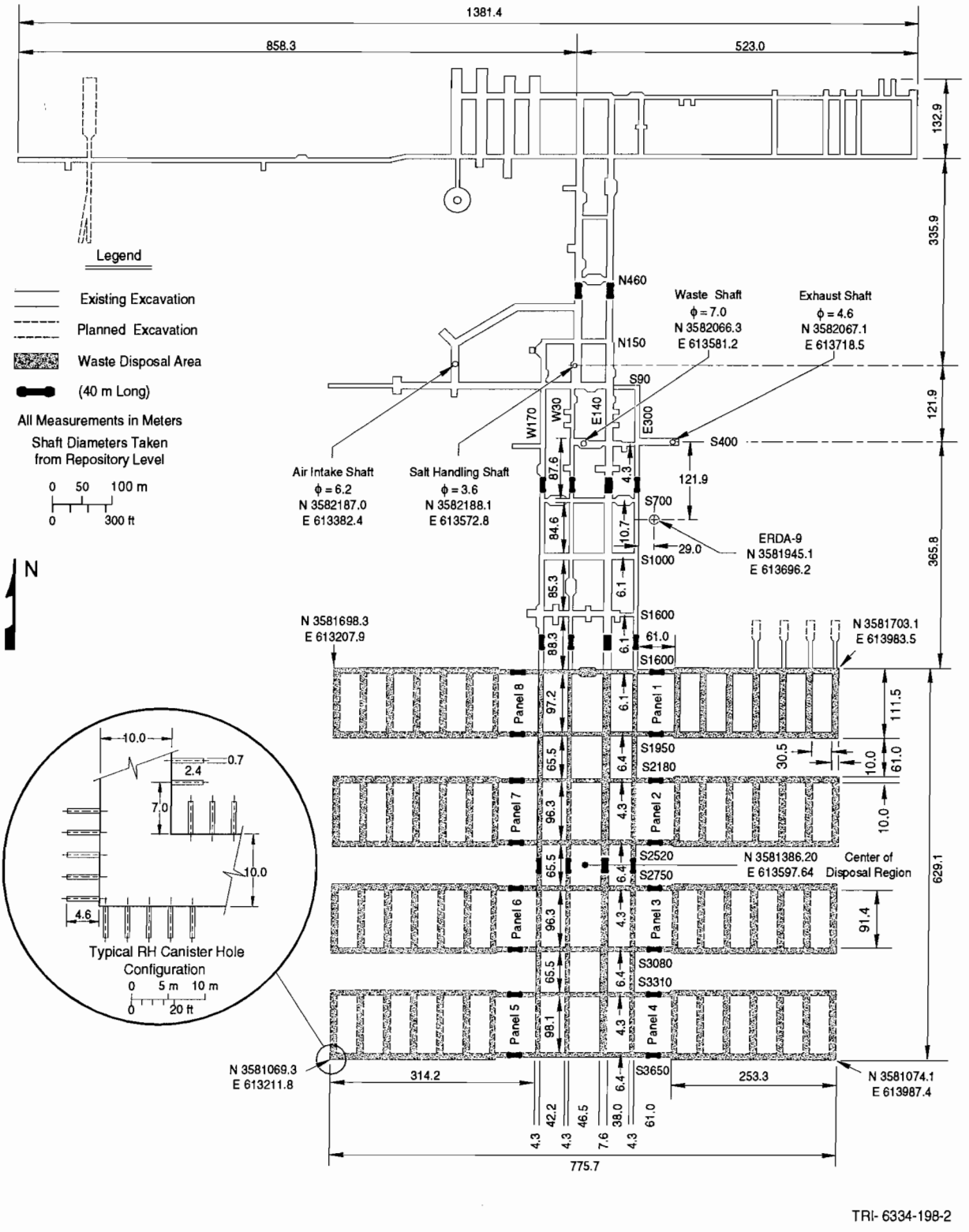

Figure 3.1-2. Planned dimensions of WIPP disposal region and access drifts. (Dimensions originally specified in units of feet.) (after Bechtel National, Inc., 1986).

Table 3.1-1. Summary of Excavated and Enclosed Areas and Initial Volumes of Excavated Regions within the WIPP Repository, Not Considering the DRZ or Closure (Rechard et al., 1990b, Table A-12)

Region*	Areas		Volume	
	Excavated (10^3 m^2)	Enclosed (10^3 m^2)	Excavated (10^3 m^3)	Enclosed (10^3 m^3)
Room (A)	0.9197	0.9197	3.644	3.644
One panel excluding seals (B)	11.64	29.42	46.10	116.59
Southern equivalent panel excluding seals (C)	8.820	49.46	32.26	180.90
Northern equivalent panel excluding seals (D)	9.564	53.68	34.98	196.34
Panel seals (20) (E)	4.133		15.119	
Total disposal region (F)	111.52	506.8	436.0	2008.0
Operations region (G)	21.84	283.6	78.07	1037.2
Four shafts (only) to base of Rustler Fm.	0.08691	0.08691	34.76	34.76
Experimental region (H)	21.61	298.1	71.90	1090
RH area canisters (7954) (I)	14.36			
Total facility (J)	152.83	1748	583.4	6926

*Regions shown in Figure 3.1-1; detailed dimensions shown in Figure 3.1-2.

3.1.1 Disposal Region

All of the underground openings are rectangular in cross section. The disposal area drifts are about 4 m (13 ft) high by 4.3 m (14 ft) wide; the disposal rooms are 4 m (13 ft) high, 10 m (33 ft) wide, and 91.4 m (300 ft) long. Tolerances for all linear dimensions are ±0.5 m. The width of the pillars between rooms is 30.5 m (100 ft). The total excavated volume in the disposal region is 4.36×10^5 m^3 (1.53×10^7 ft^3). The reported design disposal volume is 1.756×10^5 m^3 (6.2×10^6 ft^3) or about 40% of the excavated volume (Bechtel National, Inc., 1986). However, the disposal volume for waste changes depending on the type of containers, waste form, and volume of panel seals. Hence, the design volume is discussed in the description of the containers (Section 3.1.5).

3.1.2 Experimental Region

The experimental region (Figure 3.1-2) is located in the northern portion of the underground facility and consists of over ten rooms, which are used for in situ testing of salt creep and brine inflow (Matalucci, 1988, pp. 3,15). The sizes of the rooms vary, depending on the experiment. The excavated area of the experimental region is about 21.61 x 10^3 m2 (23.2 x 10^4 ft^2), and its volume is about 71.90 x 10^3 m^3 (25.3 x 10^5 ft^3) (Table 3.1-1).

3.1.3 Operations Region

The operations region (Figure 3.1-2) consists of the access drifts located in the center of the underground facility. The drifts are used for transport of equipment and personnel to the experimental area and disposal region. All four shafts are connected to the operations region. The excavated area of the operations region is 21.84 x 10^3 m^2 (23.4 x 10^4 ft^2), and its volume is 78.07 x 10^3 m^3 (27.6 x 10^5 ft^3) (Table 3.1-1).

3.1.4 Shafts

The four shafts connecting the underground facility to the surface are (1) the Air Intake Shaft, 6.2 m (20 ft) in diameter; (2) the Exhaust Shaft, 4.6 m (15 ft) in diameter, (3) the Salt Handling Shaft, 3.6 m (12 ft) in diameter, and (4) the Waste Shaft, 7 m (23 ft) in diameter (Figure 3.1-2).

During operations, the Salt-Handling Shaft will transport personnel, equipment, and salt. The Waste Shaft will transport the waste, and the Air Intake and Exhaust Shafts will provide air flow. The Air Intake Shaft will also serve as a backup for transporting personnel and equipment.

At present, the shaft functions are the same as those described above, except that the Waste Shaft is not currently used to transport waste. It serves as a backup for transport of personnel and materials.

The Air Intake Shaft, the most recently constructed shaft (1988), provides fresh air to the underground. It also serves as a backup for transporting personnel and materials. In addition, in situ testing is being performed to investigate the disturbed rock zone (DRZ) surrounding the shaft and hydrologic properties of the Rustler Formation (Nowak et al., 1990).

The Exhaust Shaft, drilled in 1983-84, serves as the primary air exhaust for the underground facility (Bechtel National, Inc., 1985).

The Salt-Handling Shaft (formerly called the Construction and Salt-Handling [C&SH] Shaft and the Exploratory Shaft [Bechtel National, Inc., 1985]) was drilled in 1981. It was used during construction of the WIPP repository to remove salt and serve as the primary transport for personnel and equipment. The Salt-Handling Shaft continues to serve as the primary transport for personnel and equipment and as a secondary air supply to the underground facility.

The Waste Shaft (initially called the Ventilation Shaft) is designed to move radioactive waste between the surface waste-handling facilities and the underground facility. The Ventilation Shaft was enlarged from 2 m (6 ft) diameter to 6 m (20 ft) diameter in 1983-84, when it was renamed the Waste Shaft (Bechtel National, Inc., 1985). Until waste transport begins, the Waste Shaft serves as a secondary means to transport personnel, materials, large, equipment, and diesel fuel. The Waste Shaft can continue to serve as backup for transporting personnel and materials whenever waste is not being transported.

All four shafts will be sealed and filled upon decommissioning of the WIPP (Nowak et al., 1990).

3.1.5 Waste Containers

Current plans for transporting contact-handled (CH) transuranic (TRU) waste to the WIPP are to ship it in 55-gal steel drums or metal standard waste boxes (SWBs). The dimensions and volumes of a 55-gal steel drum and an SWB are shown in Table 3.1-2. Waste that is currently stored in containers other than 55-gal drums and SWBs will be repackaged into SWBs. TRUPACT II, the transportation container for trucking TRU waste to the WIPP, has space for two 7-pack drums and two SWBs.

The reference canister for the remotely handled (RH) TRU waste is a 0.65-m (26-in.) O.D. (outside diameter) right-circular cylinder made of 1/4-in. carbon steel plate. Caps are welded at both ends. The canister is 3 m (10 ft) in length, including the handling pintle. Inside, the waste occupies about 0.89 m^3 (30 ft^3) (U.S. DOE, 1990c).

Table 3.1-2. CH-TRU Waste Containers (U.S. DOE, 1990a, Dwg 165-F-001-W)

Container Description	Approximate Dimensions (h x w x l) m	Volume Internal m^3	Volume External m^3	Volume Packing m^3
Approved for transportation:				
DOT 17C (metal) 55-gal steel drums	0.892 x 0.602 dia.	0.2082	0.2539	
7-Pack of 55-gal steel drums		1.4574	~ 1.47	~ 2.2
Standard waste box (Dwg 165-F-001-W)	~ 0.94 x 1.8 x 1.3	~ 1.90	~ 1.95	~ 2.34

3.1.6 Waste Placement and Backfill in Rooms

Figure 3.1-3 shows the planned packing configuration of drums in the rooms and drifts. At the waste storage room, the waste packages (7-packs) will be removed from the transporter and stacked 3 high and 6 wide across the room. In the ideal packing configuration, a total of 6,804 drums (972 7-pack units) can be placed in one panel. A 0.7-m air gap exists above the drums; also a thin plastic pallet is set between layers. For the 1991 calculations, the plastic sheet was assumed to be 0.30-cm thick, consistent with the Bechtel initial reference design report (1986). Recently developed final plans (U.S. DOE, 1990c) for the plastic sheet call for 0.004-m-thick plastic on the top and bottom; hence, slightly less salt backfill will be used.

A standard waste box (SWB) stacking configuration is shown in Figure 3.1-4. Seven-packs and SWBs may be intermixed, as practical. To reach the original design capacity of 175,600 m^3 (6.2 x 10^6 ft^3), the SWBs were also assumed to be stacked three high. However, current plans call for stacking the SWBs only two high, which substantially reduces the disposal capacity of the WIPP.

The current placement technique for RH-TRU waste in the WIPP is to emplace one canister horizontally every 2.4 m (8 ft) into the drift and room walls. Based on this technique, the capacity in each panel for RH-TRU canisters along drifts and rooms 10-m wide is 874 canisters or about 6,000 m^3. The intended capacity for RH-TRU waste is 7,080 m^3 (250,000 ft^3); hence, additional methods will be explored. Current PA calculations assume a capacity of 7,080 m^3.

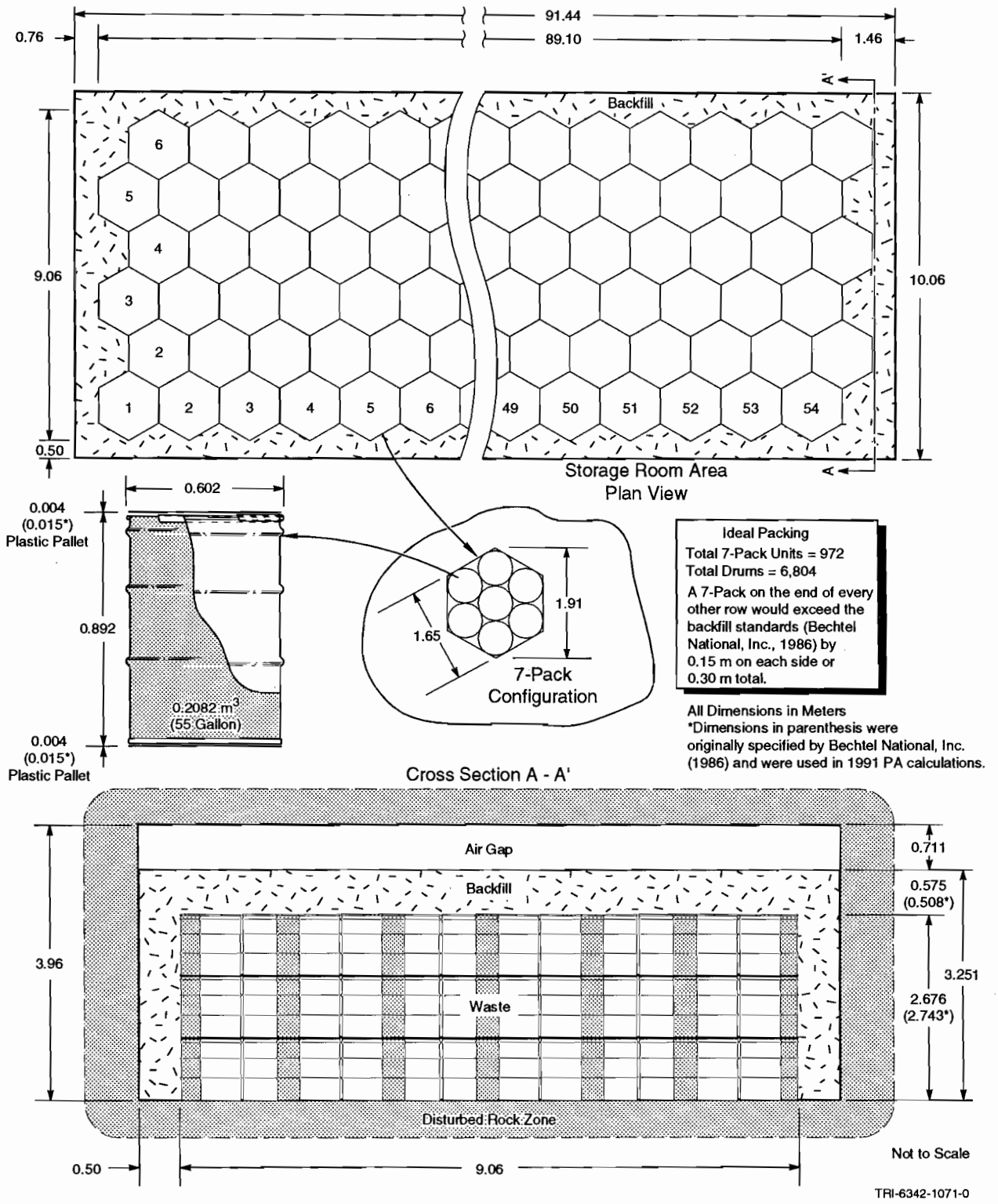

Figure 3.1-3. Ideal packing of drums in rooms and 10-m-wide drifts (not to scale).

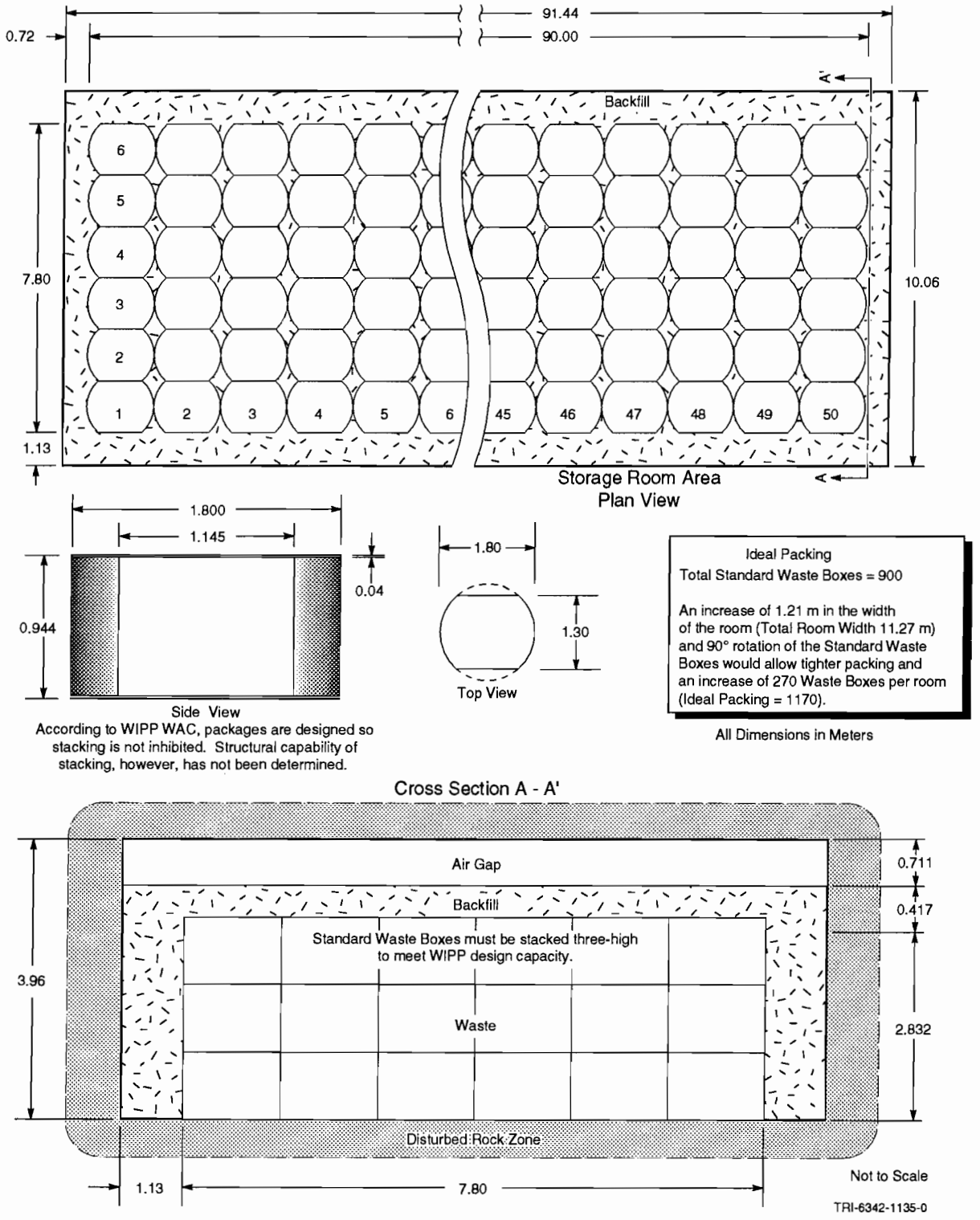

Figure 3.1-4. Ideal packing of Standard Waste Boxes in rooms and drifts (not to scale).

3.2 Parameters for Seals and Fills Outside Disposal Region

Table 3.2-1 summarizes material-property parameters (such as permeability and porosity) for seals and fills placed in the shafts and access drifts when WIPP is decommissioned.

Table 3.2-1. Parameter Values for Seals Outside Disposal Region

Parameter	Median	Range		Units	Distribution Type	Discussion and Sources in:
Preconsolidated crushed salt (Lower shaft, drifts, panels)						
Density (ρ)						
Initial	1.71×10^3 (0.8ρ Salado halite)			kg/m^3	Constant	WIPP PA Division, 1991, Vol 3, Section 3.2.2
Final	2.03×10^3 (0.95ρ Salado halite)			kg/m^3	Constant	WIPP PA Division, 1991, Vol 3, Section 3.2.2
Height (Lower shaft)	2×10^2	1×10^2	3×10^2	m	Uniform	WIPP PA Division, 1991, Vol 3, Section 3.2.2
Permeability (k)						
Initial	1×10^{-14}			m^2	Constant	WIPP PA Division, 1991, Vol 3, Section 3.2.2
Final	1×10^{-20}	3.3×10^{-21}	3.3×10^{-20}	m^2	Lognormal	WIPP PA Division, 1991, Vol 3, Section 3.2.2
Crushed salt backfill in drifts						
Density (ρ)						
Initial	1.28×10^3 (0.6ρ Salado halite)			kg/m^3	Constant	WIPP PA Division, 1991, Vol 3, Section 3.2.3
Final	2.03×10^3 (0.95ρ Salado halite)			kg/m^3	Constant	WIPP PA Division, 1991, Vol 3, Section 3.2.3
Permeability (k)						
Initial	1×10^{-11}			m^2	Constant	WIPP PA Division, 1991, Vol 3, Section 3.2.3
Final	1×10^{-20}	3.3×10^{-21}	3.3×10^{-20}	m^2	Lognormal	WIPP PA Division, 1991, Vol 3, Section 3.2.3
Partition coefficients for crushed salt						
Am	1×10^{-4}			m^3/kg	Constant	WIPP PA Division, 1991, Vol 3, Section 3.2.4
Np	1×10^{-5}			m^3/kg	Constant	WIPP PA Division, 1991, Vol 3, Section 3.2.4
Pb	1×10^{-6}			m^3/kg	Constant	WIPP PA Division, 1991, Vol 3, Section 3.2.4
Pu	1×10^{-4}			m^3/kg	Constant	WIPP PA Division, 1991, Vol 3, Section 3.2.4
Ra	1×10^{-6}			m^3/kg	Constant	WIPP PA Division, 1991, Vol 3, Section 3.2.4
Th	1×10^{-4}			m^3/kg	Constant	WIPP PA Division, 1991, Vol 3, Section 3.2.4
U	1×10^{-6}			m^3/kg	Constant	WIPP PA Division, 1991, Vol 3, Section 3.2.4
Concrete and Bentonite						
Permeability (k)						
Concrete	2.7×10^{-19}			m^2	Constant	WIPP PA Division, 1991, Vol 3, Section 3.2.5
Bentonite	1.4×10^{-19}			m^2	Constant	WIPP PA Division, 1991, Vol 3, Section 3.2.5

3.2.1 Description of the Reference Seal System Design

The purpose of the reference seal design, which Sandia has developed for sealing the WIPP repository, is to provide a common basis for calculations performed in modeling tasks such as performance assessment and sensitivity analysis (Nowak and Tyler, 1989; Nowak et al., 1990). The reference design is a starting point for developing experiments and analysis from which a detailed design will evolve.

GENERAL SEALING STRATEGY

In general, the entire underground facility and shafts will be sealed. As part of the reference design, portions of the backfill emplaced at several locations within the shafts and various drifts, which are specially prepared (i.e., preconsolidated salt with concrete plugs), are often termed "seals." However, the purpose of these prepared portions is not to act as the sole seal for the shaft or drift (in general, all the backfill fulfills this function), but instead to protect sections of the backfill from fluids (gases or liquids). Inhibiting fluids hastens backfill consolidation and thus greatly increases the probability that the salt backfill will rapidly (< 100 yr) assume properties near to those of the surrounding host rock.

The strategy for sealing specially prepared portions of the drift and shaft combines short- and long-term seal components; preconsolidated crushed salt is the principal long-term component in the Salado Formation salt. Clay -- a swelling clay material shown to be stable and to have low permeability to brines -- is the principal long-term component in the Rustler Formation. Concrete is the principal short-term component in both locations.

The combination of short- and long-term seals is used so that short-term seals provide the initial sealing functions necessary until the long-term seal components become adequately reconsolidated (Nowak et al., 1990). Preconsolidated crushed-salt and clay components are expected to become fully functional for sealing within 100 yr after emplacement (Nowak and Stormont, 1987; Arguello, 1988). Then the long-term seals take over all sealing functions.

Short-term seal components consist of concretes and clay materials developed specifically for the WIPP. The concrete components provide flow resistance to control the effects of possible gas generation in the waste disposal area and limit water inflow from above to protect the crushed salt from saturation with brine; they also provide physical containment for the swelling clay and consolidating crushed-salt materials (Nowak et al., 1990).

The long-term seals in the Salado consist of preconsolidated WIPP crushed salt in the shafts, drifts, and panel entries. The emplaced crushed-salt material is intended to have an initial density equal to 80% of the density of the intact WIPP host rock salt (80% relative density) (Nowak et al., 1990). Within 100 yr of emplacement, the preconsolidated salt backfill will be fully consolidated by creep closure of the host-rock salt to a state of low permeability, approximately 1×10^{-20} m^2 (Nowak and Stormont, 1987; Arguello, 1988; Lappin et al., 1989). This permeability value is in the expected permeability range for the host-rock salt (1×10^{-21} to 1×10^{-20}) (Nowak et al., 1988; Lappin et al., 1989), but it is on the high side of the range suggested by Gorham et al. (June 15, 1992, Memo in Appendix A). Very little compositional difference between the saturated, reconsolidated WIPP crushed-salt material and the surrounding host rock from which it was mined is anticipated. The crushed-salt seals, therefore, are expected to be mechanically and chemically stable in the WIPP environment (Nowak et al., 1990).

SEAL LOCATIONS

In the reference design, multicomponent seals between 30 and 40 m (100 and 130 ft) long will be in each of the four shafts, the entrances to the waste disposal panels, and selected access drifts (Nowak et al., 1990). (See Figures 3.1-1 and 3.1-2 for seal locations.) Seals near the Rustler Formation (upper shaft and water-bearing zone seals) serve to limit brine flow from water-bearing zones down into the crushed-salt backfill. Seals in the drifts serve to reduce fluid flow (gas and brine) from the repository area and thus limit the creation of a preferred pathway for contaminant migration. The drift entries to each filled disposal panel will be sealed during operations. The disturbed rock zone (DRZ), which occurs in the host-rock salt at the excavated openings, is expected to heal by creep closure (Nowak et

al., 1990). The extent of a DRZ in the drift entries may be reduced by the use of concrete liners during operations. If necessary, however, the conceptual design for sealing the DRZ (both in drifts and shafts) and anhydrite interbeds (e.g., MB139 directly underneath the disposal area) envisions a salt-based grout (Nowak and Tyler, 1989) using grouting techniques that are currently under development (Figure 3.2-3). When all disposal panels are filled, the drift entries to the entire disposal area will be sealed. The shafts will be backfilled upon decommissioning of the WIPP (Figures 3.2-1 and 3.2-2) (Nowak et al., 1990).

BACKFILL IN UPPER SHAFT, WATER-BEARING ZONE, AND DEWEY LAKE RED BEDS

According to current calculations, radionuclides will not reach the upper shaft in 10,000 yr. Therefore, the actual properties of the backfill in the upper shaft and above have not been used in the 1992 PA calculations and properties are not given. Instead the initial placement properties of the lower shaft have been used.

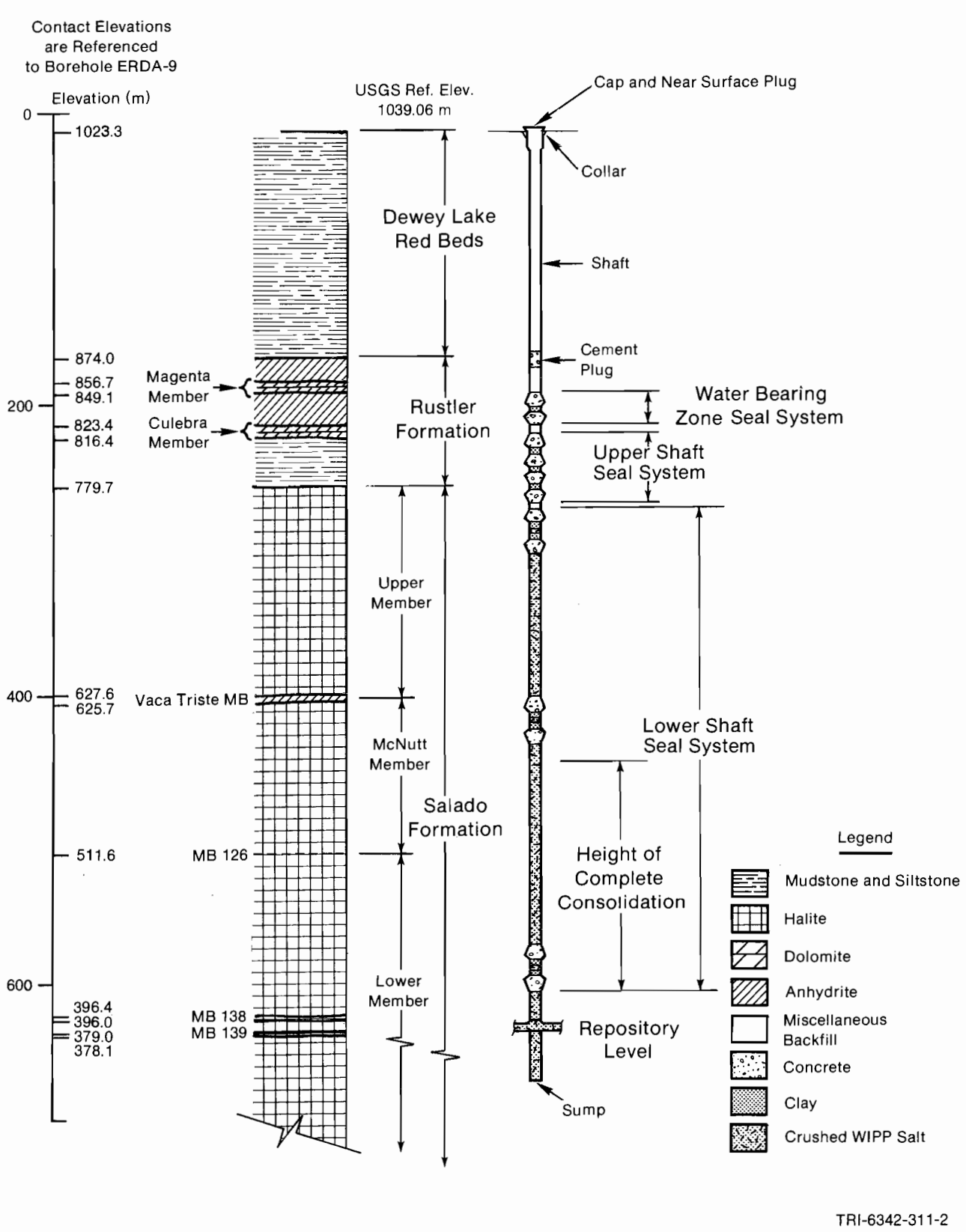

Figure 3.2-1. Diagram of typical sealed and backfilled access shaft (after Nowak et al., 1990).

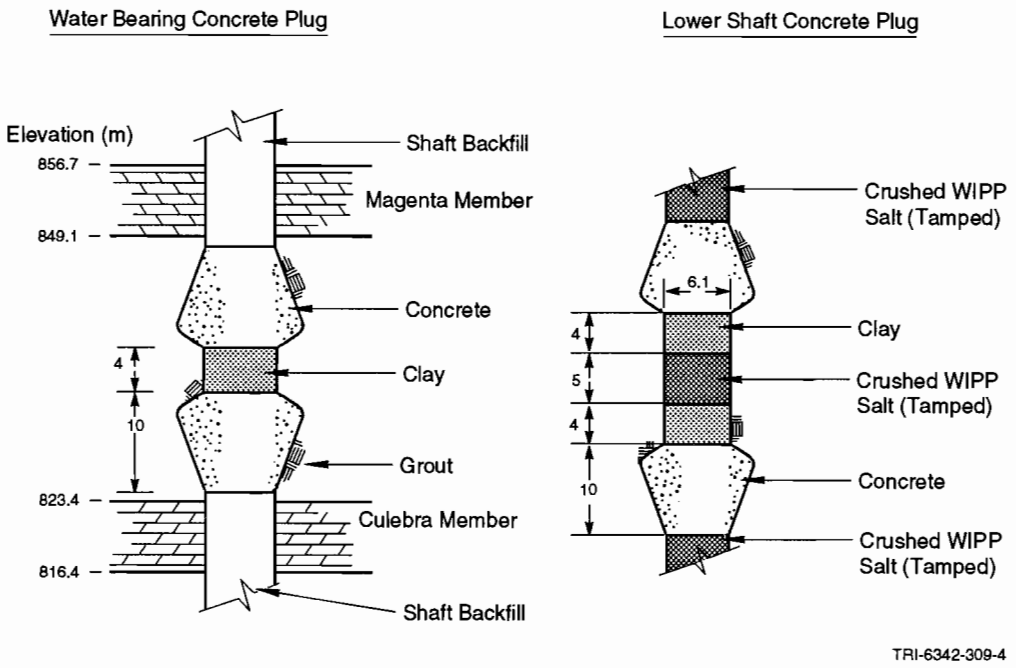

Figure 3.2-2. Diagram of typical concrete plugs in backfilled shafts. The drawing shows concrete plugs between water-bearing units (e.g., Culebra Dolomite) (left) and for the Lower Shaft Backfill (e.g., at Vaca Triste) for Waste Shaft (right) (after Nowak et al., 1990).

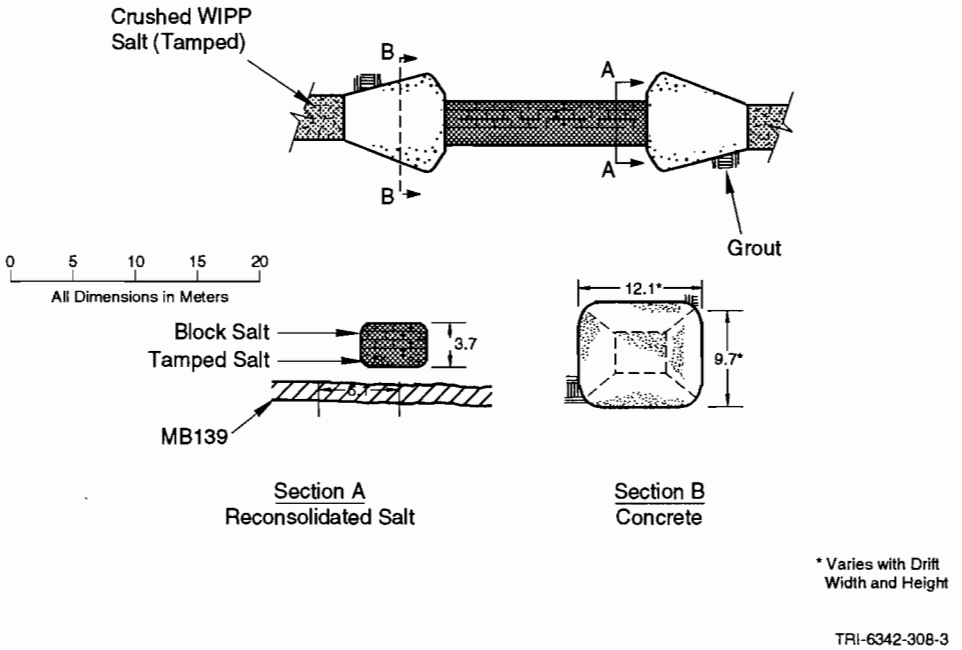

Figure 3.2-3. Diagram of typical concrete and preconsolidated salt backfill for drifts and panels (after Nowak et al., 1990). Scale applies to horizontal dimensions; vertical dimensions are exaggerated.

3.2.2 Preconsolidated Salt in Lower Shaft, Drifts, and Panels

The reference seal uses preconsolidated (tamped) crushed WIPP salt as the primary long-term seal material. For redundancy, concrete plugs and clay (Figure 3.2-2) are emplaced at three locations in the shaft: (1) near the bottom of the shaft, (2) at an intermediate position in the shaft just below the Vaca Triste Marker Bed (Figure 3.2-1), and (3) near the top of the Salado Formation.

The emplaced WIPP crushed salt is intended to have an initial density equal to 80% of the density of the intact WIPP host rock salt (80% relative density). Salt with 80% relative density will be created either by pouring and tamping crushed salt or by laying preconsolidated salt blocks. Creep closure of the lower part of the shaft will continue to consolidate this crushed salt.

3.3 Parameters for Contaminants Independent of Waste Form

The TRU waste for which the WIPP is designed is defense-program waste that has been generated at ten facilities since 1970. The waste consists of laboratory and production waste such as glassware, metal pipes, sorbed or solidified spent solvents, disposable laboratory clothing, cleaning rags, and solidified sludges. Current plans specify that most of the TRU waste generated since 1970 will be placed in the WIPP repository, with the remainder to be disposed of at other DOE facilities.

As of 1992, the ten TRU waste generator and/or storage sites that are scheduled to ship waste to the WIPP are (1) Argonne National Laboratory-East (ANL-E), Illinois; (2) Hanford Reservation (HANF), Washington; (3) Idaho National Engineering Laboratory (INEL), Idaho; (4) Los Alamos National Laboratory (LANL), New Mexico; (5) Lawrence Livermore National Laboratory (LLNL), California; (6) Mound Laboratory, Ohio; (7) Nevada Test Site (NTS), Nevada; (8) Oak Ridge National Laboratory (ORNL), Tennessee; (9) Rocky Flats Plant (RFP), Colorado; and (10) Savannah River Site (SRS), South Carolina (U.S. DOE, 1990d).

The TRU waste is contaminated by alpha-emitting transuranic elements, defined as having atomic numbers greater than uranium-92, half-lives greater than 20 yr, and curie contents greater than 100 nCi/g. Other contaminants include uranium and several radionuclides with half-lives less than 20 yr. Approximately 60% of the waste may be co-contaminated with waste considered hazardous under the RCRA, e.g., lead (WEC, 1990).

Radioactive waste that emits alpha radiation, although dangerous if inhaled or ingested, is not hazardous externally. Most of the waste, therefore, can be contact handled (CH) because the external dose rate (5.6×10^{-7} Sv/s [200 mrem/h] or less) permits people to handle drums and boxes without any special shielding.

A small portion of the TRU waste must be transported and handled in shielded casks (remotely handled [RH]), i.e., the surface dose rate exceeds 5.6×10^{-7} Sv/s (200 mrem/h). The surface dose rate of an RH-TRU canister cannot exceed 2.8×10^{-3} Sv/s (1000 rem/h); but no more than 5% of the canisters can exceed 2.8×10^{-4} Sv/s (100 rem/h) (U.S. DOE, 1990d). The volume must be less than 250,000 m^3 and the curie content must be less than 5.1×10^{6} Ci (1.89×10^{17} Bq) according to the agreement between DOE and the State of New Mexico (U.S. DOE and NM, 1984).

Subpart B of the Standard sets release limits in curies for isotopes of americium, carbon, cesium, iodine, neptunium, plutonium, radium, strontium, technetium, thorium, tin, and uranium, as well as for certain other radionuclides (Section 3.3.4 of this volume). Although the initial WIPP inventory contains little or none of some of the listed nuclides, they may be produced as a result of radioactive decay and must be accounted for in the compliance evaluation; moreover, any radionuclides not listed in Subpart B must be accounted for if those radionuclides would contribute to doses used in NEPA calculations (e.g., Pb-210).

3.3.1 Inventory of Radionuclides in Contact-Handled Transuranic Waste

The 1991 inventory (curie content) of radionuclides in the CH-TRU waste was estimated from input submitted to the 1990 Integrated Data Base (IDB) (U.S. DOE, 1990d). The information submitted to the IDB is separated into retrievably stored and newly generated (future generation) waste referred to herein as projected inventory. The anticipated total volume (stored plus projected) of CH-TRU waste submitted to the 1990 IDB was 1.0×10^5 m^3 (3.76×10^6 ft^3), which is less than the current design volume for the WIPP of about 1.8×10^5 m^3 (6.2×10^6 ft^3). To estimate the total curie content in the WIPP, if it contained a design volume of CH-TRU waste, the future-generated radionuclide inventories of the five largest future generators listed in the 1990 IDB were volume scaled to reach a design volume of waste. (Details of this volume scaling are discussed in Section 3.4.) This inventory per generator site is only a design estimate and should not be considered a statement of what they will generate.

The weight fractions reported in the 1990 IDB were used to calculate the major radionuclides of the mixes reported. The IDB did not report the inventory of each radionuclide. Rather, the inventory of each radionuclide at each site was based on the mix of waste streams reported. The Hanford submittal to the 1990 IDB indicated that the activity of some of the CH-TRU waste was currently unknown. Rather than underestimate the potential inventory, the Hanford input to the 1987 IDB was used. These inventories have not been independently checked and should be considered preliminary estimates.

Modifications to the radionuclide inventories in the 1990 IDB were made in 1992 (Peterson, October 28, 1992, Memo in Appendix A). These modifications are reflected in Table 3.3-1 which lists both CH and RH inventories.

Table 3.3-1. Inventory and Parameter Values for TRU Radioisotopes

Parameter	Median	Units	Source
Ac225			
Half-life	8.640×10^{5}	s	ICRP, Pub 38, 1983
Ac227			
Half-life	6.871×10^{8}	s	ICRP, Pub 38, 1983
Ac228			
Half-life	2.207×10^{4}	s	ICRP, Pub 38, 1983
Am241			
Activity conversion	3.43×10^{3}	Ci/kg	1.1281×10^{16}/(half-life(s)xAt.Wt.)
Half-life	1.364×10^{10}	s	ICRP, Pub 38, 1983
Inventory, Anticipated (1990)			
CH	6.65×10^{5}	Ci	
RH	1.29×10^{3}	Ci	U.S. DOE, 1990d; Peterson, 1990
Inventory, Design (1992)			
CH	7.14×10^{5}	Ci	Peterson, October 28, 1992
RH	1.06×10^{3}	Ci	(Memo in Appendix A)
Am243			
Half-life	5.822×10^{11}	s	ICRP, Pub 38, 1983
At217			
Half-life	3.230×10^{-2}	s	ICRP, Pub 38, 1983
Bi210			
Half-life	4.330×10^{5}	s	ICRP, Pub 38, 1983
Bi211			
Half-life	1.284×10^{2}	s	ICRP, Pub 38, 1983
Bi212			
Half-life	3.633×10^{3}	s	ICRP, Pub 38, 1983
Bi213			
Half-life	2.739×10^{3}	s	ICRP, Pub 38, 1983
Bi214			
Half-life	1.194×10^{3}	s	ICRP, Pub 38, 1983
Cf252			
Activity conversion	5.38×10^{5}	Ci/kg	1.1281×10^{16}/(half-life(s)xAt.Wt.)
Half-life	8.325×10^{7}	s	ICRP, Pub 38, 1983
Inventory, Anticipated (1990)			
CH	1.27×10^{4}	Ci	
RH	2.39×10^{3}	Ci	U.S. DOE, 1990d; Peterson, 1990
Inventory, Design (1992)			
CH	3.37×10^{2}	Ci	Peterson, October 28, 1992
RH	8.63×10^{1}	Ci	(Memo in Appendix A)
Cm244			
Activity conversion	8.09×10^{4}	Ci/kg	1.1281×10^{16}/(half-life(s)xAt.Wt.)
Half-life	5.715×10^{8}	s	ICRP, Pub 38, 1983

Table 3.3-1. Inventory and Parameter Values for TRU Radioisotopes (Continued)

Parameter	Median	Units	Source
Inventory, Anticipated (1990)			
CH	1.23×10^{4}	Ci	
RH	8.75×10^{3}	Ci	U.S. DOE, 1990d; Peterson, 1990
Inventory, Design (1992)			
CH	2.06×10^{4}	Ci	Peterson, October 28, 1992
RH	4.26×10^{3}	Ci	(Memo in Appendix A)
Cs137			
Activity conversion	8.70×10^{4}	Ci/kg	1.1281×10^{16}/(half-life(s)xAt.Wt.)
Half-life	9.467×10^{8}	s	ICRP, Pub 38, 1983
Inventory, Anticipated (1990)			
RH	3.33×10^{5}	Ci	U.S. DOE, 1990d; Peterson, 1990
Inventory, Design (1992)			
CH	6.30×10^{4}	Ci	Peterson, October 28, 1992
RH	5.70×10^{5}		(Memo in Appendix A)
Fr221			
Half-life	2.880×10^{2}	s	ICRP, Pub 38, 1983
Np237			
Activity conversion	7.05×10^{-1}	Ci/kg	1.1281×10^{16}/(half-life(s)xAt.Wt.)
Half-life	6.753×10^{13}	s	ICRP, Pub 38, 1983
Inventory, Anticipated (1990)			
CH	1.47	Ci	
RH	8.87×10^{-1}	Ci	U.S. DOE, 1990d; Peterson, 1990
Inventory, Design (1992)			
CH	20.8	Ci	Peterson, October 28, 1992
RH	9.20×10^{-1}	Ci	(Memo in Appendix A)
Np239			
Half-life	2.035×10^{5}	s	ICRP, Pub 38, 1983
Pa231			
Half-life	1.034×10^{12}	s	ICRP, Pub 38, 1983
Pa233			
Half-life	2.333×10^{6}	s	ICRP, Pub 38, 1983
Pb209			
Half-life	1.171×10^{4}	s	ICRP, Pub 38, 1983
Pb210			
Activity conversion	7.63×10^{4}	Ci/kg	1.1281×10^{16}/(half-life(s)xAt.Wt.)
Half-life	7.037×10^{8}	s	ICRP, Pub 38, 1983
Pb211			
Half-life	2.166×10^{3}	s	ICRP, Pub 38, 1983
Pb212			
Half-life	3.830×10^{4}	s	ICRP, Pub 38, 1983
Pb214			
Half-life	1.608×10^{3}	s	ICRP, Pub 38, 1983

Table 3.3-1. Inventory and Parameter Values for TRU Radioisotopes (Continued)

Parameter	Median	Units	Source
Pm147			
Activity conversion	9.27×10^{5}	Ci/kg	1.1281×10^{16}/(half-life(s)xAt.Wt.)
Half-life	8.279×10^{7}	s	ICRP, Pub 38, 1983
Inventory, Anticipated (1990)			
RH	3.15×10^{5}	Ci	U.S. DOE, 1990d; Peterson, 1990
Inventory, Design (1992)			
CH	7.60×10^{4}	Ci	Peterson, October 28, 1992
RH	5.36×10^{5}		(Memo in Appendix A)
Po210			
Half-life	1.196×10^{7}	s	ICRP, Pub 38, 1983
Po212			
Half-life	3.050×10^{-7}	s	ICRP, Pub 38, 1983
Po213			
Half-life	4.200×10^{-6}	s	ICRP, Pub 38, 1983
Po214			
Half-life	1.643×10^{-4}	s	ICRP, Pub 38, 1983
Po215			
Half-life	1.780×10^{-3}	s	ICRP, Pub 38, 1983
Po216			
Half-life	1.500×10^{-1}	s	ICRP, Pub 38, 1983
Po218			
Half-life	1.830×10^{2}	s	ICRP, Pub 38, 1983
Pu238			
Activity conversion	1.71×10^{4}	Ci/kg	1.1281×10^{16}/(half-life(s)xAt.Wt.)
Half-life	2.769×10^{9}	s	ICRP, Pub 38, 1983
Inventory, Anticipated (1990)			
CH	4.26×10^{6}	Ci	
RH	5.14×10^{2}	Ci	U.S. DOE, 1990d; Peterson, 1990
Inventory, Design (1992)			
CH	3.06×10^{6}	Ci	Peterson, October 28, 1992
RH	2.73×10^{4}	Ci	(Memo in Appendix A)
Pu239			
Activity conversion	6.22×10^{1}	Ci/kg	1.1281×10^{16}/(half-life(s)xAt.Wt.)
Half-life	7.594×10^{11}	s	ICRP, Pub 38, 1983
Inventory, Anticipated (1990)			
CH	4.37×10^{5}	Ci	
RH	1.16×10^{3}	Ci	U.S. DOE, 1990d; Peterson, 1990
Inventory, Design (1992)			
CH	3.35×10^{5}	Ci	Peterson, October 28, 1992
RH	8.50×10^{3}	Ci	(Memo in Appendix A)

Table 3.3-1. Inventory and Parameter Values for TRU Radioisotopes (Continued)

Parameter	Median	Units	Source
Pu240			
Activity conversion	2.28×10^{2}	Ci/kg	1.1281×10^{16}/(half-life(s)xAt.Wt.)
Half-life	2.063×10^{11}	s	ICRP, Pub 38, 1983
Inventory, Anticipated (1990)			
CH	5.91×10^{4}	Ci	
RH	2.89×10^{2}	Ci	U.S. DOE, 1990d; Peterson, 1990
Inventory, Design (1992)			
CH	1.00×10^{5}	Ci	Peterson, October 28, 1992
RH	2.28×10^{3}	Ci	(Memo in Appendix A)
Pu241			
Activity conversion	1.03×10^{5}	Ci/kg	1.1281x1016/half-life(s)xAt.Wt.)
Half-life	4.544×10^{8}	s	ICRP, Pub 38, 1983
Inventory, Anticipated (1990)			
CH	2.54×10^{6}	Ci	
RH	1.32×10^{4}	Ci	U.S. DOE, 1990d; Peterson, 1990
Inventory, Design (1992)			
CH	3.60×10^{6}	Ci	Peterson, October 28, 1992
RH	1.20×10^{5}	Ci	(Memo in Appendix A)
Pu242			
Activity conversion	3.93	Ci/kg	1.1281×10^{16}/(half-life(s)xAt.Wt.)
Half-life	1.187×10^{13}	s	ICRP, Pub 38, 1983
Inventory, Anticipated (1990)			
CH	1.84	Ci	
RH	3.31×10^{-3}	Ci	U.S. DOE, 1990d; Peterson, 1990
Inventory, Design (1992)			
CH	23.5	Ci	Peterson, October 28, 1992
RH	2.94	Ci	(Memo in Appendix A)
Ra223			
Half-life	9.879×10^{5}	s	ICRP, Pub 38, 1983
Ra224			
Half-life	3.162×10^{5}	s	ICRP, Pub 38, 1983
Ra225			
Half-life	1.279×10^{6}	s	ICRP, Pub 38, 1983
Ra226			
Activity conversion	9.89×10^{2}	Ci/kg	1.1281×10^{16}/(half-life(s)xAt.Wt.)
Half-life	5.049×10^{10}	s	ICRP, Pub 38, 1983
Ra228			
Half-life	1.815×10^{8}	s	ICRP, Pub 38, 1983
Rn219			
Half-life	3.960	s	ICRP, Pub 38, 1983
Rn220			
Half-life	5.560×10^{1}	s	ICRP, Pub 38, 1983

Table 3.3-1. Inventory and Parameter Values for TRU Radioisotopes (Continued)

Parameter	Median	Units	Source
Rn222			
Half-life	3.304×10^{5}	s	ICRP, Pub 38, 1983
Sr90			
Activity conversion	1.36×10^{5}	Ci/kg	1.1281×10^{16}/(half-life(s)xAt.Wt.)
Half-life	9.189×10^{8}	s	ICRP, Pub 38, 1983
Inventory, Anticipated (1990)			
RH	2.80×10^{5}	Ci	U.S. DOE, 1990d; Peterson, 1990
Inventory, Design (1992)			
CH	8.23×10^{4}	Ci	Peterson, October 28, 1992
RH	5.21×10^{5}		(Memo in Appendix A)
Th227			
Half-life	1.617×10^{6}	s	ICRP, Pub 38, 1983
Th228			
Half-life	6.037×10^{7}	s	ICRP, Pub 38, 1983
Th229			
Activity conversion	2.13×10^{2}	Ci/kg	1.1281×10^{16}/(half-life(s)xAt.Wt.)
Half-life	2.316×10^{11}	s	ICRP, Pub 38, 1983
Th230			
Activity conversion	2.02×10^{1}	Ci/kg	1.1281×10^{16}/(half-life(s)xAt.Wt.)
Half-life	2.430×10^{12}	s	ICRP, Pub 38, 1983
Th231			
Half-life	9.187×10^{4}	s	ICRP, Pub 38, 1983
Th232			
Activity conversion	1.10×10^{-4}	Ci/kg	1.1281×10^{16}/(half-life(s)xAt.Wt.)
Half-life	4.434×10^{17}	s	ICRP, Pub 38, 1983
Inventory, Anticipated (1990)			
CH	0.0	Ci	
RH	0.0	Ci	U.S. DOE, 1990d; Peterson, 1990
Inventory, Design (1992)			
CH	2.90×10^{-1}	Ci	Peterson, October 28, 1992
RH	5.66	Ci	(Memo in Appendix A)
Th234			
Half-life	2.082×10^{6}	s	ICRP, Pub 38, 1983
Tl207			
Half-life	2.862×10^{2}	s	ICRP, Pub 38, 1983
U233			
Activity conversion	9.68	Ci/kg	1.1281×10^{16}/(half-life(s)xAt.Wt.)
Half-life	5.002×10^{12}	s	ICRP, Pub 38, 1983
Inventory, Anticipated (1990)			
CH	7.18×10^{1}	Ci	Peterson, October 28, 1992
RH	2.86×10^{1}	Ci	(Memo in Appendix A)

Table 3.3-1. Inventory and Parameter Values for TRU Radioisotopes (Concluded)

Parameter	Median	Units	Source
Inventory, Design (1992)			
CH	1.53×10^{3}	Ci	Peterson, October 28, 1992
RH	1.99×10^{2}	Ci	(Memo in Appendix A)
U234			
Activity conversion	6.25	Ci/kg	1.1281×10^{16}/(half-life(s)xAt.Wt.)
Half-life	7.716×10^{12}	s	ICRP, Pub 38, 1983
U235			
Activity conversion	2.16×10^{-3}	Ci/kg	1.1281×10^{16}/(half-life(s)xAt.Wt.)
Half-life	2.221×10^{16}	s	ICRP, Pub 38, 1983
Inventory, Anticipated (1990)			
CH	5.54×10^{-2}	Ci	
RH	1.23×10^{-2}	Ci	U.S. DOE, 1990d; Peterson, 1990
Inventory, Design (1992)			
CH	5.38×10^{-1}	Ci	Peterson, October 28, 1992
RH	6.13×10^{-2}	Ci	(Memo in Appendix A)
U236			
Half-life	7.389×10^{14}	s	ICRP, Pub 38, 1983
U238			
Activity conversion	3.36×10^{-4}	Ci/kg	1.1281×10^{16}/(half-life(s)xAt.Wt.)
Half-life	1.410×10^{17}	s	ICRP, Pub 38, 1983
Inventory, Anticipated (1990)			
CH	0.0	Ci	
RH	7.83×10^{-2}	Ci	U.S. DOE, 1990d; Peterson, 1990
Inventory, Design (1992)			
CH	2.68	Ci	Peterson, October 28, 1992
RH	1.80	Ci	(Memo in Appendix A)

3.3.2 Inventory of Remotely Handled Waste

The 1991 inventory of TRU waste that must be transported and handled in shielded casks because of dose rates at the surface above 200 mrem/hr (remotely handled [RH]) was estimated from the input submitted to the 1990 IDB (U.S. DOE, 1990d). Estimates were made using a similar method to that used for the CH-TRU waste (discussed in Section 3.3.1).* Some differences between the methods for estimating CH and RH were in the estimation of the activity for RH waste reported as mixed fission products and the "unknown" distribution from Hanford. For the mixed fission products, a mixture of 10-yr-old fission products was assumed as the source term. For the Hanford "unknown," a slurry mixture from the Hanford high level waste tanks provided the isotopic distribution; it was estimated that a 2.15×10^{-6} C_i /(kg•s) (30 rem/hr) canister will contain about 450 Ci of gamma emitters. For other mixtures reported in the 1990 IDB, the weight fractions reported were used to calculate the major radionuclides. A volume scaling method similar to that used for CH-TRU waste was used to increase the volume from about 5,300 m^3 (estimated from the 1990 IDB) to the maximum volume of 7,079 m^3.

Modifications to the radionuclide inventories in the 1990 IDB were made in 1992 (Peterson, October 28, 1992, Memo in Appendix A). These modifications are reflected in Table 3.3-1 which lists both CH and RH inventories.

For the 1991 and 1992 PA calculations, the RH-TRU waste was included in the cuttings releases. The RH-TRU waste has not been included in the long-term performance assessment inventory for most previous calculations (Marietta et al., 1989; Lappin et al., 1989; U.S. DOE, 1990b), because RH-TRU waste constituted less than 2% of the activity. Furthermore, the current procedure for emplacing RH waste in the pillar walls will minimize the interaction of the RH waste canisters and the CH-TRU waste rooms. Also a large amount of the activity in RH waste is from radionuclides with relatively short half-lives, which have a small consequence over the long term.

* An alternative method would be to scale the radionuclides so that the activity limit agreed upon by the State of New Mexico and the DOE--5.2×10^6 Ci--would be emplaced instead of the agreed-upon volume limit.

3.3.3 Radionuclide Chains and Half-Lives

The decay chains for the initial radionuclides in the CH and RH inventory are shown in Figures 3.3-1 and 3.3-2, respectively. The half-life for each radionuclide listed in the literature by ICRP Publication 38 (ICRP, Pub 38, 1983) is also on Figure 3.3-1. For reference, the half-lives of the radionuclides in the initial WIPP inventory and decay products are tabulated in Table 3.3-2. The 1992 initial inventories (in Ci) are listed in Table 3.3-1.

Many of the daughter radionuclides have extremely short half-lives, low activities, and make a small contribution to the curie inventory. Shortened chains are used when modeling as follows.

RADIONUCLIDES FOR CUTTINGS AND REPOSITORY MODELING

From the 70 radionuclides shown in Figure 3.3-1, 23 are considered major contributors to the inventory and are used in calculating the radionuclide releases from drilling into the repository and bringing cuttings to the surface and when calculating concentrations within the repository prior to transport to the Culebra. In general, most isotopes of plutonium, thorium, americium, curium, neptunium, californium, radium, and uranium are considered.

The RH inventory decay chains include the chains in the CH inventory shown in Figure 3.3-1 plus the three chains shown in Figure 3.3-2. The radionuclides in the RH cuttings releases included cesium-137, promethium-147, and strontium-90 in addition to all of the radionuclides in the CH releases.

RADIONUCLIDES FOR TRANSPORT MODELING

Nine radionuclides are considered in 1992 PA transport calculations for CH-TRU waste and are highlighted on Figure 3.3-1.

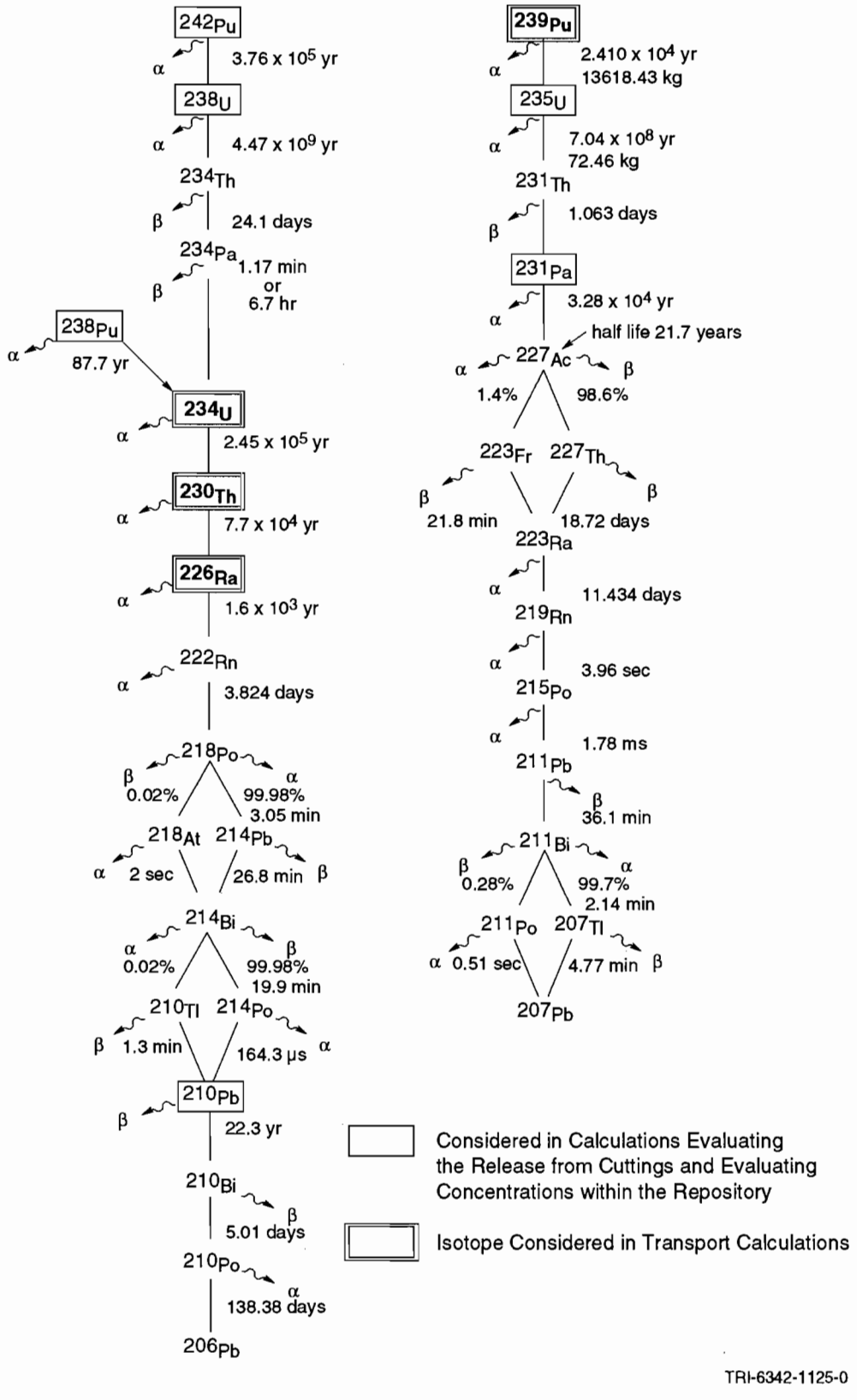

Figure 3.3-1. Decay of CH radionuclide chain in TRU-contaminated waste.

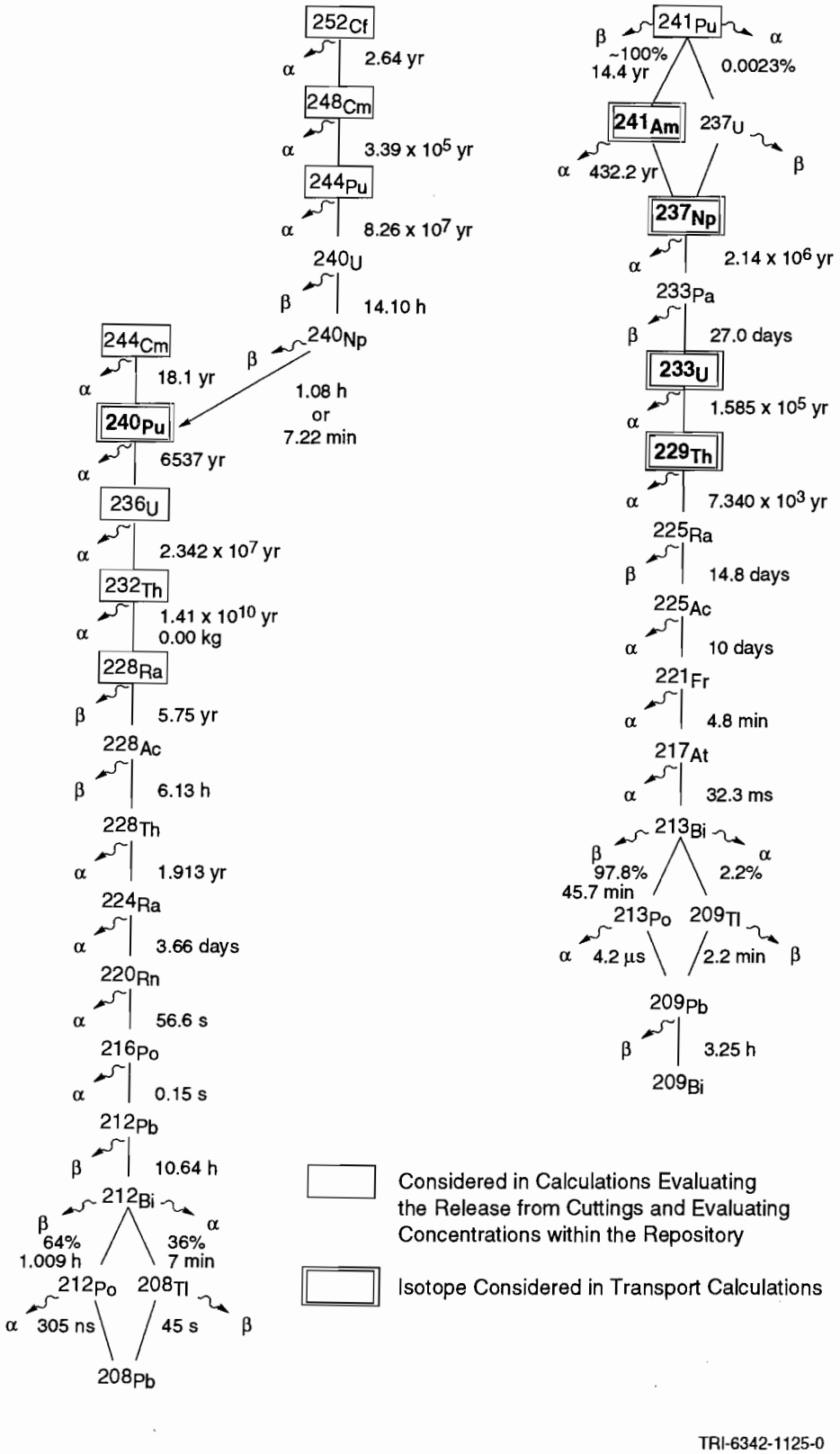

Figure 3.3-1. Decay of CH radionuclide chain in TRU-contaminated waste (concluded).

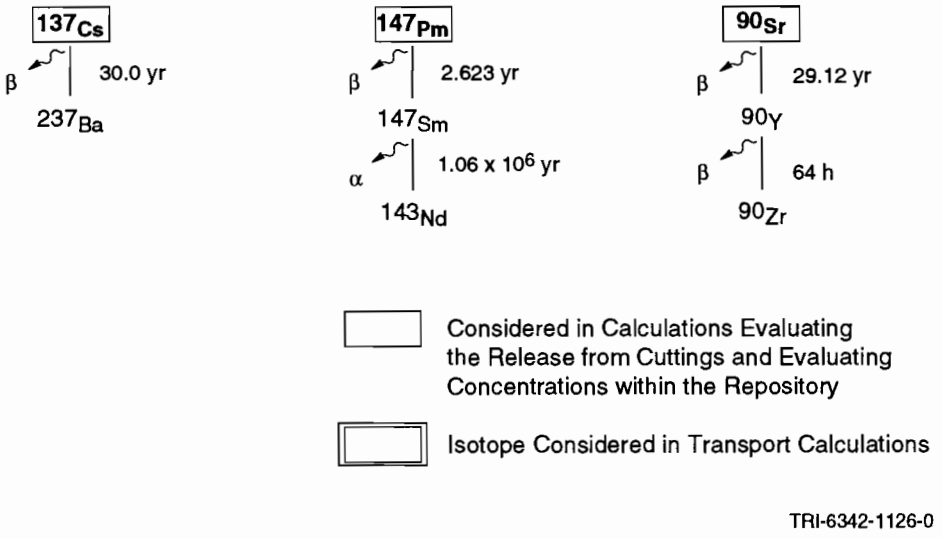

Figure 3.3-2. Decay of RH radionuclide chain in TRU-contaminated waste.

Table 3.3-2. Half-Lives of Isotopes Disposed or Created in WIPP (ICRP, Pub 38, 1983)

Radioisotope		Half-life ($t_{1/2}$) (s)	Reported
Actinium	^{228}Ac	2.207×10^{4}	6.13 h
	^{227}Ac	6.871×10^{8}	2.177×10^{1} yr
	^{225}Ac	8.64×10^{5}	10 day
Americium	^{243}Am	5.822×10^{11}	7.38×10^{3} yr
	^{241}Am	**1.364×10^{10}**	4.322×10^{2} yr
Antimony	^{125}Sb	8.741×10^{7}	2.77 yr
Astatine	^{217}At	3.23×10^{-2}	3.23×10^{-2} s
Barium	^{137m}Ba	1.531×10^{2}	2.552 min
Bismuth	^{214}Bi	1.194×10^{3}	19.9 min
	^{213}Bi	2.739×10^{3}	45.65 min
	^{212}Bi	3.633×10^{3}	60.55 min
	^{211}Bi	1.284×10^{2}	2.14 min
	^{210}Bi	4.33×10^{5}	5.012 day
Californium	**^{252}Cf**	**8.325×10^{7}**	2.638 yr
Cerium	^{144}Ce	2.456×10^{7}	284.3 day
Cesium	**^{137}Cs**	**9.467×10^{8}**	30.0 yr
	^{134}Cs	6.507×10^{7}	2.062 yr
Chromium	^{51}Cr	2.394×10^{6}	27.7 day
Cobalt	^{60}Co	1.663×10^{8}	5.221 yr
	^{58}Co	6.117×10^{6}	70.8 day
Curium	^{248}Cm	1.070×10^{13}	3.39×10^{5} yr
	^{244}Cm	**5.715×10^{8}**	18.11 yr
Europium	^{155}Eu	1.565×10^{8}	4.96 yr
	^{154}Eu	2.777×10^{8}	8.80 yr
	^{152}Eu	4.207×10^{8}	13.53 yr
Francium	^{221}Fr	2.88×10^{2}	4.8 min
Iron	^{59}Fe	3.847×10^{6}	44.53 day
Lead	^{214}Pb	1.608×10^{3}	26.8 min
	^{212}Pb	3.83×10^{4}	10.64 h
	^{211}Pb	2.166×10^{3}	3.61 min
	^{210}Pb	7.037×10^{8}	22.3 yr
	^{209}Pb	1.171×10^{4}	3.253 h
Manganese	^{54}Mn	2.7×10^{7}	312.5 day
Neptunium	^{239}Np	2.035×10^{5}	2.355 day
	^{237}Np	**6.753×10^{13}**	2.14×10^{6} yr
Niobium	^{95}Nb	3.037×10^{6}	35.15 day
Plutonium	^{244}Pu	2.607×10^{15}	8.76×10^{7} yr
	^{242}Pu	**1.187×10^{13}**	3.763×10^{5} yr
	^{241}Pu	**4.544×10^{8}**	14.4 yr
	^{240}Pu	**2.063×10^{11}**	6.537×10^{3} yr
	^{239}Pu	**7.594×10^{11}**	2.407×10^{4} yr
	^{238}Pu	**2.769×10^{9}**	87.74 yr
Polonium	^{218}Po	1.83×10^{2}	3.05 min
	^{216}Po	1.5×10^{-1}	1.5×10^{-1} s
	^{215}Po	1.78×10^{-3}	1.78×10^{-3} s
	^{214}Po	1.643×10^{-4}	1.643×10^{-4} s
	^{213}Po	4.2×10^{-6}	4.2×10^{-6} s
	^{212}Po	3.05×10^{-7}	3.05×10^{-7} s
	^{210}Po	1.196×10^{7}	138.4 day
Praseodymium	^{144}Pr	1.037×10^{3}	17.28 min
Promethium	**^{147}Pm**	**8.279×10^{7}**	2.623 yr

* Bolding indicates isotopes assumed in initial inventory for PA calculations.

Table 3.3-2. Half-Lives of Isotopes Disposed or Created in WIPP (ICRP, Pub 38, 1983) (Concluded)

Radioisotope		Half-life ($t_{1/2}$) (s)	Half-life ($t_{1/2}$) Reported
Protactinium	^{233}Pa	2.333×10^{6}	27 day
	^{231}Pa	1.034×10^{12}	3.276×10^{4} yr
Radium	^{228}Ra	1.815×10^{8}	5.75 yr
	^{226}Ra	5.049×10^{10}	1.6×10^{3} yr
	^{225}Ra	1.279×10^{6}	14.8 day
	^{224}Ra	3.162×10^{5}	3.66 day
	^{223}Ra	9.879×10^{5}	11.43 day
Radon	^{222}Rn	3.304×10^{5}	3.824 day
	^{220}Rn	5.56×10^{1}	5.56×10^{1} s
	^{219}Rn	3.96	3.96 s
Rhodium	^{106}Rh	2.99×10^{1}	2.99×10^{1} s
Ruthenium	^{106}Ru	3.181×10^{7}	3.682×10^{2} day
Strontium	**^{90}Sr***	**9.189×10^{8}**	29.12 yr
Thallium	^{207}Tl	2.862×10^{2}	4.77 min
Thorium	^{234}Th	2.082×10^{6}	24.1 day
	^{232}Th	**4.434×10^{17}**	1.405×10^{10} yr
	^{231}Th	9.187×10^{4}	25.52 h
	^{230}Th	2.43×10^{12}	7.7×10^{3} yr
	^{229}Th	2.316×10^{11}	7.34×10^{3} yr
	^{228}Th	6.037×10^{7}	1.913 yr
	^{227}Th	1.617×10^{6}	18.72 day
Uranium	^{240}U	5.076×10^{4}	1.41×10^{1} hr
	^{238}U	**1.41×10^{17}**	4.468×10^{9} yr
	^{236}U	7.389×10^{14}	2.342×10^{7} yr
	^{235}U	**2.221×10^{16}**	7.038×10^{8} yr
	^{234}U	7.716×10^{12}	2.445×10^{5} yr
	^{233}U	**5.002×10^{12}**	1.585×10^{5} yr
Yttrium	^{90}Y	2.304×10^{5}	64.0 h

* Bolding indicates isotopes assumed in initial inventory for PA calculations.

Note on half-life uncertainties:

Quoted standard errors of radioisotope half-lives are generally small relative to the mean values. This is illustrated by the examples provided below (taken from IAEA, 1986).

Radioisotope	Half-life
^{241}Am	(432.2 ± 0.5) y
^{252}Cf	(2.645 ± 0.008) y
^{244}Cm	(18.10 ± 0.02) y

For this reason, the PA Department regards radioisotope half-lives as precisely known parameters.

3.3.4 40 CFR 191 Release Limits and Waste Unit Factor

40 CFR 191 RELEASE LIMITS

The release limits (L_i) for evaluating compliance with *40 CFR 191 § 13* are provided in Table 3.3-3. These apply to the 1991 inventory: the release limits for 1992 are only slightly different.

Table 3.3-3. 1991 Cumulative Release Limits (L_i) to the Accessible Environment 10,000 Yr after Disposal for Evaluating Compliance with Containment Requirements (after EPA, 1985, Appendix A, Table 1)

Radionuclide	Release limit (Li) per 1 x 10^6 Ci α-emitting TRU nuclide with $t_{1/2}$ > 20 yr* (Ci)	1991 PA Release Limits $f_m L_i$** (Ci)
Americium (Am) -241 or -243	100	1187
Carbon (C) -14	100	1187
Cesium (Cs) -135 or -137	1000	11870
Iodine (I) -129	100	1187
Neptunium (Np) -237	100	1187
Plutonium (Pu) -238, -239, -240, or -242	100	1187
Radium (Ra) -226	100	1187
Strontium (Sr) -90	1000	11870
Technetium (Tc) -99	10000	118700
Thorium (Th) -230 or -232	10	118.7
Tin (Sn) -126	1000	11870
Uranium (U) -233, -234, -235, -236, or -238	100	1187
Any other α-emitting radionuclide with $t_{1/2}$ > 20 yr	100	1187
Any other non α-emitting radionuclide with $t_{1/2}$ > 20 yr	1000	11870

* Other units of waste described in EPA, 1985, Appendix A (40 CFR 191)
** 1992 PA release limits are not significantly different from those of 1991.

WASTE UNIT FACTOR

The waste unit factor (f_m) is the inventory in curies of transuranic (TRU) α-emitting radionuclides in the waste with half-lives greater than 20 yr divided by 10^6 Ci, where TRU is defined as radionuclides with atomic weights *greater* than uranium (92). Consequently, as currently defined in *40 CFR 191*, all TRU radioactivity in the waste cannot be included when calculating the waste unit factor. For the WIPP, 1.187 x 10^7 Ci of the 1991 radioactivity design total of 1.814 x 10^7 Ci came from TRU α-emitting radionuclides with half-lives greater than 20 yr (see Tables 3.3-5 and 3.3-6, WIPP PA Division, 1991, vol. 3). Regardless of the waste unit, the WIPP has assumed that all nuclides listed in Tables 3.3-1 and 3.3-2 are regulated and must be included in the release calculations. Therefore, the release limits (L_i) used by the WIPP are reduced somewhat (i.e., more restrictive).

3.3.5 Chemical and Physical Parameters of TRU Wastes

Some of the chemical and physical parameters needed for modeling the behavior of TRU wastes are summarized in Table 3.3-4. Other parameters connected with the waste forms plus their containers are discussed in Section 3.4.

Table 3.3-4. Chemical and Physical Parameters of TRU Waste

Parameter[a]	Median	Range		Units	Distribution Type	Source
Gas generation						
Corrosion						
Inundated rate	**6.3×10^{-9}**	**0**	**1.3×10^{-8}**	**mol/(m^2•s)[b]**	**Constructed**	**Brush, 1991**
Relative humid rate	**1×10^{-1}**	**0**	**5×10^{-1}**	**none**	**Constructed**	**Brush, 1991**
Microbiological						
Inundated rate	**3.2×10^{-9}**	**0**	**1.6×10^{-8}**	**mol/(kg•s)[c]**	**Constructed**	**Brush, 1991**
Relative humid rate	**1×10^{-1}**	**0**	**2×10^{-1}**	**none**	**Uniform**	**Brush, 1991**
Radiolysis	1×10^{-4}			mol/drum/yr	Constant	Brush, 1991
Gas generation stoichiometry factor						
Corrosion	**5×10^{-1}**	**0**	**1**	**none**	**Uniform**	**Brush and Anderson in Lappin et al., 1989, p. A-6**
Microbiological	**8.35×10^{-1}**	**0**	**1.67**	**none**	**Uniform**	**Brush and Anderson in Lappin et al., 1989, p. A-10**
Am						
Diffusion coefficient[d]	1.76×10^{-10}	5.3×10^{-11}	3×10^{-10}	m^2/s	Uniform	Lappin et al.,1989, Table E-7
Am						
Solubility	**-9.00**	**-13.3**	**0.0**	**log (Molar)**	**Constructed**	**See Section 3.3.5**
Cm						
Diffusion coefficient	1.76×10^{-10}	5.3×10^{-11}	3×10^{-10}	m^2/s	Uniform	Lappin et al.,1989, Table E-7
Cm						
Solubility	-9.00	-13.3	0.0	log (Molar)	Constructed	See Section 3.3.5
Np						
Diffusion coefficient	1.76×10^{-10}	5.2×10^{-11}	3×10^{-10}	m^2/s	Uniform	Lappin et al.,1989, Table E-7
Np						
Solubility	**-6.99**	**-15.5**	**-2.00**	**log (Molar)**	**Constructed**	**See Section 3.3.5**
Pb						
Diffusion coefficient	4×10^{-10}	2×10^{-10}	8×10^{-10}	m^2/s	Constructed	Lappin et al.,1989, Table E-7
Pb						
Solubility	0.210	-2.00	-1.00	log (Molar)	Constructed	See Section 3.3.5
Pu						
Diffusion coefficient	1.74×10^{-10}	4.8×10^{-11}	3×10^{-10}	m^2/s	Uniform	Lappin et al.,1989, Table E-7
Pu						
Solubility	**-9.22**	**-16.5**	**-3.4**	**log (Molar)**	**Constructed**	**See Section 3.3.5**
Ra						
Diffusion coefficient	3.75×10^{-10}	1.88×10^{-10}	7.5×10^{-10}	m^2/s	Constructed	Lappin et al.,1989, Table E-7
Ra						
Solubility	**1.04**	**0.3**	**1.26**	**log (Molar)**	**Constructed**	**See Section 3.3.5**
Th						
Diffusion coefficient	1×10^{-10}	5×10^{-11}	1.5×10^{-10}	m^2/s	Uniform	Lappin et al.,1989, Table E-7
Th						
Solubility	**-10.0**	**-15.2**	**-5.6**	**log (Molar)**	**Constructed**	**See Section 3.3.5**
U						
Diffusion coefficient	2.7×10^{-10}	1.1×10^{-10}	4.3×10^{-10}	m^2/s	Uniform	Lappin et al.,1989, Table E-7
U						
Solubility	**-3.27**	**-15.00**	**0.0**	**log (Molar)**	**Constructed**	**See Section 3.3.5**

[a] Parameters in bold were sampled in the 1992 calculations.
[b] mole/(m^2 - surface area steel • s)
[c] mole/(kg - cellulosics • s)
[d] Free liquid diffusion coefficient of the indicated species

Solubility of Specific Radionuclides*

Parameter: **Solubility (S) for Am, Cm, Np, Pb, Pu, Ra, Th, U**
Material: Radionuclide-bearing compounds in waste form

Definition Units: Log (Molar)

Values: See Table 3.3-4

Distribution: Constructed (see Figures 3.3-3[a] through 3.3-3[h] and discussion)
Correlation:

Data Source(s): Trauth, K. M., S. C. Hora, R. P. Rechard, and D. R. Anderson. In Review. *The Use of Expert Judgment to Quantify Uncertainty in Solubility and Sorption Parameters for Waste Isolation Pilot Plant Performance Assessment*. SAND92-0479. Albuquerque, NM: Sandia National Laboratories. (Copy on file at the Waste Management and Transportation Library, Sandia National Laboratories, Albuquerque, NM.) (Expert Panel Judgment)

Usage:

Mathematical model:
Repository Discharge, Section 1.4.4 of this volume.

Equations 1.4.4-5, 1.4.4-11.

Computational models:
PANEL

Ranking in Past Sensitivity Analyses:

40 CFR 191	High for Am, Np, Pu, Th, U; others Not tested
40 CFR 268	Not tested
NEPA	Not tested
Other	Not tested

*Key to Parameter Sheets is provided in Section 1.2.8.

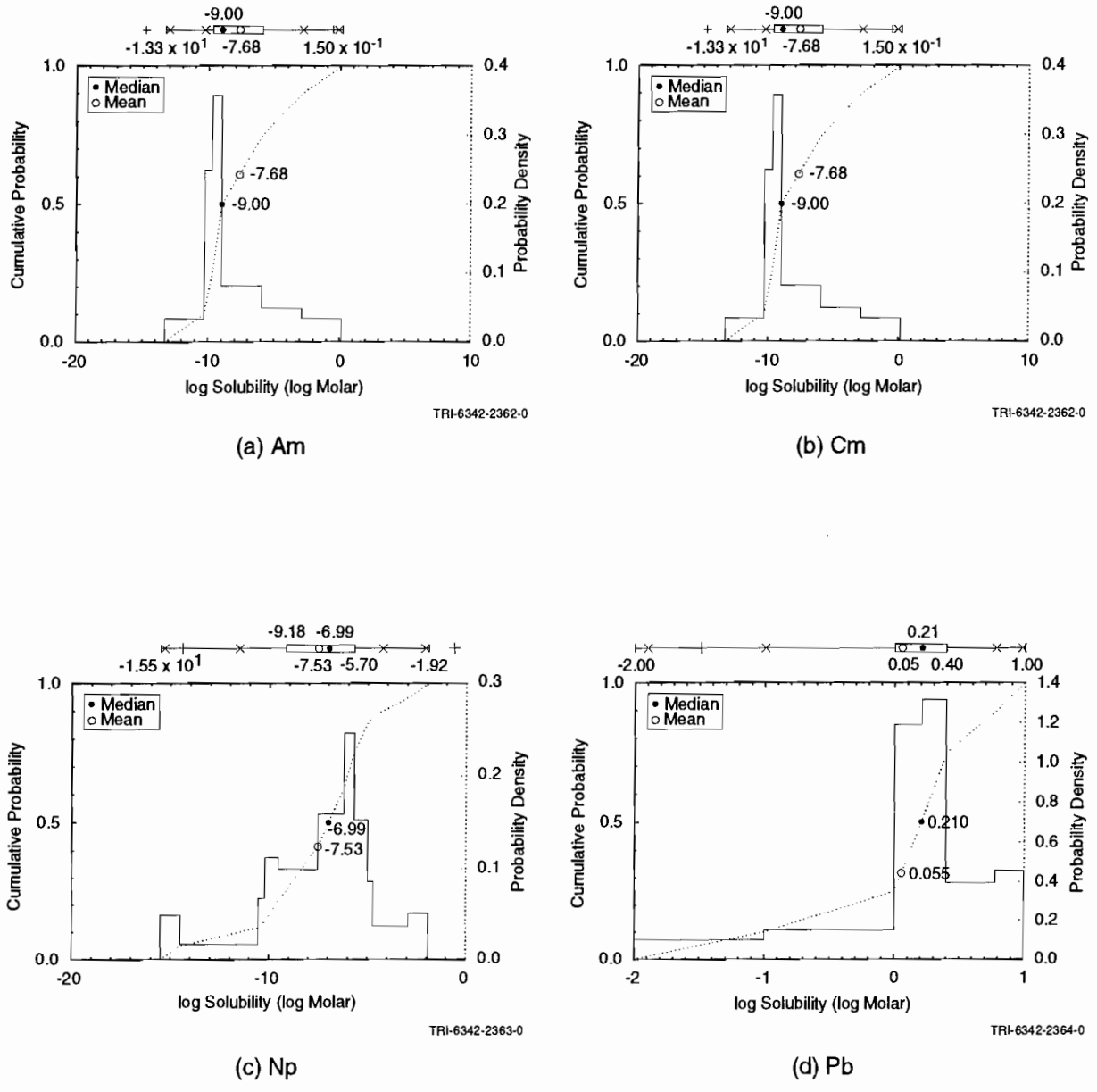

Figure 3.3-3. Constructed distribution for solubility of (a) americium (Am), (b) curium (Cm), (c) neptunium (Np), (d) lead (Pb), (e) plutonium (Pu), (f) radium (Ra), (g), thorium (Th), and (h) uranium (U).

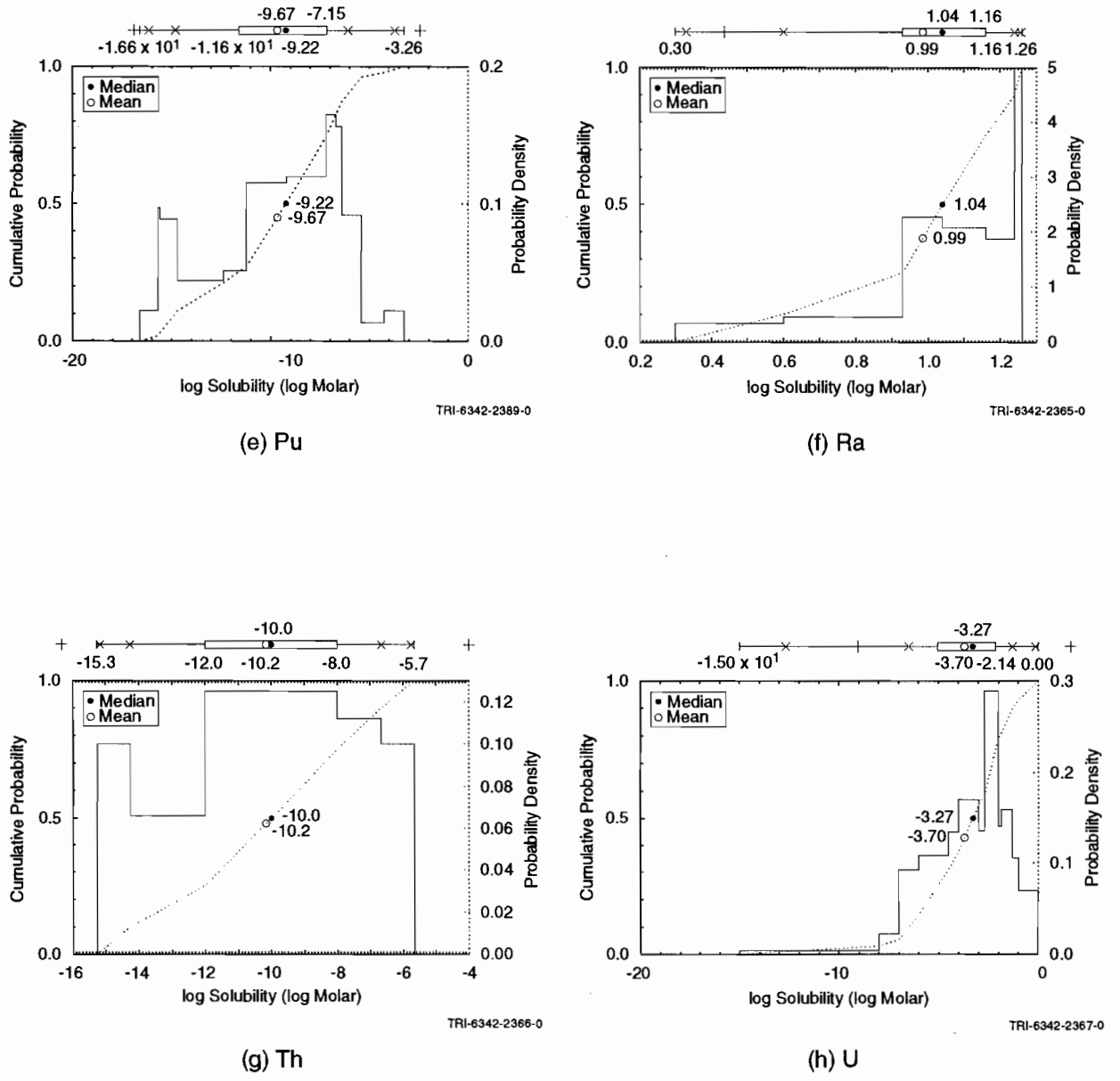

Figure 3.3-3. Constructed distribution for solubility of (a) americium (Am), (b) curium (Cm), (c) neptunium (Np), (d) lead (Pb), (e) plutonium (Pu), (f) radium (Ra), (g), thorium (Th), and (h) uranium (U) (concluded).

Discussion of Solubilities:

The distributions of solubilities elicited by Trauth et al. (1991, In Review) for the 1991 PA calculations are shown as bar diagrams in Figure 3.3-4. Different oxidation states were distinguished for Np, Pu and U; and different solution conditions were distinguished for Pb and Ra. Relative areas in pH-Eh space for the oxidation states of Np, Pu and U were also provided by the expert panel (Figure 3.3-5). No new information on solubilities was obtained in 1992.

In the 1991 PA calculations, an index variable between 0 and 1 was used to select solubilities corresponding to the several oxidation states by sampling on the relative areas in pH-Eh space. In the 1992 calculations, all solubility distributions (Figure 3.3-4) were first converted to distributions of logarithms (base 10) of Molar values; the resulting distributions having more than one oxidation state (Np, Pu, U) were then weighted according to the relative areas in pH-Eh space (Figure 3.3-5) and added to give a single distribution for each species (Figure 3.3-3). The solution condition assumed for lead (Pb) was "carbonate absent" and the solution condition assumed for radium (Ra) was "carbonate and sulfate present"; i.e., conditions giving highest values of solubility for Pb and Ra were assumed for the sake of conservatism.

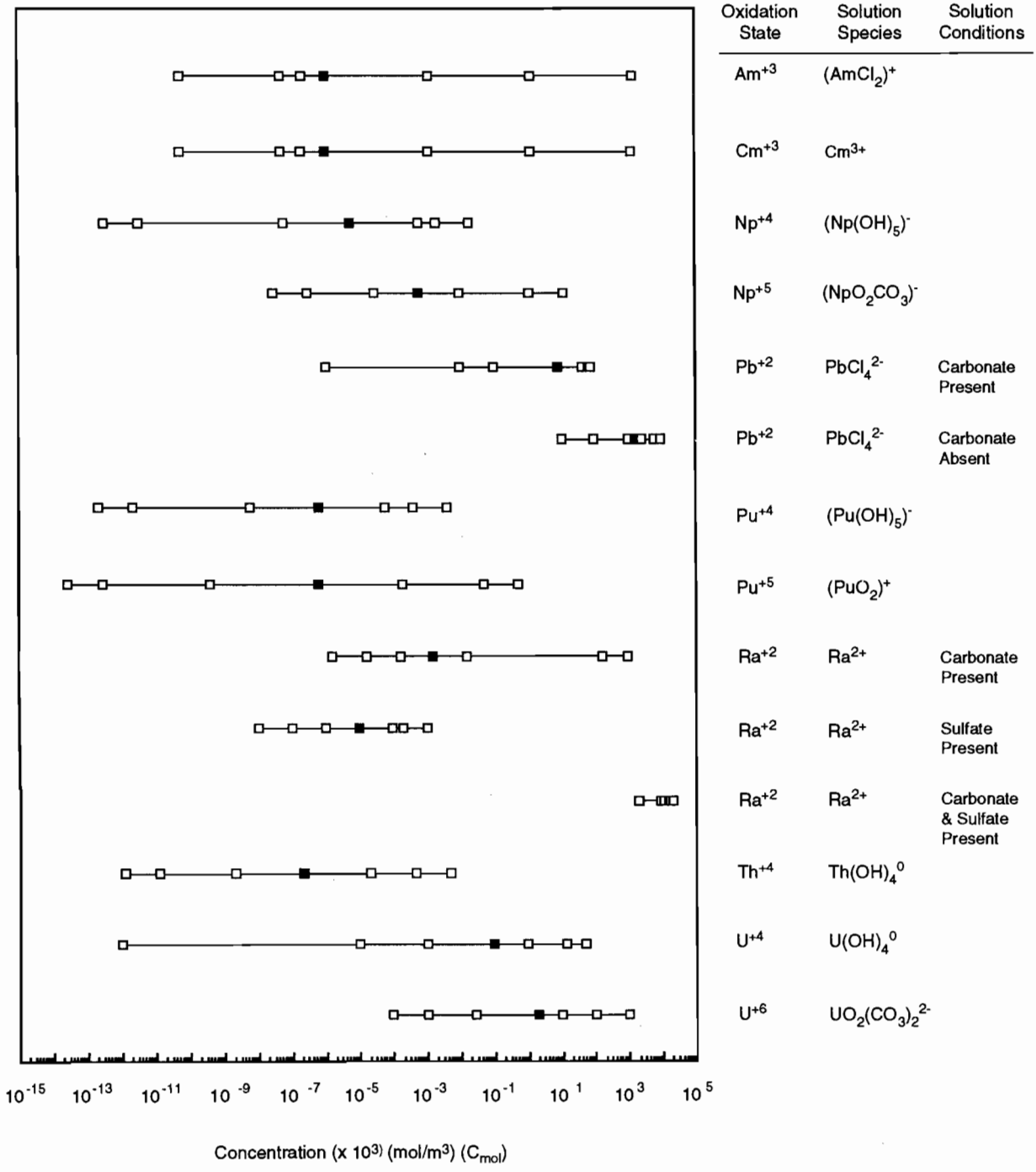

Figure 3.3-4. Bar diagrams of elicited distributions of solubility for americium, curium, lead, neptunium, plutonium, radium, thorium, and uranium (after Trauth et al., 1992).

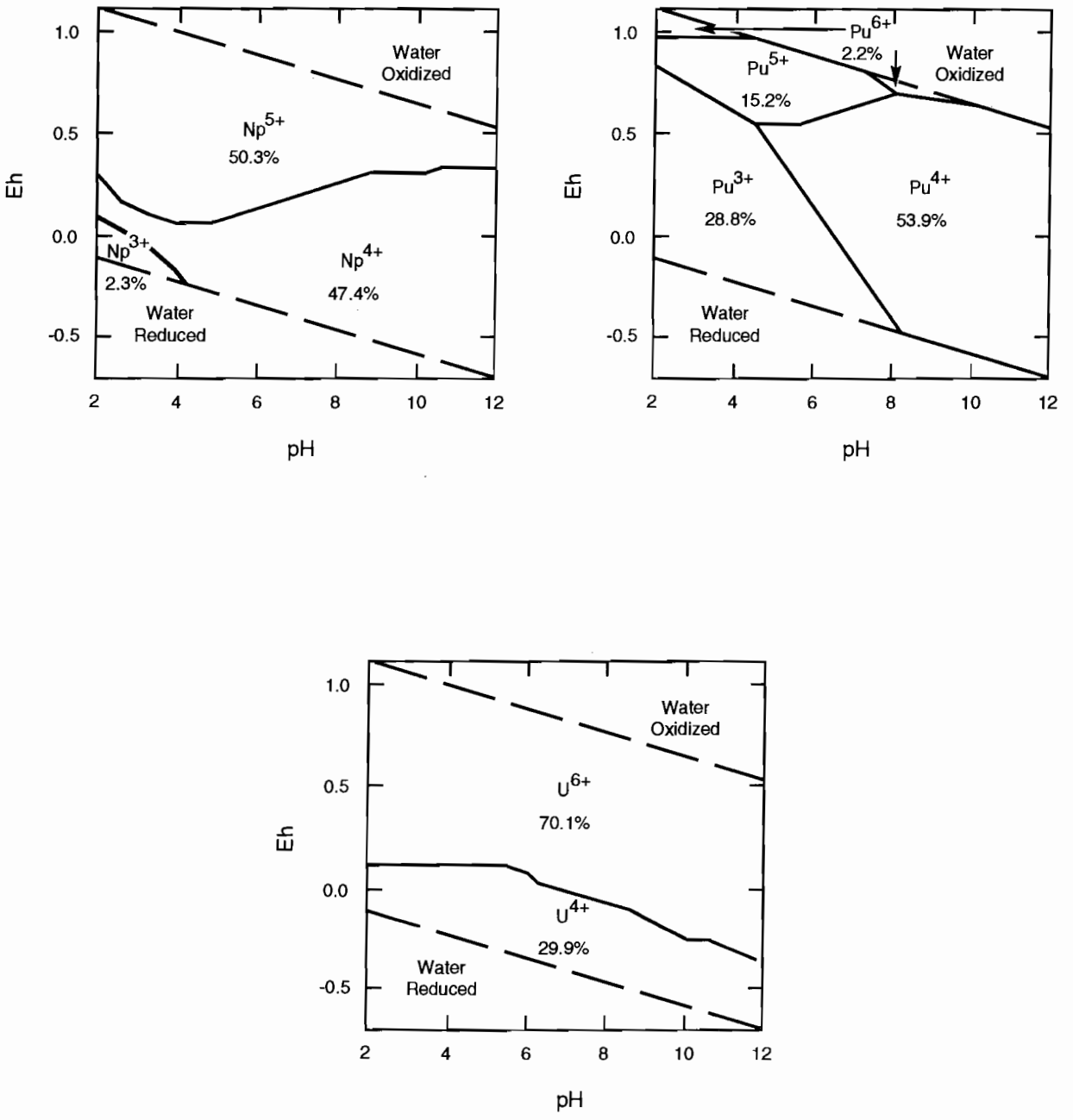

TRI--6342-1132-0

Figure 3.3-5. Estimated relative areas of stability in the pH-Eh space for neptunium, plutonium, and uranium and percentage of area of stable water.

Gas Production from Corrosion (Inundated Rate)*

Parameter: **Gas production rates, corrosion, inundated rate** ($\dot{n}'_{CI}$)
Material: Inundated, steel in waste form (WastRef, GRatCorI)

Definition Units: mol H_2/(m^2-surface area steel • s)

Values: Range: (0, 1.3×10^{-8}) Median: 6.3×10^{-9}

Distribution: Constructed (see Figure 3.3-6)
Correlation:

Data Source(s): Brush, L. H. 1991. Appendix A: "Current Estimates of Gas Production Rates, Gas Production Potentials, and Expected Chemical Conditions Relevant to Radionuclide Chemistry for the Long-Term WIPP Performance Assessment," *Preliminary Comparison with 40 CFR Part 191, Subpart B for the Waste Isolation Pilot Plant, December 1991. Volume 3: Reference Data.* WIPP Performance Assessment Division. Eds. R. P. Rechard, A. C. Peterson, J. D. Schreiber, H. J. Iuzzolino, M. S. Tierney, and J. S. Sandha. SAND91-0893/3. Albuquerque, NM: Sandia National Laboratories. A-25 through A-36. (Investigator Judgment)

Usage:

Mathematical model:
Two-Phase Flow, Section 1.4.1 of this volume.

Equation 1.4.1-12.

Computational models:
BRAGFLO

Ranking in Past Sensitivity Analyses:

40 CFR 191	Medium
40 CFR 268	Medium
NEPA	Not tested
Other	Not tested

*Key to Parameter Sheets is provided in Section 1.2.8.

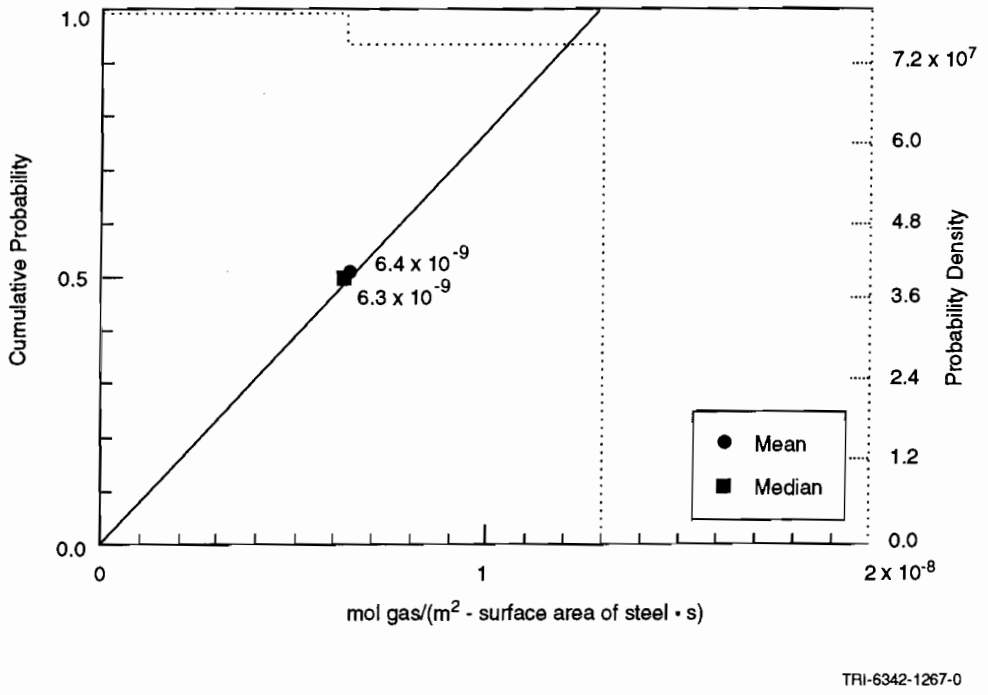

Figure 3.3-6. Constructed distribution for gas production rates from corrosion under inundated conditions.

Gas Production from Corrosion (Relative Humid Rate)*

Parameter: **Gas production rates, corrosion, relative humid rate (f)**
Material: Steel in waste form exposed to humid conditions (WastRef, GRatCorH)

Definition Units: Dimensionless

Values: Range: $(0, 5 \times 10^{-1})$ Median: 1×10^{-1}

Distribution: Constructed (see Figure 3.3-7)
Correlation:

Data Source(s): Brush, L. H. 1991. Appendix A: "Current Estimates of Gas Production Rates, Gas Production Potentials, and Expected Chemical Conditions Relevant to Radionuclide Chemistry for the Long-Term WIPP Performance Assessment," *Preliminary Comparison with 40 CFR Part 191, Subpart B for the Waste Isolation Pilot Plant, December 1991. Volume 3: Reference Data.* WIPP Performance Assessment Division. Eds. R. P. Rechard, A. C. Peterson, J. D. Schreiber, H. J. Iuzzolino, M. S. Tierney, and J. S. Sandha. SAND91-0893/3. Albuquerque, NM: Sandia National Laboratories. A-25 through A-36. (Investigator Judgment)

Usage:

Mathematical model:
Two-Phase Flow, Section 1.4.1 of this volume.

Equation 1.4.1-14.

Computational models:
BRAGFLO

Ranking in Past Sensitivity Analyses:

40 CFR 191	Low
40 CFR 268	High
NEPA	Not tested
Other	Not tested

*Key to Parameter Sheets is provided in Section 1.2.8.

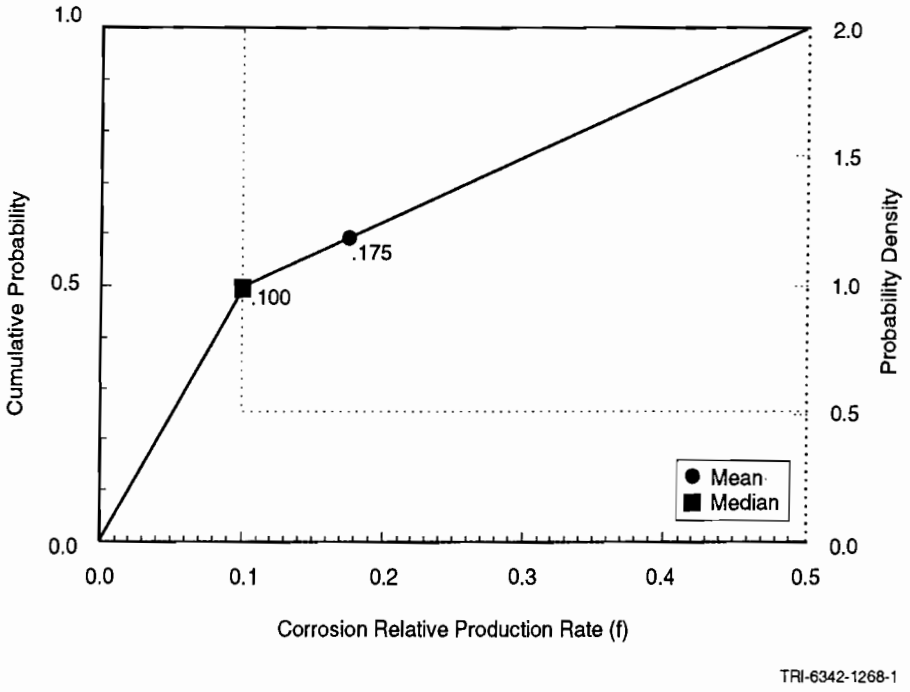

Figure 3.3-7. Constructed distribution for relative gas production rates from corrosion under humid conditions.

Gas Production from Corrosion (Stoichiometry)*

Parameter: **Anoxic iron corrosion stoichiometry (x)**
Material: Inundated steel in waste form, (WastRef, StoiCor)

Definition Units: None

Values: Range: (0, 1) Median: 0.5

Distribution: Uniform
Correlation:

Data Source(s): Brush, L. H., and D. R. Anderson. 1989. "Appendix A: Drum (Metal) Corrosion, Microbial Decomposition of Cellulose, Reactions Between Drum-Corrosion Products and Microbially Generated Gases, Reactions Between Possible Backfill Constituents and Gases and Water Chemical Reactions," *Systems Analysis, Long-Term Radionuclide Transport, and Dose Assessments, Waste Isolation Pilot Plant (WIPP), Southeastern New Mexico; March 1989*. Eds. A. R. Lappin, R. L. Hunter, D. P. Garber, and P. B. Davies. SAND89-0462. Albuquerque, NM: Sandia National Laboratories. A-3 through A-30. (Investigator Judgment)

Usage:

Mathematical model:
Two-Phase Flow, Section 1.4.1 of this volume.

Equation 1.4.1-13.

Computational models:
BRAGFLO

Ranking in Past Sensitivity Analyses:

40 CFR 191	Low
40 CFR 268	Medium
NEPA	Not tested
Other	Not tested

*Key to Parameter Sheets is provided in Section 1.2.8.

Discussion of Gas Production from Corrosion:

After waste is emplaced in the WIPP repository, some gas is expected to be generated from three types of chemical reactions: (1) anoxic corrosion, (2) biodegradation, and (3) radiolysis. In theory, the rates are dependent upon several factors, such as the chemical makeup of the waste (both organic and inorganic), the types of bacteria present, interactions among the products of the reactions, characteristics of WIPP brine, pH, and Eh. Experimental data describing these dependencies are incomplete at this time. However, some rough estimates of the range of gas generation rate values under possible WIPP environmental conditions have been made using available data.

Brush (1991) estimates gas production from corrosion for inundated and humid conditions. The estimates for inundated conditions are based on 3- and 6-month experiments by R. E. Westerman of Pacific Northwest Laboratory (PNL) on ASTM A 366 and ASTM A 570 steels by WIPP Brine A when N_2 is present at low pressures (~ 0.105 MPa [150 psig]) (Brush, 1991) (Figure 3.3-8). The following are estimated gas production and corrosion rates for inundated conditions: minimum, 0 mol H_2/m^2 steel/yr (0 mol H2/drum/yr); best estimate, 0.2 mol H_2/m^2 steel/yr (1 mol/drum/yr); and maximum, 0.4 mol H_2/m^2 steel/yr (2 mol/drum/yr) with N_2 at 0.698 MPa (1000 psig) (Brush, 1991).

Westerman also performed 3- and 6-month low-pressure humid experiments with either CO_2 or N_2 atmospheres (Brush, 1991). No H_2 production was observed except for very limited quantities from corrosion of the bottom 10% of the specimens splashed with brine during pretest preparation of the containers. Westerman is currently quantifying H_2 production from anoxic corrosion of steels in contact with noninundated backfill materials. Until further results are available, the estimated rates for humid conditions are as follows: minimum, 0 mol H_2/m^2 steel/yr (0 mol H_2/drum/yr); best estimate, 0.02 mol H_2/m^2 steel/yr (0.1 mol H_2/drum/yr); and maximum, 0.2 mol H_2/m^2 steel/yr (1 mol H_2/drum/yr) with N_2 at 0.698 MPa (1000 psig) (Brush, 1991). When expressed in terms of relative rates, the values are 0 to 0.5 with a median of 0.1.

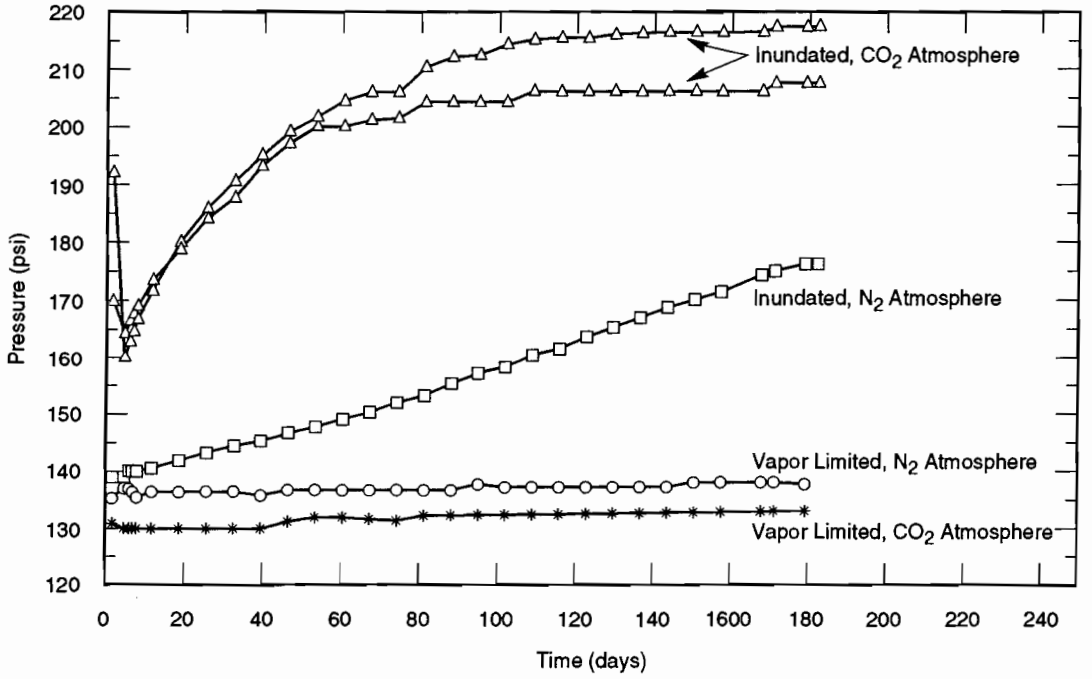

Figure 3.3-8. Pressure-time plots for 6-month anoxic corrosion experiments under brine-inundated and vapor-limited ("humid") conditions (Davies et al., 1991, Figure 6).

Gas Production from Microbiological Processes (Inundated Rate)*

Parameter: **Gas production rates, microbiological, inundated rate** ($\dot{n}_{BI}$)
Material: Inundated cellulosics in waste form (WastRef, GRatMicI)

Definition Units: mol gas/(kg - cellulosics • s)

Values: Range: (0, 1.6×10^{-8}) Median: 3.2×10^{-9}

Distribution: Constructed (see Figure 3.3-8)
Correlation:

Data Source(s): Brush, L. H. 1991. Appendix A: "Current Estimates of Gas Production Rates, Gas Production Potentials, and Expected Chemical Conditions Relevant to Radionuclide Chemistry for the Long-Term WIPP Performance Assessment," *Preliminary Comparison with 40 CFR Part 191, Subpart B for the Waste Isolation Pilot Plant, December 1991. Volume 3: Reference Data.* WIPP Performance Assessment Division. Eds. R. P. Rechard, A. C. Peterson, J. D. Schreiber, H. J. Iuzzolino, M. S. Tierney, and J. S. Sandha. SAND91-0893/3. Albuquerque, NM: Sandia National Laboratories. A-25 through A-36. (Investigator Judgment)

Usage:

Mathematical model:
Two-Phase Flow, Section 1.4.1 of this volume.

Equation 1.4.1-17.

Computational models:
BRAGFLO

Ranking in Past Sensitivity Analyses:

40 CFR 191	Low
40 CFR 268	Medium
NEPA	Not tested
Other	Not tested

*Key to Parameter Sheets is provided in Section 1.2.8.

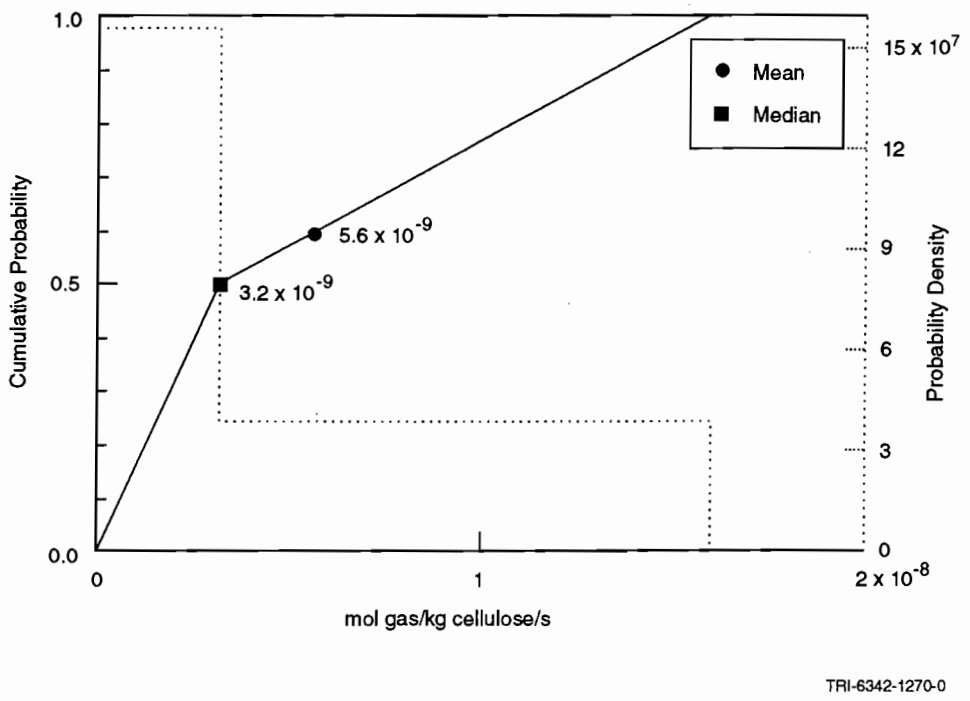

Figure 3.3-9. Constructed distribution for gas production rates from microbiological degradation under inundated conditions.

Gas Production from Microbiological Processes (Relative Humid Rate)*

Parameter: **Gas production rates, microbiological, relative humid rate (g)**
Material: Cellulosics in waste form, humid conditions (WastRef, GRatMicH)

Definition Units: Dimensionless

Values: Range: $(0, 2 \times 10^{-1})$ Median: 1×10^{-1}

Distribution: Uniform
Correlation:

Data Source(s): Brush, L. H. 1991. Appendix A: "Current Estimates of Gas Production Rates, Gas Production Potentials, and Expected Chemical Conditions Relevant to Radionuclide Chemistry for the Long-Term WIPP Performance Assessment," *Preliminary Comparison with 40 CFR Part 191, Subpart B for the Waste Isolation Pilot Plant, December 1991. Volume 3: Reference Data.* WIPP Performance Assessment Division. Eds. R. P. Rechard, A. C. Peterson, J. D. Schreiber, H. J. Iuzzolino, M. S. Tierney, and J. S. Sandha. SAND91-0893/3. Albuquerque, NM: Sandia National Laboratories. A-25 through A-36. (Investigator Judgment)

Usage:

Mathematical model:
Two-Phase Flow, Section 1.4.1 of this volume.

Equation 1.4.1-17.

Computational models:
BRAGFLO

Ranking in Past Sensitivity Analyses:

40 CFR 191	Low
40 CFR 268	High
NEPA	Not tested
Other	Not tested

*Key to Parameter Sheets is provided in Section 1.2.8.

Gas Production from Microbiological Processes (Stoichiometry Factor)*

Parameter: **Gas generation, stoichiometry factor** (S_{BH_2})

Material: Cellulosics in waste form, humid and inundated, (WastRef, StoiMic)

Definition Units: Dimensionless

Values: Range: (0, 1.67) Median: 8.35×10^{-1}

Distribution: Uniform

Correlation:

Data Source(s): Brush, L. H., and D. R. Anderson. 1989. "Appendix A: Drum (Metal) Corrosion, Microbial Decomposition of Cellulose, Reactions Between Drum-Corrosion Products and Microbially Generated Gases, Reactions Between Possible Backfill Constituents and Gases and Water Chemical Reactions," *Systems Analysis, Long-Term Radionuclide Transport, and Dose Assessments, Waste Isolation Pilot Plant (WIPP), Southeastern New Mexico; March 1989*. Eds. A. R. Lappin, R. L. Hunter, D. P. Garber, and P. B. Davies. SAND89-0462. Albuquerque, NM: Sandia National Laboratories. A-3 through A-30. (Investigator Judgment)

Usage:

Mathematical model:

Two-Phase Flow, Section 1.4.1 of this volume.

Equation 1.4.1-16.

Computational models:

BRAGFLO

Ranking in Past Sensitivity Analyses:

40 CFR 191	Low
40 CFR 268	High
NEPA	Not tested
Other	Not tested

*Key to Parameter Sheets is provided in Section 1.2.8.

Discussion of Gas Production by Microbiological Processes:

Brush (1991) estimates activity from microbiological degradation based on a recent study at Stanford University and studies carried out during the 1970s (Molecke, 1979; SNL, 1979; Barnhart et al., 1980; Caldwell et al., 1988). A test plan for laboratory experiments (Brush, 1990) and in-situ gas production experiments using real waste at the WIPP (Lappin et al., 1989) describe experiments currently underway. Although the Stanford tests seemed to suggest that microbial gas production may be significant under laboratory conditions but not under repository conditions, results from the earlier tests implied significant microbial gas production under both realistic and overtest conditions. However, until the Stanford tests are corroborated, the best estimate for microbial gas production has remained the same as first proposed by Brush and Anderson (in Lappin et al., 1989; Brush, 1990), 0.1 mole of various gases per kg cellulosics per year (1 mol gas/(drum•yr)). However, new minimum and maximum rates for inundated conditions are 0 and 0.5 mol/(kg•yr) (5 mol per drum per year), respectively.

For humid conditions, new minimum and best estimates for microbial gas production rates are 0 and 0.01 mol/(kg cellulosics•yr) (0.1 mol/(drum•yr)). The maximum estimate under humid conditions remains unchanged from the value estimated by Brush and Lappin (1990), 0.1 mol/(kg•yr) (1 mol/(drum•yr)). Expressed in terms of relative rates, the values are 0 to 0.2 with a median of 0.1.

Microbiologic Degradation Stoichiometry. The stoichiometry of the net biodegradation reaction is uncertain. About 20 reactions have been postulated and others may be possible, according to Brush and Anderson (Lappin et al., 1989, p. A-10). The reactions depend on such factors as what electron donors are available, the solubility of CO_2, and interaction with products of corrosion, pH, and Eh. It is not known at this time what effect biodegradation has on water (brine) inventory, so it is assumed to have no net effect, neither consuming water nor producing it. Some of the postulated reactions produce gas; others consume it. At present, we know that some gas (CO_2 and some H_2, H_2S, and CH_4) may be produced and that cellulose (CH_2O) will be consumed. Using the stoichiometry recommended in Lappin et al. (1989, Supplement to Appendix A.1, p. A-30) that yields the maximum gas generation per unit of cellulose (5/3 mol gas/mol CH_2O), the biodegradation reaction may be written

$$CH_2O + \text{unknowns} + \text{microbes} = 5/3\ \text{gas} + \text{unknowns}$$

However, in view of the wide variety of reactions that may occur, together with our current lack of knowledge as to precisely which reactions do occur, it is prudent to sample on the stoichiometric coefficient for gas in this reaction. If the assumption is also made that any CO_2 that is produced will dissolve in the WIPP brine, then of the reactions presented in Lappin et al. (1989) only one reaction will consume gas, that one being

$$CH_2O + O_2 = H^+ + HCO_3^-$$

This reaction requires oxygen, which will be present initially in air and will be produced by radiolysis. Neither source of oxygen is sufficient to oxidize all of the cellulose in the inventory, and oxic corrosion will compete strongly for this oxygen, so this reaction is expected to be of minor importance. None of the other reactions consumes gas, whereas most produce gas, with the net gas production ranging from 0 to 5/3 mol gas/mol CH_2O. Therefore, the stoichiometric coefficient is sampled from a uniform distribution ranging from 0 to 5/3.

3.4 Parameters for Unmodified Waste Form Including Containers

As of 1990, the currently stored CH-TRU waste that will be disposed of in the WIPP, if authorized, is estimated to be about 60,000 m^3 (2.1 x 10^6 ft^3), which is about 34% of the design storage volume of 1.756 x 10^5 m^3 (6.2 x 10^6 ft^3). The stored waste consists of about 180,000 0.21-m^3 (55-gal) drums, 5,000 1.8-m^3 (64 ft^3) Standard Waste Boxes (SWBs), and 7,000 3.2-m^3 (113-ft^3) miscellaneous containers, mostly steel and fiberglass reinforced plywood (FRP) boxes. Drums and SWBs are the only containers that can currently be transported in a TRUPACT-II. If the waste in boxes other than SWBs were repackaged into SWBs, it was estimated that 533,000 0.21-m^3 (55-gal) drums and 33,500 1.8-m^3 (64-ft^3) SWBs could be emplaced in the WIPP repository containing approximately 170,000 m^3 (6.2 x 106 ft^3) of waste, the design volume for CH-TRU waste.

The volume of RH-TRU waste is limited by the agreement between DOE and the State of New Mexico to 7.08x10^3 m^3 (0.25 x 10^6 ft^3) (U.S. DOE and NM, 1984). RH waste will likely be placed in 0.89-m^3 (31.4-ft^3) canisters in the walls of the rooms and access drifts. (Placement of canisters is discussed in Section 3.1.6.)

The parameter values for unmodified waste that is expected to be shipped (i.e., to meet the current waste acceptance criteria [WAC] discussed below) are provided in Table 3.4-1. The significant figures for masses that are reported in this table should not be interpreted as known accuracy. (Indeed, the majority of waste to be emplaced in the WIPP has not been generated; hence, the amounts are uncertain.) The significant figures in the table for masses are presented as a means to trace the work until a report detailing the assumptions and calculations pertaining to these amounts has been prepared. On the other hand, the significant figures on design volumes are important since the limits on volumes agreed upon by the DOE and the State of New Mexico (U.S. DOE and NM, 1984) were in English units and are an exact conversion.

All CH- and RH-TRU waste must meet the WIPP *Waste Acceptance Criteria* (WAC) (WEC, 1991). These criteria includes requirements for the waste form. For example, the waste material shall (1) include only residual liquids in well-drained containers (e.g., bottles, cans, etc.) in quantities less than 1% of the container volume and the total liquid shall be less than 1% of waste container volume, (2) not permit explosives or compressed gases, and (3) limit radionuclides in spontaneously combustible pyrophoric form to less than 1% by weight in each waste package. There also are limitations on the curie content in a drum, SWB, and canister based on transportation considerations (Table 3.4-2).

Table 3.4-1. Parameter Values for Unmodified TRU Waste Categories, Containers, and Salt Backfill

Parameter[a]	Median	Range		Units	Distribution Type	Source
CH-TRU waste						
Molecular weight						
Cellulose	0.030			kg/mol	Constant	CH_2; Weast and Astle, 1981
Iron	0.05585			kg/mol	Constant	Fe; Weast and Astle, 1981
Density, grain (ρ_g)						
Metal/glass	3.44×10^3			kg/m^3	Constant	Butcher, 1990, Table 2
Combustibles	1.31×10^3			kg/m^3	Constant	Butcher, 1990, Table 2
Sludge	2.15×10^3			kg/m^3	Constant	Butcher, 1990, Table 2
Salt backfill	2.14×10^3			kg/m^3	Constant	WIPP PA Division, 1991, Vol. 3, Table 2.3-1
Steel, cold-drawn	7.83×10^3			kg/m^3	Constant	Perry et al., 1969, Table 3-137
Air @ 300.15K, 1 atm	1.177			kg/m^3	Constant	Vennard and Street, 1975, p. 709
Volumes of IDB Categories[b]						
Metal/glass fraction	**3.76×10^{-1}**	**2.76×10^{-1}**	**4.76×10^{-1}**	**none**	**Normal**	**See Section 3.4.1**
Combustibles fraction	**3.84×10^{-1}**	**2.84×10^{-1}**	**4.84×10^{-1}**	**none**	**Normal**	**See Section 3.4.1**
Salt backfill	1.712×10^5			m^3	Constant	WIPP PA Division, 1991, Vol 3, Figure 3.1-3
Air @ 300.15K, 1 atm	8.908×10^4			m^3	Constant	WIPP PA Division, 1991, Vol 3, Figure 3.1-3
Average per Drum						
Metal/glass	6.44×10^1	3.05×10^1	9.83×10^1	kg/drum	Normal	Butcher, 1989, Table 7
Combustibles	4.00×10^1	1.73×10^1	6.26×10^1	kg/drum	Normal	Butcher, 1989, Table 6
Sludge	2.25×10^2			kg/drum	Constant	WIPP PA Division, 1991, Vol. 3, Table 3.4-10
Mass of IDB Categories[b]						
Metal/glass	1.984×10^7					WIPP PA Division, 1991, Vol. 3, Tables 3.4-10 and 3.4-12
Combustibles	1.348×10^7					WIPP PA Division, 1991, Vol. 3, Tables 3.4-10 and 3.4-12
Mass of Steel Containers in IDB Categories[b]						
Metal/glass	1.076×10^7			kg	Constant	WIPP PA Division, 1991, Vol. 3, Table 3.4-10
Combustibles	1.178×10^7			kg	Constant	WIPP PA Division, 1991, Vol. 3, Table 3.4-10
Sludge	3.598×10^6			kg	Constant	WIPP PA Division, 1991, Vol. 3, Table 3.4-10
Mass of Steel Containers and Liners in IDB Categories[b]						
Metal/glass	4.458×10^6			kg	Constant	WIPP PA Division, 1991, Vol. 3, Table 3.4-10
Combustibles	1.214×10^7			kg	Constant	WIPP PA Division, 1991, Vol. 3, Table 3.4-10
Sludge	1.329×10^7			kg	Constant	WIPP PA Division, 1991, Vol. 3, Table 3.4-10
Mass of Contents						
Iron, steel, paint cans, shipping cans	1.431×10^7			kg	Constant	WIPP PA Division, 1991, Vol. 3, Table 3.4-12
Steel in containers	2.613×10^7			kg	Constant	WIPP PA Division, 1991, Vol. 3, Table 3.4-10
Cellulosics, + 50% gloves, Hypalon, Neoprene, rubber	7.475×10^6			kg	Constant	WIPP PA Division, 1991, Vol 3, Table 3.4-12

[a]Parameters in bold were sampled in the 1992 calculations.
[b]IDB = Integrated Data Base

Table 3.4-1. Parameter Values for Unmodified TRU Waste Categories, Containers, and Salt Backfill (Concluded)

Parameter[a]	Median	Range		Units	Distribution Type	Source
Capillary pressure (ρ_c) and relative permeability ($k_{\ell r}$)						
Threshold displacement pressure (ρ_t)	2.02×10^{3}	2.02×10^{1}	2.02×10^{5}	Pa	Lognormal	Davies, 1991a, 1991b
Residual Saturations						
Wetting phase ($S_{\ell r}$)	2.76×10^{-1}	1.38	5.52×10^{-1}	none	Constructed	Brooks and Corey, 1964
Gas phase (S_{gr})	7×10^{-2}	3.5×10^{-2}	1.4×10^{-1}	none	Constructed	Brooks and Corey, 1964
Brooks-Corey Exponent (η)	2.89	1.44	5.78	none	Constructed	Brooks and Corey, 1964
Drilling Erosion Parameters						
Absolute roughness (ε)	2.5×10^{-2}	1×10^{-2}	4×10^{-2}	m	Uniform	Streeter and Wylie, 1975, Figure 5.32.
Shear strength (τ_{fail})	1	1×10^{-1}	1×101	Pa	Constructed	Sargunam et al., 1973; Henderson, 1966
Partition Coefficient for clays in salt backfill						
Am	1×10^{-4}			m^3/kg	Constant	Lappin et al., 1989, Table D-5 ($Kd_{clay}/1000$)
Np	1×10^{-5}			m^3/kg	Constant	Lappin et al., 1989, Table D-5 ($K_{dclay}/1000$)
Pb	1×10^{-6}			m^3/kg	Constant	Lappin et al., 1989, Table D-5 ($K_{dclay}/1000$)
Pu	1×10^{-4}			m^3/kg	Constant	Lappin et al., 1989, Table D-5 ($K_{dclay}/1000$)
Ra	1×10^{-6}			m^3/kg	Constant	Lappin et al., 1989, Table D-5 ($K_{dclay}/1000$)
Th	1×10^{-4}			m^3/kg	Constant	Lappin et al., 1989, Table D-5 ($K_{dclay}/1000$)
U	1×10^{-6}			m^3/kg	Constant	Lappin et al., 1989, Table D-5 ($K_{dclay}/1000$)
Permeability (k) [used in 1991 calculations][b]						
Average	1×10^{-13}			m^2	Constant	Lappin et al., 1989, Table 4-6
Combustibles	1.7×10^{-14}	2×10^{-15}	2×10^{-13}	m^2	Constructed	Butcher et al., 1991
Metals/glass	5×10^{-13}	4×10^{-14}	1.2×10^{-12}	m^2	Constructed	Butcher et al., 1991
Sludge	1.2×10^{-16}	1.1×10^{-17}	1.7×10^{-16}	m^2	Constructed	Butcher et al., 1991
Porosity (ϕ) [used in 1991 calculations][b]						
Average	1.9×10^{-1}			none	Constant	WIPP PA Division, 1991, Vol 3, Section 3.4.8
Combustibles	1.4×10^{-2}	8.7×10^{-2}	1.8×10^{-1}	none	Constructed	Butcher et al., 1991
Metals/glass	4×10^{-1}	3.3×10^{-1}	4.4×10^{-1}	none	Constructed	Butcher et al., 1991
Sludge	1.1×10^{-1}	1×10^{-2}	2.2×10^{-1}	none	Constructed	Butcher et al., 1991
Saturation, initial ($S_{\ell i}$)	**0.07**	**0**	**0.14**	**none**	**Uniform**	**See Section 3.4.4.**

[a]Parameters in bold were sampled in the 1992 calculations.
[b]See Sections 1.4.1 and 1.4.7 for 1992 methods of calculating permeability and porosity of unmodified waste, containers, and salt backfill.

Table 3.4-2. Summary of Waste Acceptance Criteria and Requirements Applicable to Performance Assessment

Description	Waste Type	WAC Criterion or Requirement
Particulates	CH & RH	Immobilize if greater than 1% by weight below 10 microns Immobilize if greater than 15% by weight below 200 microns
Liquids	CH & RH	Liquids that result from liquid residues remaining in well-drained containers; condensation moisture; and liquid separation from sludges or resin settling shall be less than 1% by volume of the waste container
Pyrophoric Materials	CH & RH	Radionuclides in pyrophoric form are limited to less than 1% by weight in each waste package. No non-radionuclide pyrophorics permitted.
Explosives and compressed gas	CH & RH	No explosives or compressed gases are permitted.
Specific Activity	CH	The specific activity shall be greater than 100 nCi/g TRU radionuclides, excluding the weight of added shielding, rigid liners, and waste containers.
	RH	The specific activity shall be greater than 100 nCi/g TRU radionuclides, excluding the weight of external shielding, rigid liners, and the waste containers. The container average maximum activity concentration shall not exceed 23 curies/liter.
Nuclear Criticality* (Pu-239 FGE)**	CH	The fissile or fissionable radionuclide content shall be less than 200 FGE for a 55-gallon drum. The fissile or fissionable radionuclide content shall be less than 325 FGE for a SWB. The fissile or fissionable radionuclide content shall be less than 325 FGE for a TRUPACT-II
	RH	The fissile or fissionable radionuclide content shall be less than 325 FGE.
Pu-239 Activity*	CH & RH	Waste packages shall not exceed 1000 Ci of Pu-239 equivalent activity.

* Transportation requirement
** Fissile gram equivalent of Pu-239

3.4.1 Composition of CH-TRU Waste (Non-Radionuclide/Non-RCRA Inventory)

TRU waste destined for the WIPP is generated or currently stored by ten DOE nuclear weapon facilities. Although we know that this TRU waste consists in general of laboratory and production line waste, such as glassware, metal pipes, sorbed or solidified spent solvents, disposal laboratory clothing, cleaning rags, and solidified sludges, the precise composition of the waste (e.g., percentages by weight and volume) is not well defined. Estimates of metals/glass combustible and sludge reported here were made based on information on volumes submitted annually to the IDB by the generator sites and therefore are from the same source as the radionuclide inventory. A full discussion of these estimates is given in Section 3.4.1 of WIPP PA Division (1991, Vol. 3). Only estimates of the volumes of various categories of CH-TRU contaminated waste are discussed here.

Volume Fraction, Combustibles*

Parameter: **Volume fraction, combustibles (fc)**
Material: Unmodified waste form including containers (WastRef, Vol Wood)

Definition Units: Dimensionless

Values: Range: (0.284, 0.484) Median: 0.384

Distribution: Normal
Correlation:

Data Source(s): See text and Table 3.4-6. (Investigator Judgment)

Usage:

Mathematical model:
Two-Phase Flow, Section 1.4.1 of this volume.

Equation 1.4.1-17.

Computational models:
BRAGFLO

Ranking in Past Sensitivity Analyses:

40 CFR 191	Low
40 CFR 268	Medium
NEPA	Not tested
Other	Not tested

*Key to Parameter Sheets is provided in Section 1.2.8.

Volume Fraction, Metals/Glass*

Parameter: **Volume fraction, metals/glass**
Material: Unmodified waste form including containers (WastRef,Vol Metal)

Definition Units: Dimensionless

Values: Range: (0.276, 0.476) Median: 0.376

Distribution: Normal
Correlation:

Data Source(s): See text and Table 3.4-6. (Investigator Judgment)

Usage:

Mathematical model:

Two-Phase Flow, Section 1.4.1 of this volume.

Equation 1.4.1-12 (used in computing Ad, the surface area of steel in an equivalent drum).

Computational models:

BRAGFLO

Ranking in Past Sensitivity Analyses:

40 CFR 191	Low
40 CFR 268	Medium
NEPA	Not tested
Other	Not tested

*Key to Parameter Sheets is provided in Section 1.2.8.

Discussion:

Estimates of the masses and volumes of the constituents of TRU waste that affect gas generation, transport, and room properties are required for performance assessment. Because the majority of the waste to be emplaced in the WIPP has not been generated, the waste characterization is an estimate with a potentially large uncertainty. The estimated waste characterization is used as a base for analyses that include the uncertainty in waste characterization. The following discussion presents the method that was used to estimate the characterization of the waste. The intent was to use available information and to use a reasonable method to scale it up to the design volume, which was used in performance assessment. This method resulted in estimates of volumes and masses of waste by generator site; however, these results should not necessarily be considered as indicative of the actual masses and volumes that the sites will generate.

The total anticipated volume (stored waste and projected annual volumes) of the TRU waste calculated from information reported in the yearly IDB has been decreasing over the period 1987-1990 (Table 3.4-3). The most significant change from 1987 to 1990 is the percentage of concreted or cemented sludge; the estimated volume decrease was about 30%. Furthermore, the information contained in the 1990 IDB indicates that generators anticipate there will be less volume of absorbed sludges and more volume of concreted and cemented sludges in the projected waste than is contained in the stored waste.

The 1990 IDB was used as the basis for the estimate of the total volume of CH-TRU waste for the 1991 PA calculations. Table 3.4-4 lists the stored and projected (generated in the future) waste volume by generator site listed in the 1990 IDB. The IDB uses the terms "stored" and "newly generated" waste. In the discussion that follows, the term "projected" is used in place of "newly generated."

For performance assessment calculations, we assume that a design volume of 175,564 m^3 (6.2 x 10^6 ft^3) will be emplaced in the WIPP. The following discussion presents the method that was used to estimate the volumes of the waste types if the current design volume of waste was emplaced. To estimate the volume of waste by generator site to fill the WIPP, it was assumed that the five largest generators* of projected waste would provide the additional volume. The percentage of the total projected waste for each site was calculated and, based on this percentage, volumes for the five sites were calculated to provide an additional 69,105 m^3 (2.4 x 10^6 ft^3). The scaled volume for the five sites is shown in Table 3.4-4.

Details of the volumes and physical composition of CH-TRU waste as calculated from the information from the 1990 IDB are listed in Table 3.4-5.

For performance assessment calculations, hydraulic properties of the disposal area contents are required. To estimate the volume fraction of the sludges, combustibles, and metals and glass in CH-TRU waste, it was assumed the volume of the sludges included the absorbed liquid and sludges, concreted or cemented sludges, and dirt, gravel and asphalt categories of Table 3.4-5. The volume of filter, filter media, and "other" categories of Table 3.4-5 were distributed into the volume of sludges, combustibles, and metals and glass based on the relative volume of the initial amounts of each of these categories. PA Department estimates for the volume fraction of stored; projected; projected plus scaled; and stored, projected, and scaled are tabulated in Table 3.4-6.

* These five DOE defense facilities for 1990 are Hanford Reservation (HANF), Washington; Idaho National Engineering Laboratory (INEL), Idaho; Los Alamos National Laboratory (LANL), New Mexico; Rocky Flats Plant (RFP), Colorado; and Savannah River Site (SRS), South Carolina. In 1991, INEL was reclassified as a storage site rather than a generator site because a project that would generate waste was indefinitely delayed/cancelled.

Table 3.4-3. Estimated Composition by Volume of CH-TRU Contaminated Waste from 1987 to 1990.

Year	Combustibles (%)	Metal and Glass (%)	Absorbed Liquid and Sludge (%)	Concrete/ Cemented Sludge (%	Dirt/ Gravel/ Asphalt (%)	Filters/ Filter Media (%)	Other (%)	Total Volume (m3)
1987	38.87	31.53	8.99	7.37	1.33	5.81	6.11	158,526
1988	39.84	34.18	7.28	8.00	2.44	4.53	3.73	136,402
1989	32.01	36.41	6.09	16.41	1.31	3.00	4.78	120,243
1990	34.24	34.31	6.28	14.43	1.30	3.67	5.77	106,459

* Design volume is 175,564 m^3.

Table 3.4-4. Estimate of a Design Volume for CH-TRU Waste

Site	Stored Volume (1990 IDB) (m^3)	Projected Volume (1990 IDB) (m^3)	Total Volume (1990 IDB) (m^3)	Scaled Volume* (m^3)	Estimated Design Volume (m^3)
ANL-E	--	180	180	--	180
HANF	10,041	943	10,984	1,499	12,484
INEL	37,420	4,666	42,086	7,417	49,503
LANL	7,393	4,800	12,193	7,631	19,824
LLNL	--	1,207	1,207	--	1,207
MOUND	--	945	945	--	945
NTS	606	--	606	--	606
ORNL	662	600	1,262	--	1,262
RFP	792	16,272	17,064	25,869	42,933
SRP	3,143	16,788	19,931	26,689	46,620
Total	60,057	46,402	106,459	69,105	175,564

* Assuming that HANF, INEL, LANL, RFP, and SRP provide the difference between the current total inventory and the design volume. The difference between the total volume of 106,458 m^3 in the 1990 IDB and the design volume of 175,564 m^3 (6.2x10^6 ft^3) was apportioned between the five sites based on their estimated annual generation rates. These five sites provide 94% of the estimated total annual volume of 1,993.4 m^3 per year.

Table 3.4-5. Estimated Composition of CH-TRU Contaminated Waste in 1990 by Generator (U.S. DOE, 1990d, Tables 3.5, 3.7, 3.10)

Category	ANL-E	HANF	INEL	LANL	LLNL	NTS	MOUND	ORNL	RFP	SRS	Percent	Total (m^3)	Percent of Total
STORED													
Absorbed Liquid and Sludge	--	0.0	4490.4	1626.5	--	0.0	--	0.0	122.8	0.0	10.39	--	--
Combustibles	--	4317.6	9355.0	961.1	--	312.2	--	390.3	287.5	2200.1	29.68	--	--
Concreted or Cemented Sludge	--	602.5	4864.6	2217.9	--	6.1	--	0.0	5.5	0.0	12.82	--	--
Dirt, Gravel, or Asphalt	--	301.2	0.0	0.0	--	0.0	--	6.6	5.5	0.0	0.52	--	--
Filters or Filter Media	--	0.0	1871.0	369.7	--	0.0	--	33.1	327.1	0.0	4.33	--	--
Glass/Metal/Similar Noncombustibles	--	4819.7	13097.0	2217.9	--	288.0	--	231.6	43.6	942.9	36.03	--	--
Other	--	0.0	3742.0	0.0	--	0.0	--	0.0	0.0	0.0	6.23	--	--
TOTAL	--	10041.0	37420.0	7393.1	--	606.3	--	661.6	792.0	3143.0	--	--	--
Percent of Total	--	9.43	35.15	6.94	--	0.57	--	0.62	0.74	2.95	--	--	--
PROJECTED													
Absorbed Liquid and Sludge	64.8	0.0	0.0	48.0	0.0	--	0.0	0.0	0.0	335.8	0.97	6688.2[a]	6.28[a]
Combustibles	57.6	377.3	2020.2	1944.0	881.3	--	9.5	72.0	2522.2	10744.3	40.15	36452.2	34.24
Concreted or Cemented Sludge	0.0	132.0	737.2	864.0	12.1	--	9.5	0.0	5906.7	0.0	16.51	15358.1	14.43
Dirt, Gravel, or Asphalt	0.0	113.2	0.0	0.0	0.0	--	841.6	6.0	113.9	0.0	2.32	1388.1	1.30
Filters or Filter Media	0.0	94.3	23.3	120.0	84.5	--	0.0	30.0	113.9	839.4	2.81	3906.3	3.67
Glass/Metal/Similar Noncombustibles	57.6	226.4	681.2	1824.0	181.1	--	85.1	492.0	6720.3	4616.7	32.08	36525.0	34.31
Other	0.0	0.0	1203.7	0.0	48.3	--	0.0	0.0	895.0	251.8	5.17	6140.8	5.77
TOTAL	180.0	943.2	4665.6	4800.0	1207.2	--	945.6	600.0	16272.0	16788.0		106458.6	100.00
Percent of Total	0.17	0.89	4.38	4.51	1.13	--	0.89	0.56	15.28	15.77		100.00	
PROJECTED PLUS SCALED													
Absorbed Liquid and Sludge	64.8	0.0	0.0	124.3	0.0	0.0	0.0	0.0	0.0	869.5	0.92	7298.3[b]	4.16[b]
Combustibles	57.6	977.1	5231.9	5034.5	881.3	0.0	9.5	72.0	6531.8	27825.3	40.36	64444.8	36.71
Concreted or Cemented Sludge	0.0	342.0	1909.1	2237.6	12.1	0.0	9.5	0.0	15297.1	0.0	17.15	27503.8	15.67
Dirt, Gravel, or Asphalt	0.0	293.1	0.0	0.0	0.0	0.0	841.6	6.0	295.0	0.0	1.24	1749.1	1.00
Filters or Filter Media	0.0	244.3	60.4	310.8	84.5	0.0	0.0	30.0	295.0	2173.9	2.77	5799.6	3.30
Glass/Metal/Similar Noncombustibles	57.6	586.2	1764.1	4723.7	181.1	0.0	85.1	492.0	17404.1	11956.2	32.25	58890.8	33.54
Other	0.0	0.0	3117.4	0.0	48.3	0.0	0.0	0.0	2317.7	652.2	5.31	9877.5	5.63
TOTAL	180.0	2442.7	12082.8	12430.9	1207.2	0.0	945.6	600.0	42140.7	43477.1	--	175564.0	100.00
Percent of Total	0.1	1.39	6.88	7.08	0.69	0.0	0.54	0.34	24.00	24.76	--	100.00	--

[a] Stored plus projected

[b] Stored, plus projected, plus scaled

Table 3.4-6. Calculation of Constituent Volume Distribution in CH-TRU Waste*

Category	Initial	Distributed Amount of Filter and Filter Media	Total
Stored			
Sludge**	0.2373	0.0280	0.265
Combustible	0.2968	0.0350	0.332
Glass/Metal	0.3603	0.0425	0.403
Total	0.8944	--	1.000
Projected			
Sludge**	0.1980	0.0171	0.215
Combustible	0.4015	0.0348	0.436
Glass/Metal	0.3208	0.0278	0.349
Total	0.9203	--	1.000
Stored plus Projected			
Sludge**	0.2201	0.0229	0.243
Combustible	0.3424	0.0357	0.378
Glass/Metal	0.3431	0.0358	0.379
Total	0.9056	--	1.000
Stored, Projected, plus Scaled			
Sludge**	0.2083	0.0204	0.229
Combustible	0.3671	0.0360	0.403
Glass/Metal	0.3354	0.0328	0.368
Total	0.9108	--	1.000

* The values for the initial volume percents were obtained from Table 3.4-5.
** Total of absorbed liquid and sludge, concreted and cemented sludge, and dirt, gravel, or asphalt.

3.4.2 Composition of RH-TRU Waste (Non-Radionuclide/Non-RCRA Inventory)

Estimates of the mass and volumes of RH-TRU constituents that affect gas generation, transport, and room properties are required for performance assessment. However, the mass of RH inventory was not included in the current analyses. The total RH inventory has changed considerably in the last several years. The following discussion presents a method that was used to estimate the characterization of the RH inventory. The method resulted in estimates of the volume and weights of waste by generator site; however, these results should not be interpreted as indicative of the weights and volumes that a specific site may generate.

For the current PA calculations, it was assumed that the maximum allowed RH volume of 7,079 m^3 (0.25 x 10^6 ft^3) will be emplaced in the WIPP. The following discussion presents the method that was used to estimate the total volumes of the waste constituents if the maximum volume of RH waste was emplaced. Input to the 1990 IDB was used as the basis for these estimates. The IDB presents estimates of the stored volume and projected (newly generated) volume for each generator site. The stored and projected volumes for the five sites that have or will generate RH waste are tabulated in Table 3.4-7. To estimate the additional volume required to reach the maximum volume, it was assumed that the generators of projected waste would provide the additional volume. The percentage of projected waste for each site was calculated and, based on this percentage, volumes for the five sites were calculated to provide an additional 1,735 m^3 (6.13 x 10^4 ft^3). The scaled volumes for the five sites are shown in Table 3.4-7.

The stored and newly generated (projected) RH volume in the 1990 IDB sum to about 5,300 m^3 (8.83 x 10^4 ft^3). The containers that will be placed in an RH canister have a different volume depending on the generator site. Therefore, a canister may not contain 0.89 m^3 (31.4 ft^3) of RH waste. U.S. DOE (1991) indicates that the submittals to the 1990 IDB total 7,622 canisters. The total volume based on this number of canisters is 6,784 m^3 (2.4 x 10^5 ft^3). U.S. DOE (1991) also discusses the number of uncertainties in the projection of the RH inventory and acknowledges that the details of the RH-TRU waste canister design should be revisited for re-evaluation. Because of the uncertainty in the RH inventory and the discussion in U.S. DOE (1991) on canister design, the smaller total stored plus projected volume of waste--not the volume of the canisters--was used as a scaling factor to estimate the RH radionuclide inventory for an RH design volume.

Table 3.4-7. Estimate of a Design Volume for RH-TRU Waste

Site	Stored Volume (1990 IDB) (m^3)	Projected Volume (1990 IDB) (m^3)	Total Volume (1990 IDB) (m^3)	Scaled Volume* (m^3)	Estimated Design Volume (m^3)
ANL-E	--	81.6	81.6	36.8	118.4
HANF	137	3535.2	3672.2	1,596.0	5,268.2
INEL	29.5	76.8	106.3	34.7	141.0
LANL	28.4	4.8	33.2	2.2	35.4
ORNL	1307	144.0	1,451.0	65.0	1,516.0
Total	1,501.9	3,842.4	5,344.3	1,734.7	7,079

* Assuming that ANL, HANF, INEL, LANL, and ORNL provide the difference between the current total inventory and the design volume. The difference between the total volume of 5,344 m^3 in the 1990 IDB and the design volume of 7,079 m^3 (0.25×10^6 ft^3) was ratioed between the five sites based on their estimated annual generation rates.

3.4.3 Saturation

Initial Saturation*

Parameter: **Saturation, initial ($S_{\ell i}$)**
Material: Unmodified CH-TRU waste form including containers (WastRef, BrineSat)

Definition Units: Dimensionless

Values: Range: (0, 0.14) Median: 0.07

Distribution: Uniform
Correlation:

Data Source(s): None. (PA Investigator Judgment)

Usage:

Mathematical model:
Two-Phase Flow, Section 1.4.1 of this volume.

Equations 1.4.1-1 and 1.4.1-2 (Initial condition of liquid-phase saturation in Waste material).

Computational models:
BRAGFLO

Ranking in Past Sensitivity Analyses:

40 CFR 191	Low
40 CFR 268	High
NEPA	Not tested
Other	Not tested

*Key to Parameter Sheets is provided in Section 1.2.8.

4. PARAMETERS OF GLOBAL MATERIALS AND AGENTS ACTING ON DISPOSAL SYSTEM

This chapter contains parameters for fluid properties, climate variability, and intrusion characteristics.

4.1 Fluid Properties

The fluid parameters tabulated in Table 4.1-1 include Salado and Culebra brine, drilling mud, and hydrogen gas.

Table 4.1-1. Fluid Properties

Parameter	Median	Range		Units	Distribution Type	Source
Brine, Salado (T = 27°C [300.15 K], p = 1 atm [0.101325 MPa])						
Compressibility	2.5×10^{-10}	2.4×10^{-10}	2.6×10^{-10}	Pa^{-1}	Normal	McTigue et al., 1991
Density (ρ_f)	1.23×10^{3}	1.207×10^{3}	1.253×10^{3}	kg/m^3	Normal	McTigue et al., 1991
Viscosity (μ)	1.8×10^{-3}			Pa•s	Constant	Kaufmann, 1960, p. 622
Brine, Culebra (T = 27°C [300.15 K], p = 1 atm [0.101325 MPa])						
Density (ρ_f)	1.09×10^{3}	9.99×10^{2}	1.154×10^{3}	kg/m^3	Spatial	Cauffman et al., 1990, Table E.1
Viscosity (μ)	1×10^{-3}			Pa•s	Constant	Haug et al.,1987, p.3-20
Brine, Castile (T = 27°C [300.15 K], p = 1 atm [0.101325 MPa])						
Compressibility	9×10^{-10}			Pa^{-1}	Constant	Popielak et al., 1983, p. H-32
Density	1.215×10^{3}			kg/m^3	Constant	Popielak et al., 1983, Table C-2
Hydrogen (T = 27°C [300.15 K])						
Density @	1.1037×10^{1} (15 MPa)	8.1803×10^{-2} (0.1 MPa)	1.4442×10^{1} (20 MPa)	kg/m^3	Table	WIPP PA Division, 1991, Vol. 3, Section 4.1.4
Viscosity (μ)	9.2×10^{-6}	8.92×10^{-6}	9.33×10^{-6}	Pa•s	Table	Vargaftik, 1975, p. 39.
Solubility in brine (χ)	3.84×10^{-4}	6.412×10^{-6}	4.901×10^{-4}	none	Table	WIPP PA Division, 1991, Vol. 3, Section 4.1.4; Cygan, 1991.
Drilling Mud Properties (T = 22°C [295.15 K], p = 1 atm [0.101325 MPa])						
Density (ρ_f)	1.211×10^{3}	1.139×10^{3}	1.378×10^{3}	kg/m^3	Constructed	Pace, 1990
Viscosity	9.17×10^{-3}	5×10^{-3}	3×10^{-2}	Pa•s	Constructed	Pace, 1990
Yield stress	4	2.4	1.92×10^{1}	Pa	Constructed	Fredrickson, 1960, p.252; Savins and Wallick, 1966; Pace, 1990

4.2 Human-Intrusion Borehole

Table 4.2-1 summarizes geometric and physical parameters of human-intrusion boreholes assumed by the PA Department for disturbed-scenario calculations.

Table 4.2-1. Characteristics of Human-Intrusion Borehole

Parameter[a]	Median	Range		Units	Distribution Type	Source
Borehole Fill Properties						
Creep $(r_o-r)/r_o$	n.a.	2×10^{-2}	8×10^{-1}	none	Table	Sjaardema and Krieg, 1987, Figure 4.6
Density, average (ρ_{ave})	2.3×10^{3}			kg/m^3	Constant	See Section 2.3.1
Density, bulk (ρ_{bulk})	2.14×10^{3}			kg/m^3	Constant	See Section 2.3.1
Permeability, final (k)	**3.16×10^{-12}**	**1×10^{-14}**	**1×10^{-11}**	**m^2**	**Lognormal**	**See Section 4.2.1**
Initial						
Plug in Castile Fm.	10^{-15}			m^2	Constant	Lappin et al., 1989, Table C-1
Plugs in Salado Fm.	10^{-18}			m^2	Constant	Lappin et al., 1989, Table C-1
Porosity (ϕ)	3.75×10^{-1}	2.5×10^{-1}	5×10^{-1}	none	Normal	Freeze and Cherry, 1979, Table 2.4 (sand)
Drilling Characteristics						
Drill bit diameter (d)						
Intrusion	**3.55×10^{-1}**	**2.67×10^{-1}**	**4.44×10^{-1}**	**m**	**Uniform**	**See Section 4.2.2**
Historical	2×10^{-1}	1.21×10^{-1}	4.45×10^{-1}	m	Constructed	Brinster, 1990
Drill string angular velocity ($\dot{\theta}$)	7.7	4.2	2.3×10^{1}	rad/s	Constructed	Pace, 1990; Austin, 1983
Drilling mud flowrate (Q_f)	9.935×10^{-2}	7.45×10^{-2}	1.24×10^{-1}	$m^3/(s \cdot m)$	Uniform	Pace, 1990; Austin, 1983

[a]Parameters in bold were sampled in the 1992 calculations.

4.2.1 Borehole Fill Properties

Permeability*

Parameter: **Permeability, final (k)**
Material: Fill material in a human-intrusion borehole (Borehole, Prm)

Definition Units: m^2

Values: Range: $(1 \times 10^{-14}, 1 \times 10^{-11})$ Median: 3.16×10^{-12}

Distribution: Lognormal
Correlation:

Data Source(s): Freeze, R. A., and J. A. Cherry. 1979. *Groundwater.* Englewood Cliffs, NJ: Prentice-Hall, Inc. (Table 2.2, silty sand) (Investigator Judgment)

Usage:

Mathematical model:
Two-Phase Flow, Section 1.4.1 of this volume.

Equations 1.4.1-1 and 1.4.1-2.

Computational models:
BRAGFLO

Ranking in Past Sensitivity Analyses:

40 CFR 191	High
40 CFR 268	Not applicable
NEPA	Not tested
Other	Not tested

*Key to Parameter Sheets is provided in Section 1.2.8.

Discussion:

Because of the speculative nature of inadvertent human intrusion, PA calculations depend on the guidance provided by regulations on factors such as length, severity, and resulting conditions after intrusion. The EPA Standard, *40 CFR 191*, in Appendix B states

> "...the implementing agency can assume that passive institutional controls or the intruders' own exploratory procedures are adequate for the intruders to soon detect, or be warned of, the incompatibility of the area with their activities.... Furthermore, the Agency assumes that the consequences of such inadvertent drilling need not be assumed to be more severe than: ... (2) creation of a ground water flow path with a permeability typical of a borehole filled by the soil or gravel that would normally settle into an open hole over time--not the permeability of a carefully sealed borehole."

Thus, while intruders "soon detect" the repository, the guidance in Appendix B suggests that the implementing agency should not take credit for any special precautions that the drilling company might pursue as the result of detection that could alter long-term borehole behavior.

Initial Conditions after Abandonment. Some PA calculations require that initial conditions be established for the time period immediately after intrusion; no regulatory guidance has been provided for these conditions. In defining initial conditions in the borehole, the PA calculations assume that future societies establish government regulations on drilling similar to those in effect today to protect natural resources. Thus, for any borehole through the repository and hypothetical brine reservoir, drillers would be required to place casing and several cement and sand plugs as follows:

Casing. The normal procedure for drilling an oil and gas well is to drill the hole to the base of the Rustler Formation (the top of salt) and set casing. The State Engineer Office dictates the use of casing because the WIPP is located in a closed groundwater basin, and all hydrocarbon wells are required to protect the aquifers in the basin (e.g., Culebra Dolomite). After the hole has been drilled and the casing placed in the hole, the casing is cemented from bottom to top with an API Class C grout (intended for use in oil and gas wells from surface to a depth of 2,400 m [8,000 ft] and having a sulfate resistance).

Plug Locations. The Energy, Minerals, and Natural Resources Department, Oil Conservation Commission (OCC) controls plugging when abandoning a borehole in the Delaware Basin in and around the WIPP. Exact specifications are negotiated between the drilling company and the OCC. The OCC then inspects for compliance. Because the WIPP repository is located in an area of the potash, recommended plugging procedures protect the potash horizon from foreign fluids. Prior to 1988, specifications likely included sealing off any encountered brine reservoir in the Castile Formation with cement grout and capping the seal with a 60-m (200-ft) cement-grout plug (Figure 4.2-1). About 15 m (50 ft) of sand was usually emplaced above grout plugs. Weighted drilling fluid above the sand was usually emplaced to ~60 m (~200 ft) below the potash horizon, where another plug extended through the potash horizon. A second sand cap was emplaced, followed by weighted drilling mud to within ~60 m (~200 ft) of the top of the Salado Formation salt, where another plug of cement grout was emplaced, followed by sand and weighted mud. When the base of the casing was reached, the specifications either required grouting or filling with weighted mud to the surface, where a cap and abandonment marker were often placed (Lappin et al., 1989, Appendix C).

In April 1988, the OCC amended order R-111 and specified that the plug be a "solid cement plug through the salt section" (Salado Formation); the amendment was in response to conflicts between the potash and oil/gas industries (OCC, 1989, p. 10). The 1991 PA calculations assumed these latter plugging conditions.

Initial Plug Permeability. The initial plug permeabilities depend strongly on the host rock in which the plug is emplaced (e.g., clean vs. chemically altered steel casing or anhydrite vs. halite). Because most experimental studies of plug-borehole interactions extend for only hundreds of days or less, data are limited (Christensen and Petersen, 1981; Buck, 1985; Bush and Piele, 1986; Bush and Lingle, 1986; and Scheetz et al., 1986). Any PA calculations starting from initial conditions assume permeabilities of 10^{-15} m^2 (1 mD) for plugs in the Castile Formation and 10^{-18} m^2 (10^{-3} mD) in the Salado and Rustler Formations (Lappin et al., 1989, Table C-1).

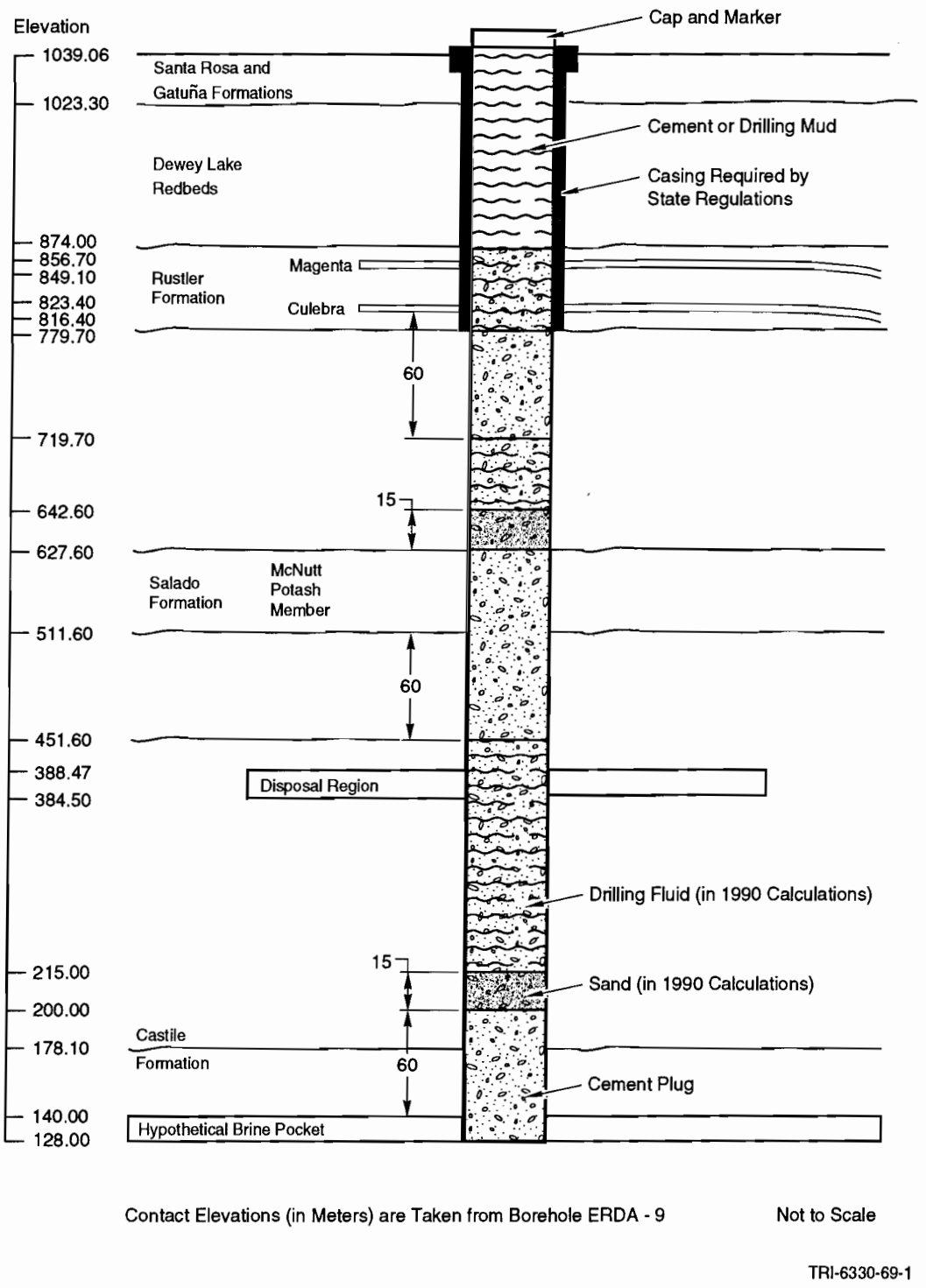

Figure 4.2-1. Required casing and plugs. New Mexico State regulations require casing through Rustler Formation when drilling exploratory boreholes; New Mexico Energy, Mineral, and Natural Resources Department currently requires solid cement plugs in Salado Formation to protect potash horizon when abandoning a borehole.

Borehole Permeability and Porosity. Of primary concern to the PA calculations is the borehole permeability over most of the 10,000 yr. Three components of these calculations are (1) the length of time that the plug and casing remain intact, (2) the change in permeability of the deteriorating plugs with time, and (3) the ultimate deformation of the borehole.

Plug Life. Cementing companies suggest that the cement plugs should last for at least 100 yr, as would the casing. PA calculations assume a life of 75 yr followed by 75 yr of degradation (Figure 4.2-2).

Degraded Plugs and Borehole Debris Permeability. PA calculations assume that the degrading concrete plugs and other debris initially present in the hole would have a permeability and porosity of silty sand (Freeze and Cherry, 1979), but with a bulk and average density equal to that of the Salado Formation (Table 4.2-1). The permeability and porosity were assumed to vary lognormally and normally, respectively, between the typical range for silty sand, typical of distributions of the parameters in the literature (Harr, 1987, Table 1.8.1).

Note that any drilling mud initially in the borehole or brine that drains into the borehole would have to be able to migrate through the degrading plugs before the borehole could be a viable conduit. In other words, if the fluid is trapped, the borehole is not a conduit.

Borehole Deformation. Because of the change in borehole abandonment procedures, the 1991 and 1992 PA calculations did not assume any borehole deformation. This assumption contributed to a more conservative calculation.

With the previous order, salt "would normally settle into an open hole" and naturally seal the hole shut in the uncemented section of the borehole. Thus, with time, the borehole would attain very low permeabilities similar to the host salt. However, if the amended orders are followed and the borehole is filled, the use of a solid cement plug through the Salado Formation greatly decreases the likelihood that the borehole will be permanently sealed by salt creep over the long term (>100 yr).

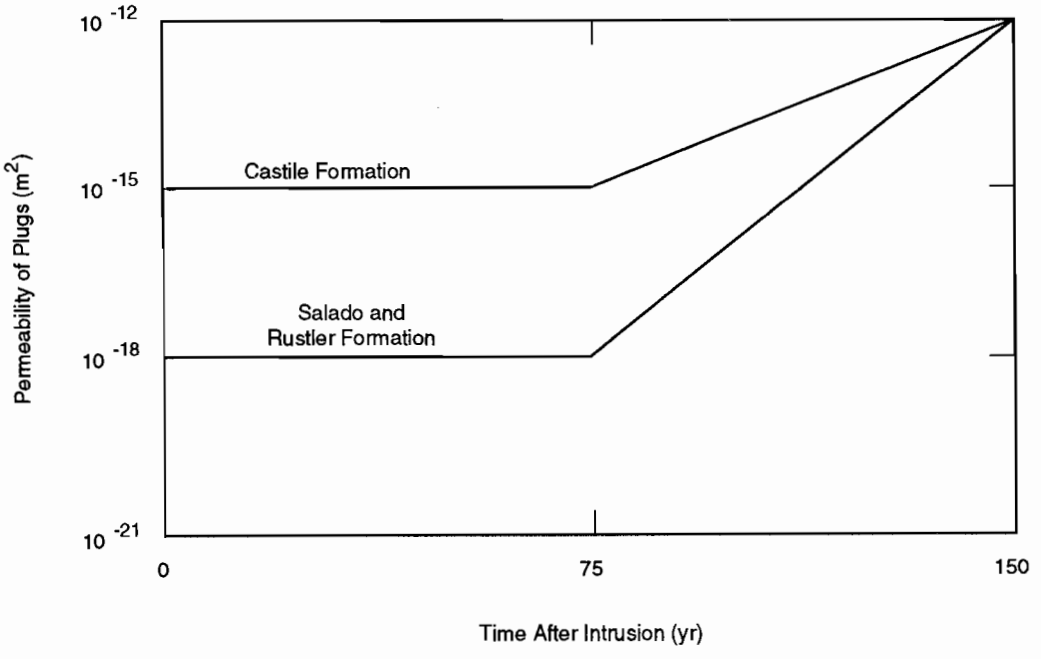

Figure 4.2-2. Increased permeability of cement grout plugs in intrusion borehole with time because of degradation.

4.2.2 Drilling Characteristics

Intrusion Drill Bit Diameter*

Parameter: **Intrusion drill bit diameter (d)**
Material: Determines initial diameter of human-intrusion borehole, (Borehole, DiamMod)

Definition Units: m

Values: Range: (2.67×10^{-1}, 4.44×10^{-1}) Median: 3.55×10^{-1}

Distribution: Uniform
Correlation:

Data Source(s): See text. (Investigator Judgment)

Usage:

Mathematical model:

Two-Phase Flow, Section 1.4.1 of this volume;
Cuttings Removal, Section 1.4.3 of this volume.

Equation: (Determines geometry of borehole in two-phase flow model; see Figure 1.4-3 for cuttings-removal model).

Computational models:

BRAGFLO
CUTTINGS

Value of Additional Information

40 CFR 191	High (CUTTINGS)
40 CFR 268	Not applicable
NEPA	Not tested
Other	Not tested

*Key to Parameter Sheets is provided in Section 1.2.8.

Discussion:

The guidance for the EPA Standard, *40 CFR 191*, (Appendix B) states that the EPA

> "...believes that the most productive consideration of inadvertent intrusion concerns those realistic possibilities that may be usefully mitigated by repository design, site selection, or use of passive controls (although passive institutional controls should not be assumed to completely rule out the possibility of intrusion). Therefore, inadvertent and intermittent intrusion by exploratory drilling for resources (other than any provided by the disposal system itself) can be the most severe intrusion scenario assumed..."

The possible futures (scenarios) that must be considered are not necessarily exhaustive, but rather those that if examined might differentiate between repository sites or perhaps identify ways to improve repository design.

Consequently, the PA Department assumes that current standard drilling procedures for gas and oil exploration will continue into the future, and that future drillers will observe regulations similar to those currently imposed by federal and state agencies to protect resources.

Drilling for oil and gas has two main objectives: to drill the hole to the target horizon as quickly and economically as safely possible, and to install casing from the reservoir to the surface for production of hydrocarbons if they are found. The procedures used to accomplish these objectives are fairly well standardized in the drilling industry.

Currently when a company drills an exploratory oil or gas well in the Delaware Basin, the operation uses a standard rotary drill rig with a mud circulation system. The differences between drilling for oil and gas depend on the depth of the well, which controls the size of drill bit used. Figure 4.2-3 shows the distribution used in the past in the Delaware Basin for oil and gas exploration. The data are reported as a discrete distribution because bit diameters cannot vary continuously between 0.1206 m and 0.4445 m diameter (4-3/4 in. and 17-1/2 in.), but must be the diameter of a bit that was actually used (Brinster, 1990). The median bit diameter is 0.2000 m (7-7/8 in. diameter).

Currently, the normal depth for an oil well in the Delaware Basin near the WIPP site ranges from 1,200 to 1,800 m (4,000 to 6,000 ft), but gas-well depths usually exceed 3,000 m (10,000 ft). Consequently, oil wells normally have a standard 0.413-m (16 1/4-in.) drilled hole to the top of salt to accommodate 0.340-m (13 3/8-in.) steel casing, and gas wells normally have a standard 0.4445-m (17 1/2-in.) drilled hole to accommodate 0.356-m (14-in.) casing. After casing is set with grout, the company drills either a standard 0.311-m (12 1/4-in.) hole, if the target is oil, or a 0.356-m (14-in.) hole, if the target is gas (Table 4.2-2). Rather than sample from the historical diameters for evaluating the borehole as was done in the 1990 PA calculations, the 1991 PA calculations sampled from a perturbation about the currently used diameter for deep gas wells (i.e., 0.356 m ± 0.0889 [14 in. ± 3.5]). This practice ensures that fairly large borehole diameters are used, and thus, is more conservative than the 1990 calculations.

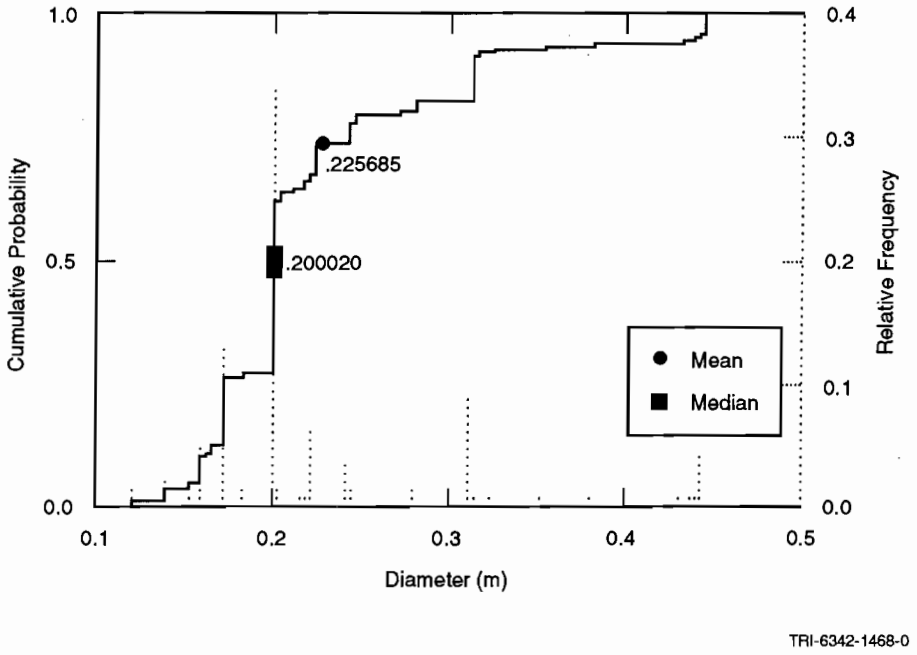

Figure 4.2-3. Distribution of historical drill bit diameter.

Table 4.2-2. Specifications for Gas and Oil Exploratory Boreholes

Parameter		Value	Units
Drilled diameter			
In Rustler Formation	(oil well)	0.413	m
	(gas well)	0.444	m
In Salado and Castile Formations,	(oil well)	0.311	m
	(gas well)	0.356	m

4.3 Parameters for Castile Formation Brine Reservoir

Pressurized brine in the northern Delaware Basin has been encountered in fractured anhydrites of the Castile Formation in boreholes both north and northeast of the WIPP over the past 50 yr. In addition, Castile brines were encountered southwest of the WIPP at the Belco Well, about 6.5 km (4 mi) from the center of the WIPP. During WIPP site characterization, Castile Formation brine reservoirs were encountered in the WIPP-12 borehole, about 1.6 km (1 mi) north of the center of the WIPP, and the ERDA-6 borehole, about 8 km (5 mi) northeast of the center of the WIPP (Figure 4.3-1).

Also, a geophysical study that correlated with the known occurrence of brine at WIPP-12 indicated the presence of brine fluid within the Castile Formation under the WIPP (Earth Technology Corp., 1988). Based on borehole experience and the geophysical study, the PA calculations assume that a brine reservoir exists underneath at least a portion of the disposal region. The assumed presence of a Castile brine reservoir beneath the repository is of concern only in the event of human intrusion. (The area, and thus, the probability of hitting a brine reservoir and the disposal area simultaneously are discussed in Chapter 5.)

Table 4.3-1 provides parameter values for the PA Department's model of the Castile Formation Brine Reservoir.

Table 4.3-1. Parameter Values for Castile Formation Brine Reservoir

Parameter[a]	Median	Range		Units	Distribution Type	Source
Elevation, top	1.4×10^{2}	-2.00×10^{2}	1.78×10^{2}	m	Constructed	WIPP PA Division, 1991, Vol. 3, Section 4.3.1
Density, grain (ρ_g)	2.963×10^{3}			kg/m^3	Constant	See anhydrite, Section 2.4
Analytic Model						
Pressure, initial (p_i)	**12.6**	**11.0**	**21.0**	**MPa**	**Constructed**	**See Section 4.3.1**
Storativity, bulk ($\hat{S}_b$)	**2×10^{-1}**	**2×10^{-2}**	**2×10^{1}**	**m^3/Pa**	**Loguniform**	**See Section 4.3.2**
Numerical Model						
Permeability						
Intact matrix	1×10^{-19}	1×10^{-20}	1×10^{-18}	m^2	Constructed	WIPP PA Division, 1991, Vol. 3, Section 4.3.2
Fractured matrix	1×10^{-13}	1×10^{-16}	1×10^{-10}	m^2	Constructed	Freeze and Cherry, 1979; Reeves et al., 1991.
Porosity	5×10^{-3}	1×10^{-3}	1×10^{-2}	none	Constructed	Reeves et al., 1991.
Radius, equivalent	2.32×10^{2}	3×10^{1}	8.6×10^{3}	m	Constructed	Reeves et al., 1991.
Thickness	1.2×10^{1}	7	6.1×10^{1}	m	Uniform	Reeves et al., 1991.

[a]Parameters in bold were sampled in the 1992 calculations.

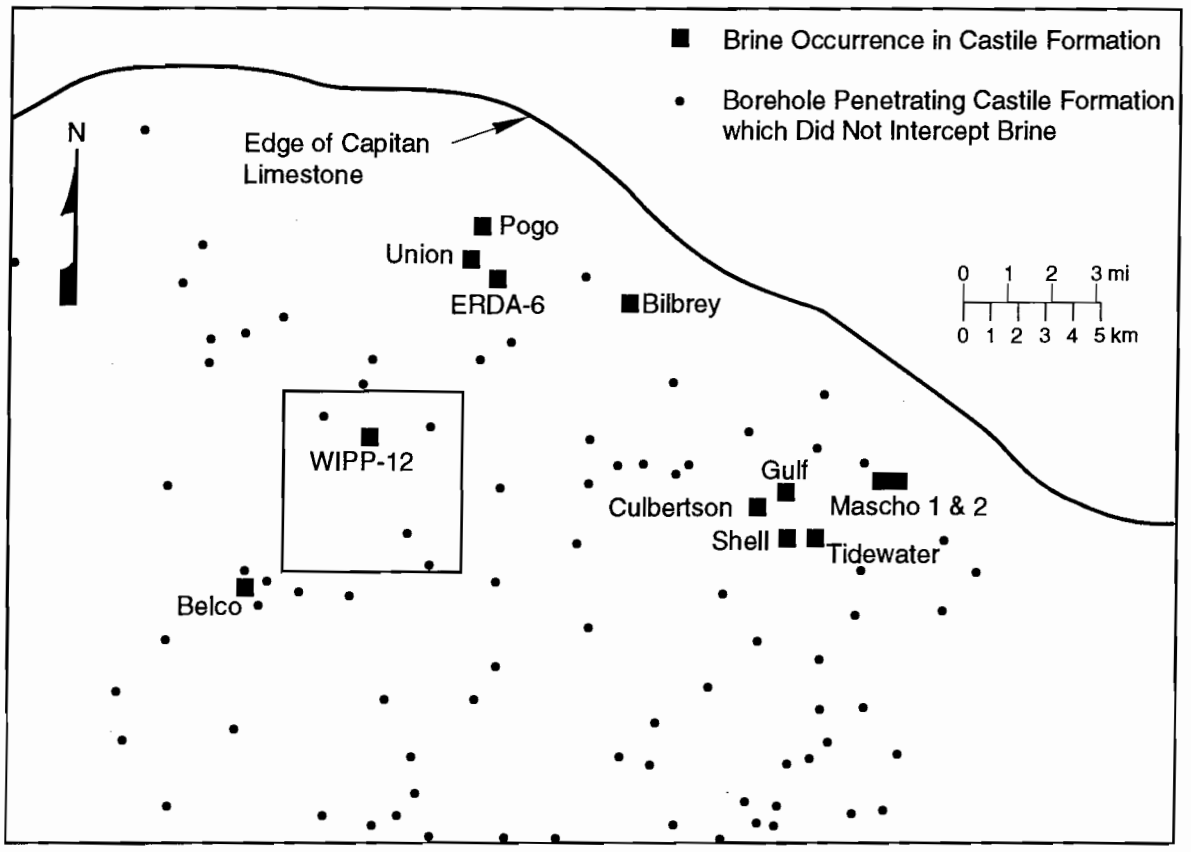

Figure 4.3-1. Deep boreholes that encountered brine reservoirs within the Castile Formation, Northern Delaware Basin (Lappin et al., 1989, Figure 3-26).

4.3.1 Brine Pressure

Pressure, Initial*

Parameter:	**Pressure, initial (p_i)**
Material:	Brine reservoirs in Castile Formation (Cstile_R, Pressure)
Definition Units:	MPa
Values:	Range: (11.0, 21.0) Median: 12.6
Distribution:	Constructed (Figure 4.3-2); see Discussion
Correlation:	

Data Source(s):

Popielak, R. S., R. L. Beauheim, S. R. Black, W. E. Coons, C. T. Ellingson, and R. L. Olsen. 1983. *Brine Reservoirs in the Castile Formation, Waste Isolation Pilot Plant (WIPP) Project, Southeastern New Mexico*. TME-3153. Carlsbad, NM: U.S. Department of Energy. (WIPP Observational Data)

Lappin, A. R., R. L. Hunter, D. P. Garber, and P. B. Davies, eds. 1989. *Systems Analysis, Long-Term Radionuclide Transport, and Dose Assessments, Waste Isolation Pilot Plant (WIPP), Southeastern New Mexico; March 1989*. SAND89-0462. Albuquerque, NM: Sandia National Laboratories. (Table 3-19) (Investigator Judgment)

Usage:

Mathematical model:

Two-Phase Flow, Section 1.4.1 of this volume.

Equations 1.4.1-1 and 1.4.1-2 (initial conditions in brine-reservoir materials).

Computational models:

BRAGFLO

Ranking in Past Sensitivity Analyses:

40 CFR 191	Medium
40 CFR 268	Not applicable
NEPA	Not tested
Other	Not tested

*Key to Parameter Sheets is provided in Section 1.2.8.

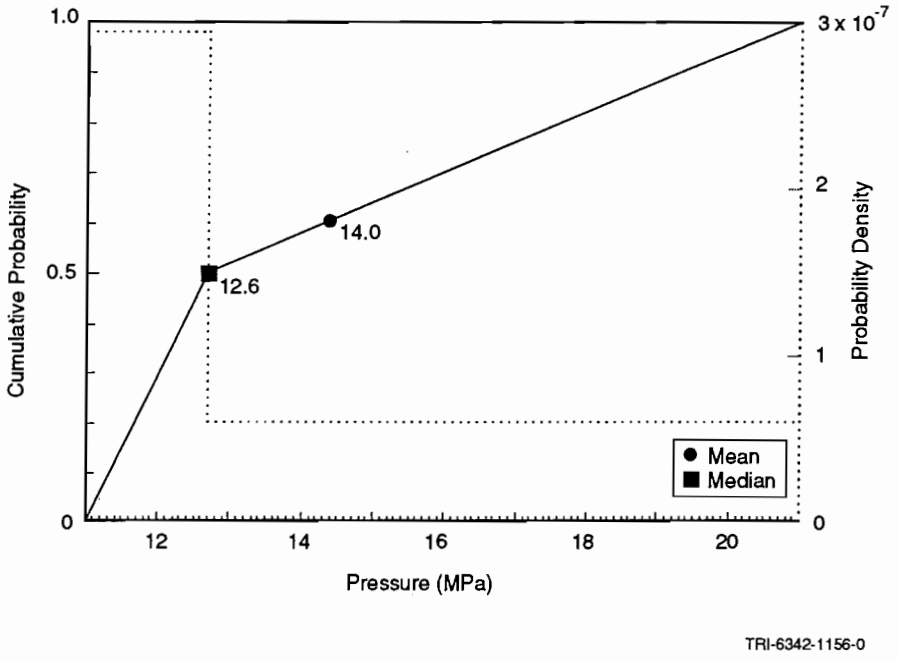

Figure 4.3-2. Constructed distribution for Castile brine reservoir initial pressure.

Discussion:

Median. The measured initial pressure of 12.6 MPa (125 atm) for WIPP-12 (Popielak et al., 1983, p. H-52) was used as the median brine reservoir initial pressure.

Range. Lappin et al. (Table 3-19, 1989, derived from Popielak et al., 1983, Table H.1) estimated the initial brine reservoir pressure from several wellhead measurements at WIPP-12 and other boreholes that encountered pressurized Castile brine. The range was between 7.0 and 17.4 MPa (69 and 172 atm). Because the range of pressures includes measurements in wells completed at various elevations, a correction for differences in elevation is required.

The origin of Castile brine reservoirs is not conclusively known. Present interpretations are that their origin is either local, by limited movement of intergranular brines from adjacent Castile halites, or regional, by the previous existence of a lateral hydraulic connection of the Castile Formation with the Capitan reef (Lappin et al., 1989). However, the initial pressure observations at other wells are only directly pertinent if (1) the reservoir fluids are from the same source (past interconnection of reservoir fluid) or (2) they had a common genesis (e.g., brine trapped along bedding planes in areas of high permeability).

For the first case (interconnection), an elevation correction assuming a hydrostatic variation with depth is most appropriate. For the second case (common genesis), an elevation correction assuming a lithostatic variation depth is most appropriate. The range using both types of elevation corrections is 10.7 to 16.8 MPa (106 to 166 atm) (Table 4.3-2). A brine density of 1,215 kg/m^3 (75.85 lb/ft^3) (Section 4.1) was assumed for the first case; an average formation density of 2,400 kg/m^3 (149.8 lb/ft^3) was assumed for the second case. Elevations (except WIPP-12 and ERDA-6) were estimated from the well location and a topographic map of the area (USGS 15 min quads, Carlsbad, NM, 1971, Nash Draw, NM, 1965).

This calculated range is similar to the maximum and minimum possible range of 11 and 21 MPa, assuming hydrostatic and lithostatic pressures at the elevation of the WIPP-12 brine reservoir (140 m [457.8 ft]) (see Figure 2.3-11), and consequently this latter range has been used in the PA calculations.

Table 4.3-2. Estimated Initial Pressures of Brine Reservoirs Encountered in the Region around the WIPP Corrected to the Depth at the WIPP-12 Brine Reservoir (after Popielak et al., 1983)

Well Name	Pressure with Hydrostatic Correction (MPa)	Pressure with Lithostatic Correction (MPa)	Reported Pressure at Observation (MPa)	Elevation of Observation (m)	Depth to Observation (m)	Surface Elevation* (m)
WIPP-12	12.7	12.7	12.7	140	918	1058
ERDA-6	15.5	16.8	14.1	253	826	1079
Belco	14.5	14.6	14.3	152	854	1006
Gulf	12.1	10.7	13.6	16	1097	1113
Pogo	>16.6	>15.8	>17.4	69	1013	1082
Tidewater	>14.0	>12.2	>16.0	-24	1137	1113
Union	>11.2	>12.2	>10.1	226	856	1082
H&W Danford 1	11.5	15.8	7.0	512	588	1100(?)
**Bilbrey	12.1	13.8	11.2	209	942	1151
**Culbreston	11.8	10.9	12.8	57	1071	1128
**Mascho 1	11.6	10.8	12.4	69	1013	1082
**Mascho 2	11.3	10.6	12.0	77	1005	1082
**Shell	11.8	10.4	13.4	9	1119	1128

* Elevation from well location and USGS 15 min quad topographic map, Carlsbad, NM, 1971, Nash

** According to Popielak et al. (1983, Table H.1), these wells should not be used to estimate static pressure.

4.3.2 Bulk Storativity

Bulk Storativity*

Parameter:	**Bulk storativity (S_b)**
Material:	Brine reservoirs in Castile Formation (Cstile_R, StorBulk)
Definition Units:	m^3/Pa
Values:	Range: $(2 \times 10^{-2}, 2)$ Median: 2×10^{-1}
Distribution:	Lognormal (Figure 4.3-3)
Correlation:	

Data Source(s): See text. (Investigator Judgment)
Popielak, R. S., R. L. Beauheim, S. R. Black, W. E. Coons, C. T. Ellingson, and R. L. Olsen. 1983. *Brine Reservoirs in the Castile Formation, Waste Isolation Pilot Plant (WIPP) Project, Southeastern New Mexico.* TME-3153. Carlsbad, NM: U.S. Department of Energy. (WIPP Observational Data)

Usage:

Mathematical model:
Two-Phase Flow, Section 1.4.1 of this volume.

Equation (used to compute time-dependent boundary conditions for Eqs. 1.4.1-1 and 1.4.1-2).

Computational models:
BRAGFLO

Ranking of Past Sensitivity Analyses:

40 CFR 191	Medium
40 CFR 268	Not applicable
NEPA	Not tested
Other	Not tested

*Key to Parameter Sheets is provided in Section 1.2.8.

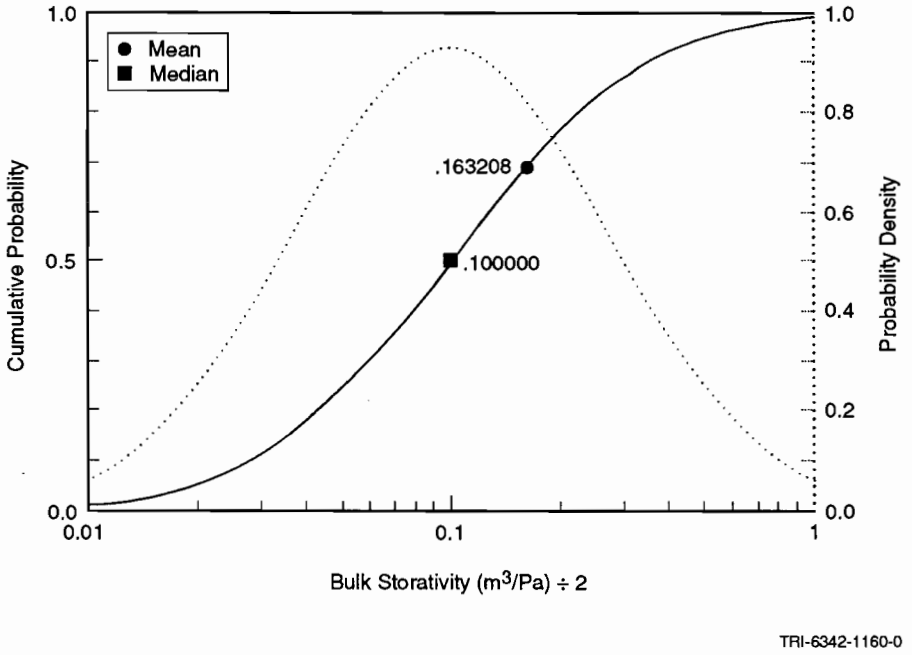

Figure 4.3-3. Estimated distribution for bulk storativity of Castile brine reservoir.

Discussion:

Bulk storativity (S_b) as defined herein is the total volume of fluid discharged from the reservoir per unit decrease in reservoir pressure ($\Delta V/\Delta p$). The bulk storativity can be estimated from wellhead measurements (long-term change in pressure and total discharge volume), or from the compressibility of the reservoir matrix and fluid and the total volume and porosity of the reservoir.

The pressure recovery of the WIPP-12 reservoir is characteristic of a dual-porosity medium. An initial rapid response is attributed to a highly permeable fracture set, whereas a more gradual component of recovery is due to repressurization of the higher permeability fracture set by intersecting lower permeability fractures. Because the human-intrusion scenarios contemplate that the Castile will be connected to the Culebra over the long term (compared to the duration of well tests), estimates of bulk storativity from long-term pressure changes are more appropriate than those made using short-term pressure changes, which may represent only the storativity of the highest permeability fractures. Estimates of bulk storativity using wellhead measurements range from 5×10^{-4} m^3/Pa (from ERDA-6 testing through October, 1982) to 2×10^{-1} m^3/Pa (from estimated total discharge volume, maximum estimated formation pressure, and apparent long-term recovery pressure at WIPP-12). Because WIPP-12 is closer to the waste disposal area than ERDA-6, the latter number is considered more appropriate for a sub-repository reservoir.

Reservoir compressibility (β_s/ϕ) and total volume (V_{tot}) may also be used to estimate bulk storativity:

$$S_b = \frac{\Delta V}{\Delta p} = V_{tot}\frac{1}{V_{tot}}\frac{\Delta V}{\Delta p} = V_{tot}\frac{1}{K} = V_{tot}\beta_s \qquad (4.3\text{-}1)$$

The area of the WIPP-12 reservoir is approximately 1.7×10^6 m^2 (Popielak et al., 1983 p. H-53). Popielak depicts brine occurrence in the lower 40% of the 100-m thickness of Anhydrite III-IV at WIPP-12 (Popielak et al., 1983, Figure G-2), giving a rough estimate of the reservoir total volume of 6.5×10^7 m^3. (Note that other published estimates of reservoir volume [e.g., Lappin et al., 1989, p. E-32] were made from wellhead measurements assuming some value of compressibility. These volume estimates will therefore not lead to independent estimates of S_b.) Estimates of the bulk modulus $K_{bulk} = E/3(1-2\upsilon)$ (where E is Young's modulus and υ is Poisson's ratio) of

Anhydrite III at WIPP-12 were used by Popielak et al. (1983, p. G-34) to derive a range of ßs from 3×10^{-11} Pa^{-1} to 1.4×10^{-10} Pa^{-1}. The resulting range in bulk storativity from Eq. 4.3-1 is 2×10^{-3} to 9×10^{-3} m^3/Pa. The reason this range does not include the wellhead estimate from WIPP-12 may be due to errors in the estimate of bulk volume or compressibility. For example, the apparent $ß_s$ may be larger than estimated here because of fractures in the anhydrite or trapped gas in the reservoir. However, at present there is no reason to suppose that bulk storativity is substantially higher than estimated from WIPP-12 wellhead measurements.

Based on the above considerations, the bulk storativity is assumed to lie between 2×10^{-2} and 2 m^3/Pa. The likelihood of the actual value falling in a given interval is described by a lognormal distribution between these limits. The median of this distribution is 0.2 m^3/Pa.

4.4 Climate Variability and Culebra Member Recharge

Climate variability is a continuous process (agent) acting on and thus affecting the state of the disposal system. The primary concerns are precipitation variation and, ultimately, recharge to strata above the Salado Formation, specifically, to the Culebra Dolomite Member. Parameters for the PA Department's models of climate variability and Culebra Member recharge are shown in Table 4.4-1. These models are discussed briefly in Section 1.4.5 and in more detail in Volume 2 of this 1992 series of reports.

Table 4.4-1. Climate Variability and Culebra Member Recharge

Parameter[a]	Median	Range		Units	Distribution Type	Source
Annual precipitation ($\bar{r}_p$)	3.436×10^{-1}	3.09×10^{-2}	6.563×10^{-1}	m	Normal	Hunter, 1985
Precipitation variation						
Amplitude factor (A_m)	2			none	Constant	Swift, 1991
Short-term fluctuation (ϕ)	2×10^{-10}			Hz	Constant	Swift, 1991
Glacial fluctuation (Θ)	1.7×10^{-12}			Hz	Constant	Swift, 1991
Index for computing recharge amplitude factor A_R	**0.5**	**0**	**1**	**none**	**Uniform**	**See Section 1.4.5.**

[a]Parameters in bold were sampled in the 1992 calculations.

Index for Computing Recharge Amplitude Factor*

Parameter: **Index for computing recharge amplitude factor (A_R)**
Material: Model of climatic variability and boundary recharge (Global, ClimtIdx)

Definition Units: None

Values: Range: (0, 1) Median: 0.5

Distribution: Uniform
Correlation:

Data Source(s): None. (Investigator Judgment), but see
Swift, P. N. 1991. Appendix A: "Climate and Recharge Variability Parameters for the 1991 WIPP PA Calculations," *Preliminary Comparison with 40 CFR Part 191, Subpart B for the Waste Isolation Pilot Plant, December 1991. Volume 3: Reference Data*. WIPP Performance Assessment Division. Eds. R. P. Rechard, A. C. Peterson, J. D. Schreiber, H. J. Iuzzolino, M. S. Tierney, and J. S. Sandha. SAND91-0893/3. Albuquerque, NM: Sandia National Laboratories. A-107 through A-121.

Usage:

Mathematical model:
Fluid Flow in Culebra, Section 1.4.5 of this volume.

Equation 1.4.5-4 and text following that equation. The recharge amplitude factor A_R is calculated from the index U by

$$A_R = 1 + (\gamma - 1)U$$

where γ is a scaling factor chosen by the PA Analyst.

Computational models:
SECO2D

Ranking in Past Sensitivity Analyses:

40 CFR 191	Medium
40 CFR 268	Not tested
NEPA	Not tested
Other	Not tested

*Key to Parameter Sheets is provided in Section 1.2.8.

5. PARAMETERS FOR SCENARIO PROBABILITY MODELS

5.1 Area of Brine Reservoirs

Parameter:	**Fraction of Area of Castile Brine Reservoirs Overlapping Disposal Area (A_b/A_t)**
Material:	Geometric Property of Castile Brine Reservoirs (Cstile_R, Area_frc)
Definition Units:	Dimensionless
Values:	Range: (0.25, 0.57) Median: 0.4
Distribution:	Constructed (by simulation; see discussion and Figure 5.1-1)
Correlation:	

Data Source(s): See text. (Investigator Judgment)

Earth Technology Corporation. 1988. *Final Report for Time Domain Electromagnetic (TDEM) Surveys at the WIPP Site.* SAND87-7144. Albuquerque, NM: Sandia National Laboratories.

Usage:

Mathematical model:

Human Intrusion; Section 1.4.2 of this volume.

Equation 1.4.2-5 and text preceding that equation.

Computational models:

CCDFPERM

Ranking in Past Sensitivity Analyses:

40 CFR 191	Low
40 CFR 268	Not applicable
NEPA	Not tested
Other	Not tested

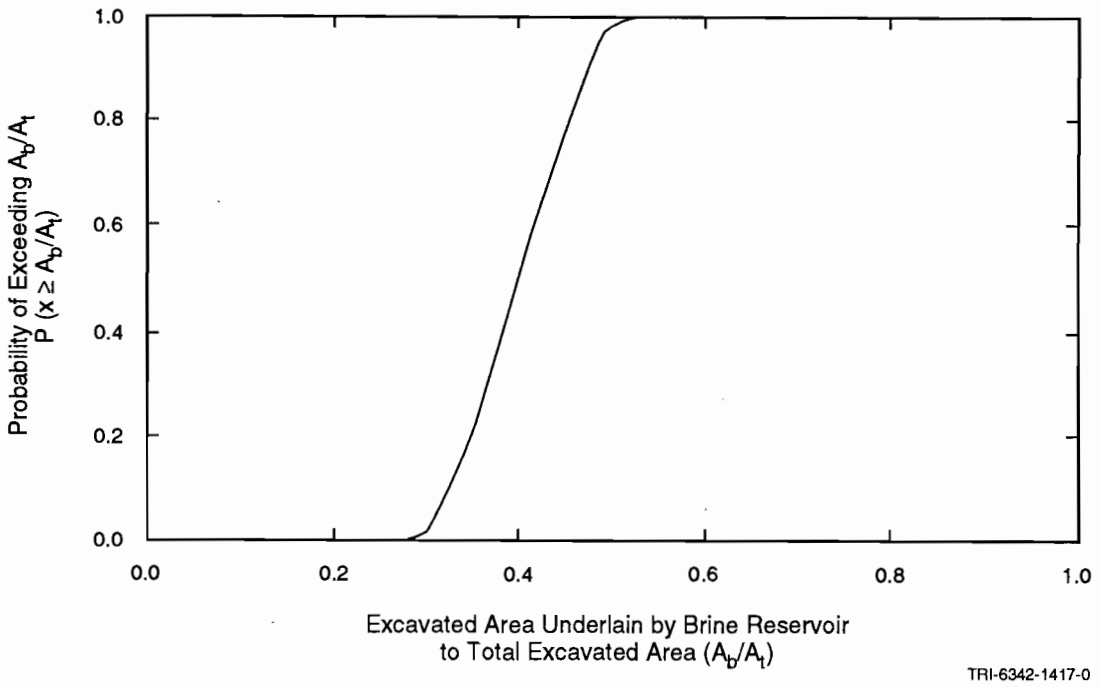

Figure 5.1-1. 1992 distribution of fraction of WIPP disposal area overlapped by brine reservoir. Simulated construction uses inclusive definition of brine reservoir and block model (see text).

Discussion:

A geophysical survey, using transient electromagnetic methods, was made in 1987 to determine the presence or absence of brines within the Castile Formation under the WIPP disposal area (Earth Technology Corp., 1988). Briefly, the electromagnetic method associates high electric conductivity with fluid. (The stated precision of depth to conducting layers was to within ±75 m.) The entire Bell Canyon Formation directly beneath the Castile Formation is a good conductor. However, in several places underneath the WIPP disposal area, the elevation to the first major conducting media detected lay above the top of the Bell Canyon Formation (~-200 ± 30 m [-654 ± 100 ft] in the ERDA-9 well) but below the bottom of the Salado Formation (178 m [582 ft] in ERDA-9) (see Figure 2.2-1 and Section 2.2).

The probability of hitting a brine reservoir can be evaluated for the waste disposal area as a whole or for subunits such as the panels. The current human-intrusion probability model (Volume 2, Chapters 1 and 2) uses the former data (the probability of hitting a brine reservoir over the entire waste panel) and assumes that this same probability applies to each panel. However, an examination of this assumption required the probability for each panel as well (Volume 2, Chapters 1 and 2). The following discussion emphasizes the probability over the entire disposal area, but provides data on a per panel basis as well.

Two methods were considered for determining the area of the brine reservoir. The first involved using the interpolated conductor elevations and the Anhydrite III of the Castile Formation and the Bell Canyon Formation elevations without considering uncertainty in the data. Although not used, it is discussed first because of its simplicity. The second method considers uncertainty in the data through geostatistics.

Area Estimate Assuming No Uncertainty in Data. Contours of the depth and elevation to the first major conductor are plotted in Figures 5.1-2 and 5.1-3. The data in Figure 5.1-2 was the interpretation originally reported (Earth Technology Corporation, 1988). However, Figure 5.1-3 is an equally valid interpretation of the data; it is somewhat more conservative and was computer generated from the same data.

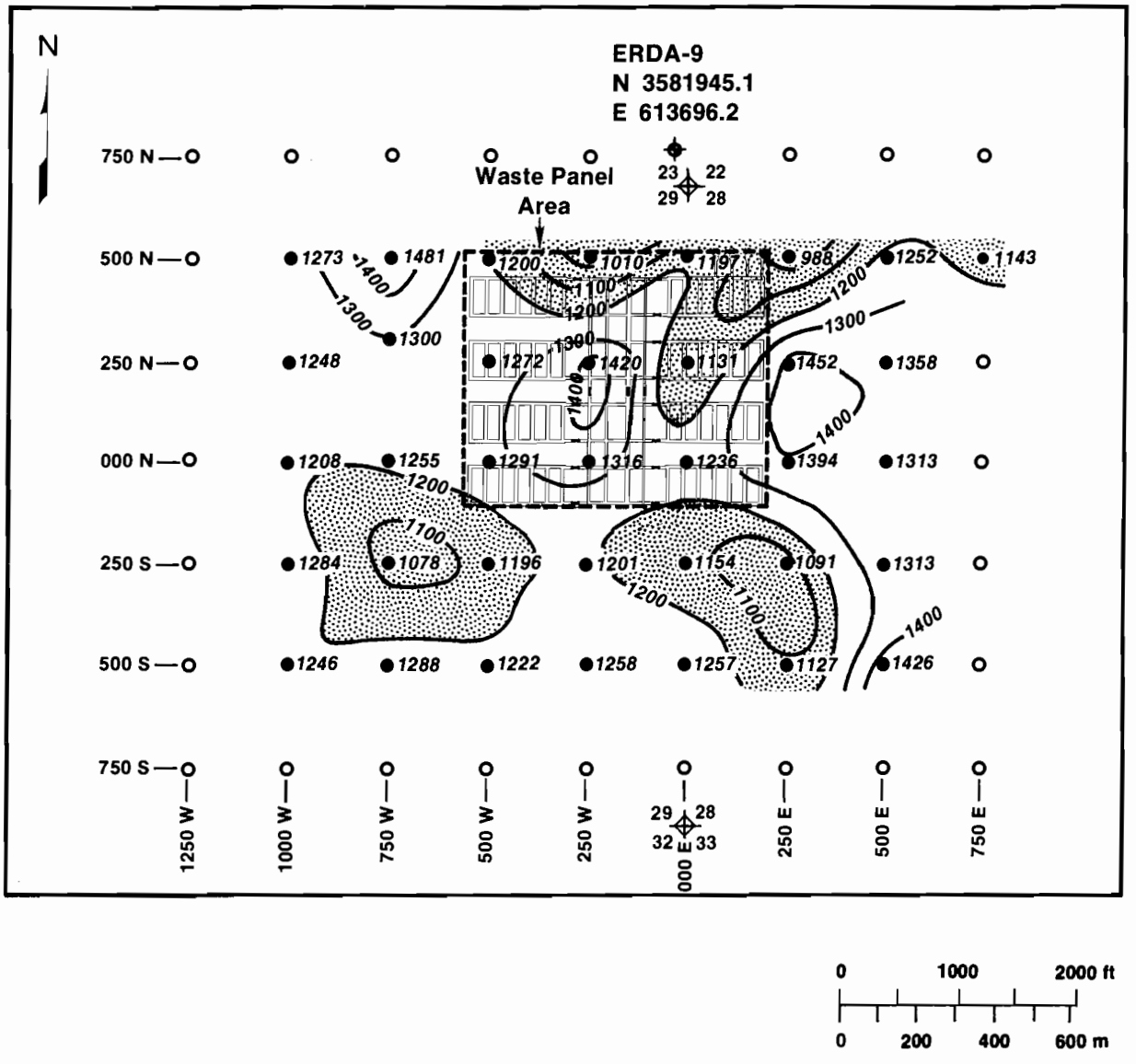

TRI-6342-256-2

Figure 5.1-2. Frequently reported contour map of depth below surface of first major conductor below WIPP disposal area. Shaded areas show extent of first major conductor. (Map drawn by hand.) (after Earth Technology Corp., 1988).

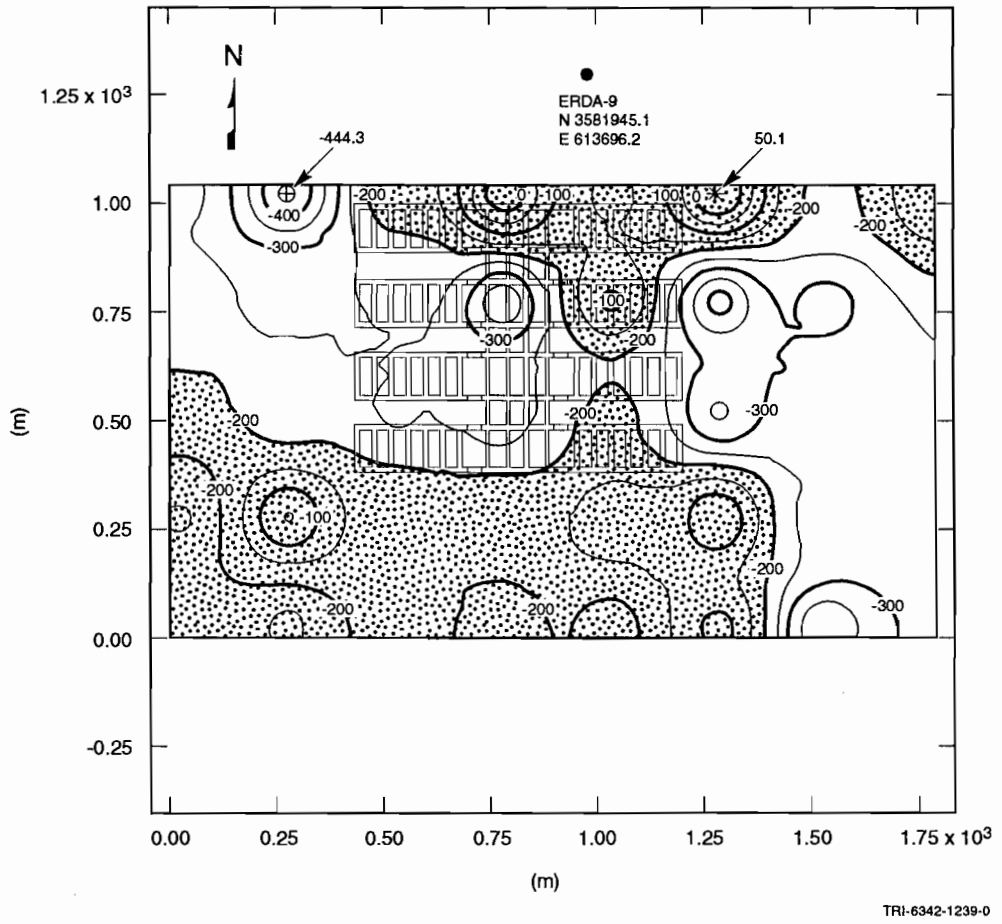

Figure 5.1-3. Conservative contour map of elevation above sea level of first major conductor below WIPP disposal area.

Minimum Area (Anhydrite III Level). The brine reservoirs are usually found in fracture zones of anticlinal structures in the uppermost anhydrite layer in the Castile (Lappin, 1988) (e.g., Anhydrite III as in WIPP-12 or when Anhydrite III is absent such as Anhydrite II in ERDA-6).

In ERDA-9, the elevation of the bottom of Anhydrite III in the Castile Formation is estimated at 90 m (295 ft). Consequently, there is a possibity that no brine is present beneath the disposal area.

Maximum Area (Bell Canyon Level). Pressurized brine reservoirs cannot be entirely discounted until the Bell Canyon Formation is reached at about -200 m (-660 ft) (Figure 2.2-1), implying that conductors higher than about -200 m (-660 ft) could indicate brine within the Castile Formation. PA calculations use the -200 m (-660 ft) contour for defining the maximum area of any brine reservoirs under the WIPP disposal area (Figure 5.1-3), resulting in a maximum area of about 40% (Table 5.1-1).

Combined Distribution. Without knowing the likelihood that either endpoint is more valid, a discrete distribution with points at 0 and 45% of equal probability is suggested.

Table 5.1-1. Cumulative Percentages of the Disposal Region Underlain by a Brine Reservoir, Assuming Various Elevations Relative to Sea Level.

Depth (m)	Cumulative Percent (%) at Indicated Elevations Relative to Sea Level										Area (m^2)
	0	-50	-100	-150	-180	-200	-250	-300	-350	-400	
Panel 1			5.37	61.95	97.80	100.00	100.00	100.00	100.00	100.00	11,530.0
Panel 2			4.00	44.57	69.33	73.08	87.47	100.00	100.00	100.00	11,530.0
Panel 3						18.23	85.73	100.00	100.00	100.00	11,530.0
Panel 4					35.85	75.57	96.17	100.00	100.00	100.00	11,530.0
Panel 5						19.76	94.80	100.00	100.00	100.00	11,530.0
Panel 6							26.57	100.00	100.00	100.00	11,530.0
Panel 7							67.45	100.00	100.00	100.00	11,530.0
Panel 8			0.79	9.01	34.64	52.86	100.00	100.00	100.00	100.00	11,530.0
Southern						3.24	45.01	100.00	100.00	100.00	8,413.0
Northern	3.97	12.49	21.67	27.49	34.86	45.29	54.79	69.25	94.52	100.00	8,701.0
Cumulative Percent	0.316	0.99	4 2.796	14.367	27.828	39.648	77.219	97.553	99.564	100.000	
Cumulative Area (m^2)	345.3	1,086.8	3,057.6	15,711.1	30,431.4	43,357.1	84,442.3	106,678.2	108,877.4	109,354.0	

Area Estimate Incorporating Uncertainty in the Data. Described above is a method of estimating the fractional area of the waste-panel region underlain by a Castile brine reservoir using contours of the conductor elevation. This method assumes that elevation contours drawn from the observed data correctly represent the variation of conductor depth between observation locations. The following discussion describes an alternative method that does not rely on reported depth contours and the resulting area fraction distribution.

Conductor elevation measurements are available at 36 points (Figure 5.1-2). These data were used to estimate conductor elevation at all points within the waste panel region. Any estimate of the conductor depth at an unmeasured location had an uncertainty associated with it. The objective of this procedure is to incorporate relevant uncertainties in the estimate of area fraction.

Spatial Variability and Interpolation. Uncertainty in interpolated elevations is a consequence of spatial variability of the observed data. Quantifying spatial variability helps in estimating the error of an interpolated value. If two observations are made close together, it is reasonable to expect that similar values will be obtained (autocorrelation function, Chapter 1). As the distance between observations increases, the similarity of observed values decreases. This behavior of spatially varying fields is often represented as a variogram (Figure 5.1-4). The variogram shows the average squared difference in observed values between observations separated by a given distance vs. the distance between observations. For a given separation distance h, the average is taken over all pairs of observations that are separated by distance h.

The variogram in Figure 5.1-4 is a generic example illustrating two common features seen in real data. Close to the origin (i.e., small separation distances), values are similar, so that the average squared difference is small. As the distance between observations increases, observed values tend to become uncorrelated, resulting in an increase in average squared difference in observed values. The distance at which observations tend to become uncorrelated is referred to as the range of the variogram. As separation distance increases beyond the range, the average squared difference tends to a limiting value, called the sill.

Not all fields exhibit clearly defined range and sill. Systematic trends in the data, for example, can produce variograms that continually increase with separation distance. In addition, the spatial variability of the data may be different along different directions, so that a variogram constructed from separations along one direction may be different from a variogram constructed along another direction.

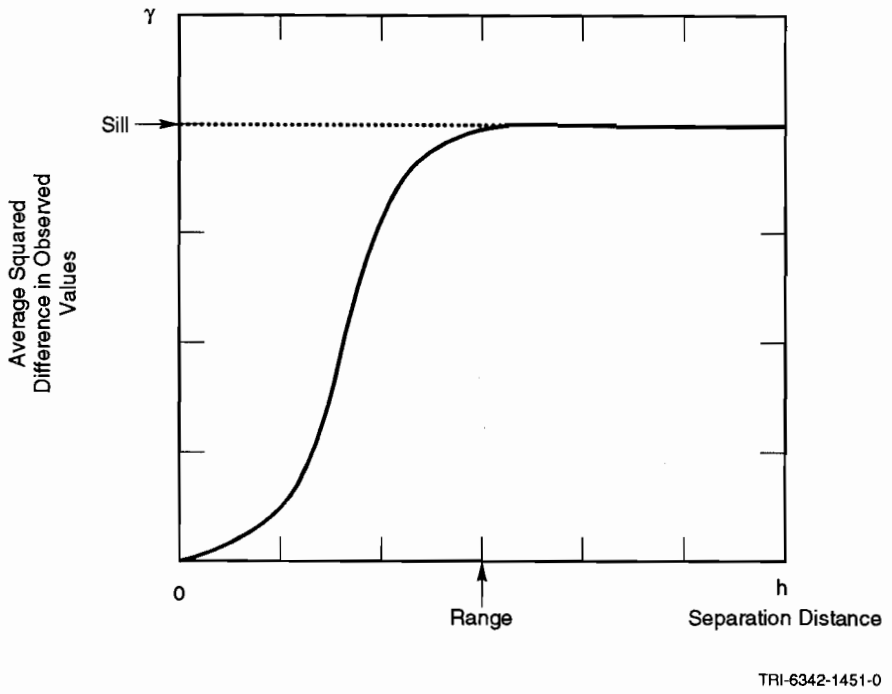

Figure 5.1-4. Example variogram illustrating typical behavior of γ with h.

Information contained in the variogram is useful in interpolating from observed values for two reasons:

(1) The range of the variogram identifies the maximum distance over which observations tend to be correlated. This information is important for selecting the data points near the interpolation location having values that may be related to the actual value at the interpolation location.

(2) The average squared difference between data values, along with the distances between the interpolation location and the locations of the selected observations, may be used to estimate the potential variability of the real value from the interpolated value.

Analysis of TDEM Data. Figure 5.1-2 shows conductor elevations interpreted from the TDEM survey at 36 locations near and within the waste panel region. Figure 5.1-5 shows a cumulative distribution of observed elevations, along with the average elevation and sample standard deviation. Scatterplots of conductor elevation vs. X (E-W) location and Y (N-S) location are shown in Figure 5.1-6. There is no suggestion of a significant simple trend in elevation along either direction.

A variogram of elevations was constructed in the E-W, N-S, NE-SW, and NW-SE directions. The regular arrangement of observation points facilitates this calculation: the variogram value for a separation of 250 m in the E-W direction, for example, is simply the average of the squared difference of elevation values at points adjacent to each other in the E-W direction. Similar averages can be made for multiples of the observation grid spacing (250 m) in the E-W and N-S directions. Points in the NE-SW and NW-SE directions are separated by multiples of ~353 m. In calculating the elevation variogram, the observation at (750W, 290N) was assumed to have been made at (750W, 250N). This displacement has no important effect on the resulting variogram.

Figure 5.1-7 shows the variogram of the elevation data along the directions mentioned. The separation distances considered were 250 m and 500 m in the E-W and N-S directions, and 353 m in the diagonal directions. Larger

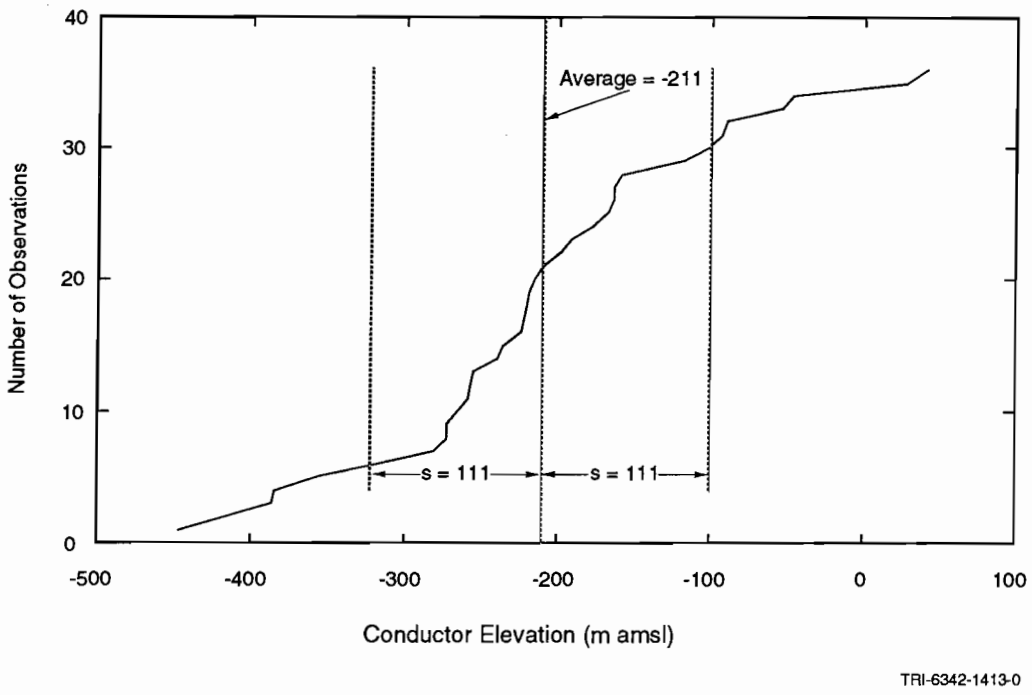

Figure 5.1-5. Population distribution and statistics for conductor elevations.

separations have too few pairs to provide a reliable estimate of mean squared difference. The horizontal line, which shows the average squared difference over all pairs of points regardless of separation, is an estimate of the variogram sill.

The striking feature of the variogram is the lack of evidence for a range of correlation of observations. The average squared difference for adjacent measurements and the expected squared difference for randomly selected measurements (i.e., the sill) are indistinguishable. In other words, there is no evidence for spatial correlation of elevation over distances as small as 250 m. (In a separate analysis, the program AKRIP was used to estimate a generalized covariance for the elevation data. The identified model contained only a "nugget" term, i.e., the generalized covariance was not found to depend on separation distance.)

Estimation of Conductor Elevation. The variogram suggests that, in attempting to estimate conductor elevation at non-measured locations, observations made 250 m from the interpolation location contain no more information about the real value at the interpolation location than more distant observations. For all points within the waste panel region, at least one observation less than 250 m away will be available. The variogram analysis does not indicate whether observations less than 250 m distant can be expected to provide information about elevation at the interpolation point. In particular, the assumption of linear variation of elevation between data points made in constructing contours of conductor elevation has no support (i.e., Figures 5.1-2 and 5.1-3).

Two bounding alternatives, corresponding to different assumptions about the behavior of the variogram between 0 and 250 m have been considered (see Figure 5.1-7):

(1) "Random elevation" assumption: Conductor elevation correlation length is very small <<250 m. The variogram is equal to the sill value between 0 and 250 m.

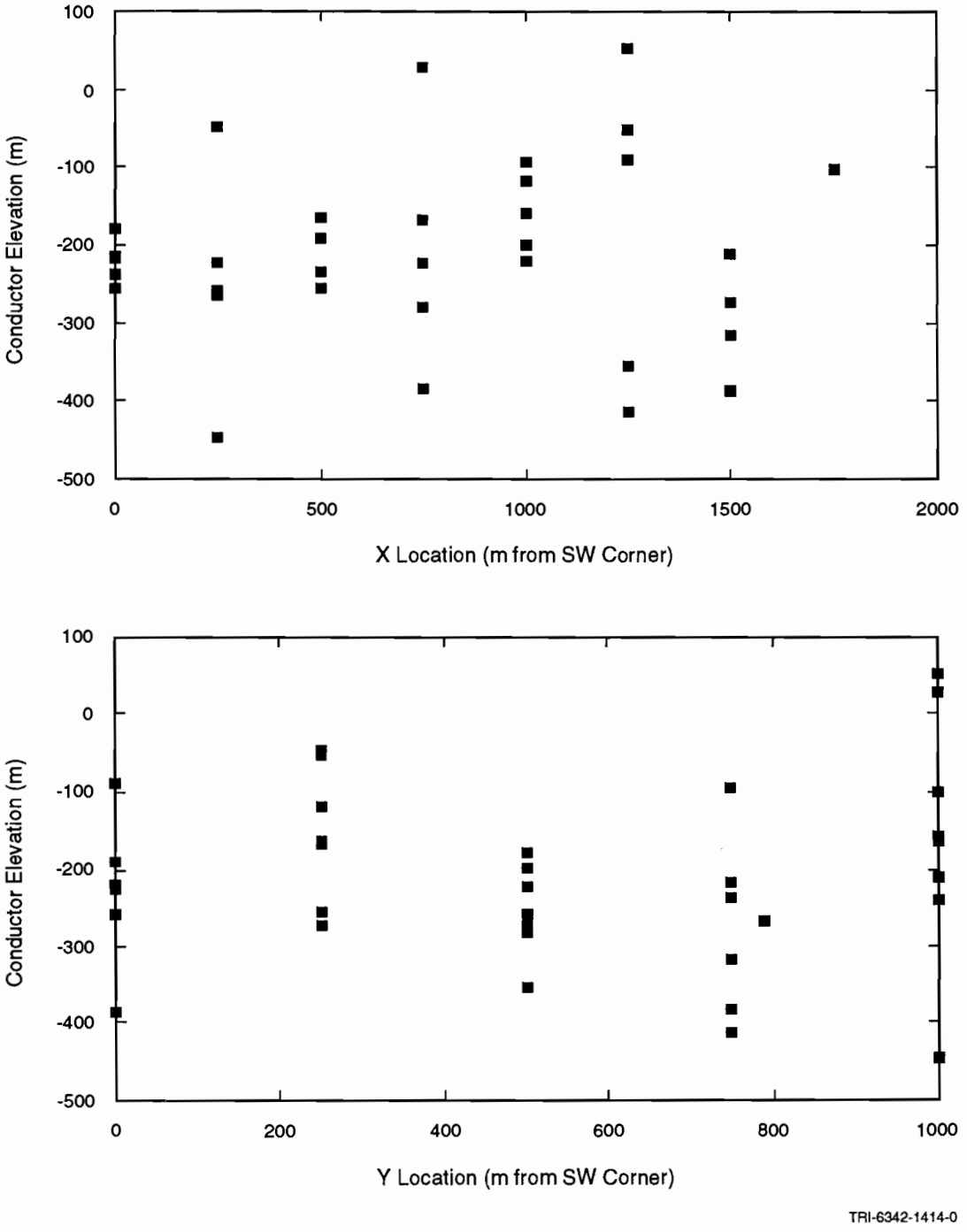

Figure 5.1-6. Scatterplots of conductor elevation vs. X and Y location.

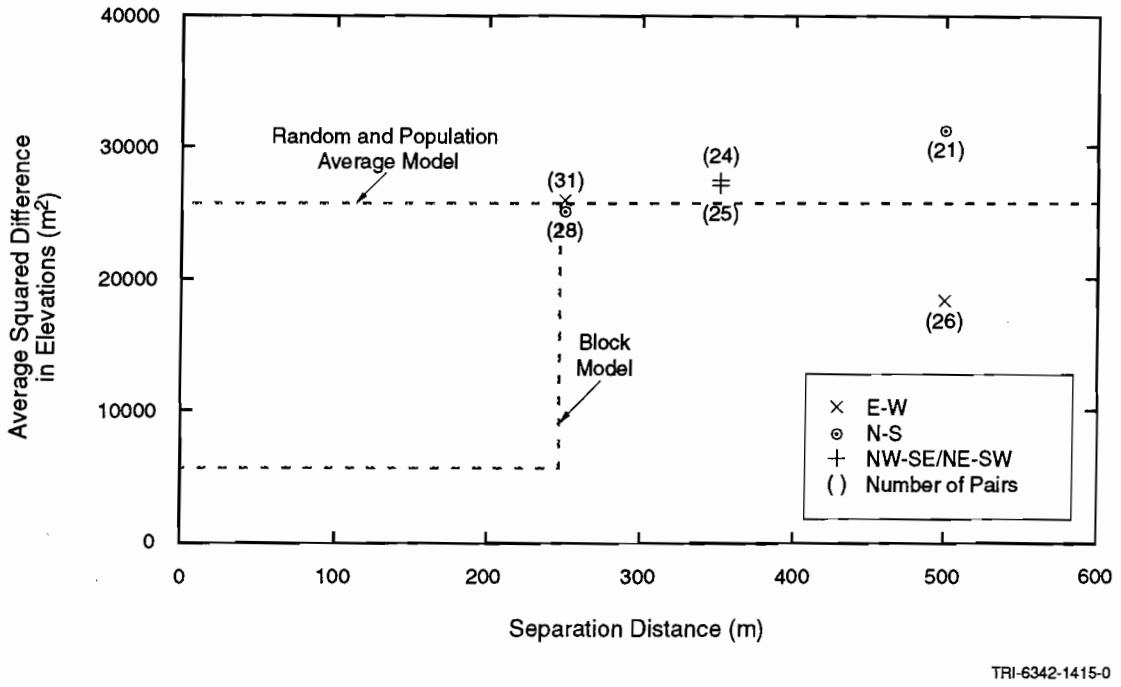

Figure 5.1-7. Empirical variogram of conductor elevations.

(2) "Block elevation" assumption: The observation grid spacing is just outside the actual correlation length. Below 250 m, observations become highly correlated, with an expected squared difference equal to twice the measurement error variance ("cookie cutter" autocorrelation).

These assumptions lead to two different methods of estimating conductor elevation. Both assumptions have been carried through in estimating brine reservoir area fraction.

In the random elevation assumption, nearby data points contribute no special information about the real value at the interpolation point in virtue of their proximity. The best estimate for elevation at any point is simply the average elevation over all observations. The variance of the error of this estimate is the population variance.

In the block elevation assumption, elevation is highly correlated over distances smaller than the measurement interval. The estimate of elevation at an interpolation point is simply the observed value at the nearest observation point. The variance of the error of this estimate is the variance of the error of the observation (75 m^2).

If the interpolated value is thought of as a weighted linear combination of observed values (as in inverse distance interpolation or in kriging), the random and block assumptions lead to the extremes of uniform weighting of all observations and exclusive weighting of the nearest observation.

Estimation of Area Fraction. The area fraction is defined as the area of the waste panel excavation overlying a brine reservoir divided by the total excavation area. A point is considered to overlie a brine reservoir if there is an electrically conductive zone in a hydrologically conductive layer of the Castile Formation. Although Castile brine reservoirs encountered during drilling appear to be always associated with the uppermost Castile anhydrite (Anhydrite III at the WIPP site), there is the possibility that brine reservoirs may occur in lower Castile anhydrites. For the purpose of estimating area fraction using the existing data, two formulations are possible:

(1) A point overlies a brine reservoir if the sub-Salado conductor elevation is greater than the elevation of the base of Anhydrite III, or

(2) A point overlies a brine reservoir if the sub-Salado conductor elevation is greater than the elevation of the base of the Castile.

For any point in the waste panel region, none of the elevations used to identify a brine reservoir by either formulation is known with certainty. In addition, there is uncertainty in which of the above formulations is appropriate. The area fraction estimate should incorporate these uncertainties.

Description of Method. Uncertainties associated with estimation of the area fraction were addressed through Monte Carlo simulations as follows:

- 200 samples from two uncorrelated uniformly distributed random variables were taken as possible values for the base elevations of the Castile and Anhydrite III. These distributions ranged from -230 m to -170 m for the base of the Castile, and from 70 m to 140 m for the base of Anhydrite III. The estimates of base elevation were uniformly distributed over the given range and were not correlated. The base elevation for the Castile and for Anhydrite III were assumed to be constant over the waste panel area.

- Along with these elevations, one of the two formulations for identifying a brine reservoir was selected at random.

- For each set of sampled base elevations and brine reservoir definition, 2000 realizations of conductor elevation were created on a uniform mesh. The relative area overlying the brine reservoir was then calculated using the sampled realizations and the selected definition of a brine reservoir.

- The relative number of simulations having a given area fraction was then used to construct an area fraction distribution. The derived area fraction distribution reflects uncertainty in conductor elevation, lithology, and the existence of brine reservoirs in lower Castile anhydrites.

The above process was applied twice, using the "random" and "block" assumptions for spatial correlation of conductor elevation in the generation of conductor realizations. In either case, conductor elevations at each mesh cell were assumed to be normally distributed around the estimated value.

Maximum Area (Bell Canyon Level). Based on the geostatistical analysis and data uncertainty described above, the use of the more conservative block model, and the assumption that a brine reservoir cannot be discounted until the Bell Canyon is reached, there is a chance that the brine reservoir has an area between 25 and 55% of the excavated area with a median of 40%. This contrasts with the best estimate of 45% from the contour method. The distribution is S-shaped (Figure 5.1-1).

Minimum Area (Anhydrite III Level). Based on the geostatistical analysis and data uncertainty described above, the probability of a brine reservoir residing in the uppermost anhydrite layer beneath the repository is very small.

50% Combination. Figure 5.1-8 shows the derived cumulative distribution of area fraction using both the "random" and "block" assumptions and assuming that 50% of the time Anhydrite III is the maximum depth and 50% of the time the Bell Canyon is the maximum depth. Both distributions show a distinct bi-modality assuming very small values of area fraction correspond to the requirement that the brine reservoir be in Anhydrite III, whereas larger area fractions correspond to the requirement that the brine reservoir be in the Castile Formation. The relative weighting of the two formulations for the brine reservoir controls the elevation of the plateau in the cumulative distribution and is clearly more important than the model of spatial variability of conductor elevation (random or block).

In the 1991 PA calculations, we used the maximum area distribution of 25 to 55% because the results are more conservative. We could not readily establish the likelihood that the elevation of Anhydrite III in the Castile

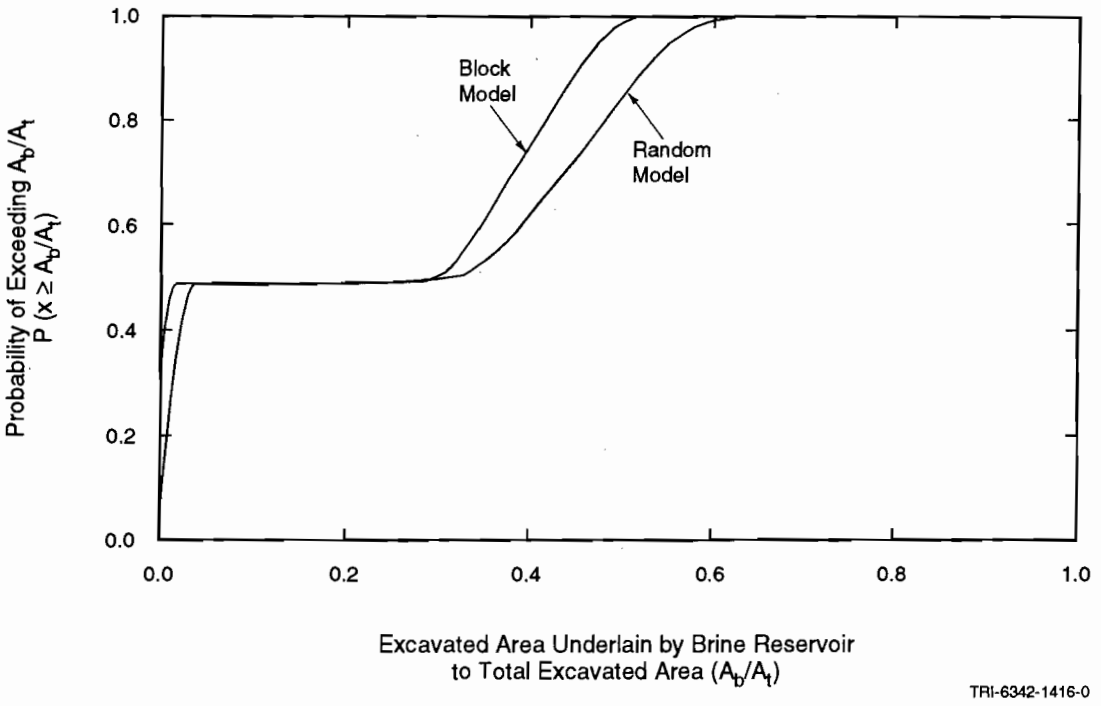

Figure 5.1-8. Cumulative distribution of area fraction using the "random" and "block" assumptions.

Formation could be used as a cutoff for indicating whether a brine reservoir existed under the disposal area without further examination of the occurrence of brine reservoirs in the region.

Lack of Spatial Correlation of Conductor Elevations. The variogram analysis suggests that conductor elevations are not correlated over a distance of 250 m. Aside from ramifications for interpolation, this result appears to place limits on the areal extent of brine reservoirs beneath WIPP. This conclusion is not entirely justified. Figure 5.1-9 shows a hypothetical arrangement of measurement points, and an underlying structure dominated by narrow features at an angle to the measurement array. Although the features are continuous over the region, observations of particular features are randomly distributed through the measurement array. In order for the underlying correlation structure of the oblong features to be revealed in this hypothetical case, the measurement array must be able to resolve the minimum characteristic dimension of the features. Note that it may still be possible for the original sampling to provide a good estimate of the relative area of each feature type.

Although Figure 5.1-9 is hypothetical, geologic considerations argue that brine reservoir location may be controlled by fracturing along Castile anticlines. In this situation, it is not unreasonable to expect brine reservoirs to be defined by long, narrow fracture zones along the anticline axis. Lack of correlation at a scale of 250 m would then place an upper limit on the minimum dimension of these fracture zones, but would not constrain maximum area extent.

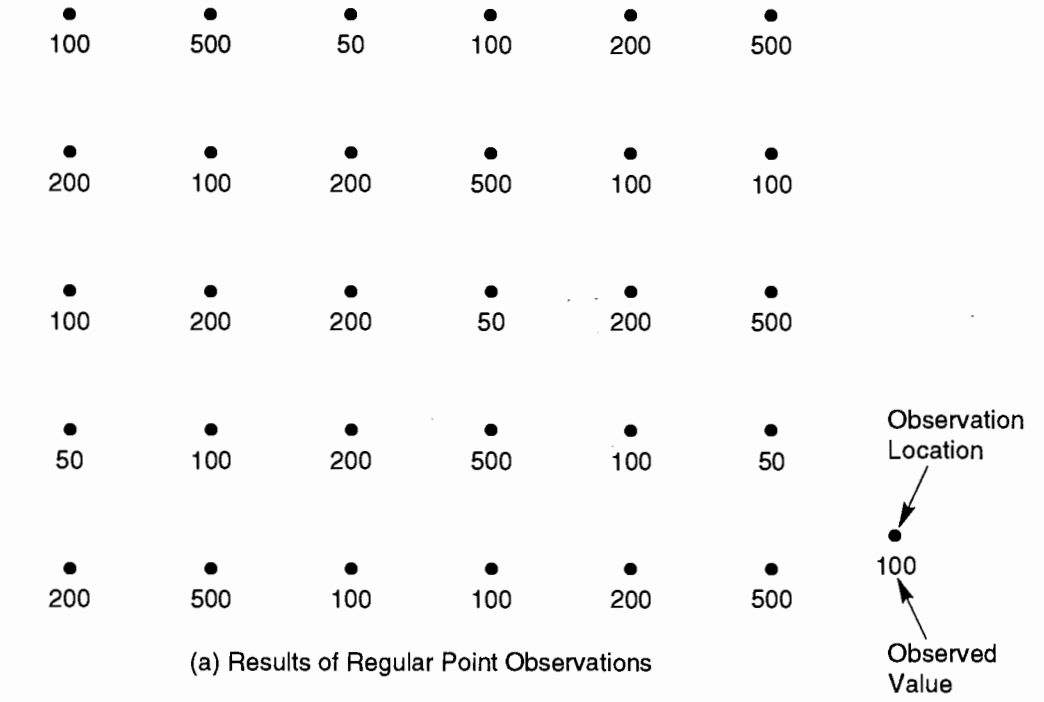

Figure 5.1-9. Illustration of hypothetical variability of regular sampling of extensive narrow features.

5.2 Human-Intrusion Probability (Drilling) Models

Index for Drilling Intensity Functions*

Parameter:	**Index for Drilling Intensity Functions**
Material:	None
Definition Units:	Dimensionless
Values:	Range: (0.0, 1.0) Median: 0.5
Distribution:	Uniform
Correlation:	

Data Source(s): See discussion in following memo:

Hora, S. C. 1992. "Probabilities of Human Intrusion into the WIPP, Methodology for the 1992 Preliminary Comparison" (see Appendix A, pp. A-69 through A-99). (Expert Panel Judgment)

Usage:

Mathematical model:

Human Intrusion, Section 1.4.2 of this volume.

Equation 1.4.2-5 and text following that equation. The index is used to make a random selection of one drilling-intensity function from among a family of equally likely drilling-intensity functions. A family of 70 drilling-intensity functions used in 1992 calculations is shown in Appendix D of this volume.

Computational models:

CCDFPERM

Ranking in Past Sensitivity Analyses:

40 CFR 191	High
40 CFR 268	Not applicable
NEPA	Not applicable
Other	Not applicable

*Key to Parameter Sheets is provided in Section 1.2.8.

6. SUMMARY OF PARAMETERS SAMPLED IN 1992

6.1 Sampled Parameters

Tables 6.0-1, 6.0-2, and 6.0-3 summarize the parameters that were sampled for the 1992 PA calculations for the geologic barriers, engineered barriers, and agents acting on the disposal system and probability models for scenarios, respectively.

Table 6.0-1. Distributions of Sample Parameters in December 1992 WIPP Performance Assessment for Geologic Barriers

Parameter	Median	Range		Units	Distribution Type	Discussed in Text Section No.
Halite within Salado Formation						
• Log permeability (log k), undisturbed	-21.2	-24.0	-19.0	log (m^2)	Constructed	2.3.5
• Relative weight, Brooks-Corey model	n.a.	(Brooks-Corey wt. = 0.67)		none	Constructed	2.3.1
• Brooks-Corey exponent (λ)	0.7	0.2	10.0	none	Constructed	2.3.1
• Residual wetting phase (liquid) saturation, $S_{\ell r}$	0.2	0.0	0.4	none	Uniform	2.3.1
• Residual gas saturation, S_{gr}	0.2	0.0	0.4	none	Uniform	2.3.1
Anhydrite within Salado Formation						
• Log permeability (log k), undisturbed	-19.3	-21.0	-16.0	log (m^2)	Constructed	2.4.2
• Pore pressure (p)	12.5	12.0	13.0	MPa	Uniform	2.4.3
• Porosity (ϕ) undisturbed	1×10^{-2}	1×10^{-3}	3×10^{-2}	none	Constructed	2.4.4
• Index for computing DRZ porosity	0.5	0	1	none	Uniform	2.4.4
Castile Formation Brine Reservoir						
• Initial pressure (p)	12.6	11.0	21.0	MPa	Constructed	4.3.1
• Storativity, bulk (S_b)	0.2	0.02	2.0	m^3/Pa	Lognormal	4.3.2
Culebra Dolomite Member						
• Fracture spacing (2B)	0.4	0.06	8.0	m	Constructed	2.6.2
• Fracture porosity (ϕ_f)	1×10^{-3}	1×10^{-4}	1×10^{-2}	none	Lognormal	2.6.2
• Clay filling fraction (b_c/b)	0.0	0.0	0.5	none	Constructed	2.6.1
• Porosity of clay lining fractures (ϕ_c)	0.275	0.05	0.5	none	Uniform	2.6.2

Table 6.0-1. Distributions of Sample Parameters in December 1992 WIPP Performance Assessment for Geologic Barriers (Concluded)

Parameter	Median	Range		Units	Distribution Type	Discussed in Text Section No.
Log partition coefficients, clay lining fractures						
• Am	1.97	-4.0	3.0	log (m^3/kg)	Constructed	2.6.4
• Np	0.0	-4.0	3.0	log (m^3/kg)	Constructed	2.6.4
• Pu	2.31	-4.0	3.0	log (m^3/kg)	Constructed	2.6.4
• Ra	-1.47	-4.0	2.0	log (m^3/kg)	Constructed	2.6.4
• Th	-1.00	-4.0	1.0	log (m^3/kg)	Constructed	2.6.4
• U	-2.12	-4.0	0.0	log (m^3/kg)	Constructed	2.6.4
• Matrix porosity (ϕ_m)	0.139	0.096	0.208	none	Constructed	2.6.2
Log partition coefficients, matrix						
• Am	-0.730	-4.0	2.0	log (m^3/kg)	Constructed	2.6.4
• Np	-1.32	-4.0	2.0	log (m^3/kg)	Constructed	2.6.4
• Pu	-5.84	-4.0	2.0	log (m^3/kg)	Constructed	2.6.4
• Ra	-2.00	-4.0	1.0	log (m^3/kg)	Constructed	2.6.4
• Th	-2.00	-4.00	0.0	log (m^3/kg)	Constructed	2.6.4
• U	-1.54	-4.00	0.0	log (m^3/kg)	Constructed	2.6.4
• Index for Culebra transmissivity fields	0.5	0	1	none	Uniform	2.6.3

Table 6.0-2. Distributions of Sample Parameters in December 1992 WIPP Performance Assessment for Engineered Barriers

Parameter	Median	Range		Units	Distribution Type	Discussed in Text Section No.
Unmodified Waste Form:						
Gas generation, corrosion						
• Inundated rate	6.3×10^{-9}	0	1.3×10^{-8}	mol/(m^2 • s)	Constructed	3.3.5
• Relative humid rate	0.1	0	0.5	none	Constructed	3.3.5
• Stoichiometry factor	0.5	0	1	none	Uniform	3.3.5
Gas Generation, Microbiological						
• Inundated rate	3.2×10^{-9}	0	1.6×10^{-8}	mol/(kg • s)	Constructed	3.3.5
• Relative humid rate	0.1	0	0.2	none	Uniform	3.3.5
• Stoichiometry factor	0.835	0	1.67	none	Uniform	3.3.5
Log Radionuclide Solubility						
• Am	-9.00	-13.3	0.0	log (Molar)	Constructed	3.3.5
• Np	-6.99	-15.5	-2.00	log (Molar)	Constructed	3.3.5
• Pu	-9.22	-16.5	-3.24	log (Molar)	Constructed	3.3.5
• Ra	1.04	0.30	1.26	log (Molar)	Constructed	3.3.5
• Th	-10.0	-15.2	-5.6	log (Molar)	Constructed	3.3.5
• U	-3.27	-15.0	0.0	log (Molar)	Constructed	3.3.5
• Initial waste saturation	0.07	0	0.14	none	Uniform	3.4.3
Volume Fractions of IDB Categories						
• Metal/glass	0.376	0.276	0.476	none	Normal	3.4.1
• Combustibles	0.384	0.284	0.484	none	Normal	3.4.1

Table 6.0-3. Distributions of Sample Parameters in December 1992 WIPP Performance Assessment for Agents Acting on Disposal System and Probability Models for Scenarios

Parameter	Median	Range		Units	Distribution Type	Discussed in Text Section No.
Agents Acting on Disposal System						
Intrusion Borehole Flow Parameters						
• Diameter	0.355	0.267	0.444	m	Uniform	4.2.2
• Permeability (k)	3.16×10^{-12}	1×10^{-14}	1×10^{-11}	m^2	Lognormal	4.2.1
Climate parameter						
• Recharge amplitude factor	0.5	0	1.0	none	Uniform	4.4
Probability Model for Intrusion Scenarios						
• Fractional overlap of brine reservoirs	0.45	0.25	0.62	none	Constructed	5.1
• Index for drilling intensity functions	0.5	0	1.0	none	Uniform	5.2

6.2 Selection Procedure for Parameters Sampled in 1992

A parameter was chosen for sampling in the 1992 series of PA calculations if it fulfilled at least one of three criteria: (1) the parameter had proved to be moderately to highly sensitive in the 1991 sensitivity analyses (Helton et al., 1992); (2) the parameter was an imprecisely known quantity in a consequence model first formally used in the present (1992) series of calculations; and (3) new data concerning an imprecisely known parameter, data sufficient to suggest significant revision of that parameter's distribution, were available by the end of April, 1992.

Most of the 49 parameters sampled in the 1992 series of PA calculations fulfilled criteria (1) and (3). For some uncertain parameters that fulfilled only criterion (2), most notably parameters specifying mechanical properties of the Salado Formation (Section 2.5), it was simply not possible to carry out an investigation of sensitivity owing to limitations on the present consequence models and on the time available for computations.

Some imprecisely known parameters are necessarily sampled in any PA calculation that uses certain intrinsically stochastic consequence models; examples of this kind of parameter are the transmissivity fields for the Culebra Dolomite Member (Section 2.6), the recharge factor for climatic change (Section 4.4), and the drilling intensity for the model of human intrusion (Section 5.2). Finally, about seven parameters found to be mildly sensitive in 1991 sensitivity analyses (Helton et al., 1992) were resampled in 1992 solely for the purpose of maintaining statistical significance of the set of sample vectors that were used in constructing CCDFs.

REFERENCES

Arguello, J.G. 1988. *WIPP Panel Entryway Seal - Numerical Simulation of Seal Composite Interaction for Preliminary Design Evaluation.* SAND87-2804. Albuquerque, NM: Sandia National Laboratories.

Austin, E.H. 1983. *Drilling Engineering Handbook.* Boston, MA: International Human Resources Development Corporation.

Avis, J.D., and G.J. Saulnier, Jr. 1990. *Analysis of the Fluid-Pressure Responses of the Rustler Formation at H-16 to the Construction of the Air-Intake Shaft at the Waste Isolation Pilot Plant (WIPP) Site.* SAND89-7067. Albuquerque, NM: Sandia National Laboratories.

Barnhart, B.J., E.W. Campbell, E. Martinez, D.E. Caldwell, and R. Hallett. 1980. *Potential Microbial Impact on Transuranic Wastes Under Conditions Expected in the Waste Isolation Pilot Plant (WIPP), Annual Report, October 1, 1978-September 30, 1979.* LA-8297-PR. Los Alamos, NM: Los Alamos Scientific Laboratory.

Bayley, S.E., M.D. Siegel, M. Moore, and S. Faith. 1990. *Sandia Sorption Data Management System Version 2 (SSDMS II) User's Manual.* SAND89-0371. Albuquerque, NM: Sandia National Laboratories.

Bear, J. 1972. *Dynamics of Fluids in Porous Media.* New York, NY: American Elsevier Publishing Company, Inc.

Bear, J., and A. Verruijt. 1987. *Modeling Groundwater Flow and Pollution.* Boston, MA: D. Reidel Publishing Company. 126.

Beauheim, R.L. 1987a. *Analysis of Pumping Tests of the Culebra Dolomite Conducted at the H-3 Hydropad at the Waste Isolation Pilot Plant (WIPP) Site.* SAND86-2311. Albuquerque, NM: Sandia National Laboratories.

Beauheim, R.L. 1987b. *Interpretation of the WIPP-13 Multipad Pumping Test of the Culebra Dolomite at the Waste Isolation Pilot Plant (WIPP) Site.* SAND87-2456. Albuquerque, NM: Sandia National Laboratories.

Beauheim, R.L. 1987c. *Interpretations of Single-Well Hydraulic Tests Conducted At and Near the Waste Isolation Pilot Plant (WIPP) Site, 1983-1987.* SAND87-0039. Albuquerque, NM: Sandia National Laboratories.

Beauheim, R.L. 1989. *Interpretation of H-11b4 Hydraulic Tests and the H-11 Multipad Pumping Test of the Culebra Dolomite at the Waste Isolation Pilot Plant (WIPP) Site.* SAND89-0536. Albuquerque, NM: Sandia National Laboratories.

Beauheim, R.[L.] 1991. Appendix A: "Review of Salado Parameter Values to be Used in 1991 Performance Assessment Calculations," *Preliminary Comparison with 40 CFR Part 191, Subpart B for the Waste Isolation Pilot Plant, December 1991. Volume 3: Reference Data.* WIPP Performance Assessment Division. Eds. R.P. Rechard, A.C. Peterson, J.D. Schreiber, H.J. Iuzzolino, M.S. Tierney, and J.S. Sandha. SAND91-0893/3. Albuquerque, NM: Sandia National Laboratories. A-19 through A-23.

Beauheim, R.L., G.J. Saulnier, Jr., and J.D. Avis. 1991a. *Interpretation of Brine-Permeability Tests of the Salado Formation at the Waste Isolation Pilot Plant Site: First Interim Report.* SAND90-0083. Albuquerque, NM: Sandia National Laboratories.

Beauheim, R.L., T.F. Corbet, P.B. Davies, and J.F. Pickens. 1991b. Appendix A: "Recommendations for the 1991 Performance Assessment Calculations on Parameter Uncertainty and Model Implementation for Culebra Transport Under Undisturbed and Brine-Reservoir-Breach Conditions," *Preliminary Comparison with 40 CFR Part 191, Subpart B for the Waste Isolation Pilot Plant, December 1991. Volume 3: Reference Data.* WIPP Performance Assessment Division. Eds. R.P. Rechard, A.C. Peterson, J.D. Schreiber, H.J. Iuzzolino, M.S. Tierney, and J.S. Sandha. SAND91-0893/3. Albuquerque, NM: Sandia National Laboratories. A-7 through A-18.

Bechtel National, Inc. 1985. *Quarterly Geotechnical Field Data Report, December 1985.* WIPP-DOE-221. Prepared for the U.S. Department of Energy. San Francisco, CA: Bechtel National, Inc.

Bechtel National, Inc. 1986. *Waste Isolation Pilot Plant Design Validation Final Report.* DOE/WIPP-86-010. Prepared for U.S. Department of Energy. San Francisco, CA: Bechtel National, Inc.

Bertram-Howery, S.G., and R.L. Hunter, eds. 1989. *Preliminary Plan for Disposal-System Characterization and Long-Term Performance Evaluation of the Waste Isolation Pilot Plant.* SAND89-0178. Albuquerque, NM: Sandia National Laboratories.

Bertram-Howery, S.G., and P.N. Swift. 1990. *Status Report: Potential for Long-Term Isolation by the Waste Isolation Pilot Plant Disposal System.* SAND90-0616. Albuquerque, NM: Sandia National Laboratories.

Bertram-Howery, S.G., M.G. Marietta, R.P. Rechard, P.N. Swift, D.R. Anderson, B.L. Baker, J.E. Bean, Jr., W. Beyeler, K.F. Brinster, R.V. Guzowski, J.C. Helton, R.D. McCurley, D.K. Rudeen, J.D. Schreiber, and P. Vaughn. 1990. *Preliminary Comparison with 40 CFR Part 191, Subpart B for the Waste Isolation Pilot Plant, December 1990.* SAND90-2347. Albuquerque, NM: Sandia National Laboratories.

Blom, G. 1989. *Probability and Statistics: Theory and Applications.* New York, NY: Springer-Verlag.

Borns, D.J. 1985. *Marker Bed 139: A Study of Drillcore From a Systematic Array.* SAND85-0023. Albuquerque, NM: Sandia National Laboratories.

Borns, D.J. 1987. *Rates of Evaporite Deformation: The Role of Pressure Solution.* SAND85-1599. Albuquerque, NM: Sandia National Laboratories.

Brinster, K.[F.] 1990. Appendix A: "Memo 10: Well Data from Electric Logs," *Data Used in Preliminary Performance Assessment of the Waste Isolation Pilot Plant (1990).* R.P. Rechard, H.[J.] Iuzzolino, and J.S. Sandha. SAND89-2408. Albuquerque, NM: Sandia National Laboratories. A-129 through A-138.

Brinster, K.F. 1991. *Preliminary Geohydrologic Conceptual Model of the Los Medaños Region Near the Waste Isolation Pilot Plant for the Purpose of Performance Assessment.* SAND89-7147. Albuquerque, NM: Sandia National Laboratories.

Broc, R., ed. 1982. *Drilling Mud and Cement Slurry Rheology Manual.* Houston, TX: Gulf Publishing Company.

Brooks, R.H., and A.T. Corey. 1964. *Hydraulic Properties of Porous Media.* Hydrology Paper No. 3. Fort Collins, CO: Colorado State University.

Brush, L.H. 1990. *Test Plan for Laboratory and Modeling Studies of Repository and Radionuclide Chemistry for the Waste Isolation Pilot Plant.* SAND90-0266. Albuquerque, NM: Sandia National Laboratories.

Brush, L.H. 1991. Appendix A: "Current Estimates of Gas Production Rates, Gas Production Potentials, and Expected Chemical Conditions Relevant to Radionuclide Chemistry for the Long-Term WIPP Performance Assessment," *Preliminary Comparison with 40 CFR Part 191, Subpart B for the Waste Isolation Pilot Plant, December 1991. Volume 3: Reference Data.* WIPP Performance Assessment Division. Eds. R.P. Rechard, A.C. Peterson, J.D.

Schreiber, H.J. Iuzzolino, M.S. Tierney, and J.S. Sandha. SAND91-0893/3. Albuquerque, NM: Sandia National Laboratories. A-25 through A-36.

Brush, L.H., and D.R. Anderson. 1989. Appendix A: "Drum (Metal) Corrosion, Microbial Decomposition of Cellulose, Reactions Between Drum-Corrosion Products and Microbially Generated Gases, Reactions Between Possible Backfill Constituents and Gases and Water Chemical Reactions," *Systems Analysis, Long-Term Radionuclide Transport, and Dose Assessments, Waste Isolation Pilot Plant (WIPP), Southeastern New Mexico; March 1989.* Eds. A.R. Lappin, R.L. Hunter, D.P. Garber, and P.B. Davies. SAND89-0462. Albuquerque, NM: Sandia National Laboratories. A-3 through A-30.

Brush, L.H., and A.R. Lappin. 1990. Appendix A: "Additional Estimates of Gas Production Rates and Radionuclide Solubilities for Use in Models of WIPP Disposal Rooms," *Data Used in Preliminary Performance Assessment of the Waste Isolation Pilot Plant (1990).* R.P. Rechard, H. Iuzzolino, and J.S. Sandha. SAND89-2408. Albuquerque, NM: Sandia National Laboratories. A-85 through A-92.

Buck, A.D. 1985. *Development of a Sanded Nonsalt Expansive Grout for Repository Sealing Application.* Miscellaneous Paper SL-85-6. Vicksburg, MS: Department of the Army, Waterways Experiment Station.

Bush, D.D., and R. Lingle. 1986. *A Full-Scale Borehole Sealing Test in Anhydrite Under Simulated Downhole Conditions. Volume 1.* BMI/ONWI-581(1). Columbus, OH: Office of Nuclear Waste Isolation, Battelle Memorial Institute.

Bush, D.D., and S. Piele. 1986. *A Full-Scale Borehole Sealing Test in Salt Under Simulated Downhole Conditions. Volume 1.* BMI/ONWI-573(1). Columbus, OH: Office of Nuclear Waste Isolation, Battelle Memorial Institute.

Butcher, B.M. 1989. *Waste Isolation Pilot Plant Simulated Waste Compositions and Mechanical Properties.* SAND89-0372. Albuquerque, NM: Sandia National Laboratories.

Butcher, B.M. 1990. Appendix A: "Memo 5: Disposal Room Porosity and Permeability Values for Disposal Room Per-formance Assessment," *Data Used in Preliminary Performance Assessment of the Waste Isolation Pilot Plant (1990).* R. P. Rechard, H. Iuzzolino, and J. S. Sandha. SAND89-2408. Albuquerque, NM: Sandia National Laboratories. A-93 through A-102.

Butcher, B.M., T.W. Thompson, R.G. VanBuskirk, and N.C. Patti. 1991. *Mechanical Compaction of Waste Isolation Pilot Plant Simulated Waste.* SAND90-1206. Albuquerque, NM: Sandia National Laboratories.

Caldwell, D.E., R.C. Hallett, M.A. Molecke, E. Martinez, and B.J. Barnhart. 1988. *Rates of Co_2 Production From the Microbial Degradation of Transuranic Wastes Under Simulated Geologic Isolation Conditions.* SAND87-7170. Albuquerque, NM: Sandia National Laboratories.

Carmichael, R.S., ed. 1984. *CRC Handbook of Physical Properties of Rocks.* Boca Raton, FL: CRC Press, Inc. Vol. III.

Cauffman, T.L., A.M. LaVenue, and J.P. McCord. 1990. *Ground-Water Flow Modeling of the Culebra Dolomite. Volume II: Data Base.* SAND89-7068/2. Albuquerque, NM: Sandia National Laboratories.

Cheeseman, R.J. 1978. "Geology and Oil/Potash Resources of Delaware Basin, Eddy and Lea Counties, New Mexico," *Geology and Mineral Deposits of Ochoan Rocks in Delaware Basin and Adjacent Areas.* New Mexico Bureau of Mines and Mineral Resources Circular 159. Socorro, NM: New Mexico Bureau of Mines and Mineral Resources. 7-14.

Christensen, C.L., and E.W. Petersen. 1981. *The Bell Canyon Test Summary Report.* SAND80-1375. Albuquerque, NM: Sandia National Laboratories.

Clark, S.P., Jr., ed. 1966. *Handbook of Physical Constants*. Memoir 97. New York, NY: The Geological Society of America, Inc.

Colebrook, C.F. 1939. "Turbulent Flow in Pipes, with Particular Reference to the Transition Region Between the Smooth and Rough Pipe Laws," *Journal of the Institution of Civil Engineers*. Vol. 11, 133-156.

Crichlow, H.B. 1977. *Modern Reservoir Engineering - A Simulation Approach*. Englewood Cliffs, NJ: Prentice-Hall, Inc.

Cygan, R.T. 1991. *The Solubility of Gases in NaCl Brine and a Critical Evaluation of Available Data*. SAND90-2848. Albuquerque, NM: Sandia National Laboratories.

Darley, H.C.H. 1969. "A Laboratory Investigation of Borehole Stability," *Journal of Petroleum Technology*. July 1969, 883-892.

Darley, H.C.H., and G.R. Gray. 1988. *Composition and Properties of Drilling and Completion Fluids*. Houston, TX: Gulf Publishing Company.

Davies, P.B. 1989. *Variable-Density Ground-Water Flow and Paleohydrology in the Waste Isolation Pilot Plant (WIPP) Region, Southeastern New Mexico*. Open-File Report 88-490. Albuquerque, NM: U.S. Geological Survey.

Davies, P.B. 1991a. *Evaluation of the Role of Threshold Pressure in Controlling Flow of Waste-Generated Gas into Bedded Salt at the Waste Isolation Pilot Plant*. SAND90-3246. Albuquerque, NM: Sandia National Laboratories.

Davies, P.B. 1991b. Appendix A: "Uncertainty Estimates for Threshold Pressure for 1991 Performance Assessment Calculations Involving Waste-Generated Gas," *Preliminary Comparison with 40 CFR Part 191, Subpart B for the Waste Isolation Pilot Plant, December 1991. Volume 3: Reference Data.* WIPP Performance Assessment Division. Eds. R.P. Rechard, A.C. Peterson, J.D. Schreiber, H.J. Iuzzolino, M.S. Tierney, and J.S. Sandha. SAND91-0893/3. Albuquerque, NM: Sandia National Laboratories. A-37 through A-41.

Davies, P.[B.], and [A.] M. LaVenue. 1990a. Appendix A: "Memo 3b: Comments on Model Implementation and Data for Use in August Performance Assessment Calculations," *Data Used in Preliminary Performance Assessment of the Waste Isolation Pilot Plant (1990).* R.P. Rechard, H. Iuzzolino, and J.S. Sandha. SAND89-2408. Albuquerque, NM: Sandia National Laboratories. A-63 through A-78.

Davies, P.B., and A.M. LaVenue. 1990b. Appendix A: "Memo 11: Additional Data for Characterizing 2-Phase Flow Behavior in Waste-Generated Gas Simulations and Pilot Point Information for Final Culebra 2-D Model," *Data Used in Preliminary Performance Assessment of the Waste Isolation Pilot Plant (1990).* R. P. Rechard, H. Iuzzolino, and J. S. Sandha. SAND89-2408. Albuquerque, NM: Sandia National Laboratories. A-139 through A-156.

Davies, P.B., L. H. Brush, and F.T. Mendenhall. 1991. "Assessing the Impact of Waste-Generated Gas from the Degradation of Transuranic Waste at the Waste Isolation Pilot Plant: An Overview of Strongly Coupled Chemical, Hydrologic, and Structural Processes," *Proceedings of NEA Workshop on Gas Generation and Release from Radioactive Waste Repositories, Aix-en-Provence, France, September 23-26, 1991.* Eds. P.B. Davies, L.H. Brush, M.A. Molecke, F.T. Mendenhall, and S.W. Webb. SAND91-2378. Albuquerque, NM: Sandia National Laboratories. 1-1 through 1-24.

Dullien, F.A.L. 1979. *Porous Media: Fluid Transport and Pore Structure*. New York, NY: Academic Press.

Earth Technology Corporation. 1988. *Final Report for Time Domain Electromagnetic (TDEM) Surveys at the WIPP Site*. SAND87-7144. Albuquerque, NM: Sandia National Laboratories.

Efron, B., and R. Tibshirani. 1991. "Statistical Data Analysis in the Computer Age," *Science*. Vol. 253, no. 5018, 390-395.

EPA (Environmental Protection Agency). 1985. "40 CFR Part 191: Environmental Standards for the Management and Disposal of Spent Nuclear Fuel, High-Level, and Transuranic Radioactive Wastes," *Federal Register*. Vol. 50, no. 182, 38066-38089.

Fanchi, J.R., J.E. Kennedy, and D.L. Dauben. 1987. *BOAST II: A Three-Dimensional, Three-Phase Black Oil Applied Simulation Tool*. DOE/BC-88/2/SP. Tulsa, OK: K and A Technology.

Finley, S.J., and D. F. McTigue. 1991. Appendix A: "Parameter Estimates from the Small-Scale Brine Inflow Experiments," *Preliminary Comparison with 40 CFR Part 191, Subpart B for the Waste Isolation Pilot Plant, December 1991. Volume 3: Reference Data.* WIPP Performance Assessment Division. Eds. R.P. Rechard, A.C. Peterson, J.D. Schreiber, H.J. Iuzzolino, M.S. Tierney, and J.S. Sandha. SAND91-0893/3. Albuquerque, NM: Sandia National Laboratories. A-55 through A-58.

Frederickson, A.G. 1960. "Helical Flow of an Annular Mass of Visco-Elastic Fluid," *Chemical Engineering Science*. Vol. 11, no. 3, 252-259.

Freeze, R.A., and J.A. Cherry. 1979. *Groundwater.* Englewood Cliffs, NJ: Prentice-Hall, Inc.

Geological Society of America, Inc. 1984. *Decade of North American Geology Geologic Time Scale*. Map and Chart Series MCH 050. Boulder, CO: Geological Society of America, Inc.

Gonzales, M.M. 1989. *Compilation and Comparison of Test-Hole Location Surveys in the Vicinity of the Waste Isolation Pilot Plant Site*. SAND88-1065. Albuquerque, NM: Sandia National Laboratories.

Harms, J.C., and C.R. Williamson. 1988. "Deep-Water Density Current Deposits of Delaware Mountain Group (Permian), Delaware Basin, Texas and New Mexico," *American Association of Petroleum Geologists Bulletin*. Vol. 72, no. 3, 299-317.

Harr, M.E. 1987. *Reliability-Based Design in Civil Engineering*. New York, NY: McGraw-Hill Book Co.

Haug, A., V.A. Kelley, A.M. LaVenue, and J.F. Pickens. 1987. *Modeling of Ground-Water Flow in the Culebra Dolomite at the Waste Isolation Pilot Plant (WIPP) Site: Interim Report*. Contractor Report SAND86-7167. Albuquerque, NM: Sandia National Laboratories.

Helton, J.C. 1991. "Drilling Intrusion Probabilities," *Preliminary Comparison with 40 CFR Part 191, Subpart B for the Waste Isolation Pilot Plant, December 1991. Volume 2: Probability and Consequence Modeling.* WIPP Performance Assessment Division. SAND91-0893/2. Albuquerque, NM: Sandia National Laboratories. 2-1 through 2-37.

Helton, J.C., J.M. Griesmeyer, F.E. Haskin, R.L. Iman, C.N. Amos, and W.B. Murfin. 1988. "Integration of the NUREG-1150 Analyses: Calculation of Risk and Propagation of Uncertainties," *Proceedings of the Fifteenth Water Reactor Safety Information Meeting, Gaithersburg, MD, October 26-30, 1987.* Ed. A.J. Weiss. Washington, DC U.S. Nuclear Regulatory Commission. Vol. 1, 151-176.

Helton. J.C., J.W. Garner, R.D. McCurley, and D.K. Rudeen. 1991. *Sensitivity Analysis Techniques and Results for Performance Assessment at the Waste Isolation Pilot Plant*. Contractor Report SAND90-7103. Albuquerque, NM: Sandia National Laboratories.

Helton, J.C., J.W. Garner, R. P. Rechard, D.K. Rudeen, and P.N. Swift. 1992. *Preliminary Comparison with 40 CFR Part 191, Subpart B for the Waste Isolation Pilot Plant, December 1991. Volume 4: Uncertainty and Sensitivity Analysis*. SAND91-0893/4. Albuquerque, NM: Sandia National Laboratories.

Henderson, F.M. 1966. *Open Channel Flow.* New York, NY: Macmillan Publishing Co.

Hills, J.M. 1984. "Sedimentation, Tectonism, and Hydrocarbon Generation in Delaware Basin, West Texas and Southeastern New Mexico," *American Association of Petroleum Geologists Bulletin*. Vol. 68, no. 3, 250-267.

Hiss, W.L. 1975. "Stratigraphy and Ground-Water Hydrology of the Capitan Aquifer, Southeastern New Mexico and West Texas." Ph.D. dissertation. Boulder, CO: University of Colorado, Hydrology Department.

Holcomb, D.J., and M. Shields. 1987. *Hydrostatic Creep Consolidation of Crushed Salt With Added Water*. SAND87-1990. Albuquerque, NM: Sandia National Laboratories.

Holt, R.M., and D.W. Powers. 1988. *Facies Variability and Post-Depositional Alteration Within the Rustler Formation in the Vicinity of the Waste Isolation Pilot Plant, Southeastern New Mexico*. DOE-WIPP 88-004. Carlsbad, NM: Westinghouse Electric Corporation.

Holt, R.M., and D.W. Powers. 1990. *Geologic Mapping of the Air Intake Shaft at the Waste Isolation Pilot Plant*. DOE-WIPP 90-051. Carlsbad, NM: Westinghouse Electric Corporation.

Hora, S.C., and R.L. Iman. 1989. "Expert Opinion in Risk Analysis: The NUREG-1150 Methodology," *Nuclear Science and Engineering*. Vol. 102, no. 4, 323-331.

Hora, S.C., D. von Winterfeldt, and K.M. Trauth. 1991. *Expert Judgment on Inadvertent Human Intrusion into the Waste Isolation Pilot Plant*. SAND90-3063. Albuquerque, NM: Sandia National Laboratories.

Howarth, S.M., E.W. Peterson, P.L. Lagus, K. Lie, S.J. Finley, and E.J. Nowak. 1991. "Interpretation of In-Situ Pressure and Flow Measurements of the Salado Formation at the Waste Isolation Pilot Plant," *Society of Petroleum Engineers Rocky Mountain Regional Meeting and Low-Permeability Reservoir Symposium, Denver, CO, April 15-17, 1991*. SPE-21840. Richardson, TX: Society of Petroleum Engineers.

Hume, H.R., and A. Shakoor. 1981. "Mechanical Properties," *Physical Properties Data for Rock Salt*. NBS Monograph 167. Washington, DC: National Bureau of Standards. 103-203.

Hunter, R.L. 1985. *A Regional Water Balance for the Waste Isolation Pilot Plant (WIPP) Site and Surrounding Area*. SAND84-2233. Albuquerque, NM: Sandia National Laboratories.

Huyakorn, P.S., H.O. White, Jr., and S. Panday. 1991. *STAFF2D: Solute Transport and Fracture Flow in Two Dimensions*. Version 3.1. Herndon, VA: Hydrogeologic, Inc.

IAEA (International Atomic Energy Agency). 1986. *Decay Data of the Transactinium Nuclides*. Technical Report No. 261. Vienna, Austria: International Atomic Energy Agency.

Ibrahim, M.A., M.R. Tek, and D.L. Katz. 1970. *Threshold Pressure in Gas Storage*. Arlington, VA: American Gas Association, Inc.

ICRP, Pub 38. 1983. "Radionuclide Transformations - Energy and Intensity of Emissions," *Annals of the International Commission on Radiological Protection (ICRP)*. Vols. 11-13. ICRP Publication No. 38.

Johnson, N.L., and S. Kotz. 1970a. *Continuous Univariate Distributions-1*. New York, NY: John Wiley & Sons.

Johnson, N.L., and S. Kotz. 1970b. *Continuous Univariate Distributions-2*. New York, NY: John Wiley & Sons.

Kaufmann, D.W., ed. 1960. *Sodium Chloride, The Production and Properties of Salt and Brine*. Monograph No. 145. Washington, DC: American Chemical Society.

Kelley, V.A., and J.F. Pickens. 1986. *Interpretation of the Convergent-Flow Tracer Tests Conducted in the Culebra Dolomite at the H-3 and H-4 Hydropads at the Waste Isolation Pilot Plant (WIPP) Site*. SAND86-7161. Albuquerque, NM: Sandia National Laboratories.

Kelley, V.A., and G.J. Saulnier, Jr. 1990. *Core Analyses for Selected Samples from the Culebra Dolomite at the Waste Isolation Pilot Plant Site*. SAND90-7011. Albuquerque, NM: Sandia National Laboratories.

Kipp, K.L., Jr. 1987. *HST3D: A Computer Code for Simulation of Heat and Solute Transport in Three-Dimensional Ground-Water Flow Systems*. WRIR 86-4095. Denver, CO: U.S. Geological Survey.

Krieg, R.D. 1984. *Reference Stratigraphy and Rock Properties for the Waste Isolation Pilot Plant (WIPP) Project*. SAND83-1908. Albuquerque, NM: Sandia National Laboratories.

Lappin, A.R. 1988. *Summary of Site-Characterization Studies Conducted from 1983 through 1987 at the Waste Isolation Pilot Plant (WIPP) Site, Southeastern New Mexico*. SAND88-0157. Albuquerque, NM: Sandia National Laboratories.

Lappin, A.R., R.L. Hunter, D.P. Garber, and P.B. Davies, eds. 1989. *Systems Analysis, Long-Term Radionuclide Transport, and Dose Assessments, Waste Isolation Pilot Plant (WIPP), Southeastern New Mexico; March 1989*. SAND89-0462. Albuquerque, NM: Sandia National Laboratories.

LaVenue, A.M., T.L. Cauffman, and J. F. Pickens. 1990. *Ground-Water Flow Modeling of the Culebra Dolomite. Volume I: Model Calibration*. SAND89-7068/1. Albuquerque, NM: Sandia National Laboratories.

Lynch, A.W., and R.G. Dosch. 1980. *Sorption Coefficients for Radionuclides on Samples from the Water-Bearing Magenta and Culebra Members of the Rustler Formation*. SAND80-1064. Albuquerque, NM: Sandia National Laboratories.

Marietta, M.G., S.G. Bertram-Howery, D.R. Anderson, K.F. Brinster, R.V. Guzowski, H.[J.] Iuzzolino, and R.P. Rechard. 1989. *Performance Assessment Methodology Demonstration: Methodology Development for Evaluating Compliance With EPA 40 CFR 191, Subpart B, for the Waste Isolation Pilot Plant*. SAND89-2027. Albuquerque, NM: Sandia National Laboratories.

Marsily, G. de. 1986. *Quantitative Hydrogeology: Groundwater Hydrology for Engineers*. Orlando, FL: Academic Press, Inc.

Matalucci, R.V. 1988. *In Situ Testing at the Waste Isolation Pilot Plant*. SAND87-2382. Albuquerque, NM: Sandia National Laboratories.

McTigue, D.F., S.J. Finley, J.H. Gieske, and K.L. Robinson. 1991. Appendix A: "Compressibility Measurements on WIPP Brines," *Preliminary Comparison with 40 CFR Part 191, Subpart B for the Waste Isolation Pilot Plant, December 1991. Volume 3: Reference Data*. WIPP Performance Assessment Division. Eds. R.P. Rechard, A.C. Peterson, J.D. Schreiber, H.J. Iuzzolino, M.S. Tierney, and J.S. Sandha. SAND91-0893/3. Albuquerque, NM: Sandia National Laboratories. A-79 through A-98.

Mendenhall, F.T., B.M. Butcher, and P.B. Davies. 1991. "Investigations into the Coupled Fluid Flow and Mechanical Creep Closure Behavior of Waste Disposal Rooms in Bedded Salt," *Waste-Generated Gas at the Waste Isolation Pilot Plant: Papers Presented at the Nuclear Energy Agency Workshop on Gas Generation and Release from Radioactive Waste Repositories, Aix-en-Provence, France, September 23-26, 1991*. Eds. P.B. Davies, L.H. Brush, M.A. Molecke, F.T. Mendenhall, and S.W. Webb. SAND91-2378. Albuquerque, NM: Sandia National Laboratories. Chapter 3.

Mercer, J. W. 1983. *Geohydrology of the Proposed Waste Isolation Pilot Plant Site, Los Medaños Area, Southeastern New Mexico*. Water-Resources Investigations Report 83-4016. Albuquerque, NM: U.S. Geological Survey.

Mercer, J.W., and B.R. Orr. 1979. *Interim Data Report on the Geohydrology of the Proposed Waste Isolation Pilot Plant Site, Southeast New Mexico.* U.S. Geological Survey Water-Resources Investigations 79-98. Albuquerque, NM: U.S. Geological Survey.

Miller, I., and J.E. Freund. 1977. *Probability and Statistics for Engineers.* 2nd ed. Englewood Cliffs, NJ: Prentice-Hall.

Molecke, M.A. 1979. *Gas Generation from Transuranic Waste Degradation: Data Summary and Interpretation.* SAND79-1245. Albuquerque, NM: Sandia National Laboratories.

Munson, D.E., A.F. Fossum, and P.E. Senseny. 1989. *Advances in Resolution of Discrepancies Between Predicted and Measured In Situ WIPP Room Closures.* SAND88-2948. Albuquerque, NM: Sandia National Laboratories.

Munson, D.E., J.R. Ball, and R.L. Jones. 1990. "Data Quality Assurance Controls Through the WIPP In Situ Data Acquisition, Analysis, and Management System," *Proceedings of the International High-Level Radioactive Waste Management Conference, Las Vegas, NV, April 8-12, 1990.* SAND88-2845C. La Grange Park, IL: American Nuclear Society. Vol. 2, 1337-1350.

NEPA. 1969. *National Environmental Policy Act of 1969.* Pub. L. No. 91-190, 83 Stat. 852.

Novak, C.F. 1991. Appendix A: "Rationale for K_d Values Provided During Elicitation of the Retardation Expert Panel, May 1991," *Preliminary Comparison with 40 CFR Part 191, Subpart B for the Waste Isolation Pilot Plant, December 1991. Volume 3: Reference Data.* WIPP Performance Assessment Division. Eds. R. P. Rechard, A.C. Peterson, J.D. Schreiber, H.J. Iuzzolino, M.S. Tierney, and J.S. Sandha. SAND91-0893/3. Albuquerque, NM: Sandia National Laboratories. A-99 through A-106.

Novak, C.F. 1992. *An Evaluation of Radionuclide Batch Sorption Data on Culebra Dolomite for Aqueous Compositions Relevant to the Human Intrusion Scenario for the Waste Isolation Pilot Plant.* SAND91-1299. Albuquerque, NM: Sandia National Laboratories.

Nowak, E.J., and J.C. Stormont. 1987. *Scoping Model Calculations of the Reconsolidation of Crushed Salt in WIPP Shafts.* SAND87-0879. Albuquerque, NM: Sandia National Laboratories.

Nowak, E.J., and L.D. Tyler. 1989. "The Waste Isolation Pilot Plant (WIPP) Seal System Performance Program," *Proceedings of the Joint NEA/CEC Workshop on Sealing of Radioactive Waste Repositories, Braunschweig, FRG, May 22-25, 1989.* SAND89-0386C. Paris, France: Organisation for Economic Co-operation and Development. 98-110.

Nowak, E.J., D.F. McTigue, and R. Beraun. 1988. *Brine Inflow to WIPP Disposal Rooms: Data, Modeling, and Assessment.* SAND88-0112. Albuquerque, NM: Sandia National Laboratories.

Nowak, E.J., J.R. Tillerson, and T.M. Torres. 1990. *Initial Reference Seal System Design: Waste Isolation Pilot Plant.* SAND90-0355. Albuquerque, NM: Sandia National Laboratories.

OCC (Oil Conservation Commission). 1989. *Application of the Oil Conservation Division Upon Its Own Motion to Revise Order R-111, As Amended, Pertaining to the Potash Areas of Eddy and Lea Counties, New Mexico.* Order No. R-111-P.

Oldroyd, J.G. 1958. "Non-Newtonian Effects in Steady Motion of Some Idealized Elastico-Viscous Liquids," *Proceedings of the Royal Society of London. Series A–Mathematical and Physical Sciences.* Vol. 245, no. 1241, 278-297.

Pace, B. O. 1990. Appendix A: "Letter 1b: Changes to Bar Graphs," *Data Used in Preliminary Performance Assessment of the Waste Isolation Pilot Plant (1990).* R. P. Rechard, H. Iuzzolino, and J. S. Sandha. SAND89-2408. Albuquerque, NM: Sandia National Laboratories. A-165 through A-170.

Parker, J.C., R.J. Lenhard, and T. Kuppusamy. 1987. "A Parametric Model for Constitutive Properties Governing Multiphase Flow in a Porous Media," *Water Resources Research*. Vol. 23, no. 4, 618-624.

Peaceman, D.W. 1977. *Fundamentals of Numerical Reservoir Simulation*. Developments in Petroleum Science, 6. New York, NY: Elsevier Scientific Publishing Company.

Perry, R.H., C.H. Chilton, and S.D. Kirkpatrick. 1969. *Chemical Engineer's Handbook*. New York, NY: McGraw-Hill Book Company.

Peterson, A.C. 1990. Appendix A: "Memo 7: Preliminary Contact Handled (CH) and Remote Handled (RH) Radionuclide Inventories," *Data Used in Preliminary Performance Assessment of the Waste Isolation Pilot Plant (1990)*. R.P. Rechard, H. Iuzzolino, and J.S. Sandha. SAND89-2408. Albuquerque, NM: Sandia National Laboratories. A-107 through A-112.

Pickens, J.F., and G.E. Grisak. 1981. "Modeling of Scale-Dependent Dispersion in Hydrogeologic Systems," *Water Resources Research*. Vol. 17, no. 6, 1701-1711.

Popielak, R.S., R.L. Beauheim, S.R. Black, W.E. Coons, C.T. Ellingson, and R.L. Olsen. 1983. *Brine Reservoirs in the Castile Formation, Waste Isolation Pilot Plant (WIPP) Project, Southeastern New Mexico*. TME-3153. Carlsbad, NM: U.S. Department of Energy.

Powers, D.W., S.J. Lambert, S-E. Shaffer, L.R. Hill, and W.D. Weart, eds. 1978. *Geological Characterization Report, Waste Isolation Pilot Plant (WIPP) Site, Southeastern New Mexico*. SAND78-1596. Albuquerque, NM: Sandia National Laboratories. Vols. 1-2.

Press, W.H., B.P. Flannery, S.A. Teukolsky, and W.T. Vetterling. 1986. *Numerical Recipes, The Art of Scientific Computing*. New York, NY: Cambridge University Press.

RCRA. 1976. *Resource Conservation and Recovery Act of 1976*. Pub. L. No. 94-580, 90 Stat. 2795.

Rechard, R.P. 1989. *Review and Discussion of Code Linkage and Data Flow in Nuclear Waste Compliance Assessments*. SAND87-2833. Albuquerque, NM: Sandia National Laboratories.

Rechard, R.P., ed. 1992. *User's Reference Manual for CAMCON: Compliance Assessment Methodology Controller, Version 3.0*. SAND90-1983. Albuquerque, NM: Sandia National Laboratories.

Rechard, R.P., H.[J.] Iuzzolino, and J.S. Sandha. 1990a. *Data Used in Preliminary Performance Assessment of the Waste Isolation Pilot Plant (1990)*. SAND89-2408. Albuquerque, NM: Sandia National Laboratories.

Rechard, R.P., W. Beyeler, R.D. McCurley, D.K. Rudeen, J.E. Bean, and J.D. Schreiber. 1990b. *Parameter Sensitivity Studies of Selected Components of the Waste Isolation Pilot Plant Repository/Shaft System*. SAND89-2030. Albuquerque, NM: Sandia National Laboratories.

Reeves, M., G.A. Freeze, V.A. Kelley, J.F. Pickens, D.T. Upton, and P.B. Davies. 1991. *Regional Double-Porosity Solute Transport in the Culebra Dolomite Under Brine-Reservoir-Breach Release Conditions: An Analysis of Parameter Sensitivity and Importance*. SAND89-7069. Albuquerque, NM: Sandia National Laboratories.

Richey, S.F., J.G. Wells, and K.T. Stephens. 1985. *Geohydrology of the Delaware Basin and Vicinity, Texas and New Mexico*. Water-Resources Investigations Report 84-4077. Albuquerque, NM: U.S. Geological Survey.

Rose, W., and W.A. Bruce. 1949. "Evaluation of Capillary Character in Petroleum Reservoir Rock," *Transactions of the American Institute of Mining and Metallurgical Engineers*. Vol. 186, 127-142.

Ross, S.M. 1985. *Introduction to Probability Models*. 3rd ed. Orlando, FL: Academic Press, Inc.

Sargunam, A., P. Riley, K. Arulanandan, and R.B. Krone. 1973. "Physico-Chemical Factors in Erosion of Cohesive Soils," *Journal of the Hydraulics Division, Proceedings of the American Society of Civil Engineers.* Vol. 99, no. HY3, 555-558.

Saulnier, G.J., Jr. 1987. *Analysis of Pumping Tests of the Culebra Dolomite Conducted at the H-11 Hydropad at the Waste Isolation Pilot Plant (WIPP) Site*. SAND87-7124. Albuquerque, NM: Sandia National Laboratories.

Savins, J.G., and G.C. Wallick. 1966. "Viscosity Profiles, Discharge Rates, Pressures, and Torques for a Rheologically Complex Fluid in a Helical Flow," *A.I.Ch.E. Journal*. Vol. 12, no. 2, 357-363.

Scheetz, B.E., P.H. Licastro, and D.M. Roy. 1986. *A Full-Scale Borehole Sealing Test in Anhydrite Under Simulated Downhole Conditions*. BMI/ONWI-581(2). Columbus, OH: Office of Nuclear Waste Isolation, Battelle Memorial Institute. Vol. 2.

Siegel, M.D. 1990. Appendix A: "Memo 3a: Representation of Radionuclide Retardation in the Culebra Dolomite in Performance Assessment Calculations," *Data Used in Preliminary Performance Assessment of the Waste Isolation Pilot Plant (1990).* R.P. Rechard, H. Iuzzolino, and J.S. Sandha. SAND89-2408. Albuquerque, NM: Sandia National Laboratories. A-43 through A-62.

Sjaardema, G.D., and R.D. Krieg. 1987. *A Constitutive Model for the Consolidation of WIPP Crushed Salt and Its Use in Analyses of Backfilled Shaft and Drift Configurations*. SAND87-1977. Albuquerque, NM: Sandia National Laboratories.

SNL (Sandia [National] Laboratories). 1979. *Summary of Research and Development Activities in Support of Waste Acceptance Criteria for WIPP.* SAND79-1305. Albuquerque, NM: Sandia National Laboratories.

SNL (Sandia National Laboratories) and U.S. Geological Survey. 1983. *Basic Data Report for Drillhole ERDA 9 (Waste Isolation Pilot Plant - WIPP)*. SAND79-0270. Albuquerque, NM: Sandia National Laboratories.

Stone, C.M., R.D. Krieg, and Z.E. Beisinger. 1985. *SANCHO: A Finite Element Computer Program for the Quasistatic, Large Deformation, Inelastic Response of Two-Dimensional Solids*. SAND84-2618. Albuquerque, NM: Sandia National Laboratories.

Streeter, V.L., and E.B. Wylie. 1975. *Fluid Mechanics*. 6th ed. New York, NY: McGraw-Hill Book Co.

Sutherland, H.J., and S. Cave. 1978. *Gas Permeability of SENM Rock Salt*. SAND78-2287. Albuquerque, NM: Sandia National Laboratories.

Swift, P.N. 1991. Appendix A: "Climate and Recharge Variability Parameters for the 1991 WIPP PA Calculations," *Preliminary Comparison with 40 CFR Part 191, Subpart B for the Waste Isolation Pilot Plant, December 1991. Volume 3: Reference Data.* WIPP Performance Assessment Division. Eds. R.P. Rechard, A.C. Peterson, J.D. Schreiber, H.J. Iuzzolino, M.S. Tierney, and J.S. Sandha. SAND91-0893/3. Albuquerque, NM: Sandia National Laboratories. A-107 through A-121.

Thomas, L.K., D.L. Katz, and M.R. Tek. 1968. "Threshold Pressure Phenomena in Porous Media," *Society of Petroleum Engineers Journal*. Vol. 8, no. 2, 174-184.

Tierney, M.S. 1990. *Constructing Probability Distributions of Uncertain Variables in Models of the Performance of the Waste Isolation Pilot Plant: The 1990 Performance Simulations*. SAND90-2510. Albuquerque, NM: Sandia National Laboratories.

Tierney, M.S. 1991. *Combining Scenarios in a Calculation of the Overall Probability Distribution of Cumulative Releases of Radioactivity from the Waste Isolation Pilot Plant, Southeastern New Mexico*. SAND90-0838. Albuquerque, NM: Sandia National Laboratories.

Trauth, K.M., R.P. Rechard, and S.C. Hora. 1991. "Expert Judgment as Input to Waste Isolation Pilot Plant Performance Assessment Calculations: Probability Distributions of Significant System Parameters," *Mixed Waste, Proceedings of the First International Symposium, Baltimore, MD, August 26-29, 1991.* SAND91-0625C. Baltimore, MD: Environmental Safety and Health, University of Maryland. 4.3.1 through 4.3.9.

Trauth, K.M., S.C. Hora, R.P. Rechard, and D.R. Anderson. 1992. *The Use of Expert Judgment to Quantify Uncertainty in Solubility and Sorption Parameters for Waste Isolation Pilot Plant Performance Assessment.* SAND92-0479. Albuquerque, NM: Sandia National Laboratories.

Tyler, L.D., R.V. Matalucci, M.A. Molecke, D.E. Munson, E.J. Nowak, and J.C. Stormont. 1988. *Summary Report for the WIPP Technology Development Program for Isolation of Radioactive Waste*. SAND88-0844. Albuquerque, NM: Sandia National Laboratories.

U.S. DOE (Department of Energy). 1983. "Brine Content of Facility Interval Strata," *Results of Site Validation Experiments.* TME 3177, Rev. 2.0. [Carlsbad, NM]: Waste Isolation Pilot Plant. Vol. II, Supporting Document 10.

U.S. DOE (Department of Energy). 1989. *Waste Isolation Pilot Plant Compliance Strategy for 40 CFR Part 191.* DOE-WIPP 86-013. Carlsbad, NM: U.S. Department of Energy.

U.S. DOE (Department of Energy). 1990a. *WIPP Test Phase Plan: Performance Assessment.* DOE/WIPP 89-011, Rev. O. Carlsbad, NM: U.S. Department of Energy.

U.S. DOE (Department of Energy). 1990b. *Final Supplement Environmental Impact Statement, Waste Isolation Pilot Plant.* DOE/EIS-0026-FS. Washington, DC: U.S. Department of Energy, Office of Environmental Restoration and Waste Management.

U.S. DOE (Department of Energy). 1990c. *Final Safety Analysis Report, Waste Isolation Pilot Plant, Carlsbad, New Mexico*. WP 02-9, Rev. 0. Carlsbad, NM: U.S. Department of Energy.

U.S. DOE (Department of Energy). 1990d. *Integrated Data Base for 1990: U.S. Spent Fuel and Radioactive Waste Inventories, Projections, and Characteristics.* DOE/RW-0006, Revision 6. Oak Ridge, TN: Oak Ridge National Laboratory for U.S. Department of Energy.

U.S. DOE (Department of Energy). 1991. *Recommended Strategy for the Remote-Handled Transuranic Waste Program.* DOE/WIPP 90-058, Revision 1. Carlsbad, NM: Waste Isolation Pilot Plant.

U.S. DOE (Department of Energy) and State of New Mexico. 1984. U.S. Department of Energy and State of New Mexico, 1981, First Modification to the July 1, 1981 "Agreement for Consultation and Cooperation" on WIPP by the State of New Mexico and U.S. Department of Energy, November 30, 1984.

Van Genuchten, R. 1978. *Calculating the Unsaturated Hydraulic Conductivity with a New Closed-Form Analytical Model.* Research Report 78-WR-08. Princeton, NJ: Princeton University, Department of Civil Engineering.

Vargaftik, N.B. 1975. *Tables on the Thermophysical Properties of Liquids and Gases in Normal and Dissociated States*. New York, NY: John Wiley & Sons, Inc.

Vennard, J.K., and R.L. Street. 1975. *Elementary Fluid Mechanics*. 5th ed. New York, NY: John Wiley & Sons, Inc.

Voss, C.I. 1984. *SUTRA (Saturated-Unsaturated TRAnsport): A Finite-Element Simulation Model for Saturated-Unsaturated Fluid-Density-Dependent Ground-Water Flow with Energy Transport or Chemically-Reactive Single-Species Solute Transport.* Reston, VA: U.S. Geological Survey National Center.

Walker, R.E. 1976. "Hydraulic Limits Are Set by Flow Restrictions," *Oil and Gas Journal.* Vol. 74, no. 40, 86-90.

Walker, R.E., and W.E. Holman. 1971. "Computer Program Predicting Drilling-Fluid Performance," *Oil and Gas Journal.* Vol. 69, no. 13, 80-90.

Ward, J.S., and N.R. Morrow. 1985. "Capillary Pressures and Gas Relative Permeabilities of Low-Permeability Sandstone," *1985 SPE/DOE Joint Symposium on Low Permeability Gas Reservoirs, Denver, CO, May 19-22, 1985.* SPE/DOE 13882. Dallas, TX: Society of Petroleum Engineers. 321-334.

Ward, R.F., C.G. St. C. Kendall, and P.M. Harris. 1986. "Upper Permian (Guadalupian) Facies and Their Association with Hydrocarbons - Permian Basin, West Texas and New Mexico," *American Association of Petroleum Geologists Bulletin.* Vol. 70, no. 3, 239-262.

Weast, R.C., and M.J. Astle, eds. 1981. *Handbook of Chemistry and Physics.* 62nd ed. Cleveland, OH: CRC Press.

WEC (Westinghouse Electric Corporation). 1990. *Waste Isolation Pilot Plant No-Migration Variance Petition.* DOE/WIPP 89-003, Rev. 1. Prepared for U.S. Department of Energy. Carlsbad, NM: Westinghouse Electric Corporation.

WEC (Westinghouse Electric Corporation). 1991. *Waste Acceptance Criteria for the Waste Isolation Pilot Plant.* WIPP-DOE-069, Rev. 4. Prepared for U.S. Department of Energy. Carlsbad, NM: Westinghouse Electric Corporation.

Williamson, C.R. 1978. "Depositional Processes, Diagenesis and Reservoir Properties of Permian Deep-Sea Sandstones, Bell Canyon Formation, Texas-New Mexico." Ph.D. dissertation. Austin, TX: University of Texas.

WIPP Act. 1979. *Department of Energy National Security and Military Applications of Nuclear Energy Authorization Act of 1980, Title II - General Provisions: Waste Isolation Pilot Plant, Delaware Basin, NM.* Pub. L. No. 96-164, 93 Stat. 1259.

WIPP PA (Performance Assessment) Department. 1992. *Long-Term Gas and Brine Migration at the Waste Isolation Pilot Plant: Preliminary Sensitivity Analyses for Post-Closure 40 CFR 268 (RCRA), May 1992.* SAND92-1933. Albuquerque, NM: Sandia National Laboratories.

WIPP PA (Performance Assessment) Division. 1991. *Preliminary Comparison with 40 CFR Part 191, Subpart B for the Waste Isolation Pilot Plant, December 1991. Volume 3: Reference Data.* SAND91-0893/3. Albuquerque, NM: Sandia National Laboratories.

Wyllie, M.R.J., and W.D. Rose. 1950. "Some Theoretical Considerations Related to the Quantitative Evaluation of the Physical Characteristics of Reservoir Rock from Electric Log Data," *Transactions of the American Institute of Mining and Metallurgical Engineers.* Vol. 189, 105-118.

Yaglom, A.M. 1962. *An Introduction to the Theory of Stationary Random Functions.* Englewood Cliffs, NJ: Prentice-Hall, Inc.

APPENDIX A:
MEMORANDA REGARDING REFERENCE DATA

Referenced Memoranda

APPENDIX A:
MEMORANDA REGARDING REFERENCE DATA

Beraún and Davies, September 12, 1991

Date: 9/12/91
To: Distribution
From: R. Beraún, 6345, and P. B. Davies, 6344
Subject: Baseline Design Input Data Base to be Used During Calculations Effort to be Performed by Division 1514 in Determining the Mechanical Creep Closure Behavior of Waste Disposal Rooms in Bedded Salt.

Butcher, September 9, 1992

Date: 9/9/92
To: M. S. Tierney, 6342
From: B. M. Butcher, 6345
Subject: Waste Compaction Properties for the Baseline Closure Surface

Davies et al., July 14, 1992 (1992a)

Date: 7/14/92
To: B. M. Butcher, J. Schreiber, and P. Vaughn (6342)
From: P. B. Davies, S. W. Webb, and E. D. Gorham (6119)
Subject: Feedback on "PA Modeling Using BRAGFLO-1992" 7-8-92 Memo by J. Schreiber

Davies et al., July 22, 1992 (1992b)

Date: 7/22/92
To: B. M. Butcher, J. Schreiber, and P. Vaughn (6342)
From: P. B. Davies, R. L. Beauheim, and E. D. Gorham (6119)
Subject: Additional Comments on Far-Field Anhydrite Permeability Distribution in "PA Modeling Using BRAGFLO -- 1992" 7-8-92 Memo by J. Schreiber"

Gorham et al., June 15, 1992

Date: 6/15/92
To: Martin Tierney, 6342
From: Elaine Gorham, Richard Beauheim, Peter Davies, Susan Howarth, and Steve Webb (6119)
Subject: Recommendations to PA on Salado Formation Intrinsic Permeability and Pore Pressure for 40 CFR 191 Subpart B Calculations

Hora, August 25, 1992

Date: 8/25/92
To: Kate Trauth, Jon Helton, Mel Marietta, Martin Tierney, Bob Guzowski, Rip Anderson
From: Steve Hora
Subject: Probabilities of Human Intrusion into the WIPP, Methodology for the 1992 Preliminary Comparison

Mendenhall and Lincoln, February 28, 1992

Date: 2/28/92
To: D. R. Anderson 6342
From: F. T. Mendenhall, 6345, R. C. Lincoln, 6345
Subject: Single Room Porosity History for Baseline Waste Form and Gas Generation Rates

Munson, October 26, 1992

Date: 10/26/92
To: M. S. Tierney, 6342
From: D. E. Munson, 6346
Subject: Mechanical Parameters for Volume 3, SAND92-0700

Novak et al., July 20, 1992

Date: 7/20/92
To: Martin S. Tierney, 6342
From: Craig F. Novak, Fred Gelbard, and Hans W. Papenguth, 6119
Subject: Parameter Recommendations for Porosity and Thickness of Clay Fracture Linings for the 1992 WIPP Performance Assessment Calculations

Peterson, October 28, 1992

Date: 10/28/92
To: Martin Tierney, 6342
From: A. Peterson, 6342
Subject: Preliminary Contact Handled (CH) Radionuclide and Nonradionuclide Inventories and Remote Handled (RH) Radionuclide Inventory for Use in 1992 Performance Assessment

Webb, March 20, 1992 (1992a)

Date: 3/20/92
To: D. R. Anderson, 6342
From: S. W. Webb, 6344
Subject: Uncertainty Estimates for Two-Phase Characteristic Curves for 1992 RCRA Calculations

Webb, April 30, 1992 (1992b)

Date: 4/30/92
To: D. R. Anderson, 6342
From: S. W. Webb, 6344
Subject: Uncertainty Estimates for Two-Phase Characteristic Curves for 1992 40 CFR 191 Calculations

Beraún and Davies, September 12, 1991

Date: 9/12/91
To: Distribution
From: R. Beraún, 6345, and P. B. Davies, 6344
Subject: Baseline Design Input Data Base to be Used During Calculations Effort to be Performed by Division 1514 in Determining the Mechanical Creep Closure Behavior of Waste Disposal Rooms in Bedded Salt.

Sandia National Laboratories
Albuquerque, New Mexico 87185

date: September 12, 1991

to: Distribution

from: R Beraún, 6345, and P. B. Davies, 6344

subject: Baseline Design Input Data Base to be Used During Calculations Effort to be Performed by Division 1514 in Determining the Mechanical Creep Closure Behavior of Waste Disposal Rooms in Bedded Salt.

Introduction

The original disposal concept for TRU waste at WIPP is to excavate disposal rooms and fill them and adjacent access drifts with waste. Under the current baseline design, the radioactive wastes to be store consist of a variety of materials (solid organics and inorganics), and sludges. The unprocessed waste in their "as-received" state will be contained in 55-gallon drums or other containers such as standard waste boxes. While the waste remains in its unprocessed state, the materials will initially have high porosities and will be highly permeable. However, over a period of time the drums may collapse due to the closure of the rooms and the consequent loading of the containers. Under these conditions the drum waste contents will compact and cause a reduction in the corresponding porosity and permeability values [1].

This memorandum documents input data base for the baseline design submitted to Division 1514, for the purpose of performing required calculations to determine the mechanical creep closure behavior of waste disposal rooms in bedded salt in the presence of gas being generated by the waste emplaced in these rooms. The results provided need to be defined as function of time to evaluate the performance of the repository.

Geometry

Each conventionally mined disposal room is 13 ft high by 33 ft wide by 300 ft long, and its internal volume is $1.287X10^5\ ft^3$ (3644.8 m^3) [2]. The baseline design calls for a total of 6804 drums to be uniformly distributed with unprocessed waste in an equivalent room. The total volume occupied by the waste and drums is, 58718.5 ft^3 (1663 m^3). With the required headspace of 28 inches [4], the total crushed salt backfill required to seal the disposal room was calculated to be approximately 1328 m^3 [2].

Waste Characteristics

The transuranic waste destined for the WIPP site is either solid or solidified material and in its "as-received" state is grouped under three major waste forms: 1) Sludges; 2) solid organics often referred to as "combustible", consist of wastes such as paper, plastic, tissues, plywood, etc and 3) solid inorganic waste consisting of metals, glass, and a small percentage of other non-combustible materials [1,5]. Table 1 summarizes the required data input to characterize the waste for the baseline case. This table shows the waste forms and their corresponding drum count, weight, density and porosities.

Table 1: **Baseline Design Database*** [2]

Waste Form	Drum Count	Drum Weight Kg	Density (Kg/m^3) Initial	Density (Kg/m^3) Stress Function	Porosity Initial	Porosity Stress Function	Elastic Modulus
Solid Organics	2722	77	380	Fig. 1	0.8	Fig 2	N/A†
Solid Inorganics	2722	102	900	Fig. 1	0.8	Fig 2	N/A†
Sludges	1360	211	1200	Fig. 1	0.5	Fig 2	N/A†

*These numbers are rounded to one significant figure.

†The waste is model as an inelastic material thus, Elastic properties are not required [12].

In an effort to understand the mechanical behavior of the waste to be emplaced in the repository, an investigation was conducted by Butcher [6] leading to the compilation of valuable experimental information about how material simulating transuranic (TRU) waste compact under axial compressive stress. Figures 1 and 2 obtained from Reference [6] are compaction curves representing the combustible, metallic, and sludge waste categories. Figure 1 depicts the waste density as a function of axial compaction stress. Figure 2 shows the waste porosity versus compressive stress for the same waste categories; also shown in this figure is an average porosity curve for the repository.

Repository Salt Backfill

Once the waste has been emplaced, the disposal room is backfilled with crushed salt leaving only a headspace of 28 inches [4]. The density of crushed salt is 1300 kg/m^3 [7, 8], the initial porosity is approximately 0.4 [2] and the corresponding elastic properties as specified in Reference 9 are:

Shear modulus $\mu = 1.24X10^{10}\ Pa$
Young's modulus $E = 3.1X10^{10}\ Pa$
Poisson's ratio $\nu = 0.25$

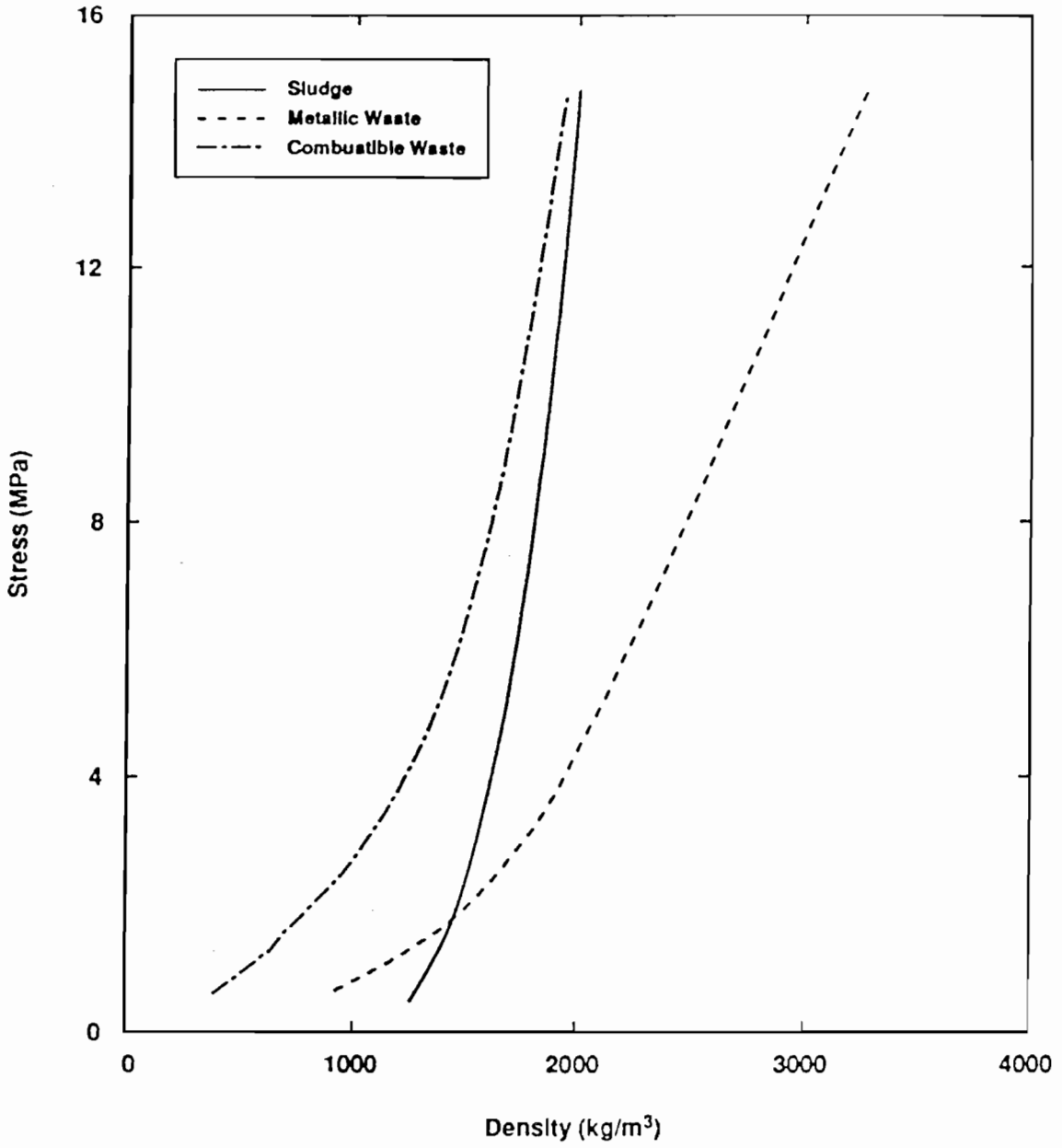

Figure 1: Compaction Stress vs Waste Densities

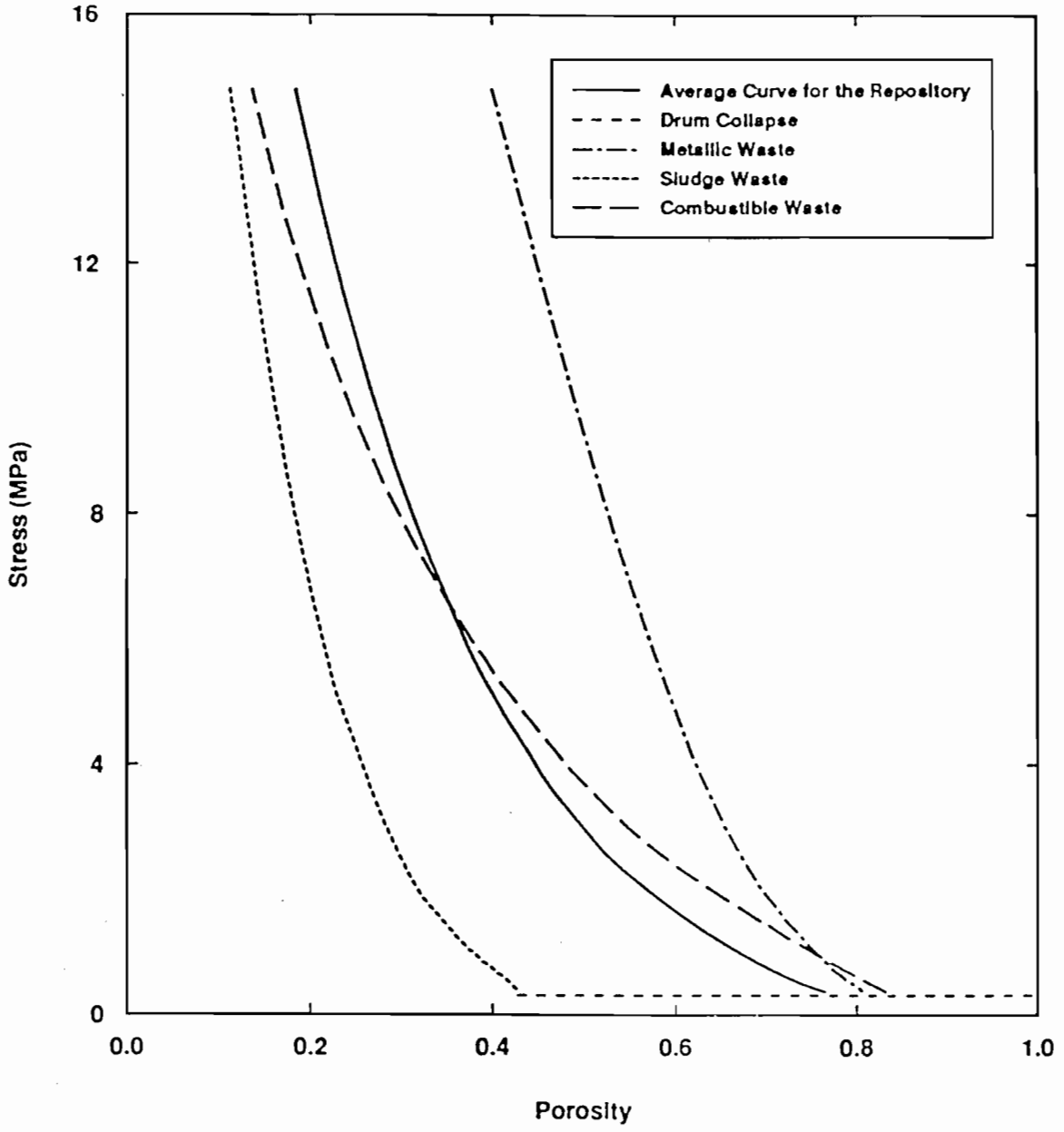

Figure 2: Waste Porosity as Function of Compressive Stress

Gas Generation

For the baseline case, Brush reported earlier [10] that H_2 production rates of 1 $mole/drum.year$ and corrosion rates of 2 $\mu m/year$ were adequate estimates for inundated conditions rounded to one significant figure. The estimated gas production potential from anoxic corrosion will be 1050 $moles/drum$ of waste [11] constituting 66 % of the total gas production potential. Brush also reports 1 mole of various gases per drum per year to be his best estimate for the microbial gas production rate under inundated conditions. The gas production potential from microbial activity is estimated to be at 550 $moles/drum$ [11], 34 % of the total gas production potential. Table 2 summarizes current estimates of gas production rates for the baseline case performed by Brush [10].

Table 2: **Gas Production Rates for the Baseline Design [10]**

Process	Gas Production Rate† ($moles/drum.year$)	
	Inundated	Humid
Anoxic corrosion	1	0.1
Microbial activity	1	0.1
Radiolysis of brine	0.0	0.0

†These numbers are rounded to one significant figure.

Number of Waste Drums

The gas generation rates as presented in Table 2 are calculated based on a baseline waste drum. The baseline design case calls for 6804 drums with "as-received" waste to be uniformly distributed in an equivalent disposal room. Thus, utilize this number (6804 drums) to calculate the amount of gas being generated in a disposal room.

References

1. Butcher, B. M., "Waste Isolation Pilot Plant Simulated Waste Compositions and Mechanical Properties," SAND89-0372, Sandia National Laboratories, Albuquerque, New Mexico, June 1989.

2. Beraun, R, " EATF Calculations to Determine Waste Form Distribution for Alternatives # 2 and # 6,"Memorandum to Distribution, Sandia National Laboratories, Albuquerque, New Mexico, In Draft.

3. Butcher, B. M., "Preliminary Evaluation of Potential Engineered Modifications for the Waste Isolation Pilot Plant (WIPP)," SAND89-3095, Sandia National Laboratories, Albuquerque, New Mexico, April 1990.

4. U. S. Department of Energy,"Waste Isolation Pilot Plant Design Validation Final Report," DOE-WIPP-86-010, Prepared by Bechtel National Inc., San Francisco, Ca. October 1986.

5. EATF, "Evaluation of the Effectiveness and Feasibility of the Waste Isolation Pilot Plant Engineered Alternatives: Final Report of the Engineered Alternatives Task Force," DOE/WIPP 91-007, U. S. Department of Commerce, Springfield, VA. July 1991.

6. Butcher, B. M., T. W. Thompson, R. G. VanBuskirk, and N. C. Patti, "Mechanical Compaction of Waste Isolation Pilot Plant Simulated Waste," SAND90-1206, Sandia National Laboratories, Albuquerque, New Mexico, In Review.

7. Gerstle, W. H., A. K. Jones, "Mechanical Properties of Crushed Salt/Bentonite Blocks," SAND86-0707, Sandia National Laboratories, Albuquerque, New Mexico, August 1986.

8. Beraun, R., M. A. Molecke, "Thermal Analysis of the WIPP In Situ Room A1 DHLW Package Experiments," SAND86-0681, Sandia National Laboratories, Albuquerque, New Mexico, May 1987.

9. Munson, D. E., A. F. Fossum and P. E. Senseny, "Advances in Resolution of Discrepancies Between Prediction and Measured in situ Room Closures," SAND88-2948, Sandia National Laboratories, Albuquerque, New Mexico, 1989.

10. Brush, L. H., "Current Estimates of Gas Production Rates, Gas production Potentials, and Expected Chemical Conditions Relevant to Radionuclide Chemistry for the Long-Term WIPP Performance Assessment," Memorandum to D. R. Anderson, Sandia National Laboratories, Albuquerque, New Mexico, July 1991.

11. Rechard, R. P. , "Data Used In Preliminary and Performance Assessment of th Waste Isolation Pilot Plant, 1991,"SAND91-0621 Volume III, Sandia National Laboratories, Albuquerque, New Mexico, In Draft.

12. Brown, W. T. amd J. R. Weatherby, " Influence of Gas Generation Potential and Gas Generation Rate on the Performance of CH-TRU Disposal Rooms," Memorandum to B. M. Butcher and F. T. Mendenhall, 6345, Sandia National Laboratories, Albuquerque, New Mexico, September 1990.

13. Beraun, R., F. T. Mendenhall, and R. P. Rechard, "Compilation of Input Data for Alternatives 2 and 6 of the EATF to be Used During Calculations Efforts to be Performed by Division 1514 in Determining the Mechanical Creep Closure Behavior of Waste Disposal Rooms in Bedded Salt," Memorandum to Distribution, Sandia National Laboratories, Albuquerque, New Mexico, September 6 1991.

Copy to:
1510 J. C. Cummings
1514 H. S. Morgan
1514 J. G. Argüello
1514 C. M. Stone
1514 J. R. Weatherby
6340 W. D. Weart
6340-A A. R. Lappin
6340 S. Y. Pickering (file) 6341 R. C. Lincoln
6342 D. R. Anderson
6342 M. G. Marietta
6342 R. P. Rechard
6343 T. M. Schultheis
6344 E. Gorham
6344 P. B. Davies
6345 B. M. Butcher
6345 R. Beraun (5)
6345 L. H. Brush
6345 F. T. Mendenhall
6345 M. A. Molecke
6346 J. R. Tillerson
6346 D. E. Munson
DOE/WPO V. Daub
DOE/WPO D. C. Blackstone
XXXDRM
J. M. Valdez, IT
M. Abashian, IT

Butcher, September 9, 1992

Date: 9/9/92
To: M. S. Tierney, 6342
From: B. M. Butcher, 6345
Subject: Waste Compaction Properties for the Baseline Closure Surface

Sandia National Laboratories

Albuquerque, New Mexico 87185

date: September 9, 1992

to: M. S. Tierney, 6342

B. M. Butcher

from: B. M. Butcher, 6345

subject: Waste Compaction Properties for the Baseline Closure Surface

This memo is in response to your question about a suitable reference source for the baseline closure mechanical properties. With the exception of the waste compaction properties, the mechanical properties listed in chapter 3 of SAND91-2378[1] are the same as those used to compute the baseline porosity surface. The baseline compaction curve data in this reference are obsolete because they were an estimate prior to acquisition of experimental compaction curves. The data define the "old" SANCHO waste compaction curve in the attached figure.

The compaction curve data for the baseline closure calculations are given in Table 1 (taken from a forthcoming memo by Stone). These data were derived from the solid line axial compaction stress versus porosity curve in Figure 2 of the memo by Beraún and Davies (1991), which represent the average response of a repository. The actual data points for the curve are tabulated in SAND90-1206, Table 3-2. Stone's curve is obtained by dividing each axial stress data value by 3 and converting porosity to the ratio ρ/ρ_0, where ρ is the current density of the waste, and ρ_0 is its initial density. The natural logarithm of the density ratio is the true (finite) volumetric strain.

As a check, Stone's pressure values were multiplied by 3, porosity values were converted to true strain, and the data replotted in the attached figure. Equivalency is demonstrated by superposition of the data on the original axial stress curve. A caution about this construction is that both curves depend on the average initial porosity of the waste, which should be 0.787 (SAND90-1206, p. A-5). This initial porosity value corresponds to an initial average waste density of 426 kg/m^3 and an average theoretical solid density of 2000 kg/m^3 (SAND90-1206, p. A-5). It differs from the value of 0.74 that can be inferred from the initial porosities of the three waste components quoted in Table 1 of Beraún's memorandum. Beraún rounded the initial waste porosities to 0.8 for combustible waste, 0.8 for metallic waste, and 0.5 for sludges, and in the process changed the average porosity for the entire repository from 0.787 to 0.74.

I am also aware that the initial waste porosity used to define the compaction curves is probably not the same as presently being assumed for PA analyses. In comparison to other assumptions that are currently necessary for the inclusion of closure in PA analysis, this difference is presently considered to be insignificant. This assumption should be checked, however, and we should attempt to better coordinate the best value for the initial density of the waste in the future.

---

1. References are given at the end of the memorandum

References

F. T. Mendenhall, B. M. Butcher, and P. B. Davies. 1991. "Investigations into the Coupled Fluid Flow and Mechanical Creep Closure Behavior of Waste Disposal Rooms in Bedded Salt" in "Waste Generated Gas at the Waste Isolation Pilot Plant: Papers presented at the Nuclear Energy Agency Workshop on Gas Generation and Release from Radioactive Waste Repositories." P. B. Davies, L. H. Brush, M. A. Molecke, F. T. Mendenhall, S. W. Webb, Editors. SAND91-2378.

R. Beraún, 6345, and P. B. Davies, 6344, "Baseline Design Input Data Base to be Used During Calculations Effort to be Performed by Division 1514 in Determining the Mechanical Creep closure Behavior of Waste Disposal Rooms in Bedded Salt", Memorandum, September 12, 1991.

B. M. Butcher, T. W. Thompson, R. G. VanBuskirk, and N. C. Patti. 1991. "Mechanical compaction of Waste Isolation Pilot Plant Simulated Waste," Sandia National Laboratories Report SAND90-1206, Albuquerque, NM.

Copy to:
6303 W. D. Weart
6340 SWCF(DRM)
6342 D. R. Anderson
6342 P. Vaughn
6345 R. C. Lincoln
6345 F. T. Mendenhall
6345 B. M. Butcher (day file)

Table 1: Pressure-Volumetric Strain Waste Compaction Data Used in The Volumetric Plasticity Model for the Waste Drums in FY92 Baseline Closure Calculations

Pressure (MPa)	$\ln(\rho/\rho_0)$
0.028	0.032
0.733	0.741
1.133	0.898
1.667	1.029
2.800	1.180
10.17	1.536

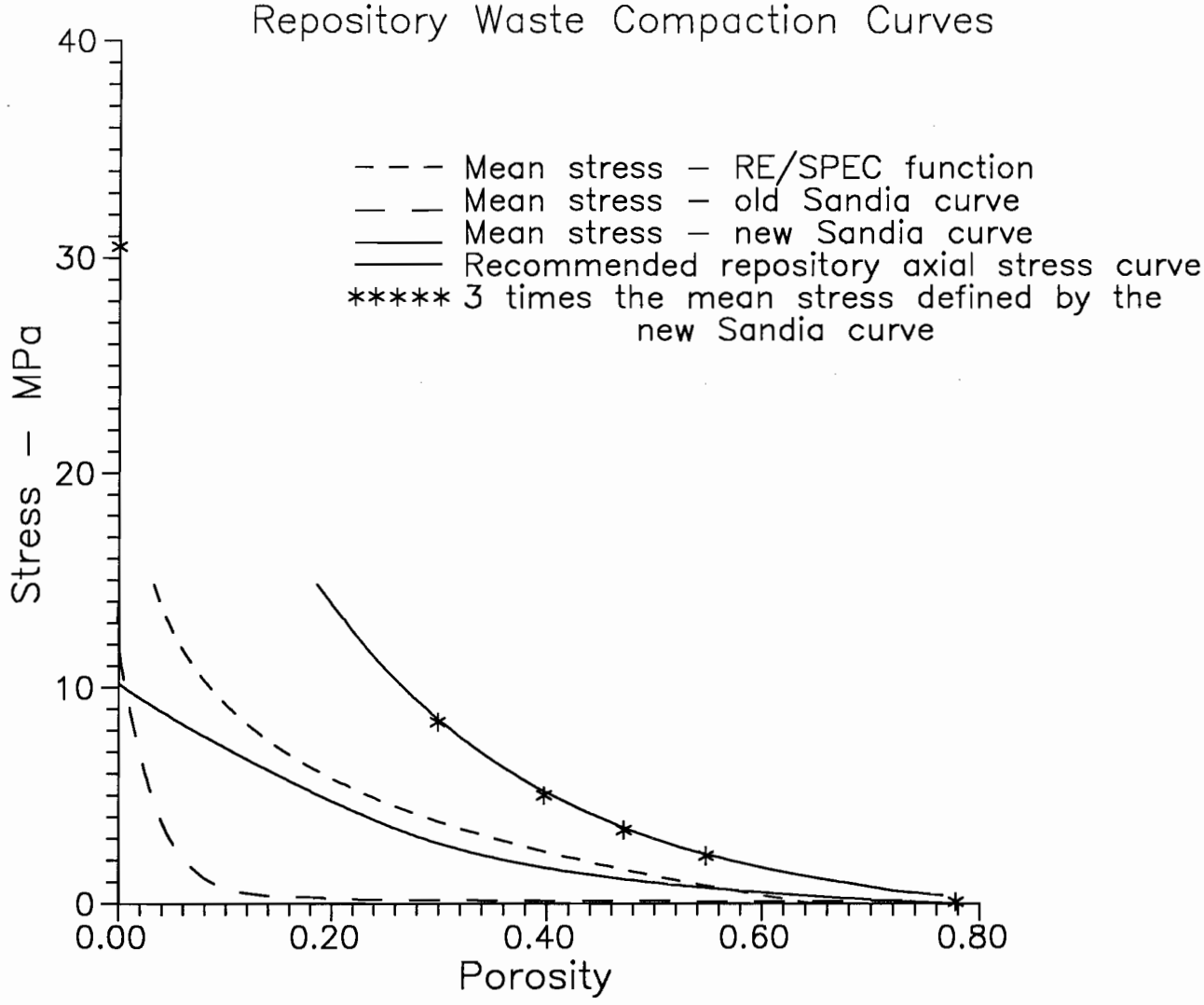

C: graph drm1 wcomp13

Davies et al., July 14, 1992 (1992a)

Date: 7/14/92
To: B. M. Butcher, J. Schreiber, and P. Vaughn (6342)
From: P. B. Davies, S. W. Webb, and E. D. Gorham (6119)
Subject: Feedback on "PA Modeling Using BRAGFLO-1992" 7-8-92 Memo by J. Schreiber

Sandia National Laboratories

Albuquerque, New Mexico 87185

Date: July 14, 1992

To: B.M. Butcher, J. Schreiber, and P. Vaughn (6342)

P.B. Davies Steve E.D. Gorham

From: P.B. Davies, S.W. Webb, E.D. Gorham (6119)

Subject: Feedback on "PA Modeling Using BRAGFLO -- 1992" 7-8-92 memo by J. Schreiber

As a follow-up to our discussions at the June 25th meeting, J. Schreiber's memo (attached) describes the configuration and rationale for repository/Salado modeling using BRAGFLO in the PA 1992 calculations. At B. Butcher's request, we have reviewed these descriptions and the following paragraphs summarize our feedback. You need to be aware that in order to respond in the very short time frame requested, this is only a brief review by those individuals that were available over the past 3 days. Therefore, this review does not cover the level of detail that should ideally be given and this review does not have input from a number of pertinent staff members. We feel that PA's effort to articulate model configuration and rationale and to incorporate feedback prior to starting simulations is a significant step forward in communications. We also feel that working through multiple iterations of this process in the months prior to calculations has the potential to significantly improve the calculations in future years. Our comments on the proposed configuration for this year are as follows:

1. The modified configuration for human intrusion scenarios is based on an "equivalent radial panel" scaled to match the initial excavated volume of a single panel. The Schreiber memo expresses concern that the 60.85 meter radius of this equivalent panel is small compared to the potential travel path distance in an actual panel (218 meters max.). Therefore, it has been suggested that the high permeability (and increased porosity) DRZ above and below the panel be extended outward to a radius of 96.78 meters. The stated rationale for this is 1) "to include some of the effect of the greater travel distances in an actual panel" and 2) to "include the DRZ above and below the pillars". There are two potential problems with this rationale. First, the original reasons for considering travel distance within an actual panel centered around the question of how much *waste* could be "accessed" by brine flow *within a panel* (Lappin et al., 1989; Marietta et al., 1989). Because there is no waste within the DRZ, extending the travel distance within the DRZ does not appear to address questions related to travel path length through waste within an actual panel. Second, the concept of "including the DRZ above and below the pillars" is confusing because other than a relatively short (roughly 1 meter) DRZ that occurs along room walls, this is no DRZ above or below the pillars. One might consider extending the DRZ in order to capture the potential increased gas storage volume if we had good information about the dimensions, porosities, and evolution of the DRZ. However, these

are poorly known and at this point do not provide a reasonable rationale for extending the DRZ. In summary, extension of the DRZ above the pillars has the effect of increasing pore volume in the DRZ to a level that cannot be substantiated by the available data. Therefore, we recommend that DRZ not be extended above the salt pillar.

2. The illustration of the model configuration is somewhat confusing in that it gives the appearance that the anhydrite interbeds start at the lateral edge of the DRZ and transition zones. Perhaps these schematics would benefit by showing how the geologic units fit into the model zones.

3. Why and how are the Culebra and the Unnamed Lower Member of the Rustler lumped in these calculations? The Unnamed Lower Member of the Rustler Formation is a dissolution residue at the contact between the Rustler and Salado. While this unit is a significant water-bearing unit in Nash Draw, it thins considerably and its transmissivities at the WIPP site are orders of magnitude lower than those in the Culebra. We do not see any good reason to lump these two units and suggest that unless there is some compelling reason not stated in the Schreiber memo as to why the Unnamed Member should be included, the Culebra Dolomite should be the only Rustler unit to be modeled explicitly.

4. Where does the 0.675 value for waste porosity (i.e. average disposal room porosity) come from? The initial porosity in the SANCHO closure calculations is 0.66. These calculations provide the basis for the creep closure porosity surface. The maximum porosity in F.T. Mendenhall's GRIDB.DAT porosity surface file is 0.565.

5. The permeability, porosity, and initial pressure are all specified in the document. What about the specific storage parameters? What are the values and what are they based on?

6. We (6119 and 6342) have not yet reached good closure on the question of the far field permeability distribution for the anhydrite interbeds. The original recommendation (model configuration and parameter distributions transmitted to PA 4-1-92 by E.D. Gorham) was to use only permeability values from a limited number of tests (3) in non-depressurized anhydrite. This approach assumed that the PA model for the 1992 calculations would be capable of including increased permeability due to fracture dilatation in response to elevated gas pressures. When it became apparent that fracture-based permeability changes will not be available in the '92 models, it was recommended that an attempt be made to crudely incorporate the effects of gas-driven increases in fracture permeability by specifying a much larger far-field permeability range for the anhydrite that included not only the non-depressurized tests, but also the group of tests in depressurized but substantially intact anhydrite and the group of tests in anhydrite that has experienced substantial fracturing in the DRZ (E.D. Gorham 6-15-92 memo). This approach was considered unrealistically conservative by performance assessment personnel in the June 25th meeting and a compromise was reached that 1) the performance assessment calculations will not attempt any representation of the interbed fracture process in the '92 calculations; 2) that explicit caveats will be placed visibly in the report that this potentially significant process was not included in the calculations; and 3) the field permeability for the anhydrite interbeds will be represented by the small group of tests in non-

depressurized anhydrite interbeds together with the much larger group of tests in depressurized but substantially intact anhydrite. While this compromise appears to be acceptable to most people, it should be recognized that this distribution is not without potential flaws that could perhaps be corrected if there were sufficient time to construct a new distribution that focused on capturing the uncertainty in whether or not some of the tests in the depressurized but substantially intact anhydrite have in fact experienced significant permeability enhancing deformation. Given the present time constraints, we suggest that the compromise distribution be used, but that it be recognized that this distribution is not without potentially important flaws.

7. Where does the DRZ porosity relationship [TZ poros + x(0.06-TZ poros)] come from and what is its purpose? We understand that in general terms, this is intend ed to relate sampled values of DRZ porosity with those from the transition zone, but there is not enough information in the Schreiber memo to fully understand this. Also, if sampled porosities between these zones are being related, shouldn't sampled permeabilities be related as well? At some point in future calculations, serious consideration should also be given to correlation of sampled permeability with sampled porosity.

8. What is the basis for the seal permeability and porosity? Are these values from recommendations from 6121?

9. We are pleased to see that the effects of depressurization of the Salado during the operation phase are being taken into account explicitly and that this appears to be a relatively straightforward task in the current PA model setup.

10. The specification of initial saturation conditions in the waste and especially in the DRZ is a difficult problem. The manual adjustment of saturations in the DRZ could lead to significant problems in correctly calculating brine mobility and gas storage volume within this zone. The approach proposed in the Schreiber memo is to start the DRZ fully brine saturated but at the end of the 20-year depressurization to manually reduce the brine volume to that which would be present prior to any adjustment (increase) of the DRZ porosity. This approach essentially assumes no substantial flow from the far field into the DRZ during the 20-year depressurization period. Given the presently specified range of anhydrite permeabilities, this is probably an unrealistic assumption. Given that this manual adjustment of the DRZ does not have a strong technical basis and that its effect is probably non-conservative (i.e. it produces less brine for gas generation and more open pore volume of gas storage), we recommend that the depressurization be run (which may produce some desaturation itself) with the specified DRZ porosity and permeability at the start of the run and that this manual saturation adjustment not be made. Another possible approach would be to not take credit for any increase in porosity in the DRZ, which we may have difficultly defending over a 10,000 year time frame.

11. The description of the relative permeability and capillary pressure curves looks good. The difficulty mentioned in defining the capillary pressure curve for a material at less than residual brine saturation is easily overcome if a maximum capillary pressure value is specified; this value can then be used if the saturation is below the brine residual

saturation value. Also, the last sentence seems to imply that a region can start out with residual saturation or higher, but the value can become below residual saturation during the calculation. We assume the only way this can happen is in the redefinition of the porosity in the DRZ regions and that it does not happen otherwise.

REFERENCES

Gorham, E.D. (6119). *Additional Suggestion for 1992 PA Calculations.* 6-15-92 Memorandum to B.Butcher and M. Tierney (6342).

Lappin, A.R., R.L. Hunter, D.P. Garber, P.B. Davies. 1989. *Systems Analysis, Long-Term Radionuclide Transport, and Dose Assessments, Waste Isolation Pilot Plant (WIPP), Southeastern New Mexico; March 1989.* SAND89-0462, Sandia National Laboratories, Albuquerque, New Mexico.

Marietta M.G., S.G. Bertram-Howery, D.R. Anderson, K.F. Brinster, R.V. Guzowski, H. Iuzzolino, R.P. Rechard. 1989. *Performance Assessment Methodology Demonstration: Methodology Development for Evaluating Compliance With EPA 40 CFR 191, Subpart B, for the Waste Isolation Pilot Plant.* SAND89-2027, Sandia National Laboratories, Albuquerque, New Mexico.

cc: R.L. Beauheim (6119)
F. Gelbard (6119)
S. Howarth (6119)
L. Jensen (6119)
R.W. Ostensen (6119)
D.R. Anderson (6342)
M.G. Marietta (6342)
W.D. Weart (6303)

ATTACHMENT: COPY OF 7-8-92 SCHREIBER MEMO

PA Modeling Using BRAGFLO -- 1992

J. Schreiber, 7/8/92

Geometry

Human Intrusion Scenarios -- Axisymmetric cylindrical equivalent panel.

The equivalent panel will preserve the initial excavated volume and the initial excavated height of a panel. The panel as modeled will be a cylinder; it will include only the initial excavated volume, and not the pillars, as was done last year. The radius of the cylindrical panel is 60.85 m. The radius used last year is that of an enclosed panel (including pillars), 96.78 m. Since the maximum travel distance in a panel will be less this year owing to the smaller equivalent panel radius, it is desirable to increase the effective radius of the cylinder to simulate more closely the greater travel distances in an actual panel. The distance from the center of an actual panel to a far corner is 138 m, while the greatest travel distance in an actual panel (from panel center to the middle of the end of a panel, going around pillars) is 218 m. To include some of the effect of the greater travel distances in an actual panel, the high-permeability DRZ above and below the cylindrical panel was extended out to last year's radius of 96.78 m, which in effect will include the DRZ above and below the pillars. At the level of the waste, the DRZ does not extend laterally beyond the panel waste; the material beyond the 60.85 m radius of the panel, which can be thought of as the pillars, is treated as intact halite. From the top of Anhydrite a+b to the top of MB138, out to a radius of 96.78 m, is a composite region, the "Transition Zone", which is 9.24 m thick and is assumed to have the same properties as intact anhydrite. The mesh extends vertically from the bottom of the Castile brine reservoir to the top of the Culebra Member of the Rustler Fm, with the Unnamed Member lumped in with the Culebra.

Undisturbed Scenario -- Entire repository, rectangular geometry

The excavated volume of the entire repository is represented by a single rectangular region, and includes no pillars or panel seals. This mesh is essentially the same as the one used in the May 1992 RCRA calculations ("Case 3"). The mesh preserves the initial excavated volume of various regions and their original excavated heights. The panel seals and backfilled drifts between the repository and the Waste Shaft are lumped into a single region of high permeability. The four shafts are consolidated into a single shaft located at a distance from the repository equal to the distance to the actual Waste Shaft. To the north of the shaft is a region that represents the initial excavated volume of the experimental region. This mesh contains the same DRZ's and Transition Zones as the cylindrical panel mesh. These regions extend laterally 1 m beyond the waste to the south and 1 m beyond the experimental region to the north, and includes a 1-m-thick DRZ at the south end of the repository and a 1-m-thick DRZ at the north end of the experimental region. This mesh extends vertically from the top of the Castile Fm to the top of the Culebra Member of the Rustler Fm; the Culebra and Unnamed Members are lumped together. The thickness of the shaft seal will vary from 10 m to 50 m.

Material Properties

The initial porosity of the waste will be fixed at 0.675, as specified by the creep closure surface. Creep closure will be simulated to account for porosity changes over time, until a human intrusion occurs. After that time, the porosity of the waste will remain fixed at the level attained at that time. The halite DRZ immediately above and beneath the panel, as well as MB139 DRZ and Anhydrite a+b DRZ are all assumed to have identical properties. The permeability of this composite DRZ will be fixed at 1.0E-13 m^2. A range of permeabilities from 1.0E-15 to 1.0E-12 m^2 was originally proposed; however, these permeabilities are so high compared with permeabilities of surrounding materials and so close to the final waste permeability of 1.0E-13 m^2 that varying them will have no noticable effect. The Transition Zone properties will be identical to those of intact far-field anhydrite: permeabilities range from 1.0E-21 to 1.0E-15 m^2; porosities range from 0.001 to 0.03. Far-field anhydrite is assumed this year not to fracture; this effect is being ignored because it cannot yet be accurately simulated. Halite permeability will be sampled over a range of 1.0E-25 to 1.0E-22 m^2. Halite porosity will be set equal to the far-field anhydrite porosity, which is sampled, ranging from 0.001 to 0.03. The final porosity of the DRZ will vary, and will depend on the far-field anhydrite porosity: it will be calculated from [TZ poros + x(0.06-TZ poros)], where x ranges from 0 to 1. In the Undisturbed calculations, the seals & backfill, shaft, and experimental regions will have a porosity of 0.075 and a permeability of 1.0E-15 m^2. The DRZ adjacent to these three regions will have a permeability of 1.0E-15 m^2. The shaft seal permeability will vary, ranging from 3.3E-21 to 3.3E-20 m^2. The seal porosity will be 0.075.

Initial and Boundary Conditions

Initial pressure distribution will be calculated over a 20-year period (see Startup Procedure -- BRAGFLO 1992 PA). This 20-year startup calculation establishes the initial pressure distribution in all regions except the waste and DRZ. The pressure distribution at the beginning of the Startup Procedure will be hydrostatic everywhere (except in the waste and in the Culebra) relative to the pore pressure in MB139. A range of MB139 pressure from 12 to 13 MPa will be used. The initial pressure in the waste will be 1 atm (0.101325 MPa); the waste pressure will be reset to this value at the end of the startup. In the Culebra, the starting pressure will be 1.053 MPa, and the far-field pressure will be held at that value over the 10,020-year calculation. (This is the pressure measured in well H-1; it is the same value as used last year.) Note that the Culebra has a fixed-pressure boundary condition, whereas the rest of the mesh uses a no-flow boundary condition. The starting brine saturation will be 1.0 everywhere except in the waste. At the end of the 20-year startup, the waste will be assigned its sampled value of initial brine saturation, which will range from 0.0 to 0.14. The DRZ will start fully brine-saturated, but at the end of the startup time, the brine saturation will be adjusted so that the brine volume is the same after the porosity is adjusted. The porosity will be adjusted at that time from its starting value (volume average based on 0.01 for halite and the sampled value for intact anhydrite) to its final sampled value. Gas will be added to the DRZ to fill in the added porosity. The pressure in the DRZ will be reset to 1 atm at this time. In the undisturbed calculations, the seal & backfill, shaft, shaft seal, and experimental region will be initialized in the same manner as the waste. All of these excavated regions will be set to be fully saturated with gas at 1 atm pressure at the end of startup. In particular, the shaft seal will initially be fully saturated with gas at atmospheric pressure; this is more conservative with regard to RCRA compliance than assuming it is fully saturated with brine, because more gas can flow through.

Relative Permeability & Capillary Pressure

The Brooks-Corey relative permeability model will be used in 2/3 of the calculations and the van Genuchten-Parker model will be used in 1/3 of the calculations. An index parameter (0 or 1) will be sampled with these probabilities, so that either one model or the other will be used in any one calculation. Relative permeability parameters will be varied and will be the same for all materials except the waste, for which a fixed set of values will be used. Residual brine and gas saturations both will range from 0.0 to 0.4. The Brooks-Corey parameter, lambda, will range from 0.2 to 10.0. The van Genuchten-Parker parameter m will be calculated from m = lambda/(1 + lambda). Threshold capillary pressures will be determined from the correlation with permeability in all regions. The van Genuchten-Parker parameter Po will be calculated by equating the capillary pressure from each of the two models at an effective saturation of 0.5, and solving the expression for Po. In the intrusion borehole, the residual gas saturation will be set to zero, which makes the intrusion calculations run much more easily. In the waste, in the DRZ, in the intrusion borehole, and in all excavated regions in the Undisturbed Scenario mesh, the capillary pressure will be zero. This has proved to be necessary because the capillary pressure curves are not defined for imbibition into a medium that has less than residual brine saturation. So any regions where the brine saturation starts out or may become less than residual have to be modeled with zero capillary pressure.

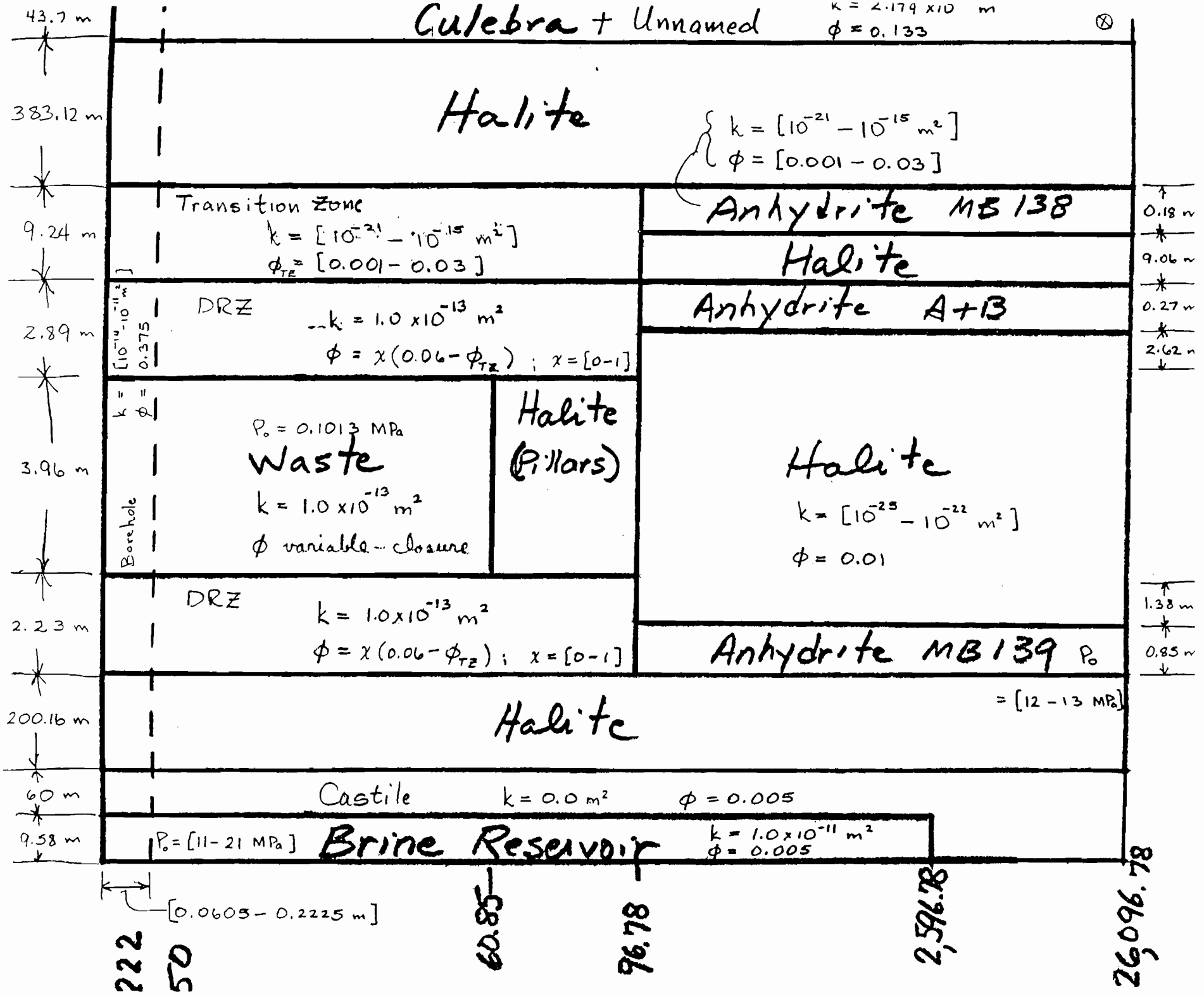
Culebra + Unnamed
k = 2.179 x10 m
φ = 0.133
43.7 m
383.12 m
Halite
k = [10^-21 – 10^-15 m²]
φ = [0.001 – 0.03]
Transition Zone
k = [10^-21 – 10^-15 m²]
φ_TZ = [0.001 – 0.03]
Anhydrite MB 138
0.18 m
9.24 m
Halite
9.06 m
DRZ
k = 1.0 x10^-13 m²
φ = χ(0.06 – φ_TZ) ; χ = [0-1]
[10^-14 – 10^-11 m²]
0.375
Anhydrite A+B
0.27 m
2.89 m
2.62 m
k =
φ =
Borehole
P_o = 0.1013 MPa
Waste
k = 1.0 x10^-13 m²
φ variable – closure
Halite (Pillars)
Halite
k = [10^-25 – 10^-22 m²]
φ = 0.01
3.96 m
DRZ
k = 1.0x10^-13 m²
φ = χ(0.06 – φ_TZ) ; χ = [0-1]
1.38 m
2.23 m
Anhydrite MB139 P_o
0.85 m
= [12 – 13 MPa]
200.16 m
Halite
60 m
Castile
k = 0.0 m²
φ = 0.005
9.58 m
P_o = [11 – 21 MPa]
Brine Reservoir
k = 1.0x10^-11 m²
φ = 0.005
[0.0605 – 0.2225 m]
222
50
60.85
96.78
2,596.78
26,096.78

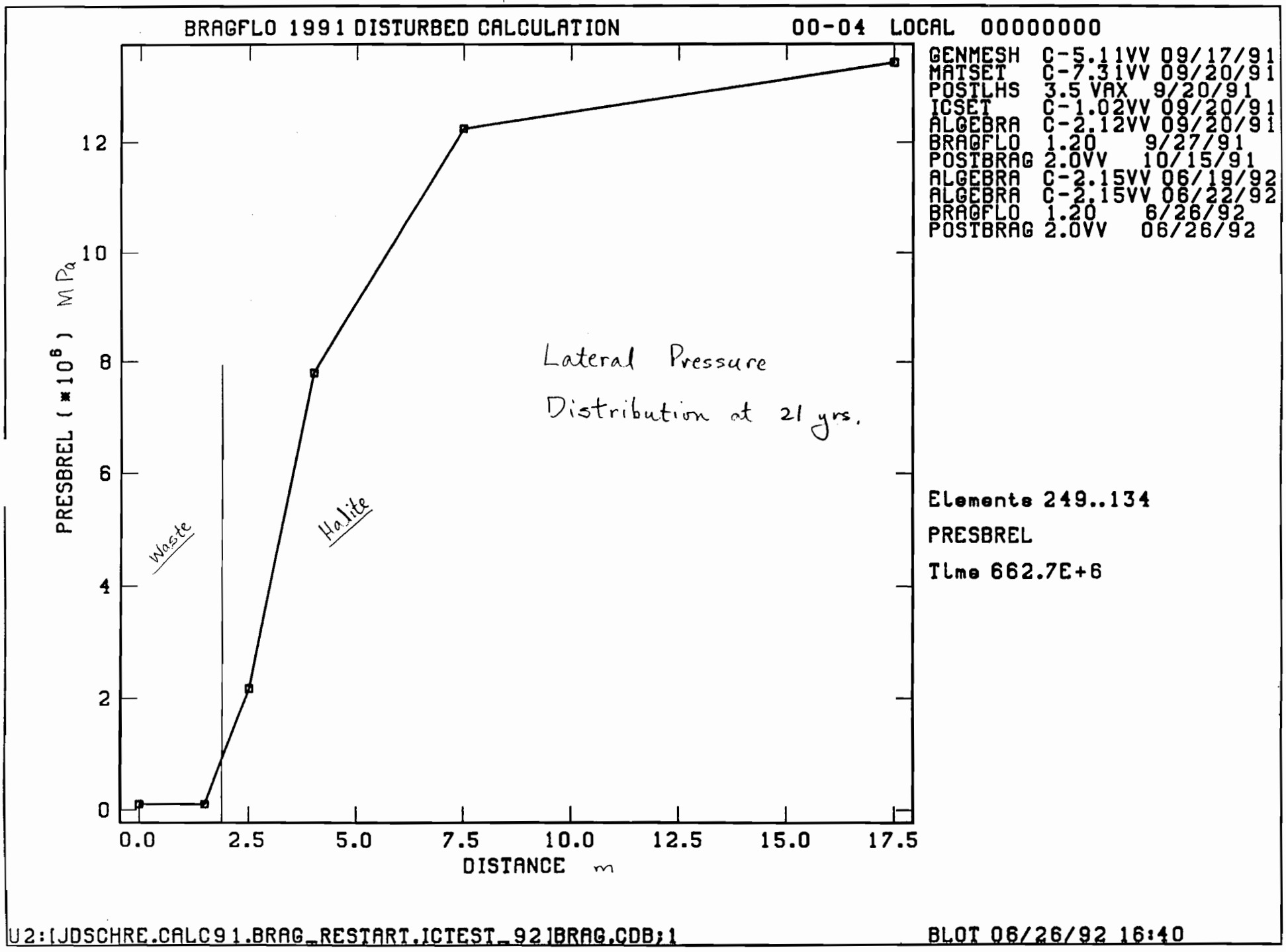
BRAGFLO 1991 DISTURBED CALCULATION
00-04 LOCAL 00000000
GENMESH C-5.11VV 09/17/91
MATSET C-7.31VV 09/20/91
POSTLHS 3.5 VAX 9/20/91
ICSET C-1.02VV 09/20/91
ALGEBRA C-2.12VV 09/20/91
BRAGFLO 1.20 9/27/91
POSTBRAG 2.0VV 10/15/91
ALGEBRA C-2.15VV 06/19/92
ALGEBRA C-2.15VV 06/22/92
BRAGFLO 1.20 6/26/92
POSTBRAG 2.0VV 06/26/92
Lateral Pressure
Distribution at 21 yrs.
PRESBREL (*10^6) MPa
0
2
4
6
8
10
12
Waste
Halite
0.0
2.5
5.0
7.5
10.0
12.5
15.0
17.5
DISTANCE m
Elements 249..134
PRESBREL
Time 662.7E+6
U2:[JDSCHRE.CALC91.BRAG_RESTART.ICTEST_92]BRAG.CDB;1
BLOT 06/26/92 16:40

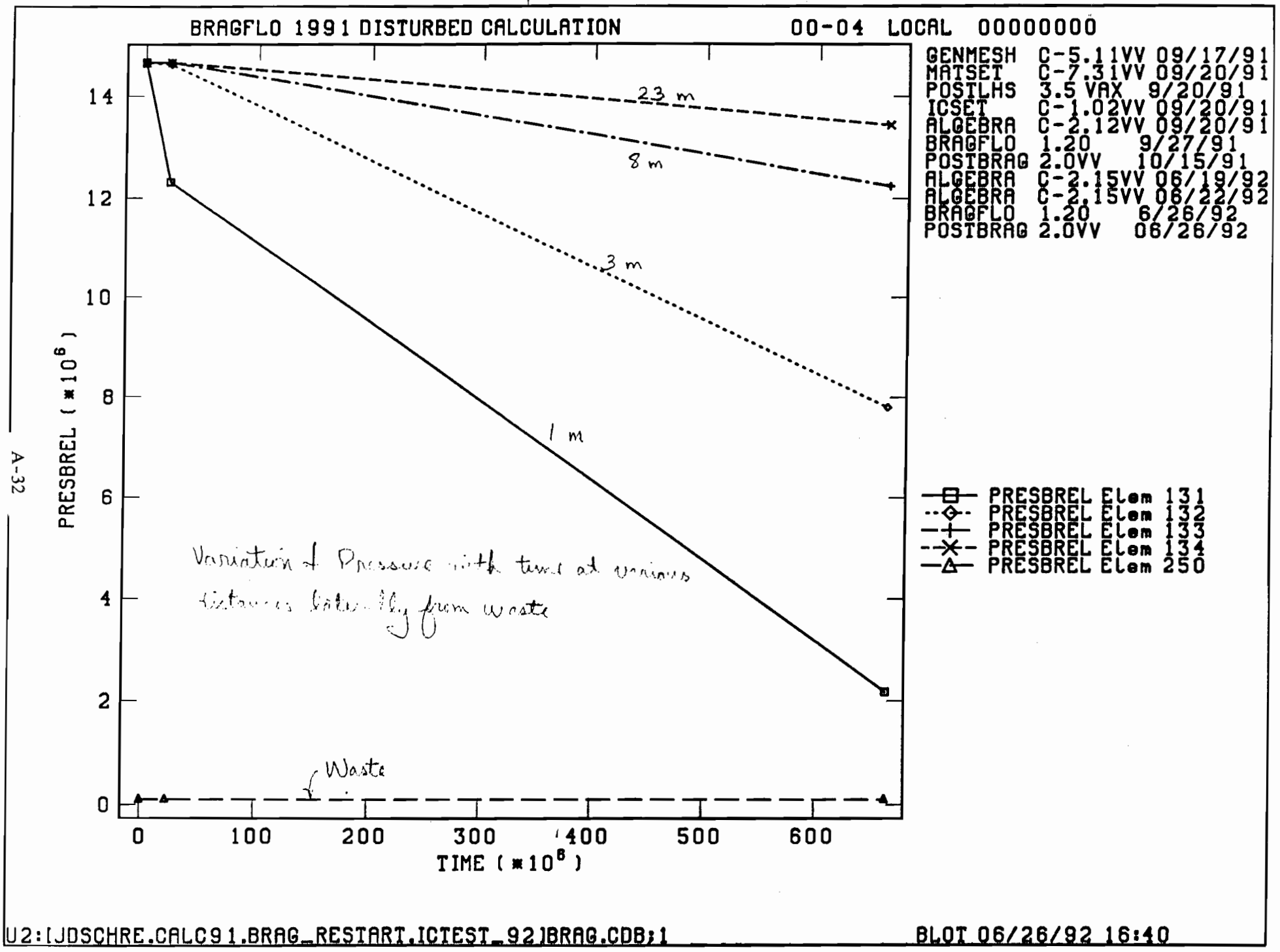
BRAGFLO 1991 DISTURBED CALCULATION
00-04 LOCAL 00000000
GENMESH C-5.11VV 09/17/91
MATSET C-7.31VV 09/20/91
POSTLHS 3.5 VAX 9/20/91
ICSET C-1.02VV 09/20/91
ALGEBRA C-2.12VV 09/20/91
BRAGFLO 1.20 9/27/91
POSTBRAG 2.0VV 10/15/91
ALGEBRA C-2.15VV 06/19/92
ALGEBRA C-2.15VV 06/22/92
BRAGFLO 1.20 6/26/92
POSTBRAG 2.0VV 06/26/92
23 m
8 m
3 m
1 m
Waste
PRESBREL (*10^6)
TIME (*10^6)
0
2
4
6
8
10
12
14
0
100
200
300
400
500
600
PRESBREL Elem 131
PRESBREL Elem 132
PRESBREL Elem 133
PRESBREL Elem 134
PRESBREL Elem 250
Variation of Pressure with time at various distances laterally from waste
U2:[JDSCHRE.CALC91.BRAG_RESTART.ICTEST_92]BRAG.CDB;1
BLOT 06/26/92 16:40

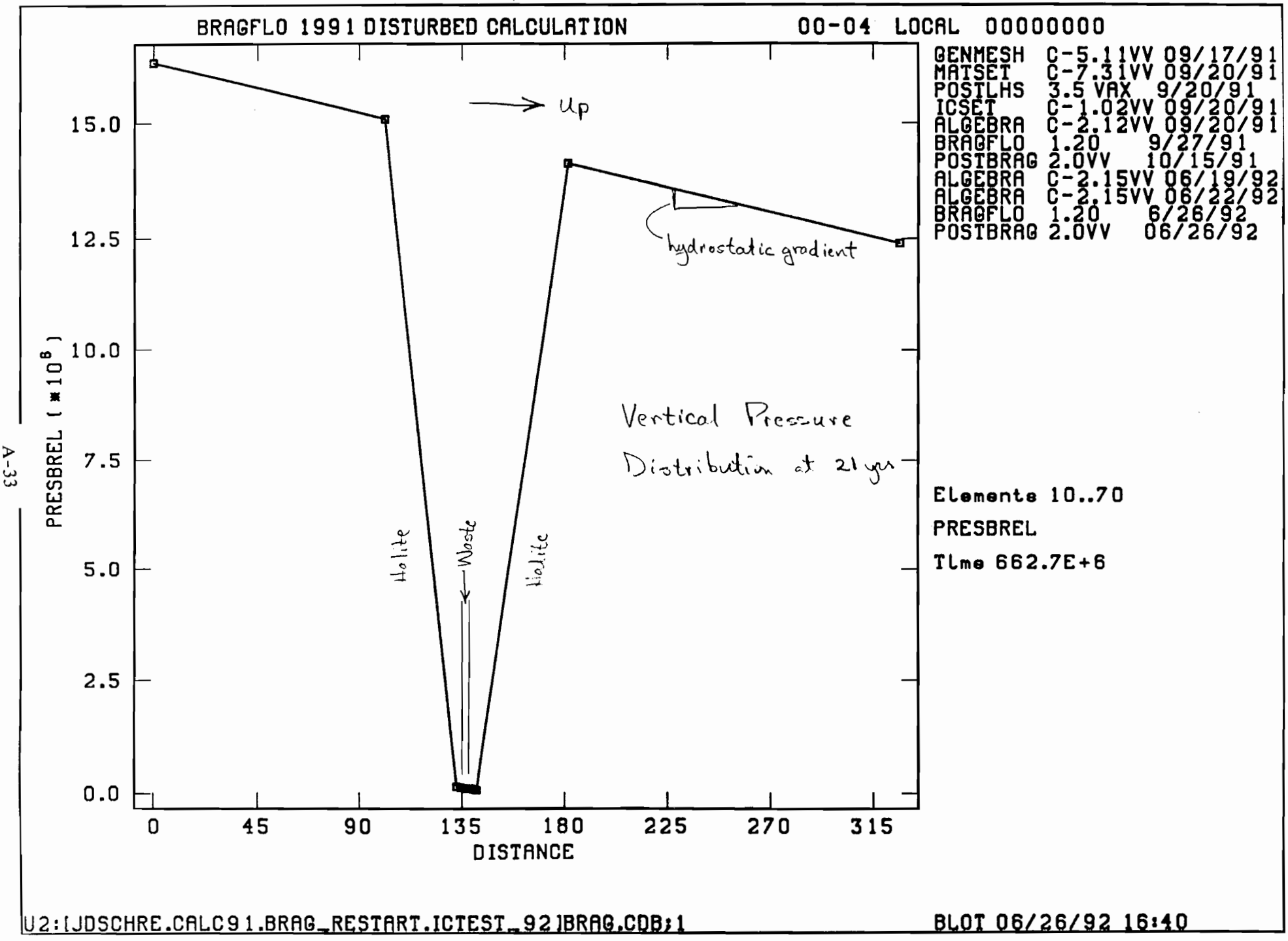
BRAGFLO 1991 DISTURBED CALCULATION
00-04 LOCAL 00000000
GENMESH C-5.11VV 09/17/91
MATSET C-7.31VV 09/20/91
POSTLHS 3.5 VAX 9/20/91
ICSET C-1.02VV 09/20/91
ALGEBRA C-2.12VV 09/20/91
BRAGFLO 1.20 9/27/91
POSTBRAG 2.0VV 10/15/91
ALGEBRA C-2.15VV 06/19/92
ALGEBRA C-2.15VV 06/22/92
BRAGFLO 1.20 6/26/92
POSTBRAG 2.0VV 06/26/92
Up
hydrostatic gradient
Vertical Pressure
Distribution at 21 yrs
Halite
Waste
Halite
PRESBREL (* 10^6)
15.0
12.5
10.0
7.5
5.0
2.5
0.0
0
45
90
135
180
225
270
315
DISTANCE
Elemente 10..70
PRESBREL
Time 662.7E+6
U2:[JDSCHRE.CALC91.BRAG_RESTART.ICTEST_92]BRAG.CDB;1
BLOT 06/26/92 16:40

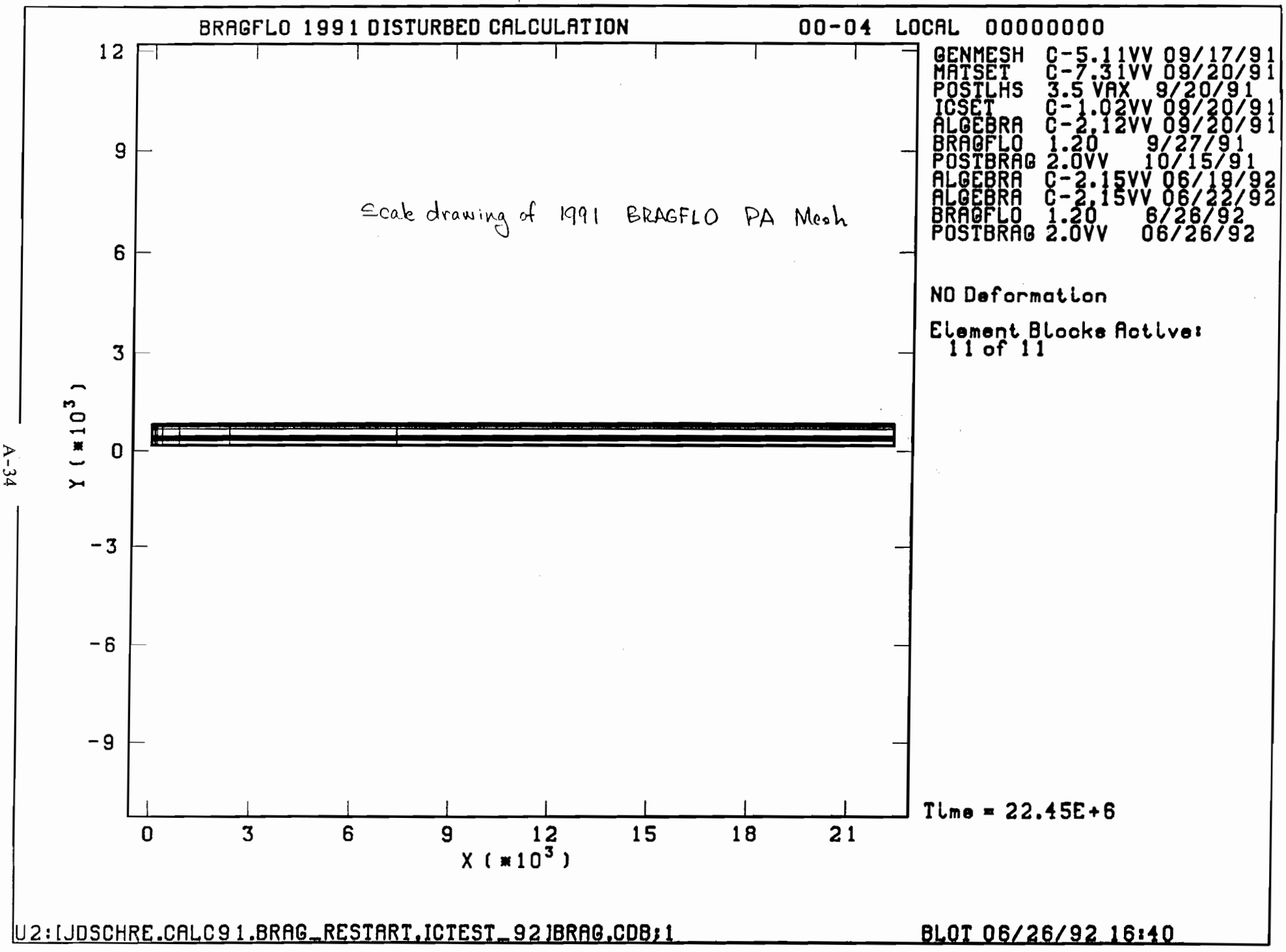
BRAGFLO 1991 DISTURBED CALCULATION
00-04 LOCAL 00000000
Scale drawing of 1991 BRAGFLO PA Mesh
GENMESH C-5.11VV 09/17/91
MATSET C-7.31VV 09/20/91
POSTLHS 3.5 VAX 9/20/91
ICSET C-1.02VV 09/20/91
ALGEBRA C-2.12VV 09/20/91
BRAGFLO 1.20 9/27/91
POSTBRAG 2.0VV 10/15/91
ALGEBRA C-2.15VV 06/19/92
ALGEBRA C-2.15VV 06/22/92
BRAGFLO 1.20 6/26/92
POSTBRAG 2.0VV 06/26/92
NO Deformation
Element Blocks Active:
11 of 11
Time = 22.45E+6
Y (*10^3)
X (*10^3)
12
9
6
3
0
-3
-6
-9
0
3
6
9
12
15
18
21
U2:[JDSCHRE.CALC91.BRAG_RESTART.ICTEST_92]BRAG.CDB;1
PLOT 06/26/92 16:40

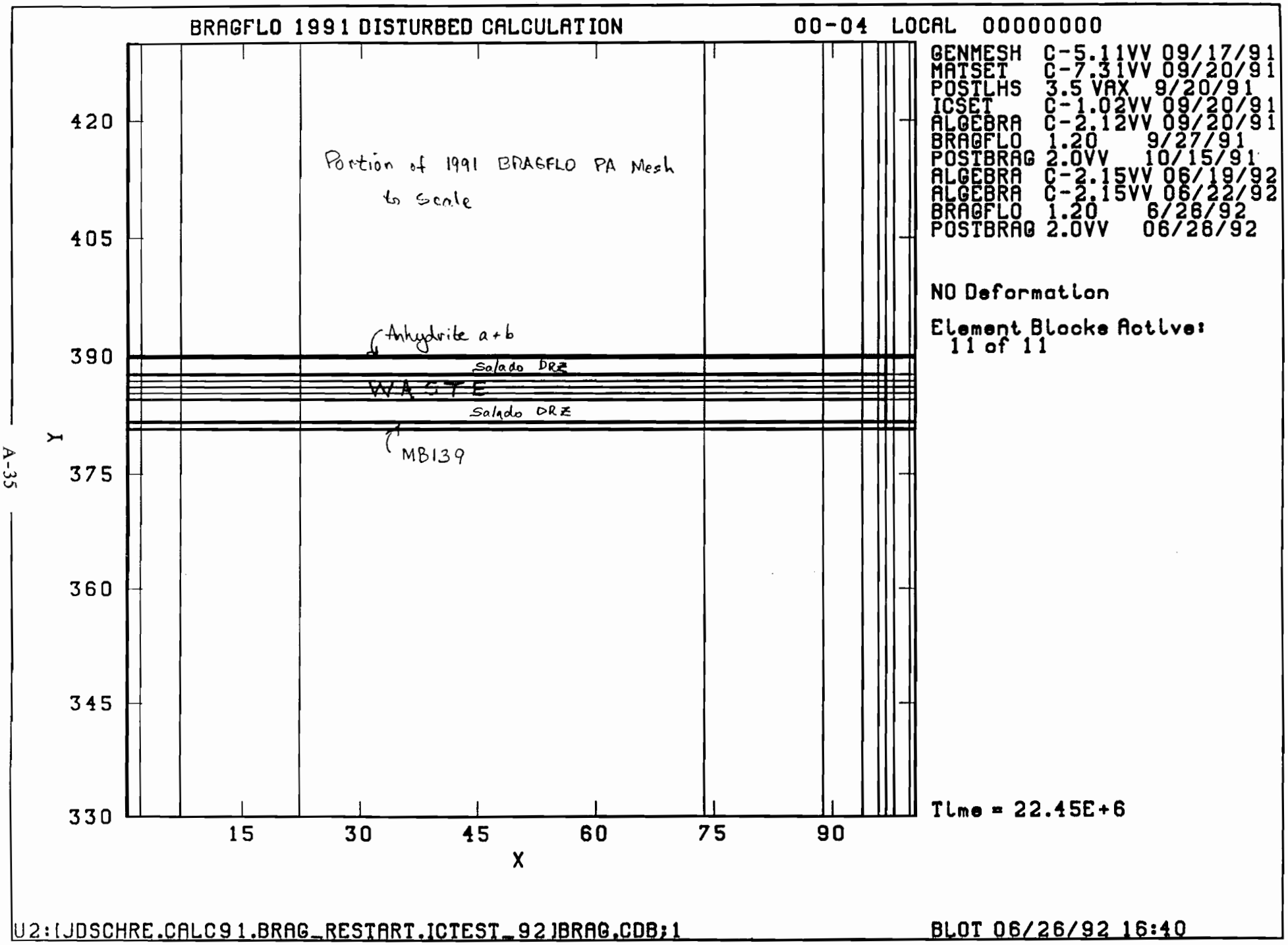
BRAGFLO 1991 DISTURBED CALCULATION
00-04 LOCAL 00000000
GENMESH C-5.11VV 09/17/91
MATSET C-7.31VV 09/20/91
POSTLHS 3.5 VAX 9/20/91
ICSET C-1.02VV 09/20/91
ALGEBRA C-2.12VV 09/20/91
BRAGFLO 1.20 9/27/91
POSTBRAG 2.0VV 10/15/91
ALGEBRA C-2.15VV 06/19/92
ALGEBRA C-2.15VV 06/22/92
BRAGFLO 1.20 6/26/92
POSTBRAG 2.0VV 06/26/92
Portion of 1991 BRAGFLO PA Mesh
to Scale
NO Deformation
Element Blocks Active:
11 of 11
Anhydrite a+b
Salado DRZ
WASTE
Salado DRZ
MB139
Time = 22.45E+6
420
405
390
375
360
345
330
Y
15
30
45
60
75
90
X
U2:[JDSCHRE.CALC91.BRAG_RESTART.ICTEST_92]BRAG.CDB;1
PLOT 06/26/92 16:40

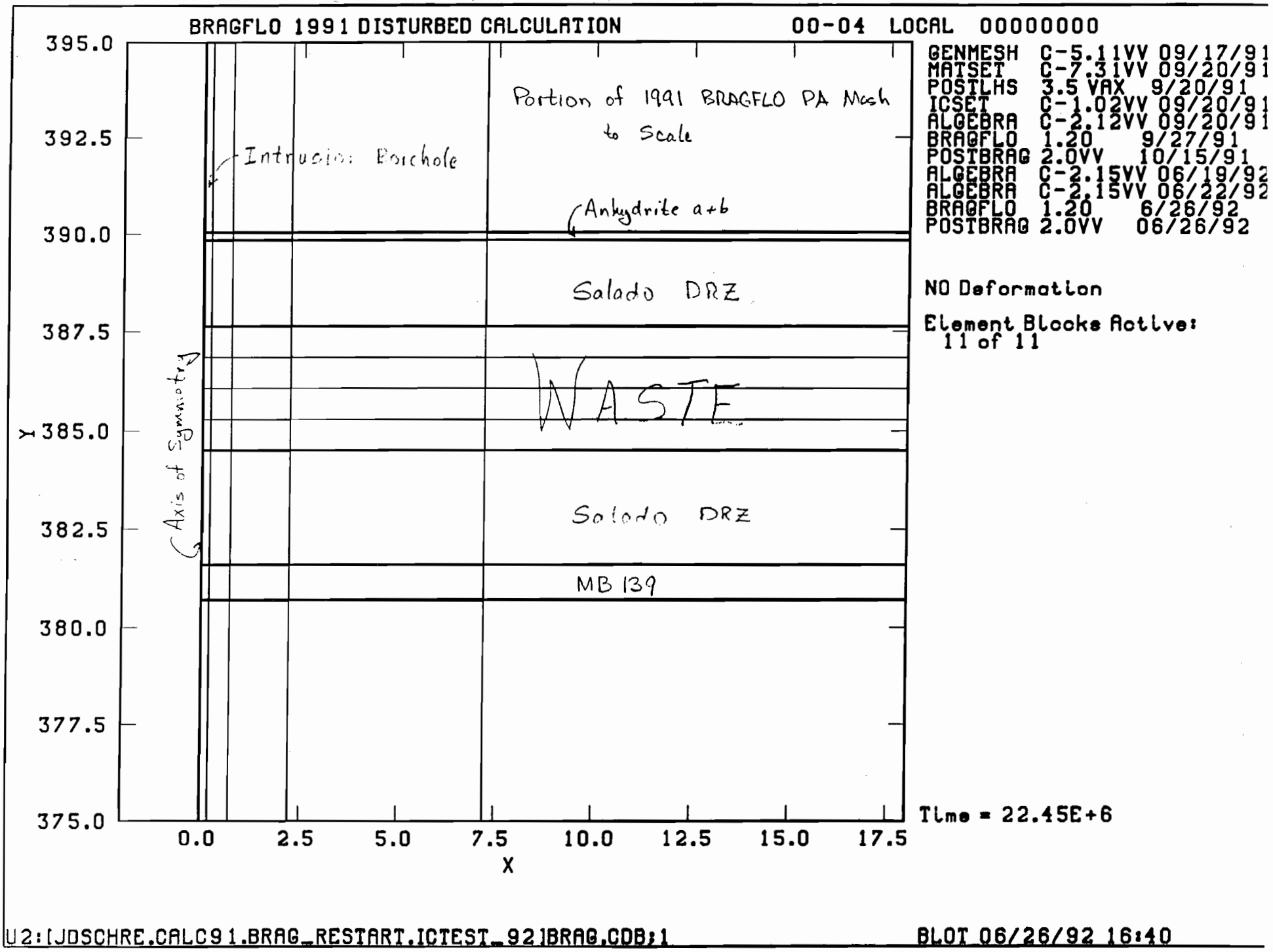
BRAGFLO 1991 DISTURBED CALCULATION
00-04 LOCAL 00000000
GENMESH C-5.11VV 09/17/91
MATSET C-7.31VV 09/20/91
POSTLHS 3.5 VAX 9/20/91
ICSET C-1.02VV 09/20/91
ALGEBRA C-2.12VV 09/20/91
BRAGFLO 1.20 9/27/91
POSTBRAG 2.0VV 10/15/91
ALGEBRA C-2.15VV 06/19/92
ALGEBRA C-2.15VV 06/22/92
BRAGFLO 1.20 6/26/92
POSTBRAG 2.0VV 06/26/92
Portion of 1991 BRAGFLO PA Mesh
to Scale
Intrusion Borehole
Anhydrite a+b
Salado DRZ
WASTE
Salado DRZ
MB 139
Axis of Symmetry
NO Deformation
Element Blocks Active:
11 of 11
Time = 22.45E+6
395.0
392.5
390.0
387.5
385.0
382.5
380.0
377.5
375.0
Y
0.0
2.5
5.0
7.5
10.0
12.5
15.0
17.5
X
U2:[JDSCHRE.CALC91.BRAG_RESTART.ICTEST_92]BRAG.CDB;1
PLOT 06/26/92 16:40

$\log_{10}$ Value	Cum. Prob.
-21.0	0
-20.0	0.05
-19.0	0.55
-18.0	0.70
-17.0	0.75
-16.0	0.80
-15.0	1.00

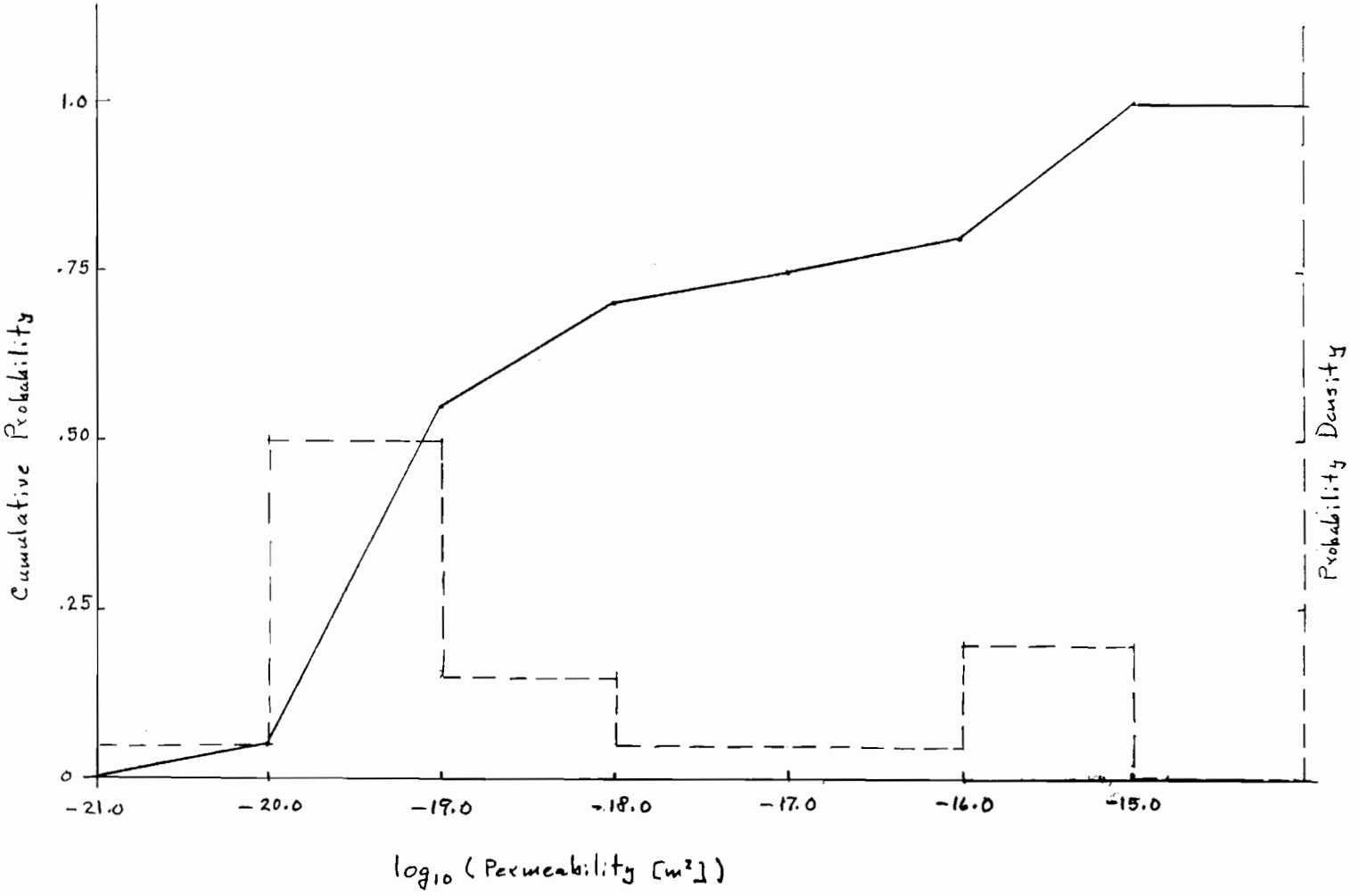

1992 Undisturbed Anhydrite Permeability

Davies et al., July 22, 1992 (1992b)

Date: 7/22/92
To: B. M. Butcher, J. Schreiber, and P. Vaughn (6342)
From: P. B. Davies, R. L. Beauheim, and E. D. Gorham (6119)
Subject: Additional Comments on Far-Field Anhydrite Permeability Distribution in "PA Modeling Using BRAGFLO -- 1992" 7-8-92 Memo by J. Schreiber"

Sandia National Laboratories

Albuquerque, New Mexico 87185

Date: July 22, 1992

To: B.M. Butcher, J. Schreiber, and P. Vaughn (6342)

From: P.B. Davies, R.L. Beauheim, E.D. Gorham (6119)

Subject: Additional Comments on Far-Field Anhydrite Permeability Distribution in "PA Modeling Using BRAGFLO -- 1992" 7-8-92 Memo by J. Schreiber

In response to a telephone conversation with Palmer Vaughn on 7-18-92, we have further reviewed the far-field anhydrite permeability distribution in the 7-8-92 Schreiber memo (Figure 1), the recommended for far-field permeability distribution in the 7-14-92 Davies et al. memo, and the experimental data that was provided with the original parameter recommendations by E.D. Gorham on 4-1-92. The experimental data have been divided into three groups: 1) anhydrite tests indicating little or no depressurization of formation fluid; 2) anhydrite tests indicating moderate depressurization of formation fluid pressure but with substantially intact anhydrite; 3) anhydrite tests with substantial depressurization of formation fluid and with substantial fracture enhancement of permeability (disturbed rock zone). The recommendation for far field anhydrite permeability as discussed at the June 25th Departments 6119/6342 meeting and reiterated in the 7-14-92 Davies et al. memo was to construct the distribution for far-field anhydrite permeability from the data in the first two of these groups (Table 1). This distribution does not encompass permeabilities representative of interbed fracturing due to gas pressurization and this caveat should be clearly stated in PA's discussions of their calculations. While it is possible that some of the permeability tests in the second group may have been slightly impacted by excavation-related deformation, it is still a distinct possibility that they have not. At present we have no objective experimental evidence that any of these tests should be eliminated from consideration.

In the 7-18-92 phone conversation, Palmer expressed PA's concern that this distribution is too high because it results in almost 25 percent of samples of far-field anhydrite permeability that are greater than 10^{-16} m^2 (Figure 1). We have gone back to the original experimental data and constructed a distribution that includes the two data groups recommended above (Figure 2 and Table 2). The distribution in the 7-8-92 Schreiber memo was apparently constructed from some other data set, as its structure is significantly different than the structure of the recommended distribution shown in Figure 2 and Table 2. The recommended distribution in Figure 2 results in no permeabilities greater than 10^{-16} m^2 and in sampling permeabilities between 10^{-18} and 10^{-16} m^2 approximately seven percent of the time.

In summary, we have carefully reviewed the experimental data base for anhydrite permeability and our recommendation for the far-field anhydrite permeability distribution is given in Figure 2 and Table 2. This distribution does not encompass permeabilities representative of interbed fracturing due to gas pressurization.

Table 1. Experimental Data from Permeability Testing of Anhydrite Interbeds

Test	*Unit*	*Permeability (m^2)*	*Pressure (MPa)*
Group 1: No substantial formation fluid depressurization			
SCP01	MB 139	3.0x10-20 m2	12.4
QPP13	pre-mineby MB 139	4.1x10-20 m2	12.5
QPP03	pre mineby anhydrite b	4.4x10-20 m2	12.6
Group 2: Moderate formation fluid depressurization			
C2H02	MB 139	7.8x10-20 m2	9.3
L4P51-B	anhydrite c	5.0x10-20 m2	5.1
S1P71-B	anhydrite c	6.8x10-20 m2	4.9
C2H01-C	MB 139	9.5x10-19 m2	8.0
C1X10	MB 139	5.0x10-17 m2	7.3
QPP03	anhydrite b post mineby	7.9x10-20 m2	7.0
QPP13	MB 139 post mine-by	4.7x10-20 m2	8.1
L4P52-A	anhydrite a	1.0x10-19 m2	6.4
QPB01	MB 139	9.6x10-21 m2	5.0 assumed
QPB02	MB 139	1.6x10-19 m2	5.0 assumed
QPB03	MB 139	1.2x10-20 m2	5.0 assumed

Table 2. Cumulative Probability for Recommended Anhydrite Far-Field Permeability Distribution

LOG10 Value	*Cumulative Probability*
-21	0.00
-20	0.07
-19	0.71
-18	0.93
-17	0.96
-61	1.00

$\log_{10}$ Value	Cum. Prob.
-21.0	0
-20.0	0.05
-19.0	0.55
-18.0	0.70
-17.0	0.75
-16.0	0.80
-15.0	1.00

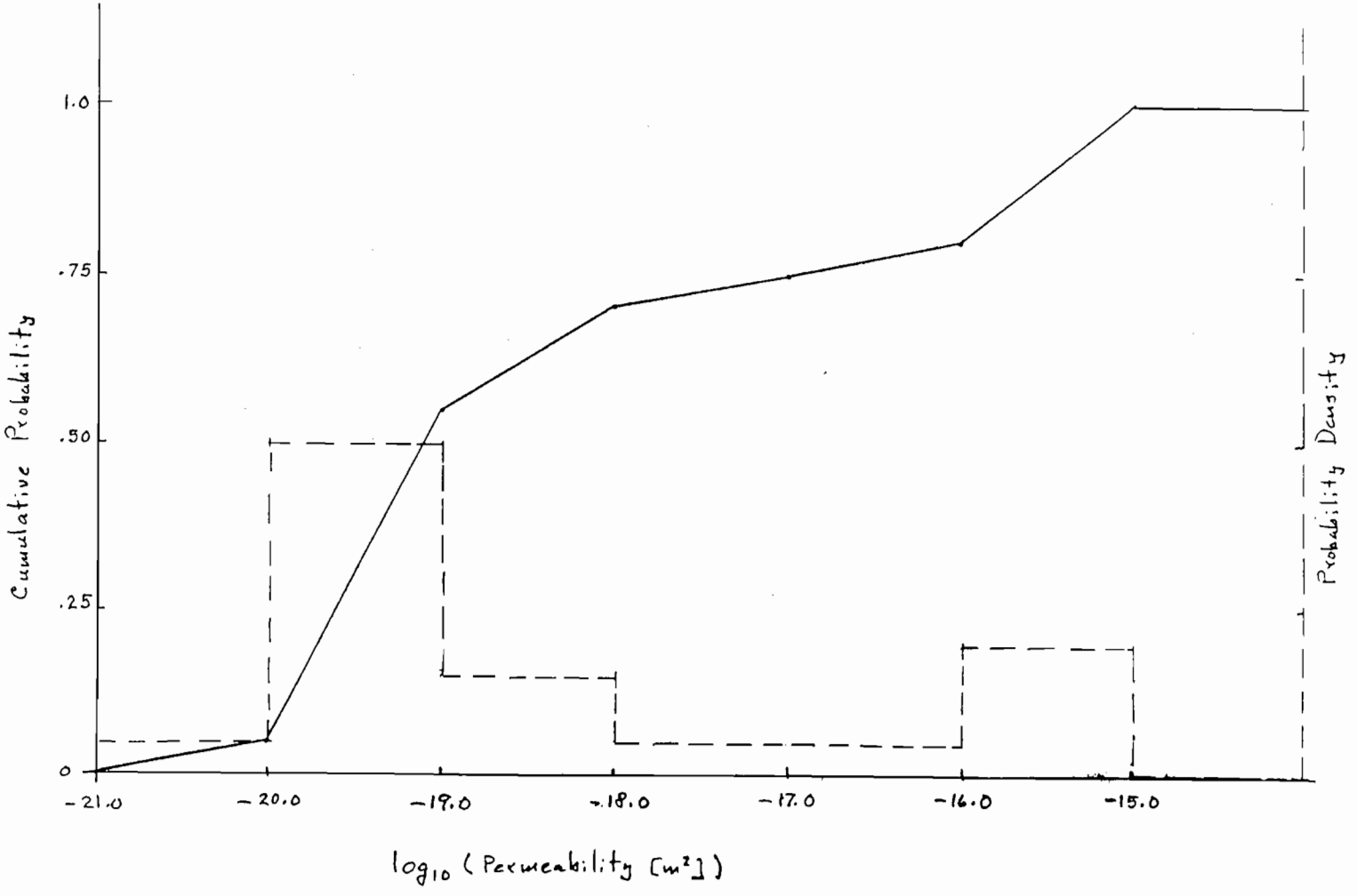

Figure 1. Undisturbed Anhydrite Permeability Distribution from 7-8-92 Schreiber Memo

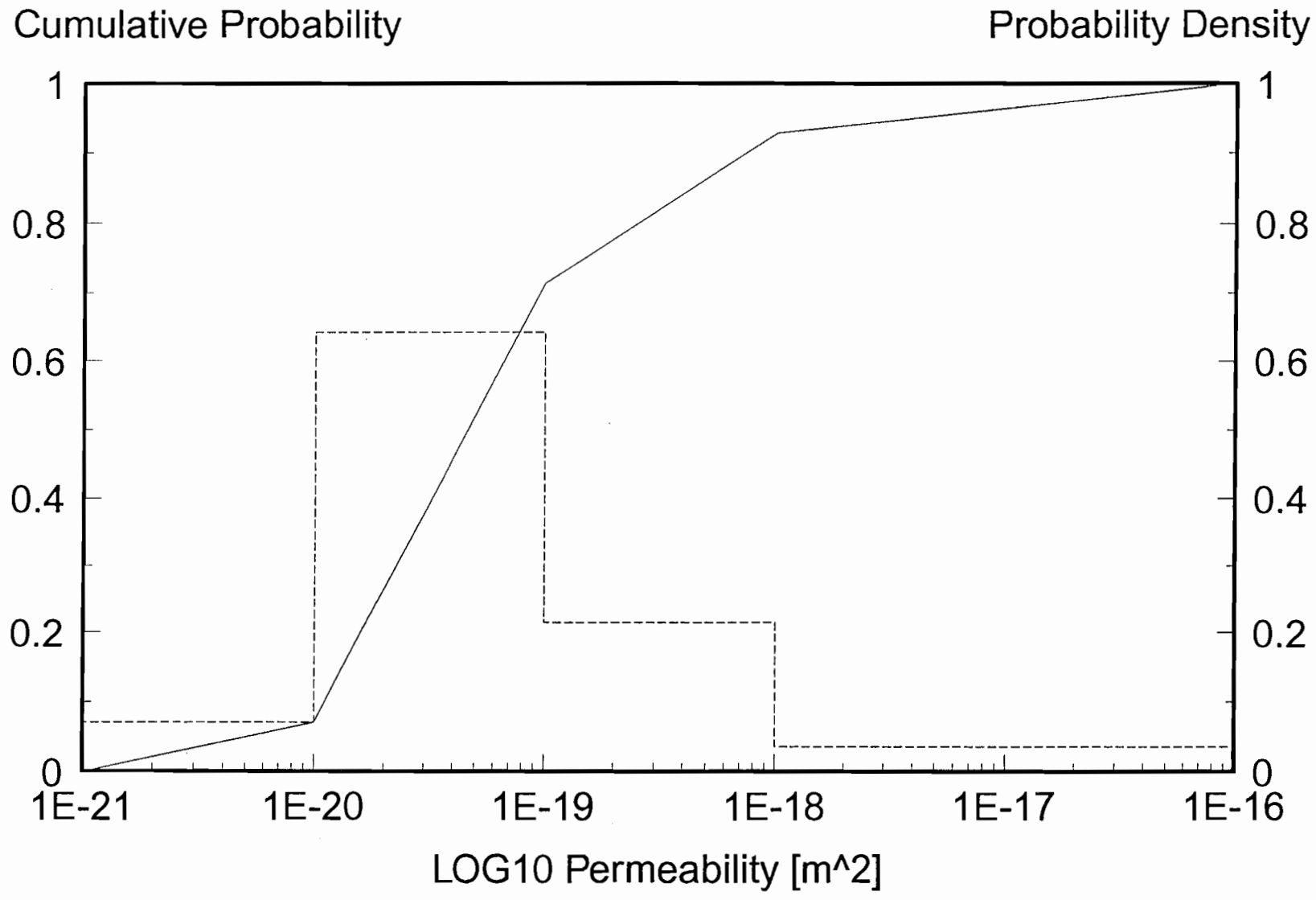

Figure 2. Recommended Undisturbed Anhydrite Permeability Distribution for 1992 PA Calculations

REFERENCES

Davies, P.B., S.W. Webb, and E.D. Gorham, *Feedback on "PA Modeling Using BRAGFLO -- 1992" 7-8-92 memo by J. Schreiber.* 7-14-92 Memorandum to B.M. Butcher, J. Schreiber, and P. Vaughn.

Schreiber, J., *PA Modeling Using BRAGFLO -- 1992.* Memorandum.

cc: F. Gelbard (6119)
S. Howarth (6119)
L. Jensen (6119)
R.W. Ostensen (6119)
S.W. Webb (6119)
D.R. Anderson (6342)
M.G. Marietta (6342)
W.D. Weart (6303)

Gorham et al., June 15, 1992

Date: 6/15/92
To: Martin Tierney, 6342
From: Elaine Gorham, Richard Beauheim, Peter Davies, Susan Howarth, and Steve Webb (6119)
Subject: Recommendations to PA on Salado Formation Intrinsic Permeability and Pore Pressure for 40 CFR 191 Subpart B Calculations

Recommendations to PA on Salado Formation Intrinsic Permeability and Pore Pressure for 40 CFR 191 Subpart B Calculations

June 15, 1992

Elaine Gorham
Richard Beauheim
Peter Davies
Susan Howarth
Stephen Webb

Department 6119

Introduction

In March 1992, the Fluid Flow and Transport Department was asked to recommend Salado Formation permeability and pore pressure probability distributions to be used in the 1992 RCRA calculations for the WIPP. The recommendations were requested and transmitted informally. Eventually a description of the rationale for the recommendations was written by the Fluid Flow and Transport Department and published in Appendix A of (WIPP Performance Assessment Division, 1992A).

Following the RCRA calculations, the Fluid Flow and Transport Department was asked to recommend Salado Formation permeability and pore pressure to be used in the 1992 40 CFR 191 Subpart B compliance calculations. The recommendations transmitted to the PA group in the attached memo by P. D. Davies et al. were based on the, earlier, RCRA recommendations.* The present description is a detailed record of the rationale for the 1992 40 CFR 191 permeability and pore pressure recommendations transmitted in the Davies et al. memo and includes some comments on the adequacy of the current PA models to accurately describe all phenomena present in the formation.

Since input parameters, such as permeability or formation pore pressure, are, for the most part, inferred from complex hydrologic tests, the interpretive model assumptions should be compatible with the predictive or performance assessment model in which the parameters will be used. Thus a suggested excavation geometry and zoning scheme was supplied along with recommended distributions for permeability and pore pressure. The recommended initial geometry is shown in Figure 1 and the distributions suggested for permeability and pore pressure (Table 1 and Figures 2-6) were referenced with respect to those zones.

* Note: The referenced memo is included in this appendix as Davies et al., July 22, 1992.

Our Assumptions

Assumptions about the models to be used in the PA calculations that were essential in formulating the 40 CFR 191 data recommendations were not included in the informal material. Our assumptions were

1. The Salado Formation was described as consisting of layers of either halite or anhydrite. Parts of the Salado Formation described as argillaceous halite were lumped with the halite; clay seams were lumped with the type of lithology in which they occurred. Anhydrites a and b were lumped together.

2. The Salado Formation is isotropic and homogeneous within each layer of halite or anhydrite. The halite and anhydrite have interconnected porosity in pressure equilibrium in the far field. Thus there can be no pre-existing hydraulic pressure differential between stratigraphic layers in the far field Salado Formation.

3. The repository will have been at atmospheric pressure for at least 20 years before final closure. PA will simulate the depressurization in the formation surrounding the repository in a start-up phase which allows brine to flow into a closed repository initially at atmospheric pressure. At the end of the start-up phase, a DRZ will be created; the repository and DRZ pressure will be re-set to atmospheric pressure; the DRZ porosity will be set to a value sampled from a probability distribution; and the brine saturation in the DRZ will be set to preserve the total volume of brine in the DRZ region at the end of the start-up calculation.

4. Excavation closure effects are **not** to be included in the PA model nor is pressurized fracture opening in the anhydrite beds. Pressurized fracture opening in the anhydrite beds may have the potential to significantly increase far-field interbed permeabilities. We were specifically requested by the PA group to **not** include the potential effects of pressurized fracture opening in our recommended permeability distribution for the anhydrite layers, as we suggested in the attached memo from E. Gorham. **Thus we believe the 1992 40 CFR 191 compliance calculations may underestimate lateral gas migration in the interbeds and overestimate repository pressurization.**

5. The nature of the disturbed rock zone (DRZ) is uncertain, reflecting the diversity of technical hypotheses that have been formulated, documented and undocumented. These include the hypothesis that the DRZ is a zone of increased porosity surrounding the excavation, that is stable in extent or increasing in extent with the age of the excavation. Other hypotheses concerning the nature of the DRZ are that the bulk properties of the halite within the DRZ are unchanged, but that within the DRZ fractures form that result in a large increase in permeability with a relatively small increase in porosity or storativity within the DRZ. The size of the DRZ can vary from a few inches into the formation from an excavation surface to a few "room-radii" away from the excavation

surface. It was assumed that all possible descriptions of the DRZ should be included in the probability distributions for permeability and porosity in the DRZ.

6. The DRZ does not reconsolidate during the post-closure calculations due to repository re-pressurization or creep closure of the excavation.

Sources of uncertainty in interpreting data.

The process of inferring permeability from a hydrologic pulse or shut-in test requires that one make an assumption about the diffusivity or specific storage in the formation, about the size of a damaged zone surrounding the test zone, and that the compressibility of the test-zone fluid is constant and can be quantified by a single measurement of fluid withdrawn from the test zone vs test zone pressure drop during withdrawal. A value of specific storage calculated using literature values for halite and and brine compressibilities may not be correct. Recent improvements in the measurement of permeability involve combining a constant-pressure flow test and a shut-in test to directly infer a value of specific storage. However, the improved interpretive technique was used only on permeability tests SCP01, S1P73-B, C1X10, L4P52-A and L4P51-B. For the remaining permeability tests, what is in reality obtained is a value of permeability **given an assumed value of specific storage.** Sensitivity calculations have shown that our inferred permeability values may range over one order of magnitude as our assumed values of specific storage range over three orders of magnitude. (Beauheim et al, 1990; Beauheim et al, 1992) Inasmuch as our assumed values of specific storage do not range over more than three orders of magnitude, we estimate our uncertainty in permeability to be about an order of magnitude.

Other assumptions in analysis of permeability tests include the assumption that gas dissolved in formation brine does not significantly affect the permeability interpretation and that significant amounts of free gas are not present in the formation. In numerous permeability tests, gas was observed to bubble from the formation shortly after the test zone was drilled. A sensitivity analysis is planned for FY93 in which the effect of these phenomena on permeability interpretation will be investigated. For the RCRA recommendations, Rick Beauheim, who has been conducting interpretations of permeability tests, provided the (subjective) input that resulted in an order of magnitude confidence in interpreted permeability values.

Uncertainties in the interpretation of brine-inflow tests are due to (a) scatter in the brine-inflow data and (b) the use of a one-dimensional model which neglects loss of fluid to the surface of the excavation and assumes a uniform pore pressure unaffected by the excavation. In a one-dimensional data analysis by McTigue (1992), it was found that the uncertainties in the inferred values of diffusivity due to data scatter could be substantial.

Uncertainties in inferred values of permeability may be smaller. (See Table 2.) In addition, recent analyses (Gelbard, 1992) indicate that the use of a one-dimensional model may introduce significant errors in the interpretation of diffusivity and permeability from brine-inflow data.

Rationale for Formulating Permeability Distributions

Table 3 represents a current (as of 1/5/92) compilation of interpreted values of permeability and formation pressure from the Permeability Testing Program, the Small-Scale Brine Inflow Program and Room Q. For the 1992 40 CFR 191 Subpart B calculations, interpreted values of permeability in Table 3 were classified according to the regional map shown in Figure 1.

The disturbed rock zone is poorly defined. For these recommendations, test zones were classified as being in the disturbed rock zone if the zone could sustain little or no formation pressure and if the permeability of the zone was clearly higher than expected in competent rock.

The tests for which a reasonable pressure could be sustained in the test zone, but the pressure was not high enough to approach our (subjective) estimate of the far field pressure, were classified as being in a "depressurized" zone. The "depressurized zone" is hypothesized as having experienced some hydraulic depressurization and possibly some elastic stress relief due to the excavation, but probably no irreversible rock damage and large permeability changes. The extent of the depressurized zone may be different in higher permeability layers, such as the Marker Beds, than in lower permeability layers, such as pure halite. It is important to note that the depressurized zone is not a disturbed rock zone; the data from the depressurized zones do not support the hypothesis that the permeability, and the interconnected porosity, are greatly different in the depressurized zones from their far field values.

The latter classifications of test zones are subjective and will be examined in more detail as the Fluid Flow and Transport Department improves interpretation techniques and understanding of the rock matrix.

For the tests in Table 3, other than the Room Q tests, the disturbed rock zone, if in fact it has a clear boundary and if it has a significant extent, was hypothesized to extend about one meter from the excavation into the formation. The boundary of the depressurized zone in the Marker Beds was hypothesized to be approximately 10 meters from the excavation. These hypotheses formed the basis for the geometrical treatment of the excavation suggested in Figure 1. Detailed repository depressurization calculations are planned for FY93.

The PA calculations did not follow the zoning scheme recommended in Figure 1. Only a disturbed rock zone was distinguished from the

far field. Thus it was recommended that the depressurized zone and far field zone tests be combined to form a single permeability distribution.

The probability distributions recommended for the PA calculations were formulated so as to reflect the true range of scientific uncertainty in the parameter values supplied, including uncertainty due to measurement error and uncertainty due to interpretation ambiguities. As mentioned above, an order of magnitude uncertainty in the interpreted value of permeability was used as a rule of thumb for creating recommended probability distributions.

All measurements of permeability were given equal weight, except those values derived from brine inflow measurements in 36" diameter holes in Room D. Those tests were considered flawed and deleted from the list because of the uncertain history of the excavation surrounding the test zone (Finley, 1992).

The hypothesis that permeabilities in the Salado Formation are heterogeneous is given much weight in the Fluid Flow and Transport Department. The use of a single uniform value for all halite and argillaceous halite regions, and a different uniform value for all marker beds implies that the permeability values used in the PA calculations should be "effective" values that are rigorously derived from our measurements. A systematic approach for defining such an "effective" value has not yet been outlined, but will be investigated in FY93. For the 1992 40 CFR 191, Subpart B calculations the values of permeability that were classified as "to low to measure were" represented by effective permeabilities in the range of 10^{-24} to 10^{-22} m^2, since it was judged that even if the halite contained regions of zero permeability, the likelihood was low that the effective permeability of the halite and argillaceous halite regions was zero.

Given the assumptions, difficulties and exceptions outlined above, differential probability distributions were formed by marking the locations along a permeability axis of the results of the tests in Table 3. Excluding the "to low to measure" permeability tests, the number of tests in each $\log_{10}$ interval were used to indicate the relative probability that the true value lay in that interval. Cumulative probability distributions listed in Table 1 can be formulated from the differential probability distributions in Figures 2-6. Test results that were "Too low to measure" are shown in Figure 2 as lying between a true 0 value and 1.0×10^{-24} m^2. Thus, the abscissa of Figure 2 is logarithmic between 10^{-24} and 10^{-21} and linear between 0 and 10^{-24}.

Rationale for Formulating Pore Pressure Distributions

The measurement of test-zone pore pressure is straightforward and is only accomplished in the Permeability Testing Program and the Room Q permeability tests. If, during a pressure build-up test or pulse-withdrawal test, the pressure reaches a steady state

pressure, that pressure is interpreted as the formation pore pressure at the location of the test zone. If a steady-state pressure is not reached before the test is terminated, some technique must be used to extrapolate the formation pore pressure from the shape of the pressure-vs-time curve.

For the tests listed in Table 3, all pressures shown are measured or estimated values of formation pore pressure. The far field formation pore pressures measured in the anhydrite layers yield a fairly consistent measurement of 12.5+-0.1 MPa. It is not understood why the pore pressure measured in the single halite far field test is significantly lower than those reached in the anhydrite far field. Possibilities include: (a) The regions in the halite that have non-zero permeability are not interconnected with higher pressure regions such as the anhydrite layers; (b) the regions in the halite that have non-zero permeability have not reached pressure equilibrium with the anhydrite layers; or (c) pore dilation (and accompanying depressurization) in response to excavation and/or drilling affects halite to a greater distance than anhydrite.

Based on current measurements, it cannot be ruled out that substantial regions of the Salado Formation will be at significantly lower initial pore pressure than the anhydrite layers. Because of potential computational difficulties the PA group did not wish to include this possibility in the 40 CFR 191 calculations. Use of a uniform hydraulic pressure throughout the formation far field allows the PA calculations to be based on the appealingly simple (although perhaps not correct) assumption of homogeneity, hydraulic equilibrium and isotropy in the undisturbed Salado Formation. (The assumption of formation hydraulic equilibrium can be tested using existing models and assumed values of halite and anhydrite permeability. Such a calculation may be performed by Department 6119 in the future.)

Since the effect of excavation on the formation is still poorly understood, from a hydrological viewpoint, it is uncertain that tests believed to be in the far field are indeed in the far field. It was recommended that the far field pore pressure reflect the average of the three far field measurements in the anhydrite, 12.5 MPa, with an uncertainty of 0.5 MPa.

Comments on the Effect of Data Recommendations on 40 CFR 191 Subpart B Compliance Calculations.

An important aspect of the current PA model for the Salado Formation is its inability to simulate pressure-induced fracturing in the anhydrite layers, a phenomenon that has been experimentally demonstrated at the WIPP. The phenomenon may enhance the migration of gas into the formation as the gas pressure in the repository builds up.

Thus it should be recognized that the data from which the permeability and pore pressure recommendations have been derived may not fully support the existing performance assessment models. While it might have been possible to adjust the input parameter distributions to crudely include effects not explicitly modeled, such as including post-fracture permeability in the far field anhydrite permeability distribution to include the phenomena of pressure-induced fracturing, this approach was unacceptable to the performance assessment group. Therefore, it is important to understand that the 1992 performance assessment calculations will not reflect the full range of potential outcomes. In other words, the calculations do not include all known or possible phenomena and outcomes.

References:

Beauheim, R. L., G. J. Saulnier, Jr. and John D. Avis. 1990. **Interpretation of Brine-Permeability Tests of the Salado Formation at the Waste Isolation Pilot Plant Site: First Interim Report.** SAND90-0083. Albuquerque, NM: Sandia National Laboratories.

Beauheim, R. L., T. F. Dale, M. D. Fort, R. M. Roberts and W. A Stensrud. 1992. **Hydraulic Testing of Salado Formation Evaporites at the Waste Isolation Pilot Plant Site: Second Interpretive Report.** SAND92-0533. Albuquerque, NM: Sandia National Laboratories.

Gelbard, F. 1992. **A Two-Dimensional Model for Brine Flow to a Borehole in a Disturbed Rock Zone.** SAND92-1303. Albuquerque, NM: Sandia National Laboratories.

McTigue, D. F. 1992. **Permeability and Hydraulic Diffusivity of WIPP Repository Salt Inferred from Small-Scale Brine Inflow Experiments.** SAND92-1911. Albuquerque, NM: Sandia National Laboratories.

WIPP Performance Assessment Division. 1992A. **Preliminary Comparison with 40 CFR Part 191, Subpart B for the Waste Isolation Pilot Plant, December 1991. SAND91-0893/6. Albuquerque, NM: Sandia National Laboratories.**

Table 1. Recommended Cumulative Probability Distributions for formation permeability (m^2), derived from Figures 2-6.

Halite Far Field and Depressurized Zones: Zones A, B and C

Permeability (m^2)	Cumulative probability
0.0	0.00
1.0×10^{-24}	0.00
1.0×10^{-23}	0.10
1.0×10^{-22}	0.19
1.0×10^{-21}	0.48
1.0×10^{-20}	0.95
1.0×10^{-19}	1.00

Halite Disturbed Zone: Zones D and E

Permeability (m^2)	Cumulative probability
1.0×10^{-18}	0.00
1.0×10^{-13}	1.00

Table 1. (Continued)

Anhydrite Far Field and Depressurized Zones: Zone F, G and H

Permeability (m^2)	Cumulative probability
$1.0x10^{-21}$	0.00
$1.0x10^{-20}$	0.07
$1.0x10^{-19}$	0.71
$1.0x10^{-18}$	0.93
$1.0x10^{-17}$	0.96
$1.0x10^{-16}$	1.00

Anhydrite Disturbed Zone: Zone J

Permeability (m^2)	Cumulative probability
$1.0x10^{-18}$	0.00
$1.0x10^{-17}$	0.12
$1.0x10^{-16}$	0.25
$1.0x10^{-15}$	0.37
$1.0x10^{-14}$	0.75
$1.0x10^{-13}$	0.87
$1.0x10^{-12}$	1.00

Anhydrite Disturbed Zone: Zone I

Permeability (m^2)	Cumulative probability
$1.0x10^{-19}$	0.00
$1.0x10^{-18}$	1.00

Table 2. Parameter Estimates from Borehole Experiments. This from information in Table 5 of an early draft of McTigue, 1992. The difference between the values from the early draft (this table) and the table in McTigue, 1992 is the use of a literature value and a WIPP-specific measured value, respectively, for brine compressibility in the data interpretation.

Borehole #	Rock Type	Permeability @Po=10 MPa (m^2)	Permeability @Po=5 MPa (m^2)	Permeability @Po=01MPa (m^2)	Diffusivity ($m2/sec$)
DBT10	Halite	2.9E-22±.18E-22	5.8E-22±.36E-22	2.9E-21±.18E-21	4.7E-11±.78E-11
DBT11	Halite	1.1E-21±.09E-21	2.3E-21±.18E-21	1.1E-20±.09E-20	3.5E-9±.63E-9
DBT12	Halite	6.4E-22±.72E-22	1.3E-21±.14E-21	6.4E-21±.72E-21	10E-8±.65E-8
DBT13	Halite	1.7E-22±.26E-22	3.4E-22±.32E-22	1.7E-21±..26E-21	5.9E-11±.2.3E-11
DBT14A	Halite	7.8E-22±.2.4E-22	1.6E-21±.48E-21	7.8E-21±.2.4E-21	2.8E-8±4.6E-8
DBT14B	Halite	2.2E-21±.28E-21	4.5E-21±.56E-21	2.2E-21±.28E-21	4.3E-8±3.3E-8
DBT15A	Halite	3.2E-22±.55E-22	6.4E-22±1.1E-22	3.2E-21±.55E-21	1.8E-10±.86E-10
DBT15B	Halite	1.8E-22±.59E-22	3.6E-22±1.1E-22	1.8E-21±.59E-21	1.3E-10±1.2E-10
L4B01	Halite	.67E-22±.43E-22	1.3E-22±.86E-22	.67E-21±.43E-21	5.8E-11±9.1E-11
DBT31A	Halite	9.0E-22±2.4E-22	1.8E-21±.48E-21	9.0E-21±.2.4E-21	1.27E-10±.22E-11
QPB01 *1	Anhydrite	4.8E-21±.3E-21	9.6E-21±.06E-21	4.8E-20±.3E-20	1.1E-8±.34E-8
QPB02 *1	Anhydrite	8.2E-20±.03E-20	1.6E-19±.006E-19	8.2E-19±.03E-19	1.2E-9±.014E-9
QPB03 *1	Anhydrite	4.8E-21±1.5E-21	9.6E-21±.3E-21	4.8E-20±1.5E-20	6.4E-7±18.8E-7*

* The lower limit of these uncertainty bounds should be assumed to be zero.

*1 For all of these borehole tests, the length of the productive unit was assumed to be equal to the average thickness of Marker Bed 139 (3-feet).

Table 3: Compilation of Interpreted Values of Permeability, 1/5/92. Zones are referenced to Figure 1.

Zone	Test	Measured Permeability	Pressure(MPA)
A. **HALITE FAR FIELD**			
	QPP12 pre-mineby		
		6.8×10^{-22} m^2	9.5
	C2HO3	Too low to measure	not measureable
	SCP01 GZ	Too low to measure	not measureable
	QPP05	Too low to measure	not measureable
	QPP02	Too low to measure	not measureable
B. **HALITE DEPRESSURIZED ZONE**			
	S1P72-A-GZ	8.6×10^{-22} m^2	5.1
	QPP21 post mineby		
		1.9×10^{-22} m^2	4.8
	C2H01-B	5.3×10^{-21} m^2	3.1
	C2H01-B-GZ	1.9×10^{-21} m^2	4.1
	L4P51-A	6.1×10^{-21} m^2	2.7
	S0P01	8.3×10^{-21} m^2	4.4
	S1P71-A	6.1×10^{-20} m^2	2.9
	QPP15	2.2×10^{-21} m^2	3.1
	DBT10	5.8×10^{-22} m^2	5.0 assumed
	DBT11	2.3×10^{-21} m^2	5.0 assumed
	DBT12	1.3×10^{-21} m^2	5.0 assumed
	DBT13	3.4×10^{-22} m^2	5.0 assumed
	DBT14A/B	3.1×10^{-21} m^2	5.0 assumed
	DBT15A/B	5.0×10^{-22} m^2	5.0 assumed
	L4B01	1.3×10^{-22} m^2	5.0 assumed
	DBT31A	not used	
	QPP12	4.4×10^{-22} m^2	9.4
C. **HALITE DEPRESSURED ZONE**			
Same as region B for permeability.			
D. **HALITE DISTURBED ROCK ZONE**			
	C2H01-A	2.7×10^{-18} m^2	0.5
	C2H01-A-GZ	unmeasureable	0.0
	S1P73-B-GZ	unmeasureable	2.5
E. **HALITE DISTURBED ROCK ZONE**			
Same as region D for permeability.			

Table 3. (Continued)

F. **ANHYDRITE FAR FIELD** (greater than 10 m from excavation)

SCP01 MB 139	3.0×10^{-20} m^2	12.4
QPP13 pre-mineby MB 139	4.1×10^{-20} m^2	12.5
QPP03 pre mineby clay b	4.4×10^{-20} m^2	12.6

G. **ANHYDRITE DEPRESSURIZED ZONE** (less than 10 meters from excavation)

C2H02 MB 139	7.8×10^{-20} m^2	9.3
L4P51-B anhydrite c	5.0×10^{-20} m^2	5.1
S1P71-B anhydrite c	6.8×10^{-20} m^2	4.9
C2H01-C MB 139	9.5×10^{-19} m^2	8.0
C1X10 MB 139	5.0×10^{-17} m^2	7.3
QPP03 anhydrite b post mineby	7.9×10^{-20} m^2	7.0
QPP13 MB 139 post mine-by	4.7×10^{-20} m^2	8.1
L4P52-A anhydrite a	1.0×10^{-19} m^2	6.4
QPB01	9.6×10^{-21} m^2	5.0 assumed
QPB02	1.6×10^{-19} m^2	5.0 assumed
QPB03	$1.2 \times 10^{--20}$ m^2	5.0 assumed
S1P72	unmeasureable	1.2

H. **ANHYDRITE DEPRESSURIZED ZONE**

Same permeability as region G.

I. **ANHYDRITE DISTURBED ROCK ZONE (138)**

S1P73-B MB 138	2.9×10^{-19} m^2	4.5

J. **ANHYDRITE DISTURBED ROCK ZONE**

SOP01 GZ	5.7×10^{-18} m^2	0.5
S1P73-A	too high to measure; estimated at 10^{-15} m^2	0.0
S1P73-A-GZ	too high to measure; estimated at 10^{-15} m^2	0.0
S1P71-A-GZ	too high to measure; estimated at 10^{-14} m^2	0.0
L4P51-A-GZ	too high to measure; estimated at 10^{-15} m^2	0.3
Crawley	1.6 to 3.2 $\times 10^{-13}$ m^2	???

YET TO BE INTERPRETED

QPP01
QPP04
QPP11
QPP14
QPP22
QPP23
QPP24
QPP25

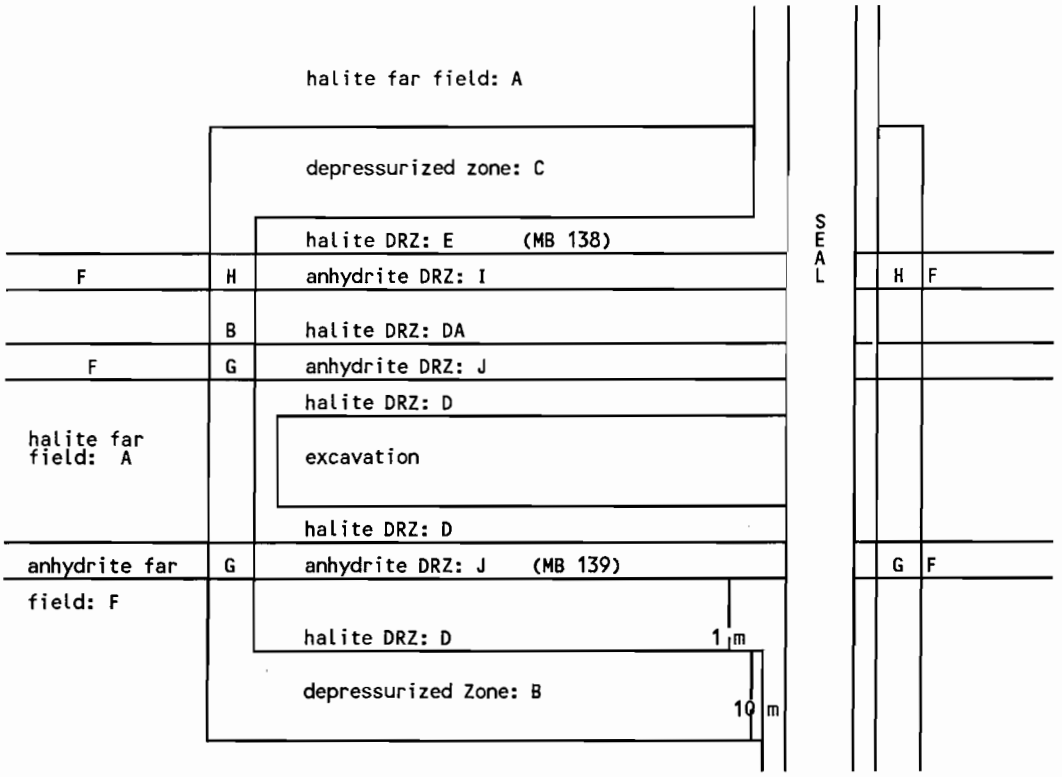

Figure 1: Schematic for assigning flow properties to Salado Formation (Not to Scale!!!!)

Halite Far Field and Halite Depressurized Zone: Zones A, B and C

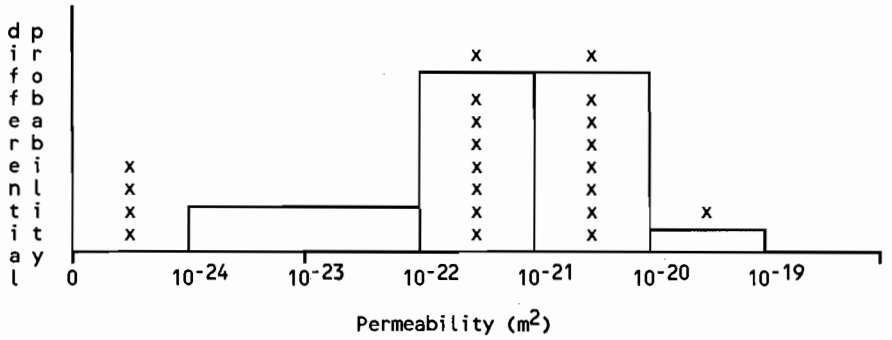

Figure 2.

Halite Disturbed Zone: Zones D and E

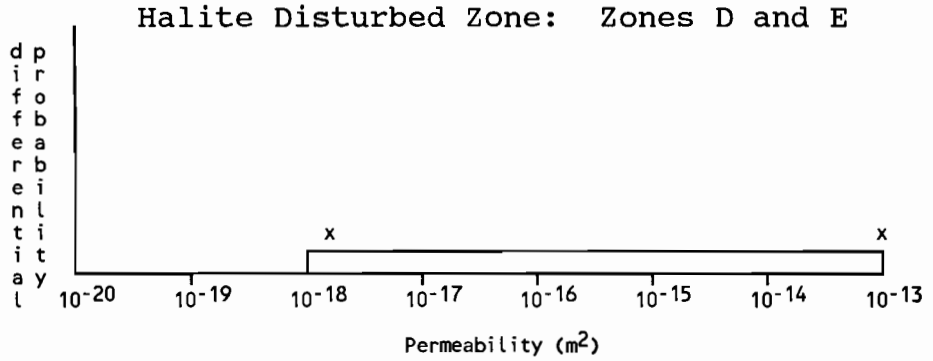

Figure 3.

Anhydrite Far Field and Anhydrite Depressurized Zone: Zones F, G and H

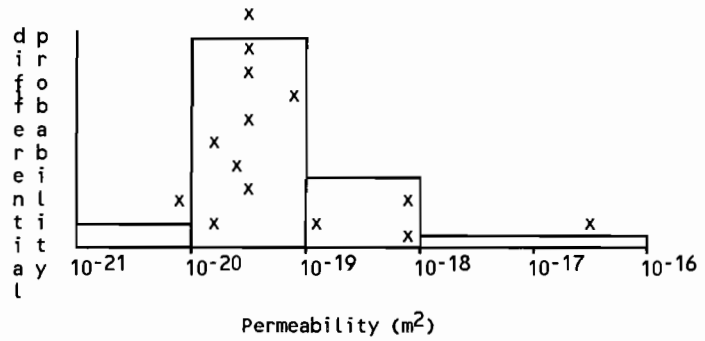

Figure 4.

Anhydrite Disturbed Zone: Zone J

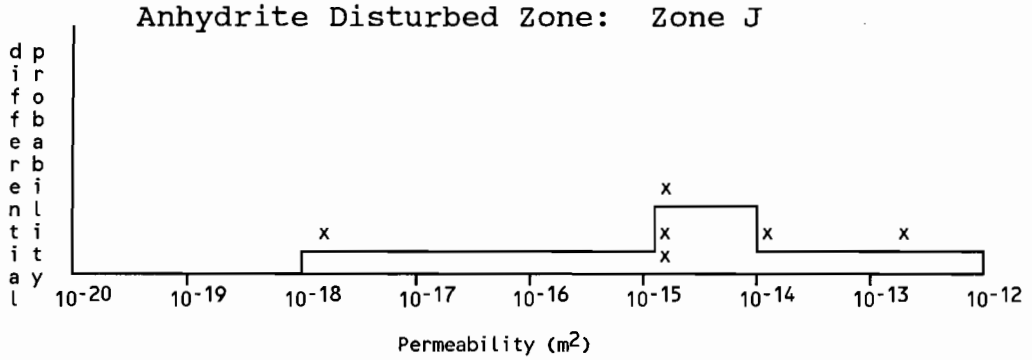

Figure 5.

Anhydrite Disturbed Zone: Zone I

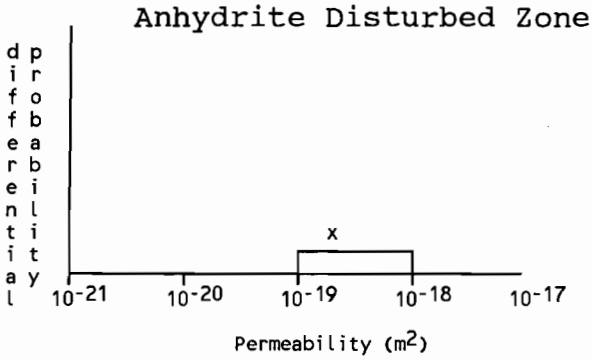

Figure 6.

Sandia National Laboratories

Albuquerque, New Mexico 87185

date: June 15, 1992

to: Barry Butcher and Martin Tierney, 6342

Elaine Gorham

from: Elaine Gorham, 6119, 4-1401

subject: Additional suggestion for 1992 PA calculations

This memo is to request a change in the parameterization of the Salado flow models for the 1992 40 CFR 191 calculations from those parameters used in the 40 CFR 268 calculations. As you have probably already heard, when we negotiated in April about probability distributions for formation parameters, we had somewhat of a misunderstanding with respect to including effects of fracture opening due to pressurization in the anhydrite layers. I (incorrectly) assumed that PA had an explicit module that would allow permeability in the anhydrite layers to increase with hydraulic pressure (to simulate fracture opening). Thus Rick and I suggested values of permeability for the far field anhydrite which were representative of unfractured anhydrite. We can discuss the implications of these assumptions on the 40 CFR 268 calculations during our June 25 meeting.

In the meantime, I'd like to suggest changes in the assumed values for far field anhydrite that would be somewhat more representative of conditions associated with pressure-generated fracturing in the anhydrite for the 1992 40 CFR 191 calculations. In particular, we (Peter Davies and myself, since Rick is on foreign travel) recommend that permeability probability distributions previously supplied for the far field anhydrite (Region F), the depressurized anhydrite (Regions G and H) and the DRZ anhydrite (Region J) be combined with equal weight to form a single probability distribution for all the anhydrite (far field, depressurized zone and DRZ). In addition, we recommend that the porosity used for our previously defined anhydrite and halite far field and depressurized zones be represented by the previously recommended far field porosity. The reason for the latter recommendation is our judgement that large increases in permeability due to fractures opening do not imply the large increases in porosity assumed for the anhydrite DRZ. This latter change is important because overestimation of Salado porosity will result in calculations that underestimate room pressure and/or lateral gas migration.

Including the DRZ permeability distribution in the distribution for the entire anhydrite, as we recommend for the 40 CFR 191 calculations, will cause about 4% of the calculations to be conducted with very high permeability values in the anhydrite

(between 10^{-14} and 10^{-12} m^2). These values correspond to our current estimates of the high end of values expected after fracturing due to overpressure. By using these values for the entire calculations you will overestimate initial brine inflow rates and gas generation rates. However, because increased gas pressure will reverse the brine inflow and gas generation, it is unclear if total gas generated will be unrealistically large. The calculation therefore has the potential to calculate reasonable values for bounding estimates of gas migration distance in the absence of fingering. Given that we are trying to simulate a missing phenomena by changing an input parameter distribution, this may be the best that can be done on short notice. A major factor in our approach to this problem has been to assure that the range of outcomes of the PA calculations provide a good representation of the true uncertainty in our understanding of the repository behavior, at least with respect to permeability and porosity values for the Salado formation. We can discuss this approach when we meet on June 25.

I would like to emphasize the importance of implementing a pressurized fracture-opening model in your codes in future years.

In the meantime, if you have any questions about these recommendations or wish to further clarify them please call either Peter or myself.

Copies:

6303 W. D. Weart
6119 R. L. Beauheim
6119 P. B. Davies
6119 S. Howarth
6117 W. R. Wawersik

Hora, August 25, 1992

Date: 8/25/92
To: Kate Trauth, Jon Helton, Mel Marietta, Martin Tierney, Bob Guzowski, Rip Anderson
From: Steve Hora
Subject: Probabilities of Human Intrusion into the WIPP, Methodology for the 1992 Preliminary Comparison

PROBABILITIES OF HUMAN INTRUSION INTO THE WIPP METHODOLOGY FOR THE 1992 PRELIMINARY COMPARISON

August 25, 1992

Prepared by
Stephen C. Hora
For
Division 6342
Sandia National Laboratories

During 1990-1992, external experts were assembled by Sandia National Laboratories to study potential inadvertent human intrusion into the Waste Isolation Pilot Plant (WIPP). These experts formed two groups -- one group studied what future societies might be like and how they might inadvertently intrude into nuclear waste. The second group, after considering the findings of the first group, studied how markers might be used to warn future societies about the presence and danger of the buried waste. Both groups provided probabilities and probability distributions for critical aspects of the human intrusion problem. This report discusses the use of these assessments in the 1992 preliminary performance assessment.

The Futures Group

The first group of experts was divided into four teams. Each team was composed of four experts from various fields of social and physical science. Each team was asked to address the same set of questions (see Hora, von Winterfeldt, and Trauth, 1992). The results of their work suggests that future societies may undertake activities that could lead to inadvertent intrusion into the WIPP. These teams judged that a number of factors (e.g. the level of technology, demand for resources, population level, the ability to retain knowledge about nuclear waste, etc.) would influence the likelihood of inadvertent intrusions.

The results of the futures teams provide a basis for developing probability distributions for inadvertent intrusion attempts into the WIPP. Because the teams used different structures for analysis and considered different factors that would influence the likelihood of inadvertent intrusion, the results of their endeavors must be individually interpreted in order to be used in the preliminary performance assessment.

The Markers Group

A second group of thirteen experts was organized into two teams to study markers for the WIPP site. These markers are to serve as warnings to future societies about the presence of nuclear waste. Such warnings, hopefully, will deter inadvertent intrusions. Each team was asked to consider the findings of the futures teams, to suggest design characteristics for a marker system, and to assess the efficacy of such a system of markers. The ability of a marker system to deter intrusions rests on the survival of the marker

system over an extended period of time, and the ability of potential intruders to detect the markers and to understand the messages that they carry.

The markers team members where asked to provide probabilities for several events. The first of these is the event that a marker and its message(s) remain intact at various times in the future. Second, for several types of intrusion, the team members were asked to provide probabilities that, given the marker and its messages are intact, the potential intruders are able to understand the message and thus become forewarned of the inherent dangers of intrusion. These assessments were made under various assumptions about the state of technology in the future.

The Standard (40 CFR 191)

The US EPA regulation (40 CFR 191), issued in 1985 and remanded in 1987, provides the rationale for performance assessment for the WIPP. Although the standard has been remanded and awaits reissue, in agreement with the State of New Mexico, the preliminary performance assessments continue to be executed as though the 1985 standard was still in place. The 1985 version of the standard provides some guidance about human intrusion. In appendix B of the standard, the frequency and severity of human intrusion is discussed:

> *The Agency believes that the most productive consideration of inadvertent intrusion concerns those realistic possibilities that may be usefully mitigated by repository design, site selection or use of passive controls (although passive institutional controls should not be assumed to completely rule out the possibility of intrusion). Therefore, inadvertent and intermittent intrusion by exploratory drilling for resources (other than any provided by the waste disposal system itself) can be the most severe intrusion scenario assumed by the implementing agencies.*
>
> *However, the Agency assumes that the likelihood of such inadvertent and intermittent drilling need not be taken to be greater than 30 boreholes per square kilometer of repository area per 10,000 years for geologic repositories in proximity to sedimentary rock formations, or more than 3 boreholes per square kilometer per 10,000 years for repositories in other geologic formations.*

From these two statements, it is concluded that the preliminary performance assessment need not consider intrusion modes such as mining or archaeological investigation that may result in more severe consequences than drilling. Moreover, the standard also provides an upper bound for the drilling intensity to be used in the performance assessment. Three modes of drilling intrusion have been identified by the experts examining human intrusion issues. These modes are exploratory drilling for mineral resources

(primarily fossil fuels) drilling water wells, and drilling for injection disposal wells. Drilling for water was found to be an insignificant threat when compared to drilling for mineral resources. Drilling for disposal wells, which was identified as a threat by one of the four futures teams, has not yet been modeled and, therefore, its affect cannot be judged. Thus, exploratory drilling for resources is the only mode of intrusion considered in the 1992 preliminary comparison.

Assembling the Judgments

The existence of markers and the ability of a society to interpret the warnings left at WIPP may depend upon the state of development of that society. In the preliminary performance assessment, the state of development of the society is represented by the level of the technological development of the society. The level of technological development (high, medium, or low) will be randomly generated from distributions provided by the futures teams.

Using a given level of technology, the frequency (λ) at which attempted inadvertent intrusions will occur at various points in time will be established. This time dependent frequency is called the raw drilling intensity and treated as a parameter of a time dependent Poisson process. The raw drilling intensity does not take into account deterrence by markers, however. For each of the several points in time that the raw drilling intensity is evaluated, the probability of the markers existing (p_1) and the probability of the markers deterring an intrusion attempt given that the markers exist (p_2) are evaluated. These two probabilities modify the raw drilling intensity to give the effective drilling intensity $\lambda(1-p_1p_2)$. The effective drilling intensity is used in the performance assessment to obtain probabilities for scenarios. The process of developing the effective drilling intensity is repeated many times in order to generate many vectors of drilling intensities. Each vector is a random realization and differences among the vectors represent the uncertainty in the drilling intensity and the effectiveness of the markers.

Because the four teams studying potential futures developed analyses independently and in different ways, there is no simple way to combine their findings. For this reason, a team will be randomly selected on each iteration of the Monte Carlo analysis. The assessments from each team represent their collective judgment. In contrast, one of the markers' teams individually provided probability assessments while the other team who provided a consensus set of probability distributions. Thus, when one of the two markers teams is randomly chosen for a Monte Carlo iteration, it may be necessary to also randomly select one of the team members for that iteration. This procedure avoids making unfounded assumptions about how to combine disparate distributions.

The algorithm for generating inadvertent intrusions can then be described by the following steps:

1. Randomly select one of the four futures teams.

The following steps use distributions conditional on the outcome of step 1.

2. Randomly select a level of technology in the future. When probabilities of levels of technology are time dependent, a rank correlation of one will be used to generate the level of technology in the several time periods.

3. Generate a random variable to determine the intrusion intensity. When intrusion intensities vary with time periods, a rank correlation of one will be used to generate the intrusion intensities in the several time periods.

4. Randomly select one of the markers teams and a marker team member, if necessary.

5. For each time period generate the probability that markers are extant given the level of technology.

6. For each time period, generate the probability that the markers deter intrusion given that the markers are extant, the level of technology, and the mode of intrusion.

7. Compute the effective drilling intensity for each time period.

There are several assumptions implicit in the above algorithm. In step 3, a single random number is used to select an intrusion intensity for all periods. This is a conservative assumption in that the variability of the performance measure will be maximized among the Monte Carlo iterations.

Future Levels of Technology

A link exists between the findings of the two groups; the futures group and the markers group. The assessments of the markers group are conditional on the findings of the futures groups. Since each of the futures teams provided a unique analysis using a different set of underlying factors, making the assessment of the markers group conditional on all of the identified factors is infeasible. However, technology emerges as an important theme in all of the analyses and has, thus, been used to capture the dependency between the state of society and the efficacy of the marker system.

The assessments of the Boston futures team provide probabilities for three levels of technology during various times in the future:

TABLE 1
LEVELS OF TECHNOLOGY - BOSTON TEAM

	Years After Closure		
Level of Technology	100-300 years	300-3000 years	3000-10000 years
High	.8	.7	.8
Medium	.15	.2	.1
Low	.05	.1	.1

The Southwest futures team provided probabilities of three scenarios for the development of society: increase, decline, and a future which alternates between these possibilities. We equate the Southwest teams pattern of steady increase in technology with a high level of technology, steady decline with a low level of technology, and the alternating or sea-saw pattern that cycles every 1000 years between increase and decline in technology with 500 years of medium technology followed by a repeating pattern of high, medium, low, and medium technology, each for a period of 500 years. The probability for the increase (high technology scenario) is .475, for the decline (low technology scenario) it is .0875, and for the alternating scenario it is .4375.

The Washington A futures team viewed the future as following a pattern of continuity, radical increase, discontinuity, or one of steady state utilization of resources. Roughly, continuity is equated with high technology while discontinuity is equated with a lower level of technology. Both radical increase and the steady state scenarios are equated with medium technology. Using these assumptions, the following table of probabilities was derived.

TABLE 2
LEVELS OF TECHNOLOGY - WASHINGTON A TEAM

Scenario	Technology	Probability
Continuity	High	.255
Radical Increase	Medium	.2275
Discontinuity	Low	.1675
Steady state	Medium	.35

The Washington B team provided assessments directly in terms of the three levels of technology as repeated in the following table:

TABLE 3
LEVELS OF TECHNOLOGY - WASHINGTON B TEAM

	Time Period	
Technology	0-200 years	200-10000 years
High	.5	.9
Medium	.5	.05
Low	.0	.05

Frequencies of Intrusion Attempts

The responses about the likelihood of intrusion vary in form from team to team. Two teams responded by providing probabilities of intrusion while the other two teams provided probability distributions for the drilling intensity. The most convenient form of information for performance assessment is to have a time dependent intensity parameter or a probability distribution on such a parameter. Therefore, the choice has been made to convert assessments from the four futures teams into a common form -- a drilling intensity parameter or probability function for such a parameter. The spacing of potential drilling intrusions is then carried out in the performance assessment simulations using a time dependent Poisson process with a random parameter.

The Boston team provided assessments for the drilling intensity that are conditional on both time and level of technology. The responses for exploratory drilling for hydrocarbons are shown in the following tables. Exploratory drilling for hydrocarbons was not thought to extend further than 300 years into the future.

TABLE 4
BOSTON TEAM -DRILLING INTENSITY DISTRIBUTIONS

Drilling Intensity	Technology High	Medium	Low
0.5	0.15	0.15	0.15
0.83	0.02	0.02	0.03
4.98	0.22	0.22	0.21
8.3	0.03	0.03	0.04
12.45	0.12	0.11	0.11
20.75	0.02	0.02	0.02
24.9	0.12	0.11	0.11
41.5	0.02	0.02	0.02
49.8	0.22	0.22	0.21
83	0.03	0.03	0.04
99.6	0.03	0.03	0.03
166	0	0	0.01
199.2	0.03	0.03	0.03
332	0	0	0.01

The Boston team also considered drilling for disposal wells as a

possible cause of inadvertent intrusion. This mode of intrusion, however, is not considered in the 1992 performance assessment. There are several reasons for this exclusion. First, this type of potential intrusion has not yet been modeled and, therefore, even if intrusion rates were developed, it would not be possible to account for the consequences. Second, the depth of such wells has not been studied and, thus, it cannot be determined if this type of activity indeed constitutes a threat. Third, only one of the four teams explicilty considered this mode of intrusion. Moreover, this team did not provide complete information at the elicitation session. A questionnaire sent later to the team members was completed by three of the four participants. There was wide disagreement on the frequency of such activity.

The Southwest team considered conventional drilling to be plausible only under the declining and alternating scenarios. In order to employ the judgments provided by this team in the performance assessment, it is necessary to interpret their conclusions. It appears that drilling should be considered only in the low and medium technology states. Moreover, since this team assessed holistic probabilities of one or more intrusions, it is necessary to convert their assessments into a drilling intensity. For the decline and see-saw scenarios, the probabilities of intrusion are given as .113 and .138 respectively. For the decline scenario (low technology) intrusion would occur, if it occurs, during the first 400 years after closure. Assuming a constant intensity during this period, we equate the Poisson probability of one or more intrusions with the assessed probability:

$$1-e^{-.00472\lambda} = .113.$$

The .00472 is the fraction (400 years/10,000 years)(.118 square miles) so that λ is expressed as per square mile per 10,000 years. The .118 arises because this is the planned footprint of the repository. The resulting drilling intensity for 100 to 500 years after closure under the decline scenario implied by the .113 probability is then 25.40 boreholes per square mile per 10,000 years.

Making the conversion under the see-saw scenario is similar with the added difficulty that drilling will not be undertaken during periods of high technology. Using the assumptions discussed in the section of this paper dealing with levels of technology, if the see-saw scenario occurs, the world will be in a high technology state about 1/3 of the time. Thus, we interpret the .138 probability of intrusion in the see-saw scenario to be applicable to 6,666 years (2/3 of 10,000). The resulting drilling intensity, again in units per square mile per 10,000 years is found from

$$1-e^{-.0787\lambda} = .138$$

The resulting drilling intensity is 1.89 boreholes per square mile per 10,000 years.

The Washington A team also provided holistic assessments of the probabilities of intrusion. Assessment were provided for both the first 200 years after closure and the ensuing 9800 years. The following table shows the assessed probabilities and intrusion intensities derived using the same procedure as was used for the Southwest Team.

TABLE 5
PROBABILITIES OF ONE OF MORE INTRUSIONS - WASHINGTON A TEAM

	0-200 years after closure		200-10,000 years after closure	
Scenario (probability)	Assessed Probability	Intrusion Intensity	Assessed Probability	Intrusion Intensity
Continuity (.255)	.076	33.5	.21	2.0
Radical Increase (.2275)	.628	419	.08	.72
Discontinuity (.1675)	.413	226	.42	4.7
Steady State (.35)	.01	4.3	.09	.82

The Washington B Team provided information which permitted the construction of a cumulative distribution function for the number of boreholes. In the near future, 0-200 years after closure, the drilling intensity follows the following CDFS:

TABLE 6
EXPECTED BOREHOLES- WASHINGTON B TEAM

Boreholes per square mile	0-200 years after closure	200-10,000 years after closure
$\lambda<0$	0	0
$\lambda=0$	0.932	0.9377
$0<\lambda\leq 2$	$0.932+0.0085\lambda^2$	$0.9377+0.007782\lambda^2$
$2<\lambda\leq 4$	$0.932+.068[\lambda-(\lambda^2/8)-1]$	$0.9377+.0623[\lambda-(\lambda^2/8)-1]$
$4<\lambda$	1.0	1.0

This team also considered the possibility of drilling for water in both the near and far futures. the probabilities of drilling for water are, however, less than 10^{-4} in both near future and the far future and thus are excluded from further analysis.

Generating the Intrusion Intensity

Let U_i be a uniform [0-1] random deviate. The following algorithm describes the generation of λ, the drilling intensity in terms of several U_i.

0. Go to step $[4*U_1]+1$ where [.] is the largest integer function.

1. (Boston) Compare U_2 to the following look up table:

TABLE 7
LOOKUP TABLE FOR TECHNOLOGY - BOSTON TEAM

U_2	100-300 years	300-3000 years	3000-10000 years
$u \leq .7$	High Tech	High Tech	High Tech
$.7 < u \leq .8$	High Tech	Medium Tech	High Tech
$.8 < u \leq .9$	Medium Tech	Medium Tech	Medium Tech
$.9 < u \leq .95$	Medium Tech	Low Tech	Low Tech
$.95 < u$	Low Tech	Low Tech	Low Tech

Given the outcome from U_2, compare U_3 to Table 8. The drilling intensity is the value having the smallest cumulative probability equal to or greater then U_3.

TABLE 8
DRILLING INENSITY CUMULATIVE PROBABILITES - BOSTON TEAM

Drilling Intensity	Cumulative Probability Technology High	Medium	Low
0.5	0.15	0.15	0.15
0.83	0.17	0.17	0.18
4.98	0.39	0.39	0.38
8.3	0.42	0.42	0.42
12.45	0.53	0.54	0.53
20.75	0.55	0.56	0.55
24.9	0.67	0.67	0.66
41.5	0.69	0.69	0.68
49.8	0.91	0.91	0.88
83	0.94	0.94	0.92
99.6	0.97	0.97	0.95
166	0.97	0.97	0.96
199.2	1.00	1.00	0.99
332	1.00	1.00	1.00

2. (Southwest) Compare U_2 to the following look-up table

TABLE 9
LOOKUP TABLE FOR TECHNOLOGY AND DRILLING INTENSITY
SOUTHWEST TEAM

U_2	Time Period	Drilling Intensity	Technology
$0 \leq u \leq .475$	0-10,000	$\lambda=0$	High
$.475 < u \leq .5625$	0-400 400-10,000	$\lambda=25.40$ $\lambda=0$	Low
$.5625 < u$	0-500 500-1000 1000-1500 1500-2000 2000-2500 2500-3000 3000-3500 3500-4000 4000-4500 4500-5000 5000-5500 5500-6000 6000-6500 6500-7000 7000-7500 7500-8000 8500-9000 9000-9500 9500-10000	1.89 0 1.89 1.89 0 1.89 1.89 0 1.89 1.89 0 1.89 1.89 0 1.89 1.89 0 1.89 1.89	Medium High Low Medium High Low Medium High Low Medium High Low Medium High Low Medium High Low Medium

3. (Washington A) Compare U_2 to the following look-up table.

TABLE 10
LOOKUP TABLE FOR TECHNOLOGY AND DRILLING INTENSITY
WASHINGTON A TEAM

U_2	Time Period	Drilling Intensity	Technology
$0 \leq u \leq .255$	0-200 200-10000	33.5 2.	High
$.255 < u \leq .4825$	0-200 200-10000	419. .72	Medium
$.4825 < u \leq .65$	0-200 200-10000	226. 4.7	Low
$.65 < u$	0-200 200-10000	4.3 .82	Medium

4. (Washington B) Compare U_2 to the following look-up table to determine the state of technology:

TABLE 11
LOOKUP TABLE FOR TECHNOLOGY - WASHINGTON B TEAM

U_2	Technology 0-200 years	Technology 200-10,000 years
$u \leq .5$	High	High
$.5 < u \leq .90$	Medium	High
$.90 < u \leq .95$	Medium	Medium
$.95 < u$	Medium	Low

Next, compare U_3 to the following two lookup tables to determine the drilling intensity which is independent of the state of technology:

TABLE 12A
DRILLING INTENSITY FOR 0-200 YEARS - WASHINGTON B TEAM

U_3	Intensity λ
$u \leq .932$	0.0
$.932 < u \leq .966$	$[(u-.932)/.0085]^{.5}$
$.966 < u$	$4(1-\{1-.5[1+(u-.932)/.068]\}^{.5})$

TABLE 12B
DRILLING INTENSITY FOR 200-500 YEARS - WASHINGTON B TEAM

U_3	Intensity λ
$u \leq .9377$	0.0
$.9377 < u \leq .96885$	$[(u-.9377)/.007782]^{.5}$
$.96885 < u$	$4(1-\{1-.5[1+(u-.9377)/.0623]\}^{.5})$

Drilling for resources does not continue beyond 500 years and thus the drilling intensity is 0 beyond 500 years.

Persistence of Markers

Markers Team A addressed probabilities of markers continuing to exist on an individual basis so that six individual assessments are available. Assessments were provided assuming three different levels of technology and at five points in time -- 200, 500, 1000, 5000, and 10000 years after closure. The following table contains the probabilities of the marker system (as defined in the report of the A team) continuing to exist at the given epoch conditional on a dominant state of technology.

TABLE 13
PROBABILITIES OF THE MARKER SYSTEM PERSISTING -TEAM A

Expert	Dominant Technology	Years After Closure				
		200	500	1000	5000	10,000
Ast	High	.99	.98	.95	.75	.50
	Medium	.99	.98	.95	.75	.60
	Low	.99	.98	.95	.75	.60
Brill	High	.99	.98	.95	.70	.50
	Medium	.99	.98	.95	.70	.50
	Low	.99	.98	.95	.85	.80
Goodenough	High	.99	.98	.90	.85	.70
	Medium	.99	.98	.95	.90	.75
	Low	.99	.98	.98	.95	.80
Kaplan	High	.95-.99	.95-.99	.90-.95	.80	.70
	Medium	.95-.99	.95-.99	.90-.95	.80	.70
	Low	.95-.99	.95-.99	.90-.95	.90	.85
Newmeyer	High	.90	.85	.70	.65	.60
	Medium	.95	.90	.85	.80	.60
	Low	.95	.90	.85	.85	.65
Sullivan	High	.90	.85	.80	.70	.50
	Medium	.95	.90	.85	.80	.70
	Low	.95	.90	.85	.80	.70

In contrast, Team B provided consensus probabilities at only three points in time -- 500, 2000, and 10,000 years. The following table contain these consensus probabilities for the three levels of technology.

TABLE 14
CONSENSUS PROBABILITIES OF THE MARKER SYSTEM PERSISTING - TEAM B

Dominant Technology	Years After Closure		
	500	2000	10000
High	.90	.85	.85
Medium	.90	.80	.60
Low	.90	.70	.40

Determining the Probabilities of Markers Deterring Intrusion

The following algorithm is based on linear interpolation of the probabilities provided by the two teams. Let k denote the level of technology and let T be the times at which probabilities are needed. V_i are uniform [0,1] random variables.

0. If $V_1 \leq .5$ go to step 1. otherwise step 2.

1. Let $i=[5*V_1]+1$ where [.] is the largest integer function. Let $t_0=0$, $t_1=200$, $t_2=500$, $t_3=1000$, $t_4=5000$, and $t_5=10000$. For each time T, calculate

$$p_1(T)=a_{i,j'-1,k}+(a_{i,j',k}-a_{i,j'-1,k})(T-t_{j'-1})/(t_{j'}-t_{j'-1})$$

and

$$p_2(T)=c_{i,j'-1,k}+(c_{i,j',k}-c_{i,j'-1,k})(T-t_{j'-1})/(t_{j'}-t_{j'-1})$$

where j' is the largest j=1,...,5 such that $T \leq t_j$. By assumption $a_{i0k}=1.0$ for all i and k.

2. Let $t_0=0$, $t_1=500$, $t_2=2000$, and $t_3=10000$. For each time T, calculate

$$p_1(T)=b_{i,j'-1,k}+(b_{i,j',k}-b_{i,j'-1,k})(T-t_{j'-1})/(t_{j'}-t_{j'-1})$$

and

$$p_2(T)=c_{m,i,j'-1,k}+(c_{m,i,j',k}-c_{m,i,j'-1,k})(T-t_{j'-1})/(t_{j'}-t_{j'-1})$$

where j' is the largest j=1,2,3 such that $T \leq t_j$. By assumption $b_{0k}=1.0$ for all k.

TABLE 15
COEFFICIENTS A_{ijk}

k=h (High Technology)					
	j=1	j=2	j=3	j=4	j=5
i=1	.99	.98	.95	.75	.50
2	.99	.98	.95	.70	.50
3	.99	.98	.90	.85	.70
4	.97	.97	.925	.80	.70
5	.90	.85	.70	.65	.60
6	.90	.85	.80	.70	.50
k=m (Medium Technology)					
i=1	.99	.98	.95	.75	.60
2	.99	.98	.95	.70	.50
3	.99	.98	.95	.90	.75
4	.97	.97	.925	.80	.70
5	.95	.90	.85	.80	.60
6	.95	.90	.85	.80	.70
k=l (Low Technology)					
i=1	.99	.98	.95	.75	.60
2	.99	.98	.95	.85	.80
3	.99	.98	.98	.95	.80
4	.97	.97	.925	.90	.85
5	.95	.90	.85	.85	.65
6	.95	.90	.85	.80	.70

TABLE 16
COEFFICIENTS b_{jk}

	j=1	j=2	j=3
k=h	.90	.85	.85
k=m	.90	.80	.60
k=l	.90	.70	.40

The Deterrence of Intrusion

The probability that the marker system will deter the potential intruders has been assessed as a function of time, the state of technology and the mode of intrusion. The following table gives the probability of deterrence of intrusion for intrusion by drilling assoicated wityh mineral exploration. The first six lines the table give the deterrence probability for the experts of Team A while the seventh line is the consensus probability for Team B.

TABLE 18

PROBABILITY OF DETERRENCE -- MINERAL EXPLORATION

COEFFICIENTS C_{mkij} WHERE M=MINERALS

	200 Years			500 Years			1000 Years			5000 Years			10000 Years		
Tech Expert	H	M	L	H	M	L	H	M	L	H	M	L	H	M	L
1	.99	.99	.98	.98	.95	.70	.95	.90	.50	.90	.20	.10	.90	.20	.05
2	.99	.99	.95	.95	.95	.90	.95	.95	.70	.95	.95	.60	.95	.95	.50
3	.99	.99	.99	.95	.95	.70	.90	.90	.50	.65	.60	.15	.50	.40	.02
4	.99	.98	.95	.98	.90	.70	.97	.85	.65	.95	.80	.50	.90	.75	.02
5	.99	.99	.90	.90	.85	.80	.80	.70	.50	.70	.60	.40	.50	.30	.20
6	.95	.95	.80	.90	.90	.60	.85	.85	.40	.70	.70	.10	.40	.40	.01
	500 Years			2000 Years			10,000 Years								
Team B	.90	.90	.80	.90	.85	.70	.99	.80	.30						

Implementation of the Algorithms

The interface between the performance assessment computer code and the findings of the two groups studying human intrusion requires the intensity of drilling activity, as a function of time, be simulated and passed to the performance assessment code. The mechanism for providing this connection is a FORTRAN code written to implement the algorithms of the preceding sections and produce vectors of time dependent drilling intensities to be used as input vectors to the performance assessment. This code is included in this report as an appendix.

The form of the output from this code is the effective drilling intensity at years 100 to 500 in increments of 100 years, and 500 to 10,000 years in increments of 500 years. The effective drilling intensity is the drilling intensity moderated by the probability of markers deterring intrusion. Let $\lambda(t)$ be the raw drilling intensity that would be expected if no markers were present. Let $p_1(t)$ be the probability that the marker systems exists at time t and let $p_2(t)$ be the probability that, given the continuing existence of the marker system, potential intruders are deterred from their intrusion attempt by the marker system. The moderated intrusion intensity, measured as expected boreholes/sq. mi./10,000 yrs., is $\lambda^*(t) = \lambda(t)[1-p_1(t)p_2(t)]$ where the factor $[1-p_1(t)p_2(t)]$ is the probability that the marker system fails to deter the potential intruders.

The FORTRAN code has been written to faithfully implement the findings of the expert teams. Several small concessions have been made to simplify the programming. These are:

1. The information for the drilling intensity from the Washington B team indicates that if minerals are extracted in the WIPP region, exploration will occur either in the first 200 years or in the next 300 years, but not in both periods. There does not seem to be adequate information from this team to model this dependence without making arbitrary assumptions. The code models this dependence by deciding if drilling occurs in the first 200 years and, if drilling does not occur, repeating the decision with the same decision rule to determine whether drilling occurs in the next 300 years.

2. There is some disparity among the time periods used by the various experts in deriving their assessments. Both the Boston and Southwest teams gave assessments that began 100 years after closure and thus allowed for a 100 year period of administrative control. In contrast, the two Washington teams gave assessments beginning immediately after closure and thus did not allow for the period of continuing administrative control. The performance assessment, however, assumes that the drilling rate is effectively nil during the first 100 years after closure.

The assessments given by the futures teams are for periods of time and thus a single, randomly chosen, intrusion rate will be effective during each period. In contrast, the assessments provided by the markers teams provide probabilities at points in time. Thus interpolation is needed to obtain probabilities for

intermediate points in time. This is accomplished in the implementation by using the middle of each time interval as the point to which interpolation is made.

In all other important respects the evaluation remains faithful to the algorithms given earlier and, hopefully, to the assessments provided by the experts.

Preliminary Evaluation of the Findings

The input to the performance assessment code from the human intrusion studies is in the form of vectors of drilling intensities. Each vector represents a different time history. The elements of the vectors are drilling intensities are various points in time.

The FORTRAN code written to create the input vectors for the performance assessment code has been modified to compute the average drilling intensity, the average marker failure probability, and the average moderated drilling intensity as a function of time. These averages are taken across the input vectors. Thus, there is an average for each time interval. Table 19 shows these three averages as a function of time since closure. Figure 1 shows these three averages on log scales to enhance the visibility of the behavior of the drilling intensities soon after closure.

Table 19 shows that the initial expected drilling intensity in the WIPP area is high for the first 500 years. After 500 years the expected intensity falls and remains fairly stable for 9500 years. The marker system, however, is shown to be most effective during this early period and, therefore, significantly moderates the drilling intensity during the first 500 years.

Figure 2 shows the empirical distribution of the time integrated drilling intensity across input vectors. This display captures the uncertainty in the overall drilling intensity since each vector is a different realization from the assessed probability distributions. Figure 2 shows that the largest time integrated drilling intensity among 1000 vectors is 2.884 boreholes/sq. mi./10,000 yr.

Figure 1

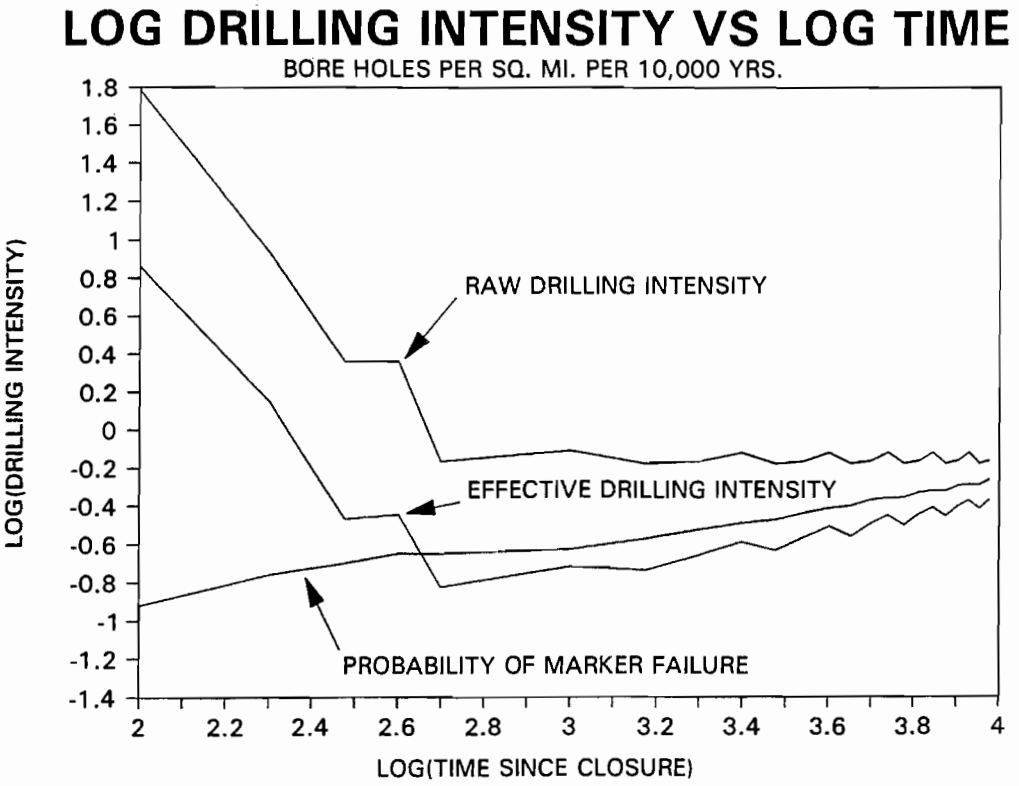

Figure 2

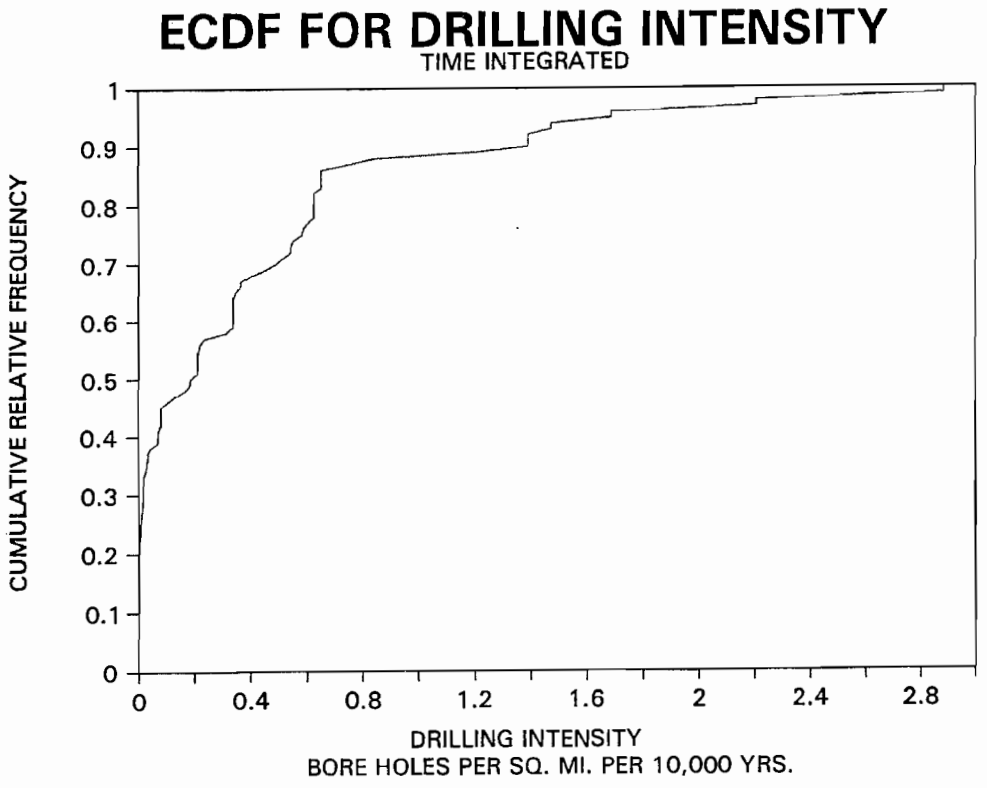

TABLE 19
COMBINED FUTURES AND MARKERS TEAMS FINDINGS
DRILLING INTENSITY PER SQUARE MILE PER 10,000 YEARS

Period	Raw Drilling Intensity	Probability of Marker Failure	Effective Drilling Intensity
0-100	55.4	0.0408	2.34
100-200	61	0.12	7.33
200-300	8.58	0.175	1.42
300-400	2.31	0.2	0.342
400-500	2.31	0.226	0.36
500-1000	0.687	0.226	0.151
1000-1500	0.781	0.237	0.192
1500-2000	0.668	0.269	0.184
2000-2500	0.687	0.301	0.222
2500-3000	0.762	0.325	0.26
3000-3500	0.668	0.338	0.234
3500-4000	0.687	0.368	0.275
4000-4500	0.762	0.389	0.313
4500-5000	0.668	0.401	0.278
5000-5500	0.687	0.43	0.323
5500-6000	0.762	0.44	0.357
6000-6500	0.668	0.443	0.317
6500-7000	0.687	0.47	0.361
7000-7500	0.762	0.479	0.392
7500-8000	0.668	0.48	0.352
8000-8500	0.687	0.509	0.397
8500-9000	0.762	0.516	0.426
9000-9500	0.668	0.515	0.386
9500-10000	0.687	0.546	0.429

REFERENCES

Hora, S.C., D. von Winterfledt, and K.M. Trauth (1991), Expert Judgment of Inadvertent Human Intrusion into the Waste Isolation Pilot Plant, Sandia National Laboratories, SAND90-3063.

Environmental Protection Agency (1985). Environmental Standards for the Management and Disposal of Spent nuclear Fuel, High-level and Transuranic Radioactive Wastes: final Rule. 40 CFR Par 191. Federal Register 50: pp. 38066-89.

APPENDIX

COMPUTER PROGRAM TO GENERATE TIME DEPENDENT DRILLING INTENSITIES

```
C
      PROGRAM HUMINT
C
C  THIS PROGRAM EVALUATES THE DRILLING INTENSITY (RATE) USING THE
C  DISTRIBUTIONS PROVIDED BY THE MARKERS AND FUTURES PANELS
C
C  THE FOLLOWING VARIABLES ARE DEFINED
C    NREPS - NUMBER OF VECTORS OF INTRUSION INTENSITIES
C    IPER  - NUMBER OF PERIODS AT WHICH THE INTENSITY IS EVALUATED
C    LAMBDA  - MINERAL DRILLING RATE FROM THE BOSTON TEAM
C    U(NREP,6) - AN ARRARY OF LHS [0,1] RANDOM DEVIATES
C    BOSTAB1 - TABLE OF DISTRIBUTIONS FROM THE BOSTON TEAM
C    ITECH(IPER) - THE LEVEL OF TECHNOLOGY 1=HIGH, 2=MEDIUM, 3=LOW
C    BTIME(5) - CHANGE TIMES FOR THE BOSTON TEAM
C    OUTPUT(6,IPER) -  AN ARRAY WITH THE FOLLOWING ROWS
C      1 - THE TIME PERIOD
C      2 - THE DRILLING INTENSITY IN HOLES/SQ MI/10,000 YRS
C      3 - THE LEVEL OF TECHNOLOGY
C      4 - THE PROBABILITY OF MARKERS SURVIVING
C      5 - THE PROBABILITY OF SURVIVING MARKERS BEING INTERPRETED
C      6 - THE EFFECTIVE DRILLING INTENSITY AFTER MARKER DETERENCE
C    TIME(NTIME) - BEGINNING YEAR OF THE TIME PERIOD
C    B & C - ARRAYS CONTANING DATA FROM THE MARKERS TEAMS
C    AMARKT, BMARKT, PROBMARK & PROBDTER - ARRAYS USED TO DETERMINE
C      MARKERS PROBABILITIES
C    SUM(3,IPER) - SUMS THE RESULTS OUTPUT VARIABLES 2, 1-4*5, AND 6
C      TO BE USED TO COMPUTE AVERAGES
C
      PARAMETER (NREP=100)
      PARAMETER (IPER=23)
      PARAMETER (NTIME=24)
      REAL LAMBDA
      COMMON /ISEEDS/IX,IY,IZ
      DIMENSION LAMBDA(10),NB(3)
      DIMENSION U(6,NREP),BOSTAB1(10,4)
      DIMENSION ITECH(0:NTIME),BTIME(2),OUTPUT(6,0:IPER)
      DIMENSION TIME(0:NTIME),B(7,6,3),C(7,6,3)
      DIMENSION AMARKT(6),BMARKT(4),PROBMARK(0:IPER),PROBDTER(0:IPER)
      DIMENSION SUM(4,0:IPER)
      DATA AMARKT/0,200,500,1000,5000,10000/
      DATA BMARKT/0,500,2000,10000/
      DATA BTIME/300,3000/
      DATA IX,IY,IZ/19345,19321,19243/
      DATA NB/11,11,8/
C
C  NU IS THE NUMBER OF UNIFORM RANDOM VARIABLES TO BE SAMPLED
C
      NU=6
C
C  COMPUTE THE TIMES AT WHICH THE VARIABLES ARE EVALUATED
C  100 TO 500 YEARS BY 100 AND 500 TO 10000 BY 500
C
      DO ITIME=0,5
       TIME(ITIME)=ITIME*100
      ENDDO
      DO ITIME=6,NTIME
       TIME(ITIME)=(ITIME-4)*500
      ENDDO
C
C  SAMPLE CREATES THE LHS SAMPLE OF NU VARIABLES WITH A VECTOR LENGTH
C  OF NREP
```

```
C
      CALL SAMPLE(NREP,NU,U)
C
C READ TABLES FROM THE BOSTON TEAM AND THE MARKERS TEAMS
C
      OPEN (UNIT=10,FILE='BOSTAB1.DAT',STATUS='OLD',MODE='READ')
      READ (10,*) ((BOSTAB1(I,J),J=1,4),I=1,10)
      CLOSE (UNIT=10)
      OPEN(UNIT=12,STATUS='OLD',FILE='MARKERS1.TAB',MODE='READ')
      READ(12,*)(((B(I,J,K),J=2,6),I=1,6),K=1,3)
      I=7
      READ(12,*) ((B(I,J,K),J=2,4),K=1,3)
      CLOSE (UNIT=12)
      OPEN (UNIT=13,FILE='MARKERS2.TAB',STATUS='OLD',MODE='READ')
      READ(13,*)(((C(I,J,K),J=2,6),I=1,6),K=1,3)
      I=7
      READ(13,*) ((C(I,J,K),J=2,4),K=1,3)
      CLOSE(13)
      OPEN (UNIT=20,FILE='HUMINT1.OUT',STATUS='UNKNOWN',MODE='WRITE')
      WRITE (20,100) (TIME(ITIME),ITIME=0,IPER)
      OPEN (UNIT=22,FILE='HUMINT3.OUT',STATUS='UNKNOWN',MODE='WRITE')
C
C SET THE PROBABILITY OF MARKERS TO 1.0 AT TIME 0
C
      DO I=1,7
       DO K=1,3
         B(I,1,K)=1.0
         C(I,1,K)=1.0
       ENDDO
      ENDDO
C
C  BEGIN SAMPLING ITERATION
C
      DO IREP=1,NREP
C
C SELECT A FUTURES TEAM (1-4)
C
      U1=U(1,IREP)
      ITEAMF=INT(4*U1)+1
C
C  BOSTON TEAM
C
    1 IF(ITEAMF.EQ.1) THEN
C
C LOOK UP LEVEL OF TECHNOLOGY 1=HIGH, 2=MEDIUM, 3=LOW
C FOR THREE TIME PERIODS
C
      U2=U(2,IREP)
      DO I=1,3
       ITECH(I)=1
      ENDDO
      IF (.7.LT.U2) ITECH(2)=2
      IF (.8.LT.U2) THEN
       ITECH(1)=2
       ITECH(3)=2
      ENDIF
      IF (.9.LT.U2) THEN
       ITECH(2)=3
       ITECH(3)=3
      ENDIF
      U3=U(3,IREP)
      IF (.95.LT.U2) ITECH(1)=3
C
C  LOOKUP THE MINERAL DRILLING RATE
```

```
C
      DO IRATE=1,10
       IF(U3.LE.BOSTAB1(IRATE,ITECH(1)+1)) THEN
         LAMBDA=BOSTAB1(IRATE,1)
         GOTO 10
       ENDIF
      ENDDO
   10 CONTINUE
C
      U4=U(4,IREP)
      DO ITIME=1,3
       DO IRATE=1,NB(ITECH(ITIME))
         IF (U4.LE.BOSTAB2(IRATE,1,ITECH(ITIME))) THEN
           DLAMBDA(ITIME)=BOSTAB2(IRATE,ITIME+1,ITECH(ITIME))
           GOTO 20
         ENDIF
       ENDDO
   20  CONTINUE
      ENDDO
C
C  CREATE OUTPUT DRILLING VECTOR, TIMES, AND TECHNOLOGIES
C
      DO ITIME=0,IPER
      IF (TIME(ITIME).EQ.0) THEN
       OUTPUT(2,ITIME)=0.0
       OUTPUT(3,ITIME)=2.0
      ELSEIF (TIME(ITIME).LT.BTIME(1)) THEN
       OUTPUT(2,ITIME)=LAMBDA(1)
       OUTPUT(3,ITIME)=ITECH(1)
      ELSEIF (TIME(ITIME).LT.BTIME(2)) THEN
       OUTPUT(2,ITIME)=0.0
       OUTPUT(3,ITIME)=ITECH(2)
      ELSE
       OUTPUT(2,ITIME)=0.0
       OUTPUT(3,ITIME)=ITECH(3)
      ENDIF
      ENDDO
      ENDIF
C
C  SOUTHWEST TEAM
C
      IF (ITEAMF.EQ.2) THEN
      U2=U(2,IREP)
      OUTPUT(2,0)=0.0
      OUTPUT(3,0)=2.0
C
C  STEADY INCREASE SCENARIO
C
      IF (U2.LE..475) THEN
       DO ITIME=0,IPER
         OUTPUT(2,ITIME)=0.0
         OUTPUT(3,ITIME)=1.0
       ENDDO
      ENDIF
C
C  STEADY DECLINE SCENARIO
C
       IF (.475.LT.U2.AND.U2.LE..5625) THEN
       DO ITIME=0,IPER
         OUTPUT(3,ITIME)=3.
         IF (TIME(ITIME).LE.400.) THEN
           OUTPUT(2,ITIME)=25.4
         ELSE
           OUTPUT(2,ITIME)=0.0
```

```
          ENDIF
        ENDDO
       ENDIF
C
C  SEE-SAW SCENARIO
C    IRAN13 ALLOWS THE SEE-SAW TO START AT A RANDOM TIME (500,1000,
C     OR 1500 YEARS
C
       IF(.5625.LT.U2) THEN
        IRAN13=INT(3*U(3,IREP))
        DO ITIME=1,6
          OUTPUT(2,ITIME)=1.89
          OUTPUT(3,ITIME)=2.0
        ENDDO
        DO ITIME=5+IRAN13,IPER
          OUTPUT(2,ITIME)=1.89
          OUTPUT(3,ITIME)=3-MOD(ITIME+IRAN13,3)
C
C NO DRILLING DURING PERIODS OF HIGH TECHNOLOGY (TECH=1.0)
C
          IF(OUTPUT(3,ITIME).EQ.1.) OUTPUT(2,ITIME)=0.0
        ENDDO
       ENDIF
       ENDIF
C
C  WASHINGTON A TEAM
C
       IF(ITEAMF.EQ.3) THEN
        U2=U(2,IREP)
C
C  SET LEVELS OF TECHNOLOGY AND DRILLING RATES FOR TWO PERIODS
C
        DO ITIME=0,IPER
C
C  CONTINUITY SCEANRIO
C
          IF(U2.LE..255) THEN
            IF (TIME(ITIME).LT.200) THEN
              OUTPUT(2,ITIME)=33.5
              OUTPUT(3,ITIME)=1
            ELSE
              OUTPUT(2,ITIME)=2
              OUTPUT(3,ITIME)=1
            ENDIF
          ENDIF
C
C  RADICAL INCREASE SCEANRIO
C
        IF (.255.LT.U2.AND.U2.LE..4825) THEN
          IF (TIME(ITIME).LT.200) THEN
              OUTPUT(2,ITIME)=419.
              OUTPUT(3,ITIME)=2
            ELSE
              OUTPUT(2,ITIME)=.72
              OUTPUT(3,ITIME)=2
          ENDIF
        ENDIF
C
C  DISCONTINUITY SCEANRIO
C
        IF(.4825.LT.U2.AND.U2.LE..65) THEN
          IF (TIME(ITIME).LT.200) THEN
              OUTPUT(2,ITIME)=226.
              OUTPUT(3,ITIME)=3
```

```
            ELSE
              OUTPUT(2,ITIME)=4.7
              OUTPUT(3,ITIME)=3
            ENDIF
          ENDIF
C
C  STEADY STATE SCEANRIO
C
          IF(.65.LT.U2) THEN
            IF (TIME(ITIME).LT.200) THEN
                OUTPUT(2,ITIME)=4.3
                OUTPUT(3,ITIME)=2
              ELSE
                OUTPUT(2,ITIME)=.82
                OUTPUT(3,ITIME)=2
            ENDIF
          ENDIF
          ENDDO
        ENDIF
C
C  WASHINGTON B TEAM
C
        IF(ITEAMF.EQ.4) THEN
          U2=U(2,IREP)
C
C  SET LEVELS OF TECHNOLOGY INDPENDENT OF DRILLING
C
          IF (U2.LE..5) THEN
            DO ITIME=0,IPER
              OUTPUT(3,ITIME)=1
            ENDDO
          ENDIF
          IF(.5.LT.U2.AND.U2.LE..9) THEN
            DO ITIME=0,IPER
              IF(TIME(ITIME).LT.200) THEN
                OUTPUT(3,ITIME)=2
              ELSE
                OUTPUT(3,ITIME)=1
              ENDIF
            ENDDO
          ENDIF
          IF(.9.LT.U2.AND.U2.LE..95) THEN
            DO ITIME=0,IPER
              OUTPUT(3,ITIME)=2
            ENDDO
          ENDIF
          IF (.95.LT.U2) THEN
            DO ITIME=0,IPER
              IF (TIME(ITIME).LT.200) THEN
                OUTPUT(3,ITIME)=2
              ELSE
               OUTPUT(3,ITIME)=3
              ENDIF
            ENDDO
          ENDIF
C
C  COMPUTE DRILLING RATE FROM THE TRIANGULAR DENSITY
C
        U3=U(3,IREP)
        U4=U(4,IREP)
        U5=U(5,IREP)
        IF (U4.LE..5) THEN
          DR=SQRT(8*U4)
        ELSE
```

```
        DR=4-SQRT(8*(1-U4))
       ENDIF
       DO ITIME=0,IPER
        IF(TIME(ITIME).LT.200) THEN
          IF(U3.LE..932) OUTPUT(2,ITIME)=0.0
          IF(U3.GT..932) OUTPUT(2,ITIME)=DR*10000./200.
        ELSE IF(TIME(ITIME).LT.500.AND.OUTPUT(2,ITIME).EQ.0.0) THEN
          IF(U5.GT.9377) OUTPUT(2,TIME)=DR*10000./300.
        ENDIF
       ENDDO
       ENDIF
C
C  CALCULATE MARKERS PROBABILITIES
C
       U6=U(6,IREP)
C
C  SELECT A MARKERS EXPERT (1-6) OR TEAM B (IMARK=7)
C
       IF(U6.LT..5) THEN
        IMARK=INT(12*U6)+1
       ELSE
        IMARK=7
       ENDIF
       DO ITIME=0,IPER
        T=(TIME(ITIME)+TIME(ITIME+1))/2
C
C CHECK THE LEVEL OF TECHNOLOGY
C
        JTECH=OUTPUT(3,ITIME)
C
C  INTERPOLATE TO FIND THE PROBABILITIES OF MARKERS EXISTING (PROBMARK)
C    AND THE PROBABILITIES OF DETERENCE (PROBDTER) AT EACH TIME
C
        IF(IMARK.LT.7) THEN
          NP=6
          JP=JNDEX(AMARKT,NP,T)
          PROBMARK(ITIME)=B(IMARK,JP-1,JTECH)
     &      +(B(IMARK,JP,JTECH)-B(IMARK,JP-1,JTECH))
     &      *(T-AMARKT(JP-1))/(AMARKT(JP)-AMARKT(JP-1))
          PROBDTER(ITIME)=C(IMARK,JP-1,JTECH)
     &      +(C(IMARK,JP,JTECH)-C(IMARK,JP-1,JTECH))
     &      *(T-AMARKT(JP-1))/(AMARKT(JP)-AMARKT(JP-1))
        ELSE
          NP=4
          JP=JNDEX(BMARKT,NP,T)
          PROBMARK(ITIME)=B(IMARK,JP-1,JTECH)
     &      +(B(IMARK,JP,JTECH)-B(IMARK,JP-1,JTECH))
     &      *(T-BMARKT(JP-1))/(BMARKT(JP)-BMARKT(JP-1))
          PROBDTER(ITIME)=C(IMARK,JP-1,JTECH)
     &      +(C(IMARK,JP,JTECH)-C(IMARK,JP-1,JTECH))
     &      *(T-BMARKT(JP-1))/(BMARKT(JP)-BMARKT(JP-1))
        ENDIF
C
C  RECORD THE MARKERS PROBS AND THE EFFECTIVE DRILLING INTENSITY
C
       OUTPUT(4,ITIME)=PROBMARK(ITIME)
       OUTPUT(5,ITIME)=PROBDTER(ITIME)
       OUTPUT(6,ITIME)=OUTPUT(2,ITIME)
     &   *(1-OUTPUT(4,ITIME)*OUTPUT(5,ITIME))
C
C  SUM THE RESULTS FOR COMPUTING MEANS
C
      SUM(1,ITIME)=SUM(1,ITIME)+OUTPUT(2,ITIME)
      SUM(2,ITIME)=SUM(2,ITIME)+(1-OUTPUT(4,ITIME)*OUTPUT(5,ITIME))
```

```
      SUM(3,ITIME)=SUM(3,ITIME)+OUTPUT(6,ITIME)
      ENDDO
C
C  THIS STATEMENT WILL WRITE OUT VECTORS FOR THE PA
C  THE FIRST VECTOR IS THE BEGINNING OF THE TIME PERIOD
C  THE RATE IS EFFECTIVE UNTIL THE START OF THE NEXT PERIOD
C
      WRITE(20,100) (OUTPUT(6,ITIME),ITIME=0,IPER)
  100 FORMAT(25(1X,F7.2))
      DRILLINT=0.
      DO ITIME=0,23
        DRILLINT=DRILLINT+(TIME(ITIME+1)-TIME(ITIME))
     & *OUTPUT(6,ITIME)/10000.
      ENDDO
       WRITE(22,300) DRILLINT
      ENDDO
  300 FORMAT(1X,F10.3)
C
C  CALCULATE MEANS
C
      DO ITIME=0,IPER
       DO J=1,3
         SUM(J,ITIME)=SUM(J,ITIME)/NREP
       ENDDO
      ENDDO
C
C  OUTPUT THE MEANS
C
      OPEN (UNIT=21,FILE='HUMINT2.OUT',STATUS='UNKNOWN',MODE='WRITE')
      DO ITIME=0,IPER
       WRITE(21,200) TIME(ITIME),(SUM(J,ITIME),J=1,3)
      ENDDO
  200 FORMAT(1X,F8.0,4(1X,G12.3))
      CLOSE(20)
      CLOSE(21)
      CLOSE(22)
      STOP
      END
C
C  FUNCTION INDEX FINDS THE INDEX OF THE LARGEST VALUE OF XI<=W
C
      INTEGER FUNCTION JNDEX(X,L,W)
      DIMENSION X(10)
      DO J=1,L
      IF(X(J).GE.W) THEN
       JNDEX=J
       RETURN
      ENDIF
      ENDDO
      JNDEX=L+1
      RETURN
      END
C
      FUNCTION RAN(DUMMY)
C  THIS PROGRAM GENERATES A RANDOM NUMBER.  THIS NUMBER IS USED IN CALCULATING
C  THE INTEGRAL OF A GIVEN FUNCTION THROUGH THE LATIN-HYPERCUBED PROCEDURE.
C  THE PARAMETERS ARE THE SEEDS TO THIS RANDOM FUNCTION.
      COMMON /ISEEDS/IX,IY,IZ
      IX=MOD(171*IX,30269)
      IY=MOD(172*IY,30307)
      IZ=MOD(170*IZ,30323)
      RAN=MOD(FLOAT(IX)/30269.0+FLOAT(IY)/30307.0
     & +FLOAT(IZ)/30323.0,1.0)
      RETURN
```

```
      END
C
C  TWO SUBROUTINES TO GENERATE A UNIFORM LATIN HYPERCUBE SAMPLE
C  IN A RANDOM ORDER
C
      SUBROUTINE SAMPLE(N,M,R)
      COMMON /ISEEDS/IX,IY,IZ
      DIMENSION YT(1000),RANDOM(1000),IPNT(1000),R(6,*)
      RINC=1./FLOAT(N)
      DO IM=1,M
      DO J=1,N
        YT(J)=(J-1)*RINC+RAN(DUMMY)*RINC
        RANDOM(J)=RAN(DUMMY)
      ENDDO
      CALL SORT2(N,RANDOM,IPNT)
      DO J=1,N
       R(IM,J)=YT(IPNT(J))
      ENDDO
      ENDDO
      RETURN
      END

      SUBROUTINE SORT2(N, XV, IPNT)
C*****FILL POINTER ARRAY IPNT
      DIMENSION XV(N), IPNT(N)
      DO I=1,N
        IPNT(I)=0
      ENDDO
      DO I=1,N
       DO J=I,N
         IF(XV(I).GE.XV(J)) THEN
             IPNT(I)=IPNT(I)+1
         ELSE
             IPNT(J)=IPNT(J)+1
         ENDIF
       ENDDO
      ENDDO
      RETURN
      END

      CC CCCCCCCCC
```

Mendenhall and Lincoln, February 28, 1992

Date: 2/28/92
To: D. R. Anderson 6342
From: F. T. Mendenhall, 6345, R. C. Lincoln, 6345
Subject: Single Room Porosity History for Baseline Waste Form and Gas Generation Rates

Sandia National Laboratories

Albuquerque, New Mexico 87185

date: February 28, 1992

to: D. R. Anderson, 6342

Fred Mendenhall R.C. Lincoln

from: F.T. Mendenhall, 6345, R.C. Lincoln, 6345

subject: Single Room Porosity History for Baseline Waste Form and Gas Generation Rates.

Attached is a topological map defining the porosity in a single WIPP disposal room, assumed to be in the middle of an infinite array of rooms, as a function of the number of moles of gas present and time. This result is expected to be representative of the majority of rooms in the repository, the exceptions being the end room of a panel where the closure rate may cause a slight time shift in the surface, i.e. a slowing of consolidation estimated to be about 25%. However, until full panel scale models are complete, we recommend that the attached porosity surface be used for any room in the repository.

This surface was constructed from a set of five SANCHO finite element runs made for the reference baseline waste form and gas generation rates as defined by Beraun and Davies 1991[1] . The finite element analysis were performed for the WIPP project by Division 1514. Detailed documentation will be prepared discussing this modeling effort and the results. However, to help the WIPP program proceed in a timely fashion, this surface is being released so that performance assessment may immediately begin to incorporate the results in their work.

After the 2000 years modeled in the finite element results attached, the porosity surface should be defined by the amount of void space required to maintain lithostatic pressure with the amount of gas contained in a room using the ideal gas law.

It should be noted that the surface is a fit to a calculational result set containing about 750 points obtained from the results of the finite element runs. After the surface was generated, a comparison of the surface to the original result set was made. The mean difference between the original result set and the topological surface, was 0.17 percent, (note porosity was plotted in percent), with a standard deviation of 1.48.

An ASCII data file of the surface grid is available for your staff should they desire it.

[1]R. Beraun and P. B. Davies, "Baseline Design Input Data Base to be Used During Calculations Effort to be Performed by Division 1514 in Determining the Mechanical Creep closure Behavior of Waste Disposal Rooms in Bedded Salt." Memorandum to Distribution, Sandia National Laboratories, Albuquerque, New Mexico, September 12, 1991.

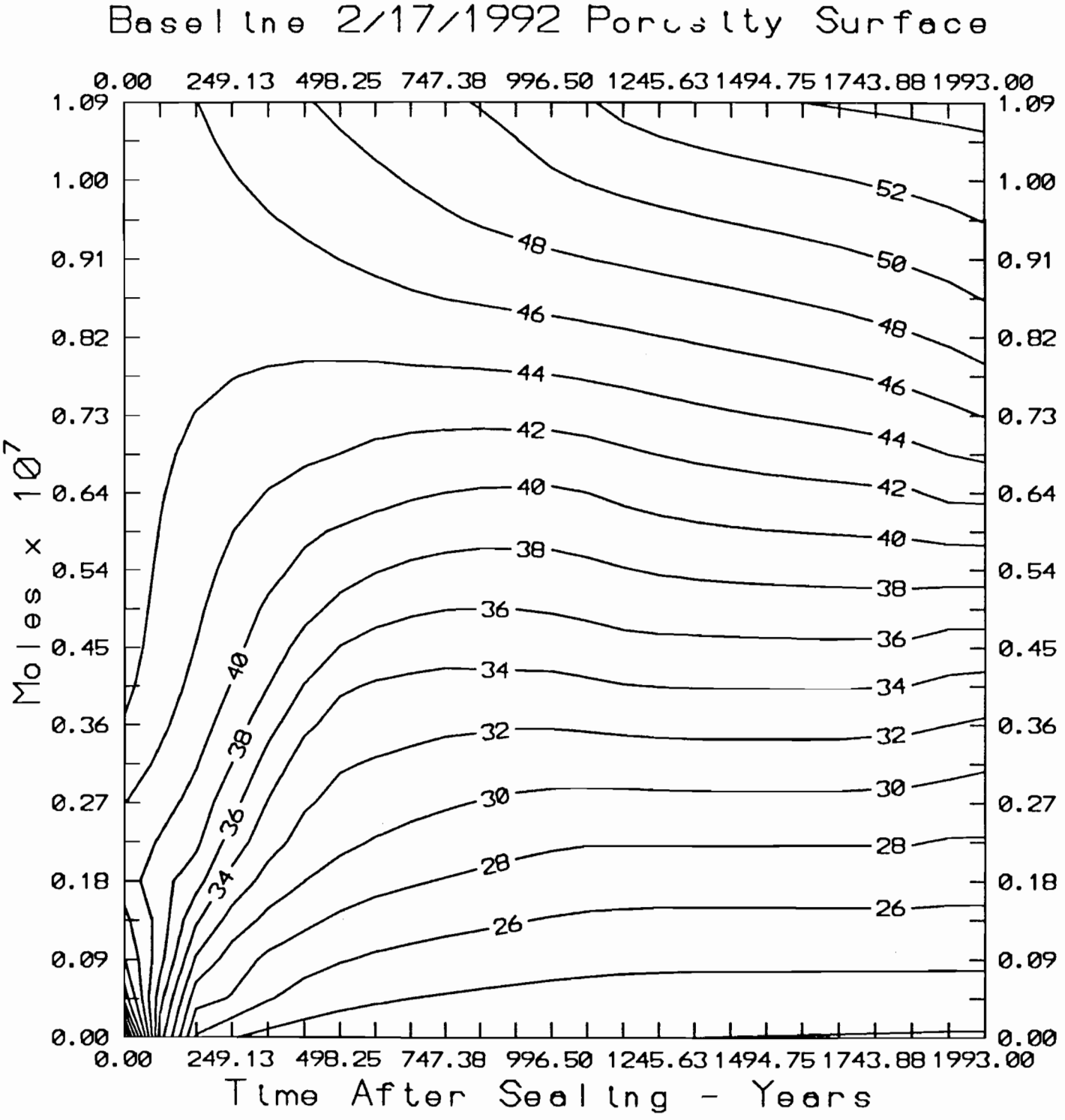
Baseline 2/17/1992 Porosity Surface
0.00
249.13
498.25
747.38
996.50
1245.63
1494.75
1743.88
1993.00
1.09
1.00
0.91
0.82
0.73
0.64
0.54
0.45
0.36
0.27
0.18
0.09
0.00
Moles x 10^7
Time After Sealing - Years
52
50
48
46
44
42
40
38
36
34
32
30
28
26

Copy to:
1561 H. S. Morgan
1561 J. G. Arguello
1561 C. M. Stone
1561 J. R. Weatherby
6340 W. D. Weart
6340 SWCF/XXXDRM (5 years)
6340 S. Y. Pickering
6341 A. L. Stevens
6342 B. M. Butcher
6342 R. D. Klett
6342 M. G. Marietta
6342 R. P. Rechard
6342 P. Vaughn
6342 M. S. Tierney
6343 T. M. Schultheis
6344 E. D. Gorham
6344 P. B. Davies
6345 ALL
6346 ALL
6347 D.R. Shafer

Munson, October 26, 1992

Date: 10/26/92
To: M. S. Tierney, 6342
From: D. E. Munson, 6346
Subject: Mechanical Parameters for Volume 3, SAND92-0700

Sandia National Laboratories

Albuquerque, New Mexico 87185

date: 10/26/92

to: M. S. Tierny, 6342

from: D. E. Munson, 6121

subject: Mechanical Parameters for Volume 3, SAND92-0700

I have attached what I believe is the correct set of mechanical parameters for use in Volume 3, SAND92-0700. These parameters are those used currently, or in the past, for thermal/structural calculations in the WIPP Program. You will note that there are actually two sets of parameters: The first set is consistent with the Modified M-D constitutive model which is the recommended model for use in any future WIPP calculations. At this stage of the program, the parameters for the Modified M-D constitutive model are well tested against in situ data. The second set is consistent with the Reduced Modulus (R-M) Steady State model based on the 1984 Reference Creep Law which is still in use, although no longer recommended as a primary model for future WIPP structural calculations. Within acceptable limits, either parameter set, with their respective constitutive models, are permissible for the purposes of performance assessment, provided the R-D model is adequately verified for a specific calculation against the more precise and better tested M-D model.

These parameters will be updated as necessary in subsequent publications of the Reference Data report.

If you have any questions please contact me.

Reviewed: Brian L. Ehgartner 10/29/92
B. L. Ehgartner, 6113

Approved: Joe R. Tillerson 10/30/92
J. R. Tillerson, 6121

Copy to:

B. L. Ehgartner, 6113
J. R. Tillerson, 6121
M. G. Marietta, 6342
R. P. Richard, 6342
WCTF--TSI/PROP

2.5 Mechanical Parameters for Material in Salado Formation

2.5.1 Halite and Argillaceous Halite

Elastic Constants (Halite and Argillaceous Halite)

Parameter	Median	Range	Units	Distribution	Source
Shear Modulus, μ	12.4	None	GPa		2.5.1
Young's Modulus, E	31.0	None	GPa		2.5.1
Poisson's Ratio, ν	0.25	None			2.5.1

Source(s): 2.5.1. Munson, D. E., A. F. Fossum, and P. E. Senseny. 1989. Advances in Resolution of Discrepancies between Predicted and Measured In Situ Room Closures. SAND88-2948. Albuquerque, NM: Sandia National Laboratories.

Creep Constants - Modified M-D Model (Halite)

Parameter	Median	Range	Units	Distribution	Source
A_1	8.386 E22	None	/s		2.5.1
Q_1	25	None	Kcal/mol		2.5.1
n_1	5.5	None			2.5.1
B_1	6.086 E06	None	/s		2.5.1
A_2	9.672 E12	None	/s		2.5.1
Q_2	10	None	Kcal/mole		2.5.1
n_2	5.0	None			2.5.1
B_2	3.034 E-2	None	/s		2.5.1
σ_0	20.57	None	MPa		2.5.1
q	5.335 E03	None			2.5.1
m	3.0	None			2.5.1
K_0	6.275 E05	None			2.5.1
c	9.198 E-3	None	/T		2.5.1
α_w	-17.37	None			2.5.1
β_w	-7.738	None			2.5.1
α_r	-2.69	None			2.5.2
β_r	-1.00	None			2.5.2
R	1.987	None	cal/mol-deg		2.5.3

Source(s):

2.5.1. Munson, D. E., A. F. Fossum, and P. E. Senseny. 1989. Advances in Resolution of Discrepancies between Predicted and Measured In Situ Room Closures. SAND88-2948. Albuquerque, NM: Sandia National Laboratories.
2.5.2. Munson, D. E., K. L. DeVries, and A. F. Fossum. 1992. Analysis of the recovery data to give these numbers is original to this memo. Albuquerque, NM: Sandia National Laboratories.
2.5.3. Munson, D. E., and P. R. Dawson. 1979. Constitutive Model for the Low Temperature Creep of Salt (with Application to WIPP). SAND79-1853. Albuquerque, NM: Sandia National Laboratories.
2.5.4. Munson, D. E. 1979. Preliminary Deformation-Mechanism Map for Salt (with Application to WIPP). SAND79-0076. Albuquerque,. NM: Sandia National Laboratories.
2.5.5. Munson, D. E., and P. R. Dawson. 1882. A Transient Creep Model for Salt during Stress Loading and Unloading. SAND82-0962. Albuquerque, NM: Sandia National Laboratories.
2.5.6. Munson, D. E., and K. L. DeVries. 1991. Development and Validation of a Predictive Technology for Creep Closure of Underground Rooms in Salt. Proc. 7th International Congress on Rock Mechanics, Aachen. Rotterdam, The Netherlands: A. A. Balkema. pp. 127-134. [SAND90-1147].
2.5.7. Callahan, G. D., A. F. Fossum, and D. K. Svalstad. 1986. Documentation of SPECTROM-32: a Finite Element Thermomechanical Stress Analysis Program. RSI-0269. Rapid City, SD: RE/SPEC Inc.

Creep Constants - Modified M-D Model (Argillaceous Halite)

Parameter	Median	Range	Units	Distribution	Source
A_1	1.407 E23	None	/s		2.5.1
Q_1	25	None	Kcal/mol		2.5.1
n_1	5.5	None			2.5.1
B_1	8.998 E06	None	/s		2.5.1
A_2	1.314 E13	None	/s		2.5.1
Q_2	10	None	Kcal/mol		2.5.1
n_2	5.0	None			2.5.1
B_2	4.289 E-2	None	/s		2.5.1
σ_0	20.57	None	MPa		2.5.1
q	5.335 E03	None			2.5.1
m	3.0	None			2.5.1
K_0	2.470 E06	None			2.5.1

c	9.198 E-3	None	/T	2.5.1
α_w	-14.96	None		2.5.1
β_w	-7.738	None		2.5.1
α_r	-2.69	None		2.5.2
β_r	-1.00	None		2.5.2
R	1.987	None	cal/mol-deg	2.5.3

Source(s):

2.5.1. Munson, D. E., A. F. Fossum, and P. E. Senseny. 1989. Advances in Resolution of Discrepancies between Predicted and Measured In Situ Room Closures. SAND88-2948. Albuquerque, NM: Sandia National Laboratories.

2.5.2. Munson, D. E., K. L. DeVries, and A. F. Fossum. 1992. Analysis of the recovery data to give these numbers is original to this memo. Albuquerque, NM: Sandia National Laboratories.

2.5.3. Munson, D. E., and P. R. Dawson. 1979. Constitutive Model for the Low Temperature Creep of Salt (with Application to WIPP). SAND79-1853. Albuquerque, NM: Sandia National Laboratories.

2.5.4. Munson, D. E. 1979. Preliminary Deformation-Mechanism Map for Salt (with Application to WIPP). SAND79-0076. Albuquerque,. NM: Sandia National Laboratories.

2.5.5. Munson, D. E., and P. R. Dawson. 1882. A Transient Creep Model for Salt during Stress Loading and Unloading. SAND82-0962. Albuquerque, NM: Sandia National Laboratories.

2.5.6. Munson, D. E., and K. L. DeVries. 1991. Development and Validation of a Predictive Technology for Creep Closure of Underground Rooms in Salt. Proc. 7th International Congress on Rock Mechanics, Aachen. Rotterdam, The Netherlands: A. A. Balkema. pp. 127-134. [SAND90-1147].

2.5.7. Callahan, G. D., A. F. Fossum, and D. K. Svalstad. 1986. Documentation of SPECTROM-32: a Finite Element Thermomechanical Stress Analysis Program. RSI-0269. Rapid City, SD: RE/SPEC Inc.

Discussion:

The constitutive model for salt creep now recommended for use is the most recent formulation of the multimechanism steady state, workhardening/recovery transient creep creep model [2.5.1], or simply the Modified M-D model. The steady state portion of the model is derived from the deformation mechanism map for salt as given by Munson [2.5.4]. Based on the mechanism map and the expected temperature and stress conditions that pertain to the potential

repository, just three of the mechanisms of salt deformation can be expected to contribute to the WIPP storage room response. These three mechanisms, not all of which are defined theoretically, but all of which are defined experimentally, form the basis of the constitutive model. The initial model, as derived by Munson and Dawson [2.5.3], included the three appropriate steady state mechanisms and a stress loading, workhardening transient response as an evolutionary process in strain. This M-D model was later improved to incorporate a stress unloading, recovery transient strain response also as an evolutionary process in strain [2.5.5].

During a major reevaluation study [2.5.1], it was found that the linear approximation used to describe the accumulation of transient strain was inadequate. As a result, the model was modified to incorporate a quadratic description of the transient strain. This resulted in the current Modified M-D creep model. Success of this model in prediction of the WIPP room closures [2.5.6] makes it the preferred constitutive model and should be taken as the definition of the reference creep property.

The total steady state creep rate of the modified model is given by:

$$\dot{\varepsilon}_s = \sum_{n=1}^{3} \dot{\varepsilon}_{s_i} \qquad 1$$

where summation is over the i^{th} individual mechanisms. Individual steady state strain rates of the three relevant mechanisms are as follows:

$$\dot{\varepsilon}_{s_1} = A_1 e^{-\frac{Q_1}{RT}} \left(\frac{\sigma}{\mu}\right)^{n_1} \qquad 2a$$

$$\dot{\varepsilon}_{s_2} = A_2 e^{-\frac{Q_2}{RT}} \left(\frac{\sigma}{\mu}\right)^{n_2} \qquad 2b$$

$$\dot{\varepsilon}_{s_3} = |H| \left[B_1 e^{-\frac{Q_1}{RT}} + B_2 e^{-\frac{Q_2}{RT}} \right] \sinh\left[\frac{q(\sigma - \sigma_0)}{\mu}\right] \qquad 2c$$

where the A's and B's are structure factors, Q's are activation energies, n's are stress exponents, σ is the stress, σ_0 is a cut off stress level for the third mechanism, μ is the shear modulus, T is the absolute temperature, and R is the universal gas constant. $|H|$ is the Heaviside step function with argument of $(\sigma-\sigma_0)$. Mechanism 1 dominates at high temperatures and low stresses, mechanism 2 controls creep at low temperatures and stresses, and mechanism 3 dominates at high stresses at all temperatures.

The total creep creep rate results from the influence of the transient creep on the steady state creep rate, as determined by:

$$\dot{\varepsilon} = F\dot{\varepsilon}_s \qquad 3$$

where the transient function, F, is

$$F=\begin{Bmatrix} e^{+\Delta\left(1-\frac{\zeta}{\varepsilon_c^*}\right)^2} ; \zeta \le \varepsilon_c^* \\ 1 \\ e^{-\delta\left(1-\frac{\zeta}{\varepsilon_c^*}\right)^2} ; \zeta \ge \varepsilon_c^* \end{Bmatrix} \quad 4$$

The transient function is composed of three branches, a workhardening branch, an equilibrium or steady state branch, and a recovery branch, respectively in order of appearance in the above equation. Here, Δ and δ are the workhardening and recovery parameters, respectively, and ε^*_t is the transient strain limit. The evolutionary equation governing the rate of change of the internal variable, ζ, is

$$\dot{\zeta}=(F-1)\dot{\varepsilon}_s \quad 5$$

The transient strain limit is a function of temperature, and we adopt the form

$$\varepsilon_t^* = K_0 e^{cT}\left(\frac{\sigma}{\mu}\right)^m \quad 6$$

where K_0, c, and m are constants.

The workhardening and recovery parameters are defined as a function of stress through

$$\Delta=\alpha_w+\beta_w \log\left(\frac{\sigma}{\mu}\right) \quad 7a$$

$$\delta=\alpha_r+\beta_r \log\left(\frac{\sigma}{\mu}\right) \quad 7b$$

where the α's and β's are constants, with the subscripts denoting either the workhardening or recovery branch.

The Modified M-D model has been incorporated into SPECTROM-32, a two dimensional finite element code [2.5.7] especially developed for solving solid mechanics problems typical of those required in the WIPP program. This code uses the Tresca flow potential for stress generalization to three dimensions [2.5.1].

Although it is strongly suggested that all final calculations be performed with the modified M-D model, the Tresca flow potential, and the above parameter set, historically, a simplified method has been used in many numerical calculations of WIPP problems. We will include the parameter set for this simplified model for completeness. This earlier method will be designated as the Reduced Modulus (R-M)

model. In this model, the elastic moduli (all except Poisson's Ratio are reduced by a factor of 12.5 [2.5.8]. This value was determined through backfitting of calculation to some of the field data.

Elastic Constants - R-M Model (Halite and Argillaceous Halite)

Parameter	Median	Range	Units	Distribution	Source
Shear Modulus, μ	0.992	None	GPa		2.5.8
Young's Modulus, E	2.480	None	GPa		2.5.8
Bulk Modulus, K	1.656	None	GPa		2.5.8
Poisson's Ratio, ν	0.25	None			2.5.9

Source(s):
2.5.8. Morgan, H. S., C. M. Stone, and R. D. Krieg. 1985. The Use of Field Data to Evaluate and Improve Drift Response Models for the Waste Isolation Pilot Plant (WIPP). Proc. 26th U.S. Symp. on Rock Mechanics, Boston, MA: A.A. Balkema.
2.5.9. Krieg, R. D. 1984. Reference Stratigraphy and Rock Properties for the Waste Isolation Pilot Plant (WIPP) Project. SAND83-1908. Albuquerque, NM: Sandia National Laboratories.

Creep Constants - R-M Model (Halite)

Parameter	Median	Range	Units	Distribution	Source
A	1.66 E14	None	/s		2.5.10
Q	12	None	Kcal/mol		2.5.9
n	4.9	None			2.5.9

Source(s):
2.5.9. Krieg, R. D. 1984. Reference Stratigraphy and Rock Properties for the Waste Isolation Pilot Plant (WIPP) Project. SAND83-1908. Albuquerque, NM: Sandia National Laboratories.
2.5.10. B. L. Ehgartner and D. E.Munson. 1992. This parameter is derived from values of D, u, and n found in Krieg [2,5,9]. Albuquerque, NM: Sandia National Laboratories.
2.5.11. Stone, C. M., R. D. Krieg, and Z. E. Beisinger. 1985. SANCHO - a Finite Element Computer Program for the Quasistatic, Large Deformation, Inelastic Response of Two-Dimensional Solids. SAND84-1618. Albuquerque, NM: Sandia National Laboratories.

Creep Constants - R-M Model (Argillaceous Halite)

Parameter	Median	Range	Units	Distribution	Source
A	4.99 E14	None	/s		2.5.10
Q	12	None	Kcal/mol		2.5.9
n	4.9	None			2.5.9

Source(s):

2.5.9. Krieg, R. D. 1984. Reference Stratigraphy and Rock Properties for the Waste Isolation Pilot Plant (WIPP) Project. SAND83-1908. Albuquerque, NM: Sandia National Laboratories.
2.5.10. B. L. Ehgartner and D. E.Munson. 1992. This parameter is derived from values of D, u, and n found in Krieg [2,5,9]. Albuquerque, NM: Sandia National Laboratories.
2.5.11. Stone, C. M., R. D. Krieg, and Z. E. Beisinger. 1985. SANCHO - a Finite Element Computer Program for the Quasistatic, Large Deformation, Inelastic Response of Two-Dimensional Solids. SAND84-1618. Albuquerque, NM: Sandia National Laboratories.

Discussion:

The R-M model is based entirely on steady state creep as described by a function of the form of Eq. 2b, which is equivalent to assuming a single thermally activated mechanism. However, evaluation of the constants of the equation utilized all of the experimental creep data for from both the unknown and climb mechanism regimes of the deformation mechanism map used in the development of the Modified M-D model. As a consequence, the constants do not match those of the steady state portion of the Modified M-D model for the unknown mechanism. Because of the use of a single function, the subscripts on the parameters have been dropped.

The general model from which the R-M model was derived [2.5.9] also provided for a first order kinetics transient response. This part of the model has not been used in WIPP calculations and will not be presented here.

Typically, the R-M model has been used most often in conjunction with the SANCHO finite element code [2.5.11], although it can be used equally with other finite element codes. In all calculations with the R-M model to date, a von Mises flow criterion has been used.

Thermal Properties (Halite and Argillaceous Halite)

Parameter	Median	Range	Units	Distribution	Source
Specific Heat	862.8	None	J/kg-K		2.5.12
Coef. Lin. Exp.	45.0 E-6	None	1/K		2.5.13
λ_{300}	5.40	None	W/mK		2.5.13
γ	1.14	None			2.5.13

Source(s): 2.5.12. Yang, J. M. 1981. Physical Properties Data for Rock Salt: Chapter 4 - Thermalphysical Properties, NBS Monograph 167. Washington, DC: National Bureau of Standards. (p. 205-221)
2.5.13. Sweet, J. N., and J. E. McCreight. 1980. Thermal Conductivity of Rocksalt and Other Geologic Materials from the Site of the Proposed Waste Isolation Pilot Plant. SAND79-1665. Albuquerque, NM: Sandia National Laboratories.
2.5.14. Moss, M., and G. M. Haseman. 1981. Thermal conductivity of Polyhalite and Anhydrite from the Site of the Proposed Waste Isolation Pilot Plant. SAND81-0856. Albuquerque, NM: Sandia National Laboratories.

Discussion:

The thermal conductivity is determined from the equation:

$$\lambda = \lambda_{300}\left(300/T\right)^{\gamma} \qquad 8$$

where the temperature, T, is in Kelvin.

2.5.2 Non-Salt Materials

Elastic Constants (Anhydrite)

Parameter	Median	Range	Units	Distribution	Source
Shear Modulus, μ	27.8	None	GPa		2.5.15
Young's Modulus, E	75.1	None	GPa		2.5.15
Bulk Modulus, K	83.4	None	GPa		2.5.15
Poisson's Ratio, ν	0.35	None			2.5.15

Source(s): 2.5.15. Munson, D. E., and H. S. Morgan. 1986. Methodology for Performing Parallel Design Calculations (Nuclear Waste Repository Application). SAND85-0324. Albuquerque, NM: Sandia National Laboratories.

Elastic Constants (Polyhalite)

Parameter	Median	Range	Units	Distribution	Source
Shear Modulus, μ	20.3	None	GPa		2.5.15
Young's Modulus, E	55.3	None	GPa		2.5.15
Bulk Modulus, K	65.8	None	GPa		2.5.15
Poisson's Ratio, ν	0.36	None			2.5.15

Source(s): 2.5.15. Munson, D. E., and H. S. Morgan. 1986. Methodology for Performing Parallel Design Calculations (Nuclear Waste Repository Application). SAND85-0324. Albuquerque, NM: Sandia National Laboratories.

Plasticity Parameters - Drucker-Prager Model Yield (Anhydite)

Parameter	Median	Range	Units	Distribution	Source
a	0.45	None			2.5.15
C	1.35	None	MPa		2.5.15

Source(s): 2.5.15. Munson, D. E., and H. S. Morgan. 1986. Methodology for Performing Parallel Design Calculations (Nuclear Waste Repository Application). SAND85-0324. Albuquerque, NM: Sandia National Laboratories.

Plasticity Parameters - Drucker-Prager Model Yield (Polyhalite)

Parameter	Median	Range	Units	Distribution	Source
a	0.473	None			2.5.15
C	1.42	None	MPa		2.5.15

Source(s): 2.5.15. Munson, D. E., and H. S. Morgan. 1986. Methodology for Performing Parallel Design Calculations (Nuclear Waste Repository Application). SAND85-0324. Albuquerque, NM: Sandia National Laboratories.

Discussion:

The Drucker-Prager model is an elastic, perfectly plastic model which has a pressure dependent yield. Typically it is given as:

$$\sqrt{J_2'} = C - aJ_1 \qquad 9$$

where $\sqrt{J_2'}$ is the second invariant and J_1 is the first invariant.

Although the Drucker-Prager model has been used almost exclusively to represent the anhydrite and polyhalite, the exact nature of the flow of these materials is under further study. In most of the analyses, the mechanical response of the polyhalite can be assumed to be elastic because the polyhalite beds are all at large distances from the WIPP horizon. The anhydrite beds however may be very close to the excavations, as in the case of MB139, and it is necessary to determine if the bed material will yield under the conditions of the analysis before it may be assumed to be elastic.

Thermal Properties (Anhydrite)

Parameter	Median	Range	Units	Distribution	Source
Specific Heat	733.3	None	J/kg-K		2.5.12
Coef. Lin. Exp.	20.0 E-6	None	1/K		2.5.13
λ_{300}	4.70	None	W/mK		2.5.13
γ	1.15	None			2.5.13

Source(s):
2.5.12. Yang, J. M. 1981. Physical Properties Data for Rock Salt: Chapter 4 - Thermalphysical Properties, NBS Monograph 167. Washington, DC: National Bureau of Standards. (p. 205-221)
2.5.13. Sweet, J. N., and J. E. McCreight. 1980. Thermal Conductivity of Rocksalt and Other Geologic Materials from the Site of the Proposed Waste Isolation Pilot Plant. SAND79-1665. Albuquerque, NM: Sandia National Laboratories.
2.5.14. Moss, M., and G. M. Haseman. 1981. Thermal conductivity of Polyhalite and Anhydrite from the Site of the Proposed Waste Isolation Pilot Plant. SAND81-0856. Albuquerque, NM: Sandia National Laboratories.

Discussion:

The thermal conductivity is determined from Eq. 8 as given previously.

Thermal Properties (Polyhalite)

Parameter	Median	Range	Units	Distribution	Source
Specific Heat	890.0	None	J/kg-K		2.5.9
Coef. Lin. Exp.	24.0 E-6	None	1/K		2.5.14
λ_{300}	1.40	None	W/mK		2.5.14
γ	0.35	None			2.5.14

Source(s):

2.5.9. Krieg, R. D. 1984. Reference Stratigraphy and Rock Properties for the Waste Isolation Pilot Plant (WIPP) Project. SAND83-1908. Albuquerque, NM: Sandia National Laboratories.
2.5.12. Yang, J. M. 1981. Physical Properties Data for Rock Salt: Chapter 4 - Thermalphysical Properties, NBS Monograph 167. Washington, DC: National Bureau of Standards. (p. 205-221)
2.5.13. Sweet, J. N., and J. E. McCreight. 1980. Thermal Conductivity of Rocksalt and Other Geologic Materials from the Site of the Proposed Waste Isolation Pilot Plant. SAND79-1665. Albuquerque, NM: Sandia National Laboratories.
2.5.14. Moss, M., and G. M. Haseman. 1981. Thermal conductivity of Polyhalite and Anhydrite from the Site of the Proposed Waste Isolation Pilot Plant. SAND81-0856. Albuquerque, NM: Sandia National Laboratories.

Discussion:

The thermal conductivity is determined from Eq. 8 as given previously.

2.5.3 Interbed Mechanical Response Parameter

Parameter	Median	Range	Units	Distribution	Source
Coef.Friction, ϕ	0.2	None			2.5.1

Source(s)

2.5.1. Munson, D. E., A. F. Fossum, and P. E. Senseny. 1989. Advances in Resolution of Discrepancies between Predicted and Measured In Situ Room Closures. SAND88-2948. Albuquerque, NM: Sandia National Laboratories.

Discussion:

The very thin interbeds that occur in the stratigraphy (as given later in Figure 2.5-1) between the major layers of salt, argillaceous salt, anhydrite, and polyhalite. These interbeds consist of either anhydrite or clay, or mixtures of these components. In structural calculations, it is not possible to model these thin interbeds as discrete layers. As a consequence they are handled as slip planes in the numerical codes. These slip planes have a coefficient of friction assigned to them which appears to be correct based on underground observations of the interbed response.

In many of the earlier calculations, especially those with the R-M model, the coefficient of friction was taken as 0.4, which is equivalent to assuming the interbeds are rigidly locked.

2.5.4 Non-Material Input Parameters

Initial Overburden Weight (Averaged)

Parameter	Median	Range	Units	Distribution	Source
Weight, G	22710	None	Pa/m		2.5.9
Source(s):	2.5.9. Krieg, R. D. 1984. Reference Stratigraphy and Rock Properties for the Waste Isolation Pilot Plant (WIPP) Project. SAND83-1908. Albuquerque, NM: Sandia National Laboratories.				

Discussion:

The lithostatic overburden pressure, P, at any depth, H, is given by:

$$P = GH \qquad 10$$

This function uses parameters based on the integrated densities of the overburden as determined from neutron logs. For the nominal facility depth of 650.45 m below ground surface, the lithostatic pressure is 14.77 MPa.

Initial Rock Temperature at Facility Horizon

Parameter	Median	Range	Units	Distribution	Source
Temperature, T_0	26.8	+/-0.5	C		2.5.16

Source(s): 2.5.16. Munson, D. E., R. L. Jones, D. L. Hoag, and J. R. Ball. 1987. Heated Axisymmetric Pillar Test (Room H): In Situ Data Report (February 1985 - April 1987). SAND87-2488. Albuquerque, NM: Sandia National Laboratories.

Local Stratigraphy for Thermal/Structural Numerical Calculations

Discussion:

The recommended stratigraphy is that given by Munson et al. [2.5.1]. This is shown in Figure 2.5-1 and has a local vertical zero referenced to anhydrite "b" (Clay G). The location of an experimental room excavation, which is a room above the WIPP facility horizon. This figure also shows the location of the room with respect to anhydrite "b" (Clay G), which is the reference zero of the stratigraphy.

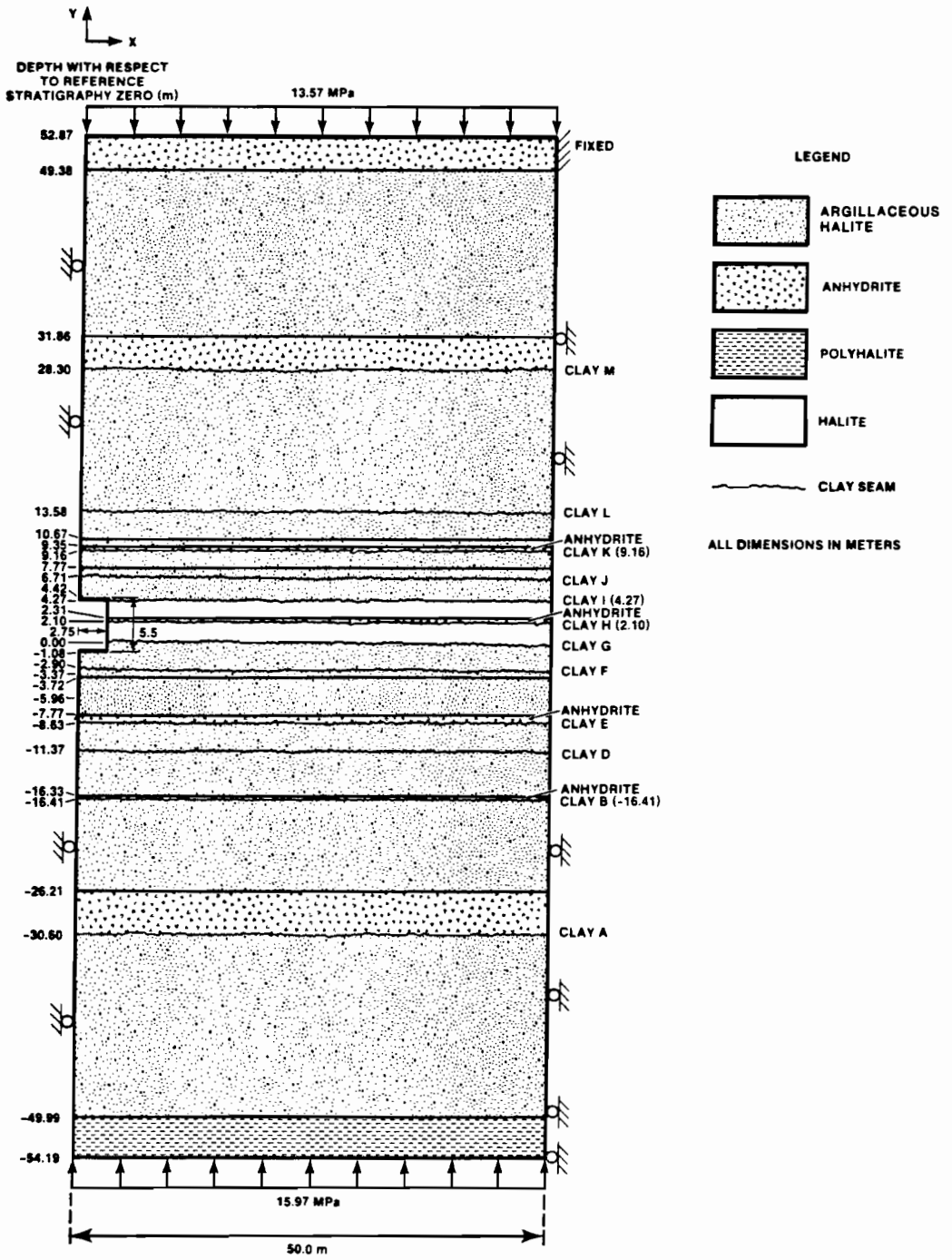

Figure 2.5-1. Local Stratigraphy for Numerical Calculations.

Novak et al., July 20, 1992

Date: 7/20/92
To: Martin S. Tierney, 6342
From: Craig F. Novak, Fred Gelbard, and Hans W. Papenguth, 6119
Subject: Parameter Recommendations for Porosity and Thickness of Clay Fracture Linings for the 1992 WIPP Performance Assessment Calculations

Sandia National Laboratories

Albuquerque, New Mexico 87185

date: 20 July 1992

to: Martin S. Tierney, 6342

from: Craig F. Novak, Fred Gelbard, and Hans W. Papenguth, 6119

subject: Parameter Recommendations for Porosity and Thickness of Clay Fracture Linings for the 1992 WIPP Performance Assessment Calculations

REQUEST FROM DEPARTMENT 6342 FOR VALUES OF CLAY POROSITY AND THICKNESS:

The 1992 WIPP Performance Assessment calculations are scheduled to use a new transport model with explicit clay linings in Culebra fractures. This model assumes there is flow through the void space in the fracture, with diffusion into the pore space of the clays lining the fractures. A schematic representation of the system is shown in Figure 1, assuming planar fractures symmetrical about the fracture centerline, with fracture half-width b and clay lining width b_c. Department 6342 has requested values for parameters necessary to implement this model, including: (1) the ratio of clay lining width to fracture half-width, $\frac{b_c}{b}$, (2) the clay porosity available for diffusive transport, ϕ_c, and (3) clay density, for which the previously recommended value of 2500 $\frac{kg}{m^3}$ (Siegel,1990) should be sufficient.

RECOMMENDATIONS:

A summary of the recommended probability distributions for the ratio of clay lining width to fracture half-width, $\frac{b_c}{b}$, and the effective clay porosity available for diffusive transport, ϕ_c, is given in Table 1.

Table 1. Recommended probability density functions for porosity and relative thickness of clay linings in Culebra fractures.

Parameter	Units	Minimum Value	Maximum Value	Probability	
$\frac{b_c}{b}$ ratio of clay lining width to fracture half-width	dimen-sionless	0.0	0.5	probability = 0.5	$\frac{b_c}{b} = 0$
				$\rho\left(\frac{b_c}{b}\right) = 0.5$	$0 < \frac{b_c}{b} \leq 0.5$
				$\rho\left(\frac{b_c}{b}\right) = 0$	$0.5 < \frac{b_c}{b} \leq 1$
ϕ_c clay porosity available for diffusive transport	volume fraction	0.05	0.50	$\rho(\phi_c) = 0$	$0 \leq \phi_c < 0.05$
				$\rho(\phi_c) = 2.22$	$0.05 \leq \phi_c \leq 0.5$
				$\rho(\phi_c) = 0$	$0.5 < \phi_c \leq 1$

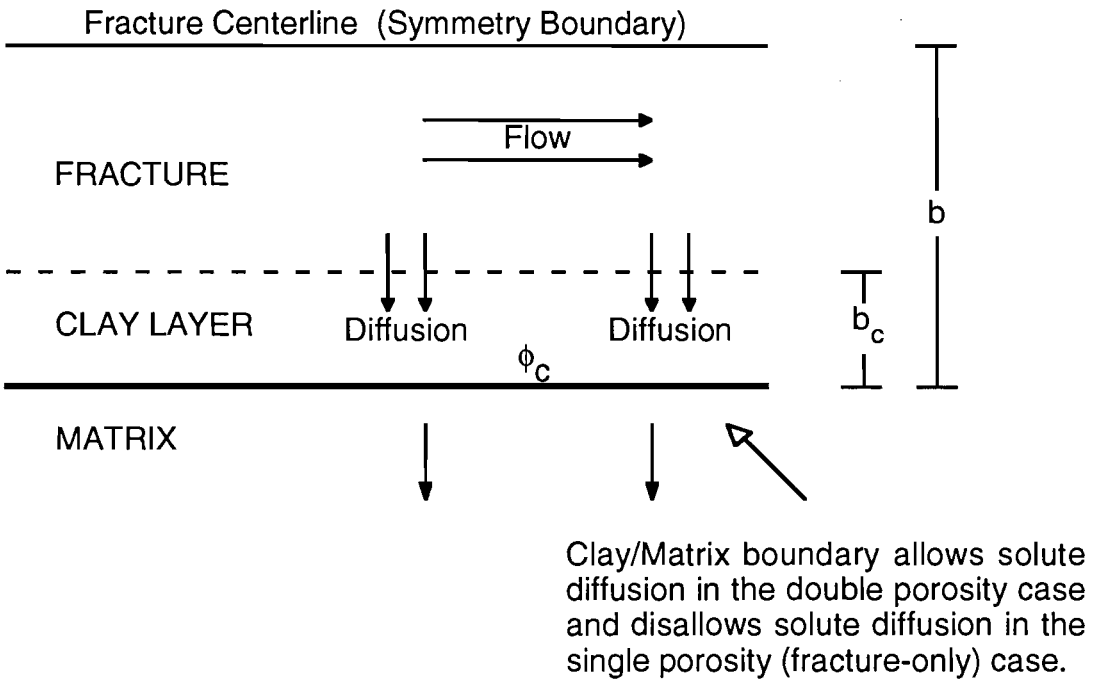

Figure 1. Schematic representation of clay-lined fracture, showing flow in the fracture with diffusion into the clay lining, with or without additional diffusion from the clay layer into the matrix.

Clay Lining Width

Previous estimates (Siegel, 1990) of the fraction of clay lining material, $\frac{b_c}{b}$, should be modified to reflect current thinking. The minimum value considered should be 0 to represent fractures with no clay lining; the maximum can be arbitrarily taken as 0.5. Also, the distribution used to represent the range should reflect a 50% probability of unlined fractures, $\frac{b_c}{b} = 0$, with an equal probability of choosing any other value in the range $0 < \frac{b_c}{b} \leq 0.5$. Defining the probability density function $\rho\left(\frac{b_c}{b}\right)$ such that

$$\int_A^B \rho\left(\frac{b_c}{b}\right) d\left(\frac{b_c}{b}\right)$$

is the fraction of fractures with $\frac{b_c}{b}$ in the range A to B, then

probability = 0.5	$\frac{b_c}{b} = 0$
$\rho\left(\frac{b_c}{b}\right) = 0.5$	$0 < \frac{b_c}{b} \leq 0.5$
$\rho\left(\frac{b_c}{b}\right) = 0$	$0.5 < \frac{b_c}{b} \leq 1$

Sewards (1991) measured and reported clay abundance for eighteen Culebra samples; thirteen from locations to the north and/or west of the WIPP site, and five from the north end of the WIPP site. None of these samples was from wells along fast transport paths. Because Sewards (1991) was focusing on clay abundance and compositional analysis, it is likely that samples were selected for analysis based on visual appearance of clays. Thus, these data may not be representative of clay abundance on fracture surfaces in the area of interest for transport modeling.

Reviews of core logs and discussions with WIPP scientists familiar with Culebra geology suggest that clays do not occur in all fractures. No statistically based studies of the occurrence of clay-lined fractures in the Culebra have been found. There are conceptual difficulties in translating the data of Sewards (1991) into the $\frac{b_c}{b}$ estimates requested by Department 6342. Therefore, the distribution and range of these values should be considered to be highly speculative.

Variation of Clay Lining Width Throughout the Culebra along Fast Transport Paths

Culebra geology and mineralogy is demonstrably variable in the vicinity of the WIPP site (Sewards et al., 1991). Probabilistic modeling of Culebra substrates such as clays should reflect this variability. The parameters provided by this memo represent possible clay occurrence and porosity on a local scale, and should be applied on the smallest scale possible, i.e., to each grid block in the discretization of the Culebra transport model. The data recommendations in this memo are not appropriately applied globally to the Culebra, as would be the case of assigning all fractures in the Culebra the same lining width and porosity for a particular realization.

Current data on clays occurring in Culebra fractures is not sufficient to construct a statistical model. However, if sensitivity studies indicate that clay occurrence and properties are sufficiently important in assessing overall repository performance, then development of a statistical model will likely be necessary.

Clay Porosity

Measurements of the second parameter of interest, the clay porosity available for transport, ϕ_c, have not been found. In the absence of direct experimental data for this parameter, values determined for other clays may serve as surrogates. Because of the short time available, a thorough literature search was not practical. Estimates for ϕ_c range from a few percent (by T. Sewards, a geologist/clay mineralogist previously associated with Culebra characterization work), to 40 to 50%. However, it is unclear whether these numbers represent total void volume fraction, or the volume fraction available for diffusive transport. The only pertinent document found in the available time* presents porosities determined from through-diffusion experiments in London clay (the composition of which was unspecified). The porosities determined with deuterated water averaged 0.47 and those determined with iodide were 0.18, indicating that there is less porosity available to large moieties such as iodide than there is available to water. It is likely that the

* Hassanizadeh, S.M. and G.C. Wijland. 1990. *Radionuclide Migration in Clay Samples by Diffusion and Advection.* INTRAVAL Project Draft Report. Bilthoven, The Netherlands: National Institute of Public Health and Environmental Protection.

lower porosity is more realistic for actinides, however, data to conclusively demonstrate this has not been found.

Applying the information described above to clays in the Culebra, it is reasonable to assume a porosity range $0.05 \leq \phi_c \leq 0.50$, with a distribution reflecting the maximum possible uncertainty (equal likelihood of any value) in the porosity. In mathematical terms, the probability density function $\rho(\phi_c)$ is given by

$$\rho(\phi_c) = 0 \qquad 0 \leq \phi_c < 0.05$$

$$\rho(\phi_c) = \frac{1}{0.50 - 0.05} \approx 2.22 \qquad 0.05 \leq \phi_c \leq 0.5$$

$$\rho(\phi_c) = 0 \qquad 0.5 < \phi_c \leq 1$$

Should sensitivity studies indicate that overall repository performance is highly dependent on the value assumed for clay porosities in the Culebra, it may be possible to implement laboratory studies to obtain these values. However, the clay porosity should be relatively constant throughout the Culebra; once experimentally determined values are available, sampling on the clay porosity may not necessary.

REFERENCES

Sewards, T. 1991. *Characterization of Fracture Surfaces in Dolomite Rock, Culebra Dolomite Member, Rustler Formation.* SAND89-7019. Albuquerque, NM: Sandia National Laboratories.

Sewards, T., M.L. Williams, and K. Keil. 1991. *Mineralogy of the Culebra Dolomite Member of the Rustler Formation.* SAND90-7008. Albuquerque, NM: Sandia National Laboratories.

Siegel, M.D. 1990. "Representation of Radionuclide Retardation in the Culebra Dolomite in Performance Assessment Calculations," Memo 3a in Appendix A of Rechard et al. 1990. *Data Used in Preliminary Performance Assessment of the Waste Isolation Pilot Plant (1990).* SAND89-2408. Albuquerque, NM: Sandia National Laboratories.

Copies to:

6303 W.D. Weart
6303 S.Y. Pickering/WIPP QA
6119 E.D. Gorham
6119 P.B. Davies
6119 C.F. Novak
6119 F. Gelbard
6119 File
6119 H.W. Papenguth
6342 D.R. Anderson
6342 M.G. Marietta
6342 R.P. Rechard

Peterson, October 28, 1992

Date: 10/28/92
To: Martin Tierney, 6342
From: A. Peterson, 6342
Subject: Preliminary Contact Handled (CH) Radionuclide and Nonradionuclide Inventories and Remote Handled (RH) Radionuclide Inventory for Use in 1992 Performance Assessment

Sandia National Laboratories

Albuquerque, New Mexico 87185

date: October 28, 1992

to: Martin Tierney, 6342

from: Andrew Peterson, 6342

subject: Preliminary Contact Handled (CH) Radionuclide and Nonradionuclide Inventories and Remote Handled (RH) Radionuclide Inventory for Use in 1992 Performance Assessment

The radioactive and nonradioactive components of the TRU waste that will be emplaced in the Waste Isolation Pilot Plant (WIPP) are not known with certainty. Most of the volume of TRU waste that could be emplaced in the WIPP has not been generated and the potential sources of TRU waste may be changing. Even though there is considerable uncertainty in the final inventory an estimate of the radioactive and nonradioactive waste inventories are required for performance assessment. The following discussion provides estimates of the radionuclide and nonradionuclide inventories for CH waste and radionuclide inventory for RH waste based on the information currently available.

CH-TRU waste consists of waste that has been generated and stored and waste that will be generated in the future. Draft report DOE/WIPP 91-058 uses input to the 1991 Integrated Data Base (IDB) (US DOE 1991) to estimate the radionuclide inventory for the stored and future generated waste. The total stored volume was about 53,700 m^3 and the future generated waste was about 42,000 m^3. The performance assessment is being analyzed assuming the design volume, 175,560 m^3 (6.2 x 10^6 ft^3) is emplaced in the WIPP. Peterson (In preparation) used the CH radionuclide inventories from Draft report DOE/WIPP 91-058 to estimate the CH radionuclide inventory for a design volume. The results of this estimate are tabulated for each radionuclide by generator site and totaled in Table 1.

Estimates of the number of drums and boxes for stored and projected waste in eight ranges of equivalent Pu-239 curie content were provided for the 1991 IDB by each generator. Peterson (In preparation) used this input to estimate the number of drums and boxes for a design volume in six curie ranges and they are listed in Table 2.

The weight and volume of the CH nonradionuclide inventory was estimated from input to the 1991 IDB for stored and future generated waste volumes and from additional information on waste weights provided by the generator sites. Peterson (In preparation) used this input to estimate

the volume and weight of sludges, metals and glass, and combustibles for the design volume of CH waste. Table 3 lists the estimated weight and volume of these constituents of CH waste.

Draft report DOE/WIPP 91-058 also used input to the 1991 IDB to estimate the RH radionuclide inventory for stored and future generated waste. The total volume of stored and future generated RH waste was nearly equal to the maximum volume of 7,089 m^3 (0.25 x 10^6 ft^3) that can currently be emplaced in the WIPP. The RH radionuclide inventory by site is tabulated in Table 4.

References:

Peterson A. C. (In preparation). Estimated CH-TRU Inventory for use in Performance Assessment for the Waste Isolation Pilot Plant.' SAND92-2023. Albuquerque NM: Sandia National Laboratories.

US DOE (Department of Energy). 1991. Integrated Data Base for 1991: U. S. Spent Fuel and Radioactive Waste Inventories, Projections, and Characteristics. DOE/RW-0006, Rev 7. September 1991.

Copy to:
SWCF (WBS 1.1.6.1.3) PA/INV

Table 1
Estimated Design Radionuclide Inventory by Waste Generator for Contact-Handled Waste (Curies)

RN91DES

Isotope	Half-life (Years)	ANL-E (Ci)	HANF (Ci)	INEL (Ci)	LANL (Ci)	LLNL (Ci)	MOUND (Ci)	NTS (Ci)	ORNL (Ci)	RFP (Ci)	SRS (Ci)	Total (Ci)	Unit Waste Factor
Sr-90	2.91E+01		8.183E+04	4.834E+02								8.231E+04	-
Y-90	7.30E-03		8.183E+04									8.183E+04	-
Ru-106	1.01E+00		9.882E+02	6.225E-01								9.888E+02	-
Rh-106	2.50E-04		9.882E+02									9.882E+02	-
Cs-137	3.00E+01		6.235E+04	6.263E+02								6.298E+04	-
Ba-137m	4.85E-06		5.579E+04									5.579E+04	-
Ce-144	7.78E-01		9.882E+03	4.610E+00								9.887E+03	-
Pr-144	3.29E-05		9.882E+03									9.882E+03	-
Pm-147	2.62E+00		7.397E+04	2.043E+03								7.601E+04	-
Th-232	1.41E+10		2.438E-02	2.600E-01					4.587E-03		5.272E-04	2.895E-01	2.895E-01
U-233	1.59E+05			7.106E+02					8.185E+02		3.072E-02	1.529E+03	-
U-235	7.04E+08	5.259E-04	2.780E-01	1.321E-01	5.315E-02				2.917E-02	6.776E-03	3.814E-02	5.378E-01	-
U-238	4.47E+09	1.534E-04	2.208E+00	1.071E-01	2.920E-01				4.490E-02		2.592E-02	2.678E+00	-
Np-237	2.14E+06			5.296E-01					8.969E+00		1.128E+01	2.078E+01	2.078E+01
Pu-238	8.77E+01		3.410E+04	5.266E+04	2.864E+05	2.973E+02	2.731E+03	3.082E+00	1.271E+04	2.665E+03	2.664E+06	3.055E+06	3.055E+06
Pu-239	2.41E+04	1.631E+02	9.882E+03	3.166E+04	1.489E+05	6.015E+03	2.025E+00	7.491E+01	4.380E+03	7.462E+04	5.940E+04	3.351E+05	3.351E+05
Pu-240	6.56E+03	3.560E+01	2.470E+03	7.897E+03	4.992E+04	1.757E+03	1.366E+00	1.728E+01	3.463E+03	1.799E+04	1.675E+04	1.003E+05	1.003E+05
Pu-241	1.44E+01	9.747E+02	6.670E+04	2.260E+05	2.097E+06	4.301E+04		7.107E+02	6.699E+04	4.917E+05	6.025E+05	3.596E+06	-
Pu-242	3.76E+05			8.305E-01	7.919E+00	1.862E-01		1.164E-03		5.237E-01	1.403E+01	2.349E+01	2.349E+01
Am-241	4.32E+02			6.904E+04	5.540E+05	1.933E+03			8.724E+02	7.929E+04	8.572E+03	7.137E+05	7.137E+05
Cm-244	1.81E+01			8.806E+02					1.290E+04		6.779E+03	2.056E+04	2.056E+04
Cf-252	2.64E+00			5.048E-02					2.515E+02		8.549E+01	3.370E+02	
Totals		1.173E+03	4.907E+05	3.920E+05	3.136E+06	5.301E+04	2.735E+03	8.060E+02	1.024E+05	6.663E+05	3.358E+06	8.203E+06	4.225E+06

Argonne National Laboratory-East (ANL-E)
Hanford Site (HANF)
Idaho National Engineering Laboratory (INEL)
Los Alamos National Laboratory (LANL)
Lawrence Livermore National Laboratory (LLNL)
Mound Plant (MOUND)
Nevada Test Site (NTS)
Oak Ridge National Laboratory (ORNL)
Rocky Flats Plant (RFP)
Savannah River Site (SRS)

Table 2
Estimate of Curie content of Drums and Standard Waste Boxes

92Acurie	0-0.5 (Ci)	0.5-1 (Ci)	1-10 (Ci)	10-20 (Ci)	20-100 (Ci)	100-1000 (Ci)
Stored Drums	30100	13642	49809	14939	11321	2600
Projected Drums	45525	11142	56936	12084	10731	885
Scaled Drums	84604	20921	107254	22786	20229	1674
Totals	160229	45705	213999	49809	42281	5159
Stored Boxes	1666	703	4453	1082	1321	305
Projected Boxes	1497	164	1838	1417	1792	600
Scaled Boxes	2572	310	3477	2524	3391	1135
Total	5735	1177	9768	5023	6504	2040
Percent	30.3	8.6	40.9	10.0	8.9	1.3

CompoRN

Table 3

Estimated composition of CH-TRU waste

	Weight (kg)	Volume Fraction	Volume (m3)	No Drums	No. SWBs	Steel Drums (kg)	SWB Steel (kg)	Poly/ PVC (kg)	Weight Reinf wood	Total Weight (kg)	Weight Fraction
Sludge	2.538E+07	0.207	36342	174720		5.084E+06		1.188E+06		3.165E+07	0.363
Metals and Glass*	1.980E+07	0.421	73912	182284	18946	5.304E+06	5.892E+06	2.034E+05		3.120E+07	0.358
Combustibles**	1.220E+07	0.372	65310	161068	16740	4.687E+06	5.206E+06	1.797E+05	1.980E+06	2.425E+07	0.278
Steel in drums	1.508E+07										
Steel in SWBs	1.110E+07										
Poly/PVC liners	1.571E+06										
Reinforced Wood	1.980E+06										
Total	8.711E+07		175564	518072	35686	1.508E+07	1.110E+07	1.571E+06	1.980E+06	8.711E+07	

*Estimate of total corrodible metals in waste = 10.7 Gg
(Iron Based Materials)

**Estimate of total biodegradable materials in waste = 5.92 Gg
(cellulosics + one half of rubbers + reinforced wood boxes)

Table 4
Estimated Design Radionuclide Inventory by Waste Generator of Remote-Handled Waste

91RHRNDES

Radio Nuclide	Halflife (Yrs)	ANL-E (Ci)	HANF (Ci)	INEL (Ci)	LANL (Ci)	ORNL (Ci)	1992 PA System Total (Ci)	PA Calculations Design 1992	Unit Waste Factors
Cr-51	7.580E-02			5.01E+00			5.01E+00		
Mn-54	8.560E-01			3.06E+05			3.06E+05		
Co-58	1.940E-01			8.03E+01			8.03E+01		
Fe-59	1.220E-01			4.89E+00			4.89E+00		
Co-60	5.270E+00		1.86E+03	3.08E+01		4.79E+03	6.69E+03		
Ni-63	1.000E+02		1.25E+01	2.85E+02			2.98E+02		
Sr-90	2.910E+01		3.02E+05	4.59E+04	5.96E+02	1.73E+05	5.22E+05	5.22E+05	
Y-90	7.306E-03		3.02E+05	1.47E+02	5.96E+02		3.03E+05		
Nb-95	9.630E-02		1.70E+03	5.14E-01			1.70E+03		
Tc-99	2.130E+05		2.42E+02	1.08E-01			2.42E+02		
Ru-106	1.010E+00		7.97E+04	1.22E+04			9.20E+04		
Rh-106	9.480E-07		7.97E+04	9.28E-01			7.97E+04		
Sb-125	2.770E+00		1.43E+04	4.35E+00			1.43E+04		
Cs-134	2.060E+00		9.29E+03	6.64E+02			9.95E+03		
Cs-137	3.000E+01	6.66E+02	3.72E+05	1.32E+04	4.47E+02	1.83E+05	5.69E+05	5.69E+05	
Ba-137m	4.855E-06		3.49E+05	1.19E+02	3.97E+02		3.49E+05		
Ce-144	7.780E-01		2.71E+05	2.80E+03			2.74E+05		
Pr-144	3.288E-05		2.71E+05	1.12E+01			2.71E+05		
Pm-147	2.623E+00		3.83E+05	1.52E+05	4.47E+02		5.36E+05	5.36E+05	
Eu-152	1.330E+01		1.20E+01			2.40E+04	2.40E+04		
Eu-154	8.800E+00		1.68E+03	1.11E+00		1.44E+04	1.61E+04		
Eu-155	4.960E+00		3.06E+03	5.55E-01			3.06E+03		
Th-232	1.410E+10		2.09E-02	5.00E-05		5.64E+00	5.66E+00	5.66E+00	5.66E+00
U-233	1.590E+05			1.72E-01		1.98E+02	1.99E+02	1.99E+02	
U-235	7.048E+08		2.18E-01	3.91E-01	3.18E-03	5.08E-04	6.13E-01	6.13E-01	
U-236	2.340E+07		2.15E-03	3.43E-03			5.59E-03	5.59E-03	
U-238	4.470E+09	1.50E-04	1.76E+00	4.21E-02	2.97E-04	1.03E-03	1.80E+00	1.80E+00	
Np-237	2.140E+07		7.28E-01	3.91E-03		1.88E-01	9.20E-01	9.20E-01	9.20E-01
Pu-238	8.770E+01		2.65E+04	5.35E+01	2.41E+00	8.14E+02	2.73E+04	2.73E+04	2.73E+04
Pu-239	2.410E+04	1.10E+01	8.07E+03	5.18E+01	2.65E+01	3.39E+02	8.50E+03	8.50E+03	8.50E+03
Pu-240	6.560E+03	7.87E+00	2.16E+03	1.04E+02	8.81E+00	4.50E-01	2.28E+03	2.28E+03	2.28E+03
Pu-241	1.440E+01	1.02E+02	6.36E+04	5.55E+04	3.72E+02	1.05E-02	1.20E+05	1.20E+05	
Pu-242	3.750E+05		1.72E-03	2.94E+00	1.66E-03		2.94E+00	2.94E+00	2.94E+00
Am-241	4.327E+02		9.81E+02	1.62E+01		6.48E+01	1.06E+03	1.06E+03	1.06E+03
Cm-244	1.810E+01		2.30E+00			4.26E+03	4.26E+03	4.26E+03	4.26E+03
Cf-252	2.638E+00					8.63E+01	8.63E+01	8.63E+01	
Totals		7.87E+02	2.54E+06	5.89E+05	2.89E+03	4.04E+05	3.54E+06	1.79E+06	4.35E+04

Argonne National Laboratory-East (ANL-E)
Hanford Site (HANF)
Idaho National Engineering Laboratory (INEL)
Los Alamos National Laboratory (LANL)
Oak Ridge National Laboratory (ORNL)

Webb, March 20, 1992 (1992a)

Date: 3/20/92
To: D. R. Anderson, 6342
From: S. W. Webb, 6344
Subject: Uncertainty Estimates for Two-Phase Characteristic Curves for 1992 RCRA Calculations

Sandia National Laboratories

Albuquerque, New Mexico 87185

date: March 20, 1992

to: D. R. Anderson, 6342

from: S. W. Webb, 6344

subject: Uncertainty Estimates for Two-Phase Characteristic Curves for 1992 RCRA Calculations

Two-phase characteristic curves (capillary pressure and relative permeability) have a large degree of uncertainty since no data on the WIPP materials have been obtained. The uncertainty in the threshold pressure has been discussed previously by Davies (Ref. 1); this variation was used by PA in the 1991 comparison with 40 CFR 191 is still considered valid for the RCRA calculations. Uncertainties in the two-phase characteristic curves were discussed by Webb (Ref. 2); these values were not used by PA in their most recent 40 CFR 191 calculations. The uncertainties given by Webb will be modified and updated in this memo.

Uncertainties in the two-phase characteristic curves fall into the following categories:

1. Conceptual Model
2. Correlation Model
3. Parameter

The conceptual model for the two-phase interface is based on standard two-phase characteristic curves. Since a lower viscosity fluid (gas) is displacing a higher viscosity fluid (brine), the displacement interface will be unstable, and viscous and capillary fingering may occur. Fingering is a very complex phenomena which has not been quantified yet for the WIPP, but the processes are not captured in standard two-phase characteristic curves. Investigation into fingering processes has recently been initiated in 6344. It is not known what the impact will be on the displacement interface, but indications are that it could be significant. In addition, these standard curves are based on a uniform porous media; fractures are expected in the Salado, especially in the anhydrite interbeds. The conceptual model uncertainty of using standard two-phase characteristic curves derived for uniform porous media is large.

Uncertainty also exists in the choice of the correlation model. At present, the modified Brooks and Corey correlation is suggested based on comparison to a single set of data for an analogue material (tight gas sands) as discussed by Davies and LaVenue (Ref. 3). As has been repeatedly emphasized, there are no measurements for any Salado lithologies, so the correlation uncertainty is large. This aspect has been addressed to a

limited extent by Webb (Ref. 4) which shows a significant influence of the two-phase characteristic curves on the gas migration distance for the undisturbed scenario.

Finally, parameter uncertainty is also large. As discussed in the preceding paragraph, there are no measurements and we rely on only one set of measurements on an analogue material. Since only one data set was used for parameter evaluation, no parameter range can be given.

With these large uncertainties in all areas, large ranges of parameters are necessary. Within the current set of RCRA calculations, PA has requested that the uncertainties fit into the modified Brooks and Corey model framework due to time constraints. While the current set of uncertainties will be molded into that framework, this restriction negates the correlation uncertainty discussed above. Thus, the real uncertainty is significantly larger than given in this memo. The parameter ranges summarized below apply to the all lithologies in the Salado. Note that the threshold pressure is different for the various units as given by Davies (Ref. 1).

Brooks and Corey

Threshold Pressure (P_t)
Expected Value and Range given by Davies (Ref. 1)
Residual Saturations (S_{lr} and S_{gr})
Expected Value = 0.2
Range between 0.0 and 0.4 with uniform distribution
Pore-Size Distribution Parameter (λ)
Expected Value = 0.7
Range between 0.2 and 10.

The residual saturation value of 0. for the critical gas saturation (S_{gr}) is the most important parameter and is specified to try to estimate possible effects of fingering. This analogy is weak at best but it is the best that can be done at present. The large range for the pore-size distribution parameter is based on values given by Mualem (Ref. 5) for real porous media. Since we do not know anything about the structure of the Salado materials, a wide range is appropriate.

The capillary and relative permeability curves are shown in Figure 1 for the λ range specified above. While the variation is significant, it is not as large as it would be if an alternative correlation model were considered.

Note that the above parameter ranges are only applicable to the RCRA calculations since the correlation has been restricted to the modified Brooks and Corey model. The uncertainty in the two-phase curves will be respecified for the 1992 comparison with 40 CFR 191 to include correlation model uncertainty.

References

1. Memo to D. R. Anderson from P. B. Davies, "Uncertainty Estimates for Threshold Pressure for 1991 Performance Assessment Calculations Involving Waste-Generated Gas," June 6, 1991.

2. Memo to D. R. Anderson from S. W. Webb, "Uncertainty Estimates for Two-Phase Characteristic Curves for 1991 PA Calculations," July 9, 1991.

3. Memo to R. P. Rechard from P. Davies and A. M. LaVenue, "Additional Data for Characterizing 2-Phase Flow Behavior in Waste-Generated Gas Simulations and Pilot Point Information for Final Culebra 2-D Model (SAND89-7068/1)," November 19, 1990.

4. Webb, S. W., "Sensitivity Studies for Gas Release from the Waste Isolation Pilot Plant," Chapter 4.0 in Waste-Generated Gas at the Waste Isolation Pilot Plant: Papers Presented at the Nuclear Energy Agency Workshop on Gas Generation and Release from Radioactive Waste Repositories, P. B. Davies et al., eds., SAND91-2378, November 1991.

5. Mualem, Y., "A New Model for Predicting the Hydraulic Conductivity of Unsaturated Porous Media," Water. Resour. Res, Vol. 12, No. 3, pp. 513-522, June 1976.

Copy to:
6340 W. D. Weart
6342 M. G. Marietta
6342 R. P. Rechard
6342 P. Vaughn
6344 E. D. Gorham
6344 P. B. Davies
6344 S. M. Howarth

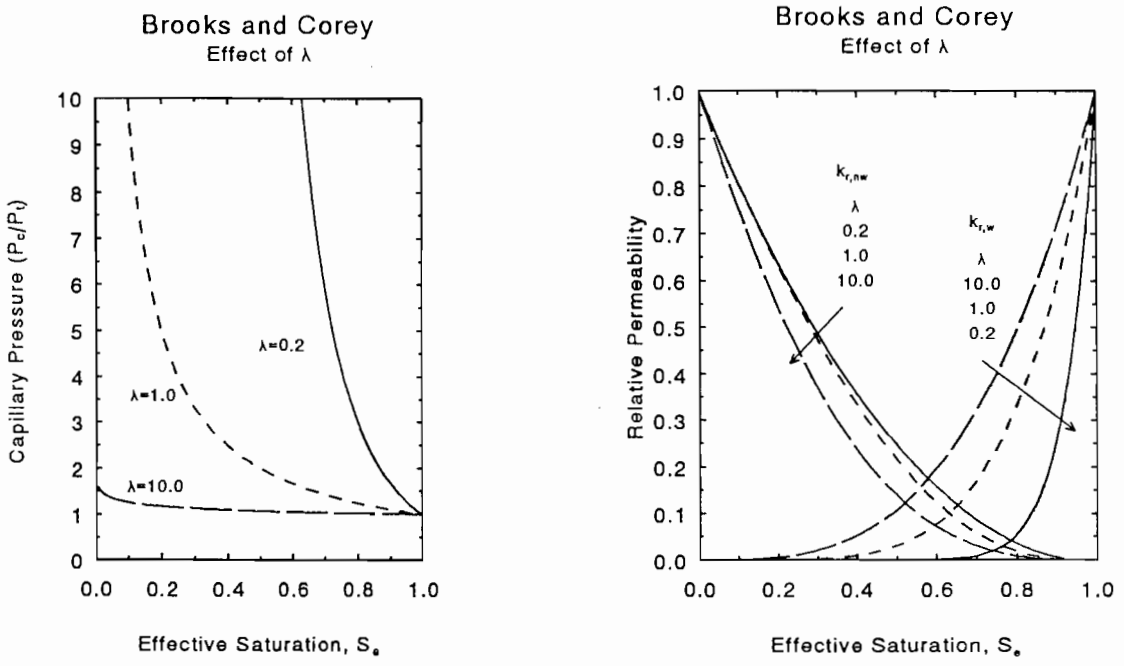

Figure 1
Range of Capillary Pressure and Relative Permeability Curves

Webb, April 30, 1992 (1992b)

Date: 4/30/92
To: D. R. Anderson, 6342
From: S. W. Webb, 6344
Subject: Uncertainty Estimates for Two-Phase Characteristic Curves for 1992 40 CFR 191 Calculations

Sandia National Laboratories

Albuquerque, New Mexico 87185

date:April 30, 1992

to:D. R. Anderson, 6342

from:S. W. Webb, 6119

subject:Uncertainty Estimates for Two-Phase Characteristic Curves for 1992 40 CFR 191 Calculations

Two-phase characteristic curves (capillary pressure and relative permeability) have a large degree of uncertainty since no data on the WIPP materials have been obtained. The uncertainty in the threshold pressure has been discussed previously by Davies (Ref. 1). Uncertainties in the two-phase characteristic curves for RCRA calculations were discussed by Webb (Ref. 2). Due to time constraints, the two-phase characteristic curves were limited to the modified Brooks and Corey format. The characteristic curves will be expanded in this memo to include correlation uncertainty.

Uncertainties in the two-phase characteristic curves fall into the following categories:

1. Conceptual Model
2. Correlation Model
3. Parameter

The conceptual model for the two-phase interface is based on standard two-phase characteristic curves. Since a lower viscosity fluid (gas) is displacing a higher viscosity fluid (brine), the displacement interface will be unstable, and viscous and capillary fingering may occur. Fingering is a very complex phenomena which has not been quantified yet for the WIPP, but the processes are not captured in standard two-phase characteristic curves. Investigation into fingering has recently been initiated in 6119. It is not known what the impact will be on the displacement interface, but indications are that it could be significant. In addition, these standard curves are based on a uniform porous media; fractures are expected in the Salado, especially in the anhydrite interbeds. The conceptual model uncertainty of using standard two-phase characteristic curves derived for uniform porous media is large.

Uncertainty also exists in the choice of the correlation model. At present, the modified Brooks and Corey correlation is suggested based on comparison to a single set of data for an analogue material (tight gas sands) as discussed by Davies and LaVenue (Ref. 3). As has been repeatedly emphasized, there are no measurements for any Salado lithologies, so the correlation uncertainty is large. This aspect has been addressed to a

limited extent by Webb (Ref. 4) which shows a significant influence of the two-phase characteristic curves on the gas migration distance for the undisturbed scenario.

As an alternative, the van Genuchten/Parker correlation (Ref. 5,6) is included. The van Genuchten relationship for capillary pressure has been used by Yucca Mountain (Ref. 7,8) to fit their data, and the curve fits the Morrow et al. data about as well as the Brooks and Corey correlation (Ref. 9). While the Brooks and Corey model also fits the limited nonwetting phase relative permeability data of Morrow et al. reasonably well, the Parker extension to the van Genuchten model is not as successful (Ref. 9). Even so, the Van Genuchten/Parker model is included as correlation uncertainty since no data are available for WIPP specific materials.

While the van Genuchten form has been successfully compared to capillary pressure data, the variation of the fitting parameter m is only given for a limited subset. However, for large values of capillary pressure, which is expected for WIPP materials, the fitting parameter m is related to the Brooks and Corey parameter λ as $m = \lambda/(1+\lambda)$. As a first approximation, the variation of λ from Brooks and Corey can be used to determine the m distribution.

No definitive threshold pressure exists for the van Genuchten curve, so the Davies' correlation described above cannot be directly used to characterize the magnitude of the capillary pressure curve. In order to include this effect, it is proposed to equate the magnitude of the Brooks and Corey and the van Genuchten curves at an effective saturation of 0.5. This procedure will at least capture the trend of the change in the magnitude of capillary pressure for different materials.

Finally, parameter uncertainty is also large. As discussed in the preceding paragraph, there are no measurements and we rely on only one set of measurements on an analogue material. Since only one data set was used for parameter evaluation, no parameter range can be given.

With these large uncertainties in all areas, large ranges of parameters are necessary. The parameter ranges summarized below apply to the all lithologies in the Salado. The Brooks and Corey model is considered more reliable than the van Genuchten/Parker model based on limited data-model comparisons (Ref. 9); therefore, a weighting factor of 0.67 for Brooks and Corey and 0.33 for van Genuchten/Parker is tentatively recommended.

<u>Brooks and Corey</u> (Weighting Factor = 0.67)

Threshold Pressure (P_t)
- Expected Value and Range given by Davies (Ref. 1)

Residual Saturations (S_{lr} and S_{gr})
- Expected Value = 0.2
- Range between 0.0 and 0.4 with uniform distribution

Pore-Size Distribution Parameter (λ)
- Expected Value = 0.7
- Range between 0.2 and 10.

van Genuchten/Parker (Weighting Factor = 0.33)

Pressure Constant (P_o)
Equate with Brooks and Corey capillary pressure at S_e=0.5
Residual Saturation (S_{lr})
Expected Value = 0.2
Range between 0.0 and 0.4 with uniform distribution
Maximum Liquid Saturation (S_{ls})
Expected Value = 1.0
No range
Pore-Size Distribution Parameter (m)
Calculate λ using Brooks and Corey distribution
Approximate m from $m = \lambda/(1+\lambda)$

The residual saturation value of 0. for the critical gas saturation (S_{gr}) is an important parameter and is specified to try to estimate possible effects of fingering. This analogy is weak at best but it is the best that can be done at present. The large range for the pore-size distribution parameter is based on values given by Mualem (Ref. 10) for real porous media. Since we do not know anything about the structure of the Salado materials, a wide range is appropriate.

The capillary and relative permeability curves are shown in Figure 1 for the λ and m ranges specified above. The equations for the correlations are summarized in the appendix.

Work is currently in progress evaluating fracture two-phase characteristic curves as well as equivalent continuum approaches which combine matrix and fracture behavior. These additional two-phase characteristic curves are expected for the 1993 PA calculations.

References

1. Memo to D. R. Anderson from P. B. Davies, "Uncertainty Estimates for Threshold Pressure for 1991 Performance Assessment Calculations Involving Waste-Generated Gas," June 6, 1991.

2. Memo to D. R. Anderson from S. W. Webb, "Uncertainty Estimates for Two-Phase Characteristic Curves for 1992 RCRA Calculations," March 20, 1992.

3. Memo to R. P. Rechard from P. Davies and A. M. LaVenue, "Additional Data for Characterizing 2-Phase Flow Behavior in Waste-Generated Gas Simulations and Pilot Point Information for Final Culebra 2-D Model (SAND89-7068/1)," November 19, 1990.

4. Webb, S. W., "Sensitivity Studies for Gas Release from the Waste Isolation Pilot Plant," Chapter 4.0 in Waste-Generated Gas at the Waste Isolation Pilot Plant: Papers Presented at the Nuclear Energy Agency Workshop on Gas Generation and Release from Radioactive Waste Repositories, P. B. Davies et al., eds., SAND91-2378, November 1991.

5. van Genuchten, R., Calculating The Unsaturated Hydraulic Conductivity With a New Closed-Form Analytical Model, Research Report 78-WR-08, Department of Civil Engineering, Princeton University, September 1978.

6. Parker, J. C., R. J. Lenhard, and T. Kuppusamy, "A Parametric Model for Constitutive Properties Regarding Multiphase Flow in Porous Media," Water Resour. Res., Vol. 23, No. 4, pp. 618-624, 1987.

7. Peters, R. R., E. A. Klavetter, I. J. Hall, S. C. Blair, P. R. Heller, and G. W. Gee, Fracture and Matrix Hydrologic Characteristics of Tuffaceous Materials from Yucca Mountain, Nye County, Nevada, SAND84-1471, Sandia National Laboratories, December 1984.

8. Klavetter, E. A., and R. R. Peters, Estimation of Hydrologic Properties of An Unsaturated, Fractured Rock Mass, SAND84-2642, Sandia National Laboratories, July 1986.

9. Webb, S. W., "Review of Two-Phase Characteristic Curves for Application to the WIPP," in progress.

10. Mualem, Y., "A New Model for Predicting the Hydraulic Conductivity of Unsaturated Porous Media," Water. Resour. Res, Vol. 12, No. 3, pp. 513-522, June 1976.

Copy to:
6340 W. D. Weart
6119 E. D. Gorham
6119 P. B. Davies
6119 S. M. Howarth
6342 M. G. Marietta
6342 R. P. Rechard
6342 M. S. Tierney
6342 P. Vaughn

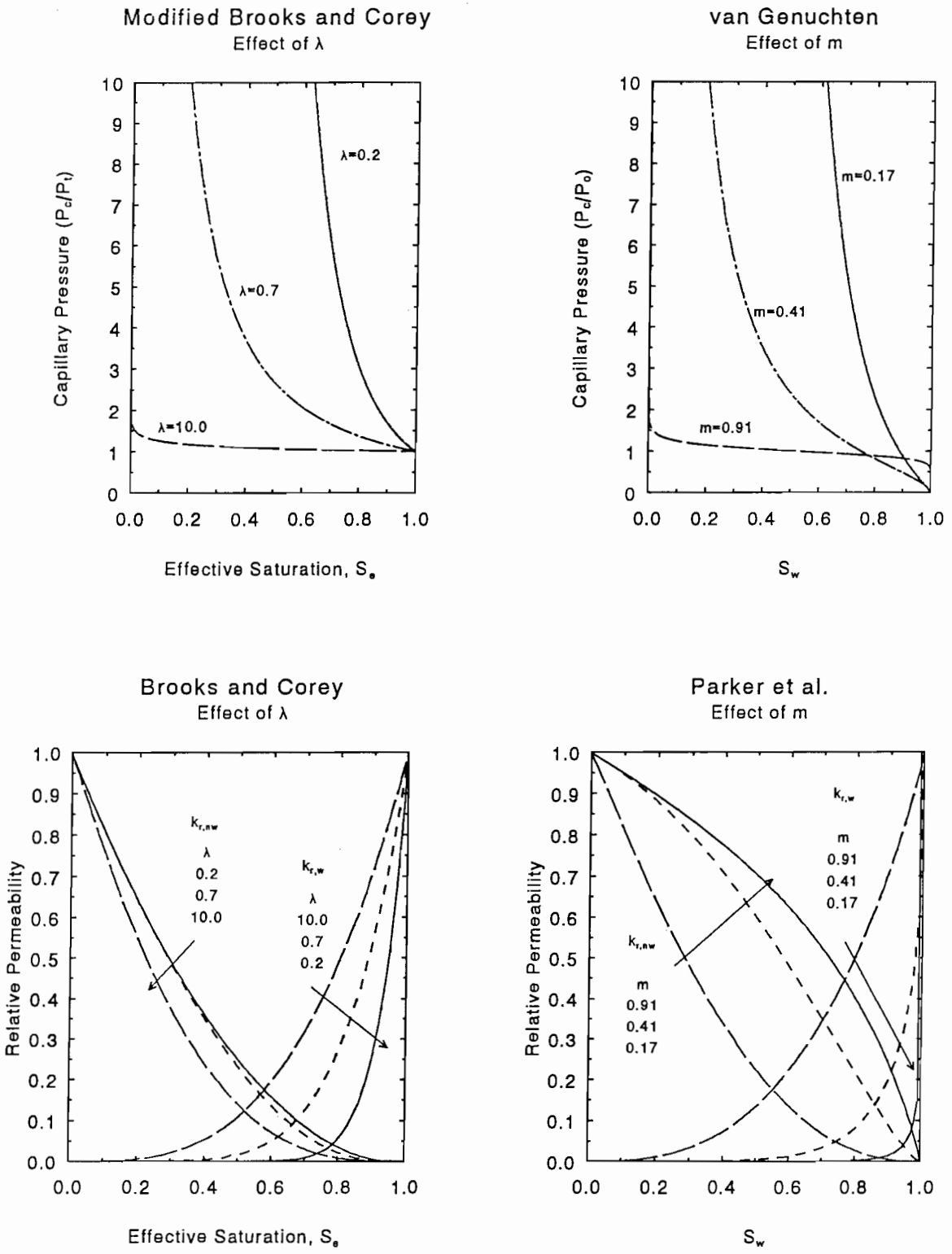

Figure 1
Capillary Pressure and
Relative Permeability Functions

Appendix
Two-Phase Characteristic Curves

The relationships defining the various sets of two-phase characteristic curves are summarized below.

Brooks and Corey

The modified Brooks and Corey relationships used by Davies and LaVenue (1991) are

Capillary Pressure

$$P_c = \frac{P_t}{S_e^{1/\lambda}} \tag{A-1}$$

Relative Permeability

$$k_{r,l} = S_e^{(2+3\lambda)/\lambda} \tag{A-2}$$

$$k_{r,g} = \left(1 - S_e\right)^2 \left[1 - S_e^{(2+\lambda)/\lambda}\right] \tag{A-3}$$

$$S_e = \frac{S_l - S_{lr}}{1 - S_{gr} - S_{lr}}. \tag{A-4}$$

The capillary pressure relationship, equation A-1, is used throughout the entire saturation region ($0. \leq S_l \leq 1.$) even though, as discussed by Corey (1986), this relationship may not be appropriate at the higher liquid saturations when $S_e > 1.0$.

van Genuchten/Parker et al.

The relationships for the van genuchten/Parker et al. (1987) characteristic curves are

Capillary Pressure

$$P_c = P_o \left[S_e^{-1/m} - 1 \right]^{1 - m}. \tag{A-5}$$

Relative Permeability

$$k_{r,l} = S_e^{1/2} \left[1 - \left(1 - S_e^{1/m} \right)^m \right]^2 \qquad \text{(A-6)}$$

$$k_{r,g} = \left(1 - S_e \right)^{1/2} \left(1 - S_e^{1/m} \right)^{2m} \qquad \text{(A-7)}$$

where

$$S_e = \frac{S_l - S_{lr}}{S_{ls} - S_{lr}} \qquad \text{(A-8)}$$

where S_{ls} is the maximum wetting phase saturation.

APPENDIX B:
WELL LOCATION DATA
AND
ELEVATIONS OF STRATIGRAPHIC LAYERS NEAR WIPP

Table B.1. Location of Wells used by WIPP (Universal Transverse Mercator [UTM], State Plan Coordinates [stpln], and Survey Sections [township, range and section])

	Well ID	x-UTM	y-UTM	x-STPLN	y-STPLN	Township	Range	Section	Source
2	AEC7	621117	3589387	691810	523142	21	32	31	Mercer, 1983, Table 1
3	AEC8	617522	3586435	679945	513555	22	31	11	Mercer, 1983, Table 1
4	B25	611695	3580609	660759	494504	22	31	20	Mercer, 1983, Table 1
5	CABIN1	613191	3578049	665559	486111	23	31	5	Gonzales, 1989, Tables 3-6 and 3-7
6	DH207	613634	3581973	667074	498589	0	0	0	Krieg, 1984, Table I
7	DH211	613637	3581784	667082	497966	0	0	0	Krieg, 1984, Table I
8	DH215	613634	3581588	667072	497326	0	0	0	Krieg, 1984, Table I
9	DH219	613636	3581448	667081	496864	0	0	0	Krieg, 1984, Table I
10	DH223	613634	3581247	667073	496207	0	0	0	Krieg, 1984, Table I
11	DH227	613632	3581071	667066	495630	0	0	0	Krieg, 1984, Table I
12	DH77	613476	3582573	666554	500556	0	0	0	Krieg, 1984, Table I
13	DO201	613581	3582062	666900	498880	0	0	0	Krieg, 1984, Table I
14	DO203	613630	3582376	667059	499910	0	0	0	Krieg, 1984, Table I
15	DO205	613587	3582616	667066	500696	0	0	0	Krieg, 1984, Table I
16	DO45	613632	3582263	667066	499540	0	0	0	Krieg, 1984, Table I
17	DO52	613586	3582231	666915	499432	0	0	0	Krieg, 1984, Table I
18	DO56	613587	3582375	666919	499907	0	0	0	Krieg, 1984, Table I
19	DO63	613587	3582524	666919	500396	0	0	0	Krieg, 1984, Table I
20	DO67	613516	3582572	666687	500551	0	0	0	Krieg, 1984, Table I
21	DO88	613435	3582572	666421	500551	0	0	0	Krieg, 1984, Table I
22	DO91	613395	3582575	666288	500561	0	0	0	Krieg, 1984, Table I
23	DOE1	615203	3580333	672206	493563	22	31	28	Gonzales, 1989, Tables 3-6 and 3-7
24	DOE2	613683	3585294	667317	509876	22	31	8	Gonzales, 1989, Tables 3-6 and 3-7
25	ENGLE	614953	3567454	671122	451297	24	31	4	Gonzales, 1989, Tables 3-6 and 3-7
26	ERDA10	606684	3570523	644057	461534	23	30	34	Mercer, 1983, Table 1
27	ERDA6	618226	3589011	682292	521975	21	31	35	Mercer, 1983, Table 1
28	ERDA9	613697	3581958	667297	498929	22	31	20	Mercer, 1983, Table 1
29	FFG_002	627231	3608400	712258	585415	20	33	3	Richey, 1989, Table 2
30	FFG_004	622022	3605526	695095	576082	20	33	7	Richey, 1989, Table 2
31	FFG_005	627356	3605486	712599	575853	20	33	10	Richey, 1989, Table 2
32	FFG_006	627658	3605587	713589	576183	20	33	11	Richey, 1989, Table 2
33	FFG_007	627758	3604682	713919	573213	20	33	14	Richey, 1989, Table 2
34	FFG_009	627959	3604782	714579	573543	20	33	14	Richey, 1989, Table 2
35	FFG_011	627658	3605184	713589	574863	20	33	14	Richey, 1989, Table 2
36	FFG_012	627255	3605184	712269	574863	20	33	15	Richey, 1989, Table 2
37	FFG_013	625249	3605163	705684	574827	20	33	16	Richey, 1989, Table 2
38	FFG_014	621225	3604704	692478	573420	20	33	18	Richey, 1989, Table 2
39	FFG_016	627303	3602758	712361	566901	20	33	22	Richey, 1989, Table 2

Table B.1. Location of Wells used by WIPP (Universal Transverse Mercator [UTM], State Plan Coordinates [stpln], and Survey Sections [township, range and section])

	Well ID	x-UTM	y-UTM	x-STPLN	y-STPLN	Township	Range	Section	Source
1	FFG_017	628494	3603697	716300	569948	20	33	23	Richey, 1989, Table 2
2	FFG_018	630636	3602305	723296	565346	20	33	24	Richey, 1989, Table 2
3	FFG_019	627720	3600778	713695	560402	20	33	26	Richey, 1989, Table 2
4	FFG_020	621672	3601468	693880	562799	20	33	30	Richey, 1989, Table 2
5	FFG_023	633058	3599616	731178	556481	20	33	33	Richey, 1989, Table 2
6	FFG_024	635469	3599257	739089	555233	20	33	34	Richey, 1989, Table 2
7	FFG_025	628538	3600381	716379	559068	20	33	35	Richey, 1989, Table 2
8	FFG_026	628122	3600375	715015	559082	20	33	35	Richey, 1989, Table 2
9	FFG_027	627820	3600074	714025	558092	20	33	35	Richey, 1989, Table 2
10	FFG_039	616468	3606754	676902	580244	20	32	10	Richey, 1989, Table 2
11	FFG_040	620041	3603892	688561	570786	20	32	13	Richey, 1989, Table 2
12	FFG_041	616805	3604246	677942	572014	20	32	15	Richey, 1989, Table 2
13	FFG_042	615263	3604535	672914	572994	20	32	16	Richey, 1989, Table 2
14	FFG_043	614824	3602618	671406	566704	20	32	21	Richey, 1989, Table 2
15	FFG_044	618435	3602658	683256	566770	20	32	23	Richey, 1989, Table 2
16	FFG_105	609126	3590258	652461	526265	21	30	25	Richey, 1989, Table 2
17	FFG_106	607630	3591218	647587	529450	21	30	26	Richey, 1989, Table 2
18	FFG_107	607832	3590109	648217	525810	21	30	26	Richey, 1989, Table 2
19	FFG_108	610586	3589854	657254	524908	21	31	31	Richey, 1989, Table 2
20	FFG_109	612822	3589796	664589	524686	21	31	32	Richey, 1989, Table 2
21	FFG_110	613636	3588341	667229	519875	21	31	32	Richey, 1989, Table 2
22	FFG_111	616209	3589857	675705	524786	21	31	34	Richey, 1989, Table 2
23	FFG_112	615312	3588335	672729	519825	21	31	34	Richey, 1989, Table 2
24	FFG_113	615319	3589869	672784	524858	21	31	34	Richey, 1989, Table 2
25	FFG_114	609458	3586996	653485	515558	22	30	1	Richey, 1989, Table 2
26	FFG_115	608243	3586900	649498	515244	22	30	2	Richey, 1989, Table 2
27	FFG_116	606902	3588088	645132	519179	22	30	3	Richey, 1989, Table 2
28	FFG_117	607132	3587086	645854	515889	22	30	3	Richey, 1989, Table 2
29	FFG_119	604055	3585149	635724	509600	22	30	9	Richey, 1989, Table 2
30	FFG_120	604750	3586261	638038	513251	22	30	9	Richey, 1989, Table 2
31	FFG_121	604134	3585930	636016	512165	22	30	9	Richey, 1989, Table 2
32	FFG_122	604165	3585505	636083	510770	22	30	9	Richey, 1989, Table 2
33	FFG_123	606439	3586110	643580	512686	22	30	10	Richey, 1989, Table 2
34	FFG_124	608252	3586096	649528	512608	22	30	11	Richey, 1989, Table 2
35	FFG_125	607631	3585457	647458	510544	22	30	11	Richey, 1989, Table 2
36	FFG_126	609341	3584606	653068	507720	22	30	13	Richey, 1989, Table 2
37	FFG_127	608226	3583523	649376	504163	22	30	14	Richey, 1989, Table 2
38	FFG_128	605614	3581894	640772	498885	22	30	21	Richey, 1989, Table 2

Table B.1. Location of Wells used by WIPP (Universal Transverse Mercator [UTM], State Plan Coordinates [stpln], and Survey Sections [township, range and section])

	Well ID	x-UTM	y-UTM	x-STPLN	y-STPLN	Township	Range	Section	Source
1	FFG_129	604814	3583050	638181	502679	22	30	21	Richey, 1989, Table 2
2	FFG_130	604412	3582244	636828	500068	22	30	21	Richey, 1989, Table 2
3	FFG_132	606479	3581068	643582	496139	22	30	27	Richey, 1989, Table 2
4	FFG_133	606462	3580266	643522	493544	22	30	27	Richey, 1989, Table 2
5	FFG_134	605663	3580407	640899	494006	22	30	27	Richey, 1989, Table 2
6	FFG_135	607211	3580978	645983	495845	22	30	27	Richey, 1989, Table 2
7	FFG_136	609279	3579410	652734	490667	22	30	36	Richey, 1989, Table 2
8	FFG_137	609955	3578869	654952	488858	22	30	36	Richey, 1989, Table 2
9	FFG_138	610827	3587071	657978	515773	22	31	6	Richey, 1989, Table 2
10	FFG_139	610665	3587722	657478	517912	22	31	6	Richey, 1989, Table 2
11	FFG_140	613648	3585123	667200	509316	22	31	8	Richey, 1989, Table 2
12	FFG_141	612120	3585114	662187	509317	22	31	8	Richey, 1989, Table 2
13	FFG_142	615288	3586667	672617	514350	22	31	9	Richey, 1989, Table 2
14	FFG_143	616006	3579286	674808	490129	22	31	34	Richey, 1989, Table 2
15	FFG_144	599879	3577828	621856	485641	23	29	1	Richey, 1989, Table 2
16	FFG_145	599320	3577132	620020	483389	23	29	1	Richey, 1989, Table 2
17	FFG_146	600363	3578186	623476	486818	23	29	1	Richey, 1989, Table 2
18	FFG_147	595499	3578188	607513	486922	23	29	4	Richey, 1989, Table 2
19	FFG_148	600569	3576193	624120	480278	23	29	12	Richey, 1989, Table 2
20	FFG_149	600707	3574718	624539	475434	23	29	13	Richey, 1989, Table 2
21	FFG_155	596597	3570664	610951	462232	23	29	27	Richey, 1989, Table 2
22	FFG_156	595692	3570883	607981	462952	23	29	28	Richey, 1989, Table 2
23	FFG_157	599212	3569453	619500	458190	23	29	35	Richey, 1989, Table 2
24	FFG_158	600510	3569436	623761	458104	23	29	36	Richey, 1989, Table 2
25	FFG_159	609539	3578101	653588	486370	23	30	1	Richey, 1989, Table 2
26	FFG_160	610084	3577670	655343	484923	23	30	1	Richey, 1989, Table 2
27	FFG_161	607676	3577068	647439	483015	23	30	2	Richey, 1989, Table 2
28	FFG_162	607342	3578605	646376	488059	23	30	2	Richey, 1989, Table 2
29	FFG_163	608127	3577850	648955	485549	23	30	2	Richey, 1989, Table 2
30	FFG_164	602541	3574598	630556	475010	23	30	17	Richey, 1989, Table 2
31	FFG_165	601827	3573070	628182	469995	23	30	19	Richey, 1989, Table 2
32	FFG_166	609182	3573205	652317	470305	23	30	24	Richey, 1989, Table 2
33	FFG_167	609012	3570846	651726	462566	23	30	26	Richey, 1989, Table 2
34	FFG_168	604202	3570581	635911	461795	23	30	28	Richey, 1989, Table 2
35	FFG_169	604034	3572065	635389	466662	23	30	29	Richey, 1989, Table 2
36	FFG_170	601537	3572060	627194	466716	23	30	30	Richey, 1989, Table 2
37	FFG_171	601959	3569718	628551	458995	23	30	31	Richey, 1989, Table 2
38	FFG_172	603366	3570098	633169	460209	23	30	32	Richey, 1989, Table 2

Table B.1. Location of Wells used by WIPP (Universal Transverse Mercator [UTM], State Plan Coordinates [stpln], and Survey Sections [township, range and section])

	Well ID	x-UTM	y-UTM	x-STPLN	y-STPLN	Township	Range	Section	Source
1	FFG_173	609960	3569937	654805	459582	23	30	36	Richey, 1989, Table 2
2	FFG_177	591351	3563822	593606	439877	24	29	19	Richey, 1989, Table 2
3	FFG_179	593084	3561340	599224	431698	24	29	29	Richey, 1989, Table 2
4	FFG_180	607488	3567427	646628	451374	24	30	2	Richey, 1989, Table 2
5	FFG_181	604028	3568585	635304	455245	24	30	5	Richey, 1989, Table 2
6	FFG_182	601542	3568281	627146	454314	24	30	6	Richey, 1989, Table 2
7	FFG_183	605177	3566738	639041	449147	24	30	9	Richey, 1989, Table 2
8	FFG_184	607564	3565857	646845	446225	24	30	11	Richey, 1989, Table 2
9	FFG_185	605866	3565683	641274	445686	24	30	15	Richey, 1989, Table 2
10	FFG_186	605016	3565698	638484	445736	24	30	16	Richey, 1989, Table 2
11	FFG_188	602948	3564040	631660	440361	24	30	20	Richey, 1989, Table 2
12	FFG_189	608405	3563679	649573	439043	24	30	23	Richey, 1989, Table 2
13	FFG_190	607685	3562746	647176	436015	24	30	23	Richey, 1989, Table 2
14	FFG_191	609337	3561151	652564	430748	24	30	25	Richey, 1989, Table 2
15	FFG_192	607401	3562442	646246	435019	24	30	27	Richey, 1989, Table 2
16	FFG_194	617718	3568422	680232	454446	24	31	2	Richey, 1989, Table 2
17	FFG_195	616941	3567615	677649	451793	24	31	3	Richey, 1989, Table 2
18	FFG_196	615316	3568812	672350	455759	24	31	4	Richey, 1989, Table 2
19	FFG_197	614612	3568483	670036	454709	24	31	4	Richey, 1989, Table 2
20	FFG_198	613807	3568888	667396	456038	24	31	5	Richey, 1989, Table 2
21	FFG_199	611628	3568640	660244	455257	24	31	6	Richey, 1989, Table 2
22	FFG_200	611273	3568414	659080	454549	24	31	6	Richey, 1989, Table 2
23	FFG_201	612154	3565951	661905	446431	24	31	7	Richey, 1989, Table 2
24	FFG_202	618692	3566653	683393	448607	24	31	11	Richey, 1989, Table 2
25	FFG_203	618143	3567223	681591	450478	24	31	11	Richey, 1989, Table 2
26	FFG_204	619790	3564834	686932	442604	24	31	13	Richey, 1989, Table 2
27	FFG_205	613734	3565566	667090	445140	24	31	17	Richey, 1989, Table 2
28	FFG_206	612171	3564340	661929	441145	24	31	18	Richey, 1989, Table 2
29	FFG_207	613776	3563957	667198	439860	24	31	20	Richey, 1989, Table 2
30	FFG_208	612992	3562725	664590	435847	24	31	20	Richey, 1989, Table 2
31	FFG_209	615380	3563980	672461	439901	24	31	21	Richey, 1989, Table 2
32	FFG_210	614199	3562745	668548	435879	24	31	21	Richey, 1989, Table 2
33	FFG_212	619811	3562825	686967	436012	24	31	24	Richey, 1989, Table 2
34	FFG_213	614915	3560252	670865	427664	24	31	33	Richey, 1989, Table 2
35	FFG_214	617438	3559994	679114	426785	24	31	35	Richey, 1989, Table 2
36	FFG_215	610576	3559150	656597	424152	25	30	1	Richey, 1989, Table 2
37	FFG_216	604853	3558664	637816	422688	25	30	4	Richey, 1989, Table 2
38	FFG_217	617694	3559360	679954	424705	25	31	2	Richey, 1989, Table 2

Table B.1. Location of Wells used by WIPP (Universal Transverse Mercator [UTM], State Plan Coordinates [stpln], and Survey Sections [township, range and section])

	Well ID	x-UTM	y-UTM	x-STPLN	y-STPLN	Township	Range	Section	Source
1	FFG_218	618235	3558795	681730	422820	25	31	2	Richey, 1989, Table 2
2	FFG_219	616649	3557179	676493	417552	25	31	10	Richey, 1989, Table 2
3	FFG_220	619057	3557584	684393	418848	25	31	12	Richey, 1989, Table 2
4	FFG_221	616028	3555913	674422	413427	25	31	15	Richey, 1989, Table 2
5	FFG_222	614248	3552703	668515	402929	25	31	28	Richey, 1989, Table 2
6	FFG_224	629257	3598870	718704	554099	21	32	1	Richey, 1989, Table 2
7	FFG_225	629076	3597979	718112	551174	21	32	1	Richey, 1989, Table 2
8	FFG_226	628708	3596750	716853	547172	21	32	1	Richey, 1989, Table 2
9	FFG_228	626669	3597926	710210	551066	21	32	2	Richey, 1989, Table 2
10	FFG_229	625894	3596724	707620	547120	21	32	3	Richey, 1989, Table 2
11	FFG_230	625486	3597502	706279	549709	21	32	3	Richey, 1989, Table 2
12	FFG_231	624249	3598303	702273	552336	21	32	4	Richey, 1989, Table 2
13	FFG_232	623880	3597479	701011	549665	21	32	4	Richey, 1989, Table 2
14	FFG_233	623730	3598370	700570	552588	21	32	4	Richey, 1989, Table 2
15	FFG_234	622268	3597867	695720	550968	21	32	5	Richey, 1989, Table 2
16	FFG_235	623075	3597479	698371	549665	21	32	5	Richey, 1989, Table 2
17	FFG_236	620626	3597834	690380	550899	21	32	6	Richey, 1989, Table 2
18	FFG_237	624279	3595893	702319	544429	21	32	9	Richey, 1989, Table 2
19	FFG_238	625894	3595919	707620	544480	21	32	10	Richey, 1989, Table 2
20	FFG_239	627919	3595147	714233	541912	21	32	11	Richey, 1989, Table 2
21	FFG_240	627501	3595945	712893	544532	21	32	11	Richey, 1989, Table 2
22	FFG_241	628322	3595549	715553	543232	21	32	12	Richey, 1989, Table 2
23	FFG_242	623510	3593053	699730	535143	21	32	21	Richey, 1989, Table 2
24	FFG_243	627958	3591122	714296	528704	21	32	26	Richey, 1989, Table 2
25	FFG_244	627169	3589486	711671	523370	21	32	35	Richey, 1989, Table 2
26	FFG_245	634293	3596014	735183	544627	21	33	9	Richey, 1989, Table 2
27	FFG_246	636300	3596435	741767	545977	21	33	11	Richey, 1989, Table 2
28	FFG_247	638785	3593673	749855	536845	21	33	13	Richey, 1989, Table 2
29	FFG_248	638754	3594075	749755	538165	21	33	13	Richey, 1989, Table 2
30	FFG_249	635538	3594033	739201	538094	21	33	15	Richey, 1989, Table 2
31	FFG_250	630707	3593573	723350	536681	21	33	18	Richey, 1989, Table 2
32	FFG_251	639185	3592056	751137	531538	21	33	24	Richey, 1989, Table 2
33	FFG_252	631978	3589148	727420	522161	21	33	32	Richey, 1989, Table 2
34	FFG_253	634373	3589591	735313	523550	21	33	33	Richey, 1989, Table 2
35	FFG_254	634776	3589591	736633	523550	21	33	34	Richey, 1989, Table 2
36	FFG_255	636385	3590012	741913	524900	21	33	35	Richey, 1989, Table 2
37	FFG_264	624541	3575777	702753	478415	23	32	9	Richey, 1989, Table 2
38	FFG_265	626158	3575003	708059	475842	23	32	15	Richey, 1989, Table 2

Table B.1. Location of Wells used by WIPP (Universal Transverse Mercator [UTM], State Plan Coordinates [stpln], and Survey Sections [township, range and section])

	Well ID	x-UTM	y-UTM	x-STPLN	y-STPLN	Township	Range	Section	Source
1	FFG_266	629827	3572644	720033	468035	23	32	24	Richey, 1989, Table 2
2	FFG_267	632644	3570662	729244	461468	23	33	32	Richey, 1989, Table 2
3	FFG_268	636682	3569503	742460	457597	23	33	35	Richey, 1989, Table 2
4	FFG_272	621266	3580141	692103	492804	22	32	31	Richey, 1989, Table 2
5	FFG_273	621714	3576972	693509	482402	23	32	7	Richey, 1989, Table 2
6	FFG_274	627262	3583857	711844	504897	22	32	14	Richey, 1989, Table 2
7	FFG_275	626055	3584259	707884	506217	22	32	15	Richey, 1989, Table 2
8	FFG_276	622836	3584196	697320	506076	22	32	17	Richey, 1989, Table 2
9	FFG_277	621627	3583775	693354	504725	22	32	18	Richey, 1989, Table 2
10	FFG_278	621646	3582157	693382	499416	22	32	19	Richey, 1989, Table 2
11	FFG_279	622836	3582989	697320	502116	22	32	20	Richey, 1989, Table 2
12	FFG_280	625245	3583022	705224	502190	22	32	22	Richey, 1989, Table 2
13	FFG_281	628878	3581872	717114	498350	22	32	25	Richey, 1989, Table 2
14	FFG_283	638822	3588438	749880	519668	22	33	1	Richey, 1989, Table 2
15	FFG_284	633260	3587655	731596	517227	22	33	4	Richey, 1989, Table 2
16	FFG_285	632916	3587152	730466	515577	22	33	5	Richey, 1989, Table 2
17	FFG_286	630045	3585511	721010	510259	22	33	7	Richey, 1989, Table 2
18	FFG_287	630815	3585934	723537	511615	22	33	7	Richey, 1989, Table 2
19	FFG_288	633218	3586749	731456	514257	22	33	9	Richey, 1989, Table 2
20	FFG_289	635668	3584383	739429	506427	22	33	15	Richey, 1989, Table 2
21	FFG_290	631649	3583118	726240	502376	22	33	20	Richey, 1989, Table 2
22	FFG_291	631716	3579091	726360	489157	22	33	32	Richey, 1989, Table 2
23	FFG_292	634513	3580338	735574	493186	22	33	33	Richey, 1989, Table 2
24	FFG_293	635741	3579152	739570	489260	22	33	34	Richey, 1989, Table 2
25	FFG_313	621557	3587797	693224	517925	22	32	6	Richey, 1989, Table 2
26	FFG_314	629670	3583902	719747	504978	22	32	13	Richey, 1989, Table 2
27	FFG_315	626522	3578214	709318	486382	23	32	3	Richey, 1989, Table 2
28	FFG_316	627739	3576635	713279	481164	23	32	11	Richey, 1989, Table 2
29	FFG_317	621734	3574920	693542	475670	23	32	18	Richey, 1989, Table 2
30	FFG_318	622977	3572533	697554	467800	23	32	20	Richey, 1989, Table 2
31	FFG_319	624161	3573735	701471	471749	23	32	21	Richey, 1989, Table 2
32	FFG_320	629107	3572102	717668	466290	23	32	25	Richey, 1989, Table 2
33	FFG_321	628524	3571093	715723	462981	23	32	25	Richey, 1989, Table 2
34	FFG_322	628222	3570892	714733	462321	23	32	26	Richey, 1989, Table 2
35	FFG_323	627420	3570965	712100	462590	23	32	26	Richey, 1989, Table 2
36	FFG_324	624184	3572130	701514	466480	23	32	28	Richey, 1989, Table 2
37	FFG_325	620546	3569268	689509	457154	23	32	31	Richey, 1989, Table 2
38	FFG_326	625008	3570140	704185	459917	23	32	33	Richey, 1989, Table 2

Table B.1. Location of Wells used by WIPP (Universal Transverse Mercator [UTM], State Plan Coordinates [stpln], and Survey Sections [township, range and section])

	Well ID	x-UTM	y-UTM	x-STPLN	y-STPLN	Township	Range	Section	Source
1	FFG_327	626737	3569761	709825	458640	23	32	34	Richey, 1989, Table 2
2	FFG_328	627719	3570289	713083	460341	23	32	35	Richey, 1989, Table 2
3	FFG_329	628625	3570188	716053	460011	23	32	36	Richey, 1989, Table 2
4	FFG_330	629464	3569834	718778	458813	23	32	36	Richey, 1989, Table 2
5	FFG_331	634557	3577522	735655	483942	23	33	4	Richey, 1989, Table 2
6	FFG_332	631443	3577384	725434	483557	23	33	6	Richey, 1989, Table 2
7	FFG_333	630183	3575856	721264	478574	23	33	7	Richey, 1989, Table 2
8	FFG_334	631791	3574262	726509	473313	23	33	17	Richey, 1989, Table 2
9	FFG_335	630204	3574250	721301	473303	23	33	18	Richey, 1989, Table 2
10	FFG_336	630611	3573046	722603	469355	23	33	19	Richey, 1989, Table 2
11	FFG_337	633022	3572674	730519	468066	23	33	20	Richey, 1989, Table 2
12	FFG_338	631435	3570650	725277	461460	23	33	31	Richey, 1989, Table 2
13	FFG_339	637863	3570326	746370	460265	23	33	35	Richey, 1989, Table 2
14	FFG_340	639497	3569942	751700	458973	23	33	36	Richey, 1989, Table 2
15	FFG_361	591407	3608036	594694	584951	20	29	1	Richey, 1989, Table 2
16	FFG_362	588581	3607624	585423	583663	20	29	3	Richey, 1989, Table 2
17	FFG_363	586158	3608022	577470	585038	20	29	4	Richey, 1989, Table 2
18	FFG_364	583878	3605062	569923	575355	20	29	7	Richey, 1989, Table 2
19	FFG_366	588498	3606300	585115	579318	20	29	10	Richey, 1989, Table 2
20	FFG_367	589516	3605699	588421	577345	20	29	11	Richey, 1989, Table 2
21	FFG_370	591027	3604798	593382	574358	20	29	13	Richey, 1989, Table 2
22	FFG_371	591334	3604826	594392	574416	20	29	13	Richey, 1989, Table 2
23	FFG_372	589730	3604102	589095	572070	20	29	14	Richey, 1989, Table 2
24	FFG_373	586192	3604773	577514	574376	20	29	16	Richey, 1989, Table 2
25	FFG_374	585392	3603561	574858	570394	20	29	17	Richey, 1989, Table 2
26	FFG_376	590555	3601690	591768	564155	20	29	25	Richey, 1989, Table 2
27	FFG_381	599172	3599246	619978	555961	20	29	36	Richey, 1989, Table 2
28	FFG_383	601077	3606916	626395	581073	20	30	1	Richey, 1989, Table 2
29	FFG_384	594213	3607648	603902	583643	20	30	5	Richey, 1989, Table 2
30	FFG_385	597883	3602444	615814	566466	20	30	22	Richey, 1989, Table 2
31	FFG_387	595912	3600331	609313	559598	20	30	28	Richey, 1989, Table 2
32	FFG_388	595864	3601219	609189	562513	20	30	28	Richey, 1989, Table 2
33	FFG_389	593453	3599602	601245	557239	20	30	31	Richey, 1989, Table 2
34	FFG_390	595208	3600029	607003	558608	20	30	32	Richey, 1989, Table 2
35	FFG_391	595208	3599627	607003	557288	20	30	32	Richey, 1989, Table 2
36	FFG_392	596612	3599732	611609	557599	20	30	33	Richey, 1989, Table 2
37	FFG_393	606297	3606985	643526	581199	20	31	4	Richey, 1989, Table 2
38	FFG_394	603077	3606946	632959	581140	20	31	6	Richey, 1989, Table 2

Table B.1. Location of Wells used by WIPP (Universal Transverse Mercator [UTM], State Plan Coordinates [stpln], and Survey Sections [township, range and section])

	Well ID	x-UTM	y-UTM	x-STPLN	y-STPLN	Township	Range	Section	Source
1	FFG_395	603098	3605631	632997	576823	20	31	7	Richey, 1989, Table 2
2	FFG_396	603243	3600398	633370	559652	20	31	30	Richey, 1989, Table 2
3	FFG_398	588017	3597286	583323	549759	21	28	2	Richey, 1989, Table 2
4	FFG_399	587111	3597387	580353	550089	21	28	3	Richey, 1989, Table 2
5	FFG_402	590847	3595289	592582	543138	21	28	12	Richey, 1989, Table 2
6	FFG_403	586424	3593240	578030	536512	21	28	15	Richey, 1989, Table 2
7	FFG_404	583988	3592021	570006	532548	21	28	20	Richey, 1989, Table 2
8	FFG_407	583988	3590814	570006	528588	21	28	29	Richey, 1989, Table 2
9	FFG_408	582473	3590320	565002	526999	21	28	30	Richey, 1989, Table 2
10	FFG_411	584828	3588367	572695	520558	21	28	33	Richey, 1989, Table 2
11	FFG_413	588470	3589234	584681	523337	21	28	35	Richey, 1989, Table 2
12	FFG_418	596362	3598010	610756	551972	21	29	3	Richey, 1989, Table 2
13	FFG_419	594776	3597648	605505	550814	21	29	4	Richey, 1989, Table 2
14	FFG_420	594662	3598348	605178	553113	21	29	4	Richey, 1989, Table 2
15	FFG_421	593556	3598412	601548	553321	21	29	5	Richey, 1989, Table 2
16	FFG_422	593958	3598000	602868	551971	21	29	5	Richey, 1989, Table 2
17	FFG_426	592398	3591591	597601	530971	21	29	19	Richey, 1989, Table 2
18	FFG_432	607401	3588903	646769	521852	21	30	35	Richey, 1989, Table 2
19	FFG_433	588569	3588121	584969	519682	22	28	2	Richey, 1989, Table 2
20	FFG_438	618629	3586910	683580	515081	22	31	1	Richey, 1989, Table 2
21	FFG_445	590526	3580760	591228	495462	22	28	25	Richey, 1989, Table 2
22	FFG_453	618415	3578487	682715	487442	23	31	2	Richey, 1989, Table 2
23	FFG_455	618558	3575680	683119	478229	23	31	11	Richey, 1989, Table 2
24	FFG_456	617677	3574462	680195	474264	23	31	14	Richey, 1989, Table 2
25	FFG_457	614456	3574425	669624	474210	23	31	16	Richey, 1989, Table 2
26	FFG_458	615274	3572430	672278	467629	23	31	21	Richey, 1989, Table 2
27	FFG_459	619295	3571652	685468	465012	23	31	25	Richey, 1989, Table 2
28	FFG_462	615699	3571221	673637	463662	23	31	27	Richey, 1989, Table 2
29	FFG_463	612475	3570378	663055	460962	23	31	32	Richey, 1989, Table 2
30	FFG_464	614894	3570416	670997	461022	23	31	33	Richey, 1989, Table 2
31	FFG_465	614090	3569999	668355	459685	23	31	33	Richey, 1989, Table 2
32	FFG_474	628677	3568183	716158	453428	24	32	1	Richey, 1989, Table 2
33	FFG_475	628244	3568580	714774	454733	24	32	2	Richey, 1989, Table 2
34	FFG_476	621409	3568885	692341	455866	24	32	6	Richey, 1989, Table 2
35	FFG_477	626275	3566554	708244	448117	24	32	10	Richey, 1989, Table 2
36	FFG_478	627890	3566569	713543	448132	24	32	11	Richey, 1989, Table 2
37	FFG_479	627468	3566954	712193	449429	24	32	11	Richey, 1989, Table 2
38	FFG_480	628677	3566976	716158	449468	24	32	12	Richey, 1989, Table 2

Table B.1. Location of Wells used by WIPP (Universal Transverse Mercator [UTM], State Plan Coordinates [stpln], and Survey Sections [township, range and section])

	Well ID	x-UTM	y-UTM	x-STPLN	y-STPLN	Township	Range	Section	Source
1	FFG_481	629921	3564597	720180	441628	24	32	13	Richey, 1989, Table 2
2	FFG_482	627482	3565749	712204	445477	24	32	14	Richey, 1989, Table 2
3	FFG_483	625893	3564517	706958	441463	24	32	15	Richey, 1989, Table 2
4	FFG_484	626601	3563741	709281	438885	24	32	22	Richey, 1989, Table 2
5	FFG_485	626323	3563337	708336	437561	24	32	22	Richey, 1989, Table 2
6	FFG_486	627104	3563741	710931	438885	24	32	23	Richey, 1989, Table 2
7	FFG_487	627003	3563842	710601	439215	24	32	23	Richey, 1989, Table 2
8	FFG_488	628618	3564276	715902	440608	24	32	24	Richey, 1989, Table 2
9	FFG_489	629141	3562161	717583	433668	24	32	25	Richey, 1989, Table 2
10	FFG_490	622290	3562046	695099	433421	24	32	29	Richey, 1989, Table 2
11	FFG_491	621485	3562046	692459	433421	24	32	30	Richey, 1989, Table 2
12	FFG_492	625107	3559688	704284	425618	24	32	33	Richey, 1989, Table 2
13	FFG_493	625912	3560090	706924	426938	24	32	34	Richey, 1989, Table 2
14	FFG_494	625912	3559688	706924	425618	24	32	34	Richey, 1989, Table 2
15	FFG_495	627126	3559716	710904	425675	24	32	35	Richey, 1989, Table 2
16	FFG_496	639095	3568735	750380	455013	24	33	1	Richey, 1989, Table 2
17	FFG_497	631494	3566228	725373	446949	24	33	7	Richey, 1989, Table 2
18	FFG_498	631883	3567428	726679	450888	24	33	8	Richey, 1989, Table 2
19	FFG_499	639536	3565513	751762	444438	24	33	13	Richey, 1989, Table 2
20	FFG_500	632702	3565844	729335	445656	24	33	17	Richey, 1989, Table 2
21	FFG_501	632345	3563004	728097	436369	24	33	20	Richey, 1989, Table 2
22	FFG_502	635140	3563849	737302	439075	24	33	22	Richey, 1989, Table 2
23	FFG_503	635586	3561835	738701	432466	24	33	27	Richey, 1989, Table 2
24	FFG_504	632771	3561413	729465	431115	24	33	29	Richey, 1989, Table 2
25	FFG_505	630239	3562683	721189	435349	24	33	30	Richey, 1989, Table 2
26	FFG_506	631576	3560189	725511	427131	24	33	31	Richey, 1989, Table 2
27	FFG_507	639607	3561088	751898	429920	24	33	36	Richey, 1989, Table 2
28	FFG_548	601155	3608819	626682	587316	19	30	36	Richey, 1989, Table 2
29	FFG_552	596378	3554488	609903	409146	25	29	15	Richey, 1989, Table 2
30	FFG_562	614317	3546624	668609	382978	26	31	9	Richey, 1989, Table 2
31	FFG_563	618774	3547092	683237	384417	26	31	11	Richey, 1989, Table 2
32	FFG_568	619132	3541724	684313	366799	26	31	25	Richey, 1989, Table 2
33	FFG_569	619132	3542127	684313	368119	26	31	25	Richey, 1989, Table 2
34	FFG_584	606879	3557091	644432	417458	25	30	10	Richey, 1989, Table 2
35	FFG_585	609769	3557118	653916	417516	25	30	12	Richey, 1989, Table 2
36	FFG_600	608992	3550622	651237	396198	25	30	35	Richey, 1989, Table 2
37	FFG_601	607790	3549783	647256	393477	25	30	35	Richey, 1989, Table 2
38	FFG_602	618235	3558795	681730	422820	25	31	2	Richey, 1989, Table 2

Table B.1. Location of Wells used by WIPP (Universal Transverse Mercator [UTM], State Plan Coordinates [stpln], and Survey Sections [township, range and section])

	Well ID	x-UTM	y-UTM	x-STPLN	y-STPLN	Township	Range	Section	Source
1	FFG_606	618324	3551156	681858	397752	25	31	35	Richey, 1989, Table 2
2	FFG_618	599392	3546376	619633	382460	26	29	11	Richey, 1989, Table 2
3	FFG_638	607809	3548155	647284	388134	26	30	2	Richey, 1989, Table 2
4	FFG_639	606187	3548136	641961	388102	26	30	3	Richey, 1989, Table 2
5	FFG_640	604548	3549331	636618	392062	26	30	4	Richey, 1989, Table 2
6	FFG_643	610657	3546572	656602	382873	26	30	12	Richey, 1989, Table 2
7	FFG_644	605816	3544896	640681	377470	26	30	16	Richey, 1989, Table 2
8	FFG_648	609863	3544129	653961	374890	26	30	24	Richey, 1989, Table 2
9	FFG_685	592502	3586828	597845	515341	22	29	6	Richey, 1989, Table 2
10	FFG_689	626339	3558413	708291	421399	25	32	3	Richey, 1989, Table 2
11	FFG_690	625251	3556776	704687	416062	25	32	9	Richey, 1989, Table 2
12	FFG_691	626238	3557256	707961	417604	25	32	10	Richey, 1989, Table 2
13	FFG_692	627982	3556520	713651	415154	25	32	11	Richey, 1989, Table 2
14	FFG_693	627068	3555594	710652	412151	25	32	14	Richey, 1989, Table 2
15	FFG_694	625965	3554867	706999	409798	25	32	15	Richey, 1989, Table 2
16	FFG_695	625955	3556071	706997	413752	25	32	15	Richey, 1989, Table 2
17	FFG_696	625955	3556134	706997	413957	25	32	15	Richey, 1989, Table 2
18	FFG_697	624748	3555669	703037	412432	25	32	16	Richey, 1989, Table 2
19	FFG_698	620989	3555992	690703	413589	25	32	18	Richey, 1989, Table 2
20	FFG_699	623679	3553534	699465	405455	25	32	20	Richey, 1989, Table 2
21	FFG_700	623679	3553131	699465	404135	25	32	20	Richey, 1989, Table 2
22	FFG_701	625090	3553358	704095	404846	25	32	21	Richey, 1989, Table 2
23	FFG_702	625492	3553761	705415	406166	25	32	22	Richey, 1989, Table 2
24	FFG_703	628006	3554508	713698	408555	25	32	23	Richey, 1989, Table 2
25	FFG_704	625492	3552956	705415	403526	25	32	27	Richey, 1989, Table 2
26	FFG_705	624099	3552123	700810	400825	25	32	28	Richey, 1989, Table 2
27	FFG_706	624300	3552123	701470	400825	25	32	28	Richey, 1989, Table 2
28	FFG_707	623679	3552427	699465	401825	25	32	29	Richey, 1989, Table 2
29	FFG_708	623679	3552930	699465	403475	25	32	29	Richey, 1989, Table 2
30	FFG_709	620746	3550770	689804	396452	25	32	31	Richey, 1989, Table 2
31	FFG_710	622771	3550799	696450	396515	25	32	32	Richey, 1989, Table 2
32	FFG_711	624012	3550012	700490	393900	25	32	33	Richey, 1989, Table 2
33	FFG_712	625263	3550440	704596	395271	25	32	33	Richey, 1989, Table 2
34	FFG_713	624830	3550038	703176	393951	25	32	33	Richey, 1989, Table 2
35	FFG_714	625626	3551242	705819	397905	25	32	34	Richey, 1989, Table 2
36	FFG_715	626840	3551268	709807	397957	25	32	34	Richey, 1989, Table 2
37	FFG_716	638420	3559464	747968	424622	25	33	1	Richey, 1989, Table 2
38	FFG_717	633193	3559403	730818	424522	25	33	5	Richey, 1989, Table 2

Table B.1. Location of Wells used by WIPP (Universal Transverse Mercator [UTM], State Plan Coordinates [stpln], and Survey Sections [township, range and section])

	Well ID	x-UTM	y-UTM	x-STPLN	y-STPLN	Township	Range	Section	Source
1	FFG_718	633234	3556994	730887	416614	25	33	8	Richey, 1989, Table 2
2	FFG_719	636829	3557836	742712	419312	25	33	11	Richey, 1989, Table 2
3	FFG_720	639698	3555152	752066	410438	25	33	13	Richey, 1989, Table 2
4	FFG_721	636045	3555837	740111	412751	25	33	15	Richey, 1989, Table 2
5	FFG_723	630458	3553740	721708	406002	25	33	19	Richey, 1989, Table 2
6	FFG_724	632860	3554578	729624	408686	25	33	20	Richey, 1989, Table 2
7	FFG_725	634859	3554589	736187	408691	25	33	21	Richey, 1989, Table 2
8	FFG_726	636908	3553407	742876	404776	25	33	23	Richey, 1989, Table 2
9	FFG_727	638515	3553426	748148	404806	25	33	24	Richey, 1989, Table 2
10	FFG_728	639741	3551836	752140	399555	25	33	25	Richey, 1989, Table 2
11	FFG_729	636519	3551797	741568	399493	25	33	27	Richey, 1989, Table 2
12	FFG_730	634908	3551777	736280	399460	25	33	28	Richey, 1989, Table 2
13	FFG_731	634882	3552983	736227	403421	25	33	28	Richey, 1989, Table 2
14	FFG_732	632068	3552542	726993	402039	25	33	29	Richey, 1989, Table 2
15	FFG_733	630508	3550122	721809	394129	25	33	31	Richey, 1989, Table 2
16	FFG_734	633325	3550558	731054	395493	25	33	32	Richey, 1989, Table 2
17	FFG_735	638531	3551412	748168	398200	25	33	36	Richey, 1989, Table 2
18	H1	613420	3581687	666391	498039	22	31	29	Mercer, 1983, Table 1
19	H10A	622949	3572457	697463	467561	23	32	20	Gonzales, 1989, Tables 3-6 and 3-7
20	H10B	622975	3572473	697549	467613	23	32	20	Gonzales, 1989, Tables 3-6 and 3-7
21	H10C	622976	3572449	697552	467525	23	32	20	Mercer, 1983, Table 1
22	H11B1	615346	3579130	672647	489617	22	31	33	Gonzales, 1989, Tables 3-6 and 3-7
23	H11B2	615348	3579107	672653	489542	22	31	33	Gonzales, 1989, Tables 3-6 and 3-7
24	H11B3	615367	3579127	672716	489608	22	31	33	Gonzales, 1989, Tables 3-6 and 3-7
25	H11B4	615301	3579131	672501	489620	22	31	33	Gonzales, 1989, Tables 3-6 and 3-7
26	H12	617023	3575452	678079	477535	23	31	15	Gonzales, 1989, Tables 3-6 and 3-7
27	H14	612341	3580354	662815	493697	22	31	29	Gonzales, 1989, Tables 3-6 and 3-7
28	H15	615315	3581859	672606	498572	22	31	28	Gonzales, 1989, Tables 3-6 and 3-7
29	H16	613369	3582212	666231	499726	22	31	20	Gonzales, 1989, Tables 3-6 and 3-7
30	H17	615718	3577513	673837	484304	23	31	3	Gonzales, 1989, Tables 3-6 and 3-7
31	H18	612264	3583166	662621	502926	22	31	20	Gonzales, 1989, Tables 3-6 and 3-7
32	H2A	612663	3581641	663897	497912	22	31	29	Gonzales, 1989, Tables 3-6 and 3-7
33	H2B1	612651	3581651	663860	497943	22	31	29	Gonzales, 1989, Tables 3-6 and 3-7
34	H2B2	612661	3581649	663890	497938	22	31	29	Gonzales, 1989, Tables 3-6 and 3-7
35	H2C	612663	3581662	663904	497992	22	31	29	Mercer, 1983, Table 1
36	H3	613735	3580895	667389	495440	22	31	29	Mercer, 1983, Table 1
37	H3B1	613729	3580895	667377	497440	22	31	29	Gonzales, 1989, Tables 3-6 and 3-7
38	H3B2	613701	3580906	667283	495476	22	31	29	Gonzales, 1989, Tables 3-6 and 3-7

Table B.1. Location of Wells used by WIPP (Universal Transverse Mercator [UTM], State Plan Coordinates [stpln], and Survey Sections [township, range and section])

	Well ID	x-UTM	y-UTM	x-STPLN	y-STPLN	Township	Range	Section	Source
1	H3B3	613705	3580876	667298	495376	22	31	29	Gonzales, 1989, Tables 3-6 and 3-7
2	H3D	613721	3580890	667350	495421	22	31	29	Gonzales, 1989, Tables 3-6 and 3-7
3	H4A	612407	3578469	662993	486962	23	31	5	Gonzales, 1989, Tables 3-6 and 3-7
4	H4B	612380	3578483	662906	487554	23	31	5	Gonzales, 1989, Tables 3-6 and 3-7
5	H4C	612404	3578497	662988	487603	23	31	5	Mercer, 1983, Table 1
6	H5A	616888	3584776	677828	508111	22	31	15	Gonzales, 1989, Tables 3-6 and 3-7
7	H5B	616872	3584801	677777	508194	22	31	15	Gonzales, 1989, Tables 3-6 and 3-7
8	H5C	616900	3584802	677873	508198	22	31	15	Mercer, 1983, Table 1
9	H6A	610580	3584982	657132	508881	22	31	18	Gonzales, 1989, Tables 3-6 and 3-7
10	H6B	610594	3585008	657180	508969	22	31	18	Gonzales, 1989, Tables 3-6 and 3-7
11	H6C	610609	3585027	657231	509066	22	31	18	Mercer, 1983, Table 1
12	H7A	608102	3574670	648790	475132	23	30	14	Gonzales, 1989, Tables 3-6 and 3-7
13	H7B1	608124	3574648	648862	475061	23	30	14	Gonzales, 1989, Tables 3-6 and 3-7
14	H7B2	608111	3574612	648837	474965	23	30	14	Gonzales, 1989, Tables 3-6 and 3-7
15	H7C	608086	3574632	648751	475020	23	30	14	Mercer, 1983, Table 1
16	H8A	608658	3563566	650392	438678	24	30	23	Gonzales, 1989, Tables 3-6 and 3-7
17	H8B	608683	3563556	650473	438646	24	30	23	Gonzales, 1989, Tables 3-6 and 3-7
18	H8C	608656	3563541	650397	438590	24	30	23	Mercer, 1983, Table 1
19	H9A	613958	3568260	667879	453977	24	31	4	Gonzales, 1989, Tables 3-6 and 3-7
20	H9B	613989	3568261	667979	453978	24	31	4	Gonzales, 1989, Tables 3-6 and 3-7
21	H9C	613965	3568233	667914	453889	24	31	4	Mercer, 1983, Table 1
22	MB139_1	613585	3582210	666913	499365	0	0	0	Krieg, 1984, Table I
23	MB139_2	613633	3582061	667069	498876	0	0	0	Krieg, 1984, Table I
24	MB139_3	613635	3582155	667076	499185	0	0	0	Krieg, 1984, Table I
25	MB139_4	613582	3582156	666902	499187	0	0	0	Krieg, 1984, Table I
26	P1	612339	3580339	662807	493649	22	31	29	Mercer, 1983, Table 1
27	P10	617074	3581193	678380	496355	22	31	26	Mercer, 1983, Table 1
28	P11	617016	3583462	678222	503799	22	31	23	Mercer, 1983, Table 1
29	P12	610454	3583452	656688	503899	22	30	24	Mercer, 1983, Table 1
30	P13	610539	3585079	657003	509237	22	31	18	Mercer, 1983, Table 1
31	P14	609083	3581974	652158	499079	22	30	24	Mercer, 1983, Table 1
32	P15	610624	3578793	657148	488609	22	31	31	Mercer, 1983, Table 1
33	P16	612704	3577312	663938	483715	23	31	5	Mercer, 1983, Table 1
34	P17	613929	3577459	667959	484166	23	31	4	Mercer, 1983, Table 1
35	P18	618367	3580352	682589	493561	22	31	26	Mercer, 1983, Table 1
36	P19	617687	3582410	680392	500348	22	31	23	Mercer, 1983, Table 1
37	P2	615315	3581850	672609	498541	22	31	28	Mercer, 1983, Table 1
38	P20	618541	3583770	683226	504775	22	31	14	Mercer, 1983, Table 1

Table B.1. Location of Wells used by WIPP (Universal Transverse Mercator [UTM], State Plan Coordinates [stpln], and Survey Sections [township, range and section])

	Well ID	x-UTM	y-UTM	x-STPLN	y-STPLN	Township	Range	Section	Source
1	P21	616901	3584847	677877	508345	22	31	15	Mercer, 1983, Table 1
2	P3	612799	3581888	664349	498733	22	31	20	Mercer, 1983, Table 1
3	P4	614936	3580324	671330	493533	22	31	28	Mercer, 1983, Table 1
4	P5	613686	3583535	667292	504105	22	31	17	Mercer, 1983, Table 1
5	P6	610591	3581133	657104	496288	22	31	30	Mercer, 1983, Table 1
6	P7	612305	3578476	662663	487535	23	31	5	Mercer, 1983, Table 1
7	P8	613827	3578467	667656	487472	23	31	4	Mercer, 1983, Table 1
8	P9	615365	3579125	672704	489600	22	31	33	Mercer, 1983, Table 1
9	SaltShft	613587	3582186	666919	499286	0	0	0	Krieg, 1984, Table I
10	USGS1	606462	3569459	643297	458066	23	30	34	Gonzales, 1989, Tables 3-6 and 3-7
11	USGS4	605841	3569887	641277	459483	23	30	34	Gonzales, 1989, Tables 3-6 and 3-7
12	USGS8	605879	3569888	641402	459483	23	30	34	Gonzales, 1989, Tables 3-6 and 3-7
13	WIPP11	613819	3586474	667796	513749	22	31	9	Mercer, 1983, Table 1
14	WIPP12	613709	3583524	667368	504067	22	31	17	Mercer, 1983, Table 1
15	WIPP13	612652	3584241	663901	506454	22	31	17	Mercer, 1983, Table 1
16	WIPP15	590057	3574585	589590	475231	23	35	18	Mercer, 1983, Table 1
17	WIPP16	602380	3597026	630458	548607	21	30	5	Mercer, 1983, Table 1
18	WIPP18	613731	3583179	667441	502935	22	31	20	Mercer, 1983, Table 1
19	WIPP19	613747	3582787	667461	501649	22	31	20	Mercer, 1983, Table 1
20	WIPP21	613747	3582349	667462	500213	22	31	20	Mercer, 1983, Table 1
21	WIPP22	613747	3582652	667462	501206	22	31	20	Mercer, 1983, Table 1
22	WIPP25	606391	3584037	643354	505885	22	30	15	Mercer, 1983, Table 1
23	WIPP26	604006	3581161	635496	496516	22	30	29	Mercer, 1983, Table 1
24	WIPP27	604425	3593073	637102	535603	21	30	21	Mercer, 1983, Table 1
25	WIPP28	611265	3594687	659578	540736	21	31	18	Mercer, 1983, Table 1
26	WIPP29	596981	3578700	612380	488570	22	29	34	Mercer, 1983, Table 1
27	WIPP30	613718	3589700	667532	524335	21	31	33	Mercer, 1983, Table 1
28	WIPP32	595909	3579081	608858	489850	22	29	33	Mercer, 1983, Table 1
29	WIPP33	609629	3584019	653981	505789	22	30	13	Mercer, 1983, Table 1
30	WIPP34	614333	3585141	669449	509375	22	31	9	Mercer, 1983, Table 1
31	WastShft	613595	3582061	666944	498876	0	0	0	Krieg, 1984, Table I

Table B.2. Elevations of Stratigraphic Layers Near WIPP

	Layer	Well ID	Elevation	Source
2	Anhydrt1	DOE2	-199.00	Mercer et al., 1987, Table 3-2
3	Anhydrt1	DOE2	-119.10	Mercer et al., 1987, Table 3-2
4	Anhydrt1	REF	-199.00	Rechard et al.,1991, Figure 2.2-1
5	Anhydrt1	REF	-119.10	Rechard et al.,1991, Figure 2.2-1
6	Anhydrt1	WIPP11	-43.90	SNL and USGS, 1982a, Table 2
7	Anhydrt1	WIPP11	-37.80	SNL and USGS, 1982a, Table 2
8	Anhydrt1	WIPP12	-139.00	SNL and D'Appolonia Consulting, 1983, Table 2
9	Anhydrt1	WIPP12	-131.10	SNL and D'Appolonia Consulting, 1983, Table 2
10	Anhydrt2	DOE1	-71.60	U.S. DOE, Sep 1982, Table 2
11	Anhydrt2	DOE1	-38.60	U.S. DOE, Sep 1982, Table 2
12	Anhydrt2	DOE2	-116.40	Mercer et al., 1987, Table 3-2
13	Anhydrt2	REF	-116.40	Rechard et al.,1991, Figure 2.2-1
14	Anhydrt2	WIPP11	-22.20	SNL and USGS, 1982a, Table 2
15	Anhydrt2	WIPP11	14.40	SNL and USGS, 1982a, Table 2
16	Anhydrt2	WIPP12	24.50	SNL and D'Appolonia Consulting, 1983, Table 2
17	Anhydrt2	WIPP12	57.80	SNL and D'Appolonia Consulting, 1983, Table 2
18	Anhydrt3	DOE1	30.00	U.S. DOE, Sep 1982, Table 2
19	Anhydrt3	DOE1	163.60	U.S. DOE, Sep 1982, Table 2
20	Anhydrt3	DOE2	102.30	Mercer et al., 1987, Table 3-2
21	Anhydrt3	ERDA9	162.00	SNL and USGS, 1982b, Table 2
22	Anhydrt3	ERDA9	178.10	SNL and USGS, 1982b, Table 2
23	Anhydrt3	REF	162.00	Rechard et al.,1991, Figure 2.2-1
24	Anhydrt3	REF	178.10	Rechard et al.,1991, Figure 2.2-1
25	Anhydrt3	WIPP11	309.40	SNL and USGS, 1982a, Table 2
26	Anhydrt3	WIPP11	334.10	SNL and USGS, 1982a, Table 2
27	Anhydrt3	WIPP12	127.30	SNL and D'Appolonia Consulting, 1983, Table 2
28	Anhydrt3	WIPP12	227.40	SNL and D'Appolonia Consulting, 1983, Table 2
29	Anhydrta	AirShft	386.41	Holt and Powers, 1990, Figure 22
30	Anhydrta	AirShft	386.70	Holt and Powers, 1990, Figure 22
31	Anhydrta	DH207	386.86	Krieg, 1984, Table I
32	Anhydrta	DH207	388.78	Krieg, 1984, Table I
33	Anhydrta	DH211	389.81	Krieg, 1984, Table I
34	Anhydrta	DH211	391.67	Krieg, 1984, Table I
35	Anhydrta	DH215	390.11	Krieg, 1984, Table I
36	Anhydrta	DH215	391.97	Krieg, 1984, Table I
37	Anhydrta	DH219	390.39	Krieg, 1984, Table I
38	Anhydrta	DH219	390.57	Krieg, 1984, Table I
39	Anhydrta	DH223	386.88	Krieg, 1984, Table I
40	Anhydrta	DH223	387.18	Krieg, 1984, Table I
41	Anhydrta	DH227	384.02	Krieg, 1984, Table I
42	Anhydrta	DH227	384.26	Krieg, 1984, Table I
43	Anhydrta	DH77	402.79	Krieg, 1984, Table I
44	Anhydrta	DH77	402.88	Krieg, 1984, Table I
45	Anhydrta	DO201	389.23	Krieg, 1984, Table I
46	Anhydrta	DO201	389.44	Krieg, 1984, Table I
47	Anhydrta	DO203	400.02	Krieg, 1984, Table I
48	Anhydrta	DO203	400.26	Krieg, 1984, Table I
49	Anhydrta	DO205	405.17	Krieg, 1984, Table I
50	Anhydrta	DO205	405.38	Krieg, 1984, Table I
51	Anhydrta	DO45	396.69	Krieg, 1984, Table I
52	Anhydrta	DO45	396.87	Krieg, 1984, Table I
53	Anhydrta	DO52	393.92	Krieg, 1984, Table I
54	Anhydrta	DO52	394.07	Krieg, 1984, Table I
55	Anhydrta	DO56	399.74	Krieg, 1984, Table I
56	Anhydrta	DO56	399.92	Krieg, 1984, Table I
57	Anhydrta	DO63	403.61	Krieg, 1984, Table I
58	Anhydrta	DO63	403.98	Krieg, 1984, Table I
59	Anhydrta	DO67	403.58	Krieg, 1984, Table I
60	Anhydrta	DO67	403.85	Krieg, 1984, Table I
61	Anhydrta	DO88	402.36	Krieg, 1984, Table I
62	Anhydrta	DO88	402.51	Krieg, 1984, Table I
63	Anhydrta	DO91	402.07	Krieg, 1984, Table I
64	Anhydrta	DO91	402.28	Krieg, 1984, Table I
65	Anhydrta	ExhtShft	389.78	Bechtel, Inc., 1986, Appendix F
66	Anhydrta	ExhtShft	390.03	Bechtel, Inc., 1986, Appendix F
67	Anhydrta	MB139_2	388.84	Krieg, 1984, Table I
68	Anhydrta	MB139_2	389.05	Krieg, 1984, Table I
69	Anhydrta	SaltShft	392.51	Bechtel, Inc., 1986, Appendix D
70	Anhydrta	SaltShft	392.74	Bechtel, Inc., 1986, Appendix D
71	Anhydrta	SaltShft	392.53	Krieg, 1984, Table I
72	Anhydrta	SaltShft	392.76	Krieg, 1984, Table I
73	Anhydrta	WastShft	388.76	Bechtel, Inc., 1986, Appendix E
74	Anhydrta	WastShft	388.97	Bechtel, Inc., 1986, Appendix E
75	Anhydrta	WastShft	389.01	Krieg, 1984, Table I
76	Anhydrta	WastShft	389.25	Krieg, 1984, Table I
77	Anhydrtb	DH207	386.65	Krieg, 1984, Table I

Table B.2. Elevations of Stratigraphic Layers Near WIPP (Continued)

	Layer	Well ID	Elevation	Source
2	Anhydrtb	DH207	386.70	Krieg, 1984, Table I
3	Anhydrtb	DH211	389.63	Krieg, 1984, Table I
4	Anhydrtb	DH211	389.66	Krieg, 1984, Table I
5	Anhydrtb	DH215	389.96	Krieg, 1984, Table I
6	Anhydrtb	DH215	390.02	Krieg, 1984, Table I
7	Anhydrtb	DH219	388.41	Krieg, 1984, Table I
8	Anhydrtb	DH219	388.42	Krieg, 1984, Table I
9	Anhydrtb	DH223	385.05	Krieg, 1984, Table I
10	Anhydrtb	DH223	385.05	Krieg, 1984, Table I
11	Anhydrtb	DH227	382.25	Krieg, 1984, Table I
12	Anhydrtb	DH227	382.25	Krieg, 1984, Table I
13	Anhydrtb	DH77	400.75	Krieg, 1984, Table I
14	Anhydrtb	DH77	400.83	Krieg, 1984, Table I
15	Anhydrtb	DO201	387.07	Krieg, 1984, Table I
16	Anhydrtb	DO201	387.13	Krieg, 1984, Table I
17	Anhydrtb	DO203	398.13	Krieg, 1984, Table I
18	Anhydrtb	DO203	398.19	Krieg, 1984, Table I
19	Anhydrtb	DO205	403.13	Krieg, 1984, Table I
20	Anhydrtb	DO205	403.19	Krieg, 1984, Table I
21	Anhydrtb	DO45	393.92	Krieg, 1984, Table I
22	Anhydrtb	DO45	393.95	Krieg, 1984, Table I
23	Anhydrtb	DO52	391.88	Krieg, 1984, Table I
24	Anhydrtb	DO52	391.94	Krieg, 1984, Table I
25	Anhydrtb	DO56	397.64	Krieg, 1984, Table I
26	Anhydrtb	DO56	397.70	Krieg, 1984, Table I
27	Anhydrtb	DO63	401.45	Krieg, 1984, Table I
28	Anhydrtb	DO63	401.51	Krieg, 1984, Table I
29	Anhydrtb	DO67	401.45	Krieg, 1984, Table I
30	Anhydrtb	DO67	401.53	Krieg, 1984, Table I
31	Anhydrtb	DO88	400.23	Krieg, 1984, Table I
32	Anhydrtb	DO88	400.30	Krieg, 1984, Table I
33	Anhydrtb	DO91	399.91	Krieg, 1984, Table I
34	Anhydrtb	DO91	399.96	Krieg, 1984, Table I
35	Anhydrtb	ExhtShft	387.66	Bechtel, Inc., 1986, Appendix F
36	Anhydrtb	ExhtShft	387.75	Bechtel, Inc., 1986, Appendix F
37	Anhydrtb	MB139_2	386.58	Krieg, 1984, Table I
38	Anhydrtb	MB139_2	386.61	Krieg, 1984, Table I
39	Anhydrtb	SaltShft	390.58	Bechtel, Inc., 1986, Appendix D
40	Anhydrtb	SaltShft	390.66	Bechtel, Inc., 1986, Appendix D
41	Anhydrtb	SaltShft	390.37	Krieg, 1984, Table I
42	Anhydrtb	SaltShft	390.45	Krieg, 1984, Table I
43	Anhydrtb	WastShft	386.57	Bechtel, Inc., 1986, Appendix E
44	Anhydrtb	WastShft	386.70	Bechtel, Inc., 1986, Appendix E
45	Anhydrtb	WastShft	386.91	Krieg, 1984, Table I
46	Anhydrtb	WastShft	386.97	Krieg, 1984, Table I
47	Anhydrtc	DH207	369.49	Krieg, 1984, Table I
48	Anhydrtc	DH207	369.55	Krieg, 1984, Table I
49	Anhydrtc	DH211	372.71	Krieg, 1984, Table I
50	Anhydrtc	DH211	372.80	Krieg, 1984, Table I
51	Anhydrtc	DH215	373.14	Krieg, 1984, Table I
52	Anhydrtc	DH215	373.20	Krieg, 1984, Table I
53	Anhydrtc	DH219	372.13	Krieg, 1984, Table I
54	Anhydrtc	DH219	372.19	Krieg, 1984, Table I
55	Anhydrtc	DH223	369.08	Krieg, 1984, Table I
56	Anhydrtc	DH223	369.17	Krieg, 1984, Table I
57	Anhydrtc	DH227	366.16	Krieg, 1984, Table I
58	Anhydrtc	DH227	366.22	Krieg, 1984, Table I
59	Anhydrtc	DH77	384.75	Krieg, 1984, Table I
60	Anhydrtc	DH77	384.81	Krieg, 1984, Table I
61	Anhydrtc	DO201	369.91	Krieg, 1984, Table I
62	Anhydrtc	DO201	370.03	Krieg, 1984, Table I
63	Anhydrtc	DO203	381.95	Krieg, 1984, Table I
64	Anhydrtc	DO203	382.01	Krieg, 1984, Table I
65	Anhydrtc	DO205	387.37	Krieg, 1984, Table I
66	Anhydrtc	DO205	387.43	Krieg, 1984, Table I
67	Anhydrtc	DO45	377.22	Krieg, 1984, Table I
68	Anhydrtc	DO45	377.28	Krieg, 1984, Table I
69	Anhydrtc	DO52	375.18	Krieg, 1984, Table I
70	Anhydrtc	DO52	375.24	Krieg, 1984, Table I
71	Anhydrtc	DO56	381.00	Krieg, 1984, Table I
72	Anhydrtc	DO56	381.09	Krieg, 1984, Table I
73	Anhydrtc	DO63	385.66	Krieg, 1984, Table I
74	Anhydrtc	DO63	385.84	Krieg, 1984, Table I
75	Anhydrtc	DO67	385.54	Krieg, 1984, Table I
76	Anhydrtc	DO67	385.63	Krieg, 1984, Table I
77	Anhydrtc	DO88	384.01	Krieg, 1984, Table I

Table B.2. Elevations of Stratigraphic Layers Near WIPP (Continued)

	Layer	Well ID	Elevation	Source
1	Anhydrtc	DO88	384.06	Krieg, 1984, Table I
2	Anhydrtc	DO91	384.03	Krieg, 1984, Table I
3	Anhydrtc	DO91	384.12	Krieg, 1984, Table I
4	Anhydrtc	SaltShft	373.09	Krieg, 1984, Table I
5	Anhydrtc	SaltShft	373.20	Krieg, 1984, Table I
6	B_CANyon	DOE2	-276.30	Mercer et al., 1987, Table 3-2
7	B_CANyon	DOE2	-199.00	Mercer et al., 1987, Table 3-2
8	B_CANyon	REF	-276.30	Rechard et al.,1991, Figure 2.2-1
9	B_CANyon	REF	-199.00	Rechard et al.,1991, Figure 2.2-1
10	Culebra	AEC7	848.50	Mercer, 1983, Table 1
11	Culebra	AEC8	822.70	Mercer, 1983, Table 1
12	Culebra	AirShft	824.48	Holt and Powers, 1990, Figure 22
13	Culebra	B25	824.50	Mercer, 1983, Table 1
14	Culebra	DOE1	806.10	U.S. DOE, Sep 1982, Table 2
15	Culebra	DOE2	790.80	Mercer et al., 1987, Table 3-2
16	Culebra	ERDA10	882.40	Mercer, 1983, Table 1
17	Culebra	ERDA6	862.60	Mercer, 1983, Table 1
18	Culebra	ERDA9	827.50	Mercer, 1983, Table 1
19	Culebra	ERDA9	823.40	SNL and USGS, 1982b, Table 2
20	Culebra	ExhtShft	821.57	Bechtel, Inc., 1986, Appendix F
21	Culebra	FFG_002	624.80	Richey, 1989, Table 2, p.21
22	Culebra	FFG_004	666.60	Richey, 1989, Table 2, p.21
23	Culebra	FFG_005	628.50	Richey, 1989, Table 2, p.21
24	Culebra	FFG_006	616.60	Richey, 1989, Table 2, p.21
25	Culebra	FFG_007	602.00	Richey, 1989, Table 2, p.21
26	Culebra	FFG_009	604.10	Richey, 1989, Table 2, p.21
27	Culebra	FFG_011	609.90	Richey, 1989, Table 2, p.21
28	Culebra	FFG_012	613.90	Richey, 1989, Table 2, p.21
29	Culebra	FFG_013	646.20	Richey, 1989, Table 2, p.21
30	Culebra	FFG_014	667.80	Richey, 1989, Table 2, p.21
31	Culebra	FFG_016	587.90	Richey, 1989, Table 2, p.21
32	Culebra	FFG_017	594.90	Richey, 1989, Table 2, p.22
33	Culebra	FFG_018	598.60	Richey, 1989, Table 2, p.22
34	Culebra	FFG_019	588.60	Richey, 1989, Table 2, p.22
35	Culebra	FFG_020	662.00	Richey, 1989, Table 2, p.22
36	Culebra	FFG_023	596.20	Richey, 1989, Table 2, p.22
37	Culebra	FFG_024	579.10	Richey, 1989, Table 2, p.22
38	Culebra	FFG_025	598.50	Richey, 1989, Table 2, p.22
39	Culebra	FFG_026	592.50	Richey, 1989, Table 2, p.22
40	Culebra	FFG_027	585.50	Richey, 1989, Table 2, p.22
41	Culebra	FFG_028	578.60	Richey, 1989, Table 2, p.22
42	Culebra	FFG_029	563.50	Richey, 1989, Table 2, p.22
43	Culebra	FFG_030	563.00	Richey, 1989, Table 2, p.22
44	Culebra	FFG_031	554.40	Richey, 1989, Table 2, p.22
45	Culebra	FFG_032	549.40	Richey, 1989, Table 2, p.22
46	Culebra	FFG_033	549.20	Richey, 1989, Table 2, p.22
47	Culebra	FFG_034	548.60	Richey, 1989, Table 2, p.23
48	Culebra	FFG_035	533.90	Richey, 1989, Table 2, p.23
49	Culebra	FFG_036	541.40	Richey, 1989, Table 2, p.23
50	Culebra	FFG_037	534.00	Richey, 1989, Table 2, p.23
51	Culebra	FFG_038	523.60	Richey, 1989, Table 2, p.23
52	Culebra	FFG_039	731.90	Richey, 1989, Table 2, p.23
53	Culebra	FFG_040	655.40	Richey, 1989, Table 2, p.23
54	Culebra	FFG_041	733.70	Richey, 1989, Table 2, p.23
55	Culebra	FFG_042	740.60	Richey, 1989, Table 2, p.23
56	Culebra	FFG_043	735.70	Richey, 1989, Table 2, p.23
57	Culebra	FFG_044	689.10	Richey, 1989, Table 2, p.23
58	Culebra	FFG_047	561.10	Richey, 1989, Table 2, p.23
59	Culebra	FFG_048	580.30	Richey, 1989, Table 2, p.23
60	Culebra	FFG_049	567.50	Richey, 1989, Table 2, p.23
61	Culebra	FFG_050	582.50	Richey, 1989, Table 2, p.24
62	Culebra	FFG_051	573.90	Richey, 1989, Table 2, p.24
63	Culebra	FFG_052	595.20	Richey, 1989, Table 2, p.24
64	Culebra	FFG_053	563.00	Richey, 1989, Table 2, p.24
65	Culebra	FFG_054	562.70	Richey, 1989, Table 2, p.24
66	Culebra	FFG_055	565.70	Richey, 1989, Table 2, p.24
67	Culebra	FFG_056	564.50	Richey, 1989, Table 2, p.24
68	Culebra	FFG_057	564.80	Richey, 1989, Table 2, p.24
69	Culebra	FFG_058	569.30	Richey, 1989, Table 2, p.24
70	Culebra	FFG_059	569.70	Richey, 1989, Table 2, p.24
71	Culebra	FFG_060	569.30	Richey, 1989, Table 2, p.24
72	Culebra	FFG_061	570.60	Richey, 1989, Table 2, p.24
73	Culebra	FFG_062	513.90	Richey, 1989, Table 2, p.24
74	Culebra	FFG_063	470.70	Richey, 1989, Table 2, p.24
75	Culebra	FFG_064	497.50	Richey, 1989, Table 2, p.24
76	Culebra	FFG_065	471.80	Richey, 1989, Table 2, p.24

Table B.2. Elevations of Stratigraphic Layers Near WIPP (Continued)

	Layer	Well ID	Elevation	Source
1	Culebra	FFG_066	434.30	Richey, 1989, Table 2, p.24
2	Culebra	FFG_067	470.00	Richey, 1989, Table 2, p.25
3	Culebra	FFG_068	430.10	Richey, 1989, Table 2, p.25
4	Culebra	FFG_069	447.50	Richey, 1989, Table 2, p.25
5	Culebra	FFG_070	484.60	Richey, 1989, Table 2, p.25
6	Culebra	FFG_071	755.00	Richey, 1989, Table 2, p.25
7	Culebra	FFG_072	681.20	Richey, 1989, Table 2, p.25
8	Culebra	FFG_073	659.30	Richey, 1989, Table 2, p.25
9	Culebra	FFG_074	666.40	Richey, 1989, Table 2, p.25
10	Culebra	FFG_075	717.90	Richey, 1989, Table 2, p.25
11	Culebra	FFG_076	777.60	Richey, 1989, Table 2, p.25
12	Culebra	FFG_078	814.70	Richey, 1989, Table 2, p.25
13	Culebra	FFG_079	787.00	Richey, 1989, Table 2, p.25
14	Culebra	FFG_080	765.60	Richey, 1989, Table 2, p.25
15	Culebra	FFG_081	683.10	Richey, 1989, Table 2, p.26
16	Culebra	FFG_082	711.10	Richey, 1989, Table 2, p.26
17	Culebra	FFG_083	638.10	Richey, 1989, Table 2, p.26
18	Culebra	FFG_084	661.40	Richey, 1989, Table 2, p.26
19	Culebra	FFG_085	655.40	Richey, 1989, Table 2, p.26
20	Culebra	FFG_086	665.00	Richey, 1989, Table 2, p.26
21	Culebra	FFG_087	636.70	Richey, 1989, Table 2, p.26
22	Culebra	FFG_088	626.10	Richey, 1989, Table 2, p.26
23	Culebra	FFG_089	613.90	Richey, 1989, Table 2, p.26
24	Culebra	FFG_091	652.30	Richey, 1989, Table 2, p.26
25	Culebra	FFG_092	670.90	Richey, 1989, Table 2, p.26
26	Culebra	FFG_093	673.60	Richey, 1989, Table 2, p.26
27	Culebra	FFG_094	674.20	Richey, 1989, Table 2, p.26
28	Culebra	FFG_095	651.60	Richey, 1989, Table 2, p.26
29	Culebra	FFG_096	635.50	Richey, 1989, Table 2, p.26
30	Culebra	FFG_097	614.80	Richey, 1989, Table 2, p.27
31	Culebra	FFG_098	587.90	Richey, 1989, Table 2, p.27
32	Culebra	FFG_099	582.50	Richey, 1989, Table 2, p.27
33	Culebra	FFG_100	564.80	Richey, 1989, Table 2, p.27
34	Culebra	FFG_101	533.70	Richey, 1989, Table 2, p.27
35	Culebra	FFG_102	549.00	Richey, 1989, Table 2, p.27
36	Culebra	FFG_103	609.30	Richey, 1989, Table 2, p.27
37	Culebra	FFG_104	508.10	Richey, 1989, Table 2, p.27
38	Culebra	FFG_105	867.50	Richey, 1989, Table 2, p.27
39	Culebra	FFG_106	902.60	Richey, 1989, Table 2, p.27
40	Culebra	FFG_107	887.90	Richey, 1989, Table 2, p.27
41	Culebra	FFG_108	878.70	Richey, 1989, Table 2, p.27
42	Culebra	FFG_109	862.30	Richey, 1989, Table 2, p.27
43	Culebra	FFG_110	832.10	Richey, 1989, Table 2, p.27
44	Culebra	FFG_111	836.60	Richey, 1989, Table 2, p.27
45	Culebra	FFG_112	824.50	Richey, 1989, Table 2, p.28
46	Culebra	FFG_113	838.50	Richey, 1989, Table 2, p.28
47	Culebra	FFG_114	870.50	Richey, 1989, Table 2, p.28
48	Culebra	FFG_115	857.40	Richey, 1989, Table 2, p.28
49	Culebra	FFG_116	871.40	Richey, 1989, Table 2, p.28
50	Culebra	FFG_117	868.70	Richey, 1989, Table 2, p.28
51	Culebra	FFG_119	870.90	Richey, 1989, Table 2, p.28
52	Culebra	FFG_120	874.20	Richey, 1989, Table 2, p.28
53	Culebra	FFG_121	882.40	Richey, 1989, Table 2, p.28
54	Culebra	FFG_122	876.30	Richey, 1989, Table 2, p.28
55	Culebra	FFG_123	867.10	Richey, 1989, Table 2, p.28
56	Culebra	FFG_124	837.90	Richey, 1989, Table 2, p.28
57	Culebra	FFG_125	851.20	Richey, 1989, Table 2, p.28
58	Culebra	FFG_126	852.70	Richey, 1989, Table 2, p.28
59	Culebra	FFG_127	860.70	Richey, 1989, Table 2, p.28
60	Culebra	FFG_128	887.00	Richey, 1989, Table 2, p.28
61	Culebra	FFG_129	858.30	Richey, 1989, Table 2, p.28
62	Culebra	FFG_130	897.60	Richey, 1989, Table 2, p.28
63	Culebra	FFG_132	898.60	Richey, 1989, Table 2, p.29
64	Culebra	FFG_133	901.60	Richey, 1989, Table 2, p.29
65	Culebra	FFG_134	904.40	Richey, 1989, Table 2, p.29
66	Culebra	FFG_135	880.90	Richey, 1989, Table 2, p.29
67	Culebra	FFG_136	882.50	Richey, 1989, Table 2, p.29
68	Culebra	FFG_137	892.80	Richey, 1989, Table 2, p.29
69	Culebra	FFG_138	844.10	Richey, 1989, Table 2, p.29
70	Culebra	FFG_139	855.60	Richey, 1989, Table 2, p.29
71	Culebra	FFG_140	792.70	Richey, 1989, Table 2, p.29
72	Culebra	FFG_141	820.10	Richey, 1989, Table 2, p.29
73	Culebra	FFG_142	795.90	Richey, 1989, Table 2, p.29
74	Culebra	FFG_143	804.00	Richey, 1989, Table 2, p.29
75	Culebra	FFG_144	894.30	Richey, 1989, Table 2, p.29
76	Culebra	FFG_145	893.10	Richey, 1989, Table 2, p.29

Table B.2. Elevations of Stratigraphic Layers Near WIPP (Continued)

	Layer	Well ID	Elevation	Source		Layer	Well ID	Elevation	Source
1	Culebra	FFG_146	906.80	Richey, 1989, Table 2, p.29	39	Culebra	FFG_194	788.50	Richey, 1989, Table 2, p.33
2	Culebra	FFG_147	882.70	Richey, 1989, Table 2, p.29	40	Culebra	FFG_195	803.50	Richey, 1989, Table 2, p.33
3	Culebra	FFG_148	900.10	Richey, 1989, Table 2, p.29	41	Culebra	FFG_196	837.00	Richey, 1989, Table 2, p.33
4	Culebra	FFG_149	910.70	Richey, 1989, Table 2, p.30	42	Culebra	FFG_197	841.00	Richey, 1989, Table 2, p.33
5	Culebra	FFG_155	901.30	Richey, 1989, Table 2, p.30	43	Culebra	FFG_198	840.90	Richey, 1989, Table 2, p.33
6	Culebra	FFG_156	906.50	Richey, 1989, Table 2, p.30	44	Culebra	FFG_199	827.00	Richey, 1989, Table 2, p.33
7	Culebra	FFG_157	904.10	Richey, 1989, Table 2, p.30	45	Culebra	FFG_200	838.20	Richey, 1989, Table 2, p.33
8	Culebra	FFG_158	928.10	Richey, 1989, Table 2, p.30	46	Culebra	FFG_201	838.20	Richey, 1989, Table 2, p.33
9	Culebra	FFG_159	898.60	Richey, 1989, Table 2, p.30	47	Culebra	FFG_202	773.80	Richey, 1989, Table 2, p.33
10	Culebra	FFG_160	895.20	Richey, 1989, Table 2, p.30	48	Culebra	FFG_203	776.00	Richey, 1989, Table 2, p.33
11	Culebra	FFG_161	901.00	Richey, 1989, Table 2, p.30	49	Culebra	FFG_204	813.50	Richey, 1989, Table 2, p.33
12	Culebra	FFG_162	891.90	Richey, 1989, Table 2, p.30	50	Culebra	FFG_205	825.10	Richey, 1989, Table 2, p.33
13	Culebra	FFG_163	897.40	Richey, 1989, Table 2, p.30	51	Culebra	FFG_206	837.00	Richey, 1989, Table 2, p.33
14	Culebra	FFG_164	937.60	Richey, 1989, Table 2, p.30	52	Culebra	FFG_207	833.60	Richey, 1989, Table 2, p.33
15	Culebra	FFG_165	912.80	Richey, 1989, Table 2, p.30	53	Culebra	FFG_208	843.10	Richey, 1989, Table 2, p.34
16	Culebra	FFG_166	900.00	Richey, 1989, Table 2, p.31	54	Culebra	FFG_209	838.20	Richey, 1989, Table 2, p.34
17	Culebra	FFG_167	887.00	Richey, 1989, Table 2, p.31	55	Culebra	FFG_210	827.50	Richey, 1989, Table 2, p.34
18	Culebra	FFG_168	906.50	Richey, 1989, Table 2, p.31	56	Culebra	FFG_212	817.50	Richey, 1989, Table 2, p.34
19	Culebra	FFG_169	919.20	Richey, 1989, Table 2, p.31	57	Culebra	FFG_213	837.90	Richey, 1989, Table 2, p.34
20	Culebra	FFG_170	903.70	Richey, 1989, Table 2, p.31	58	Culebra	FFG_214	818.40	Richey, 1989, Table 2, p.34
21	Culebra	FFG_171	922.10	Richey, 1989, Table 2, p.31	59	Culebra	FFG_215	793.10	Richey, 1989, Table 2, p.34
22	Culebra	FFG_172	915.30	Richey, 1989, Table 2, p.31	60	Culebra	FFG_216	688.80	Richey, 1989, Table 2, p.34
23	Culebra	FFG_173	876.90	Richey, 1989, Table 2, p.31	61	Culebra	FFG_217	814.80	Richey, 1989, Table 2, p.34
24	Culebra	FFG_177	889.10	Richey, 1989, Table 2, p.31	62	Culebra	FFG_218	803.50	Richey, 1989, Table 2, p.34
25	Culebra	FFG_178	718.10	Richey, 1989, Table 2, p.31	63	Culebra	FFG_219	848.80	Richey, 1989, Table 2, p.34
26	Culebra	FFG_179	886.60	Richey, 1989, Table 2, p.31	64	Culebra	FFG_220	798.60	Richey, 1989, Table 2, p.34
27	Culebra	FFG_180	883.00	Richey, 1989, Table 2, p.31	65	Culebra	FFG_221	756.50	Richey, 1989, Table 2, p.34
28	Culebra	FFG_181	930.50	Richey, 1989, Table 2, p.32	66	Culebra	FFG_222	713.30	Richey, 1989, Table 2, p.34
29	Culebra	FFG_182	812.60	Richey, 1989, Table 2, p.32	67	Culebra	FFG_224	597.80	Richey, 1989, Table 2, p.35
30	Culebra	FFG_183	904.40	Richey, 1989, Table 2, p.32	68	Culebra	FFG_225	603.50	Richey, 1989, Table 2, p.35
31	Culebra	FFG_184	891.20	Richey, 1989, Table 2, p.32	69	Culebra	FFG_226	601.80	Richey, 1989, Table 2, p.35
32	Culebra	FFG_185	899.50	Richey, 1989, Table 2, p.32	70	Culebra	FFG_228	588.30	Richey, 1989, Table 2, p.35
33	Culebra	FFG_186	827.90	Richey, 1989, Table 2, p.32	71	Culebra	FFG_229	614.70	Richey, 1989, Table 2, p.35
34	Culebra	FFG_188	845.80	Richey, 1989, Table 2, p.32	72	Culebra	FFG_230	601.10	Richey, 1989, Table 2, p.35
35	Culebra	FFG_189	867.80	Richey, 1989, Table 2, p.32	73	Culebra	FFG_231	619.90	Richey, 1989, Table 2, p.35
36	Culebra	FFG_190	843.60	Richey, 1989, Table 2, p.32	74	Culebra	FFG_232	631.50	Richey, 1989, Table 2, p.35
37	Culebra	FFG_191	845.50	Richey, 1989, Table 2, p.32	75	Culebra	FFG_233	624.00	Richey, 1989, Table 2, p.35
38	Culebra	FFG_192	774.50	Richey, 1989, Table 2, p.32	76	Culebra	FFG_234	660.20	Richey, 1989, Table 2, p.35

Table B.2. Elevations of Stratigraphic Layers Near WIPP (Continued)

	Layer	Well ID	Elevation	Source
1	Culebra	FFG_235	635.50	Richey, 1989, Table 2, p.35
2	Culebra	FFG_236	682.70	Richey, 1989, Table 2, p.35
3	Culebra	FFG_237	646.20	Richey, 1989, Table 2, p.35
4	Culebra	FFG_238	628.50	Richey, 1989, Table 2, p.36
5	Culebra	FFG_239	620.50	Richey, 1989, Table 2, p.36
6	Culebra	FFG_240	609.90	Richey, 1989, Table 2, p.36
7	Culebra	FFG_241	605.10	Richey, 1989, Table 2, p.36
8	Culebra	FFG_242	732.20	Richey, 1989, Table 2, p.36
9	Culebra	FFG_243	668.40	Richey, 1989, Table 2, p.36
10	Culebra	FFG_244	721.30	Richey, 1989, Table 2, p.36
11	Culebra	FFG_245	510.80	Richey, 1989, Table 2, p.36
12	Culebra	FFG_246	516.00	Richey, 1989, Table 2, p.36
13	Culebra	FFG_247	501.30	Richey, 1989, Table 2, p.36
14	Culebra	FFG_248	506.60	Richey, 1989, Table 2, p.36
15	Culebra	FFG_249	505.30	Richey, 1989, Table 2, p.36
16	Culebra	FFG_250	587.50	Richey, 1989, Table 2, p.36
17	Culebra	FFG_251	477.30	Richey, 1989, Table 2, p.36
18	Culebra	FFG_252	619.60	Richey, 1989, Table 2, p.36
19	Culebra	FFG_253	566.70	Richey, 1989, Table 2, p.36
20	Culebra	FFG_254	562.00	Richey, 1989, Table 2, p.36
21	Culebra	FFG_255	514.50	Richey, 1989, Table 2, p.37
22	Culebra	FFG_256	477.90	Richey, 1989, Table 2, p.37
23	Culebra	FFG_257	523.30	Richey, 1989, Table 2, p.37
24	Culebra	FFG_258	546.20	Richey, 1989, Table 2, p.37
25	Culebra	FFG_259	503.20	Richey, 1989, Table 2, p.37
26	Culebra	FFG_260	556.30	Richey, 1989, Table 2, p.37
27	Culebra	FFG_261	542.20	Richey, 1989, Table 2, p.37
28	Culebra	FFG_262	485.60	Richey, 1989, Table 2, p.37
29	Culebra	FFG_263	456.50	Richey, 1989, Table 2, p.37
30	Culebra	FFG_264	703.80	Richey, 1989, Table 2, p.37
31	Culebra	FFG_265	686.10	Richey, 1989, Table 2, p.37
32	Culebra	FFG_266	665.40	Richey, 1989, Table 2, p.37
33	Culebra	FFG_267	641.30	Richey, 1989, Table 2, p.37
34	Culebra	FFG_268	613.60	Richey, 1989, Table 2, p.37
35	Culebra	FFG_269	627.70	Richey, 1989, Table 2, p.38
36	Culebra	FFG_270	730.30	Richey, 1989, Table 2, p.38
37	Culebra	FFG_271	773.90	Richey, 1989, Table 2, p.38
38	Culebra	FFG_272	751.80	Richey, 1989, Table 2, p.38
39	Culebra	FFG_273	753.20	Richey, 1989, Table 2, p.38
40	Culebra	FFG_274	793.10	Richey, 1989, Table 2, p.38
41	Culebra	FFG_275	800.70	Richey, 1989, Table 2, p.38
42	Culebra	FFG_276	802.80	Richey, 1989, Table 2, p.38
43	Culebra	FFG_277	795.50	Richey, 1989, Table 2, p.38
44	Culebra	FFG_278	776.60	Richey, 1989, Table 2, p.38
45	Culebra	FFG_279	776.90	Richey, 1989, Table 2, p.38
46	Culebra	FFG_280	788.80	Richey, 1989, Table 2, p.38
47	Culebra	FFG_281	762.60	Richey, 1989, Table 2, p.38
48	Culebra	FFG_283	496.20	Richey, 1989, Table 2, p.39
49	Culebra	FFG_284	648.00	Richey, 1989, Table 2, p.39
50	Culebra	FFG_285	669.60	Richey, 1989, Table 2, p.39
51	Culebra	FFG_286	773.80	Richey, 1989, Table 2, p.39
52	Culebra	FFG_287	738.20	Richey, 1989, Table 2, p.39
53	Culebra	FFG_288	668.70	Richey, 1989, Table 2, p.39
54	Culebra	FFG_289	680.60	Richey, 1989, Table 2, p.39
55	Culebra	FFG_290	770.90	Richey, 1989, Table 2, p.39
56	Culebra	FFG_291	668.70	Richey, 1989, Table 2, p.39
57	Culebra	FFG_292	724.80	Richey, 1989, Table 2, p.39
58	Culebra	FFG_293	718.10	Richey, 1989, Table 2, p.39
59	Culebra	FFG_294	504.50	Richey, 1989, Table 2, p.39
60	Culebra	FFG_295	489.50	Richey, 1989, Table 2, p.39
61	Culebra	FFG_297	469.10	Richey, 1989, Table 2, p.39
62	Culebra	FFG_298	528.10	Richey, 1989, Table 2, p.40
63	Culebra	FFG_299	497.80	Richey, 1989, Table 2, p.40
64	Culebra	FFG_300	480.60	Richey, 1989, Table 2, p.40
65	Culebra	FFG_301	435.90	Richey, 1989, Table 2, p.40
66	Culebra	FFG_302	443.50	Richey, 1989, Table 2, p.40
67	Culebra	FFG_303	449.00	Richey, 1989, Table 2, p.40
68	Culebra	FFG_304	445.90	Richey, 1989, Table 2, p.40
69	Culebra	FFG_305	443.20	Richey, 1989, Table 2, p.40
70	Culebra	FFG_306	413.00	Richey, 1989, Table 2, p.40
71	Culebra	FFG_307	432.20	Richey, 1989, Table 2, p.40
72	Culebra	FFG_308	376.10	Richey, 1989, Table 2, p.40
73	Culebra	FFG_309	434.60	Richey, 1989, Table 2, p.40
74	Culebra	FFG_310	475.20	Richey, 1989, Table 2, p.40
75	Culebra	FFG_311	428.60	Richey, 1989, Table 2, p.40
76	Culebra	FFG_312	429.80	Richey, 1989, Table 2, p.40

Table B.2. Elevations of Stratigraphic Layers Near WIPP (Continued)

	Layer	Well ID	Elevation	Source
1	Culebra	FFG_313	870.30	Richey, 1989, Table 2, p.41
2	Culebra	FFG_314	788.90	Richey, 1989, Table 2, p.41
3	Culebra	FFG_315	701.50	Richey, 1989, Table 2, p.41
4	Culebra	FFG_316	678.40	Richey, 1989, Table 2, p.41
5	Culebra	FFG_317	732.40	Richey, 1989, Table 2, p.41
6	Culebra	FFG_318	710.20	Richey, 1989, Table 2, p.41
7	Culebra	FFG_319	704.60	Richey, 1989, Table 2, p.41
8	Culebra	FFG_320	669.40	Richey, 1989, Table 2, p.41
9	Culebra	FFG_321	668.40	Richey, 1989, Table 2, p.41
10	Culebra	FFG_322	669.80	Richey, 1989, Table 2, p.41
11	Culebra	FFG_323	675.20	Richey, 1989, Table 2, p.41
12	Culebra	FFG_324	699.50	Richey, 1989, Table 2, p.41
13	Culebra	FFG_325	762.30	Richey, 1989, Table 2, p.41
14	Culebra	FFG_326	706.50	Richey, 1989, Table 2, p.41
15	Culebra	FFG_327	689.80	Richey, 1989, Table 2, p.42
16	Culebra	FFG_328	673.80	Richey, 1989, Table 2, p.42
17	Culebra	FFG_329	669.00	Richey, 1989, Table 2, p.42
18	Culebra	FFG_330	669.50	Richey, 1989, Table 2, p.42
19	Culebra	FFG_331	652.90	Richey, 1989, Table 2, p.42
20	Culebra	FFG_332	639.50	Richey, 1989, Table 2, p.42
21	Culebra	FFG_333	650.60	Richey, 1989, Table 2, p.42
22	Culebra	FFG_334	644.90	Richey, 1989, Table 2, p.42
23	Culebra	FFG_335	663.30	Richey, 1989, Table 2, p.42
24	Culebra	FFG_336	658.10	Richey, 1989, Table 2, p.42
25	Culebra	FFG_337	641.90	Richey, 1989, Table 2, p.42
26	Culebra	FFG_338	646.90	Richey, 1989, Table 2, p.42
27	Culebra	FFG_339	611.70	Richey, 1989, Table 2, p.42
28	Culebra	FFG_340	617.80	Richey, 1989, Table 2, p.42
29	Culebra	FFG_342	682.70	Richey, 1989, Table 2, p.43
30	Culebra	FFG_344	659.10	Richey, 1989, Table 2, p.43
31	Culebra	FFG_345	678.60	Richey, 1989, Table 2, p.43
32	Culebra	FFG_347	699.50	Richey, 1989, Table 2, p.43
33	Culebra	FFG_348	738.50	Richey, 1989, Table 2, p.43
34	Culebra	FFG_349	714.50	Richey, 1989, Table 2, p.43
35	Culebra	FFG_350	745.20	Richey, 1989, Table 2, p.43
36	Culebra	FFG_351	629.40	Richey, 1989, Table 2, p.43
37	Culebra	FFG_352	629.40	Richey, 1989, Table 2, p.43
38	Culebra	FFG_353	651.10	Richey, 1989, Table 2, p.43
39	Culebra	FFG_354	762.00	Richey, 1989, Table 2, p.43
40	Culebra	FFG_361	955.20	Richey, 1989, Table 2, p.44
41	Culebra	FFG_362	919.30	Richey, 1989, Table 2, p.44
42	Culebra	FFG_363	947.00	Richey, 1989, Table 2, p.44
43	Culebra	FFG_364	918.30	Richey, 1989, Table 2, p.44
44	Culebra	FFG_366	911.60	Richey, 1989, Table 2, p.44
45	Culebra	FFG_367	931.70	Richey, 1989, Table 2, p.44
46	Culebra	FFG_370	968.70	Richey, 1989, Table 2, p.44
47	Culebra	FFG_371	965.70	Richey, 1989, Table 2, p.44
48	Culebra	FFG_372	949.10	Richey, 1989, Table 2, p.45
49	Culebra	FFG_373	909.00	Richey, 1989, Table 2, p.45
50	Culebra	FFG_374	908.30	Richey, 1989, Table 2, p.45
51	Culebra	FFG_376	947.60	Richey, 1989, Table 2, p.45
52	Culebra	FFG_381	914.70	Richey, 1989, Table 2, p.45
53	Culebra	FFG_383	908.30	Richey, 1989, Table 2, p.45
54	Culebra	FFG_384	921.10	Richey, 1989, Table 2, p.45
55	Culebra	FFG_385	915.90	Richey, 1989, Table 2, p.45
56	Culebra	FFG_387	911.10	Richey, 1989, Table 2, p.45
57	Culebra	FFG_388	900.70	Richey, 1989, Table 2, p.46
58	Culebra	FFG_389	924.80	Richey, 1989, Table 2, p.46
59	Culebra	FFG_390	919.60	Richey, 1989, Table 2, p.46
60	Culebra	FFG_391	919.20	Richey, 1989, Table 2, p.46
61	Culebra	FFG_392	910.50	Richey, 1989, Table 2, p.46
62	Culebra	FFG_393	785.60	Richey, 1989, Table 2, p.46
63	Culebra	FFG_394	882.40	Richey, 1989, Table 2, p.46
64	Culebra	FFG_395	874.50	Richey, 1989, Table 2, p.46
65	Culebra	FFG_396	853.80	Richey, 1989, Table 2, p.46
66	Culebra	FFG_398	771.70	Richey, 1989, Table 2, p.46
67	Culebra	FFG_399	785.20	Richey, 1989, Table 2, p.46
68	Culebra	FFG_401	839.70	Richey, 1989, Table 2, p.46
69	Culebra	FFG_402	947.10	Richey, 1989, Table 2, p.46
70	Culebra	FFG_403	914.60	Richey, 1989, Table 2, p.47
71	Culebra	FFG_404	873.30	Richey, 1989, Table 2, p.47
72	Culebra	FFG_407	908.00	Richey, 1989, Table 2, p.47
73	Culebra	FFG_408	907.10	Richey, 1989, Table 2, p.47
74	Culebra	FFG_409	943.10	Richey, 1989, Table 2, p.47
75	Culebra	FFG_411	887.30	Richey, 1989, Table 2, p.47
76	Culebra	FFG_413	915.10	Richey, 1989, Table 2, p.47

Table B.2. Elevations of Stratigraphic Layers Near WIPP (Continued)

	Layer	Well ID	Elevation	Source
1	Culebra	FFG_418	930.30	Richey, 1989, Table 2, p.48
2	Culebra	FFG_419	942.80	Richey, 1989, Table 2, p.48
3	Culebra	FFG_420	936.90	Richey, 1989, Table 2, p.48
4	Culebra	FFG_421	923.30	Richey, 1989, Table 2, p.48
5	Culebra	FFG_422	923.20	Richey, 1989, Table 2, p.48
6	Culebra	FFG_426	926.90	Richey, 1989, Table 2, p.48
7	Culebra	FFG_432	884.50	Richey, 1989, Table 2, p.48
8	Culebra	FFG_433	897.60	Richey, 1989, Table 2, p.48
9	Culebra	FFG_438	835.60	Richey, 1989, Table 2, p.49
10	Culebra	FFG_445	920.20	Richey, 1989, Table 2, p.49
11	Culebra	FFG_453	782.30	Richey, 1989, Table 2, p.50
12	Culebra	FFG_455	770.20	Richey, 1989, Table 2, p.50
13	Culebra	FFG_456	776.60	Richey, 1989, Table 2, p.50
14	Culebra	FFG_457	831.20	Richey, 1989, Table 2, p.50
15	Culebra	FFG_458	833.30	Richey, 1989, Table 2, p.50
16	Culebra	FFG_459	761.40	Richey, 1989, Table 2, p.50
17	Culebra	FFG_462	828.60	Richey, 1989, Table 2, p.50
18	Culebra	FFG_463	854.40	Richey, 1989, Table 2, p.51
19	Culebra	FFG_464	843.40	Richey, 1989, Table 2, p.51
20	Culebra	FFG_465	844.90	Richey, 1989, Table 2, p.51
21	Culebra	FFG_467	430.90	Richey, 1989, Table 2, p.51
22	Culebra	FFG_468	377.70	Richey, 1989, Table 2, p.51
23	Culebra	FFG_470	408.10	Richey, 1989, Table 2, p.51
24	Culebra	FFG_471	426.10	Richey, 1989, Table 2, p.51
25	Culebra	FFG_472	501.70	Richey, 1989, Table 2, p.51
26	Culebra	FFG_473	390.40	Richey, 1989, Table 2, p.51
27	Culebra	FFG_474	677.50	Richey, 1989, Table 2, p.51
28	Culebra	FFG_475	686.30	Richey, 1989, Table 2, p.51
29	Culebra	FFG_476	760.20	Richey, 1989, Table 2, p.51
30	Culebra	FFG_477	726.70	Richey, 1989, Table 2, p.51
31	Culebra	FFG_478	702.60	Richey, 1989, Table 2, p.52
32	Culebra	FFG_479	706.80	Richey, 1989, Table 2, p.52
33	Culebra	FFG_480	688.00	Richey, 1989, Table 2, p.52
34	Culebra	FFG_481	681.60	Richey, 1989, Table 2, p.52
35	Culebra	FFG_482	711.70	Richey, 1989, Table 2, p.52
36	Culebra	FFG_483	741.20	Richey, 1989, Table 2, p.52
37	Culebra	FFG_484	725.90	Richey, 1989, Table 2, p.52
38	Culebra	FFG_485	730.30	Richey, 1989, Table 2, p.52
39	Culebra	FFG_486	716.00	Richey, 1989, Table 2, p.52
40	Culebra	FFG_487	715.40	Richey, 1989, Table 2, p.52
41	Culebra	FFG_488	698.30	Richey, 1989, Table 2, p.52
42	Culebra	FFG_489	717.30	Richey, 1989, Table 2, p.52
43	Culebra	FFG_490	806.80	Richey, 1989, Table 2, p.52
44	Culebra	FFG_491	799.80	Richey, 1989, Table 2, p.52
45	Culebra	FFG_492	765.60	Richey, 1989, Table 2, p.52
46	Culebra	FFG_493	752.40	Richey, 1989, Table 2, p.53
47	Culebra	FFG_494	754.00	Richey, 1989, Table 2, p.53
48	Culebra	FFG_495	749.80	Richey, 1989, Table 2, p.53
49	Culebra	FFG_496	616.00	Richey, 1989, Table 2, p.53
50	Culebra	FFG_497	649.90	Richey, 1989, Table 2, p.53
51	Culebra	FFG_498	645.60	Richey, 1989, Table 2, p.53
52	Culebra	FFG_499	612.40	Richey, 1989, Table 2, p.53
53	Culebra	FFG_500	643.40	Richey, 1989, Table 2, p.53
54	Culebra	FFG_501	673.00	Richey, 1989, Table 2, p.53
55	Culebra	FFG_502	638.20	Richey, 1989, Table 2, p.53
56	Culebra	FFG_503	624.00	Richey, 1989, Table 2, p.53
57	Culebra	FFG_504	674.30	Richey, 1989, Table 2, p.53
58	Culebra	FFG_505	702.30	Richey, 1989, Table 2, p.53
59	Culebra	FFG_506	700.10	Richey, 1989, Table 2, p.53
60	Culebra	FFG_507	607.00	Richey, 1989, Table 2, p.53
61	Culebra	FFG_508	688.90	Richey, 1989, Table 2, p.53
62	Culebra	FFG_509	668.10	Richey, 1989, Table 2, p.54
63	Culebra	FFG_510	670.10	Richey, 1989, Table 2, p.54
64	Culebra	FFG_511	629.10	Richey, 1989, Table 2, p.54
65	Culebra	FFG_512	643.70	Richey, 1989, Table 2, p.54
66	Culebra	FFG_513	667.00	Richey, 1989, Table 2, p.54
67	Culebra	FFG_514	645.90	Richey, 1989, Table 2, p.54
68	Culebra	FFG_515	617.20	Richey, 1989, Table 2, p.54
69	Culebra	FFG_516	612.60	Richey, 1989, Table 2, p.54
70	Culebra	FFG_517	755.30	Richey, 1989, Table 2, p.54
71	Culebra	FFG_518	742.20	Richey, 1989, Table 2, p.54
72	Culebra	FFG_519	704.10	Richey, 1989, Table 2, p.54
73	Culebra	FFG_520	590.90	Richey, 1989, Table 2, p.54
74	Culebra	FFG_521	633.10	Richey, 1989, Table 2, p.54
75	Culebra	FFG_522	434.20	Richey, 1989, Table 2, p.54
76	Culebra	FFG_523	449.30	Richey, 1989, Table 2, p.54

Table B.2. Elevations of Stratigraphic Layers Near WIPP (Continued)

	Layer	Well ID	Elevation	Source
1	Culebra	FFG_524	616.00	Richey, 1989, Table 2, p.55
2	Culebra	FFG_525	443.90	Richey, 1989, Table 2, p.55
3	Culebra	FFG_526	950.70	Richey, 1989, Table 2, p.55
4	Culebra	FFG_527	894.20	Richey, 1989, Table 2, p.55
5	Culebra	FFG_528	896.10	Richey, 1989, Table 2, p.55
6	Culebra	FFG_530	965.90	Richey, 1989, Table 2, p.55
7	Culebra	FFG_531	894.90	Richey, 1989, Table 2, p.55
8	Culebra	FFG_532	879.70	Richey, 1989, Table 2, p.55
9	Culebra	FFG_534	892.80	Richey, 1989, Table 2, p.55
10	Culebra	FFG_535	882.10	Richey, 1989, Table 2, p.55
11	Culebra	FFG_536	892.50	Richey, 1989, Table 2, p.55
12	Culebra	FFG_537	879.90	Richey, 1989, Table 2, p.55
13	Culebra	FFG_543	932.20	Richey, 1989, Table 2, p.56
14	Culebra	FFG_548	883.30	Richey, 1989, Table 2, p.56
15	Culebra	FFG_552	732.70	Richey, 1989, Table 2, p.56
16	Culebra	FFG_562	621.80	Richey, 1989, Table 2, p.57
17	Culebra	FFG_563	537.40	Richey, 1989, Table 2, p.57
18	Culebra	FFG_568	631.90	Richey, 1989, Table 2, p.57
19	Culebra	FFG_569	632.80	Richey, 1989, Table 2, p.57
20	Culebra	FFG_584	742.70	Richey, 1989, Table 2, p.58
21	Culebra	FFG_585	686.70	Richey, 1989, Table 2, p.58
22	Culebra	FFG_600	700.10	Richey, 1989, Table 2, p.58
23	Culebra	FFG_601	580.00	Richey, 1989, Table 2, p.58
24	Culebra	FFG_602	803.50	Richey, 1989, Table 2, p.58
25	Culebra	FFG_606	673.70	Richey, 1989, Table 2, p.58
26	Culebra	FFG_607	681.30	Richey, 1989, Table 2, p.59
27	Culebra	FFG_608	663.20	Richey, 1989, Table 2, p.59
28	Culebra	FFG_609	656.50	Richey, 1989, Table 2, p.59
29	Culebra	FFG_610	649.20	Richey, 1989, Table 2, p.59
30	Culebra	FFG_611	644.00	Richey, 1989, Table 2, p.59
31	Culebra	FFG_612	679.10	Richey, 1989, Table 2, p.59
32	Culebra	FFG_613	677.90	Richey, 1989, Table 2, p.59
33	Culebra	FFG_618	686.70	Richey, 1989, Table 2, p.59
34	Culebra	FFG_638	536.80	Richey, 1989, Table 2, p.60
35	Culebra	FFG_639	508.10	Richey, 1989, Table 2, p.60
36	Culebra	FFG_640	597.80	Richey, 1989, Table 2, p.60
37	Culebra	FFG_643	642.30	Richey, 1989, Table 2, p.60
38	Culebra	FFG_644	677.20	Richey, 1989, Table 2, p.60
39	Culebra	FFG_648	513.30	Richey, 1989, Table 2, p.60
40	Culebra	FFG_652	822.90	Richey, 1989, Table 2, p.60
41	Culebra	FFG_653	822.70	Richey, 1989, Table 2, p.61
42	Culebra	FFG_654	845.80	Richey, 1989, Table 2, p.61
43	Culebra	FFG_655	847.30	Richey, 1989, Table 2, p.61
44	Culebra	FFG_656	845.20	Richey, 1989, Table 2, p.61
45	Culebra	FFG_657	862.90	Richey, 1989, Table 2, p.61
46	Culebra	FFG_658	849.40	Richey, 1989, Table 2, p.61
47	Culebra	FFG_659	856.80	Richey, 1989, Table 2, p.61
48	Culebra	FFG_660	873.40	Richey, 1989, Table 2, p.61
49	Culebra	FFG_662	843.40	Richey, 1989, Table 2, p.61
50	Culebra	FFG_664	836.40	Richey, 1989, Table 2, p.61
51	Culebra	FFG_666	890.00	Richey, 1989, Table 2, p.62
52	Culebra	FFG_667	875.70	Richey, 1989, Table 2, p.62
53	Culebra	FFG_668	926.10	Richey, 1989, Table 2, p.62
54	Culebra	FFG_669	912.90	Richey, 1989, Table 2, p.62
55	Culebra	FFG_670	897.30	Richey, 1989, Table 2, p.62
56	Culebra	FFG_671	900.00	Richey, 1989, Table 2, p.62
57	Culebra	FFG_672	897.10	Richey, 1989, Table 2, p.62
58	Culebra	FFG_673	894.20	Richey, 1989, Table 2, p.62
59	Culebra	FFG_674	893.40	Richey, 1989, Table 2, p.62
60	Culebra	FFG_675	851.50	Richey, 1989, Table 2, p.62
61	Culebra	FFG_676	862.30	Richey, 1989, Table 2, p.62
62	Culebra	FFG_677	889.70	Richey, 1989, Table 2, p.62
63	Culebra	FFG_679	891.20	Richey, 1989, Table 2, p.62
64	Culebra	FFG_685	918.10	Richey, 1989, Table 2, p.63
65	Culebra	FFG_689	764.50	Richey, 1989, Table 2, p.63
66	Culebra	FFG_690	768.70	Richey, 1989, Table 2, p.63
67	Culebra	FFG_691	760.80	Richey, 1989, Table 2, p.63
68	Culebra	FFG_692	749.90	Richey, 1989, Table 2, p.63
69	Culebra	FFG_693	760.40	Richey, 1989, Table 2, p.63
70	Culebra	FFG_694	750.40	Richey, 1989, Table 2, p.63
71	Culebra	FFG_695	756.50	Richey, 1989, Table 2, p.63
72	Culebra	FFG_696	758.30	Richey, 1989, Table 2, p.63
73	Culebra	FFG_697	760.20	Richey, 1989, Table 2, p.64
74	Culebra	FFG_698	802.00	Richey, 1989, Table 2, p.64
75	Culebra	FFG_699	755.60	Richey, 1989, Table 2, p.64
76	Culebra	FFG_700	749.30	Richey, 1989, Table 2, p.64

Table B.2. Elevations of Stratigraphic Layers Near WIPP (Continued)

	Layer	Well ID	Elevation	Source
1	Culebra	FFG_701	749.60	Richey, 1989, Table 2, p.64
2	Culebra	FFG_702	755.60	Richey, 1989, Table 2, p.64
3	Culebra	FFG_703	761.70	Richey, 1989, Table 2, p.64
4	Culebra	FFG_704	745.60	Richey, 1989, Table 2, p.64
5	Culebra	FFG_705	679.70	Richey, 1989, Table 2, p.64
6	Culebra	FFG_706	702.30	Richey, 1989, Table 2, p.64
7	Culebra	FFG_707	686.80	Richey, 1989, Table 2, p.64
8	Culebra	FFG_708	736.70	Richey, 1989, Table 2, p.64
9	Culebra	FFG_709	632.80	Richey, 1989, Table 2, p.64
10	Culebra	FFG_710	631.60	Richey, 1989, Table 2, p.64
11	Culebra	FFG_711	634.60	Richey, 1989, Table 2, p.65
12	Culebra	FFG_712	678.30	Richey, 1989, Table 2, p.65
13	Culebra	FFG_713	620.70	Richey, 1989, Table 2, p.65
14	Culebra	FFG_714	731.50	Richey, 1989, Table 2, p.65
15	Culebra	FFG_715	741.80	Richey, 1989, Table 2, p.65
16	Culebra	FFG_716	604.90	Richey, 1989, Table 2, p.65
17	Culebra	FFG_717	672.20	Richey, 1989, Table 2, p.65
18	Culebra	FFG_718	664.70	Richey, 1989, Table 2, p.65
19	Culebra	FFG_719	626.00	Richey, 1989, Table 2, p.65
20	Culebra	FFG_720	625.80	Richey, 1989, Table 2, p.65
21	Culebra	FFG_721	646.20	Richey, 1989, Table 2, p.65
22	Culebra	FFG_723	762.80	Richey, 1989, Table 2, p.65
23	Culebra	FFG_724	686.50	Richey, 1989, Table 2, p.65
24	Culebra	FFG_725	652.90	Richey, 1989, Table 2, p.65
25	Culebra	FFG_726	648.60	Richey, 1989, Table 2, p.65
26	Culebra	FFG_727	639.20	Richey, 1989, Table 2, p.66
27	Culebra	FFG_728	646.70	Richey, 1989, Table 2, p.66
28	Culebra	FFG_729	648.90	Richey, 1989, Table 2, p.66
29	Culebra	FFG_730	673.60	Richey, 1989, Table 2, p.66
30	Culebra	FFG_731	670.40	Richey, 1989, Table 2, p.66
31	Culebra	FFG_732	686.40	Richey, 1989, Table 2, p.66
32	Culebra	FFG_733	749.80	Richey, 1989, Table 2, p.66
33	Culebra	FFG_734	707.40	Richey, 1989, Table 2, p.66
34	Culebra	FFG_735	638.90	Richey, 1989, Table 2, p.66
35	Culebra	FFG_736	676.40	Richey, 1989, Table 2, p.66
36	Culebra	FFG_737	620.30	Richey, 1989, Table 2, p.66
37	Culebra	FFG_738	662.00	Richey, 1989, Table 2, p.66
38	Culebra	FFG_739	694.80	Richey, 1989, Table 2, p.66
39	Culebra	FFG_740	662.60	Richey, 1989, Table 2, p.66
40	Culebra	FFG_741	658.70	Richey, 1989, Table 2, p.66
41	Culebra	FFG_742	700.70	Richey, 1989, Table 2, p.67
42	Culebra	FFG_743	686.10	Richey, 1989, Table 2, p.67
43	Culebra	FFG_744	677.20	Richey, 1989, Table 2, p.67
44	Culebra	FFG_745	657.70	Richey, 1989, Table 2, p.67
45	Culebra	FFG_746	645.50	Richey, 1989, Table 2, p.67
46	Culebra	H1	829.70	Mercer, 1983, Table 1
47	Culebra	H10C	709.30	Mercer, 1983, Table 1
48	Culebra	H2C	839.70	Mercer, 1983, Table 1
49	Culebra	H3	828.50	Mercer, 1983, Table 1
50	Culebra	H4C	866.80	Mercer, 1983, Table 1
51	Culebra	H5C	794.90	Mercer, 1983, Table 1
52	Culebra	H6C	836.40	Mercer, 1983, Table 1
53	Culebra	H7C	891.90	Mercer, 1983, Table 1
54	Culebra	H8C	867.20	Mercer, 1983, Table 1
55	Culebra	H9C	840.90	Mercer, 1983, Table 1
56	Culebra	P1	855.60	Mercer, 1983, Table 1
57	Culebra	P10	785.70	Mercer, 1983, Table 1
58	Culebra	P11	790.00	Mercer, 1983, Table 1
59	Culebra	P12	835.50	Mercer, 1983, Table 1
60	Culebra	P13	835.50	Mercer, 1983, Table 1
61	Culebra	P14	849.40	Mercer, 1983, Table 1
62	Culebra	P15	883.00	Mercer, 1983, Table 1
63	Culebra	P16	858.90	Mercer, 1983, Table 1
64	Culebra	P17	846.70	Mercer, 1983, Table 1
65	Culebra	P18	782.70	Mercer, 1983, Table 1
66	Culebra	P19	785.80	Mercer, 1983, Table 1
67	Culebra	P2	799.20	Mercer, 1983, Table 1
68	Culebra	P20	792.50	Mercer, 1983, Table 1
69	Culebra	P21	795.50	Mercer, 1983, Table 1
70	Culebra	P3	835.40	Mercer, 1983, Table 1
71	Culebra	P4	813.50	Mercer, 1983, Table 1
72	Culebra	P5	812.90	Mercer, 1983, Table 1
73	Culebra	P6	858.60	Mercer, 1983, Table 1
74	Culebra	P7	864.40	Mercer, 1983, Table 1
75	Culebra	P8	846.10	Mercer, 1983, Table 1
76	Culebra	P9	816.30	Mercer, 1983, Table 1

Table B.2. Elevations of Stratigraphic Layers Near WIPP (Continued)

	Layer	Well ID	Elevation	Source
1	Culebra	REF	823.40	Rechard et al.,1991, Figure 2.2-1
2	Culebra	SaltShft	822.81	Bechtel, Inc., 1986, Appendix D
3	Culebra	WIPP11	786.90	Mercer, 1983, Table 1
4	Culebra	WIPP11	787.00	SNL and USGS, 1982a, Table 2
5	Culebra	WIPP12	811.30	SNL and D'Appolonia Consulting, 1983, Table 2
6	Culebra	WIPP12	811.40	Mercer, 1983, Table 1
7	Culebra	WIPP13	824.10	Mercer, 1983, Table 1
8	Culebra	WIPP16	679.70	Mercer, 1983, Table 1
9	Culebra	WIPP18	813.80	Mercer, 1983, Table 1
10	Culebra	WIPP19	816.00	Mercer, 1983, Table 1
11	Culebra	WIPP21	819.30	Mercer, 1983, Table 1
12	Culebra	WIPP22	818.00	Mercer, 1983, Table 1
13	Culebra	WIPP25	843.10	Mercer, 1983, Table 1
14	Culebra	WIPP26	904.00	Mercer, 1983, Table 1
15	Culebra	WIPP27	879.30	Mercer, 1983, Table 1
16	Culebra	WIPP28	892.20	Mercer, 1983, Table 1
17	Culebra	WIPP29	903.70	Mercer, 1983, Table 1
18	Culebra	WIPP30	852.60	Mercer, 1983, Table 1
19	Culebra	WIPP32	902.80	Mercer, 1983, Table 1
20	Culebra	WIPP33	845.30	Mercer, 1983, Table 1
21	Culebra	WIPP34	792.20	Mercer, 1983, Table 1
22	Culebra	WastShft	823.64	Bechtel, Inc., 1986, Appendix E
23	DeweyLk	AirShft	1022.02	Holt and Powers, 1990, Figure 22
24	DeweyLk	DOE1	1018.10	U.S. DOE, Sep 1982, Table 2
25	DeweyLk	DOE2	1001.30	Mercer et al., 1987, Table 3-2
26	DeweyLk	ERDA9	1023.30	SNL and USGS, 1982b, Table 2
27	DeweyLk	ExhtShft	1022.73	Bechtel, Inc., 1986, Appendix F
28	DeweyLk	REF	1023.30	Rechard et al.,1991, Figure 2.2-1
29	DeweyLk	SaltShft	1025.35	Bechtel, Inc., 1986, Appendix D
30	DeweyLk	WIPP11	995.20	SNL and USGS, 1982a, Table 2
31	DeweyLk	WIPP12	1010.90	SNL and D'Appolonia Consulting, 1983, Table 2
32	DeweyLk	WastShft	1009.97	Bechtel, Inc., 1986, Appendix E
33	Halite1	DOE1	-170.40	U.S. DOE, Sep 1982, Table 2
34	Halite1	DOE1	-71.60	U.S. DOE, Sep 1982, Table 2
35	Halite1	DOE2	-119.10	Mercer et al., 1987, Table 3-2
36	Halite1	DOE2	-116.40	Mercer et al., 1987, Table 3-2
37	Halite1	REF	-119.10	Rechard et al.,1991, Figure 2.2-1
38	Halite1	REF	-116.40	Rechard et al.,1991, Figure 2.2-1
39	Halite1	WIPP11	-37.80	SNL and USGS, 1982a, Table 2
40	Halite1	WIPP11	-22.20	SNL and USGS, 1982a, Table 2
41	Halite1	WIPP12	-131.10	SNL and D'Appolonia Consulting, 1983, Table 2
42	Halite1	WIPP12	24.50	SNL and D'Appolonia Consulting, 1983, Table 2
43	Halite2	DOE1	-38.60	U.S. DOE, Sep 1982, Table 2
44	Halite2	DOE1	30.00	U.S. DOE, Sep 1982, Table 2
45	Halite2	WIPP11	14.40	SNL and USGS, 1982a, Table 2
46	Halite2	WIPP11	309.40	SNL and USGS, 1982a, Table 2
47	Halite2	WIPP12	57.80	SNL and D'Appolonia Consulting, 1983, Table 2
48	Halite2	WIPP12	127.30	SNL and D'Appolonia Consulting, 1983, Table 2
49	L_Member	DOE1	163.60	U.S. DOE, Sep 1982, Table 2
50	L_Member	DOE2	102.30	Mercer et al., 1987, Table 3-2
51	L_Member	ERDA9	178.10	SNL and USGS, 1982b, Table 2
52	L_Member	REF	178.10	Rechard et al.,1991, Figure 2.2-1
53	L_Member	WIPP11	334.10	SNL and USGS, 1982a, Table 2
54	L_Member	WIPP12	227.40	SNL and D'Appolonia Consulting, 1983, Table 2
55	M49er	AEC7	911.90	Mercer, 1983, Table 1
56	M49er	AEC8	875.40	Mercer, 1983, Table 1
57	M49er	AirShft	877.42	Holt and Powers, 1990, Figure 22
58	M49er	B25	876.60	Mercer, 1983, Table 1
59	M49er	DOE1	855.20	U.S. DOE, Sep 1982, Table 2
60	M49er	DOE2	847.10	Mercer et al., 1987, Table 3-2
61	M49er	ERDA6	915.60	Mercer, 1983, Table 1
62	M49er	ERDA9	878.10	Mercer, 1983, Table 1
63	M49er	ERDA9	874.00	SNL and USGS, 1982b, Table 2
64	M49er	ExhtShft	872.52	Bechtel, Inc., 1986, Appendix F
65	M49er	FFG_002	686.10	Richey, 1989, Table 2, p.21
66	M49er	FFG_004	739.10	Richey, 1989, Table 2, p.21
67	M49er	FFG_005	693.80	Richey, 1989, Table 2, p.21
68	M49er	FFG_006	688.90	Richey, 1989, Table 2, p.21
69	M49er	FFG_007	678.20	Richey, 1989, Table 2, p.21
70	M49er	FFG_009	678.10	Richey, 1989, Table 2, p.21
71	M49er	FFG_011	684.60	Richey, 1989, Table 2, p.21
72	M49er	FFG_012	687.00	Richey, 1989, Table 2, p.21
73	M49er	FFG_013	696.80	Richey, 1989, Table 2, p.21
74	M49er	FFG_014	741.90	Richey, 1989, Table 2, p.21
75	M49er	FFG_016	666.90	Richey, 1989, Table 2, p.21
76	M49er	FFG_017	669.60	Richey, 1989, Table 2, p.22

Table B.2. Elevations of Stratigraphic Layers Near WIPP (Continued)

	Layer	Well ID	Elevation	Source
1	M49er	FFG_018	672.40	Richey, 1989, Table 2, p.22
2	M49er	FFG_019	666.30	Richey, 1989, Table 2, p.22
3	M49er	FFG_020	740.70	Richey, 1989, Table 2, p.22
4	M49er	FFG_023	678.50	Richey, 1989, Table 2, p.22
5	M49er	FFG_024	662.00	Richey, 1989, Table 2, p.22
6	M49er	FFG_025	674.10	Richey, 1989, Table 2, p.22
7	M49er	FFG_026	670.80	Richey, 1989, Table 2, p.22
8	M49er	FFG_027	664.20	Richey, 1989, Table 2, p.22
9	M49er	FFG_028	629.80	Richey, 1989, Table 2, p.22
10	M49er	FFG_029	616.00	Richey, 1989, Table 2, p.22
11	M49er	FFG_030	616.60	Richey, 1989, Table 2, p.22
12	M49er	FFG_031	609.60	Richey, 1989, Table 2, p.22
13	M49er	FFG_032	611.90	Richey, 1989, Table 2, p.22
14	M49er	FFG_033	607.20	Richey, 1989, Table 2, p.22
15	M49er	FFG_034	601.30	Richey, 1989, Table 2, p.23
16	M49er	FFG_035	590.30	Richey, 1989, Table 2, p.23
17	M49er	FFG_036	602.60	Richey, 1989, Table 2, p.23
18	M49er	FFG_037	592.90	Richey, 1989, Table 2, p.23
19	M49er	FFG_038	579.40	Richey, 1989, Table 2, p.23
20	M49er	FFG_039	798.60	Richey, 1989, Table 2, p.23
21	M49er	FFG_040	740.70	Richey, 1989, Table 2, p.23
22	M49er	FFG_041	801.00	Richey, 1989, Table 2, p.23
23	M49er	FFG_042	805.50	Richey, 1989, Table 2, p.23
24	M49er	FFG_043	810.00	Richey, 1989, Table 2, p.23
25	M49er	FFG_044	762.30	Richey, 1989, Table 2, p.23
26	M49er	FFG_047	633.40	Richey, 1989, Table 2, p.23
27	M49er	FFG_048	653.20	Richey, 1989, Table 2, p.23
28	M49er	FFG_049	641.90	Richey, 1989, Table 2, p.23
29	M49er	FFG_050	648.00	Richey, 1989, Table 2, p.24
30	M49er	FFG_051	648.90	Richey, 1989, Table 2, p.24
31	M49er	FFG_052	651.60	Richey, 1989, Table 2, p.24
32	M49er	FFG_053	642.80	Richey, 1989, Table 2, p.24
33	M49er	FFG_054	641.90	Richey, 1989, Table 2, p.24
34	M49er	FFG_055	641.60	Richey, 1989, Table 2, p.24
35	M49er	FFG_056	644.30	Richey, 1989, Table 2, p.24
36	M49er	FFG_057	645.60	Richey, 1989, Table 2, p.24
37	M49er	FFG_058	641.00	Richey, 1989, Table 2, p.24
38	M49er	FFG_059	643.40	Richey, 1989, Table 2, p.24
39	M49er	FFG_060	645.50	Richey, 1989, Table 2, p.24
40	M49er	FFG_061	645.90	Richey, 1989, Table 2, p.24
41	M49er	FFG_062	574.30	Richey, 1989, Table 2, p.24
42	M49er	FFG_063	534.70	Richey, 1989, Table 2, p.24
43	M49er	FFG_064	559.70	Richey, 1989, Table 2, p.24
44	M49er	FFG_065	542.90	Richey, 1989, Table 2, p.24
45	M49er	FFG_066	496.80	Richey, 1989, Table 2, p.24
46	M49er	FFG_067	537.10	Richey, 1989, Table 2, p.25
47	M49er	FFG_068	496.50	Richey, 1989, Table 2, p.25
48	M49er	FFG_069	524.30	Richey, 1989, Table 2, p.25
49	M49er	FFG_070	553.80	Richey, 1989, Table 2, p.25
50	M49er	FFG_071	811.10	Richey, 1989, Table 2, p.25
51	M49er	FFG_072	739.70	Richey, 1989, Table 2, p.25
52	M49er	FFG_073	717.80	Richey, 1989, Table 2, p.25
53	M49er	FFG_074	723.70	Richey, 1989, Table 2, p.25
54	M49er	FFG_075	773.30	Richey, 1989, Table 2, p.25
55	M49er	FFG_076	836.40	Richey, 1989, Table 2, p.25
56	M49er	FFG_078	874.40	Richey, 1989, Table 2, p.25
57	M49er	FFG_079	848.00	Richey, 1989, Table 2, p.25
58	M49er	FFG_080	827.50	Richey, 1989, Table 2, p.25
59	M49er	FFG_081	746.80	Richey, 1989, Table 2, p.26
60	M49er	FFG_082	779.10	Richey, 1989, Table 2, p.26
61	M49er	FFG_083	693.00	Richey, 1989, Table 2, p.26
62	M49er	FFG_084	721.10	Richey, 1989, Table 2, p.26
63	M49er	FFG_085	714.20	Richey, 1989, Table 2, p.26
64	M49er	FFG_086	722.60	Richey, 1989, Table 2, p.26
65	M49er	FFG_087	698.00	Richey, 1989, Table 2, p.26
66	M49er	FFG_088	694.40	Richey, 1989, Table 2, p.26
67	M49er	FFG_089	675.80	Richey, 1989, Table 2, p.26
68	M49er	FFG_091	720.00	Richey, 1989, Table 2, p.26
69	M49er	FFG_092	734.90	Richey, 1989, Table 2, p.26
70	M49er	FFG_093	737.30	Richey, 1989, Table 2, p.26
71	M49er	FFG_094	740.60	Richey, 1989, Table 2, p.26
72	M49er	FFG_095	706.50	Richey, 1989, Table 2, p.26
73	M49er	FFG_096	689.50	Richey, 1989, Table 2, p.26
74	M49er	FFG_097	671.20	Richey, 1989, Table 2, p.27
75	M49er	FFG_098	645.50	Richey, 1989, Table 2, p.27
76	M49er	FFG_099	641.60	Richey, 1989, Table 2, p.27

Table B.2. Elevations of Stratigraphic Layers Near WIPP (Continued)

	Layer	Well ID	Elevation	Source		Layer	Well ID	Elevation	Source
1	M49er	FFG_100	624.90	Richey, 1989, Table 2, p.27	39	M49er	FFG_141	873.10	Richey, 1989, Table 2, p.29
2	M49er	FFG_101	593.10	Richey, 1989, Table 2, p.27	40	M49er	FFG_142	849.30	Richey, 1989, Table 2, p.29
3	M49er	FFG_102	613.90	Richey, 1989, Table 2, p.27	41	M49er	FFG_143	855.80	Richey, 1989, Table 2, p.29
4	M49er	FFG_103	674.60	Richey, 1989, Table 2, p.27	42	M49er	FFG_159	956.20	Richey, 1989, Table 2, p.30
5	M49er	FFG_104	572.50	Richey, 1989, Table 2, p.27	43	M49er	FFG_160	950.10	Richey, 1989, Table 2, p.30
6	M49er	FFG_105	926.90	Richey, 1989, Table 2, p.27	44	M49er	FFG_161	957.40	Richey, 1989, Table 2, p.30
7	M49er	FFG_106	954.70	Richey, 1989, Table 2, p.27	45	M49er	FFG_162	955.90	Richey, 1989, Table 2, p.30
8	M49er	FFG_107	945.20	Richey, 1989, Table 2, p.27	46	M49er	FFG_163	955.30	Richey, 1989, Table 2, p.30
9	M49er	FFG_108	933.60	Richey, 1989, Table 2, p.27	47	M49er	FFG_166	954.30	Richey, 1989, Table 2, p.31
10	M49er	FFG_109	917.20	Richey, 1989, Table 2, p.27	48	M49er	FFG_167	936.70	Richey, 1989, Table 2, p.31
11	M49er	FFG_110	887.00	Richey, 1989, Table 2, p.27	49	M49er	FFG_168	967.50	Richey, 1989, Table 2, p.31
12	M49er	FFG_111	896.70	Richey, 1989, Table 2, p.27	50	M49er	FFG_169	980.20	Richey, 1989, Table 2, p.31
13	M49er	FFG_112	879.30	Richey, 1989, Table 2, p.28	51	M49er	FFG_170	933.60	Richey, 1989, Table 2, p.31
14	M49er	FFG_113	893.40	Richey, 1989, Table 2, p.28	52	M49er	FFG_173	934.80	Richey, 1989, Table 2, p.31
15	M49er	FFG_114	924.20	Richey, 1989, Table 2, p.28	53	M49er	FFG_180	943.90	Richey, 1989, Table 2, p.31
16	M49er	FFG_115	913.80	Richey, 1989, Table 2, p.28	54	M49er	FFG_182	856.50	Richey, 1989, Table 2, p.32
17	M49er	FFG_116	929.30	Richey, 1989, Table 2, p.28	55	M49er	FFG_189	922.70	Richey, 1989, Table 2, p.32
18	M49er	FFG_117	935.70	Richey, 1989, Table 2, p.28	56	M49er	FFG_190	901.60	Richey, 1989, Table 2, p.32
19	M49er	FFG_120	944.30	Richey, 1989, Table 2, p.28	57	M49er	FFG_191	901.30	Richey, 1989, Table 2, p.32
20	M49er	FFG_121	946.40	Richey, 1989, Table 2, p.28	58	M49er	FFG_192	834.50	Richey, 1989, Table 2, p.32
21	M49er	FFG_122	944.90	Richey, 1989, Table 2, p.28	59	M49er	FFG_194	839.70	Richey, 1989, Table 2, p.33
22	M49er	FFG_123	928.10	Richey, 1989, Table 2, p.28	60	M49er	FFG_195	855.30	Richey, 1989, Table 2, p.33
23	M49er	FFG_124	900.40	Richey, 1989, Table 2, p.28	61	M49er	FFG_196	897.60	Richey, 1989, Table 2, p.33
24	M49er	FFG_125	912.20	Richey, 1989, Table 2, p.28	62	M49er	FFG_197	899.50	Richey, 1989, Table 2, p.33
25	M49er	FFG_126	904.50	Richey, 1989, Table 2, p.28	63	M49er	FFG_198	898.20	Richey, 1989, Table 2, p.33
26	M49er	FFG_127	909.50	Richey, 1989, Table 2, p.28	64	M49er	FFG_199	888.80	Richey, 1989, Table 2, p.33
27	M49er	FFG_128	948.00	Richey, 1989, Table 2, p.28	65	M49er	FFG_200	902.50	Richey, 1989, Table 2, p.33
28	M49er	FFG_129	923.80	Richey, 1989, Table 2, p.28	66	M49er	FFG_201	894.60	Richey, 1989, Table 2, p.33
29	M49er	FFG_130	954.00	Richey, 1989, Table 2, p.28	67	M49er	FFG_202	834.20	Richey, 1989, Table 2, p.33
30	M49er	FFG_132	956.50	Richey, 1989, Table 2, p.29	68	M49er	FFG_203	841.30	Richey, 1989, Table 2, p.33
31	M49er	FFG_133	959.50	Richey, 1989, Table 2, p.29	69	M49er	FFG_204	864.80	Richey, 1989, Table 2, p.33
32	M49er	FFG_134	963.80	Richey, 1989, Table 2, p.29	70	M49er	FFG_205	880.60	Richey, 1989, Table 2, p.33
33	M49er	FFG_135	937.30	Richey, 1989, Table 2, p.29	71	M49er	FFG_206	895.80	Richey, 1989, Table 2, p.33
34	M49er	FFG_136	934.30	Richey, 1989, Table 2, p.29	72	M49er	FFG_207	892.20	Richey, 1989, Table 2, p.33
35	M49er	FFG_137	946.80	Richey, 1989, Table 2, p.29	73	M49er	FFG_208	902.80	Richey, 1989, Table 2, p.34
36	M49er	FFG_138	897.40	Richey, 1989, Table 2, p.29	74	M49er	FFG_210	885.80	Richey, 1989, Table 2, p.34
37	M49er	FFG_139	907.70	Richey, 1989, Table 2, p.29	75	M49er	FFG_212	870.50	Richey, 1989, Table 2, p.34
38	M49er	FFG_140	849.10	Richey, 1989, Table 2, p.29	76	M49er	FFG_213	903.50	Richey, 1989, Table 2, p.34

Table B.2. Elevations of Stratigraphic Layers Near WIPP (Continued)

	Layer	Well ID	Elevation	Source		Layer	Well ID	Elevation	Source
1	M49er	FFG_214	877.80	Richey, 1989, Table 2, p.34	39	M49er	FFG_254	651.00	Richey, 1989, Table 2, p.36
2	M49er	FFG_215	852.50	Richey, 1989, Table 2, p.34	40	M49er	FFG_255	609.90	Richey, 1989, Table 2, p.37
3	M49er	FFG_216	737.00	Richey, 1989, Table 2, p.34	41	M49er	FFG_256	557.80	Richey, 1989, Table 2, p.37
4	M49er	FFG_217	873.60	Richey, 1989, Table 2, p.34	42	M49er	FFG_257	600.40	Richey, 1989, Table 2, p.37
5	M49er	FFG_218	863.50	Richey, 1989, Table 2, p.34	43	M49er	FFG_258	615.00	Richey, 1989, Table 2, p.37
6	M49er	FFG_219	910.40	Richey, 1989, Table 2, p.34	44	M49er	FFG_259	584.90	Richey, 1989, Table 2, p.37
7	M49er	FFG_220	859.90	Richey, 1989, Table 2, p.34	45	M49er	FFG_260	621.80	Richey, 1989, Table 2, p.37
8	M49er	FFG_221	814.40	Richey, 1989, Table 2, p.34	46	M49er	FFG_261	610.20	Richey, 1989, Table 2, p.37
9	M49er	FFG_222	770.60	Richey, 1989, Table 2, p.34	47	M49er	FFG_263	553.40	Richey, 1989, Table 2, p.37
10	M49er	FFG_224	677.00	Richey, 1989, Table 2, p.35	48	M49er	FFG_264	777.60	Richey, 1989, Table 2, p.37
11	M49er	FFG_225	683.70	Richey, 1989, Table 2, p.35	49	M49er	FFG_265	775.40	Richey, 1989, Table 2, p.37
12	M49er	FFG_226	683.20	Richey, 1989, Table 2, p.35	50	M49er	FFG_266	758.90	Richey, 1989, Table 2, p.37
13	M49er	FFG_228	673.70	Richey, 1989, Table 2, p.35	51	M49er	FFG_267	736.40	Richey, 1989, Table 2, p.37
14	M49er	FFG_229	701.60	Richey, 1989, Table 2, p.35	52	M49er	FFG_268	716.00	Richey, 1989, Table 2, p.37
15	M49er	FFG_230	688.60	Richey, 1989, Table 2, p.35	53	M49er	FFG_269	729.20	Richey, 1989, Table 2, p.38
16	M49er	FFG_231	704.00	Richey, 1989, Table 2, p.35	54	M49er	FFG_270	791.80	Richey, 1989, Table 2, p.38
17	M49er	FFG_232	717.80	Richey, 1989, Table 2, p.35	55	M49er	FFG_271	833.90	Richey, 1989, Table 2, p.38
18	M49er	FFG_233	709.30	Richey, 1989, Table 2, p.35	56	M49er	FFG_272	846.60	Richey, 1989, Table 2, p.38
19	M49er	FFG_234	745.80	Richey, 1989, Table 2, p.35	57	M49er	FFG_273	816.90	Richey, 1989, Table 2, p.38
20	M49er	FFG_235	722.40	Richey, 1989, Table 2, p.35	58	M49er	FFG_274	851.00	Richey, 1989, Table 2, p.38
21	M49er	FFG_236	768.40	Richey, 1989, Table 2, p.35	59	M49er	FFG_275	858.60	Richey, 1989, Table 2, p.38
22	M49er	FFG_237	735.30	Richey, 1989, Table 2, p.35	60	M49er	FFG_276	861.60	Richey, 1989, Table 2, p.38
23	M49er	FFG_238	716.60	Richey, 1989, Table 2, p.36	61	M49er	FFG_277	853.50	Richey, 1989, Table 2, p.38
24	M49er	FFG_239	703.10	Richey, 1989, Table 2, p.36	62	M49er	FFG_278	868.40	Richey, 1989, Table 2, p.38
25	M49er	FFG_240	695.20	Richey, 1989, Table 2, p.36	63	M49er	FFG_279	860.10	Richey, 1989, Table 2, p.38
26	M49er	FFG_241	688.90	Richey, 1989, Table 2, p.36	64	M49er	FFG_280	858.60	Richey, 1989, Table 2, p.38
27	M49er	FFG_242	799.80	Richey, 1989, Table 2, p.36	65	M49er	FFG_281	835.80	Richey, 1989, Table 2, p.38
28	M49er	FFG_243	763.80	Richey, 1989, Table 2, p.36	66	M49er	FFG_283	584.60	Richey, 1989, Table 2, p.39
29	M49er	FFG_244	798.40	Richey, 1989, Table 2, p.36	67	M49er	FFG_284	730.30	Richey, 1989, Table 2, p.39
30	M49er	FFG_245	597.10	Richey, 1989, Table 2, p.36	68	M49er	FFG_285	760.20	Richey, 1989, Table 2, p.39
31	M49er	FFG_246	601.70	Richey, 1989, Table 2, p.36	69	M49er	FFG_286	837.50	Richey, 1989, Table 2, p.39
32	M49er	FFG_247	589.10	Richey, 1989, Table 2, p.36	70	M49er	FFG_287	812.00	Richey, 1989, Table 2, p.39
33	M49er	FFG_248	594.70	Richey, 1989, Table 2, p.36	71	M49er	FFG_288	765.70	Richey, 1989, Table 2, p.39
34	M49er	FFG_249	593.70	Richey, 1989, Table 2, p.36	72	M49er	FFG_289	736.30	Richey, 1989, Table 2, p.39
35	M49er	FFG_250	674.10	Richey, 1989, Table 2, p.36	73	M49er	FFG_290	825.70	Richey, 1989, Table 2, p.39
36	M49er	FFG_251	568.70	Richey, 1989, Table 2, p.36	74	M49er	FFG_291	766.20	Richey, 1989, Table 2, p.39
37	M49er	FFG_252	708.60	Richey, 1989, Table 2, p.36	75	M49er	FFG_292	774.20	Richey, 1989, Table 2, p.39
38	M49er	FFG_253	660.50	Richey, 1989, Table 2, p.36	76	M49er	FFG_293	766.00	Richey, 1989, Table 2, p.39

Table B.2. Elevations of Stratigraphic Layers Near WIPP (Continued)

	Layer	Well ID	Elevation	Source
1	M49er	FFG_294	595.30	Richey, 1989, Table 2, p.39
2	M49er	FFG_295	582.80	Richey, 1989, Table 2, p.39
3	M49er	FFG_297	567.50	Richey, 1989, Table 2, p.39
4	M49er	FFG_298	569.20	Richey, 1989, Table 2, p.40
5	M49er	FFG_299	594.40	Richey, 1989, Table 2, p.40
6	M49er	FFG_300	543.70	Richey, 1989, Table 2, p.40
7	M49er	FFG_301	514.80	Richey, 1989, Table 2, p.40
8	M49er	FFG_302	542.50	Richey, 1989, Table 2, p.40
9	M49er	FFG_303	535.90	Richey, 1989, Table 2, p.40
10	M49er	FFG_304	540.40	Richey, 1989, Table 2, p.40
11	M49er	FFG_305	534.60	Richey, 1989, Table 2, p.40
12	M49er	FFG_306	492.20	Richey, 1989, Table 2, p.40
13	M49er	FFG_307	517.90	Richey, 1989, Table 2, p.40
14	M49er	FFG_308	491.30	Richey, 1989, Table 2, p.40
15	M49er	FFG_309	535.20	Richey, 1989, Table 2, p.40
16	M49er	FFG_310	564.20	Richey, 1989, Table 2, p.40
17	M49er	FFG_311	498.70	Richey, 1989, Table 2, p.40
18	M49er	FFG_312	537.40	Richey, 1989, Table 2, p.40
19	M49er	FFG_313	934.30	Richey, 1989, Table 2, p.41
20	M49er	FFG_314	862.30	Richey, 1989, Table 2, p.41
21	M49er	FFG_315	782.90	Richey, 1989, Table 2, p.41
22	M49er	FFG_316	771.40	Richey, 1989, Table 2, p.41
23	M49er	FFG_317	792.20	Richey, 1989, Table 2, p.41
24	M49er	FFG_318	758.00	Richey, 1989, Table 2, p.41
25	M49er	FFG_319	769.30	Richey, 1989, Table 2, p.41
26	M49er	FFG_320	762.30	Richey, 1989, Table 2, p.41
27	M49er	FFG_321	760.50	Richey, 1989, Table 2, p.41
28	M49er	FFG_322	755.10	Richey, 1989, Table 2, p.41
29	M49er	FFG_323	751.10	Richey, 1989, Table 2, p.41
30	M49er	FFG_324	761.70	Richey, 1989, Table 2, p.41
31	M49er	FFG_325	819.60	Richey, 1989, Table 2, p.41
32	M49er	FFG_326	754.40	Richey, 1989, Table 2, p.41
33	M49er	FFG_327	748.30	Richey, 1989, Table 2, p.42
34	M49er	FFG_328	757.00	Richey, 1989, Table 2, p.42
35	M49er	FFG_329	755.60	Richey, 1989, Table 2, p.42
36	M49er	FFG_330	754.90	Richey, 1989, Table 2, p.42
37	M49er	FFG_331	753.50	Richey, 1989, Table 2, p.42
38	M49er	FFG_332	744.00	Richey, 1989, Table 2, p.42
39	M49er	FFG_333	746.30	Richey, 1989, Table 2, p.42
40	M49er	FFG_334	743.10	Richey, 1989, Table 2, p.42
41	M49er	FFG_335	757.10	Richey, 1989, Table 2, p.42
42	M49er	FFG_336	754.40	Richey, 1989, Table 2, p.42
43	M49er	FFG_337	738.50	Richey, 1989, Table 2, p.42
44	M49er	FFG_338	744.80	Richey, 1989, Table 2, p.42
45	M49er	FFG_339	711.10	Richey, 1989, Table 2, p.42
46	M49er	FFG_340	721.40	Richey, 1989, Table 2, p.42
47	M49er	FFG_342	747.60	Richey, 1989, Table 2, p.43
48	M49er	FFG_344	713.40	Richey, 1989, Table 2, p.43
49	M49er	FFG_345	775.50	Richey, 1989, Table 2, p.43
50	M49er	FFG_347	766.00	Richey, 1989, Table 2, p.43
51	M49er	FFG_348	790.90	Richey, 1989, Table 2, p.43
52	M49er	FFG_349	764.20	Richey, 1989, Table 2, p.43
53	M49er	FFG_350	808.90	Richey, 1989, Table 2, p.43
54	M49er	FFG_351	732.20	Richey, 1989, Table 2, p.43
55	M49er	FFG_352	731.50	Richey, 1989, Table 2, p.43
56	M49er	FFG_353	751.70	Richey, 1989, Table 2, p.43
57	M49er	FFG_354	817.80	Richey, 1989, Table 2, p.43
58	M49er	FFG_361	1011.00	Richey, 1989, Table 2, p.44
59	M49er	FFG_366	960.40	Richey, 1989, Table 2, p.44
60	M49er	FFG_367	975.90	Richey, 1989, Table 2, p.44
61	M49er	FFG_371	1012.90	Richey, 1989, Table 2, p.44
62	M49er	FFG_374	946.40	Richey, 1989, Table 2, p.45
63	M49er	FFG_383	955.30	Richey, 1989, Table 2, p.45
64	M49er	FFG_384	976.00	Richey, 1989, Table 2, p.45
65	M49er	FFG_387	966.60	Richey, 1989, Table 2, p.45
66	M49er	FFG_388	959.20	Richey, 1989, Table 2, p.46
67	M49er	FFG_390	974.40	Richey, 1989, Table 2, p.46
68	M49er	FFG_391	973.50	Richey, 1989, Table 2, p.46
69	M49er	FFG_392	967.80	Richey, 1989, Table 2, p.46
70	M49er	FFG_393	835.60	Richey, 1989, Table 2, p.46
71	M49er	FFG_394	925.90	Richey, 1989, Table 2, p.46
72	M49er	FFG_395	918.40	Richey, 1989, Table 2, p.46
73	M49er	FFG_396	901.60	Richey, 1989, Table 2, p.46
74	M49er	FFG_398	825.70	Richey, 1989, Table 2, p.46
75	M49er	FFG_402	1002.50	Richey, 1989, Table 2, p.46
76	M49er	FFG_403	963.00	Richey, 1989, Table 2, p.47

Table B.2. Elevations of Stratigraphic Layers Near WIPP (Continued)

	Layer	Well ID	Elevation	Source
1	M49er	FFG_404	925.70	Richey, 1989, Table 2, p.47
2	M49er	FFG_407	958.30	Richey, 1989, Table 2, p.47
3	M49er	FFG_419	997.00	Richey, 1989, Table 2, p.48
4	M49er	FFG_420	992.70	Richey, 1989, Table 2, p.48
5	M49er	FFG_421	983.60	Richey, 1989, Table 2, p.48
6	M49er	FFG_422	976.60	Richey, 1989, Table 2, p.48
7	M49er	FFG_432	931.80	Richey, 1989, Table 2, p.48
8	M49er	FFG_438	892.60	Richey, 1989, Table 2, p.49
9	M49er	FFG_455	837.60	Richey, 1989, Table 2, p.50
10	M49er	FFG_456	829.00	Richey, 1989, Table 2, p.50
11	M49er	FFG_457	885.10	Richey, 1989, Table 2, p.50
12	M49er	FFG_458	888.20	Richey, 1989, Table 2, p.50
13	M49er	FFG_459	816.60	Richey, 1989, Table 2, p.50
14	M49er	FFG_462	884.10	Richey, 1989, Table 2, p.50
15	M49er	FFG_463	913.50	Richey, 1989, Table 2, p.51
16	M49er	FFG_464	900.40	Richey, 1989, Table 2, p.51
17	M49er	FFG_465	902.80	Richey, 1989, Table 2, p.51
18	M49er	FFG_467	506.20	Richey, 1989, Table 2, p.51
19	M49er	FFG_468	493.50	Richey, 1989, Table 2, p.51
20	M49er	FFG_470	509.60	Richey, 1989, Table 2, p.51
21	M49er	FFG_471	525.80	Richey, 1989, Table 2, p.51
22	M49er	FFG_472	564.20	Richey, 1989, Table 2, p.51
23	M49er	FFG_473	491.60	Richey, 1989, Table 2, p.51
24	M49er	FFG_474	750.70	Richey, 1989, Table 2, p.51
25	M49er	FFG_475	749.70	Richey, 1989, Table 2, p.51
26	M49er	FFG_476	821.80	Richey, 1989, Table 2, p.51
27	M49er	FFG_477	774.50	Richey, 1989, Table 2, p.51
28	M49er	FFG_478	755.60	Richey, 1989, Table 2, p.52
29	M49er	FFG_479	752.50	Richey, 1989, Table 2, p.52
30	M49er	FFG_480	754.40	Richey, 1989, Table 2, p.52
31	M49er	FFG_481	731.80	Richey, 1989, Table 2, p.52
32	M49er	FFG_482	761.40	Richey, 1989, Table 2, p.52
33	M49er	FFG_483	785.10	Richey, 1989, Table 2, p.52
34	M49er	FFG_484	772.20	Richey, 1989, Table 2, p.52
35	M49er	FFG_485	779.40	Richey, 1989, Table 2, p.52
36	M49er	FFG_486	766.30	Richey, 1989, Table 2, p.52
37	M49er	FFG_487	763.90	Richey, 1989, Table 2, p.52
38	M49er	FFG_488	748.00	Richey, 1989, Table 2, p.52
39	M49er	FFG_489	764.60	Richey, 1989, Table 2, p.52
40	M49er	FFG_490	855.60	Richey, 1989, Table 2, p.52
41	M49er	FFG_491	855.90	Richey, 1989, Table 2, p.52
42	M49er	FFG_492	817.50	Richey, 1989, Table 2, p.52
43	M49er	FFG_493	803.60	Richey, 1989, Table 2, p.53
44	M49er	FFG_494	811.30	Richey, 1989, Table 2, p.53
45	M49er	FFG_495	799.40	Richey, 1989, Table 2, p.53
46	M49er	FFG_496	715.40	Richey, 1989, Table 2, p.53
47	M49er	FFG_497	721.50	Richey, 1989, Table 2, p.53
48	M49er	FFG_498	737.00	Richey, 1989, Table 2, p.53
49	M49er	FFG_499	715.40	Richey, 1989, Table 2, p.53
50	M49er	FFG_500	726.00	Richey, 1989, Table 2, p.53
51	M49er	FFG_501	731.50	Richey, 1989, Table 2, p.53
52	M49er	FFG_502	724.80	Richey, 1989, Table 2, p.53
53	M49er	FFG_503	705.40	Richey, 1989, Table 2, p.53
54	M49er	FFG_504	723.60	Richey, 1989, Table 2, p.53
55	M49er	FFG_505	754.70	Richey, 1989, Table 2, p.53
56	M49er	FFG_506	749.20	Richey, 1989, Table 2, p.53
57	M49er	FFG_507	712.80	Richey, 1989, Table 2, p.53
58	M49er	FFG_508	763.30	Richey, 1989, Table 2, p.53
59	M49er	FFG_509	767.80	Richey, 1989, Table 2, p.54
60	M49er	FFG_510	767.30	Richey, 1989, Table 2, p.54
61	M49er	FFG_511	728.20	Richey, 1989, Table 2, p.54
62	M49er	FFG_512	748.30	Richey, 1989, Table 2, p.54
63	M49er	FFG_513	763.00	Richey, 1989, Table 2, p.54
64	M49er	FFG_514	754.70	Richey, 1989, Table 2, p.54
65	M49er	FFG_515	722.60	Richey, 1989, Table 2, p.54
66	M49er	FFG_516	715.90	Richey, 1989, Table 2, p.54
67	M49er	FFG_517	809.30	Richey, 1989, Table 2, p.54
68	M49er	FFG_518	797.90	Richey, 1989, Table 2, p.54
69	M49er	FFG_519	765.70	Richey, 1989, Table 2, p.54
70	M49er	FFG_520	653.00	Richey, 1989, Table 2, p.54
71	M49er	FFG_521	673.30	Richey, 1989, Table 2, p.54
72	M49er	FFG_522	531.70	Richey, 1989, Table 2, p.54
73	M49er	FFG_523	541.30	Richey, 1989, Table 2, p.54
74	M49er	FFG_524	693.10	Richey, 1989, Table 2, p.55
75	M49er	FFG_525	543.30	Richey, 1989, Table 2, p.55
76	M49er	FFG_527	958.90	Richey, 1989, Table 2, p.55

Table B.2. Elevations of Stratigraphic Layers Near WIPP (Continued)

	Layer	Well ID	Elevation	Source		Layer	Well ID	Elevation	Source
1	M49er	FFG_528	951.60	Richey, 1989, Table 2, p.55	39	M49er	FFG_672	943.70	Richey, 1989, Table 2, p.62
2	M49er	FFG_535	939.70	Richey, 1989, Table 2, p.55	40	M49er	FFG_674	937.00	Richey, 1989, Table 2, p.62
3	M49er	FFG_548	930.60	Richey, 1989, Table 2, p.56	41	M49er	FFG_675	896.00	Richey, 1989, Table 2, p.62
4	M49er	FFG_562	670.60	Richey, 1989, Table 2, p.57	42	M49er	FFG_676	905.00	Richey, 1989, Table 2, p.62
5	M49er	FFG_563	582.50	Richey, 1989, Table 2, p.57	43	M49er	FFG_677	932.40	Richey, 1989, Table 2, p.62
6	M49er	FFG_569	689.20	Richey, 1989, Table 2, p.57	44	M49er	FFG_679	934.80	Richey, 1989, Table 2, p.62
7	M49er	FFG_584	773.20	Richey, 1989, Table 2, p.58	45	M49er	FFG_689	817.20	Richey, 1989, Table 2, p.63
8	M49er	FFG_600	729.10	Richey, 1989, Table 2, p.58	46	M49er	FFG_690	824.80	Richey, 1989, Table 2, p.63
9	M49er	FFG_601	645.60	Richey, 1989, Table 2, p.58	47	M49er	FFG_691	816.30	Richey, 1989, Table 2, p.63
10	M49er	FFG_606	723.00	Richey, 1989, Table 2, p.58	48	M49er	FFG_692	806.20	Richey, 1989, Table 2, p.63
11	M49er	FFG_607	743.10	Richey, 1989, Table 2, p.59	49	M49er	FFG_693	817.70	Richey, 1989, Table 2, p.63
12	M49er	FFG_608	754.60	Richey, 1989, Table 2, p.59	50	M49er	FFG_694	810.10	Richey, 1989, Table 2, p.63
13	M49er	FFG_609	758.30	Richey, 1989, Table 2, p.59	51	M49er	FFG_695	814.10	Richey, 1989, Table 2, p.63
14	M49er	FFG_610	746.70	Richey, 1989, Table 2, p.59	52	M49er	FFG_696	815.90	Richey, 1989, Table 2, p.63
15	M49er	FFG_611	731.80	Richey, 1989, Table 2, p.59	53	M49er	FFG_697	818.10	Richey, 1989, Table 2, p.64
16	M49er	FFG_612	733.40	Richey, 1989, Table 2, p.59	54	M49er	FFG_698	861.40	Richey, 1989, Table 2, p.64
17	M49er	FFG_613	728.50	Richey, 1989, Table 2, p.59	55	M49er	FFG_699	811.10	Richey, 1989, Table 2, p.64
18	M49er	FFG_620	759.80	Richey, 1989, Table 2, p.59	56	M49er	FFG_700	801.40	Richey, 1989, Table 2, p.64
19	M49er	FFG_638	591.70	Richey, 1989, Table 2, p.60	57	M49er	FFG_701	810.60	Richey, 1989, Table 2, p.64
20	M49er	FFG_639	566.30	Richey, 1989, Table 2, p.60	58	M49er	FFG_702	811.70	Richey, 1989, Table 2, p.64
21	M49er	FFG_640	649.10	Richey, 1989, Table 2, p.60	59	M49er	FFG_703	817.20	Richey, 1989, Table 2, p.64
22	M49er	FFG_643	688.90	Richey, 1989, Table 2, p.60	60	M49er	FFG_704	806.20	Richey, 1989, Table 2, p.64
23	M49er	FFG_644	723.50	Richey, 1989, Table 2, p.60	61	M49er	FFG_705	735.50	Richey, 1989, Table 2, p.64
24	M49er	FFG_648	558.40	Richey, 1989, Table 2, p.60	62	M49er	FFG_706	755.00	Richey, 1989, Table 2, p.64
25	M49er	FFG_652	878.70	Richey, 1989, Table 2, p.60	63	M49er	FFG_707	741.00	Richey, 1989, Table 2, p.64
26	M49er	FFG_653	880.00	Richey, 1989, Table 2, p.61	64	M49er	FFG_708	791.60	Richey, 1989, Table 2, p.64
27	M49er	FFG_654	899.50	Richey, 1989, Table 2, p.61	65	M49er	FFG_709	681.50	Richey, 1989, Table 2, p.64
28	M49er	FFG_655	897.30	Richey, 1989, Table 2, p.61	66	M49er	FFG_710	682.50	Richey, 1989, Table 2, p.64
29	M49er	FFG_656	894.30	Richey, 1989, Table 2, p.61	67	M49er	FFG_711	694.40	Richey, 1989, Table 2, p.65
30	M49er	FFG_657	906.20	Richey, 1989, Table 2, p.61	68	M49er	FFG_712	735.60	Richey, 1989, Table 2, p.65
31	M49er	FFG_658	898.20	Richey, 1989, Table 2, p.61	69	M49er	FFG_713	672.50	Richey, 1989, Table 2, p.65
32	M49er	FFG_659	901.90	Richey, 1989, Table 2, p.61	70	M49er	FFG_714	790.30	Richey, 1989, Table 2, p.65
33	M49er	FFG_660	919.20	Richey, 1989, Table 2, p.61	71	M49er	FFG_715	799.70	Richey, 1989, Table 2, p.65
34	M49er	FFG_662	894.60	Richey, 1989, Table 2, p.61	72	M49er	FFG_716	697.90	Richey, 1989, Table 2, p.65
35	M49er	FFG_664	888.20	Richey, 1989, Table 2, p.61	73	M49er	FFG_717	722.50	Richey, 1989, Table 2, p.65
36	M49er	FFG_666	938.10	Richey, 1989, Table 2, p.62	74	M49er	FFG_718	723.50	Richey, 1989, Table 2, p.65
37	M49er	FFG_667	923.30	Richey, 1989, Table 2, p.62	75	M49er	FFG_719	696.70	Richey, 1989, Table 2, p.65
38	M49er	FFG_670	946.10	Richey, 1989, Table 2, p.62	76	M49er	FFG_720	699.60	Richey, 1989, Table 2, p.65

Table B.2. Elevations of Stratigraphic Layers Near WIPP (Continued)

	Layer	Well ID	Elevation	Source
1	M49er	FFG_721	698.00	Richey, 1989, Table 2, p.65
2	M49er	FFG_723	808.20	Richey, 1989, Table 2, p.65
3	M49er	FFG_724	738.90	Richey, 1989, Table 2, p.65
4	M49er	FFG_725	712.30	Richey, 1989, Table 2, p.65
5	M49er	FFG_726	698.90	Richey, 1989, Table 2, p.65
6	M49er	FFG_727	702.90	Richey, 1989, Table 2, p.66
7	M49er	FFG_728	696.40	Richey, 1989, Table 2, p.66
8	M49er	FFG_729	706.60	Richey, 1989, Table 2, p.66
9	M49er	FFG_730	724.80	Richey, 1989, Table 2, p.66
10	M49er	FFG_731	720.70	Richey, 1989, Table 2, p.66
11	M49er	FFG_732	739.50	Richey, 1989, Table 2, p.66
12	M49er	FFG_733	806.50	Richey, 1989, Table 2, p.66
13	M49er	FFG_734	758.60	Richey, 1989, Table 2, p.66
14	M49er	FFG_735	704.10	Richey, 1989, Table 2, p.66
15	M49er	FFG_736	758.70	Richey, 1989, Table 2, p.66
16	M49er	FFG_737	702.60	Richey, 1989, Table 2, p.66
17	M49er	FFG_738	713.80	Richey, 1989, Table 2, p.66
18	M49er	FFG_739	753.90	Richey, 1989, Table 2, p.66
19	M49er	FFG_740	754.70	Richey, 1989, Table 2, p.66
20	M49er	FFG_741	721.20	Richey, 1989, Table 2, p.66
21	M49er	FFG_742	774.50	Richey, 1989, Table 2, p.67
22	M49er	FFG_743	757.20	Richey, 1989, Table 2, p.67
23	M49er	FFG_744	739.70	Richey, 1989, Table 2, p.67
24	M49er	FFG_745	730.30	Richey, 1989, Table 2, p.67
25	M49er	FFG_746	719.80	Richey, 1989, Table 2, p.67
26	M49er	H1	882.70	Mercer, 1983, Table 1
27	M49er	H10C	756.80	Mercer, 1983, Table 1
28	M49er	H2C	890.30	Mercer, 1983, Table 1
29	M49er	H3	880.30	Mercer, 1983, Table 1
30	M49er	H4C	920.20	Mercer, 1983, Table 1
31	M49er	H5C	845.80	Mercer, 1983, Table 1
32	M49er	H6C	890.40	Mercer, 1983, Table 1
33	M49er	H7C	937.60	Mercer, 1983, Table 1
34	M49er	H8C	924.80	Mercer, 1983, Table 1
35	M49er	H9C	899.40	Mercer, 1983, Table 1
36	M49er	P1	910.50	Mercer, 1983, Table 1
37	M49er	P10	860.40	Mercer, 1983, Table 1
38	M49er	P11	840.90	Mercer, 1983, Table 1
39	M49er	P12	887.90	Mercer, 1983, Table 1
40	M49er	P13	889.50	Mercer, 1983, Table 1
41	M49er	P14	906.10	Mercer, 1983, Table 1
42	M49er	P15	938.50	Mercer, 1983, Table 1
43	M49er	P16	915.00	Mercer, 1983, Table 1
44	M49er	P17	900.40	Mercer, 1983, Table 1
45	M49er	P18	868.40	Mercer, 1983, Table 1
46	M49er	P19	849.50	Mercer, 1983, Table 1
47	M49er	P2	850.10	Mercer, 1983, Table 1
48	M49er	P20	845.30	Mercer, 1983, Table 1
49	M49er	P21	845.80	Mercer, 1983, Table 1
50	M49er	P3	888.50	Mercer, 1983, Table 1
51	M49er	P4	864.10	Mercer, 1983, Table 1
52	M49er	P5	868.10	Mercer, 1983, Table 1
53	M49er	P6	913.50	Mercer, 1983, Table 1
54	M49er	P7	920.50	Mercer, 1983, Table 1
55	M49er	P8	898.50	Mercer, 1983, Table 1
56	M49er	P9	868.70	Mercer, 1983, Table 1
57	M49er	REF	874.00	Rechard et al.,1991, Figure 2.2-1
58	M49er	SaltShft	875.54	Bechtel, Inc., 1986, Appendix D
59	M49er	WIPP11	842.10	Mercer, 1983, Table 1
60	M49er	WIPP11	842.20	SNL and USGS, 1982a, Table 2
61	M49er	WIPP12	866.80	SNL and D'Appolonia Consulting, 1983, Table 2
62	M49er	WIPP12	866.90	Mercer, 1983, Table 1
63	M49er	WIPP13	880.20	Mercer, 1983, Table 1
64	M49er	WIPP16	681.20	Mercer, 1983, Table 1
65	M49er	WIPP18	866.60	Mercer, 1983, Table 1
66	M49er	WIPP19	866.90	Mercer, 1983, Table 1
67	M49er	WIPP21	870.80	Mercer, 1983, Table 1
68	M49er	WIPP22	869.50	Mercer, 1983, Table 1
69	M49er	WIPP25	908.60	Mercer, 1983, Table 1
70	M49er	WIPP26	957.70	Mercer, 1983, Table 1
71	M49er	WIPP27	921.70	Mercer, 1983, Table 1
72	M49er	WIPP28	954.70	Mercer, 1983, Table 1
73	M49er	WIPP30	908.00	Mercer, 1983, Table 1
74	M49er	WIPP32	921.40	Mercer, 1983, Table 1
75	M49er	WIPP33	891.60	Mercer, 1983, Table 1
76	M49er	WIPP34	846.10	Mercer, 1983, Table 1

Table B.2. Elevations of Stratigraphic Layers Near WIPP (Continued)

	Layer	Well ID	Elevation	Source
1	M49er	WastShft	875.18	Bechtel, Inc., 1986, Appendix E
2	MB126	AirShft	509.31	Holt and Powers, 1990, Figure 22
3	MB126	AirShft	509.64	Holt and Powers, 1990, Figure 22
4	MB126	DOE1	485.50	U.S. DOE, Sep 1982, Table 2
5	MB126	DOE2	484.90	Mercer et al., 1987, Table 3-2
6	MB126	DOE2	485.40	Mercer et al., 1987, Table 3-2
7	MB126	ERDA9	511.60	SNL and USGS, 1982b, Table 2
8	MB126	ExhtShft	512.54	Bechtel, Inc., 1986, Appendix F
9	MB126	ExhtShft	512.72	Bechtel, Inc., 1986, Appendix F
10	MB126	REF	511.60	Rechard et al.,1991, Figure 2.2-1
11	MB126	SaltShft	514.21	Bechtel, Inc., 1986, Appendix D
12	MB126	SaltShft	514.47	Bechtel, Inc., 1986, Appendix D
13	MB126	WIPP11	513.00	SNL and USGS, 1982a, Table 2
14	MB126	WIPP12	513.80	SNL and D'Appolonia Consulting, 1983, Table 2
15	MB126	WastShft	512.40	Bechtel, Inc., 1986, Appendix E
16	MB126	WastShft	512.75	Bechtel, Inc., 1986, Appendix E
17	MB136	AirShft	412.87	Holt and Powers, 1990, Figure 22
18	MB136	AirShft	417.16	Holt and Powers, 1990, Figure 22
19	MB136	ExhtShft	415.52	Bechtel, Inc., 1986, Appendix F
20	MB136	ExhtShft	418.86	Bechtel, Inc., 1986, Appendix F
21	MB136	SaltShft	418.84	Bechtel, Inc., 1986, Appendix D
22	MB136	SaltShft	421.37	Bechtel, Inc., 1986, Appendix D
23	MB136	WastShft	415.27	Bechtel, Inc., 1986, Appendix E
24	MB136	WastShft	419.66	Bechtel, Inc., 1986, Appendix E
25	MB138	AirShft	393.81	Holt and Powers, 1990, Figure 22
26	MB138	AirShft	393.98	Holt and Powers, 1990, Figure 22
27	MB138	DH207	395.92	Krieg, 1984, Table I
28	MB138	DH207	396.16	Krieg, 1984, Table I
29	MB138	DH211	398.83	Krieg, 1984, Table I
30	MB138	DH211	398.98	Krieg, 1984, Table I
31	MB138	DH215	399.23	Krieg, 1984, Table I
32	MB138	DH215	399.41	Krieg, 1984, Table I
33	MB138	DH219	397.58	Krieg, 1984, Table I
34	MB138	DH219	397.82	Krieg, 1984, Table I
35	MB138	DH223	394.10	Krieg, 1984, Table I
36	MB138	DH223	394.31	Krieg, 1984, Table I
37	MB138	DH227	391.03	Krieg, 1984, Table I
38	MB138	DH227	391.18	Krieg, 1984, Table I
39	MB138	DH77	409.65	Krieg, 1984, Table I
40	MB138	DH77	409.95	Krieg, 1984, Table I
41	MB138	DO201	396.40	Krieg, 1984, Table I
42	MB138	DO201	396.58	Krieg, 1984, Table I
43	MB138	DO203	406.94	Krieg, 1984, Table I
44	MB138	DO203	407.15	Krieg, 1984, Table I
45	MB138	DO205	412.06	Krieg, 1984, Table I
46	MB138	DO205	412.30	Krieg, 1984, Table I
47	MB138	DO45	403.83	Krieg, 1984, Table I
48	MB138	DO45	404.01	Krieg, 1984, Table I
49	MB138	DO52	401.39	Krieg, 1984, Table I
50	MB138	DO52	401.51	Krieg, 1984, Table I
51	MB138	DO56	406.69	Krieg, 1984, Table I
52	MB138	DO56	406.84	Krieg, 1984, Table I
53	MB138	DO63	410.47	Krieg, 1984, Table I
54	MB138	DO63	410.68	Krieg, 1984, Table I
55	MB138	DO67	410.38	Krieg, 1984, Table I
56	MB138	DO67	410.50	Krieg, 1984, Table I
57	MB138	DO88	409.07	Krieg, 1984, Table I
58	MB138	DO88	409.33	Krieg, 1984, Table I
59	MB138	DO91	408.81	Krieg, 1984, Table I
60	MB138	DO91	409.02	Krieg, 1984, Table I
61	MB138	DOE1	368.60	U.S. DOE, Sep 1982, Table 2
62	MB138	DOE2	370.40	Mercer et al., 1987, Table 3-2
63	MB138	ERDA9	396.00	SNL and USGS, 1982b, Table 2
64	MB138	ERDA9	396.40	SNL and USGS, 1982b, Table 2
65	MB138	ExhtShft	396.86	Bechtel, Inc., 1986, Appendix F
66	MB138	ExhtShft	397.03	Bechtel, Inc., 1986, Appendix F
67	MB138	MB139_2	396.15	Krieg, 1984, Table I
68	MB138	MB139_2	396.30	Krieg, 1984, Table I
69	MB138	REF	396.00	Rechard et al.,1991, Figure 2.2-1
70	MB138	REF	396.40	Rechard et al.,1991, Figure 2.2-1
71	MB138	SaltShft	399.79	Bechtel, Inc., 1986, Appendix D
72	MB138	SaltShft	399.80	Bechtel, Inc., 1986, Appendix D
73	MB138	SaltShft	399.76	Krieg, 1984, Table I
74	MB138	SaltShft	399.91	Krieg, 1984, Table I
75	MB138	WIPP11	430.40	SNL and USGS, 1982a, Table 2
76	MB138	WIPP12	411.00	SNL and D'Appolonia Consulting, 1983, Table 2

Table B.2. Elevations of Stratigraphic Layers Near WIPP (Continued)

	Layer	Well ID	Elevation	Source
1	MB138	WastShft	395.89	Bechtel, Inc., 1986, Appendix E
2	MB138	WastShft	396.07	Bechtel, Inc., 1986, Appendix E
3	MB138	WastShft	396.31	Krieg, 1984, Table I
4	MB138	WastShft	396.49	Krieg, 1984, Table I
5	MB139	DH207	377.63	Krieg, 1984, Table I
6	MB139	DH207	378.70	Krieg, 1984, Table I
7	MB139	DH211	380.73	Krieg, 1984, Table I
8	MB139	DH211	381.31	Krieg, 1984, Table I
9	MB139	DH215	381.03	Krieg, 1984, Table I
10	MB139	DH215	382.04	Krieg, 1984, Table I
11	MB139	DH219	379.91	Krieg, 1984, Table I
12	MB139	DH219	380.58	Krieg, 1984, Table I
13	MB139	DH223	376.70	Krieg, 1984, Table I
14	MB139	DH223	377.64	Krieg, 1984, Table I
15	MB139	DH227	373.78	Krieg, 1984, Table I
16	MB139	DH227	374.42	Krieg, 1984, Table I
17	MB139	DH77	392.37	Krieg, 1984, Table I
18	MB139	DH77	393.35	Krieg, 1984, Table I
19	MB139	DO201	378.26	Krieg, 1984, Table I
20	MB139	DO201	379.11	Krieg, 1984, Table I
21	MB139	DO203	389.84	Krieg, 1984, Table I
22	MB139	DO203	390.63	Krieg, 1984, Table I
23	MB139	DO205	394.29	Krieg, 1984, Table I
24	MB139	DO205	394.69	Krieg, 1984, Table I
25	MB139	DO45	385.11	Krieg, 1984, Table I
26	MB139	DO45	386.36	Krieg, 1984, Table I
27	MB139	DO52	383.44	Krieg, 1984, Table I
28	MB139	DO52	384.57	Krieg, 1984, Table I
29	MB139	DO56	388.89	Krieg, 1984, Table I
30	MB139	DO56	389.53	Krieg, 1984, Table I
31	MB139	DO63	392.79	Krieg, 1984, Table I
32	MB139	DO63	393.46	Krieg, 1984, Table I
33	MB139	DO67	393.19	Krieg, 1984, Table I
34	MB139	DO67	394.13	Krieg, 1984, Table I
35	MB139	DO88	392.06	Krieg, 1984, Table I
36	MB139	DO88	392.99	Krieg, 1984, Table I
37	MB139	DO91	391.62	Krieg, 1984, Table I
38	MB139	DO91	392.66	Krieg, 1984, Table I
39	MB139	DOE1	350.40	U.S. DOE, Sep 1982, Table 2
40	MB139	DOE2	339.00	Mercer et al., 1987, Table 3-2
41	MB139	DOE2	340.00	Mercer et al., 1987, Table 3-2
42	MB139	ERDA9	378.10	SNL and USGS, 1982b, Table 2
43	MB139	ERDA9	379.00	SNL and USGS, 1982b, Table 2
44	MB139	MB139_2	377.44	Krieg, 1984, Table I
45	MB139	MB139_2	378.42	Krieg, 1984, Table I
46	MB139	REF	378.10	Rechard et al.,1991, Figure 2.2-1
47	MB139	REF	379.00	Rechard et al.,1991, Figure 2.2-1
48	MB139	SaltShft	381.64	Bechtel, Inc., 1986, Appendix D
49	MB139	SaltShft	382.44	Bechtel, Inc., 1986, Appendix D
50	MB139	SaltShft	381.38	Krieg, 1984, Table I
51	MB139	SaltShft	382.29	Krieg, 1984, Table I
52	MB139	WIPP11	419.10	SNL and USGS, 1982a, Table 2
53	MB139	WIPP12	395.90	SNL and D'Appolonia Consulting, 1983, Table 2
54	MB139	WastShft	377.14	Bechtel, Inc., 1986, Appendix E
55	MB139	WastShft	378.22	Bechtel, Inc., 1986, Appendix E
56	MB139	WastShft	378.04	Krieg, 1984, Table I
57	MB139	WastShft	379.10	Krieg, 1984, Table I
58	Magenta	AEC7	890.30	Mercer, 1983, Table 1
59	Magenta	AEC8	858.70	Mercer, 1983, Table 1
60	Magenta	AirShft	858.82	Holt and Powers, 1990, Figure 22
61	Magenta	B25	858.40	Mercer, 1983, Table 1
62	Magenta	DOE1	838.60	U.S. DOE, Sep 1982, Table 2
63	Magenta	DOE2	829.00	Mercer et al., 1987, Table 3-2
64	Magenta	ERDA10	915.90	Mercer, 1983, Table 1
65	Magenta	ERDA6	897.60	Mercer, 1983, Table 1
66	Magenta	ERDA9	860.40	Mercer, 1983, Table 1
67	Magenta	ERDA9	856.70	SNL and USGS, 1982b, Table 2
68	Magenta	ExhtShft	855.39	Bechtel, Inc., 1986, Appendix F
69	Magenta	FFG_002	667.50	Richey, 1989, Table 2, p.21
70	Magenta	FFG_004	717.80	Richey, 1989, Table 2, p.21
71	Magenta	FFG_005	674.90	Richey, 1989, Table 2, p.21
72	Magenta	FFG_006	670.00	Richey, 1989, Table 2, p.21
73	Magenta	FFG_007	655.90	Richey, 1989, Table 2, p.21
74	Magenta	FFG_009	657.40	Richey, 1989, Table 2, p.21
75	Magenta	FFG_011	664.20	Richey, 1989, Table 2, p.21
76	Magenta	FFG_012	667.80	Richey, 1989, Table 2, p.21

Table B.2. Elevations of Stratigraphic Layers Near WIPP (Continued)

	Layer	Well ID	Elevation	Source
1	Magenta	FFG_013	674.80	Richey, 1989, Table 2, p.21
2	Magenta	FFG_014	721.10	Richey, 1989, Table 2, p.21
3	Magenta	FFG_016	644.90	Richey, 1989, Table 2, p.21
4	Magenta	FFG_017	648.30	Richey, 1989, Table 2, p.22
5	Magenta	FFG_018	652.30	Richey, 1989, Table 2, p.22
6	Magenta	FFG_019	644.70	Richey, 1989, Table 2, p.22
7	Magenta	FFG_020	718.40	Richey, 1989, Table 2, p.22
8	Magenta	FFG_023	654.10	Richey, 1989, Table 2, p.22
9	Magenta	FFG_024	638.80	Richey, 1989, Table 2, p.22
10	Magenta	FFG_025	652.20	Richey, 1989, Table 2, p.22
11	Magenta	FFG_026	649.50	Richey, 1989, Table 2, p.22
12	Magenta	FFG_027	643.10	Richey, 1989, Table 2, p.22
13	Magenta	FFG_028	612.70	Richey, 1989, Table 2, p.22
14	Magenta	FFG_029	599.20	Richey, 1989, Table 2, p.22
15	Magenta	FFG_030	598.30	Richey, 1989, Table 2, p.22
16	Magenta	FFG_031	590.10	Richey, 1989, Table 2, p.22
17	Magenta	FFG_032	592.10	Richey, 1989, Table 2, p.22
18	Magenta	FFG_033	588.30	Richey, 1989, Table 2, p.22
19	Magenta	FFG_034	582.40	Richey, 1989, Table 2, p.23
20	Magenta	FFG_035	572.60	Richey, 1989, Table 2, p.23
21	Magenta	FFG_036	582.20	Richey, 1989, Table 2, p.23
22	Magenta	FFG_037	571.80	Richey, 1989, Table 2, p.23
23	Magenta	FFG_038	559.60	Richey, 1989, Table 2, p.23
24	Magenta	FFG_039	778.80	Richey, 1989, Table 2, p.23
25	Magenta	FFG_040	720.90	Richey, 1989, Table 2, p.23
26	Magenta	FFG_041	780.60	Richey, 1989, Table 2, p.23
27	Magenta	FFG_042	785.40	Richey, 1989, Table 2, p.23
28	Magenta	FFG_043	788.10	Richey, 1989, Table 2, p.23
29	Magenta	FFG_044	741.00	Richey, 1989, Table 2, p.23
30	Magenta	FFG_047	613.90	Richey, 1989, Table 2, p.23
31	Magenta	FFG_048	630.90	Richey, 1989, Table 2, p.23
32	Magenta	FFG_049	620.90	Richey, 1989, Table 2, p.23
33	Magenta	FFG_050	627.60	Richey, 1989, Table 2, p.24
34	Magenta	FFG_051	627.30	Richey, 1989, Table 2, p.24
35	Magenta	FFG_052	630.30	Richey, 1989, Table 2, p.24
36	Magenta	FFG_053	623.30	Richey, 1989, Table 2, p.24
37	Magenta	FFG_054	620.60	Richey, 1989, Table 2, p.24
38	Magenta	FFG_055	621.10	Richey, 1989, Table 2, p.24
39	Magenta	FFG_056	621.80	Richey, 1989, Table 2, p.24
40	Magenta	FFG_057	625.20	Richey, 1989, Table 2, p.24
41	Magenta	FFG_058	623.60	Richey, 1989, Table 2, p.24
42	Magenta	FFG_059	623.60	Richey, 1989, Table 2, p.24
43	Magenta	FFG_060	627.30	Richey, 1989, Table 2, p.24
44	Magenta	FFG_061	626.00	Richey, 1989, Table 2, p.24
45	Magenta	FFG_062	553.20	Richey, 1989, Table 2, p.24
46	Magenta	FFG_063	513.70	Richey, 1989, Table 2, p.24
47	Magenta	FFG_064	538.60	Richey, 1989, Table 2, p.24
48	Magenta	FFG_065	520.60	Richey, 1989, Table 2, p.24
49	Magenta	FFG_066	473.90	Richey, 1989, Table 2, p.24
50	Magenta	FFG_067	516.40	Richey, 1989, Table 2, p.25
51	Magenta	FFG_068	481.90	Richey, 1989, Table 2, p.25
52	Magenta	FFG_069	502.40	Richey, 1989, Table 2, p.25
53	Magenta	FFG_070	532.20	Richey, 1989, Table 2, p.25
54	Magenta	FFG_071	790.70	Richey, 1989, Table 2, p.25
55	Magenta	FFG_072	721.10	Richey, 1989, Table 2, p.25
56	Magenta	FFG_073	699.50	Richey, 1989, Table 2, p.25
57	Magenta	FFG_074	703.30	Richey, 1989, Table 2, p.25
58	Magenta	FFG_075	756.00	Richey, 1989, Table 2, p.25
59	Magenta	FFG_076	818.10	Richey, 1989, Table 2, p.25
60	Magenta	FFG_078	855.20	Richey, 1989, Table 2, p.25
61	Magenta	FFG_079	829.70	Richey, 1989, Table 2, p.25
62	Magenta	FFG_080	808.30	Richey, 1989, Table 2, p.25
63	Magenta	FFG_081	727.90	Richey, 1989, Table 2, p.26
64	Magenta	FFG_082	759.30	Richey, 1989, Table 2, p.26
65	Magenta	FFG_083	674.70	Richey, 1989, Table 2, p.26
66	Magenta	FFG_084	702.20	Richey, 1989, Table 2, p.26
67	Magenta	FFG_085	695.60	Richey, 1989, Table 2, p.26
68	Magenta	FFG_086	705.60	Richey, 1989, Table 2, p.26
69	Magenta	FFG_087	680.00	Richey, 1989, Table 2, p.26
70	Magenta	FFG_088	674.60	Richey, 1989, Table 2, p.26
71	Magenta	FFG_089	656.00	Richey, 1989, Table 2, p.26
72	Magenta	FFG_091	700.40	Richey, 1989, Table 2, p.26
73	Magenta	FFG_092	716.60	Richey, 1989, Table 2, p.26
74	Magenta	FFG_093	718.10	Richey, 1989, Table 2, p.26
75	Magenta	FFG_094	720.20	Richey, 1989, Table 2, p.26
76	Magenta	FFG_095	688.80	Richey, 1989, Table 2, p.26

Table B.2. Elevations of Stratigraphic Layers Near WIPP (Continued)

	Layer	Well ID	Elevation	Source
1	Magenta	FFG_096	671.20	Richey, 1989, Table 2, p.26
2	Magenta	FFG_097	651.70	Richey, 1989, Table 2, p.27
3	Magenta	FFG_098	625.40	Richey, 1989, Table 2, p.27
4	Magenta	FFG_099	620.90	Richey, 1989, Table 2, p.27
5	Magenta	FFG_100	603.90	Richey, 1989, Table 2, p.27
6	Magenta	FFG_101	574.90	Richey, 1989, Table 2, p.27
7	Magenta	FFG_102	593.50	Richey, 1989, Table 2, p.27
8	Magenta	FFG_103	655.40	Richey, 1989, Table 2, p.27
9	Magenta	FFG_104	551.10	Richey, 1989, Table 2, p.27
10	Magenta	FFG_105	909.60	Richey, 1989, Table 2, p.27
11	Magenta	FFG_106	939.70	Richey, 1989, Table 2, p.27
12	Magenta	FFG_107	923.00	Richey, 1989, Table 2, p.27
13	Magenta	FFG_108	918.40	Richey, 1989, Table 2, p.27
14	Magenta	FFG_109	898.90	Richey, 1989, Table 2, p.27
15	Magenta	FFG_110	865.70	Richey, 1989, Table 2, p.27
16	Magenta	FFG_111	871.70	Richey, 1989, Table 2, p.27
17	Magenta	FFG_112	861.00	Richey, 1989, Table 2, p.28
18	Magenta	FFG_113	875.10	Richey, 1989, Table 2, p.28
19	Magenta	FFG_114	905.60	Richey, 1989, Table 2, p.28
20	Magenta	FFG_115	895.50	Richey, 1989, Table 2, p.28
21	Magenta	FFG_116	911.00	Richey, 1989, Table 2, p.28
22	Magenta	FFG_117	911.30	Richey, 1989, Table 2, p.28
23	Magenta	FFG_120	923.00	Richey, 1989, Table 2, p.28
24	Magenta	FFG_121	928.10	Richey, 1989, Table 2, p.28
25	Magenta	FFG_122	926.60	Richey, 1989, Table 2, p.28
26	Magenta	FFG_123	900.60	Richey, 1989, Table 2, p.28
27	Magenta	FFG_124	865.30	Richey, 1989, Table 2, p.28
28	Magenta	FFG_125	890.90	Richey, 1989, Table 2, p.28
29	Magenta	FFG_126	886.20	Richey, 1989, Table 2, p.28
30	Magenta	FFG_127	891.20	Richey, 1989, Table 2, p.28
31	Magenta	FFG_128	926.60	Richey, 1989, Table 2, p.28
32	Magenta	FFG_129	899.40	Richey, 1989, Table 2, p.28
33	Magenta	FFG_130	929.60	Richey, 1989, Table 2, p.28
34	Magenta	FFG_132	935.10	Richey, 1989, Table 2, p.29
35	Magenta	FFG_133	938.10	Richey, 1989, Table 2, p.29
36	Magenta	FFG_134	944.00	Richey, 1989, Table 2, p.29
37	Magenta	FFG_135	917.50	Richey, 1989, Table 2, p.29
38	Magenta	FFG_136	919.10	Richey, 1989, Table 2, p.29
39	Magenta	FFG_137	927.90	Richey, 1989, Table 2, p.29
40	Magenta	FFG_138	880.60	Richey, 1989, Table 2, p.29
41	Magenta	FFG_139	889.70	Richey, 1989, Table 2, p.29
42	Magenta	FFG_140	829.20	Richey, 1989, Table 2, p.29
43	Magenta	FFG_141	854.20	Richey, 1989, Table 2, p.29
44	Magenta	FFG_142	829.40	Richey, 1989, Table 2, p.29
45	Magenta	FFG_143	839.30	Richey, 1989, Table 2, p.29
46	Magenta	FFG_147	897.90	Richey, 1989, Table 2, p.29
47	Magenta	FFG_155	914.10	Richey, 1989, Table 2, p.30
48	Magenta	FFG_157	915.30	Richey, 1989, Table 2, p.30
49	Magenta	FFG_158	937.20	Richey, 1989, Table 2, p.30
50	Magenta	FFG_159	936.70	Richey, 1989, Table 2, p.30
51	Magenta	FFG_160	929.70	Richey, 1989, Table 2, p.30
52	Magenta	FFG_161	936.10	Richey, 1989, Table 2, p.30
53	Magenta	FFG_162	933.30	Richey, 1989, Table 2, p.30
54	Magenta	FFG_163	933.90	Richey, 1989, Table 2, p.30
55	Magenta	FFG_166	936.00	Richey, 1989, Table 2, p.31
56	Magenta	FFG_167	922.10	Richey, 1989, Table 2, p.31
57	Magenta	FFG_168	944.60	Richey, 1989, Table 2, p.31
58	Magenta	FFG_169	957.30	Richey, 1989, Table 2, p.31
59	Magenta	FFG_170	922.90	Richey, 1989, Table 2, p.31
60	Magenta	FFG_171	931.50	Richey, 1989, Table 2, p.31
61	Magenta	FFG_172	937.20	Richey, 1989, Table 2, p.31
62	Magenta	FFG_173	914.10	Richey, 1989, Table 2, p.31
63	Magenta	FFG_180	920.50	Richey, 1989, Table 2, p.31
64	Magenta	FFG_181	951.30	Richey, 1989, Table 2, p.32
65	Magenta	FFG_182	847.60	Richey, 1989, Table 2, p.32
66	Magenta	FFG_184	927.80	Richey, 1989, Table 2, p.32
67	Magenta	FFG_185	934.50	Richey, 1989, Table 2, p.32
68	Magenta	FFG_186	863.80	Richey, 1989, Table 2, p.32
69	Magenta	FFG_188	874.10	Richey, 1989, Table 2, p.32
70	Magenta	FFG_189	902.20	Richey, 1989, Table 2, p.32
71	Magenta	FFG_190	882.40	Richey, 1989, Table 2, p.32
72	Magenta	FFG_191	878.10	Richey, 1989, Table 2, p.32
73	Magenta	FFG_192	815.30	Richey, 1989, Table 2, p.32
74	Magenta	FFG_194	822.10	Richey, 1989, Table 2, p.33
75	Magenta	FFG_195	834.00	Richey, 1989, Table 2, p.33
76	Magenta	FFG_196	876.90	Richey, 1989, Table 2, p.33

Table B.2. Elevations of Stratigraphic Layers Near WIPP (Continued)

	Layer	Well ID	Elevation	Source		Layer	Well ID	Elevation	Source
1	Magenta	FFG_197	878.10	Richey, 1989, Table 2, p.33	39	Magenta	FFG_238	691.00	Richey, 1989, Table 2, p.36
2	Magenta	FFG_198	877.50	Richey, 1989, Table 2, p.33	40	Magenta	FFG_239	679.10	Richey, 1989, Table 2, p.36
3	Magenta	FFG_199	867.50	Richey, 1989, Table 2, p.33	41	Magenta	FFG_240	671.20	Richey, 1989, Table 2, p.36
4	Magenta	FFG_200	880.90	Richey, 1989, Table 2, p.33	42	Magenta	FFG_241	666.30	Richey, 1989, Table 2, p.36
5	Magenta	FFG_201	873.20	Richey, 1989, Table 2, p.33	43	Magenta	FFG_242	783.10	Richey, 1989, Table 2, p.36
6	Magenta	FFG_202	816.50	Richey, 1989, Table 2, p.33	44	Magenta	FFG_243	743.10	Richey, 1989, Table 2, p.36
7	Magenta	FFG_203	823.00	Richey, 1989, Table 2, p.33	45	Magenta	FFG_244	780.80	Richey, 1989, Table 2, p.36
8	Magenta	FFG_204	846.50	Richey, 1989, Table 2, p.33	46	Magenta	FFG_245	573.00	Richey, 1989, Table 2, p.36
9	Magenta	FFG_205	860.50	Richey, 1989, Table 2, p.33	47	Magenta	FFG_246	578.50	Richey, 1989, Table 2, p.36
10	Magenta	FFG_206	874.50	Richey, 1989, Table 2, p.33	48	Magenta	FFG_247	563.80	Richey, 1989, Table 2, p.36
11	Magenta	FFG_207	872.30	Richey, 1989, Table 2, p.33	49	Magenta	FFG_248	571.20	Richey, 1989, Table 2, p.36
12	Magenta	FFG_208	882.10	Richey, 1989, Table 2, p.34	50	Magenta	FFG_249	569.70	Richey, 1989, Table 2, p.36
13	Magenta	FFG_209	873.20	Richey, 1989, Table 2, p.34	51	Magenta	FFG_250	651.50	Richey, 1989, Table 2, p.36
14	Magenta	FFG_210	865.90	Richey, 1989, Table 2, p.34	52	Magenta	FFG_251	544.90	Richey, 1989, Table 2, p.36
15	Magenta	FFG_212	852.80	Richey, 1989, Table 2, p.34	53	Magenta	FFG_252	683.90	Richey, 1989, Table 2, p.36
16	Magenta	FFG_213	874.50	Richey, 1989, Table 2, p.34	54	Magenta	FFG_253	639.20	Richey, 1989, Table 2, p.36
17	Magenta	FFG_214	854.90	Richey, 1989, Table 2, p.34	55	Magenta	FFG_254	630.00	Richey, 1989, Table 2, p.36
18	Magenta	FFG_215	831.20	Richey, 1989, Table 2, p.34	56	Magenta	FFG_255	587.70	Richey, 1989, Table 2, p.37
19	Magenta	FFG_216	716.80	Richey, 1989, Table 2, p.34	57	Magenta	FFG_256	535.20	Richey, 1989, Table 2, p.37
20	Magenta	FFG_217	851.40	Richey, 1989, Table 2, p.34	58	Magenta	FFG_257	579.40	Richey, 1989, Table 2, p.37
21	Magenta	FFG_218	844.00	Richey, 1989, Table 2, p.34	59	Magenta	FFG_258	594.90	Richey, 1989, Table 2, p.37
22	Magenta	FFG_219	889.70	Richey, 1989, Table 2, p.34	60	Magenta	FFG_259	561.10	Richey, 1989, Table 2, p.37
23	Magenta	FFG_220	836.70	Richey, 1989, Table 2, p.34	61	Magenta	FFG_260	603.80	Richey, 1989, Table 2, p.37
24	Magenta	FFG_221	796.20	Richey, 1989, Table 2, p.34	62	Magenta	FFG_261	592.80	Richey, 1989, Table 2, p.37
25	Magenta	FFG_222	749.80	Richey, 1989, Table 2, p.34	63	Magenta	FFG_263	526.60	Richey, 1989, Table 2, p.37
26	Magenta	FFG_224	655.70	Richey, 1989, Table 2, p.35	64	Magenta	FFG_264	760.50	Richey, 1989, Table 2, p.37
27	Magenta	FFG_225	662.40	Richey, 1989, Table 2, p.35	65	Magenta	FFG_265	755.90	Richey, 1989, Table 2, p.37
28	Magenta	FFG_226	661.00	Richey, 1989, Table 2, p.35	66	Magenta	FFG_266	736.70	Richey, 1989, Table 2, p.37
29	Magenta	FFG_228	651.70	Richey, 1989, Table 2, p.35	67	Magenta	FFG_267	713.50	Richey, 1989, Table 2, p.37
30	Magenta	FFG_229	679.40	Richey, 1989, Table 2, p.35	68	Magenta	FFG_268	690.70	Richey, 1989, Table 2, p.37
31	Magenta	FFG_230	665.10	Richey, 1989, Table 2, p.35	69	Magenta	FFG_269	702.40	Richey, 1989, Table 2, p.38
32	Magenta	FFG_231	681.80	Richey, 1989, Table 2, p.35	70	Magenta	FFG_270	774.50	Richey, 1989, Table 2, p.38
33	Magenta	FFG_232	695.60	Richey, 1989, Table 2, p.35	71	Magenta	FFG_271	815.00	Richey, 1989, Table 2, p.38
34	Magenta	FFG_233	685.80	Richey, 1989, Table 2, p.35	72	Magenta	FFG_272	822.50	Richey, 1989, Table 2, p.38
35	Magenta	FFG_234	722.70	Richey, 1989, Table 2, p.35	73	Magenta	FFG_273	797.40	Richey, 1989, Table 2, p.38
36	Magenta	FFG_235	698.60	Richey, 1989, Table 2, p.35	74	Magenta	FFG_274	834.20	Richey, 1989, Table 2, p.38
37	Magenta	FFG_236	746.40	Richey, 1989, Table 2, p.35	75	Magenta	FFG_275	840.30	Richey, 1989, Table 2, p.38
38	Magenta	FFG_237	712.10	Richey, 1989, Table 2, p.35	76	Magenta	FFG_276	845.20	Richey, 1989, Table 2, p.38

Table B.2. Elevations of Stratigraphic Layers Near WIPP (Continued)

	Layer	Well ID	Elevation	Source
2	Magenta	FFG_277	836.70	Richey, 1989, Table 2, p.38
3	Magenta	FFG_278	845.80	Richey, 1989, Table 2, p.38
4	Magenta	FFG_279	840.90	Richey, 1989, Table 2, p.38
5	Magenta	FFG_280	837.30	Richey, 1989, Table 2, p.38
6	Magenta	FFG_281	814.20	Richey, 1989, Table 2, p.38
7	Magenta	FFG_283	563.90	Richey, 1989, Table 2, p.39
8	Magenta	FFG_284	712.00	Richey, 1989, Table 2, p.39
9	Magenta	FFG_285	741.30	Richey, 1989, Table 2, p.39
10	Magenta	FFG_286	820.20	Richey, 1989, Table 2, p.39
11	Magenta	FFG_287	793.10	Richey, 1989, Table 2, p.39
12	Magenta	FFG_288	744.90	Richey, 1989, Table 2, p.39
13	Magenta	FFG_289	719.90	Richey, 1989, Table 2, p.39
14	Magenta	FFG_290	806.50	Richey, 1989, Table 2, p.39
15	Magenta	FFG_291	742.50	Richey, 1989, Table 2, p.39
16	Magenta	FFG_292	758.40	Richey, 1989, Table 2, p.39
17	Magenta	FFG_293	750.70	Richey, 1989, Table 2, p.39
18	Magenta	FFG_294	572.80	Richey, 1989, Table 2, p.39
19	Magenta	FFG_295	560.20	Richey, 1989, Table 2, p.39
20	Magenta	FFG_297	539.20	Richey, 1989, Table 2, p.39
21	Magenta	FFG_298	552.40	Richey, 1989, Table 2, p.40
22	Magenta	FFG_299	569.10	Richey, 1989, Table 2, p.40
23	Magenta	FFG_300	520.60	Richey, 1989, Table 2, p.40
24	Magenta	FFG_301	491.10	Richey, 1989, Table 2, p.40
25	Magenta	FFG_302	518.50	Richey, 1989, Table 2, p.40
26	Magenta	FFG_303	511.20	Richey, 1989, Table 2, p.40
27	Magenta	FFG_304	517.50	Richey, 1989, Table 2, p.40
28	Magenta	FFG_305	509.30	Richey, 1989, Table 2, p.40
29	Magenta	FFG_306	469.30	Richey, 1989, Table 2, p.40
30	Magenta	FFG_307	493.50	Richey, 1989, Table 2, p.40
31	Magenta	FFG_308	465.70	Richey, 1989, Table 2, p.40
32	Magenta	FFG_309	508.10	Richey, 1989, Table 2, p.40
33	Magenta	FFG_310	539.20	Richey, 1989, Table 2, p.40
34	Magenta	FFG_311	486.50	Richey, 1989, Table 2, p.40
35	Magenta	FFG_312	510.60	Richey, 1989, Table 2, p.40
36	Magenta	FFG_313	915.10	Richey, 1989, Table 2, p.41
37	Magenta	FFG_314	843.10	Richey, 1989, Table 2, p.41
38	Magenta	FFG_315	764.30	Richey, 1989, Table 2, p.41
39	Magenta	FFG_316	747.90	Richey, 1989, Table 2, p.41
40	Magenta	FFG_317	777.00	Richey, 1989, Table 2, p.41
41	Magenta	FFG_318	742.20	Richey, 1989, Table 2, p.41
42	Magenta	FFG_319	751.60	Richey, 1989, Table 2, p.41
43	Magenta	FFG_320	741.30	Richey, 1989, Table 2, p.41
44	Magenta	FFG_321	737.90	Richey, 1989, Table 2, p.41
45	Magenta	FFG_322	733.20	Richey, 1989, Table 2, p.41
46	Magenta	FFG_323	729.50	Richey, 1989, Table 2, p.41
47	Magenta	FFG_324	745.30	Richey, 1989, Table 2, p.41
48	Magenta	FFG_325	800.40	Richey, 1989, Table 2, p.41
49	Magenta	FFG_326	736.10	Richey, 1989, Table 2, p.41
50	Magenta	FFG_327	729.10	Richey, 1989, Table 2, p.42
51	Magenta	FFG_328	734.50	Richey, 1989, Table 2, p.42
52	Magenta	FFG_329	733.90	Richey, 1989, Table 2, p.42
53	Magenta	FFG_330	733.20	Richey, 1989, Table 2, p.42
54	Magenta	FFG_331	728.50	Richey, 1989, Table 2, p.42
55	Magenta	FFG_332	719.30	Richey, 1989, Table 2, p.42
56	Magenta	FFG_333	722.80	Richey, 1989, Table 2, p.42
57	Magenta	FFG_334	718.10	Richey, 1989, Table 2, p.42
58	Magenta	FFG_335	733.70	Richey, 1989, Table 2, p.42
59	Magenta	FFG_336	730.60	Richey, 1989, Table 2, p.42
60	Magenta	FFG_337	713.80	Richey, 1989, Table 2, p.42
61	Magenta	FFG_338	720.70	Richey, 1989, Table 2, p.42
62	Magenta	FFG_339	684.80	Richey, 1989, Table 2, p.42
63	Magenta	FFG_340	694.00	Richey, 1989, Table 2, p.42
64	Magenta	FFG_342	726.90	Richey, 1989, Table 2, p.43
65	Magenta	FFG_344	692.70	Richey, 1989, Table 2, p.43
66	Magenta	FFG_345	752.10	Richey, 1989, Table 2, p.43
67	Magenta	FFG_347	744.70	Richey, 1989, Table 2, p.43
68	Magenta	FFG_348	773.30	Richey, 1989, Table 2, p.43
69	Magenta	FFG_349	742.20	Richey, 1989, Table 2, p.43
70	Magenta	FFG_350	789.10	Richey, 1989, Table 2, p.43
71	Magenta	FFG_351	705.60	Richey, 1989, Table 2, p.43
72	Magenta	FFG_352	705.60	Richey, 1989, Table 2, p.43
73	Magenta	FFG_353	726.70	Richey, 1989, Table 2, p.43
74	Magenta	FFG_354	800.80	Richey, 1989, Table 2, p.43
75	Magenta	FFG_361	986.90	Richey, 1989, Table 2, p.44
76	Magenta	FFG_366	940.60	Richey, 1989, Table 2, p.44
77	Magenta	FFG_367	954.60	Richey, 1989, Table 2, p.44

Table B.2. Elevations of Stratigraphic Layers Near WIPP (Continued)

	Layer	Well ID	Elevation	Source		Layer	Well ID	Elevation	Source
1	Magenta	FFG_371	997.70	Richey, 1989, Table 2, p.44	39	Magenta	FFG_472	538.30	Richey, 1989, Table 2, p.51
2	Magenta	FFG_374	940.90	Richey, 1989, Table 2, p.45	40	Magenta	FFG_473	468.20	Richey, 1989, Table 2, p.51
3	Magenta	FFG_383	938.80	Richey, 1989, Table 2, p.45	41	Magenta	FFG_474	729.40	Richey, 1989, Table 2, p.51
4	Magenta	FFG_384	945.80	Richey, 1989, Table 2, p.45	42	Magenta	FFG_475	728.90	Richey, 1989, Table 2, p.51
5	Magenta	FFG_387	940.30	Richey, 1989, Table 2, p.45	43	Magenta	FFG_476	805.00	Richey, 1989, Table 2, p.51
6	Magenta	FFG_388	936.70	Richey, 1989, Table 2, p.46	44	Magenta	FFG_477	760.80	Richey, 1989, Table 2, p.51
7	Magenta	FFG_390	954.00	Richey, 1989, Table 2, p.46	45	Magenta	FFG_478	739.70	Richey, 1989, Table 2, p.52
8	Magenta	FFG_391	951.50	Richey, 1989, Table 2, p.46	46	Magenta	FFG_479	736.40	Richey, 1989, Table 2, p.52
9	Magenta	FFG_392	948.60	Richey, 1989, Table 2, p.46	47	Magenta	FFG_480	732.50	Richey, 1989, Table 2, p.52
10	Magenta	FFG_393	816.10	Richey, 1989, Table 2, p.46	48	Magenta	FFG_481	715.70	Richey, 1989, Table 2, p.52
11	Magenta	FFG_394	908.60	Richey, 1989, Table 2, p.46	49	Magenta	FFG_482	744.30	Richey, 1989, Table 2, p.52
12	Magenta	FFG_395	901.60	Richey, 1989, Table 2, p.46	50	Magenta	FFG_483	767.80	Richey, 1989, Table 2, p.52
13	Magenta	FFG_396	884.30	Richey, 1989, Table 2, p.46	51	Magenta	FFG_484	753.60	Richey, 1989, Table 2, p.52
14	Magenta	FFG_398	805.60	Richey, 1989, Table 2, p.46	52	Magenta	FFG_485	762.60	Richey, 1989, Table 2, p.52
15	Magenta	FFG_402	979.40	Richey, 1989, Table 2, p.46	53	Magenta	FFG_486	749.50	Richey, 1989, Table 2, p.52
16	Magenta	FFG_403	941.40	Richey, 1989, Table 2, p.47	54	Magenta	FFG_487	746.50	Richey, 1989, Table 2, p.52
17	Magenta	FFG_404	901.60	Richey, 1989, Table 2, p.47	55	Magenta	FFG_488	731.20	Richey, 1989, Table 2, p.52
18	Magenta	FFG_407	940.00	Richey, 1989, Table 2, p.47	56	Magenta	FFG_489	748.40	Richey, 1989, Table 2, p.52
19	Magenta	FFG_408	913.20	Richey, 1989, Table 2, p.47	57	Magenta	FFG_490	838.80	Richey, 1989, Table 2, p.52
20	Magenta	FFG_419	976.60	Richey, 1989, Table 2, p.48	58	Magenta	FFG_491	836.40	Richey, 1989, Table 2, p.52
21	Magenta	FFG_420	973.50	Richey, 1989, Table 2, p.48	59	Magenta	FFG_492	798.60	Richey, 1989, Table 2, p.52
22	Magenta	FFG_421	960.10	Richey, 1989, Table 2, p.48	60	Magenta	FFG_493	785.30	Richey, 1989, Table 2, p.53
23	Magenta	FFG_422	958.30	Richey, 1989, Table 2, p.48	61	Magenta	FFG_494	792.10	Richey, 1989, Table 2, p.53
24	Magenta	FFG_432	924.10	Richey, 1989, Table 2, p.48	62	Magenta	FFG_495	783.00	Richey, 1989, Table 2, p.53
25	Magenta	FFG_438	874.60	Richey, 1989, Table 2, p.49	63	Magenta	FFG_496	688.60	Richey, 1989, Table 2, p.53
26	Magenta	FFG_455	817.50	Richey, 1989, Table 2, p.50	64	Magenta	FFG_497	701.10	Richey, 1989, Table 2, p.53
27	Magenta	FFG_456	812.50	Richey, 1989, Table 2, p.50	65	Magenta	FFG_498	714.10	Richey, 1989, Table 2, p.53
28	Magenta	FFG_457	868.10	Richey, 1989, Table 2, p.50	66	Magenta	FFG_499	689.50	Richey, 1989, Table 2, p.53
29	Magenta	FFG_458	872.60	Richey, 1989, Table 2, p.50	67	Magenta	FFG_500	704.70	Richey, 1989, Table 2, p.53
30	Magenta	FFG_459	799.50	Richey, 1989, Table 2, p.50	68	Magenta	FFG_501	710.10	Richey, 1989, Table 2, p.53
31	Magenta	FFG_462	865.80	Richey, 1989, Table 2, p.50	69	Magenta	FFG_502	702.90	Richey, 1989, Table 2, p.53
32	Magenta	FFG_463	893.10	Richey, 1989, Table 2, p.51	70	Magenta	FFG_503	684.00	Richey, 1989, Table 2, p.53
33	Magenta	FFG_464	880.00	Richey, 1989, Table 2, p.51	71	Magenta	FFG_504	706.00	Richey, 1989, Table 2, p.53
34	Magenta	FFG_465	883.00	Richey, 1989, Table 2, p.51	72	Magenta	FFG_505	739.50	Richey, 1989, Table 2, p.53
35	Magenta	FFG_467	488.20	Richey, 1989, Table 2, p.51	73	Magenta	FFG_506	730.90	Richey, 1989, Table 2, p.53
36	Magenta	FFG_468	465.50	Richey, 1989, Table 2, p.51	74	Magenta	FFG_507	692.40	Richey, 1989, Table 2, p.53
37	Magenta	FFG_470	484.90	Richey, 1989, Table 2, p.51	75	Magenta	FFG_508	744.10	Richey, 1989, Table 2, p.53
38	Magenta	FFG_471	500.50	Richey, 1989, Table 2, p.51	76	Magenta	FFG_509	745.20	Richey, 1989, Table 2, p.54

Table B.2. Elevations of Stratigraphic Layers Near WIPP (Continued)

	Layer	Well ID	Elevation	Source
1	Magenta	FFG_510	744.80	Richey, 1989, Table 2, p.54
2	Magenta	FFG_511	702.30	Richey, 1989, Table 2, p.54
3	Magenta	FFG_512	720.80	Richey, 1989, Table 2, p.54
4	Magenta	FFG_513	740.70	Richey, 1989, Table 2, p.54
5	Magenta	FFG_514	731.20	Richey, 1989, Table 2, p.54
6	Magenta	FFG_515	697.90	Richey, 1989, Table 2, p.54
7	Magenta	FFG_516	691.30	Richey, 1989, Table 2, p.54
8	Magenta	FFG_517	788.80	Richey, 1989, Table 2, p.54
9	Magenta	FFG_518	778.10	Richey, 1989, Table 2, p.54
10	Magenta	FFG_519	743.70	Richey, 1989, Table 2, p.54
11	Magenta	FFG_520	635.40	Richey, 1989, Table 2, p.54
12	Magenta	FFG_521	655.00	Richey, 1989, Table 2, p.54
13	Magenta	FFG_522	504.30	Richey, 1989, Table 2, p.54
14	Magenta	FFG_523	516.90	Richey, 1989, Table 2, p.54
15	Magenta	FFG_524	675.10	Richey, 1989, Table 2, p.55
16	Magenta	FFG_525	513.70	Richey, 1989, Table 2, p.55
17	Magenta	FFG_527	938.70	Richey, 1989, Table 2, p.55
18	Magenta	FFG_528	934.20	Richey, 1989, Table 2, p.55
19	Magenta	FFG_532	915.60	Richey, 1989, Table 2, p.55
20	Magenta	FFG_535	919.90	Richey, 1989, Table 2, p.55
21	Magenta	FFG_548	914.10	Richey, 1989, Table 2, p.56
22	Magenta	FFG_562	652.30	Richey, 1989, Table 2, p.57
23	Magenta	FFG_563	564.80	Richey, 1989, Table 2, p.57
24	Magenta	FFG_569	670.60	Richey, 1989, Table 2, p.57
25	Magenta	FFG_584	767.70	Richey, 1989, Table 2, p.58
26	Magenta	FFG_600	727.60	Richey, 1989, Table 2, p.58
27	Magenta	FFG_601	623.00	Richey, 1989, Table 2, p.58
28	Magenta	FFG_606	703.50	Richey, 1989, Table 2, p.58
29	Magenta	FFG_607	723.30	Richey, 1989, Table 2, p.59
30	Magenta	FFG_608	731.80	Richey, 1989, Table 2, p.59
31	Magenta	FFG_609	738.80	Richey, 1989, Table 2, p.59
32	Magenta	FFG_610	722.40	Richey, 1989, Table 2, p.59
33	Magenta	FFG_611	707.40	Richey, 1989, Table 2, p.59
34	Magenta	FFG_612	715.70	Richey, 1989, Table 2, p.59
35	Magenta	FFG_613	713.50	Richey, 1989, Table 2, p.59
36	Magenta	FFG_620	738.50	Richey, 1989, Table 2, p.59
37	Magenta	FFG_638	573.10	Richey, 1989, Table 2, p.60
38	Magenta	FFG_639	543.80	Richey, 1989, Table 2, p.60
39	Magenta	FFG_640	630.80	Richey, 1989, Table 2, p.60
40	Magenta	FFG_643	669.70	Richey, 1989, Table 2, p.60
41	Magenta	FFG_644	706.40	Richey, 1989, Table 2, p.60
42	Magenta	FFG_648	541.30	Richey, 1989, Table 2, p.60
43	Magenta	FFG_652	859.80	Richey, 1989, Table 2, p.60
44	Magenta	FFG_653	859.90	Richey, 1989, Table 2, p.61
45	Magenta	FFG_654	880.00	Richey, 1989, Table 2, p.61
46	Magenta	FFG_655	878.10	Richey, 1989, Table 2, p.61
47	Magenta	FFG_656	876.90	Richey, 1989, Table 2, p.61
48	Magenta	FFG_657	889.80	Richey, 1989, Table 2, p.61
49	Magenta	FFG_658	881.80	Richey, 1989, Table 2, p.61
50	Magenta	FFG_659	886.10	Richey, 1989, Table 2, p.61
51	Magenta	FFG_660	901.50	Richey, 1989, Table 2, p.61
52	Magenta	FFG_662	876.30	Richey, 1989, Table 2, p.61
53	Magenta	FFG_664	868.40	Richey, 1989, Table 2, p.61
54	Magenta	FFG_666	920.50	Richey, 1989, Table 2, p.62
55	Magenta	FFG_667	905.60	Richey, 1989, Table 2, p.62
56	Magenta	FFG_670	926.90	Richey, 1989, Table 2, p.62
57	Magenta	FFG_672	925.70	Richey, 1989, Table 2, p.62
58	Magenta	FFG_674	921.70	Richey, 1989, Table 2, p.62
59	Magenta	FFG_675	877.70	Richey, 1989, Table 2, p.62
60	Magenta	FFG_676	891.90	Richey, 1989, Table 2, p.62
61	Magenta	FFG_677	917.80	Richey, 1989, Table 2, p.62
62	Magenta	FFG_679	917.10	Richey, 1989, Table 2, p.62
63	Magenta	FFG_689	799.50	Richey, 1989, Table 2, p.63
64	Magenta	FFG_690	805.00	Richey, 1989, Table 2, p.63
65	Magenta	FFG_691	796.20	Richey, 1989, Table 2, p.63
66	Magenta	FFG_692	786.40	Richey, 1989, Table 2, p.63
67	Magenta	FFG_693	797.00	Richey, 1989, Table 2, p.63
68	Magenta	FFG_694	789.40	Richey, 1989, Table 2, p.63
69	Magenta	FFG_695	794.90	Richey, 1989, Table 2, p.63
70	Magenta	FFG_696	797.00	Richey, 1989, Table 2, p.63
71	Magenta	FFG_697	799.20	Richey, 1989, Table 2, p.64
72	Magenta	FFG_698	841.60	Richey, 1989, Table 2, p.64
73	Magenta	FFG_699	792.80	Richey, 1989, Table 2, p.64
74	Magenta	FFG_700	782.50	Richey, 1989, Table 2, p.64
75	Magenta	FFG_701	788.60	Richey, 1989, Table 2, p.64
76	Magenta	FFG_702	792.80	Richey, 1989, Table 2, p.64

Table B.2. Elevations of Stratigraphic Layers Near WIPP (Continued)

	Layer	Well ID	Elevation	Source		Layer	Well ID	Elevation	Source
1	Magenta	FFG_703	798.90	Richey, 1989, Table 2, p.64	39	Magenta	FFG_742	753.70	Richey, 1989, Table 2, p.67
2	Magenta	FFG_704	785.50	Richey, 1989, Table 2, p.64	40	Magenta	FFG_743	740.40	Richey, 1989, Table 2, p.67
3	Magenta	FFG_705	715.60	Richey, 1989, Table 2, p.64	41	Magenta	FFG_744	722.90	Richey, 1989, Table 2, p.67
4	Magenta	FFG_706	736.10	Richey, 1989, Table 2, p.64	42	Magenta	FFG_745	708.90	Richey, 1989, Table 2, p.67
5	Magenta	FFG_707	720.30	Richey, 1989, Table 2, p.64	43	Magenta	FFG_746	699.10	Richey, 1989, Table 2, p.67
6	Magenta	FFG_708	773.30	Richey, 1989, Table 2, p.64	44	Magenta	H1	864.10	Mercer, 1983, Table 1
7	Magenta	FFG_709	664.50	Richey, 1989, Table 2, p.64	45	Magenta	H10C	741.00	Mercer, 1983, Table 1
8	Magenta	FFG_710	665.40	Richey, 1989, Table 2, p.64	46	Magenta	H2C	872.60	Mercer, 1983, Table 1
9	Magenta	FFG_711	675.20	Richey, 1989, Table 2, p.65	47	Magenta	H3	862.90	Mercer, 1983, Table 1
10	Magenta	FFG_712	718.80	Richey, 1989, Table 2, p.65	48	Magenta	H4C	901.30	Mercer, 1983, Table 1
11	Magenta	FFG_713	655.80	Richey, 1989, Table 2, p.65	49	Magenta	H5C	828.70	Mercer, 1983, Table 1
12	Magenta	FFG_714	770.20	Richey, 1989, Table 2, p.65	50	Magenta	H6C	871.10	Mercer, 1983, Table 1
13	Magenta	FFG_715	783.00	Richey, 1989, Table 2, p.65	51	Magenta	H7C	928.40	Mercer, 1983, Table 1
14	Magenta	FFG_716	680.80	Richey, 1989, Table 2, p.65	52	Magenta	H8C	904.40	Mercer, 1983, Table 1
15	Magenta	FFG_717	703.30	Richey, 1989, Table 2, p.65	53	Magenta	H9C	878.70	Mercer, 1983, Table 1
16	Magenta	FFG_718	706.70	Richey, 1989, Table 2, p.65	54	Magenta	P1	890.70	Mercer, 1983, Table 1
17	Magenta	FFG_719	679.40	Richey, 1989, Table 2, p.65	55	Magenta	P10	838.80	Mercer, 1983, Table 1
18	Magenta	FFG_720	679.10	Richey, 1989, Table 2, p.65	56	Magenta	P11	824.80	Mercer, 1983, Table 1
19	Magenta	FFG_721	679.10	Richey, 1989, Table 2, p.65	57	Magenta	P12	870.20	Mercer, 1983, Table 1
20	Magenta	FFG_723	791.70	Richey, 1989, Table 2, p.65	58	Magenta	P13	870.20	Mercer, 1983, Table 1
21	Magenta	FFG_724	719.10	Richey, 1989, Table 2, p.65	59	Magenta	P14	886.00	Mercer, 1983, Table 1
22	Magenta	FFG_725	694.90	Richey, 1989, Table 2, p.65	60	Magenta	P15	919.30	Mercer, 1983, Table 1
23	Magenta	FFG_726	682.70	Richey, 1989, Table 2, p.65	61	Magenta	P16	896.70	Mercer, 1983, Table 1
24	Magenta	FFG_727	680.00	Richey, 1989, Table 2, p.66	62	Magenta	P17	883.30	Mercer, 1983, Table 1
25	Magenta	FFG_728	677.80	Richey, 1989, Table 2, p.66	63	Magenta	P18	845.20	Mercer, 1983, Table 1
26	Magenta	FFG_729	688.90	Richey, 1989, Table 2, p.66	64	Magenta	P19	832.40	Mercer, 1983, Table 1
27	Magenta	FFG_730	705.60	Richey, 1989, Table 2, p.66	65	Magenta	P2	832.40	Mercer, 1983, Table 1
28	Magenta	FFG_731	703.00	Richey, 1989, Table 2, p.66	66	Magenta	P20	827.30	Mercer, 1983, Table 1
29	Magenta	FFG_732	720.60	Richey, 1989, Table 2, p.66	67	Magenta	P21	829.30	Mercer, 1983, Table 1
30	Magenta	FFG_733	787.60	Richey, 1989, Table 2, p.66	68	Magenta	P3	869.90	Mercer, 1983, Table 1
31	Magenta	FFG_734	741.90	Richey, 1989, Table 2, p.66	69	Magenta	P4	847.90	Mercer, 1983, Table 1
32	Magenta	FFG_735	684.60	Richey, 1989, Table 2, p.66	70	Magenta	P5	848.90	Mercer, 1983, Table 1
33	Magenta	FFG_736	739.10	Richey, 1989, Table 2, p.66	71	Magenta	P6	895.20	Mercer, 1983, Table 1
34	Magenta	FFG_737	682.80	Richey, 1989, Table 2, p.66	72	Magenta	P7	901.90	Mercer, 1983, Table 1
35	Magenta	FFG_738	697.00	Richey, 1989, Table 2, p.66	73	Magenta	P8	880.50	Mercer, 1983, Table 1
36	Magenta	FFG_739	734.40	Richey, 1989, Table 2, p.66	74	Magenta	P9	851.90	Mercer, 1983, Table 1
37	Magenta	FFG_740	736.70	Richey, 1989, Table 2, p.66	75	Magenta	REF	856.70	Rechard et al.,1991, Figure 2.2-1
38	Magenta	FFG_741	702.90	Richey, 1989, Table 2, p.66	76	Magenta	SaltShft	858.77	Bechtel, Inc., 1986, Appendix D

Table B.2. Elevations of Stratigraphic Layers Near WIPP (Continued)

	Layer	Well ID	Elevation	Source
1	Magenta	WIPP11	822.60	Mercer, 1983, Table 1
2	Magenta	WIPP11	822.70	SNL and USGS, 1982a, Table 2
3	Magenta	WIPP12	847.30	SNL and D'Appolonia Consulting, 1983, Table 2
4	Magenta	WIPP12	848.00	Mercer, 1983, Table 1
5	Magenta	WIPP13	865.90	Mercer, 1983, Table 1
6	Magenta	WIPP16	668.70	Mercer, 1983, Table 1
7	Magenta	WIPP18	848.60	Mercer, 1983, Table 1
8	Magenta	WIPP19	849.20	Mercer, 1983, Table 1
9	Magenta	WIPP21	853.10	Mercer, 1983, Table 1
10	Magenta	WIPP22	852.20	Mercer, 1983, Table 1
11	Magenta	WIPP25	887.30	Mercer, 1983, Table 1
12	Magenta	WIPP26	939.40	Mercer, 1983, Table 1
13	Magenta	WIPP27	914.70	Mercer, 1983, Table 1
14	Magenta	WIPP28	933.30	Mercer, 1983, Table 1
15	Magenta	WIPP30	888.50	Mercer, 1983, Table 1
16	Magenta	WIPP32	915.60	Mercer, 1983, Table 1
17	Magenta	WIPP33	876.00	Mercer, 1983, Table 1
18	Magenta	WIPP34	827.60	Mercer, 1983, Table 1
19	Magenta	WastShft	857.36	Bechtel, Inc., 1986, Appendix E
20	RSResid	AirShft	783.13	Holt and Powers, 1990, Figure 22
21	RSResid	ExhtShft	779.98	Bechtel, Inc., 1986, Appendix F
22	RSResid	SaltShft	780.44	Bechtel, Inc., 1986, Appendix D
23	RSResid	WastShft	781.82	Bechtel, Inc., 1986, Appendix E
24	ReposFlr	AirShft	383.74	Holt and Powers, 1990, Figure 22
25	ReposFlr	ExhtShft	381.61	Bechtel, Inc., 1986, Appendix F
26	ReposFlr	SaltShft	380.08	Bechtel, Inc., 1986, Appendix D
27	ReposFlr	WastShft	380.70	Bechtel, Inc., 1986, Appendix E
28	Salado	AEC7	811.60	Mercer, 1983, Table 1
29	Salado	AEC8	776.40	Mercer, 1983, Table 1
30	Salado	B25	782.20	Mercer, 1983, Table 1
31	Salado	ERDA10	836.10	Mercer, 1983, Table 1
32	Salado	ERDA6	830.60	Mercer, 1983, Table 1
33	Salado	ERDA9	783.60	Mercer, 1983, Table 1
34	Salado	FFG_002	578.80	Richey, 1989, Table 2, p.21
35	Salado	FFG_004	627.90	Richey, 1989, Table 2, p.21
36	Salado	FFG_005	581.90	Richey, 1989, Table 2, p.21
37	Salado	FFG_007	559.00	Richey, 1989, Table 2, p.21
38	Salado	FFG_009	575.10	Richey, 1989, Table 2, p.21
39	Salado	FFG_011	570.30	Richey, 1989, Table 2, p.21
40	Salado	FFG_012	572.10	Richey, 1989, Table 2, p.21
41	Salado	FFG_013	582.50	Richey, 1989, Table 2, p.21
42	Salado	FFG_014	623.00	Richey, 1989, Table 2, p.21
43	Salado	FFG_016	545.00	Richey, 1989, Table 2, p.21
44	Salado	FFG_017	555.30	Richey, 1989, Table 2, p.22
45	Salado	FFG_018	558.40	Richey, 1989, Table 2, p.22
46	Salado	FFG_019	548.90	Richey, 1989, Table 2, p.22
47	Salado	FFG_020	622.40	Richey, 1989, Table 2, p.22
48	Salado	FFG_023	553.50	Richey, 1989, Table 2, p.22
49	Salado	FFG_024	539.20	Richey, 1989, Table 2, p.22
50	Salado	FFG_025	560.40	Richey, 1989, Table 2, p.22
51	Salado	FFG_026	552.60	Richey, 1989, Table 2, p.22
52	Salado	FFG_027	545.60	Richey, 1989, Table 2, p.22
53	Salado	FFG_028	549.60	Richey, 1989, Table 2, p.22
54	Salado	FFG_029	537.90	Richey, 1989, Table 2, p.22
55	Salado	FFG_030	532.80	Richey, 1989, Table 2, p.22
56	Salado	FFG_031	522.40	Richey, 1989, Table 2, p.22
57	Salado	FFG_032	519.00	Richey, 1989, Table 2, p.22
58	Salado	FFG_033	518.80	Richey, 1989, Table 2, p.22
59	Salado	FFG_034	517.80	Richey, 1989, Table 2, p.23
60	Salado	FFG_035	504.90	Richey, 1989, Table 2, p.23
61	Salado	FFG_036	510.30	Richey, 1989, Table 2, p.23
62	Salado	FFG_037	502.90	Richey, 1989, Table 2, p.23
63	Salado	FFG_038	491.90	Richey, 1989, Table 2, p.23
64	Salado	FFG_039	694.40	Richey, 1989, Table 2, p.23
65	Salado	FFG_040	624.90	Richey, 1989, Table 2, p.23
66	Salado	FFG_041	691.90	Richey, 1989, Table 2, p.23
67	Salado	FFG_042	695.20	Richey, 1989, Table 2, p.23
68	Salado	FFG_043	697.00	Richey, 1989, Table 2, p.23
69	Salado	FFG_044	645.60	Richey, 1989, Table 2, p.23
70	Salado	FFG_047	526.10	Richey, 1989, Table 2, p.23
71	Salado	FFG_048	527.60	Richey, 1989, Table 2, p.23
72	Salado	FFG_049	526.70	Richey, 1989, Table 2, p.23
73	Salado	FFG_050	537.40	Richey, 1989, Table 2, p.24
74	Salado	FFG_051	530.90	Richey, 1989, Table 2, p.24
75	Salado	FFG_052	565.70	Richey, 1989, Table 2, p.24
76	Salado	FFG_053	510.50	Richey, 1989, Table 2, p.24

Table B.2. Elevations of Stratigraphic Layers Near WIPP (Continued)

	Layer	Well ID	Elevation	Source
1	Salado	FFG_054	518.80	Richey, 1989, Table 2, p.24
2	Salado	FFG_055	521.20	Richey, 1989, Table 2, p.24
3	Salado	FFG_056	520.90	Richey, 1989, Table 2, p.24
4	Salado	FFG_057	524.60	Richey, 1989, Table 2, p.24
5	Salado	FFG_058	526.70	Richey, 1989, Table 2, p.24
6	Salado	FFG_059	529.70	Richey, 1989, Table 2, p.24
7	Salado	FFG_060	532.80	Richey, 1989, Table 2, p.24
8	Salado	FFG_061	532.50	Richey, 1989, Table 2, p.24
9	Salado	FFG_062	479.20	Richey, 1989, Table 2, p.24
10	Salado	FFG_063	438.40	Richey, 1989, Table 2, p.24
11	Salado	FFG_064	461.20	Richey, 1989, Table 2, p.24
12	Salado	FFG_065	449.60	Richey, 1989, Table 2, p.24
13	Salado	FFG_066	401.70	Richey, 1989, Table 2, p.24
14	Salado	FFG_067	435.90	Richey, 1989, Table 2, p.25
15	Salado	FFG_068	396.50	Richey, 1989, Table 2, p.25
16	Salado	FFG_069	407.90	Richey, 1989, Table 2, p.25
17	Salado	FFG_070	442.00	Richey, 1989, Table 2, p.25
18	Salado	FFG_071	700.20	Richey, 1989, Table 2, p.25
19	Salado	FFG_072	645.80	Richey, 1989, Table 2, p.25
20	Salado	FFG_073	623.30	Richey, 1989, Table 2, p.25
21	Salado	FFG_074	630.70	Richey, 1989, Table 2, p.25
22	Salado	FFG_075	683.40	Richey, 1989, Table 2, p.25
23	Salado	FFG_076	741.90	Richey, 1989, Table 2, p.25
24	Salado	FFG_078	776.90	Richey, 1989, Table 2, p.25
25	Salado	FFG_079	750.40	Richey, 1989, Table 2, p.25
26	Salado	FFG_080	727.50	Richey, 1989, Table 2, p.25
27	Salado	FFG_081	644.40	Richey, 1989, Table 2, p.26
28	Salado	FFG_082	673.00	Richey, 1989, Table 2, p.26
29	Salado	FFG_083	604.60	Richey, 1989, Table 2, p.26
30	Salado	FFG_084	626.00	Richey, 1989, Table 2, p.26
31	Salado	FFG_085	620.90	Richey, 1989, Table 2, p.26
32	Salado	FFG_086	630.30	Richey, 1989, Table 2, p.26
33	Salado	FFG_087	601.30	Richey, 1989, Table 2, p.26
34	Salado	FFG_088	595.30	Richey, 1989, Table 2, p.26
35	Salado	FFG_089	576.70	Richey, 1989, Table 2, p.26
36	Salado	FFG_091	614.20	Richey, 1989, Table 2, p.26
37	Salado	FFG_092	633.70	Richey, 1989, Table 2, p.26
38	Salado	FFG_093	637.70	Richey, 1989, Table 2, p.26
39	Salado	FFG_094	637.00	Richey, 1989, Table 2, p.26
40	Salado	FFG_095	618.70	Richey, 1989, Table 2, p.26
41	Salado	FFG_096	605.00	Richey, 1989, Table 2, p.26
42	Salado	FFG_097	580.60	Richey, 1989, Table 2, p.27
43	Salado	FFG_098	555.90	Richey, 1989, Table 2, p.27
44	Salado	FFG_099	550.20	Richey, 1989, Table 2, p.27
45	Salado	FFG_100	530.40	Richey, 1989, Table 2, p.27
46	Salado	FFG_101	500.20	Richey, 1989, Table 2, p.27
47	Salado	FFG_102	512.40	Richey, 1989, Table 2, p.27
48	Salado	FFG_104	474.30	Richey, 1989, Table 2, p.27
49	Salado	FFG_105	812.90	Richey, 1989, Table 2, p.27
50	Salado	FFG_106	840.70	Richey, 1989, Table 2, p.27
51	Salado	FFG_107	836.10	Richey, 1989, Table 2, p.27
52	Salado	FFG_108	836.10	Richey, 1989, Table 2, p.27
53	Salado	FFG_109	831.80	Richey, 1989, Table 2, p.27
54	Salado	FFG_110	798.60	Richey, 1989, Table 2, p.27
55	Salado	FFG_111	806.20	Richey, 1989, Table 2, p.27
56	Salado	FFG_112	784.80	Richey, 1989, Table 2, p.28
57	Salado	FFG_113	802.20	Richey, 1989, Table 2, p.28
58	Salado	FFG_114	828.80	Richey, 1989, Table 2, p.28
59	Salado	FFG_115	803.50	Richey, 1989, Table 2, p.28
60	Salado	FFG_116	795.20	Richey, 1989, Table 2, p.28
61	Salado	FFG_117	810.80	Richey, 1989, Table 2, p.28
62	Salado	FFG_119	828.20	Richey, 1989, Table 2, p.28
63	Salado	FFG_120	819.30	Richey, 1989, Table 2, p.28
64	Salado	FFG_121	830.60	Richey, 1989, Table 2, p.28
65	Salado	FFG_122	813.80	Richey, 1989, Table 2, p.28
66	Salado	FFG_123	815.30	Richey, 1989, Table 2, p.28
67	Salado	FFG_124	785.50	Richey, 1989, Table 2, p.28
68	Salado	FFG_126	813.00	Richey, 1989, Table 2, p.28
69	Salado	FFG_127	824.10	Richey, 1989, Table 2, p.28
70	Salado	FFG_128	852.60	Richey, 1989, Table 2, p.28
71	Salado	FFG_129	815.60	Richey, 1989, Table 2, p.28
72	Salado	FFG_130	854.90	Richey, 1989, Table 2, p.28
73	Salado	FFG_132	852.80	Richey, 1989, Table 2, p.29
74	Salado	FFG_133	837.60	Richey, 1989, Table 2, p.29
75	Salado	FFG_134	861.70	Richey, 1989, Table 2, p.29
76	Salado	FFG_135	844.00	Richey, 1989, Table 2, p.29

Table B.2. Elevations of Stratigraphic Layers Near WIPP (Continued)

	Layer	Well ID	Elevation	Source
1	Salado	FFG_136	844.40	Richey, 1989, Table 2, p.29
2	Salado	FFG_137	853.20	Richey, 1989, Table 2, p.29
3	Salado	FFG_138	798.30	Richey, 1989, Table 2, p.29
4	Salado	FFG_139	810.10	Richey, 1989, Table 2, p.29
5	Salado	FFG_140	750.00	Richey, 1989, Table 2, p.29
6	Salado	FFG_141	782.90	Richey, 1989, Table 2, p.29
7	Salado	FFG_142	757.80	Richey, 1989, Table 2, p.29
8	Salado	FFG_144	825.10	Richey, 1989, Table 2, p.29
9	Salado	FFG_145	830.60	Richey, 1989, Table 2, p.29
10	Salado	FFG_146	826.00	Richey, 1989, Table 2, p.29
11	Salado	FFG_147	816.30	Richey, 1989, Table 2, p.29
12	Salado	FFG_148	832.10	Richey, 1989, Table 2, p.29
13	Salado	FFG_149	842.10	Richey, 1989, Table 2, p.30
14	Salado	FFG_152	836.70	Richey, 1989, Table 2, p.30
15	Salado	FFG_155	830.90	Richey, 1989, Table 2, p.30
16	Salado	FFG_156	837.60	Richey, 1989, Table 2, p.30
17	Salado	FFG_158	856.80	Richey, 1989, Table 2, p.30
18	Salado	FFG_159	859.60	Richey, 1989, Table 2, p.30
19	Salado	FFG_160	855.60	Richey, 1989, Table 2, p.30
20	Salado	FFG_161	856.80	Richey, 1989, Table 2, p.30
21	Salado	FFG_162	857.70	Richey, 1989, Table 2, p.30
22	Salado	FFG_163	856.20	Richey, 1989, Table 2, p.30
23	Salado	FFG_164	854.70	Richey, 1989, Table 2, p.30
24	Salado	FFG_165	838.80	Richey, 1989, Table 2, p.30
25	Salado	FFG_166	858.30	Richey, 1989, Table 2, p.31
26	Salado	FFG_167	836.70	Richey, 1989, Table 2, p.31
27	Salado	FFG_168	843.10	Richey, 1989, Table 2, p.31
28	Salado	FFG_169	861.30	Richey, 1989, Table 2, p.31
29	Salado	FFG_170	839.10	Richey, 1989, Table 2, p.31
30	Salado	FFG_171	848.00	Richey, 1989, Table 2, p.31
31	Salado	FFG_172	851.90	Richey, 1989, Table 2, p.31
32	Salado	FFG_173	831.50	Richey, 1989, Table 2, p.31
33	Salado	FFG_177	812.60	Richey, 1989, Table 2, p.31
34	Salado	FFG_178	539.20	Richey, 1989, Table 2, p.31
35	Salado	FFG_179	816.80	Richey, 1989, Table 2, p.31
36	Salado	FFG_180	825.10	Richey, 1989, Table 2, p.31
37	Salado	FFG_181	869.00	Richey, 1989, Table 2, p.32
38	Salado	FFG_182	757.10	Richey, 1989, Table 2, p.32
39	Salado	FFG_183	837.30	Richey, 1989, Table 2, p.32
40	Salado	FFG_184	851.60	Richey, 1989, Table 2, p.32
41	Salado	FFG_185	840.00	Richey, 1989, Table 2, p.32
42	Salado	FFG_186	766.30	Richey, 1989, Table 2, p.32
43	Salado	FFG_188	781.20	Richey, 1989, Table 2, p.32
44	Salado	FFG_189	805.00	Richey, 1989, Table 2, p.32
45	Salado	FFG_190	793.40	Richey, 1989, Table 2, p.32
46	Salado	FFG_191	780.00	Richey, 1989, Table 2, p.32
47	Salado	FFG_192	708.00	Richey, 1989, Table 2, p.32
48	Salado	FFG_194	738.80	Richey, 1989, Table 2, p.33
49	Salado	FFG_195	753.50	Richey, 1989, Table 2, p.33
50	Salado	FFG_196	792.50	Richey, 1989, Table 2, p.33
51	Salado	FFG_197	790.10	Richey, 1989, Table 2, p.33
52	Salado	FFG_198	783.90	Richey, 1989, Table 2, p.33
53	Salado	FFG_199	780.60	Richey, 1989, Table 2, p.33
54	Salado	FFG_200	785.20	Richey, 1989, Table 2, p.33
55	Salado	FFG_201	778.70	Richey, 1989, Table 2, p.33
56	Salado	FFG_202	723.60	Richey, 1989, Table 2, p.33
57	Salado	FFG_203	727.60	Richey, 1989, Table 2, p.33
58	Salado	FFG_204	767.20	Richey, 1989, Table 2, p.33
59	Salado	FFG_205	768.50	Richey, 1989, Table 2, p.33
60	Salado	FFG_206	779.40	Richey, 1989, Table 2, p.33
61	Salado	FFG_207	775.70	Richey, 1989, Table 2, p.33
62	Salado	FFG_208	780.30	Richey, 1989, Table 2, p.34
63	Salado	FFG_209	787.30	Richey, 1989, Table 2, p.34
64	Salado	FFG_210	766.00	Richey, 1989, Table 2, p.34
65	Salado	FFG_212	768.40	Richey, 1989, Table 2, p.34
66	Salado	FFG_213	795.30	Richey, 1989, Table 2, p.34
67	Salado	FFG_214	757.70	Richey, 1989, Table 2, p.34
68	Salado	FFG_215	734.60	Richey, 1989, Table 2, p.34
69	Salado	FFG_216	520.60	Richey, 1989, Table 2, p.34
70	Salado	FFG_217	756.30	Richey, 1989, Table 2, p.34
71	Salado	FFG_218	744.00	Richey, 1989, Table 2, p.34
72	Salado	FFG_219	783.30	Richey, 1989, Table 2, p.34
73	Salado	FFG_220	742.20	Richey, 1989, Table 2, p.34
74	Salado	FFG_221	684.90	Richey, 1989, Table 2, p.34
75	Salado	FFG_222	604.50	Richey, 1989, Table 2, p.34
76	Salado	FFG_224	558.10	Richey, 1989, Table 2, p.35

Table B.2. Elevations of Stratigraphic Layers Near WIPP (Continued)

	Layer	Well ID	Elevation	Source		Layer	Well ID	Elevation	Source
1	Salado	FFG_225	566.30	Richey, 1989, Table 2, p.35	39	Salado	FFG_264	653.50	Richey, 1989, Table 2, p.37
2	Salado	FFG_226	561.90	Richey, 1989, Table 2, p.35	40	Salado	FFG_265	634.60	Richey, 1989, Table 2, p.37
3	Salado	FFG_228	549.30	Richey, 1989, Table 2, p.35	41	Salado	FFG_266	609.60	Richey, 1989, Table 2, p.37
4	Salado	FFG_229	572.10	Richey, 1989, Table 2, p.35	42	Salado	FFG_267	582.70	Richey, 1989, Table 2, p.37
5	Salado	FFG_230	558.40	Richey, 1989, Table 2, p.35	43	Salado	FFG_268	563.30	Richey, 1989, Table 2, p.37
6	Salado	FFG_231	578.20	Richey, 1989, Table 2, p.35	44	Salado	FFG_269	568.30	Richey, 1989, Table 2, p.38
7	Salado	FFG_232	586.10	Richey, 1989, Table 2, p.35	45	Salado	FFG_270	689.40	Richey, 1989, Table 2, p.38
8	Salado	FFG_233	581.90	Richey, 1989, Table 2, p.35	46	Salado	FFG_271	733.30	Richey, 1989, Table 2, p.38
9	Salado	FFG_234	616.30	Richey, 1989, Table 2, p.35	47	Salado	FFG_272	697.20	Richey, 1989, Table 2, p.38
10	Salado	FFG_235	595.90	Richey, 1989, Table 2, p.35	48	Salado	FFG_273	701.70	Richey, 1989, Table 2, p.38
11	Salado	FFG_236	641.90	Richey, 1989, Table 2, p.35	49	Salado	FFG_274	747.40	Richey, 1989, Table 2, p.38
12	Salado	FFG_237	600.80	Richey, 1989, Table 2, p.35	50	Salado	FFG_275	767.20	Richey, 1989, Table 2, p.38
13	Salado	FFG_238	584.30	Richey, 1989, Table 2, p.36	51	Salado	FFG_276	766.20	Richey, 1989, Table 2, p.38
14	Salado	FFG_239	570.50	Richey, 1989, Table 2, p.36	52	Salado	FFG_277	753.50	Richey, 1989, Table 2, p.38
15	Salado	FFG_240	568.80	Richey, 1989, Table 2, p.36	53	Salado	FFG_278	722.40	Richey, 1989, Table 2, p.38
16	Salado	FFG_241	562.70	Richey, 1989, Table 2, p.36	54	Salado	FFG_279	735.70	Richey, 1989, Table 2, p.38
17	Salado	FFG_242	681.30	Richey, 1989, Table 2, p.36	55	Salado	FFG_280	738.20	Richey, 1989, Table 2, p.38
18	Salado	FFG_243	615.10	Richey, 1989, Table 2, p.36	56	Salado	FFG_281	709.30	Richey, 1989, Table 2, p.38
19	Salado	FFG_244	689.30	Richey, 1989, Table 2, p.36	57	Salado	FFG_283	450.50	Richey, 1989, Table 2, p.39
20	Salado	FFG_245	470.60	Richey, 1989, Table 2, p.36	58	Salado	FFG_284	596.20	Richey, 1989, Table 2, p.39
21	Salado	FFG_246	473.10	Richey, 1989, Table 2, p.36	59	Salado	FFG_285	616.00	Richey, 1989, Table 2, p.39
22	Salado	FFG_247	460.10	Richey, 1989, Table 2, p.36	60	Salado	FFG_286	728.70	Richey, 1989, Table 2, p.39
23	Salado	FFG_248	464.50	Richey, 1989, Table 2, p.36	61	Salado	FFG_287	693.10	Richey, 1989, Table 2, p.39
24	Salado	FFG_249	464.20	Richey, 1989, Table 2, p.36	62	Salado	FFG_288	616.90	Richey, 1989, Table 2, p.39
25	Salado	FFG_250	545.50	Richey, 1989, Table 2, p.36	63	Salado	FFG_289	639.10	Richey, 1989, Table 2, p.39
26	Salado	FFG_251	432.20	Richey, 1989, Table 2, p.36	64	Salado	FFG_290	733.40	Richey, 1989, Table 2, p.39
27	Salado	FFG_252	567.50	Richey, 1989, Table 2, p.36	65	Salado	FFG_291	615.10	Richey, 1989, Table 2, p.39
28	Salado	FFG_253	521.90	Richey, 1989, Table 2, p.36	66	Salado	FFG_292	686.70	Richey, 1989, Table 2, p.39
29	Salado	FFG_254	517.80	Richey, 1989, Table 2, p.36	67	Salado	FFG_293	672.40	Richey, 1989, Table 2, p.39
30	Salado	FFG_255	467.30	Richey, 1989, Table 2, p.37	68	Salado	FFG_294	458.20	Richey, 1989, Table 2, p.39
31	Salado	FFG_256	438.90	Richey, 1989, Table 2, p.37	69	Salado	FFG_295	438.90	Richey, 1989, Table 2, p.39
32	Salado	FFG_257	484.00	Richey, 1989, Table 2, p.37	70	Salado	FFG_297	420.30	Richey, 1989, Table 2, p.39
33	Salado	FFG_258	497.70	Richey, 1989, Table 2, p.37	71	Salado	FFG_298	490.00	Richey, 1989, Table 2, p.40
34	Salado	FFG_259	456.80	Richey, 1989, Table 2, p.37	72	Salado	FFG_299	441.40	Richey, 1989, Table 2, p.40
35	Salado	FFG_260	515.10	Richey, 1989, Table 2, p.37	73	Salado	FFG_300	416.90	Richey, 1989, Table 2, p.40
36	Salado	FFG_261	502.60	Richey, 1989, Table 2, p.37	74	Salado	FFG_301	359.40	Richey, 1989, Table 2, p.40
37	Salado	FFG_262	440.50	Richey, 1989, Table 2, p.37	75	Salado	FFG_302	420.30	Richey, 1989, Table 2, p.40
38	Salado	FFG_263	406.80	Richey, 1989, Table 2, p.37	76	Salado	FFG_303	404.80	Richey, 1989, Table 2, p.40

Table B.2. Elevations of Stratigraphic Layers Near WIPP (Continued)

	Layer	Well ID	Elevation	Source
1	Salado	FFG_304	399.30	Richey, 1989, Table 2, p.40
2	Salado	FFG_305	399.60	Richey, 1989, Table 2, p.40
3	Salado	FFG_306	361.40	Richey, 1989, Table 2, p.40
4	Salado	FFG_307	383.80	Richey, 1989, Table 2, p.40
5	Salado	FFG_308	323.00	Richey, 1989, Table 2, p.40
6	Salado	FFG_309	388.60	Richey, 1989, Table 2, p.40
7	Salado	FFG_310	430.00	Richey, 1989, Table 2, p.40
8	Salado	FFG_311	387.40	Richey, 1989, Table 2, p.40
9	Salado	FFG_312	384.10	Richey, 1989, Table 2, p.40
10	Salado	FFG_313	832.20	Richey, 1989, Table 2, p.41
11	Salado	FFG_314	734.90	Richey, 1989, Table 2, p.41
12	Salado	FFG_315	650.90	Richey, 1989, Table 2, p.41
13	Salado	FFG_316	624.20	Richey, 1989, Table 2, p.41
14	Salado	FFG_317	693.10	Richey, 1989, Table 2, p.41
15	Salado	FFG_318	666.00	Richey, 1989, Table 2, p.41
16	Salado	FFG_319	662.00	Richey, 1989, Table 2, p.41
17	Salado	FFG_320	616.00	Richey, 1989, Table 2, p.41
18	Salado	FFG_321	612.90	Richey, 1989, Table 2, p.41
19	Salado	FFG_322	616.80	Richey, 1989, Table 2, p.41
20	Salado	FFG_323	626.80	Richey, 1989, Table 2, p.41
21	Salado	FFG_324	653.20	Richey, 1989, Table 2, p.41
22	Salado	FFG_325	713.50	Richey, 1989, Table 2, p.41
23	Salado	FFG_326	657.50	Richey, 1989, Table 2, p.41
24	Salado	FFG_327	645.30	Richey, 1989, Table 2, p.42
25	Salado	FFG_328	620.50	Richey, 1989, Table 2, p.42
26	Salado	FFG_329	613.20	Richey, 1989, Table 2, p.42
27	Salado	FFG_330	611.60	Richey, 1989, Table 2, p.42
28	Salado	FFG_331	602.60	Richey, 1989, Table 2, p.42
29	Salado	FFG_332	587.00	Richey, 1989, Table 2, p.42
30	Salado	FFG_333	598.80	Richey, 1989, Table 2, p.42
31	Salado	FFG_334	589.10	Richey, 1989, Table 2, p.42
32	Salado	FFG_335	607.80	Richey, 1989, Table 2, p.42
33	Salado	FFG_336	603.20	Richey, 1989, Table 2, p.42
34	Salado	FFG_337	584.60	Richey, 1989, Table 2, p.42
35	Salado	FFG_338	589.60	Richey, 1989, Table 2, p.42
36	Salado	FFG_339	553.80	Richey, 1989, Table 2, p.42
37	Salado	FFG_340	559.90	Richey, 1989, Table 2, p.42
38	Salado	FFG_342	651.60	Richey, 1989, Table 2, p.43
39	Salado	FFG_344	622.60	Richey, 1989, Table 2, p.43
40	Salado	FFG_345	628.60	Richey, 1989, Table 2, p.43
41	Salado	FFG_347	655.30	Richey, 1989, Table 2, p.43
42	Salado	FFG_348	686.10	Richey, 1989, Table 2, p.43
43	Salado	FFG_349	678.80	Richey, 1989, Table 2, p.43
44	Salado	FFG_350	712.30	Richey, 1989, Table 2, p.43
45	Salado	FFG_351	571.50	Richey, 1989, Table 2, p.43
46	Salado	FFG_352	573.10	Richey, 1989, Table 2, p.43
47	Salado	FFG_353	598.40	Richey, 1989, Table 2, p.43
48	Salado	FFG_354	722.40	Richey, 1989, Table 2, p.43
49	Salado	FFG_361	905.80	Richey, 1989, Table 2, p.44
50	Salado	FFG_362	841.50	Richey, 1989, Table 2, p.44
51	Salado	FFG_363	881.50	Richey, 1989, Table 2, p.44
52	Salado	FFG_366	863.80	Richey, 1989, Table 2, p.44
53	Salado	FFG_367	876.90	Richey, 1989, Table 2, p.44
54	Salado	FFG_370	919.30	Richey, 1989, Table 2, p.44
55	Salado	FFG_371	919.90	Richey, 1989, Table 2, p.44
56	Salado	FFG_374	855.00	Richey, 1989, Table 2, p.45
57	Salado	FFG_376	896.40	Richey, 1989, Table 2, p.45
58	Salado	FFG_381	875.10	Richey, 1989, Table 2, p.45
59	Salado	FFG_383	867.20	Richey, 1989, Table 2, p.45
60	Salado	FFG_385	856.50	Richey, 1989, Table 2, p.45
61	Salado	FFG_387	862.00	Richey, 1989, Table 2, p.45
62	Salado	FFG_390	863.50	Richey, 1989, Table 2, p.46
63	Salado	FFG_391	868.30	Richey, 1989, Table 2, p.46
64	Salado	FFG_392	863.20	Richey, 1989, Table 2, p.46
65	Salado	FFG_393	752.70	Richey, 1989, Table 2, p.46
66	Salado	FFG_394	846.70	Richey, 1989, Table 2, p.46
67	Salado	FFG_395	842.20	Richey, 1989, Table 2, p.46
68	Salado	FFG_396	787.30	Richey, 1989, Table 2, p.46
69	Salado	FFG_403	846.90	Richey, 1989, Table 2, p.47
70	Salado	FFG_408	827.80	Richey, 1989, Table 2, p.47
71	Salado	FFG_411	789.10	Richey, 1989, Table 2, p.47
72	Salado	FFG_413	835.20	Richey, 1989, Table 2, p.47
73	Salado	FFG_421	879.40	Richey, 1989, Table 2, p.48
74	Salado	FFG_426	856.50	Richey, 1989, Table 2, p.48
75	Salado	FFG_432	837.30	Richey, 1989, Table 2, p.48
76	Salado	FFG_433	816.80	Richey, 1989, Table 2, p.48

Table B.2. Elevations of Stratigraphic Layers Near WIPP (Continued)

	Layer	Well ID	Elevation	Source
1	Salado	FFG_438	797.50	Richey, 1989, Table 2, p.49
2	Salado	FFG_445	827.20	Richey, 1989, Table 2, p.49
3	Salado	FFG_453	726.50	Richey, 1989, Table 2, p.50
4	Salado	FFG_455	723.90	Richey, 1989, Table 2, p.50
5	Salado	FFG_456	730.90	Richey, 1989, Table 2, p.50
6	Salado	FFG_457	784.50	Richey, 1989, Table 2, p.50
7	Salado	FFG_458	785.50	Richey, 1989, Table 2, p.50
8	Salado	FFG_459	717.20	Richey, 1989, Table 2, p.50
9	Salado	FFG_462	781.30	Richey, 1989, Table 2, p.50
10	Salado	FFG_463	811.40	Richey, 1989, Table 2, p.51
11	Salado	FFG_464	787.60	Richey, 1989, Table 2, p.51
12	Salado	FFG_465	783.90	Richey, 1989, Table 2, p.51
13	Salado	FFG_467	380.30	Richey, 1989, Table 2, p.51
14	Salado	FFG_468	322.20	Richey, 1989, Table 2, p.51
15	Salado	FFG_470	360.00	Richey, 1989, Table 2, p.51
16	Salado	FFG_471	372.40	Richey, 1989, Table 2, p.51
17	Salado	FFG_472	439.30	Richey, 1989, Table 2, p.51
18	Salado	FFG_473	339.50	Richey, 1989, Table 2, p.51
19	Salado	FFG_474	634.90	Richey, 1989, Table 2, p.51
20	Salado	FFG_475	637.80	Richey, 1989, Table 2, p.51
21	Salado	FFG_476	711.40	Richey, 1989, Table 2, p.51
22	Salado	FFG_477	679.70	Richey, 1989, Table 2, p.51
23	Salado	FFG_478	655.30	Richey, 1989, Table 2, p.52
24	Salado	FFG_479	661.10	Richey, 1989, Table 2, p.52
25	Salado	FFG_480	641.60	Richey, 1989, Table 2, p.52
26	Salado	FFG_481	635.20	Richey, 1989, Table 2, p.52
27	Salado	FFG_482	665.40	Richey, 1989, Table 2, p.52
28	Salado	FFG_483	690.90	Richey, 1989, Table 2, p.52
29	Salado	FFG_484	672.20	Richey, 1989, Table 2, p.52
30	Salado	FFG_485	682.80	Richey, 1989, Table 2, p.52
31	Salado	FFG_486	668.70	Richey, 1989, Table 2, p.52
32	Salado	FFG_487	669.40	Richey, 1989, Table 2, p.52
33	Salado	FFG_488	648.90	Richey, 1989, Table 2, p.52
34	Salado	FFG_489	663.10	Richey, 1989, Table 2, p.52
35	Salado	FFG_490	765.70	Richey, 1989, Table 2, p.52
36	Salado	FFG_491	752.60	Richey, 1989, Table 2, p.52
37	Salado	FFG_492	720.50	Richey, 1989, Table 2, p.52
38	Salado	FFG_493	709.70	Richey, 1989, Table 2, p.53
39	Salado	FFG_494	713.20	Richey, 1989, Table 2, p.53
40	Salado	FFG_495	696.40	Richey, 1989, Table 2, p.53
41	Salado	FFG_496	555.40	Richey, 1989, Table 2, p.53
42	Salado	FFG_497	601.70	Richey, 1989, Table 2, p.53
43	Salado	FFG_498	589.20	Richey, 1989, Table 2, p.53
44	Salado	FFG_499	549.90	Richey, 1989, Table 2, p.53
45	Salado	FFG_500	582.80	Richey, 1989, Table 2, p.53
46	Salado	FFG_501	625.40	Richey, 1989, Table 2, p.53
47	Salado	FFG_502	567.20	Richey, 1989, Table 2, p.53
48	Salado	FFG_503	573.70	Richey, 1989, Table 2, p.53
49	Salado	FFG_504	618.80	Richey, 1989, Table 2, p.53
50	Salado	FFG_505	650.50	Richey, 1989, Table 2, p.53
51	Salado	FFG_506	649.50	Richey, 1989, Table 2, p.53
52	Salado	FFG_507	549.10	Richey, 1989, Table 2, p.53
53	Salado	FFG_508	628.80	Richey, 1989, Table 2, p.53
54	Salado	FFG_509	616.30	Richey, 1989, Table 2, p.54
55	Salado	FFG_510	615.20	Richey, 1989, Table 2, p.54
56	Salado	FFG_511	570.60	Richey, 1989, Table 2, p.54
57	Salado	FFG_512	576.70	Richey, 1989, Table 2, p.54
58	Salado	FFG_513	606.00	Richey, 1989, Table 2, p.54
59	Salado	FFG_514	577.30	Richey, 1989, Table 2, p.54
60	Salado	FFG_515	556.20	Richey, 1989, Table 2, p.54
61	Salado	FFG_516	545.90	Richey, 1989, Table 2, p.54
62	Salado	FFG_517	732.50	Richey, 1989, Table 2, p.54
63	Salado	FFG_518	720.20	Richey, 1989, Table 2, p.54
64	Salado	FFG_519	659.90	Richey, 1989, Table 2, p.54
65	Salado	FFG_520	542.70	Richey, 1989, Table 2, p.54
66	Salado	FFG_521	604.70	Richey, 1989, Table 2, p.54
67	Salado	FFG_522	382.40	Richey, 1989, Table 2, p.54
68	Salado	FFG_523	388.90	Richey, 1989, Table 2, p.54
69	Salado	FFG_524	561.70	Richey, 1989, Table 2, p.55
70	Salado	FFG_525	388.40	Richey, 1989, Table 2, p.55
71	Salado	FFG_526	911.10	Richey, 1989, Table 2, p.55
72	Salado	FFG_527	871.10	Richey, 1989, Table 2, p.55
73	Salado	FFG_528	864.10	Richey, 1989, Table 2, p.55
74	Salado	FFG_530	930.20	Richey, 1989, Table 2, p.55
75	Salado	FFG_531	855.20	Richey, 1989, Table 2, p.55
76	Salado	FFG_532	838.50	Richey, 1989, Table 2, p.55

Table B.2. Elevations of Stratigraphic Layers Near WIPP (Continued)

	Layer	Well ID	Elevation	Source
1	Salado	FFG_535	850.40	Richey, 1989, Table 2, p.55
2	Salado	FFG_536	853.50	Richey, 1989, Table 2, p.55
3	Salado	FFG_537	840.60	Richey, 1989, Table 2, p.55
4	Salado	FFG_564	557.80	Richey, 1989, Table 2, p.57
5	Salado	FFG_584	690.90	Richey, 1989, Table 2, p.58
6	Salado	FFG_585	643.40	Richey, 1989, Table 2, p.58
7	Salado	FFG_602	743.70	Richey, 1989, Table 2, p.58
8	Salado	FFG_606	603.20	Richey, 1989, Table 2, p.58
9	Salado	FFG_607	624.30	Richey, 1989, Table 2, p.59
10	Salado	FFG_608	593.70	Richey, 1989, Table 2, p.59
11	Salado	FFG_609	586.10	Richey, 1989, Table 2, p.59
12	Salado	FFG_610	588.30	Richey, 1989, Table 2, p.59
13	Salado	FFG_611	579.40	Richey, 1989, Table 2, p.59
14	Salado	FFG_612	624.90	Richey, 1989, Table 2, p.59
15	Salado	FFG_613	621.80	Richey, 1989, Table 2, p.59
16	Salado	FFG_640	519.50	Richey, 1989, Table 2, p.60
17	Salado	FFG_643	576.10	Richey, 1989, Table 2, p.60
18	Salado	FFG_652	786.40	Richey, 1989, Table 2, p.60
19	Salado	FFG_653	788.60	Richey, 1989, Table 2, p.61
20	Salado	FFG_654	812.30	Richey, 1989, Table 2, p.61
21	Salado	FFG_655	812.90	Richey, 1989, Table 2, p.61
22	Salado	FFG_656	808.90	Richey, 1989, Table 2, p.61
23	Salado	FFG_657	830.00	Richey, 1989, Table 2, p.61
24	Salado	FFG_658	816.20	Richey, 1989, Table 2, p.61
25	Salado	FFG_659	821.10	Richey, 1989, Table 2, p.61
26	Salado	FFG_660	845.10	Richey, 1989, Table 2, p.61
27	Salado	FFG_662	810.20	Richey, 1989, Table 2, p.61
28	Salado	FFG_664	794.90	Richey, 1989, Table 2, p.61
29	Salado	FFG_666	860.10	Richey, 1989, Table 2, p.62
30	Salado	FFG_667	845.80	Richey, 1989, Table 2, p.62
31	Salado	FFG_668	905.10	Richey, 1989, Table 2, p.62
32	Salado	FFG_669	890.60	Richey, 1989, Table 2, p.62
33	Salado	FFG_670	876.00	Richey, 1989, Table 2, p.62
34	Salado	FFG_671	873.50	Richey, 1989, Table 2, p.62
35	Salado	FFG_672	868.10	Richey, 1989, Table 2, p.62
36	Salado	FFG_673	870.50	Richey, 1989, Table 2, p.62
37	Salado	FFG_674	860.20	Richey, 1989, Table 2, p.62
38	Salado	FFG_675	819.20	Richey, 1989, Table 2, p.62
39	Salado	FFG_676	831.80	Richey, 1989, Table 2, p.62
40	Salado	FFG_677	857.10	Richey, 1989, Table 2, p.62
41	Salado	FFG_679	861.10	Richey, 1989, Table 2, p.62
42	Salado	FFG_685	825.70	Richey, 1989, Table 2, p.63
43	Salado	FFG_689	718.10	Richey, 1989, Table 2, p.63
44	Salado	FFG_690	718.10	Richey, 1989, Table 2, p.63
45	Salado	FFG_691	711.40	Richey, 1989, Table 2, p.63
46	Salado	FFG_693	712.60	Richey, 1989, Table 2, p.63
47	Salado	FFG_694	680.30	Richey, 1989, Table 2, p.63
48	Salado	FFG_695	702.60	Richey, 1989, Table 2, p.63
49	Salado	FFG_696	703.10	Richey, 1989, Table 2, p.63
50	Salado	FFG_697	699.90	Richey, 1989, Table 2, p.64
51	Salado	FFG_698	734.90	Richey, 1989, Table 2, p.64
52	Salado	FFG_699	691.00	Richey, 1989, Table 2, p.64
53	Salado	FFG_700	682.20	Richey, 1989, Table 2, p.64
54	Salado	FFG_701	686.50	Richey, 1989, Table 2, p.64
55	Salado	FFG_702	693.70	Richey, 1989, Table 2, p.64
56	Salado	FFG_703	716.90	Richey, 1989, Table 2, p.64
57	Salado	FFG_704	686.40	Richey, 1989, Table 2, p.64
58	Salado	FFG_705	610.80	Richey, 1989, Table 2, p.64
59	Salado	FFG_706	637.10	Richey, 1989, Table 2, p.64
60	Salado	FFG_707	616.70	Richey, 1989, Table 2, p.64
61	Salado	FFG_708	669.70	Richey, 1989, Table 2, p.64
62	Salado	FFG_710	579.20	Richey, 1989, Table 2, p.64
63	Salado	FFG_711	570.60	Richey, 1989, Table 2, p.65
64	Salado	FFG_716	553.10	Richey, 1989, Table 2, p.65
65	Salado	FFG_717	621.90	Richey, 1989, Table 2, p.65
66	Salado	FFG_718	612.80	Richey, 1989, Table 2, p.65
67	Salado	FFG_719	571.20	Richey, 1989, Table 2, p.65
68	Salado	FFG_720	570.60	Richey, 1989, Table 2, p.65
69	Salado	FFG_721	594.40	Richey, 1989, Table 2, p.65
70	Salado	FFG_723	712.50	Richey, 1989, Table 2, p.65
71	Salado	FFG_724	633.80	Richey, 1989, Table 2, p.65
72	Salado	FFG_725	610.50	Richey, 1989, Table 2, p.65
73	Salado	FFG_726	589.10	Richey, 1989, Table 2, p.65
74	Salado	FFG_727	575.50	Richey, 1989, Table 2, p.66
75	Salado	FFG_728	590.40	Richey, 1989, Table 2, p.66
76	Salado	FFG_729	595.90	Richey, 1989, Table 2, p.66

Table B.2. Elevations of Stratigraphic Layers Near WIPP (Continued)

	Layer	Well ID	Elevation	Source
1	Salado	FFG_730	622.70	Richey, 1989, Table 2, p.66
2	Salado	FFG_731	617.70	Richey, 1989, Table 2, p.66
3	Salado	FFG_733	698.30	Richey, 1989, Table 2, p.66
4	Salado	FFG_734	654.10	Richey, 1989, Table 2, p.66
5	Salado	FFG_735	584.00	Richey, 1989, Table 2, p.66
6	Salado	FFG_736	615.40	Richey, 1989, Table 2, p.66
7	Salado	FFG_737	559.30	Richey, 1989, Table 2, p.66
8	Salado	FFG_738	610.20	Richey, 1989, Table 2, p.66
9	Salado	FFG_739	628.60	Richey, 1989, Table 2, p.66
10	Salado	FFG_740	609.00	Richey, 1989, Table 2, p.66
11	Salado	FFG_741	602.30	Richey, 1989, Table 2, p.66
12	Salado	FFG_742	646.50	Richey, 1989, Table 2, p.67
13	Salado	FFG_743	630.70	Richey, 1989, Table 2, p.67
14	Salado	FFG_744	630.00	Richey, 1989, Table 2, p.67
15	Salado	FFG_745	598.30	Richey, 1989, Table 2, p.67
16	Salado	FFG_746	581.80	Richey, 1989, Table 2, p.67
17	Salado	H1	784.50	Mercer, 1983, Table 1
18	Salado	H10C	666.30	Mercer, 1983, Table 1
19	Salado	H2C	796.70	Mercer, 1983, Table 1
20	Salado	H3	783.10	Mercer, 1983, Table 1
21	Salado	H4C	825.40	Mercer, 1983, Table 1
22	Salado	H5C	751.60	Mercer, 1983, Table 1
23	Salado	H6C	800.70	Mercer, 1983, Table 1
24	Salado	H7C	877.80	Mercer, 1983, Table 1
25	Salado	H8C	823.00	Mercer, 1983, Table 1
26	Salado	H9C	797.00	Mercer, 1983, Table 1
27	Salado	P1	813.30	Mercer, 1983, Table 1
28	Salado	P10	738.50	Mercer, 1983, Table 1
29	Salado	P11	745.50	Mercer, 1983, Table 1
30	Salado	P12	800.10	Mercer, 1983, Table 1
31	Salado	P13	799.80	Mercer, 1983, Table 1
32	Salado	P14	814.70	Mercer, 1983, Table 1
33	Salado	P15	843.70	Mercer, 1983, Table 1
34	Salado	P16	814.40	Mercer, 1983, Table 1
35	Salado	P17	798.90	Mercer, 1983, Table 1
36	Salado	P18	728.20	Mercer, 1983, Table 1
37	Salado	P19	740.00	Mercer, 1983, Table 1
38	Salado	P2	753.20	Mercer, 1983, Table 1
39	Salado	P20	746.80	Mercer, 1983, Table 1
40	Salado	P21	751.60	Mercer, 1983, Table 1
41	Salado	P3	791.50	Mercer, 1983, Table 1
42	Salado	P4	766.20	Mercer, 1983, Table 1
43	Salado	P5	769.40	Mercer, 1983, Table 1
44	Salado	P6	821.40	Mercer, 1983, Table 1
45	Salado	P7	823.60	Mercer, 1983, Table 1
46	Salado	P8	799.80	Mercer, 1983, Table 1
47	Salado	P9	771.50	Mercer, 1983, Table 1
48	Salado	WIPP11	754.30	Mercer, 1983, Table 1
49	Salado	WIPP12	767.20	Mercer, 1983, Table 1
50	Salado	WIPP13	780.50	Mercer, 1983, Table 1
51	Salado	WIPP18	770.50	Mercer, 1983, Table 1
52	Salado	WIPP19	773.90	Mercer, 1983, Table 1
53	Salado	WIPP21	776.90	Mercer, 1983, Table 1
54	Salado	WIPP22	775.10	Mercer, 1983, Table 1
55	Salado	WIPP25	807.10	Mercer, 1983, Table 1
56	Salado	WIPP26	866.50	Mercer, 1983, Table 1
57	Salado	WIPP27	841.50	Mercer, 1983, Table 1
58	Salado	WIPP28	858.40	Mercer, 1983, Table 1
59	Salado	WIPP29	863.80	Mercer, 1983, Table 1
60	Salado	WIPP30	816.60	Mercer, 1983, Table 1
61	Salado	WIPP32	870.80	Mercer, 1983, Table 1
62	Salado	WIPP33	812.60	Mercer, 1983, Table 1
63	Salado	WIPP34	749.80	Mercer, 1983, Table 1
64	Supra_R	AEC7	1113.70	Mercer, 1983, Table 1
65	Supra_R	AEC8	1076.60	Mercer, 1983, Table 1
66	Supra_R	B25	1039.10	Mercer, 1983, Table 1
67	Supra_R	ERDA10	1027.50	Mercer, 1983, Table 1
68	Supra_R	ERDA6	1079.00	Mercer, 1983, Table 1
69	Supra_R	ERDA9	1042.10	Mercer, 1983, Table 1
70	Supra_R	FFG_002	1090.30	Richey, 1989, Table 2, p.21
71	Supra_R	FFG_004	1068.30	Richey, 1989, Table 2, p.21
72	Supra_R	FFG_005	1089.70	Richey, 1989, Table 2, p.21
73	Supra_R	FFG_006	1091.50	Richey, 1989, Table 2, p.21
74	Supra_R	FFG_007	1093.90	Richey, 1989, Table 2, p.21
75	Supra_R	FFG_009	1094.80	Richey, 1989, Table 2, p.21
76	Supra_R	FFG_011	1092.70	Richey, 1989, Table 2, p.21

Table B.2. Elevations of Stratigraphic Layers Near WIPP (Continued)

	Layer	Well ID	Elevation	Source
1	Supra_R	FFG_012	1092.10	Richey, 1989, Table 2, p.21
2	Supra_R	FFG_013	1080.20	Richey, 1989, Table 2, p.21
3	Supra_R	FFG_014	1068.60	Richey, 1989, Table 2, p.21
4	Supra_R	FFG_016	1099.70	Richey, 1989, Table 2, p.21
5	Supra_R	FFG_017	1100.90	Richey, 1989, Table 2, p.22
6	Supra_R	FFG_018	1116.50	Richey, 1989, Table 2, p.22
7	Supra_R	FFG_019	1111.00	Richey, 1989, Table 2, p.22
8	Supra_R	FFG_020	1091.50	Richey, 1989, Table 2, p.22
9	Supra_R	FFG_023	1109.80	Richey, 1989, Table 2, p.22
10	Supra_R	FFG_024	1124.60	Richey, 1989, Table 2, p.22
11	Supra_R	FFG_025	1117.60	Richey, 1989, Table 2, p.22
12	Supra_R	FFG_026	1116.00	Richey, 1989, Table 2, p.22
13	Supra_R	FFG_027	1117.40	Richey, 1989, Table 2, p.22
14	Supra_R	FFG_028	1183.90	Richey, 1989, Table 2, p.22
15	Supra_R	FFG_029	1145.40	Richey, 1989, Table 2, p.22
16	Supra_R	FFG_030	1154.30	Richey, 1989, Table 2, p.22
17	Supra_R	FFG_031	1168.30	Richey, 1989, Table 2, p.22
18	Supra_R	FFG_032	1158.50	Richey, 1989, Table 2, p.22
19	Supra_R	FFG_033	1143.60	Richey, 1989, Table 2, p.22
20	Supra_R	FFG_034	1139.30	Richey, 1989, Table 2, p.23
21	Supra_R	FFG_035	1121.10	Richey, 1989, Table 2, p.23
22	Supra_R	FFG_036	1147.60	Richey, 1989, Table 2, p.23
23	Supra_R	FFG_037	1129.30	Richey, 1989, Table 2, p.23
24	Supra_R	FFG_038	1118.30	Richey, 1989, Table 2, p.23
25	Supra_R	FFG_039	1046.10	Richey, 1989, Table 2, p.23
26	Supra_R	FFG_040	1077.20	Richey, 1989, Table 2, p.23
27	Supra_R	FFG_041	1065.30	Richey, 1989, Table 2, p.23
28	Supra_R	FFG_042	1069.50	Richey, 1989, Table 2, p.23
29	Supra_R	FFG_043	1067.10	Richey, 1989, Table 2, p.23
30	Supra_R	FFG_044	1080.50	Richey, 1989, Table 2, p.23
31	Supra_R	FFG_047	1112.80	Richey, 1989, Table 2, p.23
32	Supra_R	FFG_048	1106.10	Richey, 1989, Table 2, p.23
33	Supra_R	FFG_049	1119.20	Richey, 1989, Table 2, p.23
34	Supra_R	FFG_050	1132.50	Richey, 1989, Table 2, p.24
35	Supra_R	FFG_051	1131.10	Richey, 1989, Table 2, p.24
36	Supra_R	FFG_052	1132.00	Richey, 1989, Table 2, p.24
37	Supra_R	FFG_053	1137.50	Richey, 1989, Table 2, p.24
38	Supra_R	FFG_054	1150.20	Richey, 1989, Table 2, p.24
39	Supra_R	FFG_055	1145.10	Richey, 1989, Table 2, p.24
40	Supra_R	FFG_056	1136.60	Richey, 1989, Table 2, p.24
41	Supra_R	FFG_057	1134.80	Richey, 1989, Table 2, p.24
42	Supra_R	FFG_058	1147.70	Richey, 1989, Table 2, p.24
43	Supra_R	FFG_059	1156.10	Richey, 1989, Table 2, p.24
44	Supra_R	FFG_060	1138.40	Richey, 1989, Table 2, p.24
45	Supra_R	FFG_061	1137.50	Richey, 1989, Table 2, p.24
46	Supra_R	FFG_062	1122.60	Richey, 1989, Table 2, p.24
47	Supra_R	FFG_063	1118.10	Richey, 1989, Table 2, p.24
48	Supra_R	FFG_064	1127.20	Richey, 1989, Table 2, p.24
49	Supra_R	FFG_065	1110.70	Richey, 1989, Table 2, p.24
50	Supra_R	FFG_066	1113.70	Richey, 1989, Table 2, p.24
51	Supra_R	FFG_067	1127.50	Richey, 1989, Table 2, p.25
52	Supra_R	FFG_068	1125.00	Richey, 1989, Table 2, p.25
53	Supra_R	FFG_069	1130.20	Richey, 1989, Table 2, p.25
54	Supra_R	FFG_070	1130.80	Richey, 1989, Table 2, p.25
55	Supra_R	FFG_071	1115.30	Richey, 1989, Table 2, p.25
56	Supra_R	FFG_072	1105.20	Richey, 1989, Table 2, p.25
57	Supra_R	FFG_073	1107.40	Richey, 1989, Table 2, p.25
58	Supra_R	FFG_074	1107.00	Richey, 1989, Table 2, p.25
59	Supra_R	FFG_075	1108.30	Richey, 1989, Table 2, p.25
60	Supra_R	FFG_076	1097.30	Richey, 1989, Table 2, p.25
61	Supra_R	FFG_078	1087.20	Richey, 1989, Table 2, p.25
62	Supra_R	FFG_079	1091.20	Richey, 1989, Table 2, p.25
63	Supra_R	FFG_080	1082.30	Richey, 1989, Table 2, p.25
64	Supra_R	FFG_081	1097.00	Richey, 1989, Table 2, p.26
65	Supra_R	FFG_082	1084.80	Richey, 1989, Table 2, p.26
66	Supra_R	FFG_083	1115.60	Richey, 1989, Table 2, p.26
67	Supra_R	FFG_084	1107.60	Richey, 1989, Table 2, p.26
68	Supra_R	FFG_085	1108.90	Richey, 1989, Table 2, p.26
69	Supra_R	FFG_086	1107.30	Richey, 1989, Table 2, p.26
70	Supra_R	FFG_087	1107.30	Richey, 1989, Table 2, p.26
71	Supra_R	FFG_088	1108.90	Richey, 1989, Table 2, p.26
72	Supra_R	FFG_089	1108.60	Richey, 1989, Table 2, p.26
73	Supra_R	FFG_091	1091.20	Richey, 1989, Table 2, p.26
74	Supra_R	FFG_092	1097.60	Richey, 1989, Table 2, p.26
75	Supra_R	FFG_093	1097.90	Richey, 1989, Table 2, p.26
76	Supra_R	FFG_094	1095.10	Richey, 1989, Table 2, p.26

Table B.2. Elevations of Stratigraphic Layers Near WIPP (Continued)

	Layer	Well ID	Elevation	Source
1	Supra_R	FFG_095	1138.70	Richey, 1989, Table 2, p.26
2	Supra_R	FFG_096	1174.40	Richey, 1989, Table 2, p.26
3	Supra_R	FFG_097	1149.40	Richey, 1989, Table 2, p.27
4	Supra_R	FFG_098	1208.20	Richey, 1989, Table 2, p.27
5	Supra_R	FFG_099	1205.80	Richey, 1989, Table 2, p.27
6	Supra_R	FFG_100	1153.10	Richey, 1989, Table 2, p.27
7	Supra_R	FFG_101	1142.70	Richey, 1989, Table 2, p.27
8	Supra_R	FFG_102	1127.20	Richey, 1989, Table 2, p.27
9	Supra_R	FFG_103	1108.60	Richey, 1989, Table 2, p.27
10	Supra_R	FFG_104	1127.50	Richey, 1989, Table 2, p.27
11	Supra_R	FFG_105	995.20	Richey, 1989, Table 2, p.27
12	Supra_R	FFG_106	981.50	Richey, 1989, Table 2, p.27
13	Supra_R	FFG_107	987.60	Richey, 1989, Table 2, p.27
14	Supra_R	FFG_108	1015.90	Richey, 1989, Table 2, p.27
15	Supra_R	FFG_109	1039.10	Richey, 1989, Table 2, p.27
16	Supra_R	FFG_110	1045.50	Richey, 1989, Table 2, p.27
17	Supra_R	FFG_111	1062.20	Richey, 1989, Table 2, p.27
18	Supra_R	FFG_112	1056.10	Richey, 1989, Table 2, p.28
19	Supra_R	FFG_113	1054.90	Richey, 1989, Table 2, p.28
20	Supra_R	FFG_114	1014.70	Richey, 1989, Table 2, p.28
21	Supra_R	FFG_115	970.50	Richey, 1989, Table 2, p.28
22	Supra_R	FFG_116	972.00	Richey, 1989, Table 2, p.28
23	Supra_R	FFG_117	966.20	Richey, 1989, Table 2, p.28
24	Supra_R	FFG_119	950.10	Richey, 1989, Table 2, p.28
25	Supra_R	FFG_120	956.50	Richey, 1989, Table 2, p.28
26	Supra_R	FFG_121	958.60	Richey, 1989, Table 2, p.28
27	Supra_R	FFG_122	954.00	Richey, 1989, Table 2, p.28
28	Supra_R	FFG_123	961.60	Richey, 1989, Table 2, p.28
29	Supra_R	FFG_124	977.20	Richey, 1989, Table 2, p.28
30	Supra_R	FFG_125	976.20	Richey, 1989, Table 2, p.28
31	Supra_R	FFG_126	1014.20	Richey, 1989, Table 2, p.28
32	Supra_R	FFG_127	1019.20	Richey, 1989, Table 2, p.28
33	Supra_R	FFG_128	994.30	Richey, 1989, Table 2, p.28
34	Supra_R	FFG_129	961.90	Richey, 1989, Table 2, p.28
35	Supra_R	FFG_130	979.90	Richey, 1989, Table 2, p.28
36	Supra_R	FFG_132	1002.20	Richey, 1989, Table 2, p.29
37	Supra_R	FFG_133	993.00	Richey, 1989, Table 2, p.29
38	Supra_R	FFG_134	988.20	Richey, 1989, Table 2, p.29
39	Supra_R	FFG_135	1002.50	Richey, 1989, Table 2, p.29
40	Supra_R	FFG_136	1007.50	Richey, 1989, Table 2, p.29
41	Supra_R	FFG_137	1007.40	Richey, 1989, Table 2, p.29
42	Supra_R	FFG_138	1023.90	Richey, 1989, Table 2, p.29
43	Supra_R	FFG_139	1023.50	Richey, 1989, Table 2, p.29
44	Supra_R	FFG_140	1042.60	Richey, 1989, Table 2, p.29
45	Supra_R	FFG_141	1030.40	Richey, 1989, Table 2, p.29
46	Supra_R	FFG_142	1042.80	Richey, 1989, Table 2, p.29
47	Supra_R	FFG_143	1052.70	Richey, 1989, Table 2, p.29
48	Supra_R	FFG_144	905.00	Richey, 1989, Table 2, p.29
49	Supra_R	FFG_145	905.30	Richey, 1989, Table 2, p.29
50	Supra_R	FFG_146	912.90	Richey, 1989, Table 2, p.29
51	Supra_R	FFG_147	908.30	Richey, 1989, Table 2, p.29
52	Supra_R	FFG_148	907.70	Richey, 1989, Table 2, p.29
53	Supra_R	FFG_149	916.50	Richey, 1989, Table 2, p.30
54	Supra_R	FFG_152	905.30	Richey, 1989, Table 2, p.30
55	Supra_R	FFG_155	918.10	Richey, 1989, Table 2, p.30
56	Supra_R	FFG_156	908.30	Richey, 1989, Table 2, p.30
57	Supra_R	FFG_157	926.00	Richey, 1989, Table 2, p.30
58	Supra_R	FFG_158	941.80	Richey, 1989, Table 2, p.30
59	Supra_R	FFG_159	1001.30	Richey, 1989, Table 2, p.30
60	Supra_R	FFG_160	1002.50	Richey, 1989, Table 2, p.30
61	Supra_R	FFG_161	987.90	Richey, 1989, Table 2, p.30
62	Supra_R	FFG_162	988.80	Richey, 1989, Table 2, p.30
63	Supra_R	FFG_163	988.80	Richey, 1989, Table 2, p.30
64	Supra_R	FFG_164	955.90	Richey, 1989, Table 2, p.30
65	Supra_R	FFG_165	935.70	Richey, 1989, Table 2, p.30
66	Supra_R	FFG_166	993.00	Richey, 1989, Table 2, p.31
67	Supra_R	FFG_167	1019.60	Richey, 1989, Table 2, p.31
68	Supra_R	FFG_168	1001.00	Richey, 1989, Table 2, p.31
69	Supra_R	FFG_169	986.00	Richey, 1989, Table 2, p.31
70	Supra_R	FFG_170	934.80	Richey, 1989, Table 2, p.31
71	Supra_R	FFG_171	956.80	Richey, 1989, Table 2, p.31
72	Supra_R	FFG_172	986.00	Richey, 1989, Table 2, p.31
73	Supra_R	FFG_173	1022.60	Richey, 1989, Table 2, p.31
74	Supra_R	FFG_177	913.20	Richey, 1989, Table 2, p.31
75	Supra_R	FFG_178	888.20	Richey, 1989, Table 2, p.31
76	Supra_R	FFG_179	896.40	Richey, 1989, Table 2, p.31

Table B.2. Elevations of Stratigraphic Layers Near WIPP (Continued)

	Layer	Well ID	Elevation	Source
1	Supra_R	FFG_180	1062.20	Richey, 1989, Table 2, p.31
2	Supra_R	FFG_181	1016.50	Richey, 1989, Table 2, p.32
3	Supra_R	FFG_182	986.00	Richey, 1989, Table 2, p.32
4	Supra_R	FFG_183	1020.50	Richey, 1989, Table 2, p.32
5	Supra_R	FFG_184	1047.90	Richey, 1989, Table 2, p.32
6	Supra_R	FFG_185	1022.60	Richey, 1989, Table 2, p.32
7	Supra_R	FFG_186	1013.50	Richey, 1989, Table 2, p.32
8	Supra_R	FFG_188	979.00	Richey, 1989, Table 2, p.32
9	Supra_R	FFG_189	1046.10	Richey, 1989, Table 2, p.32
10	Supra_R	FFG_190	1037.80	Richey, 1989, Table 2, p.32
11	Supra_R	FFG_191	1041.50	Richey, 1989, Table 2, p.32
12	Supra_R	FFG_192	1031.40	Richey, 1989, Table 2, p.32
13	Supra_R	FFG_194	1075.40	Richey, 1989, Table 2, p.33
14	Supra_R	FFG_195	1059.20	Richey, 1989, Table 2, p.33
15	Supra_R	FFG_196	1042.40	Richey, 1989, Table 2, p.33
16	Supra_R	FFG_197	1034.50	Richey, 1989, Table 2, p.33
17	Supra_R	FFG_198	1031.40	Richey, 1989, Table 2, p.33
18	Supra_R	FFG_199	1038.80	Richey, 1989, Table 2, p.33
19	Supra_R	FFG_200	1040.90	Richey, 1989, Table 2, p.33
20	Supra_R	FFG_201	1074.10	Richey, 1989, Table 2, p.33
21	Supra_R	FFG_202	1075.60	Richey, 1989, Table 2, p.33
22	Supra_R	FFG_203	1071.40	Richey, 1989, Table 2, p.33
23	Supra_R	FFG_204	1096.40	Richey, 1989, Table 2, p.33
24	Supra_R	FFG_205	1082.00	Richey, 1989, Table 2, p.33
25	Supra_R	FFG_206	1067.70	Richey, 1989, Table 2, p.33
26	Supra_R	FFG_207	1072.60	Richey, 1989, Table 2, p.33
27	Supra_R	FFG_208	1060.10	Richey, 1989, Table 2, p.34
28	Supra_R	FFG_209	1074.10	Richey, 1989, Table 2, p.34
29	Supra_R	FFG_210	1066.20	Richey, 1989, Table 2, p.34
30	Supra_R	FFG_212	1078.40	Richey, 1989, Table 2, p.34
31	Supra_R	FFG_213	1051.60	Richey, 1989, Table 2, p.34
32	Supra_R	FFG_214	1061.60	Richey, 1989, Table 2, p.34
33	Supra_R	FFG_215	1041.80	Richey, 1989, Table 2, p.34
34	Supra_R	FFG_216	993.60	Richey, 1989, Table 2, p.34
35	Supra_R	FFG_217	1057.70	Richey, 1989, Table 2, p.34
36	Supra_R	FFG_218	1053.10	Richey, 1989, Table 2, p.34
37	Supra_R	FFG_219	1036.30	Richey, 1989, Table 2, p.34
38	Supra_R	FFG_220	1051.00	Richey, 1989, Table 2, p.34
39	Supra_R	FFG_221	1027.80	Richey, 1989, Table 2, p.34
40	Supra_R	FFG_222	1019.90	Richey, 1989, Table 2, p.34
41	Supra_R	FFG_224	1133.60	Richey, 1989, Table 2, p.35
42	Supra_R	FFG_225	1138.30	Richey, 1989, Table 2, p.35
43	Supra_R	FFG_226	1150.30	Richey, 1989, Table 2, p.35
44	Supra_R	FFG_228	1133.60	Richey, 1989, Table 2, p.35
45	Supra_R	FFG_229	1146.00	Richey, 1989, Table 2, p.35
46	Supra_R	FFG_230	1134.50	Richey, 1989, Table 2, p.35
47	Supra_R	FFG_231	1120.10	Richey, 1989, Table 2, p.35
48	Supra_R	FFG_232	1124.10	Richey, 1989, Table 2, p.35
49	Supra_R	FFG_233	1114.70	Richey, 1989, Table 2, p.35
50	Supra_R	FFG_234	1112.80	Richey, 1989, Table 2, p.35
51	Supra_R	FFG_235	1117.10	Richey, 1989, Table 2, p.35
52	Supra_R	FFG_236	1101.20	Richey, 1989, Table 2, p.35
53	Supra_R	FFG_237	1137.80	Richey, 1989, Table 2, p.35
54	Supra_R	FFG_238	1152.80	Richey, 1989, Table 2, p.36
55	Supra_R	FFG_239	1177.10	Richey, 1989, Table 2, p.36
56	Supra_R	FFG_240	1162.20	Richey, 1989, Table 2, p.36
57	Supra_R	FFG_241	1165.30	Richey, 1989, Table 2, p.36
58	Supra_R	FFG_242	1115.00	Richey, 1989, Table 2, p.36
59	Supra_R	FFG_243	1153.70	Richey, 1989, Table 2, p.36
60	Supra_R	FFG_244	1120.00	Richey, 1989, Table 2, p.36
61	Supra_R	FFG_245	1170.70	Richey, 1989, Table 2, p.36
62	Supra_R	FFG_246	1161.90	Richey, 1989, Table 2, p.36
63	Supra_R	FFG_247	1145.40	Richey, 1989, Table 2, p.36
64	Supra_R	FFG_248	1150.00	Richey, 1989, Table 2, p.36
65	Supra_R	FFG_249	1169.20	Richey, 1989, Table 2, p.36
66	Supra_R	FFG_250	1159.80	Richey, 1989, Table 2, p.36
67	Supra_R	FFG_251	1139.00	Richey, 1989, Table 2, p.36
68	Supra_R	FFG_252	1134.10	Richey, 1989, Table 2, p.36
69	Supra_R	FFG_253	1108.60	Richey, 1989, Table 2, p.36
70	Supra_R	FFG_254	1111.60	Richey, 1989, Table 2, p.36
71	Supra_R	FFG_255	1122.60	Richey, 1989, Table 2, p.37
72	Supra_R	FFG_256	1136.00	Richey, 1989, Table 2, p.37
73	Supra_R	FFG_257	1137.20	Richey, 1989, Table 2, p.37
74	Supra_R	FFG_258	1120.40	Richey, 1989, Table 2, p.37
75	Supra_R	FFG_259	1139.60	Richey, 1989, Table 2, p.37
76	Supra_R	FFG_260	1111.00	Richey, 1989, Table 2, p.37

Table B.2. Elevations of Stratigraphic Layers Near WIPP (Continued)

	Layer	Well ID	Elevation	Source		Layer	Well ID	Elevation	Source
1	Supra_R	FFG_261	1106.10	Richey, 1989, Table 2, p.37	39	Supra_R	FFG_301	1046.40	Richey, 1989, Table 2, p.40
2	Supra_R	FFG_262	1109.50	Richey, 1989, Table 2, p.37	40	Supra_R	FFG_302	1092.70	Richey, 1989, Table 2, p.40
3	Supra_R	FFG_263	1115.60	Richey, 1989, Table 2, p.37	41	Supra_R	FFG_303	1099.30	Richey, 1989, Table 2, p.40
4	Supra_R	FFG_264	1121.10	Richey, 1989, Table 2, p.37	42	Supra_R	FFG_304	1088.10	Richey, 1989, Table 2, p.40
5	Supra_R	FFG_265	1130.80	Richey, 1989, Table 2, p.37	43	Supra_R	FFG_305	1093.90	Richey, 1989, Table 2, p.40
6	Supra_R	FFG_266	1131.40	Richey, 1989, Table 2, p.37	44	Supra_R	FFG_306	1075.90	Richey, 1989, Table 2, p.40
7	Supra_R	FFG_267	1120.40	Richey, 1989, Table 2, p.37	45	Supra_R	FFG_307	1078.70	Richey, 1989, Table 2, p.40
8	Supra_R	FFG_268	1115.90	Richey, 1989, Table 2, p.37	46	Supra_R	FFG_308	1075.90	Richey, 1989, Table 2, p.40
9	Supra_R	FFG_269	1105.80	Richey, 1989, Table 2, p.38	47	Supra_R	FFG_309	1093.60	Richey, 1989, Table 2, p.40
10	Supra_R	FFG_270	1057.00	Richey, 1989, Table 2, p.38	48	Supra_R	FFG_310	1087.50	Richey, 1989, Table 2, p.40
11	Supra_R	FFG_271	1049.40	Richey, 1989, Table 2, p.38	49	Supra_R	FFG_311	1085.40	Richey, 1989, Table 2, p.40
12	Supra_R	FFG_272	1073.50	Richey, 1989, Table 2, p.38	50	Supra_R	FFG_312	1076.90	Richey, 1989, Table 2, p.40
13	Supra_R	FFG_273	1079.20	Richey, 1989, Table 2, p.38	51	Supra_R	FFG_313	1106.10	Richey, 1989, Table 2, p.41
14	Supra_R	FFG_274	1137.20	Richey, 1989, Table 2, p.38	52	Supra_R	FFG_314	1121.10	Richey, 1989, Table 2, p.41
15	Supra_R	FFG_275	1135.70	Richey, 1989, Table 2, p.38	53	Supra_R	FFG_315	1131.10	Richey, 1989, Table 2, p.41
16	Supra_R	FFG_276	1125.90	Richey, 1989, Table 2, p.38	54	Supra_R	FFG_316	1133.20	Richey, 1989, Table 2, p.41
17	Supra_R	FFG_277	1123.20	Richey, 1989, Table 2, p.38	55	Supra_R	FFG_317	1097.60	Richey, 1989, Table 2, p.41
18	Supra_R	FFG_278	1098.20	Richey, 1989, Table 2, p.38	56	Supra_R	FFG_318	1123.50	Richey, 1989, Table 2, p.41
19	Supra_R	FFG_279	1107.90	Richey, 1989, Table 2, p.38	57	Supra_R	FFG_319	1120.70	Richey, 1989, Table 2, p.41
20	Supra_R	FFG_280	1120.30	Richey, 1989, Table 2, p.38	58	Supra_R	FFG_320	1129.60	Richey, 1989, Table 2, p.41
21	Supra_R	FFG_281	1147.30	Richey, 1989, Table 2, p.38	59	Supra_R	FFG_321	1124.70	Richey, 1989, Table 2, p.41
22	Supra_R	FFG_283	1090.90	Richey, 1989, Table 2, p.39	60	Supra_R	FFG_322	1124.70	Richey, 1989, Table 2, p.41
23	Supra_R	FFG_284	1117.10	Richey, 1989, Table 2, p.39	61	Supra_R	FFG_323	1120.40	Richey, 1989, Table 2, p.41
24	Supra_R	FFG_285	1112.50	Richey, 1989, Table 2, p.39	62	Supra_R	FFG_324	1122.00	Richey, 1989, Table 2, p.41
25	Supra_R	FFG_286	1101.50	Richey, 1989, Table 2, p.39	63	Supra_R	FFG_325	1079.90	Richey, 1989, Table 2, p.41
26	Supra_R	FFG_287	1094.60	Richey, 1989, Table 2, p.39	64	Supra_R	FFG_326	1117.70	Richey, 1989, Table 2, p.41
27	Supra_R	FFG_288	1110.40	Richey, 1989, Table 2, p.39	65	Supra_R	FFG_327	1102.20	Richey, 1989, Table 2, p.42
28	Supra_R	FFG_289	1081.90	Richey, 1989, Table 2, p.39	66	Supra_R	FFG_328	1121.40	Richey, 1989, Table 2, p.42
29	Supra_R	FFG_290	1103.40	Richey, 1989, Table 2, p.39	67	Supra_R	FFG_329	1120.40	Richey, 1989, Table 2, p.42
30	Supra_R	FFG_291	1132.00	Richey, 1989, Table 2, p.39	68	Supra_R	FFG_330	1115.60	Richey, 1989, Table 2, p.42
31	Supra_R	FFG_292	1090.60	Richey, 1989, Table 2, p.39	69	Supra_R	FFG_331	1103.70	Richey, 1989, Table 2, p.42
32	Supra_R	FFG_293	1085.10	Richey, 1989, Table 2, p.39	70	Supra_R	FFG_332	1124.70	Richey, 1989, Table 2, p.42
33	Supra_R	FFG_294	1095.50	Richey, 1989, Table 2, p.39	71	Supra_R	FFG_333	1130.50	Richey, 1989, Table 2, p.42
34	Supra_R	FFG_295	1087.50	Richey, 1989, Table 2, p.39	72	Supra_R	FFG_334	1125.90	Richey, 1989, Table 2, p.42
35	Supra_R	FFG_297	1104.90	Richey, 1989, Table 2, p.39	73	Supra_R	FFG_335	1129.60	Richey, 1989, Table 2, p.42
36	Supra_R	FFG_298	1070.00	Richey, 1989, Table 2, p.40	74	Supra_R	FFG_336	1124.10	Richey, 1989, Table 2, p.42
37	Supra_R	FFG_299	1078.40	Richey, 1989, Table 2, p.40	75	Supra_R	FFG_337	1124.40	Richey, 1989, Table 2, p.42
38	Supra_R	FFG_300	1062.20	Richey, 1989, Table 2, p.40	76	Supra_R	FFG_338	1123.50	Richey, 1989, Table 2, p.42

Table B.2. Elevations of Stratigraphic Layers Near WIPP (Continued)

	Layer	Well ID	Elevation	Source
1	Supra_R	FFG_339	1107.90	Richey, 1989, Table 2, p.42
2	Supra_R	FFG_340	1107.00	Richey, 1989, Table 2, p.42
3	Supra_R	FFG_342	1056.10	Richey, 1989, Table 2, p.43
4	Supra_R	FFG_344	1040.60	Richey, 1989, Table 2, p.43
5	Supra_R	FFG_345	1073.20	Richey, 1989, Table 2, p.43
6	Supra_R	FFG_347	1039.70	Richey, 1989, Table 2, p.43
7	Supra_R	FFG_348	1035.70	Richey, 1989, Table 2, p.43
8	Supra_R	FFG_349	1034.80	Richey, 1989, Table 2, p.43
9	Supra_R	FFG_350	1041.50	Richey, 1989, Table 2, p.43
10	Supra_R	FFG_351	1102.80	Richey, 1989, Table 2, p.43
11	Supra_R	FFG_352	1103.10	Richey, 1989, Table 2, p.43
12	Supra_R	FFG_353	1095.80	Richey, 1989, Table 2, p.43
13	Supra_R	FFG_354	1051.00	Richey, 1989, Table 2, p.43
14	Supra_R	FFG_361	1012.50	Richey, 1989, Table 2, p.44
15	Supra_R	FFG_362	1010.70	Richey, 1989, Table 2, p.44
16	Supra_R	FFG_363	1009.50	Richey, 1989, Table 2, p.44
17	Supra_R	FFG_364	993.60	Richey, 1989, Table 2, p.44
18	Supra_R	FFG_366	1010.40	Richey, 1989, Table 2, p.44
19	Supra_R	FFG_367	1006.40	Richey, 1989, Table 2, p.44
20	Supra_R	FFG_370	1012.90	Richey, 1989, Table 2, p.44
21	Supra_R	FFG_371	1012.90	Richey, 1989, Table 2, p.44
22	Supra_R	FFG_372	1006.40	Richey, 1989, Table 2, p.45
23	Supra_R	FFG_373	998.10	Richey, 1989, Table 2, p.45
24	Supra_R	FFG_374	995.20	Richey, 1989, Table 2, p.45
25	Supra_R	FFG_376	1010.40	Richey, 1989, Table 2, p.45
26	Supra_R	FFG_381	1021.40	Richey, 1989, Table 2, p.45
27	Supra_R	FFG_383	1046.10	Richey, 1989, Table 2, p.45
28	Supra_R	FFG_384	976.00	Richey, 1989, Table 2, p.45
29	Supra_R	FFG_385	990.60	Richey, 1989, Table 2, p.45
30	Supra_R	FFG_387	1019.90	Richey, 1989, Table 2, p.45
31	Supra_R	FFG_388	1019.60	Richey, 1989, Table 2, p.46
32	Supra_R	FFG_389	1008.00	Richey, 1989, Table 2, p.46
33	Supra_R	FFG_390	1022.60	Richey, 1989, Table 2, p.46
34	Supra_R	FFG_391	1025.30	Richey, 1989, Table 2, p.46
35	Supra_R	FFG_392	1019.60	Richey, 1989, Table 2, p.46
36	Supra_R	FFG_393	1061.60	Richey, 1989, Table 2, p.46
37	Supra_R	FFG_394	1050.30	Richey, 1989, Table 2, p.46
38	Supra_R	FFG_395	1059.20	Richey, 1989, Table 2, p.46
39	Supra_R	FFG_396	1090.00	Richey, 1989, Table 2, p.46
40	Supra_R	FFG_398	1011.60	Richey, 1989, Table 2, p.46
41	Supra_R	FFG_399	1001.60	Richey, 1989, Table 2, p.46
42	Supra_R	FFG_401	972.30	Richey, 1989, Table 2, p.46
43	Supra_R	FFG_402	1023.10	Richey, 1989, Table 2, p.46
44	Supra_R	FFG_403	995.20	Richey, 1989, Table 2, p.47
45	Supra_R	FFG_404	976.60	Richey, 1989, Table 2, p.47
46	Supra_R	FFG_407	969.90	Richey, 1989, Table 2, p.47
47	Supra_R	FFG_408	965.00	Richey, 1989, Table 2, p.47
48	Supra_R	FFG_409	970.50	Richey, 1989, Table 2, p.47
49	Supra_R	FFG_411	957.70	Richey, 1989, Table 2, p.47
50	Supra_R	FFG_413	968.70	Richey, 1989, Table 2, p.47
51	Supra_R	FFG_418	1033.90	Richey, 1989, Table 2, p.48
52	Supra_R	FFG_419	1052.50	Richey, 1989, Table 2, p.48
53	Supra_R	FFG_420	1045.10	Richey, 1989, Table 2, p.48
54	Supra_R	FFG_421	1047.00	Richey, 1989, Table 2, p.48
55	Supra_R	FFG_422	1054.30	Richey, 1989, Table 2, p.48
56	Supra_R	FFG_426	996.10	Richey, 1989, Table 2, p.48
57	Supra_R	FFG_432	978.40	Richey, 1989, Table 2, p.48
58	Supra_R	FFG_433	968.00	Richey, 1989, Table 2, p.48
59	Supra_R	FFG_438	1082.20	Richey, 1989, Table 2, p.49
60	Supra_R	FFG_445	960.70	Richey, 1989, Table 2, p.49
61	Supra_R	FFG_453	1049.50	Richey, 1989, Table 2, p.50
62	Supra_R	FFG_455	1061.30	Richey, 1989, Table 2, p.50
63	Supra_R	FFG_456	1063.40	Richey, 1989, Table 2, p.50
64	Supra_R	FFG_457	1023.50	Richey, 1989, Table 2, p.50
65	Supra_R	FFG_458	1025.80	Richey, 1989, Table 2, p.50
66	Supra_R	FFG_459	1070.50	Richey, 1989, Table 2, p.50
67	Supra_R	FFG_462	1032.10	Richey, 1989, Table 2, p.50
68	Supra_R	FFG_463	1021.10	Richey, 1989, Table 2, p.51
69	Supra_R	FFG_464	1035.40	Richey, 1989, Table 2, p.51
70	Supra_R	FFG_465	1031.40	Richey, 1989, Table 2, p.51
71	Supra_R	FFG_467	1025.70	Richey, 1989, Table 2, p.51
72	Supra_R	FFG_468	1064.70	Richey, 1989, Table 2, p.51
73	Supra_R	FFG_470	1067.10	Richey, 1989, Table 2, p.51
74	Supra_R	FFG_471	1036.60	Richey, 1989, Table 2, p.51
75	Supra_R	FFG_472	1032.40	Richey, 1989, Table 2, p.51
76	Supra_R	FFG_473	1060.70	Richey, 1989, Table 2, p.51

Table B.2. Elevations of Stratigraphic Layers Near WIPP (Continued)

	Layer	Well ID	Elevation	Source		Layer	Well ID	Elevation	Source
1	Supra_R	FFG_474	1100.60	Richey, 1989, Table 2, p.51	39	Supra_R	FFG_512	1073.50	Richey, 1989, Table 2, p.54
2	Supra_R	FFG_475	1103.70	Richey, 1989, Table 2, p.51	40	Supra_R	FFG_513	1061.00	Richey, 1989, Table 2, p.54
3	Supra_R	FFG_476	1090.10	Richey, 1989, Table 2, p.51	41	Supra_R	FFG_514	1060.10	Richey, 1989, Table 2, p.54
4	Supra_R	FFG_477	1102.80	Richey, 1989, Table 2, p.51	42	Supra_R	FFG_515	1082.30	Richey, 1989, Table 2, p.54
5	Supra_R	FFG_478	1104.80	Richey, 1989, Table 2, p.52	43	Supra_R	FFG_516	1075.00	Richey, 1989, Table 2, p.54
6	Supra_R	FFG_479	1106.40	Richey, 1989, Table 2, p.52	44	Supra_R	FFG_517	1053.10	Richey, 1989, Table 2, p.54
7	Supra_R	FFG_480	1096.10	Richey, 1989, Table 2, p.52	45	Supra_R	FFG_518	1036.30	Richey, 1989, Table 2, p.54
8	Supra_R	FFG_481	1090.90	Richey, 1989, Table 2, p.52	46	Supra_R	FFG_519	1033.90	Richey, 1989, Table 2, p.54
9	Supra_R	FFG_482	1103.40	Richey, 1989, Table 2, p.52	47	Supra_R	FFG_520	1030.80	Richey, 1989, Table 2, p.54
10	Supra_R	FFG_483	1094.20	Richey, 1989, Table 2, p.52	48	Supra_R	FFG_521	1028.70	Richey, 1989, Table 2, p.54
11	Supra_R	FFG_484	1095.60	Richey, 1989, Table 2, p.52	49	Supra_R	FFG_522	1055.20	Richey, 1989, Table 2, p.54
12	Supra_R	FFG_485	1096.50	Richey, 1989, Table 2, p.52	50	Supra_R	FFG_523	1041.80	Richey, 1989, Table 2, p.54
13	Supra_R	FFG_486	1097.60	Richey, 1989, Table 2, p.52	51	Supra_R	FFG_524	1024.10	Richey, 1989, Table 2, p.55
14	Supra_R	FFG_487	1097.00	Richey, 1989, Table 2, p.52	52	Supra_R	FFG_525	1047.00	Richey, 1989, Table 2, p.55
15	Supra_R	FFG_488	1088.60	Richey, 1989, Table 2, p.52	53	Supra_R	FFG_526	1033.90	Richey, 1989, Table 2, p.55
16	Supra_R	FFG_489	1086.60	Richey, 1989, Table 2, p.52	54	Supra_R	FFG_527	1031.70	Richey, 1989, Table 2, p.55
17	Supra_R	FFG_490	1072.60	Richey, 1989, Table 2, p.52	55	Supra_R	FFG_528	1023.50	Richey, 1989, Table 2, p.55
18	Supra_R	FFG_491	1077.50	Richey, 1989, Table 2, p.52	56	Supra_R	FFG_530	1016.50	Richey, 1989, Table 2, p.55
19	Supra_R	FFG_492	1067.40	Richey, 1989, Table 2, p.52	57	Supra_R	FFG_531	998.20	Richey, 1989, Table 2, p.55
20	Supra_R	FFG_493	1069.20	Richey, 1989, Table 2, p.53	58	Supra_R	FFG_532	990.30	Richey, 1989, Table 2, p.55
21	Supra_R	FFG_494	1069.50	Richey, 1989, Table 2, p.53	59	Supra_R	FFG_534	1021.10	Richey, 1989, Table 2, p.55
22	Supra_R	FFG_495	1072.30	Richey, 1989, Table 2, p.53	60	Supra_R	FFG_535	995.90	Richey, 1989, Table 2, p.55
23	Supra_R	FFG_496	1108.30	Richey, 1989, Table 2, p.53	61	Supra_R	FFG_536	996.10	Richey, 1989, Table 2, p.55
24	Supra_R	FFG_497	1090.60	Richey, 1989, Table 2, p.53	62	Supra_R	FFG_537	985.40	Richey, 1989, Table 2, p.55
25	Supra_R	FFG_498	1104.90	Richey, 1989, Table 2, p.53	63	Supra_R	FFG_543	997.90	Richey, 1989, Table 2, p.56
26	Supra_R	FFG_499	1091.50	Richey, 1989, Table 2, p.53	64	Supra_R	FFG_548	1047.30	Richey, 1989, Table 2, p.56
27	Supra_R	FFG_500	1091.50	Richey, 1989, Table 2, p.53	65	Supra_R	FFG_552	922.90	Richey, 1989, Table 2, p.56
28	Supra_R	FFG_501	1075.60	Richey, 1989, Table 2, p.53	66	Supra_R	FFG_562	981.50	Richey, 1989, Table 2, p.57
29	Supra_R	FFG_502	1092.40	Richey, 1989, Table 2, p.53	67	Supra_R	FFG_563	969.90	Richey, 1989, Table 2, p.57
30	Supra_R	FFG_503	1064.10	Richey, 1989, Table 2, p.53	68	Supra_R	FFG_564	969.30	Richey, 1989, Table 2, p.57
31	Supra_R	FFG_504	1070.50	Richey, 1989, Table 2, p.53	69	Supra_R	FFG_568	957.10	Richey, 1989, Table 2, p.57
32	Supra_R	FFG_505	1077.80	Richey, 1989, Table 2, p.53	70	Supra_R	FFG_569	952.20	Richey, 1989, Table 2, p.57
33	Supra_R	FFG_506	1069.80	Richey, 1989, Table 2, p.53	71	Supra_R	FFG_584	1006.80	Richey, 1989, Table 2, p.58
34	Supra_R	FFG_507	1051.90	Richey, 1989, Table 2, p.53	72	Supra_R	FFG_585	1025.00	Richey, 1989, Table 2, p.58
35	Supra_R	FFG_508	1051.90	Richey, 1989, Table 2, p.53	73	Supra_R	FFG_600	1003.40	Richey, 1989, Table 2, p.58
36	Supra_R	FFG_509	1066.50	Richey, 1989, Table 2, p.54	74	Supra_R	FFG_601	983.90	Richey, 1989, Table 2, p.58
37	Supra_R	FFG_510	1080.50	Richey, 1989, Table 2, p.54	75	Supra_R	FFG_602	1053.10	Richey, 1989, Table 2, p.58
38	Supra_R	FFG_511	1102.80	Richey, 1989, Table 2, p.54	76	Supra_R	FFG_606	1012.90	Richey, 1989, Table 2, p.58

Table B.2. Elevations of Stratigraphic Layers Near WIPP (Continued)

	Layer	Well ID	Elevation	Source
1	Supra_R	FFG_607	1001.30	Richey, 1989, Table 2, p.59
2	Supra_R	FFG_608	1018.60	Richey, 1989, Table 2, p.59
3	Supra_R	FFG_609	1025.30	Richey, 1989, Table 2, p.59
4	Supra_R	FFG_610	1023.20	Richey, 1989, Table 2, p.59
5	Supra_R	FFG_611	1009.20	Richey, 1989, Table 2, p.59
6	Supra_R	FFG_612	977.10	Richey, 1989, Table 2, p.59
7	Supra_R	FFG_613	945.90	Richey, 1989, Table 2, p.59
8	Supra_R	FFG_618	897.00	Richey, 1989, Table 2, p.59
9	Supra_R	FFG_620	909.90	Richey, 1989, Table 2, p.59
10	Supra_R	FFG_621	905.90	Richey, 1989, Table 2, p.59
11	Supra_R	FFG_638	975.40	Richey, 1989, Table 2, p.60
12	Supra_R	FFG_639	961.50	Richey, 1989, Table 2, p.60
13	Supra_R	FFG_640	966.20	Richey, 1989, Table 2, p.60
14	Supra_R	FFG_643	975.40	Richey, 1989, Table 2, p.60
15	Supra_R	FFG_644	936.70	Richey, 1989, Table 2, p.60
16	Supra_R	FFG_648	960.70	Richey, 1989, Table 2, p.60
17	Supra_R	FFG_652	1106.40	Richey, 1989, Table 2, p.60
18	Supra_R	FFG_653	1096.10	Richey, 1989, Table 2, p.61
19	Supra_R	FFG_654	1098.50	Richey, 1989, Table 2, p.61
20	Supra_R	FFG_655	1093.00	Richey, 1989, Table 2, p.61
21	Supra_R	FFG_656	1091.80	Richey, 1989, Table 2, p.61
22	Supra_R	FFG_657	1083.30	Richey, 1989, Table 2, p.61
23	Supra_R	FFG_658	1088.10	Richey, 1989, Table 2, p.61
24	Supra_R	FFG_659	1072.60	Richey, 1989, Table 2, p.61
25	Supra_R	FFG_660	1071.10	Richey, 1989, Table 2, p.61
26	Supra_R	FFG_662	1085.70	Richey, 1989, Table 2, p.61
27	Supra_R	FFG_664	1084.50	Richey, 1989, Table 2, p.61
28	Supra_R	FFG_666	1063.10	Richey, 1989, Table 2, p.62
29	Supra_R	FFG_667	1059.20	Richey, 1989, Table 2, p.62
30	Supra_R	FFG_668	1043.30	Richey, 1989, Table 2, p.62
31	Supra_R	FFG_669	1036.30	Richey, 1989, Table 2, p.62
32	Supra_R	FFG_670	1049.10	Richey, 1989, Table 2, p.62
33	Supra_R	FFG_671	1044.90	Richey, 1989, Table 2, p.62
34	Supra_R	FFG_672	1058.00	Richey, 1989, Table 2, p.62
35	Supra_R	FFG_673	1037.20	Richey, 1989, Table 2, p.62
36	Supra_R	FFG_674	1064.70	Richey, 1989, Table 2, p.62
37	Supra_R	FFG_675	1078.40	Richey, 1989, Table 2, p.62
38	Supra_R	FFG_676	1084.50	Richey, 1989, Table 2, p.62
39	Supra_R	FFG_677	1064.40	Richey, 1989, Table 2, p.62
40	Supra_R	FFG_679	1060.70	Richey, 1989, Table 2, p.62
41	Supra_R	FFG_685	1003.50	Richey, 1989, Table 2, p.63
42	Supra_R	FFG_689	1059.20	Richey, 1989, Table 2, p.63
43	Supra_R	FFG_690	1052.20	Richey, 1989, Table 2, p.63
44	Supra_R	FFG_691	1052.50	Richey, 1989, Table 2, p.63
45	Supra_R	FFG_692	1057.70	Richey, 1989, Table 2, p.63
46	Supra_R	FFG_693	1050.60	Richey, 1989, Table 2, p.63
47	Supra_R	FFG_694	1042.40	Richey, 1989, Table 2, p.63
48	Supra_R	FFG_695	1048.50	Richey, 1989, Table 2, p.63
49	Supra_R	FFG_696	1050.60	Richey, 1989, Table 2, p.63
50	Supra_R	FFG_697	1045.80	Richey, 1989, Table 2, p.64
51	Supra_R	FFG_698	1039.70	Richey, 1989, Table 2, p.64
52	Supra_R	FFG_699	1029.60	Richey, 1989, Table 2, p.64
53	Supra_R	FFG_700	1027.10	Richey, 1989, Table 2, p.64
54	Supra_R	FFG_701	1032.10	Richey, 1989, Table 2, p.64
55	Supra_R	FFG_702	1036.60	Richey, 1989, Table 2, p.64
56	Supra_R	FFG_703	1047.00	Richey, 1989, Table 2, p.64
57	Supra_R	FFG_704	1032.70	Richey, 1989, Table 2, p.64
58	Supra_R	FFG_705	1023.80	Richey, 1989, Table 2, p.64
59	Supra_R	FFG_706	1025.70	Richey, 1989, Table 2, p.64
60	Supra_R	FFG_707	1019.30	Richey, 1989, Table 2, p.64
61	Supra_R	FFG_708	1026.60	Richey, 1989, Table 2, p.64
62	Supra_R	FFG_709	1008.60	Richey, 1989, Table 2, p.64
63	Supra_R	FFG_710	1007.40	Richey, 1989, Table 2, p.64
64	Supra_R	FFG_711	1012.90	Richey, 1989, Table 2, p.65
65	Supra_R	FFG_712	1018.00	Richey, 1989, Table 2, p.65
66	Supra_R	FFG_713	1011.30	Richey, 1989, Table 2, p.65
67	Supra_R	FFG_714	1024.10	Richey, 1989, Table 2, p.65
68	Supra_R	FFG_715	1025.30	Richey, 1989, Table 2, p.65
69	Supra_R	FFG_716	1060.60	Richey, 1989, Table 2, p.65
70	Supra_R	FFG_717	1056.10	Richey, 1989, Table 2, p.65
71	Supra_R	FFG_718	1044.90	Richey, 1989, Table 2, p.65
72	Supra_R	FFG_719	1040.40	Richey, 1989, Table 2, p.65
73	Supra_R	FFG_720	1019.90	Richey, 1989, Table 2, p.65
74	Supra_R	FFG_721	1026.90	Richey, 1989, Table 2, p.65
75	Supra_R	FFG_723	1054.30	Richey, 1989, Table 2, p.65
76	Supra_R	FFG_724	1044.20	Richey, 1989, Table 2, p.65

Table B.2. Elevations of Stratigraphic Layers Near WIPP (Continued)

	Layer	Well ID	Elevation	Source
1	Supra_R	FFG_725	1029.60	Richey, 1989, Table 2, p.65
2	Supra_R	FFG_726	1018.60	Richey, 1989, Table 2, p.65
3	Supra_R	FFG_727	1020.80	Richey, 1989, Table 2, p.66
4	Supra_R	FFG_728	1012.20	Richey, 1989, Table 2, p.66
5	Supra_R	FFG_729	1014.40	Richey, 1989, Table 2, p.66
6	Supra_R	FFG_730	1018.90	Richey, 1989, Table 2, p.66
7	Supra_R	FFG_731	1022.30	Richey, 1989, Table 2, p.66
8	Supra_R	FFG_732	1040.30	Richey, 1989, Table 2, p.66
9	Supra_R	FFG_733	1028.40	Richey, 1989, Table 2, p.66
10	Supra_R	FFG_734	1029.00	Richey, 1989, Table 2, p.66
11	Supra_R	FFG_735	1016.50	Richey, 1989, Table 2, p.66
12	Supra_R	FFG_736	1025.60	Richey, 1989, Table 2, p.66
13	Supra_R	FFG_737	1040.50	Richey, 1989, Table 2, p.66
14	Supra_R	FFG_738	1018.30	Richey, 1989, Table 2, p.66
15	Supra_R	FFG_739	1015.10	Richey, 1989, Table 2, p.66
16	Supra_R	FFG_740	1015.60	Richey, 1989, Table 2, p.66
17	Supra_R	FFG_741	1014.70	Richey, 1989, Table 2, p.66
18	Supra_R	FFG_742	1023.80	Richey, 1989, Table 2, p.67
19	Supra_R	FFG_743	1013.20	Richey, 1989, Table 2, p.67
20	Supra_R	FFG_744	1012.50	Richey, 1989, Table 2, p.67
21	Supra_R	FFG_745	1006.40	Richey, 1989, Table 2, p.67
22	Supra_R	FFG_746	1007.50	Richey, 1989, Table 2, p.67
23	Supra_R	H1	1035.70	Mercer, 1983, Table 1
24	Supra_R	H10C	1123.80	Mercer, 1983, Table 1
25	Supra_R	H2C	1029.60	Mercer, 1983, Table 1
26	Supra_R	H3	1033.30	Mercer, 1983, Table 1
27	Supra_R	H4C	1016.20	Mercer, 1983, Table 1
28	Supra_R	H5C	1068.90	Mercer, 1983, Table 1
29	Supra_R	H6C	1020.50	Mercer, 1983, Table 1
30	Supra_R	H7C	964.10	Mercer, 1983, Table 1
31	Supra_R	H8C	1046.40	Mercer, 1983, Table 1
32	Supra_R	H9C	1038.10	Mercer, 1983, Table 1
33	Supra_R	P1	1019.60	Mercer, 1983, Table 1
34	Supra_R	P10	1069.50	Mercer, 1983, Table 1
35	Supra_R	P11	1068.00	Mercer, 1983, Table 1
36	Supra_R	P12	1028.40	Mercer, 1983, Table 1
37	Supra_R	P13	1019.60	Mercer, 1983, Table 1
38	Supra_R	P14	1024.10	Mercer, 1983, Table 1
39	Supra_R	P15	1008.90	Mercer, 1983, Table 1
40	Supra_R	P16	1011.30	Mercer, 1983, Table 1
41	Supra_R	P17	1016.80	Mercer, 1983, Table 1
42	Supra_R	P18	1059.80	Mercer, 1983, Table 1
43	Supra_R	P19	1080.50	Mercer, 1983, Table 1
44	Supra_R	P2	1060.40	Mercer, 1983, Table 1
45	Supra_R	P20	1083.00	Mercer, 1983, Table 1
46	Supra_R	P21	1069.50	Mercer, 1983, Table 1
47	Supra_R	P3	1031.10	Mercer, 1983, Table 1
48	Supra_R	P4	1049.70	Mercer, 1983, Table 1
49	Supra_R	P5	1058.00	Mercer, 1983, Table 1
50	Supra_R	P6	1022.30	Mercer, 1983, Table 1
51	Supra_R	P7	1015.60	Mercer, 1983, Table 1
52	Supra_R	P8	1017.70	Mercer, 1983, Table 1
53	Supra_R	P9	1040.00	Mercer, 1983, Table 1
54	Supra_R	WIPP11	1044.20	Mercer, 1983, Table 1
55	Supra_R	WIPP12	1058.30	Mercer, 1983, Table 1
56	Supra_R	WIPP13	1037.80	Mercer, 1983, Table 1
57	Supra_R	WIPP15	996.40	Mercer, 1983, Table 1
58	Supra_R	WIPP16	1031.10	Mercer, 1983, Table 1
59	Supra_R	WIPP18	1053.40	Mercer, 1983, Table 1
60	Supra_R	WIPP19	1046.40	Mercer, 1983, Table 1
61	Supra_R	WIPP21	1041.50	Mercer, 1983, Table 1
62	Supra_R	WIPP22	1044.20	Mercer, 1983, Table 1
63	Supra_R	WIPP25	979.30	Mercer, 1983, Table 1
64	Supra_R	WIPP26	960.70	Mercer, 1983, Table 1
65	Supra_R	WIPP27	968.30	Mercer, 1983, Table 1
66	Supra_R	WIPP28	1020.20	Mercer, 1983, Table 1
67	Supra_R	WIPP29	907.40	Mercer, 1983, Table 1
68	Supra_R	WIPP30	1044.90	Mercer, 1983, Table 1
69	Supra_R	WIPP32	921.40	Mercer, 1983, Table 1
70	Supra_R	WIPP33	1012.90	Mercer, 1983, Table 1
71	Supra_R	WIPP34	1046.40	Mercer, 1983, Table 1
72	Tamarisk	AEC7	882.40	Mercer, 1983, Table 1
73	Tamarisk	AEC8	851.70	Mercer, 1983, Table 1
74	Tamarisk	AirShft	850.99	Holt and Powers, 1990, Figure 22
75	Tamarisk	B25	851.00	Mercer, 1983, Table 1
76	Tamarisk	ERDA10	910.20	Mercer, 1983, Table 1

Table B.2. Elevations of Stratigraphic Layers Near WIPP (Continued)

	Layer	Well ID	Elevation	Source
1	Tamarisk	ERDA6	889.70	Mercer, 1983, Table 1
2	Tamarisk	ERDA9	853.10	Mercer, 1983, Table 1
3	Tamarisk	ExhtShft	847.97	Bechtel, Inc., 1986, Appendix F
4	Tamarisk	FFG_002	660.50	Richey, 1989, Table 2, p.21
5	Tamarisk	FFG_004	710.80	Richey, 1989, Table 2, p.21
6	Tamarisk	FFG_005	667.90	Richey, 1989, Table 2, p.21
7	Tamarisk	FFG_006	661.40	Richey, 1989, Table 2, p.21
8	Tamarisk	FFG_007	649.80	Richey, 1989, Table 2, p.21
9	Tamarisk	FFG_009	650.10	Richey, 1989, Table 2, p.21
10	Tamarisk	FFG_011	657.10	Richey, 1989, Table 2, p.21
11	Tamarisk	FFG_012	659.60	Richey, 1989, Table 2, p.21
12	Tamarisk	FFG_013	667.80	Richey, 1989, Table 2, p.21
13	Tamarisk	FFG_014	713.50	Richey, 1989, Table 2, p.21
14	Tamarisk	FFG_016	637.60	Richey, 1989, Table 2, p.21
15	Tamarisk	FFG_017	640.70	Richey, 1989, Table 2, p.22
16	Tamarisk	FFG_018	645.90	Richey, 1989, Table 2, p.22
17	Tamarisk	FFG_019	637.60	Richey, 1989, Table 2, p.22
18	Tamarisk	FFG_020	712.30	Richey, 1989, Table 2, p.22
19	Tamarisk	FFG_023	647.40	Richey, 1989, Table 2, p.22
20	Tamarisk	FFG_024	632.10	Richey, 1989, Table 2, p.22
21	Tamarisk	FFG_025	646.10	Richey, 1989, Table 2, p.22
22	Tamarisk	FFG_026	643.40	Richey, 1989, Table 2, p.22
23	Tamarisk	FFG_027	636.40	Richey, 1989, Table 2, p.22
24	Tamarisk	FFG_028	607.50	Richey, 1989, Table 2, p.22
25	Tamarisk	FFG_029	594.00	Richey, 1989, Table 2, p.22
26	Tamarisk	FFG_030	592.90	Richey, 1989, Table 2, p.22
27	Tamarisk	FFG_031	584.00	Richey, 1989, Table 2, p.22
28	Tamarisk	FFG_032	586.00	Richey, 1989, Table 2, p.22
29	Tamarisk	FFG_033	582.80	Richey, 1989, Table 2, p.22
30	Tamarisk	FFG_034	577.90	Richey, 1989, Table 2, p.23
31	Tamarisk	FFG_035	566.50	Richey, 1989, Table 2, p.23
32	Tamarisk	FFG_036	576.70	Richey, 1989, Table 2, p.23
33	Tamarisk	FFG_037	566.90	Richey, 1989, Table 2, p.23
34	Tamarisk	FFG_038	554.10	Richey, 1989, Table 2, p.23
35	Tamarisk	FFG_039	772.10	Richey, 1989, Table 2, p.23
36	Tamarisk	FFG_040	713.60	Richey, 1989, Table 2, p.23
37	Tamarisk	FFG_041	773.60	Richey, 1989, Table 2, p.23
38	Tamarisk	FFG_042	777.80	Richey, 1989, Table 2, p.23
39	Tamarisk	FFG_043	782.00	Richey, 1989, Table 2, p.23
40	Tamarisk	FFG_044	733.60	Richey, 1989, Table 2, p.23
41	Tamarisk	FFG_047	607.50	Richey, 1989, Table 2, p.23
42	Tamarisk	FFG_048	623.30	Richey, 1989, Table 2, p.23
43	Tamarisk	FFG_049	614.80	Richey, 1989, Table 2, p.23
44	Tamarisk	FFG_050	621.50	Richey, 1989, Table 2, p.24
45	Tamarisk	FFG_051	622.10	Richey, 1989, Table 2, p.24
46	Tamarisk	FFG_052	624.20	Richey, 1989, Table 2, p.24
47	Tamarisk	FFG_053	615.40	Richey, 1989, Table 2, p.24
48	Tamarisk	FFG_054	613.30	Richey, 1989, Table 2, p.24
49	Tamarisk	FFG_055	612.60	Richey, 1989, Table 2, p.24
50	Tamarisk	FFG_056	615.40	Richey, 1989, Table 2, p.24
51	Tamarisk	FFG_057	617.60	Richey, 1989, Table 2, p.24
52	Tamarisk	FFG_058	615.10	Richey, 1989, Table 2, p.24
53	Tamarisk	FFG_059	617.50	Richey, 1989, Table 2, p.24
54	Tamarisk	FFG_060	618.10	Richey, 1989, Table 2, p.24
55	Tamarisk	FFG_061	619.90	Richey, 1989, Table 2, p.24
56	Tamarisk	FFG_062	547.10	Richey, 1989, Table 2, p.24
57	Tamarisk	FFG_063	508.50	Richey, 1989, Table 2, p.24
58	Tamarisk	FFG_064	531.90	Richey, 1989, Table 2, p.24
59	Tamarisk	FFG_065	515.40	Richey, 1989, Table 2, p.24
60	Tamarisk	FFG_066	469.40	Richey, 1989, Table 2, p.24
61	Tamarisk	FFG_067	511.20	Richey, 1989, Table 2, p.25
62	Tamarisk	FFG_068	475.80	Richey, 1989, Table 2, p.25
63	Tamarisk	FFG_069	496.30	Richey, 1989, Table 2, p.25
64	Tamarisk	FFG_070	526.10	Richey, 1989, Table 2, p.25
65	Tamarisk	FFG_071	784.30	Richey, 1989, Table 2, p.25
66	Tamarisk	FFG_072	715.00	Richey, 1989, Table 2, p.25
67	Tamarisk	FFG_073	690.60	Richey, 1989, Table 2, p.25
68	Tamarisk	FFG_074	698.40	Richey, 1989, Table 2, p.25
69	Tamarisk	FFG_075	749.20	Richey, 1989, Table 2, p.25
70	Tamarisk	FFG_076	810.50	Richey, 1989, Table 2, p.25
71	Tamarisk	FFG_078	847.00	Richey, 1989, Table 2, p.25
72	Tamarisk	FFG_079	823.60	Richey, 1989, Table 2, p.25
73	Tamarisk	FFG_080	800.40	Richey, 1989, Table 2, p.25
74	Tamarisk	FFG_081	720.90	Richey, 1989, Table 2, p.26
75	Tamarisk	FFG_082	753.20	Richey, 1989, Table 2, p.26
76	Tamarisk	FFG_083	668.60	Richey, 1989, Table 2, p.26

Table B.2. Elevations of Stratigraphic Layers Near WIPP (Continued)

	Layer	Well ID	Elevation	Source
2	Tamarisk	FFG_084	694.60	Richey, 1989, Table 2, p.26
3	Tamarisk	FFG_085	687.40	Richey, 1989, Table 2, p.26
4	Tamarisk	FFG_086	697.30	Richey, 1989, Table 2, p.26
5	Tamarisk	FFG_087	671.40	Richey, 1989, Table 2, p.26
6	Tamarisk	FFG_088	667.20	Richey, 1989, Table 2, p.26
7	Tamarisk	FFG_089	649.60	Richey, 1989, Table 2, p.26
8	Tamarisk	FFG_091	692.80	Richey, 1989, Table 2, p.26
9	Tamarisk	FFG_092	706.50	Richey, 1989, Table 2, p.26
10	Tamarisk	FFG_093	710.20	Richey, 1989, Table 2, p.26
11	Tamarisk	FFG_094	713.20	Richey, 1989, Table 2, p.26
12	Tamarisk	FFG_095	681.50	Richey, 1989, Table 2, p.26
13	Tamarisk	FFG_096	665.10	Richey, 1989, Table 2, p.26
14	Tamarisk	FFG_097	645.00	Richey, 1989, Table 2, p.27
15	Tamarisk	FFG_098	619.90	Richey, 1989, Table 2, p.27
16	Tamarisk	FFG_099	615.40	Richey, 1989, Table 2, p.27
17	Tamarisk	FFG_100	598.10	Richey, 1989, Table 2, p.27
18	Tamarisk	FFG_101	569.40	Richey, 1989, Table 2, p.27
19	Tamarisk	FFG_102	587.40	Richey, 1989, Table 2, p.27
20	Tamarisk	FFG_103	652.00	Richey, 1989, Table 2, p.27
21	Tamarisk	FFG_104	545.00	Richey, 1989, Table 2, p.27
22	Tamarisk	FFG_105	901.30	Richey, 1989, Table 2, p.27
23	Tamarisk	FFG_106	931.80	Richey, 1989, Table 2, p.27
24	Tamarisk	FFG_107	916.90	Richey, 1989, Table 2, p.27
25	Tamarisk	FFG_108	912.30	Richey, 1989, Table 2, p.27
26	Tamarisk	FFG_109	892.80	Richey, 1989, Table 2, p.27
27	Tamarisk	FFG_110	859.60	Richey, 1989, Table 2, p.27
28	Tamarisk	FFG_111	867.10	Richey, 1989, Table 2, p.27
29	Tamarisk	FFG_112	854.90	Richey, 1989, Table 2, p.28
30	Tamarisk	FFG_113	869.00	Richey, 1989, Table 2, p.28
31	Tamarisk	FFG_114	898.30	Richey, 1989, Table 2, p.28
32	Tamarisk	FFG_115	889.40	Richey, 1989, Table 2, p.28
33	Tamarisk	FFG_116	904.90	Richey, 1989, Table 2, p.28
34	Tamarisk	FFG_117	902.20	Richey, 1989, Table 2, p.28
35	Tamarisk	FFG_119	937.90	Richey, 1989, Table 2, p.28
36	Tamarisk	FFG_120	913.80	Richey, 1989, Table 2, p.28
37	Tamarisk	FFG_121	922.00	Richey, 1989, Table 2, p.28
38	Tamarisk	FFG_122	920.50	Richey, 1989, Table 2, p.28
39	Tamarisk	FFG_123	894.50	Richey, 1989, Table 2, p.28
40	Tamarisk	FFG_124	857.70	Richey, 1989, Table 2, p.28
41	Tamarisk	FFG_125	883.20	Richey, 1989, Table 2, p.28
42	Tamarisk	FFG_126	880.10	Richey, 1989, Table 2, p.28
43	Tamarisk	FFG_127	885.10	Richey, 1989, Table 2, p.28
44	Tamarisk	FFG_128	917.50	Richey, 1989, Table 2, p.28
45	Tamarisk	FFG_129	893.30	Richey, 1989, Table 2, p.28
46	Tamarisk	FFG_130	920.50	Richey, 1989, Table 2, p.28
47	Tamarisk	FFG_132	929.00	Richey, 1989, Table 2, p.29
48	Tamarisk	FFG_133	932.00	Richey, 1989, Table 2, p.29
49	Tamarisk	FFG_134	935.50	Richey, 1989, Table 2, p.29
50	Tamarisk	FFG_135	910.80	Richey, 1989, Table 2, p.29
51	Tamarisk	FFG_136	911.50	Richey, 1989, Table 2, p.29
52	Tamarisk	FFG_137	919.30	Richey, 1989, Table 2, p.29
53	Tamarisk	FFG_138	874.50	Richey, 1989, Table 2, p.29
54	Tamarisk	FFG_139	882.40	Richey, 1989, Table 2, p.29
55	Tamarisk	FFG_140	823.10	Richey, 1989, Table 2, p.29
56	Tamarisk	FFG_141	845.70	Richey, 1989, Table 2, p.29
57	Tamarisk	FFG_142	821.80	Richey, 1989, Table 2, p.29
58	Tamarisk	FFG_143	831.70	Richey, 1989, Table 2, p.29
59	Tamarisk	FFG_144	903.50	Richey, 1989, Table 2, p.29
60	Tamarisk	FFG_145	905.30	Richey, 1989, Table 2, p.29
61	Tamarisk	FFG_146	912.90	Richey, 1989, Table 2, p.29
62	Tamarisk	FFG_147	893.70	Richey, 1989, Table 2, p.29
63	Tamarisk	FFG_148	907.70	Richey, 1989, Table 2, p.29
64	Tamarisk	FFG_149	912.20	Richey, 1989, Table 2, p.30
65	Tamarisk	FFG_155	905.60	Richey, 1989, Table 2, p.30
66	Tamarisk	FFG_157	907.10	Richey, 1989, Table 2, p.30
67	Tamarisk	FFG_158	931.10	Richey, 1989, Table 2, p.30
68	Tamarisk	FFG_159	928.80	Richey, 1989, Table 2, p.30
69	Tamarisk	FFG_160	924.20	Richey, 1989, Table 2, p.30
70	Tamarisk	FFG_161	930.00	Richey, 1989, Table 2, p.30
71	Tamarisk	FFG_162	925.40	Richey, 1989, Table 2, p.30
72	Tamarisk	FFG_163	927.80	Richey, 1989, Table 2, p.30
73	Tamarisk	FFG_164	955.90	Richey, 1989, Table 2, p.30
74	Tamarisk	FFG_165	935.70	Richey, 1989, Table 2, p.30
75	Tamarisk	FFG_166	928.40	Richey, 1989, Table 2, p.31
76	Tamarisk	FFG_167	914.40	Richey, 1989, Table 2, p.31
77	Tamarisk	FFG_168	933.90	Richey, 1989, Table 2, p.31

Table B.2. Elevations of Stratigraphic Layers Near WIPP (Continued)

	Layer	Well ID	Elevation	Source
1	Tamarisk	FFG_169	949.10	Richey, 1989, Table 2, p.31
2	Tamarisk	FFG_170	916.80	Richey, 1989, Table 2, p.31
3	Tamarisk	FFG_171	924.20	Richey, 1989, Table 2, p.31
4	Tamarisk	FFG_172	933.00	Richey, 1989, Table 2, p.31
5	Tamarisk	FFG_173	906.50	Richey, 1989, Table 2, p.31
6	Tamarisk	FFG_180	915.00	Richey, 1989, Table 2, p.31
7	Tamarisk	FFG_181	946.70	Richey, 1989, Table 2, p.32
8	Tamarisk	FFG_182	842.40	Richey, 1989, Table 2, p.32
9	Tamarisk	FFG_183	939.10	Richey, 1989, Table 2, p.32
10	Tamarisk	FFG_184	924.80	Richey, 1989, Table 2, p.32
11	Tamarisk	FFG_185	929.90	Richey, 1989, Table 2, p.32
12	Tamarisk	FFG_186	857.70	Richey, 1989, Table 2, p.32
13	Tamarisk	FFG_188	869.00	Richey, 1989, Table 2, p.32
14	Tamarisk	FFG_189	894.30	Richey, 1989, Table 2, p.32
15	Tamarisk	FFG_190	874.70	Richey, 1989, Table 2, p.32
16	Tamarisk	FFG_191	870.50	Richey, 1989, Table 2, p.32
17	Tamarisk	FFG_192	806.50	Richey, 1989, Table 2, p.32
18	Tamarisk	FFG_194	815.60	Richey, 1989, Table 2, p.33
19	Tamarisk	FFG_195	828.80	Richey, 1989, Table 2, p.33
20	Tamarisk	FFG_196	869.90	Richey, 1989, Table 2, p.33
21	Tamarisk	FFG_197	870.80	Richey, 1989, Table 2, p.33
22	Tamarisk	FFG_198	871.40	Richey, 1989, Table 2, p.33
23	Tamarisk	FFG_199	859.90	Richey, 1989, Table 2, p.33
24	Tamarisk	FFG_200	873.00	Richey, 1989, Table 2, p.33
25	Tamarisk	FFG_201	865.60	Richey, 1989, Table 2, p.33
26	Tamarisk	FFG_202	808.30	Richey, 1989, Table 2, p.33
27	Tamarisk	FFG_203	815.70	Richey, 1989, Table 2, p.33
28	Tamarisk	FFG_204	837.90	Richey, 1989, Table 2, p.33
29	Tamarisk	FFG_205	853.20	Richey, 1989, Table 2, p.33
30	Tamarisk	FFG_206	867.40	Richey, 1989, Table 2, p.33
31	Tamarisk	FFG_207	865.00	Richey, 1989, Table 2, p.33
32	Tamarisk	FFG_208	874.20	Richey, 1989, Table 2, p.34
33	Tamarisk	FFG_209	866.20	Richey, 1989, Table 2, p.34
34	Tamarisk	FFG_210	858.90	Richey, 1989, Table 2, p.34
35	Tamarisk	FFG_212	845.20	Richey, 1989, Table 2, p.34
36	Tamarisk	FFG_213	868.40	Richey, 1989, Table 2, p.34
37	Tamarisk	FFG_214	848.20	Richey, 1989, Table 2, p.34
38	Tamarisk	FFG_215	823.60	Richey, 1989, Table 2, p.34
39	Tamarisk	FFG_216	710.40	Richey, 1989, Table 2, p.34
40	Tamarisk	FFG_217	843.70	Richey, 1989, Table 2, p.34
41	Tamarisk	FFG_218	835.80	Richey, 1989, Table 2, p.34
42	Tamarisk	FFG_219	879.90	Richey, 1989, Table 2, p.34
43	Tamarisk	FFG_220	832.20	Richey, 1989, Table 2, p.34
44	Tamarisk	FFG_221	787.00	Richey, 1989, Table 2, p.34
45	Tamarisk	FFG_222	741.60	Richey, 1989, Table 2, p.34
46	Tamarisk	FFG_224	648.10	Richey, 1989, Table 2, p.35
47	Tamarisk	FFG_225	656.30	Richey, 1989, Table 2, p.35
48	Tamarisk	FFG_226	654.00	Richey, 1989, Table 2, p.35
49	Tamarisk	FFG_228	643.20	Richey, 1989, Table 2, p.35
50	Tamarisk	FFG_229	672.00	Richey, 1989, Table 2, p.35
51	Tamarisk	FFG_230	658.10	Richey, 1989, Table 2, p.35
52	Tamarisk	FFG_231	674.20	Richey, 1989, Table 2, p.35
53	Tamarisk	FFG_232	688.20	Richey, 1989, Table 2, p.35
54	Tamarisk	FFG_233	678.80	Richey, 1989, Table 2, p.35
55	Tamarisk	FFG_234	715.00	Richey, 1989, Table 2, p.35
56	Tamarisk	FFG_235	691.30	Richey, 1989, Table 2, p.35
57	Tamarisk	FFG_236	738.50	Richey, 1989, Table 2, p.35
58	Tamarisk	FFG_237	704.80	Richey, 1989, Table 2, p.35
59	Tamarisk	FFG_238	685.50	Richey, 1989, Table 2, p.36
60	Tamarisk	FFG_239	673.30	Richey, 1989, Table 2, p.36
61	Tamarisk	FFG_240	664.50	Richey, 1989, Table 2, p.36
62	Tamarisk	FFG_241	659.00	Richey, 1989, Table 2, p.36
63	Tamarisk	FFG_242	776.70	Richey, 1989, Table 2, p.36
64	Tamarisk	FFG_243	735.50	Richey, 1989, Table 2, p.36
65	Tamarisk	FFG_244	773.10	Richey, 1989, Table 2, p.36
66	Tamarisk	FFG_245	566.90	Richey, 1989, Table 2, p.36
67	Tamarisk	FFG_246	573.00	Richey, 1989, Table 2, p.36
68	Tamarisk	FFG_247	558.00	Richey, 1989, Table 2, p.36
69	Tamarisk	FFG_248	566.00	Richey, 1989, Table 2, p.36
70	Tamarisk	FFG_249	564.20	Richey, 1989, Table 2, p.36
71	Tamarisk	FFG_250	644.50	Richey, 1989, Table 2, p.36
72	Tamarisk	FFG_251	538.50	Richey, 1989, Table 2, p.36
73	Tamarisk	FFG_252	677.80	Richey, 1989, Table 2, p.36
74	Tamarisk	FFG_253	632.50	Richey, 1989, Table 2, p.36
75	Tamarisk	FFG_254	623.90	Richey, 1989, Table 2, p.36
76	Tamarisk	FFG_255	580.10	Richey, 1989, Table 2, p.37

Table B.2. Elevations of Stratigraphic Layers Near WIPP (Continued)

	Layer	Well ID	Elevation	Source
1	Tamarisk	FFG_256	529.80	Richey, 1989, Table 2, p.37
2	Tamarisk	FFG_257	573.60	Richey, 1989, Table 2, p.37
3	Tamarisk	FFG_258	587.60	Richey, 1989, Table 2, p.37
4	Tamarisk	FFG_259	553.50	Richey, 1989, Table 2, p.37
5	Tamarisk	FFG_260	597.40	Richey, 1989, Table 2, p.37
6	Tamarisk	FFG_261	586.40	Richey, 1989, Table 2, p.37
7	Tamarisk	FFG_262	1109.50	Richey, 1989, Table 2, p.37
8	Tamarisk	FFG_263	521.10	Richey, 1989, Table 2, p.37
9	Tamarisk	FFG_264	753.20	Richey, 1989, Table 2, p.37
10	Tamarisk	FFG_265	749.80	Richey, 1989, Table 2, p.37
11	Tamarisk	FFG_266	730.90	Richey, 1989, Table 2, p.37
12	Tamarisk	FFG_267	708.30	Richey, 1989, Table 2, p.37
13	Tamarisk	FFG_268	684.60	Richey, 1989, Table 2, p.37
14	Tamarisk	FFG_269	696.90	Richey, 1989, Table 2, p.38
15	Tamarisk	FFG_270	769.30	Richey, 1989, Table 2, p.38
16	Tamarisk	FFG_271	808.90	Richey, 1989, Table 2, p.38
17	Tamarisk	FFG_272	816.40	Richey, 1989, Table 2, p.38
18	Tamarisk	FFG_273	790.10	Richey, 1989, Table 2, p.38
19	Tamarisk	FFG_274	827.20	Richey, 1989, Table 2, p.38
20	Tamarisk	FFG_275	834.30	Richey, 1989, Table 2, p.38
21	Tamarisk	FFG_276	837.60	Richey, 1989, Table 2, p.38
22	Tamarisk	FFG_277	829.10	Richey, 1989, Table 2, p.38
23	Tamarisk	FFG_278	838.50	Richey, 1989, Table 2, p.38
24	Tamarisk	FFG_279	833.30	Richey, 1989, Table 2, p.38
25	Tamarisk	FFG_280	830.90	Richey, 1989, Table 2, p.38
26	Tamarisk	FFG_281	807.40	Richey, 1989, Table 2, p.38
27	Tamarisk	FFG_283	558.10	Richey, 1989, Table 2, p.39
28	Tamarisk	FFG_284	705.90	Richey, 1989, Table 2, p.39
29	Tamarisk	FFG_285	734.90	Richey, 1989, Table 2, p.39
30	Tamarisk	FFG_286	814.10	Richey, 1989, Table 2, p.39
31	Tamarisk	FFG_287	786.10	Richey, 1989, Table 2, p.39
32	Tamarisk	FFG_288	738.80	Richey, 1989, Table 2, p.39
33	Tamarisk	FFG_289	713.80	Richey, 1989, Table 2, p.39
34	Tamarisk	FFG_290	799.50	Richey, 1989, Table 2, p.39
35	Tamarisk	FFG_291	736.70	Richey, 1989, Table 2, p.39
36	Tamarisk	FFG_292	752.30	Richey, 1989, Table 2, p.39
37	Tamarisk	FFG_293	744.60	Richey, 1989, Table 2, p.39
38	Tamarisk	FFG_294	567.00	Richey, 1989, Table 2, p.39
39	Tamarisk	FFG_295	554.70	Richey, 1989, Table 2, p.39
40	Tamarisk	FFG_297	532.50	Richey, 1989, Table 2, p.39
41	Tamarisk	FFG_298	546.70	Richey, 1989, Table 2, p.40
42	Tamarisk	FFG_299	564.20	Richey, 1989, Table 2, p.40
43	Tamarisk	FFG_300	515.40	Richey, 1989, Table 2, p.40
44	Tamarisk	FFG_301	485.60	Richey, 1989, Table 2, p.40
45	Tamarisk	FFG_302	514.20	Richey, 1989, Table 2, p.40
46	Tamarisk	FFG_303	505.10	Richey, 1989, Table 2, p.40
47	Tamarisk	FFG_304	512.90	Richey, 1989, Table 2, p.40
48	Tamarisk	FFG_305	503.20	Richey, 1989, Table 2, p.40
49	Tamarisk	FFG_306	465.10	Richey, 1989, Table 2, p.40
50	Tamarisk	FFG_307	488.00	Richey, 1989, Table 2, p.40
51	Tamarisk	FFG_308	460.50	Richey, 1989, Table 2, p.40
52	Tamarisk	FFG_309	503.20	Richey, 1989, Table 2, p.40
53	Tamarisk	FFG_310	534.60	Richey, 1989, Table 2, p.40
54	Tamarisk	FFG_311	481.00	Richey, 1989, Table 2, p.40
55	Tamarisk	FFG_312	504.50	Richey, 1989, Table 2, p.40
56	Tamarisk	FFG_313	908.10	Richey, 1989, Table 2, p.41
57	Tamarisk	FFG_314	836.10	Richey, 1989, Table 2, p.41
58	Tamarisk	FFG_315	758.50	Richey, 1989, Table 2, p.41
59	Tamarisk	FFG_316	742.10	Richey, 1989, Table 2, p.41
60	Tamarisk	FFG_317	772.70	Richey, 1989, Table 2, p.41
61	Tamarisk	FFG_318	734.60	Richey, 1989, Table 2, p.41
62	Tamarisk	FFG_319	745.80	Richey, 1989, Table 2, p.41
63	Tamarisk	FFG_320	735.50	Richey, 1989, Table 2, p.41
64	Tamarisk	FFG_321	732.10	Richey, 1989, Table 2, p.41
65	Tamarisk	FFG_322	727.40	Richey, 1989, Table 2, p.41
66	Tamarisk	FFG_323	723.40	Richey, 1989, Table 2, p.41
67	Tamarisk	FFG_324	738.00	Richey, 1989, Table 2, p.41
68	Tamarisk	FFG_325	793.40	Richey, 1989, Table 2, p.41
69	Tamarisk	FFG_326	729.10	Richey, 1989, Table 2, p.41
70	Tamarisk	FFG_327	723.60	Richey, 1989, Table 2, p.42
71	Tamarisk	FFG_328	728.70	Richey, 1989, Table 2, p.42
72	Tamarisk	FFG_329	728.40	Richey, 1989, Table 2, p.42
73	Tamarisk	FFG_330	728.00	Richey, 1989, Table 2, p.42
74	Tamarisk	FFG_331	722.70	Richey, 1989, Table 2, p.42
75	Tamarisk	FFG_332	713.80	Richey, 1989, Table 2, p.42
76	Tamarisk	FFG_333	717.30	Richey, 1989, Table 2, p.42

Table B.2. Elevations of Stratigraphic Layers Near WIPP (Continued)

	Layer	Well ID	Elevation	Source
1	Tamarisk	FFG_334	712.60	Richey, 1989, Table 2, p.42
2	Tamarisk	FFG_335	724.80	Richey, 1989, Table 2, p.42
3	Tamarisk	FFG_336	725.10	Richey, 1989, Table 2, p.42
4	Tamarisk	FFG_337	708.00	Richey, 1989, Table 2, p.42
5	Tamarisk	FFG_338	715.20	Richey, 1989, Table 2, p.42
6	Tamarisk	FFG_339	680.30	Richey, 1989, Table 2, p.42
7	Tamarisk	FFG_340	688.80	Richey, 1989, Table 2, p.42
8	Tamarisk	FFG_342	720.20	Richey, 1989, Table 2, p.43
9	Tamarisk	FFG_344	685.10	Richey, 1989, Table 2, p.43
10	Tamarisk	FFG_345	746.60	Richey, 1989, Table 2, p.43
11	Tamarisk	FFG_347	736.70	Richey, 1989, Table 2, p.43
12	Tamarisk	FFG_348	768.10	Richey, 1989, Table 2, p.43
13	Tamarisk	FFG_349	738.00	Richey, 1989, Table 2, p.43
14	Tamarisk	FFG_350	783.00	Richey, 1989, Table 2, p.43
15	Tamarisk	FFG_351	701.10	Richey, 1989, Table 2, p.43
16	Tamarisk	FFG_352	699.50	Richey, 1989, Table 2, p.43
17	Tamarisk	FFG_353	721.20	Richey, 1989, Table 2, p.43
18	Tamarisk	FFG_354	795.30	Richey, 1989, Table 2, p.43
19	Tamarisk	FFG_361	982.60	Richey, 1989, Table 2, p.44
20	Tamarisk	FFG_362	956.40	Richey, 1989, Table 2, p.44
21	Tamarisk	FFG_363	972.90	Richey, 1989, Table 2, p.44
22	Tamarisk	FFG_364	942.70	Richey, 1989, Table 2, p.44
23	Tamarisk	FFG_366	933.90	Richey, 1989, Table 2, p.44
24	Tamarisk	FFG_367	948.50	Richey, 1989, Table 2, p.44
25	Tamarisk	FFG_370	1012.90	Richey, 1989, Table 2, p.44
26	Tamarisk	FFG_371	994.60	Richey, 1989, Table 2, p.44
27	Tamarisk	FFG_372	1006.40	Richey, 1989, Table 2, p.45
28	Tamarisk	FFG_373	945.00	Richey, 1989, Table 2, p.45
29	Tamarisk	FFG_374	929.70	Richey, 1989, Table 2, p.45
30	Tamarisk	FFG_376	984.80	Richey, 1989, Table 2, p.45
31	Tamarisk	FFG_381	1021.40	Richey, 1989, Table 2, p.45
32	Tamarisk	FFG_383	931.20	Richey, 1989, Table 2, p.45
33	Tamarisk	FFG_384	937.90	Richey, 1989, Table 2, p.45
34	Tamarisk	FFG_385	922.00	Richey, 1989, Table 2, p.45
35	Tamarisk	FFG_387	934.60	Richey, 1989, Table 2, p.45
36	Tamarisk	FFG_388	929.40	Richey, 1989, Table 2, p.46
37	Tamarisk	FFG_389	976.60	Richey, 1989, Table 2, p.46
38	Tamarisk	FFG_390	945.50	Richey, 1989, Table 2, p.46
39	Tamarisk	FFG_391	944.50	Richey, 1989, Table 2, p.46
40	Tamarisk	FFG_392	941.90	Richey, 1989, Table 2, p.46
41	Tamarisk	FFG_393	810.60	Richey, 1989, Table 2, p.46
42	Tamarisk	FFG_394	903.10	Richey, 1989, Table 2, p.46
43	Tamarisk	FFG_395	895.80	Richey, 1989, Table 2, p.46
44	Tamarisk	FFG_396	877.20	Richey, 1989, Table 2, p.46
45	Tamarisk	FFG_398	798.50	Richey, 1989, Table 2, p.46
46	Tamarisk	FFG_399	838.50	Richey, 1989, Table 2, p.46
47	Tamarisk	FFG_401	874.80	Richey, 1989, Table 2, p.46
48	Tamarisk	FFG_402	972.00	Richey, 1989, Table 2, p.46
49	Tamarisk	FFG_403	935.30	Richey, 1989, Table 2, p.47
50	Tamarisk	FFG_404	897.40	Richey, 1989, Table 2, p.47
51	Tamarisk	FFG_407	932.40	Richey, 1989, Table 2, p.47
52	Tamarisk	FFG_408	908.60	Richey, 1989, Table 2, p.47
53	Tamarisk	FFG_409	970.50	Richey, 1989, Table 2, p.47
54	Tamarisk	FFG_418	983.30	Richey, 1989, Table 2, p.48
55	Tamarisk	FFG_419	969.00	Richey, 1989, Table 2, p.48
56	Tamarisk	FFG_420	964.30	Richey, 1989, Table 2, p.48
57	Tamarisk	FFG_421	955.00	Richey, 1989, Table 2, p.48
58	Tamarisk	FFG_422	946.10	Richey, 1989, Table 2, p.48
59	Tamarisk	FFG_426	962.00	Richey, 1989, Table 2, p.48
60	Tamarisk	FFG_432	918.00	Richey, 1989, Table 2, p.48
61	Tamarisk	FFG_433	920.50	Richey, 1989, Table 2, p.48
62	Tamarisk	FFG_438	866.70	Richey, 1989, Table 2, p.49
63	Tamarisk	FFG_453	862.20	Richey, 1989, Table 2, p.50
64	Tamarisk	FFG_455	810.40	Richey, 1989, Table 2, p.50
65	Tamarisk	FFG_456	805.20	Richey, 1989, Table 2, p.50
66	Tamarisk	FFG_457	861.30	Richey, 1989, Table 2, p.50
67	Tamarisk	FFG_458	862.30	Richey, 1989, Table 2, p.50
68	Tamarisk	FFG_459	791.90	Richey, 1989, Table 2, p.50
69	Tamarisk	FFG_462	857.50	Richey, 1989, Table 2, p.50
70	Tamarisk	FFG_463	886.40	Richey, 1989, Table 2, p.51
71	Tamarisk	FFG_464	872.30	Richey, 1989, Table 2, p.51
72	Tamarisk	FFG_465	875.30	Richey, 1989, Table 2, p.51
73	Tamarisk	FFG_467	483.30	Richey, 1989, Table 2, p.51
74	Tamarisk	FFG_468	460.00	Richey, 1989, Table 2, p.51
75	Tamarisk	FFG_470	480.10	Richey, 1989, Table 2, p.51
76	Tamarisk	FFG_471	495.00	Richey, 1989, Table 2, p.51

Table B.2. Elevations of Stratigraphic Layers Near WIPP (Continued)

	Layer	Well ID	Elevation	Source
1	Tamarisk	FFG_472	532.80	Richey, 1989, Table 2, p.51
2	Tamarisk	FFG_473	463.60	Richey, 1989, Table 2, p.51
3	Tamarisk	FFG_474	723.30	Richey, 1989, Table 2, p.51
4	Tamarisk	FFG_475	723.80	Richey, 1989, Table 2, p.51
5	Tamarisk	FFG_476	797.40	Richey, 1989, Table 2, p.51
6	Tamarisk	FFG_477	751.70	Richey, 1989, Table 2, p.51
7	Tamarisk	FFG_478	733.60	Richey, 1989, Table 2, p.52
8	Tamarisk	FFG_479	730.00	Richey, 1989, Table 2, p.52
9	Tamarisk	FFG_480	726.40	Richey, 1989, Table 2, p.52
10	Tamarisk	FFG_481	709.00	Richey, 1989, Table 2, p.52
11	Tamarisk	FFG_482	738.60	Richey, 1989, Table 2, p.52
12	Tamarisk	FFG_483	761.40	Richey, 1989, Table 2, p.52
13	Tamarisk	FFG_484	748.10	Richey, 1989, Table 2, p.52
14	Tamarisk	FFG_485	756.80	Richey, 1989, Table 2, p.52
15	Tamarisk	FFG_486	743.40	Richey, 1989, Table 2, p.52
16	Tamarisk	FFG_487	740.40	Richey, 1989, Table 2, p.52
17	Tamarisk	FFG_488	726.60	Richey, 1989, Table 2, p.52
18	Tamarisk	FFG_489	742.30	Richey, 1989, Table 2, p.52
19	Tamarisk	FFG_490	832.70	Richey, 1989, Table 2, p.52
20	Tamarisk	FFG_491	830.30	Richey, 1989, Table 2, p.52
21	Tamarisk	FFG_492	792.50	Richey, 1989, Table 2, p.52
22	Tamarisk	FFG_493	779.80	Richey, 1989, Table 2, p.53
23	Tamarisk	FFG_494	786.00	Richey, 1989, Table 2, p.53
24	Tamarisk	FFG_495	777.20	Richey, 1989, Table 2, p.53
25	Tamarisk	FFG_496	684.30	Richey, 1989, Table 2, p.53
26	Tamarisk	FFG_497	695.60	Richey, 1989, Table 2, p.53
27	Tamarisk	FFG_498	708.40	Richey, 1989, Table 2, p.53
28	Tamarisk	FFG_499	684.60	Richey, 1989, Table 2, p.53
29	Tamarisk	FFG_500	698.60	Richey, 1989, Table 2, p.53
30	Tamarisk	FFG_501	704.00	Richey, 1989, Table 2, p.53
31	Tamarisk	FFG_502	697.40	Richey, 1989, Table 2, p.53
32	Tamarisk	FFG_503	679.40	Richey, 1989, Table 2, p.53
33	Tamarisk	FFG_504	699.90	Richey, 1989, Table 2, p.53
34	Tamarisk	FFG_505	734.30	Richey, 1989, Table 2, p.53
35	Tamarisk	FFG_506	725.40	Richey, 1989, Table 2, p.53
36	Tamarisk	FFG_507	688.40	Richey, 1989, Table 2, p.53
37	Tamarisk	FFG_508	738.60	Richey, 1989, Table 2, p.53
38	Tamarisk	FFG_509	739.10	Richey, 1989, Table 2, p.54
39	Tamarisk	FFG_510	738.70	Richey, 1989, Table 2, p.54
40	Tamarisk	FFG_511	696.50	Richey, 1989, Table 2, p.54
41	Tamarisk	FFG_512	714.80	Richey, 1989, Table 2, p.54
42	Tamarisk	FFG_513	734.90	Richey, 1989, Table 2, p.54
43	Tamarisk	FFG_514	726.00	Richey, 1989, Table 2, p.54
44	Tamarisk	FFG_515	692.80	Richey, 1989, Table 2, p.54
45	Tamarisk	FFG_516	685.50	Richey, 1989, Table 2, p.54
46	Tamarisk	FFG_517	783.70	Richey, 1989, Table 2, p.54
47	Tamarisk	FFG_518	772.00	Richey, 1989, Table 2, p.54
48	Tamarisk	FFG_519	740.10	Richey, 1989, Table 2, p.54
49	Tamarisk	FFG_520	631.70	Richey, 1989, Table 2, p.54
50	Tamarisk	FFG_521	650.40	Richey, 1989, Table 2, p.54
51	Tamarisk	FFG_522	499.70	Richey, 1989, Table 2, p.54
52	Tamarisk	FFG_523	509.30	Richey, 1989, Table 2, p.54
53	Tamarisk	FFG_524	670.80	Richey, 1989, Table 2, p.55
54	Tamarisk	FFG_525	508.50	Richey, 1989, Table 2, p.55
55	Tamarisk	FFG_526	973.50	Richey, 1989, Table 2, p.55
56	Tamarisk	FFG_527	933.60	Richey, 1989, Table 2, p.55
57	Tamarisk	FFG_528	926.00	Richey, 1989, Table 2, p.55
58	Tamarisk	FFG_530	1000.30	Richey, 1989, Table 2, p.55
59	Tamarisk	FFG_531	919.30	Richey, 1989, Table 2, p.55
60	Tamarisk	FFG_532	907.10	Richey, 1989, Table 2, p.55
61	Tamarisk	FFG_534	946.40	Richey, 1989, Table 2, p.55
62	Tamarisk	FFG_535	912.80	Richey, 1989, Table 2, p.55
63	Tamarisk	FFG_536	928.40	Richey, 1989, Table 2, p.55
64	Tamarisk	FFG_537	904.60	Richey, 1989, Table 2, p.55
65	Tamarisk	FFG_543	970.90	Richey, 1989, Table 2, p.56
66	Tamarisk	FFG_548	907.70	Richey, 1989, Table 2, p.56
67	Tamarisk	FFG_562	645.30	Richey, 1989, Table 2, p.57
68	Tamarisk	FFG_563	557.50	Richey, 1989, Table 2, p.57
69	Tamarisk	FFG_568	634.60	Richey, 1989, Table 2, p.57
70	Tamarisk	FFG_569	663.20	Richey, 1989, Table 2, p.57
71	Tamarisk	FFG_584	764.30	Richey, 1989, Table 2, p.58
72	Tamarisk	FFG_585	730.90	Richey, 1989, Table 2, p.58
73	Tamarisk	FFG_600	722.10	Richey, 1989, Table 2, p.58
74	Tamarisk	FFG_601	615.70	Richey, 1989, Table 2, p.58
75	Tamarisk	FFG_602	1053.10	Richey, 1989, Table 2, p.58
76	Tamarisk	FFG_606	695.90	Richey, 1989, Table 2, p.58

Table B.2. Elevations of Stratigraphic Layers Near WIPP (Continued)

	Layer	Well ID	Elevation	Source
1	Tamarisk	FFG_607	718.40	Richey, 1989, Table 2, p.59
2	Tamarisk	FFG_608	726.60	Richey, 1989, Table 2, p.59
3	Tamarisk	FFG_609	732.70	Richey, 1989, Table 2, p.59
4	Tamarisk	FFG_610	713.20	Richey, 1989, Table 2, p.59
5	Tamarisk	FFG_611	703.20	Richey, 1989, Table 2, p.59
6	Tamarisk	FFG_612	712.70	Richey, 1989, Table 2, p.59
7	Tamarisk	FFG_613	705.90	Richey, 1989, Table 2, p.59
8	Tamarisk	FFG_618	701.90	Richey, 1989, Table 2, p.59
9	Tamarisk	FFG_638	567.30	Richey, 1989, Table 2, p.60
10	Tamarisk	FFG_639	537.40	Richey, 1989, Table 2, p.60
11	Tamarisk	FFG_640	623.10	Richey, 1989, Table 2, p.60
12	Tamarisk	FFG_643	662.40	Richey, 1989, Table 2, p.60
13	Tamarisk	FFG_644	701.20	Richey, 1989, Table 2, p.60
14	Tamarisk	FFG_648	536.10	Richey, 1989, Table 2, p.60
15	Tamarisk	FFG_652	853.70	Richey, 1989, Table 2, p.60
16	Tamarisk	FFG_653	854.10	Richey, 1989, Table 2, p.61
17	Tamarisk	FFG_654	874.80	Richey, 1989, Table 2, p.61
18	Tamarisk	FFG_655	873.20	Richey, 1989, Table 2, p.61
19	Tamarisk	FFG_656	870.80	Richey, 1989, Table 2, p.61
20	Tamarisk	FFG_657	883.70	Richey, 1989, Table 2, p.61
21	Tamarisk	FFG_658	874.40	Richey, 1989, Table 2, p.61
22	Tamarisk	FFG_659	879.70	Richey, 1989, Table 2, p.61
23	Tamarisk	FFG_660	896.90	Richey, 1989, Table 2, p.61
24	Tamarisk	FFG_662	870.80	Richey, 1989, Table 2, p.61
25	Tamarisk	FFG_664	862.00	Richey, 1989, Table 2, p.61
26	Tamarisk	FFG_666	914.40	Richey, 1989, Table 2, p.62
27	Tamarisk	FFG_667	899.50	Richey, 1989, Table 2, p.62
28	Tamarisk	FFG_668	947.70	Richey, 1989, Table 2, p.62
29	Tamarisk	FFG_669	934.20	Richey, 1989, Table 2, p.62
30	Tamarisk	FFG_670	919.30	Richey, 1989, Table 2, p.62
31	Tamarisk	FFG_671	917.70	Richey, 1989, Table 2, p.62
32	Tamarisk	FFG_672	919.90	Richey, 1989, Table 2, p.62
33	Tamarisk	FFG_673	914.70	Richey, 1989, Table 2, p.62
34	Tamarisk	FFG_674	915.00	Richey, 1989, Table 2, p.62
35	Tamarisk	FFG_675	871.60	Richey, 1989, Table 2, p.62
36	Tamarisk	FFG_676	884.20	Richey, 1989, Table 2, p.62
37	Tamarisk	FFG_677	910.50	Richey, 1989, Table 2, p.62
38	Tamarisk	FFG_679	910.40	Richey, 1989, Table 2, p.62
39	Tamarisk	FFG_689	793.70	Richey, 1989, Table 2, p.63
40	Tamarisk	FFG_690	798.90	Richey, 1989, Table 2, p.63
41	Tamarisk	FFG_691	790.40	Richey, 1989, Table 2, p.63
42	Tamarisk	FFG_692	780.30	Richey, 1989, Table 2, p.63
43	Tamarisk	FFG_693	790.90	Richey, 1989, Table 2, p.63
44	Tamarisk	FFG_694	783.30	Richey, 1989, Table 2, p.63
45	Tamarisk	FFG_695	788.80	Richey, 1989, Table 2, p.63
46	Tamarisk	FFG_696	790.60	Richey, 1989, Table 2, p.63
47	Tamarisk	FFG_697	793.70	Richey, 1989, Table 2, p.64
48	Tamarisk	FFG_698	835.50	Richey, 1989, Table 2, p.64
49	Tamarisk	FFG_699	786.70	Richey, 1989, Table 2, p.64
50	Tamarisk	FFG_700	777.00	Richey, 1989, Table 2, p.64
51	Tamarisk	FFG_701	781.90	Richey, 1989, Table 2, p.64
52	Tamarisk	FFG_702	786.70	Richey, 1989, Table 2, p.64
53	Tamarisk	FFG_703	791.60	Richey, 1989, Table 2, p.64
54	Tamarisk	FFG_704	779.40	Richey, 1989, Table 2, p.64
55	Tamarisk	FFG_705	709.60	Richey, 1989, Table 2, p.64
56	Tamarisk	FFG_706	730.70	Richey, 1989, Table 2, p.64
57	Tamarisk	FFG_707	714.20	Richey, 1989, Table 2, p.64
58	Tamarisk	FFG_708	767.20	Richey, 1989, Table 2, p.64
59	Tamarisk	FFG_709	658.70	Richey, 1989, Table 2, p.64
60	Tamarisk	FFG_710	659.30	Richey, 1989, Table 2, p.64
61	Tamarisk	FFG_711	668.20	Richey, 1989, Table 2, p.65
62	Tamarisk	FFG_712	710.90	Richey, 1989, Table 2, p.65
63	Tamarisk	FFG_713	648.10	Richey, 1989, Table 2, p.65
64	Tamarisk	FFG_714	761.90	Richey, 1989, Table 2, p.65
65	Tamarisk	FFG_715	774.80	Richey, 1989, Table 2, p.65
66	Tamarisk	FFG_716	676.60	Richey, 1989, Table 2, p.65
67	Tamarisk	FFG_717	698.10	Richey, 1989, Table 2, p.65
68	Tamarisk	FFG_718	700.90	Richey, 1989, Table 2, p.65
69	Tamarisk	FFG_719	674.20	Richey, 1989, Table 2, p.65
70	Tamarisk	FFG_720	671.50	Richey, 1989, Table 2, p.65
71	Tamarisk	FFG_721	673.60	Richey, 1989, Table 2, p.65
72	Tamarisk	FFG_723	785.30	Richey, 1989, Table 2, p.65
73	Tamarisk	FFG_724	713.60	Richey, 1989, Table 2, p.65
74	Tamarisk	FFG_725	689.70	Richey, 1989, Table 2, p.65
75	Tamarisk	FFG_726	677.50	Richey, 1989, Table 2, p.65
76	Tamarisk	FFG_727	674.90	Richey, 1989, Table 2, p.66

Table B.2. Elevations of Stratigraphic Layers Near WIPP (Continued)

	Layer	Well ID	Elevation	Source
1	Tamarisk	FFG_728	673.30	Richey, 1989, Table 2, p.66
2	Tamarisk	FFG_729	683.70	Richey, 1989, Table 2, p.66
3	Tamarisk	FFG_730	701.30	Richey, 1989, Table 2, p.66
4	Tamarisk	FFG_731	697.80	Richey, 1989, Table 2, p.66
5	Tamarisk	FFG_732	713.20	Richey, 1989, Table 2, p.66
6	Tamarisk	FFG_733	781.20	Richey, 1989, Table 2, p.66
7	Tamarisk	FFG_734	737.00	Richey, 1989, Table 2, p.66
8	Tamarisk	FFG_735	679.10	Richey, 1989, Table 2, p.66
9	Tamarisk	FFG_736	732.40	Richey, 1989, Table 2, p.66
10	Tamarisk	FFG_737	678.80	Richey, 1989, Table 2, p.66
11	Tamarisk	FFG_738	692.50	Richey, 1989, Table 2, p.66
12	Tamarisk	FFG_739	729.80	Richey, 1989, Table 2, p.66
13	Tamarisk	FFG_740	730.60	Richey, 1989, Table 2, p.66
14	Tamarisk	FFG_741	697.70	Richey, 1989, Table 2, p.66
15	Tamarisk	FFG_742	748.60	Richey, 1989, Table 2, p.67
16	Tamarisk	FFG_743	735.20	Richey, 1989, Table 2, p.67
17	Tamarisk	FFG_744	717.80	Richey, 1989, Table 2, p.67
18	Tamarisk	FFG_745	705.90	Richey, 1989, Table 2, p.67
19	Tamarisk	FFG_746	693.00	Richey, 1989, Table 2, p.67
20	Tamarisk	H1	856.20	Mercer, 1983, Table 1
21	Tamarisk	H10C	733.70	Mercer, 1983, Table 1
22	Tamarisk	H2C	864.10	Mercer, 1983, Table 1
23	Tamarisk	H3	855.30	Mercer, 1983, Table 1
24	Tamarisk	H4C	893.40	Mercer, 1983, Table 1
25	Tamarisk	H5C	821.40	Mercer, 1983, Table 1
26	Tamarisk	H6C	863.80	Mercer, 1983, Table 1
27	Tamarisk	H7C	921.40	Mercer, 1983, Table 1
28	Tamarisk	H8C	897.70	Mercer, 1983, Table 1
29	Tamarisk	H9C	869.20	Mercer, 1983, Table 1
30	Tamarisk	P1	883.00	Mercer, 1983, Table 1
31	Tamarisk	P10	831.50	Mercer, 1983, Table 1
32	Tamarisk	P11	817.10	Mercer, 1983, Table 1
33	Tamarisk	P12	862.90	Mercer, 1983, Table 1
34	Tamarisk	P13	862.90	Mercer, 1983, Table 1
35	Tamarisk	P14	878.70	Mercer, 1983, Table 1
36	Tamarisk	P15	911.10	Mercer, 1983, Table 1
37	Tamarisk	P16	889.10	Mercer, 1983, Table 1
38	Tamarisk	P17	875.70	Mercer, 1983, Table 1
39	Tamarisk	P18	837.30	Mercer, 1983, Table 1
40	Tamarisk	P19	824.80	Mercer, 1983, Table 1
41	Tamarisk	P2	824.80	Mercer, 1983, Table 1
42	Tamarisk	P20	819.00	Mercer, 1983, Table 1
43	Tamarisk	P21	822.00	Mercer, 1983, Table 1
44	Tamarisk	P3	862.50	Mercer, 1983, Table 1
45	Tamarisk	P4	840.60	Mercer, 1983, Table 1
46	Tamarisk	P5	841.30	Mercer, 1983, Table 1
47	Tamarisk	P6	887.30	Mercer, 1983, Table 1
48	Tamarisk	P7	894.30	Mercer, 1983, Table 1
49	Tamarisk	P8	873.20	Mercer, 1983, Table 1
50	Tamarisk	P9	843.70	Mercer, 1983, Table 1
51	Tamarisk	SaltShft	848.11	Bechtel, Inc., 1986, Appendix D
52	Tamarisk	WIPP11	815.60	Mercer, 1983, Table 1
53	Tamarisk	WIPP12	840.40	Mercer, 1983, Table 1
54	Tamarisk	WIPP13	860.10	Mercer, 1983, Table 1
55	Tamarisk	WIPP18	841.30	Mercer, 1983, Table 1
56	Tamarisk	WIPP19	841.60	Mercer, 1983, Table 1
57	Tamarisk	WIPP21	846.10	Mercer, 1983, Table 1
58	Tamarisk	WIPP22	844.90	Mercer, 1983, Table 1
59	Tamarisk	WIPP25	879.30	Mercer, 1983, Table 1
60	Tamarisk	WIPP26	930.50	Mercer, 1983, Table 1
61	Tamarisk	WIPP27	909.20	Mercer, 1983, Table 1
62	Tamarisk	WIPP28	925.70	Mercer, 1983, Table 1
63	Tamarisk	WIPP29	907.40	Mercer, 1983, Table 1
64	Tamarisk	WIPP30	881.20	Mercer, 1983, Table 1
65	Tamarisk	WIPP32	910.40	Mercer, 1983, Table 1
66	Tamarisk	WIPP33	870.30	Mercer, 1983, Table 1
67	Tamarisk	WIPP34	820.50	Mercer, 1983, Table 1
68	Tamarisk	WastShft	849.83	Bechtel, Inc., 1986, Appendix E
69	Tamerisk	DOE1	831.60	TME 3159, Sep 1982, Table 2
70	Tamerisk	DOE2	821.70	Mercer et al., 1987, Table 3-2
71	Tamerisk	ERDA9	849.10	SNL and USGS, 1982b, Table 2
72	Tamerisk	REF	849.10	Rechard et al.,1991, Figure 2.2-1
73	Tamerisk	WIPP11	815.70	SNL and USGS, 1982a, Table 2
74	Tamerisk	WIPP12	840.10	D'Appolonia Consulting, 1983, Table 2
75	U_Member	AirShft	782.57	IT Corporation, 1990, Figure 22
76	U_Member	DOE1	761.00	TME 3159, Sep 1982, Table 2

Table B.2. Elevations of Stratigraphic Layers Near WIPP (Continued)

	Layer	Well ID	Elevation	Source
1	U_Member	DOE2	749.00	Mercer et al., 1987, Table 3-2
2	U_Member	ERDA9	779.70	SNL and USGS, 1982b, Table 2
3	U_Member	ExhtShft	779.82	Bechtel, Inc., 1986, Appendix F
4	U_Member	REF	779.70	Rechard et al.,1991, Figure 2.2-1
5	U_Member	SaltShft	779.83	Bechtel, Inc., 1986, Appendix D
6	U_Member	WIPP11	754.40	SNL and USGS, 1982a, Table 2
7	U_Member	WIPP12	767.40	D'Appolonia Consulting, 1983, Table 2
8	U_Member	WastShft	781.32	Bechtel, Inc., 1986, Appendix E
9	Unnamed	AEC7	840.60	Mercer, 1983, Table 1
10	Unnamed	AEC8	814.80	Mercer, 1983, Table 1
11	Unnamed	AirShft	817.19	IT Corporation, 1990, Figure 22
12	Unnamed	B25	817.20	Mercer, 1983, Table 1
13	Unnamed	DOE1	799.40	TME 3159, Sep 1982, Table 2
14	Unnamed	DOE2	784.10	Mercer et al., 1987, Table 3-2
15	Unnamed	ERDA10	873.90	Mercer, 1983, Table 1
16	Unnamed	ERDA6	855.00	Mercer, 1983, Table 1
17	Unnamed	ERDA9	820.50	Mercer, 1983, Table 1
18	Unnamed	ERDA9	816.40	SNL and USGS, 1982b, Table 2
19	Unnamed	ExhtShft	814.75	Bechtel, Inc., 1986, Appendix F
20	Unnamed	FFG_002	618.10	Richey, 1989, Table 2, p.21
21	Unnamed	FFG_004	659.90	Richey, 1989, Table 2, p.21
22	Unnamed	FFG_005	622.10	Richey, 1989, Table 2, p.21
23	Unnamed	FFG_006	608.10	Richey, 1989, Table 2, p.21
24	Unnamed	FFG_007	593.70	Richey, 1989, Table 2, p.21
25	Unnamed	FFG_009	596.50	Richey, 1989, Table 2, p.21
26	Unnamed	FFG_011	603.50	Richey, 1989, Table 2, p.21
27	Unnamed	FFG_012	606.20	Richey, 1989, Table 2, p.21
28	Unnamed	FFG_013	634.30	Richey, 1989, Table 2, p.21
29	Unnamed	FFG_014	658.90	Richey, 1989, Table 2, p.21
30	Unnamed	FFG_016	579.40	Richey, 1989, Table 2, p.21
31	Unnamed	FFG_017	587.30	Richey, 1989, Table 2, p.22
32	Unnamed	FFG_018	590.70	Richey, 1989, Table 2, p.22
33	Unnamed	FFG_019	580.30	Richey, 1989, Table 2, p.22
34	Unnamed	FFG_020	655.30	Richey, 1989, Table 2, p.22
35	Unnamed	FFG_023	587.70	Richey, 1989, Table 2, p.22
36	Unnamed	FFG_024	571.80	Richey, 1989, Table 2, p.22
37	Unnamed	FFG_025	591.80	Richey, 1989, Table 2, p.22
38	Unnamed	FFG_026	585.50	Richey, 1989, Table 2, p.22
39	Unnamed	FFG_027	578.50	Richey, 1989, Table 2, p.22
40	Unnamed	FFG_028	572.50	Richey, 1989, Table 2, p.22
41	Unnamed	FFG_029	558.10	Richey, 1989, Table 2, p.22
42	Unnamed	FFG_030	557.20	Richey, 1989, Table 2, p.22
43	Unnamed	FFG_031	547.40	Richey, 1989, Table 2, p.22
44	Unnamed	FFG_032	546.10	Richey, 1989, Table 2, p.22
45	Unnamed	FFG_033	542.20	Richey, 1989, Table 2, p.22
46	Unnamed	FFG_034	542.50	Richey, 1989, Table 2, p.23
47	Unnamed	FFG_035	530.90	Richey, 1989, Table 2, p.23
48	Unnamed	FFG_036	535.60	Richey, 1989, Table 2, p.23
49	Unnamed	FFG_037	528.80	Richey, 1989, Table 2, p.23
50	Unnamed	FFG_038	517.50	Richey, 1989, Table 2, p.23
51	Unnamed	FFG_039	725.50	Richey, 1989, Table 2, p.23
52	Unnamed	FFG_040	645.30	Richey, 1989, Table 2, p.23
53	Unnamed	FFG_041	726.40	Richey, 1989, Table 2, p.23
54	Unnamed	FFG_042	730.00	Richey, 1989, Table 2, p.23
55	Unnamed	FFG_043	728.70	Richey, 1989, Table 2, p.23
56	Unnamed	FFG_044	680.90	Richey, 1989, Table 2, p.23
57	Unnamed	FFG_047	556.00	Richey, 1989, Table 2, p.23
58	Unnamed	FFG_048	573.30	Richey, 1989, Table 2, p.23
59	Unnamed	FFG_049	559.60	Richey, 1989, Table 2, p.23
60	Unnamed	FFG_050	574.90	Richey, 1989, Table 2, p.24
61	Unnamed	FFG_051	566.30	Richey, 1989, Table 2, p.24
62	Unnamed	FFG_052	589.80	Richey, 1989, Table 2, p.24
63	Unnamed	FFG_053	555.60	Richey, 1989, Table 2, p.24
64	Unnamed	FFG_054	556.60	Richey, 1989, Table 2, p.24
65	Unnamed	FFG_055	557.80	Richey, 1989, Table 2, p.24
66	Unnamed	FFG_056	556.90	Richey, 1989, Table 2, p.24
67	Unnamed	FFG_057	558.10	Richey, 1989, Table 2, p.24
68	Unnamed	FFG_058	560.80	Richey, 1989, Table 2, p.24
69	Unnamed	FFG_059	564.80	Richey, 1989, Table 2, p.24
70	Unnamed	FFG_060	563.20	Richey, 1989, Table 2, p.24
71	Unnamed	FFG_061	565.10	Richey, 1989, Table 2, p.24
72	Unnamed	FFG_062	507.20	Richey, 1989, Table 2, p.24
73	Unnamed	FFG_063	465.80	Richey, 1989, Table 2, p.24
74	Unnamed	FFG_064	488.90	Richey, 1989, Table 2, p.24
75	Unnamed	FFG_065	464.50	Richey, 1989, Table 2, p.24
76	Unnamed	FFG_066	429.10	Richey, 1989, Table 2, p.24

Table B.2. Elevations of Stratigraphic Layers Near WIPP (Continued)

	Layer	Well ID	Elevation	Source		Layer	Well ID	Elevation	Source
1	Unnamed	FFG_067	464.00	Richey, 1989, Table 2, p.25	39	Unnamed	FFG_107	878.80	Richey, 1989, Table 2, p.27
2	Unnamed	FFG_068	424.00	Richey, 1989, Table 2, p.25	40	Unnamed	FFG_108	869.60	Richey, 1989, Table 2, p.27
3	Unnamed	FFG_069	441.40	Richey, 1989, Table 2, p.25	41	Unnamed	FFG_109	856.20	Richey, 1989, Table 2, p.27
4	Unnamed	FFG_070	479.10	Richey, 1989, Table 2, p.25	42	Unnamed	FFG_110	824.50	Richey, 1989, Table 2, p.27
5	Unnamed	FFG_071	748.30	Richey, 1989, Table 2, p.25	43	Unnamed	FFG_111	830.60	Richey, 1989, Table 2, p.27
6	Unnamed	FFG_072	674.20	Richey, 1989, Table 2, p.25	44	Unnamed	FFG_112	816.80	Richey, 1989, Table 2, p.28
7	Unnamed	FFG_073	652.20	Richey, 1989, Table 2, p.25	45	Unnamed	FFG_113	830.90	Richey, 1989, Table 2, p.28
8	Unnamed	FFG_074	660.30	Richey, 1989, Table 2, p.25	46	Unnamed	FFG_114	863.20	Richey, 1989, Table 2, p.28
9	Unnamed	FFG_075	712.10	Richey, 1989, Table 2, p.25	47	Unnamed	FFG_115	848.30	Richey, 1989, Table 2, p.28
10	Unnamed	FFG_076	771.50	Richey, 1989, Table 2, p.25	48	Unnamed	FFG_116	865.30	Richey, 1989, Table 2, p.28
11	Unnamed	FFG_078	807.70	Richey, 1989, Table 2, p.25	49	Unnamed	FFG_117	856.50	Richey, 1989, Table 2, p.28
12	Unnamed	FFG_079	780.90	Richey, 1989, Table 2, p.25	50	Unnamed	FFG_119	864.80	Richey, 1989, Table 2, p.28
13	Unnamed	FFG_080	758.30	Richey, 1989, Table 2, p.25	51	Unnamed	FFG_120	865.10	Richey, 1989, Table 2, p.28
14	Unnamed	FFG_081	674.90	Richey, 1989, Table 2, p.26	52	Unnamed	FFG_121	873.30	Richey, 1989, Table 2, p.28
15	Unnamed	FFG_082	705.30	Richey, 1989, Table 2, p.26	53	Unnamed	FFG_122	868.70	Richey, 1989, Table 2, p.28
16	Unnamed	FFG_083	632.00	Richey, 1989, Table 2, p.26	54	Unnamed	FFG_123	861.00	Richey, 1989, Table 2, p.28
17	Unnamed	FFG_084	654.70	Richey, 1989, Table 2, p.26	55	Unnamed	FFG_124	830.90	Richey, 1989, Table 2, p.28
18	Unnamed	FFG_085	649.00	Richey, 1989, Table 2, p.26	56	Unnamed	FFG_125	842.10	Richey, 1989, Table 2, p.28
19	Unnamed	FFG_086	657.40	Richey, 1989, Table 2, p.26	57	Unnamed	FFG_126	846.60	Richey, 1989, Table 2, p.28
20	Unnamed	FFG_087	630.00	Richey, 1989, Table 2, p.26	58	Unnamed	FFG_127	851.60	Richey, 1989, Table 2, p.28
21	Unnamed	FFG_088	622.70	Richey, 1989, Table 2, p.26	59	Unnamed	FFG_128	877.60	Richey, 1989, Table 2, p.28
22	Unnamed	FFG_089	606.60	Richey, 1989, Table 2, p.26	60	Unnamed	FFG_129	852.20	Richey, 1989, Table 2, p.28
23	Unnamed	FFG_091	643.80	Richey, 1989, Table 2, p.26	61	Unnamed	FFG_130	888.50	Richey, 1989, Table 2, p.28
24	Unnamed	FFG_092	662.30	Richey, 1989, Table 2, p.26	62	Unnamed	FFG_132	890.90	Richey, 1989, Table 2, p.29
25	Unnamed	FFG_093	668.10	Richey, 1989, Table 2, p.26	63	Unnamed	FFG_133	895.50	Richey, 1989, Table 2, p.29
26	Unnamed	FFG_094	666.60	Richey, 1989, Table 2, p.26	64	Unnamed	FFG_134	896.80	Richey, 1989, Table 2, p.29
27	Unnamed	FFG_095	645.20	Richey, 1989, Table 2, p.26	65	Unnamed	FFG_135	875.10	Richey, 1989, Table 2, p.29
28	Unnamed	FFG_096	629.40	Richey, 1989, Table 2, p.26	66	Unnamed	FFG_136	876.40	Richey, 1989, Table 2, p.29
29	Unnamed	FFG_097	608.40	Richey, 1989, Table 2, p.27	67	Unnamed	FFG_137	884.60	Richey, 1989, Table 2, p.29
30	Unnamed	FFG_098	581.80	Richey, 1989, Table 2, p.27	68	Unnamed	FFG_138	834.90	Richey, 1989, Table 2, p.29
31	Unnamed	FFG_099	574.60	Richey, 1989, Table 2, p.27	69	Unnamed	FFG_139	847.90	Richey, 1989, Table 2, p.29
32	Unnamed	FFG_100	558.70	Richey, 1989, Table 2, p.27	70	Unnamed	FFG_140	785.00	Richey, 1989, Table 2, p.29
33	Unnamed	FFG_101	527.30	Richey, 1989, Table 2, p.27	71	Unnamed	FFG_141	812.50	Richey, 1989, Table 2, p.29
34	Unnamed	FFG_102	542.90	Richey, 1989, Table 2, p.27	72	Unnamed	FFG_142	788.30	Richey, 1989, Table 2, p.29
35	Unnamed	FFG_103	601.70	Richey, 1989, Table 2, p.27	73	Unnamed	FFG_143	797.30	Richey, 1989, Table 2, p.29
36	Unnamed	FFG_104	502.10	Richey, 1989, Table 2, p.27	74	Unnamed	FFG_144	883.70	Richey, 1989, Table 2, p.29
37	Unnamed	FFG_105	861.40	Richey, 1989, Table 2, p.27	75	Unnamed	FFG_145	887.00	Richey, 1989, Table 2, p.29
38	Unnamed	FFG_106	894.60	Richey, 1989, Table 2, p.27	76	Unnamed	FFG_146	897.70	Richey, 1989, Table 2, p.29

Table B.2. Elevations of Stratigraphic Layers Near WIPP (Continued)

	Layer	Well ID	Elevation	Source
1	Unnamed	FFG_147	875.40	Richey, 1989, Table 2, p.29
2	Unnamed	FFG_148	894.90	Richey, 1989, Table 2, p.29
3	Unnamed	FFG_149	903.10	Richey, 1989, Table 2, p.30
4	Unnamed	FFG_152	893.10	Richey, 1989, Table 2, p.30
5	Unnamed	FFG_155	894.00	Richey, 1989, Table 2, p.30
6	Unnamed	FFG_156	895.50	Richey, 1989, Table 2, p.30
7	Unnamed	FFG_157	898.60	Richey, 1989, Table 2, p.30
8	Unnamed	FFG_158	918.00	Richey, 1989, Table 2, p.30
9	Unnamed	FFG_159	891.60	Richey, 1989, Table 2, p.30
10	Unnamed	FFG_160	886.10	Richey, 1989, Table 2, p.30
11	Unnamed	FFG_161	894.90	Richey, 1989, Table 2, p.30
12	Unnamed	FFG_162	884.60	Richey, 1989, Table 2, p.30
13	Unnamed	FFG_163	888.20	Richey, 1989, Table 2, p.30
14	Unnamed	FFG_164	928.50	Richey, 1989, Table 2, p.30
15	Unnamed	FFG_165	902.20	Richey, 1989, Table 2, p.30
16	Unnamed	FFG_166	891.80	Richey, 1989, Table 2, p.31
17	Unnamed	FFG_167	877.90	Richey, 1989, Table 2, p.31
18	Unnamed	FFG_168	898.90	Richey, 1989, Table 2, p.31
19	Unnamed	FFG_169	909.20	Richey, 1989, Table 2, p.31
20	Unnamed	FFG_170	893.00	Richey, 1989, Table 2, p.31
21	Unnamed	FFG_171	909.30	Richey, 1989, Table 2, p.31
22	Unnamed	FFG_172	906.10	Richey, 1989, Table 2, p.31
23	Unnamed	FFG_173	867.80	Richey, 1989, Table 2, p.31
24	Unnamed	FFG_177	880.00	Richey, 1989, Table 2, p.31
25	Unnamed	FFG_178	711.40	Richey, 1989, Table 2, p.31
26	Unnamed	FFG_179	875.10	Richey, 1989, Table 2, p.31
27	Unnamed	FFG_180	874.70	Richey, 1989, Table 2, p.31
28	Unnamed	FFG_181	922.90	Richey, 1989, Table 2, p.32
29	Unnamed	FFG_182	804.30	Richey, 1989, Table 2, p.32
30	Unnamed	FFG_183	893.40	Richey, 1989, Table 2, p.32
31	Unnamed	FFG_184	883.60	Richey, 1989, Table 2, p.32
32	Unnamed	FFG_185	891.80	Richey, 1989, Table 2, p.32
33	Unnamed	FFG_186	819.30	Richey, 1989, Table 2, p.32
34	Unnamed	FFG_188	837.60	Richey, 1989, Table 2, p.32
35	Unnamed	FFG_189	859.60	Richey, 1989, Table 2, p.32
36	Unnamed	FFG_190	835.10	Richey, 1989, Table 2, p.32
37	Unnamed	FFG_191	839.40	Richey, 1989, Table 2, p.32
38	Unnamed	FFG_192	764.40	Richey, 1989, Table 2, p.32
39	Unnamed	FFG_194	780.60	Richey, 1989, Table 2, p.33
40	Unnamed	FFG_195	792.80	Richey, 1989, Table 2, p.33
41	Unnamed	FFG_196	827.50	Richey, 1989, Table 2, p.33
42	Unnamed	FFG_197	831.20	Richey, 1989, Table 2, p.33
43	Unnamed	FFG_198	831.80	Richey, 1989, Table 2, p.33
44	Unnamed	FFG_199	818.70	Richey, 1989, Table 2, p.33
45	Unnamed	FFG_200	828.10	Richey, 1989, Table 2, p.33
46	Unnamed	FFG_201	830.00	Richey, 1989, Table 2, p.33
47	Unnamed	FFG_202	763.20	Richey, 1989, Table 2, p.33
48	Unnamed	FFG_203	767.50	Richey, 1989, Table 2, p.33
49	Unnamed	FFG_204	805.30	Richey, 1989, Table 2, p.33
50	Unnamed	FFG_205	816.60	Richey, 1989, Table 2, p.33
51	Unnamed	FFG_206	828.10	Richey, 1989, Table 2, p.33
52	Unnamed	FFG_207	826.00	Richey, 1989, Table 2, p.33
53	Unnamed	FFG_208	834.50	Richey, 1989, Table 2, p.34
54	Unnamed	FFG_209	829.70	Richey, 1989, Table 2, p.34
55	Unnamed	FFG_210	818.70	Richey, 1989, Table 2, p.34
56	Unnamed	FFG_212	809.00	Richey, 1989, Table 2, p.34
57	Unnamed	FFG_213	828.80	Richey, 1989, Table 2, p.34
58	Unnamed	FFG_214	808.60	Richey, 1989, Table 2, p.34
59	Unnamed	FFG_215	784.90	Richey, 1989, Table 2, p.34
60	Unnamed	FFG_216	682.70	Richey, 1989, Table 2, p.34
61	Unnamed	FFG_217	805.60	Richey, 1989, Table 2, p.34
62	Unnamed	FFG_218	794.30	Richey, 1989, Table 2, p.34
63	Unnamed	FFG_219	840.30	Richey, 1989, Table 2, p.34
64	Unnamed	FFG_220	789.50	Richey, 1989, Table 2, p.34
65	Unnamed	FFG_221	744.30	Richey, 1989, Table 2, p.34
66	Unnamed	FFG_222	705.00	Richey, 1989, Table 2, p.34
67	Unnamed	FFG_224	590.10	Richey, 1989, Table 2, p.35
68	Unnamed	FFG_225	598.00	Richey, 1989, Table 2, p.35
69	Unnamed	FFG_226	594.80	Richey, 1989, Table 2, p.35
70	Unnamed	FFG_228	580.70	Richey, 1989, Table 2, p.35
71	Unnamed	FFG_229	607.10	Richey, 1989, Table 2, p.35
72	Unnamed	FFG_230	595.00	Richey, 1989, Table 2, p.35
73	Unnamed	FFG_231	613.80	Richey, 1989, Table 2, p.35
74	Unnamed	FFG_232	625.80	Richey, 1989, Table 2, p.35
75	Unnamed	FFG_233	617.90	Richey, 1989, Table 2, p.35
76	Unnamed	FFG_234	653.50	Richey, 1989, Table 2, p.35

Table B.2. Elevations of Stratigraphic Layers Near WIPP (Continued)

	Layer	Well ID	Elevation	Source
1	Unnamed	FFG_235	628.50	Richey, 1989, Table 2, p.35
2	Unnamed	FFG_236	677.20	Richey, 1989, Table 2, p.35
3	Unnamed	FFG_237	634.40	Richey, 1989, Table 2, p.35
4	Unnamed	FFG_238	621.50	Richey, 1989, Table 2, p.36
5	Unnamed	FFG_239	613.50	Richey, 1989, Table 2, p.36
6	Unnamed	FFG_240	602.60	Richey, 1989, Table 2, p.36
7	Unnamed	FFG_241	598.10	Richey, 1989, Table 2, p.36
8	Unnamed	FFG_242	724.20	Richey, 1989, Table 2, p.36
9	Unnamed	FFG_243	659.30	Richey, 1989, Table 2, p.36
10	Unnamed	FFG_244	715.20	Richey, 1989, Table 2, p.36
11	Unnamed	FFG_245	503.50	Richey, 1989, Table 2, p.36
12	Unnamed	FFG_246	508.10	Richey, 1989, Table 2, p.36
13	Unnamed	FFG_247	493.70	Richey, 1989, Table 2, p.36
14	Unnamed	FFG_248	498.30	Richey, 1989, Table 2, p.36
15	Unnamed	FFG_249	498.30	Richey, 1989, Table 2, p.36
16	Unnamed	FFG_250	580.50	Richey, 1989, Table 2, p.36
17	Unnamed	FFG_251	470.00	Richey, 1989, Table 2, p.36
18	Unnamed	FFG_252	612.60	Richey, 1989, Table 2, p.36
19	Unnamed	FFG_253	561.50	Richey, 1989, Table 2, p.36
20	Unnamed	FFG_254	554.70	Richey, 1989, Table 2, p.36
21	Unnamed	FFG_255	506.30	Richey, 1989, Table 2, p.37
22	Unnamed	FFG_256	470.90	Richey, 1989, Table 2, p.37
23	Unnamed	FFG_257	517.20	Richey, 1989, Table 2, p.37
24	Unnamed	FFG_258	536.40	Richey, 1989, Table 2, p.37
25	Unnamed	FFG_259	494.90	Richey, 1989, Table 2, p.37
26	Unnamed	FFG_260	548.90	Richey, 1989, Table 2, p.37
27	Unnamed	FFG_261	537.30	Richey, 1989, Table 2, p.37
28	Unnamed	FFG_262	477.00	Richey, 1989, Table 2, p.37
29	Unnamed	FFG_263	448.50	Richey, 1989, Table 2, p.37
30	Unnamed	FFG_264	696.20	Richey, 1989, Table 2, p.37
31	Unnamed	FFG_265	677.30	Richey, 1989, Table 2, p.37
32	Unnamed	FFG_266	656.80	Richey, 1989, Table 2, p.37
33	Unnamed	FFG_267	632.70	Richey, 1989, Table 2, p.37
34	Unnamed	FFG_268	606.30	Richey, 1989, Table 2, p.37
35	Unnamed	FFG_269	617.60	Richey, 1989, Table 2, p.38
36	Unnamed	FFG_270	721.10	Richey, 1989, Table 2, p.38
37	Unnamed	FFG_271	767.80	Richey, 1989, Table 2, p.38
38	Unnamed	FFG_272	743.90	Richey, 1989, Table 2, p.38
39	Unnamed	FFG_273	745.30	Richey, 1989, Table 2, p.38
40	Unnamed	FFG_274	785.80	Richey, 1989, Table 2, p.38
41	Unnamed	FFG_275	794.60	Richey, 1989, Table 2, p.38
42	Unnamed	FFG_276	795.80	Richey, 1989, Table 2, p.38
43	Unnamed	FFG_277	789.10	Richey, 1989, Table 2, p.38
44	Unnamed	FFG_278	765.40	Richey, 1989, Table 2, p.38
45	Unnamed	FFG_279	767.70	Richey, 1989, Table 2, p.38
46	Unnamed	FFG_280	780.00	Richey, 1989, Table 2, p.38
47	Unnamed	FFG_281	754.40	Richey, 1989, Table 2, p.38
48	Unnamed	FFG_283	489.20	Richey, 1989, Table 2, p.39
49	Unnamed	FFG_284	641.30	Richey, 1989, Table 2, p.39
50	Unnamed	FFG_285	660.50	Richey, 1989, Table 2, p.39
51	Unnamed	FFG_286	766.20	Richey, 1989, Table 2, p.39
52	Unnamed	FFG_287	733.30	Richey, 1989, Table 2, p.39
53	Unnamed	FFG_288	662.60	Richey, 1989, Table 2, p.39
54	Unnamed	FFG_289	673.90	Richey, 1989, Table 2, p.39
55	Unnamed	FFG_290	760.80	Richey, 1989, Table 2, p.39
56	Unnamed	FFG_291	660.80	Richey, 1989, Table 2, p.39
57	Unnamed	FFG_292	717.80	Richey, 1989, Table 2, p.39
58	Unnamed	FFG_293	710.50	Richey, 1989, Table 2, p.39
59	Unnamed	FFG_294	497.50	Richey, 1989, Table 2, p.39
60	Unnamed	FFG_295	480.00	Richey, 1989, Table 2, p.39
61	Unnamed	FFG_297	455.40	Richey, 1989, Table 2, p.39
62	Unnamed	FFG_298	520.40	Richey, 1989, Table 2, p.40
63	Unnamed	FFG_299	489.80	Richey, 1989, Table 2, p.40
64	Unnamed	FFG_300	473.00	Richey, 1989, Table 2, p.40
65	Unnamed	FFG_301	430.40	Richey, 1989, Table 2, p.40
66	Unnamed	FFG_302	436.80	Richey, 1989, Table 2, p.40
67	Unnamed	FFG_303	442.00	Richey, 1989, Table 2, p.40
68	Unnamed	FFG_304	438.90	Richey, 1989, Table 2, p.40
69	Unnamed	FFG_305	434.60	Richey, 1989, Table 2, p.40
70	Unnamed	FFG_306	405.30	Richey, 1989, Table 2, p.40
71	Unnamed	FFG_307	424.30	Richey, 1989, Table 2, p.40
72	Unnamed	FFG_308	367.80	Richey, 1989, Table 2, p.40
73	Unnamed	FFG_309	427.90	Richey, 1989, Table 2, p.40
74	Unnamed	FFG_310	469.10	Richey, 1989, Table 2, p.40
75	Unnamed	FFG_311	420.30	Richey, 1989, Table 2, p.40
76	Unnamed	FFG_312	424.00	Richey, 1989, Table 2, p.40

Table B.2. Elevations of Stratigraphic Layers Near WIPP (Continued)

	Layer	Well ID	Elevation	Source
1	Unnamed	FFG_313	862.00	Richey, 1989, Table 2, p.41
2	Unnamed	FFG_314	781.60	Richey, 1989, Table 2, p.41
3	Unnamed	FFG_315	694.20	Richey, 1989, Table 2, p.41
4	Unnamed	FFG_316	670.20	Richey, 1989, Table 2, p.41
5	Unnamed	FFG_317	725.10	Richey, 1989, Table 2, p.41
6	Unnamed	FFG_318	702.60	Richey, 1989, Table 2, p.41
7	Unnamed	FFG_319	696.40	Richey, 1989, Table 2, p.41
8	Unnamed	FFG_320	662.00	Richey, 1989, Table 2, p.41
9	Unnamed	FFG_321	661.70	Richey, 1989, Table 2, p.41
10	Unnamed	FFG_322	662.20	Richey, 1989, Table 2, p.41
11	Unnamed	FFG_323	667.90	Richey, 1989, Table 2, p.41
12	Unnamed	FFG_324	692.20	Richey, 1989, Table 2, p.41
13	Unnamed	FFG_325	753.20	Richey, 1989, Table 2, p.41
14	Unnamed	FFG_326	698.00	Richey, 1989, Table 2, p.41
15	Unnamed	FFG_327	681.90	Richey, 1989, Table 2, p.42
16	Unnamed	FFG_328	664.70	Richey, 1989, Table 2, p.42
17	Unnamed	FFG_329	661.40	Richey, 1989, Table 2, p.42
18	Unnamed	FFG_330	661.00	Richey, 1989, Table 2, p.42
19	Unnamed	FFG_331	646.80	Richey, 1989, Table 2, p.42
20	Unnamed	FFG_332	632.80	Richey, 1989, Table 2, p.42
21	Unnamed	FFG_333	643.00	Richey, 1989, Table 2, p.42
22	Unnamed	FFG_334	637.00	Richey, 1989, Table 2, p.42
23	Unnamed	FFG_335	655.00	Richey, 1989, Table 2, p.42
24	Unnamed	FFG_336	650.40	Richey, 1989, Table 2, p.42
25	Unnamed	FFG_337	634.30	Richey, 1989, Table 2, p.42
26	Unnamed	FFG_338	639.00	Richey, 1989, Table 2, p.42
27	Unnamed	FFG_339	604.10	Richey, 1989, Table 2, p.42
28	Unnamed	FFG_340	609.30	Richey, 1989, Table 2, p.42
29	Unnamed	FFG_342	676.30	Richey, 1989, Table 2, p.43
30	Unnamed	FFG_344	650.90	Richey, 1989, Table 2, p.43
31	Unnamed	FFG_345	671.30	Richey, 1989, Table 2, p.43
32	Unnamed	FFG_347	692.80	Richey, 1989, Table 2, p.43
33	Unnamed	FFG_348	733.00	Richey, 1989, Table 2, p.43
34	Unnamed	FFG_349	709.30	Richey, 1989, Table 2, p.43
35	Unnamed	FFG_350	739.70	Richey, 1989, Table 2, p.43
36	Unnamed	FFG_351	621.20	Richey, 1989, Table 2, p.43
37	Unnamed	FFG_352	621.80	Richey, 1989, Table 2, p.43
38	Unnamed	FFG_353	644.10	Richey, 1989, Table 2, p.43
39	Unnamed	FFG_354	756.00	Richey, 1989, Table 2, p.43
40	Unnamed	FFG_361	948.50	Richey, 1989, Table 2, p.44
41	Unnamed	FFG_362	911.00	Richey, 1989, Table 2, p.44
42	Unnamed	FFG_363	937.90	Richey, 1989, Table 2, p.44
43	Unnamed	FFG_364	909.80	Richey, 1989, Table 2, p.44
44	Unnamed	FFG_366	904.00	Richey, 1989, Table 2, p.44
45	Unnamed	FFG_367	922.60	Richey, 1989, Table 2, p.44
46	Unnamed	FFG_370	962.60	Richey, 1989, Table 2, p.44
47	Unnamed	FFG_371	958.60	Richey, 1989, Table 2, p.44
48	Unnamed	FFG_372	941.50	Richey, 1989, Table 2, p.45
49	Unnamed	FFG_373	902.00	Richey, 1989, Table 2, p.45
50	Unnamed	FFG_374	902.20	Richey, 1989, Table 2, p.45
51	Unnamed	FFG_376	939.70	Richey, 1989, Table 2, p.45
52	Unnamed	FFG_381	908.60	Richey, 1989, Table 2, p.45
53	Unnamed	FFG_383	902.20	Richey, 1989, Table 2, p.45
54	Unnamed	FFG_384	912.30	Richey, 1989, Table 2, p.45
55	Unnamed	FFG_385	906.80	Richey, 1989, Table 2, p.45
56	Unnamed	FFG_387	901.60	Richey, 1989, Table 2, p.45
57	Unnamed	FFG_388	893.70	Richey, 1989, Table 2, p.46
58	Unnamed	FFG_389	917.50	Richey, 1989, Table 2, p.46
59	Unnamed	FFG_390	913.50	Richey, 1989, Table 2, p.46
60	Unnamed	FFG_391	913.10	Richey, 1989, Table 2, p.46
61	Unnamed	FFG_392	904.40	Richey, 1989, Table 2, p.46
62	Unnamed	FFG_393	781.00	Richey, 1989, Table 2, p.46
63	Unnamed	FFG_394	877.20	Richey, 1989, Table 2, p.46
64	Unnamed	FFG_395	867.50	Richey, 1989, Table 2, p.46
65	Unnamed	FFG_396	847.10	Richey, 1989, Table 2, p.46
66	Unnamed	FFG_398	767.20	Richey, 1989, Table 2, p.46
67	Unnamed	FFG_399	780.60	Richey, 1989, Table 2, p.46
68	Unnamed	FFG_401	833.60	Richey, 1989, Table 2, p.46
69	Unnamed	FFG_402	936.70	Richey, 1989, Table 2, p.46
70	Unnamed	FFG_403	903.30	Richey, 1989, Table 2, p.47
71	Unnamed	FFG_404	867.20	Richey, 1989, Table 2, p.47
72	Unnamed	FFG_407	898.90	Richey, 1989, Table 2, p.47
73	Unnamed	FFG_408	901.00	Richey, 1989, Table 2, p.47
74	Unnamed	FFG_409	932.40	Richey, 1989, Table 2, p.47
75	Unnamed	FFG_411	873.90	Richey, 1989, Table 2, p.47
76	Unnamed	FFG_413	906.20	Richey, 1989, Table 2, p.47

Table B.2. Elevations of Stratigraphic Layers Near WIPP (Continued)

	Layer	Well ID	Elevation	Source
1	Unnamed	FFG_418	923.00	Richey, 1989, Table 2, p.48
2	Unnamed	FFG_419	936.70	Richey, 1989, Table 2, p.48
3	Unnamed	FFG_420	927.80	Richey, 1989, Table 2, p.48
4	Unnamed	FFG_421	913.80	Richey, 1989, Table 2, p.48
5	Unnamed	FFG_422	915.60	Richey, 1989, Table 2, p.48
6	Unnamed	FFG_426	919.30	Richey, 1989, Table 2, p.48
7	Unnamed	FFG_432	876.90	Richey, 1989, Table 2, p.48
8	Unnamed	FFG_433	892.40	Richey, 1989, Table 2, p.48
9	Unnamed	FFG_438	829.80	Richey, 1989, Table 2, p.49
10	Unnamed	FFG_445	911.60	Richey, 1989, Table 2, p.49
11	Unnamed	FFG_453	772.90	Richey, 1989, Table 2, p.50
12	Unnamed	FFG_455	761.40	Richey, 1989, Table 2, p.50
13	Unnamed	FFG_456	769.90	Richey, 1989, Table 2, p.50
14	Unnamed	FFG_457	822.60	Richey, 1989, Table 2, p.50
15	Unnamed	FFG_458	825.10	Richey, 1989, Table 2, p.50
16	Unnamed	FFG_459	752.30	Richey, 1989, Table 2, p.50
17	Unnamed	FFG_462	820.70	Richey, 1989, Table 2, p.50
18	Unnamed	FFG_463	843.70	Richey, 1989, Table 2, p.51
19	Unnamed	FFG_464	833.60	Richey, 1989, Table 2, p.51
20	Unnamed	FFG_465	835.10	Richey, 1989, Table 2, p.51
21	Unnamed	FFG_467	423.00	Richey, 1989, Table 2, p.51
22	Unnamed	FFG_468	373.10	Richey, 1989, Table 2, p.51
23	Unnamed	FFG_470	402.60	Richey, 1989, Table 2, p.51
24	Unnamed	FFG_471	420.60	Richey, 1989, Table 2, p.51
25	Unnamed	FFG_472	495.60	Richey, 1989, Table 2, p.51
26	Unnamed	FFG_473	383.70	Richey, 1989, Table 2, p.51
27	Unnamed	FFG_474	671.70	Richey, 1989, Table 2, p.51
28	Unnamed	FFG_475	677.70	Richey, 1989, Table 2, p.51
29	Unnamed	FFG_476	751.70	Richey, 1989, Table 2, p.51
30	Unnamed	FFG_477	718.80	Richey, 1989, Table 2, p.51
31	Unnamed	FFG_478	694.00	Richey, 1989, Table 2, p.52
32	Unnamed	FFG_479	698.90	Richey, 1989, Table 2, p.52
33	Unnamed	FFG_480	681.30	Richey, 1989, Table 2, p.52
34	Unnamed	FFG_481	674.50	Richey, 1989, Table 2, p.52
35	Unnamed	FFG_482	703.80	Richey, 1989, Table 2, p.52
36	Unnamed	FFG_483	732.70	Richey, 1989, Table 2, p.52
37	Unnamed	FFG_484	720.70	Richey, 1989, Table 2, p.52
38	Unnamed	FFG_485	723.00	Richey, 1989, Table 2, p.52
39	Unnamed	FFG_486	708.40	Richey, 1989, Table 2, p.52
40	Unnamed	FFG_487	706.90	Richey, 1989, Table 2, p.52
41	Unnamed	FFG_488	692.50	Richey, 1989, Table 2, p.52
42	Unnamed	FFG_489	708.80	Richey, 1989, Table 2, p.52
43	Unnamed	FFG_490	801.30	Richey, 1989, Table 2, p.52
44	Unnamed	FFG_491	793.10	Richey, 1989, Table 2, p.52
45	Unnamed	FFG_492	757.10	Richey, 1989, Table 2, p.52
46	Unnamed	FFG_493	743.20	Richey, 1989, Table 2, p.53
47	Unnamed	FFG_494	747.00	Richey, 1989, Table 2, p.53
48	Unnamed	FFG_495	743.10	Richey, 1989, Table 2, p.53
49	Unnamed	FFG_496	604.20	Richey, 1989, Table 2, p.53
50	Unnamed	FFG_497	642.20	Richey, 1989, Table 2, p.53
51	Unnamed	FFG_498	637.60	Richey, 1989, Table 2, p.53
52	Unnamed	FFG_499	603.20	Richey, 1989, Table 2, p.53
53	Unnamed	FFG_500	635.20	Richey, 1989, Table 2, p.53
54	Unnamed	FFG_501	665.60	Richey, 1989, Table 2, p.53
55	Unnamed	FFG_502	630.90	Richey, 1989, Table 2, p.53
56	Unnamed	FFG_503	616.30	Richey, 1989, Table 2, p.53
57	Unnamed	FFG_504	667.60	Richey, 1989, Table 2, p.53
58	Unnamed	FFG_505	696.20	Richey, 1989, Table 2, p.53
59	Unnamed	FFG_506	690.60	Richey, 1989, Table 2, p.53
60	Unnamed	FFG_507	599.40	Richey, 1989, Table 2, p.53
61	Unnamed	FFG_508	680.70	Richey, 1989, Table 2, p.53
62	Unnamed	FFG_509	662.30	Richey, 1989, Table 2, p.54
63	Unnamed	FFG_510	658.80	Richey, 1989, Table 2, p.54
64	Unnamed	FFG_511	619.40	Richey, 1989, Table 2, p.54
65	Unnamed	FFG_512	634.60	Richey, 1989, Table 2, p.54
66	Unnamed	FFG_513	659.30	Richey, 1989, Table 2, p.54
67	Unnamed	FFG_514	637.00	Richey, 1989, Table 2, p.54
68	Unnamed	FFG_515	610.80	Richey, 1989, Table 2, p.54
69	Unnamed	FFG_516	601.60	Richey, 1989, Table 2, p.54
70	Unnamed	FFG_517	750.70	Richey, 1989, Table 2, p.54
71	Unnamed	FFG_518	735.80	Richey, 1989, Table 2, p.54
72	Unnamed	FFG_519	696.50	Richey, 1989, Table 2, p.54
73	Unnamed	FFG_520	585.40	Richey, 1989, Table 2, p.54
74	Unnamed	FFG_521	628.20	Richey, 1989, Table 2, p.54
75	Unnamed	FFG_522	427.50	Richey, 1989, Table 2, p.54
76	Unnamed	FFG_523	443.20	Richey, 1989, Table 2, p.54

Table B.2. Elevations of Stratigraphic Layers Near WIPP (Continued)

	Layer	Well ID	Elevation	Source
1	Unnamed	FFG_524	607.40	Richey, 1989, Table 2, p.55
2	Unnamed	FFG_525	436.60	Richey, 1989, Table 2, p.55
3	Unnamed	FFG_526	943.10	Richey, 1989, Table 2, p.55
4	Unnamed	FFG_527	888.10	Richey, 1989, Table 2, p.55
5	Unnamed	FFG_528	891.50	Richey, 1989, Table 2, p.55
6	Unnamed	FFG_530	957.70	Richey, 1989, Table 2, p.55
7	Unnamed	FFG_531	888.80	Richey, 1989, Table 2, p.55
8	Unnamed	FFG_532	873.00	Richey, 1989, Table 2, p.55
9	Unnamed	FFG_534	883.30	Richey, 1989, Table 2, p.55
10	Unnamed	FFG_535	875.70	Richey, 1989, Table 2, p.55
11	Unnamed	FFG_536	884.50	Richey, 1989, Table 2, p.55
12	Unnamed	FFG_537	872.60	Richey, 1989, Table 2, p.55
13	Unnamed	FFG_543	926.70	Richey, 1989, Table 2, p.56
14	Unnamed	FFG_548	877.20	Richey, 1989, Table 2, p.56
15	Unnamed	FFG_552	722.00	Richey, 1989, Table 2, p.56
16	Unnamed	FFG_562	614.50	Richey, 1989, Table 2, p.57
17	Unnamed	FFG_563	528.20	Richey, 1989, Table 2, p.57
18	Unnamed	FFG_564	663.00	Richey, 1989, Table 2, p.57
19	Unnamed	FFG_568	625.80	Richey, 1989, Table 2, p.57
20	Unnamed	FFG_569	624.20	Richey, 1989, Table 2, p.57
21	Unnamed	FFG_584	736.60	Richey, 1989, Table 2, p.58
22	Unnamed	FFG_585	678.40	Richey, 1989, Table 2, p.58
23	Unnamed	FFG_600	692.50	Richey, 1989, Table 2, p.58
24	Unnamed	FFG_601	572.70	Richey, 1989, Table 2, p.58
25	Unnamed	FFG_602	794.30	Richey, 1989, Table 2, p.58
26	Unnamed	FFG_606	667.60	Richey, 1989, Table 2, p.58
27	Unnamed	FFG_607	671.80	Richey, 1989, Table 2, p.59
28	Unnamed	FFG_608	654.70	Richey, 1989, Table 2, p.59
29	Unnamed	FFG_609	646.70	Richey, 1989, Table 2, p.59
30	Unnamed	FFG_610	640.10	Richey, 1989, Table 2, p.59
31	Unnamed	FFG_611	635.50	Richey, 1989, Table 2, p.59
32	Unnamed	FFG_612	669.70	Richey, 1989, Table 2, p.59
33	Unnamed	FFG_613	668.70	Richey, 1989, Table 2, p.59
34	Unnamed	FFG_618	679.10	Richey, 1989, Table 2, p.59
35	Unnamed	FFG_620	731.20	Richey, 1989, Table 2, p.59
36	Unnamed	FFG_621	695.00	Richey, 1989, Table 2, p.59
37	Unnamed	FFG_638	530.10	Richey, 1989, Table 2, p.60
38	Unnamed	FFG_639	498.40	Richey, 1989, Table 2, p.60
39	Unnamed	FFG_640	586.60	Richey, 1989, Table 2, p.60
40	Unnamed	FFG_643	637.10	Richey, 1989, Table 2, p.60
41	Unnamed	FFG_644	670.50	Richey, 1989, Table 2, p.60
42	Unnamed	FFG_648	500.50	Richey, 1989, Table 2, p.60
43	Unnamed	FFG_652	815.90	Richey, 1989, Table 2, p.60
44	Unnamed	FFG_653	815.70	Richey, 1989, Table 2, p.61
45	Unnamed	FFG_654	839.10	Richey, 1989, Table 2, p.61
46	Unnamed	FFG_655	840.30	Richey, 1989, Table 2, p.61
47	Unnamed	FFG_656	838.50	Richey, 1989, Table 2, p.61
48	Unnamed	FFG_657	856.20	Richey, 1989, Table 2, p.61
49	Unnamed	FFG_658	842.70	Richey, 1989, Table 2, p.61
50	Unnamed	FFG_659	848.60	Richey, 1989, Table 2, p.61
51	Unnamed	FFG_660	866.40	Richey, 1989, Table 2, p.61
52	Unnamed	FFG_662	837.30	Richey, 1989, Table 2, p.61
53	Unnamed	FFG_664	830.90	Richey, 1989, Table 2, p.61
54	Unnamed	FFG_666	883.90	Richey, 1989, Table 2, p.62
55	Unnamed	FFG_667	869.30	Richey, 1989, Table 2, p.62
56	Unnamed	FFG_668	919.40	Richey, 1989, Table 2, p.62
57	Unnamed	FFG_669	905.80	Richey, 1989, Table 2, p.62
58	Unnamed	FFG_670	889.10	Richey, 1989, Table 2, p.62
59	Unnamed	FFG_671	891.20	Richey, 1989, Table 2, p.62
60	Unnamed	FFG_672	889.80	Richey, 1989, Table 2, p.62
61	Unnamed	FFG_673	887.50	Richey, 1989, Table 2, p.62
62	Unnamed	FFG_674	885.50	Richey, 1989, Table 2, p.62
63	Unnamed	FFG_675	844.20	Richey, 1989, Table 2, p.62
64	Unnamed	FFG_676	854.70	Richey, 1989, Table 2, p.62
65	Unnamed	FFG_677	883.30	Richey, 1989, Table 2, p.62
66	Unnamed	FFG_679	883.90	Richey, 1989, Table 2, p.62
67	Unnamed	FFG_685	911.10	Richey, 1989, Table 2, p.63
68	Unnamed	FFG_689	756.80	Richey, 1989, Table 2, p.63
69	Unnamed	FFG_690	760.80	Richey, 1989, Table 2, p.63
70	Unnamed	FFG_691	752.90	Richey, 1989, Table 2, p.63
71	Unnamed	FFG_692	741.60	Richey, 1989, Table 2, p.63
72	Unnamed	FFG_693	753.70	Richey, 1989, Table 2, p.63
73	Unnamed	FFG_694	743.10	Richey, 1989, Table 2, p.63
74	Unnamed	FFG_695	749.20	Richey, 1989, Table 2, p.63
75	Unnamed	FFG_696	751.60	Richey, 1989, Table 2, p.63
76	Unnamed	FFG_697	754.10	Richey, 1989, Table 2, p.64

Table B.2. Elevations of Stratigraphic Layers Near WIPP (Continued)

	Layer	Well ID	Elevation	Source
1	Unnamed	FFG_698	795.30	Richey, 1989, Table 2, p.64
2	Unnamed	FFG_699	749.50	Richey, 1989, Table 2, p.64
3	Unnamed	FFG_700	744.40	Richey, 1989, Table 2, p.64
4	Unnamed	FFG_701	740.80	Richey, 1989, Table 2, p.64
5	Unnamed	FFG_702	747.00	Richey, 1989, Table 2, p.64
6	Unnamed	FFG_703	753.80	Richey, 1989, Table 2, p.64
7	Unnamed	FFG_704	737.30	Richey, 1989, Table 2, p.64
8	Unnamed	FFG_705	671.80	Richey, 1989, Table 2, p.64
9	Unnamed	FFG_706	694.40	Richey, 1989, Table 2, p.64
10	Unnamed	FFG_707	677.00	Richey, 1989, Table 2, p.64
11	Unnamed	FFG_708	728.80	Richey, 1989, Table 2, p.64
12	Unnamed	FFG_709	625.80	Richey, 1989, Table 2, p.64
13	Unnamed	FFG_710	625.20	Richey, 1989, Table 2, p.64
14	Unnamed	FFG_711	626.10	Richey, 1989, Table 2, p.65
15	Unnamed	FFG_712	669.50	Richey, 1989, Table 2, p.65
16	Unnamed	FFG_713	613.70	Richey, 1989, Table 2, p.65
17	Unnamed	FFG_714	725.10	Richey, 1989, Table 2, p.65
18	Unnamed	FFG_715	735.10	Richey, 1989, Table 2, p.65
19	Unnamed	FFG_716	597.30	Richey, 1989, Table 2, p.65
20	Unnamed	FFG_717	665.20	Richey, 1989, Table 2, p.65
21	Unnamed	FFG_718	656.10	Richey, 1989, Table 2, p.65
22	Unnamed	FFG_719	618.70	Richey, 1989, Table 2, p.65
23	Unnamed	FFG_720	614.50	Richey, 1989, Table 2, p.65
24	Unnamed	FFG_721	639.50	Richey, 1989, Table 2, p.65
25	Unnamed	FFG_723	755.10	Richey, 1989, Table 2, p.65
26	Unnamed	FFG_724	678.00	Richey, 1989, Table 2, p.65
27	Unnamed	FFG_725	646.50	Richey, 1989, Table 2, p.65
28	Unnamed	FFG_726	641.00	Richey, 1989, Table 2, p.65
29	Unnamed	FFG_727	630.70	Richey, 1989, Table 2, p.66
30	Unnamed	FFG_728	638.20	Richey, 1989, Table 2, p.66
31	Unnamed	FFG_729	641.00	Richey, 1989, Table 2, p.66
32	Unnamed	FFG_730	665.30	Richey, 1989, Table 2, p.66
33	Unnamed	FFG_731	662.80	Richey, 1989, Table 2, p.66
34	Unnamed	FFG_732	678.20	Richey, 1989, Table 2, p.66
35	Unnamed	FFG_733	741.90	Richey, 1989, Table 2, p.66
36	Unnamed	FFG_734	699.20	Richey, 1989, Table 2, p.66
37	Unnamed	FFG_735	630.30	Richey, 1989, Table 2, p.66
38	Unnamed	FFG_736	667.80	Richey, 1989, Table 2, p.66
39	Unnamed	FFG_737	611.80	Richey, 1989, Table 2, p.66
40	Unnamed	FFG_738	654.40	Richey, 1989, Table 2, p.66
41	Unnamed	FFG_739	683.80	Richey, 1989, Table 2, p.66
42	Unnamed	FFG_740	653.20	Richey, 1989, Table 2, p.66
43	Unnamed	FFG_741	651.10	Richey, 1989, Table 2, p.66
44	Unnamed	FFG_742	690.70	Richey, 1989, Table 2, p.67
45	Unnamed	FFG_743	675.20	Richey, 1989, Table 2, p.67
46	Unnamed	FFG_744	670.80	Richey, 1989, Table 2, p.67
47	Unnamed	FFG_745	650.40	Richey, 1989, Table 2, p.67
48	Unnamed	FFG_746	637.20	Richey, 1989, Table 2, p.67
49	Unnamed	H1	822.60	Mercer, 1983, Table 1
50	Unnamed	H10C	699.80	Mercer, 1983, Table 1
51	Unnamed	H2C	833.00	Mercer, 1983, Table 1
52	Unnamed	H3	821.80	Mercer, 1983, Table 1
53	Unnamed	H4C	858.90	Mercer, 1983, Table 1
54	Unnamed	H5C	787.30	Mercer, 1983, Table 1
55	Unnamed	H6C	829.40	Mercer, 1983, Table 1
56	Unnamed	H7C	880.60	Mercer, 1983, Table 1
57	Unnamed	H8C	859.30	Mercer, 1983, Table 1
58	Unnamed	H9C	831.80	Mercer, 1983, Table 1
59	Unnamed	P1	847.40	Mercer, 1983, Table 1
60	Unnamed	P10	777.80	Mercer, 1983, Table 1
61	Unnamed	P11	782.10	Mercer, 1983, Table 1
62	Unnamed	P12	828.50	Mercer, 1983, Table 1
63	Unnamed	P13	828.50	Mercer, 1983, Table 1
64	Unnamed	P14	842.70	Mercer, 1983, Table 1
65	Unnamed	P15	876.30	Mercer, 1983, Table 1
66	Unnamed	P16	851.90	Mercer, 1983, Table 1
67	Unnamed	P17	839.10	Mercer, 1983, Table 1
68	Unnamed	P18	773.90	Mercer, 1983, Table 1
69	Unnamed	P19	776.60	Mercer, 1983, Table 1
70	Unnamed	P2	791.30	Mercer, 1983, Table 1
71	Unnamed	P20	784.60	Mercer, 1983, Table 1
72	Unnamed	P21	787.90	Mercer, 1983, Table 1
73	Unnamed	P3	828.40	Mercer, 1983, Table 1
74	Unnamed	P4	805.30	Mercer, 1983, Table 1
75	Unnamed	P5	805.90	Mercer, 1983, Table 1
76	Unnamed	P6	851.60	Mercer, 1983, Table 1

Table B.2. Elevations of Stratigraphic Layers Near WIPP (Continued)

	Layer	Well ID	Elevation	Source
1	Unnamed	P7	856.50	Mercer, 1983, Table 1
2	Unnamed	P8	838.50	Mercer, 1983, Table 1
3	Unnamed	P9	809.30	Mercer, 1983, Table 1
4	Unnamed	REF	816.40	Rechard et al.,1991, Figure 2.2-1
5	Unnamed	SaltShft	813.97	Bechtel, Inc., 1986, Appendix D
6	Unnamed	WIPP11	779.90	Mercer, 1983, Table 1
7	Unnamed	WIPP11	780.00	SNL and USGS, 1982a, Table 2
8	Unnamed	WIPP12	803.90	D'Appolonia Consulting, 1983, Table 2
9	Unnamed	WIPP12	803.80	Mercer, 1983, Table 1
10	Unnamed	WIPP13	817.10	Mercer, 1983, Table 1
11	Unnamed	WIPP15	996.40	Mercer, 1983, Table 1
12	Unnamed	WIPP16	672.70	Mercer, 1983, Table 1
13	Unnamed	WIPP18	807.10	Mercer, 1983, Table 1
14	Unnamed	WIPP19	809.60	Mercer, 1983, Table 1
15	Unnamed	WIPP21	812.00	Mercer, 1983, Table 1
16	Unnamed	WIPP22	811.30	Mercer, 1983, Table 1
17	Unnamed	WIPP25	835.40	Mercer, 1983, Table 1
18	Unnamed	WIPP26	897.00	Mercer, 1983, Table 1
19	Unnamed	WIPP27	871.40	Mercer, 1983, Table 1
20	Unnamed	WIPP28	884.30	Mercer, 1983, Table 1
21	Unnamed	WIPP29	894.60	Mercer, 1983, Table 1
22	Unnamed	WIPP30	845.60	Mercer, 1983, Table 1
23	Unnamed	WIPP32	894.00	Mercer, 1983, Table 1
24	Unnamed	WIPP33	836.70	Mercer, 1983, Table 1
25	Unnamed	WIPP34	784.30	Mercer, 1983, Table 1
26	Unnamed	WastShft	817.02	Bechtel, Inc., 1986, Appendix E
27	V_Triste	AirShft	622.89	IT Corporation, 1990, Figure 22
28	V_Triste	AirShft	625.30	IT Corporation, 1990, Figure 22
29	V_Triste	DOE1	604.50	TME 3159, Sep 1982, Table 2
30	V_Triste	DOE1	605.70	TME 3159, Sep 1982, Table 2
31	V_Triste	DOE2	598.10	Mercer et al., 1987, Table 3-2
32	V_Triste	DOE2	600.30	Mercer et al., 1987, Table 3-2
33	V_Triste	ERDA9	625.70	SNL and USGS, 1982b, Table 2
34	V_Triste	ERDA9	627.60	SNL and USGS, 1982b, Table 2
35	V_Triste	ExhtShft	625.11	Bechtel, Inc., 1986, Appendix F
36	V_Triste	ExhtShft	626.66	Bechtel, Inc., 1986, Appendix F
37	V_Triste	REF	625.70	Rechard et al.,1991, Figure 2.2-1
38	V_Triste	REF	627.60	Rechard et al.,1991, Figure 2.2-1
39	V_Triste	SaltShft	627.89	Bechtel, Inc., 1986, Appendix D
40	V_Triste	SaltShft	628.33	Bechtel, Inc., 1986, Appendix D
41	V_Triste	WIPP11	611.20	SNL and USGS, 1982a, Table 2
42	V_Triste	WIPP11	612.70	SNL and USGS, 1982a, Table 2
43	V_Triste	WIPP12	620.80	D'Appolonia Consulting, 1983, Table 2
44	V_Triste	WIPP12	621.70	D'Appolonia Consulting, 1983, Table 2
45				

REFERENCES FOR APPENDIX B

Bechtel, Inc. 1986. *WIPP Design Validation Final Report.* DOE/WIPP-86-010. Prepared for U.S. Department of Energy. San Francisco, CA: Bechtel National, Inc.

Gonzales, M. 1989. *Compilation and Comparison of Test-Hole Location Surveys in the Vicinity of the Waste Isolation Pilot Plant Site.* SAND88-1065. Albuquerque, NM: Sandia National Laboratories.

Holt, R. M. and D. W. Powers. 1990. *Geologic Mapping of the Air Intake Shaft at the Waste Isolation Pilot Plant.* DOE-WIPP 90-051. Carlsbad, NM: U.S. Department of Energy.

Krieg, R. D. 1984. *Reference Stratigraphy and Rock Properties for the Waste Isolation Pilot Plant (WIPP) Project.* SAND83-1908. Albuquerque, NM: Sandia National Laboratories.

Mercer, J. W. 1983. *Geohydrology of the Proposed Waste Isolation Pilot Plant Site, Los Medaños Area, Southeastern New Mexico.* U.S. Geological Survey Water Resources Investigation 83-4016.

Mercer, J. W., R. L. Beauheim, R. P. Snyder, and G. M. Fairer. 1987. *Basic Data Report for Drilling and Hydrologic Testing of Drillhole DOE-2 at the Waste Isolation Pilot Plant (WIPP) Site.* SAND86-0611. Albuquerque, NM: Sandia National Laboratories.

Rechard, R. P., H. J. Iuzzolino, J. S. Rath, R. D. McCurley, and D. K. Rudeen. 1989. *User's Manual for CAMCON: Compliance Assessment Methodology Controller.* SAND88-1496. Albuquerque, NM: Sandia National Laboratories.

Richey, S. F. 1989. *Geologic and Hydrologic Data for the Rustler Formation near the Waste Isolation Pilot Plant, Southeastern New Mexico.* Albuquerque, NM: U.S. Geological Survey Open-File Report 89-32.

SNL (Sandia National Laboratories) and U.S. Geological Survey. 1982a. *Basic Data Report for Drillhole WIPP 11 (Waste Isolation Pilot Plant - WIPP).* SAND79-0272. Albuquerque, NM: Sandia National Laboratories.

SNL (Sandia National Laboratories) and U.S. Geological Survey. 1982b. *Basic Data Report for Drillhole ERDA 9 (Waste Isolation Pilot Plant - WIPP).* SAND79-0270. Albuquerque, NM: Sandia National Laboratories.

SNL (Sandia National Laboratories) and D'Appolonia Consulting Engineers. 1983. *Basic Data Report for Drillhole WIPP 12 (Waste Isolation Pilot Plant - WIPP).* SAND82-2336. Albuquerque, NM: Sandia National Laboratories.

U.S. DOE (Department of Energy). 1982. *Basic Data Report for Borehole DOE-1, Waste Isolation Pilot Plant (WIPP) Project, Southeastern New Mexico.* TME 3159. Albuquerque, NM: Sandia National Laboratories.

APPENDIX C:
REALIZATIONS OF TRANSMISSIVITY FIELDS IN THE CULEBRA DOLOMITE MEMBER OF THE RUSTLER FORMATION

APPENDIX C

APPENDIX C: REALIZATIONS OF TRANSMISSIVITY FIELDS IN THE CULEBRA DOLOMITE MEMBER OF THE RUSTLER FORMATION

The following 70 figures are grey-scale representations of the 70 realizations of Culebra transmissivity field generated for use in the 1992 series of PA calculations. The realizations are ordered by increasing travel time (marked at the bottom of each figure).

The origins of these representations of transmissivity field are briefly explained in Section 2.6.3 of this report, and in more detail in Volume 2 of the 1992 series of reports.

Note: On all figures, the grey-scale values are in units of $\log_{10}$ (m^2/s).

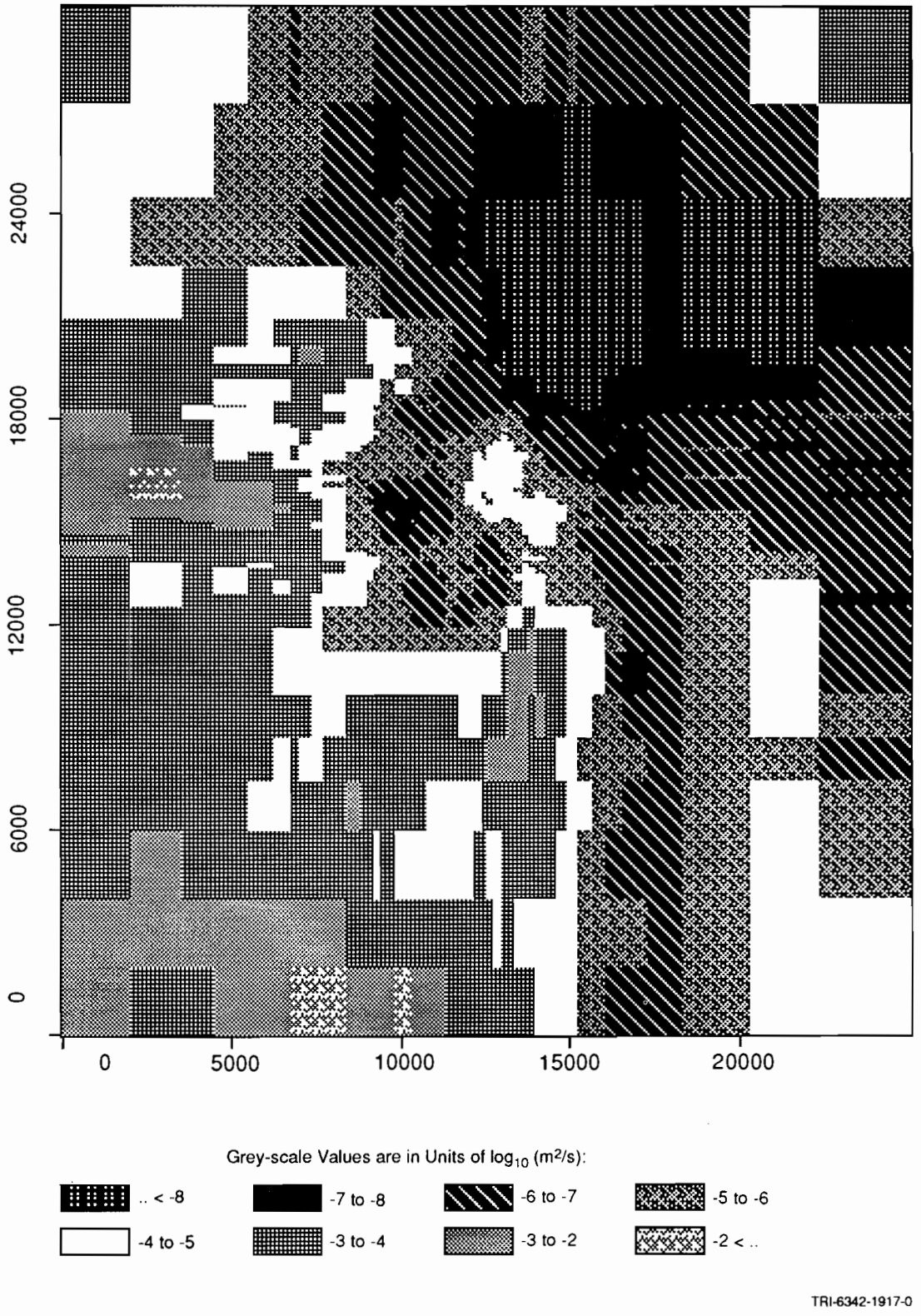

Figure C-1. Realization 12 of Culebra transmissivity.

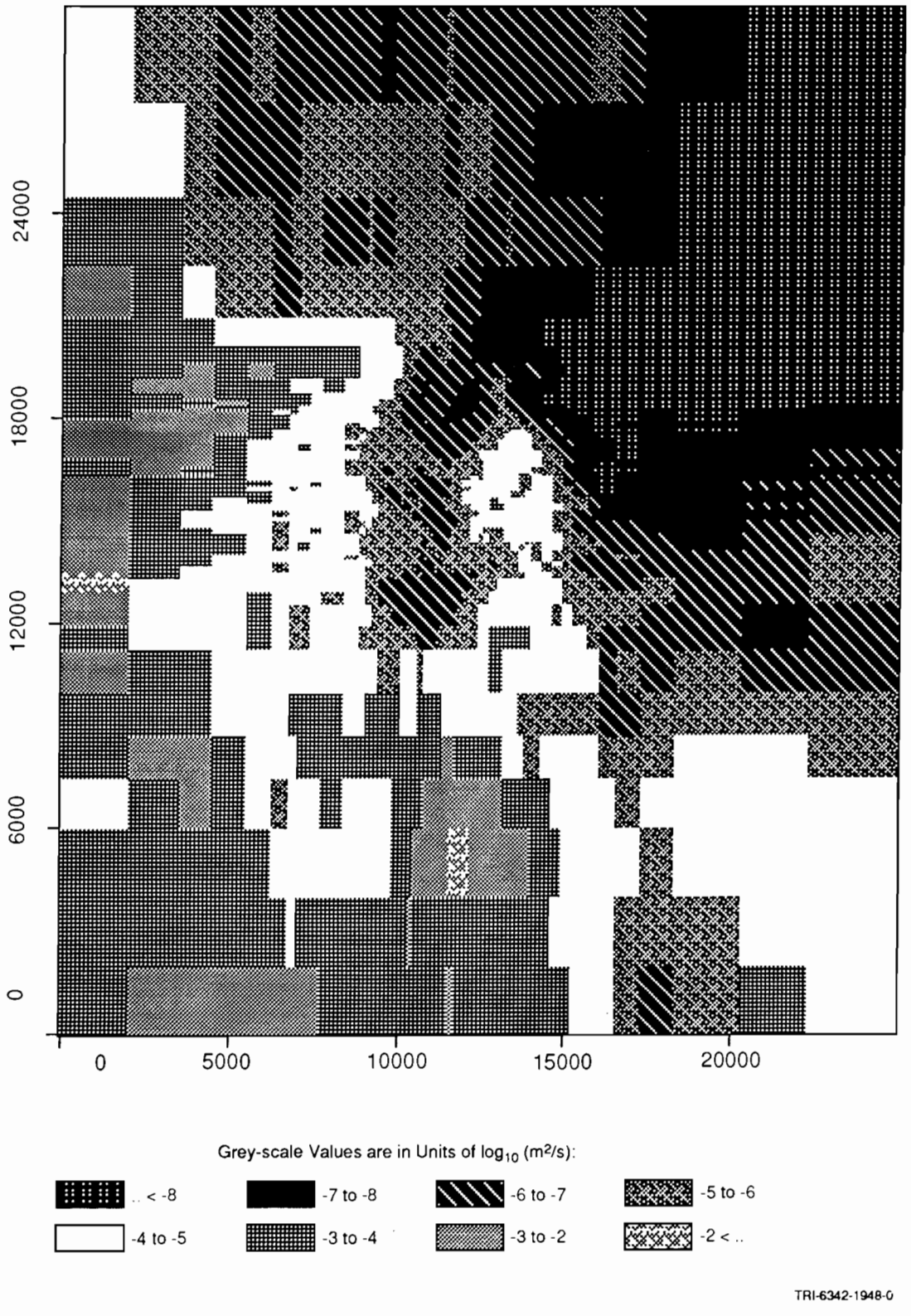

Figure C-2. Realization 64 of Culebra transmissivity.

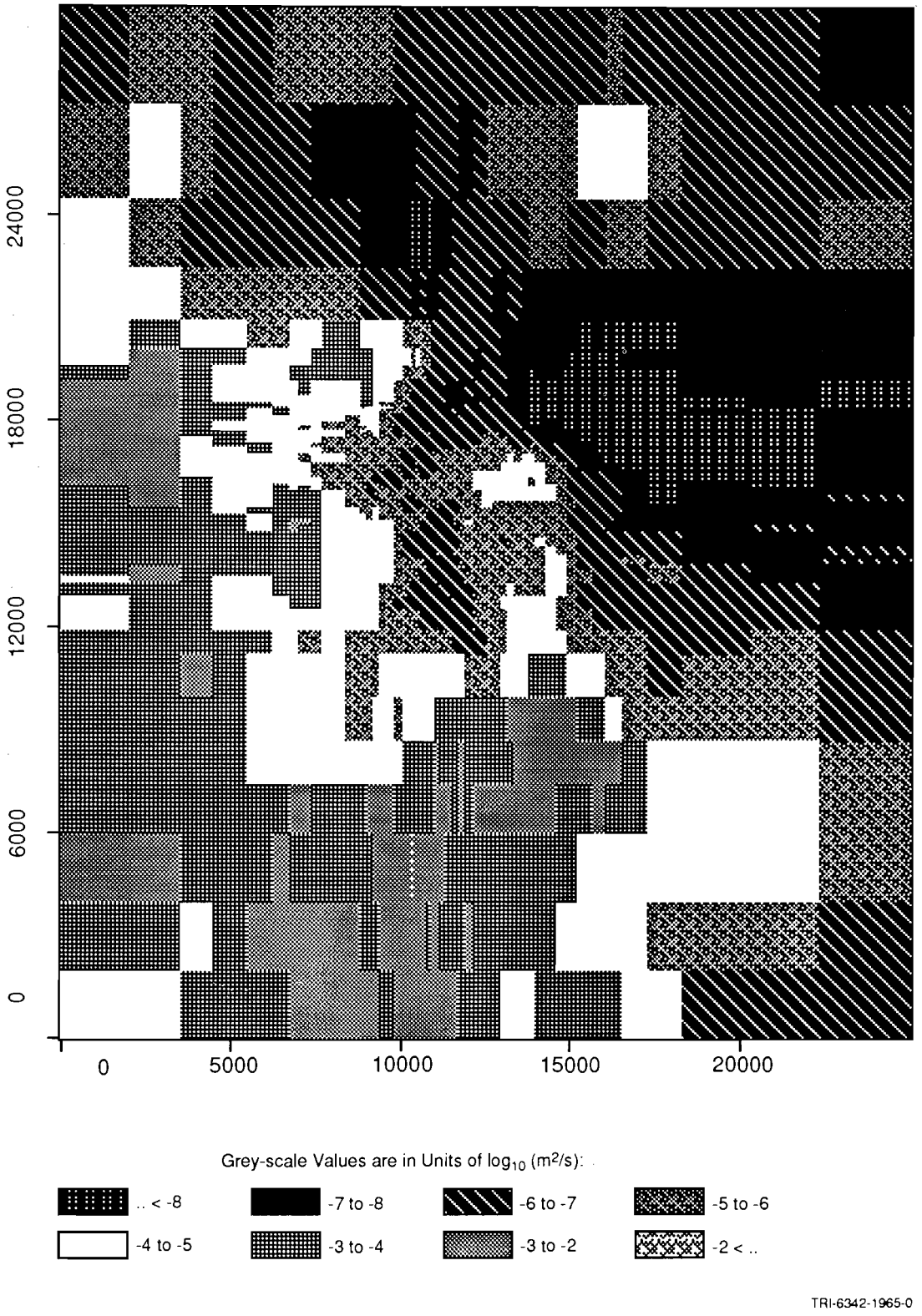

Figure C-3. Realization 25 of Culebra transmissivity.

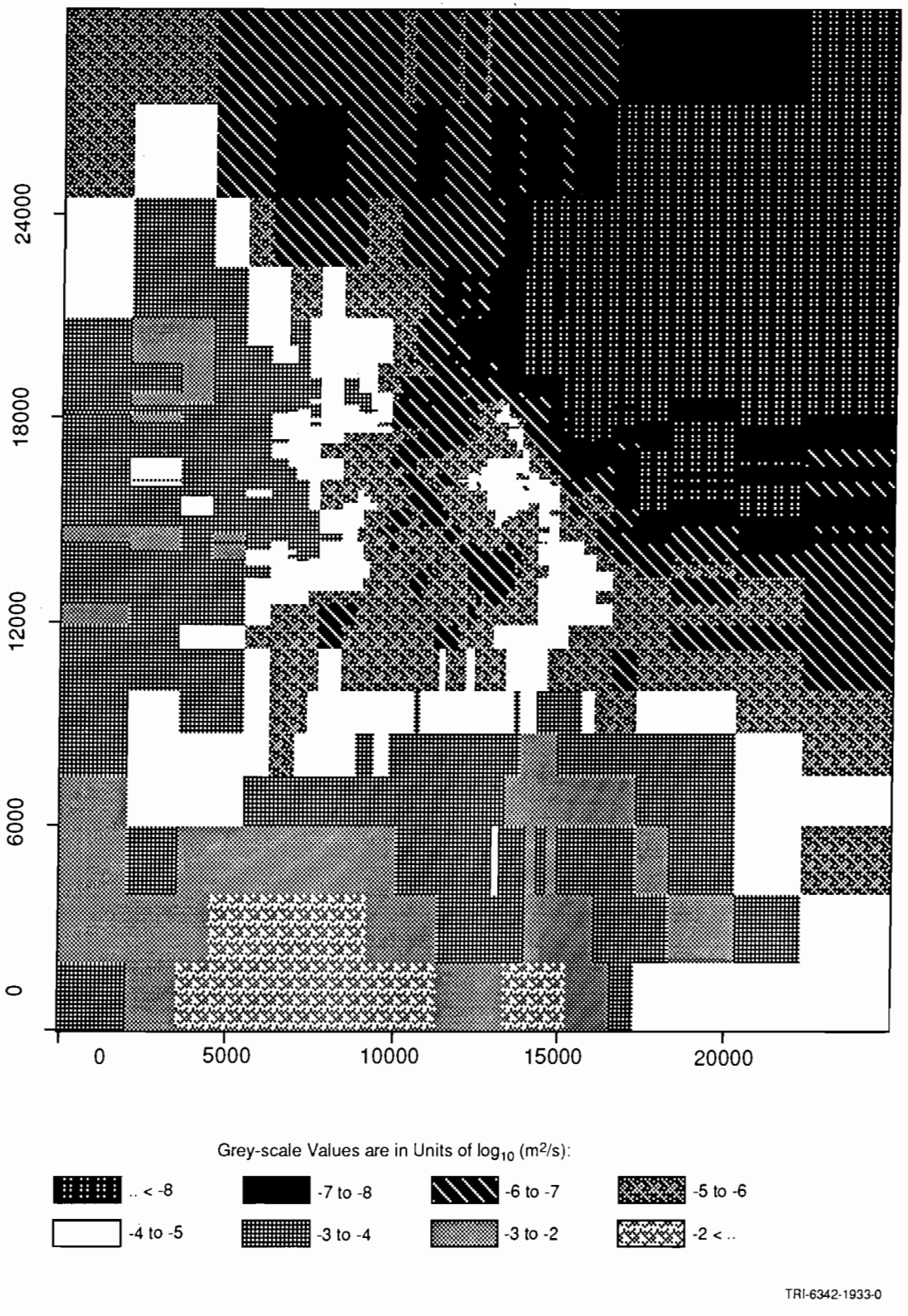

Figure C-4. Realization 23 of Culebra transmissivity.

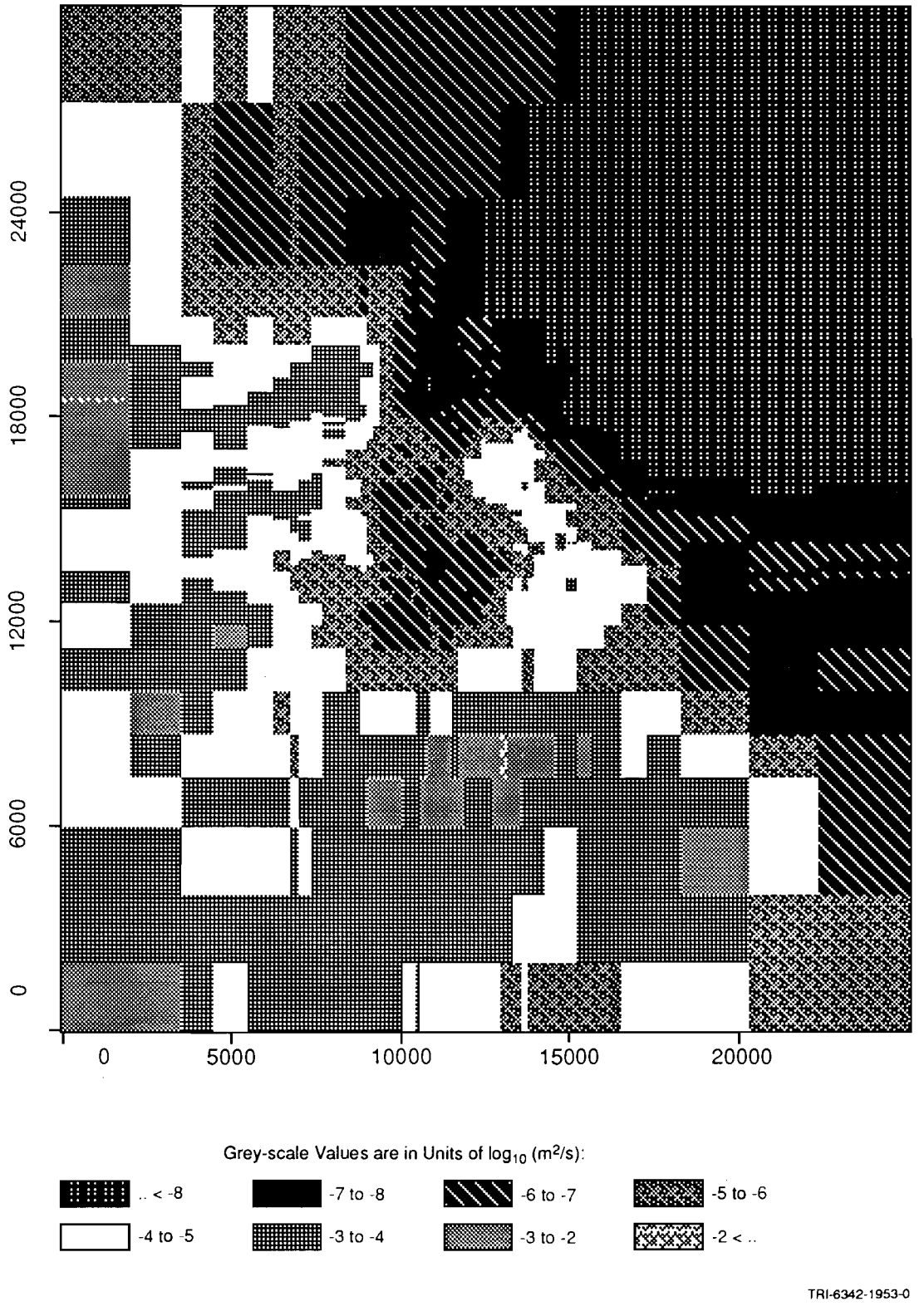

Figure C-5. Realization 15 of Culebra transmissivity.

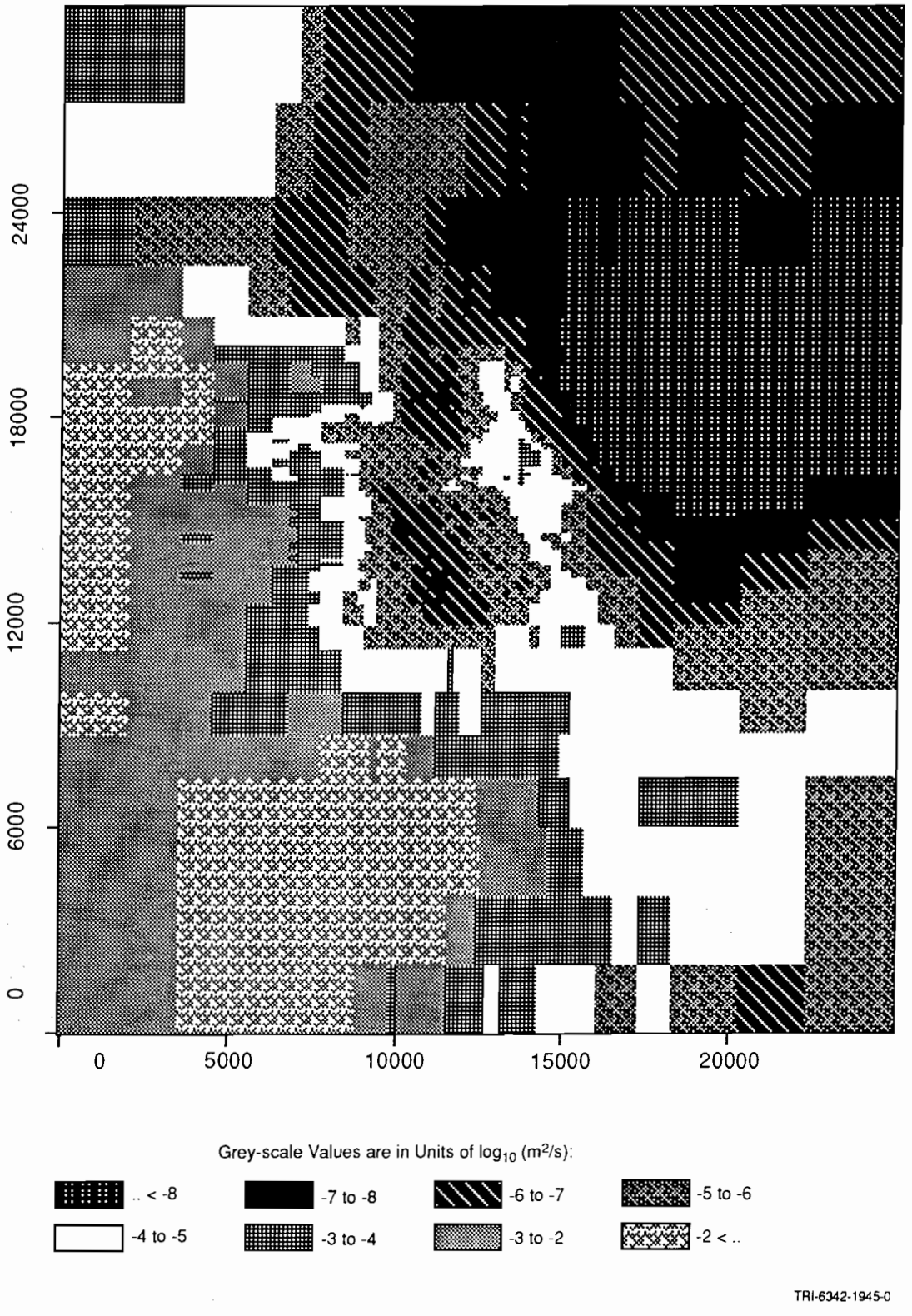

Figure C-6. Realization 18 of Culebra transmissivity.

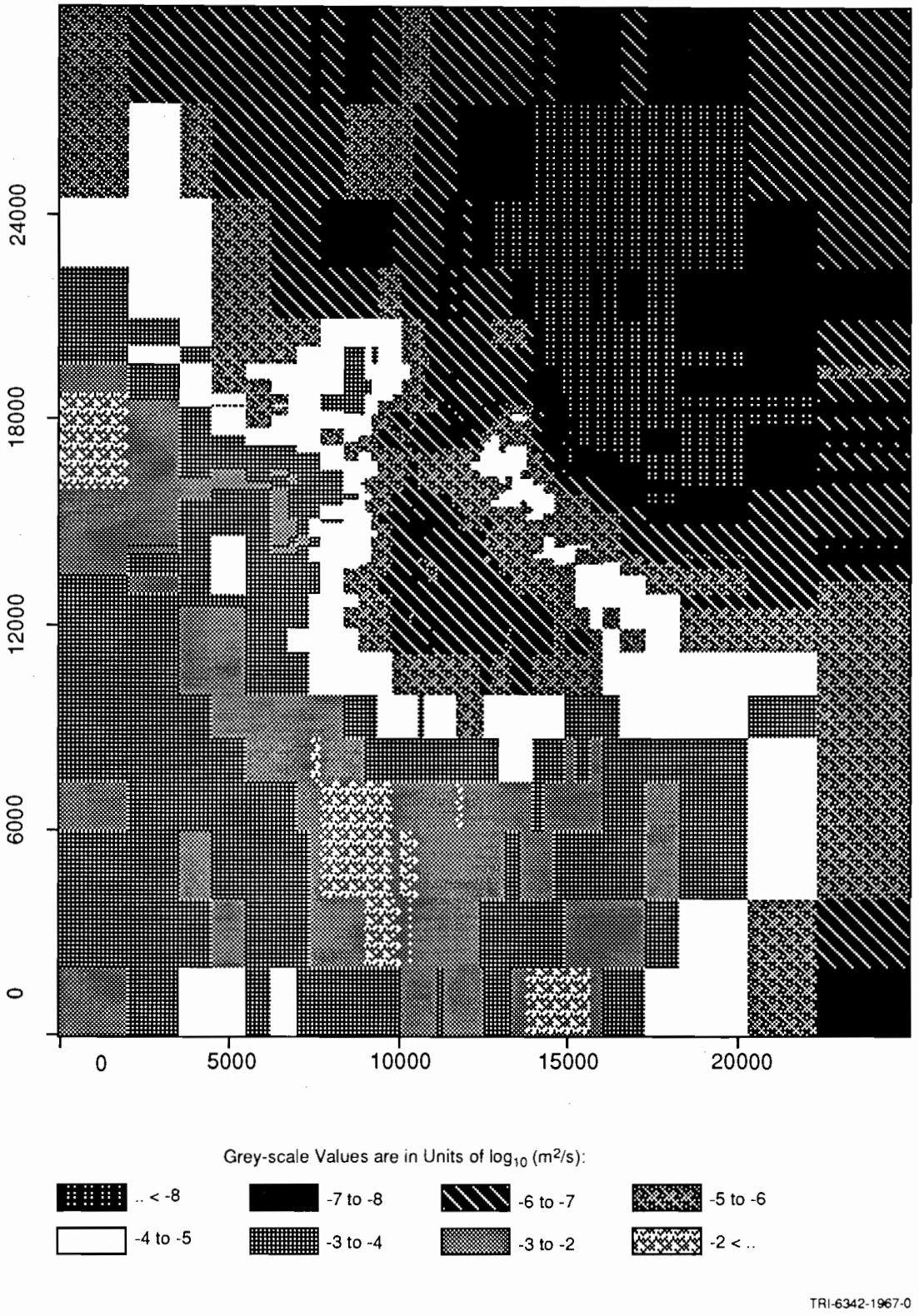

Figure C-7. Realization 53 of Culebra transmissivity.

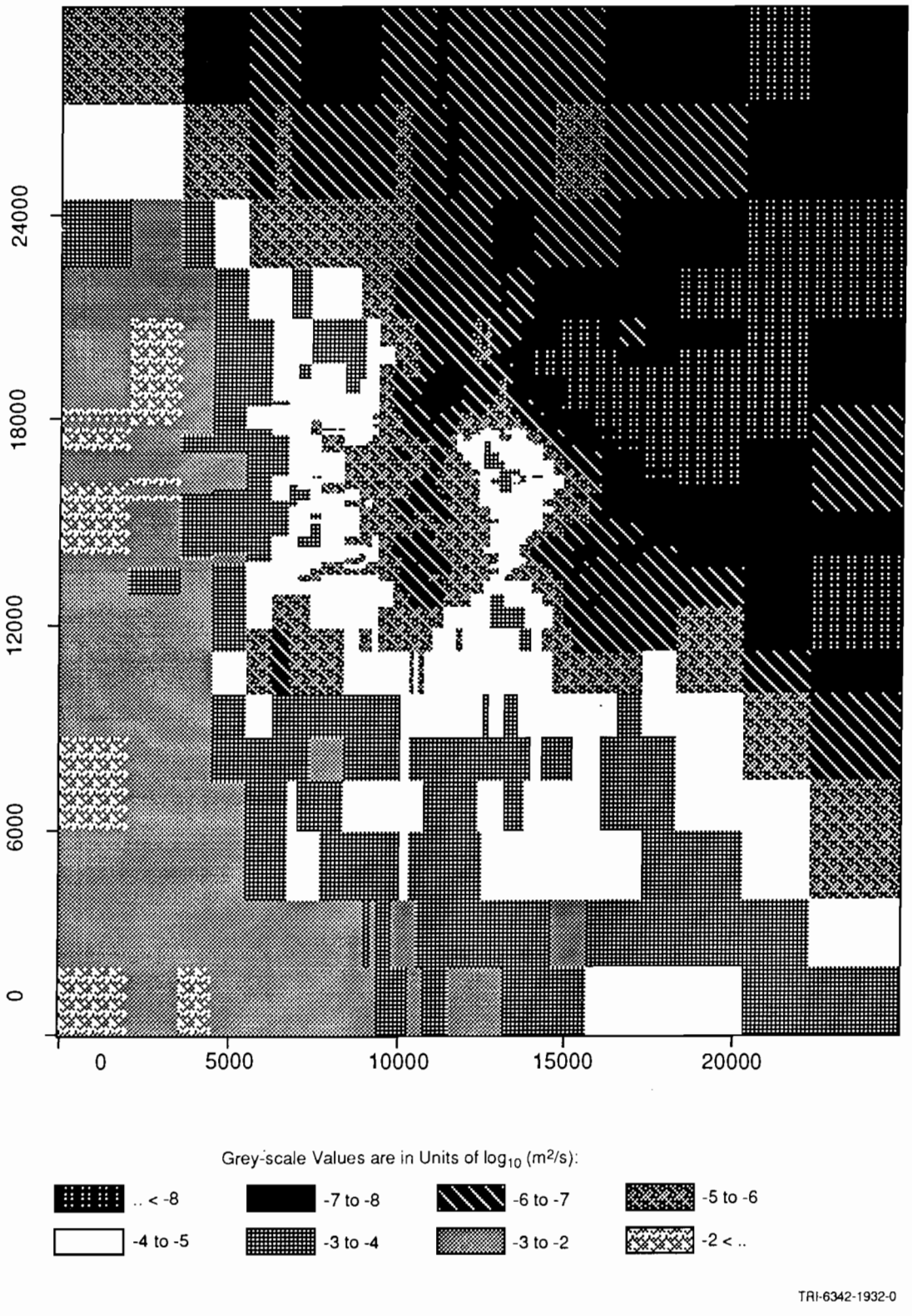

Figure C-8. Realization 16 of Culebra transmissivity.

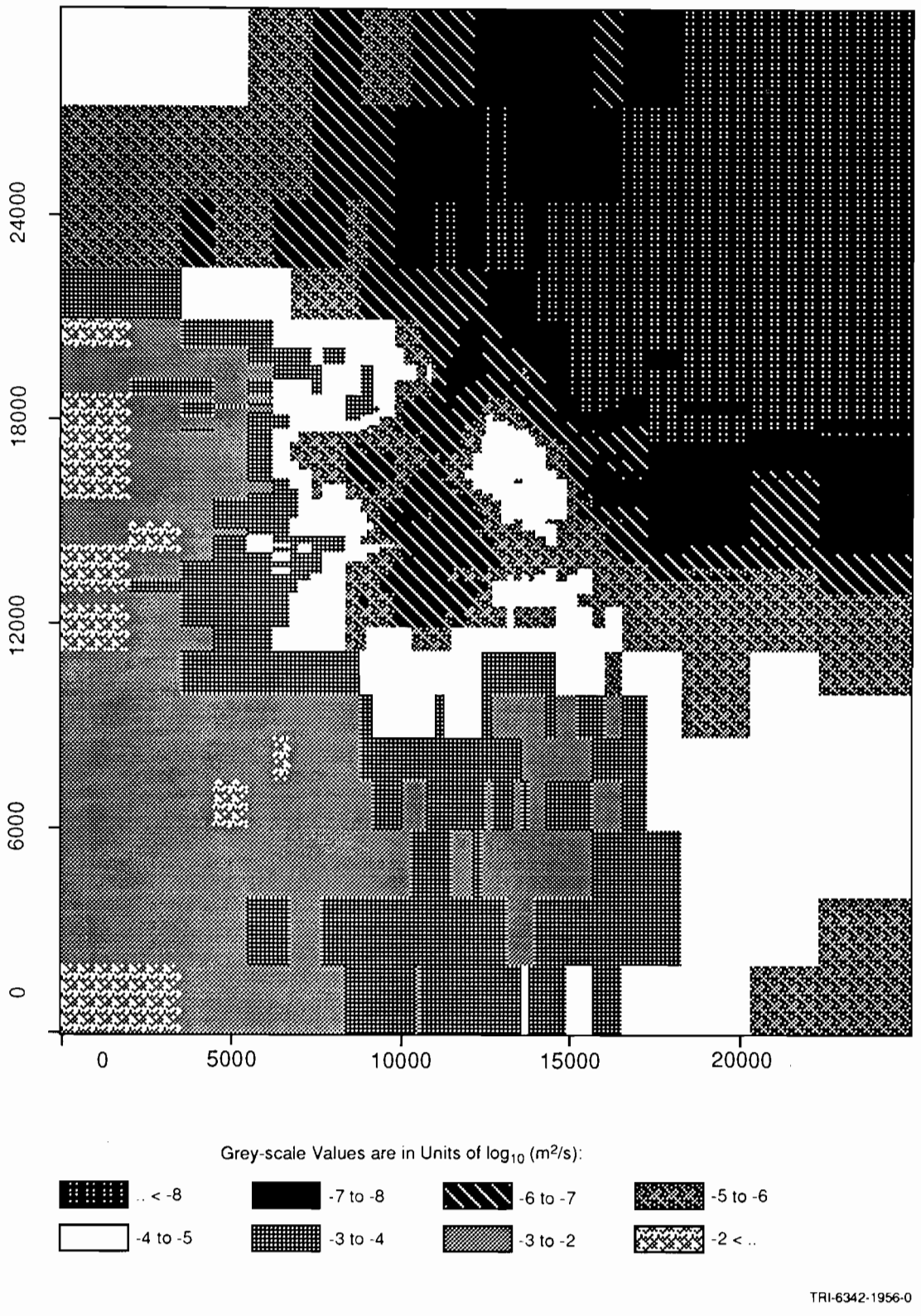

Figure C-9. Realization 36 of Culebra transmissivity.

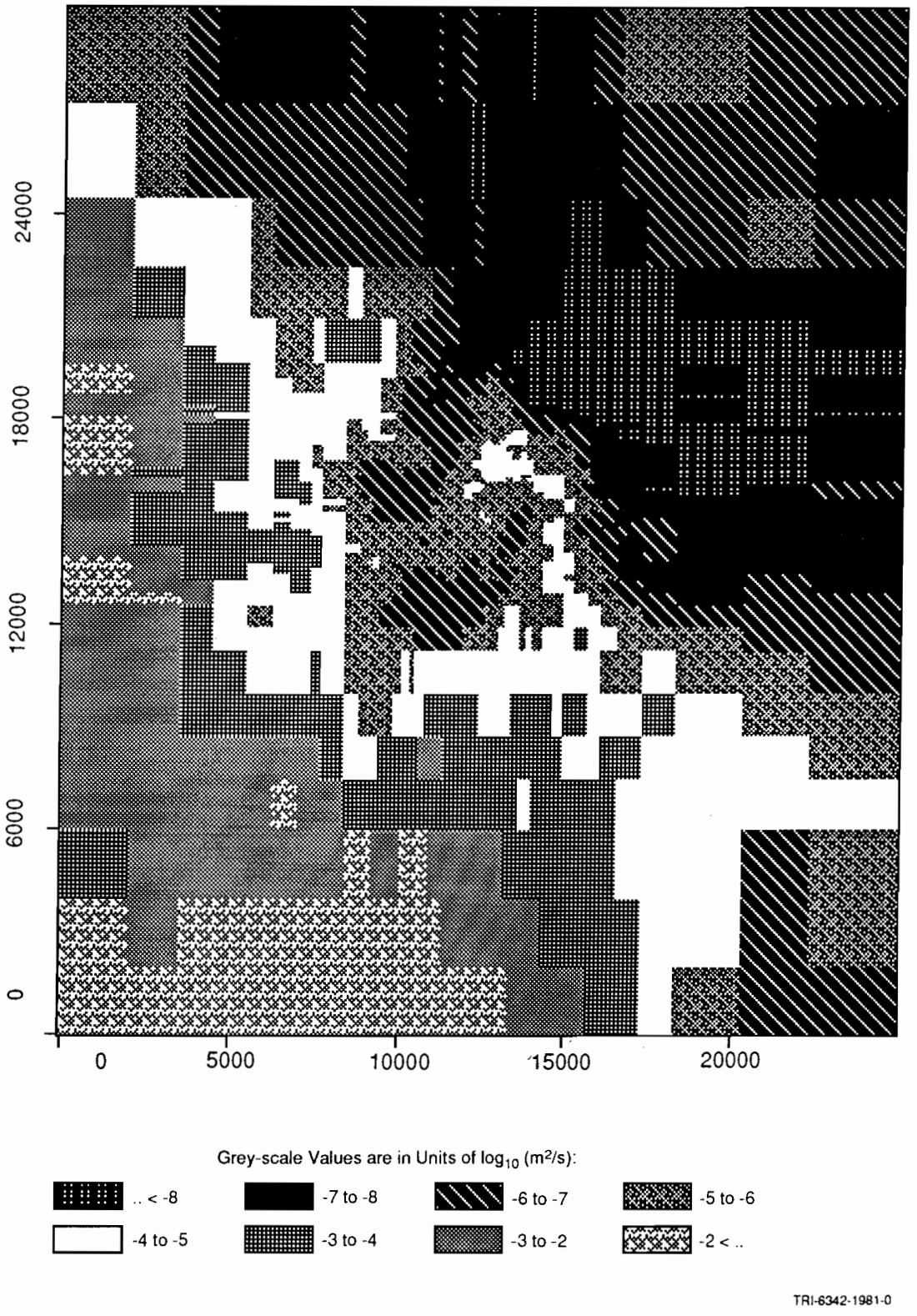

Figure C-10. Realization 19 of Culebra transmissivity.

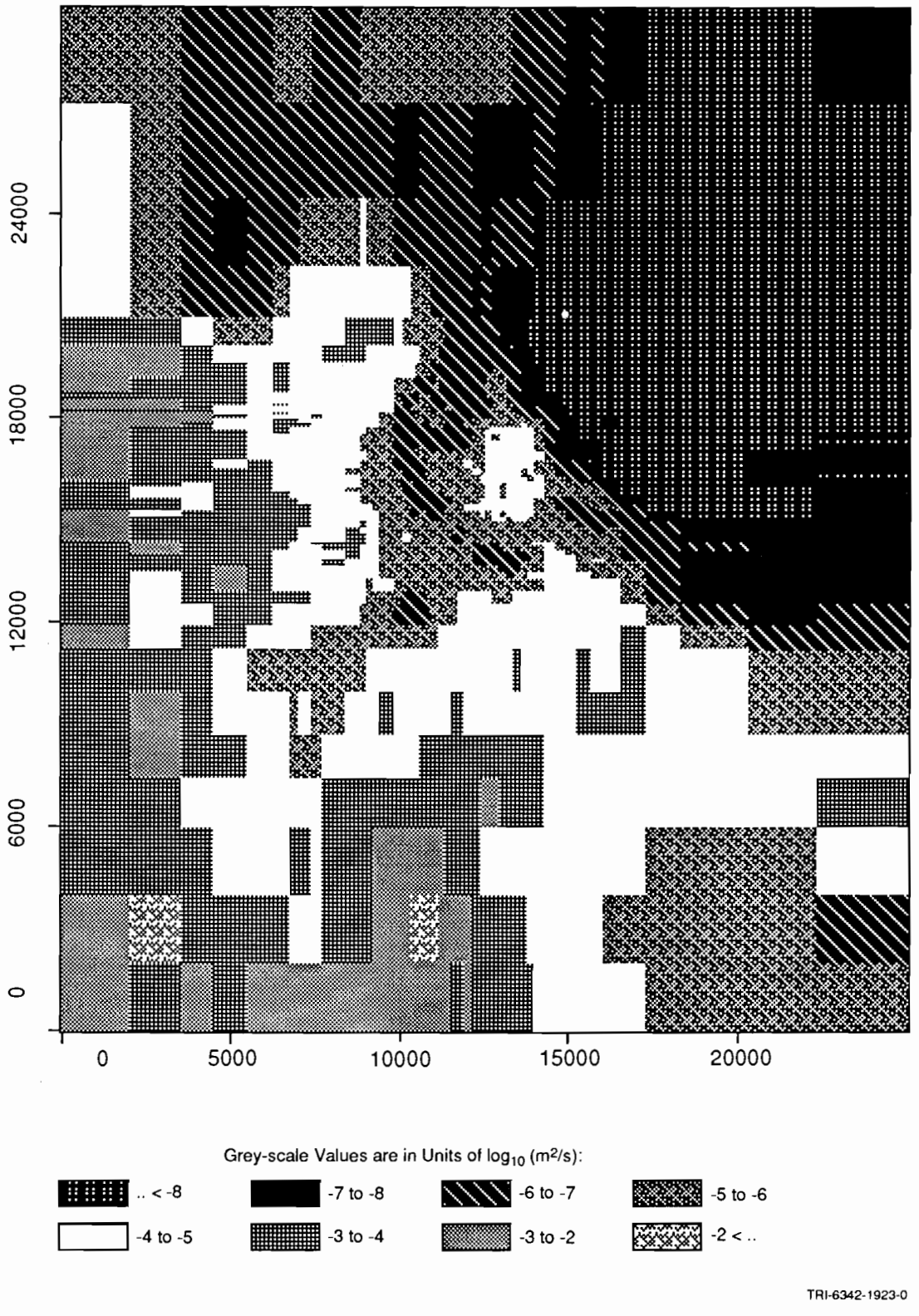

Figure C-11. Realization 66 of Culebra transmissivity.

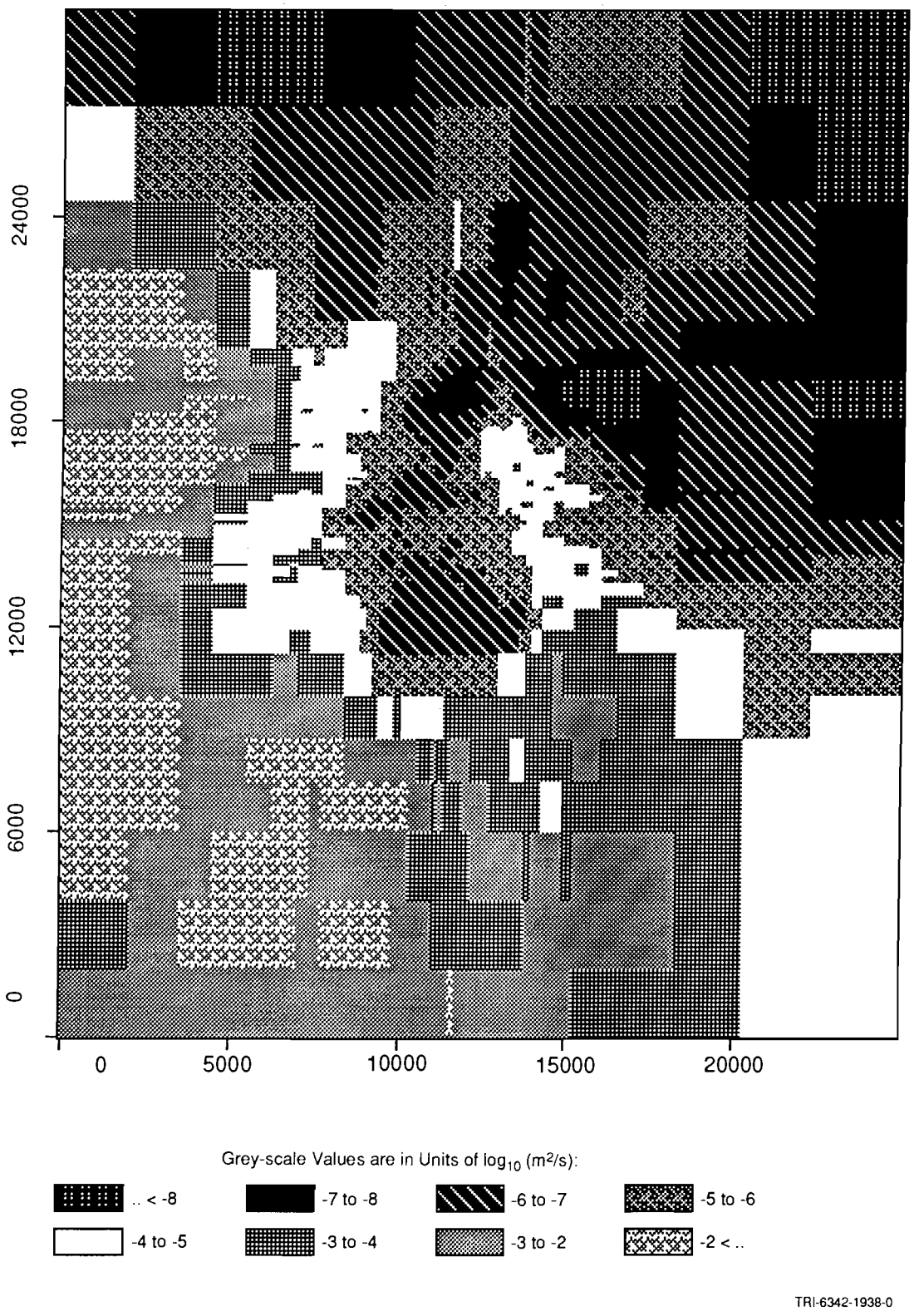

Figure C-12. Realization 45 of Culebra transmissivity.

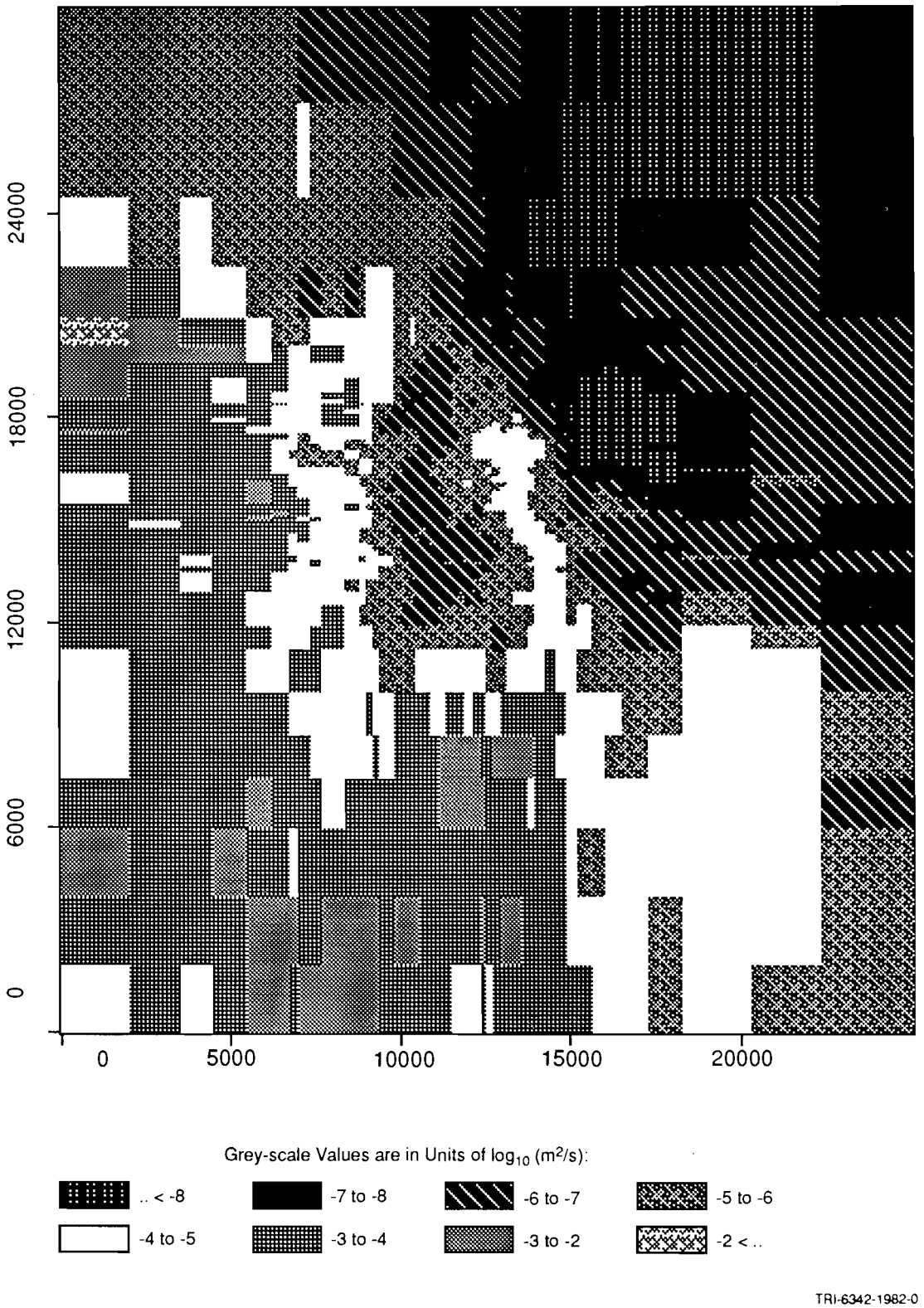

Figure C-13. Realization 34 of Culebra transmissivity.

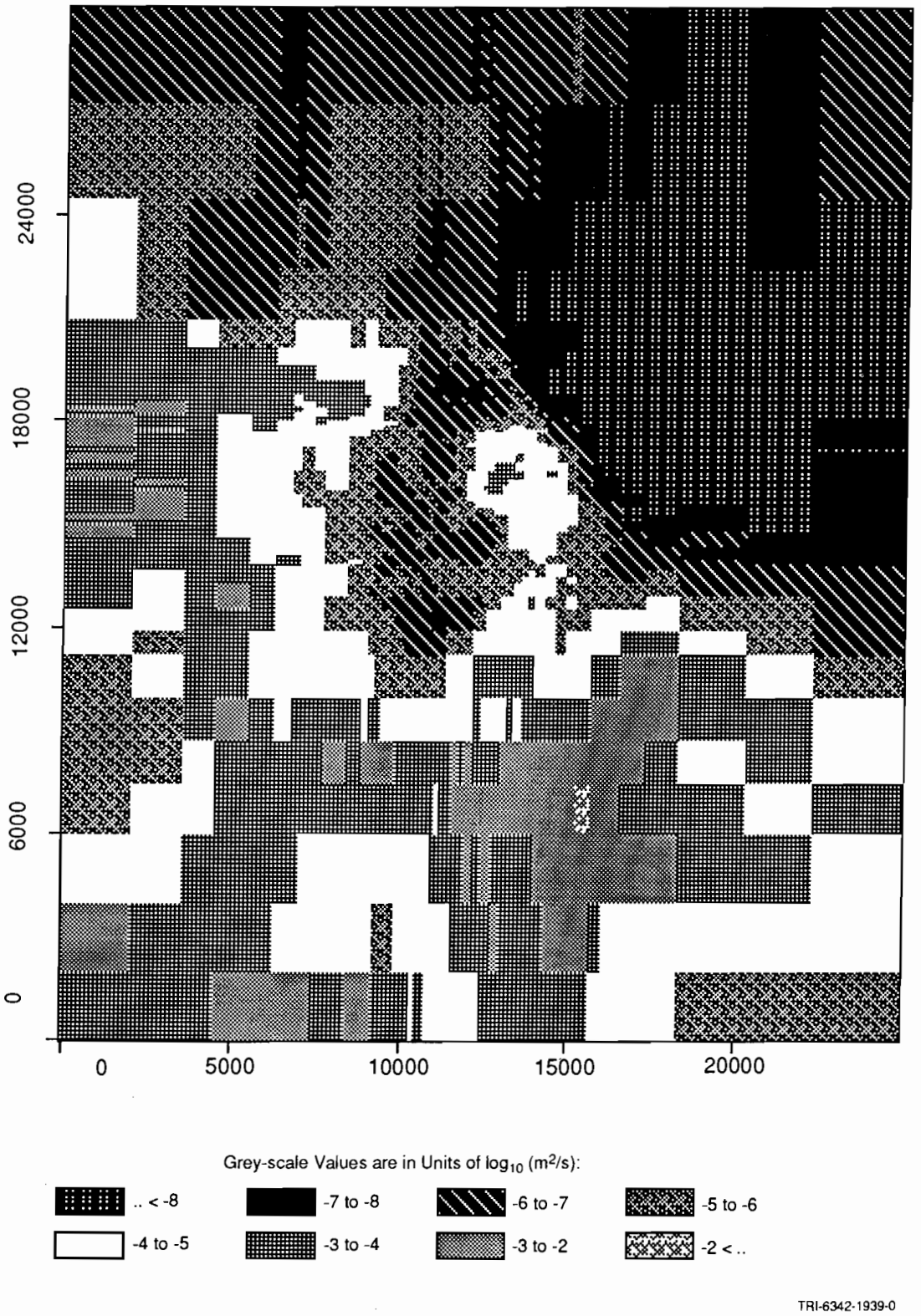

Figure C-14. Realization 24 of Culebra transmissivity.

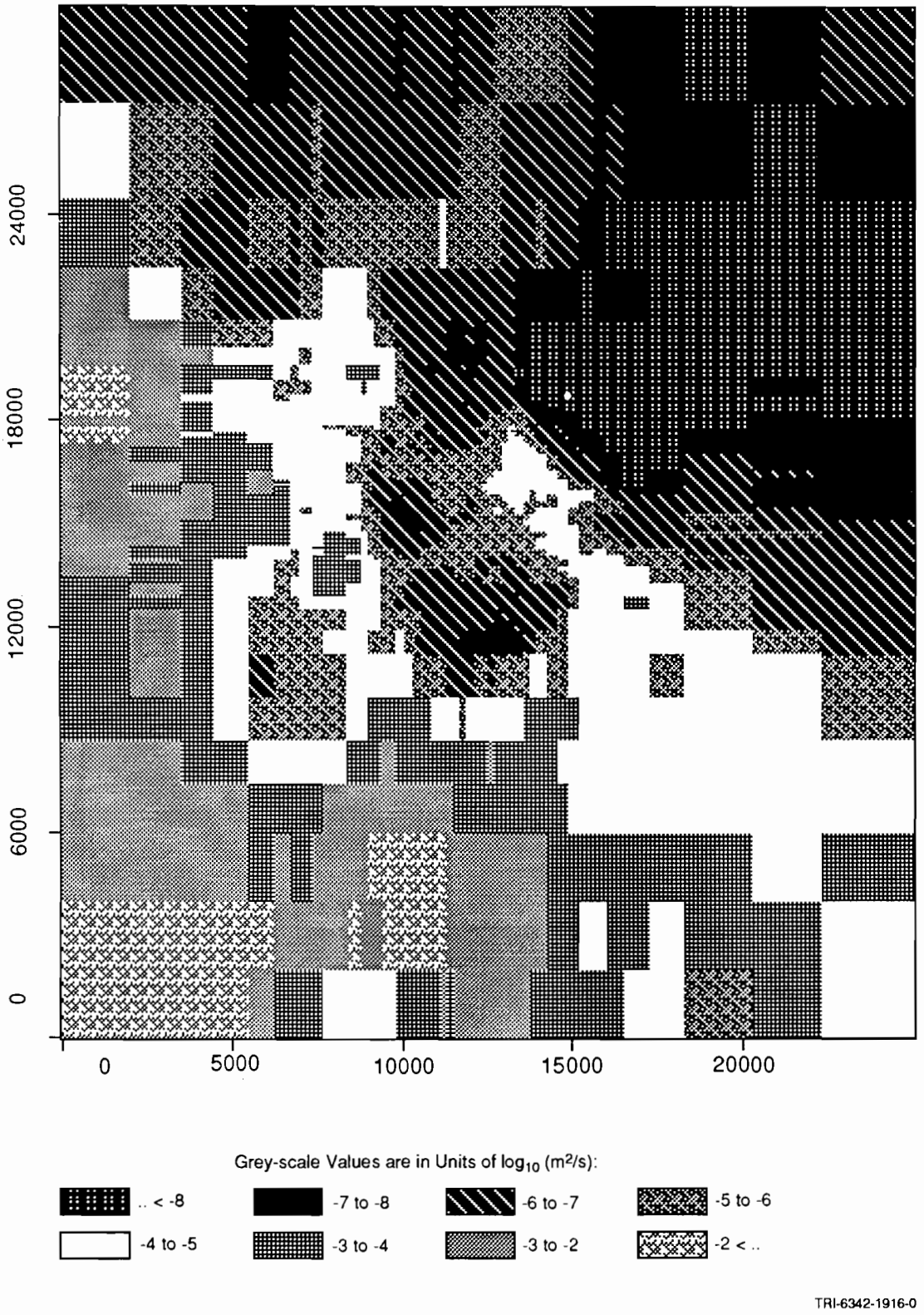

Figure C-15. Realization 63 of Culebra transmissivity.

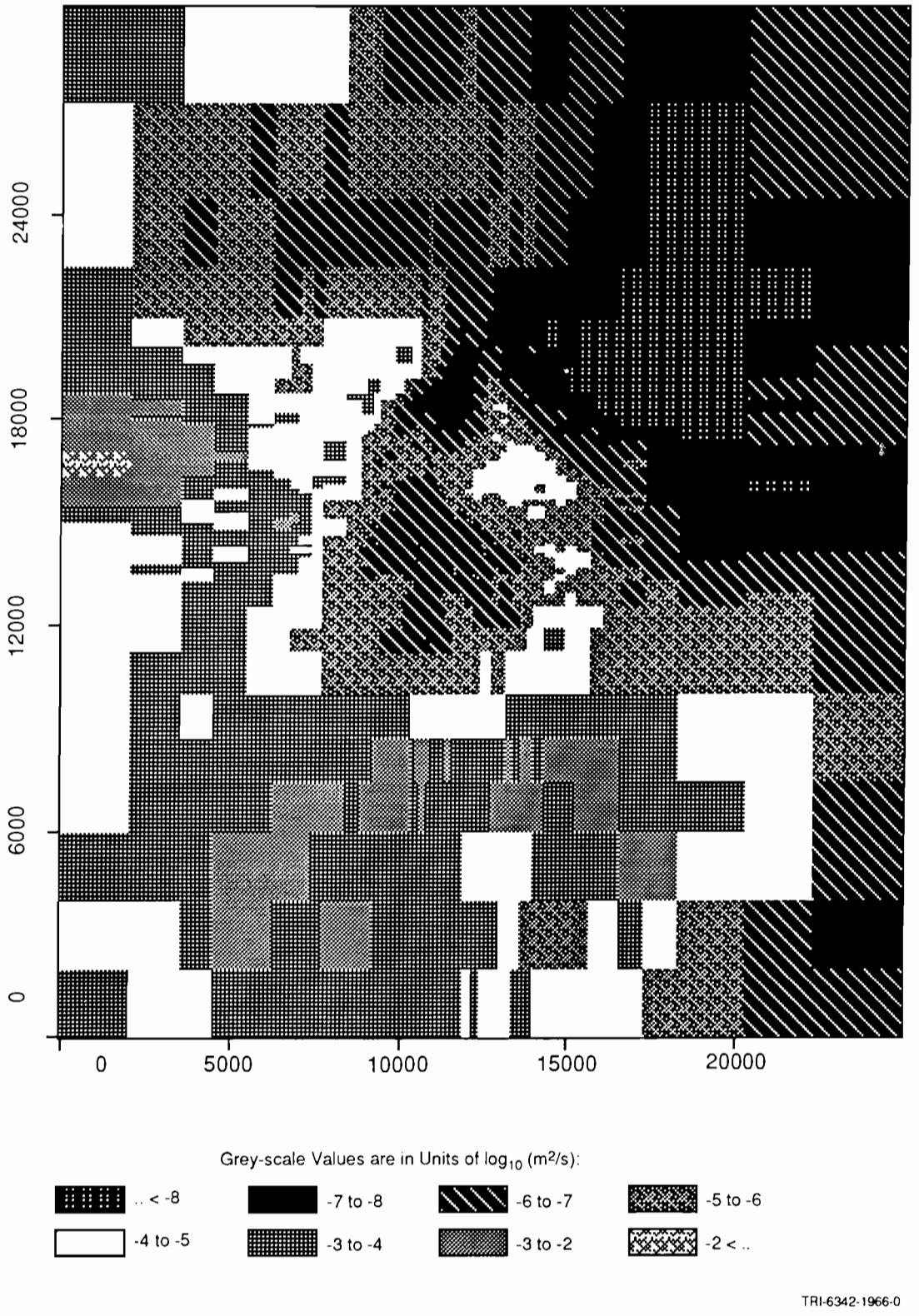

Figure C-16. Realization 70 of Culebra transmissivity.

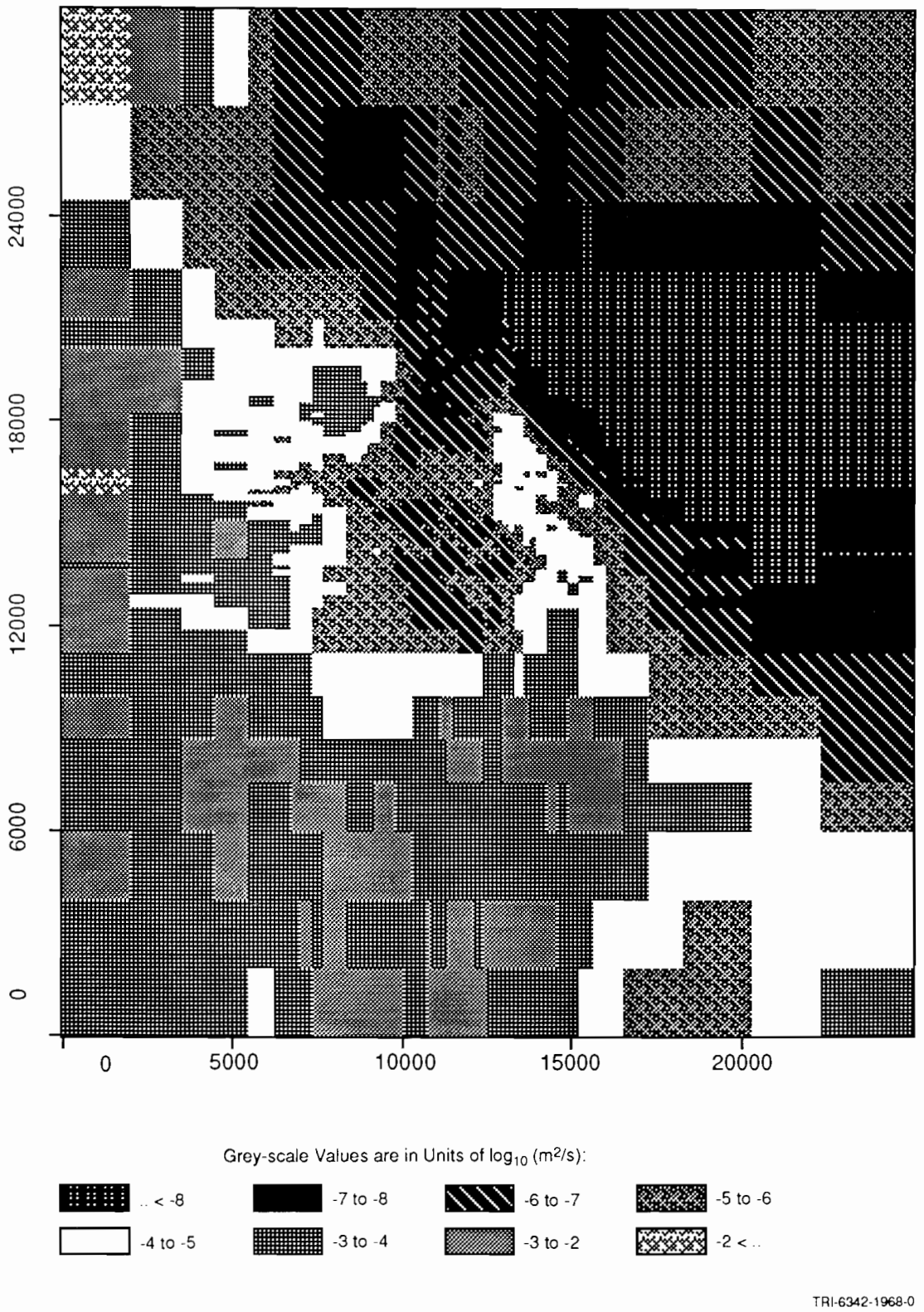

Figure C-17. Realization 42 of Culebra transmissivity.

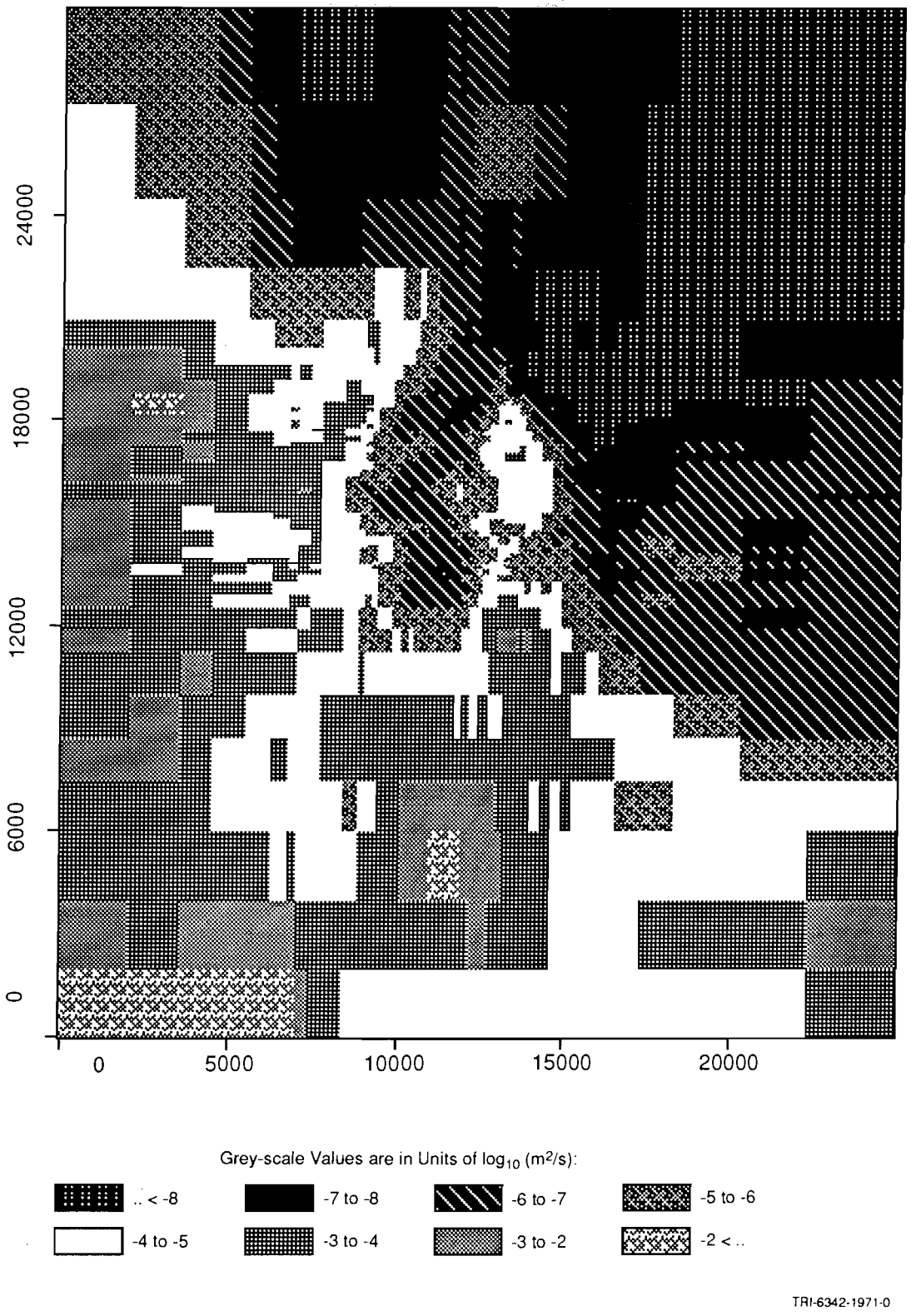

Figure C-18. Realization 56 of Culebra transmissivity.

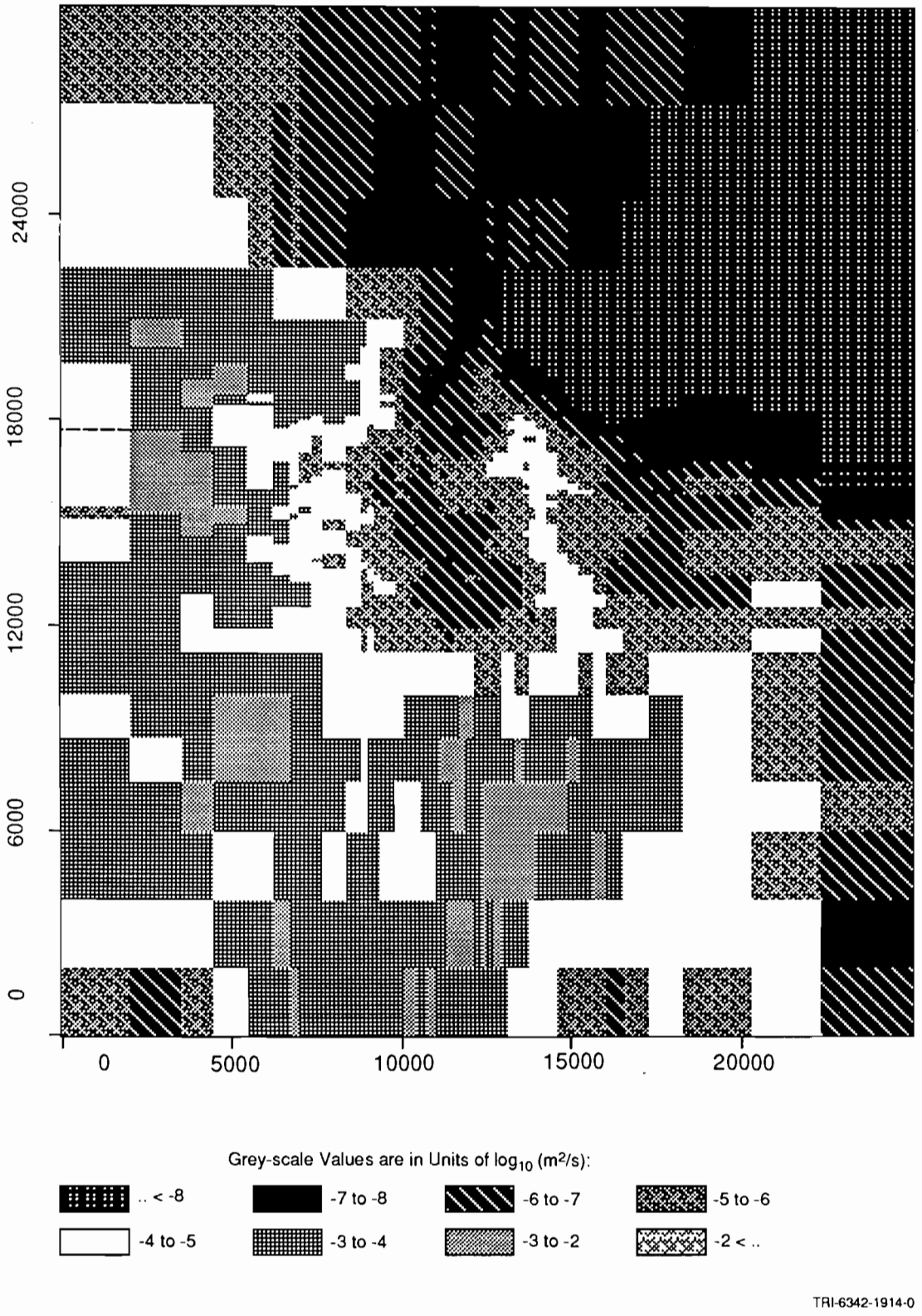

Figure C-19. Realization 69 of Culebra transmissivity.

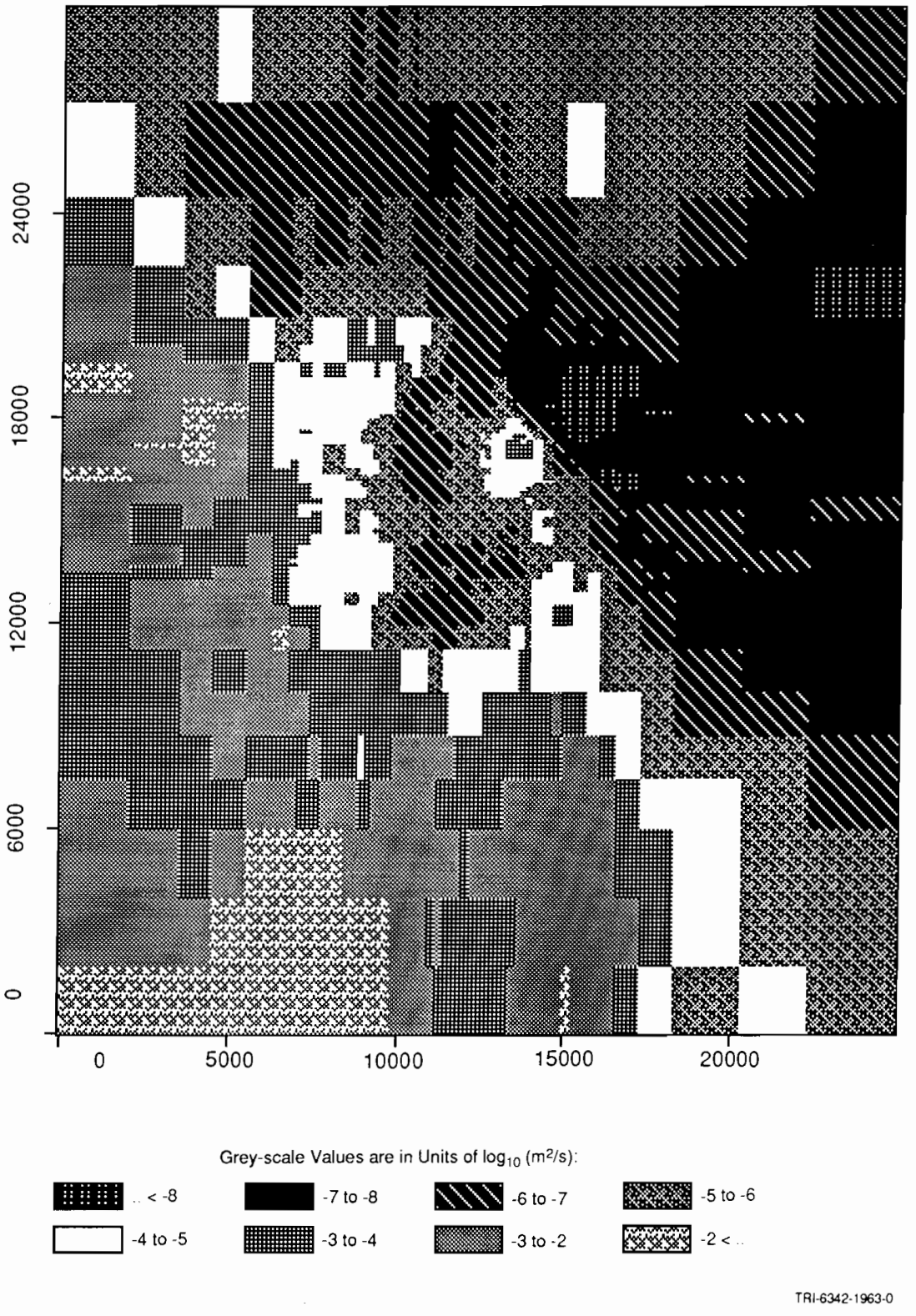

Figure C-20. Realization 7 of Culebra transmissivity.

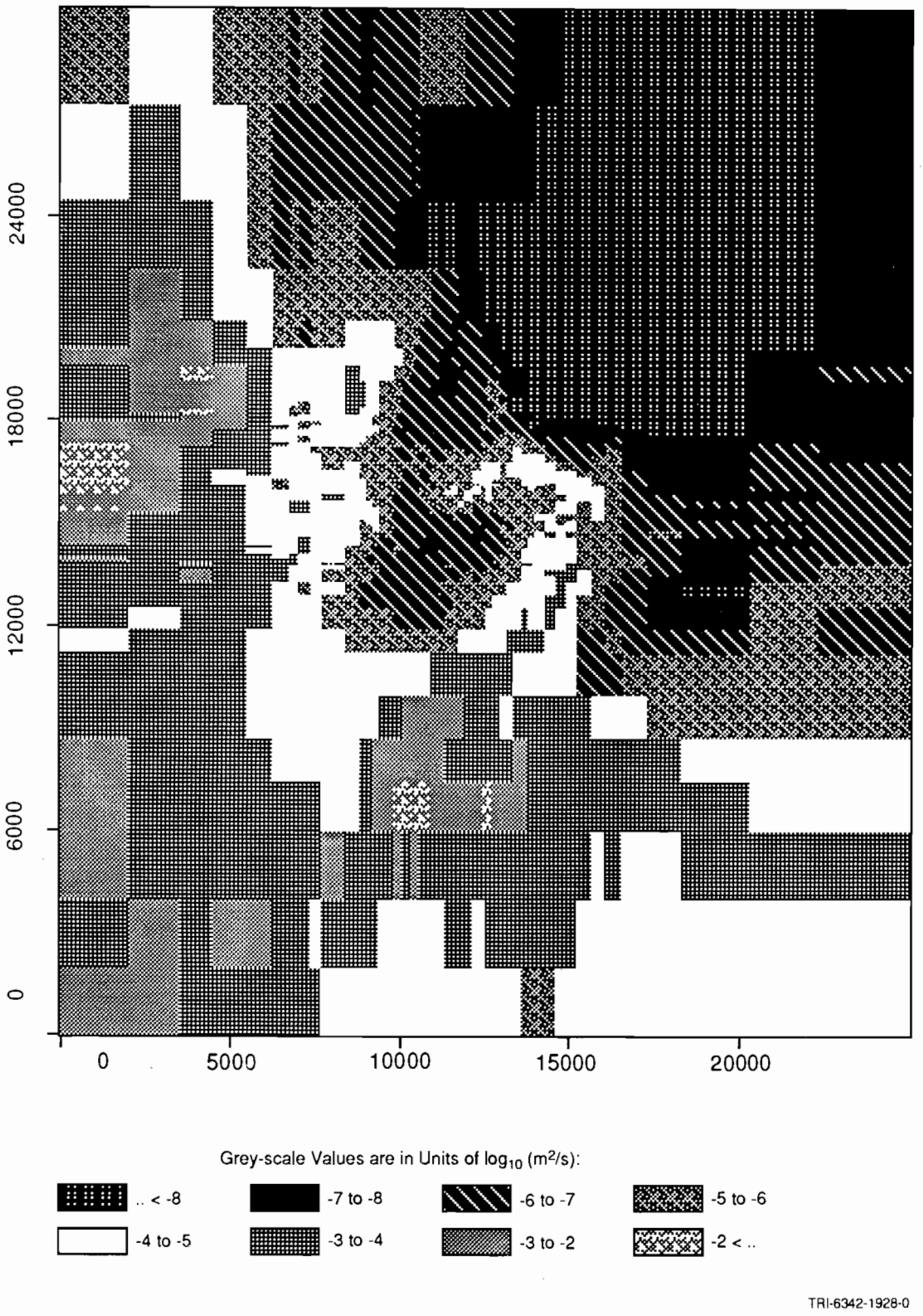

Figure C-21. Realization 52 of Culebra transmissivity.

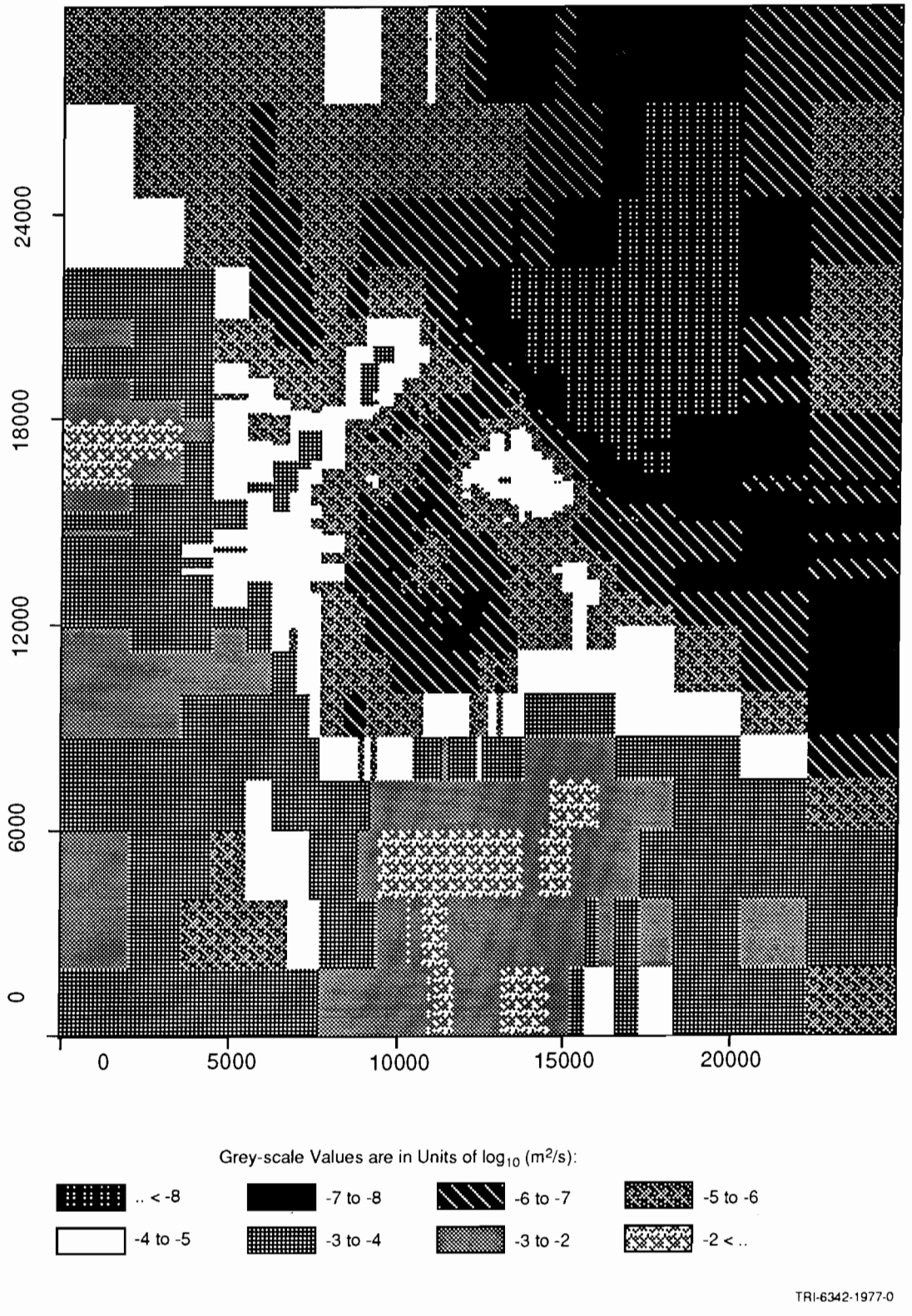

Figure C-22. Realization 20 of Culebra transmissivity.

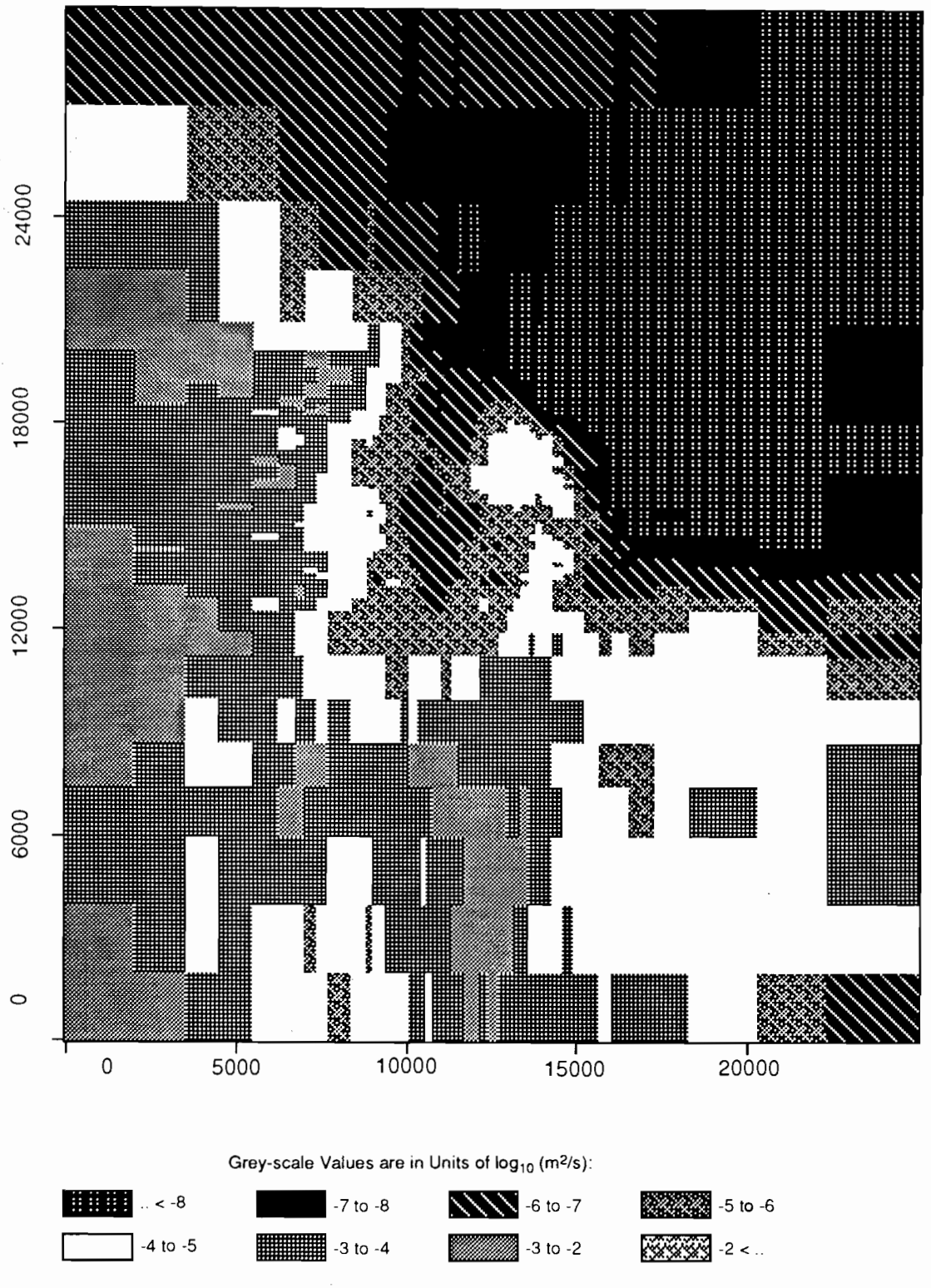

Figure C-23. Realization 33 of Culebra transmissivity.

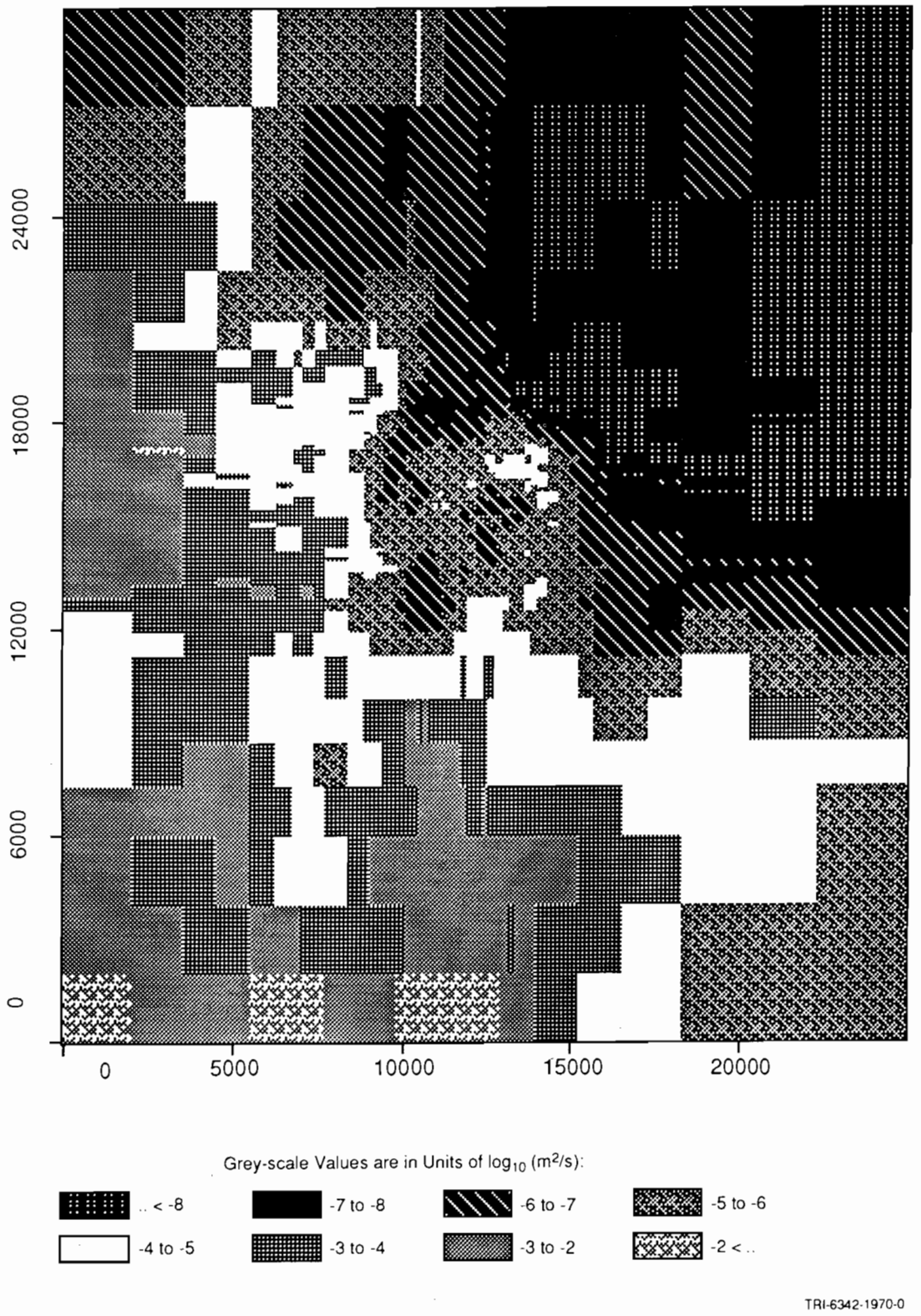

Figure C-24. Realization 39 of Culebra transmissivity.

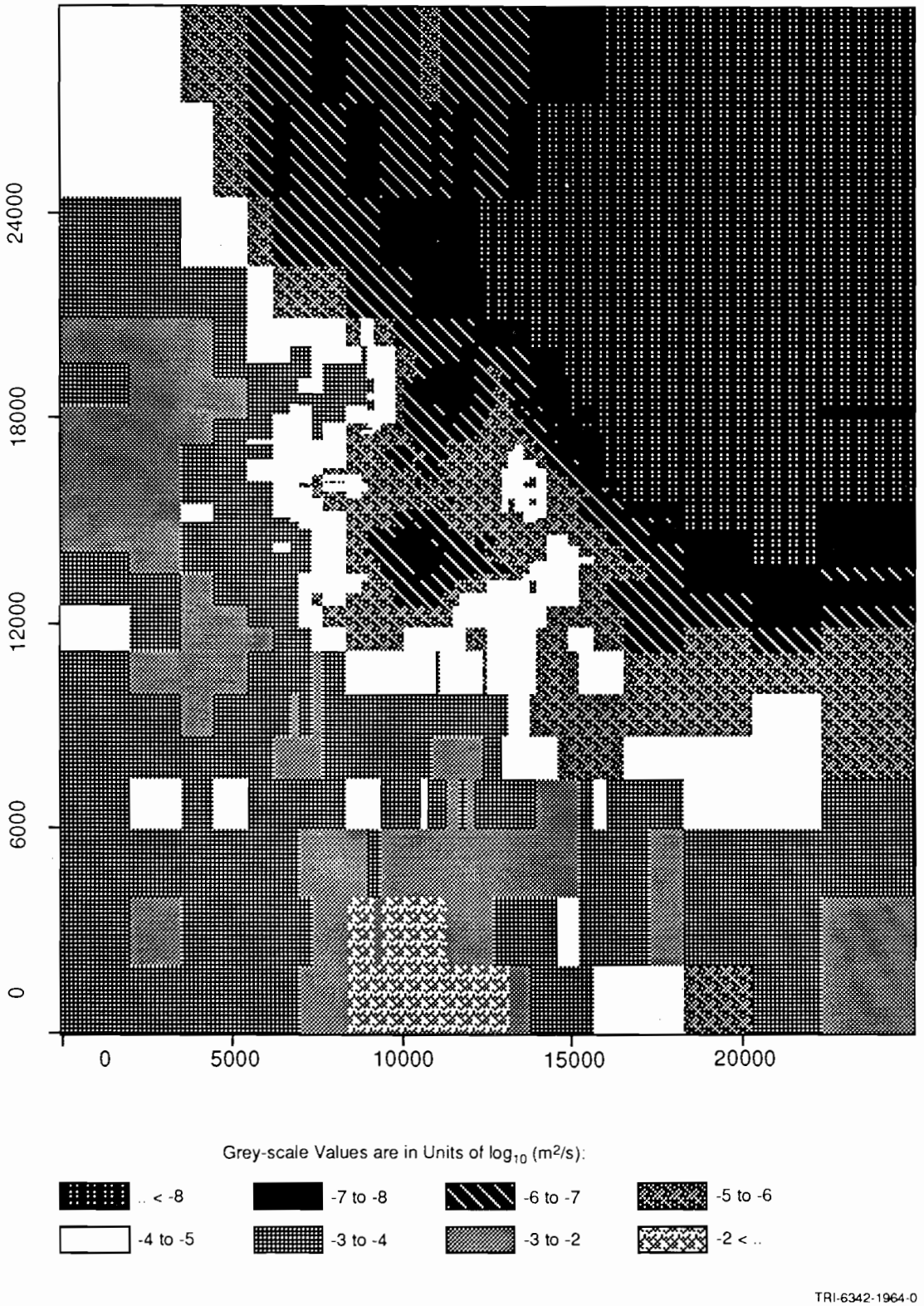

Figure C-25. Realization 28 of Culebra transmissivity.

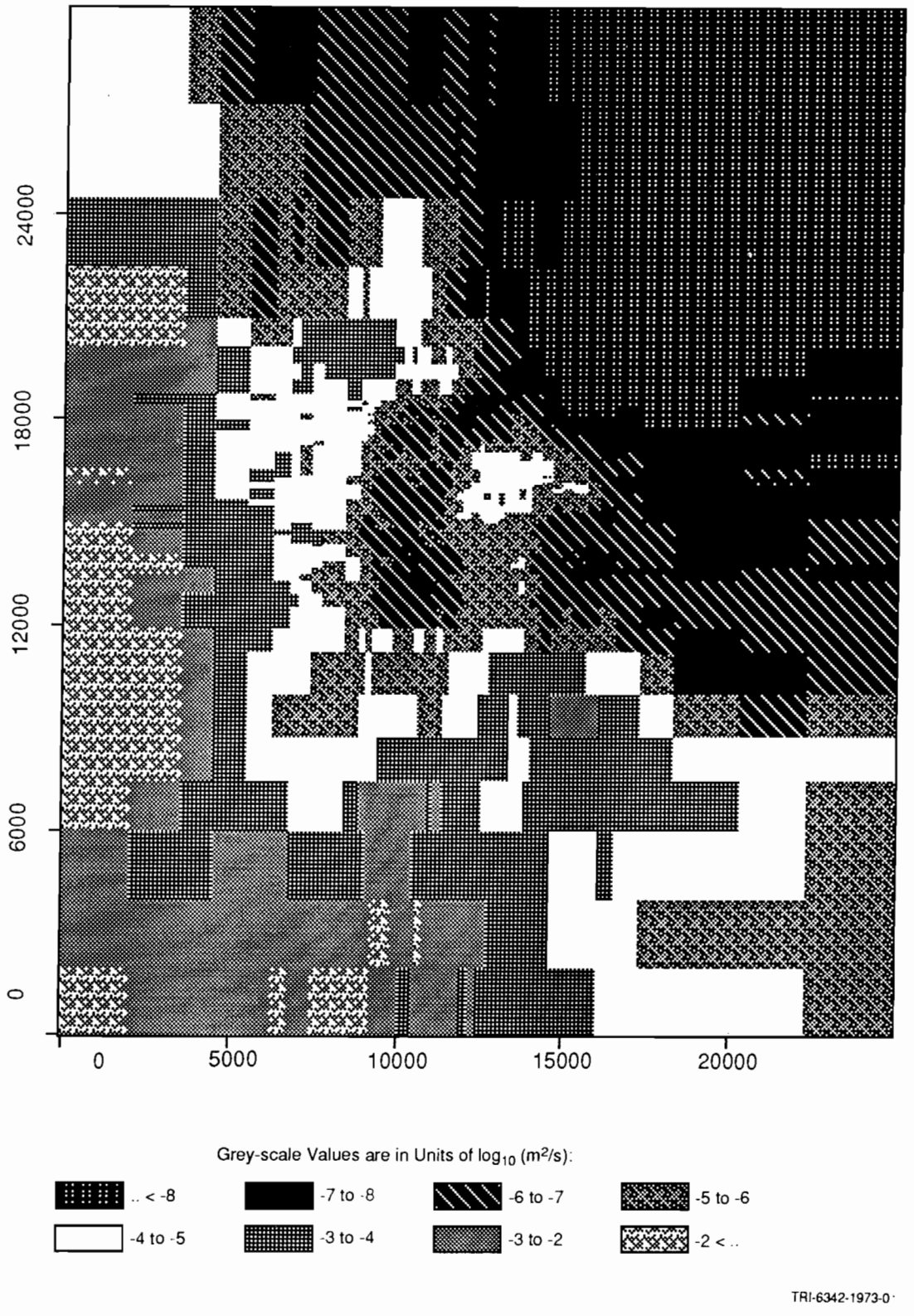

Figure C-26. Realization 1 of Culebra transmissivity.

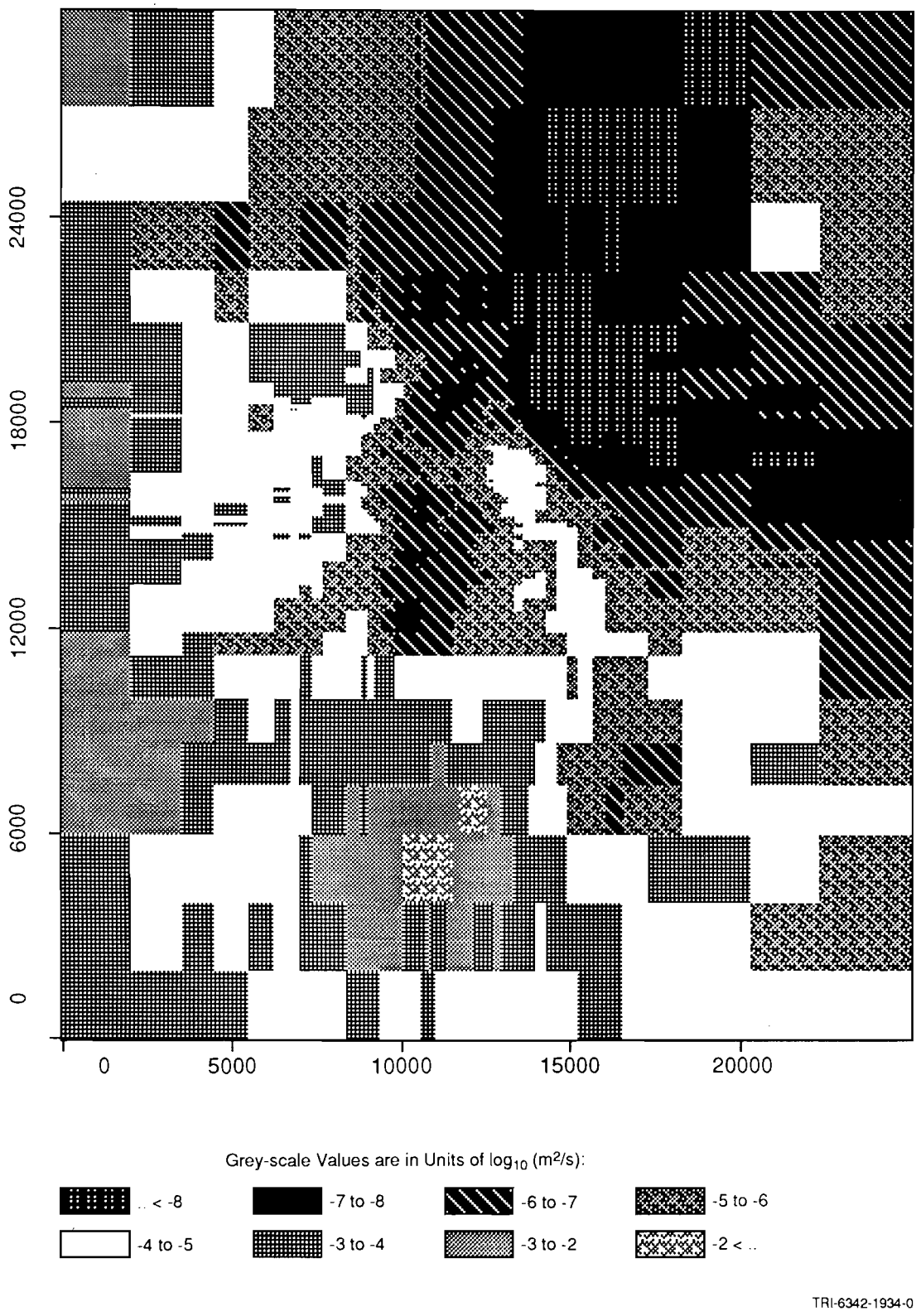

Figure C-27. Realization 55 of Culebra transmissivity.

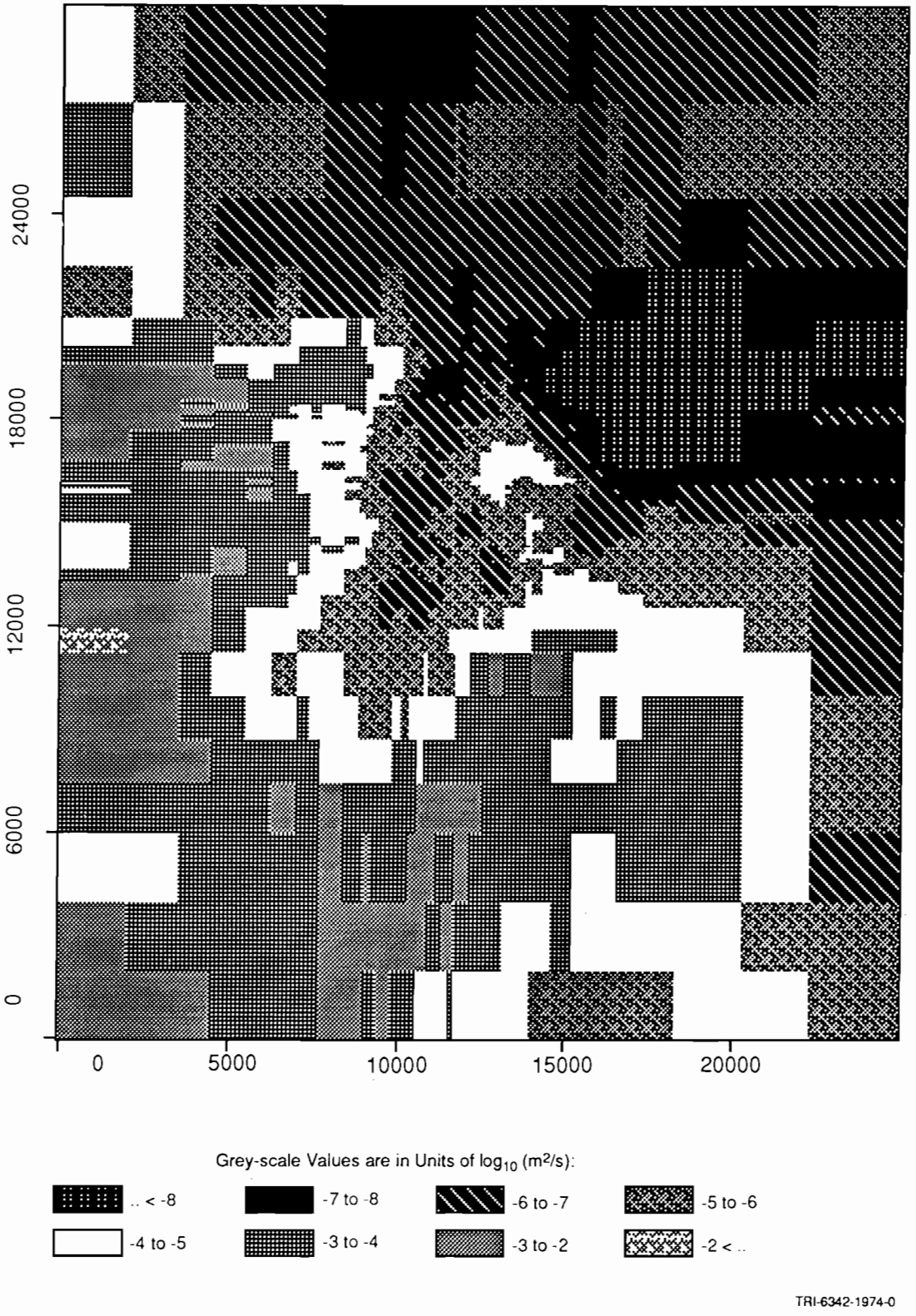

Figure C-28. Realization 43 of Culebra transmissivity.

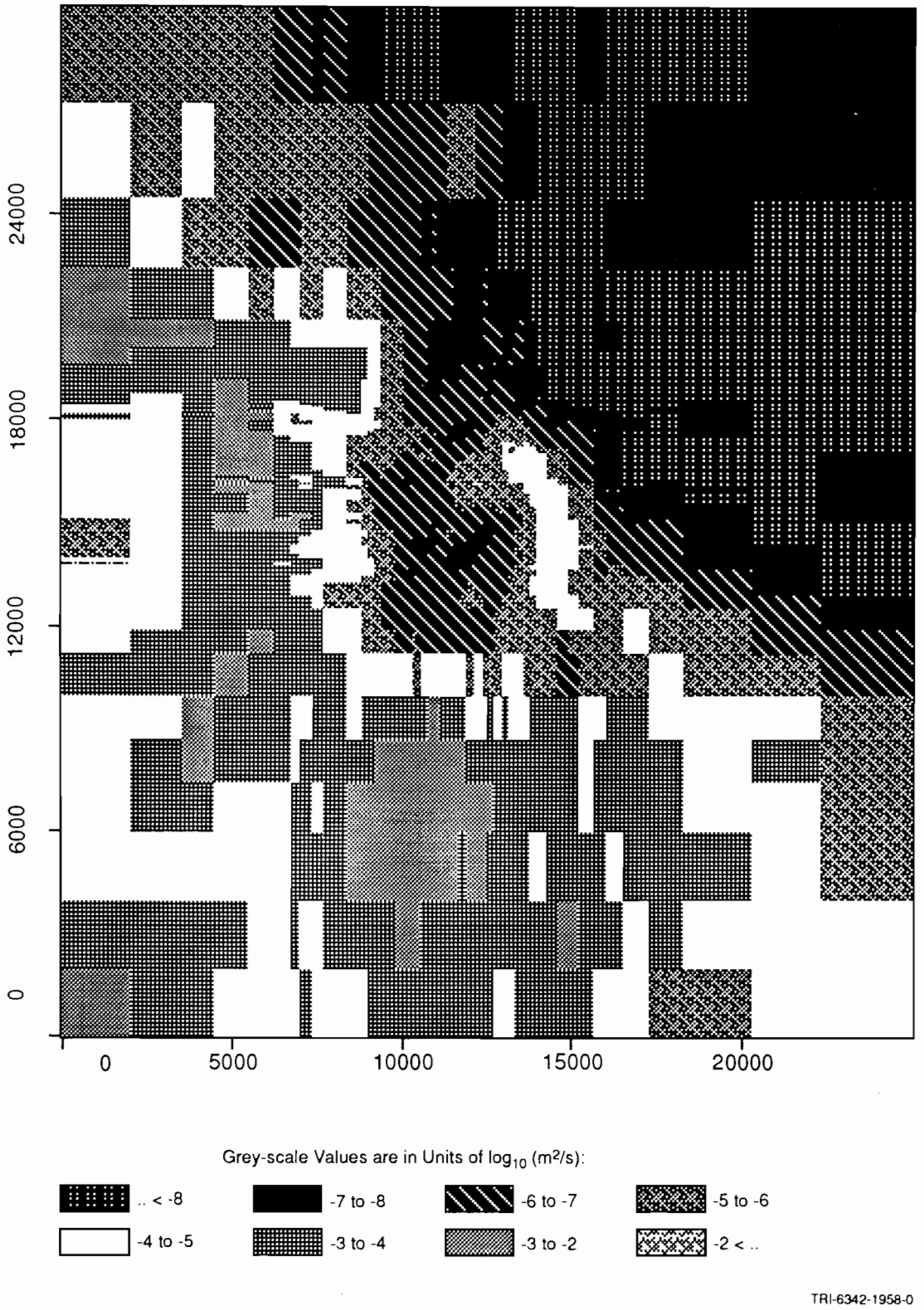

Figure C-29. Realization 2 of Culebra transmissivity.

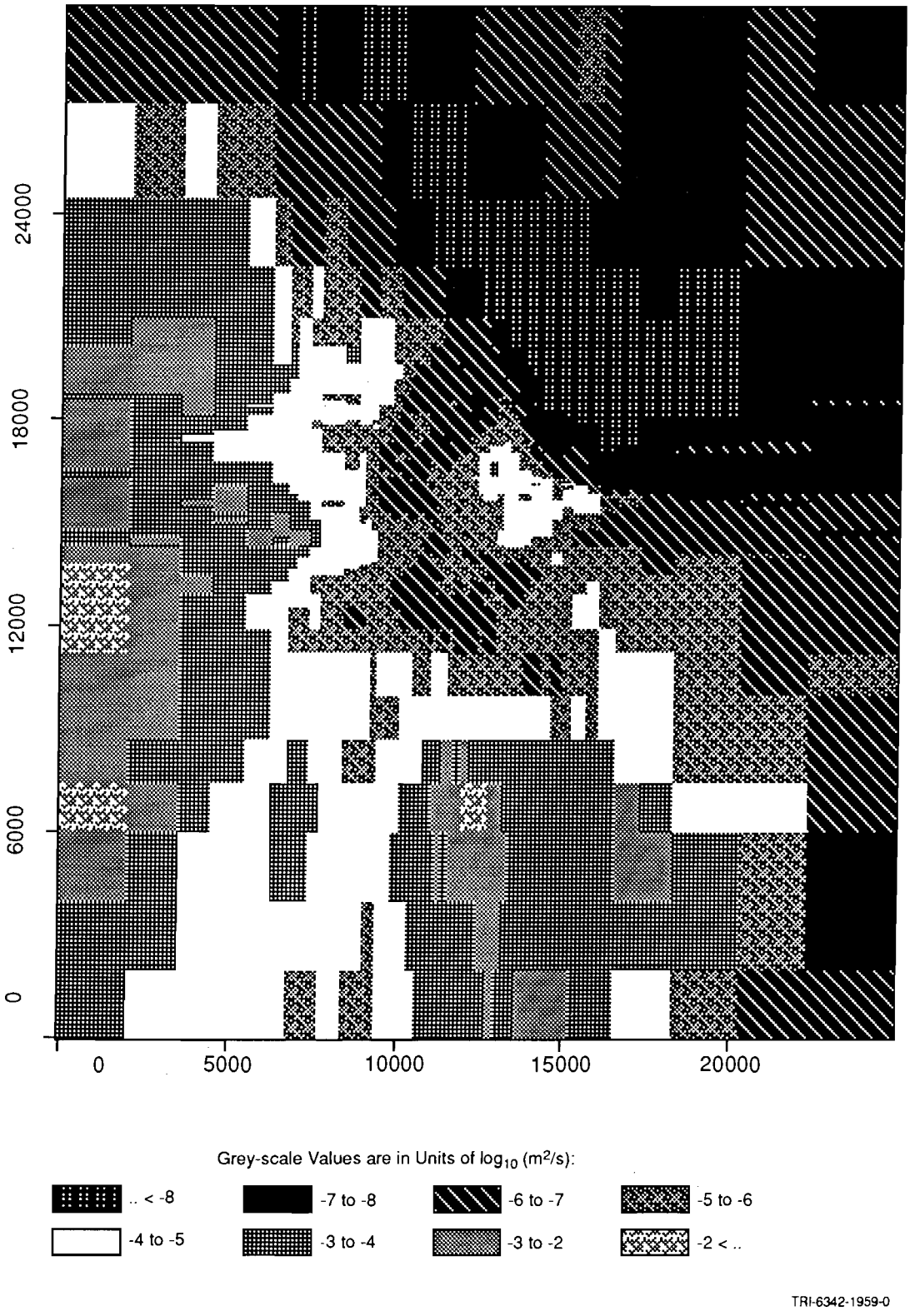

Figure C-30. Realization 47 of Culebra transmissivity.

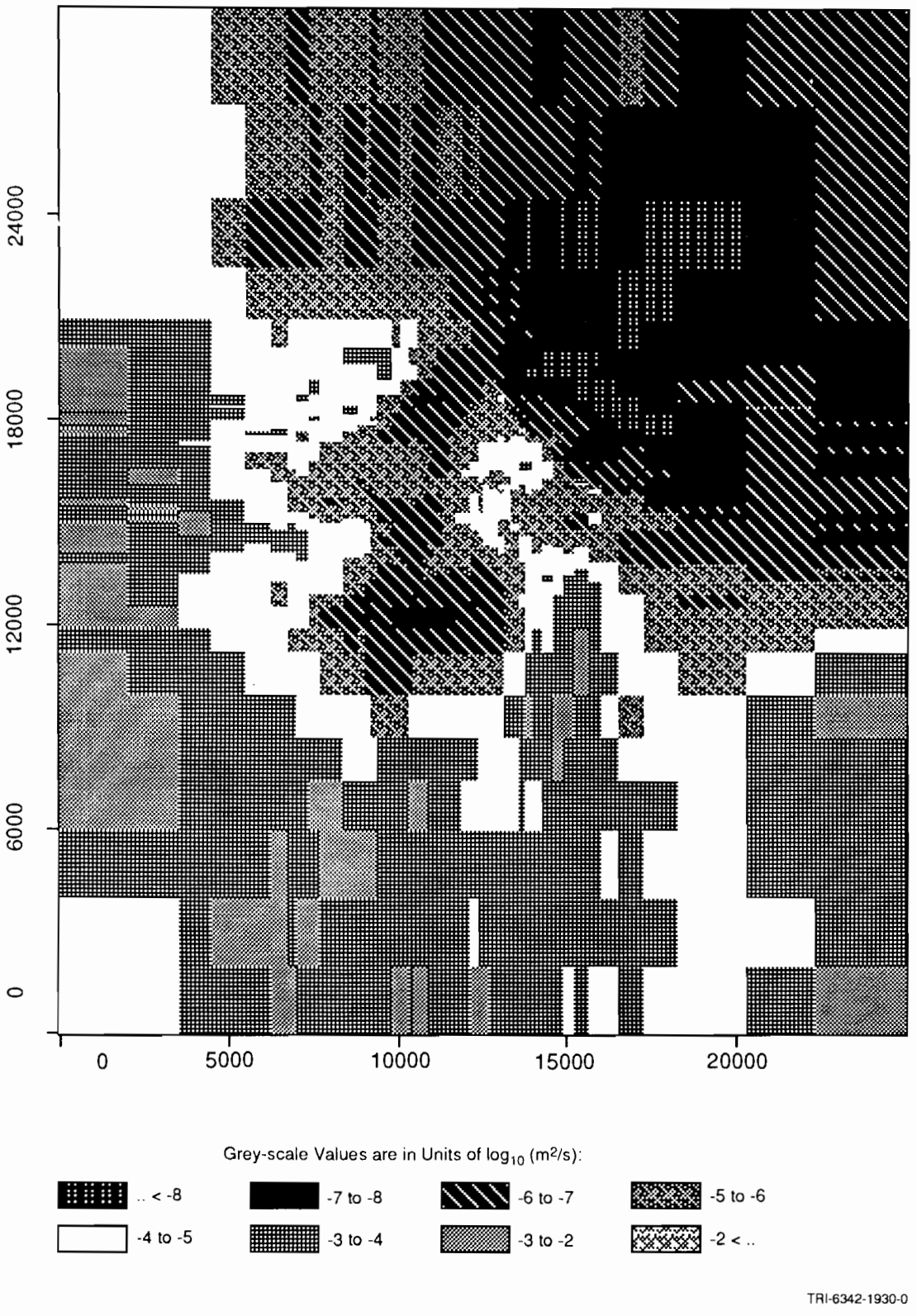

Figure C-31. Realization 48 of Culebra transmissivity.

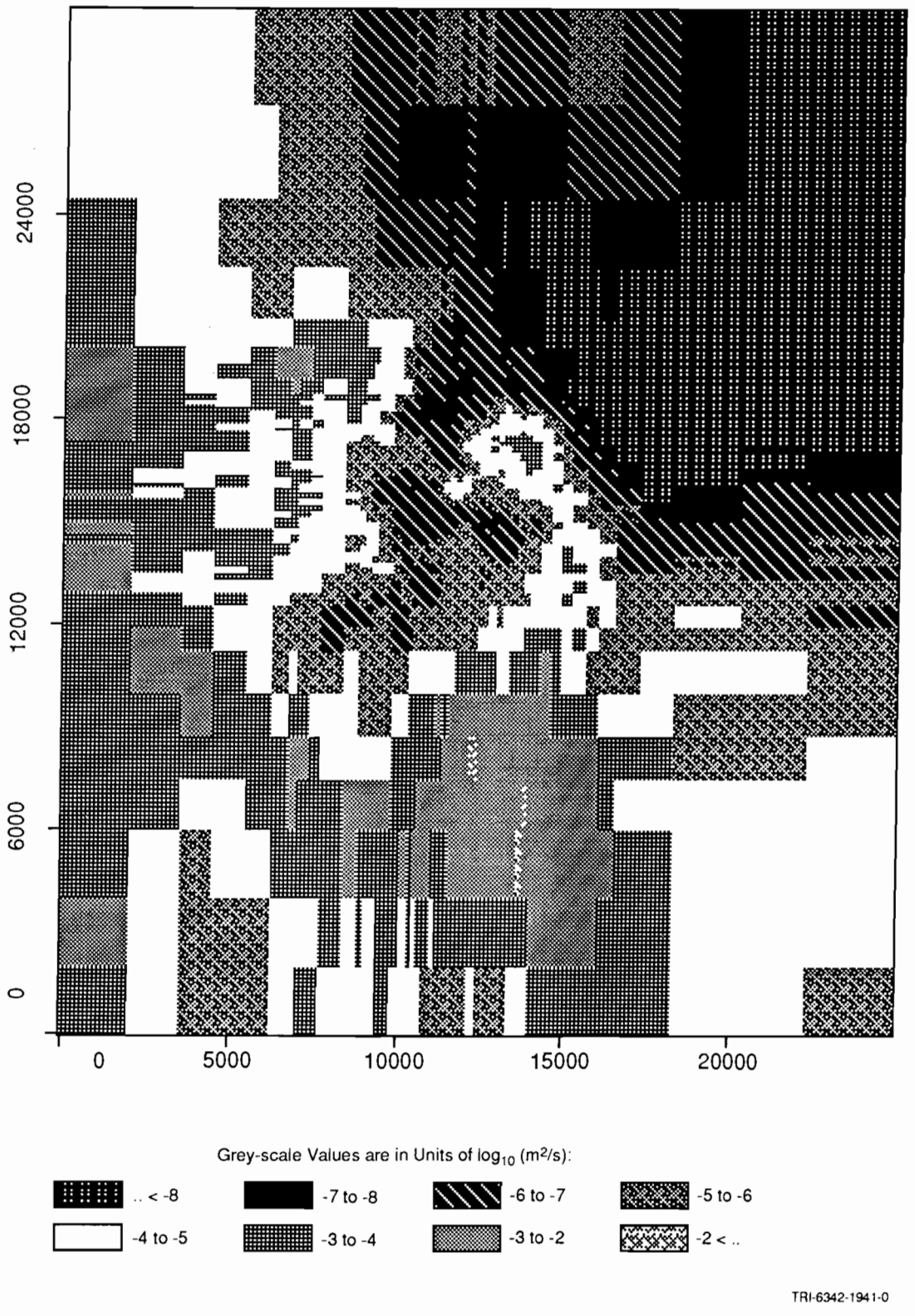

Figure C-32. Realization 29 of Culebra transmissivity.

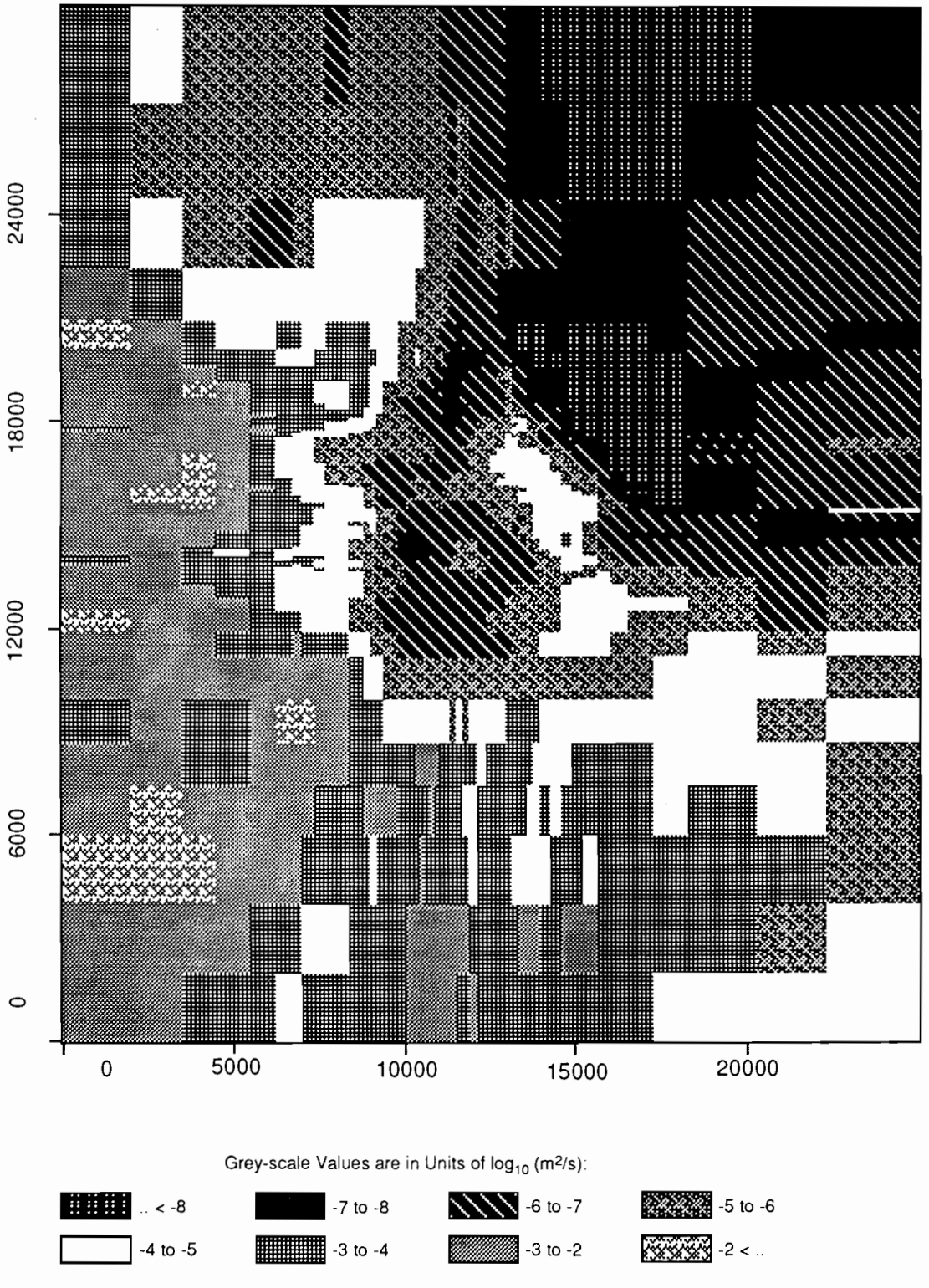

Figure C-33. Realization 68 of Culebra transmissivity.

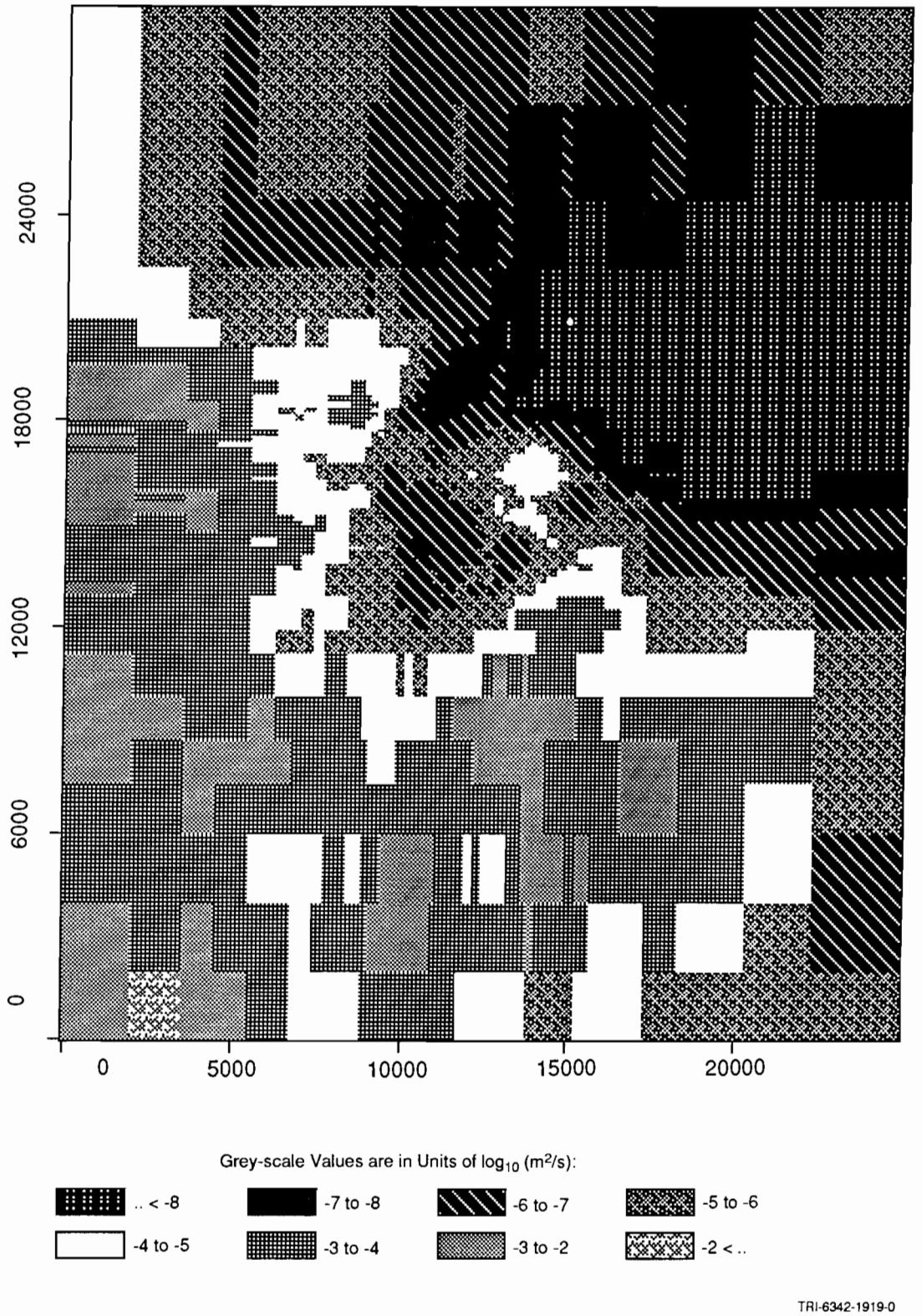

Figure C-34. Realization 40 of Culebra transmissivity.

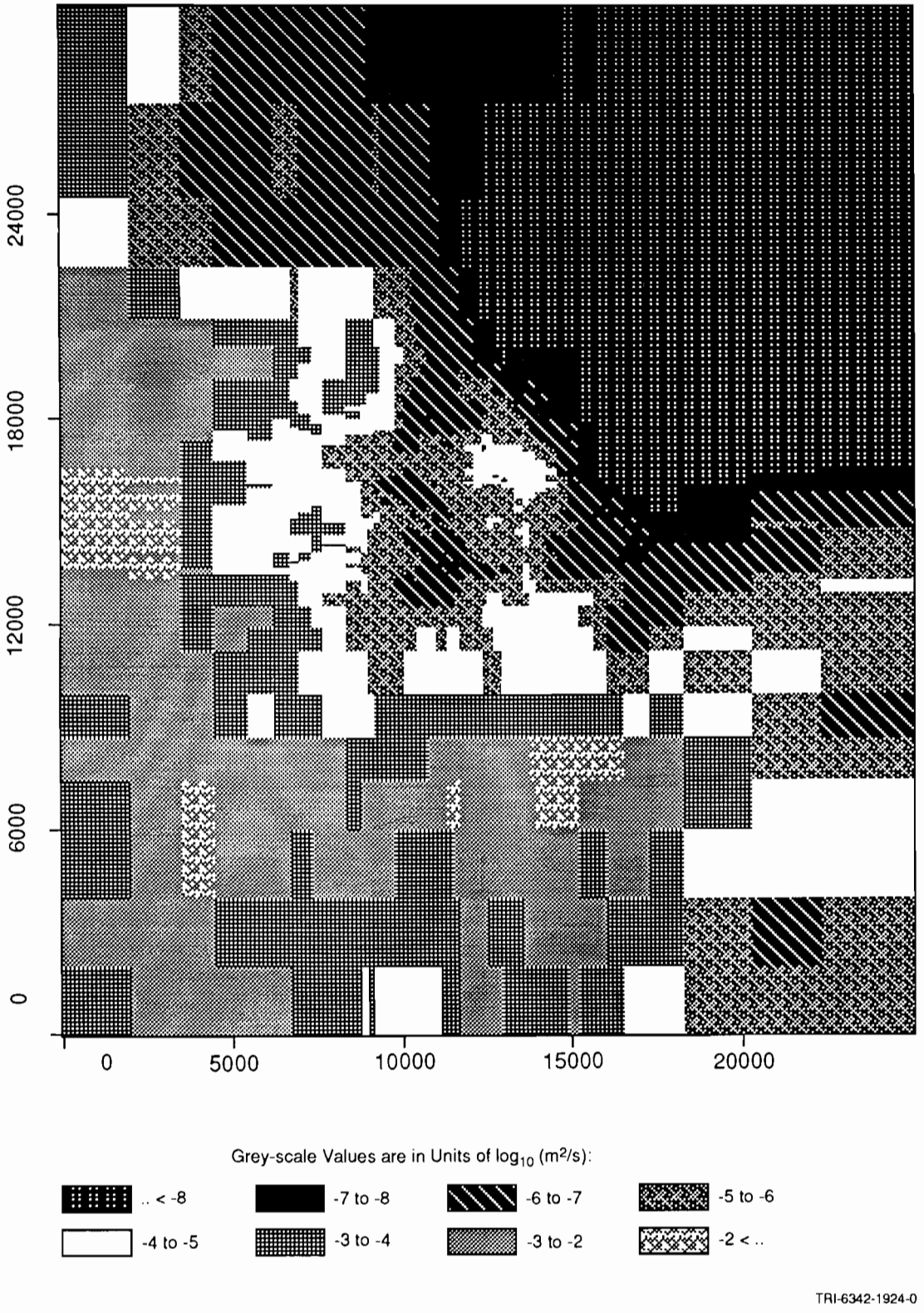

Figure C-35. Realization 5 of Culebra transmissivity.

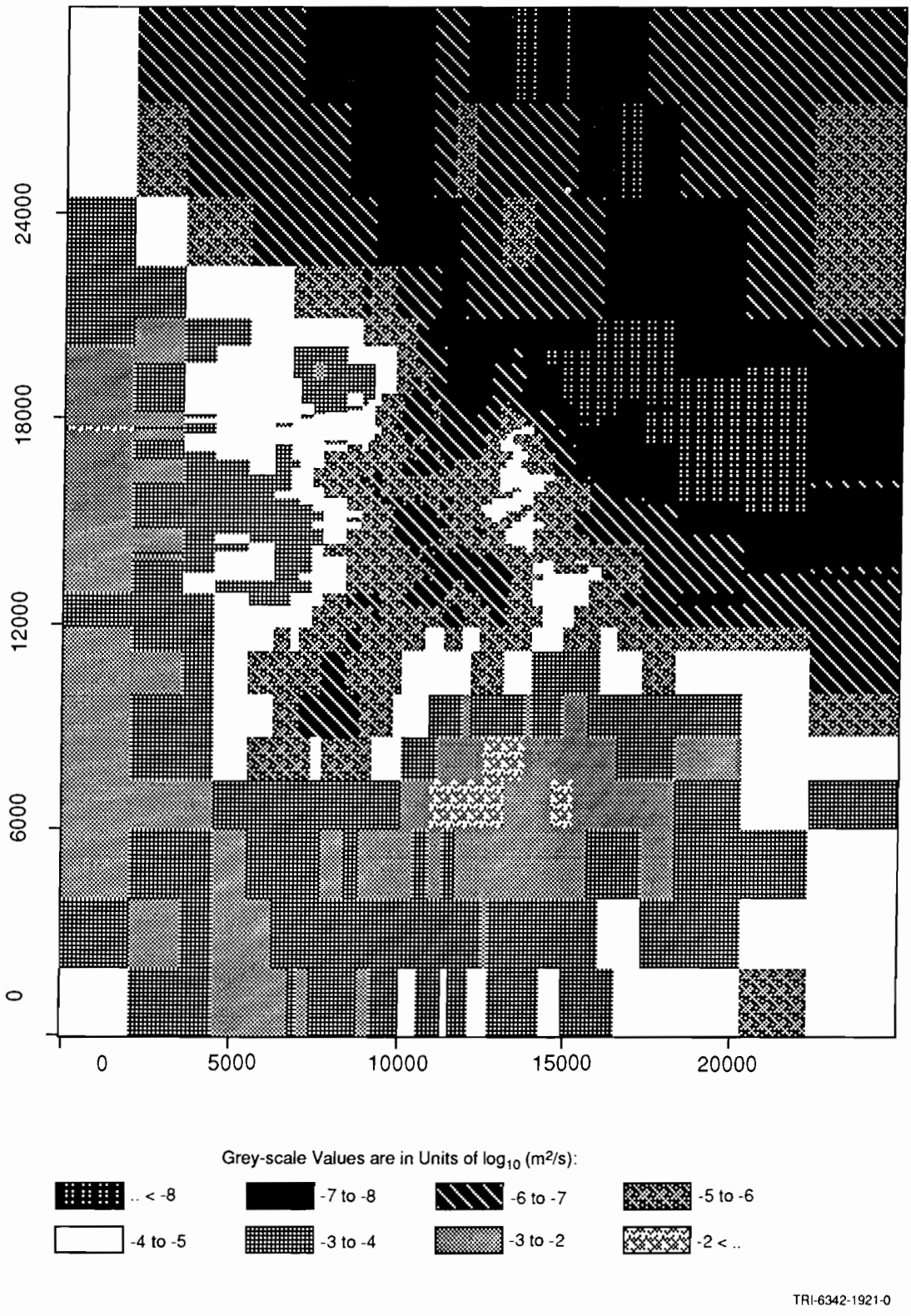

Figure C-36. Realization 61 of Culebra transmissivity.

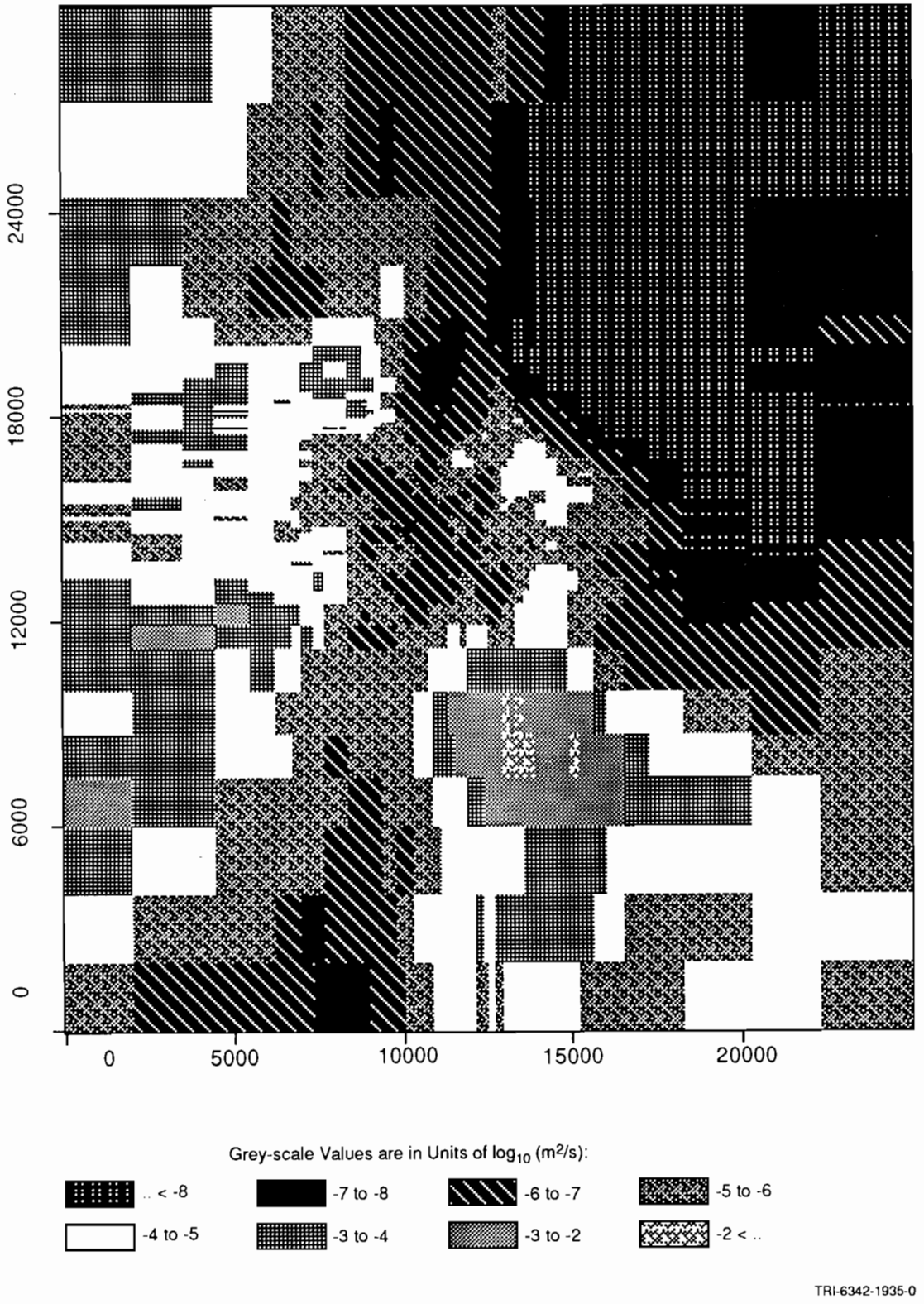

Figure C-37. Realization 14 of Culebra transmissivity.

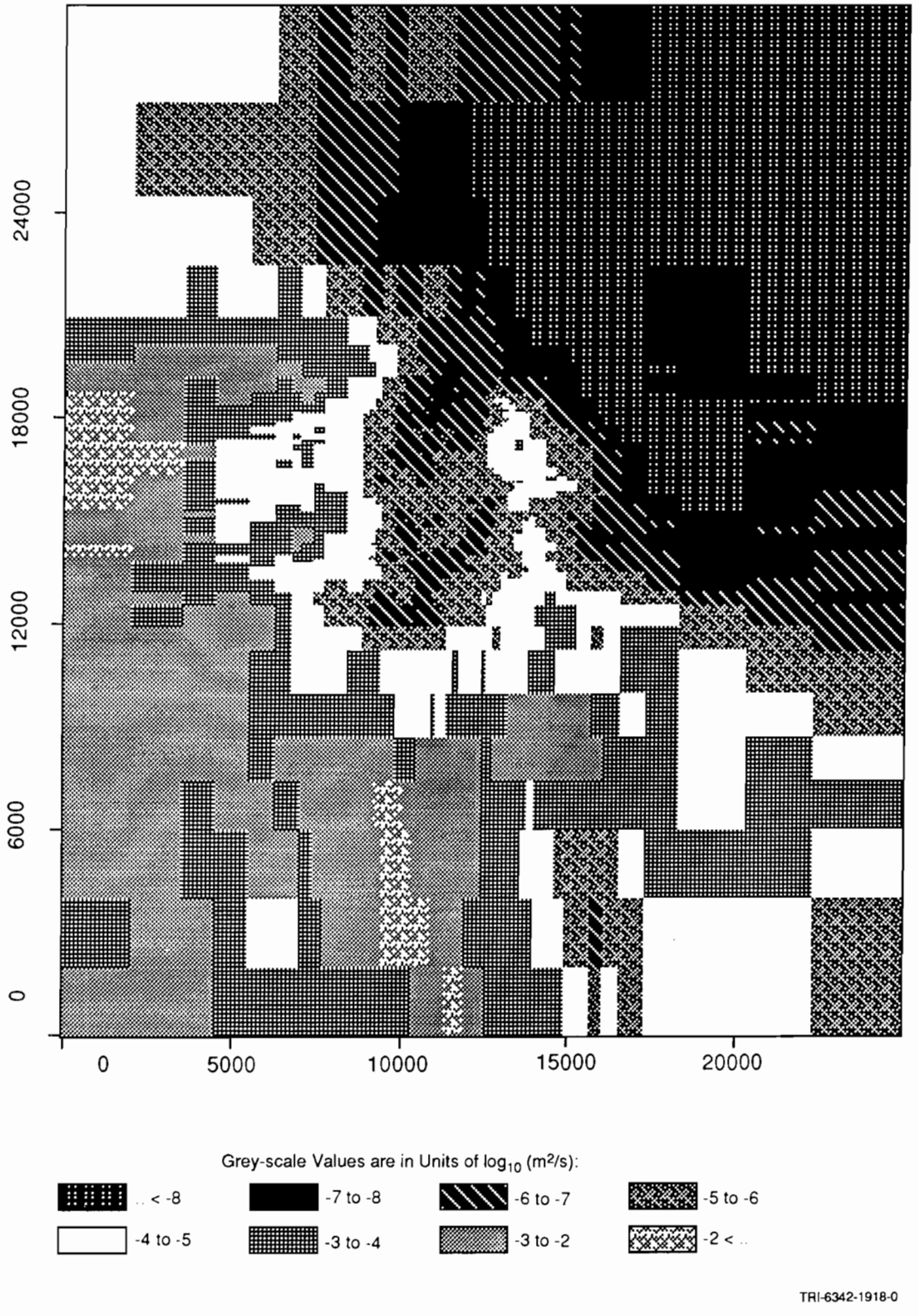

Figure C-38. Realization 31 of Culebra transmissivity.

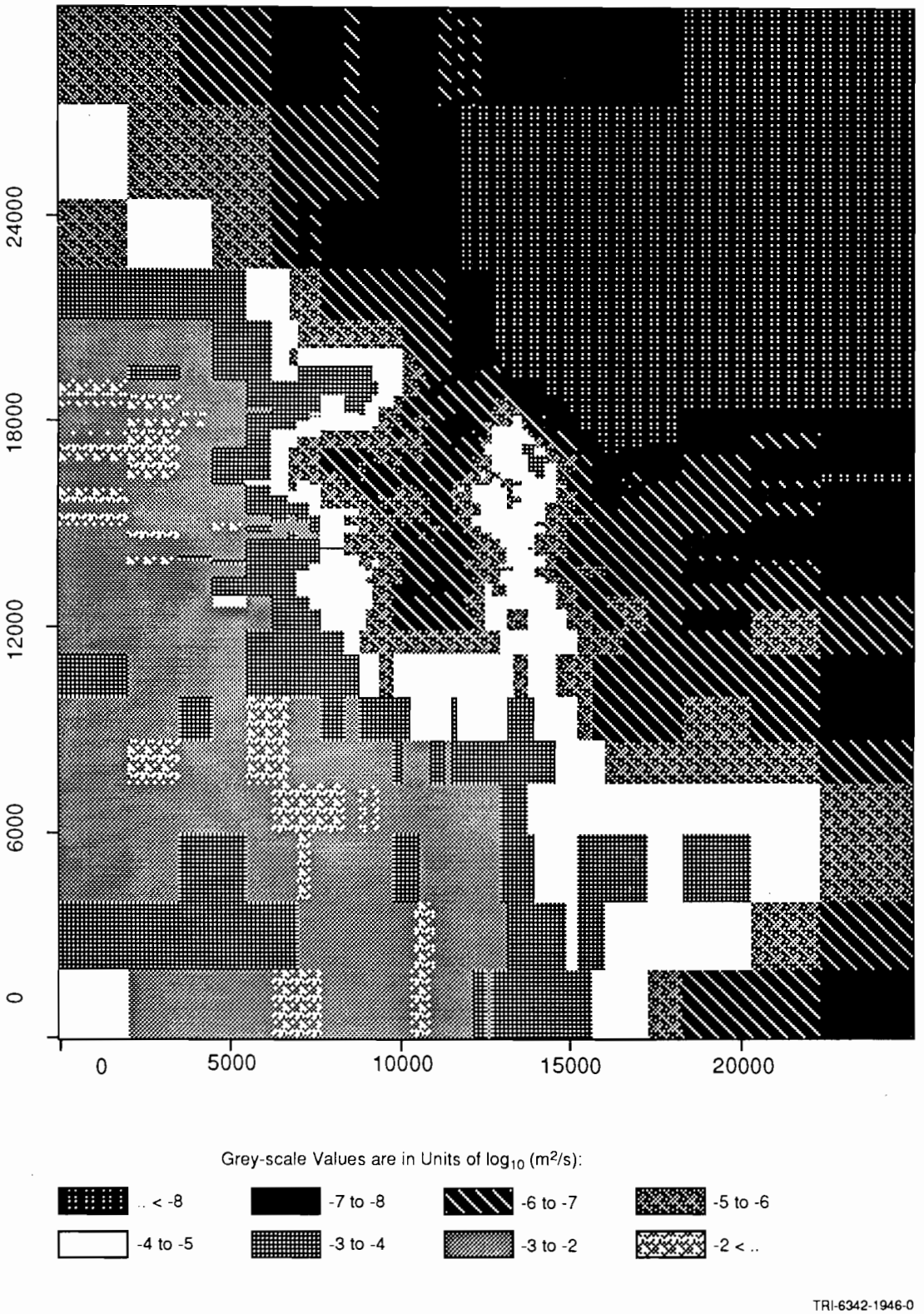

Figure C-39. Realization 38 of Culebra transmissivity.

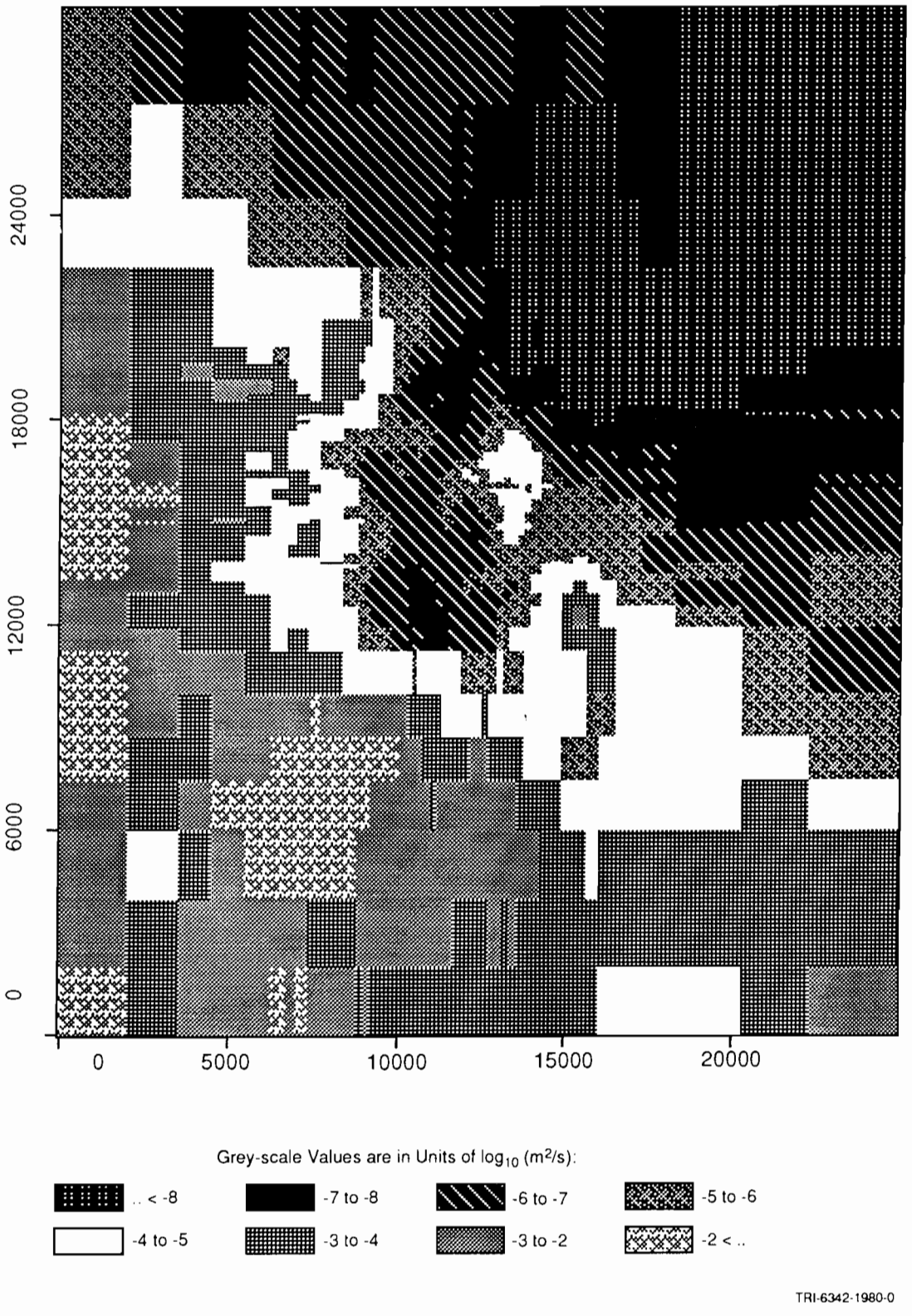

Figure C-40. Realization 27 of Culebra transmissivity.

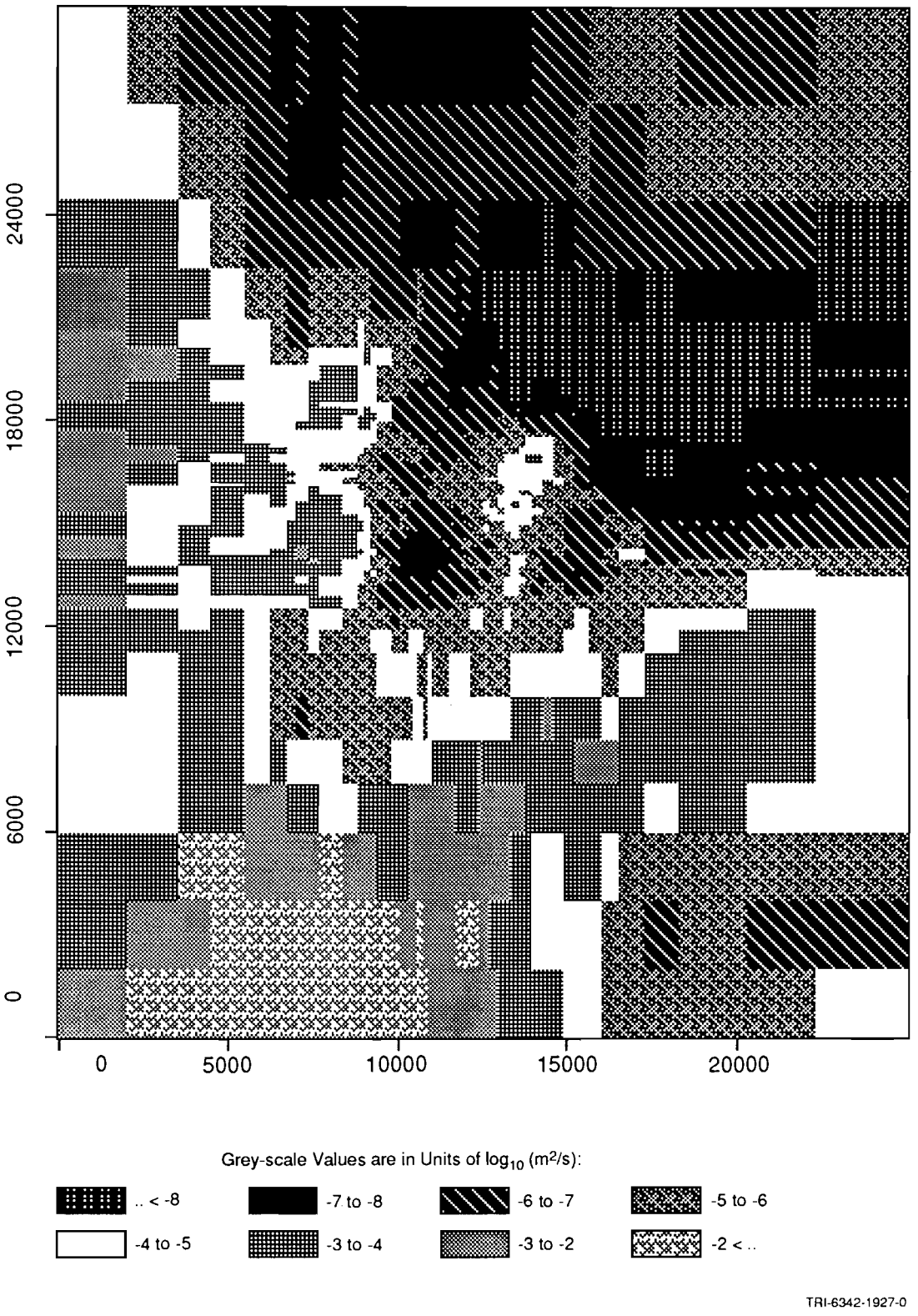

Figure C-41. Realization 4 of Culebra transmissivity.

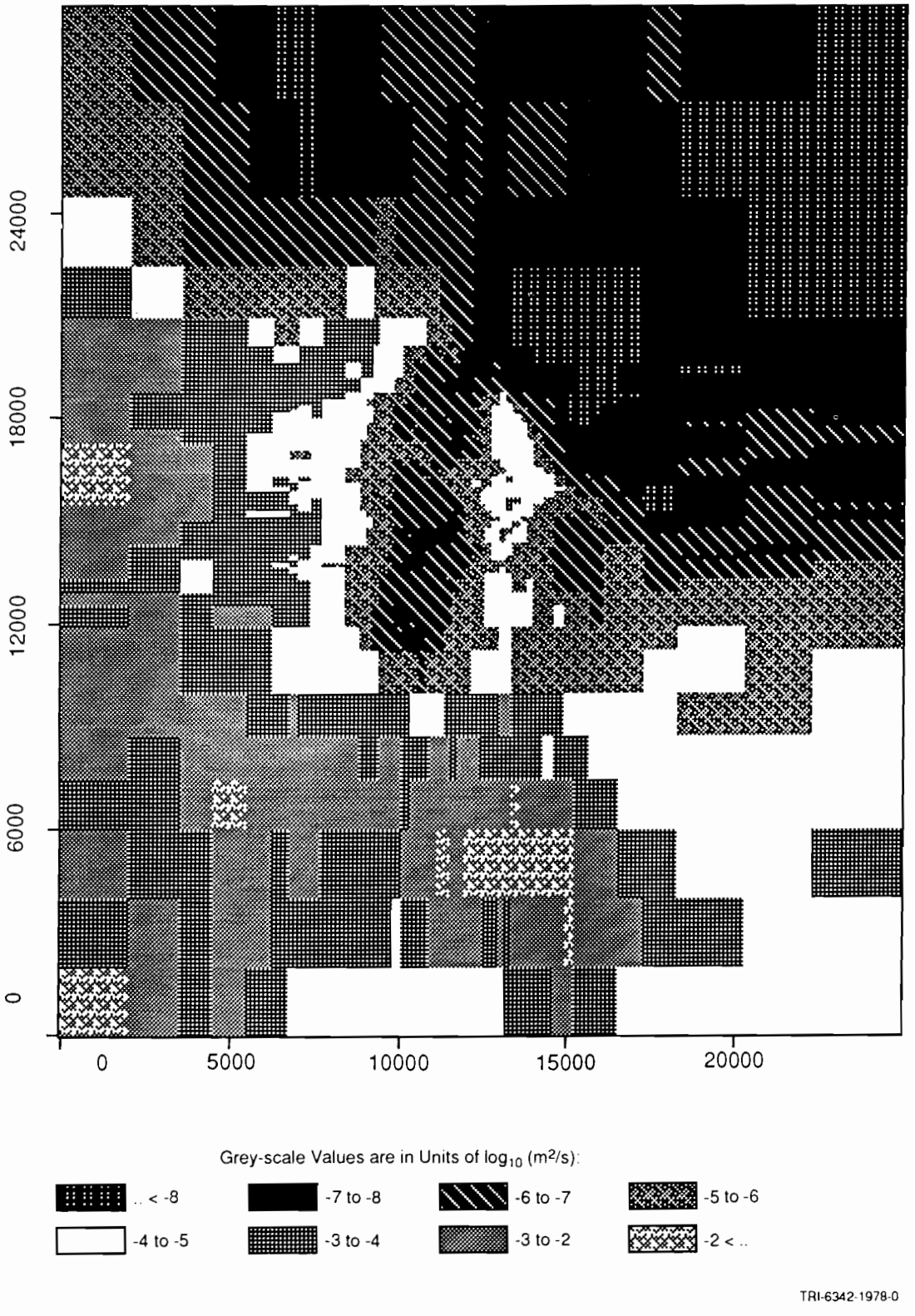

Figure C-42. Realization 59 of Culebra transmissivity.

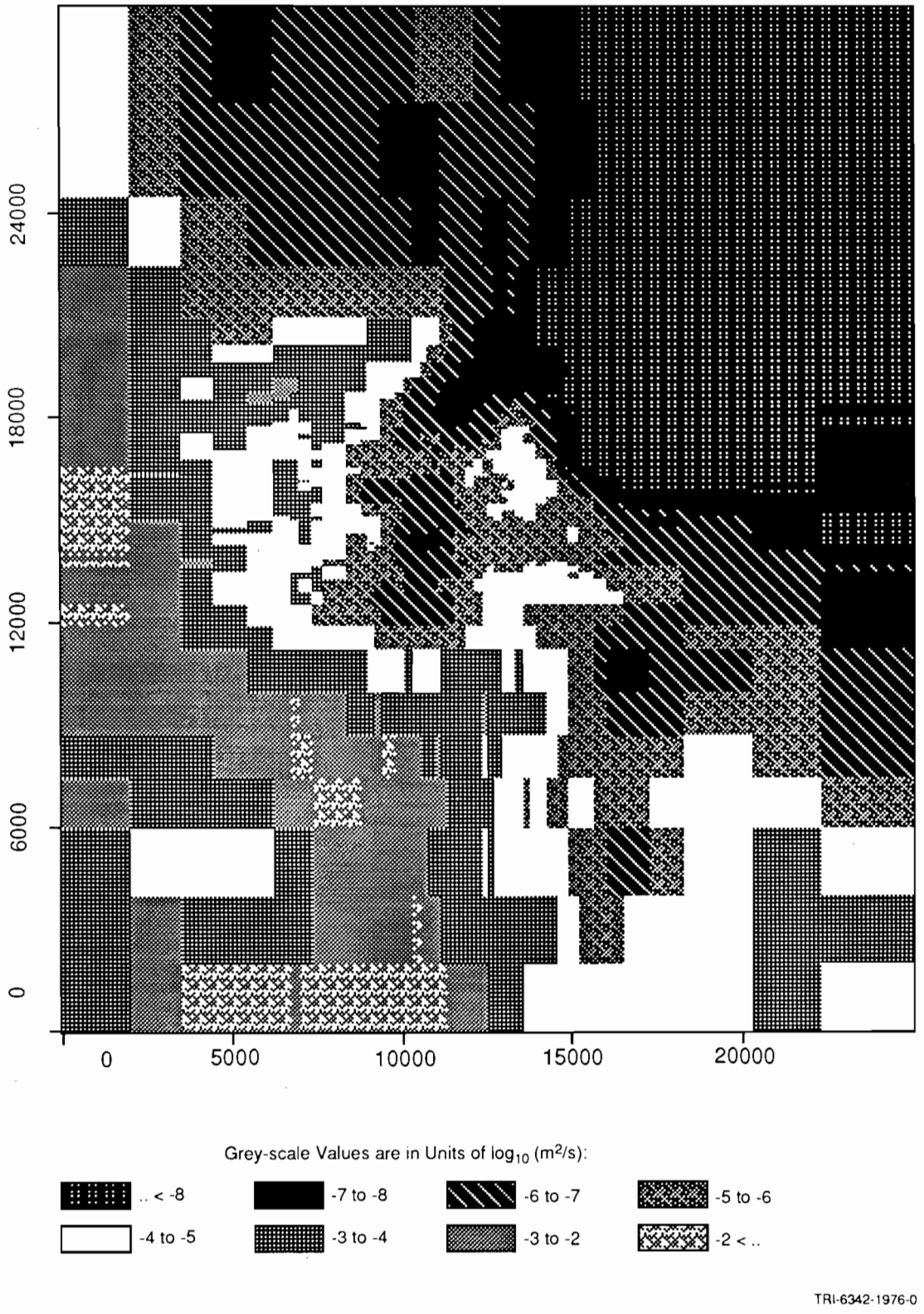

Figure C-43. Realization 17 of Culebra transmissivity.

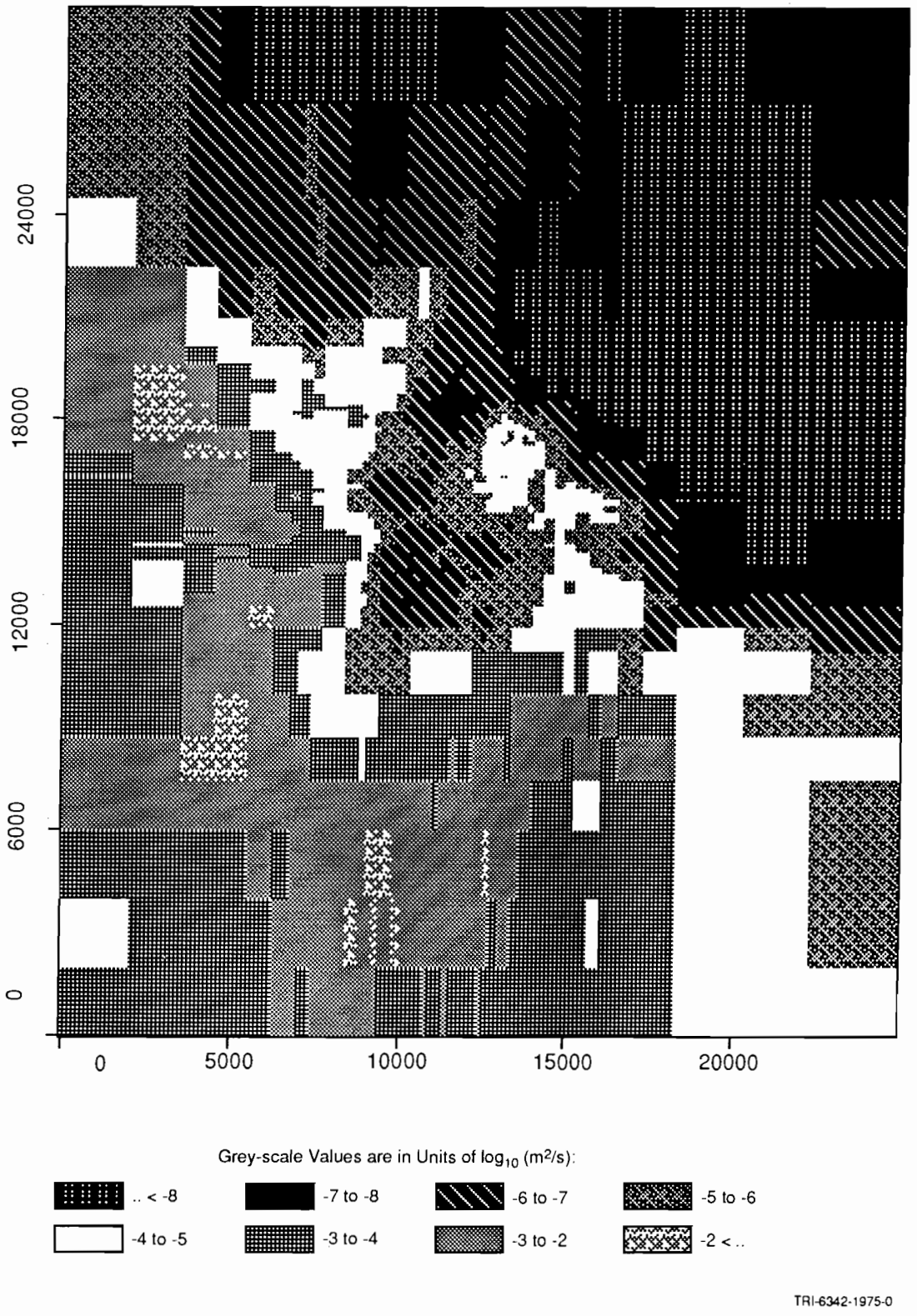

Figure C-44. Realization 51 of Culebra transmissivity.

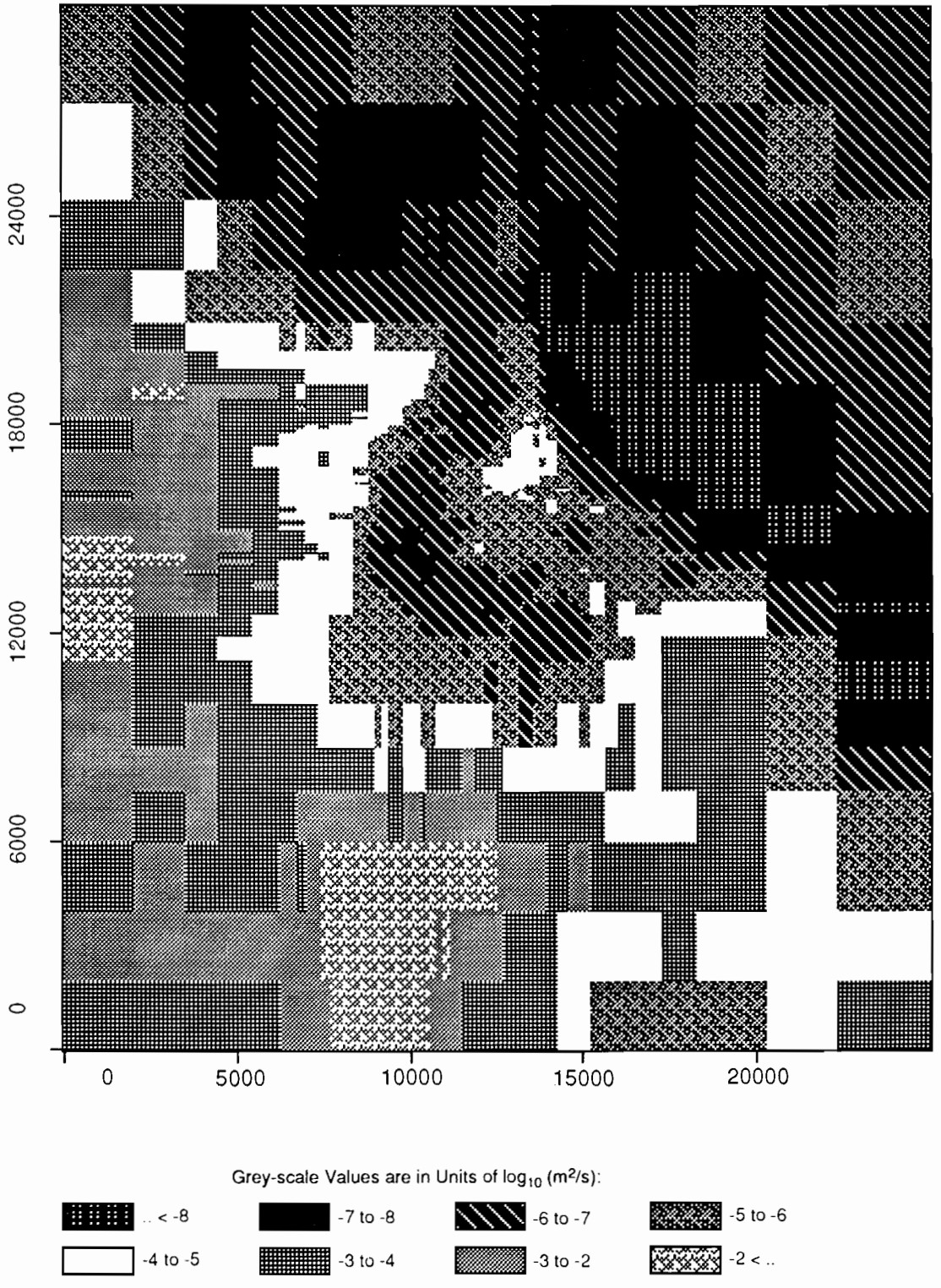

Figure C-45. Realization 9 of Culebra transmissivity.

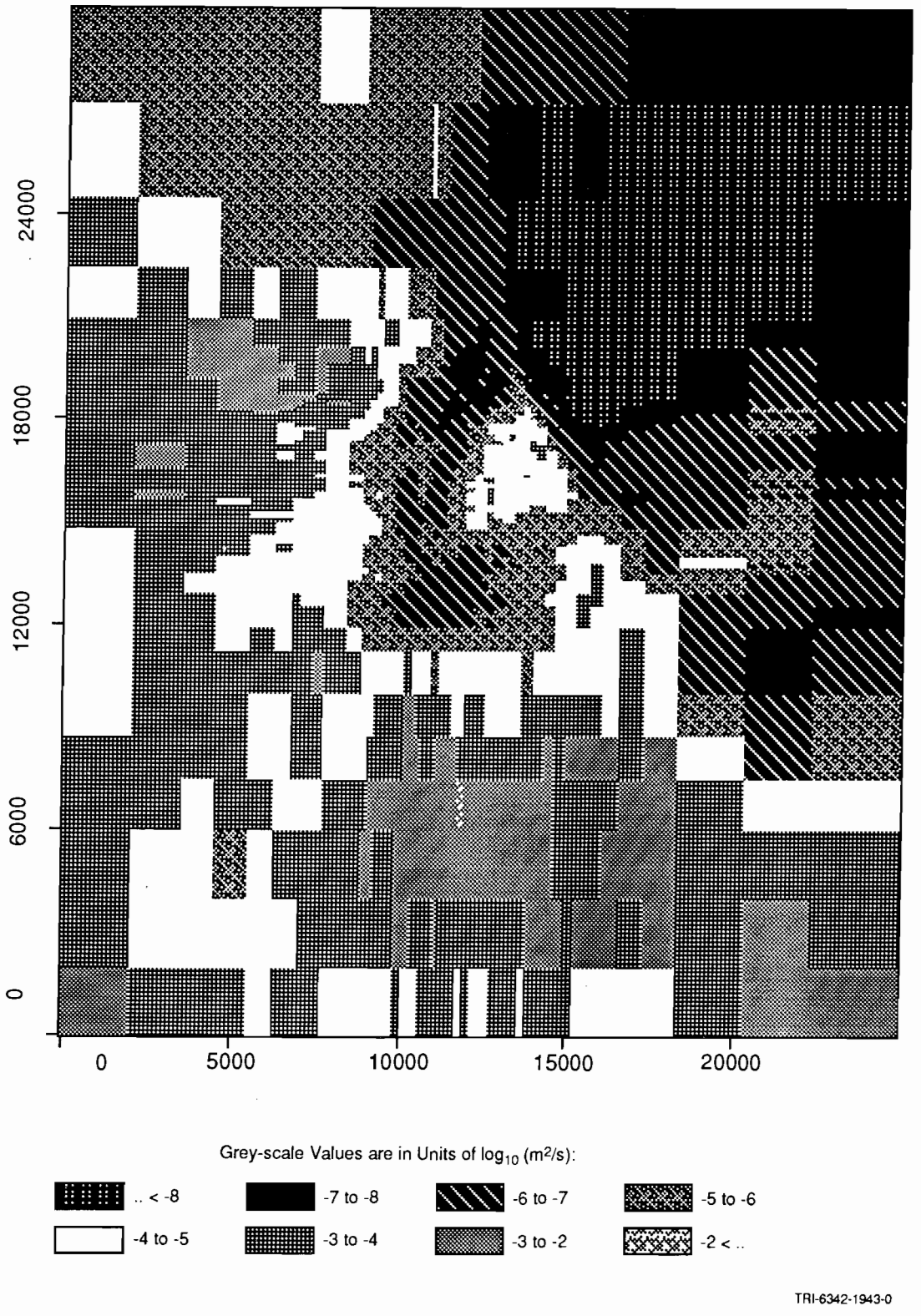

Figure C-46. Realization 30 of Culebra transmissivity.

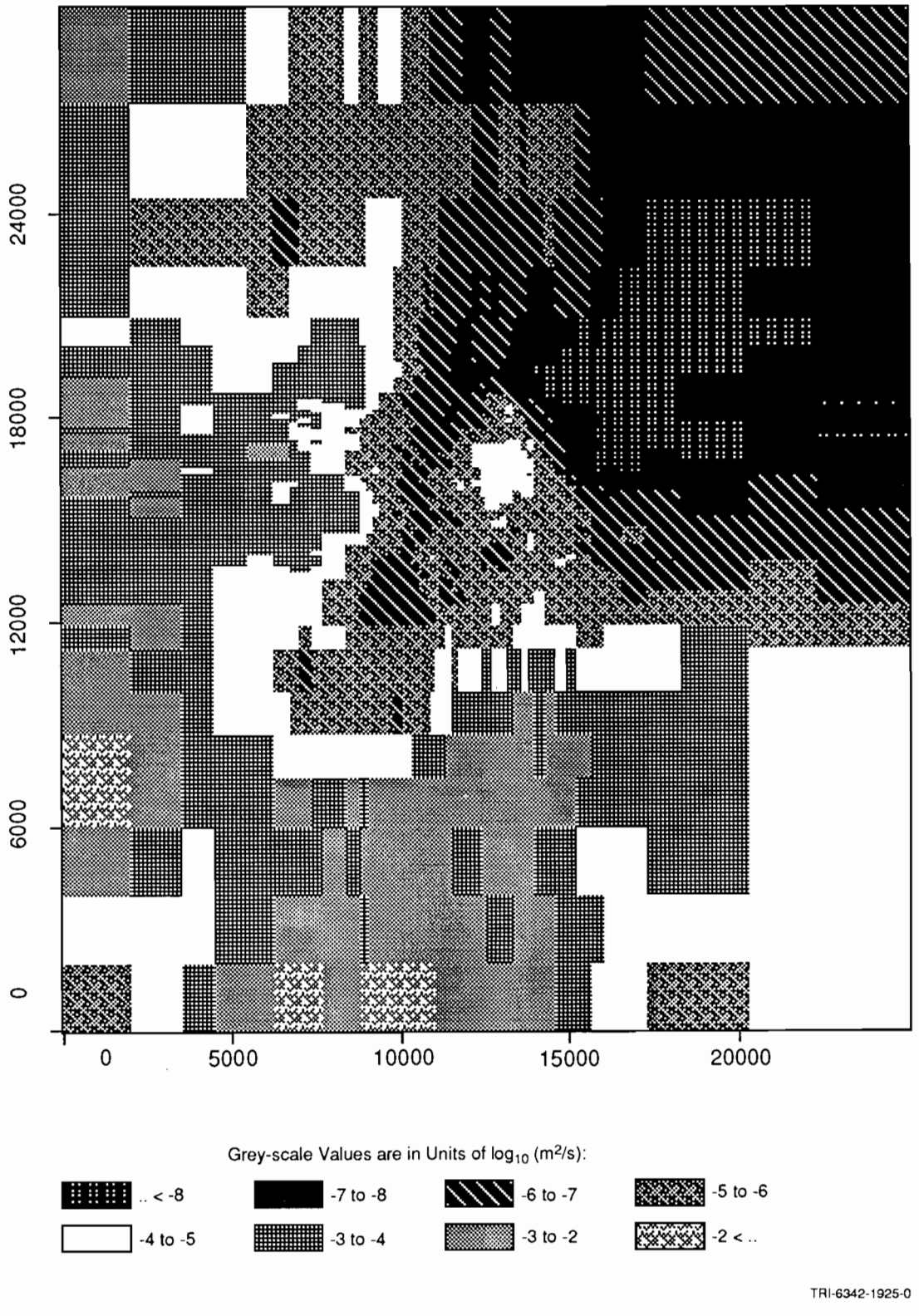

Figure C-47. Realization 46 of Culebra transmissivity.

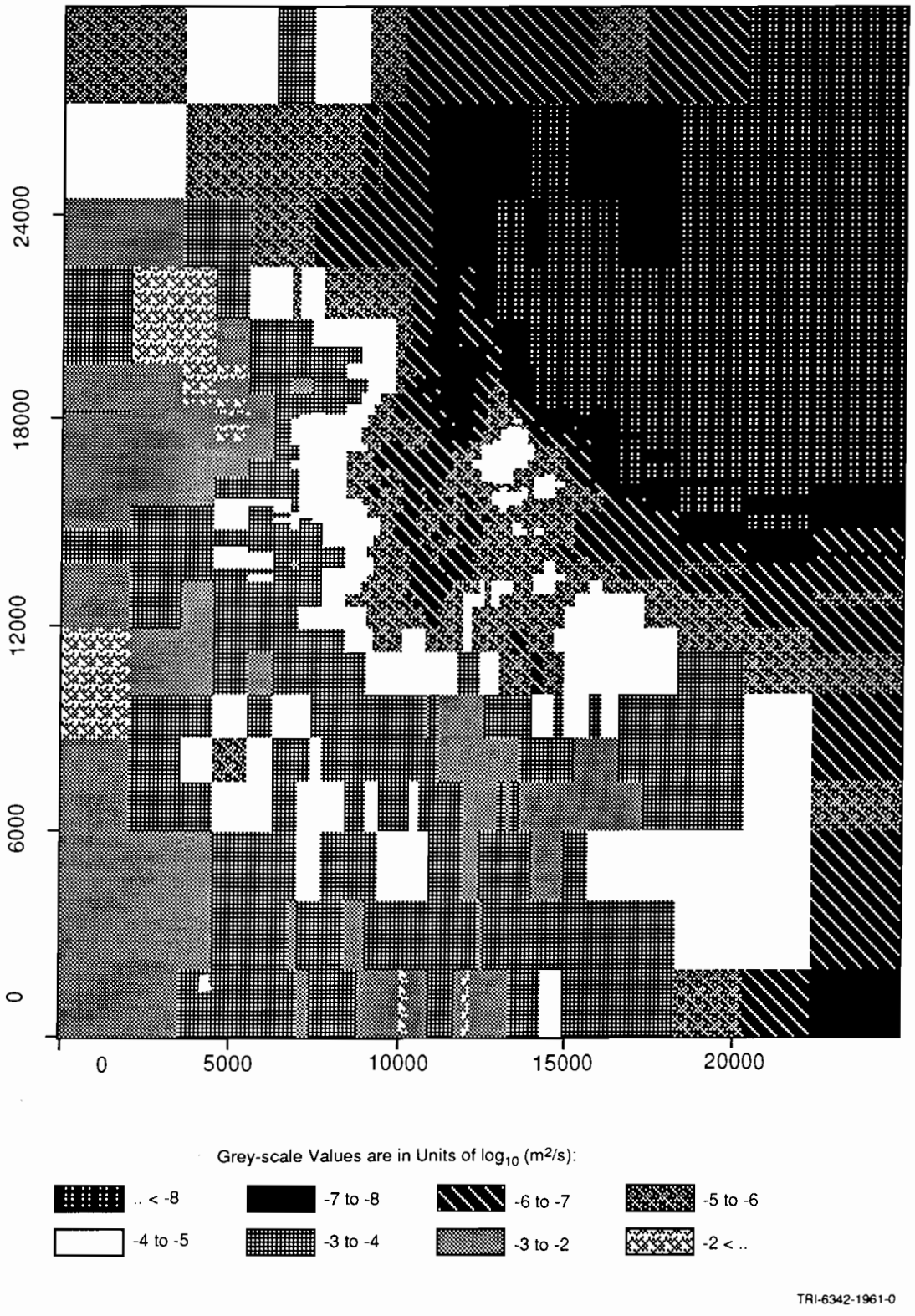

Figure C-48. Realization 3 of Culebra transmissivity.

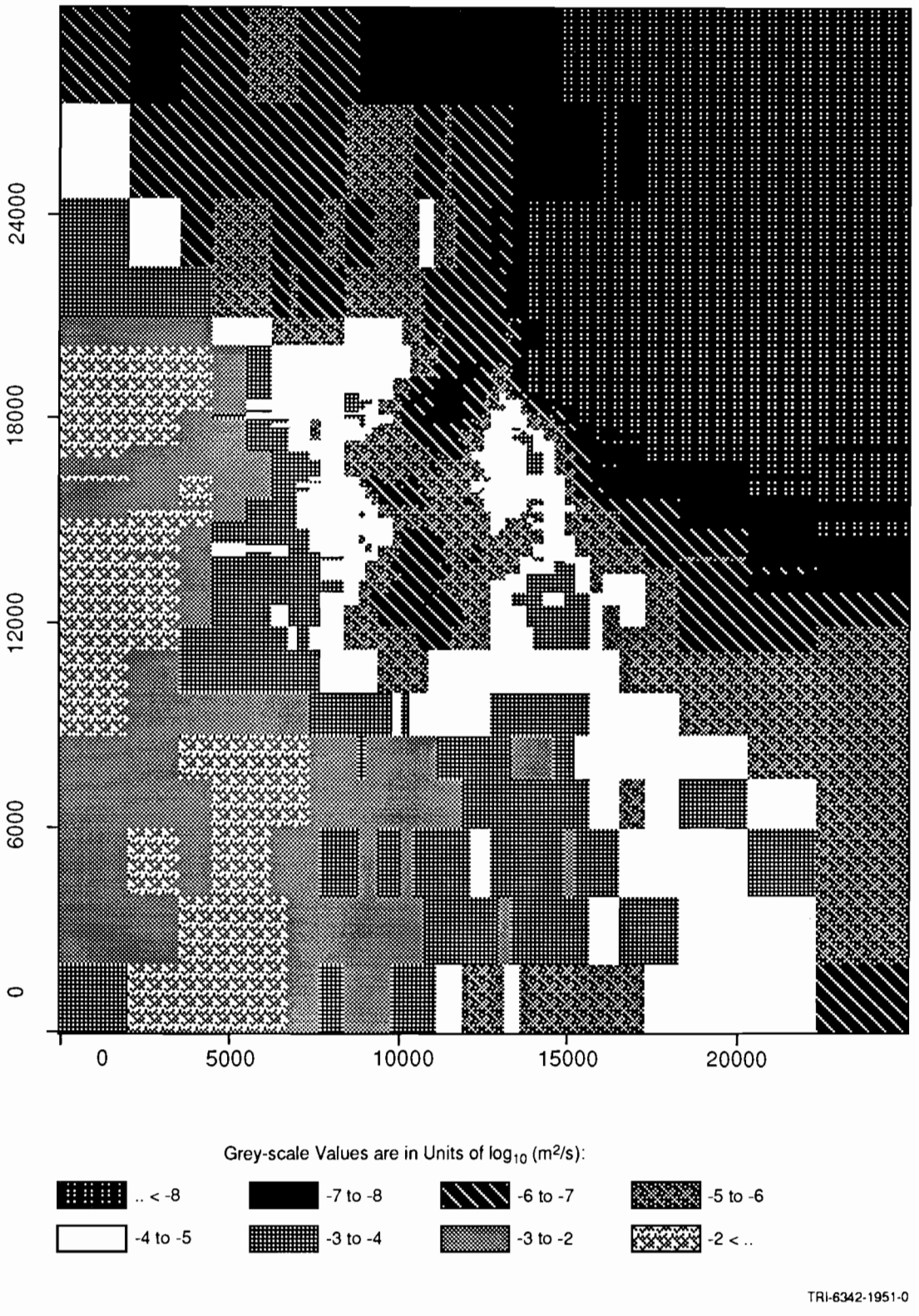

Figure C-49. Realization 62 of Culebra transmissivity.

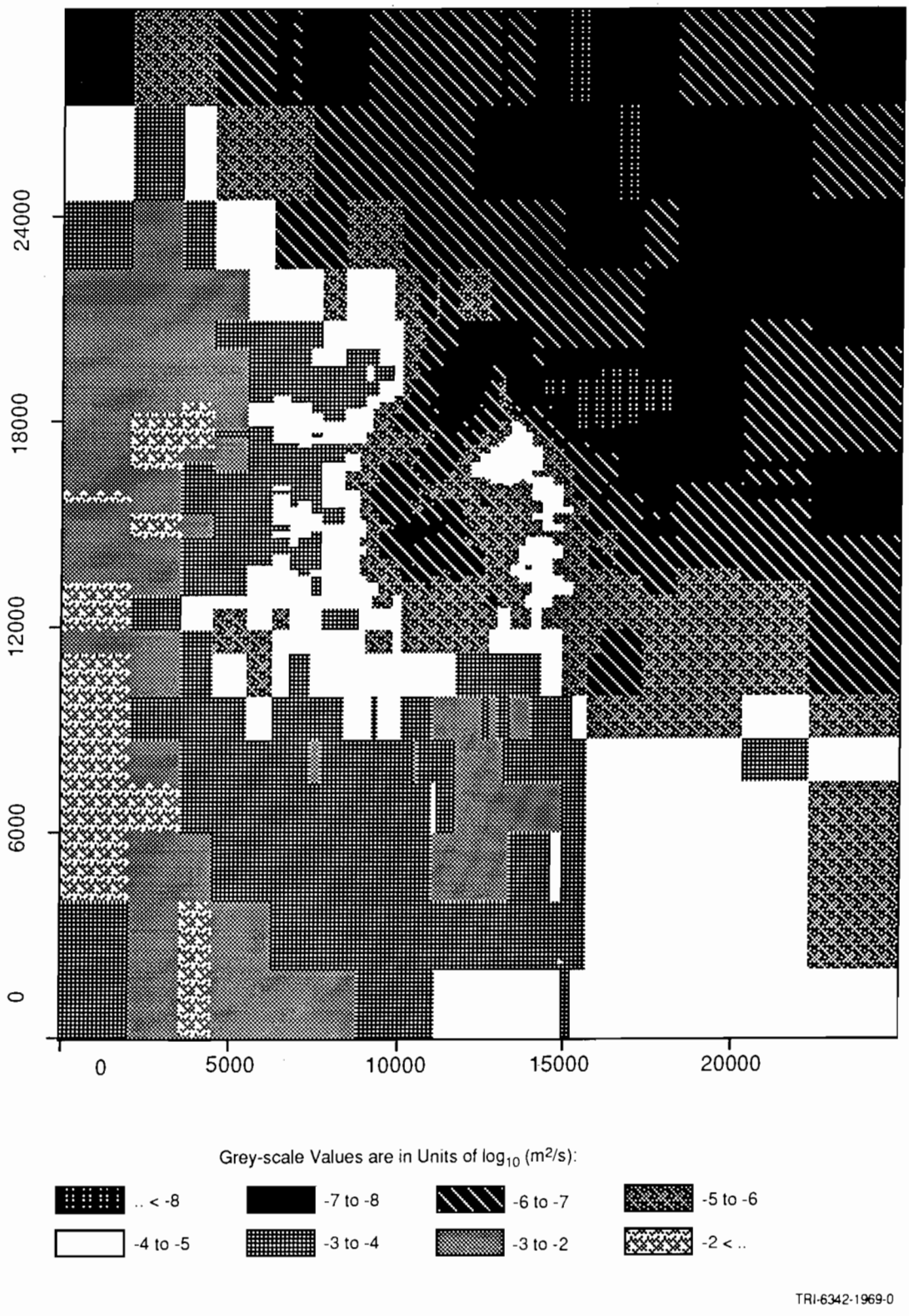

Figure C-50. Realization 22 of Culebra transmissivity.

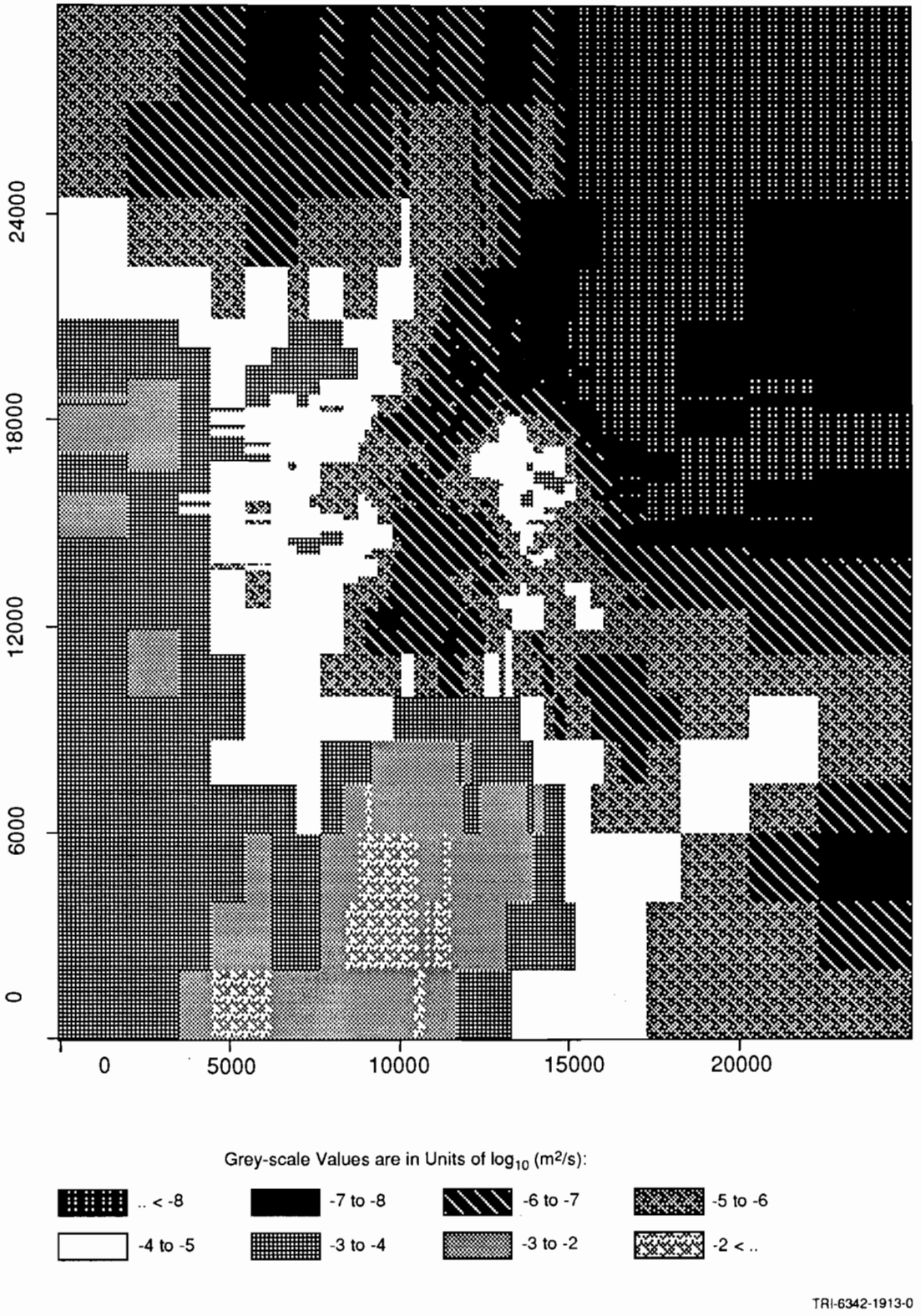

Figure C-51. Realization 50 of Culebra transmissivity.

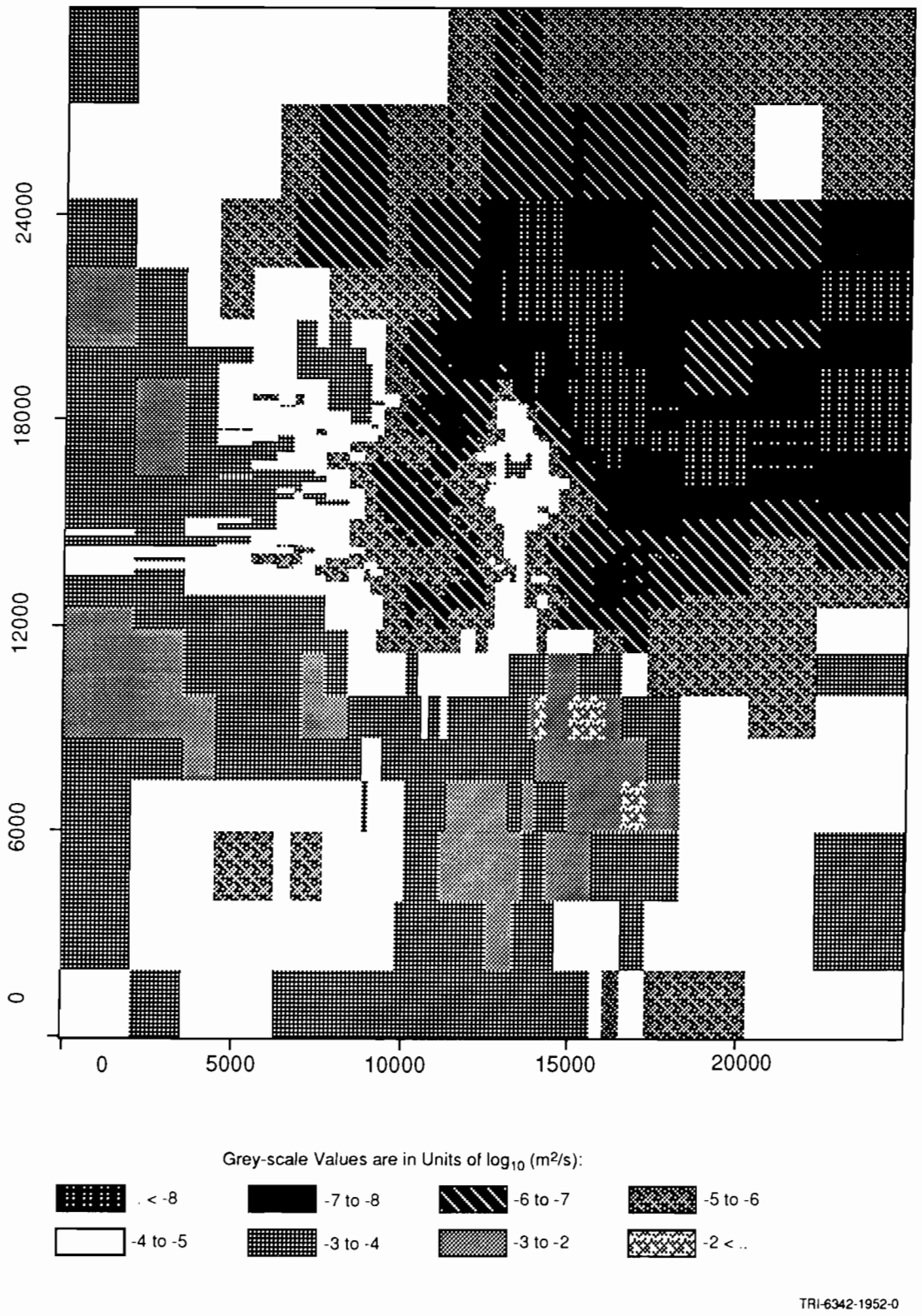

Figure C-52. Realization 35 of Culebra transmissivity.

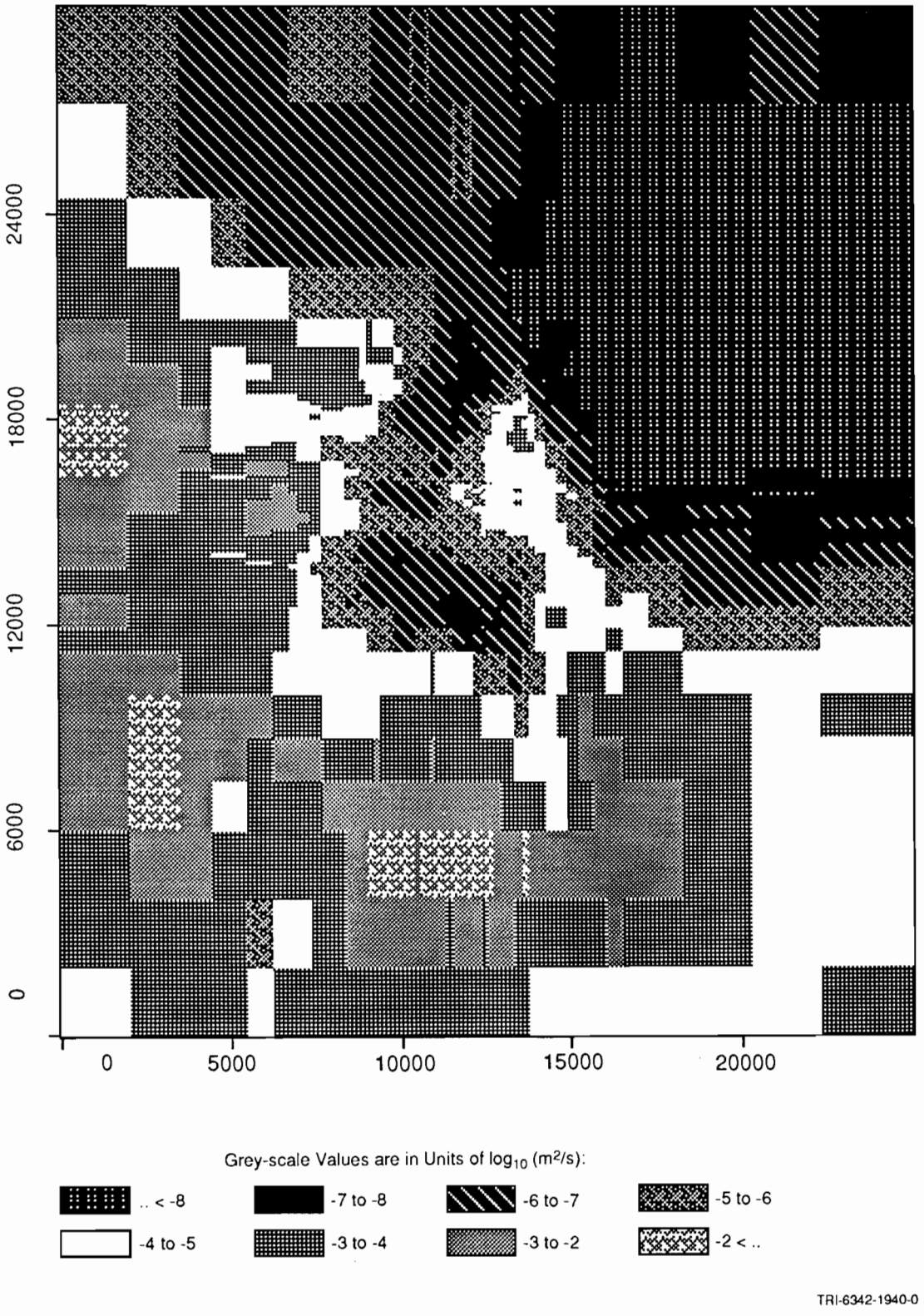

Figure C-53. Realization 57 of Culebra transmissivity.

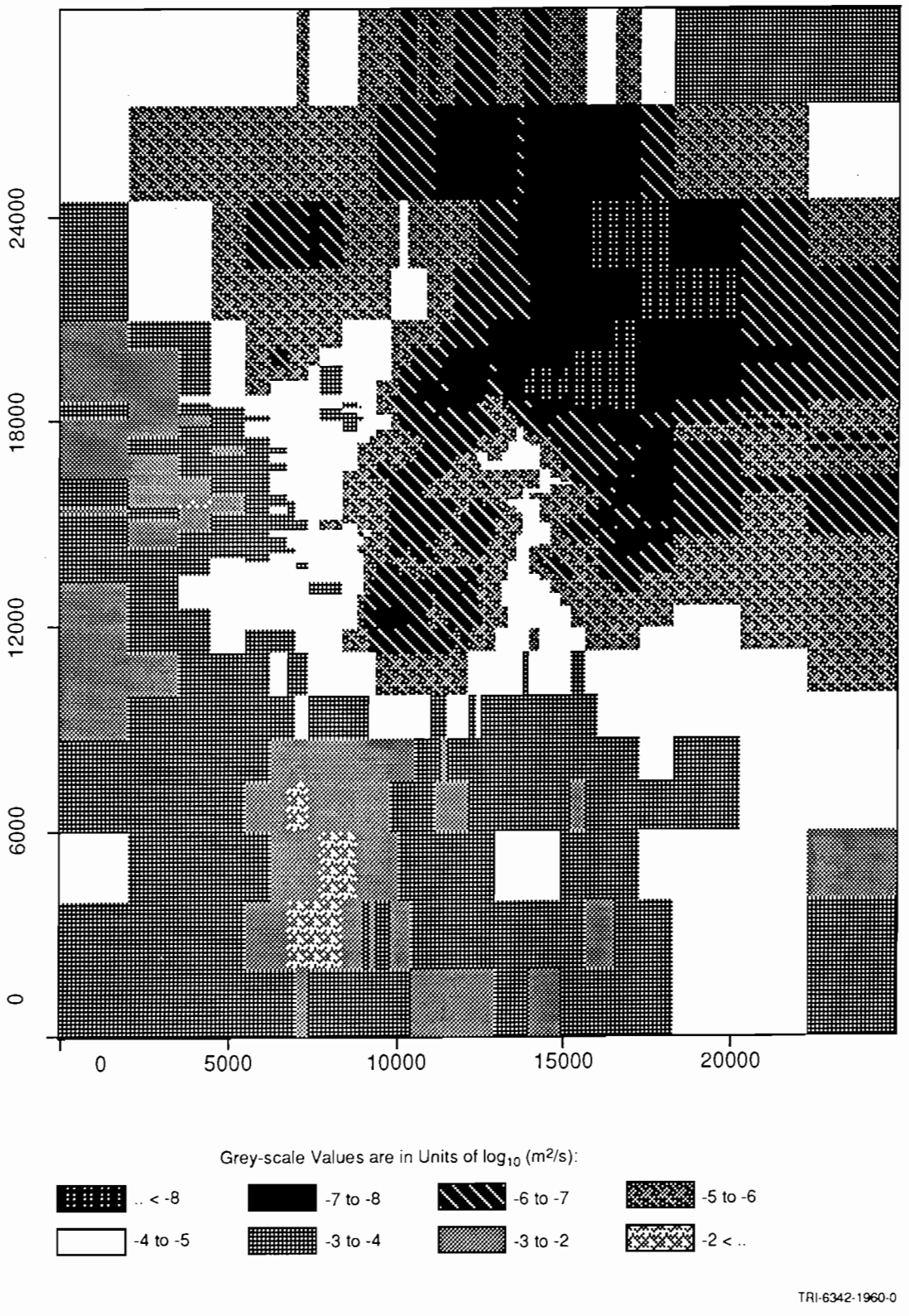

Figure C-54. Realization 49 of Culebra transmissivity.

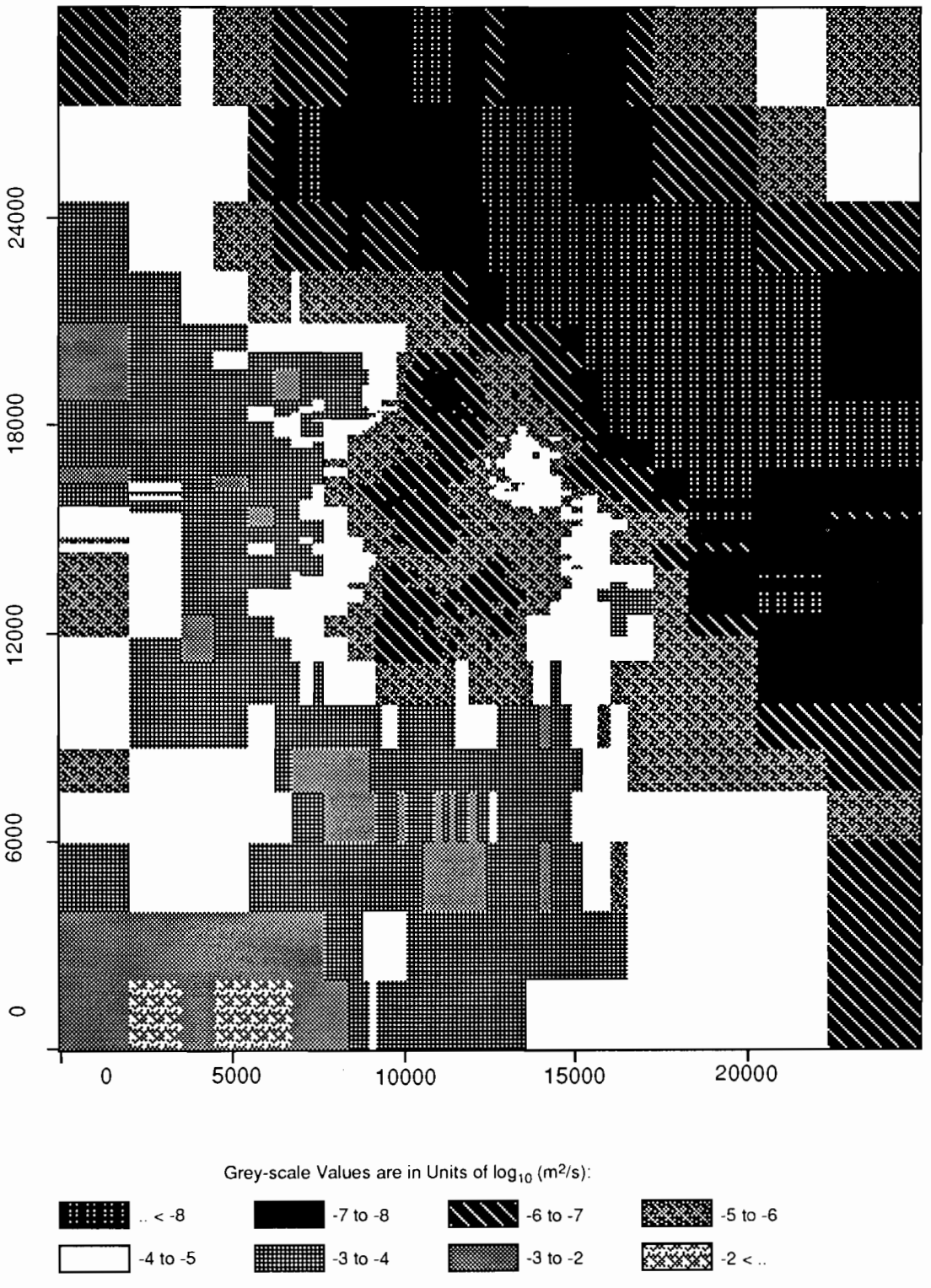

Figure C-55. Realization 65 of Culebra transmissivity.

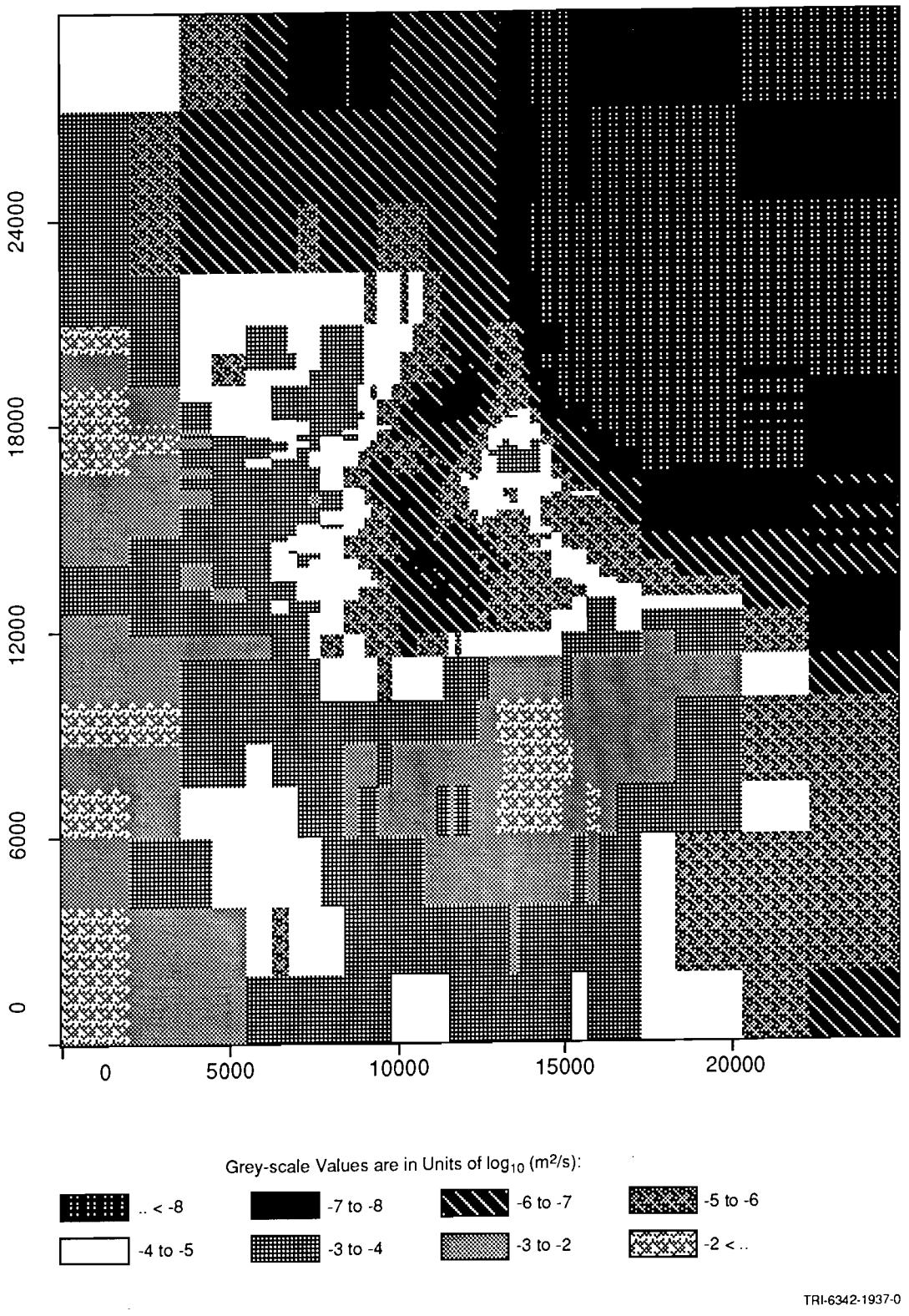

Figure C-56. Realization 41 of Culebra transmissivity.

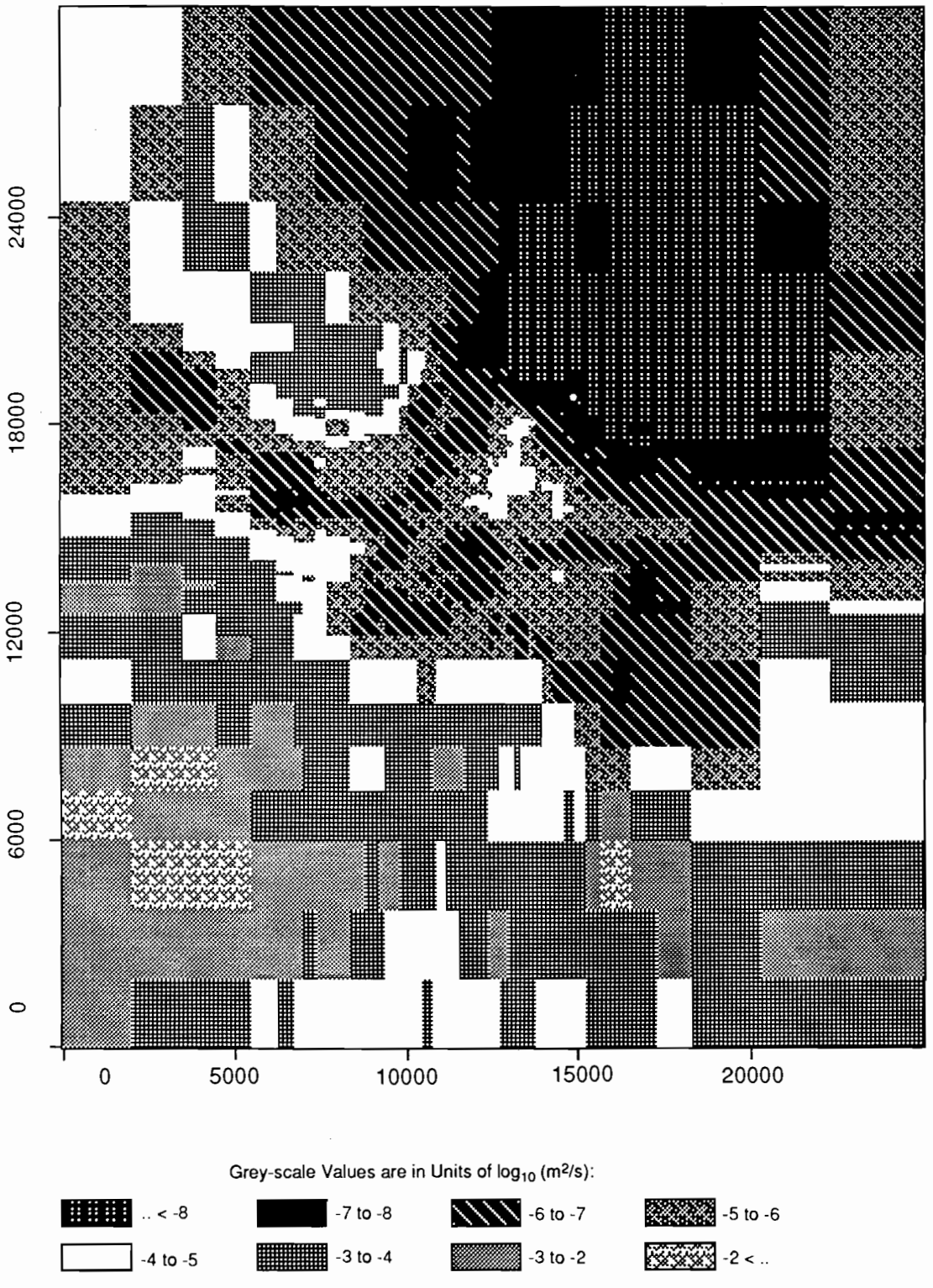

Figure C-57. Realization 26 of Culebra transmissivity.

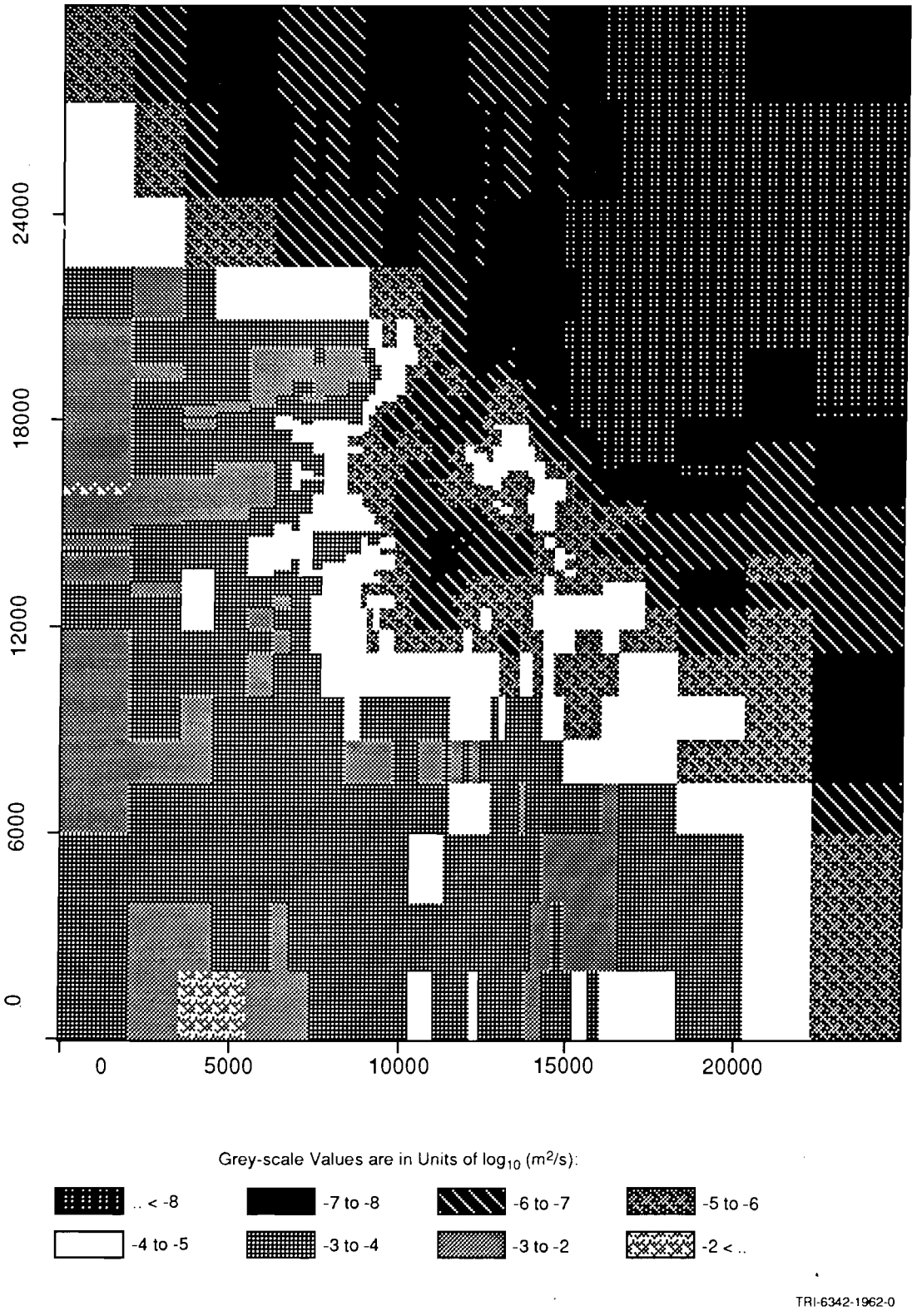

Figure C-58. Realization 37 of Culebra transmissivity.

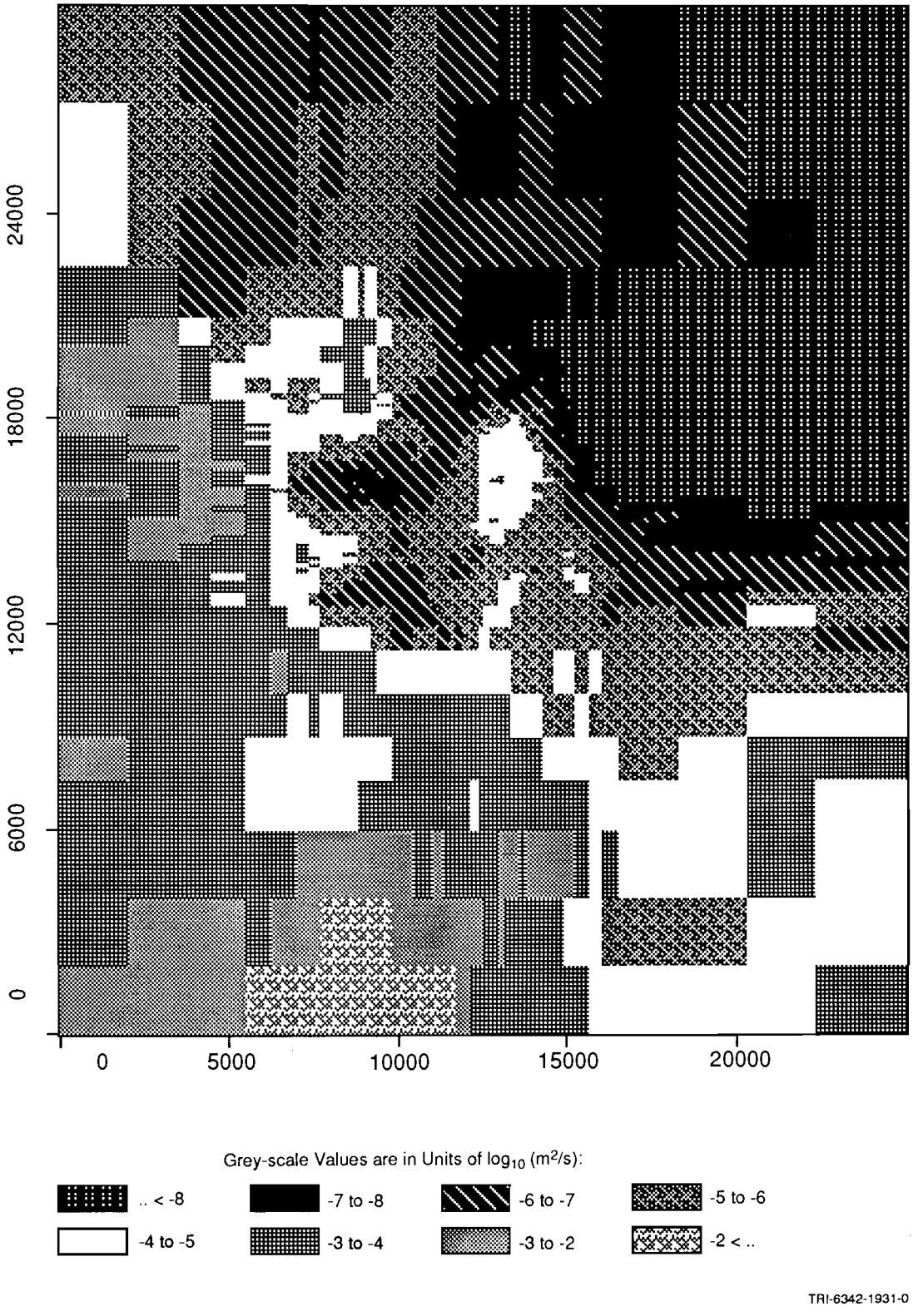

Figure C-59. Realization 44 of Culebra transmissivity.

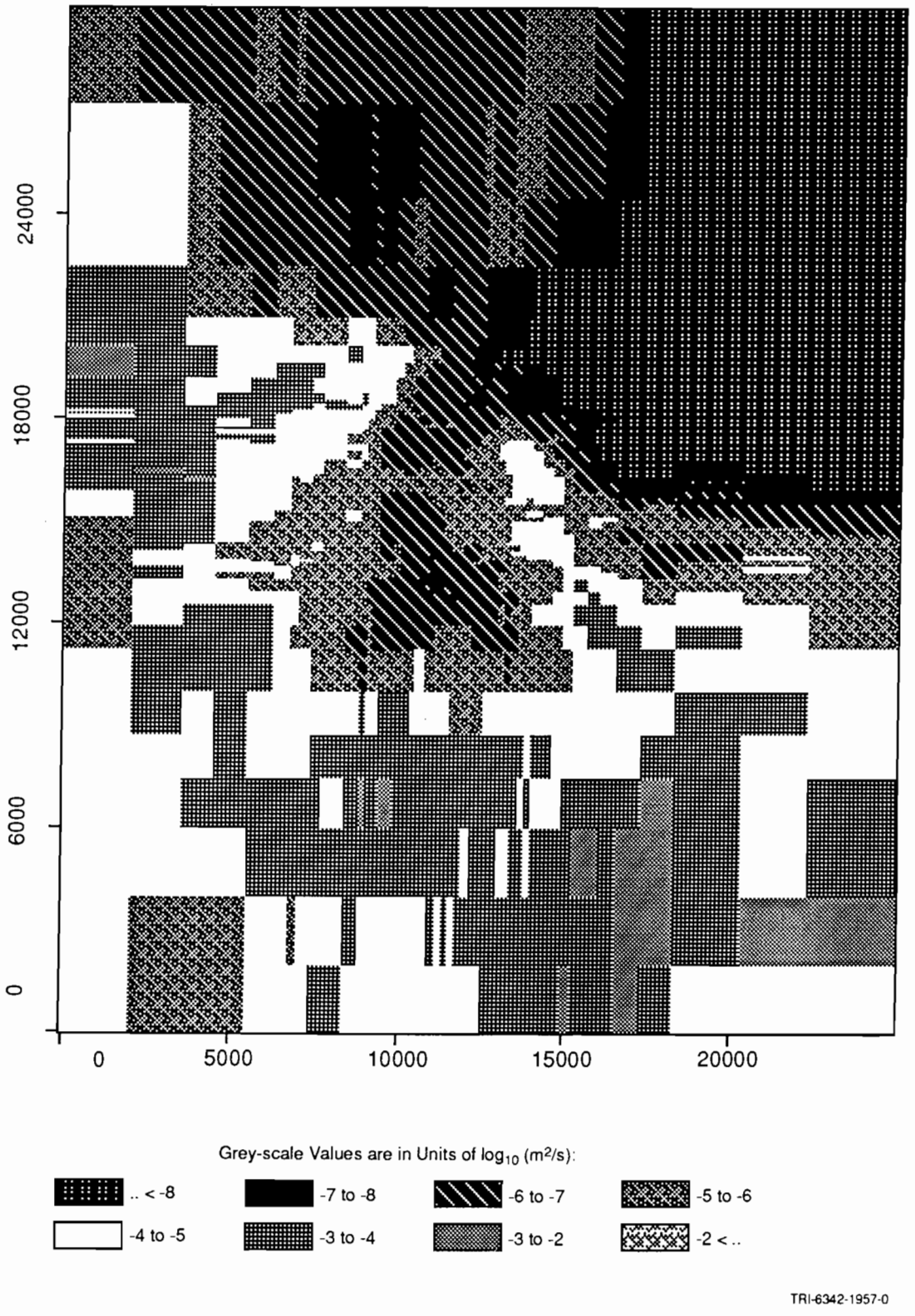

Figure C-60. Realization 60 of Culebra transmissivity.

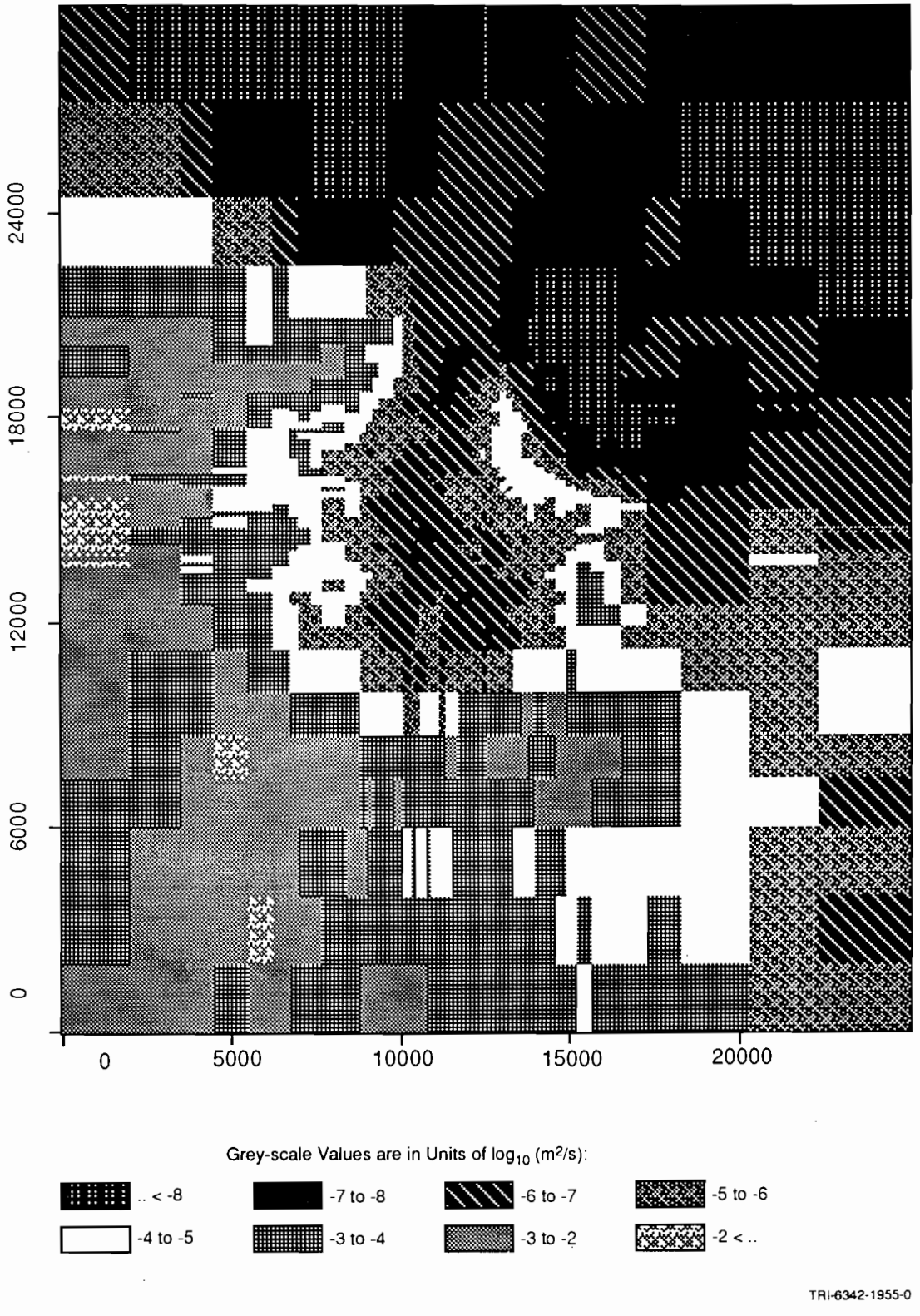

Figure C-61. Realization 21 of Culebra transmissivity.

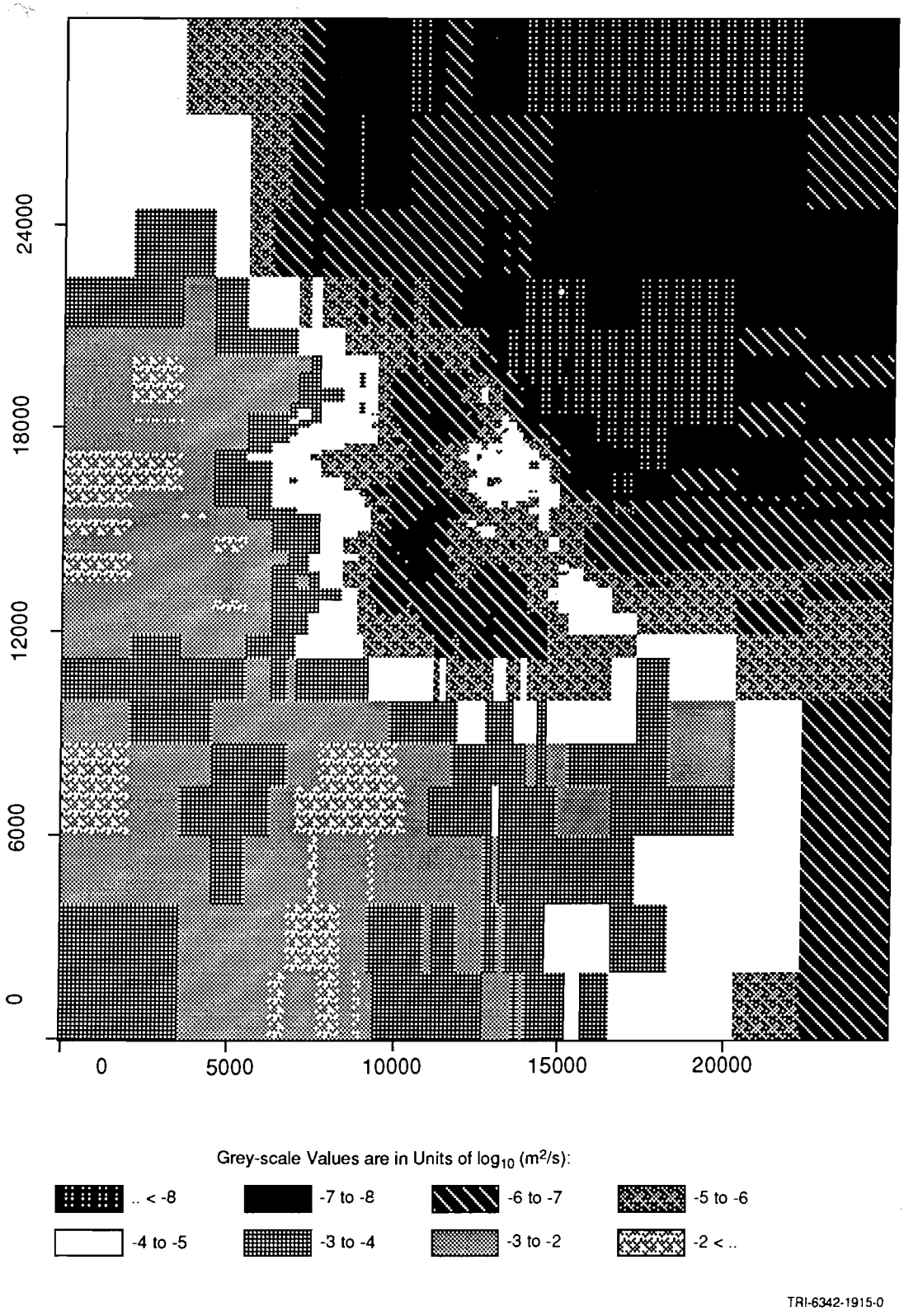

Figure C-62. Realization 13 of Culebra transmissivity.

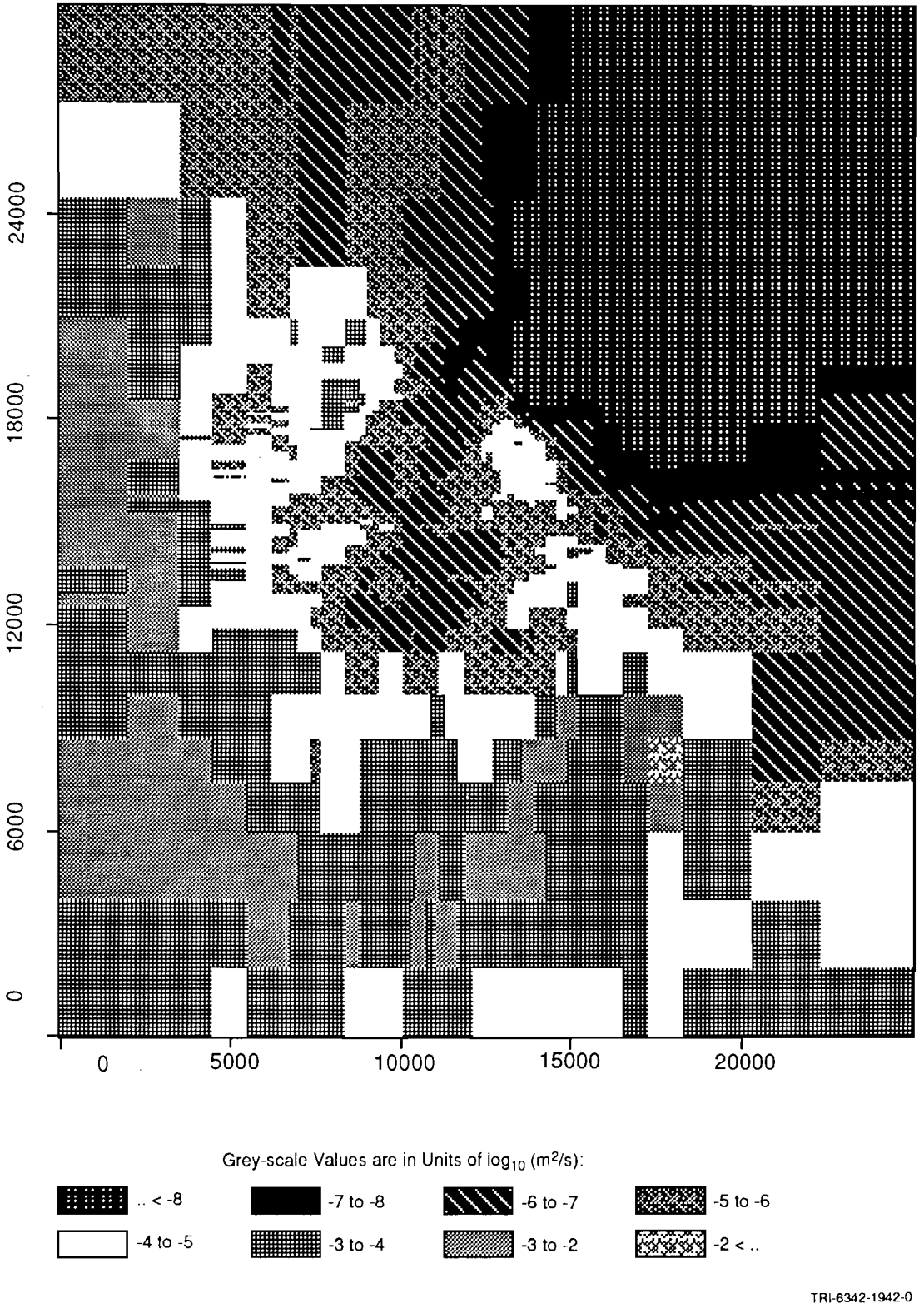

Figure C-63. Realization 10 of Culebra transmissivity.

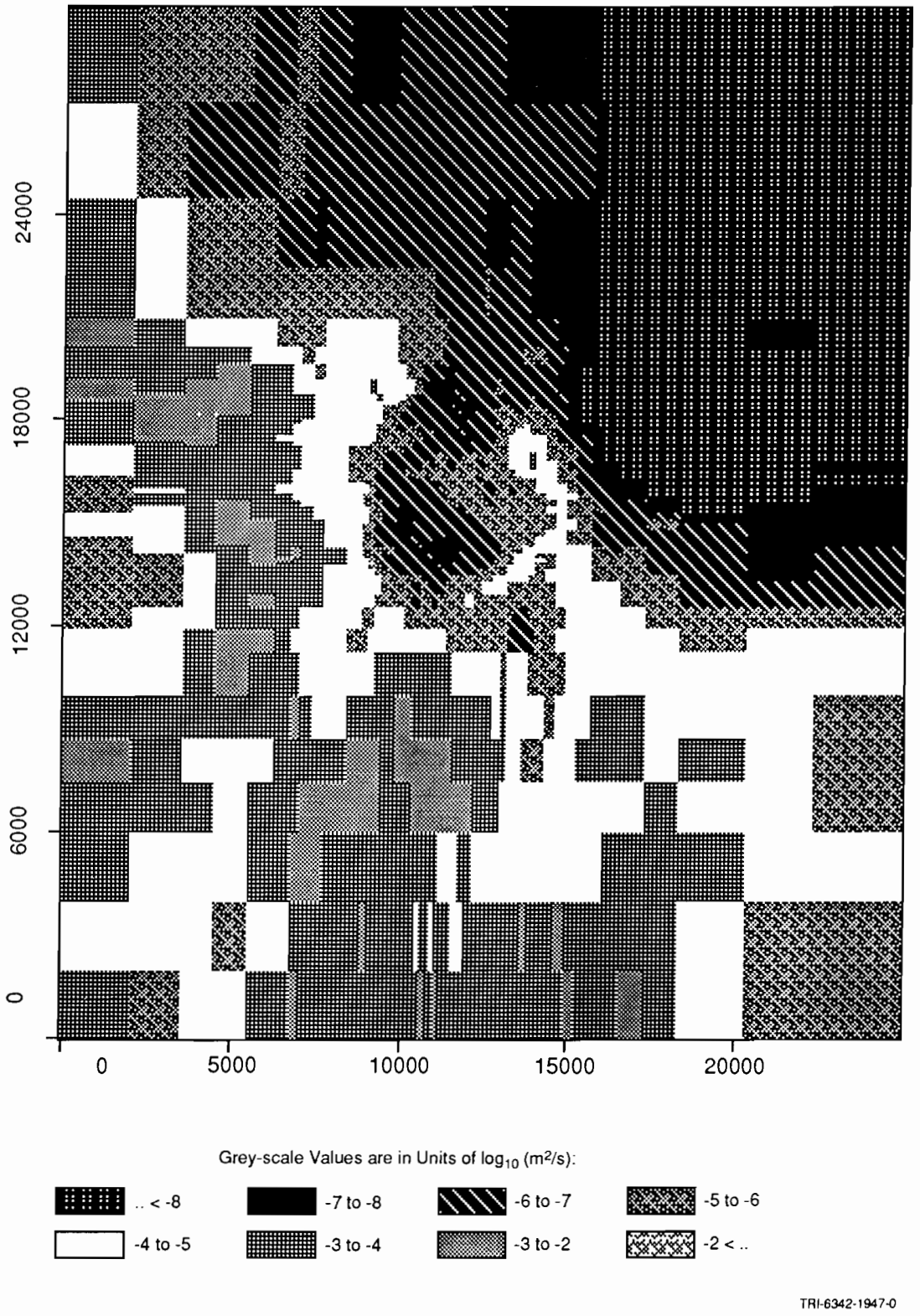

Figure C-64. Realization 32 of Culebra transmissivity.

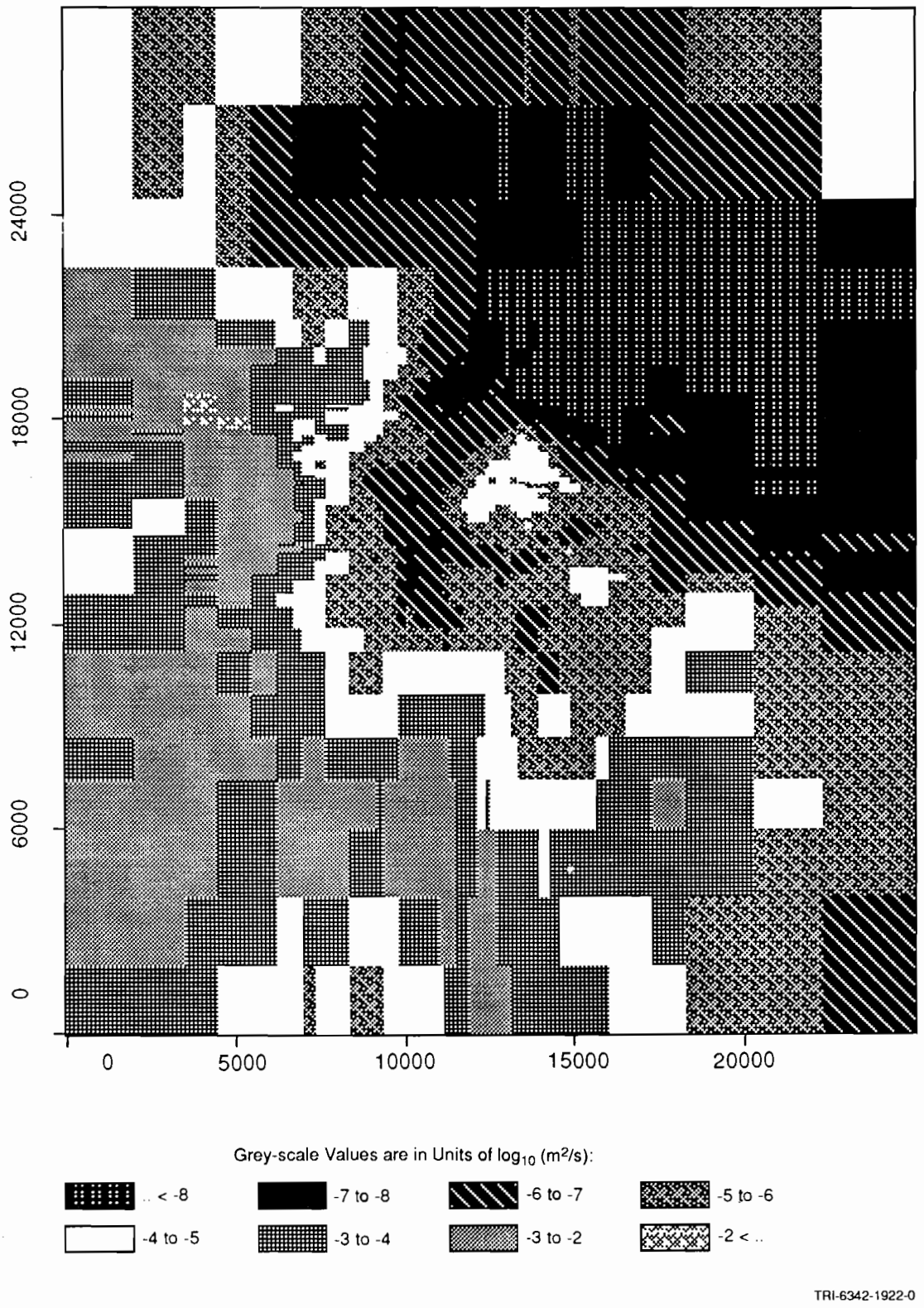

Figure C-65. Realization 8 of Culebra transmissivity.

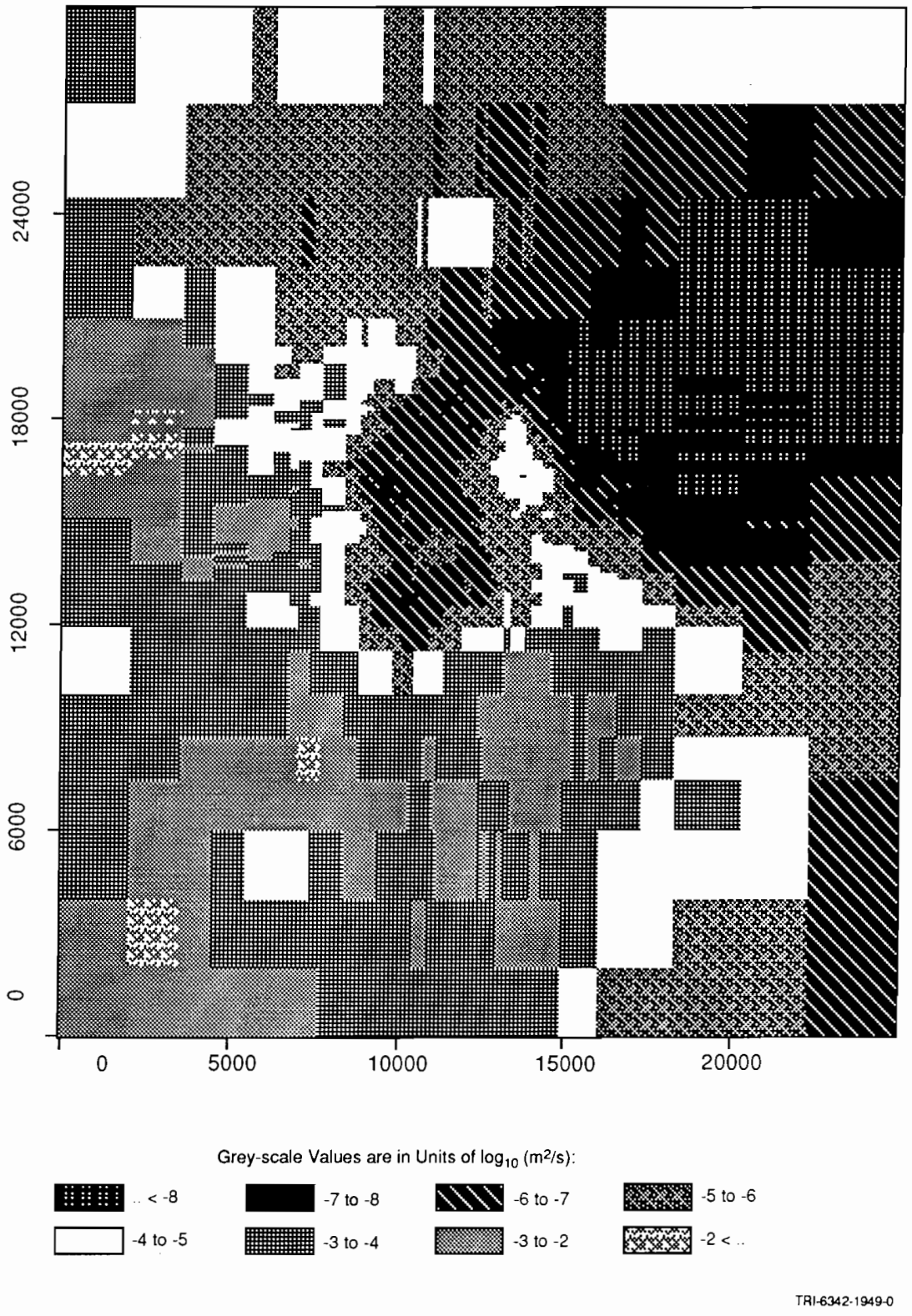

Figure C-66. Realization 11 of Culebra transmissivity.

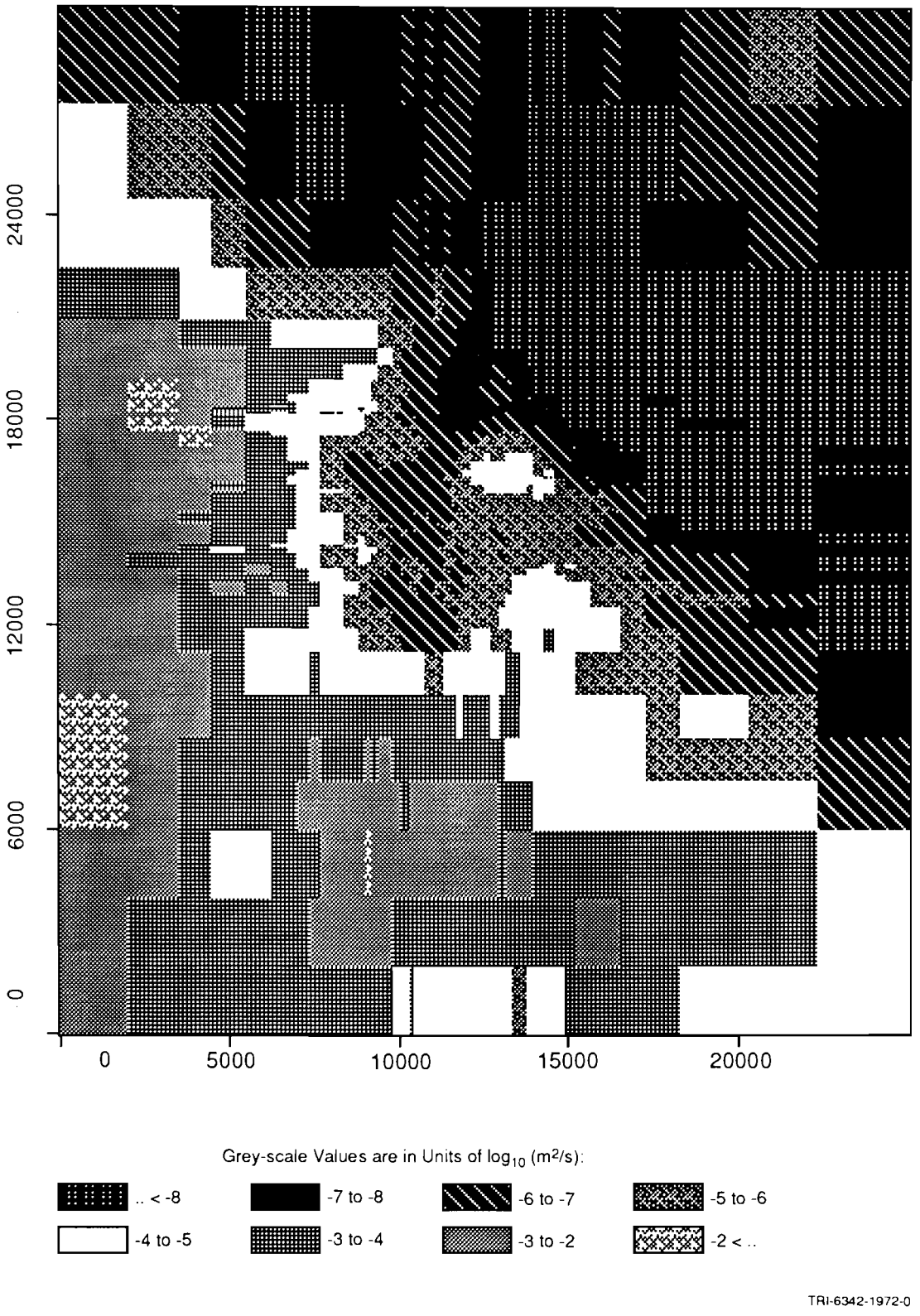

Figure C-67. Realization 54 of Culebra transmissivity.

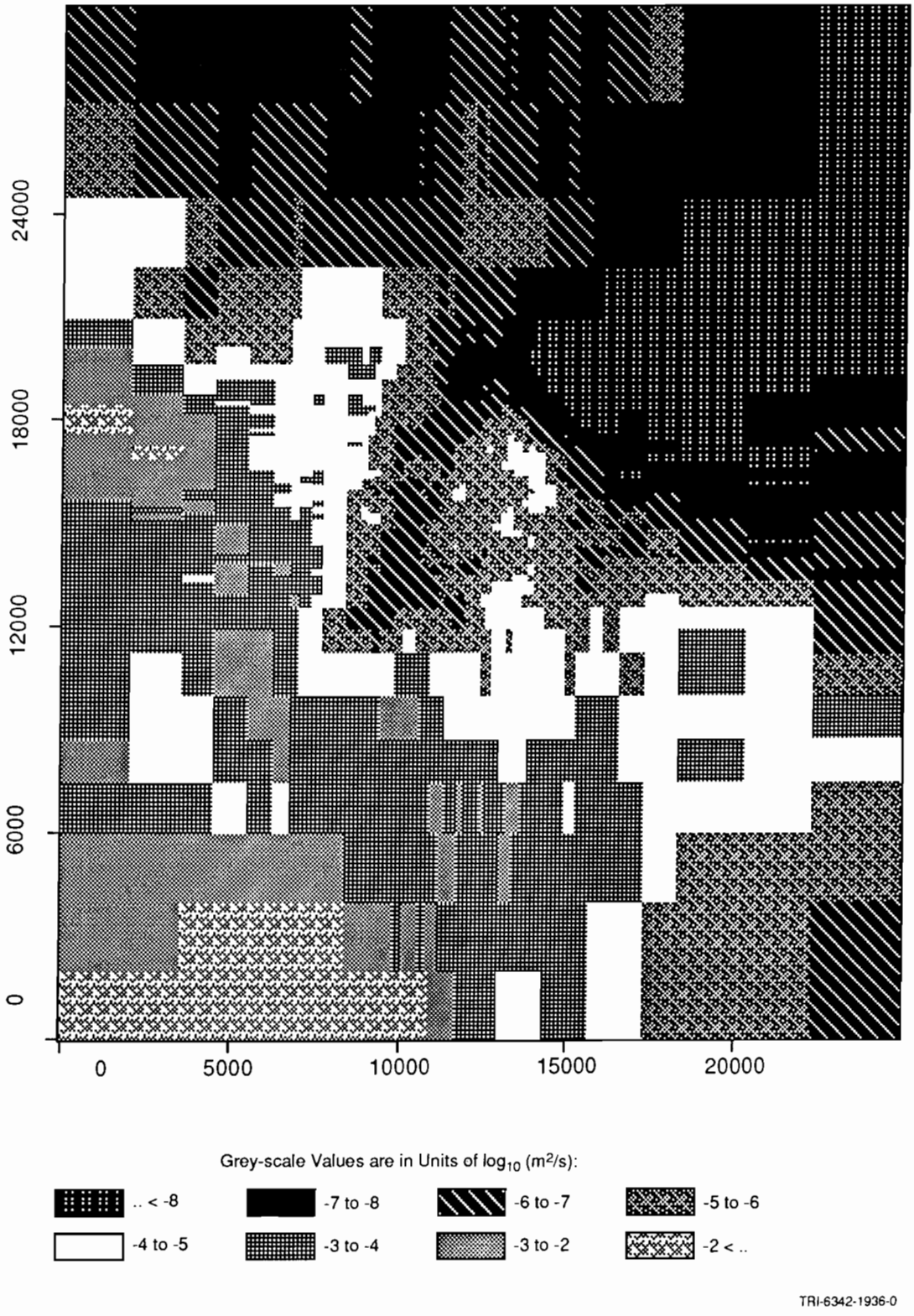

Figure C-68. Realization 6 of Culebra transmissivity.

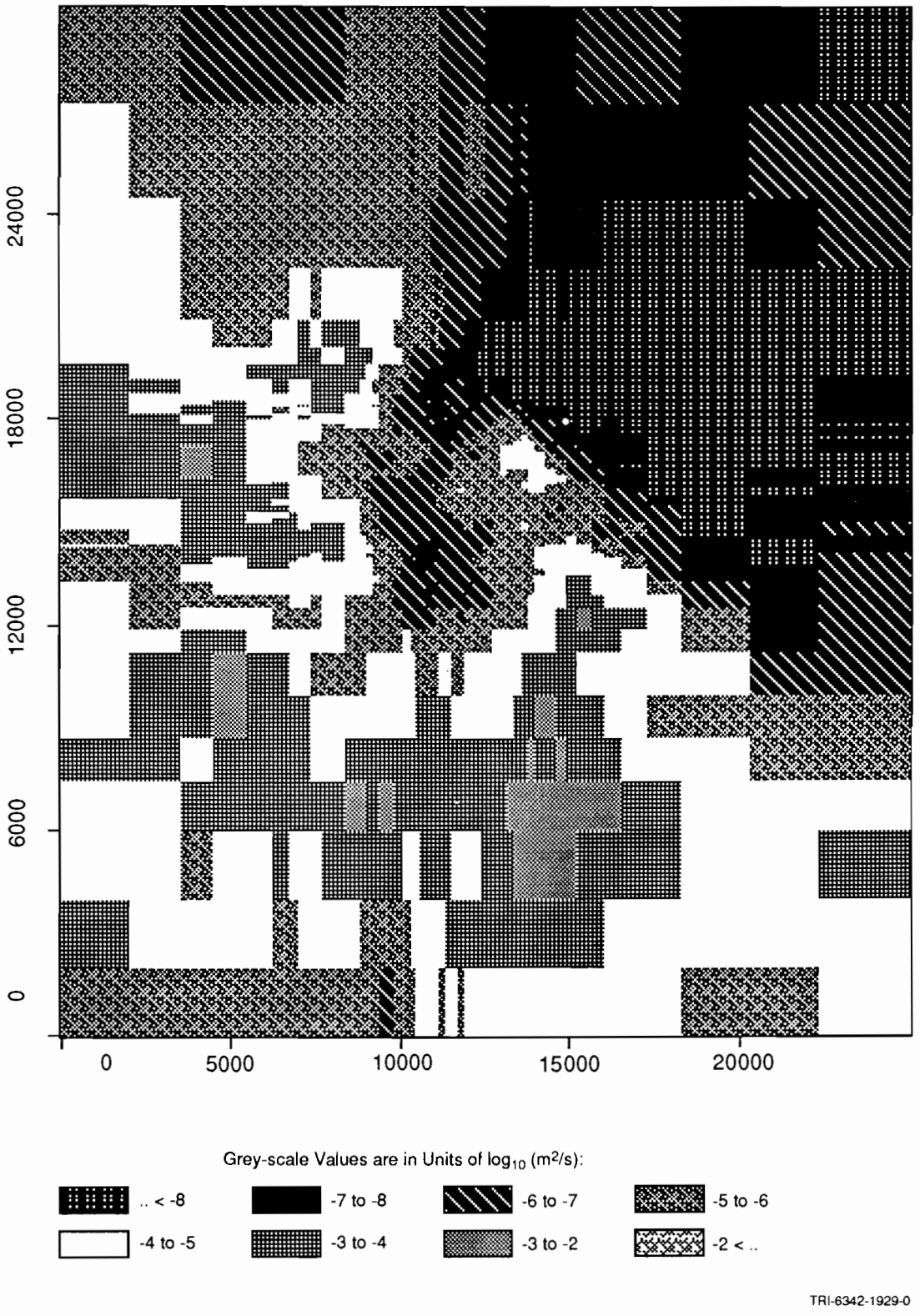

Figure C-69. Realization 67 of Culebra transmissivity.

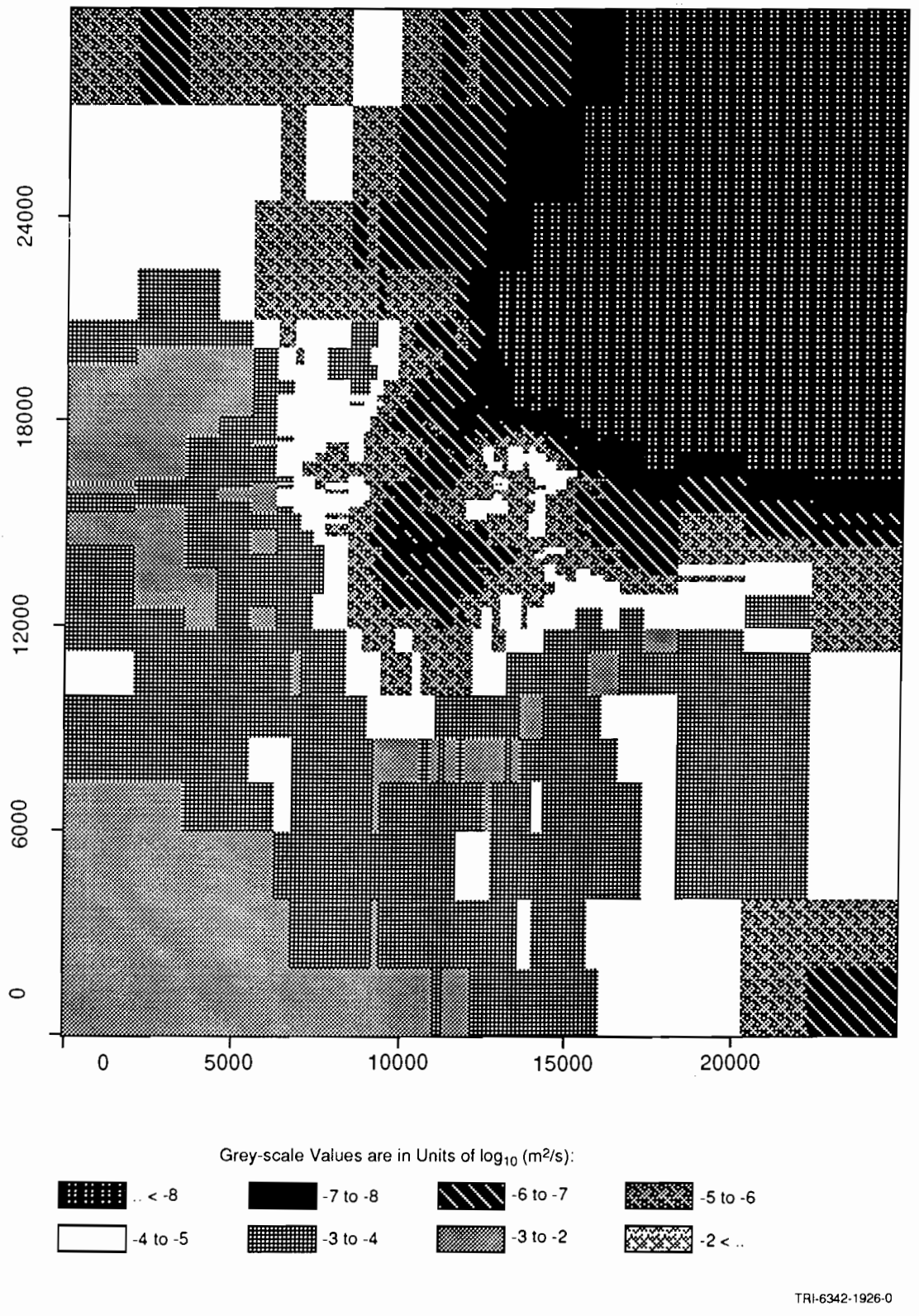

Figure C-70. Realization 58 of Culebra transmissivity.

APPENDIX D:
REALIZATIONS OF
DRILLING INTENSITY FUNCTIONS
FOR HUMAN INTRUSION

APPENDIX D

APPENDIX D: REALIZATIONS OF DRILLING INTENSITY FUNCTIONS FOR HUMAN INTRUSION

The following figures are graphs of the 70 representations of drilling intensity functions used in the 1992 Performance Assessment (PA) calculations to calculate probabilities of inadvertent drilling at the Waste Isolation Pilot Plant (WIPP) site (Section 1.4.2 of this volume). The genesis of these representations is explained in Section 5.2. Each graph of a representation shows two quantities: the intrusion rate, measured in boreholes/($km^2 \cdot 10^4$ yr), which is also the function $\lambda_s(t)$ mentioned in Eq. 1.4.2-5 of Section 1.4.2; and the time-integrated intrusion rate,

$$\int_0^t \lambda_s(x)\,dx, \text{ for any t such that } 0 < t < 10{,}000 \text{ yr},$$

which is also called *intrusions* and is measured in boreholes/km^2.

The 70 graphs are ordered by increasing values of intrusions measured at 10,000 yr. The ordering is specified by "sequence" number; note that many graphs are identical and so will correspond to more than one sequence number. Note also that only those representations that were not identically zero are included in this collection.

Note on scaling of graphs: The ordinates and abscissas of each graph have been scaled to improve resolution; the scaling used is

$$y = \sinh^{-1}\left(\frac{x}{a}\right)$$

where x is the variable noted on the ordinate (or abscissa) and y is the distance from origin of graph along ordinate (or abscissa). The constant a is chosen to make numbered intervals (e.g., $[0,10^2]$, $[10^2, 10^3]$) of approximately the same size.

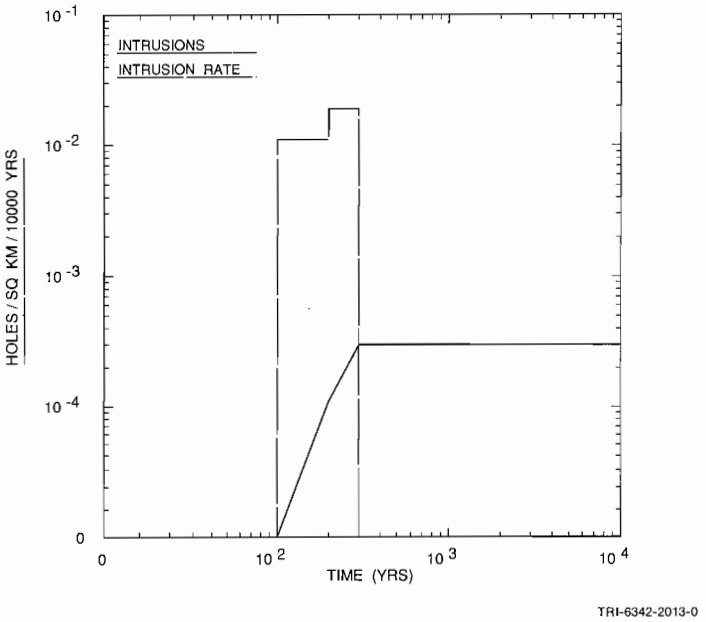

Figure D-1. Realization of drilling intensity function, Sequence 1.

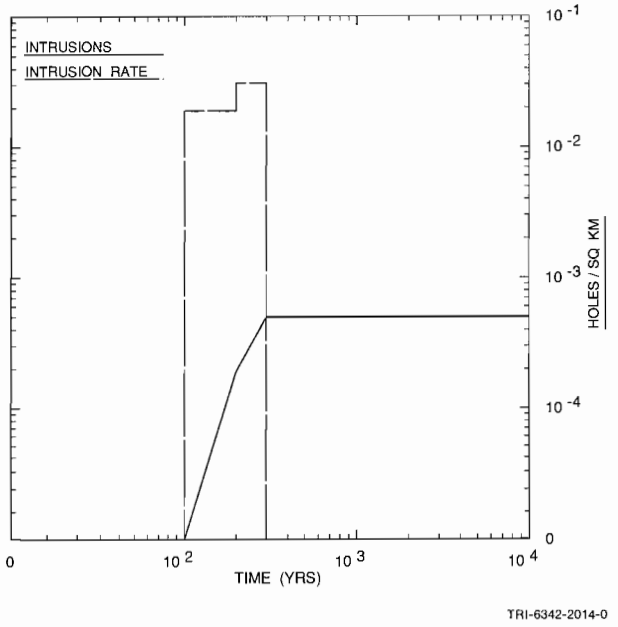

Figure D-2. Realization of drilling intensity function, Sequence 2.

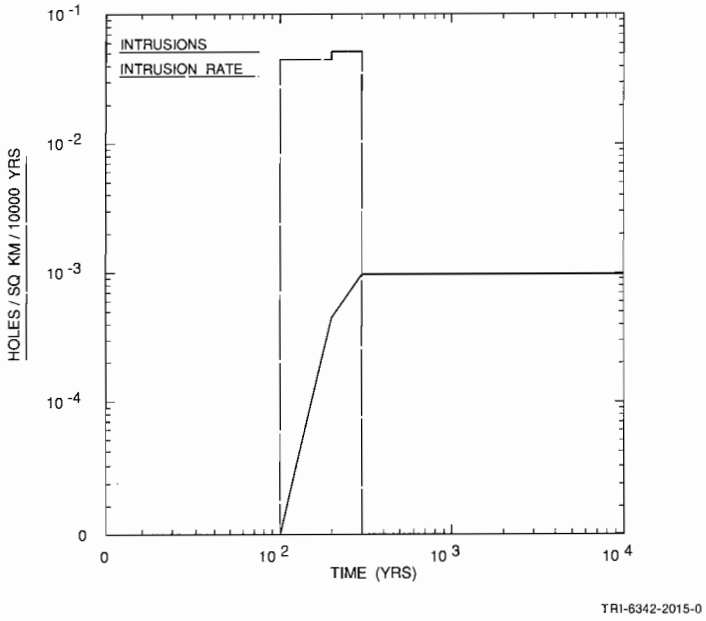

Figure D-3. Realization of drilling intensity function, Sequence 3.

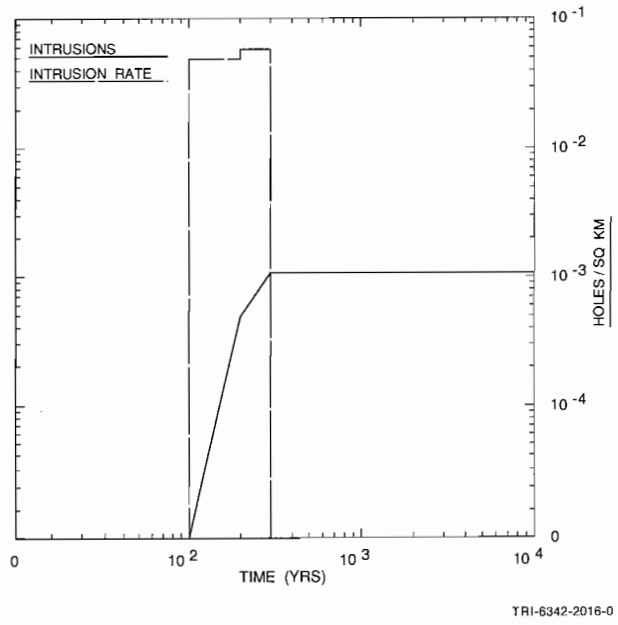

Figure D-4. Realization of drilling intensity function, Sequence 4.

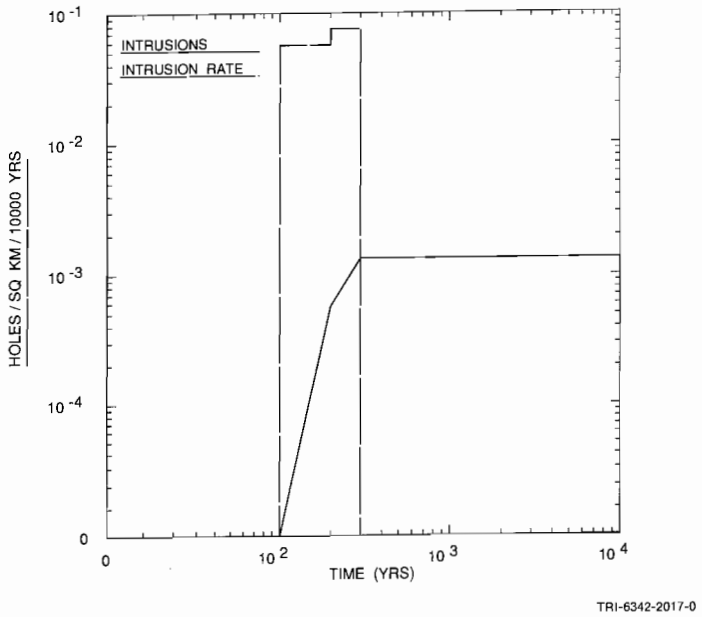

Figure D-5. Realization of drilling intensity function, Sequence 5.

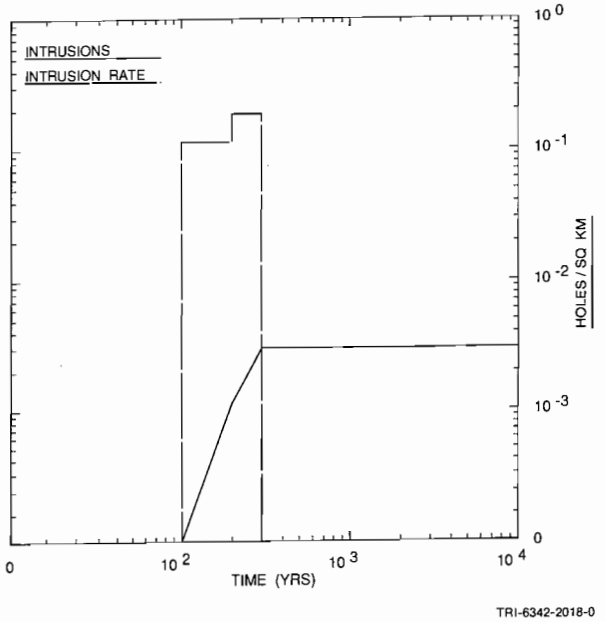

Figure D-6. Realization of drilling intensity function, Sequences 6 and 7.

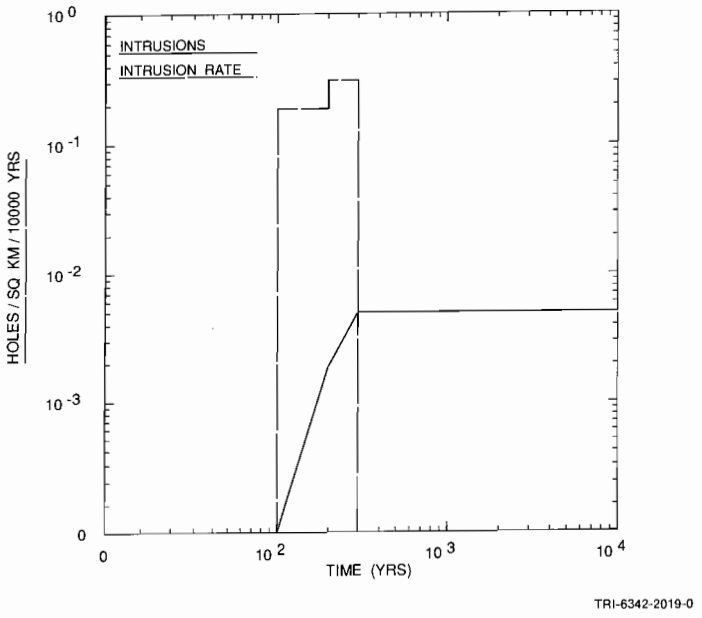

Figure D-7. Realization of drilling intensity function, Sequences 8 and 9.

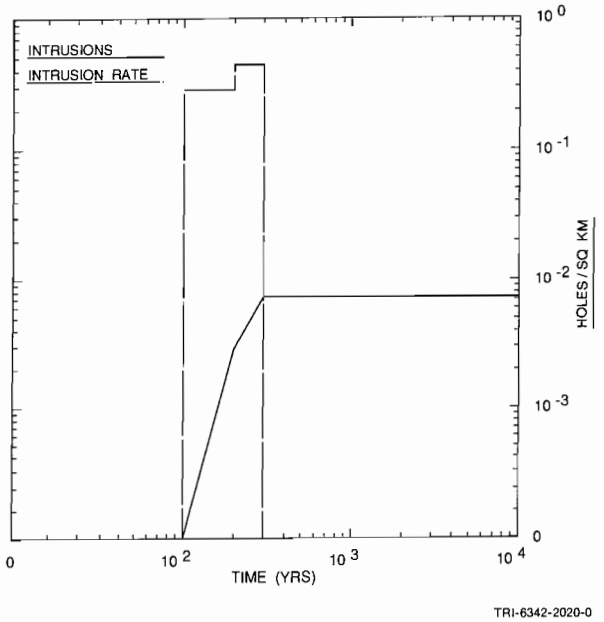

Figure D-8. Realization of drilling intensity function, Sequence 10.

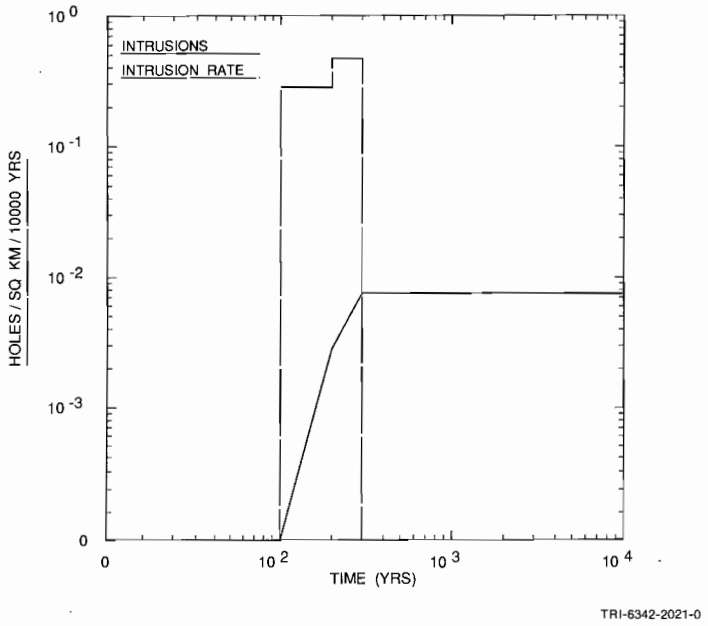

Figure D-9. Realization of drilling intensity function, Sequences 11 and 12.

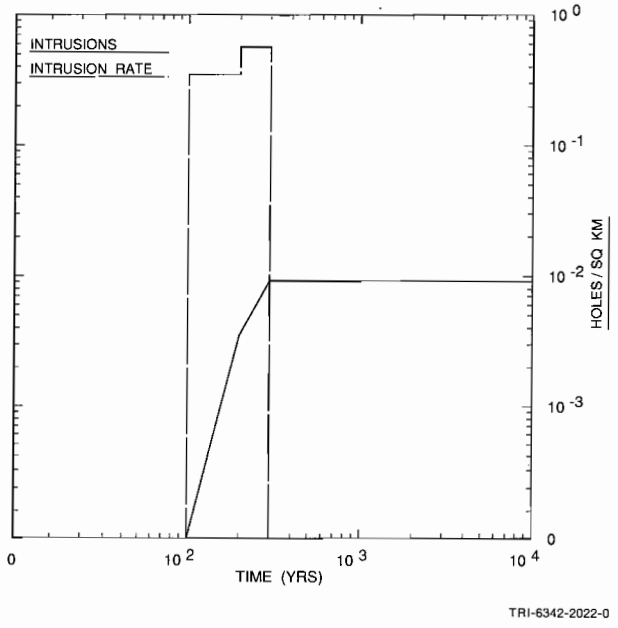

Figure D-10. Realization of drilling intensity function, Sequence 13.

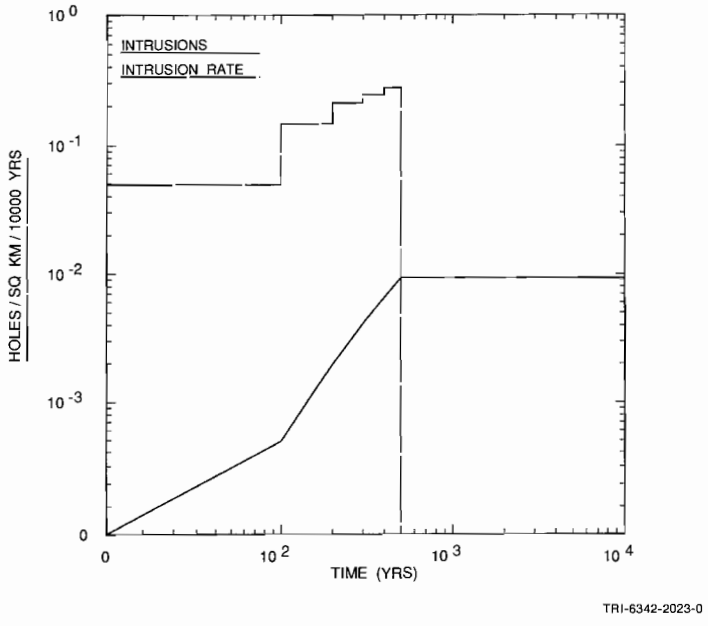

Figure D-11. Realization of drilling intensity function, Sequence 14.

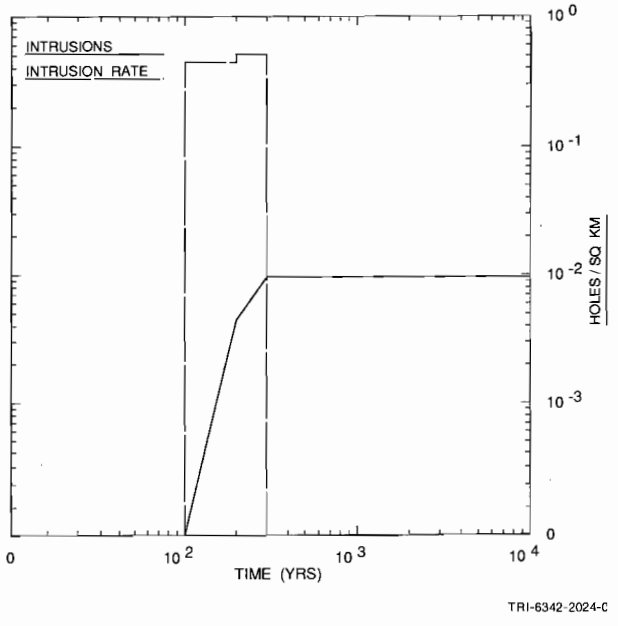

Figure D-12. Realization of drilling intensity function, Sequence 15.

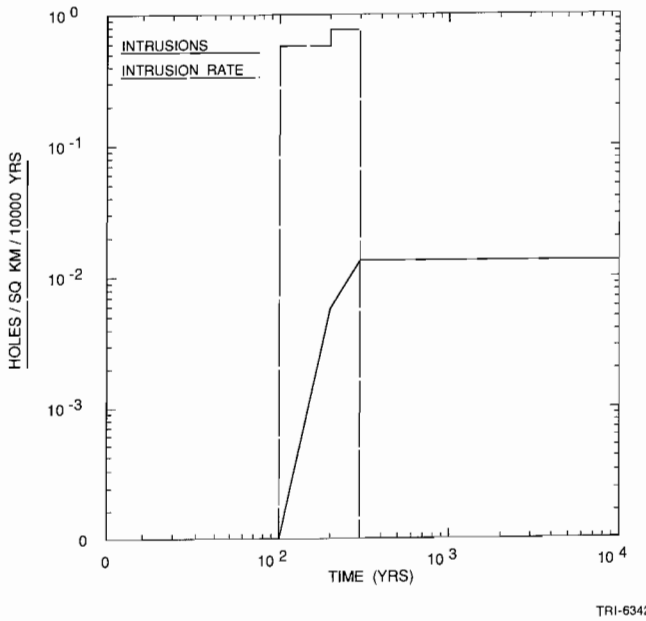

Figure D-13. Realization of drilling intensity function, Sequence 16.

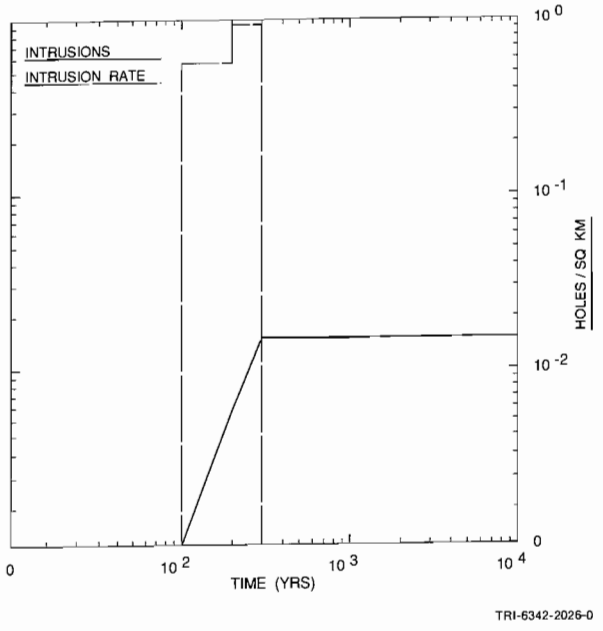

Figure D-14. Realization of drilling intensity function, Sequences 17, 18 and 19.

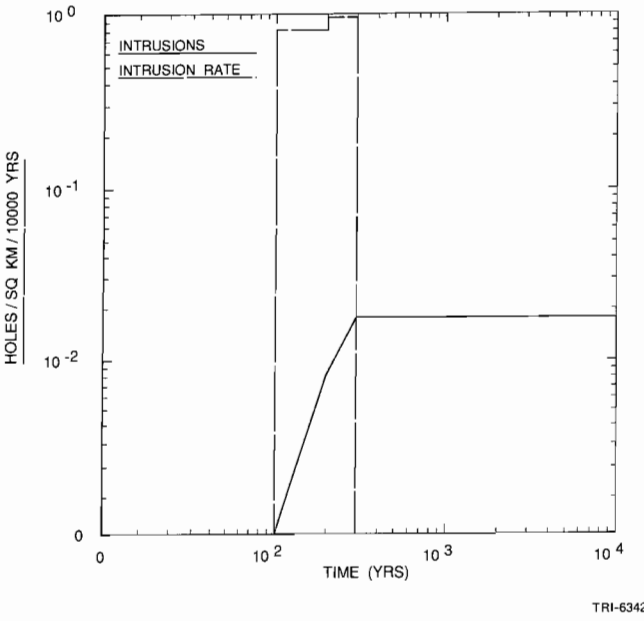

Figure D-15. Realization of drilling intensity function, Sequence 20.

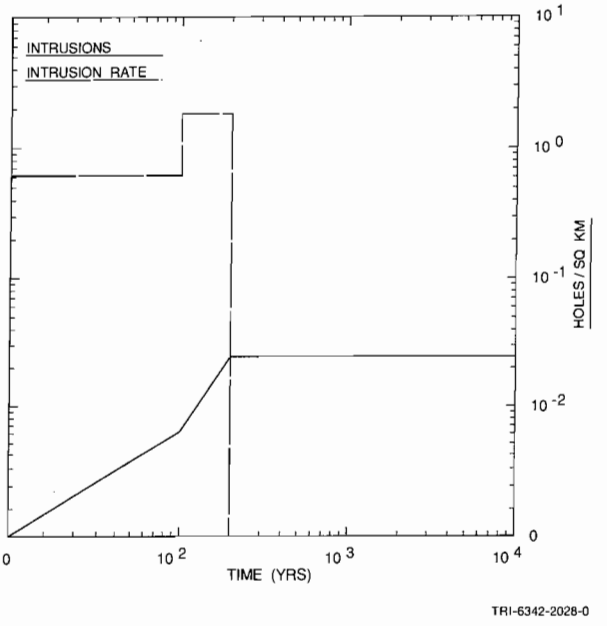

Figure D-16. Realization of drilling intensity function, Sequence 21.

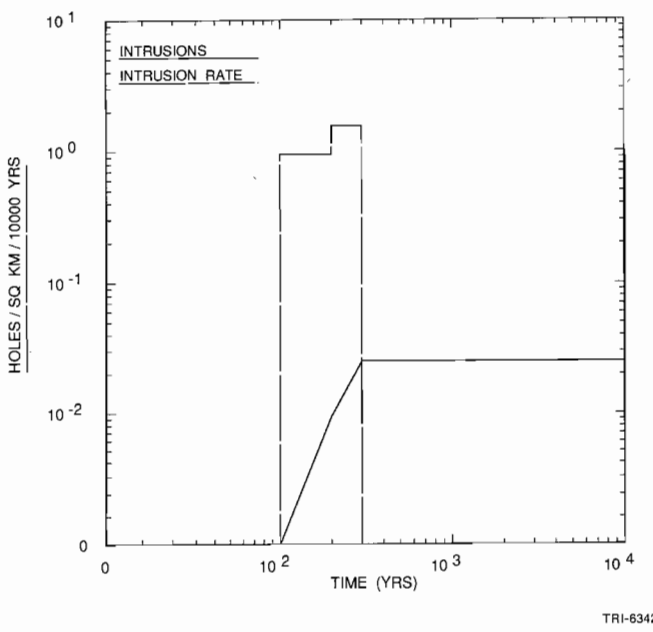

Figure D-17. Realization of drilling intensity function, Sequence 22.

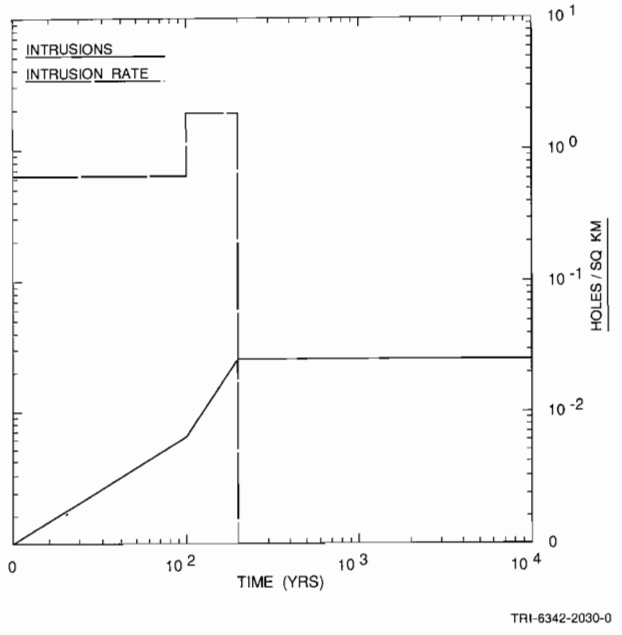

Figure D-18. Realization of drilling intensity function, Sequence 23.

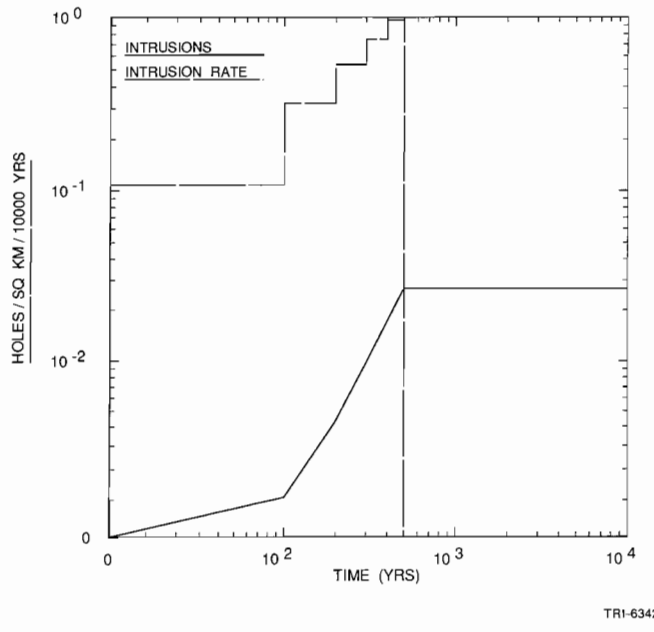

Figure D-19. Realization of drilling intensity function, Sequences 24 and 25.

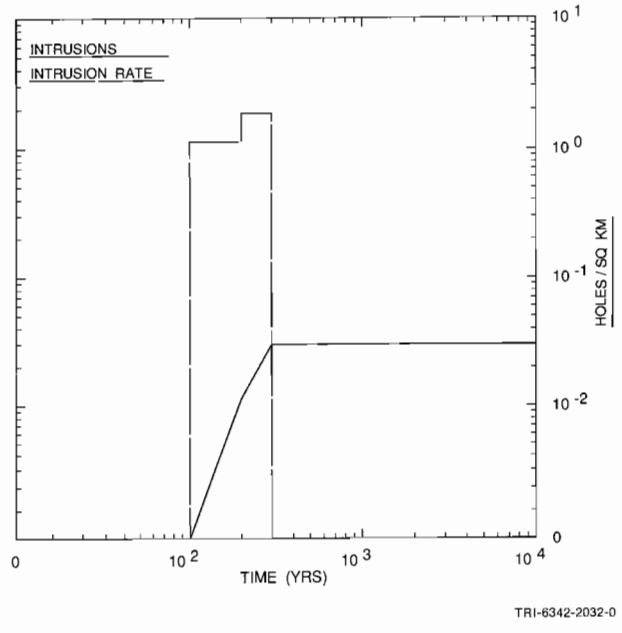

Figure D-20. Realization of drilling intensity function, Sequences 26 and 27.

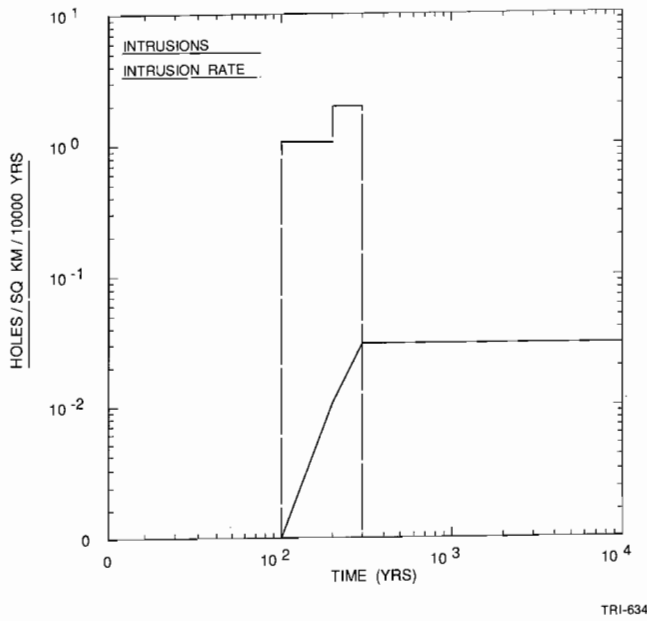

Figure D-21. Realization of drilling intensity function, Sequence 28.

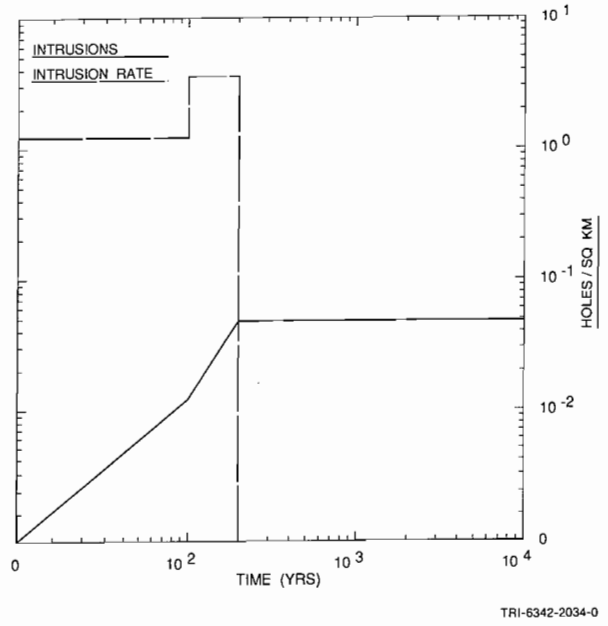

Figure D-22. Realization of drilling intensity function, Sequence 29.

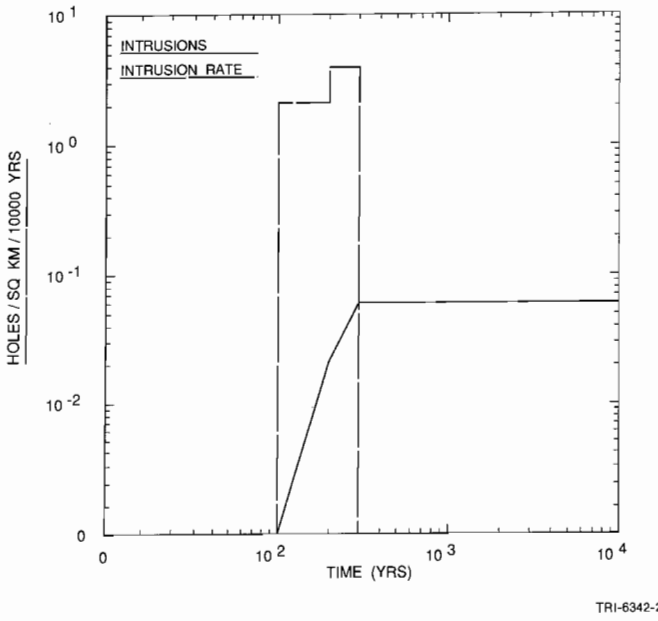

Figure D-23. Realization of drilling intensity function, Sequence 30.

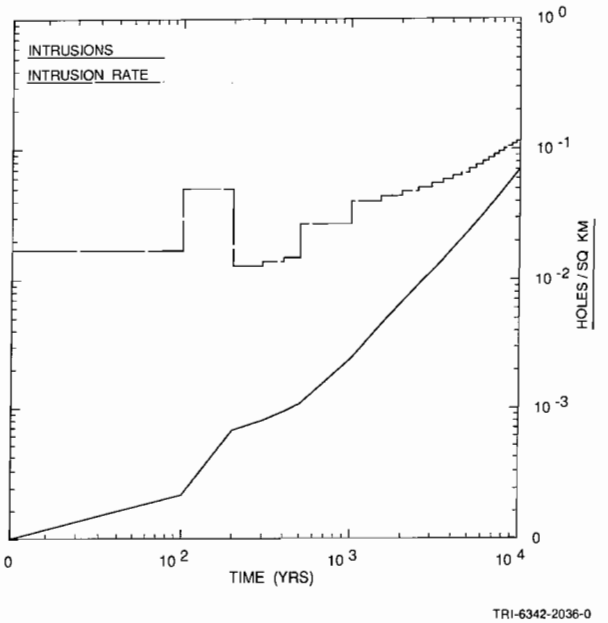

Figure D-24. Realization of drilling intensity function, Sequence 31.

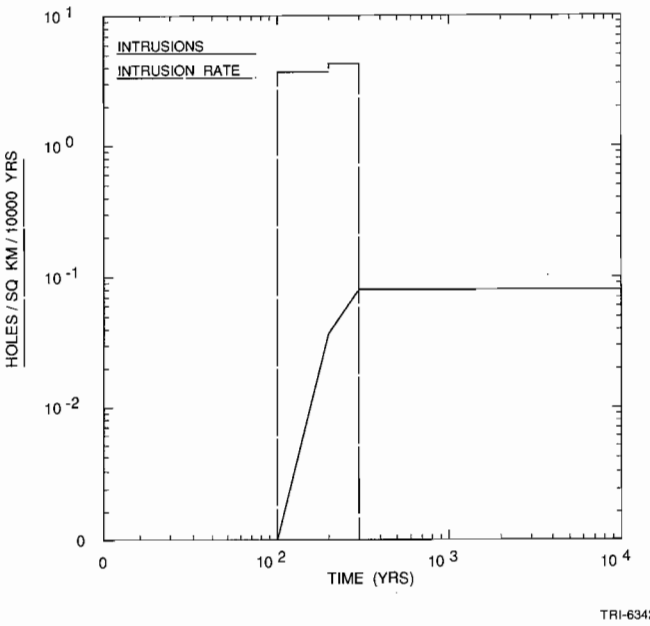

Figure D-25. Realization of drilling intensity function, Sequence 32.

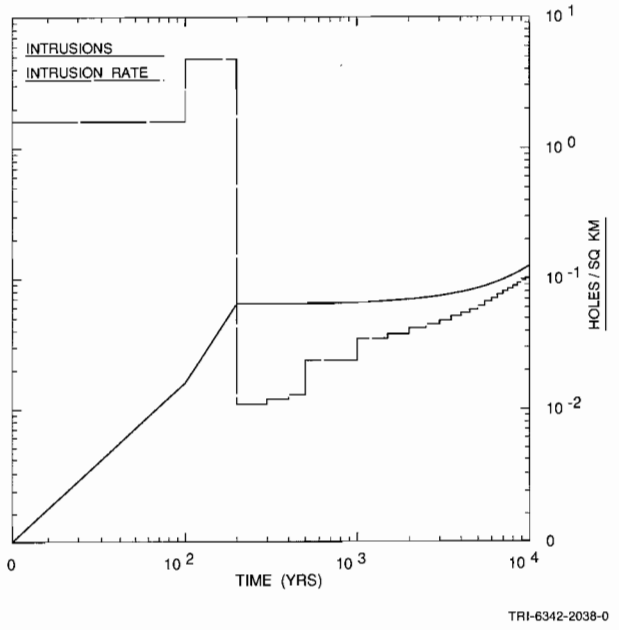

Figure D-26. Realization of drilling intensity function, Sequence 33.

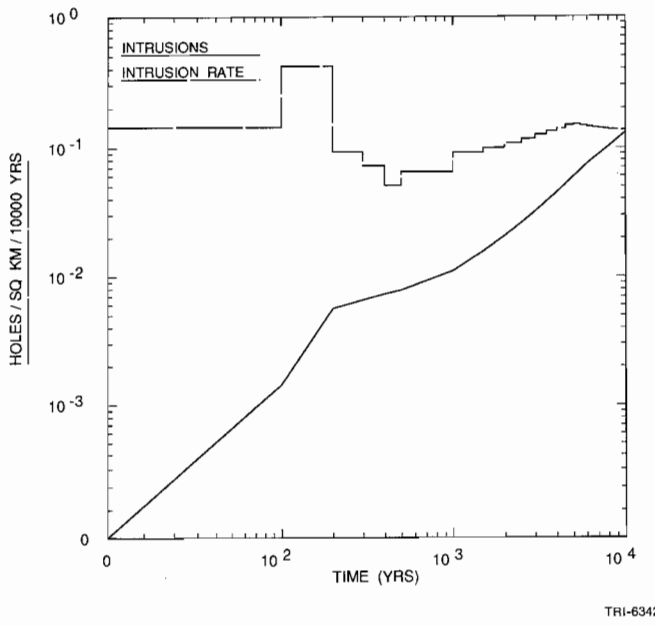

Figure D-27. Realization of drilling intensity function, Sequences 34, 35 and 36.

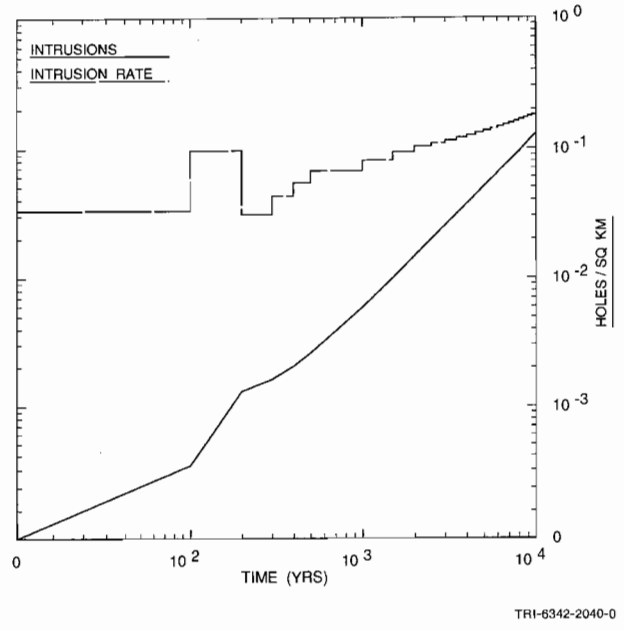

Figure D-28. Realization of drilling intensity function, Sequences 37, 38, 39 and 40.

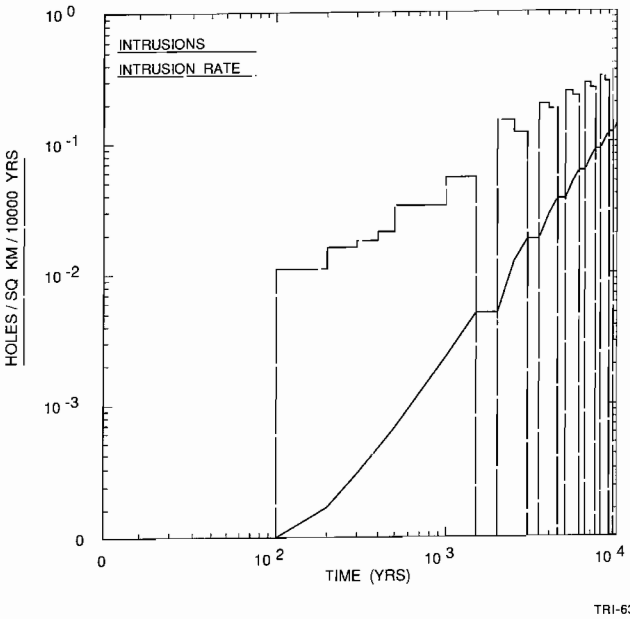

Figure D-29. Realization of drilling intensity function, Sequence 41.

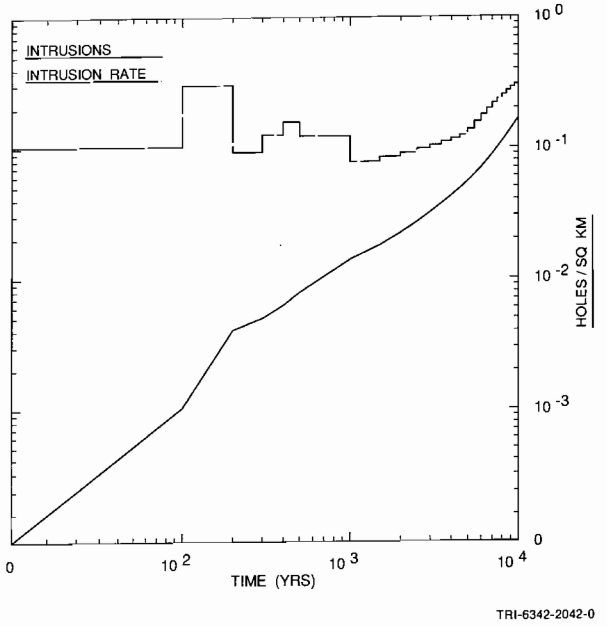

Figure D-30. Realization of drilling intensity function, Sequence 42.

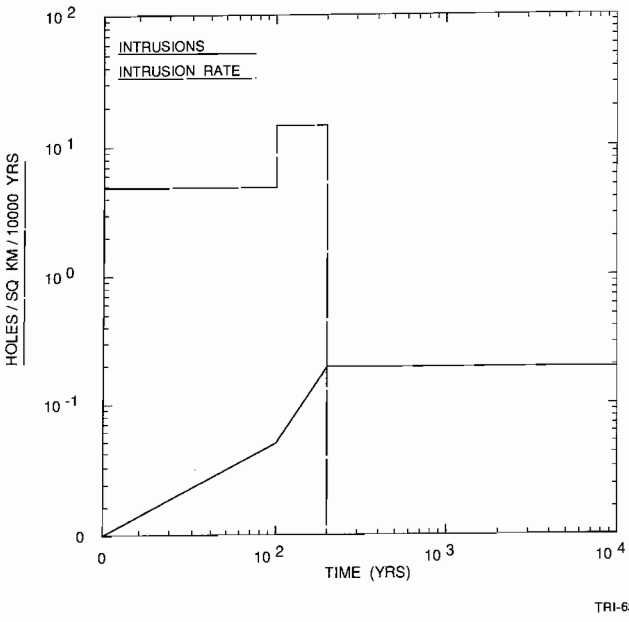

Figure D-31. Realization of drilling intensity function, Sequence 43.

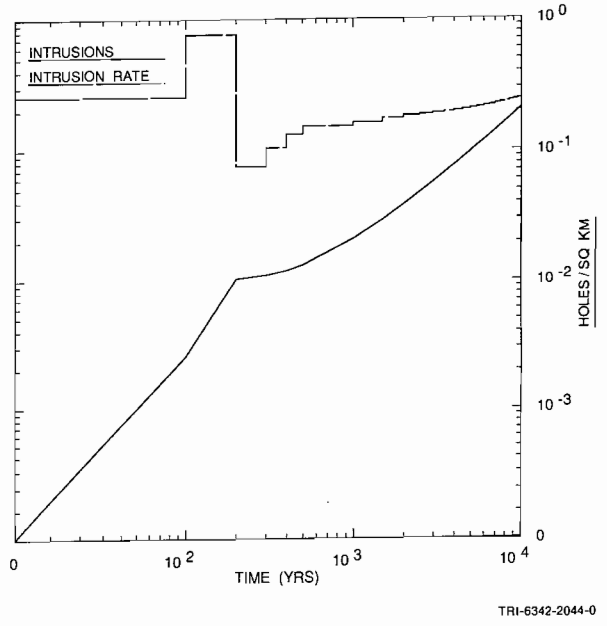

Figure D-32. Realization of drilling intensity function, Sequences 44, 45, 46, 47 and 48.

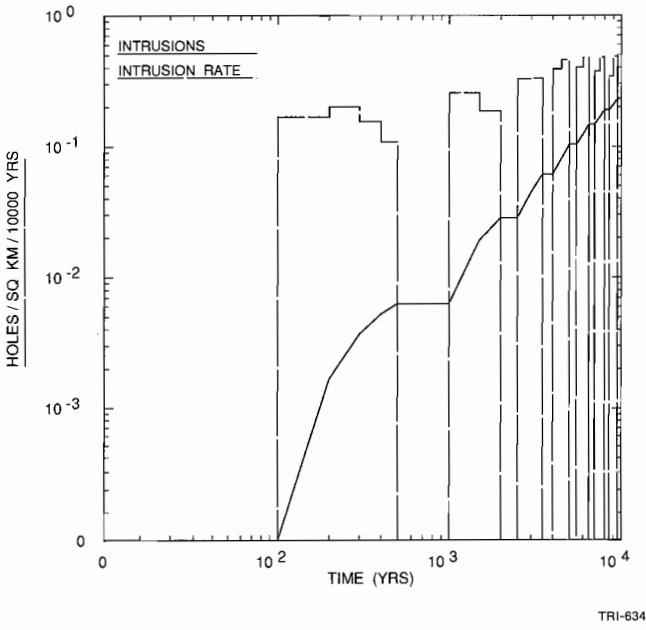

Figure D-33. Realization of drilling intensity function, Sequence 49.

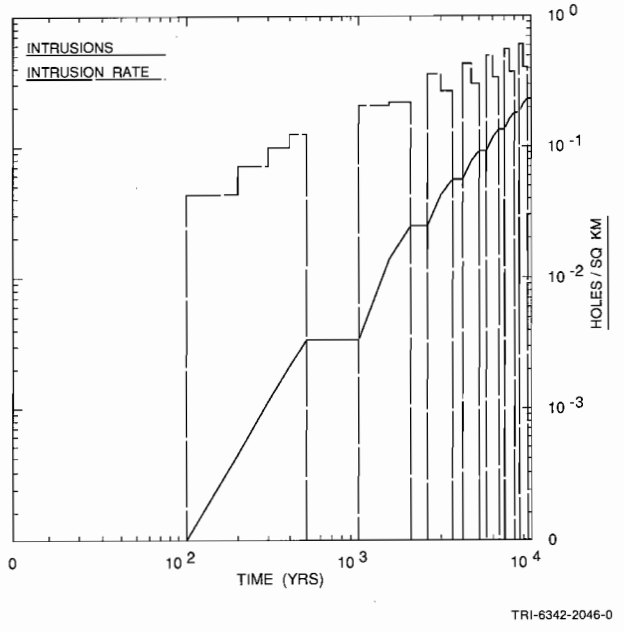

Figure D-34. Realization of drilling intensity function, Sequence 50.

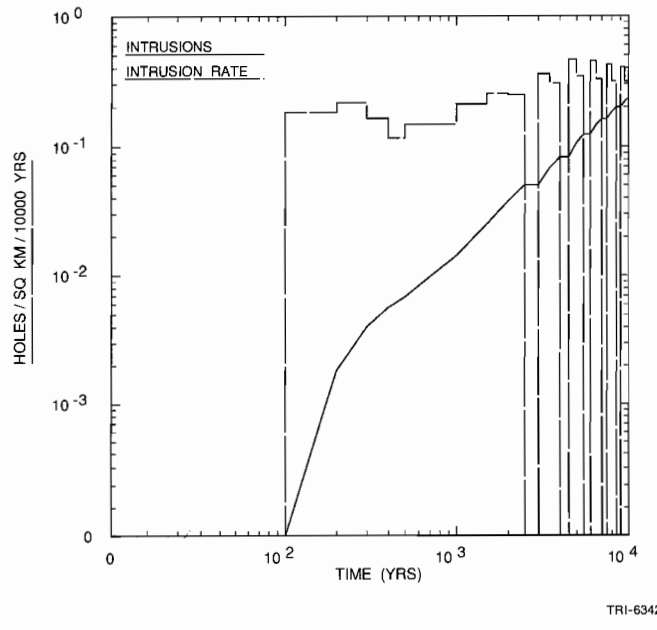

Figure D-35. Realization of drilling intensity function, Sequence 51.

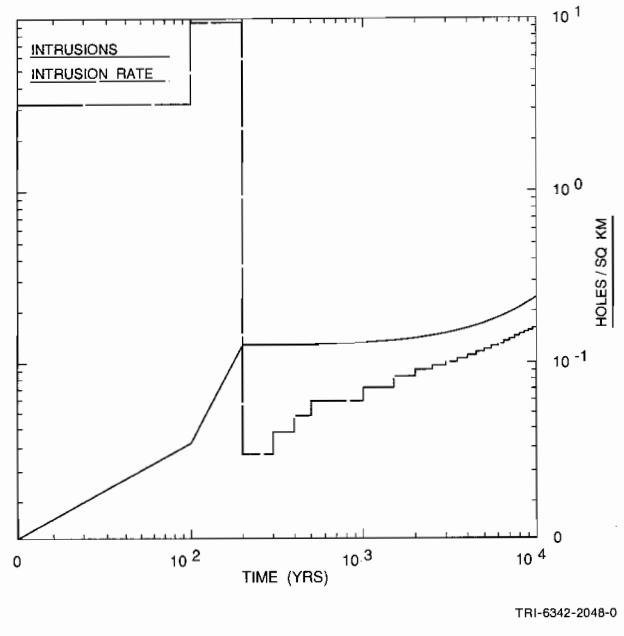

Figure D-36. Realization of drilling intensity function, Sequences 52, 53, 54, 55 and 56.

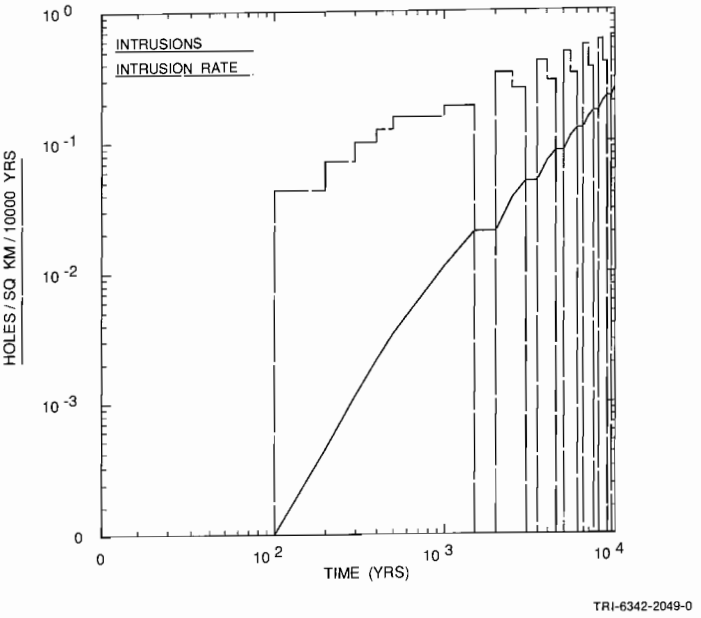

Figure D-37. Realization of drilling intensity function, Sequence 57.

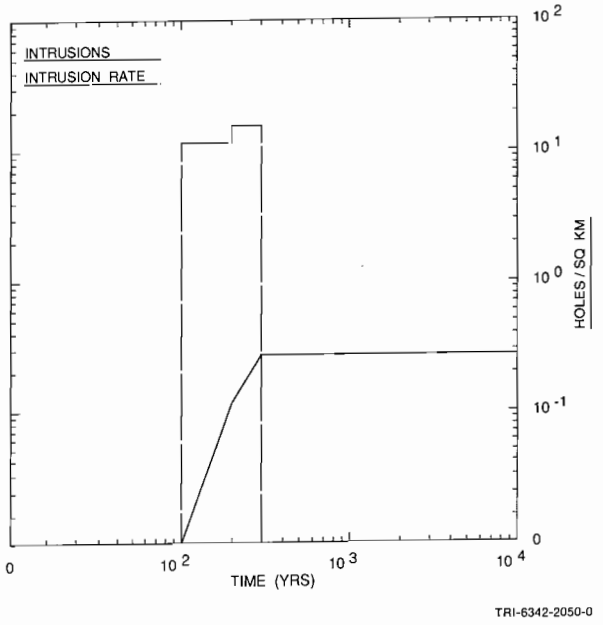

Figure D-38. Realization of drilling intensity function, Sequence 58.

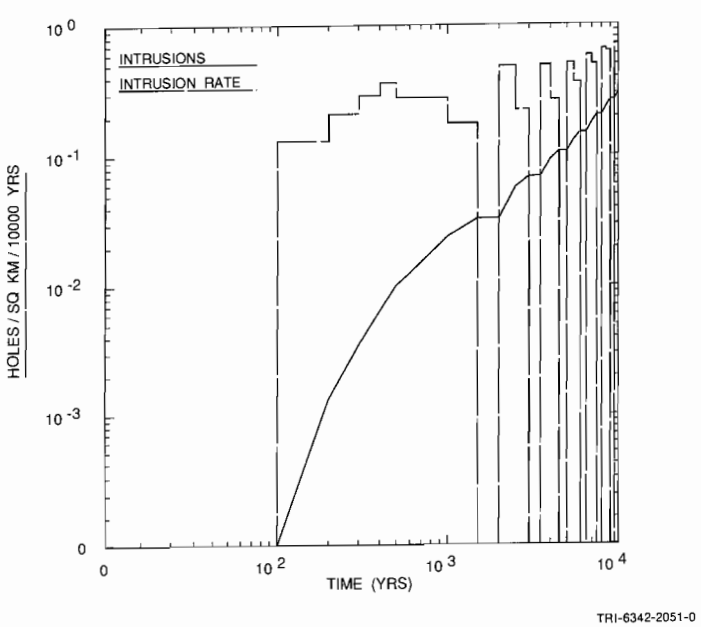

Figure D-39. Realization of drilling intensity function, Sequences 59 and 60.

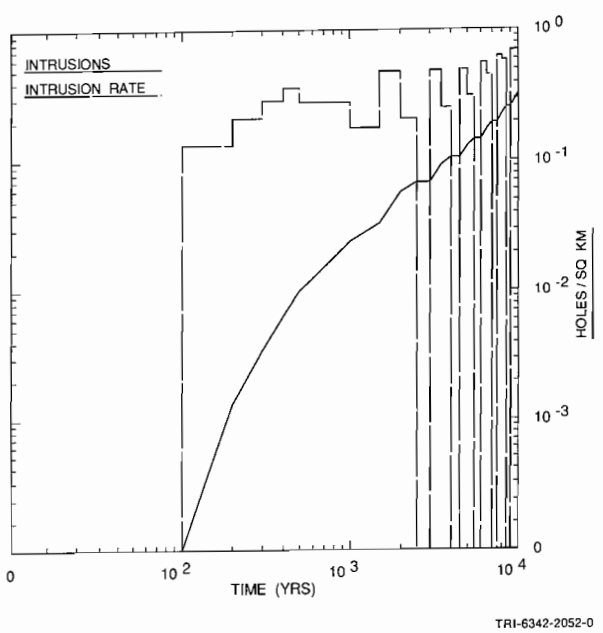

Figure D-40. Realization of drilling intensity function, Sequence 61.

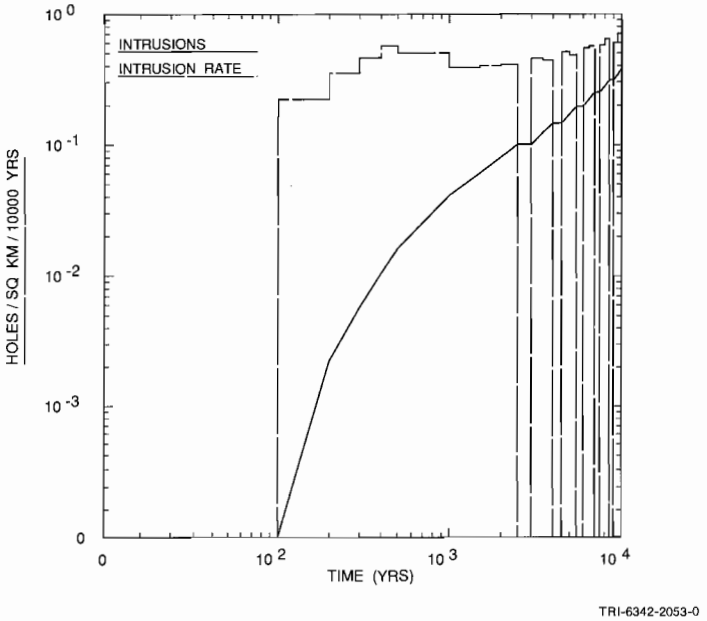

Figure D-41. Realization of drilling intensity function, Sequences 62 and 63.

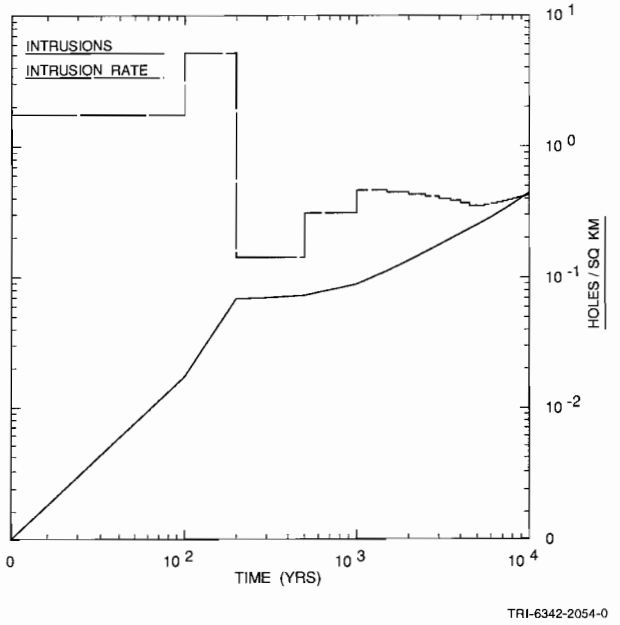

Figure D-42. Realization of drilling intensity function, Sequence 64.

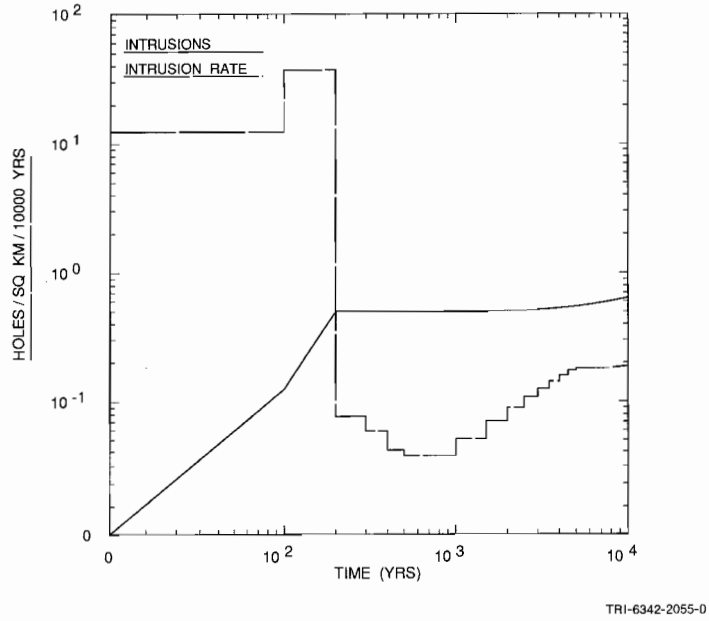

Figure D-43. Realization of drilling intensity function, Sequences 65 and 66.

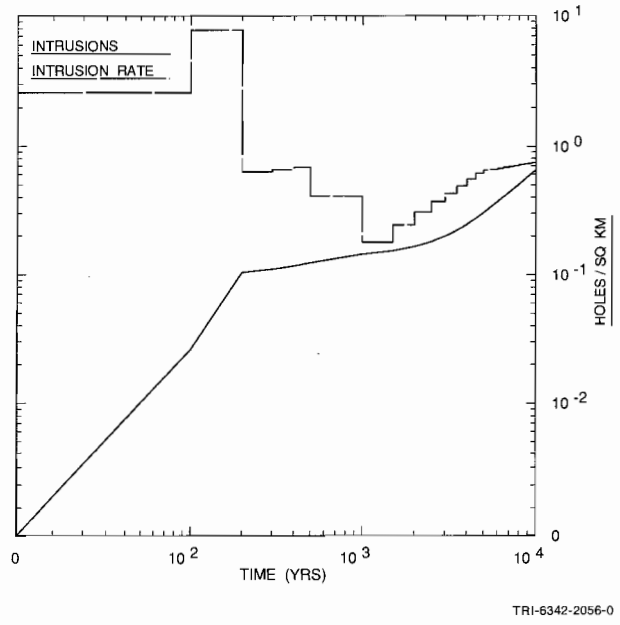

Figure D-44. Realization of drilling intensity function, Sequences 67 and 68.

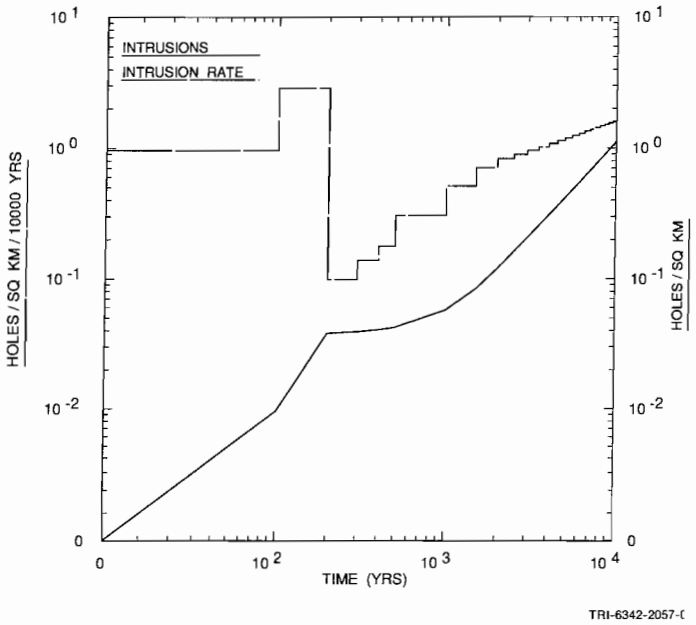

Figure D-45. Realization of drilling intensity function, Sequences 69 and 70.

NOMENCLATURE

Mathematical Symbols

A	-	cross-sectional area (m^2)
A_m	-	amplitude scaling factor for precipitation variation
a	-	minimum of range of distribution
$2B$	-	characteristic fracture spacing or block length (m)
B_ℓ, B_g	-	formation volume factor (reservoir conditions/standard conditions) for liquid or gas, respectively
b	-	maximum of range of distribution
$2b_\ell$	-	fracture aperature (m)
C	-	concentration (kg/m^3)
C_w	-	total concentration of water in solution (e.g., brine)
$\hat{C}$	-	mass fraction (kg/kg)
C°	-	solubility (kg chemical/m^3 fluid)
c	-	capacitance ($ß_b + \phi ß_\ell$) (Pa^{-1})
D_m	-	molecular diffusion in porous media matrix ($D^\square \bullet \tau$) (m^2/s)
$D^\square$	-	molecular diffusion in pure fluid (m^2/s)
D_L, D_T	-	hydrodynamic dispersion $D_m + \alpha_L \bar{V}$ and $D_m + \alpha_T \bar{V}$, respectively (m^2/s)
D	-	hydrodynamic dispersion tensor
d	-	diameter
d_i	-	separation distance to grid point i, e.g., separation distance between interpolated point and a nearby point
d_s	-	distance traveled by solute
E	-	Young's modulus (Pa)
e	-	weighting power for inverse-distance interpolation
f	-	fanning friction factor
f_w	-	waste unit factor
f_c, f_m, f_s	-	volume fraction of combustibles, metals/glass, and sludge, respectively
f_{rchg}	-	recharge factor evaluated from precipitation fluctuation
$F(x)$	-	cumulative distribution function, integral of f(x), probability density function of parameter x
$f(x)$	-	distribution of x

1	g	-	acceleration due to gravity = ~9.8 m/s^2 or 9.80616 - 2.5928 x 10^{-2} $\cos 2\phi_{lat}$ + 6.9 x 10^{-5} $\cos^2 2\phi_{lat}$ - 3.086 x $10^{-6} z_{sur}$ - 1.543 x $10^{-6} \Delta z$, where ϕ_{lat} is the latitude, z_{sur} is the surface elevation in meters, and Δz is the depth in meters below the surface (Helmert's equation) (Weast and Astle, 1981, F-78) (9.792 m/s^2 at 1039.06 m [surface] and 9.791 m/s^2 at 351 m [repository level])
7	h	-	multiplier factor
9	h^*	-	Plank's constant, 6.6262×10^{-34} J • s
11	K	-	hydraulic conductivity (m/s)
13	K_d	-	distribution (or partition) coefficient (m^3/kg)
15	K_{bulk}	-	bulk modulus $(E/(3(1-2\nu))$ (Pa)
17	k^*	-	Boltzmann's constant 1.3806×10^{-23} (J/K)
19	k	-	permeability (m^2)
21	$k_{r\ell}, k_{rg}$	-	relative liquid and gas permeability, respectively
23	L_i	-	release limit for radionuclide i (from *40 CFR 191* Appendix A, Table 1)
25	M	-	molecular weight (g/mol)
27	M_{dc}, M_{dm}, M_{ds}	-	average mass of combustibles, metals/glass, and sludge, respectively, per drum (kg)
29	m_A	-	atomic mass
31	$\dot{m}_b, \dot{m}_c, \dot{m}_t$	-	gas generation rate, biodegradation (mol/kg cellulose/s), corrosion (mol/m^2 surface area steel/s), and total, respectively
34	N_R	-	Reynold's number, $\frac{\rho_f v d}{\mu}$
36	Np	-	Peclet number, $\bar{V} d_{50} / \tau D^{\square}$, where d_{50} is average particle diameter (length dimension)
38	N	-	molarity (mol/ℓ)
40	n	-	number of moles
42	n_g	-	number of grid points used for interpolation
44	$P(r>R)$	-	probability of r > R
46	p	-	pressure (Pa)
48	p_c	-	capillary pressure (Pa)
50	p_{cr}	-	critical pressure (Pa)
52	p_t	-	threshold displacement pressure (Pa)
54	Q	-	flow rate
56	R_m, R_f	-	retardation, matrix and fracture, respectively
59	R^*	-	universal gas constant $\left(8.31441 \frac{Pa \bullet m^3}{mol \bullet K}\right)$
62	r_g/ℓ	-	gas (nonwetting phase)/liquid (wetting phase) ratio
64	$\bar{r}_p$, $\bar{r}_f$	-	average annual precipitation (m/s), present and future, respectively

S_s	-	specific storage (γc) (m^{-1})
S_b	-	bulk storativity $\left(\frac{A \bullet \Delta z \bullet S_s}{\rho g}\right)$ (m^3/Pa)
s	-	sample standard deviation, (s^2 is sample variance)
s_g,s_ℓ	-	saturation (ratio of gas or liquid volume to total void volume), gas (nonwetting phase) and liquid (wetting phase), respectively (V/V_v)
s_{gr},$s_{\ell r}$	-	residual saturation, gas (nonwetting phase) and liquid (wetting phase), respectively
T_K	-	transmissivity (m^2/s)
T	-	temperature (K)
T_{cr}	-	critical temperature (Pa)
T_r	-	reduced temperature (T/T_{cr})
t	-	time (s)
$t_{1/2}$	-	radionuclide half life (s)
V	-	volume (m^3)
V_{cr}	-	theoretical volume of gas assuming ideal gas behavior at critical temperature and pressure of the gas
V_d, V_s, V_w	-	volume of the drum, solids, and design capacity of the repository, respectively (m^3)
v	-	velocity (m/s)
x,y,z	-	variable or parameter
$\bar{x}$	-	mean or expected value
x_{50},x_{99}	-	value of x at 50% (0.50) quantile and 99% (0.99) quantile
Z	-	gas compressibility factor
Δz	-	thickness
α	-	parameter of probability density function
α_L, α_T	-	dispersivity, longitudinal or transverse, respectively (m)
$ß_s$, $ß_b$, $ß_\ell$	-	material compressibility solid, bulk [$(1 - \phi)ß_s$], and liquid, respectively (Pa^{-1})
Γ	-	strain rate (dv/dy) (s^{-1})
γ	-	unit weight (ρg)
ε	-	roughness height (m)
ξ_1,ξ_2	-	Oldroyd viscosity parameter
θ	-	Pleistocene glaciation frequency (s^{-1})
$\dot{\theta}$	-	angular velocity of drill bit (m/s)
λ	-	failure rate function for probability model of human intrusion
μ_ℓ,μ_g	-	viscosity, liquid or gas, respectively (Pa • s)

ρ_s, ρ_b, ρ_f	-	density, solid, bulk, and fluid, respectively (kg/m^3)
τ	-	tortuosity $(\ell / \ell_{path})^2$
Φ	-	Holocene precipitation fluctuation frequency (s^{-1})
ϕ_{lat}	-	latitude
ϕ_m, ϕ_f	-	porosity, matrix and fracture (b/[B + b]), respectively
ζ	-	skin resistance from materials lining fractures, (b_s/D_s)
υ	-	molar volume (m^3/mol)
ν	-	Poisson's ratio
χ	-	mole fraction
η	-	Brooks-Corey relative permeability model parameter exponent

Superscripts

*	-	physical constants
°	-	property at reference conditions
□	-	property in pure fluid
•	-	parameter with respect to time (rate)
–	-	mean of parameter

Subscripts

g	-	gas
ℓ	-	liquid
f	-	fracture
m	-	matrix

Acronyms

ANL-E	-	Argonne National Laboratories, East
ASCII	-	American Standard Code for Information Interchange
ALGEBRA	-	support program for manipulating data in CAMDAT
BLOT	-	a mesh and curve plot program for CAMDAT data
BOAST	-	Black Oil Applied Simulation Tool; 3-D, 3-phase code for flow-through porous media
BRAGFLO	-	Brine And Gas Flow; 2-D, 2-phase code for flow-through porous media
CAM	-	Compliance Assessment Methodology
CAMCON	-	Compliance Assessment Methodology CONtroller–controller (driver) for compliance evaluations developed for WIPP
CAMDAT	-	Compliance Assessment Methodology DATa–computational data base developed for WIPP (modification of GENESIS and EXODUS)
CCDF	-	Complementary Cumulative Distribution Function
CCDFPLT	-	program to calculate and display complementary cumulative distribution function
CH	-	Contact Handled (TRU waste)
DCL	-	Digital Equipment Corporation Command Language
DOE	-	U.S. Department of Energy
DRZ	-	Disturbed Rock Zone
EPA	-	U.S. Environmental Protection Agency
EOS	-	equation of state
FD	-	Finite-Difference numerical analysis
FE	-	Finite-Element numerical analysis
Fm	-	formation
GENMESH	-	rectilinear three-dimensional finite-difference grid generator
HANF	-	Hanford Reservation
HLW	-	High-Level Waste
HST3D	-	a program to simulate heat and solute transport in a three-dimensional groundwater flow system
INEL	-	Idaho National Engineering Laboratory
LANL	-	Los Alamos National Laboratory
LHS	-	Latin Hypercube Sampling (efficient, stratified Monte Carlo sampling)
LLNL	-	Lawrence Livermore National Laboratory
MATSET	-	a program to insert user-selected parameter or material values into the computational data base
MOUND	-	Mound Laboratory

NEFTRAN	-	NEtwork Flow and TRANsport code
NRC	-	U.S. Nuclear Regulatory Commission
NTS	-	Nevada Test Site
ORNL	-	Oak Ridge National Laboratory
PCCSRC	-	program for calculating partial correlation coefficients (PCC) and standardized regression coefficients (SRC)
PREBOAST	-	preprocessor (translator) for input to BOAST
PREBRAG	-	preprocessor (translator) for input to BRAGFLO
PREHST	-	preprocessor (translator) for input to HST3D
PRELHS	-	preprocessor (translator) for input to LHS
PREPCC	-	preprocessor (translator) for input to PCC/SRC
PRENEF	-	preprocessor (translator) for input to NEFTRAN
PRESTEP	-	preprocessor (translator) for input to STEPWISE
PRESUTRA	-	preprocessor (translator) for input to SUTRA
PRESWFT	-	preprocessor (translator) for input to SWIFT II
POSTBOAST	-	postprocessor (translator) of output from BOAST to CAMDAT
POSTBRAG	-	postprocessor (translator) of output from BRAGFLO to CAMDAT
POSTHST	-	postprocessor (translator) of output from HST3D to CAMDAT
POSTLHS	-	postprocessor (translator) of output from LHS to CAMDAT
POSTSUTRA	-	postprocessor (translator) of output from SUTRA to CAMDAT
POSTSWFT	-	postprocessor (translator) of output from SWIFT II to CAMDAT
QA	-	Quality Assurance
RCRA	-	Resource, Conservation, and Recovery Act of 1976 (Public Law 94-580) and subsequent amendments (e.g., HSWA–Hazardous and Solid Waste Amendments of 1984)
RFP	-	Rocky Flats Plant
RH	-	Remotely Handled (TRU waste)
SNL	-	Sandia National Laboratories, Albuquerque, NM
SRS	-	Savannah River Site
STEPWISE	-	stepwise regression program with rank regression and predicted error sum of squares criterion
SWIFTII	-	Sandia Waste-Isolation, Flow and Transport code for solving transient, three-dimensional, coupled equations for fluid flow, heat transport, brine-miscible displacement, and radionuclide-miscible displacement in porous and fractured media
SUTRA	-	Saturated-Unsaturated TRAnsport code
TRACKER	-	a support program to estimate the pathway of a particle released in a fluid velocity field

TRU	-	Transuranic
WIPP	-	Waste Isolation Pilot Plant
40 CFR 191	-	Code of Federal Regulations, Title 40, Part 191

CONVERSION TABLES
FOR SI AND COMMON ENGLISH UNITS

Table 1. Base and Derived SI Units

	Quantity	Name	Symbol	Expression in Terms of Other Units	Expression in Terms of SI Base Units
Base SI Units					
	length	meter	m		
	time	second	s		
	mass	kilogram	kg		
	temperature	kelvin	K		
	amount of substance	mole	mol		
	electric current	ampere	A		
SI-Derived Units					
	force	newton	N		$kg \cdot m \cdot s^{-2}$
	pressure, stress	pascal	Pa	N/m^2	$kg \cdot m^{-1} \cdot s^{-2}$
	energy, work, quantity of heat	joule	J	$N \cdot m$	$kg \cdot m^2 \cdot s^{-2}$
	power, radiant flux	watt	W	J/s	$kg \cdot m^2 \cdot s^{-3}$
	electric potential	volt	V	W/A	$kg \cdot m^2 \cdot s^{-3} \cdot A^{-1}$
	electric resistance	ohm	Ω	V/A	$kg \cdot m^2 \cdot s^{-3} \cdot A^{-2}$
	frequency	hertz	Hz		s^{-1}
	activity (of a radionuclide)	bequerel	Bq		s^{-1}
	absorbed dose	gray	Gy	J/kg	$m^2 \cdot s^{-2}$
	quantity of electricity, electric charge	coulomb	C		$A \cdot s$

Table 2. List of Prefixes

Factor	Prefix	Symbol*
10^{12}	tera	T
10^{9}	giga	G
10^{6}	mega	M
10^{3}	kilo	k
10^{2}	hecto	h
10	deka	da
10^{-1}	deci	d
10^{-2}	centi	c
10^{-3}	milli	m
10^{-6}	micro	µ
10^{-9}	nano	n
10^{-12}	pico	p
10^{-15}	femto	f
10^{-18}	atto	a

* Only the symbols T (tera), G (giga), and M (mega) are capitalized. Compound prefixes are not allowed — for example, use nm (*nano*metre) rather than mµm (*millimicro*metre).

Table 3. Length Conversions

	m	cm	Å	in.	ft	mi	nmi
meter (m)	1	*100	$*1x10^{10}$	39.37	3.281	$6.214x10^{-4}$	$5.400x10^{-4}$
centimeter (cm)	*0.01	1	$*1x10^{8}$	0.3937	$3.281x10^{-2}$	$6.214x10^{-6}$	$5.400x10^{-6}$
angstrom (Å)	$*1x10^{-10}$	$*1x10^{-8}$	1	$3.937x10^{-9}$	$3.281x10^{-10}$	$6.214x10^{-14}$	$5.400x10^{-14}$
inch (in.)	*0.0254	*2.54	$*2.54x10^{8}$	1	$8.333x10^{-2}$	$1.578x10^{-5}$	$1.371x10^{-5}$
foot (ft)	*0.3048	*30.48	$*3.048x10^{9}$	*12	1	$1.894x10^{-4}$	$1.646x10^{-4}$
mile (U.S.) (mi)	1609	$1.609x10^{5}$	$1.609x10^{13}$	$*6.336x10^{4}$	*5280	1	0.8690
nautical mile (nmi)	*1852	$*1.852x10^{5}$	$*1.852x10^{13}$	$7.291x10^{4}$	$6.076x10^{3}$	1.151	1

* Exact

Table 4. Area or Permeability

	m^2	ha	$in.^2$	ft^2	ac	mi^2	Darcy	cm^2
square meters (m^2)	1	$*1x10^{-4}$	1550	10.76	$2.471x10^{-4}$	$3.861x10^{-7}$	$1.013x10^{12}$	$*1.000x10^{4}$
hectare (ha)	$*1x10^{4}$	1	$1.550x10^{7}$	$1.076x10^{5}$	2.471	$3.861x10^{-3}$	$1.013x10^{16}$	$*1.000x10^{8}$
square inches ($in.^2$)	$6.452x10^{-4}$	$6.452x10^{-8}$	1	$6.944x10^{-3}$	$1.594x10^{-7}$	$2.491x10^{-10}$	$6.537x10^{8}$	6.452
square feet (ft^2)	$9.290x10^{-2}$	$9.290x10^{-6}$	144	1	$2.296x10^{-5}$	$3.587x10^{-8}$	$9.413x10^{10}$	929
acre (ac)	4047	0.4047	$6.273x10^{6}$	$*4.356x10^{4}$	1	$1.563x10^{-3}$	$4.100x10^{15}$	$4.047x10^{7}$
square miles (mi^2)	$2.590x10^{6}$	2590	$4.015x10^{9}$	$2.788x10^{7}$	*640	1	2.624	$2.590x10^{10}$
darcy (D)	$9.869x10^{-13}$	$9.869x10^{-17}$	$1.530x10^{-9}$	$1.062x10^{-11}$	$2.439x10^{-16}$	$3.811x10^{-19}$	1	$9.864x10^{-9}$
square centimeters (cm^2)	$*1x10^{-4}$	$1x10^{-8}$	0.1550	$1.076x10^{-3}$	$2.471x10^{-8}$	$3.861x10^{-11}$	$1.013x10^{8}$	1

*Exact

Table 5. Volume

	m^3	l	ft^3	yd^3	gal (U.S.)	bbl	drum	std bx	room	panel	disposal	ac•ft	sec•ft•day	bushel
cubic meters (m^3)	1	*1000	35.31	1.308	264.2	6.290	4.803	0.5618	$2.744x10^{-4}$	$2.169x10^{-5}$	$2.293x10^{-6}$	$8.107x10^{-4}$	$4.087x10^{-4}$	28.38
liter (l)	*$1x10^{-3}$	1	$3.531x10^{-2}$	$1.308x10^{-3}$	0.2642	$6.290x10^{-3}$	$4.803x10^{-3}$	$5.618x10^{-4}$	$2.744x10^{-7}$	$2.169x10^{-8}$	$2.293x10^{-9}$	$8.107x10^{-7}$	$4.087x10^{-7}$	$2.838x10^{-2}$
cubic feet (ft^3)	$2.832x10^{-2}$	28.32	1	$3.704x10^{-2}$	7.481	0.1781	0.1360	$1.591x10^{-2}$	$7.770x10^{-6}$	$6.143x10^{-7}$	$6.494x10^{-8}$	$2.296x10^{-5}$	$1.157x10^{-5}$	0.8036
cubic yard (yd^3)	0.7646	7646	*27	1	201.97	4.809	3.672	0.4295	$2.098x10^{-4}$	$1.659x10^{-5}$	$1.753x10^{-6}$	$6.198x10^{-4}$	$3.125x10^{-4}$	21.70
U.S. gallon (gal)	$3.785x10^{-3}$	3.785	0.1337	$4.951x10^{-3}$	1	$2.381x10^{-2}$	$1.818x10^{-2}$	$2.127x10^{-3}$	$1.039x10^{-6}$	$8.212x10^{-8}$	$8.682x10^{-9}$	$3.069x10^{-6}$	$1.547x10^{-6}$	0.1074
barrel (bbl)	0.1590	159	5.615	0.2079	*42	1	0.7636	$8.932x10^{-2}$	$4.363x10^{-5}$	$3.449x10^{-6}$	$3.646x10^{-7}$	$1.289x10^{-4}$	$6.498x10^{-5}$	4.512
drum (55-gal)	0.2082	208.2	7.352	0.2723	*55	1.310	1	0.1170	$5.713x10^{-5}$	$4.556x10^{-6}$	$4.804x10^{-7}$	$1.688x10^{-4}$	$8.510x10^{-5}$	5.908
standard-waste box (std bx)	1.9	1780	62.86	2.328	470.2	1.120	8.550	1	$4.884x10^{-4}$	$3.895x10^{-5}$	$4.107x10^{-6}$	$1.443x10^{-3}$	$7.275x10^{-4}$	50.51
room volume (room)	3644	$3.644x10^{6}$	$1.287x10^{5}$	4767	$9.627x10^{5}$	$2.292x10^{4}$	$1.750x10^{4}$	2047	1	$7.906x10^{-2}$	$8.358x10^{-3}$	2.955	1.490	$1.034x10^{5}$
panel volume (panel)	$4.610x10^{4}$	$4.610x10^{7}$	$1.628x10^{6}$	$6.029x10^{4}$	$1.218x10^{7}$	$2.899x10^{5}$	$2.214x10^{5}$	$2.590x10^{4}$	12.65	1	0.1057	37.37	18.84	$1.308x10^{6}$
disposal area (disposal)	$4.360x10^{5}$	$4.360x10^{8}$	$1.540x10^{7}$	$5.703x10^{5}$	$1.152x10^{8}$	$2.730x10^{5}$	$2.094x10^{6}$	$2.450x10^{5}$	119.6	9.459	1	353.5	178.2	$1.237x10^{7}$
acre•foot (ac•ft)	1233	$1.233x10^{6}$	*43560	1613	$3.259x10^{5}$	7758	5925	6.930	0.3385	$2.699x10^{-2}$	$2.846x10^{-3}$	1	0.5042	$3.500x10^{4}$
second•foot•day (sec•ft•day)	2447	$2.447x10^{6}$	*86400	*3200	$6.463x10^{5}$	$1.539x10^{4}$	$1.175x10^{4}$	1374	0.6713	$5.353x10^{-2}$	$5.645x10^{-3}$	1.983	1	$6.943x10^{4}$
bushel (bu)	$3.524x10^{-2}$	35.24	1.244	$4.609x10^{-2}$	9.309	0.2216	0.1693	$1.980x10^{-2}$	$9.669x10^{-6}$	$7.711x10^{-7}$	$8.131x10^{-8}$	$2.857x10^{-5}$	$1.440x10^{-5}$	1

*Exact

Table 6. Discharge (Volume/Time)

	m^3/s	m^3/yr	l	ft^3/s	ft^3/min	ft^3/day	acre•ft/day	gal/min	gal/day	bbl/day
cubic meters per second (m^3/s)	1	3.156×10^{7}	*1000	35.31	2119	3.051×10^{6}	70.05	1.585×10^{4}	2.282×10^{7}	5.434×10^{5}
cubic meters per year (m^3/yr)	3.169×10^{-8}	1	3.169×10^{-5}	1.119×10^{-6}	6.714×10^{-5}	9.669×10^{-2}	2.220×10^{-6}	5.023×10^{-4}	0.7233	1.722×10^{-2}
liters per second (l/s)	$*1 \times 10^{-3}$	3.156×10^{4}	1	3.531×10^{-2}	2.119	3051	7.005×10^{-2}	15.85	2.282×10^{4}	543.4
cubic feet per second (ft^3/s)	2.832×10^{-2}	8.936×10^{5}	28.32	1	*60	$*8.640 \times 10^{4}$	1.983	448.8	6.463×10^{5}	1.539×10^{4}
cubic feet per minute (ft^3/min)	4.719×10^{-4}	1.489×10^{4}	0.4719	1.667×10^{-2}	1	1440	3.306×10^{-2}	7.481	1.077×10^{4}	256.5
cubic feet per day (ft^3/day)	3.277×10^{-7}	10.34	3.277×10^{-4}	1.157×10^{-5}	6.944×10^{-4}	1	2.296×10^{-5}	5.195×10^{-3}	7.481	0.1781
acre•foot per day (acre• ft/day)	1.428×10^{-2}	4.505×10^{5}	14.28	0.5042	30.25	4.356×10^{4}	1	226.3	3.259×10^{5}	7758
gallons per minute (gal/min)	6.309×10^{-5}	1991	6.309×10^{-2}	2.228×10^{-3}	0.1337	19.25	4.419×10^{-3}	1	1440	34.29
gallons per day (gal/day)	4.381×10^{-8}	1.383	4.381×10^{-5}	1.547×10^{-6}	9.283×10^{-5}	0.1337	3.069×10^{-6}	6.944×10^{-4}	1	2.381×10^{-2}
barrels per day (bbl/day)	1.840×10^{-6}	58.07	1.840×10^{-3}	6.498×10^{-5}	3.899×10^{-3}	5.615	1.289×10^{-4}	2.917×10^{-2}	*42	1

*Exact

Table 7. Velocity, Hydraulic Conductivity, Precipitation

	m/s	m/yr	in./yr	cm/yr	km/yr	ft/s	ft/day	mph	knots	gal/(day•ft^2)
meters per second (m/s)	1	3.156×10^{7}	1.242×10^{9}	3.156×10^{9}	3.156×10^{4}	3.281	2.835×10^{5}	2.237	1.944	2.120×10^{6}
meters per year (m/yr)	3.169×10^{-8}	1	39.37	*100	$*1 \times 10^{-3}$	1.040×10^{-7}	8.983×10^{-3}	7.089×10^{-8}	6.160×10^{-8}	6.719×10^{-2}
inches per year (in./yr)	8.049×10^{-10}	$*2.540 \times 10^{-2}$	1	*2.540	$*2.540 \times 10^{-5}$	2.641×10^{-9}	2.282×10^{-4}	1.800×10^{-9}	1.565×10^{-9}	1.707×10^{-3}
centimeters per year (cm/yr)	3.169×10^{-10}	$*1 \times 10^{-2}$	0.3937	1	$*1 \times 10^{-5}$	1.040×10^{-9}	8.983×10^{-5}	7.089×10^{-10}	6.160×10^{-10}	6.719×10^{-4}
kilometers per year (km/yr)	3.169×10^{-5}	*1000	3.937×10^{4}	$*1 \times 10^{5}$	1	1.040×10^{-4}	8.983	7.089×10^{-5}	6.160×10^{-5}	67.19
feet per second (ft/s)	*0.3048	9.619×10^{6}	3.787×10^{8}	9.619×10^{8}	9619	1	$*8.640 \times 10^{4}$	0.6818	0.5925	6.463×10^{5}
feet per day (ft/day)	3.528×10^{-6}	111.3	4383	1.113×10^{4}	0.1113	1.157×10^{-5}	1	7.891×10^{-6}	6.857×10^{-6}	7.481
miles per hour (mph)	0.4470	1.411×10^{7}	5.554×10^{8}	1.411×10^{9}	1.411×10^{4}	1.467	1.267×10^{5}	1	0.8690	9.479×10^{5}
knots	0.5144	1.623×10^{7}	6.391×10^{8}	1.623×10^{9}	1.623×10^{4}	1.688	1.458×10^{5}	1.151	1	1.091×10^{6}
gallons per day per square foot (gal/(day•ft^2))	4.716×10^{-7}	14.88	585.9	1488	1.488×10^{-2}	1.547×10^{-6}	0.1337	$.055 \times 10^{-6}$	9.167×10^{-7}	1

*Exact

Table 8. Force

	N	kg-force	dyne	lbf
Newton (N)	1	0.1020	*$1x10^5$	0.2248
kilogram-force (kg-force)	9.807	1	$9.807x10^5$	2.205
dyne	*$1.00x10^{-5}$	$1.020x10^{-6}$	1	$2.248x10^{-6}$
pound force (lbf)	4.448	0.4536	$4.448x10^5$	1

*Exact

Table 9. Pressure and Stress

	Pa	bar	dyne/cm^2	atm	mm Hg	psi	lb/ft^2
pascal (Pa)	1	*$1x10^{-5}$	*10	$9.869x10^{-6}$	$7.501x10^{-3}$	$1.450x10^{-4}$	$2.089x10^{-2}$
bar	*$1x10^5$	1	*$1x10^6$	0.9869	750.1	14.50	2089
dyne per square centimeters (dyne/cm^2)	*0.1	*$1x10^{-6}$	1	$9.869x10^{-7}$	$7.501x10^{-4}$	$1.450x10^{-5}$	$2.089x10^{-3}$
atmosphere (atm)	$1.013x10^5$	1.013	$1.013x10^6$	1	*760	14.70	2116
millimeter of Mercury (mm Hg)	1333	$1.333x10^{-3}$	1333	$1.316x10^{-3}$	1	$1.934x10^{-2}$	2.785
pound per square inch (psi)	698.5	$6.895x10^{-2}$	$6.895x10^4$	$6.805x10^{-2}$	51.71	1	*144
pounds per square foot (lb/ft^2)	47.88	$4.788x10^{-4}$	478.8	$4.725x10^{-4}$	0.3591	$6.944x10^{-3}$	1

*Exact

Table 10. Absolute Viscosity

	Pa•s (kg/(m•s))	cP	lbm/ft/s	slug/(ft•s) lbf • ft/s^2
Pascal-second (Pa•s) (kg/(m•s))	1	*1000	0.6720	2.089×10^{-2}
centipoise (cP)	$*1 \times 10^{-3}$	1	6.720×10^{-4}	2.089×10^{-5}
pound mass per foot per second (lbm/ft/s)	1.488	1488	1	3.108×10^{-2}
slug per foot per second (slug/(ft•s) or lbf • ft/s^2)	47.88	4.788×10^4	32.17	1

*Exact

Table 11. Mass

	kg	metric tonne	oz	lbm	short ton	long ton	slug
kilogram (kg)	1	$*1 \times 10^{-3}$	35.27	2.205	1.102×10^{-3}	9.842×10^{-4}	6.852×10^{-2}
metric tonne (t)	*1000	1	3.527×10^4	2205	1.102	0.9842	68.52
avoirdupois ounce (oz)	2.835×10^{-2}	2.835×10^{-5}	1	*0.0625	$*3.125 \times 10^{-5}$	2.790×10^{-5}	1.943×10^{-3}
pound mass (lbm)	0.4536	4.536×10^{-4}	*16	1	$*5.000 \times 10^{-4}$	4.464×10^{-4}	3.108×10^{-2}
short ton	907.2	9.072	*32000	*2000	1	0.8927	62.16
long ton	1016	1.016	*35840	*2240	*1.12	1	69.62
slug	14.59	1.459×10^{-2}	514.8	32.17	1.609×10^{-2}	1.436×10^{-2}	1

*Exact

Table 12. Density

	kg/m^3	g/cm^3	lb/ft^3	lb/gal	lb/bbl
kilogram per cubic meters (kg/m^3)	1	$*1x10^{-3}$	$6.243x10^{-2}$	$8.345x10^{-3}$	2.853
grams per cubic centimeters (g/cm^3)	*1000	1	62.43	8.345	350.5
pounds per cubic feet (lb/ft^3)	16.02	$1.602x10^{-2}$	1	0.1337	5.615
pounds per gallon (lb/gal)	119.8	0.1198	7.481	1	*42
pounds per barrel (lb/bbl)	2.853	$2.853x10^{-3}$	0.1781	$2.381x10^{-2}$	1

*Exact

Table 13. Time

	s	min	h	day	yr
mean solar second (s)	1	$1.6667x10^{-2}$	$2.7779x10^{-4}$	$1.15741x10^{-5}$	$3.1689x10^{-8}$
mean solar minute (min)	*60	1	$1.6667x10^{-2}$	$6.9444x10^{-4}$	$1.9013x10^{-6}$
mean solar hour (h)	*3600	*60	1	$4.16667x10^{-2}$	$1.1408x10^{-4}$
mean solar day	$*8.640x10^4$	*1440	*24	1	$2.7379x10^{-3}$
tropical time year (yr)	$3.1557x10^7$	$5.2595x10^5$	8765.8	365.24	1

*Exact

Table 14. Temperature (T)

	K	°C	°R	°F
kelvin (K)	1	K-273.15	K x 9/5	(K-273.15) x 9/5 +32
Celsius (°C)	°C + 273.15	1	(°C + 273.15) x 9/5	°C x 9/5 +32
Rankine (°R)	°R x 5/9	(°R x 5/9) -273.15	1	°R -459.67
Fahrenheit (°F)	(°F + 459.67) x 5/9	(°F - 32) x 5/9	°F + 459.67	1

Table 15. Specific Activity(1)

	Bq	Ci	kg
becquerel (Bq)	1	2.703×10^{-11}	$\frac{\ln^2}{t_{1/2}} \times \frac{6.022 \times 10^{23}}{M} \times \frac{10^3 g}{kg} = \frac{4.174 \times 10^{26}}{t_{1/2} \times M}$
curie (Ci)	*3.7×10^{10}	1	$\frac{1.128 \times 10^{16}}{t_{1/2} \times M}$
kg	$2.396 \times 10^{-27} \times t_{1/2}^{(2)} \times M^{(3)}$	$8.864 \times 10^{-17} \times t_{1/2} \times M$	1

(1) Specific Activity is $\frac{ds_A}{s_A}$; where $s_A = s_{OA}\, e^{-\lambda t}$; $\frac{\lambda = \ln^2}{t_{1/2}}$

(2) $t_{1/2}$ is half life in seconds

(3) M is gram molecular weight (g/mol)

*Exact

Table 16. Miscellaneous

To convert:	to	Multiply by	Inverse
1. Angular velocity rad/s	rpm	$\frac{30}{\pi} = 9.549$	$\frac{\pi}{30} = 0.1047$
2. Radioactivity			
a. Dose equivalent Sv	rem	100	0.01
b. Absorbed dose Gy (gray) (1J/kg)	rad	100	0.01
c. Activity (1 disintegration/s) becquerel (Bq)	Ci	2.703×10^{-11}	3.7×10^{10}
d. Charge roentgen (R)	c/kg	2.58×10^{-4}	3876

DISTRIBUTION

(Send Distribution list changes to M.M. Gruebel, Dept. 6342, Sandia National Laboratories, PO Box 5800, Albuquerque, NM 87185-5800)

Federal Agencies

US Department of Energy (2)
Office of Environmental Restoration and Waste Management
Attn: L.P. Duffy, EM-1
C. Frank, EM-50
Washington, DC 20585

US Department of Energy (3)
Office of Environmental Restoration and Waste Management
Attn: M. Frei, EM-34 (Trevion II)
Director, Waste Management Projects
Washington, DC 20585-0002

US Department of Energy
Office of Environmental Restoration and Waste Management
Attn: J. Lytle, EM-30 (Trevion II)
Washington, DC 20585-0002

US Department of Energy
Office of Environmental Restoration and Waste Management
Attn: S. Schneider, EM-342 (Trevion II)
Washington, DC 20585-0002

US Department of Energy (3)
WIPP Task Force
Attn: G.H. Daly
S. Fucigna
B. Bower
12800 Middlebrook Rd.
Suite 400
Germantown, MD 20874

US Department of Energy (4)
Office of Environment, Safety and Health
Attn: R.P. Berube, EH-20
C. Borgstrum, EH-25
R. Pelletier, EH-231
K. Taimi, EH-232
Washington, DC 20585

US Department of Energy (5)
WIPP Project Integration Office
Attn: W.J. Arthur III
R. Becker
P. Dickman
L.W. Gage
P.J. Higgins
D.A. Olona
PO Box 5400
Albuquerque, NM 87115-5400

US Department of Energy (10)
WIPP Project Site Office (Carlsbad)
Attn: A. Hunt (4)
V. Daub (4)
J. Lippis
K. Hunter
PO Box 3090
Carlsbad, NM 88221-3090

US Department of Energy, (5)
Office of Civilian Radioactive Waste Management
Attn: Deputy Director, RW-2
Associate Director, RW-10
Office of Program Administration and Resources Management
Associate Director, RW-20
Office of Facilities Siting and Development
Associate Director, RW-30
Office of Systems Integration and Regulations
Associate Director, RW-40
Office of External Relations and Policy
Office of Geologic Repositories
Forrestal Building
Washington, DC 20585

US Department of Energy
Attn: National Atomic Museum Library
Albuquerque Operations Office
PO Box 5400
Albuquerque, NM 87185

US Department of Energy
Research & Waste Management Division
Attn: Director
PO Box E
Oak Ridge, TN 37831

US Department of Energy (2)
Idaho Operations Office
Fuel Processing and Waste
Management Division
785 DOE Place
Idaho Falls, ID 83402

US Department of Energy
Savannah River Operations Office
Defense Waste Processing
Facility Project Office
Attn: W.D. Pearson
PO Box A
Aiken, SC 29802

US Department of Energy (2)
Richland Operations Office
Nuclear Fuel Cycle & Production
Division
Attn: R.E. Gerton
825 Jadwin Ave.
PO Box 500
Richland, WA 99352

US Department of Energy (3)
Nevada Operations Office
Attn: J.R. Boland
D. Livingston
P.K. Fitzsimmons
2753 S. Highland Drive
Las Vegas, NV 89183-8518

US Department of Energy (2)
Technical Information Center
PO Box 62
Oak Ridge, TN 37831

US Department of Energy (2)
Chicago Operations Office
Attn: J.C. Haugen
9800 South Cass Avenue
Argonne, IL 60439

US Department of Energy
Los Alamos Area Office
528 35th Street
Los Alamos, NM 87544

US Department of Energy (3)
Rocky Flats Area Office
Attn: W.C. Rask
G. Huffman
T. Lukow
PO Box 928
Golden, CO 80402-0928

US Department of Energy
Dayton Area Office
Attn: R. Grandfield
PO Box 66
Miamisburg, OH 45343-0066

US Department of Energy
Attn: E. Young
Room E-178
GAO/RCED/GTN
Washington, DC 20545

US Bureau of Land Management
101 E. Mermod
Carlsbad, NM 88220

US Bureau of Land Management
New Mexico State Office
PO Box 1449
Santa Fe, NM 87507

US Environmental Protection
Agency (2)
Office of Radiation Protection Programs
(ANR-460)
Washington, DC 20460

US Nuclear Regulatory Commission
Division of Waste Management
Attn: H. Marson
Mail Stop 4-H-3
Washington, DC 20555

US Nuclear Regulatory Commission (4)
Advisory Committee on Nuclear Waste
Attn: D. Moeller
M.J. Steindler
P.W. Pomeroy
W.J. Hinze
7920 Norfolk Avenue
Bethesda, MD 20814

Defense Nuclear Facilities Safety Board
Attn: D. Winters
625 Indiana Avenue, NW
Suite 700
Washington, DC 20004

Nuclear Waste Technical Review
Board (2)
Attn: Library
Suite 910
1100 Wilson Blvd.
Arlington, VA 22209-2297

Energy and Science Division
Office of Management and Budget
Attn: K. Yuracko
725 17th Street NW
Washington, DC 20503

US Geological Survey (2)
Water Resources Division
Attn: C. Peters
Suite 200
4501 Indian School NE
Albuquerque, NM 87110

New Mexico Congressional Delegation

Jeff Bingaman
U.S. Senate
110 Hart SOB
Washington, DC 20510-3102

Pete V. Domenici
U.S. Senate
427 Dirksen Bldg.
Washington, DC 20510-3101

Bill Richardson
House of Representatives
2349 Rayburn HOB
Washington, DC 20515

Steven H. Schiff
House of Representatives
1009 Longworth HOB
Washington, DC 20515

Joe Skeen
House of Representatives
2367 Rayburn HOB
Washington, DC 20515

State Agencies

New Mexico Bureau of Mines
and Mineral Resources
Socorro, NM 87801

New Mexico Energy, Minerals and Natural
Resources Department
Attn: Librarian
2040 South Pacheco
Santa Fe, NM 87505

New Mexico Energy, Minerals and Natural
Resources Department
New Mexico Radioactive Task Force (2)
(Governor's WIPP Task Force)
Attn: A. Lockwood, Chairman
C. Wentz, Coordinator/Policy Analyst
2040 South Pacheco
Santa Fe, NM 87505

Bob Forrest
Mayor, City of Carlsbad
PO Box 1569
Carlsbad, NM 88221

Executive Director
Carlsbad Department of Development
Attn: C. Bernard
PO Box 1090
Carlsbad, NM 88221

New Mexico Environment Department
Secretary of the Environment (3)
Attn: J. Espinosa
PO Box 968
1190 St. Francis Drive
Santa Fe, NM 87503-0968

New Mexico Environment Department
Attn: P. McCasland
WIPP Project Site Office
PO Box 3090
Carlsbad, NM 88221-3090

New Mexico State Engineer's Office
Attn: M. Chudnoff
PO Box 25102
Santa Fe, NM 87504-5102

Environmental Evaluation Group (5)
Attn: R. Neill
Suite F-2
7007 Wyoming Blvd. NE
Albuquerque, NM 87109

Advisory Committee on Nuclear Facility Safety

John F. Ahearne
Executive Director, Sigma Xi
99 Alexander Drive
Research Triangle Park, NC 27709

James E. Martin
109 Observatory Road
Ann Arbor, MI 48109

WIPP Panel of National Research Council's Board on Radioactive Waste Management

Charles Fairhurst, Chairman
Department of Civil and
Mineral Engineering
University of Minnesota
500 Pillsbury Dr., SE
Minneapolis, MN 55455-0220

John O. Blomeke
3833 Sandy Shore Drive
Lenoir City, TN 37771-9803

John D. Bredehoeft
Western Region Hydrologist
Water Resources Division
US Geological Survey (M/S 439)
345 Middlefield Road
Menlo Park, CA 94025

Fred M. Ernsberger
1325 NW 10th Avenue
Gainsville, FL 32601

Rodney C. Ewing
Department of Geology
University of New Mexico
200 Yale, NE
Albuquerque, NM 87131

B. John Garrick
PLG, Inc.
Suite 400
4590 MacArthur Blvd.
Newport Beach, CA 92660-2027

Leonard F. Konikow
US Geological Survey
431 National Center
Reston, VA 22092

Jeremiah O'Driscoll
505 Valley Hill Drive
Atlanta, GA 30350

Christopher Whipple
Clement International Corp.
160 Spear St.
Suite 1380
San Francisco, CA 94105-1535

National Research Council (3)
Board on Radioactive
Waste Management
RM HA456
Attn: P.B. Myers,
Staff Director (2)
G.J. Grube
2101 Constitution Avenue
Washington, DC 20418

Performance Assessment Peer Review Panel

G. Ross Heath
College of Ocean and
Fishery Sciences HN-15
583 Henderson Hall
University of Washington
Seattle, WA 98195

Thomas H. Pigford
Department of Nuclear Engineering
4159 Etcheverry Hall
University of California
Berkeley, CA 94720

Thomas A. Cotton
JK Research Associates, Inc.
4429 Butterworth Place, NW
Washington, DC 20016

Robert J. Budnitz
President, Future Resources
Associates, Inc.
2000 Center Street
Suite 418
Berkeley, CA 94704

C. John Mann
Department of Geology
245 Natural History Bldg.
1301 West Green Street
University of Illinois
Urbana, IL 61801

Frank W. Schwartz
Department of Geology and Mineralogy
The Ohio State University
Scott Hall
1090 Carmack Rd.
Columbus, OH 43210

National Laboratories

Argonne National Laboratory (2)
Attn: A. Smith
D. Tomasko
9700 South Cass, Bldg. 201
Argonne, IL 60439

Battelle Pacific Northwest Laboratory (3)
Attn: R.E. Westerman
S. Bates
H.C. Burkholder
Battelle Boulevard
Richland, WA 99352

Idaho National Engineering Laboratory (2)
Attn: H. Loo
R. Klinger
Mail Stop 5108
Idaho Falls, ID 83403-4000

Los Alamos National Laboratory
Attn: B. Erdal, CNC-11
PO Box 1663
Los Alamos, NM 87545

Los Alamos National Laboratory
Attn: A. Meijer
PO Box 1663, Mail Stop J514
Los Alamos, NM 87545

Los Alamos National Laboratory (3)
HSE-8
Attn: M. Enoris
L. Soholt
J. Wenzel
PO Box 1663
Los Alamos, NM 87545

Los Alamos National Laboratory
EM-7
Attn: S. Kosiewicz
PO Box 1663, Mail Stop J595
Los Alamos, NM 87545

Oak Ridge National Laboratory
Transuranic Waste Manager
Attn: D.W. Turner
PO Box 2008, Bldg. 3047
Oak Ridge, TN 37831-6060

Pacific Northwest Laboratory
Attn: B. Kennedy
PO Box 999
Richland, WA 99352

Savannah River Laboratory (3)
Attn: N. Bibler
M.J. Plodinec
G.G. Wicks
Aiken, SC 29801

Savannah River Plant (2)
Attn: R.G. Baxter
Bldg. 704-S
K.W. Wierzbicki
Bldg. 703-H
Aiken, SC 29808-0001

Corporations/Members of the Public

Benchmark Environmental Corp.
Attn: C. Frederickson
4501 Indian School NE
Suite 105
Albuquerque, NM 87110

City of Albuquerque
Public Works Department
Utility Planning Division
Attn: W.K. Summers
PO Box 1293
Albuquerque, NM 87103

Deuel and Associates, Inc.
Attn: R.W. Prindle
7208 Jefferson NE
Albuquerque, NM 87109

Disposal Safety, Inc.
Attn: B. Ross
1660 L Street NW
Suite 314
Washington, DC 20036

Ecodynamics (2)
Attn: P. Roache
R. Blaine
PO Box 9229
Albuquerque, NM 87119-9229

EG & G Idaho (3)
1955 Fremont Street
Attn: C. Atwood
C. Hertzler
T.I. Clements
Idaho Falls, ID 83415

Geomatrix
Attn: K. Coppersmith
100 Pine Street, Suite 1000
San Francisco, CA 94111

Golder Associates, Inc. (3)
Attn: M. Cunnane
R. Kossik
I. Miller
4104 148th Avenue NE
Redmond, WA 98052

INTERA, Inc. (2)
Attn: J.F. Pickens
A.M. LaVenve
6850 Austin Center Blvd.
Suite 300
Austin, TX 78731

INTERA, Inc.
Attn: W. Stensrud
PO Box 2123
Carlsbad, NM 88221

INTERA, Inc.
Attn: W. Nelson
101 Convention Center Drive
Suite 540
Las Vegas, NV 89109

IT Corporation (2)
Attn: R.F. McKinney
J. Myers
Regional Office, Suite 700
5301 Central Avenue NE
Albuquerque, NM 87108

John Hart and Associates, P.A.
Attn: J.S. Hart
2815 Candelaria Road NW
Albuquerque, NM 87107

John Hart and Associates, P.A.
Attn: K. Lickliter
1009 North Washington
Tacoma, WA 98406

MACTEC (2)
Attn: J.A. Thies
D.K. Duncan
8418 Zuni Road SE, Suite 200
Albuquerque, NM 87108

Newman and Holtzinger
Attn: C. Mallon
1615 L Street NW, Suite 1000
Washington, DC 20036

RE/SPEC, Inc. (2)
Attn: W. Coons
4775 Indian School NE, Suite 300
Albuquerque, NM 87110

RE/SPEC, Inc.
Attn: J.L. Ratigan
PO Box 725
Rapid City, SD 57709

Reynolds Elect/Engr. Co., Inc.
Attn: E.W. Kendall
Building 790, Warehouse Row
PO Box 98521
Las Vegas, NV 89193-8521

Roy F. Weston, Inc.
CRWM Tech. Supp. Team
Attn: C.J. Noronha
955 L'Enfant Plaza SW
North Building, Eighth Floor
Washington, DC 20024

Science Applications International Corporation (SAIC)
Attn: H.R. Pratt
10260 Campus Point Drive
San Diego, CA 92121

Science Applications International Corporation (2)
Attn: D.C.Royer
C.G. Pflum
101 Convention Center Dr.
Las Vegas, NV 89109

Science Applications International Corporation (2)
Attn: M. Davis
J. Tollison
2109 Air Park Road SE
Albuquerque, NM 87106

Science Applications International Corporation (2)
Attn: J. Young
D. Lester
18706 North Creek Parkway, Suite 110
Bothell, WA 98011

Southwest Research Institute
Center for Nuclear Waste Regulatory Analysis (2)
Attn: P.K. Nair
6220 Culebra Road
San Antonio, TX 78228-0510

Systems, Science, and Software (2)
Attn: E. Peterson
P. Lagus
Box 1620
La Jolla, CA 92038

TASC
Attn: S.G. Oston
55 Walkers Brook Drive
Reading, MA 01867

Tech Reps, Inc. (6)
Attn: J. Chapman
C. Crawford
D. Marchand
J. Stikar
P. Oliver
D. Scott
5000 Marble NE, Suite 222
Albuquerque, NM 87110

Tolan, Beeson & Associates
Attn: T.L. Tolan
2320 W. 15th Avenue
Kennewick, WA 99337

TRW Environmental Safety Systems
Attn: I. Sacks
2650 Park Tower Drive, Suite 800
Vienna, VA 22180

Westinghouse Electric Corporation (5)
Attn: Library
L. Trego
C. Cox
L. Fitch
R.F. Kehrman
PO Box 2078
Carlsbad, NM 88221

Westinghouse Hanford Company
Attn: D. E. Wood
MSIN HO-32
PO Box 1970
Richland, WA 99352

Western Water Consultants
Attn: D. Fritz
1949 Sugarland Drive #134
Sheridan, WY 82801-5720

Western Water Consultants
Attn: P.A. Rechard
PO Box 4128
Laramie, WY 82071

P. Drez
8816 Cherry Hills Road, NE
Albuquerque, NM 87111

D.W. Powers
Star Route Box 87
Anthony, TX 79821

Shirley Thieda
PO Box 2109, RR1
Bernalillo, NM 87004

Jack Urich
c/o CARD
144 Harvard SE
Albuquerque, NM 87106

Universities

University of California
Mechanical, Aerospace, and
Nuclear Engineering Department (2)
Attn: W. Kastenberg
D. Browne
5532 Boelter Hall
Los Angeles, CA 90024

University of California
Mine Engineering Dept.
Attn: Neville Cook
Rock Mechanics Engineering
Berkeley, CA 94720

University of Hawaii at Hilo
Attn: S. Hora
Business Administration
Hilo, HI 96720-4091

University of New Mexico
Geology Department
Attn: Library
Albuquerque, NM 87131

University of New Mexico
Research Administration
Attn: H. Schreyer
102 Scholes Hall
Albuquerque, NM 87131

University of Wyoming
Department of Civil Engineering
Attn: V.R. Hasfurther
Laramie, WY 82071

University of Wyoming
Department of Geology
Attn: J.I. Drever
Laramie, WY 82071

University of Wyoming
Department of Mathematics
Attn: R.E. Ewing
Laramie, WY 82071

Libraries

Thomas Brannigan Library
Attn: D. Dresp
106 W. Hadley St.
Las Cruces, NM 88001

Hobbs Public Library
Attn: M. Lewis
509 N. Ship Street
Hobbs, NM 88248

New Mexico State Library
Attn: N. McCallan
325 Don Gaspar
Santa Fe, NM 87503

New Mexico Tech
Martin Speere Memorial Library
Campus Street
Socorro, NM 87810

New Mexico Junior College
Pannell Library
Attn: R. Hill
Lovington Highway
Hobbs, NM 88240

Carlsbad Municipal Library
WIPP Public Reading Room
Attn: L. Hubbard
101 S. Halagueno St.
Carlsbad, NM 88220

University of New Mexico
General Library
Government Publications Department
Albuquerque, NM 87131

NEA/Performance Assessment Advisory Group (PAAG)

P. Duerden
ANSTO
Lucas Heights Research Laboratories
Private Mail Bag No. 1
Menai, NSW 2234, AUSTRALIA

Gordon S. Linsley
Division of Nuclear Fuel Cycle and Waste Management
International Atomic Energy Agency
PO Box 100
A-1400 Vienna, AUSTRIA

Nicolo Cadelli
Commission of the European Communities
200, Rue de la Loi
B-1049 Brussels, BELGIUM

R. Heremans
Organisme Nationale des Déchets Radioactifs et des Matiéres Fissiles
ONDRAF
Place Madou 1, Boitec 24/25
B-1030 Brussels, BELGIUM

J. Marivoet
Centre d'Etudes de l'Energie Nucléaire
CEN/SCK
Boeretang 200
B-2400 Mol, BELGIUM

P. Conlon
Waste Management Division
Atomic Energy Control Board (AECB)
PO Box 1046
Ottawa, Canada KIP 559, CANADA

A.G. Wikjord
Manager, Environmental and Safety Assessment Branch
Atomic Energy of Canada Limited
Whiteshell Nuclear Research Establishment
Pinewa, Manitoba ROE 1LO, CANADA

Jukka-Pekka Salo
Teollisuuden Voima Oy (TVO)
Fredrikinkatu 51-53 B
SF-00100 Helsinki, FINLAND

Timo Vieno
Technical Research Centre of Finland (VTT)
Nuclear Energy Laboratory
PO Box 208
SF-02151 Espoo, FINLAND

Timo Äikäs
Teollisuuden Voima Oy (TVO)
Fredrikinkatu 51-53 B
SF-00100 Helsinki, FINLAND

M. Claude Ringeard
Division de la Sécurité et de la Protection de l'Environment (DSPE)
Commissariat á l'Energie Atomique
Agence Nationale pour la Gestion des Déchets Radioactifs (ANDRA)
Route du Panorama Robert Schuman
B. P. No. 38
F-92266 Fontenay-aux-Roses Cedex
FRANCE

Gérald Ouzounian
Agence Nationale pour la Gestion des Déchets Radioactifs (ANDRA)
Route du Panorama Robert Schuman
B. P. No. 38
F-92266 Fontenay-aux-Roses Cedex
FRANCE

Claudio Pescatore
Division of Radiation Protection and Waste Management
OECD Nuclear Energy Agency
38, Boulevard Suchet
F-75016 Paris, FRANCE

M. Dominique Greneche
Commissariat á l'Energie Atomique
IPSN/DAS/SASICC/SAED
B. P. No. 6
F-92265 Fontenay-aux-Roses Cedex,
FRANCE

Robert Fabriol
Bureau de Recherches Géologiques et Miniéres (BRGM)
B. P. 6009
45060 Orléans Cedex 2, FRANCE

P. Bogorinski
Gesellschaft für Reaktorsicherheit (GRS) mbH
Schwertnergasse 1
D-5000 Köln 1, GERMANY

R. Storck
GSF - Institut für Tieflagerung
Theodor-Heuss-Strabe 4
D-3300 Braunschweig, GERMANY

Ferrucio Gera
ISMES S.p.A
Via del Crociferi 44
I-00187 Rome, ITALY

Hiroyuki Umeki
Isolation System Research Program
Radioactive Waste Management Project
Power Reactor and Nuclear Fuel Development Corporation (PNC)
1-9-13, Akasaka
Minato-ku
Tokyo 107, JAPAN

P. Carboneras Martinez
ENRESA
Calle Emilio Vargas 7
R-28043 Madrid, SPAIN

Tönis Papp
Swedish Nuclear Fuel and Waste Management Co.
Box 5864
S 102 48 Stockholm, SWEDEN

Conny Hägg
Swedish Radiation Protection Institute (SSI)
Box 60204
S-104 01 Stockholm, SWEDEN

J. Hadermann
Paul Scherrer Institute
Waste Management Programme
CH-5232 Villigen PSI, SWITZERLAND

J. Vigfusson
USK- Swiss Nuclear Safety Inspectorate
Federal Office of Energy
CH-5303 Würenlingen, SWITZERLAND

D.E. Billington
Departmental Manager - Assessment Studies
Radwaste Disposal R&D Division
AEA Decommissioning & Radwaste
Harwell Laboratory, B60
Didcot Oxfordshire OX11 ORA
UNITED KINGDOM

P. Grimwood
Waste Management Unit
BNFL
Sellafield
Seascale, Cumbria CA20 1PG
UNITED KINGDOM

Alan J. Hooper
UK Nirex Ltd
Curie Avenue
Harwell, Didcot
Oxfordshire, OX11 ORH
UNITED KINGDOM

Jerry M. Boak
Yucca Mountain Project Office
US Department of Energy
PO Box 98608
Las Vegas, NV 89193

Seth M. Coplan (Chairman)
US Nuclear Regulatory Commission
Division of High-Level Waste Management
Mail Stop 4-H-3
Washington, DC 20555

A.E. Van Luik
INTERA/M&O
The Valley Bank Center
101 Convention Center Dr.
Las Vegas, NV 89109

NEA/PSAG User's Group

Shaheed Hossain
Division of Nuclear Fuel Cycle and Waste Management
International Atomic Energy Agency
Wagramerstrasse 5
PO Box 100
A-1400 Vienna, AUSTRIA

Alexander Nies (PSAC Chairman)
Gesellschaft für Strahlen- und
Institut für Tieflagerung
Abteilung für Endlagersicherheit
Theodor-Heuss-Strasse 4
D-3300 Braunschweig, GERMANY

Eduard Hofer
Gesellschaft für Reaktorsicherheit (GRS) MBH
Forschungsgelände
D-8046 Garching, GERMANY

Andrea Saltelli
Commission of the European Communities
Joint Resarch Centre of Ispra
I-21020 Ispra (Varese), ITALY

Alejandro Alonso
Cátedra de Tecnología Nuclear
E.T.S. de Ingenieros Industriales
José Gutiérrez Abascal, 2
E-28006 Madrid, SPAIN

Pedro Prado
CIEMAT
Instituto de Tecnología Nuclear
Avenida Complutense, 22
E-28040 Madrid, SPAIN

Miguel Angel Cuñado
ENRESA
Emilio Vargas, 7
E-28043 Madrid, SPAIN

Francisco Javier Elorza
ENRESA
Emilio Vargas, 7
E-28043 Madrid, SPAIN

Nils A. Kjellbert
Swedish Nuclear Fuel and Waste Management Company (SKB)
Box 5864
S-102 48 Stockholm, SWEDEN

Björn Cronhjort
Swedish National Board for Spent Nuclear Fuel (SKN)
Sehlsedtsgatan 9
S-115 28 Stockholm, SWEDEN

Richard A. Klos
Paul-Scherrer Institute (PSI)
CH-5232 Villingen PSI
SWITZERLAND

NAGRA (2)
Attn: C. McCombie
F. Van Dorp
Parkstrasse 23
CH-5401 Baden, SWITZERLAND

N. A. Chapman
Intera Information Technologies
Park View House, 14B Burton Street
Melton Mowbray
Leicestershire, LE13 1AE
UNITED KINGDOM

Daniel A. Galson
Galson Sciences Ltd.
35, Market Place
Oakham
Leicestershire LE15 6DT
UNITED KINGDOM

David P. Hodgkinson
Intera Information Technologies
Chiltern House
45 Station Road
Henley-on-Thames
Oxfordshire RG9 1AT, UNITED KINGDOM

Brian G.J. Thompson
Department of the Environment: Her Majesty's Inspectorate of Pollution
Room A5.33, Romney House
43 Marsham Street
London SW1P 2PY, UNITED KINGDOM

Intera Information Technologies
Attn: M.J.Apted
3609 South Wadsworth Blvd.
Denver, CO 80235

US Nuclear Regulatory Commission (2)
Attn: R. Codell
N. Eisenberg
Mail Stop 4-H-3
Washington, DC 20555

Battelle Pacific Northwest Laboratories
Attn: P.W. Eslinger
PO Box 999, MS K2-32
Richland, WA 99352

Center for Nuclear Waste Regulatory Analysis (CNWRA)
Southwest Research Institute
Attn: B. Sagar
PO Drawer 28510
6220 Culebra Road
San Antonio, TX 78284

Geostatistics Expert Working Group (GXG)

Rafael L. Bras
R.L. Bras Consulting Engineers
44 Percy Road
Lexington, MA 02173

Jesus Carrera
Universidad Politêcnica de Cataluña
E.T.S.I. Caminos
Jordi, Girona 31
E-08034 Barcelona, SPAIN

Gedeon Dagan
Department of Fluid Mechanics and Heat Transfer
Tel Aviv University
PO Box 39040
Ramat Aviv, Tel Aviv 69978, ISRAEL

Ghislain de Marsily (GXG Chairman)
University Pierre et Marie Curie
Laboratorie de Geologie Applique
4, Place Jussieu - T.26 - 5^{e} etage
75252 Paris Cedex 05, FRANCE

Alain Galli
Centre de Geostatistique
Ecole des Mines de Paris
35 Rue St. Honore
77035 Fontainebleau, FRANCE

Steve Gorelick
Department of Applied Earth Sciences
Stanford University
Stanford, CA 94305-2225

Peter Grindrod
INTERA Information Technologies Ltd.
Chiltern House, 45 Station Road
Henley-on-Thames
Oxfordshire, RG9 1AT
UNITED KINGDOM

Alan Gutjahr
Department of Mathematics
New Mexico Institute of Mining and Technology
Socorro, NM 87801

C. Peter Jackson
Harwell Laboratory
Theoretical Studies Department
Radwaste Disposal Division
Bldg. 424.4
Oxfordshire Didcot Oxon OX11 ORA
UNITED KINDGOM

Peter Kitanidis
60 Peter Coutts Circle
Stanford, CA 94305

Rae Mackay
Department of Civil Engineering
University of Newcastle Upon Tyne
Newcastle Upon Tyne NE1 7RU
UNITED KINGDOM

Dennis McLaughlin
Parsons Laboratory
Room 48-209
Department of Civil Engineering
Massachusetts Institute of Technology
Cambridge, MA 02139

Shlomo P. Neuman
College of Engineering and Mines
Department of Hydrology and Water Resources
University of Arizona
Tucson, AZ 85721

Christian Ravenne
Geology and Geochemistry Division
Institut Francais du Pétrole
1 & 4, av. de Bois-Préau BP311
92506 Rueil Malmaison Cedex
FRANCE

Yoram Rubin
Department of Civil Engineering
University of California
Berkeley, CA 94720

Foreign Addresses

Studiecentrum Voor Kernenergie
Centre D'Energie Nucleaire
Attn: A. Bonne
SCK/CEN
Boeretang 200
B-2400 Mol, BELGIUM

Atomic Energy of Canada, Ltd. (3)
Whiteshell Research Estab.
Attn: M.E. Stevens
B.W. Goodwin
D. Wushke
Pinewa, Manitoba
ROE 1L0, CANADA

Esko Peltonen
Industrial Power Company Ltd.
TVO
Fredrikinkatu 51-53
SF-00100 Helsinki 10, FINLAND

Jean-Pierre Olivier
OECD Nuclear Energy Agency (2)
38, Boulevard Suchet
F-75016 Paris, FRANCE

D. Alexandre, Deputy Director
ANDRA
31 Rue de la Federation
75015 Paris, FRANCE

Claude Sombret
Centre D'Etudes Nucleaires
De La Vallee Rhone
CEN/VALRHO
S.D.H.A. BP 171
30205 Bagnols-Sur-Ceze, FRANCE

Bundesministerium fur Forschung und
Technologie
Postfach 200 706
5300 Bonn 2, GERMANY

Bundesanstalt fur Geowissenschaften
und Rohstoffe
Attn: M. Langer
Postfach 510 153
3000 Hanover 51, GERMANY

Gesellschaft fur Reaktorsicherheit (GRS) (2)
Attn: B. Baltes
W. Muller
Schwertnergasse 1
D-5000 Cologne, GERMANY

Institut fur Tieflagerung (2)
Attn: K. Kuhn
Theodor-Heuss-Strasse 4
D-3300 Braunschweig, GERMANY

Physikalisch-Technische
Bundesanstalt
Attn: P. Brenneke
Postfach 33 45
D-3300 Braunschweig, GERMANY

Shingo Tashiro
Japan Atomic Energy Research Institute
Tokai-Mura, Ibaraki-Ken
319-11, JAPAN

Netherlands Energy Research
Foundation (ECN)
Attn: L.H. Vons
3 Westerduinweg
PO Box 1
1755 ZG Petten, THE NETHERLANDS

Johan Andersson
Swedish Nuclear Power Inspectorate
Statens Kärnkraftinspektion (SKI)
Box 27106
S-102 52 Stockholm, SWEDEN

Fred Karlsson
Svensk Karnbransleforsorjning
AB SKB
Box 5864
S-102 48 Stockholm, SWEDEN

Nationale Genossenschaft fur die Lagerung
Radioaktiver Abfalle (NAGRA) (2)
Attn: S. Vomvoris
P. Zuidema
Hardstrasse 73
CH-5430 Wettingen, SWITZERLAND

AEA Technology
Attn: J.H. Rees
D5W/29 Culham Laboratory
Abington
Oxfordshire OX14 3DB, UNITED KINGDOM

AEA Technology
Attn: W.R. Rodwell
O44/A31 Winfrith Technical Centre
Dorchester
Dorset DT2 8DH, UNITED KINGDOM

AEA Technology
Attn: J.E. Tinson
B4244 Harwell Laboratory
Didcot, Oxfordshire OX11 ORA
UNITED KINGDOM

D.R. Knowles
British Nuclear Fuels, plc
Risley, Warrington
Cheshire WA3 6AS, 1002607
UNITED KINGDOM

Internal

1	A. Narath
20	O.E. Jones
1502	J.C. Cummings
1511	D.K. Gartling
6000	D.L. Hartley
6115	P.B. Davies
6119	E.D. Gorham
6119	Staff (14)
6121	J.R. Tillerson
6121	Staff (7)
6233	J.C. Eichelberger
6300	D.E. Ellis
6302	L.E. Shephard
6303	S.Y. Pickering
6303	W.D. Weart
6305	S.A. Goldstein
6306	A.L. Stevens
6312	F.W. Bingham
6313	L.S. Costin
6331	P.A. Davis
6341	Sandia WIPP Central Files (300)
6342	D.R. Anderson
6342	Staff (30)
6343	S.A. Orrell, Acting
6343	Staff (3)
6345	R.C. Lincoln
6345	Staff (9)
6347	D.R. Schafer
6348	J.T. Holmes
6351	R.E. Thompson
6352	D.P. Garber
6352	S.E. Sharpton
6400	N.R. Ortiz
6613	R.M. Cranwell
6613	R.L. Iman
6613	C. Leigh
6622	M.S.Y. Chu
6641	R.E. Luna, Acting
7141	Technical Library (5)
7151	Technical Publications
7613-2	Document Processing for DOE/OSTI (10)
8523-2	Central Technical Files
9300	J.E. Powell
9310	J.D. Plimpton
9330	J.D. Kennedy

☆ U.S. GOVERNMENT PRINTING OFFICE 1992—774-122/80127

Org.	Bldg.	Name	Rec'd by	Org.	Bldg.	Name	Rec'd by

Sandia National Laboratories

SANDIA REPORT

SAND92–0700/4 • UC–721
Unlimited Release
Printed August 1993

Preliminary Performance Assessment for the Waste Isolation Pilot Plant, December 1992

Volume 4: Uncertainty and Sensitivity Analyses for 40 CFR 191, Subpart B

WIPP Performance Assessment Department

Prepared by
Sandia National Laboratories
Albuquerque, New Mexico 87185 and Livermore, California 94550
for the United States Department of Energy
under Contract DE-AC04-76DP00789

Issued by Sandia National Laboratories, operated for the United States Department of Energy by Sandia Corporation.

Available to DOE and DOE contractors from
Office of Scientific and Technical Information
PO Box 62
Oak Ridge, TN 37831

Prices available from (615) 576-8401, FTS 626-8401

Available to the public from
National Technical Information Service
US Department of Commerce
5285 Port Royal Rd
Springfield, VA 22161

NTIS price codes
Printed copy: A18
Microfiche copy: A01

SAND92-0700/4
Unlimited Release
Printed August 1993

Distribution
Category UC-721

Preliminary Performance Assessment for the Waste Isolation Pilot Plant, December 1992

Volume 4: Uncertainty and Sensitivity Analyses for 40 CFR 191, Subpart B

WIPP Performance Assessment Department
Sandia National Laboratories
Albuquerque, New Mexico 87185

ABSTRACT

Before disposing of transuranic radioactive waste in the Waste Isolation Pilot Plant (WIPP), the United States Department of Energy (DOE) must evaluate compliance with applicable long-term regulations of the United States Environmental Protection Agency (EPA). Sandia National Laboratories is conducting iterative performance assessments (PAs) of the WIPP for the DOE to provide interim guidance while preparing for a final compliance evaluation. This volume of the 1992 PA contains results of uncertainty and sensitivity analyses with respect to the EPA's *Environmental Protection Standards for Management and Disposal of Spent Nuclear Fuel, High-Level and Transuranic Radioactive Wastes* (40 CFR 191, Subpart B). Additional information about the 1992 PA is provided in other volumes. Volume 1 contains an overview of WIPP PA and results of a preliminary comparison with 40 CFR 191, Subpart B. Volume 2 describes the technical basis for the PA, including descriptions of the linked computational models used in the Monte Carlo analyses. Volume 3 contains values for input parameters used in consequence and probability modeling. Volume 5 contains uncertainty and sensitivity analyses of gas and brine migration for undisturbed performance. Finally, guidance derived from the entire 1992 PA is presented in Volume 6.

Results of the 1992 uncertainty and sensitivity analyses indicate that, conditional on the modeling assumptions, the choice of parameters selected for sampling, and the assigned parameter-value distributions, the most important parameters for which uncertainty has the potential to affect compliance with 40 CFR 191B are: drilling intensity, intrusion borehole permeability, halite and anhydrite permeabilities, radionuclide solubilities and distribution coefficients, fracture spacing in the Culebra Dolomite Member of the Rustler Formation, porosity of the Culebra, and spatial variability of Culebra transmissivity. Performance with respect to 40 CFR 191B is insensitive to uncertainty in other parameters; however, additional data are needed to confirm that reality lies within the assigned distributions.

ACKNOWLEDGMENTS

The Waste Isolation Pilot Plant (WIPP) Performance Assessment (PA) Department is comprised of both Sandia National Laboratories (SNL) and contractor employees working as a team to produce preliminary comparisons with Environmental Protection Agency (EPA) regulations, assessments of overall long-term safety of the repository, and interim technical guidance to the program. The on-site team, affiliations, and contributions to the 1992 performance assessment are listed in alphabetical order:

Performance Assessment Department

Name	Affil.*	Primary Author of Major Code	Area of Responsibility
R. Anderson	SNL		Department Manager
B. Baker	TEC		SECO2D, Hydrology, Office Manager
J. Bean	UNM		BRAGFLO, 2-Phase Flow
J. Berglund	UNM	CUTTINGS	Task Ldr., Cuttings/Cavings/ Spallings, Engr. Mech.
S. Bertram-Howery	SNL		PA Liaison with DOE, Criteria Document, Test Phase Plan
W. Beyeler	SAI	PANEL, GARFIELD	Geostatistics, Analytical Models, CAMCON Systems Codes
K. Brinster	SAI		Geohydrology, Conceptual Models
R. Blaine	ECO		SECO2D, SECOTP, & CAMCON Systems Codes
T. Blaine	GC		Drilling Technology, Exposure Pathways Data
K. Byle	UNM		Software and Analysis QA
J. Chapman	TRI		Documentation V.3
D. Duncan	MAC		Data QA
K. Economy	ECO		SECO2D, SECOTP, Hydrology &
D. Gallegos	SNL		Transport Task Ldr., Hydrology, Geostatistics, NEA, PSAG
D. Galson	GS		NEA Working Groups, PSAG, PAAG, Human Intrusion
J. Garner	API	PANEL	Source Term, Sens. Anal.
A. Gilkey	UNM		CAMCON Systems Codes
L. Gomez	SNL		Task Ldr., Safety Assessments
M. Gruebel	TRI		EPA Regulations, Documentation V.1, Editor V.1
R. Guzowski	SAI		Geology, Scenario Construction
J. Helton	ASU	CCDFPERM	Task Ldr., Uncert./Sens. Anal., Probability Models, Editor V.4
S. Hora	UHH		Expert Elicitation, Probability Models
H. Iuzzolino	GC	CCDFCALC CCDFPERM	LHS, CAMCON System Codes, Probability Models
R. Klett	SNL		EPA Regulations
P. Knupp	ECO	SECOTP	Comp. Fluid Dyn.
M. LaVenue	INT	GRASP-INV	Hydrology/Geostatistics
C. Leigh	SNL	GENII-S	Exposure Pathways

M. Marietta	SNL		Dep. Dept. Manager, Tech. Coord.
G. de Marsily	UP		Geostatistics Expert Group Chair
R. McCurley	UNM		CAMCON System Codes
B. Napier	PNL	GENII	Safety Assessments
A. Peterson	SNL		Task Ldr., Inventory
B. RamaRao	INT	GRASP-INV	Geostatistics
J. Rath	UNM		CAMCON System Codes
R. Rechard	SNL		Task Ldr., CAMCON, QA
P. Roache	ECO	SECO	Task Ldr., Comp. Fluid Dyn.
D. Rudeen	UNM		STAFF2D, SECOTP, Transport
J. Ruge	ECO		Multigrid Methods/BRAGFLO
T. Russell	ECO		Upscaling
K. Salari	ECO	SECOTP	Transport, Computational Fluid Dynamics
J. Sandha	SAI		INGRES, PA Data Base
J. Schreiber	SAI		BRAGFLO, 2-Phase Flow
D. Scott	TRI		Documentation V.2
P. Swift	TRI		Task Ldr., Geology, Climate Var., Editor V.1, 2, 4, & 5
M. Tierney	SNL		Task Ldr., CDF Constr., Probability Models, Ref. Data, Editor V.2 & 3
K. Trauth	SNL		Task Ldr., Expert Panels
P. Vaughn	API	BRAGFLO	Task Ldr., 2-Phase Flow & Waste Panel Chemistry, Editor V. 4 & 5
T. Zimmerman	GRA		Geostatistics Test Problem

The foundation of the annual WIPP performance assessment is the underlying data set and understanding of the important processes in the engineered and natural barrier systems. Other SNL Departments are the primary source of these data and understanding. Assistance with the waste inventory comes from Westinghouse Electric Corporation and its contractors. We gratefully acknowledge the support of our departmental and project colleagues. Some individuals have worked closely with the performance assessment team, and we wish to acknowledge their contributions individually:

H. Batchelder	WEC	CH & RH Inventories
R. Beauheim	SNL	Natural Barrier System, Hydrologic Parameters
D. Borns	SNL	Geology, Geophysics
B. Butcher	SNL	Engineered Barrier System, Unmodified Waste-Form Parameters, Disposal Room Systems Parameters
L. Brush	SNL	Engineered Barrier System, Source Term (Solubility) and Gas Generation Parameters
L. Clements	ReS	Computer System Support
T. Corbet	SNL	Natural Barrier System, Geologic & Hydrologic Parameters, Conceptual Models
P. Davies	SNL	Natural Barrier System, Hydrologic & Transport Parameters, & 2-Phase Flow Mechanistic Modeling
P. Drez	DEA	CH & RH Inventories
R. Finley	SNL	Repository Isolation Systems Parameters
F. Gelbard	SNL	Natural Barrier System, Retardation

E. Gorham	SNL	Natural Barrier System, Fluid Flow & Transport Parameters
R. Holt	CON	Geology
S. Howarth	SNL	Natural Barrier System, Hydrologic Parameters
R. Kehrman	WEC	CH & RH Waste Characterization
K. Lickliter	BEC	EPA Regulations
R. Lincoln	SNL	Room Modeling
F. Mendenhall	SNL	Engineered Barrier System, Unmodified Waste Form Parameters, Waste Panel Closure (Expansion)
D. Munson	SNL	Reference Stratigraphy, Constitutive Models, Physical & Mechanical Parameters
C. Novak	SNL	Natural Barrier Systems, Chemistry
E. Nowak	SNL	Room Modeling, Source Term
J. Orona	ReS	Computer System Support
A. Stevens	SNL	DOE Liaison
J. Tillerson	SNL	Repository Isolation Systems Parameters
W. Wawersik	SNL	Fracturing
S. Webb	SNL	2-Phase Flow Sensitivity Analysis & Benchmarking

* Affiliation

API = Applied Physics Incorporated
ASU = Arizona State University
BEC = Benchmark Environmental Corp.
CON = Consultant
DEA = Drez Environmental Associates
ECO = Ecodynamics Research Associates
GC = Geo-Centers Incorporated
GRA = GRAM, Inc.
GS = Galson Sciences
INT = Intera
MAC = MACTEC
PNL = Pacific Northwest Laboratory
ReS = ReSpec
SAI = Scientific Applications International Corporation
SNL = Sandia National Laboratories
TEC = Technadyne Engineering Consultants
TRI = Tech Reps, Inc.
UHH = University of Hawaii at Hilo
UNM = Univ. of New Mexico/New Mexico Engineering Research Institute
UP = University of Paris
WEC = Westinghouse Electric Corporation

Expert Panels

Futures

M. Baram	Boston University
W. Bell	Yale University
G. Benford	University of California, Irvine
D. Chapman	The World Bank, Cornell University
B. Cohen	University of Pittsburgh
V. Ferkiss	Georgetown University
T. Glickman	Resources for the Future
T. Gordon	Futures Group
C. Kirkwood	Arizona State University
H. Otway	Joint Research Center (Ispra), Los Alamos National Laboratory
M. Pasqualetti	Arizona State University
D. Reicher	Natural Resources Defense Council
N. Rosenberg	Resources for the Future
M. Singer	The Potomac Organization

Volume 3: J. Chapman (text); D. Pulliam (illustrations)
Volume 4: V. Gilliland, M. Minahan (text); S. Laundre-Woerner, A. Montano (illustrations)

D. Rivard and the Word Processing Department
R. Rohac, R. Andree, and the Illustration and Computer Graphics Departments
S. Tullar and the Production Department

Peer Review

Internal/Sandia
F. Mendenhall
L. Gomez

Management/Sandia
W. Weart

PA Peer Review Panel

R. Heath, Chair	University of Washington
R. Budnitz	Future Resources Associates, Inc.
T. Cotton	JK Research Associates, Inc.
J. Mann	University of Illinois
T. Pigford	University of California, Berkeley
F. Schwartz	Ohio State University

Department of Energy
J. Coffey

PREFACE

The *Preliminary Performance Assessment for the Waste Isolation Pilot Plant, December 1992* is currently planned to consist of six volumes. The titles of the volumes are listed below. All analyses reported in the 1992 Preliminary Performance Assessment, including those described in this volume, are based on computer modeling of disposal-system performance that was completed in November 1992.

This report is the fourth in a series of annual reports that document ongoing assessments of the predicted long-term performance of the Waste Isolation Pilot Plant (WIPP); this documentation will continue during the WIPP Test Phase. However, the Test Phase schedule and projected budget may change; if so, the content of the *1992 Preliminary Performance Assessment* report and its production schedule may also change.

Volume 1: Third Comparison with 40 CFR 191, Subpart B

Volume 2: Technical Basis

Volume 3: Model Parameters

Volume 4: Uncertainty and Sensitivity Analyses for 40 CFR 191, Subpart B

Volume 5: Uncertainty and Sensitivity Analyses of Gas and Brine Migration for Undisturbed Performance

Volume 6: Guidance to the WIPP Project from the December 1992 Performance Assessment

CONTENTS

FIGURES

Figure Page

Figure Page

Figure Page

TABLES

1. INTRODUCTION

The Waste Isolation Pilot Plant (WIPP) is planned as a research and development facility to demonstrate the safe disposal of transuranic (TRU) wastes generated by defense programs of the United States Department of Energy (DOE). Before disposing of waste in the WIPP, the DOE must evaluate compliance with applicable long-term regulations of the United States Environmental Protection Agency (EPA), including 40 CFR 191, Subpart B *(Environmental Radiation Protection Standards for the Management and Disposal of Spent Nuclear Fuel, High-Level and Transuranic Radioactive Wastes)* (EPA, 1985) and *40 CFR 268.6 (Petitions to Allow Land Disposal of a Waste Prohibited Under Subpart C of Part 268)* (EPA, 1986), which is the regulation implementing the *Resource Conservation and Recovery Act (RCRA)* that states the conditions for disposal of specified hazardous wastes. Performance assessment (PA) will form the basis for evaluations of compliance with these regulations.

The WIPP Performance Assessment Department of Sandia National Laboratories (SNL) is performing iterative preliminary PAs to provide guidance to the WIPP Project while preparing for final compliance evaluation. This volume is part of a multi-volume report documenting the third preliminary performance assessment for the WIPP, completed in December 1992. Preparation for preliminary performance assessments began with the December 1989 *Draft Forecast of the Final Report for the Comparison to 40 CFR Part 191, Subpart B for the Waste Isolation Pilot Plant* (Bertram-Howery et al., 1989) and *Performance Assessment Methodology Demonstration: Methodology Development for Evaluating Compliance with EPA 40 CFR 191, Subpart B, for the Waste Isolation Pilot Plant* (Marietta et al., 1989). The 1990 report (Bertram-Howery et al., 1990) and two supporting volumes (Rechard et al., 1990; Helton et al., 1991) presented preliminary results of evaluations that addressed only the long-term performance criteria for disposal specified in the radioactive-waste disposal standards (*40 CFR 191, Subpart B*, EPA, 1985). The 1991 version of the report (WIPP PA Division, 1991a, 1991b, 1991c; Helton et al., 1992) presented preliminary evaluations for comparison with the regulatory requirements of *40 CFR 191, Subpart B*. Results of the 1992 performance assessment are not suitable for final compliance evaluations because portions of the modeling system and data base are incomplete, and the level of confidence in the defensibility of the performance estimates has not been established. Results are, however, suitable for providing interim guidance to the WIPP Project as it moves toward final compliance evaluations.

Previous volumes of the December 1992 *Preliminary Performance Assessment* have provided an overview of the performance assessment and results of a preliminary comparison with Subpart B of *40 CFR 191* (Volume 1), a description of the technical basis for probability and consequence modeling (Volume 2), and the data base of parameter values used in modeling (Volume 3). This volume contains the results of uncertainty and sensitivity analyses performed with respect to *40 CFR 191B*. These analyses provide quantitative and qualitative insights on the relationships between uncertainty in the models and data used in the performance assessment and the resultant uncertainty in the results of the performance assessment. Additional uncertainty and sensitivity analyses of gas and brine migration for undisturbed conditions relevant to compliance evaluations for *40 CFR 268.6* are contained in Volume 5. Finally, Volume 6 contains guidance to the WIPP Project based on the 1992 performance assessment.

Uncertainty and sensitivity analysis is an important part of the WIPP PA and contributes to the overall analysis in the following areas: (1) assessment of the uncertainty in performance assessment results that must be used in regulatory compliance evaluations, (2) identification of modeling areas where reductions in uncertainty can increase confidence in performance assessment results, and (3) partial verification that the computational models used in the performance assessment system are operating properly. Because uncertainty and sensitivity analyses are inherently conditional on the models, data distributions, and techniques used to generate them, they cannot provide insight about parameters not sampled, conceptual and computational models not used in the analysis in question, or processes that have been oversimplified in the analysis. As discussed further in Volume 6, qualitative judgment about the modeling system must be used in combination with the results of analyses presented in this volume to set priorities for additional data acquisition and model development.

Organization of this volume is as follows:

- Chapter 2 provides an overview of the structure of the WIPP PA, including an introduction to the Kaplan and Garrick (1981) ordered-triple representation for risk. The definition of scenarios, the determination of scenario probabilities, and the calculation of scenario consequences are described in the context of the ordered-triple representation for risk. Additional information about the PA methodology is provided in Chapters 3 and 4 in Volume 2 of this report.

- Chapter 3 provides information about the imprecisely known variables selected for sampling in the 1992 PA. Detailed information about parameter values is provided in Volume 3 of this report.

- Chapter 4 contains a discussion of the modeling of undisturbed performance using a rectangular cross-section representation of the entire repository. Results are presented in terms of cumulative gas and brine migration and other two-phase flow performance measures. Radionuclide transport is not modeled because no brine that has been in contact with waste reaches the accessible environment during 10,000 yr of undisturbed performance. Discussions of two-phase flow and creep closure and detailed information about the BRAGFLO and SANCHO codes used in the modeling are provided in Chapter 7 and Appendices A and B in Volume 2 of this report.

- Chapter 5 contains a discussion of the modeling of disturbed performance (i.e., scenarios in which the waste-disposal region is intruded by an exploratory borehole) using a cylindrical representation of a single panel. Results in this chapter are presented in terms of cumulative gas and brine migration and other two-phase flow performance measures. Uncertainty and sensitivity analyses using radionuclide releases as the primary performance measure are discussed in Chapter 8. Modeling for disturbed performance uses the BRAGFLO and SANCHO codes, and also uses the PANEL code to model radionuclide mobilization in the waste-emplacement panel. PANEL is described in Chapter 7 and Appendix A in Volume 2 of this report.

- Chapter 6 contains a discussion of the modeling of groundwater flow and radionuclide transport in the Culebra Dolomite Member of the Rustler Formation above the repository. Radionuclide transport in the Culebra occurs only in human intrusion scenarios. Modeling is done using the SECO flow and transport codes, as described in Chapter 7 and Appendix C in Volume 2 of this report.

- Chapter 7 contains a discussion of the modeling of the release of radionuclides directly at the ground surface during the drilling of an exploratory borehole that intrudes into the waste-disposal region. As modeled, particulate waste is brought to the surface in the drilling fluid both as cuttings (material intersected by the drill bit) and cavings (material eroded from the borehole wall by the circulating drilling fluid). Cuttings and cavings are collectively referred to as cuttings in this report. Modeling is done using the CUTTINGS code, as described by Berglund (1992) and Chapter 7 in Volume 2 of this report.

- Chapter 8 contains uncertainty and sensitivity analysis results for radionuclide releases both from cuttings and groundwater transport. Alternative conceptual models are examined for transport in the Culebra, including transport in a single-porosity, fracture-only medium and transport in a dual-porosity, fracture plus porous-matrix system. For dual-porosity transport, releases are examined with and without the physical effect of clay linings in fractures and with and without chemical retardation by sorption. Cases considered here are a more complete set of those for which results were presented in Chapter 5 of Volume 1 of this report for preliminary comparison with the Containment Requirements of *40 CFR 191B*. Dual-porosity transport with both chemical and physical retardation in matrix and clay linings is the conceptual model believed by the WIPP PA Department to provide the most realistic representation for transport in the Culebra. Experimental and field data are not sufficient at this time to eliminate alternative conceptual models, and other cases are therefore analyzed here for comparison.

- Chapter 9 summarizes the results of the 1992 uncertainty and sensitivity analyses for *40 CFR 191B*, and identifies overall importance of individual parameters.

2. STRUCTURE OF WIPP PERFORMANCE ASSESSMENT

2.1 Conceptual Model

As proposed by Kaplan and Garrick (1981), the outcome of a performance assessment can be represented by a set R of ordered triples of the form

$$R = \{(S_i, pS_i, \mathbf{cS}_i), i=1, \ldots, nS\}, \qquad (2.1\text{-}1)$$

where

S_i = a set of similar occurrences,

pS_i = probability that an occurrence in the set S_i will take place,

$\mathbf{cS}_i$ = a vector of consequences associated with S_i,

nS = number of sets selected for consideration,

and the sets S_i have no occurrences in common (i.e., the S_i are disjoint sets). This representation formally decomposes the outcome of a performance assessment into what can happen (the S_i), how likely things are to happen (the pS_i), and the consequences of what can happen (the $\mathbf{cS}_i$). The S_i are typically referred to as "scenarios" in radioactive waste disposal. Similarly, the pS_i are scenario probabilities, and the vector $\mathbf{cS}_i$ contains environmental releases for individual isotopes, the normalized EPA release for all isotopes, and possibly other information associated with scenario S_i. The set R in Eq. 2.1-1 is used as the conceptual model for the WIPP performance assessment.

Although the expression in Eq. 2.1-1 provides a logical conceptual representation for risk, the set R by itself can be difficult to examine. For this reason, the risk results in R are often summarized with complementary cumulative distribution functions (CCDFs). These functions provide a display of the information contained in the probabilities pS_i and the consequences $\mathbf{cS}_i$. With the assumption that a particular consequence result cS in the vector $\mathbf{cS}$ has been ordered so that $cS_i \leq cS_{i+1}$ for i=1, ..., nS-1, the associated CCDF is shown in Figure 2.1-1. A consequence result of particular interest in performance assessments for radioactive waste disposal is the EPA normalized release to the accessible environment (EPA, 1985). As indicated in Figure 2.1-1, the EPA places a bound on the CCDF for normalized release to the accessible environment.

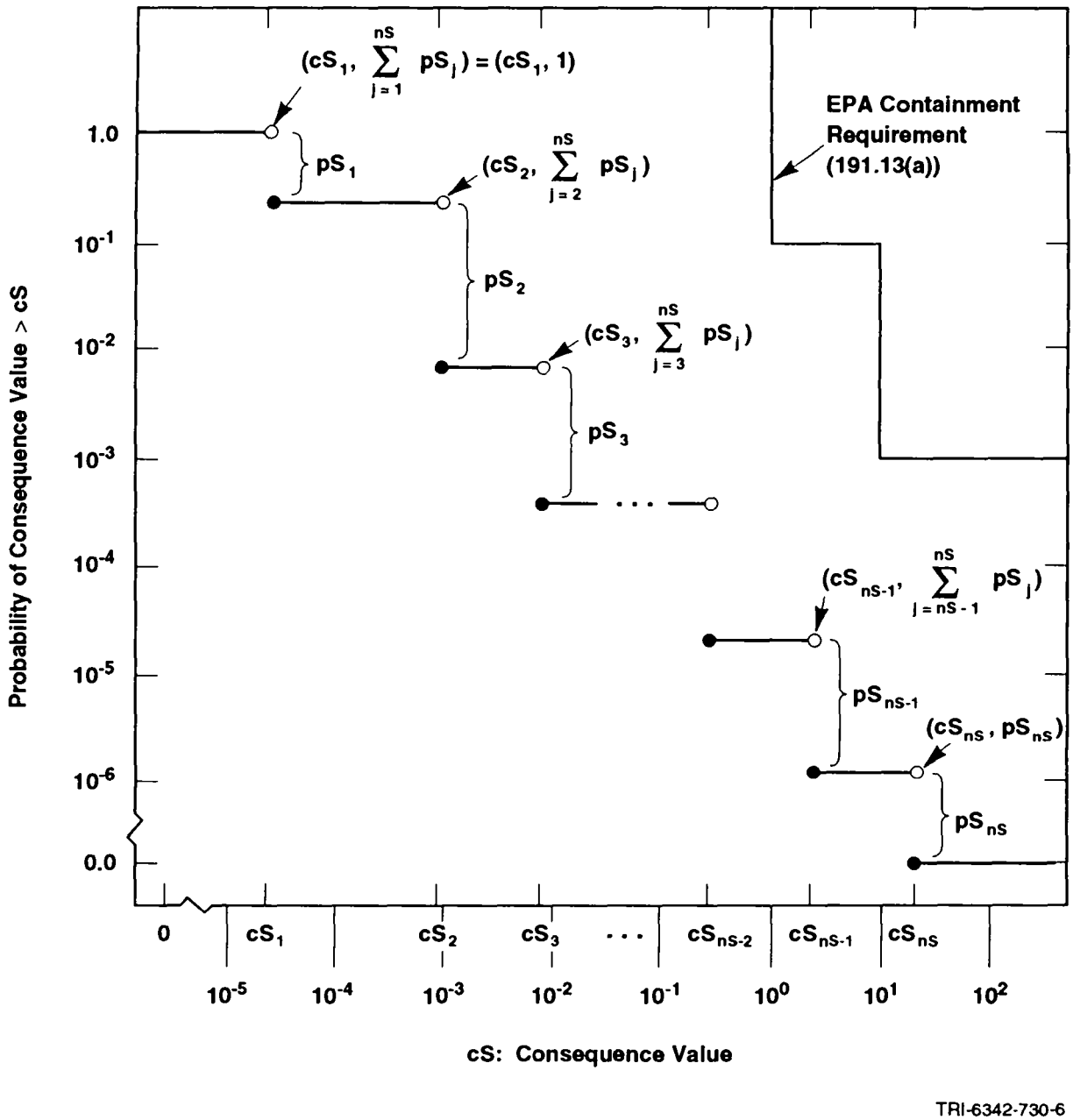

Figure 2.1-1. Estimated complementary cumulative distribution function (CCDF) for consequence result cS (Helton et al., 1991). The open and solid circles at the discontinuities indicate the points included on (solid circles) and excluded from (open circles) the CCDF.

In practice, the outcome of a performance assessment depends on many imprecisely known variables. These imprecisely known variables can be represented by a vector

$$\mathbf{x} = [x_1, x_2, \ldots, x_{nV}], \tag{2.1-2}$$

where each x_j is an imprecisely known input required in the performance assessment and nV is the total number of such inputs. As a result, the set R is actually a function of $\mathbf{x}$:

$$R(\mathbf{x}) = \{[S_i(\mathbf{x}), pS_i(\mathbf{x}), \mathbf{cS}_i(\mathbf{x})], i=1, \ldots, nS(\mathbf{x})\}. \tag{2.1-3}$$

As $\mathbf{x}$ changes, so will $R(\mathbf{x})$ and all summary measures that can be derived from $R(\mathbf{x})$. Thus, rather than a single CCDF for each consequence value contained in $\mathbf{cS}$, there will be a distribution of CCDFs that results from the possible values that $\mathbf{x}$ can take on.

The uncertainty in $\mathbf{x}$ can be characterized by a sequence of probability distributions

$$D_1, D_2, \ldots, D_{nV}, \tag{2.1-4}$$

where D_j is the distribution for the variable x_j contained in $\mathbf{x}$. The definition of these distributions may also be accompanied by the specification of correlations and various restrictions that further define the relations between the x_j. These distributions and other restrictions probabilistically characterize where the appropriate input to use in a performance assessment might fall given that the analysis has been structured so that only one value can be used for each variable.

Once the distributions in Eq. 2.1-4 have been developed, Monte Carlo techniques can be used to determine the uncertainty in $R(\mathbf{x})$ that results from the uncertainty in $\mathbf{x}$. First, a sample

$$\mathbf{x}_k = [x_{k1}, x_{k2}, \ldots, x_{k,nV}], k=1, \ldots, nK, \tag{2.1-5}$$

is generated according to the specified distributions and restrictions, where nK is the size of the sample. A performance assessment is then conducted for each sample element $\mathbf{x}_k$, which yields a sequence of risk results of the form

$$R(\mathbf{x}_k) = \{[S_i(\mathbf{x}_k), pS_i(\mathbf{x}_k), \mathbf{cS}_i(\mathbf{x}_k)], i=1, \ldots, nS(\mathbf{x}_k)\} \tag{2.1-6}$$

for k=1, ..., nK. Each set $R(\mathbf{x}_k)$ is the result of one complete performance assessment conducted with a set of inputs (i.e., $\mathbf{x}_k$) that the review process producing the distributions in Eq. 2.1-4 concluded was possible. Further, associated with each risk result $R(\mathbf{x}_k)$ in Eq. 2.1-6 is a probability or weight that can be used in making probabilistic statements about the distribution of $R(\mathbf{x})$. When random or Latin hypercube sampling is used, this weight is the reciprocal of the sample size (i.e., 1/nK).

In most performance assessments, CCDFs are the results of greatest interest. For a particular consequence result, a CCDF will be produced for each set $R(\mathbf{x}_k)$ shown in Eq. 2.1-6. This yields a distribution of CCDFs of the form shown in Figure 2.1-2.

An important distinction exists between the uncertainty that gives rise to a single CCDF in Figure 2.1-2 and the uncertainty that gives rise to the distribution of CCDFs in this figure. A single CCDF arises from the fact that a number of different occurrences (e.g., borehole intrusions) have a real possibility of taking place. This type of uncertainty is referred to as stochastic variation or uncertainty in this report. A distribution of CCDFs arises from the fact that fixed, but unknown, quantities (e.g., hydrologic properties) are needed in the estimation of a CCDF. The development of distributions that characterize what the values for these fixed quantities might be leads to a distribution of CCDFs. In essence, a performance assessment can be viewed as a very complex function that estimates a CCDF. As there is uncertainty in the values of some of the variables operated on by this function, there will also be uncertainty in the dependent variable produced by this function, where this dependent variable is a CCDF.

Both Kaplan and Garrick (1981) and a recent report by the International Atomic Energy Agency (IAEA, 1989) distinguish between these two types of uncertainty. Specifically, Kaplan and Garrick distinguish between probabilities derived from frequencies and probabilities that characterize degrees of belief. Probabilities derived from frequencies correspond to the probabilities pS_i in Eq. 2.1-1, while probabilities that characterize degrees of belief (i.e., subjective probabilities) correspond to the distributions indicated in Eq. 2.1-4. The IAEA report distinguishes between what it calls Type A uncertainty and Type B uncertainty. The IAEA report defines Type A uncertainty to be stochastic variation; as such, this uncertainty corresponds to the frequency-based probability of Kaplan and Garrick and the pS_i of Eq. 2.1-1. Type B uncertainty is defined to be uncertainty that is due to lack of knowledge about fixed quantities; thus, this uncertainty corresponds to the subjective probability of Kaplan and Garrick and the distributions indicated in Equation 2.1-4. Expressed another way, Type A uncertainty

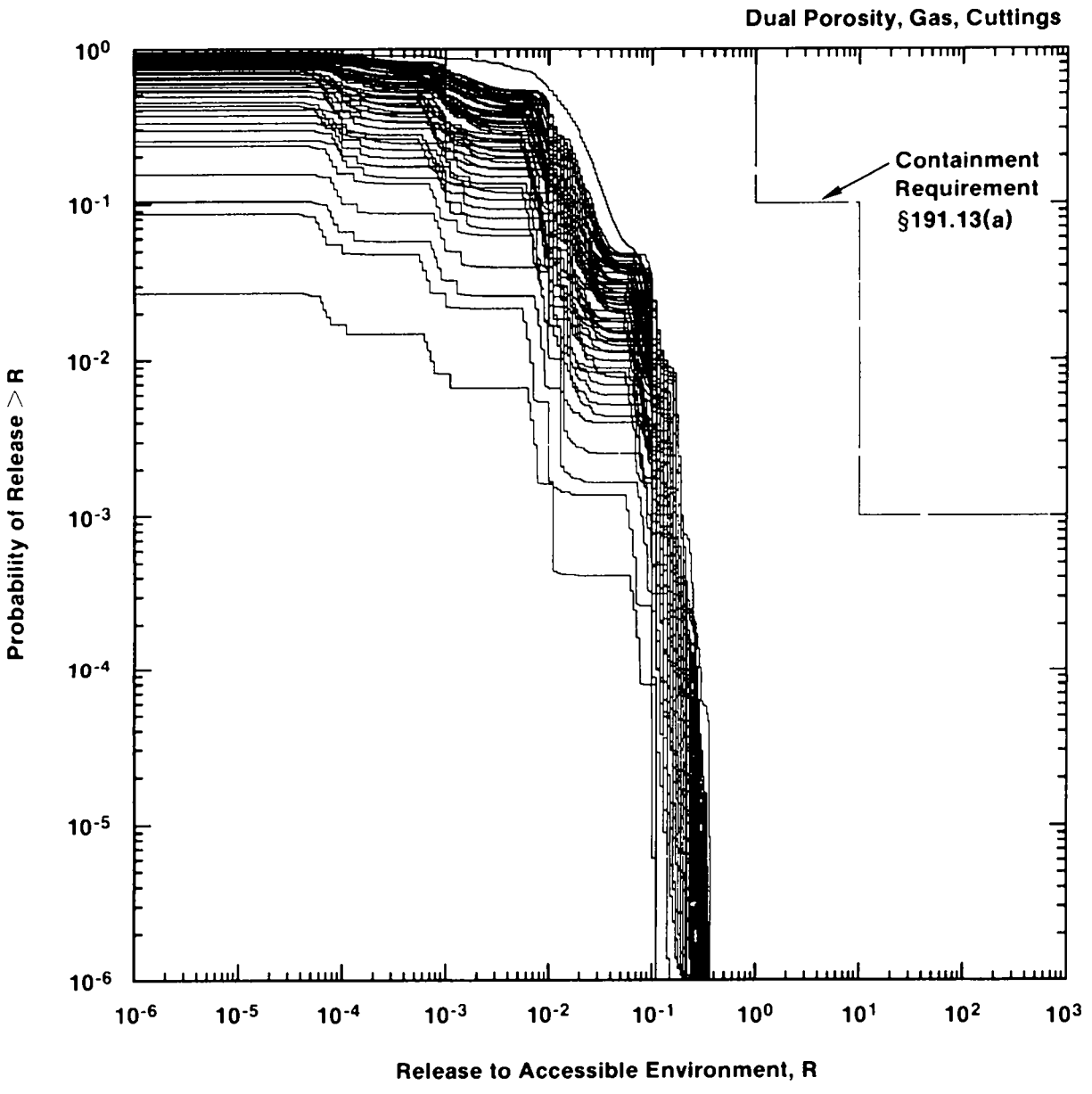

TRI-6342-1293-1

Figure 2.1-2. Distribution of complementary cumulative distribution functions (CCDFs) for normalized release to the accessible environment obtained in the 1991 WIPP performance assessment including both cuttings removal and groundwater transport with gas generation in the repository and a dual-porosity transport model in the Culebra Dolomite (Helton et al., 1992, Figure 2.1-2).

designates variability in a population; Type B uncertainty designates a lack of knowledge about this population and how to appropriately calculate associated results of interest. For the WIPP performance assessment, Type A uncertainty refers to all possible patterns of disruption that could occur over a 10,000 yr period, and Type B uncertainty refers to our lack of knowledge on how to characterize these patterns and calculate their consequences. This distinction has also been made by other authors, including Vesely and Rasmuson (1984), Paté-Cornell (1986), Parry (1988), Helton (1993b), and Helton and Breeding (1993).

As already indicated, the ordered-triple representation shown in Eq. 2.1-1 is used as the conceptual model for the WIPP performance assessment. In consistency with this representation, the scenarios S_i, scenario probabilities pS_i and scenario consequences $\mathbf{cS}_i$ used in the 1991 preliminary WIPP performance assessment are discussed in Sections 2.2, 2.3 and 2.4, respectively. Several specific definitions used for R in the 1992 WIPP performance assessment are then presented in Section 2.5.

The WIPP performance assessment endeavors to maintain a distinction between stochastic (i.e., Type A) uncertainty and subjective (i.e., Type B) uncertainty. The effect of stochastic uncertainty is represented by the probabilities pS_i discussed in Section 2.3. The characterization of the subjective uncertainty in the inputs to the 1992 WIPP performance assessment is discussed in Chapter 3. The primary focus of this report is the impact of subjective uncertainties on the outcomes of the 1992 WIPP performance assessment. These impacts will be investigated in Chapters 4 through 8. A concluding discussion is given in Chapter 9.

2.2 Definition of Scenarios

Scenarios constitute the first element S_i of the ordered triples contained in the set R shown in Eq. 2.1-1 and are obtained by subdividing the set

$$S = \{x\text{: } x \text{ a single 10,000-yr history beginning at decommissioning of the WIPP}\}. \qquad (2.2\text{-}1)$$

Each 10,000-yr history is complete in the sense that it includes a full specification, including time of occurrence, for everything of importance to performance assessment that happens in this time period. In the terminology of Cranwell et al. (1990), each history would contain a characterization for a specific sequence of "naturally occurring and/or human-induced conditions

that represent realistic future states of the repository, geologic systems, and ground-water flow systems that could affect the release and transport of radionuclides from the repository to humans." In the terminology of probability theory, the set S is called the sample space, the members of S are called elementary events, and the individual scenarios S_i are called events.

The WIPP performance assessment uses a two-stage procedure for scenario development (Chapter 4 of Volume 2). The purpose of the first stage is to develop a comprehensive set of scenarios that includes all occurrences that might reasonably take place at the WIPP. The result of this stage is a set of scenarios, called summary scenarios, that summarize what might happen at the WIPP. These summary scenarios provide a basis for discussing the future behavior of the WIPP and a starting point for the second stage of the procedure, which is the definition of scenarios at a level of detail that is appropriate for use with the computational models employed in the WIPP performance assessment. The scenarios obtained in this second stage of scenario development are referred to as computational scenarios. The development of summary scenarios is directed at understanding what might happen at the WIPP and answering completeness questions. The development of computational scenarios is directed at organizing the actual calculations that must be performed to obtain the consequences $\mathbf{cS}_i$ appearing in Eq. 2.1-1, and as a result, must provide a structure that both permits the $\mathbf{cS}_i$ to be calculated at a reasonable cost and holds the amount of aggregation error that enters the analysis to a reasonable level. Here, aggregation error refers to the inevitable loss of resolution that occurs when an infinite number of occurrences (i.e., the elements of S) must be divided into a finite number of sets for analysis (i.e., the subsets S_i of S). The following discussion describes the computational scenarios used in the 1992 WIPP performance assessment.

The development of summary scenarios for the 1992 WIPP performance assessment led to a set S of the form shown in Eq. 2.2-1 in which all disruptions were due to drilling intrusions (Chapter 4 of Volume 2). As a result, computational scenarios were defined to provide a systematic coverage of drilling intrusions. Specifically, computational scenarios were defined on the basis of (1) number of drilling intrusions, (2) time of the drilling intrusions, (3) whether or not a single waste panel is penetrated by two or more boreholes, of which at least one penetrates a pressurized brine pocket and at least one does not, and (4) activity level of the waste penetrated by the boreholes.

The construction of computational scenarios started with the division of the 10,000-yr time period appearing in the EPA regulations into a sequence

$[t_{i-1}, t_i]$, i = 1, 2, ..., nT, (2.2-2)

of disjoint time intervals. When the activity levels of the waste are not considered, these time intervals lead to computational scenarios of the form

$$S(\mathbf{n}) = \{x: x \text{ an element of } S \text{ for which exactly n(i) intrusions occur in time interval } [t_{i-1}, t_i] \text{ for i=1, 2, ..., nT (i.e., an E1 or E2-type scenario as described in Section 4.2.3.2 of Volume 2.)}\} \quad (2.2\text{-}3)$$

and

$$S^{+-}(t_{i-1},t_i) = \{x: x \text{ an element of } S \text{ for which two or more boreholes penetrate the same waste panel during the time interval } [t_{i-1}, t_i], \text{ with at least one of these boreholes penetrating a pressurized brine pocket and at least one not penetrating a pressurized brine pocket (i.e., an E1E2-type scenario as described in Section 4.2.3.2 of Volume 2)}\}, \quad (2.2\text{-}4)$$

where

$$\mathbf{n} = [n(1), n(2), \ldots, n(nT)]. \quad (2.2\text{-}5)$$

As discussed in Section 2.5, the 1992 WIPP performance assessment uses two different subdivisions of the 10,000-yr time period in the EPA regulations. In turn, these different subdivisions lead to different definitions for the set R in Eq. 2.1-1.

When the activity levels of the waste are considered, the preceding time intervals lead to computational scenarios of the form

$$S(\mathbf{l},\mathbf{n}) = \{x: x \text{ an element of } S(\mathbf{n}) \text{ for which the } j^{th} \text{ borehole encounters waste of activity level } \ell(j) \text{ for j=1, 2, ..., nBH, where nBH is the total number of boreholes associated with a time history in } S(\mathbf{n})\} \quad (2.2\text{-}6)$$

and

$$S^{+-}(\mathbf{l};t_{i-1},t_i) = \{x: x \text{ an element of } S^{+-}(t_{i-1},t_i) \text{ for which the } j^{th} \text{ borehole encounters waste of activity level } \ell(j) \text{ for j=1, 2, ..., nBH, where nBH is the total number of boreholes associated with a time history in } S^{+-}(t_{i-1},t_i)\}, \quad (2.2\text{-}7)$$

where

$$\mathbf{l} = [\ell(1), \ell(2), \ldots, \ell(nBH)] \text{ and } nBH = \sum_{i=1}^{nT} n(i). \qquad (2.2\text{-}8)$$

The computational scenarios $S(\mathbf{l},\mathbf{n})$ and $S^{+-}(\mathbf{l};t_{i-1},t_i)$ are used as the basis for the CCDFs for normalized release to the accessible environment presented in the 1992 WIPP performance assessment.

The definitions of $S^{+-}(t_{i-1},t_i)$ and $S^{+-}(\mathbf{l};t_{i-1},t_i)$ appearing in Eqs. 2.2-4 and 2.2-7 do not use the vector $\mathbf{n}$ designating the time intervals in which drilling intrusions occur that appears in the definitions of $S(\mathbf{n})$ and $S(\mathbf{l},\mathbf{n})$. However, vectors of this form can be incorporated into the definitions of $S^{+-}(t_{i-1},t_i)$ and $S^{+-}(\mathbf{l};t_{i-1},t_i)$. Specifically, let

$$S_i^{+-}(\mathbf{n}) = \{x: \text{ x an element of } S(\mathbf{n}) \text{ for which 2 or more boreholes penetrate the same waste panel during the time interval } [t_{i-1},t_i] \text{ (i.e., } n(i)\geq 2\text{), with at least one of these boreholes penetrating a pressurized brine pocket and at least one not penetrating a pressurized brine pocket}\}. \qquad (2.2\text{-}9)$$

Then,

$$S^{+-}(t_{i-1},t_i) = \bigcup_{\mathbf{n}\in A(i)} S_i^{+-}(\mathbf{n}), \qquad (2.2\text{-}10)$$

where $\mathbf{n}\in A(i)$ only if $\mathbf{n}$ is a vector of the form defined in Eq. 2.2-5 with $n(i)\geq 2$. The computational scenarios $S_i^{+-}(\mathbf{l},\mathbf{n})$ and $S^{+-}(\mathbf{l};t_{i-1},t_i)$ can be defined analogously for the vector $\mathbf{l}$ indicated in Eq. 2.2-8. In Section 2.3, conservative relations are presented (i.e., Eqs. 2.3-3 and 2.3-4) that bound the probabilities for $S^{+-}(t_{i-1},t_i)$ and $S^{+-}(\mathbf{l};t_{i-1},t_i)$ and are used in the construction of CCDFs of the form appearing in Figure 2.1-2. In Section 2.4, $S^{+-}(t_{i-1},t_i)$ and $S^{+-}(\mathbf{l};t_{i-1},t_i)$, $i = 1, \ldots, nT$, are assigned the groundwater releases (i.e., Eqs. 2.4-13 and 2.4-14) associated with

$$S_1^{+-}(2,0,\ldots,0),\ S_2^{+-}(0,2,\ldots,0),\ \ldots,\ S_{nT}^{+-}(0,0,\ldots,2), \qquad (2.2\text{-}11)$$

respectively; these releases are used in the construction of CCDFs of the form appearing in Figure 2.1-2. The subscripts in the preceding notation for $S_1^{+-}(2,0,\ldots,0)$ through $S_{nT}^{+-}(0,0,\ldots,2)$ are redundant and will be omitted in the remainder of this report.

Additional information on the construction of computational scenarios for the 1992 WIPP performance assessment is available elsewhere (Chapter 5 of Volume 2).

2.3 Determination of Scenario Probabilities

As discussed in Chapter 5 of Volume 2 and Helton (1993a), probabilities for computational scenarios were determined under the assumption that the occurrence of boreholes through the repository follows a Poisson process with a rate term λ. The probabilities $pS(\mathbf{n})$ and $pS(\mathbf{I},\mathbf{n})$ for the computational scenarios $S(\mathbf{n})$ and $S(\mathbf{I},\mathbf{n})$ are given by

$$pS(\mathbf{n}) = \left\{ \prod_{i=1}^{nT} \left[\int_{t_{i-1}}^{t_i} \lambda(t)dt \right]^{n(i)} / n(i)! \right\} \exp\left[-\int_{t_0}^{t_{nT}} \lambda(t)dt \right] \tag{2.3-1}$$

and

$$pS(\mathbf{I},\mathbf{n}) = \left[\prod_{j=1}^{nBH} pL_{\ell(j)} \right] pS(\mathbf{n}), \tag{2.3-2}$$

where $\mathbf{n}$ and $\mathbf{I}$ are defined in Eqs. 2.2-5 and 2.2-8, respectively, and pL_ℓ is the probability that a randomly placed borehole through a waste panel will encounter waste of activity level ℓ. Examples of probabilities $pS(\mathbf{n})$ calculated as shown in Eq. 2.3-1 are given in Section 2.5.

The probabilities $pS^{+-}(t_{i-1},t_i)$ and $pS^{+-}(\mathbf{I};t_{i-1},t_i)$ for the computational scenarios $S^{+-}(t_{i-1},t_i)$ and $S^{+-}(\mathbf{I};t_{i-1},t_i)$ are given by

$$pS^{+-}(t_{i-1},t_i) \triangleq \sum_{\ell=1}^{nP} \left\{ 1 - \exp\left[-\int_{t_{i-1}}^{t_i} \alpha_\ell(t)dt \right] \right\} \left\{ 1 - \exp\left[-\int_{t_{i-1}}^{t_i} \beta_\ell(t)dt \right] \right\} \tag{2.3-3}$$

and

$$pS^{+-}(\mathbf{I};t_{i-1},t_i) \triangleq \left[\prod_{j=1}^{nBH} pL_{\ell(j)} \right] pS^{+-}(t_{i-1},t_i), \tag{2.3-4}$$

where

$$\alpha_\ell(t) = [aBP_\ell]\lambda(t)/aTOT,$$

$$\beta_\ell(t) = [aTOT_\ell - aBP_\ell]\lambda(t)/aTOT,$$

aBP_ℓ = area (m^2) of pressurized brine pocket under waste panel ℓ,

$aTOT_\ell$ = total area (m^2) of waste panel ℓ,

aTOT = total area (m^2) of waste panels,

and

nP = number of waste panels.

For the 1992 WIPP performance assessment, each of the areas $aTOT_\ell$ and aBP_ℓ is assumed to be the same for all waste panels. This assumption is conservative in the sense that it increases the probability of E1E2-type scenarios as defined in Eq. 2.2-4 as the probability of the necessary pattern of drilling intrusions is zero for a waste panel that is underlain by no pressurized brine pocket or entirely underlain by a pressurized brine pocket.

The relations appearing in Eqs. 2.3-1 through 2.3-4 are derived in Chapter 5 of Volume 2 of this report and also in Helton (1993a) under the assumption that drilling intrusions follow a Poisson process (i.e., are random in time and space).

2.4 Calculation of Scenario Consequences

As indicated in Figure 2.4-1, the following nine computer models were used to estimate scenario consequences in the 1992 WIPP performance assessment: CUTTINGS, BRAGFLO, PANEL, SECO2D, SECOTP, GRASP-INV, CCDFPERM, GENII-S and SANCHO. Brief descriptions of these models are given in Table 2.4-1. More detailed descriptions of some of these models and their use in the 1992 WIPP performance assessment are provided in Chapters 4 through 7 and in additional references indicated in Table 2.4-1.

There are too many computational scenarios (e.g., $S(\mathbf{n})$ and $S(\mathbf{l},\mathbf{n})$) to perform a detailed calculation for each scenario with the models summarized in Table 2.4-1. For example, 3003 scenarios of the form $S(\mathbf{n})$ are required to reach a cumulative probability of 0.9994 when $\lambda = 3.28 \times 10^{-4}$ yr^{-1} and five time intervals of length 2000 yr are used (Helton et al., 1992, Table 2.3-1).

Construction of a CCDF for comparison against the EPA release limits requires the estimation of cumulative probability through at least the 0.999 level. Thus, depending on the value for the rate λ in the Poisson model for drilling intrusions, this may require the inclusion of computational scenarios involving as many as 10 to 12 drilling intrusions, which results in a total of several thousand computational scenarios. Further, this number does not include the effects of different activity levels in the waste. To obtain results for such a large number of computational scenarios, it is necessary to plan and implement the overall calculations very carefully. The following describes the approach used in the 1992 WIPP performance assessment (Helton and Iuzzolino, 1993).

As indicated in Eq. 2.2-2, the 10,000-yr time interval that must be considered in the construction of CCDFs for comparison with the EPA release limits is divided into disjoint subintervals $[t_{i-1}, t_i]$, $i = 1, 2, \ldots, nT$, in the definition of computational scenarios. The following results can be calculated for each time interval:

rC_i = EPA normalized release to the surface environment for cuttings removal due to a single borehole in time interval i with the assumption that the waste is homogeneous (i.e., waste of different activity levels is not present), (2.4-1)

rC_{ij} = EPA normalized release to the surface environment for cuttings removal due to a single borehole in time interval i that penetrates waste of activity level j, (2.4-2)

$rGW1_i$ = EPA normalized release to the accessible environment due to groundwater transport initiated by a single borehole in time interval i (i.e., an E2-type scenario), (2.4-3)

$rGW2_i$ = EPA normalized release to the accessible environment due to groundwater transport initiated by two boreholes in the same waste panel in time interval i, of which one penetrates a pressurized brine pocket and one does not (i.e., an E1E2-type scenario), (2.4-4)

with the assumption that the intrusions occur at the midpoints of the time intervals (e.g., at 1000 yr for the time interval [0, 2000 yr]). For the calculation of $rGW1_i$ and $rGW2_i$ in the 1992 WIPP performance assessment, the accessible environment is assumed to begin 2.65 km from the center of the waste panels (i.e., at the land-withdrawal boundary as shown in Figure 1-2 of Volume 1 of this report).

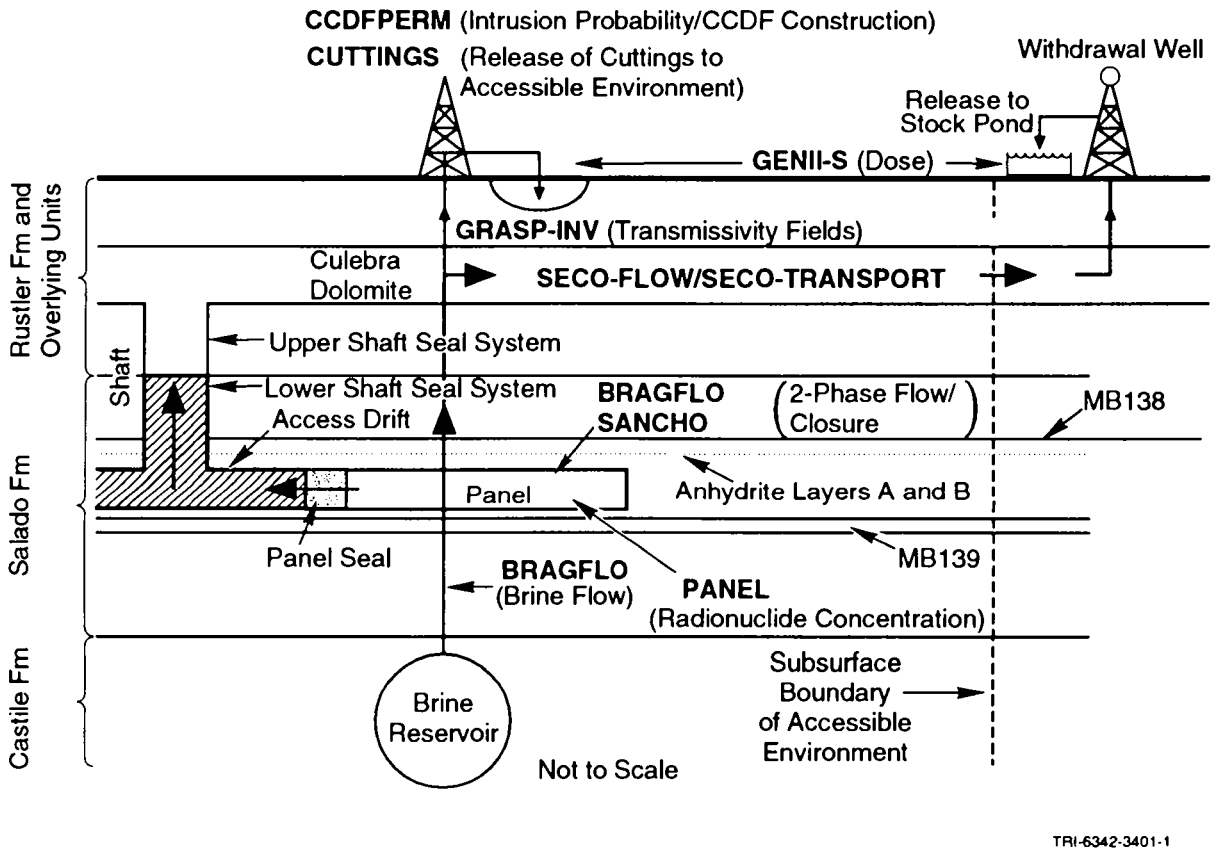

Figure 2.4-1. Models used in 1992 WIPP performance assessment to calculate scenario consequences. The names for computer models (i.e., computer codes) are shown in capital letters.

Table 2.4-1. Summary of Computer Models Used in the 1992 WIPP Performance Assessment to Calculate Scenario Consequences

Model	Description
BRAGFLO	Describes the multiphase flow of gas and brine through a porous, heterogenous reservoir. BRAGFLO solves simultaneously the coupled partial differential equations that describe the mass conservation of gas and brine along with appropriate constraint equations, initial conditions, and boundary conditions. Additional information: Chapters 4 and 5.
CCDFPERM	Constructs probabilities and consequences for various computational scenarios associated with human intrusion by exploratory drilling. Also constructs CCDFS. Additional information: Section 1.4.2 of Volume 3 and Helton and Iuzzolino, 1993.
CUTTINGS	Calculates the quantity of radioactive material brought to the surface in cuttings and cavings generated by an exploratory borehole that penetrates a waste panel. Additional information: Chapter 7.
GENII-S	Estimates potential radiation doses to humans from radionuclides in the environment. Additional information: Leigh et al., 1993.
GRASP-INV	Generates transmissivity fields (estimates of transmissivity values) conditioned on measured transmissivity values and calibrated to steady-state and transient pressure data at well locations using an adjoint sensitivity and pilot-point technique. Additional information: LaVenue and RamaRao, 1992.
PANEL	Calculates rate of discharge and cumulative discharge of radionuclides from a repository panel through an intrusion borehole. Discharge is a function of fluid flow rate, elemental solubility, and radionuclide inventory. Additional information: WIPP PA Division 1991b, Section 5.3.
SECO-FLOW	Calculates single-phase Darcy flow for groundwater-flow problems in two dimensions. The formulation is based on a single partial differential equation for hydraulic head using fully implicit time differencing. Additional information: Chapter 6.
SECO-TRANSPORT	Simulates fluid flow and transport of radionuclides in fractured porous media. Additional information: Chapter 6.
SANCHO	Solves quasistatic, large deformation, inelastic response of two-dimensional solids with finite element techniques. Used in the 1992 performance assessment to determine porosity of the waste as a function of time and cumulative gas generation. Additional information: Section 1.4.7 of Volume 3, Stone et al., 1985.

In general, rC_i, rC_{ij}, $rGW1_i$ and $rGW2_i$ will be vectors containing a large variety of information; however, for notational simplicity, a vector representation will not be used. For the 1992 WIPP performance assessment, the cuttings release to the accessible environment (i.e., rC_i and rC_{ij}) is determined by the CUTTINGS program, and the groundwater release to the accessible environment (i.e., $rGW1_i$ and $rGW2_i$) is determined through a sequence of linked calculations involving the BRAGFLO, PANEL, SECO-FLOW and SECO-TRANSPORT programs.

The cuttings releases

$$rC_1, rC_2, \ldots, rC_{nT} \tag{2.4-5}$$

correspond to the cuttings releases associated with the computational scenarios

$$S(1,0,\ldots,0), S(0,1,\ldots,0), \ldots, S(0,0,\ldots,1) \tag{2.4-6}$$

under the assumption that all waste is of the same average activity level. Similarly, the groundwater releases

$$rGW1_1, rGW1_2, \ldots, rGW1_{nT} \tag{2.4-7}$$

correspond to the groundwater releases associated with the preceding five scenarios, while

$$rGW2_1, rGW2_2, \ldots, rGW2_{nT} \tag{2.4-8}$$

correspond to the groundwater releases associated with the computational scenarios

$$S^{+-}(2,0,\ldots,0),\ S^{+-}(0,2,\ldots,0),\ \ldots,\ S^{+-}(0,0,\ldots,2). \tag{2.4-9}$$

In like manner, rC_{1j} corresponds to the cuttings release associated with the computational scenario $S(j;\ 1,0,\ldots,0)$; rC_{2j} corresponds to the cuttings release associated with $S(j;\ 0,1,\ldots,0)$, and so on.

The releases rC_i, rC_{ij}, $rGW1_i$ and $rGW2_i$ are used to construct the releases associated with the many individual computational scenarios that are used in the construction of a CCDF for comparison with the EPA release limits. The following assumptions are made:

(1) With the exception of E1E2-type scenarios, no synergistic effects result from multiple boreholes, and thus, the total release for a scenario involving multiple intrusions can be obtained by adding the releases associated with the individual intrusions.

(2) An E1E2-type scenario can take place only when the necessary boreholes occur within the same time interval $[t_{i-1}, t_i]$.

(3) An E1E2-type scenario involving more than two boreholes will have the same subsurface release as an E1E2-type scenario involving exactly two boreholes.

The preceding assumptions are used to construct the releases for individual computational scenarios.

For cuttings removal, Assumption (1) is the only pertinent assumption. As the only release associated with cuttings removal is the direct removal of cuttings and spallings to the surface, this assumption seems reasonable; the relatively small cross-sectional area intersected by a drilling intrusion makes the interaction of two or more drilling intrusions very unlikely. Further, should such an intersection occur, the assumption is conservative in the sense that it would tend to overestimate the total size of the release. For E2-type scenarios, Assumption (1) is again the only pertinent assumption. When one, and only one intrusion occurs into each of several waste panels, this assumption seems to be appropriate as there is little reason to believe that the release taking place from one waste panel would affect the release taking place from another waste panel. If anything, the assumption in this case would be conservative due to the limited amount of brine in the region surrounding the waste panels that is available for the potential transport of radionuclides up an intruding borehole; specifically, a single borehole may experience more brine flow than each of several boreholes. For several drilling intrusions into the same waste panel, Assumption (1) is probably conservative due to the limited amount of brine available for radionuclide transport and the possible inventory limits on the releases of some radionuclides. Assumptions (2) and (3) relate to E1E2-type scenarios. Assumption (2) places a limit on how far apart in time two drilling intrusions can occur and still give rise to an E1E2-type scenario. Such a limitation seems reasonable due to both the plugging of boreholes by natural processes and the depletion of the brine in a pressurized brine pocket. If anything, the relatively long time intervals (e.g., 2000 yrs) used in the WIPP performance assessment in conjunction with this assumption lead to overestimates of the probability of E1E2-type scenarios. Further, given this assumption, the relationships used in the WIPP performance assessment tend to overestimate the probability of an E1E2-type scenario. Assumption (3) should have a neutral effect on the analysis as multiple drilling intrusions do not

affect the amount of brine available for radionuclide transport up the intruding boreholes and the effect of the increased borehole cross-sectional area is small compared to the uncertainties that result from borehole permeability and elemental solubilities.

The normalized releases rC_i, rC_{ij} and $rGWl_i$ can be used to construct the EPA normalized releases for the scenarios $S(\mathbf{n})$ and $S(\mathbf{l},\mathbf{n})$. For $S(\mathbf{n})$, the normalized release to the accessible environment, $cS(\mathbf{n})$, can be approximated by

$$cS(\mathbf{n}) = \sum_{j=1}^{nBH} (rC_{m(j)} + rGWl_{m(j)}), \tag{2.4-10}$$

where m(j) designates the time interval in which the j^{th} borehole occurs. The vector

$$\mathbf{m} = [m(1), m(2), \ldots, m(nBH)] \tag{2.4-11}$$

is uniquely determined once the vector $\mathbf{n}$ appearing in the definition of $S(\mathbf{n})$ is specified. The definition of $S(\mathbf{n})$ in Eq. 2.2-3 contains no information on the activity levels encountered by the individual boreholes, and so $cS(\mathbf{n})$ was constructed with the assumption that all waste is of the same average activity. However, the definition of $S(\mathbf{l},\mathbf{n})$ in Eq. 2.2-6 does contain information on activity levels, and the associated normalized release to the accessible environment, $cS(\mathbf{l},\mathbf{n})$, can be approximated by

$$cS(\mathbf{l},\mathbf{n}) = \sum_{j=1}^{nBH} \left[rC_{m(j),\ell(j)} + rGWl_{m(j)} \right], \tag{2.4-12}$$

which does incorporate the activity levels encountered by the individual boreholes.

For $S^{+-}(t_{i-1},t_i)$, the normalized release to the accessible environment, $cS^{+-}(t_{i-1},t_i)$, can be approximated by

$$cS^{+-}(t_{i-1},t_i) = 2\, rC_i + rGW2_i, \tag{2.4-13}$$

where it is assumed that all waste is of the same average activity for cuttings removal. Similarly, the normalized release $cS^{+-}(\mathbf{I};t_{i-1},t_i)$ for $S^{+-}(\mathbf{I};t_{i-1},t_i)$ can be approximated by

$$cS^{+-}(\mathbf{I};t_{i-1},t_i) = \sum_{j=1}^{2} rC_{i,\ell(j)} + rGW2_i, \qquad (2.4\text{-}14)$$

which incorporates the activity level of the waste. The approximations for $cS^{+-}(t_{i-1},t_i)$ and $cS^{+-}(\mathbf{I};t_{i-1},t_i)$ in Eqs. 2.4-13 and 2.4-14 are based on exactly two intrusions in the time interval $[t_{i-1},t_i]$. More complicated expressions could be developed to define releases for multiple E1E2-type intrusions. However, due to the low probability of such patterns of intrusion (e.g., the probabilities for 2 and ≥2 boreholes in Table 2-6 of WIPP PA Division (1991b) for the time interval [0,2000 yr] with 100 yr of administrative control are 0.009022 and 0.009315, respectively), the use of such expressions would have little impact on the CCDFs used for comparison with the EPA release limits.

The construction process shown in Eqs. 2.4-10 and 2.4-13 to obtain the normalized releases $cS(\mathbf{n})$and $cS^{+-}(t_{i-1},t_i)$ for scenarios $S(\mathbf{n})$ and $S^{+-}(t_{i-1},t_i)$ is illustrated in Table 3-4 of Volume 3. Further, the construction process shown in Eqs. 2.4-12 and 2.4-14 to obtain normalized releases $cS(\mathbf{I},\mathbf{n})$ and $cS^{+-}(\mathbf{I};t_{i-1},t_i)$ for scenarios $S(\mathbf{I},\mathbf{n})$ and $S^{+-}(\mathbf{I};t_{i-1},t_i)$ is illustrated in Table 3-5 of Volume 3.

2.5 Performance Assessment Representations Used in 1992

As discussed in conjunction with Eq. 2.1-1, the outcome of a performance assessment can be represented by a set R of ordered triples. Sections 2.2, 2.3 and 2.4 provide general descriptions of the manner in which the individual elements of these triples are defined in the 1992 WIPP performance assessment. Due to computational constraints and the desire to present results obtained with different modeling assumptions, the set R is actually defined in two different ways in the 1992 WIPP performance assessment.

The computational cost of performing groundwater transport calculations precluded the consideration of a large number of intrusion times in the 1992 WIPP performance assessment. Specifically, the decision was made to consider intrusions at only a single time (i.e., 1000 yr) for the initiation of groundwater transport. A relatively early intrusion time was selected because of the reduced releases that occur for later intrusion times due to both increased radioactive decay and reduced time for groundwater transport

to the accessible environment. This decision led to scenarios defined on the basis of the time intervals [0, 2000 yr] and [2000, 10,000 yr], with the rate term (i.e., $\lambda(t)$) in the Poisson model for drilling intrusions assumed to be zero after 2000 yr. This definition produced a set R_1 defined by

$$R_1 = \{(S_i, pS_i, \mathbf{cS}_i), i=1,\ldots, nS\}, \tag{2.5-1}$$

where the intervals indicated in Eq. 2.2-2 are

$$[0, 2000 \text{ yr}], [2000, 10{,}000 \text{ yr}] \tag{2.5-2}$$

and the vector $\mathbf{n}$ appearing in Eq. 2.2-5 is of the form

$$\mathbf{n} = [n(1), n(2)]. \tag{2.5-3}$$

The scenarios $S(\mathbf{n})$, $S^{+-}(t_{i-1}, t_i)$, $S(\mathbf{l},\mathbf{n})$ and $S^{+-}(\mathbf{l}; t_{i-1}, t_i)$ in Eqs. 2.2-3, 2.2-4, 2.2-6 and 2.2-7 are then defined accordingly.

As already indicated, the rate term $\lambda(t)$ in the Poisson model for drilling intrusions is assumed to be zero for $t > 2000$ yr. With this assumption, the expressions in Eqs. 2.3-1 and 2.3-3 for scenario probability become

$$pS(n(1),n(2)) = \begin{cases} \{[\int_0^{2000} \lambda(t)dt]^{n(1)}/n(1)!\}\exp[-\int_0^{2000} \lambda(t)dt] & \text{if } n(2) = 0 \\ 0 & \text{if } n(2) \neq 0 \end{cases} \tag{2.5-4}$$

and

$$pS^{+-}(t_{i-1},t_i) \doteq \begin{cases} \sum_{\ell=1}^{nP} \{1-\exp[-\int_0^{2000} \alpha_\ell(t)dt]\}\{1-\exp[-\int_0^{2000} \beta_\ell(t)dt]\} & \text{if } i = 1 \\ 0 & \text{if } i = 2 \end{cases}, \tag{2.5-5}$$

respectively. As a reminder, the assumption of 100 yr of administrative control in which no drilling intrusions can occur is equivalent to assuming that $\lambda(t) = 0$ for $0 \leq t \leq 100$ yr. Thus, the assumptions of 100 yr of administrative control and a constant value λ for $\lambda(t)$ in the time interval [100, 2000 yr] leads to the scenario probabilities

$$pS(n(1),n(2)) = \begin{cases} [(1900\ \lambda)^{n(1)}/n(1)!]\exp[-1900\lambda] & \text{if } n(2) = 0 \\ 0 & \text{if } n(2) \neq 0 \end{cases} \quad (2.5\text{-}6)$$

and

$$pS^{+-}(t_{i-1},t_i) \doteq \begin{cases} \sum_{\ell=1}^{nP} (1-\exp[-1900\ \alpha_\ell])(1-\exp[-1900\ \beta_\ell]) & \text{if } i = 1 \\ 0 & \text{if } i = 2 \end{cases}, \quad (2.5\text{-}7)$$

where α_ℓ and β_ℓ are defined in conjunction with Eq. 2.3-3 with $\lambda(t) = \lambda$. Examples of the scenario probabilities pS(n(1),n(2)) defined in Eqs. 2.5-4 and 2.5-6 are given in Tables 2.5-1 and 2.5-2, respectively. Further, the time-dependent λ used in the determination of the probabilities in Table 2.5-1 is based on the time-dependent drilling rate shown in Figure 2.5-1. In particular, the drilling rate in Figure 2.5-1 is expressed in units of drilling intrusions per square kilometer per 10,000 yr (i.e., $1/(km^2 \times 10^4$ yr) or $(km^2 \times 10^4\ yr)^{-1}$). As used in this report, λ has units of drilling intrusions per year (i.e., 1/yr or yr^{-1}) and is obtained by multiplying the drilling rate in Figure 2.5-1 by 0.126 km^2 and performing the indicated division by 10^4 where 0.126 km^2 is the area of emplaced waste used in the 1992 WIPP performance assessment.

The scenario consequences $\mathbf{cS}_i$ for R_1 appearing in Eq. 2.5-1 are constructed as shown in Eqs. 2.4-10 through 2.4-14 for the scenarios S_i that have nonzero probabilities.

Once R_1 is determined, the information contained in the probabilities pS_i and consequences $\mathbf{cS}_i$ can be summarized in CCDFs as shown in Figure 2.1-1. The set R_1 and its associated CCDFs are determined with the assumption that $\lambda(t)=0$ for $t > 2{,}000$ yr. Except for small effects due to the approximations used for the probabilities of the scenarios $S^{+-}(0, 2000)$ and $S^{+-}(2000, 10{,}000)$, the same CCDFs result when $\lambda(t)$ is unchanged (i.e., $\lambda(t)$ is not set to 0 for $t > 2000$ yr) but the environmental releases rC_2, rC_{2j}, rGW_2 and $rGW2_2$ for intrusions in the time interval [2000, 10,000 yr] are set to 0.

The calculation of releases to the accessible environment due to cuttings removal was significantly less computationally demanding than the calculation of releases due to groundwater transport. As a result, the decision was made to consider the effects of cuttings removal at a sequence of intrusion times rather than only at the single intrusion time considered

Table 2.5-1. Probabilities for Scenarios Involving Multiple Intrusions over 10,000 yr for the Time-Dependent λ Shown in Figure 2.5-1, 100 yr Administrative Control, and the Time Intervals [0, 2000 yr], [2000, 10,000 yr]. The scenarios shown in this table are contained in the set R_1 defined in Eq. 2.5-1.

Scenario[a]	Prob with $\lambda \neq 0$[b]	Prob with $\lambda \to 0$[c]
	0 intrusions	
	(# Scenarios = 1)	
$S(0,0)$	8.703E-01	9.863E-01
Prob 0 intr[d]	8.703E-01	9.863E-01
Cum Prob[e]	8.703E-01	9.863E-01
	1 intrusions	
	(# Scenarios = 2)	
$S(1,0)$	1.199E-02	1.358E-02
$S(0,1)$	1.090E-01	0.000E+00
Prob 1 intr	1.209E-01	1.358E-02
Cum Prob	9.912E-01	9.999E-01
	2 intrusions	
	(# Scenarios = 3)	
$S(2,0)$	8.253E-05	9.353E-05
$S(1,1)$	1.500E-03	0.000E+00
$S(0,2)$	6.820E-03	0.000E+00
Prob 2 intr	8.403E-03	9.353E-05
Cum Prob	9.996E-01	1.000E+00
	3 intrusions	
	(# Scenarios = 4)	
$S(3,0)$	3.789E-07	4.294E-07
$S(2,1)$	1.033E-05	0.000E+00
$S(1,2)$	9.392E-05	0.000E+00
$S(0,3)$	2.846E-04	0.000E+00
Prob 3 intr	3.892E-04	4.294E-07
Cum Prob	1.000E+00	1.000E+00
	4 intrusions	
	(# Scenarios = 5)	
$S(4,0)$	1.304E-09	1.478E-09
$S(3,1)$	4.743E-08	0.000E+00
$S(2,2)$	6.467E-07	0.000E+00
$S(1,3)$	3.919E-06	0.000E+00
$S(0,4)$	8.907E-06	0.000E+00
Prob 4 intr	1.352E-05	1.478E-09
Cum Prob	1.000E+00	1.000E+00
	5 intrusions	
	(# Scenarios = 6)	
$S(5,0)$	3.593E-12	4.072E-12
$S(4,1)$	1.633E-10	0.000E+00
$S(3,2)$	2.969E-09	0.000E+00
$S(2,3)$	2.699E-08	0.000E+00
$S(1,4)$	1.227E-07	0.000E+00
$S(0,5)$	2.230E-07	0.000E+00
Prob 5 intr	3.758E-07	4.072E-12
Cum Prob	1.000E+00	1.000E+00
	6 intrusions	
	(# Scenarios = 7)	
$S(6,0)$	8.246E-15	9.346E-15
$S(5,1)$	4.498E-13	0.000E+00
$S(4,2)$	1.022E-11	0.000E+00
$S(3,3)$	1.239E-10	0.000E+00
$S(2,4)$	8.447E-10	0.000E+00
$S(1,5)$	3.072E-09	0.000E+00
$S(0,6)$	4.654E-09	0.000E+00
Prob 6 intr	8.704E-09	9.346E-15
Cum Prob	1.000E+00	1.000E+00

[a] $S(i,j)$ represents the scenario in which i and j drilling intrusions occur in the time intervals [0, 2000 yr], and [2000, 10,000 yr], respectively.
[b] Scenario probability calculated with $\lambda \neq 0$ over the time interval [100, 10,000 yr].
[c] Scenario probability calculated with $\lambda \neq 0$ over the time interval [100, 2000 yr] and $\lambda = 0$ over the time interval [2000, 10,000 yr].
[d] Probability of indicated number of intrusions.
[e] Cumulative probability for all scenarios.

Table 2.5-1. Probabilities for Scenarios Involving Multiple Intrusions over 10,000 yr for the Time-Dependent λ Shown in Figure 2.5-1, 100 yr Administrative Control, and the Time Intervals [0, 2000 yr], [2000, 10,000 yr]. The scenarios shown in this table are contained in the set R_1 defined in Eq. 2.5-1. (concluded)

Scenario[a]	Prob with $\lambda \neq 0$[b]	Prob with $\lambda \rightarrow 0$[c]
	7 intrusions (# Scenarios = 8)	
S(7,0)	1.622E-17	1.839E-17
S(6,1)	1.032E-15	0.000E+00
S(5,2)	2.815E-14	0.000E+00
S(4,3)	4.266E-13	0.000E+00
S(3,4)	3.878E-12	0.000E+00
S(2,5)	2.115E-11	0.000E+00
S(1,6)	6.409E-11	0.000E+00
S(0,7)	8.323E-11	0.000E+00
Prob 7 intr	1.728E-10	1.839E-17
Cum Prob	1.000E+00	1.000E+00
	8 intrusions (# Scenarios = 9)	
S(8,0)	2.793E-20	3.165E-20
S(7,1)	2.031E-18	0.000E+00
S(6,2)	6.462E-17	0.000E+00
S(5,3)	1.175E-15	0.000E+00
S(4,4)	1.335E-14	0.000E+00
S(3,5)	9.709E-14	0.000E+00
S(2,6)	4.413E-13	0.000E+00
S(1,7)	1.146E-12	0.000E+00
S(0,8)	1.302E-12	0.000E+00
Prob 8 intr[d]	3.002E-12	3.165E-20
Cum Prob[e]	1.000E+00	1.000E+00
	9 intrusions (# Scenarios = 10)	
S(9,0)	4.274E-23	4.844E-23
S(8,1)	3.497E-21	0.000E+00
S(7,2)	1.271E-19	0.000E+00
S(6,3)	2.697E-18	0.000E+00
S(5,4)	3.677E-17	0.000E+00
S(4,5)	3.343E-16	0.000E+00
S(3,6)	2.026E-15	0.000E+00
S(2,7)	7.893E-15	0.000E+00
S(1,8)	1.794E-14	0.000E+00
S(0,9)	1.812E-14	0.000E+00
Prob 9 intr	4.635E-14	4.844E-23
Cum Prob	1.000E+00	1.000E+00
	10 intrusions (# Scenarios = 11)	
S(10,0)	5.886E-26	6.671E-26
S(9,1)	5.350E-24	0.000E+00
S(8,2)	2.189E-22	0.000E+00
S(7,3)	5.306E-21	0.000E+00
S(6,4)	8.440E-20	0.000E+00
S(5,5)	9.207E-19	0.000E+00
S(4,6)	6.975E-18	0.000E+00
S(3,7)	3.623E-17	0.000E+00
S(2,8)	1.235E-16	0.000E+00
S(1,9)	2.495E-16	0.000E+00
S(0,10)	2.268E-16	0.000E+00
Prob 10 intr	6.441E-16	6.671E-26
Cum Prob	1.000E+00	1.000E+00

[a] S(i,j) represents the scenario in which i and j drilling intrusions occur in the time intervals [0, 2000 yr], and [2000, 10,000 yr], respectively.
[b] Scenario probability calculated with $\lambda \neq 0$ over the time interval [100, 10,000 yr].
[c] Scenario probability calculated with $\lambda \neq 0$ over the time interval [100, 2000 yr] and $\lambda = 0$ over the time interval [2000, 10,000 yr].
[d] Probability of indicated number of intrusions.
[e] Cumulative probability for all scenarios.

Table 2.5-2. Probabilities for Scenarios Involving Multiple Intrusions over 10,000 yr for $\lambda = 3.78 \times 10^{-4}$ yr^{-1}, 100 yr Administrative Control, and the Time Intervals [0, 2000 yr], [2000, 10,000 yr]. The scenarios shown in this table are contained in the set R_1 defined in Eq. 2.5-1, and $\lambda = 3.78 \times 10^{-4}$ yr^{-1} is the largest drilling rate considered in the 1992 WIPP PA.

Scenario[a]	Prob with $\lambda \neq 0$[b]	Prob with $\lambda \rightarrow 0$[c]
	0 intrusions	
	(# Scenarios = 1)	
$S(0,0)$	2.378E-02	4.879E-01
Prob 0 intr[d]	2.378E-02	4.879E-01
Cum Prob[e]	2.378E-02	4.879E-01
	1 intrusions	
	(# Scenarios = 2)	
$S(1,0)$	1.707E-02	3.501E-01
$S(0,1)$	7.185E-02	0.000E+00
Prob 1 intr	8.892E-02	3.501E-01
Cum Prob	1.127E-01	8.381E-01
	2 intrusions	
	(# Scenarios = 3)	
$S(2,0)$	6.123E-03	1.256E-01
$S(1,1)$	5.156E-02	0.000E+00
$S(0,2)$	1.085E-01	0.000E+00
Prob 2 intr	1.662E-01	1.256E-01
Cum Prob	2.789E-01	9.637E-01
	3 intrusions	
	(# Scenarios = 4)	
$S(3,0)$	1.464E-03	3.004E-02
$S(2,1)$	1.850E-02	0.000E+00
$S(1,2)$	7.789E-02	0.000E+00
$S(0,3)$	1.093E-01	0.000E+00
Prob 3 intr	2.072E-01	3.004E-02
Cum Prob	4.861E-01	9.937E-01
	4 intrusions	
	(# Scenarios = 5)	
$S(4,0)$	2.627E-04	5.390E-03
$S(3,1)$	4.424E-03	0.000E+00
$S(2,2)$	2.794E-02	0.000E+00
$S(1,3)$	7.844E-02	0.000E+00
$S(0,4)$	8.257E-02	0.000E+00
Prob 4 intr	1.936E-01	5.390E-03
Cum Prob	6.797E-01	9.991E-01
	5 intrusions	
	(# Scenarios = 6)	
$S(5,0)$	3.770E-05	7.735E-04
$S(4,1)$	7.937E-04	0.000E+00
$S(3,2)$	6.683E-03	0.000E+00
$S(2,3)$	2.814E-02	0.000E+00
$S(1,4)$	5.924E-02	0.000E+00
$S(0,5)$	4.989E-02	0.000E+00
Prob 5 intr	1.448E-01	7.735E-04
Cum Prob	8.245E-01	9.999E-01
	6 intrusions	
	(# Scenarios = 7)	
$S(6,0)$	4.508E-06	9.250E-05
$S(5,1)$	1.139E-04	0.000E+00
$S(4,2)$	1.199E-03	0.000E+00
$S(3,3)$	6.731E-03	0.000E+00
$S(2,4)$	2.126E-02	0.000E+00
$S(1,5)$	3.580E-02	0.000E+00
$S(0,6)$	2.512E-02	0.000E+00
Prob 6 intr	9.022E-02	9.250E-05
Cum Prob	9.147E-01	1.000E+00

[a] $S(i,j)$ represents the scenario in which i and j drilling intrusions occur in the time intervals [0, 2000 yr] and [2000, 10,000 yr], respectively.
[b] Scenario probability calculated with $\lambda = 3.78 \times 10^{-4}$ yr^{-1} over the time interval [100, 10,000 yr].
[c] Scenario probability calculated with $\lambda = 3.78 \times 10^{-4}$ yr^{-1} over the time interval [100, 2000 yr] and $\lambda = 0$ over the time interval [2000, 10,000 yr].
[d] Probability of indicated number of intrusions.
[e] Cumulative probability for all scenarios.

Table 2.5-2. Probabilities for Scenarios Involving Multiple Intrusions over 10,000 yr for $\lambda = 3.78 \times 10^{-4}$ yr^{-1}, 100 yr Administrative Control, and the Time Intervals [0, 2000 yr], [2000, 10,000 yr]. The scenarios shown in this table are contained in the set R_1 defined in Eq. 2.5-1, and $\lambda = 3.78 \times 10^{-4}$ yr^{-1} is the largest drilling rate considered in the 1992 WIPP PA. (concluded)

Scenario[a]	Prob with $\lambda \neq 0$[b]	Prob with $\lambda \to 0$[c]
	7 intrusions	
	(# Scenarios = 8)	
S(7,0)	4.621E-07	9.482E-06
S(6,1)	1.362E-05	0.000E+00
S(5,2)	1.721E-04	0.000E+00
S(4,3)	1.207E-03	0.000E+00
S(3,4)	5.084E-03	0.000E+00
S(2,5)	1.284E-02	0.000E+00
S(1,6)	1.803E-02	0.000E+00
S(0,7)	1.084E-02	0.000E+00
Prob 7 intr	4.819E-02	9.482E-06
Cum Prob	9.629E-01	1.000E+00
	8 intrusions	
	(# Scenarios = 9)	
S(8,0)	4.145E-08	8.504E-07
S(7,1)	1.396E-06	0.000E+00
S(6,2)	2.058E-05	0.000E+00
S(5,3)	1.733E-04	0.000E+00
S(4,4)	9.120E-04	0.000E+00
S(3,5)	3.072E-03	0.000E+00
S(2,6)	6.467E-03	0.000E+00
S(1,7)	7.780E-03	0.000E+00
S(0,8)	4.095E-03	0.000E+00
Prob 8 intr[d]	2.252E-02	8.504E-07
Cum Prob[e]	9.854E-01	1.000E+00
	9 intrusions	
	(# Scenarios = 10)	
S(9,0)	3.305E-09	6.780E-08
S(8,1)	1.252E-07	0.000E+00
S(7,2)	2.109E-06	0.000E+00
S(6,3)	2.072E-05	0.000E+00
S(5,4)	1.309E-04	0.000E+00
S(4,5)	5.511E-04	0.000E+00
S(3,6)	1.547E-03	0.000E+00
S(2,7)	2.791E-03	0.000E+00
S(1,8)	2.938E-03	0.000E+00
S(0,9)	1.375E-03	0.000E+00
Prob 9 intr	9.356E-03	6.780E-08
Cum Prob	9.948E-01	1.000E+00
	10 intrusions	
	(# Scenarios = 11)	
S(10,0)	2.371E-10	4.865E-09
S(9,1)	9.985E-09	0.000E+00
S(8,2)	1.892E-07	0.000E+00
S(7,3)	2.124E-06	0.000E+00
S(6,4)	1.565E-05	0.000E+00
S(5,5)	7.908E-05	0.000E+00
S(4,6)	2.775E-04	0.000E+00
S(3,7)	6.676E-04	0.000E+00
S(2,8)	1.054E-03	0.000E+00
S(1,9)	9.863E-04	0.000E+00
S(0,10)	4.153E-04	0.000E+00
Prob 10 intr	3.498E-03	4.865E-09
Cum Prob	9.983E-01	1.000E+00

[a] S(i,j) represents the scenario in which i and j drilling intrusions occur in the time intervals [0, 2000 yr] and [2000, 10,000 yr], respectively.
[b] Scenario probability calculated with $\lambda = 3.78 \times 10^{-4}$ yr^{-1} over the time interval [100, 10,000 yr].
[c] Scenario probability calculated with $\lambda = 3.78 \times 10^{-4}$ yr^{-1} over the time interval [100, 2000 yr] and $\lambda = 0$ over the time interval [2000, 10,000 yr].
[d] Probability of indicated number of intrusions.
[e] Cumulative probability for all scenarios.

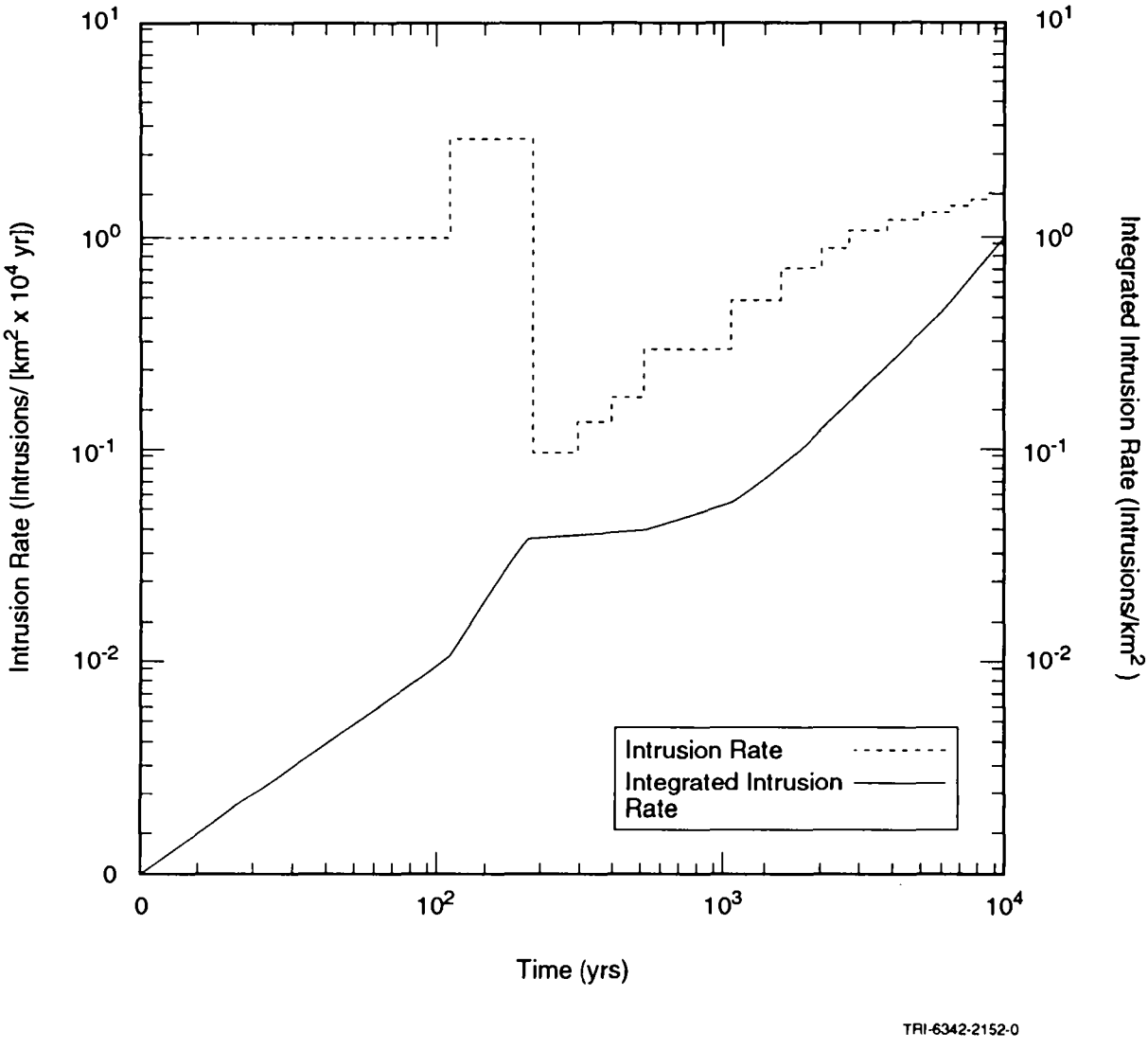

Figure 2.5-1. Example time-dependent rate term used in Poisson model for drilling intrusions in the 1992 WIPP performance assessment (Volume 3, Appendix D, Figure D-45). The rate $\lambda(t)$ as used in this chapter has units of yr^{-1} and is obtained by multiplying the rate indicated in this figure by 0.126 km^2 (i.e., the area of emplaced waste) and performing the indicated division by 10^4; further, $\lambda(t)$ is set to zero for the first 100 yrs when 100 yrs of administrative control is assumed. The rate $\lambda(t)$ was a sampled variable in the 1992 WIPP performance assessment; this figure shows the drilling rate with the largest integrated value (i.e., expected number of drilling intrusions) over 10,000 yr. In this and other similar figures, a hyperbolic sine transformation is used to generate the scales on the abscissa and ordinate; this transformation allows the plotting of zero, which is not possible when a logarithmic transformation is used.

for the initiation of groundwater transport. In particular, a set R_2 defined by

$$R_2 = \{(S_i, pS_i, \mathbf{cS}_i), i=1, \ldots, nS\} \tag{2.5-8}$$

was used in the 1992 WIPP performance assessment to investigate the effects of cuttings removal, where the time intervals indicated in Eq. 2.2-2 are

$$[0, 150 \text{ yr}], [150, 200 \text{ yr}], [200, 500 \text{ yr}], [500, 1500 \text{ yr}], [1500, 4500 \text{ yr}], [4500, 10{,}000 \text{ yr}] \tag{2.5-9}$$

and the vector $\mathbf{n}$ appearing in Eq. 2.2-5 is of the form

$$\mathbf{n} = [n(1), n(2), n(3), n(4), n(5), n(6)] \; . \tag{2.5-10}$$

The time intervals in Eq. 2.5-9 were selected to provide increased resolution at early times when the inventory of radionuclides with relatively short half lives (e.g., Pu-238 and Am-241) is changing rapidly. With the assumption of 100 yr of administrative control, the first time interval in Eq. 2.5-9 (i.e., [0, 150 yr]) effectively becomes [100, 150 yr].

The set R_2 is used to show only the effects of cuttings removal. As a result, the only scenarios used in the definition of R_2 are of the form $S(\mathbf{n})$ and $S(\mathbf{I},\mathbf{n})$ shown in Eqs. 2.2-3 and 2.2-6. The probabilities $pS(\mathbf{n})$ and $pS(\mathbf{I},\mathbf{n})$ for these scenarios with a time-dependent rate term (i.e., $\lambda(t)$) in the Poisson model for drilling intrusions are defined in Eqs. 2.3-1 and 2.3-2, respectively, with the times t_i, i=0, 1, ..., 6, equal to

$$0, 150, 200, 500, 1500, 4500, 10{,}000 \text{ yr}. \tag{2.5-11}$$

Examples of the probabilities $pS(\mathbf{n})$ calculated with the rate term shown in Figure 2.5-1 are presented in Table 2.5-3. Further, the resultant probabilities for a constant-valued λ are illustrated in Table 2.5-4.

The scenario consequences $\mathbf{cS}_i$ for R_2 appearing in Eq. 2.5-8 are constructed as shown in Eqs. 2.4-10 and 2.4-12. As R_2 is used to show only the effects of cuttings removal to the accessible environment, the term $rGWl_{m(j)}$ corresponding to the groundwater release in Eqs. 2.4-10 and 2.4-12 is assumed to equal zero.

Table 2.5-3. Probabilities for Scenarios Involving Multiple Intrusions over 10,000 yr for the Time-Dependent λ Shown in Figure 2.5-1, 100 yr Administrative Control, and the Time Intervals [0, 150 yr], [150, 200 yr], [200, 500 yr], [500, 1500 yr], [1500, 4500 yr] and [4500, 10,000 yr]. The scenarios shown in this table are contained in the set R_2 defined in Eq. 2.5-8.

Scenario[a]	Prob with $\lambda \neq 0$[b]	Prob with $\lambda \to 0$[c]
	0 intrusions	
	(# Scenarios = 1)	
S(0,0,0,0,0,0)	8.703E-01	9.863E-01
Prob 0 intr[d]	8.703E-01	9.863E-01
Cum Prob[e]	8.703E-01	9.863E-01
	1 intrusion	
	(# Scenarios = 6)	
S(1,0,0,0,0,0)	1.572E-03	1.782E-03
S(0,1,0,0,0,0)	1.572E-03	1.782E-03
S(0,0,1,0,0,0)	4.601E-04	5.215E-04
S(0,0,0,1,0,0)	4.503E-03	5.103E-03
S(0,0,0,0,1,0)	3.009E-02	4.395E-03
S(0,0,0,0,0,1)	8.273E-02	0.000E+00
Prob 1 intr	1.209E-01	1.358E-02
Cum Prob	9.912E-01	9.999E-01
	2 intrusions	
	(# Scenarios = 21)	
S(2,0,0,0,0,0)	1.420E-06	1.609E-06
S(1,1,0,0,0,0)	2.840E-06	3.219E-06
S(1,0,1,0,0,0)	8.312E-07	9.420E-07
S(1,0,0,1,0,0)	8.134E-06	9.219E-06
S(1,0,0,0,1,0)	5.436E-05	7.940E-06
S(1,0,0,0,0,1)	1.495E-04	0.000E+00
S(0,2,0,0,0,0)	1.420E-06	1.609E-06
S(0,1,1,0,0,0)	8.312E-07	9.420E-07
S(0,1,0,1,0,0)	8.134E-06	9.219E-06
S(0,1,0,0,1,0)	5.436E-05	7.940E-06
S(0,1,0,0,0,1)	1.495E-04	0.000E+00
S(0,0,2,0,0,0)	1.216E-07	1.379E-07
S(0,0,1,1,0,0)	2.381E-06	2.698E-06
S(0,0,1,0,1,0)	1.591E-05	2.324E-06
S(0,0,1,0,0,1)	4.374E-05	0.000E+00
S(0,0,0,2,0,0)	1.165E-05	1.320E-05
S(0,0,0,1,1,0)	1.557E-04	2.274E-05
S(0,0,0,1,0,1)	4.281E-04	0.000E+00
S(0,0,0,0,2,0)	5.203E-04	9.794E-06
S(0,0,0,0,1,1)	2.861E-03	0.000E+00
S(0,0,0,0,0,2)	3.933E-03	0.000E+00
Prob 2 intr	8.403E-03	9.353E-05
Cum Prob	9.996E-01	1.000E+00
	3 intrusions	
	(# Scenarios = 56)	
S(3,0,0,0,0,0)	8.550E-10	9.690E-10
S(2,1,0,0,0,0)	2.565E-09	2.907E-09
S(2,0,1,0,0,0)	7.507E-10	8.509E-10
S(2,0,0,1,0,0)	7.347E-09	8.326E-09
S(2,0,0,0,1,0)	4.910E-08	7.172E-09
S(2,0,0,0,0,1)	1.350E-07	0.000E+00
S(1,2,0,0,0,0)	2.565E-09	2.907E-09
S(1,1,1,0,0,0)	1.501E-09	1.702E-09
S(1,1,0,1,0,0)	1.469E-08	1.665E-08
S(1,1,0,0,1,0)	9.820E-08	1.434E-08
S(1,1,0,0,0,1)	2.700E-07	0.000E+00
S(1,0,2,0,0,0)	2.197E-10	2.490E-10
S(1,0,1,1,0,0)	4.300E-09	4.874E-09
S(1,0,1,0,1,0)	2.874E-08	4.198E-09
S(1,0,1,0,0,1)	7.902E-08	0.000E+00
S(1,0,0,2,0,0)	2.104E-08	2.385E-08
S(1,0,0,1,1,0)	2.813E-07	4.108E-08
S(1,0,0,1,0,1)	7.733E-07	0.000E+00
S(1,0,0,0,2,0)	9.400E-07	1.769E-08
S(1,0,0,0,1,1)	5.168E-06	0.000E+00
S(1,0,0,0,0,2)	7.104E-06	0.000E+00
S(0,3,0,0,0,0)	8.550E-10	9.690E-10
S(0,2,1,0,0,0)	7.507E-10	8.509E-10
S(0,2,0,1,0,0)	7.347E-09	8.326E-09
S(0,2,0,0,1,0)	4.910E-08	7.172E-09
S(0,2,0,0,0,1)	1.350E-07	0.000E+00
S(0,1,2,0,0,0)	2.197E-10	2.490E-10
S(0,1,1,1,0,0)	4.300E-09	4.874E-09
S(0,1,1,0,1,0)	2.874E-08	4.198E-09
S(0,1,1,0,0,1)	7.902E-08	0.000E+00

[a] S(i,j,k,l,m,n) represents the scenario in which i,j,k,l,m, and n drilling intrusions occur in the time intervals [0, 150 yr], [150, 200 yr], [200, 500 yr], and [500, 1500 yr], [1500, 4500 yr], and [4500, 10,000 yr], respectively.

[b] Scenario probability calculated with $\lambda \neq 0$ over the time interval [100, 10,000 yr].

[c] Scenario probability calculated with $\lambda \neq 0$ over the time interval [100, 2000 yr] and $\lambda = 0$ over the time interval [2000, 10,000 yr].

[d] Probability of indicated number of intrusions.

[e] Cumulative probability for all scenarios.

Table 2.5-3. Probabilities for Scenarios Involving Multiple Intrusions over 10,000 yr for the Time-Dependent λ Shown in Figure 2.5-1, 100 yr Administrative Control, and the Time Intervals [0, 150 yr], [150, 200 yr], [200, 500 yr], [500, 1500 yr], [1500, 4500 yr] and [4500, 10,000 yr]. The scenarios shown in this table are contained in the set R_2 defined in Eq. 2.5-8. (concluded)

Scenario[a]	Prob with $\lambda \neq 0$[b]	Prob with $\lambda \rightarrow 0$[c]
S(0,1,0,2,0,0)	2.104E-08	2.385E-08
S(0,1,0,1,1,0)	2.813E-07	4.108E-08
S(0,1,0,1,0,1)	7.733E-07	0.000E+00
S(0,1,0,0,2,0)	9.400E-07	1.769E-08
S(0,1,0,0,1,1)	5.168E-06	0.000E+00
S(0,1,0,0,0,2)	7.104E-06	0.000E+00
S(0,0,3,0,0,0)	2.144E-11	2.430E-11
S(0,0,2,1,0,0)	6.293E-10	7.133E-10
S(0,0,2,0,1,0)	4.206E-09	6.143E-10
S(0,0,2,0,0,1)	1.156E-08	0.000E+00
S(0,0,1,2,0,0)	6.158E-09	6.980E-09
S(0,0,1,1,1,0)	8.232E-08	1.202E-08
S(0,0,1,1,0,1)	2.263E-07	0.000E+00
S(0,0,1,0,2,0)	2.751E-07	5.178E-09
S(0,0,1,0,1,1)	1.513E-06	0.000E+00
S(0,0,1,0,0,2)	2.079E-06	0.000E+00
S(0,0,0,3,0,0)	2.009E-08	2.277E-08
S(0,0,0,2,1,0)	4.028E-07	5.883E-08
S(0,0,0,2,0,1)	1.107E-06	0.000E+00
S(0,0,0,1,2,0)	2.692E-06	5.067E-08
S(0,0,0,1,1,1)	1.480E-05	0.000E+00
S(0,0,0,1,0,2)	2.035E-05	0.000E+00
S(0,0,0,0,3,0)	5.998E-06	1.455E-08
S(0,0,0,0,2,1)	4.947E-05	0.000E+00
S(0,0,0,0,1,2)	1.360E-04	0.000E+00
S(0,0,0,0,0,3)	1.246E-04	0.000E+00
Prob 3 intr[d]	3.892E-04	4.294E-07
Cum Prob[e]	1.000E+00	1.000E+00
	4 intrusions	
	(# Scenarios = 126)	
S(4,0,0,0,0,0)	3.861E-13	4.376E-13
S(3,1,0,0,0,0)	1.545E-12	1.751E-12
.	.	.
.	.	.
.	.	.
S(1,1,1,1,0,0)	7.769E-12	8.805E-12
.	.	.
.	.	.
.	.	.
S(0,0,0,0,1,3)	4.310E-06	0.000E+00
S(0,0,0,0,0,4)	2.962E-06	0.000E+00
Prob 4 intr	1.352E-05	1.478E-09
Cum Prob	1.000E+00	1.000E+00
	5 intrusions	
	(# Scenarios = 252)	
Prob 5 intr	3.758E-07	4.072E-12
Cum Prob	1.000E+00	1.000E+00
	6 intrusions	
	(# Scenarios = 462)	
Prob 6 intr	8.704E-09	9.346E-15
Cum Prob	1.000E+00	1.000E+00
	7 intrusions	
	(# Scenarios = 792)	
Prob 7 intr	1.728E-10	1.839E-17
Cum Prob	1.000E+00	1.000E+00
	8 intrusions	
	(# Scenarios = 1287)	
Prob 8 intr	3.002E-12	3.165E-20
Cum Prob	1.000E+00	1.000E+00
	9 intrusions	
	(# Scenarios = 2002)	
Prob 9 intr	4.635E-14	4.844E-23
Cum Prob	1.000E+00	1.000E+00
	10 intrusions	
	(# Scenarios = 3003)	
Prob 10 intr	6.441E-16	6.671E-26
Cum Prob	1.000E+00	1.000E+00

[a] S(i,j,k,l,m,n) represents the scenario in which i,j,k,l,m, and n drilling intrusions occur in the time intervals [0, 150 yr], [150, 200 yr], [200, 500 yr], and [500, 1500 yr], [1500, 4500 yr], and [4500, 10,000 yr], respectively.

[b] Scenario probability calculated with $\lambda \neq 0$ over the time interval [100, 10,000 yr].

[c] Scenario probability calculated with $\lambda \neq 0$ over the time interval [100, 2000 yr] and $\lambda = 0$ over the time interval [2000, 10,000 yr].

[d] Probability of indicated number of intrusions.

[e] Cumulative probability for all scenarios.

Table 2.5-4. Probabilities for Scenarios Involving Multiple Intrusions over 10,000 years for $\lambda = 3.78 \times 10^{-4}$ yr^{-1}, 100 yr Administrative Control, and the Time Intervals [0, 150 yr], [150, 200 yr], [200, 500 yr], [500, 1500 yr], [1500, 4500 yr] and [4500, 10,000 yr]. The scenarios shown in this table are contained in the set R_2 defined in Eq. 2.5-8, and $\lambda = 3.78 \times 10^{-4}$ yr^{-1} is the largest drilling rate considered in the 1992 WIPP PA.

Scenario[a]	Prob with $\lambda \neq 0$[b]	Prob with $\lambda \rightarrow 0$[c]
	0 intrusions	
	(# Scenarios = 1)	
S(0,0,0,0,0,0)	2.378E-02	4.879E-01
Prob 0 intr[d]	2.378E-02	4.879E-01
Cum Prob[e]	2.378E-02	4.879E-01
	1 intrusion	
	(# Scenarios = 6)	
S(1,0,0,0,0,0)	4.491E-04	9.214E-03
S(0,1,0,0,0,0)	4.491E-04	9.214E-03
S(0,0,1,0,0,0)	2.695E-03	5.528E-02
S(0,0,0,1,0,0)	8.982E-03	1.843E-01
S(0,0,0,0,1,0)	2.695E-02	9.214E-02
S(0,0,0,0,0,1)	4.940E-02	0.000E+00
Prob 1 intr	8.892E-02	3.501E-01
Cum Prob	1.127E-01	8.381E-01
	2 intrusions	
	(# Scenarios = 21)	
S(2,0,0,0,0,0)	4.240E-06	8.699E-05
S(1,1,0,0,0,0)	8.480E-06	1.740E-04
S(1,0,1,0,0,0)	5.088E-05	1.044E-03
S(1,0,0,1,0,0)	1.696E-04	3.480E-03
S(1,0,0,0,1,0)	5.088E-04	1.740E-03
S(1,0,0,0,0,1)	9.328E-04	0.000E+00
S(0,2,0,0,0,0)	4.240E-06	8.699E-05
S(0,1,1,0,0,0)	5.088E-05	1.044E-03
S(0,1,0,1,0,0)	1.696E-04	3.480E-03
S(0,1,0,0,1,0)	5.088E-04	1.740E-03
S(0,1,0,0,0,1)	9.328E-04	0.000E+00
S(0,0,2,0,0,0)	1.526E-04	3.132E-03
S(0,0,1,1,0,0)	1.018E-03	2.088E-02
S(0,0,1,0,1,0)	3.053E-03	1.044E-02
S(0,0,1,0,0,1)	5.597E-03	0.000E+00
S(0,0,0,2,0,0)	1.696E-03	3.480E-02
S(0,0,0,1,1,0)	1.018E-02	3.480E-02
S(0,0,0,1,0,1)	1.866E-02	0.000E+00
S(0,0,0,0,2,0)	1.526E-02	8.699E-03
S(0,0,0,0,1,1)	5.597E-02	0.000E+00
S(0,0,0,0,0,2)	5.130E-02	0.000E+00
Prob 2 intr	1.662E-01	1.256E-01
Cum Prob	2.789E-01	9.637E-01
	3 intrusions	
	(# Scenarios = 56)	
S(3,0,0,0,0,0)	2.669E-08	5.475E-07
S(2,1,0,0,0,0)	8.006E-08	1.643E-06
S(2,0,1,0,0,0)	4.804E-07	9.856E-06
S(2,0,0,1,0,0)	1.601E-06	3.285E-05
S(2,0,0,0,1,0)	4.804E-06	1.643E-05
S(2,0,0,0,0,1)	8.807E-06	0.000E+00
S(1,2,0,0,0,0)	8.006E-08	1.643E-06
S(1,1,1,0,0,0)	9.608E-07	1.971E-05
S(1,1,0,1,0,0)	3.203E-06	6.571E-05
S(1,1,0,0,1,0)	9.608E-06	3.285E-05
S(1,1,0,0,0,1)	1.761E-05	0.000E+00
S(1,0,2,0,0,0)	2.882E-06	5.913E-05
S(1,0,1,1,0,0)	1.922E-05	3.942E-04
S(1,0,1,0,1,0)	5.765E-05	1.971E-04
S(1,0,1,0,0,1)	1.057E-04	0.000E+00
S(1,0,0,2,0,0)	3.203E-05	6.571E-04
S(1,0,0,1,1,0)	1.922E-04	6.571E-04
S(1,0,0,1,0,1)	3.523E-04	0.000E+00
S(1,0,0,0,2,0)	2.882E-04	1.643E-04
S(1,0,0,0,1,1)	1.057E-03	0.000E+00
S(1,0,0,0,0,2)	9.688E-04	0.000E+00
S(0,3,0,0,0,0)	2.669E-08	5.475E-07
S(0,2,1,0,0,0)	4.804E-07	9.856E-06
S(0,2,0,1,0,0)	1.601E-06	3.285E-05
S(0,2,0,0,1,0)	4.804E-06	1.643E-05
S(0,2,0,0,0,1)	8.807E-06	0.000E+00
S(0,1,2,0,0,0)	2.882E-06	5.913E-05
S(0,1,1,1,0,0)	1.922E-05	3.942E-04
S(0,1,1,0,1,0)	5.765E-05	1.971E-04
S(0,1,1,0,0,1)	1.057E-04	0.000E+00
S(0,1,0,2,0,0)	3.203E-05	6.571E-04

[a] S(i,j,k,l,m,n) represents the scenario in which i,j,k,l,m, and n drilling intrusions occur in the time intervals [0, 150 yr], [150, 200 yr], [200, 500 yr], and [500, 1500 yr], [1500, 4500 yr], and [4500, 10,000 yr], respectively.

[b] Scenario probability calculated with $\lambda = 3.78 \times 10^{-4}$ yr^{-1} over the time interval [100, 10,000 yr].

[c] Scenario probability calculated with $\lambda = 3.78 \times 10^{-4}$ yr^{-1} over the time interval [100, 2000 yr] and $\lambda = 0$ over the time interval [2000, 10,000 yr].

[d] Probability of indicated number of intrusions.

[e] Cumulative probability for all scenarios.

Table 2.5-4. Probabilities for Scenarios Involving Multiple Intrusions over 10,000 years for $\lambda = 3.78 \times 10^{-4}$ yr^{-1}, 100 yr Administrative Control, and the Time Intervals [0, 150 yr], [150, 200 yr], [200, 500 yr], [500, 1500 yr], [1500, 4500 yr] and [4500, 10,000 yr]. The scenarios shown in this table are contained in the set R_2 defined in Eq. 2.5-8, and $\lambda = 3.78 \times 10^{-4}$ yr^{-1} is the largest drilling rate considered in the 1992 WIPP PA. (concluded)

Scenario[a]	Prob with $\lambda \neq 0$[b]	Prob with $\lambda \to 0$[c]
S(0,1,0,1,1,0)	1.922E-04	6.571E-04
S(0,1,0,1,0,1)	3.523E-04	0.000E+00
S(0,1,0,0,2,0)	2.882E-04	1.643E-04
S(0,1,0,0,1,1)	1.057E-03	0.000E+00
S(0,1,0,0,0,2)	9.688E-04	0.000E+00
S(0,0,3,0,0,0)	5.765E-06	1.183E-04
S(0,0,2,1,0,0)	5.765E-05	1.183E-03
S(0,0,2,0,1,0)	1.729E-04	5.913E-04
S(0,0,2,0,0,1)	3.170E-04	0.000E+00
S(0,0,1,2,0,0)	1.922E-04	3.942E-03
S(0,0,1,1,1,0)	1.153E-03	3.942E-03
S(0,0,1,1,0,1)	2.114E-03	0.000E+00
S(0,0,1,0,2,0)	1.729E-03	9.856E-04
S(0,0,1,0,1,1)	6.341E-03	0.000E+00
S(0,0,1,0,0,2)	5.813E-03	0.000E+00
S(0,0,0,3,0,0)	2.135E-04	4.380E-03
S(0,0,0,2,1,0)	1.922E-03	6.571E-03
S(0,0,0,2,0,1)	3.523E-03	0.000E+00
S(0,0,0,1,2,0)	5.765E-03	3.285E-03
S(0,0,0,1,1,1)	2.114E-02	0.000E+00
S(0,0,0,1,0,2)	1.938E-02	0.000E+00
S(0,0,0,0,3,0)	5.765E-03	5.475E-04
S(0,0,0,0,2,1)	3.170E-02	0.000E+00
S(0,0,0,0,1,2)	5.813E-02	0.000E+00
S(0,0,0,0,0,3)	3.552E-02	0.000E+00
Prob 3 intr	2.072E-01	3.004E-02
Cum Prob	4.861E-01	9.937E-01
	4 intrusions	
	(# Scenarios = 126)	
S(4,0,0,0,0,0)	1.260E-10	2.585E-09
S(3,1,0,0,0,0)	5.039E-10	1.034E-08
.	.	.
.	.	.
.	.	.
S(1,1,1,1,0,0)	3.628E-07	7.444E-06
.	.	.
.	.	.
.	.	.
S(0,0,0,0,1,3)	4.024E-02	0.000E+00
S(0,0,0,0,0,4)	1.845E-02	0.000E+00
Prob 4 intr	1.936E-01	5.390E-03
Cum Prob	6.797E-01	9.991E-01
	5 intrusions	
	(# Scenarios = 252)	
Prob 5 intr	1.448E-01	7.735E-04
Cum Prob	8.245E-01	9.999E-01
	6 intrusions	
	(# Scenarios = 462)	
Prob 6 intr	9.022E-02	9.250E-05
Cum Prob	9.147E-01	1.000E+00
	7 intrusions	
	(# Scenarios = 792)	
Prob 7 intr	4.819E-02	9.482E-06
Cum Prob	9.629E-01	1.000E+00
	8 intrusions	
	(# Scenarios = 1287)	
Prob 8 intr	2.252E-02	8.504E-07
Cum Prob	9.854E-01	1.000E+00
	9 intrusions	
	(# Scenarios = 2002)	
Prob 9 intr	9.356E-03	6.780E-08
Cum Prob	9.948E-01	1.000E+00
	10 intrusions	
	(# Scenarios = 3003)	
Prob 10 intr	3.498E-03	4.865E-09
Cum Prob	9.983E-01	1.000E+00

[a] S(i,j,k,l,m,n) represents the scenario in which i,j,k,l,m, and n drilling intrusions occur in the time intervals [0, 150 yr], [150, 200 yr], [200, 500 yr], and [500, 1500 yr], [1500, 4500 yr], and [4500, 10,000 yr], respectively.

[b] Scenario probability calculated with $\lambda = 3.78 \times 10^{-4}$ yr^{-1} over the time interval [100, 10,000 yr].

[c] Scenario probability calculated with $\lambda = 3.78 \times 10^{-4}$ yr^{-1} over the time interval [100, 2000 yr] and $\lambda = 0$ over the time interval [2000, 10,000 yr].

[d] Probability of indicated number of intrusions.

[e] Cumulative probability for all scenarios.

The sets R_1 and R_2 in Eqs. 2.5-1 and 2.5-8 provide two different summaries of the results of the WIPP performance assessment based on different partitioning of the sample space S shown in Eq. 2.2-1. These sets actually depend on both the partitioning of S into the scenarios S_i and the determination of the scenario probabilities pS_i and the scenario consequences $\mathbf{cS}_i$. Thus, a full specification of R_1 and R_2 would also contain subscripts indicating the manner in which the probabilities pS_i and the consequences $\mathbf{cS}_i$ are determined. To avoid the use of unnecessarily cumbersome notation, such subscripting is not employed in this presentation. However, the manner in which the pS_i and $\mathbf{cS}_i$ are defined for use with the risk representations R_1 and R_2 is indicated in Chapter 8 when analysis results are presented.

3. UNCERTAIN VARIABLES SELECTED FOR SAMPLING

The 1992 WIPP performance assessment selected 49 imprecisely known variables for consideration. These variables are listed in Table 3-1 and correspond to the elements x_j, j=1, 2, ..., nV = 49, of the vector **x** shown in Eq. 2.1-2. The distributions indicated in Table 3-1 and shown more explicitly in Figure 3-1 correspond to the distributions appearing in Eq. 2.1-4 and characterize subjective, or type B, uncertainty. The variables in Table 3-1 and the rationale for their distributions are discussed extensively in Volume 3 of this report, which can be consulted for more detailed information than is presented here.

Table 3-1. Variables Sampled in 1992 WIPP Performance Assessment (adapted from Tables 6.0-1, 6.0-2, and 6.0-3 of Volume 3 of this report)

Variable	Definition
BCBRSAT	Residual brine saturation for Salado Formation (S_{lr}) (dimensionless). Used in BRAGFLO. Range: 0.0 to 0.4. Median 0.2. Distribution: Uniform. Additional information: Section 2.3.1, Volume 3. Variable 13 in Latin hypercube sample (LHS).
BCEXP	Brooks and Corey pore-size distribution parameter for Salado Formation (λ) (dimensionless). Used in BRAGFLO. Range: 0.2 to 10. Median 0.7. Distribution: Piecewise uniform. Additional information: Same as BCBRSAT. Variable 11 in LHS.
BCFLG	Pointer variable (flag) for selection of characteristic curve for capillary behavior. Used in BRAGFLO. Range: {0, 1}. Distribution: 33% 0, 67% 1. Value of 0 selects van Genuchten-Parker model; value of 1 selects Brooks-Corey model. Additional information: Section 2.3.1, Volume 3. Variable 12 in LHS.
BCGSSAT	Brooks and Corey residual gas saturation for Salado Formation (S_{gr}) (dimensionless). Used in BRAGFLO. Range: 0.0 to 0.4. Median: 0.2. Distribution: Uniform. Additional information: Same as BCBRSAT. Variable 14 in LHS.
BHPERM	Borehole permeability (k) (m^2). Used in BRAGFLO. Range: 1×10^{-14} to 1×10^{-11}. Median: 3.16×10^{-12}. Distribution: Lognormal. Additional information: Freeze and Cherry, 1979, Table 2-2 (silty sand); Section 4.2.1 Volume 3. Variable 21 in LHS.
BPPRES	Initial pressure (p) of pressurized brine pocket in Castile Formation (Pa). Used in BRAGFLO. Range: 1.3×10^7 to 2.1×10^7. Median: 1.7×10^7. Distribution: Piecewise linear. Additional information: Popielak et al., 1983, p. H-52; Lappin et al., 1989, Table 3-19; Section 4.3.1, Volume 3. Variable 19 in LHS.

Table 3-1. Variables Sampled in 1992 WIPP Performance Assessment (adapted from Tables 6.0-1, 6.0-2, and 6.0-3 of Volume 3 of this report) (continued)

Variable	Definition
BPSTOR	Bulk storativity (S_b) of pressurized brine pocket in Castile Formation (m^3/Pa). Used in BRAGFLO. Range: 0.02 to 2. Median: 0.2. Distribution: Lognormal. Additional information: Section 4.3.1, Volume 3. Variable 20 in LHS.
BPAREAFR	Fraction of waste panel area underlain by a pressurized brine pocket (dimensionless). Used in CCDFPERM in calculation of probability of E1E2-type scenarios. Range: 0.24 to 0.568. Median: 0.40. Distribution: Piecewise Linear. Additional information: Section 5.1, Volume 3. Variable 24 in LHS.
BRSAT	Initial fluid (brine) saturation of waste (dimensionless). Used in BRAGFLO. Range: 0 to 0.14. Median: 0.07. Distribution: Uniform. Additional information: Section 3.4.3, Volume 3. Variable 1 in LHS.
CULCLIM	Recharge amplitude factor (A_m) for Culebra (dimensionless). Used in SECO-FLOW. Range: 1 to 1.07. Median: 1.035. Distribution: Uniform. Used in definition of time dependent boundary heads in Culebra, with the maximum head increasing from the estimated present-day head in the Culebra in the northern most element of the regional model domain for CULCLIM = 1 to the elevation of the Clayton Basin spill point (1007m) for CULCLIM = 1.07. Additional information: Section 6.4, of this Volume. Variable 32 in LHS is uniformly distributed on [0,1] and used to select value for CULCLIM by preprocessor to SECO-FLOW.
CULFRPOR	Fracture porosity (Θ_f) in Culebra (dimensionless). Used in SECO-FLOW and SECO-TRANSPORT. Range: 1×10^{-4} to 1×10^{-2}. Median: 1×10^{-3}. Distribution: Lognormal. Additional information: Tables 1-2 and E-6, Lappin et al., 1989; Section 2.6.2, Volume 3. Variable 33 in LHS.
CULFRSP	Fracture spacing (2B) in Culebra (m). Used in SECO-TRANSPORT. Range: 6×10^{-2} to 8. Median: 4×10^{-1}. Distribution: Piecewise uniform. Additional information: Beauheim et al., 1991b. Variable 34 in LHS.
CULCLYF	Clay filling fraction (b_c/b) in Culebra (dimensionless), where 2b is the fracture aperture and $2b_c$ is the total thickness of the clay lining in the fracture. Used in SECO-TRANSPORT. Range: 0 to 0.5. Median: 0. Distribution: $b_c/b=0$ has probability 0.5 and $b_c/b\neq0$ is uniformly distributed between 0 and 0.5. Additional information: Section 2.6.1, Volume 3. Variable 35 in LHS.
CULCLYP	Porosity of clay lining fractures in Culebra (dimensionless). Used in SECOTP. Range: 0.05 to 0.5. Median: 0.275. Distribution: Uniform. Additional information: Section 2.6.2, Volume 3. Variable 36 in LHS.

Table 3-1. Variables Sampled in 1992 WIPP Performance Assessment (adapted from Tables 6.0-1, 6.0-2, and 6.0-3 of Volume 3 of this report) (continued)

Variable	Definition
CULPOR	Matrix porosity (θ_m) in Culebra (dimensionless). Used in BRAGFLO and SECO-TRANSPORT. Range: 5.8×10^{-2} to 2.53×10^{-1}. Median: 1.39×10^{-1}. Distribution: Piecewise uniform. Additional information: Table 4.4, Kelley and Saulnier, 1990; Table E-8, Lappin et al., 1989; Section 2.6.2, Volume 3. Variable 43 in LHS.
CULTRFLD	Transmissivity field for Culebra. Seventy transmissivity fields consistent with available field data were constructed and ranked with respect to travel time to the accessible environment. CULTRFLD is a pointer variable used to select from these 70 fields, with travel time increasing monotonically with CULTRFLD. Used in STAFF2D and SECO-TRANSPORT. Range: 0 to 1. Median: 0.5. Distribution: Uniform. Additional information: Section 7.5, Volume 2; Section 2.6.3, Volume 3. Variable 31 in LHS.
DBDIAM	Drill bit diameter (m). Used in CUTTINGS and BRAGFLO. Range: 0.267 to 0.444. Median: 0.355. Distribution: Uniform. Additional information: Section 4.2.2, Volume 3. Variable 22 in LHS.
FKDAM	Fracture distribution coefficient (K_d) for Am in Culebra (m^3/ kg). Used in SECO-TRANSPORT. Range: 1×10^{-4} to 1×10^{3}. Median: 9.33×10^{1}. Distribution: Piecewise loguniform. Additional information: Section 2.6.4, Volume 3. Variable 37 in LHS.
FKDNP	Fracture distribution coefficient (K_d) for Np in Culebra (m^3/kg). Used in SECO-TRANSPORT. Range: 1×10^{-4} to 1×10^{3}. Median: 1. Distribution: Piecewise loguniform. Additional information: Section 2.6.4, Volume 3. Variable 38 in LHS.
FKDPU	Fracture distribution coefficient (K_d) for Pu in Culebra (m^3/kg). Used in SECO-TRANSPORT. Range: 1×10^{-4} to 1×10^{3}. Median: 2.04×10^{2}. Distribution: Piecewise loguniform. Additional information: Section 2.6.4, Volume 3. Variable 39 in LHS.
FKDRA	Fracture distribution coefficient (K_d) for Ra in Culebra (m^3/kg). Used in SECO-TRANSPORT. Range: 1×10^{-4} to 1×10^{2}. Median: 3.31×10^{-2}. Distribution: Piecewise loguniform. Additional information: Section 2.6.4, Volume 3. Variable 42 in LHS.
FKDTH	Fracture distribution coefficient (K_d) for Th in Culebra (m^3/kg). Used in SECO-TRANSPORT. Range: 1×10^{-4} to 1×10^{1}. Median: 1×10^{-1}. Distribution: Piecewise loguniform. Additional information: Section 2.6.4, Volume 3. Variable 40 in LHS.

Table 3-1. Variables Sampled in 1992 WIPP Performance Assessment (adapted from Tables 6.0-1, 6.0-2, and 6.0-3 of Volume 3 of this report) (continued)

Variable	Definition
FKDU	Fracture distribution coefficient (K_d) for U in Culebra (m^3/kg). Used in SECO-TRANSPORT. Range: 1×10^{-4} to 1. Median: 7.94×10^{-3}. Distribution: Piecewise loguniform. Additional information: Section 2.6.4, Volume 3. Variable 41 in LHS.
GRCORHF	Scale factor used in definition of gas generation rate for corrosion of steel under humid conditions (dimensionless). Actual gas generation rate is GRCORH = GRCORHF • GRCORI. Used in BRAGFLO. Range: 0 to 0.5. Median: 0.1. Distribution: Piecewise uniform. Additional information: Brush, 1991. Variable 3 in LHS.
GRCORI	Gas generation rate for corrosion of steel under inundated conditions (mol/m^2 surface area steel • s). Used in BRAGFLO. Range: 0 to 1.3×10^{-8}. Median: 6.3×10^{-9}. Distribution: Piecewise uniform. Additional information: Same as GRCORHF. Variable 2 in LHS.
GRMICHF	Scale factor used in definition of gas generation rate due to microbial degradation of cellulosics under humid conditions (mol/kg cellulosics • s). Actual gas generation rate is GRMICH = GRMICHF • GRMICI. Used in BRAGFLO. Range: 0 to 0.2. Median: 0.1. Distribution: Uniform. Additional information: Same as GRCORHF. Variable 6 in LHS.
GRMICI	Gas generation rate due to microbial degradation of cellulosics under inundated conditions (mol/kg cellulosics • s). Used in BRAGFLO. Range: 0 to 1.6×10^{-8}. Median: 3.2×10^{-9}. Distribution: Piecewise uniform. Additional information: Same as GRCORHF. Variable 5 in LHS.
LAMBDA	Pointer variable used to select rate term (λ or $\lambda(t)$, units: yr^{-1}) in Poisson model for drilling intrusions. Used in CCDFPERM. Range: 0 to 1. Median: 0.5. Distribution: Uniform. Additional information: Section 5.2, Volume 3. Variable 23 in LHS.
MBPERM	Permeability (k) in intact anhydrite marker beds in Salado Formation (m^2). Used in BRAGFLO. Range: 1×10^{-21} to 1×10^{-16}. Median: 5.0×10^{-20}. Distribution: Piecewise loguniform. Correlation: 0.3 rank correlation with SALPERM. Additional information: Section 2.4.2, Volume 3. Variable 15 in LHS.
MBPOR	Porosity (ϕ) in intact anhydrite marker beds in Salado Formation (dimensionless). Used in BRAGFLO. Range: 1×10^{-3} to 3×10^{-2}. Median: 1×10^{-2}. Distribution: Piecewise uniform. Additional information: Section 2.4.4, Volume 3. Variable 16 in LHS.

Table 3-1. Variables Sampled in 1992 WIPP Performance Assessment (adapted from Tables 6.0-1, 6.0-2, and 6.0-3 of Volume 3 of this report) (continued)

Variable	Definition
MBPRES	Far field pressure (p) in Salado Formation at the MB139 elevation. Used in BRAGFLO. Range: 1.2×10^{7} to 1.3×10^{7}. Median: 1.25×10^{7}. Distribution: Uniform. Additional information: Section 2.4.3, Volume 3. Variable 18 in LHS.
MKDAM	Matrix distribution coefficient (K_d) Am in Culebra (m^3/kg). Used in SECO-TRANSPORT. Range: 1×10^{-4} to 1×10^{2}. Median: 1.86×10^{-1}. Distribution: Piecewise loguniform. Additional information: Section 2.6.4, Volume 3. Variable 44 in LHS.
MKDNP	Matrix distribution coefficient (K_d) for Np in Culebra (m^3/kg). Used in SECO-TRANSPORT. Range: 1×10^{-4} to 1×10^{2}. Median: 4.78×10^{-2}. Distribution: Piecewise loguniform. Additional information: Section 2.6.4, Volume 3. Variable 45 in LHS.
MKDPU	Matrix distribution coefficient (K_d) for Pu in Culebra (m^3/kg). Used in SECO-TRANSPORT. Range: 1×10^{-4} to 1×10^{2}. Median: 2.61×10^{-1}. Distribution: Piecewise loguniform. Additional information: Section 2.6.4, Volume 3. Variable 46 in LHS.
MKDRA	Matrix distribution coefficient (K_d) for Ra in Culebra (m^3/kg). Used in SECO-TRANSPORT. Range: 1×10^{-4} to 1×10^{1}. Median: 1×10^{-2}. Distribution: Piecewise loguniform. Additional information: Section 2.6.4, Volume 3. Variable 49 in LHS.
MKDTH	Matrix distribution coefficient (K_d) for Th in Culebra (m^3/kg). Used in SECO-TRANSPORT. Range: 1×10^{-4} to 1. Median: 1×10^{-2}. Distribution: Piecewise loguniform. Additional information: Section 2.6.4, Volume 3. Variable 47 in LHS.
MKDU	Matrix distribution coefficient (K_d) for U in Culebra (m^3/kg). Used in SECO-TRANSPORT. Range: 1×10^{-4} to 1. Median: 2.88×10^{-2}. Distribution: Piecewise loguniform. Additional information: Section 2.6.4, Volume 3. Variable 48 in LHS.
SALPERM	Permeability (k) in intact halite component of Salado Formation (m^2). Used in BRAGFLO. Range: 1×10^{-24} to 1×10^{-19}. Median: 2×10^{-21}. Distribution: Piecewise loguniform. Correlation: 0.3 rank correlation with MBPERM. Additional information: Gorham et al., 1992; Howarth et al., 1991; Beauheim et al., 1991a; Section 2.3.5, Volume 3. Variable 10 in LHS.
SOLAM	Solubility of Am in brine (mol/ℓ). Used in PANEL. Range: 5×10^{-14} to 1.4. Median: 1×10^{-9}. Distribution: Piecewise loguniform. Additional information: Trauth et al., 1991; Section 3.3.5, Volume 3. Variable 25 in LHS.

Table 3-1. Variables Sampled in 1992 WIPP Performance Assessment (adapted from Tables 6.0-1, 6.0-2, and 6.0-3 of Volume 3 of this report) (continued)

Variable	Definition
SOLNP	Solubility of Np in brine (mol/ℓ). Used in PANEL. Range: 3×10^{-16} to 1.2×10^{-2}. Median: 1.0×10^{-7}. Distribution: Piecewise loguniform. Additional information: Same as SOLAM. Variable 26 in LHS.
SOLPU	Solubility of Pu in brine (mol/ℓ). Used in PANEL. Range: 2.5×10^{-17} to 5.5×10^{-4}. Median: 6×10^{-10}. Distribution: Piecewise loguniform. Additional information: Same as SOLAM. Variable 27 in LHS.
SOLRA	Solubility of Ra in brine (mol/ℓ). Used in PANEL. Range: 2 to 18.2. Median: 11. Distribution: Piecewise loguniform. Additional information: Same as SOLAM. Variable 28 in LHS.
SOLTH	Solubility of Th in brine (mol/ℓ). Used in PANEL. Range: 5.5×10^{-16} to 2.2×10^{-6}. Median: 1×10^{-10}. Distribution: Piecewise loguniform. Additional information: Same as SOLAM. Variable 29 in LHS.
SOLU	Solubility of U in brine (mol/ℓ). Used in PANEL. Range: 1×10^{-15} to 1. Median: 5.4×10^{-4}. Distribution: Piecewise loguniform. Additional information: Same as SOLAM. Variable 30 in LHS.
STOICCOR	Stoichiometric coefficient for corrosion of steel (dimensionless). Defines proportion of two different chemical reactions taking place during the corrosion process. Used in BRAGFLO. Range: 0 to 1. Median: 0.5. Distribution: Uniform. Additional information: Brush and Anderson, 1989. Variable 4 in LHS.
STOICMIC	Stoichiometric coefficient for microbial degradation of cellulosics (mol gas/mol CH_2O). Used in BRAGFLO. Range: 0 to 1.67. Median: 0.835. Distribution: Uniform. Additional information: Brush and Anderson, 1989. Variable 7 in LHS.
TZPORF	Scale factor used in definition of transition zone and disturbed rock zone porosity (ϕ_Z), with the transition zone and disturbed rock zone porosity defined by TZPOR = SALPOR + (0.06 - SALPOR)•TZPORF. Used in BRAGFLO. Range: 0 to 1. Median: 0.5. Distribution: Uniform. Additional information: Section 2.4.4, Volume 3. Variable 17 in LHS.
VMETAL	Fraction of total waste volume that is occupied by IDB (Integrated Data Base) metals and glass waste category (dimensionless). Used in BRAGFLO. Range: 0.276 to 0.476. Median: 0.376. Distribution: Normal. Additional information: Section 3.4.1, Volume 3. Variable 9 in LHS.

Table 3-1. Variables Sampled in 1992 WIPP Performance Assessment (adapted from Tables 6.0-1, 6.0-2, and 6.0-3 of Volume 3 of this report) (concluded)

Variable	Definition
VWOOD	Fraction of total waste volume that is occupied by IDB combustible waste category (dimensionless). Used in BRAGFLO. Range: 0.284 to 0.484. Median: 0.384. Distribution: Normal. Additional information: Section 3.4.1, Volume 3. Variable 8 in LHS.

As discussed in conjunction with Eq. 2.1-5, a Latin hypercube sample (McKay et al., 1979; Iman and Shortencarier, 1984) of size nK = 70 was generated from the variables listed in Table 3-1. The restricted pairing technique developed by Iman and Conover (1982) was used to induce the correlations between variables indicated in Table 3-1 and also to assure that the correlations between other variables were close to zero. The values used for each variable in the Latin hypercube sample are shown in Figure 3-1.

Once the sample indicated in Eq. 2.1-5 was generated from the variables in Table 3-1, the individual sample elements $\mathbf{x}_k$, k=1, ..., 70, were used in the generation of the risk results shown in Eq. 2.1-6. An overview of this process is provided in Sections 2.2, 2.3 and 2.4. In addition to many intermediate results, the final outcome of this process is a distribution of CCDFs of the form shown in Figure 2.1-2.

The analyses leading to the risk results shown in Eq. 2.1-6 were actually repeated a number of times with different modeling assumptions. The specific cases considered are listed in Table 3-2 (following Figure 3-1). Of the cases listed in Table 3-2, number 13, which is a dual-porosity transport model in the Culebra Dolomite with chemical sorption in both the dolomite matrix and clay-lined fractures, is believed by the WIPP performance assessment team to be the most credible and is presented as the best-estimate analysis in the 1992 WIPP performance assessment (see Section 2.2.4 of Volume 2 of this report). The other cases listed in Table 3-2 can be viewed as sensitivity studies that explore various perturbations on this best-estimate analysis.

In addition to the variation between the cases listed in Table 3-2, the sampling-based approach to the treatment of subjective uncertainty also produces uncertainty and sensitivity results for the individual cases. In Chapter 8, box plots and distributions of CCDFs are used to display the effect of subjective uncertainty on the cases listed in

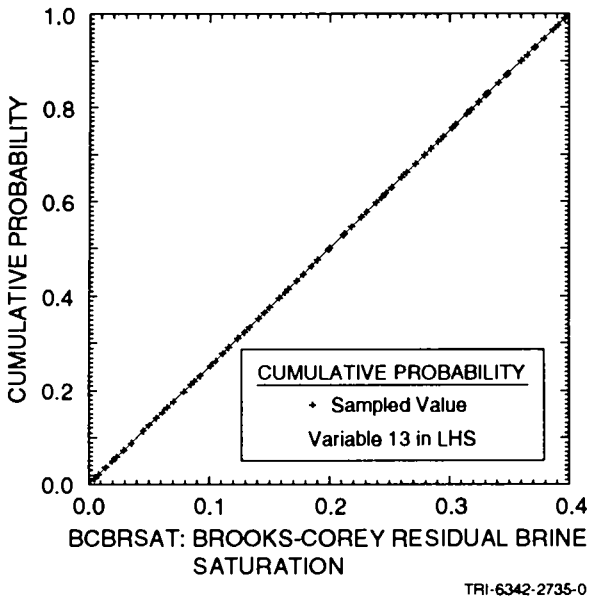

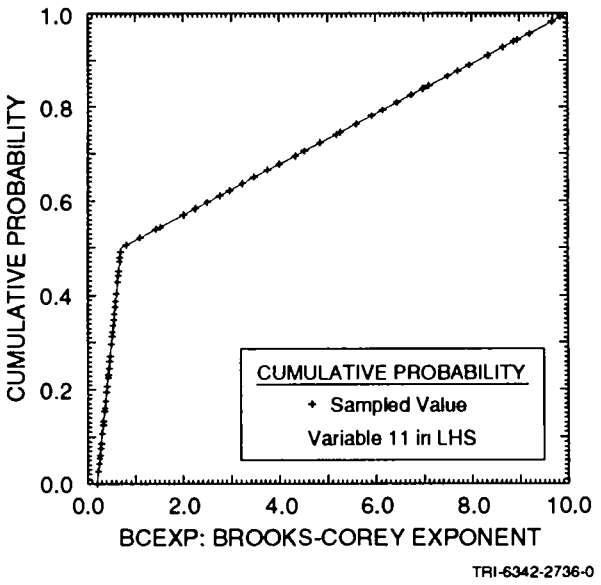

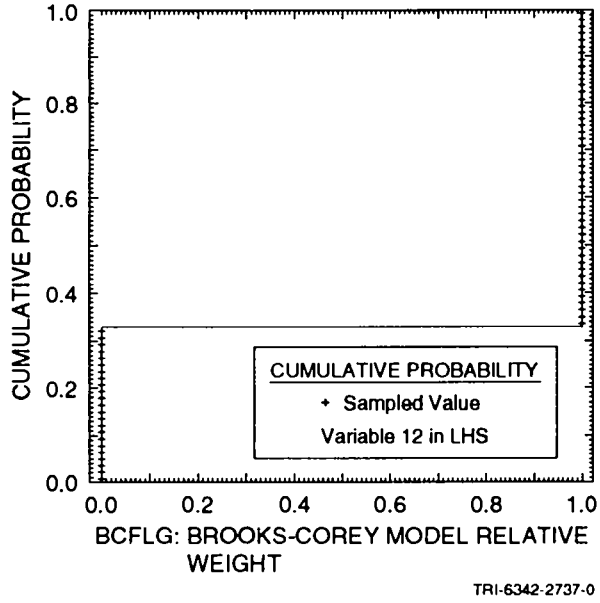

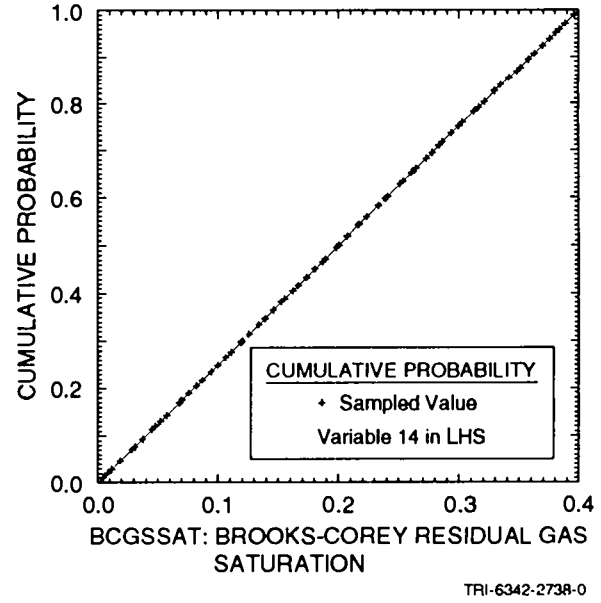

Figure 3-1. Distributions used for sampled variables in 1992 WIPP performance assessment.

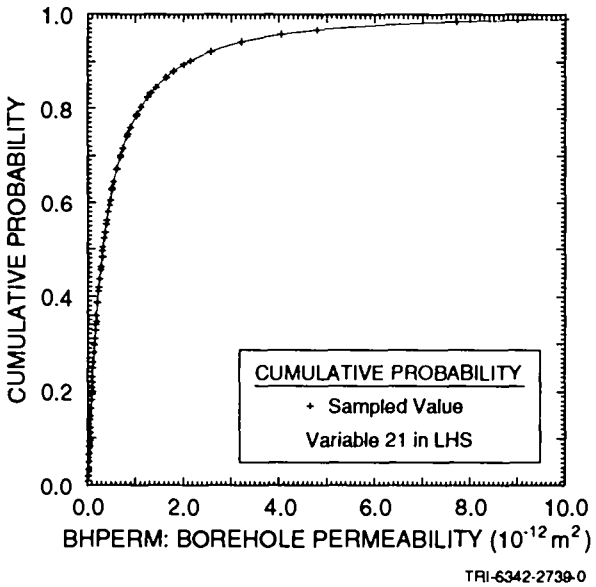

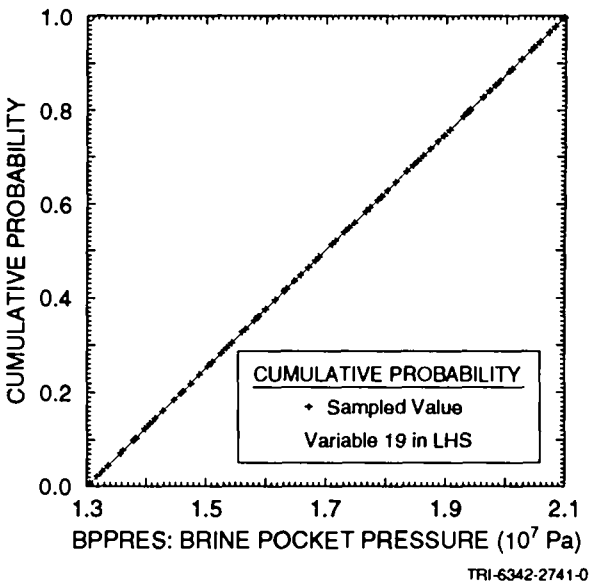

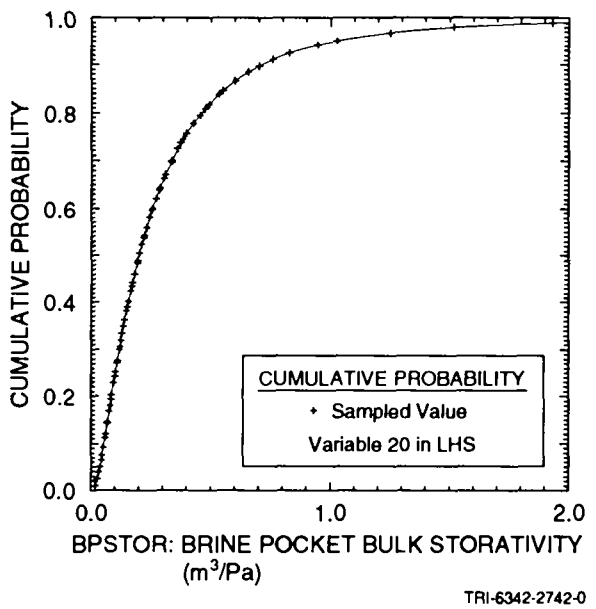

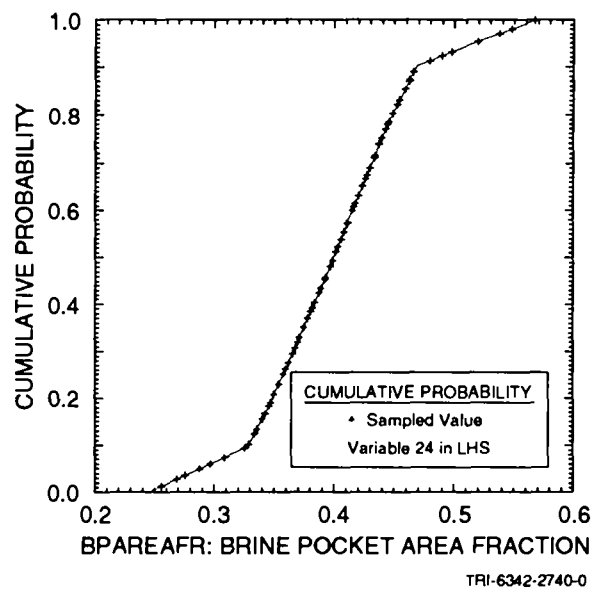

Figure 3-1. Distributions used for sampled variables in 1992 WIPP performance assessment. (continued)

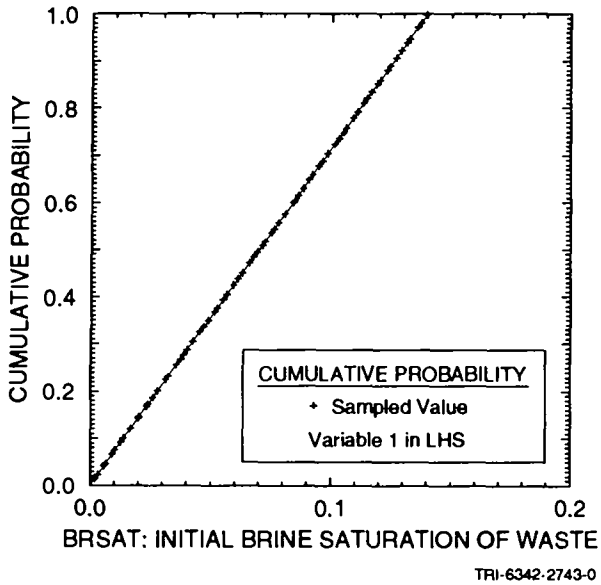

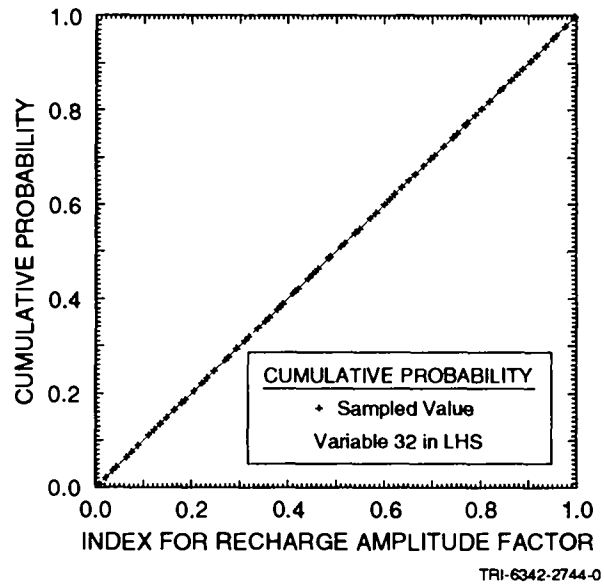

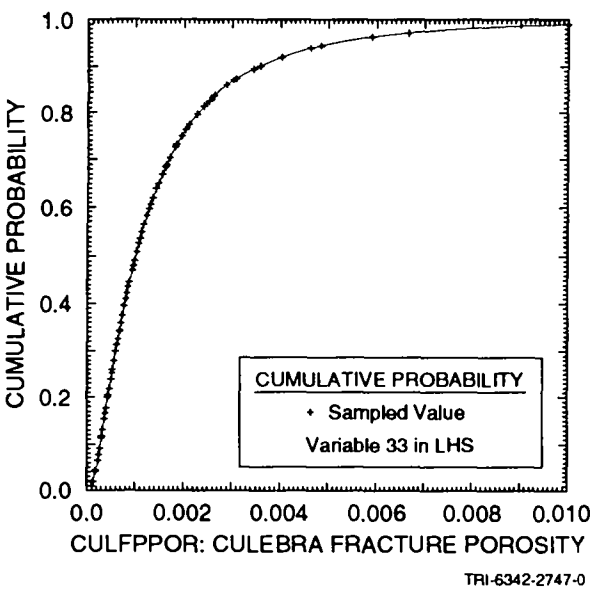

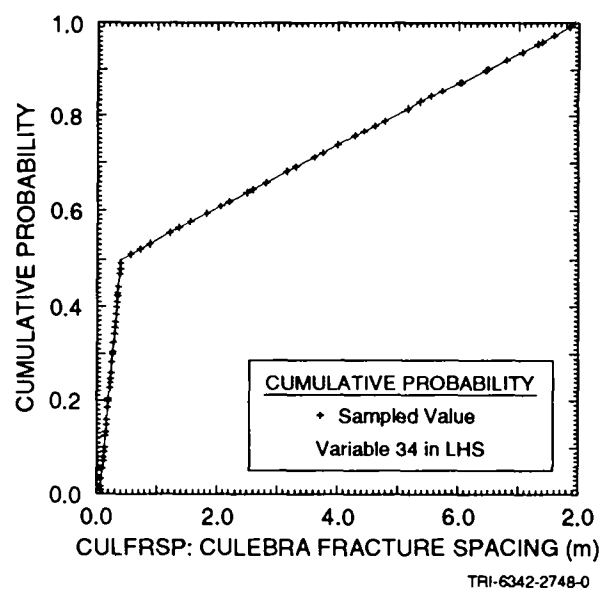

Figure 3-1. Distributions used for sampled variables in 1992 WIPP performance assessment. (continued)

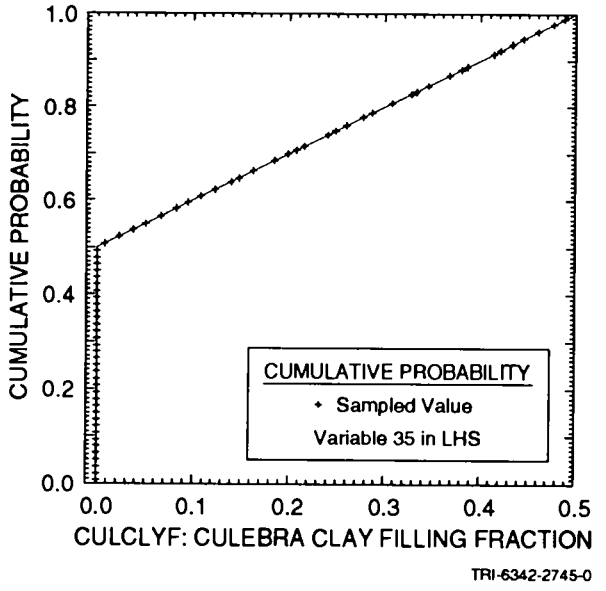

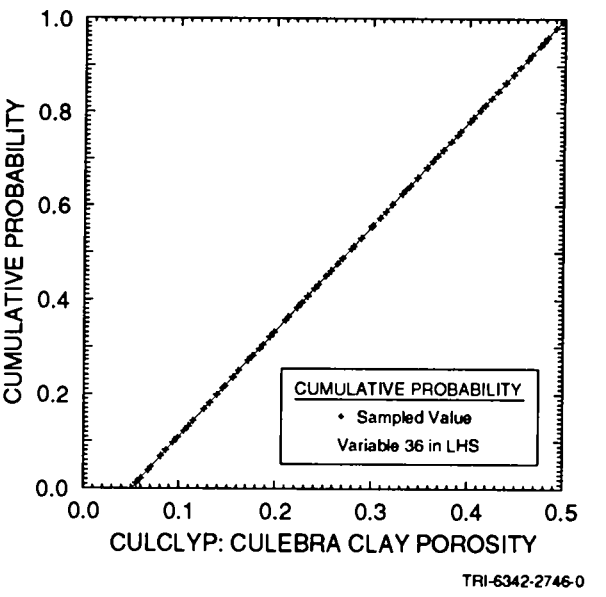

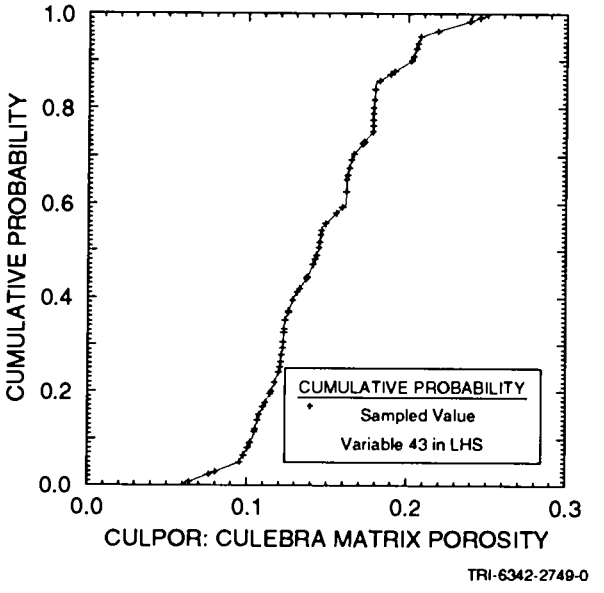

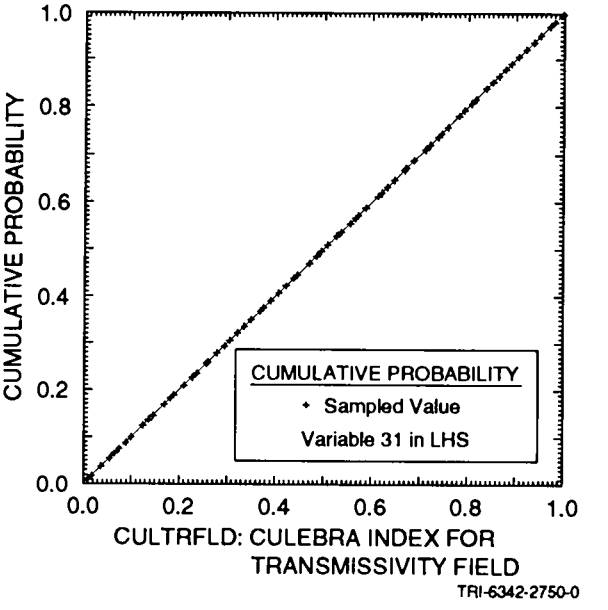

Figure 3-1. Distributions used for sampled variables in 1992 WIPP performance assessment. (continued)

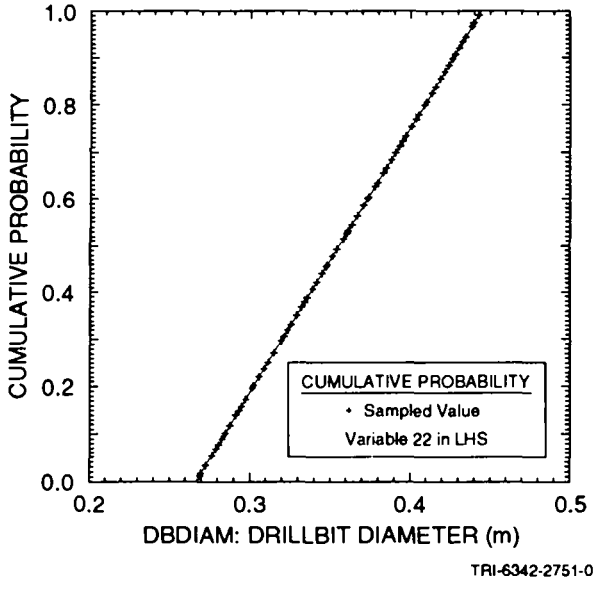

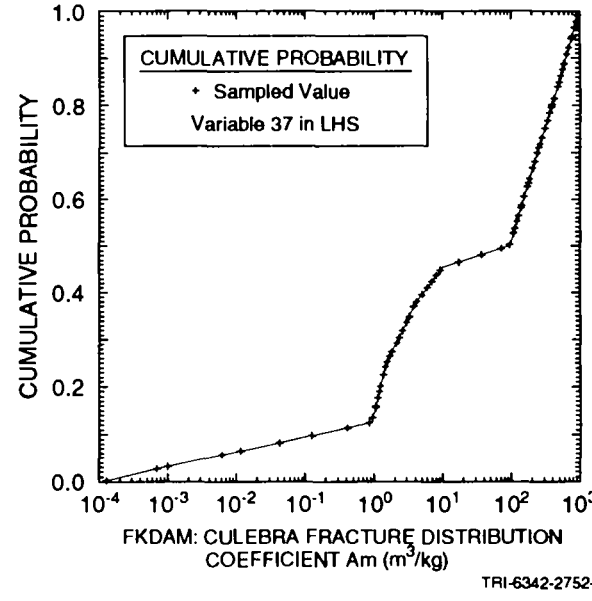

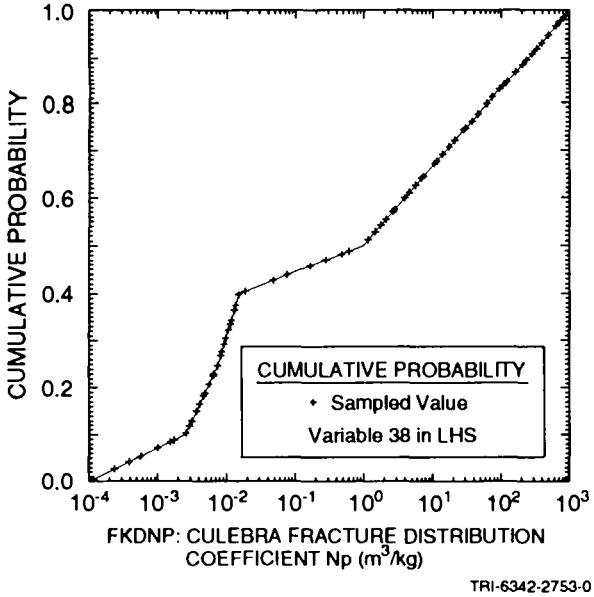

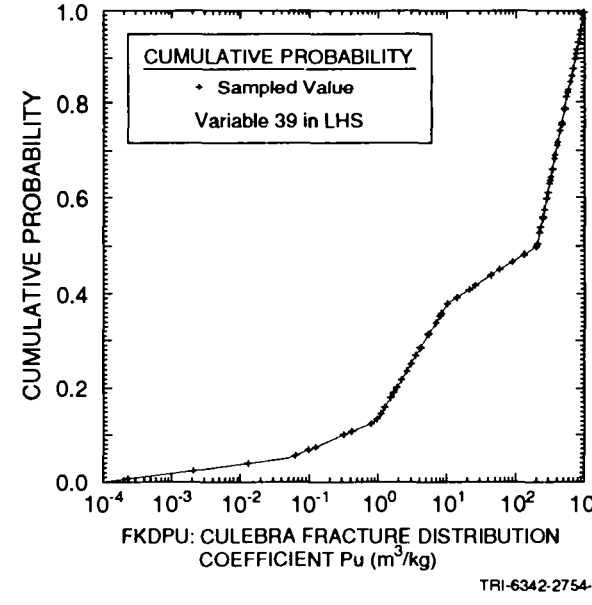

Figure 3-1. Distributions used for sampled variables in 1992 WIPP performance assessment. (continued)

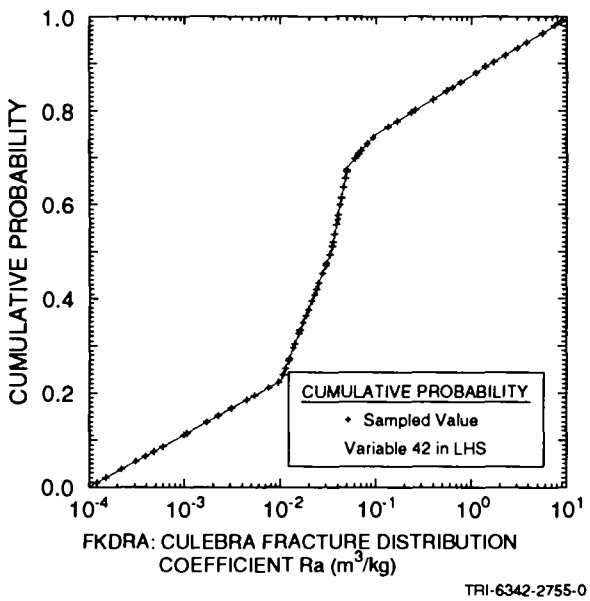

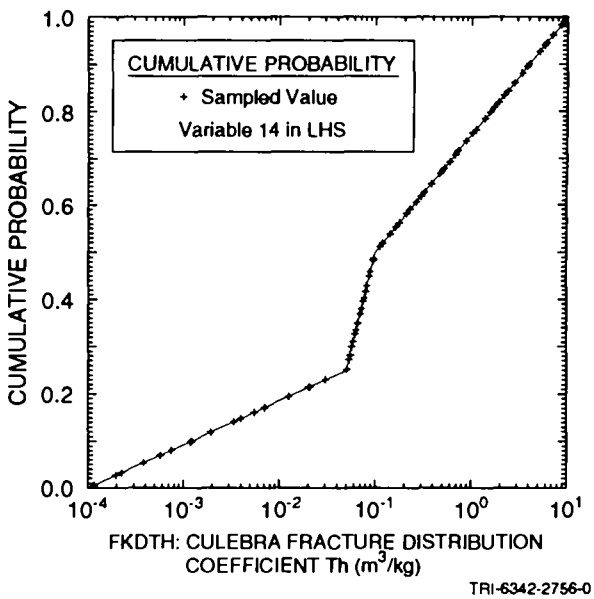

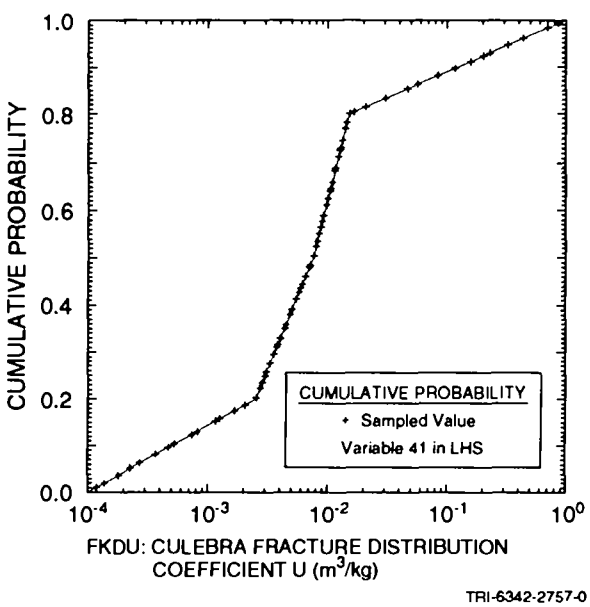

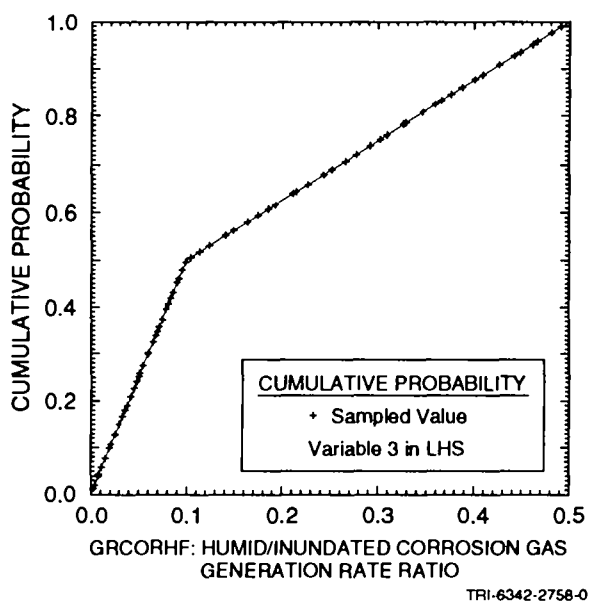

Figure 3-1. Distributions used for sampled variables in 1992 WIPP performance assessment. (continued)

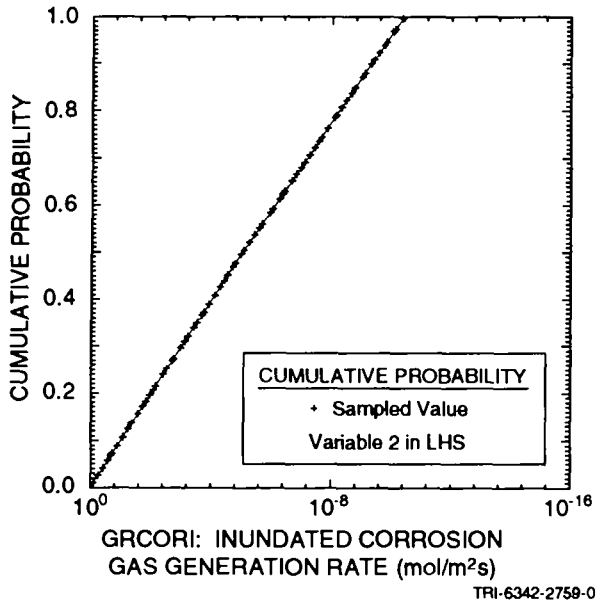

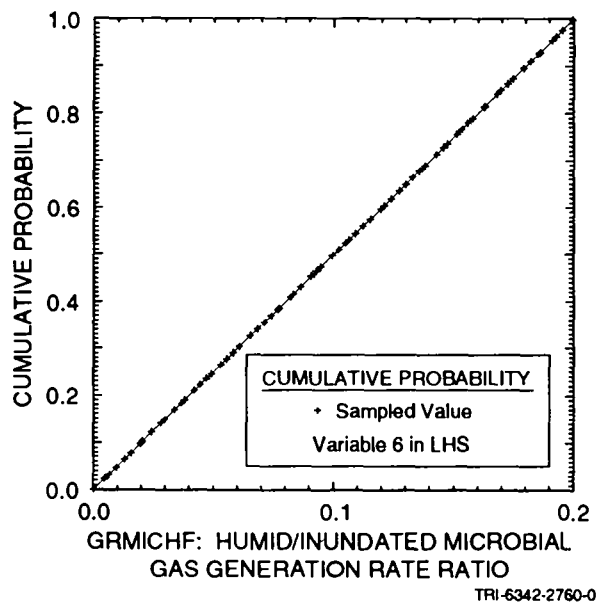

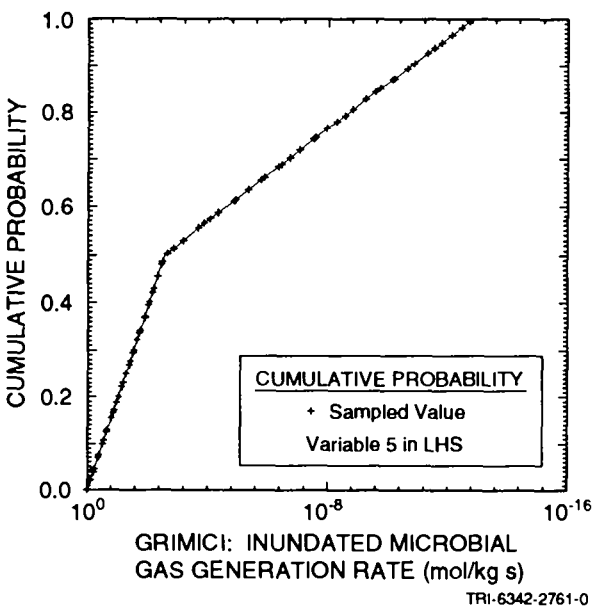

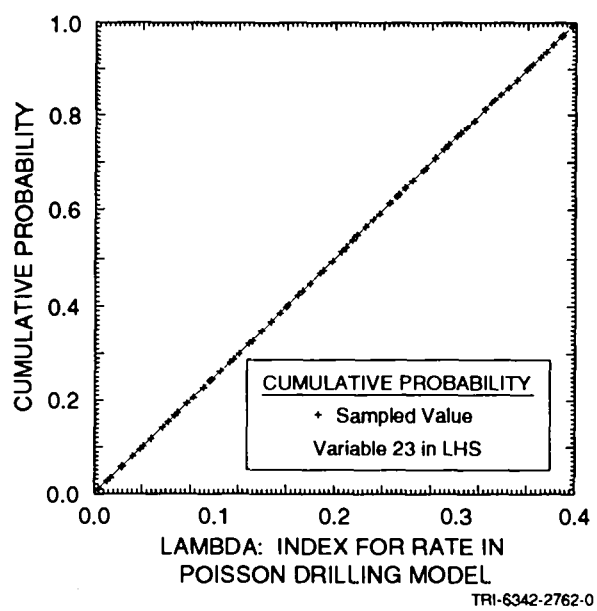

Figure 3-1. Distributions used for sampled variables in 1992 WIPP performance assessment. (continued)

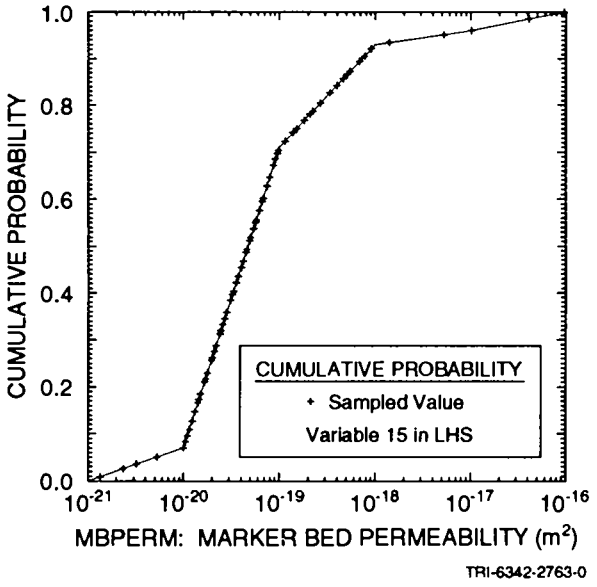

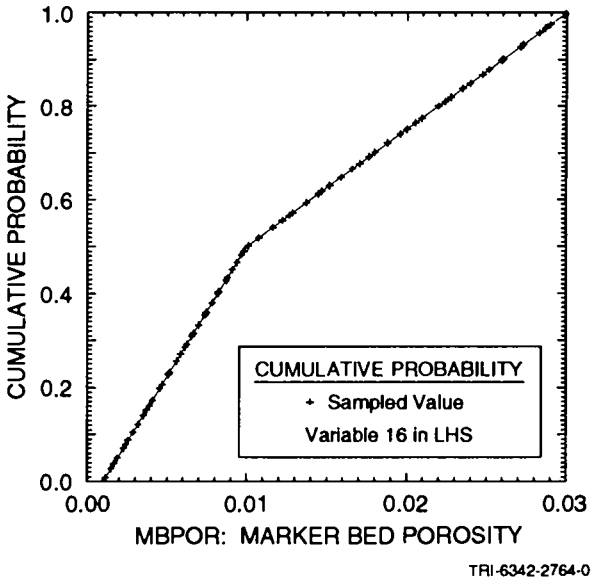

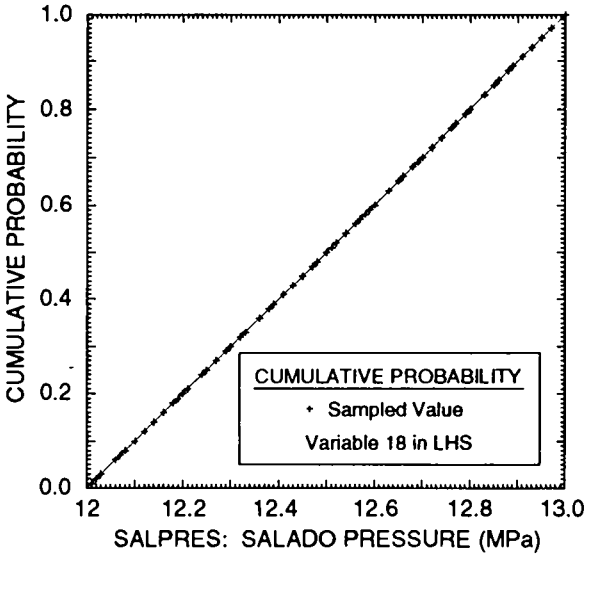

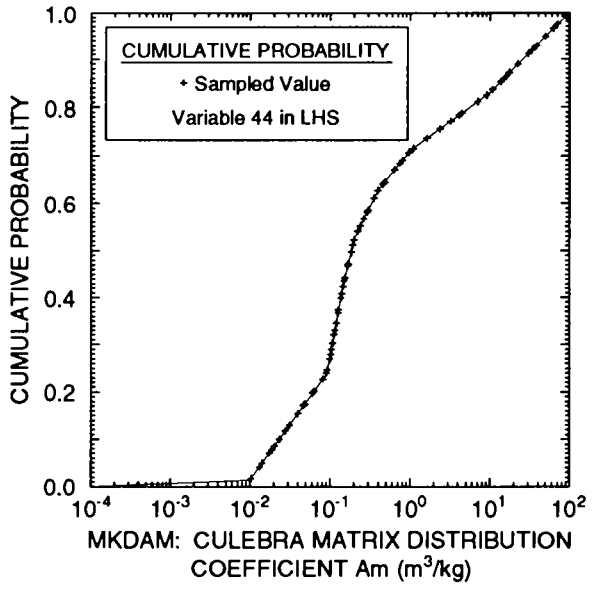

Figure 3-1. Distributions used for sampled variables in 1992 WIPP performance assessment. (continued)

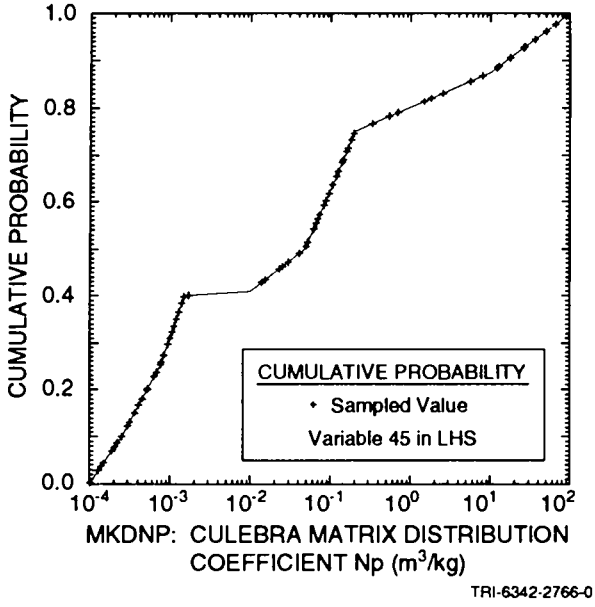

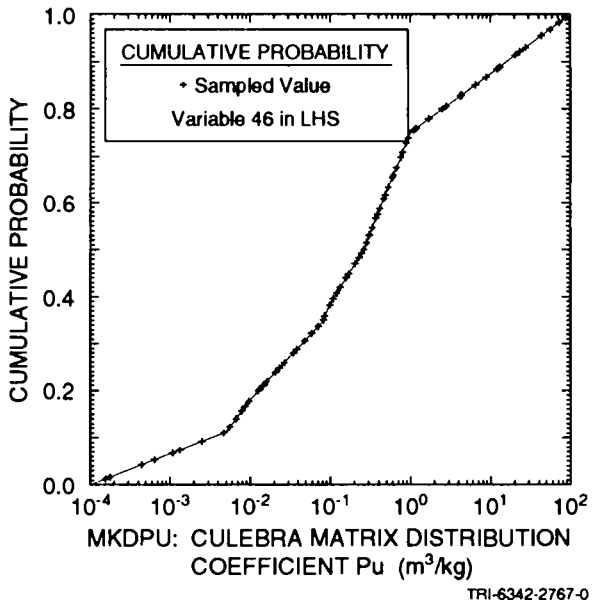

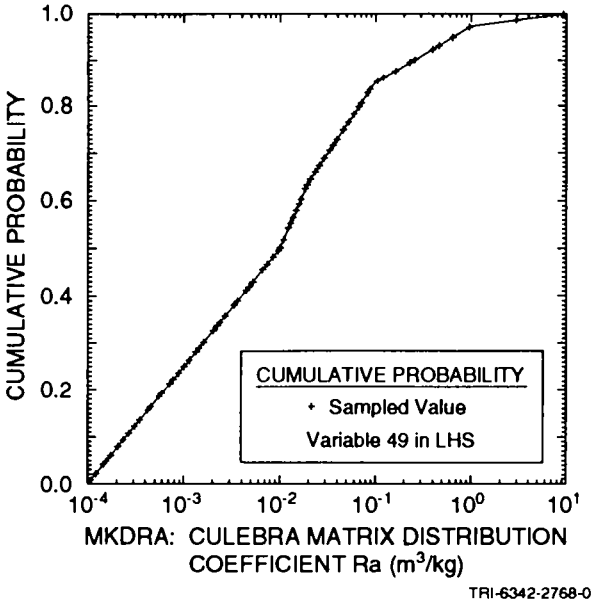

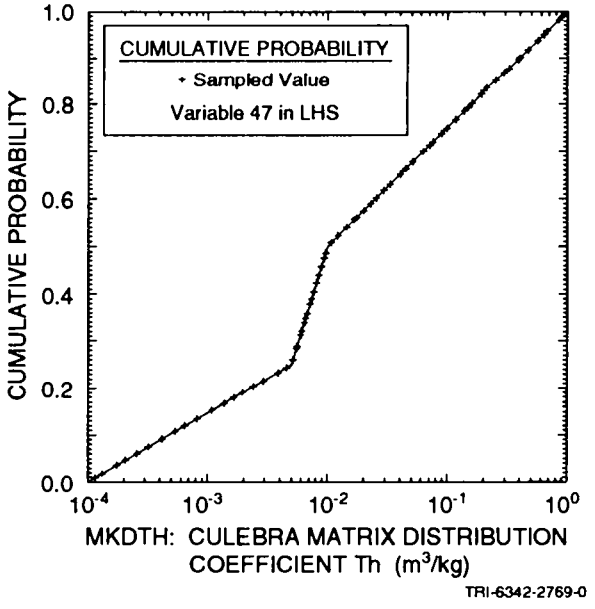

Figure 3-1. Distributions used for sampled variables in 1992 WIPP performance assessment. (continued)

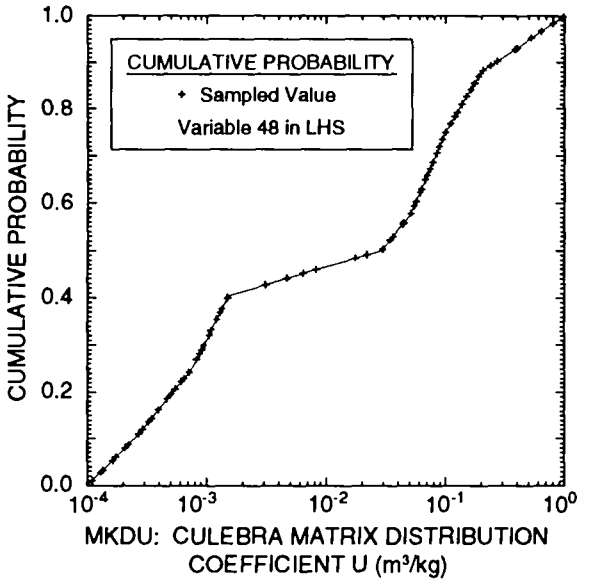

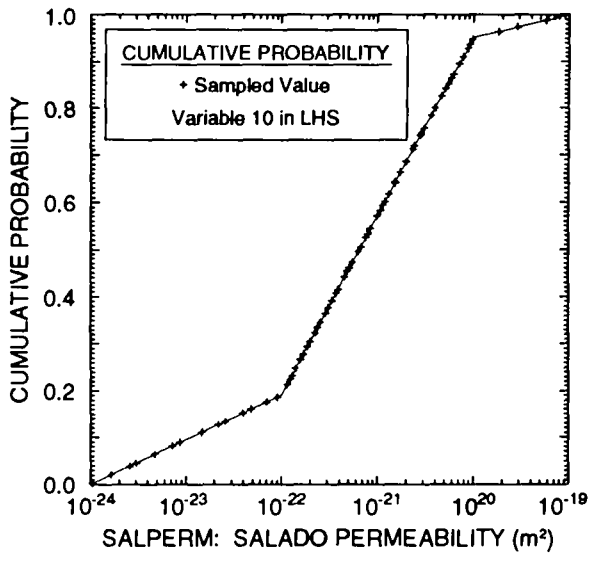

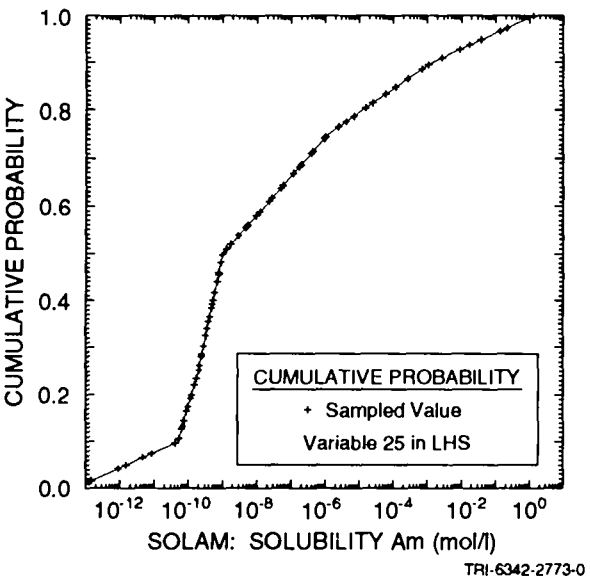

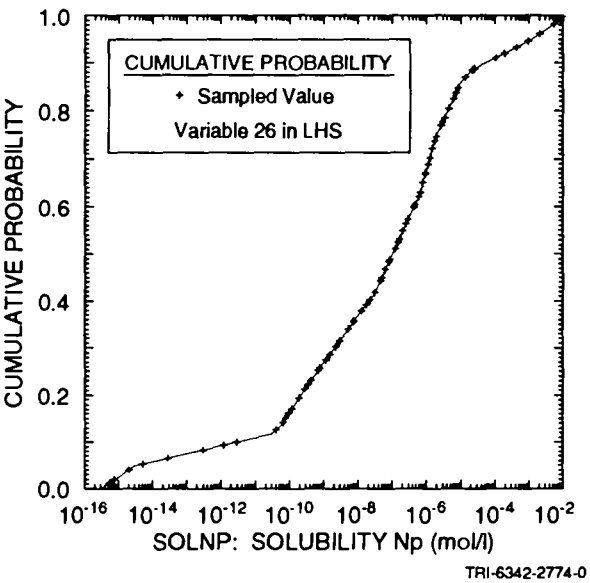

Figure 3-1. Distributions used for sampled variables in 1992 WIPP performance assessment. (continued)

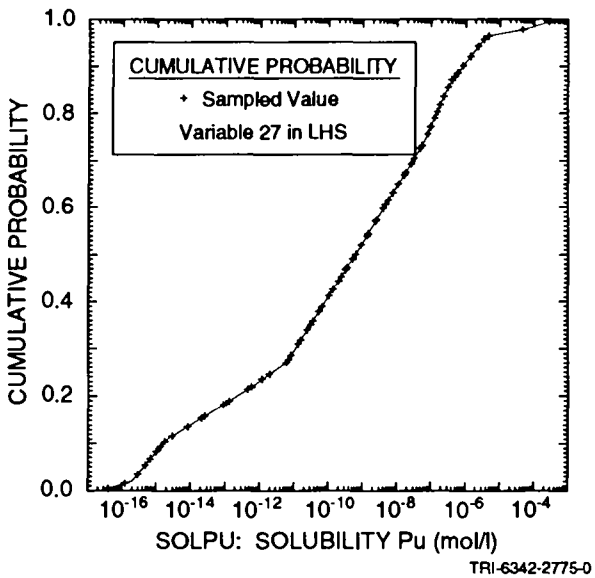

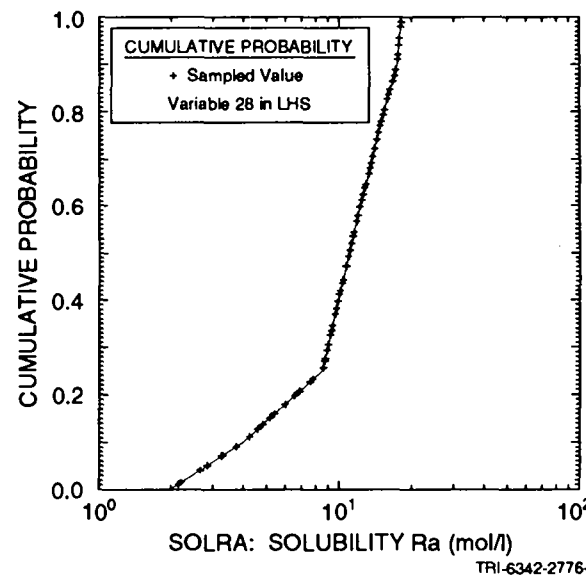

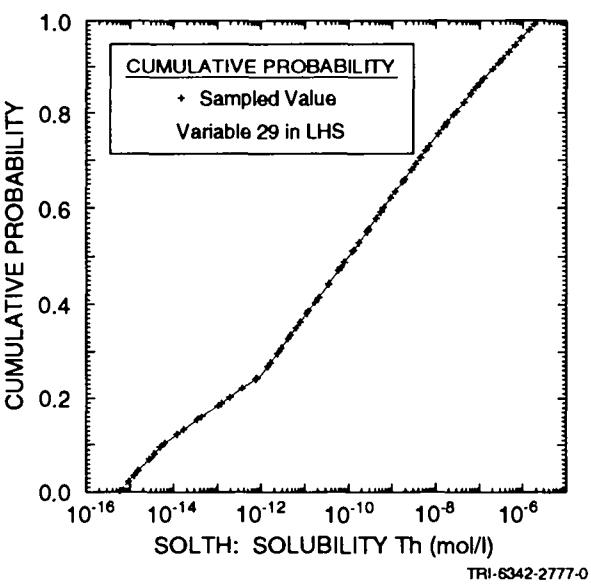

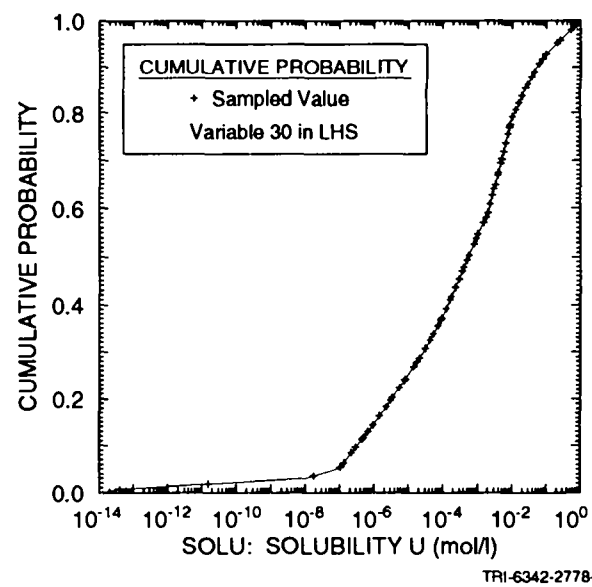

Figure 3-1. Distributions used for sampled variables in 1992 WIPP performance assessment. (continued)

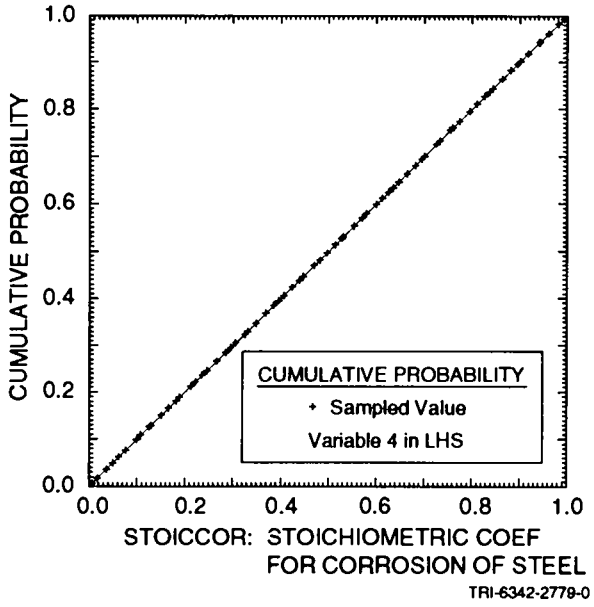

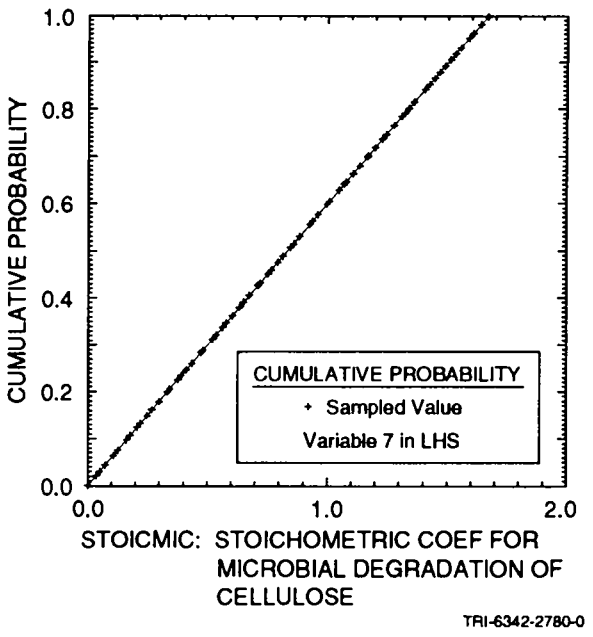

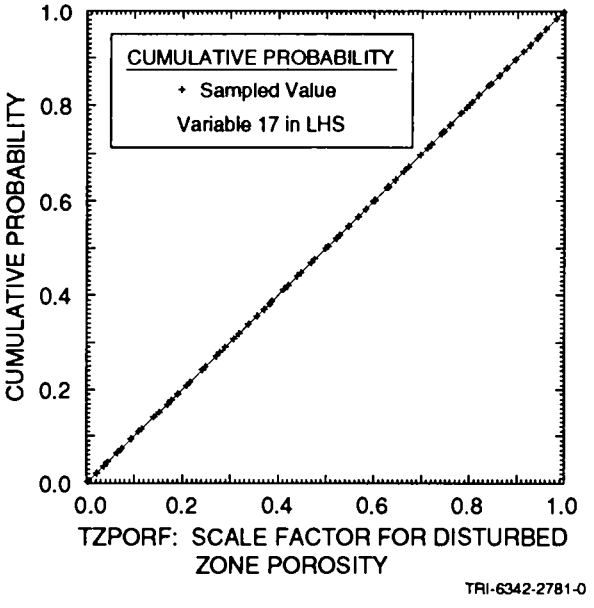

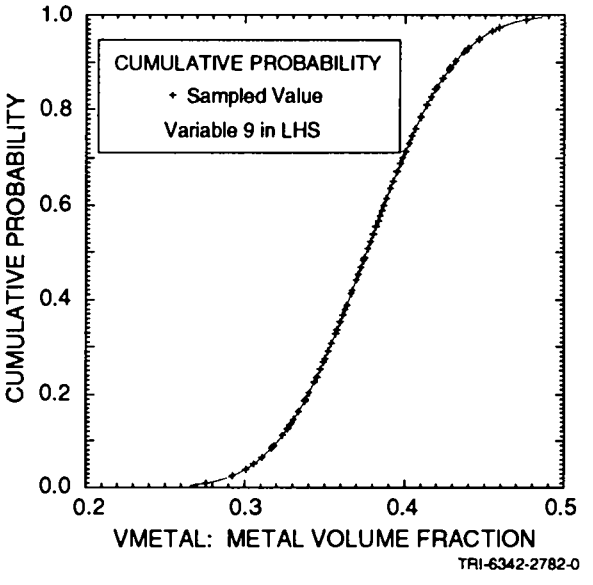

Figure 3-1. Distributions used for sampled variables in 1992 WIPP performance assessment. (continued)

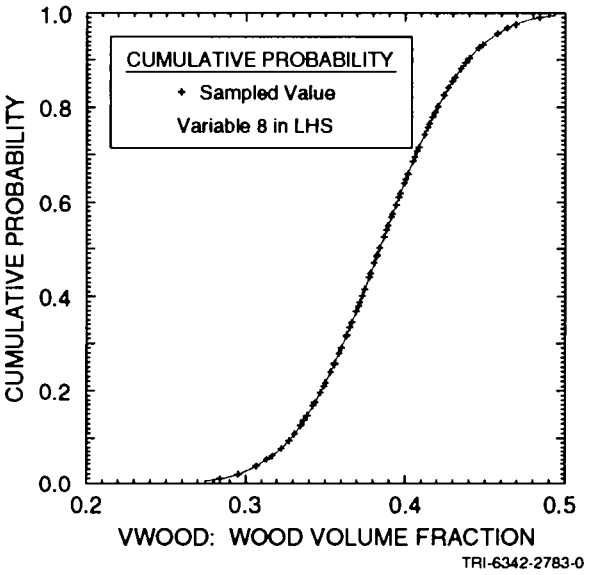

Figure 3-1. Distributions used for sampled variables in 1992 WIPP performance assessment. (continued)

Table 3-2. Further, the impact of individual variables are investigated with sensitivity analysis techniques based on scatterplots, regression analysis and partial correlation analysis. Scatterplots are also used to compare results obtained with the different analysis cases listed in Table 3-2.

Before concluding this chapter, it is perhaps worth emphasizing that the WIPP performance assessment uses two different experimental designs in the treatment of uncertainty. The division of the sample space S in Eq. 2.2-1 into the scenarios S_i indicated in Eq. 2.1-1, and more explicitly in Tables 2.5-1 through 2.5-4, is an experimental design based on importance sampling and is used to assure that the exceedance probabilities associated with the EPA release limits (i.e., 0.1 and 0.001) are approximately estimated (Helton and Iuzzolino, 1993). Such designs are used in analyses where it is important to include the effects of low probability, but possibly high consequence, occurrences. The generation of a Latin hypercube sample of size 70 from the 49 variables in Table 3-1 is a type of random design. Such designs, especially Latin hypercube sampling, are often used in uncertainty/sensitivity studies because of their efficient stratification across the range of each variable under consideration. Thus, the WIPP performance assessment is using an experimental design based on importance sampling to incorporate the effects of stochastic uncertainty and an experimental design based on Latin hypercube sampling to assess the effects of subjective uncertainty. In particular, the use of a Latin hypercube sample of size 70 to assess the effects of subjective uncertainty has no effect on the estimation of the 0.1 and 0.001 exceedance probabilities in the individual CCDFs used in comparison with the EPA release limits.

Additional information on the uncertainty and sensitivity analysis techniques in use is available elsewhere (Chapter 3 in Volume 2; Helton et al., 1991).

Table 3-2. Alternative Modeling Assumptions Considered in the 1992 WIPP Performance Assessment. "CUTTINGS" refers to direct releases at the ground surface during drilling. "GW TO ACC ENV" refers to releases at the subsurface boundary of the accessible environment due to groundwater transport in the Culebra Dolomite Member of the Rustler Formation.

	TYPE OF RELEASE	CUTTINGS	CHEMICAL RETARDATION	CLAY LINING IN FRACTURES	MATRIX DIFFUSION
1	CUTTINGS	+			
2	GW TO CULEBRA	-			
3	GW TO ACC ENV	-	-	-	-
4	GW TO ACC ENV	-	+	+	-
5	GW TO ACC ENV	-	+	-	+
6	GW TO ACC ENV	-	+	+	+
7	GW TO ACC ENV	-	-	+	-
8	GW TO ACC ENV	-	-	-	+
9	GW TO ACC ENV	-	-	+	+
10	CUTTINGS + GW TO ACC ENV	+	-	-	-
11	CUTTINGS + GW TO ACC ENV	+	+	+	-
12	CUTTINGS + GW TO ACC ENV	+	+	-	+
13	CUTTINGS + GW TO ACC ENV	+	+	+	+
14	CUTTINGS + GW TO ACC ENV	+	-	+	-
15	CUTTINGS + GW TO ACC ENV	+	-	-	+
16	CUTTINGS + GW TO ACC ENV	+	-	+	+

4. UNDISTURBED PERFORMANCE (REPOSITORY/SHAFT)

4.1 Model Geometry

For undisturbed performance of the repository/shaft system, BRAGFLO simulates two-phase flow[1] in a geometry very similar to that used in previous gas and brine migration analyses (Case 3 in WIPP PA Department, 1992) related to the Resource Conservation and Recovery Act (RCRA) (EPA, 1986). This model represents the three-dimensional repository (Figure 4.1-1) using a two-dimensional rectangular grid oriented vertically north-south through the disposal system (Figure 4.1-2). This grid preserves the initial excavated volume of various regions and their original excavated heights. Major assumptions made in the construction of this grid include:

- All waste is lumped into one region immediately south of the seals and backfill region. The volume of the waste-emplacement block equals the excavated volume of all the panels in the WIPP repository.

- The access and ventilation drifts are lumped into one region of high permeability immediately south of the shaft system. The volume of this region equals that of the original excavated volume of all of the drifts south of the Waste Shaft.

- The four shafts are consolidated into a single shaft at the location of the Waste Shaft. The volume and cross-sectional area of the consolidated shaft equals that of the four shafts. The single modeled shaft is divided vertically into two segments with a single seal in between. Thickness of the shaft seal is assumed to vary between 10 and 50 m.

- The experimental rooms are combined into a region directly north of the single shaft. The volume of this region equals that of all the excavated region north of the shafts.

---

1. The BRAGFLO computational model is described in detail in Appendix A in Volume 2 of this report, and in literature cited therein; a discussion of multiphase flow through porous media, which BRAGFLO models, is provided in Section 7.2 in Volume 2 of this report.

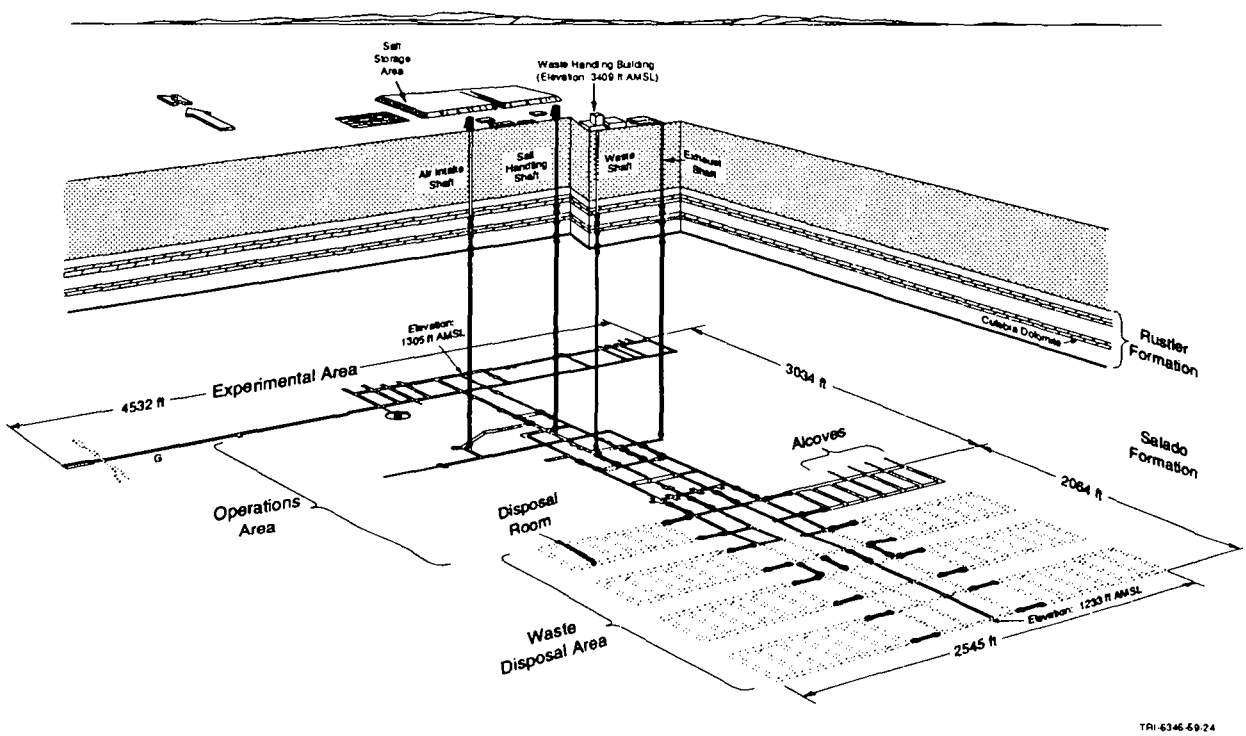

Figure 4.1-1. Proposed WIPP repository showing the 10 waste-disposal regions (panels) (after Waste Management Technology Department, 1987).

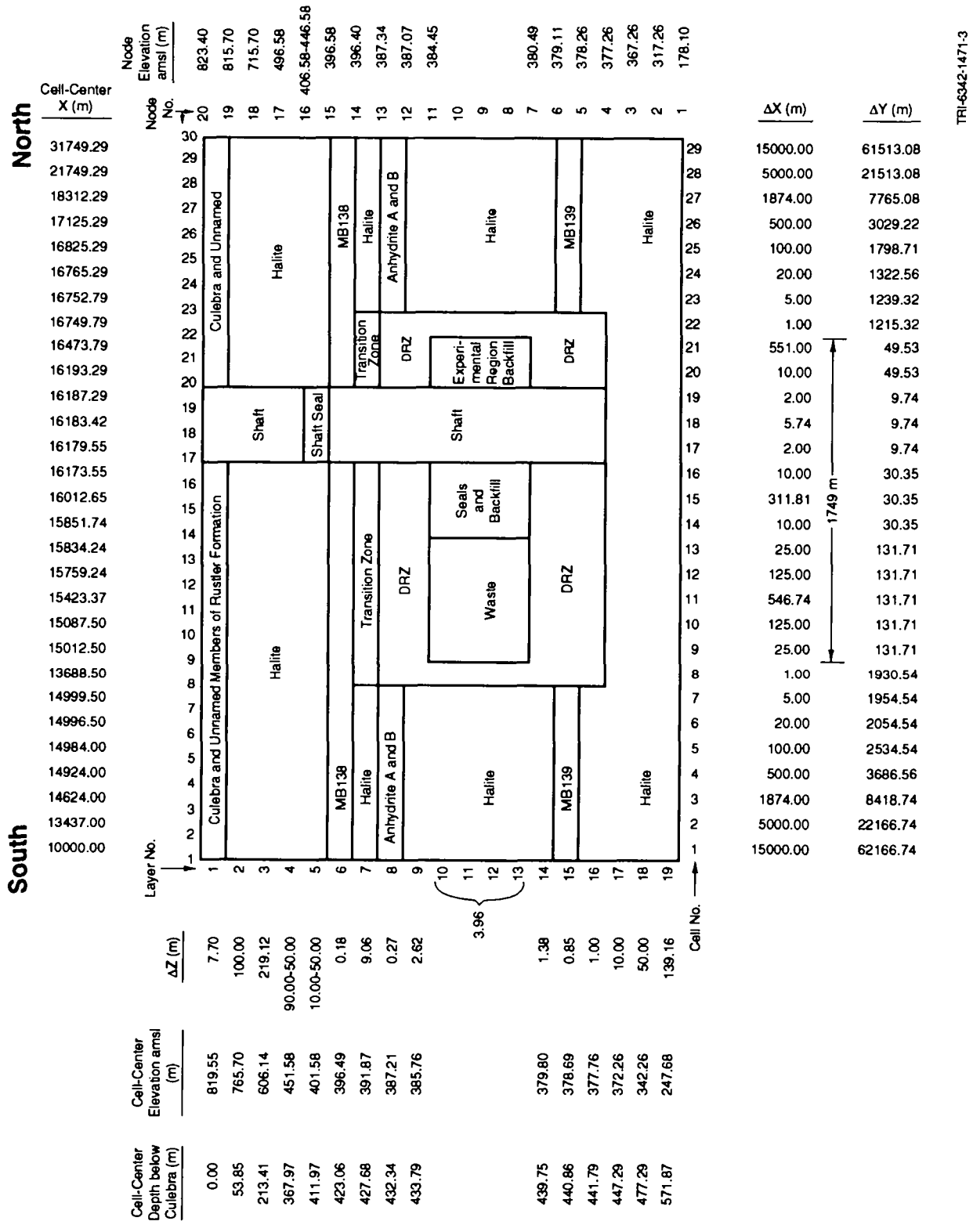

Cell-Center X (m)
31749.29
21749.29
18312.29
17125.29
16825.29
16765.29
16752.79
16749.79
16473.79
16193.29
16187.29
16183.42
16179.55
16173.55
16012.65
15851.74
15834.24
15759.24
15423.37
15087.50
15012.50
13688.50
14999.50
14996.50
14984.00
14924.00
14624.00
13437.00
10000.00

Node No.	Node Elevation amsl (m)
20	823.40
19	815.70
18	715.70
17	496.58
16	406.58-446.58
15	396.58
14	396.40
13	387.34
12	387.07
11	384.45
10	
9	
8	
7	380.49
6	379.11
5	378.26
4	377.26
3	367.26
2	317.26
1	178.10

Layer No.	Cell-Center Depth below Culebra (m)	Cell-Center Elevation amsl (m)	ΔZ (m)
1	0.00	819.55	7.70
2	53.85	765.70	100.00
3	213.41	606.14	219.12
4	367.97	451.58	90.00-50.00
5	411.97	401.58	10.00-50.00
6	423.06	396.49	0.18
7	427.68	391.87	9.06
8	432.34	387.21	0.27
9	433.79	385.76	2.62
10			3.96
11			
12			
13			
14	439.75	379.80	1.38
15	440.86	378.69	0.85
16	441.79	377.76	1.00
17	447.29	372.26	10.00
18	477.29	342.26	50.00
19	571.87	247.68	139.16

Cell No.	ΔX (m)	ΔY (m)
29	15000.00	61513.08
28	5000.00	21513.08
27	1874.00	7765.08
26	500.00	3029.22
25	100.00	1798.71
24	20.00	1322.56
23	5.00	1239.32
22	1.00	1215.32
21	551.00	49.53
20	10.00	49.53
19	2.00	9.74
18	5.74	9.74
17	2.00	9.74
16	10.00	30.35
15	311.81	30.35
14	10.00	30.35
13	25.00	131.71
12	125.00	131.71
11	546.74	131.71
10	125.00	131.71
9	25.00	131.71
8	1.00	1930.54
7	5.00	1954.54
6	20.00	2054.54
5	100.00	2534.54
4	500.00	3686.56
3	1874.00	8418.74
2	5000.00	22166.74
1	15000.00	62166.74

Figure 4.1-2. Plan view of the geometry of the two-dimensional vertical cross-section model used for modeling undisturbed performance of the repository/shaft system.

- Stratigraphic layers are assumed to be parallel and horizontal; the repository elevation actually follows the marker beds at the WIPP, which are slightly undulatory and dip less than 1 degree to the southeast. The elevation of the repository, excavated at a constant stratigraphic horizon, drops about 7 m between the Waste Shaft and the southernmost panel. The model does not include this change in elevation.

Figure 4.1-2 shows the model grid in the vertical (z), north-south (x) plane. The region extends vertically 645 m from the top of the Culebra Dolomite Member of the Rustler Formation to the bottom of the Salado Formation. The total north-south length is approximately 47 km. Stratigraphic units included in the model are the Culebra Dolomite, the intact halite of the Salado Formation, MB138, anhydrites A and B lumped into a single anhydrite layer, MB139, a disturbed rock zone (DRZ) surrounding the waste-emplacement and experimental areas, and a transition zone immediately above the DRZ that provides a potential pathway to MB138.

The width of the elements (the out-of-plane [y] dimension in Figure 4.1-2) varies significantly in the x direction, from as little as 9.74 m at the location of the shaft to as much as 62 km in the intact Salado Formation. The y dimension, however, does not vary vertically. For example, the Δy value for cell 20 (49.53 m), which is comparatively small because of the small excavated volume, remains the same regardless of the vertical (z) location specified by the node number. Figures 4.1-3 and 4.1-4 show a scaled plan view of the grid in the horizontal (x-y) plane containing the repository.

The out-of-plane grid block y dimension is included in the model only to allow for variable storage volumes in each block. Flow is not modeled in the y direction, and occurs only in the x and z directions (in the plane of Figure 4.1-2).

The y dimension at the ends of the mesh, south of the waste block and north of the experimental region backfill, increases in a cylindrical manner away from the model to simulate some of the three-dimensional behavior using a two-dimensional model. Close to the repository, flow paths will have complex orientations determined by the variable geometry of the excavations; fluid flow will be primarily horizontal and mostly through the anhydrite layers. Farther away from the repository, at a distance perhaps several times the maximum horizontal dimension of the repository (about 1.7 km), flow will be nearly radial. All flow is assumed to result from the disturbances introduced by the repository; i.e., there is no regional flow field that predates excavation of the repository. Flow to and from the repository in

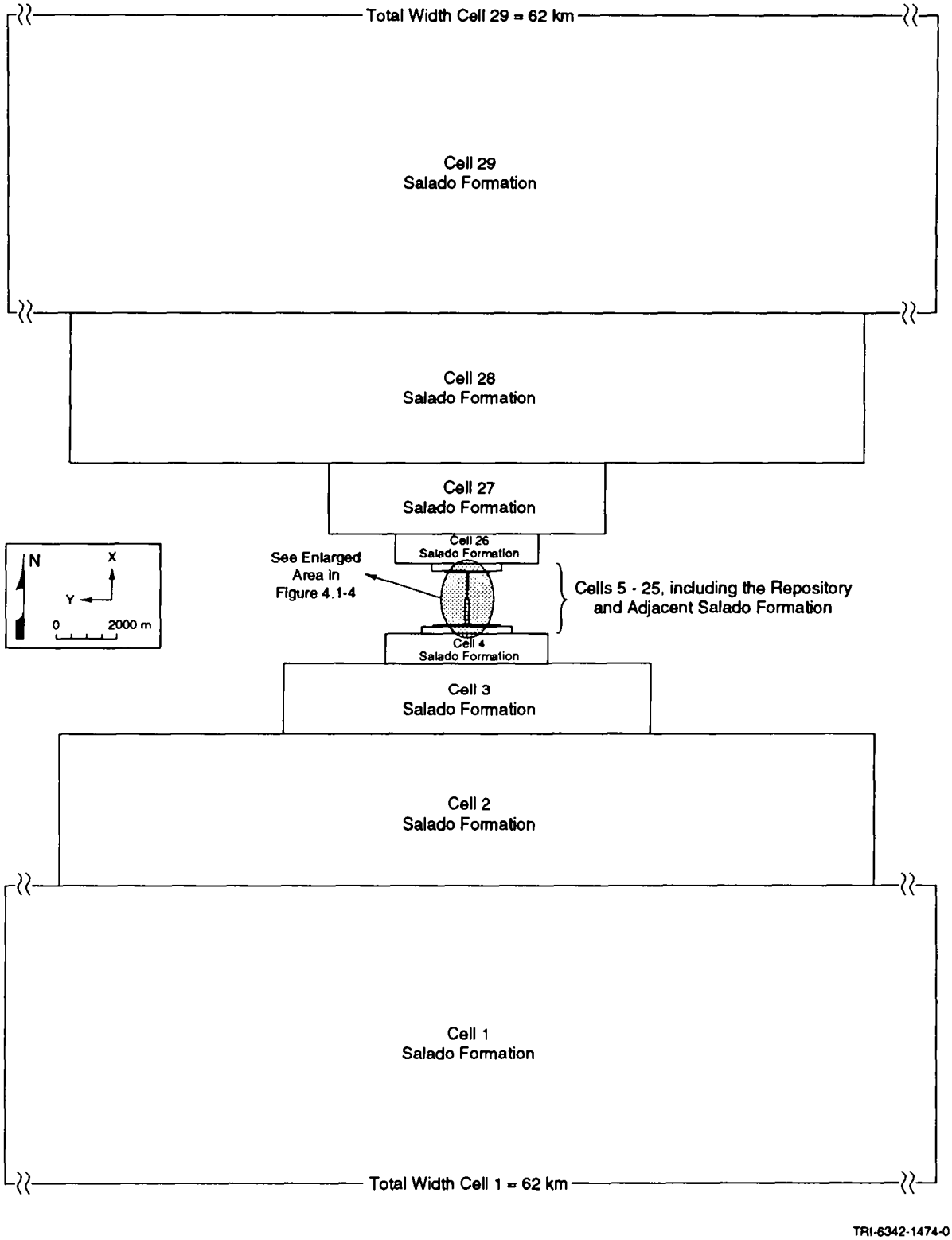

Figure 4.1-3. Scaled view of layer 12 of Figure 4.1-2. Cells representing the repository and its immediate vicinity are too small to plot individually at this scale.

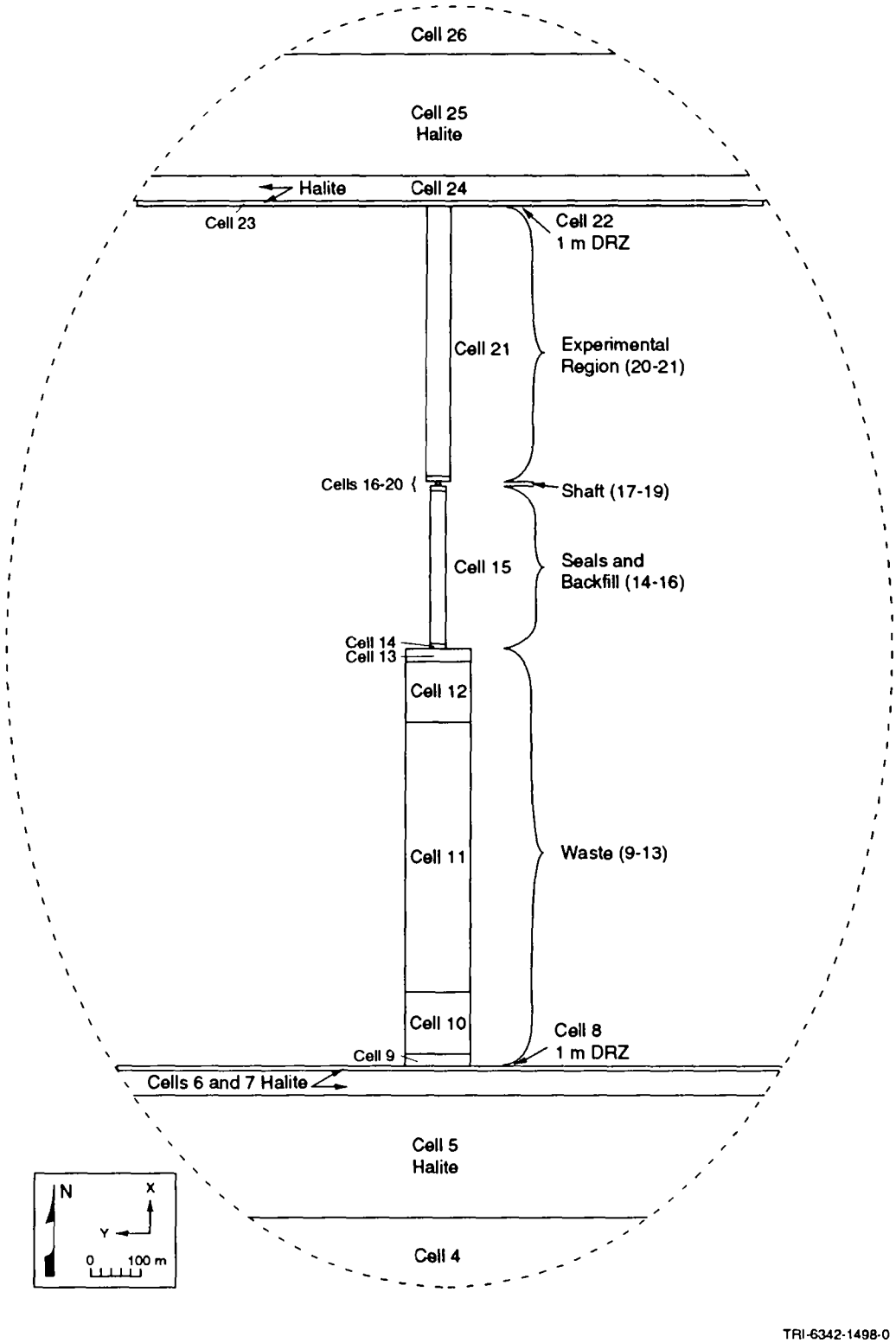

Figure 4.1-4. Enlargement of the central portion of Figure 4.1-3.

the surrounding region can be approximated with the two-dimensional model if the y dimension of the grid blocks increases away from the repository by a factor of approximately $2\pi r$, where r is the distance from the center of the grid (Voss, 1984).

In a strict sense, the $2\pi r$ relationship is valid only if it is applied to the entire mesh. Such a mesh represents a vertical cylinder that allows a two-dimensional model to simulate radial flow in a three-dimensional cylinder. In the mesh used for undisturbed performance of the repository/shaft system, only the north and south ends of the modeled regions are treated in this fashion, and the results are not expected to be precise in modeling all flow north and south of the repository/shaft system. However, as a first approximation, this procedure accounts for the radial increase in pore volume away from the central region. This radial increase in pore volume is important because brine and gas will not flow in only two dimensions (x and z) as they flow from (or towards) the repository. Rather, at a distance of a few kilometers from the repository (approximately the disposal-unit boundary), flow will be radial into (or from) an increasingly larger pore volume.

4.2 Material Properties

Material properties for undisturbed performance of the repository/shaft system are discussed in detail throughout Volume 3 of this report and are summarized in Chapter 6 of Volume 3. The following material properties that apply specifically to undisturbed performance of the repository/shaft system are discussed below in the indicated sections:

- permeability (Sections 4.1.2.1 and 4.1.2.4),
- porosity (Section 4.1.2.2),
- specific storage (Section 4.1.2.3),
- brine and gas saturations (Sections 4.1.2.4),
- capillary pressure (Section 4.1.2.4).

Radionuclide transport is not modeled for the undisturbed case because releases into the Culebra Dolomite Member of the Rustler Formation do not occur (see Section 4.4), and therefore, parameter values for radionuclide inventory and solubilities are not input for the undisturbed performance calculations.

4.2.1 Permeability

4.2.1.1 PERMEABILITY RANGES

Permeability values used for the undisturbed repository/shaft model are shown in Figure 4.2-1 and listed below in order of increasing permeability:

- Halite is assigned a range of permeability values from 1.0×10^{-24} to 1.0×10^{-19} m^2.
- The shaft seal is assigned a range from 3.3×10^{-21} to 3.3×10^{-20} m^2.
- Anhydrite interbeds (MB138, MB139, and anhydrite A and B) and the transition zone above the DRZ are assigned a range from 1.0×10^{-21} to 1.0×10^{-16} m^2.
- The DRZ, the upper and lower shaft, the seals and backfill for the waste storage rooms, and the backfill for the experimental region are assigned a value of 1.0×10^{-15} m^2.
- The Culebra is assigned a value of 2.1×10^{-14} m^2.
- The waste is assigned a value of 1.0×10^{-13} m^2.

The permeability range for the anhydrite interbeds (1.0×10^{-21} to 1.0×10^{-16} m^2) is larger than that estimated for undisturbed anhydrite, but does not explicitly take into account pressure dependent fracturing of these interbeds. Interbed fracturing as a result of gas pressurization is not modeled in the 1992 calculations. Implications of not modeling interbed fracturing are uncertain. The phenomenon will be modeled in future PAs.

4.2.1.2 CULEBRA PERMEABILITY

Culebra permeability above the repository/shaft system, which is an important material property primarily for the disturbed calculations, is explained in Section 5.1.2.2. Culebra permeability above the repository/shaft system for undisturbed conditions is determined in the same manner as for disturbed conditions.

4.2.2 Porosity

4.2.2.1 FIXED (TIME-INVARIANT) POROSITY

Assumed porosity values for materials in the undisturbed repository/shaft simulation that do not change with respect to time are listed below and shown in Figure 4.2-2:

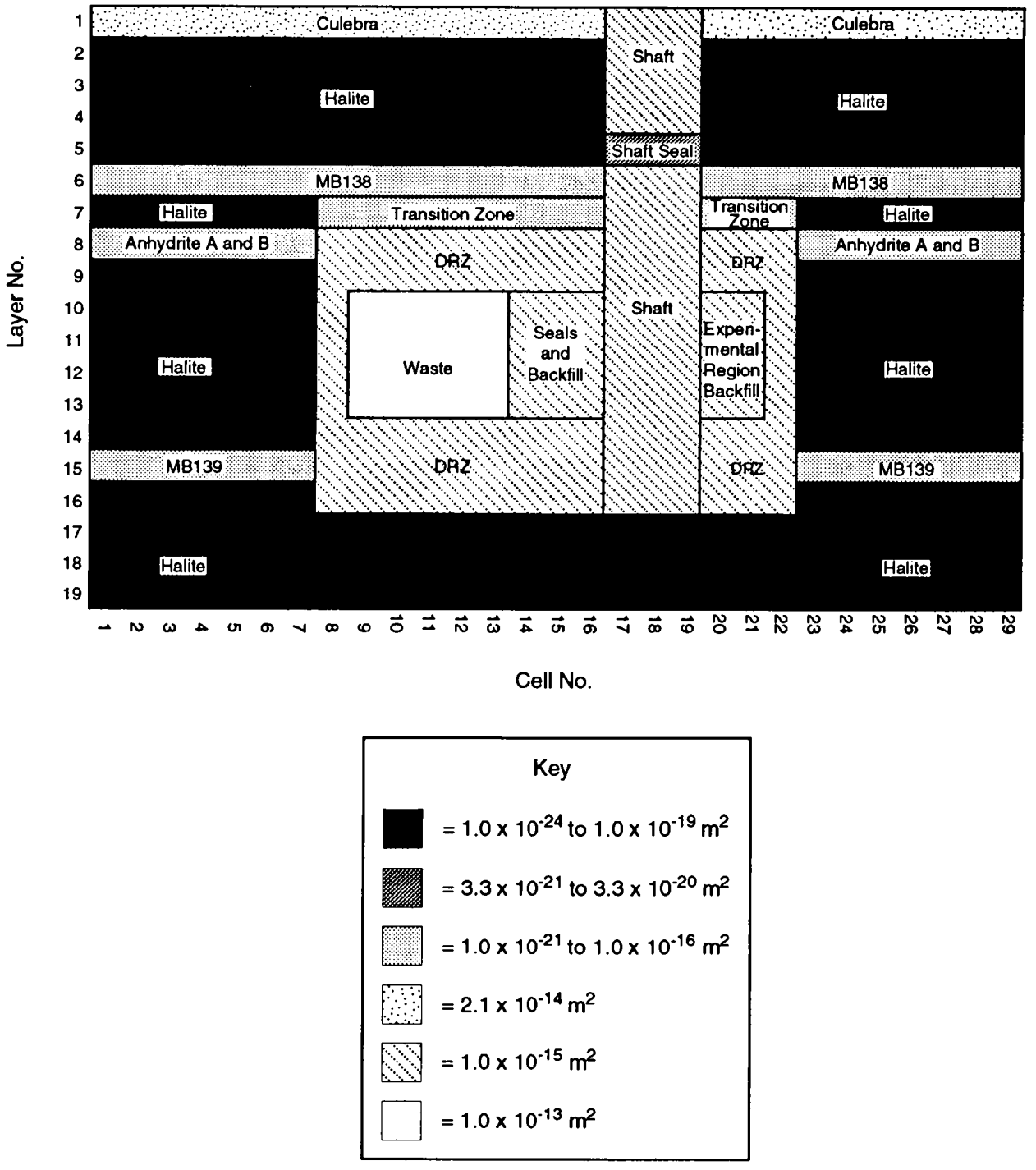

Figure 4.2-1. Permeability values for the undisturbed repository/shaft system.

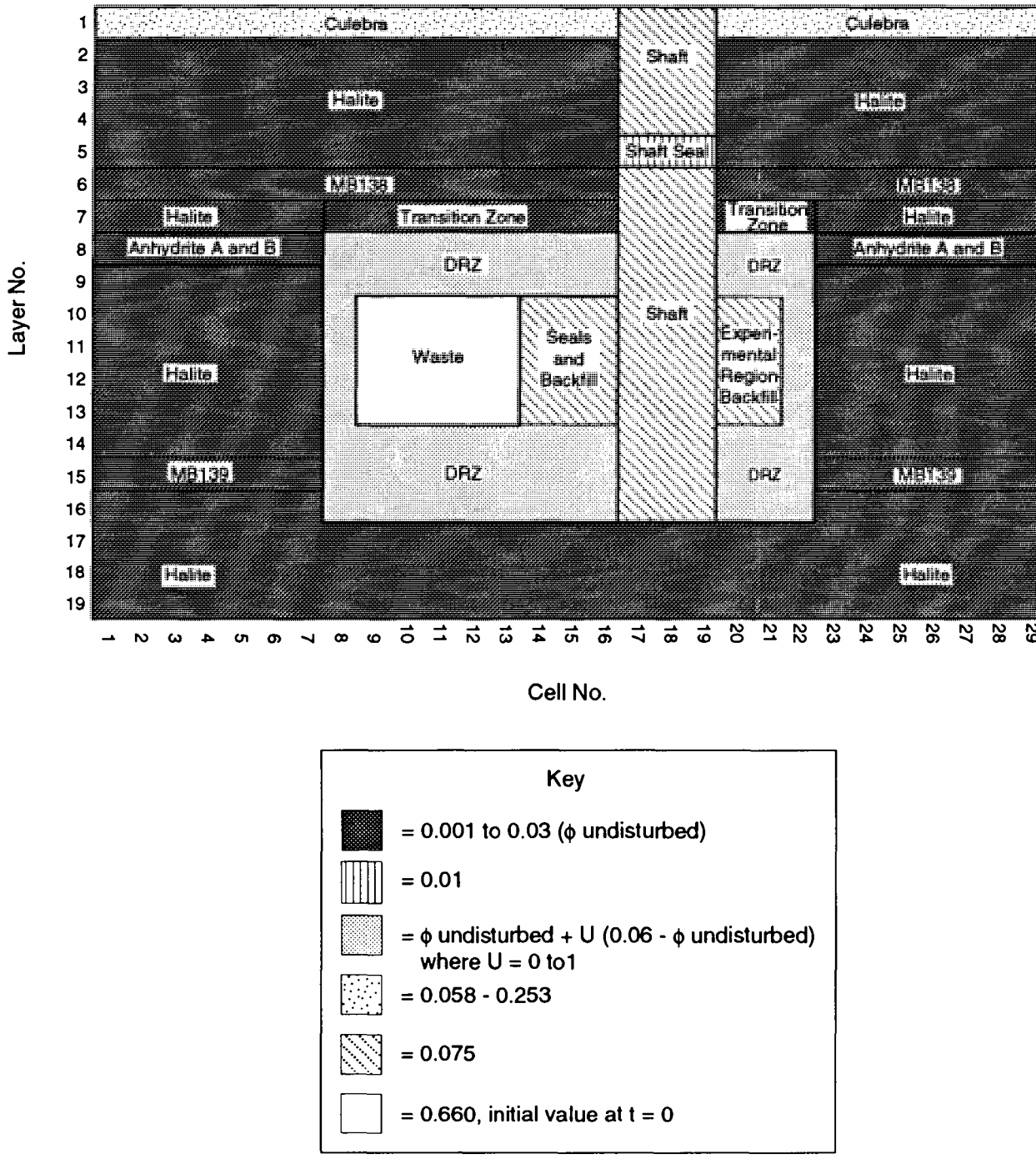

Figure 4.2-2. Time-invariant porosity values for the undisturbed repository/shaft system.

- Halite, the anhydrite interbeds, and the transition zone are assigned a range of porosity values from 0.001 to 0.03.

- The shaft seal is assigned a value of 0.01.

- A slightly higher range of porosity values is assigned to the DRZ. As is explained in Section 2.4.4 of Volume 3 of this report, the DRZ range is determined by the relationship

$$\phi_{disturbed} = \phi_{undisturbed} + U(0.06-\phi_{undisturbed}), \qquad (4.2\text{-}1)$$

where U is a number uniformly distributed between 0 and 1, and $\phi_{undisturbed}$ is the porosity range of the undisturbed halite (0.001 to 0.03). This relationship forces the DRZ porosity, $\phi_{disturbed}$, to fall within a range bounded by $\phi_{undisturbed}$ and 0.06, which is the maximum DRZ porosity considered (see WIPP PA Division 1991c, Section 2.3.7).

- A porosity value of 0.075 is assigned to the entire shaft (except the shaft seal) and the seals for the waste storage area, and the backfill for both the waste storage and experimental areas.

- The Culebra is assigned a range from 0.058 to 0.253.

- The waste prior to closure modeling is assigned a value of 0.660.

4.2.2.2 TIME-VARYING POROSITY

Background

In the 1991 and previous BRAGFLO simulations of the repository/shaft system (WIPP PA Division, 1991b; WIPP PA Department, 1992), porosity in the waste-emplacement panels was assumed to be constant in time. The effect of halite creep on waste-panel porosity was not accounted for. The porosities assigned to the waste panel for each of the 1991 realizations were determined in an external calculation (WIPP PA Division, 1991c). These porosities were calculated as the post-compaction pore volume required to store all of the waste-generated gas at lithostatic pressure in a brine-free repository. These "lithostatic equilibrium" porosities varied with sampled values for waste composition, gas-generation rates, and stoichiometry. Although these externally calculated porosities did not limit panel pressure to lithostatic, they may have overestimated the void volume available for gas for cases where the panel does not re-expand significantly beyond the closed state.

Another shortcoming of the 1991 approach was that the external calculation of porosities correlated porosity only to the theoretical gas-generation potential, which is the amount of gas that would be generated if all ferrous metal and cellulosic material was completely consumed (see Sections 1.4.1 and 3.3 of Volume 3 of this report for additional information about the gas-generation model). In some realizations, brine availability limits the amount of gas generated to less than the theoretical potential and not all ferrous metal or cellulose is consumed. Modeling studies using the finite element program SANCHO[2] for simulating quasistatic, large-deformation, inelastic response of two-dimensional solids indicate that low gas-generation rates result in more rapid closure and lower porosities at full compaction.

1992 Approach for Accounting for Time-Dependent Panel Porosity

The 1992 BRAGFLO calculations include a simple first attempt at accounting for time-dependent panel porosity. This time dependence is indirect in the sense that results from this application of SANCHO indicate that panel porosity varies with the amount of gas generated and the pore pressure in the waste area, each of which in turn varies with time.

The discussion that follows describes the implementation of the SANCHO halite deformation results in BRAGFLO for the 1992 PA calculations. The SANCHO results and data of importance for use in BRAGFLO, discussed in detail below, are

- moles of gas generated,
- time after sealing of repository,
- panel pressure, and
- panel porosity.

The porosity contours appearing in Figure 7-2 in Volume 2 of this report result from interpolation of the SANCHO results that describe the dependence of panel porosity on cumulative moles of gas produced and time after sealing. The direct (not interpolated) SANCHO porosity results are presented in Figure 4.2-3. "Noise" visible in the solutions are an artifact of the approach used

---

2. The SANCHO computational model is described by Stone et al., 1985, and summarized in Appendix B in Volume 2 of this report; a discussion of room closure, which SANCHO models, is provided in Section 7.3 in Volume 2 of this report. SANCHO is also discussed in Sections 1.4.1 and 1.4.7 of Volume 3 of this report.

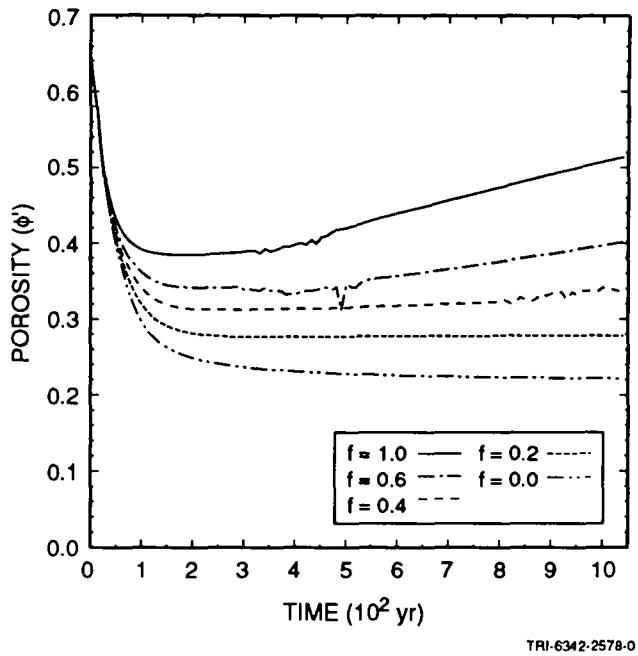

Figure 4.2-3. SANCHO results: porosity as a function of time for f=1.0, 0.6, 0.4 and 0.2; piecewise constant gas-generation rates; porosity based on SANCHO definition of porosity (ratio of void volume to instantaneous room volume); f is the fraction of the piecewise constant gas-generation rate and potential, where f=1.0 is defined as the sum of the corrosion rate (1 mole/drum-yr for 1050 yr) and the biodegradation rate (1 mole/drum-yr for 550 yr) (Brush, 1991; memorandum by Beraun and Davies in Appendix A of Volume 3 of this report).

to model separation at the surface between the waste/backfill and the overlying halite as pressure in the room exceeds lithostatic, and are not attributed to a physical process. This "noise" has been filtered out of the SANCHO solution prior to its use in BRAGFLO. Smoothed SANCHO results form the basis of accounting for the effect of halite creep on waste room porosity and are used within BRAGFLO.

The difference in definition of porosity by SANCHO and BRAGFLO requires further manipulation of the data presented in Figure 4.2-3. In SANCHO, as the halite creeps, the numerical mesh deforms; in BRAGFLO, the mesh dimensions are fixed with time. In the SANCHO room model, the porosity (ϕ' of Figure 4.2-3) is therefore defined as the ratio of the void volume to the current total volume of the panel. In BRAGFLO, the porosity (ϕ, Eq. 4.2-2) is therefore defined as the ratio of the void volume to the initial volume of the panel. If the mass and volume of the solids contained within the deforming panel does not change with time, the two differently defined porosities can be related by

$$\phi(t) = \phi'(t) \left[\frac{1-\phi'(t_o)}{1-\phi'(t)} \right] . \qquad (4.2\text{-}2)$$

A derivation of Eq. 4.2-2 is provided in Appendix B. The porosities as defined by SANCHO (Figure 4.2-3) are converted to porosity as defined by BRAGFLO by using Equation 4.2-2 and are presented in Figure 4.2-4.

Conceptual Modeling Differences Between SANCHO Room Model and BRAGFLO Panel/Repository Model

Because SANCHO and BRAGFLO simulate fundamentally different processes (large-scale quasistatic deformation of solids versus multi-phase fluid flow in nondeforming porous media), some differences have arisen in the conceptual models for the disposal system used in applications of the two codes. Differences between the SANCHO and BRAGFLO conceptualizations used in the 1992 PA that have important implications for the representation of time-varying porosity are as follows:

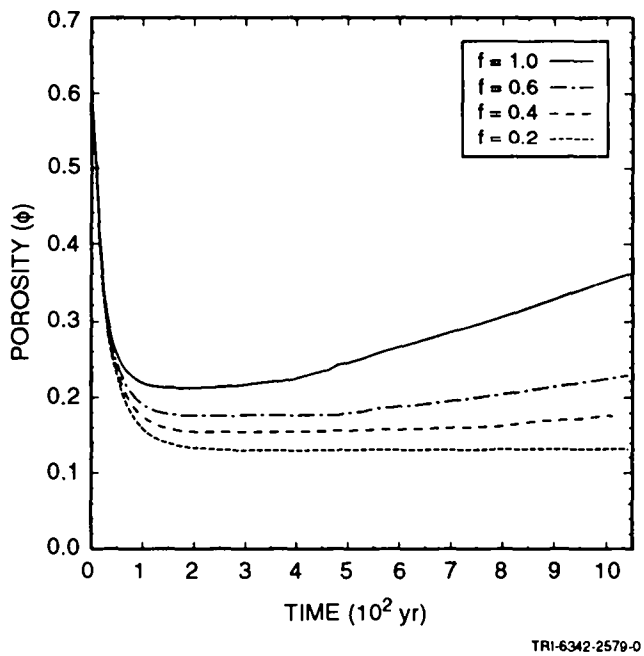

Figure 4.2-4. SANCHO results: porosity as a function of time for f=1.0, 0.6, 0.4, 0.2 and 0.1; piecewise constant gas-generation rates and potentials; porosity based on BRAGFLO definition of porosity (ratio of void volume to initial room volume); f is defined in Figure 4.2-3.

- This application of SANCHO models the behavior of a single room in an infinite array of rooms, simulating behavior of the middle rooms in a panel; BRAGFLO models the behavior of the entire repository for undisturbed conditions and an axisymmetric cylindrical-equivalent single panel for disturbed conditions.

- In the SANCHO room model, pressure and gas generation rates within the waste storage area are spatially uniform; in BRAGFLO, they vary spatially.

- In the SANCHO room model, the void space is completely occupied by waste-generated gas; in BRAGFLO, this space is occupied by two fluid phases, brine and gas.

- In the SANCHO room model, gas was not allowed to flow into or out of the waste area; in BRAGFLO, gas and brine flow into or out of the waste area.

- In the SANCHO room model, gas is generated at a constant rate for each reaction (corrosion and biodegradation) for fixed periods of time; in BRAGFLO, gas generation is not constant: it varies with degree of brine saturation in the waste area and continues until all of the corrodible metal and cellulose or brine are consumed.

- This application of the SANCHO room model simulates undisturbed repository performance for 2000 yr; these BRAGFLO simulations describe both undisturbed and disturbed performance for 10,000 yr.

Modeling Assumptions

The differences discussed above between the conceptual models used in the applications of the two codes led to difficulties in using the SANCHO porosity results in BRAGFLO. Specifically, the implementation of time-varying porosity in BRAGFLO for the 1992 PA required the following assumptions:

- Halite creep is assumed to affect the porosity of the waste storage area until the time of maximum repository pressure. Results were produced for cases in which pressure in the room increases from its initial level at various rates, dependent on gas-generation rates. Stress gradients between the host halite and the waste-filled room were not determined when waste-room pressure fell as gas escaped.

Rather than speculate on the halite response during decreasing waste-panel pore pressure, porosity in BRAGFLO is held constant at the value it has when pressure begins to fall. Porosity is maintained at this value unless and until pressure rises above its previous temporary maximum. This treatment of porosity may somewhat underestimate the degree of closure (overestimate porosity) by neglecting continuing creep closure. However, errors introduced by this treatment are believed to be small because reexpansion of the room is a relatively slow process compared to room closure/ consolidation, which is largely complete before pressures rise sufficiently to cause increases in porosity. Figure 4.2-4 indicates rather modest rates of increases in porosity after maximum consolidation, particularly at the lower gas-generation rates, compared to the dramatic decrease in porosity prior to maximum closure. As discussed in the following section, significant increases in waste-area porosity resulting from the reversal of creep closure require pressures in excess of lithostatic. As long as repository pore pressure is close to or below lithostatic, porosity in the waste panel is close to its fully compacted value. Limiting waste-panel porosity at this value somewhat limits the void volume available to store inflowing brine and generated gas.

- The effect of halite deformation on the porosity of material in a disposal room is assumed to be representative of the effect on the porosity of material in an excavated panel or the entire disposal region. It is recognized that the stress fields surrounding a single room do differ depending on where in the panel the room is located. The gross response of the halite resulting from the spatially varying deviatoric and room stress on porosity is assumed to be independent of the size or geometry of the WIPP excavation when implemented in BRAGFLO.

- In this application of SANCHO, pore pressure and gas-generation rate do not vary spatially within the waste-filled room. In BRAGFLO, pore pressure and gas-generation rate vary spatially throughout the waste-disposal region. Porosity in the panels is assumed to be spatially invariant in BRAGFLO despite spatial variations in pressure and gas-generation rate because the effective (representative) porosity is correlated to the effective panel pore pressure and gas-generation rate. This correlation is implemented by volume-averaging BRAGFLO pore pressures and gas-generation rates within the disposal region and using the average values to determine the porosity within the waste at any point in time.

- It is assumed that interpolation of the data in Figure 4.2-3 yields valid porosity results. The porosity surface (Figure 7-1 in Volume 2

of this report) and the data of Figure 4.2-3 were generated under specific constant rates of gas generation by corrosion and biodegradation and resulting pressure histories. It is assumed that all pressure and gas-generation histories that can be constructed within the bounds of the SANCHO results will yield valid predictions of the effect of halite deformation on waste-storage area porosity.

- Results of the SANCHO simulations indicate that room porosity varies with the gas-generation rate and the time. This is reasonable, because in this application of SANCHO, brine is assumed not to be present and gas cannot escape from the room. However, in BRAGFLO, where both brine and gas occupy void space and can flow into or out of the waste-storage area, the specification of time and gas-generation rate will not in general result in a unique porosity. The difficulty in using the porosity dependency from the no-flow, single-phase fluid system of SANCHO in the multiphase system of BRAGFLO is that Figure 4.2-4 fails to account for the change in pressure due to the flow of brine and gas into or out of the waste room. In addition, because this application of SANCHO did not include a brine phase, any effect the presence of brine in the waste area might have had on halite creep is not captured explicitly. If it is reasonable to assume that the halite responds in part to the degree of back pressure in the waste-storage area as well as the waste-storage area pore-pressure history, then it follows that the porosity associated with the no-flow single-phase system of SANCHO will differ from the porosity in the flowing two-phase system of BRAGFLO, at the same time following sealing and given the same gas-generation rate.

The results from the SANCHO room model strictly apply only to the case where the pore space in the waste-disposal room is occupied by gas and the gas remains in this volume. Additional SANCHO simulations are required to describe more adequately the deformation of the halite when the pore space in the waste area is occupied by both brine and gas and each phase is capable of flowing into or out of the waste. An improved way of dealing with these inconsistencies is planned for future performance assessments. As implemented for 1992, the use of SANCHO results in BRAGFLO are based on the following assumptions about the SANCHO modeling.

- Halite deformation can be correlated in part to pore-pressure history and is independent of the fluid that occupies the pore space.

- Halite deformation is independent of the amount of brine present in the pore space within the room.

- Porosity is parameterized in terms of the rate of gas generation and pore pressure, but not in terms of the amount of gas present in the pore space of the waste panel as calculated by BRAGFLO because gas may flow out of panel in BRAGFLO but is confined to the room in these SANCHO simulations.

The validity of these assumptions and their impact on repository performance are uncertain and still under evaluation. As a result, this extension of the SANCHO-calculated porosities into BRAGFLO should be viewed as an initial attempt to describe the effect of halite deformation on waste-storage area porosity for two-phase flow modeling.

The SANCHO results described in this section represent only a small portion of the types of calculations that have been addressed with this code. Although the closure inputs for the BRAGFLO calculations were derived assuming a single disposal room in an infinite array of rooms, calculations for a full panel of empty rooms are being completed by the Waste Isolation Pilot Plant (WIPP) Disposal Room Systems Department at Sandia National Laboratories (SNL). These calculations will be a first step in examination of the error introduced by using single room closure to approximate the response of larger portions of the repository. The results will be used to examine both porosity variations within a given room and porosity variations from room to room. Calculations for other two-dimensional representations of the repository or its components are equally feasible, depending on the required computer time. Computer time for WIPP closure solutions over hundreds of years is a pressing constraint on mechanical closure analyses because of the complex finite-element mesh that must be constructed to represent disposal room components.

A number of calculations with SANCHO also are being completed by the WIPP Disposal Room Systems Department at SNL to examine the consequences of a human intrusion on post-intrusion closure. Other studies will examine various features of the room model, including the effect of existing cracks in halite and interbeds on gas pressurization. The effect on closure caused by different waste forms will be examined. Although the current SANCHO calculations did not include any fluid flow, calculations are also being completed coupling the mechanical response of the room with single-phase brine flow, and this coupling will be further extended to two-phase fluid flow.

How SANCHO Pore Pressure Data Are Used

In SANCHO a unique pore-pressure history exists for each gas-generation rate. These pressure histories are presented in Figure 4.2-5. This

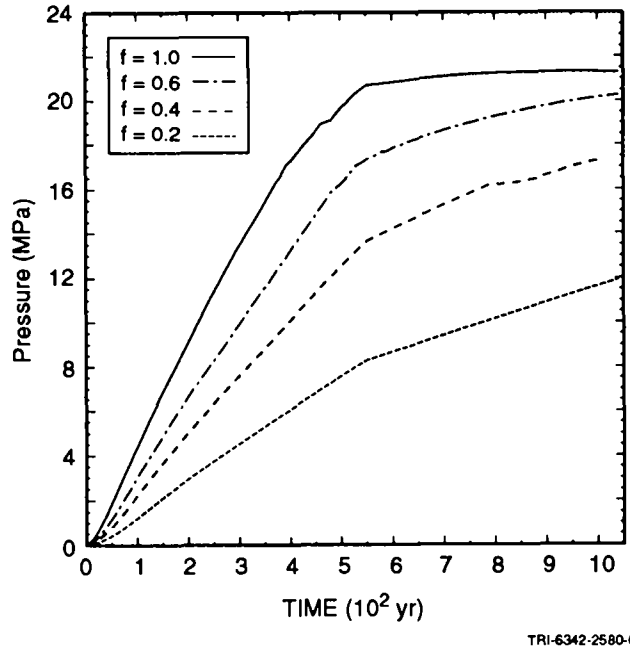

Figure 4.2-5. SANCHO results: pressure as a function of time for f=1.0, 0.6, 0.4 and 0.2; constant gas-generation rates for corrosion and biodegradation; f is defined in Figure 4.2-3.

relationship permits the unique determination of porosity given the gas-generation rate and the pore pressure instead of time, as is shown in Figure 4.2-6. In light of the assumptions mentioned above, the data presented in Figure 4.2-6 are used directly in BRAGFLO. The discussion that follows describes how the data in Figure 4.2-6 are used in the 1992 version of BRAGFLO.

First, the current fraction of gas potential is calculated by summing across all waste the cumulative moles of gas generated and normalizing this sum to the moles of gas that would have been generated under the baseline gas-generation conditions assumed in the SANCHO calculations. These conditions are

- for corrosion: 1 mole gas/(drum•yr) for 1050 yr, and
- for biodegradation: 1 mole gas/(drum•yr) for 550 yr.

To avoid extrapolation of data, this fraction is constrained to fall between a value of 1.0 and 0.1.

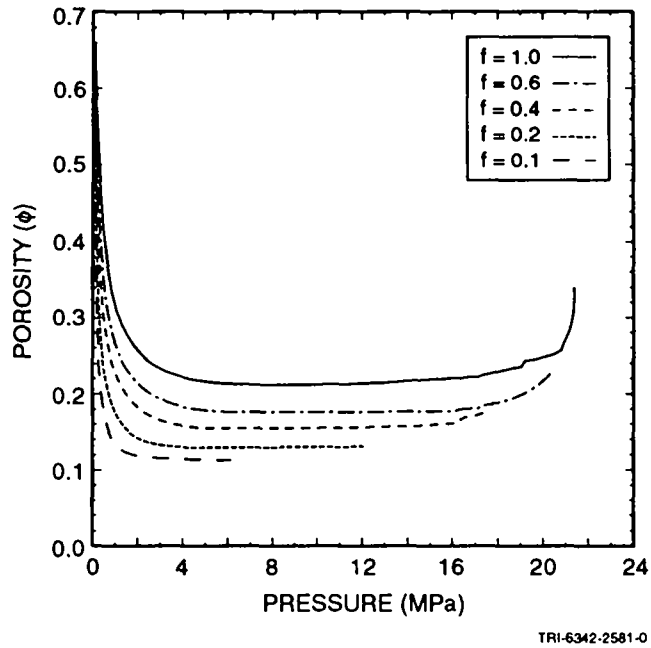

Figure 4.2-6. Modified SANCHO results as used in BRAGFLO: porosity as a function of pressure for constant gas-generation rates; porosity based on initial room brine; f is defined in Figure 4.2-3.

Second, the volume-averaged pore pressure in the waste area is calculated in BRAGFLO by

$$\bar{P} = \frac{\sum_{i=1}^{N} P_i V_i}{\sum_{i=1}^{N} V_i}, \qquad (4.2\text{-}3)$$

where the summation is over all waste grid blocks.

Third, the porosity associated with the BRAGFLO-calculated gas-generation rate fraction (f) and volume-averaged pressure is determined by linear interpolation of the data displayed in Figure 4.2-6. The gas-generation rate fraction is calculated by first accumulating the amount of gas generated in the waste over a given period of time, dividing by the length of time to give an average rate, and finally normalizing to the rates associated with f=1.0. These rates are given previously in this section and also in Figures 4.2-3 through 4.2-7. Some restrictions on the selection of the porosity are made to further avoid extrapolation of the data. These restrictions, depicted on Figure 4.2-7, are described below:

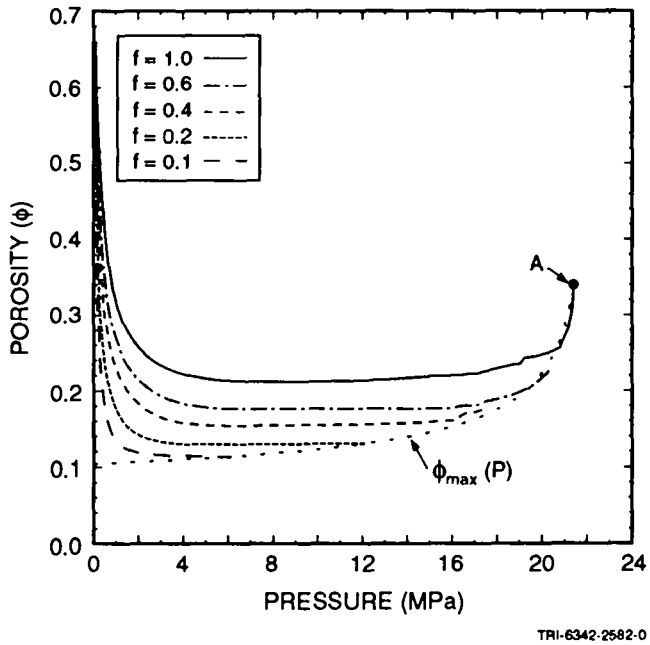

Figure 4.2-7. Limiting porosity, pressure, and gas generation in BRAGFLO implementation; f is as defined in Figure 4.2-3. Point A indicates maximum expanded porosity of waste (0.34), occurring at a pressure of 21.43 MPa.

- The maximum expanded porosity of the waste is limited to a value of 0.34, which occurs at a pore pressure of 21.4 MPa, at Point A in Figure 4.2-7.

- A bounding curve of porosity versus pore pressure, $\overline{P}$ (Pa), is constructed by connecting the points of maximum pressure for each of the gas-generation rate curves. The equation for this bounding curve is

$$\phi_{max} = 0.04991601 + \frac{0.2562233}{\sqrt{22.2 - (\overline{P})(1.0 \times 10^{-6})}} \quad , \qquad (4.2\text{-}4)$$

where $0.1 < \phi < 0.34$, $0 < P < 22$ MPa, and using the positive root.

If the pore pressure during a BRAGFLO simulation exceeds the maximum pressure associated with the current gas-generation fraction, then the dependence of porosity on pressure is restricted to this bounding curve.

- The curves are followed along the direction of low to high pressure only. The porosity results of SANCHO are generated only as waste pore pressure increases. The response of the halite to decreases in pore pressure is not simulated. This is not due to a limitation in SANCHO, but rather to scheduling constraints. Rather than speculate on a possible hysteresis effect, porosity is assumed to remain constant if waste pore pressure decreases and does not vary again until pressure exceeds the level at which it first began to decrease (Figure 4.2-8). If the direction path in which the data were generated is not preserved, physically unreal situations can result. For instance, consider the 10% base gas-generation curve at a pressure of 1 MPa (f = 0.1 on Figure 4.2-7). If the pressure were to decrease and the curve were followed, the porosity would actually increase even though pressure was well below lithostatic. Similarly, if the pressure were well above lithostatic and began to fall but still remained above lithostatic, the porosity from Figure 4.2-6 would decrease when in fact it would be expected still to increase but perhaps at a decreasing rate.

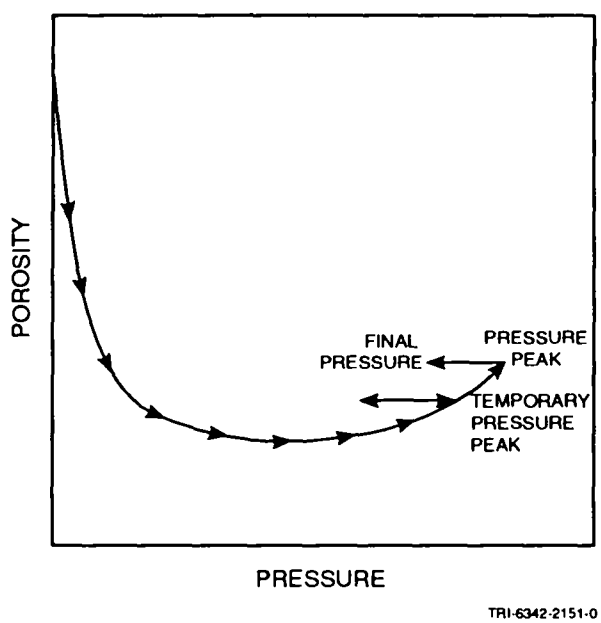

Figure 4.2-8. Hypothetical porosity/pressure path showing porosity treatment when pressure has a maximum.

Time-Step Considerations

Porosity is determined using the values of gas generation and pressure as outlined above at the beginning of a time step. In BRAGFLO, the initial values at a time step are converged values at the end of the previous time step. The porosity so determined is assumed to remain fixed across the current time step even though pressure and gas generation (via saturation) change during the intra-time iterations. The porosity is then updated at the start of the next time step. This explicit treatment of porosity is necessary because the more desirable implicit dating of porosity currently produces convergence difficulties for some of the input sets. In implicit dating, porosity would change with pressure and saturation during the intra-time-step iterations, and thus would change continuously across the time step rather than in step changes at the beginning of each time step, as in the explicit treatment. The more accurate implicit treatment is expected to be included in the 1993 PA BRAGFLO calculations.

4.2.3 Specific Storage

The mathematical relationship defining specific storage is

$$S_s = \rho g(\alpha + \phi\beta), \tag{4.2-5}$$

where S_s is specific storage (m^{-1}), ϕ is porosity, β is fluid compressibility (Pa^{-1}), and α is rock compressibility (Pa^{-1}). It is assumed that α is related to porosity change according to

$$\alpha = \frac{\partial \phi}{\partial p}, \tag{4.2-6}$$

where p is the fluid pressure in Pa.

BRAGFLO actually uses a modified rock compressibility, α',

$$\alpha' = \frac{1}{\phi}\frac{\partial \phi}{\partial p} = \frac{1}{\phi}\alpha. \tag{4.2-7}$$

Therefore, given the values for S_s, ρ, g, ϕ, and β, then α and α' can be computed. In the 1992 PA calculations, the following parameter values were used:

S_s = 1.0×10^{-6} m^{-1} (anhydrite)
S_s = 1.4×10^{-6} m^{-1} (halite)
ρ = 1230 kg/m^3
g = 9.79 m/s^2
ϕ = [0.001-0.03].

4.2.4 Relative Permeability [3] and Capillary Pressure[4]

In modeling two-phase phenomena, characteristic curves for surrogate materials using either the modified Brooks-Corey formulae (Equations 4.2-8 to 4.2-11) (Brooks and Corey, 1964) or the van Genuchten-Parker formulae (Equations 4.2-12 and 4.2-15) (van Genuchten, 1978; Parker et al., 1987) are used (see Section 2.3.1 of Volume 3 of this report). The Brooks-Corey relative permeability model is used for two-thirds of the calculations and the van Genuchten-Parker model is used for the remaining one-third of the calculations. An index parameter (0 or 1) is sampled with these probabilities, so that either one model or the other is used in any one realization. The rationale for treating model uncertainty (Brooks-Corey vs. van Genuchten-Parker) in this manner is discussed in the memorandum by Webb dated April 30, 1992, in Appendix A of Volume 3 of this report.

The modified Brooks-Corey relationships used are as follows:

Capillary pressure, P_c, is given by

$$P_c = \frac{P_t}{S_e^{1/\lambda}} \quad . \tag{4.2-8}$$

Threshold capillary pressure, P_t, is correlated to permeability (see Section 2.3.1 of Volume 3 of this report). S_e is the effective saturation in the modified Brooks-Corey model:

---

3. Relative permeability is a function of saturation of the phase of interest. It is a value between 0 and 1 that is multiplied by the absolute permeability to yield the effective permeability for that phase. Relative permeabilities are empirical fits of pressure drop and flow data to extensions of Darcy's law, and measurements taken at different degrees of saturation result in differing relative permeabilities (see Section 7.2 of Volume 2 and Section 2.3.1 of Volume 3 of this report).

4. Capillary pressure differences arise when immiscible phases exist simultaneously in a porous network (see Section 7.2 of Volume 2 and Section 2.3.1 of Volume 3 of this report).

$$S_e = \frac{S_l - S_{lr}}{1 - S_{gr} - S_{lr}} , \qquad (4.2\text{-}9)$$

where S_l is the liquid saturation, S_{gr} and S_{lr} are the residual gas saturation and residual liquid (brine) saturation, respectively, and λ is the pore size distribution parameter.

Relative permeability to liquid, $k_{r,l}$, and to gas, $k_{r,g}$, are given by

$$k_{r,l} = S_e^{(2+3\lambda)/\lambda} \qquad (4.2\text{-}10)$$

and

$$k_{r,g} = \left(1 - S_e\right)^2 \left(1 - S_e^{(2+\lambda)/\lambda}\right) . \qquad (4.2\text{-}11)$$

The capillary pressure relationship, Equation 4.2-8, is used throughout the entire saturation region ($0. \le S_l \le 1.$) even though, as discussed by Corey (1986), this relationship may not be appropriate at the higher liquid saturations when $S_e > 1.0$.

The relationship for the van Genuchten-Parker (van Genuchten, 1978; Parker et al., 1987) characteristic curves are as follows:

Capillary pressure is

$$P_c = P_o \left(S_e^{-1/m} - 1\right)^{1-m} , \qquad (4.2\text{-}12)$$

where $m = \lambda/(1+\lambda)$, and P_o is a capillary pressure constant discussed later.

Relative permeability is

$$k_{r,l} = S_e^{1/2}\left(1 - \left(1 - S_e^{1/m}\right)^m\right)^2 \qquad (4.2\text{-}13)$$

and

$$k_{r,g} = \left(1 - S_e\right)^{1/2} \left(1 - S_e^{1/m}\right)^{2m} , \qquad (4.2\text{-}14)$$

where the effective saturation, S_e, is now defined as

$$S_e = \frac{S_l - S_{lr}}{S_{ls} - S_{lr}} \qquad (4.2\text{-}15)$$

where S_{ls} is the maximum wetting phase saturation; a value of $S_{ls} = 1$ is used.

The same sampled values of relative permeability parameters are used for halite, anhydrite, the transition zone, and the DRZ. The waste, seals and backfill, experimental region, and all shaft sections use a fixed set of values and the Brooks-Corey model only. Residual brine and gas saturations range from 0.0 to 0.4. The Brooks-Corey pore-size distribution parameter, λ, ranges from 0.2 to 10.0. The van Genuchten-Parker parameter m is calculated from $m=\lambda/(1+\lambda)$ and ranges from 0.167 to 0.909. These parameter ranges are based on parameter values for surrogate materials, as discussed in Section 2.3.1 of Volume 3 of this report. These parameters have not yet been measured for WIPP materials.

The choice of the characteristic curve model has important implications on the expected behavior of multiphase flow in porous media. The most obvious effect stems from differences in the capillary pressure curve at high values of brine saturation. The Brooks-Corey model assumes an irreducible gas saturation, S_{gr}. When the gas saturation is below this residual value, the capillary pressure is assumed to remain at some fixed, non-zero value, known as the threshold capillary pressure. According to this model, in order for gas to penetrate a brine-filled pore, the gas pressure must first exceed this threshold value. This constraint effectively prohibits gas from flowing into a liquid-saturated medium until it overcomes this "barrier" to flow.

In the van Genuchten-Parker model, there is no residual gas saturation, and the capillary pressure is zero when the medium is fully brine saturated. Thus, there is no resistance to gas flow under fully brine-saturated conditions, and there is no "barrier" pressure to overcome. One incentive to using the van Genuchten-Parker model is to account in a simplistic way for the effects of fingering, which is the unstable displacement interface that occurs when a lower-viscosity fluid (gas) displaces a higher-viscosity fluid (brine). While this complex phenomenon cannot currently be modeled accurately by any method, its gross effects, such as unexpectedly rapid movement of gas, can be more closely approximated using a characteristic curve model such as the van Genuchten-Parker model that imposes no barrier to gas penetration into a brine-saturated medium. Conceptually, the van Genuchten-Parker model allows gas to migrate farther from the source (i.e., the waste) at a lower pressure than would occur under otherwise identical conditions using the Brooks-Corey model.

The characteristic curve model also affects brine flow, especially with the van Genuchten-Parker model when m is small (see Figure 4.2-9). Capillary pressures then rise steeply as the gas saturation increases from zero, and

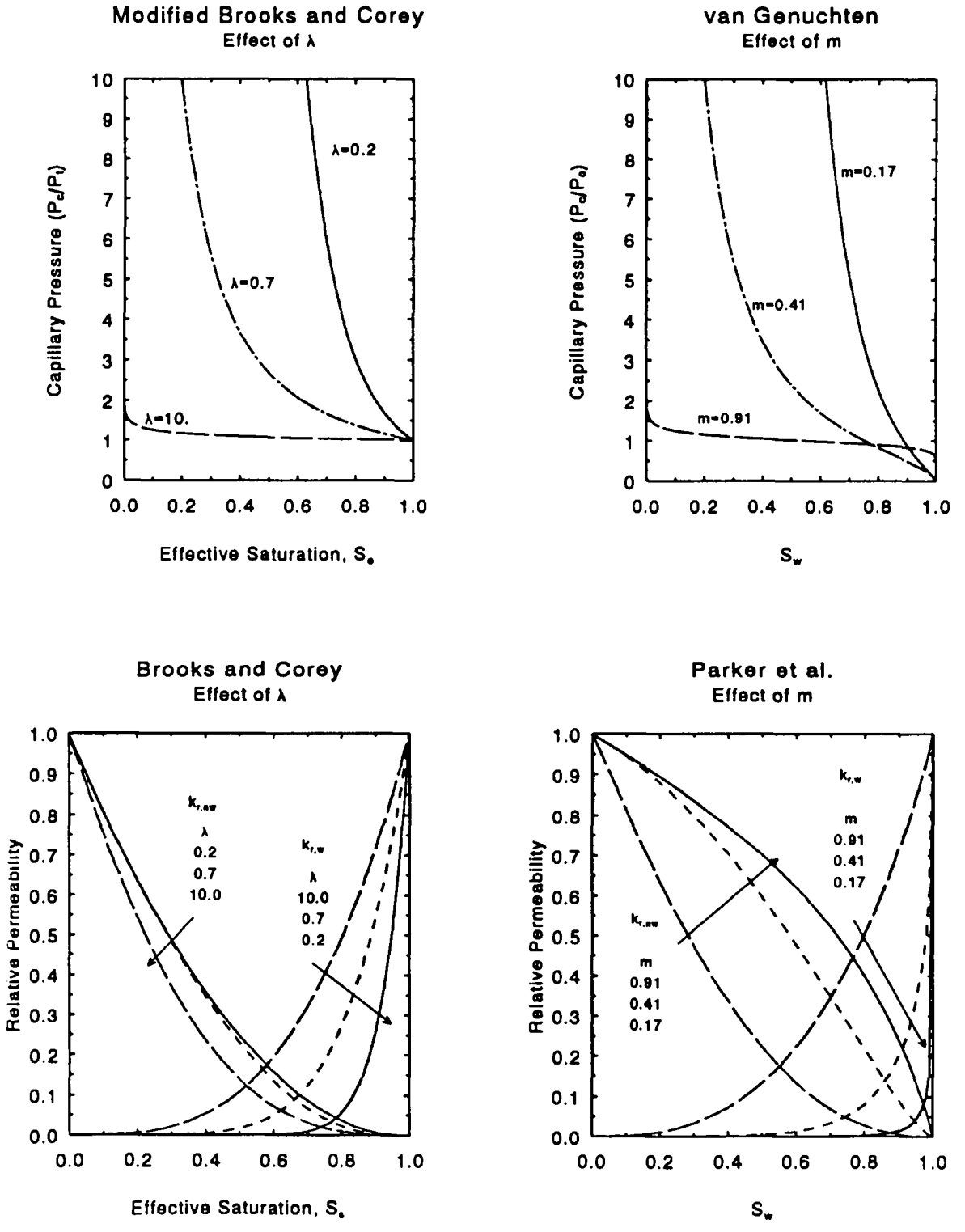

Figure 4.2-9. Capillary pressure and relative permeability functions (from memo from Webb to Anderson, 1992; in Appendix A of Volume 3).

the relative permeability curves are very steep at high brine saturations. Sampled values of m that are small effectively prevent brine from flowing when even a small amount of gas is present. With the Brooks-Corey model, even the smallest sampled values of λ have no inhibitory effect on brine flow until the gas saturation is below the residual value.

Threshold capillary pressures are determined from the correlation with permeability in all regions. The van Genuchten-Parker capillary pressure constant, p_o, is calculated by equating the capillary pressure from each of the two models at an effective saturation of 0.5, and solving the expression for Po. In the waste, in the DRZ, and in all excavated regions, capillary pressure is assumed to be zero. Zero capillary pressure for these regions is necessary because the capillary pressure curves are not defined for imbibition into a medium that has less than residual brine saturation. Any regions where the brine saturation starts out or may become less than residual (e.g., as a result of brine-consuming reactions that occur due to reactions in the waste region) were modeled with zero capillary pressure. However, if a maximum capillary pressure is specified and used at brine saturations less than residual, assuming zero capillary pressure is not necessary. Though this latter approach was not taken in the 1992 performance assessment it may be adopted for future calculations so that non-zero capillary pressure can be used without causing numerical problems when brine saturations below residual are encountered.

4.3 Initial and Boundary Conditions

A major difference between the 1992 and 1991 PA calculations for undisturbed conditions is in the treatment of initial conditions. The primary objective of taking a new approach in modeling initial conditions has been to establish a more realistic pressure distribution in the formations surrounding the waste at the time the repository will be sealed. This time is referred to here as time zero. The 1992 undisturbed calculations achieve more realistic time-zero conditions by varying the initial conditions in the repository over a 50-yr period immediately preceding time zero.

Before the 1992 calculations, it was always assumed that excavated regions were initially at atmospheric pressure with some arbitrary degree of brine saturation (various combinations of saturations were considered), while all other regions were fully brine saturated at hydrostatic pressure (relative to a sampled pressure at the level of MB139). These assumptions were unrealistic and produced results that may have been unrealistic for the following reasons:

- Brine in the DRZ above the waste could immediately drain down into the waste, presumably having been suspended there while the repository was excavated and filled. In many cases, brine from the DRZ was sufficient to corrode all ferrous metal in the waste, without any brine from the far field reaching the waste.

- The assumed pressure distribution imposed a large pressure gradient from the Salado halite to the shaft, which at time zero resulted in improbably large quantities of brine flowing from the halite into the shaft, despite the low permeability of the halite.

- The unrealistically high initial pressures surrounding the repository retarded migration of brine or gas from waste for much longer periods of time than could reasonably be expected, although the exact effect is unpredictable.

- Higher external pressures could raise the pressure in the waste more quickly, in part because of the higher pressure gradient near the waste, and in part because a faster influx of brine would cause gas generation by corrosion to occur more rapidly.

In reality, brine will seep in continually from the surrounding formations during the disposal phase of the WIPP. Water in the brine will evaporate into the well-ventilated atmosphere of the excavations or will be pumped out as standard mining practice if it accumulates anywhere. Thus, formations surrounding the excavations will be dewatered and depressurized while the panels are in use. Therefore, the initial conditions used in BRAGFLO now reflect the impact that the time between excavation and sealing of the panels will have on fluid saturations and pressures in the surrounding formations.

In 1992, the time between excavation and decommissioning is modeled explicitly, as detailed in Table 4.3-1. For the full repository, this phase is assumed to last 50 yr. The important features of conditions during this time are as follows:

- Except for the waste, the excavated regions, and the Culebra, the pressure distribution at 50 yr before time zero is hydrostatic relative to the pore pressure of MB139, which is sampled from a range of 12 to 13 MPa.

- Pressure at 50 yr before time zero in the waste and excavated regions is atmospheric, and the waste pressure is reset to this value at the end of the 50-yr period.

Table 4.3-1. Startup Procedure for Undisturbed Calculations

I. Don't allow brine inflow from the Culebra during initialization	1)	Set Culebra permeability to zero
II. Simulate the panels, seals, backfill, shaft, and experimental region as empty, newly excavated, gas-filled cavities	1)	Set initial porosity to 1.0
	2)	Set initial brine saturation to 0.0
	3)	Set initial pressure to 1 atm
	4)	Set residual brine and gas saturation to 0.0
	5)	Set permeability to 1.0×10^{-10} m^2
III. Simulate DRZ as initially pressurized, but partially fractured	1)	Set initial pressure to hydrostatic relative to sampled value of MB139 pore pressure
	2)	Set permeability to 1.0×10^{-17} m^2
	3)	Set initial porosity to volume average of sampled value of intact far field anhydrite and intact halite porosities (since DRZ has both)
	4)	Set initial brine saturation to 1.0
	5)	Set capillary pressure to 0.0 (so gas and brine pressures are same)
IV. Let the system equilibrate for 50 yr, the approximate time span between excavation and sealing of the repository	1)	Brine pressure in the excavation will increase slightly (~0.5%)
	2)	Brine will drain down from DRZ, approaching residual saturation
	3)	DRZ pressure will drop precipitously, approaching equal waste pressure
	4)	Let no creep closure occur
V. Instantly add the waste at 50 yr	1)	Reset waste pressure to 1 atm
	2)	Set brine saturation of waste to sampled "initial" brine saturation
	3)	Set waste residual brine and gas saturations to their sampled values
	4)	Set waste permeability to 1.0×10^{-13} m^2
	5)	Set waste porosity to "initial" value calculated from sampled values of volume fractions of metal and combustibles
	6)	Set reactant concentrations to "initial" values
VI. Adjust parameters for the DRZ and excavated regions	1)	Change porosity to final sampled values (except for creep closure and rock compressibility, simulating time-dependent porosity is beyond current modeling capability)
	2)	Adjust brine saturation so brine content of DRZ is unchanged; add gas to fill added pore volume
	3)	Reset DRZ and excavated region pressure to 1 atm
	4)	Reset brine saturation in excavated regions
	5)	Set DRZ permeability to 1.0×10^{-15} m^2 to account for fracturing
	6)	Set Culebra permeability to 2.1×10^{-14} m^2
VII. Resume calculation at 50 yr; this is the time normally called t=0	1)	Begin creep closure of repository
	2)	Allow gas generation to begin in waste
	3)	Pressures outside waste, DRZ, and excavated regions start from 50-yr values (t = 0)
VIII. Continue out to 10,050 yr, i.e., 10,000 yr past the time normally called t=0		

- Pressure in the Culebra at 50 yr before time zero is 1.053 MPa, and the far-field pressure is held at that value over the 10,050-yr calculation. (The Culebra has a fixed-pressure boundary condition, whereas the rest of the mesh uses a no-flow boundary condition.)

- The starting brine saturation is 1.0 everywhere except in the waste and other excavated regions, where the brine saturation starts at 0.0.

- At the end of the 50-yr period, the waste is assigned its sampled value of initial brine saturation, which ranges from 0.0 to 0.14.

The initial condition calculations themselves begin with initial conditions similar to those used in 1991; perhaps the greatest difference is simply in interpretation. What was called time zero in 1991 is now called -50 yr; this is the time of initial excavation. The performance calculations begin at time zero (50 yr after the initial condition calculation as started); this corresponds to the time of sealing of the repository.

During the initial conditions calculation, the permeability of the excavated regions is assumed to be very high (1×10^{-10} m^2), to simulate cavities. At the end of the 50-yr period, any brine that has flowed into the excavated regions is ignored, since it will have evaporated or will have been pumped out of the repository. The sampled initial brine saturation in the waste is introduced. Pressures in all the excavated regions are reset to atmospheric. Pressures there are generally barely above atmospheric (by a few hundred pascals) after the 50-yr emplacement period; they are reset to atmospheric to reestablish realistic conditions at time zero, since at the time of sealing, the excavated regions should be at atmospheric pressure. Except in the DRZ, pressures in all the surrounding formations, including the transition zone and the intact ahydrite interbeds, remain as they are at the end of the 50-yr period.

In the DRZ, at least the residual saturation of brine, and possibly more, will remain, the rest having drained into the excavated region that will later be filled with waste. At time zero, the brine remaining in the DRZ is left there; however, the porosity is assumed to change from the initial intact halite value to the final sampled DRZ porosity. This porosity change increases the void volume. In order to conserve the volume of brine in the DRZ, the additional void volume is assumed to be filled with gas. The pressures in the DRZ will typically be slightly above atmospheric at time zero. If the pressures were left at those values when additional gas is introduced at time zero, it could result in a gas-drive condition that would cause brine to be expelled suddenly from the DRZ into the waste at time zero. To prevent this unrealistic behavior, the pressure in the DRZ is also reset to atmospheric at time zero.

The previously excavated regions will contain no brine except for the initial brine brought in with the waste. The surrounding formations will be depressurized and dewatered to the extent expected after being exposed to ventilated air at atmospheric pressure for 50 yr. All surrounding formations are fully saturated with brine at time -50 yr. Generally, at time zero, they will still be fully brine-saturated (except for the DRZ). Except for the DRZ, brine saturation in surrounding formations is not modified to reflect a change in porosity at time zero.

The calculations proceed from this calculated initial condition for the 10,000-yr performance period. The most important effect of these more realistic initial condition is that less brine will flow into the excavated regions (including the waste), since the initial "surge" of brine that occurs upon excavation has been eliminated, and the pressure gradients in the immediate vicinity of excavations have been greatly reduced.

4.4 Results and Discussion (Undisturbed Performance)

General observations are described in this section that pertain to all of the calculations. Detailed statistical analyses that specific results relate to specific parameter values will be discussed in a later section.

The plots presented in this section show results as a function of time for all 70 realizations (vectors) on a single plot. These results enable trends to be easily observed if present. Although the plots are sometimes cluttered, they are useful for illuminating general behavior and allowing comparisons to be made among all of the realizations.

4.4.1 Repository Behavior

Pressures in the repository (Figure 4.4-1) invariably rise from the initial value of one atmosphere, primarily because of gas generation. The rise is not always monotonic. In many of the vectors, the pressure in the waste peaks relatively early, in 1000 to 2000 yr, then levels off at a slightly lower value. This leveling off may be the result of gas breaking through a lower-permeability barrier, such as the shaft seal, or it may occur simply as gas generation ceases. Either the reactants are fully consumed or no more brine can make its way into the waste to allow gas generation to continue. The peak pressure among all vectors was about 22 MPa. In the vectors in which the pressure peaked early, the peak was almost always greater than the far-field pore pressure, so even if gas did not break through any kind of barrier, the pressure would always tend to decrease. In a

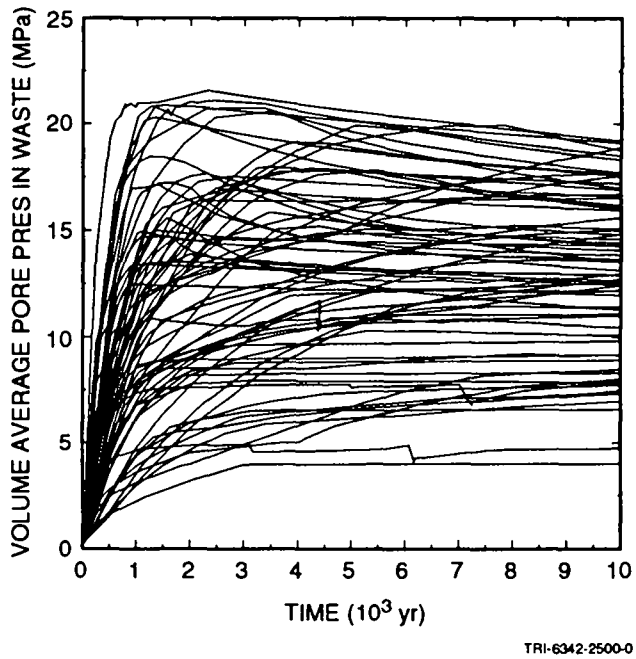

Figure 4.4-1. Volume average gas pressure in waste.

few vectors, the pressure rose continually over the 10,000-yr performance period, in some cases to pressures in excess of lithostatic (14.8 MPa), without ever peaking. This behavior is expected when the gas-generation rate is low, but the initial brine content of the waste is high enough to sustain reactions continuously without additional brine influx from outside the repository. At 10,000 yr, the range of pressures in the waste is very large, from 4 MPa to 19 MPa. For those realizations in which final pressures are at the lower end of the range, little gas has been generated and all of the surrounding formations have extremely low permeability, thereby preventing brine inflow from equalizing pressure with the far field. For those realizations in which pressures are at the upper end of the range, gas generation has been vigorous, resulting in pressures well above lithostatic.

Because of the implementation of the porosity surface (see Section 7.3 in Volume 2, of this report), pore volume (Figure 4.4-2) or porosity in the waste behaves similarly among all realizations. In all cases, the porosity drops from the initial value of 66% during the first few hundred years, as the repository creeps shut. The porosity reaches a minimum between 12% and 21%, depending on the rate at which the pressure in the repository increases, primarily as a result of gas generation. In the extreme case, in which the

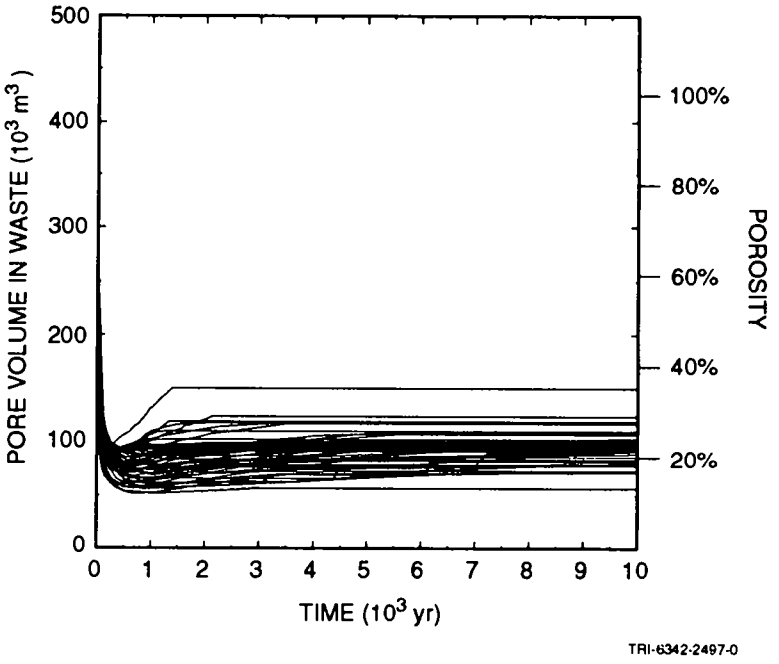

Figure 4.4-2. Pore volume in waste.

pressure rises rapidly to about 21 MPa, the repository reopens to a porosity of 34%, which is the maximum porosity resulting from reopening that is allowed in the current implementation of the porosity surface. Most vectors show much less expansion, generally to porosities of 15% to 21%. In the other extreme, pressures in the repository remain so low that almost no inflation occurs, and the porosity at 10,000 yr is still only 12.6%. Note that in the current model, porosity cannot decrease when pressure decreases. This explains why, after the initial expansion that typically occurs between 500 and 1500 yr, there is no decrease in pore volume, despite the fact that in many realizations pressures in the repository decrease after that. See Section 4.4.3 for further discussions of the effects of creep closure.

Although the average brine saturation in the waste varies greatly from vector to vector (Figure 4.4-3), the variations with time show nearly the same trends in all of the realizations. There is an initial period when the brine saturation increases rapidly, peaking in 500 to 1500 yr. This rise in brine saturation is a direct result of the rapid drop in porosity. As the pore volume decreases, gas, but not brine, is compressed, and as a result the brine saturation increases. During this same period, brine volume (or mass) generally decreases, as a result of consumption by corrosion (See

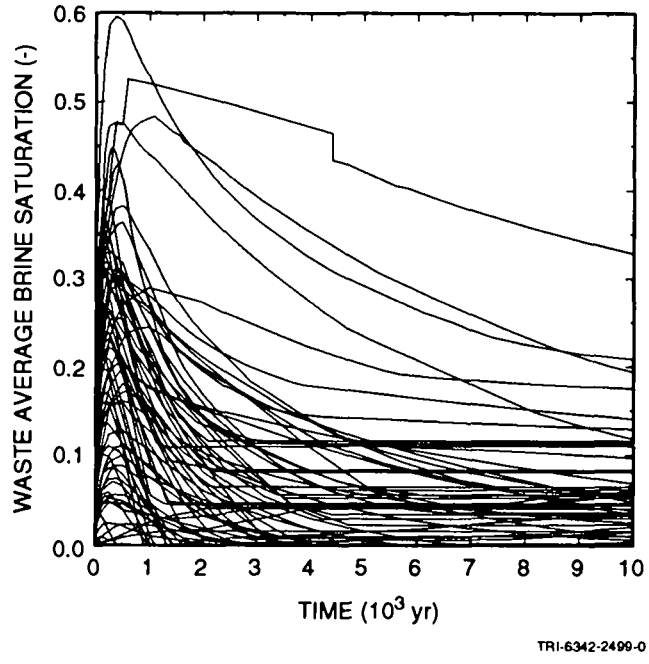

Figure 4.4-3. Waste average brine saturation.

Figure 4.4-4). Brine saturation increases initially in large part because porosity reduction resulting from creep closure occurs at a faster rate than brine consumption by corrosion. Once creep closure effectively ceases, in most cases within 500 yr, brine saturation is no longer influenced by porosity changes, although brine inflow causes brine saturation to continue to rise for as much as 1000 more years. Thereafter, the brine saturation generally decreases--rapidly at first, at a slower rate later--as brine is consumed by corrosion. Corrosion consumes as much as 29,000 m^3 of brine, as shown in Figure 4.4-5. Some brine may flow out of the waste; the maximum among the 70 realizations was 11,000 m^3 (Figure 4.4-6), but in 87% of the vectors, less than 2000 m^3 flows from the waste. Only in one vector is less than 2000 m^3 of brine consumed (Figure 4.4-5). Thus, in a general sense, most of the brine that disappears from the waste is consumed by reaction, rather than by outflow.

The rate and amount of gas generation varies greatly, as shown in Figure 4.4-7. Among the 70 realizations, the quantity of gas generated varies over more than an order magnitude, from 2 x 10^6 m^3 to 32 x 10^6 m^3 of hydrogen, at reference conditions (30°C, 1.01325 x 10^5 Pa). In almost all cases, gas generation ceases in less than 10,000 yr. (The curves in Figure 4.4-7 become flat at that point.) Apparently, gas generation as modeled ceases because

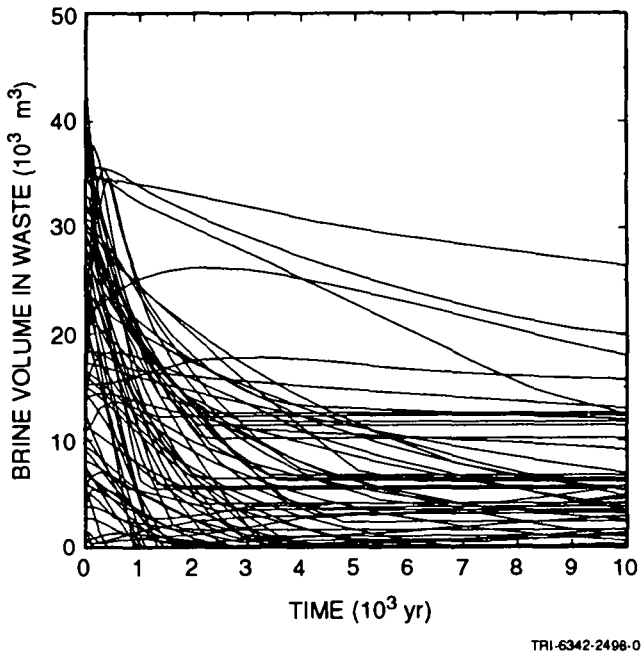

Figure 4.4-4. Brine volume in waste.

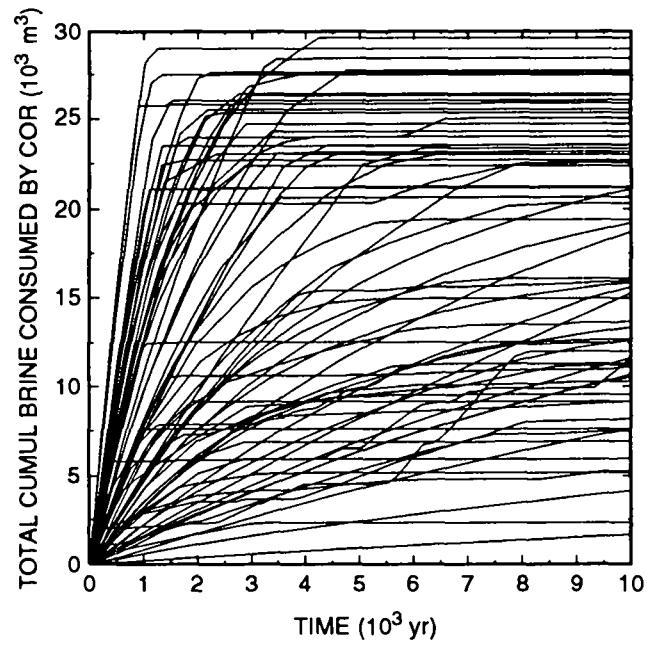

Figure 4.4-5. Total cumulative brine consumed by corrosion.

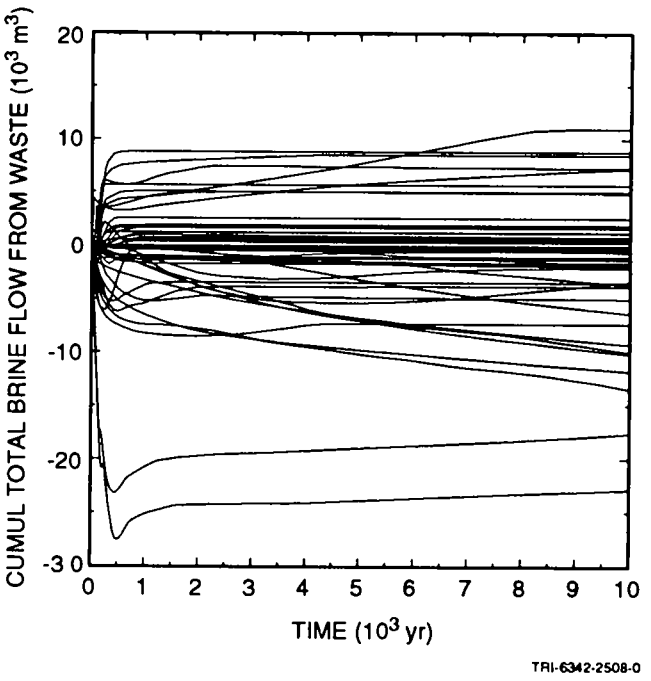

Figure 4.4-6. Cumulative net brine flow from waste.

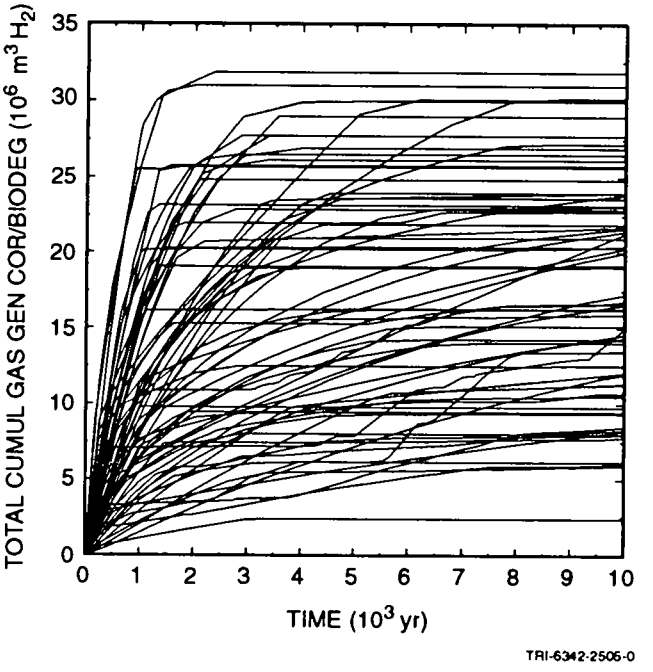

Figure 4.4-7. Total cumulative gas generated from corrosion and biodegradation.

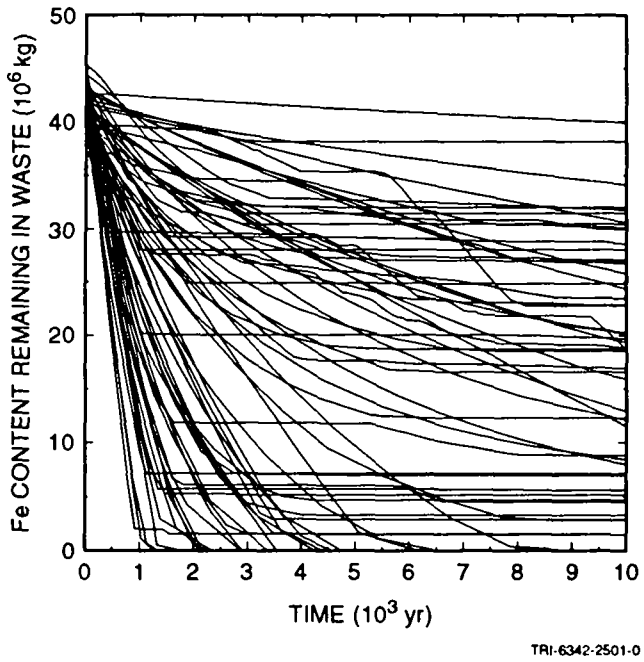

Figure 4.4-8. Iron content remaining in waste.

brine is no longer available for corrosion or biodegradation in those cells where iron and cellulosics remain. As shown in Figure 4.4-8, iron is still present in the waste in 53 of the 70 realizations after 10,000 yr, yet the rate of gas generation by corrosion (Figure 4.4-9) has decreased greatly from the rate at earlier times. Similarly, cellulose is still available in 17 realizations after 10,000 yr (see Figure 4.4-10) even though the biodegradation gas-generation rate has dropped nearly to zero for all realizations, as shown in Figure 4.4-11.

4.4.2 Conditions Outside of the Waste

As discussed in Volume 2, Section 4.2.3.1, the dominant pathways for contaminated brine flow from the waste to the accessible environment are: (1) along MB139 to the shaft and up the shaft to the Culebra; (2) through degraded drift and shaft seals to the shaft and up the shaft to the Culebra; and (3) along MB139 laterally outward toward the accessible environment. In addition, the anhydrite layers above the repository could provide a pathway for brine flow in the same manner as MB139.

Because BRAGFLO models only flow and does not simulate transport, it is difficult to state with certainty where contaminated brine has flowed.

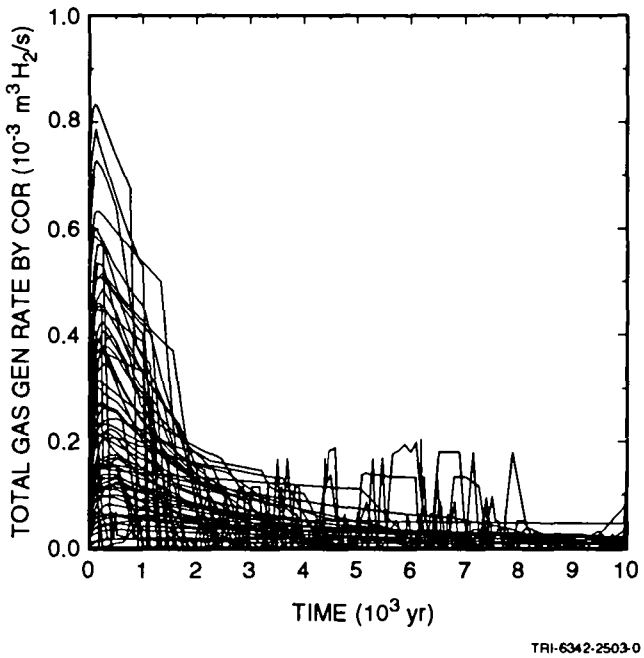

Figure 4.4-9. Rate of gas generation by corrosion.

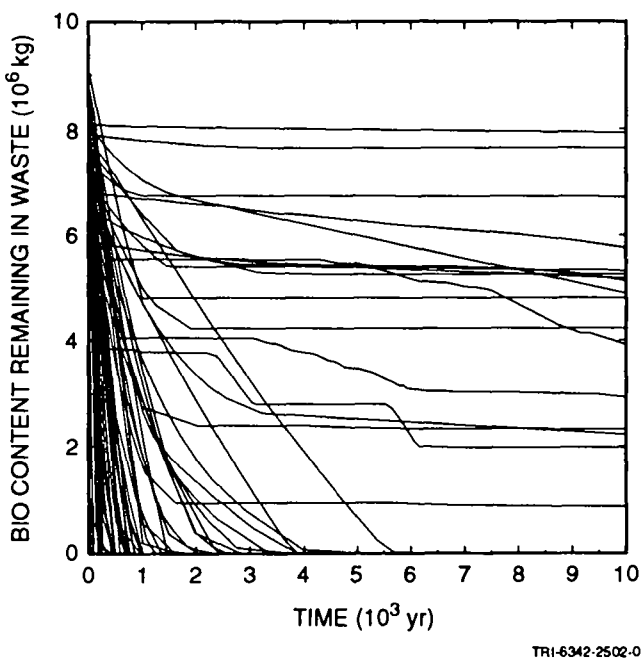

Figure 4.4-10. Biological content remaining in waste.

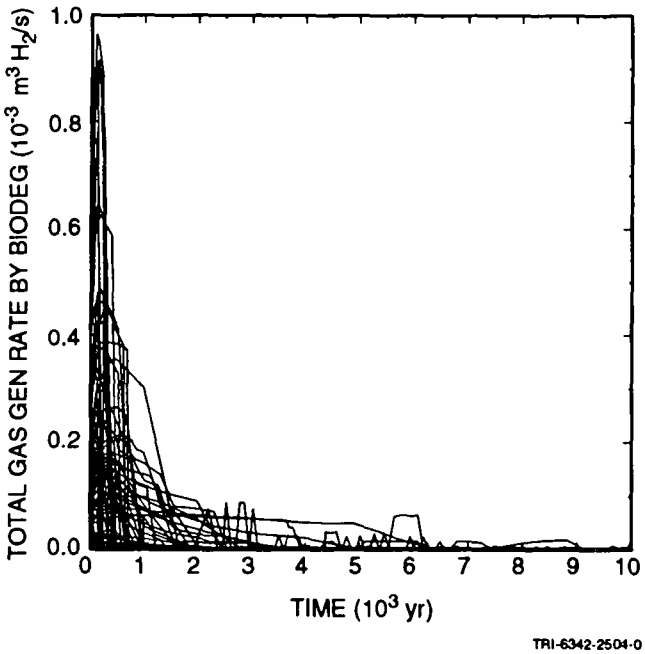

Figure 4.4-11. Rate of gas generation from biodegradation.

However, Figures 4.4-12 to 4.4-17 strongly suggest that no contaminated brine has flowed up the shaft. Figures 4.4-18 to 4.4-20 suggest that no contaminated brine has reached the accessible environment by way of lateral outward flow through the anhydrite layers or marker beds.

For contaminated brine to flow up the shaft, it must first flow either through the drift seals and backfill and into the shaft, or through the DRZ above and below the waste (see Figure 4.1-2). As Figure 4.4-12 shows, although some brine (less than 300 m^3) has flowed from the waste into the seals and backfill (in only four realizations), none has flowed from the seals and backfill into the shaft (Figure 4.4-13). In fact, as shown in Figure 4.4-13, for the assumptions used inthe 1992 PA, there was flow between these two regions in only two realizations, and it was <u>from</u> the shaft, rather than into the shaft. In more than 60 realizations, there was no flow between these two regions.

These results do not preclude the flow of contaminated brine from the waste through the DRZ and into the shaft. However, Figure 4.4-14 shows only a momentary (from the perspective of the 10,000-yr regulatory period) flow of brine from the DRZ into the shaft and in only two of the realizations. Brine

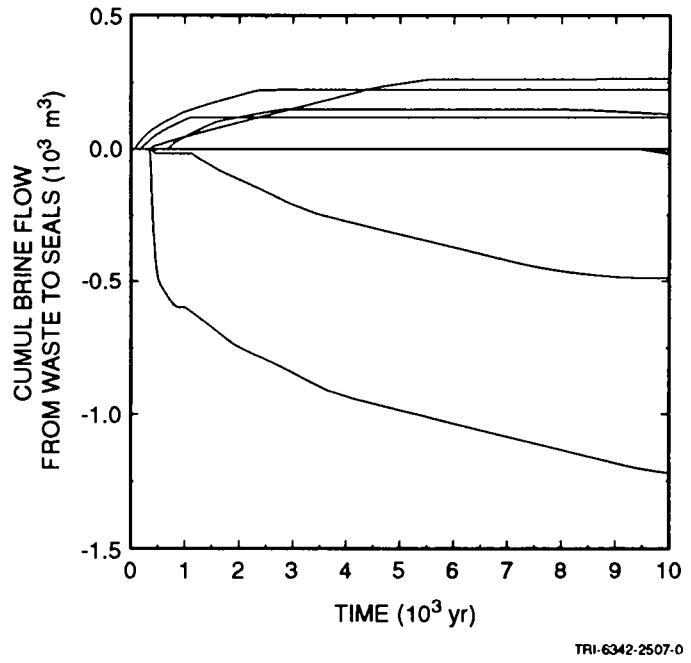

Figure 4.4-12. Cumulative brine flow from waste to seals.

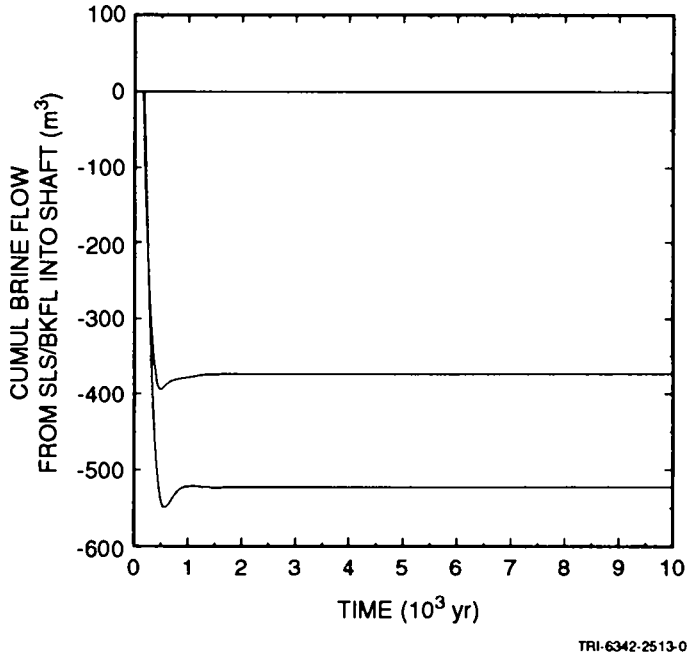

Figure 4.4-13. Cumulative brine flow from seals and backfill into shaft.

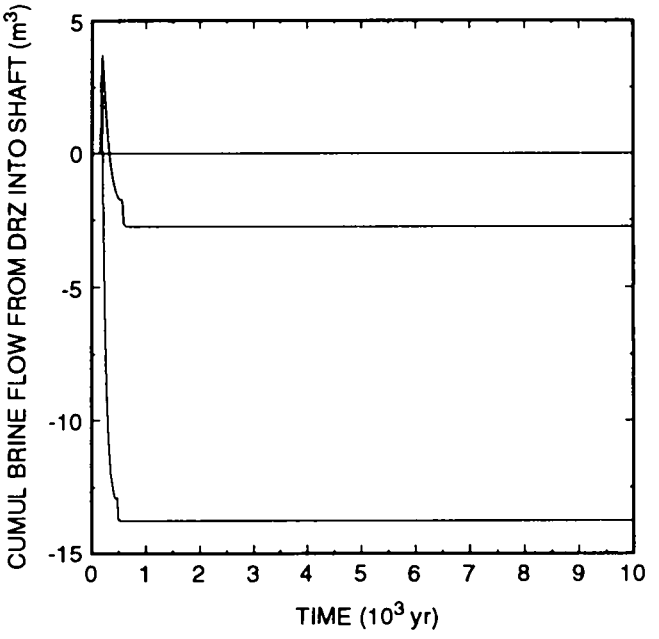

Figure 4.4-14. Cumulative flow from DRZ into shaft.

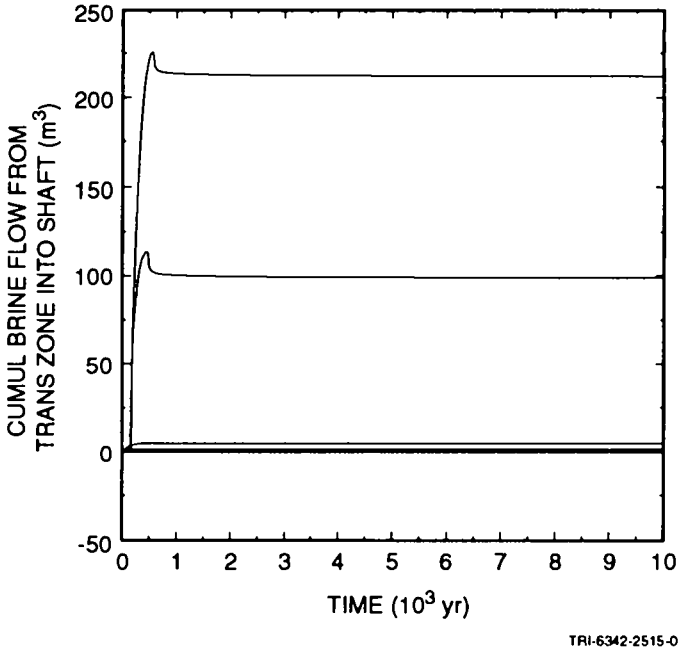

Figure 4.4-15. Cumulative brine flow from transition zone into shaft.

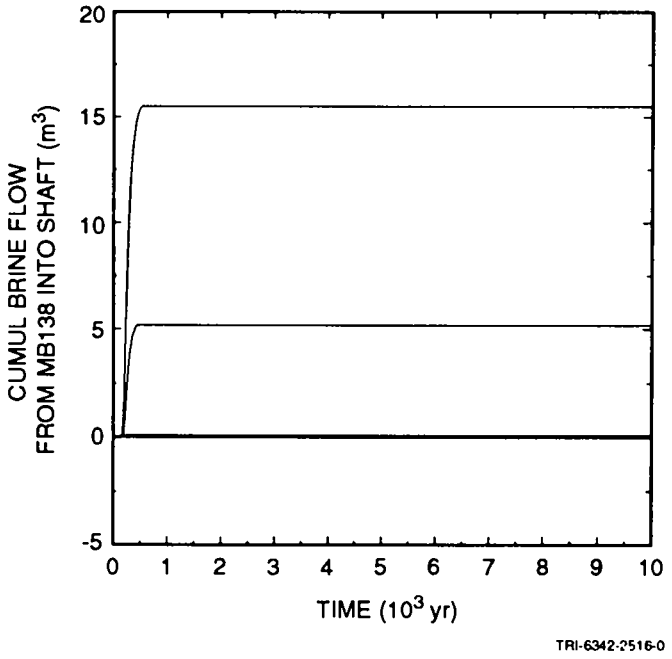

Figure 4.4-16. Cumulative brine flow from MB138 into shaft.

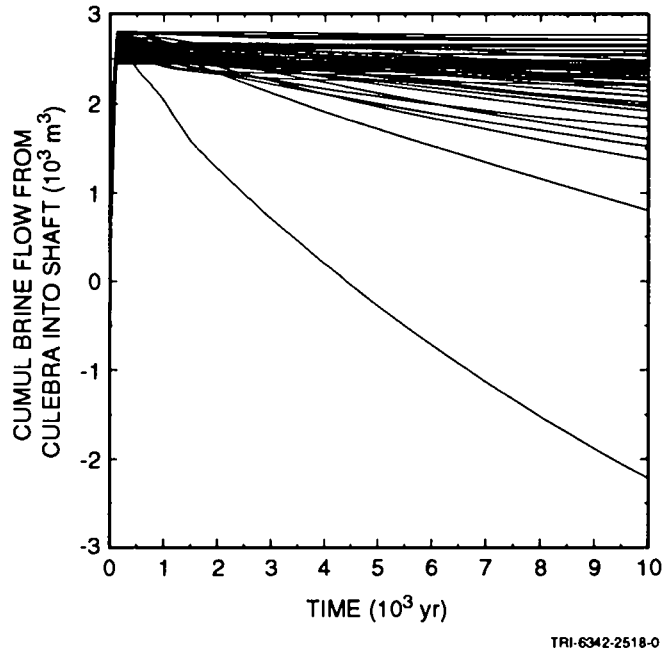

Figure 4.4-17. Cumulative brine flow from Culebra into shaft.

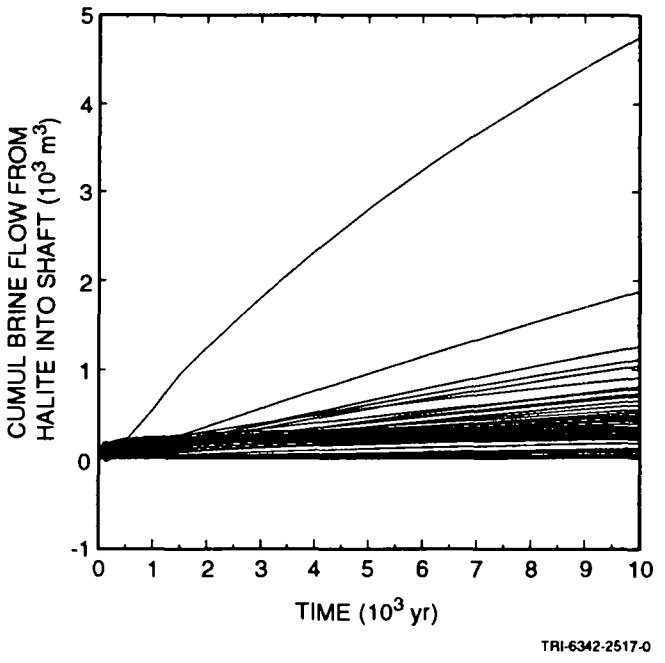

Figure 4.4-18. Cumulative brine flow from intact halite into the shaft.

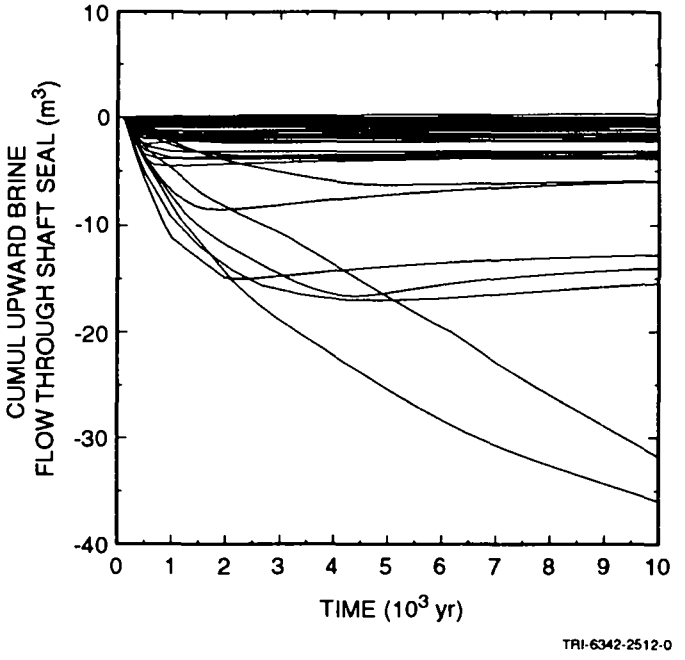

Figure 4.4-19. Cumulative brine flow upward through the shaft seal.

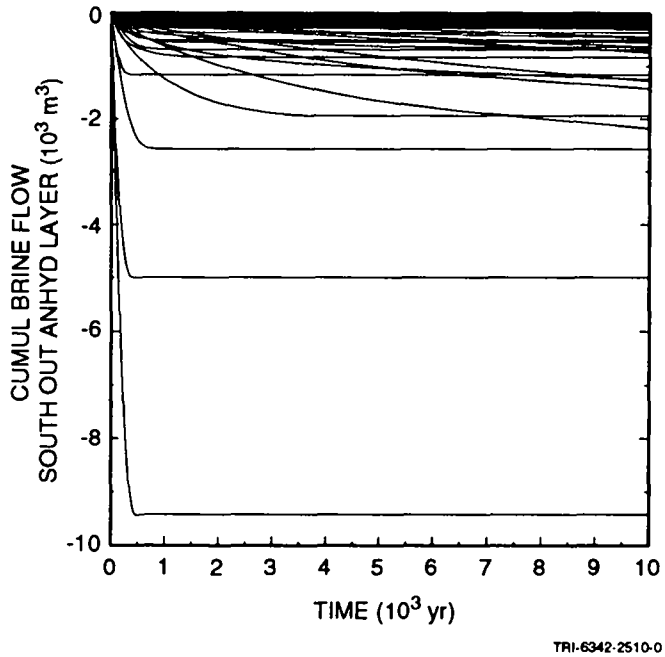

Figure 4.4-20. Cumulative brine flow south out of anhydrite layers A and B.

flow from the transition zone and MB138 into the shaft does occur in a few realizations (Figures 4.4-15 and 4.4-16), but it is unlikely that that brine has come from the waste, since these beds are several meters above the waste, and the waste is never fully saturated with brine (Figure 4.4-3). Figure 4.4-17 shows that there is a large net flow of brine from the Culebra into the shaft in all but one realization, and in that one realization, the brine flow comes from the halite, and not from the shaft seal (Figure 4.4-18). Finally, Figure 4.4-19 shows upward flow of brine through the shaft seal. In only one realization was there any pitive upward flow, and it amounted to only 0.26 m^3 of brine. In all other cases, there was either no flow through the seal, or there was flow downward. Thus, it appears highly unlikely that any brine originating in the waste could have flowed up and out of the shaft and into the Culebra.

In Figures 4.4-12 to 4.4-16, two realizations display behavior that is markedly different from all the rest. In these two realizations, the anhydrite permeability, a sampled parameter, is higher than in all the others, having values of 9.5×10^{-17} m^2 and 4.1×10^{-17} m^2. Apparently, this permeability is just high enough to allow sufficient influx of brine from the far field to flood the portion of the shaft below the shaft seal. Brine

flows into the shaft from MB138 and the transition zone and from the shaft into the seals, backfill region, and the DRZ. This occurs only in these two realizations. It does not occur in the realization having the next highest anhydrite permeability, 1.0×10^{-17} m^2, even though none of the other sampled parameters in this realization differs radically from the other two realizations. Evidently, the model is quite sensitive to anhydrite permeability when the permeability is greater than 1.0×10^{-17} m^2.

It is more difficult to establish that contaminated brine has not flowed laterally out the anhydrite layers beyond the WIPP boundaries without more detailed examination of the results, but an indirect argument can be made. First, note that since the likelihood of contaminated brine flowing into the shaft is negligible, it is even less likely that it could have flowed beyond the shaft to the north. (As Figure 4.1-2 shows, the shaft intersects all of the anhydrite layers, which are the only significant lateral flow paths.) As for the southern direction, Figure 4.4-20 shows that there was no brine flow south laterally out the anhydrite A and B layer. While there was some flow to the south out MB138 in some realizations (Figure 4.4-21), it is unlikely that this brine came from the waste. In order for contaminated brine to flow out the top of the waste, the repository must be saturated with brine, with the remaining gas at the residual gas saturation of 0.07. As Figure 4.4-3 showed, brine saturation never exceeded 60%, and was generally less than 40%. Therefore, contaminated brine flow out the top of the repository and laterally out MB138 is highly unlikely. In most realizations, there was a large flow of brine toward the repository through MB138. The only remaining possibility for lateral migration of contaminated brine is south out MB139. Among the nine realizations having a positive southward brine flow (Figure 4.4-22), the maximum cumulative southward flow was less than 1800 m^3. Assuming radial plug flow and a minimum porosity of 0.001, the farthest this amount of brine could have flowed south out MB139 is 626 m. In Figure 4.4-22, some of the curves (especially the bottom two) increase after passing through a minimum typically within the first 1000 yr. This indicates that even though the cumulative net brine flow is inward (toward the waste), there can still be a large outward flow of contaminated brine. In the worst case – the bottom curve - 6600 m^3 of brine flows out of the waste into MB139. However, in this particular realization, the porosity of MB139 is 0.0041 and the maximum gas saturation of MB139 is only 0.065, so the 6600 m^3 still flows out no farther than 626 m. (The distance of 626 m is the distance to the far end of the farthest grid block into which contaminated brine could have flowed.) In fact, this quantity of brine would not have flowed past the WIPP site boundary even with the minimum MB139 porosity of 0.001 and an improbable gas saturation throughout MB139 of 50%. Thus, it is unlikely that any contaminated brine could have flowed laterally beyond the WIPP site

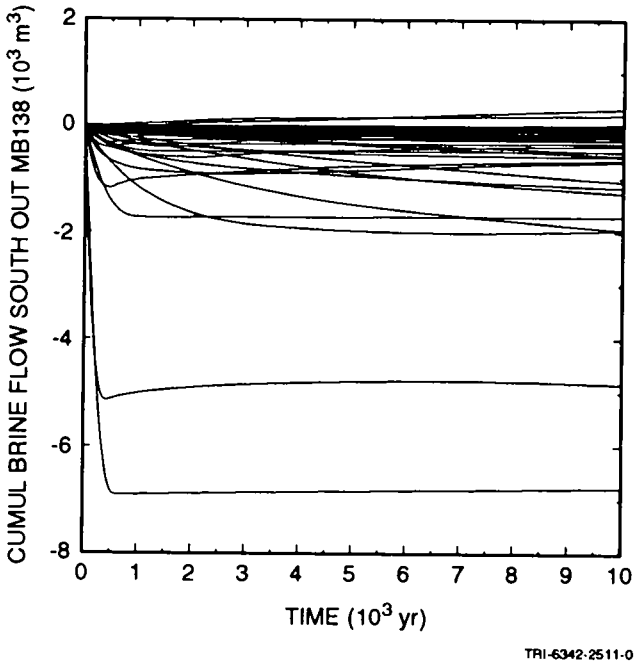

Figure 4.4-21. Cumulative brine flow south out of MB138.

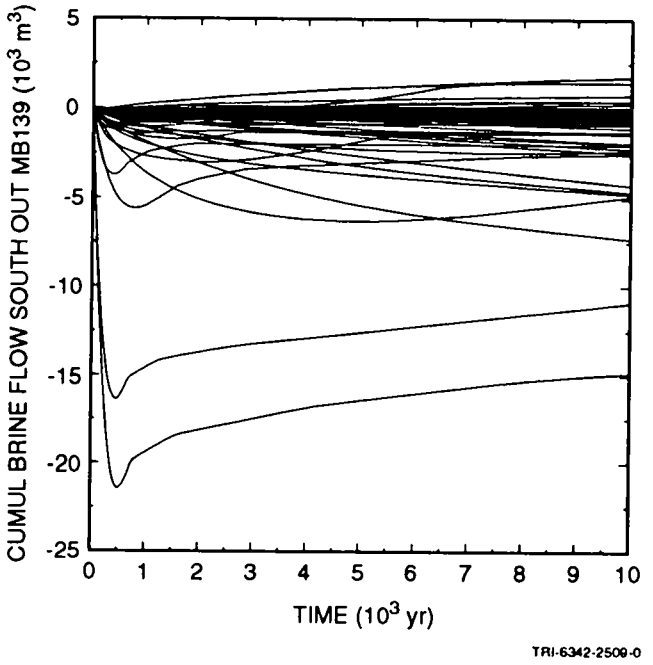

Figure 4.4-22. Cumulative brine flow south out of MB139.

boundaries (approximately 2400 m beyond the repository) in the undisturbed scenario.

4.4.3 Creep Closure Effects

The same set of 70 calculations that was described above was repeated with the only change being that creep closure of the waste was not allowed to take place dynamically. Instead, the porosity of the waste was held constant at a partially closed state (except for very small pressure-dependent compressibility effects). These calculations were done to determine what effect creep closure dynamics, as currently implemented, have on the results. These calculations will be referred to as "fixed-porosity" calculations to indicate that dynamic closure was not modeled, even though the repository is actually assumed to have crept to a final-state porosity.

The overall effect of modeling creep closure dynamically was minor. Pressures in the waste are generally higher without dynamic closure, but only because the fixed value of porosity is lower than the porosity calculated dynamically. Higher pressures result in gas flowing farther out the anhydrite layers. However, potentially contaminated brine still does not reach the disposal-unit boundary when a fixed porosity is used.

With creep closure modeled dynamically, the panel porosity was initially 66% and dropped as creep progressed, leveling off at 12% to 21%. In the fixed-porosity calculations, the waste panel porosity was initially 19%, which is the median final-state porosity of the waste. (See Table 3.4-1 in Volume 3 of this report.) The porosity was allowed to vary only as a result of the non-zero compressibility of the waste; because the value used for compressibility of the waste is very small (1.6×10^{-9} Pa^{-1}), the porosity increased only 1.1 percentage points even under the maximum pressures (Figure 4.4-23). This analysis helps to illustrate the significance of creep closure in assessing the performance of the WIPP. Although only the early time dynamics are accounted for in the current implementation, that is the period during which the greatest changes occur and during which transient effects of closure should have the greatest impact on the performance of the WIPP.

Pressure profiles from the fixed-porosity runs (Figure 4.4-24) are very similar to the calculations that include closure. The most apparent differences are in the peak pressures, which now are as high as 34 MPa, compared with 22 MPa with creep closure. Pressures are generally higher when the creep closure process is not modeled. This occurs because, as mentioned above, the porosity used in the fixed-porosity calculations is lower initially but the brine volume is the same, so with less pore volume in which

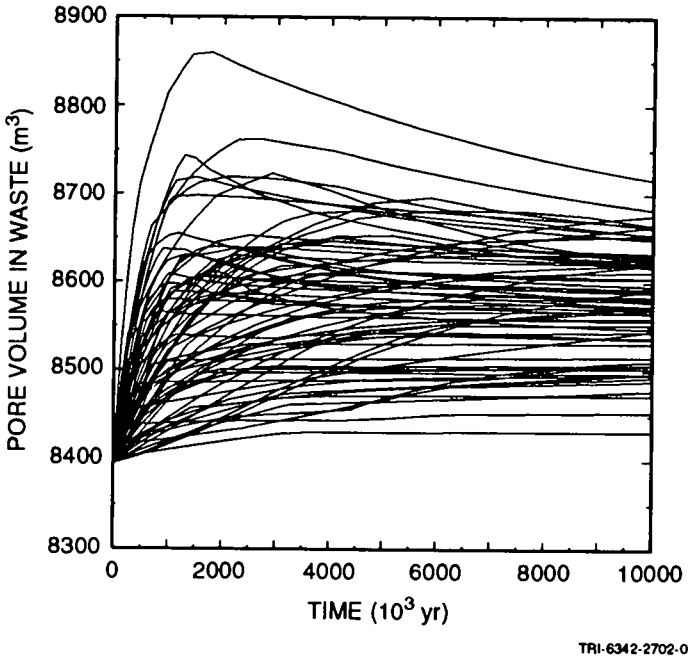

Figure 4.4-23. Waste porosity without creep closure.

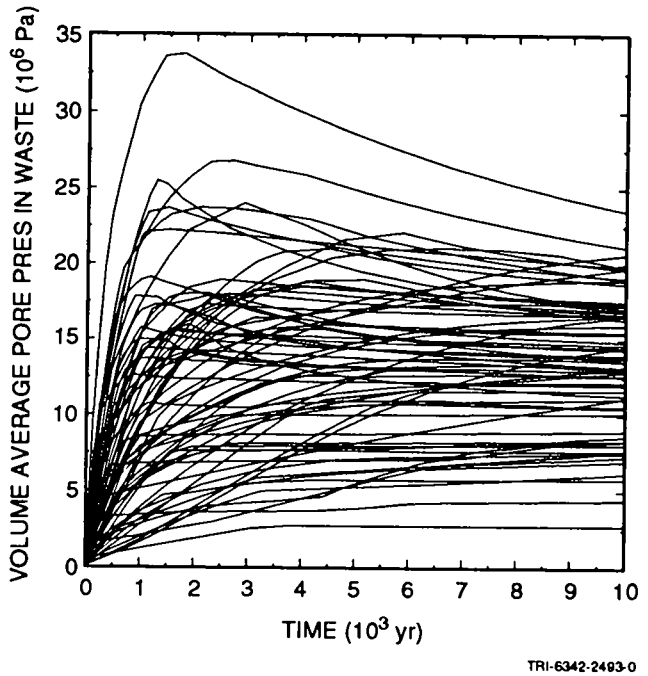

Figure 4.4-24. Panel pressure without creep closure.

to store the gas, pressures increase much more rapidly and go much higher, even though the amount of gas generated is roughly the same. Note that the pressure profiles and the pore volume profiles are identical in shape. The porosity is calculated as an exponential function of pressure, but because the compressibility is so low the function is essentially linear in pressure.

Most of the results from the BRAGFLO fixed-porosity calculations are nearly identical to the results that included creep closure dynamics. Compared with the 10,000-yr regulatory period, creep closure transients are brief; a nearly constant final closed state is reached in only a few hundred yr (as currently modeled). Most flow phenomena in the vicinity of the repository take place at very low rates because of the low permeabilities of the surrounding strata. Only the chemical reactions (corrosion and biodegradation) occur rapidly. The initial brine volume was the same (for a given realization) in both calculations, and the low inflow and outflow rates changed that volume little over the first few hundred years, so the extent of the reactions was largely unaffected by the different porosities in the two sets of calculations. Thus, profiles of the remaining iron and cellulose content of the waste (Figures 4.4-25 and 4.4-26), and the total cumulative gas generated (Figure 4.4-27), look very similar in both the closure and fixed-porosity calculations (Figures 4.4-8, 4.4-10, and 4.4-7, respectively). After a few hundred years, conditions in the fixed-porosity calculations are very close to those in the closure runs, because by then porosities in the creep closure calculations have reached stable values that range from about 13% to 25%, similar to those in the fixed-porosity calculations (19%). The exceptions are those few realizations in which the pressure rose rapidly and sufficiently high in the closure calculations to result in significant reinflation. In these, the stable final-state porosities are much higher (26% to 34%) than the porosities used in the fixed-porosity calculations, so pressures and other responses differed more substantially in the two sets of calculations.

Where the two calculations differed most was in the pressure-sensitive fluid-flow behavior, including gas flow out the Culebra, MB138, and the anhydrite A and B layer, and brine flow out MB139. Differences resulted from the lower average porosity in the fixed-porosity calculations, which produced higher pressures in the waste. The higher pressures forced gas farther out the gas flow paths, and pushed brine farther out MB139. However, the maximum volume of brine that flowed laterally out MB139 (3540 m^3) was still not enough to reach the accessible environment boundary, even if the porosity of MB139 had been 0.001 (the low end of the sampled range) in the realization producing the highest brine flow.

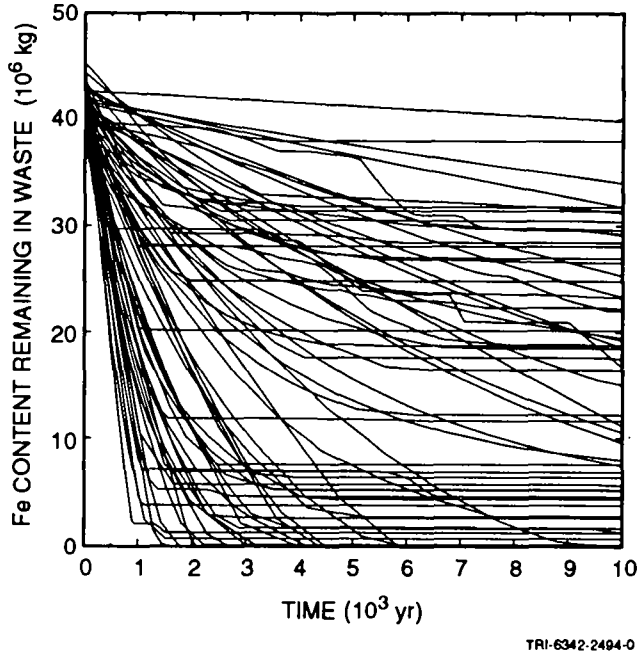

Figure 4.4-25. Iron content remaining in the waste without creep closure.

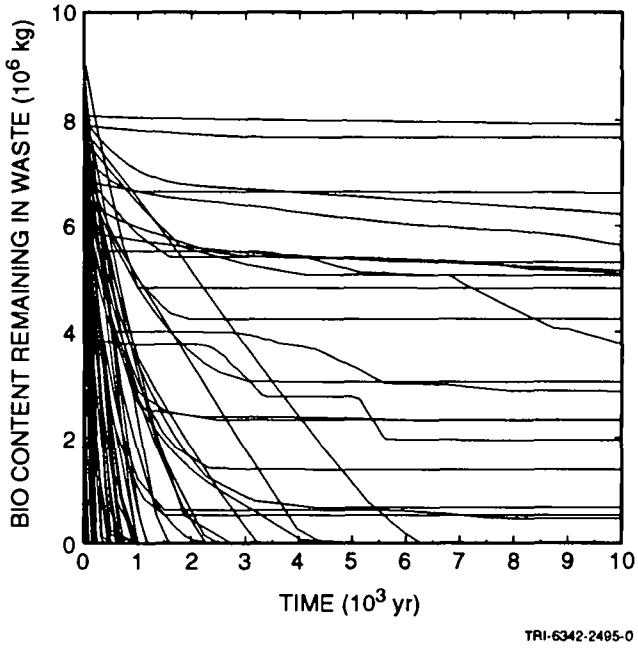

Figure 4.4-26. Cellulosic content remaining in the waste without creep closure.

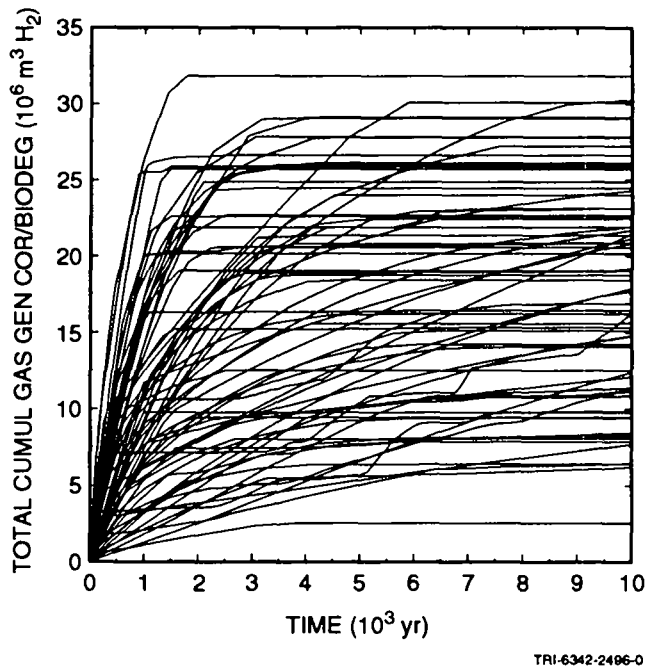

Figure 4.4-27. Total cumulative gas generated from corrosion and biodegradation, without creep closure.

4.4.4 Comparisons with 1991 Results

The 1992 undisturbed performance calculations can be compared with two earlier sets of calculations (WIPP PA Department, 1992), the first done on a single panel scale (similar to the 1992 disturbed performance calculations), and the second done on a full repository scale (similar to the 1992 undisturbed performance calculations).

The implementation of creep closure in the 1992 performance assessment resulted in significant differences in repository behavior, particularly in the pressure histories. Whereas peak pressures in the 1992 calculations are around 22 MPa, in the previous analyses they peaked at 17 MPa in the panel-scale calculations and 16 MPa in the full-repository (undisturbed) calculations. This resulted from the lower porosities obtained from creep closure. With creep closure, final waste porosities ranged from 13% to 34%. In the previous analyses without creep, closure porosities ranged from 33% to 60%. Waste pore volumes were nearly constant through time in all previous calculations, the only variation resulting from compressibility of the waste.

There was, however, no net effect on performance. Neither in previous analyses nor in the 1992 PA was there any release of contaminated brine to the accessible environment in the undisturbed scenario. This result could change when pressure-dependent fracturing of anhydrite interbeds is implemented in the model in 1993, because pressures exceeding lithostatic could cause greater migration through fractured marker beds. However, because of the high degree of nonlinearity in the model, it is impossible to predict with any certainty what effect fracturing will have until the calculations are performed.

5. DISTURBED PERFORMANCE

5.1 Repository/Shaft

5.1.1 Model Geometry

The model geometry for disturbed performance (i.e., scenarios in which the waste-disposal region is intruded by an exploratory borehole) of the repository/shaft system modeled by BRAGFLO[1] differs from that used for undisturbed performance (Section 4.1), and is based on a radial-panel approximation scaled to match the initial excavated volume of a single equivalent panel. The model uses axisymmetric geometry with the intruding borehole as the axis of symmetry (Figure 5.1-1) to represent one of the ten waste-disposal panels (labeled 1 through 10 in Figure 4.1-1) and the surrounding stratigraphy (also shown in Figure 4.1-1). Differences between this model geometry and the rectangular geometry used to simulate undisturbed performance reflect the different purposes of the two sets of analyses, and result in performance estimates from the two geometries that are not in all regards directly comparable.

Several assumptions are implicit in the axisymmetric model:

- As Figure 4.1-1 shows, the intruding borehole is located along the axis of symmetry of the cylindrically shaped equivalent panel. Strata directly above and below the panel are also represented by cylindrical elements. Strata adjacent to the panel are ring-shaped cylindrical elements surrounding the panel cylinder.

- The volume of the equivalent panel equals approximately one-tenth of the total storage volume of the repository. This smaller volume is based on the assumption that the panel seals will prevent fluid flow between each of the ten panels; therefore only one of the repository's ten panels is compromised by a borehole intrusion. The volume of this equivalent panel is assumed to equal the volume of one of the eight full-size waste-emplacement panels. The impact of allowing no flow between panels following human intrusion will be examined in future PAs.

---

1. The BRAGFLO computational model is described in Appendix A of Volume 2 of this report and in the literature cited therein. A discussion of multiphase flow through porous media, which BRAGFLO models, is provided in Section 7.2 in Volume 2 of this report.

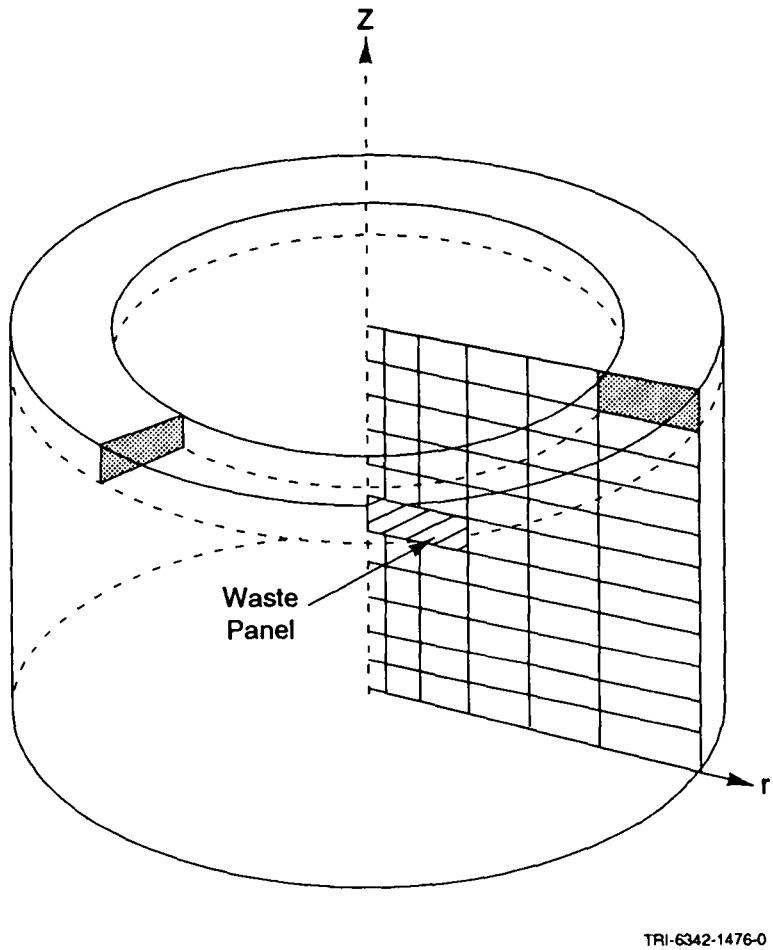

Figure 5.1-1. Schematic representation of the axisymmetric cylindrical model used for calculating disturbed performance of the repository/shaft system.

- Because flow of radionuclides up the exploratory borehole is the dominant radionuclide transport mechanism, radionuclide transport through the panel seals towards the existing shafts can be ignored. Therefore, the drift and shaft systems are omitted entirely from the model, and the mesh resolution is coarse in the strata surrounding the repository.

Figure 5.1-2 shows a vertical slice of the axisymmetric model. The region extends vertically 695 m from the top of the Culebra Dolomite Member of the Rustler Formation down to a hypothetical brine reservoir in the Castile Formation underlying the repository. The total radius is approximately 26 km. Stratigraphic units included in the model are the Culebra Dolomite, the intact halite of the Salado Formation, MB138, anhydrites A and B lumped into a single anhydrite layer, MB139, a disturbed rock zone (DRZ) surrounding the waste-storage area, and a transition zone above the DRZ overlying the waste-storage area.

5.1.2 Material Properties

Material properties for disturbed performance of the repository/shaft system are discussed in detail in Volume 3 of this report. The following material properties, which apply specifically to disturbed performance of the repository/shaft system, are discussed below in the following order:

- permeability,
- porosity,
- specific storage,
- relative permeability,
- brine and gas saturations,
- capillary pressure,
- Castile Formation brine reservoir pressure and storativity,
- radionuclide inventory, and
- radionuclide solubility.

All of the above material properties except radionuclide inventory and radionuclide solubility are used by BRAGFLO. These two material properties

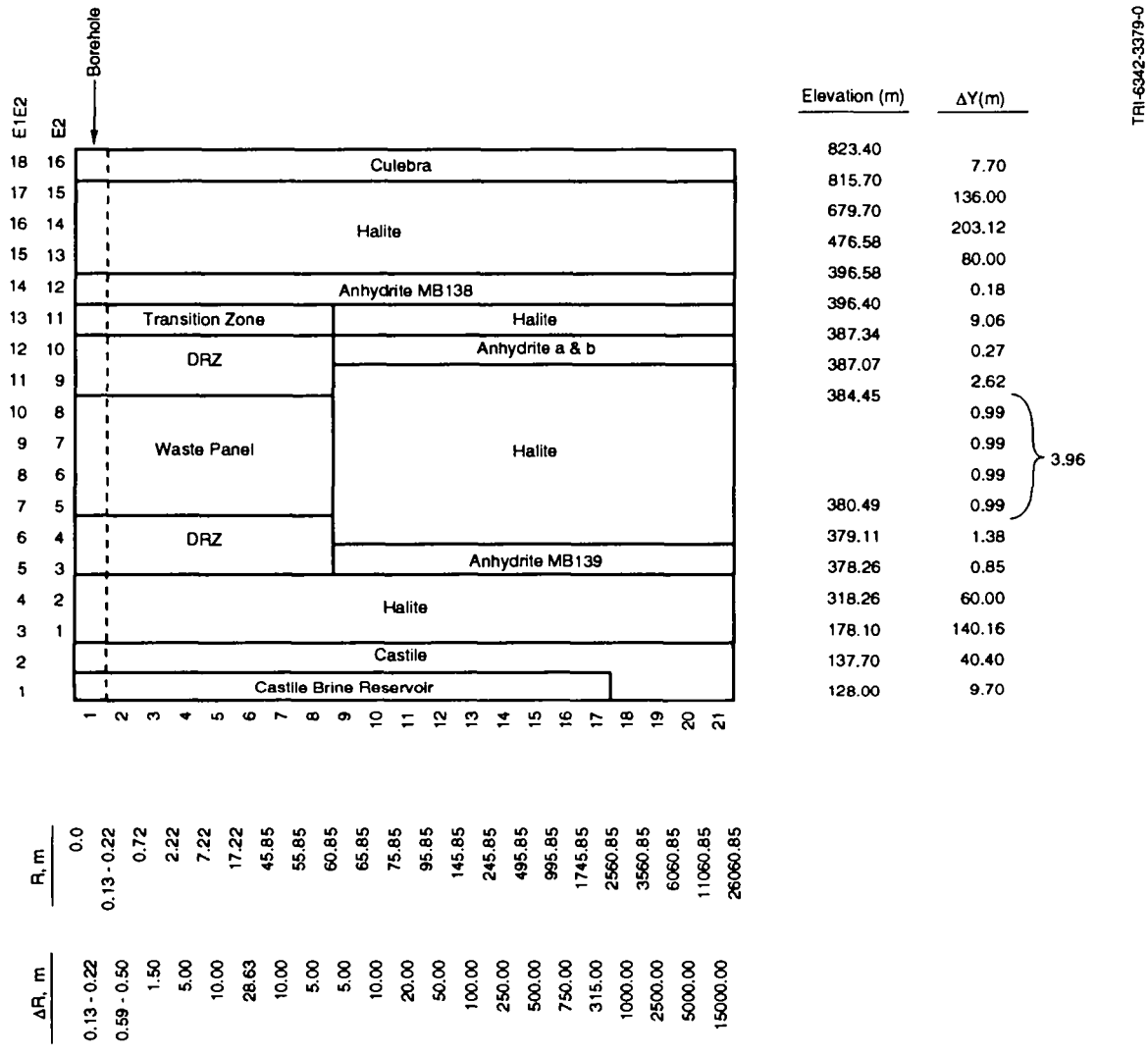

Figure 5.1-2. Geometry of the cylindrical equivalent panel model used for calculating disturbed performance of the repository/shaft system.

are input to the PANEL computational model, which is used to model radionuclide dissolution and mixing with brine flow up the intrusion borehole. PANEL is discussed further in Section 7.4 in Volume 2 of this report.

5.1.2.1 PERMEABILITY

Permeability Ranges

Assumed permeability values for the disturbed repository/shaft, shown in Figure 5.1-3, are listed below in order of increasing permeability

- Halite is assigned a range of permeability values from 1.0×10^{-24} to 1.0×10^{-19} m^2.
- The anhydrite interbeds (MB138, MB139, and anhydrite A and B) and the transition zone above the DRZ overlying the waste-disposal panel are assigned a range from 1.0×10^{-21} to 1.0×10^{-16} m^2.
- 1.0×10^{-15} m^2 is assigned to the DRZ.
- 2.1×10^{-14} m^2 is assigned to the Culebra.
- 1.0×10^{-13} m^2 is assigned to the waste.
- 1.0×10^{-11} m^2 is assigned to the Castile brine reservoir.

The Castile Formation (except for the brine reservoir) is assigned a permeability of zero. This is necessary to prevent the pressure in the brine reservoir from decaying before an intrusion occurs.

As discussed in Section 4.2.1, the permeability range for the anhydrite interbeds (1.0×10^{-21} to 1.0×10^{-16} m^2) is extended to reflect some increase in permeability associated with fracturing. The interbed fracturing process, however, is not modeled in the 1992 calculations.

Culebra Permeability

For each of the 70 transmissivity fields used in the 1992 PA analysis, an area-weighted hydraulic conductivity was computed for the repository/shaft calculations. The conductivity was estimated for a circular region 5 km in radius centered at the intrusion borehole location.[2]

2. For undisturbed calculations, this region is a 5-km-radius region centered about the waste storage area.

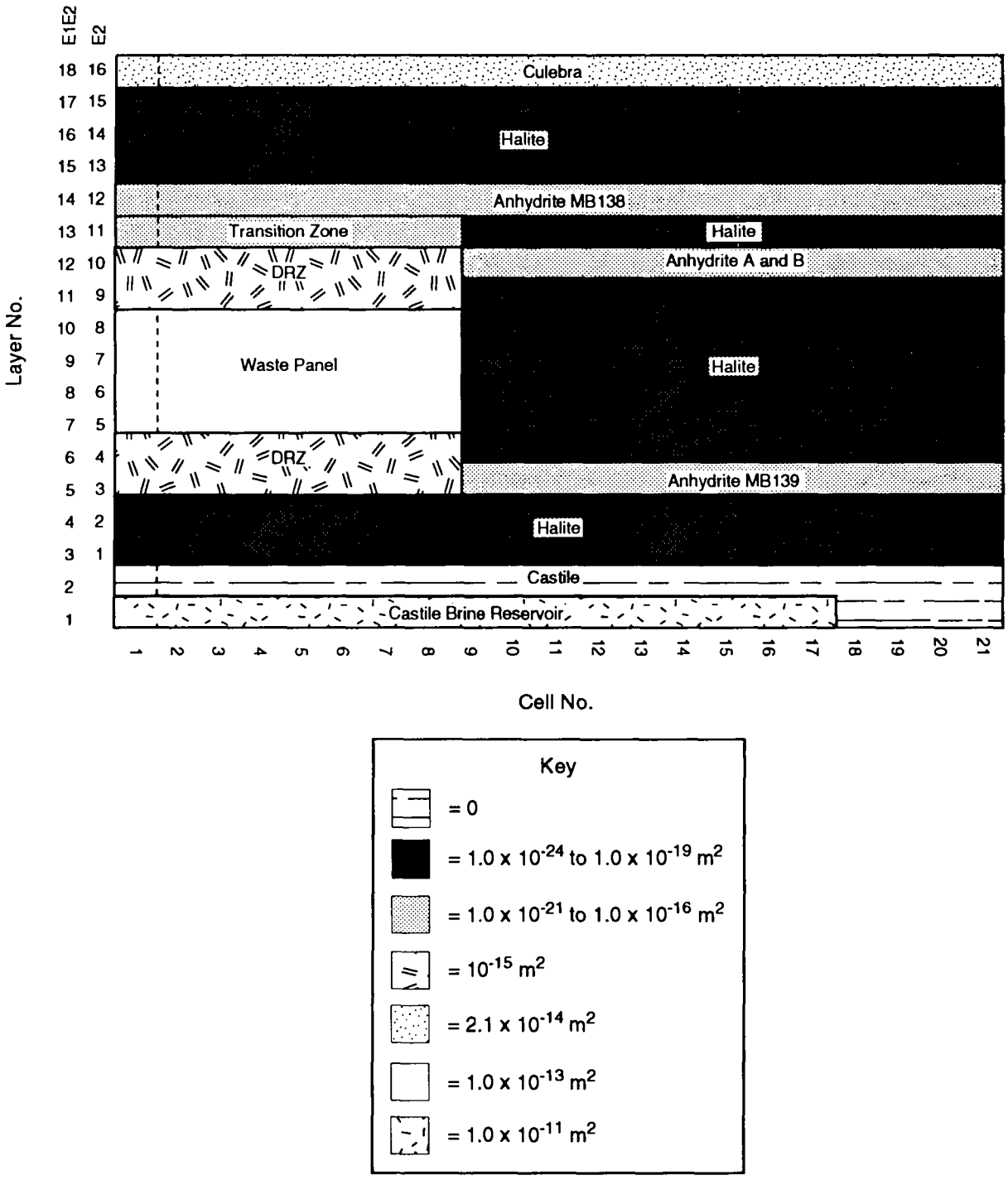

Figure 5.1-3. Permeability values for the disturbed repository/shaft system.

BRAGFLO uses intrinsic permeability (a property of the medium alone; usually referred to in this report simply as permeability) rather than hydraulic conductivity (which includes properties of the fluid) for the Culebra Dolomite above the repository. The relationship is given by

$$k = \frac{K\mu}{\rho g}, \qquad (5.1\text{-}1)$$

where k is intrinsic permeability (m^2), K is hydraulic conductivity (m/s), μ is fluid viscosity (Pa•s), ρ is fluid mass density (kg/m^3), and g is the gravitational constant (m/s^2). The median value of hydraulic conductivity was used and fluid properties for Culebra brine were obtained from the property data base. The following values were used:

$K = 2.24 \times 10^{-7}$ m/s,

$\mu = 0.001$ Pa•s,

$\rho = 1090$ kg/m^3, and

$g = 9.79$ m/s^2.

resulting in an intrinsic permeability, k, of 2.1×10^{-14} m^2.

5.1.2.2 POROSITY

Fixed (Time-Invariant) Porosity

Assumed porosity values for the disturbed repository/shaft that do not change in time, shown in Figure 5.1-4, are listed below:

- Halite, the anhydrite interbeds, and the transition zone are assigned a range of porosity values from 0.001 to 0.03.
- A slightly larger range of porosity values is assigned to the DRZ. As is explained in Section 2.4.4 of Volume 3 of this report, the DRZ range is determined by Equation 4.2-1 (Section 4.2.2.1)
- The waste prior to closure modeling is assigned a value of 0.660.

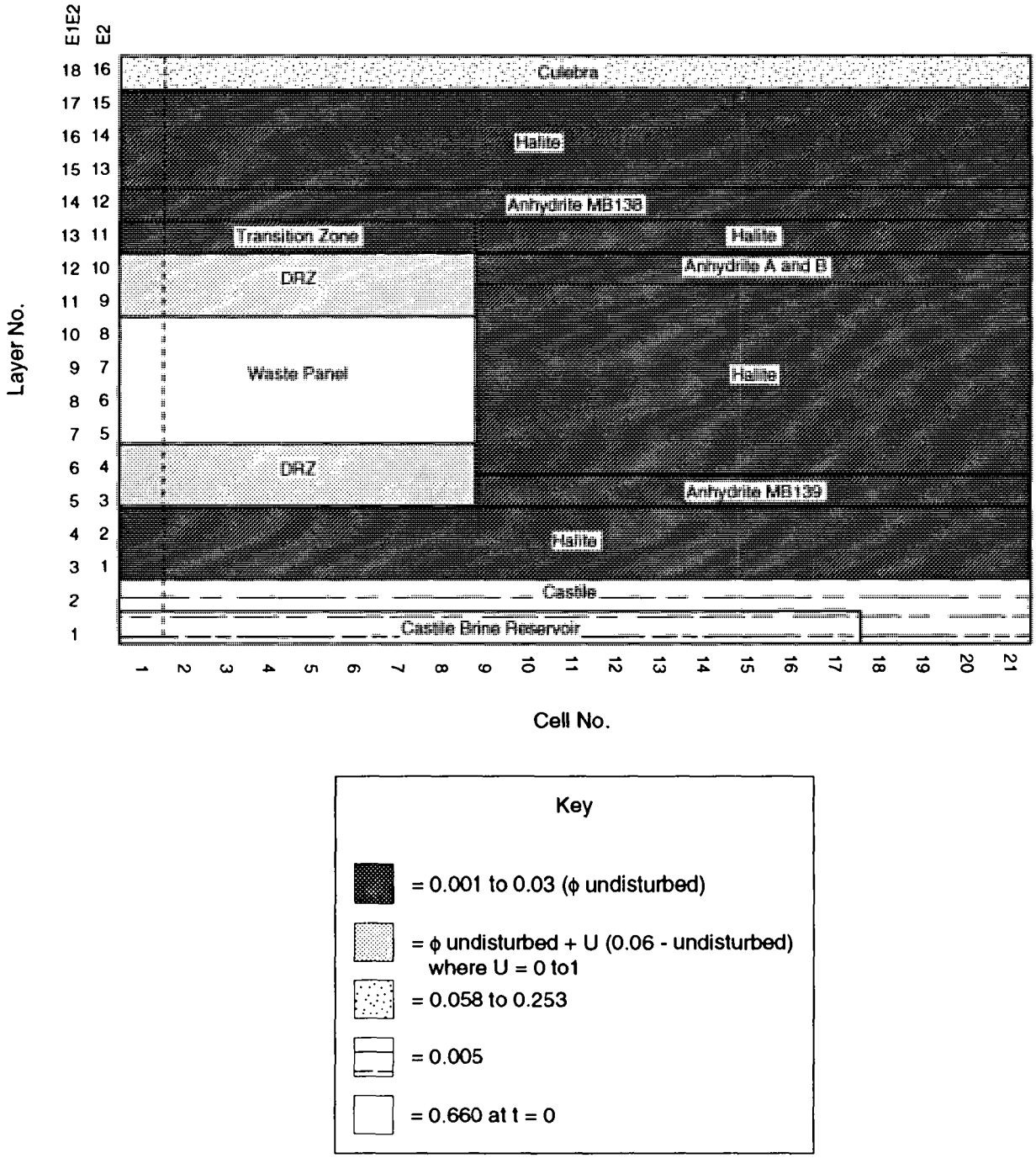

Figure 5.1-4. Porosity values for the disturbed repository/shaft system.

Variable (Time-Varying) Porosity

The 1992 calculations for the first time take into account time-varying changes in panel porosity caused by creep closure of the panel. Input is from the computer code SANCHO. The reader is referred to Section 4.2.2.2 for a complete discussion of how the SANCHO porosity results are incorporated into BRAGFLO. Observations applying specifically to the disturbed repository/shaft environment appear as footnotes to the text in Section 4.2.2.

5.1.2.3 SPECIFIC STORAGE

Specific storage values for the disturbed repository/shaft system are calculated based on the relations presented by Equations 4.2-5, 4.2-6, and 4.2-7 (Section 4.2.3).

5.1.2.4 RELATIVE PERMEABILITY[3] AND CAPILLARY PRESSURE[4]

In modeling two-phase phenomena, characteristic curves using either the Brooks-Corey formulae (Brooks and Corey, 1964) or the van Genuchten-Parker formulae (van Genuchten, 1978; Parker et al., 1987) are used (see Section 2.3.1 of Volume 3 of this report). The Brooks-Corey relative permeability model is used for two-thirds of the calculations and the van Genuchten-Parker model is used for the remaining one-third of the calculations. An index parameter (0 or 1) is sampled with these probabilities, so that either one model or the other is used in any one calculation.

Relative permeability parameters are varied and are the same for all materials except the waste and DRZ, which use a fixed set of values and the Brooks-Corey model. Residual brine and gas saturations range from 0.0 to

---

3. Relative permeability is a function of the saturation. It is a value between 0 and 1 that is multiplied by the absolute permeability to yield the effective permeability. Relative permeabilities are empirical fits of pressure drop and flow data to extensions of Darcy's law, and measurements taken at different degrees of saturation result in differing relative permeabilities (see Chapter 7 of Volume 2 and Section 2.3.1 of Volume 3 of this report).

4. Capillary pressure differences arise when the gas and brine phases flow simultaneously through a porous network (see Chapter 7 of Volume 2 and Section 2.3.1 of Volume 3 of this report).

0.4. The Brooks-Corey parameter, λ, ranges from 0.2 to 10.0. The van Genuchten-Parker parameter m is calculated from $m=\lambda/1+\lambda$. The choice of the characteristic curve model has important implications for the expected behavior of multiphase flow in porous media (see discussion in Section 4.2.4).

Threshold capillary pressures are determined from the correlation with permeability in all regions, as described in Section 2.3.1 of Volume 3 of this report. The van Genuchten-Parker capillary pressure constant, P_o, is calculated by equating the capillary pressure from each of the two models at an effective saturation of 0.5, and solving the expression for P_o. In the waste, in the DRZ, and in all excavated regions, the capillary pressure is assumed to be zero. In the 1992 performance assessment, zero capillary pressure for these regions is assumed because the capillary pressure curves are not defined for imbibition into a medium that has less than residual brine saturation. Any regions where the brine saturation starts out or may become less than residual (e.g., as a result of brine-consuming reactions) were modeled with zero capillary pressure. However, assuming zero capillary pressure may not be necessary in future calculations (see Section 4.2.4).

5.1.2.5 CASTILE BRINE RESERVOIR PRESSURE AND STORATIVITY

In disturbed performance of the repository/shaft system, an exploratory borehole can penetrate a pressurized brine pocket in the Castile Formation underlying the repository (see Section 4.3.3.2 in Volume 2 of this report). In order to calculate the effects of Castile brine flow through the waste following intrusion, brine pressure and storativity are required inputs. Initial pressure is assumed to range between 12.6 and 21.0 MPa; storativity is assumed to range between 0.2 and 2.0 m^3/Pa.

5.1.2.6 RADIONUCLIDE INVENTORY

Radionuclide inventory ranges for remote-handled (RH) and contact-handled (CH) waste vary by radioisotope. A complete list of ranges by isotope is provided in Table 3.3-1 of Volume 3 of this report.

5.1.2.7 RADIONUCLIDE SOLUBILITY

Radionuclide solubility varies by element. The lowest value is -16.5 log(molar) for plutonium and the highest value is 1.26 log(molar) for radium.

Complete information on radionuclide solubilities is provided in Section 3.3.5 of Volume 3 of this report.

5.1.3 Initial and Boundary Conditions

As with the calculations for undisturbed conditions, a major difference between the 1992 and 1991 PA calculations for disturbed conditions of the repository/shaft system is in the treatment of initial conditions (Section 4.3). The primary objective of taking a new approach in modeling the initial conditions has been to establish a more realistic pressure distribution in the formations surrounding the waste at the time the repository will be sealed. This time is referred to here as time zero. The 1992 calculations achieve more realistic time-zero initial conditions by varying the initial conditions in the repository over a 20-yr period immediately preceding time zero.

As explained in Section 4.3, it was previously assumed that excavated regions were initially at atmospheric pressure with some arbitrary degree of brine-saturation, while all other regions were fully brine-saturated at hydrostatic pressure. In reality, brine will seep in continually from the surrounding formations during the operational phase of the WIPP. Water in the brine will evaporate into the well-ventilated atmosphere of the excavations, or will be pumped out as a standard mining practice if it accumulates anywhere. Thus, formations surrounding the excavations will be partially dewatered and depressurized during the operation.

The operational phase for disturbed conditions is now modeled more explicitly, as detailed in Table 5.1-1. The important features of conditions during the operational phase are as follows:

- Because the disturbed-performance calculations are performed on a panel scale (Section 5.1.1), the operational phase is assumed to last 20 yr rather than the 50-yr period used for the repository-scale undisturbed calculations (Section 4.3). The 20-yr time period was chosen to incorporate some of the effects of other panels. While a single panel will not be likely to be open for 20 yr (except for the North and South Equivalent Panels), adjacent panels will be undergoing excavation or completing operations while each panel is being filled, and the formations surrounding a panel will be disturbed during operation.

- Except for the waste, the excavated regions, and the Culebra, the pressure distribution at 20 yr before time zero is hydrostatic

Table 5.1-1. Startup Procedure for Disturbed Calculations

I. Simulate the panel as an empty, newly excavated, gas-filled cavity	1) Set initial waste porosity to 1.0 2) Set initial waste brine saturation to 0.0 3) Set initial waste pressure to 1 atm 4) Set initial waste residual brine and gas saturation to 0.0 5) Set initial permeability to 1.0×10^{-10} m^2
II. Simulate DRZ as initially pressurized, but partially fractured	1) Set initial pressure to hydrostatic relative to sampled value of MB139 pore pressure 2) Set initial permeability to 1.0×10^{-17} m^2 3) Set initial porosity to volume average of sampled value of intact far field anhydrite and intact halite porosities (since DRZ has both) 4) Set initial brine saturation to 1.0 5) Set capillary pressure to 0.0 (so gas and brine pressures are same)
III. Let the system equilibrate for 20 yr, the approximate time span between excavation and sealing of the repository	1) Waste pressure will increase slightly (~-0.5%) 2) Brine will drain down from DRZ, leaving residual saturation 3) DRZ pressure will drop precipitously, to equal waste pressure 4) Let no creep closure occur
IV. Instantly add the waste at 20 yr	1) Reset waste pressure to 1 atm 2) Set brine saturation of waste to sampled "initial" brine saturation 3) Set waste residual brine and gas saturations to their sampled values 4) Set waste permeability to 1.0×10^{-13} m^2 5) Set waste porosity to "initial" value calculated from sampled values of volume fractions of metal and combustibles 6) Set reactant concentrations to "initial" values
V. Adjust parameters for the DRZ and Culebra	1) Change porosity to final sampled values (except for the creep closure and rock compressibility, simulating time-dependent porosity is beyond current modeling capability) 2) Adjust brine saturation so brine content of DRZ is unchanged; add gas to fill added pore volume 3) Reset DRZ pressure to 1 atm 4) Set DRZ permeability to 1.0×10^{-15} m^2 to account for fracturing
VI. Resume calculation at 20 yr, this is the time normally called t=0	1) Begin creep closure 2) Allow gas generation to begin 3) Pressures outside waste and DRZ start from 20- yr values
VII. Continue out to 10,020 yr, i.e., 10,000 yr past the time normally called t=0	

relative to the pore pressure of MB139, for which a sampled range of 12 to 13 MPa is used.

- Pressure at 20 yr before time zero in the waste and excavated regions is atmospheric, and the waste pressure is reset to this value at the end of the 20-yr period.

- Pressure in the Culebra at 20 yr before time zero is 1.053 MPa, and the far-field pressure is held at that value over the 10,020-yr calculation. (The Culebra has a fixed-pressure boundary condition, whereas the rest of the mesh uses a no-flow boundary condition.)

- The starting brine saturation will be 1.0 everywhere except in the waste panel (there are no other excavated regions in disturbed scenarios except maybe the borehole, but it doesn't exist until 1000 yr have elapsed), where the brine saturation starts at 0.0.

- At the end of the 20-yr operational period, the waste is emplaced instantaneously and assigned its sampled value of initial brine saturation, which will range from 0.0 to 0.14.

The initial-condition calculations themselves begin with initial conditions similar to those used in 1991; perhaps the greatest difference is simply in interpretation. What was called time zero last year is now called -20 yr; this is the time of initial excavation. The performance calculations begin at time zero (20 yr after the initial-condition calculation has started); this corresponds to the time of sealing of the repository.

For the initial-conditions calculation, the permeability of the excavated regions is assumed to be very high (1×10^{-10} m^2) to simulate cavities. At the end of the 20-yr operational period, any brine that has flowed into the excavated regions is ignored, since it will have evaporated or will have been pumped out of the repository. The sampled initial liquid saturation in the waste is introduced. Pressures in all the excavated regions are reset to atmospheric. Pressures there will generally be barely above atmospheric (by a few hundred pascals); they are reset to atmospheric to reestablish realistic conditions at time zero, since at the time of sealing, the excavated regions should really be at atmospheric pressure. With the exception of the DRZ pressures in all the surrounding formations, including the transition zone and the anhydrite interbeds, remain as they are at the end of the 20 yr.

In the DRZ, at least the residual saturation of brine, and possibly more, will remain, the rest having drained into the excavated region that will later be filled with waste. At time zero, porosity is assumed to change from

the initial intact halite value to the final sampled DRZ porosity. This porosity change increases the void volume. In order to conserve the volume of brine in the DRZ, the additional void volume is assumed to be filled with gas. The pressures in the DRZ will typically be slightly above atmospheric at time zero. If the pressures were left at those values when additional gas is introduced at time zero, it could result in a gas-drive condition that would cause brine to be expelled suddenly from the DRZ into the waste at time zero. To prevent this unrealistic behavior, the pressure in the DRZ is also reset to atmospheric at time zero.

The previously excavated regions will contain no brine except for the initial liquid brought in with the waste. The surrounding formations will be depressurized and dewatered to the extent expected after being exposed to ventilated air at atmospheric pressure for 20 yr. All surrounding formations are fully saturated with brine at time -20 yr. Generally, at time zero, they will still be fully brine-saturated (except for the DRZ). Except for the DRZ, the brine saturation in surrounding formations is not modified due to a change in porosity at time zero.

The calculations proceed from this calculated initial condition for the 10,000-yr performance period. The most important effect of these more realistic initial conditions is that less brine will flow into the excavated regions (including the waste), since the initial "surge" of brine that occurs upon excavation has been eliminated, and the pressure gradients in the immediate vicinity of excavations have been greatly reduced.

5.2 Results and Discussion (Disturbed Performance)

As with the results of the undisturbed performance calculations, some general descriptions of the results for disturbed performance calculations are provided here. Plots showing the time dependence of various results include all 70 realizations (vectors), which allows trends to be observed and gross behavior comparisons to be made among all the vectors. Scenarios analyzed (E2 and E1E2) are defined in Section 2.2 of this volume and described in more detail in Section 4.2.3.2 of Volume 2 of this report.

5.2.1 E2 Scenario

5.2.1.1 WASTE PANEL BEHAVIOR

The time dependence of pressures in the waste panel is shown in Figure 5.2-1 for all 70 realizations. In only two of the vectors does the peak

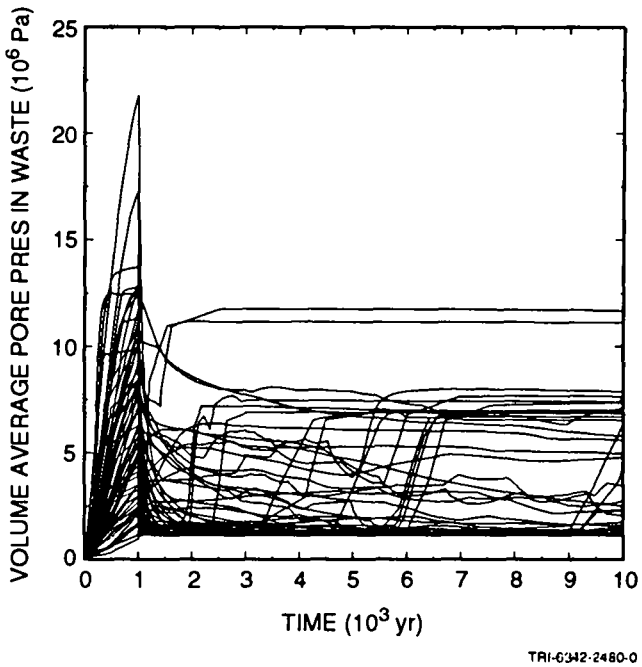

Figure 5.2-1. E2 scenario, intrusion at 1000 yr: volume average gas pressure in waste.

pressure exceed lithostatic (~14.8 MPa), probably as a result of rapid gas-generation rates and high initial brine content in the waste.

At the time of human intrusion, 1000 yr, the waste panel pressure in all of the vectors drops precipitously (except for two cases in which the pressure was so low that intrusion had no immediate effect). After intrusion, two general types of behavior can be seen. The more common response is for the pressure to continue to decrease after the intrusion. The other response is for the pressure to rise again relatively rapidly following a period of low or slowly decreasing pressure. The time lag between intrusion and repressurization lasts from 500 to over 8000 yr. During this time, gas that has filled the panel is driven up the intrusion borehole as brine flows into the waste through the anhydrite layers (principally MB139). Once the panel is filled with brine (except for residual gas and, in some cases, large trapped bubbles), brine begins to flow up the borehole, eventually filling the borehole to the Culebra. Once the borehole is filled with brine, the pressure in the waste reaches hydrostatic relative to the Culebra pressure, and then levels off. Pressure fluctuations can be seen in the pressure profiles in Figure 5.2-1 with a rapid buildup in pressure as the borehole fills with brine followed by the pressure leveling off at hydrostatic, approximately 7 MPa. There are two realizations in which

the pressure levels off at much higher values. It is not clear why in these two realizations, the pressures level off at such high values. The only parameter that distinguishes these two from the other 68 is that they have the highest sampled anhydrite permeabilities, which would have provided good communication to the higher far-field pressures. In these two vectors, there are no other extreme values among all other parameters that were sampled. However, vectors having similarly high anhydrite permeabilities did not result in final pressures intermediate between the two high ones (>11.1 MPa) and all the rest (<7.8 MPa). This may be a case where the model is extremely sensitive to certain combinations of sampled parameters, and the sampling was not sufficiently detailed in the range of parameters over which the model is most sensitive.

Panel porosities follow the same trends as seen in the undisturbed performance calculations. From the initial waste porosity of 66%, the porosity drops rapidly, bottoming out at 12% to 21% in 300 to 1000 yr. All vectors behave quite similarly, since the creep closure process, as currently modeled, does not allow much deviation from a median closure rate. Only vector 59 shows a different response; in this case, very high pressures were obtained as a result of high gas-generation rates before the human intrusion occurred, and the panel inflated to the maximum allowed porosity, 34%. None of the other vectors indicated sufficient pressure before the intrusion to cause inflation. As Figure 4.2-7 shows, the pressure in the waste must reach at least 6 MPa at low gas-generation rates and as high as 18 MPa at high gas-generation rates before expansion of the panel is noticeable. After intrusion occurs, creep closure is no longer allowed; only compressibility of the waste affects the porosity, and that effect can barely be detected in the plots of waste pore volume (Figure 5.2-2). Thus, the porosity is nearly constant after intrusion.

5.2.1.2 BOREHOLE INTRUSION EFFECTS

In 14 of the 70 realizations, brine from the waste flowed up the borehole into the Culebra. The maximum cumulative brine flow from the waste was 16,300 m^3. As Figure 5.2-3 shows, a group of five vectors has substantial flows up the borehole over the 10,000-yr performance period (ranging from 7200 m^3 to 16,300 m^3); another group of nine vectors had much lower flows (from 800 m^3 to 2600 m^3). Judging from the pressure profiles (Figure 5.2-1) there were two more vectors in which brine flow occurred into the borehole, but which had no release to the Culebra within 10,000 yr. In all of the other vectors, the panel did not fill with brine, and therefore there was no release up the borehole. In most of these cases, the permeability of the surrounding formations was simply too low to allow enough brine to flow in to fill the panel.

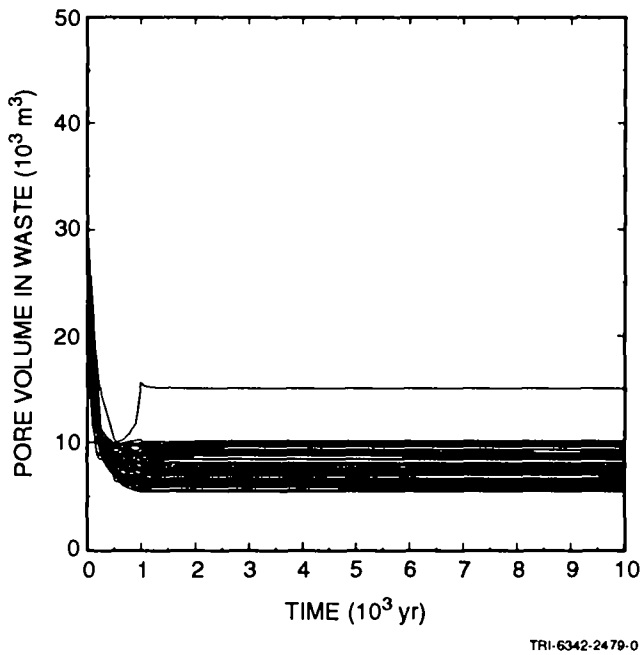

Figure 5.2-2. E2 scenario, intrusion at 1000 yr: pore volume in waste.

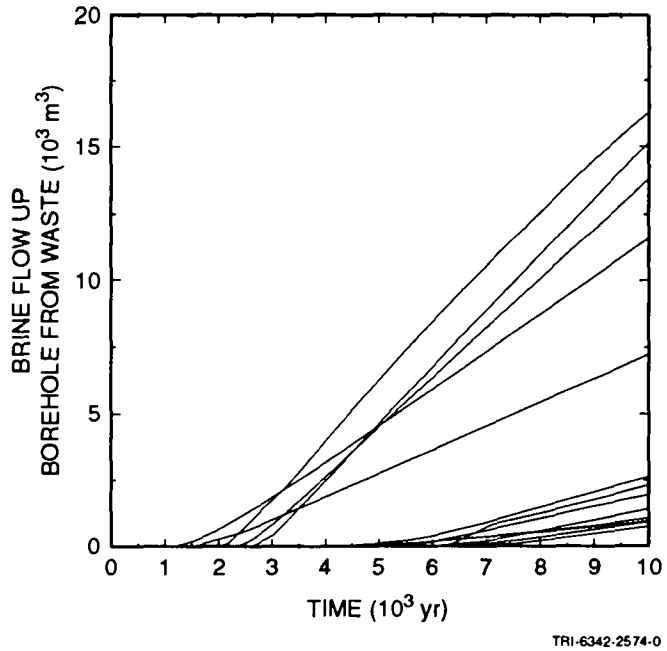

Figure 5.2-3. E2 scenario, intrusion at 1000 yr: cumulative brine flow up borehole.

5.2.1.3 FLOW IN ANHYDRITE LAYERS

It is hypothetically possible for contaminated brine to flow out one of the anhydrite layers to beyond the WIPP boundaries. This possibility cannot be ruled out completely based upon these BRAGFLO simulations alone, since specific particles within the brine have not been tracked. However, it can be shown to be highly unlikely given the assumptions of these calculations using information on the amount of brine flow from the panel. Figures 5.2-4 and 5.2-5 show cumulative brine flow from and toward the panel, respectively, in MB138. The greatest outflow was only 120 m^3, which is not enough to fill the pore space in MB138 between the panel and the WIPP boundary. The quantity of brine that flowed toward the panel in MB138 varied from zero to 8000 m^3. Given the low probability of contaminated brine even reaching MB138, which lies nearly 12 m above the panel, it appears to be unlikely that contaminated brine can flow out as far as the WIPP boundary. Similarly, Figure 5.2-6 shows that almost no brine flows out the anhydrite A and B layer, while as much as 12,000 m^3 may flow in (Figure 5.2-7). The most likely conduit for contaminated brine flow from the waste is MB139. Figure 5.2-8 shows that in one case 2500 m^3 of brine flowed out MB139 from the waste panel. Without tracking particles, it cannot be stated with complete certainty that contaminated brine has not flowed out MB139 to the WIPP boundary. However, if the porosity is as low as can be expected, 0.001, this brine would travel only 935 m radially from the panel, well short of the WIPP boundaries. Note that MB139 is the major conduit for brine inflow; as much as 38,000 m^3 of brine flowed into the waste via MB139 in these calculations (Figure 5.2-9). Based on these calculations, the only probable release conduit from the waste is up the borehole. Some contaminated brine may migrate outward along the marker beds, but not enough to constitute a release to the accessible environment. This assumes that the anhydrite layers do not fracture as the pressure in the waste increases and radial flow occurs along a uniform front. The effects of fracturing will be accounted for in the 1993 PA calculations.

5.2.1.4 EFFECTS OF CREEP CLOSURE

The same set of 70 realizations described above was repeated with the only change being that creep closure of the waste was not allowed to take place. The objective was to determine what effect creep closure, as currently implemented, has on the results. With creep closure, the panel porosity was initially 66% and dropped to 12% to 21%. In the calculations without dynamic creep closure, the waste-panel porosity was initially 19%, which is the median final-state porosity of the waste. (See Table 3.4-1 in Volume 3 of this report.) The porosity was allowed to vary only as a result of the non-zero compressibility of the waste; because the value used for

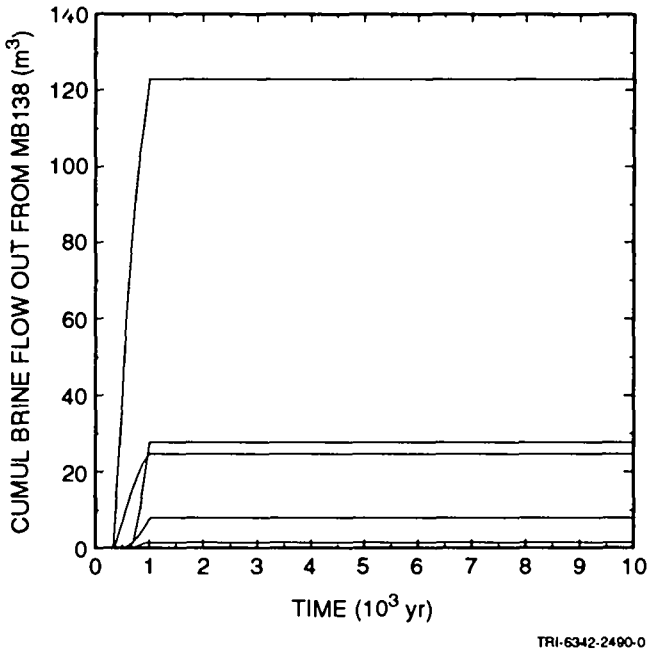

Figure 5.2-4. E2 scenario, intrusion at 1000 yr: cumulative brine flow out MB138.

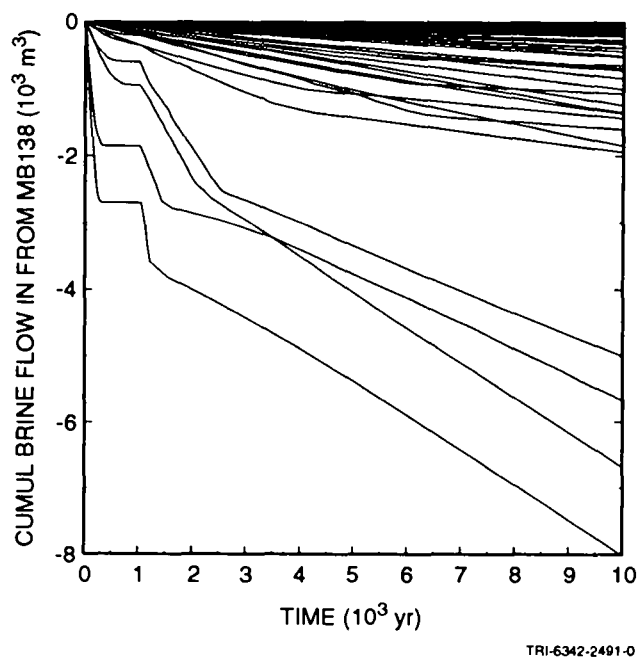

Figure 5.2-5. E2 scenario, intrusion at 1000 yr: cumulative brine flow in from MB138.

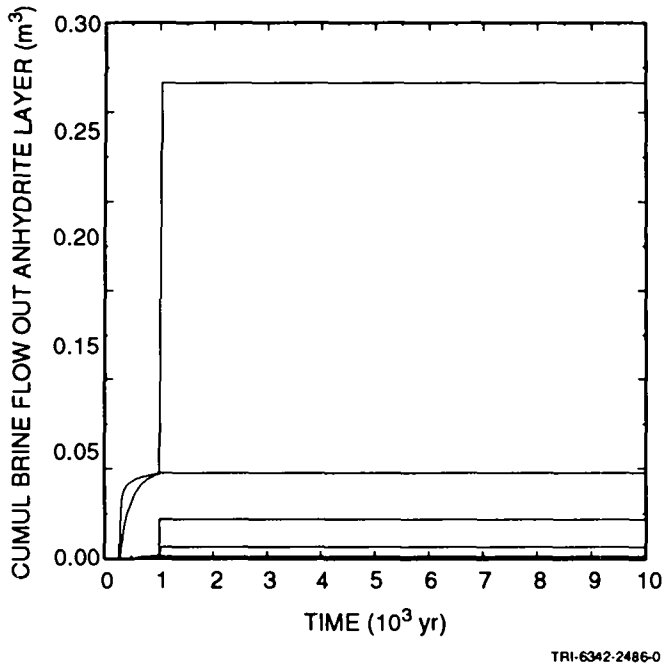

Figure 5.2-6. E2 scenario, intrusion at 1000 yr: cumulative brine flow out anhydrite layers A and B.

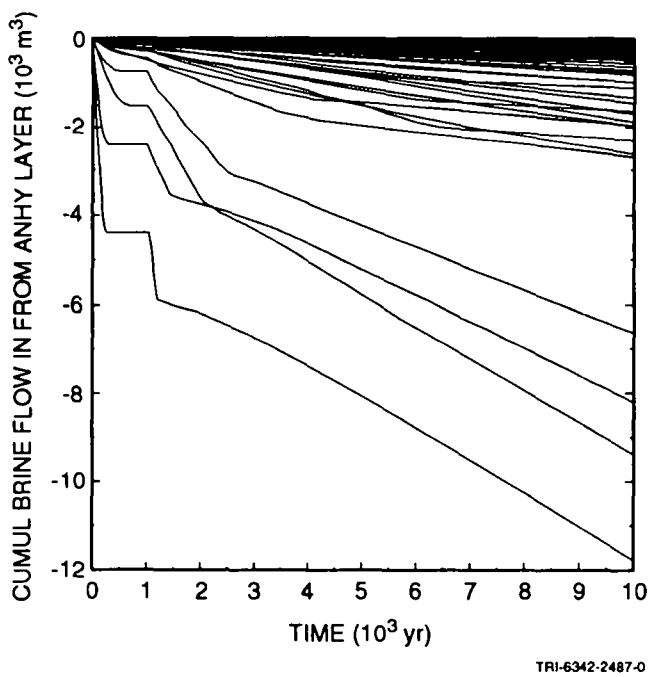

Figure 5.2-7. E2 scenario, intrusion at 1000 yr: cumulative brine flow in from anhydrite layers A and B.

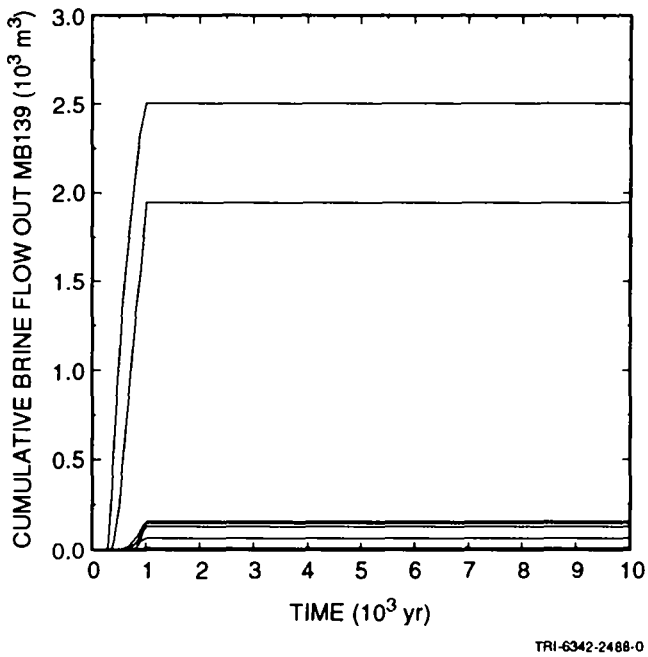

Figure 5.2-8. E2 scenario, intrusion at 1000 yr: cumulative brine flow out MB139.

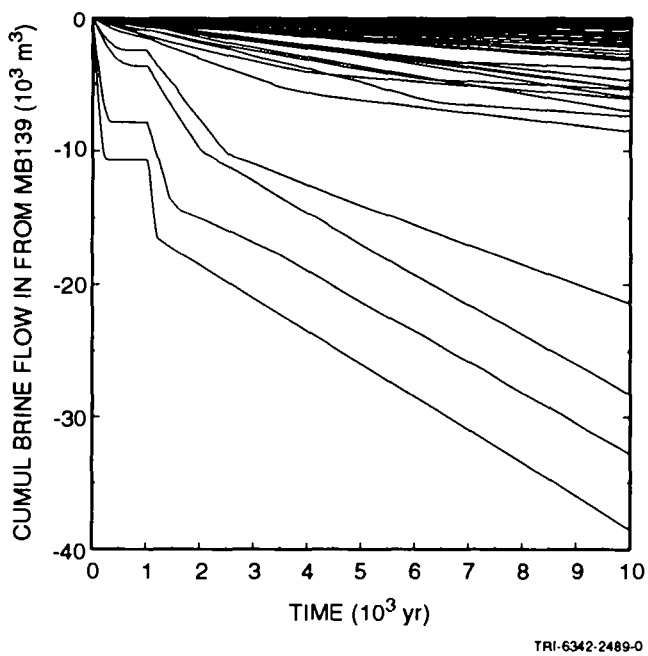

Figure 5.2-9. E2 scenario, intrusion at 1000 yr: cumulative brine flow in from MB139.

compressibility of the waste is very small (1.6×10^{-9} Pa^{-1}), the porosity varied less than 1.2% even under high pressures (Figure 5.2-10). These simulations are therefore referred to as the "fixed-porosity" case. This analysis illustrates the significance of creep closure, to the limit of current modeling assumptions, in assessing the performance of the WIPP. Although only the early time dynamics are accounted for in the current implementation, it is during that time period when the greatest changes occur, so it should be the period during which closure should have a major impact on the performance of the WIPP.

Overall, dynamically modeling creep closure results in only minor differences compared with using a fixed porosity. Transient behavior prior to the intrusion, such as pressure in the repository, may be very different. However, after 10,000 yr, total gas production is nearly identical, and the release of contaminated brine to the Culebra averages about 1% less with dynamic creep closure. Comparisons of results are complicated because the two sets of calculations must start with different initial conditions. The closure calculations start with 66% porosity and a sampled initial brine saturation in the waste, which translates into a certain initial brine volume. Because the rate and volume of gas production is strongly dependent on the initial brine volume, the fixed-porosity calculations were initialized with this same brine volume, rather than the same brine saturation. However, because the pore volume in the fixed-porosity calculations is initially much lower, the pressure in the waste rises more rapidly and much higher, even to unrealistic values. The alternative would be to start with the same initial brine saturation, but then the initial brine volume would be less, so pressures would rise much more slowly, and much less gas would be produced.

As expected, pressure profiles from the fixed-porosity runs (Figure 5.2-11) show some major differences prior to human intrusion. The most obvious differences are in the peak pressures, which now are as high as 38 MPa, compared with 22 MPa with creep closure. Pressures are generally higher without dynamic closure until the intrusion occurs. This results, as mentioned above, because the porosity used in the fixed-porosity calculations is lower initially while the brine volume is the same. With less pore volume in which to store the gas, pressures increase more rapidly and go higher, even though the amount generated is roughly the same.

Following intrusion, the waste pressures are very similar in both the dynamic closure and fixed-porosity results, since by then the porosities are of similar magnitude, much of the brine that is initially present has been consumed, and the gas has been vented to the same low-pressure sink (the

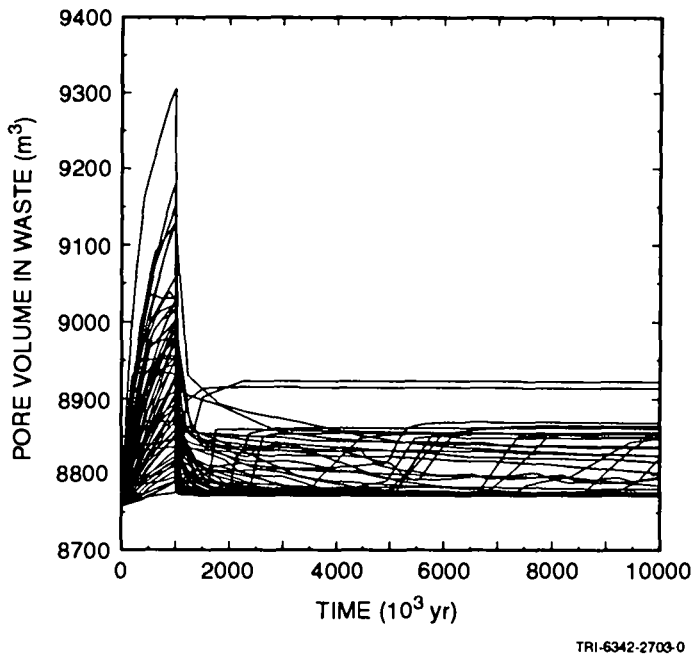

Figure 5.2-10. E2 scenario, intrusion at 1000 yr, no dynamic creep closure: waste porosity.

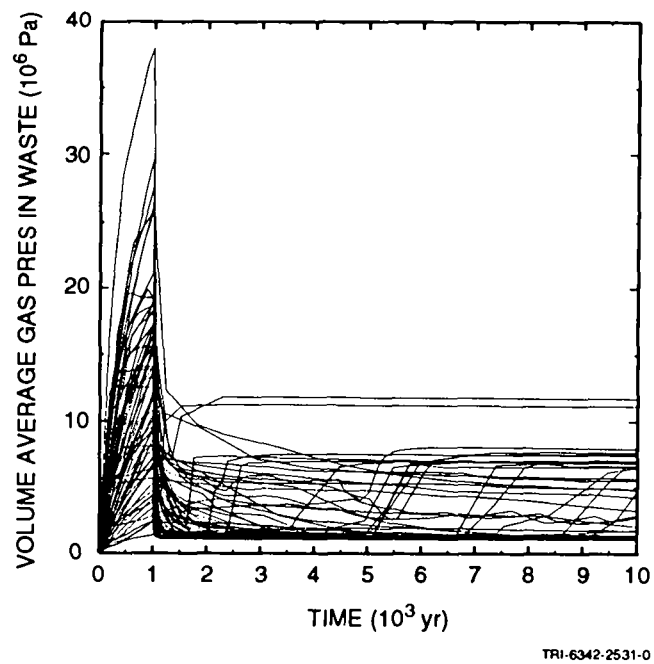

Figure 5.2-11. E2 scenario, intrusion at 1000 yr, no dynamic creep closure: panel pressure.

Culebra). Comparison of plots of the remaining iron and cellulose content for the fixed-porosity runs with those for the runs that include dynamic creep closure reveals a greater extent of reaction early on in the fixed porosity set that seemed to affect about a third of the realizations (Figure 5.2-12). However, except for lowering those particular curves, the general shape of most of the plots is quite similar. This further illustrates that the behavior in the two sets of runs differs little after intrusion.

Plots of the total cumulative gas generated show some distinct differences (Figure 5.2-13), especially in the rate of gas generation (i.e., the slopes of the curves). However, after 10,000 yr, the amount of gas that has been produced is approximately the same in both the dynamic closure and fixed-porosity calculations. The fixed-porosity calculations started with higher brine saturation. Since the gas generation rate is dependent on the brine saturation, the rate is higher initially in the fixed-porosity runs. The initial reactant concentrations are the same in both calculations, as is the initial brine volume in the waste. Thus, the total gas produced is nearly the same with and without dynamic closure.

The maximum amount of brine that flowed up the borehole is slightly less with dynamic closure (Figure 5.2-14). The largest cumulative brine flow up the borehole in the calculations with closure was 16,300 m^3; in the fixed-porosity calculations, it was 17,800 m^3. Among the nonzero flows, the average cumulative flow was 5490 m^3 in the dynamic closure calculations and 4850 m^3 in the fixed-porosity runs. In the dynamic closure calculations, 14 of the 70 vectors showed some positive flow of brine to the Culebra; in the fixed-porosity calculations, 16 vectors had some positive cumulative flow, although two of those amounted to less than 20 m^3. Among the other 14 fixed-porosity nonzero-flow vectors, the average cumulative flow was 5540 m^3, slightly more than the closure average. The net effect of including dynamic creep closure as it is currently implemented, therefore, is to decrease slightly the estimated release of contaminated brine to the Culebra, although the difference is very small, averaging less than 1%.

5.2.1.5 COMPARISONS WITH THE 1991 PA RESULTS

It is useful to compare the 1992 disturbed performance calculations with those from the 1991 performance assessment. Significant changes since 1991 include some parameter value changes (in most cases, only the range of sampled values changed; there was still some overlap in the parameter ranges), and the inclusion of creep closure in 1992. In the 1991 performance

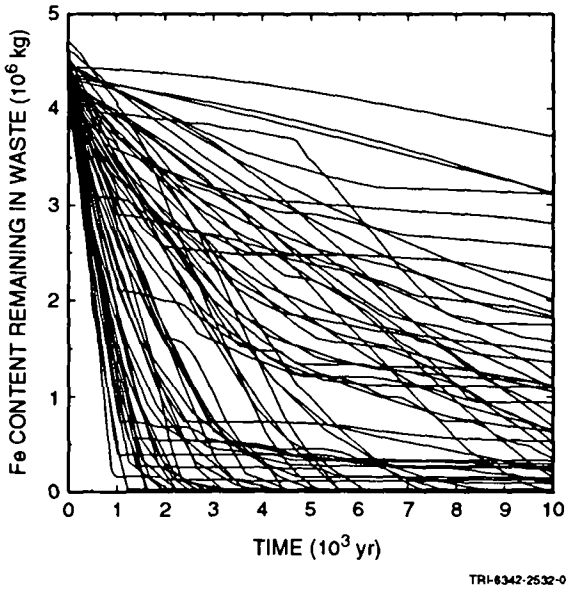

(a)

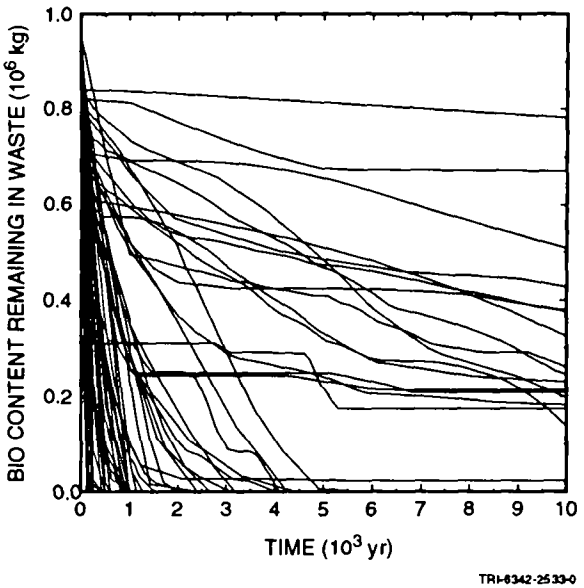

(b)

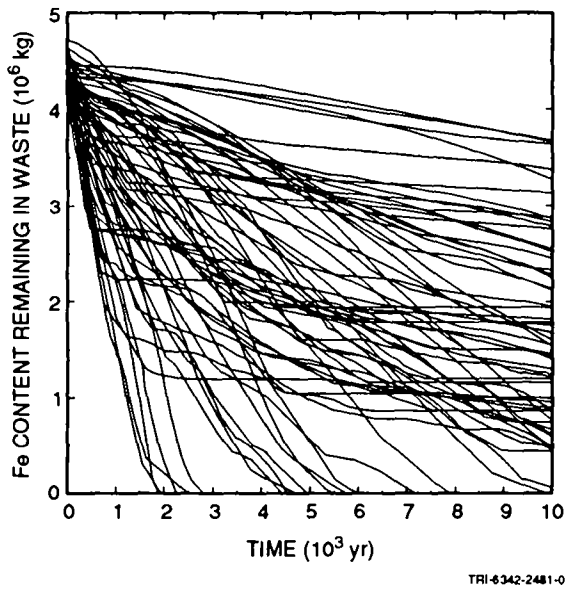

(c)

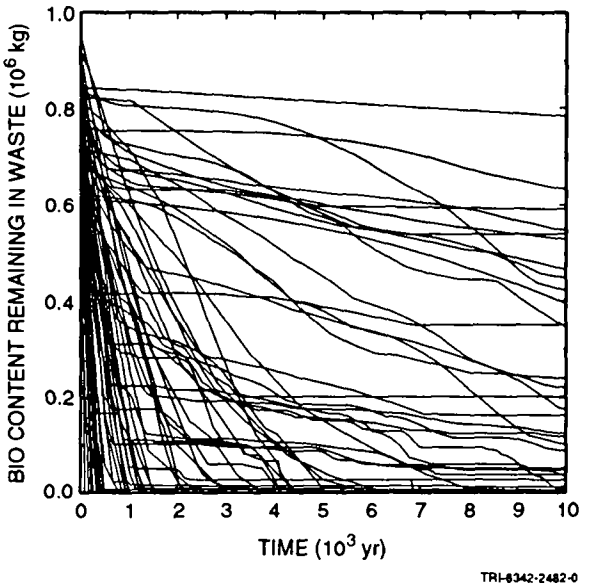

(d)

Figure 5.2-12. E2 scenario, intrusion at 1000 yr: iron and cellulosic content remaining with fixed porosity (5.2-12a and 5.2-12b) and with dynamic creep closure (5.2-12c and 5.2-12d).

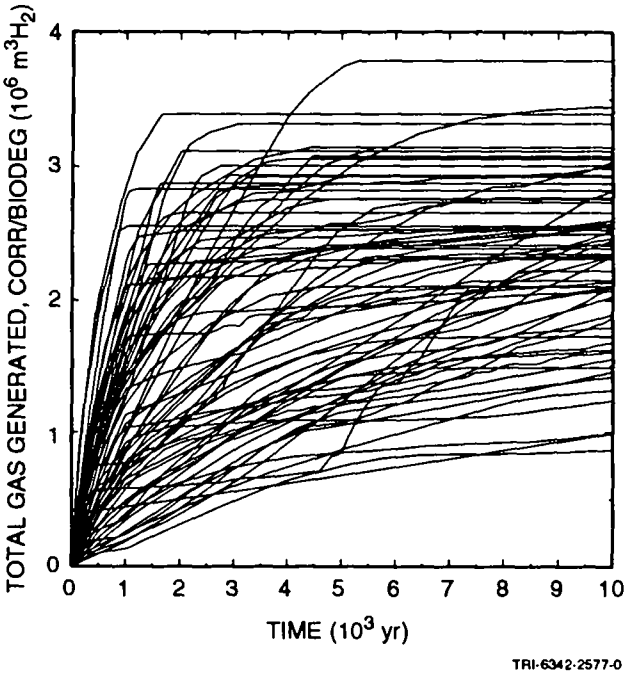

(a)

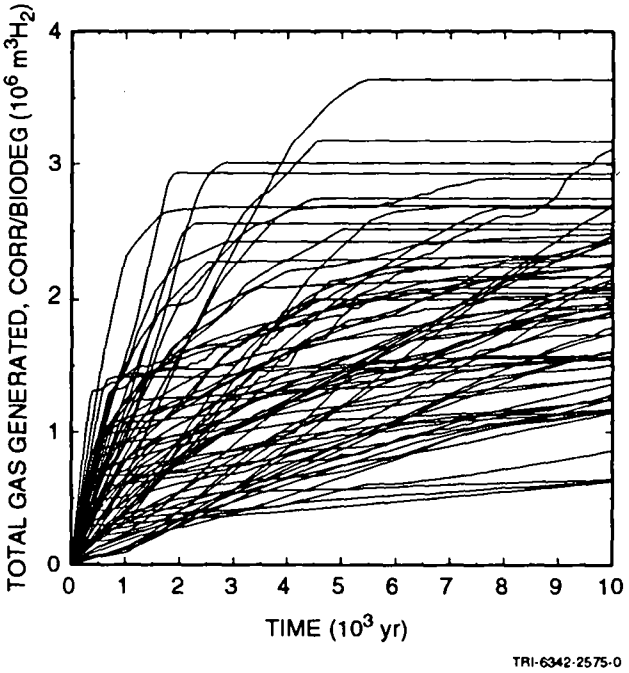

(b)

Figure 5.2-13. E2 scenario, intrusion at 1000 yr: total cumulative gas generated by corrosion and microbial degradation with fixed porosity (Figure 5.2-13a) and with dynamic creep closure (Figure 5.2-13b).

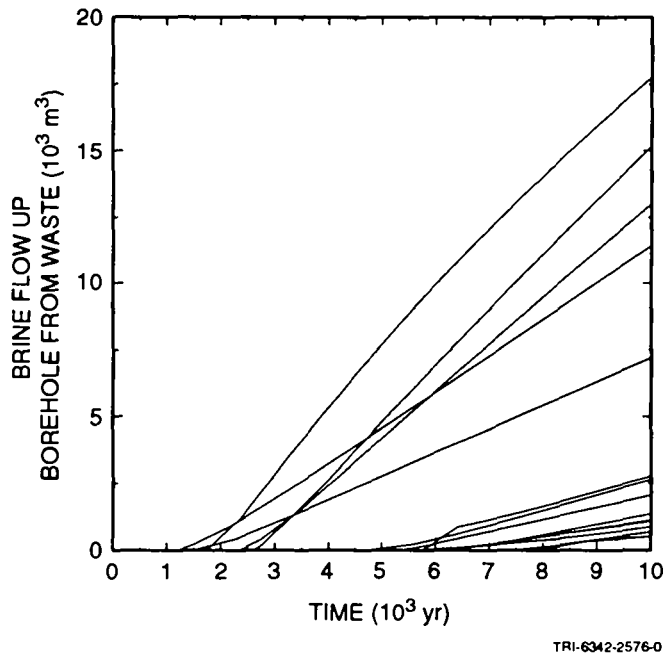

(a)

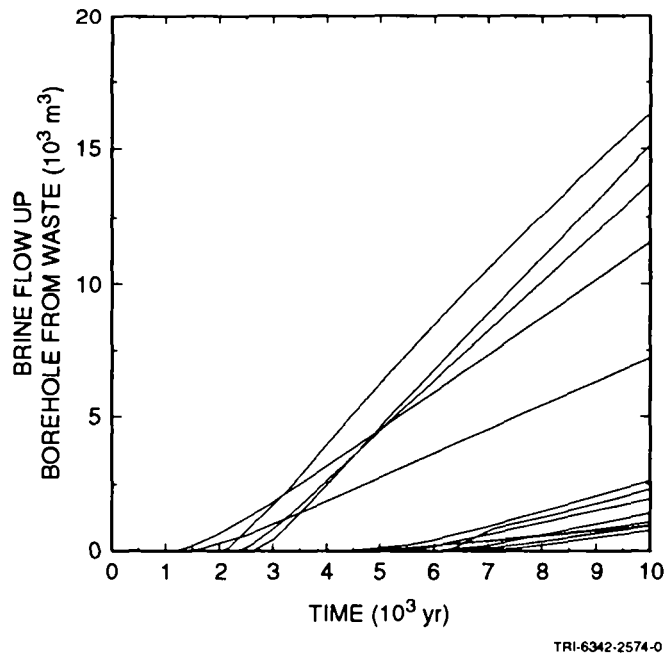

(b)

Figure 5.2-14. E2 scenario, intrusion at 1000 yr: cumulative brine flow up the borehole with fixed porosity (Figure 5.2-14a) and with dynamic creep closure (Figure 5.2-14b).

assessment, in the E2 scenario with an intrusion at 1000 years, there were 17 instances of brine release up the borehole among the 60 vectors, or 28%. In the 1992 performance assessment, 14 of 70 vectors resulted in borehole releases, or 20%. The more detailed analyses described later in this report indicate what parameter changes or conceptual model changes produced this small difference in the number of releases. In 1991, the maximum release in an E2 scenario was about 45,000 m^3; in 1992 it is 16,300 m^3. Both volumes are small relative to brine releases from the E1E2 scenario (Section 5.2.2).

The maximum pressure observed in the 1992 performance assessment, 22 MPa, is higher than that obtained in 1991, when the maximum was less than 17 MPa. However, peak pressures in excess of lithostatic were seen in only two vectors in 1992; except for those two, the highest pressures seen were about 13 MPa. And except for the two vectors in which the pressure remained at 11 to 12 MPa for most of the 10,000 yr, the pressures in the waste settled into a range from 1 to 7 MPa. In the 1991 performance assessment, more than 10% of the vectors maintained pressures higher than 7 MPa. Under "normal" circumstances, if the borehole fills with brine, the waste pressure should level off at around 7 MPa, which is hydrostatic relative to the Culebra, where the pressure is modeled as constant at 1.05 MPa. When pressures remain in excess of 7 MPa, the waste is either over-pressured with gas, or it is in excellent communication with the far field, where fluid pressures may exceed hydrostatic.

5.2.2 E1E2 Scenario

5.2.2.1 WASTE PANEL BEHAVIOR

The time dependence of pressures in the waste panel is shown in Figure 5.2-15. Up to the time of intrusion, 1000 yr, the behavior is identical to that in the E2 scenario. In only two vectors does the pressure rise above lithostatic. In most cases, the pressure rises steadily, at widely varying rates, until the intrusion occurs. From that point on, the behavior differs greatly from the E2 scenario. In the majority of vectors, the pressure undergoes some rapid transients immediately following the intrusion. In some cases, there is a sudden depressurization when the intrusion borehole connects the pressurized panel with the lower-pressure Culebra. In other instances, the pressure in the waste is still low at the time of intrusion, and it increases suddenly when the borehole connects the panel with the pressurized Castile brine reservoir. In most of the runs, a relatively steady pressure is attained fairly quickly at a value intermediate between the pressure in the Castile and in the Culebra. These pressures range from about 7.5 MPa to 13.7 MPa. In about one-third of the vectors,

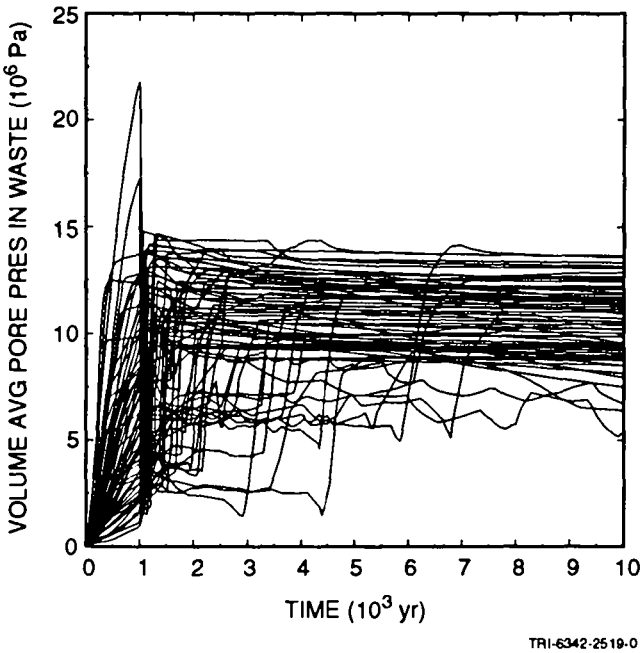

Figure 5.2-15. E1E2 scenario, intrusion at 1000 yr: panel pressure.

there is a time lag between the intrusion and attainment of this steady pressure. During this period, panel pressure is not yet strongly influenced by the Castile pressure because of low borehole permeability, small borehole diameter, or sufficient gas generation in the waste to retard flow of brine up the borehole. Whatever the cause, it takes anywhere from a few hundred to several thousand years for good communication to be established between the Castile and the Culebra, which will occur once the borehole becomes completely filled with brine from the Castile to the Culebra. A few vectors show erratic pressure behavior over the full 10,000 yr. This behavior results from borehole permeabilities that are too low to keep the waste panel filled with Castile brine. Pressures in the waste in these realizations fluctuate as some brine starts to flow up the borehole from the waste, but then is displaced as gas generation consumes brine and newly generated gas refills the borehole. Given sufficient time (perhaps tens of thousands to hundreds of thousands of years), these pressures would eventually level out at hydrostatic pressure relative to the Culebra, after all gas generation ceases and brine from the far field refills the panel.

Because creep closure is not modeled after the intrusion occurs, the waste porosities in the E1E2 scenario are nearly identical to those in the E2 scenario. The only differences result from different pressure histories after the intrusion, which affects porosity because the waste is still

assumed to be compressible. However, the effects on porosity are insignificant.

5.2.2.2 BOREHOLE INTRUSION EFFECTS

In all but two realizations, brine flows up the intrusion borehole from the waste (Figure 5.2-16). Cumulative nonzero brine flows at 10,000 yr range from 156 to 9.8 x 10^5 m^3. There is a strong correlation between borehole permeability and cumulative brine flow up the borehole. The three vectors with the highest brine flows also have the highest sampled borehole permeabilities. It is assumed that all of this brine is contaminated with radionuclides from the waste. As currently modeled, most of this brine would flow directly from the Castile to the Culebra with little mixing with the waste unless mixing was assumed. However, the E1E2 scenario involves lateral flow through the waste, rather than simply vertical flow through the waste, so all of the brine flowing up the borehole is assumed to flow through the waste. (Calculation of radionuclide releases, using PANEL [see Table 2.4-1], involves elemental solubility and radionuclide inventory, in addition to brine flow rate.)

The amount of brine that flows through the waste is large compared to the E2 scenario; the maximum cumulative flow is a factor of 60 higher. This

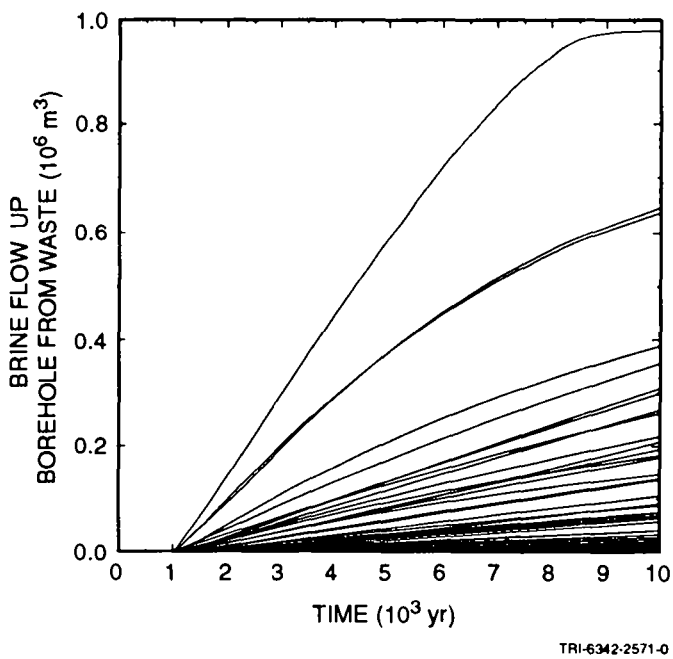

Figure 5.2-16. E1E2 scenario, intrusion at 1000 yr: cumulative brine flow up the borehole.

has a major effect on corrosion and biodegradation. The ready availability of brine results in all of the iron content in the waste being consumed in all but five realizations, and all of the cellulose being consumed in all but two realizations (Figures 5.2-17 and 5.2-18). Compare this with the E2 scenario, in which the only brine available had to flow in from the far field through the relatively impermeable (compared to the intrusion borehole) anhydrite layers. In the E2 scenario, iron remained in the waste after 10,000 yr in 55 of the vectors (Figure 5.2-17) and cellulose was unreacted in 30 vectors (Figure 5.2-18).

The effect of this greater consumption of degradable materials in the waste is to generate more gas. Whereas the maximum cumulative gas generated in the E1E2 scenario is nearly identical to that in the E2 scenario (3.60×10^6 m^3 H_2 at reference conditions vs. 3.64×10^6 m^3), the average cumulative gas generated was 2.6×10^6 m^3, compared with 2.0×10^6 m^3 in the E2 scenario. Most vectors in the E1E2 scenario resulted in 1.4×10^6 m^3 to 3.3×10^6 m^3 H_2 (Figure 5.2-19), compared to a lower and broader range of 0.6×10^6 m^3 to 3.1×10^6 m^3 for the E2 scenario (Figure 5.2-19b). However, because of the much higher brine flow rates in the E1E2 scenario, the higher gas-generation rates and volumes affected the release of brine up the borehole less than in the E2 scenario, in which the presence of gas tended more to interfere with the flow of brine.

5.2.2.3 BRINE FLOW IN ANHYDRITE LAYERS

The behavior of the anhydrite layers in the E1E2 scenario is essentially identical to the E2 scenario. Only in four vectors was there any net outward flow of brine from the waste panel, and the maximum amounted to only 68 m^3. In all other vectors, the net cumulative flows were inward (Figures 5.2-20), and ranged up to 36,000 m^3. The bulk of the flow (typically 65%), came in from MB139; about 20% came in through anhydrite A and B, and the remainder (about 15%) came through MB138. In considering possible lateral flow of contaminated brine to the accessible environment, it may be more useful to look at absolute outward flows, rather than net flows, since brine that has flowed outward may leave adsorbed contaminants even after the flow has been reversed. In this case, there were four vectors in which there was no outward flow at all. The maximum cumulative outward flow in any of the anhydrite layers was 2500 m^3 in MB139 (Figure 5.2-21). Even at the minimum porosity of 0.001, under the present modeling assumptions this brine could have traveled out MB139 no more than 500 m. So, as with the E2 scenario, it is improbable that contaminated brine can reach the accessible environment (2500 m from the panel) by means of lateral flow through the anhydrite layers, assuming again that these layers do not fracture as the pressure in

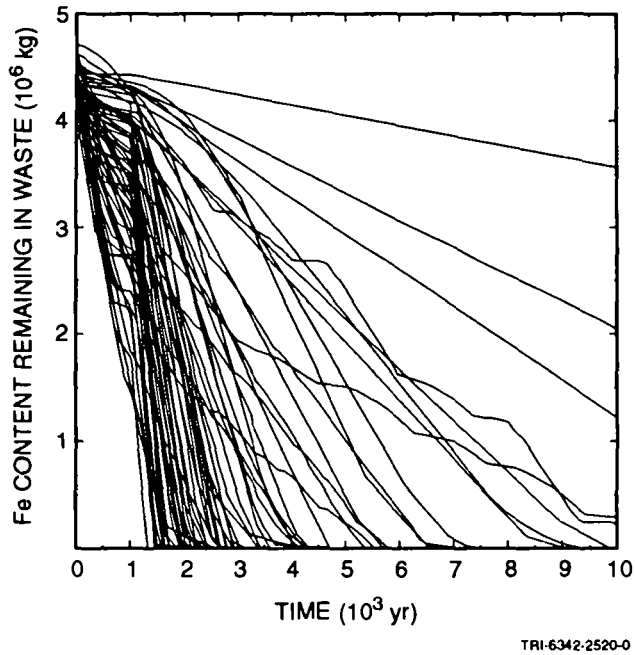

Figure 5.2-17. E1E2 scenario, intrusion at 1000 yr: iron remaining in waste.

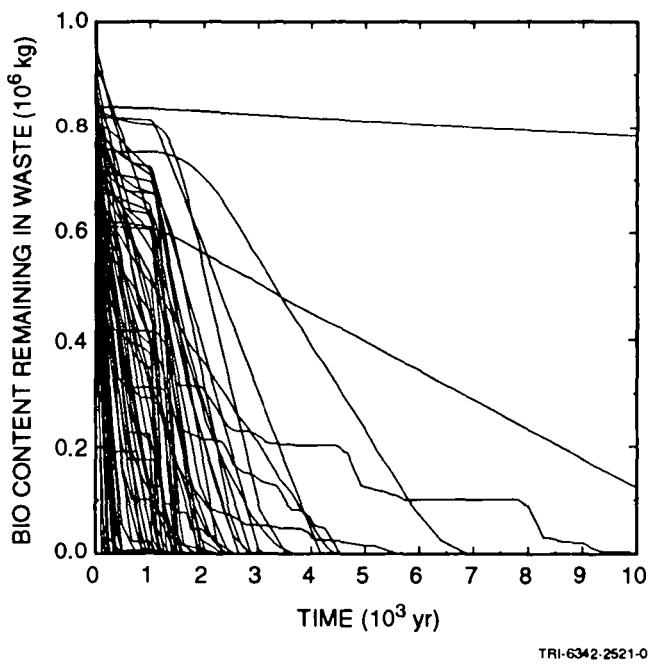

Figure 5.2-18. E1E2 scenario, intrusion at 1000 yr: cellulosics remaining in waste.

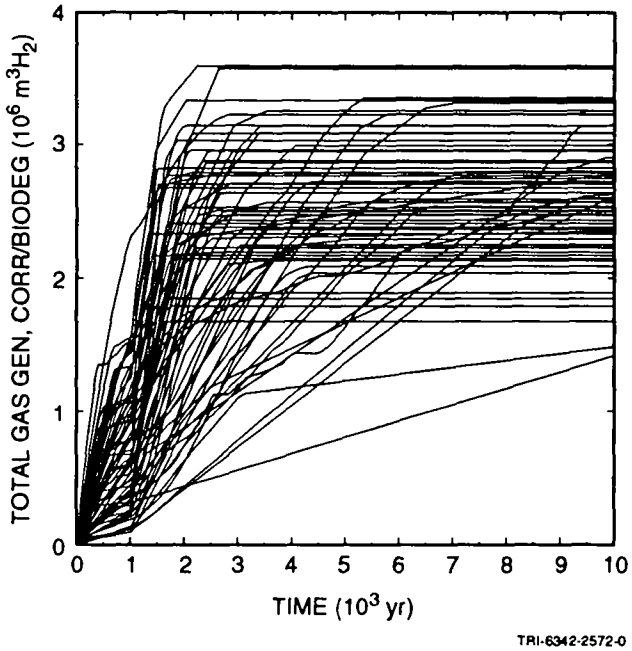

Figure 5.2-19. E1E2 scenario, intrusion at 1000 yr: total cumulative gas generated by corrosion and microbial biodegradation.

the waste increases. (However, note that the pressure in the waste exceeded lithostatic in only two of the vectors, so it is difficult to determine how much impact fracturing may have on radionuclide releases resulting from the E1E2 scenario. Fracturing of anhydrite layers will be included in next year's PA calculations.)

5.2.2.4 EFFECTS OF CREEP CLOSURE

The comments made above on the results of the E2 scenario calculations apply to E1E2 scenario almost without change. In the fixed-porosity calculations, the pressures reach similarly unrealistically high values, up to 38 MPa (Figure 5.2-22). The reasons are the same: The initial pore volume has been decreased as the initial porosity was reduced from 66% in the closure calculations to 19% in the fixed porosity calculations, while initial brine volume, rather than brine saturation, was conserved. Gas was produced at roughly the same rate, but with less storage volume in the panel, the pressure rose more rapidly. As a result of this pressure increase, the porosity increased, but only slightly (to a maximum of 20.2% at the maximum peak pressure). Unlike the E2 scenario, however, most of the reactants (iron and cellulose) are consumed within 10,000 yr in the E1E2 scenario, regardless of how the waste porosity is modeled, so the cumulative gas volume

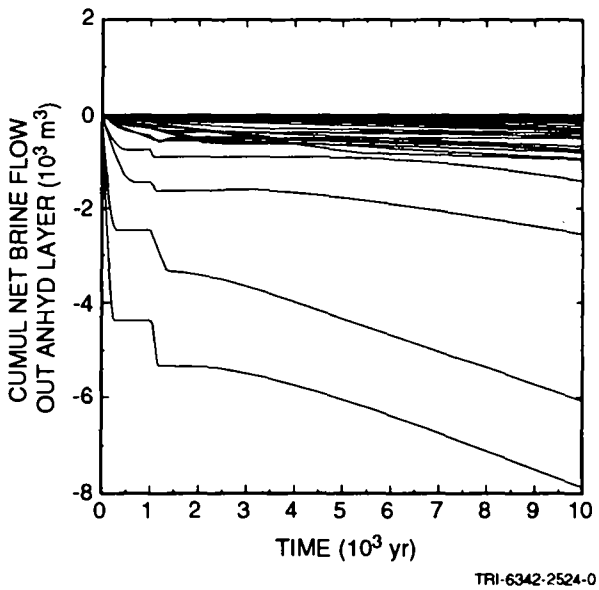

(a)

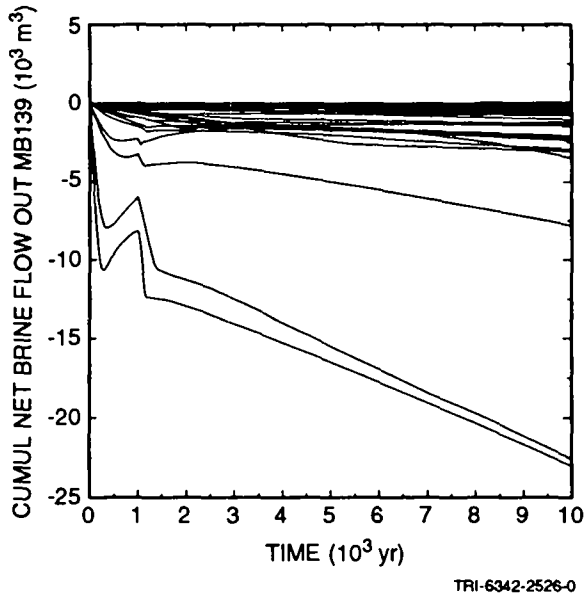

(b)

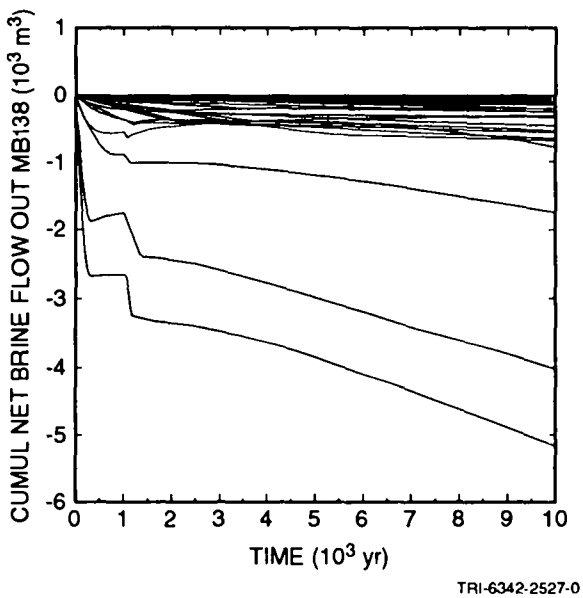

(c)

Figure 5.2-20. E1E2 scenario, intrusion at 1000 yr: cumulative net brine flow out anhydrite A and B (Figure 5.2-20a), MB139 (Figure 5.2-20b), and MB138 (Figure 5.2-20c).

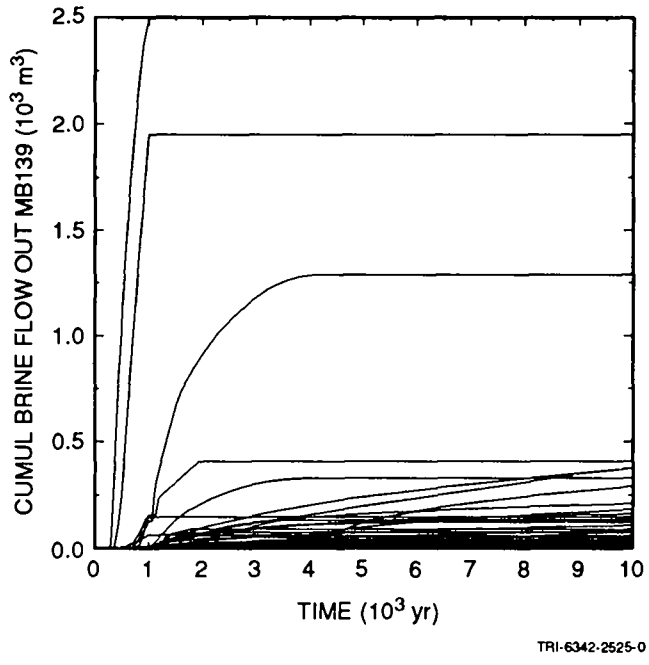

Figure 5.2-21. E1E2 scenario, intrusion at 1000 yr: cumulative absolute brine flow out MB139.

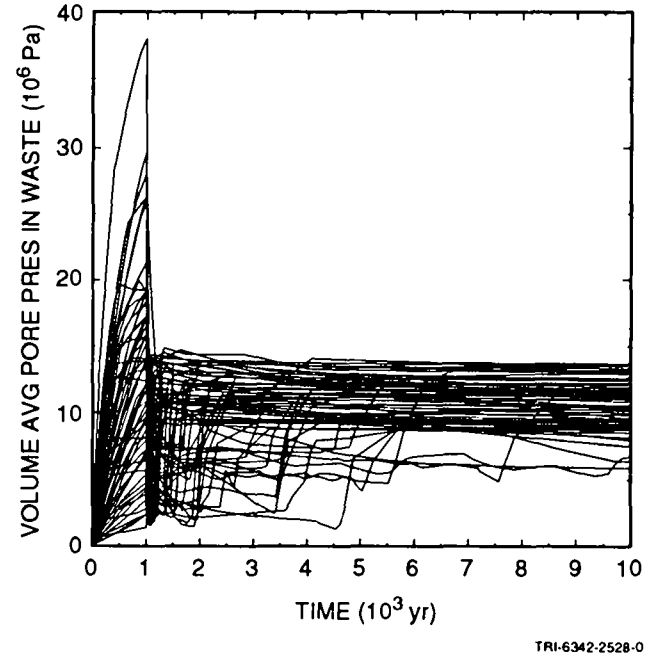

Figure 5.2-22. E1E2 scenario, intrusion at 1000 yr: pressure in waste, without dynamic creep closure.

generated differs very little in the fixed-porosity calculations from the calculations with dynamic creep closure.

The fixed-porosity calculations resulted in cumulative brine flows up the borehole that were nearly identical to those from the closure calculations (Figures 5.2-16 and 5.2-23). Whereas the maximum cumulative flow in the closure calculations was 9.79×10^5 m^3, it was 9.77×10^5 m^3 in the fixed porosity calculations. The average flow in the closure calculations was 9.71×10^4 m^3 and 9.70×10^4 m^3 in the fixed porosity calculations. In both sets of runs there were only two vectors that produced zero brine flow to the Culebra. Despite some major effects on transient behavior (such as waste pressures), the current dynamic creep closure model has no net effect on the performance assessment compared with the fixed-porosity model.

5.2.2.5 COMPARISON WITH THE 1991 PA RESULTS

The maximum cumulative release of contaminated brine to the Culebra is higher than in the 1991 performance assessment: 1.24×10^6 m^3, compared with 6.75×10^5 m^3 in the 1991 performance assessment. This can be attributed almost entirely to the borehole permeabilities used in those particular vectors. As long as pressure in the Castile is high enough to drive brine all the way to the Culebra, and borehole permeability is high, then cumulative flows to the Culebra are proportional to borehole permeability. This observation reflects the dominant role that borehole permeability plays in controlling flows in an E1E2 intrusion. Confirmation of that observation is provided by the following results: The ratio of the maximum flow in the 1992 performance assessment to the maximum flow in the 1991 performance assessment is 1.84; the ratio of the borehole permeability in the 1992 vector with maximum flow (1.0×10^{-11} m^2) to the borehole permeability in the 1991 vector with maximum flow (5.5×10^{-12} m^2) is 1.82. Under these conditions (high borehole permeability and sufficiently high Castile pressure), none of the other sampled parameters has much impact on releases to the Culebra. However, when the borehole permeability is not high, other parameters come into play. This is apparent when one considers that the average cumulative flow to the Culebra calculated in the 1992 performance assessment is 126,000 m^3, whereas the average obtained last year was 70,400 m^3, even though the ranges of borehole permeabilities and diameters and Castile pressures that were sampled were the same in 1992 as in 1991.

In the 1992 performance assessment, only two of the 70 realizations resulted in zero flow to the Culebra. In the 1991 performance assessment, there were also only two realizations (out of 60) with zero flow. In both the 1991 and 1992 calculations, E1E2 intrusions almost always result in releases to the Culebra.

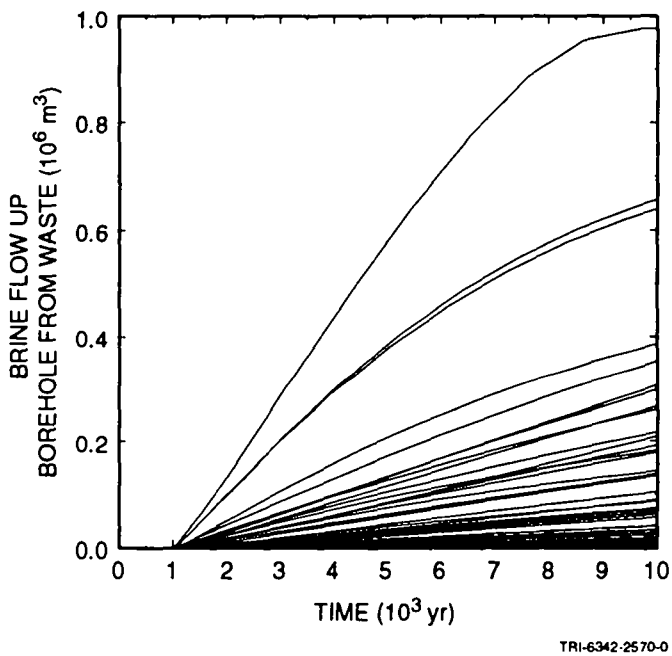

Figure 5.2-23. E1E2 scenario, intrusion at 1000 yr: cumulative brine flow up borehole without dynamic creep closure.

6. DISTURBED PERFORMANCE: CULEBRA GROUNDWATER FLOW AND TRANSPORT

This chapter describes the implementation of the 1992 PA model for groundwater flow and radionuclide transport in the Culebra Dolomite Member of the Rustler Formation. The computer codes used are SECO-FLOW for groundwater flow and SECO-TRANSPORT for radionuclide transport. Both codes are described in Chapter 7 and Appendix C of Volume 2 of this report. Flow is calculated in seventy different transmissivity fields that are described in Chapter 7 and Appendix D of Volume 2 of this report and by LaVenue and RamaRao (1992).

6.1 Conceptual Model

The conceptual model for flow in the Culebra Dolomite Member of the Rustler Formation is essentially unchanged from that used in the 1990 and 1991 PA (Bertram-Howery et al., 1990; WIPP PA Division, 1991b, Section 6.1). As discussed in Chapter 7 of Volume 2 of this report, conceptual models for transport have been modified to allow a more complete representation of the possible affect of clay linings in fractures on both physical and chemical retardation. Geologic and hydrologic information supporting the flow and transport models are described in Chapter 2 of Volume 2 of this report. Major aspects of the models are as follows.

- **Single-porosity Darcian flow.** Results of hydrologic tests on wells completed in the Culebra are consistent with the response of a heterogeneous medium obeying Darcy's law (Jones et al., 1992). Results of some well tests indicate dual-porosity response during the early part of the tests (Beauheim, 1987; Jones et al., 1992). This is interpreted to be caused by disequilibrium between pressure in coextensive fracture and matrix porosity sets. Because the time of pressure equilibration between the porosity sets is much smaller than the time scale of processes considered in the human-intrusion scenario, the Culebra is modeled as a heterogeneous single-porosity medium for the purpose of fluid-flow calculations. (Dual-porosity effects on transport are considered, however, as discussed below.)

- **Two-dimensional flow.** Most hydrologic test wells in the Culebra are completed across the entire vertical extent of the unit. Parameters derived from tests on these wells are therefore composite or average values over the vertical extent of the member. Although flow is known to be localized to particular elevations within the Culebra at several wells (Mercer and Orr, 1979), there is insufficient information to

characterize vertical variability of hydrologic properties within the Culebra. A vertically integrated two-dimensional model has therefore been adopted.

- **No flow through upper and lower boundaries.** Potentiometric differences between the Culebra and other members of the Rustler Formation suggest that vertical flow between the members is extremely slow over the WIPP and in much of the surrounding study area (Beauheim, 1987; Brinster, 1991). The present conceptual model includes impermeable upper and lower boundaries on the Culebra. The validity of the assumption that leakage between the Culebra and the over- and underlying units can be neglected is uncertain, and the importance of possible vertical flux will be examined when information is available from regional three-dimensional hydrologic modeling being conducted by the SNL Fluid Flow and Transport Department.

- **Flow in Nash Draw parallel to the axis of the draw.** Nash Draw is believed to be a major sub-surface drain for the Rustler Formation west of the WIPP (Davies, 1989; Brinster, 1991). Groundwater flow in the draw is therefore assumed to parallel the topographic axis of the draw.

- **Pressure equilibrium and flow prior to WIPP construction.** Time constants of pressure changes due to compression of the fluid and matrix are small compared to time constants of fluid density changes, transmissivity changes, or other transient processes affecting pressure. For any subdomain of the Culebra, and in the absence of fluid sources or sinks within the subdomain, the Culebra pressure is assumed to be currently in equilibrium with pressures around the boundary of the subdomain.

- **Future flow-field transients induced by external changes.** The future state of the Culebra flow field is assumed to differ from the present state through regional climate change. Climate change is assumed to affect recharge and discharge rates external to the model domain, and therefore to influence flow within the model domain through a change in boundary pressures (memorandum by Swift in WIPP PA Division, 1991c; WIPP PA Division, 1991b; Swift, 1993).

- **Transport decoupled from flow.** In the human intrusion scenario, one or more boreholes create a long-term connection between the repository and the Culebra. Hydrologic properties of the borehole limit potential fluid discharge to the Culebra to approximately 80 m^3/yr. This rate of fluid injection is assumed to have no impact on the prevailing Culebra flow field (Reeves et al., 1991). Fluid injected from the repository

is also assumed to have no effect on Culebra fluid density. Estimation of the Culebra flow field and estimation of radionuclide transport through this flow field are, therefore, considered as separate problems.

- **Dual-porosity transport.** Matrix and fracture porosities that are coextensive and communicating can result in local disequilibrium between radionuclide concentrations between the fracture and matrix (Jones et al., 1992). The time constant associated with this disequilibrium is determined by the rate of exchange of radionuclides between the porosity sets and the radionuclide storage capacity of the fracture and matrix. Because this equilibration time may be significant in comparison to the time scale of source-term concentration change, a dual-porosity transport model has been adopted. The 1992 conceptual model for dual-porosity transport differs from that used in 1991 in that porosity of the clay linings within fracture is modeled explicitly, and diffusion may occur in both the clay linings and the dolomite matrix (see Section 7.6 of Volume 2 of this report). Alternative conceptual models are examined with and without clay linings and dolomite matrix porosity (see Section 5.1 of Volume 1 of this report and Chapter 8 of this volume). Available information is insufficient to confirm or refute these alternative conceptual models at this time. Proposed tracer tests may provide additional information to support a choice of transport model (Beauheim and Davies, 1992).

- **Linear equilibrium sorption of radionuclides.** In addition to hydrodynamic processes, radionuclide concentrations in Culebra groundwater are assumed to be affected by geochemical interactions with the host rock. Reversible sorption is assumed to be the only mechanism on interaction of the radionuclides with the rock (Trauth et al., 1992). Sorption is further assumed to follow a linear Freundlich isotherm, with different coefficients describing sorption on the dolomite matrix and the clay linings in fractures. Chemical retardation of radionuclides by sorption is believed realistic, but, by agreement between the DOE and the State of New Mexico, cannot be considered in a final compliance evaluation unless supported by experimental data (US DOE and the State of New Mexico, 1981, as modified). Experimental programs are in progress or planned to reduce these uncertainties, including laboratory-scale radioactive tracer tests in core samples (US DOE, 1992, and references cited therein) and nonradioactive tracer tests between well locations in the Culebra (Beauheim and Davies, 1992).

6.2 Model Geometry

6.2.1 Regional Domain

The regional domain (Figure 6.2-1) is 25 x 30 km, with the long axis oriented 38 degrees east of north. The grid (Figure 6.2-2) consists of 50 x 57 x 1 (x,y,z) blocks and has varying spacing in the x-y plane, reflecting the spatial distribution of transmissivity data from wells. Grid spacing is finer in the central portion of the model in the vicinity of H-3, H-11, WIPP-13, and the shafts. Grid-block dimensions range from 50 m near the center of the site to approximately 2800 m at the model boundary. The vertical dimension of the grid is 7.7 m, and is the mean thickness of the Culebra Dolomite Member of the Rustler Formation in the WIPP area (LaVenue et al., 1988).

The rotated orientation of the grid and the location of a model boundary along the axis of Nash Draw were chosen to take advantage of the draw as a natural no-flow symmetry boundary. Locations and orientations of the regional model boundaries are the same as those used in the 1991 PA (WIPP PA Division, 1991b).

6.2.2 Local Domain

The 5.75 x 6.625 km local domain (Figure 6.2-1) is oriented with its long dimension north-south, and the grid (Figure 6.2-2) consists of 46 x 53 x 1 (x,y,z) blocks, each of which is 125 x 125 m. The vertical thickness of the blocks is 7.7 m, and is the same as the thickness of the regional grid. The intrusion borehole is assumed to intersect the Culebra directly over the center of the disposal region (see the following Section 6.2.3 for a discussion of the location of this point). The local grid is positioned to place the intrusion borehole at a grid-block center. Fluid flow and mass transport in the local domain are solved using regional head solutions as input boundary conditions.

6.2.3 Location of the Intrusion Borehole

The location of the intrusion borehole in the local domain is held constant in all 70 realizations at a point directly above the center of the waste-disposal region. Specifically, the intersection of the intrusion borehole and the Culebra is located above the center of the central pillar separating the southern and northern equivalent panels (panels 9 and 10 on Figure 4.1-1). See Figure 3.1.2 in Volume 3 of this volume for a scale drawing providing coordinates for this point.

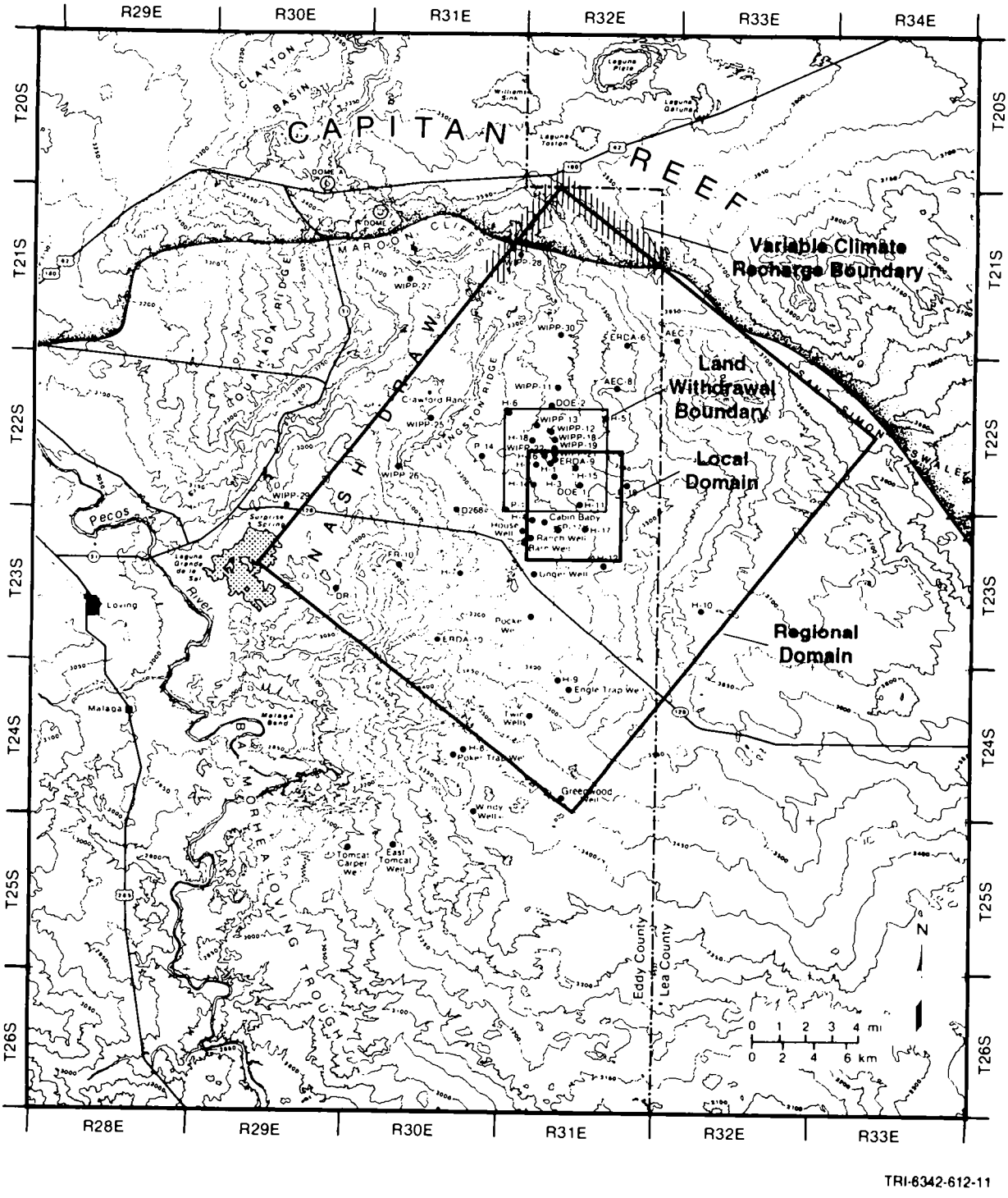

Figure 6.2-1. Regional and local domains for groundwater flow and transport calculations.

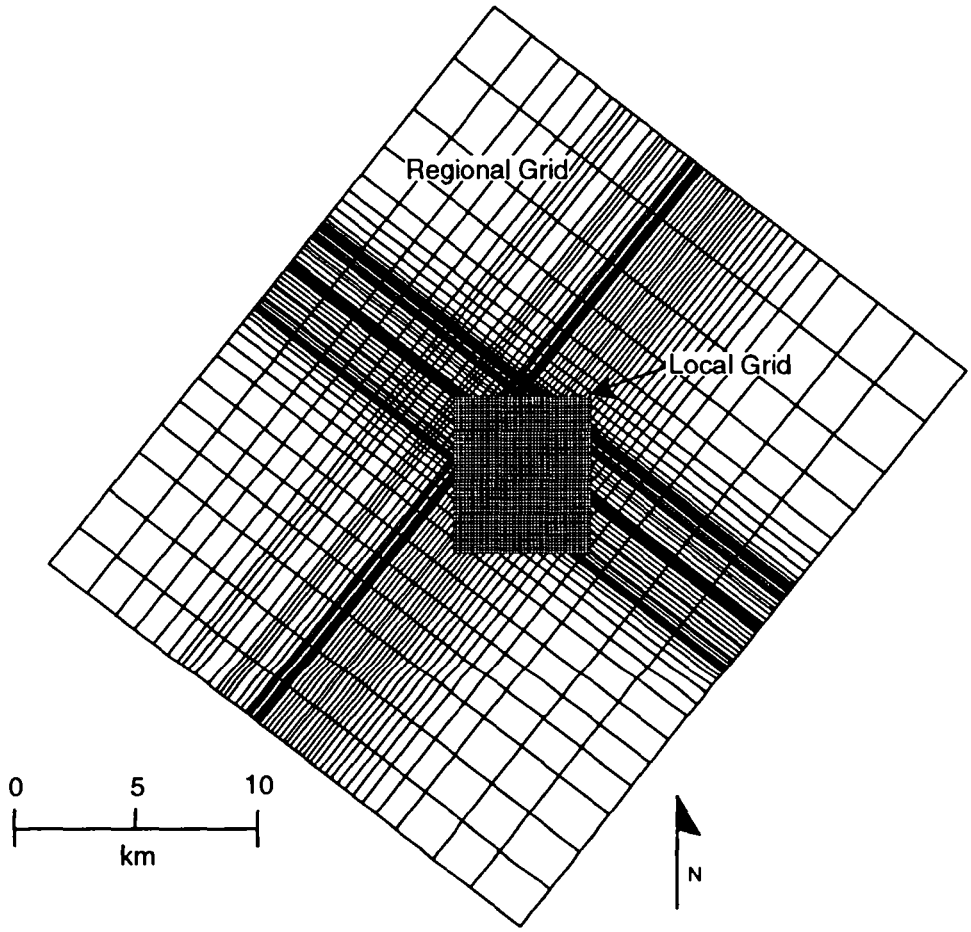

TRI-6342-2680-0

Figure 6.2-2. Grids for regional and local domains for groundwater flow and transport calculations.

The choice of a fixed location for the intrusion borehole is an assumption made for convenience in defining computational scenarios and determining scenario probabilities (WIPP PA Division, 1991b, Chapter 2). Spatial variability of future drilling events is assumed to be uniform, and the straight-line distance between the center of the waste-disposal region and the subsurface boundary of the accessible environment is therefore the mean distance between an intrusion and a regulatory release point. As discussed in the following paragraphs, this distance is approximately 2.4 km. Based on the planned dimensions of the waste-disposal region (Figure 3.1.2 in Volume 3 of this report), the actual straight-line distance from a randomly-located intrusion borehole to the accessible environment boundary may be as much as approximately 315 m more or less than this mean distance. As shown in Section 6.8.3 of this report, modeled flow does not occur along straight lines, and transport distances are therefore somewhat greater than the minimum distance.

The shortest horizontal distance from waste to the accessible environment is a straight line south from any of the southern panels to the WIPP land-withdrawal boundary at the southern edge of either sections 32 or 33, T22S, R31E (Figure 6.2-3). Based on the surveyed location of the southern end of the South Drift (WEC, 1988) and the north-south dimensions of sections 29 and 32, T22S, R31E, as scaled from the Los Medaños 7.5 minute topographic quadrangle (USGS, 1985a), this distance is estimated to be 2414 m (7916 ft). Possible sources of error in this estimate are as follows:

- Gonzales (1989) noted that the WIPP survey coordinates for the northeast corner of section 29, T22S, R31E give a location about 12 m south of that indicated by the USGS coordinates for the same point. Gonzales (1989) concluded that the WIPP survey was more reliable, and the distance reported here is based on WIPP survey coordinates.

- Accuracy in scaling from the topographic map is estimated to be ± 10 m.

- No estimate is made here of the accuracy of either the WIPP survey or the topographic map.

- No estimate is made of the precision with which future excavations will match present design.

- Possible horizontal emplacement of remote-handled transuranic (RH-TRU waste) in the southern walls of the southern panels is not included in this estimate.

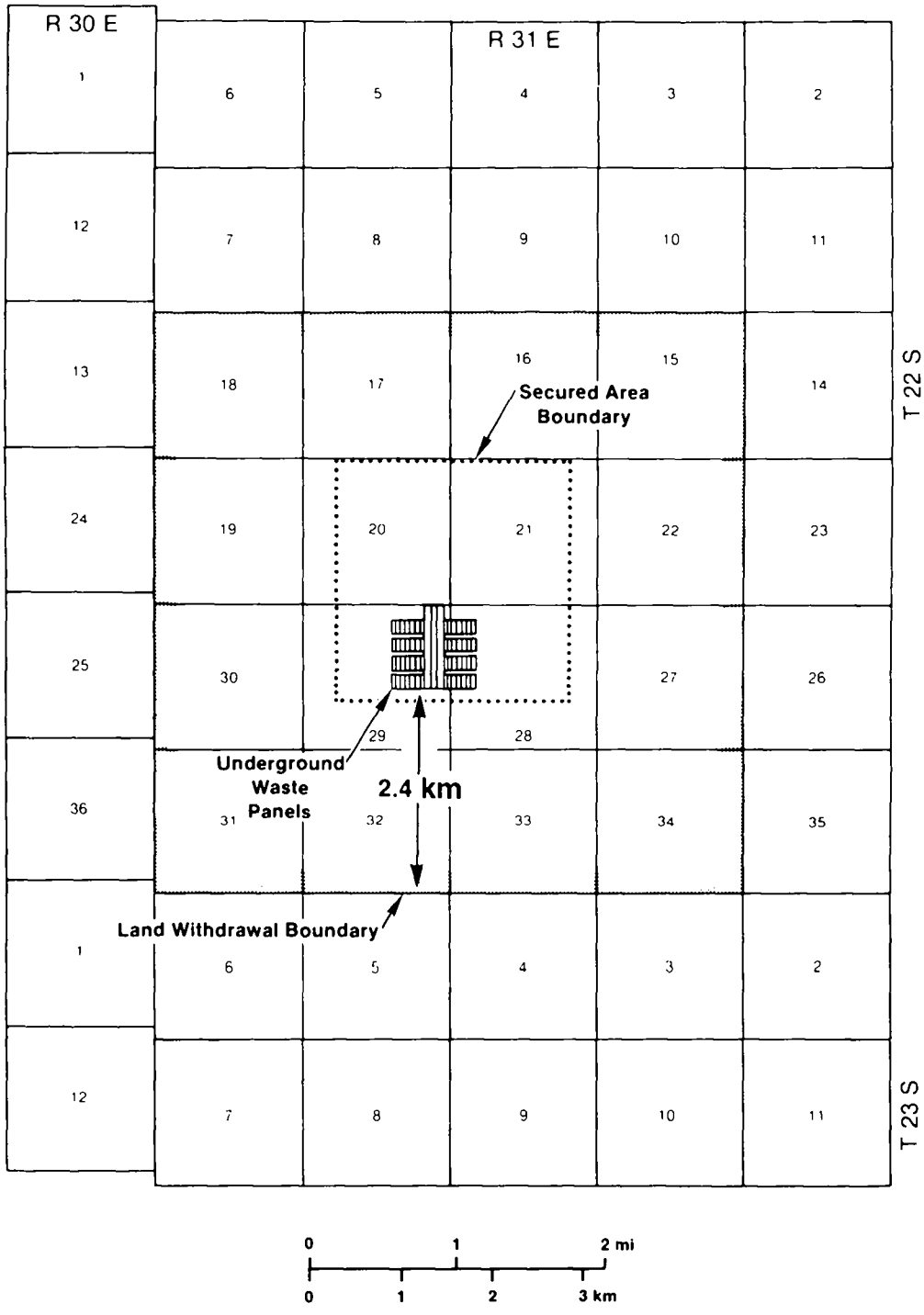

Figure 6.2-3. Position of the waste-emplacement panels relative to the WIPP boundaries and surveyed section lines (US DOE, 1989).

6.3. Material Properties

The most important hydrologic property used in modeling the flow and transport pathways is the transmissivity of the Culebra. In the 1992 PA, 70 groundwater transmissivity fields (presented in Appendix C of Volume 3 of this report) were generated using a multiple-realization technique to account for spatial variability of the transmissivity field within the Culebra (LaVenue and RamaRao, 1992; see also Section 6.8 of this volume and Section 7.5 of Volume 2 of this report). Each of the 70 realizations in the 1992 PA used a different transmissivity field and a corresponding different flow solution. All other hydrologic parameters were held constant, at values described in Volume 3 of this report. The only sampled parameter affecting flow within the transmissivity fields was the climate factor, discussed in the following section. Sampled parameters affecting radionuclide transport are described in Chapter 3 of this volume, and include distribution coefficients for each radionuclide, fracture porosity and spacing, matrix porosity, the fraction of fracture openings lined with clay, and the porosity of the clay linings.

6.4 Boundary and Initial Conditions

Three different types of boundary conditions were used for the regional domain: no-flow, time-dependent head, and fixed head. Locations in which these boundary conditions were applied are shown in Figure 6.4-1. As previously noted (Section 6.2.1), a no-flow boundary was used along a portion of the northwest side of the domain, coinciding with the axis of Nash Draw beginning 4.0 km NE of the origin of the domain at its western corner and continuing to 18.595 km NE. No-flow boundaries were also assigned to the NE portion of the domain, from 30 km NE, 17.3 km SE to 27.240 km NE, 25 km SE. These northeastern no-flow boundary segments correspond to a region of low permeability in the Culebra (see Chapter 2 of Volume 2 of this report).

Time-dependent heads were used to simulate possible effects of climatically varying recharge (see Sections 6.4.1 and 6.4.2, following), and were assigned to a 21.505 km "recharge strip" surrounding the northern apex of the regional domain. Specifically, time-dependent heads were used along the northwestern boundary between 18.595 km NE, 0 km SE and 30 km NE, 0 km SE, and along the northeastern boundary from 30 km NE, 0 km SE to 30 km NE, 10 km SE. Heads within this strip were prescribed as a function of a sinusoidal climate function applied to the initial calibrated heads derived from the steady-state solution for each transmissivity field (see Sections 6.4.1 and 6.4.2).

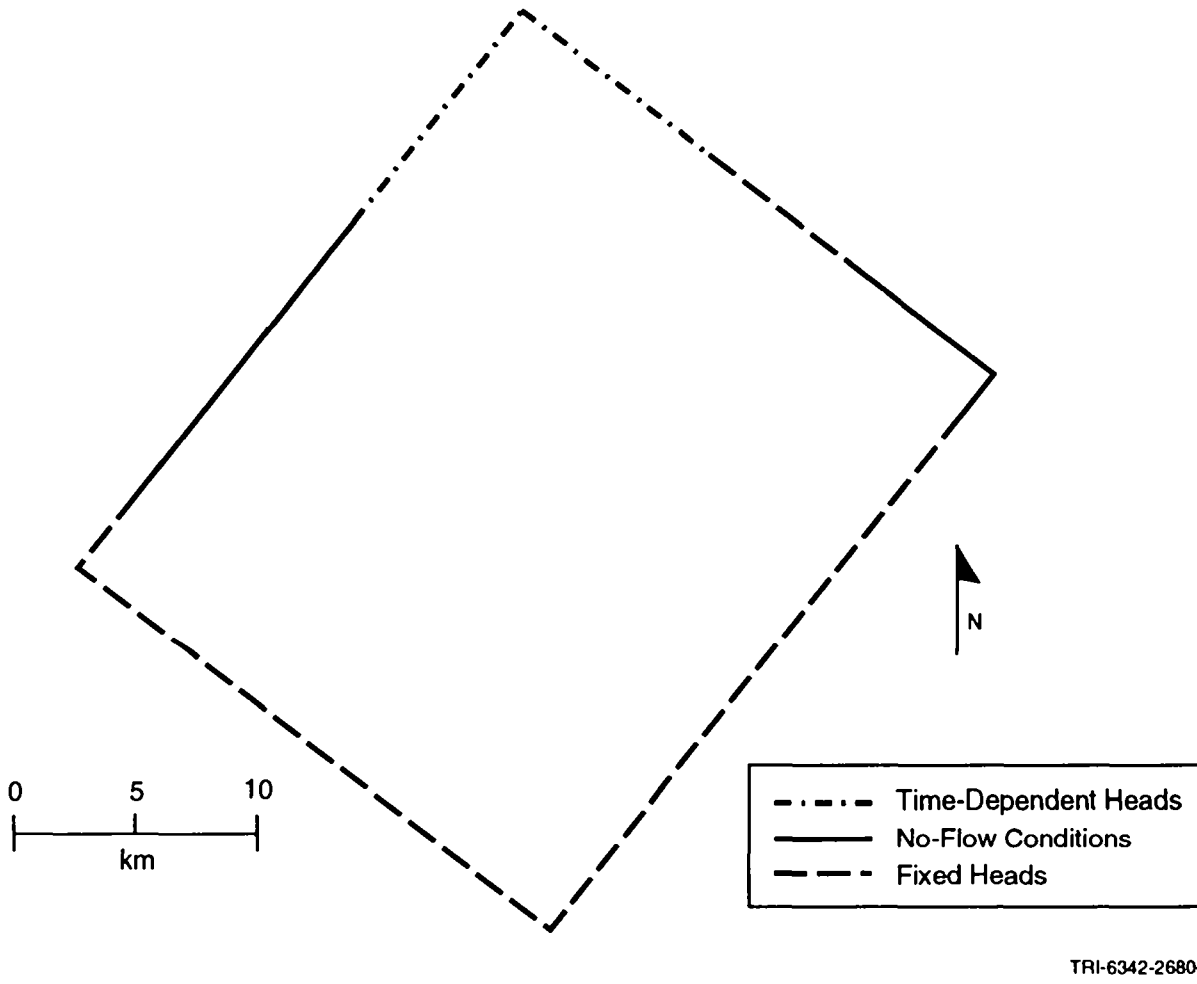

Figure 6.4-1. Boundary conditions for regional domain.

All other boundary conditions were fixed (time-invariant) heads based on the steady-state solution for each transmissivity field (see Section 6.8.2), and therefore were different for each realization.

As with the fixed boundary heads, initial heads within the regional domain were determined from the steady-state solution for each transmissivity field. No vertical flow (i.e., leakage) was allowed within the model domain. Possible effects of leakage into or out of the Culebra will be examined in future PAs when a three-dimensional model for regional groundwater flow is available.

As previously noted, boundary and initial conditions for the local domain were determined by the solution of flow in the regional domain. Because the the local grid elements do not exactly overlay the regional grid elements, SECO-FLOW interpolates boundary conditions for the local grid.

6.4.1 Climatic Variability

As discussed in more detail in Swift (1993) and Section 2.2.3.2 of Volume 2 of this report, climate in southeastern New Mexico is likely to be wetter than that of the present at some times during the next 10,000 yr. The timing of future climatic changes is unknown, but the wettest plausible climate during the next 10,000 yr is expected to be no wetter than that of the late Pleistocene (20,000 yr ago), which was approximately twice as wet as that of the present (Swift, 1993).

The effect of climatic changes on regional boundary conditions cannot be modeled directly because of uncertainty in the location of present and future recharge and uncertainty in the hydrologic properties affecting the flow path from the recharge area to the regional domain boundary. Climatic effects are instead approximated indirectly using information about hydrologic conditions during past climatic conditions. Geologic evidence (Bachman, 1985, p. 20-21) indicates that at some time or times during the Pleistocene the water table was sufficiently high to sustain springs along the east margin of Nash Draw and a lake in Clayton Basin north of Nash Draw (see Figure 6.2-1). Rustler Formation outcrops in Clayton Basin have been identified as a possible recharge area for groundwater in the Culebra at the WIPP (Mercer, 1983), and the 1992 PA therefore uses the highest possible lake elevation in Clayton Basin as a maximum boundary head condition that could result from climatic change. The present elevation of the Clayton Basin spill point (1007 m, in section 11, T20S,R29E [USGS, 1885b]) is assumed to be the maximum possible lake elevation. This elevation is used as the maximum head elevation at the northern apex of the regional model domain, reached during future wet climates. Heads elsewhere along the

"recharge strip" are scaled upward during wet climates proportional to the amount head at the apex is raised.

The choice of the elevation of the Clayton Basin spill point as the maximum head value represents a change from the 1991 PA, in which maximum heads were allowed to rise to the ground surface (1030 m), scaled according to the same climate function. The change was made to improve consistency with the confined-aquifer conceptual model.

Scaling of heads along the recharge strip is based on the calibrated initial heads for each transmissivity field, a "climate factor" (CULCLIM in Chapter 3 of this volume) derived from a sampled index parameter, and the following sinusoidal function (Swift, 1991, memorandum in Appendix A of WIPP PA Division, 1991c).

$$\frac{h_f(t)}{h_p} = \frac{3A + 1}{4} - \frac{A - 1}{2}\left(\cos \Theta t + \frac{1}{2}\cos \Phi t - \sin \frac{1}{2} \Phi t\right) \qquad (6.4\text{-}1)$$

defines time-dependent heads in the Culebra, where

$h_f(t)$ = head (m) in Culebra at time t (s),
h_p = estimate of present-day boundary head in Culebra (e.g., 880 m),
A = recharge amplitude factor (dimensionless) for Culebra (i.e., CULCLIM),
Θ = frequency (Hz) for Pleistocene glaciations: 1.7×10^{-12} Hz (5.4×10^{-5} yr^{-1}),
Φ = frequency (Hz) for second-order climatic fluctuations: 1.0×10^{-10} Hz (3.2×10^{-3} yr^{-1}),

and

t = time (s), with t=0 corresponding to decommissioning of the WIPP.

This function is not used to predict future climates, but rather is designed to provide a simple way to examine the influence of possible climatic changes during the next 10,000 yr. The periodicity of the function is based on approximately 30,000 yr of paleoclimatic data from southeastern New Mexico and the surrounding region and the global record of Pleistocene glaciations (Swift, 1993). The glacial frequency term Θ produces a maximum value of the function $h_f(t)$ at 60,000 yr, and has little effect during the regulatory period. Most of the introduced variability results from second-

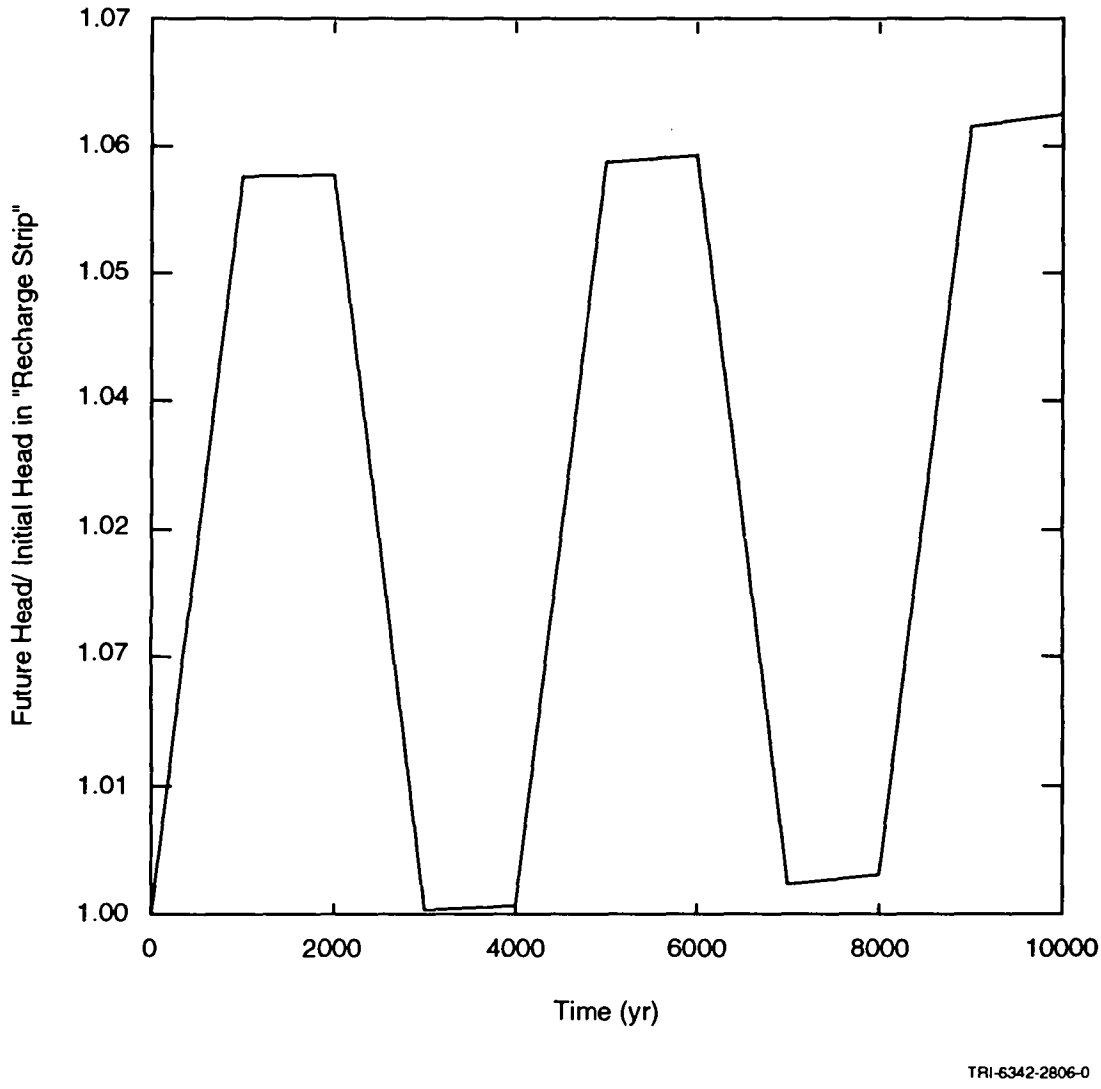

Figure 6.4-2. 10,000-yr history of climate function, evaluated at 1000-yr time steps for the maximum value of CULCLIM.

order fluctuations controlled by the higher-frequency term Φ. This variability corresponds to the frequency of nonglacial climatic fluctuations observed in both late Pleistocene and Holocene paleoclimatic data. The chosen value for Φ results in a sinusoidal curve with three peaks in 10,000 years. Figure 6.4-2 illustrates the function as applied in the 1992 SECO-FLOW calculations, with values calculated only at the 1000 yr time steps.

6.4.2 Time-Dependant Boundary Heads

The recharge amplitude factor CULCLIM used in Equation 6.4-1 is a dimensionless scaling factor that varies uniformly between 1.07 and 1.00, and is derived from a sampled climate index variable that varies uniformly between 0 and 1 (see Section 4.4 of Volume 3 of this report). At 1500 yr (not simulated by the 1000 yr time steps), a maximum value of 1.07 for CULCLIM results in the maximum head in the grid block at the northern apex of the regional domain to rise from its initial elevation of 942.5 m (LaVenue and RamaRao, 1992) to the elevation of the spill point of Clayton Basin, 1007 m. Heads in other grid blocks within the "recharge strip" are scaled using the same value for CULCLIM, and may therefore reach a maximum elevation somewhat higher or lower than the head in the northernmost block, depending on their initial elevations. At its minimum value (1.00), CULCLIM results in no change in boundary heads throughout the 10,000 years. Intermediate values of CULCLIM result in intermediate increases in boundary heads. For all values of CULCLIM greater than 1.00, the maximum head elevation occurs at the final, 10,000 yr climatic peak. Heads in earlier peaks are slightly less, because of the effect of the glacial term in the climate function.

6.5 Effect of Climatic Change on Groundwater Flow

The effects of climatically varying heads along the "recharge strip" is different in each of the 70 realizations, because each realization uses a different transmissivity field (Section 6.8). Changes in groundwater flow are discussed here for two realizations that contained the largest sampled value for the climate index factor and an intermediate value. The largest sampled value for the climate index factor, 0.9966, occurred in realization 11 and resulted in a value for CULCLIM of 1.068. The calculated head field for this realization is displayed for time zero (initial conditions) (Figure 6.5-1a) and for 10,000 yr (Figure 6.5-1b). Vector representations of the specific discharge (i.e., volume of fluid moving through a unit area in a unit time) are shown for the corresponding velocity fields in Figures 6.5-1c and 6.5-1d. Similar plots are shown in Figure 6.5-2 for realization 20, which contained a sampled value for the climate index factor of 0.4519,

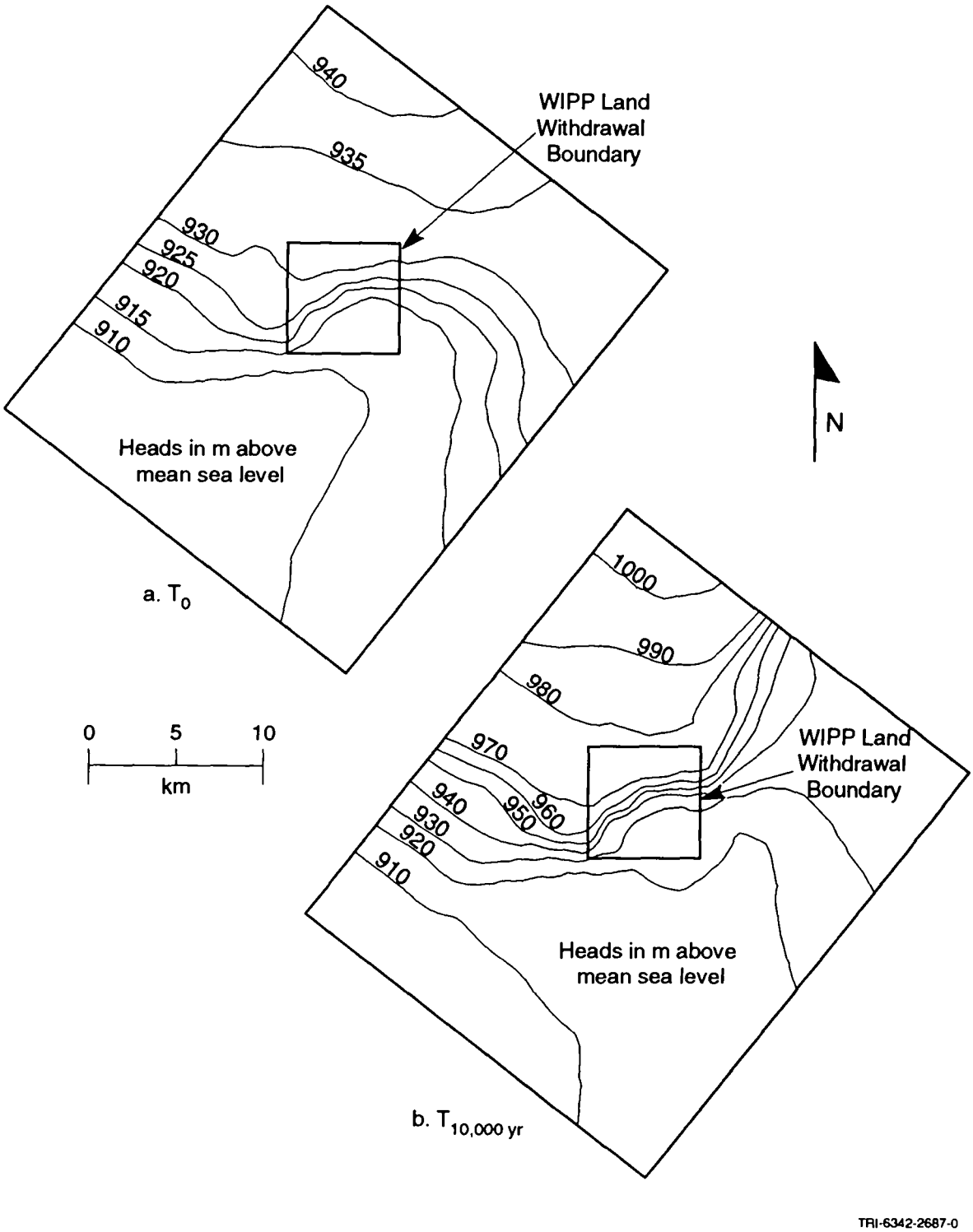

Figure 6.5-1. Head (Figures 6.5-1a,b) and specific discharge (Figures 6.5-1c,d) plots for the SECO-FLOW regional domain for realization 11 at time zero and 10,000 yr. This realization contains the largest value for CULCLIM.

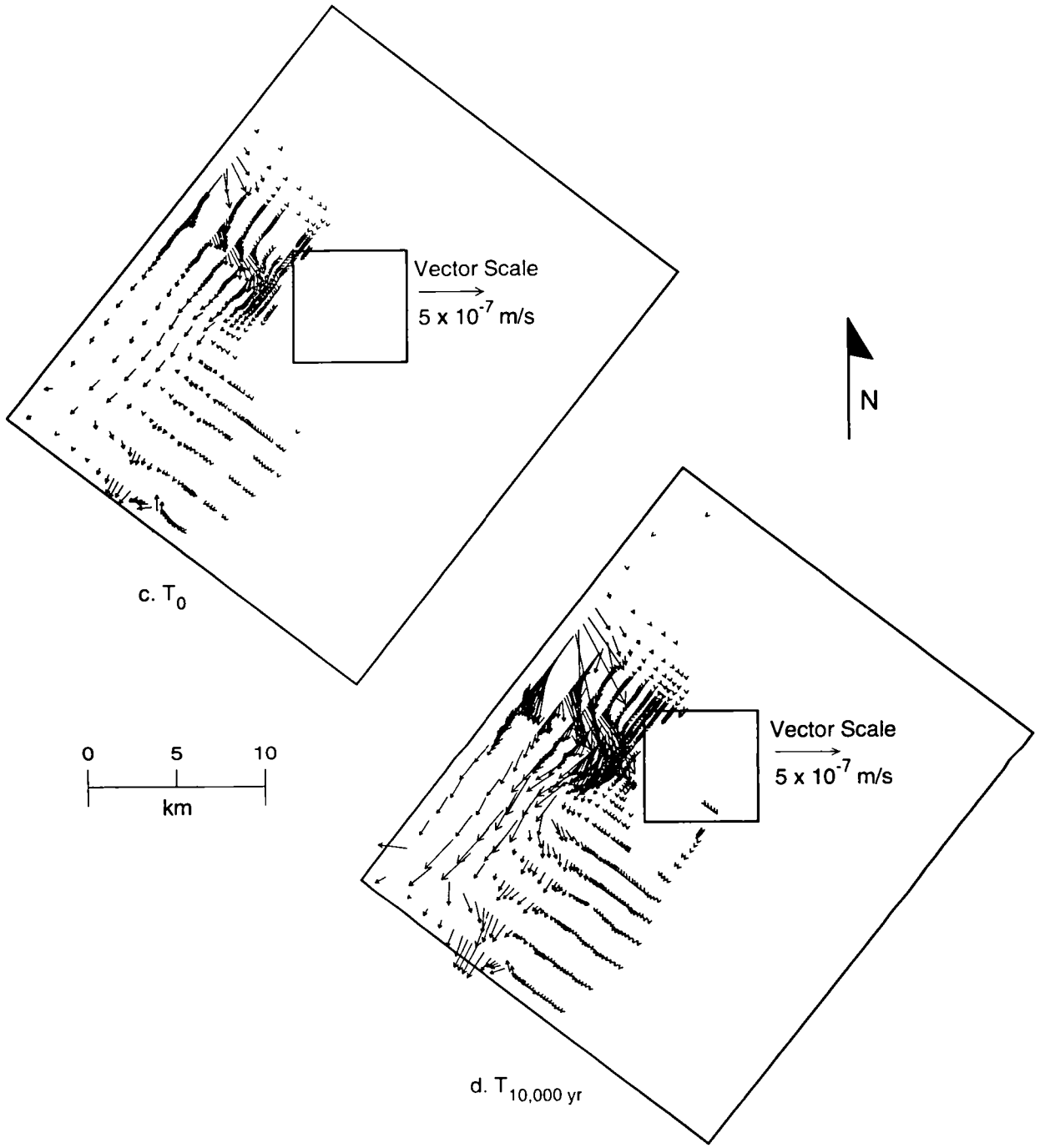

Figure 6.5-1. Head (Figures 6.5-1a,b) and specific discharge (Figures 6.5-1c,d) plots for the SECO-FLOW regional domain for realization 11 at time zero and 10,000 yr. This realization contains the largest value for CULCLIM. (continued)

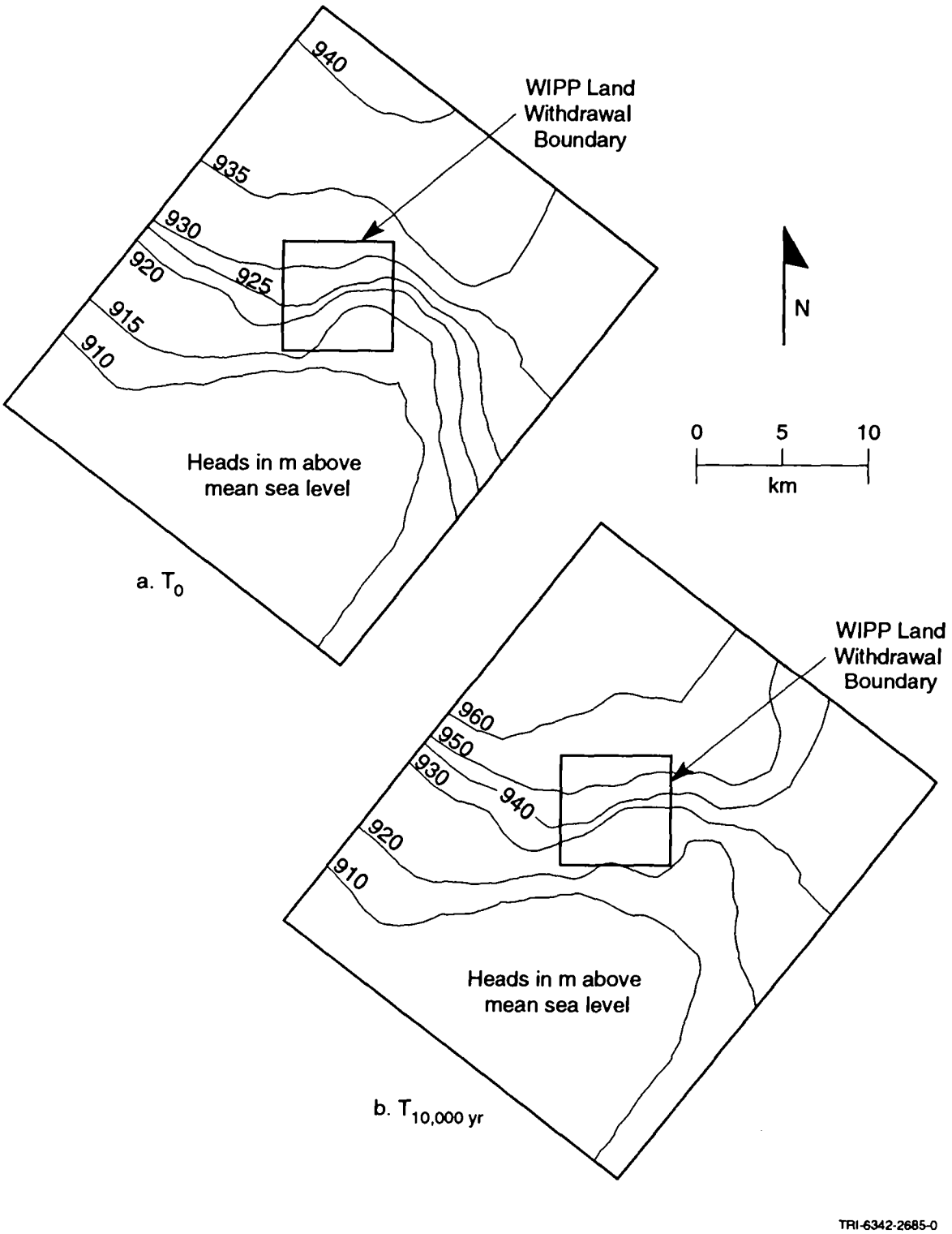

Figure 6.5-2. Head (Figures 6.5-2a,b) and specific discharge (Figures 6.5-2c,d) plots for the SECO-FLOW regional domain for realization 20 at time zero and 10,000 yr. This realization contains an intermediate value for CULCLIM.

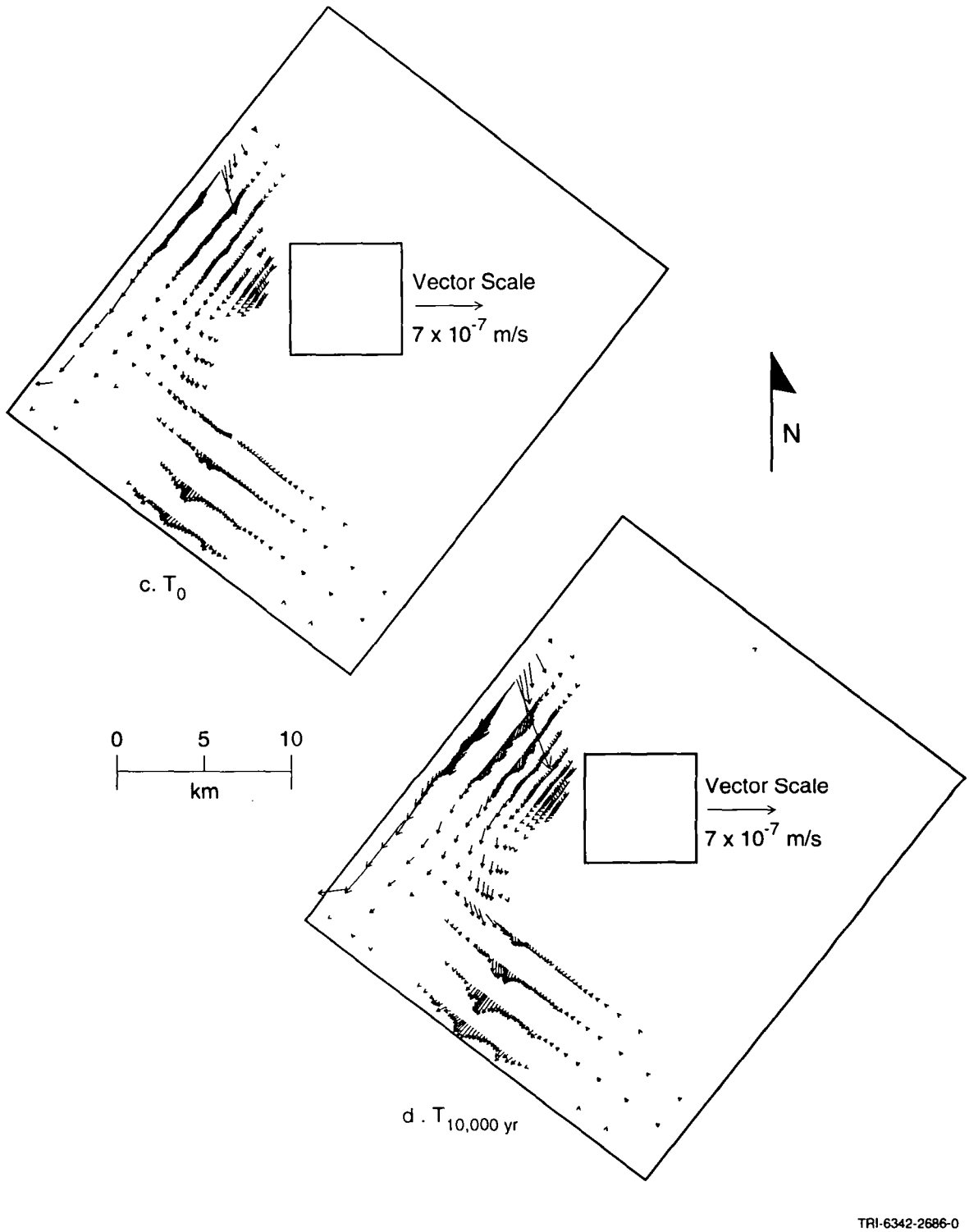

Figure 6.5-2. Head (Figures 6.5-2a,b) and specific discharge (Figures 6.5-2c,d) plots for the SECO-FLOW regional domain for realization 20 at time zero and 10,000 yr. This realization contains an intermediate value for CULCLIM. (continued)

resulting in a value for CULCLIM of 1.031. Examination of these figures shows that the largest increases in head occur in the northern and northwestern portion of the regional domain, and that most of the increase in groundwater flow occurs in and near Nash Draw. Some increase in groundwater flow is observed within the land-withdrawal boundary. CULCLIM does not, however, appear as an important parameter in stepwise linear regression analyses (see Chapter 8), and subsurface releases of radionuclides are not sensitive to climatic variation of heads along the modeled "recharge strip."

6.6 Flow and Transport Model Coupling

Radionuclide transport was modeled on the same computational grid used for the local flow calculations. Flow fields generated from the first time step by SECO-FLOW were used as the initial and boundary conditions by SECO-TRANSPORT. The transient SECO-FLOW flow fields from subsequent time steps, starting at 1000 yr, were used for solute transport modeling. Radionuclide release from the repository to the Culebra was from a single, time-dependent source term located above the center of the waste-disposal region. Density and volume of liquid injected into the Culebra was assumed to be negligible relative to the total flow within the aquifer. Source-term flux was therefore disregarded, and did not affect flux in the flow fields. Volume and density affects of injecting brine into the Culebra will be examined in future PAs.

SECO-FLOW solves the time-dependent partial differential equation for hydraulic head for a heterogeneous, isotropic aquifer, and provides the specific discharge (volume of fluid moving through a unit area in a unit time) for each grid element. Heterogeneity is introduced through each spatially-varying transmissivity field. SECO-TRANSPORT models radionuclide transport in a fractured medium under a variety of assumptions (see Section 7.6 of Volume 2 of this report). The fluid is transported in fracture porosity only, and not in the matrix porosity of the dolomite or clay fracture linings. Matrix porosity affects diffusion into and storage in the matrix. Therefore, dividing the specific discharge by fracture porosity to obtain pore-water velocity within the fractures can result in relatively fast travel times to the accessible environment boundary if other processes (e.g., matrix diffusion and sorption) are not effective in retarding radionuclide transport. However, if matrix diffusion and/or sorption are effective in retarding radionuclide transport, travel times may be orders of magnitude longer.

6.7 Coupling the Repository/Shaft and Culebra Models

Radionuclide releases into the Culebra were modeled for E2- and E1E2-type intrusions (see Section 4.4.2.4 of Volume 2 of this report). Solute concentration and rate of discharge was dependent on parametrically described geochemical and physical processes and interactions. The code PANEL (see Section 7.4 of Volume 2 of this report) calculated the solute concentration and pulse length. Sampled parameters affecting these processes were used in both PANEL and BRAGFLO, and each realization therefore had a specific suite of source files which consisted of a source term having varying pulse lengths and concentrations for each radionuclide. The source files, from PANEL and located on a separate CAMDAT data base, were imported and attached to the local velocity flow fields by the SECO-TRANSPORT preprocessor for the transport calculations.

6.8 Transmissivity Fields

The synthetic transmissivity fields generated by LaVenue and RamaRao (1992) represent an improvement over the fields used in 1991 (WIPP PA Division, 1991b), in that they more accurately characterize the uncertainty due to spatial variability in aquifer properties, and, therefore, result in better characterization of uncertainty in groundwater flow. A discussion of the 1992 transmissivity field results, extracted from LaVenue and RamaRao (1992), follows.

6.8.1 Ensemble Mean Transmissivities

Each of the 70 fields were calibrated to steady-state and transient head data using conditionally simulated (CS) fields (presented in Appendix C of Volume 3 of this report) composed of an underlying kriged field to which different conditional random error fields were added. Thus, each of the calibrated CS transmissivity fields has a different spatial distribution of transmissivities. For example, in some cases there is a broad zone of higher transmissivity that extends from the DOE-1 borehole west to H-14 (see Figure 6.2-1 for borehole locations). In other cases, the high-transmissivity zone has a narrow, tortuous and in some instances, discontinuous nature.

An ensemble mean calculation was performed across the realizations to determine the average transmissivity value at each grid block. The resulting ensemble transmissivity field (Figure 6.8-1) has features which are very similar to the 1990 kriged transmissivity field that was used as

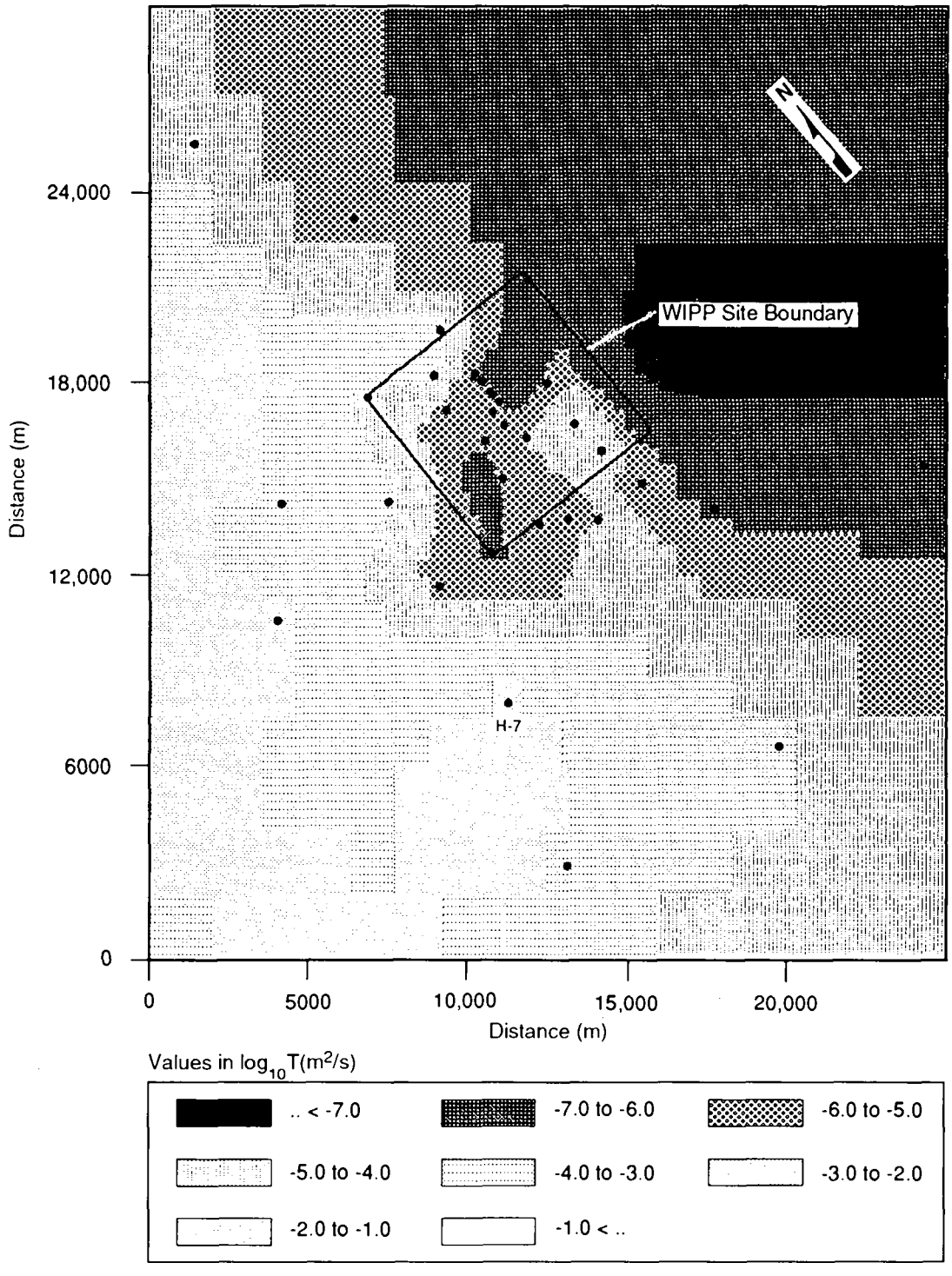

Figure 6.8-1. Ensemble transmissivity field resulting from a mean calculation performed across the realizations.

the basis for generating the transmissivity fields for the 1991 PA calculations. Outside the land-withdrawal area, the re-entry of high transmissivities from the Nash Draw area occurs south of the WIPP near the H-7 borehole in both the 1990 results and in the ensemble mean field. The high-transmissivity zone within the land-withdrawal boundary, as represented in the ensemble mean field (Figure 6.8-2), extends northward from the P-17 borehole where it narrowly lies between the P-17 and H-17 boreholes. Once crossing the southern land-withdrawal boundary, the high-transmissivity zone widens significantly extending westward to the H-3 borehole. The eastern extent terminates approximately 100 m east of the H-11 and DOE-1 boreholes. The nature of the high-transmissivity zone as determined in the 1990 study (Figure 6.8-3) is quite similar to the ensemble mean field with a narrow width toward the southern land-withdrawal boundary, which widens in both the east and west directions as it extends northward toward the H-15 borehole.

6.8.2 Ensemble Steady-State Head Differences

A root-mean squared error (RMSE) between calculated and observed steady-state heads was calculated in order to summarize the fit of each realization to the steady-state data. The RMSE values at each of the boreholes that had steady-state observed head data were then summed within each simulation to obtain an average RMSE. A histogram of the average RMSE value for each of the 70 simulations (Figure 6.8-4) depicts a mean RMSE value within the simulations between 2.0 and 5.0 m. Uncertainty in the steady-state heads is approximately 1.5 m. The simulation with the worst steady-state head fit is shown to have an average RMSE value between 6.5 and 7.5 m. This particular realization illustrates a situation in which the difference field (added to the kriged field during the CS process) significantly reduced the ability of the code to calibrate the field to steady-state conditions within 50 calibration steps. This situation occurs when the initial CS field generated has features that produce significantly high initial-head differences. The code then has to add more pilot points to modify the CS field to bring the head field into agreement with the observed data than may be necessary for an initial CS field which produces initial head differences that are low. Because a fixed number of pilot points were specified for calibrating to the steady-state data, some fields had smaller RMSE values than others.

RMSE values were also calculated to determine average head differences over the ensemble of realizations at each borehole location. Figure 6.8-5

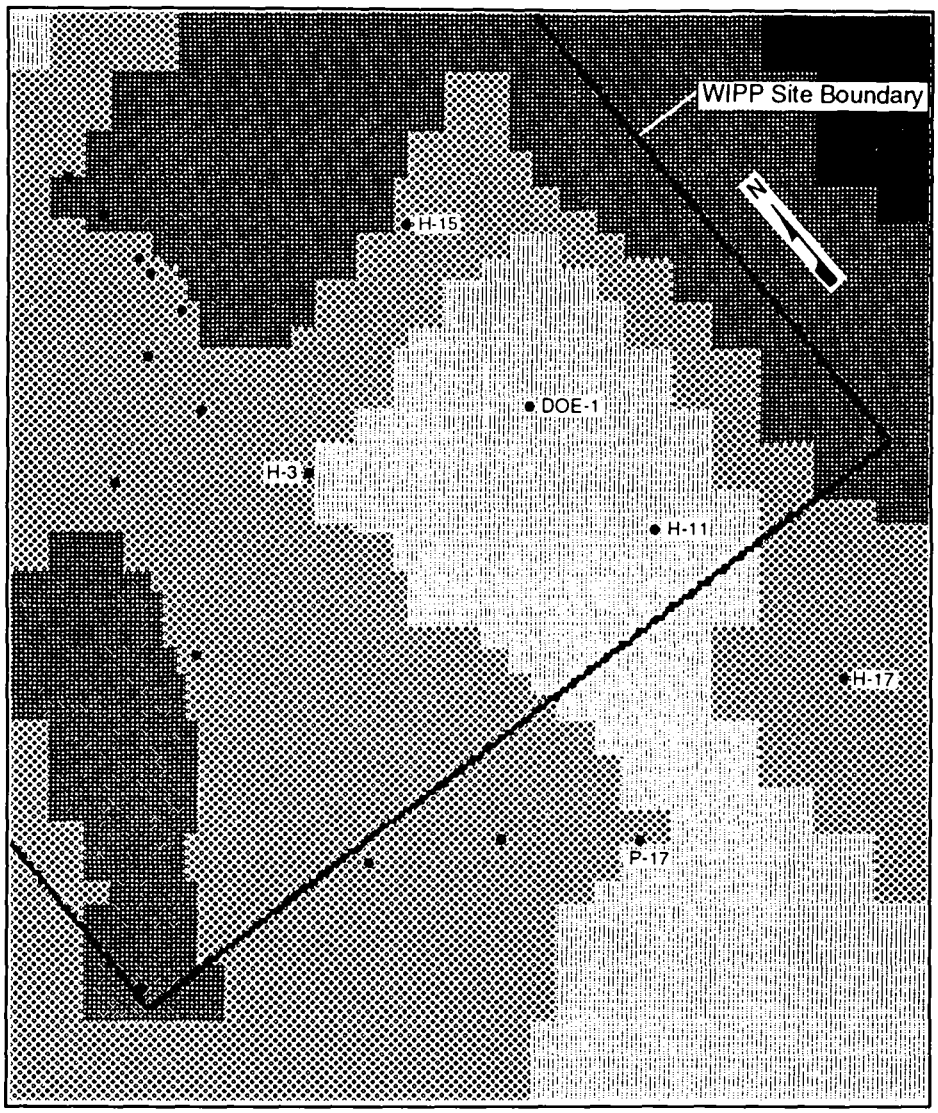

Figure 6.8-2. Ensemble transmissivity field in the vicinity of the southern land-withdrawal boundary.

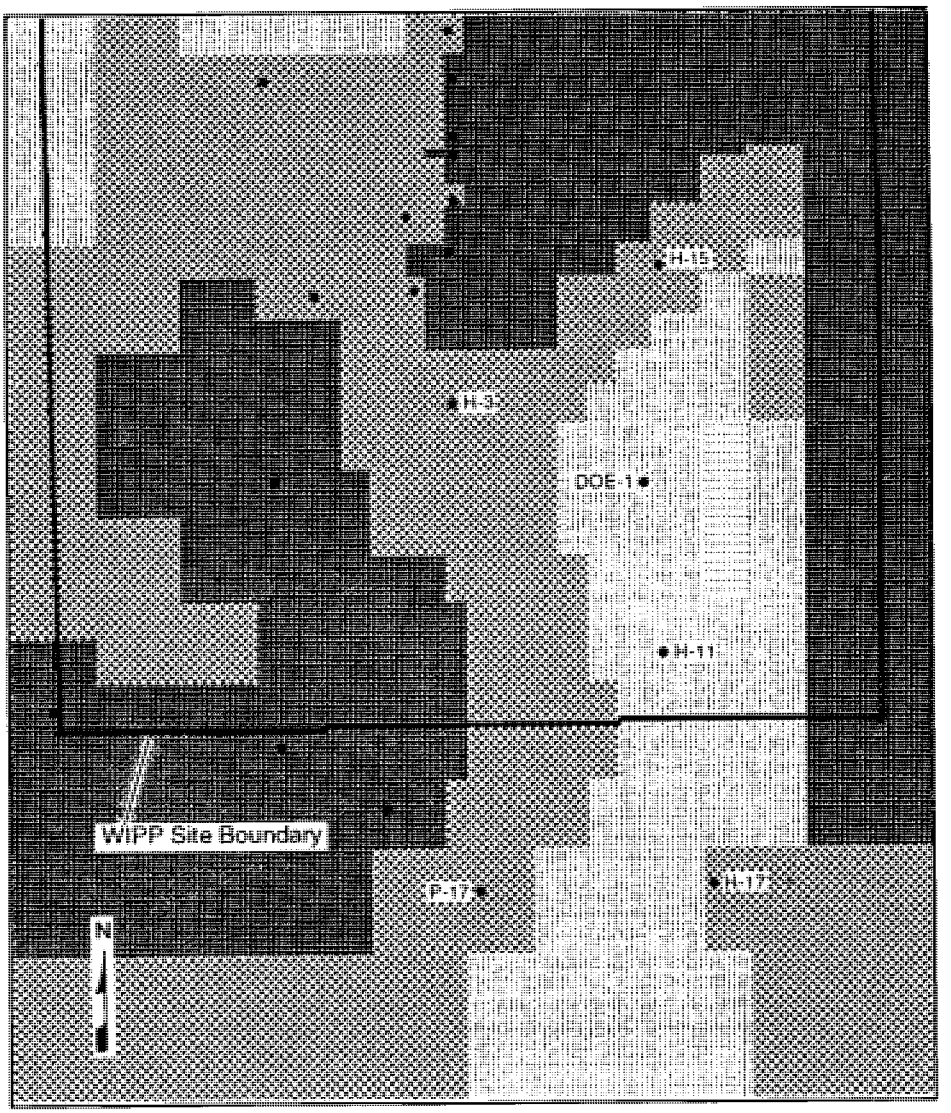

Figure 6.8-3. Calibrated transmissivities in the vicinity of southern land-withdrawal boundary.

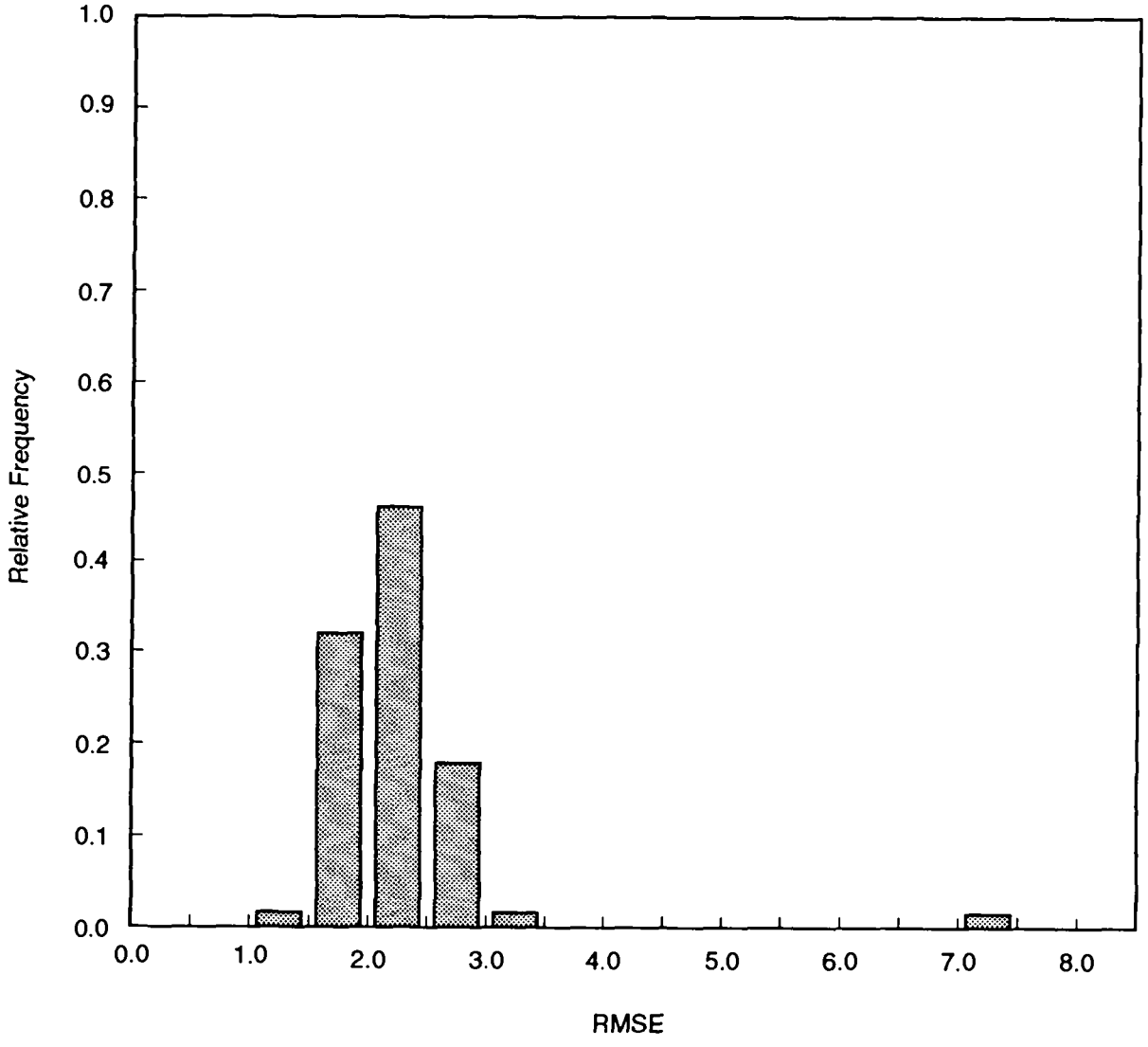

Figure 6.8-4. Histogram of the average RMSE value for each of the 70 simulations.

contains a contour surface of the RMSE values over the model domain. The maximum average difference between the calculated and observed data occurs at the H-7 borehole where the RMSE value is -4.3 m. (Note: The sign of the RMSE was assigned after evaluating the ensemble differences.) The head differences in the southern portion of the regional domain and the central portion of the land-withdrawal area also have negative signs with average values ranging between -0.7 m and -2.8 m. The regions that have positive head differences occur in the area immediately adjacent to the H-11 borehole and in the area between the P-14 and WIPP-26 boreholes. The average head differences in these regions are less than 2.0 m. The difference at the H-17 borehole is the highest with a positive value of 3.4 m.

The average head differences illustrated in Figure 6.8-5 indicate that the boundary conditions specified along the southern and western boundaries are not consistent with the observed heads. Several iterations were made to the boundary conditions prior to beginning the calibration exercise. The iterations were necessary due to the difficulty in matching the H-7, USGS-1, and H-9 observed heads while properly fitting the heads in the rest of the model domain. The difficulty arises from the existence of the no-flow region along the Nash Draw axis and the extremely flat hydraulic gradients in the southern area. If the specified heads are increased along the southern boundary to fit H-7 and USGS-1, the southern boundary converts from a discharge boundary to a recharge boundary. However, the Pecos River, and the Malaga Bend region in particular, has been determined to behave as a discharge region for regional flux from the Rustler (Mercer, 1983). While no absolute conclusions may be made yet concerning the direction of groundwater flow in the southern portion of the regional domain, the results determined in this study have indicated that there is an inconsistency between the observed heads in this area if regional groundwater flow is to the south. This may indicate a groundwater divide occurs between the H-9 borehole and the H-8 borehole south of the model domain.

6.8.3 Ensemble Groundwater Travel Times

The groundwater travel time from a point above the center of the waste-disposal region (Section 6.2.3) to the land-withdrawal boundary was calculated for each of the calibrated CS fields. This groundwater travel time is not the same as the radionuclide transport travel times calculated by SECO-TRANSPORT, which are used as input to the CCDF calculations. The purpose of the groundwater-travel-time calculations described here is to characterize the transmissivity fields, not to predict transport of radionuclides. These travel times were calculated assuming advection of groundwater through a single-porosity medium without fracture flow--i.e.,

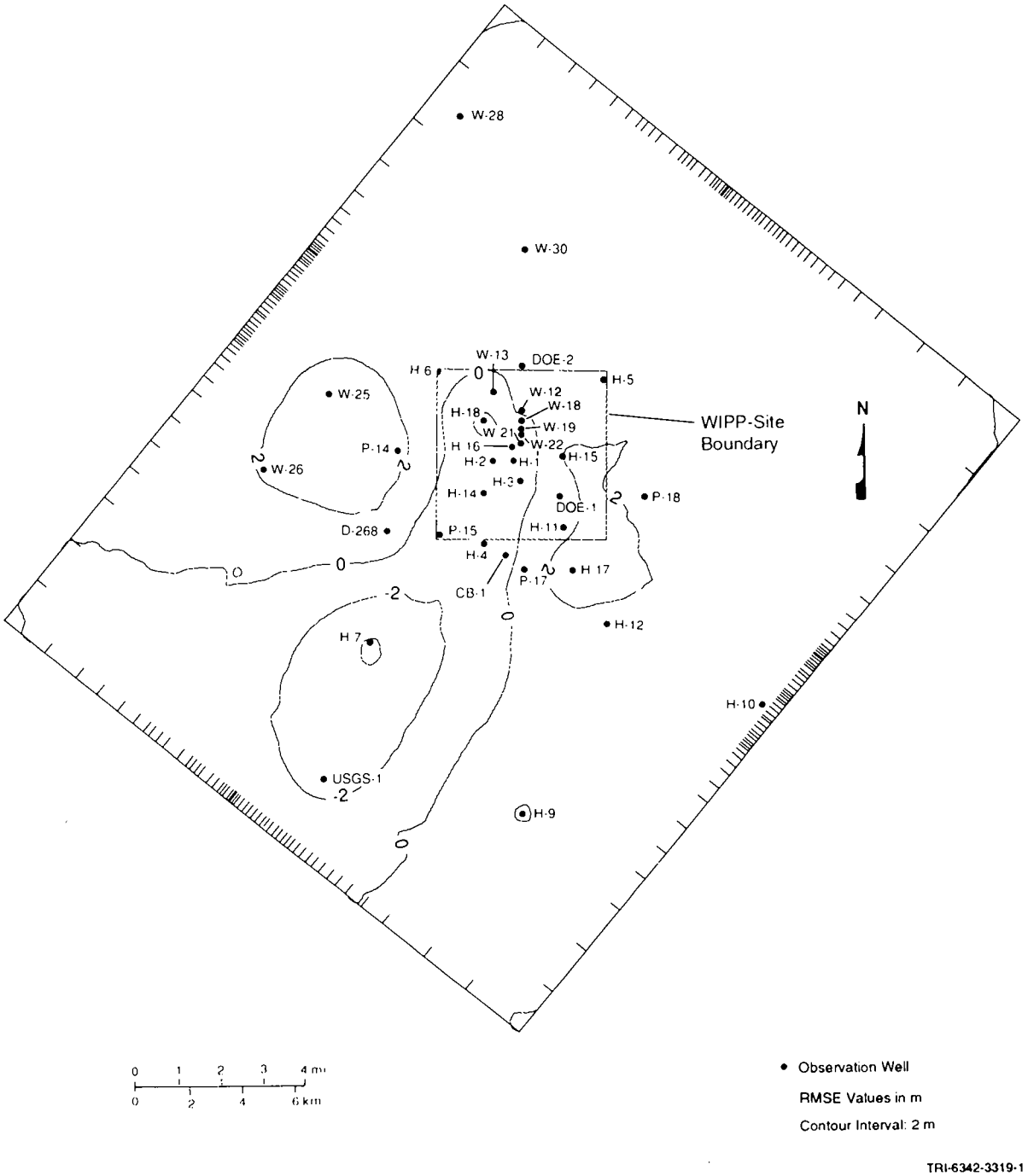

Figure 6.8-5. Contour surface of the RMSE values over the model domain.

total porosity was equal to a matrix porosity of 0.16. Travel times are therefore substantially longer than those calculated assuming transport in fractures, with an average fracture porosity of 0.001.

Matrix travel-time distributions are displayed as a cumulative distribution function (CDF) that represents the probability of various travel times occurring (Figure 6.8-6). This CDF shows, for example, that 90% of the travel times were longer than 12,000 yr, 50% of the travel times were longer than 18,000 yr, and 10% of the travel times were longer than 27,000 yr. The histogram shown in Figure 6.8-7 also conveys the narrow distribution of groundwater travel times.

The travel paths that correspond to the travel times contained in the CDF are illustrated in Figure 6.8-8. Most of the travel paths follow a southeasterly direction until reaching the DOE-1 vicinity at which point the paths travel directly south to the land-withdrawal boundary. A few paths travel directly south from the starting point while several others have an east-southeasterly direction prior to moving south toward the land-withdrawal boundary. The travel paths are indicative of the southerly groundwater-flow direction observed today. Should significant changes occur in the future in the direction of the hydraulic gradient, travel paths would also change.

Assuming the numerical model used to simulate a system properly accounts for the physics and scale of the problem of interest, the uncertainty of model results should decrease as the data set to which the model is conditioned increases. Conditioning a transmissivity field used in a model to observed steady-state pressure data reduces uncertainty in the transmissivity estimates away from the observed locations. Conditioning to transient-pressure data further reduces uncertainty in the transmissivity estimates between pressure-measurement locations due to the increase in information regarding the transmissivity between these two locations. The reduction in the uncertainty of the travel time due to the conditioning of the Culebra model to the transient pressure data base is illustrated in Figure 6.8-9 where the CDF of travel times determined from the transient-calibrated model (referred to herein as the TCDF) and the CDF determined from the steady-state calibrated model (referred to herein as the SCDF) are shown. The CDF of the steady-state model was calculated by removing all the pilot points added during transient calibration from the input data sets of each of the realizations.

As illustrated in Figure 6.8-9, the SCDF has a much broader range of travel times than the TCDF. The minimum values between the two are approximately the same; however, the median and maximum travel times are

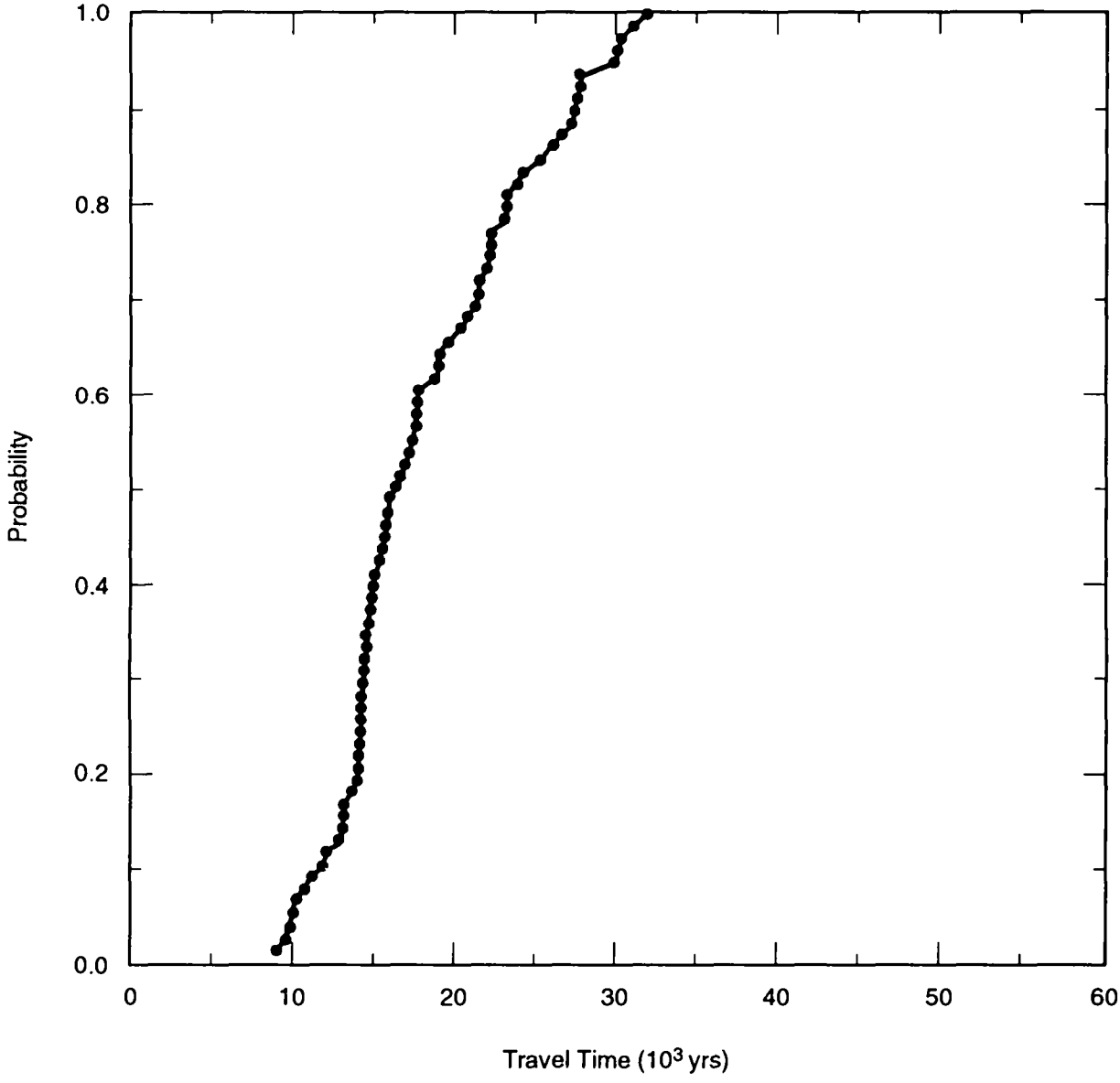

Figure 6.8-6. Travel time cumulative distribution function (CDF) determined from the 70 calibrated fields (assuming matrix porosity of 16%).

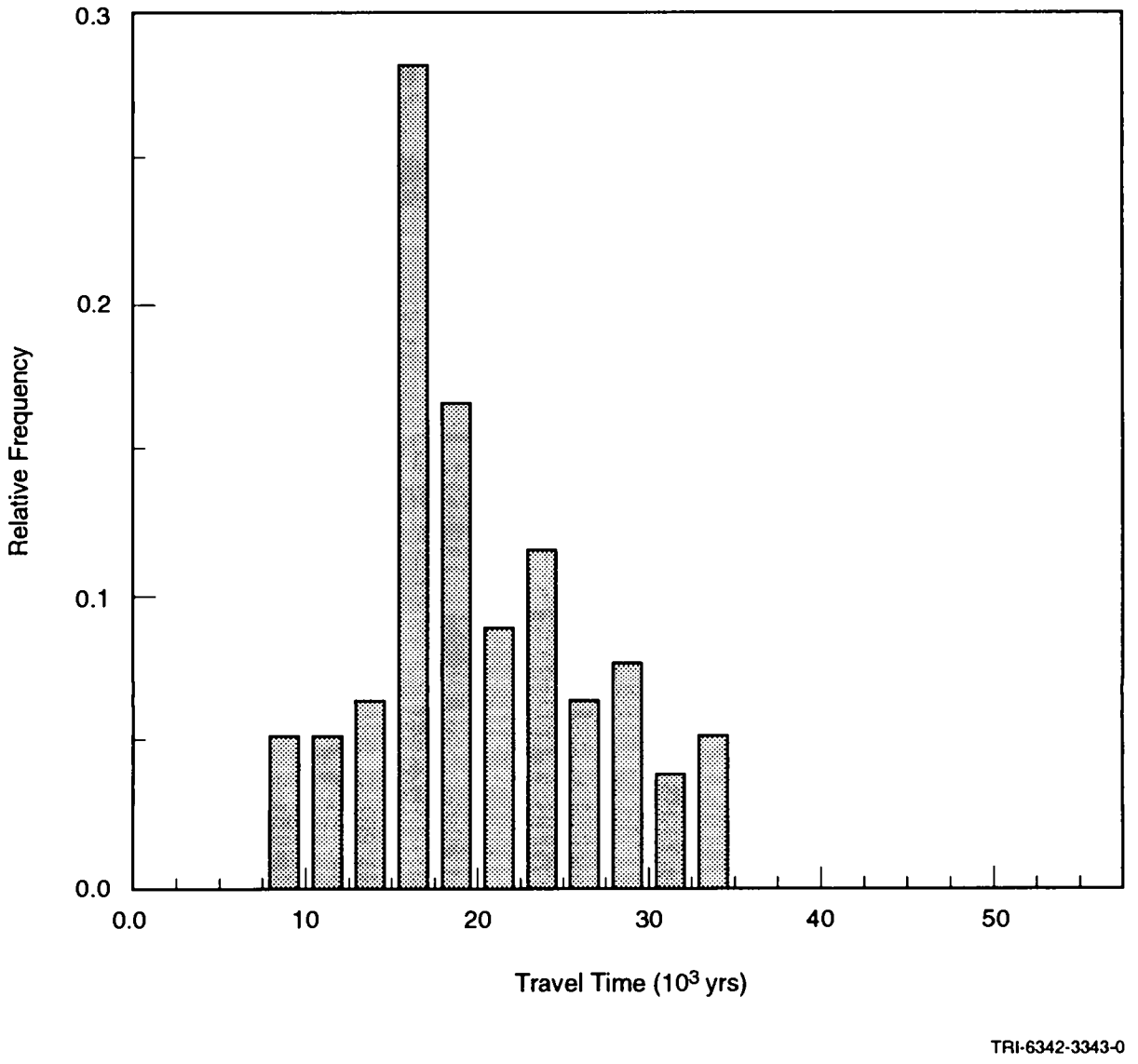

Figure 6.8-7. Histogram of travel times from ensemble of transient calibrated fields.

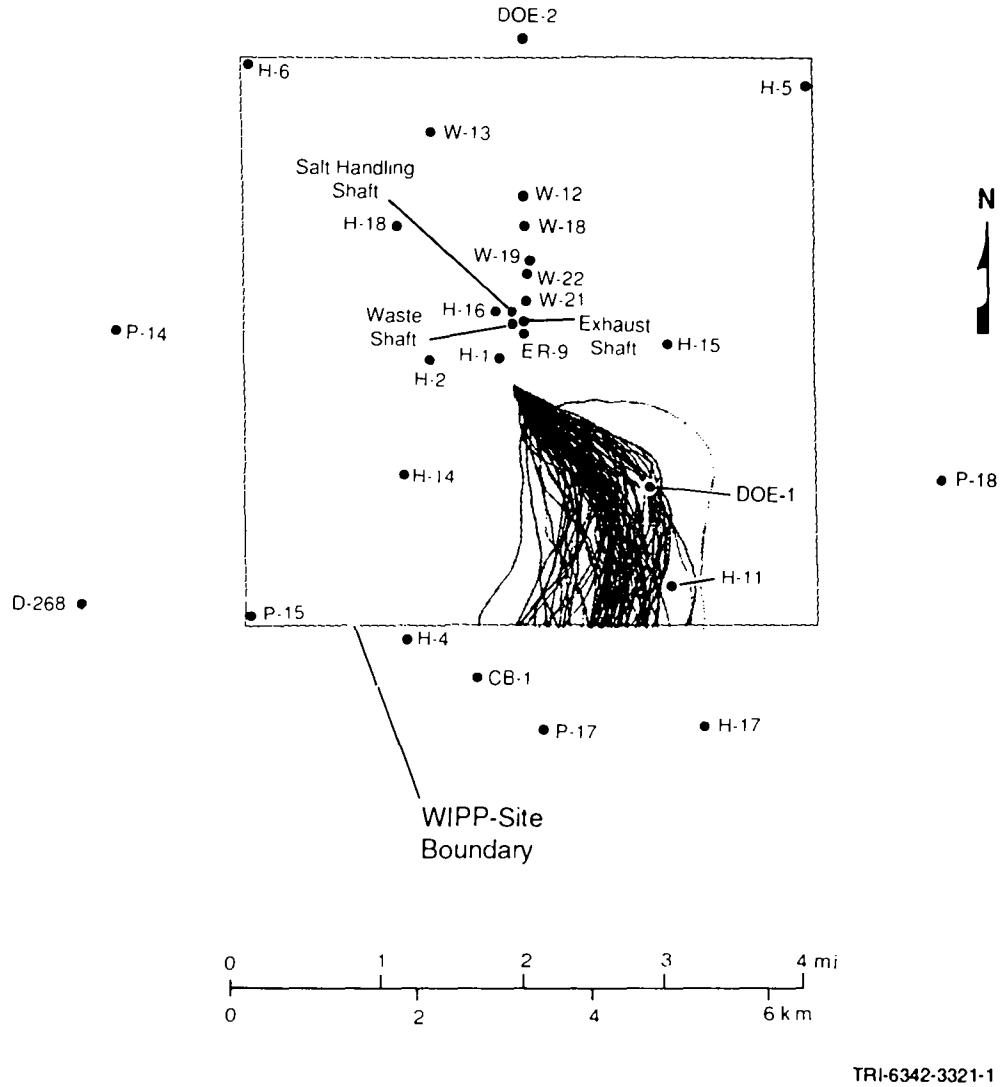

Figure 6.8-8. Travel paths that correspond to the travel times contained in the cumulative distribution function (CDF) shown in Figure 6.8-4.

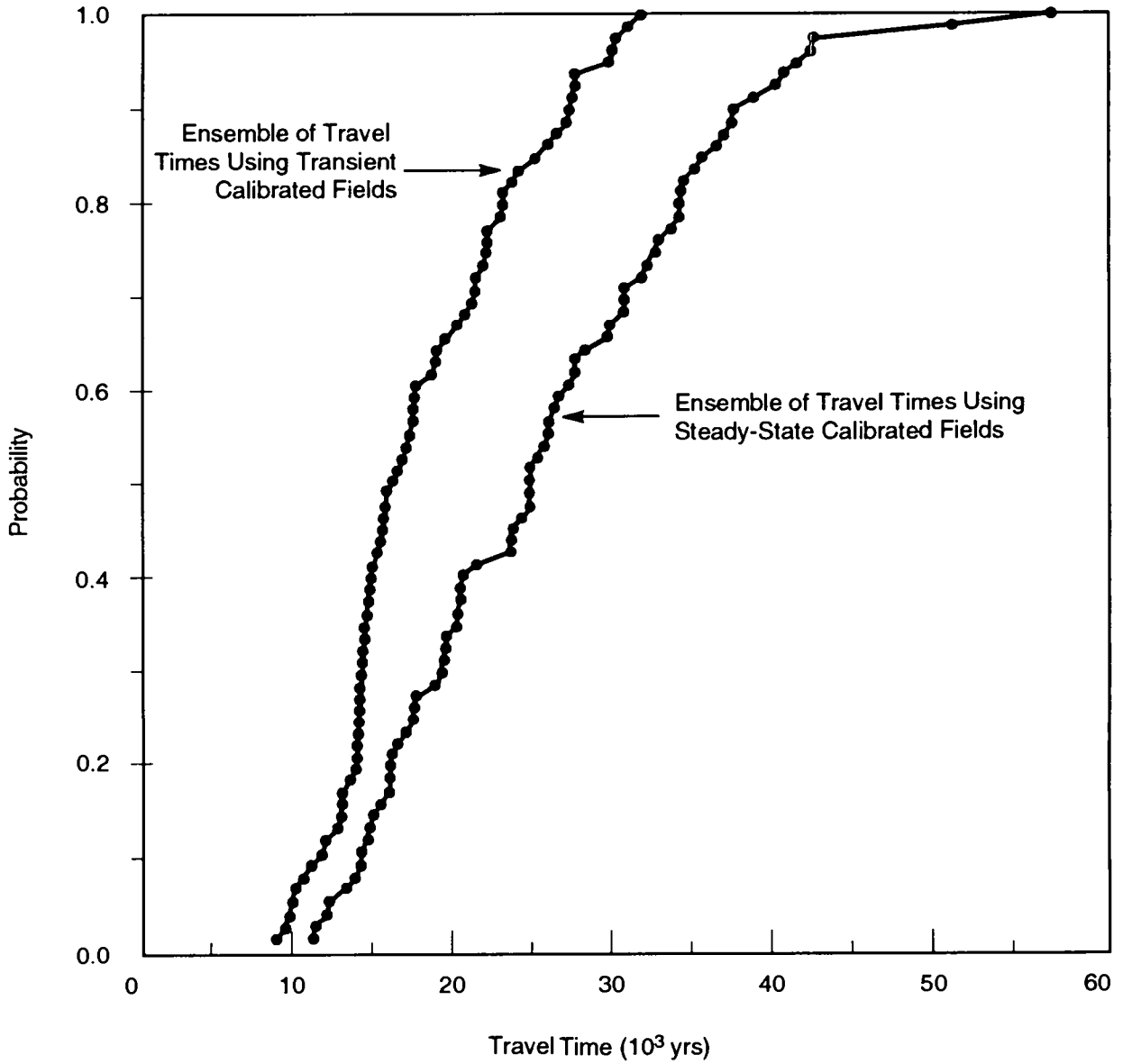

Figure 6.8-9. Cumulative distribution function (CDF) of travel times determined from the transient-calibrated model (TCDF) and the CDF determined from the steady-state calibrated model (SCDF).

quite different. As mentioned above, 50% of the travel times in the TCDF were greater than 18,000 yr and 10% were greater than 27,000 yr. In the SCDF, 50% of the travel times are greater than 25,000 yr and 10% are greater than 37,500 yr. The maximum travel times for the steady-state and transient-calibrated fields are 57,000 yr and 33,000 yr, respectively. The histogram of travel times using only the steady-state calculated models also illustrates this point (Figure 6.8-10).

Thus, the calibration to the transient-pressure data has significantly reduced the magnitude and range of observed travel times. The extension of the high-transmissivity zone toward the H-15 borehole and the subsequent effect the extension has upon the reduction in travel distance from the starting point (above the center of the waste-disposal region) to a region of higher transmissivities has reduced the uncertainty in the travel times. The reduction in uncertainty occurs, as stated above, because of the modifications to the CS transmissivity fields in the southeastern region of the land-withdrawal area, which are necessary to match the observed transient pressures in this region.

For comparison purposes, the travel paths that correspond to the travel times contained in the SCDF are illustrated in Figure 6.8-11. Like the travel paths shown in Figure 6.8-8, most of the travel paths follow a southeasterly direction until reaching the DOE-1 vicinity at which time the paths travel directly south to the land-withdrawal boundary. A few more paths traveldirectly south from the starting point while several others have an east-southeasterly direction prior to moving south toward the land-withdrawal boundary. In general though, the distribution of paths seems very similar to those illustrated in Figure 6.8-8.

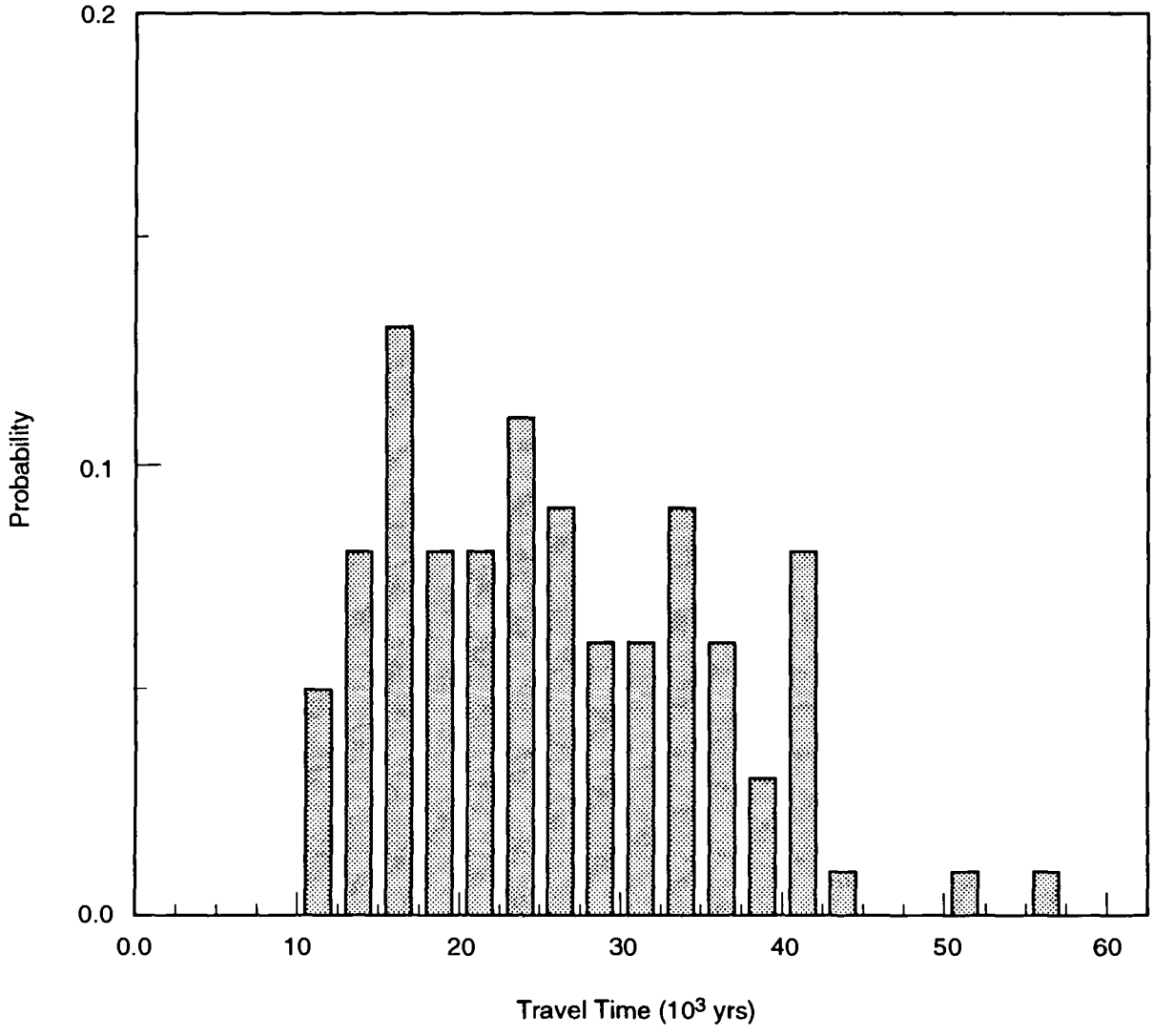

Figure 6.8-10. Histogram of travel times from ensemble of fields calibrated only to steady-state head data.

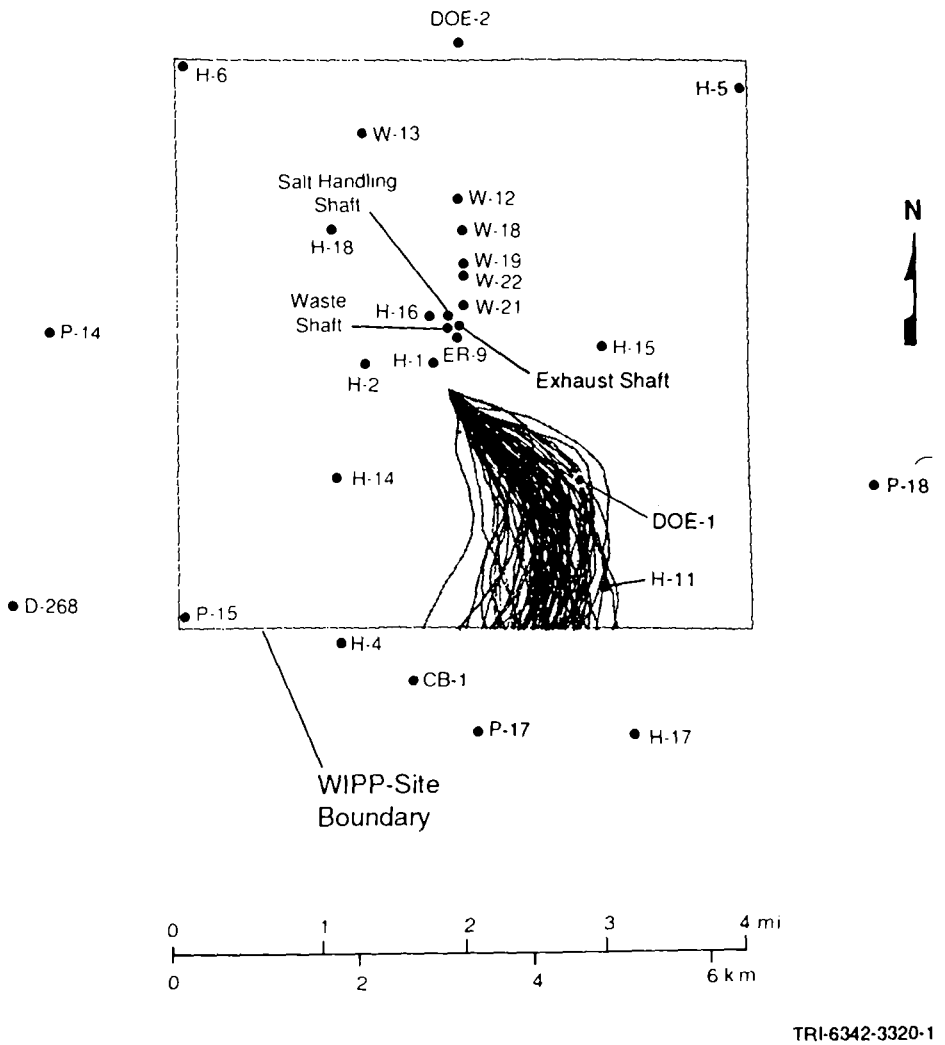

Figure 6.8-11. Travel paths associated with ensemble of transmissivity fields calibrated only to steady-state head data.

7. DISTURBED PERFORMANCE: DIRECT RELEASES TO THE GROUND SURFACE DURING DRILLING

This chapter describes the implementation of the 1992 PA model CUTTINGS for calculating the quantity of radionuclides removed directly to the surface due to an intrusion event. Only exploratory drilling for hydrocarbons is considered. Present-day rotary drilling methods are assumed to persist throughout the regulatory period. Cuttings are estimated based on the drill-bit diameter which is a sampled variable with a CDF constructed from past drilling history in the Delaware Basin (Section 4.4.2 of Volume 3 of this report). Cavings, comprised of waste material eroded from the borehole wall by drilling fluid, are also removed to the surface with the cuttings. The amount of cavings removed depends on the assumption that erosion occurs when the calculated drilling fluid shear stress exceeds the effective shear strength of the consolidated waste, as estimated from analogue data (Table 3.4.1 of Volume 3 of this report). The quantity of waste material spalled from the borehole wall when the drill bit penetrates a gas-pressurized waste panel has not been included because this mechanism is not yet sufficiently understood. Modeling and laboratory work are presently investigating this phenomenon. When constant λs are used, the assumption that present-day drilling technology and practice persists for 10,000 yr is consistent with the philosophy that the risk to future generations should be equally weighted with that to the present generation. The assumptions concerning future levels of technology made by the Futures Panel (memorandum by Hora in Appendix A of Volume 3 of this report) and used for constructing time-varying λs, however, indicate a lower risk to future generations that is not wholly consistent with this philosophy. The volume of waste brought to the ground surface will depend upon the physical properties of the compacted, decomposed wastes, the drilling procedures used, and the pore pressures encountered. Because of radioactive decay, the radioactivity of the removed waste (in curies) will also depend upon the time of intrusion.

7.1 Current Drilling Practices

In standard rotary drilling, a cutting bit attached to a series of hollow drill collars and drill pipes is rotated at a fixed angular velocity and is directed to cut downward through the underlying strata. To remove the drill cuttings, a fluid is pumped down the drill pipe, through and around the drill bit, and up to the surface within the annulus formed by the drillpipe and the borehole wall (Figure 7.1-1). In addition to the removal of cuttings, the drilling fluid (mud) serves to cool and clean the bit, reduce drilling friction, maintain borehole stability, prevent the inflow of

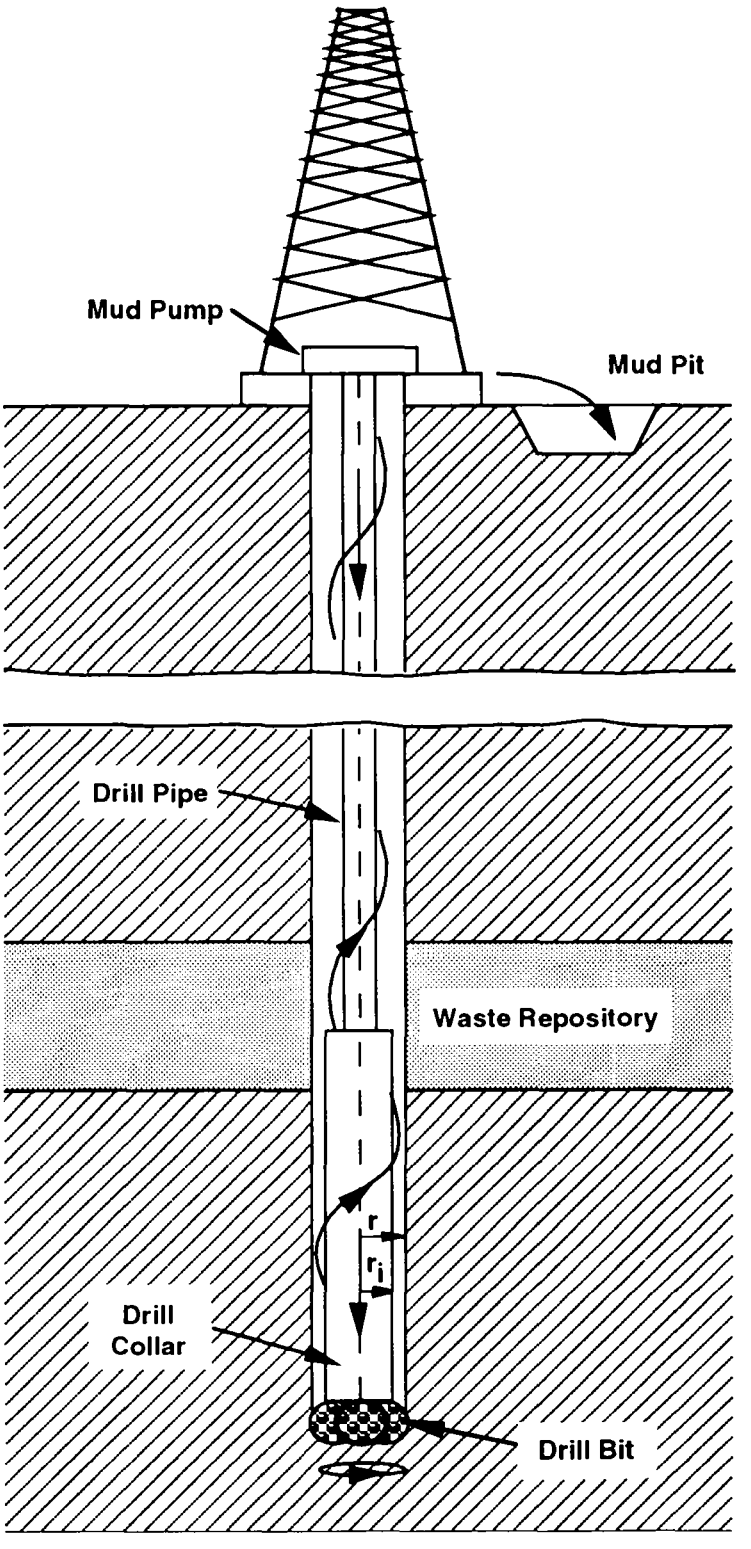

Figure 7.1-1. Rotary drilling.

unwanted fluids from permeable formations, and form a thin, low-permeability barrier on the surface of penetrated formations. When drilling through salt, a saturated brine is often used as the drilling fluid to prevent excessive erosion of the borehole wall through dissolution (Berglund, 1990; Pace, 1990). For a gauge borehole, the volume of cuttings removed and transported to the surface is equal to the product of the drill-bit area and the drill depth. Thus, to estimate the total volume of waste removed due to the cutting action of the drill-bit, it is only necessary to know the compacted repository height and the drill-bit area. The cuttings volume calculated in this manner is a lower bound to the total quantity of waste removed by drilling.

After passing through the drill bit, the drilling fluid flows up the annulus formed by the borehole wall and the drill collar (or drill pipe). In the annulus, the motion of the drilling fluid has both a vertical and rotational component, the latter caused by the rotating drill string. Depending on fluid properties, annulus geometry, and flow rates, the fluid flow within the annulus may be smooth and laminar or turbulent.

7.2 Mechanisms for Waste Removal

There are at least two mechanisms that can be identified as contributing to the removal of waste to the accessible environment over and above that transported by the direct cutting of a gauge borehole. The first is the erosion of the borehole wall caused by the action of the upward-flowing drilling fluid within the annulus. This eroded material is referred to as cavings. The second arises from the effect on the waste of waste-generated gas escaping to the lower-pressure borehole. Material released by this mechanism is referred to as spallings. Both of these phenomena and models for them are discussed in detail by Berglund (1992). In the case of erosion, Berglund (1992) has developed a quantitative model that is based on an effective shear strength for erosion of the compacted, decomposed waste. In the absence of specific experimental data, waste removal from the borehole wall into the drilling fluid due to gas flow is much more difficult to address. For this latter mechanism, Berglund (1992) discusses the general phenomenology, but no quantitative model is available.

7.2.1 Mechanism I: Erosion within the Borehole Annulus

Although a number of factors exist that may influence borehole erosion, Berglund (1992) identifies the effects of fluid shear acting on the borehole wall and the character of the fluid flow (laminar or turbulent) as the most important. To consider these effects, it is necessary to know the threshold

fluid shear stress acting on the borehole wall that will initiate erosion. This "effective" borehole shear strength for erosion must be determined by experiment and may be different for laminar and turbulent flow. In Berglund's (1992) analysis, it is assumed that borehole erosion is caused primarily by the magnitude of the fluid shear stress acting on the borehole wall. Other effects are generally ignored, except insofar as they may influence the experimentally determined effective shear strength for erosion of the repository material.

In the annulus formed by the collars or drill pipe and the borehole wall, the flow of the drilling fluid has both a vertical and rotational component. Within this helical flow pattern, shear stresses are generated by the relative motion of adjacent fluid regions and by the action of the fluid on the borehole wall. It is assumed that if the fluid shear stress at the wall exceeds the effective shear strength for erosion of the wall material (caked drilling fluid or compacted repository wastes), erosion of the wall material will occur, increasing the diameter of the bored hole. The eroded material will then be passed to the surface in the flowing drilling fluid.

Flow in the annulus between the drill pipe and borehole wall is usually laminar (Darley and Gray, 1988). Adjacent to the collars (Figure 1-1), however, the flow may be either laminar or turbulent as a consequence of the larger collar diameter and resulting higher mud velocities (Berglund, 1990; Pace, 1990). For laminar flow, the analysis lends itself to classical solution methods. Turbulent flow, where the flow is assumed to be axial with no rotational component, requires a more approximate approach. For both cases, erosion is assumed to be axisymmetric. The following discussion of these two cases is taken from Berglund (1992).

7.2.1.1 LAMINAR FLOW

Below Reynolds numbers[1] of about 2100 for Newtonian fluids and 2400 for some non-Newtonian fluids (Walker, 1976), experiments have shown that the flow of a fluid in a circular pipe or annulus is well behaved and can be

---

1. The Reynolds number (R_e) is defined as

$$R_e = \frac{\overline{\rho} V D_e}{\overline{\eta}} \qquad (7.2\text{-}1)$$

where D_e is the equivalent hydraulic diameter, $\overline{\rho}$ is the drill fluid density, V is the average fluid velocity, and $\overline{\eta}$ is the average fluid viscosity.

described using a well-defined relationship between the velocity field and the fluid shear stress. This type of flow is called laminar.

Some of the early work on laminar helical flow of a non-Newtonian fluid in an annulus was performed by Coleman and Noll (1959), and Fredrickson (1960). The laminar helical flow solution procedure used in the CUTTINGS code is, for the most part, an adaptation of methods described in a paper by Savins and Wallick (1966).

One of the principal difficulties in solving for the shear stresses within a helically flowing drilling fluid is the shear-rate dependence of the fluid viscosity. This non-Newtonian fluid behavior necessitates choosing a functional form for the variation of viscosity with shear rate for the fluid. There are several functional forms for the viscosity of drilling fluids that can be assumed. For example, in the oil and gas industry, the Bingham and power law models are often used to approximate the shear rate dependence of the fluid viscosity. An alternative form is that chosen by Oldroyd (1958) and used in the analysis by Savins and Wallick (1966). Oldroyd assumed that the viscosity varied according to the functional relation

$$\eta = \eta_o \left[\frac{1+\sigma_2 \Gamma^2}{1+\sigma_1 \Gamma^2} \right] , \qquad (7.2\text{-}2)$$

where σ_1 and σ_2 are constants, η_o is the limiting viscosity at zero rate of shear and Γ is the shear rate. The viscous shear stress is described by $\tau = \eta\Gamma$.

Using the Oldroyd viscosity, Eq. 7.2-2, the viscous shear stress can be illustrated graphically as in Figure 7.2-2. This is a rate softening (pseudoplastic) model that has an initial slope of η_o and a limiting slope of η_∞ for large shear rates, where η_∞ (defined as $\eta_o(\sigma_2/\sigma_1)$) is the limiting viscosity at infinite rate of shear.

The Oldroyd model cannot account for drilling fluids that exhibit a yield stress. However, above a shear rate of zero, parameters can be chosen so that the model can be made to approximate the pseudoplastic rate response of many drilling fluids (see Figure 7.2-1).

Savins and Wallick (1966), expanding on the work of Coleman and Noll (1959) and Fredrickson (1960), showed that the solution for laminar helical flow of a non-Newtonian fluid in an annulus could be written in terms of three nonlinear integral equations.

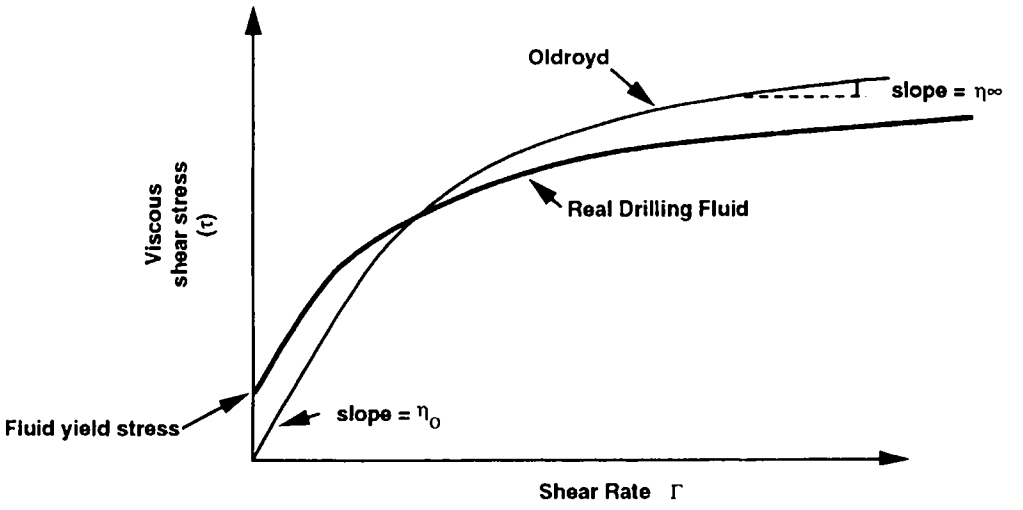

Figure 7.2-1. Viscous shear stress for Oldroyd and real drilling fluids.

These three nonlinear integral equations must be solved numerically (Berglund, 1992). A Fortran computer CUTTINGS code was written to perform the necessary computations for a solution to the problem of laminar helical flow in an annulus. This code was partially verified by comparing its results against those published by Savins and Wallick (1966).

For the specific case of borehole erosion, once a solution to the three integral equations is found, the shear stress in the fluid at the wall can be calculated. By changing the outer radius of the hole, the fluid shear stress can be forced to equal the repository effective shear strength for erosion. The required outer hole radius is determined by iteration as shown in Figure 7.2-2.

The effective shear strength for erosion equals the threshold value of fluid shear stress required to sustain general erosion at the borehole wall. Partheniades and Paaswell (1970), in discussing investigations on the erosion of seabed sediments and in channels, have noted that this effective soil shear strength is not related to the soil shear strength as normally

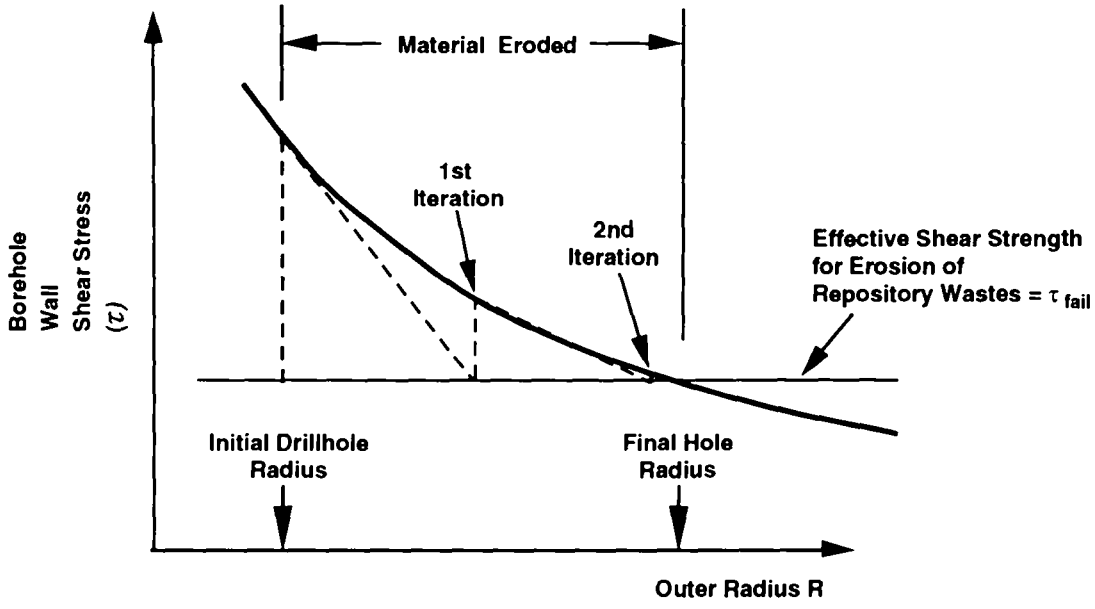

Figure 7.2-2. Iteration procedure for finding the final hole radius.

determined from conventional soil tests. The effective shear strength for erosion based on seabed data, as determined by Partheniades and Paaswell (1970), is on the order of 1 to 5 Pa and is thus smaller by several orders of magnitude than the macroscopic soil shear strength.

7.2.1.2 TURBULENT FLOW

For Newtonian fluids with Reynolds numbers greater than about 2100, flow in a circular pipe or annulus starts to become more or less random in character, which makes orderly mathematical analysis of the flow difficult, if not impossible. With increasing Reynolds numbers, this random behavior increases until, at a Reynolds number of about 3000, the flow becomes fully turbulent. In fully turbulent flow, momentum effects dominate and the fluid viscosity is no longer important in characterizing pressure losses.

For Newtonian fluids, the value to use for the viscosity is clear because the viscosity is constant for all rates of shear. Non-Newtonian fluids exhibit a changing viscosity with shear rate and present a special problem in calculating R_e. For fluids that exhibit a limiting viscosity at high rates of shear (such as the Bingham model and in our case the Oldroyd

model), it has been suggested (Broc, 1982) that the limiting viscosity ($\bar{\eta} = \eta_\infty$) be used in calculating the Reynolds number.

The Reynolds number for an Oldroyd fluid in an annulus can then be written as (Broc, 1982)

$$R_e = \frac{0.8165 D \bar{V} \rho}{\bar{\eta}} , \qquad (7.2\text{-}3)$$

where the hydraulic diameter is expressed as $D = 2(r - r_i)$, where r is the radius of the drill bit and r_i is the radius of the drill collar (see Figure 7.1-1).

The most important influence viscosity has on the calculation of pressure losses in fully turbulent flow of non-Newtonian fluids appears to be in the calculation of the Reynolds number. A far more important parameter is the surface roughness past which the fluid must flow. As previously noted, the Reynolds number, however, does have a role in determining the onset of turbulence; for Newtonian fluids this critical number R_{ec} is about 2100. For non-Newtonian, rate-thinning fluids, R_{ec} tends to be greater than 2100 but less than 2400 (Walker, 1976). For our purposes, a value of 2100 will be used to represent R_{ec} for the Oldroyd fluid model. Because turbulent flow is more effective in generating fluid shear stresses at the borehole wall, this assumption is conservative.

A transition region exists beyond R_{ec} before the development of fully turbulent flow. In this regime, the flow has the character of both laminar and turbulent flow. However, because pressure losses increase rapidly in turbulent flow and affect borehole shear stresses more severely, it will be assumed that beyond R_{ec} the flow is fully turbulent.

Turbulent flow is very complex and, thus, to characterize the turbulent flow regime, the great bulk of analysis has concentrated on empirical procedures. For axial flow in an annulus, the pressure loss under turbulent conditions can be approximated by (Broc, 1982)

$$\Delta P = \frac{2 f L \bar{\rho} \bar{V}^2}{(0.8165) D} , \qquad (7.2\text{-}4)$$

where f is the coefficient of pressure head loss (Fanning friction factor) and L is the borehole length.

If the shear stress due to the flowing fluid is assumed to be uniformly distributed on the inner and outer surfaces of the annulus, it can be easily

shown using Eq. 7.2-4 that the shear stress is related to the average fluid velocity through the relation

$$\tau = \frac{f\overline{\rho V^2}}{2(0.8165)} \quad , \tag{7.2-5}$$

The Fanning friction factor is empirically related to the Reynolds number and relative roughness by the equation (Whittaker, 1985)

$$\frac{1}{\sqrt{f}} = -4\log_{10}\left(\frac{\varepsilon}{3.72D} + \frac{1.255}{Re\sqrt{f}}\right) \quad , \tag{7.2-6}$$

where ε/D is the relative roughness. For circular pipes, D in this equation represents the inside diameter and ε is the absolute roughness or the average depth of pipe wall irregularities. In the absence of a similar equation for flow in an annulus, it will be assumed that this equation also applies here, where D is the hydraulic diameter as defined earlier and ε is the absolute roughness of the waste-borehole interface.

Using a relative roughness and a calculated Reynolds number, a Fanning friction factor can be determined by iteratively solving Eq. 7.2-5. The value of the shear stress acting on the borehole wall can then be determined from Eq. 7.2-4. Using an iterative procedure similar to that for the laminar flow problem (Figure 7.2-2), the fluid shear stress can be forced to equal the repository shear strength for erosion (τ_{fail}) to obtain the final eroded borehole radius.

In the actual solution sequence employed in CUTTINGS, the Reynolds number is calculated first to determine which solution regime (laminar or turbulent) should be initiated. For Reynolds numbers initially less than R_{ec}, the code calculates the flow as laminar. Any increase in diameter of the borehole calculated during the laminar calculation will cause the Reynolds number to decrease as a result of a velocity decrease, ensuring that the calculation remains laminar. If the initial Reynolds number is greater than R_{ec}, the turbulent formulation is used to calculate borehole erosion. When the turbulent calculation is complete, a check is again made to determine whether the Reynolds number still exceeds R_{ec}. If it does not, the laminar calculation is performed starting with a "critical" borehole radius. The critical borehole radius corresponds to a Reynolds number of R_{ec} and is given by

$$R_{crit} = \frac{\overline{\rho}Q}{1286\pi\eta_{\infty}} - R_i, \tag{7.2-7}$$

7.2.1.3 EROSION CALCULATIONS

The equations governing erosion based on laminar and turbulent flow were combined into a single Fortran computer code called CUTTINGS. Using appropriately selected input based on the physical properties of the waste and other drilling parameters, this code calculates the final eroded diameter of the borehole that passes through the waste. The drilling parameters chosen must reflect data typical of that valid near the WIPP repository. Berglund (1992) provides a discussion of suitable parameter values and model sensitivity to uncertainty in those parameters. Drill bit diameter (DBDIAM) is the most important parameter, and is the only parameter used with the CUTTINGS code that is sampled in the 1992 PA. Values for other model parameters are given in Berglund (1992) and Chapter 4 of Volume 3 of this report.

7.2.2 Mechanism II: Waste-Gas-Induced Borehole Spall

The storage, compaction, and brine-induced corrosive degradation of transuranic waste is not directly analogous to any known phenomenon that has occurred in nature. However, considerable information exists in the literature on the exploration for and production of fossil fuels and the problems encountered during these activities. The failure, sloughing, or spalling of borehole walls is a common occurrence in oil and gas drilling and can be caused by a number of different mechanisms, including an encounter with a geopressurized formation. Available literature, summarized by Berglund (1992), supports the need to study the potential for gas-induced spall in waste. The problem is complex, involving the flow of gas in a moving waste matrix, changing stress states, changing porosity and permeability of the waste, waste failure, and, when the waste interacts with the drill bit, turbulent mixing of the three phases – solid waste, drilling fluid, and gas. Berglund (1992) describes simplifying assumptions and modeling approaches that could be used for the WIPP PA. Spalling has not been included in the 1992 PA, and implementation of any of the available models will require additional information about the material properties of decomposed and compacted wastes. Tests are planned to provide this information (US DOE, 1990, in revision). Until such information is available, estimates of releases due to spalling are speculative. Berglund (1992) concludes, however, that "it does not appear unreasonable that volumes of waste several times greater than the lower bound volume [bit area times waste thickness] could eventually reach the ground surface" as a result of spalling. The volumes of waste removed as cavings in the 1991 and 1992 PAs are also several times greater than cuttings volumes. As shown in

Section 5.1 of Volume 1 and Section 8.5 of this volume, the cuttings releases (including cavings but not yet including spallings) control the location of the CCDF (and therefore regulatory compliance) if retardation by either matrix diffusion or sorption occurs in the Culebra Dolomite Member of the Rustler Formation.

7.3 Radionuclide Inventory Available for Removal

Figure 7.3-1 shows the EPA-normalized inventory of the repository, radionuclide by radionuclide, as a function of time (based on the most recent Integrated Data Base [IDB; US DOE, 1991] as reported in the memorandum by Peterson in Appendix A of Volume 3). Time-dependent inventories are shown to 10^4 yr, which is the end of the regulatory period specified by 40 CFR 191B. All radionuclides shown in Figure 7.3-1 are included in the estimation for cuttings release in the 1992 PA. Radionuclides whose normalized inventories never exceed 10^{-2} during 10^4 yr cannot result in releases greater than 10^{-2}, and are not considered in analyses of subsurface transport for 40 CFR 191B.

Figure 7.3-1a shows that the normalized inventories of Pu-239, Pu-240, Am-241, U-233, U-234, Np-237, Th-229, Th-230, and Ra-226 all exceed 10^{-2} during the 10^4-yr period. Figure 7.3-1b shows an additional radionuclide with normalized inventory exceeding 10^{-2}, Pu-238, which is significant only early in the regulatory period. PA modeling for 1991 examined subsurface transport to the accessible environment of 7 of these radionuclides (Pu-239, Pu-240, Am-241, U-233, U-234, Np-237, and Th-230) (WIPP PA Division, 1991c, Section 6.5.2.10). Subsurface transport of two of the remaining radionuclides is modeled in 1992, Th-229 and Ra-226. Transport of Pu-238 in the Culebra will not be modeled because of its short half-life (87.7 yr). Pb-210, which reaches an EPA-normalized inventory of 10^{-2} at late times approaching 10^5 yr, may be considered for subsurface transport in future dose calculations as a daughter product created in the Culebra. Groundwater transport of Pb-210 is not modeled here because of its low inventory at 10^4 yr and short half-life (22.3 yr), and consequent low impact on 40 CFR 191B compliance. Transport of both Pu-238 and Pb-210 in brine brought directly to the ground surface following intrusion (not yet included in performance assessments) also has the potential to contribute to doses.

Table 7.3-1 lists the initial inventory of waste used in the 1992 calculations, Table 7.3-2 lists the decay chains used for transport calculations in the Culebra Dolomite, and Table 7.3-3 lists the activity levels considered in the estimation of cuttings releases.

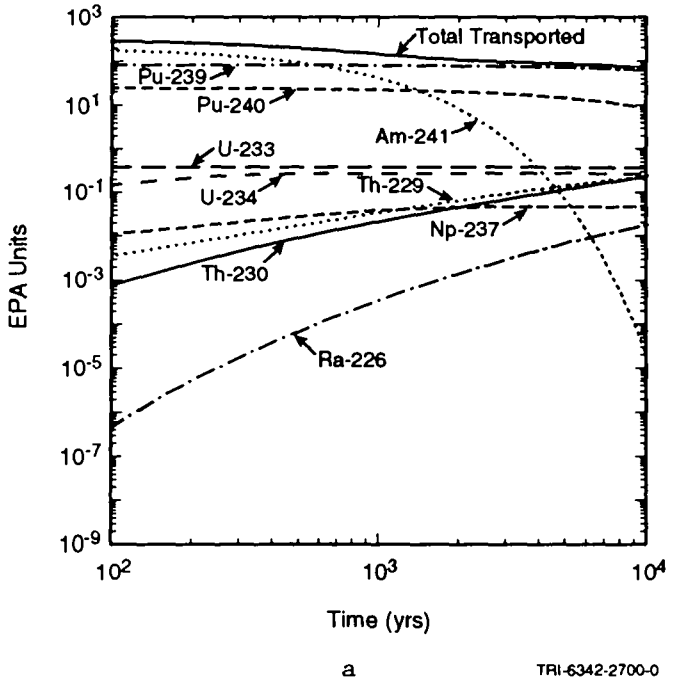

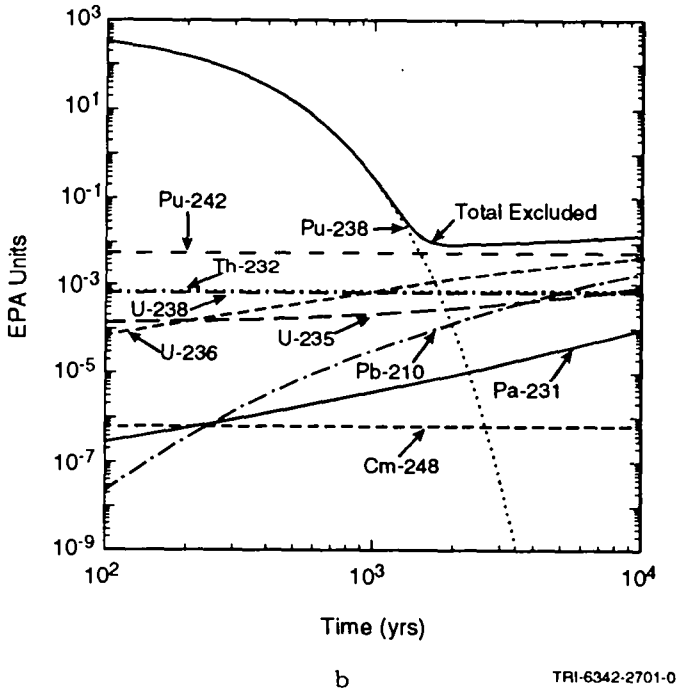

Figure 7.3-1. Decay histories expressed in EPA units (i.e., the normalized units used in showing compliance with 40 CFR 191) for the present IDB inventory for a single waste panel. The total WIPP inventory used in the 1992 PA is ten times the values shown in this figure. Figure 7.3-1a shows radionuclides included in groundwater transport calculations. Figure 7.3-1b shows radionuclides not included in groundwater transport because of low inventory or short half-life. All radionuclides shown are included in estimates of cuttings releases.

The cuttings releases used in the 1992 WIPP performance assessment were calculated with the program CUTTINGS for waste of average activity level. Then, the releases for activity levels 1 through 5 shown in Table 7.3-3 were obtained by multiplying the average activity level releases by scale factors of the form

$$SF_{i\ell} = AL_{i\ell}/AL_i, \tag{7.3-1}$$

where

$AL_{i\ell}$ = projected radioactivity (Ci/m^2) contained in waste of activity level ℓ at time i, where 1 ~ 125 yr, 2 ~ 175 yr, 3 ~ 350 yr, 4 ~ 1000 yr, 5 ~ 3000 yr, and 6 ~ 7250 yr,

and

AL_i = projected radioactivity (Ci/m^2) contained in waste of average activity at time i.

For example, the scale factor

$$SF_{24} = 184.01/7.9658 = 23.100 \tag{7.3-2}$$

is used to convert from a release of average activity at 3000 yr to a release of activity level 4 at 3000 yr.

Table 7.3-1. Potentially Important Radionuclides Associated with Initial Contact-Handled Waste Inventory Used in Calculations for Cuttings Removal and Release to Culebra Dolomite (from memorandum by Peterson in Appendix A of Volume 3)

Radionuclide	$t_{1/2}$(yr)	Curies
Pu-238	8.77×10^{1}	3.06×10^{6}
Pu-239	2.41×10^{4}	3.35×10^{5}
Pu-240	6.53×10^{3}	1.00×10^{5}
Pu-242	3.76×10^{5}	2.35×10^{1}
U-233	1.59×10^{5}	1.53×10^{3}
U-234	2.44×10^{5}	0
U-236	2.34×10^{7}	0
Am-241	4.32×10^{2}	7.14×10^{5}
Np-237	2.14×10^{6}	2.08×10^{1}
Th-229	7.43×10^{3}	0
Th-230	7.70×10^{4}	0
Ra-226	1.60×10^{3}	0

Table 7.3-2. Simplified Radionuclide Decay Chains Used for Transport Calculations in the Culebra Dolomite (from Figure 3.3.1 of Volume 3 of this report)

(1) Pu-240

(2) Am-241 → Np-237 → U-233 → Th-229

(3) U-234 → Th-230 → Ra-226

(4) Pu-239

Table 7.3-3. Projected Activity Levels (Ci/m^2) in the WIPP Due to Waste that is Currently Stored and May Be Shipped to the WIPP (based on Memorandum by Peterson in Appendix A of Volume 3 of this report)

Activity Level	Type[a]	Probability[b]	Time (yr) 0	125	175	350	1000	3000	7250
1	CH[c]	0.3968	2.7578	0.7994	0.6468	0.3884	0.2078	0.1387	0.1156
2	CH	0.3572	27.578	7.9941	6.4683	3.8844	2.0782	1.3867	1.1559
3	CH	0.1259	275.78	79.941	64.683	38.844	20.782	13.867	11.559
4	CH	0.0060	2757.8	799.41	646.83	388.44	207.82	138.67	115.59
5	RH[d]	0.1141	124.70	7.7110	3.3430	1.1180	0.8210	0.7080	0.6280
Average for CH Waste:			70.145	20.333	16.452	9.8800	5.2860	3.5270	2.9400

a CH designates contact-handled waste; RH designates remotely-handled waste

b Probability that a randomly placed borehole through the waste panels will intersect waste of activity level ℓ, $\ell = 1,2,3,4,5$.

c CH activity levels based on 111,520 m^2 total surface area

d RH activity levels based on 14,360 m^2 total surface area

8. UNCERTAINTY AND SENSITIVITY ANALYSIS RESULTS

8.1 Scenario Probability

As indicated in Section 2.3, drilling intrusions into the repository are assumed to follow a Poisson process in the 1992 WIPP performance assessment. Both stationary (i.e., constant λ) and nonstationary (i.e., time-dependent λ) processes are considered. The rate term in these processes is treated as being uncertain; the sampled variable LAMBDA in Table 3-1 is used to identify the λ used for each sample element. For the stationary case, the actual λ used in the analysis is assumed to be uniformly distributed on the interval $[0, 3.78 \times 10^{-4}\ \text{yr}^{-1}]$. For the nonstationary case, the $\lambda(t)$'s used in the analysis were developed in an expert review process (memorandum by Hora, Appendix A, pp. A-69 to A-99, of Volume 3) and are listed in Appendix D of Volume 3.

This section contains two illustrations of the uncertainty in scenario probability. Probabilities for the scenarios

$$S(0,0),\ S(1,0),\ \ldots,\ S(6,0) \tag{8.1-1}$$

used in conjunction with the risk representation R_1 defined in Eq. 2.5-1 are shown in Figure 8.1-1. Figure 8.1-1 shows scenario probabilities determined with both constant λ's and time-dependent λ's. As a reminder, the risk representation R_1 uses time intervals of [0, 2000 yr] and [2000, 10,000 yr] as indicated in Eq. 2.5-2. For both the constant and time-dependent cases, the individual λ's are assumed to equal 0 yr^{-1} after 2000 yr. The actual formulas used to calculate the probabilities are given in Eqs. 2.5-4 and 2.5-6. As examination of Figure 8.1-1 shows, scenario probability decreases rapidly with increasing number of drilling intrusions. Further, the use of the time-dependent λ's results in considerably lower scenario probabilities for scenarios involving drilling intrusions than the use of constant λ's.

Probabilities for the scenarios

$$S(0,0,0,0,0,0), S(1,0,0,0,0,0), S(0,1,0,0,0,0), \ldots, S(0,0,0,0,0,1) \tag{8.1-2}$$

used in conjunction with the risk representation R_2 defined in Eq. 2.5-8 are shown in Figure 8.1-2. Figure 8.1-2 shows scenario probabilities determined with both constant λ's and time-dependent λ's. As a reminder, the risk representation R_2 uses time intervals of [0, 150 yr], [150, 200 yr],

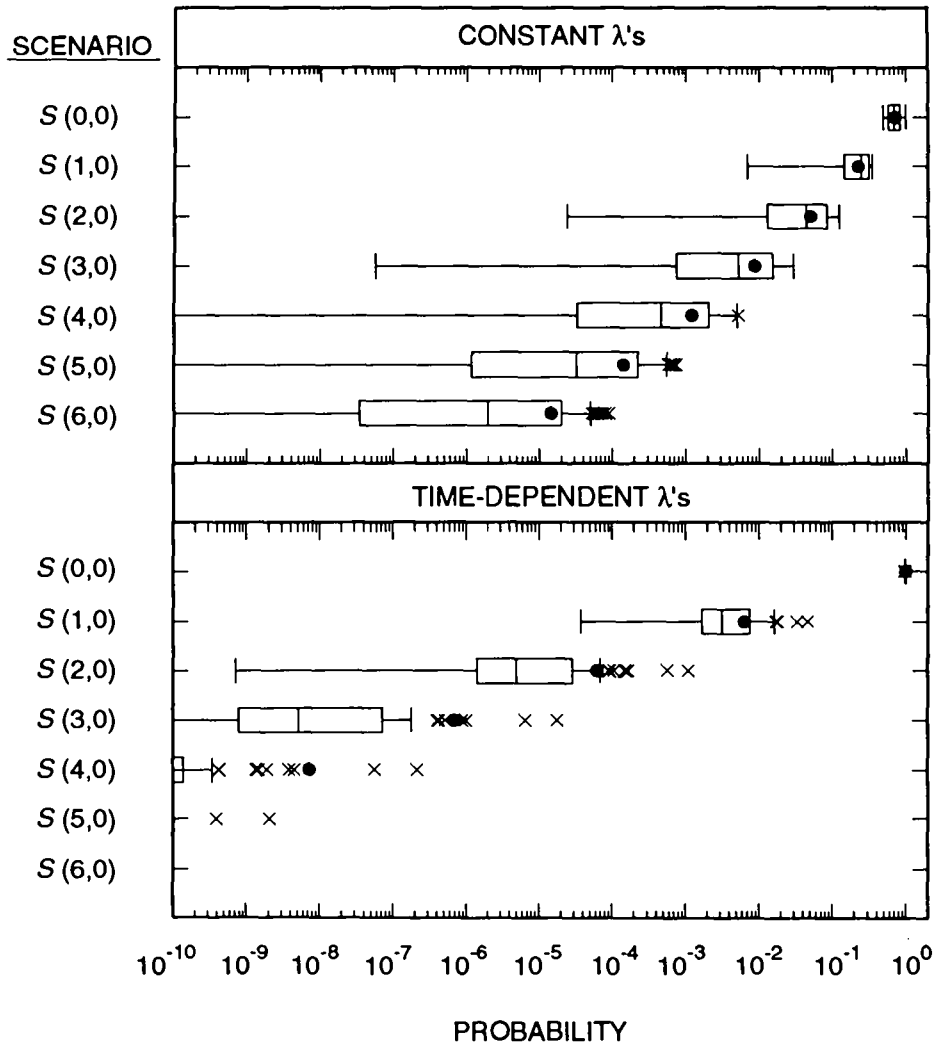

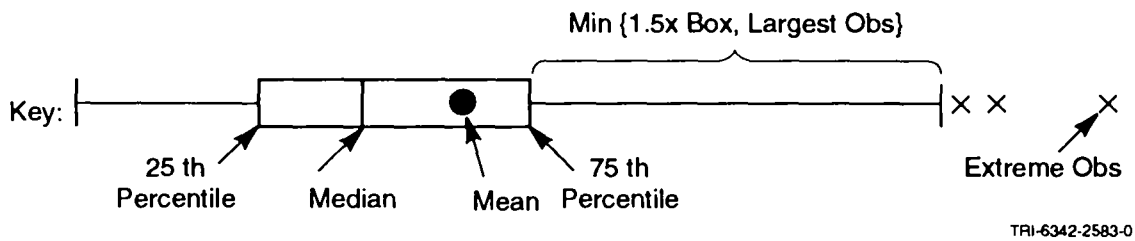

Figure 8.1-1. Uncertainty in probability of scenarios $S(0,0)$, $S(1,0)$, ..., $S(6,0)$ used in conjunction with the risk representation R_1 defined in Eq. 2.5-1 with an assumed 100 yr period of administrative control in which drilling intrusions cannot occur.

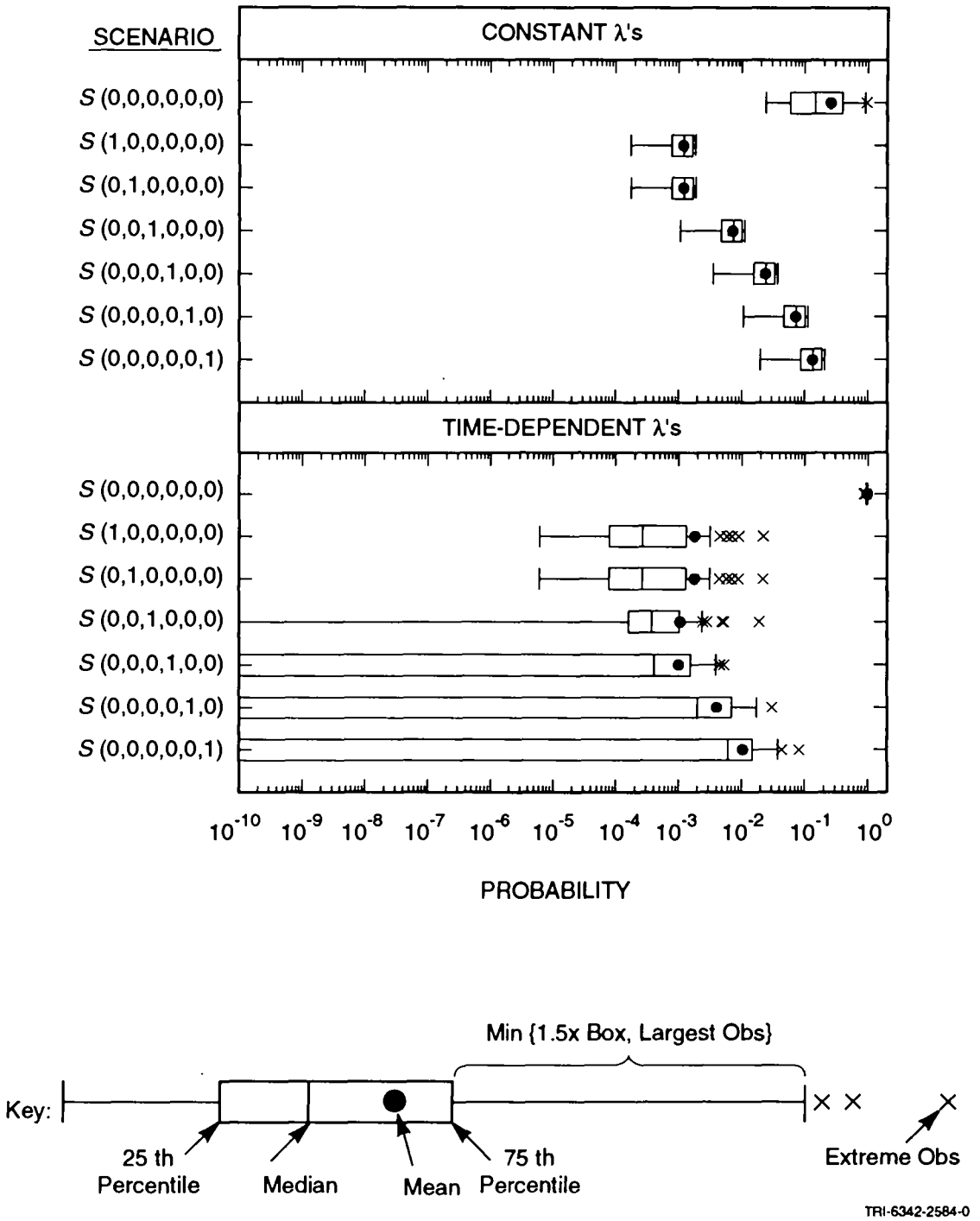

Figure 8.1-2. Uncertainty in probability of scenarios $S(0,0,0,0,0,0)$, $S(1,0,0,0,0,0)$, $S(0,1,0,0,0,0)$, ... , $S(0,0,0,0,0,1)$ used in conjunction with the risk representation R_2 defined in Eq. 2.5-8 with an assumed 100 yr period of administrative control in which drilling intrusions cannot occur.

[200, 500 yr], [500, 1500 yr], [1500, 4500 yr] and [4500, 10,000 yr] as indicated in Eq. 2.5-9. The formula used to calculate the probabilities is given in Eq. 2.3-1 and specializes to

$$pS(\mathbf{n}) = \left\{ \prod_{i=1}^{nT} [\lambda(t_i - t_{i-1})]^{n(i)}/n(i)! \right\} \exp[-\lambda(t_{nT} - t_0)] \qquad (8.1\text{-}3)$$

for the constant λ case. The differences in probability between scenarios in Figure 8.1-2 result from the use of unequal time intervals in scenario definition.

The probabilities in Figure 8.1-2 are for exactly 1 intrusion over 10,000 yr, with that intrusion occurring in a specified time interval. As indicated in Tables 2.5-3 and 2.5-4, many different combinations of drilling intrusion times are used in the definition of the risk representation R_2 given in Eq. 2.5-8. Because of the large number of scenarios involved, box plots of the form shown in Figure 8.1-2 cannot be presented for all scenarios contained in R_2. However, due to the effects of radioactive decay, the cuttings releases for a scenario are often dominated by the time at which the first drilling intrusion occurs. For this reason, it is useful to examine the probability of drilling intrusions in specified time intervals regardless of the drilling intrusions that may occur in subsequent time intervals. Specifically, Figure 8.1-3 presents probabilities for the scenarios

$$S(\geq 1,\geq 0,\geq 0,\geq 0,\geq 0,\geq 0),\ S(0,\geq 1,\geq 0,\geq 0,\geq 0,\geq 0),\ S(0,0,\geq 1,\geq 0,\geq 0,\geq 0),$$
$$S(0,0,0,\geq 1,\geq 0,\geq 0),\ S(0,0,0,0,\geq 1,\geq 0),\ S(0,0,0,0,0,\geq 1), \qquad (8.1\text{-}4)$$

where the notation $\geq n(i)$ in expressions of the form

$$S(\geq n(1),\ \geq n(2),\ \geq n(3),\ \geq n(4),\ \geq n(5),\ \geq n(6)) \qquad (8.1\text{-}5)$$

indicates that the number of drilling intrusions in the i^{th} time interval (i.e., $[t_{i-1}, t_i]$) equals or exceeds n(i). For example, the scenario $S(0,\geq 1,\geq 0,\geq 0,\geq 0,\geq 0)$ appearing in Eq. 8.1-4 consists of all time histories contained in the sample space S defined in Eq. 2.2-1 in which 0 drilling intrusions occur in the time interval [0, 150 yr], 1 or more drilling intrusions occur in the time interval [150, 200 yr], and 0 or more drilling intrusions occur in each of the time intervals [200, 500 yr], [500, 1500 yr], [1500, 4500 yr], and [4500, 10,000 yr]. The defining formulas for the scenario probabilities in Figure 8.1-3 are given in Table 8.1-1. The box plots in Figure 8.1-3 are displaying the uncertainty in the probability that the first drilling intrusion occurs in each of the time intervals used in the definition of the risk representation R_2. As shown in Section 8.2, the size of the cuttings removal release decreases with time.

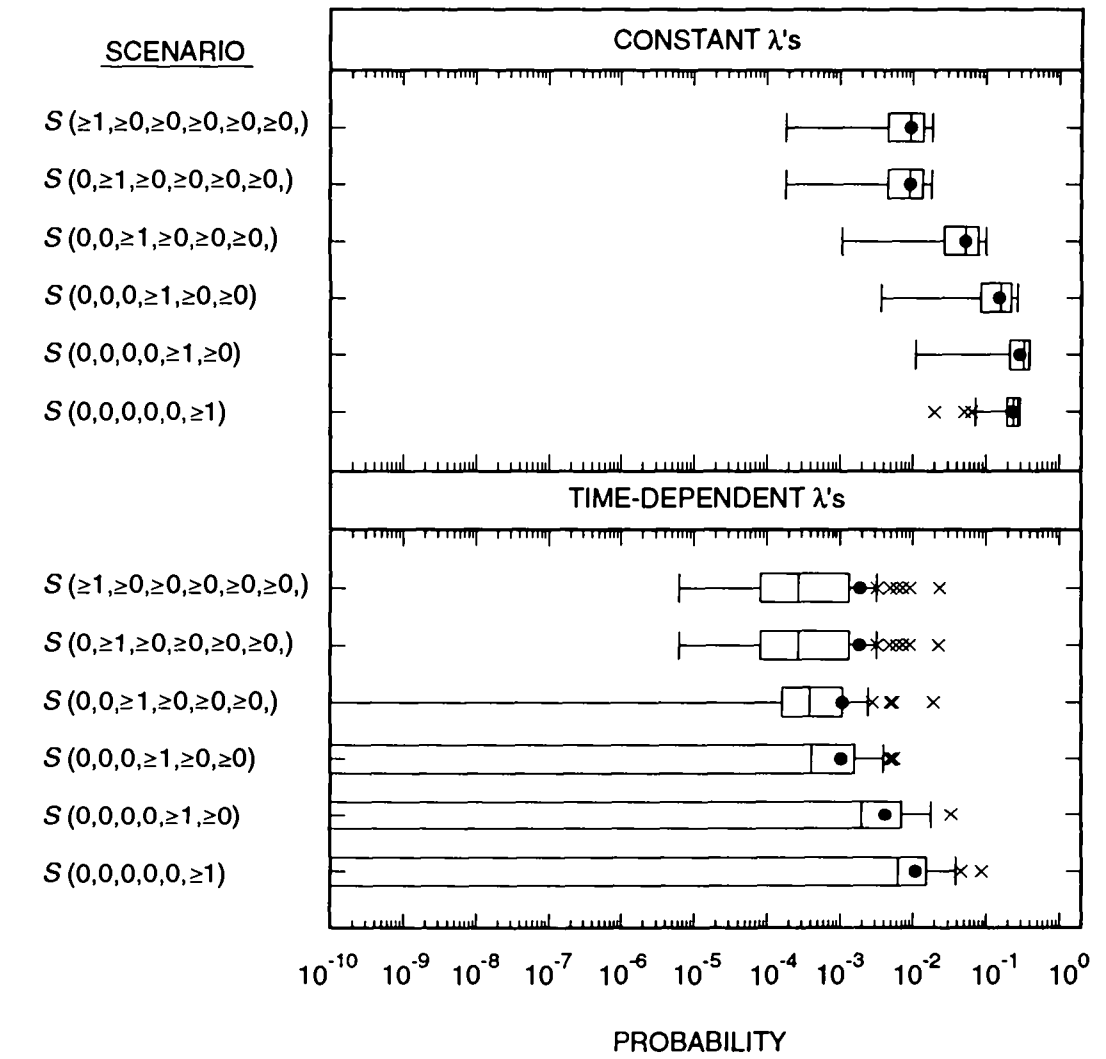

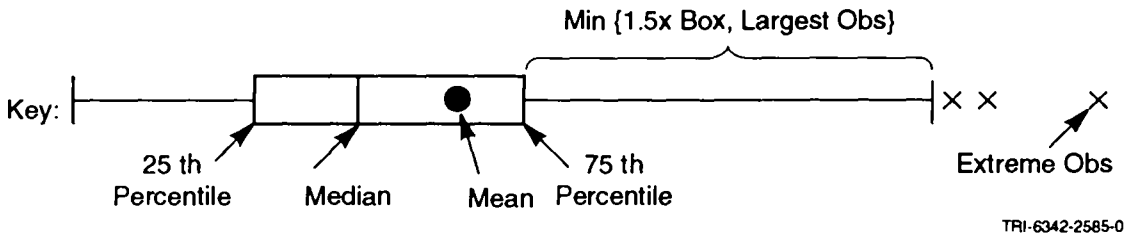

Figure 8.1-3. Uncertainty in probabilities of scenarios $S(\geq 1,\geq 0,\geq 0,\geq 0,\geq 0,\geq 0)$, $S(0,\geq 1,\geq 0,\geq 0,\geq 0,\geq 0)$, ..., $S(0,0,0,0,0,\geq 1)$ associated with risk representation R_2 defined in Eq. 2.5-8 with an assumed 100 yr period of administrative control in which drilling intrusions cannot occur.

Table 8.1-1. Probability of Scenarios $S(\geq 1,\geq 0,\geq 0,\geq 0,\geq 0)$, $S(0,\geq 1,\geq 0,\geq 0,\geq 0)$, ..., $S(0,0,0,0,0,\geq 1)$ Associated with the Risk Representation R_2 Defined in Eq. 2.5-8.

$$pS(\geq 1,\geq 0,\geq 0,\geq 0,\geq 0,\geq 0)$$

$$= \sum_{i=1}^{\infty} \sum_{j=0}^{\infty} \sum_{k=0}^{\infty} \sum_{l=0}^{\infty} \sum_{m=0}^{\infty} \sum_{n=0}^{\infty} pS(i,j,k,l,m,n)$$

$$= 1 - \exp\left[-\int_{t_0}^{t_1} \lambda(t)dt\right]$$

$$pS(0,\geq 1,\geq 0,\geq 0,\geq 0,\geq 0)$$

$$= \sum_{j=1}^{\infty} \sum_{k=0}^{\infty} \sum_{l=0}^{\infty} \sum_{m=0}^{\infty} \sum_{n=0}^{\infty} pS(0,j,k,l,m,n)$$

$$= \left\{\exp\left[-\int_{t_0}^{t_1} \lambda(t)dt\right]\right\} \left\{1-\exp\left[-\int_{t_1}^{t_2} \lambda(t)dt\right]\right\}$$

$$pS(0,0,\geq 1,\geq 0,\geq 0,\geq 0)$$

$$= \sum_{k=1}^{\infty} \sum_{l=0}^{\infty} \sum_{m=0}^{\infty} \sum_{n=0}^{\infty} pS(0,0,k,l,m,n)$$

$$= \left\{\exp\left[-\int_{t_0}^{t_2} \lambda(t)dt\right]\right\} \left\{1-\exp\left[-\int_{t_2}^{t_3} \lambda(t)dt\right]\right\}$$

$$\bullet$$

$$\bullet$$

$$\bullet$$

$$pS(0,0,0,0,0,\geq 1)$$

$$= \sum_{n=1}^{\infty} pS(0,0,0,0,0,n)$$

$$= \left\{\exp\left[-\int_{t_0}^{t_5} \lambda(t)dt\right]\right\} \left\{1-\exp\left[-\int_{t_5}^{t_6} \lambda(t)dt\right]\right\}$$

8.2 Cuttings Removal

The risk representation R_2 defined in Eq. 2.5-8 is used to display the effects of cuttings removal. The releases associated with single intrusions into waste of average activity at different times are summarized in Figure 8.2-1. As discussed in Section 7.3, the releases shown in Figure 8.2-1 are then scaled to determine the releases associated with intrusions into waste of different activity levels. Further, as discussed in Section 2.4, the releases in Figure 8.2-1 are also used in the construction of the cuttings releases assigned to scenarios that involve more than one drilling intrusion.

The cuttings releases shown in Figure 8.2-1 are initially (i.e., at 100 yr) centered around approximately 3.2×10^{-2} EPA release units. The size of the release then decreases due to radioactive decay, with release being reduced to values centered around 5.5×10^{-3} EPA release units by 3000 yr. An additional reduction to about 4×10^{-3} EPA release units occurs by 10,000 yr.

The isotopes associated with the releases at 100 yr and 1000 yr are shown in Figure 8.2-2. The release at 100 yr is dominated by Pu-238, with additional contributions from Am-241, Pu-239 and Pu-240. Due to the short half-life of Pu-238 (i.e., 88 yr), the dominant contributor to the cuttings release at 1000 yr is Pu-239, with additional contributions from Am-241 and Pu-240. Due to the 432 yr half-life of Am-241, the cuttings releases at later times are dominated by Pu-239, with a small contribution from Pu-240.

The only sampled variable that affects cuttings removal is DBDIAM (drillbit diameter). As shown in Figure 4.3-1 of Helton et al. (1992), an almost linear relationship exists between DBDIAM and the cuttings release to the accessible environment. The relationship is actually quadratic. However, due to the range of values for drillbit diameter under consideration (i.e., 0.267-0.444 m), the relationship is close to being linear.

For a given set of analysis input, the risk representation R_2 defined in Eq. 2.5-8 leads to a single CCDF for cuttings removal to the accessible environment. The 1992 WIPP performance assessment considered two imprecisely known variables that affected the CCDF for cuttings removal: drillbit diameter (DBDIAM) and the rate term in the Poisson model for drilling intrusions (LAMBDA). As discussed in Section 2.1, the uncertainty in these variables leads to a distribution of CCDFs. Actually, two cases were considered: constant rate terms and time-dependent rate terms. The

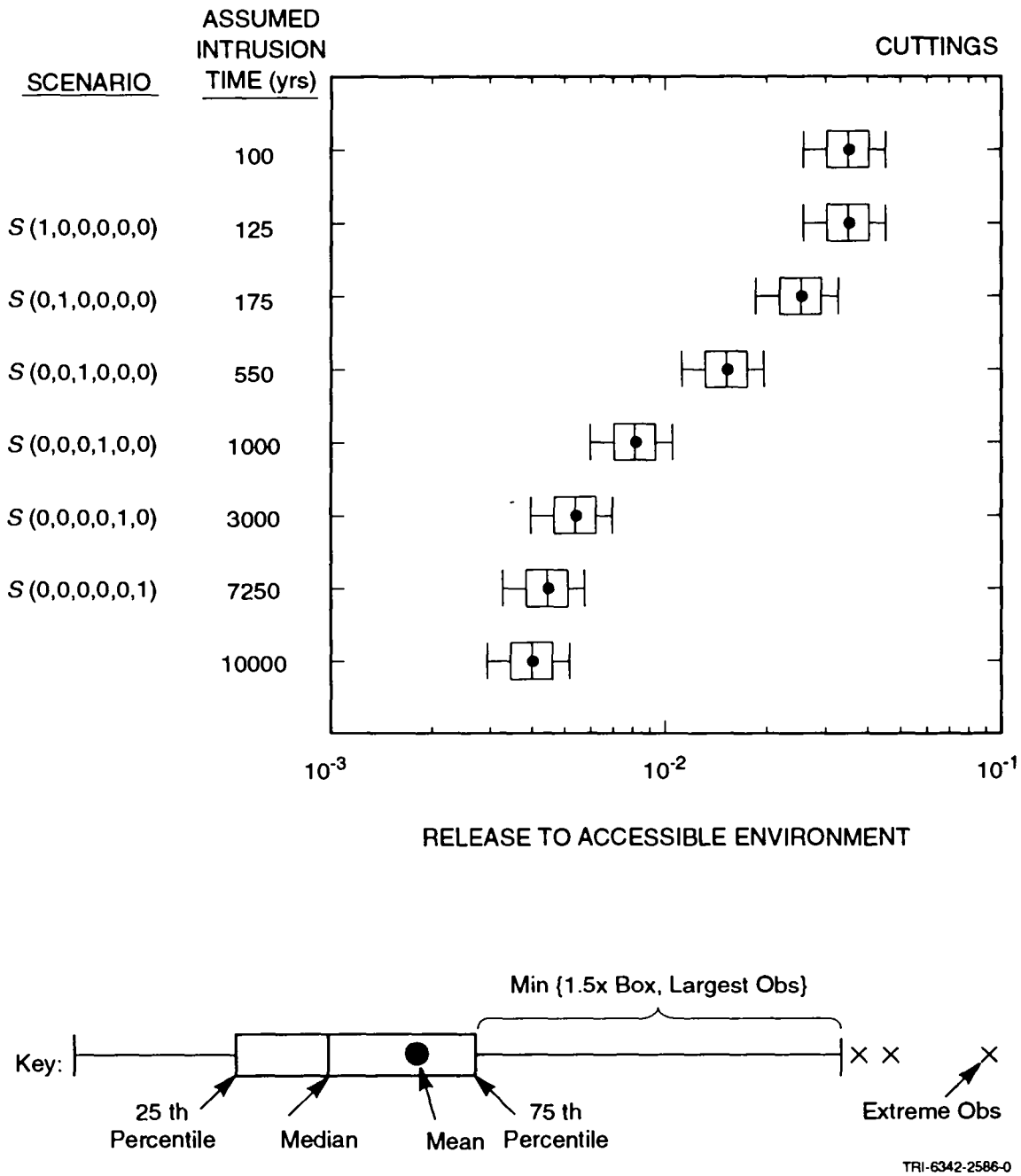

Figure 8.2-1. Total normalized release to the accessible environment due to cuttings removal from waste of average activity level.

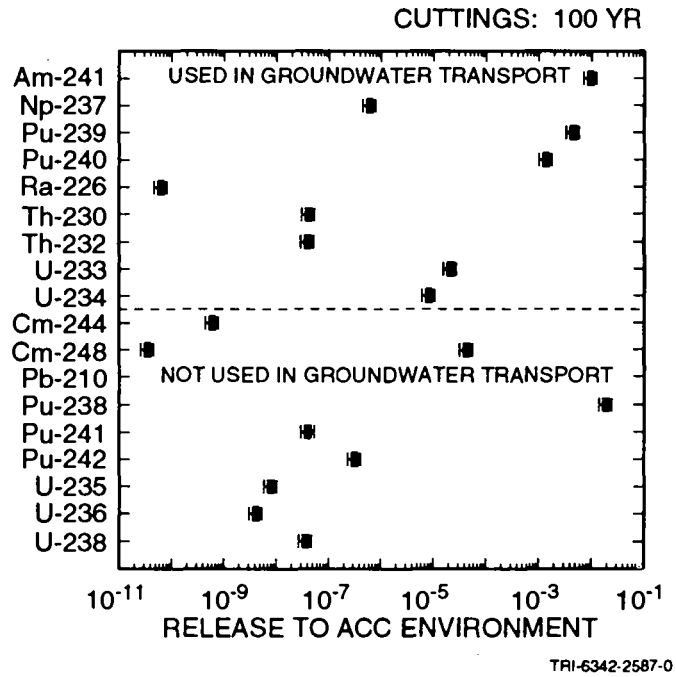

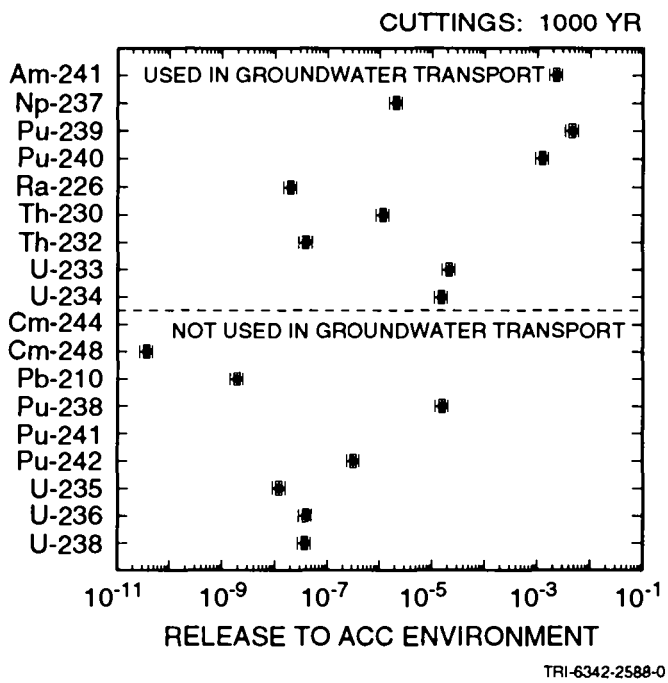

Figure 8.2-2. Normalized releases to the accessible environment for individual isotopes for cuttings removal resulting from a single borehole intersecting waste of average activity level at 100 yr and 1000 yr.

distributions of CCDFs that result for these two cases are shown in the two left frames of Figure 8.2-3; summaries based on mean and percentile curves are shown in the two right frames. Due to the use of a sample of size 70 in the 1992 WIPP performance assessment, the individual plots in Figure 8.2-3 are based on 70 CCDFs.

As examination of Figure 8.2-3 shows, the CCDFs for cuttings removal fall substantially below the EPA release limits. Further, the CCDFs constructed with the time-dependent rate terms obtained through an expert-review process fall below the CCDFs constructed with constant rate terms. As a reminder, the constant rate terms were obtained by generating a uniformly-distributed sample from the interval $[0, 3.75 \times 10^{-4}\ yr^{-1}]$, where $3.75 \times 10^{-4}\ yr^{-1}$ corresponds to the maximum drilling rate of 30 boreholes/km^2/10,000 yr specified by the EPA.

The variability in the CCDFs shown in Figure 8.2-3 is due primarily to uncertainty in the rate term in the Poisson model for drilling intrusions (i.e., in the function $\lambda(t)$ appearing in Eq. 2.3-1), with a small additional contribution from drillbit diameter (DBDIAM). Sensitivity analyses based on partial correlation analysis or regression analysis produce results similar to those shown in Figures 4.6-1 and 4.6-2 of Helton et al. (1992). In particular, there is a strong positive correlation between exceedance probability and the rate term in the Poisson model for drilling intrusions (LAMBDA), and a positive but less strong correlation between exceedance probability and drillbit diameter.

The steps appearing in the individual CCDFs in Figure 8.2-3 result from the discretization of the waste into five activity levels for the calculation of cuttings removal. The use of more activity levels would cause these steps to be eliminated but would not significantly alter the distributions of CCDFs for cuttings removal. Additional discussion of this pattern is provided in conjunction with Figure 4.6-3 of Helton et al. (1992).

8.3 Release to Culebra

Due to constraints imposed by computational cost, the 1992 WIPP performance assessment performed groundwater transport calculations only for intrusions occurring at 1000 yr. As discussed in Section 2.4 and in more detail in Chapters 4 and 5, the first step in these calculations is the use of the BRAGFLO model to determine time-dependent releases into the Culebra Dolomite. The integrated (i.e., total) values for these releases over 10,000 yr are summarized in Figure 8.3-1 for scenarios $S(1,0)$ and $S^{+-}(2,0)$, which

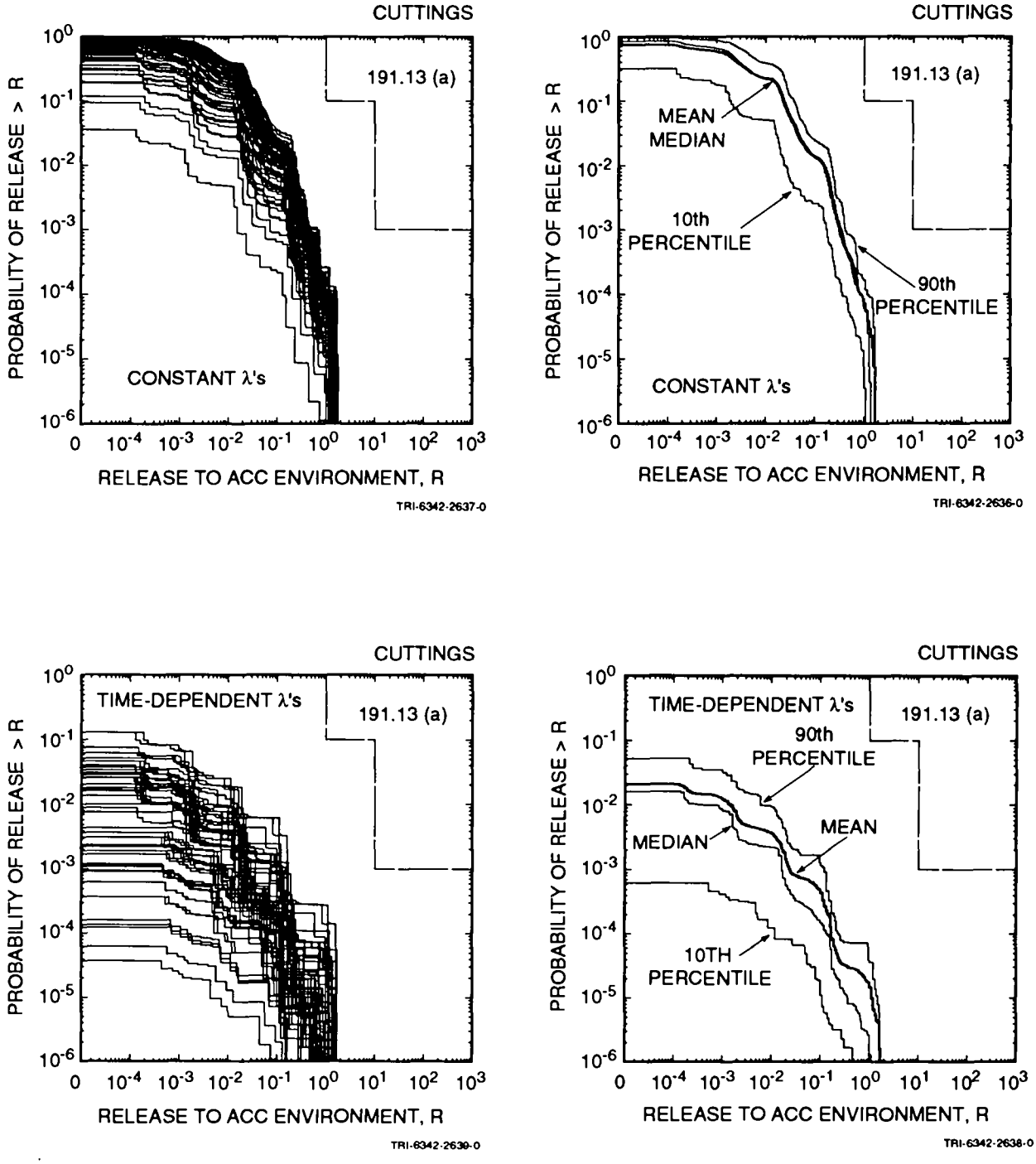

Figure 8.2-3. Distribution of CCDFs for normalized release to the accessible environment over 10,000 yr for cuttings removal constructed for the risk representation R_2 defined in Eq. 2.5-8 with constant (upper two frames) and time-dependent (lower two frames) rate terms in the Poisson model for drilling intrusions.

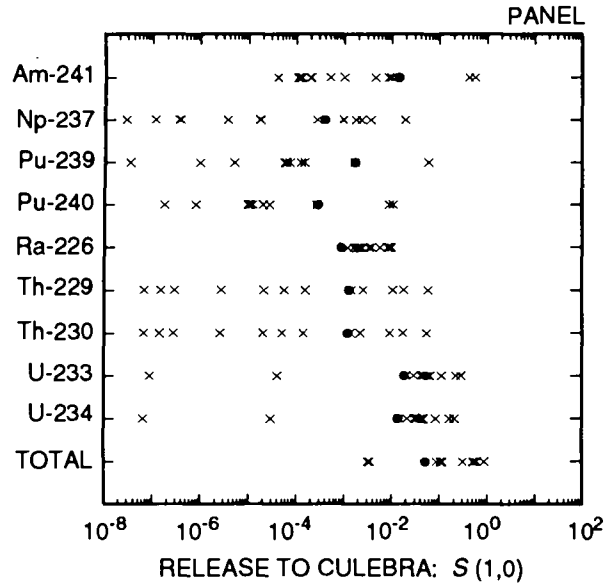

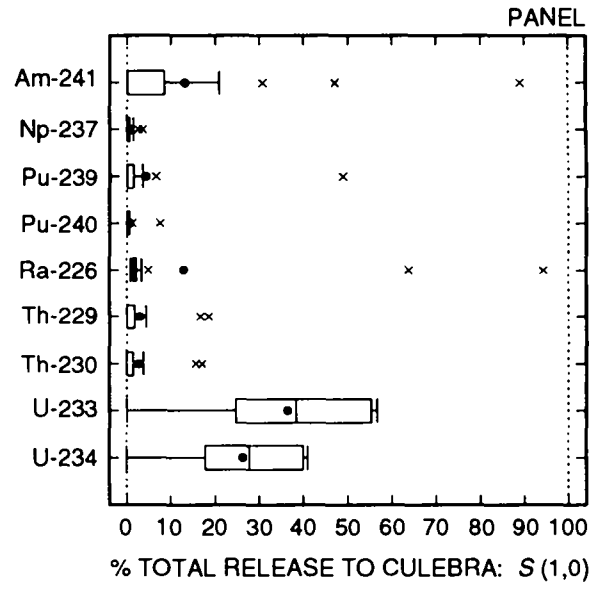

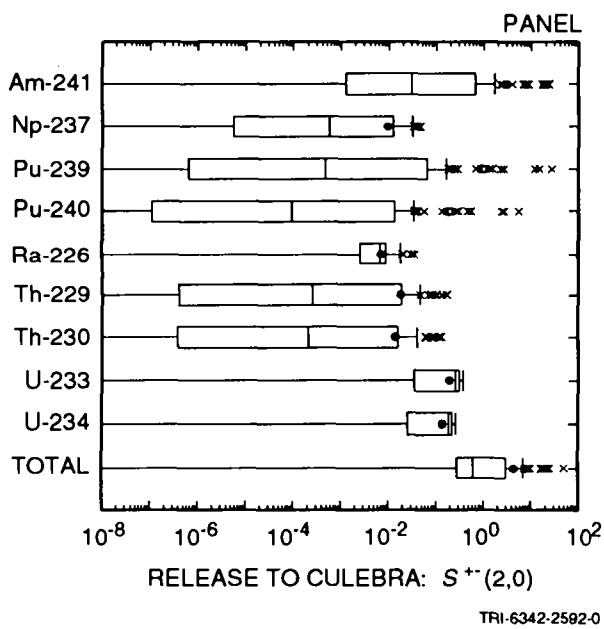

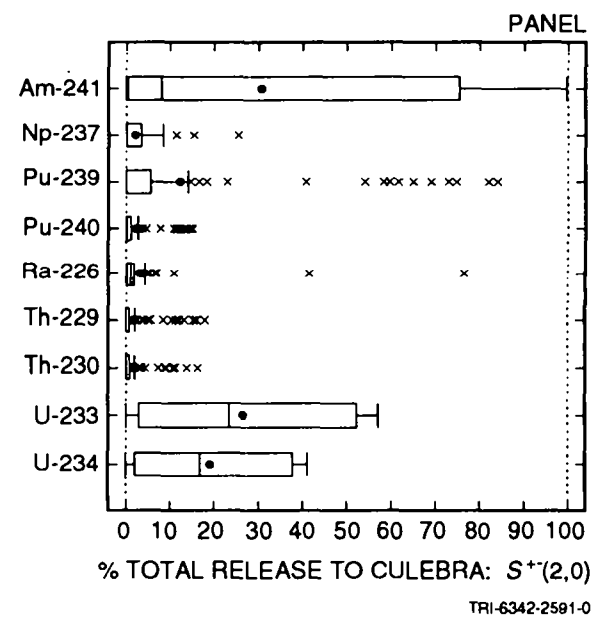

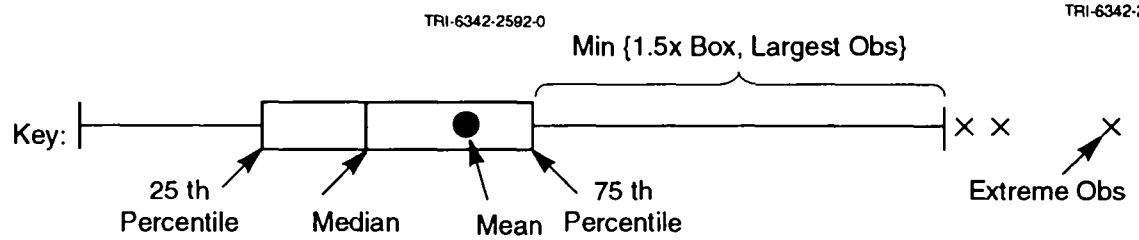

Figure 8.3-1. Normalized releases to the Culebra Dolomite over 10,000 yr due to groundwater transport for scenarios $S(1,0)$ and $S^{+-}(2,0)$ used in conjunction with the risk representation R_1 defined in Eq. 2.5-1 with intrusion occurring at 1000 yr.

are used in conjunction with the risk representation R_1 defined in Eq. 2.5-1 to develop CCDFs for normalized release to the accessible environment due to groundwater transport.

Only 14 of the 70 sample elements used in the analysis resulted in nonzero releases to the Culebra for scenario $S(1,0)$. Thus, the individual box plots in Figure 8.3-1 for scenario $S(1,0)$ are based on a maximum of 14 nonzero normalized releases. The total normalized release to the Culebra for scenario $S(1,0)$ is always less than 1, with the total release being dominated by U-233, U-234 and Am-241. As shown by the scatterplot in Figure 8.3-2, zero releases to the Culebra tend to be associated with the smaller values for Salado halite permeability (SALPERM). This pattern occurs because the repository fails to fill with brine for small values of SALPERM, with the result that there is no brine flow, and hence no radionuclide transport, up an intruding borehole.

In contrast to scenario $S(1,0)$, only two sample elements resulted in no release to the Culebra for scenario $S^{+-}(2,0)$. As examination of Figure 8.3-1 shows, half the sample elements have total normalized releases to the Culebra that exceed 0.6 EPA release units. Further, 9 sample elements have total normalized releases that exceed 10. As for scenario $S(1,0)$, the total release tends to be dominated by Am-241, U-233 and U-234, with Pu-239 also making a large contribution to the total release for some sample elements. The larger brine flows associated with scenario $S^{+-}(2,0)$ permit radionuclides with short half-lives to be transported out of the repository before they are lost due to radioactive decay. Because of this, Am-241 is a larger contributor to the total release for scenario $S^{+-}(2,0)$ than it is for scenario $S(1,0)$.

As shown in Table 8.3-1, stepwise regression analysis can be used to investigate which of the sampled variables listed in Table 3.1 dominate the uncertainty in the releases to the Culebra summarized in Figure 8.3-1 for scenario $S^{+-}(2,0)$. The results contained in Table 8.3-1 and other similar presentations in this report were calculated with the STEPWISE program (Iman et al., 1980) with rank-transformed data (Iman and Conover, 1979). The rationale for using rank-transformed data is that this transform enables the analysis to identify the extent to which variables tend to increase and decrease together, which is typically the question of interest in a sensitivity analysis. Further, use of the rank transform avoids some of the technical problems associated with other transforms (e.g., appropriately weighting outliers and the treatment of zeros).

For Am-241, the uncertainty in the integrated release to the Culebra is dominated by BHPERM (borehole permeability) and SOLAM (solubility for Am),

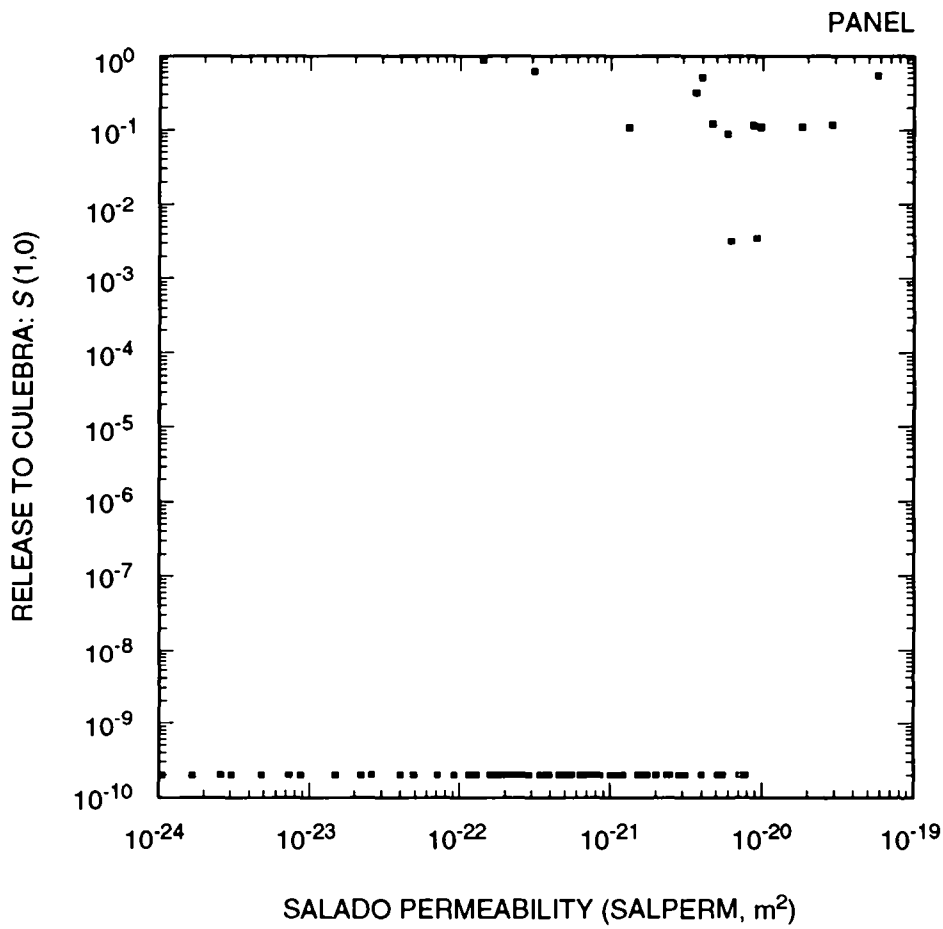

Figure 8.3-2. Scatterplot for total normalized release to the Culebra Dolomite over 10,000 yr versus Salado Permeability (SALPERM) for scenario $S(1,0)$ with intrusion occurring at 1000 yr.

Table 8.3-1. Stepwise Regression Analyses with Rank-Transformed Data for Integrated Release to the Culebra Dolomite over 10,000 yr for Scenario S^{+-}(2,0) with Intrusion Occurring 1000 yr after Repository Closure.

	Variable[a]	R^{2b}	Variable	R^2	Variable	R^2	Variable	R^2
Step[c]	Am-241		Np-237		Pu-239		Pu-240	
1	BHPERM	0.42(+)	SOLNP	0.75(+)	SOLPU	0.86(+)	SOLPU	0.86(+)
2	SOLAM	0.81(+)	BHPERM	0.90(+)	BHPERM	0.94(+)	BHPERM	0.94(+)
3	DBDIAM	0.83(+)			DBDIAM	0.95(+)	DBDIAM	0.95(+)
Step	Ra-226		Th-229		Th-230		U-233	
1	BHPERM	0.21(+)	SOLTH	0.77(+)	SOLTH	0.77(+)	BHPERM	0.41(+)
2	SOLTH	0.33(-)	BHPERM	0.89(+)	BHPERM	0.88(+)	SOLU	0.60(+)
Step	U-234		Total					
1	BHPERM	0.41(+)	BHPERM	0.48(+)				
2	SOLU	0.60(+)	SOLAM	0.60(+)				

[a]Variables listed in order of selection in regression analysis
[b]Cumulative R^2 value with entry of each variable into regression model, with "+" and "-" indicating positive and negative regression coefficients, respectively
[c]Steps in stepwise regression analysis

with the release tending to increase as each of these variables increases. These positive effects result because increasing BHPERM reduces resistance to flow up the boreholes and increasing SOLAM increases the amount of Am-241 that can be dissolved in brine. The regression model with BHPERM and SOLAM can account for 81% (i.e., R^2 = 0.81) of the variability in the Am-241 release to the Culebra. The release patterns that result in the selection of BHPERM and SOLAM in the regression analysis for Am-241 summarized in Table 8.3-1 are shown in Figure 8.3-3 for both log-transformed and rank-transformed data. The flattening associated with large values of SOLAM is due to inventory limits; as shown in Figure 7.3-1, the amount of Am-241 in one waste panel at 1000 yr is approximately 40 EPA release units. The regression analysis for Am-241 in Table 8.3-1 also indicates a small positive effect for DBDIAM (drillbit diameter), which results because increasing DBDIAM increases the diameter of the intruding boreholes and thus produces a larger area through which brine flow can take place.

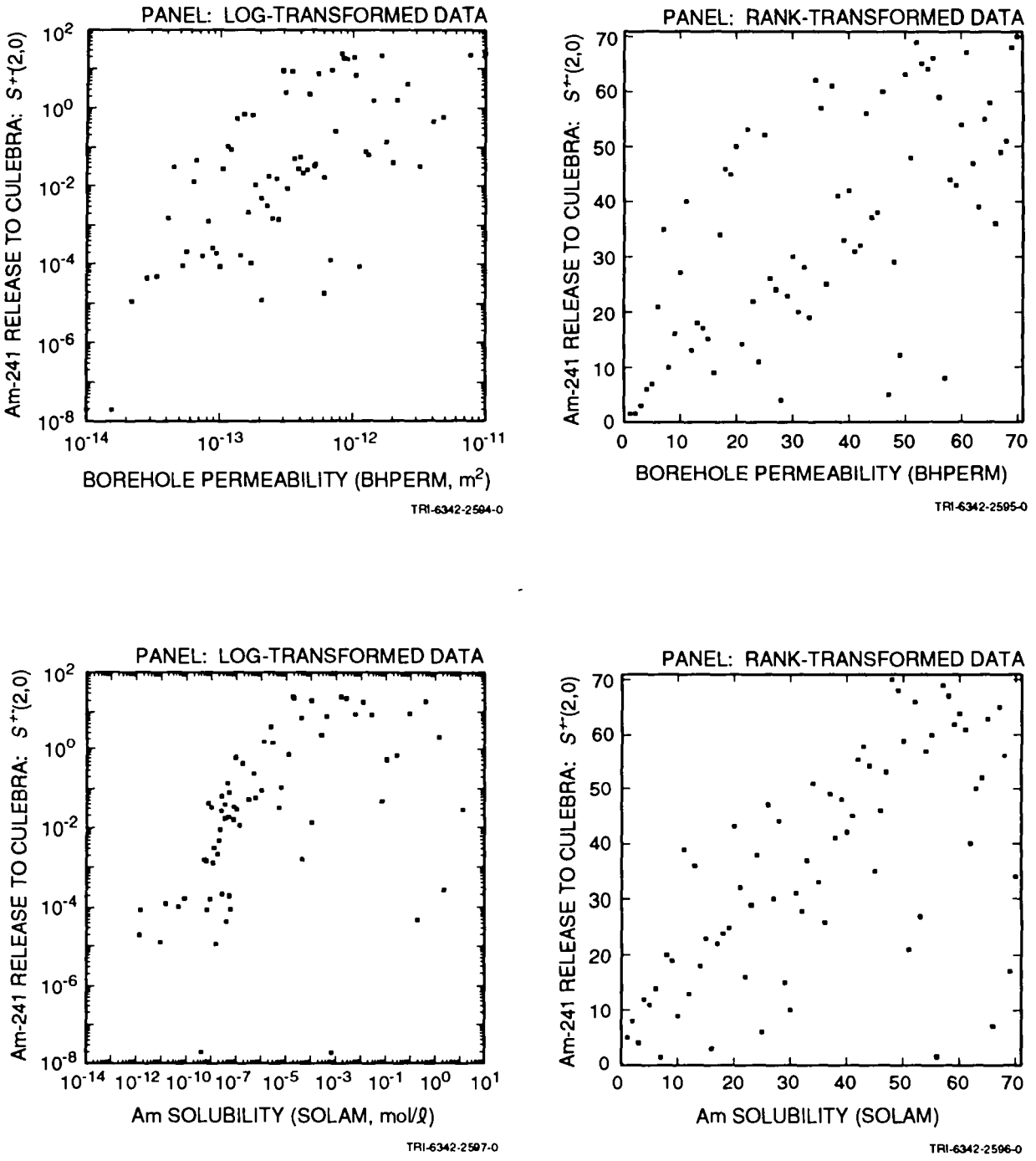

Figure 8.3-3. Scatterplots with log-transformed and rank-transformed data for normalized release of Am-241 to the Culebra Dolomite over 10,000 yr for variables BHPERM (borehole permeability) and SOLAM (solubility of Am) and scenario $S^{+-}(2,0)$ with intrusion occurring 1000 yr after repository closure.

The radionuclides Np-237, Pu-239, Pu-240, Th-229 and Th-230 show release patterns similar to those shown by Am-241, although the solubility limits (i.e., SOLNP, SOLPU, SOLTH) tend to be more important than borehole permeability (BHPERM). In the analysis for Am-241, solubility and borehole permeability were of approximately equal importance. This difference in importance for BHPERM results from the relatively short half-life of Am-241 (i.e., 432 yr), which makes reduced flow rates up an intruding borehole more important for Am-241 than for Np-237, Pu-239, Pu-240, Th-229 and Th-230 due to loss resulting from radioactive decay. As an example, the scatterplot for Pu-239 release to the Culebra versus SOLPU in Figure 8.3-4 shows less spread than the corresponding scatterplot for Am-241 in Figure 8.3-3. Also, the scatterplot for Pu-239 in Figure 8.3-4 does not suggest the presence of any effects due to inventory limitations as is the case for Am-241 in Figure 8.3-3.

The regression analysis for Ra-226 summarized in Table 8.3-1 is not very successful, with two variables selected and an R^2 value of only 0.33. In particular, the analysis indicates that the release of Ra-226 to the Culebra tends to increase as BHPERM (borehole permeability) increases and tends to decrease as SOLTH (solubility of Th) increases. The patterns that give rise to these selections are shown in the scatterplots in Figure 8.3-5 with both log-transformed and rank-transformed data. The positive effect indicated for BHPERM in Table 8.3-1 and Figure 8.3-5 results because increasing BHPERM increases brine flow out the intruding boreholes, and the negative effect indicated for SOLTH results because increasing SOLTH increases the amount of Th-230 removed from the waste panel and thus decreases the amount of Ra-226 that will be produced within the panel by radioactive decay. The solubility limit for radium (SOLRA) is assigned a high range of values (i.e., 2 to 18.2 mol/L). As a result, all available Ra-226 goes into solution, and thus SOLRA does not show up as an important variable in the regression analysis for Ra-226 release to the Culebra. As examination of the box plots for Ra-226 in Figure 8.3-1 and the range of Ra-226 releases on the coordinates in Figure 8.3-5 shows, the high values for SOLRA result in a smaller range of release values for Ra-226 than is the case for the other isotopes considered in this study due to a complete removal of the available Ra-226.

The scatterplots in Figure 8.3-5 suggest that a regression analysis with log-transformed data may indicate a stronger relationship between Ra-226 release to the Culebra and the variables BHPERM (borehole permeability) and SOLTH (solubility of Th) than was observed with rank-transformed data. The two sample elements with zero release to the Culebra were dropped from the analysis and the remaining 68 sample elements were used in a regression analysis with log-transformed data. This produced the regression model

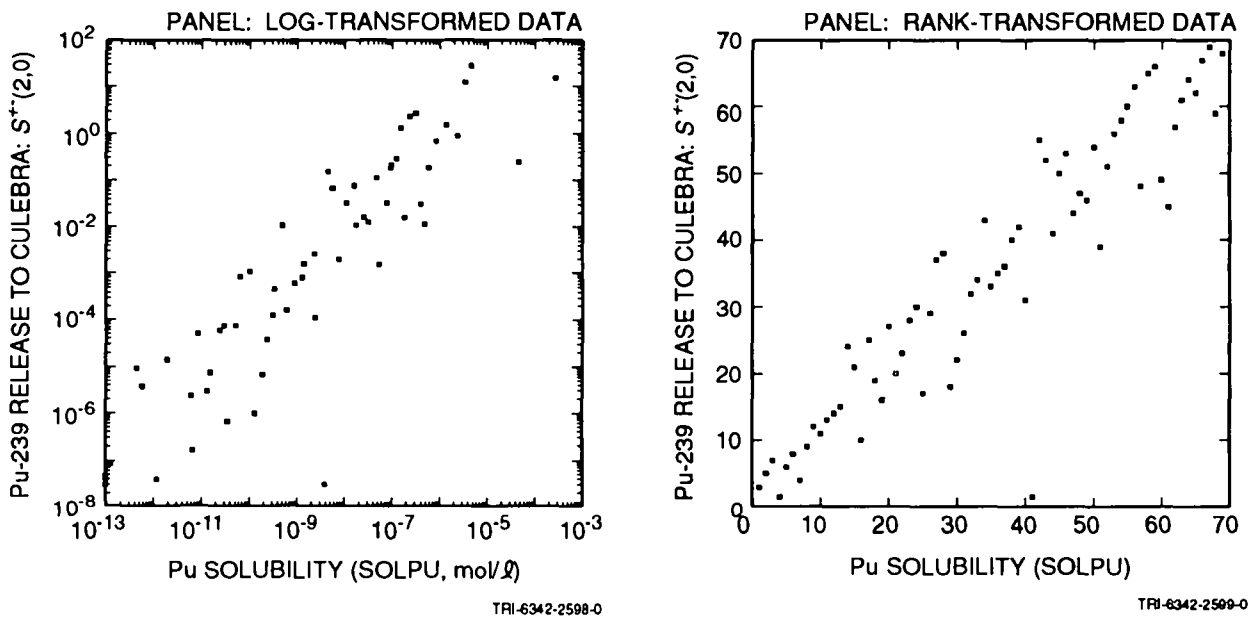

Figure 8.3-4. Scatterplots with log-transformed and rank-transformed data for normalized release of Pu-239 to the Culebra Dolomite over 10,000 yr versus plutonium solubility (SOLPU) for scenario $S^{+-}(2,0)$ with intrusion occurring 1000 yr after repository closure.

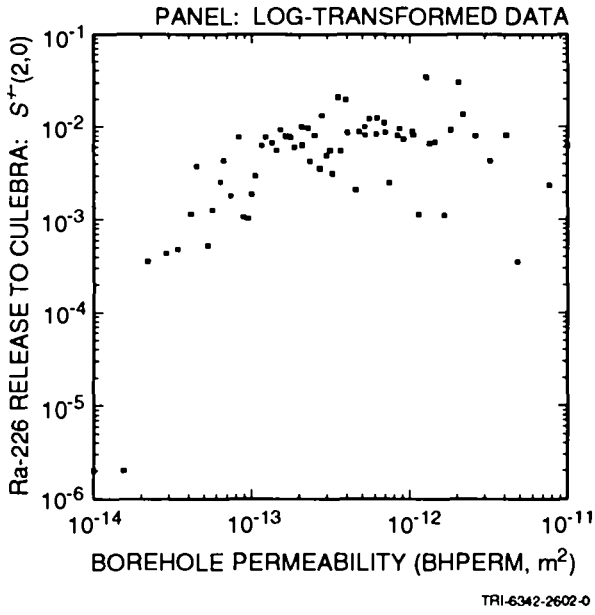

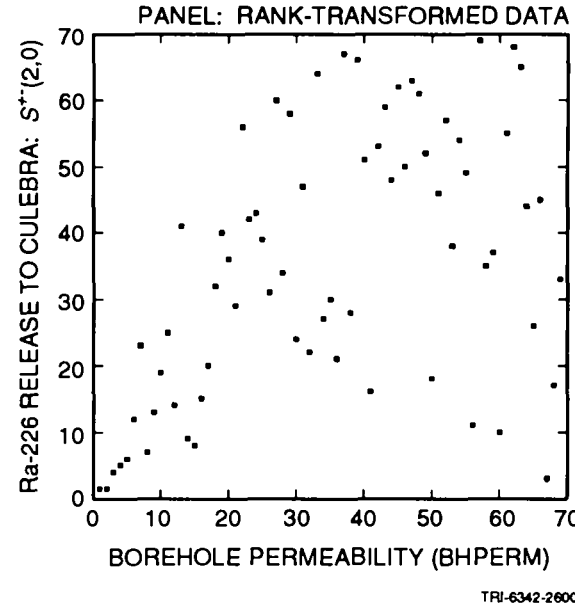

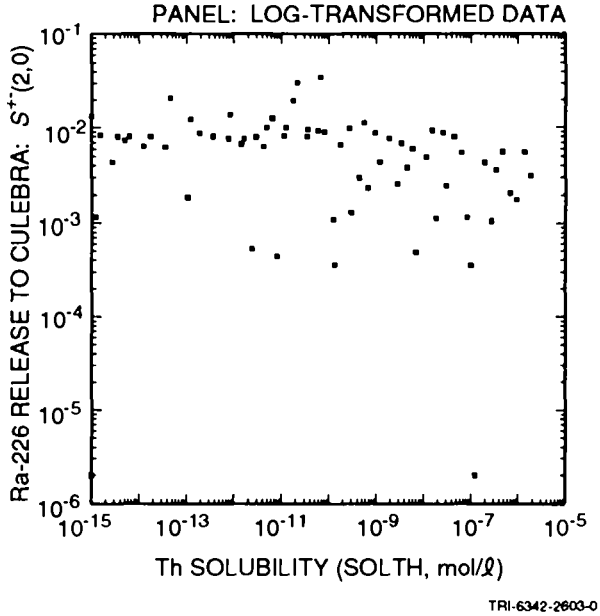

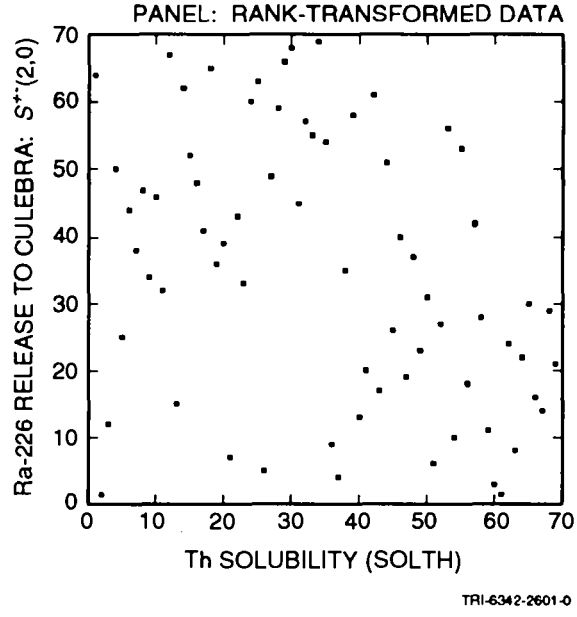

Figure 8.3-5. Scatterplots with log-transformed and rank-transformed data for normalized release of Ra-226 to the Culebra Dolomite over 10,000 yr for variables BHPERM (borehole permeability) and SOLTH (solubility of Th) and scenario $S^{+-}(2,0)$ with intrusion occurring 1000 yr after repository closure.

$$\log y = 0.762 + 0.289 \log \text{BHPERM} - 0.052 \log \text{SOLTH}, \quad R^2 = 0.24 \qquad (8.3\text{-}1)$$

where y is the normalized release of Ra-226 to the Culebra. Thus, the use of log-transformed data does not improve the regression results for Ra-226 (i.e., R^2 = 0.33 with rank-transformed data and R^2 = 0.24 with log-transformed data).

The regression analyses for U-233 and U-234 summarized in Table 8.3-1 produce similar results, with release tending to increase as BHPERM (borehole permeability) and SOLU (solubility for U) increase. However, the regressions with these two variables have R^2 values of only 0.60. Scatterplots for U-233 release to the Culebra versus BHPERM and SOLU are shown in Figure 8.3-6. The lines of approximately equal releases across the tops of these scatterplots correspond to the U-233 inventory in a single waste panel (i.e., approximately 0.4 EPA release units as shown in Figure 7.3-1). A similar pattern also occurs in the corresponding scatterplots for U-234. Thus, the larger values for both BHPERM and SOLU result in a complete removal of U-233 and U-234 from the waste panel, which creates a pattern that is not well-captured by the regression techniques in use. Similar behavior was also observed for U-233 and U-234 in the 1991 WIPP performance assessment (e.g., see Helton et al., 1992, Figures 4.5-2 and 5.1-6).

The last regression analysis summarized in Table 8.3-1 is for the total normalized release to the Culebra. This analysis indicates that the total release tends to increase as each of BHPERM (borehole permeability) and SOLAM (solubility for Am) increases. The regression model with these two variables has an R^2 value of 0.60, which is not particularly good. As shown in Figure 8.3-1, U-233 and U-234 are important contributors to total release. Thus, the low R^2 value in the regression analysis for total release is due in part to the inventory-related patterns shown in Figure 8.3-6 for U-233 and similar patterns for U-234.

The radionuclide releases to the Culebra analyzed in Table 8.3-1 result from brine flow up the two intruding boreholes associated with scenario S^{+-} (2,0). These flows are summarized in Figure 5.2-16. The uncertainty in the cumulative brine flow to the Culebra shown in Figure 5.2-16 results from the uncertainty in the following 21 variables contained in Table 3-1: BHPERM, BPPRES, BPSTOR, BRSAT, BCBRSAT, BCEXP, BCFLG, BCGSSAT, DBDIAM, GRCORHF, GRCORI, GRMICHF, GRMICI, MBPERM, MBPOR, SALPERM, SALPRES, STOICCOR, STOICMIC, VMETAL AND VWOOD. The PCCSRC program (Iman et al., 1985) can be used to determine which of the sampled variables dominates the uncertainty in the cumulative brine flows shown in Figure 5.2-16. In particular, PCCSRC can be used to calculate the partial rank correlation coefficients (PRCCs) between the cumulative brine flow appearing above fixed times on the abcissa

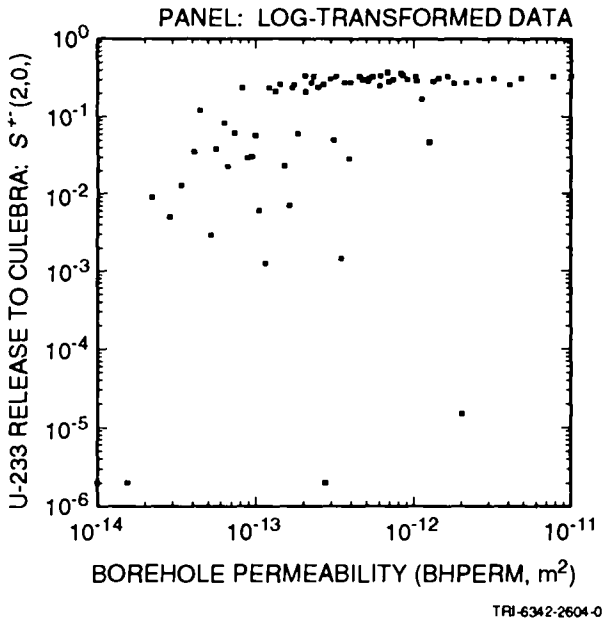

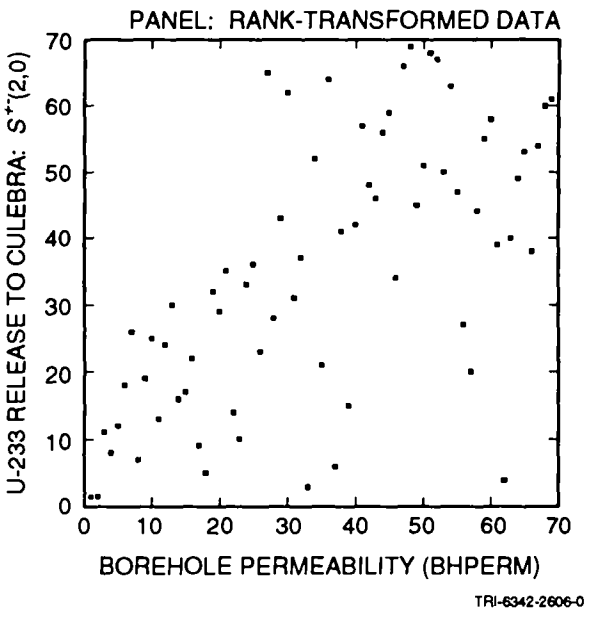

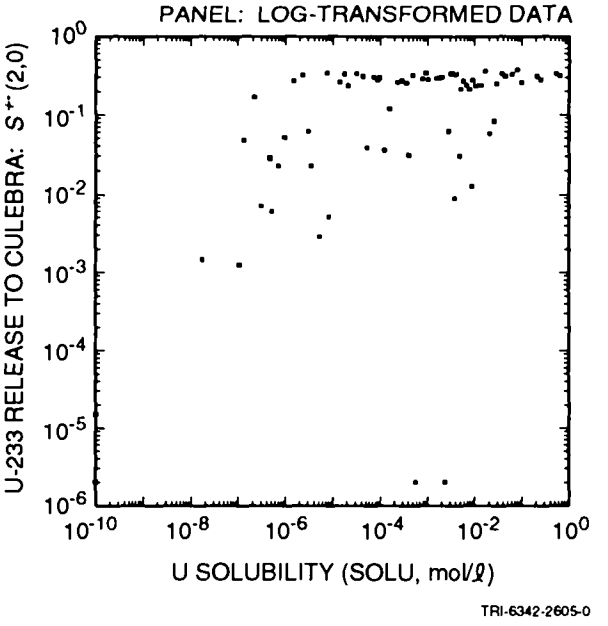

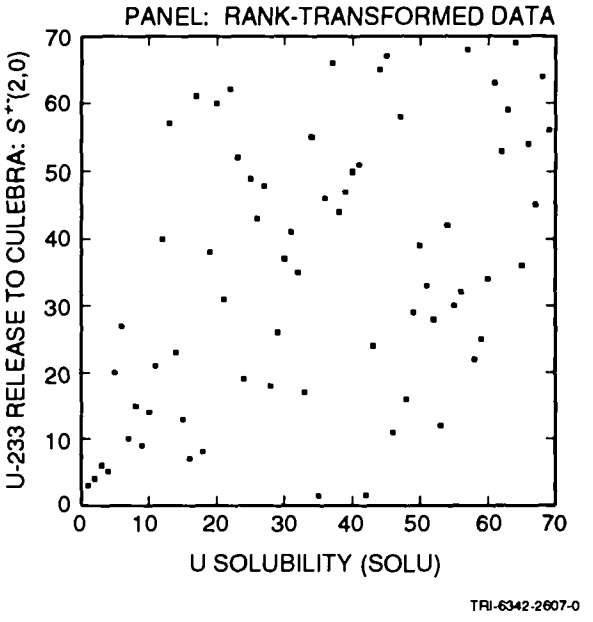

Figure 8.3-6. Scatterplots with log-transformed data and rank-transformed data for normalized release of U-233 to the Culebra Dolomite over 10,000 yr for variables BHPERM (borehole permeability) and SOLU (solubility of U) for scenario $S^{+-}(2,0)$ with intrusion occurring 1000 yr after repository closure.

and the previously indicated variables in Table 3-1. The values for these PRCCs can be plotted above the corresponding times and then connected to form continuous curves. As shown in Figure 8.3-7, the most important variables identified in this analysis are BHPERM (borehole permeability), DBDIAM (drillbit diameter) and BPPRES (brine pocket pressure), with cumulative brine flow tending to increase as each of these variables increases. These positive effects result because increasing BHPERM reduces the resistance to brine flow in the intruding boreholes, increasing DBDIAM increases the diameter of the intruding boreholes, and increasing BPPRES increases brine pressure within the waste panel. A small negative effect is also indicated for GRCORI (gas-generation rate for corrosion of steel under inundated conditions) between 1500 and 3000 yr, although GRCORI appears to have little or no effect on cumulative brine flow at later times. This pattern probably results from the effect of GRCORI in reducing the amount of brine in the waste at the assumed intrusion time of 1000 yr, with the result that more brine is required to enter the repository before flow up the boreholes can commence than might be the case otherwise. As indicated by PRCCs of approximately one, BHPERM is the most important variable with respect to the uncertainty in brine flow.

Stepwise regression analysis can also be used to investigate brine flow out of a waste panel through the intruding boreholes associated with scenario $S^{+-}(2,0)$. In particular, a stepwise regression analysis for cumulative brine flow over 10,000 yr (i.e., for the cumulative brine flows appearing above 10,000 yr in Figure 5.2-16 is presented in Table 8.3-2. As previously indicated by the PRCCs in Figure 8.3-7, BHPERM (borehole permeability) is the dominant variable with an R^2 value of 0.94. Further, the addition of DBDIAM (drillbit diameter), BPPRES (brine pocket pressure) and BPSTOR (brine pocket storativity) results in a regression model with an R^2 value of 0.99. These results indicate that brine flow is dominated by variables affecting borehole properties (BHPERM, DBDIAM), with small additional effects coming from variables that define brine pocket properties (BPPRES, BPSTOR). The relationship between BHPERM and cumulative brine flow is shown in the scatterplot in Figure 8.3-8.

For a given set of analysis input, the risk representation R_1 defined in Eq. 2.5-1 leads to a single CCDF for release to the Culebra. The 1992 WIPP performance assessment considered the following 29 imprecisely known variables defined in Table 3-1 that affect the CCDF for release to the Culebra: BHPERM, BPPRES, BPSTOR, BPAREAFR, BRSAT, BCBRSAT, BCEXP, BCFLG, BCGSSAT, DBDIAM, GRCORHF, GRCORI, GRMICHF, GRMICI, LAMBDA, MBPERM, MBPOR, SALPERM, SALPRES, SOLAM, SOLNP, SOLPU, SOLRA, SOLTH, SOLU, STOICCOR, STOICMIC, VMETAL and VWOOD. As discussed in Section 2.1, the uncertainty in

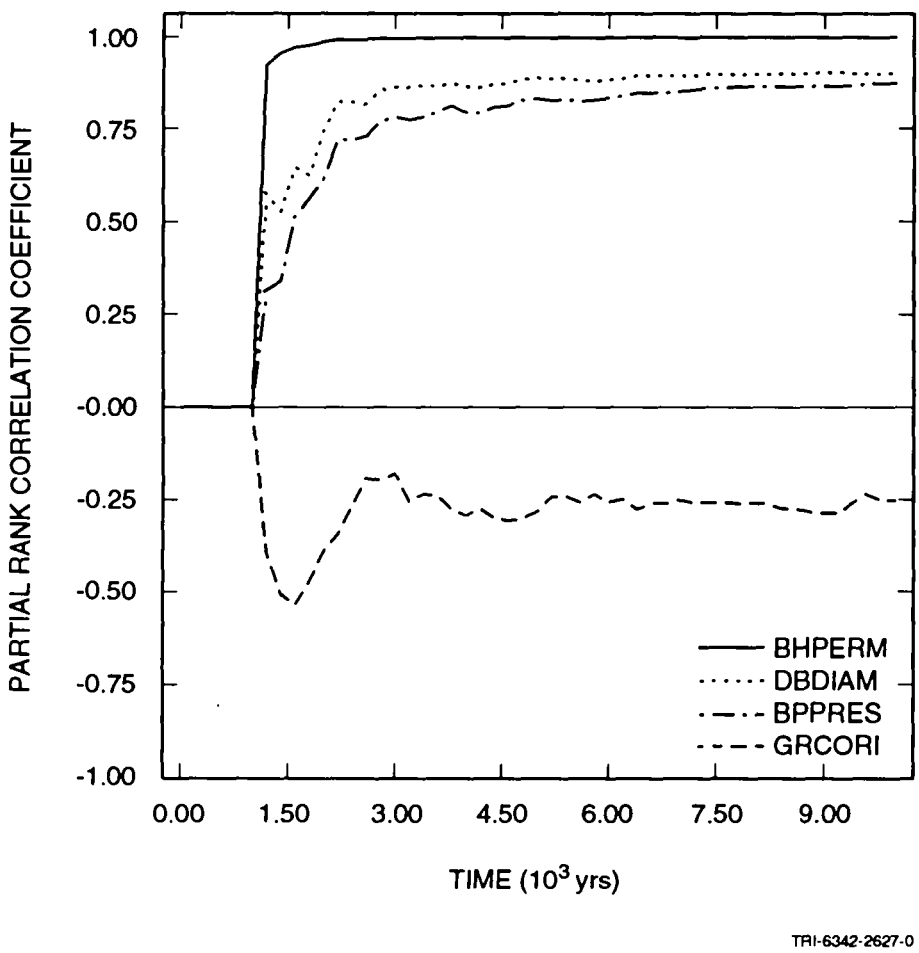

Figure 8.3-7. Partial rank correlation coefficients for cumulative flow of brine into a borehole over 10,000 yr for scenario $S^{+-}(2,0)$ with intrusion occurring at 1000 yr.

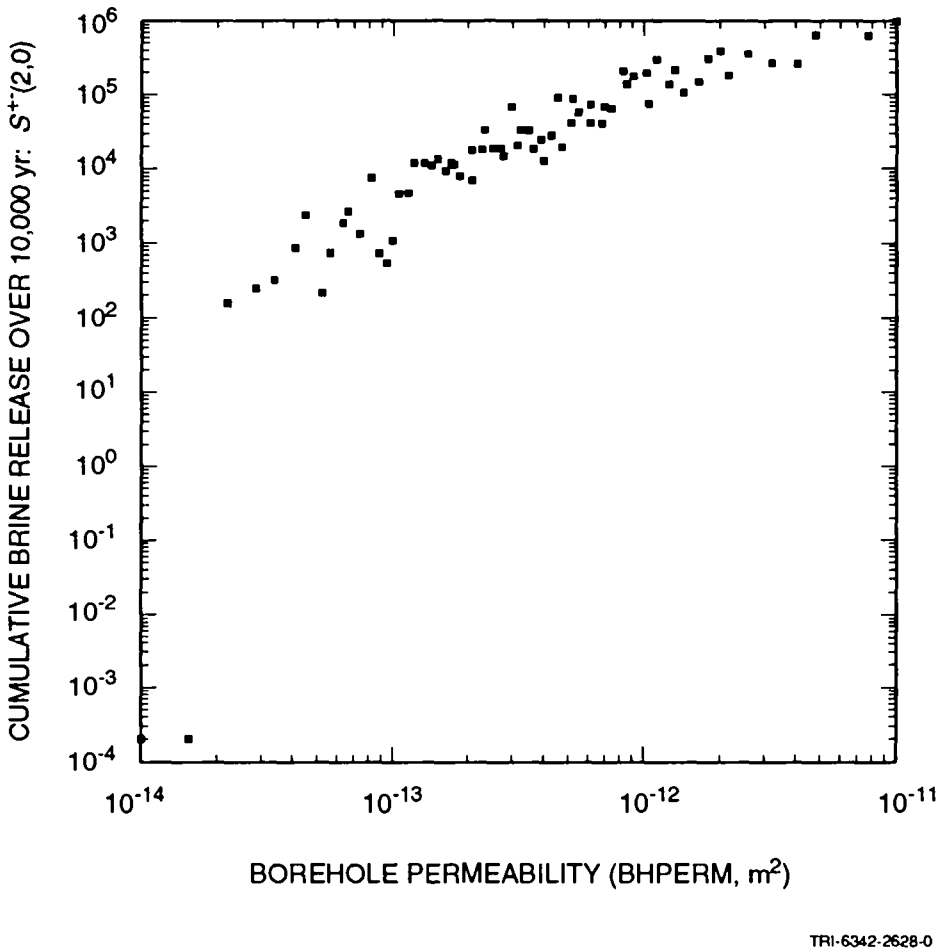

Figure 8.3-8 Scatterplot for borehole permeability (BHPERM, m^2) and volume of brine (m^3) released into a borehole over 10,000 yr for Scenario $S^{+-}(2,0)$ with intrusion occurring at 1,000 yr.

Table 8.3-2 Stepwise Regression Analysis with Rank-Transformed Data for Cumulative Flow of Brine into a Borehole Over 10,000 yr for Scenario S^{+-}(2,0) with Intrusion at 1,000 years.

Steps[a]	Variable[b]	R^2 [c]
1	BHPERM	0.94 (+)
2	DBDIAM	0.97 (+)
3	BPPRES	0.99 (+)
4	BPSTOR	0.99 (+)

[a]Steps in stepwise regression analysis
[b]Variables listed in order of selection in regression analysis
[c]Cumulative R^2 value with entry of each variable into regression model, with "+" and "-" indicating positive and negative regression coefficients, respectively

these variables leads to a distribution of CCDFs. As previously noted in the discussion of cuttings releases, two cases were considered in the analysis for the rate term (i.e., λ) in the Poisson model for drilling intrusions: constant rate terms and time-dependent rate terms. The distribution of CCDFs that result for these two cases are shown in the two left frames of Figure 8.3-9; further, summaries based on mean and percentile curves are shown in the two right frames. Because a sample size of 70 is used in the 1992 WIPP performance assessment, the individual plots in Figure 8.3-9 are based on 70 CCDFs.

As examination of the upper two frames in Figure 8.3-9 shows, the use of constant-valued rate terms in the Poisson model for drilling intrusions results in most CCDFs falling below the EPA release limits. Further, the mean and percentile curves also fall beneath the EPA release limits, although both the mean and 90^{th} percentile curves come close to intercepting the release limit at the (10, 0.001) point. As shown in the two lower frames in Figure 8.3-9, the use of time-dependent rate terms in the Poisson model for drilling intrusions produces CCDFs that are shifted down from those obtained with constant-valued rate terms. In particular, the mean and 90^{th} percentile curves obtained with time-dependent rate terms fall approximately two orders of magnitude below the corresponding curves obtained with constant-valued rate terms. Due to the skewed nature of the distributions shown in Figure 8.3-9 and other similar figures, it is possible for parts of the mean curve to be located above the 90^{th} percentile curve. Such behavior occurs when a distribution has a few very large values and many small values.

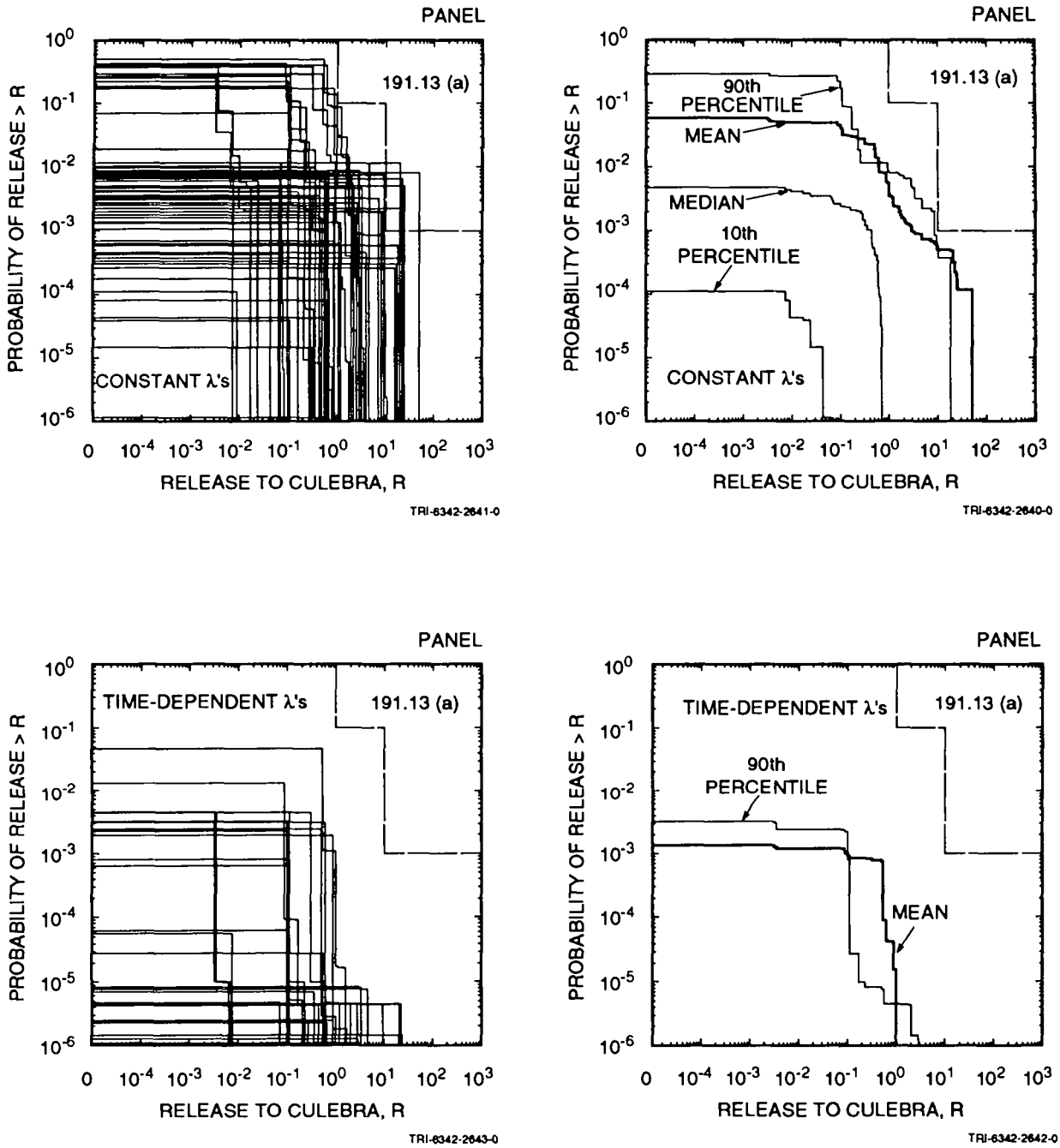

Figure 8.3-9. Distribution of CCDFs for normalized release to the Culebra Dolomite over 10,000 yr constructed for the risk representation R_1 defined in Eq. 2.5-1 with constant (upper two frames) and time-dependent (lower two frames) rate terms in the Poisson model for drilling intrusions. As the release under consideration is to the Culebra, the CCDFs shown in this figure are not the CCDFs used for comparison with the bounds given in 40 CFR 191, Subpart B.

As discussed in conjunction with Figure 8.3-7, the PCCSRC program (Iman et al., 1985) can be used to determine which of the sampled variables dominates the uncertainty in the CCDFs shown in the upper left frame of Figure 8.3-9. In particular, PCCSRC can be used to calculate PRCCs between the exceedance probabilities appearing above fixed release values on the abcissa and the variables in Table 3.1. The values for these PRCCs can be plotted above the corresponding release values and then connected to form continuous curves. As shown in Figure 8.3-10, the three most important variables identified in this analysis were LAMBDA (rate constant in Poisson model for drilling intrusions), BHPERM (borehole permeability), and SOLAM (solubility for Am). No other variables were identified as having a substantial effect on the indicated distribution of CCDFs. The variable LAMBDA defines the probability of having one or more drilling intrusions and hence controls the initial horizontal section of the CCDFs. The variables BHPERM and SOLAM control the size of releases and hence determine how far the individual CCDFs extend to the right before they drop to the abcissa.

The two lower plots in Figure 8.3-9 were generated with the same releases to the Culebra as the upper two plots but with time-dependent rather than constant rate terms in the Poisson model for drilling intrusions. Thus, the downward shift of the CCDFs associated with the two lower frames is indicative of the impact of the time-dependent rate terms developed in an expert review process as part of the WIPP performance assessment (Hora et al., 1991; memorandum by Hora in Appendix A, pp. A-69 to A-99, in Volume 3 of this report).

8.4 Groundwater Transport to Accessible Environment

As indicated in Table 8.4-1, seven alternative modeling assumptions for radionuclide transport in the Culebra were evaluated. Transport results without chemical retardation are presented in Sections 8.4.1 and 8.4.5 and transport results with chemical retardation are presented in Sections 8.4.2, 8.4.3 and 8.4.4. The results in Section 8.4.1 are for no chemical retardation, no clay lining in fractures and no matrix diffusion, with the result that releases to the Culebra are transported unimpeded to the accessible environment. This is believed to be the most conservative set of assumptions for modeling radionuclide transport in the Culebra. Several variants on the assumption of no chemical retardation are presented in Section 8.4.5. The most important of these variants assumes diffusion into the Dolomite matrix and thus illustrates the effect of physical retardation (i.e., retardation in the Dolomite matrix) in the absence of chemical retardation. The analyses in Sections 8.4.2, 8.4.3 and 8.4.4 with chemical retardation illustrate the effects of assuming fracture only (i.e., no matrix

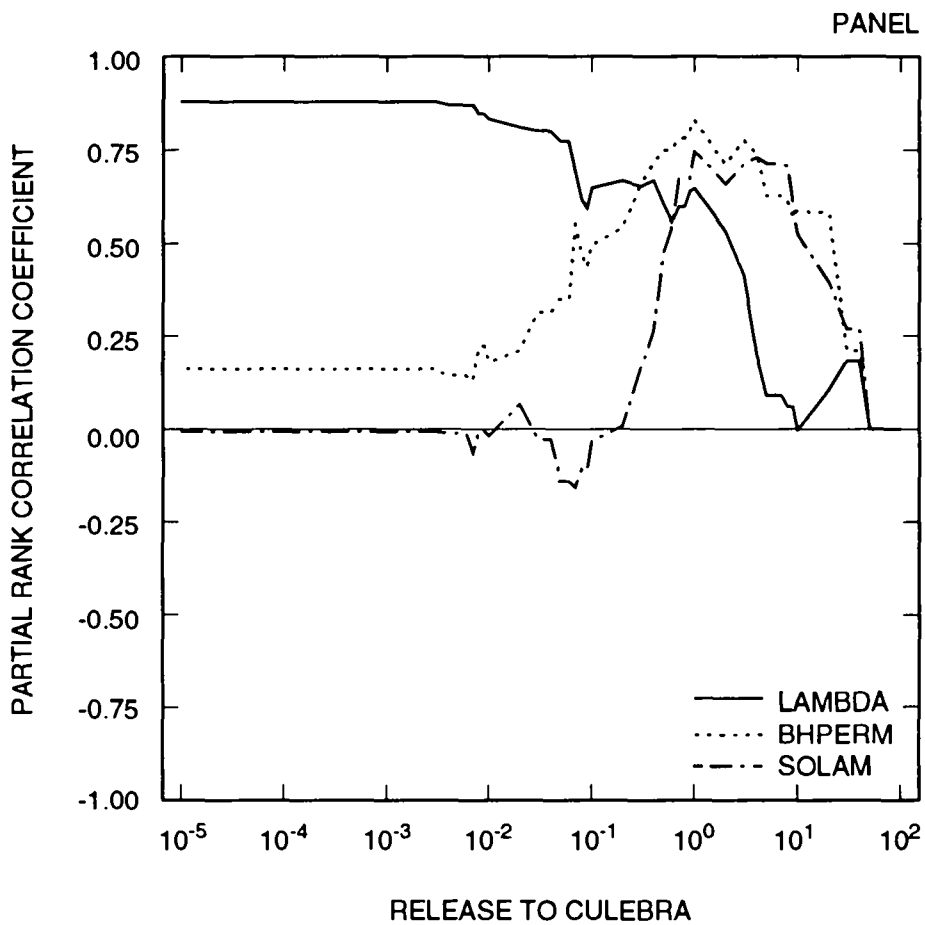

Figure 8.3-10. Partial rank correlation coefficients for exceedance probabilites associated with individual CCDFs in Figure 8.3-9 for release to the Culebra Dolomite with constant rate terms in the Poisson model for drilling intrusions.

Table 8.4-1. Alternative Modeling Assumptions for Radionuclide Transport in the Culebra Dolomite.

Section	Chemical Retardation	Clay Lining in Fractures	Matrix Diffusion	Comment
8.4.1	-	-	-	No chemical sorption and no movement to dolomite matrix. Illustrates most conservative modeling assumptions.
8.4.2	+	+	-	Chemical sorption in fractures only and no movement of dolomite matrix. Illustrates transport in fractures only.
8.4.3	+	-	+	Chemical sorption in dolomite matrix only.
8.4.4	+	+	+	Chemical sorption in fractures and dolomite matrix. Believed to be most realistic case.
8.4.5	-	+	-	No chemical sorption and no movement to dolomite matrix.
8.4.5	-	-	+	No chemical sorption with movement to dolomite matrix. Illustrates physical retardation in dolomite matrix.
8.4.5	-	+	+	No chemical sorption with movement to dolomite matrix.

diffusion) and dual porosity (i.e., diffusion into the dolomite matrix) transport. The case in Section 8.4.4 with chemical retardation in both the fractures and the dolomite matrix is believed by the WIPP performance assessment project to be the most appropriate model for radionuclide transport in the Culebra.

8.4.1 No Chemical Retardation, No Clay in Fractures, No Matrix Diffusion

This section presents results calculated with the assumptions that all fluid flow within the Culebra takes place in fractures, no clay is present in the fractures, and no chemical retardation occurs within the fractures. Thus, radionuclides released into the Culebra are transported unimpeded to the accessible environment. As shown by the scatterplot in Figure 8.4-1, these assumptions result in the releases to the accessible environment being essentially identical to the releases to the Culebra. Thus, the discussions in Section 8.3 for release to the Culebra also apply to release to the accessible environment for no chemical retardation and no matrix diffusion. In particular, the distribution of CCDFs for release to the accessible environment due to groundwater transport with no chemical retardation, no clay and no matrix diffusion are visually indistinguishable from those appearing in Figure 8.3-9 for release to the Culebra.

8.4.2 Chemical Retardation, Clay-Lined Fractures, No Matrix Diffusion

This section presents results calculated with the assumptions that all fluid flow within the Culebra takes place in fractures and that these fractures are lined with clay that can sorb radionuclides. The variable CULCLYF (clay-filling fraction in Culebra) determines the total thickness of the clay lining in fractures in the Culebra Dolomite. As indicated in Table 3-1 and Figure 3-1, this variable was assigned a distribution in the 1992 WIPP performance assessment that implies with a certain degree of belief (i.e., 0.5) that no fractures in the Culebra have a clay lining. As the purpose of this section is specifically to investigate the effects of clay-lined fractures, only calculations performed for the 35 sample elements that have a non-zero value for CULCLYF will be considered. The calculations performed for the 35 sample elements in which CULCLYF = 0 produce results identical to the results obtained for these sample elements in the calculations for Section 8.4.1.

The scatterplot in Figure 8.4-2 provides a comparison of releases to the accessible environment calculated with and without a clay lining in the fractures. The significance of the presence of a clay lining is that

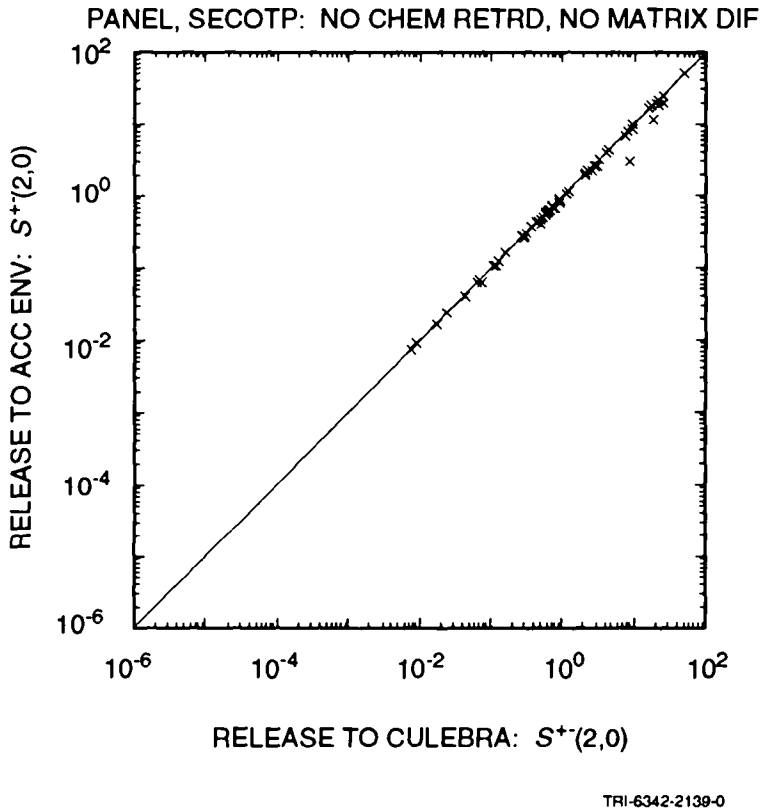

Figure 8.4-1. Scatterplot for total normalized release to Culebra over 10,000 yr versus total normalized release to the accessible environment due to groundwater transport with no chemical retardation and no matrix diffusion for scenario $S^{+-}(2,0)$ used in conjunction with the risk representation R_1 defined in Eq. 2.5-1 with intrusion occurring at 1000 yr after repository closure.

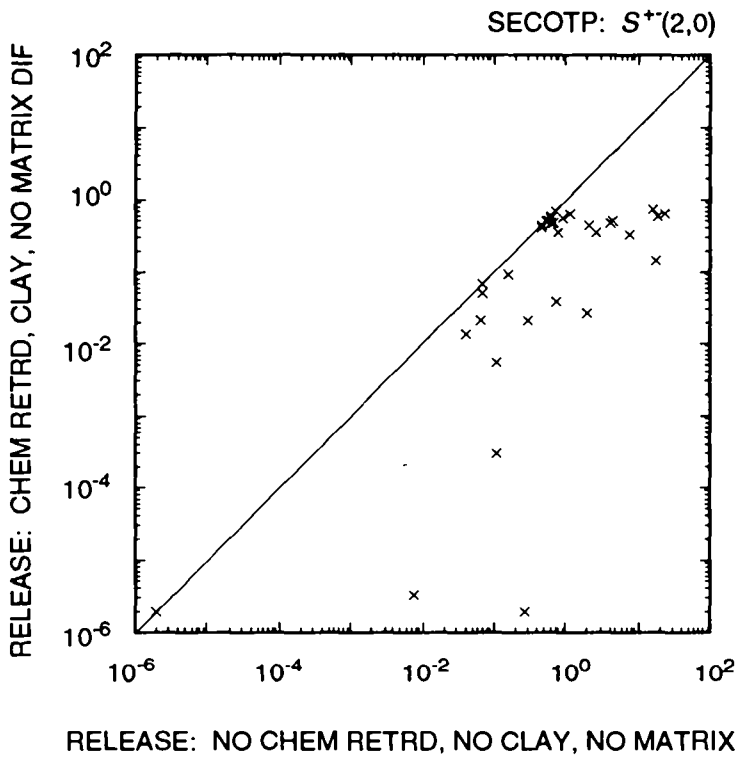

Figure 8.4-2. Scatterplot for total normalized release to the accessible environment over 10,000 yr due to groundwater transport with no chemical retardation and no matrix diffusion versus total normalized release to the accessible environment over 10,000 yr due to groundwater transport with chemical retardation, clay-lined fractures and no matrix diffusion for scenario $S^{+-}(2,0)$ used in conjunction with the risk representation R_1 defined in Eq. 2.5-1 with intrusion occurring 1000 yr after repository closure.

chemical retardation takes place in the presence of clay-lined fractures but is assumed not to take place in the absence of a clay lining in the fractures. As indicated in the preceding paragraph, this scatterplot is based on the 35 sample elements for which CULCLYF $\neq$ 0. The large number of points falling below the diagonal line in Figure 8.4-2 indicate that the presence of a clay lining in fractures has the potential to reduce releases from those that would be obtained without a clay lining. This reduction is due to radionuclide sorption.

As shown by the box plots in Figure 8.4-3, the releases to the accessible environment for this case are dominated by U-234 and U-233, with additional contributions from Np-237, Th-230 and Th-229. In contrast, the corresponding release to the accessible environment in the absence of clay-lined fractures is dominated by Am-241, with lesser contributions from Pu-239, U-233 and U-234 (i.e., see Figure 8.3-1 and discussion in Section 8.4.1).

As indicated by the scatterplot in Figure 8.4-4 for U-233, the entire uranium release to the Culebra is transported to the accessible environment over the 10,000-yr period under consideration for most sample elements. A more extensive reduction between release to the Culebra and release to the accessible environment is shown by the scatterplot for Np-237. This difference in behavior results from the fracture distribution coefficients (FKDU and FKDNP) assigned to uranium and neptunium, which have median values of 0.001 and 1 m^3/kg, respectively. The points in Figure 8.4-4 that indicate that the Np-237 release to the accessible environment exceeds the Np-237 release to the Culebra result from the decay of Am-241 to Np-237 within the Culebra. As shown by the scatterplot in Figure 8.4-5, the releases of Np-237 to the accessible environment are zero for values of FKDNP above 0.1 m^3/kg. The higher fracture distribution coefficients assigned to americium and plutonium result in essentially no Am-241, Pu-239 and Pu-240 being transported to the accessible environment. Radium and thorium display patterns intermediate to those displayed by uranium and neptunium.

As shown in Figure 8.4-6, the CCDFs for release to the accessible environment generated for groundwater transport with chemical retardation, clay-lined fractures, no matrix diffusion and constant rate terms in the Poisson model for drilling intrusions fall below the EPA release limits. Further, these CCDFs are shifted down and to the left when time-dependent rate terms are used.

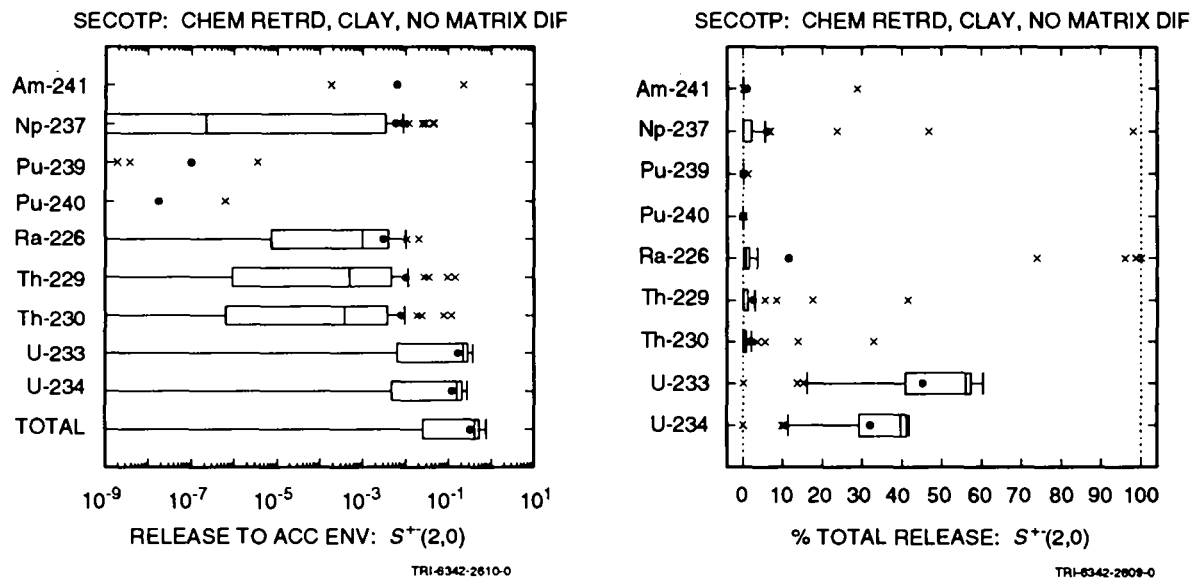

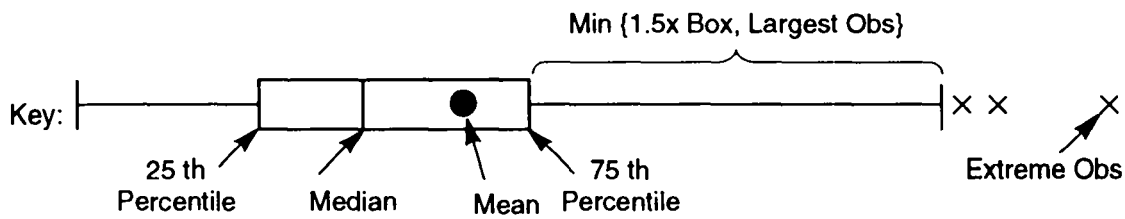

Figure 8.4-3. Normalized releases to the accessible environment over 10,000 yr due to groundwater transport with chemical retardation, clay lining in fractures and no matrix diffusion for scenario $S^{+-}(2,0)$ used in conjunction with the risk representation R_1 defined in Eq. 2.5-1 with intrusion occurring 1000 yr after repository closure.

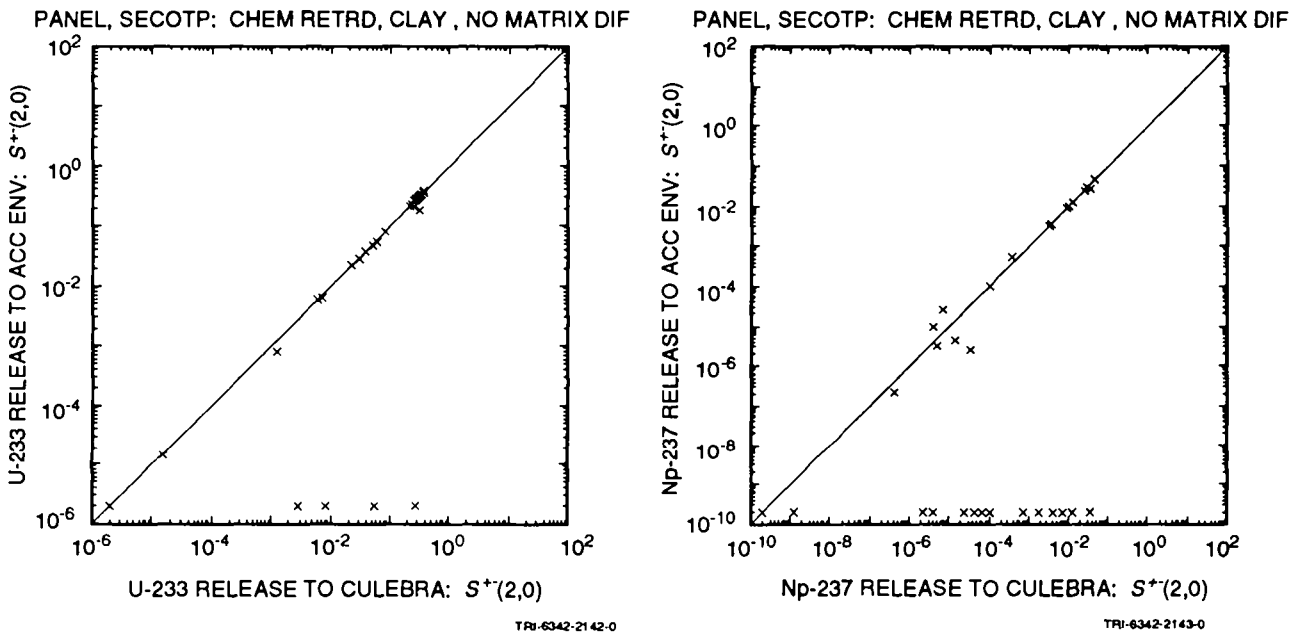

Figure 8.4-4. Scatterplots for total normalized release to the Culebra over 10,000 yr versus total normalized release to the accessible environment over 10,000 yr due to groundwater transport with chemical retardation, clay-lined fractures and no matrix diffusion for U-233 and Np-237 for scenario $S^{+-}(2,0)$ used in conjunction with the risk representation R_1 defined in Eq. 2.5-1 with intrusion occurring 1000 yr after closure.

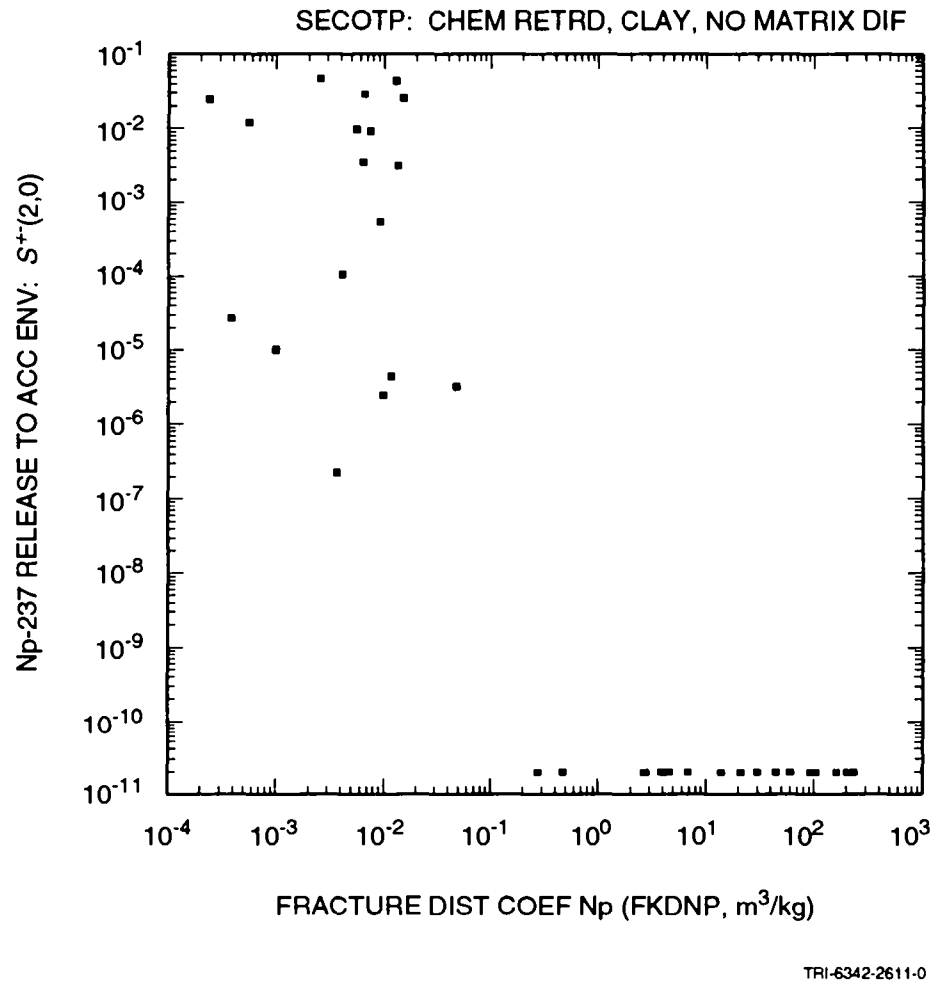

Figure 8.4-5. Scatterplot for normalized release of Np-237 to the accessible environment over 10,000 yr due to groundwater transport with chemical retardation, clay-lined fractures and no matrix diffusion versus FKDNP (fracture distribution coefficient for Np) for scenario $S^{+-}(2,0)$ used in conjunction with the risk representation R_1 defined in Eq. 2.5-1 with intrusion occurring 1000 yr after repository closure.

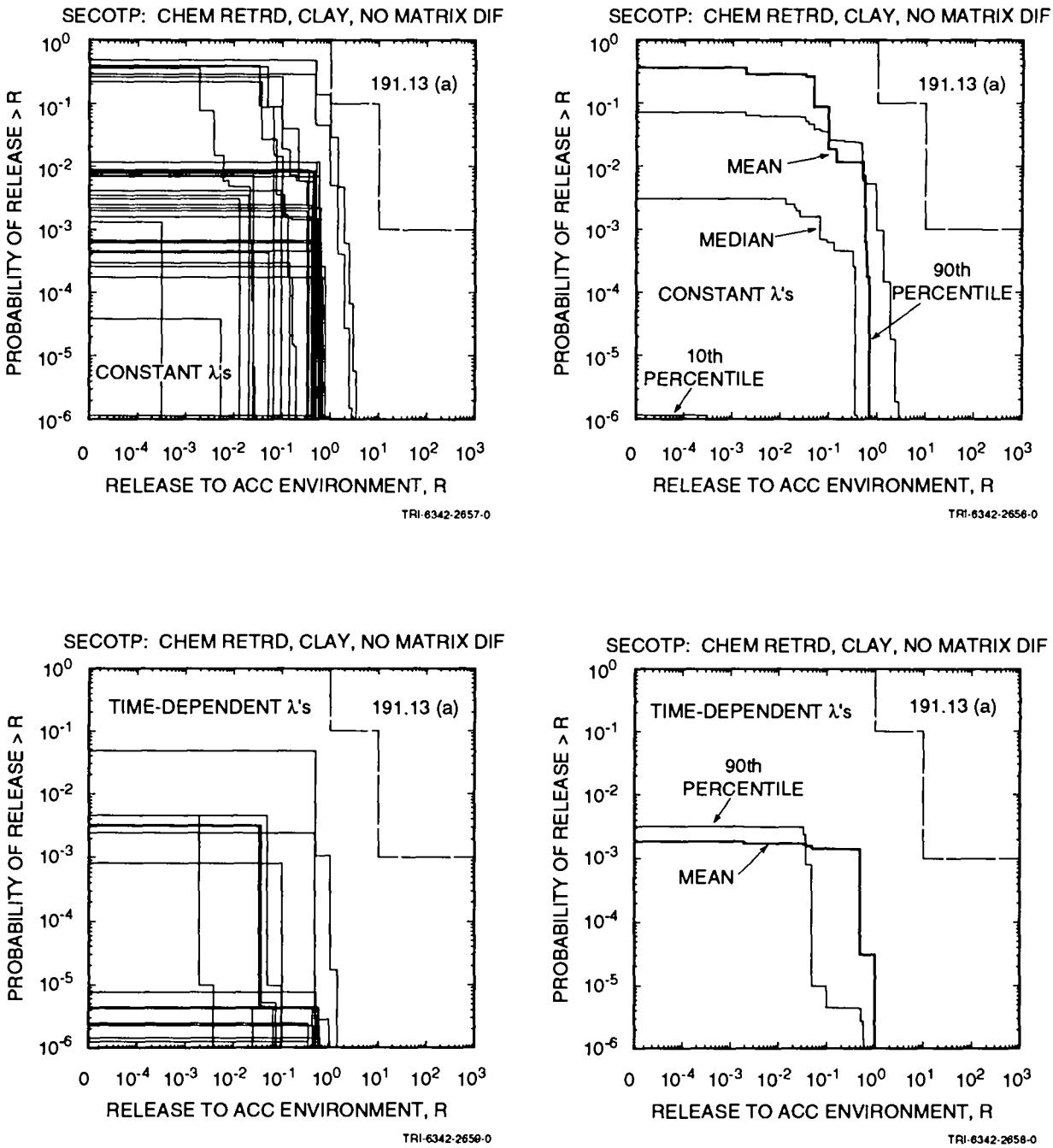

Figure 8.4-6. Distribution of CCDFs for normalized release to the accessible environment over 10,000 yr due to groundwater transport with chemical retardation, clay-lined fractures and no matrix diffusion for risk representation R_1 defined in Eq. 2.5-1 with constant (upper two frames) and time-dependent (lower two frames) rate terms in the Poisson model for drilling intrusions.

8.4.3 Chemical Retardation, No Clay Lining in Fractures, Matrix Diffusion

This section presents results calculated with the assumptions that diffusion occurs into the dolomite matrix, chemical retardation occurs in the dolomite matrix, and no clay lining is present in the fractures. Due to the absence of a clay lining, no chemical retardation occurs in the fractures. As shown by the scatterplot in Figure 8.4-7 for scenario $S^{+-}(2,0)$, these assumptions result in releases to the accessible environment that are substantially less than the releases to the Culebra. Specifically, only 21 sample elements result in releases to the accessible environment that exceed 1×10^{-10} EPA release units and the largest release is approximately 0.1 EPA release units. As shown by the box plots in Figure 8.4-8, the nonzero releases to the accessible environment tend to be dominated by U-233, U-234, Th-229, Th-230 and Ra-226, although all the releases tend to be small (i.e., less than 0.1 EPA release units).

As indicated by the two scatterplots in Figure 8.4-9 for U-233, release to the accessible environment is controlled primarily by processes associated with the dolomite matrix. In particular, the left scatterplot indicates that U-233 releases occur only for values of MKDU (matrix distribution coefficient for U) that are less than approximately 10^{-3} m^3/kg, and the right scatterplot indicates that releases occur only for values of CULFRSP (Culebra fracture spacing) that exceed 1 m. Increasing CULFRSP decreases the number of fractures and thus also decreases the total surface area through which diffusion can take place from the fractures to the dolomite matrix. As a result, the nonzero releases associated with the larger values of CULFRSP result from decreased diffusion into the dolomite matrix. The effect of distribution coefficients is element specific but increasing surface area for diffusion affects all elements. As shown in Figure 8.4-10, the occurrence of nonzero releases to the accessible environment is strongly associated with the larger values for CULFRSP.

The CCDFs for release to the accessible environment due to groundwater transport with diffusion into the dolomite matrix, chemical retardation in the dolomite matrix, and no clay lining in the fractures are presented in Figure 8.4-11. As examination of this figure shows, the indicated assumptions lead to CCDFs that are significantly below the EPA release limits. Indeed, only 8 out a possible 70 CCDFs appear in the upper left frame when constant rate terms are used, and only 1 out of a possible 70 CCDFs appear in the lower right frame when time-dependent rate terms are

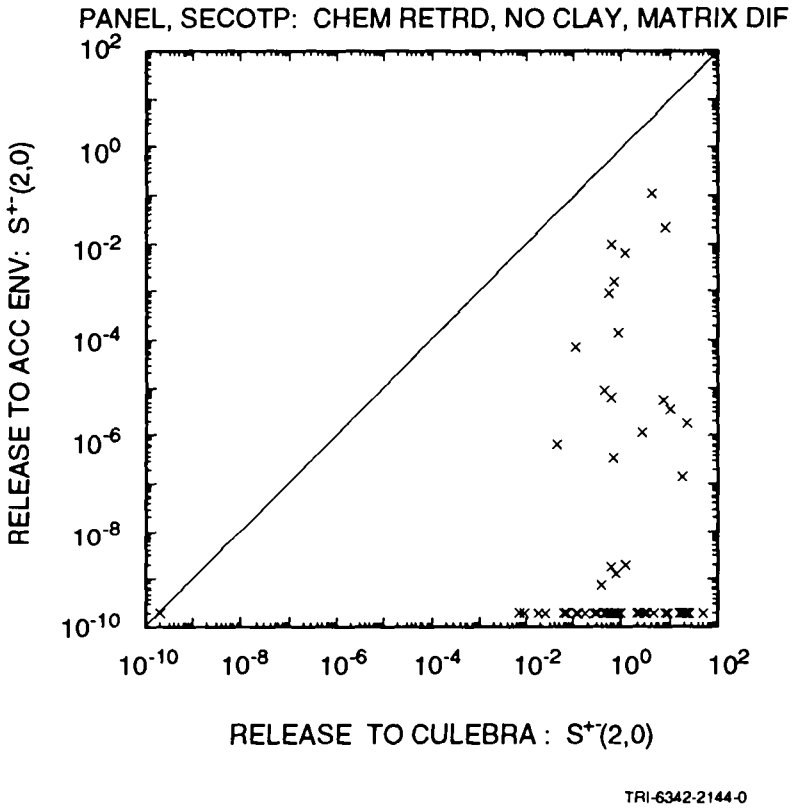

Figure 8.4-7. Scatterplot for total normalized release to Culebra over 10,000 yr versus total normalized release to accessible environment over 10,000 yr due to groundwater transport with chemical retardation, no clay lining in fractures and matrix diffusion for scenario $S^{+-}(2,0)$ used in conjunction with the risk representation R_1 defined in Eq. 2.5-1 with intrusion occurring at 1000 yr.

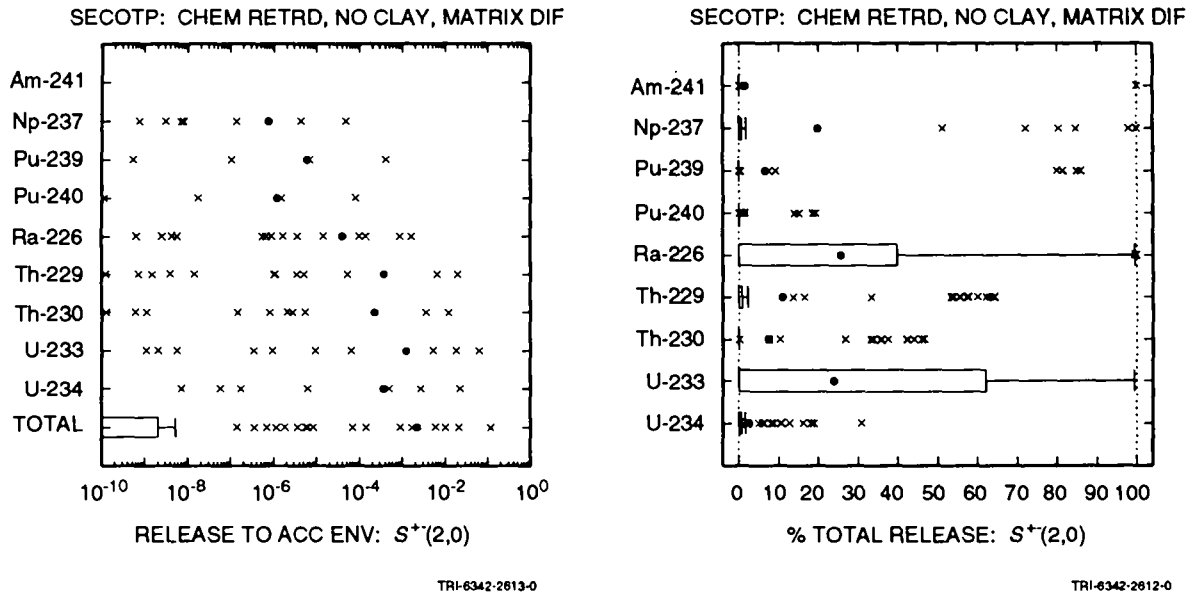

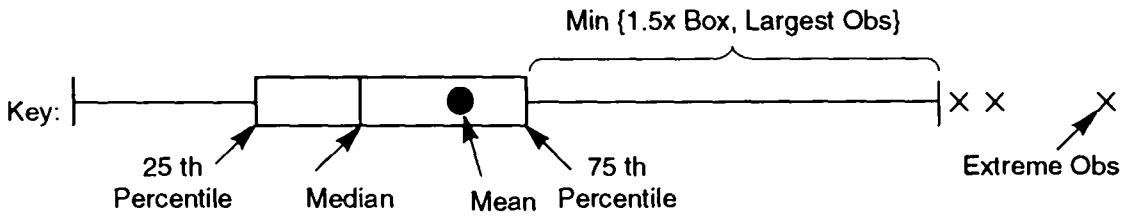

Figure 8.4-8. Normalized releases to accessible environment over 10,000 yr due to groundwater transport with chemical retardation, no clay lining in fractures and matrix diffusion for scenario $S^{+-}(2,0)$ used in conjunction with the risk representation R_1 defined in Eq. 2.5-1 with intrusion occurring at 1000 yr after repository closure.

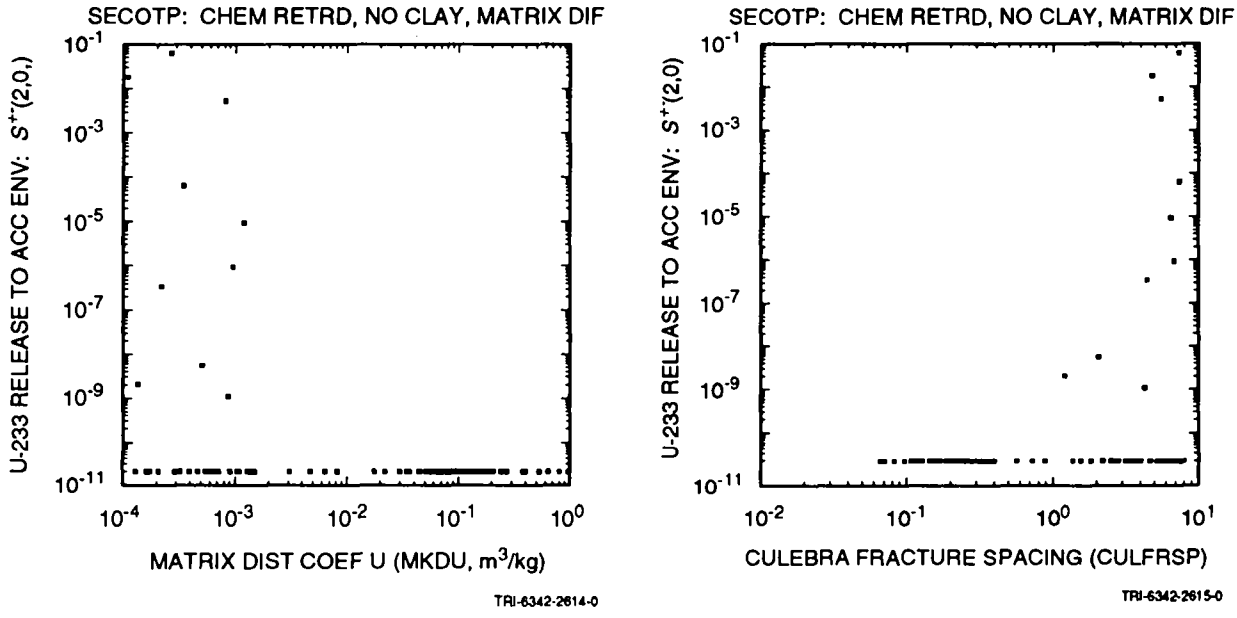

Figure 8.4-9. Scatterplots for normalized release of U-233 to the accessible environment over 10,000 yr due to groundwater transport with chemical retardation, no clay lining in fractures and matrix diffusion versus variables MKDU (matrix distribution coefficient for U) and CULFRSP (Culebra fracture spacing) for scenario $S^{+-}(2,0)$ used in conjunction with the risk representation R_1 defined in Eq. 2.5-1 with intrusion occurring 1000 yr after repository closure.

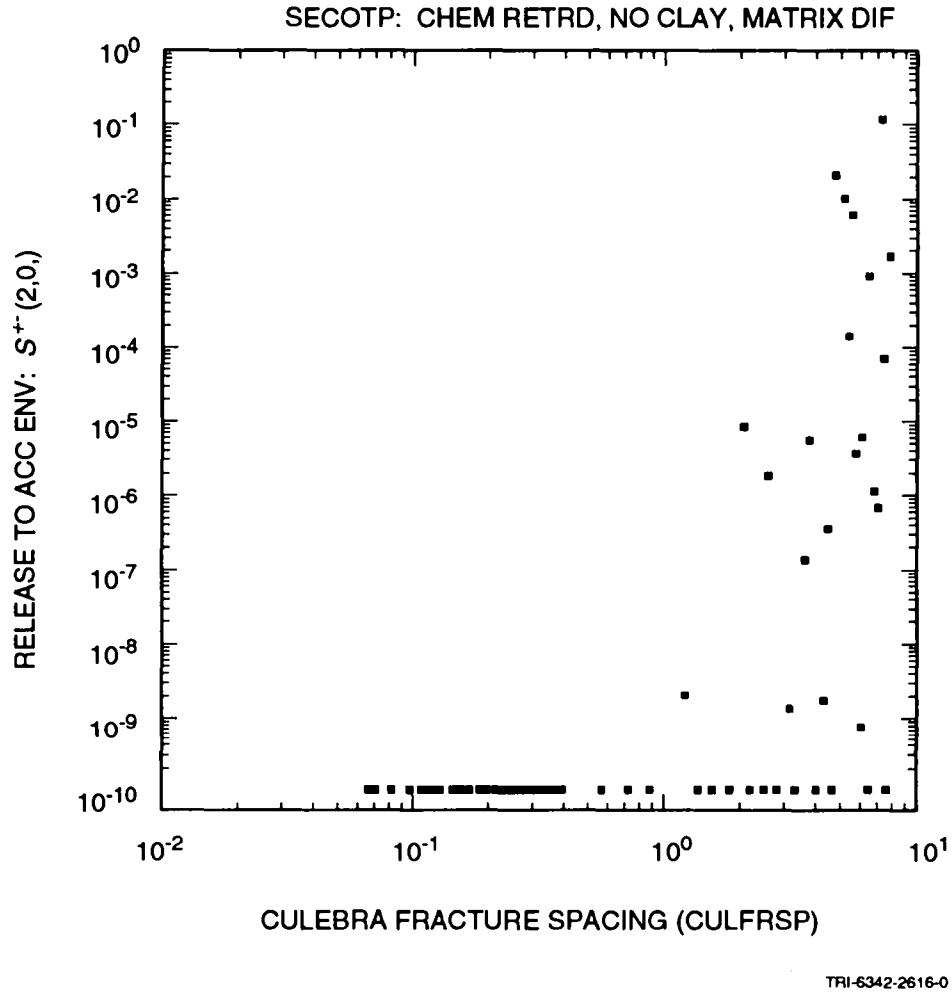

Figure 8.4-10. Scatterplot for total normalized release to the accessible environment over 10,000 yr due to groundwater transport with chemical retardation, no clay lining in fractures and matrix diffusion versus CULFRSP (Culebra fracture spacing) for scenario $S^{+-}(2,0)$ used in conjunction with the risk representation R_1 defined in Eq. 2.5-1 with intrusion occurring 1000 yr after repository closure.

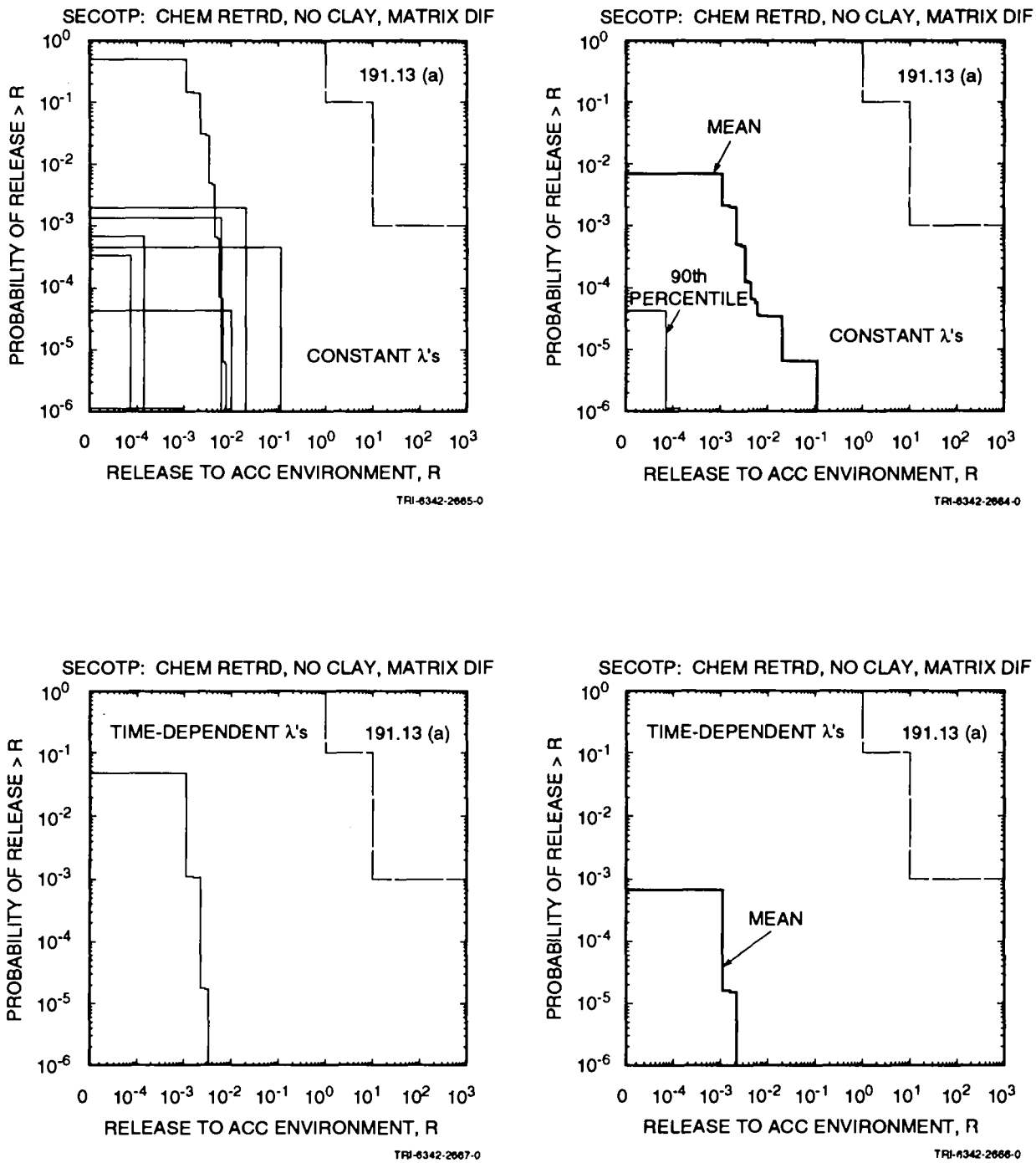

Figure 8.4-11. Distribution of CCDFs for normalized release to the accessible environment over 10,000 yr due to groundwater transport with chemical retardation, no clay lining in fractures and matrix diffusion constructed for the risk representation R_1 defined in Eq. 2.5-1 with constant (upper two frames) and time-dependent (lower two frames) rate terms in the Poisson model for drilling intrusions.

used. As a reminder, only 21 sample elements produce releases to the accessible environment that exceed 1 x 10^{-10} EPA release units for scenario $S^{+-}(2,0)$, and only 14 sample elements produce nonzero releases to the Culebra for scenario $S(1,0)$, with these releases being smaller than the corresponding releases for scenario $S^{+-}(2,0)$.

8.4.4 Chemical Retardation, Clay Lining in Fractures, Matrix Diffusion

This section presents results calculated with the assumptions that diffusion occurs into the dolomite matrix, clay-lined fractures are present, and sorption takes place in both the dolomite matrix and the clay lining of the fractures. As discussed in Section 8.4.2, only half the sample elements used in the 1992 WIPP performance assessment have clay-lined fractures. Therefore, the results presented in this section involve only the 35 sample elements that have clay-lined fractures (i.e., those sample elements for which CULCLYF≠0). At present, the WIPP performance assessment project believes this is the most appropriate set of assumptions to use for radionuclide transport in the Culebra.

As a reminder, only 21 out of 70 sample elements result in releases to the accessible environment that exceed 1 x 10^{-10} EPA release units for chemical retardation, no clay lining in fractures and matrix diffusion. Thus, approximately two-thirds of the sample elements produce no release to the accessible environment in the absence of clay-lined fractures. As shown by the scatterplot in Figure 8.4-12, the releases calculated with clay-lined fractures tend to equal or exceed the releases calculated without clay-lined fractures. This pattern probably results because the clay lining of the fractures slows diffusion into the dolomite matrix. However, it should be recognized that this comparison is based on only 9 nonzero releases to the accessible environment out of a total of 35 sample elements that have clay-lined fractures.

As 26 of the 35 sample elements with clay-lined fractures result in no releases to the accessible environment for scenario $S^{+-}(2,0)$, most of the resultant CCDFs for comparison with the EPA release limits are degenerate. The few nonzero CCDFs that do result are shown in Figure 8.4-13. As comparison of Figures 8.4-11 and 8.4-13 shows, the presence of matrix diffusion in conjunction with chemical retardation results in releases that fall substantially below the EPA release limits regardless of whether or not a clay lining is present in the fractures.

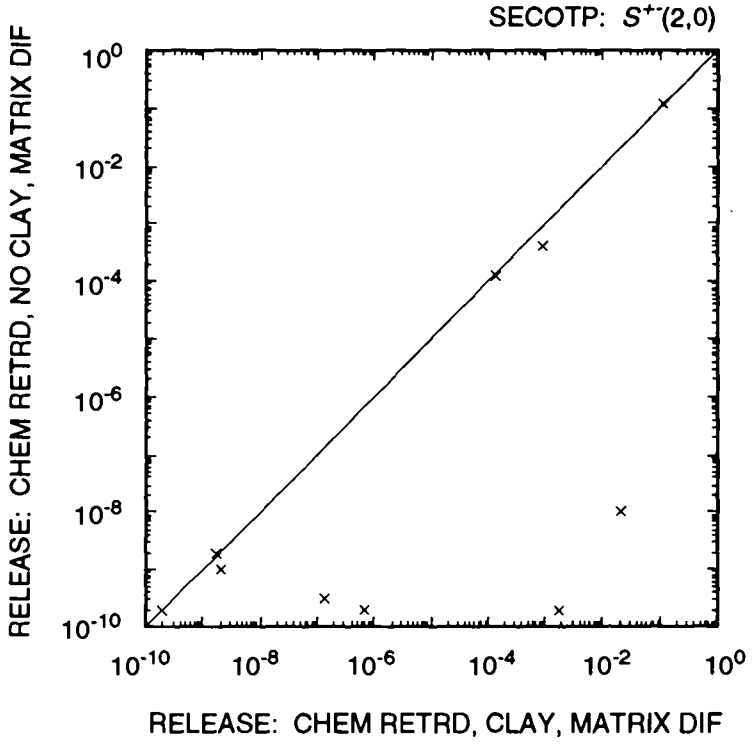

Figure 8.4-12. Scatterplot for total normalized release to the accessible environment over 10,000 yr due to groundwater transport with chemical retardation, no clay-lined fractures and matrix diffusion versus total normalized release to the accessible environment over 10,000 yr due to groundwater transport with chemical retardation, clay-lined fractures and matrix diffusion for scenario $S^{+-}(2,0)$ used in conjunction with the risk representation R_1 defined in Eq. 2.5-1 with intrusion occurring 1000 yr after repository closure.

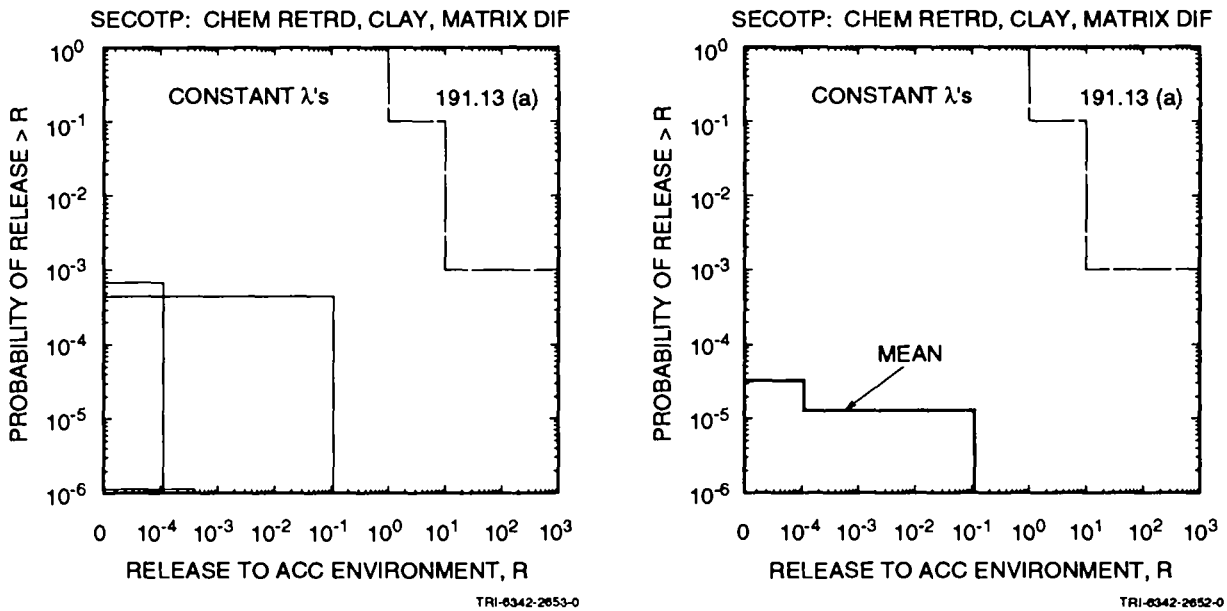

Figure 8.4-13. Distribution of CCDFs for normalized release to the accessible environment over 10,000 yr due to groundwater transport with chemical retardation, clay-lined fractures and matrix diffusion for risk representation R_1 defined in Eq. 2.5-1 with constant terms in the Poisson model for drilling intrusions. The use of time-dependent rate terms in the Poisson model results in all CCDFs being outside the plotting limits in use. The plots in this figure are based on 35 sample elements rather than 70 sample elements as in Figure 8.4-1 and other similar figures.

8.4.5 No Chemical Retardation

Calculations without chemical retardation were performed for three additional sets of assumptions: (1) clay-lined fractures and no matrix diffusion, (2) no clay lining in fractures and matrix diffusion, and (3) clay-lined fractures and matrix diffusion. The releases to the accessible environment for Assumption (1) were essentially identical to the results obtained for release to the Culebra (Section 8.3) and for release to the accessible environment with no chemical retardation, no clay lining in fractures and no matrix diffusion (Section 8.4.1). The releases to the accessible environment for Assumptions (2) and (3) were similar to each other. Further, as shown in Figure 8.4-14, the releases for Assumptions (2) and (3) were larger than the corresponding releases obtained with chemical retardation and matrix diffusion (Sections 8.4.3 and 8.4.4) and, as shown in Figure 8.4-15, often smaller than the releases obtained with chemical retardation and no matrix diffusion (Section 8.4.2).

The releases of the individual radionuclides to the accessible environment due to groundwater transport with no chemical retardation, no clay lining in fractures and matrix diffusion are summarized in Figure 8.4-16. As examination of this figure shows, the total release is dominated by Pu-239, with additional contributions from Am-241 and U-233. The corresponding results for chemical retardation, no clay-lining in fractures and matrix diffusion appear in Figure 8.4-8, while the results for chemical retardation, clay-lined fractures and no matrix diffusion appear in Figure 8.4-3. As comparison with Figures 8.4-3 and 8.4-8 shows, the removal of chemical retardation increases the importance of Pu-239 in the release to the accessible environment.

Because of the large number of zero releases, no regression-based sensitivity analyses were presented for groundwater transport to the accessible environment with chemical retardation. However, such analyses have the potential to be more revealing for the transport results in the absence of chemical retardation due to the occurrence of a larger number of nonzero releases. The results of such analyses for no chemical retardation, no clay lining in fractures and matrix diffusion are presented in Table 8.4-1. As examination of Table 8.4-1 shows, the variable with the largest influence on release to the accessible environment is CULFRSP (Culebra fracture spacing), with release tending to increase as CULFRSP increases. This positive effect results because increasing CULFRSP reduces the surface area over which diffusion into the dolomite matrix can take place. Positive effects are also indicated for BHPERM (borehole permeability) and the solubilities of individual elements (i.e., SOLAM, SOLNP, SOLPU, SOLTH, SOLU). Increasing BHPERM decreases resistance to brine flow up an intruding

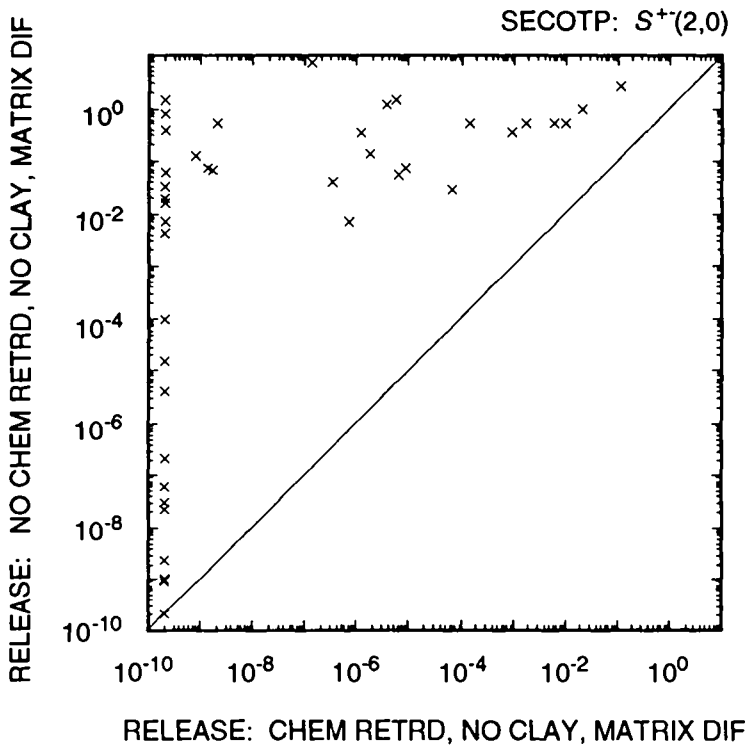

Figure 8.4-14. Scatterplot for total normalized release to the accessible environment over 10,000 yr with and without chemical retardation for groundwater transport with matrix diffusion and no clay lining in fractures for scenario $S^{+-}(2,0)$ used in conjunction with the risk representation R_1 defined in Eq. 2.5-1 with intrusion occurring 1000 yr after repository closure.

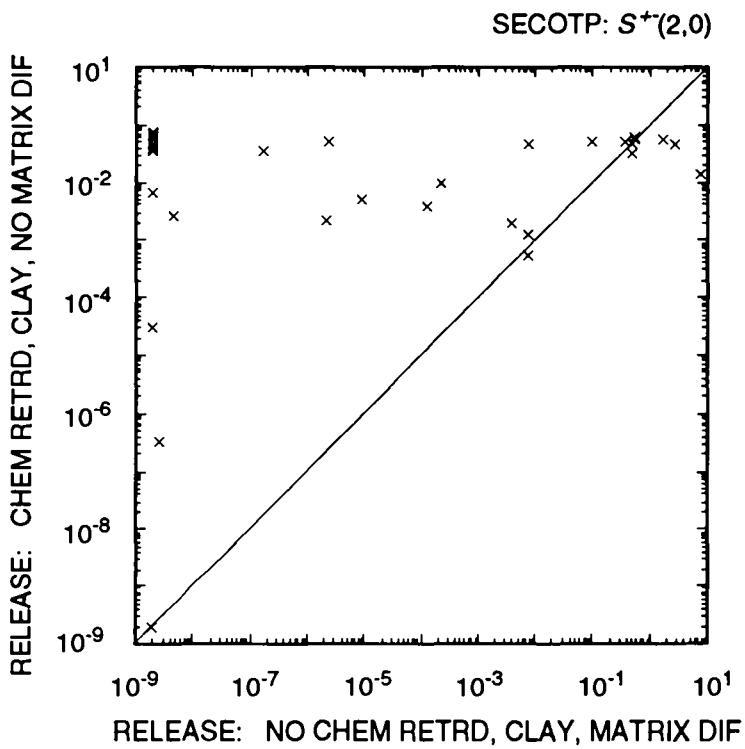

Figure 8.4-15. Scatterplot for total normalized release to the accessible environment over 10,000 yr due to groundwater transport with no chemical retardation, clay-lined fractures and matrix diffusion versus total normalized release to the accessible environment over 10,000 yr due to groundwater transport with chemical retardation, clay-lined fractures and no matrix diffusion for scenario $S^{+-}(2,0)$ used in conjunction with the risk representation R_1 defined in Eq. 2.5-1 with intrusion occurring 1000 yr after repository closure.

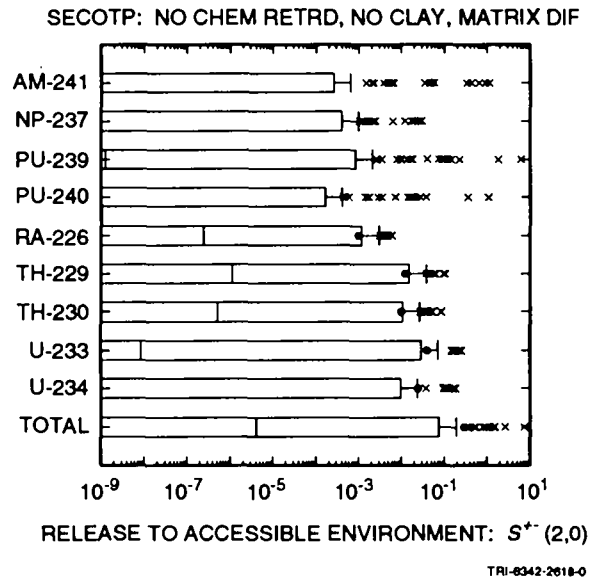

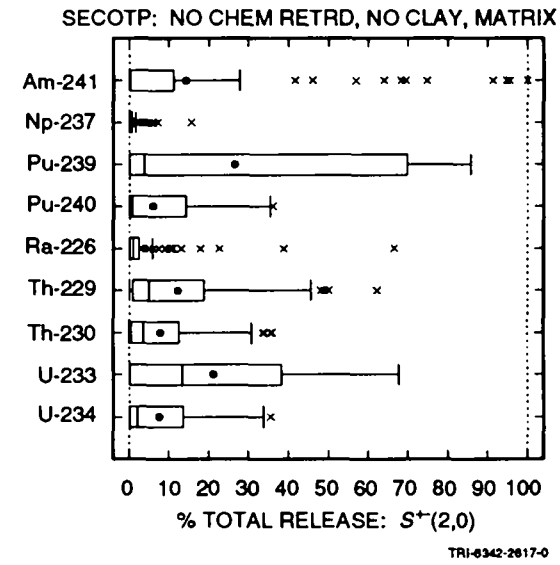

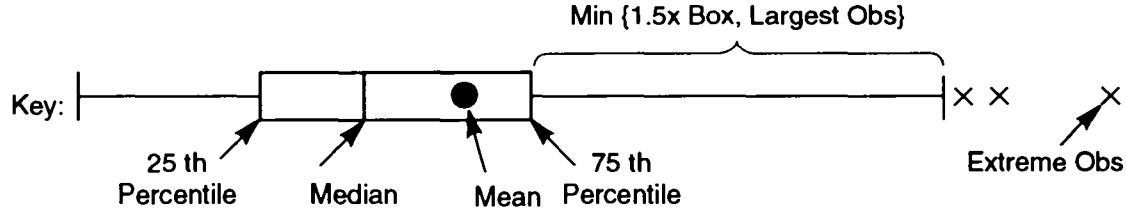

Figure 8.4-16. Normalized releases to accessible environment over 10,000 yr due to groundwater transport with no chemical retardation, no clay lining in fractures and matrix diffusion for scenario $S^{+-}(2,0)$ used in conjunction with the risk representation R_1 defined in Eq. 2.5-1 with intrusion occurring at 1000 yr after repository closure.

Table 8.4-1. Stepwise Regression Analyses with Rank-Transformed Data for Integrated Release to the Accessible Environment over 10,000 yr due to Groundwater Transport with No Chemical Retardation, No Clay Lining in Fractures and Matrix Diffusion for Scenario S^{+-}(2,0) with Intrusion Occurring 1000 yr after Repository Closure.

	Variable[a]	R^{2b}	Variable	R^2	Variable	R^2	Variable	R^2
Step[c]	Am-241		Np-237		Pu-239		Pu-240	
1	CULFRSP	0.54(+)	CULFRSP	0.56(+)	CULFRSP	0.42(+)	CULFRSP	0.42(+)
2	BHPERM	0.64(+)	BHPERM	0.64(+)	SOLPU	0.64(+)	SOLPU	0.64(+)
3	SOLAM	0.70(+)	SOLNP	0.68(+)	BHPERM	0.71(+)	BHPERM	0.71(+)
4	CULPOR	0.74 (-)			CULTRFLD	0.74 (-)	CULTRFLD	0.74 (-)
Step	Ra-226		Th-229		Th-230		U-233	
1	CULFRSP	0.60(+)	CULFRSP	0.53(+)	CULFRSP	0.54(+)	CULFRSP	0.57(+)
2	BHPERM	0.69(+)	BHPERM	0.63(+)	BHPERM	0.64(+)	BHPERM	0.67(+)
3	CULPOR	0.72 (-)	SOLTH	0.68(+)	SOLTH	0.69(+)	SOLU	0.70(+)
4	CULTRFLD	0.74 (-)						
Step	U-234		Total					
1	CULFRSP	0.58(+)	CULFRSP	0.58(+)				
2	BHPERM	0.68(+)	BHPERM	0.68(+)				
3			CULTRFLD	0.72 (-)				
4			SOLPU	0.74(+)				

[a]Variables listed in order of selection in regression analysis

[b]Cumulative R^2 value with entry of each variable into regression model, with "+" and "-" indicating positive and negative regression coefficients, respectively

[c]Steps in stepwise regression analysis

borehole, and increasing the solubilities increases the amount of dissolved radionuclides that can be transported by a given volume of brine. Small negative effects are indicated for CULPOR (matrix porosity in Culebra) and CULTRFLD (transmissivity field for Culebra). Increasing CULPOR increases the amount of radionuclide that can be held in the dolomite matrix and thus tends to decrease release. The variable CULTRFLD is actually the travel time to the accessible environment for the individual transmissivity fields used in the analysis. Thus, increasing CULTRFLD increases the amount of time required to transport a radionuclide from its release point into the Culebra to the accessible environment, which in turn tends to decrease the amount of a radionuclide that can be transported to the accessible environment over 10,000 yr.

Examination of scatterplots often provides an additional perspective on regression-based sensitivity analysis results of the form presented in Table 8.4-1. The regression analyses in Table 8.4-1 consistently identify CULFRSP (Culebra fracture spacing) and BHPERM (borehole permeability) as being important variables, with CULFRSP being the first variable selected in every analysis. As an example, scatterplots for CULFRSP and BHPERM for the release of Am-241 to the accessible environment are presented in Figure 8.4-17. Consistent with the regression results in Table 8.4-1, a stronger positive relationship between release to the accessible environment and CULFRSP can be seen in Figure 8.4-17 than between release to the accessible environment and BHPERM.

The analyses for Pu-239 and Pu-240 in Table 8.4-1 differ from the analyses for the other radionuclides in that solubility of plutonium (SOLPU) is indicated as being more important for release to the accessible environment than is solubility for the other elements (i.e., SOLAM, SOLNP, SOLRA, SOLTH, SOLU). To a great extent, this importance results from the very large range of values (i.e., 2.5×10^{-17} to 5.5×10^{-4} mol/ℓ) assigned to SOLPU. As shown in Figure 8.4-18, there is an interplay between the effects of CULFRSP (Culebra fracture spacing) and SOLPU. In particular, the value assigned to CULFRSP is a major determinant of whether or not a release to the accessible environment will occur. However, given that there is a release, the size of this release tends to increase as SOLPU increases.

Distributions of CCDFs for release to the accessible environment generated for groundwater transport with no chemical retardation, no clay lining in fractures and matrix diffusion are shown in Figure 8.4-19. The upper two frames show results for constant rate terms in the Poisson model for drilling intrusion, and the lower two frames show results for time-dependent rate terms. As already suggested by the comparison in Figure 8.4-14, the assumptions of no chemical retardation and matrix diffusion lead

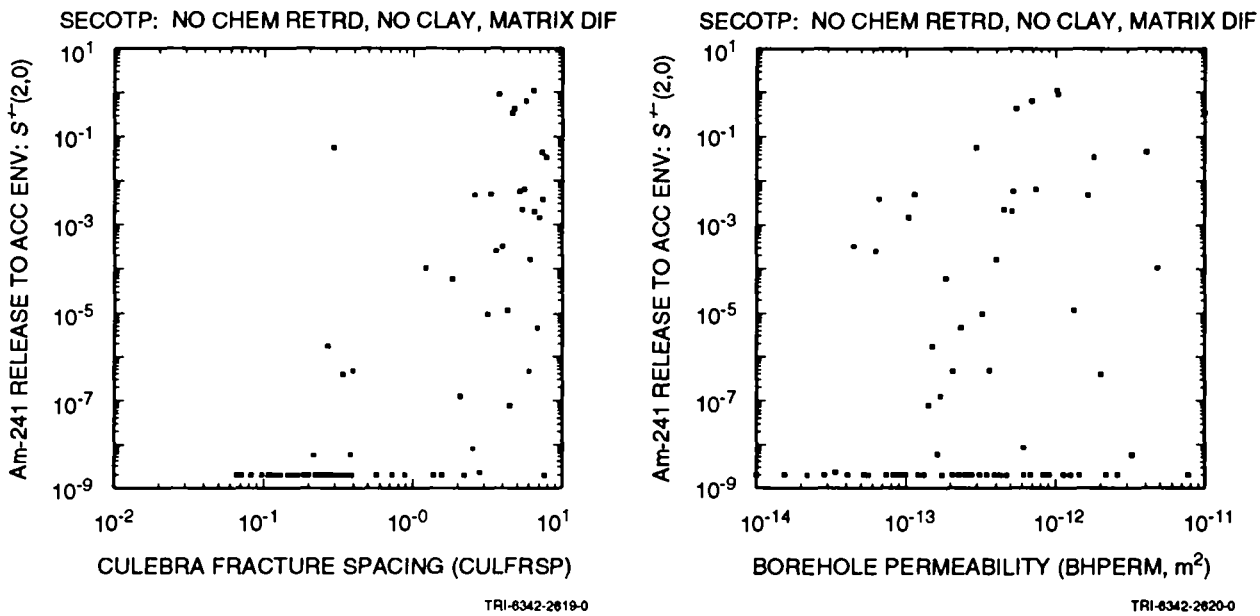

Figure 8.4-17. Scatterplots for normalized release of Am-241 to the accessible environment over 10,000 yr due to groundwater transport with no chemical retardation, no clay lining in fractures and matrix diffusion versus variables CULFRSP (Culebra fracture spacing) and BHPERM (borehole permeability) for scenario $S^{+-}(2,0)$ used in conjunction with the risk representation R_1 defined in Eq. 2.5-1 with intrusion occurring 1000 yr after repository closure.

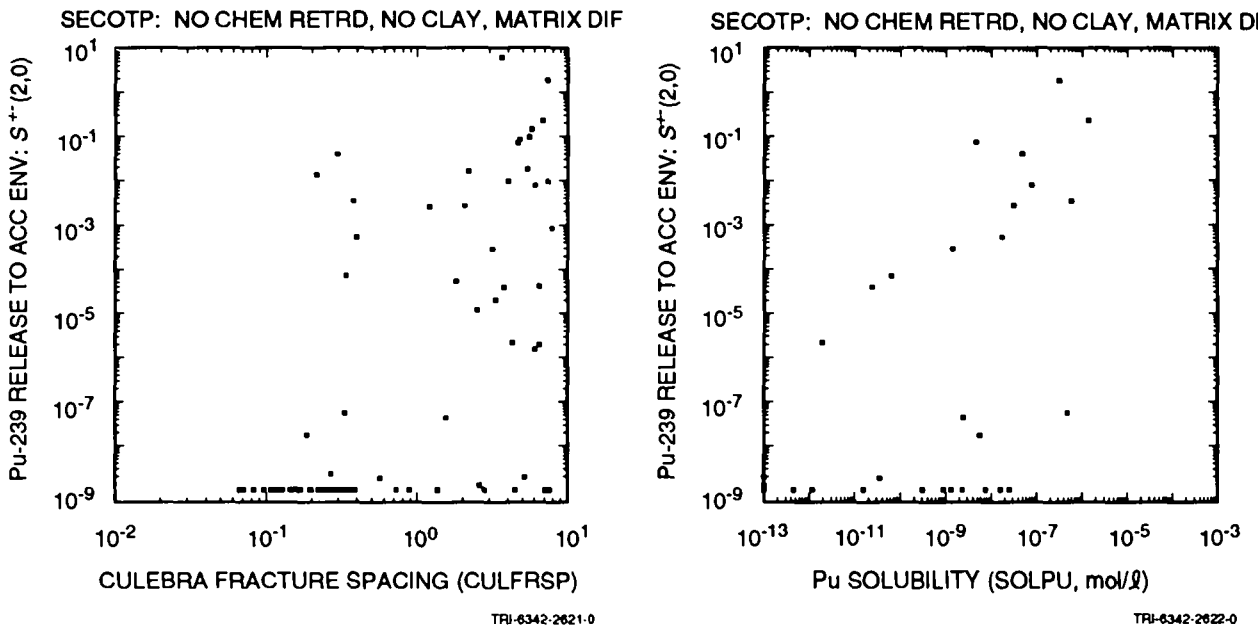

Figure 8.4-18. Scatterplots for normalized release of Pu-239 to the accessible environment over 10,000 yr due to groundwater transport with no chemical retardation, no clay lining in fractures and matrix diffusion versus variables CULFRSP (Culebra fracture spacing) and SOLPU (solubility of plutonium) for scenario $S^{+-}(2,0)$ used in conjunction with the risk representation R_1 defined in Eq. 2.5-1 with intrusion occurring 1000 yr after repository closure.

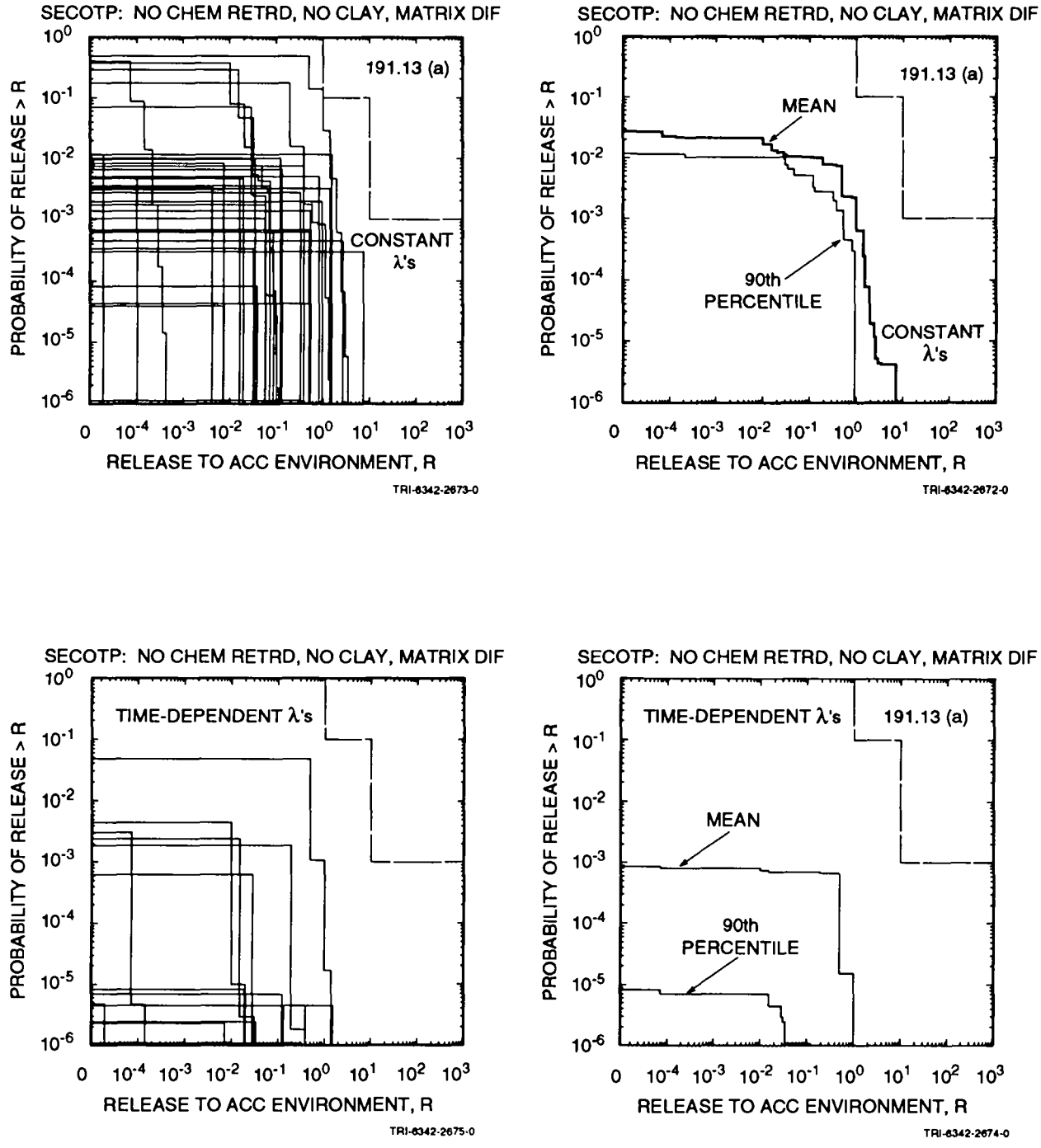

Figure 8.4-19. Distribution of CCDFs for normalized release to the accessible environment over 10,000 yr due to groundwater transport with no chemical retardation, no clay lining in fractures and matrix diffusion constructed for the risk representation R_1 defined in Eq. 2.5-1 with constant (upper two frames) and time-dependent (lower two frames) rate terms in the Poisson model for drilling intrusions.

to CCDFs that are closer to the EPA release limits than the CCDFs in Figure 8.4-11 obtained with chemical retardation and matrix diffusion. Further, as suggested by the comparison in Figure 8.4-15, the assumptions of no chemical retardation and matrix diffusion leads to a distribution that is similar to the one obtained with chemical retardation, clay-lined fractures and no matrix diffusion, although the assumption of matrix diffusion produces more small releases.

8.5 Total Release to Accessible Environment

As shown in Eqs. 2.4-10 through 2.4-14, the total release to the accessible environment is obtained by combining a release due to cuttings removal and a release due to groundwater transport. Summaries of this total release, and the cuttings removal and groundwater transport components from which it is constructed, are given in Figures 8.5-1 and 8.5-2 for scenarios $S(1,0)$ and $S^{+-}(2,0)$ used in conjunction with the risk representation R_1 defined in Eq. 2.5-1 and the various alternative modeling assumptions considered in the 1992 WIPP performance assessment.

For scenario $S(1,0)$, only 14 out of the 70 sample elements result in a release to the Culebra. Further, most of these releases (i.e., 11 out of 14) fall between 0.1 and 1 EPA release units. This narrow range of nonzero releases results from an almost complete removal of U-233 and U-234 from the waste (i.e., see Figures 8.3-1 and 7-4). As a result, the releases for the alternative modeling assumptions shown in Figure 8.5-1 for scenario $S(1,0)$ tend to be dominated by the cuttings release component, although in a few sample elements the groundwater transport release does exceed the cuttings release.

For scenario $S^{+-}(2,0)$, 68 out of the 70 sample elements result in releases to the Culebra. Further, most (i.e., 58 out of 68) exceed 0.1 EPA release units. As a result, scenario $S^{+-}(2,0)$ provides a more revealing comparison of releases than scenario $S(1,0)$. Each of the alternative modeling assumptions without matrix diffusion produces releases that are dominated by the groundwater transport component. In contrast, the release is almost completely dominated by the cuttings component when chemical retardation and matrix diffusion are assumed. For no chemical retardation and matrix diffusion, both the groundwater component and the cuttings component are important contributors to the total release.

Due to the large number of nonzero releases to the Culebra that result for scenario $S^{+-}(2,0)$, Figure 8.5-2 also provides a convenient

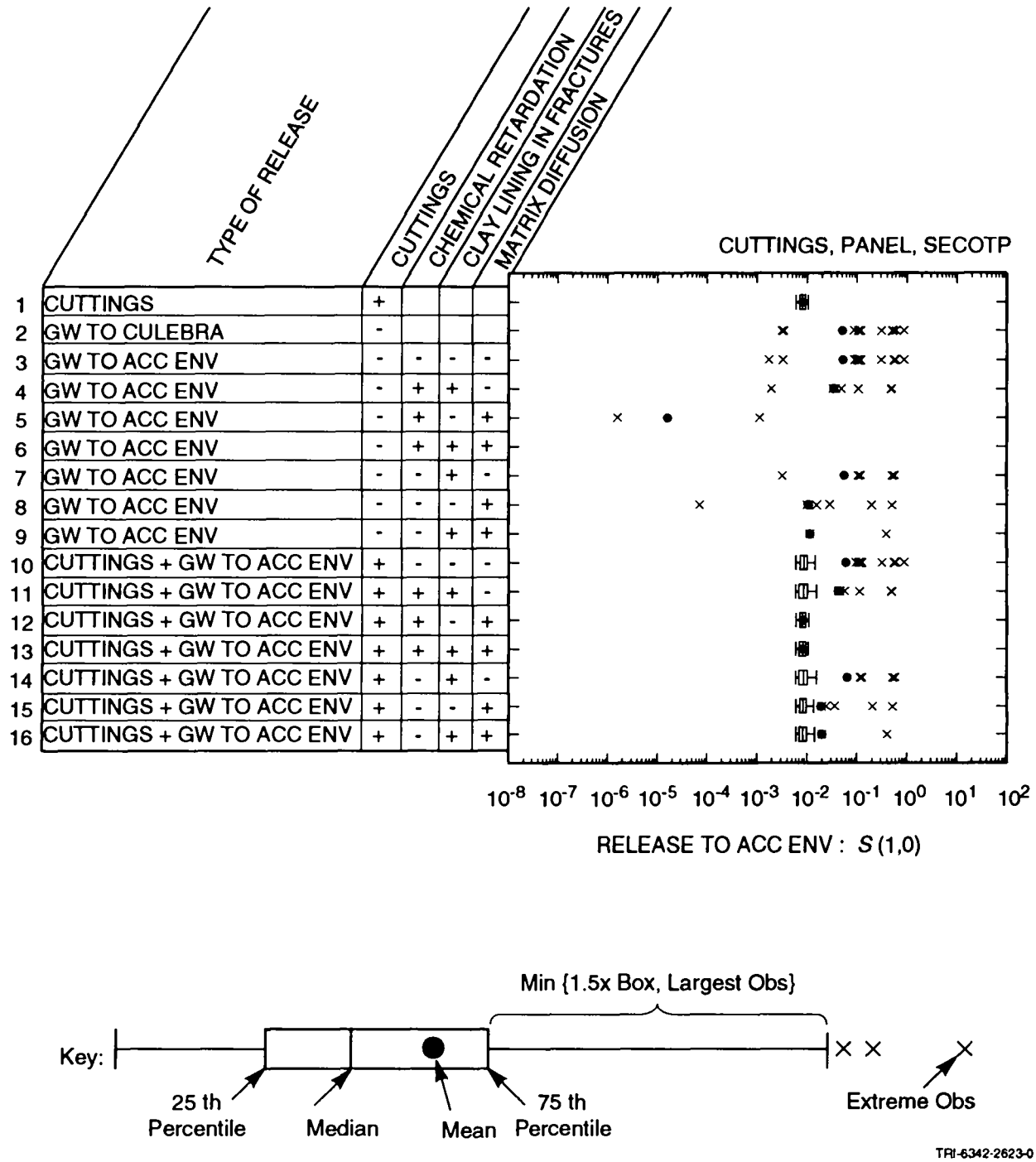

Figure 8.5-1. Summary of total normalized releases to the accessible environment over 10,000 yr for scenario $S(1,0)$ used in conjunction with the risk representation R_1 defined in Eq. 2.5-1 with intrusion occurring 1000 yr after repository closure. Box plots for results without a clay lining in fractures in the Culebra Dolomite are generated with 70 observations; box plots for results with a clay lining are generated with 35 observations (i.e., the observations in which CULCLYF=0 have been dropped).

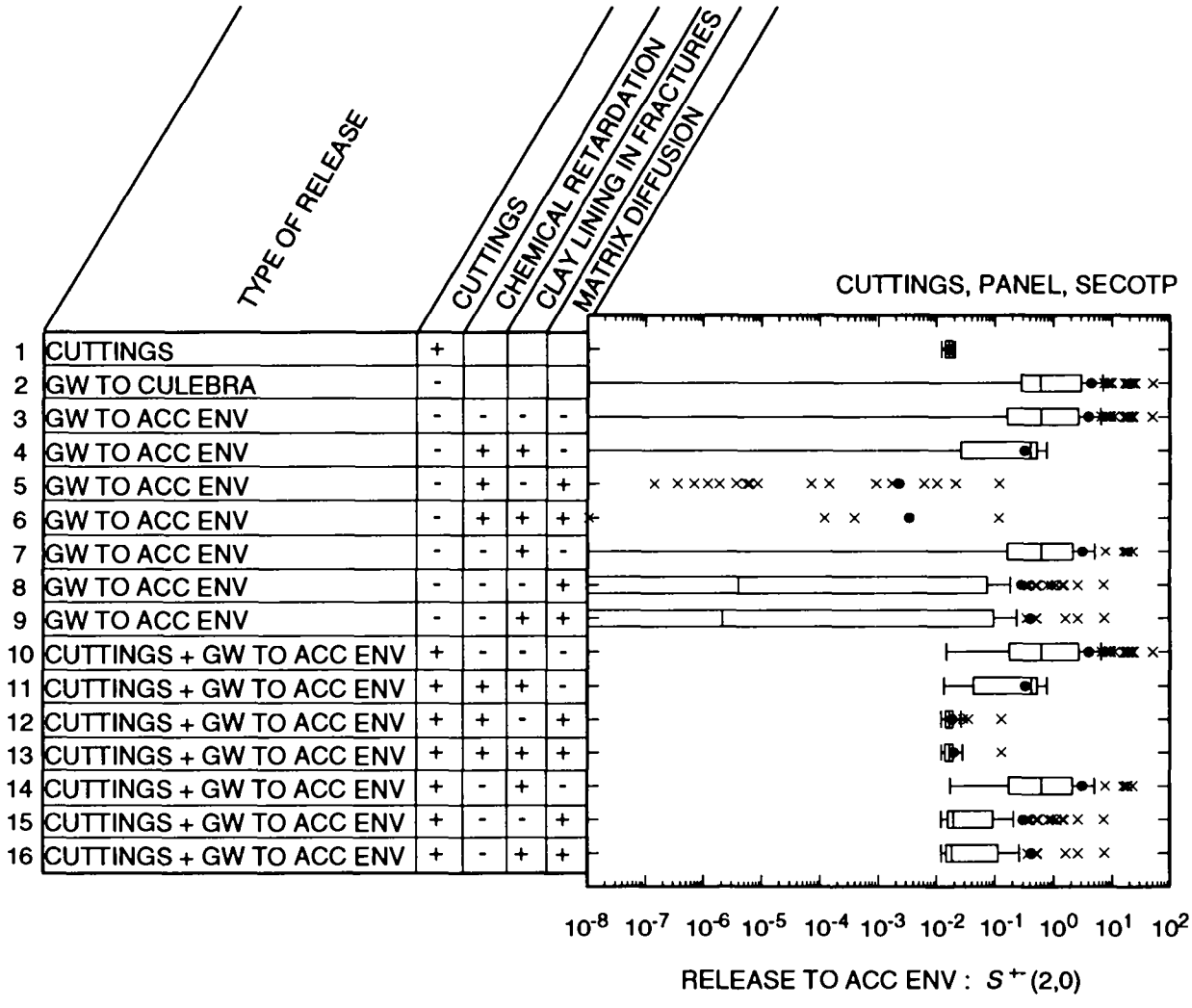

Figure 8.5-2. Summary of total normalized releases to the accessible environment over 10,000 yr for scenario $S^{+-}(2,0)$ used in conjunction with the risk representation R_1 defined in Eq. 2.5-1 with intrusion occurring 1000 yr after repository closure. Box plots for results without a clay lining in fractures in the Culebra Dolomite are generated with 70 observations; box plots for results with a clay lining are generated with 35 observations (i.e., the observations in which CULCLYF=0 have been dropped).

comparison of the effects of the alternative modeling assumptions. In particular, no chemical retardation and no matrix diffusion produce releases to the accessible environment that are essentially identical to the release to the Culebra. The assumption of chemical retardation and no matrix diffusion lowers the releases to the accessible environment somewhat and has a noticeable effect on reducing the largest releases. Further, the assumption of chemical retardation and matrix diffusion leads to very small releases, with most releases being less than 1×10^{-8} EPA release units. The assumption of matrix diffusion in conjunction with no chemical retardation produces releases that are generally larger than those obtained with chemical retardation and matrix diffusion and smaller than those obtained with chemical retardation and no matrix diffusion, although the largest releases for matrix diffusion in conjunction with no chemical retardation exceed the largest releases for chemical retardation and no matrix diffusion.

The CCDFs constructed in the 1992 WIPP performance assessment for comparison with the EPA release limits are based on releases for each scenario that include both groundwater transport and cuttings removal components. As suggested by the results in Figures 8.5-1 and 8.5-2, the CCDFs for a particular set of modeling assumptions are often dominated by either the cuttings release or the groundwater release.

Before presenting CCDFs for total releases due to both cuttings removal and groundwater transport, it is useful to review the cuttings removal results presented in Section 8.2. In particular, the CCDFs for cuttings removal presented in Figure 8.2-3 were constructed for the risk representation R_2 defined in Eq. 2.5-8. This representation uses the six time intervals in Eq. 2.5-9 in the definition of scenarios. Due to computational constraints, the CCDFs presented in Sections 8.4 and 8.5 for releases due to groundwater transport are constructed for the risk representation R_1 defined in Eq. 2.5-1, which uses the two time intervals in Eq. 2.5-2. Further, the rate term λ in the Poisson model for drilling intrusion is assumed to equal 0 yr^{-1} after 2000 yr in the calculation of scenario probabilities for R_1. In contrast, no such constraint is placed on the λ's in the determination of scenario probabilities for R_2, although some of the time-dependent λ's obtained in the expert review process do go to zero before 10,000 yr (see Appendix D in Volume 3).

The CCDFs for total release (i.e., cuttings removal and groundwater transport) presented in this section use the risk representation R_1 defined in Eq. 2.5-1. To facilitate comparisons between groundwater releases, cuttings releases and total releases, CCDFs are presented in Figure 8.5-3 for the cuttings release to the accessible environment constructed for R_1 with

the rate term λ in the Poisson model for drilling intrusions equal to 0 yr^{-1} after 2000 yr. The corresponding results for the risk representation R_2 defined in Eq. 2.5-8 with no restrictions on λ are presented in Figure 8.2-3. As the more explicit comparison in Figure 8.5-4 shows, use of the risk representation R_1 with constant λ's produces mean and 90th percentile curves for cuttings removal that are shifted down and to the left by factors of approximately 3 or less from the corresponding curves obtained with the risk representation R_2; similar shifts also occur for time-dependent λ's.

The CCDFs for total release to the accessible environment with no chemical retardation, no clay lining in fractures and no matrix diffusion are presented in Figure 8.5-5. For comparison, the associated releases due to cuttings removal only and groundwater transport only appear in Figures 8.5-3 and 8.3-9, respectively. As a reminder, the CCDFs for release to the Culebra shown in Figure 8.3-9 are essentially identical to the CCDFs for release to the accessible environment for groundwater transport with no chemical retardation, no clay lining in fractures and no matrix diffusion (see Section 8.4.1). As comparison with Figure 8.5-3 shows, the larger releases to the accessible environment associated with the CCDFs in Figure 8.5-5 are due to groundwater transport. However, because of the zero releases associated with scenarios of the form $S(1,0)$, $S(2,0)$, ... for many sample elements, large parts of many CCDFs are still dominated by the cuttings release. This effect can be seen in the similarity of parts of the CCDF plots on the left side of Figure 8.5-5 to the corresponding plots in Figure 8.5-3. Although the inclusion of groundwater transport releases does cause a shift to the right of the cuttings removal only CCDFs in Figure 8.5-3, most CCDFs still fall below the EPA release limits for constant rate terms in the Poisson model for drilling intrusion, and all CCDFs fall considerably below the EPA release limits for time-dependent rate terms.

The removal of the assumption that the rate term in the Poisson model for drilling intrusions is equal to 0 yr^{-1} after 2000 yr would cause the CCDFs in Figure 8.5-5 and other similar figures in this section to be shifted up and to the right. However, as the comparisons in Figure 8.5-4 show, these shifts would probably not move the CCDFs up or to the right by more than a factor of 3. The shifts in the CCDFs for groundwater transport are anticipated to be similar to those for cuttings removal because the scenario probabilities are undergoing the same change. Thus, although the use of the risk representation R_1, defined in Eq. 2.5-1, does produce lower risk results than the representation R_2, defined in Eq. 2.5-8, results obtained with R_1 do provide insights in comparisons with the EPA release limits.

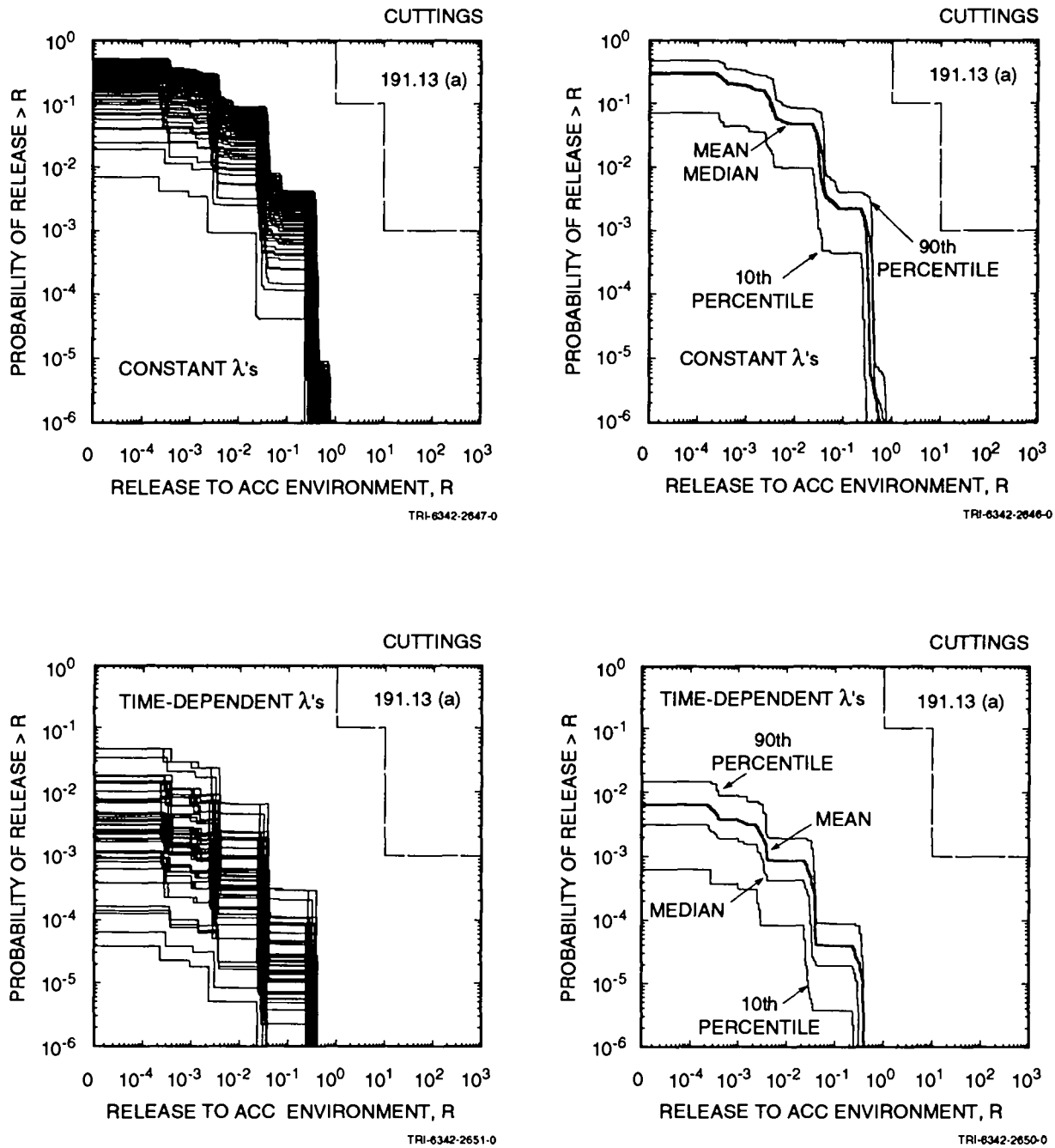

Figure 8.5-3. Distribution of CCDFs for normalized release to the accessible environment over 10,000 yr for cuttings removal constructed with the risk representation R_1 defined in Eq. 2.5-1 with constant (upper two frames) and time-dependent (lower two frames) rate terms in the Poisson model for drilling intrusions.

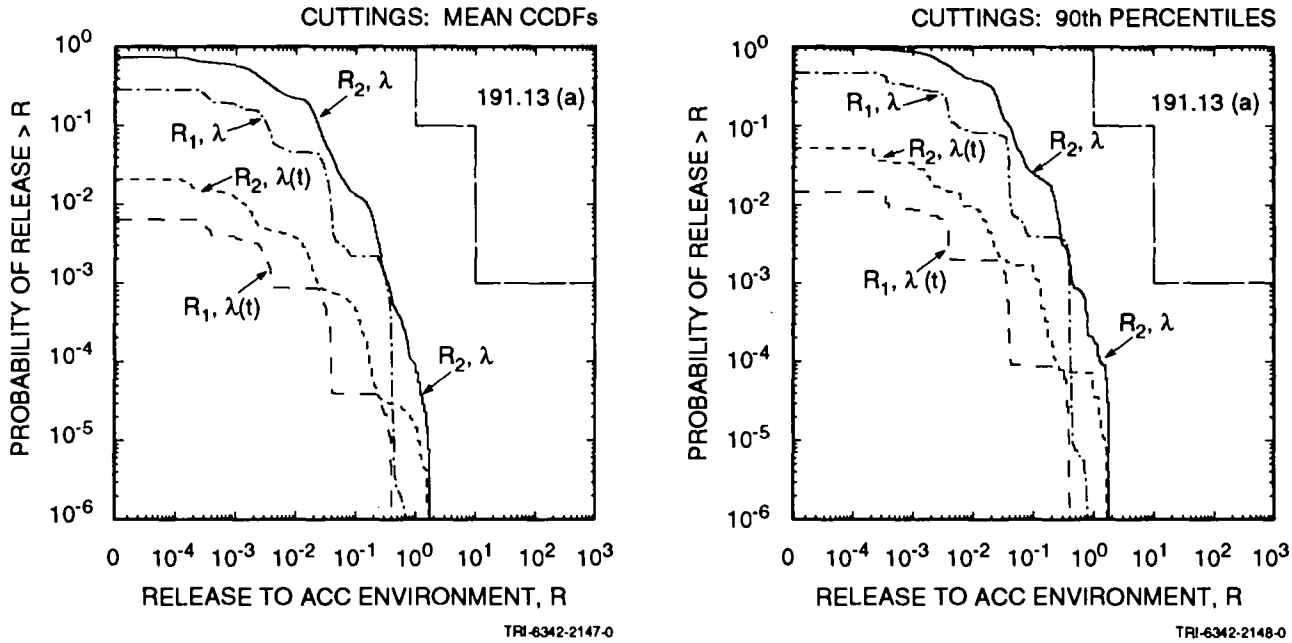

Figure 8.5-4. Comparison of mean and 90th percentile curves for cuttings removal over 10,000 yr obtained for risk representations R_1 (Eq. 2.5-1) and R_2 (Eq. 2.5-8) with constant (λ) and time-dependent ($\lambda(t)$) rate terms in the Poisson model for drilling intrusion.

The CCDFs for total release to the accessible environment with chemical retardation, clay-lined fractures and no matrix diffusion are presented in Figure 8.5-6. As discussed in Section 8.4.2, these CCDFs are based on 35 sample elements. As shown by the box plots in Figures 8.5-1 and 8.5-2, this analysis alternative produces releases to the accessible environment that are somewhat smaller than the corresponding releases to the Culebra. Further, when releases to the Culebra occur, they are often larger than the corresponding cuttings release for waste of average activity level. However, as is the case for all of the alternative analyses, most sample elements (i.e., 56 out of 70) result in no release to the Culebra for scenarios of the form $S(1,0)$, $S(2,0)$, ... The overall result is that the CCDFs in Figure 8.5-6 tend to fall somewhat farther to the right than the CCDFs for cuttings removal only in Figure 8.5-3 and yet display much of the structure present in Figure 8.5-3 for CCDFs based on cuttings removal only. The mean and 90th percentile curves in Figure 8.5-6 constructed with constant values

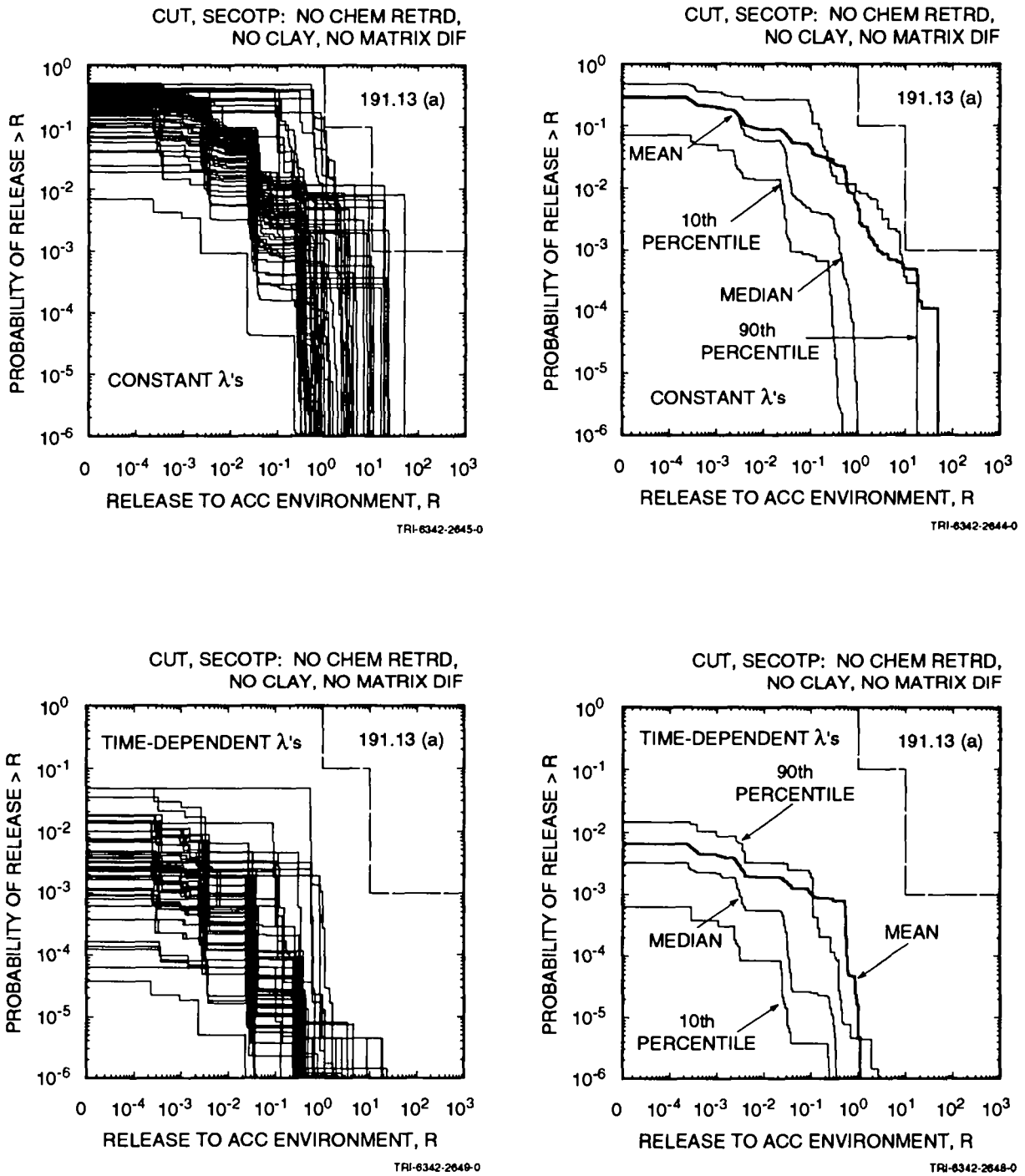

Figure 8.5-5. Distribution of CCDFs for normalized release to the accessible environment over 10,000 yr due to cuttings removal and groundwater transport with no chemical retardation, no clay lining in fractures and no matrix diffusion for risk representation R_1 defined in Eq. 2.5-1 with constant (upper two frames) and time-dependent (lower two frames) rate terms in the Poisson model for drilling intrusions.

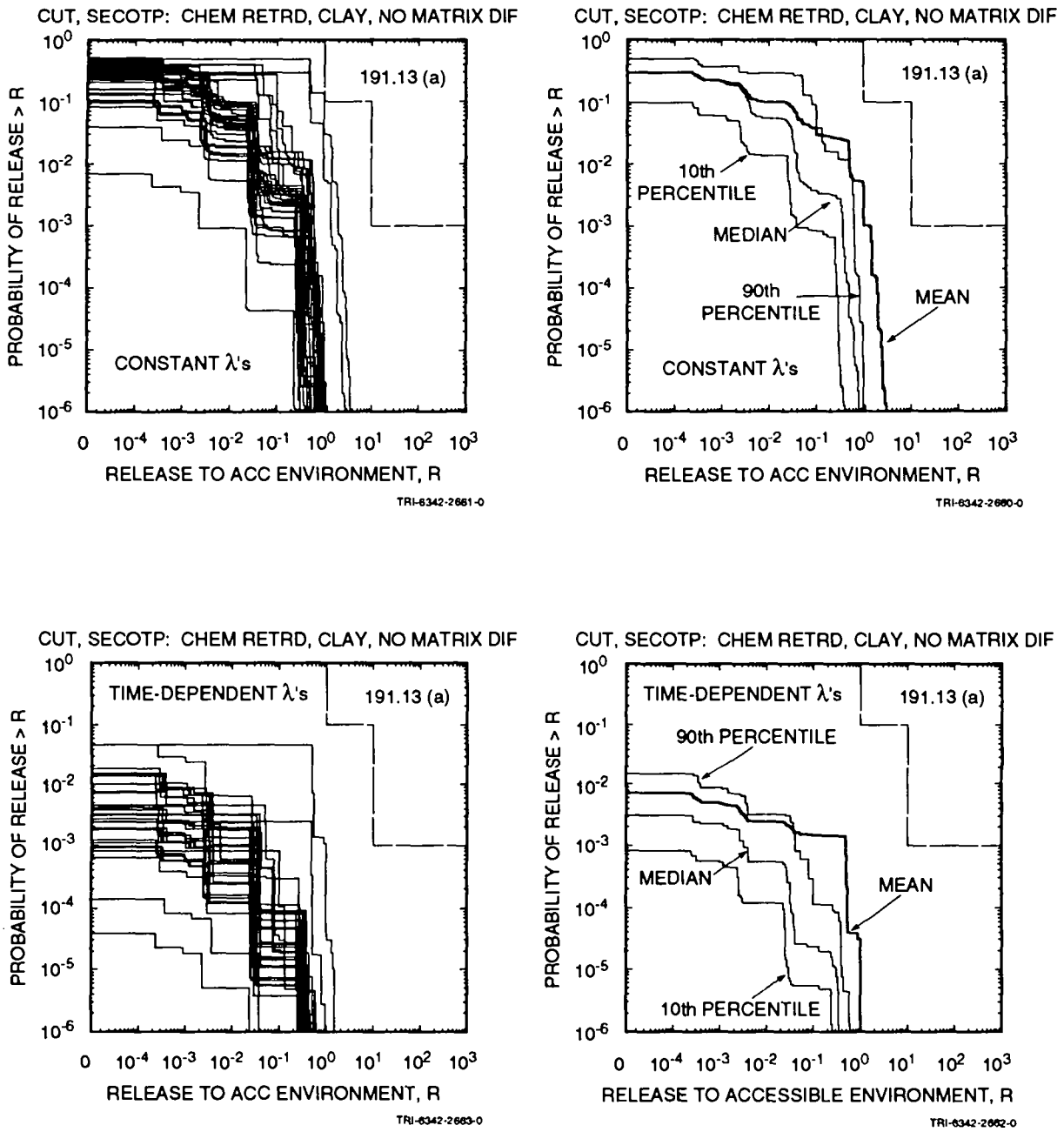

Figure 8.5-6. Distribution of CCDFs for normalized release to the accessible environment over 10,000 yr due to cuttings removal and groundwater transport with chemical retardation, clay-lined fractures and no matrix diffusion for risk representation R_1 defined in Eq. 2.5-1 with constant (upper two frames) and time-dependent (lower two frames) rate terms in the Poisson model for drilling intrusions.

for the rate constant λ in the Poisson model for drilling intrusions fall substantially below the EPA release limits. Further, as is the case throughout this analysis, the use of the time-dependent λ's produces CCDFs that are farther from the EPA release limits than those obtained with the constant λ's. As comparison with the results in Figure 8.5-5 for groundwater transport with no chemical retardation, no clay lining in fractures and no matrix diffusion shows, the addition of chemical retardation causes a noticeable shift of the CCDFs away from the EPA release limits.

The CCDFs for total release to the accessible environment with chemical retardation, no clay lining in fractures and matrix diffusion are presented in Figure 8.5-7. As suggested by the very small releases shown in Figures 8.5-1 and 8.5-2 for this analysis alternative, the CCDFs in Figure 8.5-7 for total release are essentially identical to the CCDFs in Figure 8.5-3 for cuttings removal only. Although not shown, the CCDFs for total release to the accessible environment with chemical retardation, clay-lined fractures and matrix diffusion are also essentially identical to the CCDFs for cuttings removal only in Figure 8.5-3.

The CCDFs for total release to the accessible environment with no chemical retardation, no clay lining in fractures and matrix diffusion are presented in Figure 8.5-8. As shown in Figures 8.5-1 and 8.5-2, most releases due to groundwater transport for this analysis alternative are less than the corresponding releases due to cuttings removal, although there are some sample elements for which the groundwater release exceeds the cuttings removal release. The result is that the CCDFs in Figure 8.5-8 for total release are similar to the CCDFs in Figure 8.5-3 for cuttings removal only, with a few CCDFs for total release being shifted closer to the EPA release limits than the corresponding CCDFs for cuttings removal only.

As shown in Figures 8.5-1 and 8.5-2, releases to the accessible environment due to groundwater transport calculated with and without a clay lining in fractures in conjunction with no chemical retardation and matrix diffusion are similar. The box plot in Figure 8.5-2 for groundwater transport with no chemical retardation, no clay lining in fractures and matrix diffusion appears to have more extreme values than the corresponding plot for results obtained with clay-lined fractures. This difference is due to the use of 35 and 70 sample elements, respectively, to generate the box plots for the cases with and without clay-lined fractures. As comparison of the box plots shows, similar mean, median and 75th percentile values are obtained for releases calculated with and without clay-lined fractures. As a result, the CCDFs for total release to the accessible environment with no chemical retardation, clay-lined fractures and matrix diffusion are essentially the same as the CCDFs in Figure 8.5-8 for total release to the accessible environment with no chemical retardation, no clay lining in fractures and matrix diffusion, and thus are not shown.

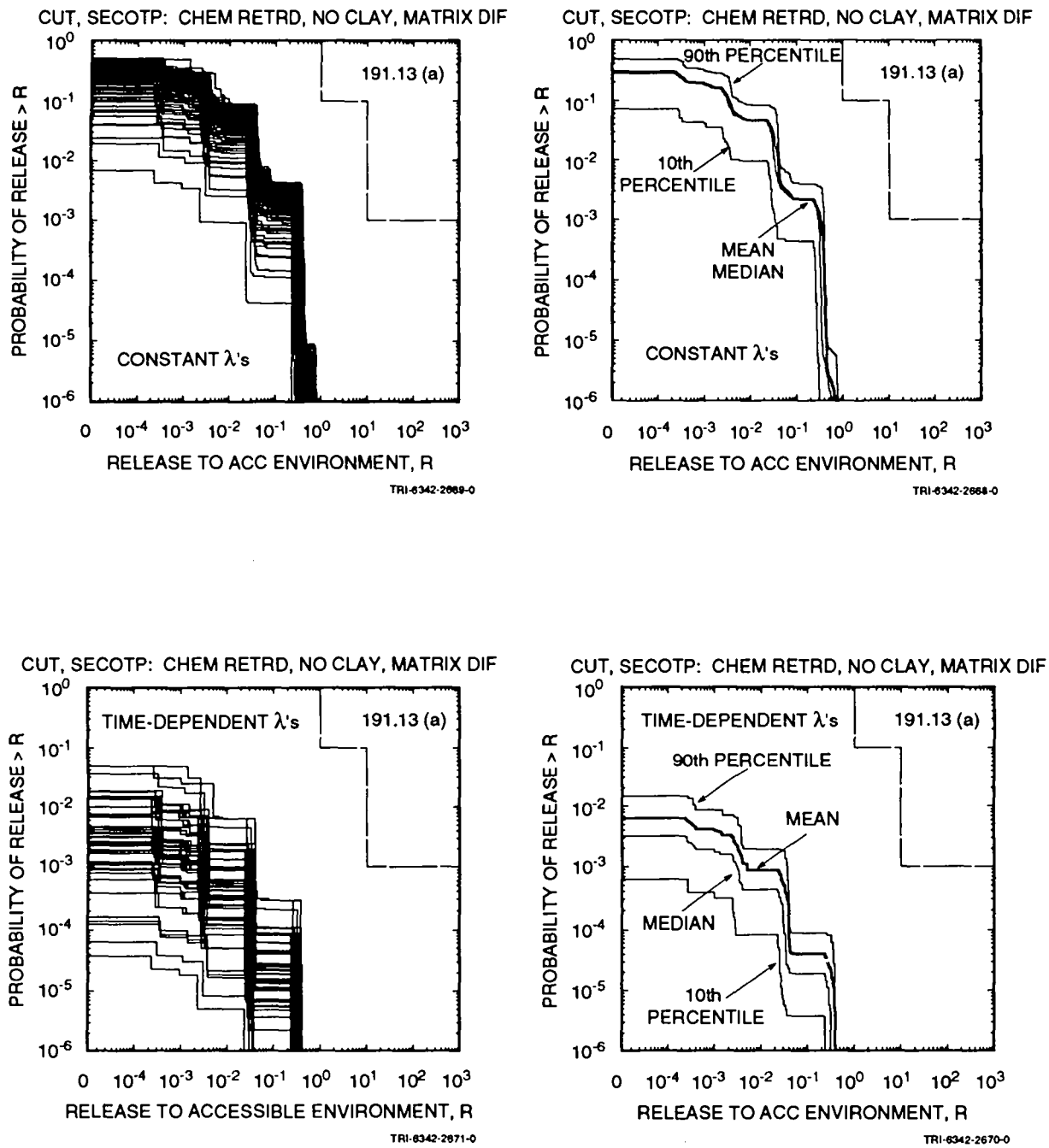

Figure 8.5-7. Distribution of CCDFs for normalized release to the accessible environment over 10,000 yr due to cuttings removal and groundwater transport with chemical retardation, no clay lining in fractures and matrix diffusion for risk representation R_1 defined in Eq. 2.5-1 with constant (upper two frames) and time-dependent (lower two frames) rate terms in the Poisson model for drilling intrusions.

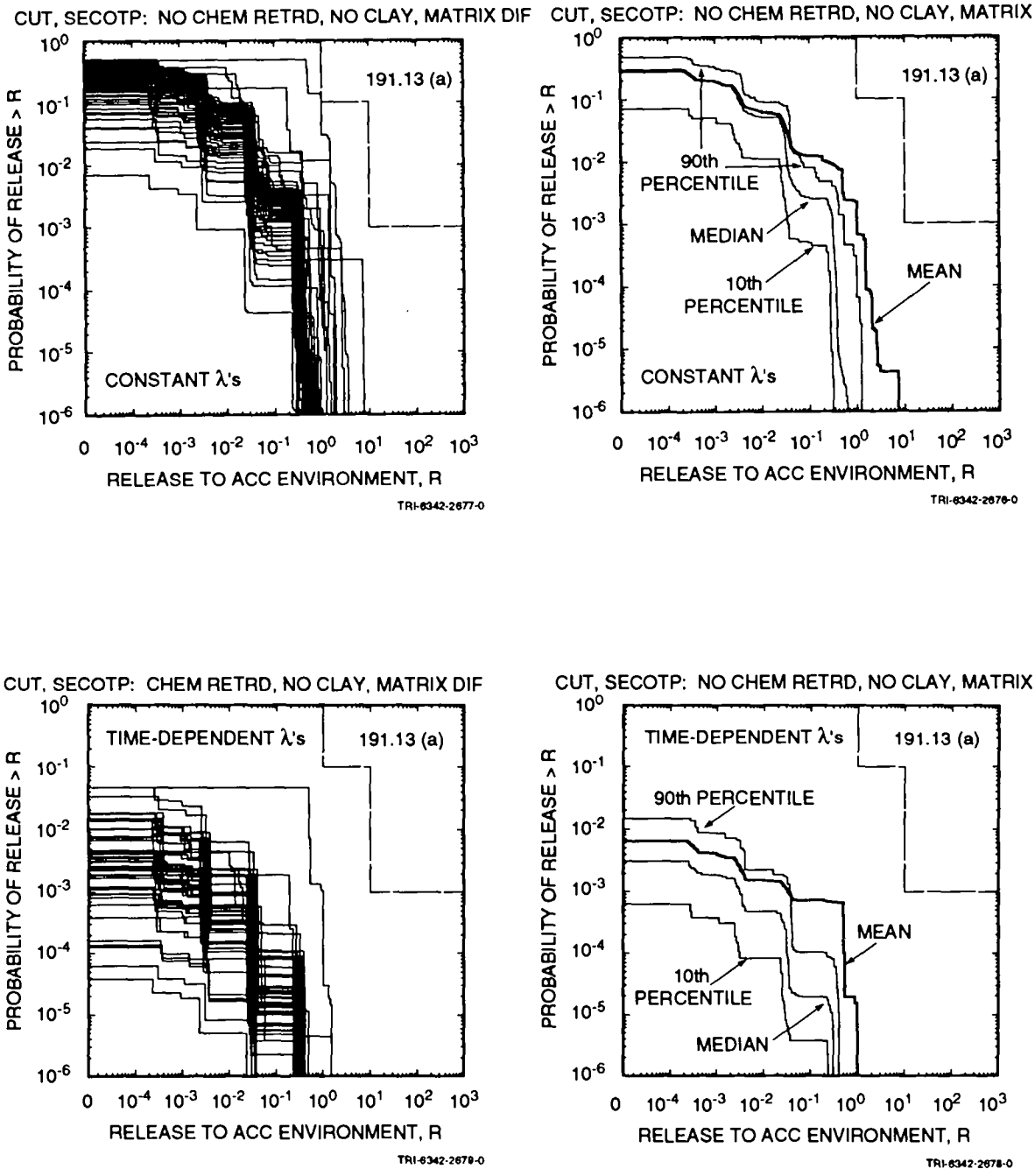

Figure 8.5-8. Distribution of CCDFs for normalized release to the accessible environment over 10,000 yr due to cuttings removal and groundwater transport with no chemical retardation, no clay lining in fractures and matrix diffusion for risk representation R_1 defined in Eq. 2.5-1 with constant (upper two frames) and time-dependent (lower two frames) rate terms in the Poisson model for drilling intrusions.

9. DISCUSSION

As described in Volumes 1 and 2 of this report, major modeling improvements have been made since the 1991 preliminary comparison with 40 CFR 191 (WIPP PA Division, 1991a, 1991b, 1991c). These improvements include the following: coupling creep closure of the repository to gas generation and two-phase flow; accounting for spatial variability in the transmissivity fields of the Culebra Dolomite Member of the Rustler Formation in a way that each field reproduces exactly measured transmissivity data at well locations and is also calibrated to steady-state and transient-pump data; more accurately simulating radionuclide transport in the Culebra; and accounting for the effects of passive marker systems through time-varying drilling intensities within the Poisson model for calculating intrusion probabilities. As described in Volumes 2 and 3 of this report, other improvements have been made throughout the modeling system and data base. Improvements remain to be made in many areas, including the following: modeling of possible pressure-dependent fracturing of anhydrite interbeds in the Salado Formation; modeling of three-dimensional groundwater flow in the Rustler Formation including the effects of subsidence of potash mine excavations; incorporating effects of plug degradation in intrusion boreholes; understanding and modeling spalling phenomena; modeling of gas-generation processes; acquiring experimental data for actinide solubilities and retardations; and determining the most appropriate conceptual model for radionuclide transport in the Culebra.

Consideration of alternative models for the probability of human intrusion and radionuclide transport in the Culebra provides insights into the relative impacts on performance of specific components of the natural and engineered barrier system and institutional controls at the Waste Isolation Pilot Plant (WIPP). Resulting CCDFs, grouped into major barrier effects, are presented in Figure 9-1.

The uppermost CCDF in Figure 9-1, labeled (1) and calculated without any transport in the Culebra and with constant rate term λ, represents an estimate of the performance of the disposal system with no contribution from the natural barrier provided by retardation in the Culebra and no contribution from the potential institutional barrier that could be provided by passive markers, as required by the Assurance Requirements (§ 191.14c). For the modeling system and data base used in 1992, the mean CCDF for this case lies below the EPA limits.

The CCDF in Figure 9-1 labeled (2) represents an estimate of the performance of the disposal system if physical retardation by diffusion into

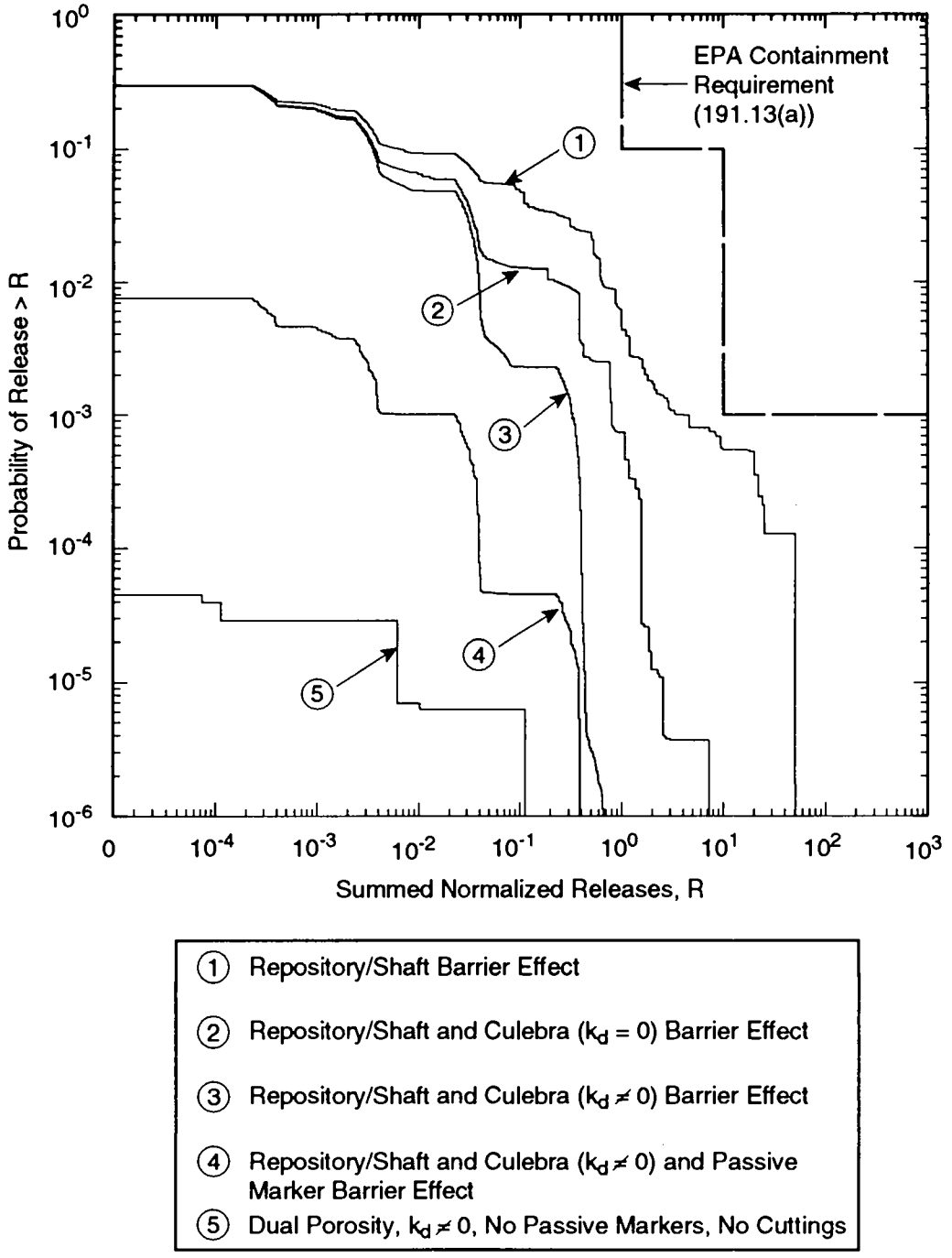

Figure 9-1. A comparison of mean CCDFs by barrier effect. CCDFs are constructed using releases from intrusions occurring at 1000 yr. CCDFs display the impact of including specific components of the engineered, natural, and institutional barrier systems as shown.

the pore volume of the Culebra is included as a part of the natural barrier system. The area between the first and second CCDFs is a measure of the potential regulatory impact of including physical retardation. Similarly, the next CCDF in Figure 9-1, labeled (3), represents an estimate of performance of the disposal system if both physical and chemical retardation in the Culebra are included in the natural barrier system. Because the location of this CCDF is determined entirely by cuttings releases, it represents the largest possible shift to the left because of including the barrier effect of non-Salado units.

The CCDF in Figure 9-1 labeled (5) represents an estimate of the performance of the disposal system only considering subsurface releases to the accessible environment, i.e., cuttings are not included. These subsurface releases plus cuttings releases result in the previous CCDF, labeled (3). Comparison of these two CCDFs shows the importance of cuttings releases in the CCDF labeled with (3) representing the combined barrier effect of sorption and physical retardation.

The CCDF in Figure 9-1 labeled (4) shows the effect of including expert judgment on the efficacy of passive markers in reducing the probability of human intrusion. This final CCDF (number 4) in Figure 9-1, also determined entirely by cuttings releases, was calculated using what the WIPP PA Department believes at this time to be the most realistic conceptual model for the disposal system, based on models and data available in 1992. As indicated previously, results are preliminary, and none of the curves shown in Figure 9-1 are believed sufficiently defensible for use in a final compliance evaluation.

The CCDFs in Figure 9-1 represent a barrier-effect display of the status of WIPP PA with respect to the Containment Requirements (§ 191.13). The barrier effects are represented by "total" (cuttings plus subsurface) CCDFs for the repository/shaft barrier labeled (1); the zero-sorption, physical retardation barrier effect of the Culebra labeled (2); the nonzero sorption, physical retardation barrier effect of the Culebra labeled (3); and the passive-marker-barrier effect CCDF labeled (4). Other important displays are CCDFs for cuttings alone [coincident with (3)] and subsurface releases alone (5). Important parameters for each of these cases will now be discussed barrier by barrier in the context of a possible approach to defending a closure decision for compliance.

Cuttings are a part of each CCDF that represents a viable comparison with the Containment Requirements. As seen in Figure 8.2-2, the important radionuclides contributing to releases in excess of 10^{-2} that would have any chance of contributing to the CCDF near the limit $(1, 10^{-1})$ and $(10, 10^{-3})$ are Pu-238, Am-241, and Pu-239. The important parameter that dominates virtually

all of the variability up to EPA Sums of 10^{-1} is the drilling intensity. Clearly, if no intrusion occurs, there are no cuttings releases.

The repository/shaft barrier-effect, mean CCDF (1) lies close to but below the regulatory criterion of (10, 10^{-3}). From Figure 8.3-1, it is evident that the important radionuclides (EPA Sums greater than 10^{-2}) are, in descending order, Am-241, Pu-239, Pu-240, U-233, U-234, Th-229, Th-230, Np-237, and Ra-226. Comparison with Figure 7.3-1 shows that this list includes all radionuclides in the inventory that have not decayed below 10^{-2} by the 1000-yr intrusion time except Pu-238. Regression analyses (Table 8.3-1) indicated that the important parameters are intrusion borehole permeability, radionuclide solubilities, and Salado halite and anhydrite permeabilities (correlated at 0.8). If intrusion occurs, the permeability of the borehole fill is the most important parameter affecting releases because it is a direct determinant of the quantity of brine released. The assumptions about the range and distribution of this parameter are determined by regulatory guidance. After assumptions about the intrusion event, the next most important parameters are related to how much brine flows through the waste and the solubility of radionuclides in that brine. With the present conceptual model for the Salado and its interbeds, the permeabilities of these units determine brine inflow and outflow. In fact, Figure 8.3-2 shows a threshold of permeability (10^{-22} m^2) below which brine inflow will not occur in sufficient amount to result in any release to the Culebra. The scatterplot emphasizes the importance of this parameter, and is the reason for placing halite and anhydrite permeabilities equal to solubilities in importance. If brine flows through the waste and borehole to the Culebra, then radionuclide solubilities determine the quantity of radionuclides released. Note that drill-bit diameter is the next most important parameter in the regression analysis, but only accounts for a very small amount of the variability in releases.

Table 9-1 shows the important parameters and radionuclides for only the repository/shaft barrier. These results are based on 68/70 nonzero releases for E1E2-type scenarios and 14/70 nonzero releases for E1- and E2-type scenarios. The family of CCDFs (Figure 8.3-9) that gave rise to the mean CCDF as a summary measure contained 6/70 sample elements resulting in CCDFs above the regulatory limit and resulting in the 90th-percentile curve falling just below the (10,10^{-3}) limit. Therefore, defending a compliance decision would be strongly influenced by the list of parameters in Table 9-1. Note that of the five parameters listed, only one parameter, solubility, can be changed by action taken within the repository. Only one parameter (permeabilities of halite and anhydrite) can be reduced in uncertainty with continued in-situ investigation. Three parameters are determined by regulatory guidance. Further, the list of important radionuclides requiring

Table 9-1. Important Radionuclides and Parameters for the Repository/Shaft Barrier

Radionuclides	Parameters
Am-241	Drilling Intensity
Pu-239, Pu-240	Intrusion Borehole Permeability
U-233, U-234	Salado (Marker Bed) Permeabilities
Th-229, Th-230	Radionuclide Solubilities
Np-237, Ra-226	Drill-Bit Diameter

solubility estimates has not changed from last year's guidance (Memorandum by Marietta and Nowak in Appendix D of this volume) to the solubility/leachate experimental program.

The next barrier-effect CCDF, labeled (2), represents only physical retardation or zero sorption in the Culebra as specified in the Consultation and Cooperation Agreement (US DOE and State of New Mexico, 1981, as modified) in the absence of in-situ measurements. Inspection of Figure 8.4-16 shows a change in important radionuclides from the repository/shaft barrier-effect CCDF. Am-241 and Pu-238 have dropped in importance because of increased travel times in the Culebra and their subsequent decay. The same radionuclides, Pu-239, Pu-240, Am-241, U-233, U-234, Th-229, Th-230, and Np-237, are released at amounts greater than EPA Sums of 10^{-2} for a few sample elements, but with lower values. All sample elements show Ra-226 below 10^{-2}, and Pu-239, Pu-240, and Am-241 have exchanged positions. Because physical retardation in the Culebra now represents the last retardation effect in the system, parameters related to this effect move to the top of the list resulting from the regression analysis (see Table 9-2). Thus, Culebra fracture spacing accounts for most of the variability in releases, followed closely by intrusion borehole permeability. Radionuclide solubility accounts for less variability. The effect of Culebra transmissivity fields and Culebra porosity accounts for a small amount of the variability.

The next barrier-effect CCDF, labeled (3), represents the full Culebra barrier effect with both physical retardation and sorption. Inspection of Figure 8.4-8 shows another change in important radionuclides from the previous two barrier-effect CCDFs. Am and Pu do not appear because they have been sorbed within the land-withdrawal boundary in the Culebra. Only U-233, U-234, Th-229, and Th-230 are released for a few sample elements at amounts greater, but only slightly greater, than EPA Sums of 10^{-2}. Parameters related to sorption comprise the list resulting from the regression analysis. Thus, Culebra fracture spacing and matrix K_ds are the only parameters

Table 9-2. Important Radionuclides and Parameters for the Culebra

Radionuclides	Parameters
Pu-239, Pu-240	Culebra Fracture Spacing
Am-241	Intrusion Borehole Permeability
U-233, U-234	Radionuclide Solubilities
Th-229, Th-230	Culebra Transmissivity Fields
Np-237	Culebra Porosity

selected during the regression analysis. Because only a few nonzero releases occur, very little variability can be accounted for. Further, the list of important radionuclides requiring retardation estimates has not changed from the last year's guidance to the tracer-column experimental program (Memorandum by Marietta and Gelbard in Appendix D of this volume).

Now the problem is how to summarize the results of the above barrier-by-barrier analyses in a list of important parameters. Compiling such a list is a subjective process that assumes a strategy for building a defensible PA, and it must rely on setting priorities to reach a closure decision on compliance. This list of important parameters by barrier effect is assembled in the following sense. Conditional on the present analysis, the repository/shaft CCDF falls below the criteria with a level of confidence of 90%. Therefore, increasing the defensibility of the assumptions that were involved in constructing the repository/shaft barrier-effect CCDF should get highest priority for building defensibility of the overall PA. Only some of these assumptions can actually be impacted by additional investigations and/or programmatic decisions, whereas the others are impacted by regulatory guidance.

Next, the Culebra barrier effect provides an additional margin of safety. This margin of safety is important in providing an additional shift of the CCDF to the compliance side of the criteria. Because the repository/shaft case is already essentially in compliance, this additional safety margin of the Culebra should assume a lower priority in compiling the summary list. However, no matter how well the Culebra and other non-Salado units are characterized, the resulting CCDFs will never fall to the right of the repository/shaft case or to the left of the cuttings-only case. This represents a spread in uncertainty over about two orders of magnitude with respect to normalized release. Of course, reduction of uncertainty within the repository, such as that associated with actinide solubilities, will shrink this spread because cuttings will not be affected by such a reduction. Cuttings-only CCDFs could, in fact, move to the right slightly with the

inclusion of spalled material from the waste. Thus, for defending a closure decision, a small spread in uncertainty exists that could be affected by additional characterization of non-Salado units.

The separate issue of assessing long-term safety of the repository from a health-effects point of view requires additional consideration. Because the subsurface-to-stock-well-to-cow-to-human pathway, is the important exposure pathway (conditional on an assumption that present-day conditions persist), the shift from zero-sorption to nonzero-sorption cases is important. Defending this shift between zero-sorption and nonzero-sorption CCDFs is analogous to defending a shift in overall, long-term safety of the repository of about four orders of magnitude. Even though the CCDF labeled (3) is the one that should be compared to the regulatory criteria, the CCDF labeled (5) can lead to a site-specific measure of long-term safety in terms of human risk.

Next, the passive-marker barrier effect provides a second additional margin of safety with respect to both compliance with 40 CFR 191 and site-specific, long-term safety (health effects), representing a shift of another two orders of magnitude.

Taking the above barrier-by-barrier reasoning into account, the regression, partial correlation, and scatterplot sensitivity analysis results are compiled into the list of important parameters in Table 9-3. Parameters in the first three categories are those for which reductions in uncertainty have the potential to affect the location of the mean CCDF near the compliance criteria. Conditional on the present modeling assumptions and parameter-value distributions, long-term disposal-system performance with regard to 40 CFR 191 is not sensitive to uncertainty in parameters included in the "Less Important" category. Defensibility of a compliance decision will require, however, that uncertainties assigned to all parameters, including those identified as less important, adequately capture reality. Specifically, wherever practical, site-specific information should be collected to verify with sufficient confidence that reality lies within the assigned range and distribution for each parameter.

With respect to 40 CFR 191, improvements to be made in either the next or following PA are expected to have the following effects on these results. (1) The addition of pressure-dependent fracturing in anhydrite interbeds of the Salado Formation: No effect on the shape of the CCDF near the criteria because brine flow into a borehole for high-consequence sample elements will not be impacted. (2) Modeling of three-dimensional groundwater flow innon-Salado units: The inclusion of vertical flow and effects on vertical flow because of climate variability and subsidence events may create changes in the list of important parameters for the natural-barrier system. However,

Table 9-3. Importance of Sampled Parameters with Respect to 40 CFR 191B. Results apply only to disturbed performance of the repository (human intrusion), and are conditional on modeling assumptions, the choice of parameters sampled, and the assumed parameter-value distributions. Comparable results for 40 CFR 268.6 (undisturbed performance) can be found in Volume 5 of this report.

Parameter Name	Parameter Description
Critically Important Parameters (listed in order of importance)	
LAMBDA	Drilling intensity
BHPERM	Intrusion borehole permeability
Very Important Parameters (listed in order of importance)	
SALPERM	Salado halite permeability
MBPERM	Salado anhydrite permeability
SOLx	Radionuclide solubilities (6, x = AM,NP,PU, RA,TH,U)
CULFRSP	Culebra fracture spacing
MKDx	Matrix K_ds (6, x = AM,NP,PU,RA,TH,U)
Important Parameters (listed in order of importance)	
CULTRFLD	Culebra transmissivity fields
CULPOR	Culebra matrix porosity
Less Important Parameters (listed in alphabetical order)	
BCBRSAT	Residual brine saturation in Salado Fm.
BCEXP	Brooks-Corey relative permeability model exponent
BCFLG	Brooks-Corey/van Genuchten-Parker pointer
BCGSSAT	Brooks-Corey residual gas saturation for Salado Fm.
BPPRES	Castile brine pressure
BPSTOR	Castile brine reservoir storativity
BPAREAFR	Castile brine reservoir area fraction
BRSAT	Initial brine saturation in waste
CULCLIM	Climatic recharge factor
CULFRPOR	Culebra fracture porosity
CULCLYF	Culebra fracture clay filling fraction
CULCLYP	Culebra fracture clay filling porosity
FKDx	Fracture K_ds (6, x = AM,NP,PU,RA,TH,U)
GRCORHF	Corrosion gas-generation rate factor, humid conditions

Table 9-3. Importance of Sampled Parameters with Respect to 40 CFR 191B. Results apply only to disturbed performance of the repository (human intrusion), and are conditional on modeling assumptions, the choice of parameters sampled, and the assumed parameter-value distributions. Comparable results for 40 CFR 268.6 (undisturbed performance) can be found in Volume 5 of this report (concluded).

Parameter Name	Parameter Description
GRCORI	Corrosion gas-generation rate, inundated conditions
GRMICHF	Biodegradation gas-generation rate factor, humid conditions
GRMICI	Biodegradation gas-generation rate, inundated conditions
MBPOR	Salado anhydrite porosity
MBPRES	Far-field pressure in Salado Fm.
STOICCOR	Corrosion stoichiometric coefficient
STOICMIC	Biodegradation stoichiometric coefficient
TZPORF	Transition Zone and DRZ porosity factor
VMETAL	Volume fraction of metals and glass in waste
VWOOD	Volume fraction of combustibles in waste

the resulting CCDFs will always lie between the repository/shaft barrier-effect CCDF (number 1 in Figure 9-1) and the cuttings-only CCDF (number 3). (3) Modeling of gas-generation processes: This model is primarily a RCRA issue, and gas-generation model parameters have little importance in the regression analyses for 40 CFR 191. For the Containment Requirements, the important issue is whether gas is generated or not because gas generation diminishes brine and radionuclide releases. Once some gas generation occurs, the uncertainty associated with the gas-generation model is relatively unimportant compared to other system parameters listed in Table 9-3. (4) Actinide source-term modeling: Inspection of Table 9-3 shows that radionuclide solubilities are the parameters affecting the repository/shaft barrier that are ranked in the first two categories, and that can most readily be impacted by programmatic decisions and an experimental program. Based on the present wide range of uncertainty in the PA data base for solubilities, more project effort here has the potential for improving the compliance picture by shifting the CCDF labeled (1) to the left in Figure 9-1. (5) Addition of releases because of spalling of waste material into an intruding borehole: The mechanism for this phenomenon is poorly understood. Preliminary estimates indicate that cuttings releases could be increased significantly (Berglund, 1992). If the experimental program corroborates this estimate, the CCDF labeled

(3) will shift to the right slightly. This shift would not significantly impact the compliance picture, but as these improvements in the PA system move CCDFs (1) and (3) closer together, the range of uncertainty that can be impacted by further work in the Culebra and non-Salado units shrinks. (6) Addition of plug degradation in the intrusion boreholes: Allowing plugs to degrade to essentially borehole-fill properties should result in two effects. The probability of E1E2-type flow paths will diminish, and flow directly to the surface may occur. The latter effect cannot result in a shift of the CCDF past the repository/shaft barrier-effect CCDF because calculating EPA Sums at the discharge point in the Culebra is equivalent with transporting directly to the surface. (7) The use of time-varying drilling intensities: The above discussion of uncertainty and sensitivity analyses relied primarily on the use of time-invariant drilling intensities, within the Poisson model that have been used for calculating scenario probabilities. The constant rate term is a sampled parameter that has a different value, constant for 10,000 yr, for each sample element, whereas the time-dependant rate term is a different function of time for each sample element. The time-dependant rate term incorporates the deterrent effect and estimated efficacy of possible passive marker systems for future societies of different levels of technology. The passive-marker barrier effect does not depend on the Culebra (or non-Salado) barrier effect and can be used equally well with the repository/shaft, barrier-effect CCDF or the cuttings-only CCDF to provide additional safety margins. In any case, a shift of about two orders of magnitude is indicated. Again, defense of the PA and compliance assessment should be based on defending the repository/shaft barrier-effect CCDF (number 1) and determining the potential contribution of the natural barrier system (displayed here as the region between CCDFs 1 and 3). In addition, passive marker systems could provide a convincing and effective margin of safety without requiring extensive reduction of uncertainty in the natural-barrier system.

10. REFERENCES

Bachman, G.O. 1985. *Assessment of Near-Surface Dissolution At and Near the Waste Isolation Pilot Plant (WIPP), Southeastern New Mexico.* SAND84-7178. Albuquerque, NM: Sandia National Laboratories.

Beauheim, R.L. 1987. *Interpretations of Single-Well Hydraulic Tests Conducted At and Near The Waste Isolation Pilot Plant (WIPP) Site, 1983-1987.* SAND87-0039. Albuquerque, NM: Sandia National Laboratories.

Beauheim, R.L., and P.B. Davies. 1992. "Experimental Plan for Tracer Testing in the Culebra Dolomite at the WIPP Site." Revision A. Albuquerque, NM: Sandia National Laboratories.

Beauheim, R.L., G.J. Saulnier, Jr., and J.D. Avis. 1991a. *Interpretation of Brine-Permeability Tests of the Salado Formation at the Waste Isolation Pilot Plant Site: First Interim Report.* SAND90-0083. Albuquerque, NM: Sandia National Laboratories.

Beauheim, R.L., T.F. Corbet, P.B. Davies, and J.F. Pickens. 1991b. "Appendix A: Recommendations for the 1991 Performance Assessment Calculations on Parameter Uncertainty and Model Implementation for Culebra Transport Under Undisturbed and Brine-Reservoir-Breach Conditions," *Preliminary Comparison with 40 CFR Part 191, Subpart B for the Waste Isolation Pilot Plant, December 1991. Volume 3: Reference Data.* WIPP Performance Assessment Division. Eds. R.P. Rechard, A.C. Peterson, J.D. Schreiber, H.J. Iuzzolino, M.S. Tierney, and J.S. Sandha. SAND91-0893/3. Albuquerque, NM: Sandia National Laboratories. A-7 through A-18.

Berglund, J.W. 1990. Appendix A: "Letter 1a: Bar Graphs Representing Range of Values for Drilling Operations Near WIPP Site," *Data Used in Preliminary Performance Assessment of the Waste Isolation Pilot Plant (1990).* R.P. Rechard, H.J. Iuzzolino, and J.S. Sandha. SAND89-2408. Albuquerque, NM: Sandia National Laboratories. A-157 through A-164.

Berglund, J.W. 1992. *Mechanisms Governing the Direct Removal of Wastes from the Waste Isolation Pilot Plant Repository Caused by Exploratory Drilling.* SAND92-7295. Albuquerque, NM: Sandia National Laboratories.

Bertram-Howery, S.G., M.G. Marietta, D.R. Anderson, K.F. Brinster, L.S. Gomez, R.V. Guzowski, and R.P. Rechard. 1989. *Draft Forecast of the Final Report for the Comparison to 40 CFR Part 191, Subpart B, for the Waste Isolation Pilot Plant.* SAND88-1452. Albuquerque, NM: Sandia National Laboratories.

Bertram-Howery, S.G., M.G. Marietta, R.P. Rechard, P.N. Swift, D.R. Anderson, B.L. Baker, J.E. Bean, Jr., W. Beyeler, K.F. Brinster, R.V. Guzowski, J.C. Helton, R.D. McCurley, D.K. Rudeen, J.D. Schreiber, and P. Vaughn. 1990. *Preliminary Comparison with 40 CFR Part 191, Subpart B for the Waste Isolation Pilot Plant, December 1990.* SAND90-2347. Albuquerque, NM: Sandia National Laboratories.

Brinster, K.F. 1991. *Preliminary Geohydrologic Conceptual Model of the Los Medaños Region Near the Waste Isolation Pilot Plant for the Purpose of Performance Assessment.* SAND89-7147. Albuquerque, NM: Sandia National Laboratories.

Broc, R., ed. 1982. *Drilling Mud and Cement Slurry Rheology Manual.* Houston, TX: Gulf Publishing Company.

Brooks, R.H., and A.T. Corey. 1964. *Hydraulic Properties of Porous Media.* Hydrology Paper No. 3. Fort Collins, CO: Civil Engineering Department, Colorado State University.

Brush, L.H. 1991. "Appendix A: Current Estimates of Gas Production Rates, Gas Production Potentials, and Expected Chemical Conditions Relevant to Radionuclide Chemistry for the Long-Term WIPP Performance Assessment," *Preliminary Comparison with 40 CFR Part 191, Subpart B for the Waste Isolation Pilot Plant, December 1991. Volume 3: Reference Data.* WIPP Performance Assessment Division. Eds. R.P. Rechard, A.C. Peterson, J.D. Schreiber, H.J. Iuzzolino, M.S. Tierney, and J.S. Sandha. SAND91-0893/3. Albuquerque, NM: Sandia National Laboratories. A-25 through A-36.

Brush, L.H., and D.R. Anderson. 1989. "A.1: Drum (Metal) Corrosion, Microbial Decomposition of Cellulose, Reactions Between Drum-Corrosion Products and Microbially Generated Gases, Reactions on WIPP Gas and Water Budgets," *Systems Analysis, Long-Term Radionuclide Transport, and Dose Assessments, Waste Isolation Pilot Plant (WIPP), Southeastern New Mexico; March 1989.* Eds. A.R. Lappin, R.L. Hunter, D.P. Garber, and P.B. Davies. SAND89-0462. Albuquerque, NM: Sandia National Laboratories. A-3 through A-30.

Coleman, B.D., and W. Noll. 1959. "Helical Flow of General Fluids," *Journal of Applied Physics.* Vol. 30, no. 10, 1508-1515.

Corey, A.T. 1986. *Mechanics of Immiscible Fluids in Porous Media.* Littleton, CO: Water Resources Publications.

Cranwell, R.M., R.V. Guzowski, J.E. Campbell, and N.R. Ortiz. 1990. *Risk Methodology for Geologic Disposal of Radioactive Waste: Scenario Selection Procedure.* NUREG/CR-1667, SAND80-1429. Albuquerque, NM: Sandia National Laboratories.

Darley, H.C.H., and G.R. Gray. 1988. *Composition and Properties of Drilling and Completion Fluids.* Houston, TX: Gulf Publishing Company. 243.

Davies, P.B. 1989. *Variable-Density Ground-Water Flow and Paleohydrology in the Waste Isolation Pilot Plant (WIPP) Region, Southeastern New Mexico*. Open-File Report 88-490. Albuquerque, NM: US Geological Survey.

EPA (Environmental Protection Agency). 1985. "40 CFR Part 191: Environmental Standards for the Management and Disposal of Spent Nuclear Fuel, High-Level and Transuranic Radioactive Wastes; Final Rule," *Federal Register*. Vol. 50, no. 182, 38066-38089.

EPA (Environmental Protection Agency). 1986. "40 CFR Part 268: Land Disposal Restrictions," as amended and published in the most recent *Code of Federal Regulations*. Washington, DC: Office of the Federal Register, National Archives and Records Administration.

Fredrickson, A.G. 1960. "Helical Flow of an Annular Mass of Visco-Elastic Fluid," *Chemical Engineering Science*. Vol. 11, no. 3, 252-259.

Freeze, R.A., and J.A. Cherry. 1979. *Groundwater*. Englewood Cliffs, NJ: Prentice-Hall, Inc.

Gonzales, M.M. 1989. *Compilation and Comparison of Test-Hole Location Surveys in the Vicinity of the Waste Isolation Pilot Plant Site*. SAND88-1065. Albuquerque, NM: Sandia National Laboratories.

Gorham, E., R. Beauheim, P. Davies, S. Howarth, and S. Webb. 1992. "Appendix A: Recommendations to PA on Salado Formation Intrinsic Permeability and Pore Pressure for 40 CFR 191 Subpart B Calculations," *Preliminary Performance Assessment for the Waste Isolation Pilot Plant, December 1992. Volume 3: Model Parameters*. Sandia WIPP Project. SAND92-0700/3. Albuquerque, NM: Sandia National Laboratories. A-47 through A-67.

Helton, J.C. 1993a. "Drilling Intrusion Probabilities for Use in Performance Assessment for Radioactive Waste Disposal," *Reliability Engineering and System Safety*. Vol. 40, no. 3, 259-275.

Helton, J.C. 1993b. "Risk, Uncertainty in Risk, and the EPA Release Limits for Radioactive Waste Disposal," *Nuclear Technology*. Vol. 101, no. 1, 18-39.

Helton, J.C., and R.J. Breeding. 1993. "Calculation of Reactor Accident Safety Goals," *Reliability Engineering and System Safety*. Vol. 39, no. 2, 129-158.

Helton, J.C., and H.J. Iuzzolino. 1993. "Construction of Complementary Cumulative Distribution Functions for Comparison with the EPA Release Limits for Radioactive Waste Disposal," *Reliability Engineering and System Safety*. Vol. 40, no. 3, 277-293.

Helton, J.C., J.W. Garner, R.D. McCurley, and D.K. Rudeen. 1991. *Sensitivity Analysis Techniques and Results for Performance Assessment at the Waste Isolation Pilot Plant*. SAND90-7103. Albuquerque, NM: Sandia National Laboratories.

Helton, J.C., J.W. Garner, R.P. Rechard, D.K. Rudeen, and P.N. Swift. 1992. *Preliminary Comparison with 40 CFR Part 191, Subpart B for the Waste Isolation Pilot Plant, December 1991—Volume 4: Uncertainty and Sensitivity Analysis Results*. SAND91-0893/4. Albuquerque, NM: Sandia National Laboratories.

Hora, S.C., D. von Winterfeldt, and K.M. Trauth. 1991. *Expert Judgment on Inadvertent Human Intrusion into the Waste Isolation Pilot Plant*. SAND90-3063. Albuquerque, NM: Sandia National Laboratories.

Howarth, S.M., E.W. Peterson, P.L. Lagus, K-H. Lie, S.J. Finley, and E.J. Nowak. 1991. "Interpretation of In-Situ Pressure and Flow Measurements of the Salado Formation at the Waste Isolation Pilot Plant," *1991 Joint Rocky Mountain Regional Meeting, Society of Petroleum Engineers and Low Permeability Reservoirs Symposium, Denver, CO, April 15-17, 1991*. SPE-21840; SAND90-2334C. Richardson, TX: Society of Petroleum Engineers.

Huyakorn, P.S., H.O. White, Jr., and S. Panday. 1991. *STAFF2D, Version 3.1, A Two-Dimensional Finite Element Code for Simulating Fluid Flow and Transport of Radionuclides in Fractured Porous Media with Water Table Boundary Conditions*. Herndon, VA: HydroGeoLogic, Inc. (Copy on file in the Waste Management and Transportation Library, Sandia National Laboratories, Albuquerque, NM.)

IAEA (International Atomic Energy Agency). 1989. *Evaluating the Reliability of Predictions Made Using Environmental Transfer Models*. Safety Series Report No. 100. Vienna, Austria: International Atomic Energy Agency.

Iman, R.L., and W.J. Conover. 1979. "The Use of the Rank Transform in Regression," *Technometrics*. Vol. 21, no. 4, 499-509.

Iman, R.L., and W.J. Conover. 1982. "A Distribution-Free Approach to Inducing Rank Correlation Among Input Variables," *Communications in Statistics: Simulation and Computation*. Vol. B11, no. 3, 311-334.

Iman, R.L., and M.J. Shortencarier. 1984. *A FORTRAN 77 Program and User's Guide for the Generation of Latin Hypercube and Random Samples for Use with Computer Models*. NUREG/CR-3624, SAND83-2365. Albuquerque, NM: Sandia National Laboratories.

Iman, R.L., J.M. Davenport, E.L. Frost, and M.J. Shortencarier. 1980. *Stepwise Regression with PRESS and Rank Regression (Program User's Guide)*. SAND79-1472. Albuquerque, NM: Sandia National Laboratories.

Iman, R.L., M.J. Shortencarier, and J.D. Johnson. 1985. *A FORTRAN 77 Program and User's Guide for the Calculation of Partial Correlation and Standardized Regression Coefficients*. NUREG/CR-4122, SAND85-0044. Albuquerque, NM: Sandia National Laboratories.

Jones, T.L., V.A. Kelley, J.F. Pickens, D.T. Upton, R.L. Beauheim, and P.B. Davies. 1992. *Integration of Interpretation Results of Tracer Tests Performed in the Culebra Dolomite at the Waste Isolation Pilot Plant Site*. SAND92-1579. Albuquerque, NM: Sandia National Laboratories.

Kaplan, S., and B.J. Garrick. 1981. "On the Quantitative Definition of Risk," *Risk Analysis*. Vol. 1, no. 1, 11-27.

Kelley, V.A., and G.J. Saulnier, Jr. 1990. *Core Analyses for Selected Samples from the Culebra Dolomite at the Waste Isolation Pilot Plant Site*. SAND90-7011. Albuquerque, NM: Sandia National Laboratories.

Lappin, A.R., R.L. Hunter, D.P. Garber, P.B. Davies, R.L. Beauheim, D.J. Borns, L.H. Brush, B.M. Butcher, T. Cauffman, M.S.Y. Chu, L.S. Gomez, R.V. Guzowski, H.J. Iuzzolino, V. Kelley, S.J. Lambert, M.G. Marietta, J.W. Mercer, E.J. Nowak, J. Pickens, R.P. Rechard, M. Reeves, K.L. Robinson, and M.D. Siegel. 1989. *Systems Analysis, Long-Term Radionuclide Transport, and Dose Assessments, Waste Isolation Pilot Plant (WIPP), Southeastern New Mexico; March 1989*. SAND89-0462. Albuquerque, NM: Sandia National Laboratories.

LaVenue, A.M., and B.S. RamaRao. 1992. *A Modeling Approach To Address Spatial Variability within the Culebra Dolomite Transmissivity Field*. SAND92-7306. Albuquerque, NM: Sandia National Laboratories.

LaVenue, A.M., A. Haug, and V.A. Kelley. 1988. *Numerical Simulation of Ground-Water Flow in the Culebra Dolomite at the Waste Isolation Pilot Plant (WIPP) Site: Second Interim Report*. SAND88-7002. Albuquerque, NM: Sandia National Laboratories.

Leigh, C.D., B.M. Thompson, J.E. Campbell, D.E. Longsine, R.A. Kennedy, and B.A. Napier. 1993. *User's Guide for GENII-S: A Code for Statistical and Deterministic Simulations of Radiation Doses to Humans from Radionuclides in the Environment*. SAND91-0561. Albuquerque, NM: Sandia National Laboratories.

Marietta, M.G., S.G. Bertram-Howery, D.R. Anderson, K.F. Brinster, R.V. Guzowski, H. Iuzzolino, and R.P. Rechard. 1989. *Performance Assessment Methodology Demonstration: Methodology Development for Evaluating Compliance with EPA 40 CFR 191, Subpart B, for the Waste Isolation Pilot Plant*. SAND89-2027. Albuquerque, NM: Sandia National Laboratories.

McKay, M.D., R.J. Beckman, and W.J. Conover. 1979. "A Comparison of Three Methods for Selecting Values of Input Variables in the Analysis of Output from a Computer Code," *Technometrics*. Vol. 21, no. 2, 239-245.

Mercer, J.W. 1983. *Geohydrology of the Proposed Waste Isolation Pilot Plant Site, Los Medaños Area, Southeastern New Mexico.* Water-Resources Investigations Report 83-4016. Albuquerque, NM: US Geological Survey.

Mercer, J.W., and B.R. Orr. 1979. *Interim Data Report on the Geohydrology of the Proposed Waste Isolation Pilot Plant Site, Southeast New Mexico.* US Geological Survey Water-Resources Investigations 79-98. Albuquerque, NM: US Geological Survey.

Oldroyd, J.G. 1958. "Non-Newtonian Effects in Steady Motion of Some Idealized Elastico-Viscous Liquids," *Proceedings of the Royal Society of London.* Series A, Vol. 245, no. 1241, 278-297.

Pace, B.O. 1990. Appendix A: "Letter 1b: Changes to Bar Graphs," *Data Used in Preliminary Performance Assessment of the Waste Isolation Pilot Plant (1990).* R.P. Rechard, H. Iuzzolino, and J.S. Sandha. SAND89-2408. Albuquerque, NM: Sandia National Laboratories. A-165 through A-170.

Parker, J.C., R.J. Lenhard, and T. Kuppusamy. 1987. "A Parametric Model for Constitutive Properties Governing Multiphase Flow in Porous Media," *Water Resources Research.* Vol. 23, no. 4, 618-624.

Parry, G.W. 1988. "On the Meaning of Probability in Probabilistic Safety Assessment," *Reliability Engineering and System Safety.* Vol. 23, no. 4, 309-314.

Partheniades, E., and R.E. Paaswell. 1970. "Erodibility of Channels with Cohesive Boundary," *Journal of the Hydraulics Division, Proceedings of the American Society of Civil Engineers.* Vol. 96, no. HY3, 755-771.

Paté-Cornell, M.E. 1986. "Probability and Uncertainty in Nuclear Safety Decisions," *Nuclear Engineering and Design.* Vol. 93, nos. 2-3, 319-327.

Popielak, R.S., R.L. Beauheim, S.R. Black, W.E. Coons, C.T. Ellingson, and R.L. Olsen. 1983. *Brine Reservoirs in the Castile Formation, Waste Isolation Pilot Plant (WIPP) Project, Southeastern New Mexico.* TME-3153. Carlsbad, NM: US Department of Energy.

Rechard, R.P., H. Iuzzolino, and J.S. Sandha. 1990. *Data Used in Preliminary Performance Assessment of the Waste Isolation Pilot Plant (1990).* SAND89-2408. Albuquerque, NM: Sandia National Laboratories.

Reeves, M., G.A. Freeze, V.A. Kelley, J.F. Pickens, D.T. Upton, and P.B. Davies. 1991. *Regional Double-Porosity Solute Transport in the Culebra Dolomite Under Brine-Reservoir-Breach Release Conditions: An Analysis of Parameter Sensitivity and Importance.* SAND89-7069. Albuquerque, NM: Sandia National Laboratories.

Savins, J.G., and G.C. Wallick. 1966. "Viscosity Profiles, Discharge Rates, Pressures, and Torques for a Rheologically Complex Fluid in a Helical Flow," *A.I.Ch.E. Journal*. Vol. 12, no. 2, 357-363.

Stone, C.M., R.D. Krieg, and Z.E. Beisinger. 1985. *SANCHO: A Finite Element Computer Program for the Quasistatic, Large Deformation, Inelastic Response of Two-Dimensional Solids*. SAND84-2618. Albuquerque, NM: Sandia National Laboratories.

Swift, P.N. 1991. Appendix A: "Climate and Recharge Variability Parameters for the 1991 WIPP PA Calculations," *Preliminary Comparison with 40 CFR Part 191, Subpart B for the Waste Isolation Pilot Plant, December 1991. Volume 3: Reference Data*. WIPP Performance Assessment Division. Eds. R.P. Rechard, A.C. Peterson, J.D. Schreiber, H.J. Iuzzolino, M.S. Tierney, and J.S. Sandha. SAND91-0893/3. Albuquerque, NM: Sandia National Laboratories. A-107 through A-121.

Swift, P.N. 1993. "Long-Term Climate Variability at the Waste Isolation Pilot Plant, Southeastern New Mexico, USA," *Environmental Management*. SAND91-7055. Vol. 17, no. 1, 83-97.

Tierney, M.S. 1990. *Constructing Probability Distributions of Uncertain Variables in Models of the Performance of the Waste Isolation Pilot Plant: The 1990 Performance Simulations*. SAND90-2510. Albuquerque, NM: Sandia National Laboratories.

Trauth, K.M., S.C. Hora, R.P. Rechard, and D.R. Anderson. 1992. *The Use of Expert Judgment to Quantify Uncertainty in Solubility and Sorption Parameters for Waste Isolation Pilot Plant Performance Assessment*. SAND92-0479. Albuquerque, NM: Sandia National Laboratories.

US DOE (Department of Energy). 1989. *Waste Isolation Pilot Plant Compliance Strategy for 40 CFR Part 191, March 17, 1989*. DOE-WIPP 86-013. Carlsbad, NM: WIPP Project Office.

US DOE (Department of Energy). 1990. *WIPP Test Phase Plan: Performance Assessment*. DOE/WIPP 89-011, Rev. 0. Carlsbad, NM: US Department of Energy, Waste Isolation Pilot Plant.

US DOE (Department of Energy). 1991. *Integrated Data Base for 1991: U.S. Spent Fuel and Radioactive Waste Inventories, Projections, and Characteristics*. DOE/RW-0006, Rev. 7. Oak Ridge, TN: Oak Ridge National Laboratory.

US DOE (Department of Energy). 1992. *WIPP Test Phase Activities in Support of Critical Performance Assessment Information Needs (40 CFR 191, Subpart B)*. Washington, DC: US Department of Energy. Attachment I.

US DOE (Department of Energy) and State of New Mexico. 1981, as modified. "Agreement for Consultation and Cooperation" on WIPP by the State of New Mexico and US Department of Energy, modified 11/30/84, 8/4/87, and 4/18/88.

USGS (United States Geological Survey). 1985a. *Los Medaños Quadrangle, New Mexico-Eddy Co.* 7.5 Minute Series (Topographic). Provisional Edition. Reston, VA: US Geological Survey. (Copy on file in the Waste Management and Transportation Library, Sandia National Laboratories, Albuquerque, NM.)

USGS (United States Geological Survey). 1985b. *Illinois Camp SE Quandrangle, New Mexico-Eddy Co.* 7.5 Minute Series (Topographic). Provisional Edition. Reston, VA: US Geological Survey. (Copy on file in the Waste Management and Transportation Library, Sandia National Laboratories, Albuquerque, NM.)

van Genuchten, R. 1978. *Calculating the Unsaturated Hydraulic Conductivity with a New Closed-Form Analytical Model.* Research Report 78-WR-08. Princeton, NJ: Princeton University, Department of Civil Engineering.

Vesely, W.E., and D.M. Rasmuson. 1984. "Uncertainties in Nuclear Probabilistic Risk Analyses," *Risk Analysis.* Vol. 4, no. 4, 313-322.

Voss, C.I. 1984. *SUTRA (Saturated-Unsaturated Transport): A Finite-Element Simulation Model for Saturated-Unsaturated, Fluid-Density-Dependent Ground-Water Flow with Energy Transport or Chemically-Reactive Single-Species Solute Transport.* Water-Resources Investigations Report 84-4369. Reston, VA: US Geological Survey.

Walker, R.E. 1976. "Hydraulic Limits Are Set by Flow Restrictions," *Oil and Gas Journal.* Vol. 74, no. 40, 86-90.

Waste Management Technology Department. 1987. *The Scientific Program at the Waste Isolation Pilot Plant.* SAND85-1699. Albuquerque, NM: Sandia National Laboratories.

WEC (Westinghouse Electric Corporation). 1988. *WIPP Underground Mine Plan, Bulkhead Locations and Numbers.* Drawing 54-W-012-W, Rev. A. Carlsbad, NM: Westinghouse Waste Isolation Division. (Copy on file in the Waste Management and Transportation Library, Sandia National Laboratories, Albuquerque, NM.)

Whittaker, A., ed. 1985. *Theory and Application of Drilling Fluid Hydraulics.* Boston, MA: International Human Resources Development Corporation.

WIPP PA (Performance Assessment) Department. 1992. *Long-Term Gas and Brine Migration at the Waste Isolation Pilot Plant: Preliminary Sensitivity Analyses for Post-Closure 40 CFR 268 (RCRA), May 1992.* SAND92-1933. Albuquerque, NM: Sandia National Laboratories.

WIPP PA (Performance Assessment) Department. 1993. *Preliminary Comparison with 40 CFR Part 191, Subpart B for the Waste Isolation Pilot Plant, December 1991. Volume 6: Guidance to the WIPP Project from the December 1991 Performance Assessment*. SAND91-0893/6. Albuquerque, NM: Sandia National Laboratories. (draft)

WIPP PA (Performance Assessment) Division. 1991a. *Preliminary Comparison with 40 CFR Part 191, Subpart B for the Waste Isolation Pilot Plant, December 1991. Volume 1: Methodology and Results*. SAND91-0893/1. Albuquerque, NM: Sandia National Laboratories.

WIPP PA (Performance Assessment) Division. 1991b. *Preliminary Comparison with 40 CFR Part 191, Subpart B for the Waste Isolation Pilot Plant, December 1991. Volume 2: Probability and Consequence Modeling*. SAND91-0893/2. Albuquerque, NM: Sandia National Laboratories.

WIPP PA (Performance Assessment) Division. 1991c. *Preliminary Comparison with 40 CFR Part 191, Subpart B for the Waste Isolation Pilot Plant, December 1991. Volume 3: Reference Data*. Eds. R.P. Rechard, A.C. Peterson, J.D. Schreiber, H.J. Iuzzolino, M.S. Tierney, and J.S. Sandha. SAND91-0893/3. Albuquerque, NM: Sandia National Laboratories.

APPENDIX A: VERIFICATION OF THE SECO-TRANSPORT CODE

Verification of the SECO-TRANSPORT Code

Kambiz Salari

April 2, 1993

Contents

1 SECO-TRANSPORT Code

1.1 Transport Model

The code predicts solute transport in fractured porous media using the dual-porosity approach. It allows for radioactive decay and generation of daughter products. In addition, the matrix block equation can model both the matrix material and the clay lining.

For the fracture-with-matrix block system, transport in the fracture is produced by the combined effect of convection and hydrodynamic dispersion, while transport in the matrix block is dominated by molecular diffusion. Two sets of governing equations are used to describe the concentration in the fracture and matrix block.

The equation for the transport of kth radionuclide component in the fracture (N species) can be written

$k = 1, \ldots, N$:

$$\begin{aligned} \nabla \cdot [\mathbf{D}\nabla C_k - \mathbf{V}C_k] &= \phi R_k \frac{\partial C_k}{\partial t} + \phi R_k \lambda_k C_k - \phi R_{k-1}\lambda_{k-1} C_{k-1} \\ &\quad -Q\tilde{C}_k - \Gamma_k \end{aligned} \tag{1}$$

where the dependent variables are C_k, the concentration of the kth radionuclide. For $k = 1$, the term involving C_{k-1} is omitted. Physical parameters include $\mathbf{D}(\mathbf{x}, t)$, a 2×2 hydrodynamic dispersion tensor (velocity-dependent); $\mathbf{V}(\mathbf{x}, t)$, the Darcy velocity, $\phi(\mathbf{x})$; the fracture porosity; R_k, the retardation coefficient; λ_k, the species decay constant; and $\tilde{C}_k$, the concentration of the kth injected radionuclide. The well injection rate is Q. Detailed physical descriptions of these terms can be found in [1, 2].

The N fracture equations are linear and sequentially-coupled. A general Robin boundary condition is assumed

$$\alpha C_k + \beta \frac{\partial C_k}{\partial n} = \gamma \tag{2}$$

on a planar rectangular domain Ω. For various choice of α, β, and γ, one may obtain Dirichlet, Neumann, or Cauchy boundary conditions on different portions of the boundary. For example, the commonly used flux boundary condition is

$$\mathbf{V}C_k - \mathbf{D}\nabla C_k = \mathbf{V}f(t) \tag{3}$$

where f is a known function.

The flow-field $\mathbf{V}$ is assumed to be independent of the solute concentration. In practice, the flow-field is obtained from the SECO-FLOW code [6].

Since the dual-continuum model [3, 4, 5] includes the exchange of mass between the matrix block and the fracture, it is necessary to solve a transport equation in the matrix block. Assuming that there is no fluid flow, the equation for the concentration of the kth species, is given (for a slab block model) by

$$\frac{\partial}{\partial \chi}(D' \frac{\partial C'_k}{\partial \chi}) = \phi' R'_k \frac{\partial C'_k}{\partial t} + \phi' R'_k \lambda_k C'_k - \phi' R'_{k-1} \lambda_{k-1} C'_{k-1} \tag{4}$$

where χ is the coordinate originating from the symmetry line of the matrix block, the prime is denoting matrix block, D' is the coefficient of the molecular diffusion, and the remaining symbols have the same meaning as those in the equation for fracture transport (Eq. 1).

The equations for the fracture and the matrix block are coupled through the mass transfer term Γ_k which is given by

$$\Gamma_k = -\frac{2}{b}(D' \frac{\partial C'_k}{\partial \chi}|_{\chi=0}) \tag{5}$$

where b is the fracture aperture.

For a typical matrix slab of thickness b', the initial and boundary conditions are given by

$$C'_k(\chi, t=0) = C'^0_k \tag{6}$$

$$D' \frac{\partial C'_k}{\partial \chi}(0,t) = 0 \tag{7}$$

$$C'_k(b',t) = C_k - \zeta D' \frac{\partial C'_k}{\partial \chi} \tag{8}$$

where ζ is a parameter characterizing the resistance of the thin skin adjacent to the fracture. This parameter is defined as $\zeta = b_s/D_s$, where b_s and D_s are the skin thickness and the skin diffusion coefficient, respectively.

1.2 Numerical Discretization, Algorithm

1.2.1 Fracture Equation

Equation (1) has been transformed into stretched Cartesian coordinates

$$t = \tau, \tag{9}$$

$$x = x(\xi), \tag{10}$$

$$y = y(\eta) \tag{11}$$

where metric transformations are $\xi_x = Jy_\eta$, $\eta_y = Jx_\xi$, and $J = \xi_x\eta_y$. The transformed equation, with further algebraic manipulations, was put into a strong conservation form [7, 8]. This is done to ensure mass conservation, which is essential here. The transformed equation is given by

$$\begin{aligned}\phi R_k\frac{\partial}{\partial t}(\hat{C}_k) + \frac{\partial}{\partial\xi}(\hat{E}) + \frac{\partial}{\partial\eta}(\hat{F}) &= \frac{\partial}{\partial\xi}(\hat{E}_{v1}) + \frac{\partial}{\partial\xi}(\hat{E}_{v2}) \\ &+ \frac{\partial}{\partial\eta}(\hat{F}_{v1}) + \frac{\partial}{\partial\eta}(\hat{F}_{v2}) \\ &+ \phi R_k\lambda_k\hat{C}_k + \phi R_{k-1}\lambda_{k-1}\hat{C}_{k-1} \\ &+ \hat{Q} + \hat{\Gamma}\end{aligned} \tag{12}$$

where

$$\hat{C}_k = \frac{C_k}{J}, \tag{13}$$

$$\hat{E} = \xi_x u\hat{C}_k, \tag{14}$$

$$\hat{F} = \eta_y v\hat{C}_k, \tag{15}$$

$$\hat{E}_{v1} = \frac{\xi_x^2 D_{11}}{J}\frac{\partial\hat{C}_k}{\partial\xi}, \tag{16}$$

$$\hat{E}_{v2} = \frac{\xi_x\eta_y D_{12}}{J}\frac{\partial\hat{C}_k}{\partial\eta}, \tag{17}$$

$$\hat{F}_{v1} = \frac{\xi_x\eta_y D_{21}}{J}\frac{\partial\hat{C}_k}{\partial\xi}, \tag{18}$$

$$\hat{F}_{v2} = \frac{\eta_y^2 D_{22}}{J}\frac{\partial\hat{C}_k}{\partial\eta}, \tag{19}$$

$$\hat{Q} = \frac{Q\tilde{C}_k}{J}, \tag{20}$$

$$\hat{\Gamma} = \frac{\Gamma}{J}. \tag{21}$$

Equation (12) is solved using an implicit Approximate Factorization procedure [9]. The convective terms are modeled by TVD [10] and the remaining terms by central differencing. A general two-level implicit finite volume scheme, in delta form [9], can be written as

$$\phi R_k \triangle \hat{C}_k^n = \frac{\theta \triangle t}{1+\varphi}(\phi R_k \triangle \hat{C}_k^n)_t + \frac{\triangle t}{1+\varphi}(\phi R_k \hat{C}_k^n)_t + \frac{\varphi}{1+\varphi}(\phi R_k \triangle \hat{C}_k^{n-1}) \tag{22}$$

where

$$\triangle \hat{C}_k^n = \hat{C}_k^{n+1} - \hat{C}_k^n$$

The $\triangle \hat{C}_k^n$ can be thought of as a correction to advance the solution to a new time-level (n+1). The time difference equation (22), with appropriate choice of the parameters θ and φ, produces many two- and three-level implicit schemes as shown in Table 1. Applying equation (22) to equation (12) we have

$$\begin{aligned}
\phi R_k \triangle \hat{C}_k^n &= \frac{\theta \triangle t}{1+\varphi}[-(\triangle \hat{E}^n)_\xi - (\triangle \hat{F}^n)_\eta + (\triangle \hat{E}_{v1}^n)_\xi + (\triangle \hat{F}_{v2}^n)_\eta \\
&\qquad -\phi R_k \lambda_k \triangle \hat{C}_k^n] \\
&+ \frac{\theta \triangle t}{1+\varphi}[(\triangle \hat{E}_{v2}^{n-1})_\xi + (\triangle \hat{F}_{v1}^{n-1})_\eta] \\
&+ \frac{\triangle t}{1+\varphi}[-\hat{E}_\xi^n - \hat{F}_\eta^n + (\hat{E}_{v1}^n)_\xi + (\hat{E}_{v2}^n)_\xi + (\hat{F}_{v1}^n)_\eta + (\hat{F}_{v2}^n)_\eta \\
&\qquad -\phi R_k \lambda_k \hat{C}_k^n + \phi R_{k-1} \lambda_{k-1} \hat{C}_{k-1}^n + \hat{Q}^n + \hat{\Gamma}^n] \\
&+ \frac{\varphi}{1+\varphi}[\phi R_k \triangle \hat{C}_k^{n-1}]
\end{aligned} \tag{23}$$

The cross derivative terms are time-lagged to facilitate the factorization of the right-hand-side operator. The error introduced by lagging these terms can be corrected through an intra-time step iteration. This procedure has been employed here.

The convective terms are modeled using the following TVD flux which we have developed for staggered meshes. The flux is a combination of upwind and centered schemes.

$$\begin{aligned}
\hat{E}_{j-\frac{1}{2},k}^n &= \frac{1}{2}(1 - \Phi_{j-\frac{1}{2},k})[(C_{j,k}^n + C_{j-1,k}^n)u_{j-\frac{1}{2},k}^n - (C_{j,k}^n - C_{j-1,k}^n) \mid u_{j-\frac{1}{2},k}^n \mid] \\
&\quad + \frac{1}{2}\Phi_{j-\frac{1}{2},k}(\hat{C}_{j,k}^n + \hat{C}_{j-1,k}^n)(\tilde{\xi}_x^n)_{j-\frac{1}{2},k} u_{j-\frac{1}{2},k}^n
\end{aligned} \tag{24}$$

Table 1: Partial list of schemes available

θ	φ	Schemes	Truncation error
1	0	Euler, implicit	O($\triangle t$)
$\frac{1}{2}$	0	Trapezoidal, implicit	O($\triangle t^2$)
1	$\frac{1}{2}$	3-point-backward, implicit	O($\triangle t^2$)

where

$$(\tilde{\xi}_x^n)_{j-\frac{1}{2},k} = \frac{2(\xi_x)_{j,k}(\xi_x)_{j-1,k}}{(\xi_x)_{j,k} + (\xi_x)_{j-1,k}}$$

The function Φ is called a limiter function. There are a number of limiter functions available ranging from very compressive (Roe superbee) to very dissipative (minmod) [10].

After the explicit portion (RHS) of equation (23) has been evaluated, the solution at the new time level is obtained through the following sequence

$$(I + \alpha_x L_{xx})\triangle \bar{C}_{j,k} = RHS, \tag{25}$$

$$(I + \alpha_y L_{yy})\triangle \hat{C}_{j,k} = \triangle \bar{C}_{j,k}, \tag{26}$$

$$\hat{C}_{j,k}^{n+1} = \hat{C}_{j,k}^{n} + \triangle \hat{C}_{j,k}^{n} \tag{27}$$

where I is an identity matrix and L_{xx}, L_{yy} are the x and y operators, respectively. The first sweep in either the x or y direction produces intermediate results, denoted by $\bar{C}_{j,k}$. The second sweep uses the intermediate results to complete the cycle. The order of the sweep can be symmetrized by alternating the direction. After both sweeps are complete, the solution is updated.

The boundary conditions (Dirichlet, Neumann, and Robin) are all implicitly implemented in the 1-D operator in both directions. This ensures the second-order accuracy of the scheme. The implicit construction of boundary conditions requires an intermediate boundary condition for the initial sweep. The intermediate boundary condition is subtle, and is evaluated by applying either the x or y operator, depending on the boundary, to

the equation of the ghost cell. The stencils of these operators will be different near the boundaries.

This algorithm uses a finite-volume mesh where fluxes are evaluated at cell faces and concentrations at cell centers.

1.2.2 Matrix Block Equation

Using a similar procedure oulined for the fracture equation (1), equation (4) is first mapped to a computational space

$$\phi' R'_k \frac{\partial \hat{C}'_k}{\partial t} = \frac{\partial \hat{F}'_v}{\partial \xi} - \phi' R'_k \lambda_k \hat{C}'_k + \phi' R'_{k-1} \lambda_{k-1} \hat{C}'_{k-1} \tag{28}$$

where

$$\hat{C}'_k = \frac{C'_k}{J} \tag{29}$$

$$\hat{F}'_v = D' \xi_x \frac{\partial C'_k}{\partial \xi} \tag{30}$$

Then, the above equation is discretized using the general implicit finite volume scheme, in a delta form given by equation 22.

$$\begin{aligned} \phi' R'_k \triangle \hat{C}'^n_k &= \frac{\theta \triangle t}{1+\varphi}[(\triangle \hat{F}'^n_v)_\xi - \phi' R'_k \lambda_k \hat{C}'^n_k] \\ &+ \frac{\triangle t}{1+\varphi}[(\hat{F}'^n)_\xi - \phi' R'_k \lambda_k \hat{C}'^n_k + \phi' R'_{k-1} \lambda_{k-1} \hat{C}'^n_{k-1}] \\ &+ \frac{\varphi}{1+\varphi}[\phi' R'_k \triangle \hat{C}'^{n-1}_k] \end{aligned} \tag{31}$$

where

$$(\hat{F}'^n_v)_{j-\frac{1}{2}} = D'_{j-\frac{1}{2}} (\xi_x)_{j-\frac{1}{2}} (C'^n_j - C'^n_{j-1}) \tag{32}$$

$$(\triangle \hat{F}'^n_v)_{j-\frac{1}{2}} = D'_{j-\frac{1}{2}} (\xi_x)_{j-\frac{1}{2}} [J_j \triangle \hat{C}'^n_j - J_{j-1} \triangle \hat{C}'^n_{j-1}] \tag{33}$$

Equation (31) is solved using a tridiagonal inversion with implicit boundary conditions.

1.2.3 Fracture-Matrix Coupling

The equations for the fracture and the matrix block are coupled through a mass transfer term Γ_k. This term is proportional to the gradient of the solute concentration in a matrix

block at their interface. A simple approach to couple these equations is to time lag the Γ term or, in other words, treat the coupling term explicitly. Our experience with the matrix block equation has shown if the molecular diffusion coefficient is high, if there exists a clay lining, or if there is high resolution at the interface, the solution for the coupled system would be unstable. To make the coupling more robust, the equations must be coupled in a fully implicit manner. A procedure outlined in reference [1] was adapted and modified to work with the approximate factorization and delta formulation of the transport equation. This new procedure would couple the equations implicitly and has shown to be quite robust.

Even with implicit coupling, a problem can arise if the characteristic time for the matrix block, i.e., the time in which the solution in the matrix would approximately reach steady state, is much smaller than the time step used to advance the fracture solution. In such a case, the coupling term Γ can exhibit an oscillatory behavior in time which is not physical. To avoid such a behavior the fracture time step must resolve or be smaller than the characteristic time of the matrix block.

1.3 Improvements / Issues

The present code uses a TVD scheme with three-level time differencing and directional splitting to improve accuracy and execution time. The code is second-order accurate both in time and space. Problems with moderately-high Peclet number would greatly benefit from this scheme by avoiding spurious oscillations commonly associated with the central differencing schemes. The long time-scales of the problems to which the code is to be applied dictate the use of fully-implicit algorithms.

The flow field is computed by the SECO-flow code. It is important to note that the convergence tolerance on the flow must be smaller in magnitude than the *source* for the transport calculation. Lack of proper iterative convergence in the flow calculation can show up as a source term in the transport calculation due to its conservation formulation and in some cases can lead to instabilities.

In practice the computational boundaries for transport and the flow are not the same.

This difference in the location of the far-field boundaries can pose a difficult problem (unbounded source) for the transport calculation. The SECO-transport code can eliminate this difficulty by automatically assigning the boundary conditions using the flow field.

The code is capable of computing the history of integrated discharge around any number of defined closed boundaries within the computational mesh.

2 Analytic Solutions & Convergence Test

2.1 Fracture Transport

The code, which has been developed based on the scheme described in the algorithm section (section 1.2), is verified for temporal and spatial accuracy using the following unsteady equation and its solution, with $\mathbf{V} = u\mathbf{i}$.

$$C_t + uC_x = \alpha_L u C_{xx} + \alpha_T u C_{yy} - g(x, y, t), \tag{34}$$

where

$$g(x, y, t) = (x - ut)^2 + y^2, \tag{35}$$

and $0 < x < 1$, $0 < y < 1$. The initial condition is given by

$$C(x, y, 0) = \frac{1}{12u}\left[\frac{x^4}{\alpha_L} + \frac{y^4}{\alpha_T}\right]. \tag{36}$$

The exact solution to equation (34) is

$$C(x, y, t) = \frac{1}{12u}\left[\frac{(x - ut)^4}{\alpha_L} + \frac{y^4}{\alpha_T}\right]. \tag{37}$$

Since the computational domain is finite, the Dirichlet boundary conditions are time dependent and may be obtained from the exact solution.

Table 2 presents the computed solution to equation (34) at time=$25sec$, for four different grid sizes and time steps. The magnitude of coefficients are $u = 0.1m/s$, $\alpha_L = 1.0m$, $\alpha_T = 0.1m$. By examining the ratio of Root Mean Square (RMS) of errors, it is evident that the overall solution is second-order accurate in time and space.

Table 2: Convergence results, uniform grid

Size	$\triangle x$	$\triangle t$	RMS	RMS ratio
20x20	.05	.25	7.697E-3	
40x40	.025	.125	1.954E-3	3.94
80x80	.0125	.0625	4.921E-4	3.97
160x160	.00625	.03125	1.234E-4	3.99

To illustrate the advantages of this algorithm, we have chosen to solve a two-dimensional convection-dispersion problem for which we have an exact solution [11]. The medium is assumed to be homogeneous and isotropic with unidirectional steady state flow. The initial solute concentration is zero. At a certain time, a strip-type source with a finite length (2a) along the y-axis is introduced. For detailed information regarding this problem see Reference [11]. In our test problems, the solute concentration at the source remains constant with time.

The solution is obtained for two cases. A uniform grid 80x80 where $0 < x < 200m$, $-100 < y < 100m$ and Van Leer MUSCL limiter [10] are used for both cases. Case 1: low mesh Peclet number, $Pe = 2$, $u = 1.0m/s$, $\alpha_L = 0.5m$, $\alpha_T = 0.1m$, $\lambda = 0.0$, and $a = 50$. Figures 1a and 1b present the numerical solution and the absolute error at time=$100sec$, respectively. The maximum error is 6.1E-2 and is located in the vicinity of the discontinuity on the boundary and RMS=6.389E-3. Figures 2a and 2b show the same calculation using implicit upwind differencing. The latter computations serve as a representative solution computed by the majority of existing codes. The maximum error is .1847 and is located around the front as one would expect and the RMS=5.111E-2. The maximum error is about three times and the RMS about 8 times larger than TVD solution. Case 2: moderately high mesh Peclet number, $Pe = 10$, $u = 1.0$, $\alpha_L = \alpha_T = 0.1$, and $a = 50$. Figure 3 shows solute concentration computed using TVD at Time=100. Figure 4 presents the same calculation using upwinding. The difference between the two solutions is dramatic. As expected, the TVD scheme retained a sharp front as opposed

to a very diffused front generated by the implicit upwind differencing. Unfortunately, we encountered numerical difficulties in computing the exact solution at Peclet numbers higher than 4; hence, we have no comparison to exact solution. However, if Case 1 is any indication, the error introduced by implicit upwinding should be much higher than was observed in the previous case.

As we have shown above, the TVD scheme in conjunction with second-order time discretization is more accurate in tracking sharp changes in solute concentration even for low-Peclet number cases.

2.2 Dual Porosity Transport

To verify both fracture and the matrix finite volume discretization as a system and the coupling procedure, we have chosen a dual porosity problem in one dimension with the analytical solution given by Tang [12]. The fracture equation is

$$\frac{\partial c}{\partial t} + \frac{v}{R}\frac{\partial c}{\partial z} - \frac{D}{R}\frac{\partial^2 c}{\partial z^2} + \lambda c - \frac{\theta D'}{bR}\frac{\partial c'}{\partial x}|_{x=b} = 0 \tag{38}$$

where $0 \leq z < \infty$. The initial and boundary conditions are

$$c(0,t) = 0 \tag{39}$$

$$c(\infty,t) = 0 \tag{40}$$

$$c(z,0) = 0 \tag{41}$$

The matrix equation is given by

$$\frac{\partial c'}{\partial t} - \frac{D'}{R'}\frac{\partial^2 c'}{\partial x^2} + \lambda c' = 0 \tag{42}$$

where $b \leq x < \infty$. The initial and boundary conditions are

$$c'(b,z,t) = c(z,t) \tag{43}$$

$$c'(\infty,z,t) = 0 \tag{44}$$

$$c'(x,z,0) = 0 \tag{45}$$

for further explanation of the problem and the definition of parameters and the analytical solution see reference [12].

The test problem is set up by defining the required parameters as follows. Fracture length, $x_0 = 10m$, fracture spacing $2.4m$. *Fracture properties:* aperture, $b = 10^{-4}m$, seepage velocity, $V = 0.01m/d$, longitudinal dispersivity, $\alpha_L = 0.50m$, molecular diffusion coefficient, $D = 1.382 \times 10^{-4}m^2/d$, and fracture porosity, $\phi_f = 0.42 \times 10^{-4}$. *Matrix properties:* matrix porosity, $\phi' = 0.01$, and matrix diffusion coefficient, $D' = 1.382 \times 10^{-7}m^2/d$. *Radionuclide properties:* decay constant, $\lambda = 0.154 \times 10^{-3} 1/d$, and retardation factor, $R = R' = 1$. *Initial condition:* $c(x,0) = c'(x,z,0) = 0$. The boundary conditions are

$$c(0,t) = 1 \tag{46}$$

$$\frac{\partial c}{\partial x}(x,0,t) = c(x,t) \tag{47}$$

$$c'(x,0,t) = c(x,t) \tag{48}$$

$$\frac{\partial c'}{\partial x}(x,z_0,t) = 0 \tag{49}$$

Fracture length is discretized using 80 stretched cells and 15 stretched cells was used for the matrix block. The calculation was stopped at time equal to 100 days to test both spatial and temporal accuracy of the computed solution. Figures 5 and 6 present the comparison of the fracture and matrix solution to the analytical solution, respectively. The computed solution in both regions seems to be quite accurate which also verifies the accuray of the coupling procedure. Further mesh refinement in both fracture and the matrix block reproduced the same results.

Unfortunately, proper grid convergence test is not possible since in the above transport problem the size of the matrix block is infinite whereas in computation we have a finite matrix block length.

3 Convergence Test on PA Problems

To verify the code on a realistic problem (excluding extreme cases), we will use one of the 1992 PA calculations [14].

3.1 Fracture Transport

For grid convergence test on fracture transport we have chosen vector 2 (E1E2 scenario). This vector has moderate parameters, such as, fracture aperture and realistic fracture travel time with climate from the source to the far field boundary of 72 years

Since we do not have an exact solution for vector 2, to check the convergence of the solution on different grids we rely on contours of the solution for judging convergence. We will use three different grid sizes, 46×53, 93×107, and 187×215. For each grid size three different time steps are used, $\triangle t = 10, 5$, and 2.5 years, for time convergence.

Figure 7 shows temporal behavior of the source function over 10,000 years. Figures 8a,8c, and 8e present the contours of solute concentrations on the first grid at t=10,000 years for three different time steps, respectively. The time resolution for this mesh is quite adequate since there is hardly any change between contour plots. Figures 8b,8d, and 8f present breakthrough curves, with each plot presenting integrated discharges through three closed boundaries. As is the case for solute concentrations, there are no massive changes in the solution as the time accuracy of the computation is increased. Figures 9 and 10 show similar plot for grids number 2 and 3. As we refine the grid, the plume becomes narrower and the concentration front becomes sharper. This is due to improved effectiveness of the TVD algorithm.

These sequences of grid and time steps clearly show that we have resolved this problem adequately.

3.2 Dual-Porosity Transport

For a dual-porosity transport calculation vector 52 (E1E2 scenario) is a realistic example, which has no extremes in its parameters, for grid convergence test. Some of the parameters are calculation time, 10,000 years; fracture travel time with climate, 219 years; and matrix characteristic time, 8076 years.

We will use the same grid sizes as in the fracture transport case, However, vector 52 has different time scales for both fracture and the matrix block, and requires different time steps, with $\triangle t = 2, 1$, and 0.66 years.

Figure 11 shows temporal behavior of the source function over 10,000 years. Figures 12a,12c, and 12e present the solute concentration on the first grid at t=10,000 years for different time steps, respectively. Similar to the fracture calculation, the time resolution is satisfactory. Figures 12b,12d, and 12f present breakthrough curves. Again, there are no massive changes in the solution as the time accuracy of the computation is increased. Figures 13 and 14 show a similar plot for grids number 2 and 3. As the grid becomes finer the concentration front becomes sharper as we have observed in the fracture calculation. Figure 12c show some discharge on the side boundary where on the finer meshes there are no discharges. This points out that the first grid is not resolving the solution well. However, the other grids seem to be adequate.

3.3 Recommendations for Input Parameters

As our grid convergence test on fracture and fracture-matrix calculations have shown, the coarse grid (46×53), which has been used for the 1992 PA caculations, is not adequate in both cases. This grid was not dense enough to properly resolve the gradients in the solution. However, the time-step sizes have all resolved the time scales in both cases adequately.

4 Improvements

A three-dimensional version of the SECO-TRANSPORT code in stretched cartesian coordinates will be available for the next PA cycle. Other improvements will be general coordinate transformation in both two and three dimensions in conjunction with solution adaptivity. Also, more benchmark tests; for example, the Sudicky problem [13] for which an analytical solution exists for a dual-porosity assumption with a specified finite matrix block length.

References

[1] Huyakorn, P.S. and Pinder, G.F. *Computational Methods in Subsurface Flow*, Academic Press, New York, 1983.

[2] Bear, J. and Bachmat, Y. *Introduction to Modeling of Transport Phenomena in Porous Media*, Kluwer Academic Publishers, Dordrecht, Netherlands, 1990.

[3] Streltsova-Adams, T.D. 'Well Hydraulics in Heterogeneous Aquifer Formations' *Advances in Hydroscience*, Vol. 11, (Ed., Chow, V.T.), pp. 357-423, Academic Press, New York, 1978.

[4] Huyakorn, P.S., Lester, B.H., and Mercer, J.W. 'An Efficient Finite Element Technique for Modeling Transport in Fractured Porous Media: Single Species Transport' *Water Res. Res.*, Vol. 19, No. 3, pp. 841 - 854, 1983.

[5] Huyakorn, P.S., Lester, B.H., and Mercer, J.W. 'An Efficient Finite Element Technique for Modeling Transport in Fractured Porous Media: Nuclide Decay Chain Transport' *Water Res. Res.*, Vol. 19, No. 5, pp. 1286-1296, 1983.

[6] Roache, P.J., Knupp, P.M., Steinberg, S., and Blaine, R.L. 'Experience with Benchmark Test Cases for Groundwater Flow' in ASME FED Vol. 93 (Ed. Celik, I. and Freitas, C.J.), *Benchmark Test Cases for Computational Fluid Dynamics*, 1990.

[7] Pulliam, T.H. 'Efficient Solution Methods for the Navier-Stokes Equations', *Lecture Notes for the Von Karman Institute for Fluid Dynamics Lecture Series*, Brusses, Belgium, 1986.

[8] Steinberg, S., and Roache, P.J. '*Discretizing Symmetric Operators in General Coordinates*', to appear.

[9] Fletcher, C.A.J. *Computational Techniques for Fluid Dynamics*, Volumes I and II, Springer-Verlag, 1988.

[10] Yee, H.C. 'Construction of Explicit and Implicit Symmetric TVD Schemes and Their Applications' *J. Comp. Phys.*, Vol. 68, pp. 151-179, 1987.

[11] Javandel, I., Doughty, C., and Tsang, C.F. *Groundwater Transport: Handbook of Mathematical Models*, American Geophysical Union, Washington, D.C. , 1984.

[12] Tang, D.H., Frind, E.O., and Sudicky, E.A. 'Contaminant Transport in Fractured Porous Media: Analytical Solution for a Single Fracture' *Water Resources Research*, Vol. 17, No. 3, pp. 555-564, 1981.

[13] Sudicky, E.A., and Frind, E.O. 'Contaminant Transport in Fractured Porous Media: Analytical Solutions for a System of Parallel Fractures' *Water Resources Research*, Vol. 18, No. 6, pp. 1634-1642, 1982.

[14] Proper ref. for appendix in volume 4

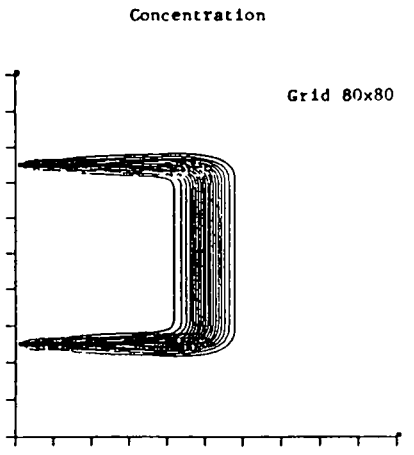

Figure 1a. TVD scheme, MUSCL limiter, Pe = 2.

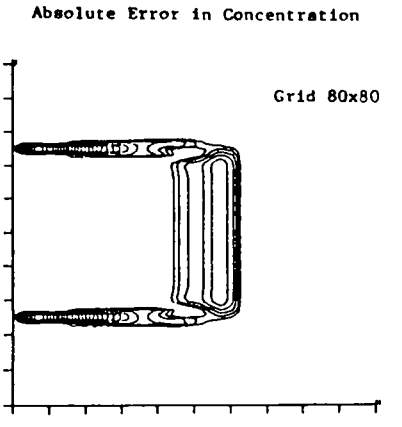

Figure 1b. TVD scheme, MUSCL limiter, Pe = 2.

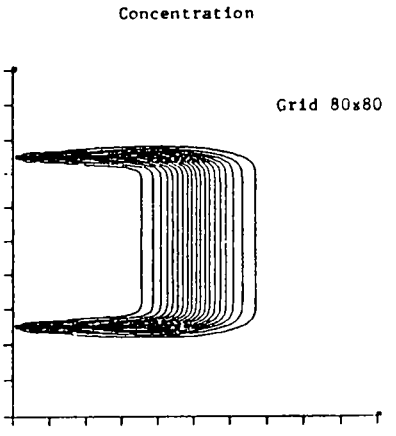

Figure 2a. Upwind, Pe = 2.

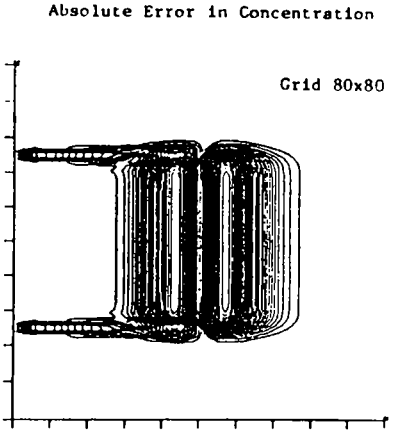

Figure 2b. Upwind, Pe = 2.

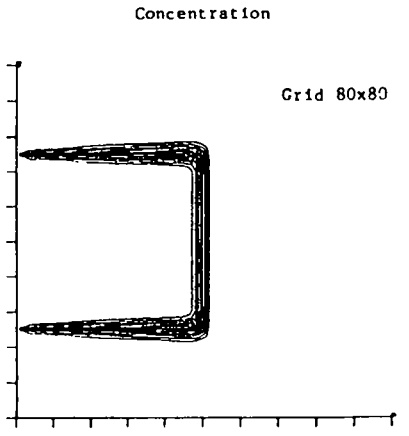

Figure 3. TVD scheme, MUSCL limiter, Pe = 10.

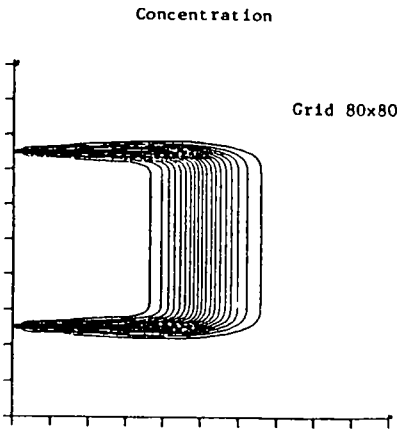

Figure 4. Upwind, Pe = 10.

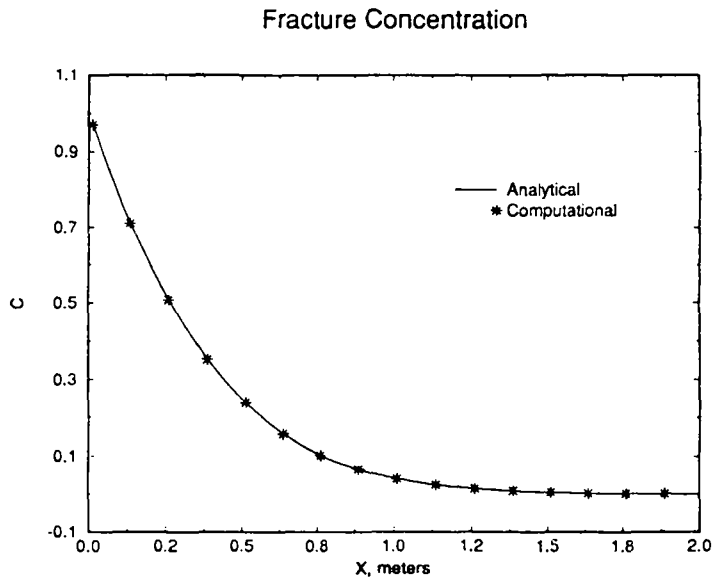

Figure 5

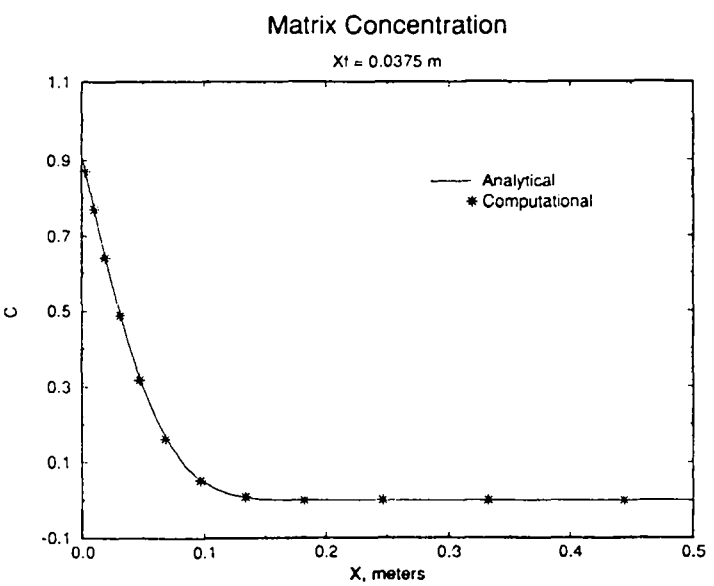

Figure 6

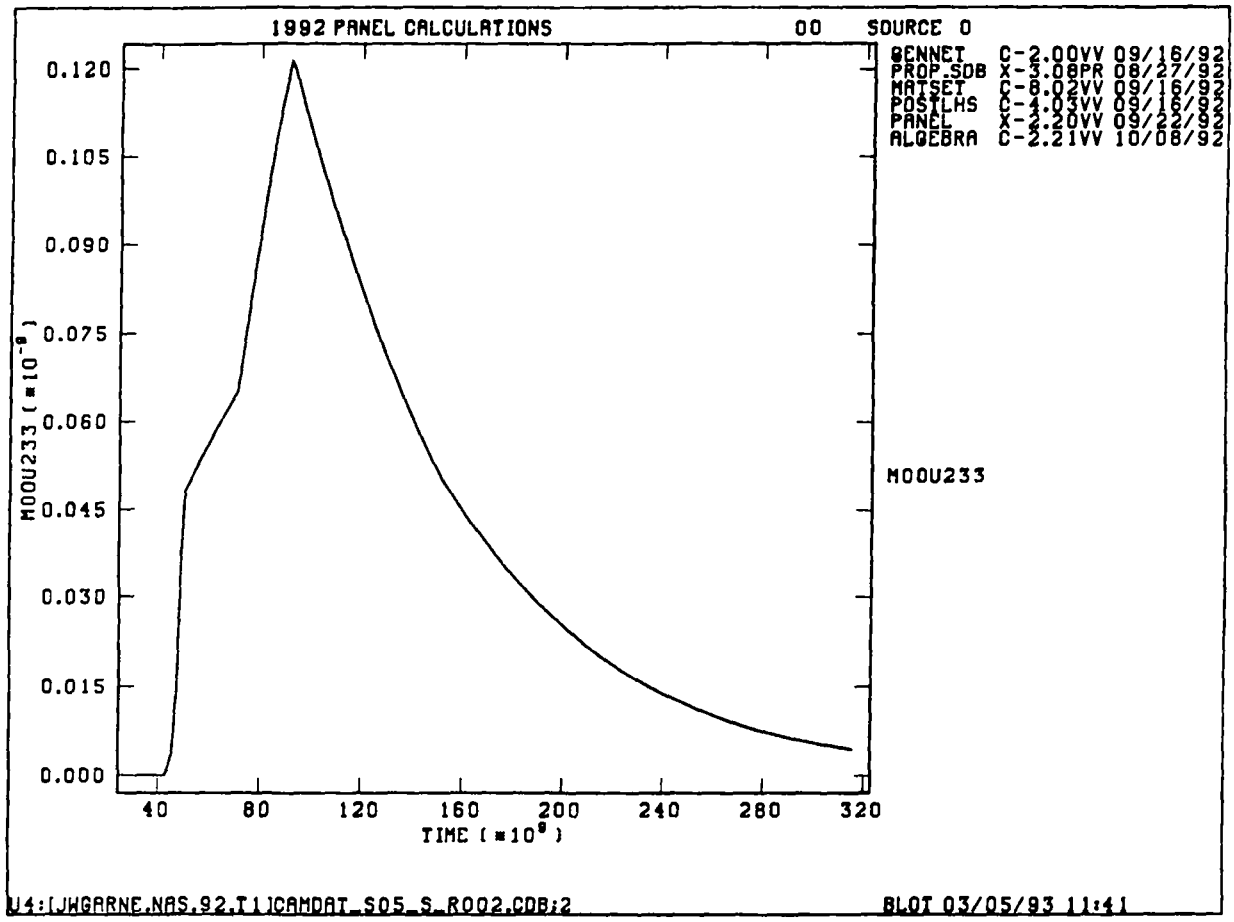
1992 PANEL CALCULATIONS
00 SOURCE 0
GENNET C-2.00VV 09/16/92
PROP.SDB X-3.08PR 08/27/92
MATSET C-8.02VV 09/16/92
POSTLHS C-4.03VV 09/16/92
PANEL X-2.20VV 09/22/92
ALGEBRA C-2.21VV 10/08/92
M00U233
M00U233 (*10^-6)
0.120
0.105
0.090
0.075
0.060
0.045
0.030
0.015
0.000
40
80
120
160
200
240
280
320
TIME (*10^6)
U4:[JWGARNE.NAS.92.T1]CAMDAT_S05_S_R002.CDB;2
PLOT 03/05/93 11:41

Figure 7

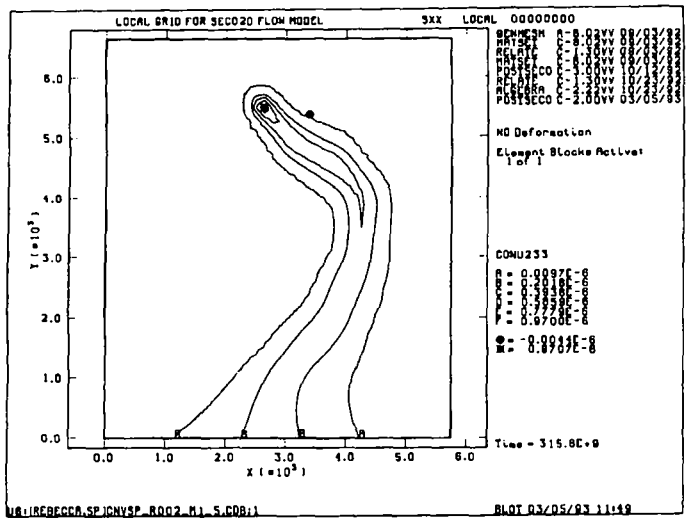

(a)

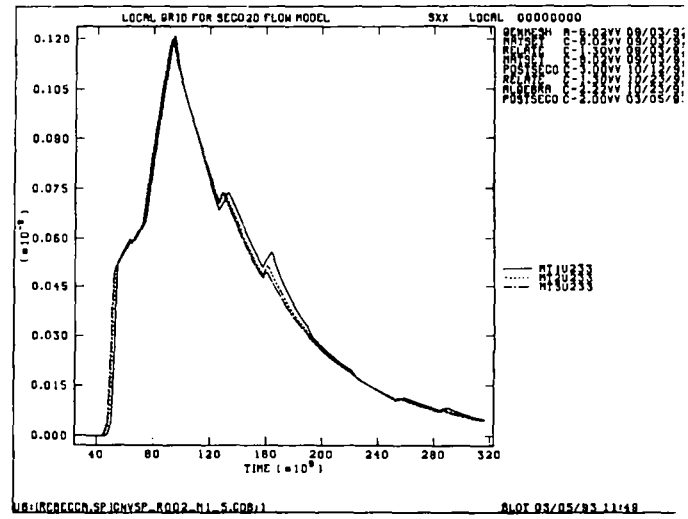

(b)

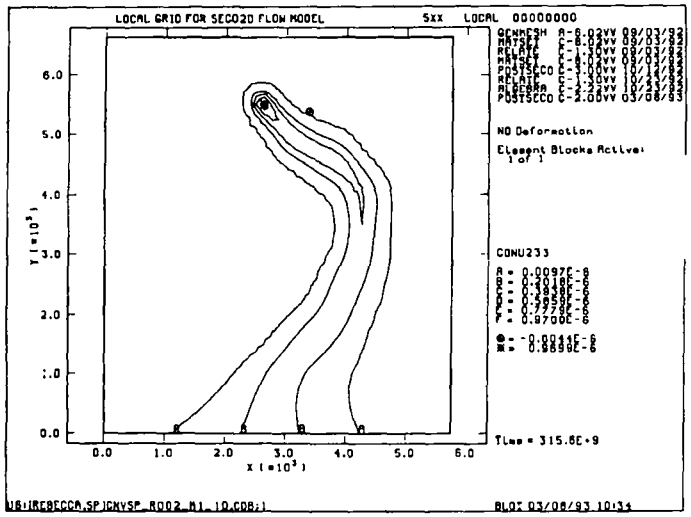

(c)

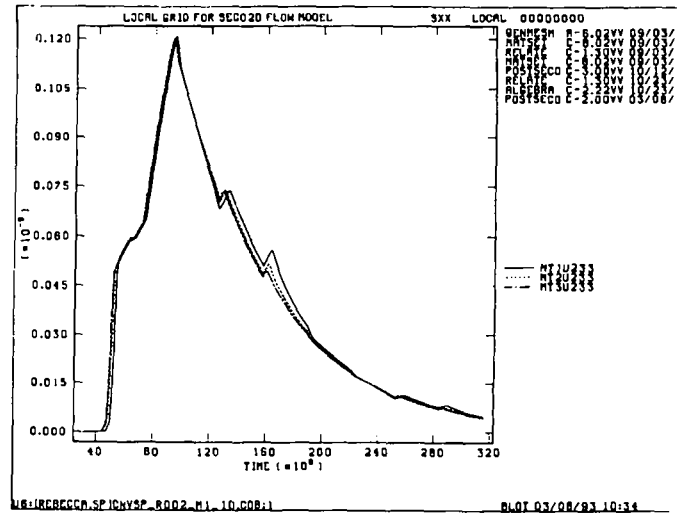

(d)

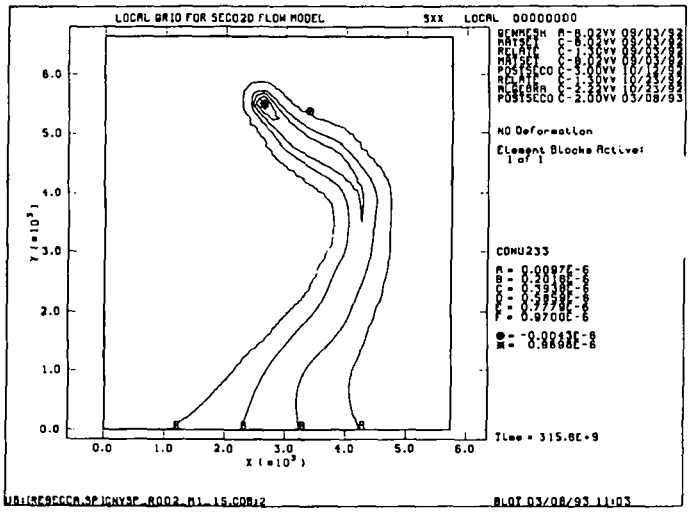

(e)

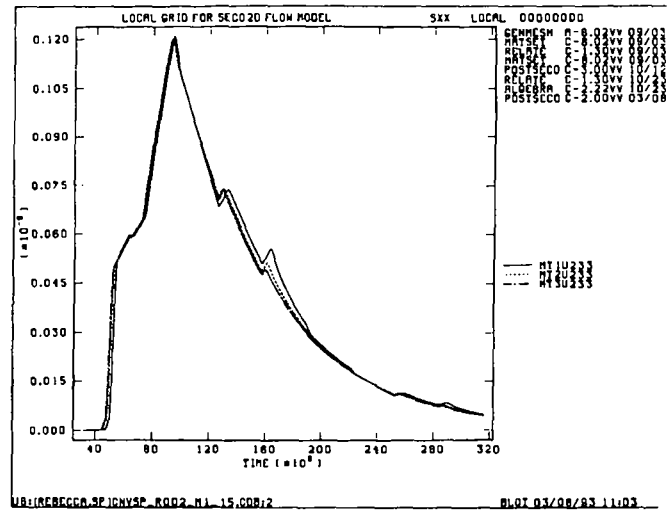

(f)

Figure 8

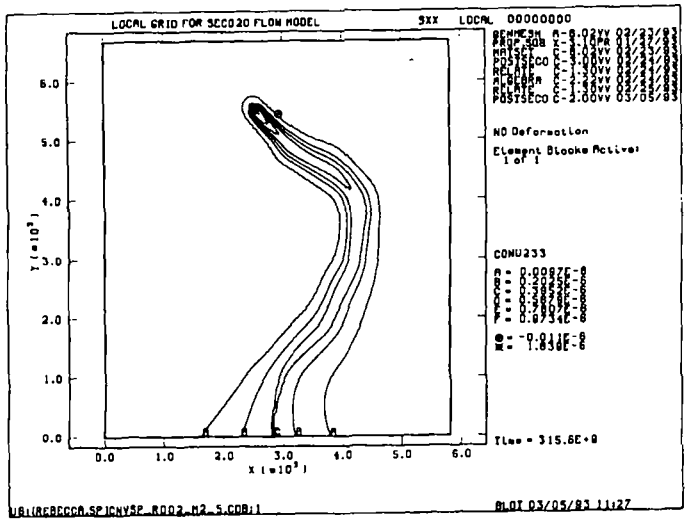

(a)

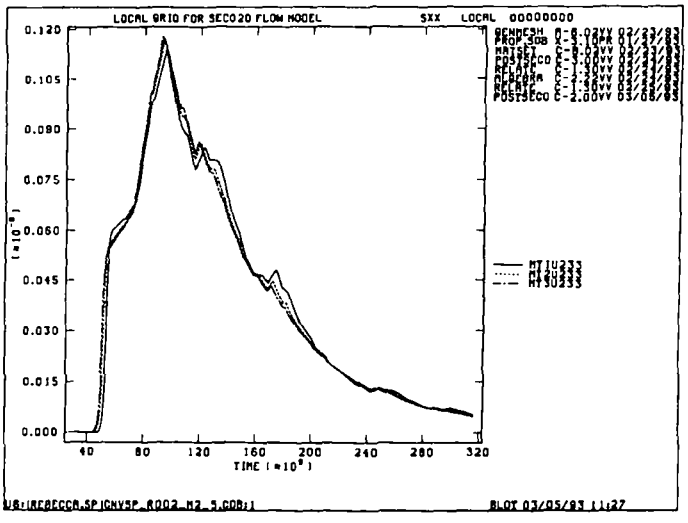

(b)

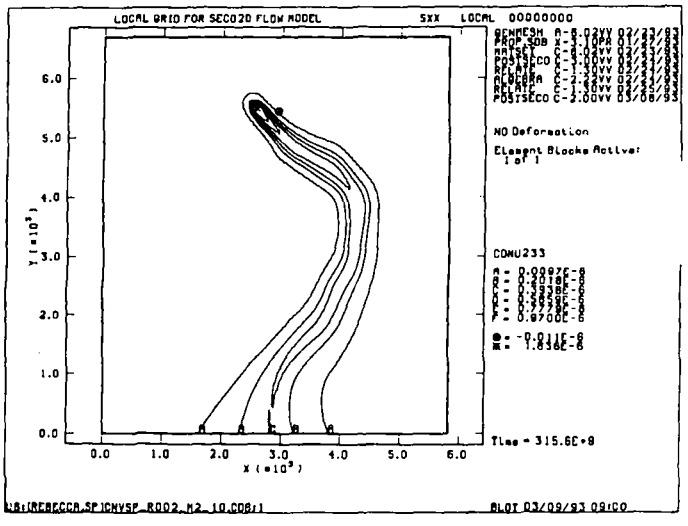

(c)

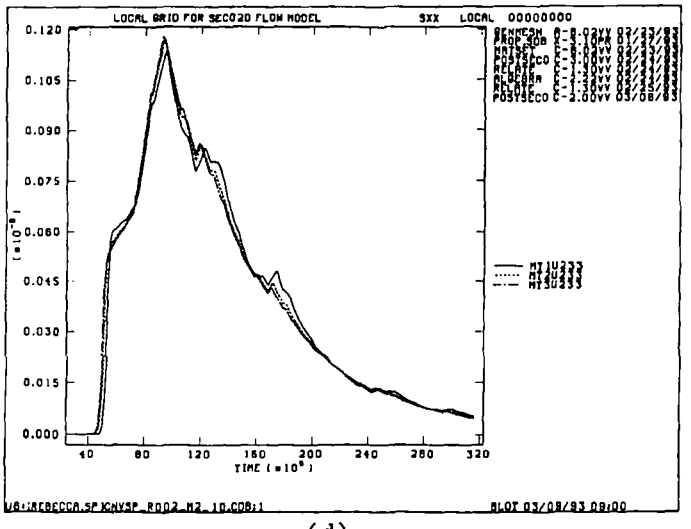

(d)

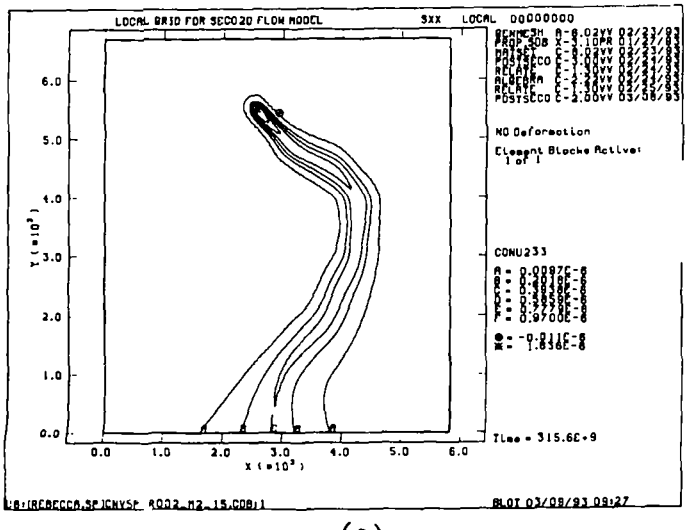

(e)

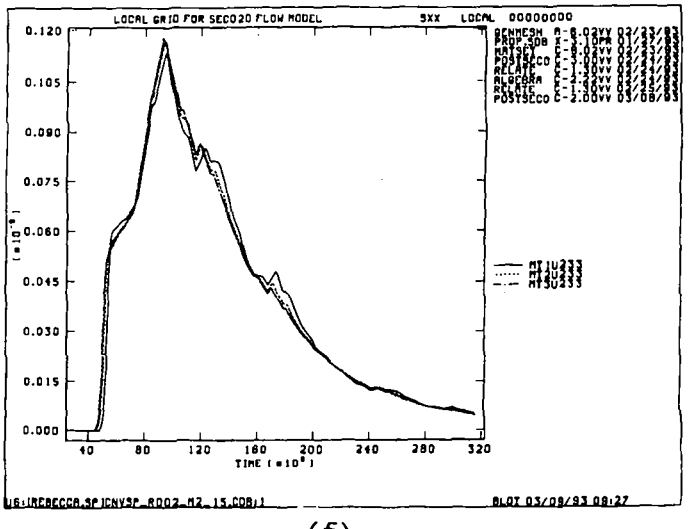

(f)

Figure 9

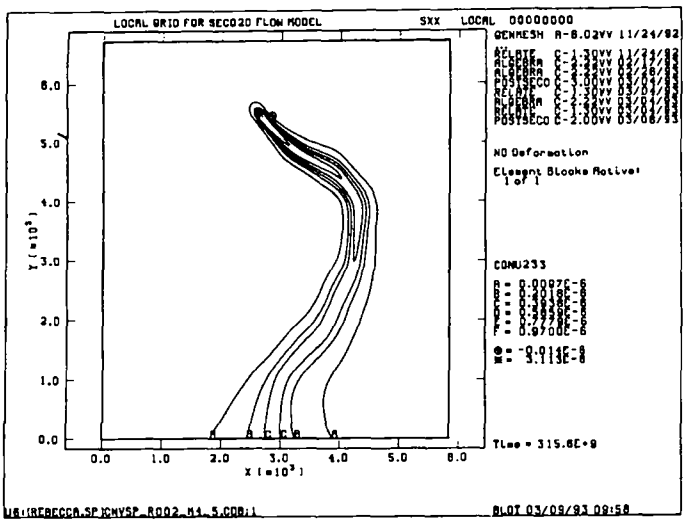

(a)

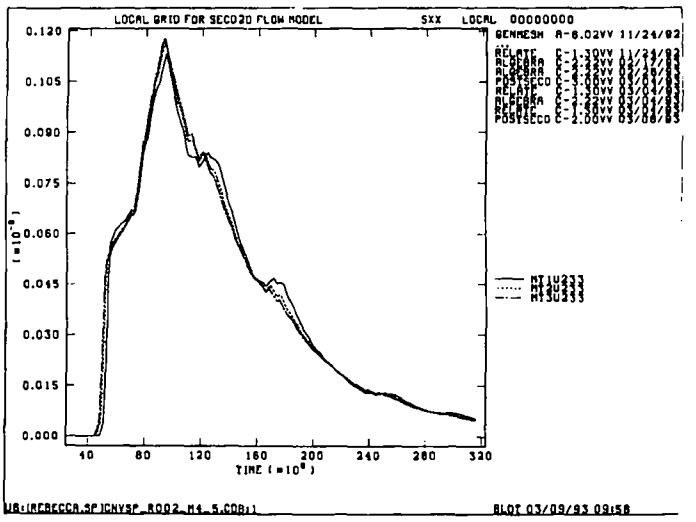

(b)

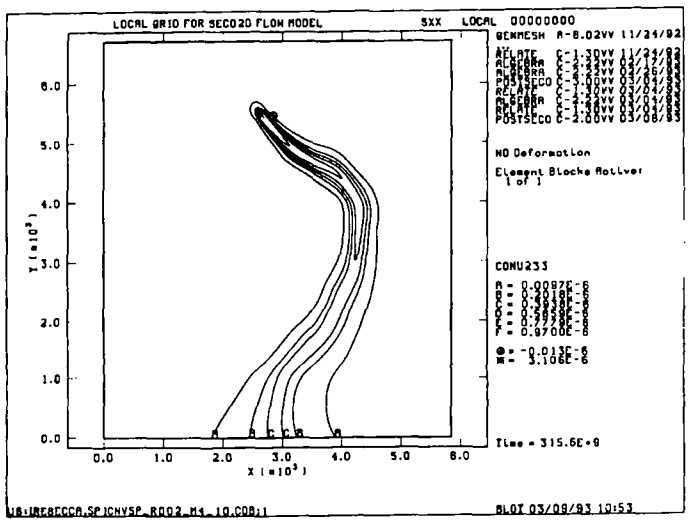

(c)

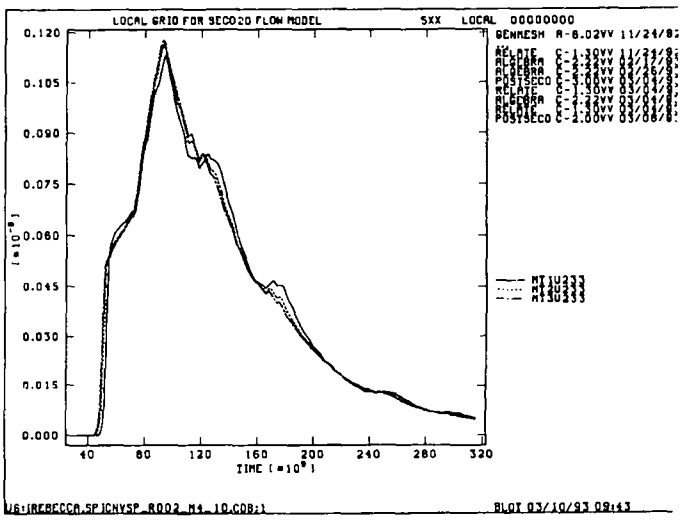

(d)

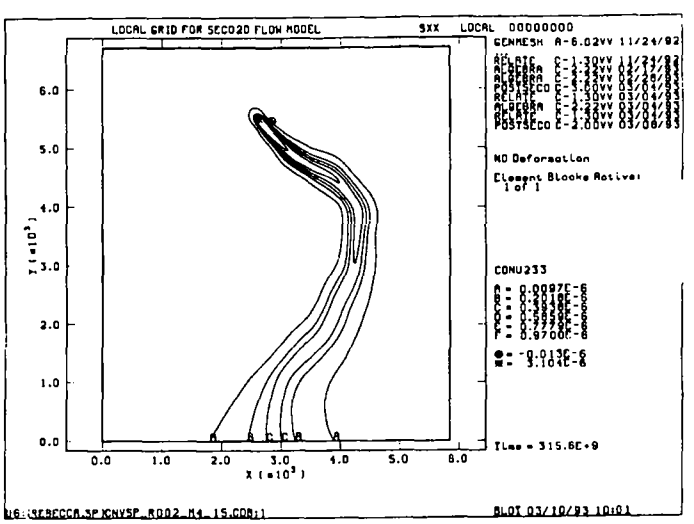

(e)

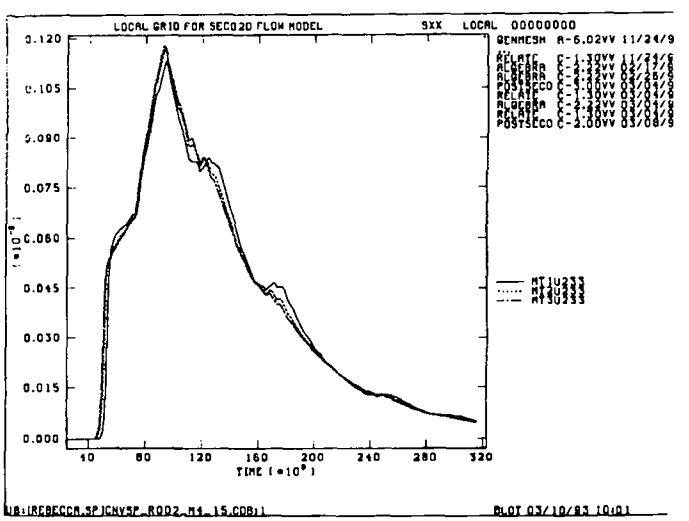

(f)

Figure 10

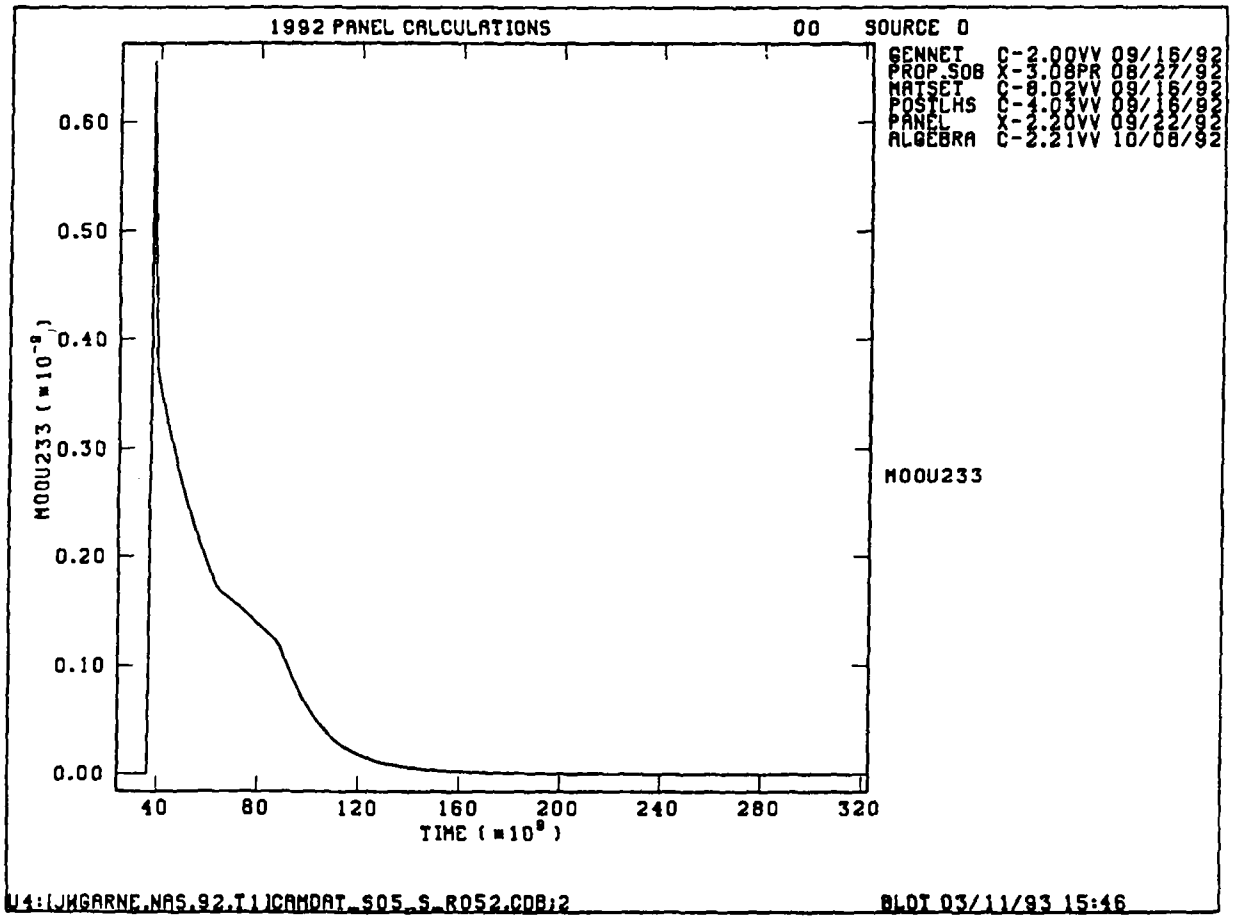
1992 PANEL CALCULATIONS
00
SOURCE 0
GENNET C-2.00VV 09/16/92
PROP.SOB X-3.08PR 08/27/92
MATSET C-8.02VV 09/16/92
POSTLHS C-4.03VV 09/16/92
PANEL X-2.20VV 09/22/92
ALGEBRA C-2.21VV 10/08/92
MOOU233
MOOU233 (*10^-9)
0.60
0.50
0.40
0.30
0.20
0.10
0.00
40
80
120
160
200
240
280
320
TIME (*10^9)
U4:[JHGARNE.NAS.92.T1]CAMDAT_S05_S_R052.CDB;2
PLOT 03/11/93 15:46

Figure 11

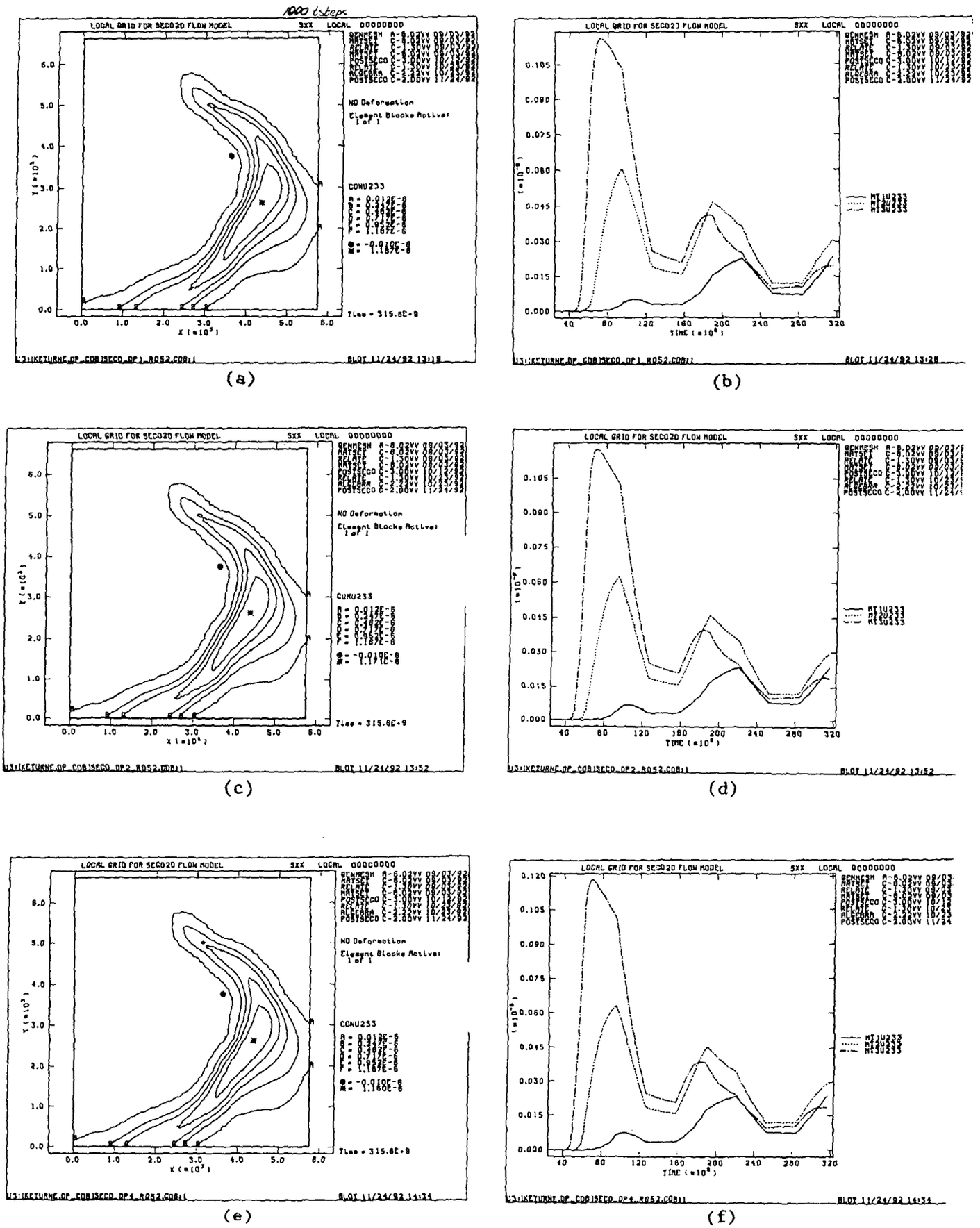
1000 tsteps
LOCAL GRID FOR SECO3D FLOW MODEL
SXX LOCAL 00000000
NO Deformation
CONU233
TLee = 315.8E+9
X (*10³)
Y (*10³)
TIME (*10⁸)
(a)
(b)
(c)
(d)
(e)
(f)

Figure 12

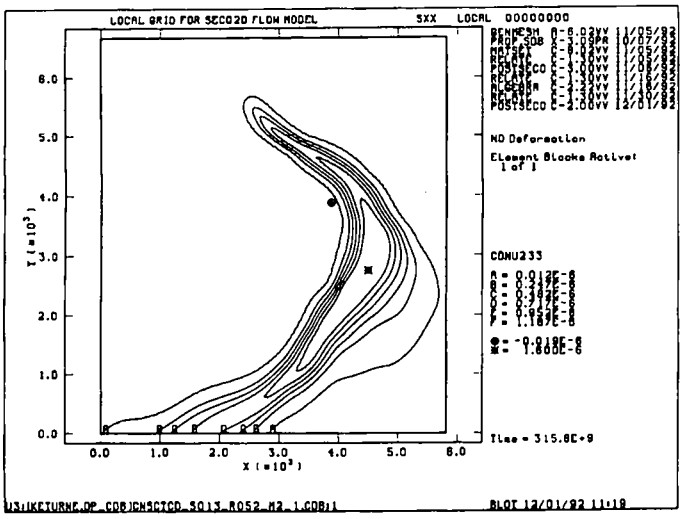

(a)

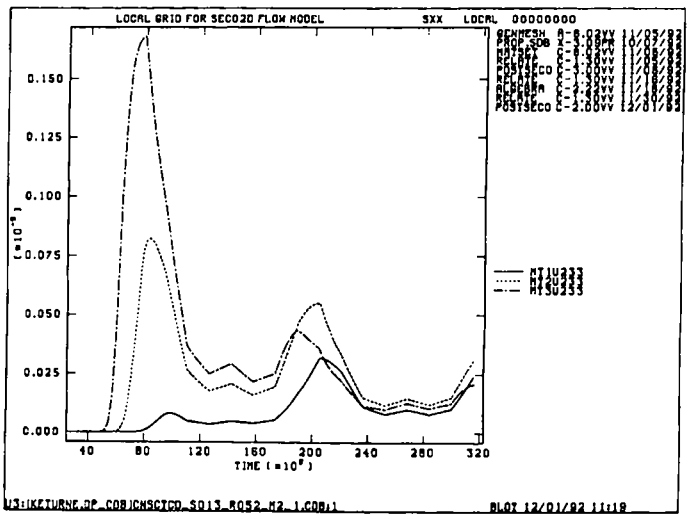

(b)

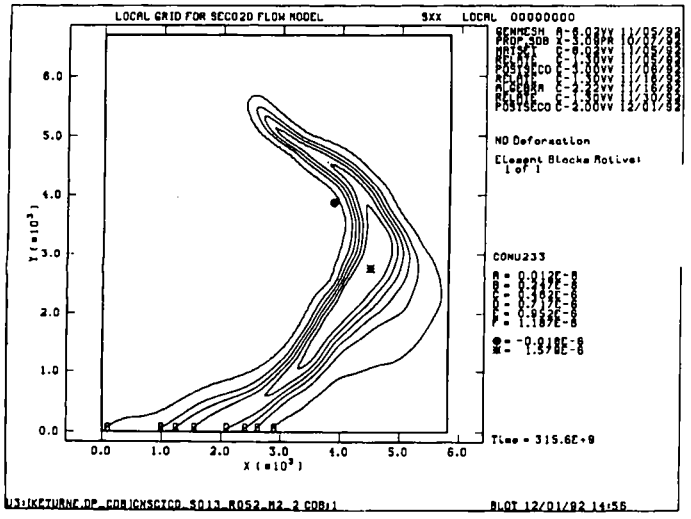

(c)

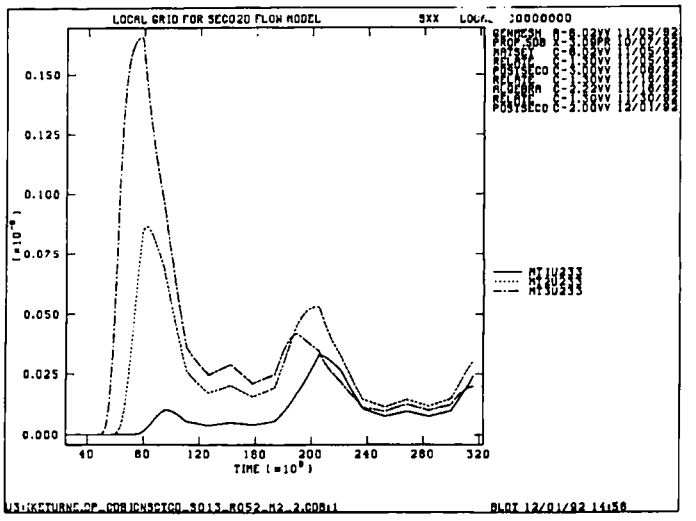

(d)

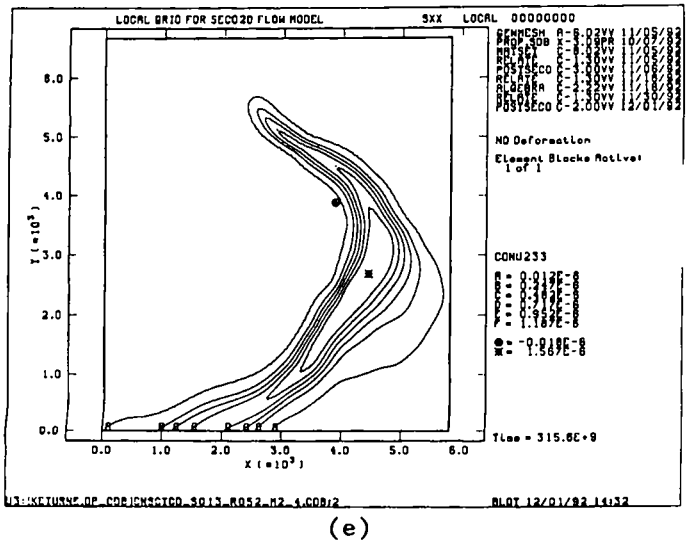

(e)

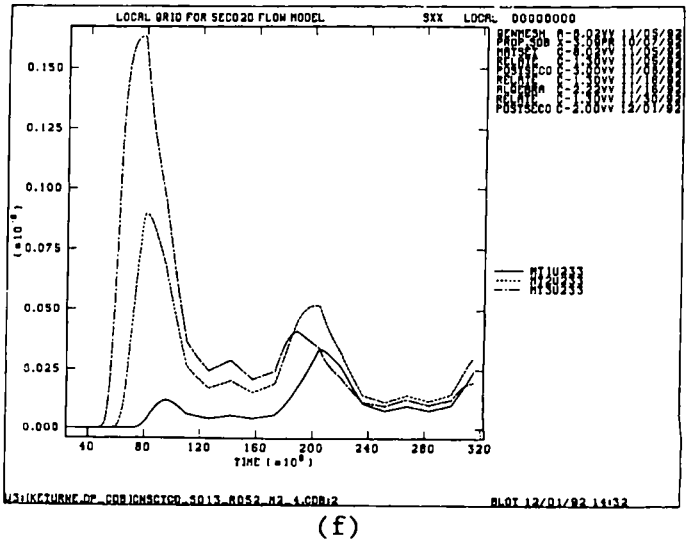

(f)

Figure 13

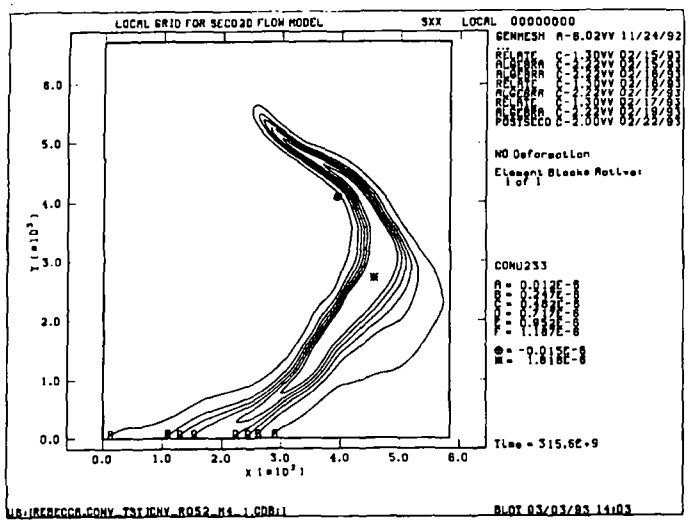

(a)

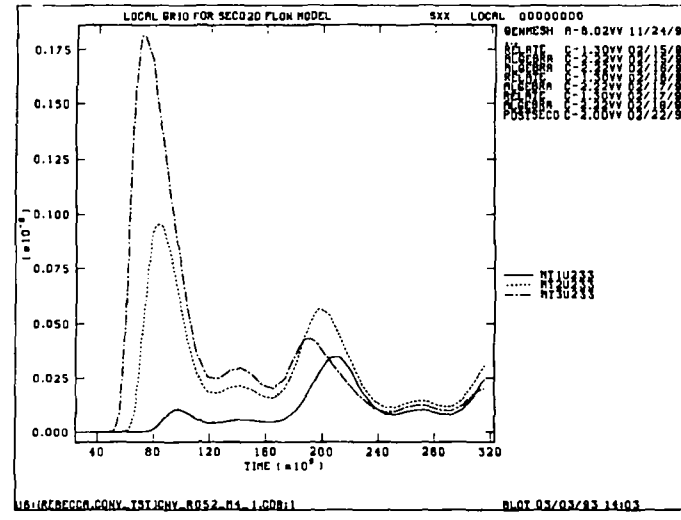

(b)

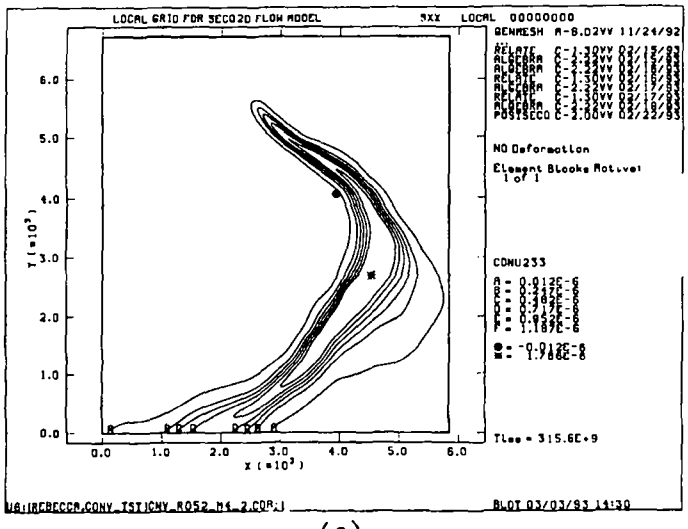

(c)

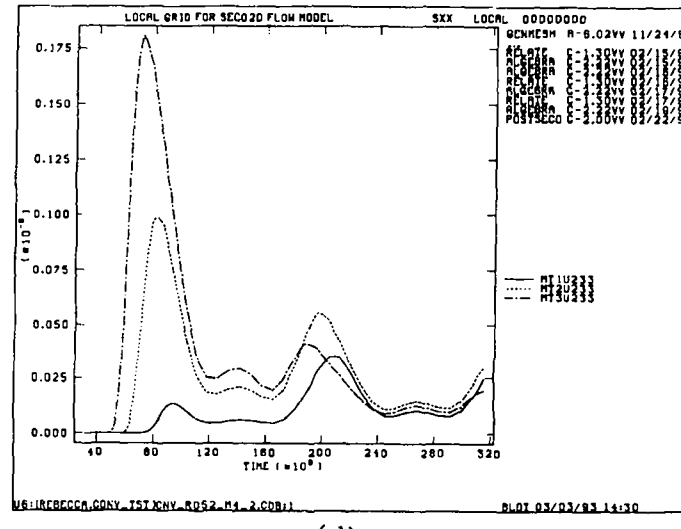

(d)

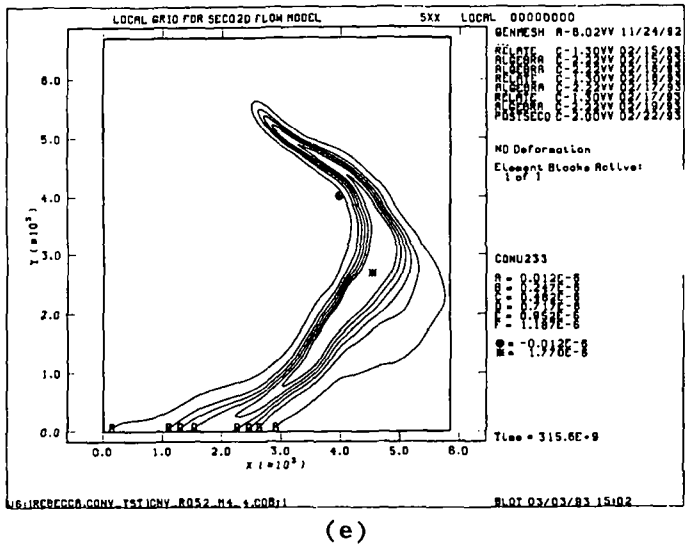

(e)

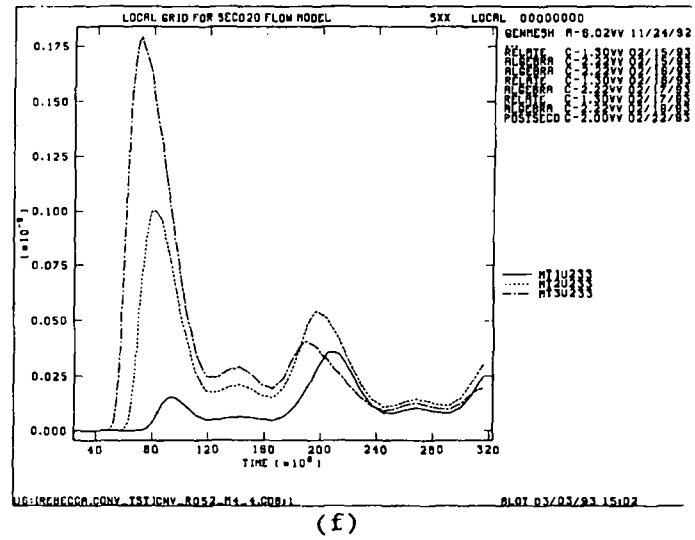

(f)

Figure 14

APPENDIX B: ASSUMPTIONS AND DERIVATION OF EQUATION 4.2-2 RELATING SANCHO POROSITY TO BRAGFLO POROSITY

APPENDIX B: ASSUMPTIONS AND DERIVATION OF EQUATION 4.2-2 RELATING SANCHO POROSITY TO BRAGFLO POROSITY

Inherent in Equation 4.2-2 is that the compressibility of halite is small compared to the compressibility of the gas that occupies the voids within the waste panel. Making this assumption permits the conclusion that the mass and volume occupied by the solid (waste and backfill) within the moving boundary defining the time variant dimensions of the waste panel remains constant. The volume of solids within the waste panel, at any time, is the same as the volume of solids that are present initially in the waste panel prior to compaction (Equation B-1).

$$V_s\ (t=0) = V_s(t) \tag{B-1}$$

where

V_s = volume of solids within the boundaries defining the waste panel.

Figure B-1 depicts the waste panel in two states, the top figure, a, depicts the waste panel initially, at t=0, while the bottom figure, b, depicts the waste-panel after some consolidation, at time t. While the figure implies compaction of the waste panel by movement of the upper boundary or roof, this is for convenience only; movement of the other boundaries may also participate in the compaction process.

The porosity, ϕ', of the waste panel is defined, at any time, as the ratio of the void volume (V_v) to the total volume, V_t, where V_t is the sum of the void volume and solid volume, Equations B-2 and B-3, respectively,

$$\phi'(t) = \frac{V_v\ (t)}{V_t\ (t)} \tag{B-2}$$

and

$$V_t(t) = V_v(t) + V_s(t). \tag{B-3}$$

Substitution of Equation B-3 into Equation B-2 allows the solid volume to be expressed in terms of porosity and total panel volume, Equation B-4,

$$V_s = (1 - \phi')\ V_t. \tag{B-4}$$

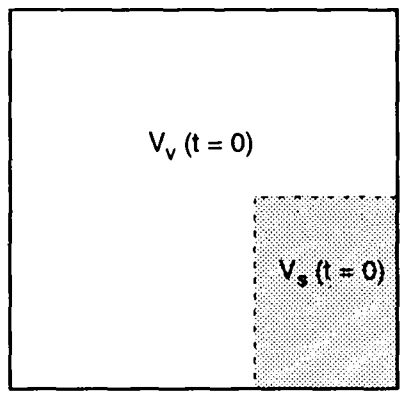

a) Waste-panel at initial state.

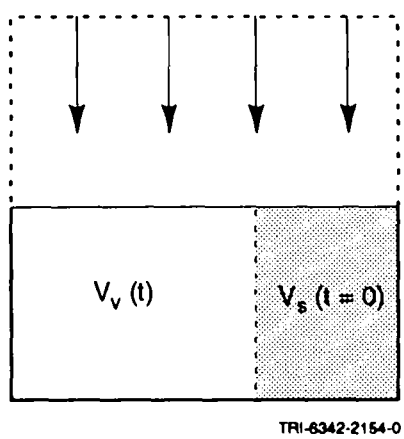

b) Waste-panel at compacted state.

Figure B-1. Waste-Panel at two states of compaction, showing volume of voids (V_V) and volume of solids (V_S).

Applying Equation B-4 at time, t=0, and at an arbitrary time, t, and using the equality of Equation B-1, after some rearrangement yields Equation B-5,

$$\frac{1 - \phi'(t=0)}{1 - \phi'(t)} = \frac{V_t(t)}{V_t(t=0)} \quad . \tag{B-5}$$

Now, define an alternate porosity, ϕ, as the ratio of the void volume at any given time to the total initial volume of the waste panel prior to compaction, Equation B-6,

$$\phi(t) = \frac{V_v(t)}{V_t(t=0)} \quad . \tag{B-6}$$

It is desired to relate ϕ and ϕ' in a way that conserves void volume. This can be done by determining the porosity associated with the waste panel of initial dimensions and volume that is equivalent to the void volume of the compacted and collapsed representation of the waste panel. Combining Equations B-2 and B-6 and solving for $\phi(t)$ yields the desired result, Equation B-7,

$$\phi(t) = \frac{\phi'(t)\, V_t(t)}{V_t(t=0)} \quad . \tag{B-7}$$

Equation B-8, reproduced as Equation 4.2-2, is obtained by substituting the left hand side of B-5 for the ratio, $V_t(t)/V_t(t=0)$ in Equation B-7,

$$\phi(t) = \phi'(t) \left[\frac{1 - \phi'(t=0)}{1 - \phi'(t)} \right] \quad . \tag{B-8}$$

Equation B-8 relates ϕ to only ϕ' at a given value of time and is used to transform the porosities resulting from the Segrangian treatment of the numerical mesh in SANCHO to the Eulerian treatment in BRAGFLO, while conserving void volume.

APPENDIX C: LHS SAMPLES AND CALCULATED NORMALIZED RELEASES

Contents For Appendix C

Tables

APPENDIX C: LHS SAMPLES AND CALCULATED NORMALIZED RELEASES

This appendix contains the 70 sample elements for each of the 49 parameters varied and sampled by LHS and summaries of EPA-normalized radionuclide releases to the 2.9-km, accessible environment boundary south of the WIPP for the E1 and E1E2 scenarios with an intrusion at 1000 yr. Releases are given for simulations assuming a dual porosity model with chemical retardation for transport in the Culebra Dolomite Member of the Rustler Formation.

This appendix also contains the summaries of release to the accessible environment from initially drilling into the repository and bringing up cuttings from one average activity of CH waste and one average activity of RH waste. (The CH waste activity is subsequently multiplied by a factor to account for the four CH activity levels. This modified activity along with the probability of actually hitting these various CH activity levels is used when constructing the CCDF). Cuttings were calculated for six different intrusion times. Releases are the same for the E1, E2 or E1E2 scenarios, and different scenarios are accounted for by the CCDFPERM program.

The output tables were created by the CCDFCALC computer code from output databases created by SECO-TRANSPORT and CUTTINGS and are the input to the CCDFPERM program which calculates the final CCDF.

Table C-1 lists the 49 parameters sampled and the distribution type used.

Table C-1. Numerical ID and Distributions of 49 Sampled Parameters In December 1992 WIPP PA Calculations

Parameter	Range		Distribution
1 Initial Brine Saturation of Waste (BRSAT)	0.	0.14	Uniform
2 Inundated Corrosion Gas Generation Rate (mol/m^2•s) (GRCORI)	0.	1.3E-08	Cumulative
3 Humid/Inundated Corrosion Gas Generation Rate Ratio (GRCORHF)	0.	0.5	Cumulative
4 Stoichiometric For Corrosion of Steel (STOICCOR)	0.	1.	Uniform
5 Inundated Microbial Gas Generation Rate (mol/kg•s) (GRMICI)	0.	1.6E-08	Cumulative
6 Humid/Inundated Microbial Gas Generation Rate Ratio (GRMICHF)	0.	0.2	Uniform
7 Stoichiometric Coef For Biodegradation of Cellulose (STOICMIC)	0.	1.67	Uniform
8 Wood Volume Fraction (VWOOD)	0.284	0.484	Normal
9 Metal Volume Fraction (VMETAL)	0.276	0.476	Normal
10 Log Salado Permeability (m^2) (SALPERM)	-24.	-19.	Cumulative
11 Brooks-Corey Exponent (BCEXP)	0.2	10.	Cumulative
12 Brooks-Corey Model Relative Weight (BCFLG)	0.	1.	Delta
13 Brooks-Corey Residual Brine Saturation (BCBRSAT)	0.	0.4	Uniform
14 Brooks-Corey Residual Gas Saturation (BCGSSAT)	0.	0.4	Uniform
15 Log Marker Bed Permeability (m^2) (MBPERM)	-21.	-16.	Cumulative
16 Marker Bed Porosity (MBPOR)	0.001	0.03	Cumulative
17 Scale Factor For Disturbed Zone Porosity (TZPORF)	0.	1.	Uniform
18 Salado Pressure (Pa) (MBPRES)	1.2E+07	1.3E+07	Uniform
19 Brine Pocket Pressure (Pa) (BPPRES)	1.3E+07	2.1E+07	Uniform

Table C-1. Numerical ID and Distributions of 49 Sampled Parameters In December 1992 WIPP PA Calculations (Continued)

	Parameter	Range		Distribution
20	Brine Pocket Bulk Storativity (m^3/Pa) (BPSTOR)	0.02	2.	Lognormal
21	Borehole Permeability (m^2) (BHPERM)	1.0E-14	1.0E-11	Lognormal
22	Drillbit Diameter (m) (DBDIAM)	0.2667	0.4445	Uniform
23	Index for Rate in Poisson Drilling Model (LAMBDA)	0.	1.	Uniform
24	Brine Pocket Area Fraction (BPAREAFR)	0.24479	0.56771	Cumulative
25	Log Solubility Am (mol/l) (SOLAM)	-13.3	0.15	Cumulative
26	Log Solubility Np (mol/l) (SOLNP)	-15.52	-1.92	Cumulative
27	Log Solubility Pu (mol/l) (SOLPU)	-16.6	-3.26	Cumulative
28	Log Solubility Ra (mol/l) (SOLRA)	0.3	1.26	Cumulative
29	Log Solubility Th (mol/l) (SOLTH)	-15.26	-5.66	Cumulative
30	Log Solubility U (mol/l) (SOLU)	-15.	0.	Cumulative
31	Culebra Index for Transmissivity Field (CULTRFLD)	0.	1.	Uniform
32	Index for Recharge Amplitude Factor (CULCLIM)	0.	1.	Uniform
33	Culebra Fracture Porosity (CULFRPOR)	0.0001	0.01	Lognormal
34	Culebra Fracture Spacing (m) (CULFRSP)	0.06	8.	Cumulative
35	Culebra Clay Filling Fraction (CULCLYF)	0.	0.5	Cumulative
36	Culebra Clay Porosity (CULCLYP)	0.05	0.5	Uniform
37	Log Culebra Fracture Dist Coef Am (m^3/kg) (FKDAM)	-4.	3.	Cumulative
38	Log Culebra Fracture Dist Coef Np (m^3/kg) (FKDNP)	-4.	3.	Cumulative
39	Log Culebra Fracture Dist Coef Pu (m^3/kg) (FKDPU)	-4.	3.	Cumulative
40	Log Culebra Fracture Dist Coef Th (m^3/kg) (FKDTH)	-4.	1.	Cumulative
41	Log Culebra Fracture Dist Coef U (m^3/kg) (FKDU)	-4.	0.	Cumulative
42	Log Culebra Fracture Dist Coef Ra (m^3/kg) (FKDRA)	-4.	2.	Cumulative
43	Culebra Matrix Porosity (CULPOR)	.058056	0.2525	Data
44	Log Culebra Matrix Dist Coef Am (m^3/kg) (MKDAM)	-4.	2.	Cumulative
45	Log Culebra Matrix Dist Coef Np (m^3/kg) (MKDNP)	-4.	2.	Cumulative
46	Log Culebra Matrix Dist Coef Pu (m^3/kg) (MKDPU)	-4.	2.	Cumulative
47	Log Culebra Matrix Dist Coef Th (m^3/kg) (MKDTH)	-4.	0.	Cumulative
48	Log Culebra Matrix Dist Coef U (m^3/kg) (MKDU)	-4.	0.	Cumulative
49	Log Culebra Matrix Dist Coef Ra (m^3/kg) (MKDRA)	-4.	1.	Cumulative

Table C-2 lists the Latin Hypercube sampled (LHS) values for each of the 49 parameters.

Table C-2. Seventy Values Sampled by LHS for 49 Parameters that Were Varied in December 1992 PA Calculations

Material Parameter RUN NO.	BRSAT X(1)	GRCORI X(2)	GRCORHF X(3)	STOICCOR X(4)	GRMICI X(5)	GRMICHF X(6)	STOICMIC X(7)	VWOOD X(8)	VMETAL X(9)	SALPERM X(10)
1	4.023E-02	1.570E-09	1.238E-01	4.810E-01	1.154E-08	8.629E-02	7.677E-01	3.601E-01	3.741E-01	-2.044E+01
2	1.269E-01	3.730E-09	2.775E-01	2.119E-01	1.588E-08	1.696E-01	1.264E-01	4.242E-01	3.910E-01	-2.001E+01
3	8.612E-02	8.501E-10	7.155E-02	4.965E-02	3.585E-09	1.532E-01	7.179E-04	3.914E-01	3.452E-01	-2.088E+01
4	3.242E-02	1.013E-08	8.783E-03	4.382E-01	9.379E-09	4.926E-02	2.213E-01	3.425E-01	4.137E-01	-2.082E+01
5	1.149E-01	3.321E-10	1.539E-02	6.945E-01	1.195E-08	5.316E-02	4.741E-01	3.808E-01	3.928E-01	-2.154E+01
6	1.373E-01	1.176E-08	3.287E-01	6.461E-01	3.979E-09	9.957E-02	1.322E+00	4.637E-01	4.465E-01	-2.314E+01

Table C-2. Seventy Values Sampled by LHS for 49 Parameters that Were Varied in December 1992 PA Calculations (Continued)

Material Parameter RUN NO.	BRSAT X(1)	GRCORI X(2)	GRCORHF X(3)	STOICCOR X(4)	GRMICI X(5)	GRMICHF X(6)	STOICMIC X(7)	VWOOD X(8)	VMETAL X(9)	SALPERM X(10)
7	1.395E-01	1.041E-08	3.263E-01	6.245E-01	1.421E-09	1.238E-01	4.816E-01	3.225E-01	3.987E-01	-2.194E+01
8	8.068E-02	6.341E-09	4.805E-01	7.551E-01	7.905E-09	4.721E-02	5.214E-01	3.502E-01	3.437E-01	-2.131E+01
9	5.937E-02	1.715E-09	3.813E-02	3.057E-01	8.037E-09	5.041E-05	1.425E+00	4.689E-01	4.191E-01	-2.332E+01
10	7.619E-02	8.712E-09	2.143E-01	7.950E-01	6.070E-09	1.297E-02	1.229E+00	3.587E-01	3.578E-01	-2.040E+01
11	1.202E-01	9.067E-09	2.269E-01	6.636E-03	2.159E-09	1.064E-01	3.519E-02	3.065E-01	4.027E-01	-2.011E+01
12	8.396E-02	1.127E-08	9.043E-02	4.057E-01	3.123E-09	6.075E-02	1.490E+00	3.632E-01	3.785E-01	-2.004E+01
13	3.577E-02	4.420E-09	2.111E-01	9.610E-01	6.352E-10	1.559E-01	7.945E-01	3.733E-01	4.369E-01	-2.306E+01
14	1.272E-02	1.138E-08	3.582E-02	1.254E-01	2.820E-10	1.745E-01	3.435E-01	4.060E-01	3.886E-01	-2.215E+01
15	1.315E-01	2.155E-09	3.880E-01	3.308E-01	8.800E-09	8.200E-02	1.339E+00	4.120E-01	3.523E-01	-2.352E+01
16	4.263E-02	5.910E-09	4.610E-01	3.478E-01	1.216E-08	1.580E-01	1.667E+00	3.436E-01	3.820E-01	-2.070E+01
17	5.151E-02	2.705E-09	1.751E-01	9.018E-01	7.343E-09	4.462E-02	9.611E-01	4.016E-01	3.183E-01	-2.189E+01
18	6.297E-02	5.140E-10	3.003E-02	2.212E-01	1.285E-09	1.021E-01	1.446E+00	3.556E-01	3.845E-01	-2.117E+01
19	5.652E-02	8.036E-09	4.058E-03	3.615E-02	1.413E-08	2.054E-02	5.646E-01	4.048E-01	3.375E-01	-2.240E+01
20	3.744E-02	5.687E-09	2.713E-03	1.508E-01	5.405E-09	4.216E-02	1.606E+00	3.995E-01	4.760E-01	-1.974E+01
21	1.046E-02	1.095E-08	3.090E-01	1.887E-01	1.268E-08	6.836E-02	1.108E+00	3.841E-01	3.952E-01	-1.954E+01
22	7.499E-02	1.962E-09	5.486E-02	6.810E-01	2.061E-09	1.300E-01	9.990E-01	4.185E-01	3.697E-01	-2.026E+01
23	8.469E-02	7.970E-09	4.012E-01	7.260E-01	2.704E-09	1.680E-01	3.339E-01	4.075E-01	4.277E-01	-2.126E+01
24	7.128E-02	4.287E-09	2.143E-02	5.270E-01	2.922E-09	1.995E-01	8.854E-01	3.275E-01	3.802E-01	-2.092E+01
25	7.809E-02	7.428E-09	9.208E-02	5.991E-01	3.319E-09	1.195E-01	5.792E-01	3.560E-01	2.760E-01	-2.015E+01
26	1.014E-01	1.164E-08	1.136E-01	5.786E-01	4.518E-10	4.783E-03	7.210E-01	4.269E-01	3.382E-01	-2.076E+01
27	2.606E-02	1.061E-08	1.638E-01	2.359E-01	1.602E-09	1.821E-01	6.518E-01	4.840E-01	3.869E-01	-2.129E+01
28	2.351E-02	6.576E-09	5.147E-02	5.697E-01	5.082E-09	7.677E-02	4.355E-01	3.970E-01	3.748E-01	-2.134E+01
29	6.911E-02	1.295E-08	8.140E-02	9.815E-01	2.366E-09	1.852E-01	5.370E-01	3.868E-01	3.236E-01	-2.063E+01
30	8.819E-02	1.196E-08	4.481E-01	5.139E-01	1.556E-08	9.290E-02	7.124E-01	4.171E-01	4.237E-01	-2.110E+01
31	1.292E-01	6.995E-09	4.523E-02	9.431E-01	6.670E-09	7.725E-02	3.767E-01	3.943E-01	3.568E-01	-2.147E+01
32	5.255E-02	1.368E-10	7.907E-02	3.954E-01	7.986E-10	1.859E-01	1.553E+00	4.151E-01	4.101E-01	-2.021E+01
33	9.849E-02	3.385E-09	2.919E-01	4.463E-01	1.200E-09	1.427E-01	2.698E-01	4.349E-01	3.108E-01	-2.100E+01
34	9.053E-02	1.081E-08	7.457E-02	8.960E-01	7.207E-09	9.077E-02	1.079E+00	3.784E-01	4.395E-01	-2.162E+01
35	2.035E-02	4.618E-09	6.518E-02	8.269E-01	1.067E-08	1.631E-01	1.468E+00	3.823E-01	3.402E-01	-2.051E+01
36	7.227E-02	9.288E-09	3.464E-01	6.634E-01	9.881E-10	1.971E-02	1.277E+00	3.922E-01	3.170E-01	-2.180E+01
37	3.864E-02	7.111E-09	3.316E-02	6.227E-02	6.134E-09	9.403E-03	4.126E-01	3.894E-01	3.058E-01	-2.107E+01
38	4.888E-02	1.119E-09	9.576E-02	7.598E-01	4.617E-09	6.536E-02	1.049E+00	4.085E-01	4.099E-01	-2.029E+01
39	1.031E-01	3.905E-09	2.661E-01	8.822E-01	1.884E-09	2.835E-02	1.532E+00	3.717E-01	4.067E-01	-2.112E+01
40	4.701E-02	1.228E-08	7.826E-03	6.342E-01	1.442E-08	1.152E-01	8.155E-01	4.003E-01	3.834E-01	-2.259E+01
41	1.689E-02	3.028E-09	3.656E-01	8.111E-01	9.466E-09	2.958E-02	2.491E-01	3.775E-01	4.046E-01	-2.023E+01
42	1.994E-02	1.218E-08	3.757E-01	1.081E-01	2.577E-09	1.627E-01	1.199E+00	3.388E-01	3.639E-01	-2.120E+01
43	3.326E-03	5.150E-09	1.927E-01	8.371E-01	1.101E-08	1.090E-01	1.782E-01	4.140E-01	3.627E-01	-2.061E+01
44	1.359E-01	9.052E-10	1.171E-02	4.237E-01	6.858E-10	3.679E-02	6.056E-01	3.635E-01	3.725E-01	-2.040E+01
45	1.326E-01	7.140E-10	4.905E-01	7.660E-02	2.197E-09	1.121E-01	7.530E-01	3.748E-01	3.710E-01	-2.054E+01
46	9.242E-03	3.435E-09	3.021E-01	1.721E-02	4.856E-09	1.792E-01	1.245E+00	3.667E-01	3.543E-01	-2.398E+01
47	1.167E-01	1.019E-08	6.963E-02	2.849E-01	2.386E-09	1.724E-01	9.291E-01	4.484E-01	3.285E-01	-1.924E+01
48	1.406E-02	2.606E-09	4.659E-01	8.438E-01	1.769E-09	6.468E-03	8.594E-01	3.471E-01	3.267E-01	-2.055E+01
49	9.471E-02	9.572E-09	6.801E-02	7.736E-01	2.535E-09	1.910E-01	1.588E+00	3.309E-01	4.285E-01	-2.170E+01
50	3.147E-02	1.265E-08	6.036E-02	2.953E-01	1.106E-09	2.437E-02	2.987E-01	3.884E-01	3.672E-01	-2.173E+01
51	6.122E-02	5.379E-09	2.432E-01	7.003E-01	1.180E-11	1.356E-01	1.407E+00	4.295E-01	3.614E-01	-2.006E+01
52	2.412E-02	3.170E-09	2.522E-01	7.324E-01	3.087E-09	1.577E-02	1.628E-01	2.953E-01	4.004E-01	-2.070E+01

Table C-2. Seventy Values Sampled by LHS for 49 Parameters that Were Varied in December 1992 PA Calculations (Continued)

Material Parameter RUN NO.	BRSAT X(1)	GRCORI X(2)	GRCORHF X(3)	STOICCOR X(4)	GRMICI X(5)	GRMICHF X(6)	STOICMIC X(7)	VWOOD X(8)	VMETAL X(9)	SALPERM X(10)
53	1.190E-01	1.257E-08	8.368E-02	4.961E-01	1.480E-09	3.382E-02	6.351E-01	3.825E-01	4.589E-01	-2.033E+01
54	1.048E-01	4.903E-09	8.608E-02	9.416E-01	1.032E-08	1.952E-01	1.009E+00	4.310E-01	2.923E-01	-2.143E+01
55	6.768E-02	5.538E-09	4.791E-02	1.810E-01	1.717E-09	1.272E-01	9.388E-01	4.399E-01	3.493E-01	-2.185E+01
56	6.598E-02	6.245E-09	2.555E-02	8.643E-01	2.762E-09	1.049E-01	3.921E-01	2.840E-01	3.337E-01	-2.378E+01
57	1.244E-01	8.522E-09	1.496E-01	5.302E-01	1.922E-09	7.123E-02	1.071E+00	3.493E-01	3.502E-01	-2.141E+01
58	9.213E-02	7.530E-09	1.041E-01	9.933E-02	1.514E-08	1.209E-01	1.167E+00	3.654E-01	3.306E-01	-2.266E+01
59	1.232E-01	8.353E-09	3.593E-01	2.458E-01	1.274E-08	7.395E-02	1.512E+00	3.961E-01	3.769E-01	-2.283E+01
60	1.061E-01	4.043E-09	5.023E-02	1.658E-01	1.330E-08	1.378E-01	1.171E+00	3.709E-01	3.951E-01	-2.204E+01
61	1.108E-01	9.816E-09	2.580E-02	5.530E-01	8.393E-09	9.473E-02	1.637E+00	3.369E-01	3.007E-01	-2.097E+01
62	1.090E-01	5.998E-09	5.971E-02	2.666E-01	1.377E-10	3.802E-02	1.361E+00	3.136E-01	3.665E-01	-2.191E+01
63	4.544E-02	6.794E-09	9.919E-02	6.120E-01	2.423E-10	1.513E-01	1.073E-01	4.460E-01	3.857E-01	-2.151E+01
64	5.499E-02	4.681E-09	1.980E-02	9.927E-01	1.357E-08	1.455E-01	6.761E-01	4.375E-01	3.473E-01	-2.177E+01
65	2.810E-02	2.293E-09	1.413E-01	9.178E-01	9.936E-09	8.331E-02	5.036E-02	3.535E-01	4.544E-01	-2.081E+01
66	9.633E-02	8.857E-09	4.421E-01	1.287E-01	2.928E-09	5.813E-02	2.075E-01	4.576E-01	4.164E-01	-2.231E+01
67	5.864E-03	9.458E-09	1.858E-01	3.687E-01	8.269E-10	1.328E-01	1.136E+00	3.695E-01	3.597E-01	-2.094E+01
68	1.134E-01	2.460E-09	4.183E-02	4.695E-01	1.067E-09	1.927E-01	7.354E-02	3.347E-01	4.317E-01	-2.165E+01
69	6.604E-03	7.825E-09	4.264E-01	3.850E-01	1.472E-08	1.471E-01	8.473E-01	3.170E-01	4.200E-01	-2.159E+01
70	1.904E-03	1.351E-09	4.095E-01	3.248E-01	4.814E-10	5.544E-02	1.310E+00	4.204E-01	3.972E-01	-2.359E+01

Material Parameter RUN NO.	BCEXP X(11)	BCFLG X(12)	BCBRSAT X(13)	BCGSSAT X(14)	MBPERM X(15)	MBPOR X(16)	TZPORF X(17)	MBPRES X(18)	BPPRES X(19)	BPSTOR X(20)
1	9.679E+00	0.000E+00	8.789E-02	2.330E-01	-1.785E+01	2.866E-02	2.165E-02	1.202E+07	1.543E+07	1.947E-01
2	4.966E-01	1.000E+00	1.457E-01	1.259E-01	-1.977E+01	6.990E-03	4.764E-01	1.300E+07	1.458E+07	3.996E-01
3	6.790E-01	1.000E+00	1.849E-01	2.166E-01	-1.804E+01	2.897E-02	7.123E-01	1.260E+07	1.561E+07	1.364E-01
4	5.182E+00	1.000E+00	1.726E-01	1.890E-01	-1.930E+01	5.613E-03	9.978E-01	1.201E+07	1.511E+07	9.468E-01
5	4.071E-01	1.000E+00	1.988E-01	1.459E-01	-1.994E+01	2.056E-02	6.428E-02	1.233E+07	1.600E+07	1.657E-01
6	6.142E+00	0.000E+00	3.317E-01	4.793E-02	-1.982E+01	1.375E-02	9.602E-01	1.256E+07	2.082E+07	3.368E-01
7	1.099E+00	0.000E+00	3.543E-02	1.622E-01	-1.975E+01	2.593E-02	2.709E-01	1.245E+07	1.407E+07	2.578E-01
8	6.448E+00	1.000E+00	3.866E-01	2.852E-02	-1.874E+01	3.185E-03	5.669E-01	1.250E+07	1.874E+07	1.565E-01
9	4.261E-01	1.000E+00	3.408E-01	1.869E-01	-1.991E+01	2.727E-02	4.401E-01	1.230E+07	1.306E+07	1.483E-01
10	1.517E+00	1.000E+00	7.900E-02	3.481E-01	-1.728E+01	9.677E-03	2.896E-01	1.238E+07	1.972E+07	8.469E-02
11	5.125E-01	0.000E+00	2.717E-01	2.003E-01	-1.988E+01	2.573E-03	6.303E-01	1.227E+07	2.010E+07	8.790E-02
12	7.496E+00	1.000E+00	1.410E-01	2.862E-01	-1.865E+01	9.827E-03	5.472E-01	1.236E+07	2.097E+07	8.068E-02
13	2.249E+00	1.000E+00	3.650E-01	2.937E-01	-1.931E+01	1.661E-02	7.349E-02	1.277E+07	1.845E+07	7.603E-01
14	3.062E-01	1.000E+00	8.366E-03	1.736E-01	-2.000E+01	1.960E-02	4.472E-01	1.272E+07	1.683E+07	4.436E-02
15	4.462E-01	0.000E+00	2.310E-01	3.835E-01	-1.968E+01	1.159E-03	8.622E-01	1.279E+07	1.535E+07	4.805E-02
16	5.359E-01	1.000E+00	3.789E-01	2.172E-01	-1.829E+01	5.870E-03	7.594E-01	1.220E+07	1.357E+07	2.458E-01
17	5.919E+00	0.000E+00	1.113E-01	3.806E-01	-1.924E+01	2.395E-02	8.442E-01	1.297E+07	1.803E+07	1.258E-01
18	5.873E-01	0.000E+00	2.947E-01	8.612E-03	-1.918E+01	6.137E-03	3.866E-01	1.248E+07	2.042E+07	1.308E-01
19	2.005E+00	1.000E+00	1.164E-01	1.667E-01	-1.934E+01	6.255E-03	7.942E-01	1.286E+07	2.047E+07	3.845E-01
20	6.709E-01	1.000E+00	1.294E-01	3.211E-01	-1.935E+01	1.707E-02	7.418E-01	1.295E+07	1.817E+07	3.349E-01
21	2.259E-01	0.000E+00	1.977E-02	2.233E-01	-1.894E+01	2.350E-02	2.158E-01	1.207E+07	1.961E+07	1.515E-01
22	1.434E+00	1.000E+00	2.183E-01	1.871E-02	-1.913E+01	2.603E-02	7.201E-01	1.216E+07	1.990E+07	1.931E+00
23	7.099E+00	1.000E+00	2.388E-01	4.523E-02	-1.945E+01	2.992E-02	8.192E-01	1.210E+07	1.929E+07	1.816E-01

Table C-2. Seventy Values Sampled by LHS for 49 Parameters that Were Varied in December 1992 PA Calculations (Continued)

Material Parameter RUN NO.	BCEXP X(11)	BCFLG X(12)	BCBRSAT X(13)	BCGSSAT X(14)	MBPERM X(15)	MBPOR X(16)	TZPORF X(17)	MBPRES X(18)	BPPRES X(19)	BPSTOR X(20)
24	4.327E-01	1.000E+00	6.127E-02	2.643E-01	-1.921E+01	1.471E-02	1.909E-01	1.243E+07	2.006E+07	3.497E-02
25	2.761E+00	1.000E+00	3.051E-01	9.990E-02	-1.949E+01	2.472E-02	8.779E-01	1.214E+07	1.379E+07	5.503E-01
26	5.266E+00	1.000E+00	2.470E-01	6.806E-02	-1.962E+01	1.882E-02	8.054E-01	1.252E+07	1.490E+07	3.907E-02
27	8.333E+00	1.000E+00	2.128E-01	7.573E-02	-1.966E+01	2.274E-03	4.993E-01	1.268E+07	1.773E+07	8.291E-01
28	7.946E+00	0.000E+00	3.474E-01	1.527E-01	-1.971E+01	2.883E-03	2.091E-01	1.219E+07	1.793E+07	2.722E-01
29	6.041E-01	1.000E+00	3.304E-01	3.578E-01	-1.951E+01	1.268E-02	1.152E-01	1.277E+07	1.382E+07	1.189E-01
30	2.004E-01	0.000E+00	1.405E-02	1.553E-01	-1.913E+01	8.791E-03	9.132E-01	1.221E+07	1.566E+07	3.610E-01
31	3.316E-01	1.000E+00	2.113E-01	2.405E-01	-2.049E+01	1.765E-02	3.827E-01	1.212E+07	1.887E+07	5.362E-02
32	8.880E+00	1.000E+00	3.143E-01	3.755E-01	-1.998E+01	2.093E-02	9.418E-01	1.257E+07	1.428E+07	7.034E-02
33	5.220E-01	1.000E+00	1.053E-01	3.419E-01	-1.833E+01	6.664E-03	9.820E-01	1.206E+07	1.853E+07	1.092E-01
34	8.652E+00	0.000E+00	2.515E-01	3.628E-01	-1.991E+01	9.103E-03	5.828E-01	1.224E+07	1.398E+07	2.319E-01
35	3.947E-01	1.000E+00	2.907E-01	1.339E-01	-1.955E+01	2.423E-03	7.825E-01	1.218E+07	1.786E+07	6.246E-02
36	2.750E-01	1.000E+00	3.709E-01	3.696E-01	-1.970E+01	2.712E-02	6.279E-01	1.241E+07	2.056E+07	2.884E-01
37	6.978E+00	1.000E+00	2.265E-01	3.079E-02	-1.959E+01	5.096E-03	5.286E-01	1.270E+07	1.767E+07	9.572E-02
38	2.964E+00	1.000E+00	1.781E-01	3.962E-01	-1.882E+01	1.894E-03	6.447E-01	1.243E+07	1.447E+07	1.412E-01
39	2.606E-01	1.000E+00	1.633E-01	3.724E-02	-1.925E+01	1.009E-02	6.724E-01	1.283E+07	1.635E+07	2.122E-01
40	2.416E-01	1.000E+00	2.434E-01	1.110E-01	-1.868E+01	2.276E-02	1.097E-01	1.254E+07	1.504E+07	7.721E-02
41	5.749E-01	1.000E+00	1.334E-01	1.065E-01	-1.840E+01	1.802E-02	1.518E-01	1.251E+07	1.475E+07	2.549E-01
42	5.484E-01	0.000E+00	3.964E-01	3.350E-01	-2.063E+01	2.199E-02	4.115E-01	1.274E+07	1.581E+07	7.030E-01
43	4.000E+00	0.000E+00	3.907E-01	1.204E-01	-1.857E+01	5.179E-03	4.205E-01	1.227E+07	1.588E+07	6.006E-02
44	3.605E-01	0.000E+00	2.598E-01	5.735E-02	-1.927E+01	3.901E-03	2.482E-01	1.208E+07	1.462E+07	6.582E-01
45	3.239E-01	1.000E+00	1.583E-01	9.419E-02	-1.901E+01	9.387E-03	2.787E-01	1.265E+07	1.361E+07	1.209E-01
46	4.606E-01	1.000E+00	6.517E-02	2.388E-01	-1.978E+01	2.828E-02	8.963E-01	1.232E+07	1.897E+07	4.544E-01
47	3.476E+00	1.000E+00	3.178E-01	2.606E-01	-1.904E+01	6.570E-03	1.412E-01	1.293E+07	1.648E+07	5.341E-01
48	7.708E+00	0.000E+00	4.551E-02	2.075E-01	-1.985E+01	2.239E-02	9.268E-01	1.288E+07	1.940E+07	1.113E-01
49	3.753E-01	1.000E+00	5.011E-02	6.990E-02	-1.816E+01	1.682E-03	9.470E-01	1.229E+07	1.415E+07	1.703E-01
50	3.539E-01	1.000E+00	1.899E-01	1.985E-01	-1.961E+01	1.289E-02	6.970E-01	1.266E+07	1.318E+07	2.231E-01
51	5.600E-01	1.000E+00	2.318E-02	1.181E-02	-1.639E+01	7.844E-03	3.078E-01	1.293E+07	1.631E+07	6.020E-01
52	3.237E+00	0.000E+00	1.504E-01	3.886E-01	-1.906E+01	4.713E-03	7.463E-01	1.297E+07	1.716E+07	1.251E+00
53	6.741E+00	1.000E+00	2.847E-01	1.806E-01	-1.811E+01	1.590E-02	3.382E-01	1.263E+07	1.731E+07	2.000E-02
54	4.720E-01	0.000E+00	1.659E-01	2.729E-01	-1.984E+01	1.450E-02	3.559E-01	1.259E+07	1.982E+07	1.000E-01
55	6.503E-01	0.000E+00	3.245E-01	3.033E-01	-1.699E+01	2.003E-02	5.037E-01	1.247E+07	1.689E+07	3.050E-01
56	4.848E+00	0.000E+00	9.277E-02	5.221E-02	-1.996E+01	1.165E-02	8.402E-01	1.276E+07	1.336E+07	3.112E-01
57	9.211E+00	1.000E+00	5.116E-03	2.777E-01	-2.028E+01	4.563E-03	4.489E-02	1.210E+07	1.907E+07	4.921E-01
58	6.406E-01	1.000E+00	3.488E-01	3.298E-01	-1.847E+01	8.711E-03	3.184E-01	1.239E+07	1.937E+07	2.852E-01
59	8.958E+00	1.000E+00	8.512E-02	3.127E-01	-1.910E+01	2.516E-02	9.379E-02	1.269E+07	1.711E+07	4.277E-01
60	9.862E+00	1.000E+00	7.038E-02	8.194E-02	-1.902E+01	8.260E-03	6.020E-01	1.283E+07	1.526E+07	2.881E-02
61	8.049E-01	1.000E+00	2.791E-01	1.389E-01	-1.938E+01	7.384E-03	1.695E-01	1.216E+07	1.835E+07	1.518E+00
62	2.863E-01	1.000E+00	3.599E-01	2.512E-01	-1.826E+01	1.225E-02	3.707E-01	1.289E+07	1.748E+07	1.920E-01
63	3.754E+00	0.000E+00	2.001E-01	2.836E-01	-1.602E+01	4.109E-03	6.620E-01	1.225E+07	1.616E+07	1.739E-01
64	2.495E+00	1.000E+00	2.932E-02	8.702E-02	-1.957E+01	3.739E-03	4.692E-01	1.285E+07	1.739E+07	4.756E-01
65	2.541E-01	1.000E+00	2.641E-01	3.510E-01	-1.943E+01	7.470E-03	5.998E-01	1.280E+07	2.072E+07	3.755E-01
66	6.915E-01	0.000E+00	1.238E-01	3.163E-01	-1.940E+01	3.533E-03	3.140E-03	1.236E+07	1.671E+07	1.027E+00
67	5.589E+00	0.000E+00	5.635E-02	2.537E-01	-1.886E+01	8.191E-03	2.424E-01	1.258E+07	1.326E+07	2.200E-01
68	4.520E+00	0.000E+00	3.024E-01	2.997E-01	-1.917E+01	1.076E-02	5.214E-01	1.263E+07	2.026E+07	2.027E-01

Table C-2. Seventy Values Sampled by LHS for 49 Parameters that Were Varied in December 1992 PA Calculations (Continued)

Material Parameter RUN NO.	BCEXP X(11)	BCFLG X(12)	BCBRSAT X(13)	BCGSSAT X(14)	MBPERM X(15)	MBPOR X(16)	TZPORF X(17)	MBPRES X(18)	BPPRES X(19)	BPSTOR X(20)
69	4.327E+00	1.000E+00	3.715E-01	4.839E-03	-1.948E+01	1.519E-02	1.780E-01	1.291E+07	1.658E+07	6.938E-02
70	6.277E-01	1.000E+00	1.013E-01	1.192E-01	-2.087E+01	1.489E-03	3.635E-02	1.203E+07	1.862E+07	1.034E-01

Material Parameter RUN NO.	BHPERM X(21)	DBDIAM X(22)	LAMBDA X(23)	BPAREAFR X(24)	SOLAM X(25)	SOLNP X(26)	SOLPU X(27)	SOLRA X(28)	SOLTH X(29)	SOLU X(30)
1	3.223E-13	4.087E-01	6.459E-01	2.756E-01	-9.664E+00	-9.454E+00	-8.853E+00	1.256E+00	-5.739E+00	-2.746E-01
2	2.683E-13	3.780E-01	3.485E-01	3.806E-01	-9.123E+00	-1.513E+01	-1.368E+01	1.094E+00	-6.470E+00	-3.643E+00
3	2.054E-13	4.214E-01	2.818E-01	3.888E-01	-9.693E+00	-6.185E+00	-1.359E+01	1.248E+00	-1.132E+01	-2.513E+00
4	1.000E-11	3.908E-01	6.879E-01	3.087E-01	-6.752E+00	-1.192E+01	-8.339E+00	1.110E+00	-1.138E+01	-5.123E+00
5	4.051E-12	2.788E-01	2.059E-01	2.964E-01	-8.758E+00	-6.916E+00	-6.509E+00	9.393E-01	-1.046E+01	-4.858E+00
6	2.328E-13	3.668E-01	4.707E-01	4.151E-01	-9.320E+00	-5.710E+00	-5.862E+00	1.251E+00	-6.704E+00	-4.508E+00
7	1.257E-12	4.100E-01	3.375E-02	4.445E-01	-9.300E+00	-4.863E+00	-7.801E+00	1.132E+00	-1.019E+01	-6.874E+00
8	7.713E-12	2.949E-01	1.731E-01	4.110E-01	-6.699E+00	-7.652E+00	-1.235E+01	1.043E+00	-9.188E+00	-4.763E+00
9	9.434E-14	2.762E-01	9.720E-01	4.628E-01	-9.277E+00	-1.019E+01	-1.045E+01	5.121E-01	-6.572E+00	-3.402E+00
10	1.322E-12	3.603E-01	4.759E-01	4.793E-01	-9.613E+00	-6.526E+00	-1.172E+01	1.107E+00	-9.756E+00	-2.987E+00
11	3.378E-14	3.320E-01	7.262E-01	3.501E-01	-1.740E+00	-4.591E+00	-1.193E+01	9.632E-01	-8.166E+00	-2.066E+00
12	2.016E-12	3.950E-01	6.321E-01	3.695E-01	-1.012E+01	-9.369E+00	-1.019E+01	1.015E+00	-1.068E+01	-1.081E+01
13	8.206E-14	4.189E-01	9.091E-01	2.689E-01	-9.926E+00	-3.360E+00	-8.118E+00	1.127E+00	-1.212E+01	-1.980E+00
14	1.646E-12	3.416E-01	7.358E-01	4.108E-01	-4.602E+00	-7.190E+00	-1.475E+01	1.234E+00	-7.740E+00	-2.399E+00
15	1.042E-12	3.357E-01	5.136E-01	4.016E-01	-6.398E+00	-9.919E+00	-1.062E+01	1.072E+00	-1.095E+01	-2.817E+00
16	8.788E-14	2.932E-01	1.927E-01	3.455E-01	-6.618E-01	-2.674E+00	-6.321E+00	1.258E+00	-9.910E+00	-2.327E+00
17	2.761E-13	2.847E-01	6.611E-01	3.468E-01	-1.019E+01	-6.337E+00	-1.081E+01	1.176E+00	-1.523E+01	-1.339E+01
18	2.585E-12	3.234E-01	9.689E-01	4.896E-01	-7.632E+00	-1.428E+01	-8.256E+00	1.163E+00	-1.444E+01	-4.146E+00
19	2.966E-13	4.262E-01	7.876E-01	4.204E-01	-4.225E+00	-2.066E+00	-7.325E+00	1.028E+00	-7.944E+00	-4.375E+00
20	2.257E-13	3.390E-01	2.651E-02	3.653E-01	-9.898E+00	-7.503E+00	-8.882E+00	9.832E-01	-9.571E+00	-4.058E+00
21	2.489E-13	3.090E-01	4.326E-01	3.356E-01	-1.027E+01	-5.897E+00	-7.599E+00	9.884E-01	-1.420E+01	-4.687E+00
22	8.276E-13	4.158E-01	4.229E-01	4.176E-01	-4.820E+00	-6.835E+00	-1.555E+01	8.333E-01	-1.376E+01	-1.781E+00
23	1.624E-13	3.058E-01	5.226E-01	4.589E-01	-9.760E+00	-5.568E+00	-6.234E+00	6.281E-01	-7.353E+00	-6.526E+00
24	3.118E-13	2.804E-01	8.593E-01	3.926E-01	-5.607E+00	-3.709E+00	-9.050E+00	1.057E+00	-6.334E+00	-6.016E+00
25	1.708E-13	4.326E-01	5.463E-01	3.837E-01	-1.132E+01	-5.467E+00	-7.503E+00	8.892E-01	-1.154E+01	-2.181E+00
26	4.007E-13	2.697E-01	3.010E-01	3.538E-01	-8.257E+00	-5.816E+00	-7.110E+00	1.242E+00	-9.030E+00	-2.048E+00
27	6.130E-13	2.689E-01	7.530E-01	3.966E-01	-9.486E+00	-8.816E+00	-1.518E+01	1.228E+00	-1.120E+01	-3.036E+00
28	8.499E-13	3.707E-01	2.271E-01	3.336E-01	-1.403E+00	-7.086E+00	-1.454E+01	8.135E-01	-1.045E+01	-2.485E+00
29	3.628E-13	3.340E-01	8.769E-01	3.255E-01	-8.532E+00	-1.355E+01	-7.762E+00	7.736E-01	-7.196E+00	-3.542E+00
30	1.334E-13	4.280E-01	4.486E-01	4.236E-01	-2.966E+00	-8.271E+00	-9.508E+00	9.546E-01	-1.185E+01	-2.299E+00
31	5.200E-13	3.932E-01	5.816E-02	5.669E-01	-9.447E+00	-9.102E+00	-1.500E+01	9.722E-01	-1.244E+01	-1.965E-01
32	3.473E-13	4.428E-01	4.029E-01	4.427E-01	-3.580E+00	-7.308E+00	-8.633E+00	6.622E-01	-1.335E+01	-7.758E+00
33	7.358E-14	2.877E-01	5.914E-01	3.673E-01	-1.004E+01	-6.684E+00	-8.610E+00	4.520E-01	-6.046E+00	-2.560E+00
34	4.264E-13	3.581E-01	8.248E-01	4.057E-01	-9.162E+00	-7.894E+00	-1.409E+01	1.201E+00	-8.763E+00	-3.749E+00
35	1.422E-13	3.740E-01	8.017E-02	4.330E-01	-1.107E+01	-7.348E+00	-1.591E+01	1.156E+00	-5.862E+00	-3.444E+00
36	2.846E-14	3.194E-01	9.552E-02	3.818E-01	-9.405E+00	-6.590E+00	-1.488E+01	1.100E+00	-1.110E+01	-5.092E+00
37	2.197E-14	3.832E-01	4.946E-01	3.291E-01	-9.817E+00	-1.154E+01	-4.335E+00	6.835E-01	-9.880E+00	-2.416E+00
38	9.957E-14	2.975E-01	3.215E-01	4.661E-01	-1.017E+01	-4.659E+00	-9.720E+00	1.171E+00	-1.299E+01	-1.695E+00

Table C-2. Seventy Values Sampled by LHS for 49 Parameters that Were Varied in December 1992 PA Calculations (Continued)

Material Parameter RUN NO.	BHPERM X(21)	DBDIAM X(22)	LAMBDA X(23)	BPAREAFR X(24)	SOLAM X(25)	SOLNP X(26)	SOLPU X(27)	SOLRA X(28)	SOLTH X(29)	SOLU X(30)
39	4.797E-12	4.398E-01	2.449E-01	2.877E-01	-9.050E+00	-5.345E+00	-9.307E+00	1.005E+00	-7.002E+00	-6.833E-01
40	2.160E-12	3.635E-01	7.612E-01	4.456E-01	-7.907E+00	-5.953E+00	-1.108E+01	1.206E+00	-1.209E+01	-5.830E+00
41	4.710E-13	2.826E-01	7.731E-01	4.525E-01	-8.640E-01	-5.218E+00	-1.290E+01	5.719E-01	-7.589E+00	-4.022E+00
42	3.221E-12	2.914E-01	6.280E-01	4.486E-01	-1.000E+01	-3.013E+00	-6.828E+00	3.350E-01	-8.923E+00	-1.357E+00
43	6.646E-14	3.968E-01	1.669E-01	3.749E-01	-3.156E+00	-6.788E+00	-6.742E+00	9.415E-01	-1.455E+01	-5.469E+00
44	5.226E-14	3.016E-01	9.254E-01	4.166E-01	-9.232E+00	-2.260E+00	-9.871E+00	1.183E+00	-1.163E+01	-5.276E+00
45	3.887E-13	4.034E-01	8.107E-01	3.986E-01	-9.006E+00	-8.645E+00	-6.077E+00	1.139E+00	-1.076E+01	-6.340E+00
46	5.483E-13	3.114E-01	3.988E-01	4.273E-01	-5.388E+00	-1.470E+01	-7.027E+00	1.189E+00	-1.291E+01	-1.213E+00
47	1.802E-12	4.134E-01	9.369E-01	4.336E-01	-9.372E+00	-5.527E+00	-9.985E+00	1.221E+00	-1.023E+01	-2.244E+00
48	1.023E-12	3.883E-01	9.918E-01	3.872E-01	-6.016E+00	-8.125E+00	-1.224E+01	1.087E+00	-1.010E+01	-1.434E+00
49	2.071E-13	3.150E-01	9.525E-01	3.422E-01	-1.204E+01	-7.061E+00	-1.088E+01	3.447E-01	-1.391E+01	-2.114E+00
50	1.146E-13	4.051E-01	5.620E-02	3.920E-01	-7.225E+00	-8.524E+00	-9.635E+00	1.244E+00	-1.345E+01	-6.980E+00
51	1.853E-13	3.150E-01	1.018E-01	3.712E-01	-8.886E+00	-1.039E+01	-9.217E+00	9.675E-01	-8.234E+00	-5.521E+00
52	7.378E-13	3.024E-01	3.290E-01	5.479E-01	-8.310E+00	-5.064E+00	-7.013E+00	1.027E+00	-7.531E+00	-2.687E+00
53	1.754E-13	3.516E-01	6.830E-01	4.295E-01	-2.568E+00	-1.001E+01	-5.636E+00	1.001E+00	-1.179E+01	-1.011E+00
54	9.068E-13	3.851E-01	8.436E-01	3.540E-01	-3.924E+00	-5.136E+00	-5.334E+00	1.147E+00	-1.430E+01	-2.736E+00
55	6.937E-13	3.293E-01	2.628E-01	4.032E-01	-2.032E+00	-9.169E+00	-6.906E+00	9.326E-01	-1.272E+01	-6.019E-01
56	5.605E-14	3.612E-01	8.309E-01	3.399E-01	-9.552E+00	-7.756E+00	-1.117E+01	1.121E+00	-9.535E+00	-4.278E+00
57	4.087E-14	3.450E-01	5.791E-01	4.975E-01	-6.351E+00	-1.010E+01	-7.276E+00	8.800E-01	-1.491E+01	-3.903E+00
58	1.125E-12	4.304E-01	6.134E-01	4.375E-01	-1.283E+01	-9.544E+00	-6.632E+00	5.178E-01	-7.088E+00	-6.654E+00
59	1.049E-13	3.476E-01	5.638E-01	2.559E-01	1.125E-01	-5.750E+00	-1.640E+01	4.217E-01	-9.366E+00	-6.291E+00
60	6.800E-13	3.257E-01	1.180E-01	4.259E-01	-1.181E+01	-3.981E+00	-9.468E+00	1.061E+00	-9.261E+00	-1.105E+00
61	1.546E-14	3.212E-01	2.890E-01	4.622E-01	-5.153E+00	-1.252E+01	-8.405E+00	1.251E+00	-6.910E+00	-3.247E+00
62	1.214E-13	4.239E-01	3.673E-01	3.780E-01	-8.009E+00	-8.928E+00	-1.122E+01	7.132E-01	-8.726E+00	-1.871E+00
63	1.511E-13	4.346E-01	7.078E-01	5.198E-01	-6.916E+00	-6.103E+00	-1.306E+01	1.012E+00	-7.818E+00	-6.161E+00
64	6.340E-14	3.483E-01	1.539E-01	4.396E-01	-5.982E+00	-6.030E+00	-3.565E+00	7.319E-01	-8.564E+00	-1.593E+00
65	4.483E-14	4.005E-01	8.983E-01	4.081E-01	-7.295E+00	-1.526E+01	-6.406E+00	1.212E+00	-8.355E+00	-3.795E+00
66	6.107E-13	3.543E-01	3.857E-01	3.620E-01	-1.288E+01	-6.225E+00	-1.052E+01	1.037E+00	-1.481E+01	-1.535E+00
67	1.434E-12	3.734E-01	1.422E-01	5.376E-01	-7.557E+00	-8.103E+00	-5.464E+00	9.945E-01	-8.466E+00	-3.316E+00
68	5.128E-13	2.726E-01	9.745E-03	3.596E-01	-9.110E+00	-9.712E+00	-1.028E+01	9.491E-01	-1.091E+01	-3.105E+00
69	1.000E-14	3.795E-01	5.364E-01	4.543E-01	-1.038E+01	-6.366E+00	-1.533E+01	1.050E+00	-1.503E+01	-2.625E+00
70	4.531E-13	4.387E-01	2.411E-01	3.577E-01	-9.599E+00	-6.020E+00	-7.968E+00	1.078E+00	-6.183E+00	-5.649E+00

Material Parameter RUN NO.	CULTRFLD X(31)	CULCLIM X(32)	CULFRPOR X(33)	CULFRSP X(34)	CULCLYF X(35)	CULCLYP X(36)	FKDAM X(37)	FKDNP X(38)	FKDPU X(39)	FKDTH X(40)
1	3.689E-01	1.347E-01	1.307E-03	3.149E+00	0.000E+00	9.844E-02	2.100E+00	-2.194E-01	1.137E+00	-1.263E+00
2	4.068E-01	5.823E-01	1.356E-03	1.078E-01	1.848E-01	4.169E-01	2.284E-01	-2.437E+00	2.874E+00	-3.127E+00
3	6.714E-01	8.879E-01	3.436E-03	3.478E-01	0.000E+00	3.011E-01	-9.079E-01	2.591E+00	-9.157E-01	9.695E-01
4	5.721E-01	3.106E-01	2.102E-03	4.629E+00	0.000E+00	2.892E-01	2.045E+00	-2.084E+00	2.942E+00	-7.889E-01
5	4.952E-01	5.394E-01	2.416E-03	7.314E+00	4.601E-01	4.119E-01	2.249E+00	2.370E+00	-1.004E-01	-1.208E+00
6	9.702E-01	1.115E-01	1.000E-02	6.791E+00	0.000E+00	1.458E-01	3.185E-01	1.058E+00	2.723E-01	3.758E-01
7	2.787E-01	2.758E-01	3.077E-04	3.104E-01	0.000E+00	3.002E-01	-2.487E-02	2.917E+00	2.668E+00	-2.930E+00
8	9.213E-01	7.240E-01	2.443E-04	1.133E-01	0.000E+00	2.134E-01	8.402E-01	2.522E+00	2.572E+00	2.835E-01

Table C-2. Seventy Values Sampled by LHS for 49 Parameters that Were Varied in December 1992 PA Calculations (Continued)

Material Parameter RUN NO.	CULTRFLD X(31)	CULCLIM X(32)	CULFRPOR X(33)	CULFRSP X(34)	CULCLYF X(35)	CULCLYP X(36)	FKDAM X(37)	FKDNP X(38)	FKDPU X(39)	FKDTH X(40)
9	6.322E-01	8.636E-01	1.471E-03	5.667E-01	0.000E+00	1.050E-01	1.631E-01	-2.822E+00	2.830E+00	-2.469E+00
10	8.899E-01	1.227E-01	3.077E-03	4.288E+00	2.777E-01	6.018E-02	2.138E+00	-3.622E+00	8.307E-01	-1.198E+00
11	9.365E-01	9.966E-01	4.324E-04	2.807E+00	0.000E+00	8.102E-02	9.633E-01	6.463E-02	-1.486E-02	-3.422E+00
12	9.128E-03	9.358E-01	3.571E-03	3.387E-01	8.276E-02	1.836E-01	2.314E+00	4.235E-01	6.207E-01	-1.693E+00
13	8.782E-01	9.174E-01	1.844E-03	9.675E-02	5.057E-02	1.946E-01	5.097E-01	-2.184E+00	2.114E+00	-1.676E+00
14	5.275E-01	7.538E-03	1.275E-03	2.589E+00	0.000E+00	4.739E-01	2.839E+00	2.420E-01	2.413E+00	5.278E-01
15	6.464E-02	4.629E-01	1.944E-03	3.750E+00	0.000E+00	4.237E-01	-1.944E+00	-2.335E+00	9.381E-02	3.394E-01
16	1.002E-01	5.997E-01	1.175E-03	3.312E-01	2.076E-01	2.446E-01	5.779E-01	-2.194E+00	2.888E+00	-1.085E+00
17	6.130E-01	5.713E-01	7.672E-04	2.635E-01	0.000E+00	3.395E-01	2.747E+00	2.686E+00	2.362E+00	-3.245E+00
18	7.468E-02	6.964E-01	9.308E-04	1.853E-01	6.629E-02	2.409E-01	2.077E+00	-2.010E+00	2.601E+00	8.519E-01
19	1.358E-01	6.647E-01	1.098E-03	2.927E-01	0.000E+00	4.047E-01	2.198E-02	-2.068E+00	8.928E-01	-2.913E+00
20	3.055E-01	4.519E-01	1.292E-04	8.809E-01	0.000E+00	1.478E-01	1.851E+00	1.662E-01	1.407E+00	7.119E-01
21	8.639E-01	6.504E-01	2.871E-03	1.981E-01	3.766E-02	4.654E-01	-3.934E-01	-2.127E+00	2.931E+00	7.650E-01
22	7.117E-01	5.489E-01	2.659E-04	1.685E-01	4.767E-01	4.013E-01	4.069E-01	-3.252E+00	-3.630E+00	-1.514E+00
23	5.492E-02	3.609E-01	1.427E-03	3.799E-01	1.475E-01	4.972E-01	7.533E-02	-2.254E+00	2.708E+00	2.400E-01
24	1.891E-01	6.105E-01	1.817E-03	1.610E-01	1.991E-01	2.791E-01	2.266E+00	5.886E-01	1.633E+00	-1.903E+00
25	3.704E-02	6.827E-01	1.701E-03	2.060E+00	0.000E+00	3.211E-01	2.672E+00	-7.864E-01	3.397E-01	-1.060E+00
26	8.072E-01	9.053E-01	5.944E-04	6.057E+00	0.000E+00	3.680E-01	2.443E+00	-1.975E+00	9.984E-01	-1.099E+00
27	5.662E-01	5.105E-01	2.522E-03	2.364E-01	1.629E-01	3.630E-01	1.231E+00	4.460E-01	7.365E-01	-3.938E+00
28	3.500E-01	2.168E-02	4.626E-03	6.637E-02	0.000E+00	3.145E-01	2.718E+00	1.864E+00	4.774E-01	-1.348E-01
29	4.453E-01	8.028E-01	3.027E-03	3.953E-01	3.330E-01	3.569E-01	2.403E+00	6.590E-01	1.783E-01	5.844E-01
30	6.472E-01	6.217E-01	2.274E-03	1.219E-01	3.679E-01	1.395E-01	2.930E+00	2.308E+00	9.142E-01	-1.227E+00
31	5.367E-01	9.768E-01	2.613E-03	5.169E+00	0.000E+00	3.088E-01	2.522E+00	7.498E-01	2.739E+00	-1.021E+00
32	9.048E-01	2.698E-01	5.894E-03	3.207E-01	0.000E+00	1.097E-01	2.592E+00	2.081E+00	2.497E+00	-2.254E+00
33	3.218E-01	4.387E-02	1.839E-04	1.555E+00	2.868E-01	2.228E-01	2.881E+00	-2.390E+00	2.392E+00	-1.016E+00
34	1.817E-01	8.466E-01	1.000E-04	2.277E-01	0.000E+00	4.303E-01	2.487E+00	-1.119E+00	1.944E+00	1.410E-01
35	7.374E-01	2.333E-01	6.994E-04	4.443E+00	0.000E+00	2.647E-01	-3.894E+00	1.026E+00	2.295E+00	-1.050E+00
36	1.243E-01	1.795E-01	6.654E-04	7.070E-02	0.000E+00	2.275E-01	1.335E-01	1.244E+00	2.764E+00	-1.181E+00
37	8.156E-01	3.528E-01	4.016E-03	1.444E-01	4.450E-01	1.561E-01	-7.678E-02	2.211E+00	2.445E+00	4.460E-01
38	5.551E-01	6.568E-02	2.028E-03	1.945E-01	2.488E-01	4.386E-01	9.195E-02	1.654E+00	-1.884E+00	-5.709E-01
39	3.355E-01	4.421E-01	1.546E-03	1.212E+00	9.509E-02	4.534E-01	1.803E-02	-1.891E+00	2.347E+00	-1.297E+00
40	4.853E-01	2.227E-01	1.024E-03	3.612E-01	2.600E-01	5.556E-02	1.870E-01	-1.825E+00	-1.014E+00	-1.241E+00
41	7.923E-01	9.005E-02	8.515E-04	2.800E-01	0.000E+00	7.060E-02	2.380E+00	2.798E+00	2.860E+00	-5.004E-02
42	2.366E-01	1.481E-01	6.353E-04	2.144E-01	0.000E+00	9.389E-02	4.665E-01	-1.735E+00	-2.685E+00	1.949E-01
43	3.907E-01	1.870E-01	5.579E-04	7.386E+00	0.000E+00	4.771E-01	7.765E-01	-2.771E+00	4.188E-02	-3.708E+00
44	8.378E-01	3.195E-01	4.624E-04	1.368E+00	4.333E-01	4.610E-01	2.579E+00	1.145E+00	2.462E+00	-6.334E-01
45	1.691E-01	1.642E-01	6.700E-04	2.524E-01	0.000E+00	1.320E-01	2.417E+00	-2.508E+00	-1.200E+00	-7.496E-01
46	6.676E-01	7.674E-01	7.987E-04	4.783E+00	3.280E-01	3.349E-01	2.187E+00	1.785E+00	2.487E+00	-3.650E+00
46	6.676E-01	7.674E-01	7.987E-04	4.783E+00	3.280E-01	3.349E-01	2.187E+00	1.785E+00	2.487E+00	-3.650E+00
47	4.224E-01	4.110E-01	3.989E-04	7.852E+00	3.862E-01	1.763E-01	2.562E-01	1.966E+00	2.994E+00	-1.274E+00
48	4.385E-01	3.782E-01	3.626E-04	6.452E+00	4.207E-01	2.578E-01	2.232E+00	8.375E-01	5.452E-01	-2.831E-01
49	7.578E-01	7.722E-01	8.756E-04	6.025E+00	0.000E+00	2.700E-01	3.579E-01	2.455E+00	7.299E-01	-1.713E-01
50	7.210E-01	5.186E-01	6.171E-04	3.304E+00	4.881E-01	1.261E-01	2.692E+00	-3.413E+00	4.172E-01	1.715E-02
51	6.205E-01	8.187E-01	1.611E-03	1.823E+00	0.000E+00	1.619E-01	1.977E+00	-1.950E+00	6.136E-01	-2.148E+00
52	2.939E-01	9.520E-01	6.659E-03	5.554E+00	0.000E+00	2.815E-01	2.148E+00	-2.317E+00	2.643E+00	-5.250E-01

Table C-2. Seventy Values Sampled by LHS for 49 Parameters that Were Varied in December 1992 PA Calculations (Continued)

Material Parameter RUN NO.	CULTRFLD X(31)	CULCLIM X(32)	CULFRPOR X(33)	CULFRSP X(34)	CULCLYF X(35)	CULCLYP X(36)	FKDAM X(37)	FKDNP X(38)	FKDPU X(39)	FKDTH X(40)
53	8.836E-02	2.940E-01	3.815E-04	1.281E-01	1.084E-01	3.886E-01	5.221E-02	2.020E+00	2.314E+00	-2.400E+00
54	9.512E-01	6.366E-01	3.283E-04	1.501E-01	0.000E+00	2.107E-01	2.027E+00	-3.932E+00	2.908E+00	7.848E-01
55	3.754E-01	7.419E-01	3.014E-04	5.735E+00	0.000E+00	1.989E-01	-2.214E+00	2.865E+00	2.704E+00	-9.494E-01
56	2.569E-01	2.058E-01	4.414E-04	2.211E-01	2.312E-02	1.147E-01	-3.157E+00	-1.324E+00	2.754E+00	-1.159E+00
57	7.443E-01	7.629E-02	1.070E-03	7.231E-01	0.000E+00	2.526E-01	-2.999E+00	-2.543E+00	2.387E+00	-1.126E+00
58	9.975E-01	4.856E-01	2.223E-04	2.199E+00	0.000E+00	4.464E-01	2.769E+00	1.453E+00	1.758E+00	-2.715E+00
59	5.879E-01	7.044E-01	9.522E-04	7.052E+00	1.229E-01	3.820E-01	6.146E-01	-1.870E+00	1.317E+00	9.363E-01
60	8.512E-01	7.893E-01	5.273E-04	8.214E-02	7.808E-03	3.472E-01	2.981E+00	-2.593E+00	2.662E+00	-6.702E-01
61	5.085E-01	7.507E-01	1.630E-03	3.520E-01	0.000E+00	3.738E-01	2.954E+00	1.567E+00	-4.994E-01	6.040E-01
62	6.872E-01	3.605E-02	4.837E-03	3.871E-01	2.159E-01	4.813E-01	2.889E+00	-1.934E+00	2.976E+00	-1.117E+00
63	2.096E-01	8.759E-01	9.785E-04	2.673E-01	3.076E-01	1.873E-01	6.946E-01	-5.562E-01	2.809E+00	4.670E-02
64	1.725E-02	4.210E-01	5.152E-04	3.611E+00	4.137E-01	8.630E-02	2.810E+00	1.325E+00	2.562E+00	-2.293E-01
65	7.809E-01	3.890E-01	1.775E-04	4.006E+00	0.000E+00	3.917E-01	9.076E-01	8.677E-01	-3.815E-01	-4.160E-01
66	1.453E-01	3.381E-01	7.300E-04	2.497E+00	0.000E+00	1.719E-01	2.554E+00	3.185E-01	2.508E+00	-8.453E-01
67	9.797E-01	8.423E-01	8.231E-04	3.017E-01	3.453E-01	4.905E-01	-1.380E+00	-2.036E+00	2.246E-01	-1.144E+00
68	4.706E-01	2.480E-01	1.134E-03	6.490E+00	2.408E-01	6.800E-02	1.563E+00	-3.004E+00	2.530E+00	-9.225E-01
69	2.602E-01	4.888E-01	1.228E-03	7.588E+00	1.395E-01	3.317E-01	2.618E+00	-3.263E-01	2.790E+00	-3.250E-01
70	2.270E-01	9.583E-01	4.925E-04	5.379E+00	3.802E-01	2.334E-01	2.345E+00	1.477E+00	2.609E+00	-4.852E-01

Material Parameter RUN NO.	FKDU X(41)	FKDRA X(42)	CULPOR X(43)	MKDAM X(44)	MKDNP X(45)	MKDPU X(46)	MKDTH X(47)	MKDU X(48)	MKDRA X(49)
1	-1.973E+00	-3.324E+00	1.143E-01	-5.213E-01	-2.949E+00	1.081E+00	-2.961E+00	-9.568E-01	-7.915E-01
2	-1.328E+00	-1.909E+00	1.822E-01	-1.557E+00	-3.164E+00	-1.633E+00	-1.348E+00	-3.044E+00	-1.630E+00
3	-2.687E+00	-2.978E+00	1.726E-01	-7.160E-01	-3.525E+00	-1.898E+00	-1.997E-01	-2.512E+00	-1.828E+00
4	-2.085E+00	-1.178E+00	1.284E-01	-9.199E-01	-1.183E+00	-1.090E+00	-3.000E-02	-4.026E-01	-6.370E-01
5	-2.208E+00	-1.406E+00	1.220E-01	1.583E+00	9.019E-01	-2.061E+00	-3.493E+00	-3.570E+00	-1.886E+00
6	-2.260E+00	-3.510E+00	1.783E-01	-8.983E-01	-2.889E+00	-2.012E+00	-1.968E+00	-3.023E+00	-9.798E-01
7	-2.393E+00	-2.639E-01	1.206E-01	-4.012E-01	-3.499E+00	-1.232E+00	-1.641E+00	-6.873E-01	-5.865E-01
8	-2.150E+00	-1.846E+00	1.045E-01	1.199E+00	-3.115E+00	1.638E+00	-2.146E+00	-2.873E+00	-2.569E+00
9	-2.221E+00	-8.716E-01	1.210E-01	-8.154E-01	-3.275E+00	-2.104E+00	-8.599E-01	-1.108E+00	-1.797E+00
10	-3.274E+00	5.759E-01	1.634E-01	-9.658E-01	-1.305E+00	-1.152E+00	-2.052E+00	-3.061E+00	-3.144E+00
11	-2.008E+00	-7.792E-01	1.788E-01	9.574E-01	1.949E+00	-1.230E-01	-2.225E+00	-1.026E+00	4.770E-01
12	-1.851E+00	-1.648E+00	1.374E-01	2.117E-01	-3.437E+00	-1.792E+00	-2.029E+00	-3.787E+00	-2.693E+00
13	-2.182E+00	2.384E-01	1.115E-01	1.799E+00	-9.035E-01	-7.714E-01	-2.412E+00	-2.830E+00	-2.651E+00
14	-2.042E+00	1.483E-01	1.259E-01	8.448E-01	1.102E+00	-3.750E+00	-3.756E+00	-3.262E+00	-3.232E+00
15	-2.115E+00	-1.763E+00	1.075E-01	-3.158E-01	-2.825E+00	9.417E-01	-2.862E+00	-6.235E-01	-2.179E+00
16	-2.414E+00	-1.397E+00	1.229E-01	-5.761E-01	-7.990E-01	-3.805E+00	-3.379E+00	-1.077E+00	-9.146E-01
17	-2.479E+00	7.485E-01	1.446E-01	-3.411E+00	-1.597E+00	-8.047E-01	-2.073E+00	-1.248E+00	9.659E-01
18	-3.923E+00	-1.916E+00	1.782E-01	1.136E+00	1.558E+00	-2.176E+00	-2.169E+00	-1.131E+00	-1.056E+00
19	-2.931E+00	-1.805E+00	7.602E-02	-8.255E-01	-1.283E+00	1.113E+00	-1.008E+00	-1.291E+00	-2.474E+00
20	-2.447E+00	-1.377E+00	2.052E-01	-8.912E-01	7.450E-01	1.309E+00	-3.085E+00	-1.154E+00	-4.022E-01
21	-2.311E+00	-1.599E+00	1.050E-01	3.747E-01	-3.720E+00	6.354E-01	-2.706E+00	-3.192E+00	-3.458E+00
22	-2.899E+00	-1.306E+00	1.311E-01	-1.002E+00	-3.196E+00	-2.878E+00	-2.133E+00	-9.999E-01	-1.586E+00
23	-1.685E+00	8.752E-01	1.422E-01	-1.254E-01	1.817E+00	1.748E+00	-1.699E+00	-1.364E-02	-1.859E+00

Table C-2. Seventy Values Sampled by LHS for 49 Parameters that Were Varied in December 1992 PA Calculations (Continued)

Material Parameter RUN NO.	FKDU X(41)	FKDRA X(42)	CULPOR X(43)	MKDAM X(44)	MKDNP X(45)	MKDPU X(46)	MKDTH X(47)	MKDU X(48)	MKDRA X(49)
24	-2.521E+00	-3.915E+00	1.451E-01	-1.690E+00	-3.683E+00	-9.208E-01	-1.124E+00	-9.652E-02	-1.960E+00
25	-1.892E+00	-1.516E+00	2.034E-01	-9.375E-01	-7.844E-01	8.066E-01	-3.880E+00	-3.297E+00	-3.759E+00
26	-3.430E+00	-1.341E+00	2.078E-01	-1.197E+00	-3.990E+00	-5.145E-01	-2.781E+00	-8.614E-01	-3.628E+00
27	-2.772E+00	-2.646E+00	1.647E-01	5.074E-01	-1.389E+00	1.863E+00	-3.269E+00	-1.216E+00	-3.257E+00
28	-3.605E-01	3.550E-01	1.889E-01	-9.915E-01	-3.889E+00	-3.191E+00	-2.616E+00	-4.194E-01	-1.908E+00
29	-3.642E+00	-1.452E+00	1.554E-01	1.352E+00	1.414E+00	-2.277E-01	-1.699E-01	-3.213E+00	-1.663E-02
30	-3.740E+00	-1.223E+00	1.662E-01	-6.191E-01	-1.020E+00	-4.121E-01	-8.300E-01	-1.051E+00	-3.835E+00
31	-2.054E+00	-1.674E+00	1.020E-01	-1.088E+00	2.580E-01	-3.806E-01	-3.684E+00	-2.781E-01	-1.538E+00
32	-2.507E+00	-2.124E+00	1.224E-01	6.149E-01	-3.105E+00	4.431E-01	-1.594E+00	-2.981E+00	-3.372E+00
33	-1.874E+00	-1.948E+00	1.255E-01	6.488E-01	-2.998E+00	-2.965E+00	-1.530E+00	-1.755E+00	-2.131E+00
34	-1.930E+00	-3.411E+00	1.458E-01	-7.348E-01	-3.074E+00	-5.174E-02	-2.254E+00	-3.536E+00	-3.572E+00
35	-2.595E+00	9.350E-01	2.021E-01	1.480E+00	-2.973E+00	2.266E-01	-5.313E-01	-3.657E+00	-1.402E+00
36	-1.839E+00	-3.820E+00	1.718E-01	1.699E+00	1.430E+00	-3.356E+00	-1.291E+00	-2.961E+00	-2.790E+00
37	-1.782E+00	-5.875E-01	1.099E-01	-1.399E+00	1.651E-01	-8.768E-01	-3.588E+00	-2.193E+00	-2.627E+00
38	-6.954E-01	-1.709E+00	1.196E-01	-1.214E+00	1.700E+00	-1.769E-01	-7.181E-01	-1.951E-01	-2.348E+00
39	-1.978E+00	-3.008E+00	1.328E-01	-1.986E+00	-2.677E-01	-6.431E-01	-2.050E+00	-3.868E+00	-1.443E+00
40	-6.488E-02	-1.734E+00	1.916E-01	-9.715E-02	-1.641E+00	1.368E+00	-1.840E+00	-1.358E+00	-1.995E+00
41	-3.132E+00	-3.663E+00	1.431E-01	-1.327E+00	1.246E+00	-9.698E-02	-2.342E+00	-3.402E+00	-2.321E+00
42	-2.357E+00	-1.363E+00	9.562E-02	-1.720E+00	-3.653E+00	-1.069E+00	-9.338E-01	-3.148E+00	-1.082E+00
43	-3.325E+00	-2.766E+00	1.215E-01	-7.704E-01	-1.136E+00	-9.655E-01	-7.951E-01	-3.463E+00	-1.712E+00
44	-4.902E-01	-1.416E+00	1.593E-01	-7.772E-01	-2.918E+00	-2.830E-02	-4.897E-01	-3.887E+00	-1.778E+00
45	-2.235E+00	4.820E-01	1.617E-01	-6.506E-01	-1.814E+00	4.050E-02	-2.534E+00	-2.826E+00	-2.944E+00
46	-1.243E+00	-1.155E-01	1.368E-01	-1.034E+00	-1.854E+00	1.440E+00	-1.202E+00	-3.958E+00	-1.147E+00
47	-2.096E+00	4.563E-02	7.999E-02	-7.023E-01	-1.082E+00	-2.603E+00	-1.394E+00	-7.574E-01	-3.807E+00
48	-1.514E+00	-2.353E+00	1.462E-01	-3.391E-01	4.024E-01	6.585E-02	-6.711E-01	-7.236E-01	-1.681E+00
49	-1.889E+00	-1.526E+00	1.231E-01	-8.642E-01	-3.026E+00	-1.417E+00	-2.215E+00	-1.529E+00	-2.282E+00
50	-1.820E+00	-2.019E+00	6.405E-02	-1.943E-01	-1.213E+00	-2.758E-01	-2.114E+00	-1.265E+00	-1.226E+00
51	-1.544E-01	-1.863E+00	1.065E-01	4.152E-02	-1.058E+00	-5.830E-01	-3.304E-01	-8.211E-01	-1.732E+00
52	-6.399E-01	-1.361E+00	2.452E-01	1.529E+00	-2.852E+00	-1.575E+00	-2.016E+00	-3.086E+00	-3.108E+00
53	-2.031E+00	-1.153E+00	1.618E-01	-1.312E+00	-8.421E-01	-6.104E-01	-4.110E-01	-3.330E+00	-2.997E+00
54	-9.314E-01	-1.558E+00	2.184E-01	-1.631E+00	-1.158E+00	6.242E-01	-1.051E+00	-1.466E+00	-2.069E+00
55	-8.030E-01	-1.089E+00	1.793E-01	1.036E+00	-3.343E+00	-5.505E-01	-1.913E+00	-1.350E+00	-3.343E+00
56	-3.560E+00	-1.482E+00	1.617E-01	-8.378E-01	-8.552E-01	-1.008E+00	-2.258E+00	-1.444E+00	-3.914E+00
57	-1.935E+00	-2.511E+00	1.488E-01	-4.477E-01	-3.388E+00	-1.318E+00	-2.183E+00	-3.487E+00	-3.368E-01
58	-1.906E+00	-3.232E+00	1.784E-01	-8.554E-01	1.081E+00	-1.844E+00	-3.188E+00	-7.868E-01	-2.875E+00
59	-1.995E+00	-6.297E-01	1.409E-01	-5.343E-01	-9.310E-01	-6.923E-01	-1.757E+00	-2.086E+00	-2.843E+00
60	-2.069E+00	-1.029E+00	9.787E-02	1.958E+00	-9.753E-01	-2.254E+00	-2.489E-01	-3.758E+00	-2.014E+00
61	-2.423E+00	-2.027E-01	1.171E-01	-1.755E+00	-7.094E-01	-3.331E-01	-5.990E-01	-2.889E+00	-3.511E+00
62	-3.083E+00	-1.624E+00	1.781E-01	1.244E+00	-3.853E+00	1.945E+00	-1.480E+00	-9.237E-01	-1.283E+00
63	-2.143E+00	-1.309E+00	1.151E-01	-1.849E+00	-2.768E+00	-3.154E-01	-3.938E+00	-3.683E+00	-1.921E-01
64	-2.544E+00	-1.436E+00	1.624E-01	1.851E+00	-3.598E+00	-2.137E-01	-2.092E+00	-2.327E+00	-1.336E+00
65	-2.346E+00	-3.999E-01	1.004E-01	-1.470E-02	-3.825E+00	-1.460E+00	-2.193E+00	-1.204E+00	-3.052E+00
66	-3.859E+00	-1.793E+00	2.062E-01	-9.802E-01	-4.791E-01	-4.331E-01	-3.969E-01	-1.660E+00	-1.175E+00
67	-2.563E+00	-2.268E+00	2.387E-01	-9.478E-01	-7.412E-01	-2.326E+00	-2.288E+00	-5.709E-01	-2.441E+00
68	-2.293E+00	-1.459E+00	1.238E-01	-1.881E+00	-1.606E-01	3.982E-01	-1.149E+00	-2.917E+00	-3.971E+00
69	-1.076E+00	-1.974E+00	1.780E-01	-1.045E+00	-3.282E+00	-1.684E+00	-1.774E+00	-9.031E-01	-1.480E+00
70	-1.960E+00	-1.322E+00	1.617E-01	-1.504E+00	-1.530E+00	-4.783E-01	-7.179E-02	-1.171E+00	-3.685E+00

Table C-3 lists the ranks of samples.

Table C-3. Ranks of 70 Values Sampled

Material Parameter RUN NO.	BRSAT X(1)	GRCORI X(2)	GRCORHF X(3)	STOICCOR X(4)	GRMICI X(5)	GRMICHF X(6)	STOICMIC X(7)	VWOOD X(8)	VMETAL X(9)	SALPERM X(10)
1	21.	9.	38.	34.	58.	31.	33.	21.	34.	55.
2	64.	21.	51.	15.	70.	60.	6.	58.	45.	67.
3	44.	5.	26.	4.	37.	54.	1.	40.	17.	44.
4	17.	55.	4.	31.	52.	18.	10.	12.	57.	45.
5	58.	2.	6.	49.	59.	19.	20.	33.	46.	26.
6	69.	64.	56.	46.	38.	35.	56.	68.	67.	6.
7	70.	57.	55.	44.	16.	44.	21.	6.	50.	15.
8	41.	36.	69.	53.	48.	17.	22.	16.	16.	32.
9	30.	10.	14.	22.	49.	1.	60.	69.	59.	5.
10	39.	48.	46.	56.	43.	5.	52.	20.	24.	56.
11	61.	50.	47.	1.	24.	38.	2.	3.	52.	64.
12	42.	61.	32.	29.	35.	22.	63.	22.	37.	66.
13	18.	25.	45.	68.	7.	55.	34.	29.	65.	7.
14	7.	62.	13.	9.	4.	62.	15.	49.	44.	13.
15	66.	12.	61.	24.	51.	29.	57.	52.	21.	4.
16	22.	33.	67.	25.	60.	56.	70.	13.	39.	48.
17	26.	16.	42.	64.	47.	16.	41.	47.	7.	17.
18	32.	3.	11.	16.	15.	36.	61.	18.	41.	36.
19	29.	45.	2.	3.	65.	8.	24.	48.	13.	11.
20	19.	32.	1.	11.	42.	15.	68.	45.	70.	68.
21	6.	60.	54.	14.	61.	24.	47.	36.	48.	69.
22	38.	11.	20.	48.	23.	46.	42.	56.	31.	60.
23	43.	44.	62.	51.	30.	59.	14.	50.	62.	34.
24	36.	24.	8.	37.	32.	70.	38.	7.	38.	43.
25	40.	41.	33.	42.	36.	42.	25.	19.	1.	63.
26	51.	63.	37.	41.	5.	2.	31.	59.	14.	47.
27	14.	58.	41.	17.	18.	64.	28.	70.	43.	33.
28	12.	37.	19.	40.	41.	27.	19.	44.	35.	31.
29	35.	70.	29.	69.	26.	65.	23.	37.	8.	50.
30	45.	65.	66.	36.	69.	33.	30.	55.	61.	38.
31	65.	39.	16.	67.	45.	28.	16.	42.	23.	28.
32	27.	1.	28.	28.	9.	66.	66.	54.	56.	62.
33	50.	19.	52.	32.	14.	50.	12.	62.	5.	40.
34	46.	59.	27.	63.	46.	32.	46.	32.	66.	24.
35	11.	26.	23.	58.	56.	58.	62.	34.	15.	54.
36	37.	51.	57.	47.	11.	7.	54.	41.	6.	19.
37	20.	40.	12.	5.	44.	4.	18.	39.	4.	39.
38	25.	7.	34.	54.	39.	23.	44.	51.	55.	59.
39	52.	22.	50.	62.	21.	10.	65.	28.	54.	37.
40	24.	67.	3.	45.	66.	41.	35.	46.	40.	10.
41	9.	17.	59.	57.	53.	11.	11.	31.	53.	61.
42	10.	66.	60.	8.	29.	57.	51.	11.	28.	35.
43	2.	29.	44.	59.	57.	39.	8.	53.	27.	51.
44	68.	6.	5.	30.	8.	13.	26.	23.	33.	57.
45	67.	4.	70.	6.	25.	40.	32.	30.	32.	53.

Table C-3. Ranks of 70 Values Sampled (Continued)

Material Parameter / RUN NO.	BRSAT X(1)	GRCORI X(2)	GRCORHF X(3)	STOICCOR X(4)	GRMICI X(5)	GRMICHF X(6)	STOICMIC X(7)	VWOOD X(8)	VMETAL X(9)	SALPERM X(10)
46	5.	20.	53.	2.	40.	63.	53.	25.	22.	1.
47	59.	56.	25.	20.	27.	61.	39.	66.	10.	70.
48	8.	15.	68.	60.	20.	3.	37.	14.	9.	52.
49	48.	53.	24.	55.	28.	67.	67.	8.	63.	22.
50	16.	69.	22.	21.	13.	9.	13.	38.	30.	21.
51	31.	30.	48.	50.	1.	48.	59.	60.	26.	65.
52	13.	18.	49.	52.	34.	6.	7.	2.	51.	49.
53	60.	68.	30.	35.	17.	12.	27.	35.	69.	58.
54	53.	28.	31.	66.	55.	69.	43.	61.	2.	29.
55	34.	31.	17.	13.	19.	45.	40.	64.	19.	18.
56	33.	35.	9.	61.	31.	37.	17.	1.	12.	2.
57	63.	47.	40.	38.	22.	25.	45.	15.	20.	30.
58	47.	42.	36.	7.	68.	43.	49.	24.	11.	9.
59	62.	46.	58.	18.	62.	26.	64.	43.	36.	8.
60	54.	23.	18.	12.	63.	49.	50.	27.	47.	14.
61	56.	54.	10.	39.	50.	34.	69.	10.	3.	41.
62	55.	34.	21.	19.	2.	14.	58.	4.	29.	16.
63	23.	38.	35.	43.	3.	53.	5.	65.	42.	27.
64	28.	27.	7.	70.	64.	51.	29.	63.	18.	20.
65	15.	13.	39.	65.	54.	30.	3.	17.	68.	46.
66	49.	49.	65.	10.	33.	21.	9.	67.	58.	12.
67	3.	52.	43.	26.	10.	47.	48.	26.	25.	42.
68	57.	14.	15.	33.	12.	68.	4.	9.	64.	23.
69	4.	43.	64.	27.	67.	52.	36.	5.	60.	25.
70	1.	8.	63.	23.	6.	20.	55.	57.	49.	3.

Material Parameter / RUN NO.	BCEXP X(11)	BCFLG X(12)	BCBRSAT X(13)	BCGSSAT X(14)	MBPERM X(15)	MBPOR X(16)	TZPORF X(17)	MBPRES X(18)	BPPRES X(19)	BPSTOR X(20)
1	69.	12.	16.	41.	66.	68.	2.	2.	22.	35.
2	21.	47.	26.	23.	16.	24.	34.	70.	14.	54.
3	34.	47.	33.	38.	65.	69.	50.	43.	23.	25.
4	52.	47.	31.	34.	37.	18.	70.	1.	19.	66.
5	15.	47.	35.	26.	8.	54.	5.	24.	27.	30.
6	56.	12.	59.	9.	14.	42.	68.	39.	69.	50.
7	37.	12.	7.	29.	17.	63.	19.	32.	10.	43.
8	57.	47.	68.	5.	54.	9.	40.	35.	51.	29.
9	16.	47.	60.	33.	10.	66.	31.	22.	1.	27.
10	39.	47.	14.	61.	67.	34.	21.	27.	59.	14.
11	22.	12.	48.	36.	11.	7.	45.	20.	63.	15.
12	61.	47.	25.	51.	56.	35.	39.	26.	70.	13.
13	41.	47.	64.	52.	36.	47.	6.	54.	48.	64.
14	8.	47.	2.	31.	5.	52.	32.	51.	34.	5.
15	18.	12.	41.	68.	20.	1.	61.	56.	21.	6.
16	24.	47.	67.	39.	61.	19.	54.	15.	5.	41.
17	55.	12.	20.	67.	40.	60.	60.	69.	45.	23.

Table C-3. Ranks of 70 Values Sampled (Continued)

Material Parameter RUN NO.	BCEXP X(11)	BCFLG X(12)	BCBRSAT X(13)	BCGSSAT X(14)	MBPERM X(15)	MBPOR X(16)	TZPORF X(17)	MBPRES X(18)	BPPRES X(19)	BPSTOR X(20)
18	28.	12.	52.	2.	42.	20.	28.	34.	65.	24.
19	40.	47.	21.	30.	35.	21.	56.	61.	66.	53.
20	33.	47.	23.	57.	34.	48.	52.	67.	46.	49.
21	2.	12.	4.	40.	51.	59.	16.	5.	58.	28.
22	38.	47.	39.	4.	44.	64.	51.	11.	61.	70.
23	60.	47.	42.	8.	30.	70.	58.	8.	55.	33.
24	17.	47.	11.	47.	41.	44.	14.	31.	62.	3.
25	43.	47.	54.	18.	28.	61.	62.	10.	7.	60.
26	53.	47.	44.	12.	22.	51.	57.	37.	17.	4.
27	64.	47.	38.	14.	21.	5.	35.	48.	42.	65.
28	63.	12.	61.	27.	18.	8.	15.	14.	44.	44.
29	29.	47.	58.	63.	27.	40.	9.	55.	8.	21.
30	1.	12.	3.	28.	45.	31.	64.	16.	24.	51.
31	10.	47.	37.	43.	3.	49.	27.	9.	52.	7.
32	66.	47.	55.	66.	6.	55.	66.	40.	12.	11.
33	23.	47.	19.	60.	60.	23.	69.	4.	49.	19.
34	65.	12.	45.	64.	9.	32.	41.	17.	9.	40.
35	14.	47.	51.	24.	26.	6.	55.	13.	43.	9.
36	6.	47.	65.	65.	19.	65.	44.	29.	67.	46.
37	59.	47.	40.	6.	24.	16.	38.	50.	41.	16.
38	44.	47.	32.	70.	53.	4.	46.	30.	13.	26.
39	5.	47.	29.	7.	39.	36.	48.	59.	30.	37.
40	3.	47.	43.	20.	55.	58.	8.	38.	18.	12.
41	27.	47.	24.	19.	59.	50.	11.	36.	16.	42.
42	25.	12.	70.	59.	2.	56.	29.	52.	25.	63.
43	48.	12.	69.	22.	57.	17.	30.	19.	26.	8.
44	12.	12.	46.	11.	38.	12.	18.	6.	15.	62.
45	9.	47.	28.	17.	50.	33.	20.	46.	6.	22.
46	19.	47.	12.	42.	15.	67.	63.	23.	53.	56.
47	46.	47.	56.	46.	48.	22.	10.	65.	31.	59.
48	62.	12.	8.	37.	12.	57.	65.	62.	57.	20.
49	13.	47.	9.	13.	63.	3.	67.	21.	11.	31.
50	11.	47.	34.	35.	23.	41.	49.	47.	2.	39.
51	26.	47.	5.	3.	69.	27.	22.	66.	29.	61.
52	45.	12.	27.	69.	47.	15.	53.	68.	37.	68.
53	58.	47.	50.	32.	64.	46.	24.	44.	38.	1.
54	20.	12.	30.	48.	13.	43.	25.	42.	60.	17.
55	32.	12.	57.	54.	68.	53.	36.	33.	35.	47.
56	51.	12.	17.	10.	7.	38.	59.	53.	4.	48.
57	68.	47.	1.	49.	4.	14.	4.	7.	54.	58.
58	31.	47.	62.	58.	58.	30.	23.	28.	56.	45.
59	67.	47.	15.	55.	46.	62.	7.	49.	36.	55.
60	70.	47.	13.	15.	49.	29.	43.	58.	20.	2.
61	36.	47.	49.	25.	33.	25.	12.	12.	47.	69.
62	7.	47.	63.	44.	62.	39.	26.	63.	40.	34.

Table C-3. Ranks of 70 Values Sampled (Continued)

Material Parameter / RUN NO.	BCEXP X(11)	BCFLG X(12)	BCBRSAT X(13)	BCGSSAT X(14)	MBPERM X(15)	MBPOR X(16)	TZPORF X(17)	MBPRES X(18)	BPPRES X(19)	BPSTOR X(20)
63	47.	12.	36.	50.	70.	13.	47.	18.	28.	32.
64	42.	47.	6.	16.	25.	11.	33.	60.	39.	57.
65	4.	47.	47.	62.	31.	26.	42.	57.	68.	52.
66	35.	12.	22.	56.	32.	10.	1.	25.	33.	67.
67	54.	12.	10.	45.	52.	28.	17.	41.	3.	38.
68	50.	12.	53.	53.	43.	37.	37.	45.	64.	36.
69	49.	47.	66.	1.	29.	45.	13.	64.	32.	10.
70	30.	47.	18.	21.	1.	2.	3.	3.	50.	18.

Material Parameter / RUN NO.	BHPERM X(21)	DBDIAM X(22)	LAMBDA X(23)	BPAREAFR X(24)	SOLAM X(25)	SOLNP X(26)	SOLPU X(27)	SOLRA X(28)	SOLTH X(29)	SOLU X(30)
1	36.	56.	46.	3.	19.	16.	39.	69.	70.	69.
2	32.	44.	25.	27.	32.	2.	11.	43.	65.	31.
3	27.	61.	20.	31.	18.	45.	12.	66.	24.	45.
4	70.	49.	49.	6.	48.	7.	43.	46.	23.	17.
5	67.	5.	15.	5.	37.	36.	60.	19.	31.	19.
6	30.	40.	33.	42.	27.	53.	65.	67.	63.	22.
7	58.	57.	3.	55.	28.	61.	47.	49.	34.	5.
8	69.	12.	13.	41.	49.	29.	15.	36.	43.	20.
9	15.	4.	69.	62.	29.	10.	26.	5.	64.	34.
10	59.	37.	34.	64.	20.	41.	18.	45.	38.	39.
11	5.	26.	51.	15.	66.	63.	17.	23.	52.	54.
12	63.	51.	45.	23.	11.	17.	28.	32.	30.	2.
13	13.	60.	64.	2.	14.	66.	45.	48.	17.	56.
14	61.	30.	52.	40.	58.	33.	8.	63.	55.	48.
15	56.	28.	36.	36.	50.	13.	24.	40.	27.	40.
16	14.	11.	14.	13.	69.	68.	62.	70.	36.	49.
17	33.	8.	47.	14.	9.	43.	23.	55.	1.	1.
18	65.	23.	68.	65.	43.	4.	44.	53.	6.	25.
19	34.	63.	56.	45.	59.	70.	51.	34.	53.	23.
20	29.	29.	2.	21.	15.	30.	38.	26.	39.	26.
21	31.	17.	31.	10.	8.	50.	49.	27.	8.	21.
22	52.	59.	30.	44.	57.	37.	3.	15.	10.	58.
23	23.	16.	37.	60.	17.	54.	63.	8.	58.	7.
24	35.	6.	61.	33.	54.	65.	37.	38.	66.	11.
25	24.	66.	39.	29.	5.	56.	50.	17.	22.	52.
26	40.	2.	22.	16.	40.	51.	53.	64.	44.	55.
27	48.	1.	53.	34.	23.	21.	5.	62.	25.	38.
28	53.	41.	16.	9.	67.	34.	9.	14.	32.	46.
29	38.	27.	62.	7.	38.	5.	48.	13.	59.	32.
30	20.	64.	32.	46.	63.	24.	33.	22.	19.	50.
31	45.	50.	5.	70.	24.	19.	6.	25.	16.	70.
32	37.	70.	29.	54.	61.	32.	40.	9.	12.	3.
33	12.	9.	42.	22.	12.	39.	41.	4.	68.	44.
34	41.	36.	58.	38.	31.	27.	10.	58.	46.	30.

Table C-3. Ranks of 70 Values Sampled (Continued)

Material Parameter RUN NO.	BHPERM X(21)	DBDIAM X(22)	LAMBDA X(23)	BPAREAFR X(24)	SOLAM X(25)	SOLNP X(26)	SOLPU X(27)	SOLRA X(28)	SOLTH X(29)	SOLU X(30)
35	21.	43.	6.	50.	6.	31.	2.	52.	69.	33.
36	4.	21.	7.	28.	25.	40.	7.	44.	26.	18.
37	3.	46.	35.	8.	16.	8.	69.	10.	37.	47.
38	16.	13.	23.	63.	10.	62.	31.	54.	13.	59.
39	68.	69.	18.	4.	34.	57.	35.	30.	61.	67.
40	64.	39.	54.	56.	42.	49.	21.	59.	18.	12.
41	43.	7.	55.	58.	68.	58.	14.	7.	56.	27.
42	66.	10.	44.	57.	13.	67.	57.	1.	45.	63.
43	11.	52.	12.	25.	62.	38.	58.	20.	5.	15.
44	8.	14.	65.	43.	30.	69.	30.	56.	21.	16.
45	39.	54.	57.	35.	35.	22.	64.	50.	29.	8.
46	46.	18.	28.	48.	55.	3.	54.	57.	14.	64.
47	62.	58.	66.	51.	26.	55.	29.	61.	33.	51.
48	55.	48.	70.	30.	52.	25.	16.	42.	35.	62.
49	28.	20.	67.	12.	3.	35.	22.	2.	9.	53.
50	18.	55.	4.	32.	46.	23.	32.	65.	11.	4.
51	26.	19.	8.	24.	36.	9.	36.	24.	51.	14.
52	51.	15.	24.	69.	39.	60.	55.	33.	57.	42.
53	25.	34.	48.	49.	64.	12.	66.	29.	20.	66.
54	54.	47.	60.	17.	60.	59.	68.	51.	7.	41.
55	50.	25.	19.	37.	65.	18.	56.	18.	15.	68.
56	9.	38.	59.	11.	22.	28.	20.	47.	40.	24.
57	6.	31.	41.	66.	51.	11.	52.	16.	3.	28.
58	57.	65.	43.	52.	2.	15.	59.	6.	60.	6.
59	17.	32.	40.	1.	70.	52.	1.	3.	41.	9.
60	49.	24.	9.	47.	4.	64.	34.	39.	42.	65.
61	2.	22.	21.	61.	56.	6.	42.	68.	62.	36.
62	19.	62.	26.	26.	41.	20.	19.	11.	47.	57.
63	22.	67.	50.	67.	47.	46.	13.	31.	54.	10.
64	10.	33.	11.	53.	53.	47.	70.	12.	48.	60.
65	7.	53.	63.	39.	45.	1.	61.	60.	50.	29.
66	47.	35.	27.	20.	1.	44.	25.	35.	4.	61.
67	60.	42.	10.	68.	44.	26.	67.	28.	49.	35.
68	44.	3.	1.	19.	33.	14.	27.	21.	28.	37.
69	1.	45.	38.	59.	7.	42.	4.	37.	2.	43.
70	42.	68.	17.	18.	21.	48.	46.	41.	67.	13.

Material Parameter RUN NO.	CULTRFLD X(31)	CULCLIM X(32)	CULFRPOR X(33)	CULFRSP X(34)	CULCLYF X(35)	CULCLYP X(36)	FKDAM X(37)	FKDNP X(38)	FKDAM X(39)	FKDTH X(40)
1	26.	10.	43.	48.	18.	8.	40.	35.	28.	20.
2	29.	41.	44.	5.	48.	58.	19.	11.	64.	6.
3	48.	63.	63.	30.	18.	40.	7.	66.	6.	70.
4	41.	22.	55.	55.	18.	38.	38.	19.	68.	39.
5	35.	38.	57.	67.	68.	57.	45.	63.	9.	23.
6	68.	8.	70.	65.	18.	15.	21.	48.	15.	60.

Table C-3. Ranks of 70 Values Sampled (Continued)

Material Parameter RUN NO.	CULTRFLD X(31)	CULCLIM X(32)	CULFRPOR X(33)	CULFRSP X(34)	CULCLYF X(35)	CULCLYP X(36)	FKDAM X(37)	FKDNP X(38)	FKDAM X(39)	FKDTH X(40)
7	20.	20.	9.	26.	18.	39.	10.	70.	54.	7.
8	65.	51.	6.	6.	18.	26.	30.	65.	49.	58.
9	45.	61.	46.	36.	18.	9.	17.	6.	62.	10.
10	63.	9.	62.	53.	55.	2.	41.	2.	24.	24.
11	66.	70.	14.	47.	18.	5.	32.	36.	10.	4.
12	1.	66.	64.	29.	41.	21.	47.	40.	21.	15.
13	62.	65.	52.	4.	39.	23.	25.	17.	34.	16.
14	37.	1.	42.	46.	18.	66.	65.	38.	41.	62.
15	5.	33.	53.	51.	18.	59.	5.	13.	12.	59.
16	8.	42.	40.	28.	50.	31.	26.	16.	65.	31.
17	43.	40.	28.	21.	18.	46.	62.	67.	38.	5.
18	6.	49.	33.	13.	40.	30.	39.	22.	50.	68.
19	10.	47.	38.	24.	18.	56.	12.	20.	25.	8.
20	22.	32.	2.	38.	18.	16.	35.	37.	30.	65.
21	61.	46.	60.	15.	38.	65.	8.	18.	67.	66.
22	50.	39.	7.	12.	69.	55.	23.	4.	1.	17.
23	4.	26.	45.	33.	46.	70.	14.	15.	56.	57.
24	14.	43.	51.	11.	49.	36.	46.	42.	31.	14.
25	3.	48.	50.	43.	18.	43.	59.	32.	16.	32.
26	57.	64.	21.	62.	18.	50.	52.	23.	27.	30.
27	40.	36.	58.	19.	47.	49.	33.	41.	23.	1.
28	25.	2.	66.	1.	18.	42.	61.	57.	18.	51.
29	32.	57.	61.	35.	59.	48.	50.	43.	13.	63.
30	46.	44.	56.	7.	61.	14.	68.	62.	26.	22.
31	38.	69.	59.	57.	18.	41.	54.	44.	57.	34.
32	64.	19.	68.	27.	18.	10.	57.	60.	45.	12.
33	23.	4.	4.	41.	56.	27.	66.	12.	40.	35.
34	13.	60.	1.	18.	18.	60.	53.	31.	33.	55.
35	52.	17.	26.	54.	18.	34.	1.	47.	35.	33.
36	9.	13.	24.	2.	18.	28.	16.	50.	59.	25.
37	58.	25.	65.	9.	67.	17.	9.	61.	42.	61.
38	39.	5.	54.	14.	53.	61.	15.	55.	3.	43.
39	24.	31.	47.	39.	42.	63.	11.	26.	37.	18.
40	34.	16.	36.	32.	54.	1.	18.	28.	5.	21.
41	56.	7.	31.	23.	18.	4.	49.	68.	63.	52.
42	17.	11.	23.	16.	18.	7.	24.	29.	2.	56.
43	28.	14.	20.	68.	18.	67.	29.	7.	11.	2.
44	59.	23.	16.	40.	66.	64.	56.	49.	43.	42.
45	12.	12.	25.	20.	18.	13.	51.	10.	4.	40.
46	47.	54.	29.	56.	58.	45.	43.	56.	44.	3.
47	30.	29.	13.	70.	63.	20.	20.	58.	70.	19.
48	31.	27.	11.	63.	65.	33.	44.	45.	19.	48.
49	54.	55.	32.	61.	18.	35.	22.	64.	22.	50.
50	51.	37.	22.	49.	70.	12.	60.	3.	17.	53.
51	44.	58.	48.	42.	18.	18.	36.	24.	20.	13.
52	21.	67.	69.	59.	18.	37.	42.	14.	52.	44.

Table C-3. Ranks of 70 Values Sampled (Continued)

Material Parameter RUN NO.	CULTRFLD X(31)	CULCLIM X(32)	CULFRPOR X(33)	CULFRSP X(34)	CULCLYF X(35)	CULCLYP X(36)	FKDAM X(37)	FKDNP X(38)	FKDAM X(39)	FKDTH X(40)
53	7.	21.	12.	8.	43.	53.	13.	59.	36.	11.
54	67.	45.	10.	10.	18.	25.	37.	1.	66.	67.
55	27.	52.	8.	60.	18.	24.	4.	69.	55.	36.
56	18.	15.	15.	17.	37.	11.	2.	30.	58.	26.
57	53.	6.	37.	37.	18.	32.	3.	9.	39.	28.
58	70.	34.	5.	44.	18.	62.	63.	52.	32.	9.
59	42.	50.	34.	66.	44.	52.	27.	27.	29.	69.
60	60.	56.	19.	3.	36.	47.	70.	8.	53.	41.
61	36.	53.	49.	31.	18.	51.	69.	54.	7.	64.
62	49.	3.	67.	34.	51.	68.	67.	25.	69.	29.
63	15.	62.	35.	22.	57.	22.	28.	33.	61.	54.
64	2.	30.	18.	50.	64.	6.	64.	51.	48.	49.
65	55.	28.	3.	52.	18.	54.	31.	46.	8.	46.
66	11.	24.	27.	45.	18.	19.	55.	39.	46.	38.
67	69.	59.	30.	25.	60.	69.	6.	21.	14.	27.
68	33.	18.	39.	64.	52.	3.	34.	5.	47.	37.
69	19.	35.	41.	69.	45.	44.	58.	34.	60.	47.
70	16.	68.	17.	58.	62.	29.	48.	53.	51.	45.

Material *Parameter* RUN NO.	FKDU X(41)	FKDRA X(42)	CULPOR X(43)	MKDAM X(44)	MKDNP X(45)	MKDPU X(46)	MKDTH X(47)	MKDU X(48)	MKDRA X(49)
1	46.	6.	14.	42.	24.	62.	11.	54.	62.
2	60.	20.	60.	9.	17.	18.	47.	21.	47.
3	14.	9.	52.	36.	9.	14.	67.	30.	41.
4	38.	50.	28.	25.	39.	25.	70.	66.	63.
5	32.	40.	21.	66.	61.	12.	6.	8.	39.
6	29.	4.	56.	26.	26.	13.	36.	22.	60.
7	24.	59.	18.	44.	10.	23.	42.	62.	64.
8	34.	22.	8.	61.	18.	67.	27.	27.	26.
9	31.	54.	19.	32.	15.	11.	55.	49.	42.
10	8.	67.	48.	22.	36.	24.	32.	20.	15.
11	43.	55.	58.	58.	70.	49.	22.	52.	69.
12	54.	29.	32.	52.	11.	16.	34.	4.	23.
13	33.	64.	13.	68.	47.	32.	17.	28.	24.
14	41.	63.	27.	57.	63.	2.	3.	15.	14.
15	36.	25.	11.	46.	28.	61.	12.	63.	32.
16	23.	41.	23.	40.	50.	1.	7.	50.	61.
17	20.	68.	36.	1.	33.	31.	31.	43.	70.
18	1.	19.	55.	60.	67.	10.	26.	48.	59.
19	11.	23.	2.	31.	37.	63.	53.	41.	27.
20	21.	42.	65.	27.	60.	64.	10.	47.	65.
21	27.	31.	9.	53.	5.	59.	14.	17.	10.
22	12.	48.	29.	19.	16.	6.	28.	53.	48.
23	58.	69.	34.	48.	69.	68.	41.	70.	40.

Table C-3. Ranks of 70 Values Sampled (Continued)

Material Parameter RUN NO.	FKDU X(41)	FKDRA X(42)	CULPOR X(43)	MKDAM X(44)	MKDNP X(45)	MKDPU X(46)	MKDTH X(47)	MKDU X(48)	MKDRA X(49)
24	18.	1.	37.	7.	6.	29.	51.	69.	37.
25	51.	34.	64.	24.	51.	60.	2.	14.	5.
26	6.	45.	67.	15.	1.	38.	13.	57.	7.
27	13.	11.	49.	54.	35.	69.	8.	44.	13.
28	68.	65.	61.	20.	2.	4.	15.	65.	38.
29	4.	37.	41.	63.	65.	46.	68.	16.	68.
30	3.	49.	50.	39.	44.	41.	56.	51.	3.
31	40.	28.	7.	16.	58.	42.	4.	67.	49.
32	19.	15.	22.	55.	19.	57.	43.	23.	11.
33	53.	18.	26.	56.	22.	5.	44.	34.	33.
34	49.	5.	38.	35.	20.	51.	21.	9.	8.
35	15.	70.	63.	64.	23.	55.	61.	7.	52.
36	55.	2.	51.	67.	66.	3.	48.	24.	22.
37	57.	57.	12.	11.	57.	30.	5.	32.	25.
38	65.	27.	17.	14.	68.	48.	58.	68.	29.
39	45.	8.	30.	2.	55.	34.	33.	3.	51.
40	70.	26.	62.	49.	32.	65.	38.	39.	36.
41	9.	3.	35.	12.	64.	50.	18.	12.	30.
42	25.	43.	4.	6.	7.	26.	54.	18.	58.
43	7.	10.	20.	34.	41.	28.	57.	11.	45.
44	67.	39.	42.	33.	25.	52.	62.	2.	43.
45	30.	66.	44.	38.	31.	53.	16.	29.	19.
46	61.	61.	31.	18.	30.	66.	49.	1.	57.
47	37.	62.	3.	37.	42.	7.	46.	60.	4.
48	59.	13.	39.	45.	59.	54.	59.	61.	46.
49	52.	33.	24.	28.	21.	21.	23.	36.	31.
50	56.	16.	1.	47.	38.	45.	29.	42.	55.
51	69.	21.	10.	51.	43.	36.	65.	58.	44.
52	66.	44.	70.	65.	27.	19.	35.	19.	16.
53	42.	51.	46.	13.	49.	35.	63.	13.	18.
54	63.	32.	68.	8.	40.	58.	52.	37.	34.
55	64.	52.	59.	59.	13.	37.	37.	40.	12.
56	5.	35.	45.	30.	48.	27.	20.	38.	2.
57	48.	12.	40.	43.	12.	22.	25.	10.	66.
58	50.	7.	57.	29.	62.	15.	9.	59.	20.
59	44.	56.	33.	41.	46.	33.	40.	33.	21.
60	39.	53.	5.	70.	45.	9.	66.	5.	35.
61	22.	60.	16.	5.	53.	43.	60.	26.	9.
62	10.	30.	54.	62.	3.	70.	45.	55.	54.
63	35.	47.	15.	4.	29.	44.	1.	6.	67.
64	17.	38.	47.	69.	8.	47.	30.	31.	53.
65	26.	58.	6.	50.	4.	20.	24.	45.	17.
66	2.	24.	66.	21.	54.	40.	64.	35.	56.
67	16.	14.	69.	23.	52.	8.	19.	64.	28.
68	28.	36.	25.	3.	56.	56.	50.	25.	1.
69	62.	17.	53.	17.	14.	17.	39.	56.	50.
70	47.	46.	43.	10.	34.	39.	69.	46.	6.

Table C-4 lists the total and percentage release for the 3 radionuclides contributing the most for each vector showing integrated discharge to the accessible environment for the E2 scenario assuming the dual porosity with chemical retardation conceptual model for contaminant transport in the Culebra Dolomite Member. Values are normalized by the EPA factor for each radionuclide. Vectors are ordered from most to least release. Vectors that have no release are omitted.

Table C-4. Vectors with Integrated Discharge through the Culebra Dolomite Member to the Accessible Environment for Scenario E2 and Assuming a Conceptual Model with Dual Porosity, Retardation, Clay, Matrix Diffusion, Intrusion at 1000 yr

Comp. Scen. ID	Vector	Total EPA-normalized, Integrated Discharge	Top 3 Radionuclides Contribution to Integrated Discharge								
01	55	1.5601E-06	RA226	1.5592E-06	100%	NP237	8.7829E-10	0%	PU239	7.2127E-12	0%
	10	1.2951E-10	RA226	9.4533E-11	73%	U233	3.3887E-11	26%	U234	9.8343E-13	1%
	1	1.8060E-11	TH229	9.2657E-12	51%	TH230	8.7942E-12	49%	RA226	8.0844E-17	0%
	47	3.9772E-12	TH229	2.9440E-12	74%	TH230	9.8663E-13	25%	U233	4.5353E-14	1%
	63	1.2484E-17	U233	1.0999E-17	88%	U234	1.4825E-18	12%	TH229	1.5601E-21	0%
	51	3.2655E-19	RA226	3.2653E-19	100%	U233	1.7647E-23	0%	PU239	3.8685E-24	0%
	32	2.1158E-20	RA226	2.1157E-20	100%	NP237	9.3466E-25	0%	U233	5.4155E-25	0%
	21	1.1627E-21	NP237	6.3619E-22	55%	RA226	4.4290E-22	38%	U233	7.7841E-23	7%
	12	1.2747E-22	RA226	6.6260E-23	52%	U233	5.6530E-23	44%	U234	2.5981E-24	2%
	41	5.0185E-23	U233	4.6164E-23	92%	U234	4.0125E-24	8%	TH229	7.2193E-27	0%
	20	2.0522E-23	TH229	1.1004E-23	54%	TH230	9.5181E-24	46%	U233	1.8413E-30	0%
	53	1.8459E-27	U233	1.5152E-27	82%	U234	3.2534E-28	18%	RA226	5.3614E-30	0%
	2	1.3229E-27	U233	1.0991E-27	83%	U234	2.2383E-28	17%			
	55	8.6746E-01	AM241	4.0456E-01	47%	U233	2.2463E-01	26%	U234	1.6182E-01	19%
	63	5.8316E-01	AM241	5.1702E-01	89%	U233	1.9999E-02	3%	U234	1.4437E-02	2%
	10	5.6803E-01	U233	2.8043E-01	49%	U234	2.0115E-01	35%	AM241	3.6609E-02	6%
	47	5.3812E-01	U233	2.9088E-01	54%	U234	2.0964E-01	39%	NP237	1.9271E-02	4%
	1	3.0538E-01	U233	1.1123E-01	36%	U234	8.0423E-02	26%	TH229	5.6951E-02	19%
	53	1.1882E-01	PU239	5.7959E-02	49%	U233	2.9360E-02	25%	U234	2.1251E-02	18%
	21	1.1481E-01	U233	6.2304E-02	54%	U234	4.5067E-02	39%	RA226	2.0227E-03	2%
	51	1.1373E-01	U233	5.4729E-02	48%	U234	3.9510E-02	35%	AM241	8.4059E-03	7%
	2	1.0707E-01	U233	4.0889E-02	38%	U234	2.9590E-02	28%	TH229	1.7937E-02	17%
	3	1.0372E-01	U233	5.7465E-02	55%	U234	4.1564E-02	40%	RA226	1.7829E-03	2%
	20	1.0007E-01	U233	9.9260E-02	99%	PU239	7.2152E-04	1%	AM241	3.7963E-05	0%
	41	8.8558E-02	U233	4.7047E-02	53%	U234	3.4002E-02	38%	NP237	2.2922E-03	3%
	12	3.2740E-03	RA226	3.0988E-03	95%	AM241	1.6372E-04	5%	PU239	4.8928E-06	0%
	32	1.7216E-03	RA226	1.2015E-03	70%	AM241	3.6873E-04	21%	PU239	6.1195E-05	4%
	47	3.9283E-01	U233	2.0411E-01	52%	U234	1.3539E-01	34%	TH229	1.8711E-02	5%
	55	1.9484E-01	U233	7.7691E-02	40%	U234	3.9633E-02	20%	PU239	2.7302E-02	14%
	51	2.8577E-02	U233	1.2640E-02	44%	U234	7.1274E-03	25%	TH229	4.5987E-03	16%
	10	1.1650E-02	U233	5.7654E-03	49%	TH229	3.0936E-03	27%	TH230	1.6631E-03	14%
	1	1.0092E-02	TH229	3.5024E-03	35%	TH230	3.1794E-03	32%	U233	2.5898E-03	26%
	63	6.0843E-10	AM241	3.8981E-10	64%	TH229	1.0160E-10	17%	TH230	7.7372E-11	13%
	12	2.6788E-10	RA226	2.1076E-10	79%	PU239	3.1347E-11	12%	PU240	2.3450E-11	9%
	3	1.1364E-11	U233	7.2824E-12	64%	U234	2.8670E-12	25%	TH229	6.3320E-13	6%

Table C-4. Vectors with Integrated Discharge through the Culebra Dolomite Member to the Accessible Environment for Scenario E2 and Assuming a Conceptual Model with Dual Porosity, Retardation, Clay, Matrix Diffusion, Intrusion at 1000 yr (Continued)

Comp. Scen. ID	Vector	Total EPA-normalized, Integrated Discharge	Top 3 Radionuclides Contribution to Integrated Discharge								
	21	3.3155E-14	U233	1.8388E-14	55%	U234	8.9303E-15	27%	PU239	3.0273E-15	9%
	32	1.9654E-14	PU239	9.4868E-15	48%	RA226	6.7524E-15	34%	PU240	1.8496E-15	9%
	20	2.1770E-16	PU239	1.1824E-16	54%	PU240	5.2106E-17	24%	U233	2.9388E-17	13%
	41	1.2839E-16	U233	4.8078E-17	37%	TH229	3.1209E-17	24%	TH230	2.3807E-17	19%
	2	6.9351E-18	U233	2.5481E-18	37%	U234	1.5823E-18	23%	TH229	1.4046E-18	20%
	53	2.2487E-19	PU239	1.5996E-19	71%	PU240	2.6297E-20	12%	U233	2.3418E-20	10%

Table C-5 lists the total and percentage release for the 3 radionuclides contributing the most for each vector showing integrated discharge to the accessible environment for the E1E2 scenario assuming the dual porosity with chemical retardation conceptual model for contaminant transport in the Culebra Dolomite Member. Values are normalized by the EPA factor for each radionuclide. Vectors are ordered from most to least release. Vectors that have no release are omitted.

Table C-5. Vectors with Integrated Discharge through the Culebra Dolomite Member to the Accessible Environment for Scenario E1E2 and Assuming a Conceptual Model with Dual Porosity, Retardation, Clay, Matrix Diffusion, Intrusion at 1000 yr

Comp. Scen. ID	Vector	Total EPA-normalized, Integrated Discharge	Top 3 Radionuclides Contribution to Integrated Discharge								
02	5	1.1828E-01	U233	6.3491E-02	54%	U234	2.2618E-02	19%	TH229	1.9558E-02	17%
	31	1.0155E-02	TH229	6.5324E-03	64%	TH230	3.6215E-03	36%	RA226	8.9532E-07	0%
	52	6.0021E-03	U233	5.3036E-03	88%	U234	4.9025E-04	8%	RA226	1.0069E-04	2%
	68	3.9493E-04	U233	3.8109E-04	96%	U234	1.1554E-05	3%	RA226	1.4480E-06	0%
	70	1.1963E-04	RA226	1.1963E-04	100%	NP237	1.0256E-16	0%	U233	7.4618E-17	0%
	43	7.0064E-05	U233	6.3893E-05	91%	U234	6.1699E-06	9%	TH229	1.4683E-09	0%
	25	8.3413E-06	TH229	5.0085E-06	60%	TH230	2.7607E-06	33%	RA226	5.6645E-07	7%
	26	6.0574E-06	NP237	4.3598E-06	72%	RA226	1.6974E-06	28%	TH229	1.2307E-10	0%
	15	5.6070E-06	TH229	3.4898E-06	62%	TH230	2.1084E-06	38%	RA226	5.7817E-09	0%
	55	3.6315E-06	RA226	3.6244E-06	100%	NP237	7.0716E-09	0%	U233	1.4572E-14	0%
	14	1.8426E-06	TH229	1.0264E-06	56%	TH230	8.1182E-07	44%	RA226	4.3964E-09	0%
	6	1.1396E-06	U233	9.3545E-07	82%	PU239	1.0569E-07	9%	U234	5.7744E-08	5%
	35	3.5419E-07	U233	3.4704E-07	98%	U234	7.1424E-09	2%	TH229	1.1195E-12	0%
	46	1.0551E-08	U233	9.2165E-09	87%	U234	1.3042E-09	12%	TH229	2.6075E-11	0%
	10	1.9074E-09	U233	1.1957E-09	63%	RA226	6.9553E-10	36%	U234	1.1530E-11	1%
	1	1.3264E-09	TH229	7.1628E-10	54%	TH230	6.1014E-10	46%	RA226	9.1101E-15	0%
	39	9.8486E-10	U233	9.7633E-10	99%	U234	8.3454E-12	1%	TH229	1.8781E-13	0%
	49	7.6570E-10	NP237	7.6493E-10	100%	RA226	5.2987E-13	0%	TH229	1.5280E-13	0%

Table C-5. Vectors with Integrated Discharge through the Culebra Dolomite Member to the Accessible Environment for Scenario E1E2 and Assuming a Conceptual Model with Dual Porosity, Retardation, Clay, Matrix Diffusion, Intrusion at 1000 yr (Continued)

Comp. Scen. ID	Vector	Total EPA-normalized, Integrated Discharge	Top 3 Radionuclides Contribution to Integrated Discharge								
	64	3.0805E-10	U233	3.0586E-10	99%	U234	1.7844E-12	1%	TH229	3.2846E-13	0%
	47	3.2280E-11	TH229	2.3698E-11	73%	TH230	8.3160E-12	26%	U233	2.5458E-13	1%
	4	3.0631E-11	PU239	2.6332E-11	86%	PU240	4.2924E-12	14%	AM241	5.6472E-15	0%
	59	2.3598E-11	U233	2.3405E-11	99%	U234	1.8425E-13	1%	RA226	5.8968E-15	0%
	48	9.5001E-13	RA226	9.5001E-13	100%	U234	1.3993E-19	0%	TH230	1.7653E-20	0%
	65	1.0586E-13	NP237	5.8251E-14	55%	RA226	4.7593E-14	45%	PU239	5.1619E-18	0%
	58	3.0946E-14	TH229	1.7760E-14	57%	TH230	1.3142E-14	42%	RA226	4.1869E-17	0%
	29	6.7815E-17	U233	6.3840E-17	94%	U234	3.9754E-18	6%	TH229	6.1612E-23	0%
	63	1.5077E-17	U233	1.3290E-17	88%	U234	1.7854E-18	12%	TH229	1.9138E-21	0%
	50	1.2251E-17	RA226	1.2121E-17	99%	U233	1.2432E-19	1%	U234	3.5309E-21	0%
	12	1.8679E-18	U233	1.8347E-18	98%	U234	2.1588E-20	1%	NP237	8.2324E-21	0%
	32	1.1875E-18	RA226	1.1870E-18	100%	NP237	3.2289E-22	0%	U233	1.6037E-22	0%
	57	4.0887E-19	U233	3.8426E-19	94%	U234	2.4527E-20	6%	TH229	7.8421E-23	0%
	51	3.5073E-19	RA226	3.5070E-19	100%	U233	1.9957E-23	0%	PU239	4.3904E-24	0%
	66	6.0965E-20	U233	5.7009E-20	94%	U234	3.9062E-21	6%	RA226	3.4558E-23	0%
	33	5.6963E-20	NP237	5.4450E-20	96%	RA226	2.1994E-21	4%	U233	1.6844E-22	0%
	42	1.9346E-20	NP237	1.8950E-20	98%	U233	3.7176E-22	2%	U234	2.3762E-23	0%
	11	3.8308E-21	TH229	2.0436E-21	53%	TH230	1.7854E-21	47%	U233	1.2593E-24	0%
	21	3.1981E-21	U233	2.4925E-21	78%	RA226	3.6286E-22	11%	U234	3.4266E-22	11%
	34	3.1981E-21	U233	2.4925E-21	78%	RA226	3.6286E-22	11%	U234	3.4266E-22	11%
	27	2.9053E-21	RA226	2.1703E-21	75%	TH229	4.7573E-22	16%	TH230	2.5929E-22	9%
	62	2.8047E-21	NP237	2.8047E-21	100%	U233	1.0084E-27	0%	TH229	2.3834E-28	0%
	60	2.0768E-21	U233	1.4616E-21	70%	U234	6.1526E-22	30%	RA226	4.7559E-28	0%
	20	9.1047E-22	TH229	5.2577E-22	58%	TH230	3.8470E-22	42%	RA226	5.9309E-29	0%
	24	8.0686E-22	NP237	8.0686E-22	100%	TH229	9.9112E-30	0%	U233	2.3114E-30	0%
	56	4.2492E-22	RA226	4.2492E-22	100%						
	44	3.3833E-22	U233	2.4447E-22	72%	U234	9.3438E-23	28%	RA226	4.1767E-25	0%
	28	6.1027E-23	NP237	6.1027E-23	100%	TH229	1.4684E-29	0%	U233	1.0105E-32	0%
	41	6.1027E-23	NP237	6.1027E-23	100%	TH229	1.4684E-29	0%	U233	1.0105E-32	0%
	30	5.3950E-23	RA226	5.3950E-23	100%						
	17	2.1233E-23	AM241	2.1233E-23	100%	NP237	1.3391E-30	0%			
	16	1.8958E-23	TH229	1.1168E-23	59%	TH230	7.7901E-24	41%	RA226	1.8494E-29	0%
	7	8.7737E-24	NP237	8.7737E-24	100%	TH229	2.8720E-31	0%			
	9	1.4889E-24	NP237	1.2603E-24	85%	PU239	1.1273E-25	8%	RA226	9.4959E-26	6%
	19	1.2786E-24	RA226	1.2786E-24	100%	U233	5.9915E-30	0%			
	45	5.8283E-25	RA226	5.5385E-25	95%	U233	2.7106E-26	5%	U234	1.6430E-27	0%
	67	3.1973E-25	RA226	1.1826E-25	37%	PU239	1.0921E-25	34%	TH229	3.7671E-26	12%
	53	1.9971E-25	U233	1.6527E-25	83%	U234	3.4201E-26	17%	RA226	2.3306E-28	0%
	2	9.5792E-26	U233	8.0505E-26	84%	U234	1.5286E-26	16%	TH229	1.2829E-30	0%
	22	9.7373E-27	NP237	9.7373E-27	100%						
	40	5.2502E-27	RA226	5.1259E-27	98%	TH229	5.8592E-29	1%	NP237	4.0679E-29	1%
	23	6.2438E-28	RA226	2.4878E-28	40%	TH229	2.0823E-28	33%	TH230	1.6737E-28	27%
	8	3.3002E-29	NP237	3.3002E-29	100%						

Table C-5. Vectors with Integrated Discharge through the Culebra Dolomite Member to the Accessible Environment for Scenario E1E2 and Assuming a Conceptual Model with Dual Porosity, Retardation, Clay, Matrix Diffusion, Intrusion at 1000 yr (Continued)

Comp. Scen. ID	Vector	Total EPA-normalized, Integrated Discharge	Top 3 Radionuclides Contribution to Integrated Discharge								
	36	1.3894E-30	U233	1.3573E-30	98%	U234	3.2119E-32	2%			
	38	9.1987E-31	RA226	9.1987E-31	100%						
02	54	5.0300E+01	PU239	2.7662E+01	55%	AM241	1.6566E+01	33%	PU240	5.5098E+00	11%
	22	2.3592E+01	AM241	2.2964E+01	97%	U233	3.5322E-01	1%	U234	2.5314E-01	1%
	8	2.1797E+01	AM241	2.1186E+01	97%	U233	3.2907E-01	2%	U234	2.3574E-01	1%
	4	1.9332E+01	AM241	1.8560E+01	96%	U233	3.3371E-01	2%	U234	2.3899E-01	1%
	48	1.9143E+01	AM241	1.8567E+01	97%	U233	3.2829E-01	2%	U234	2.3491E-01	1%
	14	1.8735E+01	AM241	1.8108E+01	97%	U233	3.2275E-01	2%	U234	2.3123E-01	1%
	64	1.8123E+01	PU239	1.5233E+01	84%	PU240	2.7304E+00	15%	U233	8.3300E-02	0%
	67	1.6270E+01	PU239	1.1978E+01	74%	PU240	2.3449E+00	14%	AM241	1.3633E+00	8%
	28	1.1190E+01	AM241	1.0576E+01	95%	U233	3.3862E-01	3%	U234	2.4268E-01	2%
	55	9.6472E+00	AM241	8.8167E+00	91%	PU239	2.8487E-01	3%	U233	2.8006E-01	3%
	19	8.8337E+00	AM241	8.0633E+00	91%	U233	3.0567E-01	3%	U234	2.1985E-01	2%
	46	7.8671E+00	AM241	7.0795E+00	90%	U233	3.2616E-01	4%	U234	2.3378E-01	3%
	15	6.6504E+00	AM241	6.1418E+00	92%	U233	2.8958E-01	4%	U234	2.0758E-01	3%
	18	4.4919E+00	AM241	3.8971E+00	87%	U233	2.9499E-01	7%	U234	2.1083E-01	5%
	5	4.0360E+00	PU239	2.6736E+00	66%	PU240	5.3952E-01	13%	AM241	3.4492E-01	9%
	58	3.3798E+00	PU239	2.3358E+00	69%	PU240	4.6454E-01	14%	TH229	1.7070E-01	5%
	32	3.0265E+00	AM241	3.0066E+00	99%	RA226	1.3014E-02	0%	PU239	2.3076E-03	0%
	41	2.6822E+00	AM241	2.0646E+00	77%	U233	2.9897E-01	11%	U234	2.1454E-01	8%
	24	2.6710E+00	AM241	2.2550E+00	84%	TH229	1.6329E-01	6%	TH230	1.2764E-01	5%
	6	2.2398E+00	PU239	1.2093E+00	54%	U233	3.2245E-01	14%	U234	2.3239E-01	10%
	42	2.2350E+00	PU239	1.3299E+00	60%	U233	3.0902E-01	14%	PU240	2.6319E-01	12%
	53	2.1395E+00	PU239	8.7786E-01	41%	AM241	6.4127E-01	30%	U233	2.5846E-01	12%
	40	1.9444E+00	AM241	1.4252E+00	73%	U233	2.7280E-01	14%	U234	1.9630E-01	10%
	39	1.1568E+00	AM241	5.1098E-01	44%	U233	3.1071E-01	27%	U234	2.2325E-01	19%
	52	1.0484E+00	U233	3.0219E-01	29%	U234	2.1733E-01	21%	PU239	2.0287E-01	19%
	45	9.0755E-01	PU239	6.8001E-01	75%	PU240	1.3384E-01	15%	U233	2.8106E-02	3%
	70	8.8969E-01	U233	3.2313E-01	36%	U234	2.3268E-01	26%	TH229	1.3685E-01	15%
	30	8.0558E-01	AM241	4.3508E-01	54%	U233	2.0857E-01	26%	U234	1.5027E-01	19%
	1	7.3146E-01	U233	3.3002E-01	45%	U234	2.3696E-01	32%	TH229	8.5585E-02	12%
	63	7.1551E-01	AM241	6.4078E-01	90%	U233	2.2719E-02	3%	U234	1.6400E-02	2%
	60	7.0063E-01	U233	3.7112E-01	53%	U234	2.6711E-01	38%	NP237	4.6131E-02	7%
	29	6.6141E-01	U233	2.7253E-01	41%	U234	1.9599E-01	30%	TH229	7.1920E-02	11%
	47	6.4328E-01	U233	2.6967E-01	42%	U234	1.9376E-01	30%	AM241	1.3012E-01	20%
	35	6.3165E-01	U233	2.5361E-01	40%	U234	1.8288E-01	29%	TH229	1.0164E-01	16%
	27	6.0961E-01	U233	3.3583E-01	55%	U234	2.4099E-01	40%	AM241	1.2347E-02	2%
	2	6.0892E-01	U233	2.5822E-01	42%	U234	1.8575E-01	31%	TH229	8.1899E-02	13%
	3	5.9995E-01	U233	3.3174E-01	55%	U234	2.3855E-01	40%	RA226	8.5920E-03	1%
	26	5.7868E-01	U233	2.7287E-01	47%	U234	1.9658E-01	34%	AM241	5.0188E-02	9%
	31	5.7764E-01	U233	3.1091E-01	54%	U234	2.2280E-01	39%	AM241	3.0944E-02	5%

Table C-5. Vectors with Integrated Discharge through the Culebra Dolomite Member to the Accessible Environment for Scenario E1E2 and Assuming a Conceptual Model with Dual Porosity, Retardation, Clay, Matrix Diffusion, Intrusion at 1000 yr (Continued)

Comp. Scen. ID	Vector	Total EPA-normalized, Integrated Discharge	Top 3 Radionuclides Contribution to Integrated Discharge								
	10	5.6803E-01	U233	2.8043E-01	49%	U234	2.0115E-01	35%	AM241	3.6609E-02	6%
	68	5.3173E-01	U233	2.8485E-01	54%	U234	2.0417E-01	38%	AM241	2.9595E-02	6%
	62	4.7248E-01	U233	2.3342E-01	49%	U234	1.6803E-01	36%	AM241	4.8164E-02	10%
	66	4.5604E-01	U233	2.4992E-01	55%	U234	1.7923E-01	39%	NP237	1.7269E-02	4%
	21	4.4697E-01	U233	2.3355E-01	52%	U234	1.6819E-01	38%	PU239	1.5544E-02	3%
	13	4.4662E-01	U233	2.3243E-01	52%	U234	1.6771E-01	38%	NP237	2.9304E-02	7%
	25	4.4433E-01	U233	2.3441E-01	53%	U234	1.6891E-01	38%	NP237	1.6014E-02	4%
	20	4.0991E-01	U234	4.0128E-01	98%	AM241	4.6955E-03	1%	TH229	3.4309E-03	1%
	49	3.6689E-01	U233	2.0807E-01	57%	U234	1.5011E-01	41%	RA226	6.1160E-03	2%
	7	3.1454E-01	AM241	7.4657E-02	24%	PU239	7.2978E-02	23%	U233	4.6748E-02	15%
	23	2.9013E-01	PU239	1.7934E-01	62%	PU240	3.3597E-02	12%	TH229	2.4695E-02	9%
	65	2.7809E-01	U233	1.1942E-01	43%	U234	8.6289E-02	31%	PU239	3.1322E-02	11%
	37	2.6454E-01	PU239	2.1702E-01	82%	PU240	3.2911E-02	12%	U233	8.0237E-03	3%
	33	1.6210E-01	U233	6.0685E-02	37%	U234	4.3846E-02	27%	TH229	2.9083E-02	18%
	51	1.2475E-01	U233	6.0116E-02	48%	U234	4.3395E-02	35%	AM241	9.2960E-03	7%
	43	1.0729E-01	AM241	4.4342E-02	41%	U233	2.2834E-02	21%	U234	1.6497E-02	15%
	50	1.0717E-01	AM241	9.8895E-02	92%	RA226	6.0852E-03	6%	U233	1.2382E-03	1%
	38	1.0622E-01	U233	5.5296E-02	52%	U234	3.9976E-02	38%	NP237	7.0201E-03	7%
	9	6.9506E-02	U233	3.0044E-02	43%	U234	2.1726E-02	31%	TH229	8.6543E-03	12%
	16	6.8157E-02	U233	2.8944E-02	42%	U234	2.0936E-02	31%	PU239	1.1265E-02	17%
	56	6.7705E-02	U233	3.8211E-02	56%	U234	2.7625E-02	41%	RA226	1.2161E-03	2%
	57	6.4570E-02	U233	3.4748E-02	54%	U234	2.5120E-02	39%	PU239	1.4873E-03	2%
	12	6.4309E-02	AM241	3.4036E-02	53%	RA226	2.8281E-02	44%	PU239	8.2614E-04	1%
	59	4.1731E-02	AM241	2.5102E-02	60%	U233	5.9522E-03	14%	U234	4.3001E-03	10%
	11	2.4469E-02	U233	1.2764E-02	52%	U234	9.2353E-03	38%	NP237	1.6258E-03	7%
	17	1.6855E-02	RA226	1.2892E-02	76%	NP237	2.6671E-03	16%	AM241	1.2859E-03	8%
	36	9.0879E-03	U233	4.9695E-03	55%	U234	3.5957E-03	40%	RA226	4.2488E-04	5%
	44	7.4099E-03	U233	2.8507E-03	38%	U234	2.0615E-03	28%	NP237	1.8861E-03	25%
02	64	7.4398E+00	PU239	6.3272E+00	85%	PU240	1.0757E+00	14%	U233	1.8908E-02	0%
	5	2.6223E+00	PU239	1.8323E+00	70%	PU240	3.5809E-01	14%	U233	1.8591E-01	7%
	48	1.5998E+00	AM241	1.2074E+00	75%	U233	1.8819E-01	12%	U234	1.1950E-01	7%
	15	1.4192E+00	AM241	9.0606E-01	64%	U233	2.4204E-01	17%	U234	1.7830E-01	13%
	55	1.1245E+00	AM241	6.3912E-01	57%	U233	1.5497E-01	14%	PU239	1.4422E-01	13%
	4	8.1018E-01	AM241	3.3669E-01	42%	U233	1.6562E-01	20%	U234	1.0902E-01	13%
	52	5.3199E-01	U233	1.6629E-01	31%	U234	1.0756E-01	20%	PU239	9.6773E-02	18%
	31	5.2176E-01	U233	2.5468E-01	49%	U234	1.8483E-01	35%	TH229	3.7762E-02	7%
	39	5.0865E-01	U233	1.8365E-01	36%	U234	1.1461E-01	23%	TH229	9.5212E-02	19%
	70	5.0663E-01	U233	1.7125E-01	34%	U234	1.0458E-01	21%	TH229	1.0453E-01	21%
	47	4.9744E-01	U233	2.2141E-01	45%	U234	1.5632E-01	31%	AM241	3.5945E-02	7%
	46	4.9697E-01	U233	2.2074E-01	44%	U234	1.5659E-01	32%	AM241	3.6518E-02	7%
	19	3.8423E-01	U233	1.4682E-01	38%	TH229	6.1683E-02	16%	AM241	5.6854E-02	15%
	68	3.5157E-01	U233	1.7063E-01	49%	U234	1.1140E-01	32%	TH229	3.4456E-02	10%

Table C-5. Vectors with Integrated Discharge through the Culebra Dolomite Member to the Accessible Environment for Scenario E1E2 and Assuming a Conceptual Model with Dual Porosity, Retardation, Clay, Matrix Diffusion, Intrusion at 1000 yr (Continued)

Comp. Scen. ID	Vector	Total EPA-normalized, Integrated Discharge	Top 3 Radionuclides Contribution to Integrated Discharge								
	6	3.2714E-01	PU239	2.2525E-01	69%	PU240	3.7739E-02	12%	U233	2.1199E-02	6%
	14	1.3659E-01	U233	5.2046E-02	38%	TH229	3.3106E-02	24%	TH230	2.5103E-02	18%
	49	1.2935E-01	U233	6.8289E-02	53%	U234	3.7181E-02	29%	TH229	1.2854E-02	10%
	10	9.5365E-02	U233	3.9891E-02	42%	TH229	2.1184E-02	22%	U234	1.5944E-02	17%
	1	7.3931E-02	U233	2.7756E-02	38%	TH229	2.2514E-02	30%	TH230	1.6522E-02	22%
	25	7.0795E-02	U233	3.2985E-02	47%	TH229	1.2671E-02	18%	U234	1.1847E-02	17%
	66	5.8591E-02	U233	2.8356E-02	48%	TH229	1.4991E-02	26%	TH230	8.6782E-03	15%
	26	5.6905E-02	U233	2.4752E-02	43%	TH229	9.0774E-03	16%	PU239	7.9224E-03	14%
	35	3.8868E-02	TH229	1.2217E-02	31%	U233	1.2050E-02	31%	TH230	1.0461E-02	27%
	65	3.4223E-02	U233	1.2769E-02	37%	PU239	9.9092E-03	29%	U234	3.6726E-03	11%
	51	3.1533E-02	U233	1.3969E-02	44%	U234	7.8247E-03	25%	TH229	5.1002E-03	16%
	43	3.1122E-02	PU239	9.5341E-03	31%	U233	8.3647E-03	27%	U234	4.5549E-03	15%
	58	1.9514E-02	PU239	1.6448E-02	84%	PU240	2.8386E-03	15%	TH229	1.1116E-04	1%
	42	1.6532E-02	PU239	1.3677E-02	83%	PU240	2.8462E-03	17%	TH229	4.2986E-06	0%
	50	7.5564E-03	AM241	5.2142E-03	69%	RA226	1.3324E-03	18%	U233	4.9539E-04	7%
	59	7.5457E-03	U233	2.1848E-03	29%	AM241	1.5770E-03	21%	U234	1.2179E-03	16%
	29	7.4028E-03	TH229	2.9104E-03	39%	U233	1.8528E-03	25%	TH230	1.7509E-03	24%
	23	3.9549E-03	PU239	3.3333E-03	84%	PU240	5.6213E-04	14%	TH229	2.6880E-05	1%
	33	2.2398E-04	TH229	9.8575E-05	44%	TH230	8.8017E-05	39%	U233	2.3950E-05	11%
	63	1.2267E-04	TH229	5.4031E-05	44%	TH230	4.5323E-05	37%	AM241	9.2966E-06	8%
	9	1.4765E-05	TH229	5.6827E-06	38%	TH230	4.9635E-06	34%	U233	3.3129E-06	22%
	16	8.8900E-06	PU239	7.6626E-06	86%	PU240	1.1887E-06	13%	TH229	1.4055E-08	0%
	11	4.0238E-06	U233	1.8497E-06	46%	TH229	1.1237E-06	28%	TH230	5.0738E-07	13%
	18	2.4501E-06	PU239	2.0224E-06	83%	PU240	4.2713E-07	17%	TH229	3.3858E-10	0%
	12	2.1123E-06	PU239	1.4349E-06	68%	PU240	3.0961E-07	15%	RA226	2.9390E-07	14%
	24	1.7199E-07	PU239	6.0899E-08	35%	TH229	5.1494E-08	30%	TH230	4.2481E-08	25%
	40	4.5393E-09	TH229	2.2883E-09	50%	TH230	8.8384E-10	19%	U233	4.5053E-10	10%
	44	2.5787E-09	TH229	8.1549E-10	32%	U233	4.9601E-10	19%	TH230	3.9865E-10	15%
	3	1.5489E-09	U233	9.4857E-10	61%	U234	3.7179E-10	24%	TH229	1.3461E-10	9%
	32	1.3706E-09	AM241	1.2268E-09	90%	PU239	8.9295E-11	7%	PU240	1.8095E-11	1%
	57	1.0122E-09	PU239	7.9878E-10	79%	PU240	1.5931E-10	16%	U233	3.0336E-11	3%
	67	9.6018E-11	PU239	7.8296E-11	82%	PU240	1.7638E-11	18%	U233	2.9731E-14	0%
	7	5.3780E-11	PU239	4.3661E-11	81%	PU240	1.0117E-11	19%	RA226	4.2362E-16	0%
	21	1.0735E-11	U233	4.8143E-12	45%	U234	2.2874E-12	21%	PU239	2.1974E-12	20%
	20	7.3981E-12	PU239	6.0215E-12	81%	PU240	1.3398E-12	18%	U233	1.5176E-14	0%
	45	6.4161E-12	PU239	5.2204E-12	81%	PU240	1.1932E-12	19%	RA226	1.3834E-15	0%
	13	3.4304E-12	U233	1.8367E-12	54%	U234	1.1541E-12	34%	NP237	2.2407E-13	7%
	62	2.4448E-12	U233	9.9724E-13	41%	TH229	7.3057E-13	30%	TH230	3.1740E-13	13%
	41	1.2315E-12	AM241	8.5370E-13	69%	U233	1.5725E-13	13%	TH229	1.1752E-13	10%
	28	6.1138E-13	U233	2.3314E-13	38%	AM241	1.7063E-13	28%	U234	1.6292E-13	27%
	27	2.0458E-13	U233	1.3850E-13	68%	U234	3.3816E-14	17%	TH229	1.9067E-14	9%
	53	6.8844E-14	PU239	5.6094E-14	81%	PU240	1.2691E-14	18%	AM241	4.4416E-17	0%
	22	2.0337E-14	AM241	1.9410E-14	95%	U233	5.8864E-16	3%	TH229	1.9363E-16	1%

Table C-5. Vectors with Integrated Discharge through the Culebra Dolomite Member to the Accessible Environment for Scenario E1E2 and Assuming a Conceptual Model with Dual Porosity, Retardation, Clay, Matrix Diffusion, Intrusion at 1000 yr (Continued)

Comp. Scen. ID	Vector	Total EPA-normalized, Integrated Discharge	Top 3 Radionuclides Contribution to Integrated Discharge								
	8	1.6813E-14	AM241	1.5920E-14	95%	U233	4.4742E-16	3%	TH229	2.4006E-16	1%
	30	1.2627E-14	AM241	8.4374E-15	67%	U233	2.6757E-15	21%	U234	1.2602E-15	10%
	37	7.6926E-15	PU239	6.5873E-15	86%	PU240	1.0775E-15	14%	U233	1.7715E-17	0%
	17	7.1648E-15	RA226	4.7673E-15	67%	PU239	1.3183E-15	18%	PU240	7.5391E-16	11%
	60	6.3257E-15	U233	3.7468E-15	59%	PU239	6.9432E-16	11%	TH229	5.3069E-16	8%
	2	1.6995E-15	U233	7.6826E-16	45%	U234	4.7135E-16	28%	TH229	2.4665E-16	15%
	38	1.0373E-15	U233	3.6615E-16	35%	PU240	2.4939E-16	24%	PU239	1.5507E-16	15%
	34	8.5961E-16	U233	5.2466E-16	61%	TH229	1.4732E-16	17%	RA226	8.8110E-17	10%
	54	2.6880E-16	PU239	2.1514E-16	80%	PU240	5.3100E-17	20%	AM241	5.4714E-19	0%
	56	3.0443E-18	U233	1.8870E-18	62%	RA226	6.8848E-19	23%	TH229	2.3680E-19	8%
	36	2.1027E-23	U233	1.2969E-23	62%	U234	5.2115E-24	25%	RA226	2.2437E-24	11%

Table C-6 lists total EPA summed normalized release and the percentages contribution for the 3 radionuclides contributing the most release for each vector when drilling into a CH waste drum with an average activity level. Vectors are ordered from most to least release. All vectors have some release when intruding into the repository from drilling.

Table C-6. Vectors with CH Cuttings Discharged to the Ground Surface

Comp. Scen. ID	Vector	Total EPA-normalized Cuttings	Top 3 Radionuclides Contribution to Integrated Discharge								
			(Time of Intrusion, 125 years)								
01	32	4.5271E-02	PU238	2.4764E-02	55%	AM241	1.2726E-02	28%	PU239	5.9680E-03	13%
	39	4.4913E-02	PU238	2.4568E-02	55%	AM241	1.2626E-02	28%	PU239	5.9208E-03	13%
	70	4.4782E-02	PU238	2.4496E-02	55%	AM241	1.2589E-02	28%	PU239	5.9035E-03	13%
	63	4.4294E-02	PU238	2.4230E-02	55%	AM241	1.2452E-02	28%	PU239	5.8392E-03	13%
	25	4.4057E-02	PU238	2.4100E-02	55%	AM241	1.2385E-02	28%	PU239	5.8079E-03	13%
	58	4.3796E-02	PU238	2.3957E-02	55%	AM241	1.2312E-02	28%	PU239	5.7735E-03	13%
	30	4.3512E-02	PU238	2.3802E-02	55%	AM241	1.2232E-02	28%	PU239	5.7361E-03	13%
	19	4.3299E-02	PU238	2.3685E-02	55%	AM241	1.2172E-02	28%	PU239	5.7080E-03	13%
	62	4.3028E-02	PU238	2.3537E-02	55%	AM241	1.2096E-02	28%	PU239	5.6723E-03	13%
	3	4.2733E-02	PU238	2.3376E-02	55%	AM241	1.2013E-02	28%	PU239	5.6334E-03	13%
	13	4.2439E-02	PU238	2.3215E-02	55%	AM241	1.1930E-02	28%	PU239	5.5947E-03	13%
	22	4.2076E-02	PU238	2.3016E-02	55%	AM241	1.1828E-02	28%	PU239	5.5467E-03	13%
	47	4.1794E-02	PU238	2.2862E-02	55%	AM241	1.1749E-02	28%	PU239	5.5096E-03	13%
	7	4.1397E-02	PU238	2.2645E-02	55%	AM241	1.1637E-02	28%	PU239	5.4572E-03	13%
	1	4.1245E-02	PU238	2.2562E-02	55%	AM241	1.1594E-02	28%	PU239	5.4372E-03	13%

Table C-6. Vectors with CH Cuttings Discharged to the Ground Surface (Continued)

Comp. Scen. ID	Vector	Total EPA-normalized Cuttings	Top 3 Radionuclides Contribution to Integrated Discharge								
			(Time of Intrusion, 125 years)								
	50	4.0826E-02	PU238	2.2332E-02	55%	AM241	1.1477E-02	28%	PU239	5.3820E-03	13%
	45	4.0628E-02	PU238	2.2224E-02	55%	AM241	1.1421E-02	28%	PU239	5.3559E-03	13%
	65	4.0291E-02	PU238	2.2040E-02	55%	AM241	1.1326E-02	28%	PU239	5.3115E-03	13%
	43	3.9863E-02	PU238	2.1806E-02	55%	AM241	1.1206E-02	28%	PU239	5.2550E-03	13%
	12	3.9655E-02	PU238	2.1692E-02	55%	AM241	1.1147E-02	28%	PU239	5.2276E-03	13%
	31	3.9447E-02	PU238	2.1578E-02	55%	AM241	1.1089E-02	28%	PU239	5.2002E-03	13%
	4	3.9170E-02	PU238	2.1427E-02	55%	AM241	1.1011E-02	28%	PU239	5.1637E-03	13%
	48	3.8883E-02	PU238	2.1269E-02	55%	AM241	1.0930E-02	28%	PU239	5.1258E-03	13%
	54	3.8515E-02	PU238	2.1068E-02	55%	AM241	1.0827E-02	28%	PU239	5.0773E-03	13%
	37	3.8297E-02	PU238	2.0949E-02	55%	AM241	1.0766E-02	28%	PU239	5.0486E-03	13%
	69	3.7874E-02	PU238	2.0718E-02	55%	AM241	1.0647E-02	28%	PU239	4.9928E-03	13%
	2	3.7703E-02	PU238	2.0624E-02	55%	AM241	1.0599E-02	28%	PU239	4.9702E-03	13%
	35	3.7247E-02	PU238	2.0375E-02	55%	AM241	1.0470E-02	28%	PU239	4.9101E-03	13%
	67	3.7179E-02	PU238	2.0337E-02	55%	AM241	1.0451E-02	28%	PU239	4.9011E-03	13%
	28	3.6872E-02	PU238	2.0169E-02	55%	AM241	1.0365E-02	28%	PU239	4.8607E-03	13%
	6	3.6430E-02	PU238	1.9928E-02	55%	AM241	1.0241E-02	28%	PU239	4.8024E-03	13%
	40	3.6056E-02	PU238	1.9723E-02	55%	AM241	1.0136E-02	28%	PU239	4.7532E-03	13%
	56	3.5797E-02	PU238	1.9581E-02	55%	AM241	1.0063E-02	28%	PU239	4.7190E-03	13%
	10	3.5695E-02	PU238	1.9526E-02	55%	AM241	1.0034E-02	28%	PU239	4.7056E-03	13%
	34	3.5448E-02	PU238	1.9390E-02	55%	AM241	9.9647E-03	28%	PU239	4.6730E-03	13%
	66	3.5021E-02	PU238	1.9157E-02	55%	AM241	9.8447E-03	28%	PU239	4.6167E-03	13%
	53	3.4718E-02	PU238	1.8991E-02	55%	AM241	9.7596E-03	28%	PU239	4.5768E-03	13%
	64	3.4349E-02	PU238	1.8790E-02	55%	AM241	9.6559E-03	28%	PU239	4.5282E-03	13%
	59	3.4271E-02	PU238	1.8747E-02	55%	AM241	9.6339E-03	28%	PU239	4.5179E-03	13%
	57	3.3981E-02	PU238	1.8588E-02	55%	AM241	9.5524E-03	28%	PU239	4.4796E-03	13%
	14	3.3603E-02	PU238	1.8381E-02	55%	AM241	9.4461E-03	28%	PU239	4.4298E-03	13%
	20	3.3314E-02	PU238	1.8223E-02	55%	AM241	9.3649E-03	28%	PU239	4.3917E-03	13%
	15	3.2948E-02	PU238	1.8023E-02	55%	AM241	9.2621E-03	28%	PU239	4.3435E-03	13%
	29	3.2760E-02	PU238	1.7920E-02	55%	AM241	9.2093E-03	28%	PU239	4.3187E-03	13%
	11	3.2539E-02	PU238	1.7800E-02	55%	AM241	9.1472E-03	28%	PU239	4.2896E-03	13%
	55	3.2242E-02	PU238	1.7637E-02	55%	AM241	9.0635E-03	28%	PU239	4.2504E-03	13%
	60	3.1846E-02	PU238	1.7420E-02	55%	AM241	8.9522E-03	28%	PU239	4.1982E-03	13%
	18	3.1593E-02	PU238	1.7282E-02	55%	AM241	8.8812E-03	28%	PU239	4.1649E-03	13%
	61	3.1352E-02	PU238	1.7150E-02	55%	AM241	8.8135E-03	28%	PU239	4.1331E-03	13%
	36	3.1155E-02	PU238	1.7043E-02	55%	AM241	8.7581E-03	28%	PU239	4.1071E-03	13%
	51	3.0675E-02	PU238	1.6780E-02	55%	AM241	8.6231E-03	28%	PU239	4.0438E-03	13%
	49	3.0675E-02	PU238	1.6780E-02	55%	AM241	8.6231E-03	28%	PU239	4.0438E-03	13%
	46	3.0283E-02	PU238	1.6565E-02	55%	AM241	8.5130E-03	28%	PU239	3.9922E-03	13%
	21	3.0023E-02	PU238	1.6423E-02	55%	AM241	8.4397E-03	28%	PU239	3.9578E-03	13%
	23	2.9676E-02	PU238	1.6233E-02	55%	AM241	8.3422E-03	28%	PU239	3.9121E-03	13%
	52	2.9309E-02	PU238	1.6032E-02	55%	AM241	8.2389E-03	28%	PU239	3.8637E-03	13%
	44	2.9222E-02	PU238	1.5985E-02	55%	AM241	8.2147E-03	28%	PU239	3.8523E-03	13%
	38	2.8781E-02	PU238	1.5743E-02	55%	AM241	8.0905E-03	28%	PU239	3.7941E-03	13%
	8	2.8501E-02	PU238	1.5591E-02	55%	AM241	8.0120E-03	28%	PU239	3.7573E-03	13%

Table C-6. Vectors with CH Cuttings Discharged to the Ground Surface (Continued)

Comp. Scen. ID	Vector	Total EPA-normalized Cuttings	Top 3 Radionuclides Contribution to Integrated Discharge								
			(Time of Intrusion, 125 years)								
	16	2.8319E-02	PU238	1.5491E-02	55%	AM241	7.9607E-03	28%	PU239	3.7332E-03	13%
	42	2.8126E-02	PU238	1.5385E-02	55%	AM241	7.9065E-03	28%	PU239	3.7078E-03	13%
	33	2.7731E-02	PU238	1.5169E-02	55%	AM241	7.7953E-03	28%	PU239	3.6557E-03	13%
	17	2.7411E-02	PU238	1.4994E-02	55%	AM241	7.7054E-03	28%	PU239	3.6135E-03	13%
	41	2.7187E-02	PU238	1.4872E-02	55%	AM241	7.6426E-03	28%	PU239	3.5840E-03	13%
	24	2.6953E-02	PU238	1.4744E-02	55%	AM241	7.5769E-03	28%	PU239	3.5532E-03	13%
	5	2.6784E-02	PU238	1.4651E-02	55%	AM241	7.5292E-03	28%	PU239	3.5308E-03	13%
	9	2.6508E-02	PU238	1.4500E-02	55%	AM241	7.4517E-03	28%	PU239	3.4945E-03	13%
	68	2.6128E-02	PU238	1.4292E-02	55%	AM241	7.3448E-03	28%	PU239	3.4444E-03	13%
	26	2.5822E-02	PU238	1.4125E-02	55%	AM241	7.2589E-03	28%	PU239	3.4041E-03	13%
	27	2.5738E-02	PU238	1.4079E-02	55%	AM241	7.2352E-03	28%	PU239	3.3930E-03	13%
			(Time of Intrusion, 175 years)								
02	32	3.2751E-02	PU238	1.3693E-02	42%	AM241	1.1299E-02	35%	PU239	5.9551E-03	18%
	39	3.2492E-02	PU238	1.3585E-02	42%	AM241	1.1210E-02	35%	PU239	5.9080E-03	18%
	70	3.2397E-02	PU238	1.3545E-02	42%	AM241	1.1177E-02	35%	PU239	5.8908E-03	18%
	63	3.2044E-02	PU238	1.3398E-02	42%	AM241	1.1056E-02	35%	PU239	5.8266E-03	18%
	25	3.1873E-02	PU238	1.3326E-02	42%	AM241	1.0996E-02	35%	PU239	5.7954E-03	18%
	58	3.1684E-02	PU238	1.3247E-02	42%	AM241	1.0931E-02	35%	PU239	5.7611E-03	18%
	30	3.1478E-02	PU238	1.3161E-02	42%	AM241	1.0860E-02	35%	PU239	5.7237E-03	18%
	19	3.1325E-02	PU238	1.3097E-02	42%	AM241	1.0807E-02	35%	PU239	5.6957E-03	18%
	62	3.1128E-02	PU238	1.3015E-02	42%	AM241	1.0740E-02	35%	PU239	5.6600E-03	18%
	3	3.0915E-02	PU238	1.2926E-02	42%	AM241	1.0666E-02	35%	PU239	5.6213E-03	18%
	13	3.0702E-02	PU238	1.2837E-02	42%	AM241	1.0593E-02	35%	PU239	5.5826E-03	18%
	22	3.0439E-02	PU238	1.2727E-02	42%	AM241	1.0502E-02	35%	PU239	5.5347E-03	18%
	47	3.0236E-02	PU238	1.2642E-02	42%	AM241	1.0432E-02	35%	PU239	5.4978E-03	18%
	7	2.9948E-02	PU238	1.2521E-02	42%	AM241	1.0332E-02	35%	PU239	5.4455E-03	18%
	1	2.9839E-02	PU238	1.2476E-02	42%	AM241	1.0295E-02	35%	PU239	5.4255E-03	18%
	50	2.9535E-02	PU238	1.2349E-02	42%	AM241	1.0190E-02	35%	PU239	5.3703E-03	18%
	45	2.9392E-02	PU238	1.2289E-02	42%	AM241	1.0141E-02	35%	PU239	5.3443E-03	18%
	65	2.9148E-02	PU238	1.2187E-02	42%	AM241	1.0056E-02	35%	PU239	5.3000E-03	18%
	43	2.8838E-02	PU238	1.2057E-02	42%	AM241	9.9495E-03	35%	PU239	5.2437E-03	18%
	12	2.8688E-02	PU238	1.1994E-02	42%	AM241	9.8976E-03	35%	PU239	5.2163E-03	18%
	31	2.8538E-02	PU238	1.1932E-02	42%	AM241	9.8457E-03	35%	PU239	5.1890E-03	18%
	4	2.8337E-02	PU238	1.1848E-02	42%	AM241	9.7767E-03	35%	PU239	5.1526E-03	18%
	48	2.8129E-02	PU238	1.1761E-02	42%	AM241	9.7048E-03	35%	PU239	5.1147E-03	18%
	54	2.7863E-02	PU238	1.1650E-02	42%	AM241	9.6131E-03	35%	PU239	5.0664E-03	18%
	37	2.7706E-02	PU238	1.1584E-02	42%	AM241	9.5588E-03	35%	PU239	5.0377E-03	18%
	69	2.7400E-02	PU238	1.1456E-02	42%	AM241	9.4531E-03	35%	PU239	4.9820E-03	18%
	2	2.7276E-02	PU238	1.1404E-02	42%	AM241	9.4103E-03	35%	PU239	4.9595E-03	18%
	35	2.6946E-02	PU238	1.1266E-02	42%	AM241	9.2966E-03	35%	PU239	4.8996E-03	18%
	67	2.6897E-02	PU238	1.1246E-02	42%	AM241	9.2795E-03	35%	PU239	4.8906E-03	18%
	28	2.6675E-02	PU238	1.1153E-02	42%	AM241	9.2029E-03	35%	PU239	4.8502E-03	18%

Table C-6. Vectors with CH Cuttings Discharged to the Ground Surface (Continued)

Comp. Scen. ID	Vector	Total EPA-normalized Cuttings	Top 3 Radionuclides Contribution to Integrated Discharge								
(Time of Intrusion, 175 years)											
	6	2.6355E-02	PU238	1.1019E-02	42%	AM241	9.0926E-03	35%	PU239	4.7920E-03	18%
	40	2.6085E-02	PU238	1.0906E-02	42%	AM241	8.9995E-03	35%	PU239	4.7430E-03	18%
	56	2.5897E-02	PU238	1.0828E-02	42%	AM241	8.9347E-03	35%	PU239	4.7088E-03	18%
	10	2.5824E-02	PU238	1.0797E-02	42%	AM241	8.9094E-03	35%	PU239	4.6955E-03	18%
	34	2.5644E-02	PU238	1.0722E-02	42%	AM241	8.8475E-03	35%	PU239	4.6629E-03	18%
	66	2.5336E-02	PU238	1.0593E-02	42%	AM241	8.7410E-03	35%	PU239	4.6067E-03	18%
	53	2.5117E-02	PU238	1.0501E-02	42%	AM241	8.6655E-03	35%	PU239	4.5669E-03	18%
	64	2.4850E-02	PU238	1.0390E-02	42%	AM241	8.5734E-03	35%	PU239	4.5184E-03	18%
	59	2.4793E-02	PU238	1.0366E-02	42%	AM241	8.5538E-03	35%	PU239	4.5081E-03	18%
	57	2.4583E-02	PU238	1.0278E-02	42%	AM241	8.4815E-03	35%	PU239	4.4700E-03	18%
	14	2.4310E-02	PU238	1.0164E-02	42%	AM241	8.3870E-03	35%	PU239	4.4202E-03	18%
	20	2.4101E-02	PU238	1.0077E-02	42%	AM241	8.3150E-03	35%	PU239	4.3822E-03	18%
	15	2.3836E-02	PU238	9.9660E-03	42%	AM241	8.2237E-03	35%	PU239	4.3341E-03	18%
	29	2.3700E-02	PU238	9.9091E-03	42%	AM241	8.1768E-03	35%	PU239	4.3094E-03	18%
	11	2.3540E-02	PU238	9.8423E-03	42%	AM241	8.1217E-03	35%	PU239	4.2803E-03	18%
	55	2.3325E-02	PU238	9.7523E-03	42%	AM241	8.0474E-03	35%	PU239	4.2412E-03	18%
	60	2.3039E-02	PU238	9.6325E-03	42%	AM241	7.9485E-03	35%	PU239	4.1891E-03	18%
	18	2.2856E-02	PU238	9.5562E-03	42%	AM241	7.8855E-03	35%	PU239	4.1559E-03	18%
	61	2.2682E-02	PU238	9.4833E-03	42%	AM241	7.8254E-03	35%	PU239	4.1242E-03	18%
	36	2.2539E-02	PU238	9.4237E-03	42%	AM241	7.7762E-03	35%	PU239	4.0983E-03	18%
	51	2.2192E-02	PU238	9.2784E-03	42%	AM241	7.6563E-03	35%	PU239	4.0351E-03	18%
	49	2.2192E-02	PU238	9.2784E-03	42%	AM241	7.6563E-03	35%	PU239	4.0351E-03	18%
	46	2.1908E-02	PU238	9.1599E-03	42%	AM241	7.5586E-03	35%	PU239	3.9836E-03	18%
	21	2.1720E-02	PU238	9.0811E-03	42%	AM241	7.4935E-03	35%	PU239	3.9493E-03	18%
	23	2.1469E-02	PU238	8.9762E-03	42%	AM241	7.4070E-03	35%	PU239	3.9037E-03	18%
	52	2.1203E-02	PU238	8.8651E-03	42%	AM241	7.3153E-03	35%	PU239	3.8553E-03	18%
	44	2.1141E-02	PU238	8.8390E-03	42%	AM241	7.2937E-03	35%	PU239	3.8440E-03	18%
	38	2.0821E-02	PU238	8.7054E-03	42%	AM241	7.1835E-03	35%	PU239	3.7859E-03	18%
	8	2.0619E-02	PU238	8.6209E-03	42%	AM241	7.1138E-03	35%	PU239	3.7491E-03	18%
	16	2.0487E-02	PU238	8.5657E-03	42%	AM241	7.0682E-03	35%	PU239	3.7252E-03	18%
	42	2.0348E-02	PU238	8.5074E-03	42%	AM241	7.0201E-03	35%	PU239	3.6998E-03	18%
	33	2.0061E-02	PU238	8.3878E-03	42%	AM241	6.9214E-03	35%	PU239	3.6478E-03	18%
	17	1.9830E-02	PU238	8.2910E-03	42%	AM241	6.8415E-03	35%	PU239	3.6057E-03	18%
	41	1.9668E-02	PU238	8.2234E-03	42%	AM241	6.7858E-03	35%	PU239	3.5763E-03	18%
	24	1.9499E-02	PU238	8.1527E-03	42%	AM241	6.7274E-03	35%	PU239	3.5455E-03	18%
	5	1.9376E-02	PU238	8.1014E-03	42%	AM241	6.6850E-03	35%	PU239	3.5232E-03	18%
	9	1.9177E-02	PU238	8.0180E-03	42%	AM241	6.6163E-03	35%	PU239	3.4870E-03	18%
	68	1.8902E-02	PU238	7.9030E-03	42%	AM241	6.5214E-03	35%	PU239	3.4369E-03	18%
	26	1.8681E-02	PU238	7.8105E-03	42%	AM241	6.4451E-03	35%	PU239	3.3967E-03	18%
	27	1.8620E-02	PU238	7.7850E-03	42%	AM241	6.4240E-03	35%	PU239	3.3856E-03	18%
(Time of Intrusion, 350 years)											
03	32	1.9671E-02	AM241	8.5346E-03	43%	PU239	5.9252E-03	30%	PU238	3.4362E-03	17%
	39	1.9516E-02	AM241	8.4671E-03	43%	PU239	5.8783E-03	30%	PU238	3.4090E-03	17%

Table C-6. Vectors with CH Cuttings Discharged to the Ground Surface (Continued)

Comp. Scen. ID	Vector	Total EPA-normalized Cuttings	Top 3 Radionuclides Contribution to Integrated Discharge								
(Time of Intrusion, 350 years)											
	70	1.9459E-02	AM241	8.4424E-03	43%	PU239	5.8611E-03	30%	PU238	3.3991E-03	17%
	63	1.9247E-02	AM241	8.3504E-03	43%	PU239	5.7973E-03	30%	PU238	3.3621E-03	17%
	25	1.9144E-02	AM241	8.3057E-03	43%	PU239	5.7662E-03	30%	PU238	3.3441E-03	17%
	58	1.9030E-02	AM241	8.2565E-03	43%	PU239	5.7321E-03	30%	PU238	3.3243E-03	17%
	30	1.8907E-02	AM241	8.2030E-03	43%	PU239	5.6949E-03	30%	PU238	3.3027E-03	17%
	19	1.8815E-02	AM241	8.1629E-03	43%	PU239	5.6671E-03	30%	PU238	3.2866E-03	17%
	62	1.8697E-02	AM241	8.1117E-03	43%	PU239	5.6316E-03	30%	PU238	3.2659E-03	17%
	3	1.8569E-02	AM241	8.0562E-03	43%	PU239	5.5930E-03	30%	PU238	3.2436E-03	17%
	13	1.8441E-02	AM241	8.0007E-03	43%	PU239	5.5545E-03	30%	PU238	3.2213E-03	17%
	22	1.8283E-02	AM241	7.9321E-03	43%	PU239	5.5069E-03	30%	PU238	3.1937E-03	17%
	47	1.8161E-02	AM241	7.8791E-03	43%	PU239	5.4701E-03	30%	PU238	3.1723E-03	17%
	7	1.7988E-02	AM241	7.8042E-03	43%	PU239	5.4181E-03	30%	PU238	3.1422E-03	17%
	1	1.7922E-02	AM241	7.7756E-03	43%	PU239	5.3982E-03	30%	PU238	3.1306E-03	17%
	50	1.7740E-02	AM241	7.6965E-03	43%	PU239	5.3433E-03	30%	PU238	3.0988E-03	17%
	45	1.7654E-02	AM241	7.6593E-03	43%	PU239	5.3175E-03	30%	PU238	3.0838E-03	17%
	65	1.7508E-02	AM241	7.5958E-03	43%	PU239	5.2734E-03	30%	PU238	3.0582E-03	17%
	43	1.7321E-02	AM241	7.5150E-03	43%	PU239	5.2173E-03	30%	PU238	3.0257E-03	17%
	12	1.7231E-02	AM241	7.4758E-03	43%	PU239	5.1901E-03	30%	PU238	3.0099E-03	17%
	31	1.7141E-02	AM241	7.4366E-03	43%	PU239	5.1629E-03	30%	PU238	2.9941E-03	17%
	4	1.7020E-02	AM241	7.3844E-03	43%	PU239	5.1267E-03	30%	PU238	2.9731E-03	17%
	48	1.6895E-02	AM241	7.3302E-03	43%	PU239	5.0890E-03	30%	PU238	2.9513E-03	17%
	54	1.6736E-02	AM241	7.2609E-03	43%	PU239	5.0409E-03	30%	PU238	2.9234E-03	17%
	37	1.6641E-02	AM241	7.2199E-03	43%	PU239	5.0124E-03	30%	PU238	2.9069E-03	17%
	69	1.6457E-02	AM241	7.1401E-03	43%	PU239	4.9570E-03	30%	PU238	2.8747E-03	17%
	2	1.6383E-02	AM241	7.1078E-03	43%	PU239	4.9346E-03	30%	PU238	2.8617E-03	17%
	35	1.6185E-02	AM241	7.0218E-03	43%	PU239	4.8749E-03	30%	PU238	2.8271E-03	17%
	67	1.6155E-02	AM241	7.0090E-03	43%	PU239	4.8660E-03	30%	PU238	2.8220E-03	17%
	28	1.6022E-02	AM241	6.9511E-03	43%	PU239	4.8258E-03	30%	PU238	2.7987E-03	17%
	6	1.5829E-02	AM241	6.8678E-03	43%	PU239	4.7680E-03	30%	PU238	2.7651E-03	17%
	40	1.5667E-02	AM241	6.7974E-03	43%	PU239	4.7191E-03	30%	PU238	2.7368E-03	17%
	56	1.5555E-02	AM241	6.7485E-03	43%	PU239	4.6851E-03	30%	PU238	2.7171E-03	17%
	10	1.5510E-02	AM241	6.7294E-03	43%	PU239	4.6719E-03	30%	PU238	2.7094E-03	17%
	34	1.5403E-02	AM241	6.6827E-03	43%	PU239	4.6395E-03	30%	PU238	2.6906E-03	17%
	66	1.5217E-02	AM241	6.6022E-03	43%	PU239	4.5836E-03	30%	PU238	2.6582E-03	17%
	53	1.5086E-02	AM241	6.5451E-03	43%	PU239	4.5440E-03	30%	PU238	2.6352E-03	17%
	64	1.4926E-02	AM241	6.4756E-03	43%	PU239	4.4957E-03	30%	PU238	2.6072E-03	17%
	59	1.4892E-02	AM241	6.4608E-03	43%	PU239	4.4854E-03	30%	PU238	2.6013E-03	17%
	57	1.4766E-02	AM241	6.4062E-03	43%	PU239	4.4475E-03	30%	PU238	2.5793E-03	17%
	14	1.4601E-02	AM241	6.3348E-03	43%	PU239	4.3980E-03	30%	PU238	2.5505E-03	17%
	20	1.4476E-02	AM241	6.2804E-03	43%	PU239	4.3602E-03	30%	PU238	2.5286E-03	17%
	15	1.4317E-02	AM241	6.2115E-03	43%	PU239	4.3123E-03	30%	PU238	2.5009E-03	17%
	29	1.4235E-02	AM241	6.1760E-03	43%	PU239	4.2877E-03	30%	PU238	2.4866E-03	17%
	11	1.4139E-02	AM241	6.1344E-03	43%	PU239	4.2588E-03	30%	PU238	2.4698E-03	17%
	55	1.4010E-02	AM241	6.0783E-03	43%	PU239	4.2199E-03	30%	PU238	2.4473E-03	17%

Table C-6. Vectors with CH Cuttings Discharged to the Ground Surface (Continued)

Comp. Scen. ID	Vector	Total EPA-normalized Cuttings	Top 3 Radionuclides Contribution to Integrated Discharge								
			(Time of Intrusion, 350 years)								
	60	1.3838E-02	AM241	6.0036E-03	43%	PU239	4.1680E-03	30%	PU238	2.4172E-03	17%
	18	1.3728E-02	AM241	5.9560E-03	43%	PU239	4.1350E-03	30%	PU238	2.3980E-03	17%
	61	1.3623E-02	AM241	5.9106E-03	43%	PU239	4.1034E-03	30%	PU238	2.3797E-03	17%
	36	1.3538E-02	AM241	5.8735E-03	43%	PU239	4.0777E-03	30%	PU238	2.3648E-03	17%
	51	1.3329E-02	AM241	5.7829E-03	43%	PU239	4.0148E-03	30%	PU238	2.3283E-03	17%
	49	1.3329E-02	AM241	5.7829E-03	43%	PU239	4.0148E-03	30%	PU238	2.3283E-03	17%
	46	1.3159E-02	AM241	5.7091E-03	43%	PU239	3.9635E-03	30%	PU238	2.2986E-03	17%
	21	1.3046E-02	AM241	5.6600E-03	43%	PU239	3.9294E-03	30%	PU238	2.2788E-03	17%
	23	1.2895E-02	AM241	5.5946E-03	43%	PU239	3.8841E-03	30%	PU238	2.2525E-03	17%
	52	1.2735E-02	AM241	5.5253E-03	43%	PU239	3.8360E-03	30%	PU238	2.2246E-03	17%
	44	1.2698E-02	AM241	5.5090E-03	43%	PU239	3.8247E-03	30%	PU238	2.2181E-03	17%
	38	1.2506E-02	AM241	5.4258E-03	43%	PU239	3.7669E-03	30%	PU238	2.1845E-03	17%
	8	1.2384E-02	AM241	5.3731E-03	43%	PU239	3.7303E-03	30%	PU238	2.1633E-03	17%
	16	1.2305E-02	AM241	5.3387E-03	43%	PU239	3.7064E-03	30%	PU238	2.1495E-03	17%
	42	1.2221E-02	AM241	5.3024E-03	43%	PU239	3.6812E-03	30%	PU238	2.1349E-03	17%
	33	1.2050E-02	AM241	5.2278E-03	43%	PU239	3.6294E-03	30%	PU238	2.1048E-03	17%
	17	1.1911E-02	AM241	5.1675E-03	43%	PU239	3.5876E-03	30%	PU238	2.0806E-03	17%
	41	1.1813E-02	AM241	5.1254E-03	43%	PU239	3.5583E-03	30%	PU238	2.0636E-03	17%
	24	1.1712E-02	AM241	5.0813E-03	43%	PU239	3.5277E-03	30%	PU238	2.0458E-03	17%
	5	1.1638E-02	AM241	5.0493E-03	43%	PU239	3.5055E-03	30%	PU238	2.0330E-03	17%
	9	1.1518E-02	AM241	4.9974E-03	43%	PU239	3.4694E-03	30%	PU238	2.0121E-03	17%
	68	1.1353E-02	AM241	4.9257E-03	43%	PU239	3.4197E-03	30%	PU238	1.9832E-03	17%
	26	1.1220E-02	AM241	4.8680E-03	43%	PU239	3.3796E-03	30%	PU238	1.9600E-03	17%
	27	1.1184E-02	AM241	4.8522E-03	43%	PU239	3.3686E-03	30%	PU238	1.9536E-03	17%
			(Time of Intrusion, 1000 years)								
04	32	1.0509E-02	PU239	5.8153E-03	55%	AM241	3.0092E-03	29%	PU240	1.6121E-03	15%
	39	1.0425E-02	PU239	5.7693E-03	55%	AM241	2.9854E-03	29%	PU240	1.5994E-03	15%
	70	1.0395E-02	PU239	5.7524E-03	55%	AM241	2.9767E-03	29%	PU240	1.5947E-03	15%
	63	1.0282E-02	PU239	5.6898E-03	55%	AM241	2.9443E-03	29%	PU240	1.5774E-03	15%
	25	1.0227E-02	PU239	5.6593E-03	55%	AM241	2.9285E-03	29%	PU240	1.5689E-03	15%
	58	1.0166E-02	PU239	5.6258E-03	55%	AM241	2.9112E-03	29%	PU240	1.5596E-03	15%
	30	1.0100E-02	PU239	5.5893E-03	55%	AM241	2.8923E-03	29%	PU240	1.5495E-03	15%
	19	1.0051E-02	PU239	5.5620E-03	55%	AM241	2.8782E-03	29%	PU240	1.5419E-03	15%
	62	9.9878E-03	PU239	5.5271E-03	55%	AM241	2.8601E-03	29%	PU240	1.5323E-03	15%
	3	9.9194E-03	PU239	5.4893E-03	55%	AM241	2.8405E-03	29%	PU240	1.5218E-03	15%
	13	9.8512E-03	PU239	5.4515E-03	55%	AM241	2.8210E-03	29%	PU240	1.5113E-03	15%
	22	9.7667E-03	PU239	5.4048E-03	55%	AM241	2.7968E-03	29%	PU240	1.4983E-03	15%
	47	9.7014E-03	PU239	5.3687E-03	55%	AM241	2.7781E-03	29%	PU240	1.4883E-03	15%
	7	9.6092E-03	PU239	5.3176E-03	55%	AM241	2.7517E-03	29%	PU240	1.4742E-03	15%
	1	9.5740E-03	PU239	5.2981E-03	55%	AM241	2.7416E-03	29%	PU240	1.4688E-03	15%
	50	9.4766E-03	PU239	5.2442E-03	55%	AM241	2.7137E-03	29%	PU240	1.4538E-03	15%
	45	9.4307E-03	PU239	5.2188E-03	55%	AM241	2.7006E-03	29%	PU240	1.4468E-03	15%
	65	9.3526E-03	PU239	5.1756E-03	55%	AM241	2.6782E-03	29%	PU240	1.4348E-03	15%
	43	9.2531E-03	PU239	5.1205E-03	55%	AM241	2.6497E-03	29%	PU240	1.4195E-03	15%
	12	9.2048E-03	PU239	5.0938E-03	55%	AM241	2.6359E-03	29%	PU240	1.4121E-03	15%
	31	9.1565E-03	PU239	5.0671E-03	55%	AM241	2.6221E-03	29%	PU240	1.4047E-03	15%
	4	9.0923E-03	PU239	5.0316E-03	55%	AM241	2.6037E-03	29%	PU240	1.3949E-03	15%

Table C-6. Vectors with CH Cuttings Discharged to the Ground Surface (Continued)

Comp. Scen. ID	Vector	Total EPA-normalized Cuttings	Top 3 Radionuclides Contribution to Integrated Discharge								
			(Time of Intrusion, 1000 years)								
	48	9.0255E-03	PU239	4.9946E-03	55%	AM241	2.5846E-03	29%	PU240	1.3846E-03	15%
	54	8.9402E-03	PU239	4.9474E-03	55%	AM241	2.5601E-03	29%	PU240	1.3715E-03	15%
	37	8.8897E-03	PU239	4.9194E-03	55%	AM241	2.5457E-03	29%	PU240	1.3638E-03	15%
	69	8.7914E-03	PU239	4.8651E-03	55%	AM241	2.5175E-03	29%	PU240	1.3487E-03	15%
	2	8.7517E-03	PU239	4.8431E-03	55%	AM241	2.5061E-03	29%	PU240	1.3426E-03	15%
	35	8.6458E-03	PU239	4.7845E-03	55%	AM241	2.4758E-03	29%	PU240	1.3264E-03	15%
	67	8.6300E-03	PU239	4.7757E-03	55%	AM241	2.4713E-03	29%	PU240	1.3240E-03	15%
	28	8.5588E-03	PU239	4.7363E-03	55%	AM241	2.4509E-03	29%	PU240	1.3130E-03	15%
	6	8.4561E-03	PU239	4.6795E-03	55%	AM241	2.4215E-03	29%	PU240	1.2973E-03	15%
	40	8.3695E-03	PU239	4.6316E-03	55%	AM241	2.3967E-03	29%	PU240	1.2840E-03	15%
	56	8.3093E-03	PU239	4.5982E-03	55%	AM241	2.3795E-03	29%	PU240	1.2747E-03	15%
	10	8.2857E-03	PU239	4.5852E-03	55%	AM241	2.3727E-03	29%	PU240	1.2711E-03	15%
	34	8.2282E-03	PU239	4.5534E-03	55%	AM241	2.3562E-03	29%	PU240	1.2623E-03	15%
	66	8.1291E-03	PU239	4.4986E-03	55%	AM241	2.3279E-03	29%	PU240	1.2471E-03	15%
	53	8.0589E-03	PU239	4.4597E-03	55%	AM241	2.3078E-03	29%	PU240	1.2363E-03	15%
	64	7.9732E-03	PU239	4.4123E-03	55%	AM241	2.2832E-03	29%	PU240	1.2232E-03	15%
	59	7.9551E-03	PU239	4.4023E-03	55%	AM241	2.2780E-03	29%	PU240	1.2204E-03	15%
	57	7.8878E-03	PU239	4.3650E-03	55%	AM241	2.2588E-03	29%	PU240	1.2101E-03	15%
	14	7.8000E-03	PU239	4.3164E-03	55%	AM241	2.2336E-03	29%	PU240	1.1966E-03	15%
	20	7.7330E-03	PU239	4.2793E-03	55%	AM241	2.2144E-03	29%	PU240	1.1863E-03	15%
	15	7.6481E-03	PU239	4.2324E-03	55%	AM241	2.1901E-03	29%	PU240	1.1733E-03	15%
	29	7.6044E-03	PU239	4.2082E-03	55%	AM241	2.1776E-03	29%	PU240	1.1666E-03	15%
	11	7.5532E-03	PU239	4.1798E-03	55%	AM241	2.1629E-03	29%	PU240	1.1588E-03	15%
	55	7.4841E-03	PU239	4.1416E-03	55%	AM241	2.1431E-03	29%	PU240	1.1482E-03	15%
	60	7.3922E-03	PU239	4.0907E-03	55%	AM241	2.1168E-03	29%	PU240	1.1341E-03	15%
	18	7.3336E-03	PU239	4.0583E-03	55%	AM241	2.1000E-03	29%	PU240	1.1251E-03	15%
	61	7.2776E-03	PU239	4.0273E-03	55%	AM241	2.0840E-03	29%	PU240	1.1165E-03	15%
	36	7.2319E-03	PU239	4.0020E-03	55%	AM241	2.0709E-03	29%	PU240	1.1095E-03	15%
	51	7.1204E-03	PU239	3.9404E-03	55%	AM241	2.0390E-03	29%	PU240	1.0924E-03	15%
	49	7.1204E-03	PU239	3.9404E-03	55%	AM241	2.0390E-03	29%	PU240	1.0924E-03	15%
	46	7.0295E-03	PU239	3.8900E-03	55%	AM241	2.0130E-03	29%	PU240	1.0784E-03	15%
	21	6.9690E-03	PU239	3.8566E-03	55%	AM241	1.9956E-03	29%	PU240	1.0691E-03	15%
	23	6.8885E-03	PU239	3.8120E-03	55%	AM241	1.9726E-03	29%	PU240	1.0568E-03	15%
	52	6.8032E-03	PU239	3.7648E-03	55%	AM241	1.9482E-03	29%	PU240	1.0437E-03	15%
	44	6.7832E-03	PU239	3.7537E-03	55%	AM241	1.9424E-03	29%	PU240	1.0406E-03	15%
	38	6.6807E-03	PU239	3.6970E-03	55%	AM241	1.9131E-03	29%	PU240	1.0249E-03	15%
	8	6.6158E-03	PU239	3.6611E-03	55%	AM241	1.8945E-03	29%	PU240	1.0149E-03	15%
	16	6.5735E-03	PU239	3.6377E-03	55%	AM241	1.8824E-03	29%	PU240	1.0085E-03	15%
	42	6.5287E-03	PU239	3.6129E-03	55%	AM241	1.8696E-03	29%	PU240	1.0016E-03	15%
	33	6.4369E-03	PU239	3.5621E-03	55%	AM241	1.8433E-03	29%	PU240	9.8750E-04	15%
	17	6.3627E-03	PU239	3.5210E-03	55%	AM241	1.8220E-03	29%	PU240	9.7611E-04	15%
	41	6.3108E-03	PU239	3.4923E-03	55%	AM241	1.8072E-03	29%	PU240	9.6815E-04	15%
	24	6.2565E-03	PU239	3.4623E-03	55%	AM241	1.7916E-03	29%	PU240	9.5983E-04	15%
	5	6.2171E-03	PU239	3.4405E-03	55%	AM241	1.7803E-03	29%	PU240	9.5379E-04	15%
	9	6.1532E-03	PU239	3.4051E-03	55%	AM241	1.7620E-03	29%	PU240	9.4398E-04	15%
	68	6.0649E-03	PU239	3.3562E-03	55%	AM241	1.7367E-03	29%	PU240	9.3043E-04	15%
	26	5.9939E-03	PU239	3.3170E-03	55%	AM241	1.7164E-03	29%	PU240	9.1954E-04	15%
	27	5.9744E-03	PU239	3.3061E-03	55%	AM241	1.7108E-03	29%	PU240	9.1654E-04	15%
			(Time of Intrusion, 3000 years)								
05	32	6.9712E-03	PU239	5.4897E-03	79%	PU240	1.3041E-03	19%	AM241	1.2175E-04	2%
	39	6.9161E-03	PU239	5.4463E-03	79%	PU240	1.2938E-03	19%	AM241	1.2078E-04	2%
	70	6.8959E-03	PU239	5.4304E-03	79%	PU240	1.2900E-03	19%	AM241	1.2043E-04	2%
	63	6.8208E-03	PU239	5.3713E-03	79%	PU240	1.2759E-03	19%	AM241	1.1912E-04	2%

Table C-6. Vectors with CH Cuttings Discharged to the Ground Surface (Continued)

Comp. Scen. ID	Vector	Total EPA-normalized Cuttings	Top 3 Radionuclides Contribution to Integrated Discharge								
(Time of Intrusion, 3000 years)											
	25	6.7842E-03	PU239	5.3425E-03	79%	PU240	1.2691E-03	19%	AM241	1.1848E-04	2%
	58	6.7441E-03	PU239	5.3109E-03	79%	PU240	1.2616E-03	19%	AM241	1.1778E-04	2%
	30	6.7003E-03	PU239	5.2764E-03	79%	PU240	1.2534E-03	19%	AM241	1.1702E-04	2%
	19	6.6676E-03	PU239	5.2506E-03	79%	PU240	1.2473E-03	19%	AM241	1.1644E-04	2%
	62	6.6258E-03	PU239	5.2177E-03	79%	PU240	1.2395E-03	19%	AM241	1.1571E-04	2%
	3	6.5804E-03	PU239	5.1820E-03	79%	PU240	1.2310E-03	19%	AM241	1.1492E-04	2%
	13	6.5352E-03	PU239	5.1463E-03	79%	PU240	1.2225E-03	19%	AM241	1.1413E-04	2%
	22	6.4791E-03	PU239	5.1022E-03	79%	PU240	1.2120E-03	19%	AM241	1.1315E-04	2%
	47	6.4358E-03	PU239	5.0681E-03	79%	PU240	1.2039E-03	19%	AM241	1.1240E-04	2%
	7	6.3746E-03	PU239	5.0199E-03	79%	PU240	1.1925E-03	19%	AM241	1.1133E-04	2%
	1	6.3513E-03	PU239	5.0015E-03	79%	PU240	1.1881E-03	19%	AM241	1.1092E-04	2%
	50	6.2867E-03	PU239	4.9507E-03	79%	PU240	1.1760E-03	19%	AM241	1.0979E-04	2%
	45	6.2562E-03	PU239	4.9267E-03	79%	PU240	1.1703E-03	19%	AM241	1.0926E-04	2%
	65	6.2044E-03	PU239	4.8859E-03	79%	PU240	1.1606E-03	19%	AM241	1.0836E-04	2%
	43	6.1384E-03	PU239	4.8339E-03	79%	PU240	1.1483E-03	19%	AM241	1.0720E-04	2%
	12	6.1064E-03	PU239	4.8087E-03	79%	PU240	1.1423E-03	19%	AM241	1.0664E-04	2%
	31	6.0744E-03	PU239	4.7835E-03	79%	PU240	1.1363E-03	19%	AM241	1.0608E-04	2%
	4	6.0317E-03	PU239	4.7499E-03	79%	PU240	1.1283E-03	19%	AM241	1.0534E-04	2%
	48	5.9874E-03	PU239	4.7150E-03	79%	PU240	1.1200E-03	19%	AM241	1.0457E-04	2%
	54	5.9309E-03	PU239	4.6705E-03	79%	PU240	1.1095E-03	19%	AM241	1.0358E-04	2%
	37	5.8973E-03	PU239	4.6441E-03	79%	PU240	1.1032E-03	19%	AM241	1.0299E-04	2%
	69	5.8321E-03	PU239	4.5927E-03	79%	PU240	1.0910E-03	19%	AM241	1.0185E-04	2%
	2	5.8058E-03	PU239	4.5720E-03	79%	PU240	1.0861E-03	19%	AM241	1.0139E-04	2%
	35	5.7356E-03	PU239	4.5167E-03	79%	PU240	1.0729E-03	19%	AM241	1.0017E-04	2%
	67	5.7250E-03	PU239	4.5084E-03	79%	PU240	1.0710E-03	19%	AM241	9.9984E-05	2%
	28	5.6778E-03	PU239	4.4712E-03	79%	PU240	1.0621E-03	19%	AM241	9.9159E-05	2%
	6	5.6097E-03	PU239	4.4176E-03	79%	PU240	1.0494E-03	19%	AM241	9.7970E-05	2%
	40	5.5523E-03	PU239	4.3723E-03	79%	PU240	1.0386E-03	19%	AM241	9.6966E-05	2%
	56	5.5123E-03	PU239	4.3408E-03	79%	PU240	1.0312E-03	19%	AM241	9.6268E-05	2%
	10	5.4967E-03	PU239	4.3285E-03	79%	PU240	1.0282E-03	19%	AM241	9.5996E-05	2%
	34	5.4585E-03	PU239	4.2985E-03	79%	PU240	1.0211E-03	19%	AM241	9.5329E-05	2%
	66	5.3928E-03	PU239	4.2467E-03	79%	PU240	1.0088E-03	19%	AM241	9.4181E-05	2%
	53	5.3462E-03	PU239	4.2101E-03	79%	PU240	1.0001E-03	19%	AM241	9.3368E-05	2%
	64	5.2894E-03	PU239	4.1653E-03	79%	PU240	9.8946E-04	19%	AM241	9.2375E-05	2%
	59	5.2773E-03	PU239	4.1558E-03	79%	PU240	9.8721E-04	19%	AM241	9.2165E-05	2%
	57	5.2327E-03	PU239	4.1207E-03	79%	PU240	9.7885E-04	19%	AM241	9.1385E-05	2%
	14	5.1744E-03	PU239	4.0748E-03	79%	PU240	9.6795E-04	19%	AM241	9.0368E-05	2%
	20	5.1300E-03	PU239	4.0398E-03	79%	PU240	9.5964E-04	19%	AM241	8.9591E-05	2%
	15	5.0737E-03	PU239	3.9954E-03	79%	PU240	9.4911E-04	19%	AM241	8.8608E-05	2%
	29	5.0447E-03	PU239	3.9726E-03	79%	PU240	9.4369E-04	19%	AM241	8.8102E-05	2%
	11	5.0107E-03	PU239	3.9458E-03	79%	PU240	9.3733E-04	19%	AM241	8.7508E-05	2%
	55	4.9649E-03	PU239	3.9098E-03	79%	PU240	9.2875E-04	19%	AM241	8.6708E-05	2%
	60	4.9039E-03	PU239	3.8617E-03	79%	PU240	9.1735E-04	19%	AM241	8.5643E-05	2%
	18	4.8650E-03	PU239	3.8311E-03	79%	PU240	9.1008E-04	19%	AM241	8.4964E-05	2%
	61	4.8279E-03	PU239	3.8019E-03	79%	PU240	9.0313E-04	19%	AM241	8.4316E-05	2%
	36	4.7976E-03	PU239	3.7780E-03	79%	PU240	8.9746E-04	19%	AM241	8.3786E-05	2%
	51	4.7236E-03	PU239	3.7198E-03	79%	PU240	8.8363E-04	19%	AM241	8.2495E-05	2%
	49	4.7236E-03	PU239	3.7198E-03	79%	PU240	8.8363E-04	19%	AM241	8.2495E-05	2%
	46	4.6633E-03	PU239	3.6723E-03	79%	PU240	8.7234E-04	19%	AM241	8.1441E-05	2%
	21	4.6232E-03	PU239	3.6407E-03	79%	PU240	8.6483E-04	19%	AM241	8.0740E-05	2%
	23	4.5698E-03	PU239	3.5986E-03	79%	PU240	8.5485E-04	19%	AM241	7.9808E-05	2%
	52	4.5132E-03	PU239	3.5541E-03	79%	PU240	8.4426E-04	19%	AM241	7.8820E-05	2%
	44	4.4999E-03	PU239	3.5436E-03	79%	PU240	8.4177E-04	19%	AM241	7.8587E-05	2%
	38	4.4319E-03	PU239	3.4900E-03	79%	PU240	8.2905E-04	19%	AM241	7.7400E-05	2%
	8	4.3889E-03	PU239	3.4562E-03	79%	PU240	8.2100E-04	19%	AM241	7.6648E-05	2%

Table C-6. Vectors with CH Cuttings Discharged to the Ground Surface (Continued)

Comp. Scen. ID	Vector	Total EPA-normalized Cuttings	Top 3 Radionuclides Contribution to Integrated Discharge								
(Time of Intrusion, 1000 years)											
	16	4.3608E-03	PU239	3.4341E-03	79%	PU240	8.1575E-04	19%	AM241	7.6158E-05	2%
	42	4.3311E-03	PU239	3.4107E-03	79%	PU240	8.1020E-04	19%	AM241	7.5640E-05	2%
	33	4.2702E-03	PU239	3.3627E-03	79%	PU240	7.9880E-04	19%	AM241	7.4576E-05	2%
	17	4.2209E-03	PU239	3.3239E-03	79%	PU240	7.8959E-04	19%	AM241	7.3715E-05	2%
	41	4.1865E-03	PU239	3.2968E-03	79%	PU240	7.8315E-04	19%	AM241	7.3114E-05	2%
	24	4.1505E-03	PU239	3.2685E-03	79%	PU240	7.7642E-04	19%	AM241	7.2486E-05	2%
	5	4.1244E-03	PU239	3.2479E-03	79%	PU240	7.7153E-04	19%	AM241	7.2029E-05	2%
	9	4.0820E-03	PU239	3.2145E-03	79%	PU240	7.6359E-04	19%	AM241	7.1289E-05	2%
	68	4.0234E-03	PU239	3.1684E-03	79%	PU240	7.5264E-04	19%	AM241	7.0266E-05	2%
	26	3.9763E-03	PU239	3.1313E-03	79%	PU240	7.4383E-04	19%	AM241	6.9443E-05	2%
	27	3.9633E-03	PU239	3.1211E-03	79%	PU240	7.4140E-04	19%	AM241	6.9217E-05	2%
(Time of Intrusion, 7250 years)											
06	32	5.7513E-03	PU239	4.8572E-03	84%	PU240	8.3097E-04	14%	U233	2.6554E-05	0%
	39	5.7058E-03	PU239	4.8188E-03	84%	PU240	8.2440E-04	14%	U233	2.6344E-05	0%
	70	5.6891E-03	PU239	4.8047E-03	84%	PU240	8.2199E-04	14%	U233	2.6268E-05	0%
	63	5.6272E-03	PU239	4.7524E-03	84%	PU240	8.1304E-04	14%	U233	2.5981E-05	0%
	25	5.5970E-03	PU239	4.7269E-03	84%	PU240	8.0868E-04	14%	U233	2.5842E-05	0%
	58	5.5639E-03	PU239	4.6990E-03	84%	PU240	8.0389E-04	14%	U233	2.5689E-05	0%
	30	5.5278E-03	PU239	4.6685E-03	84%	PU240	7.9868E-04	14%	U233	2.5523E-05	0%
	19	5.5007E-03	PU239	4.6457E-03	84%	PU240	7.9478E-04	14%	U233	2.5398E-05	0%
	62	5.4663E-03	PU239	4.6165E-03	84%	PU240	7.8979E-04	14%	U233	2.5239E-05	0%
	3	5.4289E-03	PU239	4.5849E-03	84%	PU240	7.8439E-04	14%	U233	2.5066E-05	0%
	13	5.3915E-03	PU239	4.5534E-03	84%	PU240	7.7899E-04	14%	U233	2.4893E-05	0%
	22	5.3453E-03	PU239	4.5143E-03	84%	PU240	7.7231E-04	14%	U233	2.4680E-05	0%
	47	5.3096E-03	PU239	4.4842E-03	84%	PU240	7.6715E-04	14%	U233	2.4515E-05	0%
	7	5.2591E-03	PU239	4.4415E-03	84%	PU240	7.5986E-04	14%	U233	2.4282E-05	0%
	1	5.2398E-03	PU239	4.4253E-03	84%	PU240	7.5707E-04	14%	U233	2.4193E-05	0%
	50	5.1865E-03	PU239	4.3803E-03	84%	PU240	7.4937E-04	14%	U233	2.3947E-05	0%
	45	5.1614E-03	PU239	4.3590E-03	84%	PU240	7.4574E-04	14%	U233	2.3831E-05	0%
	65	5.1186E-03	PU239	4.3229E-03	84%	PU240	7.3956E-04	14%	U233	2.3633E-05	0%
	43	5.0642E-03	PU239	4.2769E-03	84%	PU240	7.3170E-04	14%	U233	2.3382E-05	0%
	12	5.0377E-03	PU239	4.2546E-03	84%	PU240	7.2788E-04	14%	U233	2.3260E-05	0%
	31	5.0113E-03	PU239	4.2323E-03	84%	PU240	7.2406E-04	14%	U233	2.3138E-05	0%
	4	4.9762E-03	PU239	4.2026E-03	84%	PU240	7.1898E-04	14%	U233	2.2976E-05	0%
	48	4.9396E-03	PU239	4.1718E-03	84%	PU240	7.1370E-04	14%	U233	2.2807E-05	0%
	54	4.8929E-03	PU239	4.1323E-03	84%	PU240	7.0696E-04	14%	U233	2.2591E-05	0%
	37	4.8653E-03	PU239	4.1090E-03	84%	PU240	7.0296E-04	14%	U233	2.2464E-05	0%
	69	4.8115E-03	PU239	4.0635E-03	84%	PU240	6.9519E-04	14%	U233	2.2215E-05	0%
	2	4.7897E-03	PU239	4.0452E-03	84%	PU240	6.9205E-04	14%	U233	2.2115E-05	0%
	35	4.7318E-03	PU239	3.9963E-03	84%	PU240	6.8368E-04	14%	U233	2.1848E-05	0%
	67	4.7232E-03	PU239	3.9889E-03	84%	PU240	6.8243E-04	14%	U233	2.1808E-05	0%
	28	4.6842E-03	PU239	3.9560E-03	84%	PU240	6.7679E-04	14%	U233	2.1628E-05	0%
	6	4.6280E-03	PU239	3.9086E-03	84%	PU240	6.6868E-04	14%	U233	2.1368E-05	0%
	40	4.5806E-03	PU239	3.8685E-03	84%	PU240	6.6183E-04	14%	U233	2.1149E-05	0%
	56	4.5476E-03	PU239	3.8407E-03	84%	PU240	6.5706E-04	14%	U233	2.0997E-05	0%
	10	4.5347E-03	PU239	3.8298E-03	84%	PU240	6.5520E-04	14%	U233	2.0938E-05	0%
	34	4.5033E-03	PU239	3.8032E-03	84%	PU240	6.5066E-04	14%	U233	2.0792E-05	0%
	66	4.4490E-03	PU239	3.7574E-03	84%	PU240	6.4282E-04	14%	U233	2.0542E-05	0%
	53	4.4106E-03	PU239	3.7250E-03	84%	PU240	6.3727E-04	14%	U233	2.0364E-05	0%
	64	4.3637E-03	PU239	3.6854E-03	84%	PU240	6.3049E-04	14%	U233	2.0148E-05	0%
	59	4.3538E-03	PU239	3.6770E-03	84%	PU240	6.2906E-04	14%	U233	2.0102E-05	0%
	57	4.3170E-03	PU239	3.6459E-03	84%	PU240	6.2374E-04	14%	U233	1.9932E-05	0%

Table C-6. Vectors with CH Cuttings Discharged to the Ground Surface (Continued)

Comp. Scen. ID	Vector	Total EPA-normalized Cuttings	Top 3 Radionuclides Contribution to Integrated Discharge								
(Time of Intrusion, 7250 years)											
	14	4.2689E-03	PU239	3.6053E-03	84%	PU240	6.1679E-04	14%	U233	1.9710E-05	0%
	20	4.2322E-03	PU239	3.5743E-03	84%	PU240	6.1149E-04	14%	U233	1.9541E-05	0%
	15	4.1858E-03	PU239	3.5351E-03	84%	PU240	6.0478E-04	14%	U233	1.9326E-05	0%
	29	4.1619E-03	PU239	3.5149E-03	84%	PU240	6.0133E-04	14%	U233	1.9216E-05	0%
	11	4.1338E-03	PU239	3.4912E-03	84%	PU240	5.9727E-04	14%	U233	1.9086E-05	0%
	55	4.0960E-03	PU239	3.4593E-03	84%	PU240	5.9181E-04	14%	U233	1.8912E-05	0%
	60	4.0457E-03	PU239	3.4168E-03	84%	PU240	5.8454E-04	14%	U233	1.8680E-05	0%
	18	4.0136E-03	PU239	3.3897E-03	84%	PU240	5.7991E-04	14%	U233	1.8532E-05	0%
	61	3.9830E-03	PU239	3.3638E-03	84%	PU240	5.7548E-04	14%	U233	1.8390E-05	0%
	36	3.9580E-03	PU239	3.3427E-03	84%	PU240	5.7187E-04	14%	U233	1.8275E-05	0%
	51	3.8970E-03	PU239	3.2912E-03	84%	PU240	5.6305E-04	14%	U233	1.7993E-05	0%
	49	3.8970E-03	PU239	3.2912E-03	84%	PU240	5.6305E-04	14%	U233	1.7993E-05	0%
	46	3.8472E-03	PU239	3.2492E-03	84%	PU240	5.5586E-04	14%	U233	1.7763E-05	0%
	21	3.8141E-03	PU239	3.2212E-03	84%	PU240	5.5108E-04	14%	U233	1.7610E-05	0%
	23	3.7701E-03	PU239	3.1840E-03	84%	PU240	5.4472E-04	14%	U233	1.7407E-05	0%
	52	3.7234E-03	PU239	3.1446E-03	84%	PU240	5.3797E-04	14%	U233	1.7191E-05	0%
	44	3.7124E-03	PU239	3.1353E-03	84%	PU240	5.3639E-04	14%	U233	1.7141E-05	0%
	38	3.6563E-03	PU239	3.0879E-03	84%	PU240	5.2828E-04	14%	U233	1.6882E-05	0%
	8	3.6208E-03	PU239	3.0579E-03	84%	PU240	5.2315E-04	14%	U233	1.6718E-05	0%
	16	3.5976E-03	PU239	3.0384E-03	84%	PU240	5.1981E-04	14%	U233	1.6611E-05	0%
	42	3.5731E-03	PU239	3.0177E-03	84%	PU240	5.1627E-04	14%	U233	1.6498E-05	0%
	33	3.5229E-03	PU239	2.9753E-03	84%	PU240	5.0901E-04	14%	U233	1.6266E-05	0%
	17	3.4823E-03	PU239	2.9409E-03	84%	PU240	5.0313E-04	14%	U233	1.6078E-05	0%
	41	3.4539E-03	PU239	2.9170E-03	84%	PU240	4.9903E-04	14%	U233	1.5947E-05	0%
	24	3.4242E-03	PU239	2.8919E-03	84%	PU240	4.9474E-04	14%	U233	1.5810E-05	0%
	5	3.4026E-03	PU239	2.8737E-03	84%	PU240	4.9162E-04	14%	U233	1.5710E-05	0%
	9	3.3676E-03	PU239	2.8441E-03	84%	PU240	4.8657E-04	14%	U233	1.5549E-05	0%
	68	3.3193E-03	PU239	2.8033E-03	84%	PU240	4.7959E-04	14%	U233	1.5326E-05	0%
	26	3.2804E-03	PU239	2.7705E-03	84%	PU240	4.7398E-04	14%	U233	1.5146E-05	0%
	27	3.2697E-03	PU239	2.7615E-03	84%	PU240	4.7243E-04	14%	U233	1.5097E-05	0%

Table C-7 lists total EPA summed normalized release and the percentage contribution for the top 3 radionuclides for each vector when drilling into RH waste with an average activity level. Vectors are ordered from most to least release. All vectors have some small release when intruding into the repository from drilling.

Table C-7. Vectors with RH Cuttings Discharged to the Ground Surface

Comp. Scen. ID	Vector	Total EPA-normalized Cuttings	Top 3 Radionuclides Contribution to Integrated Discharge								
			(Time of Intrusion, 125 years)								
01	32	5.3080E-03	PU238	1.7186E-03	32%	PU239	1.1756E-03	22%	CS137	7.8303E-04	15%
	39	5.2660E-03	PU238	1.7050E-03	32%	PU239	1.1663E-03	22%	CS137	7.7684E-04	15%
	70	5.2507E-03	PU238	1.7000E-03	32%	PU239	1.1629E-03	22%	CS137	7.7457E-04	15%
	63	5.1935E-03	PU238	1.6815E-03	32%	PU239	1.1503E-03	22%	CS137	7.6614E-04	15%
	25	5.1656E-03	PU238	1.6725E-03	32%	PU239	1.1441E-03	22%	CS137	7.6203E-04	15%
	58	5.1351E-03	PU238	1.6626E-03	32%	PU239	1.1373E-03	22%	CS137	7.5752E-04	15%
	30	5.1018E-03	PU238	1.6518E-03	32%	PU239	1.1299E-03	22%	CS137	7.5260E-04	15%
	19	5.0768E-03	PU238	1.6437E-03	32%	PU239	1.1244E-03	22%	CS137	7.4893E-04	15%
	62	5.0450E-03	PU238	1.6334E-03	32%	PU239	1.1174E-03	22%	CS137	7.4423E-04	15%
	3	5.0105E-03	PU238	1.6222E-03	32%	PU239	1.1097E-03	22%	CS137	7.3914E-04	15%
	13	4.9760E-03	PU238	1.6111E-03	32%	PU239	1.1021E-03	22%	CS137	7.3405E-04	15%
	22	4.9333E-03	PU238	1.5973E-03	32%	PU239	1.0926E-03	22%	CS137	7.2776E-04	15%
	47	4.9004E-03	PU238	1.5866E-03	32%	PU239	1.0853E-03	22%	CS137	7.2290E-04	15%
	7	4.8538E-03	PU238	1.5715E-03	32%	PU239	1.0750E-03	22%	CS137	7.1602E-04	15%
	1	4.8360E-03	PU238	1.5658E-03	32%	PU239	1.0711E-03	22%	CS137	7.1340E-04	15%
	50	4.7868E-03	PU238	1.5498E-03	32%	PU239	1.0602E-03	22%	CS137	7.0614E-04	15%
	45	4.7636E-03	PU238	1.5423E-03	32%	PU239	1.0551E-03	22%	CS137	7.0272E-04	15%
	65	4.7241E-03	PU238	1.5295E-03	32%	PU239	1.0463E-03	22%	CS137	6.9690E-04	15%
	43	4.6739E-03	PU238	1.5133E-03	32%	PU239	1.0352E-03	22%	CS137	6.8949E-04	15%
	12	4.6495E-03	PU238	1.5054E-03	32%	PU239	1.0298E-03	22%	CS137	6.8589E-04	15%
	31	4.6251E-03	PU238	1.4975E-03	32%	PU239	1.0244E-03	22%	CS137	6.8229E-04	15%
	4	4.5927E-03	PU238	1.4870E-03	32%	PU239	1.0172E-03	22%	CS137	6.7751E-04	15%
	48	4.5590E-03	PU238	1.4761E-03	32%	PU239	1.0097E-03	22%	CS137	6.7253E-04	15%
	54	4.5159E-03	PU238	1.4621E-03	32%	PU239	1.0002E-03	22%	CS137	6.6617E-04	15%
	37	4.4903E-03	PU238	1.4538E-03	32%	PU239	9.9453E-04	22%	CS137	6.6241E-04	15%
	69	4.4407E-03	PU238	1.4378E-03	32%	PU239	9.8353E-04	22%	CS137	6.5508E-04	15%
	2	4.4206E-03	PU238	1.4313E-03	32%	PU239	9.7908E-04	22%	CS137	6.5212E-04	15%
	35	4.3672E-03	PU238	1.4140E-03	32%	PU239	9.6725E-04	22%	CS137	6.4424E-04	15%
	67	4.3592E-03	PU238	1.4114E-03	32%	PU239	9.6547E-04	22%	CS137	6.4306E-04	15%
	28	4.3232E-03	PU238	1.3997E-03	32%	PU239	9.5751E-04	22%	CS137	6.3775E-04	15%
	6	4.2713E-03	PU238	1.3829E-03	32%	PU239	9.4602E-04	22%	CS137	6.3010E-04	15%
	40	4.2276E-03	PU238	1.3688E-03	32%	PU239	9.3633E-04	22%	CS137	6.2365E-04	15%
	56	4.1972E-03	PU238	1.3589E-03	32%	PU239	9.2959E-04	22%	CS137	6.1916E-04	15%
	10	4.1853E-03	PU238	1.3551E-03	32%	PU239	9.2696E-04	22%	CS137	6.1740E-04	15%
	34	4.1562E-03	PU238	1.3457E-03	32%	PU239	9.2053E-04	22%	CS137	6.1312E-04	15%
	66	4.1062E-03	PU238	1.3295E-03	32%	PU239	9.0944E-04	22%	CS137	6.0574E-04	15%
	53	4.0707E-03	PU238	1.3180E-03	32%	PU239	9.0158E-04	22%	CS137	6.0050E-04	15%
	64	4.0274E-03	PU238	1.3040E-03	32%	PU239	8.9200E-04	22%	CS137	5.9412E-04	15%
	59	4.0183E-03	PU238	1.3010E-03	32%	PU239	8.8997E-04	22%	CS137	5.9277E-04	15%
	57	3.9843E-03	PU238	1.2900E-03	32%	PU239	8.8244E-04	22%	CS137	5.8775E-04	15%
	14	3.9399E-03	PU238	1.2756E-03	32%	PU239	8.7262E-04	22%	CS137	5.8121E-04	15%
	20	3.9060E-03	PU238	1.2647E-03	32%	PU239	8.6512E-04	22%	CS137	5.7621E-04	15%
	15	3.8632E-03	PU238	1.2508E-03	32%	PU239	8.5562E-04	22%	CS137	5.6989E-04	15%
	29	3.8411E-03	PU238	1.2436E-03	32%	PU239	8.5074E-04	22%	CS137	5.6664E-04	15%
	11	3.8152E-03	PU238	1.2353E-03	32%	PU239	8.4501E-04	22%	CS137	5.6282E-04	15%
	55	3.7803E-03	PU238	1.2240E-03	32%	PU239	8.3728E-04	22%	CS137	5.5767E-04	15%
	60	3.7339E-03	PU238	1.2089E-03	32%	PU239	8.2699E-04	22%	CS137	5.5082E-04	15%
	18	3.7043E-03	PU238	1.1993E-03	32%	PU239	8.2044E-04	22%	CS137	5.4645E-04	15%

Table C-7. Vectors with RH Cuttings Discharged to the Ground Surface (Continued)

Comp. Scen. ID	Vector	Total EPA-normalized Cuttings	Top 3 Radionuclides Contribution to Integrated Discharge								
			(Time of Intrusion, 125 years)								
	61	3.6760E-03	PU238	1.1902E-03	32%	PU239	8.1418E-04	22%	CS137	5.4229E-04	15%
	36	3.6530E-03	PU238	1.1827E-03	32%	PU239	8.0906E-04	22%	CS137	5.3888E-04	15%
	51	3.5966E-03	PU238	1.1645E-03	32%	PU239	7.9659E-04	22%	CS137	5.3057E-04	15%
	49	3.5966E-03	PU238	1.1645E-03	32%	PU239	7.9659E-04	22%	CS137	5.3057E-04	15%
	46	3.5507E-03	PU238	1.1496E-03	32%	PU239	7.8642E-04	22%	CS137	5.2380E-04	15%
	21	3.5202E-03	PU238	1.1397E-03	32%	PU239	7.7965E-04	22%	CS137	5.1929E-04	15%
	23	3.4795E-03	PU238	1.1266E-03	32%	PU239	7.7065E-04	22%	CS137	5.1329E-04	15%
	52	3.4364E-03	PU238	1.1126E-03	32%	PU239	7.6110E-04	22%	CS137	5.0694E-04	15%
	44	3.4263E-03	PU238	1.1093E-03	32%	PU239	7.5886E-04	22%	CS137	5.0544E-04	15%
	38	3.3745E-03	PU238	1.0926E-03	32%	PU239	7.4739E-04	22%	CS137	4.9780E-04	15%
	8	3.3418E-03	PU238	1.0820E-03	32%	PU239	7.4014E-04	22%	CS137	4.9297E-04	15%
	16	3.3204E-03	PU238	1.0750E-03	32%	PU239	7.3540E-04	22%	CS137	4.8982E-04	15%
	42	3.2978E-03	PU238	1.0677E-03	32%	PU239	7.3040E-04	22%	CS137	4.8648E-04	15%
	33	3.2514E-03	PU238	1.0527E-03	32%	PU239	7.2012E-04	22%	CS137	4.7964E-04	15%
	17	3.2139E-03	PU238	1.0406E-03	32%	PU239	7.1182E-04	22%	CS137	4.7411E-04	15%
			(Time of Intrusion, 175 years)								
02	32	3.2678E-03	PU239	1.1731E-03	36%	PU238	9.5030E-04	29%	AM241	5.4423E-04	17%
	39	3.2420E-03	PU239	1.1638E-03	36%	PU238	9.4278E-04	29%	AM241	5.3992E-04	17%
	70	3.2325E-03	PU239	1.1604E-03	36%	PU238	9.4003E-04	29%	AM241	5.3835E-04	17%
	63	3.1973E-03	PU239	1.1478E-03	36%	PU238	9.2979E-04	29%	AM241	5.3248E-04	17%
	25	3.1802E-03	PU239	1.1416E-03	36%	PU238	9.2481E-04	29%	AM241	5.2963E-04	17%
	58	3.1614E-03	PU239	1.1349E-03	36%	PU238	9.1933E-04	29%	AM241	5.2649E-04	17%
	30	3.1409E-03	PU239	1.1275E-03	36%	PU238	9.1337E-04	29%	AM241	5.2308E-04	17%
	19	3.1255E-03	PU239	1.1220E-03	36%	PU238	9.0890E-04	29%	AM241	5.2052E-04	17%
	62	3.1059E-03	PU239	1.1150E-03	36%	PU238	9.0321E-04	29%	AM241	5.1726E-04	17%
	3	3.0847E-03	PU239	1.1073E-03	36%	PU238	8.9702E-04	29%	AM241	5.1372E-04	17%
	13	3.0634E-03	PU239	1.0997E-03	36%	PU238	8.9085E-04	29%	AM241	5.1018E-04	17%
	22	3.0372E-03	PU239	1.0903E-03	36%	PU238	8.8322E-04	29%	AM241	5.0581E-04	17%
	47	3.0169E-03	PU239	1.0830E-03	36%	PU238	8.7731E-04	29%	AM241	5.0243E-04	17%
	7	2.9882E-03	PU239	1.0727E-03	36%	PU238	8.6897E-04	29%	AM241	4.9765E-04	17%
	1	2.9772E-03	PU239	1.0688E-03	36%	PU238	8.6579E-04	29%	AM241	4.9583E-04	17%
	50	2.9470E-03	PU239	1.0579E-03	36%	PU238	8.5698E-04	29%	AM241	4.9079E-04	17%
	45	2.9327E-03	PU239	1.0528E-03	36%	PU238	8.5283E-04	29%	AM241	4.8841E-04	17%
	65	2.9084E-03	PU239	1.0441E-03	36%	PU238	8.4576E-04	29%	AM241	4.8436E-04	17%
	43	2.8774E-03	PU239	1.0329E-03	36%	PU238	8.3677E-04	29%	AM241	4.7921E-04	17%
	12	2.8624E-03	PU239	1.0276E-03	36%	PU238	8.3240E-04	29%	AM241	4.7671E-04	17%
	31	2.8474E-03	PU239	1.0222E-03	36%	PU238	8.2804E-04	29%	AM241	4.7421E-04	17%
	4	2.8275E-03	PU239	1.0150E-03	36%	PU238	8.2223E-04	29%	AM241	4.7088E-04	17%
	48	2.8067E-03	PU239	1.0075E-03	36%	PU238	8.1619E-04	29%	AM241	4.6743E-04	17%
	54	2.7802E-03	PU239	9.9802E-04	36%	PU238	8.0848E-04	29%	AM241	4.6301E-04	17%
	37	2.7644E-03	PU239	9.9238E-04	36%	PU238	8.0390E-04	29%	AM241	4.6039E-04	17%
	69	2.7339E-03	PU239	9.8141E-04	36%	PU238	7.9502E-04	29%	AM241	4.5530E-04	17%
	2	2.7215E-03	PU239	9.7697E-04	36%	PU238	7.9142E-04	29%	AM241	4.5324E-04	17%
	35	2.6886E-03	PU239	9.6516E-04	36%	PU238	7.8185E-04	29%	AM241	4.4776E-04	17%
	67	2.6837E-03	PU239	9.6339E-04	36%	PU238	7.8042E-04	29%	AM241	4.4694E-04	17%
	28	2.6615E-03	PU239	9.5544E-04	36%	PU238	7.7398E-04	29%	AM241	4.4325E-04	17%
	6	2.6296E-03	PU239	9.4398E-04	36%	PU238	7.6470E-04	29%	AM241	4.3794E-04	17%
	40	2.6027E-03	PU239	9.3431E-04	36%	PU238	7.5687E-04	29%	AM241	4.3345E-04	17%

Table C-7. Vectors with RH Cuttings Discharged to the Ground Surface (Continued)

Comp. Scen. ID	Vector	Total EPA-normalized Cuttings	Top 3 Radionuclides Contribution to Integrated Discharge								
			(Time of Intrusion, 175 years)								
	56	2.5840E-03	PU239	9.2759E-04	36%	PU238	7.5142E-04	29%	AM241	4.3033E-04	17%
	10	2.5766E-03	PU239	9.2496E-04	36%	PU238	7.4929E-04	29%	AM241	4.2911E-04	17%
	34	2.5588E-03	PU239	9.1854E-04	36%	PU238	7.4409E-04	29%	AM241	4.2613E-04	17%
	66	2.5279E-03	PU239	9.0748E-04	36%	PU238	7.3513E-04	29%	AM241	4.2100E-04	17%
	53	2.5061E-03	PU239	8.9964E-04	36%	PU238	7.2878E-04	29%	AM241	4.1736E-04	17%
	64	2.4795E-03	PU239	8.9008E-04	36%	PU238	7.2103E-04	29%	AM241	4.1293E-04	17%
	59	2.4738E-03	PU239	8.8805E-04	36%	PU238	7.1939E-04	29%	AM241	4.1199E-04	17%
	57	2.4529E-03	PU239	8.8054E-04	36%	PU238	7.1330E-04	29%	AM241	4.0850E-04	17%
	14	2.4256E-03	PU239	8.7073E-04	36%	PU238	7.0536E-04	29%	AM241	4.0395E-04	17%
	20	2.4047E-03	PU239	8.6325E-04	36%	PU238	6.9930E-04	29%	AM241	4.0048E-04	17%
	15	2.3783E-03	PU239	8.5378E-04	36%	PU238	6.9163E-04	29%	AM241	3.9609E-04	17%
	29	2.3648E-03	PU239	8.4891E-04	36%	PU238	6.8768E-04	29%	AM241	3.9383E-04	17%
	11	2.3488E-03	PU239	8.4318E-04	36%	PU238	6.8304E-04	29%	AM241	3.9117E-04	17%
	55	2.3273E-03	PU239	8.3547E-04	36%	PU238	6.7679E-04	29%	AM241	3.8759E-04	17%
	60	2.2988E-03	PU239	8.2521E-04	36%	PU238	6.6848E-04	29%	AM241	3.8283E-04	17%
	18	2.2805E-03	PU239	8.1867E-04	36%	PU238	6.6318E-04	29%	AM241	3.7980E-04	17%
	61	2.2631E-03	PU239	8.1242E-04	36%	PU238	6.5812E-04	29%	AM241	3.7690E-04	17%
	36	2.2489E-03	PU239	8.0732E-04	36%	PU238	6.5399E-04	29%	AM241	3.7453E-04	17%
	51	2.2143E-03	PU239	7.9487E-04	36%	PU238	6.4391E-04	29%	AM241	3.6876E-04	17%
	49	2.2143E-03	PU239	7.9487E-04	36%	PU238	6.4391E-04	29%	AM241	3.6876E-04	17%
	46	2.1860E-03	PU239	7.8472E-04	36%	PU238	6.3568E-04	29%	AM241	3.6405E-04	17%
	21	2.1672E-03	PU239	7.7797E-04	36%	PU238	6.3021E-04	29%	AM241	3.6092E-04	17%
	23	2.1421E-03	PU239	7.6898E-04	36%	PU238	6.2294E-04	29%	AM241	3.5675E-04	17%
	52	2.1156E-03	PU239	7.5946E-04	36%	PU238	6.1522E-04	29%	AM241	3.5233E-04	17%
	44	2.1094E-03	PU239	7.5722E-04	36%	PU238	6.1341E-04	29%	AM241	3.5129E-04	17%
	38	2.0775E-03	PU239	7.4578E-04	36%	PU238	6.0414E-04	29%	AM241	3.4599E-04	17%
	8	2.0573E-03	PU239	7.3854E-04	36%	PU238	5.9828E-04	29%	AM241	3.4263E-04	17%
	16	2.0442E-03	PU239	7.3382E-04	36%	PU238	5.9445E-04	29%	AM241	3.4044E-04	17%
	42	2.0302E-03	PU239	7.2882E-04	36%	PU238	5.9040E-04	29%	AM241	3.3812E-04	17%
	33	2.0017E-03	PU239	7.1857E-04	36%	PU238	5.8210E-04	29%	AM241	3.3336E-04	17%
	17	1.9786E-03	PU239	7.1028E-04	36%	PU238	5.7538E-04	29%	AM241	3.2952E-04	17%
	41	1.9625E-03	PU239	7.0449E-04	36%	PU238	5.7069E-04	29%	AM241	3.2683E-04	17%
	24	1.9456E-03	PU239	6.9843E-04	36%	PU238	5.6578E-04	29%	AM241	3.2402E-04	17%
	5	1.9333E-03	PU239	6.9403E-04	36%	PU238	5.6222E-04	29%	AM241	3.2198E-04	17%
	9	1.9135E-03	PU239	6.8690E-04	36%	PU238	5.5644E-04	29%	AM241	3.1867E-04	17%
	68	1.8860E-03	PU239	6.7704E-04	36%	PU238	5.4845E-04	29%	AM241	3.1410E-04	17%
	26	1.8639E-03	PU239	6.6912E-04	36%	PU238	5.4204E-04	29%	AM241	3.1042E-04	17%
	27	1.8579E-03	PU239	6.6694E-04	36%	PU238	5.4027E-04	29%	AM241	3.0941E-04	17%
			(Time of Intrusion, 350 years)								
03	32	2.1649E-03	PU239	1.1672E-03	54%	AM241	4.1114E-04	19%	PU240	3.0632E-04	14%
	39	2.1478E-03	PU239	1.1580E-03	54%	AM241	4.0789E-04	19%	PU240	3.0389E-04	14%
	70	2.1415E-03	PU239	1.1546E-03	54%	AM241	4.0670E-04	19%	PU240	3.0301E-04	14%
	63	2.1182E-03	PU239	1.1420E-03	54%	AM241	4.0227E-04	19%	PU240	2.9971E-04	14%
	25	2.1069E-03	PU239	1.1359E-03	54%	AM241	4.0011E-04	19%	PU240	2.9810E-04	14%
	58	2.0944E-03	PU239	1.1292E-03	54%	AM241	3.9774E-04	19%	PU240	2.9633E-04	14%
	30	2.0808E-03	PU239	1.1218E-03	54%	AM241	3.9516E-04	19%	PU240	2.9441E-04	14%
	19	2.0706E-03	PU239	1.1164E-03	54%	AM241	3.9323E-04	19%	PU240	2.9297E-04	14%
	62	2.0577E-03	PU239	1.1094E-03	54%	AM241	3.9077E-04	19%	PU240	2.9114E-04	14%
	3	2.0436E-03	PU239	1.1018E-03	54%	AM241	3.8809E-04	19%	PU240	2.8914E-04	14%
	13	2.0295E-03	PU239	1.0942E-03	54%	AM241	3.8542E-04	19%	PU240	2.8715E-04	14%
	22	2.0121E-03	PU239	1.0848E-03	54%	AM241	3.8212E-04	19%	PU240	2.8469E-04	14%
	47	1.9987E-03	PU239	1.0776E-03	54%	AM241	3.7956E-04	19%	PU240	2.8279E-04	14%
	7	1.9797E-03	PU239	1.0673E-03	54%	AM241	3.7595E-04	19%	PU240	2.8010E-04	14%
	1	1.9724E-03	PU239	1.0634E-03	54%	AM241	3.7458E-04	19%	PU240	2.7907E-04	14%

Table C-7. Vectors with RH Cuttings Discharged to the Ground Surface (Continued)

Comp. Scen. ID	Vector	Total EPA-normalized Cuttings	Top 3 Radionuclides Contribution to Integrated Discharge								
(Time of Intrusion, 350 years)											
	50	1.9523E-03	PU239	1.0526E-03	54%	AM241	3.7077E-04	19%	PU240	2.7624E-04	14%
	45	1.9429E-03	PU239	1.0475E-03	54%	AM241	3.6897E-04	19%	PU240	2.7490E-04	14%
	65	1.9268E-03	PU239	1.0388E-03	54%	AM241	3.6591E-04	19%	PU240	2.7262E-04	14%
	43	1.9063E-03	PU239	1.0278E-03	54%	AM241	3.6202E-04	19%	PU240	2.6972E-04	14%
	12	1.8963E-03	PU239	1.0224E-03	54%	AM241	3.6013E-04	19%	PU240	2.6831E-04	14%
	31	1.8864E-03	PU239	1.0170E-03	54%	AM241	3.5824E-04	19%	PU240	2.6691E-04	14%
	4	1.8732E-03	PU239	1.0099E-03	54%	AM241	3.5573E-04	19%	PU240	2.6503E-04	14%
	48	1.8594E-03	PU239	1.0025E-03	54%	AM241	3.5312E-04	19%	PU240	2.6309E-04	14%
	54	1.8418E-03	PU239	9.9301E-04	54%	AM241	3.4978E-04	19%	PU240	2.6060E-04	14%
	37	1.8314E-03	PU239	9.8739E-04	54%	AM241	3.4780E-04	19%	PU240	2.5913E-04	14%
	69	1.8112E-03	PU239	9.7648E-04	54%	AM241	3.4396E-04	19%	PU240	2.5626E-04	14%
	2	1.8030E-03	PU239	9.7206E-04	54%	AM241	3.4240E-04	19%	PU240	2.5510E-04	14%
	35	1.7812E-03	PU239	9.6031E-04	54%	AM241	3.3826E-04	19%	PU240	2.5202E-04	14%
	67	1.7779E-03	PU239	9.5855E-04	54%	AM241	3.3764E-04	19%	PU240	2.5156E-04	14%
	28	1.7633E-03	PU239	9.5064E-04	54%	AM241	3.3486E-04	19%	PU240	2.4948E-04	14%
	6	1.7421E-03	PU239	9.3924E-04	54%	AM241	3.3084E-04	19%	PU240	2.4649E-04	14%
	40	1.7243E-03	PU239	9.2962E-04	54%	AM241	3.2745E-04	19%	PU240	2.4397E-04	14%
	56	1.7119E-03	PU239	9.2292E-04	54%	AM241	3.2510E-04	19%	PU240	2.4221E-04	14%
	10	1.7070E-03	PU239	9.2031E-04	54%	AM241	3.2417E-04	19%	PU240	2.4152E-04	14%
	34	1.6952E-03	PU239	9.1392E-04	54%	AM241	3.2193E-04	19%	PU240	2.3985E-04	14%
	66	1.6747E-03	PU239	9.0292E-04	54%	AM241	3.1805E-04	19%	PU240	2.3696E-04	14%
	53	1.6603E-03	PU239	8.9512E-04	54%	AM241	3.1530E-04	19%	PU240	2.3491E-04	14%
	64	1.6426E-03	PU239	8.8560E-04	54%	AM241	3.1195E-04	19%	PU240	2.3241E-04	14%
	59	1.6389E-03	PU239	8.8359E-04	54%	AM241	3.1124E-04	19%	PU240	2.3189E-04	14%
	57	1.6250E-03	PU239	8.7611E-04	54%	AM241	3.0861E-04	19%	PU240	2.2992E-04	14%
	14	1.6069E-03	PU239	8.6635E-04	54%	AM241	3.0517E-04	19%	PU240	2.2736E-04	14%
	20	1.5931E-03	PU239	8.5891E-04	54%	AM241	3.0255E-04	19%	PU240	2.2541E-04	14%
	15	1.5756E-03	PU239	8.4948E-04	54%	AM241	2.9923E-04	19%	PU240	2.2294E-04	14%
	29	1.5666E-03	PU239	8.4464E-04	54%	AM241	2.9752E-04	19%	PU240	2.2166E-04	14%
	11	1.5561E-03	PU239	8.3894E-04	54%	AM241	2.9551E-04	19%	PU240	2.2017E-04	14%
	55	1.5419E-03	PU239	8.3127E-04	54%	AM241	2.9281E-04	19%	PU240	2.1816E-04	14%
	60	1.5229E-03	PU239	8.2106E-04	54%	AM241	2.8921E-04	19%	PU240	2.1548E-04	14%
	18	1.5108E-03	PU239	8.1455E-04	54%	AM241	2.8692E-04	19%	PU240	2.1377E-04	14%
	61	1.4993E-03	PU239	8.0834E-04	54%	AM241	2.8473E-04	19%	PU240	2.1214E-04	14%
	36	1.4899E-03	PU239	8.0326E-04	54%	AM241	2.8294E-04	19%	PU240	2.1080E-04	14%
	51	1.4669E-03	PU239	7.9088E-04	54%	AM241	2.7858E-04	19%	PU240	2.0756E-04	14%
	49	1.4669E-03	PU239	7.9088E-04	54%	AM241	2.7858E-04	19%	PU240	2.0756E-04	14%
	46	1.4482E-03	PU239	7.8078E-04	54%	AM241	2.7502E-04	19%	PU240	2.0490E-04	14%
	21	1.4357E-03	PU239	7.7406E-04	54%	AM241	2.7266E-04	19%	PU240	2.0314E-04	14%
	23	1.4192E-03	PU239	7.6512E-04	54%	AM241	2.6951E-04	19%	PU240	2.0080E-04	14%
	52	1.4016E-03	PU239	7.5564E-04	54%	AM241	2.6617E-04	19%	PU240	1.9831E-04	14%
	44	1.3975E-03	PU239	7.5342E-04	54%	AM241	2.6539E-04	19%	PU240	1.9772E-04	14%
	38	1.3763E-03	PU239	7.4203E-04	54%	AM241	2.6138E-04	19%	PU240	1.9474E-04	14%
	8	1.3630E-03	PU239	7.3483E-04	54%	AM241	2.5884E-04	19%	PU240	1.9285E-04	14%
	16	1.3543E-03	PU239	7.3013E-04	54%	AM241	2.5718E-04	19%	PU240	1.9161E-04	14%
	42	1.3450E-03	PU239	7.2516E-04	54%	AM241	2.5543E-04	19%	PU240	1.9031E-04	14%
	33	1.3261E-03	PU239	7.1496E-04	54%	AM241	2.5184E-04	19%	PU240	1.8763E-04	14%
	17	1.3108E-03	PU239	7.0671E-04	54%	AM241	2.4894E-04	19%	PU240	1.8547E-04	14%
	41	1.3001E-03	PU239	7.0095E-04	54%	AM241	2.4691E-04	19%	PU240	1.8395E-04	14%
	24	1.2890E-03	PU239	6.9492E-04	54%	AM241	2.4478E-04	19%	PU240	1.8237E-04	14%
	5	1.2808E-03	PU239	6.9054E-04	54%	AM241	2.4324E-04	19%	PU240	1.8122E-04	14%
	9	1.2677E-03	PU239	6.8344E-04	54%	AM241	2.4074E-04	19%	PU240	1.7936E-04	14%
	68	1.2495E-03	PU239	6.7364E-04	54%	AM241	2.3728E-04	19%	PU240	1.7679E-04	14%
	26	1.2349E-03	PU239	6.6575E-04	54%	AM241	2.3451E-04	19%	PU240	1.7472E-04	14%
	27	1.2308E-03	PU239	6.6358E-04	54%	AM241	2.3374E-04	19%	PU240	1.7415E-04	14%

Table C-7. Vectors with RH Cuttings Discharged to the Ground Surface (Continued)

Comp. Scen. ID	Vector	Total EPA-normalized Cuttings	Top 3 Radionuclides Contribution to Integrated Discharge								
			(Time of Intrusion, 1000 years)								
04	32	1.6156E-03	PU239	1.1455E-03	71%	PU240	2.8591E-04	18%	AM241	1.4496E-04	9%
	39	1.6028E-03	PU239	1.1365E-03	71%	PU240	2.8365E-04	18%	AM241	1.4382E-04	9%
	70	1.5982E-03	PU239	1.1332E-03	71%	PU240	2.8282E-04	18%	AM241	1.4340E-04	9%
	63	1.5808E-03	PU239	1.1208E-03	71%	PU240	2.7974E-04	18%	AM241	1.4184E-04	9%
	25	1.5723E-03	PU239	1.1148E-03	71%	PU240	2.7825E-04	18%	AM241	1.4108E-04	9%
	58	1.5630E-03	PU239	1.1082E-03	71%	PU240	2.7660E-04	18%	AM241	1.4024E-04	9%
	30	1.5528E-03	PU239	1.1010E-03	71%	PU240	2.7480E-04	18%	AM241	1.3933E-04	9%
	19	1.5452E-03	PU239	1.0957E-03	71%	PU240	2.7346E-04	18%	AM241	1.3865E-04	9%
	62	1.5356E-03	PU239	1.0888E-03	71%	PU240	2.7175E-04	18%	AM241	1.3778E-04	9%
	3	1.5250E-03	PU239	1.0813E-03	71%	PU240	2.6989E-04	18%	AM241	1.3684E-04	9%
	13	1.5146E-03	PU239	1.0739E-03	71%	PU240	2.6803E-04	18%	AM241	1.3590E-04	9%
	22	1.5016E-03	PU239	1.0647E-03	71%	PU240	2.6573E-04	18%	AM241	1.3473E-04	9%
	47	1.4915E-03	PU239	1.0576E-03	71%	PU240	2.6396E-04	18%	AM241	1.3383E-04	9%
	7	1.4774E-03	PU239	1.0475E-03	71%	PU240	2.6145E-04	18%	AM241	1.3256E-04	9%
	1	1.4719E-03	PU239	1.0437E-03	71%	PU240	2.6049E-04	18%	AM241	1.3207E-04	9%
	50	1.4570E-03	PU239	1.0331E-03	71%	PU240	2.5784E-04	18%	AM241	1.3073E-04	9%
	45	1.4499E-03	PU239	1.0281E-03	71%	PU240	2.5659E-04	18%	AM241	1.3010E-04	9%
	65	1.4379E-03	PU239	1.0195E-03	71%	PU240	2.5446E-04	18%	AM241	1.2902E-04	9%
	43	1.4226E-03	PU239	1.0087E-03	71%	PU240	2.5176E-04	18%	AM241	1.2765E-04	9%
	12	1.4152E-03	PU239	1.0034E-03	71%	PU240	2.5044E-04	18%	AM241	1.2698E-04	9%
	31	1.4078E-03	PU239	9.9817E-04	71%	PU240	2.4913E-04	18%	AM241	1.2631E-04	9%
	4	1.3979E-03	PU239	9.9117E-04	71%	PU240	2.4738E-04	18%	AM241	1.2543E-04	9%
	48	1.3876E-03	PU239	9.8389E-04	71%	PU240	2.4557E-04	18%	AM241	1.2451E-04	9%
	54	1.3745E-03	PU239	9.7459E-04	71%	PU240	2.4324E-04	18%	AM241	1.2333E-04	9%
	37	1.3667E-03	PU239	9.6908E-04	71%	PU240	2.4187E-04	18%	AM241	1.2263E-04	9%
	69	1.3516E-03	PU239	9.5836E-04	71%	PU240	2.3920E-04	18%	AM241	1.2128E-04	9%
	2	1.3455E-03	PU239	9.5403E-04	71%	PU240	2.3811E-04	18%	AM241	1.2073E-04	9%
	35	1.3292E-03	PU239	9.4250E-04	71%	PU240	2.3524E-04	18%	AM241	1.1927E-04	9%
	67	1.3268E-03	PU239	9.4077E-04	71%	PU240	2.3480E-04	18%	AM241	1.1905E-04	9%
	28	1.3159E-03	PU239	9.3300E-04	71%	PU240	2.3287E-04	18%	AM241	1.1807E-04	9%
	6	1.3001E-03	PU239	9.2182E-04	71%	PU240	2.3007E-04	18%	AM241	1.1665E-04	9%
	40	1.2868E-03	PU239	9.1237E-04	71%	PU240	2.2772E-04	18%	AM241	1.1546E-04	9%
	56	1.2775E-03	PU239	9.0581E-04	71%	PU240	2.2608E-04	18%	AM241	1.1463E-04	9%
	10	1.2739E-03	PU239	9.0324E-04	71%	PU240	2.2544E-04	18%	AM241	1.1430E-04	9%
	34	1.2650E-03	PU239	8.9697E-04	71%	PU240	2.2387E-04	18%	AM241	1.1351E-04	9%
	66	1.2498E-03	PU239	8.8617E-04	71%	PU240	2.2118E-04	18%	AM241	1.1214E-04	9%
	53	1.2390E-03	PU239	8.7851E-04	71%	PU240	2.1927E-04	18%	AM241	1.1117E-04	9%
	64	1.2258E-03	PU239	8.6917E-04	71%	PU240	2.1694E-04	18%	AM241	1.0999E-04	9%
	59	1.2230E-03	PU239	8.6720E-04	71%	PU240	2.1644E-04	18%	AM241	1.0974E-04	9%
	57	1.2127E-03	PU239	8.5986E-04	71%	PU240	2.1461E-04	18%	AM241	1.0881E-04	9%
	14	1.1992E-03	PU239	8.5028E-04	71%	PU240	2.1222E-04	18%	AM241	1.0760E-04	9%
	20	1.1889E-03	PU239	8.4298E-04	71%	PU240	2.1040E-04	18%	AM241	1.0668E-04	9%
	15	1.1758E-03	PU239	8.3373E-04	71%	PU240	2.0809E-04	18%	AM241	1.0550E-04	9%
	29	1.1691E-03	PU239	8.2897E-04	71%	PU240	2.0690E-04	18%	AM241	1.0490E-04	9%
	11	1.1613E-03	PU239	8.2338E-04	71%	PU240	2.0551E-04	18%	AM241	1.0420E-04	9%
	55	1.1506E-03	PU239	8.1585E-04	71%	PU240	2.0363E-04	18%	AM241	1.0324E-04	9%
	60	1.1365E-03	PU239	8.0583E-04	71%	PU240	2.0113E-04	18%	AM241	1.0197E-04	9%
	18	1.1275E-03	PU239	7.9944E-04	71%	PU240	1.9953E-04	18%	AM241	1.0117E-04	9%
	61	1.1189E-03	PU239	7.9334E-04	71%	PU240	1.9801E-04	18%	AM241	1.0039E-04	9%
	36	1.1119E-03	PU239	7.8836E-04	71%	PU240	1.9676E-04	18%	AM241	9.9764E-05	9%
	51	1.0947E-03	PU239	7.7621E-04	71%	PU240	1.9373E-04	18%	AM241	9.8226E-05	9%
	49	1.0947E-03	PU239	7.7621E-04	71%	PU240	1.9373E-04	18%	AM241	9.8226E-05	9%
	46	1.0807E-03	PU239	7.6629E-04	71%	PU240	1.9126E-04	18%	AM241	9.6971E-05	9%
	21	1.0714E-03	PU239	7.5970E-04	71%	PU240	1.8961E-04	18%	AM241	9.6137E-05	9%
	23	1.0591E-03	PU239	7.5093E-04	71%	PU240	1.8742E-04	18%	AM241	9.5026E-05	9%

Table C-7. Vectors with RH Cuttings Discharged to the Ground Surface (Continued)

Comp. Scen. ID	Vector	Total EPA-normalized Cuttings	Top 3 Radionuclides Contribution to Integrated Discharge								
			(Time of Intrusion, 100 years)								
	52	1.0460E-03	PU239	7.4163E-04	71%	PU240	1.8510E-04	18%	AM241	9.3850E-05	9%
	44	1.0429E-03	PU239	7.3944E-04	71%	PU240	1.8456E-04	18%	AM241	9.3573E-05	9%
	38	1.0271E-03	PU239	7.2827E-04	71%	PU240	1.8177E-04	18%	AM241	9.2159E-05	9%
	8	1.0171E-03	PU239	7.2120E-04	71%	PU240	1.8000E-04	18%	AM241	9.1265E-05	9%
	16	1.0106E-03	PU239	7.1658E-04	71%	PU240	1.7885E-04	18%	AM241	9.0681E-05	9%
	42	1.0038E-03	PU239	7.1171E-04	71%	PU240	1.7763E-04	18%	AM241	9.0063E-05	9%
	33	9.8964E-04	PU239	7.0170E-04	71%	PU240	1.7513E-04	18%	AM241	8.8797E-05	9%
	17	9.7822E-04	PU239	6.9360E-04	71%	PU240	1.7311E-04	18%	AM241	8.7772E-05	9%
	41	9.7024E-04	PU239	6.8795E-04	71%	PU240	1.7170E-04	18%	AM241	8.7057E-05	9%
	24	9.6190E-04	PU239	6.8203E-04	71%	PU240	1.7023E-04	18%	AM241	8.6308E-05	9%
	5	9.5584E-04	PU239	6.7774E-04	71%	PU240	1.6915E-04	18%	AM241	8.5765E-05	9%
	9	9.4601E-04	PU239	6.7077E-04	71%	PU240	1.6742E-04	18%	AM241	8.4883E-05	9%
	68	9.3244E-04	PU239	6.6114E-04	71%	PU240	1.6501E-04	18%	AM241	8.3665E-05	9%
	26	9.2153E-04	PU239	6.5341E-04	71%	PU240	1.6308E-04	18%	AM241	8.2686E-05	9%
	27	9.1852E-04	PU239	6.5127E-04	71%	PU240	1.6255E-04	18%	AM241	8.2416E-05	9%
			(Time of Intrusion, 3000 years)								
05	32	1.3564E-03	PU239	1.0814E-03	80%	PU240	2.3128E-04	17%	U233	2.7246E-05	2%
	39	1.3457E-03	PU239	1.0729E-03	80%	PU240	2.2945E-04	17%	U233	2.7031E-05	2%
	70	1.3418E-03	PU239	1.0697E-03	80%	PU240	2.2878E-04	17%	U233	2.6952E-05	2%
	63	1.3271E-03	PU239	1.0581E-03	80%	PU240	2.2629E-04	17%	U233	2.6658E-05	2%
	25	1.3200E-03	PU239	1.0524E-03	80%	PU240	2.2508E-04	17%	U233	2.6515E-05	2%
	58	1.3122E-03	PU239	1.0462E-03	80%	PU240	2.2374E-04	17%	U233	2.6359E-05	2%
	30	1.3037E-03	PU239	1.0394E-03	80%	PU240	2.2229E-04	17%	U233	2.6188E-05	2%
	19	1.2973E-03	PU239	1.0343E-03	80%	PU240	2.2121E-04	17%	U233	2.6060E-05	2%
	62	1.2892E-03	PU239	1.0278E-03	80%	PU240	2.1982E-04	17%	U233	2.5896E-05	2%
	3	1.2804E-03	PU239	1.0208E-03	80%	PU240	2.1831E-04	17%	U233	2.5719E-05	2%
	13	1.2716E-03	PU239	1.0138E-03	80%	PU240	2.1681E-04	17%	U233	2.5542E-05	2%
	22	1.2607E-03	PU239	1.0051E-03	80%	PU240	2.1495E-04	17%	U233	2.5323E-05	2%
	47	1.2522E-03	PU239	9.9837E-04	80%	PU240	2.1352E-04	17%	U233	2.5154E-05	2%
	7	1.2403E-03	PU239	9.8887E-04	80%	PU240	2.1149E-04	17%	U233	2.4915E-05	2%
	1	1.2358E-03	PU239	9.8525E-04	80%	PU240	2.1071E-04	17%	U233	2.4823E-05	2%
	50	1.2232E-03	PU239	9.7523E-04	80%	PU240	2.0857E-04	17%	U233	2.4571E-05	2%
	45	1.2173E-03	PU239	9.7051E-04	80%	PU240	2.0756E-04	17%	U233	2.4452E-05	2%
	65	1.2072E-03	PU239	9.6246E-04	80%	PU240	2.0584E-04	17%	U233	2.4249E-05	2%
	43	1.1944E-03	PU239	9.5223E-04	80%	PU240	2.0365E-04	17%	U233	2.3991E-05	2%
	12	1.1881E-03	PU239	9.4726E-04	80%	PU240	2.0259E-04	17%	U233	2.3866E-05	2%
	31	1.1819E-03	PU239	9.4229E-04	80%	PU240	2.0152E-04	17%	U233	2.3741E-05	2%
	4	1.1736E-03	PU239	9.3568E-04	80%	PU240	2.0011E-04	17%	U233	2.3574E-05	2%
	48	1.1650E-03	PU239	9.2881E-04	80%	PU240	1.9864E-04	17%	U233	2.3401E-05	2%
	54	1.1540E-03	PU239	9.2003E-04	80%	PU240	1.9676E-04	17%	U233	2.3180E-05	2%
	37	1.1475E-03	PU239	9.1483E-04	80%	PU240	1.9565E-04	17%	U233	2.3049E-05	2%
	69	1.1348E-03	PU239	9.0472E-04	80%	PU240	1.9349E-04	17%	U233	2.2794E-05	2%
	2	1.1296E-03	PU239	9.0063E-04	80%	PU240	1.9261E-04	17%	U233	2.2691E-05	2%
	35	1.1160E-03	PU239	8.8974E-04	80%	PU240	1.9028E-04	17%	U233	2.2417E-05	2%
	67	1.1139E-03	PU239	8.8811E-04	80%	PU240	1.8994E-04	17%	U233	2.2376E-05	2%
	28	1.1047E-03	PU239	8.8078E-04	80%	PU240	1.8837E-04	17%	U233	2.2191E-05	2%
	6	1.0915E-03	PU239	8.7021E-04	80%	PU240	1.8611E-04	17%	U233	2.1925E-05	2%
	40	1.0803E-03	PU239	8.6130E-04	80%	PU240	1.8420E-04	17%	U233	2.1700E-05	2%
	56	1.0725E-03	PU239	8.5510E-04	80%	PU240	1.8288E-04	17%	U233	2.1544E-05	2%
	10	1.0695E-03	PU239	8.5268E-04	80%	PU240	1.8236E-04	17%	U233	2.1483E-05	2%
	34	1.0621E-03	PU239	8.4676E-04	80%	PU240	1.8109E-04	17%	U233	2.1334E-05	2%
	66	1.0493E-03	PU239	8.3656E-04	80%	PU240	1.7891E-04	17%	U233	2.1077E-05	2%
	53	1.0402E-03	PU239	8.2934E-04	80%	PU240	1.7737E-04	17%	U233	2.0895E-05	2%

Table C-7. Vectors with RH Cuttings Discharged to the Ground Surface (Continued)

Comp. Scen. ID	Vector	Total EPA-normalized Cuttings	Top 3 Radionuclides Contribution to Integrated Discharge								
			(Time of Intrusion, 3000 years)								
	64	1.0292E-03	PU239	8.2052E-04	80%	PU240	1.7548E-04	17%	U233	2.0673E-05	2%
	59	1.0268E-03	PU239	8.1865E-04	80%	PU240	1.7508E-04	17%	U233	2.0626E-05	2%
	57	1.0181E-03	PU239	8.1173E-04	80%	PU240	1.7360E-04	17%	U233	2.0451E-05	2%
	14	1.0068E-03	PU239	8.0269E-04	80%	PU240	1.7167E-04	17%	U233	2.0224E-05	2%
	20	9.9815E-04	PU239	7.9579E-04	80%	PU240	1.7019E-04	17%	U233	2.0050E-05	2%
	15	9.8719E-04	PU239	7.8706E-04	80%	PU240	1.6832E-04	17%	U233	1.9830E-05	2%
	29	9.8156E-04	PU239	7.8257E-04	80%	PU240	1.6736E-04	17%	U233	1.9717E-05	2%
	11	9.7494E-04	PU239	7.7729E-04	80%	PU240	1.6624E-04	17%	U233	1.9584E-05	2%
	55	9.6602E-04	PU239	7.7018E-04	80%	PU240	1.6472E-04	17%	U233	1.9405E-05	2%
	60	9.5416E-04	PU239	7.6072E-04	80%	PU240	1.6269E-04	17%	U233	1.9166E-05	2%
	18	9.4660E-04	PU239	7.5469E-04	80%	PU240	1.6140E-04	17%	U233	1.9014E-05	2%
	61	9.3937E-04	PU239	7.4893E-04	80%	PU240	1.6017E-04	17%	U233	1.8869E-05	2%
	36	9.3347E-04	PU239	7.4423E-04	80%	PU240	1.5917E-04	17%	U233	1.8751E-05	2%
	51	9.1908E-04	PU239	7.3276E-04	80%	PU240	1.5671E-04	17%	U233	1.8462E-05	2%
	49	9.1908E-04	PU239	7.3276E-04	80%	PU240	1.5671E-04	17%	U233	1.8462E-05	2%
	46	9.0735E-04	PU239	7.2340E-04	80%	PU240	1.5471E-04	17%	U233	1.8226E-05	2%
	21	8.9954E-04	PU239	7.1717E-04	80%	PU240	1.5338E-04	17%	U233	1.8069E-05	2%
	23	8.8915E-04	PU239	7.0889E-04	80%	PU240	1.5161E-04	17%	U233	1.7860E-05	2%
	52	8.7814E-04	PU239	7.0011E-04	80%	PU240	1.4973E-04	17%	U233	1.7639E-05	2%
	44	8.7555E-04	PU239	6.9805E-04	80%	PU240	1.4929E-04	17%	U233	1.7587E-05	2%
	38	8.6232E-04	PU239	6.8750E-04	80%	PU240	1.4703E-04	17%	U233	1.7322E-05	2%
	8	8.5395E-04	PU239	6.8083E-04	80%	PU240	1.4561E-04	17%	U233	1.7153E-05	2%
	16	8.4849E-04	PU239	6.7647E-04	80%	PU240	1.4467E-04	17%	U233	1.7044E-05	2%
	42	8.4271E-04	PU239	6.7187E-04	80%	PU240	1.4369E-04	17%	U233	1.6928E-05	2%
	33	8.3086E-04	PU239	6.6242E-04	80%	PU240	1.4167E-04	17%	U233	1.6690E-05	2%
	17	8.2127E-04	PU239	6.5478E-04	80%	PU240	1.4003E-04	17%	U233	1.6497E-05	2%
	41	8.1458E-04	PU239	6.4944E-04	80%	PU240	1.3889E-04	17%	U233	1.6363E-05	2%
	24	8.0757E-04	PU239	6.4385E-04	80%	PU240	1.3770E-04	17%	U233	1.6222E-05	2%
	5	8.0249E-04	PU239	6.3980E-04	80%	PU240	1.3683E-04	17%	U233	1.6120E-05	2%
	9	7.9424E-04	PU239	6.3322E-04	80%	PU240	1.3542E-04	17%	U233	1.5954E-05	2%
	68	7.8284E-04	PU239	6.2413E-04	80%	PU240	1.3348E-04	17%	U233	1.5725E-05	2%
	26	7.7368E-04	PU239	6.1683E-04	80%	PU240	1.3192E-04	17%	U233	1.5541E-05	2%
	27	7.7116E-04	PU239	6.1482E-04	80%	PU240	1.3149E-04	17%	U233	1.5490E-05	2%
			(Time of Intrusion, 7250 years)								
06	32	1.1421E-03	PU239	9.5682E-04	84%	PU240	1.4737E-04	13%	U233	2.6750E-05	2%
	39	1.1331E-03	PU239	9.4925E-04	84%	PU240	1.4621E-04	13%	U233	2.6538E-05	2%
	70	1.1298E-03	PU239	9.4648E-04	84%	PU240	1.4578E-04	13%	U233	2.6461E-05	2%
	63	1.1174E-03	PU239	9.3617E-04	84%	PU240	1.4419E-04	13%	U233	2.6172E-05	2%
	25	1.1115E-03	PU239	9.3115E-04	84%	PU240	1.4342E-04	13%	U233	2.6032E-05	2%
	58	1.1049E-03	PU239	9.2564E-04	84%	PU240	1.4257E-04	13%	U233	2.5878E-05	2%
	30	1.0977E-03	PU239	9.1964E-04	84%	PU240	1.4165E-04	13%	U233	2.5710E-05	2%
	19	1.0923E-03	PU239	9.1514E-04	84%	PU240	1.4095E-04	13%	U233	2.5584E-05	2%
	62	1.0855E-03	PU239	9.0941E-04	84%	PU240	1.4007E-04	13%	U233	2.5424E-05	2%
	3	1.0781E-03	PU239	9.0318E-04	84%	PU240	1.3911E-04	13%	U233	2.5250E-05	2%
	13	1.0707E-03	PU239	8.9697E-04	84%	PU240	1.3815E-04	13%	U233	2.5076E-05	2%
	22	1.0615E-03	PU239	8.8928E-04	84%	PU240	1.3697E-04	13%	U233	2.4861E-05	2%
	47	1.0544E-03	PU239	8.8334E-04	84%	PU240	1.3606E-04	13%	U233	2.4695E-05	2%
	7	1.0444E-03	PU239	8.7494E-04	84%	PU240	1.3476E-04	13%	U233	2.4460E-05	2%
	1	1.0405E-03	PU239	8.7173E-04	84%	PU240	1.3427E-04	13%	U233	2.4371E-05	2%
	50	1.0299E-03	PU239	8.6286E-04	84%	PU240	1.3290E-04	13%	U233	2.4123E-05	2%
	45	1.0250E-03	PU239	8.5869E-04	84%	PU240	1.3226E-04	13%	U233	2.4006E-05	2%
	65	1.0165E-03	PU239	8.5157E-04	84%	PU240	1.3116E-04	13%	U233	2.3807E-05	2%
	43	1.0057E-03	PU239	8.4251E-04	84%	PU240	1.2977E-04	13%	U233	2.3554E-05	2%

Table C-7. Vectors with RH Cuttings Discharged to the Ground Surface (Continued)

Comp. Scen. ID	Vector	Total EPA-normalized Cuttings	Top 3 Radionuclides Contribution to Integrated Discharge								
			(Time of Intrusion, 7250 years)								
	12	1.0004E-03	PU239	8.3811E-04	84%	PU240	1.2909E-04	13%	U233	2.3431E-05	2%
	31	9.9516E-04	PU239	8.3372E-04	84%	PU240	1.2841E-04	13%	U233	2.3308E-05	2%
	4	9.8818E-04	PU239	8.2787E-04	84%	PU240	1.2751E-04	13%	U233	2.3145E-05	2%
	48	9.8092E-04	PU239	8.2179E-04	84%	PU240	1.2658E-04	13%	U233	2.2975E-05	2%
	54	9.7165E-04	PU239	8.1403E-04	84%	PU240	1.2538E-04	13%	U233	2.2757E-05	2%
	37	9.6616E-04	PU239	8.0942E-04	84%	PU240	1.2467E-04	13%	U233	2.2629E-05	2%
	69	9.5548E-04	PU239	8.0048E-04	84%	PU240	1.2329E-04	13%	U233	2.2379E-05	2%
	2	9.5116E-04	PU239	7.9686E-04	84%	PU240	1.2274E-04	13%	U233	2.2277E-05	2%
	35	9.3966E-04	PU239	7.8722E-04	84%	PU240	1.2125E-04	13%	U233	2.2008E-05	2%
	67	9.3793E-04	PU239	7.8578E-04	84%	PU240	1.2103E-04	13%	U233	2.1968E-05	2%
	28	9.3019E-04	PU239	7.7929E-04	84%	PU240	1.2003E-04	13%	U233	2.1786E-05	2%
	6	9.1904E-04	PU239	7.6995E-04	84%	PU240	1.1859E-04	13%	U233	2.1525E-05	2%
	40	9.0962E-04	PU239	7.6206E-04	84%	PU240	1.1738E-04	13%	U233	2.1305E-05	2%
	56	9.0308E-04	PU239	7.5658E-04	84%	PU240	1.1653E-04	13%	U233	2.1151E-05	2%
	10	9.0052E-04	PU239	7.5443E-04	84%	PU240	1.1620E-04	13%	U233	2.1091E-05	2%
	34	8.9427E-04	PU239	7.4920E-04	84%	PU240	1.1539E-04	13%	U233	2.0945E-05	2%
	66	8.8350E-04	PU239	7.4018E-04	84%	PU240	1.1400E-04	13%	U233	2.0693E-05	2%
	53	8.7587E-04	PU239	7.3378E-04	84%	PU240	1.1302E-04	13%	U233	2.0514E-05	2%
	64	8.6656E-04	PU239	7.2598E-04	84%	PU240	1.1182E-04	13%	U233	2.0296E-05	2%
	59	8.6458E-04	PU239	7.2433E-04	84%	PU240	1.1156E-04	13%	U233	2.0250E-05	2%
	57	8.5727E-04	PU239	7.1820E-04	84%	PU240	1.1062E-04	13%	U233	2.0078E-05	2%
	14	8.4772E-04	PU239	7.1020E-04	84%	PU240	1.0939E-04	13%	U233	1.9855E-05	2%
	20	8.4044E-04	PU239	7.0410E-04	84%	PU240	1.0845E-04	13%	U233	1.9684E-05	2%
	15	8.3122E-04	PU239	6.9637E-04	84%	PU240	1.0726E-04	13%	U233	1.9468E-05	2%
	29	8.2647E-04	PU239	6.9240E-04	84%	PU240	1.0665E-04	13%	U233	1.9357E-05	2%
	11	8.2090E-04	PU239	6.8773E-04	84%	PU240	1.0593E-04	13%	U233	1.9227E-05	2%
	55	8.1339E-04	PU239	6.8144E-04	84%	PU240	1.0496E-04	13%	U233	1.9051E-05	2%
	60	8.0340E-04	PU239	6.7307E-04	84%	PU240	1.0367E-04	13%	U233	1.8817E-05	2%
	18	7.9703E-04	PU239	6.6774E-04	84%	PU240	1.0285E-04	13%	U233	1.8668E-05	2%
	61	7.9095E-04	PU239	6.6264E-04	84%	PU240	1.0206E-04	13%	U233	1.8525E-05	2%
	36	7.8598E-04	PU239	6.5848E-04	84%	PU240	1.0142E-04	13%	U233	1.8409E-05	2%
	51	7.7387E-04	PU239	6.4833E-04	84%	PU240	9.9858E-05	13%	U233	1.8125E-05	2%
	49	7.7387E-04	PU239	6.4833E-04	84%	PU240	9.9858E-05	13%	U233	1.8125E-05	2%
	46	7.6399E-04	PU239	6.4005E-04	84%	PU240	9.8583E-05	13%	U233	1.7894E-05	2%
	21	7.5741E-04	PU239	6.3454E-04	84%	PU240	9.7735E-05	13%	U233	1.7740E-05	2%
	23	7.4866E-04	PU239	6.2721E-04	84%	PU240	9.6606E-05	13%	U233	1.7535E-05	2%
	52	7.3939E-04	PU239	6.1945E-04	84%	PU240	9.5410E-05	13%	U233	1.7318E-05	2%
	44	7.3722E-04	PU239	6.1762E-04	84%	PU240	9.5129E-05	13%	U233	1.7267E-05	2%
	38	7.2607E-04	PU239	6.0829E-04	84%	PU240	9.3691E-05	13%	U233	1.7006E-05	2%
	8	7.1903E-04	PU239	6.0238E-04	84%	PU240	9.2782E-05	13%	U233	1.6841E-05	2%
	16	7.1443E-04	PU239	5.9853E-04	84%	PU240	9.2188E-05	13%	U233	1.6733E-05	2%
	42	7.0956E-04	PU239	5.9445E-04	84%	PU240	9.1560E-05	13%	U233	1.6619E-05	2%
	33	6.9958E-04	PU239	5.8609E-04	84%	PU240	9.0273E-05	13%	U233	1.6385E-05	2%
	17	6.9151E-04	PU239	5.7933E-04	84%	PU240	8.9231E-05	13%	U233	1.6196E-05	2%
	41	6.8587E-04	PU239	5.7461E-04	84%	PU240	8.8504E-05	13%	U233	1.6064E-05	2%
	24	6.7998E-04	PU239	5.6967E-04	84%	PU240	8.7743E-05	13%	U233	1.5926E-05	2%
	5	6.7569E-04	PU239	5.6608E-04	84%	PU240	8.7190E-05	13%	U233	1.5826E-05	2%
	9	6.6875E-04	PU239	5.6026E-04	84%	PU240	8.6294E-05	13%	U233	1.5663E-05	2%
	68	6.5915E-04	PU239	5.5222E-04	84%	PU240	8.5055E-05	13%	U233	1.5438E-05	2%
	26	6.5144E-04	PU239	5.4576E-04	84%	PU240	8.4060E-05	13%	U233	1.5258E-05	2%
	27	6.4931E-04	PU239	5.4398E-04	84%	PU240	8.3786E-05	13%	U233	1.5208E-05	2%

APPENDIX D: MEMORANDA REGARDING REFERENCE DATA

Referenced Memoranda

APPENDIX D: MEMORANDA REGARDING REFERENCE DATA

Marietta and Nowak, November 25, 1992

Date: 11/25/92
To: Distribution
From: M.G. Marietta, 6342, and E.J. Nowak, 6345
Subject: Joint Memorandum from SNL Departments 6342 and 6345 on WIPP Performance Assessment Needs, Priorities, and Thresholds for Solubility Tests

Marietta and Gelbard, December 14, 1992

Date: 12/14/92
To: Distribution
From: M.G. Marietta, 6342, and F. Gelbard, 6119
Subject: Joint Memorandum from SNL Departments 6342 and 6119 on WIPP Performance Assessment Needs, Priorities, and Thresholds for Tracer Column Experiments

Marietta and Nowak, November 25, 1992

Date: 11/25/92
To: Distribution
From: M.G. Marietta, 6342, and E.J. Nowak, 6345
Subject: Joint Memorandum from SNL Departments 6342 and 6345 on WIPP Performance Assessment Needs, Priorities, and Thresholds for Solubility Tests

Sandia National Laboratories

Albuquerque, New Mexico 87185

date: November 25, 1992

to: Distribution

from: M. G. Marietta (6342) and E. J. Nowak (6345)

subject: Joint Memorandum from SNL Departments 6342 and 6345 on WIPP Performance Assessment Needs, Priorities, and Thresholds for Solubility Tests

This memo (1) records present WIPP Performance Assessment (PA) needs concerning radionuclide concentrations in the waste-disposal panels and priorities of these needs, (2) documents PA guidance and requests for information from the radionuclide source term activities, and (3) discusses feasibility of providing these critical information needs.

BACKGROUND
(M. G. Marietta, 6342)

PA's needs for a quantitative understanding of radionuclide concentrations in the waste-disposal panels should be considered in the context of the present understanding of the Project's status with regard to regulatory compliance.

Performance assessments to date (Marietta et al., 1989; Bertram-Howery et al., 1990; WIPP PA Division, 1991) indicate that radionuclides will reach the accessible environment only if the repository is breached by human intrusion, and therefore only the Containment Requirements of 40 CFR 191B and the safety assessments needed for NEPA evaluations are of concern. The long-term requirements of RCRA (40 CFR 268.6) apply to the release of non-radioactive contaminants at the disposal-unit boundary (i.e., the top of the Salado Formation and the subsurface extension of the land-withdrawal boundary), and, as presently interpreted by the WIPP Project, only to the undisturbed performance of the disposal system. Calculations of undisturbed performance indicate that brine (and, by implication, radionuclides) does not migrate from the disturbed rock zone surrounding the panels (WIPP PA Department, 1992). Therefore, concentrations in brine are not needed for assessing compliance with the long-term requirements of RCRA.

Assessments to date indicate that, for the preferred choice of conceptual model (i.e., including gas generation in the waste and dual-porosity transport in the Culebra with chemical retardation), the shape and position of the CCDF used for comparison with 40 CFR 191B are determined primarily by the direct releases at the ground surface during drilling (cuttings) (WIPP PA Division, 1991; Helton et al., 1992). Figure 1 shows the CCDFs calculated for the 1991 performance assessment with and without groundwater transport in the Culebra. Note that the mean, median, and 10 and 90 quantile curves are relatively close together, their positions are essentially unchanged by the inclusion of subsurface groundwater releases, and normalized releases in the region of regulatory interest are approximately 10^{-1}. If subsurface releases are to affect the position of the CCDF, they must result in normalized releases comparable in magnitude to those caused by cuttings. Releases of radionuclides mobilized in brine that may flow directly to the ground surface following

borehole intrusion have not been included in CCDFs to date, but preliminary estimates indicate that they will be significantly less than particulate releases of cuttings.

These observations about the magnitude of the releases that may affect compliance lead to a recognition of PA priorities for information on radionuclide concentrations in disposal rooms. Releases orders of magnitude below the predicted cuttings releases are of little regulatory interest. Because radionuclide concentrations do not affect the quantity of particulate waste brought to the surface as cuttings and cavings, the primary impact of changes in concentrations will be on subsurface releases, and changes that result in relatively small changes in the subsurface release will have little effect on compliance. PA therefore recommends concentrating solubility research on those radionuclides with the potential to result in normalized releases greater than 10^{-2} (approximately one order of magnitude below the presently predicted cuttings releases).

Figure 2 shows the EPA-normalized inventory of the repository, radionuclide by radionuclide, as a function of time (based on the most recent IDB, as will be reported in Volume 3 of the 1992 Preliminary Performance Assessment). Note that the two portions of the figure are plotted at different scales, and that a horizontal line is drawn on each at an EPA-normalized value of 10^{-2}. Time-dependent inventories are shown to 10^5 yr, although a vertical line is drawn on each figure at 10^4 yr, indicating the end of the regulatory period specified by 40 CFR 191B. Radionuclides whose normalized inventories never exceed 10^{-2} during 10^4 yr cannot result in releases greater than 10^{-2}, and can therefore be dropped from further consideration in analyses for 40 CFR 191B.

Figure 2a shows that the normalized inventories of ^{239}Pu, ^{240}Pu, ^{241}Am, ^{233}U, ^{234}U, ^{237}Np, ^{229}Th, ^{230}Th, and ^{226}Ra all exceed 10^{-2} during the 10^4-yr period. Figure 2b shows normalized inventories for two additional radionuclides exceeding 10^{-2}; ^{238}Pu (which is high early in the regulatory period) and ^{210}Pb (which barely reaches 10^{-2} at very late times approaching 10^5 yr) exceeding 10^{-2}. PA modeling for 1991 examined transport to the accessible environment of 7 of these radionuclides (^{239}Pu, ^{240}Pu, ^{241}Am, ^{233}U, ^{234}U, ^{237}Np, and ^{230}Th) (WIPP PA Division, 1991, volume 2, section 6.5.2.10). Subsurface transport of two of the remaining radionuclides will be modeled in 1992, ^{229}Th and ^{226}Ra. Transport of ^{238}Pu in the Culebra will not be modeled because of its short half-life (87.7 yr). Subsurface transport of ^{210}Pb will not be modeled because of its low inventory at 10^4 yr and short half-life (22.3 yr), and consequent low impact on 40 CFR 191B compliance. ^{210}Pb may be considered for subsurface transport in future dose calculations as a daughter product created in the Culebra. Transport of both ^{238}Pu and ^{210}Pb in brine brought directly to the ground surface following intrusion (not yet included in performance assessments) also has the potential to contribute to doses.

Figure 3 shows cumulative (10^4 yr) normalized releases into the Culebra resulting from an intrusion borehole that occurs at 10^3 yr (1991 PA, as reported in Helton et al., 1992) for the seven transported radionuclides for the E1E2 scenario (upper row) and E1 scenario (lower row) for three different assumptions. Figure 4 shows the corresponding CCDF plots.

The first column in Figure 3 plots releases into the Culebra from the borehole, before any retardation can occur in the Culebra. The corresponding CCDFs are shown in the top row of Figure 4. The second column of Figure 3 shows releases to the accessible environment (5 km for this analysis) assuming no chemical retardation in the Culebra (i.e., $K_d = 0$, as stipulated in the Consultation and Cooperation (C & C) agreement between DOE and the State of New Mexico [US DOE and State of New Mexico, 1981 as modified]). Note that because a dual-porosity transport model was used, physical retardation does occur because of diffusion into the dolomite matrix. The corresponding CCDFs are shown in the middle row of Figure 4. The third column of Figure 3 shows releases to the accessible environment calculated using the sampled values for K_d, and the corresponding CCDFs are shown in the bottom row of Figure 4. These curves are incorporated in the total release CCDFs shown in

the top half of Figure 1, although the contribution of the groundwater release can be observed in only one realization shown in Figure 1a.

(In interpreting Figure 3, note that upper and lower bounds of the boxes for each radionuclide indicate the 25th and 75th percentiles from the total number of realizations, the vertical line within the box is the median value, and the black dot is the mean. The horizontal lines extending above the boxes extend to either the maximum value or the value representing $x_{.75} + 1.5(x_{.75} - x_{.25})$, which ever is lower, and the lines extending below the boxes indicate the comparable lower value. Observations falling outside these ranges are shown with individual "x" symbols. These plots do not contain information about the probability of scenario occurrence, and therefore assign equal weight to each scenario. [Helton et al., 1992])

Clearly, retardation in the Culebra may be an important contributor to increasing our confidence of complying with 40 CFR 191B and of defending the overall long-term safety of the WIPP. Given the stipulations of the C & C agreement, however, chemical retardation in the Culebra will not be assumed for a final compliance evaluation until confirmed by the tracer column experiments. To insure a defensible multi-barrier system, we recommend that radionuclide concentration research be designed assuming no credit for retardation in the Culebra. Therefore, we recommend that radionuclide concentration research be designed with respect to releases into the Culebra, as shown in the first column of Figure 3. These releases are calculated before any retardation can occur in the Culebra, and are primarily dependent on the available inventory and the sampled values for solubility limits (and quantity of brine flowing up the borehole, as calculated by the two-phase flow code BRAGFLO). Note that cumulative normalized releases of all seven radionuclides into the Culebra have the potential to exceed 10^{-2} for both scenarios. Cumulative releases for many radionuclides exceed 10^{0} in some realizations, resulting in the potential for a violation of 40 CFR 191B and causing some individual CCDFs in the top row of Figure 4 to exceed the EPA limits.

Concentrations of all radionuclides shown in Figure 3 are therefore important to PA, although special importance falls to U (which is the major contributor to the 1991 subsurface releases at the accessible environment assuming chemical retardation in the Culebra, as shown in the third column of Figure 3) and to Pu (which is an important contributor to releases into the Culebra, as shown in the first column of Figure 3, and could dominate releases to the accessible environment if chemical retardation were not allowed). Of the remaining radionuclides, Ra and Pb are relatively less important for compliance with 40 CFR 191B because of their lower inventories. Ra and Pb are important, however, in safety assessments because of their potential contributions to doses to humans through either subsurface transport or the direct release of brine at the ground surface during drilling. Because of the relatively short half-lives of ^{226}Ra and ^{210}Pb (1600 yr and 22.3 yr, respectively) their concentrations in disposal-room brine are primarily of concern for direct releases at the ground surface. Most subsurface transport of these isotopes will be of decay products of other radionuclides.

Solubility distributions used in the 1991 PA were based on the judgment of an expert panel (Trauth et al., 1992), and are shown in Figure 5. Distributions were provided for different oxidation states for the major radionuclides, reflecting uncertainty in the chemical conditions in the waste-panel environment. Solubilities used in the multiple simulations were selected from these distributions by Latin hypercube sampling after first sampling on Eh-pH conditions within the panel to determine the oxidation states present. (For additional information, see Sections 3.3.5 and 3.3.6 of Volume 3 of WIPP PA Division, 1991.) Concentrations of elements dissolved in waste-panel brine were then calculated assuming equilibrium conditions and uniform distribution of waste. Concentrations of individual isotopes of each element were proportional to their relative abundance in the solid phase of the element. (For additional information, see Section 5.3.2 of Volume 2 of WIPP PA Division, 1991).

As noted above, solubility, inventory, and the quantity of brine flowing up the borehole are the main factors controlling the magnitude of the releases into the Culebra shown in Figure 3. Sensitivity analyses provide a means to separate the relative contribution of brine flow and isolate the effects of uncertainty in solubility. As shown in Figure 6, far-field halite permeability in the Salado Formation (SALPERM) was one of the most important two-phase flow parameter affecting radionuclide migration up the borehole under the assumptions of the 1991 PA (Helton et al., 1992). Releases of ^{239}Pu do not occur for an E1-type intrusion at 10^3 yr for sampled values of SALPERM below approximately 5×10^{-21}. Above that value, the magnitude of release shows no apparent correlation with SALPERM. This "switch" effect, which is also observed for releases of other radionuclides, reflects the control of SALPERM over brine inflow from the far-field. At low values of SALPERM, the panel never becomes brine-saturated, in part because inflow is restricted by elevated gas pressures within the panel and in part because corrosion consumes what brine does enter, and less brine is available to transport radionuclides up the borehole.

Figure 7 (Helton et al., 1992) shows scatterplots of releases versus sampled values for solubility for ^{239}Pu for E1 and E1E2 intrusions at 10^3 yr. Releases on the vertical axis of Figure 7a, the E1 intrusion, are the same as those shown in Figure 6. Note the zero releases (plotted at 10^{-8}) corresponding to low values of SALPERM. Figure 7b shows the same relationship for the E1E2 intrusion at 10^3 yr. Note that there are far fewer zero releases, reflecting the abundant supply of brine from the Castile reservoir assumed in the E1E2 scenario. In both plots, for those realizations that do result in a release, the log of the magnitude of the release is linearly dependent on the log of the sampled value for solubility. Both plots show a solubility threshold for ^{239}Pu for releases of regulatory interest (above approximately 10^{-2}) between 10^{-8} and 10^{-7} mol/ℓ. PA therefore recommends that radionuclide concentration research concentrate on possible values above this threshold.

Figure 8 (Helton et al., 1992) shows a scatterplot of releases versus sampled values for solubility for ^{234}U for an E1E2 intrusion at 10^3 yr. In this case, sampled solubilities were high enough (see Figure 5, U^{+6}) and the inventory low enough that releases were in many realizations limited by the available inventory rather than by the sampled solubility value. Only below solubilities of approximately 10^{-5} mol/ℓ was a log-log linear relationship present between releases and solubilities, and a threshold of regulatory interest (i.e., releases below approximately 10^{-2}) does not occur until solubilities drop below approximately 10^{-6} mol/ℓ. The cutoff recommended for U is the same as that suggested above for Pu, between approximately 10^{-8} and 10^{-7} mol/ℓ.

RECOMMENDATIONS FROM PA FOR THE EXPERIMENTAL PROGRAM
(M. G. Marietta, 6342)

40 CFR 191B

With regard to 40 CFR 191B, PA needs data on concentrations above approximately 10^{-7} mol/ℓ for

U and Pu (highest priority)
Am, Np, and Th (high priority)
Ra and Pb (lower priority--not essential)

For all radionuclides, data on concentrations less than approximately 10^{-7} mol/ℓ are less important, because releases from this range will have essentially no impact on the location of the CCDF.

NEPA

With regard to NEPA, PA needs data for

U and Pu (highest priority)
Np and Th (high priority)
Am, Ra, and Pb (low priority)

Again, data on concentrations less than approximately 10^{-7} mol/ℓ will have little effect on the determination of disposal-system safety. Ra and Pb are given low priority here despite their potential to contribute to doses from subsurface releases because most transport of these radionuclides in the Culebra will be of decay products formed during transport of other radionuclides. Low initial inventories and relatively short half-lives of ^{226}Ra and ^{210}Pb will cause the amount of these radionuclides dissolved in repository brine to have little affect on doses following transport in the Culebra.

Overall Recommendations

Taking into account relative priorities of compliance evaluations with 40 CFR 191B (high) and safety evaluations (relatively lower), our composite recommendations are as follows:

U and Pu data are critical (highest priority)

Am, Np, and Th are important (high priority)

Ra and Pb should be included if possible and if their inclusion does not add significantly to the cost of the experiments or detract from the ultimate defensibility of data for the other elements. This judgement is based on some remaining uncertainty regarding possible brine flow directly to the surface during drilling. Assumptions about future drilling techniques and practices will be a concern of regulators and could change.

ACTINIDE SOURCE TERM PROGRAM RESPONSE TO RECOMMENDATIONS FROM PA

(E. J. Nowak, 6345)

The actinide source term program consists of laboratory tests with radionuclides in WIPP brines, source term model development, and a source term waste test program (STTP) with actual waste in WIPP brines. The laboratory tests produce data on species identification, stability constants of chemical complexes, solubilities, sorption on backfill materials that may be used in the WIPP, and colloid formation. An actinide source term model will be developed with data produced by laboratory tests. The model will predict the concentrations of actinide species in brines within the disposal rooms and panels, with particular emphasis on upper bounds. Results from the tests with actual waste (STTP) will be used to test the validity of the source term model. STTP data will be interpreted with the aid of the laboratory test data.

The actinide source term model will include isotopes of plutonium, americium, neptunium, thorium, and uranium. The model will reflect the complex chemical behavior of these elements, including radionuclide-containing colloid formation and sensitivities to parameters such as Eh, pH, and the concentrations of organic and inorganic ligands that can act as complexing agents. Numerical models that incorporate these parameters and thermodynamic relationships are being evaluated in the modeling effort.

Inclusion of radium and lead is not planned at this time, because significant additional resources would be required to do so, and the priority for data on these elements has not been established at a sufficiently high level to warrant the required expansion of the actinide source term program.

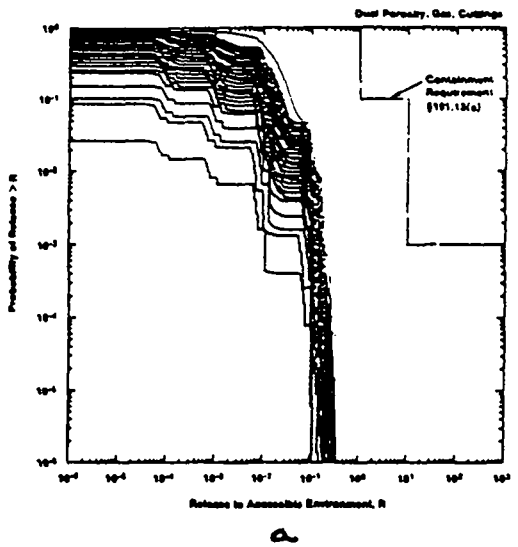

a

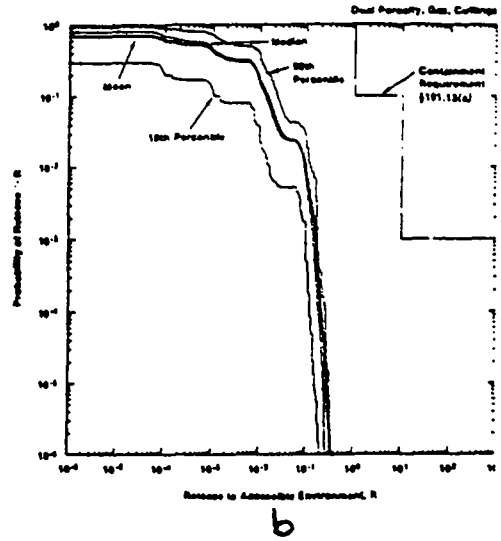

b

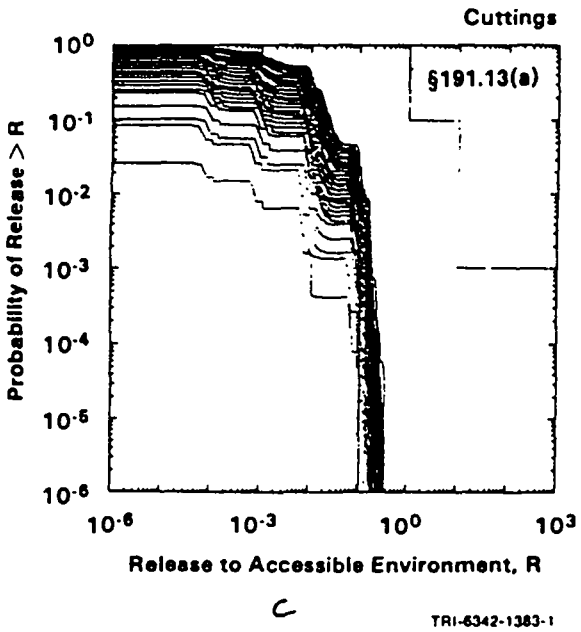

c

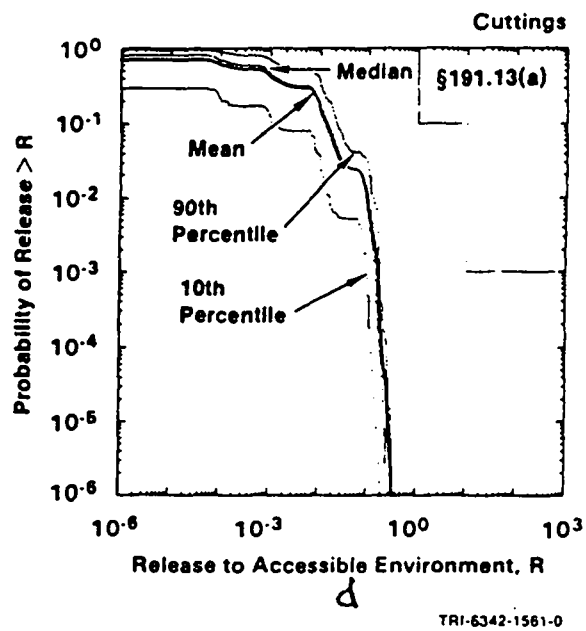

d

Figure 1. Distributions of CCDFs and summary CCDFs from the 1991 WIPP preliminary performance assessment. Figures 1a and 1b show total releases (subsurface and cuttings) assuming dual porosity transport with chemical retardation in the Culebra (Figures 2.1-2 and 4.1-1 in Helton et al., 1992). Figures 1c and 1d show the same curves without subsurface releases (i.e., cuttings only) (Figure 4-1.2 in Helton et al., 1992).

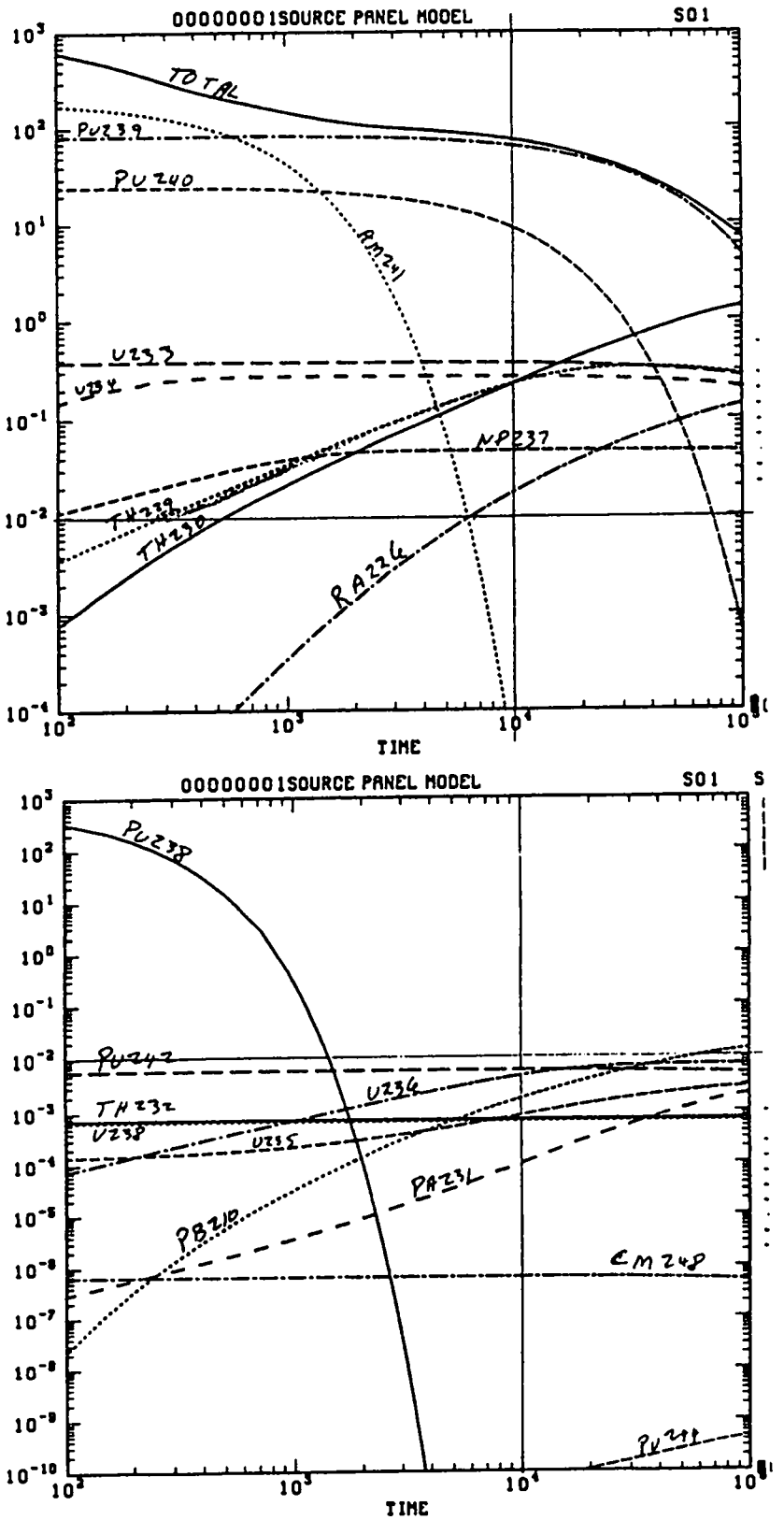

Figure 2. Decay histories for the present IDB inventory. Note scale change between Figures 2a and 2b. Horizontal line at 10^{-2} indicates threshold of importance for PA. Vertical line at 10^{4} yr indicates EPA regulatory time period.

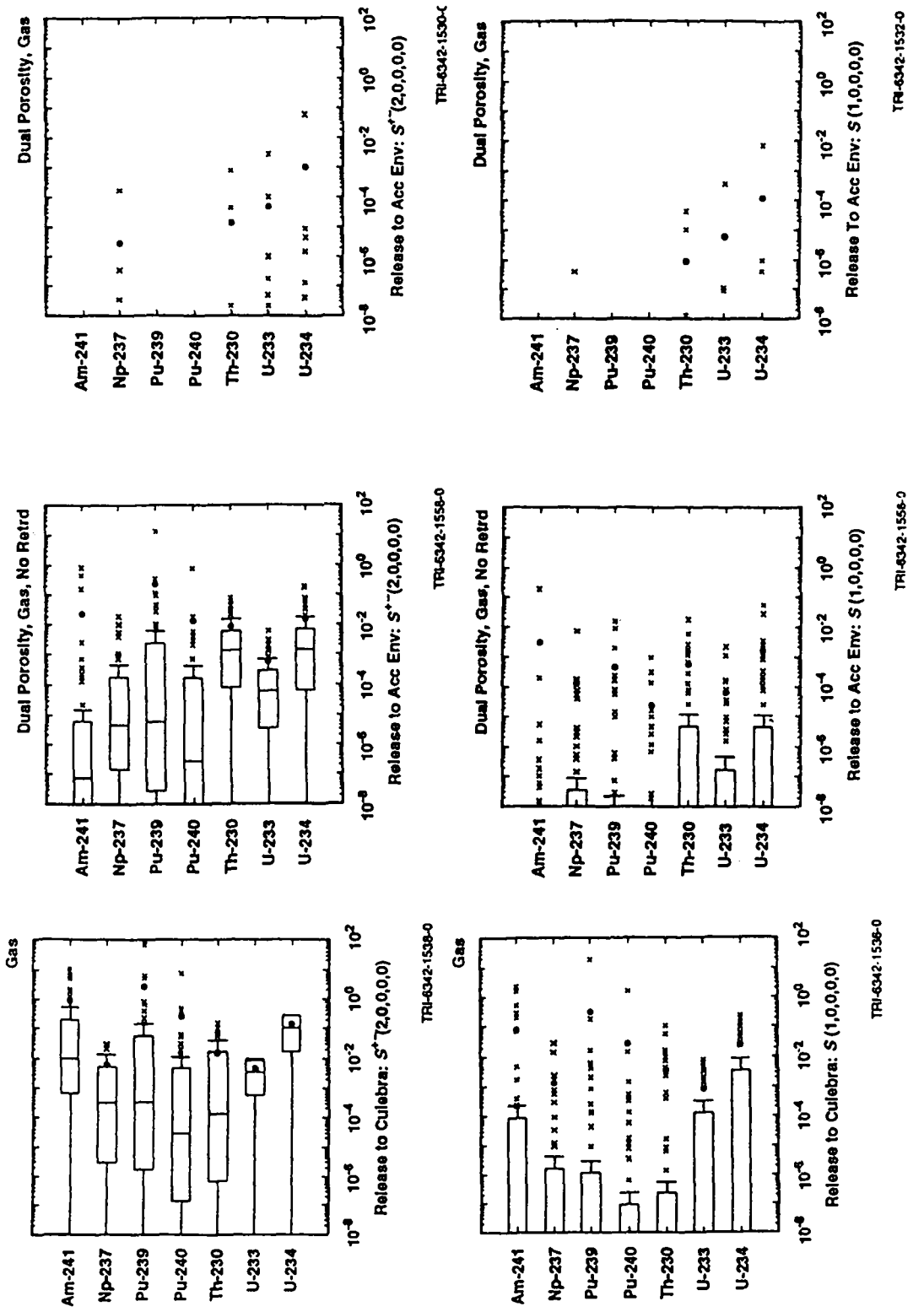

Figure 3. Cumulative normalized releases for radionuclides from E1E2 (upper row) and E1 (lower row) intrusions at 10^3 yr. (1991 WIPP preliminary performance assessment) (Helton et al., 1992).

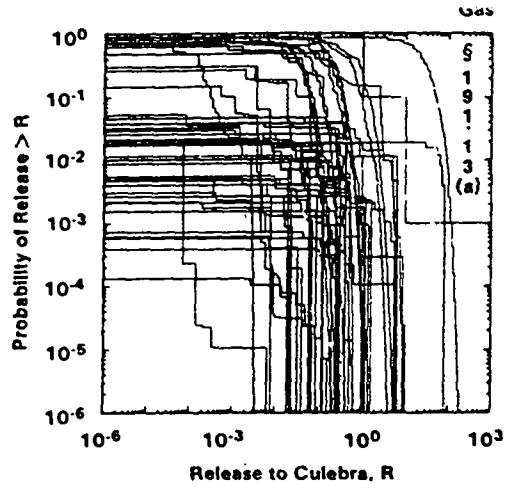

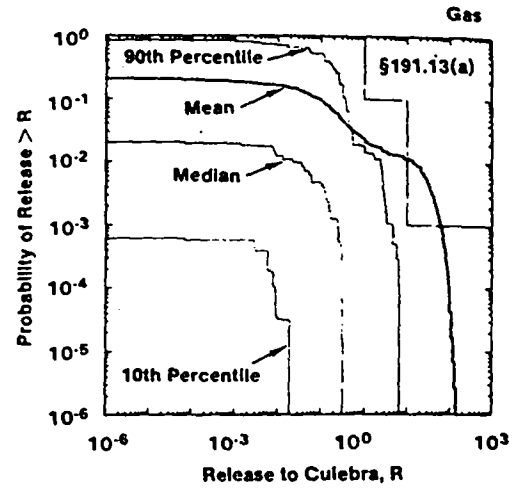

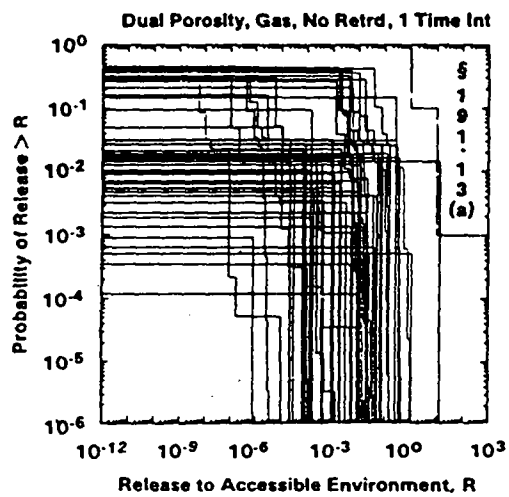

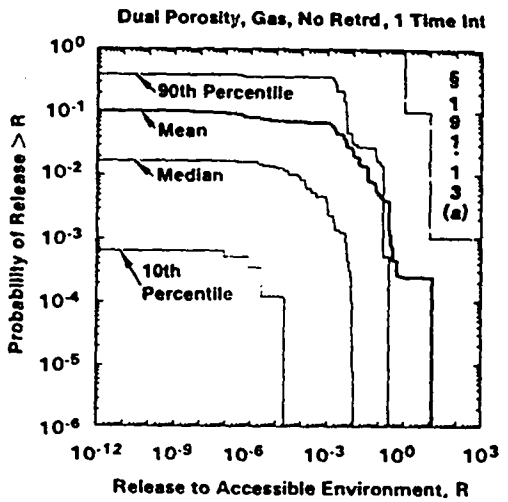

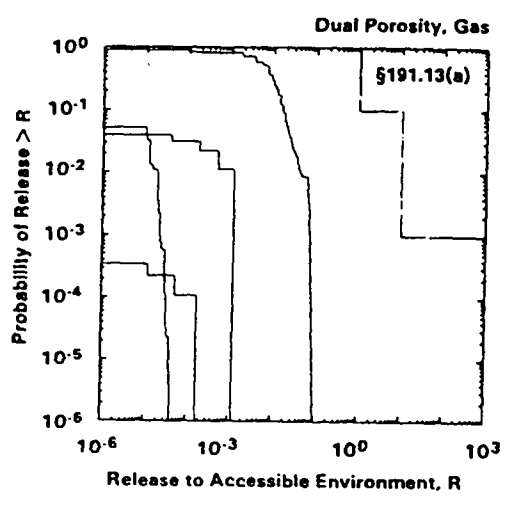

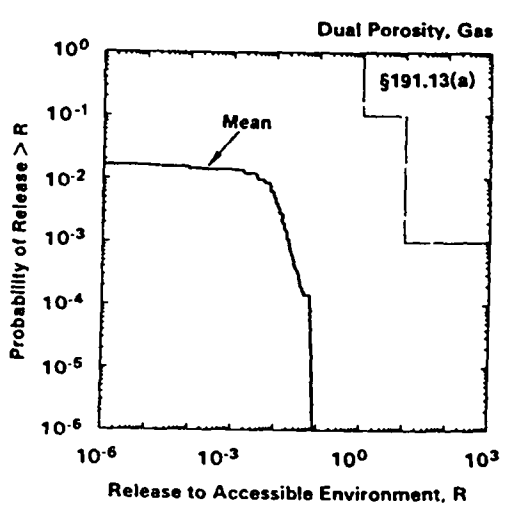

Figure 4. CCDFs corresponding to the releases plotted in Figure 3 (Helton et al., 1992).

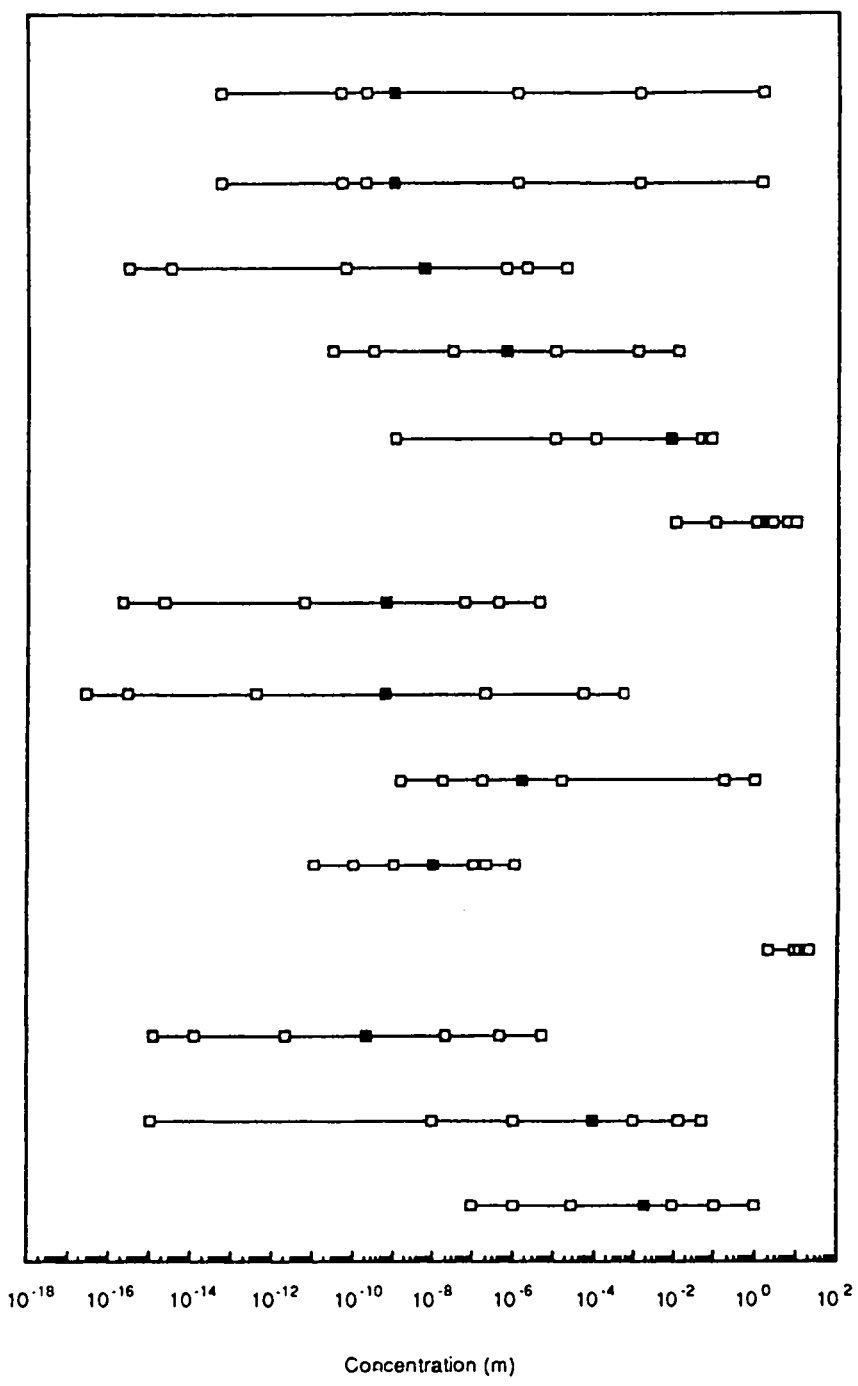

The blocks represent, from left to right, the 0.00, 0.10, 0.25, 0.50, 0.75, 0.90 and 1.00 fractiles

TRI-6342-1410-0

Figure 5. Distributions used for elemental solubilities in the 1991 PA (WIPP PA Division, 1991, Volume 3).

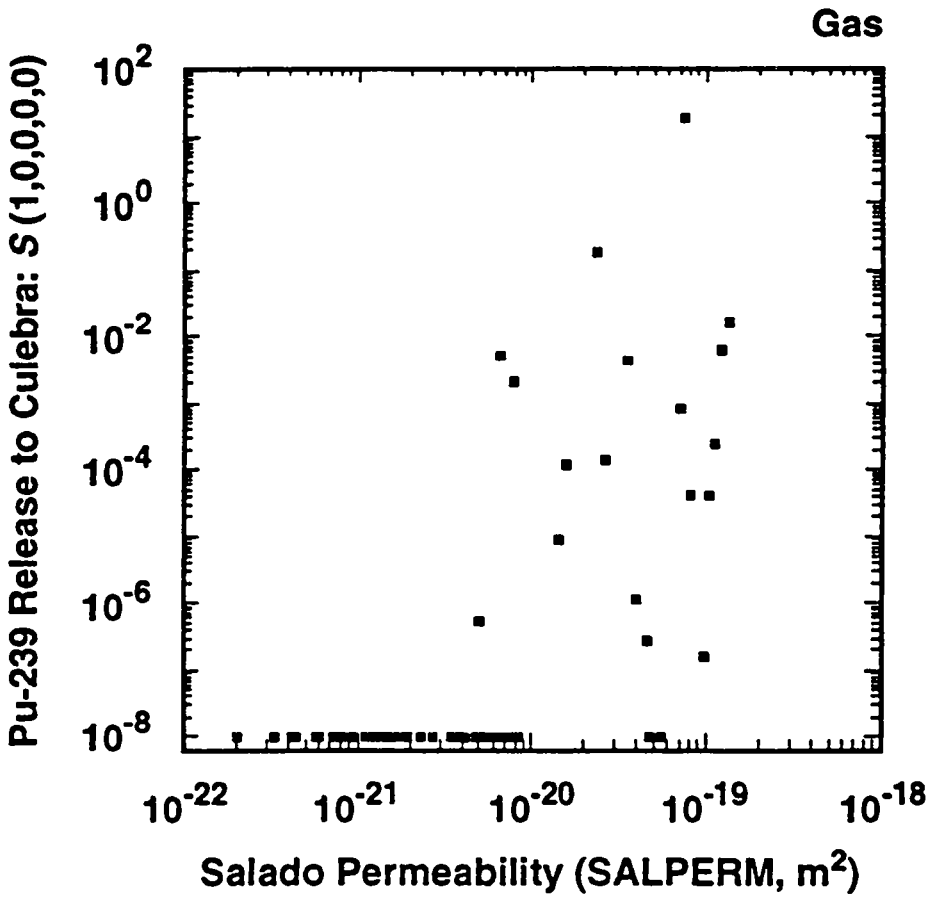

Figure 6. Scatterplot showing relationship between release of ^{239}Pu to the Culebra and sampled value for far-field halite permeability in the Salado Formation (Helton et al., 1992).

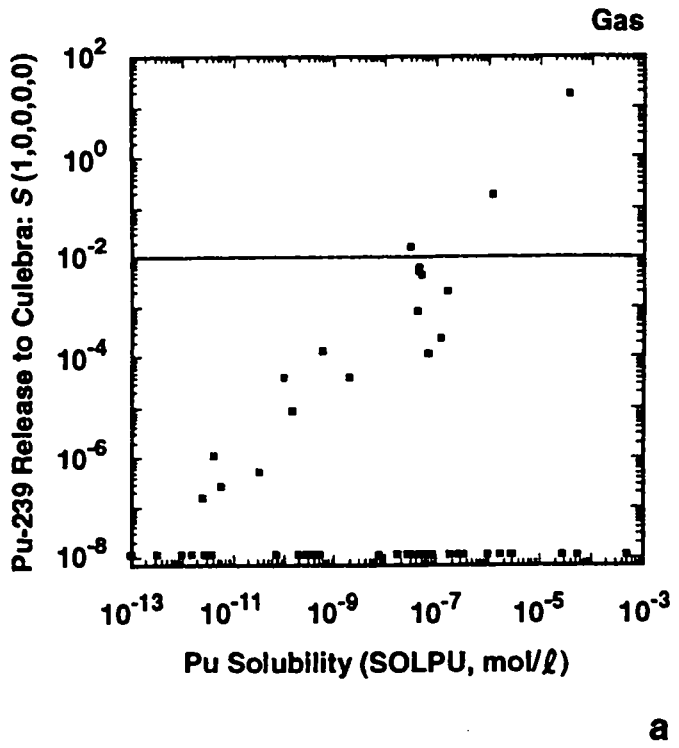

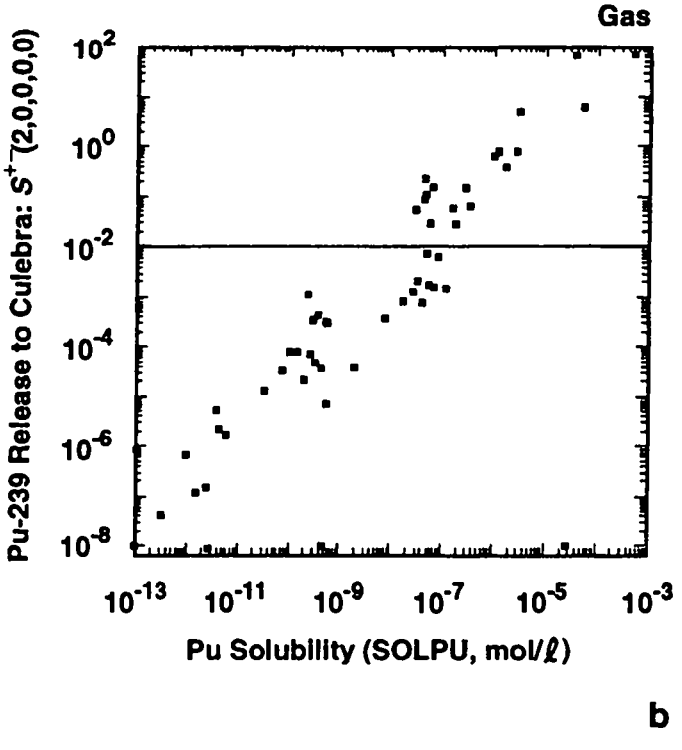

Figure 7. Scatterplots showing relationship between release of ^{239}Pu to the Culebra and sampled value for Pu solubility for E1 (Figure 7a) and E1E2 (Figure 7b) intrusions at 1000 yr (Helton et al, 1992). Horizontal lines at 10^{-2} indicate threshold of importance to PA.

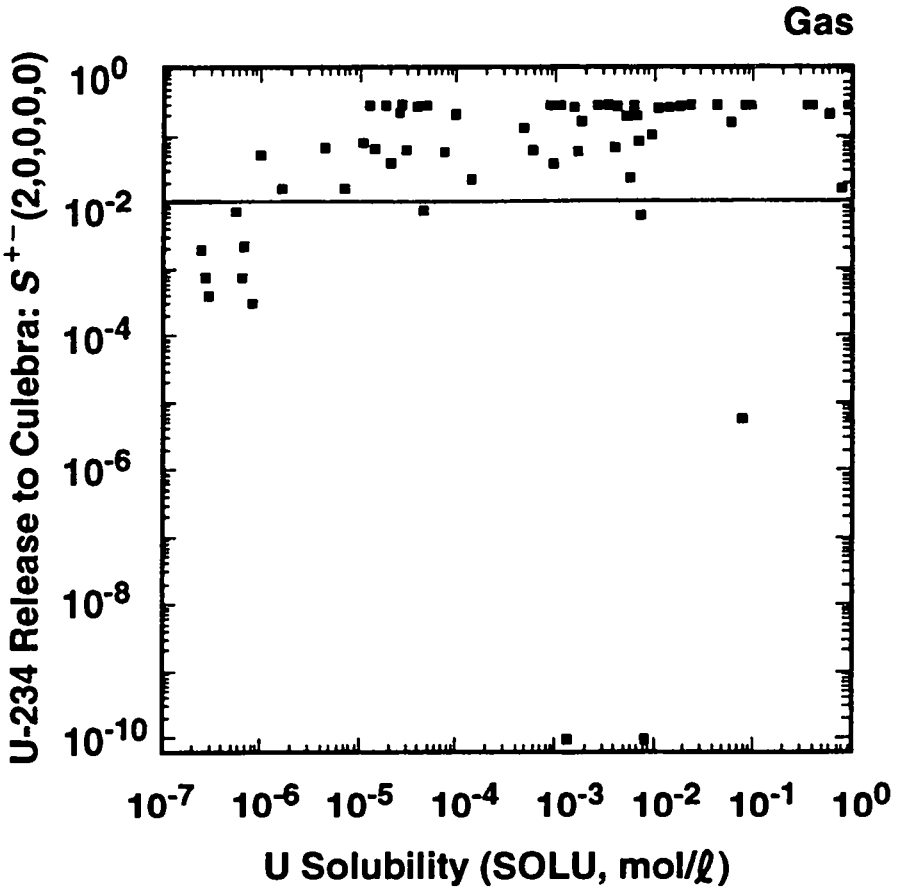

Figure 8. Scatterplot showing relationship between release of ^{234}U to the Culebra and sampled value for U solubility for E1E2 intrusion at 10^{3} yr (Helton et al., 1992). Horizontal line at 10^{-2} indicates threshold of importance to PA.

REFERENCES

Bertram-Howery, S. G., M. G. Marietta, R. P. Rechard, P. N. Swift, D. R. Anderson, B. L. Baker, J. E. Bean, W. Beyeler, K. F. Brinster, R. V. Guzowski, J. C. Helton, R. D. McCurley, D. K. Rudeen, J. D. Schreiber, and P. Vaughn. 1990. *Preliminary Comparison with 40 CFR Part 191, Subpart B for the Waste Isolation Pilot Plant, December 1990.* SAND90-2347. Albuquerque, NM: Sandia National Laboratories.

Marietta, M. G., S. G. Bertram Howery, D. R. Anderson, K. F. Brinster, R. V. Guzowski, H. Iuzzolino, and R. P. Rechard. 1989. *Performance Assessment Methodology Demonstration: Methodology Development for Purposes of Evaluating Compliance with EPA 40 CFR Part 191, Subpart B, for the Waste Isolation Pilot Plant.* SAND89-2027. Albuquerque, NM: Sandia National Laboratories.

Helton, J. C., J. W. Garner, R. P. Rechard, D. K. Rudeen, and P. N. Swift. 1992. *Preliminary Comparison with 40 CFR Part 191, Subpart B for the Waste Isolation Pilot Plant, December 1991. Volume 4: Uncertainty and Sensitivity Analysis Results.* SAND91-0893/4. Albuquerque, NM: Sandia National Laboratories.

Trauth, K. M., S. C. Hora, R. P. Rechard, and D. R. Anderson. 1992. *The Use of Expert Judgment to Quantify Uncertainty in Solubility and Sorption Parameters for Waste Isolation Pilot Plant Performance Assessment.* SAND92-0479. Albuquerque, NM: Sandia National Laboratories. (in review).

US DOE (Department of Energy). 1991. *Integrated Data Base for 1991: Spent Fuel and Radioactive Waste Inventories, Projects and Characterizations.* DOE/RW-006, Rev. 7.

US DOE (Department of Energy) and State of New Mexico. 1981, as modified. "Agreement for Consultation and Cooperation" on WIPP by the State of New Mexico and the U.S. Department of Energy, modified 11/30/84, 8/4/87, and 4/18/88.

WIPP PA (Performance Assessment) Department. 1992. *Long-Term Gas and Brine Migration at the Waste Isolation Pilot Plant: Preliminary Sensitivity Analyses for Post-Closure 40 CFR 268 (RCRA), May 1992.*SAND92-1933. Albuquerque, NM: Sandia National Laboratories.

WIPP PA (Performance Assessment) Division. 1991. *Preliminary Comparison with 40 CFR Part 191, Subpart B for the Waste Isolation Pilot Plant, December 1991. Volumes 1-3.* SAND91-0893/1,2,3. Albuquerque, NM: Sandia National Laboratories.

Distribution

D. E. Miller, 6300
W. D. Weart, 6303
D. R. Anderson, 6342
R. C. Lincoln, 6345
M. L. F. Phillips, 6345
SWCF/GENEXP

Marietta and Gelbard, December 14, 1992

Date: 12/14/92
To: Distribution
From: M.G. Marietta, 6342, and F. Gelbard, 6119
Subject: Joint Memorandum from SNL Departments 6342 and 6119 on WIPP Performance Assessment Needs, Priorities, and Thresholds for Tracer Column Experiments

Sandia National Laboratories

Albuquerque, New Mexico 87185

date: December 14, 1992

to: Distribution

from: M. G. Marietta, 6342, and F. Gelbard, 6119

subject: Joint Memorandum from SNL Departments 6342 and 6119 on WIPP Performance Assessment Needs, Priorities, and Thresholds for Tracer Column Experiments

This memo records present WIPP Performance Assessment (PA) needs concerning radionuclide retardation measurements in the Culebra Dolomite and priorities of these needs. The importance of both physical and chemical retardation is discussed, and threshold values for matrix distribution coefficients (assuming double porosity transport can be justified), as observed in sensitivity analyses of the 1991 preliminary PA, are provided. The feasibility of fulfilling PA needs is briefly discussed. The memo documents PA guidance and requests for information from the tracer column experiments.

BACKGROUND
(M. G. Marietta)

PA's needs for a quantitative understanding of radionuclide retardation in the Culebra should be considered in the context of the present understanding of the Project's status with regard to regulatory compliance.

Performance assessments to date (Marietta et al., 1989; Bertram-Howery et al., 1990; WIPP PA Division, 1991) indicate that radionuclides will reach the Culebra only if the repository is breached by human intrusion, and therefore only the Containment Requirements of 40 CFR 191B and the safety assessments needed for NEPA evaluations are of concern. The long-term requirements of RCRA (40 CFR 268.6) apply to the release of non-radioactive contaminants at the disposal-unit boundary (i.e., the top of the Salado Formation and the subsurface extension of the land-withdrawal boundary), and as presently interpreted by the WIPP Project, only to the undisturbed performance of the disposal system.

The conceptual model used in assessments to date has assumed that radionuclide transport in the Culebra occurs in a double-porosity medium, with both physical and chemical retardation occurring in the dolomite matrix (WIPP PA Division, 1991; Helton et al., 1992). Given the assumptions of this model, retardation during groundwater transport is sufficient to reduce subsurface releases in the Culebra below those estimated to occur directly at the ground surface during drilling (i.e., cuttings).

If present assumptions about transport mechanisms and retardation in the Culebra can be justified experimentally, subsurface releases may continue to have little affect on the position of the CCDF. If, however, assumptions about retardation change or cannot be defended, estimates of subsurface releases comparable in magnitude to or greater than those estimated for cuttings may result, and may affect regulatory compliance.

For the purposes of setting priorities, PA recommends concentrating retardation research on those radionuclides with the potential to result in normalized releases greater than 10^{-2} (approximately one order of magnitude below the presently predicted cutting releases). Figure 1 shows the EPA normalized inventory of the repository, radionuclide by radionuclide, as a function of time (based on the most recent IDB [US DOE, 1991], as will be reported in Volume 3 of the 1992 Preliminary Performance Assessment). Note that the two portions of the figure are plotted at different scales, and that a horizontal line is drawn on each at an EPA normalized value of 10^{-2}. Time-dependent inventories are shown to 10^5 yr, although a vertical line is drawn at 10^4 yr, indicating the end of the regulatory period specified by 40 CFR 191B. Radionuclides with normalized inventories that never exceed 10^{-2} during 10^4 yr cannot result in releases greater than 10^{-2}, and can therefore be dropped from further consideration.

Figure 1a shows that the normalized inventories of ^{239}Pu, ^{240}Pu, ^{241}Am, ^{233}U, ^{234}U, ^{237}Np, ^{229}Th, ^{230}Th, and ^{226}Ra all exceed 10^{-2} during the 10^4 yr period. Figure 1b shows ^{238}Pu and ^{210}Pb (just barely at very late times approaching 10^5 yr) exceeding 10^{-2}. PA modeling for 1991 examined transport of 7 of these radionuclides (^{239}Pu, ^{240}Pu, ^{241}Am, ^{233}U, ^{234}U, ^{237}Np, and ^{230}Th) (WIPP PA Division, 1991, volume 2, section 6.5.2.10). Subsurface transport of two of the remaining radionuclides will be modeled in 1992, ^{229}Th and ^{226}Ra. Transport of ^{238}Pu in the Culebra will not be modeled because of its short half-life (87.7 yr). Subsurface transport of ^{210}Pb will not be modeled because of its low inventory at 10^4 yr and therefore low impact on 40 CFR 191B compliance. ^{210}Pb may be considered for subsurface transport in future dose calculations as a daughter product created in the Culebra by the decay of ^{226}Ra. Transport of both ^{238}Pu and ^{210}Pb in brine brought directly to the ground surface following intrusion (not yet included in performance assessments) also has the potential to contribute to doses.

Figure 2 shows cumulative normalized releases (1991 PA, as reported in Helton et al., 1992) for the seven transported radionuclides for the E1E2 scenario (upper row) and E1 scenario (lower row) at 1000 yr for three different assumptions. Figure 3 shows the corresponding CCDF plots.

The first column in Figure 4 plots releases into the Culebra from the borehole, before any retardation can occur in the Culebra. These releases are calculated assuming gas generation in the repository and no pressure-dependent fracturing of anhydrite layers in the Salado Formation, which may underestimate radionuclide releases to the Culebra. The corresponding CCDFs are shown in the top row of Figure 3. The second column of Figure 2 shows releases to the accessible environment (5 km for this analysis) assuming no chemical retardation (i.e., $K_d = 0$, as stipulated in the Consultation and Cooperation agreement between DOE and the State of New Mexico [US DOE and State of New Mexico, 1981 as modified]). Note that because a double-porosity transport model was used, physical retardation does occur because of diffusion into the dolomite matrix. The corresponding CCDFs are shown in the middle row of Figure 3. The third column of Figure 2 shows releases to the accessible environment calculated using the sampled values for K_d. The corresponding CCDFs are shown in the bottom row of Figure 3.

(In interpreting Figure 2, note that upper and lower bounds of the boxes for each radionuclide indicate the 25th and 75th percentiles from the total number of realizations, the vertical line within the box is the median value, and the black dot is the mean. The horizontal lines extending above the boxes extend to either the maximum value or the value representing $x_{.75} + 1.5(x_{.75} - x_{.25})$, which ever is lower, and the lines extending below the boxes indicate the comparable lower value. Observations falling outside these ranges are shown with individual "x" symbols. These plots do not contain information about the probability of scenario occurrence, and therefore assign equal weight to each scenario. [Helton et al., 1992])

The first column of Figure 2 shows that cumulative normalized releases of all seven radionuclides into the Culebra have the potential to exceed 10^{-2} for both scenarios. Therefore, transport of all seven in the Culebra has the potential to affect regulatory compliance. (Note that cumulative releases for many radionuclides exceed 10^{0} in some realizations, resulting in the potential for a violation of 40 CFR 191B).

The second column of Figure 2 ($K_d = 0$) shows that physical retardation by matrix diffusion significantly lowers cumulative normalized releases. Most radionuclides still exceed 10^{-1} for some realizations, but mean values are now in all cases within the EPA limit. This observation indicates that verification of physical retardation may be important to defending compliance with 191B, and that physical retardation should receive special attention in the experimental program.

The third column of Figure 2 (sampled values for K_ds) shows that using chemical retardation estimates based on judgment from two experts (C. Novak and R. Dosch, as reported in Trauth et al., 1992) resulted in only one value close to 10^{-1} (^{234}U in a single E1E2 realization) and very few values greater than 10^{-3}. Although the experts' values represent the best information available at this point, there are no actual data to support these values rigorously. Chemical retardation has the potential to greatly reduce releases to the accessible environment, and defensible values for K_ds in the Culebra may be very important for building confidence in a demonstration of compliance with 191B.

All of the radionuclides listed in Figure 2 are important for consideration in the experimental program. Special importance falls to U, which is the main contributor to releases, and to Pu, which dominates the inventory but makes no subsurface contribution to the 1991 CCDF because of its assumed high chemical retardation in the Culebra (compare columns 2 and 3 of Figure 2). It may be critically important for PA to be able to defend the high K_d values for Pu. (Although not shown in Figure 2 and not discussed further in this memo, releases of Pu into the Culebra [column 1] are limited by the assumed solubility of Pu in the repository brine, and defensible solubilities are therefore also important.)

Figure 4 provides additional insight into the sensitivity of PA results to the assumed values for K_ds. As seen in the upper left scatterplot, K_d values greater than 10^{-2} m^3/kg imply essentially zero release of ^{234}U to the accessible environment. (Note that, in these scatterplots, cumulative normalized releases are given at one-quarter of the distance to the accessible environment, rather than at the accessible environment boundary.) K_d values greater than approximately 10^{-1} m^3/kg imply essentially zero release of ^{239}Pu and ^{241}Am.

A major purpose of the column experiments is to generate defensible information on chemical retardation in the Culebra. Therefore, column experiments should include all radionuclides that, in the absence of chemical and physical retardation, have the potential to reach the accessible environment in quantities large enough to violate the Standard. These include isotopes of Pu, Am, U, Np, Th, and Ra. Pb should be included because of its potential to contribute to long-term doses.

RECOMMENDATIONS FROM PA FOR THE EXPERIMENTAL PROGRAM
(M. G. Marietta)

1. With regard to 40 CFR 191B, PA needs transport data for:

   U and Pu (highest priority)
   Am, Np, and Th (high priority)
   Ra (lower priority--not essential)

2. With regard to NEPA, PA needs transport data for

   U (highest priority)
   Ra and Pb (high priority)
   Np and Th (low priority)
   (assuming retardation of Pu is defensible)

3. Taking into account relative priorities of compliance evaluations with 40 CFR 191B (high) and safety evaluations (relatively lower), PA's composite recommendations are as follows:

   U and Pu data are critical (highest priority)

   Am, Np, and Th are important (high priority)

   Ra and Pb should be included if possible and if their inclusion does not add significantly to the cost of the experiment or detract from the ultimate defensibility of data for the other elements.

FEASIBILITY
(F. Gelbard)

The radiation detectors purchased for the experiment are designed to detect, identify, and measure the concentration of individual radioisotopes in a mixture of radioisotopes. A germanium detector, cooled with liquid nitrogen, is used to analyze gamma radiation from a sample. Although in principle, our system should be able to distinguish an arbitrary number of radionuclides, we have not yet tested the system. Obviously, the fewer the number of radionuclides, the easier to distinguish a specific radionuclide. Furthermore, for ES&H considerations, we would like to minimize the total radioactivity, and thus reduce the number of radionuclides.

With these considerations, we expect that a mixture with the following radioisotopes can be measured with our equipment: ^{232}U, ^{228}Th, ^{241}Am and/or ^{243}Am, ^{237}Np, ^{226}Ra, ^{210}Pb, and ^{22}Na (nonsorbing tracer). We are investigating which isotope of Pu would be best to use. In addition, we may also include the following isotopes, ^{133}Ba (analog for Ra), a radioactive rare-earth metal (analog for radionuclides in the +3 oxidation state), and ^{243}Cm. If we encounter difficulty in the measurements, Ra, Ba, and/or Pb may be excluded from our measurements.

The number of experiments that can be performed is limited not only by time and cost, but also because it would be virtually impossible to obtain more core. Furthermore, ES&H requirements limit the number of experiments. All the liquid radioactive effluent, regardless of the activity level, is considered radioactive waste and must be stored in the laboratory indefinitely (or until SNL has an acceptable means for disposal). Because of the large volume of waste generated for each experiment, and our plans to perform destructive post-test analysis on the cores, it is crucial that the above list of radioisotopes be complete.

Based on the composite recommendations of the PA Department (6342) given previously, the only elements requiring retardation measurements in Culebra rock are U, Pu, Th, Am, Np, Ra, and Pb, with Ra and Pb of least importance. Both physical and chemical retardation measurements are needed for these elements. The oxidation states of the radionuclides in solution is determined by the brine composition, pH, and temperature. In the experiments these three variables will be controlled to be the same as that found in the Culebra from which the cores were taken. Therefore, retardation factors will be obtained for the radionuclides in whatever oxidation state they would be in in the field, but the oxidation state will not be measured.

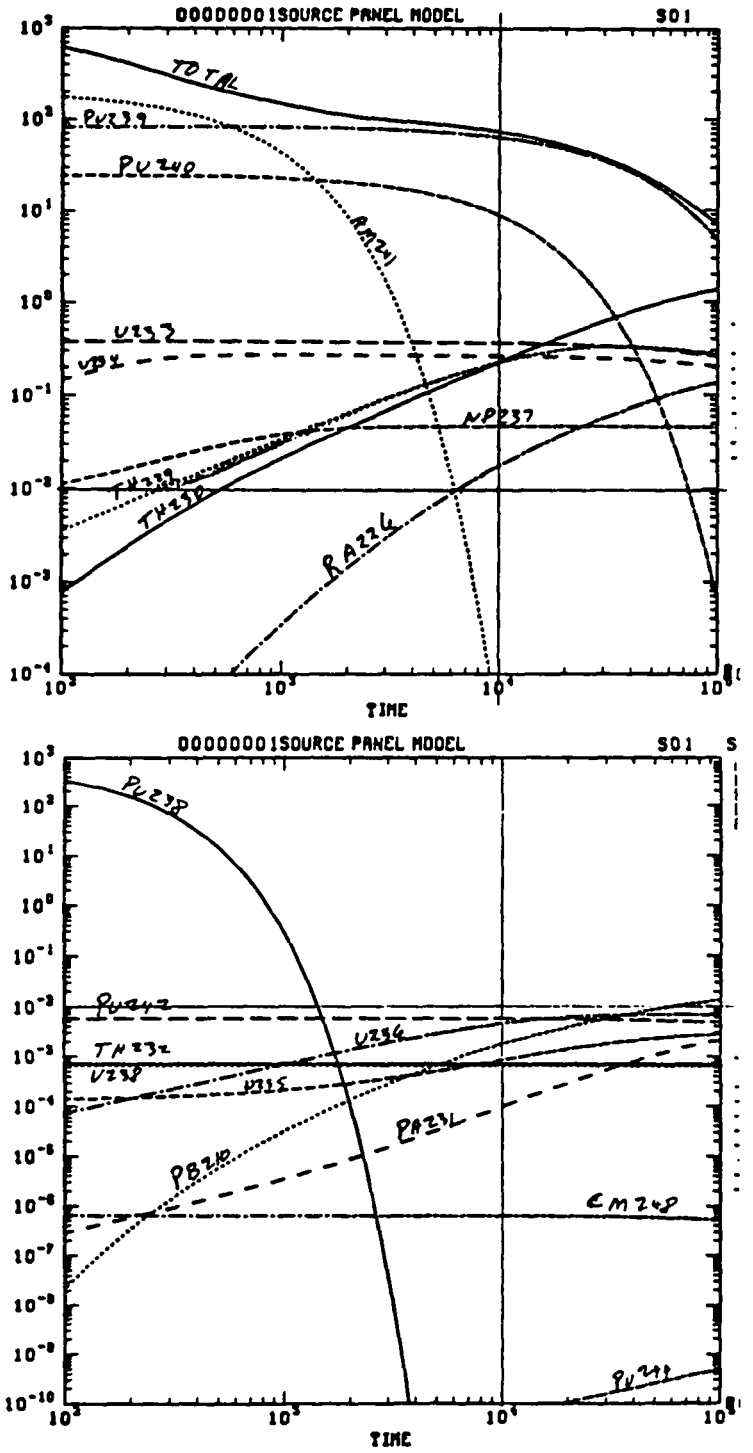

Figure 1. Decay histories for the present IDB inventory. Note scale change between Figures 2a and 2b. Horizontal line at 10^{-2} indicates threshold of importance for PA. Vertical line at 10^{4} yr indicates EPA regulatory time period.

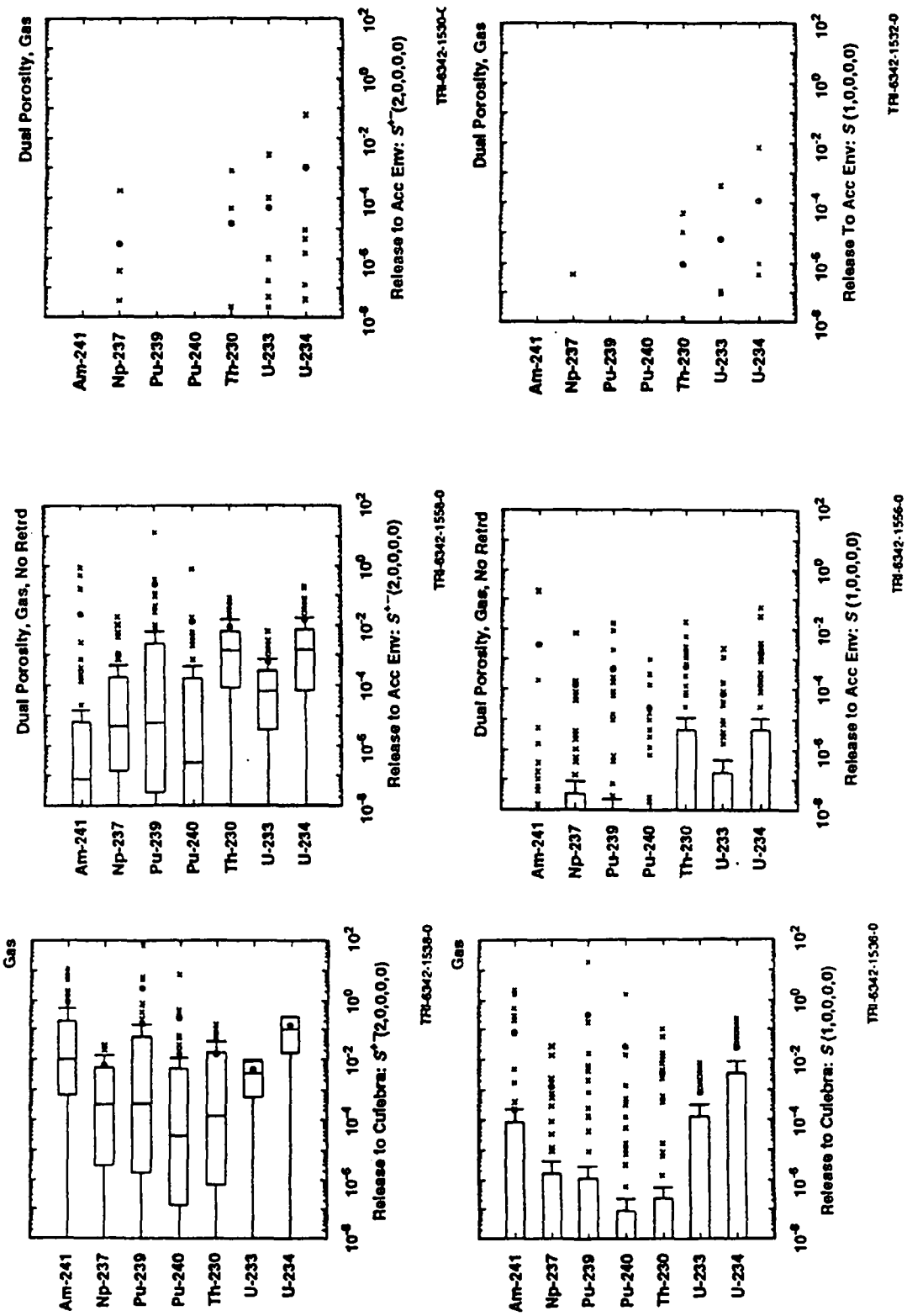

Figure 2. Cumulative normalized releases for radionuclides from E1E2 (upper row) and E1 (lower row) intrusions at 10^3 yr (1991 WIPP preliminary performance assessment) (Helton et al., 1992).

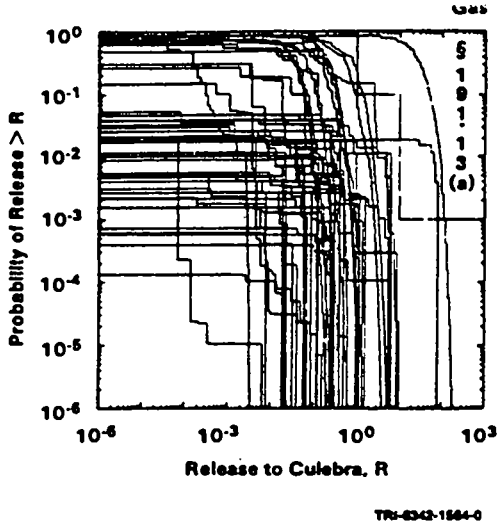

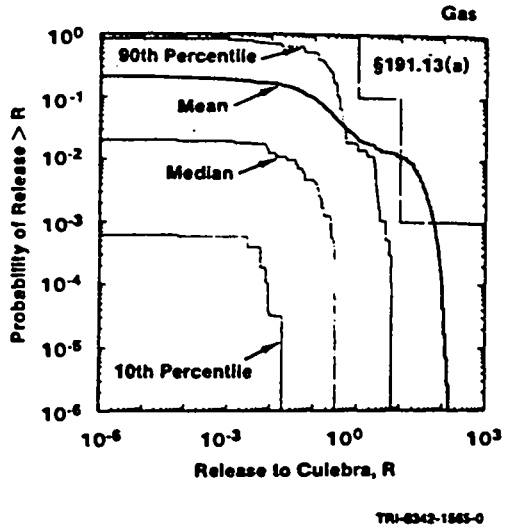

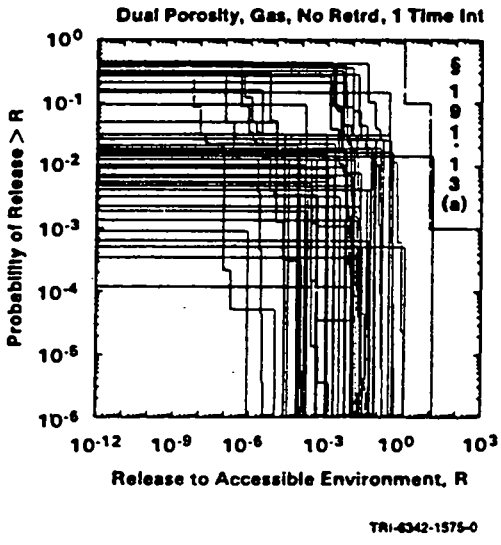

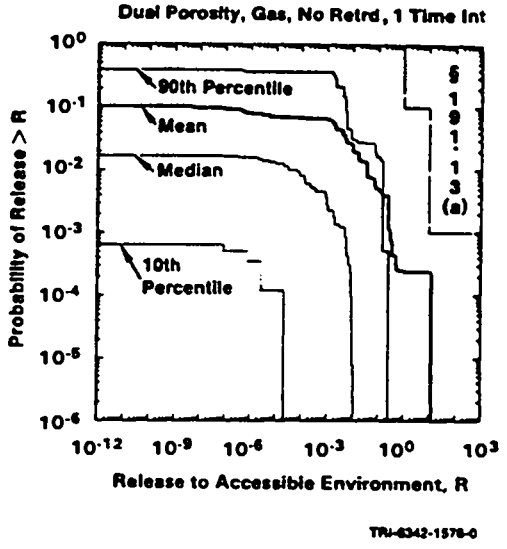

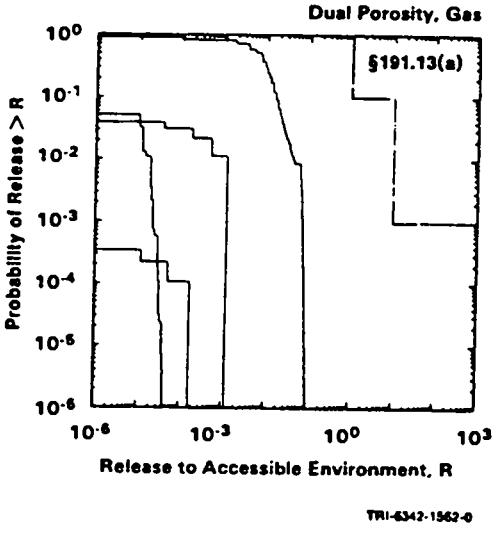

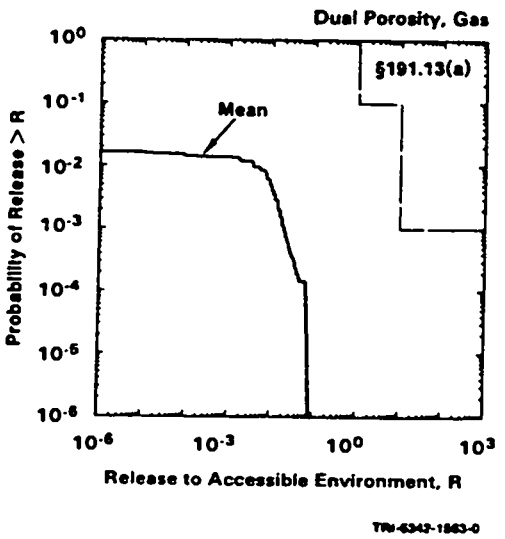

Figure 3. CCDFs corresponding to the releases plotted in Figure 2 (Helton et al., 1992).

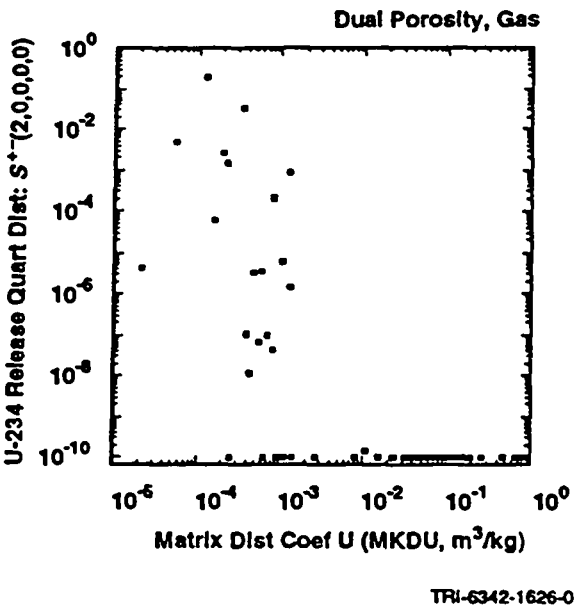

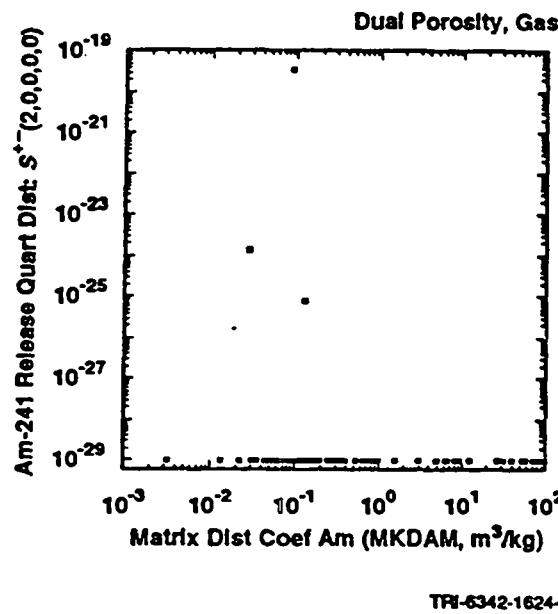

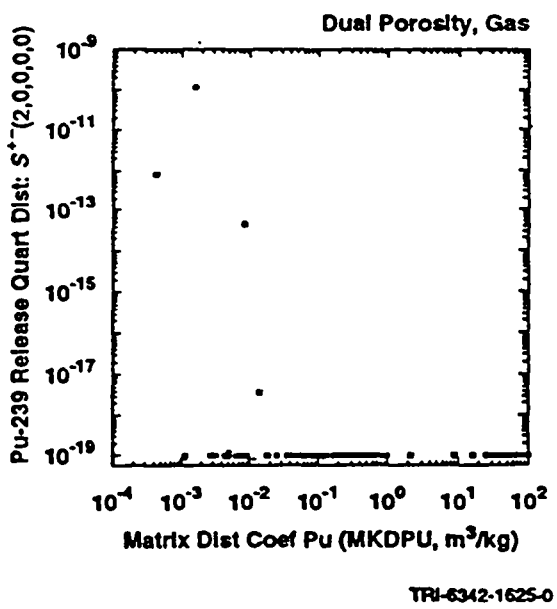

Figure 4. Scatterplots for radioisotope release versus matrix K_ds showing thresholds.

REFERENCES

Bertram-Howery, S. G., M. G. Marietta, R. P. Rechard, P. N. Swift, D. R. Anderson, B. L. Baker, J. E. Bean, W. Beyeler, K. F. Brinster, R. V. Guzowski, J. C. Helton, R. D. McCurley, D. K. Rudeen, J. D. Schreiber, and P. Vaughn. 1990. *Preliminary Comparison with 40 CFR Part 191, Subpart B for the Waste Isolation Pilot Plant, December 1990.* SAND90-2347. Albuquerque, NM: Sandia National Laboratories.

Marietta, M. G., S. G. Bertram Howery, D. R. Anderson, K. F. Brinster, R. V. Guzowski, H. Iuzzolino, and R. P. Rechard. 1989. *Performance Assessment Methodology Demonstration: Methodology Development for Purposes of Evaluating Compliance with EPA 40 CFR Part 191, Subpart B, for the Waste Isolation Pilot Plant.* SAND89-2027. Albuquerque, NM: Sandia National Laboratories.

Helton, J. C., J. W. Garner, R. P. Rechard, D. K. Rudeen, and P. N. Swift. 1992. *Preliminary Comparison with 40 CFR Part 191, Subpart B for the Waste Isolation Pilot Plant, December 1991. Volume 4: Uncertainty and Sensitivity Analysis Results.* SAND91-0893/4. Albuquerque, NM: Sandia National Laboratories.

Trauth, K. M., S. C. Hora, R. P. Rechard, and D. R. Anderson. 1992. *The Use of Expert Judgment to Quantify Uncertainty in Solubility and Sorption Parameters for Waste Isolation Pilot Plant Performance Assessment.* SAND92-0479. Albuquerque, NM: Sandia National Laboratories. (in review).

US DOE (Department of Energy). 1991. *Integrated Data Base for 1991: Spent Fuel and Radioactive Waste Inventories, Projects and Characterizations.* DOE/RW-006, Rev. 7.

US DOE (Department of Energy) and State of New Mexico. 1981, as modified. "Agreement for Consultation and Cooperation" on WIPP by the State of New Mexico and the U.S. Department of Energy, modified 11/30/84, 8/4/87, and 4/18/88.

WIPP PA (Performance Assessment) Department. 1992. *Long-Term Gas and Brine Migration at the Waste Isolation Pilot Plant: Preliminary Sensitivity Analyses for Post-Closure 40 CFR 268 (RCRA), May 1992.*SAND92-1933. Albuquerque, NM: Sandia National Laboratories.

WIPP PA (Performance Assessment) Division. 1991. *Preliminary Comparison with 40 CFR Part 191, Subpart B for the Waste Isolation Pilot Plant, December 1991. Volumes 1-3.* SAND91-0893/1,2,3. Albuquerque, NM: Sandia National Laboratories.

Distribution

R. W. Lynch, 6100
D. E. Miller, 6300
W. D. Weart, 6303
E. D. Gorham, 6119
C. F. Novak, 6119
D. R. Anderson, 6342
SWCF/GENEXP

DISTRIBUTION

(Send Distribution list changes to M.M. Gruebel, Dept. 6342, Sandia National Laboratories, PO Box 5800, Albuquerque, NM 87185-5800)

Federal Agencies

US Department of Energy (6)
Office of Civilian Radioactive Waste Management
Attn: Deputy Director, RW-2
Associate Director, RW-10/50
Office of Program and Resources Management
Office of Contract Business Management
Director, Analysis and Verification Division, RW-22
Associate Director, RW-30
Office of Systems and Compliance
Associate Director, RW-40
Office of Storage and Transportation
Director, RW-4/5
Office of Strategic Planning and International Programs
Office of External Relations
Forrestal Building
Washington, DC 20585

US Department of Energy
Albuquerque Operations Office
Attn: National Atomic Museum Library
PO Box 5400
Albuquerque, NM 87185

US Department of Energy (2)
Office of Environmental Restoration and Waste Management
Attn: EM-1
C. Frank, EM-50
Washington, DC 20585

US Department of Energy (3)
Office of Environmental Restoration and Waste Management
Attn: M. Frei, EM-34, Trevion II
Director, Waste Management Projects
Washington, DC 20585-0002

US Department of Energy
Office of Environmental Restoration and Waste Management
Attn: J. Lytle, EM-30, Trevion II
Washington, DC 20585-0002

US Department of Energy
Office of Environmental Restoration and Waste Management
Attn: S. Schneider, EM-342, Trevion II
Washington, DC 20585-0002

US Department of Energy (3)
WIPP Task Force
Attn: G.H. Daly
S. Fucigna
B. Bower
12800 Middlebrook Rd., Suite 400
Germantown, MD 20874

US Department of Energy (4)
Office of Environment, Safety and Health
Attn: R.P. Berube, EH-20
C. Borgstrum, EH-25
R. Pelletier, EH-231
K. Taimi, EH-232
Washington, DC 20585

US Department of Energy (6)
WIPP Project Integration Office
Attn: S. Alcorn
W.J. Arthur III
J. Coffey
L.W. Gage
P.J. Higgins
D.A. Olona
PO Box 5400
Albuquerque, NM 87115-5400

US Department of Energy (2)
WIPP Project Integration Satellite Office
Attn: R. Batra
R. Becker
PO Box 3090, Mail Stop 525
Carlsbad, NM 88221-3090

US Department of Energy (10)
WIPP Project Site Office (Carlsbad)
Attn: A. Hunt (4)
V. Daub (4)
J. Lippis
K. Hunter
PO Box 3090
Carlsbad, NM 88221-3090

US Department of Energy
Research & Waste Management Division
Attn: Director
PO Box E
Oak Ridge, TN 37831

US Department of Energy (2)
Idaho Operations Office
Fuel Processing and Waste
Management Division
785 DOE Place
Idaho Falls, ID 83402

US Department of Energy
Savannah River Operations Office
Defense Waste Processing
Facility Project Office
Attn: W.D. Pearson
PO Box A
Aiken, SC 29802

US Department of Energy (2)
Richland Operations Office
Nuclear Fuel Cycle & Production
Division
Attn: R.E. Gerton
825 Jadwin Ave.
PO Box 500
Richland, WA 99352

US Department of Energy
Office of Geologic Disposal
Yucca Mountain Project Office
Attn: Associate Director, RW-20
PO Box 98608
Las Vegas, NV 89193-8608

US Department of Energy (3)
Nevada Operations Office
Attn: J.R. Boland
D. Livingston
P.K. Fitzsimmons
2753 S. Highland Drive
Las Vegas, NV 89183-8518

US Department of Energy (2)
Technical Information Center
PO Box 62
Oak Ridge, TN 37831

US Department of Energy
Los Alamos Area Office
528 35th Street
Los Alamos, NM 87544

US Department of Energy (2)
Chicago Operations Office
Attn: J.C. Haugen
9800 South Cass Avenue
Argonne, IL 60439

US Department of Energy (3)
Rocky Flats Area Office
Attn: W.C. Rask
G. Huffman
T. Lukow
PO Box 928
Golden, CO 80402-0928

US Department of Energy
Dayton Area Office
Attn: R. Grandfield
PO Box 66
Miamisburg, OH 45343-0066

US Department of Energy
Attn: E. Young
Room E-178
GAO/RCED/GTN
Washington, DC 20545

US Bureau of Land Management
Carlsbad Office
101 E. Mermod
Carlsbad, NM 88220

US Bureau of Land Management
New Mexico State Office
PO Box 1449
Santa Fe, NM 87507

US Environmental Protection
Agency (2)
Radiation Protection Programs
Attn: M. Oge
ANR-460
Washington, DC 20460

US Environmental Protection
Agency, Region 6
Attn: C. Byrum, 6T-ET
1445 Ross Ave.
Dallas, TX 75202

US Geological Survey (2)
Water Resources Division
Attn: C. Peters
4501 Indian School NE
Suite 200
Albuquerque, NM 87110

US Nuclear Regulatory Commission
Division of Waste Management
Attn: H. Marson
Mail Stop 4-H-3
Washington, DC 20555

US Nuclear Regulatory Commission (4)
Advisory Committee on Nuclear Waste
Attn: D. Moeller
M.J. Steindler
P.W. Pomeroy
W.J. Hinze
7920 Norfolk Ave.
Bethesda, MD 20814

Defense Nuclear Facilities Safety Board
Attn: D. Winters
625 Indiana Ave. NW
Suite 700
Washington, DC 20004

Nuclear Waste Technical Review Board
Attn: Library (2)
1100 Wilson Blvd.
Suite 910
Arlington, VA 22209-2297

Energy and Science Division
Office of Management and Budget
Attn: K. Yuracko
725 17th Street NW
Washington, DC 20503

State Agencies

New Mexico Bureau of Mines
and Mineral Resources
Socorro, NM 87801

New Mexico Energy, Minerals and Natural Resources Department
Attn: Librarian
2040 South Pacheco
Santa Fe, NM 87505

New Mexico Energy, Minerals and Natural Resources Department
New Mexico Radioactive Task Force (2)
(Governor's WIPP Task Force)
Attn: A. Lockwood, Chairman
C. Wentz, Policy Analyst
2040 South Pacheco
Santa Fe, NM 87505

Bob Forrest
Mayor, City of Carlsbad
PO Box 1569
Carlsbad, NM 88221

Carlsbad Department of Development
Executive Director
Attn: C. Bernard
PO Box 1090
Carlsbad, NM 88221

New Mexico Environment Department
Secretary of the Environment (3)
Attn: J. Espinosa
PO Box 968
1190 St. Francis Drive
Santa Fe, NM 87503-0968

New Mexico Environment Department
Attn: P. McCasland
WIPP Project Site Office
PO Box 3090
Carlsbad, NM 88221-3090

New Mexico State Engineer's Office
Attn: M. Chudnoff
PO Box 25102
Santa Fe, NM 87504-5102

Environmental Evaluation Group (5)
Attn: R. Neill
7007 Wyoming Blvd. NE, Suite F-2
Albuquerque, NM 87109

Advisory Committee on Nuclear Facility Safety

John F. Ahearne
Executive Director, Sigma Xi
99 Alexander Drive
Research Triangle Park, NC 27709

James E. Martin
109 Observatory Road
Ann Arbor, MI 48109

WIPP Panel of National Research Council's Board on Radioactive Waste Management

Charles Fairhurst, Chairman
Department of Civil and
Mineral Engineering
University of Minnesota
500 Pillsbury Dr. SE
Minneapolis, MN 55455-0220

John O. Blomeke
3833 Sandy Shore Drive
Lenoir City, TN 37771-9803

John D. Bredehoeft
Western Region Hydrologist
Water Resources Division
US Geological Survey (M/S 439)
345 Middlefield Road
Menlo Park, CA 94025

Rodney C. Ewing
Department of Geology
University of New Mexico
Albuquerque, NM 87131

B. John Garrick
PLG, Inc.
4590 MacArthur Blvd.
Suite 400
Newport Beach, CA 92660-2027

Leonard F. Konikow
US Geological Survey
431 National Center
Reston, VA 22092

Jeremiah O'Driscoll
505 Valley Hill Drive
Atlanta, GA 30350

Chris G. Whipple
ICF Kaiser Engineers
1800 Harrison St.
Oakland, CA 94612-3430

National Research Council (3)
Board on Radioactive
Waste Management
RM HA456
Attn: P.B. Myers (2)
G.J. Grube
2101 Constitution Ave.
Washington, DC 20418

Performance Assessment Peer Review Panel

G. Ross Heath
College of Ocean and Fishery
Sciences, HN-15
583 Henderson Hall
University of Washington
Seattle, WA 98195

Thomas H. Pigford
Department of Nuclear Engineering
4159 Etcheverry Hall
University of California
Berkeley, CA 94720

Thomas A. Cotton
JK Research Associates, Inc.
4429 Butterworth Place NW
Washington, DC 20016

Robert J. Budnitz
President, Future Resources
Associates, Inc.
2000 Center Street, Suite 418
Berkeley, CA 94704

C. John Mann
Department of Geology
245 Natural History Bldg.
1301 West Green Street
University of Illinois
Urbana, IL 61801

Frank W. Schwartz
Department of Geology and Mineralogy
The Ohio State University
Scott Hall
1090 Carmack Rd.
Columbus, OH 43210

National Laboratories

Argonne National Laboratory (2)
Attn: A. Smith
D. Tomasko
9700 South Cass, Bldg. 201
Argonne, IL 60439

Battelle Pacific Northwest
Laboratory (2)
Attn: S. Bates
R.E. Westerman
MSIN P8-44
Battelle Boulevard
Richland, WA 99352

Idaho National Engineering
Laboratory (2)
Attn: H. Loo
R. Klinger
Mail Stop 5108
Idaho Falls, ID 83403-4000

Los Alamos National Laboratory (5)
Attn: B. Erdal, CNC-11
M. Ennis, HS-12
Mail Stop J900
S. Kosiewicz, EM-7
Mail Stop J595
L. Soholt, EM-13
Mail Stop M992
J. Wenzel, HS-12
Mail Stop K482
PO Box 1663
Los Alamos, NM 87545

Oak Ridge National Laboratory
Transuranic Waste Manager
Attn: D.W. Turner
Bldg. 3047
PO Box 2008
Oak Ridge, TN 37831-6060

Pacific Northwest Laboratory
Attn: B. Kennedy
PO Box 999
Richland, WA 99352

Westinghouse-Savannah River
Technology Center (4)
Attn: N. Bibler
J.R. Harbour
M.J. Plodinec
G.G. Wicks
Aiken, SC 29802

Corporations/Members of the Public

Battelle Memorial Institute
Attn: R. Root
J. Kircher
505 Marquette NW
Suite 1
Albuquerque, NM 87102

Benchmark Environmental Corp.
Attn: C. Frederickson
4501 Indian School NE
Suite 105
Albuquerque, NM 87110

Beta Corporation Int.
Attn: E. Bonano
6613 Esther NE
Albuquerque, NM 87109

City of Albuquerque
Public Works Department
Utility Planning Division
Attn: W.K. Summers
PO Box 1293
Albuquerque, NM 87103

Deuel and Associates, Inc.
Attn: R.W. Prindle
7208 Jefferson NE
Albuquerque, NM 87109

Disposal Safety, Inc.
Attn: B. Ross
1660 L Street NW, Suite 314
Washington, DC 20036

Ecodynamics (2)
Attn: P. Roache
R. Blaine
PO Box 9229
Albuquerque, NM 87119-9229

EG & G Idaho (3)
1955 Fremont Street
Attn: C. Atwood
C. Hertzler
T.I. Clements
Idaho Falls, ID 83415

Geomatrix
Attn: K. Coppersmith
100 Pine St., Suite 1000
San Francisco, CA 94111

Golder Associates, Inc.
Attn: R. Kossik
4104 148th Avenue NE
Redmond, WA 98052

INTERA, Inc.
Attn: A.M. LaVenue
1650 University Blvd. NE, Suite 300
Albuquerque, NM 87102

INTERA, Inc.
Attn: J.F. Pickens
6850 Austin Center Blvd., Suite 300
Austin, TX 78731

INTERA, Inc.
Attn: W. Stensrud
PO Box 2123
Carlsbad, NM 88221

INTERA, Inc.
Attn: W. Nelson
101 Convention Center Drive
Suite 540
Las Vegas, NV 89109

IT Corporation (2)
Attn: R.F. McKinney
J. Myers
Regional Office
Suite 700
5301 Central Avenue NE
Albuquerque, NM 87108

John Hart and Associates, P.A.
Attn: J.S. Hart
2815 Candelaria Road NW
Albuquerque, NM 87107

John Hart and Associates, P.A.
Attn: K. Lickliter
1009 North Washington
Tacoma, WA 98406

MAC Technical Services Co.
Attn: D.K. Duncan
8418 Zuni Road SE
Suite 200
Albuquerque, NM 87108

Newman and Holtzinger
Attn: C. Mallon
1615 L Street NW
Suite 1000
Washington, DC 20036

RE/SPEC, Inc. (2)
Attn: W. Coons
4775 Indian School NE
Suite 300
Albuquerque, NM 87110

RE/SPEC, Inc.
Attn: J.L. Ratigan
PO Box 725
Rapid City, SD 57709

Reynolds Electric and Engineering
Company, Inc.
Attn: E.W. Kendall
Building 790
Warehouse Row
PO Box 98521
Las Vegas, NV 89193-8521

Science Applications International
Corporation (SAIC)
Attn: H.R. Pratt
10260 Campus Point Drive
San Diego, CA 92121

Science Applications International
Corporation (2)
Attn: D.C.Royer
C.G. Pflum
101 Convention Center Dr.
Las Vegas, NV 89109

Science Applications International
Corporation (3)
Attn: M. Davis
R. Guzowski
J. Tollison
2109 Air Park Road SE
Albuquerque, NM 87106

Science Applications International
Corporation (2)
Attn: J. Young
D. Lester
18706 North Creek Parkway, Suite 110
Bothell, WA 98011

Southwest Research Institute
Center for Nuclear Waste Regulatory
Analysis (2)
Attn: P.K. Nair
6220 Culebra Road
San Antonio, TX 78228-0510

Systems, Science, and Software (2)
Attn: E. Peterson
P. Lagus
Box 1620
La Jolla, CA 92038

TASC
Attn: S.G. Oston
55 Walkers Brook Drive
Reading, MA 01867

Tech Reps, Inc. (7)
Attn: J. Chapman
C. Crawford
D. Marchand
T. Peterson
J. Stikar
D. Scott
M. Minahan
5000 Marble NE, Suite 222
Albuquerque, NM 87110

Tolan, Beeson & Associates
Attn: T.L. Tolan
2320 W. 15th Avenue
Kennewick, WA 99337

TRW Environmental Safety Systems (2)
Attn: I. Sacks, Suite 800
L. Wildman, Suite 1300
2650 Park Tower Drive
Vienna, VA 22180-7306

Sanford Cohen and Associates
Attn: J. Channell
7101 Carriage Rd NE
Albuquerque, NM 87109

Westinghouse Electric Corporation (5)
Attn: Library
C. Cox
L. Fitch
B.A. Howard
R.F. Kehrman
PO Box 2078
Carlsbad, NM 88221

Westinghouse Hanford Company
Attn: D.E. Wood, MSIN HO-32
PO Box 1970
Richland, WA 99352

Western Water Consultants
Attn: P.A. Rechard
PO Box 4128
Laramie, WY 82071

Western Water Consultants
Attn: D. Fritz
1949 Sugarland Drive #134
Sheridan, WY 82801-5720

P. Drez
8816 Cherry Hills Road NE
Albuquerque, NM 87111

David Lechel
9600 Allende Rd. NE
Albuquerque, NM 87109

C.A. Marchese
PO Box 21790
Albuquerque, NM 87154

Arend Meijer
3821 Anderson SE
Albuquerque, NM 87108

D.W. Powers
Star Route Box 87
Anthony, TX 79821

Shirley Thieda
PO Box 2109, RR1
Bernalillo, NM 87004

Jack Urich
c/o CARD
144 Harvard SE
Albuquerque, NM 87106

Universities

University of California
Mechanical, Aerospace, and
Nuclear Engineering Department (2)
Attn: W. Kastenberg
D. Browne
5532 Boelter Hall
Los Angeles, CA 90024

University of California
Engineering and Applied Science Attn:
D. Okrent
48-121A Engineering IV
Los Angeles, CA 90024-1597

University of California
Mine Engineering Department
Rock Mechanics Engineering
Attn: N. Cook
Berkeley, CA 94720

University of Hawaii at Hilo
Business Administration
Attn: S. Hora
Hilo, HI 96720-4091

University of New Mexico
Geology Department
Attn: Library
Albuquerque, NM 87131

University of New Mexico
Research Administration
Attn: H. Schreyer
102 Scholes Hall
Albuquerque, NM 87131

University of Wyoming
Department of Civil Engineering
Attn: V.R. Hasfurther
Laramie, WY 82071

University of Wyoming
Department of Geology
Attn: J.I. Drever
Laramie, WY 82071

University of Wyoming
Department of Mathematics
Attn: R.E. Ewing
Laramie, WY 82071

Libraries

Thomas Brannigan Library
Attn: D. Dresp
106 W. Hadley St.
Las Cruces, NM 88001

New Mexico State Library
Attn: N. McCallan
325 Don Gaspar
Santa Fe, NM 87503

New Mexico Tech
Martin Speere Memorial Library
Campus Street
Socorro, NM 87810

New Mexico Junior College
Pannell Library
Attn: R. Hill
Lovington Highway
Hobbs, NM 88240

Carlsbad Municipal Library
WIPP Public Reading Room
Attn: L. Hubbard
101 S. Halagueno St.
Carlsbad, NM 88220

University of New Mexico
Zimmerman Library
Government Publications Department
Albuquerque, NM 87131

NEA/Performance Assessment Advisory Group (PAAG)

P. Duerden
ANSTO
Lucas Heights Research Laboratories
Private Mail Bag No. 1
Menai, NSW 2234
AUSTRALIA

Gordon S. Linsley
Division of Nuclear Fuel Cycle and Waste Management
International Atomic Energy Agency
PO Box 100
A-1400 Vienna, AUSTRIA

Nicolo Cadelli
Commission of the European Communities
200, Rue de la Loi
B-1049 Brussels, BELGIUM

R. Heremans
Organisme Nationale des Déchets Radioactifs et des Matiéres Fissiles (ONDRAF)
Place Madou 1, Boitec 24/25
B-1030 Brussels, BELGIUM

J. Marivoet
Centre d'Etudes de l'Energie Nucléaire (CEN/SCK)
Boeretang 200
B-2400 Mol, BELGIUM

P. Conlon
Waste Management Division
Atomic Energy Control Board (AECB)
PO Box 1046
Ottawa, Ontario KIP 559, CANADA

A.G. Wikjord
Manager, Environmental and Safety Assessment Branch
Atomic Energy of Canada Limited
Whiteshell Research Establishment
Pinewa, Manitoba ROE 1LO
CANADA

Teollisuuden Voima Oy (TVO) (2)
Attn: Timo Äikäs
Jukka-Pekka Salo
Annankatu 42 C
SF-00100 Helsinki Suomi
FINLAND

Timo Vieno
Technical Research Centre of Finland (VTT)
Nuclear Energy Laboratory
PO Box 208
SF-02151 Espoo, FINLAND

Division de la Sécurité et de la
Protection de l'Environment (DSPE)
Commissariat á l'Energie Atomique
Agence Nationale pour la Gestion des
Déchets Radioactifs (ANDRA) (2)
Attn: Gérald Ouzounian
M. Claude Ringeard
Route du Panorama Robert Schuman
B. P. No. 38
F-92266 Fontenay-aux-Roses Cedex
FRANCE

Claudio Pescatore
Division of Radiation Protection and
Waste Management
OECD Nuclear Energy Agency
38, Boulevard Suchet
F-75016 Paris, FRANCE

M. Dominique Greneche
Commissariat á l'Energie Atomique
IPSN/DAS/SASICC/SAED
B.P. No. 6
F-92265 Fontenay-aux-Roses Cedex
FRANCE

Robert Fabriol
Bureau de Recherches Géologiques et
Miniéres (BRGM)
B.P. 6009
45060 Orléans Cedex 2, FRANCE

P. Bogorinski
Gesellschaft für Reaktorsicherheit
(GRS) MBH
Schwertnergasse 1
D-5000 Köln 1, GERMANY

R. Storck
GSF - Institut für Tieflagerung
Theodor-Heuss-Strabe 4
D-3300 Braunschweig, GERMANY

Ferrucio Gera
ISMES S.p.A
Via del Crociferi 44
I-00187 Rome, ITALY

Hiroyuki Umeki
Isolation System Research Program
Radioactive Waste Management Project
Power Reactor and Nuclear Fuel
Development Corporation (PNC)
1-9-13, Akasaka, Minato-ku
Tokyo 107, JAPAN

P. Carboneras Martinez
ENRESA
Calle Emilio Vargas, 7
R-28043 Madrid
SPAIN

Tönis Papp
Swedish Nuclear Fuel and Waste
Management Co.
Box 5864
S 102 48 Stockholm
SWEDEN

Conny Hägg
Swedish Radiation Protection
Institute (SSI)
Box 60204
S-104 01 Stockholm
SWEDEN

J. Hadermann
Paul Scherrer Institute
Waste Management Programme
CH-5232 Villigen PSI
SWITZERLAND

J. Vigfusson
HSK-Swiss Nuclear Safety Inspectorate
Federal Office of Energy
CH-5232 Villigen-HSK
SWITZERLAND

D.E. Billington
Departmental Manager—Assessment
Studies
Radwaste Disposal R&D Division
AEA Decommissioning & Radwaste
Harwell Laboratory, B60
Didcot Oxfordshire OX11 ORA
UNITED KINGDOM

P. Grimwood
Waste Management Unit
BNFL
Sellafield
Seascale, Cumbria CA20 1PG
UNITED KINGDOM

Alan J. Hooper
UK Nirex Ltd
Curie Avenue
Harwell, Didcot
Oxfordshire, OX11 ORH
UNITED KINGDOM

Jerry M. Boak
Yucca Mountain Project Office
US Department of Energy
PO Box 98608
Las Vegas, NV 89193

Seth M. Coplan (Chairman)
US Nuclear Regulatory Commission
Division of High-Level Waste Management
Mail Stop 4-H-3
Washington, DC 20555

A.E. Van Luik
INTERA/M&O
The Valley Bank Center
101 Convention Center Dr.
Las Vegas, NV 89109

NEA/Probabilistic System Assessment Group (PSAG)

Shaheed Hossain
Division of Nuclear Fuel Cycle and Waste Management
International Atomic Energy Agency
Wagramerstrasse 5
PO Box 100
A-1400 Vienna, AUSTRIA

Alexander Nies (PSAC Chairman)
Gesellschaft für Strahlen- und Institut für Tieflagerung
Abteilung für Endlagersicherheit
Theodor-Heuss-Strasse 4
D-3300 Braunschweig, GERMANY

Eduard Hofer
Gesellschaft für Reaktorsicherheit (GRS) MBH
Forschungsgelände
D-8046 Garching, GERMANY

Andrea Saltelli
Commission of the European Communities
Joint Resarch Centre of Ispra
I-21020 Ispra (Varese)
ITALY

Alejandro Alonso
Cátedra de Tecnología Nuclear
E.T.S. de Ingenieros Industriales
José Gutiérrez Abascal, 2
E-28006 Madrid, SPAIN

ENRESA (2)
Attn: M. A. Cuñado
F. J. Elorza
Calle Emilio Vargas, 7
E-28043 Madrid, SPAIN

Pedro Prado
CIEMAT
Instituto de Tecnología Nuclear
Avenida Complutense, 22
E-28040 Madrid, SPAIN

Nils A. Kjellbert
Swedish Nuclear Fuel and Waste Management Company (SKB)
Box 5864
S-102 48 Stockholm, SWEDEN

Björn Cronhjort
Royal Institute of Technology
Automatic Control
S-100 44 Stockholm, SWEDEN

Richard A. Klos
Paul-Scherrer Institute (PSI)
CH-5232 Villingen PSI, SWITZERLAND

Nationale Genossenschaft für die Lagerung Radioaktiver Abfälle (2)
Attn: C. McCombie
F. Van Dorp
Hardstrasse 73
CH-5430 Wettingen, SWITZERLAND

N. A. Chapman
Intera Information Technologies
Park View House
14B Burton Street
Melton Mowbray
Leicestershire LE13 1AE
UNITED KINGDOM

Daniel A. Galson
Galson Sciences Ltd.
35, Market Place
Oakham
Leicestershire LE15 6DT
UNITED KINGDOM

David P. Hodgkinson
Intera Information Technologies
45 Station Road, Chiltern House
Henley-on-Thames
Oxfordshire RG9 1AT
UNITED KINGDOM

Brian G.J. Thompson
Department of the Environment: Her Majesty's Inspectorate of Pollution
Room A5.33, Romney House
43 Marsham Street
London SW1P 2PY
UNITED KINGDOM

Intera Information Technologies
Attn: M.J.Apted
3609 South Wadsworth Blvd.
Denver, CO 80235

US Nuclear Regulatory Commission (2)
Attn: R. Codell
N. Eisenberg
Mail Stop 4-H-3
Washington, DC 20555

Battelle Pacific Northwest Laboratories
Attn: P.W. Eslinger
MS K2-32
PO Box 999
Richland, WA 99352

Center for Nuclear Waste Regulatory Analysis (CNWRA)
Southwest Research Institute
Attn: B. Sagar
PO Drawer 28510
6220 Culebra Road
San Antonio, TX 78284

Geostatistics Expert Working Group (GXG)

Rafael L. Bras
R.L. Bras Consulting Engineers
44 Percy Road
Lexington, MA 02173

Jesus Carrera
Universidad Politécnica de Cataluña
E.T.S.I. Caminos
Jordi, Girona 31
E-08034 Barcelona
SPAIN

Gedeon Dagan
Department of Fluid Mechanics and Heat Transfer
Tel Aviv University
PO Box 39040
Ramat Aviv, Tel Aviv 69978
ISRAEL

Ghislain de Marsily (GXG Chairman)
University Pierre et Marie Curie
Laboratorie de Geologie Applique
4, Place Jussieu
T.26 - 5^{e} etage
75252 Paris Cedex 05, FRANCE

Alain Galli
Centre de Geostatistique
Ecole des Mines de Paris
35 Rue St. Honore
77035 Fontainebleau, FRANCE

Christian Ravenne
Geology and Geochemistry Division
Institut Francais du Pétrole
1 & 4, Av. de Bois-Préau B.P. 311
92506 Rueil Malmaison Cedex
FRANCE

Peter Grindrod
INTERA Information Technologies Ltd.
Chiltern House
45 Station Road
Henley-on-Thames
Oxfordshire, RG9 1AT, UNITED KINGDOM

Alan Gutjahr
Department of Mathematics
New Mexico Institute of Mining and Technology
Socorro, NM 87801

C. Peter Jackson
Harwell Laboratory
Theoretical Studies Department
Radwaste Disposal Division
Bldg. 424.4
Oxfordshire Didcot Oxon OX11 ORA
UNITED KINDGOM

Rae Mackay
Department of Civil Engineering
University of Newcastle Upon Tyne
Newcastle Upon Tyne NE1 7RU
UNITED KINGDOM

Steve Gorelick
Department of Applied Earth Sciences
Stanford University
Stanford, CA 94305-2225

Peter Kitanidis
60 Peter Coutts Circle
Stanford, CA 94305

Dennis McLaughlin
Parsons Laboratory
Room 48-209
Department of Civil Engineering
Massachusetts Institute of Technology
Cambridge, MA 02139

Shlomo P. Neuman
College of Engineering and Mines
Department of Hydrology and Water Resources
University of Arizona
Tucson, AZ 85721

Yoram Rubin
Department of Civil Engineering
University of California
Berkeley, CA 94720

Foreign Addresses

Studiecentrum Voor Kernenergie
Centre D'Energie Nucleaire
Attn: A. Bonne
SCK/CEN
Boeretang 200
B-2400 Mol
BELGIUM

Atomic Energy of Canada, Ltd. (3)
Whiteshell Research Establishment
Attn: M.E. Stevens
B.W. Goodwin
D. Wushke
Pinewa, Manitoba ROE 1LO, CANADA

Juhani Vira
Teollisuuden Voima Oy (TVO)
Annankatu 42 C
SF-00100 Helsinki Suomi
FINLAND

Jean-Pierre Olivier
OECD Nuclear Energy Agency (2)
38, Boulevard Suchet
F-75016 Paris
FRANCE

D. Alexandre, Deputy Director
ANDRA
31 Rue de la Federation
75015 Paris
FRANCE

Claude Sombret
Centre D'Etudes Nucleaires
De La Vallee Rhone
CEN/VALRHO
S.D.H.A. B.P. 171
30205 Bagnols-Sur-Ceze, FRANCE

Bundesministerium fur Forschung und Technologie
Postfach 200 706
5300 Bonn 2, GERMANY

Bundesanstalt fur Geowissenschaften und Rohstoffe
Attn: M. Langer
Postfach 510 153
3000 Hanover 51, GERMANY

Gesellschaft fur Reaktorsicherheit (GRS) (2)
Attn: B. Baltes
W. Muller
Schwertnergasse 1
D-5000 Cologne, GERMANY

Institut fur Tieflagerung (2)
Attn: K. Kuhn
Theodor-Heuss-Strasse 4
D-3300 Braunschweig, GERMANY

Physikalisch-Technische Bundesanstalt
Attn: P. Brenneke
Postfach 33 45
D-3300 Braunschweig, GERMANY

Shingo Tashiro
Japan Atomic Energy Research Institute
Tokai-Mura, Ibaraki-Ken
319-11, JAPAN

Netherlands Energy Research Foundation (ECN)
Attn: L.H. Vons
3 Westerduinweg
PO Box 1
1755 ZG Petten, THE NETHERLANDS

Johan Andersson
Swedish Nuclear Power Inspectorate
Statens Kärnkraftinspektion (SKI)
Box 27106
S-102 52 Stockholm, SWEDEN

Fred Karlsson
Svensk Karnbransleforsorjning
AB SKB
Box 5864
S-102 48 Stockholm, SWEDEN

Nationale Genossenschaft für die
Lagerung Radioaktiver Abfälle (2)
Attn: S. Vomvoris
P. Zuidema
Hardstrasse 73
CH-5430 Wettingen, SWITZERLAND

AEA Technology
Attn: J.H. Rees
D5W/29 Culham Laboratory
Abington
Oxfordshire OX14 3DB, UNITED KINGDOM

AEA Technology
Attn: W.R. Rodwell
044/A31 Winfrith Technical Centre
Dorchester
Dorset DT2 8DH, UNITED KINGDOM

AEA Technology
Attn: J.E. Tinson
B4244 Harwell Laboratory
Didcot, Oxfordshire OX11 ORA
UNITED KINGDOM

D.R. Knowles
British Nuclear Fuels, plc
Risley, Warrington
Cheshire WA3 6AS, 1002607
UNITED KINGDOM

Internal

1 A. Narath
20 O.E. Jones
1502 J.C. Cummings
1511 D.K. Gartling
6000 D.L. Hartley
6115 P.B. Davies
6115 R.L. Beauheim
6119 E.D. Gorham
6119 Staff (14)
6121 J.R. Tillerson
6121 Staff (7)
6233 J.C. Eichelberger
6300 D.E. Ellis
6302 L.E. Shephard
6303 S.Y. Pickering
6303 W.D. Weart
6305 S.A. Goldstein
6305 A.R. Lappin
6306 A.L. Stevens
6312 F.W. Bingham
6313 L.S. Costin
6331 P.A. Davis
6341 Sandia WIPP Central Files (100)
6342 D.R. Anderson
6342 Staff (30)
6343 V. Harper-Slaboszewicz
6343 Staff (3)
6345 R.C. Lincoln
6345 Staff (9)
6347 D.R. Schafer
6348 J.T. Holmes
6348 Staff (4)
6351 R.E. Thompson
6352 D.P. Garber
6352 S.E. Sharpton
6400 N.R. Ortiz
6613 R.M. Cranwell
6613 R.L. Iman
6613 C. Leigh
6622 M.S.Y. Chu
6641 R.E. Luna, Acting
7141 Technical Library (5)
7151 Technical Publications
7613-2 Document Processing for
DOE/OSTI (10)
8523-2 Central Technical Files

☆ U.S. GOVERNMENT PRINTING OFFICE 1993—774-122/80240

THIS PAGE INTENTIONALLY LEFT BLANK

SANDIA REPORT

SAND92–0700/5 • UC–721
Unlimited Release
Printed August 1993

Preliminary Performance Assessment for the Waste Isolation Pilot Plant, December 1992

Volume 5: Uncertainty and Sensitivity Analyses of Gas and Brine Migration for Undisturbed Performance

WIPP Performance Assessment Department

Prepared by
Sandia National Laboratories
Albuquerque, New Mexico 87185 and Livermore, California 94550
for the United States Department of Energy
under Contract DE-AC04-76DP00789

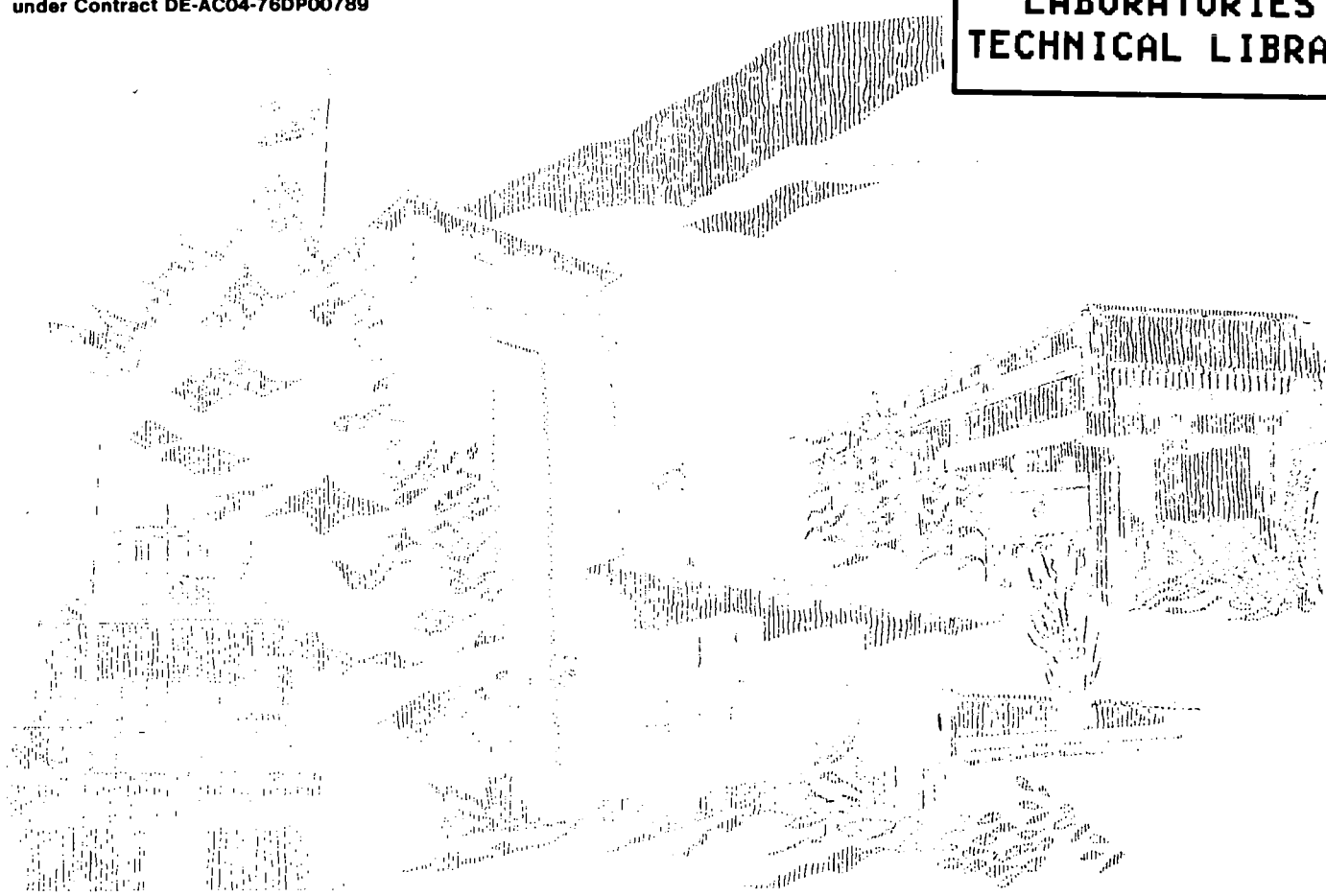

Issued by Sandia National Laboratories, operated for the United States Department of Energy by Sandia Corporation.

Available to DOE and DOE contractors from
Office of Scientific and Technical Information
PO Box 62
Oak Ridge, TN 37831

Prices available from (615) 576-8401, FTS 626-8401

Available to the public from
National Technical Information Service
US Department of Commerce
5285 Port Royal Rd
Springfield, VA 22161

NTIS price codes
Printed copy: A07
Microfiche copy: A01

Record Copy

TECH REPS, inc. 5000 MARBLE, N.E. ● ALBUQUERQUE, NEW MEXICO 87110 ● (505) 255-5678/262-2077

Date: November 3, 1993

To: Distribution

From: Faith Puffer, Tech Reps, Inc.

Subject: Addition to Volume 5 of SAND93-0700, *Preliminary Performance Assessment for the Waste Isolation Pilot Plant, December 1992*

To whom it may concern:

The following pages were omitted from your copy of *Volume 5: Uncertainty and Sensitivity Analyses of Gas and Brine Migration for Undisturbed Performance*. Please insert these pages into your copy.

Thank you.

Faith Puffer

encl: Pages A-5 through A-8

~~NOS 11/01/94~~

SAND92-0700/5
Unlimited Release
Printed August 1993

Distribution
Category UC-721

Preliminary Performance Assessment for the Waste Isolation Pilot Plant, December 1992

Volume 5: Uncertainty and Sensitivity Analyses of Gas and Brine Migration for Undisturbed Performance

WIPP Performance Assessment Department
Sandia National Laboratories
Albuquerque, New Mexico 87185

ABSTRACT

Before disposing of transuranic radioactive waste in the Waste Isolation Pilot Plant (WIPP), the United States Department of Energy (DOE) must evaluate compliance with applicable long-term regulations of the United States Environmental Protection Agency (EPA). Sandia National Laboratories is conducting iterative performance assessments (PAs) of the WIPP for the DOE to provide interim guidance while preparing for a final compliance evaluation. This volume of the 1992 PA contains results of uncertainty and sensitivity analyses with respect to migration of gas and brine from the undisturbed repository. Additional information about the 1992 PA is provided in other volumes. Volume 1 contains an overview of WIPP PA and results of a preliminary comparison with 40 CFR 191, Subpart B. Volume 2 describes the technical basis for the performance assessment, including descriptions of the linked computational models used in the Monte Carlo analyses. Volume 3 contains the reference data base and values for input parameters used in consequence and probability modeling. Volume 4 contains uncertainty and sensitivity analyses with respect to the EPA's *Environmental Standards for the Management and Disposal of Spent Nuclear Fuel, High-Level and Transuranic Radioactive Wastes* (40 CFR 191, Subpart B). Finally, guidance derived from the entire 1992 PA is presented in Volume 6.

Results of the 1992 uncertainty and sensitivity analyses indicate that, conditional on the modeling assumptions and the assigned parameter-value distributions, the most important parameters for which uncertainty has the potential to affect gas and brine migration from the undisturbed repository are: initial liquid saturation in the waste, anhydrite permeability, biodegradation-reaction stoichiometry, gas-generation rates for both corrosion and biodegradation under inundated conditions, and the permeability of the long-term shaft seal. Gas and brine migration are less sensitive to other parameters, although additional information is needed to confirm that the preferred conceptual models and assigned parameter distributions adequately describe reality.

ACKNOWLEDGMENTS

The Waste Isolation Pilot Plant (WIPP) Performance Assessment (PA) Department is comprised of both Sandia National Laboratories (SNL) and contractor employees working as a team to produce preliminary comparisons with Environmental Protection Agency (EPA) regulations, assessments of overall long-term safety of the repository, and interim technical guidance to the program. The on-site team, affiliations, and contributions to the 1992 performance assessment are listed in alphabetical order:

Performance Assessment Department

Name	Affil.*	Primary Author of Major Code	Area of Responsibility
R. Anderson	SNL		Department Manager
B. Baker	TEC		SEC02D, Hydrology, Office Manager
J. Bean	UNM		BRAGFLO, 2-Phase Flow
J. Berglund	UNM	CUTTINGS	Task Ldr., Cuttings/Cavings/ Spallings, Engr. Mech.
S. Bertram-Howery	SNL		PA Liaison with DOE, Criteria Document, Test Phase Plan
W. Beyeler	SAI	PANEL, GARFIELD	Geostatistics, Analytical Models, CAMCON Systems Codes
K. Brinster	SAI		Geohydrology, Conceptual Models
R. Blaine	ECO		SEC02D, SECOTP, & CAMCON Systems Codes
T. Blaine	GC		Drilling Technology, Exposure Pathways Data
K. Byle	UNM		Software and Analysis QA
J. Chapman	TRI		Documentation V.3
D. Duncan	MAC		Data QA
K. Economy	ECO		SECO2D, SECOTP, Hydrology &
D. Gallegos	SNL		Transport Task Ldr., Hydrology, Geostatistics, NEA, PSAG
D. Galson	GS		NEA Working Groups, PSAG, PAAG, Human Intrusion
J. Garner	API	PANEL	Source Term, Sens. Anal.
A. Gilkey	UNM		CAMCON Systems Codes
L. Gomez	SNL		Task Ldr., Safety Assessments
M. Gruebel	TRI		EPA Regulations, Documentation V.I, Editor V.I
R. Guzowski	SAI		Geology, Scenario Construction
J. Helton	ASU	CCDFPERM	Task Ldr., Uncert./Sens. Anal., Probability Models, Editor V.4
S. Hora	UHH		Expert Elicitation, Probability Models
H. Iuzzolino	GC	CCDFCALC CCDFPERM	LHS, CAMCON System Codes, Probability Models
R. Klett	SNL		EPA Regulations
P. Knupp	ECO	SECOTP	Comp. Fluid Dyn.
M. LaVenue	INT	GRASP-INV	Hydrology/Geostatistics
C. Leigh	SNL	GENII-S	Exposure Pathways
M. Marietta	SNL		Dep. Dept. Manager, Tech. Coord.
G. de Marsily	UP		Geostatistics Expert Group Chair
R. McCurley	UNM		CAMCON System Codes
B. Napier	PNL	GENII	Safety Assessments
A. Peterson	SNL		Task Ldr., Inventory
B. RamaRao	INT	GRASP-INV	Geostatistics

J. Rath	UNM		CAMCON System Codes
R. Rechard	SNL		Task Ldr., CAMCON, QA
P. Roache	ECO	SECO	Task Ldr., Comp. Fluid Dyn.
D. Rudeen	UNM		STAFF2D, SECOTP, Transport
J. Ruge	ECO		Multigrid Methods/BRAGFLO
T. Russell	ECO		Upscaling
K. Salari	ECO	SECOTP	Transport, Computational Fluid Dynamics
J. Sandha	SAI		INGRES, PA Data Base
J. Schreiber	SAI		BRAGFLO, 2-Phase Flow, Editor V.5
D. Scott	TRI		Documentation V.2
P. Swift	TRI		Task Ldr., Geology, Climate Var., Editor V.1, 2, 4, & 5
M. Tierney	SNL		Task Ldr., CDF Constr., Probability Models, Ref. Data, Editor V.2 & 3
K. Trauth	SNL		Task Ldr., Expert Panels
P. Vaughn	API	BRAGFLO	Task Ldr., 2-Phase Flow & Waste Panel Chemistry, Editor V. 4 & 5
T. Zimmerman	GRA		Geostatistics Test Problem

The foundation of the annual WIPP performance assessment is the underlying data set and understanding of the important processes in the engineered and natural barrier systems. Other SNL Departments are the primary source of these data and understanding. Assistance with the waste inventory comes from Westinghouse Electric Corporation and its contractors. We gratefully acknowledge the support of our departmental and project colleagues. Some individuals have worked closely with the performance assessment team, and we wish to acknowledge their contributions individually:

H. Batchelder	WEC	CH & RH Inventories
R. Beauheim	SNL	Natural Barrier System, Hydrologic Parameters
D. Borns	SNL	Geology, Geophysics
B. Butcher	SNL	Engineered Barrier System, Unmodified Waste-Form Parameters, Disposal Room Systems Parameters
L. Brush	SNL	Engineered Barrier System, Source Term (Solubility) and Gas Generation Parameters
L. Clements	ReS	Computer System Support
T. Corbet	SNL	Natural Barrier System, Geologic & Hydrologic Parameters, Conceptual Models
P. Davies	SNL	Natural Barrier System, Hydrologic & Transport Parameters, & 2-Phase Flow Mechanistic Modeling
P. Drez	DE	CH & RH Inventories
R. Finley	SNL	Repository Isolation Systems Parameters
F. Gelbard	SNL	Natural Barrier System, Retardation
E. Gorham	SNL	Natural Barrier System, Fluid Flow & Transport Parameters
R. Holt	CON	Geology
S. Howarth	SNL	Natural Barrier System, Hydrologic Parameters
R. Kehrman	WEC	CH & RH Waste Characterization
K. Lickliter	BEC	EPA Regulations
R. Lincoln	SNL	Room Modeling
F. Mendenhall	SNL	Engineered Barrier System, Unmodified Waste Form Parameters, Waste Panel Closure (Expansion)
D. Munson	SNL	Reference Stratigraphy, Constitutive Models, Physical & Mechanical Parameters
C. Novak	SNL	Natural Barrier Systems, Chemistry
E. Nowak	SNL	Room Modeling, Source Term
J. Orona	ReS	Computer System Support
A. Stevens	SNL	DOE Liaison

J. Tillerson	SNL	Repository Isolation Systems Parameters
W. Wawersik	SNL	Fracturing
S. Webb	SNL	2-Phase Flow Sensitivity Analysis & Benchmarking

* Affiliation

API	= Applied Physics Incorporated	ReS	= ReSpec
ASU	= Arizona State University	SAI	= Scientific Applications International Corporation
BEC	= Benchmark Environmental Corp.	SNL	= Sandia National Laboratories
CON	= Consultant	TEC	= Technadyne Engineering Consultants
DE	= Drez Environmental	TRI	= Tech Reps, Inc.
ECO	= Ecodynamics Research Associates	UHH	= University of Hawaii at Hilo
GC	= Geo-Centers Incorporated	UNM	= Univ. of New Mexico/New Mexico Engineering Research Institute
GRA	= GRAM, Inc.	UP	= University of Paris
GS	= Galson Sciences	WEC	= Westinghouse Electric Corporation
INT	= Intera		
MAC	= MACTEC		
PNL	= Pacific Northwest Laboratory		

Expert Panels

Futures

M. Baram	Boston University
W. Bell	Yale University
G. Benford	University of California, Irvine
D. Chapman	The World Bank, Cornell University
B. Cohen	University of Pittsburgh
V. Ferkiss	Georgetown University
T. Glickman	Resources for the Future
T. Gordon	Futures Group
C. Kirkwood	Arizona State University
H. Otway	Joint Research Center (Ispra), Los Alamos National Laboratory
M. Pasqualetti	Arizona State University
D. Reicher	Natural Resources Defense Council
N. Rosenberg	Resources for the Future
M. Singer	The Potomac Organization
T. Taylor	Consultant
M. Vinovski	University of Michigan

Markers

D. Ast	Cornell University
V. Baker	University of Arizona
M. Brill	Buffalo Organization for Social and Technological Innovation
F. Drake	University of California at Santa Cruz
B. Finney	University of Hawaii at Manoa
D. Givens	American Anthropological Association
W. Goodenough	University of Pennsylvania
M. Kaplan	Eastern Research Group
J. Lomberg	Consultant
L. Narens	University of California at Irvine
F. Newmeyer	University of Washington
W. Sullivan	University of Washington
W. Williams	Case Western Reserve University

Source Term

C. Bruton	Lawrence Livermore National Laboratory
I-Ming Chou	U.S. Geological Survey
D. Hobart	Los Alamos National Laboratory
F. Millero	University of Miami

Retardation

R. Dosch	Sandia National Laboratories
C. Novak	Sandia National Laboratories
M. Siegel	Sandia National Laboratories

Geostatistics Expert Group

G. de Marsily, Chair	U. of Paris
R. Bras	Massachusetts Inst. of Tech.
J. Carrera	U. Politécnica de Cataluña
G. Dagan	Tel Aviv U.
A. Galli	Ecole des Mines de Paris
S. Gorelick	Stanford U.
P. Grindrod	Intera Sciences
A. Gutjahr	New Mexico Tech.
D. McLaughlin	Massachusetts Inst. of Tech.
S. Neuman	U. of Arizona
C. Ravenne	Institut Français du Pétrole
Y. Rubin	U. of California, Berkeley

Report Preparation (TRI)

Editors:

Volume 1: M. Minahan (text); D. Marchand (illustrations)
Volume 2: M. Minahan (text); D. Marchand (illustrations)
Volume 3: J. Chapman (text); D. Pulliam (illustrations)
Volume 4: V. Gilliland, M. Minahan (text); S. Laundre-Woerner (illustrations)
Volume 5: S. Strong, F. Puffer (text); D. Marchand (illustrations)

D. Rivard and the Word Processing Department
R. Rohac, R. Andree, and the Illustration and Computer Graphics Departments
S. Tullar and the Production Department

Peer Review

Internal/Sandia

F. Mendenhall
L. Gomez

Management/Sandia

W. Weart

PA Peer Review Panel

R. Heath, Chair	University of Washington
R. Budnitz	Future Resources Associates, Inc.
T. Cotton	JK Research Associates, Inc.
J. Mann	University of Illinois
T. Pigford	University of California, Berkeley
F. Schwartz	Ohio State University

Department of Energy

J. Coffey

PREFACE

The *Preliminary Performance Assessment for the Waste Isolation Pilot Plant, December 1992* is currently planned to consist of six volumes. The titles of the volumes are listed below. All analyses reported in the 1992 Preliminary Performance Assessment, including those described in this volume, are based on computer modeling of disposal-system performance that was completed in November 1992.

This report is the fifth in a series of annual reports that document ongoing assessments of the predicted long-term performance of the Waste Isolation Pilot Plant (WIPP); this documentation will continue during the WIPP Test Phase. However, the Test Phase schedule and projected budget may change; if so, the content of the *1992 Preliminary Performance Assessment* report and its production schedule may also change.

Volume 1: Third Comparison with 40 CFR 191, Subpart B

Volume 2: Technical Basis

Volume 3: Model Parameters

Volume 4: Uncertainty and Sensitivity Analyses for 40 CFR 191, Subpart B

Volume 5: Uncertainty and Sensitivity Analyses of Gas and Brine Migration for Undisturbed Performance

Volume 6: Guidance to the WIPP Project from the December 1992 Performance Assessment

CONTENTS

Figures

Tables

1. INTRODUCTION

The Waste Isolation Pilot Plant (WIPP) is planned as a research and development facility to demonstrate the safe disposal of transuranic (TRU) wastes generated by defense programs of the United States Department of Energy (DOE). Before disposing of waste in the WIPP, the DOE must evaluate compliance with applicable long-term regulations of the United States Environmental Protection Agency (EPA), including 40 CFR 191, Subpart B (*Environmental Standards for the Management and Disposal of Spent Nuclear Fuel, High-Level and Transuranic Radioactive Wastes, Final Rule* [U.S. EPA, 1985]) and 40 CFR 268.6 (Petitions to allow land disposal of a waste prohibited under Subpart C of Part 268 [U.S. EPA, 1986]), which is the portion of the regulations implementing the Resource Conservation and Recovery Act (RCRA) that states the conditions for disposal of specified hazardous wastes. Performance assessments (PAs) will form the basis for evaluating compliance with all applicable long-term regulations of the EPA. The WIPP Performance Assessment (PA) Department of Sandia National Laboratories (SNL) is performing iterative preliminary PAs to provide guidance to the Project while preparing for final compliance evaluation. Previous preliminary PAs for 40 CFR 191, Subpart B, have been documented for 1990 (Bertram-Howery et al., 1990; Rechard et al., 1990; Helton et al., 1991) and 1991 (WIPP PA Division, 1991 a,b,c; Helton et al., 1992).

1.1 Purpose of Volume 5

This volume describes uncertainty and sensitivity analyses of gas and brine migration for undisturbed performance only (i.e., without a breach of the repository by human intrusion). The volume is part of a set documenting the 1992 preliminary PA, and is not intended to provide a stand-alone description of the WIPP or of the compliance-assessment modeling system. Some essential information from other volumes of the 1992 PA is repeated here as necessary, but in general, cross-references are given throughout to more complete discussions elsewhere. Volume 1 of the 1992 PA provides an overview of the 1992 preliminary comparison with 40 CFR 191, Subpart B. Volume 2 describes the technical basis for the compliance assessment modeling system, including conceptual model development, probability modeling, and consequence modeling. Volume 3 compiles model parameters, constructs cumulative distribution functions (CDFs), and discusses their derivation from the pertinent data of disposal-system characterization. Uncertainty and sensitivity analyses specifically related to 40 CFR 191, Subpart B, (including analyses of consequences of human intrusion) are contained in Volume 4. Volume 6 contains guidance to the WIPP Project derived from the entire 1992 PA. Similar analyses of undisturbed performance based on simulations completed earlier in 1992 are documented elsewhere (WIPP PA Department, 1992).

Analyses of undisturbed performance are of interest for both the Individual Protection Requirements (§ 191.15) of 40 CFR 191 and 40 CFR 268.6. As discussed in Volume 4 of this report, brine migration is of interest for 40 CFR 191 because of the potential for radionuclide transport in the liquid phase. Both gas and brine migration are of interest for 40 CFR 268.6 because of the potential for transport of regulated hazardous constituents in both gas and brine phases. However, the preliminary results reported are intended to provide interim guidance to the WIPP Project as it develops a compliance strategy for 40 CFR 268.6, and should not be used as the basis for regulatory decisions. The modeling system and data base remain incomplete, and one potentially important process, the pressure-dependent fracturing of anhydrite interbeds above and below the waste-emplacement region, has not been included in the 1992 PA. Furthermore, transport of radionuclides and heavy metals in brine and volatile organic compounds in gas is not modeled. Performance measures described here apply only to the migration of the fluid

phases and do not provide information about potential concentrations of contaminants within the fluids. If additional analyses of gas and brine migration continue to show a potential for gas migration beyond regulatory boundaries, a compliance determination for 40 CFR 268.6 will be based on evaluations of hazardous constituent concentrations using expanded data bases and more detailed computational models.

1.2 Requirements of 40 CFR 268.6

The *Land Disposal Restrictions* (40 CFR 268) regulate disposal of specified hazardous wastes. For the WIPP, hazardous constituents mixed with the radioactive transuranic waste can include solids such as lead and other heavy metals, and semivolatile and volatile organic compounds (VOCs) as residual liquids sorbed on waste materials or as gases associated with the waste in waste containers. A detailed inventory of the 40 CFR 268 contaminants anticipated for the WIPP is not available at this time, but a preliminary list of anticipated hazardous constituents were documented in the *Waste Isolation Pilot Plant No-Migration Variance Petition* (DOE, 1990). The Environmental Protection Agency (EPA) subsequently issued the *Conditional No-Migration Determination for the Department of Energy Waste Isolation Pilot Plant (WIPP),* which mandated waste characterization requirements for the WIPP Test Phase and recommended waste characterization data needs in support of any long-term performance assessment. Methods of sampling and analysis for volatile and semivolatile constituents have been developed for headspace gases (DOE, 1991a) and additional methods for analysis of hazardous constituents in homogeneous solid waste forms are under development as part of the *Waste Characterization Program Plan for WIPP Experimental Waste* (DOE, 1991b).

In general, 40 CFR 268 prohibits the disposal of hazardous wastes unless the owner or operator of the facility petitions for a variance and successfully demonstrates "to a reasonable degree of certainty, that there will be no migration of hazardous constituents from the disposal unit or injection zone for as long as the wastes remain hazardous" or the waste is treated in accordance with applicable standards (40 CFR 268.6 (a), U.S. EPA, 1986). General guidance provided by the EPA on the interpretation of this wording indicates that "no migration" will be defined to be concentrations of hazardous constituents below health-based or environmentally based levels at the disposal-unit boundary (U.S. EPA, 1992). Following guidance from the EPA (U.S. EPA, 1990a, p. 13073) the SNL WIPP PA Department has assumed for the purposes of these analyses that the length of the regulatory period is 10,000 yr.

1.2.1 Status of WIPP Compliance with 40 CFR 268.6

In response to a no-migration variance petition from the DOE (U.S. DOE, 1990a) the EPA issued a conditional no-migration determination (U.S. EPA, 1990b) allowing the emplacement of a limited amount of transuranic mixed waste in the WIPP for experimental purposes during the Test Phase (U.S. DOE, 1993). However, as the EPA states in the supplementary information included with the no-migration determination "[b]efore DOE may move from the test phase to full-scale operations, it must petition EPA again and demonstrate no migration over the long term, that is, it must successfully address current uncertainties about long-term WIPP performance" (U.S. EPA, 1990b, p. 47704). Long-term uncertainties specifically identified by the EPA include "the extent and effects of gas generation, the effects of brine inflow into the repository, and the influence of a 'disturbed rock zone' surrounding the mined repository" (ibid.).

1.2.2 The 40 CFR 268 Disposal Unit

The "disposal unit" for the WIPP as applied to 40 CFR 268.6 (RCRA) is defined to include the entire volume of the Salado Formation from top to bottom within the 41 km^2 (16 mi^2) WIPP land-withdrawal area (U.S. DOE, 1990b) (Figure 1-1). The SNL WIPP PA Department assumes for the purpose of PA modeling that the disposal-unit boundaries will remain unchanged for long-term performance. The RCRA disposal unit contains a smaller volume than that contained within the boundary of the accessible environment used in preliminary comparisons with 40 CFR 191, Subpart B (see Section 3.2 of Volume 1 of this report). As is the case for radionuclides regulated under 40 CFR 191, migration of hazardous constituents is allowed into the Salado Formation within the land-withdrawal area. Unlike the requirements of 40 CFR 191, however, migration of hazardous constituents into the Rustler Formation and other overlying strata within land-withdrawal area constitutes a potential violation.

1.2.3 Human Intrusion and 40 CFR 268.6

The extent to which estimates of the consequences of human intrusion will be required for long-term compliance evaluations has not been determined. The EPA has determined that human intrusion need not be considered for the Test Phase, and describes it as a long-term issue to "be addressed at the time a petition is considered for permanent disposal" (U.S. EPA, 1990b, p. 47720). Consideration of inadvertent human intrusion is required for compliance with 40 CFR 191, Subpart B, and analyses of the consequences of intrusion during exploratory drilling for hydrocarbons are described in detail in Volumes 1 and 4 of this report.

1.3 PA Methodology

Analyses have been performed using the Monte Carlo methodology and modeling system described in detail in Volume 2 of this report. In keeping with the requirement in 40 CFR 191.13 for probabilistic estimates of performance and a consideration of uncertainty in the results, this methodology relies on multiple realizations using deterministic models of physical processes and a Latin hypercube sampling (LHS) strategy to incorporate uncertainty for input parameters. Values for selected parameters are described by a range and distribution based on available data, and each simulation uses a separate input vector of sampled values drawn from the assigned distributions. The methodology is well suited for conducting uncertainty and sensitivity analyses that provide quantitative and qualitative insights about the potential variability in model results caused by uncertainty in specific input data (Helton et al., 1991, 1992; Helton, 1993). Sensitivity analysis techniques and methods for displaying their results have been summarized by Helton et al. (1991). Scatterplots and stepwise linear regression analyses are used in this volume to evaluate model sensitivity to uncertainty in sampled parameters.

Analyses described in this volume have been performed using the same modeling system and same vectors of sampled input parameters used for the analyses described in other volumes of the 1992 PA. As discussed in Chapter 3, selected parameters have been changed from the previous simulations to examine specific aspects of the disposal-system, such as shaft-seal system performance. Because these analyses are otherwise unchanged from those reported in Volume 4, direct comparisons may be made between specific realizations.

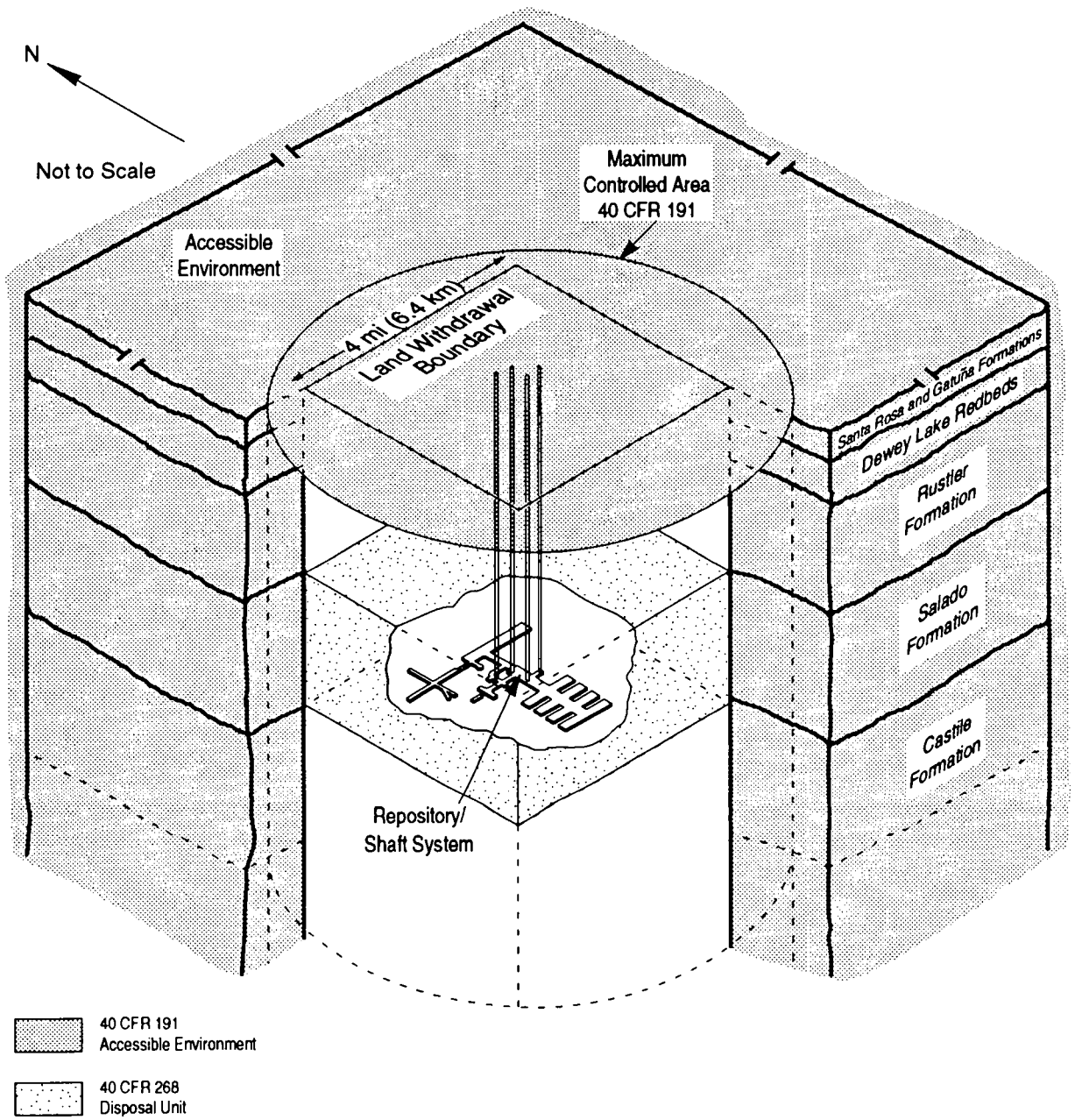

Figure 1-1. Artist's concept of the WIPP disposal system, showing the boundaries of the 40 CFR 268 disposal unit. Boundaries of the accessible environment as defined by 40 CFR 191, Subpart B, are shown for comparison. The scale of the repository/shaft system is exaggerated.

1.4 Cases Selected for Analysis

All analyses reported in this volume use a two-dimensional representation of the repository and surrounding strata as a vertical, north-south cross-section (described in detail in Chapter 2). This geometry is similar to that used in the analyses of undisturbed performance reported in Chapter 4 of Volume 4 of this report, differing only in the representation used for the shaft-seal system. Model stratigraphy is unchanged, and flow of both gas and brine is simulated in lithologies within the Salado Formation including halite, anhydrite Marker Beds 138 and 139, and anhydrite interbeds a and b (combined into a single model unit, anhydrite a + b) (Figure 1-2), as well as in the excavated regions of the repository and the overlying Rustler Formation (represented in the simplified model geometry only by the Culebra Member) (Figure 1-3).

Variations of the modeling system are used to simulate three separate cases: one in which the total volume of all four existing shafts is combined into a single shaft with the total cross-sectional area and the four-shaft-equivalent volume (as was done in Volume 4 of this report); a second case in which the volume and cross-sectional area of only a single shaft was modeled; and a third case using the four-shaft-equivalent-volume geometry in which the dynamic creep closure model was not used, and instead the waste-emplacement regions were assumed to have closed to a final porosity before gas-generation began. The first case represents the PA Department's preferred conceptual model for the behavior of the repository/shaft system. The second case was examined to simulate flow under conditions where only one shaft functioned as a migration pathway. The third case, analogous to cases analyzed in Volume 2 for human intrusion scenarios, was analyzed to provide insight into the effect of including dynamic creep closure on disposal-system performance.

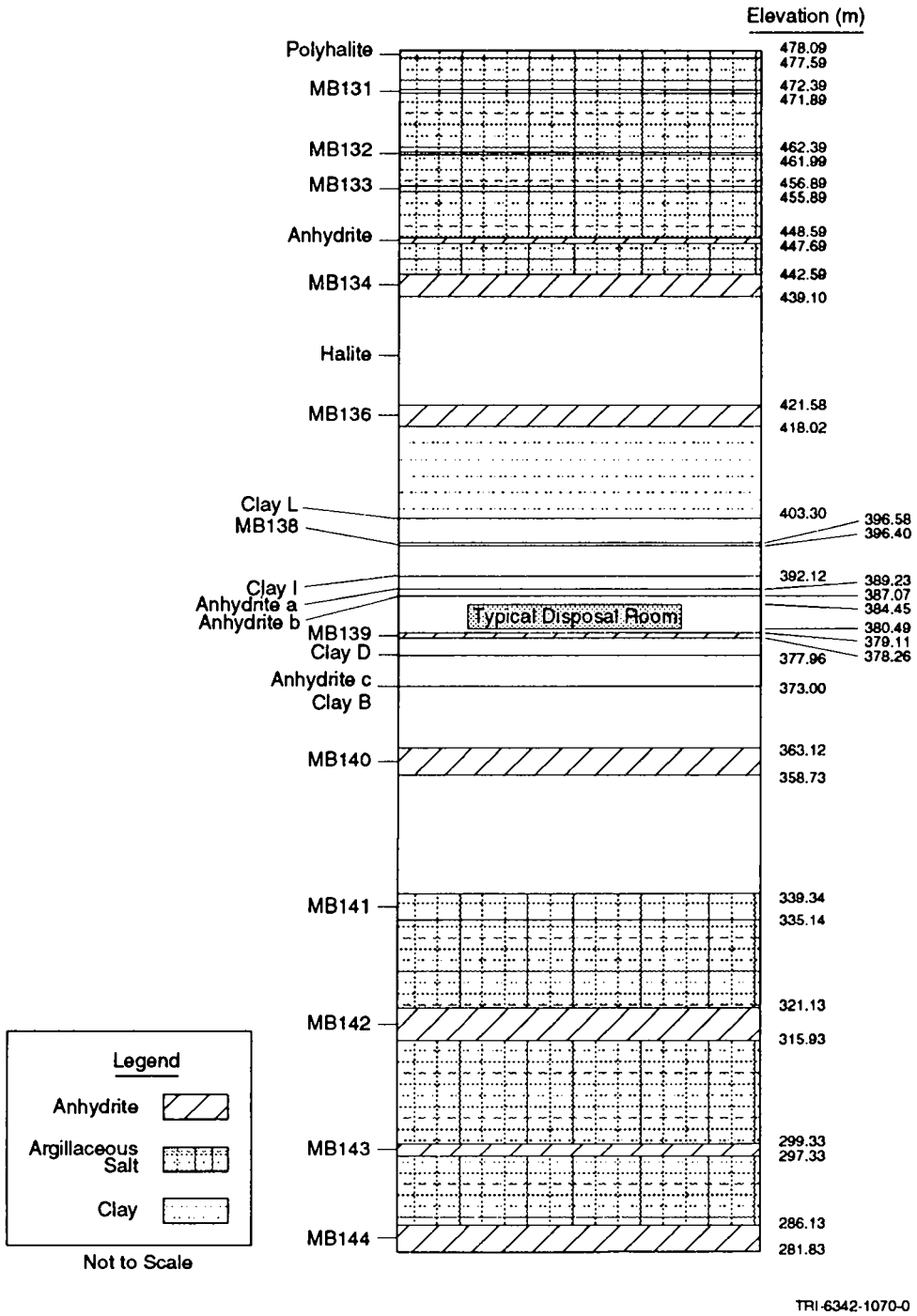

Figure 1-2. Stratigraphy within the Salado Formation near the repository elevation (after Munson et al., 1989).

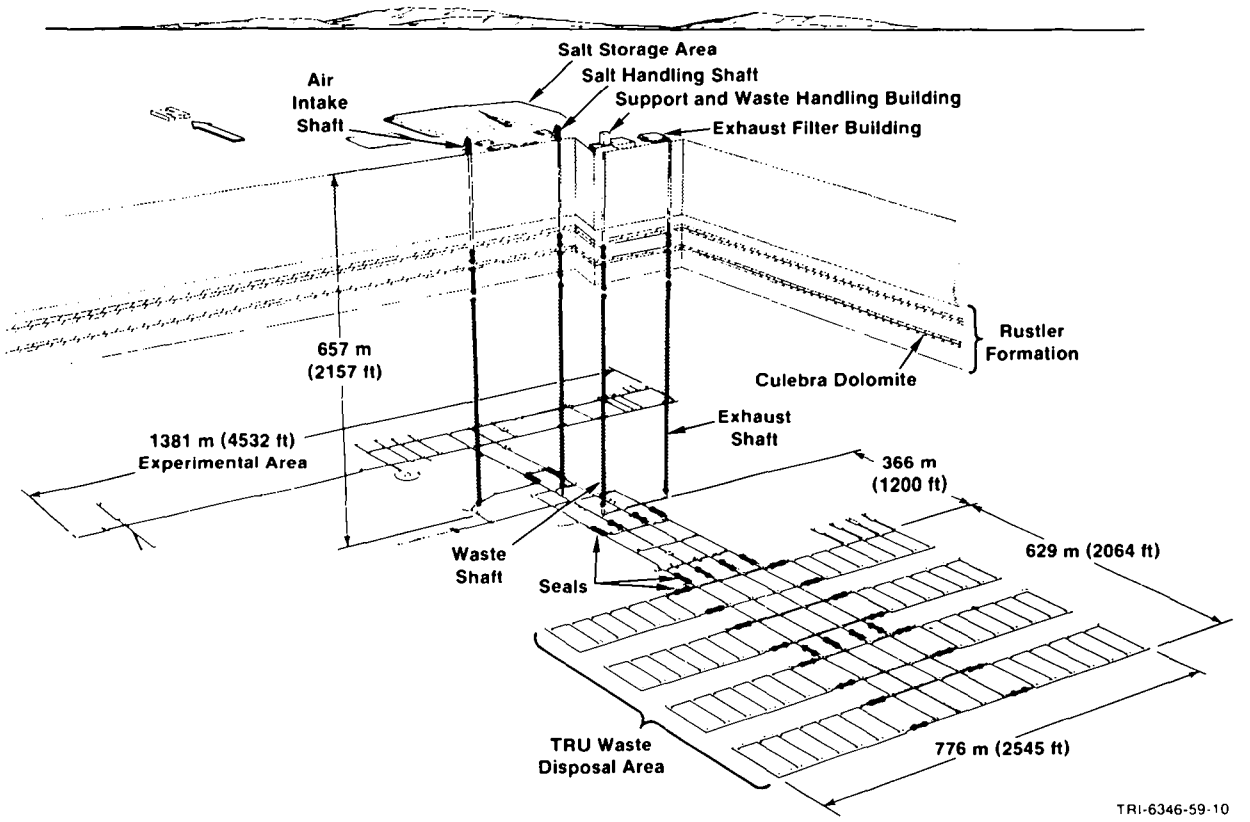

Figure 1-3. Proposed WIPP repository, showing transuranic-waste emplacement regions and location of the shafts.

2. MODEL DESCRIPTION

This chapter contains descriptions of the geometry, boundary conditions, and initial conditions for the repository model used in these simulations, as well as a brief discussion of the approach used to incorporate dynamic creep closure of the repository into the analysis. In general, the conceptual and computational models used to simulate the disposal system are essentially unchanged from those used in the previous volumes of the 1992 PA, and therefore much of the discussion has not been repeated here. Parameter values used to characterize the various components within the model are described in Chapter 3.

2.1 Conceptual Model for the Repository

The conceptual model used for the repository includes gas generation by corrosion of iron and microbial degradation of cellulosic waste; pressure-dependent two-phase (brine and gas) Darcy flow in the repository and the surrounding strata; development of a disturbed rock zone (DRZ) around the excavated area before the repository is sealed; dynamic pressure-dependent closure of the waste-emplacement region by halite creep after the repository is sealed; isolation of the waste by both panel and shaft seals; and possible fluid migration from the waste through anhydrite interbeds above and below the emplacement region and through the panel- and shaft-seal systems. Brine is assumed initially (i.e., before development of the DRZ) to fill the pore space in all strata surrounding the repository. Pressure-dependent fracturing of anhydrite interbeds as a result of gas generation is not yet included in the conceptual or computational model, but will be included in future PAs. Discussions of the other processes included in the conceptual model can be found in previous volumes of this report, together with extensive references to primary documents: gas generation is described in Sections 1.4.1 and 3.3 of Volume 3; two-phase flow is described in Section 7.2 of Volume 2; properties of the strata around the repository and the DRZ are described in Section 2.3.1 of Volume 2 and Chapter 2 of Volume 3; development of the DRZ and closure by halite creep is described in Chapter 4 of Volume 4; the panel- and shaft-seal systems are described in Section 2.3.2 of Volume 2 and Section 3.2 of Volume 3; and migration pathways are described in Section 4.2.3.1 of Volume 2.

2.2 Computational Model for the Repository/Shaft System

Analyses reported in this volume do not include radionuclide transport or human intrusion, and therefore the computational model for the repository/shaft system uses only two of the computer codes described in previous volumes, BRAGFLO and SANCHO. BRAGFLO (WIPP PA Division, 1991b) simulates gas generation and two-phase flow in the entire model domain, and is described in Appendix A of Volume 2 of this report. SANCHO (Stone et al., 1985) is a finite-element program for the quasistatic, large deformation, inelastic response of two-dimensional solids, and is used to simulate halite creep. The implementation of SANCHO results in BRAGFLO, in terms of emplacement-room porosity as a function of pressure, is described in Chapter 4 of Volume 4.

2.3 Model Geometry

The mesh used in the BRAGFLO simulations attempts to incorporate radial flow phenomena at large distances from the repository and to include the full accessible volume available for multiphase flow. Time and cost constraints currently preclude a full three-dimensional representation of the repository and surrounding strata, so a two-dimensional approximation to the actual geometry was made. In reducing the three dimensions to two, certain measures were preserved. The single most important measure is the volume of various regions. In constructing the mesh (Figure 2-1), the full initial excavated volumes of all excavated regions were preserved. This includes the repository, the drift seals and drift backfill, the shaft, and the experimental region. In addition, the volume of the formations surrounding the repository and other excavated regions could be preserved. In order to include the true volumes of each of these regions, but still reduce the dimensionality to two, other measures had to be compromised. Which of these were preserved and which were compromised in some fashion determined how the mesh was constructed.

The mesh was developed as follows. The repository was modeled as a single large room, with a volume the same as currently planned for the entire waste disposal region, including all rooms and drifts. The initial excavated height, 3.96 m, was preserved. This was desirable because the creep closure treatment is based on porosity changes in a newly excavated and filled room. The height of the room, along with its initial porosity, is one of the few features that can be maintained identically between the original salt creep model done using SANCHO and the model as implemented in BRAGFLO. (This is described briefly in Section 2.1 and in more detail in Section 4.2.2.2 in Volume 4 of this report). It was also considered desirable to preserve the overall length in the north-south direction (847 m). This distance was somewhat arbitrary; it represents a compromise in the maximum distance that contaminated brine must flow from one end of the repository to the access drifts leading to the shaft. In the true repository configuration, some brine could flow a greater distance (e.g., starting from the far southwest corner of the southwest panel). On the other hand, some of this brine is already *at* the drift seals leading to the shaft, so some compromise was necessary. Having fixed the volume, height, and length of the repository, the east-west dimension must be 131.7 m.

The dimensions of the other excavated regions were established in a similar fashion. The distance from the north end of the repository to the nearest shaft (the Waste Shaft) was maintained at 332 m. The height of the access drifts, as well as of the experimental region, was fixed at the same initial excavated height of the waste-disposal region to simplify the mesh. In reality, access drifts and experimental rooms vary in height from about 3.7 to 4.9 m. Having specified the length, height, and volume of the sealed and backfilled access drifts, the width of that region was fixed at 30.35 m, which was approximately the combined widths of the four north-south drifts. Similarly, the distance from the Waste Shaft to the northernmost end of the experimental region was preserved at 561 m, so the east-west width of that region is 49.5 m.

In the base case, the shaft is a composite of the four existing shafts. The volume of the four combined shafts was preserved, and the height was set by the stratigraphy. The horizontal cross-sectional area was therefore the sum of the cross-sectional areas of the four shafts, 94.9 m^2. It seemed most reasonable to model the shaft as having a square cross section, although the shape is not likely to be important. Thus, the shaft is modeled as a square column 9.74 m on each side. The portion of the shaft below the Rustler Formation but above the shaft seal is referred to as the lower shaft. The upper shaft, above the Culebra, is not modeled here.

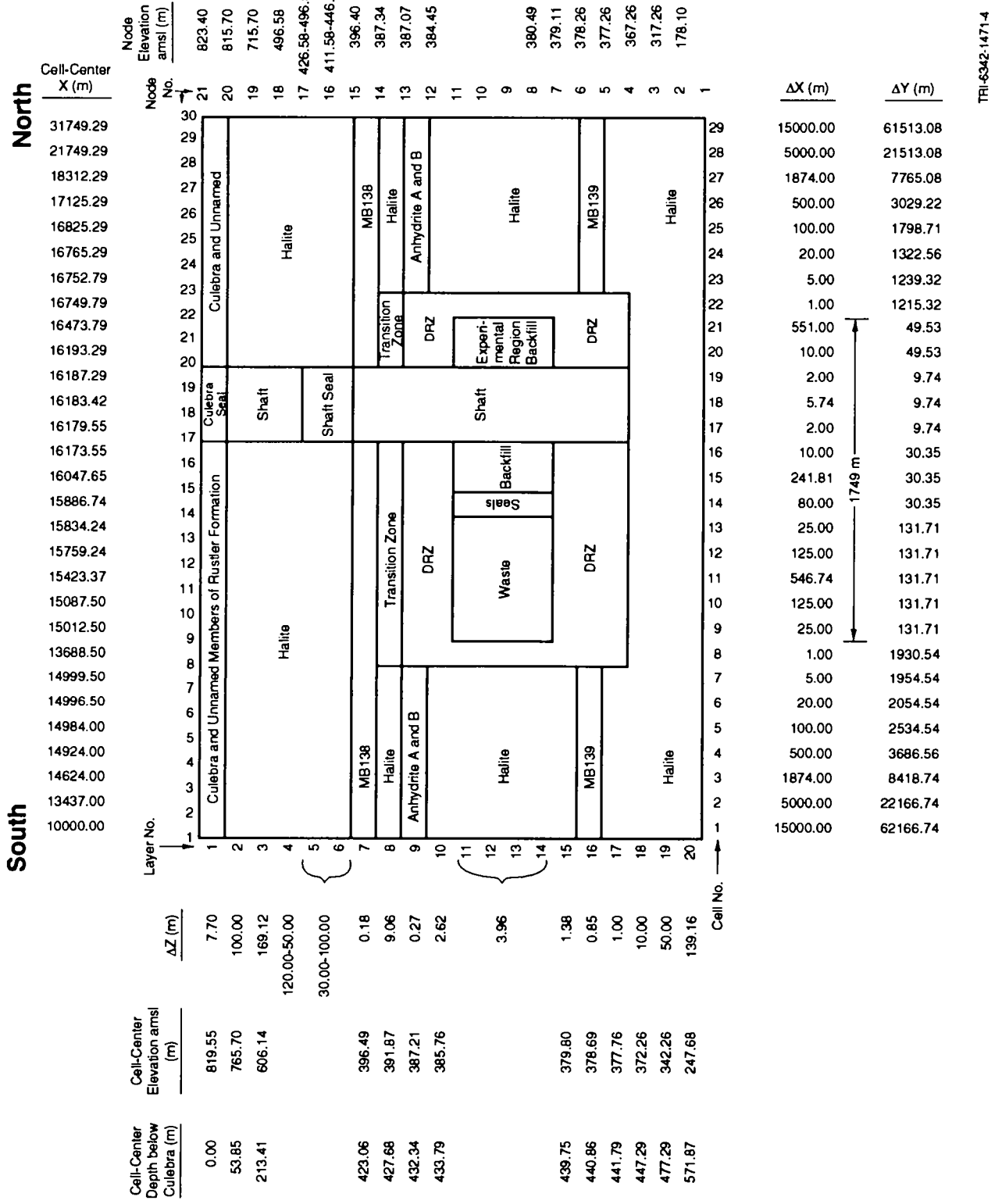

Figure 2-1. North-south vertical cross-section showing dimensions of the mesh used in BRAGFLO calculations for this volume.

This completely specifies the sizes and shapes of the excavated regions. The next step was to build the mesh surrounding these regions. The objective was to include at any given horizon the entire accessible pore space as far as the mesh extended, that is, to include the pore volume in the east-west direction to the same extent as in the north-south direction. In a plan view at the repository horizon, Figure 2-2, this is done by including volume east and west of the excavated region in the volume of grid cells to the north and south of the excavated regions.

If the model were radially symmetrical, this would be easily accomplished by requiring that the east-west dimension, or Δy, be equal to $2\pi r$, where r is the radial distance from the axis of symmetry. Voss (1984) shows that when Δy is varied in this manner using rectilinear geometry, the results are exactly equivalent to solving a true radial problem. This geometry was used in the WIPP PA for human intrusion scenarios, as described in Volumes 2 and 4 of this report. Unfortunately, the geometry that has to be used in the undisturbed scenario is not radially symmetrical. It is not clear how the mesh should be "flared" in the Δy-direction at each end of the excavated regions in order to mimic radial symmetry with complete accuracy, if indeed it can be done rigorously. The procedure used in the current calculations essentially divides the excavated regions in two along a vertical east-west plane. Then layers of thickness Δx are "unwrapped" from the outside of the excavated region. The total length of each unwrapped layer becomes the Δy corresponding to that grid cell. Figure 2-3 illustrates this unwrapping. At a given elevation, a layer in the vertical direction of thickness Δz and horizontal north-south width Δx includes the volume of a segment with cross section $\Delta x \Delta z$ both from the east side and the west side of the excavated region.

An example will help clarify the procedure. The first grid block south of the repository, Cell 8, is $\Delta x_8 = 1$ m long in the north-south dimension (Figure 2-3). In the east-west direction, the dimension Δy_8 is the sum of the lengths of five segments: 8S, 8E, 8W, 8NE, and 8NW. The first segment (8S in Figure 2-2) is the east-west width of the repository, 131.7 m. The second is the length of a Δx_8-thick segment, 8E, that extends along the entire east side of the repository, plus $2\Delta x_8$, or 848.7 m. The third segment, 8NE, wraps around the north end of the repository, ending at the seals and backfill regions, for a length of 50.7 m. The fourth and fifth segments, 8W and 8NW, are duplicates of the second and third, respectively, except that they wrap around the west side of the repository. Thus, the total width of Cell 8 after it is unwrapped is $\Delta y_8 = 131.7 + 2(848.7 + 50.7) = 1930.5$ m. For Cells 7, 6, and 5, Δy is evaluated in exactly the same manner. Because the same process is carried out at the north end of the mesh, the segments along the east and west sides of the repository will eventually run into the line dividing the north and south ends of the mesh, and will no longer wrap around the north end of the repository. Only Cells 5-8 will wrap around the north end of the repository. Beginning with Cell 4, the segments along the east and west sides of the repository (before being unwrapped) now intersect the north-south midpoint of the mesh, but otherwise each Δy is evaluated the same as for Cells 5-8. Thus, all of the volume of the strata surrounding the excavated regions is included in the mesh. This representation is not strictly equivalent to cylindrical geometry, but is reasonably accurate at large distances from the repository. Very near the repository, this representation requires all flow to go past the end of the repository, rather than through the sides, producing some loss of accuracy.

This two-dimensional approximation to three-dimensional geometry will be necessary until full three-dimensional simulations become technically and economically feasible. It is doubtful that the full suite of PA simulations can ever be carried out in three dimensions. However, a more limited set will necessarily be done in three dimensions to confirm the approximations used in the two-dimensional calculations. A fast, robust, iterative solver combining a conjugate gradient preconditioner with a multigrid solution algorithm is being adapted to BRAGFLO. Together with newer machines that are more than an order of magnitude faster that those currently used, full three-dimensional simulations should be more practical by next year.

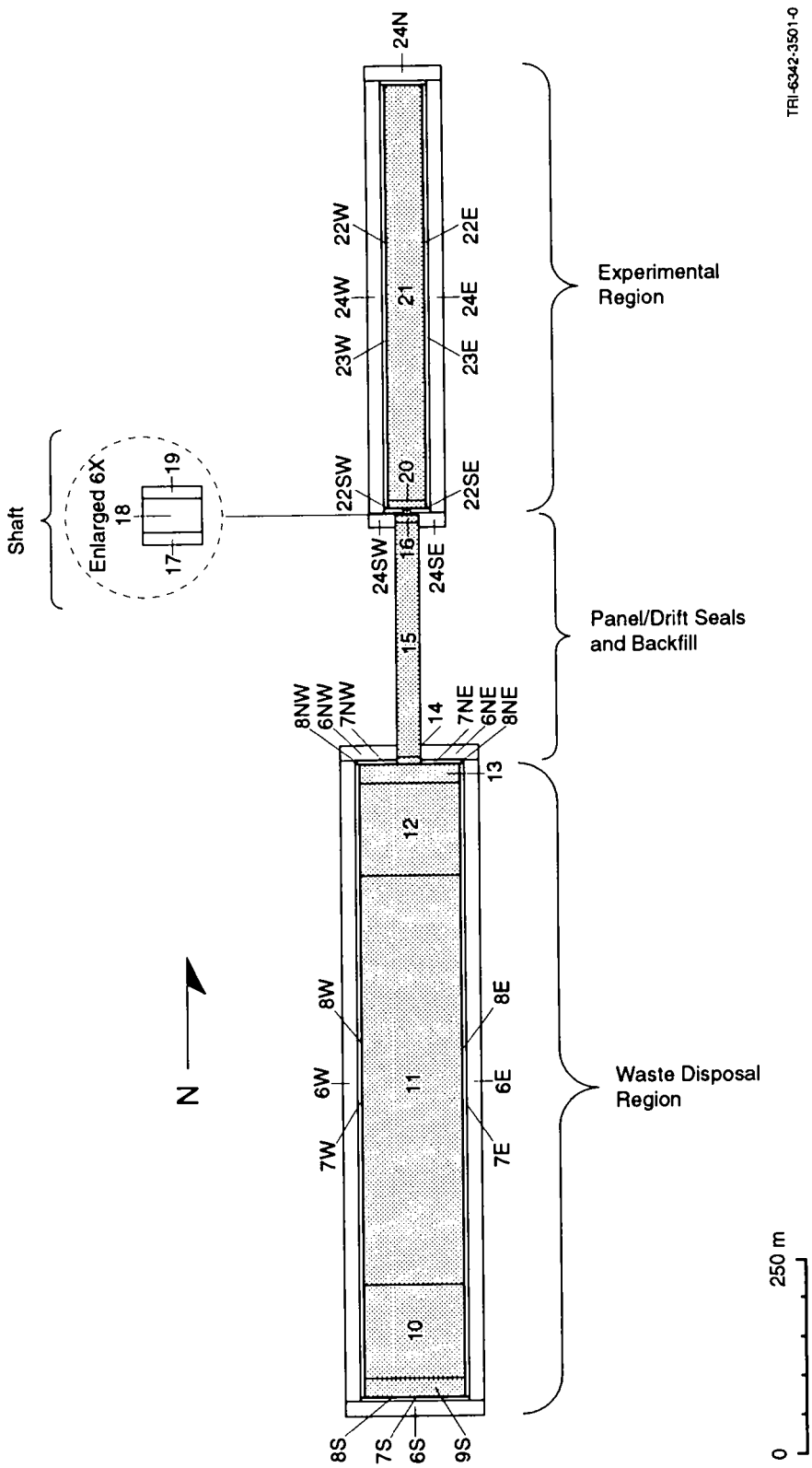

Figure 2-2. Plan view of grid cells 6-8 and 22-24 as initially wrapped around excavated regions.

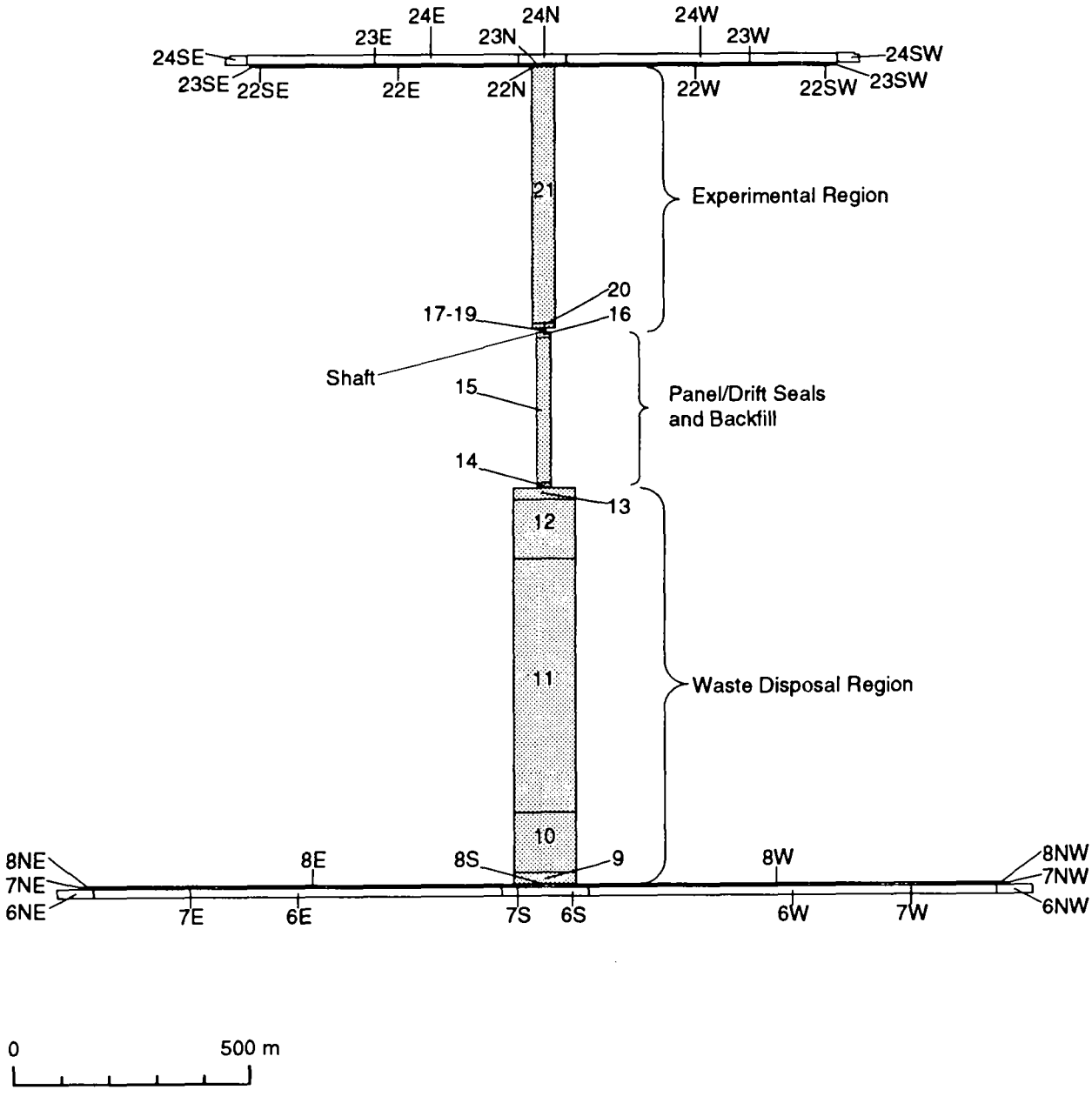

Figure 2-3. Plan view of grid cells after they are unwrapped from around the excavated region.

2.4 Boundary and Initial Conditions

Boundary conditions were the same as in all previous BRAGFLO calculations done for PA: there was no flow in the normal directions across all far-field boundaries except the lateral boundaries of the Culebra, where the initial pressure of 1.053 MPa was held constant throughout the simulations. Initial far-field pressure in the Salado Formation was varied hydrostatically from the sampled value for pressure in MB139. This resulted in a pressure discontinuity at the boundary between the Salado and the Culebra that had little effect on fluid flow because of the low permeability of the halite.

Initial conditions were treated the same as for the undisturbed performance calculations discussed in Volume 4 of this report. Rather than simply specifying uniform pressures and saturations in each region at time zero, spatially varying initial conditions were computed over a 50-yr operational or disposal period. This enabled more realistic pressure and saturation distributions to be established in the formations surrounding the repository at the time when the repository is sealed. The procedure used to calculate initial conditions will be summarized here; a more detailed description can be found in Section 4.3 of Volume 4.

During the disposal phase of the WIPP, brine will seep in continually from the surrounding formations, reducing the pressure in the vicinity of the excavated regions. Water in the brine will evaporate into the well-ventilated atmosphere of the excavations or will be pumped out if it accumulates anywhere. Thus, the formations surrounding the excavations will be dewatered and depressurized during the operation. By modeling the time between excavation and decommissioning explicitly, the conditions at decommissioning (time zero) will be much more realistic. In the absence of this calculation, certain unrealistic results are obtained. Foremost among these is the large quantity of brine that immediately drains into excavated regions, in particular the waste, owing to the large pressure gradient between the initially pressurized surrounding formations and the atmospheric excavations. Because brine will be continuously removed during the time each panel is open, it would be incorrect to assume that it is still available to react with waste components to produce gas. When this brine is assumed to react with waste the result is erroneously large estimates of gas generation and inaccuracies in the predicted interaction of gas generation and brine and gas flow throughout the modeled region.

The duration of the disposal phase of the WIPP was assumed to be 50 yr. This may be excessively long for this calculation even if it is an accurate estimate of the duration of the disposal phases because panels will be excavated as needed, not simultaneously, and will be scaled after only a few years. Therefore, only a portion of the excavation is open to the atmosphere at any given time. However, the initial condition calculation does not appear to be highly sensitive to the duration. Most of the depressurization and drainage occurs during the first 20 yr, the duration used in the disturbed performance assessment. A longer duration was used in the undisturbed performance assessment to be consistent with the longer duration of the disposal phase when considering the entire repository instead of a single panel.

The important features of this 50-yr disposal phase or initial condition calculation are as follows. At the beginning of this calculation, pressure in the shaft, drifts, waste, and experimental region are atmospheric (0.101 MPa) and fully gas-saturated. In all other regions, the pressure is hydrostatic relative to the pore pressure in MB139, which is sampled from a range of 12 to 13 MPa. These regions are assumed to be fully brine-saturated. So far, this is how previous PA calculations started at time zero; now they are starting at -50 yr. After 50 yr (i.e., at time zero when the disposal region is sealed), pressure in the waste is reset to atmospheric from the calculated value

(in most realizations very slightly above atmospheric), and the brine saturation in the waste is set to its sampled value. Any brine in the waste in excess of the sampled saturation is ignored, simulating its disappearance by evaporation or pumping. In all other excavated regions, the brine saturation is set to 1.0, and the pressure is reset to atmospheric. (A hydrostatic gradient would be more accurate, but because of the high permeability of these regions, this is achieved very quickly and much more conveniently in the course of the calculations after time zero.) The permeability of each region is reset at this time. Excavated regions were originally given a very high permeability (1.0×10^{-10} m^2) and a porosity of 1.0 to simulate cavities. At time zero, these regions take on different characteristics, becoming seals or backfill, each with different permeabilities and porosities, as described in Section 3.

The DRZ receives special treatment. The porosity of the DRZ is assumed to increase at time zero from the porosity of intact halite to the porosity of the highly fractured disturbed zone. One of the more important objectives of this initial condition calculation is to account more accurately for mobile brine content of the DRZ. In previous PA calculations, the DRZ was assumed to be fully saturated at time zero, with a relatively large permeability. This allowed large quantities of brine to drain from the DRZ into the waste, providing much of the brine source for gas generation. The current initial condition calculation recognizes that much of this brine will have been removed during the disposal phase of the WIPP. Therefore, when the porosity of the DRZ increases at time zero, the brine volume is held constant, and the additional pore volume is filled with gas. The pressure in the DRZ, already very close to atmospheric, is set to atmospheric (0.101 MPa) to preclude any gas drive from being artificially created when the DRZ porosity is changed. Such a gas drive could force an immediate and unrealistic surge of remaining DRZ brine into the waste.

The calculations proceed from this calculated initial condition for the 10,000-yr performance period. The most important effect of these more realistic initial conditions is that less brine will flow into the excavated regions (including the waste), because the initial "surge" of brine that occurs upon excavation has been eliminated, and the pressure gradients in the immediate vicinity of excavations have been greatly reduced.

At time zero, waste is assumed to have some initial brine saturation that is available for waste degradation. This is a sampled parameter, ranging from 0.0 to 0.14. When it arrives at the WIPP, waste is expected to contain some small quantity of free liquid. For BRAGFLO simulations, this liquid is assumed to be Salado brine; its actual composition is unknown. The actual liquid content, or saturation, is also unknown. In 1991, the initial brine saturation was varied from 0.0 to 0.276. The maximum (0.276) is the assumed residual brine saturation of the waste (WIPP PA, 1991c). In the absence of real data, residual saturation was selected as the maximum liquid that the waste could contain and still comply with transportation regulations (U.S. DOE, 1991c) that prohibit transporting any waste that contains significant quantities of mobile liquids, i.e., liquids that can flow and, therefore, exceed residual saturation. In 1992, the maximum initial brine saturation was reduced to 0.14. This reduction was necessitated by numerical constraints imposed by the creep closure model that was implemented in 1992. Thus, the range of values over which the initial brine saturation is sampled (0.0 to 0.14) is somewhat arbitrary. However, the range does satisfy two other important criteria: (1) It includes values of initial brine saturation that are physically reasonable and possible. (2) It is sufficiently broad to enable sensitivity analyses to determine how initial brine saturation affects the performance of the WIPP.

2.5 Summary of Model Assumptions

Table 2-1 contains a list of important assumptions made in modeling for the sensitivity analyses reported in this volume. In general, the impact of these assumptions on disposal-system performance is difficult to quantify. Complexities of the coupled processes affecting two-phase flow preclude predictions about how the system will respond to specific changes in modeling assumptions. Assumptions that have a high potential to affect performance, such as the omission of pressure-dependent fracturing of anhydrite interbeds, will be investigated in future analyses as improvements are made in the PA modeling system.

Table 2-1. Partial List of Assumptions Used in the BRAGFLO Analyses of Undisturbed Performance Reported in Volume 5 of the 1992 WIPP PA

General Assumptions
Brine and gas flow obeys generalized Darcy's Law for compressible fluids in all media. Pore space is fully interconnected in all regions.
Dimensions of all regions are fixed and do not change with time.
All gas is assumed to have the physical properties of hydrogen.
All liquid is assumed to be Salado Formation brine.
Gas does not dissolve in brine.
Pressure-dependent fracturing of anhydrite interbeds does not occur.
Stratigraphy is simplified as shown in Section 2.1.
Initial conditions calculated by simulating a 50-yr operational period during which the repository remains open. Time t_0 for the 10,000 yr simulations is at the end of the operational phase, when the repository is sealed. Permeabilities, porosities, and saturations are adjusted at this time as described in Ch. 4 of Volume 4 of this report.
Permeabilities and porosities of selected regions are adjusted at 200 yr to reflect consolidation of the seal system (this volume only).
No hysteresis in capillary pressure curves.
Permeabilities and porosities sampled independently. (Sufficient data are not yet available to correlate permeability with porosity.)
No-flow boundaries everywhere except far-field Culebra, where pressure is specified.
Klinkenberg effect is ignored.

Table 2-1. Partial List of Assumptions Used in the BRAGFLO Analyses of Undisturbed Performance Reported in Volume 5 of the 1992 WIPP PA (Continued).

Halite Assumptions
Permeability specified, and constant in time.
Initial (pre-excavation) porosity specified; varies with pressure (because of compressibility); unchanged at t_0.
Initial brine saturation specified; unchanged at t_0.
Initial pressures specified, vary with depth; pressures at t_0 are calculated.
Threshold capillary pressure a function of permeability; constant in time.
Anhydrite Assumptions
Permeability specified and constant in time.
Initial porosity specified as same as intact halite; varies with pressure (because of compressibility).
Initial saturation specified.
Initial pressure specified.
Threshold capillary pressure a function of permeability; constant in time.
MB138 not included in the DRZ above the repository.
Disturbed Rock Zone (DRZ) Assumptions
Includes what was originally intact halite between the repository and MB139 and anhydrite a + b; also includes what was originally intact MB139 and anhydrite a + b directly above and below the repository; also includes (for this volume only) one meter of what was originally intact halite below MB139 beneath the repository.
Permeability specified and constant during operational phase; changes at t_0 and is constant thereafter; the DRZ does not "heal."
Threshold capillary pressure is zero and constant in time.

Table 2-1. Partial List of Assumptions Used in the BRAGFLO Analyses of Undisturbed Performance Reported in Volume 5 of the 1992 WIPP PA (Continued).

Initial porosity specified as same as intact halite; varies with pressure (because of compressibility); changes at t_0.
Initial brine saturation specified, variation calculated during operational phase as brine flows in or out. At t_0, brine volume is conserved when porosity changes; brine saturation changes and added pore volume is filled with gas.
Initial pressure same as that of intact halite at the same elevation; calculated during operational phase. Pressure set to atmospheric at t_0.
Transition Zone Assumptions
Located in what was originally intact halite between anhydrite a+b and MB138 above the repository.
Permeability specified as same as that of anhydrite; constant in time.
Initial porosity specified as same as intact halite; varies with pressure (because of compressibility).
Initial saturation specified.
Initial pressure specified.
Threshold capillary pressure a function of permeability; constant in time.
Culebra Assumptions
Initial permeability zero; at t_0, nonzero permeability specified, uniform, and constant in time.
Initial porosity specified, varies with pressure (because of compressibility).
Initial saturation specified.
Initial pressure specified, <u>not</u> in hydrostatic equilibrium with underlying halite; far-field pressure constant.
Threshold capillary pressure a function of permeability; constant in time.

Table 2-1. Partial List of Assumptions Used in the BRAGFLO Analyses of Undisturbed Performance Reported in Volume 5 of the 1992 WIPP PA (Concluded).

Waste/Disposal Region Assumptions
Initially treated as an empty cavity; very high permeability, porosity equals 1.0 and is constant in time; threshold capillary pressure zero and constant in time; pressure is atmospheric; no gas generation.
At t_0, waste and all panel seals are emplaced simultaneously, and all properties change.
Permeability specified, constant in time, independent of porosity.
Threshold capillary pressure zero and constant in time.
Pressure at t_0 is atmospheric, calculated for later times.
Brine content at end of operational phase is discarded (assumed to be removed by ventilation); brine saturation at t_0 is saturation of the newly emplaced waste.
Gas-generation rate is dependent on degree of brine saturation, ranging from humid rate to inundated rate; rate is zero if brine saturation is zero. If brine is present, gas continues to be generated until all corrodible and biodegradable material is consumed. No functional dependence of rate on pressure or chemistry. Corrosion consumes water. Biodegradation requires the presence of water. Mineral precipitation is ignored.
Dynamic creep closure as a function of pressure in waste results in large porosity changes from the initial specified porosity; porosity changes only as pressure increases, and varies slightly (because of compressibility) if pressure decreases. Dimensions of the modeled waste-disposal region remain constant in time regardless of porosity.

3. UNCERTAIN VARIABLES USED IN SIMULATIONS OF UNDISTURBED PERFORMANCE

Previous volumes of the 1992 WIPP performance assessment selected 49 imprecisely known variables for consideration (see Table 3-1 of Volume 4 of this report). Nineteen of these parameters are used in simulations of gas and brine migration for undisturbed performance, either directly or to derive the parameters used as BRAGFLO input. Sampled values for these 19 parameters are unchanged in this volume from those used in other analyses in the 1992 PA and are as reported in Appendix C of Volume 4. Six additional parameters related specifically to the performance of the shaft-seal system have been included in sampling for this volume. Values for these parameters are provided in Appendix B of this report, together with values of parameters derived from sampled variables and used directly in BRAGFLO.

Table 3-1 identifies the 25 variables sampled for these analyses, and provides information about ranges, distributions, and sources of additional information for each. The nineteen variables unchanged from earlier volumes are listed first, and are followed by the six additional variables added for these analyses.

Table 3-1. Variables Sampled in 1992 WIPP Performance Assessment[a]

Variable	Definition
BCBRSAT	Residual brine saturation for Salado Formation (S_{lr}) (dimensionless). Range: 0.0 to 0.4. Median: 0.2. Distribution: Uniform. Additional information: Section 2.3.1, Volume 3. Variable 13 in Latin hypercube sample (LHS).
BCEXP	Brooks-Corey pore-size distribution parameter for Salado Formation (λ) (dimensionless). Range: 0.2 to 10. Median: 0.7. Distribution: Piecewise uniform. Additional information: Same as BCBRSAT. Variable 11 in LHS.
BCFLG	Pointer variable (flag) for selection of characteristic curve sub-model. Range: 0 or 1. Distribution: 33% 0, 67% 1. Value of 0 selects Van Genuchten/Parker Model; value of 1 selects Brooks-Corey model. Additional information: Section 2.3.1, Volume 3. Variable 12 in LHS.
BCGSSAT	Brooks-Corey residual gas saturation for Salado Formation (S_{gr}) (dimensionless). Range: 0.0 to 0.4. Median: 0.2. Distribution: Uniform. Additional information: Same as BCBRSAT. Variable 14 in LHS.

Table 3-1. Variables Sampled in 1992 WIPP Performance Assessment (Continued)

Variable	Definition
BRSAT	Initial liquid (brine) saturation of waste (dimensionless). Range: 0 to 0.14. Median: 0.07. Distribution: Uniform. Additional information: Section 3.4.3, Volume 3. Variable 1 in LHS.
CULPOR	Matrix porosity (Θ_m) in Culebra (dimensionless). Range: 5.8×10^{-2} to 2.53×10^{-1}. Median: 1.39×10^{-1}. Distribution: Piecewise uniform. Additional information: Table 4.4, Kelley and Saulnier, 1990; Table E-8, Lappin et al., 1989; Section 2.6.2, Volume 3. Variable 43 in LHS.
GRCORHF	Scale factor used in definition of gas generation rate for corrosion of steel under humid conditions (dimensionless). Actual gas generation rate is GRCORH=GRCORHF • GRCORI. Range: 0 to 0.5. Median: 0.1. Distribution: Piecewise uniform. Additional information: Memo from Brush, July 8, 1991, contained in Appendix A, WIPP PA Division, 1991c; Section 3.3.5, Volume 3. Variable 3 in LHS.
GRCORI	Gas generation rate for corrosion of steel under inundated conditions (mol/m^2•s surface area steels). Range: 0 to 1.3×10^{-8}•s. Median: 6.3×10^{-9}. Distribution: Piecewise uniform. Additional information: Same as GRCORHF. Variable 2 in LHS.
GRMICHF	Scale factor used in definition of gas generation rate due to microbial degradation of cellulosics under humid conditions (mol/kg cellulosics•s). Actual gas generation rate is GRMICH = GRMICHF • GRMICI. Range: 0 to 0.2. Median: 0.1. Distribution: Uniform. Additional information: Same as GRCORHF. Variable 6 in LHS.
GRMICI	Gas generation rate due to microbial degradation of cellulosics under inundated conditions (mol/kg•s cellulosics). Range: 0 to 1.6×10^{-8}. Median: 3.2×10^{-9}. Distribution: Piecewise uniform. Additional information: Same as GRCORHF. Variable 5 in LHS.
MBPERM	Permeability (k) in intact anhydrite marker beds in Salado Formation (m^2). Range: 1×10^{-21} to 1×10^{-16}. Median: 5.0×10^{-20}. Distribution: Piecewise loguniform. Correlation: 0.3 rank correlation with SALPERM. Additional information: Section 2.4.2, Volume 3. Variable 15 in LHS.
MBPOR	Porosity (ϕ) in intact anhydrite marker beds in Salado Formation (dimensionless). Range: 1×10^{-3} to 3×10^{-2}. Median 1×10^{-2}. Distribution: Piecewise uniform. Additional information: Section 2.4.4, Volume 3. Variable 16 in LHS.

Table 3-1. Variables Sampled in 1992 WIPP Performance Assessment (Continued)

Variable	Definition
MBPRES	Far Field Pressure (p) in Salado formation at the MB139 elevation. Range: 1.2×10^7 to 1.3×10^7. Median: 1.25×10^7. Distribution: Uniform. Additional information: Section 2.4.3, Volume 3. Variable 18 in LHS.
SALPERM	Permeability (k) in intact halite component of Salado Formation (m^2). Range: 1×10^{-24} to 1×10^{-19}. Median: 2×10^{-21}. Distribution: Piecewise loguniform. Correlation: 0.3 rank correlation with MBPERM. Additional information: Memo from Gorham et al., June 15, 1992, contained in Appendix A, Volume 3; Howarth et al., 1991; Beauheim et al., 1991; Section 2.3.5, Volume 3. Variable 10 in LHS.
STOICCOR	Stoichiometric coefficient for corrosion of steel (dimensionless). Defines proportion of two different chemical reactions taking place during the corrosion process. Range: 0 to 1. Median: 0.5. Distribution: Uniform. Additional information: Brush and Anderson in Lappin et al., 1989, p. A-6; Section 3.3.5, Volume 3. Variable 4 in LHS.
STOICMIC	Stoichiometric coefficient for microbial degradation of cellulosics (mol gas/mol CH_2O). Range: 0 to 1.67. Median: 0.835. Distribution: Uniform. Additional information: Brush and Anderson in Lappin et al., 1989, p. A-10; Section 3.3.5, Volume 3. Variable 7 in LHS.
TZPORF	Scale factor used in definition of transition zone and disturbed rock zone porosity (ϕ_z), with the transition zone and disturbed rock zone porosity defined by TZPOR = SALPOR + (0.06 - SALPOR) • TZPORF. Range 0 to 1. Median: 0.5. Distribution: Uniform. Additional information: Section 2.4.4, Volume 3. Variable 17 in LHS.
VMETAL	Fraction of total waste volume that is occupied by IDB (Integrated Data Base) metals and glass waste category (dimensionless). Range: 0.276 to 0.476. Median: 0.376. Distribution: Normal. Additional information: Section 3.4.1, Volume 3. Variable 9 in LHS.
VWOOD	Fraction of total waste volume that is occupied by IDB combustible waste category (dimensionless). Range: 0.285 to 0.484. Median: 0.384. Distribution: Normal. Additional information: Section 3.4.1, Volume 3. Variable 8 in LHS.

The following variables were sampled for the undisturbed calculations reported in this volume only, and were not used in the calculations reported in Volume 4. Sampled values for these variables are given in Appendix B of this volume.

Table 3-1. Variables Sampled in 1992 WIPP Performance Assessment (Concluded)

Variable	Definition
BKFLPOR	Porosity of backfill materials in drifts and experimental region and in the shaft below the shaft seal (dimensionless). Range: 0.01 to 0.075. Median: 0.0425. Distribution: Uniform. Additional information: Memorandum by Finley and Vaughn, Appendix A of this volume. Variable 26 in LHS for the Volume 5 calculations
DSEALPRM	Permeability of panel and drift seals (m^2). Range: 1.0×10^{-21} to 1.0×10^{-18}. Also used to define porosity for panel and drift seals (see Appendix B of this volume for definition of relationship). Distribution: lognormal. Additional information: Same as BKFLPOR. Variable 25 in LHS for the Volume 5 calculations.
SEALPRM1	Permeability of the shaft for the time period from 0 to 200 yr (m^2). Range: 1.0×10^{-19} to 5.0×10^{-16}. Median: 7.0×10^{-18}. Distribution: lognormal. Additional information: Same as BKFLPOR. Variable 22 in LHS for the Volume 5 calculations.
SEALPRM2	Permeability of the shaft seal and shaft-fill material within the Salado Formation for the time period from 200 to 10,000 yr (m^2). Range: 1.0×10^{-21} to 1.0×10^{-18}. Median: 3.2×10^{-20}. Distribution: lognormal. Also used to define porosity for the shaft seal and shaft-fill material (see Appendix B of this volume for relationship). Additional information: Same as BKFLPOR. Variable 23 in LHS for the Volume 5 calculations.
SHFTPRM	Permeability of the shaft-fill material within the Salado Formation for the period from 0 to 200 yr (m^2). Range: 1.0×10^{-19} to 1.0×10^{-15}. Median: 1.0×10^{-17}. Distribution: lognormal. Additional information: Same as BKFLPOR. Variable 24 in LHS for the Volume 5 calculations.
SEALTHK	Thickness of the shaft seal within the Salado Formation, as modeled (m). Range: 30 to 100. Median: 65. Distribution: Uniform. Additional information: Same as BKFLPOR. Variable 21 in LHS for the Volume 5 calculations.

[a] Adapted from Table 3-1 of Volume 4 and Tables 6.0-1, 6.0-2, and 6.0-3 of Volume 3 of this report.

4. GAS AND BRINE MIGRATION

In this chapter, results are discussed for three cases. In the first, the base case, the shaft is modeled as a composite of the four existing shafts. The second case considers a single shaft instead of combining all four shafts into one, but is otherwise identical to the base case. In the third case, the base case is repeated but without dynamic creep closure; instead, the porosity of the repository is fixed at the median final-state porosity of 19%. This is the best current estimate for the repository-wide average porosity of waste compacted to lithostatic pressure (14.8 MPa) (Butcher, 1990).

In all three cases, the behavior of the repository and the responses of the surrounding strata to changes in the repository is largely determined by the initial brine saturation in the waste. If gas generation is relatively low, primarily as a result of low initial brine content in the waste, the pressure in the repository rises slowly as brine from the far field flows in to equilibrate repository pressure with the far field. Under these conditions, the direction of flow is mostly in toward the repository, and the repository behaves simply as a brine sink. A more common response (in 70% of the realizations) is for gas to be generated sufficiently rapidly so that the pressure in the repository builds quickly, exceeding the far-field pore pressure. In about half of the realizations, the disposal-region pressure exceeds lithostatic pressure. In these cases, brine and gas are driven away from the repository out the most permeable pathways: the three anhydrite layers, and the sealed and backfilled shaft. Despite the high pressures reached in the repository, cumulative brine flow outward through the anhydrite layers is never enough to reach the disposal-unit boundary. Brine flows up the sealed shaft are also small and do not reach the Culebra. Cumulative gas flow out the anhydrite layers is sufficient in 6 of the 70 realizations for gas to flow beyond the disposal-unit boundary. Gas reaches the Culebra in 12 of the 70 realizations.

Results for the single-shaft case differ little from the base case. Cumulative brine flows up the shaft are lower than in the base case in proportion to the cross sectional area of the shaft. Cumulative gas flows into the Culebra are also proportionately lower. Flows of brine and gas out the anhydrite layers are indistinguishable from those of the base case.

Results for the fixed-porosity case differ from the base case primarily in the pressures obtained in the repository. Peak pressures are considerably higher, reaching 39 MPa versus 24 MPa in the base case. However, in the absence of a model for pressure-dependent fracturing of anhydrite interbeds, the higher repository pressures have essentially no effect on the other performance measures examined. Brine and gas flows out the anhydrite layers and up the shaft are unaffected by the use of a fixed repository porosity instead of a time-varying porosity. This conclusion may change in future performance assessments when pressure-dependent fracturing is included in simulations.

4.1 Four-Shaft Equivalent Geometry

Repository behavior is largely dictated by the amount of water initially present in the waste. Pressure in the repository initially increases, either rapidly, as a result of gas generation, or slowly, while gradually equilibrating with far-field pressure if the gas generation rate is low. Peak pressures range from 5.8 to 23.8 MPa. Brine saturation in the waste rises steeply during the first 100-300 yr as creep closure reduces the pore volume of the waste more rapidly than corrosion consumes brine. After peaking at about 300 yr, the brine saturation generally

decreases continuously during the remainder of the 10,000 yr (unless the initial brine saturation and the corrosion rate are both very low) because corrosion consumes brine faster than it flows into the repository from the far field. Because sufficient brine is not available, the initial iron inventory of the repository is usually not fully consumed within 10,000 yr. The opposite is true for cellulose. As a result of its lower initial inventory and higher reaction rate, cellulose generally is fully consumed fairly early (within the first 3000 yr), when sufficient brine is still available for biodegradation to take place. Although the amount of brine that flows into the repository is usually greater than the amount that flows out, brine inflow has little effect on gas generation because it tends to accumulate in regions of the repository that are depleted of reactants. Thus, the initial brine content of the waste has a far greater impact than brine inflow on how much gas is generated.

Cumulative brine flow out the high-permeability pathways — the three anhydrite layers and the shaft — impacts directly on regulatory compliance. In none of the realizations did sufficient brine flow out any of these pathways to reach the disposal-unit boundary. Because transport was not modeled, the analysis is based on quantities of brine flow relative to pathway pore volumes and residual saturations. As expected, the largest volumes of brine flow out MB139. None flows out anhydrite a + b. Although enough brine flowed out MB138 to warrant some concern, it is not clear that the brine there could originate in the waste; it is possible that brine in MB138, as currently modeled, is not contaminated, but instead originates in MB138 or the transition zone above the repository. Small amounts of brine flowed upward through the shaft seal, but not enough to fill the rest of the lower shaft between the seal and the Culebra. Although almost no brine flows *through* the drift seals, it bypasses the drift seals by flowing through the DRZ above and below the seals.

Sufficient quantities of gas are produced in 6 of the 70 realizations for gas to flow beyond the disposal-unit boundary. The largest amounts of gas flow out MB139, even though this pathway is also the main conduit for brine flow. Smaller quantities flow out anhydrite a + b and MB138; in the six realizations having flow past the disposal-unit boundary, such flow occurs in all three anhydrite layers. Gas also flows up the shaft into the Culebra in the same six realizations. The panel and drift seals were not completely effective in stopping gas flow: less than 0.01% of the total gas flow from the waste entered the panel and drift seals.

4.1.1 Repository Behavior

Pressures in the waste (Figure 4-1) increase for at least the first 1000 yr in all realizations. In all cases, the pressures start at atmospheric (0.101 MPa). Some of the increase in pressure results from brine inflow from the far field, and some small component from the reduction of void volume by creep closure. Most of the increase, particularly in those realizations in which pressure rises above the far-field pore pressure (12 to 13 MPa), is caused by gas generation by corrosion and biodegradation of the waste. After 10,000 yr, pressures range from 5.8 to 22.3 MPa; peak pressures range from 5.8 to 23.8 MPa. Two general types of behavior can be observed. In about two-thirds of the cases, the pressure profile peaks in less than 10,000 yr, often fairly early — between 1000 and 3000 yr. In these instances, gas is generated faster than pressure can be relieved by fluids flowing out of the anhydrite layers or up the sealed shaft. Eventually, either reactants are fully consumed or brine is no longer available for corrosion, and gas generation stops or slows greatly. From that time on, pressures in the waste gradually equilibrate with the far-field pressures. If the pressure has exceeded the far-field pressure at the elevation of the repository, then the pressure will drop.

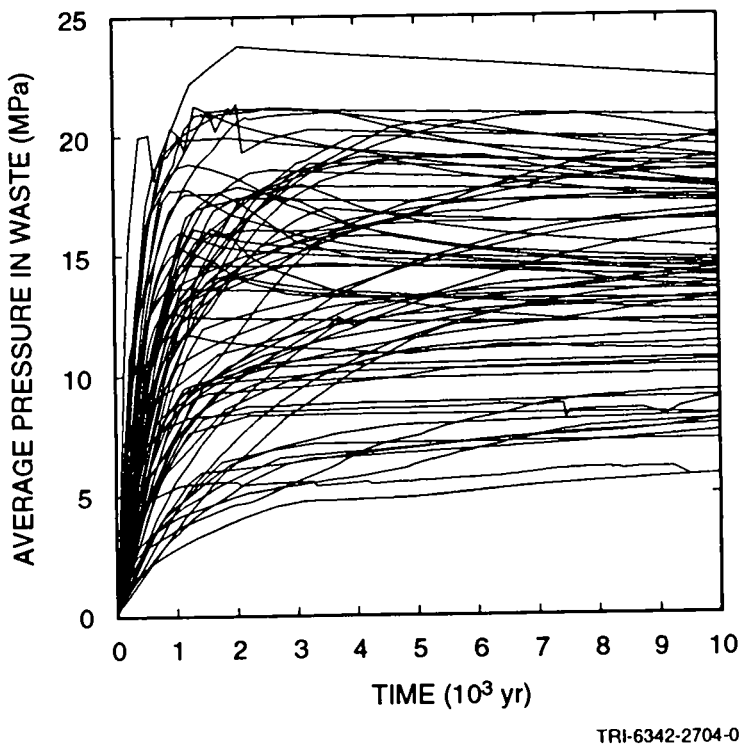

Figure 4-1. Volume Average Pressure in the Waste Repository.

Otherwise, the pressure will continue to rise. This is seen in about one-third of the runs, where the pressure has not yet reached the far-field pressure within 10,000 yr, and is increasing so slowly that it may never exceed the far-field pressure. Lithostatic pressure is exceeded in about half of the realizations. Until fracturing of the anhydrite layers is included in the model (planned for 1993), these high repository pressures will always be obtained in some of the realizations.

Pressures in the waste can also increase as a result of creep closure reducing the pore volume. In the current implementation of creep closure, it is difficult to determine how much creep closure contributes to pressure increases in the presence of other phenomena. This will be discussed further in Section 4.3. In order for creep closure to have a significant effect, pressures in the waste must first increase independently of creep closure, as a result of either gas generation or influx of fluid from outside the repository.

There are a few realizations in which the pressure fluctuates. This generally results when gas generation rates vary rapidly. For example, in the realization producing the highest pressures (see Figure 4-1), the pressure peaks very early at 20 MPa, drops briefly, then rises again to peak at 23.8 MPa. In this case, biodegradation is very rapid, causing pressures to rise rapidly. But when the biodegradable inventory is fully consumed (in about 600 yr), gas generation slows dramatically, resulting in a rapid drop in pressure as gas continues to migrate into the far field. Eventually, gas generation from corrosion brings the pressures back up to the higher peak, when all corrodible materials are finally consumed.

Brine saturation in the waste also generally increases initially (Figure 4-2), peaking quite early — within a few hundred years after the repository is sealed. The saturation increase is a direct result of the rapid creep closure during these early times and results in a sharp decrease in pore volume in the waste (Figure 4-3). Although corrosion consumes brine during this time period, which causes the brine volume in the waste to drop (Figure 4-4), the decrease in pore volume is more rapid than the decrease in brine volume. Consequently, brine saturation undergoes a rapid increase initially. Once the repository has crept shut about as far as it can in the current creep closure implementation, brine consumption causes the brine saturation to decrease. Generally, the rate of decrease in brine saturation is quite rapid, dropping to less than 20% of its peak value within 2000 yr. In most cases, once brine saturation begins to decrease, it never rises again during the remainder of the 10,000 yr. Only in a few realizations in which the brine saturation is always quite low (less than 0.05) does the saturation increase after 1000 yr. In these cases, the pressure in the repository remains fairly low, typically below hydrostatic (about 7 MPa), because little gas has been generated, and some brine is still able to flow in from outside the repository. However, in most cases, the rate of brine flow in from the far field is quite low as a result of low interbed permeabilities and pressures within the repository that are comparable to the far-field pressures. Any brine that does flow into the repository is usually consumed by corrosion as quickly as it flows in. Thus, there is generally no increase in brine saturation after about 1000 yr.

The two reactants, iron and cellulose, differ markedly in their time-dependent behavior (Figures 4-5 and 4-6, respectively). In 18 of the 70 realizations, all of the iron is consumed. The initial corrosion rate is generally the highest rate; however, the initial brine content is consumed in most of the realizations, and, given the generally low flow of brine into the waste, much iron is often unreacted after 10,000 yr. In contrast, cellulose is fully consumed in 52 of the 70 realizations. This stems from the lower initial content and higher reaction rate for cellulose compared with iron. The median value for the initial mass of cellulose is about 17% that of iron. The median biodegradation

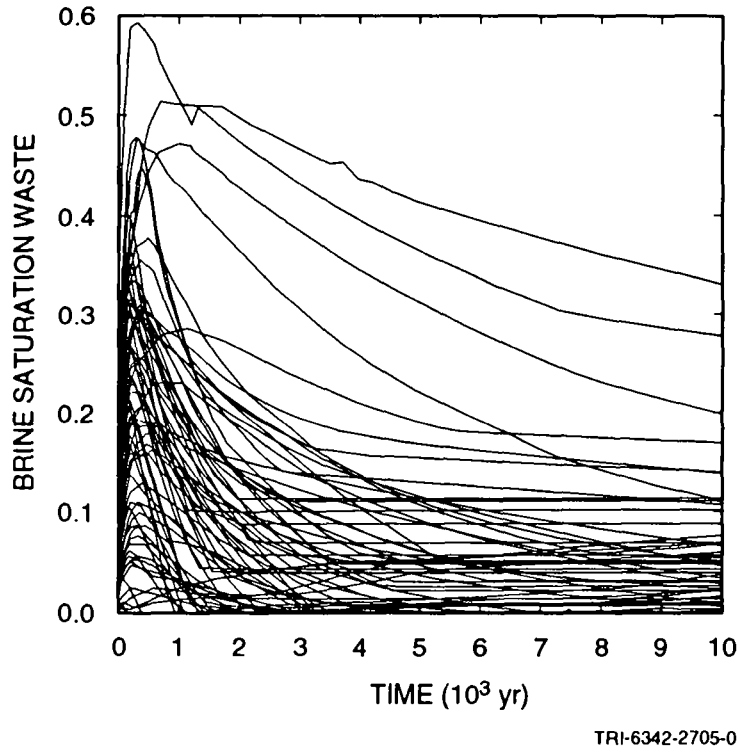

Figure 4-2. Volume Average Brine Saturation in the Waste Repository.

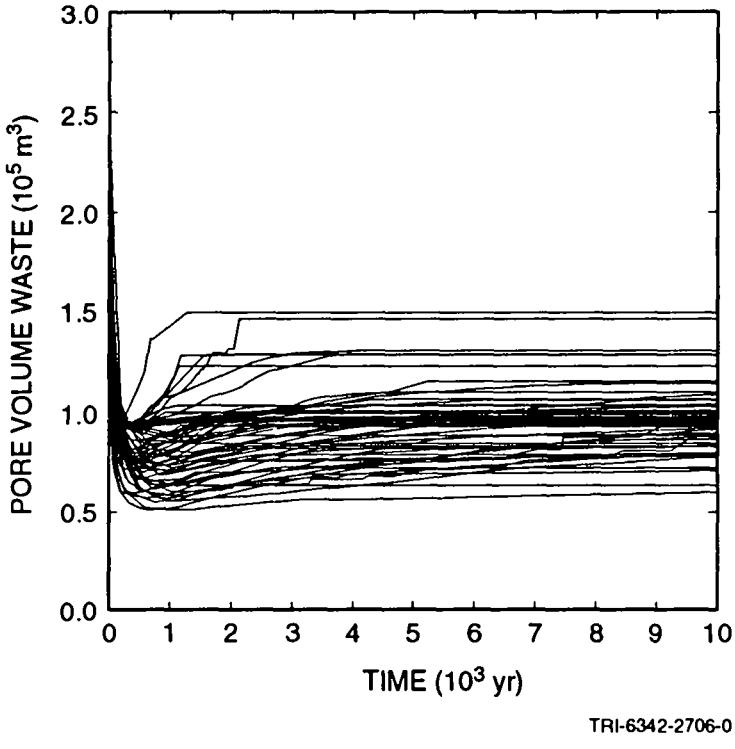

Figure 4-3. Pore Volume in the Waste Repository.

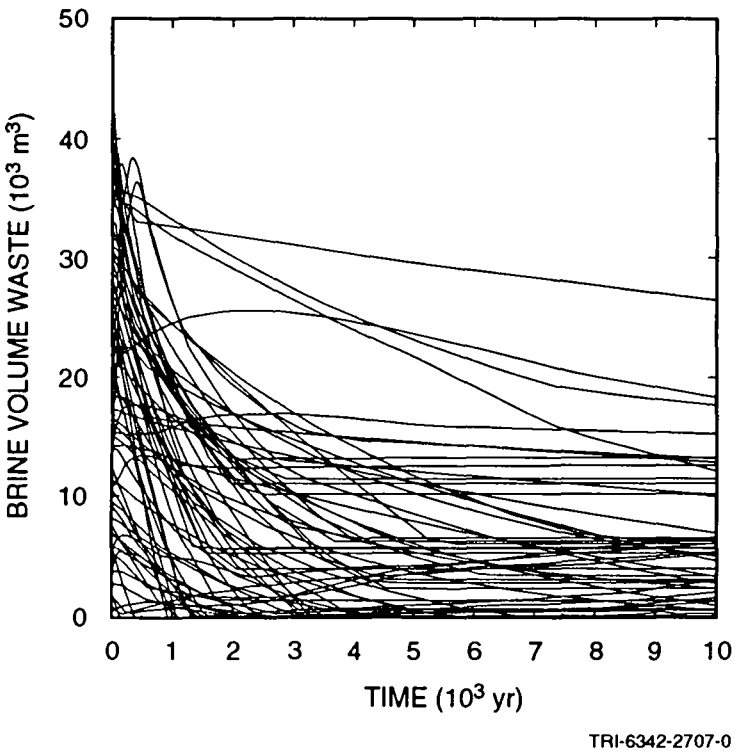

Figure 4-4. Brine Volume in the Waste Repository.

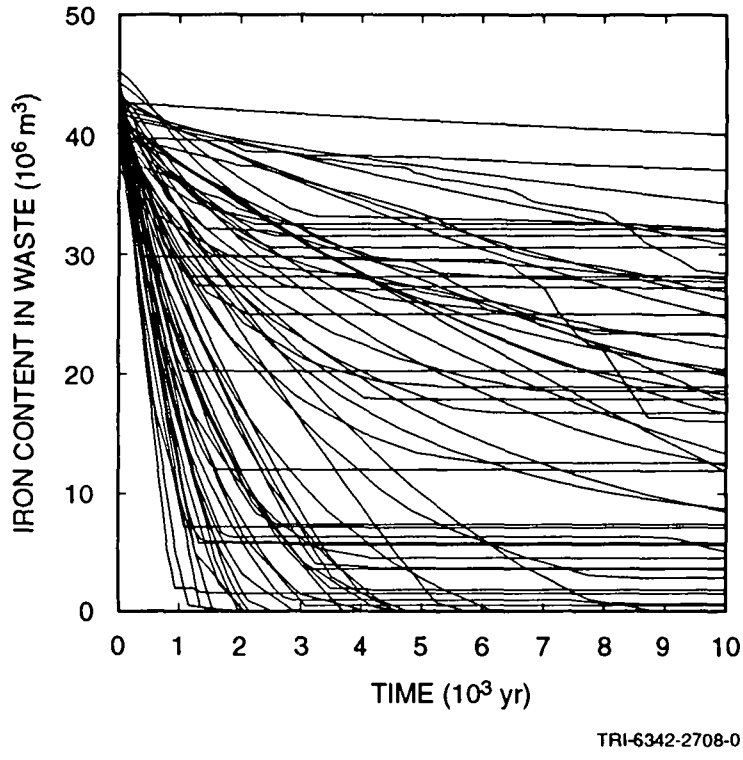

Figure 4-5. Iron Remaining in the Waste Repository.

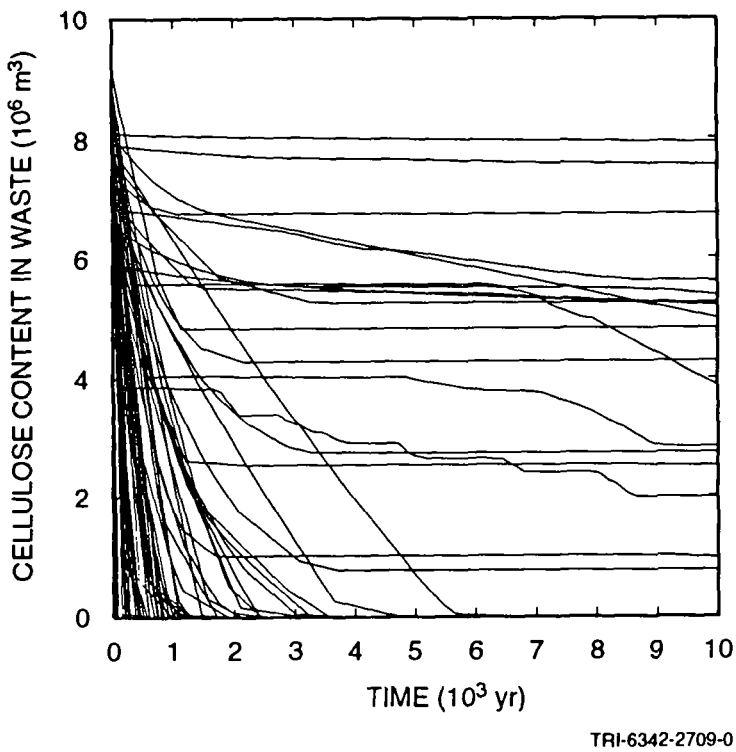

Figure 4-6. Cellulose Remaining in the Waste Repository.

rate among the 70 realizations is about 6 times higher than the median corrosion rate on a mass basis under inundated conditions. Thus, cellulose is expected to be fully consumed in approximately 1/40th of the time required for corrosion, at their full rates. Because of the smaller initial content and higher rate, biodegradation is not inhibited by lack of brine as much as corrosion because it is largely completed while brine is still present in the waste, whereas, brine is depleted in the waste long before corrosion is completed. (Note that although biodegradation is currently assumed not to consume water, there still must be water present in order for biodegradation to occur. Corrosion, as currently modeled, consumes water, so water must also be present for corrosion to take place. These statements are true for both the inundated reactions and the humid reactions. See Sections 1.4.1 and 3.3 of Volume 3 of this report for additional discussions of the gas-generation model.) Averaging over the 70 realizations, 32% of the total initial iron content of the waste remains unreacted after 10,000 yr, whereas, only 16% of the total initial biodegradable content remains at that time.

The amount of gas generated, Figure 4-7, ranges from 3.0×10^6 to 3.2×10^7 m^3 (at reference conditions: 30 °C and 0.101 MPa). This corresponds to 1.3×10^8 to 1.3×10^9 mol H_2 total, or nominally 160 to 1600 mol/drum (based on 6804 drums/room, as modeled). The full potential as currently modeled is 2.0×10^7 to 3.5×10^7 m^3 (at reference conditions), or equivalently 8.1×10^8 to 1.4×10^9 mol H_2 total, or 1000 to 1770 mol/drum. Because so much iron remains after 10,000 yr, the average cumulative gas generated (1.8×10^7 m^3) is relatively low, only 70 percent of the average potential (2.6×10^7 m^3).

Total brine consumed by corrosion, Figure 4-8, ranges from 1600 to 29,600 m^3; compared with the total brine required to complete corrosion, 19,700 to 32,200 m^3. In 45 realizations (or 64%), sufficient brine is available in the waste initially to corrode all the iron in the waste without any brine flowing in from outside the waste. However, only in 18 of the realizations (or 26%) was all of the iron fully consumed. In the other 27 realizations, the corrosion rate was too low to consume all of the iron within 10,000 yr, even though enough brine was always available.

As shown in Figure 4-9, there were more realizations (39) in which the net brine flow was *into* the waste, rather than *from* the waste (19), and in 12 of the 70 realizations, there was no brine flow either into or out of the waste. The maximum brine outflow was 11,400 m^3. In some realizations, the net cumulative flow of brine was inward because of an early surge of inflowing brine, but there was still a substantial amount of brine outflow. However, even in the most extreme case (the second curve from the bottom in Figure 4-9), only about 7100 m^3 of brine flowed back out after having flowed into the waste. It is interesting that in the ten realizations with the highest inflow of brine, none had all the iron fully corroded. This suggests that brine inflow has only a marginal impact, at best, on corrosion, and that corrosion rate is a more important factor influencing corrosion and gas generation, rather than the availability of brine. In contrast, those realizations with the highest brine inflow generally had among the lowest initial brine present in the waste, so, whereas brine inflow may not be important, initial brine content is. Brine inflow has little effect on corrosion because it tends to flow in just at the edges of the repository and then pool in the bottom of the repository. Iron may be largely consumed there, but not enough brine flows in to fill the repository to the top, so iron remains relatively unreacted in the upper portion of the repository.

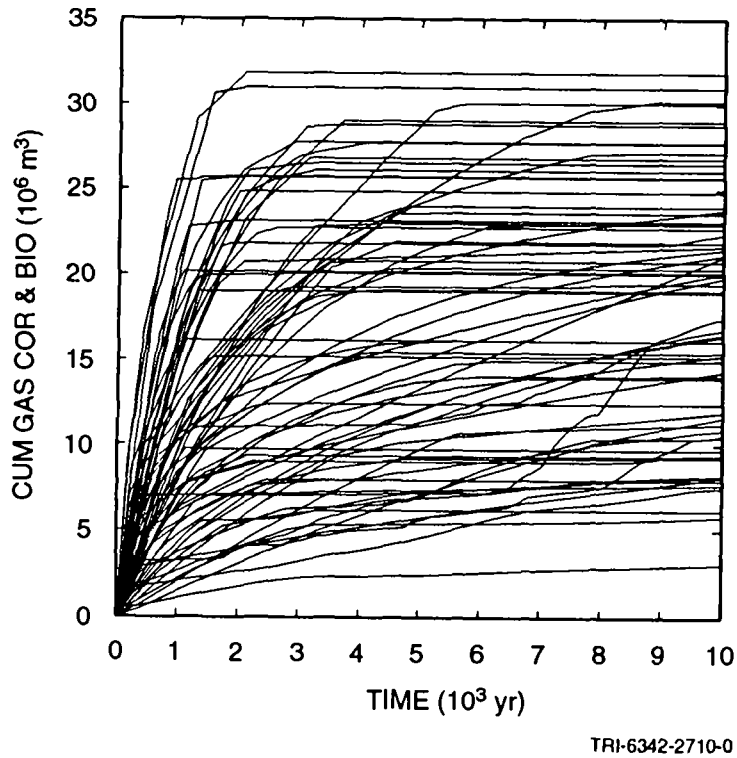

Figure 4-7. Cumulative Gas Volume Generated (at 30 °C; 0.101 MPa).

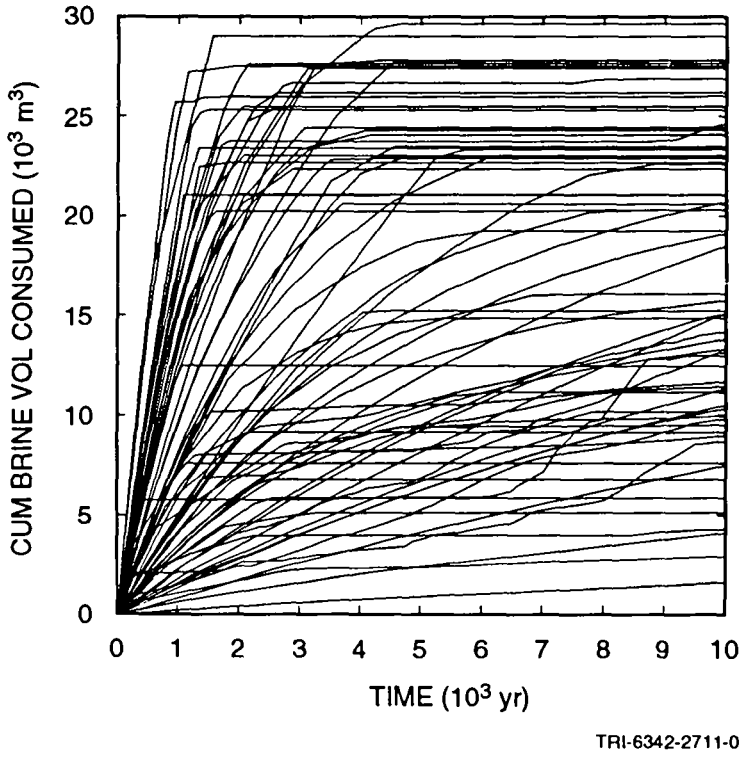

Figure 4-8. Cumulative Brine Volume Consumed.

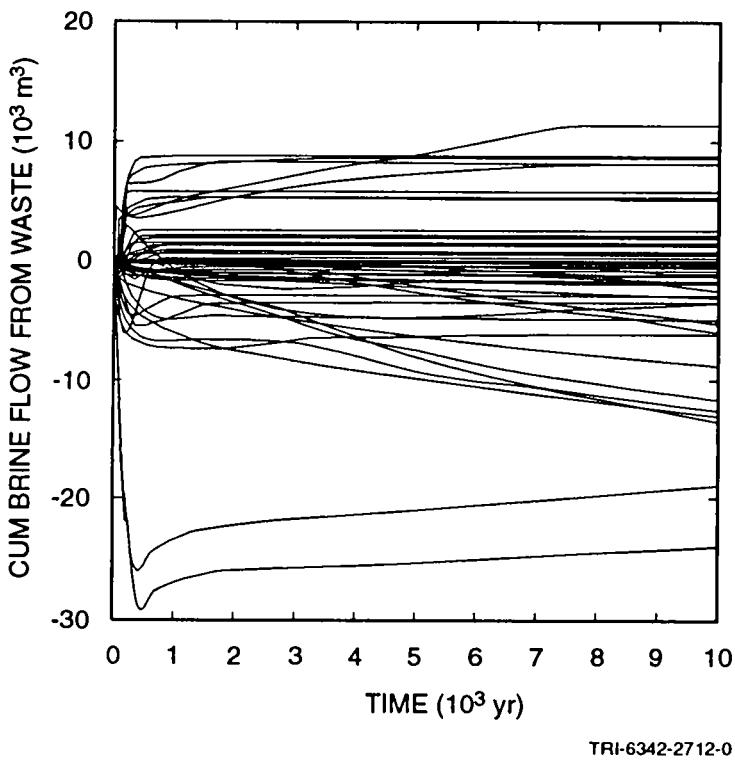

Figure 4-9. Cumulative Brine Flow from the Waste Repository. (Positive values indicate flow OUT from the repository.)

4.1.2 Brine Flow Behavior

A key question for PA to answer is: Where does contaminated brine flow to? Because the presence of brine in the waste results in gas generation, it is also desirable to know where brine comes from, specifically, what are the flow paths taken by brine near the WIPP site over the thousands of years following the sealing of the repository. As discussed above, as much as 11,400 m^3 of brine flowed out of the waste. This brine is presumably contaminated with radioactive isotopes and hazardous constituents. Although the model used does not simulate transport, the extent and directions of contaminated brine flow can be estimated, in addition to the sources of brine that flows into the waste. Figure 4-10 shows that almost no brine flowed through the drift seals. The maximum cumulative flow of contaminated brine from the waste into the seals was 0.03 m^3. In most realizations, brine flowed from the seals into the waste, but the maximum was still only 0.9 m^3. The bulk of flow into or out of the waste was through the DRZ. The drift seals, as currently modeled, are very effective in blocking brine flow from the waste through the seals, but they do not prevent fluids from bypassing the seals by way of the DRZ.

Fluids do not migrate significant distances in the low-permeability halite, and to get to the disposal-unit boundary, contaminated brine must flow through one of the permeable units: the anhydrite layers (Marker Beds 138 or 139 or the combined anhydrite "a" and "b" layer), or up the sealed shaft. As described below, the results of the BRAGFLO simulations show that no contaminated brine would have reached the unit boundaries. This conclusion is based on examinations of the quantities of brine and gas that flowed into various regions, rather than on actual transport calculations because those calculations were not performed.

For these model results, it can safely be stated that no contaminated brine reached the Culebra upward through the shaft seal system. As Figure 4-11 shows, in most realizations, brine flowed downward through the modeled shaft seal, not upward, and did not provide a potential transport medium away from the waste. In seven realizations there was a positive net upward flow of brine, and the maximum flow was only 25 m^3. In addition, there were several realizations in which brine flowed downward initially but flowed upward later. To be conservative, it must be assumed that all of this upward-flowing brine is contaminated, although this may not be true. In the worst cases, approximately 40 m^3 of brine flows upward (even though in one of those realizations the *net* cumulative flow was 30 m^3 downward). However, Figure 4-12 shows that the minimum brine volume in the lower shaft (above the shaft seal but below the Culebra seal) is 370 m^3. This figure also shows that the brine volume in the lower shaft is nearly constant in most cases even though that portion of the shaft is never fully saturated with brine after 200 yr, so brine in the lower shaft is never completely displaced by the small amount of brine flowing up through the seal. Therefore, 40 m^3 of brine flowing through the shaft seal would flow only about 1/10th of the distance from the seal to the Culebra, never actually reaching the Culebra. In fact, when individual realizations are examined, the quantity of brine that flows through the shaft seal never amounts to more than 1.7% of the brine volume in the lower shaft. (In Figure 4-12, the small drop in brine volume that occurs in every realization at 200 yr results from the change in porosity in the Culebra seal at that time, as described in the memorandum by Finley and Vaughn in Appendix A of this volume.)

Before considering the other flow paths — the three anhydrite layers — it must be pointed out that the fundamental assumption of plug flow in a porous medium requires that any outward flow of contaminated brine from the waste must displace all the brine-saturated pore volume in a grid block before it can move to he next grid block. Because of the quasi-cylindrical geometry used in the mesh, the volume of grid blocks increases greatly as one moves outward from the repository (see Section 2.3). Table 4-1 lists the cumulative grid block volumes in each anhydrite layer for the mesh used in these calculations, along with the distance from the repository to the outer edge

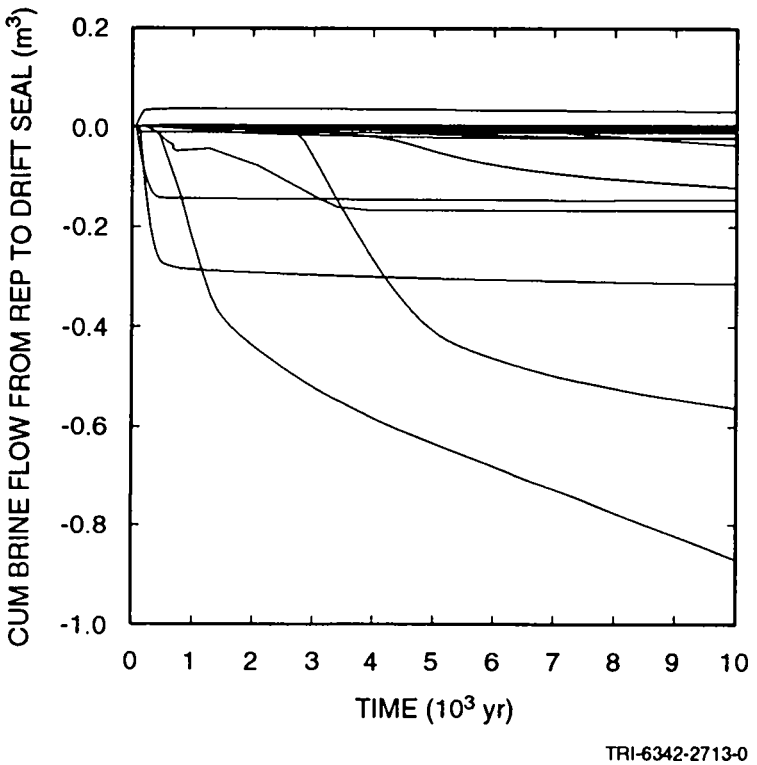

Figure 4-10. Cumulative Brine Flow from the Repository to the Drift Seals. (Positive values indicate flow OUT from the repository, into the drift seals.)

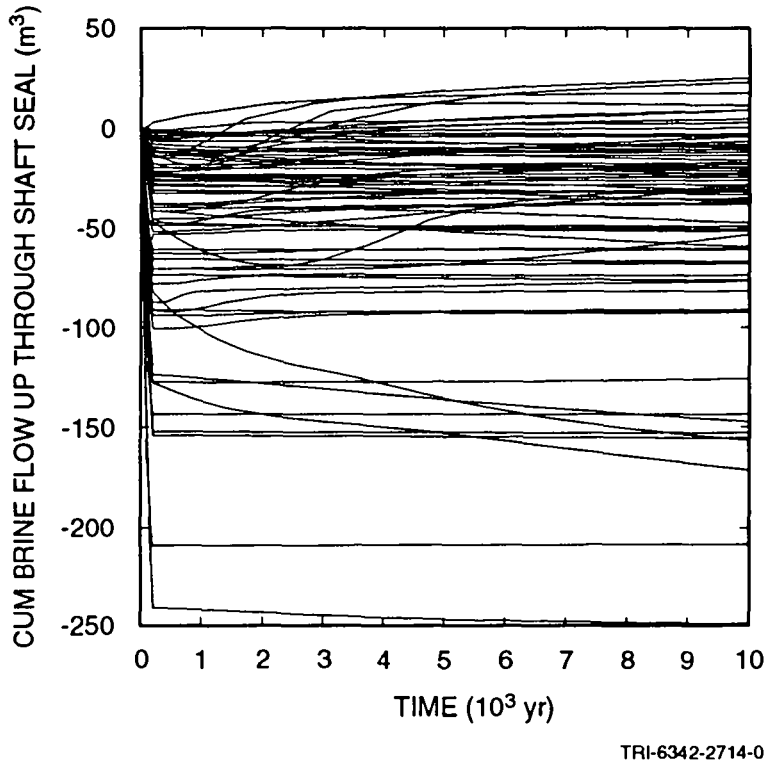

Figure 4-11. Cumulative Upward Brine Flow through Shaft Seal. (Positive values indicate upward flow.)

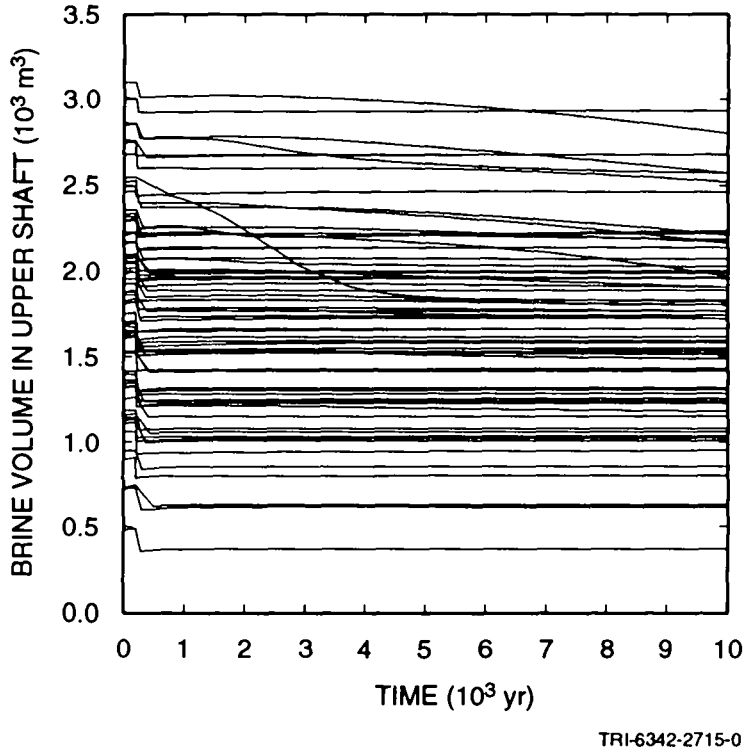

Figure 4-12. Brine Volume in Lower Shaft.

Table 4-1. Cumulative Volumes in Anhydrite Layers in BRAGFLO Mesh (South of Repository) (see Figure 2-1)

		Volume (m^3)		
Cell No.	Distance (m)	Layer 7 MB138	Layer 9 Anhydrite a + b	Layer 16 MB139
8	1	347	521	1,640
7	6	2,110	3,160	9,950
6	26	9,500	14,300	44,900
5	126	55,100	82,700	260,000
4	626	387,000	580,000	1,830,000
3	2,500	3,230,000	4,840,000	15,200,000
2	7,500	23,200,000	34,800,000	109,000,000
1	22,500	191,000,000	287,000,000	902,000,000

of the grid block. Table 4-2 lists initial pore volumes in the same grid blocks. This is the actual volume of brine that must be displaced by contaminated brine and gas flowing out from the repository. This will help to put into perspective the large amount of brine that has to be displaced in order for contaminated brine to reach the disposal-unit boundary. If some of the pore volume is occupied by gas, then the estimates of travel distances must be increased proportionately. The tables give volumes only for the portion of the mesh to the south of the repository. Generally, the cumulative flows of gas and brine are greater south of the repository, so only flows to the south are examined.

Cumulative brine flow southward out through Marker Bed 138 is shown in Figure 4-13. The amount of brine that flows inward toward the repository is generally far greater than the amount that flows outward. In eight realizations was there a net outward flow to the south of the repository, with the maximum being 320 m^3. However, in many other cases large quantities of brine flowed in toward the repository initially, but flowed outward later as pressures within the repository built up. This occurred in 40 of the 70 realizations. Although the most brine that flowed south from the repository was 520 m^3, which would occupy 54,000 m^3 of MB138 volume (at a porosity in this realization of 0.0097), another realization that had 350 m^3 brine flow at a lower porosity (0.0046), so that brine occupied 77,000 m^3 of the marker bed. Table 4-1 shows that this brine would flow as far south as Cell 4, or 626 m, provided that the marker bed was fully saturated with brine. However, this is generally not true. If some contaminated brine flowed out early on, followed by a large quantity of gas, even small amounts of contaminated brine could be pushed far out. A more accurate way to estimate the distance contaminated brine has flowed is to sum the volumes of brine and gas (at local pressures) that flowed out. The maximum gas flow out through MB138 is 2.8×10^6 m^3 at reference conditions of 0.101 MPa, as shown in Figure 4-14. The repository pressure must exceed the far-field fluid pressure in order for gas to flow out from the repository, so gas pressures in MB138 must be at least 12 MPa, which is the low end of the sampled range of far-field pressures. Thus, the maximum cumulative gas volume that has flowed south out of MB138 is approximately 2.3×10^4 m^3, which, at the minimum sampled marker bed porosity of 0.001159, would occupy 20×10^6 m^3 of the marker bed. Table 4-1 shows that when gas and brine flows are combined, they could flow out into Cell 2, 7500 m south of the repository, or 5 km beyond the disposal-unit boundary, using all the most unfavorable parameter values from the Latin hypercube sampling. Because these extreme combinations of parameter values did not occur in the Latin Hypercube Sample (LHS), the maximum gas

Table 4-2. Pore Volumes in Grid Blocks in Anhydrite Layers in BRAGFLO Mesh (South of Repository)[a] (see Figure 2-1)

		Layer 7 MB138		Layer 9 Anhydrite a + b		Layer 16 MB139	
Cell No.	Distance (m)	Minimum Volume (m^3)	Maximum Volume (m^3)	Minimum Volume (m^3)	Maximum Volume (m^3)	Minimum Volume (m^3)	Maximum Volume (m^3)
8	1	0	10	1	16	2	49
7	6	2	63	4	95	12	298
6	26	11	284	17	426	52	1,340
5	126	64	1,650	96	2,470	302	7,790
4	626	448	11,600	673	17,400	2,120	54,700
3	2,500	3,740	96,500	5,610	145,000	17,700	456,000
2	7,500	26,900	693,000	40,300	1,040,000	127,000	3,270,000
1	22,500	221,000	5,720,000	332,000	8,570,000	1,050,000	27,000,000

[a] Based on actual *sampled* minimum and maximum anhydrite porosity: 0.001159 and 0.02992; *not* on minimum and maximum reported in Volume 3, Table in Volume 3, Table 2.4.4: 0.001 and 0.03.

and brine flow out through MB138 is much less. In only one realization does enough gas flow out through MB138 to occupy all the pore volume in MB138 to a distance beyond the disposal-unit boundary. In this one case, 19,700 m^3 of gas at local pressures flows out of MB138, occupying only 4.8×10^6 m^3 of marker bed volume, which would only extend into Cell 2 in MB138, the first cell beyond the disposal-unit boundary.

It still cannot be stated with certainty whether contaminated brine actually reached the boundary, however. First, MB138 is not fully saturated with either gas or brine. The residual brine saturation in the realization that potentially crosses the boundary is 0.2001. (This parameter was sampled and is constant in any given realization.) Thus, some brine, contaminated or not, remains as residual saturation rather than being pushed ahead of the gas. This residual brine results in a smaller volume for gas storage in the marker bed, and causes gas to migrate approximately 25% farther than it would if the unit were fully gas-saturated.

Residual brine volume in MB138 in the realization in which brine potentially reached the unit boundary is 2650 m^3, whereas the calculated volume of cumulative brine flow past the disposal-unit boundary is far less at 150 m^3. Second, it is necessary to know the history of release of contaminated brine from the waste to know whether the underlying assumption that contaminated brine preceded gas flow out MB138 is true. No brine actually flowed out of the waste in this realization; therefore, no contaminated brine could have reached the disposal-unit boundary. This realization illustrates the hazards involved in making conservative assumptions. With enough bad

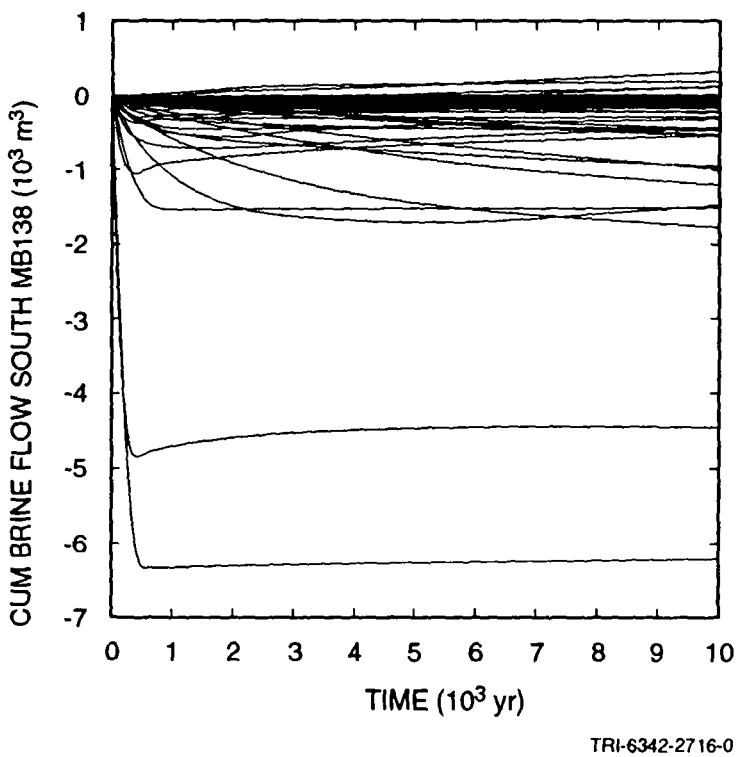

Figure 4-13. Cumulative Brine Flow South out MB138. (Positive values indicate flow southward away from the repository.)

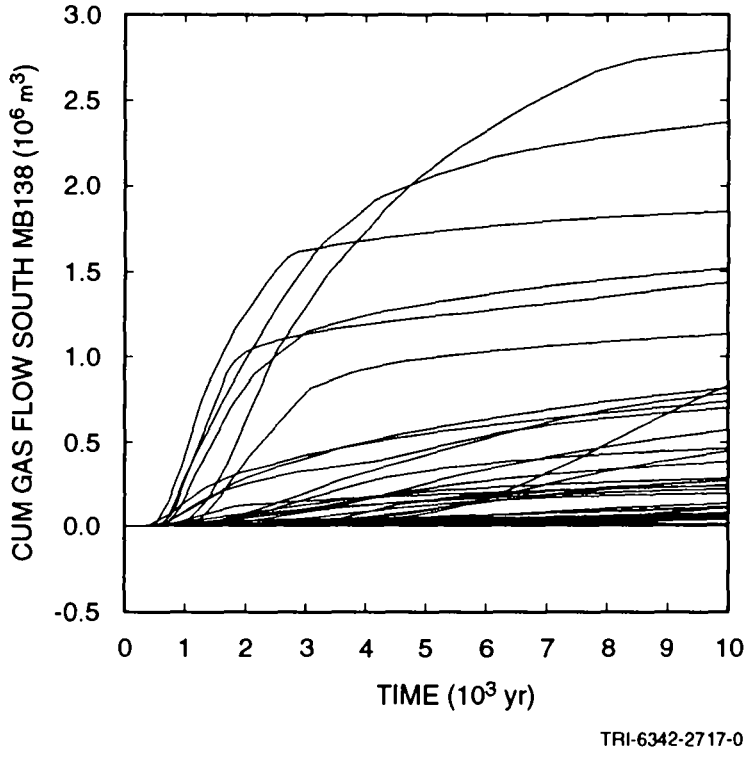

Figure 4-14. Cumulative Gas Flow South out MB138 (at 30 °C; 0.101 MPa). (Positive values indicate flow southward away from the repository.)

assumptions about the results, it would appear that brine crossed the disposal-unit boundary in at least one realization, when in fact, this did not occur.

This analysis can be repeated for the anhydrite a + b layer, which is expected to have a larger cumulative gas flow than MB138. The brine flow should be greater simply because this layer is thicker, and, being slightly closer to the repository, the driving pressures are higher. Surprisingly, Figure 4-15 shows that no outward brine flow occurred south of the repository in this layer. Brine flowed only in toward the repository. As pressures quickly built up in the waste, inward brine flow ceased. In more than half of the realizations, this occurred within the first 1000 yr. At the same time, gas began to flow outward (Figure 4-16). As expected, the volume of gas flow out through this layer is somewhat higher than in MB138, ranging up to 3.5×10^6 m^3, compared with 2.3×10^4 m^3 in MB138.

The analysis for MB139 is similar in complexity to MB138. The net cumulative brine flow out of MB139 (Figure 4-17) is positive (i.e., outward) in 13 realizations, with a maximum of 2030 m^3. From Table 4-2, it can be seen that if MB139 were fully brine saturated, this maximum quantity of brine, which may or may not be contaminated, would flow only as far as Cell 4, or 626 m from the repository, assuming the minimum value for porosity. However, as seen in MB138, more than half of the realizations that had net inward cumulative flows actually had a substantial amount of outward brine flow following a large initial inward surge. The largest of these was 6700 m^3. In a brine-saturated MB139, assuming minimum porosity, this brine would reach Cell 3, which extends to the disposal-unit boundary. In fact, the realizations having the greatest outward flow of brine do not have the lowest porosity. The realization with the largest brine flow has a porosity of 0.0041, meaning that the brine flows only to Cell 4, or 626 m from the repository, not to the disposal-unit boundary.

As shown in the analysis for MB138, gas flow has a major impact on how far contaminated brine might flow. Figure 4-18 shows that as much as 3.6×10^6 m^3 of gas flowed out through MB139. That large quantities of gas flow out through MB139 is surprising; previous work has suggested that brine will tend to pool in the lower portion of the waste and beneath the repository (Bertram-Howery et al., 1990; WIPP PA Division, 1991b; WIPP PA Department, 1992). The main flow path for brine inflow is MB139, but if gas generation in the repository raises the pressure there rapidly enough, little brine ever flows in. Generally, model results indicate that any brine initially present in the repository is converted to gas, which raises the pressure, preventing any further significant influx of brine, and driving large amounts of gas out through MB139. If it is again assumed that contaminated brine precedes any outflowing gas, then it must be concluded that contaminated brine flows past the disposal-unit boundary through MB139. However, at least a residual saturation of brine will remain throughout the anhydrite layers. In the case in which the maximum brine outflow was 6700 m^3, residual brine volume out to the disposal-unit boundary is 12,500 m^3, nearly double the actual contaminated brine volume that flowed into MB139. So again, no contaminated brine could have reached the disposal-unit boundary through any of the anhydrite layers.

The results show that except for flow out the anhydrite layers, there is little movement of brine in the vicinity of the repository. Figure 4-19 shows that almost no brine flowed from the seals and backfill regions into the shaft, while flow in the other direction, cumulative brine flow amounted to less than 800 m^3. Flow from the experimental region into the shaft, Figure 4-20, is almost a mirror image of flow from the seals and backfill into the shaft, indicating that the shaft does little to impede flow from the experimental region to the seals and backfill. Considering the small volume of the lower shaft, this result is expected. The flow behavior in these regions stems directly from the initial conditions. At time zero, all of the excavated regions except for the repository were assumed to be fully saturated with brine. This assumption was based on the expected brine content of the halite

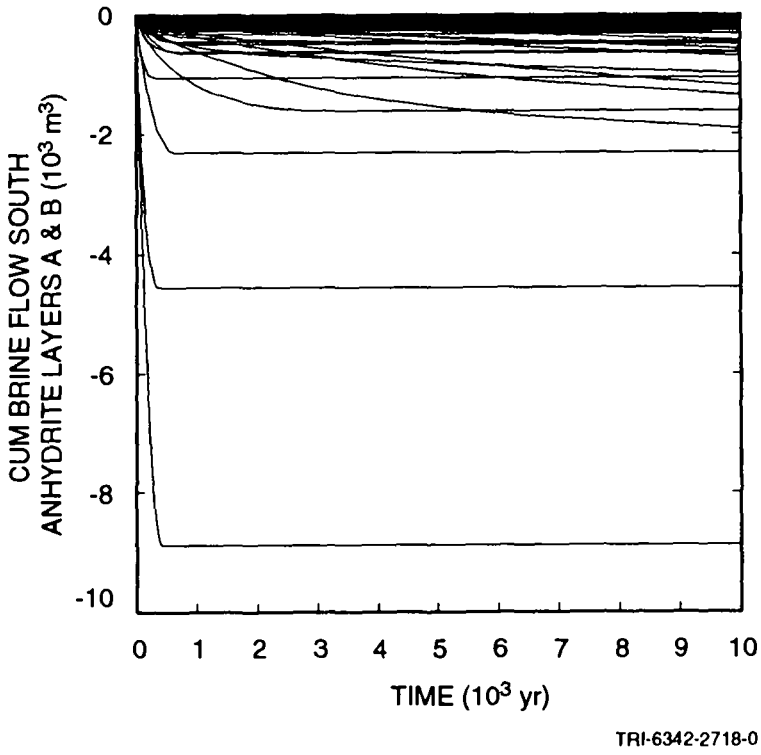

Figure 4-15. Cumulative Brine Flow South out Anhydrite Layers a + b. (Negative values indicate flow northward toward the repository.)

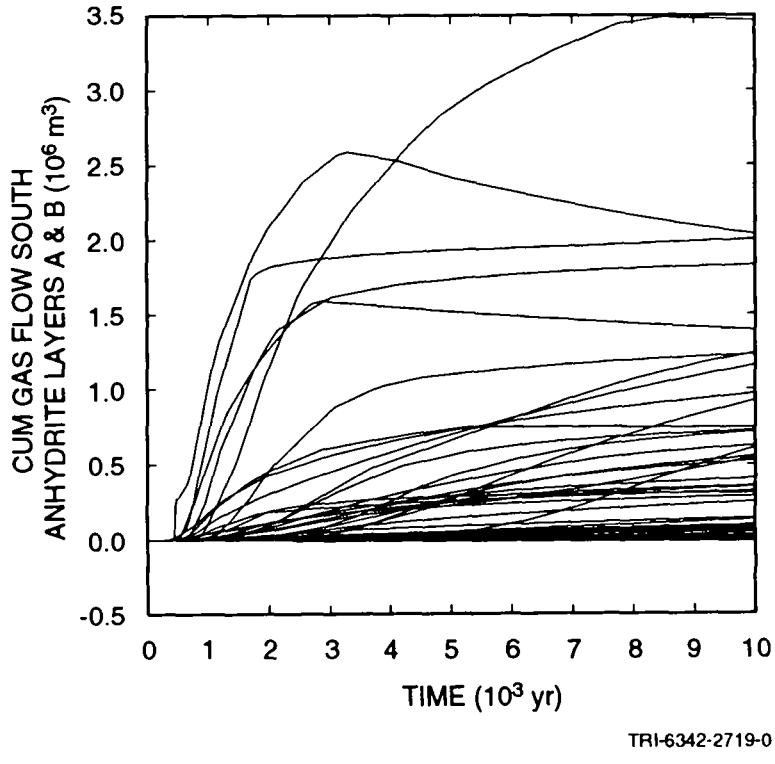

Figure 4-16. Cumulative Gas Flow South out Anhydrite Layers a + b (at 30 °C; 0.101 MPa). (Positive values indicate flow southward away from the repository.)

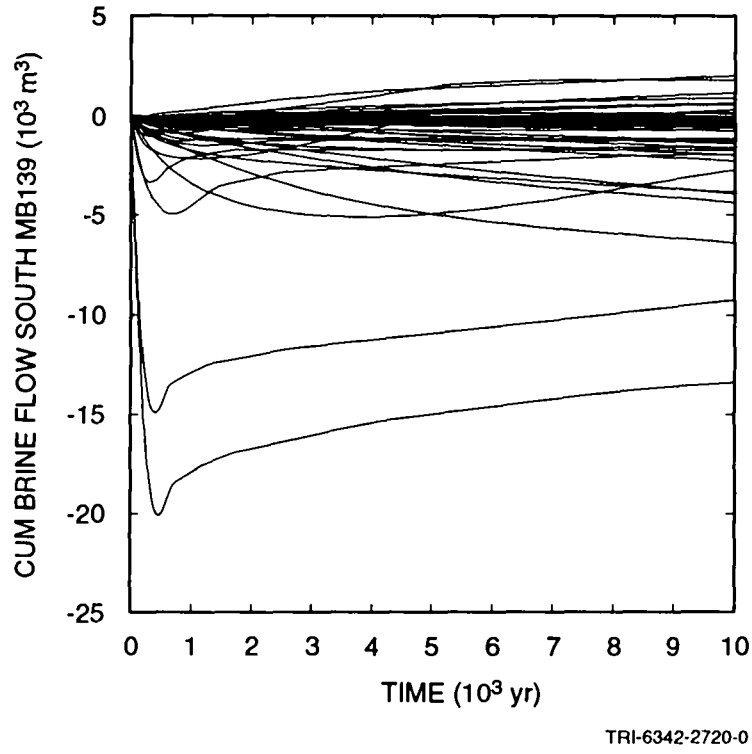

Figure 4-17. Cumulative Brine Flow South out MB139. (Positive values indicate flow southward away from the repository.)

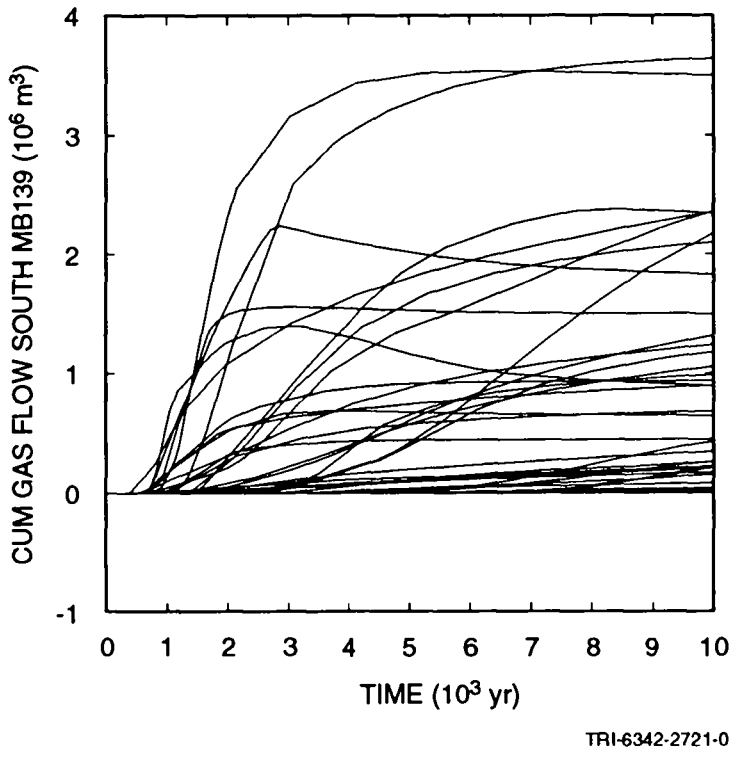

Figure 4-18. Cumulative Gas Flow South out MB139 (at 30 °C; 0.101 MPa). (Positive values indicate flow southward away from the repository.)

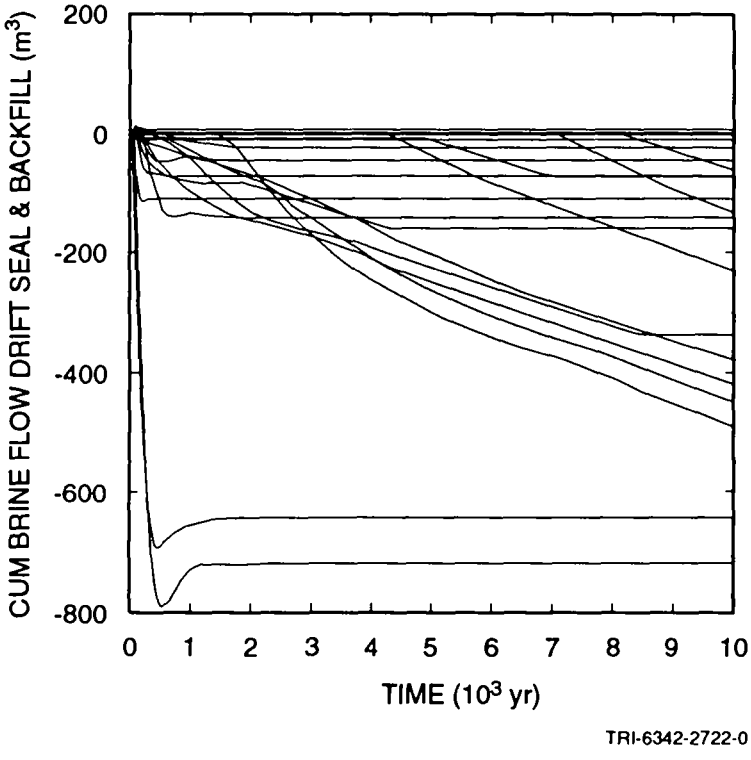

Figure 4-19. Cumulative Brine Flow from Drift Seals and Backfill into Shaft. (Positive values indicate flow from seals and backfill into shaft.)

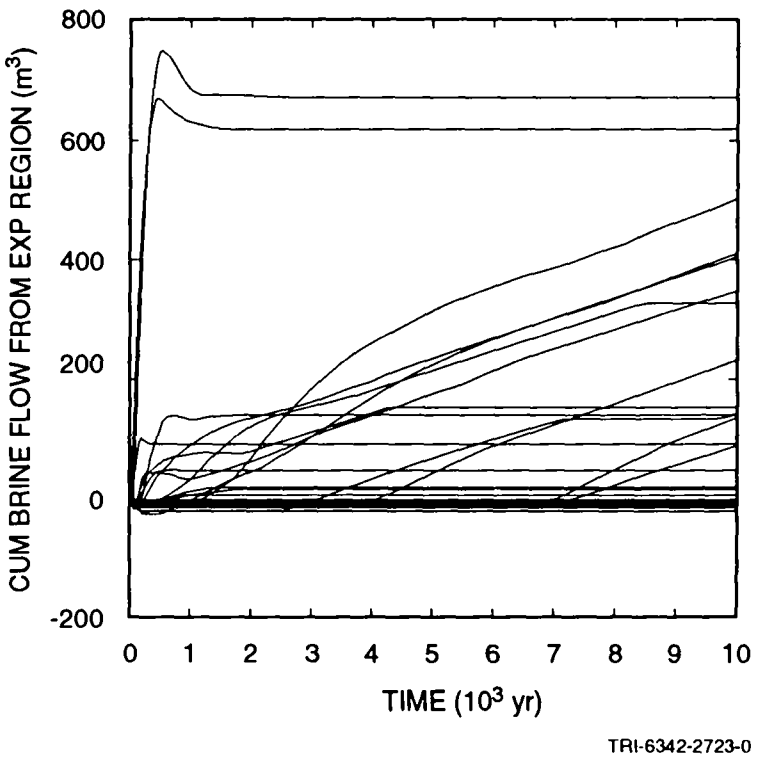

Figure 4-20. Cumulative Brine Flow from Experimental Region into Shaft.

backfill, estimated to be 5 to 8 weight percent (see memorandum by Finley and Vaughn in Appendix A). Depending on the porosity of the backfill (a sampled parameter), this corresponds to nearly 100% brine saturation. The brine saturation of the DRZ, however, was calculated during the 50-yr operational simulation, then adjusted downward to account for the increased porosity of the DRZ at time zero, when the repository is sealed. The result is that whereas the backfilled excavated regions are fully saturated with brine at time zero, the surrounding DRZ has a relatively low brine saturation, so an immediate flux of brine occurs from the backfilled regions into the DRZ, particularly that portion of the DRZ beneath the seals and backfilled regions. In the majority of realizations, this flow of brine is small, less than 1 m^3. But in about 15% of the cases, more than 100 m^3 flows into the DRZ.

Flow between other regions is generally much smaller. Less than 15 m^3 flows between the DRZ and the shaft (Figure 4-21). Except for two realizations, almost no brine flows between MB138 and the shaft (Figure 4-22) or between the transition zone and the shaft (Figure 4-23). Up to 400 m^3 of brine flows from the Salado halite into the shaft (Figure 4-24). Although the permeability of the halite is extremely low, the large surface area of the shaft allows a substantial amount of brine to flow in. The one realization in which 700 m^3 flows from the shaft into the halite is characterized by the highest halite permeability among the 70 realizations, a highly permeable shaft seal, and large quantities of gas generation that cause the shaft to pressurize much more than in other realizations, thus providing a greater driving force out of the shaft and into the halite. Only seven other realizations have a net flow of brine from the shaft into the halite. Flow through the shaft seal was discussed earlier. In two-thirds of the realizations, brine flows from the shaft into the Culebra (Figure 4-25). This flow is largely driven by gas flowing up the shaft. In the other one-third of the realizations, the shaft is never pressurized enough to prevent brine from draining from the Culebra into the shaft.

4.1.3 Gas Flow Behavior

Gas flow in the anhydrite layers was discussed earlier in connection with its impact on brine flow. It was mentioned then that gas may flow beyond the disposal-unit boundaries in some realizations. This issue will be clarified here. For brevity, the discussion will be restricted to flow in the mesh south of the repository because the cumulative flows are greater there than to the north. Figures 4-26, 4-27, and 4-28 show the cumulative gas flows past the southern disposal-unit boundary in MB139, anhydrite a + b, and in MB138, respectively. Significant volumes of gas (i.e., greater than one m^3) flow past the boundary in six realizations. The maximum gas flow past a boundary occurs in MB138, with 1.7×10^6 m^3 of gas (at reference conditions). All gas is assumed to have the physical properties of hydrogen. Because the viscosity of hydrogen is lower than that of other gases likely to be present or produced in the waste (CO_2, CH_4, N_2), this assumption should result in greater and more extensive gas flows than if other gases were used.

Although no gas flowed past the disposal-unit boundary in the Culebra, it is interesting to see how effective the shaft seal is in preventing gas flow into the Culebra. The cumulative gas flow up through the shaft seal is shown in Figure 4-29. With a maximum of 1.9×10^5 m^3, gas flows through the shaft seal are small compared with the flows out the anhydrite layers, where the maxima are more than an order of magnitude higher. Why the upper curve in Figure 4-29 stands out from the others is difficult to explain. The only exceptional parameter in this realization is the halite permeability, which is the highest among the 70 realizations. That the cumulative flow is a factor of five higher than the next highest result suggests that sampling should be more detailed in order to fill in the gap between the one outstanding result and all the rest. The drift seals were relatively ineffective in stopping gas flow toward the shaft for the time scales of this study (Figure 4-30). Nearly as much gas flows through these seals as out each of the

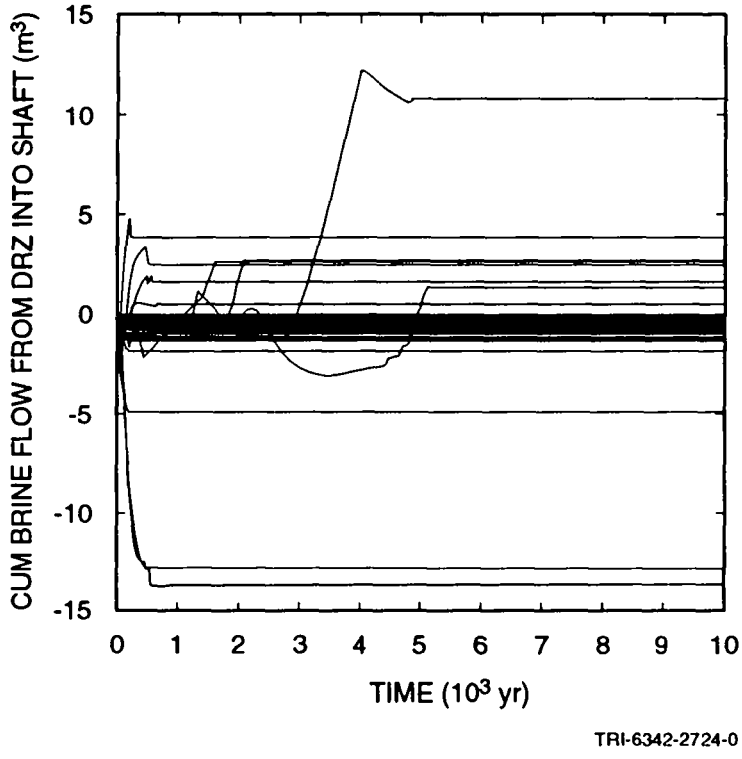

Figure 4-21. Cumulative Brine Flow from DRZ into Shaft.

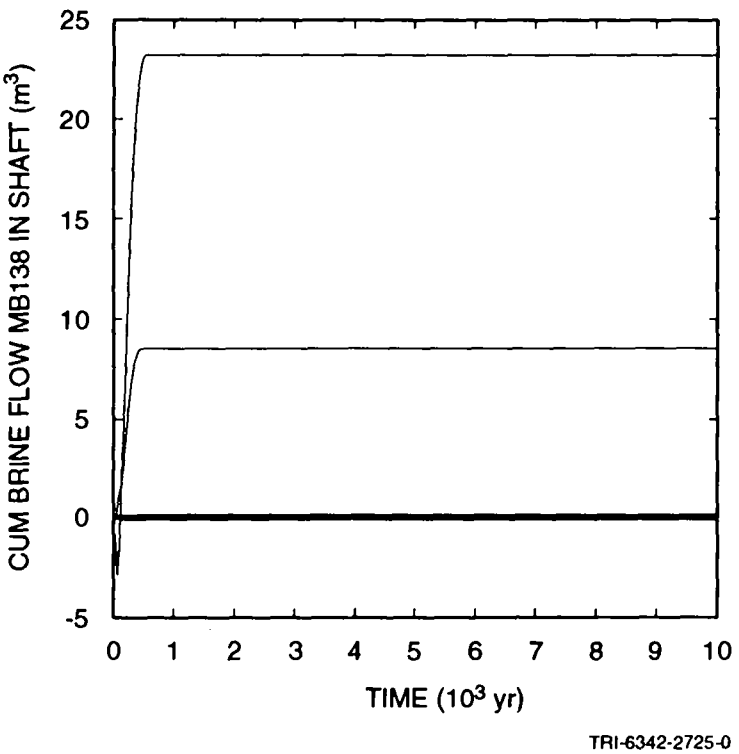

Figure 4-22. Cumulative Brine Flow from MB138 into Shaft.

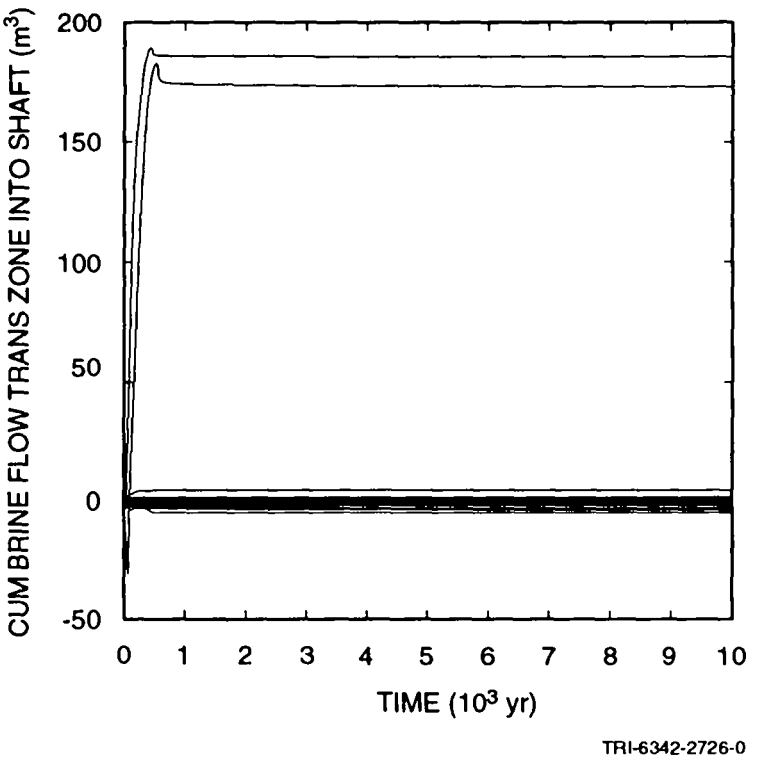

Figure 4-23. Cumulative Brine Flow from Transition Zone into Shaft.

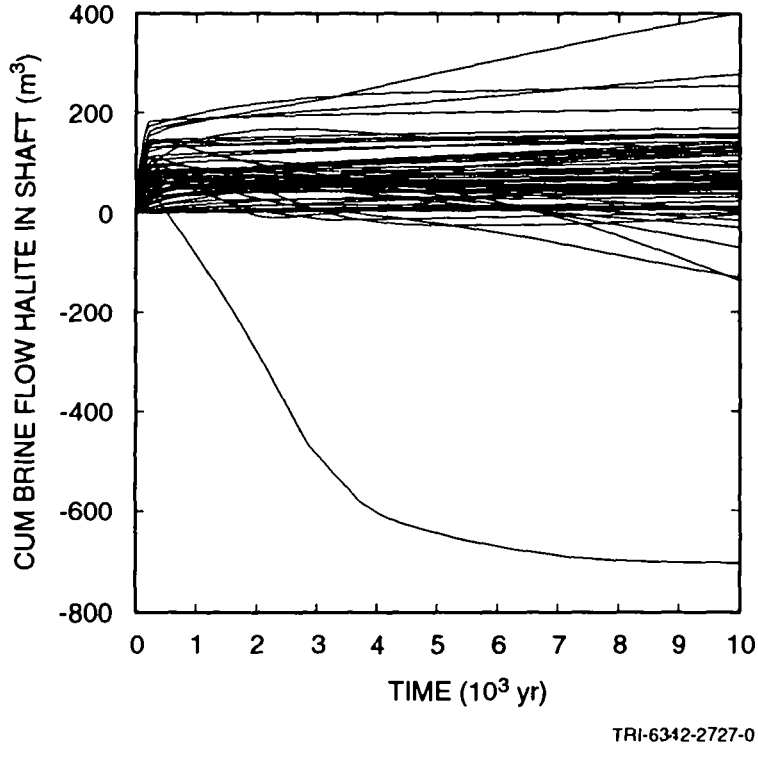

Figure 4-24. Cumulative Brine Flow from Halite into Shaft.

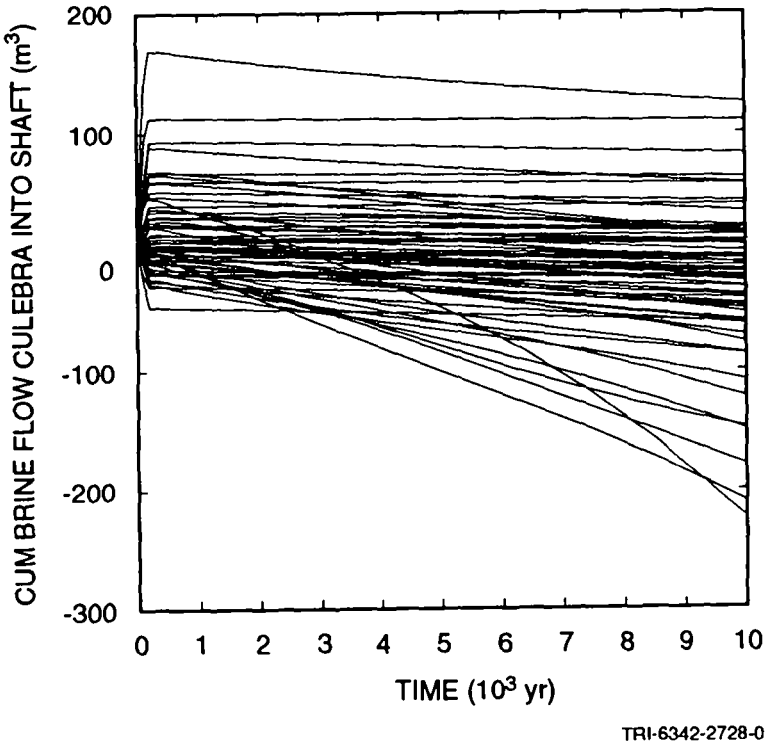

Figure 4-25. Cumulative Brine Flow from Culebra into Shaft.

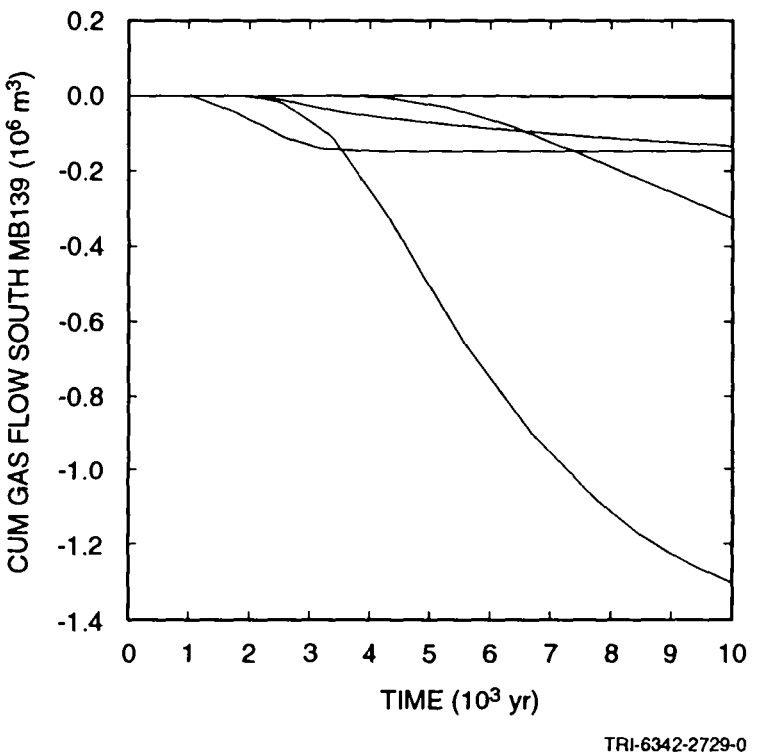

Figure 4-26. Cumulative Gas Flow South in MB139 Past the WIPP Boundary (at 30°C; 0.101 MPa). (Negative values indicate flow southward away from the repository.)

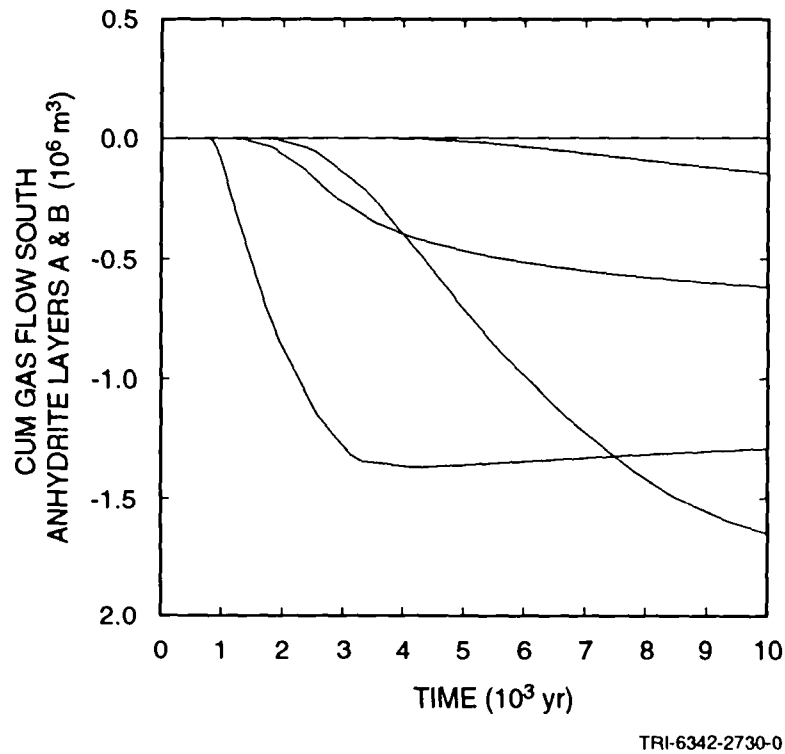

Figure 4-27. Cumulative Gas Flow South in Anhydrite Layers a + b Past the WIPP Boundary (at 30 °C; 0.101 MPa). (Negative values indicate flow southward away from the repository.)

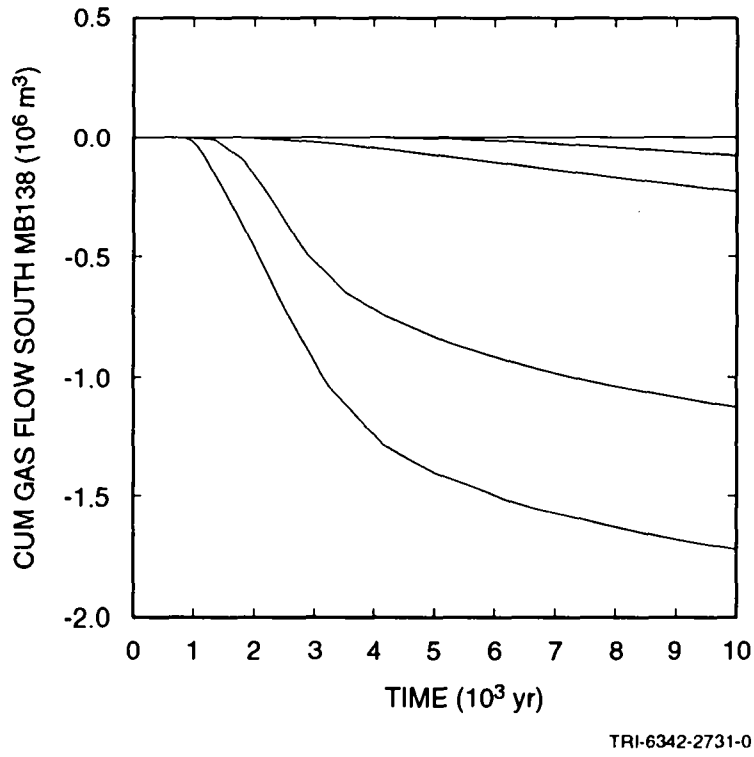

Figure 4-28. Cumulative Gas Flow South in MB138 Past the WIPP Boundary (at 30 °C; 0.101 MPa). (Negative values indicate flow southward away from the repository.)

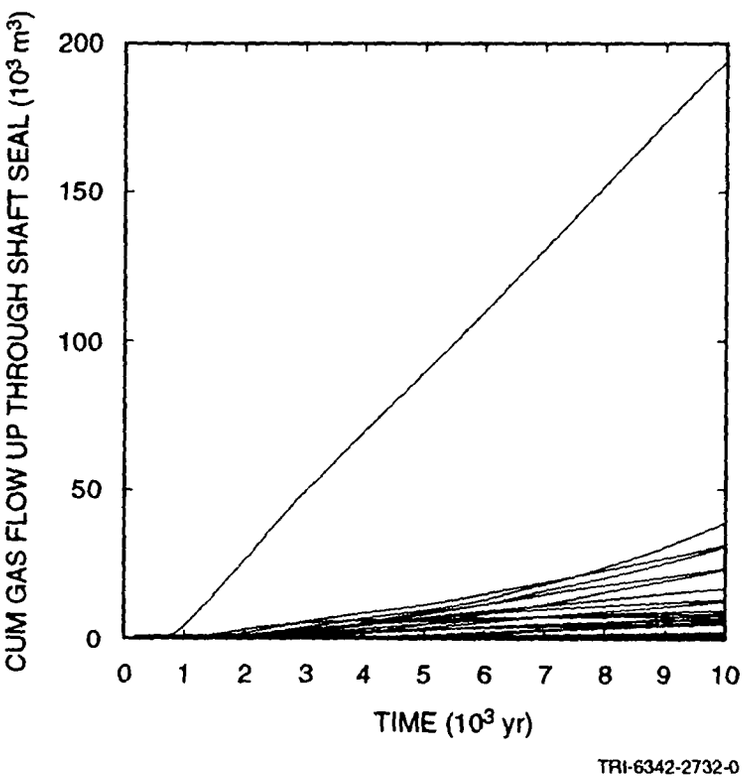

Figure 4-29. Cumulative Upward Gas Flow through Shaft Seal (at 30 °C; 0.101 MPa).

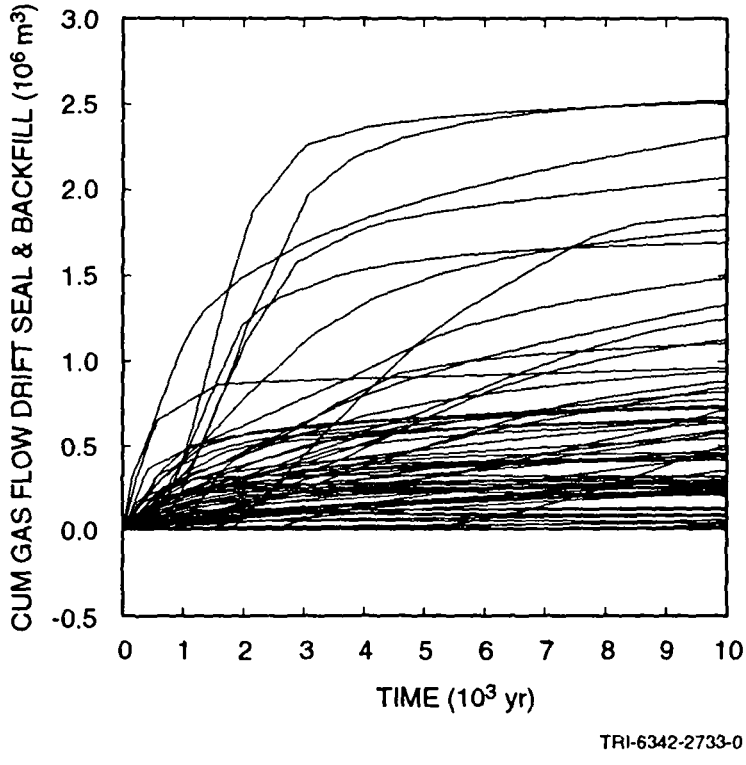

Figure 4-30. Cumulative Gas Flow from Drift Seals and Backfill into Shaft (*at 30 °C; 0.101 MPa*).

three anhydrite layers: a maximum of 2.5×10^6 m^3 versus an average maximum of 3.3×10^6 m^3 to the south in each anhydrite layer. A somewhat greater amount flows through the DRZ into the shaft below the shaft seal (Figure 4-31), up to 3.9×10^6 m^3. Gas encounters little resistance between the repository and the shaft, which leaves the shaft seal to prevent gas migration into the Culebra. (It is assumed that there is no DRZ around the shaft above MB138 through which gas could bypass the shaft seal [see Figure 2-1].) Other flow paths between the repository and the shaft are insignificant. Less than 50,000 m^3 of gas flows into the shaft via the transition zone, and less than 8000 m^3 by way of MB138; in fact, in some realizations, the flow is in the opposite direction, *from* the shaft, rather than *into* the shaft.

4.2 Single-Shaft Geometry

In these calculations, the shaft was changed from the original configuration (in which all four shafts were combined into one), to a single shaft the size of the Salt Handling Shaft. All other parameters are identical to those used in the four-shaft equivalent geometry calculations. As shown in the following discussion, the affect of reducing the size of the shaft is negligible. Fluid flows up the shaft were reduced in proportion to the shaft cross section reduction. However, shaft flows had only a small effect on the overall performance of the repository in the original calculations. There were no flows of brine and small flows of gas to the top of the Salado Formation in both four-shafts-in-one geometry or the single-shaft geometry. In particular, the shaft seal performance was good enough that the presence of the shaft was of no consequence in either performance assessment, whether there was one shaft or four.

4.2.1 Repository Behavior

Although minor differences occurred between individual realizations, on the whole, the pressures in the repository differ insignificantly between these single-shaft calculations and the base case (see Figure 4-32). The peak pressure was still 23.8 MPa; after 10,000 yr, pressures ranged from 5.4 to 22.3 MPa, compared with 5.8 to 22.3 MPa in the base case. Because the transient pressure behavior in the repository differed little from the base case, other performance measures would also be expected to differ little. Plots of remaining corrodible content, biodegradable content, and total gas generated — Figures 4-33, 4-34, and 4-35, respectively — are nearly indistinguishable from their base case counterparts. Other results describing conditions in the waste are also very similar: pore volumes, cumulative brine consumption, and brine and gas saturations. These results are not surprising. The shaft is a relatively small region located more than 600 m from the waste-disposal region. Its diameter should not and does not have any significant effect on processes that occur in the waste, particularly because the behavior of the repository is largely determined by the amount of brine initially present and by marker bed permeability. Shaft diameter would be expected to have a noticeable effect only on flows up the shaft, although fluid flow in other regions should be considered.

4.2.2 Brine Flow Behavior

Cumulative brine flow from the repository, Figure 4-36, is virtually identical to the base case, Figure 4-9, which was expected because all other repository responses are unchanged. Plots of cumulative brine flow out each of the

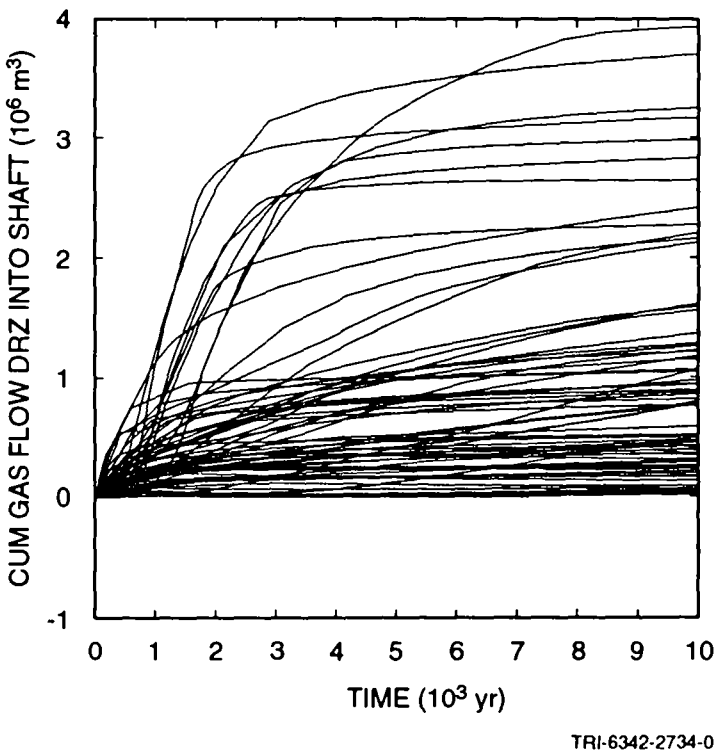

Figure 4-31. Cumulative Gas Flow from DRZ into Shaft (at 30 °C; 0.101 MPa).

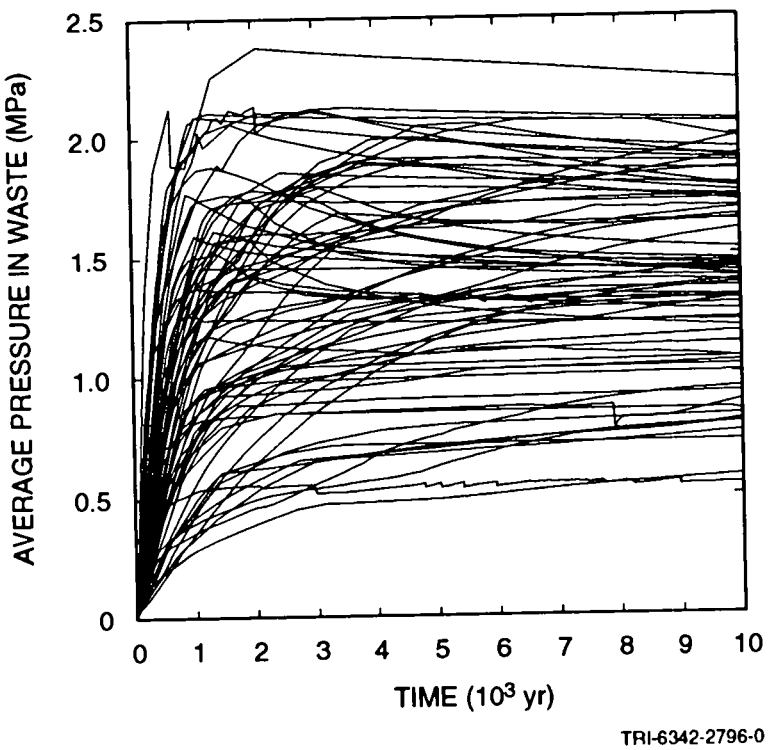

Figure 4-32. Volume Average Pressure in the Waste Repository, Single Shaft Model.

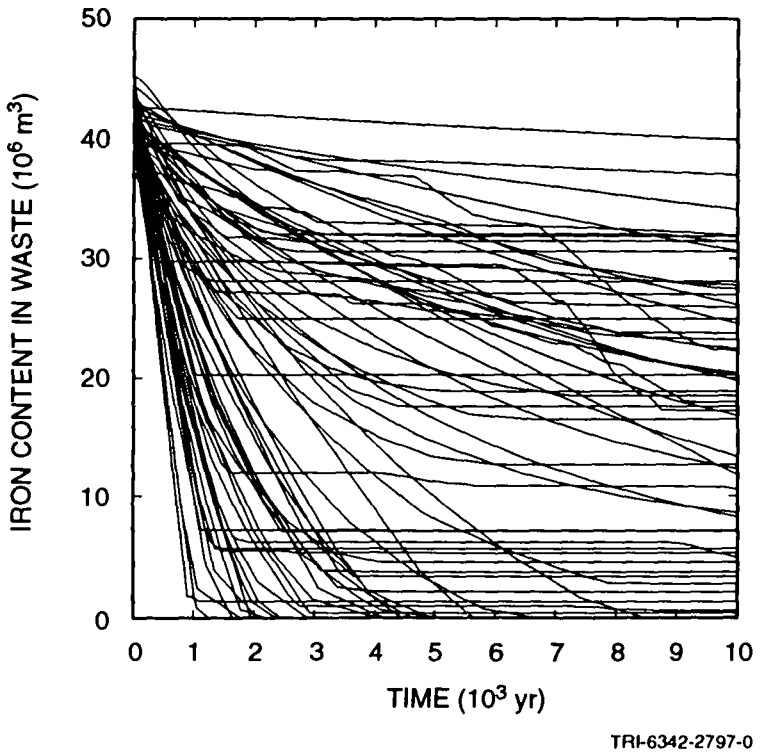

Figure 4-33. Iron Remaining in the Waste Repository, Single Shaft Model.

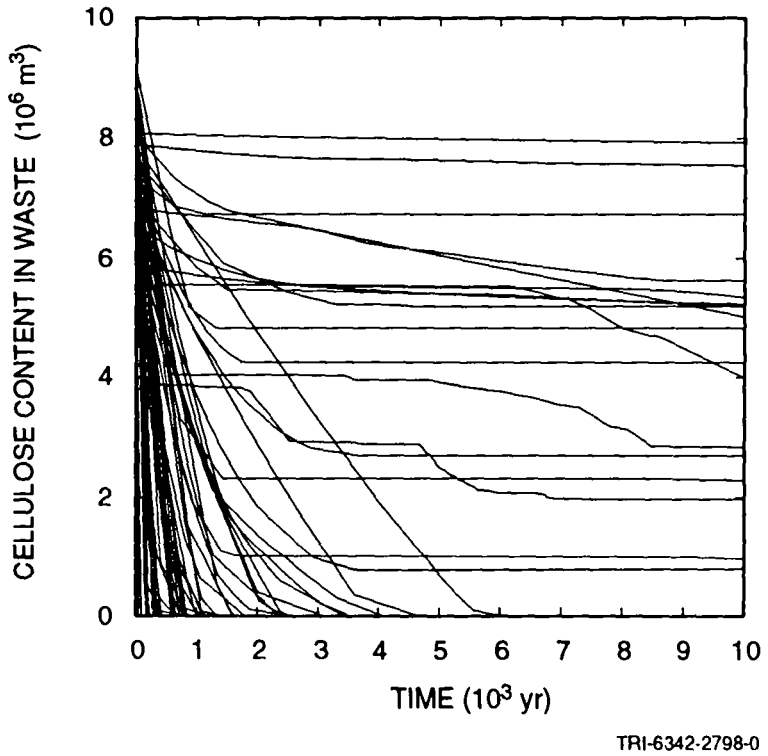

Figure 4-34. Cellulose Remaining in the Waste Repository, Single Shaft Model.

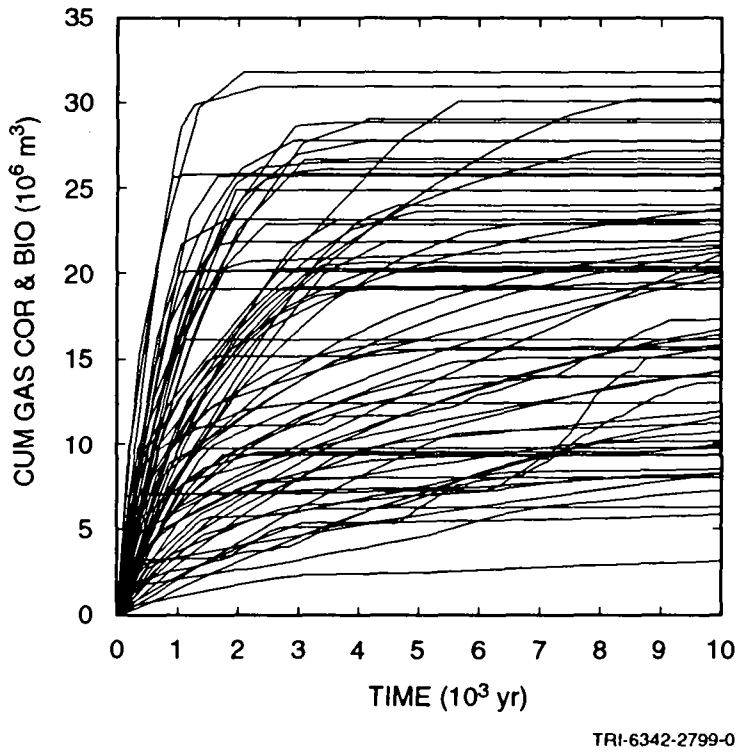

Figure 4-35. Cumulative Gas Volume Generated (at 30 °C; 0.101 MPa), Single Shaft Model.

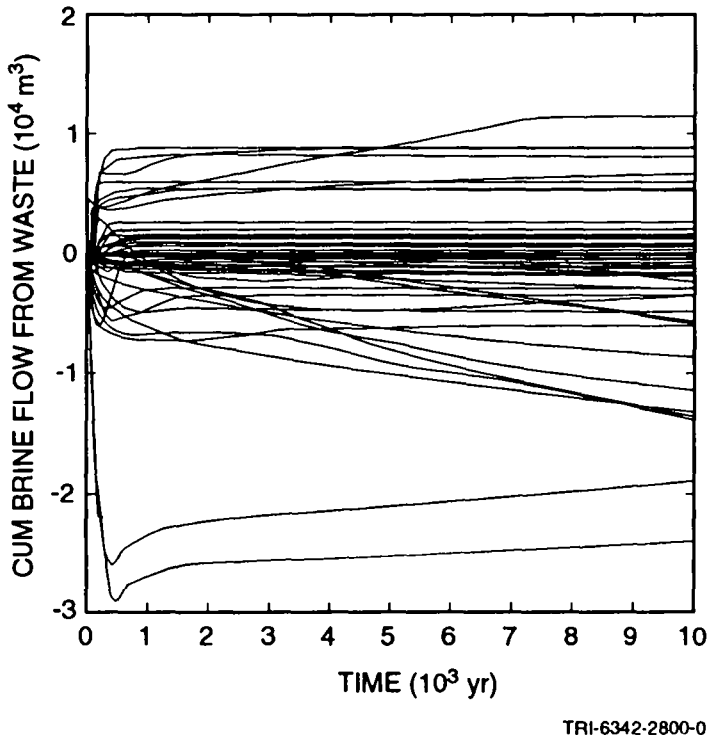

Figure 4-36. Cumulative Brine Flow from the Waste Repository, Single Shaft Model. (Positive values indicate flow away from the repository.)

three anhydrite layers overlay plots of the base case exactly and are not repeated here. Where differences are expected is in flow up the shaft. The most apparent difference between the single-shaft results and the results with four shafts combined is in flows through the shaft seal, Figure 4-37. Comparing this with the earlier plot, Figure 4-11, the flow of brine through the shaft seal is reduced by the smaller shaft cross section. The maximum net upward flow is now 3 m^3 versus 25 m^3 with four combined shafts. However, the minimum pore volume of the lower shaft, 37 m^3, is still 10 times the volume of brine that flowed up through the shaft seal, just as in the base case. Although the lower shaft pore volume is smaller with the single shaft, the amount of brine that flowed up the shaft is reduced proportionately. (Although there were a few realizations in which brine initially flowed downward but later reversed direction, as in the base case, the total upward flow was still less than 5 m^3.)

The amount of brine that flows out through the anhydrite layers is negligibly different when the shaft is modeled as a single shaft the size of the Salt Handling Shaft compared to modeling it as all four shafts combined. Brine flow up the shaft is proportionately smaller when a single shaft is used. Thus, shaft diameter has no effect on releases of contaminated brine as far as 40 CFR 191B is concerned.

4.2.3 Gas Flow Behavior

As with brine flow, gas flow is largely determined by the behavior of the repository. The shaft has only a minor impact on repository behavior, since it is more than 600 m away, whereas the anhydrite layers provide flow paths of much greater capacity. Thus, the same conclusions arrived at with the base case hold true for the single-shaft case. Cumulative gas flows out each of the anhydrite layers are nearly identical with the base case: Maximum southward gas flows past the Disposal unit boundary in MB139 are 1.30×10^6 m^3 in both cases; southward flows out of anhydrite a + b are 1.65×10^6 m^3. Only in MB138 are maximum flows slightly lower: 1.65×10^6 m^3 versus 1.72×10^6 m^3 in the base case. In the single-shaft calculations, gas flows into the Culebra in twelve realizations, compared with six realizations in the combined-shafts case. However, the maximum cumulative gas flow are now 1.9×10^4 m^3, instead of 1.4×10^5 m^3 with combined shafts. With a single shaft, the average cumulative gas flow is 5400 m^3 (for 12 realizations), which is about one-fourth of the four-shaft average, 22,900 m^3 (for 6 realizations).

The main difference when using a smaller versus a larger shaft is the flow up through the shaft seal, Figure 4-38. The obvious difference is the smaller cumulative flows through the seal. The maximum is now 30,000 m^3, compared with 194,000 m^3 in the base case. In both cases, there were 37 realizations in which the cumulative flow was greater than 1 m^3. The average flow among those 37 was 4500 m^3, compared with 12,400 m^3 in the base case.

4.3 Four-Shaft Equivalent Geometry without Dynamic Creep Closure

This set of calculations is identical to the base case, with all four shafts combined into one, except that the repository does not undergo creep closure. Instead, the initial porosity is set at 19%, which is the median final closed porosity of the repository. Small changes in porosity are allowed as a result of compressibility effects. However, unlike the case of dynamic creep closure, in which the repository porosity varies from an initial value of 66% to as low as 12%, the "fixed porosity" varies by no more than 1.2 percentage points from its initial value (i. e., from 19 to 20.2%). This has a major effect on the behavior of the repository, especially on pressures within the repository. However, the net effect over the 10,000-yr compliance period is negligible, because, ultimately, what

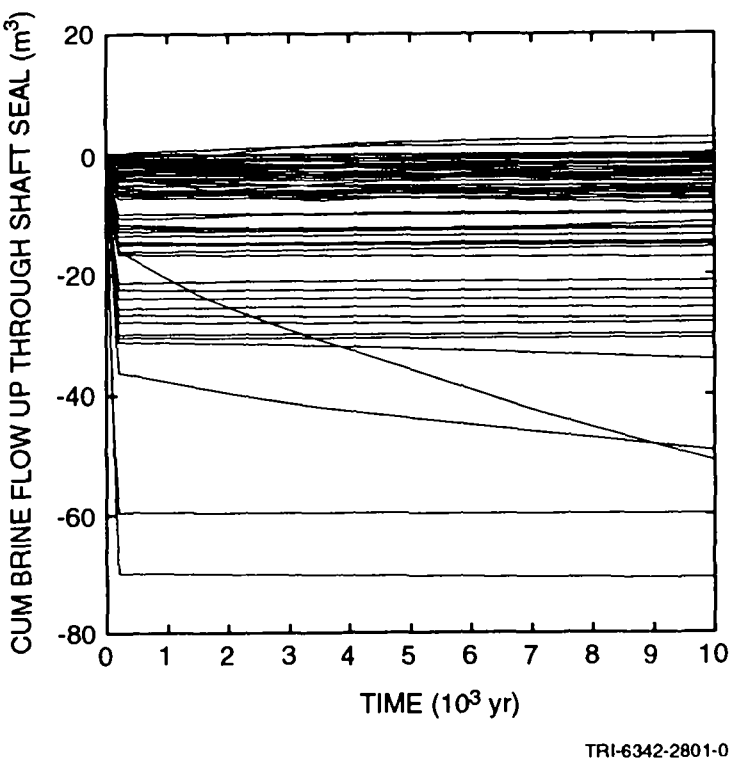

Figure 4-37. Cumulative Upward Brine Flow through Shaft Seal, Single Shaft Model

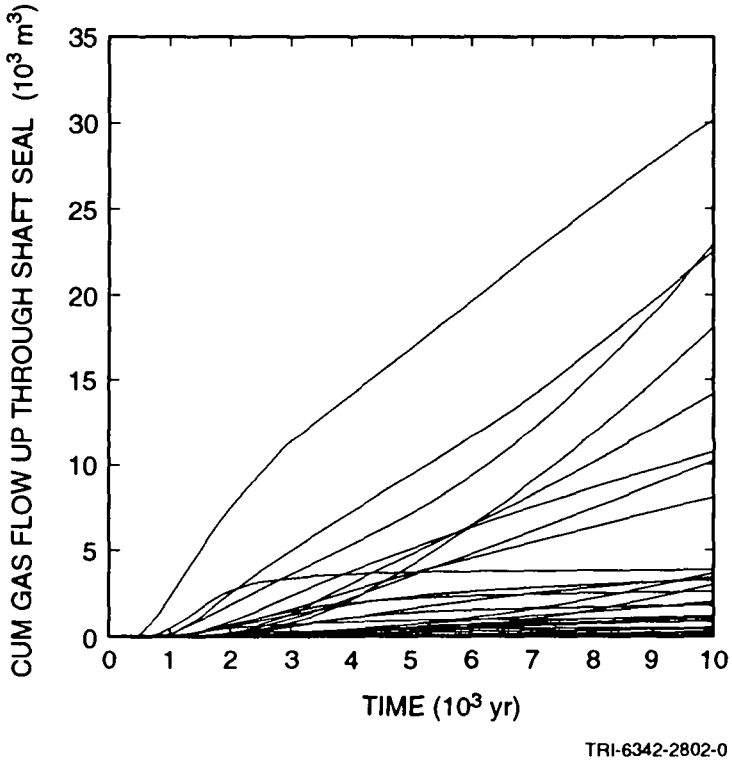

Figure 4-38. Cumulative Upward Gas Flow through Shaft Seal (at 30°C; 0.101 MPa), Single Shaft Model.

drives gas migration is the number of moles of gas generated in the waste, which is primarily dependent on the amount of brine present there initially. Conditional on the conceptual models and parameter distributions used in these analyses, results described have suggested that detailed modeling of the dynamics of creep closure may be unnecessary.

4.3.1 Repository Behavior

Pressures in the waste generally peak at much higher values than in the calculations with dynamic creep closure (Figure 4-39). In order to maintain the gas generation potential in the fixed porosity calculations to be the same as in the dynamic creep closure calculations, the same initial repository brine volume is used. This results in approximately the same amount of gas being generated. (Compare Figures 4-40 and 4-7). With dynamic creep closure, final porosities greater than the median value are often obtained, particularly when large amounts of gas are generated and pressures are relatively high. In fact, in one dynamic closure realization, the repository is forced open to 34% porosity after closing down to 21%. When the porosity in this realization is fixed at 19%, the pressure is proportionately higher. Instead of peaking at 23.8 MPa, it now peaks at 38.8 MPa. At the other extreme, some realizations that result in very low porosities with dynamic closure (as low as 11.6%) because little gas is generated now have lower pressures because the porosity is fixed at 19%. Over time, the differences become less significant. After 10,000 yr, pressures within the repository range from 5.8 to 22.3 MPa using dynamic creep closure, compared with 4.0 to 29.2 MPa with fixed porosities. Even more similar are the averages over the 70 realizations: 14.9 MPa with dynamic closure versus 14.2 MPa with fixed porosity. Thus, it would be expected that a few realizations will display significantly different behavior, but that overall, the results using fixed porosity will not differ much from using dynamic creep closure.

Other performance measures for waste behavior are less affected by the dynamics of porosity changes. Based on the data currently available, gas generation is modeled as a direct function only of brine saturation, not of pressure. As shown earlier, the amount of gas generated, as well as the rate, is strongly influenced by the amount of brine present initially and relatively little by the amount of brine that flows into the repository over time. Porosities and pressures therefore have little effect on the amount of gas generated. Since gas generation is unaffected, the amount of reactants remaining in the waste over time is also unaffected by how the porosity of the waste is modeled.

4.3.2 Brine Flow Behavior

Differences in how the waste porosity is modeled should manifest themselves in fluid flow behavior outside the waste, as a result of differences in peak pressures. Because the initial brine volume is fixed between the two sets of calculations, the initial brine saturation is about 3.5 times higher in the fixed-porosity calculations. Whereas the original brine saturations range from zero to 0.14, where the maximum is half the residual brine saturation, now the initial saturations ranges as high as 0.48, well above residual saturation. This enables brine to flow from the waste in several of the realizations from the start (Figure 4-41), in contrast to the dynamic closure model, in which brine could flow out of the waste only after the repository has crept shut enough to raise the brine saturation above residual. (Brine could also flow out after first flowing in; this behavior is seen in both models.) With the porosity fixed, the number of realizations in which there is a net positive flow of brine from the repository is larger (25 versus 19), and the maximum outflow is greater (13,300 m^3 compared with 11,400 m^3 with dynamic closure). While this constitutes a larger source of contaminated brine, the key measure remains the distance this brine flows

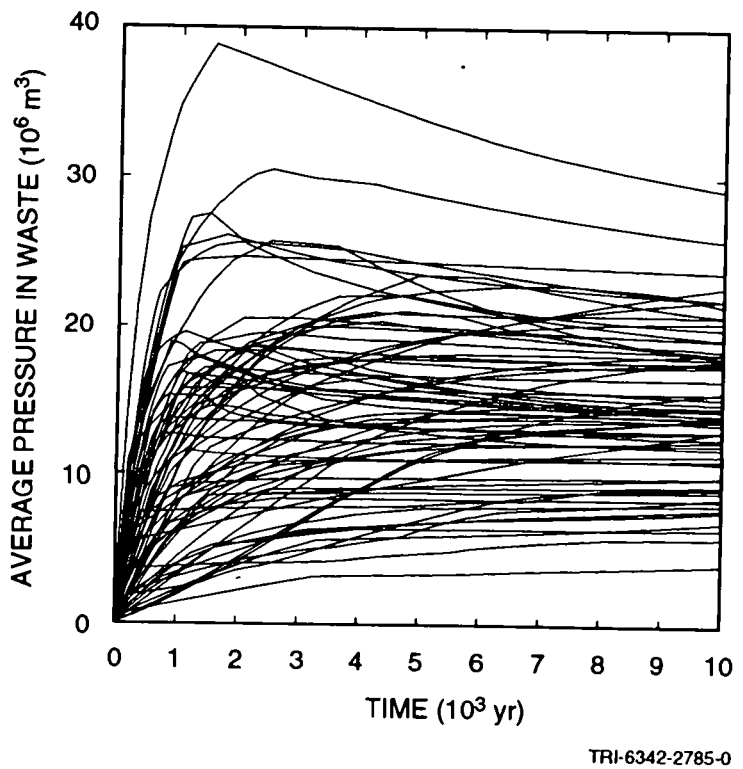

Figure 4-39. Volume Average Pressure in the Waste Repository, Fixed Waste Porosity Model.

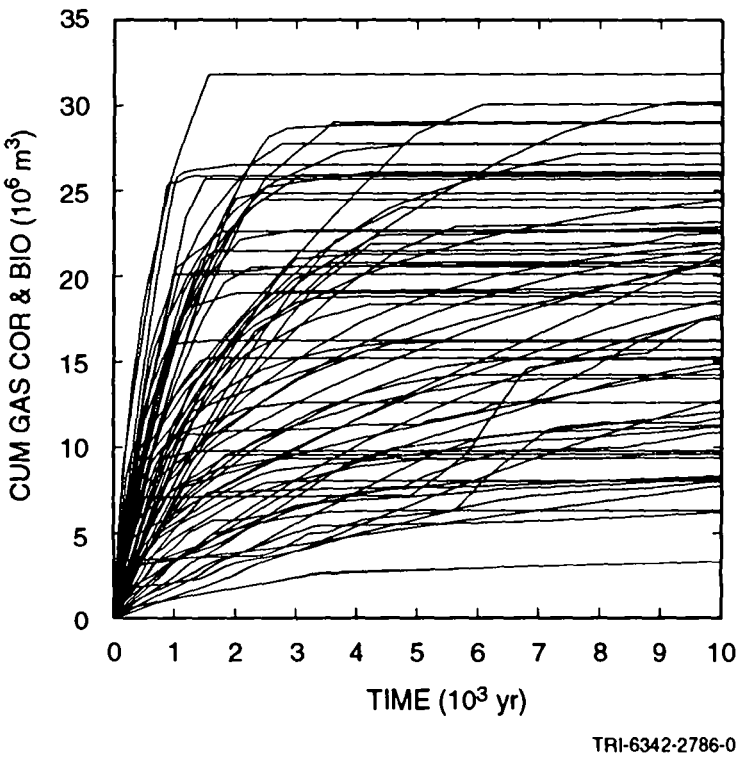

Figure 4-40. Cumulative Gas Volume Generated (at 30 °C; 0.101 MPa), Fixed Waste Porosity Model.

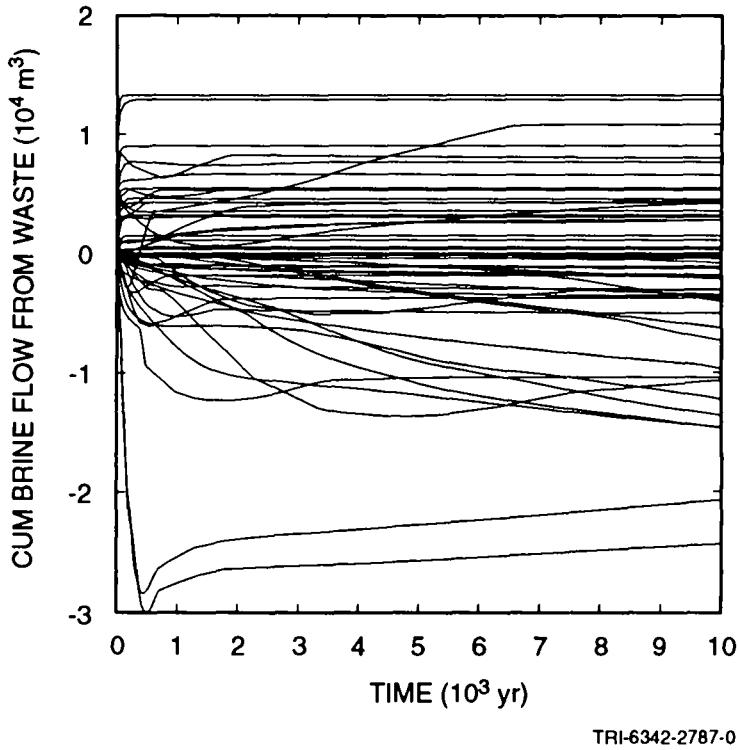

Figure 4-41. Cumulative Brine Flow from the Waste Repository, Fixed Waste Porosity Model. (Positive values indicate flow away from the repository.)

toward the disposal-unit boundaries, and whether it reached the boundaries. In the fixed porosity results, the maximum cumulative brine flows out each of the anhydrite layers in the southern direction are 7200 m^3 out MB139 (the lowest curve in Figure 4-42, outflow occurs only after approximately 600 yr), zero out anhydrite a + b layer (Figure 4-43), and 540 m^3 out MB138 (Figure 4-44). These values differ little from the dynamic closure results reported in Section 4.1.2 (6700 m^3 for MB139, zero for anhydrite a + b, and 520 m^3 for MB138). In MB139, the realization having the greatest outflow has an anhydrite porosity of 0.0041 and a residual saturation of 0.20, both sampled parameters. Thus, the residual brine in MB139 out to the disposal-unit boundary is 12,500 m^3. Even if all of the brine flowing out MB139 is contaminated, it will not even occupy all the volume required for residual brine saturation, and will not reach the disposal-unit boundary. Residual brine occupies 2650 m^3 of pore volume in MB138 between the repository and the southern boundary in the realization with the maximum brine outflow, so, again, the amount of potentially contaminated brine flowing south out MB138 will not reach the boundary. The maximum upward brine flow through the shaft seal (Figure 4-45) is 58 m^3, somewhat more than the 40 m^3 in the dynamic closure calculation, but still not enough to fill the lower shaft to the top of the Salado. Thus, none of the brine flow performance measures shows any significant difference between dynamic creep closure and fixed waste porosity.

4.3.3 Gas Flow Behavior

Cumulative gas flows out the anhydrite layers and through the shaft seal are similarly unaffected by repository porosity dynamics. The high peak pressures that are obtained when the waste porosity is fixed occur because the low permeability of these pathways prevents significant outflow of gas from the waste. It is only when the permeability of the anhydrite is high that large volumes of gas can flow out these pathways, and in those cases, the driving pressure remains relatively low. As pointed out earlier, it is ultimately the amount of gas generated that causes the driving force for gas migration from the repository. After 10,000 yr, the pore volume of the waste differs little regardless of how the pore volume dynamics are modeled because nearly the same final porosity is attained, so the quantity of gas generated and the permeability of flow paths away from the waste are the controlling factors in determining how far gas migrates. Figures 4-46, 4-47, 4-48, and 4-49 show the amount of gas that flows past the disposal-unit boundary in MB139, anhydrite a + b, MB138, and the shaft seal, respectively. Comparing these with their counterparts in Section 4.1.3 shows that the number of realizations in which gas migrated past the boundary is the same and the total volumes are insignificantly different. Thus, none of the gas flow performance measures shows any significant difference between fixed waste porosity and dynamic creep closure as currently modeled. This conclusion may change when pressure-dependent fracturing of anhydrite interbeds is included in future performance assessments, potentially lowering peak repository pressures and allowing for additional gas migration.

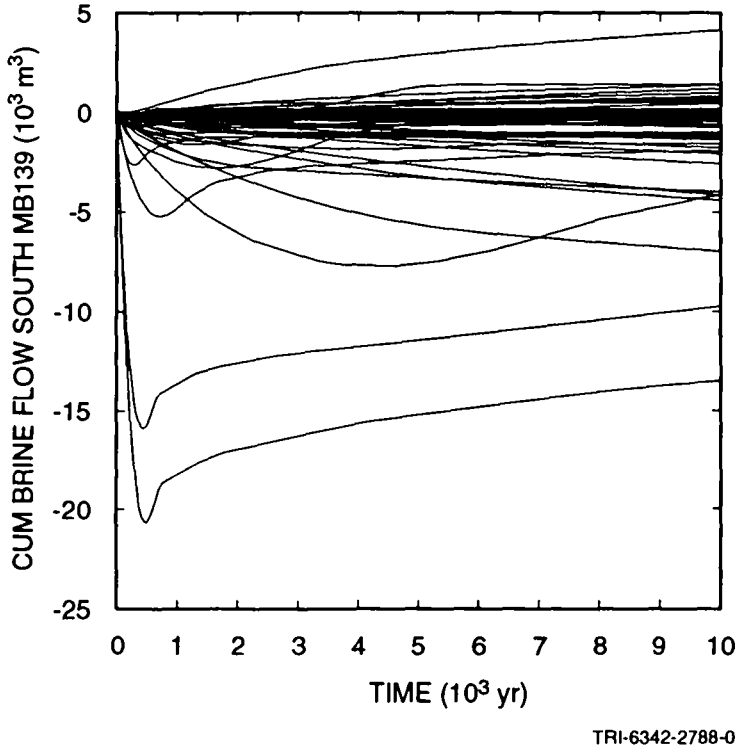

Figure 4-42. Cumulative Brine Flow South out MB139, Fixed Waste Porosity Model. (Positive values indicate flow southward away from the repository.)

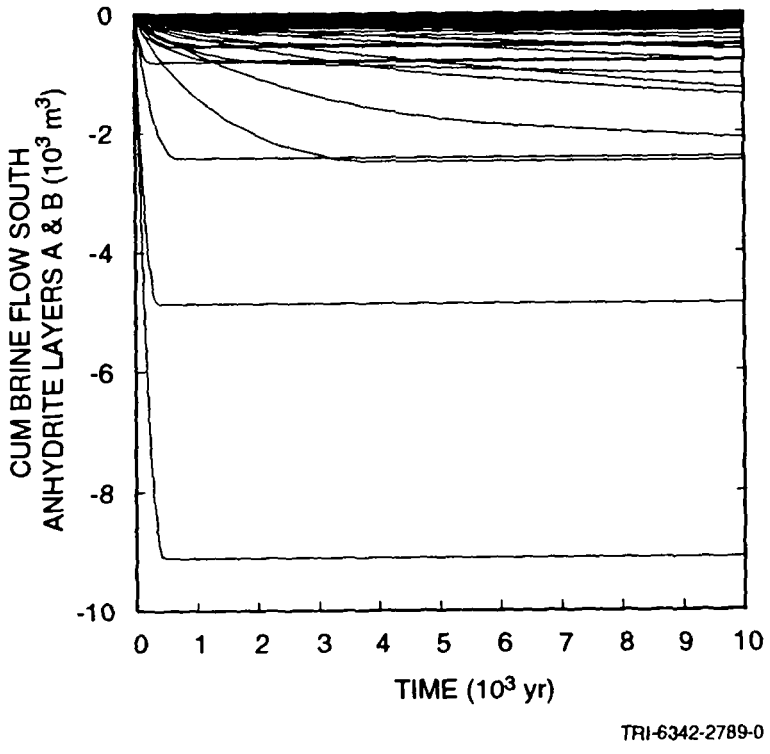

Figure 4-43. Cumulative Brine Flow South out Anhydrite Layers a + b, Fixed Waste Porosity Model. (Negative values indicate flow northward toward repository.)

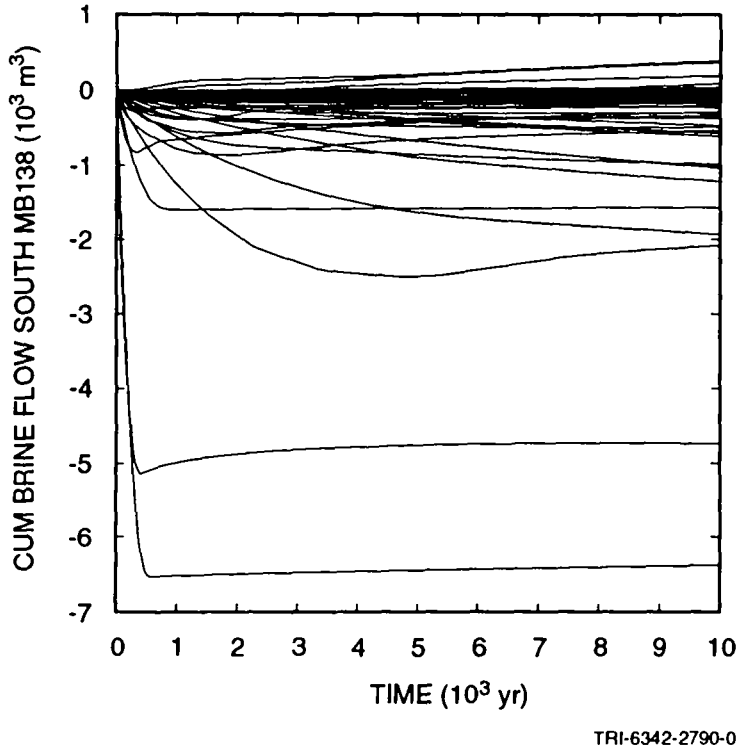

Figure 4-44. Cumulative Brine Flow South out MB138, Fixed Waste Porosity Model. (Negative values indicate flow northward toward repository.)

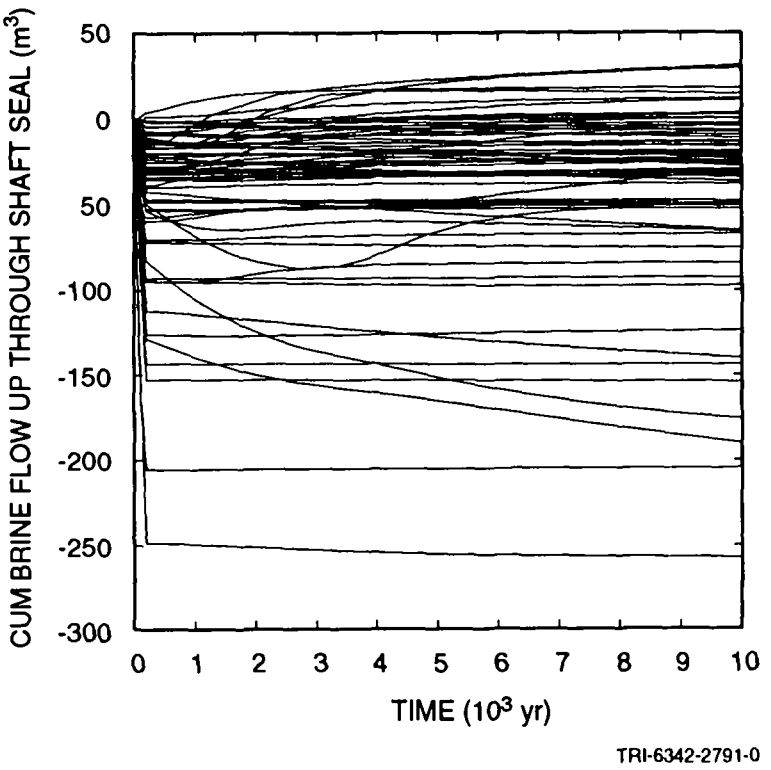

Figure 4-45. Cumulative Upward Brine Flow through Shaft Seal, Fixed Waste Porosity Model. (Positive values indicate flow upward through shaft seal.)

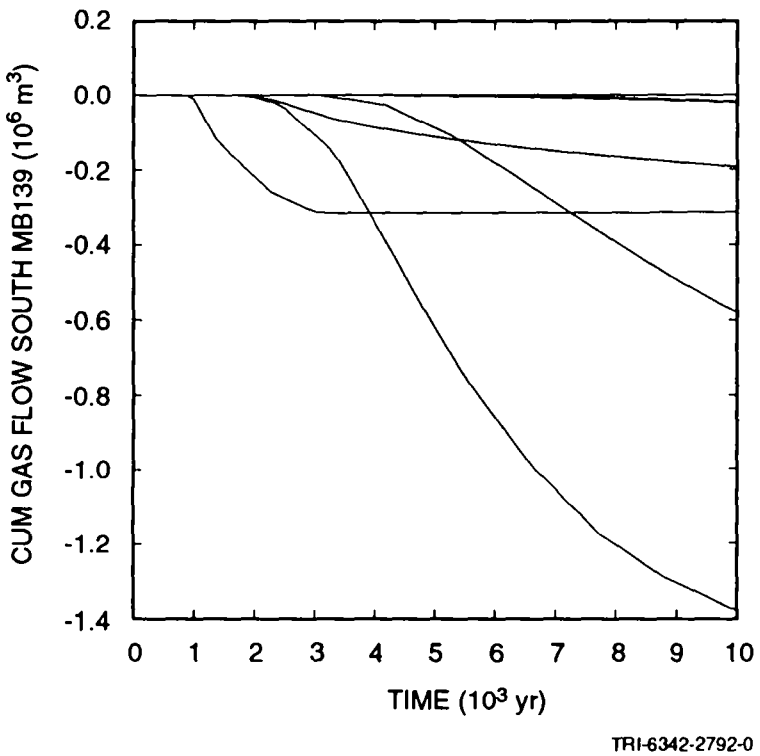

Figure 4-46. Cumulative Gas Flow South in Marker Bed 139 Past the WIPP Boundary (at 30 °C; 0.101 MPa), Fixed Waste Porosity Model. (Negative values indicate flow southward away from repository.)

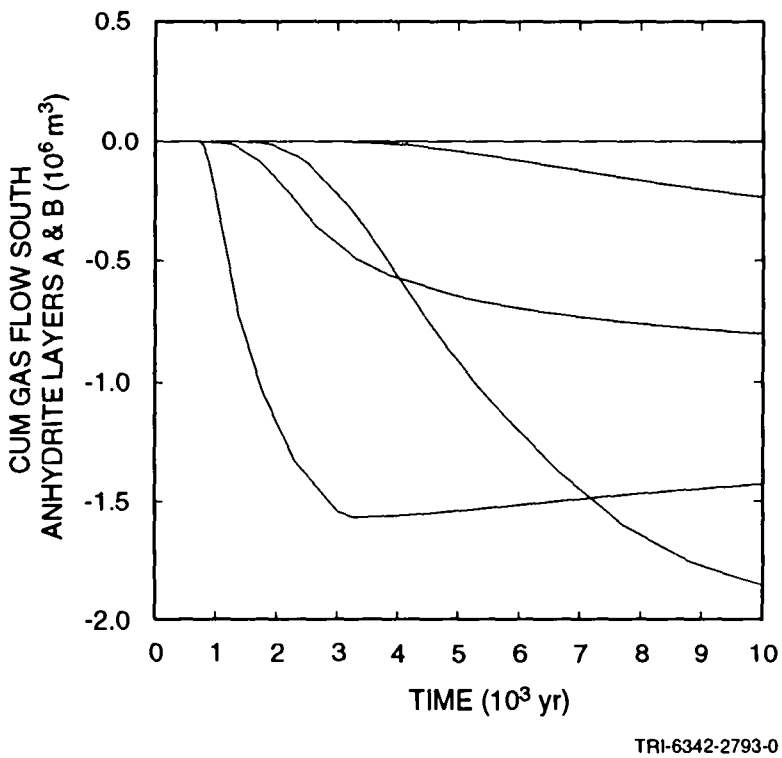

Figure 4-47. Cumulative Gas Flow South in Anhydrite Layers a + b Past the WIPP Boundary (at 30 °C; 0.101 MPa), Fixed Waste Porosity Model. (Negative values indicate flow southward away from repository.)

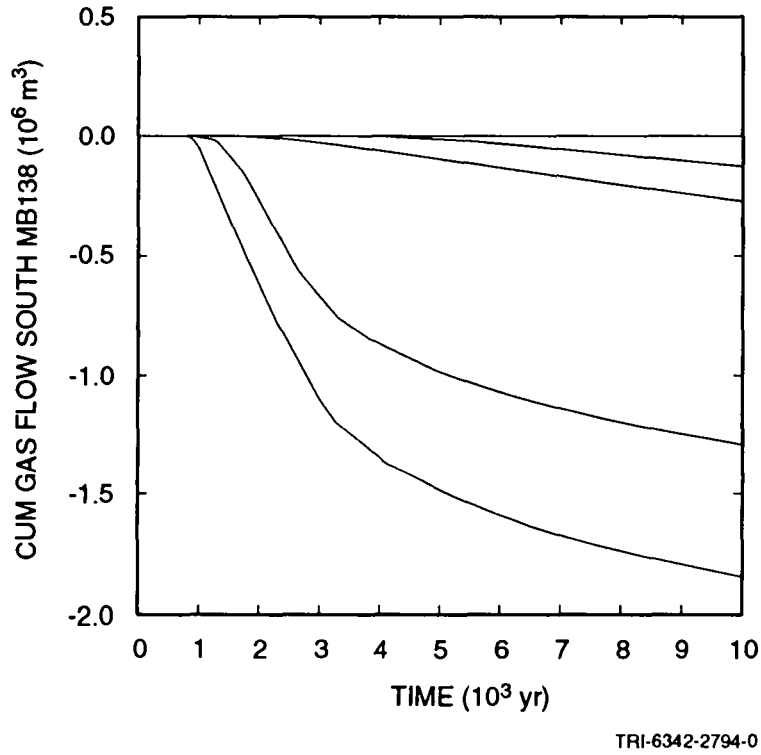

Figure 4-48. Cumulative Gas Flow South in MB138 Past the WIPP Boundary (at 30 °C; 0.101 MPa), Fixed Waste Porosity Model. (Negative values indicate flow southward away from the repository.)

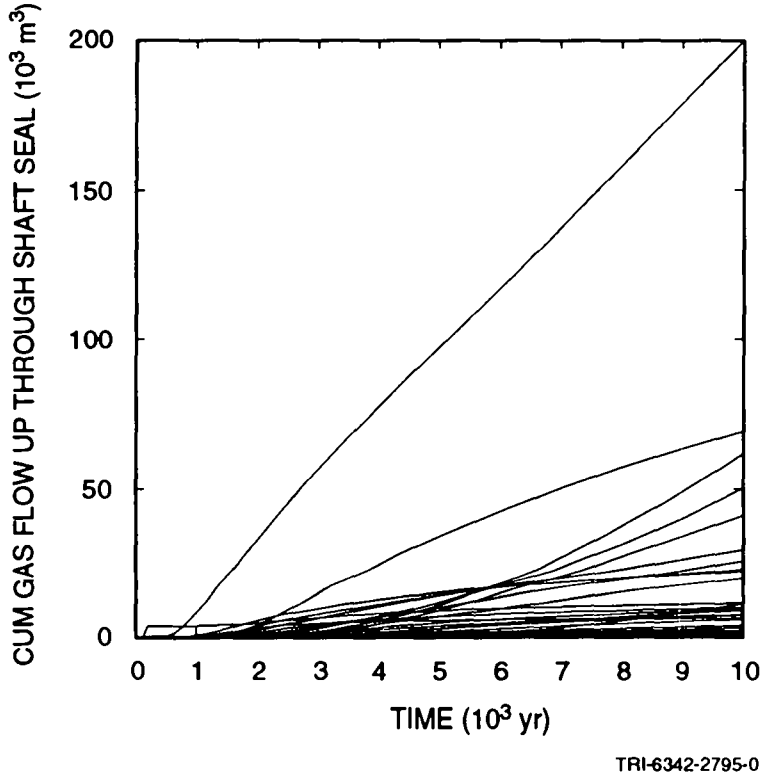

Figure 4-49. Cumulative Upward Gas Flow through Shaft Seal (at 30 °C; 0.101 MPa), Fixed Waste Porosity Model.

5. UNCERTAINTY AND SENSITIVITY ANALYSIS RESULTS

Uncertainty and sensitivity analyses were performed to determine factors that affect gas generation and movement of gas and brine away from the repository. The uncertainty and sensitivity analyses in this presentation use techniques based on Latin hypercube sampling, including examination of scatterplots, partial correlation analysis, and stepwise regression analysis. Specific performance measures examined were cumulative gas and brine flows out through the three anhydrite layers to the south of the repository, cumulative gas and brine flows up through the shaft seal and the distance that gas flowed out through the three anhydrite layers. Only the base case, in which the four shafts were combined into one, was analyzed. Gas and brine flows to the north of the repository were not analyzed because they were generally smaller and, therefore, of less importance from a regulatory standpoint. Also examined were various measures of the behavior of the repository itself, including cumulative gas generation by means of corrosion and biodegradation, pressure in the repository, and repository pore volume. These were analyzed to show how gas generation is affected by variability in the sampled parameters, because gas generation is the driving force behind gas and brine migration away from the repository in the undisturbed scenario.

The results show that the most important parameter affecting gas and brine migration from the repository is the initial brine saturation in the waste. This one parameter has the greatest impact on total gas generation, which effectively controls gas and brine flow into and out of the waste. Other important parameters include the gas-generation rates for corrosion and biodegradation under inundated conditions and the biodegradation stoichiometry. These parameters also affect gas generation, but are secondary to initial brine content in determining the total amount of gas produced. Over the 10,000-yr regulatory period, it is the total volume of gas generated, rather than transient behavior such as pressure in the repository, that most affects how far gas and brine migrate. Thus, *rates* of gas generation are most important only if sufficient brine is available to consume all the reactants in the waste. Biodegradation stoichiometry (i. e., the moles of gas produced per mole of cellulose consumed) is important because its sampled range extends to zero, which can completely nullify the effect of biodegradation. Because the amount of gas produced by biodegradation is directly proportional to the stoichiometric coefficient, gas generation by biodegradation can vary greatly, and, all other things being equal, this parameter can have a major impact. The only other parameter of significance was the shaft-seal permeability, which, for the range sampled, impacts gas flow, but not brine flow, up the shaft. These conclusions are valid only over the ranges of all the parameters used in the calculations and within the limits of the conceptual and numerical models.

Numerous sampled parameters had no noticeable effect on any of the performance measures. These include all four of the relative permeability model parameters (Brooks-Corey exponent, Brooks-Corey weight factor, residual brine saturation, and residual gas saturation for all regions except the waste), the far-field pressure in MB139, the shaft seal thickness, drift seal permeability, shaft porosity, and Culebra porosity. As modeled, drift seals were not effective; higher-permeability DRZ layers above and below the drift seals allowed gas and brine to flow around, rather than through the drift seals, so performance was insensitive the permeability of the seals. The porosity of the Culebra was also not tested adequately, because little gas and no brine from the waste reached the Culebra; when few realizations result in nonzero flow, the sensitivity to porosity cannot be properly analyzed.

The remaining 10 sampled parameters had, at most, a minor effect on these performance measures. These parameters include: the gas-generation rates for corrosion and biodegradation under humid conditions; corrosion stoichiometry; the initial volume fractions of biodegradables and metals in the waste; the porosity of anhydrite interbeds; the DRZ porosity; the permeabilities of halite and the shaft seal during the first 200 yr; and the permeability of the shaft between the shaft seal and the Culebra during the first 200 yr.

These results are strongly dependent on the conceptual models that are currently used. If the conceptual models were modified, the results could differ from those presented here.

Each of the performance measures is discussed separately below.

5.1 Sensitivity Analysis Techniques

The purpose of sensitivity analysis is to determine the relationships between the uncertainty in the independent variables used in an analysis and the uncertainty in the resultant dependent variables. Uncertainty analysis provides measures of the uncertainty in estimates for dependent variables of interest, including means, variances, and distribution functions. A formal uncertainty analysis is not presented here because such an analysis is not particularly useful in determining relationships among variables. However, uncertainty analysis is incorporated in the sensitivity analysis. This section describes briefly the sensitivity analysis techniques used, including scatterplots, stepwise regression analysis, and partial correlation analysis. A more detailed discussion of these techniques and their application to the WIPP project can be found in Helton et al. (1991).

The generation of scatterplots is the simplest sensitivity analysis technique. This approach consists of generating plots of dependent variable value versus independent variable value, with each point on the plot representing one realization. When there is no relationship between the independent and dependent variable, the individual points will be randomly spread over the plot. In contrast, the existence of a well-defined relationship between the independent and dependent variable often will be revealed by the distribution of the individual points. The examination of such plots when Latin hypercube sampling is used can be particularly revealing because of the full stratification over the range of each independent variable. For each dependent variable examined in this chapter, scatterplots are presented only for the two most influential independent variables. As the contribution of additional independent variables to the variability of the dependent variable decreases, the distribution of points in the scatterplots becomes more random and less useful, so additional plots are not presented.

In stepwise regression analysis, a sequence of regression models is constructed. The first regression model contains the single independent variable that has the largest impact on the dependent variable. The second regression model contains the two independent variables that have the largest impact on the dependent variable — the independent variable from the first step plus whichever of the remaining variables has the largest impact on the variation not accounted for by the first step. Additional models in the sequence are constructed in the same manner until a point is reached at which further models are unable to increase meaningfully the amount of variation in the dependent variable that can be accounted for. The order in which the variables are selected in the stepwise procedure provides an indication of variable importance, with the most important variables being selected first, the next most important variable being selected second, and so on. The R^2 values (coefficients of determination) indicate how much variation in the dependent variable can be accounted for by all variables selected through that

another step in the regression analysis. When the variables are independent and uncorrelated, as they are assumed to be here, the differences in the R^2 values for each step in the regression models equals the fraction of the total variability in the dependent variable that can be accounted for by the individual independent variable added at each step. When the variation about the regression model is small, the corresponding R^2 value is close to 1, which indicates that the regression model is accounting for most of the variability in the dependent variable. Conversely, an R^2 value close to zero indicates that the regression model is not very successful in accounting for the variability in the dependent variable. In addition to R^2 values, standardized regression coefficients (SRCs) in the individual regression models provide an indication of variable importance, and the sign of the SRC indicates whether the independent and dependent variable tend to increase and decrease together (a positive SRC) or tend to move in opposite directions (a negative SRC).

The statistical program, STEPWISE (Iman et al., 1980; Rechard, 1992), was used to evaluate variable importance using the stepwise regression procedure on rank-transformed data. Regression analyses often perform poorly when the relationships between the independent and dependent variables are nonlinear. Poor linear fits to nonlinear data can often be avoided when the data are replaced with their corresponding ranks and the regression procedures are performed on these ranks (Iman and Conover, 1979). In most cases, the analyses were tried with both raw and ranked data. The rank regressions generally gave better results, meaning that the rank regression models could account for higher percentages of the observed variability in the dependent variables. Only the rank regression analyses are reported, although raw data are shown in the scatterplots.

Stepwise regression analyses were performed on results at the end of the 10,000-yr simulations. Tables 5-1 and 5-2 summarize the variables used in the stepwise regression analysis. It is necessary to have some criterion to stop the regression model construction process. These are discussed in Helton et. al. (1991). In the analyses reported here, an α-value of 0.02 was used to add a variable to the regression model and a value of 0.05 to drop a variable from the model. (The α-value is the probability of obtaining a stronger relationship than the one identified in the analysis as a result of chance variation.) In addition, the Predicted Error Sum of Squares (PRESS) criterion was used to protect against overfit.

Partial correlation analysis provides measures of the linear relationship between a dependent variable and an independent variable when the linear effects of the other independent variables are removed. When a well-defined linear relationship exists between an independent variable and a dependent variable, the partial correlation coefficient will be close to +1 or -1, regardless of the distribution assigned to the independent variable or the magnitude of the impact that the independent variable has on the dependent variable. A positive partial correlation coefficient indicates that two variables tend to increase and decrease together, whereas a negative correlation coefficient indicates that, as one variable increases, the other decreases. Partial correlation coefficients were calculated using time-dependent results, such as those shown in figures in Chapter 4, and show how the impact of different independent variables changes over time. These analyses complement the stepwise regression analyses, which provide more detailed statistics but at a single time. Note that because variables change in importance through time the regression analyses and partial correlation coefficient analyses may identify different variables as being important.

The partial correlation analyses were done using the statistical module PCCSRC (Iman et al., 1985; Rechard, 1992). As with the stepwise regression analyses, these analyses were performed on rank-transformed data. For each dependent variable, a plot of the partial rank correlation coefficients is presented that shows the time dependence of the coefficient for the four most influential independent variables.

Table 5-1. Latin Hypercube Sampled Independent Variables Used in Stepwise Regression and Partial Correlation Analyses[a]

Independent Variables	LHS No.	Description
BCBRSAT	13	Residual brine saturation in all regions except waste
BCEXP	11	Brooks-Corey exponent
BCFLG	12	Brooks-Corey/van Genuchten-Parker weighting factor
BCGSSAT	14	Residual gas saturation in all regions except waste
BKFLPOR	26	Porosity of backfill material in drifts, the experimental region, and in the shaft below the seal
BRSAT	1	Initial brine saturation in waste
CULPOR	27	Culebra porosity
DSEALPRM	25	Permeability of drift seals
GRCORHF	3	Humid corrosion rate factor
GRCORI	2	Inundated corrosion rate
GRMICHF	6	Humid biodegradation rate factor
GRMICI	5	Inundated biodegradation rate
MBPERM	15	Log of anhydrite interbeds permeability
MBPOR	16	Undisturbed anhydrite interbeds porosity
MBPRES	18	Far-field pressure in MB139
SALPERM	10	Intact Salado halite permeability
SEALPRM1	22	Initial shaft seal permeability
SEALPRM2	23	Shaft seal permeability after 200 yr

Table 5-1. Latin Hypercube Sampled Independent Variables Used in Stepwise Regression and Partial Correlation Analyses (Concluded)

Independent Variables	LHS No.	Description
SEALTHK	21	Shaft seal thickness
SHFTPRM	24	Permeability of shaft-fill material above shaft seal
STOICCOR	4	Corrosion stoichiometry factor
STOICMIC	7	Biodegradation stoichiometric coefficient
TZPORF	17	Factor used in calculating DRZ and transition zone porosity
VMETAL	9	Initial volume fraction iron in waste
VWOOD	8	Initial volume fraction cellulose in waste

[a] Ranges of values for independent variables are given in Table 3-1. Sampled values are given in Appendix B

Table 5-2. Latin Hypercube Sample Dependent Variables Used in Stepwise Regression and Partial Correlation Analyses

Dependent Variables	Description
BIOCONT	Cellulose remaining in waste
BRNANHSC	Cumulative brine flow south of repository out anhydrite layers a + b
BRNMB8SC	Cumulative brine flow south of repository out MB138

Table 5-2. Latin Hypercube Sample Dependent Variables Used in Stepwise Regression and Partial Correlation Analyses (Continued)

Dependent Variables	Description
BRNMB9SC	Cumulative brine flow south of repository out MB139
BSHSLUPC	Cumulative brine flow up through shaft seal
BWSTC	Cumulative brine flow from waste
FECONT	Iron remaining in waste
GASANHSC	Cumulative gas flow south of repository out anhydrite layers a + b
GASGENVC	Cumulative gas generated by corrosion and biodegradation
GASMB8SC	Cumulative gas flow south of repository out MB138
GASMB9SC	Cumulative gas flow south of repository out MB139
GASCULTC	Cumulative gas flow into Culebra from shaft
GDSTANHS	Distance from waste that gas flowed south in anhydrite layers a + b
GDSTCULS	Distance from shaft that gas flowed south in Culebra
GDSTMB8S	Distance from waste that gas flowed south in MB138
GDSTMB9S	Distance from waste that gas flowed south in MB139
GSHSLUPC	Cumulative gas flow up through shaft seal
GWSTC	Cumulative gas flow from waste
PORVOLW	Pore volume in waste
PRESWAST	Average pressure in waste
QRGBIOVC	Cumulative gas generated by inundated and humid biodegradation
QRGCORVC	Cumulative gas generated by inundated and humid corrosion
QRHCUMGB	Cumulative gas generated by humid biodegradation

Table 5-2. Latin Hypercube Sample Dependent Variables Used in Stepwise Regression and Partial Correlation Analyses (Concluded)

Dependent Variables	Description
QRHCUMGC	Cumulative gas generated by humid corrosion
QRSCUMGB	Cumulative gas generated by inundated biodegradation
QRSCUMGC	Cumulative gas generated by inundated corrision
SBAVW	Volume-average brine saturation in waste

5.2 Gas Generation and Repository Performance

In this section, factors that affect gas generation are examined. The focus is on parameters influencing corrosion and microbial degradation. In addition, variables that affect repository performance, including pressure, reactant concentrations, pore volume, and brine saturation, will be determined. Although gas generation and repository behavior are not compliance measures *per se*, it is useful to know how these are affected so that they can, if necessary, be controlled.

5.2.1 Gas Generation from Inundated Corrosion

The regression analysis results in Table 5-3 are for cumulative gas generation resulting from inundated corrosion over 10,000 yr. The first variable selected in the analysis is BRSAT, the initial brine saturation in the waste, which has a positive regression coefficient and can account for 49% of the variability in gas generation by inundated corrosion. The partial rank correlation coefficients shown in Figure 5-1 further support the dominatingeffect that initial brine saturation has on inundated corrosion. This result is discussed in Section 4.1.1, in which it is apparent even in the behavior of brine saturation in the repository over time that initial brine saturation is the controlling factor.

The next variable selected in the regression analysis is GRCORHF, the humid corrosion rate factor that is multiplied by the inundated rate to give the actual humid corrosion rate. This variable has a negative regression coefficient, indicating that it has an inhibiting effect on gas generation by inundated corrosion. This effect continues increasingly over the 10,000-yr simulation period, as shown in the plot of partial rank correlation coefficients in Figure 5-1. This increasing effect occurs because humid corrosion competes with inundated corrosion. It dominates inundated corrosion, especially later on, because inundated corrosion is limited by the amount of brine present. As long an any amount of brine is present, humid corrosion can proceed at a rate that is proportional to the gas saturation. Except at early times when the brine saturation is relatively large it is more common for the waste to be mostly dry, so humid corrosion will generate gas faster than inundated corrosion. The humid corrosion rate factor contributes another 20% of the variability in gas generation by inundated corrosion.

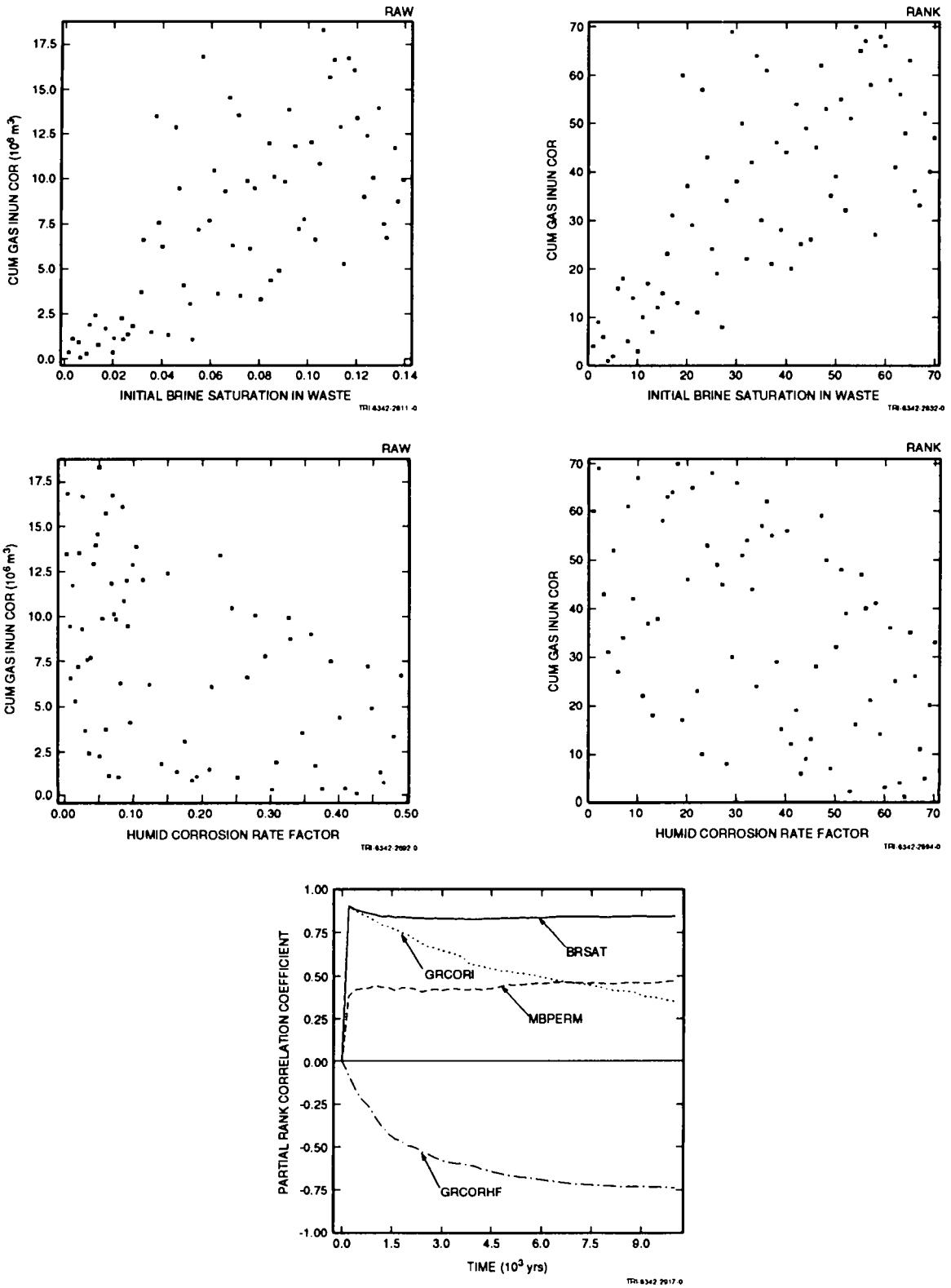

Figure 5-1. Scatterplots and partial rank correlation coefficients for gas generation from inundated corrosion.

The other two variables selected in the analysis, MBPERM (anhydrite permeability) and GRCORI (inundated corrosion rate), play a relatively minor role in affecting inundated corrosion. The small effect of the inundated corrosion rate on inundated corrosion is, in part, a result of the current model used for gas generation and corrosion, in which the inundated rate is proportional to the brine saturation. Because brine saturation tends to decrease over time, the net inundated rate decreases, becoming relatively unimportant after 10,000 yr. These results may not hold true using a different corrosion model, but sufficient data do not yet exist to warrant changing the model.

Scatterplots relating cumulative gas generation to the two dominant variables, BRSAT and GRCORHF, are shown in Figure 5-1. While these two together account for 69% of the variability in gas generation by inundated corrosion, it is apparent from these plots that neither variable is a reliable predictor of gas generation, even though some correlation is evident.

Table 5-3. Stepwise Regression Analysis with Rank-Transformed Data for Total Gas Production Resulting from Inundated Corrosion (QRSCUMGC)

Step	Variable	Description	SRC[a]	R^{2b}
1	BRSAT	Initial brine saturation in waste	0.68	0.49
2	GRCORHF	Humid corrosion rate factor	-0.47	0.69
3	MBPERM	Log of anhydrite interbeds permeability	0.25	0.75
4	GRCORI	Inundated corrosion rate	0.16	0.78

[a] Standard regression coefficients (SRC) for variables in the regression model at each step

[b] R^2 value for the regression model at each step

5.2.2 Gas Generation from Humid Corrosion

Unlike gas generation by inundated corrosion, gas generation by humid corrosion is a fairly strong function of the rate of humid corrosion. (See Volume 3, Section 3.3.5 for a description of the current gas generation model and parameters used in the model.) In Table 5-4, the first variable selected in the regression analysis for gas generation by humid corrosion is GRCORHF, the factor multiplying the inundated rate to obtain the humid corrosion rate. This variable accounts for 64% of the variability in gas generation by humid corrosion. The next variable selected is the inundated corrosion rate, GRCORI. Together, these rate parameters account for 75% of the variability. The regression coefficient for GRCORI is positive now, because humid corrosion does not occur unless inundated corrosion is taking place at the same time. Recall that the corrosion model requires brine to be present for humid corrosion to occur, even though the humid corrosion rate is modeled as proportional to *gas* saturation.

The initial brine saturation in the waste, BRSAT, is a less-important variable, accounting for only an additional 8% of the variability in gas generation by humid corrosion. The plot of partial rank correlation coefficients in Figure 5-2 shows that BRSAT had a negative effect at first, becoming significantly positive only after about 3000 yr. This results from the changing relative importance of inundated corrosion compared with humid corrosion. Initially, when the brine saturation is usually highest, the total reaction rate is dominated by the inundated reaction. Later, as the brine saturation in the waste decreases, having been consumed predominantly by inundated corrosion, humid corrosion becomes more important.

Scatterplots of the first two variables selected in the regression analysis, Figure 5-2, show some clear trends for the first variable, GRCORHF. The correlation is much weaker for the second variable, GRCORI.

Table 5-4. Stepwise Regression Analysis with Rank-Transformed Data for Total Gas Production Resulting from Humid Corrosion (QRHCUMGC)

Step	Variable	Description	SRC	R^2
1	GRCORHF	Humid corrosion rate factor	0.79	0.64
2	GRCORI	Inundated corrosion rate	0.32	0.75
3	BRSAT	Initial brine saturation in waste	0.29	0.83

5.2.3 Gas Generation from Inundated and Humid Corrosion

When both inundated and humid corrosion are considered together, the regression analysis selects BRSAT first, accounting for 56% of the variability in gas generation by corrosion. This suggests that corrosion under inundated conditions contributes more to the amount of gas produced by corrosion than humid conditions, since BRSAT has a strong positive impact on inundated corrosion, but only a weak effect on humid corrosion. The scatterplot relating cumulative gas generation by corrosion to initial brine saturation in the waste, Figure 5-3, shows a clear trend, even more so than for inundated corrosion alone, with the amount of gas generated increasing as the initial brine saturation increases. The plot of partial rank correlation coefficients in Figure 5-3 shows that BRSAT has a strong effect throughout the 10,000 yr, although other variables were slightly more important at first, when inundated corrosion was not yet inhibited by a lack of brine.

The inundated corrosion rate, GRCORI, was selected next, accounting for an additional 11% of the variability in gas generation by corrosion. The scatterplot relating cumulative gas generation by corrosion after 10,000 yr to inundated corrosion rate in Figure 5-3, however, shows only the slightest of trends to increasing gas generation as the rate increases. As shown in the plot of partial rank correlation coefficients, Figure 5-3, GRCORI has the greatest impact during the first 3000 yr, when adequate sources of brine remain from the initial brine saturation. Its influence gradually decreases from the start, as brine is consumed.

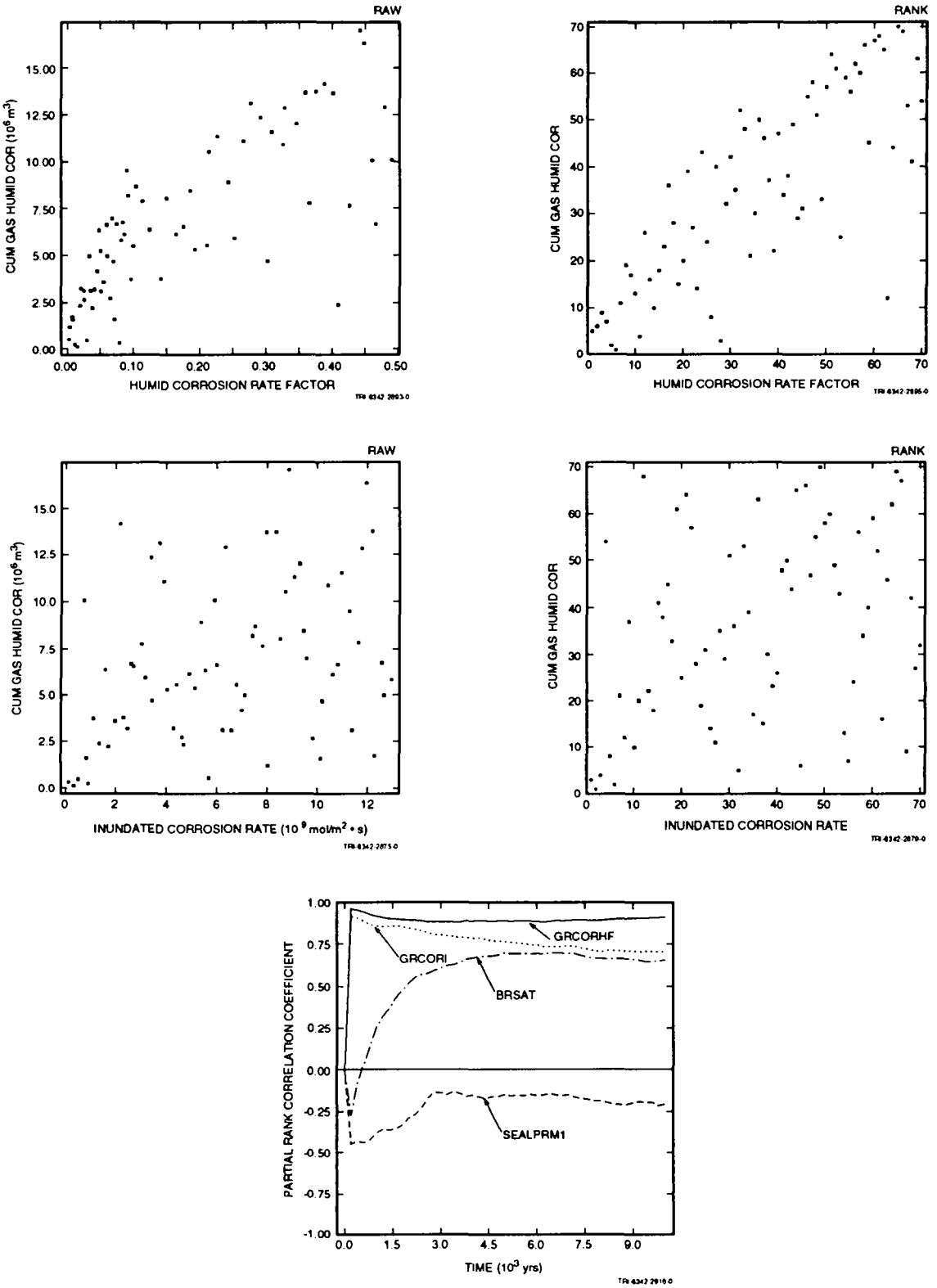

Figure 5-2. Scatterplots and partial rank correlation coefficients for gas generation from humid corrosion.

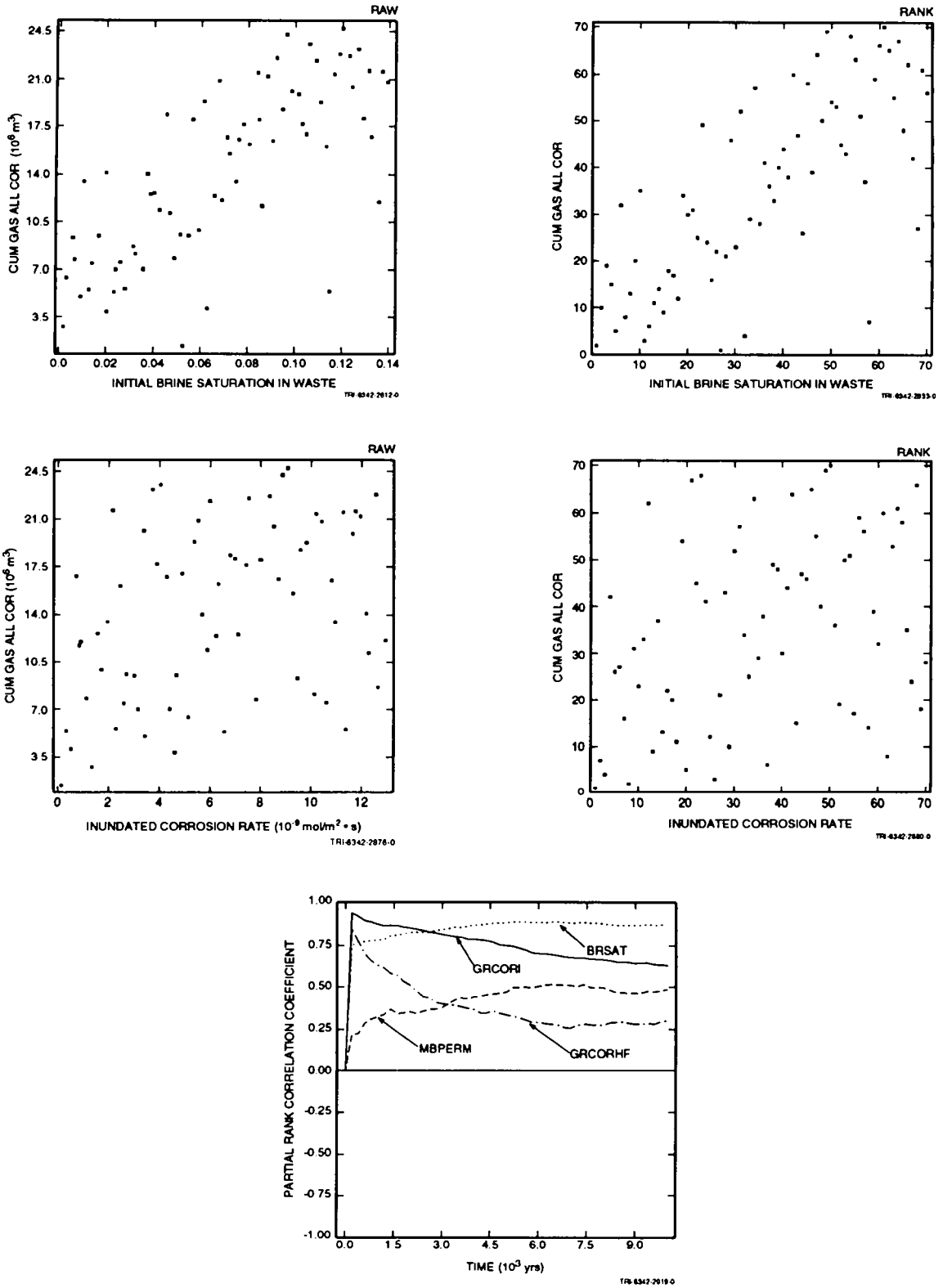

Figure 5-3. Scatterplots and partial rank correlation coefficients for gas generation from inundated and humid corrosion.

The regression analysis (Table 5-5) selected three more variables as having some measurable effect on total gas generation by corrosion: MBPERM, the permeability of anhydrite interbeds; STOICCOR, a factor that determines the relative importance of two corrosion reactions and thus the stoichiometry for corrosion; and GRCORHF, the humid corrosion rate factor. Together, these three account for an additional 12% of the variability in gas generation by corrosion. The linear correlation with five variables accounts for 79% of the variability. STOICCOR has a negative correlation coefficient, indicating that as this variable increases, gas generation decreases. This occurs because the corrosion stoichiometric coefficient, or the moles of gas generated per mole of iron consumed, decreases as STOICCOR increases: the stoichiometric coefficient has a value of 1.333 when STOICCOR is 1.0, and a value of 1.0 when STOICCOR is 0. The minor effect of STOICCOR stems from the relatively narrow range of values taken by the stoichiometric coefficient. Anhydrite permeability has a small effect on gas generation by affecting the amount of brine that can flow into the repository and contribute to additional corrosion. As discussed in Section 4.1.1, little brine flows into the waste in general, so the effect is not great.

Table 5-5. Stepwise Regression Analysis with Rank-Transformed Data for Total Gas Production Resulting from Both Inundated and Humid Corrosion (QRGCORVC)

Step	Variable	Description	SRC	R^2
1	BRSAT	Initial brine saturation in waste	0.74	0.56
2	GRCORI	Inundated corrosion rate	0.33	0.67
3	MBPERM	Log of anhydrite interbeds permeability	0.24	0.73
4	STOICCOR	Corrosion stoichiometry factor	-0.17	0.76
5	GRCORHF	Humid corrosion rate factor	0.16	0.79

5.2.4 Gas Generation from Inundated Biodegradation

The sensitivity analysis done for gas generation by corrosion is repeated for gas generation by biodegradation. For inundated biodegradation, the regression analysis in Table 5-6 selected STOICMIC, the biodegradation stoichiometric coefficient, as the most important variable. This variable accounts for 36% of the variability in gas generation by inundated biodegradation. The scatterplot relating cumulative gas generation to this variable, Figure 5-4, shows a definite trend, with the amount of gas generated increasing as STOICMIC increases. This result is exactly as expected, since this is the definition of the stoichiometric coefficient (moles of gas produced per mole of cellulose consumed).

This analysis found eight variables having a measurable effect, although the additional influence of each of the last five is very slight. As with inundated corrosion, biodegradation under inundated conditions requires brine to be present, although biodegradation is currently assumed not to consume water. Thus, the next most important variable selected is BRSAT, which shows a trend similar to that for STOICMIC, but less pronounced. As expected, the inundated biodegradation rate, GRMICI, is one of the more important variables, but it is surprising that it accounts for only 8% of the variability in gas production by inundated biodegradation. As the partial rank correlation coefficient plot in Figure 5-4 shows, GRMICI was the dominant variable early, but its influenced decreased steadily over the first 1000 yr as brine in the waste was consumed. In addition, as seen earlier in Figure 4-6, much of the cellulose in the waste was fully consumed within that same time period, which explains why the curves in the plot of partial rank correlation coefficients are flat after about 1500 yr. GRCORHF has a negative regression coefficient, indicating that humid corrosion competes with inundated biodegradation by consuming brine needed for inundated biodegradation. As the partial rank correlation coefficient plot shows, GRCORHF becomes significant only after the microbial rate becomes less significant. At later times, humid corrosion tends to consume the remaining brine required for any further inundated biodegradation.

Table 5-6. Stepwise Regression Analysis with Rank-Transformed Data for Total Gas Production Resulting from Inundated Biodegradation (QRSCUMGB)

Step	Variable	Description	SRC	R^2
1	STOICMIC	Biodegradation stoichiometric coefficient	0.61	0.36
2	BRSAT	Initial brine saturation in waste	0.42	0.53
3	GRMICI	Inundated biodegradation rate	0.28	0.61
4	GRCORHF	Humid corrosion rate factor	-0.22	0.65
5	BCEXP	Brooks-Corey exponent	0.18	0.69
6	GRMICHF	Humid biodegration rate factor	0.20	0.72
7	VWOOD	Initial volume fraction cellulose in waste	-0.18	0.75
8	SEALPRM2	Shaft seal permeability after 200 yr	0.17	0.78

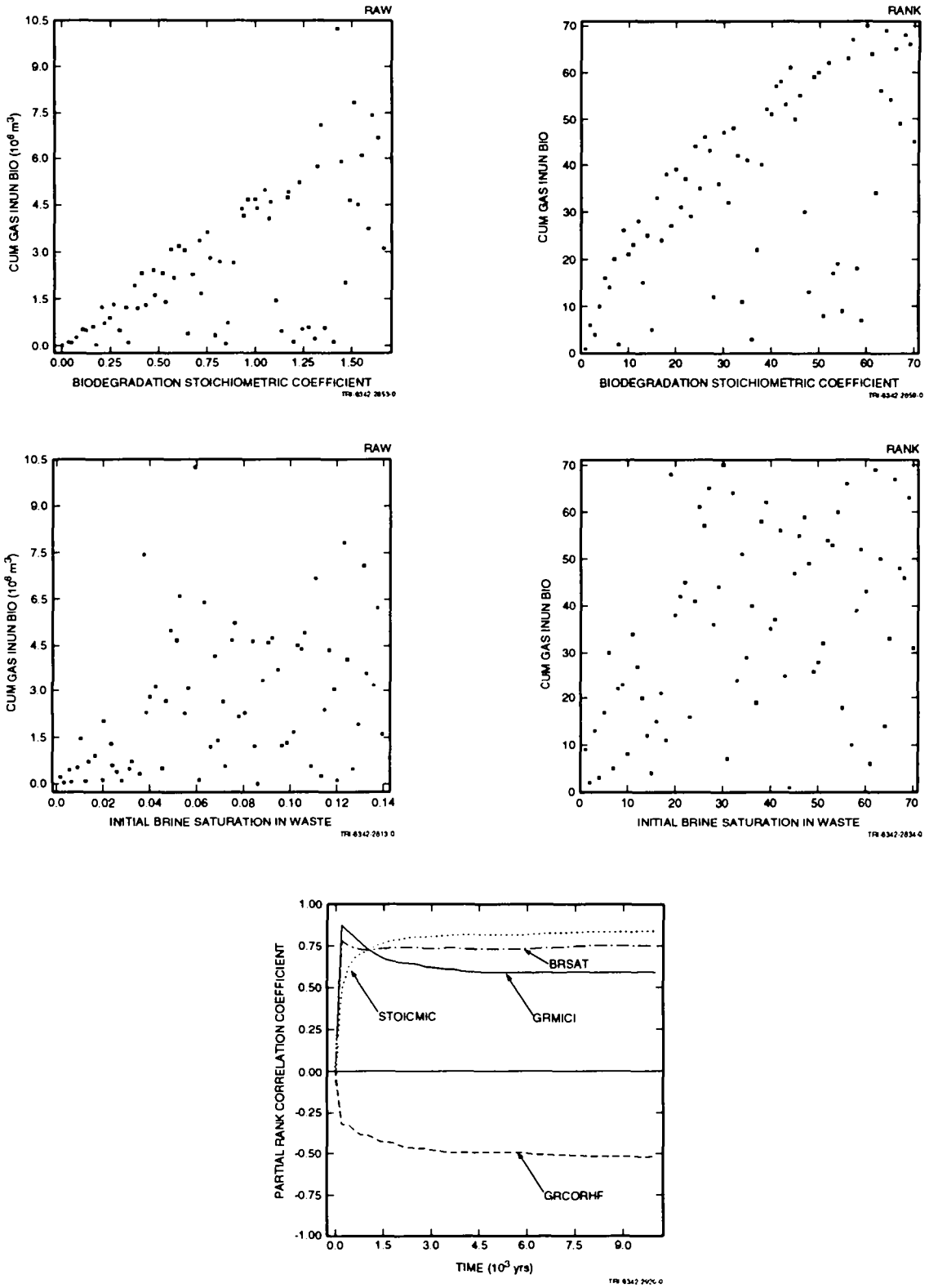

Figure 5-4. Scatterplots and partial rank correlation coefficients for gas generation from inundated biodegradation.

5.2.5 Gas Generation from Humid Biodegradation

The regression analysis in Table 5-7 is for cumulative gas generation by humid biodegradation. As with humid corrosion, humid biodegradation, as currently modeled, requires brine to be present. However, as with inundated biodegradation, it is assumed to consume no brine, in contrast to corrosion, in which both inundated and humid reactions consume brine. The first variable selected in the regression analysis is STOICMIC, the biodegradation stoichiometric coefficient. It accounts for only 29% of the variability in gas generation by humid biodegradation, making it somewhat less important here than in inundated biodegradation, although the scatterplot in Figure 5-5 still shows a clear trend. As it was under inundated conditions, STOICMIC is important because it strongly affects the amount of gas produced for a given amount of reactants. The second variable selected, GRMICHF (humid biodegradation rate factor), contributes nearly as much as STOICMIC to the variability in cumulative gas generation by humid biodegradation. The scatterplot for this variable also shows an apparent trend, but with more scatter than shown by STOICMIC. The partial rank correlation coefficients in Figure 5-5 show STOICMIC becoming more important apparently at the expense of the inundated biodegradation rate, GRMICI, which dominated at first. The inundated corrosion rate, GRCORI, has a very small positive effect on gas generation by humid biodegradation by consuming brine, thereby increasing the gas saturation, which results in more gas production under humid, rather than inundated conditions.

Table 5-7. Stepwise Regression Analysis with Rank-Transformed Data for Total Gas Production Resulting from Humid Biodegradation (QRHCUMGB)

Step	Variable	Description	SRC	R^2
1	STOICMIC	Biodegradation stoichiometric coefficient	0.55	0.29
2	GRMICHF	Humid biodegradation rate factor	0.50	0.53
3	GRMICI	Inundated biodegradation rate	0.34	0.64
4	GRCORI	Inundated corrosion rate	0.20	0.68

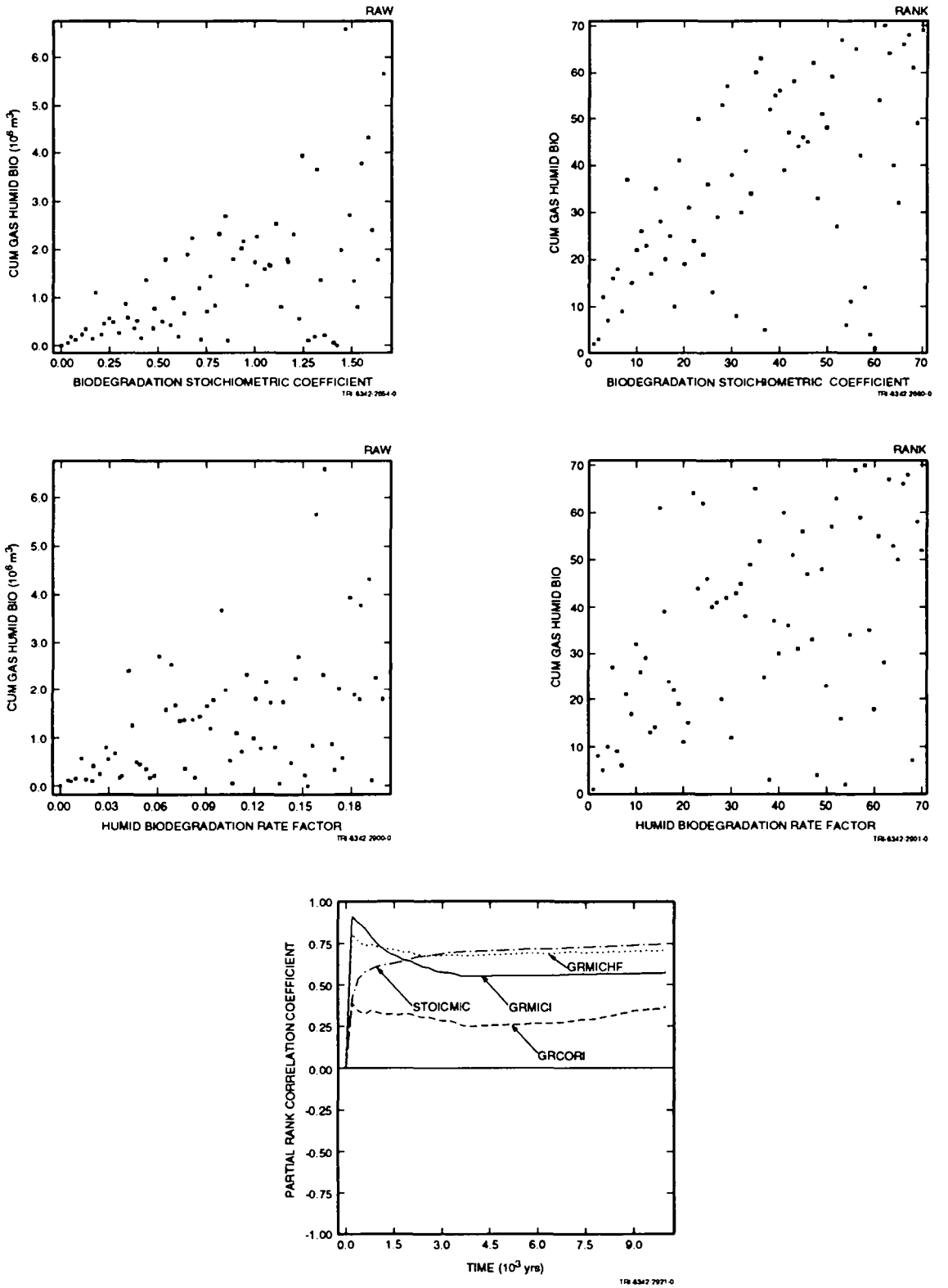

Figure 5-5. Scatterplots and partial rank correlation coefficients for gas generation from humid biodegradation.

5.2.6 Gas Generation from Inundated and Humid Biodegradation

The regression analysis for cumulative gas generation by both inundated and humid biodegradation, shown in Table 5-8, selected STOICMIC as the dominant variable in determining the variability of gas generation. It accounts for 50% of the variability. The scatterplot relating gas generation to biodegradation stoichiometry, in Figure 5-6, confirms the strong influence that stoichiometry has on the amount of gas generated. Because STOICMIC was most influential under both inundated and humid conditions, this result is not surprising.

The next variable selected, GRMICI, contributes another 14% to the variability in gas generation. GRMICI plays a measurably significant, if minor, role because a large portion of the gas produced by biodegradation takes place under inundated conditions. This can be deduced from Figures 4-2 and 4-6, which show the time-dependent behavior of brine saturation in the waste and cellulose content remaining in the waste, respectively. However, its scatterplot indicates that the effect is not very strong.

The influence of initial brine saturation, BRSAT, is understandable, because, in the absence of a large influx of brine from outside the waste, initial brine saturation essentially provides the driving force for biodegradation. However, it actually contributes very little to the variability of total gas generation from biodegradation, only 4%.The partial rank correlation coefficients in Figure 5-6 show the same trends as for inundated and humid biodegradation separately, with the inundated rate, GRMICI, dominating at first, to be superseded later by STOICMIC. This ordering of influence consistently occurs because, as brine and reactants (cellulose) are depleted, the amount of gas produced per unit quantity of reactant has an increasingly greater impact on total gas generated, whereas the *rate* becomes irrelevant. Gas generation per unit of reactant, as measured by the stoichiometric coefficient, also has a far greater impact than potential. The original basis for potential, VWOOD (the volume fraction of cellulose in the initial inventory), has no discernible effect because the stoichiometry, which ranges from 0.0 to 1.67, completely determines how much of this initial cellulose inventory will be converted to gas. This will be true as long as any cellulose is present initially. If the initial cellulose content of the waste were also varied over a range that extended to zero, it could possibly become as important as STOICMIC in determining the variability in

Table 5-8. Stepwise Regression Analysis with Rank-Transformed Data for Total Gas Production Resulting from Both Inundated and Humid Biodegradation (QRGBIOVC)

Step	Variable	Description	SRC	R^2
1	STOICMIC	Biodegradation stoichiometric coefficient	0.70	0.50
2	GRMICI	Inundated biodegradation rateor	0.38	0.64
3	BRSAT	Initial brine saturation in waste	0.23	0.69
4	GRCORHF	Humid corrosion rate factor	-0.18	0.72

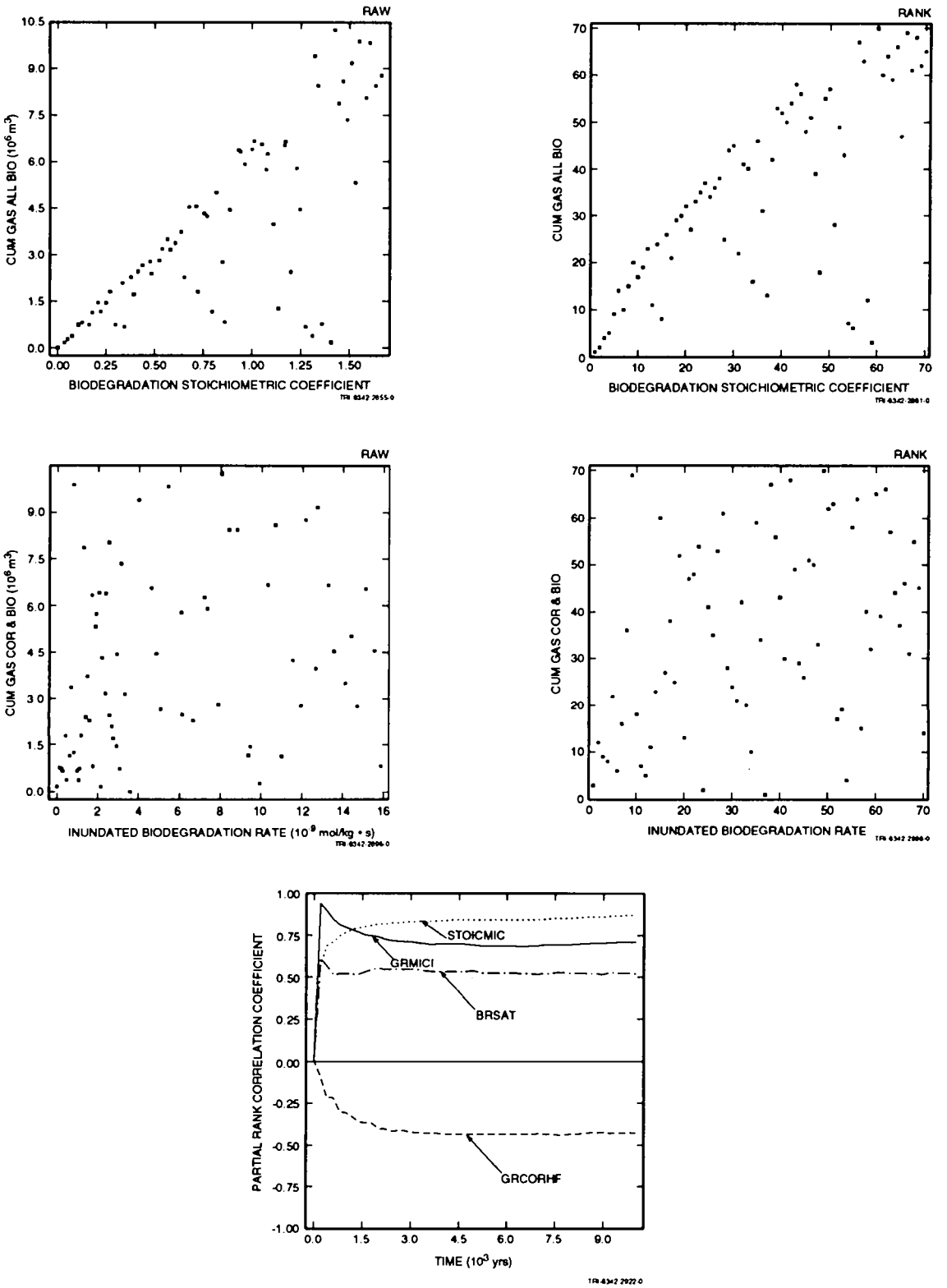

Figure 5-6. Scatterplots and partial rank correlation coefficients for gas generation from inundated and humid biodegradation.

gas generation. However, cellulose will be present in some of the waste (as wood and paper products), and the fraction of cellulosics in the initial waste inventory, VWOOD, is assumed to range from 0.284 to 0.484. Therefore, the sampled value for initial cellulose content will always be nonzero, and its range will be relatively narrow compared to the currently assumed range of stoichiometric coefficients.

The other two variables selected in the regression analysis contribute very little to the variability in gas generation. BRSAT continues to have some influence, but is dominated by the stoichiometry and inundated biodegradation rate. The correlation coefficient for GRCORHF is negative, indicating that it continues to show a competing effect on gas generation by consuming brine that must be present for biodegradation to take place.

5.2.7 Gas Generation from Corrosion and Biodegradation

When gas generation by both corrosion and biodegradation are considered, the regression analysis, Table 5-9, shows that the initial brine saturation of the waste is the dominant variable, accounting for 55% of the variability in the amount of gas generated. The plot of partial rank correlation coefficients in Figure 5-7 indicates that this is true almost from the beginning. The scatterplot relating the amount of gas generated to initial brine saturation (Figure 5-7) shows a clear trend. The biodegradation stoichiometry, which is dominant in determining gas generation by biodegradation, also has a significant impact on the total gas generation, although the scatterplot is less convincing. The inundated biodegradation rate, GRMICI, is a major influence at first, but, as cellulose is rapidly consumed, its effect decreases greatly, as seen in the plot of partial rank correlation coefficients. The inundated corrosion rate is also a dominant variable at first, but its influence gradually decreases over time, as the amount of gas generated under more prevalent humid conditions increases.

Anhydrite permeability continues to show up in the regression analysis. Accounting for 5% of the variability in gas generation, it is clearly not a dominant variable, but still cannot be ignored, because it controls the flow of brine into the waste as well as the flow of gas out of the repository. Gas flow does not affect gas generation directly, but when the pressure in the repository approaches that of the far field, it can strongly inhibit the influx of brine from outside the waste. Higher anhydrite permeability over the range of sampled values can allow the pressure in the repository to be relieved, in turn allowing more brine to flow inward. However, because the permeability is so low, little brine can flow under any circumstances, and these mechanisms are relatively unimportant. Thus, the overall impact of anhydrite permeability on gas generation is minor. Knowing that absolute permeability has only a small effect over the range of sampled values, it is understandable that *relative* permeability has no discernible effect. Neither of the relative permeability parameters, BCEXP and BCFLG, was selected in the stepwise regression analysis. Scatterplots relating cumulative gas generation to these two variables, Figure 5-8, show completely random scatter and suggest no trends. These results reinforce the conclusions that brine flow has little effect on gas generation and that the initial state of the waste, along with parameters directly affecting gas generation, largely control how much gas is generated.

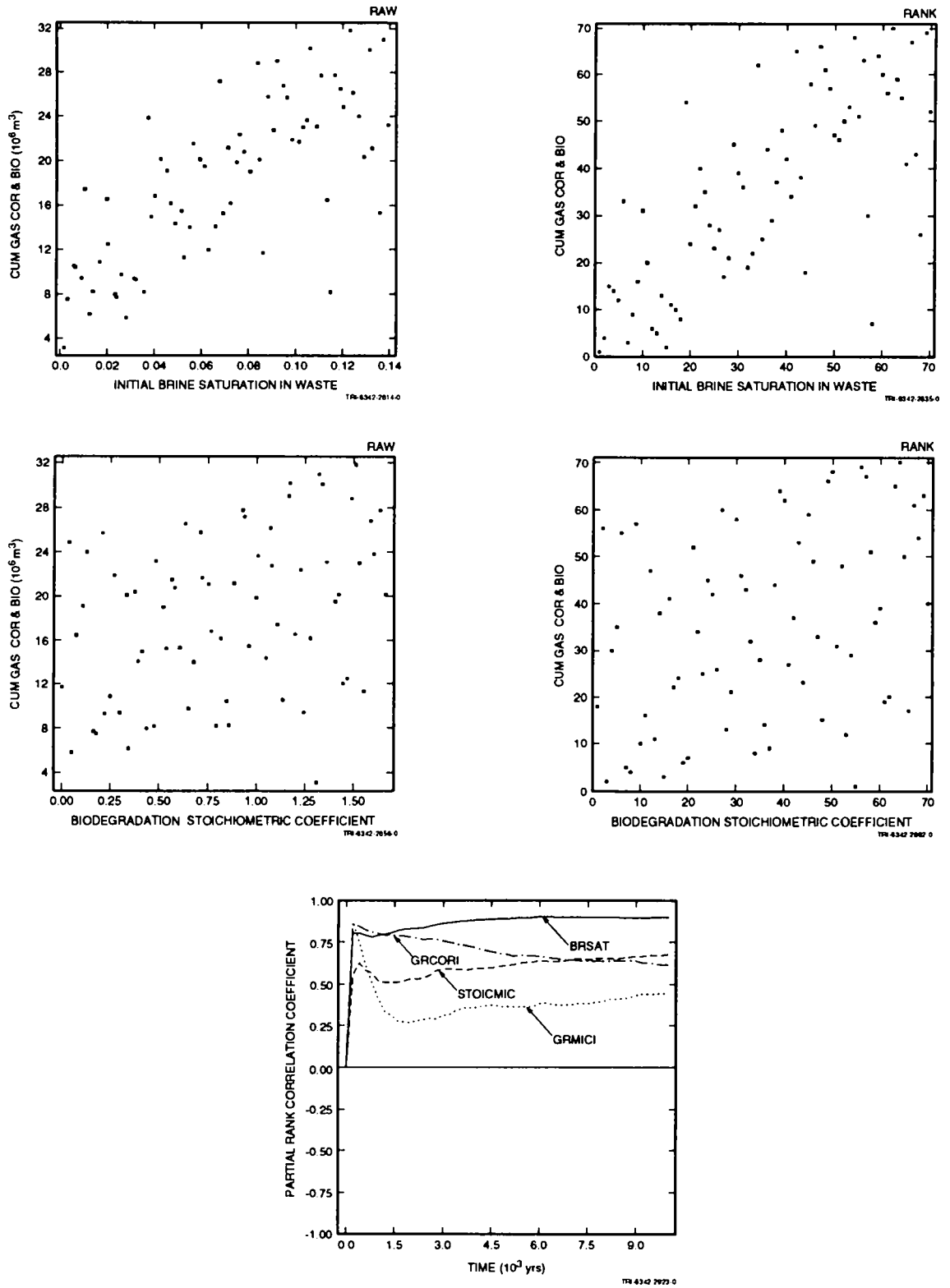

Figure 5-7. Partial rank correlation coefficients for gas generation from corrosion and biodegradation.

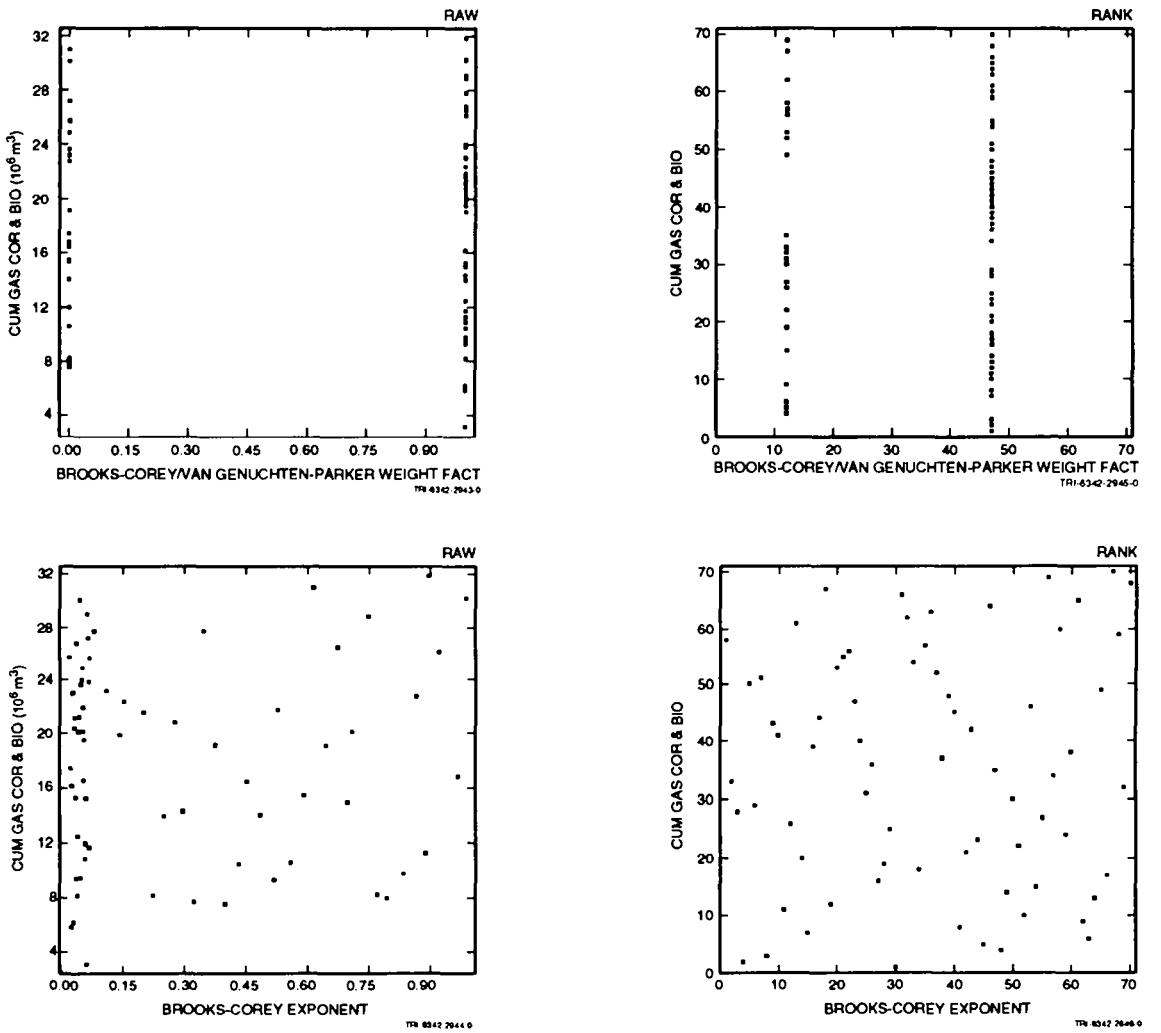

Figure 5-8. Scatterplots for coefficients for gas generation from corrosion and biodegradation.

Table 5-9. Stepwise Regression Analysis with Rank-Transformed Data for Total Gas Production Resulting from Corrosion and Biodegradation (GASGENVC)

Step	Variable	Description	SRC	R^2
1	BRSAT	Initial brine saturation in waste	0.73	0.55
2	STOICMIC	Biodegradation stoichiometric coefficient	0.32	0.66
3	GRCORI	Inundated corrosion rate	0.28	0.73
4	MBPERM	Log of anhydrite interbeds permeability	0.20	0.78
5	GRMICI	Inundated biodegradation rate	0.16	0.80
6	STOICCOR	Corrosion stoichiometry factor	-0.15	0.83

5.2.8 Iron Remaining in the Waste

Analysis of other performance measures will help to understand the behavior of the repository. Table 5-10 shows the regression analysis for iron content remaining in the waste, FECONT. Initial brine saturation in the waste, BRSAT, is the first variable selected, accounting for 61% of the variability in FECONT. The correlation coefficient is negative, indicating, as expected, that the more brine present initially in the waste, the less iron will remain after 10,000 yr. The corrosion rate under inundated conditions, GRCORI, also has some influence, but the rate is sufficiently high that if the waste were fully inundated at all times, all of the iron would be consumed in most realizations within 10,000 yr. As seen earlier with gas generation, potentials become more important over the long term than rates. In the case of corrosion, initial brine content in the waste is one of these potentials, because so little brine flows in from outside the waste. Another potential measure, VMETAL, the initial volume fraction of corrodible metal in the waste, also shows up in the regression analysis, but accounts for only 3% of the variability in FECONT because the limiting potential is the amount of brine available.

Anhydrite permeability, MBPERM, has a small effect, accounting for 4% of the variability in FECONT. The correlation coefficient is negative, so higher permeabilities result in more iron being consumed, indicating that brine influx does contribute to gas generation. However, because anhydrite permeability has so little influence on remaining iron content, it is clear that brine influx has at most a minor impact on gas generation.

The plot of partial rank correlation coefficients in Figure 5-9 illustrates the dominating effect that initial brine saturation has on the amount of iron remaining in the repository.

The scatterplot relating iron content to initial brine saturation, Figure 5-9, shows the strong negative effect that brine saturation has on the amount of iron that remains after 10,000 yr. The relationship between remaining iron content and the next most influential variable, inundated corrosion rate, also in Figure 5-9, shows the large amount of random scatter typical of an independent variable that accounts for only 11% of the variability of a dependent variable.

Table 5-10. Stepwise Regression Analysis with Rank-Transformed Data for Iron Remaining in the Repository after 10,000 yr (FECONT)

Step	Variable	Description	SRC	R^2
1	BRSAT	Initial brine saturation in waste	-0.77	0.61
2	GRCORI	Inundated corrosion rate	-0.33	0.72
3	VMETAL	Initial volume fraction iron in waste	0.20	0.75
4	MBPERM	Log of anhydrite interbeds permeability	-0.18	0.79
5	GRCORHF	Humid corrosion rate factor	-0.17	0.82

5.2.9 Cellulose Remaining in the Waste

The amount of cellulose remaining after 10,000 yr, BIOCONT, is not strongly dependent on any single variable. The most influential, GRMICI, accounts for only 29% of the variability in BIOCONT, as shown in the regression analysis in Table 5-11. BRSAT appears once again, with nearly as much influence as the biodegradation rate. The scatterplots for each of these two variables, Figure 5-10, show some correlation for GRMICI and less for BRSAT. The partial rank correlation coefficients in Figure 5-10 show that these variables, as well as STOICMIC, dominate at very early times, but their influence degrades over time.

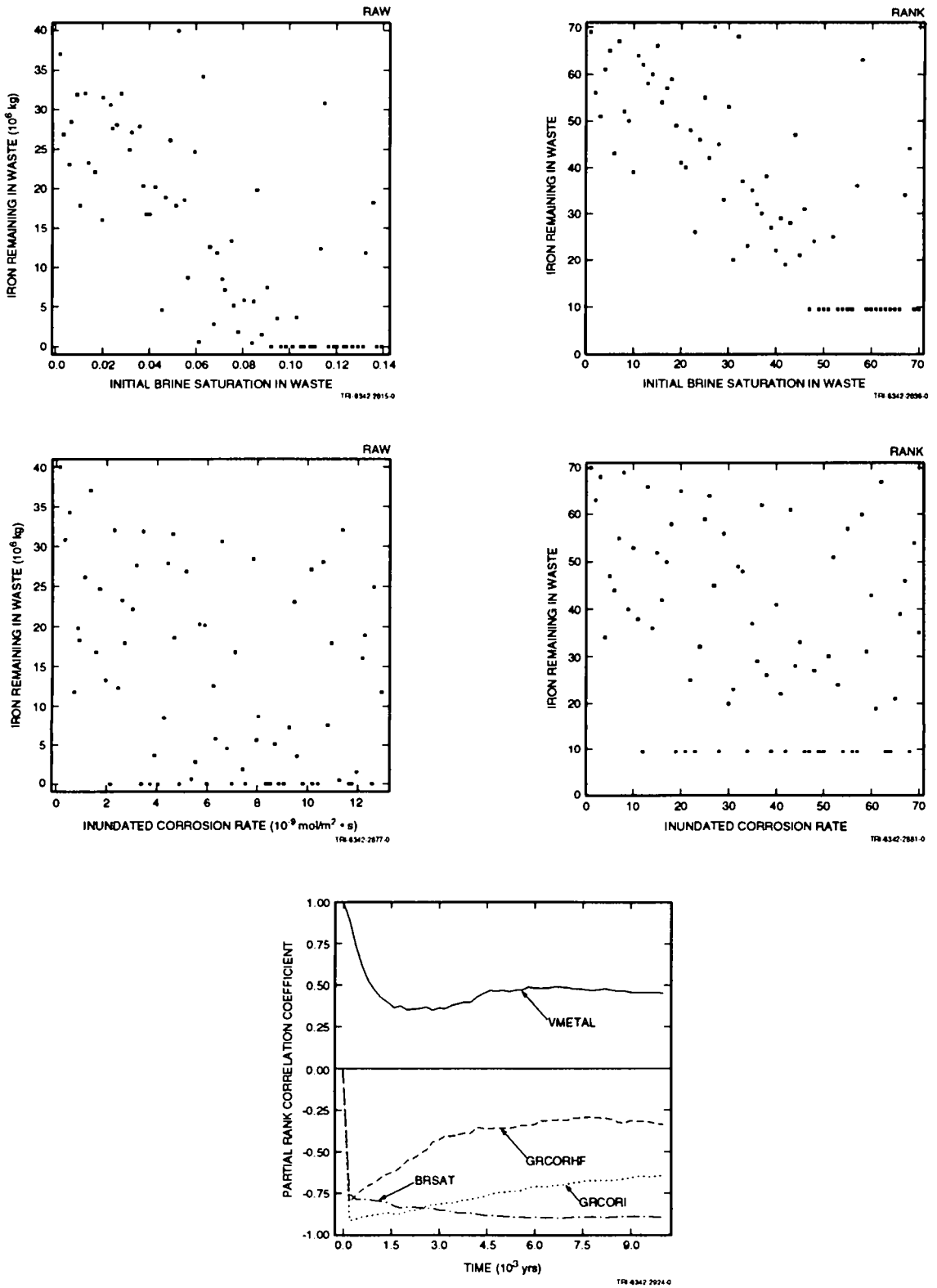

Figure 5-9. Scatterplots and partial rank correlation coefficients for iron remaining in the waste. (Rows of points in the rank plots with identical ranks result from the convention used to assign ranks to realizations with identical raw results [i.e., zero]).

Table 5-11. Stepwise Regression Analysis with Rank-Transformed Data for Cellulosics Remaining in the Repository (BIOCONT)

Step	Variable	Description	SRC	R^2
1	GRMICI	Inundated biodegradation rate	-0.47	0.21
2	BRSAT	Initial brine saturation in waste	-0.42	0.38
3	GRCORHF	Humid corrosion rate factor	0.25	0.45
4	STOICMIC	Biodegradation stoichiometric coefficient	0.25	0.51
5	GRCORI	Inundated corrosion rate	0.22	0.56

5.2.10 Repository Pore Volume

Pore volume in the repository is of interest primarily as a measure of the impact of creep closure on repository performance. The stepwise regression analysis (Table 5-12) selected initial brine saturation in the waste as the first variable, accounting for 57% of the variability in PORVOLW. The strength of this correlation is confirmed by the scatterplot shown in Figure 5-11, in which there is a clear trend to increasing the pore volume as the brine saturation increases. The effect is actually an indirect one. Higher initial brine saturation results in more gas being generated, which in turn raises the pressure in the repository. This initially coincides with a decrease in pore volume. Thus, the partial rank correlation coefficient, Figure 5-11, shows that brine saturation initially has a negative correlation with pore volume. However, as seen in Figure 4-3, the porosity in the waste quickly reaches a miminum and then starts to increase again as the pressure continues to rise. The reduction in pore volume, in itself, contributes to this pressure rise. Three other variables influence the pressure measurably at early times: STOICMIC, GRCORI, and GRMICI. The impact of these variables decreases over time, leaving BRSAT to dominate over the 10,000-yr period, as the plot of partial rank correlations shows. According to the creep closure model as currently implemented, once the pressure begins to decline, the porosity is fixed (except for small compressibility effects). Thus, the pore volume at 10,000 yr is strongly affected by the peak pressure attained, usually fairly early, which is heavily influenced by initial brine saturation.

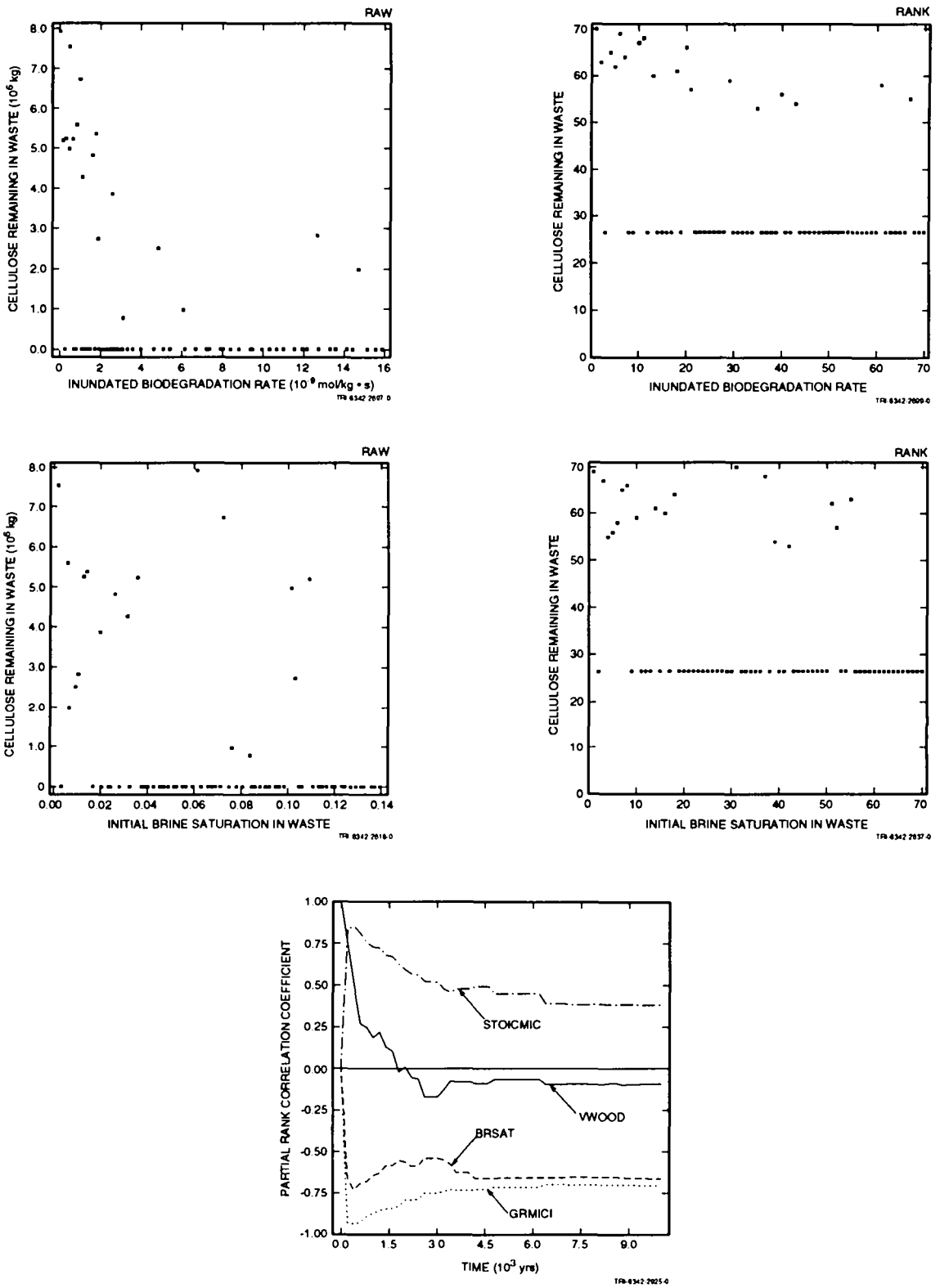

Figure 5-10. Scatterplots and partial rank correlation coefficients for cellulose remaining in the waste. (Rows of points in the rank plots with identical ranks result from the convention used to assign ranks to realizations with identical raw results [i.e., zero]).

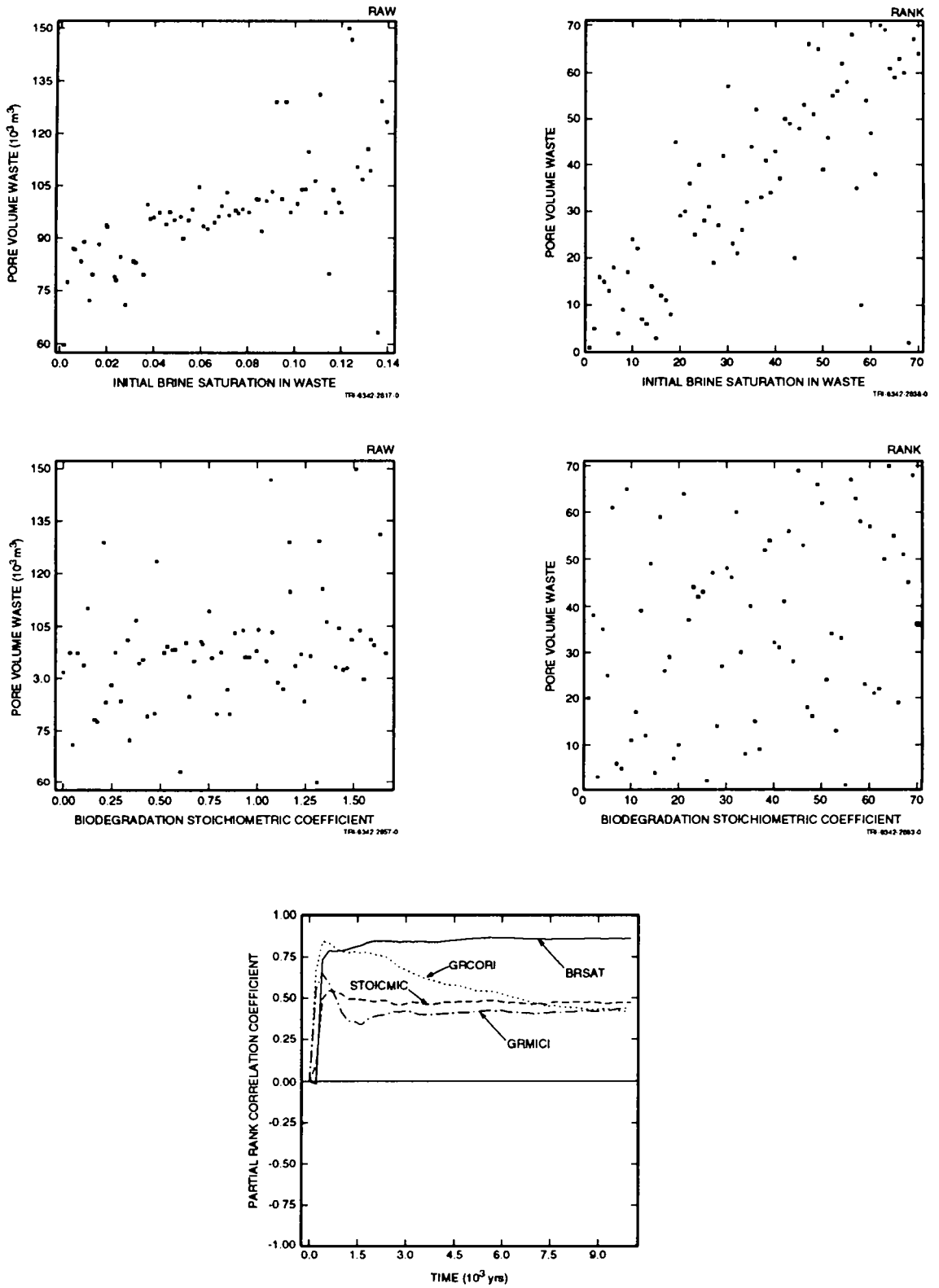

Figure 5-11. Scatterplots and partial rank correlation coefficients for repository pore volume.

Table 5-12. Stepwise Regression Analysis with Rank-Transformed Data for Pore Volume in the Waste (PORVOLW)

Step	Variable	Description	SRC	R^2
1	BRSAT	Initial brine saturation in waste	0.75	0.57
2	STOICMIC	Biodegradation stoichiometric coefficient	0.28	0.65
3	GRCORI	Inundated corrosion rate	0.23	0.70
4	GRMICI	Inundated biodegradation rate	0.22	0.75

5.2.11 Average Brine Saturation in the Waste

The stepwise regression analysis (Table 5-13) found seven variables that have some impact on the average brine saturation in the waste, SBAVW. However, none of them alone contributes greatly to the variability. Scatterplots of the two variables that affect SBAVW most strongly, Figure 5-12, confirm that the relationships are weak. The plot of partial rank correlation coefficients shows that, at first, initial brine saturation in the waste dominates; by definition, there should be a perfect correlation initially. Later, as corrosion consumed brine, the inundated corrosion rate has a strong influence. However, by 10,000 yr, no variable dominates, even though many have some small effect.

Table 5-13. Stepwise Regression Analysis with Rank-Transformed Data for Average Brine Saturation in the Waste (SBAVW)

Step	Variable	Description	SRC	R^2
1	BRSAT	Initial brine saturation in waste	0.39	0.14
2	GRCORI	Inundated corrosion rate	-0.36	0.26
3	TZPORF	Factor used in calculating DRZ and transition zone porosity	-0.29	0.35

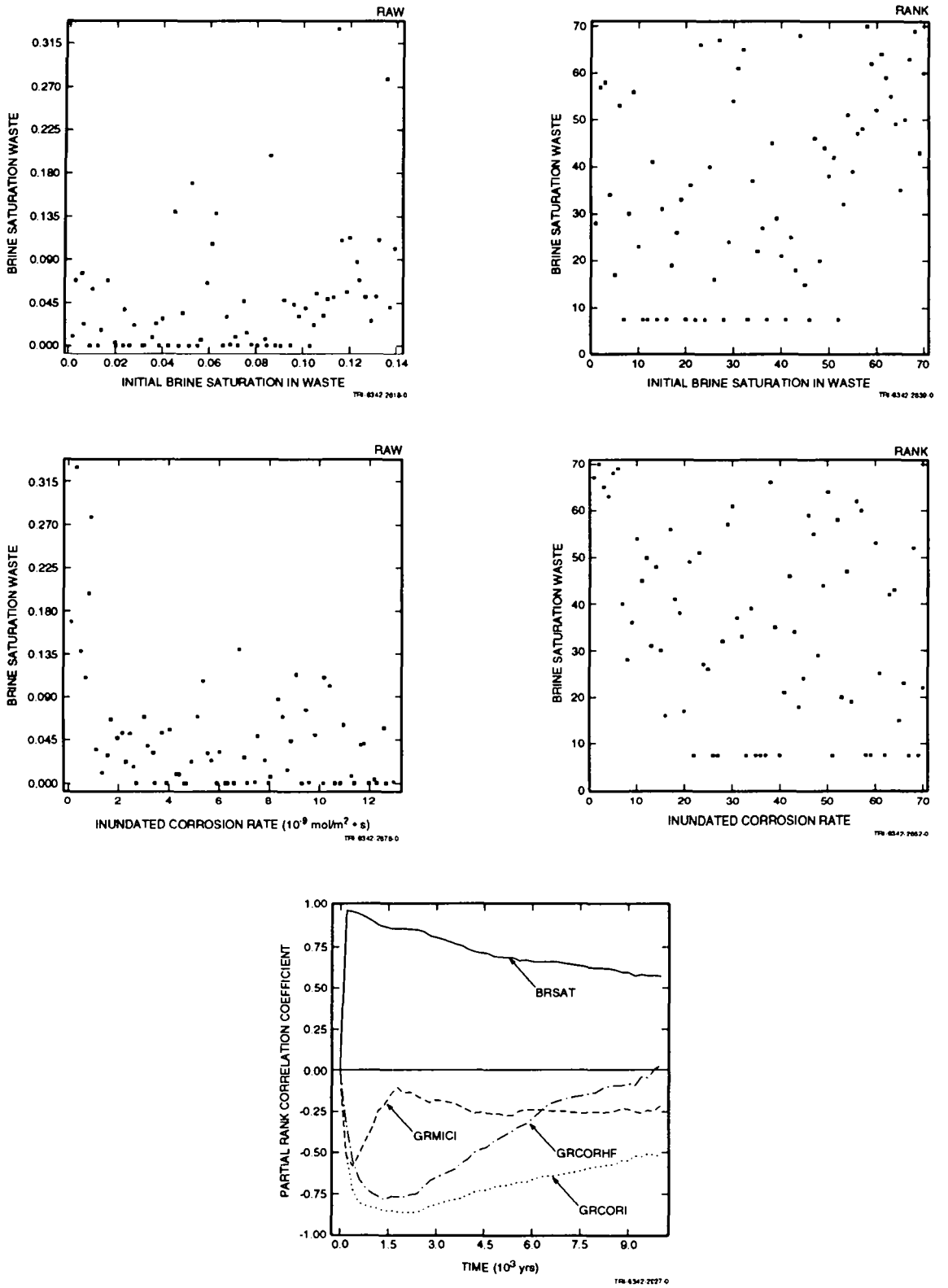

Figure 5-12. Scatterplots and partial rank correlation coefficients for average brine saturation in the waste. (Rows of points in the rank plots with identical ranks result from the convention used to assign ranks to realizations with identical raw results [i.e., zero]).

Table 5-13. Stepwise Regression Analysis with Rank-Transformed Data for Average Brine Saturation in the Waste (SBAVW) (Concluded)

Step	Variable	Description	SRC	R^2
4	SALPERM	Intact Salado halite permeability	0.29	0.41
5	STOICCOR	Corrosion stoichiometry factor	-0.28	0.49
6	SHFTPRM	Permeability of shaft-fill material above shaft seal	0.23	0.54
7	BCFLG	Brooks-Corey/van Genuchten-Parker weighting factor	-0.23	0.59

5.2.12 Pore Pressure in the Waste

Because the pressure in the waste results from gas generation, the variables that affect gas generation, reactant content, and pore volume should also affect pressure. The regression analysis, Table 5-14, confirms this. Once again, the dominant variable is the initial brine saturation in the waste, accounting for 62% of the variability in repository pressure. The scatterplot relating pressure to initial brine saturation shows the strong correlation between them. Two other variables have only minor impacts, although their influence was considerably greater at early times, as shown by the partial rank correlation coefficients in Figure 5-13

Table 5-14. Stepwise Regression Analysis with Rank-Transformed Data for Average Pore Pressure in the Waste (PRESWAST)

Step	Variable	Description	SRC	R^2
1	BRSAT	Initial brine saturation in waste	0.79	0.62
2	STOICMIC	Biodegradation stoichiometric coefficient	0.24	0.68
3	GRMICI	Inundated biodegradation rate	0.21	0.72

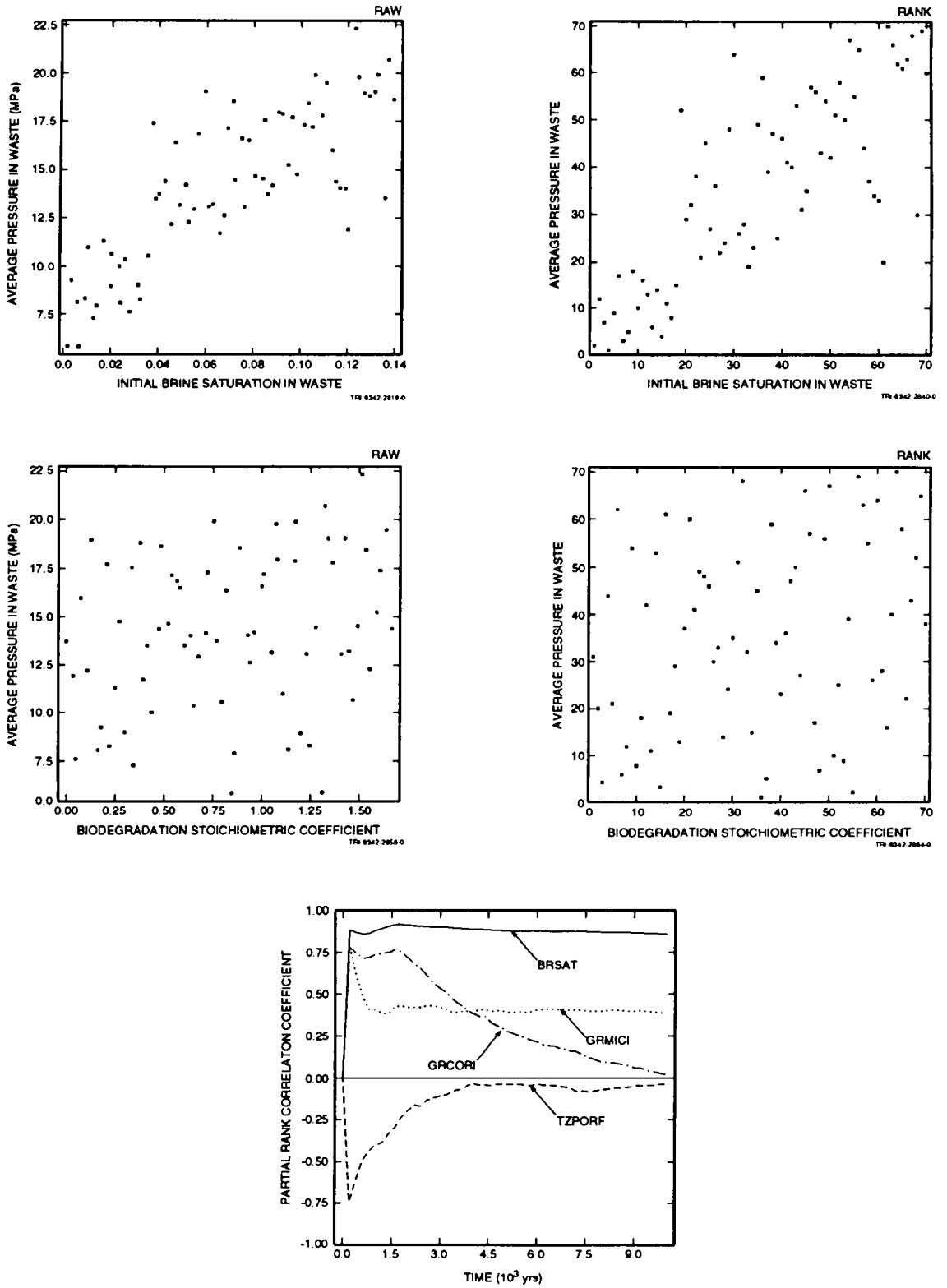

Figure 5-13. Scatterplots and partial rank correlation coefficients for pore pressure in the waste.

5.3 Brine Flow

A key performance measure for the WIPP under undisturbed conditions is the amount of contaminants (either radionuclides or hazardous chemical constituents) in brine that flows beyond the disposal unit boundaries. In the absence of actual modeling of contaminant transport, surrogate key measures are simply the amounts of brine that flow out the various flow paths from the repository, including the three anhydrite layers and the sealed shafts. In this section, these performance measures are examined to determine which sampled parameters affect them. This analysis provides insight into which parameters require more attention (and perhaps more measured data), and which conceptual features of the model may require more sophisticated treatment. It also identifies parameters or conceptual models that are *not* important and can therefore be further simplified.

5.3.1 Cumulative Net Brine Flow from the Repository

In Table 5-15, the regression analysis for cumulative net brine flow from the repository selected the initial brine saturation of the waste as the first variable. The scatterplot relating brine flow to brine saturation, Figure 5-14, shows brine flow tending to increase as initial brine saturation increases. Net brine flows out of the repository range from -24,000 m^3 to +11,400 m^3, implying that some minimum initial brine saturation is necessary for brine to flow out of the waste. Because the initial brine saturation is at most half of the residual brine saturation of the waste, the initial saturation itself is not sufficient to cause flow from the waste. Rather, when more brine is present initially, less inflow is required to exceed residual before allowing brine to flow out. Also affecting this correlation is the creep closure model. Brine saturation is increased more rapidly and residual saturation is reached more quickly, allowing some of the initial brine content of the waste to flow out in some realizations. Under these circumstances, it is not necessary for any brine to flow in first, although, as seen in Figure 4-9, this does occur in some realizations. The partial rank correlation coefficients in Figure 5-14 confirm that BRSAT is the dominant variable affecting net flow from the waste.

Anhydrite porosity accounts for an additional 8% of the variability in brine flow from the waste. It has a negative correlation coefficient, indicating that brine outflow decreases as the anhydrite porosity increases. Higher porosities allow more brine to flow in toward the repository because the storage capacity of the anhydrite is greater, so the distance over which the brine must travel is less. Similarly, brine flowing out of the repository must displace brine in the anhydrite over a greater distance when the porosity is lower.

Anhydrite permeability also has a small influence on brine flow from the waste. It has a negative correlation coefficient, as anhydrite porosity does, for the same reasons. High permeabilities contribute to brine flow in from the far field. This brine inflow eventually fills the DRZ enough to allow brine to flow into the waste, where it may be consumed by corrosion. Although some brine does flow out of the repository in some realizations, it most often occurs because creep closure has increased the brinesaturation in the waste independently of brine inflow from the far field. Thus, anhydrite permeability enhances brine flow into the waste, and inhibits outflow by filling the DRZ that surrounds the repository with brine.

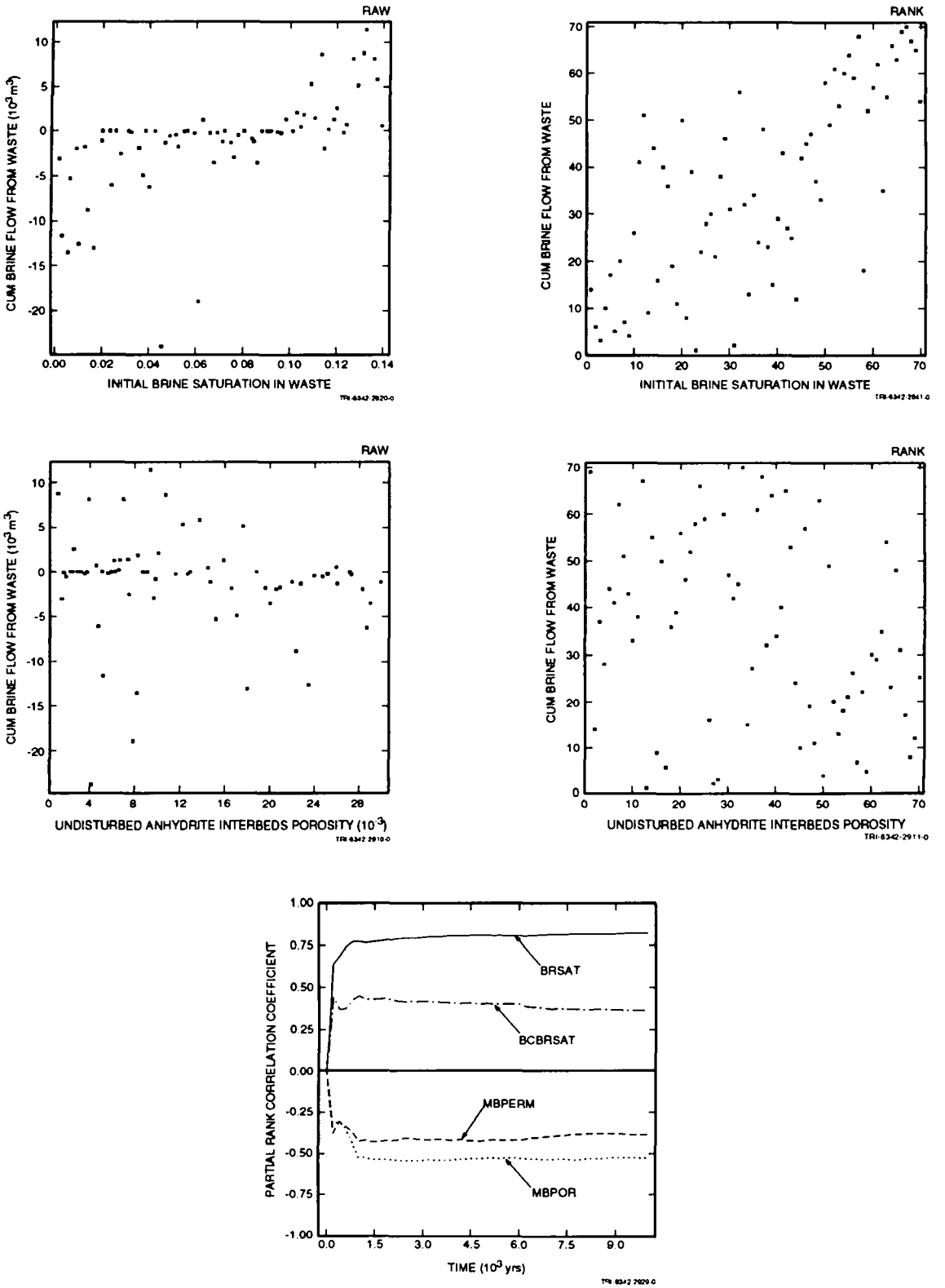

Figure 5-14. Scatterplots and partial rank correlation coefficients for cumulative net brine flow from the repository.

Table 5-15. Stepwise Regression Analysis with Rank-Transformed Data for Cumulative Net Brine Flow from the Repository (BWSTC)

Step	Variable	Description	SRC	R^2
1	BRSAT	Initial brine saturation in waste	0.72	0.53
2	MBPOR	Undisturbed anhydrite interbeds porosity	-0.30	0.61
3	MBPERM	Log of anhydrite interbeds permeability	-0.24	0.67
4	BCBRSAT	Residual brine saturation in all regions except waste	0.18	0.70

5.3.2 Cumulative Net Brine Flow Out MB139

The stepwise regression analysis (Table 5-16) for cumulative net brine flow out MB139 to the south of the repository (from Cell 8 to Cell 7 in Figure 2-2) selected BRSAT as the first variable. It accounts for 45% of the variability in brine flow. The scatterplot relating MB139 brine flow to initial waste brine saturation, in Figure 5-15, shows that brine flow out is negative in most realizations, that is, brine flows toward the repository. Generally, the inward brine flow is greatest when the initial brine saturation is lowest because less gas is generated in the waste, leaving the pressure in the waste lower, and thereby offering less resistance to brine flow from the far field.

Anhydrite permeability is also an influential parameter affecting brine flow in MB139, accounting for an additional 16% of the variability in brine flow. The scatterplot in Figure 5-15 shows that when the permeability is high, net brine outflow is more likely to be negative, or toward the repository, especially at early times when the pressure gradient from the far field to the repository is greatest. This is the same effect that was seen on the cumulative brine flow from the waste. Intermediate values of permeability (10^{-18} to 10^{-20} m^2) can allow some outward flow, which is a concern from a regulatory standpoint. In these cases, creep closure and gas generation may reverse the pressure gradient while elevating the waste brine saturation to the point where brine can flow from the waste. If the rate at which these processes take place is faster than the rate of brine inflow through MB139 when the anhydrite permeability is intermediate in value, brine flow out MB139 will result. When the permeability is less than 10^{-20} m^2, brine movement in the anhydrite layers tends to become insignificant. The partial rank correlation coefficients show that permeability is more important at early times, but its influence gradually decreases over the first 2000 yr. This occurs because, when there is a large quantity of brine flow, it generally takes place early, when the waste pressure is still very low and the pressure gradient from the far field to the waste is largest. As the pressure in the waste builds, the relative importance of permeability decreases compared with the initial brine saturation, which strongly influences pressure buildup.

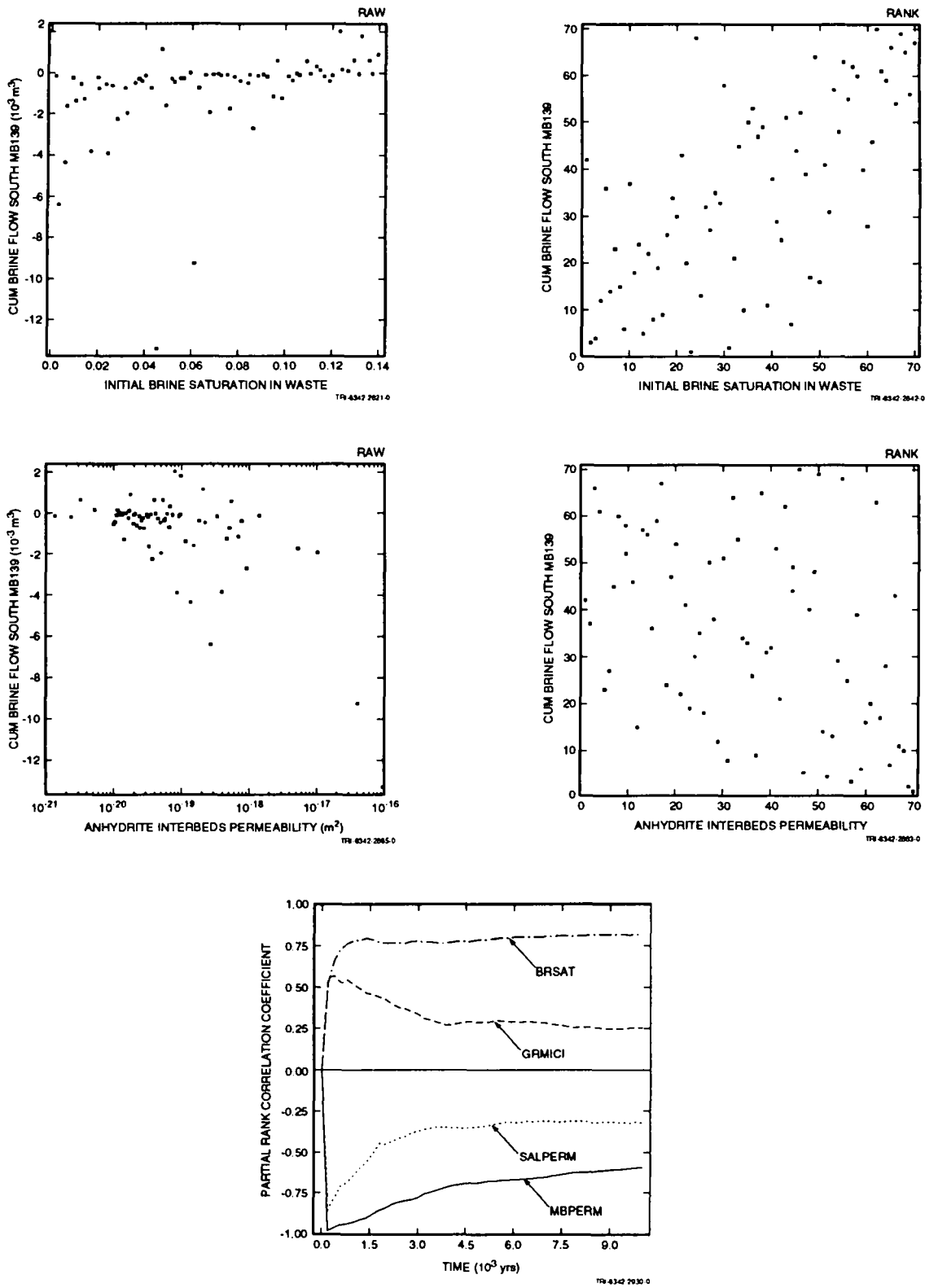

Figure 5-15. Scatterplots and partial rank correlation coefficients for cumulative net brine flow out MB139.

The third variable selected in the regression analysis, TZPORF, is a measure of the DRZ porosity. It has a small negative effect on brine flow out MB139 for the same reason that BCBRSAT affects brine flow from the repository, BWSTC. A high DRZ porosity constitutes a larger storage capacity in the DRZ, effectively damping out the interchange of fluids between the repository and the anhydrite layers. For brine flow out MB139 to occur, the DRZ must first fill at least to residual saturation with brine. Whether that brine comes from initial inflow from MB139 or, as it must eventually, from the waste, the more pore volume in the DRZ, the longer brine flow out MB139 will be delayed.

Anhydrite porosity and halite permeability each account for 3% of the variability in brine flow out MB139. Higher porosity tends to result in greater brine flows by providing more source and sink capacity close to the repository. Higher halite permeability allows brine to flow vertically out of the anhydrite layer and into halite instead of through the anhydrite, thus reducing flow out MB139.

Table 5-16. Stepwise Regression Analysis with Rank-Transformed Data for Cumulative Net Brine Flow South into MB139 (BRNMB9SC)

Step	Variable	Description	SRC	R^2
1	BRSAT	Initial brine saturation in waste	0.65	0.45
2	MBPERM	Log of anhydrite interbeds permeability	-0.35	0.61
3	TZPORF	Factor used in calculating DRZ and transition zone porosity	-0.26	0.68
4	MBPOR	Undisturbed anhydrite interbeds porosity	0.17	0.71
5	SALPERM	Intact Salado halite permeability	-0.18	0.74

5.3.3 Cumulative Net Brine Flow Out Anhydrite a + b

Brine flow out through the anhydrite a + b layer differs in one major respect from flow in MB139: there is no net outward brine flow in any of the 70 realizations. Brine flows in early when the pressure gradient from the far field to the waste is high. But this brine either flows into the repository or ends up further down in the DRZ or MB139. When the pressure in the waste exceeds the far-field pressure, there is no "pool" of brine at the repository end of anhydrite a + b to flow back out. Anhydrite permeability, as might be expected, is the dominant variable affecting brine flow. The scatterplot (Figure 5-16) shows that, as with MB139, cumulative flows into the waste can be large when the anhydrite permeability is greater than 10^{-18} m^2, and are nearly zero when the permeability is less than 10^{-20} m^2.

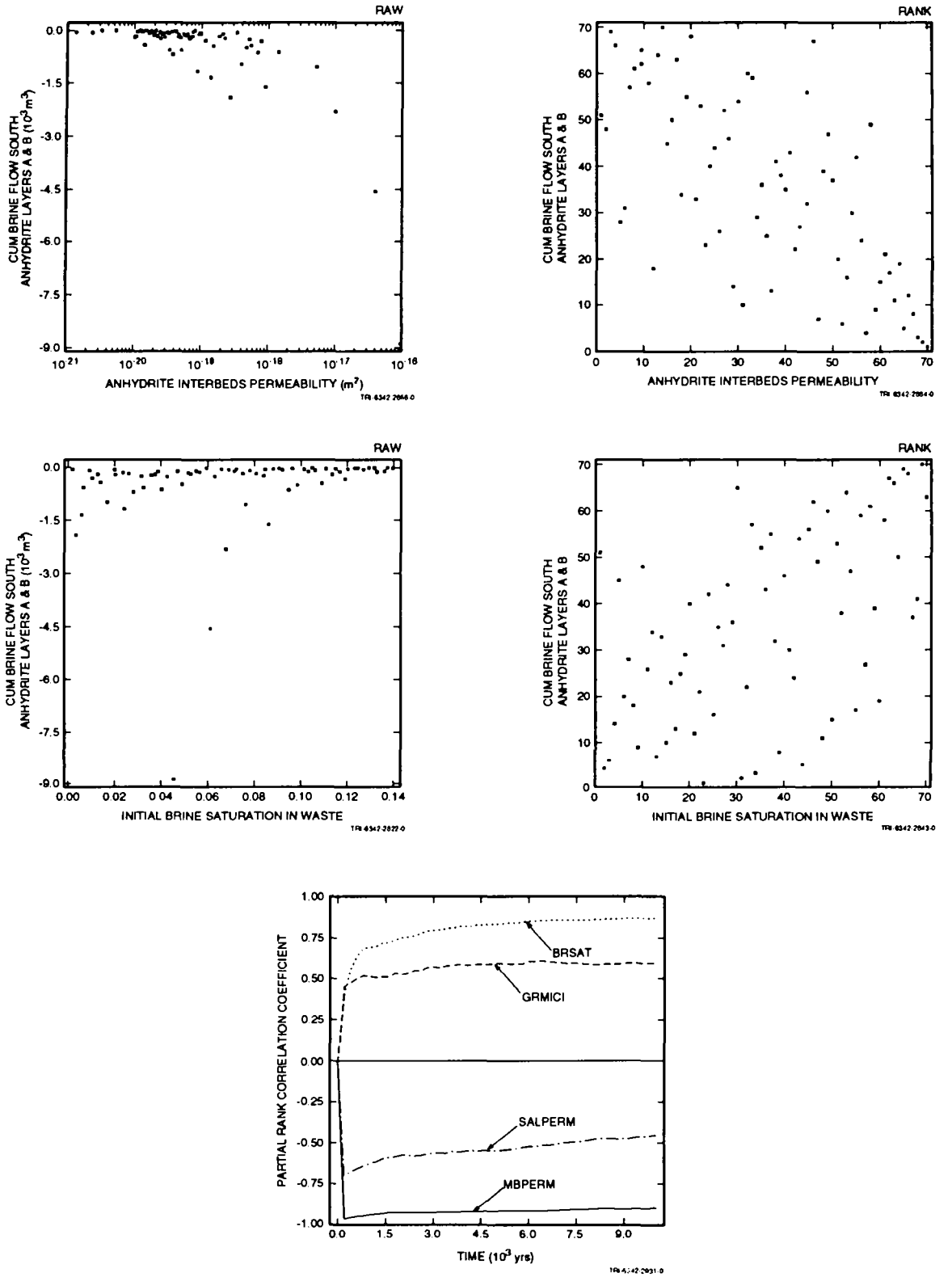

Figure 5-16. Scatterplots and partial rank correlation coefficients for cumulative net brine flow out anhydrite a + b.

Although the regression analysis (Tables 5-17) indicates that the initial brine saturation also has a moderate influence on brine flow in anhydrite a + b , the scatterplot in Figure 5-16 suggests that the effect is not really very predictable. Intermediate values of brine saturation can result in large flows toward the repository, but low values of initial brine saturation have a more consistent effect. When there is little brine in the waste, the back pressure created in the waste remains low, allowing more brine to flow inward through anhydrite a + b. The plot of partial rank correlation coefficients in Figure 5-16 indicates that the effect of initial waste brine saturation grows slightly over 10,000 yr, while the influence of permeability starts high and remains steady.

Other gas-generation-related variables also have a small effect, essentially contributing to the increase in back pressure that eventually stops the flow of brine through anhydrite a + b. As in MB139, higher halite permeability tends to reduce flow through the anhydrite layer by allowing some brine to enter the halite instead of continuing to flow through the anhydrite.

Table 5-17. Stepwise Regression Analysis with Rank-Transformed Data for Cumulative Net Brine Flow South into Anhydrite Layers a + b (BRNANHSC)

Step	Variable	Description	SRC	R^2
1	MBPERM	Log of anhydrite interbeds permeability	-0.64	0.46
2	BRSAT	Initial brine saturation in waste	0.52	0.74
3	GRMICI	Inundated biodegradation rate	0.23	0.79
4	SALPERM	Intact Salado halite permeability	-0.17	0.82
5	STOICMIC	Biodegradation stoichiometric coefficient	0.12	0.84
6	GRCORI	Inundated corrosion rate	0.12	0.85

5.3.4 Cumulative Net Brine Flow Out MB138

The regression analysis for net brine flow out MB138, Table 5-18, shows that the initial brine saturation in the waste and anhydrite permeability are about equally influential variables, although neither one provides a very strong correlation. Scatterplots for these variables in Figure 5-17 look very similar to those for the same variables in anhydrite a + b. The partial rank correlation coefficients, Figure 5-17, show similar trends, although the effect of permeability decreases slightly more over time than for anhydrite a + b.

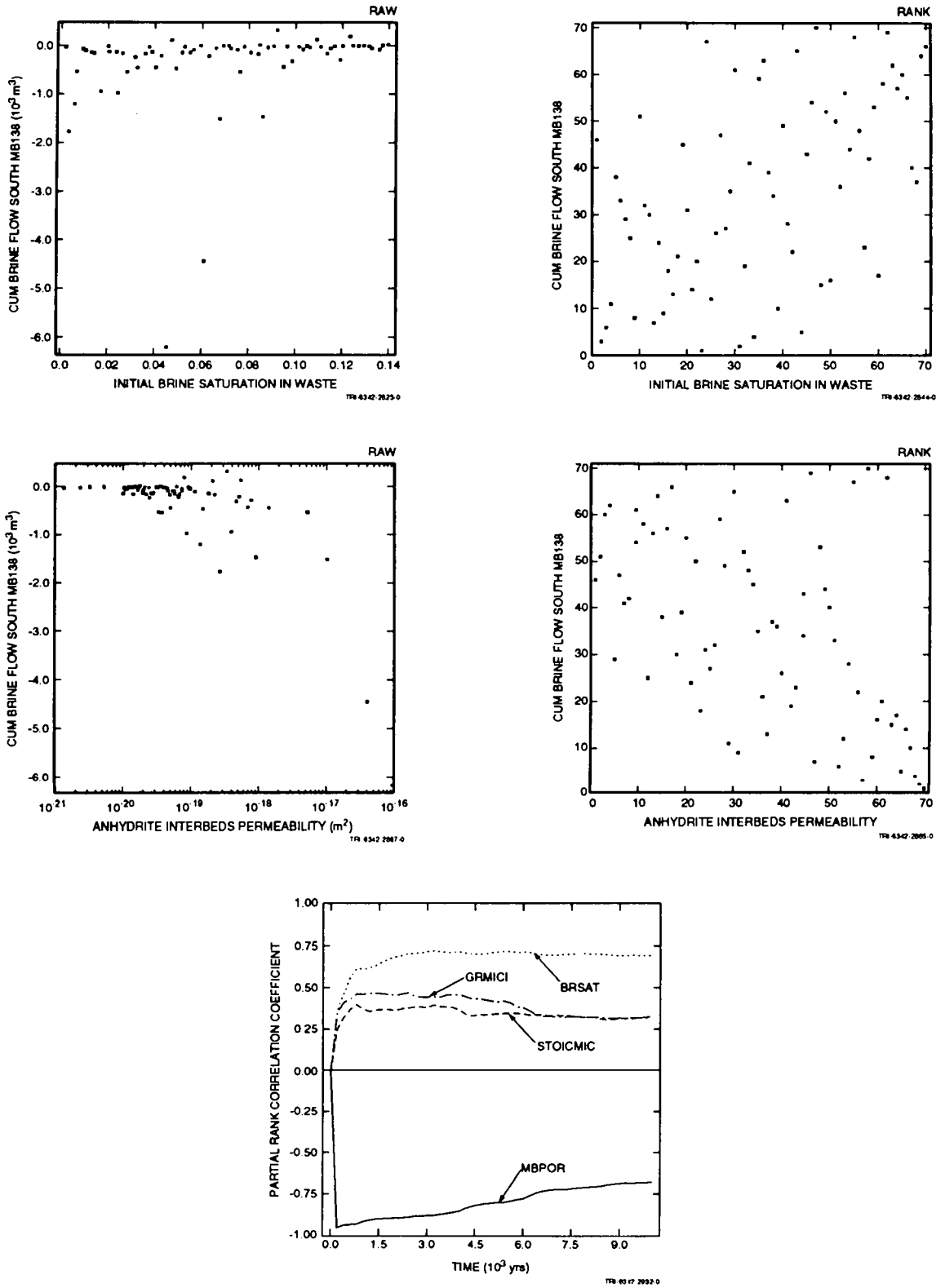

Figure 5-17. Scatterplots and partial rank correlation coefficients for cumulative net brine flow out MB138.

Table 5-18. Stepwise Regression Analysis with Rank-Transformed Data for Cumulative Net Brine Flow South into MB138 (BRNMB8SC)

Step	Variable	Description	SRC	R^2
1	BRSAT	Initial brine saturation in waste	0.51	0.27
2	MBPERM	Log of anhydrite interbeds permeability	-0.51	0.52
3	STOICMIC	Biodegradation stoichiometric coefficient	0.22	0.57

5.3.5 Cumulative Net Brine Flow Upward through Shaft Seal

The stepwise regression analysis (Table 5-19) performed for cumulative net upward flow of brine through the shaft seal, BSHSLUPC, shows that the dominant variable is the permeability during the first 200 yr of the shaft above the shaft seal but below the Culebra (SHFTPRM), not the long-term shaft seal permeability, as one might expect. However, this accounts for only 33% of the variability in brine flow through the shaft seal. Shaft seal permeability during the first 200 yr (SEALPRM1) is nearly as important, contributing another 26% to the variability in brine flow. Scatterplots in Figure 5-18 confirm that neither variable alone is very strongly correlated to brine flow. Shaft permeability during the first 200 yr (SHFTPRM) was sampled from a range that is nearly identical to the range of seal permeability for that same time period. Because that portion of the shaft is 319 to 389 m long compared to 30 to 100 m for the shaft seal (a sampled parameter, SEALTHK), it is reasonable to believe that permeability of the lower shaft is slightly more significant than seal permeability in determining brine flow through the seal. However, the impact of these variables is somewhat distorted because most of the cumulative flow through the shaft seal was downward drainage by gravity during the first 200 yr. In more than half of the realizations, the flow direction eventually reverses. Upward flow that takes place over the last 9000 yr or so is small compared to the initial downward surge, but is potentially much more important to regulatory compliance. (See Section 4.1.2 for additional discussion of brine flow.)

Halite permeability has an additional effect, but it is of secondary importance. Because of the large surface area of the shaft-halite interface, some brine drains into the shaft from the surrounding halite, even though the highest surge of brine occurred during the 50-yr disposal phase. That brine was removed from the simulation at time zero (reflecting evaporation before the repository is sealed), leaving a depressurized zone around the shaft at time zero. Despite this, when the permeability of halite is sufficiently high, some seepage from the Salado into the shaft often continues, as seen in Figure 4-24. This contributes to the downward flow of brine through the shaft seal, but should not greatly impact upward flow.

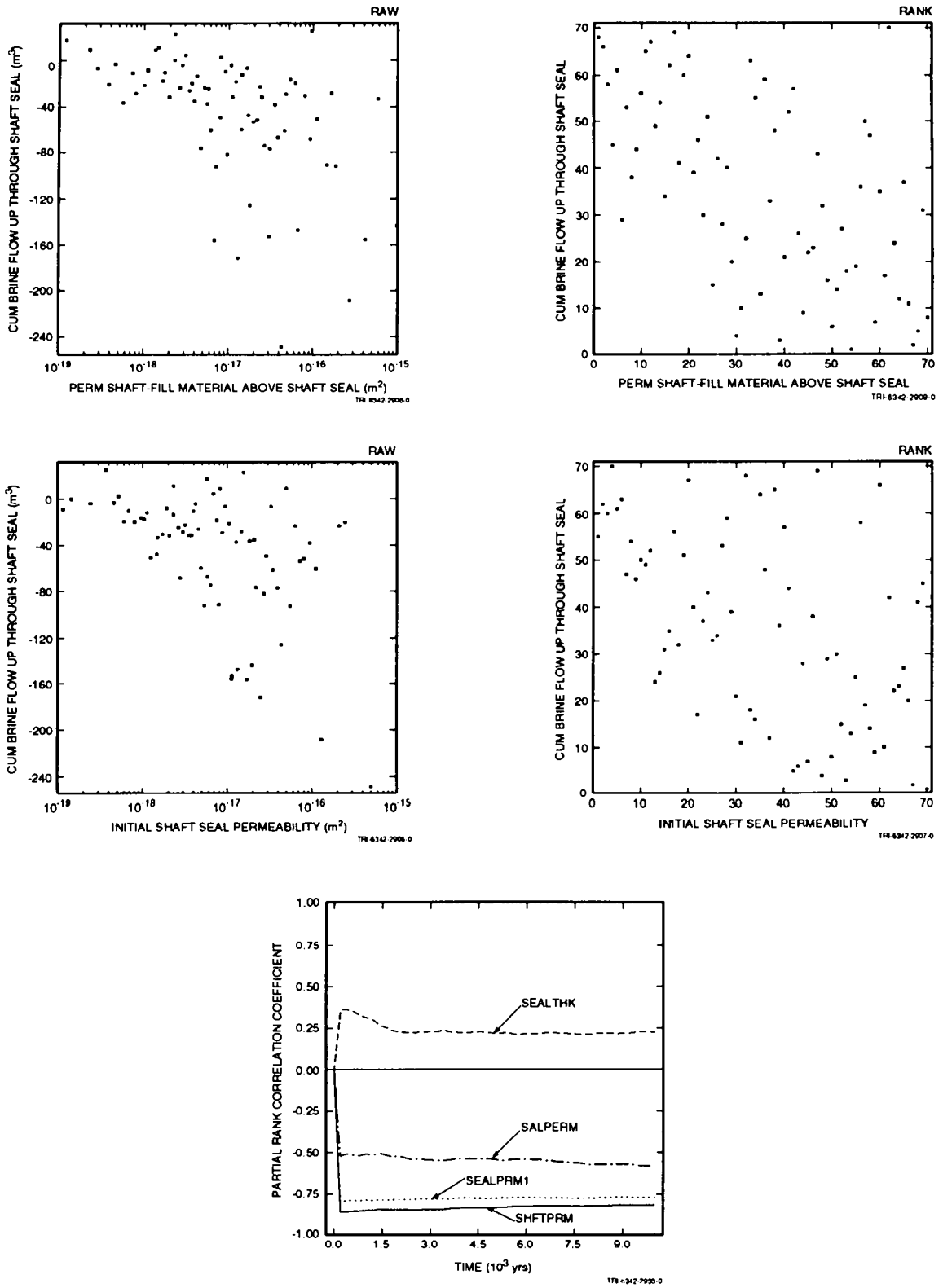

Figure 5-18. Scatterplots and partial rank correlation coefficients for cumulative net brine flow upward through shaft seal.

All three variables have negative correlation coefficients, indicating that larger values result in larger downward flows. The process being observed here is gravity drainage, which would be aided by higher seal and shaft permeabilities. If only the upward component of brine flow during 10,000 yr was analyzed, positive correlation coefficients would be expected.

Table 5-19. Stepwise Regression Analysis with Rank-Transformed Data for Cumulative Net Brine Flow Upward through Shaft Seal (BSHSLUPC)

Step	Variable	Description	SRC	R^2
1	SHFTPRM	Permeability of shaft-fill material above shaft seal	-0.58	0.33
2	SEALPRM1	Initial shaft seal permeability	-0.51	0.59
3	SALPERM	Intact Salado halite permeability	-0.34	0.71

5.4 Gas Flow

A key performance measure for the WIPP under undisturbed conditions is the amount of volatile organic compounds (VOCs) dissolved in gas that flows beyond the disposal unit boundaries. Because transport of VOCs has not yet been modeled using the two-phase flow model, measures discussed here are the amount and distance that gas flows out the various flow paths from the repository, including the three anhydrite layers and the sealed shaft leading to the Culebra. These measures provide insight into which parameters control migration of VOCs, which parameters require more attention (and perhaps more measured data), and which conceptual features of the model may require more sophisticated treatment. Two-phase flow modeling also provides insight into parameters or conceptual models that are *not* important and can therefore be further simplified or omitted in future performance assessments.

5.4.1 Cumulative Net Gas Flow Out MB139

The first three performance measures to be examined are the cumulative flows southward out each of the anhydrite layers. The stepwise regression analysis for flow out MB139, shown in Table 5-20, selected BRSAT, the initial brine saturation in the waste, as the first variable. The correlation is not strong, but it is reasonable that the key parameter affecting gas generation plays an important role in determining how much gas flows out MB139. The second variable selected, the permeability of the anhydrite layers, is also an obvious choice to affect gas flow. Another gas-generation parameter, the biodegradation stoichiometric coefficient, STOICMIC, also has a small effect. Altogether, the three variables selected account for only half of the variability in cumulative gas flow. The scatterplots for the first two variables, BRSAT and MBPERM, in Figure 5-19, illustrate the relatively poor

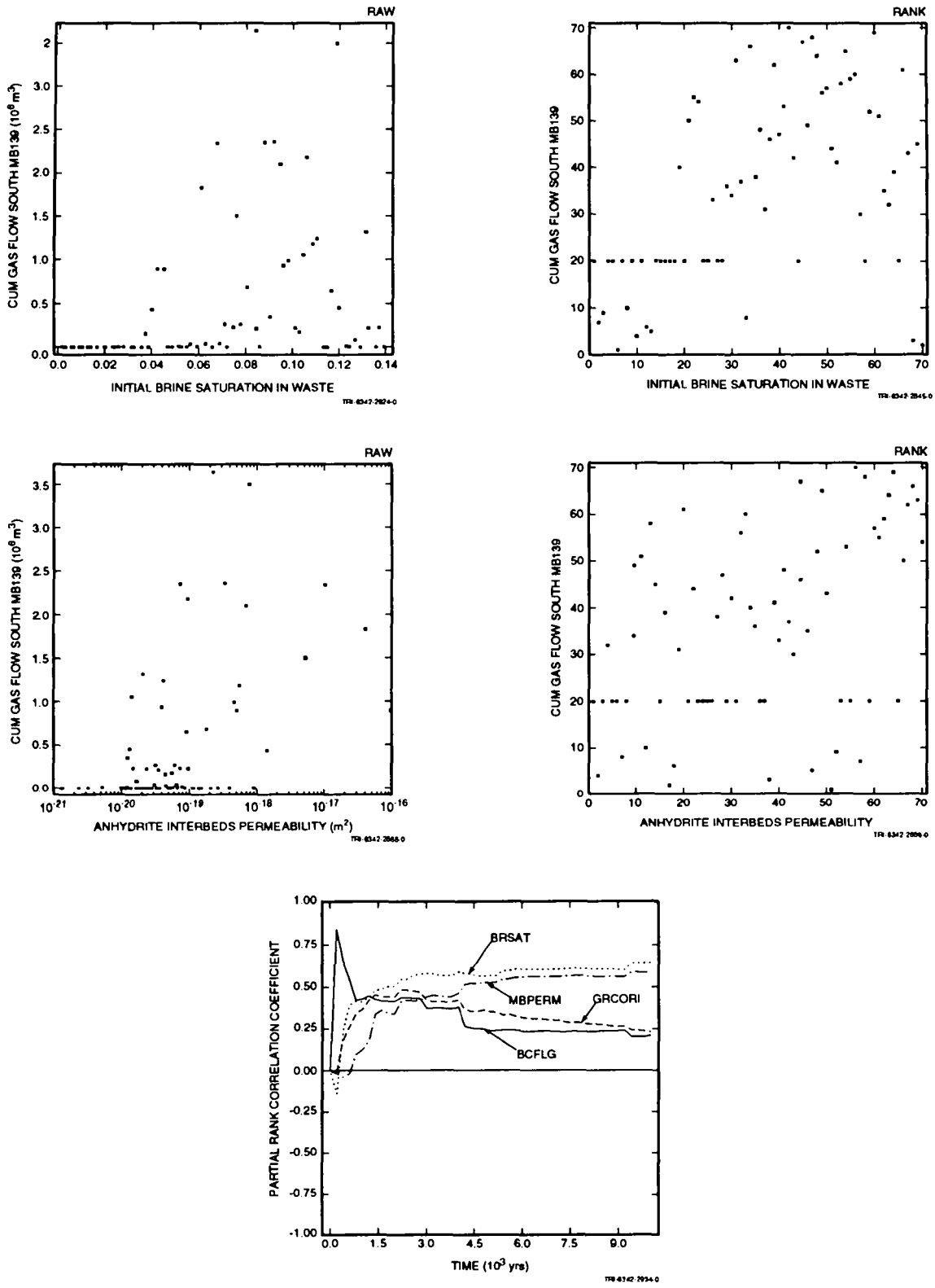

Figure 5-19. Scatterplots and partial rank correlation coefficients for cumulative net gas flow out MB139. (Rows of points in the rank plots with identical ranks result from the convention used to assign ranks to realizations with identical raw results [i.e., zero]).

correlation between cumulative gas flows and each variable. The partial rank correlation coefficients in Figure 5-19 show that BRSAT was most important over the last 9000 yr, but that it really does not dominate the other variables. Very early on, all three variables actually had small negative correlation coefficients, with higher values resulting in smaller gas flows out MB139. However, the effects may have been too small to be significant at that time because almost no gas had flowed out in any realization. One interesting feature that shows up in the scatterplots is that there appear to be cutoff values in both BRSAT and MBPERM below which there is no gas flow out MB139. For BRSAT, this value is about 4% initial brine saturation in the waste. When the initial brine saturation is too low, insufficient gas is generated to raise the pressure in the repository and push gas out the anhydrite layers. For anhydrite permeability, the cutoff is about 10^{-20} m^2, the same value below which brine flow becomes insignificant.

Table 5-20. Stepwise Regression Analysis with Rank-Transformed Data for Cumulative Net Gas Flow South into MB139 (GASMB9SC)

Step	Variable	Description	SRC	R^2
1	BRSAT	Initial brine saturation in waste	0.49	0.25
2	MBPERM	Log of anhydrite interbeds permeability	0.41	0.43
3	STOICMIC	Biodegradation stoichiometric coefficient	0.27	0.50

5.4.2 Cumulative Net Gas Flow Out Anhydrite a + b

The regression analysis for cumulative gas flow south out through anhydrite layers a + b, in Table 5-21, also selected BRSAT as the first variable. The correlation is somewhat stronger than it was in MB139. Because gas flow is not competing with brine outflow, gas generation, which is largely controlled by the initial brine saturation, has a more direct impact on gas flow. Anhydrite permeability and biodegradation stoichiometry were again selected. Together, these three account for 66% of the variability in gas flow out anhydrite a + b. Gas generation, again, has a strong influence on the amount of gas that flows out the anhydrite layer. The plot of partial rank correlation coefficients, Figure 5-20, shows that BRSAT and MBPERM dominate in determining the cumulative gas flows over the last 8000 yr. Scatterplots of BRSAT and MBPERM, in Figure 5-20, show lower limits below which gas does not flow out anhydrite a+ b, the values again being 4% for brine saturation and 10^{-20} m^2 for permeability.

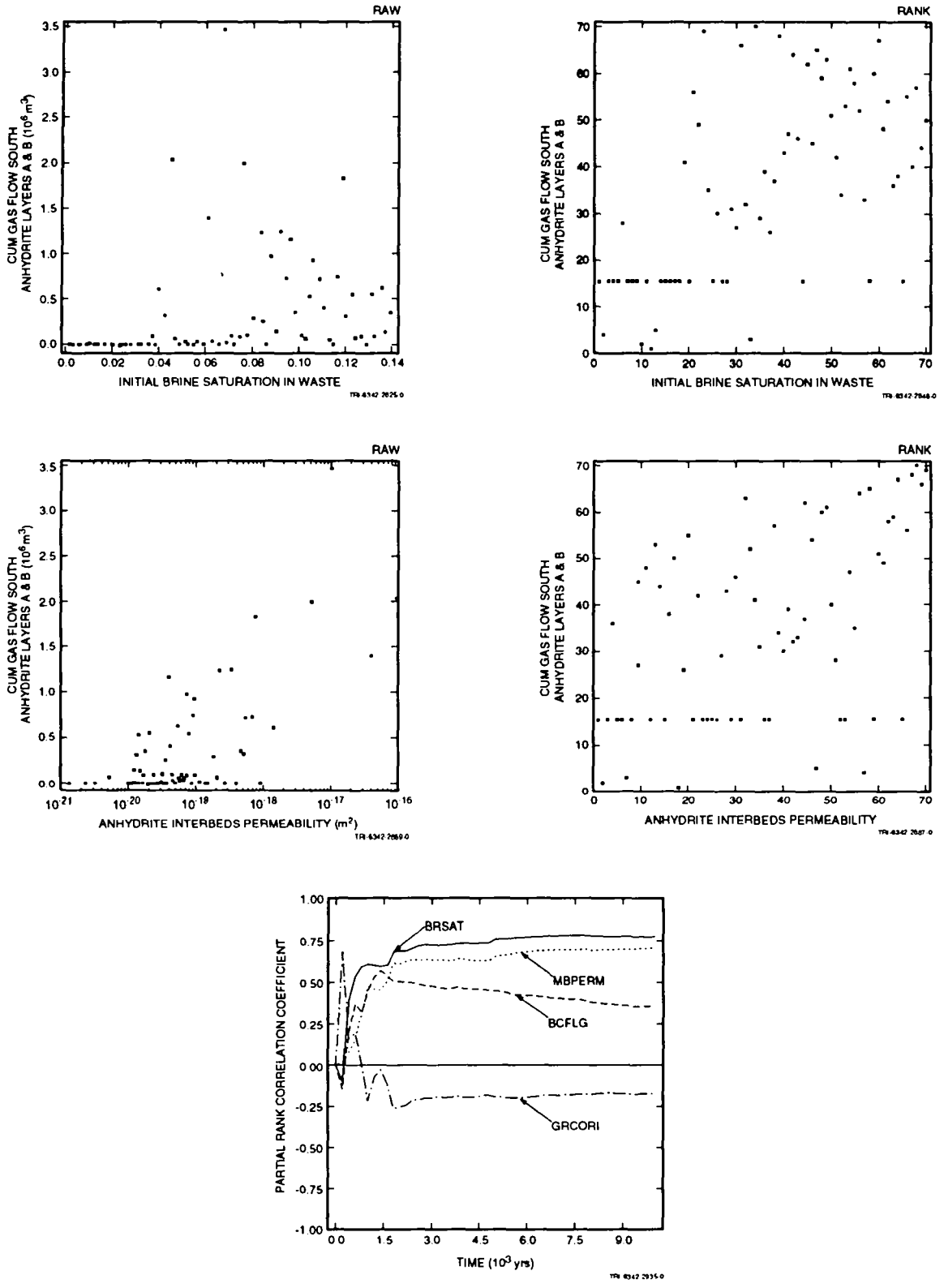

Figure 5-20. Scatterplots and partial rank correlation coefficients for cumulative net gas flow out anhydrite a + b. (Rows of points in the rank plots with identical ranks result from the convention used to assign ranks to realizations with identical raw results [i.e., zero]).

Table 5-21. Stepwise Regression Analysis with Rank-Transformed Data for Cumulative Net Gas Flow Out Anhydrite Layers a + b (GASANHSC)

Step	Variable	Description	SRC	R^2
1	BRSAT	Initial brine saturation in waste	0.59	0.37
2	MBPERM	Log of anhydrite interbeds permeability	0.50	0.61
3	STOICMIC	Biodegradation stoichiometric coefficient	0.22	0.66
4	GRCORI	Inundated corrosion rate	0.20	0.69

5.4.3 Cumulative Net Gas Flow Out MB138

The regression analysis for cumulative gas flow south out through MB138, Table 5-22, as for the other two anhydrite layers, selected BRSAT and MBPERM as the two most important variables affecting gas flow (Figure 5-21). Two other gas generation parameters, STOICMIC and GRCORI (inundated corrosion rate), also made small contributions to the variability of gas flow out MB138. Comments made above regarding the other two anhydrite layers apply also to MB138.

One other parameter, BCFLG, which is the weighting factor that determines which relative permeability model to use, showed a small influence in all three anhydrite layers (but only in the plots of partial rank correlation coefficients for MB139 and anhydrite a + b). When BCFLG = 0, the van Genuchten-Parker model is used; when BCFLG = 1, the Brooks-Corey model is used. In MB139, BCFLG had a positive correlation coefficient, whereas in anhydrite a + b and in MB138, it had a negative correlation. It is positive during the first 500 yr or so in all three layers, but there is almost no gas flow during this period in any realization. Therefore, the high value that seems to dominate all other variables over that time period is apparently spurious. Once gas flows have started in most realizations, the influence of BCFLG quickly becomes insignificant.

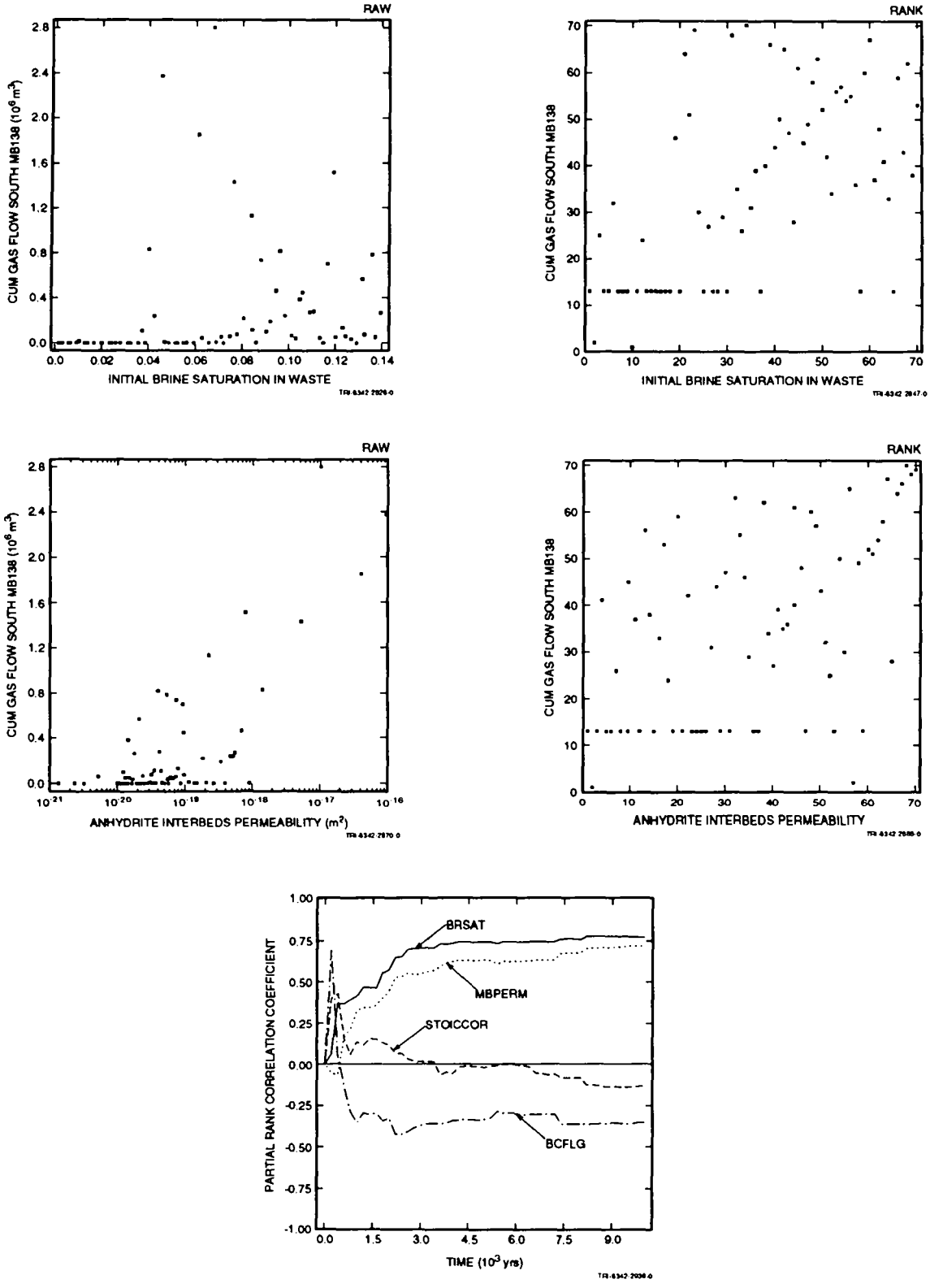

Figure 5-21. Scatterplots and partial rank correlation coefficients for cumulative net gas flow out of MB138. (Rows of points in the rank plots with identical ranks result from the convention used to assign ranks to realizations with identical raw results [i.e., zero]).

Table 5-22. Stepwise Regression Analysis with Rank-Transformed Data for Cumulative Net Gas Flow Out MB138 (GASMB8SC)

Step	Variable	Description	SRC	R^2
1	BRSAT	Initial brine saturation in waste	0.58	0.34
2	MBPERM	Log of anhydrite interbeds permeability	0.53	0.61
3	BCFLG	Brooks-Corey/van Genuchten-Parker weighting factor	-0.22	0.64
4	STOICMIC	Biodegradation stoichiometric coefficient	0.20	0.68
5	GRCORI	Inundated corrosion rate	0.17	0.71

5.4.4 Distance Gas Flows Out Anhydrite Layers

Three additional performance measures test the possible impact of the storage capacity of various regions. These measures are the distances that gas flows out each of the three anhydrite layers. Factors that affect storage or retention of fluids would be expected to influence how far gas can flow.

The results of the stepwise regression analyses and partial rank correlation analyses continue to show that the initial brine saturation in the waste is the most important variable affecting how far gas flows away from the repository. No storage factors, such as anhydrite porosity and DRZ porosity, and no retention parameters, such as residual saturations, have any measurable effect on the distance that gas migrates from the repository.

The stepwise regression analysis for distance that gas flows out MB139, shown in Table 5-23, selected BRSAT as the first variable. Although it has greater influence than any other variable, its impact is fairly weak, accounting for only 27% of the variability in gas flow distance. Nearly as influential is anhydrite permeability. As seen in preceding analyses, initial brine saturation in the waste results in the main driving force for gas migration away from the repository, whereas anhydrite permeability determines the ease with which gas flows out as it is generated. Scatterplots relating gas flow distance to these two variables, Figure 5-22, confirm the slight trends in the raw data. Gas migration distances appear at a small number of fixed values. These are the distances from the repository to the outer edge of the grid cells in the mesh, as shown in Table 4-1. Gas is assumed to have reached that distance when the saturation in a grid cell exceeds 1.0×10^{-12}. Volumes of gas in grid cells at this minimum saturation are extremely small (i.e., less than one m^3).

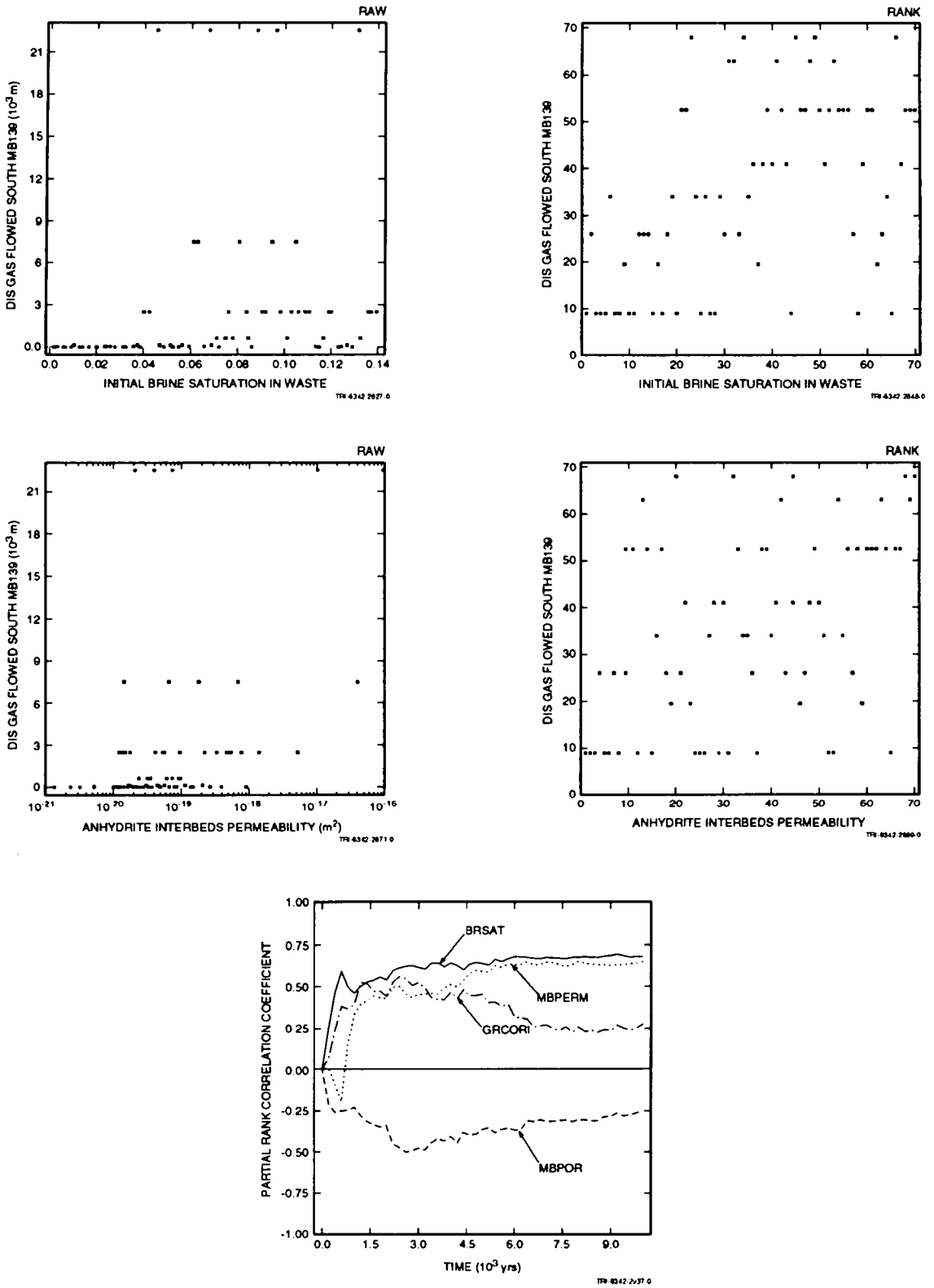

Figure 5-22. Scatterplots and partial rank correlation coefficients for distance gas flows out MB139. (Rows of points in the rank plots with identical ranks result from the convention used to assign ranks to realizations with identical raw results [i.e., zero]).

The next variable selected in the regression analysis is the relative permeability model weight factor, BCFLG. This variable has a negative regression coefficient, indicating that gas migration distance tends to be less when BCFLG = 1 (i. e., when the Brooks-Corey model is used), and migration distances tend to be greater when the van Genuchten-Parker model is used. The effect is minor, but seems to stem from the differences in capillary pressure between the two models. Unlike the Brooks-Corey model, the van Genuchten-Parker model uses a threshold capillary pressure of zero, so there is no minimum gas pressure required for flow to occur. The slightly greater ease with which gas flow is initiated using the van Genuchten-Parker model results in greater migration distances.

The last variable selected in the regression analysis is STOICMIC, the biodegradation stoichiometric coefficient. Although its influence is slight, it contributes to the driving force behind gas migration in the same way that BRSAT does.

The plots of partial rank correlation coefficients shown in Figure 5-22 indicate that the influence of the first three variables increases slowly over at least the last 8000 yr. The inundated corrosion rate shows some impact during the first 3000 yr, but its influence wanes after that.

Table 5-23. Stepwise Regression Analysis with Rank-Transformed Data for Distance Gas Flows Out MB139 (GDSTMB9S)

Step	Variable	Description	SRC	R^2
1	BRSAT	Initial brine saturation in waste	0.52	0.27
2	MBPERM	Log of anhydrite interbeds permeability	0.45	0.46
3	BCFLG	Brooks-Corey/van Genuchten-Parker weighting factor	-0.36	0.56
4	STOICMIC	Biodegradation stoichiometric coefficient	0.21	0.60

The regression analysis (Table 5-24) for gas migration distance out through anhydrite a + b is essentially identical to that of MB139, but with slightly better correlations.

The regression analysis (Table 5-25) for gas migration distance out through MB138 is also nearly identical to that of MB139 and anhydrite a + b, but with still slightly better correlations. An additional gas generation parameter has been added, although its effect is barely measurable.

Table 5-24. Stepwise Regression Analysis with Rank-Transformed Data for Gas Migration Distance South Out Anhydrite Layers a + b (GDSTANHS)

Step	Variable	Description	SRC	R^2
1	BRSAT	Initial brine saturation in waste	0.59	0.34
2	MBPERM	Log of anhydrite interbeds permeability	0.45	0.53
3	BCFLG	Brooks-Corey/van Genuchten-Parker weighting factor	-0.35	0.62
4	STOICMIC	Biodegradation stoichiometric coefficient	0.24	0.68

Table 5-25. Stepwise Regression Analysis with Rank-Transformed Data for Gas Migration Distance South Out MB138 (GDSTMB8S)

Step	Variable	Description	SRC	R^2
1	BRSAT	Initial brine saturation in waste	0.58	0.34
2	MBPERM	Log of anhydrite interbeds permeability	0.51	0.57
3	BCFLG	Brooks-Corey/van Genuchten-Parker weighting factor	-0.41	0.71
4	STOICMIC	Biodegradation stoichiometric coefficient	0.19	0.75

The regression analysis for gas migration distance out through the Culebra, shown in Table 5-26, selected BCFLG as the most influential variable, although its effect is minor. The low values of R^2 are obtained because only eight realizations resulted in gas migration distances from the shaft into the Culebra that were greater than zero. With so few non-zero responses, little significance can be assigned to this analysis.

Table 5-26. Stepwise Regression Analysis with Rank-Transformed Data for Gas Migration Distance South Out the Culebra (GDSTCULS)

Step	Variable	Description	SRC	R^2
1	BCFLG	Brooks-Corey/van Genuchten-Parker weighting factor	-0.49	0.18
2	BCEXP	Brooks-Corey exponent	-0.35	0.29
3	SALPERM	Intact Salado halite permeability	0.27	0.36

5.4.5 Cumulative Net Gas Flow Upward through Shaft Seal

Two more crucial performance measures are flow through the shaft seal and flow into the Culebra layer of the BRAGFLO model. Since the lower shaft is assumed to have zero residual gas saturation, any amount of gas that gets through the shaft seal can, in principle, reach the Culebra layer, which is outside the disposal unit boundary. (The top of the Salado Formation is the boundary for purposes of evaluating gas migration.) Cumulative flow into the Culebra, GASCULTC (which is actually measured from the Culebra shaft seal into the Culebra), is greater than zero in 6 of the 70 realizations. Flows range from 109 to 136,000 m^3.

The regression analysis for cumulative gas flow through the shaft seal, Table 5-27, once again selected the initial brine saturation in the waste as the first variable. As in the anhydrite analyses, the correlation between gas flow and brine saturation is not particularly strong, but the scatterplot, Figure 5-23, shows an apparent minimum value of brine saturation (6%) below which no gas flows through the shaft seal. This again stems from a minimum gas and pressure generation required for gas to migrate beyond the repository. The plot of partial rank correlation coefficients, Figure 5-23, shows that BRSAT is the dominant variable over the full 10,000 yr. Together with STOICMIC, gas generation parameters account for at least 47% of the variability in gas flow through the shaft seal.

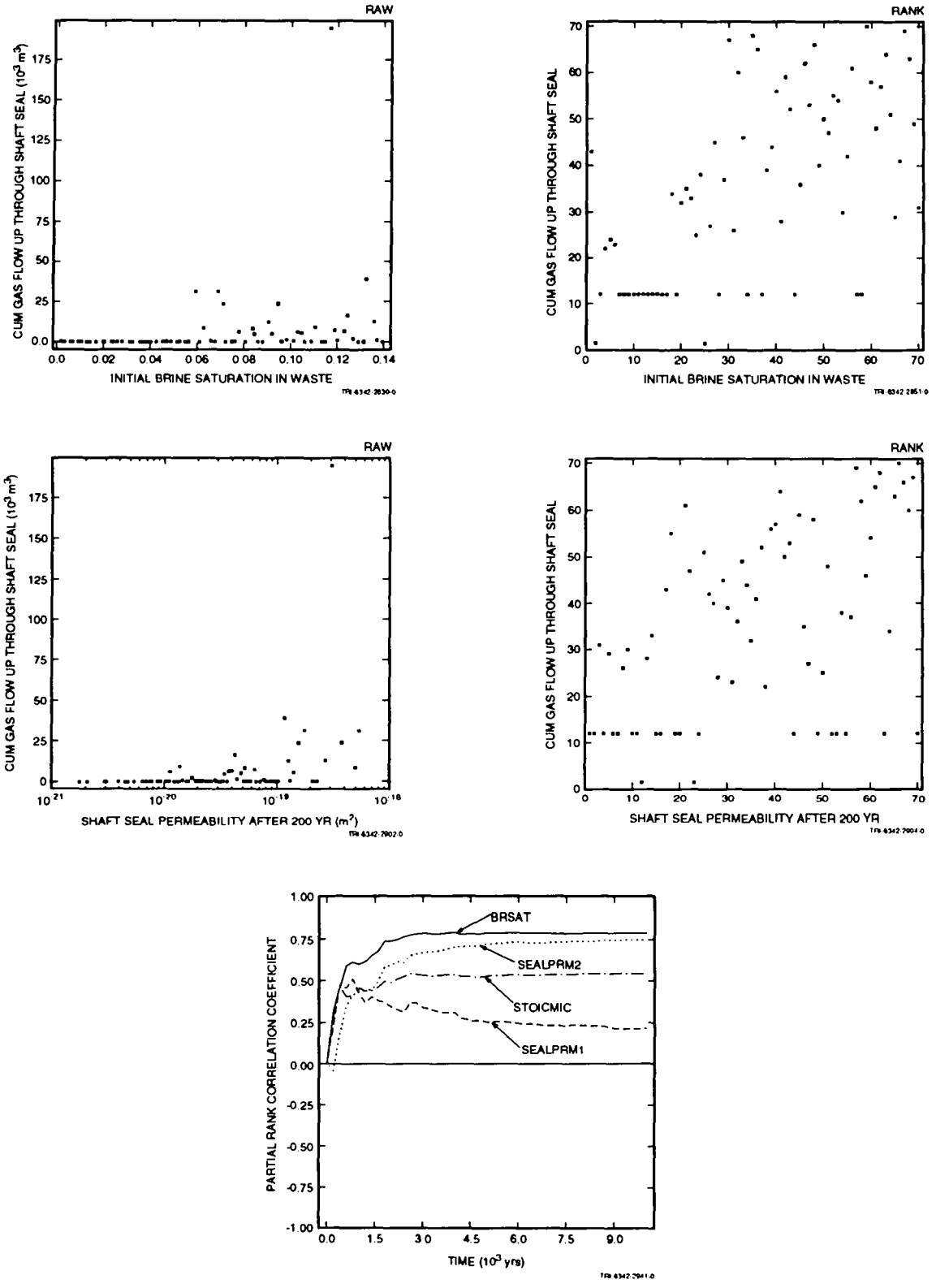

Figure 5-23. Scatterplots and partial rank correlation coefficients for cumulative net gas flow upward through the shaft seal. (Rows of points in the rank plots with identical ranks result from the convention used to assign ranks to realizations with identical raw results [i.e., zero]).

Table 5-27. Stepwise Regression Analysis with Rank-Transformed Data for Cumulative Net Upward Gas Flow through Shaft Seal (GSHSLUPC)

Step	Variable	Description	SRC	R^2
1	BRSAT	Initial brine saturation in waste	0.60	0.37
2	SEALPRM2	Shaft seal permeability after 200 yr	0.50	0.60
3	STOICMIC	Biodegradation stoichiometric coefficient	0.31	0.70

5.4.6 Cumulative Net Gas Flow Upward into the Culebra

The regression analysis for cumulative net gas flow into the Culebra from the Culebra shaft seal, in Table 5-28, selected the permeability of the shaft seal after 200 yr as the first variable. As expected, the higher the permeability, the more gas flowed into the Culebra. The correlation is not strong, accounting for only 30% of the variability in GASCULTC, but this is largely a result of the few occurrences of flow into the Culebra; there were only six realizations in which there was any significant flow. (Two more realizations had minute quantities of gas flow into the Culebra — enough to result in measurable gas migration distances.) Whereas five of these ranged from 110 m^3 to 1070 m^3, there was one realization that resulted in 136,000 m^3. The scatterplots shown in Figure 5-24 illustrate how this correlation is unduly weighted by a single outlying data point, although the regression analysis supports intuitively finding that seal permeability and parameters that control gas generation have the most influence on the amount of gas that flows into the Culebra. The partial rank correlation coefficients, Figure 5-24, indicate that the influence of these two parameters is growing with time. The step-like behavior of the curves is indicative of the few realizations in which flow into the Culebra actually resulted.

Table 5-28. Stepwise Regression Analysis with Rank-Transformed Data for Cumulative Net Gas Flow into the Culebra (GASCULTC)

Step	Variable	Description	SRC	R^2
1	SEALPRM2	Shaft seal permeability after 200 yr	0.55	0.30
2	BRSAT	Initial brine saturation in waste	0.38	0.45

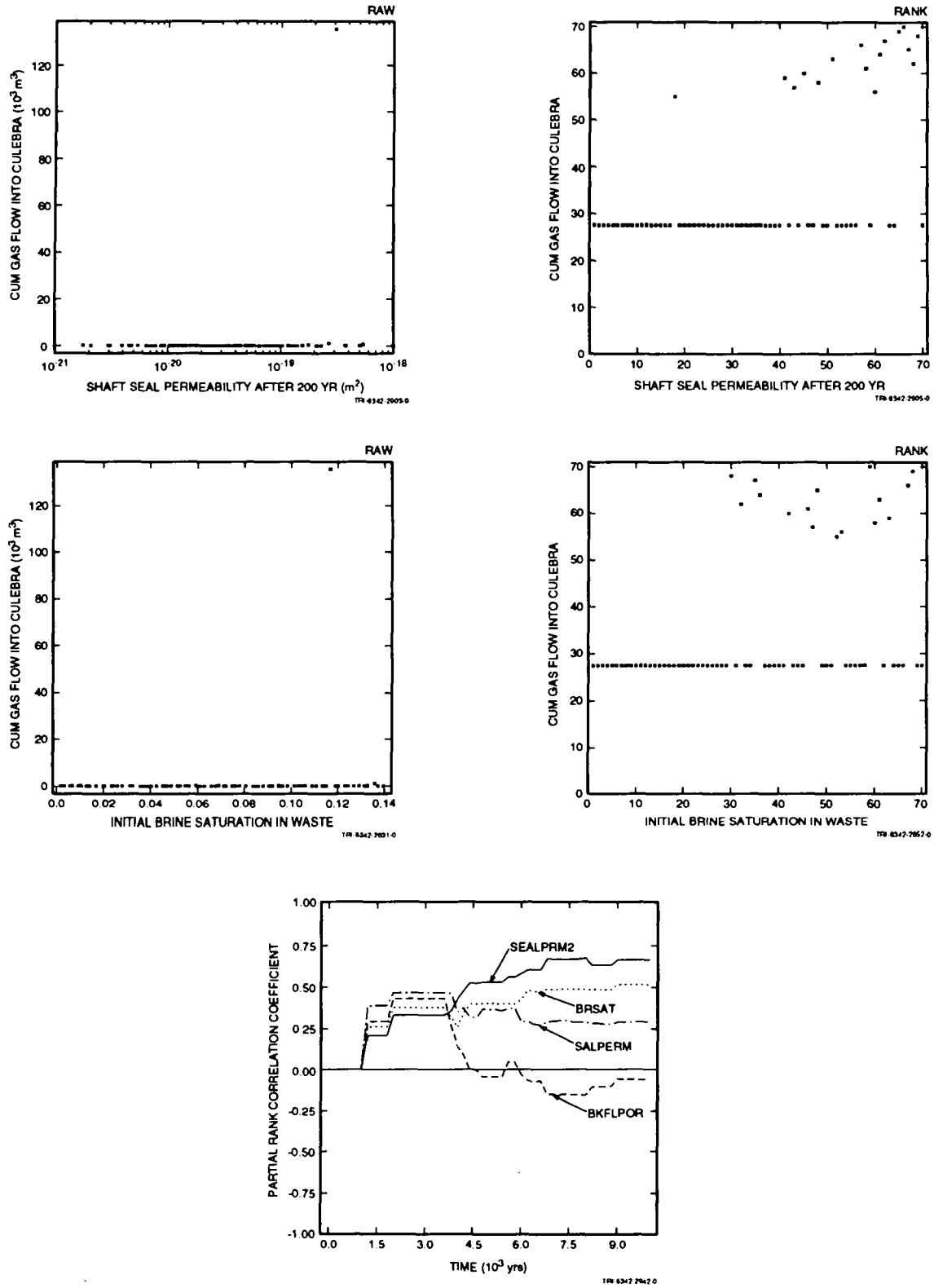

Figure 5-24. Scatterplots and partial rank correlation coefficients for cumulative net gas flow upward through the shaft seal. (Rows of points in the rank plots with identical ranks result from the convention used to assign ranks to realizations with identical raw results [i.e., zero]).

6. SUMMARY AND CONCLUSIONS

Conclusions based on these analyses are conditional on the modeling assumptions and parameter-value distributions used in the 1992 preliminary PA. These analyses do not represent a final performance assessment, and results should not be used for comparisons to regulatory standards. The 1992 PA modeling system does not yet include all potentially important physical processes that may affect disposal-system performance (e.g., pressure-dependent fracturing of anhydrites and effects of possible channeling of fluid flow are not included in 1992, and will be included in future PAs), nor are all portions of the data base complete. Results are presented here to provide interim guidance to the WIPP Project as it plans for a final compliance evaluation.

Of the 25 parameters that were selected for sampling in the analyses of undisturbed performance, 6 have significant effects on the performance measures considered. These 6 parameters are listed in Table 6-1 as "very important," reflecting their potential impact on gas and brine migration from the repository. The single most important parameter, as shown in the sensitivity analyses described in Chapter 5 of this volume, is the initial brine saturation in the waste. Few data are available for this parameter (see Section 2.4 of this volume), but for the range of values sampled here, the initial water content of the waste effectively controls the amount of gas that is generated. The total amount of gas generated, in turn, controls how much gas flows out through the various release pathways. Unless the overall gas-generation rate is very small, the full gas-generation potential allowed by the amount of water initially present will be realized over 10,000 yr. Unless the permeability of the anhydrite layers is near the lower limit of the sampled range, this time period is sufficient for gas to flow to the disposal-unit boundaries as long as enough water is initially present to generate the amount of gas required to flow that far. The other five parameters listed as "very important" also play a major role in influencing gas and brine migration from the repository, but their effect is secondary to that of the initial brine saturation. The range of initial brine saturation currently used does not have a sound basis in measured data, and is expected to change. Because this one parameter so dominates the undisturbed performance, a different range of values may produce different results, and even the conclusions with the strongest statistical support in this report should be regarded as preliminary.

Most of the other sampled parameters had a smaller impact on gas and brine migration, and are listed as "important" in Table 6-1. These parameters each appear in only a few of the regression analyses reported in Chapter 5. Their importance, however, is conditional on the conceptual models used to describe the repository and its surroundings, and may change in future analyses as conceptual models are refined.

The final category of parameters listed in Table 6-1, "less important," includes those that were not identified in any of the regression analyses reported in Chapter 5. Conditional on all assumptions of the 1992 PA, the distributions used for these parameters had no effect on the undisturbed performance measures considered. Essentially any value could have been selected from the distributions and used as a fixed value throughout without affecting performance, implying that, unless conceptual models change significantly, these parameters could be omitted from future samplings if the present ranges are shown to be defensible. However, these conclusions apply only to undisturbed performance; some parameters that are insignificant here (e.g., Culebra matrix porosity) may be more important in assessing performance following human intrusion.

Table 6-1. Importance of Sampled Parameters with Respect to 40 CFR 268.6. Results apply only to undisturbed performance of the repository (no human intrusion), and are conditional on modeling assumptions, the choice of parameters sampled, and the assumed parameter-value distributions. Comparable results for 40 CFR 191B (disturbed performance) can be found in Volume 4 of this report.

Parameter Name	Parameter Description
Very Important Parameters (listed in order of importance)	
BRSAT	Initial brine saturation in waste*
MBPERM	Salado anhydrite permeability
STOICMIC	Biodegradation stoichiometric coefficient
GRCORI	Corrosion gas-generation rate, inundated conditions
GRMICI	Biodegradation gas-generation rate, inundated conditions
SEALPERM2	Shaft seal permeability after 200 yr
Important Parameters (lisited in alphabetical order)	
BCFLG	Brooks-Corey/van Genuchten-Parker pointer
GRCORHF	Corrosion gas-generation rate factor, humid conditions
GRMICHF	Biodegradation gas-generation rate factor, humid conditions
MBPOR	Salado anhydrite porosity
SALPERM	Salado halite permeability
SEALPERM1	Shaft seal permeability, 0-200 yr
SHFTPRM	Lower shaft permeability, 0-200 yr
STOICCOR	Corrosion stoichiometric coefficient
TZPORF	Transition zone and DRZ porosity factor
VMETAL	Initial volume fraction of metals and glass in waste
VWOOD	Initial volume fraction of combustibles in waste
Less Important Parameters (listed in alphabetical order)	
BCBRSAT	Residual brine saturation in Salado Fm.
BCEXP	Brooks-Corey relative permeability model exponent
BCGSSAT	Residual gas saturation in Salado Fm.
BKFLPOR	Porosity of backfill in drifts, experimental region, and shaft below seal
CULPOR	Matrix porosity of Culebra
DSEALPRM	Drift and panel seal permeability
MBPRES	Far-field pressure in Salado Fm.
SEALTHK	Shaft seal vertical thickness

* Importance of initial brine saturation in the waste may be highly sensitive to the assumed parameter-value distribution. See text for additional information.

7. REFERENCES

Beauheim, R.L., G.J. Saulnier, Jr., and J.D. Avis. 1991 *Interpretation of Brine-Permeability Tests of the Salado Formation at the Waste Isolation Pilot Plant Site: First Interim Report.* SAND90-0083. Albuquerque, NM: Sandia National Laboratories.

Bertram-Howery, S.G., M.G. Marietta, R.P. Rechard, P.N. Swift, D.R. Anderson, B.L. Baker, J.E. Bean, Jr., W. Beyeler, K.F. Brinster, R.V. Guzowski, J.C. Helton, R.D. McCurley, D.K. Rudeen, J.D. Schreiber, and P. Vaughn. 1990. *Preliminary Comparison with 40 CFR Part 191, Subpart B for the Waste Isolation Pilot Plant, December 1990.* SAND90-2347. Albuquerque, NM: Sandia National Laboratories.

Butcher, B.M. 1990. Appendix A: "Memo 5: Disposal Room Porosity and Permeability Values for Disposal Room Performance Assessment," *Data Used in Preliminary Performance Assessment of the Waste Isolation Pilot Plant (1990).* R.P. Rechard, H. Iuzzolino, and J.S. Sandha. SAND89-2408. Albuquerque, NM: Sandia National Laboratories. A-93 through A-102.

Helton, J.C. 1993. "Risk, Uncertainty in Risk, and the EPA Release Limits for Radioactive Waste Disposal," *Nuclear Technology.* SAND91-1255J. Vol. 101, no. 1, 18-39.

Helton, J.C., J.W. Garner, R.D. McCurley, and D.K. Rudeen. 1991. *Sensitivity Analysis Techniques and Results for Performance Assessment at the Waste Isolation Pilot Plant.* SAND90-7103. Albuquerque, NM: Sandia National Laboratories.

Helton, J.C., J.W. Garner, R.P. Rechard, D.K. Rudeen, and P.N. Swift. 1992. *Preliminary Comparison with 40 CFR Part 191, Subpart B for the Waste Isolation Pilot Plant, December 1991—Volume 4: Uncertainty and Sensitivity Analysis Results.* SAND91-0893/4. Albuquerque, NM: Sandia National Laboratories.

Howarth, S.M., E.W. Peterson, P.L. Lagus, K. Lie, S.J. Finley, and E.J. Nowak. 1991. "Interpretation of In-Situ Pressure and Flow Measurements of the Salado Formation at the Waste Isolation Pilot Plant," *1991 Joint Rocky Mountain Regional Meeting and Low Permeability Reservoirs Symposium, Society of Petroleum Engineers, Denver, CO, April 15-17, 1991.* SPE-21840. Richardson, TX: Society of Petroleum Engineers. 355-369.

Iman, R.L., and W.J. Conover. 1979. "The Use of the Rank Transform in Regression," *Technometrics.* Vol. 21, No. 4, 499-509.

Iman, R.L., J.M. Davenport, E.L. Frost, and M.J. Shortencarier. 1980. *Stepwise Regression with PRESS and Rank Regression (Program and User's Guide).* SAND79-1472. Albuquerque, NM: Sandia National Laboratories.

Iman, R.L., M.J. Shortencarier, and J.D. Johnson. 1985. *A FORTRAN 77 Program and User's Guide for the Calculation of Partial Correlation and Standardized Regression Coefficients.* NUREG/CR-4122, SAND85-0044. Albuquerque, NM: Sandia National Laboratories.

Kelley, V.A., and G.J. Saulnier, Jr. 1990 *Core Analyses for Selected Samples from the Culebra Dolomite at the Waste Isolation Pilot Plant Site.* SAND90-7011. Albuquerque, NM: Sandia National Laboratories.

Lappin, A.R., R.L. Hunter, D.P. Garber, P.B. Davies, R.L. Beauheim, D.J. Borns, L.H. Brush, B.M. Butcher, T. Cauffman, M.S.Y. Chu, L.S. Gomez, R.V. Guzowski, H.J. Iuzzolino, V. Kelley, S.J. Lambert, M.G. Marietta, J.W. Mercer, E.J. Nowak, J. Pickens, R.P. Rechard, M. Reeves, K.L. Robinson, and M.D. Siegel. 1989. *Systems Analysis, Long-Term Radionuclide Transport, and Dose Assessments, Waste Isolation Pilot Plant (WIPP), Southeastern New Mexico; March 1989.* SAND89-0462. Albuquerque, NM: Sandia National Laboratories.

Munson, D.E., A.F. Fossum, and P.E. Senseny. 1989. *Advances in Resolution of Discrepancies Between Predicted and Measured In Situ WIPP Room Closures.* SAND88-2948. Albuquerque, NM: Sandia National Laboratories.

Rechard, R.P., ed. 1992. *User's Reference Manual for CAMCON: Compliance Assessment Methodology Controller Version 3.0.* SAND90-1983. Albuquerque, NM: Sandia National Laboratories.

Rechard, R.P., W. Beyeler, R.D. McCurley, D.K. Rudeen, J.E. Bean, and J.D. Schreiber. 1990. *Parameter Sensitivity Studies of Selected Components of the Waste Isolation Pilot Plant Repository/Shaft System.* SAND89-2030. Albuquerque, NM: Sandia National Laboratories.

Stone, C.M., R.D. Krieg, and Z.E. Beisinger. 1985. *SANCHO: A Finite Element Computer Program for the Quasistatic, Large Deformation, Inelastic Response of Two-Dimensional Solids.* SAND84-2618. Albuquerque, NM: Sandia National Laboratories.

U.S. DOE (Department of Energy). 1990a. *Waste Isolation Pilot Plant No-Migration Variance Petition.* DOE/WIPP 89-003, Revision 1. Carlsbad, NM: Westinghouse Electric Corporation, Waste Isolation Division.

U.S. DOE (Department of Energy). 1990b. *Draft Plan for the Waste Isolation Pilot Plant Test Phase: Performance Assessment and Operations Demonstration.* DOE/WIPP 89-011. Carlsbad, NM: U.S. Department of Energy, Waste Isolation Pilot Plant. (Copy on file at the Waste Management and Transportation Library, Sandia National Laboratories, Albuquerque, NM.)

U.S. DOE (Department of Energy). 1991a. *Quality Assurance Program Plan for the Waste Isolation Pilot Plant Experimental Waste-Characterization Program.* DOE/EM/48063-1, Rev. 1, Washington, D.C.

U.S. DOE (Department of Energy). 1991b. *Waste Characterization Program Plan for WIPP Experimental Waste.* DOE/WIPP 89-025, Rev. 1, Carlsbad, NM: Westinghouse Electric Corporation.

U.S. DOE (Department of Energy). 1991c. *Waste Acceptance Criteria for the Waste Isolation Pilot Plant, December 1991.* DOE/WIPP-069, Rev. 4. Carlsbad, NM: Westinghouse Electric Corporation.

U.S. DOE (Department of Energy). 1993. *Test Phase Plan for the Waste Isolation Pilot Plant.* DOE/WIPP 89-011, Rev. 1. Albuquerque, NM: U.S. Department of Energy, WIPP Project Integration Office.

U.S. EPA (Environmental Protection Agency). 1985. "40 CFR 191: Environmental Standards for the Management and Disposal of Spent Nuclear Fuel, High-Level and Transuranic Radioactive Wastes, Final Rule," *Federal Register.* Vol. 50, no. 182, 38066-38089.

U.S. EPA (Environmental Protection Agency). 1986. "Land Disposal Restrictions," *Code of Federal Regulations 40, Part 268.* Washington, DC: Office of the Federal Register, National Archives and Records Administration.

U.S. EPA (Environmental Protection Agency). 1990a. "Hazardous and Solid Waste; Conditional Variance to Department of Energy Waste Isolation Pilot Plant; Notice of Proposed Decision," *Federal Register*, V. 55, No. 67, 13068-13094.

U.S. EPA (Environmental Protection Agency). 1990b. "Conditional No-Migration Determination for the Department of Energy Waste Isolation Pilot Plant (WIPP)," *Federal Register.* Vol. 55. no. 220, 47700-47721.

U.S. EPA (Environmental Protection Agency). 1992. *"No Migration" Variances to the Hazardous Waste Land Disposal Prohibitions: A Guidance Manual for Petitioners, Draft, July 1992.* EPA 530/R/92/03. Washington, DC: U.S. Environmental Protection Agency, Office of Solid Waste. (Copy on file at the Waste Management and Transportation Library, Sandia National Laboratories, Albuquerque, NM.)

Voss, C. I. 1984. *SUTRA (Saturated-Unsaturated TRAnsport): A Finite-Element Simulation Model for Saturated-Unsaturated, Fluid-Density-Dependent Ground-Water Flow with Energy Transport or Chemically-Reactive Single-Species Solute Transport.* Water-Resources Investigations Report 84-4369. Reston, VA: U. S. Geological Survey National Center.

WIPP PA (Performance Assessment) Department. 1992. *Long-Term Gas and Brine Migration at the Waste Isolation Pilot Plant: Preliminary Sensitivity Analyses for Post-Closure 40 CFR 268 (RCRA), May 1992.* SAND92-1933. Albuquerque, NM: Sandia National Laboratories.

WIPP PA (Performance Assessment) Division. 1991a. *Preliminary Comparison with 40 CFR Part 191, Subpart B for the Waste Isolation Pilot Plant, December 1991. Volume 1: Methodology and Results.* SAND91-0893/1. Albuquerque, NM: Sandia National Laboratories.

WIPP PA (Performance Assessment) Division. 1991b. *Preliminary Comparison with 40 CFR Part 191, Subpart B for the Waste Isolation Pilot Plant, December 1991. Volume 2: Probability and Consequence Modeling.* SAND91-0893/2. Albuquerque, NM: Sandia National Laboratories.

WIPP PA (Performance Assessment) Division. 1991c. *Preliminary Comparison with 40 CFR Part 191, Subpart B for the Waste Isolation Pilot Plant, December 1991. Volume 3: Reference Data.* SAND91-0893/3. Albuquerque, NM: Sandia National Laboratories.

APPENDIX A: MEMORANDUM REGARDING REFERENCE DATA

APPENDIX A: MEMORANDUM REGARDING REFERENCE DATA

Referenced Manorandum

2/17/93

WIPP Performance Assessment Dept. 6342

Ray E. Finley, 6121, and Palmer Vaughn, 6342

Seal and Backfill Information

A series of meetings was held between the Repository Isolation Systems Dept. (6121) and the WIPP Performance Assessment Dept. (6342) personnel to develop seal and backfill parameters for the 1993 gas migration calculations to be performed by Dept. 6342. Estimates for seal and backfill parameters were developed from available literature for two time periods: 0-200 years, and 200-10,000 years. The modeling to be done by 6342 requires upper and lower bound estimates, and in some cases "best guess" estimates for each parameter of interest for each time period. Table 1 (attached) lists the various seal and backfill locations and parameters required for the Gas Migration calculations.

The estimates listed in Table 1 assume that the water-bearing-zone seals are effective at limiting water inflow into the facility. Also, these estimates do not take into consideration the DRZ in the surrounding halite or in the interbeds (primarily MB139).

It should be stressed that the values in Table 1 are estimates and could change as our understanding of the nature and behavior of the seal materials changes. Also, the estimates are limited by the assumptions used in the reference materials.

Implicit in Table 1 are various assumptions of correlations between certain parameters; e.g., porosities are correlated to permeabilities, although the correlation is not stated. The threshold capillary pressure is assumed to be correlated to permeability.

Although the values shown in Table 1 represent the current best estimates, modeling constraints and the need to be more consistent in making assumptions resulted in some changes in values. The values actually used in the calculations are shown in Table 2. Correlations implicit in Table 1 were clarified and are shown more explicitly in Table 2. In particular, note that porosities are correlated to the log of permeabilities.

Initial brine saturations were originally assumed to correspond to 5-8 wt% of the salt and backfill. However, given the ranges of porosities in Table 2 and using values of bulk density and brine density measured for WIPP halite and Salado brine (2140 kg/m^3 and 1230 kg/m^3, respectively, it was found that 5-8 wt% brine corresponds to more than 90% brine saturation. The lowest brine saturation corresponds to 5 wt% brine added to halite having a compacted porosity of 9%. If 5 wt% brine is added to crush halite having a porosity of 9% after compaction, the pore space will be 90% saturated with brine. Rather than sample a narrow

range of initial brine saturations in the backfill/seal/shaft components (90-100%) a fixed value of 100% is assumed (1.0, Table 2).

In Table 1, the porosity of the Shaft Seal is shown changing after 200 years, and the Shaft Fill porosity differs from that of the Shaft Seal. Furthermore, it is anticipated that the Shaft Fill porosity will become identical to that of the Shaft Seal after 200 years. However, these changes create problems in modeling because they constitute instantaneous changes in brine mass that introduce mass balance errors into the calculations. It is difficult to rationalize these errors, which are artifacts of the model. To avoid this difficulty, the porosities of these two materials will be assumed to be equal and constant in time, rather than changing at 200 years. This is expected to result in more accurate results even though the porosity change that is actually believed to occur is ignored.

The parameter values listed in Table 1 were developed from information contained in the following references:

Arguello, J.G., 1988, "WIPP Panel Entryway Seal - Numerical Simulation of Seal Composite Interaction for Preliminary Design Evaluation," SAND87-2804, Sandia National Laboratories, Albuquerque, NM.

Butcher, B.M., 1991, "The Advantages of a Salt/Bentonite Backfill for Waste Isolation Pilot Plant Disposal Rooms," SAND90-3074, Sandia National Laboratories, Albuquerque, NM.

Ehgartner, B., 1990, "Geomechanical Analyses in Support of the Waste Isolation Pilot Plant (WIPP)," SAND90-0285, Sandia National Laboratories, Albuquerque, NM.

Ehgartner, B., 1991, "A Coupled Mechanical/Hydrological Model for WIPP Shaft Seals," SAND90-2826, Sandia National Laboratories, Albuquerque, NM.

Finley, R.E., and J.R. Tillerson, 1992, "WIPP Small Scale Seal Performance Tests - Status and Impacts" SAND91-2247, Sandia National Laboratories, Albuquerque, NM.

Morgan, H.S., 1987, "TRU Storage Room Calculation with Stratigraphy," Memo to D.E. Munson, December 9, 1987, Sandia National Laboratories, Albuquerque, NM.

Nowak, E.J., J.R. Tillerson, and T.M. Torres, 1990, "Initial Reference Seal System Design: Waste Isolation Pilot Plant," SAND90-0355, Sandia National Laboratories, Albuquerque, NM.

Stormont, J.C., and C.L. Howard, 1987, "Development, Implementation, and Early Results: Test Series C of the Small-Scale Seal Performance Tests," SAND87-2203, Sandia National Laboratories, Albuquerque, NM.

Weatherby, J.R., W.T. Brown, and B.M. Butcher, 1991, "The Closure of WIPP Disposal Rooms Filled with Various Waste and Backfill Combination," Proceedings of the 33rd U.S. Rock Mechanics Symposium, A.A. Balkema, Pub.

Table 1. Parameter Values Initially Determined for Use in Gas Migration Calculations Using BRAGFLO.

Material	Time Period 1 0-200 yrs	Time Period 2 200-10,000 yrs
Shaft Seal		
Permeability (m^2)	$5.0x10^{-16} > 1.0x10^{-18} > 1.0x10^{-19}$	$1.0x10^{-18}$ - $1.0x10^{-21}$
Porosity	12% > 9% > 7%	9% - 1%
Brine saturation	5% - 8% (wt.)	---
Capillary pressure	Correlation	Correlation
Length (m)	30 - 90	Remainder of Shaft
Shaft Fill		
Permeability (m^2)	$1.0x10^{-15}$ - $1.0x10^{-19}$	Same
Porosity	16% - 7%	as
Brine saturation	5% - 8% (wt.)	Shaft
Capillary pressure	Correlation	Seal
Backfill/Experimental/Lower Shaft		
Permeability (m^2)	$1.0x10^{-15}$ - $1.0x10^{-17}$	$1.0x10^{-15}$ - $1.0x10^{-17}$
Porosity	2% < 10% < 12%	1% - 7.5%
Brine saturation	5% - 8% (wt.)	---
Capillary pressure	Correlation	Correlation
Culebra Seal		
Permeability (m^2)	$1.0x10^{-18}$	Same
Porosity	Values for concrete	as
Brine saturation	100%	Shaft
Capillary pressure	Correlation	Fill
Panel Seals		
Permeability (m^2)	$1.0x10^{-18}$ - $1.0x10^{-21}$	Same
Porosity	5% - 9%	as
Brine saturation	5% - 8%	Time
Capillary pressure	---	Period 1

Note: All values based on water-bearing zone seals being effective at minimizing inflow and no significant contribution to saturation from halite.

Table 2. Modified Parameter Values to be Used in Gas Migration Calculations Using BRAGFLO.

Material/Property	Time Period 1 0-200 yrs	Time Period 2 200-10,000 yrs
Shaft Seal		
Permeability (m^2)	$1.0x10^{-19}$ - $5.0x10^{-16}$	$1.0x10^{-21}$ - $1.0x10^{-18}$
Porosity	Same as period 2	0.01 - 0.09
Brine saturation	1.00	---
Length (m)	30 - 100	Rest of Upper Shaft
Shaft Fill		
Permeability (m^2)	$1.0x10^{-19}$ - $1.0x10^{-15}$	Same as
Porosity	same as Shaft Seal	Shaft Seal
Brine saturation	1.00	---
Backfill/Experimental/Lower Shaft		
Permeability (m^2)	$1.0x10^{-15}$	Same as
Porosity	0.01 - 0.075	Period 1
Brine saturation	1.00	---
Culebra Seal		
Permeability (m^2)	$1.0x10^{-18}$	Same as
Porosity	0.20[a]	Shaft Seal
Brine saturation	100	---
Length (m)	7.7	7.7
Panel Seals		
Permeability (m^2)	$1.0x10^{-21}$ - $1.0x10^{-18}$	Same as
Porosity	0.05 - 0.09	Period 1
Brine saturation	1.00	---

Note: 1) "Brine saturation" is Initial Brine Saturation.
2) Porosity of Shaft Seal (Period 2) correlated linearly to log of Shaft Seal permeability (Period 2).
3) Porosity of Panel Seal correlated linearly to log of Panel Seal permeability.
a) Value for concrete from Neville, A.M., 'Properties of Concrete', John Wiley & Sons, NY, 1973

APPENDIX B: BRAGFLO REFERENCE TABLES

APPENDIX B: BRAGFLO REFERENCE TABLES

Table B-1. Variable Parameters for Volume 5 BRAGFLO Calculations

Halite

(1) Permeability	$= 10^{k}$	[m^2]
k	= Sampled variable (LHS variable #10) LHS distribution type: Cumulative Range: -24.0 to -19.0	
(2) Porosity	= Sampled anhydrite porosity (LHS variable #16) LHS distribution type: Cumulative Range: 1.0×10^{-3} to 3.0×10^{-2}	[dimensionless]
(3) Compressibility	$= \left(\frac{S_s}{\rho_f g \phi} - \beta_f \right)$	[Pa^{-1}]
S_s	= Specific storage $= 1.4 \times 10^{-6}$	[m^{-1}]
ρ_f	= Salado brine fluid density $= 1.23 \times 10^{3}$	[kg/m^3]
g	= Acceleration due to gravity = 9.79	[m/s^2]
ϕ	= Porosity	[dimensionless]
β_f	= Salado brine fluid compressibility $= 2.5 \times 10^{-10}$	[Pa^{-1}]
(4) BCEXP	= Sampled Brooks-Corey exponent (LHS variable #11) LHS distribution type: Cumulative Range: 2.0×10^{-2} to 1.0	[dimensionless]
(5) BCBRSAT	= Sampled residual brine saturation (LHS variable #13) LHS distribution type: Uniform Range: 0.0 to 0.4	[dimensionless]
(6) BCGSSAT	= Sampled residual gas saturation (LHS variable #14) LHS distribution type: Uniform Range: 0.0 to 0.4	[dimensionless]
(7) BCFLG	= Sampled Brooks-Corey weighting factor (LHS variable #12) LHS distribution type: Delta Range: 0.0 to 1.0	[dimensionless]
(8) BC_PCT	= Brooks-Corey Threshold Capillary Pressure $= 0.56 \cdot (\text{Permeability})^{-0.346}$	[Pa]

Table B-1. Variable Parameters for Volume 5 BRAGFLO Calculations (Continued)

Initial Disturbed Rock Zone (DRZ)
(Initial DRZ used during time period of -50 years to 0 years)

(1) Permeability = 1.0×10^{-17}

(2) Porosity = Sampled anhydrite porosity [dimensionless]
(LHS variable #16)
LHS distribution type: Cumulative
Range: 1.0×10^{-3} to 3.0×10^{-2}

(3) Compressibility $= \left(\frac{S_s}{\rho_f g \phi} - \beta_f \right)$ [Pa^{-1}]

S_s = Specific storage [m^{-1}]
= 1.4×10^{-6}

ρ_f = Salado brine fluid density [kg/m^3]
= 1.23×10^3

g = Acceleration due to gravity [m/s^2]
= 9.79

ϕ = Porosity [dimensionless]

β_f = Salado brine fluid compressibility [Pa^{-1}]
= 2.5×10^{-10}

(4) BCEXP = Sampled halite Brooks-Corey exponent [dimensionless]
(LHS variable #11)
LHS distribution type: Cumulative
Range: 2.0×10^{-2} to 1.0

(5) BCBRSAT = Sampled halite residual brine saturation [dimensionless]
(LHS variable #13)
LHS distribution type: Uniform
Range: 0.0 to 0.4

(6) BCGSSAT = Sampled halite residual gas saturation [dimensionless]
(LHS variable #14)
LHS distribution type: Uniform
Range: 0.0 to 0.4

(7) BCFLG = Brooks-Corey weighting factor [dimensionless]
= 1.0

(8) BC_PCT = Brooks-Corey Threshold Capillary Pressure [Pa]
= $0.56 \cdot (\text{Permeability})^{-0.346}$

Table B-1. Variable Parameters for Volume 5 BRAGFLO Calculations (Continued)

Transition Zone

(1) Permeability	$= 10^k$	[m^2]
k	= Sampled variable (LHS variable #15) LHS distribution type: Cumulative Range: -21.0 to -16.0	
(2) Porosity	= Sampled anhydrite porosity (LHS variable #16) LHS distribution type: Cumulative Range: 1.0×10^{-3} to 3.0×10^{-2}	[dimensionless]
(3) Compressibility	$= \left(\frac{S_s}{\rho_f g \phi} - \beta_f \right)$	[Pa^{-1}]
S_s	= Specific storage $= 1.4 \times 10^{-6}$	[m^{-1}]
ρ_f	= Salado brine fluid density $= 1.23 \times 10^3$	[kg/m^3]
g	= Acceleration due to gravity = 9.79	[m/s^2]
ϕ	= Porosity	[dimensionless]
β_f	= Salado brine fluid compressibility $= 2.5 \times 10^{-10}$	[Pa^{-1}]
(4) BCEXP	= Sampled halite Brooks-Corey exponent (LHS variable #11) LHS distribution type: Cumulative Range: 2.0×10^{-2} to 1.0	[dimensionless]
(5) BCBRSAT	= Sampled halite residual brine saturation (LHS variable #13) LHS distribution type: Uniform Range: 0.0 to 0.4	[dimensionless]
(6) BCGSSAT	= Sampled halite residual gas saturation (LHS variable #14) LHS distribution type: Uniform Range: 0.0 to 0.4	[dimensionless]
(7) BCFLG	= Brooks-Corey weighting factor = 1.0	[dimensionless]
(8) BC_PCT	= Brooks-Corey Threshold Capillary Pressure $= 0.56 \cdot (\text{Permeability})^{-0.346}$	[Pa]

Table B-1. Variable Parameters for Volume 5 BRAGFLO Calculations (Continued)

Anhydrite

(1) Permeability	$= 10^k$	[m^2]
k	= Sampled variable (LHS variable #15) LHS distribution type: Cumulative Range: -21.0 to -16.0	
(2) Porosity	= Sampled variable (LHS variable #16) LHS distribution type: Cumulative Range: 1.0×10^{-3} to 3.0×10^{-2}	[dimensionless]
(3) Compressibility	$= \left(\frac{S_s}{\rho_f g \phi} - \beta_f \right)$	[Pa^{-1}]
S_s	= Specific storage $= 1.0 \times 10^{-6}$	[m^{-1}]
ρ_f	= Salado brine fluid density $= 1.23 \times 10^3$	[kg/m^3]
g	= Acceleration due to gravity = 9.79	[m/s^2]
ϕ	= Porosity	[dimensionless]
β_f	= Salado brine fluid compressibility $= 2.5 \times 10^{-10}$	
(4) BCEXP	= Sampled halite Brooks-Corey exponent (LHS variable #11) LHS distribution type: Cumulative Range: 2.0×10^{-2} to 1.0	[dimensionless]
(5) BCBRSAT	= Sampled halite residual brine saturation (LHS variable #13) LHS distribution type: Uniform Range: 0.0 to 0.4	[dimensionless]
(6) BCGSSAT	= Sampled halite residual gas saturation (LHS variable #14) LHS distribution type: Uniform Range: 0.0 to 0.4	[dimensionless]
(7) BCFLG	= Sampled SALADO Brooks-Corey weighting factor (LHS variable #12) LHS distribution type: Delta Range: 0.0 to 1.0	[dimensionless]

Table B-1. Variable Parameters for Volume 5 BRAGFLO Calculations (Continued)

Anhydrite (Concluded)

(8) BC_PCT = Brooks-Corey Threshold Capillary Pressure [Pa]

$= 0.56 \cdot (\text{Permeability})^{-0.346}$

Table B-1. Variable Parameters for Volume 5 BRAGFLO Calculations (Continued)

Cavity 1
(Cavity 1 used to describe waste-emplacement region during time period of -50 years to 0 years)

(1) Permeability	= 1.0×10^{-10}	[m^2]
(2) Porosity	= 1.0	[dimensionless]
(3) Compressibility	= 0.0	[Pa^{-1}]
(4) BCEXP	= Sampled halite Brooks-Corey exponent (LHS variable #11) LHS distribution type: Cumulative Range: 2.0×10^{-2} to 1.0	[dimensionless]
(5) BCBRSAT	= Residual brine saturation = 0.0	[dimensionless]
(6) BCGSSAT	= Residual gas saturation = 0.0	[dimensionless]
(7) BCFLG	= Brooks-Corey weighting factor = 1.0	[dimensionless]
(8) BC_PCT	= Brooks-Corey Threshold Capillary Pressure = 0.0	[Pa]

Table B-1. Variable Parameters for Volume 5 BRAGFLO Calculations (Continued)

Culebra 1
(Culebra 1 used during time period of -50 years to 0 years)

(1) Permeability	= 0.0	[m^2]
(2) Porosity	= Sampled Culebra porosity (LHS variable #43) LHS distribution type: Data Range: 5.80565×10^{-2} to 2.5250×10^{-1}	[dimensionless]
(3) Compressibility	= 0.0	[Pa^{-1}]
(4) BCEXP	= Brooks-Corey exponent = 0.7	[dimensionless]
(5) BCBRSAT	= Residual brine saturation = 0.2	[dimensionless]
(6) BCGSSAT	= Residual gas saturation = 0.2	[dimensionless]
(7) BCFLG	= Brooks-Corey weighting factor = 1.0	[dimensionless]
(8) BC_PCT	= Brooks-Corey Threshold Capillary Pressure = 0.0	[Pa]

Table B-1. Variable Parameters for Volume 5 BRAGFLO Calculations (Continued)

Cavity 2
(Cavity 2 used to describe excavated volume other than waste-emplacement region during time period of -50 years to 0 years)

(1) Permeability	= 1.0×10^{-10}	[m^2]
(2) Porosity	= 1.0	[dimensionless]
(3) Compressibility	= 0.0	[Pa^{-1}]
(4) BCEXP	= Sampled halite Brooks-Corey exponent (LHS variable #11) LHS distribution type: Cumulative Range: 2.0×10^{-2} to 1.0	[dimensionless]
(5) BCBRSAT	= Residual brine saturation = 0.0	[dimensionless]
(6) BCGSSAT	= Residual gas saturation = 0.0	[dimensionless]
(7) BCFLG	= Brooks-Corey weighting factor = 1.0	[dimensionless]
(8) BC_PCT	= Brooks-Corey Threshold Capillary Pressure = 0.0	[Pa]

Table B-1. Variable Parameters for Volume 5 BRAGFLO Calculations (Continued)

Waste
(Waste replaces Cavity 1 at time=0 years)

(1) Permeability	= 1.0×10^{-13}	[m^2]
(2) Porosity	= 6.601785×10^{-1}	[dimensionless]
(3) Compressibility	= 1.6×10^{-9}	[Pa^{-1}]
(4) BCEXP	= Brooks-Corey exponent = 2.89	[dimensionless]
(5) BCBRSAT	= Residual brine saturation = 2.76×10^{-1}	[dimensionless]
(6) BCGSSAT	= Residual gas saturation = 0.7	[dimensionless]
(7) BCFLG	= Brooks-Corey weighting factor = 1.0	[dimensionless]
(8) BC_PCT	= Brooks-Corey Threshold Capillary Pressure = 0.0	[Pa]
(9) Initial Iron (Fe) Concentration:		[kg/m^3]

$$= \frac{WTDRMET \cdot (WTFRFE/VDRUM) \cdot \omega \cdot VWASTE + WTFECONT}{VREPOS}$$

WTDRMET	= Mass of contents of one drum of metal+glass = 64.5	[kg]
WTFRFE	= Mass fraction of corrodable metal in metal+glass = 0.7210021	[dimensionless]
ω	= Volume fraction of metal (i.e. Fe) = Sampled variable (LHS variable #9) LHS distribution type: Normal Range: 2.76×10^{-1} to 4.76×10^{-1}	[dimensionless]
VDRUM	= Volume (internal capacity) of one drum = 0.21	[m^3]
VWASTE	= Design volume of waste in repository = 1.75564×10^5	[m^3]
WTFECONT	= Mass of Fe in containers = 2.6132656×10^7	[kg]
VREPOS	= Total excavated storage volume of repository = $4.36023214418 \times 10^5$	[m^3]

Table B-1. Variable Parameters for Volume 5 BRAGFLO Calculations (Continued)

Waste (Continued)
(Waste replaces Cavity 1 at time=0 years)

(10) Initial Cellulose Concentration: [kg/m^3]

$$= CONCBIOI$$

$$= \frac{WTDRCOMB \cdot WTFRBIO \cdot \omega \cdot (VWASTE/VDRUM) + WTBIOCONT}{VREPOS}$$

WTDRCOMB	= Mass of contents of one drum of combustibles = 40.0	[kg]
WTFRBIO	= Mass fraction of biodegradables in combustibles = 0.5546459	[dimensionless]
ω	= Volume fraction of combustibles = Sampled variable (LHS variable #8) LHS distribution type: Normal Range: 2.84 x 10^{-1} to 4.84 x 10^{-1}	[dimensionless]
VWASTE	= Design volume of waste in repository = 1.75564 x 10^5	[m^3]
VDRUM	= Volume (internal capacity) of one drum = 0.21	[m^3]
WTBIOCONT	= Mass of biodegradables in containers = 0.0	[kg]
VREPOS	= Total excavated storage volume of repository = 4.36023214418 x 10^5	[m^3]

(11) Gas Production Rate, Corrosion, Inundated [mol Fe/(m^3·s)]

$$= \lambda \cdot \frac{(ASDRUM \cdot DRPANEL)}{((4.0 - \omega)/3.0) \cdot VPANELX}$$

λ	= Sampled variable (LHS variable #2) LHS distribution type: Cumulative Range: 0.0 to 1.3 x 10^{-8}	[mol Fe/(m^2·s)]
ASDRUM	= Surface area of corrodable metal per drum = 6.0	[m^2]
DRPANEL	= Number of Drums in one Panel = 8.606362 x 10^4	[dimensionless]
VPANELX	= Excavated volume of one panel = 46097.6458546	[m^3]
$\frac{4.0-\omega}{3.0}$	= Anoxic Iron Corrosion Stoichiometry	[dimensionless]
ω	= Sampled variable (LHS variable #4) LHS distribution type: Uniform Range: 0.0 to 1.0	[dimensionless]

Table B-1. Variable Parameters for Volume 5 BRAGFLO Calculations (Continued)

Waste (Continued)
(Waste replaces Cavity 1 at time=0 years)

(12) Gas Production Rate, Microbial, Inundated: [mol cellulose/(m^3·s)]

$$= \lambda \cdot CONCBIOI / STOIMIC$$

λ = Sampled variable [mol cellulose/(kg·s)]
(LHS variable #5)
LHS distribution type: Cumulative
Range: 0.0 to 1.6×10^{-8}

CONCBIOI = Initial Cellulose Concentration [kg/m^3]
(same as equation (10))

$$= \frac{WTDRCOMB \cdot WTFRBIO \cdot \omega \cdot (VWASTE/VDRUM) + WTBIOCONT}{VREPOS}$$

WTDRCOMB = Mass of contents of one drum of combustibles [kg]
= 40.0

WTFRBIO = Mass fraction of biodegradables in combustibles [dimensionless]
= 0.5546459

ω = Volume fraction of combustibles [dimensionless]
= Sampled variable (LHS variable #8)
LHS distribution type: Normal
Range: 2.84×10^{-1} to 4.84×10^{-1}

VWASTE = Design volume of waste in repository [m^3]
= 1.75564×10^5

VDRUM = Volume (internal capacity) of one drum [m^3]
= 0.21

WTBIOCONT = Mass of biodegradables in containers [kg]
= 0.0

VREPOS = Total excavated storage volume of repository [m^3]
= $4.36023214418 \times 10^5$

STOIMIC = Microbial Stoichiometry [dimensionless]
= Sampled variable
(LHS variable #7)
LHS distribution type: Uniform
Range: 0.0 to 1.67

(13) Humidity Factor, Corrosion = Sampled variable [dimensionless]
(LHS variable #3)
LHS distribution type: Cumulative
Range: 0.0 to 0.5

(14) Humidity Factor, Microbial = Sampled variable [dimensionless]
(LHS variable #6)
LHS distribution type: Uniform
Range: 0.0 to 0.2

Table B-1. Variable Parameters for Volume 5 BRAGFLO Calculations (Continued)

Waste (Concluded)
(Waste replaces Cavity 1 at time=0 years)

(15) Anoxic Iron Corrosion Stoichiometry = $\frac{4.0 - \omega}{3.0}$ [dimensionless]

ω = Sampled variable (LHS variable #4)
LHS distribution type: Uniform
Range: 0.0 to 1.0

(16) Microbial Stoichiometry = Sampled variable [dimensionless]
(LHS variable #7)
LHS distribution type: Uniform
Range: 0.0 to 1.67

Table B-1. Variable Parameters for Volume 5 BRAGFLO Calculations (Continued)

Final Disturbed Rock Zone (DRZ)
(Final DRZ replaces Initial DRZ at time=0 years)

(1) Permeability	$= 10^k$	[m^2]
k	= Sampled variable (LHS variable #10) LHS distribution type: Cumulative Range: -24.0 to -19.0	
(2) Porosity	$= \phi_A + \omega(0.06 - \phi_A)$	[dimensionless]
ϕ_A	= Sampled anhydrite (LHS variable #16)	[dimensionless]
ω	= Sampled variable (LHS variable #17) LHS distribution type: Uniform Range: 0.0 to 1.0	[dimensionless]
(3) Compressibility	$= \left(\frac{S_s}{\rho_f g \phi} - \beta_f \right)$	[Pa^{-1}]
S_S	= Specific storage = 1.4 x 10^{-6}	[m^{-1}]
ρ_f	= Salado brine fluid density = 1.23 x 10^3	[kg/m^3]
g	= Acceleration due to gravity = 9.79	[m/s^2]
ϕ	= Porosity	[dimensionless]
β_f	= Salado brine fluid compressibility = 2.5 x 10^{-10}	[Pa^{-1}]
(4) BCEXP	= Sampled halite Brooks-Corey exponent (LHS variable #11) LHS distribution type: Cumulative Range: 2.0 x 10^{-2} to 1.0	[dimensionless]
(5) BCBRSAT	= Sampled halite residual brine saturation (LHS variable #13) LHS distribution type: Uniform Range: 0.0 to 0.4	[dimensionless]
(6) BCGSSAT	= Sampled halite residual gas saturation (LHS variable #14) LHS distribution type: Uniform Range: 0.0 to 0.4	[dimensionless]
(7) BCFLG	= Brooks-Corey weighting factor = 1.0	[dimensionless]

Table B-1. Variable Parameters for Volume 5 BRAGFLO Calculations (Continued)

Final Disturbed Rock Zone (DRZ) (Concluded)
(Final DRZ replaces Initial DRZ at time=0 years)

(8) BC_PCT = Brooks-Corey Threshold Capillary Pressure [Pa]

$$= 0.56 \cdot (\text{Permeability})^{-0.346}$$

Table B-1. Variable Parameters for Volume 5 BRAGFLO Calculations (Continued)

Culebra
(Culebra replaces Culebra 1 at time=0 years)

(1) Permeability	$= \frac{\kappa\mu}{\rho_f g}$	[m^2]
κ	= Hydraulic Conductivity = 2.24×10^{-7}	[m/s]
μ	= Culebra brine viscosity = 1.0×10^{-3}	[kg/(m•s)]
ρ_f	= Culebra brine fluid density = 1.09×10^{3}	[kg/m^3]
g	= Acceleration due to gravity = 9.79	[m/s^2]
(2) Porosity	= Sampled variable (LHS variable #43) LHS distrribution type: Data Range: 5.80565×10^{-2} to 2.52500×10^{-1}	[dimensionless]
(3) Compressibility	$= \frac{S}{t\rho_f \phi g} - \beta_f$	[Pa^{-1}]
S	= Storage coefficient (= Specific storage x thickness) = 2.0×10^{-5}	[dimensionless]
t	= Culebra layer thickness = 7.7	[m]
ρ_f	= Culebra brine fluid density = 1.09×10^{3}	[kg/m^3]
ϕ	= Porosity	[dimensionless]
g	= Acceleration due to gravity = 9.79	[m/s^2]
β_f	= Culebra brine fluid compressibility = 2.5×10^{-10}	[Pa^{-1}]
(4) BCEXP	= Brooks-Corey exponent = 0.7	[dimensionless]
(5) BCBRSAT	= Residual brine saturation = 0.2	[dimensionless]
(6) BCGSSAT	= Residual gas saturation = 0.2	[dimensionless]
(7) BCFLG	= Brooks-Corey weighting factor = 1.0	[dimensionless]

Table B-1. Variable Parameters for Volume 5 BRAGFLO Calculations (Continued)

Culebra (Concluded)
(Culebra replaces Culebra 1 at time=0 years)

(8) BC_PCT = Brooks-Corey Threshold Capillary Pressure [Pa]

$$= 0.56 \cdot (\text{Permeability})^{-0.346}$$

Table B-1. Variable Parameters for Volume 5 BRAGFLO Calculations (Continued)

Shaft Seal
(Shaft Seal, Upper Shaft, Lower Shaft, Backfill, Culebra Seal, and Experimental Region replaces Cavity 2 at time=0 years)

(1) Permeability = Sampled variable [m^2]
(LHS variable #22)
LHS distribution type: Lognormal
Range: 1.0×10^{-19} to 5.0×10^{-16}

(2) Porosity $= \left(\frac{LOG_{10}\omega - LOG_{10}(1.0x10^{-21})}{LOG_{10}(1.0x10^{-18}) - LOG_{10}(1.0x10^{-21})} \right)(0.09 - 0.01) + 0.01$ [dimensionless]

ω = Sampled variable [m^2]
(LHS variable #23)
LHS distribution type: Lognormal
Range: 1.0×10^{-21} to 1.0×10^{-18}

(3) Compressibility $= \left(\frac{S_s}{\rho_f g \phi} - \beta_f \right)$ [Pa^{-1}]

S_s = Specific storage [m^{-1}]
$= 1.4 \times 10^{-6}$

ρ_f = Salado brine fluid density [kg/m^3]
$= 1.23 \times 10^3$

ϕ = Porosity [dimensionless]

g = Acceleration due to gravity [m/s^2]
$= 9.79$

β_f = Salado brine fluid compressibility [Pa^{-1}]
$= 2.5 \times 10^{-10}$

(4) BCEXP = Brooks-Corey exponent [dimensionless]
$= 0.7$

(5) BCBRSAT = Residual brine saturation [dimensionless]
$= 0.2$

(6) BCGSSAT = Residual gas saturation [dimensionless]
$= 0.0$

(7) BCFLG = Brooks-Corey weighting factor [dimensionless]
$= 1.0$

(8) BC_PCT = Brooks-Corey Threshold Capillary Pressure [Pa]
$= 0.56 \cdot (\text{Permeability})^{-0.346}$

Table B-1. Variable Parameters for Volume 5 BRAGFLO Calculations (Continued)

Upper Shaft
(Shaft Seal, Upper Shaft, Lower Shaft, Backfill, Culebra Seal, and Experimental Region replaces Cavity 2 at time=0 years)

(1) Permeability = Sampled variable [m^2]
(LHS variable #24)
LHS distribution type: Lognormal
Range: 1.0×10^{-19} to 5.0×10^{-15}

(2) Porosity $= \left(\frac{LOG_{10}\omega - LOG_{10}(1.0x10^{-21})}{LOG_{10}(1.0x10^{-18}) - LOG_{10}(1.0x10^{-21})} \right)(0.09 - 0.01) + 0.01$ [dimensionless]

ω = Sampled variable [m^2]
(LHS variable #23)
LHS distribution type: Lognormal
Range: 1.0×10^{-21} to 1.0×10^{-18}

(3) Compressibility $= \left(\frac{S_s}{\rho_f g \phi} - \beta_f \right)$ [Pa^{-1}]

S_s = Specific storage [m^{-1}]
$= 1.4 \times 10^{-6}$

ρ_f = Salado brine fluid density [kg/m^3]
$= 1.23 \times 10^3$

ϕ = Porosity [dimensionless]

g = Acceleration due to gravity [m/s^2]
$= 9.79$

β_f = Salado brine fluid compressibility [Pa^{-1}]
$= 2.5 \times 10^{-10}$

(4) BCEXP = Brooks-Corey exponent [dimensionless]
$= 0.7$

(5) BCBRSAT = Residual brine saturation [dimensionless]
$= 0.2$

(6) BCGSSAT = Residual gas saturation [dimensionless]
$= 0.0$

(7) BCFLG = Brooks-Corey weighting factor [dimensionless]
$= 1.0$

(8) BC_PCT = Brooks-Corey Threshold Capillary Pressure [Pa]
$= 0.56 \cdot (\text{Permeability})^{-0.346}$

Table B-1. Variable Parameters for Volume 5 BRAGFLO Calculations (Continued)

Lower Shaft
(Shaft Seal, Upper Shaft, Lower Shaft, Backfill, Culebra Seal, and Experimental Region replaces Cavity 2 at time=0 years)

(1) Permeability	= 1.0×10^{-15}	[m^2]
(2) Porosity	= Sampled variable (LHS variable #26) LHS distribution type: Uniform Range: 1.0×10^{-2} to 7.5×10^{-2}	[dimensionless]
(3) Compressibility	$= \left(\frac{S_s}{\rho_f g \phi} - \beta_f \right)$	[Pa^{-1}]
S_s	= Specific storage = 1.4×10^{-6}	[m^{-1}]
ρ_f	= Salado brine fluid density = 1.23×10^{3}	[kg/m^3]
ϕ	= Porosity	[dimensionless]
g	= Acceleration due to gravity = 9.79	[m/s^2]
β_f	= Salado brine fluid compressibility = 2.5×10^{-10}	[Pa^{-1}]
(4) BCEXP	= Brooks-Corey exponent = 0.7	[dimensionless]
(5) BCBRSAT	= Residual brine saturation = 0.2	[dimensionless]
(6) BCGSSAT	= Residual gas saturation = 0.0	[dimensionless]
(7) BCFLG	= Brooks-Corey weighting factor = 1.0	[dimensionless]
(8) BC_PCT	= Brooks-Corey Threshold Capillary Pressure $= 0.56 \cdot (\text{Permeability})^{-0.346}$	[Pa]

Table B-1. Variable Parameters for Volume 5 BRAGFLO Calculations (Continued)

Backfill
(Shaft Seal, Upper Shaft, Lower Shaft, Backfill, Culebra Seal, and Experimental Region replaces Cavity 2 at time=0 years)

(1) Permeability	= 1.0×10^{-15}	[m^2]
(2) Porosity	= Sampled LOWER SHAFT porosity (LHS variable #26) LHS distribution type: Uniform Range: 1.0×10^{-2} to 7.5×10^{-2}	[dimensionless]
(3) Compressibility	$= \left(\frac{S_s}{\rho_f g \phi} - \beta_f \right)$	[Pa^{-1}]
S_s	= Specific storage = 1.4×10^{-6}	[m^{-1}]
ρ_f	= Salado brine fluid density = 1.23×10^3	[kg/m^3]
ϕ	= Porosity	[dimensionless]
g	= Acceleration due to gravity = 9.79	[m/s^2]
β_f	= Salado brine fluid compressibility = 2.5×10^{-10}	[Pa^{-1}]
(4) BCEXP	= Brooks-Corey exponent = 0.7	[dimensionless]
(5) BCBRSAT	= Residual brine saturation = 0.2	[dimensionless]
(6) BCGSSAT	= Residual gas saturation = 0.0	[dimensionless]
(7) BCFLG	= Brooks-Corey weighting factor = 1.0	[dimensionless]
(8) BC_PCT	= Brooks-Corey Threshold Capillary Pressure $= 0.56 \cdot (\text{Permeability})^{-0.346}$	[Pa]

Table B-1. Variable Parameters for Volume 5 BRAGFLO Calculations (Continued)

Experimental Region
(Shaft Seal, Upper Shaft, Lower Shaft, Backfill, Culebra Seal, and Experimental Region replaces Cavity 2 at time=0 years)

(1) Permeability	= 1.0×10^{-15}	[m^2]
(2) Porosity	= Sampled Lower Shaft porosity (LHS variable #26) LHS distribution type: Uniform Range: 1.0×10^{-2} to 7.5×10^{-2}	[dimensionless]
(3) Compressibility	$= \left(\frac{S_s}{\rho_f g \phi} - \beta_f \right)$	[Pa^{-1}]
S_s	= Specific storage = 1.4×10^{-6}	[m^{-1}]
ρ_f	= Salado brine fluid density = 1.23×10^{3}	[kg/m^3]
ϕ	= Porosity	[dimensionless]
g	= Acceleration due to gravity = 9.79	[m/s^2]
β_f	= Salado brine fluid compressibility = 2.5×10^{-10}	[Pa^{-1}]
(4) BCEXP	= Brooks-Corey exponent = 0.7	[dimensionless]
(5) BCBRSAT	= Residual brine saturation = 0.2	[dimensionless]
(6) BCGSSAT	= Residual gas saturation = 0.0	[dimensionless]
(7) BCFLG	= Brooks-Corey weighting factor = 1.0	[dimensionless]
(8) BC_PCT	= Brooks-Corey Threshold Capillary Pressure $= 0.56 \cdot (\text{Permeability})^{-0.346}$	[Pa]

Table B-1. Variable Parameters for Volume 5 BRAGFLO Calculations (Continued)

Shaft Seal 2
(Shaft Seal 2 replaces Culebra Seal, Upper Shaft, and Shaft Seal at time=200 years)

(1) Permeability = Sampled Shaft Seal permeability [m^2]
(LHS variable #22)
LHS distribution type: Lognormal
Range: 1.0×10^{-19} to 5.0×10^{-16}

(2) Porosity = $\left(\frac{LOG_{10}\omega - LOG_{10}(1.0x10^{-21})}{LOG_{10}(1.0x10^{-18}) - LOG_{10}(1.0x10^{-21})}\right)(0.09-0.01)+0.01$ [dimensionless]

ω = Sampled variable [dimensionless]
(LHS variable #23)
LHS distribution type: Lognormal
Range: 1.0×10^{-21} to 1.0×10^{-18}

(3) Compressibility = $\left(\frac{S_s}{\rho_f g \phi} - \beta_f\right)$ [Pa^{-1}]

S_s = Specific storage [m^{-1}]
$= 1.4 \times 10^{-6}$

ρ_f = Salado brine fluid density [kg/m^3]
$= 1.23 \times 10^{3}$

ϕ = Porosity [dimensionless]

g = Acceleration due to gravity [m/s^2]
$= 9.79$

β_f = Salado brine fluid compressibility [Pa^{-1}]
$= 2.5 \times 10^{-10}$

(4) BCEXP = Brooks-Corey exponent [dimensionless]
$= 0.7$

(5) BCBRSAT = Residual brine saturation [dimensionless]
$= 0.2$

(6) BCGSSAT = Residual gas saturation [dimensionless]
$= 0.0$

(7) BCFLG = Brooks-Corey weighting factor [dimensionless]
$= 1.0$

(8) BC_PCT = Brooks-Corey Threshold Capillary Pressure [Pa]
$= 0.56 \cdot (\text{Permeability})^{-0.346}$

Table B-1. Variable Parameters for Volume 5 BRAGFLO Calculations (Continued)

Panel Seal

(1) Permeability	= Sampled variable (LHS variable #25) LHS distribution type: Lognormal Range: 1.0×10^{-21} to 1.0×10^{-18}	[m^2]
(2) Porosity	$= \left(\frac{LOG_{10}(\text{Permeability}) - LOG_{10}(1.0x10^{-21})}{LOG_{10}(1.0x10^{-18}) - LOG_{10}(1.0x10^{-21})} \right)(0.09 - 0.05) + 0.05$	[dimensionless]
(3) Compressibility	$= \left(\frac{S_s}{\rho_f g \phi} - \beta_f \right)$	[Pa^{-1}]
S_s	= Specific storage = 1.4×10^{-6}	[m^{-1}]
ρ_f	= Salado brine fluid density = 1.23×10^{3}	[kg/m^3]
ϕ	= Porosity	[dimensionless]
g	= Acceleration due to gravity = 9.79	[m/s^2]
β_f	= Salado brine fluid compressibility = 2.5×10^{-10}	[Pa^{-1}]
(4) BCEXP	= Brooks-Corey exponent = 0.7	[dimensionless]
(5) BCBRSAT	= Residual brine saturation = 0.2	[dimensionless]
(6) BCGSSAT	= Residual gas saturation = 0.0	[dimensionless]
(7) BCFLG	= Brooks-Corey weighting factor = 1.0	[dimensionless]
(8) BC_PCT	= Brooks-Corey Threshold Capillary Pressure $= 0.56 \cdot (\text{Permeability})^{-0.346}$	[Pa]

Table B-1. Variable Parameters for Volume 5 BRAGFLO Calculations (Concluded)

Culebra Seal

(1) Permeability	= 1.0×10^{-18}	[m^2]
(2) Porosity	= 0.2	[dimensionless]
(3) Compressibility	$= \left(\frac{S_s}{\rho_f g \phi} - \beta_f \right)$	[Pa^{-1}]
S_s	= Specific storage = 1.4×10^{-6}	[m^{-1}]
ρ_f	= Salado brine fluid density = 1.23×10^{3}	[kg/m^3]
ϕ	= Porosity	[dimensionless]
g	= Acceleration due to gravity = 9.79	[m/s^2]
β_f	= Salado brine fluid compressibility = 2.5×10^{-10}	[Pa^{-1}]
(4) BCEXP	= Brooks-Corey exponent = 0.7	[dimensionless]
(5) BCBRSAT	= Residual brine saturation = 0.2	[dimensionless]
(6) BCGSSAT	= Residual gas saturation = 0.0	[dimensionless]
(7) BCFLG	= Brooks-Corey weighting factor = 1.0	[dimensionless]
(8) BC_PCT	= Brooks-Corey Threshold Capillary Pressure = $0.56 \cdot (\text{Permeability})^{-0.346}$	[Pa]

Table B-2. 1992 BRAGFLO Computed Variable Values for ANHYDRITE

Run No.	Porosity	Permeability	Compressibility	BCEXP	BCBRSAT	BCGSSAT	BCFLG	BC PCT
1	2.8660×10^{-2}	1.4125×10^{-18}	2.6476×10^{-9}	9.6790	8.7890×10^{-2}	2.3300×10^{-1}	0.0000	8.4002×10^{5}
2	6.9900×10^{-3}	1.6982×10^{-20}	1.1631×10^{-8}	4.9660×10^{-1}	1.4570×10^{-1}	1.2590×10^{-1}	1.0000	3.8780×10^{6}
3	2.8970×10^{-2}	9.1201×10^{-19}	2.6166×10^{-9}	6.7900×10^{-1}	1.8490×10^{-1}	2.1660×10^{-1}	1.0000	9.7730×10^{5}
4	5.6130×10^{-3}	5.0119×10^{-20}	1.4545×10^{-8}	5.1820	1.7260×10^{-1}	1.8900×10^{-1}	1.0000	2.6668×10^{6}
5	2.0560×10^{-2}	1.1482×10^{-20}	3.7891×10^{-9}	4.0710×10^{-1}	1.9880×10^{-1}	1.4590×10^{-1}	1.0000	4.4405×10^{6}
6	1.3750×10^{-2}	1.5136×10^{-20}	5.7896×10^{-9}	6.1420	3.3170×10^{-1}	4.7930×10^{-2}	0.0000	4.0356×10^{6}
7	2.5930×10^{-2}	1.7783×10^{-20}	2.9526×10^{-9}	1.0990	3.5430×10^{-2}	1.6220×10^{-1}	0.0000	3.8167×10^{6}
8	3.1850×10^{-3}	1.8197×10^{-19}	2.5824×10^{-8}	6.4480	3.8660×10^{-1}	2.8520×10^{-2}	1.0000	1.7070×10^{6}
9	2.7270×10^{-2}	1.2303×10^{-20}	2.7953×10^{-9}	4.2610×10^{-1}	3.4080×10^{-1}	1.8690×10^{-1}	1.0000	4.3356×10^{6}
10	9.6770×10^{-3}	5.2481×10^{-18}	8.3317×10^{-9}	1.5170	7.9000×10^{-2}	3.4810×10^{-1}	1.0000	5.3342×10^{5}
11	2.5730×10^{-3}	1.3183×10^{-20}	3.2026×10^{-8}	5.1250×10^{-1}	2.7170×10^{-1}	2.0030×10^{-1}	0.0000	4.2332×10^{6}
12	9.8270×10^{-3}	2.2387×10^{-19}	8.2007×10^{-9}	7.4960	1.4100×10^{-1}	2.8620×10^{-1}	1.0000	1.5889×10^{6}
13	1.6610×10^{-2}	4.8978×10^{-20}	4.7497×10^{-9}	2.2490	3.6500×10^{-1}	2.9370×10^{-1}	1.0000	2.6881×10^{6}
14	1.9600×10^{-2}	1.0000×10^{-20}	3.9870×10^{-9}	3.0620×10^{-1}	8.3660×10^{-3}	1.7360×10^{-1}	1.0000	4.6579×10^{6}
15	1.1590×10^{-3}	2.0893×10^{-20}	7.1402×10^{-8}	4.4620×10^{-1}	2.3100×10^{-1}	3.8350×10^{-1}	0.0000	3.6097×10^{6}
16	5.8700×10^{-3}	5.1286×10^{-19}	1.3897×10^{-8}	5.3590×10^{-1}	3.7890×10^{-1}	2.1720×10^{-1}	1.0000	1.1927×10^{6}
17	2.3950×10^{-2}	5.7544×10^{-20}	3.2174×10^{-9}	5.9190	1.1130×10^{-1}	3.8060×10^{-1}	0.0000	2.5423×10^{6}
18	6.1370×10^{-3}	6.6069×10^{-20}	1.3282×10^{-8}	5.8730×10^{-1}	2.9470×10^{-1}	8.6120×10^{-3}	0.0000	2.4236×10^{6}
19	6.2550×10^{-3}	4.5709×10^{-20}	1.3026×10^{-8}	2.0050	1.1640×10^{-1}	1.6670×10^{-1}	1.0000	2.7531×10^{6}
20	1.7070×10^{-2}	4.4668×10^{-20}	4.6150×10^{-9}	6.7090×10^{-1}	1.2940×10^{-1}	3.2110×10^{-1}	1.0000	2.7752×10^{6}
21	2.3500×10^{-2}	1.1481×10^{-19}	3.2838×10^{-9}	2.2590×10^{-1}	1.9770×10^{-2}	2.2330×10^{-1}	0.0000	2.0018×10^{6}
22	2.6030×10^{-2}	7.4131×10^{-20}	2.9403×10^{-9}	1.4340	2.1830×10^{-1}	1.8710×10^{-2}	1.0000	2.3290×10^{6}
23	2.9920×10^{-2}	3.5481×10^{-20}	2.5256×10^{-9}	7.0990	2.3880×10^{-1}	4.5230×10^{-2}	1.0000	3.0053×10^{6}
24	1.4710×10^{-2}	6.1660×10^{-20}	5.3955×10^{-9}	4.3270×10^{-1}	6.1270×10^{-2}	2.6430×10^{-1}	1.0000	2.4823×10^{6}
25	2.4720×10^{-2}	3.2359×10^{-20}	3.1094×10^{-9}	2.7610	3.0510×10^{-1}	9.9900×10^{-2}	1.0000	3.1026×10^{6}
26	1.8820×10^{-2}	2.3988×10^{-20}	4.1626×10^{-9}	5.2660	2.4700×10^{-1}	6.8060×10^{-2}	1.0000	3.4412×10^{6}
27	2.2740×10^{-3}	2.1878×10^{-20}	3.6269×10^{-8}	8.3330	2.1280×10^{-1}	7.5730×10^{-2}	1.0000	3.5526×10^{6}
28	2.8830×10^{-3}	1.9499×10^{-20}	2.8555×10^{-8}	7.9460	3.4740×10^{-1}	1.5270×10^{-1}	0.0000	3.6970×10^{6}
29	1.2680×10^{-2}	3.0903×10^{-20}	6.2993×10^{-9}	6.0410×10^{-1}	3.3040×10^{-1}	3.5780×10^{-1}	1.0000	3.1525×10^{6}
30	8.7910×10^{-3}	7.4131×10^{-20}	9.1966×10^{-9}	2.0040×10^{-1}	1.4050×10^{-2}	1.5530×10^{-1}	0.0000	2.3290×10^{6}
31	1.7650×10^{-2}	3.2359×10^{-21}	4.4551×10^{-9}	3.3160×10^{-1}	2.1130×10^{-1}	2.4050×10^{-1}	1.0000	6.8822×10^{6}
32	2.0930×10^{-2}	1.0471×10^{-20}	3.7177×10^{-9}	8.8800	3.1430×10^{-1}	3.7550×10^{-1}	1.0000	4.5842×10^{6}
33	6.6640×10^{-3}	4.6774×10^{-19}	1.2212×10^{-8}	5.2200×10^{-1}	1.0530×10^{-1}	3.4190×10^{-1}	1.0000	1.2313×10^{6}
34	9.1030×10^{-3}	1.2303×10^{-20}	8.8728×10^{-9}	8.6520	2.5150×10^{-1}	3.6280×10^{-1}	0.0000	4.3356×10^{6}
35	2.4230×10^{-3}	2.8184×10^{-20}	3.4024×10^{-8}	3.9470×10^{-1}	2.9070×10^{-1}	1.3390×10^{-1}	1.0000	3.2545×10^{6}
36	2.7120×10^{-2}	1.9953×10^{-20}	2.8121×10^{-9}	2.7500×10^{-1}	3.7090×10^{-1}	3.6960×10^{-1}	1.0000	3.6677×10^{6}
37	5.0960×10^{-3}	2.5704×10^{-20}	1.6046×10^{-8}	6.9780	2.2650×10^{-1}	3.0790×10^{-2}	1.0000	3.3599×10^{6}
38	1.8940×10^{-3}	1.5136×10^{-19}	4.3596×10^{-8}	2.9640	1.7810×10^{-1}	3.9620×10^{-1}	1.0000	1.8193×10^{6}
39	1.0090×10^{-2}	5.6234×10^{-20}	7.9804×10^{-9}	2.6060×10^{-1}	1.6330×10^{-1}	3.7240×10^{-2}	1.0000	2.5626×10^{6}
40	2.2760×10^{-2}	2.0893×10^{-19}	3.3987×10^{-9}	2.4160×10^{-1}	2.4340×10^{-1}	1.1100×10^{-1}	1.0000	1.6273×10^{6}
41	1.8020×10^{-2}	3.9811×10^{-19}	4.3585×10^{-9}	5.7490×10^{-1}	1.3340×10^{-1}	1.0650×10^{-1}	1.0000	1.3019×10^{6}
42	2.1990×10^{-2}	2.3442×10^{-21}	3.5265×10^{-9}	5.4840×10^{-1}	3.9640×10^{-1}	3.3500×10^{-1}	0.0000	7.6943×10^{6}
43	5.1790×10^{-3}	2.6915×10^{-19}	1.5785×10^{-8}	4.0000	3.9070×10^{-1}	1.2040×10^{-1}	0.0000	1.4908×10^{6}
44	3.9010×10^{-3}	5.3703×10^{-20}	2.1038×10^{-8}	3.6050×10^{-1}	2.5980×10^{-1}	5.7350×10^{-2}	0.0000	2.6038×10^{6}
45	9.3870×10^{-3}	9.7724×10^{-20}	8.5968×10^{-9}	3.2390×10^{-1}	1.5830×10^{-1}	9.4190×10^{-2}	1.0000	2.1166×10^{6}
46	2.8280×10^{-2}	1.6596×10^{-20}	2.6865×10^{-9}	4.6060×10^{-1}	6.5170×10^{-2}	2.3880×10^{-1}	1.0000	3.9090×10^{6}
47	6.5700×10^{-3}	9.1201×10^{-20}	1.2390×10^{-8}	3.4760	3.1780×10^{-1}	2.6060×10^{-1}	1.0000	2.1678×10^{6}
48	2.2390×10^{-2}	1.4125×10^{-20}	3.4590×10^{-9}	7.7080	4.5510×10^{-2}	2.0750×10^{-1}	0.0000	4.1332×10^{6}
49	1.6820×10^{-3}	6.9183×10^{-19}	4.9123×10^{-8}	3.7530×10^{-1}	5.0110×10^{-2}	6.9900×10^{-2}	1.0000	1.0753×10^{6}
50	1.2890×10^{-2}	2.4547×10^{-20}	6.1926×10^{-9}	3.5390×10^{-1}	1.8990×10^{-1}	1.9850×10^{-1}	1.0000	3.4139×10^{6}
51	7.8440×10^{-3}	4.0738×10^{-17}	1.0337×10^{-8}	5.6000×10^{-1}	2.3180×10^{-2}	1.1810×10^{-2}	1.0000	2.6250×10^{5}
52	4.7130×10^{-3}	8.7097×10^{-20}	1.7370×10^{-8}	3.2370	1.5040×10^{-1}	3.8860×10^{-1}	0.0000	2.2027×10^{6}

Table B-2. 1992 BRA GFLO Computed Variable Values for ANHYDRITE (Concluded)

Run No.	Porosity	Permeability	Compressibility	BCEXP	BCBRSAT	BCGSSAT	BCFLG	BC PCT
53	1.5900×10^{-2}	7.7625×10^{-19}	4.9729×10^{-9}	6.7410	2.8470×10^{-1}	1.8060×10^{-1}	1.0000	1.0334×10^{6}
54	1.4500×10^{-2}	1.4454×10^{-20}	5.4772×10^{-9}	4.7200×10^{-1}	1.6590×10^{-1}	2.7290×10^{-1}	0.0000	4.1004×10^{6}
55	2.0030×10^{-2}	1.0233×10^{-17}	3.8960×10^{-9}	6.5030×10^{-1}	3.2450×10^{-1}	3.0330×10^{-1}	0.0000	4.2338×10^{5}
56	1.1650×10^{-2}	1.0965×10^{-20}	6.8783×10^{-9}	4.8480	9.2770×10^{-2}	5.2210×10^{-2}	0.0000	4.5118×10^{6}
57	4.5630×10^{-3}	5.2481×10^{-21}	1.7950×10^{-8}	9.2110	5.1160×10^{-3}	2.7770×10^{-1}	1.0000	5.8219×10^{6}
58	8.7110×10^{-3}	3.3884×10^{-19}	9.2833×10^{-9}	6.4060×10^{-1}	3.4880×10^{-1}	3.2980×10^{-1}	1.0000	1.3766×10^{6}
59	2.5160×10^{-2}	7.9433×10^{-20}	3.0507×10^{-9}	8.9580	8.5120×10^{-2}	3.1270×10^{-1}	1.0000	2.2740×10^{6}
60	8.2600×10^{-3}	9.5499×10^{-20}	9.8038×10^{-9}	9.8620	7.0380×10^{-2}	8.1940×10^{-2}	1.0000	2.1336×10^{6}
61	7.3840×10^{-3}	4.1687×10^{-20}	1.0997×10^{-8}	8.0490×10^{-1}	2.7910×10^{-1}	1.3890×10^{-1}	1.0000	2.8423×10^{6}
62	1.2250×10^{-2}	5.4954×10^{-19}	6.5292×10^{-9}	2.8630×10^{-1}	3.5990×10^{-1}	2.5120×10^{-1}	1.0000	1.1645×10^{6}
63	4.1090×10^{-3}	9.5499×10^{-17}	1.9961×10^{-8}	3.7540	2.0010×10^{-1}	2.8360×10^{-1}	0.0000	1.9548×10^{5}
64	3.7390×10^{-3}	2.6915×10^{-20}	2.1960×10^{-8}	2.4950	2.9320×10^{-2}	8.7020×10^{-2}	1.0000	3.3068×10^{6}
65	7.4700×10^{-3}	3.7153×10^{-20}	1.0867×10^{-8}	2.5410×10^{-1}	2.6410×10^{-1}	3.5100×10^{-1}	1.0000	2.9578×10^{6}
66	3.5330×10^{-3}	3.9811×10^{-20}	2.3255×10^{-8}	6.9150×10^{-1}	1.2380×10^{-1}	3.1630×10^{-1}	0.0000	2.8879×10^{6}
67	8.1910×10^{-3}	1.3804×10^{-19}	9.8885×10^{-9}	5.5890	5.6350×10^{-2}	2.5370×10^{-1}	0.0000	1.8782×10^{6}
68	1.0760×10^{-2}	6.7608×10^{-20}	7.4679×10^{-9}	4.5200	3.0240×10^{-1}	2.9970×10^{-1}	0.0000	2.4044×10^{6}
69	1.5190×10^{-2}	3.3113×10^{-20}	5.2171×10^{-9}	4.3270	3.7150×10^{-1}	4.8390×10^{-3}	1.0000	3.0780×10^{6}
70	1.4890×10^{-3}	1.3490×10^{-21}	5.5522×10^{-8}	6.2770×10^{-1}	1.0130×10^{-1}	1.1920×10^{-1}	1.0000	9.3155×10^{6}

Table B-2 1992 BRAGFLO Ranks of Computed Variable Values for ANHYDRITE

Run No.	Porosity	Permeability	Compressibility	BCEXP	BCBRSAT	BCGSSAT	BCFLG	BC PCT
1	68.	66.	3.	69.	16.	41.	1.	5.
2	24.	16.	47.	21.	26.	23.	24.	55.
3	69.	65.	2.	34.	33.	38.	24.	6.
4	18.	37.	53.	52.	31.	34.	24.	34.
5	54.	8.	17.	15.	35.	26.	24.	63.
6	42.	14.	29.	56.	59.	9.	1.	57.
7	63.	17.	8.	37.	7.	29.	1.	54.
8	9.	54.	62.	57.	68.	5.	24.	17.
9	66.	9.	5.	16.	60.	33.	24.	61.
10	34.	67.	37.	39.	14.	61.	24.	4.
11	7.	11.	64.	22.	48.	36.	1.	60.
12	35.	56.	36.	61.	25.	51.	24.	15.
13	47.	36.	24.	41.	64.	52.	24.	35.
14	52.	5.	19.	8.	2.	31.	24.	66.
15	1.	20.	70.	18.	41.	68.	1.	51.
16	19.	61.	52.	24.	67.	39.	24.	10.
17	60.	40.	11.	55.	20.	67.	1.	31.
18	20.	42.	51.	28.	52.	2.	1.	29.
19	21.	35.	50.	40.	21.	30.	24.	36.
20	48.	34.	23.	33.	23.	57.	24.	37.
21	59.	51.	12.	2.	4.	40.	1.	20.
22	64.	44.	7.	38.	39.	4.	24.	26.
23	70.	30.	1.	60.	42.	8.	24.	41.
24	44.	41.	27.	17.	11.	47.	24.	30.
25	61.	28.	10.	43.	54.	18.	24.	43.
26	51.	22.	20.	53.	44.	12.	24.	49.
27	5.	21.	66.	64.	38.	14.	24.	50.
28	8.	18.	63.	63.	61.	27.	1.	53.
29	40.	27.	31.	29.	58.	63.	24.	44.
30	31.	44.	40.	1.	3.	28.	1.	26.
31	49.	3.	22.	10.	37.	43.	24.	68.
32	55.	6.	16.	66.	55.	66.	24.	65.
33	23.	60.	48.	23.	19.	60.	24.	11.
34	32.	9.	39.	65.	45.	64.	1.	61.
35	6.	26.	65.	14.	51.	24.	24.	45.
36	65.	19.	6.	6.	65.	65.	24.	52.
37	16.	24.	55.	59.	40.	6.	24.	47.
38	4.	53.	67.	44.	32.	70.	24.	18.
39	36.	39.	35.	5.	29.	7.	24.	32.
40	58.	55.	13.	3.	43.	20.	24.	16.
41	50.	59.	21.	27.	24.	19.	24.	12.
42	56.	2.	15.	25.	70.	59.	1.	69.
43	17.	57.	54.	48.	69.	22.	1.	14.
44	12.	38.	59.	12.	46.	11.	1.	33.
45	33.	50.	38.	9.	28.	17.	24.	21.
46	67.	15.	4.	19.	12.	42.	24.	56.
47	22.	48.	49.	46.	56.	46.	24.	23.
48	57.	12.	14.	62.	8.	37.	1.	59.
49	3.	63.	68.	13.	9.	13.	24.	8.
50	41.	23.	30.	11.	34.	35.	24.	48.
51	27.	69.	44.	26.	5.	3.	24.	2.
52	15.	47.	56.	45.	27.	69.	1.	24.

Table B-2 1992 BRAGFLO Ranks of Computed Variable Values for ANHYDRITE (Concluded)

Run No.	Porosity	Permeability	Compressibility	BCEXP	BCBRSAT	BCGSSAT	BCFLG	BC PCT
53	46.	64.	25.	58.	50.	32.	24.	7.
54	43.	13.	28.	20.	30.	48.	1.	58.
55	53.	68.	18.	32.	57.	54.	1.	3.
56	38.	7.	33.	51.	17.	10.	1.	64.
57	14.	4.	57.	68.	1.	49.	24.	67.
58	30.	58.	41.	31.	62.	58.	24.	13.
59	62.	46.	9.	67.	15.	55.	24.	25.
60	29.	49.	42.	70.	13.	15.	24.	22.
61	25.	33.	46.	36.	49.	25.	24.	38.
62	39.	62.	32.	7.	63.	44.	24.	9.
63	13.	70.	58.	47.	36.	50.	1.	1.
64	11.	25.	60.	42.	6.	16.	24.	46.
65	26.	31.	45.	4.	47.	62.	24.	40.
66	10.	32.	61.	35.	22.	56.	1.	39.
67	28.	52.	43.	54.	10.	45.	1.	19.
68	37.	43.	34.	50.	53.	53.	1.	28.
69	45.	29.	26.	49.	66.	1.	24.	42.
70	2.	1.	69.	30.	18.	21.	24.	70.

Table B-2 1992 BRAGFLO Computed Variable Values for BACKFILL

Run No.	Porosity	Permeability	Compressibility	BCEXP	BCBRSAT	BCGSSAT	BCFLG	BC PCT
1	2.4490×10^{-2}	1.0000×10^{-15}	4.4974×10^{-9}	7.0000×10^{-1}	2.0000×10^{-1}	0.0000	1.0000	8.6734×10^{4}
2	1.1240×10^{-2}	1.0000×10^{-15}	1.0094×10^{-8}	7.0000×10^{-1}	2.0000×10^{-1}	0.0000	1.0000	8.6734×10^{4}
3	5.1030×10^{-2}	1.0000×10^{-15}	2.0283×10^{-9}	7.0000×10^{-1}	2.0000×10^{-1}	0.0000	1.0000	8.6734×10^{4}
4	1.6070×10^{-2}	1.0000×10^{-15}	6.9848×10^{-9}	7.0000×10^{-1}	2.0000×10^{-1}	0.0000	1.0000	8.6734×10^{4}
5	4.3250×10^{-2}	1.0000×10^{-15}	2.4381×10^{-9}	7.0000×10^{-1}	2.0000×10^{-1}	0.0000	1.0000	8.6734×10^{4}
6	5.8630×10^{-2}	1.0000×10^{-15}	1.7330×10^{-9}	7.0000×10^{-1}	2.0000×10^{-1}	0.0000	1.0000	8.6734×10^{4}
7	6.6520×10^{-2}	1.0000×10^{-15}	1.4978×10^{-9}	7.0000×10^{-1}	2.0000×10^{-1}	0.0000	1.0000	8.6734×10^{4}
8	3.6140×10^{-2}	1.0000×10^{-15}	2.9670×10^{-9}	7.0000×10^{-1}	2.0000×10^{-1}	0.0000	1.0000	8.6734×10^{4}
9	1.9210×10^{-2}	1.0000×10^{-15}	5.8022×10^{-9}	7.0000×10^{-1}	2.0000×10^{-1}	0.0000	1.0000	8.6734×10^{4}
10	4.7300×10^{-2}	1.0000×10^{-15}	2.2080×10^{-9}	7.0000×10^{-1}	2.0000×10^{-1}	0.0000	1.0000	8.6734×10^{4}
11	6.7690×10^{-2}	1.0000×10^{-15}	1.4676×10^{-9}	7.0000×10^{-1}	2.0000×10^{-1}	0.0000	1.0000	8.6734×10^{4}
12	2.5040×10^{-2}	1.0000×10^{-15}	4.3931×10^{-9}	7.0000×10^{-1}	2.0000×10^{-1}	0.0000	1.0000	8.6734×10^{4}
13	7.0630×10^{-2}	1.0000×10^{-15}	1.3961×10^{-9}	7.0000×10^{-1}	2.0000×10^{-1}	0.0000	1.0000	8.6734×10^{4}
14	4.0420×10^{-2}	1.0000×10^{-15}	2.6264×10^{-9}	7.0000×10^{-1}	2.0000×10^{-1}	0.0000	1.0000	8.6734×10^{4}
15	2.1150×10^{-2}	1.0000×10^{-15}	5.2470×10^{-9}	7.0000×10^{-1}	2.0000×10^{-1}	0.0000	1.0000	8.6734×10^{4}
16	7.2500×10^{-2}	1.0000×10^{-15}	1.3536×10^{-9}	7.0000×10^{-1}	2.0000×10^{-1}	0.0000	1.0000	8.6734×10^{4}
17	4.9250×10^{-2}	1.0000×10^{-15}	2.1107×10^{-9}	7.0000×10^{-1}	2.0000×10^{-1}	0.0000	1.0000	8.6734×10^{4}
18	1.3450×10^{-2}	1.0000×10^{-15}	8.3941×10^{-9}	7.0000×10^{-1}	2.0000×10^{-1}	0.0000	1.0000	8.6734×10^{4}
19	7.4520×10^{-2}	1.0000×10^{-15}	1.3101×10^{-9}	7.0000×10^{-1}	2.0000×10^{-1}	0.0000	1.0000	8.6734×10^{4}
20	3.7170×10^{-2}	1.0000×10^{-15}	2.8779×10^{-9}	7.0000×10^{-1}	2.0000×10^{-1}	0.0000	1.0000	8.6734×10^{4}
21	5.5630×10^{-2}	1.0000×10^{-15}	1.8399×10^{-9}	7.0000×10^{-1}	2.0000×10^{-1}	0.0000	1.0000	8.6734×10^{4}
22	4.4090×10^{-2}	1.0000×10^{-15}	2.3869×10^{-9}	7.0000×10^{-1}	2.0000×10^{-1}	0.0000	1.0000	8.6734×10^{4}
23	6.0100×10^{-2}	1.0000×10^{-15}	1.6845×10^{-9}	7.0000×10^{-1}	2.0000×10^{-1}	0.0000	1.0000	8.6734×10^{4}
24	6.9800×10^{-2}	1.0000×10^{-15}	1.4157×10^{-9}	7.0000×10^{-1}	2.0000×10^{-1}	0.0000	1.0000	8.6734×10^{4}
25	6.1100×10^{-2}	1.0000×10^{-15}	1.6528×10^{-9}	7.0000×10^{-1}	2.0000×10^{-1}	0.0000	1.0000	8.6734×10^{4}
26	5.6930×10^{-2}	1.0000×10^{-15}	1.7922×10^{-9}	7.0000×10^{-1}	2.0000×10^{-1}	0.0000	1.0000	8.6734×10^{4}
27	2.8620×10^{-2}	1.0000×10^{-15}	3.8123×10^{-9}	7.0000×10^{-1}	2.0000×10^{-1}	0.0000	1.0000	8.6734×10^{4}
28	4.1490×10^{-2}	1.0000×10^{-15}	2.5522×10^{-9}	7.0000×10^{-1}	2.0000×10^{-1}	0.0000	1.0000	8.6734×10^{4}
29	1.4260×10^{-2}	1.0000×10^{-15}	7.9031×10^{-9}	7.0000×10^{-1}	2.0000×10^{-1}	0.0000	1.0000	8.6734×10^{4}
30	3.2140×10^{-2}	1.0000×10^{-15}	3.3674×10^{-9}	7.0000×10^{-1}	2.0000×10^{-1}	0.0000	1.0000	8.6734×10^{4}
31	2.6760×10^{-2}	1.0000×10^{-15}	4.0946×10^{-9}	7.0000×10^{-1}	2.0000×10^{-1}	0.0000	1.0000	8.6734×10^{4}
32	3.9190×10^{-2}	1.0000×10^{-15}	2.7166×10^{-9}	7.0000×10^{-1}	2.0000×10^{-1}	0.0000	1.0000	8.6734×10^{4}
33	4.5660×10^{-2}	1.0000×10^{-15}	2.2963×10^{-9}	7.0000×10^{-1}	2.0000×10^{-1}	0.0000	1.0000	8.6734×10^{4}
34	3.4580×10^{-2}	1.0000×10^{-15}	3.1121×10^{-9}	7.0000×10^{-1}	2.0000×10^{-1}	0.0000	1.0000	8.6734×10^{4}
35	3.8780×10^{-2}	1.0000×10^{-15}	2.7480×10^{-9}	7.0000×10^{-1}	2.0000×10^{-1}	0.0000	1.0000	8.6734×10^{4}
36	4.6630×10^{-2}	1.0000×10^{-15}	2.2433×10^{-9}	7.0000×10^{-1}	2.0000×10^{-1}	0.0000	1.0000	8.6734×10^{4}
37	1.6500×10^{-2}	1.0000×10^{-15}	6.7962×10^{-9}	7.0000×10^{-1}	2.0000×10^{-1}	0.0000	1.0000	8.6734×10^{4}
38	6.7530×10^{-2}	1.0000×10^{-15}	1.4716×10^{-9}	7.0000×10^{-1}	2.0000×10^{-1}	0.0000	1.0000	8.6734×10^{4}
39	6.2320×10^{-2}	1.0000×10^{-15}	1.6156×10^{-9}	7.0000×10^{-1}	2.0000×10^{-1}	0.0000	1.0000	8.6734×10^{4}
40	5.4740×10^{-2}	1.0000×10^{-15}	1.8739×10^{-9}	7.0000×10^{-1}	2.0000×10^{-1}	0.0000	1.0000	8.6734×10^{4}
41	6.3580×10^{-2}	1.0000×10^{-15}	1.5786×10^{-9}	7.0000×10^{-1}	2.0000×10^{-1}	0.0000	1.0000	8.6734×10^{4}
42	7.1460×10^{-2}	1.0000×10^{-15}	1.3770×10^{-9}	7.0000×10^{-1}	2.0000×10^{-1}	0.0000	1.0000	8.6734×10^{4}
43	4.4580×10^{-2}	1.0000×10^{-15}	2.3580×10^{-9}	7.0000×10^{-1}	2.0000×10^{-1}	0.0000	1.0000	8.6734×10^{4}
44	7.3870×10^{-2}	1.0000×10^{-15}	1.3239×10^{-9}	7.0000×10^{-1}	2.0000×10^{-1}	0.0000	1.0000	8.6734×10^{4}
45	2.9730×10^{-2}	1.0000×10^{-15}	3.6606×10^{-9}	7.0000×10^{-1}	2.0000×10^{-1}	0.0000	1.0000	8.6734×10^{4}
46	1.2610×10^{-2}	1.0000×10^{-15}	8.9699×10^{-9}	7.0000×10^{-1}	2.0000×10^{-1}	0.0000	1.0000	8.6734×10^{4}
47	6.0510×10^{-2}	1.0000×10^{-15}	1.6714×10^{-9}	7.0000×10^{-1}	2.0000×10^{-1}	0.0000	1.0000	8.6734×10^{4}
48	3.3090×10^{-2}	1.0000×10^{-15}	3.2635×10^{-9}	7.0000×10^{-1}	2.0000×10^{-1}	0.0000	1.0000	8.6734×10^{4}
49	4.1760×10^{-2}	1.0000×10^{-15}	2.5341×10^{-9}	7.0000×10^{-1}	2.0000×10^{-1}	0.0000	1.0000	8.6734×10^{4}
50	3.0510×10^{-2}	1.0000×10^{-15}	3.5606×10^{-9}	7.0000×10^{-1}	2.0000×10^{-1}	0.0000	1.0000	8.6734×10^{4}
51	1.8180×10^{-2}	1.0000×10^{-15}	6.1451×10^{-9}	7.0000×10^{-1}	2.0000×10^{-1}	0.0000	1.0000	8.6734×10^{4}
52	6.5110×10^{-2}	1.0000×10^{-15}	1.5356×10^{-9}	7.0000×10^{-1}	2.0000×10^{-1}	0.0000	1.0000	8.6734×10^{4}

Table B-2 1992 BRAGFLO Computed Variable Values for BACKFILL (Concluded)

Run No.	Porosity	Permeability	Compressibility	BCEXP	BCBRSAT	BCGSSAT	BCFLG	BC PCT
53	2.0520×10^{-2}	1.0000×10^{-15}	5.4158×10^{-9}	7.0000×10^{-1}	2.0000×10^{-1}	0.0000	1.0000	8.6734×10^{4}
54	6.4400×10^{-2}	1.0000×10^{-15}	1.5553×10^{-9}	7.0000×10^{-1}	2.0000×10^{-1}	0.0000	1.0000	8.6734×10^{4}
55	2.6330×10^{-2}	1.0000×10^{-15}	4.1656×10^{-9}	7.0000×10^{-1}	2.0000×10^{-1}	0.0000	1.0000	8.6734×10^{4}
56	3.5470×10^{-2}	1.0000×10^{-15}	3.0278×10^{-9}	7.0000×10^{-1}	2.0000×10^{-1}	0.0000	1.0000	8.6734×10^{4}
57	1.9820×10^{-2}	1.0000×10^{-15}	5.6159×10^{-9}	7.0000×10^{-1}	2.0000×10^{-1}	0.0000	1.0000	8.6734×10^{4}
58	2.3880×10^{-2}	1.0000×10^{-15}	4.6186×10^{-9}	7.0000×10^{-1}	2.0000×10^{-1}	0.0000	1.0000	8.6734×10^{4}
59	5.7990×10^{-2}	1.0000×10^{-15}	1.7549×10^{-9}	7.0000×10^{-1}	2.0000×10^{-1}	0.0000	1.0000	8.6734×10^{4}
60	6.9150×10^{-2}	1.0000×10^{-15}	1.4313×10^{-9}	7.0000×10^{-1}	2.0000×10^{-1}	0.0000	1.0000	8.6734×10^{4}
61	1.5400×10^{-2}	1.0000×10^{-15}	7.2995×10^{-9}	7.0000×10^{-1}	2.0000×10^{-1}	0.0000	1.0000	8.6734×10^{4}
62	2.7890×10^{-2}	1.0000×10^{-15}	3.9186×10^{-9}	7.0000×10^{-1}	2.0000×10^{-1}	0.0000	1.0000	8.6734×10^{4}
63	5.2340×10^{-2}	1.0000×10^{-15}	1.9713×10^{-9}	7.0000×10^{-1}	2.0000×10^{-1}	0.0000	1.0000	8.6734×10^{4}
64	5.3500×10^{-2}	1.0000×10^{-15}	1.9231×10^{-9}	7.0000×10^{-1}	2.0000×10^{-1}	0.0000	1.0000	8.6734×10^{4}
65	1.0820×10^{-2}	1.0000×10^{-15}	1.0495×10^{-8}	7.0000×10^{-1}	2.0000×10^{-1}	0.0000	1.0000	8.6734×10^{4}
66	5.0410×10^{-2}	1.0000×10^{-15}	2.0563×10^{-9}	7.0000×10^{-1}	2.0000×10^{-1}	0.0000	1.0000	8.6734×10^{4}
67	3.3230×10^{-2}	1.0000×10^{-15}	3.2487×10^{-9}	7.0000×10^{-1}	2.0000×10^{-1}	0.0000	1.0000	8.6734×10^{4}
68	2.2660×10^{-2}	1.0000×10^{-15}	4.8807×10^{-9}	7.0000×10^{-1}	2.0000×10^{-1}	0.0000	1.0000	8.6734×10^{4}
69	4.8950×10^{-2}	1.0000×10^{-15}	2.1251×10^{-9}	7.0000×10^{-1}	2.0000×10^{-1}	0.0000	1.0000	8.6734×10^{4}
70	5.3660×10^{-2}	1.0000×10^{-15}	1.9166×10^{-9}	7.0000×10^{-1}	2.0000×10^{-1}	0.0000	1.0000	8.6734×10^{4}

Table B-2 1992 BRAGFLO Ranks of Computed Variable Values for BACKFILL

Run No.	Porosity	Permeability	Compressibility	BCEXP	BCBRSAT	BCGSSAT	BCFLG	BC PCT
1	16.	1.	55.	1.	1.	1.	1.	1.
2	2.	1.	69.	1.	1.	1.	1.	1.
3	45.	1.	26.	1.	1.	1.	1.	1.
4	7.	1.	64.	1.	1.	1.	1.	1.
5	36.	1.	35.	1.	1.	1.	1.	1.
6	53.	1.	18.	1.	1.	1.	1.	1.
7	61.	1.	10.	1.	1.	1.	1.	1.
8	29.	1.	42.	1.	1.	1.	1.	1.
9	10.	1.	61.	1.	1.	1.	1.	1.
10	41.	1.	30.	1.	1.	1.	1.	1.
11	63.	1.	8.	1.	1.	1.	1.	1.
12	17.	1.	54.	1.	1.	1.	1.	1.
13	66.	1.	5.	1.	1.	1.	1.	1.
14	33.	1.	38.	1.	1.	1.	1.	1.
15	13.	1.	58.	1.	1.	1.	1.	1.
16	68.	1.	3.	1.	1.	1.	1.	1.
17	43.	1.	28.	1.	1.	1.	1.	1.
18	4.	1.	67.	1.	1.	1.	1.	1.
19	70.	1.	1.	1.	1.	1.	1.	1.
20	30.	1.	41.	1.	1.	1.	1.	1.
21	50.	1.	21.	1.	1.	1.	1.	1.
22	37.	1.	34.	1.	1.	1.	1.	1.
23	54.	1.	17.	1.	1.	1.	1.	1.
24	65.	1.	6.	1.	1.	1.	1.	1.
25	56.	1.	15.	1.	1.	1.	1.	1.
26	51.	1.	20.	1.	1.	1.	1.	1.
27	21.	1.	50.	1.	1.	1.	1.	1.
28	34.	1.	37.	1.	1.	1.	1.	1.
29	5.	1.	66.	1.	1.	1.	1.	1.
30	24.	1.	47.	1.	1.	1.	1.	1.
31	19.	1.	52.	1.	1.	1.	1.	1.
32	32.	1.	39.	1.	1.	1.	1.	1.
33	39.	1.	32.	1.	1.	1.	1.	1.
34	27.	1.	44.	1.	1.	1.	1.	1.
35	31.	1.	40.	1.	1.	1.	1.	1.
36	40.	1.	31.	1.	1.	1.	1.	1.
37	8.	1.	63.	1.	1.	1.	1.	1.
38	62.	1.	9.	1.	1.	1.	1.	1.
39	57.	1.	14.	1.	1.	1.	1.	1.
40	49.	1.	22.	1.	1.	1.	1.	1.
41	58.	1.	13.	1.	1.	1.	1.	1.
42	67.	1.	4.	1.	1.	1.	1.	1.
43	38.	1.	33.	1.	1.	1.	1.	1.
44	69.	1.	2.	1.	1.	1.	1.	1.
45	22.	1.	49.	1.	1.	1.	1.	1.
46	3.	1.	68.	1.	1.	1.	1.	1.
47	55.	1.	16.	1.	1.	1.	1.	1.
48	25.	1.	46.	1.	1.	1.	1.	1.
49	35.	1.	36.	1.	1.	1.	1.	1.
50	23.	1.	48.	1.	1.	1.	1.	1.
51	9.	1.	62.	1.	1.	1.	1.	1.
52	60.	1.	11.	1.	1.	1.	1.	1.

Table B-2 1992 BRAGFLO Ranks of Computed Variable Values for BACKFILL (Concluded)

Run No.	Porosity	Permeability	Compressibility	BCEXP	BCBRSAT	BCGSSAT	BCFLG	BC PCT
53	12.	1.	59.	1.	1.	1.	1.	1.
54	59.	1.	12.	1.	1.	1.	1.	1.
55	18.	1.	53.	1.	1.	1.	1.	1.
56	28.	1.	43.	1.	1.	1.	1.	1.
57	11.	1.	60.	1.	1.	1.	1.	1.
58	15.	1.	56.	1.	1.	1.	1.	1.
59	52.	1.	19.	1.	1.	1.	1.	1.
60	64.	1.	7.	1.	1.	1.	1.	1.
61	6.	1.	65.	1.	1.	1.	1.	1.
62	20.	1.	51.	1.	1.	1.	1.	1.
63	46.	1.	25.	1.	1.	1.	1.	1.
64	47.	1.	24.	1.	1.	1.	1.	1.
65	1.	1.	70.	1.	1.	1.	1.	1.
66	44.	1.	27.	1.	1.	1.	1.	1.
67	26.	1.	45.	1.	1.	1.	1.	1.
68	14.	1.	57.	1.	1.	1.	1.	1.
69	42.	1.	29.	1.	1.	1.	1.	1.
70	48.	1.	23.	1.	1.	1.	1.	1.

Table B-2 1992 BRAGFLO Computed Variable Values for CAVITY_1

Run No.	Porosity	Permeability	Compressibility	BCEXP	BCBRSAT	BCGSSAT	BCFLG	BC PCT
1	1.0000	1.0000×10^{-10}	0.0000	9.6790	0.0000	0.0000	1.0000	0.0000
2	1.0000	1.0000×10^{-10}	0.0000	4.9660×10^{-1}	0.0000	0.0000	1.0000	0.0000
3	1.0000	1.0000×10^{-10}	0.0000	6.7900×10^{-1}	0.0000	0.0000	1.0000	0.0000
4	1.0000	1.0000×10^{-10}	0.0000	5.1820	0.0000	0.0000	1.0000	0.0000
5	1.0000	1.0000×10^{-10}	0.0000	4.0710×10^{-1}	0.0000	0.0000	1.0000	0.0000
6	1.0000	1.0000×10^{-10}	0.0000	6.1420	0.0000	0.0000	1.0000	0.0000
7	1.0000	1.0000×10^{-10}	0.0000	1.0990	0.0000	0.0000	1.0000	0.0000
8	1.0000	1.0000×10^{-10}	0.0000	6.4480	0.0000	0.0000	1.0000	0.0000
9	1.0000	1.0000×10^{-10}	0.0000	4.2610×10^{-1}	0.0000	0.0000	1.0000	0.0000
10	1.0000	1.0000×10^{-10}	0.0000	1.5170	0.0000	0.0000	1.0000	0.0000
11	1.0000	1.0000×10^{-10}	0.0000	5.1250×10^{-1}	0.0000	0.0000	1.0000	0.0000
12	1.0000	1.0000×10^{-10}	0.0000	7.4960	0.0000	0.0000	1.0000	0.0000
13	1.0000	1.0000×10^{-10}	0.0000	2.2490	0.0000	0.0000	1.0000	0.0000
14	1.0000	1.0000×10^{-10}	0.0000	3.0620×10^{-1}	0.0000	0.0000	1.0000	0.0000
15	1.0000	1.0000×10^{-10}	0.0000	4.4620×10^{-1}	0.0000	0.0000	1.0000	0.0000
16	1.0000	1.0000×10^{-10}	0.0000	5.3590×10^{-1}	0.0000	0.0000	1.0000	0.0000
17	1.0000	1.0000×10^{-10}	0.0000	5.9190	0.0000	0.0000	1.0000	0.0000
18	1.0000	1.0000×10^{-10}	0.0000	5.8730×10^{-1}	0.0000	0.0000	1.0000	0.0000
19	1.0000	1.0000×10^{-10}	0.0000	2.0050	0.0000	0.0000	1.0000	0.0000
20	1.0000	1.0000×10^{-10}	0.0000	6.7090×10^{-1}	0.0000	0.0000	1.0000	0.0000
21	1.0000	1.0000×10^{-10}	0.0000	2.2590×10^{-1}	0.0000	0.0000	1.0000	0.0000
22	1.0000	1.0000×10^{-10}	0.0000	1.4340	0.0000	0.0000	1.0000	0.0000
23	1.0000	1.0000×10^{-10}	0.0000	7.0990	0.0000	0.0000	1.0000	0.0000
24	1.0000	1.0000×10^{-10}	0.0000	4.3270×10^{-1}	0.0000	0.0000	1.0000	0.0000
25	1.0000	1.0000×10^{-10}	0.0000	2.7610	0.0000	0.0000	1.0000	0.0000
26	1.0000	1.0000×10^{-10}	0.0000	5.2660	0.0000	0.0000	1.0000	0.0000
27	1.0000	1.0000×10^{-10}	0.0000	8.3330	0.0000	0.0000	1.0000	0.0000
28	1.0000	1.0000×10^{-10}	0.0000	7.9460	0.0000	0.0000	1.0000	0.0000
29	1.0000	1.0000×10^{-10}	0.0000	6.0410×10^{-1}	0.0000	0.0000	1.0000	0.0000
30	1.0000	1.0000×10^{-10}	0.0000	2.0040×10^{-1}	0.0000	0.0000	1.0000	0.0000
31	1.0000	1.0000×10^{-10}	0.0000	3.3160×10^{-1}	0.0000	0.0000	1.0000	0.0000
32	1.0000	1.0000×10^{-10}	0.0000	8.8800	0.0000	0.0000	1.0000	0.0000
33	1.0000	1.0000×10^{-10}	0.0000	5.2200×10^{-1}	0.0000	0.0000	1.0000	0.0000
34	1.0000	1.0000×10^{-10}	0.0000	8.6520	0.0000	0.0000	1.0000	0.0000
35	1.0000	1.0000×10^{-10}	0.0000	3.9470×10^{-1}	0.0000	0.0000	1.0000	0.0000
36	1.0000	1.0000×10^{-10}	0.0000	2.7500×10^{-1}	0.0000	0.0000	1.0000	0.0000
37	1.0000	1.0000×10^{-10}	0.0000	6.9780	0.0000	0.0000	1.0000	0.0000
38	1.0000	1.0000×10^{-10}	0.0000	2.9640	0.0000	0.0000	1.0000	0.0000
39	1.0000	1.0000×10^{-10}	0.0000	2.6060×10^{-1}	0.0000	0.0000	1.0000	0.0000
40	1.0000	1.0000×10^{-10}	0.0000	2.4160×10^{-1}	0.0000	0.0000	1.0000	0.0000
41	1.0000	1.0000×10^{-10}	0.0000	5.7490×10^{-1}	0.0000	0.0000	1.0000	0.0000
42	1.0000	1.0000×10^{-10}	0.0000	5.4840×10^{-1}	0.0000	0.0000	1.0000	0.0000
43	1.0000	1.0000×10^{-10}	0.0000	4.0000	0.0000	0.0000	1.0000	0.0000
44	1.0000	1.0000×10^{-10}	0.0000	3.6050×10^{-1}	0.0000	0.0000	1.0000	0.0000
45	1.0000	1.0000×10^{-10}	0.0000	3.2390×10^{-1}	0.0000	0.0000	1.0000	0.0000
46	1.0000	1.0000×10^{-10}	0.0000	4.6060×10^{-1}	0.0000	0.0000	1.0000	0.0000
47	1.0000	1.0000×10^{-10}	0.0000	3.4760	0.0000	0.0000	1.0000	0.0000
48	1.0000	1.0000×10^{-10}	0.0000	7.7080	0.0000	0.0000	1.0000	0.0000
49	1.0000	1.0000×10^{-10}	0.0000	3.7530×10^{-1}	0.0000	0.0000	1.0000	0.0000
50	1.0000	1.0000×10^{-10}	0.0000	3.5390×10^{-1}	0.0000	0.0000	1.0000	0.0000
51	1.0000	1.0000×10^{-10}	0.0000	5.6000×10^{-1}	0.0000	0.0000	1.0000	0.0000
52	1.0000	1.0000×10^{-10}	0.0000	3.2370	0.0000	0.0000	1.0000	0.0000

Table B-2 1992 BRAGFLO Computed Variable Values for CAVITY_1 (Concluded)

Run No.	Porosity	Permeability	Compressibility	BCEXP	BCBRSAT	BCGSSAT	BCFLG	BC PCT
53	1.0000	1.0000×10^{-10}	0.0000	6.7410	0.0000	0.0000	1.0000	0.0000
54	1.0000	1.0000×10^{-10}	0.0000	4.7200×10^{-1}	0.0000	0.0000	1.0000	0.0000
55	1.0000	1.0000×10^{-10}	0.0000	6.5030×10^{-1}	0.0000	0.0000	1.0000	0.0000
56	1.0000	1.0000×10^{-10}	0.0000	4.8480	0.0000	0.0000	1.0000	0.0000
57	1.0000	1.0000×10^{-10}	0.0000	9.2110	0.0000	0.0000	1.0000	0.0000
58	1.0000	1.0000×10^{-10}	0.0000	6.4060×10^{-1}	0.0000	0.0000	1.0000	0.0000
59	1.0000	1.0000×10^{-10}	0.0000	8.9580	0.0000	0.0000	1.0000	0.0000
60	1.0000	1.0000×10^{-10}	0.0000	9.8620	0.0000	0.0000	1.0000	0.0000
61	1.0000	1.0000×10^{-10}	0.0000	8.0490×10^{-1}	0.0000	0.0000	1.0000	0.0000
62	1.0000	1.0000×10^{-10}	0.0000	2.8630×10^{-1}	0.0000	0.0000	1.0000	0.0000
63	1.0000	1.0000×10^{-10}	0.0000	3.7540	0.0000	0.0000	1.0000	0.0000
64	1.0000	1.0000×10^{-10}	0.0000	2.4950	0.0000	0.0000	1.0000	0.0000
65	1.0000	1.0000×10^{-10}	0.0000	2.5410×10^{-1}	0.0000	0.0000	1.0000	0.0000
66	1.0000	1.0000×10^{-10}	0.0000	6.9150×10^{-1}	0.0000	0.0000	1.0000	0.0000
67	1.0000	1.0000×10^{-10}	0.0000	5.5890	0.0000	0.0000	1.0000	0.0000
68	1.0000	1.0000×10^{-10}	0.0000	4.5200	0.0000	0.0000	1.0000	0.0000
69	1.0000	1.0000×10^{-10}	0.0000	4.3270	0.0000	0.0000	1.0000	0.0000
70	1.0000	1.0000×10^{-10}	0.0000	6.2770×10^{-1}	0.0000	0.0000	1.0000	0.0000

Table B-2 1992 BRAGFLO Ranks of Computed Variable Values for CAVITY_1

Run No.	Porosity	Permeability	Compressibility	BCEXP	BCBRSAT	BCGSSAT	BCFLG	BC PCT
1	1.	1.	1.	69.	1.	1.	1.	1.
2	1.	1.	1.	21.	1.	1.	1.	1.
3	1.	1.	1.	34.	1.	1.	1.	1.
4	1.	1.	1.	52.	1.	1.	1.	1.
5	1.	1.	1.	15.	1.	1.	1.	1.
6	1.	1.	1.	56.	1.	1.	1.	1.
7	1.	1.	1.	37.	1.	1.	1.	1.
8	1.	1.	1.	57.	1.	1.	1.	1.
9	1.	1.	1.	16.	1.	1.	1.	1.
10	1.	1.	1.	39.	1.	1.	1.	1.
11	1.	1.	1.	22.	1.	1.	1.	1.
12	1.	1.	1.	61.	1.	1.	1.	1.
13	1.	1.	1.	41.	1.	1.	1.	1.
14	1.	1.	1.	8.	1.	1.	1.	1.
15	1.	1.	1.	18.	1.	1.	1.	1.
16	1.	1.	1.	24.	1.	1.	1.	1.
17	1.	1.	1.	55.	1.	1.	1.	1.
18	1.	1.	1.	28.	1.	1.	1.	1.
19	1.	1.	1.	40.	1.	1.	1.	1.
20	1.	1.	1.	33.	1.	1.	1.	1.
21	1.	1.	1.	2.	1.	1.	1.	1.
22	1.	1.	1.	38.	1.	1.	1.	1.
23	1.	1.	1.	60.	1.	1.	1.	1.
24	1.	1.	1.	17.	1.	1.	1.	1.
25	1.	1.	1.	43.	1.	1.	1.	1.
26	1.	1.	1.	53.	1.	1.	1.	1.
27	1.	1.	1.	64.	1.	1.	1.	1.
28	1.	1.	1.	63.	1.	1.	1.	1.
29	1.	1.	1.	29.	1.	1.	1.	1.
30	1.	1.	1.	1.	1.	1.	1.	1.
31	1.	1.	1.	10.	1.	1.	1.	1.
32	1.	1.	1.	66.	1.	1.	1.	1.
33	1.	1.	1.	23.	1.	1.	1.	1.
34	1.	1.	1.	65.	1.	1.	1.	1.
35	1.	1.	1.	14.	1.	1.	1.	1.
36	1.	1.	1.	6.	1.	1.	1.	1.
37	1.	1.	1.	59.	1.	1.	1.	1.
38	1.	1.	1.	44.	1.	1.	1.	1.
39	1.	1.	1.	5.	1.	1.	1.	1.
40	1.	1.	1.	3.	1.	1.	1.	1.
41	1.	1.	1.	27.	1.	1.	1.	1.
42	1.	1.	1.	25.	1.	1.	1.	1.
43	1.	1.	1.	48.	1.	1.	1.	1.
44	1.	1.	1.	12.	1.	1.	1.	1.
45	1.	1.	1.	9.	1.	1.	1.	1.
46	1.	1.	1.	19.	1.	1.	1.	1.
47	1.	1.	1.	46.	1.	1.	1.	1.
48	1.	1.	1.	62.	1.	1.	1.	1.
49	1.	1.	1.	13.	1.	1.	1.	1.
50	1.	1.	1.	11.	1.	1.	1.	1.
51	1.	1.	1.	26.	1.	1.	1.	1.
52	1.	1.	1.	45.	1.	1.	1.	1.

Table B-2 1992 BRAGFLO Ranks of Computed Variable Values for CAVITY_1 (Concluded)

Run No.	Porosity	Permeability	Compressibility	BCEXP	BCBRSAT	BCGSSAT	BCFLG	BC PCT
53	1.	1.	1.	58.	1.	1.	1.	1.
54	1.	1.	1.	20.	1.	1.	1.	1.
55	1.	1.	1.	32.	1.	1.	1.	1.
56	1.	1.	1.	51.	1.	1.	1.	1.
57	1.	1.	1.	68.	1.	1.	1.	1.
58	1.	1.	1.	31.	1.	1.	1.	1.
59	1.	1.	1.	67.	1.	1.	1.	1.
60	1.	1.	1.	70.	1.	1.	1.	1.
61	1.	1.	1.	36.	1.	1.	1.	1.
62	1.	1.	1.	7.	1.	1.	1.	1.
63	1.	1.	1.	47.	1.	1.	1.	1.
64	1.	1.	1.	42.	1.	1.	1.	1.
65	1.	1.	1.	4.	1.	1.	1.	1.
66	1.	1.	1.	35.	1.	1.	1.	1.
67	1.	1.	1.	54.	1.	1.	1.	1.
68	1.	1.	1.	50.	1.	1.	1.	1.
69	1.	1.	1.	49.	1.	1.	1.	1.
70	1.	1.	1.	30.	1.	1.	1.	1.

Table B-2 1992 BRAGFLO Computed Variable Values for CAVITY_2

Run No.	Porosity	Permeability	Compressibility	BCEXP	BCBRSAT	BCGSSAT	BCFLG	BC PCT
1	1.0000	1.0000×10^{-10}	0.0000	9.6790	0.0000	0.0000	1.0000	0.0000
2	1.0000	1.0000×10^{-10}	0.0000	4.9660×10^{-1}	0.0000	0.0000	1.0000	0.0000
3	1.0000	1.0000×10^{-10}	0.0000	6.7900×10^{-1}	0.0000	0.0000	1.0000	0.0000
4	1.0000	1.0000×10^{-10}	0.0000	5.1820	0.0000	0.0000	1.0000	0.0000
5	1.0000	1.0000×10^{-10}	0.0000	4.0710×10^{-1}	0.0000	0.0000	1.0000	0.0000
6	1.0000	1.0000×10^{-10}	0.0000	6.1420	0.0000	0.0000	1.0000	0.0000
7	1.0000	1.0000×10^{-10}	0.0000	1.0990	0.0000	0.0000	1.0000	0.0000
8	1.0000	1.0000×10^{-10}	0.0000	6.4480	0.0000	0.0000	1.0000	0.0000
9	1.0000	1.0000×10^{-10}	0.0000	4.2610×10^{-1}	0.0000	0.0000	1.0000	0.0000
10	1.0000	1.0000×10^{-10}	0.0000	1.5170	0.0000	0.0000	1.0000	0.0000
11	1.0000	1.0000×10^{-10}	0.0000	5.1250×10^{-1}	0.0000	0.0000	1.0000	0.0000
12	1.0000	1.0000×10^{-10}	0.0000	7.4960	0.0000	0.0000	1.0000	0.0000
13	1.0000	1.0000×10^{-10}	0.0000	2.2490	0.0000	0.0000	1.0000	0.0000
14	1.0000	1.0000×10^{-10}	0.0000	3.0620×10^{-1}	0.0000	0.0000	1.0000	0.0000
15	1.0000	1.0000×10^{-10}	0.0000	4.4620×10^{-1}	0.0000	0.0000	1.0000	0.0000
16	1.0000	1.0000×10^{-10}	0.0000	5.3590×10^{-1}	0.0000	0.0000	1.0000	0.0000
17	1.0000	1.0000×10^{-10}	0.0000	5.9190	0.0000	0.0000	1.0000	0.0000
18	1.0000	1.0000×10^{-10}	0.0000	5.8730×10^{-1}	0.0000	0.0000	1.0000	0.0000
19	1.0000	1.0000×10^{-10}	0.0000	2.0050	0.0000	0.0000	1.0000	0.0000
20	1.0000	1.0000×10^{-10}	0.0000	6.7090×10^{-1}	0.0000	0.0000	1.0000	0.0000
21	1.0000	1.0000×10^{-10}	0.0000	2.2590×10^{-1}	0.0000	0.0000	1.0000	0.0000
22	1.0000	1.0000×10^{-10}	0.0000	1.4340	0.0000	0.0000	1.0000	0.0000
23	1.0000	1.0000×10^{-10}	0.0000	7.0990	0.0000	0.0000	1.0000	0.0000
24	1.0000	1.0000×10^{-10}	0.0000	4.3270×10^{-1}	0.0000	0.0000	1.0000	0.0000
25	1.0000	1.0000×10^{-10}	0.0000	2.7610	0.0000	0.0000	1.0000	0.0000
26	1.0000	1.0000×10^{-10}	0.0000	5.2660	0.0000	0.0000	1.0000	0.0000
27	1.0000	1.0000×10^{-10}	0.0000	8.3330	0.0000	0.0000	1.0000	0.0000
28	1.0000	1.0000×10^{-10}	0.0000	7.9460	0.0000	0.0000	1.0000	0.0000
29	1.0000	1.0000×10^{-10}	0.0000	6.0410×10^{-1}	0.0000	0.0000	1.0000	0.0000
30	1.0000	1.0000×10^{-10}	0.0000	2.0040×10^{-1}	0.0000	0.0000	1.0000	0.0000
31	1.0000	1.0000×10^{-10}	0.0000	3.3160×10^{-1}	0.0000	0.0000	1.0000	0.0000
32	1.0000	1.0000×10^{-10}	0.0000	8.8800	0.0000	0.0000	1.0000	0.0000
33	1.0000	1.0000×10^{-10}	0.0000	5.2200×10^{-1}	0.0000	0.0000	1.0000	0.0000
34	1.0000	1.0000×10^{-10}	0.0000	8.6520	0.0000	0.0000	1.0000	0.0000
35	1.0000	1.0000×10^{-10}	0.0000	3.9470×10^{-1}	0.0000	0.0000	1.0000	0.0000
36	1.0000	1.0000×10^{-10}	0.0000	2.7500×10^{-1}	0.0000	0.0000	1.0000	0.0000
37	1.0000	1.0000×10^{-10}	0.0000	6.9780	0.0000	0.0000	1.0000	0.0000
38	1.0000	1.0000×10^{-10}	0.0000	2.9640	0.0000	0.0000	1.0000	0.0000
39	1.0000	1.0000×10^{-10}	0.0000	2.6060×10^{-1}	0.0000	0.0000	1.0000	0.0000
40	1.0000	1.0000×10^{-10}	0.0000	2.4160×10^{-1}	0.0000	0.0000	1.0000	0.0000
41	1.0000	1.0000×10^{-10}	0.0000	5.7490×10^{-1}	0.0000	0.0000	1.0000	0.0000
42	1.0000	1.0000×10^{-10}	0.0000	5.4840×10^{-1}	0.0000	0.0000	1.0000	0.0000
43	1.0000	1.0000×10^{-10}	0.0000	4.0000	0.0000	0.0000	1.0000	0.0000
44	1.0000	1.0000×10^{-10}	0.0000	3.6050×10^{-1}	0.0000	0.0000	1.0000	0.0000
45	1.0000	1.0000×10^{-10}	0.0000	3.2390×10^{-1}	0.0000	0.0000	1.0000	0.0000
46	1.0000	1.0000×10^{-10}	0.0000	4.6060×10^{-1}	0.0000	0.0000	1.0000	0.0000
47	1.0000	1.0000×10^{-10}	0.0000	3.4760	0.0000	0.0000	1.0000	0.0000
48	1.0000	1.0000×10^{-10}	0.0000	7.7080	0.0000	0.0000	1.0000	0.0000
49	1.0000	1.0000×10^{-10}	0.0000	3.7530×10^{-1}	0.0000	0.0000	1.0000	0.0000
50	1.0000	1.0000×10^{-10}	0.0000	3.5390×10^{-1}	0.0000	0.0000	1.0000	0.0000
51	1.0000	1.0000×10^{-10}	0.0000	5.6000×10^{-1}	0.0000	0.0000	1.0000	0.0000
52	1.0000	1.0000×10^{-10}	0.0000	3.2370	0.0000	0.0000	1.0000	0.0000

Table B-2 1992 BRAGFLO Computed Variable Values for CAVITY_2 (Concluded)

Run No.	Porosity	Permeability	Compressibility	BCEXP	BCBRSAT	BCGSSAT	BCFLG	BC PCT
53	1.0000	1.0000×10^{-10}	0.0000	6.7410	0.0000	0.0000	1.0000	0.0000
54	1.0000	1.0000×10^{-10}	0.0000	4.7200×10^{-1}	0.0000	0.0000	1.0000	0.0000
55	1.0000	1.0000×10^{-10}	0.0000	6.5030×10^{-1}	0.0000	0.0000	1.0000	0.0000
56	1.0000	1.0000×10^{-10}	0.0000	4.8480	0.0000	0.0000	1.0000	0.0000
57	1.0000	1.0000×10^{-10}	0.0000	9.2110	0.0000	0.0000	1.0000	0.0000
58	1.0000	1.0000×10^{-10}	0.0000	6.4060×10^{-1}	0.0000	0.0000	1.0000	0.0000
59	1.0000	1.0000×10^{-10}	0.0000	8.9580	0.0000	0.0000	1.0000	0.0000
60	1.0000	1.0000×10^{-10}	0.0000	9.8620	0.0000	0.0000	1.0000	0.0000
61	1.0000	1.0000×10^{-10}	0.0000	8.0490×10^{-1}	0.0000	0.0000	1.0000	0.0000
62	1.0000	1.0000×10^{-10}	0.0000	2.8630×10^{-1}	0.0000	0.0000	1.0000	0.0000
63	1.0000	1.0000×10^{-10}	0.0000	3.7540	0.0000	0.0000	1.0000	0.0000
64	1.0000	1.0000×10^{-10}	0.0000	2.4950	0.0000	0.0000	1.0000	0.0000
65	1.0000	1.0000×10^{-10}	0.0000	2.5410×10^{-1}	0.0000	0.0000	1.0000	0.0000
66	1.0000	1.0000×10^{-10}	0.0000	6.9150×10^{-1}	0.0000	0.0000	1.0000	0.0000
67	1.0000	1.0000×10^{-10}	0.0000	5.5890	0.0000	0.0000	1.0000	0.0000
68	1.0000	1.0000×10^{-10}	0.0000	4.5200	0.0000	0.0000	1.0000	0.0000
69	1.0000	1.0000×10^{-10}	0.0000	4.3270	0.0000	0.0000	1.0000	0.0000
70	1.0000	1.0000×10^{-10}	0.0000	6.2770×10^{-1}	0.0000	0.0000	1.0000	0.0000

Table B-2 1992 BRAGFLO Ranks of Computed Variable Values for CAVITY_2

Run No.	Porosity	Permeability	Compressibility	BCEXP	BCBRSAT	BCGSSAT	BCFLG	BC PCT
1	1.	1.	1.	69.	1.	1.	1.	1.
2	1.	1.	1.	21.	1.	1.	1.	1.
3	1.	1.	1.	34.	1.	1.	1.	1.
4	1.	1.	1.	52.	1.	1.	1.	1.
5	1.	1.	1.	15.	1.	1.	1.	1.
6	1.	1.	1.	56.	1.	1.	1.	1.
7	1.	1.	1.	37.	1.	1.	1.	1.
8	1.	1.	1.	57.	1.	1.	1.	1.
9	1.	1.	1.	16.	1.	1.	1.	1.
10	1.	1.	1.	39.	1.	1.	1.	1.
11	1.	1.	1.	22.	1.	1.	1.	1.
12	1.	1.	1.	61.	1.	1.	1.	1.
13	1.	1.	1.	41.	1.	1.	1.	1.
14	1.	1.	1.	8.	1.	1.	1.	1.
15	1.	1.	1.	18.	1.	1.	1.	1.
16	1.	1.	1.	24.	1.	1.	1.	1.
17	1.	1.	1.	55.	1.	1.	1.	1.
18	1.	1.	1.	28.	1.	1.	1.	1.
19	1.	1.	1.	40.	1.	1.	1.	1.
20	1.	1.	1.	33.	1.	1.	1.	1.
21	1.	1.	1.	2.	1.	1.	1.	1.
22	1.	1.	1.	38.	1.	1.	1.	1.
23	1.	1.	1.	60.	1.	1.	1.	1.
24	1.	1.	1.	17.	1.	1.	1.	1.
25	1.	1.	1.	43.	1.	1.	1.	1.
26	1.	1.	1.	53.	1.	1.	1.	1.
27	1.	1.	1.	64.	1.	1.	1.	1.
28	1.	1.	1.	63.	1.	1.	1.	1.
29	1.	1.	1.	29.	1.	1.	1.	1.
30	1.	1.	1.	1.	1.	1.	1.	1.
31	1.	1.	1.	10.	1.	1.	1.	1.
32	1.	1.	1.	66.	1.	1.	1.	1.
33	1.	1.	1.	23.	1.	1.	1.	1.
34	1.	1.	1.	65.	1.	1.	1.	1.
35	1.	1.	1.	14.	1.	1.	1.	1.
36	1.	1.	1.	6.	1.	1.	1.	1.
37	1.	1.	1.	59.	1.	1.	1.	1.
38	1.	1.	1.	44.	1.	1.	1.	1.
39	1.	1.	1.	5.	1.	1.	1.	1.
40	1.	1.	1.	3.	1.	1.	1.	1.
41	1.	1.	1.	27.	1.	1.	1.	1.
42	1.	1.	1.	25.	1.	1.	1.	1.
43	1.	1.	1.	48.	1.	1.	1.	1.
44	1.	1.	1.	12.	1.	1.	1.	1.
45	1.	1.	1.	9.	1.	1.	1.	1.
46	1.	1.	1.	19.	1.	1.	1.	1.
47	1.	1.	1.	46.	1.	1.	1.	1.
48	1.	1.	1.	62.	1.	1.	1.	1.
49	1.	1.	1.	13.	1.	1.	1.	1.
50	1.	1.	1.	11.	1.	1.	1.	1.
51	1.	1.	1.	26.	1.	1.	1.	1.
52	1.	1.	1.	45.	1.	1.	1.	1.

Table B-2 1992 BRAGFLO Ranks of Computed Variable Values for CAVITY_2 (Concluded)

Run No.	Porosity	Permeability	Compressibility	BCEXP	BCBRSAT	BC GSSAT	BCFLG	BC PCT
53	1.	1.	1.	58.	1.	1.	1.	1.
54	1.	1.	1.	20.	1.	1.	1.	1.
55	1.	1.	1.	32.	1.	1.	1.	1.
56	1.	1.	1.	51.	1.	1.	1.	1.
57	1.	1.	1.	68.	1.	1.	1.	1.
58	1.	1.	1.	31.	1.	1.	1.	1.
59	1.	1.	1.	67.	1.	1.	1.	1.
60	1.	1.	1.	70.	1.	1.	1.	1.
61	1.	1.	1.	36.	1.	1.	1.	1.
62	1.	1.	1.	7.	1.	1.	1.	1.
63	1.	1.	1.	47.	1.	1.	1.	1.
64	1.	1.	1.	42.	1.	1.	1.	1.
65	1.	1.	1.	4.	1.	1.	1.	1.
66	1.	1.	1.	35.	1.	1.	1.	1.
67	1.	1.	1.	54.	1.	1.	1.	1.
68	1.	1.	1.	50.	1.	1.	1.	1.
69	1.	1.	1.	49.	1.	1.	1.	1.
70	1.	1.	1.	30.	1.	1.	1.	1.

Table B-2 1992 BRAGFLO Computed Variable Values for CULEBRA

Run No.	Porosity	Permeability	Compressibility	BCEXP	BCBRSAT	BCGSSAT	BCFLG	BC PCT
1	1.1430×10^{-1}	2.0991×10^{-14}	1.8795×10^{-9}	7.0000×10^{-1}	2.0000×10^{-1}	2.0000×10^{-1}	1.0000	3.0253×10^{4}
2	1.8220×10^{-1}	2.0991×10^{-14}	1.0859×10^{-9}	7.0000×10^{-1}	2.0000×10^{-1}	2.0000×10^{-1}	1.0000	3.0253×10^{4}
3	1.7260×10^{-1}	2.0991×10^{-14}	1.1602×10^{-9}	7.0000×10^{-1}	2.0000×10^{-1}	2.0000×10^{-1}	1.0000	3.0253×10^{4}
4	1.2840×10^{-1}	2.0991×10^{-14}	1.6457×10^{-9}	7.0000×10^{-1}	2.0000×10^{-1}	2.0000×10^{-1}	1.0000	3.0253×10^{4}
5	1.2200×10^{-1}	2.0991×10^{-14}	1.7451×10^{-9}	7.0000×10^{-1}	2.0000×10^{-1}	2.0000×10^{-1}	1.0000	3.0253×10^{4}
6	1.7830×10^{-1}	2.0991×10^{-14}	1.1151×10^{-9}	7.0000×10^{-1}	2.0000×10^{-1}	2.0000×10^{-1}	1.0000	3.0253×10^{4}
7	1.2060×10^{-1}	2.0991×10^{-14}	1.7683×10^{-9}	7.0000×10^{-1}	2.0000×10^{-1}	2.0000×10^{-1}	1.0000	3.0253×10^{4}
8	1.0450×10^{-1}	2.0991×10^{-14}	2.0792×10^{-9}	7.0000×10^{-1}	2.0000×10^{-1}	2.0000×10^{-1}	1.0000	3.0253×10^{4}
9	1.2100×10^{-1}	2.0991×10^{-14}	1.7616×10^{-9}	7.0000×10^{-1}	2.0000×10^{-1}	2.0000×10^{-1}	1.0000	3.0253×10^{4}
10	1.6340×10^{-1}	2.0991×10^{-14}	1.2396×10^{-9}	7.0000×10^{-1}	2.0000×10^{-1}	2.0000×10^{-1}	1.0000	3.0253×10^{4}
11	1.7880×10^{-1}	2.0991×10^{-14}	1.1113×10^{-9}	7.0000×10^{-1}	2.0000×10^{-1}	2.0000×10^{-1}	1.0000	3.0253×10^{4}
12	1.3740×10^{-1}	2.0991×10^{-14}	1.5215×10^{-9}	7.0000×10^{-1}	2.0000×10^{-1}	2.0000×10^{-1}	1.0000	3.0253×10^{4}
13	1.1150×10^{-1}	2.0991×10^{-14}	1.9330×10^{-9}	7.0000×10^{-1}	2.0000×10^{-1}	2.0000×10^{-1}	1.0000	3.0253×10^{4}
14	1.2590×10^{-1}	2.0991×10^{-14}	1.6833×10^{-9}	7.0000×10^{-1}	2.0000×10^{-1}	2.0000×10^{-1}	1.0000	3.0253×10^{4}
15	1.0750×10^{-1}	2.0991×10^{-14}	2.0142×10^{-9}	7.0000×10^{-1}	2.0000×10^{-1}	2.0000×10^{-1}	1.0000	3.0253×10^{4}
16	1.2290×10^{-1}	2.0991×10^{-14}	1.7305×10^{-9}	7.0000×10^{-1}	2.0000×10^{-1}	2.0000×10^{-1}	1.0000	3.0253×10^{4}
17	1.4460×10^{-1}	2.0991×10^{-14}	1.4333×10^{-9}	7.0000×10^{-1}	2.0000×10^{-1}	2.0000×10^{-1}	1.0000	3.0253×10^{4}
18	1.7820×10^{-1}	2.0991×10^{-14}	1.1159×10^{-9}	7.0000×10^{-1}	2.0000×10^{-1}	2.0000×10^{-1}	1.0000	3.0253×10^{4}
19	7.6020×10^{-2}	2.0991×10^{-14}	2.9519×10^{-9}	7.0000×10^{-1}	2.0000×10^{-1}	2.0000×10^{-1}	1.0000	3.0253×10^{4}
20	2.0520×10^{-1}	2.0991×10^{-14}	9.3619×10^{-10}	7.0000×10^{-1}	2.0000×10^{-1}	2.0000×10^{-1}	1.0000	3.0253×10^{4}
21	1.0500×10^{-1}	2.0991×10^{-14}	2.0682×10^{-9}	7.0000×10^{-1}	2.0000×10^{-1}	2.0000×10^{-1}	1.0000	3.0253×10^{4}
22	1.3110×10^{-1}	2.0991×10^{-14}	1.6066×10^{-9}	7.0000×10^{-1}	2.0000×10^{-1}	2.0000×10^{-1}	1.0000	3.0253×10^{4}
23	1.4220×10^{-1}	2.0991×10^{-14}	1.4617×10^{-9}	7.0000×10^{-1}	2.0000×10^{-1}	2.0000×10^{-1}	1.0000	3.0253×10^{4}
24	1.4510×10^{-1}	2.0991×10^{-14}	1.4275×10^{-9}	7.0000×10^{-1}	2.0000×10^{-1}	2.0000×10^{-1}	1.0000	3.0253×10^{4}
25	2.0340×10^{-1}	2.0991×10^{-14}	9.4668×10^{-10}	7.0000×10^{-1}	2.0000×10^{-1}	2.0000×10^{-1}	1.0000	3.0253×10^{4}
26	2.0780×10^{-1}	2.0991×10^{-14}	9.2134×10^{-10}	7.0000×10^{-1}	2.0000×10^{-1}	2.0000×10^{-1}	1.0000	3.0253×10^{4}
27	1.6470×10^{-1}	2.0991×10^{-14}	1.2279×10^{-9}	7.0000×10^{-1}	2.0000×10^{-1}	2.0000×10^{-1}	1.0000	3.0253×10^{4}
28	1.8890×10^{-1}	2.0991×10^{-14}	1.0385×10^{-9}	7.0000×10^{-1}	2.0000×10^{-1}	2.0000×10^{-1}	1.0000	3.0253×10^{4}
29	1.5540×10^{-1}	2.0991×10^{-14}	1.3163×10^{-9}	7.0000×10^{-1}	2.0000×10^{-1}	2.0000×10^{-1}	1.0000	3.0253×10^{4}
30	1.6620×10^{-1}	2.0991×10^{-14}	1.2145×10^{-9}	7.0000×10^{-1}	2.0000×10^{-1}	2.0000×10^{-1}	1.0000	3.0253×10^{4}
31	1.0200×10^{-1}	2.0991×10^{-14}	2.1363×10^{-9}	7.0000×10^{-1}	2.0000×10^{-1}	2.0000×10^{-1}	1.0000	3.0253×10^{4}
32	1.2240×10^{-1}	2.0991×10^{-14}	1.7386×10^{-9}	7.0000×10^{-1}	2.0000×10^{-1}	2.0000×10^{-1}	1.0000	3.0253×10^{4}
33	1.2550×10^{-1}	2.0991×10^{-14}	1.6895×10^{-9}	7.0000×10^{-1}	2.0000×10^{-1}	2.0000×10^{-1}	1.0000	3.0253×10^{4}
34	1.4580×10^{-1}	2.0991×10^{-14}	1.4195×10^{-9}	7.0000×10^{-1}	2.0000×10^{-1}	2.0000×10^{-1}	1.0000	3.0253×10^{4}
35	2.0210×10^{-1}	2.0991×10^{-14}	9.5438×10^{-10}	7.0000×10^{-1}	2.0000×10^{-1}	2.0000×10^{-1}	1.0000	3.0253×10^{4}
36	1.7180×10^{-1}	2.0991×10^{-14}	1.1668×10^{-9}	7.0000×10^{-1}	2.0000×10^{-1}	2.0000×10^{-1}	1.0000	3.0253×10^{4}
37	1.0990×10^{-1}	2.0991×10^{-14}	1.9648×10^{-9}	7.0000×10^{-1}	2.0000×10^{-1}	2.0000×10^{-1}	1.0000	3.0253×10^{4}
38	1.1960×10^{-1}	2.0991×10^{-14}	1.7852×10^{-9}	7.0000×10^{-1}	2.0000×10^{-1}	2.0000×10^{-1}	1.0000	3.0253×10^{4}
39	1.3280×10^{-1}	2.0991×10^{-14}	1.5829×10^{-9}	7.0000×10^{-1}	2.0000×10^{-1}	2.0000×10^{-1}	1.0000	3.0253×10^{4}
40	1.9160×10^{-1}	2.0991×10^{-14}	1.0204×10^{-9}	7.0000×10^{-1}	2.0000×10^{-1}	2.0000×10^{-1}	1.0000	3.0253×10^{4}
41	1.4310×10^{-1}	2.0991×10^{-14}	1.4510×10^{-9}	7.0000×10^{-1}	2.0000×10^{-1}	2.0000×10^{-1}	1.0000	3.0253×10^{4}
42	9.5620×10^{-2}	2.0991×10^{-14}	2.2955×10^{-9}	7.0000×10^{-1}	2.0000×10^{-1}	2.0000×10^{-1}	1.0000	3.0253×10^{4}
43	1.2150×10^{-1}	2.0991×10^{-14}	1.7533×10^{-9}	7.0000×10^{-1}	2.0000×10^{-1}	2.0000×10^{-1}	1.0000	3.0253×10^{4}
44	1.5930×10^{-1}	2.0991×10^{-14}	1.2780×10^{-9}	7.0000×10^{-1}	2.0000×10^{-1}	2.0000×10^{-1}	1.0000	3.0253×10^{4}
45	1.6170×10^{-1}	2.0991×10^{-14}	1.2553×10^{-9}	7.0000×10^{-1}	2.0000×10^{-1}	2.0000×10^{-1}	1.0000	3.0253×10^{4}
46	1.3680×10^{-1}	2.0991×10^{-14}	1.5293×10^{-9}	7.0000×10^{-1}	2.0000×10^{-1}	2.0000×10^{-1}	1.0000	3.0253×10^{4}
47	7.9990×10^{-2}	2.0991×10^{-14}	2.7930×10^{-9}	7.0000×10^{-1}	2.0000×10^{-1}	2.0000×10^{-1}	1.0000	3.0253×10^{4}
48	1.4620×10^{-1}	2.0991×10^{-14}	1.4149×10^{-9}	7.0000×10^{-1}	2.0000×10^{-1}	2.0000×10^{-1}	1.0000	3.0253×10^{4}
49	1.2310×10^{-1}	2.0991×10^{-14}	1.7273×10^{-9}	7.0000×10^{-1}	2.0000×10^{-1}	2.0000×10^{-1}	1.0000	3.0253×10^{4}
50	6.4050×10^{-2}	2.0991×10^{-14}	3.5502×10^{-9}	7.0000×10^{-1}	2.0000×10^{-1}	2.0000×10^{-1}	1.0000	3.0253×10^{4}
51	1.0650×10^{-1}	2.0991×10^{-14}	2.0355×10^{-9}	7.0000×10^{-1}	2.0000×10^{-1}	2.0000×10^{-1}	1.0000	3.0253×10^{4}
52	2.4520×10^{-1}	2.0991×10^{-14}	7.4268×10^{-10}	7.0000×10^{-1}	2.0000×10^{-1}	2.0000×10^{-1}	1.0000	3.0253×10^{4}

Table B-2 1992 BRAGFLO Computed Variable Values for CULEBRA (Concluded)

Run No.	Porosity	Permeability	Compressibility	BCEXP	BCBRSAT	BCGSSAT	BCFLG	BC PCT
53	1.6180×10^{-1}	2.0991×10^{-14}	1.2544×10^{-9}	7.0000×10^{-1}	2.0000×10^{-1}	2.0000×10^{-1}	1.0000	3.0253×10^{4}
54	2.1840×10^{-1}	2.0991×10^{-14}	8.6449×10^{-10}	7.0000×10^{-1}	2.0000×10^{-1}	2.0000×10^{-1}	1.0000	3.0253×10^{4}
55	1.7930×10^{-1}	2.0991×10^{-14}	1.1075×10^{-9}	7.0000×10^{-1}	2.0000×10^{-1}	2.0000×10^{-1}	1.0000	3.0253×10^{4}
56	1.6170×10^{-1}	2.0991×10^{-14}	1.2553×10^{-9}	7.0000×10^{-1}	2.0000×10^{-1}	2.0000×10^{-1}	1.0000	3.0253×10^{4}
57	1.4880×10^{-1}	2.0991×10^{-14}	1.3858×10^{-9}	7.0000×10^{-1}	2.0000×10^{-1}	2.0000×10^{-1}	1.0000	3.0253×10^{4}
58	1.7840×10^{-1}	2.0991×10^{-14}	1.1144×10^{-9}	7.0000×10^{-1}	2.0000×10^{-1}	2.0000×10^{-1}	1.0000	3.0253×10^{4}
59	1.4090×10^{-1}	2.0991×10^{-14}	1.4775×10^{-9}	7.0000×10^{-1}	2.0000×10^{-1}	2.0000×10^{-1}	1.0000	3.0253×10^{4}
60	9.7870×10^{-2}	2.0991×10^{-14}	2.2370×10^{-9}	7.0000×10^{-1}	2.0000×10^{-1}	2.0000×10^{-1}	1.0000	3.0253×10^{4}
61	1.1710×10^{-1}	2.0991×10^{-14}	1.8286×10^{-9}	7.0000×10^{-1}	2.0000×10^{-1}	2.0000×10^{-1}	1.0000	3.0253×10^{4}
62	1.7810×10^{-1}	2.0991×10^{-14}	1.1167×10^{-9}	7.0000×10^{-1}	2.0000×10^{-1}	2.0000×10^{-1}	1.0000	3.0253×10^{4}
63	1.1510×10^{-1}	2.0991×10^{-14}	1.8647×10^{-9}	7.0000×10^{-1}	2.0000×10^{-1}	2.0000×10^{-1}	1.0000	3.0253×10^{4}
64	1.6240×10^{-1}	2.0991×10^{-14}	1.2488×10^{-9}	7.0000×10^{-1}	2.0000×10^{-1}	2.0000×10^{-1}	1.0000	3.0253×10^{4}
65	1.0040×10^{-1}	2.0991×10^{-14}	2.1744×10^{-9}	7.0000×10^{-1}	2.0000×10^{-1}	2.0000×10^{-1}	1.0000	3.0253×10^{4}
66	2.0620×10^{-1}	2.0991×10^{-14}	9.3043×10^{-10}	7.0000×10^{-1}	2.0000×10^{-1}	2.0000×10^{-1}	1.0000	3.0253×10^{4}
67	2.3870×10^{-1}	2.0991×10^{-14}	7.6971×10^{-10}	7.0000×10^{-1}	2.0000×10^{-1}	2.0000×10^{-1}	1.0000	3.0253×10^{4}
68	1.2380×10^{-1}	2.0991×10^{-14}	1.7161×10^{-9}	7.0000×10^{-1}	2.0000×10^{-1}	2.0000×10^{-1}	1.0000	3.0253×10^{4}
69	1.7800×10^{-1}	2.0991×10^{-14}	1.1175×10^{-9}	7.0000×10^{-1}	2.0000×10^{-1}	2.0000×10^{-1}	1.0000	3.0253×10^{4}
70	1.6170×10^{-1}	2.0991×10^{-14}	1.2553×10^{-9}	7.0000×10^{-1}	2.0000×10^{-1}	2.0000×10^{-1}	1.0000	3.0253×10^{4}

Table B-2 1992 BRAGFLO Ranks of Computed Variable Values for CULEBRA

Run No.	Porosity	Permeability	Compressibility	BCEXP	BCBRSAT	BCGSSAT	BCFLG	BC PCT
1	14.	1.	57.	1.	1.	1.	1.	1.
2	60.	1.	11.	1.	1.	1.	1.	1.
3	52.	1.	19.	1.	1.	1.	1.	1.
4	28.	1.	43.	1.	1.	1.	1.	1.
5	21.	1.	50.	1.	1.	1.	1.	1.
6	56.	1.	15.	1.	1.	1.	1.	1.
7	18.	1.	53.	1.	1.	1.	1.	1.
8	8.	1.	63.	1.	1.	1.	1.	1.
9	19.	1.	52.	1.	1.	1.	1.	1.
10	48.	1.	23.	1.	1.	1.	1.	1.
11	58.	1.	13.	1.	1.	1.	1.	1.
12	32.	1.	39.	1.	1.	1.	1.	1.
13	13.	1.	58.	1.	1.	1.	1.	1.
14	27.	1.	44.	1.	1.	1.	1.	1.
15	11.	1.	60.	1.	1.	1.	1.	1.
16	23.	1.	48.	1.	1.	1.	1.	1.
17	36.	1.	35.	1.	1.	1.	1.	1.
18	55.	1.	16.	1.	1.	1.	1.	1.
19	2.	1.	69.	1.	1.	1.	1.	1.
20	65.	1.	6.	1.	1.	1.	1.	1.
21	9.	1.	62.	1.	1.	1.	1.	1.
22	29.	1.	42.	1.	1.	1.	1.	1.
23	34.	1.	37.	1.	1.	1.	1.	1.
24	37.	1.	34.	1.	1.	1.	1.	1.
25	64.	1.	7.	1.	1.	1.	1.	1.
26	67.	1.	4.	1.	1.	1.	1.	1.
27	49.	1.	22.	1.	1.	1.	1.	1.
28	61.	1.	10.	1.	1.	1.	1.	1.
29	41.	1.	30.	1.	1.	1.	1.	1.
30	50.	1.	21.	1.	1.	1.	1.	1.
31	7.	1.	64.	1.	1.	1.	1.	1.
32	22.	1.	49.	1.	1.	1.	1.	1.
33	26.	1.	45.	1.	1.	1.	1.	1.
34	38.	1.	33.	1.	1.	1.	1.	1.
35	63.	1.	8.	1.	1.	1.	1.	1.
36	51.	1.	20.	1.	1.	1.	1.	1.
37	12.	1.	59.	1.	1.	1.	1.	1.
38	17.	1.	54.	1.	1.	1.	1.	1.
39	30.	1.	41.	1.	1.	1.	1.	1.
40	62.	1.	9.	1.	1.	1.	1.	1.
41	35.	1.	36.	1.	1.	1.	1.	1.
42	4.	1.	67.	1.	1.	1.	1.	1.
43	20.	1.	51.	1.	1.	1.	1.	1.
44	42.	1.	29.	1.	1.	1.	1.	1.
45	43.	1.	26.	1.	1.	1.	1.	1.
46	31.	1.	40.	1.	1.	1.	1.	1.
47	3.	1.	68.	1.	1.	1.	1.	1.
48	39.	1.	32.	1.	1.	1.	1.	1.
49	24.	1.	47.	1.	1.	1.	1.	1.
50	1.	1.	70.	1.	1.	1.	1.	1.
51	10.	1.	61.	1.	1.	1.	1.	1.
52	70.	1.	1.	1.	1.	1.	1.	1.

Table B-2 1992 BRAGFLO Ranks of Computed Variable Values for CULEBRA (Concluded)

Run No.	Porosity	Permeability	Compressibility	BCEXP	BCBRSAT	BGSSAT	BCFLG	BC PCT
53	46.	1.	25.	1.	1.	1.	1.	1.
54	68.	1.	3.	1.	1.	1.	1.	1.
55	59.	1.	12.	1.	1.	1.	1.	1.
56	43.	1.	26.	1.	1.	1.	1.	1.
57	40.	1.	31.	1.	1.	1.	1.	1.
58	57.	1.	14.	1.	1.	1.	1.	1.
59	33.	1.	38.	1.	1.	1.	1.	1.
60	5.	1.	66.	1.	1.	1.	1.	1.
61	16.	1.	55.	1.	1.	1.	1.	1.
62	54.	1.	17.	1.	1.	1.	1.	1.
63	15.	1.	56.	1.	1.	1.	1.	1.
64	47.	1.	24.	1.	1.	1.	1.	1.
65	6.	1.	65.	1.	1.	1.	1.	1.
66	66.	1.	5.	1.	1.	1.	1.	1.
67	69.	1.	2.	1.	1.	1.	1.	1.
68	25.	1.	46.	1.	1.	1.	1.	1.
69	53.	1.	18.	1.	1.	1.	1.	1.
70	43.	1.	26.	1.	1.	1.	1.	1.

Table B-2 1992 BRAGFLO Computed Variable Values for CULEBRA1

Run No.	Porosity	Permeability	Compressibility	BCEXP	BCBRSAT	BCGSSAT	BCFLG	BC PCT
1	1.1430×10^{-1}	0.0000	0.0000	7.0000×10^{-1}	2.0000×10^{-1}	2.0000×10^{-1}	1.0000	0.0000
2	1.8220×10^{-1}	0.0000	0.0000	7.0000×10^{-1}	2.0000×10^{-1}	2.0000×10^{-1}	1.0000	0.0000
3	1.7260×10^{-1}	0.0000	0.0000	7.0000×10^{-1}	2.0000×10^{-1}	2.0000×10^{-1}	1.0000	0.0000
4	1.2840×10^{-1}	0.0000	0.0000	7.0000×10^{-1}	2.0000×10^{-1}	2.0000×10^{-1}	1.0000	0.0000
5	1.2200×10^{-1}	0.0000	0.0000	7.0000×10^{-1}	2.0000×10^{-1}	2.0000×10^{-1}	1.0000	0.0000
6	1.7830×10^{-1}	0.0000	0.0000	7.0000×10^{-1}	2.0000×10^{-1}	2.0000×10^{-1}	1.0000	0.0000
7	1.2060×10^{-1}	0.0000	0.0000	7.0000×10^{-1}	2.0000×10^{-1}	2.0000×10^{-1}	1.0000	0.0000
8	1.0450×10^{-1}	0.0000	0.0000	7.0000×10^{-1}	2.0000×10^{-1}	2.0000×10^{-1}	1.0000	0.0000
9	1.2100×10^{-1}	0.0000	0.0000	7.0000×10^{-1}	2.0000×10^{-1}	2.0000×10^{-1}	1.0000	0.0000
10	1.6340×10^{-1}	0.0000	0.0000	7.0000×10^{-1}	2.0000×10^{-1}	2.0000×10^{-1}	1.0000	0.0000
11	1.7880×10^{-1}	0.0000	0.0000	7.0000×10^{-1}	2.0000×10^{-1}	2.0000×10^{-1}	1.0000	0.0000
12	1.3740×10^{-1}	0.0000	0.0000	7.0000×10^{-1}	2.0000×10^{-1}	2.0000×10^{-1}	1.0000	0.0000
13	1.1150×10^{-1}	0.0000	0.0000	7.0000×10^{-1}	2.0000×10^{-1}	2.0000×10^{-1}	1.0000	0.0000
14	1.2590×10^{-1}	0.0000	0.0000	7.0000×10^{-1}	2.0000×10^{-1}	2.0000×10^{-1}	1.0000	0.0000
15	1.0750×10^{-1}	0.0000	0.0000	7.0000×10^{-1}	2.0000×10^{-1}	2.0000×10^{-1}	1.0000	0.0000
16	1.2290×10^{-1}	0.0000	0.0000	7.0000×10^{-1}	2.0000×10^{-1}	2.0000×10^{-1}	1.0000	0.0000
17	1.4460×10^{-1}	0.0000	0.0000	7.0000×10^{-1}	2.0000×10^{-1}	2.0000×10^{-1}	1.0000	0.0000
18	1.7820×10^{-1}	0.0000	0.0000	7.0000×10^{-1}	2.0000×10^{-1}	2.0000×10^{-1}	1.0000	0.0000
19	7.6020×10^{-2}	0.0000	0.0000	7.0000×10^{-1}	2.0000×10^{-1}	2.0000×10^{-1}	1.0000	0.0000
20	2.0520×10^{-1}	0.0000	0.0000	7.0000×10^{-1}	2.0000×10^{-1}	2.0000×10^{-1}	1.0000	0.0000
21	1.0500×10^{-1}	0.0000	0.0000	7.0000×10^{-1}	2.0000×10^{-1}	2.0000×10^{-1}	1.0000	0.0000
22	1.3110×10^{-1}	0.0000	0.0000	7.0000×10^{-1}	2.0000×10^{-1}	2.0000×10^{-1}	1.0000	0.0000
23	1.4220×10^{-1}	0.0000	0.0000	7.0000×10^{-1}	2.0000×10^{-1}	2.0000×10^{-1}	1.0000	0.0000
24	1.4510×10^{-1}	0.0000	0.0000	7.0000×10^{-1}	2.0000×10^{-1}	2.0000×10^{-1}	1.0000	0.0000
25	2.0340×10^{-1}	0.0000	0.0000	7.0000×10^{-1}	2.0000×10^{-1}	2.0000×10^{-1}	1.0000	0.0000
26	2.0780×10^{-1}	0.0000	0.0000	7.0000×10^{-1}	2.0000×10^{-1}	2.0000×10^{-1}	1.0000	0.0000
27	1.6470×10^{-1}	0.0000	0.0000	7.0000×10^{-1}	2.0000×10^{-1}	2.0000×10^{-1}	1.0000	0.0000
28	1.8890×10^{-1}	0.0000	0.0000	7.0000×10^{-1}	2.0000×10^{-1}	2.0000×10^{-1}	1.0000	0.0000
29	1.5540×10^{-1}	0.0000	0.0000	7.0000×10^{-1}	2.0000×10^{-1}	2.0000×10^{-1}	1.0000	0.0000
30	1.6620×10^{-1}	0.0000	0.0000	7.0000×10^{-1}	2.0000×10^{-1}	2.0000×10^{-1}	1.0000	0.0000
31	1.0200×10^{-1}	0.0000	0.0000	7.0000×10^{-1}	2.0000×10^{-1}	2.0000×10^{-1}	1.0000	0.0000
32	1.2240×10^{-1}	0.0000	0.0000	7.0000×10^{-1}	2.0000×10^{-1}	2.0000×10^{-1}	1.0000	0.0000
33	1.2550×10^{-1}	0.0000	0.0000	7.0000×10^{-1}	2.0000×10^{-1}	2.0000×10^{-1}	1.0000	0.0000
34	1.4580×10^{-1}	0.0000	0.0000	7.0000×10^{-1}	2.0000×10^{-1}	2.0000×10^{-1}	1.0000	0.0000
35	2.0210×10^{-1}	0.0000	0.0000	7.0000×10^{-1}	2.0000×10^{-1}	2.0000×10^{-1}	1.0000	0.0000
36	1.7180×10^{-1}	0.0000	0.0000	7.0000×10^{-1}	2.0000×10^{-1}	2.0000×10^{-1}	1.0000	0.0000
37	1.0990×10^{-1}	0.0000	0.0000	7.0000×10^{-1}	2.0000×10^{-1}	2.0000×10^{-1}	1.0000	0.0000
38	1.1960×10^{-1}	0.0000	0.0000	7.0000×10^{-1}	2.0000×10^{-1}	2.0000×10^{-1}	1.0000	0.0000
39	1.3280×10^{-1}	0.0000	0.0000	7.0000×10^{-1}	2.0000×10^{-1}	2.0000×10^{-1}	1.0000	0.0000
40	1.9160×10^{-1}	0.0000	0.0000	7.0000×10^{-1}	2.0000×10^{-1}	2.0000×10^{-1}	1.0000	0.0000
41	1.4310×10^{-1}	0.0000	0.0000	7.0000×10^{-1}	2.0000×10^{-1}	2.0000×10^{-1}	1.0000	0.0000
42	9.5620×10^{-2}	0.0000	0.0000	7.0000×10^{-1}	2.0000×10^{-1}	2.0000×10^{-1}	1.0000	0.0000
43	1.2150×10^{-1}	0.0000	0.0000	7.0000×10^{-1}	2.0000×10^{-1}	2.0000×10^{-1}	1.0000	0.0000
44	1.5930×10^{-1}	0.0000	0.0000	7.0000×10^{-1}	2.0000×10^{-1}	2.0000×10^{-1}	1.0000	0.0000
45	1.6170×10^{-1}	0.0000	0.0000	7.0000×10^{-1}	2.0000×10^{-1}	2.0000×10^{-1}	1.0000	0.0000
46	1.3680×10^{-1}	0.0000	0.0000	7.0000×10^{-1}	2.0000×10^{-1}	2.0000×10^{-1}	1.0000	0.0000
47	7.9990×10^{-2}	0.0000	0.0000	7.0000×10^{-1}	2.0000×10^{-1}	2.0000×10^{-1}	1.0000	0.0000
48	1.4620×10^{-1}	0.0000	0.0000	7.0000×10^{-1}	2.0000×10^{-1}	2.0000×10^{-1}	1.0000	0.0000
49	1.2310×10^{-1}	0.0000	0.0000	7.0000×10^{-1}	2.0000×10^{-1}	2.0000×10^{-1}	1.0000	0.0000
50	6.4050×10^{-2}	0.0000	0.0000	7.0000×10^{-1}	2.0000×10^{-1}	2.0000×10^{-1}	1.0000	0.0000
51	1.0650×10^{-1}	0.0000	0.0000	7.0000×10^{-1}	2.0000×10^{-1}	2.0000×10^{-1}	1.0000	0.0000
52	2.4520×10^{-1}	0.0000	0.0000	7.0000×10^{-1}	2.0000×10^{-1}	2.0000×10^{-1}	1.0000	0.0000

Table B-2 1992 BRAGFLO Computed Variable Values for CULEBRA1 (Concluded)

Run No.	Porosity	Permeability	Compressibility	BCEXP	BCBRSAT	BCGSSAT	BCFLG	BC PCT
53	1.6180×10^{-1}	0.0000	0.0000	7.0000×10^{-1}	2.0000×10^{-1}	2.0000×10^{-1}	1.0000	0.0000
54	2.1840×10^{-1}	0.0000	0.0000	7.0000×10^{-1}	2.0000×10^{-1}	2.0000×10^{-1}	1.0000	0.0000
55	1.7930×10^{-1}	0.0000	0.0000	7.0000×10^{-1}	2.0000×10^{-1}	2.0000×10^{-1}	1.0000	0.0000
56	1.6170×10^{-1}	0.0000	0.0000	7.0000×10^{-1}	2.0000×10^{-1}	2.0000×10^{-1}	1.0000	0.0000
57	1.4880×10^{-1}	0.0000	0.0000	7.0000×10^{-1}	2.0000×10^{-1}	2.0000×10^{-1}	1.0000	0.0000
58	1.7840×10^{-1}	0.0000	0.0000	7.0000×10^{-1}	2.0000×10^{-1}	2.0000×10^{-1}	1.0000	0.0000
59	1.4090×10^{-1}	0.0000	0.0000	7.0000×10^{-1}	2.0000×10^{-1}	2.0000×10^{-1}	1.0000	0.0000
60	9.7870×10^{-2}	0.0000	0.0000	7.0000×10^{-1}	2.0000×10^{-1}	2.0000×10^{-1}	1.0000	0.0000
61	1.1710×10^{-1}	0.0000	0.0000	7.0000×10^{-1}	2.0000×10^{-1}	2.0000×10^{-1}	1.0000	0.0000
62	1.7810×10^{-1}	0.0000	0.0000	7.0000×10^{-1}	2.0000×10^{-1}	2.0000×10^{-1}	1.0000	0.0000
63	1.1510×10^{-1}	0.0000	0.0000	7.0000×10^{-1}	2.0000×10^{-1}	2.0000×10^{-1}	1.0000	0.0000
64	1.6240×10^{-1}	0.0000	0.0000	7.0000×10^{-1}	2.0000×10^{-1}	2.0000×10^{-1}	1.0000	0.0000
65	1.0040×10^{-1}	0.0000	0.0000	7.0000×10^{-1}	2.0000×10^{-1}	2.0000×10^{-1}	1.0000	0.0000
66	2.0620×10^{-1}	0.0000	0.0000	7.0000×10^{-1}	2.0000×10^{-1}	2.0000×10^{-1}	1.0000	0.0000
67	2.3870×10^{-1}	0.0000	0.0000	7.0000×10^{-1}	2.0000×10^{-1}	2.0000×10^{-1}	1.0000	0.0000
68	1.2380×10^{-1}	0.0000	0.0000	7.0000×10^{-1}	2.0000×10^{-1}	2.0000×10^{-1}	1.0000	0.0000
69	1.7800×10^{-1}	0.0000	0.0000	7.0000×10^{-1}	2.0000×10^{-1}	2.0000×10^{-1}	1.0000	0.0000
70	1.6170×10^{-1}	0.0000	0.0000	7.0000×10^{-1}	2.0000×10^{-1}	2.0000×10^{-1}	1.0000	0.0000

Table B-2 1992 BRAGFLO Ranks of Computed Variable Values for CULEBRA1

Run No.	Porosity	Permeability	Compressibility	BCEXP	BCBRSAT	BCGSSAT	BCFLG	BC PCT
1	14.	1.	1.	1.	1.	1.	1.	1.
2	60.	1.	1.	1.	1.	1.	1.	1.
3	52.	1.	1.	1.	1.	1.	1.	1.
4	28.	1.	1.	1.	1.	1.	1.	1.
5	21.	1.	1.	1.	1.	1.	1.	1.
6	56.	1.	1.	1.	1.	1.	1.	1.
7	18.	1.	1.	1.	1.	1.	1.	1.
8	8.	1.	1.	1.	1.	1.	1.	1.
9	19.	1.	1.	1.	1.	1.	1.	1.
10	48.	1.	1.	1.	1.	1.	1.	1.
11	58.	1.	1.	1.	1.	1.	1.	1.
12	32.	1.	1.	1.	1.	1.	1.	1.
13	13.	1.	1.	1.	1.	1.	1.	1.
14	27.	1.	1.	1.	1.	1.	1.	1.
15	11.	1.	1.	1.	1.	1.	1.	1.
16	23.	1.	1.	1.	1.	1.	1.	1.
17	36.	1.	1.	1.	1.	1.	1.	1.
18	55.	1.	1.	1.	1.	1.	1.	1.
19	2.	1.	1.	1.	1.	1.	1.	1.
20	65.	1.	1.	1.	1.	1.	1.	1.
21	9.	1.	1.	1.	1.	1.	1.	1.
22	29.	1.	1.	1.	1.	1.	1.	1.
23	34.	1.	1.	1.	1.	1.	1.	1.
24	37.	1.	1.	1.	1.	1.	1.	1.
25	64.	1.	1.	1.	1.	1.	1.	1.
26	67.	1.	1.	1.	1.	1.	1.	1.
27	49.	1.	1.	1.	1.	1.	1.	1.
28	61.	1.	1.	1.	1.	1.	1.	1.
29	41.	1.	1.	1.	1.	1.	1.	1.
30	50.	1.	1.	1.	1.	1.	1.	1.
31	7.	1.	1.	1.	1.	1.	1.	1.
32	22.	1.	1.	1.	1.	1.	1.	1.
33	26.	1.	1.	1.	1.	1.	1.	1.
34	38.	1.	1.	1.	1.	1.	1.	1.
35	63.	1.	1.	1.	1.	1.	1.	1.
36	51.	1.	1.	1.	1.	1.	1.	1.
37	12.	1.	1.	1.	1.	1.	1.	1.
38	17.	1.	1.	1.	1.	1.	1.	1.
39	30.	1.	1.	1.	1.	1.	1.	1.
40	62.	1.	1.	1.	1.	1.	1.	1.
41	35.	1.	1.	1.	1.	1.	1.	1.
42	4.	1.	1.	1.	1.	1.	1.	1.
43	20.	1.	1.	1.	1.	1.	1.	1.
44	42.	1.	1.	1.	1.	1.	1.	1.
45	43.	1.	1.	1.	1.	1.	1.	1.
46	31.	1.	1.	1.	1.	1.	1.	1.
47	3.	1.	1.	1.	1.	1.	1.	1.
48	39.	1.	1.	1.	1.	1.	1.	1.
49	24.	1.	1.	1.	1.	1.	1.	1.
50	1.	1.	1.	1.	1.	1.	1.	1.
51	10.	1.	1.	1.	1.	1.	1.	1.
52	70.	1.	1.	1.	1.	1.	1.	1.

Table B-2 1992 BRAGFLO Ranks of Computed Variable Values for CULEBRA1 (Concluded)

Run No.	Porosity	Permeability	Compressibility	BCEXP	BCBRSAT	BCGSSAT	BCFLG	BC PCT
53	46.	1.	1.	1.	1.	1.	1.	1.
54	68.	1.	1.	1.	1.	1.	1.	1.
55	59.	1.	1.	1.	1.	1.	1.	1.
56	43.	1.	1.	1.	1.	1.	1.	1.
57	40.	1.	1.	1.	1.	1.	1.	1.
58	57.	1.	1.	1.	1.	1.	1.	1.
59	33.	1.	1.	1.	1.	1.	1.	1.
60	5.	1.	1.	1.	1.	1.	1.	1.
61	16.	1.	1.	1.	1.	1.	1.	1.
62	54.	1.	1.	1.	1.	1.	1.	1.
63	15.	1.	1.	1.	1.	1.	1.	1.
64	47.	1.	1.	1.	1.	1.	1.	1.
65	6.	1.	1.	1.	1.	1.	1.	1.
66	66.	1.	1.	1.	1.	1.	1.	1.
67	69.	1.	1.	1.	1.	1.	1.	1.
68	25.	1.	1.	1.	1.	1.	1.	1.
69	53.	1.	1.	1.	1.	1.	1.	1.
70	43.	1.	1.	1.	1.	1.	1.	1.

Table B-2 1992 BRAGFLO Computed Variable Values for CULEBRA_SEAL

Run No.	Porosity	Permeability	Compressibility	BCEXP	BCBRSAT	BCGSSAT	BCFLG	BC PCT
1	2.0000×10^{-1}	1.0000×10^{-18}	3.3131×10^{-10}	7.0000×10^{-1}	2.0000×10^{-1}	0.0000	1.0000	9.4665×10^{5}
2	2.0000×10^{-1}	1.0000×10^{-18}	3.3131×10^{-10}	7.0000×10^{-1}	2.0000×10^{-1}	0.0000	1.0000	9.4665×10^{5}
3	2.0000×10^{-1}	1.0000×10^{-18}	3.3131×10^{-10}	7.0000×10^{-1}	2.0000×10^{-1}	0.0000	1.0000	9.4665×10^{5}
4	2.0000×10^{-1}	1.0000×10^{-18}	3.3131×10^{-10}	7.0000×10^{-1}	2.0000×10^{-1}	0.0000	1.0000	9.4665×10^{5}
5	2.0000×10^{-1}	1.0000×10^{-18}	3.3131×10^{-10}	7.0000×10^{-1}	2.0000×10^{-1}	0.0000	1.0000	9.4665×10^{5}
6	2.0000×10^{-1}	1.0000×10^{-18}	3.3131×10^{-10}	7.0000×10^{-1}	2.0000×10^{-1}	0.0000	1.0000	9.4665×10^{5}
7	2.0000×10^{-1}	1.0000×10^{-18}	3.3131×10^{-10}	7.0000×10^{-1}	2.0000×10^{-1}	0.0000	1.0000	9.4665×10^{5}
8	2.0000×10^{-1}	1.0000×10^{-18}	3.3131×10^{-10}	7.0000×10^{-1}	2.0000×10^{-1}	0.0000	1.0000	9.4665×10^{5}
9	2.0000×10^{-1}	1.0000×10^{-18}	3.3131×10^{-10}	7.0000×10^{-1}	2.0000×10^{-1}	0.0000	1.0000	9.4665×10^{5}
10	2.0000×10^{-1}	1.0000×10^{-18}	3.3131×10^{-10}	7.0000×10^{-1}	2.0000×10^{-1}	0.0000	1.0000	9.4665×10^{5}
11	2.0000×10^{-1}	1.0000×10^{-18}	3.3131×10^{-10}	7.0000×10^{-1}	2.0000×10^{-1}	0.0000	1.0000	9.4665×10^{5}
12	2.0000×10^{-1}	1.0000×10^{-18}	3.3131×10^{-10}	7.0000×10^{-1}	2.0000×10^{-1}	0.0000	1.0000	9.4665×10^{5}
13	2.0000×10^{-1}	1.0000×10^{-18}	3.3131×10^{-10}	7.0000×10^{-1}	2.0000×10^{-1}	0.0000	1.0000	9.4665×10^{5}
14	2.0000×10^{-1}	1.0000×10^{-18}	3.3131×10^{-10}	7.0000×10^{-1}	2.0000×10^{-1}	0.0000	1.0000	9.4665×10^{5}
15	2.0000×10^{-1}	1.0000×10^{-18}	3.3131×10^{-10}	7.0000×10^{-1}	2.0000×10^{-1}	0.0000	1.0000	9.4665×10^{5}
16	2.0000×10^{-1}	1.0000×10^{-18}	3.3131×10^{-10}	7.0000×10^{-1}	2.0000×10^{-1}	0.0000	1.0000	9.4665×10^{5}
17	2.0000×10^{-1}	1.0000×10^{-18}	3.3131×10^{-10}	7.0000×10^{-1}	2.0000×10^{-1}	0.0000	1.0000	9.4665×10^{5}
18	2.0000×10^{-1}	1.0000×10^{-18}	3.3131×10^{-10}	7.0000×10^{-1}	2.0000×10^{-1}	0.0000	1.0000	9.4665×10^{5}
19	2.0000×10^{-1}	1.0000×10^{-18}	3.3131×10^{-10}	7.0000×10^{-1}	2.0000×10^{-1}	0.0000	1.0000	9.4665×10^{5}
20	2.0000×10^{-1}	1.0000×10^{-18}	3.3131×10^{-10}	7.0000×10^{-1}	2.0000×10^{-1}	0.0000	1.0000	9.4665×10^{5}
21	2.0000×10^{-1}	1.0000×10^{-18}	3.3131×10^{-10}	7.0000×10^{-1}	2.0000×10^{-1}	0.0000	1.0000	9.4665×10^{5}
22	2.0000×10^{-1}	1.0000×10^{-18}	3.3131×10^{-10}	7.0000×10^{-1}	2.0000×10^{-1}	0.0000	1.0000	9.4665×10^{5}
23	2.0000×10^{-1}	1.0000×10^{-18}	3.3131×10^{-10}	7.0000×10^{-1}	2.0000×10^{-1}	0.0000	1.0000	9.4665×10^{5}
24	2.0000×10^{-1}	1.0000×10^{-18}	3.3131×10^{-10}	7.0000×10^{-1}	2.0000×10^{-1}	0.0000	1.0000	9.4665×10^{5}
25	2.0000×10^{-1}	1.0000×10^{-18}	3.3131×10^{-10}	7.0000×10^{-1}	2.0000×10^{-1}	0.0000	1.0000	9.4665×10^{5}
26	2.0000×10^{-1}	1.0000×10^{-18}	3.3131×10^{-10}	7.0000×10^{-1}	2.0000×10^{-1}	0.0000	1.0000	9.4665×10^{5}
27	2.0000×10^{-1}	1.0000×10^{-18}	3.3131×10^{-10}	7.0000×10^{-1}	2.0000×10^{-1}	0.0000	1.0000	9.4665×10^{5}
28	2.0000×10^{-1}	1.0000×10^{-18}	3.3131×10^{-10}	7.0000×10^{-1}	2.0000×10^{-1}	0.0000	1.0000	9.4665×10^{5}
29	2.0000×10^{-1}	1.0000×10^{-18}	3.3131×10^{-10}	7.0000×10^{-1}	2.0000×10^{-1}	0.0000	1.0000	9.4665×10^{5}
30	2.0000×10^{-1}	1.0000×10^{-18}	3.3131×10^{-10}	7.0000×10^{-1}	2.0000×10^{-1}	0.0000	1.0000	9.4665×10^{5}
31	2.0000×10^{-1}	1.0000×10^{-18}	3.3131×10^{-10}	7.0000×10^{-1}	2.0000×10^{-1}	0.0000	1.0000	9.4665×10^{5}
32	2.0000×10^{-1}	1.0000×10^{-18}	3.3131×10^{-10}	7.0000×10^{-1}	2.0000×10^{-1}	0.0000	1.0000	9.4665×10^{5}
33	2.0000×10^{-1}	1.0000×10^{-18}	3.3131×10^{-10}	7.0000×10^{-1}	2.0000×10^{-1}	0.0000	1.0000	9.4665×10^{5}
34	2.0000×10^{-1}	1.0000×10^{-18}	3.3131×10^{-10}	7.0000×10^{-1}	2.0000×10^{-1}	0.0000	1.0000	9.4665×10^{5}
35	2.0000×10^{-1}	1.0000×10^{-18}	3.3131×10^{-10}	7.0000×10^{-1}	2.0000×10^{-1}	0.0000	1.0000	9.4665×10^{5}
36	2.0000×10^{-1}	1.0000×10^{-18}	3.3131×10^{-10}	7.0000×10^{-1}	2.0000×10^{-1}	0.0000	1.0000	9.4665×10^{5}
37	2.0000×10^{-1}	1.0000×10^{-18}	3.3131×10^{-10}	7.0000×10^{-1}	2.0000×10^{-1}	0.0000	1.0000	9.4665×10^{5}
38	2.0000×10^{-1}	1.0000×10^{-18}	3.3131×10^{-10}	7.0000×10^{-1}	2.0000×10^{-1}	0.0000	1.0000	9.4665×10^{5}
39	2.0000×10^{-1}	1.0000×10^{-18}	3.3131×10^{-10}	7.0000×10^{-1}	2.0000×10^{-1}	0.0000	1.0000	9.4665×10^{5}
40	2.0000×10^{-1}	1.0000×10^{-18}	3.3131×10^{-10}	7.0000×10^{-1}	2.0000×10^{-1}	0.0000	1.0000	9.4665×10^{5}
41	2.0000×10^{-1}	1.0000×10^{-18}	3.3131×10^{-10}	7.0000×10^{-1}	2.0000×10^{-1}	0.0000	1.0000	9.4665×10^{5}
42	2.0000×10^{-1}	1.0000×10^{-18}	3.3131×10^{-10}	7.0000×10^{-1}	2.0000×10^{-1}	0.0000	1.0000	9.4665×10^{5}
43	2.0000×10^{-1}	1.0000×10^{-18}	3.3131×10^{-10}	7.0000×10^{-1}	2.0000×10^{-1}	0.0000	1.0000	9.4665×10^{5}
44	2.0000×10^{-1}	1.0000×10^{-18}	3.3131×10^{-10}	7.0000×10^{-1}	2.0000×10^{-1}	0.0000	1.0000	9.4665×10^{5}
45	2.0000×10^{-1}	1.0000×10^{-18}	3.3131×10^{-10}	7.0000×10^{-1}	2.0000×10^{-1}	0.0000	1.0000	9.4665×10^{5}
46	2.0000×10^{-1}	1.0000×10^{-18}	3.3131×10^{-10}	7.0000×10^{-1}	2.0000×10^{-1}	0.0000	1.0000	9.4665×10^{5}
47	2.0000×10^{-1}	1.0000×10^{-18}	3.3131×10^{-10}	7.0000×10^{-1}	2.0000×10^{-1}	0.0000	1.0000	9.4665×10^{5}
48	2.0000×10^{-1}	1.0000×10^{-18}	3.3131×10^{-10}	7.0000×10^{-1}	2.0000×10^{-1}	0.0000	1.0000	9.4665×10^{5}
49	2.0000×10^{-1}	1.0000×10^{-18}	3.3131×10^{-10}	7.0000×10^{-1}	2.0000×10^{-1}	0.0000	1.0000	9.4665×10^{5}
50	2.0000×10^{-1}	1.0000×10^{-18}	3.3131×10^{-10}	7.0000×10^{-1}	2.0000×10^{-1}	0.0000	1.0000	9.4665×10^{5}
51	2.0000×10^{-1}	1.0000×10^{-18}	3.3131×10^{-10}	7.0000×10^{-1}	2.0000×10^{-1}	0.0000	1.0000	9.4665×10^{5}
52	2.0000×10^{-1}	1.0000×10^{-18}	3.3131×10^{-10}	7.0000×10^{-1}	2.0000×10^{-1}	0.0000	1.0000	9.4665×10^{5}

Table B-2 1992 BRAGFLO Computed Variable Values for CULEBRA_SEAL (Concluded)

Run No.	Porosity	Permeability	Compressibility	BCEXP	BCBRSAT	BCGSSAT	BCFLG	BC PCT
53	2.0000×10^{-1}	1.0000×10^{-18}	3.3131×10^{-10}	7.0000×10^{-1}	2.0000×10^{-1}	0.0000	1.0000	9.4665×10^{5}
54	2.0000×10^{-1}	1.0000×10^{-18}	3.3131×10^{-10}	7.0000×10^{-1}	2.0000×10^{-1}	0.0000	1.0000	9.4665×10^{5}
55	2.0000×10^{-1}	1.0000×10^{-18}	3.3131×10^{-10}	7.0000×10^{-1}	2.0000×10^{-1}	0.0000	1.0000	9.4665×10^{5}
56	2.0000×10^{-1}	1.0000×10^{-18}	3.3131×10^{-10}	7.0000×10^{-1}	2.0000×10^{-1}	0.0000	1.0000	9.4665×10^{5}
57	2.0000×10^{-1}	1.0000×10^{-18}	3.3131×10^{-10}	7.0000×10^{-1}	2.0000×10^{-1}	0.0000	1.0000	9.4665×10^{5}
58	2.0000×10^{-1}	1.0000×10^{-18}	3.3131×10^{-10}	7.0000×10^{-1}	2.0000×10^{-1}	0.0000	1.0000	9.4665×10^{5}
59	2.0000×10^{-1}	1.0000×10^{-18}	3.3131×10^{-10}	7.0000×10^{-1}	2.0000×10^{-1}	0.0000	1.0000	9.4665×10^{5}
60	2.0000×10^{-1}	1.0000×10^{-18}	3.3131×10^{-10}	7.0000×10^{-1}	2.0000×10^{-1}	0.0000	1.0000	9.4665×10^{5}
61	2.0000×10^{-1}	1.0000×10^{-18}	3.3131×10^{-10}	7.0000×10^{-1}	2.0000×10^{-1}	0.0000	1.0000	9.4665×10^{5}
62	2.0000×10^{-1}	1.0000×10^{-18}	3.3131×10^{-10}	7.0000×10^{-1}	2.0000×10^{-1}	0.0000	1.0000	9.4665×10^{5}
63	2.0000×10^{-1}	1.0000×10^{-18}	3.3131×10^{-10}	7.0000×10^{-1}	2.0000×10^{-1}	0.0000	1.0000	9.4665×10^{5}
64	2.0000×10^{-1}	1.0000×10^{-18}	3.3131×10^{-10}	7.0000×10^{-1}	2.0000×10^{-1}	0.0000	1.0000	9.4665×10^{5}
65	2.0000×10^{-1}	1.0000×10^{-18}	3.3131×10^{-10}	7.0000×10^{-1}	2.0000×10^{-1}	0.0000	1.0000	9.4665×10^{5}
66	2.0000×10^{-1}	1.0000×10^{-18}	3.3131×10^{-10}	7.0000×10^{-1}	2.0000×10^{-1}	0.0000	1.0000	9.4665×10^{5}
67	2.0000×10^{-1}	1.0000×10^{-18}	3.3131×10^{-10}	7.0000×10^{-1}	2.0000×10^{-1}	0.0000	1.0000	9.4665×10^{5}
68	2.0000×10^{-1}	1.0000×10^{-18}	3.3131×10^{-10}	7.0000×10^{-1}	2.0000×10^{-1}	0.0000	1.0000	9.4665×10^{5}
69	2.0000×10^{-1}	1.0000×10^{-18}	3.3131×10^{-10}	7.0000×10^{-1}	2.0000×10^{-1}	0.0000	1.0000	9.4665×10^{5}
70	2.0000×10^{-1}	1.0000×10^{-18}	3.3131×10^{-10}	7.0000×10^{-1}	2.0000×10^{-1}	0.0000	1.0000	9.4665×10^{5}

Table B-2 1992 BRAGFLO Ranks of Computed Variable Values for CULEBRA_SEAL

Run No.	Porosity	Permeability	Compressibility	BCEXP	BCBRSAT	BCGSSAT	BCFLG	BC PCT
1	1.	1.	1.	1.	1.	1.	1.	1.
2	1.	1.	1.	1.	1.	1.	1.	1.
3	1.	1.	1.	1.	1.	1.	1.	1.
4	1.	1.	1.	1.	1.	1.	1.	1.
5	1.	1.	1.	1.	1.	1.	1.	1.
6	1.	1.	1.	1.	1.	1.	1.	1.
7	1.	1.	1.	1.	1.	1.	1.	1.
8	1.	1.	1.	1.	1.	1.	1.	1.
9	1.	1.	1.	1.	1.	1.	1.	1.
10	1.	1.	1.	1.	1.	1.	1.	1.
11	1.	1.	1.	1.	1.	1.	1.	1.
12	1.	1.	1.	1.	1.	1.	1.	1.
13	1.	1.	1.	1.	1.	1.	1.	1.
14	1.	1.	1.	1.	1.	1.	1.	1.
15	1.	1.	1.	1.	1.	1.	1.	1.
16	1.	1.	1.	1.	1.	1.	1.	1.
17	1.	1.	1.	1.	1.	1.	1.	1.
18	1.	1.	1.	1.	1.	1.	1.	1.
19	1.	1.	1.	1.	1.	1.	1.	1.
20	1.	1.	1.	1.	1.	1.	1.	1.
21	1.	1.	1.	1.	1.	1.	1.	1.
22	1.	1.	1.	1.	1.	1.	1.	1.
23	1.	1.	1.	1.	1.	1.	1.	1.
24	1.	1.	1.	1.	1.	1.	1.	1.
25	1.	1.	1.	1.	1.	1.	1.	1.
26	1.	1.	1.	1.	1.	1.	1.	1.
27	1.	1.	1.	1.	1.	1.	1.	1.
28	1.	1.	1.	1.	1.	1.	1.	1.
29	1.	1.	1.	1.	1.	1.	1.	1.
30	1.	1.	1.	1.	1.	1.	1.	1.
31	1.	1.	1.	1.	1.	1.	1.	1.
32	1.	1.	1.	1.	1.	1.	1.	1.
33	1.	1.	1.	1.	1.	1.	1.	1.
34	1.	1.	1.	1.	1.	1.	1.	1.
35	1.	1.	1.	1.	1.	1.	1.	1.
36	1.	1.	1.	1.	1.	1.	1.	1.
37	1.	1.	1.	1.	1.	1.	1.	1.
38	1.	1.	1.	1.	1.	1.	1.	1.
39	1.	1.	1.	1.	1.	1.	1.	1.
40	1.	1.	1.	1.	1.	1.	1.	1.
41	1.	1.	1.	1.	1.	1.	1.	1.
42	1.	1.	1.	1.	1.	1.	1.	1.
43	1.	1.	1.	1.	1.	1.	1.	1.
44	1.	1.	1.	1.	1.	1.	1.	1.
45	1.	1.	1.	1.	1.	1.	1.	1.
46	1.	1.	1.	1.	1.	1.	1.	1.
47	1.	1.	1.	1.	1.	1.	1.	1.
48	1.	1.	1.	1.	1.	1.	1.	1.
49	1.	1.	1.	1.	1.	1.	1.	1.
50	1.	1.	1.	1.	1.	1.	1.	1.
51	1.	1.	1.	1.	1.	1.	1.	1.
52	1.	1.	1.	1.	1.	1.	1.	1.

Table B-2 1992 BRAGFLO Ranks of Computed Variable Values for CULEBRA_SEAL (Concluded)

Run No.	Porosity	Permeability	Compressibility	BCEXP	BCBRSAT	BCGSSAT	BCFLG	BC PCT
53	1.	1.	1.	1.	1.	1.	1.	1.
54	1.	1.	1.	1.	1.	1.	1.	1.
55	1.	1.	1.	1.	1.	1.	1.	1.
56	1.	1.	1.	1.	1.	1.	1.	1.
57	1.	1.	1.	1.	1.	1.	1.	1.
58	1.	1.	1.	1.	1.	1.	1.	1.
59	1.	1.	1.	1.	1.	1.	1.	1.
60	1.	1.	1.	1.	1.	1.	1.	1.
61	1.	1.	1.	1.	1.	1.	1.	1.
62	1.	1.	1.	1.	1.	1.	1.	1.
63	1.	1.	1.	1.	1.	1.	1.	1.
64	1.	1.	1.	1.	1.	1.	1.	1.
65	1.	1.	1.	1.	1.	1.	1.	1.
66	1.	1.	1.	1.	1.	1.	1.	1.
67	1.	1.	1.	1.	1.	1.	1.	1.
68	1.	1.	1.	1.	1.	1.	1.	1.
69	1.	1.	1.	1.	1.	1.	1.	1.
70	1.	1.	1.	1.	1.	1.	1.	1.

Table B-2 1992 BRAGFLO Computed Variable Values for EXPERIMENTAL_REGION

Run No.	Porosity	Permeability	Compressibility	BCEXP	BCBRSAT	BCGSSAT	BCFLG	BCPCT
1	2.4490×10^{-2}	1.0000×10^{-15}	4.4974×10^{-9}	7.0000×10^{-1}	2.0000×10^{-1}	0.0000	1.0000	8.6734×10^{4}
2	1.1240×10^{-2}	1.0000×10^{-15}	1.0094×10^{-8}	7.0000×10^{-1}	2.0000×10^{-1}	0.0000	1.0000	8.6734×10^{4}
3	5.1030×10^{-2}	1.0000×10^{-15}	2.0283×10^{-9}	7.0000×10^{-1}	2.0000×10^{-1}	0.0000	1.0000	8.6734×10^{4}
4	1.6070×10^{-2}	1.0000×10^{-15}	6.9848×10^{-9}	7.0000×10^{-1}	2.0000×10^{-1}	0.0000	1.0000	8.6734×10^{4}
5	4.3250×10^{-2}	1.0000×10^{-15}	2.4381×10^{-9}	7.0000×10^{-1}	2.0000×10^{-1}	0.0000	1.0000	8.6734×10^{4}
6	5.8630×10^{-2}	1.0000×10^{-15}	1.7330×10^{-9}	7.0000×10^{-1}	2.0000×10^{-1}	0.0000	1.0000	8.6734×10^{4}
7	6.6520×10^{-2}	1.0000×10^{-15}	1.4978×10^{-9}	7.0000×10^{-1}	2.0000×10^{-1}	0.0000	1.0000	8.6734×10^{4}
8	3.6140×10^{-2}	1.0000×10^{-15}	2.9670×10^{-9}	7.0000×10^{-1}	2.0000×10^{-1}	0.0000	1.0000	8.6734×10^{4}
9	1.9210×10^{-2}	1.0000×10^{-15}	5.8022×10^{-9}	7.0000×10^{-1}	2.0000×10^{-1}	0.0000	1.0000	8.6734×10^{4}
10	4.7300×10^{-2}	1.0000×10^{-15}	2.2080×10^{-9}	7.0000×10^{-1}	2.0000×10^{-1}	0.0000	1.0000	8.6734×10^{4}
11	6.7690×10^{-2}	1.0000×10^{-15}	1.4676×10^{-9}	7.0000×10^{-1}	2.0000×10^{-1}	0.0000	1.0000	8.6734×10^{4}
12	2.5040×10^{-2}	1.0000×10^{-15}	4.3931×10^{-9}	7.0000×10^{-1}	2.0000×10^{-1}	0.0000	1.0000	8.6734×10^{4}
13	7.0630×10^{-2}	1.0000×10^{-15}	1.3961×10^{-9}	7.0000×10^{-1}	2.0000×10^{-1}	0.0000	1.0000	8.6734×10^{4}
14	4.0420×10^{-2}	1.0000×10^{-15}	2.6264×10^{-9}	7.0000×10^{-1}	2.0000×10^{-1}	0.0000	1.0000	8.6734×10^{4}
15	2.1150×10^{-2}	1.0000×10^{-15}	5.2470×10^{-9}	7.0000×10^{-1}	2.0000×10^{-1}	0.0000	1.0000	8.6734×10^{4}
16	7.2500×10^{-2}	1.0000×10^{-15}	1.3536×10^{-9}	7.0000×10^{-1}	2.0000×10^{-1}	0.0000	1.0000	8.6734×10^{4}
17	4.9250×10^{-2}	1.0000×10^{-15}	2.1107×10^{-9}	7.0000×10^{-1}	2.0000×10^{-1}	0.0000	1.0000	8.6734×10^{4}
18	1.3450×10^{-2}	1.0000×10^{-15}	8.3941×10^{-9}	7.0000×10^{-1}	2.0000×10^{-1}	0.0000	1.0000	8.6734×10^{4}
19	7.4520×10^{-2}	1.0000×10^{-15}	1.3101×10^{-9}	7.0000×10^{-1}	2.0000×10^{-1}	0.0000	1.0000	8.6734×10^{4}
20	3.7170×10^{-2}	1.0000×10^{-15}	2.8779×10^{-9}	7.0000×10^{-1}	2.0000×10^{-1}	0.0000	1.0000	8.6734×10^{4}
21	5.5630×10^{-2}	1.0000×10^{-15}	1.8399×10^{-9}	7.0000×10^{-1}	2.0000×10^{-1}	0.0000	1.0000	8.6734×10^{4}
22	4.4090×10^{-2}	1.0000×10^{-15}	2.3869×10^{-9}	7.0000×10^{-1}	2.0000×10^{-1}	0.0000	1.0000	8.6734×10^{4}
23	6.0100×10^{-2}	1.0000×10^{-15}	1.6845×10^{-9}	7.0000×10^{-1}	2.0000×10^{-1}	0.0000	1.0000	8.6734×10^{4}
24	6.9800×10^{-2}	1.0000×10^{-15}	1.4157×10^{-9}	7.0000×10^{-1}	2.0000×10^{-1}	0.0000	1.0000	8.6734×10^{4}
25	6.1100×10^{-2}	1.0000×10^{-15}	1.6528×10^{-9}	7.0000×10^{-1}	2.0000×10^{-1}	0.0000	1.0000	8.6734×10^{4}
26	5.6930×10^{-2}	1.0000×10^{-15}	1.7922×10^{-9}	7.0000×10^{-1}	2.0000×10^{-1}	0.0000	1.0000	8.6734×10^{4}
27	2.8620×10^{-2}	1.0000×10^{-15}	3.8123×10^{-9}	7.0000×10^{-1}	2.0000×10^{-1}	0.0000	1.0000	8.6734×10^{4}
28	4.1490×10^{-2}	1.0000×10^{-15}	2.5522×10^{-9}	7.0000×10^{-1}	2.0000×10^{-1}	0.0000	1.0000	8.6734×10^{4}
29	1.4260×10^{-2}	1.0000×10^{-15}	7.9031×10^{-9}	7.0000×10^{-1}	2.0000×10^{-1}	0.0000	1.0000	8.6734×10^{4}
30	3.2140×10^{-2}	1.0000×10^{-15}	3.3674×10^{-9}	7.0000×10^{-1}	2.0000×10^{-1}	0.0000	1.0000	8.6734×10^{4}
31	2.6760×10^{-2}	1.0000×10^{-15}	4.0946×10^{-9}	7.0000×10^{-1}	2.0000×10^{-1}	0.0000	1.0000	8.6734×10^{4}
32	3.9190×10^{-2}	1.0000×10^{-15}	2.7166×10^{-9}	7.0000×10^{-1}	2.0000×10^{-1}	0.0000	1.0000	8.6734×10^{4}
33	4.5660×10^{-2}	1.0000×10^{-15}	2.2963×10^{-9}	7.0000×10^{-1}	2.0000×10^{-1}	0.0000	1.0000	8.6734×10^{4}
34	3.4580×10^{-2}	1.0000×10^{-15}	3.1121×10^{-9}	7.0000×10^{-1}	2.0000×10^{-1}	0.0000	1.0000	8.6734×10^{4}
35	3.8780×10^{-2}	1.0000×10^{-15}	2.7480×10^{-9}	7.0000×10^{-1}	2.0000×10^{-1}	0.0000	1.0000	8.6734×10^{4}
36	4.6630×10^{-2}	1.0000×10^{-15}	2.2433×10^{-9}	7.0000×10^{-1}	2.0000×10^{-1}	0.0000	1.0000	8.6734×10^{4}
37	1.6500×10^{-2}	1.0000×10^{-15}	6.7962×10^{-9}	7.0000×10^{-1}	2.0000×10^{-1}	0.0000	1.0000	8.6734×10^{4}
38	6.7530×10^{-2}	1.0000×10^{-15}	1.4716×10^{-9}	7.0000×10^{-1}	2.0000×10^{-1}	0.0000	1.0000	8.6734×10^{4}
39	6.2320×10^{-2}	1.0000×10^{-15}	1.6156×10^{-9}	7.0000×10^{-1}	2.0000×10^{-1}	0.0000	1.0000	8.6734×10^{4}
40	5.4740×10^{-2}	1.0000×10^{-15}	1.8739×10^{-9}	7.0000×10^{-1}	2.0000×10^{-1}	0.0000	1.0000	8.6734×10^{4}
41	6.3580×10^{-2}	1.0000×10^{-15}	1.5786×10^{-9}	7.0000×10^{-1}	2.0000×10^{-1}	0.0000	1.0000	8.6734×10^{4}
42	7.1460×10^{-2}	1.0000×10^{-15}	1.3770×10^{-9}	7.0000×10^{-1}	2.0000×10^{-1}	0.0000	1.0000	8.6734×10^{4}
43	4.4580×10^{-2}	1.0000×10^{-15}	2.3580×10^{-9}	7.0000×10^{-1}	2.0000×10^{-1}	0.0000	1.0000	8.6734×10^{4}
44	7.3870×10^{-2}	1.0000×10^{-15}	1.3239×10^{-9}	7.0000×10^{-1}	2.0000×10^{-1}	0.0000	1.0000	8.6734×10^{4}
45	2.9730×10^{-2}	1.0000×10^{-15}	3.6606×10^{-9}	7.0000×10^{-1}	2.0000×10^{-1}	0.0000	1.0000	8.6734×10^{4}
46	1.2610×10^{-2}	1.0000×10^{-15}	8.9699×10^{-9}	7.0000×10^{-1}	2.0000×10^{-1}	0.0000	1.0000	8.6734×10^{4}
47	6.0510×10^{-2}	1.0000×10^{-15}	1.6714×10^{-9}	7.0000×10^{-1}	2.0000×10^{-1}	0.0000	1.0000	8.6734×10^{4}
48	3.3090×10^{-2}	1.0000×10^{-15}	3.2635×10^{-9}	7.0000×10^{-1}	2.0000×10^{-1}	0.0000	1.0000	8.6734×10^{4}
49	4.1760×10^{-2}	1.0000×10^{-15}	2.5341×10^{-9}	7.0000×10^{-1}	2.0000×10^{-1}	0.0000	1.0000	8.6734×10^{4}
50	3.0510×10^{-2}	1.0000×10^{-15}	3.5606×10^{-9}	7.0000×10^{-1}	2.0000×10^{-1}	0.0000	1.0000	8.6734×10^{4}
51	1.8180×10^{-2}	1.0000×10^{-15}	6.1451×10^{-9}	7.0000×10^{-1}	2.0000×10^{-1}	0.0000	1.0000	8.6734×10^{4}
52	6.5110×10^{-2}	1.0000×10^{-15}	1.5356×10^{-9}	7.0000×10^{-1}	2.0000×10^{-1}	0.0000	1.0000	8.6734×10^{4}

Table B-2 1992 BRAGFLO Computed Variable Values for EXPERIMENTAL_REGION (Concluded)

Run No.	Porosity	Permeability	Compressibility	BCEXP	BCBRSAT	BCGSSAT	BCFLG	BCPCT
53	2.0520×10^{-2}	1.0000×10^{-15}	5.4158×10^{-9}	7.0000×10^{-1}	2.0000×10^{-1}	0.0000	1.0000	8.6734×10^{4}
54	6.4400×10^{-2}	1.0000×10^{-15}	1.5553×10^{-9}	7.0000×10^{-1}	2.0000×10^{-1}	0.0000	1.0000	8.6734×10^{4}
55	2.6330×10^{-2}	1.0000×10^{-15}	4.1656×10^{-9}	7.0000×10^{-1}	2.0000×10^{-1}	0.0000	1.0000	8.6734×10^{4}
56	3.5470×10^{-2}	1.0000×10^{-15}	3.0278×10^{-9}	7.0000×10^{-1}	2.0000×10^{-1}	0.0000	1.0000	8.6734×10^{4}
57	1.9820×10^{-2}	1.0000×10^{-15}	5.6159×10^{-9}	7.0000×10^{-1}	2.0000×10^{-1}	0.0000	1.0000	8.6734×10^{4}
58	2.3880×10^{-2}	1.0000×10^{-15}	4.6186×10^{-9}	7.0000×10^{-1}	2.0000×10^{-1}	0.0000	1.0000	8.6734×10^{4}
59	5.7990×10^{-2}	1.0000×10^{-15}	1.7549×10^{-9}	7.0000×10^{-1}	2.0000×10^{-1}	0.0000	1.0000	8.6734×10^{4}
60	6.9150×10^{-2}	1.0000×10^{-15}	1.4313×10^{-9}	7.0000×10^{-1}	2.0000×10^{-1}	0.0000	1.0000	8.6734×10^{4}
61	1.5400×10^{-2}	1.0000×10^{-15}	7.2995×10^{-9}	7.0000×10^{-1}	2.0000×10^{-1}	0.0000	1.0000	8.6734×10^{4}
62	2.7890×10^{-2}	1.0000×10^{-15}	3.9186×10^{-9}	7.0000×10^{-1}	2.0000×10^{-1}	0.0000	1.0000	8.6734×10^{4}
63	5.2340×10^{-2}	1.0000×10^{-15}	1.9713×10^{-9}	7.0000×10^{-1}	2.0000×10^{-1}	0.0000	1.0000	8.6734×10^{4}
64	5.3500×10^{-2}	1.0000×10^{-15}	1.9231×10^{-9}	7.0000×10^{-1}	2.0000×10^{-1}	0.0000	1.0000	8.6734×10^{4}
65	1.0820×10^{-2}	1.0000×10^{-15}	1.0495×10^{-8}	7.0000×10^{-1}	2.0000×10^{-1}	0.0000	1.0000	8.6734×10^{4}
66	5.0410×10^{-2}	1.0000×10^{-15}	2.0563×10^{-9}	7.0000×10^{-1}	2.0000×10^{-1}	0.0000	1.0000	8.6734×10^{4}
67	3.3230×10^{-2}	1.0000×10^{-15}	3.2487×10^{-9}	7.0000×10^{-1}	2.0000×10^{-1}	0.0000	1.0000	8.6734×10^{4}
68	2.2660×10^{-2}	1.0000×10^{-15}	4.8807×10^{-9}	7.0000×10^{-1}	2.0000×10^{-1}	0.0000	1.0000	8.6734×10^{4}
69	4.8950×10^{-2}	1.0000×10^{-15}	2.1251×10^{-9}	7.0000×10^{-1}	2.0000×10^{-1}	0.0000	1.0000	8.6734×10^{4}
70	5.3660×10^{-2}	1.0000×10^{-15}	1.9166×10^{-9}	7.0000×10^{-1}	2.0000×10^{-1}	0.0000	1.0000	8.6734×10^{4}

Table B-2 1992 BRAGFLO Ranks of Computed Variable Values for EXPERIMENTAL_REGION

Run No.	Porosity	Permeability	Compressibility	BCEXP	BCBRSAT	BCGSSAT	BCFLG	BCPCT
1	16.	1.	55.	1.	1.	1.	1.	1.
2	2.	1.	69.	1.	1.	1.	1.	1.
3	45.	1.	26.	1.	1.	1.	1.	1.
4	7.	1.	64.	1.	1.	1.	1.	1.
5	36.	1.	35.	1.	1.	1.	1.	1.
6	53.	1.	18.	1.	1.	1.	1.	1.
7	61.	1.	10.	1.	1.	1.	1.	1.
8	29.	1.	42.	1.	1.	1.	1.	1.
9	10.	1.	61.	1.	1.	1.	1.	1.
10	41.	1.	30.	1.	1.	1.	1.	1.
11	63.	1.	8.	1.	1.	1.	1.	1.
12	17.	1.	54.	1.	1.	1.	1.	1.
13	66.	1.	5.	1.	1.	1.	1.	1.
14	33.	1.	38.	1.	1.	1.	1.	1.
15	13.	1.	58.	1.	1.	1.	1.	1.
16	68.	1.	3.	1.	1.	1.	1.	1.
17	43.	1.	28.	1.	1.	1.	1.	1.
18	4.	1.	67.	1.	1.	1.	1.	1.
19	70.	1.	1.	1.	1.	1.	1.	1.
20	30.	1.	41.	1.	1.	1.	1.	1.
21	50.	1.	21.	1.	1.	1.	1.	1.
22	37.	1.	34.	1.	1.	1.	1.	1.
23	54.	1.	17.	1.	1.	1.	1.	1.
24	65.	1.	6.	1.	1.	1.	1.	1.
25	56.	1.	15.	1.	1.	1.	1.	1.
26	51.	1.	20.	1.	1.	1.	1.	1.
27	21.	1.	50.	1.	1.	1.	1.	1.
28	34.	1.	37.	1.	1.	1.	1.	1.
29	5.	1.	66.	1.	1.	1.	1.	1.
30	24.	1.	47.	1.	1.	1.	1.	1.
31	19.	1.	52.	1.	1.	1.	1.	1.
32	32.	1.	39.	1.	1.	1.	1.	1.
33	39.	1.	32.	1.	1.	1.	1.	1.
34	27.	1.	44.	1.	1.	1.	1.	1.
35	31.	1.	40.	1.	1.	1.	1.	1.
36	40.	1.	31.	1.	1.	1.	1.	1.
37	8.	1.	63.	1.	1.	1.	1.	1.
38	62.	1.	9.	1.	1.	1.	1.	1.
39	57.	1.	14.	1.	1.	1.	1.	1.
40	49.	1.	22.	1.	1.	1.	1.	1.
41	58.	1.	13.	1.	1.	1.	1.	1.
42	67.	1.	4.	1.	1.	1.	1.	1.
43	38.	1.	33.	1.	1.	1.	1.	1.
44	69.	1.	2.	1.	1.	1.	1.	1.
45	22.	1.	49.	1.	1.	1.	1.	1.
46	3.	1.	68.	1.	1.	1.	1.	1.
47	55.	1.	16.	1.	1.	1.	1.	1.
48	25.	1.	46.	1.	1.	1.	1.	1.
49	35.	1.	36.	1.	1.	1.	1.	1.
50	23.	1.	48.	1.	1.	1.	1.	1.
51	9.	1.	62.	1.	1.	1.	1.	1.
52	60.	1.	11.	1.	1.	1.	1.	1.

Table B-2 1992 BRAGFLO Ranks of Computed Variable Values for EXPERIMENTAL_REGION (Concluded)

Run No.	Porosity	Permeability	Compressibility	BCEXP	BCBRSAT	BCGSSAT	BCFLG	BCPCT
53	12.	1.	59.	1.	1.	1.	1.	1.
54	59.	1.	12.	1.	1.	1.	1.	1.
55	18.	1.	53.	1.	1.	1.	1.	1.
56	28.	1.	43.	1.	1.	1.	1.	1.
57	11.	1.	60.	1.	1.	1.	1.	1.
58	15.	1.	56.	1.	1.	1.	1.	1.
59	52.	1.	19.	1.	1.	1.	1.	1.
60	64.	1.	7.	1.	1.	1.	1.	1.
61	6.	1.	65.	1.	1.	1.	1.	1.
62	20.	1.	51.	1.	1.	1.	1.	1.
63	46.	1.	25.	1.	1.	1.	1.	1.
64	47.	1.	24.	1.	1.	1.	1.	1.
65	1.	1.	70.	1.	1.	1.	1.	1.
66	44.	1.	27.	1.	1.	1.	1.	1.
67	26.	1.	45.	1.	1.	1.	1.	1.
68	14.	1.	57.	1.	1.	1.	1.	1.
69	42.	1.	29.	1.	1.	1.	1.	1.
70	48.	1.	23.	1.	1.	1.	1.	1.

Table B-2 1992 BRAGFLO Computed Variable Values for FINAL_SALADO_DRZ

Run No.	Porosity	Permeability	Compressibility	BCEXP	BCBRSAT	BCGSSAT	BCFLG	BCPCT
1	2.9338×10^{-2}	1.0000×10^{-15}	3.7128×10^{-9}	9.6790	8.7890×10^{-2}	2.3300×10^{-1}	1.0000	8.6734×10^{4}
2	3.2244×10^{-2}	1.0000×10^{-15}	3.3557×10^{-9}	4.9660×10^{-1}	1.4570×10^{-1}	1.2590×10^{-1}	1.0000	8.6734×10^{4}
3	5.1073×10^{-2}	1.0000×10^{-15}	2.0264×10^{-9}	6.7900×10^{-1}	1.8490×10^{-1}	2.1660×10^{-1}	1.0000	8.6734×10^{4}
4	5.9880×10^{-2}	1.0000×10^{-15}	1.6916×10^{-9}	5.1820	1.7260×10^{-1}	1.8900×10^{-1}	1.0000	8.6734×10^{4}
5	2.3095×10^{-2}	1.0000×10^{-15}	4.7841×10^{-9}	4.0710×10^{-1}	1.9880×10^{-1}	1.4590×10^{-1}	1.0000	8.6734×10^{4}
6	5.8159×10^{-2}	1.0000×10^{-15}	1.7490×10^{-9}	6.1420	3.3170×10^{-1}	4.7930×10^{-2}	1.0000	8.6734×10^{4}
7	3.5160×10^{-2}	1.0000×10^{-15}	3.0567×10^{-9}	1.0990	3.5430×10^{-2}	1.6220×10^{-1}	1.0000	8.6734×10^{4}
8	3.5393×10^{-2}	1.0000×10^{-15}	3.0349×10^{-9}	6.4480	3.8660×10^{-1}	2.8520×10^{-2}	1.0000	8.6734×10^{4}
9	4.1674×10^{-2}	1.0000×10^{-15}	2.5398×10^{-9}	4.2610×10^{-1}	3.4080×10^{-1}	1.8690×10^{-1}	1.0000	8.6734×10^{4}
10	2.4250×10^{-2}	1.0000×10^{-15}	4.5442×10^{-9}	1.5170	7.9000×10^{-2}	3.4810×10^{-1}	1.0000	8.6734×10^{4}
11	3.8769×10^{-2}	1.0000×10^{-15}	2.7488×10^{-9}	5.1250×10^{-1}	2.7170×10^{-1}	2.0030×10^{-1}	1.0000	8.6734×10^{4}
12	3.7282×10^{-2}	1.0000×10^{-15}	2.8685×10^{-9}	7.4960	1.4100×10^{-1}	2.8620×10^{-1}	1.0000	8.6734×10^{4}
13	1.9799×10^{-2}	1.0000×10^{-15}	5.6222×10^{-9}	2.2490	3.6500×10^{-1}	2.9370×10^{-1}	1.0000	8.6734×10^{4}
14	3.7667×10^{-2}	1.0000×10^{-15}	2.8366×10^{-9}	3.0620×10^{-1}	8.3660×10^{-3}	1.7360×10^{-1}	1.0000	8.6734×10^{4}
15	5.1892×10^{-2}	1.0000×10^{-15}	1.9905×10^{-9}	4.4620×10^{-1}	2.3100×10^{-1}	3.8350×10^{-1}	1.0000	8.6734×10^{4}
16	4.6976×10^{-2}	1.0000×10^{-15}	2.2249×10^{-9}	5.3590×10^{-1}	3.7890×10^{-1}	2.1720×10^{-1}	1.0000	8.6734×10^{4}
17	5.4383×10^{-2}	1.0000×10^{-15}	1.8878×10^{-9}	5.9190	1.1130×10^{-1}	3.8060×10^{-1}	1.0000	8.6734×10^{4}
18	2.6960×10^{-2}	1.0000×10^{-15}	4.0623×10^{-9}	5.8730×10^{-1}	2.9470×10^{-1}	8.6120×10^{-3}	1.0000	8.6734×10^{4}
19	4.8939×10^{-2}	1.0000×10^{-15}	2.1257×10^{-9}	2.0050	1.1640×10^{-1}	1.6670×10^{-1}	1.0000	8.6734×10^{4}
20	4.8916×10^{-2}	1.0000×10^{-15}	2.1268×10^{-9}	6.7090×10^{-1}	1.2940×10^{-1}	3.2110×10^{-1}	1.0000	8.6734×10^{4}
21	3.1377×10^{-2}	1.0000×10^{-15}	3.4554×10^{-9}	2.2590×10^{-1}	1.9770×10^{-2}	2.2330×10^{-1}	1.0000	8.6734×10^{4}
22	5.0492×10^{-2}	1.0000×10^{-15}	2.0526×10^{-9}	1.4340	2.1830×10^{-1}	1.8710×10^{-2}	1.0000	8.6734×10^{4}
23	5.4561×10^{-2}	1.0000×10^{-15}	1.8808×10^{-9}	7.0990	2.3880×10^{-1}	4.5230×10^{-2}	1.0000	8.6734×10^{4}
24	2.3356×10^{-2}	1.0000×10^{-15}	4.7279×10^{-9}	4.3270×10^{-1}	6.1270×10^{-2}	2.6430×10^{-1}	1.0000	8.6734×10^{4}
25	5.5692×10^{-2}	1.0000×10^{-15}	1.8376×10^{-9}	2.7610	3.0510×10^{-1}	9.9900×10^{-2}	1.0000	8.6734×10^{4}
26	5.1986×10^{-2}	1.0000×10^{-15}	1.9864×10^{-9}	5.2660	2.4700×10^{-1}	6.8060×10^{-2}	1.0000	8.6734×10^{4}
27	3.1097×10^{-2}	1.0000×10^{-15}	3.4888×10^{-9}	8.3330	2.1280×10^{-1}	7.5730×10^{-2}	1.0000	8.6734×10^{4}
28	1.4826×10^{-2}	1.0000×10^{-15}	7.5917×10^{-9}	7.9460	3.4740×10^{-1}	1.5270×10^{-1}	1.0000	8.6734×10^{4}
29	1.8131×10^{-2}	1.0000×10^{-15}	6.1623×10^{-9}	6.0410×10^{-1}	3.3040×10^{-1}	3.5780×10^{-1}	1.0000	8.6734×10^{4}
30	5.5555×10^{-2}	1.0000×10^{-15}	1.8427×10^{-9}	2.0040×10^{-1}	1.4050×10^{-2}	1.5530×10^{-1}	1.0000	8.6734×10^{4}
31	3.3857×10^{-2}	1.0000×10^{-15}	3.1839×10^{-9}	3.3160×10^{-1}	2.1130×10^{-1}	2.4050×10^{-1}	1.0000	8.6734×10^{4}
32	5.7726×10^{-2}	1.0000×10^{-15}	1.7640×10^{-9}	8.8800	3.1430×10^{-1}	3.7550×10^{-1}	1.0000	8.6734×10^{4}
33	5.9040×10^{-2}	1.0000×10^{-15}	1.7192×10^{-9}	5.2200×10^{-1}	1.0530×10^{-1}	3.4190×10^{-1}	1.0000	8.6734×10^{4}
34	3.8766×10^{-2}	1.0000×10^{-15}	2.7491×10^{-9}	8.6520	2.5150×10^{-1}	3.6280×10^{-1}	1.0000	8.6734×10^{4}
35	4.7477×10^{-2}	1.0000×10^{-15}	2.1988×10^{-9}	3.9470×10^{-1}	2.9070×10^{-1}	1.3390×10^{-1}	1.0000	8.6734×10^{4}
36	4.7765×10^{-2}	1.0000×10^{-15}	2.1840×10^{-9}	2.7500×10^{-1}	3.7090×10^{-1}	3.6960×10^{-1}	1.0000	8.6734×10^{4}
37	3.4118×10^{-2}	1.0000×10^{-15}	3.1576×10^{-9}	6.9780	2.2650×10^{-1}	3.0790×10^{-2}	1.0000	8.6734×10^{4}
38	3.9355×10^{-2}	1.0000×10^{-15}	2.7042×10^{-9}	2.9640	1.7810×10^{-1}	3.9620×10^{-1}	1.0000	8.6734×10^{4}
39	4.3649×10^{-2}	1.0000×10^{-15}	2.4136×10^{-9}	2.6060×10^{-1}	1.6330×10^{-1}	3.7240×10^{-2}	1.0000	8.6734×10^{4}
40	2.6845×10^{-2}	1.0000×10^{-15}	4.0808×10^{-9}	2.4160×10^{-1}	2.4340×10^{-1}	1.1100×10^{-1}	1.0000	8.6734×10^{4}
41	2.4393×10^{-2}	1.0000×10^{-15}	4.5163×10^{-9}	5.7490×10^{-1}	1.3340×10^{-1}	1.0650×10^{-1}	1.0000	8.6734×10^{4}
42	3.7631×10^{-2}	1.0000×10^{-15}	2.8395×10^{-9}	5.4840×10^{-1}	3.9640×10^{-1}	3.3500×10^{-1}	1.0000	8.6734×10^{4}
43	2.8231×10^{-2}	1.0000×10^{-15}	3.8682×10^{-9}	4.0000	3.9070×10^{-1}	1.2040×10^{-1}	1.0000	8.6734×10^{4}
44	1.7825×10^{-2}	1.0000×10^{-15}	6.2725×10^{-9}	3.6050×10^{-1}	2.5980×10^{-1}	5.7350×10^{-2}	1.0000	8.6734×10^{4}
45	2.3493×10^{-2}	1.0000×10^{-15}	4.6989×10^{-9}	3.2390×10^{-1}	1.5830×10^{-1}	9.4190×10^{-2}	1.0000	8.6734×10^{4}
46	5.6711×10^{-2}	1.0000×10^{-15}	1.8001×10^{-9}	4.6060×10^{-1}	6.5170×10^{-2}	2.3880×10^{-1}	1.0000	8.6734×10^{4}
47	1.4114×10^{-2}	1.0000×10^{-15}	7.9872×10^{-9}	3.4760	3.1780×10^{-1}	2.6060×10^{-1}	1.0000	8.6734×10^{4}
48	5.7247×10^{-2}	1.0000×10^{-15}	1.7809×10^{-9}	7.7080	4.5510×10^{-2}	2.0750×10^{-1}	1.0000	8.6734×10^{4}
49	5.6909×10^{-2}	1.0000×10^{-15}	1.7930×10^{-9}	3.7530×10^{-1}	5.0110×10^{-2}	6.9900×10^{-2}	1.0000	8.6734×10^{4}
50	4.5726×10^{-2}	1.0000×10^{-15}	2.2926×10^{-9}	3.5390×10^{-1}	1.8990×10^{-1}	1.9850×10^{-1}	1.0000	8.6734×10^{4}
51	2.3898×10^{-2}	1.0000×10^{-15}	4.6150×10^{-9}	5.6000×10^{-1}	2.3180×10^{-2}	1.1810×10^{-2}	1.0000	8.6734×10^{4}
52	4.5974×10^{-2}	1.0000×10^{-15}	2.2789×10^{-9}	3.2370	1.5040×10^{-1}	3.8860×10^{-1}	1.0000	8.6734×10^{4}

Table B-2 1992 BRAGFLO Computed Variable Values for FINAL_SALADO_DRZ (Concluded)

Run No.	Porosity	Permeability	Compressibility	BCEXP	BCBRSAT	BCGSSAT	BCFLG	BCPCT
53	3.0815×10^{-2}	1.0000×10^{-15}	3.5230×10^{-9}	6.7410	2.8470×10^{-1}	1.8060×10^{-1}	1.0000	8.6734×10^{4}
54	3.0693×10^{-2}	1.0000×10^{-15}	3.5379×10^{-9}	4.7200×10^{-1}	1.6590×10^{-1}	2.7290×10^{-1}	1.0000	8.6734×10^{4}
55	4.0163×10^{-2}	1.0000×10^{-15}	2.6448×10^{-9}	6.5030×10^{-1}	3.2450×10^{-1}	3.0330×10^{-1}	1.0000	8.6734×10^{4}
56	5.2274×10^{-2}	1.0000×10^{-15}	1.9741×10^{-9}	4.8480	9.2770×10^{-2}	5.2210×10^{-2}	1.0000	8.6734×10^{4}
57	7.0516×10^{-3}	1.0000×10^{-15}	1.6238×10^{-8}	9.2110	5.1160×10^{-3}	2.7770×10^{-1}	1.0000	8.6734×10^{4}
58	2.5041×10^{-2}	1.0000×10^{-15}	4.3928×10^{-9}	6.4060×10^{-1}	3.4880×10^{-1}	3.2980×10^{-1}	1.0000	8.6734×10^{4}
59	2.8428×10^{-2}	1.0000×10^{-15}	3.8398×10^{-9}	8.9580	8.5120×10^{-2}	3.1270×10^{-1}	1.0000	8.6734×10^{4}
60	3.9407×10^{-2}	1.0000×10^{-15}	2.7003×10^{-9}	9.8620	7.0380×10^{-2}	8.1940×10^{-2}	1.0000	8.6734×10^{4}
61	1.6302×10^{-2}	1.0000×10^{-15}	6.8816×10^{-9}	8.0490×10^{-1}	2.7910×10^{-1}	1.3890×10^{-1}	1.0000	8.6734×10^{4}
62	2.9951×10^{-2}	1.0000×10^{-15}	3.6318×10^{-9}	2.8630×10^{-1}	3.5990×10^{-1}	2.5120×10^{-1}	1.0000	8.6734×10^{4}
63	4.1109×10^{-2}	1.0000×10^{-15}	2.5782×10^{-9}	3.7540	2.0010×10^{-1}	2.8360×10^{-1}	1.0000	8.6734×10^{4}
64	3.0137×10^{-2}	1.0000×10^{-15}	3.6079×10^{-9}	2.4950	2.9320×10^{-2}	8.7020×10^{-2}	1.0000	8.6734×10^{4}
65	3.8978×10^{-2}	1.0000×10^{-15}	2.7328×10^{-9}	2.5410×10^{-1}	2.6410×10^{-1}	3.5100×10^{-1}	1.0000	8.6734×10^{4}
66	3.7103×10^{-3}	1.0000×10^{-15}	3.1085×10^{-8}	6.9150×10^{-1}	1.2380×10^{-1}	3.1630×10^{-1}	1.0000	8.6734×10^{4}
67	2.0750×10^{-2}	1.0000×10^{-15}	5.3531×10^{-9}	5.5890	5.6350×10^{-2}	2.5370×10^{-1}	1.0000	8.6734×10^{4}
68	3.6434×10^{-2}	1.0000×10^{-15}	2.9411×10^{-9}	4.5200	3.0240×10^{-1}	2.9970×10^{-1}	1.0000	8.6734×10^{4}
69	2.3166×10^{-2}	1.0000×10^{-15}	4.7686×10^{-9}	4.3270	3.7150×10^{-1}	4.8390×10^{-3}	1.0000	8.6734×10^{4}
70	3.6159×10^{-3}	1.0000×10^{-15}	3.1903×10^{-8}	6.2770×10^{-1}	1.0130×10^{-1}	1.1920×10^{-1}	1.0000	8.6734×10^{4}

Table B-2 1992 BRAGFLO Ranks of Computed Variable Values for FINAL_SALADO_DRZ

Run No.	Porosity	Permeability	Compressibility	BCEXP	BCBRSAT	BCGSSAT	BCFLG	BCPCT
1	23.	1.	48.	69.	16.	41.	1.	1.
2	30.	1.	41.	21.	26.	23.	1.	1.
3	56.	1.	15.	34.	33.	38.	1.	1.
4	70.	1.	1.	52.	31.	34.	1.	1.
5	11.	1.	60.	15.	35.	26.	1.	1.
6	68.	1.	3.	56.	59.	9.	1.	1.
7	33.	1.	38.	37.	7.	29.	1.	1.
8	34.	1.	37.	57.	68.	5.	1.	1.
9	46.	1.	25.	16.	60.	33.	1.	1.
10	16.	1.	55.	39.	14.	61.	1.	1.
11	40.	1.	31.	22.	48.	36.	1.	1.
12	36.	1.	35.	61.	25.	51.	1.	1.
13	9.	1.	62.	41.	64.	52.	1.	1.
14	38.	1.	33.	8.	2.	31.	1.	1.
15	57.	1.	14.	18.	41.	68.	1.	1.
16	50.	1.	21.	24.	67.	39.	1.	1.
17	60.	1.	11.	55.	20.	67.	1.	1.
18	20.	1.	51.	28.	52.	2.	1.	1.
19	54.	1.	17.	40.	21.	30.	1.	1.
20	53.	1.	18.	33.	23.	57.	1.	1.
21	29.	1.	42.	2.	4.	40.	1.	1.
22	55.	1.	16.	38.	39.	4.	1.	1.
23	61.	1.	10.	60.	42.	8.	1.	1.
24	13.	1.	58.	17.	11.	47.	1.	1.
25	63.	1.	8.	43.	54.	18.	1.	1.
26	58.	1.	13.	53.	44.	12.	1.	1.
27	28.	1.	43.	64.	38.	14.	1.	1.
28	5.	1.	66.	63.	61.	27.	1.	1.
29	8.	1.	63.	29.	58.	63.	1.	1.
30	62.	1.	9.	1.	3.	28.	1.	1.
31	31.	1.	40.	10.	37.	43.	1.	1.
32	67.	1.	4.	66.	55.	66.	1.	1.
33	69.	1.	2.	23.	19.	60.	1.	1.
34	39.	1.	32.	65.	45.	64.	1.	1.
35	51.	1.	20.	14.	51.	24.	1.	1.
36	52.	1.	19.	6.	65.	65.	1.	1.
37	32.	1.	39.	59.	40.	6.	1.	1.
38	42.	1.	29.	44.	32.	70.	1.	1.
39	47.	1.	24.	5.	29.	7.	1.	1.
40	19.	1.	52.	3.	43.	20.	1.	1.
41	17.	1.	54.	27.	24.	19.	1.	1.
42	37.	1.	34.	25.	70.	59.	1.	1.
43	21.	1.	50.	48.	69.	22.	1.	1.
44	7.	1.	64.	12.	46.	11.	1.	1.
45	14.	1.	57.	9.	28.	17.	1.	1.
46	64.	1.	7.	19.	12.	42.	1.	1.
47	4.	1.	67.	46.	56.	46.	1.	1.
48	66.	1.	5.	62.	8.	37.	1.	1.
49	65.	1.	6.	13.	9.	13.	1.	1.
50	48.	1.	23.	11.	34.	35.	1.	1.
51	15.	1.	56.	26.	5.	3.	1.	1.
52	49.	1.	22.	45.	27.	69.	1.	1.

Table B-2 1992 BRAGFLO Ranks of Computed Variable Values for FINAL_SALADO_DRZ (Concluded)

Run No.	Porosity	Permeability	Compressibility	BCEXP	BCBRSAT	BCGSSAT	BCFLG	BCPCT
53	27.	1.	44.	58.	50.	32.	1.	1.
54	26.	1.	45.	20.	30.	48.	1.	1.
55	44.	1.	27.	32.	57.	54.	1.	1.
56	59.	1.	12.	51.	17.	10.	1.	1.
57	3.	1.	68.	68.	1.	49.	1.	1.
58	18.	1.	53.	31.	62.	58.	1.	1.
59	22.	1.	49.	67.	15.	55.	1.	1.
60	43.	1.	28.	70.	13.	15.	1.	1.
61	6.	1.	65.	36.	49.	25.	1.	1.
62	24.	1.	47.	7.	63.	44.	1.	1.
63	45.	1.	26.	47.	36.	50.	1.	1.
64	25.	1.	46.	42.	6.	16.	1.	1.
65	41.	1.	30.	4.	47.	62.	1.	1.
66	2.	1.	69.	35.	22.	56.	1.	1.
67	10.	1.	61.	54.	10.	45.	1.	1.
68	35.	1.	36.	50.	53.	53.	1.	1.
69	12.	1.	59.	49.	66.	1.	1.	1.
70	1.	1.	70.	30.	18.	21.	1.	1.

Table B-2 1992 BRAGFLO Computed Variable Values for INITIAL_SALADO_DRZ

Run No.	Porosity	Permeability	Compressibility	BCEXP	BCBRSAT	BCGSSAT	BCFLG	BCPCT
1	2.8660×10^{-2}	1.0000×10^{-17}	3.8066×10^{-9}	9.6790	8.7890×10^{-2}	2.3300×10^{-1}	1.0000	4.2676×10^{5}
2	6.9900×10^{-3}	1.0000×10^{-17}	1.6383×10^{-8}	4.9660×10^{-1}	1.4570×10^{-1}	1.2590×10^{-1}	1.0000	4.2676×10^{5}
3	2.8970×10^{-2}	1.0000×10^{-17}	3.7632×10^{-9}	6.7900×10^{-1}	1.8490×10^{-1}	2.1660×10^{-1}	1.0000	4.2676×10^{5}
4	5.6130×10^{-3}	1.0000×10^{-17}	2.0463×10^{-8}	5.1820	1.7260×10^{-1}	1.8900×10^{-1}	1.0000	4.2676×10^{5}
5	2.0560×10^{-2}	1.0000×10^{-17}	5.4048×10^{-9}	4.0710×10^{-1}	1.9880×10^{-1}	1.4590×10^{-1}	1.0000	4.2676×10^{5}
6	1.3750×10^{-2}	1.0000×10^{-17}	8.2055×10^{-9}	6.1420	3.3170×10^{-1}	4.7930×10^{-2}	1.0000	4.2676×10^{5}
7	2.5930×10^{-2}	1.0000×10^{-17}	4.2337×10^{-9}	1.0990	3.5430×10^{-2}	1.6220×10^{-1}	1.0000	4.2676×10^{5}
8	3.1850×10^{-3}	1.0000×10^{-17}	3.6253×10^{-8}	6.4480	3.8660×10^{-1}	2.8520×10^{-2}	1.0000	4.2676×10^{5}
9	2.7270×10^{-2}	1.0000×10^{-17}	4.0134×10^{-9}	4.2610×10^{-1}	3.4080×10^{-1}	1.8690×10^{-1}	1.0000	4.2676×10^{5}
10	9.6770×10^{-3}	1.0000×10^{-17}	1.1764×10^{-8}	1.5170	7.9000×10^{-2}	3.4810×10^{-1}	1.0000	4.2676×10^{5}
11	2.5730×10^{-3}	1.0000×10^{-17}	4.4936×10^{-8}	5.1250×10^{-1}	2.7170×10^{-1}	2.0030×10^{-1}	1.0000	4.2676×10^{5}
12	9.8270×10^{-3}	1.0000×10^{-17}	1.1581×10^{-8}	7.4960	1.4100×10^{-1}	2.8620×10^{-1}	1.0000	4.2676×10^{5}
13	1.6610×10^{-2}	1.0000×10^{-17}	6.7496×10^{-9}	2.2490	3.6500×10^{-1}	2.9370×10^{-1}	1.0000	4.2676×10^{5}
14	1.9600×10^{-2}	1.0000×10^{-17}	5.6818×10^{-9}	3.0620×10^{-1}	8.3660×10^{-3}	1.7360×10^{-1}	1.0000	4.2676×10^{5}
15	1.1590×10^{-3}	1.0000×10^{-17}	1.0006×10^{-7}	4.4620×10^{-1}	2.3100×10^{-1}	3.8350×10^{-1}	1.0000	4.2676×10^{5}
16	5.8700×10^{-3}	1.0000×10^{-17}	1.9556×10^{-8}	5.3590×10^{-1}	3.7890×10^{-1}	2.1720×10^{-1}	1.0000	4.2676×10^{5}
17	2.3950×10^{-2}	1.0000×10^{-17}	4.6044×10^{-9}	5.9190	1.1130×10^{-1}	3.8060×10^{-1}	1.0000	4.2676×10^{5}
18	6.1370×10^{-3}	1.0000×10^{-17}	1.8695×10^{-8}	5.8730×10^{-1}	2.9470×10^{-1}	8.6120×10^{-3}	1.0000	4.2676×10^{5}
19	6.2550×10^{-3}	1.0000×10^{-17}	1.8337×10^{-8}	2.0050	1.1640×10^{-1}	1.6670×10^{-1}	1.0000	4.2676×10^{5}
20	1.7070×10^{-2}	1.0000×10^{-17}	6.5609×10^{-9}	6.7090×10^{-1}	1.2940×10^{-1}	3.2110×10^{-1}	1.0000	4.2676×10^{5}
21	2.3500×10^{-2}	1.0000×10^{-17}	4.6974×10^{-9}	2.2590×10^{-1}	1.9770×10^{-2}	2.2330×10^{-1}	1.0000	4.2676×10^{5}
22	2.6030×10^{-2}	1.0000×10^{-17}	4.2165×10^{-9}	1.4340	2.1830×10^{-1}	1.8710×10^{-2}	1.0000	4.2676×10^{5}
23	2.9920×10^{-2}	1.0000×10^{-17}	3.6358×10^{-9}	7.0990	2.3880×10^{-1}	4.5230×10^{-2}	1.0000	4.2676×10^{5}
24	1.4710×10^{-2}	1.0000×10^{-17}	7.6537×10^{-9}	4.3270×10^{-1}	6.1270×10^{-2}	2.6430×10^{-1}	1.0000	4.2676×10^{5}
25	2.4720×10^{-2}	1.0000×10^{-17}	4.4532×10^{-9}	2.7610	3.0510×10^{-1}	9.9900×10^{-2}	1.0000	4.2676×10^{5}
26	1.8820×10^{-2}	1.0000×10^{-17}	5.9276×10^{-9}	5.2660	2.4700×10^{-1}	6.8060×10^{-2}	1.0000	4.2676×10^{5}
27	2.2740×10^{-3}	1.0000×10^{-17}	5.0877×10^{-8}	8.3330	2.1280×10^{-1}	7.5730×10^{-2}	1.0000	4.2676×10^{5}
28	2.8830×10^{-3}	1.0000×10^{-17}	4.0077×10^{-8}	7.9460	3.4740×10^{-1}	1.5270×10^{-1}	1.0000	4.2676×10^{5}
29	1.2680×10^{-2}	1.0000×10^{-17}	8.9190×10^{-9}	6.0410×10^{-1}	3.3040×10^{-1}	3.5780×10^{-1}	1.0000	4.2676×10^{5}
30	8.7910×10^{-3}	1.0000×10^{-17}	1.2975×10^{-8}	2.0040×10^{-1}	1.4050×10^{-2}	1.5530×10^{-1}	1.0000	4.2676×10^{5}
31	1.7650×10^{-2}	1.0000×10^{-17}	6.3371×10^{-9}	3.3160×10^{-1}	2.1130×10^{-1}	2.4050×10^{-1}	1.0000	4.2676×10^{5}
32	2.0930×10^{-2}	1.0000×10^{-17}	5.3048×10^{-9}	8.8800	3.1430×10^{-1}	3.7550×10^{-1}	1.0000	4.2676×10^{5}
33	6.6640×10^{-3}	1.0000×10^{-17}	1.7196×10^{-8}	5.2200×10^{-1}	1.0530×10^{-1}	3.4190×10^{-1}	1.0000	4.2676×10^{5}
34	9.1030×10^{-3}	1.0000×10^{-17}	1.2522×10^{-8}	8.6520	2.5150×10^{-1}	3.6280×10^{-1}	1.0000	4.2676×10^{5}
35	2.4230×10^{-3}	1.0000×10^{-17}	4.7733×10^{-8}	3.9470×10^{-1}	2.9070×10^{-1}	1.3390×10^{-1}	1.0000	4.2676×10^{5}
36	2.7120×10^{-2}	1.0000×10^{-17}	4.0370×10^{-9}	2.7500×10^{-1}	3.7090×10^{-1}	3.6960×10^{-1}	1.0000	4.2676×10^{5}
37	5.0960×10^{-3}	1.0000×10^{-17}	2.2564×10^{-8}	6.9780	2.2650×10^{-1}	3.0790×10^{-2}	1.0000	4.2676×10^{5}
38	1.8940×10^{-3}	1.0000×10^{-17}	6.1135×10^{-8}	2.9640	1.7810×10^{-1}	3.9620×10^{-1}	1.0000	4.2676×10^{5}
39	1.0090×10^{-2}	1.0000×10^{-17}	1.1273×10^{-8}	2.6060×10^{-1}	1.6330×10^{-1}	3.7240×10^{-2}	1.0000	4.2676×10^{5}
40	2.2760×10^{-2}	1.0000×10^{-17}	4.8582×10^{-9}	2.4160×10^{-1}	2.4340×10^{-1}	1.1100×10^{-1}	1.0000	4.2676×10^{5}
41	1.8020×10^{-2}	1.0000×10^{-17}	6.2019×10^{-9}	5.7490×10^{-1}	1.3340×10^{-1}	1.0650×10^{-1}	1.0000	4.2676×10^{5}
42	2.1990×10^{-2}	1.0000×10^{-17}	5.0371×10^{-9}	5.4840×10^{-1}	3.9640×10^{-1}	3.3500×10^{-1}	1.0000	4.2676×10^{5}
43	5.1790×10^{-3}	1.0000×10^{-17}	2.2199×10^{-8}	4.0000	3.9070×10^{-1}	1.2040×10^{-1}	1.0000	4.2676×10^{5}
44	3.9010×10^{-3}	1.0000×10^{-17}	2.9553×10^{-8}	3.6050×10^{-1}	2.5980×10^{-1}	5.7350×10^{-2}	1.0000	4.2676×10^{5}
45	9.3870×10^{-3}	1.0000×10^{-17}	1.2135×10^{-8}	3.2390×10^{-1}	1.5830×10^{-1}	9.4190×10^{-2}	1.0000	4.2676×10^{5}
46	2.8280×10^{-2}	1.0000×10^{-17}	3.8611×10^{-9}	4.6060×10^{-1}	6.5170×10^{-2}	2.3880×10^{-1}	1.0000	4.2676×10^{5}
47	6.5700×10^{-3}	1.0000×10^{-17}	1.7446×10^{-8}	3.4760	3.1780×10^{-1}	2.6060×10^{-1}	1.0000	4.2676×10^{5}
48	2.2390×10^{-2}	1.0000×10^{-17}	4.9426×10^{-9}	7.7080	4.5510×10^{-2}	2.0750×10^{-1}	1.0000	4.2676×10^{5}
49	1.6820×10^{-3}	1.0000×10^{-17}	6.8872×10^{-8}	3.7530×10^{-1}	5.0110×10^{-2}	6.9900×10^{-2}	1.0000	4.2676×10^{5}
50	1.2890×10^{-2}	1.0000×10^{-17}	8.7696×10^{-9}	3.5390×10^{-1}	1.8990×10^{-1}	1.9850×10^{-1}	1.0000	4.2676×10^{5}
51	7.8440×10^{-3}	1.0000×10^{-17}	1.4572×10^{-8}	5.6000×10^{-1}	2.3180×10^{-2}	1.1810×10^{-2}	1.0000	4.2676×10^{5}
52	4.7130×10^{-3}	1.0000×10^{-17}	2.4418×10^{-8}	3.2370	1.5040×10^{-1}	3.8860×10^{-1}	1.0000	4.2676×10^{5}

Table B-2 1992 BRAGFLO Computed Variable Values for INITIAL_SALADO_DRZ (Concluded)

Run No.	Porosity	Permeability	Compressibility	BCEXP	BCBRSAT	BCGSSAT	BCFLG	BCPCT
53	1.5900×10^{-2}	1.0000×10^{-17}	7.0621×10^{-9}	6.7410	2.8470×10^{-1}	1.8060×10^{-1}	1.0000	4.2676×10^{5}
54	1.4500×10^{-2}	1.0000×10^{-17}	7.7681×10^{-9}	4.7200×10^{-1}	1.6590×10^{-1}	2.7290×10^{-1}	1.0000	4.2676×10^{5}
55	2.0030×10^{-2}	1.0000×10^{-17}	5.5544×10^{-9}	6.5030×10^{-1}	3.2450×10^{-1}	3.0330×10^{-1}	1.0000	4.2676×10^{5}
56	1.1650×10^{-2}	1.0000×10^{-17}	9.7296×10^{-9}	4.8480	9.2770×10^{-2}	5.2210×10^{-2}	1.0000	4.2676×10^{5}
57	4.5630×10^{-3}	1.0000×10^{-17}	2.5229×10^{-8}	9.2110	5.1160×10^{-3}	2.7770×10^{-1}	1.0000	4.2676×10^{5}
58	8.7110×10^{-3}	1.0000×10^{-17}	1.3097×10^{-8}	6.4060×10^{-1}	3.4880×10^{-1}	3.2980×10^{-1}	1.0000	4.2676×10^{5}
59	2.5160×10^{-2}	1.0000×10^{-17}	4.3709×10^{-9}	8.9580	8.5120×10^{-2}	3.1270×10^{-1}	1.0000	4.2676×10^{5}
60	8.2600×10^{-3}	1.0000×10^{-17}	1.3825×10^{-8}	9.8620	7.0380×10^{-2}	8.1940×10^{-2}	1.0000	4.2676×10^{5}
61	7.3840×10^{-3}	1.0000×10^{-17}	1.5495×10^{-8}	8.0490×10^{-1}	2.7910×10^{-1}	1.3890×10^{-1}	1.0000	4.2676×10^{5}
62	1.2250×10^{-2}	1.0000×10^{-17}	9.2408×10^{-9}	2.8630×10^{-1}	3.5990×10^{-1}	2.5120×10^{-1}	1.0000	4.2676×10^{5}
63	4.1090×10^{-3}	1.0000×10^{-17}	2.8045×10^{-8}	3.7540	2.0010×10^{-1}	2.8360×10^{-1}	1.0000	4.2676×10^{5}
64	3.7390×10^{-3}	1.0000×10^{-17}	3.0845×10^{-8}	2.4950	2.9320×10^{-2}	8.7020×10^{-2}	1.0000	4.2676×10^{5}
65	7.4700×10^{-3}	1.0000×10^{-17}	1.5314×10^{-8}	2.5410×10^{-1}	2.6410×10^{-1}	3.5100×10^{-1}	1.0000	4.2676×10^{5}
66	3.5330×10^{-3}	1.0000×10^{-17}	3.2658×10^{-8}	6.9150×10^{-1}	1.2380×10^{-1}	3.1630×10^{-1}	1.0000	4.2676×10^{5}
67	8.1910×10^{-3}	1.0000×10^{-17}	1.3944×10^{-8}	5.5890	5.6350×10^{-2}	2.5370×10^{-1}	1.0000	4.2676×10^{5}
68	1.0760×10^{-2}	1.0000×10^{-17}	1.0555×10^{-8}	4.5200	3.0240×10^{-1}	2.9970×10^{-1}	1.0000	4.2676×10^{5}
69	1.5190×10^{-2}	1.0000×10^{-17}	7.4039×10^{-9}	4.3270	3.7150×10^{-1}	4.8390×10^{-3}	1.0000	4.2676×10^{5}
70	1.4890×10^{-3}	1.0000×10^{-17}	7.7831×10^{-8}	6.2770×10^{-1}	1.0130×10^{-1}	1.1920×10^{-1}	1.0000	4.2676×10^{5}

Table B-2 1992 BRAGFLO Ranks of Computed Variable Values for INITIAL_SALADO_DRZ

Run No.	Porosity	Permeability	Compressibility	BCEXP	BCBRSAT	BCGSSAT	BCFLG	BCPCT
1	68.	1.	3.	69.	16.	41.	1.	1.
2	24.	1.	47.	21.	26.	23.	1.	1.
3	69.	1.	2.	34.	33.	38.	1.	1.
4	18.	1.	53.	52.	31.	34.	1.	1.
5	54.	1.	17.	15.	35.	26.	1.	1.
6	42.	1.	29.	56.	59.	9.	1.	1.
7	63.	1.	8.	37.	7.	29.	1.	1.
8	9.	1.	62.	57.	68.	5.	1.	1.
9	66.	1.	5.	16.	60.	33.	1.	1.
10	34.	1.	37.	39.	14.	61.	1.	1.
11	7.	1.	64.	22.	48.	36.	1.	1.
12	35.	1.	36.	61.	25.	51.	1.	1.
13	47.	1.	24.	41.	64.	52.	1.	1.
14	52.	1.	19.	8.	2.	31.	1.	1.
15	1.	1.	70.	18.	41.	68.	1.	1.
16	19.	1.	52.	24.	67.	39.	1.	1.
17	60.	1.	11.	55.	20.	67.	1.	1.
18	20.	1.	51.	28.	52.	2.	1.	1.
19	21.	1.	50.	40.	21.	30.	1.	1.
20	48.	1.	23.	33.	23.	57.	1.	1.
21	59.	1.	12.	2.	4.	40.	1.	1.
22	64.	1.	7.	38.	39.	4.	1.	1.
23	70.	1.	1.	60.	42.	8.	1.	1.
24	44.	1.	27.	17.	11.	47.	1.	1.
25	61.	1.	10.	43.	54.	18.	1.	1.
26	51.	1.	20.	53.	44.	12.	1.	1.
27	5.	1.	66.	64.	38.	14.	1.	1.
28	8.	1.	63.	63.	61.	27.	1.	1.
29	40.	1.	31.	29.	58.	63.	1.	1.
30	31.	1.	40.	1.	3.	28.	1.	1.
31	49.	1.	22.	10.	37.	43.	1.	1.
32	55.	1.	16.	66.	55.	66.	1.	1.
33	23.	1.	48.	23.	19.	60.	1.	1.
34	32.	1.	39.	65.	45.	64.	1.	1.
35	6.	1.	65.	14.	51.	24.	1.	1.
36	65.	1.	6.	6.	65.	65.	1.	1.
37	16.	1.	55.	59.	40.	6.	1.	1.
38	4.	1.	67.	44.	32.	70.	1.	1.
39	36.	1.	35.	5.	29.	7.	1.	1.
40	58.	1.	13.	3.	43.	20.	1.	1.
41	50.	1.	21.	27.	24.	19.	1.	1.
42	56.	1.	15.	25.	70.	59.	1.	1.
43	17.	1.	54.	48.	69.	22.	1.	1.
44	12.	1.	59.	12.	46.	11.	1.	1.
45	33.	1.	38.	9.	28.	17.	1.	1.
46	67.	1.	4.	19.	12.	42.	1.	1.
47	22.	1.	49.	46.	56.	46.	1.	1.
48	57.	1.	14.	62.	8.	37.	1.	1.
49	3.	1.	68.	13.	9.	13.	1.	1.
50	41.	1.	30.	11.	34.	35.	1.	1.
51	27.	1.	44.	26.	5.	3.	1.	1.
52	15.	1.	56.	45.	27.	69.	1.	1.

Table B-2 1992 BRAGFLO Ranks of Computed Variable Values for INITIAL_SALADO_DRZ (Concluded)

Run No.	Porosity	Permeability	Compressibility	BCEXP	BCBRSAT	BCGSSAT	BCFLG	BCPCT
53	46.	1.	25.	58.	50.	32.	1.	1.
54	43.	1.	28.	20.	30.	48.	1.	1.
55	53.	1.	18.	32.	57.	54.	1.	1.
56	38.	1.	33.	51.	17.	10.	1.	1.
57	14.	1.	57.	68.	1.	49.	1.	1.
58	30.	1.	41.	31.	62.	58.	1.	1.
59	62.	1.	9.	67.	15.	55.	1.	1.
60	29.	1.	42.	70.	13.	15.	1.	1.
61	25.	1.	46.	36.	49.	25.	1.	1.
62	39.	1.	32.	7.	63.	44.	1.	1.
63	13.	1.	58.	47.	36.	50.	1.	1.
64	11.	1.	60.	42.	6.	16.	1.	1.
65	26.	1.	45.	4.	47.	62.	1.	1.
66	10.	1.	61.	35.	22.	56.	1.	1.
67	28.	1.	43.	54.	10.	45.	1.	1.
68	37.	1.	34.	50.	53.	53.	1.	1.
69	45.	1.	26.	49.	66.	1.	1.	1.
70	2.	1.	69.	30.	18.	21.	1.	1.

Table B-2 1992 BRAGFLO Computed Variable Values for LOWER_SHAFT

Run No.	Porosity	Permeability	Compressibility	BCEXP	BCBRSAT	BCGSSAT	BCFLG	BCPCT
1	2.4490×10^{-2}	1.0000×10^{-15}	4.4974×10^{-9}	7.0000×10^{-1}	2.0000×10^{-1}	0.0000	1.0000	8.6734×10^{4}
2	1.1240×10^{-2}	1.0000×10^{-15}	1.0094×10^{-8}	7.0000×10^{-1}	2.0000×10^{-1}	0.0000	1.0000	8.6734×10^{4}
3	5.1030×10^{-2}	1.0000×10^{-15}	2.0283×10^{-9}	7.0000×10^{-1}	2.0000×10^{-1}	0.0000	1.0000	8.6734×10^{4}
4	1.6070×10^{-2}	1.0000×10^{-15}	6.9848×10^{-9}	7.0000×10^{-1}	2.0000×10^{-1}	0.0000	1.0000	8.6734×10^{4}
5	4.3250×10^{-2}	1.0000×10^{-15}	2.4381×10^{-9}	7.0000×10^{-1}	2.0000×10^{-1}	0.0000	1.0000	8.6734×10^{4}
6	5.8630×10^{-2}	1.0000×10^{-15}	1.7330×10^{-9}	7.0000×10^{-1}	2.0000×10^{-1}	0.0000	1.0000	8.6734×10^{4}
7	6.6520×10^{-2}	1.0000×10^{-15}	1.4978×10^{-9}	7.0000×10^{-1}	2.0000×10^{-1}	0.0000	1.0000	8.6734×10^{4}
8	3.6140×10^{-2}	1.0000×10^{-15}	2.9670×10^{-9}	7.0000×10^{-1}	2.0000×10^{-1}	0.0000	1.0000	8.6734×10^{4}
9	1.9210×10^{-2}	1.0000×10^{-15}	5.8022×10^{-9}	7.0000×10^{-1}	2.0000×10^{-1}	0.0000	1.0000	8.6734×10^{4}
10	4.7300×10^{-2}	1.0000×10^{-15}	2.2080×10^{-9}	7.0000×10^{-1}	2.0000×10^{-1}	0.0000	1.0000	8.6734×10^{4}
11	6.7690×10^{-2}	1.0000×10^{-15}	1.4676×10^{-9}	7.0000×10^{-1}	2.0000×10^{-1}	0.0000	1.0000	8.6734×10^{4}
12	2.5040×10^{-2}	1.0000×10^{-15}	4.3931×10^{-9}	7.0000×10^{-1}	2.0000×10^{-1}	0.0000	1.0000	8.6734×10^{4}
13	7.0630×10^{-2}	1.0000×10^{-15}	1.3961×10^{-9}	7.0000×10^{-1}	2.0000×10^{-1}	0.0000	1.0000	8.6734×10^{4}
14	4.0420×10^{-2}	1.0000×10^{-15}	2.6264×10^{-9}	7.0000×10^{-1}	2.0000×10^{-1}	0.0000	1.0000	8.6734×10^{4}
15	2.1150×10^{-2}	1.0000×10^{-15}	5.2470×10^{-9}	7.0000×10^{-1}	2.0000×10^{-1}	0.0000	1.0000	8.6734×10^{4}
16	7.2500×10^{-2}	1.0000×10^{-15}	1.3536×10^{-9}	7.0000×10^{-1}	2.0000×10^{-1}	0.0000	1.0000	8.6734×10^{4}
17	4.9250×10^{-2}	1.0000×10^{-15}	2.1107×10^{-9}	7.0000×10^{-1}	2.0000×10^{-1}	0.0000	1.0000	8.6734×10^{4}
18	1.3450×10^{-2}	1.0000×10^{-15}	8.3941×10^{-9}	7.0000×10^{-1}	2.0000×10^{-1}	0.0000	1.0000	8.6734×10^{4}
19	7.4520×10^{-2}	1.0000×10^{-15}	1.3101×10^{-9}	7.0000×10^{-1}	2.0000×10^{-1}	0.0000	1.0000	8.6734×10^{4}
20	3.7170×10^{-2}	1.0000×10^{-15}	2.8779×10^{-9}	7.0000×10^{-1}	2.0000×10^{-1}	0.0000	1.0000	8.6734×10^{4}
21	5.5630×10^{-2}	1.0000×10^{-15}	1.8399×10^{-9}	7.0000×10^{-1}	2.0000×10^{-1}	0.0000	1.0000	8.6734×10^{4}
22	4.4090×10^{-2}	1.0000×10^{-15}	2.3869×10^{-9}	7.0000×10^{-1}	2.0000×10^{-1}	0.0000	1.0000	8.6734×10^{4}
23	6.0100×10^{-2}	1.0000×10^{-15}	1.6845×10^{-9}	7.0000×10^{-1}	2.0000×10^{-1}	0.0000	1.0000	8.6734×10^{4}
24	6.9800×10^{-2}	1.0000×10^{-15}	1.4157×10^{-9}	7.0000×10^{-1}	2.0000×10^{-1}	0.0000	1.0000	8.6734×10^{4}
25	6.1100×10^{-2}	1.0000×10^{-15}	1.6528×10^{-9}	7.0000×10^{-1}	2.0000×10^{-1}	0.0000	1.0000	8.6734×10^{4}
26	5.6930×10^{-2}	1.0000×10^{-15}	1.7922×10^{-9}	7.0000×10^{-1}	2.0000×10^{-1}	0.0000	1.0000	8.6734×10^{4}
27	2.8620×10^{-2}	1.0000×10^{-15}	3.8123×10^{-9}	7.0000×10^{-1}	2.0000×10^{-1}	0.0000	1.0000	8.6734×10^{4}
28	4.1490×10^{-2}	1.0000×10^{-15}	2.5522×10^{-9}	7.0000×10^{-1}	2.0000×10^{-1}	0.0000	1.0000	8.6734×10^{4}
29	1.4260×10^{-2}	1.0000×10^{-15}	7.9031×10^{-9}	7.0000×10^{-1}	2.0000×10^{-1}	0.0000	1.0000	8.6734×10^{4}
30	3.2140×10^{-2}	1.0000×10^{-15}	3.3674×10^{-9}	7.0000×10^{-1}	2.0000×10^{-1}	0.0000	1.0000	8.6734×10^{4}
31	2.6760×10^{-2}	1.0000×10^{-15}	4.0946×10^{-9}	7.0000×10^{-1}	2.0000×10^{-1}	0.0000	1.0000	8.6734×10^{4}
32	3.9190×10^{-2}	1.0000×10^{-15}	2.7166×10^{-9}	7.0000×10^{-1}	2.0000×10^{-1}	0.0000	1.0000	8.6734×10^{4}
33	4.5660×10^{-2}	1.0000×10^{-15}	2.2963×10^{-9}	7.0000×10^{-1}	2.0000×10^{-1}	0.0000	1.0000	8.6734×10^{4}
34	3.4580×10^{-2}	1.0000×10^{-15}	3.1121×10^{-9}	7.0000×10^{-1}	2.0000×10^{-1}	0.0000	1.0000	8.6734×10^{4}
35	3.8780×10^{-2}	1.0000×10^{-15}	2.7480×10^{-9}	7.0000×10^{-1}	2.0000×10^{-1}	0.0000	1.0000	8.6734×10^{4}
36	4.6630×10^{-2}	1.0000×10^{-15}	2.2433×10^{-9}	7.0000×10^{-1}	2.0000×10^{-1}	0.0000	1.0000	8.6734×10^{4}
37	1.6500×10^{-2}	1.0000×10^{-15}	6.7962×10^{-9}	7.0000×10^{-1}	2.0000×10^{-1}	0.0000	1.0000	8.6734×10^{4}
38	6.7530×10^{-2}	1.0000×10^{-15}	1.4716×10^{-9}	7.0000×10^{-1}	2.0000×10^{-1}	0.0000	1.0000	8.6734×10^{4}
39	6.2320×10^{-2}	1.0000×10^{-15}	1.6156×10^{-9}	7.0000×10^{-1}	2.0000×10^{-1}	0.0000	1.0000	8.6734×10^{4}
40	5.4740×10^{-2}	1.0000×10^{-15}	1.8739×10^{-9}	7.0000×10^{-1}	2.0000×10^{-1}	0.0000	1.0000	8.6734×10^{4}
41	6.3580×10^{-2}	1.0000×10^{-15}	1.5786×10^{-9}	7.0000×10^{-1}	2.0000×10^{-1}	0.0000	1.0000	8.6734×10^{4}
42	7.1460×10^{-2}	1.0000×10^{-15}	1.3770×10^{-9}	7.0000×10^{-1}	2.0000×10^{-1}	0.0000	1.0000	8.6734×10^{4}
43	4.4580×10^{-2}	1.0000×10^{-15}	2.3580×10^{-9}	7.0000×10^{-1}	2.0000×10^{-1}	0.0000	1.0000	8.6734×10^{4}
44	7.3870×10^{-2}	1.0000×10^{-15}	1.3239×10^{-9}	7.0000×10^{-1}	2.0000×10^{-1}	0.0000	1.0000	8.6734×10^{4}
45	2.9730×10^{-2}	1.0000×10^{-15}	3.6606×10^{-9}	7.0000×10^{-1}	2.0000×10^{-1}	0.0000	1.0000	8.6734×10^{4}
46	1.2610×10^{-2}	1.0000×10^{-15}	8.9699×10^{-9}	7.0000×10^{-1}	2.0000×10^{-1}	0.0000	1.0000	8.6734×10^{4}
47	6.0510×10^{-2}	1.0000×10^{-15}	1.6714×10^{-9}	7.0000×10^{-1}	2.0000×10^{-1}	0.0000	1.0000	8.6734×10^{4}
48	3.3090×10^{-2}	1.0000×10^{-15}	3.2635×10^{-9}	7.0000×10^{-1}	2.0000×10^{-1}	0.0000	1.0000	8.6734×10^{4}
49	4.1760×10^{-2}	1.0000×10^{-15}	2.5341×10^{-9}	7.0000×10^{-1}	2.0000×10^{-1}	0.0000	1.0000	8.6734×10^{4}
50	3.0510×10^{-2}	1.0000×10^{-15}	3.5606×10^{-9}	7.0000×10^{-1}	2.0000×10^{-1}	0.0000	1.0000	8.6734×10^{4}
51	1.8180×10^{-2}	1.0000×10^{-15}	6.1451×10^{-9}	7.0000×10^{-1}	2.0000×10^{-1}	0.0000	1.0000	8.6734×10^{4}
52	6.5110×10^{-2}	1.0000×10^{-15}	1.5356×10^{-9}	7.0000×10^{-1}	2.0000×10^{-1}	0.0000	1.0000	8.6734×10^{4}

Table B-2 1992 BRAGFLO Computed Variable Values for LOWER_SHAFT (Concluded)

Run No.	Porosity	Permeability	Compressibility	BCEXP	BCBRSAT	BCGSSAT	BCFLG	BCPCT
53	2.0520×10^{-2}	1.0000×10^{-15}	5.4158×10^{-9}	7.0000×10^{-1}	2.0000×10^{-1}	0.0000	1.0000	8.6734×10^{4}
54	6.4400×10^{-2}	1.0000×10^{-15}	1.5553×10^{-9}	7.0000×10^{-1}	2.0000×10^{-1}	0.0000	1.0000	8.6734×10^{4}
55	2.6330×10^{-2}	1.0000×10^{-15}	4.1656×10^{-9}	7.0000×10^{-1}	2.0000×10^{-1}	0.0000	1.0000	8.6734×10^{4}
56	3.5470×10^{-2}	1.0000×10^{-15}	3.0278×10^{-9}	7.0000×10^{-1}	2.0000×10^{-1}	0.0000	1.0000	8.6734×10^{4}
57	1.9820×10^{-2}	1.0000×10^{-15}	5.6159×10^{-9}	7.0000×10^{-1}	2.0000×10^{-1}	0.0000	1.0000	8.6734×10^{4}
58	2.3880×10^{-2}	1.0000×10^{-15}	4.6186×10^{-9}	7.0000×10^{-1}	2.0000×10^{-1}	0.0000	1.0000	8.6734×10^{4}
59	5.7990×10^{-2}	1.0000×10^{-15}	1.7549×10^{-9}	7.0000×10^{-1}	2.0000×10^{-1}	0.0000	1.0000	8.6734×10^{4}
60	6.9150×10^{-2}	1.0000×10^{-15}	1.4313×10^{-9}	7.0000×10^{-1}	2.0000×10^{-1}	0.0000	1.0000	8.6734×10^{4}
61	1.5400×10^{-2}	1.0000×10^{-15}	7.2995×10^{-9}	7.0000×10^{-1}	2.0000×10^{-1}	0.0000	1.0000	8.6734×10^{4}
62	2.7890×10^{-2}	1.0000×10^{-15}	3.9186×10^{-9}	7.0000×10^{-1}	2.0000×10^{-1}	0.0000	1.0000	8.6734×10^{4}
63	5.2340×10^{-2}	1.0000×10^{-15}	1.9713×10^{-9}	7.0000×10^{-1}	2.0000×10^{-1}	0.0000	1.0000	8.6734×10^{4}
64	5.3500×10^{-2}	1.0000×10^{-15}	1.9231×10^{-9}	7.0000×10^{-1}	2.0000×10^{-1}	0.0000	1.0000	8.6734×10^{4}
65	1.0820×10^{-2}	1.0000×10^{-15}	1.0495×10^{-8}	7.0000×10^{-1}	2.0000×10^{-1}	0.0000	1.0000	8.6734×10^{4}
66	5.0410×10^{-2}	1.0000×10^{-15}	2.0563×10^{-9}	7.0000×10^{-1}	2.0000×10^{-1}	0.0000	1.0000	8.6734×10^{4}
67	3.3230×10^{-2}	1.0000×10^{-15}	3.2487×10^{-9}	7.0000×10^{-1}	2.0000×10^{-1}	0.0000	1.0000	8.6734×10^{4}
68	2.2660×10^{-2}	1.0000×10^{-15}	4.8807×10^{-9}	7.0000×10^{-1}	2.0000×10^{-1}	0.0000	1.0000	8.6734×10^{4}
69	4.8950×10^{-2}	1.0000×10^{-15}	2.1251×10^{-9}	7.0000×10^{-1}	2.0000×10^{-1}	0.0000	1.0000	8.6734×10^{4}
70	5.3660×10^{-2}	1.0000×10^{-15}	1.9166×10^{-9}	7.0000×10^{-1}	2.0000×10^{-1}	0.0000	1.0000	8.6734×10^{4}

Table B-2 1992 BRAGFLO Ranks of Computed Variable Values for LOWER_SHAFT

Run No.	Porosity	Permeability	Compressibility	BCEXP	BCBRSAT	BCGSSAT	BCFLG	BCPCT
1	16.	1.	55.	1.	1.	1.	1.	1.
2	2.	1.	69.	1.	1.	1.	1.	1.
3	45.	1.	26.	1.	1.	1.	1.	1.
4	7.	1.	64.	1.	1.	1.	1.	1.
5	36.	1.	35.	1.	1.	1.	1.	1.
6	53.	1.	18.	1.	1.	1.	1.	1.
7	61.	1.	10.	1.	1.	1.	1.	1.
8	29.	1.	42.	1.	1.	1.	1.	1.
9	10.	1.	61.	1.	1.	1.	1.	1.
10	41.	1.	30.	1.	1.	1.	1.	1.
11	63.	1.	8.	1.	1.	1.	1.	1.
12	17.	1.	54.	1.	1.	1.	1.	1.
13	66.	1.	5.	1.	1.	1.	1.	1.
14	33.	1.	38.	1.	1.	1.	1.	1.
15	13.	1.	58.	1.	1.	1.	1.	1.
16	68.	1.	3.	1.	1.	1.	1.	1.
17	43.	1.	28.	1.	1.	1.	1.	1.
18	4.	1.	67.	1.	1.	1.	1.	1.
19	70.	1.	1.	1.	1.	1.	1.	1.
20	30.	1.	41.	1.	1.	1.	1.	1.
21	50.	1.	21.	1.	1.	1.	1.	1.
22	37.	1.	34.	1.	1.	1.	1.	1.
23	54.	1.	17.	1.	1.	1.	1.	1.
24	65.	1.	6.	1.	1.	1.	1.	1.
25	56.	1.	15.	1.	1.	1.	1.	1.
26	51.	1.	20.	1.	1.	1.	1.	1.
27	21.	1.	50.	1.	1.	1.	1.	1.
28	34.	1.	37.	1.	1.	1.	1.	1.
29	5.	1.	66.	1.	1.	1.	1.	1.
30	24.	1.	47.	1.	1.	1.	1.	1.
31	19.	1.	52.	1.	1.	1.	1.	1.
32	32.	1.	39.	1.	1.	1.	1.	1.
33	39.	1.	32.	1.	1.	1.	1.	1.
34	27.	1.	44.	1.	1.	1.	1.	1.
35	31.	1.	40.	1.	1.	1.	1.	1.
36	40.	1.	31.	1.	1.	1.	1.	1.
37	8.	1.	63.	1.	1.	1.	1.	1.
38	62.	1.	9.	1.	1.	1.	1.	1.
39	57.	1.	14.	1.	1.	1.	1.	1.
40	49.	1.	22.	1.	1.	1.	1.	1.
41	58.	1.	13.	1.	1.	1.	1.	1.
42	67.	1.	4.	1.	1.	1.	1.	1.
43	38.	1.	33.	1.	1.	1.	1.	1.
44	69.	1.	2.	1.	1.	1.	1.	1.
45	22.	1.	49.	1.	1.	1.	1.	1.
46	3.	1.	68.	1.	1.	1.	1.	1.
47	55.	1.	16.	1.	1.	1.	1.	1.
48	25.	1.	46.	1.	1.	1.	1.	1.
49	35.	1.	36.	1.	1.	1.	1.	1.
50	23.	1.	48.	1.	1.	1.	1.	1.
51	9.	1.	62.	1.	1.	1.	1.	1.
52	60.	1.	11.	1.	1.	1.	1.	1.

Table B-2 1992 BRAGFLO Ranks of Computed Variable Values for LOWER_SHAFT (Concluded)

Run No.	Porosity	Permeability	Compressibility	BCEXP	BCBRSAT	BCGSSAT	BCFLG	BCPCT
53	12.	1.	59.	1.	1.	1.	1.	1.
54	59.	1.	12.	1.	1.	1.	1.	1.
55	18.	1.	53.	1.	1.	1.	1.	1.
56	28.	1.	43.	1.	1.	1.	1.	1.
57	11.	1.	60.	1.	1.	1.	1.	1.
58	15.	1.	56.	1.	1.	1.	1.	1.
59	52.	1.	19.	1.	1.	1.	1.	1.
60	64.	1.	7.	1.	1.	1.	1.	1.
61	6.	1.	65.	1.	1.	1.	1.	1.
62	20.	1.	51.	1.	1.	1.	1.	1.
63	46.	1.	25.	1.	1.	1.	1.	1.
64	47.	1.	24.	1.	1.	1.	1.	1.
65	1.	1.	70.	1.	1.	1.	1.	1.
66	44.	1.	27.	1.	1.	1.	1.	1.
67	26.	1.	45.	1.	1.	1.	1.	1.
68	14.	1.	57.	1.	1.	1.	1.	1.
69	42.	1.	29.	1.	1.	1.	1.	1.
70	48.	1.	23.	1.	1.	1.	1.	1.

Table B-2 1992 BRAGFLO Computed Variable Values for PANEL_SEAL

Run No.	Porosity	Permeability	Compressibility	BCEXP	BCBRSAT	BCGSSAT	BCFLG	BCPCT
1	6.4546×10^{-2}	1.2330×10^{-20}	1.5512×10^{-9}	7.0000×10^{-1}	2.0000×10^{-1}	0.0000	1.0000	4.3323×10^{6}
2	6.9050×10^{-2}	2.6840×10^{-20}	1.4337×10^{-9}	7.0000×10^{-1}	2.0000×10^{-1}	0.0000	1.0000	3.3100×10^{6}
3	6.4267×10^{-2}	1.1750×10^{-20}	1.5591×10^{-9}	7.0000×10^{-1}	2.0000×10^{-1}	0.0000	1.0000	4.4051×10^{6}
4	7.4080×10^{-2}	6.3970×10^{-20}	1.3194×10^{-9}	7.0000×10^{-1}	2.0000×10^{-1}	0.0000	1.0000	2.4509×10^{6}
5	7.0423×10^{-2}	3.4020×10^{-20}	1.4009×10^{-9}	7.0000×10^{-1}	2.0000×10^{-1}	0.0000	1.0000	3.0494×10^{6}
6	6.7501×10^{-2}	2.0540×10^{-20}	1.4724×10^{-9}	7.0000×10^{-1}	2.0000×10^{-1}	0.0000	1.0000	3.6310×10^{6}
7	6.7660×10^{-2}	2.1110×10^{-20}	1.4683×10^{-9}	7.0000×10^{-1}	2.0000×10^{-1}	0.0000	1.0000	3.5968×10^{6}
8	7.4185×10^{-2}	6.5140×10^{-20}	1.3172×10^{-9}	7.0000×10^{-1}	2.0000×10^{-1}	0.0000	1.0000	2.4356×10^{6}
9	6.7849×10^{-2}	2.1810×10^{-20}	1.4636×10^{-9}	7.0000×10^{-1}	2.0000×10^{-1}	0.0000	1.0000	3.5564×10^{6}
10	6.5015×10^{-2}	1.3370×10^{-20}	1.5382×10^{-9}	7.0000×10^{-1}	2.0000×10^{-1}	0.0000	1.0000	4.2126×10^{6}
11	8.3154×10^{-2}	3.0660×10^{-19}	1.1482×10^{-9}	7.0000×10^{-1}	2.0000×10^{-1}	0.0000	1.0000	1.4251×10^{6}
12	6.0920×10^{-2}	6.5920×10^{-21}	1.6584×10^{-9}	7.0000×10^{-1}	2.0000×10^{-1}	0.0000	1.0000	5.3803×10^{6}
13	6.2562×10^{-2}	8.7530×10^{-21}	1.6084×10^{-9}	7.0000×10^{-1}	2.0000×10^{-1}	0.0000	1.0000	4.8776×10^{6}
14	7.7689×10^{-2}	1.1930×10^{-19}	1.2465×10^{-9}	7.0000×10^{-1}	2.0000×10^{-1}	0.0000	1.0000	1.9755×10^{6}
15	7.4789×10^{-2}	7.2300×10^{-20}	1.3046×10^{-9}	7.0000×10^{-1}	2.0000×10^{-1}	0.0000	1.0000	2.3492×10^{6}
16	8.6557×10^{-2}	5.5180×10^{-19}	1.0932×10^{-9}	7.0000×10^{-1}	2.0000×10^{-1}	0.0000	1.0000	1.1629×10^{6}
17	6.0226×10^{-2}	5.8470×10^{-21}	1.6805×10^{-9}	7.0000×10^{-1}	2.0000×10^{-1}	0.0000	1.0000	5.6083×10^{6}
18	7.2424×10^{-2}	4.8060×10^{-20}	1.3553×10^{-9}	7.0000×10^{-1}	2.0000×10^{-1}	0.0000	1.0000	2.7058×10^{6}
19	7.8301×10^{-2}	1.3260×10^{-19}	1.2348×10^{-9}	7.0000×10^{-1}	2.0000×10^{-1}	0.0000	1.0000	1.9045×10^{6}
20	6.2783×10^{-2}	9.0940×10^{-21}	1.6018×10^{-9}	7.0000×10^{-1}	2.0000×10^{-1}	0.0000	1.0000	4.8135×10^{6}
21	5.9353×10^{-2}	5.0290×10^{-21}	1.7088×10^{-9}	7.0000×10^{-1}	2.0000×10^{-1}	0.0000	1.0000	5.9085×10^{6}
22	7.7349×10^{-2}	1.1250×10^{-19}	1.2531×10^{-9}	7.0000×10^{-1}	2.0000×10^{-1}	0.0000	1.0000	2.0160×10^{6}
23	6.3790×10^{-2}	1.0820×10^{-20}	1.5726×10^{-9}	7.0000×10^{-1}	2.0000×10^{-1}	0.0000	1.0000	4.5326×10^{6}
24	7.6220×10^{-2}	9.2570×10^{-20}	1.2754×10^{-9}	7.0000×10^{-1}	2.0000×10^{-1}	0.0000	1.0000	2.1567×10^{6}
25	5.7045×10^{-2}	3.3760×10^{-21}	1.7881×10^{-9}	7.0000×10^{-1}	2.0000×10^{-1}	0.0000	1.0000	6.7820×10^{6}
26	7.1304×10^{-2}	3.9610×10^{-20}	1.3805×10^{-9}	7.0000×10^{-1}	2.0000×10^{-1}	0.0000	1.0000	2.8930×10^{6}
27	6.6134×10^{-2}	1.6220×10^{-20}	1.5080×10^{-9}	7.0000×10^{-1}	2.0000×10^{-1}	0.0000	1.0000	3.9401×10^{6}
28	8.3995×10^{-2}	3.5450×10^{-19}	1.1342×10^{-9}	7.0000×10^{-1}	2.0000×10^{-1}	0.0000	1.0000	1.3553×10^{6}
29	7.0821×10^{-2}	3.6440×10^{-20}	1.3916×10^{-9}	7.0000×10^{-1}	2.0000×10^{-1}	0.0000	1.0000	2.9777×10^{6}
30	8.0747×10^{-2}	2.0230×10^{-19}	1.1898×10^{-9}	7.0000×10^{-1}	2.0000×10^{-1}	0.0000	1.0000	1.6456×10^{6}
31	6.6460×10^{-2}	1.7160×10^{-20}	1.4994×10^{-9}	7.0000×10^{-1}	2.0000×10^{-1}	0.0000	1.0000	3.8641×10^{6}
32	7.9457×10^{-2}	1.6190×10^{-19}	1.2132×10^{-9}	7.0000×10^{-1}	2.0000×10^{-1}	0.0000	1.0000	1.7774×10^{6}
33	6.1584×10^{-2}	7.3930×10^{-21}	1.6379×10^{-9}	7.0000×10^{-1}	2.0000×10^{-1}	0.0000	1.0000	5.1710×10^{6}
34	6.8752×10^{-2}	2.5490×10^{-20}	1.4410×10^{-9}	7.0000×10^{-1}	2.0000×10^{-1}	0.0000	1.0000	3.3696×10^{6}
35	5.7582×10^{-2}	3.7040×10^{-21}	1.7691×10^{-9}	7.0000×10^{-1}	2.0000×10^{-1}	0.0000	1.0000	6.5679×10^{6}
36	6.6807×10^{-2}	1.8220×10^{-20}	1.4903×10^{-9}	7.0000×10^{-1}	2.0000×10^{-1}	0.0000	1.0000	3.7848×10^{6}
37	6.3385×10^{-2}	1.0090×10^{-20}	1.5842×10^{-9}	7.0000×10^{-1}	2.0000×10^{-1}	0.0000	1.0000	4.6435×10^{6}
38	6.0375×10^{-2}	6.0000×10^{-21}	1.6757×10^{-9}	7.0000×10^{-1}	2.0000×10^{-1}	0.0000	1.0000	5.5584×10^{6}
39	6.9617×10^{-2}	2.9600×10^{-20}	1.4200×10^{-9}	7.0000×10^{-1}	2.0000×10^{-1}	0.0000	1.0000	3.1998×10^{6}
40	7.1929×10^{-2}	4.4120×10^{-20}	1.3664×10^{-9}	7.0000×10^{-1}	2.0000×10^{-1}	0.0000	1.0000	2.7870×10^{6}
41	8.5712×10^{-2}	4.7690×10^{-19}	1.1064×10^{-9}	7.0000×10^{-1}	2.0000×10^{-1}	0.0000	1.0000	1.2231×10^{6}
42	6.1966×10^{-2}	7.8970×10^{-21}	1.6262×10^{-9}	7.0000×10^{-1}	2.0000×10^{-1}	0.0000	1.0000	5.0544×10^{6}
43	8.0322×10^{-2}	1.8800×10^{-19}	1.1975×10^{-9}	7.0000×10^{-1}	2.0000×10^{-1}	0.0000	1.0000	1.6878×10^{6}
44	6.8201×10^{-2}	2.3180×10^{-20}	1.4547×10^{-9}	7.0000×10^{-1}	2.0000×10^{-1}	0.0000	1.0000	3.4822×10^{6}
45	6.9955×10^{-2}	3.1380×10^{-20}	1.4120×10^{-9}	7.0000×10^{-1}	2.0000×10^{-1}	0.0000	1.0000	3.1358×10^{6}
46	7.6523×10^{-2}	9.7550×10^{-20}	1.2693×10^{-9}	7.0000×10^{-1}	2.0000×10^{-1}	0.0000	1.0000	2.1180×10^{6}
47	6.7080×10^{-2}	1.9100×10^{-20}	1.4832×10^{-9}	7.0000×10^{-1}	2.0000×10^{-1}	0.0000	1.0000	3.7235×10^{6}
48	7.5590×10^{-2}	8.3030×10^{-20}	1.2881×10^{-9}	7.0000×10^{-1}	2.0000×10^{-1}	0.0000	1.0000	2.2394×10^{6}
49	5.5156×10^{-2}	2.4360×10^{-21}	1.8579×10^{-9}	7.0000×10^{-1}	2.0000×10^{-1}	0.0000	1.0000	7.5927×10^{6}
50	7.3176×10^{-2}	5.4730×10^{-20}	1.3388×10^{-9}	7.0000×10^{-1}	2.0000×10^{-1}	0.0000	1.0000	2.5868×10^{6}
51	7.0199×10^{-2}	3.2730×10^{-20}	1.4062×10^{-9}	7.0000×10^{-1}	2.0000×10^{-1}	0.0000	1.0000	3.0904×10^{6}
52	7.1211×10^{-2}	3.8980×10^{-20}	1.3826×10^{-9}	7.0000×10^{-1}	2.0000×10^{-1}	0.0000	1.0000	2.9091×10^{6}

Table B-2 1992 BRAGFLO Computed Variable Values for PANEL_SEAL (Concluded)

Run No.	Porosity	Permeability	Compressibility	BCEXP	BCBRSAT	BCGSSAT	BCFLG	BCPCT
53	8.1495×10^{-2}	2.3020×10^{-19}	1.1766×10^{-9}	7.0000×10^{-1}	2.0000×10^{-1}	0.0000	1.0000	1.5736×10^{6}
54	7.8822×10^{-2}	1.4510×10^{-19}	1.2250×10^{-9}	7.0000×10^{-1}	2.0000×10^{-1}	0.0000	1.0000	1.8461×10^{6}
55	8.2516×10^{-2}	2.7460×10^{-19}	1.1590×10^{-9}	7.0000×10^{-1}	2.0000×10^{-1}	0.0000	1.0000	1.4805×10^{6}
56	6.5560×10^{-2}	1.4690×10^{-20}	1.5234×10^{-9}	7.0000×10^{-1}	2.0000×10^{-1}	0.0000	1.0000	4.0775×10^{6}
57	7.4885×10^{-2}	7.3510×10^{-20}	1.3026×10^{-9}	7.0000×10^{-1}	2.0000×10^{-1}	0.0000	1.0000	2.3358×10^{6}
58	5.1492×10^{-2}	1.2940×10^{-21}	2.0079×10^{-9}	7.0000×10^{-1}	2.0000×10^{-1}	0.0000	1.0000	9.4506×10^{6}
59	9.0000×10^{-2}	1.0000×10^{-18}	1.0418×10^{-9}	7.0000×10^{-1}	2.0000×10^{-1}	0.0000	1.0000	9.4665×10^{5}
60	5.5835×10^{-2}	2.7390×10^{-21}	1.8323×10^{-9}	7.0000×10^{-1}	2.0000×10^{-1}	0.0000	1.0000	7.2909×10^{6}
61	7.6860×10^{-2}	1.0340×10^{-19}	1.2626×10^{-9}	7.0000×10^{-1}	2.0000×10^{-1}	0.0000	1.0000	2.0757×10^{6}
62	7.1746×10^{-2}	4.2750×10^{-20}	1.3705×10^{-9}	7.0000×10^{-1}	2.0000×10^{-1}	0.0000	1.0000	2.8176×10^{6}
63	7.3762×10^{-2}	6.0550×10^{-20}	1.3262×10^{-9}	7.0000×10^{-1}	2.0000×10^{-1}	0.0000	1.0000	2.4979×10^{6}
64	7.5663×10^{-2}	8.4080×10^{-20}	1.2866×10^{-9}	7.0000×10^{-1}	2.0000×10^{-1}	0.0000	1.0000	2.2297×10^{6}
65	7.3045×10^{-2}	5.3500×10^{-20}	1.3417×10^{-9}	7.0000×10^{-1}	2.0000×10^{-1}	0.0000	1.0000	2.6072×10^{6}
66	5.1070×10^{-2}	1.2030×10^{-21}	2.0265×10^{-9}	7.0000×10^{-1}	2.0000×10^{-1}	0.0000	1.0000	9.6921×10^{6}
67	7.2562×10^{-2}	4.9220×10^{-20}	1.3523×10^{-9}	7.0000×10^{-1}	2.0000×10^{-1}	0.0000	1.0000	2.6835×10^{6}
68	6.9149×10^{-2}	2.7300×10^{-20}	1.4313×10^{-9}	7.0000×10^{-1}	2.0000×10^{-1}	0.0000	1.0000	3.2906×10^{6}
69	5.8844×10^{-2}	4.6060×10^{-21}	1.7258×10^{-9}	7.0000×10^{-1}	2.0000×10^{-1}	0.0000	1.0000	6.0909×10^{6}
70	6.5148×10^{-2}	1.3680×10^{-20}	1.5346×10^{-9}	7.0000×10^{-1}	2.0000×10^{-1}	0.0000	1.0000	4.1793×10^{6}

Table B-2 1992 BRAGFLO Ranks of Computed Variable Values for PANEL_SEAL

Run No.	Porosity	Permeability	Compressibility	BCEXP	BCBRSAT	BCGSSAT	BCFLG	BCPCT
1	19.	19.	52.	1.	1.	1.	1.	52.
2	32.	32.	39.	1.	1.	1.	1.	39.
3	18.	18.	53.	1.	1.	1.	1.	53.
4	48.	48.	23.	1.	1.	1.	1.	23.
5	37.	37.	34.	1.	1.	1.	1.	34.
6	27.	27.	44.	1.	1.	1.	1.	44.
7	28.	28.	43.	1.	1.	1.	1.	43.
8	49.	49.	22.	1.	1.	1.	1.	22.
9	29.	29.	42.	1.	1.	1.	1.	42.
10	20.	20.	51.	1.	1.	1.	1.	51.
11	66.	66.	5.	1.	1.	1.	1.	5.
12	11.	11.	60.	1.	1.	1.	1.	60.
13	14.	14.	57.	1.	1.	1.	1.	57.
14	58.	58.	13.	1.	1.	1.	1.	13.
15	50.	50.	21.	1.	1.	1.	1.	21.
16	69.	69.	2.	1.	1.	1.	1.	2.
17	9.	9.	62.	1.	1.	1.	1.	62.
18	43.	43.	28.	1.	1.	1.	1.	28.
19	59.	59.	12.	1.	1.	1.	1.	12.
20	15.	15.	56.	1.	1.	1.	1.	56.
21	8.	8.	63.	1.	1.	1.	1.	63.
22	57.	57.	14.	1.	1.	1.	1.	14.
23	17.	17.	54.	1.	1.	1.	1.	54.
24	54.	54.	17.	1.	1.	1.	1.	17.
25	5.	5.	66.	1.	1.	1.	1.	66.
26	40.	40.	31.	1.	1.	1.	1.	31.
27	23.	23.	48.	1.	1.	1.	1.	48.
28	67.	67.	4.	1.	1.	1.	1.	4.
29	38.	38.	33.	1.	1.	1.	1.	33.
30	63.	63.	8.	1.	1.	1.	1.	8.
31	24.	24.	47.	1.	1.	1.	1.	47.
32	61.	61.	10.	1.	1.	1.	1.	10.
33	12.	12.	59.	1.	1.	1.	1.	59.
34	31.	31.	40.	1.	1.	1.	1.	40.
35	6.	6.	65.	1.	1.	1.	1.	65.
36	25.	25.	46.	1.	1.	1.	1.	46.
37	16.	16.	55.	1.	1.	1.	1.	55.
38	10.	10.	61.	1.	1.	1.	1.	61.
39	34.	34.	37.	1.	1.	1.	1.	37.
40	42.	42.	29.	1.	1.	1.	1.	29.
41	68.	68.	3.	1.	1.	1.	1.	3.
42	13.	13.	58.	1.	1.	1.	1.	58.
43	62.	62.	9.	1.	1.	1.	1.	9.
44	30.	30.	41.	1.	1.	1.	1.	41.
45	35.	35.	36.	1.	1.	1.	1.	36.
46	55.	55.	16.	1.	1.	1.	1.	16.
47	26.	26.	45.	1.	1.	1.	1.	45.
48	52.	52.	19.	1.	1.	1.	1.	19.
49	3.	3.	68.	1.	1.	1.	1.	68.
50	46.	46.	25.	1.	1.	1.	1.	25.
51	36.	36.	35.	1.	1.	1.	1.	35.
52	39.	39.	32.	1.	1.	1.	1.	32.

Table B-2 1992 BRAGFLO Ranks of Computed Variable Values for PANEL_SEAL (Concluded)

Run No.	Porosity	Permeability	Compressibility	BCEXP	BCBRSAT	BCGSSAT	BCFLG	BCPCT
53	64.	64.	7.	1.	1.	1.	1.	7.
54	60.	60.	11.	1.	1.	1.	1.	11.
55	65.	65.	6.	1.	1.	1.	1.	6.
56	22.	22.	49.	1.	1.	1.	1.	49.
57	51.	51.	20.	1.	1.	1.	1.	20.
58	2.	2.	69.	1.	1.	1.	1.	69.
59	70.	70.	1.	1.	1.	1.	1.	1.
60	4.	4.	67.	1.	1.	1.	1.	67.
61	56.	56.	15.	1.	1.	1.	1.	15.
62	41.	41.	30.	1.	1.	1.	1.	30.
63	47.	47.	24.	1.	1.	1.	1.	24.
64	53.	53.	18.	1.	1.	1.	1.	18.
65	45.	45.	26.	1.	1.	1.	1.	26.
66	1.	1.	70.	1.	1.	1.	1.	70.
67	44.	44.	27.	1.	1.	1.	1.	27.
68	33.	33.	38.	1.	1.	1.	1.	38.
69	7.	7.	64.	1.	1.	1.	1.	64.
70	21.	21.	50.	1.	1.	1.	1.	50.

Table B-2 1992 BRAGFLO Computed Variable Values for SALADO

Run No.	Porosity	Permeability	Compressibility	BCEXP	BCBRSAT	BCGSSAT	BCFLG	BCPCT
1	2.8660×10^{-2}	3.6308×10^{-21}	3.8066×10^{-9}	9.6790	8.7890×10^{-2}	2.3300×10^{-1}	0.0000	6.6135×10^{6}
2	6.9900×10^{-3}	9.7724×10^{-21}	1.6383×10^{-8}	4.9660×10^{-1}	1.4570×10^{-1}	1.2590×10^{-1}	1.0000	4.6951×10^{6}
3	2.8970×10^{-2}	1.3183×10^{-21}	3.7632×10^{-9}	6.7900×10^{-1}	1.8490×10^{-1}	2.1660×10^{-1}	1.0000	9.3900×10^{6}
4	5.6130×10^{-3}	1.5136×10^{-21}	2.0463×10^{-8}	5.1820	1.7260×10^{-1}	1.8900×10^{-1}	1.0000	8.9517×10^{6}
5	2.0560×10^{-2}	2.8840×10^{-22}	5.4048×10^{-9}	4.0710×10^{-1}	1.9880×10^{-1}	1.4590×10^{-1}	1.0000	1.5887×10^{7}
6	1.3750×10^{-2}	7.2444×10^{-24}	8.2055×10^{-9}	6.1420	3.3170×10^{-1}	4.7930×10^{-2}	0.0000	5.6837×10^{7}
7	2.5930×10^{-2}	1.1481×10^{-22}	4.2337×10^{-9}	1.0990	3.5430×10^{-2}	1.6220×10^{-1}	0.0000	2.1849×10^{7}
8	3.1850×10^{-3}	4.8978×10^{-22}	3.6253×10^{-8}	6.4480	3.8660×10^{-1}	2.8520×10^{-2}	1.0000	1.3227×10^{7}
9	2.7270×10^{-2}	4.7863×10^{-24}	4.0134×10^{-9}	4.2610×10^{-1}	3.4080×10^{-1}	1.8690×10^{-1}	1.0000	6.5601×10^{7}
10	9.6770×10^{-3}	3.9811×10^{-21}	1.1764×10^{-8}	1.5170	7.9000×10^{-2}	3.4810×10^{-1}	1.0000	6.4060×10^{6}
11	2.5730×10^{-3}	7.7625×10^{-21}	4.4936×10^{-8}	5.1250×10^{-1}	2.7170×10^{-1}	2.0030×10^{-1}	0.0000	5.0845×10^{6}
12	9.8270×10^{-3}	9.1201×10^{-21}	1.1581×10^{-8}	7.4960	1.4100×10^{-1}	2.8620×10^{-1}	1.0000	4.8087×10^{6}
13	1.6610×10^{-2}	8.7096×10^{-24}	6.7496×10^{-9}	2.2490	3.6500×10^{-1}	2.9370×10^{-1}	1.0000	5.3327×10^{7}
14	1.9600×10^{-2}	7.0795×10^{-23}	5.6818×10^{-9}	3.0620×10^{-1}	8.3660×10^{-3}	1.7360×10^{-1}	1.0000	2.5828×10^{7}
15	1.1590×10^{-3}	3.0200×10^{-24}	1.0006×10^{-7}	4.4620×10^{-1}	2.3100×10^{-1}	3.8350×10^{-1}	0.0000	7.6932×10^{7}
16	5.8700×10^{-3}	1.9953×10^{-21}	1.9556×10^{-8}	5.3590×10^{-1}	3.7890×10^{-1}	2.1720×10^{-1}	1.0000	8.1356×10^{6}
17	2.3950×10^{-2}	1.2882×10^{-22}	4.6044×10^{-9}	5.9190	1.1130×10^{-1}	3.8060×10^{-1}	0.0000	2.0996×10^{7}
18	6.1370×10^{-3}	6.7608×10^{-22}	1.8695×10^{-8}	5.8730×10^{-1}	2.9470×10^{-1}	8.6120×10^{-3}	0.0000	1.1831×10^{7}
19	6.2550×10^{-3}	3.9811×10^{-23}	1.8337×10^{-8}	2.0050	1.1640×10^{-1}	1.6670×10^{-1}	1.0000	3.1520×10^{7}
20	1.7070×10^{-2}	1.8197×10^{-20}	6.5609×10^{-9}	6.7090×10^{-1}	1.2940×10^{-1}	3.2110×10^{-1}	1.0000	3.7864×10^{6}
21	2.3500×10^{-2}	2.8840×10^{-20}	4.6974×10^{-9}	2.2590×10^{-1}	1.9770×10^{-2}	2.2330×10^{-1}	0.0000	3.2287×10^{6}
22	2.6030×10^{-2}	5.4954×10^{-21}	4.2165×10^{-9}	1.4340	2.1830×10^{-1}	1.8710×10^{-2}	1.0000	5.7299×10^{6}
23	2.9920×10^{-2}	5.4954×10^{-22}	3.6358×10^{-9}	7.0990	2.3880×10^{-1}	4.5230×10^{-2}	1.0000	1.2710×10^{7}
24	1.4710×10^{-2}	1.2023×10^{-21}	7.6537×10^{-9}	4.3270×10^{-1}	6.1270×10^{-2}	2.6430×10^{-1}	1.0000	9.6941×10^{6}
25	2.4720×10^{-2}	7.0795×10^{-21}	4.4532×10^{-9}	2.7610	3.0510×10^{-1}	9.9900×10^{-2}	1.0000	5.2491×10^{6}
26	1.8820×10^{-2}	1.7378×10^{-21}	5.9276×10^{-9}	5.2660	2.4700×10^{-1}	6.8060×10^{-2}	1.0000	8.5339×10^{6}
27	2.2740×10^{-3}	5.1286×10^{-22}	5.0877×10^{-8}	8.3330	2.1280×10^{-1}	7.5730×10^{-2}	1.0000	1.3018×10^{7}
28	2.8830×10^{-3}	4.5709×10^{-22}	4.0077×10^{-8}	7.9460	3.4740×10^{-1}	1.5270×10^{-1}	0.0000	1.3547×10^{7}
29	1.2680×10^{-2}	2.3442×10^{-21}	8.9190×10^{-9}	6.0410×10^{-1}	3.3040×10^{-1}	3.5780×10^{-1}	1.0000	7.6943×10^{6}
30	8.7910×10^{-3}	7.9433×10^{-22}	1.2975×10^{-8}	2.0040×10^{-1}	1.4050×10^{-2}	1.5530×10^{-1}	0.0000	1.1189×10^{7}
31	1.7650×10^{-2}	3.3884×10^{-22}	6.3371×10^{-9}	3.3160×10^{-1}	2.1130×10^{-1}	2.4050×10^{-1}	1.0000	1.5025×10^{7}
32	2.0930×10^{-2}	6.1660×10^{-21}	5.3048×10^{-9}	8.8800	3.1430×10^{-1}	3.7550×10^{-1}	1.0000	5.5061×10^{6}
33	6.6640×10^{-3}	1.0000×10^{-21}	1.7196×10^{-8}	5.2200×10^{-1}	1.0530×10^{-1}	3.4190×10^{-1}	1.0000	1.0332×10^{7}
34	9.1030×10^{-3}	2.3988×10^{-22}	1.2522×10^{-8}	8.6520	2.5150×10^{-1}	3.6280×10^{-1}	0.0000	1.6932×10^{7}
35	2.4230×10^{-3}	3.0903×10^{-21}	4.7733×10^{-8}	3.9470×10^{-1}	2.9070×10^{-1}	1.3390×10^{-1}	1.0000	6.9928×10^{6}
36	2.7120×10^{-2}	1.5849×10^{-22}	4.0370×10^{-9}	2.7500×10^{-1}	3.7090×10^{-1}	3.6960×10^{-1}	1.0000	1.9543×10^{7}
37	5.0960×10^{-3}	8.5114×10^{-22}	2.2564×10^{-8}	6.9780	2.2650×10^{-1}	3.0790×10^{-2}	1.0000	1.0925×10^{7}
38	1.8940×10^{-3}	5.1286×10^{-21}	6.1135×10^{-8}	2.9640	1.7810×10^{-1}	3.9620×10^{-1}	1.0000	5.8685×10^{6}
39	1.0090×10^{-2}	7.5858×10^{-22}	1.1273×10^{-8}	2.6060×10^{-1}	1.6330×10^{-1}	3.7240×10^{-2}	1.0000	1.1369×10^{7}
40	2.2760×10^{-2}	2.5704×10^{-23}	4.8582×10^{-9}	2.4160×10^{-1}	2.4340×10^{-1}	1.1100×10^{-1}	1.0000	3.6671×10^{7}
41	1.8020×10^{-2}	5.8884×10^{-21}	6.2019×10^{-9}	5.7490×10^{-1}	1.3340×10^{-1}	1.0650×10^{-1}	1.0000	5.5946×10^{6}
42	2.1990×10^{-2}	6.3096×10^{-22}	5.0371×10^{-9}	5.4840×10^{-1}	3.9640×10^{-1}	3.3500×10^{-1}	0.0000	1.2117×10^{7}
43	5.1790×10^{-3}	2.4547×10^{-21}	2.2199×10^{-8}	4.0000	3.9070×10^{-1}	1.2040×10^{-1}	0.0000	7.5727×10^{6}
44	3.9010×10^{-3}	3.9811×10^{-21}	2.9553×10^{-8}	3.6050×10^{-1}	2.5980×10^{-1}	5.7350×10^{-2}	0.0000	6.4060×10^{6}
45	9.3870×10^{-3}	2.8840×10^{-21}	1.2135×10^{-8}	3.2390×10^{-1}	1.5830×10^{-1}	9.4190×10^{-2}	1.0000	7.1619×10^{6}
46	2.8280×10^{-2}	1.0471×10^{-24}	3.8611×10^{-9}	4.6060×10^{-1}	6.5170×10^{-2}	2.3880×10^{-1}	1.0000	1.1099×10^{8}
47	6.5700×10^{-3}	5.7544×10^{-20}	1.7446×10^{-8}	3.4760	3.1780×10^{-1}	2.6060×10^{-1}	1.0000	2.5423×10^{6}
48	2.2390×10^{-2}	2.8184×10^{-21}	4.9426×10^{-9}	7.7080	4.5510×10^{-2}	2.0750×10^{-1}	0.0000	7.2192×10^{6}
49	1.6820×10^{-3}	1.9953×10^{-22}	6.8872×10^{-8}	3.7530×10^{-1}	5.0110×10^{-2}	6.9900×10^{-2}	1.0000	1.8046×10^{7}
50	1.2890×10^{-2}	1.8621×10^{-22}	8.7696×10^{-9}	3.5390×10^{-1}	1.8990×10^{-1}	1.9850×10^{-1}	1.0000	1.8483×10^{7}
51	7.8440×10^{-3}	8.7096×10^{-21}	1.4572×10^{-8}	5.6000×10^{-1}	2.3180×10^{-2}	1.1810×10^{-2}	1.0000	4.8859×10^{6}
52	4.7130×10^{-3}	1.9953×10^{-21}	2.4418×10^{-8}	3.2370	1.5040×10^{-1}	3.8860×10^{-1}	0.0000	8.1356×10^{6}

Table B-2 1992 BRAGFLO Computed Variable Values for SALADO (Concluded)

Run No.	Porosity	Permeability	Compressibility	BCEXP	BCBRSAT	BCGSSAT	BCFLG	BCPCT
53	1.5900×10^{-2}	4.6774×10^{-21}	7.0621×10^{-9}	6.7410	2.8470×10^{-1}	1.8060×10^{-1}	1.0000	6.0585×10^{6}
54	1.4500×10^{-2}	3.7154×10^{-22}	7.7681×10^{-9}	4.7200×10^{-1}	1.6590×10^{-1}	2.7290×10^{-1}	0.0000	1.4554×10^{7}
55	2.0030×10^{-2}	1.4125×10^{-22}	5.5544×10^{-9}	6.5030×10^{-1}	3.2450×10^{-1}	3.0330×10^{-1}	0.0000	2.0337×10^{7}
56	1.1650×10^{-2}	1.6596×10^{-24}	9.7296×10^{-9}	4.8480	9.2770×10^{-2}	5.2210×10^{-2}	0.0000	9.4639×10^{7}
57	4.5630×10^{-3}	3.8904×10^{-22}	2.5229×10^{-8}	9.2110	5.1160×10^{-3}	2.7770×10^{-1}	1.0000	1.4324×10^{7}
58	8.7110×10^{-3}	2.1878×10^{-23}	1.3097×10^{-8}	6.4060×10^{-1}	3.4880×10^{-1}	3.2980×10^{-1}	1.0000	3.8775×10^{7}
59	2.5160×10^{-2}	1.4791×10^{-23}	4.3709×10^{-9}	8.9580	8.5120×10^{-2}	3.1270×10^{-1}	1.0000	4.4398×10^{7}
60	8.2600×10^{-3}	9.1201×10^{-23}	1.3825×10^{-8}	9.8620	7.0380×10^{-2}	8.1940×10^{-2}	1.0000	2.3661×10^{7}
61	7.3840×10^{-3}	1.0715×10^{-21}	1.5495×10^{-8}	8.0490×10^{-1}	2.7910×10^{-1}	1.3890×10^{-1}	1.0000	1.0088×10^{7}
62	1.2250×10^{-2}	1.2303×10^{-22}	9.2408×10^{-9}	2.8630×10^{-1}	3.5990×10^{-1}	2.5120×10^{-1}	1.0000	2.1333×10^{7}
63	4.1090×10^{-3}	3.0903×10^{-22}	2.8045×10^{-8}	3.7540	2.0010×10^{-1}	2.8360×10^{-1}	0.0000	1.5511×10^{7}
64	3.7390×10^{-3}	1.6982×10^{-22}	3.0845×10^{-8}	2.4950	2.9320×10^{-2}	8.7020×10^{-2}	1.0000	1.9081×10^{7}
65	7.4700×10^{-3}	1.5488×10^{-21}	1.5314×10^{-8}	2.5410×10^{-1}	2.6410×10^{-1}	3.5100×10^{-1}	1.0000	8.8807×10^{6}
66	3.5330×10^{-3}	4.8978×10^{-23}	3.2658×10^{-8}	6.9150×10^{-1}	1.2380×10^{-1}	3.1630×10^{-1}	0.0000	2.9339×10^{7}
67	8.1910×10^{-3}	1.1482×10^{-21}	1.3944×10^{-8}	5.5890	5.6350×10^{-2}	2.5370×10^{-1}	0.0000	9.8498×10^{6}
68	1.0760×10^{-2}	2.2387×10^{-22}	1.0555×10^{-8}	4.5200	3.0240×10^{-1}	2.9970×10^{-1}	0.0000	1.7342×10^{7}
69	1.5190×10^{-2}	2.5704×10^{-22}	7.4039×10^{-9}	4.3270	3.7150×10^{-1}	4.8390×10^{-3}	1.0000	1.6532×10^{7}
70	1.4890×10^{-3}	2.5704×10^{-24}	7.7831×10^{-8}	6.2770×10^{-1}	1.0130×10^{-1}	1.1920×10^{-1}	1.0000	8.1344×10^{7}

Table B-2 1992 BRAGFLO Ranks of Computed Variable Values for SALADO

Run No.	Porosity	Permeability	Compressibility	BCEXP	BCBRSAT	BCGSSAT	BCFLG	BCPCT
1	68.	55.	3.	69.	16.	41.	1.	16.
2	24.	67.	47.	21.	26.	23.	24.	4.
3	69.	44.	2.	34.	33.	38.	24.	27.
4	18.	45.	53.	52.	31.	34.	24.	26.
5	54.	26.	17.	15.	35.	26.	24.	45.
6	42.	6.	29.	56.	59.	9.	1.	65.
7	63.	15.	8.	37.	7.	29.	1.	56.
8	9.	32.	62.	57.	68.	5.	24.	39.
9	66.	5.	5.	16.	60.	33.	24.	66.
10	34.	56.	37.	39.	14.	61.	24.	14.
11	7.	64.	64.	22.	48.	36.	1.	7.
12	35.	66.	36.	61.	25.	51.	24.	5.
13	47.	7.	24.	41.	64.	52.	24.	64.
14	52.	13.	19.	8.	2.	31.	24.	58.
15	1.	4.	70.	18.	41.	68.	1.	67.
16	19.	48.	52.	24.	67.	39.	24.	22.
17	60.	17.	11.	55.	20.	67.	1.	54.
18	20.	36.	51.	28.	52.	2.	1.	35.
19	21.	11.	50.	40.	21.	30.	24.	60.
20	48.	68.	23.	33.	23.	57.	24.	3.
21	59.	69.	12.	2.	4.	40.	1.	2.
22	64.	60.	7.	38.	39.	4.	24.	11.
23	70.	34.	1.	60.	42.	8.	24.	37.
24	44.	43.	27.	17.	11.	47.	24.	28.
25	61.	63.	10.	43.	54.	18.	24.	8.
26	51.	47.	20.	53.	44.	12.	24.	24.
27	5.	33.	66.	64.	38.	14.	24.	38.
28	8.	31.	63.	63.	61.	27.	1.	40.
29	40.	50.	31.	29.	58.	63.	24.	21.
30	31.	38.	40.	1.	3.	28.	1.	33.
31	49.	28.	22.	10.	37.	43.	24.	43.
32	55.	62.	16.	66.	55.	66.	24.	9.
33	23.	40.	48.	23.	19.	60.	24.	31.
34	32.	24.	39.	65.	45.	64.	1.	47.
35	6.	54.	65.	14.	51.	24.	24.	17.
36	65.	19.	6.	6.	65.	65.	24.	52.
37	16.	39.	55.	59.	40.	6.	24.	32.
38	4.	59.	67.	44.	32.	70.	24.	12.
39	36.	37.	35.	5.	29.	7.	24.	34.
40	58.	10.	13.	3.	43.	20.	24.	61.
41	50.	61.	21.	27.	24.	19.	24.	10.
42	56.	35.	15.	25.	70.	59.	1.	36.
43	17.	51.	54.	48.	69.	22.	1.	20.
44	12.	56.	59.	12.	46.	11.	1.	14.
45	33.	53.	38.	9.	28.	17.	24.	18.
46	67.	1.	4.	19.	12.	42.	24.	70.
47	22.	70.	49.	46.	56.	46.	24.	1.
48	57.	52.	14.	62.	8.	37.	1.	19.
49	3.	22.	68.	13.	9.	13.	24.	49.
50	41.	21.	30.	11.	34.	35.	24.	50.
51	27.	65.	44.	26.	5.	3.	24.	6.
52	15.	48.	56.	45.	27.	69.	1.	22.

Table B-2 1992 BRAGFLO Ranks of Computed Variable Values for SALADO (Concluded)

Run No.	Porosity	Permeability	Compressibility	BCEXP	BCBRSAT	BCGSSAT	BCFLG	BCPCT
53	46.	58.	25.	58.	50.	32.	24.	13.
54	43.	29.	28.	20.	30.	48.	1.	42.
55	53.	18.	18.	32.	57.	54.	1.	53.
56	38.	2.	33.	51.	17.	10.	1.	69.
57	14.	30.	57.	68.	1.	49.	24.	41.
58	30.	9.	41.	31.	62.	58.	24.	62.
59	62.	8.	9.	67.	15.	55.	24.	63.
60	29.	14.	42.	70.	13.	15.	24.	57.
61	25.	41.	46.	36.	49.	25.	24.	30.
62	39.	16.	32.	7.	63.	44.	24.	55.
63	13.	27.	58.	47.	36.	50.	1.	44.
64	11.	20.	60.	42.	6.	16.	24.	51.
65	26.	46.	45.	4.	47.	62.	24.	25.
66	10.	12.	61.	35.	22.	56.	1.	59.
67	28.	42.	43.	54.	10.	45.	1.	29.
68	37.	23.	34.	50.	53.	53.	1.	48.
69	45.	25.	26.	49.	66.	1.	24.	46.
70	2.	3.	69.	30.	18.	21.	24.	68.

Table B-2 1992 BRAGFLO Computed Variable Values for SHAFT_SEAL

Run No.	Porosity	Permeability	Compressibility	BCEXP	BCBRSAT	BCGSSAT	BCFLG	BCPCT
1	5.6433×10^{-2}	3.2690×10^{-17}	1.8102×10^{-9}	7.0000×10^{-1}	2.0000×10^{-1}	0.0000	1.0000	2.8327×10^{5}
2	4.3305×10^{-2}	1.2730×10^{-17}	2.4347×10^{-9}	7.0000×10^{-1}	2.0000×10^{-1}	0.0000	1.0000	3.9257×10^{5}
3	4.0073×10^{-2}	5.5560×10^{-17}	2.6512×10^{-9}	7.0000×10^{-1}	2.0000×10^{-1}	0.0000	1.0000	2.3578×10^{5}
4	5.8422×10^{-2}	1.8260×10^{-17}	1.7400×10^{-9}	7.0000×10^{-1}	2.0000×10^{-1}	0.0000	1.0000	3.4650×10^{5}
5	3.5889×10^{-2}	4.6190×10^{-19}	2.9895×10^{-9}	7.0000×10^{-1}	2.0000×10^{-1}	0.0000	1.0000	1.2367×10^{6}
6	4.8739×10^{-2}	9.4430×10^{-18}	2.1354×10^{-9}	7.0000×10^{-1}	2.0000×10^{-1}	0.0000	1.0000	4.3531×10^{5}
7	1.8565×10^{-2}	3.4350×10^{-17}	6.0125×10^{-9}	7.0000×10^{-1}	2.0000×10^{-1}	0.0000	1.0000	2.7846×10^{5}
8	3.3804×10^{-2}	1.1320×10^{-18}	3.1893×10^{-9}	7.0000×10^{-1}	2.0000×10^{-1}	0.0000	1.0000	9.0690×10^{5}
9	8.2847×10^{-2}	3.6880×10^{-19}	1.1533×10^{-9}	7.0000×10^{-1}	2.0000×10^{-1}	0.0000	1.0000	1.3368×10^{6}
10	4.8961×10^{-2}	7.9740×10^{-18}	2.1246×10^{-9}	7.0000×10^{-1}	2.0000×10^{-1}	0.0000	1.0000	4.6154×10^{5}
11	6.0343×10^{-2}	3.8050×10^{-18}	1.6767×10^{-9}	7.0000×10^{-1}	2.0000×10^{-1}	0.0000	1.0000	5.9619×10^{5}
12	5.5800×10^{-2}	2.0750×10^{-17}	1.8336×10^{-9}	7.0000×10^{-1}	2.0000×10^{-1}	0.0000	1.0000	3.3151×10^{5}
13	7.2964×10^{-2}	4.9500×10^{-17}	1.3434×10^{-9}	7.0000×10^{-1}	2.0000×10^{-1}	0.0000	1.0000	2.4539×10^{5}
14	6.0840×10^{-2}	4.9160×10^{-18}	1.6610×10^{-9}	7.0000×10^{-1}	2.0000×10^{-1}	0.0000	1.0000	5.4562×10^{5}
15	5.0585×10^{-2}	4.2050×10^{-18}	2.0484×10^{-9}	7.0000×10^{-1}	2.0000×10^{-1}	0.0000	1.0000	5.7592×10^{5}
16	3.5074×10^{-2}	1.0530×10^{-18}	3.0648×10^{-9}	7.0000×10^{-1}	2.0000×10^{-1}	0.0000	1.0000	9.2988×10^{5}
17	5.7146×10^{-2}	6.8710×10^{-19}	1.7845×10^{-9}	7.0000×10^{-1}	2.0000×10^{-1}	0.0000	1.0000	1.0779×10^{6}
18	8.2074×10^{-2}	2.9880×10^{-18}	1.1666×10^{-9}	7.0000×10^{-1}	2.0000×10^{-1}	0.0000	1.0000	6.4820×10^{5}
19	6.3721×10^{-2}	7.1460×10^{-17}	1.5746×10^{-9}	7.0000×10^{-1}	2.0000×10^{-1}	0.0000	1.0000	2.1611×10^{5}
20	1.6736×10^{-2}	4.5930×10^{-18}	6.6967×10^{-9}	7.0000×10^{-1}	2.0000×10^{-1}	0.0000	1.0000	5.5860×10^{5}
21	4.7082×10^{-2}	1.9190×10^{-18}	2.2194×10^{-9}	7.0000×10^{-1}	2.0000×10^{-1}	0.0000	1.0000	7.5552×10^{5}
22	4.6655×10^{-2}	4.3250×10^{-17}	2.2420×10^{-9}	7.0000×10^{-1}	2.0000×10^{-1}	0.0000	1.0000	2.5712×10^{5}
23	5.0975×10^{-2}	1.7220×10^{-18}	2.0308×10^{-9}	7.0000×10^{-1}	2.0000×10^{-1}	0.0000	1.0000	7.8437×10^{5}
24	6.8520×10^{-2}	5.2090×10^{-19}	1.4468×10^{-9}	7.0000×10^{-1}	2.0000×10^{-1}	0.0000	1.0000	1.1863×10^{6}
25	5.1999×10^{-2}	1.1040×10^{-16}	1.9859×10^{-9}	7.0000×10^{-1}	2.0000×10^{-1}	0.0000	1.0000	1.8592×10^{5}
26	4.1033×10^{-2}	1.4510×10^{-19}	2.5834×10^{-9}	7.0000×10^{-1}	2.0000×10^{-1}	0.0000	1.0000	1.8461×10^{6}
27	6.1762×10^{-2}	1.1630×10^{-19}	1.6324×10^{-9}	7.0000×10^{-1}	2.0000×10^{-1}	0.0000	1.0000	1.9930×10^{6}
28	3.7132×10^{-2}	1.0480×10^{-17}	2.8811×10^{-9}	7.0000×10^{-1}	2.0000×10^{-1}	0.0000	1.0000	4.1990×10^{5}
29	6.9933×10^{-2}	4.0080×10^{-18}	1.4125×10^{-9}	7.0000×10^{-1}	2.0000×10^{-1}	0.0000	1.0000	5.8557×10^{5}
30	4.7777×10^{-2}	7.9680×10^{-17}	2.1834×10^{-9}	7.0000×10^{-1}	2.0000×10^{-1}	0.0000	1.0000	2.0812×10^{5}
31	2.2998×10^{-2}	1.9610×10^{-17}	4.8054×10^{-9}	7.0000×10^{-1}	2.0000×10^{-1}	0.0000	1.0000	3.3806×10^{5}
32	4.5772×10^{-2}	5.0000×10^{-16}	2.2901×10^{-9}	7.0000×10^{-1}	2.0000×10^{-1}	0.0000	1.0000	1.1024×10^{5}
33	5.3975×10^{-2}	8.1000×10^{-19}	1.9040×10^{-9}	7.0000×10^{-1}	2.0000×10^{-1}	0.0000	1.0000	1.0182×10^{6}
34	6.6056×10^{-2}	7.5340×10^{-18}	1.5101×10^{-9}	7.0000×10^{-1}	2.0000×10^{-1}	0.0000	1.0000	4.7069×10^{5}
35	2.5859×10^{-2}	1.1420×10^{-17}	4.2460×10^{-9}	7.0000×10^{-1}	2.0000×10^{-1}	0.0000	1.0000	4.0760×10^{5}
36	2.7519×10^{-2}	2.6550×10^{-18}	3.9748×10^{-9}	7.0000×10^{-1}	2.0000×10^{-1}	0.0000	1.0000	6.7525×10^{5}
37	4.9770×10^{-2}	1.4690×10^{-17}	2.0860×10^{-9}	7.0000×10^{-1}	2.0000×10^{-1}	0.0000	1.0000	3.7359×10^{5}
38	4.2030×10^{-2}	1.2620×10^{-18}	2.5162×10^{-9}	7.0000×10^{-1}	2.0000×10^{-1}	0.0000	1.0000	8.7342×10^{5}
39	3.8123×10^{-2}	2.4400×10^{-16}	2.7997×10^{-9}	7.0000×10^{-1}	2.0000×10^{-1}	0.0000	1.0000	1.4130×10^{5}
40	6.2212×10^{-2}	8.6700×10^{-18}	1.6188×10^{-9}	7.0000×10^{-1}	2.0000×10^{-1}	0.0000	1.0000	4.4837×10^{5}
41	6.2879×10^{-2}	6.0530×10^{-19}	1.5990×10^{-9}	7.0000×10^{-1}	2.0000×10^{-1}	0.0000	1.0000	1.1262×10^{6}
42	5.5614×10^{-2}	9.7010×10^{-19}	1.8405×10^{-9}	7.0000×10^{-1}	2.0000×10^{-1}	0.0000	1.0000	9.5664×10^{5}
43	3.3383×10^{-2}	2.1950×10^{-17}	3.2327×10^{-9}	7.0000×10^{-1}	2.0000×10^{-1}	0.0000	1.0000	3.2513×10^{5}
44	7.4798×10^{-2}	1.4780×10^{-18}	1.3044×10^{-9}	7.0000×10^{-1}	2.0000×10^{-1}	0.0000	1.0000	8.2695×10^{5}
45	6.5132×10^{-2}	2.7170×10^{-17}	1.5350×10^{-9}	7.0000×10^{-1}	2.0000×10^{-1}	0.0000	1.0000	3.0199×10^{5}
46	4.5591×10^{-2}	2.0720×10^{-18}	2.3001×10^{-9}	7.0000×10^{-1}	2.0000×10^{-1}	0.0000	1.0000	7.3573×10^{5}
47	7.6297×10^{-2}	3.9130×10^{-17}	1.2738×10^{-9}	7.0000×10^{-1}	2.0000×10^{-1}	0.0000	1.0000	2.6618×10^{5}
48	9.0000×10^{-2}	1.6990×10^{-17}	1.0418×10^{-9}	7.0000×10^{-1}	2.0000×10^{-1}	0.0000	1.0000	3.5526×10^{5}
49	7.8712×10^{-2}	2.3260×10^{-18}	1.2271×10^{-9}	7.0000×10^{-1}	2.0000×10^{-1}	0.0000	1.0000	7.0687×10^{5}
50	2.2704×10^{-2}	2.8780×10^{-17}	4.8708×10^{-9}	7.0000×10^{-1}	2.0000×10^{-1}	0.0000	1.0000	2.9604×10^{5}
51	2.8140×10^{-2}	2.3210×10^{-18}	3.8816×10^{-9}	7.0000×10^{-1}	2.0000×10^{-1}	0.0000	1.0000	7.0740×10^{5}
52	4.2389×10^{-2}	1.5210×10^{-18}	2.4928×10^{-9}	7.0000×10^{-1}	2.0000×10^{-1}	0.0000	1.0000	8.1879×10^{5}

Table B-2 1992 BRAGFLO Computed Variable Values for SHAFT_SEAL (Concluded)

Run No.	Porosity	Permeability	Compressibility	BCEXP	BCBRSAT	BCGSSAT	BCFLG	BCPCT
53	5.8188×10^{-2}	6.3790×10^{-18}	1.7480×10^{-9}	7.0000×10^{-1}	2.0000×10^{-1}	0.0000	1.0000	4.9859×10^{5}
54	6.7354×10^{-2}	1.5510×10^{-17}	1.4762×10^{-9}	7.0000×10^{-1}	2.0000×10^{-1}	0.0000	1.0000	3.6664×10^{5}
55	3.9083×10^{-2}	3.5290×10^{-18}	2.7248×10^{-9}	7.0000×10^{-1}	2.0000×10^{-1}	0.0000	1.0000	6.1193×10^{5}
56	6.6469×10^{-2}	8.1660×10^{-18}	1.4991×10^{-9}	7.0000×10^{-1}	2.0000×10^{-1}	0.0000	1.0000	4.5775×10^{5}
57	5.3429×10^{-2}	5.3740×10^{-18}	1.9260×10^{-9}	7.0000×10^{-1}	2.0000×10^{-1}	0.0000	1.0000	5.2906×10^{5}
58	5.4958×10^{-2}	9.3590×10^{-17}	1.8655×10^{-9}	7.0000×10^{-1}	2.0000×10^{-1}	0.0000	1.0000	1.9685×10^{5}
59	5.2762×10^{-2}	5.7450×10^{-18}	1.9535×10^{-9}	7.0000×10^{-1}	2.0000×10^{-1}	0.0000	1.0000	5.1698×10^{5}
60	2.9620×10^{-2}	3.1910×10^{-18}	3.6751×10^{-9}	7.0000×10^{-1}	2.0000×10^{-1}	0.0000	1.0000	6.3362×10^{5}
61	4.0430×10^{-2}	2.8000×10^{-18}	2.6256×10^{-9}	7.0000×10^{-1}	2.0000×10^{-1}	0.0000	1.0000	6.6294×10^{5}
62	4.4173×10^{-2}	6.3220×10^{-17}	2.3820×10^{-9}	7.0000×10^{-1}	2.0000×10^{-1}	0.0000	1.0000	2.2547×10^{5}
63	5.9404×10^{-2}	1.2980×10^{-16}	1.7071×10^{-9}	7.0000×10^{-1}	2.0000×10^{-1}	0.0000	1.0000	1.7579×10^{5}
64	3.2463×10^{-2}	5.8550×10^{-18}	3.3314×10^{-9}	7.0000×10^{-1}	2.0000×10^{-1}	0.0000	1.0000	5.1360×10^{5}
65	7.1865×10^{-2}	2.4680×10^{-17}	1.3678×10^{-9}	7.0000×10^{-1}	2.0000×10^{-1}	0.0000	1.0000	3.1220×10^{5}
66	4.5003×10^{-2}	6.8400×10^{-18}	2.3335×10^{-9}	7.0000×10^{-1}	2.0000×10^{-1}	0.0000	1.0000	4.8670×10^{5}
67	3.1590×10^{-2}	1.1240×10^{-17}	3.4304×10^{-9}	7.0000×10^{-1}	2.0000×10^{-1}	0.0000	1.0000	4.0985×10^{5}
68	1.0000×10^{-2}	2.4420×10^{-19}	1.1376×10^{-8}	7.0000×10^{-1}	2.0000×10^{-1}	0.0000	1.0000	1.5418×10^{6}
69	5.1572×10^{-2}	1.3260×10^{-17}	2.0044×10^{-9}	7.0000×10^{-1}	2.0000×10^{-1}	0.0000	1.0000	3.8707×10^{5}
70	3.7917×10^{-2}	2.0800×10^{-16}	2.8162×10^{-9}	7.0000×10^{-1}	2.0000×10^{-1}	0.0000	1.0000	1.4933×10^{5}

Table B-2 1992 BRAGFLO Ranks of Computed Variable Values for SHAFT_SEAL

Run No.	Porosity	Permeability	Compressibility	BCEXP	BCBRSAT	BCGSSAT	BCFLG	BCPCT
1	46.	56.	25.	1.	1.	1.	1.	15.
2	25.	44.	46.	1.	1.	1.	1.	27.
3	20.	61.	51.	1.	1.	1.	1.	10.
4	49.	49.	22.	1.	1.	1.	1.	22.
5	15.	5.	56.	1.	1.	1.	1.	66.
6	33.	40.	38.	1.	1.	1.	1.	31.
7	3.	57.	68.	1.	1.	1.	1.	14.
8	13.	12.	58.	1.	1.	1.	1.	59.
9	69.	4.	2.	1.	1.	1.	1.	67.
10	34.	37.	37.	1.	1.	1.	1.	34.
11	51.	26.	20.	1.	1.	1.	1.	45.
12	45.	51.	26.	1.	1.	1.	1.	20.
13	64.	60.	7.	1.	1.	1.	1.	11.
14	52.	30.	19.	1.	1.	1.	1.	41.
15	36.	28.	35.	1.	1.	1.	1.	43.
16	14.	11.	57.	1.	1.	1.	1.	60.
17	47.	8.	24.	1.	1.	1.	1.	63.
18	68.	23.	3.	1.	1.	1.	1.	48.
19	56.	63.	15.	1.	1.	1.	1.	8.
20	2.	29.	69.	1.	1.	1.	1.	42.
21	31.	17.	40.	1.	1.	1.	1.	54.
22	30.	59.	41.	1.	1.	1.	1.	12.
23	37.	16.	34.	1.	1.	1.	1.	55.
24	61.	6.	10.	1.	1.	1.	1.	65.
25	39.	66.	32.	1.	1.	1.	1.	5.
26	22.	2.	49.	1.	1.	1.	1.	69.
27	53.	1.	18.	1.	1.	1.	1.	70.
28	16.	41.	55.	1.	1.	1.	1.	30.
29	62.	27.	9.	1.	1.	1.	1.	44.
30	32.	64.	39.	1.	1.	1.	1.	7.
31	5.	50.	66.	1.	1.	1.	1.	21.
32	29.	70.	42.	1.	1.	1.	1.	1.
33	42.	9.	29.	1.	1.	1.	1.	62.
34	58.	36.	13.	1.	1.	1.	1.	35.
35	6.	43.	65.	1.	1.	1.	1.	28.
36	7.	21.	64.	1.	1.	1.	1.	50.
37	35.	46.	36.	1.	1.	1.	1.	25.
38	23.	13.	48.	1.	1.	1.	1.	58.
39	18.	69.	53.	1.	1.	1.	1.	2.
40	54.	39.	17.	1.	1.	1.	1.	32.
41	55.	7.	16.	1.	1.	1.	1.	64.
42	44.	10.	27.	1.	1.	1.	1.	61.
43	12.	52.	59.	1.	1.	1.	1.	19.
44	65.	14.	6.	1.	1.	1.	1.	57.
45	57.	54.	14.	1.	1.	1.	1.	17.
46	28.	18.	43.	1.	1.	1.	1.	53.
47	66.	58.	5.	1.	1.	1.	1.	13.
48	70.	48.	1.	1.	1.	1.	1.	23.
49	67.	20.	4.	1.	1.	1.	1.	51.
50	4.	55.	67.	1.	1.	1.	1.	16.
51	8.	19.	63.	1.	1.	1.	1.	52.
52	24.	15.	47.	1.	1.	1.	1.	56.

Table B-2 1992 BRAGFLO Ranks of Computed Variable Values for SHAFT_SEAL (Concluded)

Run No.	Porosity	Permeability	Compressibility	BCEXP	BCBRSAT	BCGSSAT	BCFLG	BCPCT
53	48.	34.	23.	1.	1.	1.	1.	37.
54	60.	47.	11.	1.	1.	1.	1.	24.
55	19.	25.	52.	1.	1.	1.	1.	46.
56	59.	38.	12.	1.	1.	1.	1.	33.
57	41.	31.	30.	1.	1.	1.	1.	40.
58	43.	65.	28.	1.	1.	1.	1.	6.
59	40.	32.	31.	1.	1.	1.	1.	39.
60	9.	24.	62.	1.	1.	1.	1.	47.
61	21.	22.	50.	1.	1.	1.	1.	49.
62	26.	62.	45.	1.	1.	1.	1.	9.
63	50.	67.	21.	1.	1.	1.	1.	4.
64	11.	33.	60.	1.	1.	1.	1.	38.
65	63.	53.	8.	1.	1.	1.	1.	18.
66	27.	35.	44.	1.	1.	1.	1.	36.
67	10.	42.	61.	1.	1.	1.	1.	29.
68	1.	3.	70.	1.	1.	1.	1.	68.
69	38.	45.	33.	1.	1.	1.	1.	26.
70	17.	68.	54.	1.	1.	1.	1.	3.

Table B-2 1992 BRAGFLO Computed Variable Values for SHAFT_SEAL_2

Run No.	Porosity	Permeability	Compressibility	BCEXP	BCBRSAT	BCGSSAT	BCFLG	BCPCT
1	5.6433×10^{-2}	5.5110×10^{-20}	1.8102×10^{-9}	7.0000×10^{-1}	2.0000×10^{-1}	0.0000	1.0000	2.5806×10^{6}
2	4.3305×10^{-2}	1.7740×10^{-20}	2.4347×10^{-9}	7.0000×10^{-1}	2.0000×10^{-1}	0.0000	1.0000	3.8199×10^{6}
3	4.0073×10^{-2}	1.3420×10^{-20}	2.6512×10^{-9}	7.0000×10^{-1}	2.0000×10^{-1}	0.0000	1.0000	4.2071×10^{6}
4	5.8422×10^{-2}	6.5440×10^{-20}	1.7400×10^{-9}	7.0000×10^{-1}	2.0000×10^{-1}	0.0000	1.0000	2.4317×10^{6}
5	3.5889×10^{-2}	9.3510×10^{-21}	2.9895×10^{-9}	7.0000×10^{-1}	2.0000×10^{-1}	0.0000	1.0000	4.7673×10^{6}
6	4.8739×10^{-2}	2.8360×10^{-20}	2.1354×10^{-9}	7.0000×10^{-1}	2.0000×10^{-1}	0.0000	1.0000	3.2475×10^{6}
7	1.8565×10^{-2}	2.0950×10^{-21}	6.0125×10^{-9}	7.0000×10^{-1}	2.0000×10^{-1}	0.0000	1.0000	7.9994×10^{6}
8	3.3804×10^{-2}	7.8100×10^{-21}	3.1893×10^{-9}	7.0000×10^{-1}	2.0000×10^{-1}	0.0000	1.0000	5.0738×10^{6}
9	8.2847×10^{-2}	5.3920×10^{-19}	1.1533×10^{-9}	7.0000×10^{-1}	2.0000×10^{-1}	0.0000	1.0000	1.1722×10^{6}
10	4.8961×10^{-2}	2.8910×10^{-20}	2.1246×10^{-9}	7.0000×10^{-1}	2.0000×10^{-1}	0.0000	1.0000	3.2260×10^{6}
11	6.0343×10^{-2}	7.7240×10^{-20}	1.6767×10^{-9}	7.0000×10^{-1}	2.0000×10^{-1}	0.0000	1.0000	2.2961×10^{6}
12	5.5800×10^{-2}	5.2180×10^{-20}	1.8336×10^{-9}	7.0000×10^{-1}	2.0000×10^{-1}	0.0000	1.0000	2.6299×10^{6}
13	7.2964×10^{-2}	2.2970×10^{-19}	1.3434×10^{-9}	7.0000×10^{-1}	2.0000×10^{-1}	0.0000	1.0000	1.5748×10^{6}
14	6.0840×10^{-2}	8.0630×10^{-20}	1.6610×10^{-9}	7.0000×10^{-1}	2.0000×10^{-1}	0.0000	1.0000	2.2623×10^{6}
15	5.0585×10^{-2}	3.3260×10^{-20}	2.0484×10^{-9}	7.0000×10^{-1}	2.0000×10^{-1}	0.0000	1.0000	3.0733×10^{6}
16	3.5074×10^{-2}	8.7150×10^{-21}	3.0648×10^{-9}	7.0000×10^{-1}	2.0000×10^{-1}	0.0000	1.0000	4.8849×10^{6}
17	5.7146×10^{-2}	5.8610×10^{-20}	1.7845×10^{-9}	7.0000×10^{-1}	2.0000×10^{-1}	0.0000	1.0000	2.5262×10^{6}
18	8.2074×10^{-2}	5.0440×10^{-19}	1.1666×10^{-9}	7.0000×10^{-1}	2.0000×10^{-1}	0.0000	1.0000	1.1996×10^{6}
19	6.3721×10^{-2}	1.0340×10^{-19}	1.5746×10^{-9}	7.0000×10^{-1}	2.0000×10^{-1}	0.0000	1.0000	2.0757×10^{6}
20	1.6736×10^{-2}	1.7890×10^{-21}	6.6967×10^{-9}	7.0000×10^{-1}	2.0000×10^{-1}	0.0000	1.0000	8.4486×10^{6}
21	4.7082×10^{-2}	2.4580×10^{-20}	2.2194×10^{-9}	7.0000×10^{-1}	2.0000×10^{-1}	0.0000	1.0000	3.4123×10^{6}
22	4.6655×10^{-2}	2.3690×10^{-20}	2.2420×10^{-9}	7.0000×10^{-1}	2.0000×10^{-1}	0.0000	1.0000	3.4561×10^{6}
23	5.0975×10^{-2}	3.4400×10^{-20}	2.0308×10^{-9}	7.0000×10^{-1}	2.0000×10^{-1}	0.0000	1.0000	3.0377×10^{6}
24	6.8520×10^{-2}	1.5650×10^{-19}	1.4468×10^{-9}	7.0000×10^{-1}	2.0000×10^{-1}	0.0000	1.0000	1.7984×10^{6}
25	5.1999×10^{-2}	3.7580×10^{-20}	1.9859×10^{-9}	7.0000×10^{-1}	2.0000×10^{-1}	0.0000	1.0000	2.9461×10^{6}
26	4.1033×10^{-2}	1.4580×10^{-20}	2.5834×10^{-9}	7.0000×10^{-1}	2.0000×10^{-1}	0.0000	1.0000	4.0882×10^{6}
27	6.1762×10^{-2}	8.7310×10^{-20}	1.6324×10^{-9}	7.0000×10^{-1}	2.0000×10^{-1}	0.0000	1.0000	2.2008×10^{6}
28	3.7132×10^{-2}	1.0410×10^{-20}	2.8811×10^{-9}	7.0000×10^{-1}	2.0000×10^{-1}	0.0000	1.0000	4.5936×10^{6}
29	6.9933×10^{-2}	1.7680×10^{-19}	1.4125×10^{-9}	7.0000×10^{-1}	2.0000×10^{-1}	0.0000	1.0000	1.7241×10^{6}
30	4.7777×10^{-2}	2.6100×10^{-20}	2.1834×10^{-9}	7.0000×10^{-1}	2.0000×10^{-1}	0.0000	1.0000	3.3422×10^{6}
31	2.2998×10^{-2}	3.0720×10^{-21}	4.8054×10^{-9}	7.0000×10^{-1}	2.0000×10^{-1}	0.0000	1.0000	7.0071×10^{6}
32	4.5772×10^{-2}	2.1950×10^{-20}	2.2901×10^{-9}	7.0000×10^{-1}	2.0000×10^{-1}	0.0000	1.0000	3.5486×10^{6}
33	5.3975×10^{-2}	4.4570×10^{-20}	1.9040×10^{-9}	7.0000×10^{-1}	2.0000×10^{-1}	0.0000	1.0000	2.7773×10^{6}
34	6.6056×10^{-2}	1.2650×10^{-19}	1.5101×10^{-9}	7.0000×10^{-1}	2.0000×10^{-1}	0.0000	1.0000	1.9358×10^{6}
35	2.5859×10^{-2}	3.9330×10^{-21}	4.2460×10^{-9}	7.0000×10^{-1}	2.0000×10^{-1}	0.0000	1.0000	6.4330×10^{6}
36	2.7519×10^{-2}	4.5390×10^{-21}	3.9748×10^{-9}	7.0000×10^{-1}	2.0000×10^{-1}	0.0000	1.0000	6.1218×10^{6}
37	4.9770×10^{-2}	3.1000×10^{-20}	2.0860×10^{-9}	7.0000×10^{-1}	2.0000×10^{-1}	0.0000	1.0000	3.1490×10^{6}
38	4.2030×10^{-2}	1.5890×10^{-20}	2.5162×10^{-9}	7.0000×10^{-1}	2.0000×10^{-1}	0.0000	1.0000	3.9683×10^{6}
39	3.8123×10^{-2}	1.1340×10^{-20}	2.7997×10^{-9}	7.0000×10^{-1}	2.0000×10^{-1}	0.0000	1.0000	4.4596×10^{6}
40	6.2212×10^{-2}	9.0770×10^{-20}	1.6188×10^{-9}	7.0000×10^{-1}	2.0000×10^{-1}	0.0000	1.0000	2.1714×10^{6}
41	6.2879×10^{-2}	9.6150×10^{-20}	1.5990×10^{-9}	7.0000×10^{-1}	2.0000×10^{-1}	0.0000	1.0000	2.1286×10^{6}
42	5.5614×10^{-2}	5.1350×10^{-20}	1.8405×10^{-9}	7.0000×10^{-1}	2.0000×10^{-1}	0.0000	1.0000	2.6445×10^{6}
43	3.3383×10^{-2}	7.5310×10^{-21}	3.2327×10^{-9}	7.0000×10^{-1}	2.0000×10^{-1}	0.0000	1.0000	5.1380×10^{6}
44	7.4798×10^{-2}	2.6910×10^{-19}	1.3044×10^{-9}	7.0000×10^{-1}	2.0000×10^{-1}	0.0000	1.0000	1.4909×10^{6}
45	6.5132×10^{-2}	1.1680×10^{-19}	1.5350×10^{-9}	7.0000×10^{-1}	2.0000×10^{-1}	0.0000	1.0000	1.9900×10^{6}
46	4.5591×10^{-2}	2.1610×10^{-20}	2.3001×10^{-9}	7.0000×10^{-1}	2.0000×10^{-1}	0.0000	1.0000	3.5678×10^{6}
47	7.6297×10^{-2}	3.0630×10^{-19}	1.2738×10^{-9}	7.0000×10^{-1}	2.0000×10^{-1}	0.0000	1.0000	1.4256×10^{6}
48	9.0000×10^{-2}	1.0000×10^{-18}	1.0418×10^{-9}	7.0000×10^{-1}	2.0000×10^{-1}	0.0000	1.0000	9.4665×10^{5}
49	7.8712×10^{-2}	3.7730×10^{-19}	1.2271×10^{-9}	7.0000×10^{-1}	2.0000×10^{-1}	0.0000	1.0000	1.3263×10^{6}
50	2.2704×10^{-2}	2.9950×10^{-21}	4.8708×10^{-9}	7.0000×10^{-1}	2.0000×10^{-1}	0.0000	1.0000	7.0689×10^{6}
51	2.8140×10^{-2}	4.7890×10^{-21}	3.8816×10^{-9}	7.0000×10^{-1}	2.0000×10^{-1}	0.0000	1.0000	6.0093×10^{6}
52	4.2389×10^{-2}	1.6390×10^{-20}	2.4928×10^{-9}	7.0000×10^{-1}	2.0000×10^{-1}	0.0000	1.0000	3.9259×10^{6}

Table B-2 1992 BRAGFLO Computed Variable Values for SHAFT_SEAL_2 (Concluded)

Run No.	Porosity	Permeability	Compressibility	BCEXP	BCBRSAT	BCGSSAT	BCFLG	BCPCT
53	5.8188×10^{-2}	6.4130×10^{-20}	1.7480×10^{-9}	7.0000×10^{-1}	2.0000×10^{-1}	0.0000	1.0000	2.4488×10^{6}
54	6.7354×10^{-2}	1.4150×10^{-19}	1.4762×10^{-9}	7.0000×10^{-1}	2.0000×10^{-1}	0.0000	1.0000	1.8622×10^{6}
55	3.9083×10^{-2}	1.2320×10^{-20}	2.7248×10^{-9}	7.0000×10^{-1}	2.0000×10^{-1}	0.0000	1.0000	4.3335×10^{6}
56	6.6469×10^{-2}	1.3110×10^{-19}	1.4991×10^{-9}	7.0000×10^{-1}	2.0000×10^{-1}	0.0000	1.0000	1.9120×10^{6}
57	5.3429×10^{-2}	4.2520×10^{-20}	1.9260×10^{-9}	7.0000×10^{-1}	2.0000×10^{-1}	0.0000	1.0000	2.8229×10^{6}
58	5.4958×10^{-2}	4.8520×10^{-20}	1.8655×10^{-9}	7.0000×10^{-1}	2.0000×10^{-1}	0.0000	1.0000	2.6969×10^{6}
59	5.2762×10^{-2}	4.0140×10^{-20}	1.9535×10^{-9}	7.0000×10^{-1}	2.0000×10^{-1}	0.0000	1.0000	2.8797×10^{6}
60	2.9620×10^{-2}	5.4420×10^{-21}	3.6751×10^{-9}	7.0000×10^{-1}	2.0000×10^{-1}	0.0000	1.0000	5.7493×10^{6}
61	4.0430×10^{-2}	1.3840×10^{-20}	2.6256×10^{-9}	7.0000×10^{-1}	2.0000×10^{-1}	0.0000	1.0000	4.1625×10^{6}
62	4.4173×10^{-2}	1.9120×10^{-20}	2.3820×10^{-9}	7.0000×10^{-1}	2.0000×10^{-1}	0.0000	1.0000	3.7221×10^{6}
63	5.9404×10^{-2}	7.1230×10^{-20}	1.7071×10^{-9}	7.0000×10^{-1}	2.0000×10^{-1}	0.0000	1.0000	2.3614×10^{6}
64	3.2463×10^{-2}	6.9560×10^{-21}	3.3314×10^{-9}	7.0000×10^{-1}	2.0000×10^{-1}	0.0000	1.0000	5.2812×10^{6}
65	7.1865×10^{-2}	2.0890×10^{-19}	1.3678×10^{-9}	7.0000×10^{-1}	2.0000×10^{-1}	0.0000	1.0000	1.6274×10^{6}
66	4.5003×10^{-2}	2.0540×10^{-20}	2.3335×10^{-9}	7.0000×10^{-1}	2.0000×10^{-1}	0.0000	1.0000	3.6310×10^{6}
67	3.1590×10^{-2}	6.4510×10^{-21}	3.4304×10^{-9}	7.0000×10^{-1}	2.0000×10^{-1}	0.0000	1.0000	5.4207×10^{6}
68	1.0000×10^{-2}	1.0000×10^{-21}	1.1376×10^{-8}	7.0000×10^{-1}	2.0000×10^{-1}	0.0000	1.0000	1.0332×10^{7}
69	5.1572×10^{-2}	3.6220×10^{-20}	2.0044×10^{-9}	7.0000×10^{-1}	2.0000×10^{-1}	0.0000	1.0000	2.9840×10^{6}
70	3.7917×10^{-2}	1.1140×10^{-20}	2.8162×10^{-9}	7.0000×10^{-1}	2.0000×10^{-1}	0.0000	1.0000	4.4871×10^{6}

Table B-2 1992 BRAGFLO Ranks of Computed Variable Values for SHAFT_SEAL_2

Run No.	Porosity	Permeability	Compressibility	BCEXP	BCBRSAT	BCGSSAT	BCFLG	BCPCT
1	46.	46.	25.	1.	1.	1.	1.	25.
2	25.	25.	46.	1.	1.	1.	1.	46.
3	20.	20.	51.	1.	1.	1.	1.	51.
4	49.	49.	22.	1.	1.	1.	1.	22.
5	15.	15.	56.	1.	1.	1.	1.	56.
6	33.	33.	38.	1.	1.	1.	1.	38.
7	3.	3.	68.	1.	1.	1.	1.	68.
8	13.	13.	58.	1.	1.	1.	1.	58.
9	69.	69.	2.	1.	1.	1.	1.	2.
10	34.	34.	37.	1.	1.	1.	1.	37.
11	51.	51.	20.	1.	1.	1.	1.	20.
12	45.	45.	26.	1.	1.	1.	1.	26.
13	64.	64.	7.	1.	1.	1.	1.	7.
14	52.	52.	19.	1.	1.	1.	1.	19.
15	36.	36.	35.	1.	1.	1.	1.	35.
16	14.	14.	57.	1.	1.	1.	1.	57.
17	47.	47.	24.	1.	1.	1.	1.	24.
18	68.	68.	3.	1.	1.	1.	1.	3.
19	56.	56.	15.	1.	1.	1.	1.	15.
20	2.	2.	69.	1.	1.	1.	1.	69.
21	31.	31.	40.	1.	1.	1.	1.	40.
22	30.	30.	41.	1.	1.	1.	1.	41.
23	37.	37.	34.	1.	1.	1.	1.	34.
24	61.	61.	10.	1.	1.	1.	1.	10.
25	39.	39.	32.	1.	1.	1.	1.	32.
26	22.	22.	49.	1.	1.	1.	1.	49.
27	53.	53.	18.	1.	1.	1.	1.	18.
28	16.	16.	55.	1.	1.	1.	1.	55.
29	62.	62.	9.	1.	1.	1.	1.	9.
30	32.	32.	39.	1.	1.	1.	1.	39.
31	5.	5.	66.	1.	1.	1.	1.	66.
32	29.	29.	42.	1.	1.	1.	1.	42.
33	42.	42.	29.	1.	1.	1.	1.	29.
34	58.	58.	13.	1.	1.	1.	1.	13.
35	6.	6.	65.	1.	1.	1.	1.	65.
36	7.	7.	64.	1.	1.	1.	1.	64.
37	35.	35.	36.	1.	1.	1.	1.	36.
38	23.	23.	48.	1.	1.	1.	1.	48.
39	18.	18.	53.	1.	1.	1.	1.	53.
40	54.	54.	17.	1.	1.	1.	1.	17.
41	55.	55.	16.	1.	1.	1.	1.	16.
42	44.	44.	27.	1.	1.	1.	1.	27.
43	12.	12.	59.	1.	1.	1.	1.	59.
44	65.	65.	6.	1.	1.	1.	1.	6.
45	57.	57.	14.	1.	1.	1.	1.	14.
46	28.	28.	43.	1.	1.	1.	1.	43.
47	66.	66.	5.	1.	1.	1.	1.	5.
48	70.	70.	1.	1.	1.	1.	1.	1.
49	67.	67.	4.	1.	1.	1.	1.	4.
50	4.	4.	67.	1.	1.	1.	1.	67.
51	8.	8.	63.	1.	1.	1.	1.	63.
52	24.	24.	47.	1.	1.	1.	1.	47.

Table B-2 1992 BRAGFLO Ranks of Computed Variable Values for SHAFT_SEAL_2 (Concluded)

Run No.	Porosity	Permeability	Compressibility	BCEXP	BCBRSAT	BCGSSAT	BCFLG	BCPCT
53	48.	48.	23.	1.	1.	1.	1.	23.
54	60.	60.	11.	1.	1.	1.	1.	11.
55	19.	19.	52.	1.	1.	1.	1.	52.
56	59.	59.	12.	1.	1.	1.	1.	12.
57	41.	41.	30.	1.	1.	1.	1.	30.
58	43.	43.	28.	1.	1.	1.	1.	28.
59	40.	40.	31.	1.	1.	1.	1.	31.
60	9.	9.	62.	1.	1.	1.	1.	62.
61	21.	21.	50.	1.	1.	1.	1.	50.
62	26.	26.	45.	1.	1.	1.	1.	45.
63	50.	50.	21.	1.	1.	1.	1.	21.
64	11.	11.	60.	1.	1.	1.	1.	60.
65	63.	63.	8.	1.	1.	1.	1.	8.
66	27.	27.	44.	1.	1.	1.	1.	44.
67	10.	10.	61.	1.	1.	1.	1.	61.
68	1.	1.	70.	1.	1.	1.	1.	70.
69	38.	38.	33.	1.	1.	1.	1.	33.
70	17.	17.	54.	1.	1.	1.	1.	54.

Table B-2 1992 BRAGFLO Computed Variable Values for TRANSITION_ZONE

Run No.	Porosity	Permeability	Compressibility	BCEXP	BCBRSAT	BCGSSAT	BCFLG	BCPCT
1	2.8660×10^{-2}	1.4125×10^{-18}	3.8066×10^{-9}	9.6790	8.7890×10^{-2}	2.3300×10^{-1}	0.0000	8.4002×10^{5}
2	6.9900×10^{-3}	1.6982×10^{-20}	1.6383×10^{-8}	4.9660×10^{-1}	1.4570×10^{-1}	1.2590×10^{-1}	1.0000	3.8780×10^{6}
3	2.8970×10^{-2}	9.1201×10^{-19}	3.7632×10^{-9}	6.7900×10^{-1}	1.8490×10^{-1}	2.1660×10^{-1}	1.0000	9.7730×10^{5}
4	5.6130×10^{-3}	5.0119×10^{-20}	2.0463×10^{-8}	5.1820	1.7260×10^{-1}	1.8900×10^{-1}	1.0000	2.6668×10^{6}
5	2.0560×10^{-2}	1.1482×10^{-20}	5.4048×10^{-9}	4.0710×10^{-1}	1.9880×10^{-1}	1.4590×10^{-1}	1.0000	4.4405×10^{6}
6	1.3750×10^{-2}	1.5136×10^{-20}	8.2055×10^{-9}	6.1420	3.3170×10^{-1}	4.7930×10^{-2}	0.0000	4.0356×10^{6}
7	2.5930×10^{-2}	1.7783×10^{-20}	4.2337×10^{-9}	1.0990	3.5430×10^{-2}	1.6220×10^{-1}	0.0000	3.8167×10^{6}
8	3.1850×10^{-3}	1.8197×10^{-19}	3.6253×10^{-8}	6.4480	3.8660×10^{-1}	2.8520×10^{-2}	1.0000	1.7070×10^{6}
9	2.7270×10^{-2}	1.2303×10^{-20}	4.0134×10^{-9}	4.2610×10^{-1}	3.4080×10^{-1}	1.8690×10^{-1}	1.0000	4.3356×10^{6}
10	9.6770×10^{-3}	5.2481×10^{-18}	1.1764×10^{-8}	1.5170	7.9000×10^{-2}	3.4810×10^{-1}	1.0000	5.3342×10^{5}
11	2.5730×10^{-3}	1.3183×10^{-20}	4.4936×10^{-8}	5.1250×10^{-1}	2.7170×10^{-1}	2.0030×10^{-1}	0.0000	4.2332×10^{6}
12	9.8270×10^{-3}	2.2387×10^{-19}	1.1581×10^{-8}	7.4960	1.4100×10^{-1}	2.8620×10^{-1}	1.0000	1.5889×10^{6}
13	1.6610×10^{-2}	4.8978×10^{-20}	6.7496×10^{-9}	2.2490	3.6500×10^{-1}	2.9370×10^{-1}	1.0000	2.6881×10^{6}
14	1.9600×10^{-2}	1.0000×10^{-20}	5.6818×10^{-9}	3.0620×10^{-1}	8.3660×10^{-3}	1.7360×10^{-1}	1.0000	4.6579×10^{6}
15	1.1590×10^{-3}	2.0893×10^{-20}	1.0006×10^{-7}	4.4620×10^{-1}	2.3100×10^{-1}	3.8350×10^{-1}	0.0000	3.6097×10^{6}
16	5.8700×10^{-3}	5.1286×10^{-19}	1.9556×10^{-8}	5.3590×10^{-1}	3.7890×10^{-1}	2.1720×10^{-1}	1.0000	1.1927×10^{6}
17	2.3950×10^{-2}	5.7544×10^{-20}	4.6044×10^{-9}	5.9190	1.1130×10^{-1}	3.8060×10^{-1}	0.0000	2.5423×10^{6}
18	6.1370×10^{-3}	6.6069×10^{-20}	1.8695×10^{-8}	5.8730×10^{-1}	2.9470×10^{-1}	8.6120×10^{-3}	0.0000	2.4236×10^{6}
19	6.2550×10^{-3}	4.5709×10^{-20}	1.8337×10^{-8}	2.0050	1.1640×10^{-1}	1.6670×10^{-1}	1.0000	2.7531×10^{6}
20	1.7070×10^{-2}	4.4668×10^{-20}	6.5609×10^{-9}	6.7090×10^{-1}	1.2940×10^{-1}	3.2110×10^{-1}	1.0000	2.7752×10^{6}
21	2.3500×10^{-2}	1.1481×10^{-19}	4.6974×10^{-9}	2.2590×10^{-1}	1.9770×10^{-2}	2.2330×10^{-1}	0.0000	2.0018×10^{6}
22	2.6030×10^{-2}	7.4131×10^{-20}	4.2165×10^{-9}	1.4340	2.1830×10^{-1}	1.8710×10^{-2}	1.0000	2.3290×10^{6}
23	2.9920×10^{-2}	3.5481×10^{-20}	3.6358×10^{-9}	7.0990	2.3880×10^{-1}	4.5230×10^{-2}	1.0000	3.0053×10^{6}
24	1.4710×10^{-2}	6.1660×10^{-20}	7.6537×10^{-9}	4.3270×10^{-1}	6.1270×10^{-2}	2.6430×10^{-1}	1.0000	2.4823×10^{6}
25	2.4720×10^{-2}	3.2359×10^{-20}	4.4532×10^{-9}	2.7610	3.0510×10^{-1}	9.9900×10^{-2}	1.0000	3.1026×10^{6}
26	1.8820×10^{-2}	2.3988×10^{-20}	5.9276×10^{-9}	5.2660	2.4700×10^{-1}	6.8060×10^{-2}	1.0000	3.4412×10^{6}
27	2.2740×10^{-3}	2.1878×10^{-20}	5.0877×10^{-8}	8.3330	2.1280×10^{-1}	7.5730×10^{-2}	1.0000	3.5526×10^{6}
28	2.8830×10^{-3}	1.9499×10^{-20}	4.0077×10^{-8}	7.9460	3.4740×10^{-1}	1.5270×10^{-1}	0.0000	3.6970×10^{6}
29	1.2680×10^{-2}	3.0903×10^{-20}	8.9190×10^{-9}	6.0410×10^{-1}	3.3040×10^{-1}	3.5780×10^{-1}	1.0000	3.1525×10^{6}
30	8.7910×10^{-3}	7.4131×10^{-20}	1.2975×10^{-8}	2.0040×10^{-1}	1.4050×10^{-2}	1.5530×10^{-1}	0.0000	2.3290×10^{6}
31	1.7650×10^{-2}	3.2359×10^{-21}	6.3371×10^{-9}	3.3160×10^{-1}	2.1130×10^{-1}	2.4050×10^{-1}	1.0000	6.8822×10^{6}
32	2.0930×10^{-2}	1.0471×10^{-20}	5.3048×10^{-9}	8.8800	3.1430×10^{-1}	3.7550×10^{-1}	1.0000	4.5842×10^{6}
33	6.6640×10^{-3}	4.6774×10^{-19}	1.7196×10^{-8}	5.2200×10^{-1}	1.0530×10^{-1}	3.4190×10^{-1}	1.0000	1.2313×10^{6}
34	9.1030×10^{-3}	1.2303×10^{-20}	1.2522×10^{-8}	8.6520	2.5150×10^{-1}	3.6280×10^{-1}	0.0000	4.3356×10^{6}
35	2.4230×10^{-3}	2.8184×10^{-20}	4.7733×10^{-8}	3.9470×10^{-1}	2.9070×10^{-1}	1.3390×10^{-1}	1.0000	3.2545×10^{6}
36	2.7120×10^{-2}	1.9953×10^{-20}	4.0370×10^{-9}	2.7500×10^{-1}	3.7090×10^{-1}	3.6960×10^{-1}	1.0000	3.6677×10^{6}
37	5.0960×10^{-3}	2.5704×10^{-20}	2.2564×10^{-8}	6.9780	2.2650×10^{-1}	3.0790×10^{-2}	1.0000	3.3599×10^{6}
38	1.8940×10^{-3}	1.5136×10^{-19}	6.1135×10^{-8}	2.9640	1.7810×10^{-1}	3.9620×10^{-1}	1.0000	1.8193×10^{6}
39	1.0090×10^{-2}	5.6234×10^{-20}	1.1273×10^{-8}	2.6060×10^{-1}	1.6330×10^{-1}	3.7240×10^{-2}	1.0000	2.5626×10^{6}
40	2.2760×10^{-2}	2.0893×10^{-19}	4.8582×10^{-9}	2.4160×10^{-1}	2.4340×10^{-1}	1.1100×10^{-1}	1.0000	1.6273×10^{6}
41	1.8020×10^{-2}	3.9811×10^{-19}	6.2019×10^{-9}	5.7490×10^{-1}	1.3340×10^{-1}	1.0650×10^{-1}	1.0000	1.3019×10^{6}
42	2.1990×10^{-2}	2.3442×10^{-21}	5.0371×10^{-9}	5.4840×10^{-1}	3.9640×10^{-1}	3.3500×10^{-1}	0.0000	7.6943×10^{6}
43	5.1790×10^{-3}	2.6915×10^{-19}	2.2199×10^{-8}	4.0000	3.9070×10^{-1}	1.2040×10^{-1}	0.0000	1.4908×10^{6}
44	3.9010×10^{-3}	5.3703×10^{-20}	2.9553×10^{-8}	3.6050×10^{-1}	2.5980×10^{-1}	5.7350×10^{-2}	0.0000	2.6038×10^{6}
45	9.3870×10^{-3}	9.7724×10^{-20}	1.2135×10^{-8}	3.2390×10^{-1}	1.5830×10^{-1}	9.4190×10^{-2}	1.0000	2.1166×10^{6}
46	2.8280×10^{-2}	1.6596×10^{-20}	3.8611×10^{-9}	4.6060×10^{-1}	6.5170×10^{-2}	2.3880×10^{-1}	1.0000	3.9090×10^{6}
47	6.5700×10^{-3}	9.1201×10^{-20}	1.7446×10^{-8}	3.4760	3.1780×10^{-1}	2.6060×10^{-1}	1.0000	2.1678×10^{6}
48	2.2390×10^{-2}	1.4125×10^{-20}	4.9426×10^{-9}	7.7080	4.5510×10^{-2}	2.0750×10^{-1}	0.0000	4.1332×10^{6}
49	1.6820×10^{-3}	6.9183×10^{-19}	6.8872×10^{-8}	3.7530×10^{-1}	5.0110×10^{-2}	6.9900×10^{-2}	1.0000	1.0753×10^{6}
50	1.2890×10^{-2}	2.4547×10^{-20}	8.7696×10^{-9}	3.5390×10^{-1}	1.8990×10^{-1}	1.9850×10^{-1}	1.0000	3.4139×10^{6}
51	7.8440×10^{-3}	4.0738×10^{-17}	1.4572×10^{-8}	5.6000×10^{-1}	2.3180×10^{-2}	1.1810×10^{-2}	1.0000	2.6250×10^{5}
52	4.7130×10^{-3}	8.7097×10^{-20}	2.4418×10^{-8}	3.2370	1.5040×10^{-1}	3.8860×10^{-1}	0.0000	2.2027×10^{6}

Table B-2 1992 BRAGFLO Computed Variable Values for TRANSITION_ZONE (Concluded)

Run No.	Porosity	Permeability	Compressibility	BCEXP	BCBRSAT	BCGSSAT	BCFLG	BCPCT
53	1.5900×10^{-2}	7.7625×10^{-19}	7.0621×10^{-9}	6.7410	2.8470×10^{-1}	1.8060×10^{-1}	1.0000	1.0334×10^{6}
54	1.4500×10^{-2}	1.4454×10^{-20}	7.7681×10^{-9}	4.7200×10^{-1}	1.6590×10^{-1}	2.7290×10^{-1}	0.0000	4.1004×10^{6}
55	2.0030×10^{-2}	1.0233×10^{-17}	5.5544×10^{-9}	6.5030×10^{-1}	3.2450×10^{-1}	3.0330×10^{-1}	0.0000	4.2338×10^{5}
56	1.1650×10^{-2}	1.0965×10^{-20}	9.7296×10^{-9}	4.8480	9.2770×10^{-2}	5.2210×10^{-2}	0.0000	4.5118×10^{6}
57	4.5630×10^{-3}	5.2481×10^{-21}	2.5229×10^{-8}	9.2110	5.1160×10^{-3}	2.7770×10^{-1}	1.0000	5.8219×10^{6}
58	8.7110×10^{-3}	3.3884×10^{-19}	1.3097×10^{-8}	6.4060×10^{-1}	3.4880×10^{-1}	3.2980×10^{-1}	1.0000	1.3766×10^{6}
59	2.5160×10^{-2}	7.9433×10^{-20}	4.3709×10^{-9}	8.9580	8.5120×10^{-2}	3.1270×10^{-1}	1.0000	2.2740×10^{6}
60	8.2600×10^{-3}	9.5499×10^{-20}	1.3825×10^{-8}	9.8620	7.0380×10^{-2}	8.1940×10^{-2}	1.0000	2.1336×10^{6}
61	7.3840×10^{-3}	4.1687×10^{-20}	1.5495×10^{-8}	8.0490×10^{-1}	2.7910×10^{-1}	1.3890×10^{-1}	1.0000	2.8423×10^{6}
62	1.2250×10^{-2}	5.4954×10^{-19}	9.2408×10^{-9}	2.8630×10^{-1}	3.5990×10^{-1}	2.5120×10^{-1}	1.0000	1.1645×10^{6}
63	4.1090×10^{-3}	9.5499×10^{-17}	2.8045×10^{-8}	3.7540	2.0010×10^{-1}	2.8360×10^{-1}	0.0000	1.9548×10^{5}
64	3.7390×10^{-3}	2.6915×10^{-20}	3.0845×10^{-8}	2.4950	2.9320×10^{-2}	8.7020×10^{-2}	1.0000	3.3068×10^{6}
65	7.4700×10^{-3}	3.7153×10^{-20}	1.5314×10^{-8}	2.5410×10^{-1}	2.6410×10^{-1}	3.5100×10^{-1}	1.0000	2.9578×10^{6}
66	3.5330×10^{-3}	3.9811×10^{-20}	3.2658×10^{-8}	6.9150×10^{-1}	1.2380×10^{-1}	3.1630×10^{-1}	0.0000	2.8879×10^{6}
67	8.1910×10^{-3}	1.3804×10^{-19}	1.3944×10^{-8}	5.5890	5.6350×10^{-2}	2.5370×10^{-1}	0.0000	1.8782×10^{6}
68	1.0760×10^{-2}	6.7608×10^{-20}	1.0555×10^{-8}	4.5200	3.0240×10^{-1}	2.9970×10^{-1}	0.0000	2.4044×10^{6}
69	1.5190×10^{-2}	3.3113×10^{-20}	7.4039×10^{-9}	4.3270	3.7150×10^{-1}	4.8390×10^{-3}	1.0000	3.0780×10^{6}
70	1.4890×10^{-3}	1.3490×10^{-21}	7.7831×10^{-8}	6.2770×10^{-1}	1.0130×10^{-1}	1.1920×10^{-1}	1.0000	9.3155×10^{6}

Table B-2 1992 BRAGFLO Ranks of Computed Variable Values for TRANSITION_ZONE

Run No.	Porosity	Permeability	Compressibility	BCEXP	BCBRSAT	BCGSSAT	BCFLG	BCPCT
1	68.	66.	3.	69.	16.	41.	1.	5.
2	24.	16.	47.	21.	26.	23.	24.	55.
3	69.	65.	2.	34.	33.	38.	24.	6.
4	18.	37.	53.	52.	31.	34.	24.	34.
5	54.	8.	17.	15.	35.	26.	24.	63.
6	42.	14.	29.	56.	59.	9.	1.	57.
7	63.	17.	8.	37.	7.	29.	1.	54.
8	9.	54.	62.	57.	68.	5.	24.	17.
9	66.	9.	5.	16.	60.	33.	24.	61.
10	34.	67.	37.	39.	14.	61.	24.	4.
11	7.	11.	64.	22.	48.	36.	1.	60.
12	35.	56.	36.	61.	25.	51.	24.	15.
13	47.	36.	24.	41.	64.	52.	24.	35.
14	52.	5.	19.	8.	2.	31.	24.	66.
15	1.	20.	70.	18.	41.	68.	1.	51.
16	19.	61.	52.	24.	67.	39.	24.	10.
17	60.	40.	11.	55.	20.	67.	1.	31.
18	20.	42.	51.	28.	52.	2.	1.	29.
19	21.	35.	50.	40.	21.	30.	24.	36.
20	48.	34.	23.	33.	23.	57.	24.	37.
21	59.	51.	12.	2.	4.	40.	1.	20.
22	64.	44.	7.	38.	39.	4.	24.	26.
23	70.	30.	1.	60.	42.	8.	24.	41.
24	44.	41.	27.	17.	11.	47.	24.	30.
25	61.	28.	10.	43.	54.	18.	24.	43.
26	51.	22.	20.	53.	44.	12.	24.	49.
27	5.	21.	66.	64.	38.	14.	24.	50.
28	8.	18.	63.	63.	61.	27.	1.	53.
29	40.	27.	31.	29.	58.	63.	24.	44.
30	31.	44.	40.	1.	3.	28.	1.	26.
31	49.	3.	22.	10.	37.	43.	24.	68.
32	55.	6.	16.	66.	55.	66.	24.	65.
33	23.	60.	48.	23.	19.	60.	24.	11.
34	32.	9.	39.	65.	45.	64.	1.	61.
35	6.	26.	65.	14.	51.	24.	24.	45.
36	65.	19.	6.	6.	65.	65.	24.	52.
37	16.	24.	55.	59.	40.	6.	24.	47.
38	4.	53.	67.	44.	32.	70.	24.	18.
39	36.	39.	35.	5.	29.	7.	24.	32.
40	58.	55.	13.	3.	43.	20.	24.	16.
41	50.	59.	21.	27.	24.	19.	24.	12.
42	56.	2.	15.	25.	70.	59.	1.	69.
43	17.	57.	54.	48.	69.	22.	1.	14.
44	12.	38.	59.	12.	46.	11.	1.	33.
45	33.	50.	38.	9.	28.	17.	24.	21.
46	67.	15.	4.	19.	12.	42.	24.	56.
47	22.	48.	49.	46.	56.	46.	24.	23.
48	57.	12.	14.	62.	8.	37.	1.	59.
49	3.	63.	68.	13.	9.	13.	24.	8.
50	41.	23.	30.	11.	34.	35.	24.	48.
51	27.	69.	44.	26.	5.	3.	24.	2.
52	15.	47.	56.	45.	27.	69.	1.	24.

Table B-2 1992 BRAGFLO Ranks of Computed Variable Values for TRANSITION_ZONE (Concluded)

Run No.	Porosity	Permeability	Compressibility	BCEXP	BCBRSAT	BCGSSAT	BCFLG	BCPCT
53	46.	64.	25.	58.	50.	32.	24.	7.
54	43.	13.	28.	20.	30.	48.	1.	58.
55	53.	68.	18.	32.	57.	54.	1.	3.
56	38.	7.	33.	51.	17.	10.	1.	64.
57	14.	4.	57.	68.	1.	49.	24.	67.
58	30.	58.	41.	31.	62.	58.	24.	13.
59	62.	46.	9.	67.	15.	55.	24.	25.
60	29.	49.	42.	70.	13.	15.	24.	22.
61	25.	33.	46.	36.	49.	25.	24.	38.
62	39.	62.	32.	7.	63.	44.	24.	9.
63	13.	70.	58.	47.	36.	50.	1.	1.
64	11.	25.	60.	42.	6.	16.	24.	46.
65	26.	31.	45.	4.	47.	62.	24.	40.
66	10.	32.	61.	35.	22.	56.	1.	39.
67	28.	52.	43.	54.	10.	45.	1.	19.
68	37.	43.	34.	50.	53.	53.	1.	28.
69	45.	29.	26.	49.	66.	1.	24.	42.
70	2.	1.	69.	30.	18.	21.	24.	70.

Table B-2 1992 BRAGFLO Computed Variable Values for UPPER_SHAFT

Run No.	Porosity	Permeability	Compressibility	BCEXP	BCBRSAT	BCGSSAT	BCFLG	BCPCT
1	5.6433×10^{-2}	2.8110×10^{-19}	1.8102×10^{-9}	7.0000×10^{-1}	2.0000×10^{-1}	0.0000	1.0000	1.4685×10^{6}
2	4.3305×10^{-2}	5.6030×10^{-18}	2.4347×10^{-9}	7.0000×10^{-1}	2.0000×10^{-1}	0.0000	1.0000	5.2148×10^{5}
3	4.0073×10^{-2}	7.1940×10^{-18}	2.6512×10^{-9}	7.0000×10^{-1}	2.0000×10^{-1}	0.0000	1.0000	4.7827×10^{5}
4	5.8422×10^{-2}	5.6960×10^{-19}	1.7400×10^{-9}	7.0000×10^{-1}	2.0000×10^{-1}	0.0000	1.0000	1.1502×10^{6}
5	3.5889×10^{-2}	4.5850×10^{-19}	2.9895×10^{-9}	7.0000×10^{-1}	2.0000×10^{-1}	0.0000	1.0000	1.2398×10^{6}
6	4.8739×10^{-2}	1.6410×10^{-17}	2.1354×10^{-9}	7.0000×10^{-1}	2.0000×10^{-1}	0.0000	1.0000	3.5955×10^{5}
7	1.8565×10^{-2}	4.5900×10^{-17}	6.0125×10^{-9}	7.0000×10^{-1}	2.0000×10^{-1}	0.0000	1.0000	2.5188×10^{5}
8	3.3804×10^{-2}	1.4360×10^{-17}	3.1893×10^{-9}	7.0000×10^{-1}	2.0000×10^{-1}	0.0000	1.0000	3.7654×10^{5}
9	8.2847×10^{-2}	9.5250×10^{-17}	1.1533×10^{-9}	7.0000×10^{-1}	2.0000×10^{-1}	0.0000	1.0000	1.9566×10^{5}
10	4.8961×10^{-2}	1.4640×10^{-16}	2.1246×10^{-9}	7.0000×10^{-1}	2.0000×10^{-1}	0.0000	1.0000	1.6862×10^{5}
11	6.0343×10^{-2}	1.9920×10^{-18}	1.6767×10^{-9}	7.0000×10^{-1}	2.0000×10^{-1}	0.0000	1.0000	7.4582×10^{5}
12	5.5800×10^{-2}	3.9570×10^{-18}	1.8336×10^{-9}	7.0000×10^{-1}	2.0000×10^{-1}	0.0000	1.0000	5.8817×10^{5}
13	7.2964×10^{-2}	2.2680×10^{-19}	1.3434×10^{-9}	7.0000×10^{-1}	2.0000×10^{-1}	0.0000	1.0000	1.5817×10^{6}
14	6.0840×10^{-2}	1.4270×10^{-17}	1.6610×10^{-9}	7.0000×10^{-1}	2.0000×10^{-1}	0.0000	1.0000	3.7736×10^{5}
15	5.0585×10^{-2}	1.0660×10^{-17}	2.0484×10^{-9}	7.0000×10^{-1}	2.0000×10^{-1}	0.0000	1.0000	4.1743×10^{5}
16	3.5074×10^{-2}	1.6750×10^{-18}	3.0648×10^{-9}	7.0000×10^{-1}	2.0000×10^{-1}	0.0000	1.0000	7.9192×10^{5}
17	5.7146×10^{-2}	1.7580×10^{-18}	1.7845×10^{-9}	7.0000×10^{-1}	2.0000×10^{-1}	0.0000	1.0000	7.7877×10^{5}
18	8.2074×10^{-2}	1.6710×10^{-16}	1.1666×10^{-9}	7.0000×10^{-1}	2.0000×10^{-1}	0.0000	1.0000	1.6108×10^{5}
19	6.3721×10^{-2}	1.9530×10^{-17}	1.5746×10^{-9}	7.0000×10^{-1}	2.0000×10^{-1}	0.0000	1.0000	3.3854×10^{5}
20	1.6736×10^{-2}	3.4450×10^{-18}	6.6967×10^{-9}	7.0000×10^{-1}	2.0000×10^{-1}	0.0000	1.0000	6.1705×10^{5}
21	4.7082×10^{-2}	1.1130×10^{-18}	2.2194×10^{-9}	7.0000×10^{-1}	2.0000×10^{-1}	0.0000	1.0000	9.1222×10^{5}
22	4.6655×10^{-2}	1.7830×10^{-17}	2.2420×10^{-9}	7.0000×10^{-1}	2.0000×10^{-1}	0.0000	1.0000	3.4937×10^{5}
23	5.0975×10^{-2}	8.0220×10^{-17}	2.0308×10^{-9}	7.0000×10^{-1}	2.0000×10^{-1}	0.0000	1.0000	2.0764×10^{5}
24	6.8520×10^{-2}	8.1030×10^{-18}	1.4468×10^{-9}	7.0000×10^{-1}	2.0000×10^{-1}	0.0000	1.0000	4.5898×10^{5}
25	5.1999×10^{-2}	6.1670×10^{-18}	1.9859×10^{-9}	7.0000×10^{-1}	2.0000×10^{-1}	0.0000	1.0000	5.0446×10^{5}
26	4.1033×10^{-2}	2.2930×10^{-18}	2.5834×10^{-9}	7.0000×10^{-1}	2.0000×10^{-1}	0.0000	1.0000	7.1038×10^{5}
27	6.1762×10^{-2}	9.1500×10^{-18}	1.6324×10^{-9}	7.0000×10^{-1}	2.0000×10^{-1}	0.0000	1.0000	4.4009×10^{5}
28	3.7132×10^{-2}	1.0160×10^{-18}	2.8811×10^{-9}	7.0000×10^{-1}	2.0000×10^{-1}	0.0000	1.0000	9.4146×10^{5}
29	6.9933×10^{-2}	7.3210×10^{-19}	1.4125×10^{-9}	7.0000×10^{-1}	2.0000×10^{-1}	0.0000	1.0000	1.0545×10^{6}
30	4.7777×10^{-2}	2.1720×10^{-17}	2.1834×10^{-9}	7.0000×10^{-1}	2.0000×10^{-1}	0.0000	1.0000	3.2631×10^{5}
31	2.2998×10^{-2}	1.0000×10^{-15}	4.8054×10^{-9}	7.0000×10^{-1}	2.0000×10^{-1}	0.0000	1.0000	8.6734×10^{4}
32	4.5772×10^{-2}	4.2740×10^{-17}	2.2901×10^{-9}	7.0000×10^{-1}	2.0000×10^{-1}	0.0000	1.0000	2.5818×10^{5}
33	5.3975×10^{-2}	3.6810×10^{-18}	1.9040×10^{-9}	7.0000×10^{-1}	2.0000×10^{-1}	0.0000	1.0000	6.0306×10^{5}
34	6.6056×10^{-2}	1.2150×10^{-17}	1.5101×10^{-9}	7.0000×10^{-1}	2.0000×10^{-1}	0.0000	1.0000	3.9896×10^{5}
35	2.5859×10^{-2}	3.0210×10^{-17}	4.2460×10^{-9}	7.0000×10^{-1}	2.0000×10^{-1}	0.0000	1.0000	2.9111×10^{5}
36	2.7519×10^{-2}	5.8240×10^{-18}	3.9748×10^{-9}	7.0000×10^{-1}	2.0000×10^{-1}	0.0000	1.0000	5.1454×10^{5}
37	4.9770×10^{-2}	8.0100×10^{-19}	2.0860×10^{-9}	7.0000×10^{-1}	2.0000×10^{-1}	0.0000	1.0000	1.0222×10^{6}
38	4.2030×10^{-2}	1.1200×10^{-16}	2.5162×10^{-9}	7.0000×10^{-1}	2.0000×10^{-1}	0.0000	1.0000	1.8499×10^{5}
39	3.8123×10^{-2}	3.8250×10^{-19}	2.7997×10^{-9}	7.0000×10^{-1}	2.0000×10^{-1}	0.0000	1.0000	1.3201×10^{6}
40	6.2212×10^{-2}	4.8060×10^{-17}	1.6188×10^{-9}	7.0000×10^{-1}	2.0000×10^{-1}	0.0000	1.0000	2.4791×10^{5}
41	6.2879×10^{-2}	6.2130×10^{-17}	1.5990×10^{-9}	7.0000×10^{-1}	2.0000×10^{-1}	0.0000	1.0000	2.2683×10^{5}
42	5.5614×10^{-2}	5.3950×10^{-17}	1.8405×10^{-9}	7.0000×10^{-1}	2.0000×10^{-1}	0.0000	1.0000	2.3819×10^{5}
43	3.3383×10^{-2}	4.7020×10^{-18}	3.2327×10^{-9}	7.0000×10^{-1}	2.0000×10^{-1}	0.0000	1.0000	5.5409×10^{5}
44	7.4798×10^{-2}	1.7210×10^{-17}	1.3044×10^{-9}	7.0000×10^{-1}	2.0000×10^{-1}	0.0000	1.0000	3.5368×10^{5}
45	6.5132×10^{-2}	9.7080×10^{-18}	1.5350×10^{-9}	7.0000×10^{-1}	2.0000×10^{-1}	0.0000	1.0000	4.3116×10^{5}
46	4.5591×10^{-2}	2.4720×10^{-17}	2.3001×10^{-9}	7.0000×10^{-1}	2.0000×10^{-1}	0.0000	1.0000	3.1203×10^{5}
47	7.6297×10^{-2}	3.0790×10^{-17}	1.2738×10^{-9}	7.0000×10^{-1}	2.0000×10^{-1}	0.0000	1.0000	2.8920×10^{5}
48	9.0000×10^{-2}	6.8540×10^{-18}	1.0418×10^{-9}	7.0000×10^{-1}	2.0000×10^{-1}	0.0000	1.0000	4.8635×10^{5}
49	7.8712×10^{-2}	1.4730×10^{-18}	1.2271×10^{-9}	7.0000×10^{-1}	2.0000×10^{-1}	0.0000	1.0000	8.2792×10^{5}
50	2.2704×10^{-2}	7.9550×10^{-18}	4.8708×10^{-9}	7.0000×10^{-1}	2.0000×10^{-1}	0.0000	1.0000	4.6192×10^{5}
51	2.8140×10^{-2}	4.1850×10^{-18}	3.8816×10^{-9}	7.0000×10^{-1}	2.0000×10^{-1}	0.0000	1.0000	5.7687×10^{5}
52	4.2389×10^{-2}	5.9300×10^{-16}	2.4928×10^{-9}	7.0000×10^{-1}	2.0000×10^{-1}	0.0000	1.0000	1.0392×10^{5}

Table B-2 1992 BRAGFLO Computed Variable Values for UPPER_SHAFT (Concluded)

Run No.	Porosity	Permeability	Compressibility	BCEXP	BCBRSAT	BCGSSAT	BCFLG	BCPCT
53	5.8188×10^{-2}	2.6650×10^{-17}	1.7480×10^{-9}	7.0000×10^{-1}	2.0000×10^{-1}	0.0000	1.0000	3.0402×10^{5}
54	6.7354×10^{-2}	2.3110×10^{-18}	1.4762×10^{-9}	7.0000×10^{-1}	2.0000×10^{-1}	0.0000	1.0000	7.0846×10^{5}
55	3.9083×10^{-2}	1.1210×10^{-17}	2.7248×10^{-9}	7.0000×10^{-1}	2.0000×10^{-1}	0.0000	1.0000	4.1023×10^{5}
56	6.6469×10^{-2}	1.3450×10^{-18}	1.4991×10^{-9}	7.0000×10^{-1}	2.0000×10^{-1}	0.0000	1.0000	8.5438×10^{5}
57	5.3429×10^{-2}	1.8690×10^{-16}	1.9260×10^{-9}	7.0000×10^{-1}	2.0000×10^{-1}	0.0000	1.0000	1.5496×10^{5}
58	5.4958×10^{-2}	3.5380×10^{-17}	1.8655×10^{-9}	7.0000×10^{-1}	2.0000×10^{-1}	0.0000	1.0000	2.7562×10^{5}
59	5.2762×10^{-2}	1.2070×10^{-19}	1.9535×10^{-9}	7.0000×10^{-1}	2.0000×10^{-1}	0.0000	1.0000	1.9675×10^{6}
60	2.9620×10^{-2}	2.3520×10^{-17}	3.6751×10^{-9}	7.0000×10^{-1}	2.0000×10^{-1}	0.0000	1.0000	3.1745×10^{5}
61	4.0430×10^{-2}	9.2530×10^{-17}	2.6256×10^{-9}	7.0000×10^{-1}	2.0000×10^{-1}	0.0000	1.0000	1.9763×10^{5}
62	4.4173×10^{-2}	5.1730×10^{-18}	2.3820×10^{-9}	7.0000×10^{-1}	2.0000×10^{-1}	0.0000	1.0000	5.3608×10^{5}
63	5.9404×10^{-2}	2.7290×10^{-16}	1.7071×10^{-9}	7.0000×10^{-1}	2.0000×10^{-1}	0.0000	1.0000	1.3594×10^{5}
64	3.2463×10^{-2}	3.8080×10^{-17}	3.3314×10^{-9}	7.0000×10^{-1}	2.0000×10^{-1}	0.0000	1.0000	2.6870×10^{5}
65	7.1865×10^{-2}	1.3080×10^{-17}	1.3678×10^{-9}	7.0000×10^{-1}	2.0000×10^{-1}	0.0000	1.0000	3.8890×10^{5}
66	4.5003×10^{-2}	3.0810×10^{-18}	2.3335×10^{-9}	7.0000×10^{-1}	2.0000×10^{-1}	0.0000	1.0000	6.4136×10^{5}
67	3.1590×10^{-2}	4.1580×10^{-16}	3.4304×10^{-9}	7.0000×10^{-1}	2.0000×10^{-1}	0.0000	1.0000	1.1750×10^{5}
68	1.0000×10^{-2}	2.8300×10^{-18}	1.1376×10^{-8}	7.0000×10^{-1}	2.0000×10^{-1}	0.0000	1.0000	6.6050×10^{5}
69	5.1572×10^{-2}	6.6500×10^{-17}	2.0044×10^{-9}	7.0000×10^{-1}	2.0000×10^{-1}	0.0000	1.0000	2.2156×10^{5}
70	3.7917×10^{-2}	2.6470×10^{-18}	2.8162×10^{-9}	7.0000×10^{-1}	2.0000×10^{-1}	0.0000	1.0000	6.7595×10^{5}

Table B-2 1992 BRAGFLO Ranks of Computed Variable Values for UPPER_SHAFT

Run No.	Porosity	Permeability	Compressibility	BCEXP	BCBRSAT	BCGSSAT	BCFLG	BCPCT
1	46.	3.	25.	1.	1.	1.	1.	68.
2	25.	27.	46.	1.	1.	1.	1.	44.
3	20.	31.	51.	1.	1.	1.	1.	40.
4	49.	6.	22.	1.	1.	1.	1.	65.
5	15.	5.	56.	1.	1.	1.	1.	66.
6	33.	42.	38.	1.	1.	1.	1.	29.
7	3.	55.	68.	1.	1.	1.	1.	16.
8	13.	41.	58.	1.	1.	1.	1.	30.
9	69.	62.	2.	1.	1.	1.	1.	9.
10	34.	64.	37.	1.	1.	1.	1.	7.
11	51.	15.	20.	1.	1.	1.	1.	56.
12	45.	23.	26.	1.	1.	1.	1.	48.
13	64.	2.	7.	1.	1.	1.	1.	69.
14	52.	40.	19.	1.	1.	1.	1.	31.
15	36.	36.	35.	1.	1.	1.	1.	35.
16	14.	13.	57.	1.	1.	1.	1.	58.
17	47.	14.	24.	1.	1.	1.	1.	57.
18	68.	65.	3.	1.	1.	1.	1.	6.
19	56.	45.	15.	1.	1.	1.	1.	26.
20	2.	21.	69.	1.	1.	1.	1.	50.
21	31.	10.	40.	1.	1.	1.	1.	61.
22	30.	44.	41.	1.	1.	1.	1.	27.
23	37.	60.	34.	1.	1.	1.	1.	11.
24	61.	33.	10.	1.	1.	1.	1.	38.
25	39.	29.	32.	1.	1.	1.	1.	42.
26	22.	16.	49.	1.	1.	1.	1.	55.
27	53.	34.	18.	1.	1.	1.	1.	37.
28	16.	9.	55.	1.	1.	1.	1.	62.
29	62.	7.	9.	1.	1.	1.	1.	64.
30	32.	46.	39.	1.	1.	1.	1.	25.
31	5.	70.	66.	1.	1.	1.	1.	1.
32	29.	54.	42.	1.	1.	1.	1.	17.
33	42.	22.	29.	1.	1.	1.	1.	49.
34	58.	38.	13.	1.	1.	1.	1.	33.
35	6.	50.	65.	1.	1.	1.	1.	21.
36	7.	28.	64.	1.	1.	1.	1.	43.
37	35.	8.	36.	1.	1.	1.	1.	63.
38	23.	63.	48.	1.	1.	1.	1.	8.
39	18.	4.	53.	1.	1.	1.	1.	67.
40	54.	56.	17.	1.	1.	1.	1.	15.
41	55.	58.	16.	1.	1.	1.	1.	13.
42	44.	57.	27.	1.	1.	1.	1.	14.
43	12.	25.	59.	1.	1.	1.	1.	46.
44	65.	43.	6.	1.	1.	1.	1.	28.
45	57.	35.	14.	1.	1.	1.	1.	36.
46	28.	48.	43.	1.	1.	1.	1.	23.
47	66.	51.	5.	1.	1.	1.	1.	20.
48	70.	30.	1.	1.	1.	1.	1.	41.
49	67.	12.	4.	1.	1.	1.	1.	59.
50	4.	32.	67.	1.	1.	1.	1.	39.
51	8.	24.	63.	1.	1.	1.	1.	47.
52	24.	69.	47.	1.	1.	1.	1.	2.

Table B-2 1992 BRAGFLO Ranks of Computed Variable Values for UPPER_SHAFT (Concluded)

Run No.	Porosity	Permeability	Compressibility	BCEXP	BCBRSAT	BCGSSAT	BCFLG	BCPCT
53	48.	49.	23.	1.	1.	1.	1.	22.
54	60.	17.	11.	1.	1.	1.	1.	54.
55	19.	37.	52.	1.	1.	1.	1.	34.
56	59.	11.	12.	1.	1.	1.	1.	60.
57	41.	66.	30.	1.	1.	1.	1.	5.
58	43.	52.	28.	1.	1.	1.	1.	19.
59	40.	1.	31.	1.	1.	1.	1.	70.
60	9.	47.	62.	1.	1.	1.	1.	24.
61	21.	61.	50.	1.	1.	1.	1.	10.
62	26.	26.	45.	1.	1.	1.	1.	45.
63	50.	67.	21.	1.	1.	1.	1.	4.
64	11.	53.	60.	1.	1.	1.	1.	18.
65	63.	39.	8.	1.	1.	1.	1.	32.
66	27.	20.	44.	1.	1.	1.	1.	51.
67	10.	68.	61.	1.	1.	1.	1.	3.
68	1.	19.	70.	1.	1.	1.	1.	52.
69	38.	59.	33.	1.	1.	1.	1.	12.
70	17.	18.	54.	1.	1.	1.	1.	53.

DISTRIBUTION

(Send Distribution list changes to M.M. Gruebel, Dept. 6342, Sandia National Laboratories, PO Box 5800, Albuquerque, NM 87185-5800)

Federal Agencies

US Department of Energy (6)
Office of Civilian Radioactive Waste Management
Attn: Deputy Director, RW-2
Associate Director, RW-10/50
Office of Program and Resources Management
Office of Contract Business Management
Director, Analysis and Verification Division, RW-22
Associate Director, RW-30
Office of Systems and Compliance
Associate Director, RW-40
Office of Storage and Transportation
Director, RW-4/5
Office of Strategic Planning and International Programs
Office of External Relations
Forrestal Building
Washington, DC 20585

US Department of Energy
Albuquerque Operations Office
Attn: National Atomic Museum Library
PO Box 5400
Albuquerque, NM 87185

US Department of Energy (2)
Office of Environmental Restoration and Waste Management
Attn: EM-1
C. Frank, EM-50
Washington, DC 20585

US Department of Energy (3)
Office of Environmental Restoration and Waste Management
Attn: M. Frei, EM-34, Trevion II
Director, Waste Management Projects
Washington, DC 20585-0002

US Department of Energy
Office of Environmental Restoration and Waste Management
Attn: J. Lytle, EM-30, Trevion II
Washington, DC 20585-0002

US Department of Energy
Office of Environmental Restoration and Waste Management
Attn: S. Schneider, EM-342, Trevion II
Washington, DC 20585-0002

US Department of Energy (3)
WIPP Task Force
Attn: G.H. Daly
S. Fucigna
B. Bower
12800 Middlebrook Rd., Suite 400
Germantown, MD 20874

US Department of Energy (4)
Office of Environment, Safety and Health
Attn: R.P. Berube, EH-20
C. Borgstrum, EH-25
R. Pelletier, EH-231
K. Taimi, EH-232
Washington, DC 20585

US Department of Energy (6)
WIPP Project Integration Office
Attn: S. Alcorn
W.J. Arthur III
J. Coffey
L.W. Gage
P.J. Higgins
D.A. Olona
PO Box 5400
Albuquerque, NM 87115-5400

US Department of Energy (2)
WIPP Project Integration Satellite Office
Attn: R. Batra
R. Becker
PO Box 3090, Mail Stop 525
Carlsbad, NM 88221-3090

US Department of Energy (10)
WIPP Project Site Office (Carlsbad)
Attn: A. Hunt (4)
V. Daub (4)
J. Lippis
K. Hunter
PO Box 3090
Carlsbad, NM 88221-3090

US Department of Energy
Research & Waste Management Division
Attn: Director
PO Box E
Oak Ridge, TN 37831

US Department of Energy (2)
Idaho Operations Office
Fuel Processing and Waste
Management Division
785 DOE Place
Idaho Falls, ID 83402

US Department of Energy
Savannah River Operations Office
Defense Waste Processing
Facility Project Office
Attn: W.D. Pearson
PO Box A
Aiken, SC 29802

US Department of Energy (2)
Richland Operations Office
Nuclear Fuel Cycle & Production
Division
Attn: R.E. Gerton
825 Jadwin Ave.
PO Box 500
Richland, WA 99352

US Department of Energy
Office of Geologic Disposal
Yucca Mountain Project Office
Attn: Associate Director, RW-20
PO Box 98608
Las Vegas, NV 89193-8608

US Department of Energy (3)
Nevada Operations Office
Attn: J.R. Boland
D. Livingston
P.K. Fitzsimmons
2753 S. Highland Drive
Las Vegas, NV 89183-8518

US Department of Energy (2)
Technical Information Center
PO Box 62
Oak Ridge, TN 37831

US Department of Energy
Los Alamos Area Office
528 35th Street
Los Alamos, NM 87544

US Department of Energy (2)
Chicago Operations Office
Attn: J.C. Haugen
9800 South Cass Avenue
Argonne, IL 60439

US Department of Energy (3)
Rocky Flats Area Office
Attn: W.C. Rask
G. Huffman
T. Lukow
PO Box 928
Golden, CO 80402-0928

US Department of Energy
Dayton Area Office
Attn: R. Grandfield
PO Box 66
Miamisburg, OH 45343-0066

US Department of Energy
Attn: E. Young
Room E-178
GAO/RCED/GTN
Washington, DC 20545

US Bureau of Land Management
Carlsbad Office
101 E. Mermod
Carlsbad, NM 88220

US Bureau of Land Management
New Mexico State Office
PO Box 1449
Santa Fe, NM 87507

US Environmental Protection
Agency (2)
Radiation Protection Programs
Attn: M. Oge
ANR-460
Washington, DC 20460

US Environmental Protection
Agency, Region 6
Attn: C. Byrum, 6T-ET
1445 Ross Ave.
Dallas, TX 75202

US Geological Survey (2)
Water Resources Division
Attn: C. Peters
4501 Indian School NE
Suite 200
Albuquerque, NM 87110

US Nuclear Regulatory Commission
Division of Waste Management
Attn: H. Marson
Mail Stop 4-H-3
Washington, DC 20555

US Nuclear Regulatory Commission (4)
Advisory Committee on Nuclear Waste
Attn: D. Moeller
M.J. Steindler
P.W. Pomeroy
W.J. Hinze
7920 Norfolk Ave.
Bethesda, MD 20814

Defense Nuclear Facilities Safety Board
Attn: D. Winters
625 Indiana Ave. NW
Suite 700
Washington, DC 20004

Nuclear Waste Technical Review Board
Attn: Library (2)
1100 Wilson Blvd.
Suite 910
Arlington, VA 22209-2297

Energy and Science Division
Office of Management and Budget
Attn: K. Yuracko
725 17th Street NW
Washington, DC 20503

State Agencies

New Mexico Bureau of Mines
and Mineral Resources
Socorro, NM 87801

New Mexico Energy, Minerals and Natural Resources Department
Attn: Librarian
2040 South Pacheco
Santa Fe, NM 87505

New Mexico Energy, Minerals and Natural Resources Department
New Mexico Radioactive Task Force (2)
(Governor's WIPP Task Force)
Attn: A. Lockwood, Chairman
C. Wentz, Policy Analyst
2040 South Pacheco
Santa Fe, NM 87505

Bob Forrest
Mayor, City of Carlsbad
PO Box 1569
Carlsbad, NM 88221

Carlsbad Department of Development
Executive Director
Attn: C. Bernard
PO Box 1090
Carlsbad, NM 88221

New Mexico Environment Department
Secretary of the Environment (3)
Attn: J. Espinosa
PO Box 968
1190 St. Francis Drive
Santa Fe, NM 87503-0968

New Mexico Environment Department
Attn: P. McCasland
WIPP Project Site Office
PO Box 3090
Carlsbad, NM 88221-3090

New Mexico State Engineer's Office
Attn: M. Chudnoff
PO Box 25102
Santa Fe, NM 87504-5102

Environmental Evaluation Group (5)
Attn: R. Neill
7007 Wyoming Blvd. NE, Suite F-2
Albuquerque, NM 87109

Advisory Committee on Nuclear Facility Safety

John F. Ahearne
Executive Director, Sigma Xi
99 Alexander Drive
Research Triangle Park, NC 27709

James E. Martin
109 Observatory Road
Ann Arbor, MI 48109

WIPP Panel of National Research Council's Board on Radioactive Waste Management

Charles Fairhurst, Chairman
Department of Civil and
Mineral Engineering
University of Minnesota
500 Pillsbury Dr. SE
Minneapolis, MN 55455-0220

John O. Blomeke
3833 Sandy Shore Drive
Lenoir City, TN 37771-9803

John D. Bredehoeft
Western Region Hydrologist
Water Resources Division
US Geological Survey (M/S 439)
345 Middlefield Road
Menlo Park, CA 94025

Rodney C. Ewing
Department of Geology
University of New Mexico
Albuquerque, NM 87131

B. John Garrick
PLG, Inc.
4590 MacArthur Blvd.
Suite 400
Newport Beach, CA 92660-2027

Leonard F. Konikow
US Geological Survey
431 National Center
Reston, VA 22092

Jeremiah O'Driscoll
505 Valley Hill Drive
Atlanta, GA 30350

Chris G. Whipple
ICF Kaiser Engineers
1800 Harrison St.
Oakland, CA 94612-3430

National Research Council (3)
Board on Radioactive
Waste Management
RM HA456
Attn: P.B. Myers (2)
G.J. Grube
2101 Constitution Ave.
Washington, DC 20418

Performance Assessment Peer Review Panel

G. Ross Heath
College of Ocean and Fishery
Sciences, HN-15
583 Henderson Hall
University of Washington
Seattle, WA 98195

Thomas H. Pigford
Department of Nuclear Engineering
4159 Etcheverry Hall
University of California
Berkeley, CA 94720

Thomas A. Cotton
JK Research Associates, Inc.
4429 Butterworth Place NW
Washington, DC 20016

Robert J. Budnitz
President, Future Resources
Associates, Inc.
2000 Center Street, Suite 418
Berkeley, CA 94704

C. John Mann
Department of Geology
245 Natural History Bldg.
1301 West Green Street
University of Illinois
Urbana, IL 61801

Frank W. Schwartz
Department of Geology and Mineralogy
The Ohio State University
Scott Hall
1090 Carmack Rd.
Columbus, OH 43210

National Laboratories

Argonne National Laboratory (2)
Attn: A. Smith
D. Tomasko
9700 South Cass, Bldg. 201
Argonne, IL 60439

Battelle Pacific Northwest
Laboratory (2)
Attn: S. Bates
R.E. Westerman
MSIN P8-44
Battelle Boulevard
Richland, WA 99352

Idaho National Engineering
Laboratory (2)
Attn: H. Loo
R. Klinger
Mail Stop 5108
Idaho Falls, ID 83403-4000

Los Alamos National Laboratory (5)
Attn: B. Erdal, CNC-11
M. Ennis, HS-12
Mail Stop J900
S. Kosiewicz, EM-7
Mail Stop J595
L. Soholt, EM-13
Mail Stop M992
J. Wenzel, HS-12
Mail Stop K482
PO Box 1663
Los Alamos, NM 87545

Oak Ridge National Laboratory
Transuranic Waste Manager
Attn: D.W. Turner
Bldg. 3047
PO Box 2008
Oak Ridge, TN 37831-6060

Pacific Northwest Laboratory
Attn: B. Kennedy
PO Box 999
Richland, WA 99352

Westinghouse—Savannah River
Technology Center (4)
Attn: N. Bibler
J.R. Harbour
M.J. Plodinec
G.G. Wicks
Aiken, SC 29802

Corporations/Members of the Public

Battelle Memorial Institute
Attn: R. Root
J. Kircher
505 Marquette NW
Suite 1
Albuquerque, NM 87102

Benchmark Environmental Corp.
Attn: C. Frederickson
4501 Indian School NE
Suite 105
Albuquerque, NM 87110

Beta Corporation Int.
Attn: E. Bonano
6613 Esther NE
Albuquerque, NM 87109

City of Albuquerque
Public Works Department
Utility Planning Division
Attn: W.K. Summers
PO Box 1293
Albuquerque, NM 87103

Deuel and Associates, Inc.
Attn: R.W. Prindle
7208 Jefferson NE
Albuquerque, NM 87109

Disposal Safety, Inc.
Attn: B. Ross
1660 L Street NW, Suite 314
Washington, DC 20036

Ecodynamics (2)
Attn: P. Roache
R. Blaine
PO Box 9229
Albuquerque, NM 87119-9229

EG & G Idaho (3)
1955 Fremont Street
Attn: C. Atwood
C. Hertzler
T.I. Clements
Idaho Falls, ID 83415

Geomatrix
Attn: K. Coppersmith
100 Pine St., Suite 1000
San Francisco, CA 94111

Golder Associates, Inc.
Attn: R. Kossik
4104 148th Avenue NE
Redmond, WA 98052

INTERA, Inc.
Attn: A.M. LaVenue
1650 University Blvd. NE, Suite 300
Albuquerque, NM 87102

INTERA, Inc.
Attn: J.F. Pickens
6850 Austin Center Blvd., Suite 300
Austin, TX 78731

INTERA, Inc.
Attn: W. Stensrud
PO Box 2123
Carlsbad, NM 88221

INTERA, Inc.
Attn: W. Nelson
101 Convention Center Drive
Suite 540
Las Vegas, NV 89109

IT Corporation (2)
Attn: R.F. McKinney
J. Myers
Regional Office
Suite 700
5301 Central Avenue NE
Albuquerque, NM 87108

John Hart and Associates, P.A.
Attn: J.S. Hart
2815 Candelaria Road NW
Albuquerque, NM 87107

John Hart and Associates, P.A.
Attn: K. Lickliter
1009 North Washington
Tacoma, WA 98406

MAC Technical Services Co.
Attn: D.K. Duncan
8418 Zuni Road SE
Suite 200
Albuquerque, NM 87108

Newman and Holtzinger
Attn: C. Mallon
1615 L Street NW
Suite 1000
Washington, DC 20036

RE/SPEC, Inc. (2)
Attn: W. Coons
4775 Indian School NE
Suite 300
Albuquerque, NM 87110

RE/SPEC, Inc.
Attn: J.L. Ratigan
PO Box 725
Rapid City, SD 57709

Reynolds Electric and Engineering
Company, Inc.
Attn: E.W. Kendall
Building 790
Warehouse Row
PO Box 98521
Las Vegas, NV 89193-8521

Science Applications International
Corporation (SAIC)
Attn: H.R. Pratt
10260 Campus Point Drive
San Diego, CA 92121

Science Applications International
Corporation (2)
Attn: D.C.Royer
C.G. Pflum
101 Convention Center Dr.
Las Vegas, NV 89109

Science Applications International
Corporation (3)
Attn: M. Davis
R. Guzowski
J. Tollison
2109 Air Park Road SE
Albuquerque, NM 87106

Science Applications International
Corporation (2)
Attn: J. Young
D. Lester
18706 North Creek Parkway, Suite 110
Bothell, WA 98011

Southwest Research Institute
Center for Nuclear Waste Regulatory
Analysis (2)
Attn: P.K. Nair
6220 Culebra Road
San Antonio, TX 78228-0510

Systems, Science, and Software (2)
Attn: E. Peterson
P. Lagus
Box 1620
La Jolla, CA 92038

TASC
Attn: S.G. Oston
55 Walkers Brook Drive
Reading, MA 01867

Tech Reps, Inc. (7)
Attn: J. Chapman
C. Crawford
D. Marchand
T. Peterson
J. Stikar
D. Scott
F. Puffer
5000 Marble NE, Suite 222
Albuquerque, NM 87110

Tolan, Beeson & Associates
Attn: T.L. Tolan
2320 W. 15th Avenue
Kennewick, WA 99337

TRW Environmental Safety Systems (2)
Attn: I. Sacks, Suite 800
L. Wildman, Suite 1300
2650 Park Tower Drive
Vienna, VA 22180-7306

Sanford Cohen and Associates
Attn: J. Channell
7101 Carriage Rd NE
Albuquerque, NM 87109

Westinghouse Electric Corporation (5)
Attn: Library
C. Cox
L. Fitch
B.A. Howard
R.F. Kehrman
PO Box 2078
Carlsbad, NM 88221

Westinghouse Hanford Company
Attn: D.E. Wood, MSIN HO-32
PO Box 1970
Richland, WA 99352

Western Water Consultants
Attn: P.A. Rechard
PO Box 4128
Laramie, WY 82071

Western Water Consultants
Attn: D. Fritz
1949 Sugarland Drive #134
Sheridan, WY 82801-5720

P. Drez
8816 Cherry Hills Road NE
Albuquerque, NM 87111

David Lechel
9600 Allende Rd. NE
Albuquerque, NM 87109

C.A. Marchese
PO Box 21790
Albuquerque, NM 87154

Arend Meijer
3821 Anderson SE
Albuquerque, NM 87108

D.W. Powers
Star Route Box 87
Anthony, TX 79821

Shirley Thieda
PO Box 2109, RR1
Bernalillo, NM 87004

Jack Urich
c/o CARD
144 Harvard SE
Albuquerque, NM 87106

Universities

University of California
Mechanical, Aerospace, and
Nuclear Engineering Department (2)
Attn: W. Kastenberg
D. Browne
5532 Boelter Hall
Los Angeles, CA 90024

University of California
Engineering and Applied Science Attn:
D. Okrent
48-121A Engineering IV
Los Angeles, CA 90024-1597

University of California
Mine Engineering Department
Rock Mechanics Engineering
Attn: N. Cook
Berkeley, CA 94720

University of Hawaii at Hilo
Business Administration
Attn: S. Hora
Hilo, HI 96720-4091

University of New Mexico
Geology Department
Attn: Library
Albuquerque, NM 87131

University of New Mexico
Research Administration
Attn: H. Schreyer
102 Scholes Hall
Albuquerque, NM 87131

University of Wyoming
Department of Civil Engineering
Attn: V.R. Hasfurther
Laramie, WY 82071

University of Wyoming
Department of Geology
Attn: J.I. Drever
Laramie, WY 82071

University of Wyoming
Department of Mathematics
Attn: R.E. Ewing
Laramie, WY 82071

Libraries

Thomas Brannigan Library
Attn: D. Dresp
106 W. Hadley St.
Las Cruces, NM 88001

New Mexico State Library
Attn: N. McCallan
325 Don Gaspar
Santa Fe, NM 87503

New Mexico Tech
Martin Speere Memorial Library
Campus Street
Socorro, NM 87810

New Mexico Junior College
Pannell Library
Attn: R. Hill
Lovington Highway
Hobbs, NM 88240

Carlsbad Municipal Library
WIPP Public Reading Room
Attn: L. Hubbard
101 S. Halagueno St.
Carlsbad, NM 88220

University of New Mexico
Zimmerman Library
Government Publications Department
Albuquerque, NM 87131

NEA/Performance Assessment Advisory Group (PAAG)

P. Duerden
ANSTO
Lucas Heights Research Laboratories
Private Mail Bag No. 1
Menai, NSW 2234
AUSTRALIA

Gordon S. Linsley
Division of Nuclear Fuel Cycle and Waste Management
International Atomic Energy Agency
PO Box 100
A-1400 Vienna, AUSTRIA

Nicolo Cadelli
Commission of the European Communities
200, Rue de la Loi
B-1049 Brussels, BELGIUM

R. Heremans
Organisme Nationale des Déchets Radioactifs et des Matiéres Fissiles (ONDRAF)
Place Madou 1, Boitec 24/25
B-1030 Brussels, BELGIUM

J. Marivoet
Centre d'Etudes de l'Energie Nucléaire (CEN/SCK)
Boeretang 200
B-2400 Mol, BELGIUM

P. Conlon
Waste Management Division
Atomic Energy Control Board (AECB)
PO Box 1046
Ottawa, Ontario KIP 559, CANADA

A.G. Wikjord
Manager, Environmental and Safety Assessment Branch
Atomic Energy of Canada Limited
Whiteshell Research Establishment
Pinewa, Manitoba ROE 1LO
CANADA

Teollisuuden Voima Oy (TVO) (2)
Attn: Timo Äikäs
Jukka-Pekka Salo
Annankatu 42 C
SF-00100 Helsinki Suomi
FINLAND

Timo Vieno
Technical Research Centre of Finland (VTT)
Nuclear Energy Laboratory
PO Box 208
SF-02151 Espoo, FINLAND

Division de la Sécurité et de la
Protection de l'Environment (DSPE)
Commissariat á l'Energie Atomique
Agence Nationale pour la Gestion des
Déchets Radioactifs (ANDRA) (2)
Attn: Gérald Ouzounian
M. Claude Ringeard
Route du Panorama Robert Schuman
B. P. No. 38
F-92266 Fontenay-aux-Roses Cedex
FRANCE

Claudio Pescatore
Division of Radiation Protection and
Waste Management
OECD Nuclear Energy Agency
38, Boulevard Suchet
F-75016 Paris, FRANCE

M. Dominique Greneche
Commissariat á l'Energie Atomique
IPSN/DAS/SASICC/SAED
B.P. No. 6
F-92265 Fontenay-aux-Roses Cedex
FRANCE

Robert Fabriol
Bureau de Recherches Géologiques et
Miniéres (BRGM)
B.P. 6009
45060 Orléans Cedex 2, FRANCE

P. Bogorinski
Gesellschaft für Reaktorsicherheit
(GRS) MBH
Schwertnergasse 1
D-5000 Köln 1, GERMANY

R. Storck
GSF - Institut für Tieflagerung
Theodor-Heuss-Strabe 4
D-3300 Braunschweig, GERMANY

Ferrucio Gera
ISMES S.p.A
Via del Crociferi 44
I-00187 Rome, ITALY

Hiroyuki Umeki
Isolation System Research Program
Radioactive Waste Management Project
Power Reactor and Nuclear Fuel
Development Corporation (PNC)
1-9-13, Akasaka, Minato-ku
Tokyo 107, JAPAN

P. Carboneras Martinez
ENRESA
Calle Emilio Vargas, 7
R-28043 Madrid
SPAIN

Tönis Papp
Swedish Nuclear Fuel and Waste
Management Co.
Box 5864
S 102 48 Stockholm
SWEDEN

Conny Hägg
Swedish Radiation Protection
Institute (SSI)
Box 60204
S-104 01 Stockholm
SWEDEN

J. Hadermann
Paul Scherrer Institute
Waste Management Programme
CH-5232 Villigen PSI
SWITZERLAND

J. Vigfusson
HSK-Swiss Nuclear Safety Inspectorate
Federal Office of Energy
CH-5232 Villigen-HSK
SWITZERLAND

D.E. Billington
Departmental Manager—Assessment
Studies
Radwaste Disposal R&D Division
AEA Decommissioning & Radwaste
Harwell Laboratory, B60
Didcot Oxfordshire OX11 ORA
UNITED KINGDOM

P. Grimwood
Waste Management Unit
BNFL
Sellafield
Seascale, Cumbria CA20 1PG
UNITED KINGDOM

Alan J. Hooper
UK Nirex Ltd
Curie Avenue
Harwell, Didcot
Oxfordshire, OX11 ORH
UNITED KINGDOM

Jerry M. Boak
Yucca Mountain Project Office
US Department of Energy
PO Box 98608
Las Vegas, NV 89193

Seth M. Coplan (Chairman)
US Nuclear Regulatory Commission
Division of High-Level Waste Management
Mail Stop 4-H-3
Washington, DC 20555

A.E. Van Luik
INTERA/M&O
The Valley Bank Center
101 Convention Center Dr.
Las Vegas, NV 89109

NEA/Probabilistic System Assessment Group (PSAG)

Shaheed Hossain
Division of Nuclear Fuel Cycle and Waste Management
International Atomic Energy Agency
Wagramerstrasse 5
PO Box 100
A-1400 Vienna, AUSTRIA

Alexander Nies (PSAC Chairman)
Gesellschaft für Strahlen- und Institut für Tieflagerung
Abteilung für Endlagersicherheit
Theodor-Heuss-Strasse 4
D-3300 Braunschweig, GERMANY

Eduard Hofer
Gesellschaft für Reaktorsicherheit (GRS) MBH
Forschungsgelände
D-8046 Garching, GERMANY

Andrea Saltelli
Commission of the European Communities
Joint Resarch Centre of Ispra
I-21020 Ispra (Varese)
ITALY

Alejandro Alonso
Cátedra de Tecnología Nuclear
E.T.S. de Ingenieros Industriales
José Gutiérrez Abascal, 2
E-28006 Madrid, SPAIN

ENRESA (2)
Attn: M. A. Cuñado
F. J. Elorza
Calle Emilio Vargas, 7
E-28043 Madrid, SPAIN

Pedro Prado
CIEMAT
Instituto de Tecnología Nuclear
Avenida Complutense, 22
E-28040 Madrid, SPAIN

Nils A. Kjellbert
Swedish Nuclear Fuel and Waste Management Company (SKB)
Box 5864
S-102 48 Stockholm, SWEDEN

Björn Cronhjort
Royal Institute of Technology
Automatic Control
S-100 44 Stockholm, SWEDEN

Richard A. Klos
Paul-Scherrer Institute (PSI)
CH-5232 Villingen PSI, SWITZERLAND

Nationale Genossenschaft für die Lagerung Radioaktiver Abfälle (2)
Attn: C. McCombie
F. Van Dorp
Hardstrasse 73
CH-5430 Wettingen, SWITZERLAND

N. A. Chapman
Intera Information Technologies
Park View House
14B Burton Street
Melton Mowbray
Leicestershire LE13 1AE
UNITED KINGDOM

Daniel A. Galson
Galson Sciences Ltd.
35, Market Place
Oakham
Leicestershire LE15 6DT
UNITED KINGDOM

David P. Hodgkinson
Intera Information Technologies
45 Station Road, Chiltern House
Henley-on-Thames
Oxfordshire RG9 1AT
UNITED KINGDOM

Brian G.J. Thompson
Department of the Environment: Her Majesty's Inspectorate of Pollution
Room A5.33, Romney House
43 Marsham Street
London SW1P 2PY
UNITED KINGDOM

Intera Information Technologies
Attn: M.J.Apted
3609 South Wadsworth Blvd.
Denver, CO 80235

US Nuclear Regulatory Commission (2)
Attn: R. Codell
N. Eisenberg
Mail Stop 4-H-3
Washington, DC 20555

Battelle Pacific Northwest Laboratories
Attn: P.W. Eslinger
MS K2-32
PO Box 999
Richland, WA 99352

Center for Nuclear Waste Regulatory Analysis (CNWRA)
Southwest Research Institute
Attn: B. Sagar
PO Drawer 28510
6220 Culebra Road
San Antonio, TX 78284

Geostatistics Expert Working Group (GXG)

Rafael L. Bras
R.L. Bras Consulting Engineers
44 Percy Road
Lexington, MA 02173

Jesus Carrera
Universidad Politécnica de Cataluña
E.T.S.I. Caminos
Jordi, Girona 31
E-08034 Barcelona
SPAIN

Gedeon Dagan
Department of Fluid Mechanics and Heat Transfer
Tel Aviv University
PO Box 39040
Ramat Aviv, Tel Aviv 69978
ISRAEL

Ghislain de Marsily (GXG Chairman)
University Pierre et Marie Curie
Laboratorie de Geologie Applique
4, Place Jussieu
T.26 - 5^{e} etage
75252 Paris Cedex 05, FRANCE

Alain Galli
Centre de Geostatistique
Ecole des Mines de Paris
35 Rue St. Honore
77035 Fontainebleau, FRANCE

Christian Ravenne
Geology and Geochemistry Division
Institut Francais du Pétrole
1 & 4, Av. de Bois-Préau B.P. 311
92506 Rueil Malmaison Cedex
FRANCE

Peter Grindrod
INTERA Information Technologies Ltd.
Chiltern House
45 Station Road
Henley-on-Thames
Oxfordshire, RG9 1AT, UNITED KINGDOM

Alan Gutjahr
Department of Mathematics
New Mexico Institute of Mining and Technology
Socorro, NM 87801

C. Peter Jackson
Harwell Laboratory
Theoretical Studies Department
Radwaste Disposal Division
Bldg. 424.4
Oxfordshire Didcot Oxon OX11 ORA
UNITED KINDGOM

Rae Mackay
Department of Civil Engineering
University of Newcastle Upon Tyne
Newcastle Upon Tyne NE1 7RU
UNITED KINGDOM

Steve Gorelick
Department of Applied Earth Sciences
Stanford University
Stanford, CA 94305-2225

Peter Kitanidis
60 Peter Coutts Circle
Stanford, CA 94305

Dennis McLaughlin
Parsons Laboratory
Room 48-209
Department of Civil Engineering
Massachusetts Institute of Technology
Cambridge, MA 02139

Shlomo P. Neuman
College of Engineering and Mines
Department of Hydrology and Water Resources
University of Arizona
Tucson, AZ 85721

Yoram Rubin
Department of Civil Engineering
University of California
Berkeley, CA 94720

Foreign Addresses

Studiecentrum Voor Kernenergie
Centre D'Energie Nucleaire
Attn: A. Bonne
SCK/CEN
Boeretang 200
B-2400 Mol
BELGIUM

Atomic Energy of Canada, Ltd. (3)
Whiteshell Research Establishment
Attn: M.E. Stevens
B.W. Goodwin
D. Wushke
Pinewa, Manitoba ROE 1LO, CANADA

Juhani Vira
Teollisuuden Voima Oy (TVO)
Annankatu 42 C
SF-00100 Helsinki Suomi
FINLAND

Jean-Pierre Olivier
OECD Nuclear Energy Agency (2)
38, Boulevard Suchet
F-75016 Paris
FRANCE

D. Alexandre, Deputy Director
ANDRA
31 Rue de la Federation
75015 Paris
FRANCE

Claude Sombret
Centre D'Etudes Nucleaires
De La Vallee Rhone
CEN/VALRHO
S.D.H.A. B.P. 171
30205 Bagnols-Sur-Ceze, FRANCE

Bundesministerium fur Forschung und Technologie
Postfach 200 706
5300 Bonn 2, GERMANY

Bundesanstalt fur Geowissenschaften und Rohstoffe
Attn: M. Langer
Postfach 510 153
3000 Hanover 51, GERMANY

Gesellschaft fur Reaktorsicherheit (GRS) (2)
Attn: B. Baltes
W. Muller
Schwertnergasse 1
D-5000 Cologne, GERMANY

Institut fur Tieflagerung (2)
Attn: K. Kuhn
Theodor-Heuss-Strasse 4
D-3300 Braunschweig, GERMANY

Physikalisch-Technische Bundesanstalt
Attn: P. Brenneke
Postfach 33 45
D-3300 Braunschweig, GERMANY

Shingo Tashiro
Japan Atomic Energy Research Institute
Tokai-Mura, Ibaraki-Ken
319-11, JAPAN

Netherlands Energy Research Foundation (ECN)
Attn: L.H. Vons
3 Westerduinweg
PO Box 1
1755 ZG Petten, THE NETHERLANDS

Johan Andersson
Swedish Nuclear Power Inspectorate
Statens Kärnkraftinspektion (SKI)
Box 27106
S-102 52 Stockholm, SWEDEN

Fred Karlsson
Svensk Karnbransleforsorjning
AB SKB
Box 5864
S-102 48 Stockholm, SWEDEN

Nationale Genossenschaft für die
Lagerung Radioaktiver Abfälle (2)
Attn: S. Vomvoris
P. Zuidema
Hardstrasse 73
CH-5430 Wettingen, SWITZERLAND

AEA Technology
Attn: J.H. Rees
D5W/29 Culham Laboratory
Abington
Oxfordshire OX14 3DB, UNITED KINGDOM

AEA Technology
Attn: W.R. Rodwell
044/A31 Winfrith Technical Centre
Dorchester
Dorset DT2 8DH, UNITED KINGDOM

AEA Technology
Attn: J.E. Tinson
B4244 Harwell Laboratory
Didcot, Oxfordshire OX11 ORA
UNITED KINGDOM

D.R. Knowles
British Nuclear Fuels, plc
Risley, Warrington
Cheshire WA3 6AS, 1002607
UNITED KINGDOM

Internal

1 A. Narath
20 O.E. Jones
1502 J.C. Cummings
1511 D.K. Gartling
6000 D.L. Hartley
6115 P.B. Davies
6115 R.L. Beauheim
6119 E.D. Gorham
6119 Staff (14)
6121 J.R. Tillerson
6121 Staff (7)
6233 J.C. Eichelberger
6300 D.E. Ellis
6302 L.E. Shephard
6303 S.Y. Pickering
6303 W.D. Weart
6305 S.A. Goldstein
6305 A.R. Lappin
6306 A.L. Stevens
6312 F.W. Bingham
6313 L.S. Costin
6331 P.A. Davis
6341 Sandia WIPP Central Files (100)
6342 D.R. Anderson
6342 Staff (30)
6343 V. Harper-Slaboszewicz
6343 Staff (3)
6345 R.C. Lincoln
6345 Staff (9)
6347 D.R. Schafer
6348 J.T. Holmes
6348 Staff (4)
6351 R.E. Thompson
6352 D.P. Garber
6352 S.E. Sharpton
6400 N.R. Ortiz
6613 R.M. Cranwell
6613 R.L. Iman
6613 C. Leigh
6622 M.S.Y. Chu
6641 R.E. Luna, Acting
7141 Technical Library (5)
7151 Technical Publications
7613-2 Document Processing for
DOE/OSTI (10)
8523-2 Central Technical Files

☆ U.S. GOVERNMENT PRINTING OFFICE 1993—774-122/80241

Revised: 17 AUG 93

THIS PAGE INTENTIONALLY LEFT BLANK